PERGAMON

Phytochemistry 57 (2001) 1–5

PHYTOCHEMISTRY

www.elsevier.com/locate/phytochem

A serine endopeptidase from the fruits of *Melothria japonica* (Thunb.) Maxim.

Tetsuya Uchikoba [a,*], Saburo Hosoyamada [b], Michio Onjyo [c], Kazunari Arima [a], Hiroo Yonezawa [a], Makoto Kaneda [a]

[a] *Department of Chemistry, Faculty of Science, Kagoshima University, Korimoto, Kagoshima, Kagoshima 890-0065, Japan*
[b] *Terayama Natural Education Institute, Faculty of Education, Kagoshima University, Korimoto 1-20-6, Kagoshima 890-0065, Japan*
[c] *Ibusuki Experimental Botanical Garden, Faculty of Agriculture, Kagoshima University, 1291 Ju-cho, Ibusuki, 891-0402, Japan*

Received 22 August 2000; received in revised form 1 December 2000

Abstract

An endopeptidase from the fruits of *Melothria japonica* (Thunb.) Maxim. has been purified by DEAE-Sepharose chromatography and gel-filtration by a Sephacryl S-300. The enzyme has M_r of 61 kDa. The optimum pH of the enzyme was 8. The enzyme activity was inhibited by diisopropyl fluorophosphate and phenylmethanesulfonylfluoride, but not by EDTA. Casein was a poor substrate, but angiotensin I was cleaved by the enzyme within 30 min at four different sites. These results indicated that the enzyme was a serine oligopeptidase of broad substrate specificity. © 2001 Elsevier Science Ltd. All rights reserved.

Keywords: *Melothria japonica*; Cucurbitaceae; Fruits; Oligopeptidase; Plant peptidase

1. Introduction

Several fruits of the Cucurbitaceae species have large amounts of proteolytic enzymes within them. Among them, cucumisin [EC.3.4.21.25], a serine protease from the fruit of prince melons, has been well characterized (Kaneda and Tominaga, 1975; Yamagata et al., 1994; Uchikoba et al., 1995). Screening for proteolytic activity revealed that various fruits of the Cucurbitaceae had this activity in their juice, but as of yet there is no way of knowing whether or not the proteases are identical in content and specific activity.

Proteases having strong caseinolytic activity have been found in the fruits of Cucurbitaceae (Uchikoba et al., 1995; Arima et al., 2000); however, oligopeptidases from fruits of the Cucurbitaceae are unknown.

Here, we report that the peptidyl-*p*NA, Glt-Ala-Ala-Pro-Leu-*p*NA is hydrolyzed by the juice from the fruits of *Melothria japonica* (Thunb.) Maxim., called suzumeuri in Japan. However, the caseinolytic activity of the juice from the fruits was insignificant. The isolation of the general properties of the new peptidase from the fruits of *Melothria japonica* are described.

2. Results and discussion

The elution profile of the enzyme, using Glt-Ala-Ala-Pro-Leu-*p*NA as substrate, from a DEAE-Sepharose column is shown in Fig. 1. We term this activity *Melothria* peptidase. The fractions containing *Melthoria* peptidase were collected and then the enzyme was further purified by gel filtration of a Sephacryl S-300. From 100 g of the fruits of *Melthoria japonica*, 3.2 mg of the purified enzyme was obtained in a final yield of 11% (Table 1). The final preparation shown as a single band on the SDS-PAGE, having a M_r of 61 kDa (Fig. 2A), and the hydrolysis activity of Glt-Ala-Ala-Pro-Leu-*p*NA by the enzyme in the gel was detected at the same position as the band of purified *Melthoria* peptidase on SDS-PAGE (Fig. 2B).

Abbreviations: Boc, *t*-butyloxycarbonyl; Bz, benzoyl; DFP, diisopropyl fluorophosphate; Glt, glutaryl; MCA, 4-methy-coumaryl-7-amide; MIA, monoiodoacetic acid; PCMPS, *p*-chloromercuriphenylsulfonic acid; PMSF, phenylmethanesulfonylfluoride; *p*NA, *p*-nitroanilide; Pyr, pyroglutamyl-; SDS-PAGE, sodium dodecylsulfate polyacrylamide gel electrophoresis; STI, soybean trypsin inhibitor; Tos-Lys-CH_2Cl, *N*-Tosyl-L-lysine chloromethylketone

* Corresponding author. Fax: +81-99-285-8117.
E-mail address: uchik@sci.kagoshima-u.ac.jp (T. Uchikoba).

0031-9422/01/$ - see front matter © 2001 Elsevier Science Ltd. All rights reserved.
PII: S0031-9422(00)00511-2

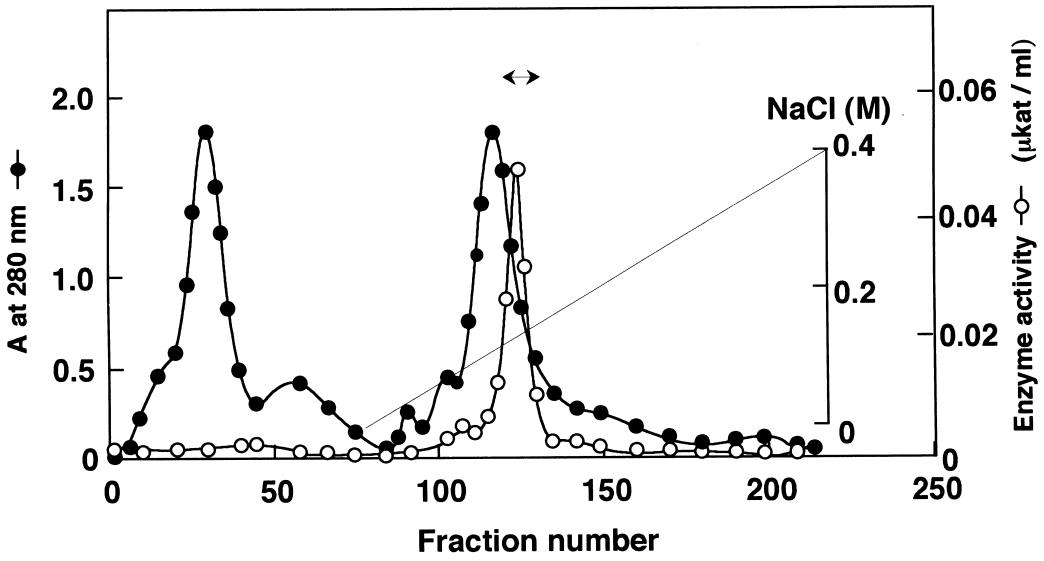

Fig. 1. Elution profile of *Melothria* peptidase from DEAE-Sepharose. Protein (*A* 280 nm) (closed circles), hydrolytic activity of Glt-Ala-Ala-Pro-Leu-*p*NA (open circles). The flow rate of the column was 72 ml/h and the fraction size is 8 ml. Double headed arrow shows fractions which were pooled.

Table 1
Purification of *Melothria* peptidase[a]

Purification step	Total protein (mg)	Total activity (μkat)	Specific activity (nkat/mg)	Recovery (%)	Purity (fold)
Juice	1130	5.62	4.98	100	1
DEAE-Sepharose	46	5.00	109	89	22
SephacrylS-300	3.2	0.594	186	11	37

[a] Peptidase was purified from 100 g of *Melothria japonica* fruits.

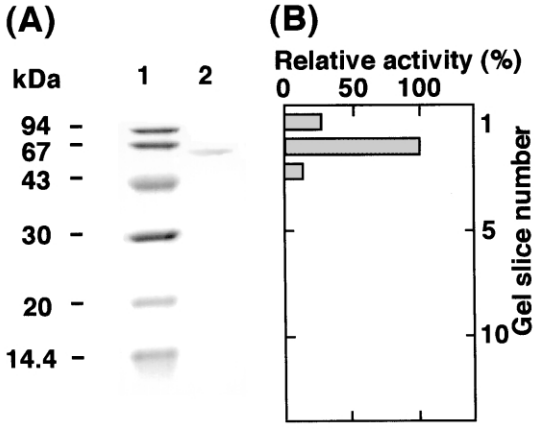

Fig. 2. SDS-PAGE and the activity assay in the gel of purified *Melothria* peptidase. (A) SDS-PAGE analysis. To avoid autolysis, the purified enzyme was inactivated by a treatment of 10 mM DFP. The iinactivated enzyme was subjected to a SDS-PAGE using the method of Laemmli (1970) in a 15% polyacrylamide gel. The gel was stained and Coomassie Brilliant Blue R-250. Lane 1, M_r markers, Lane 2, 10 μg of purified *Melothria* peptidase from Sephacryl S-300 gel-filtration. (B) The activity assay in the gel. Purified *Melothria* peptidase on a Sephacryl S-300 gel-filtration was subjected to SDS-PAGE and the acrylamide gel was cut in 3 mm slices. Each gel slice was incubated with 67 mMK, Na-Pi buffer, pH 7.5 containing 0.1 mM Glt-Ala-Ala-Pro-Leu-*p*NA at 30°. After 3 h the gel was taken out of the mixture, *A* 405 nm of the remaining solution was assayed in a Hitachi spectrophotometer U-1100.

The optimum pH for the hydrolysis of Glt-Ala-Ala-Pro-Leu-*p*NA was found to be pH8 (Fig. 3).

The enzyme (50 μl, 60 μg/ml) was incubated with 50 μl of 67 mM sodium, potassium-phosphate buffer, pH 7.5, containing various inhibitors at 37°. After 120 min, the remaining hydrolysis activity of Glt-Ala-Ala-Pro-Leu-*p*NA was measured (Table 2). The peptidase was completely inactivated by incubation with DFP, PMSF, and STI. The activity was strongly inhibited by phenylbutylamine. PCMPS, MIA, and pepstatin had a definite effect on the over-all activity, and EDTA caused no inhibition. These results indicated that the peptidase was a serine-type enzyme.

Angiotensin I was cleaved by *Melothria* peptidase within 30 min at four different sites (Arg^2-Val^3-, Tyr^4-Ile^5, Ile^5-His^6, and Phe^8-His^9) (Fig. 4). Among these cleavage sites, Arg^2-Val^3 was the most susceptible position for the enzyme. The cleavage rate of the position Arg^2-Val^3 by *Melthoria* peptidase was 0.3 nmol of the digestive product per min. The hydrolysis rates of other cleavage sites were less than 0.3 nmol of the digestive product per min. The cleaved sites, Tyr^4-Ile^5 and Phe^8-His^9, were identical to those of cucumisin. It seems that *Melthoria* peptidase has a broader substrate specifity than cucumisin. Casein was strongly hydrolyzed by cucumisin, but it was a poor substrate for *Melthoria* peptidase (data not shown). It seems that *Melthoria* peptidase belongs to oligopeptidase (Tsuru, 1998).

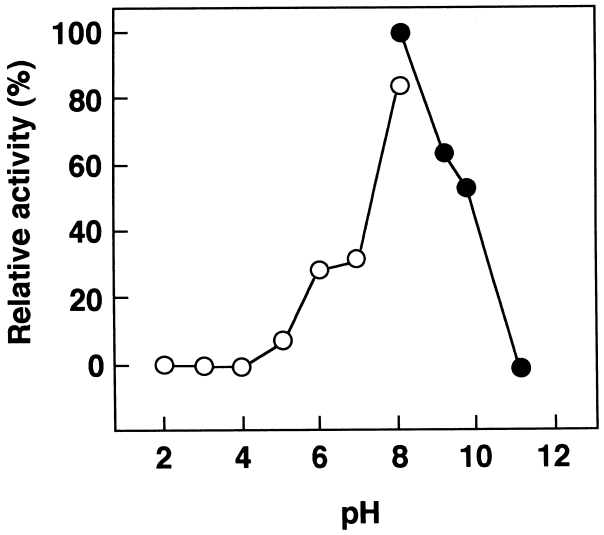

Fig. 3. The effect of pH on peptidase activity. Buffers: 0.2 M sodium phosphate-citric acid buffer (open circles, pH 2.0–8.0), 0.2 M glycine-NaOH buffer (closed circles, pH 8.0–11.0).

Table 2
Effect of various compounds on the enzyme activity of *Melothria* peptidase

Compounds	Concentration[a] (mM)	Class	Relative activity (%)
None	–	–	100[b]
DFP	2.0	Serine	0
PMSF	2.0	Serine	0
STI	0.01	Serine trypsin-like	0
Phenylbutylamine	10	Chymotrypsin-like	16
Tos-Lys-CH_2Cl	2.0	Serine trypsin-like/ cysteine	52
PCMPS	0.7	Cysteine	30
MIA	1.0	Cysteine	44
Peptstatin	0.01	Aspartic	57
EDTA	2.0	Metallo	109

[a] Final concentration. These results are for a 120-min incubation of 37°C.

[b] Activity of a control with no addition was taken as 100%.

Glt-Ala-Ala-Pro-Leu-*p*NA appears to be more active as a substrate with *Melthoria* peptidase compared to a commercial peptidyl-*p*NA, such as Suc-Ala-Ala-Pro-Phe-*p*NA. Leu-*p*NA was not hydrolyzed by the enzyme. Several peptidyl-MCAs were slightly hydrolyzed by *Melthoria* peptidase as shown in Table 3. However, those hydrolytic activities of the enzyme were inferior to that of Glt-Ala-Ala-Pro-Leu-*p*NA. Hydrolytic activity of Bz-Arg-MCA by the enzyme was the highest among the peptide-MCAs tested, but the relative activity on Bz-Arg-MCA was only 4.58% of that on Glt-Ala-Ala-Pro-Leu-*p*NA. Among those peptide-MCAs, the acidic charged residue, such as Glu or Asp at the P_1 position (the amino acid residue of the carboxyl site of the cleavage bond), was not preferred by the enzyme. Substrate

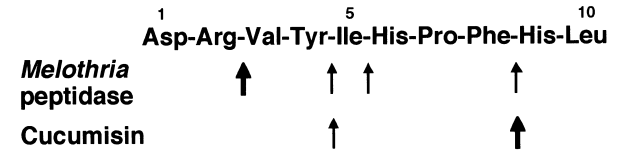

Fig. 4. Sites of human angiotensin I cleaved by *Melothria* peptidase or cucumisin (Uchikoba et al., 1995). The cleavage sites were predicted from the N-terminal sequence analysis of the digestion of angiotensin I. The thin arrows mark the cleavage sites with less than 10% recovery from the initial substrate (10 nmol), and the thick arrows indicate cleavage with more than a 10% recovery.

Table 3
Hydrolysis of peptidyl-(*p*NA/MCA) with *Melothria* peptidase

Substrates	Hydrolysis rate (nkat/ml)	Relative activity (%)
Glt-Ala-Ala-Pro-Leu-*p*NA	30.0	100[a]
Bz-Arg-MCA	0.172	5.73
Bz-Phe-Arg-MCA	0.138	4.58
Pyr-Gly-Arg-MCA	0.108	3.61
Boc-Leu-Gly-Arg-MCA	0.105	3.50
Boc-Gln-Ala-Arg-MCA	0.0774	2.58
Boc-Phe-Ser-Arg-MCA	0.0482	1.60
Boc-Val-Leu-Lys-MCA	0.0396	1.32
Boc-Val-Pro-Arg-MCA	0.0258	0.86
Glt-Ala-Ala-Phe-MCA	0.0258	0.86
Suc-Leu-Leu-Val-Tyr-MCA	0.0017	0.06
Suc-Ala-Glu-MCA	0	0
Suc-Ala-Pro-Ala-MCA	0	0
Ac-Tyr-Val-Ala-Asp-MCA	0	0

[a] Activity with glt-Ala-Ala-Pro-Leu-*p*NA was taken as 100%.

specifity studies indicate that the enzyme has a broad specifity at the P_1 position. Substrate specifity of *Melthoria* peptidase toward peptidyl-MCAs (or peptidyl-*p*NAs) was similar to that of *Euphorbia supina* protease (Arima et al., 2000).

The amino-terminal sequence of the first 10 residues of *Melthoria* peptidase was determined as shown in Fig. 5. The amino-terminal sequence of *Melthoria* peptidase was aligned with those of the eight plant serine proteases: that which is expressed in melon fruit (Yamagata et al., 1994); white gourd protease (Uchikoba et al., 1998); *Euphorbia supina* protease B (Armina et al., 2000); lily protease, induced in meiotic prophase (Kobayashi et al., 1994; Taylor et al., 1998); *Arabidopsis thaliana* protease, which are expressed in the precursor cells that are initiated upon auxin-induced lateral root formation (Neuteboom et al., 1999); ag12, which is expressed in the early stages of actinorhizal nodule formation in *Alnus glutinosa* (Ribeiro et al., 1995); and PR-P69 (also known as P69A) and P69B, a pathogen-induced in tomatoes (Tornero et al., 1996, 1997). Six out of 10 amino-terminal residues in *Melthoria* peptidase were identical to those of each protease of *E. supina*, *A. thaliana*, *A. glutinosa*, and P69B. The amino-terminal sequence, T-T-R/H-X-X-X-F/Y-L- was considered among the nine serine proteases shown in Fig. 5.

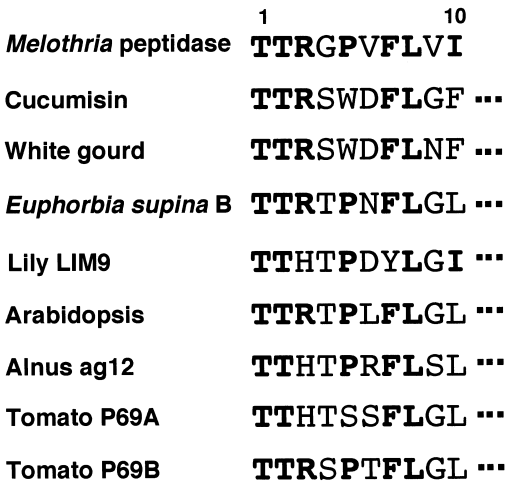

Fig. 5. Comparison of the N-terminal amino acid sequences of nine plant serine proteases. The proteases are *Melothria* peptidase in the present study. The bolds show identical amino acid residues to the sequence of *Melothria* peptidase.

Melthoria japonica is a plant of the Cucurbitaceae family. Cucumisin has already been isolated from the fruits of *Cucumis melov* var. Prince (Uchikoba et al., 1995). The M_r of *Melthoria* peptidase (61 kDa) was slightly smaller than that of cucumisin (67 kDa) (Uchikoba et al., 1995), and was similar to that of a serine protease (60 kDa) from spinach leaves (Aduccia et al., 1986).

3. Experimental

3.1. Material

Fruits of *Melthoria japonica* were collected in Kaseda City, Japan. DEAE-Sepharose was a product of Pharmacia. Tos-Lys-CH_2Cl was a product of Sigma. Peptidyl-MCAs and peptidyl-*p*NAs were purchased from the Peptide Institute. Other reagents were purchased from Wako Pure Chemical.

3.2. Enzymatic activity assay

Enzymatic hydrolysis of peptidyl-*p*NA, peptidyl-MCAs, and casein were performed by previously described methods (Uchikoba et al., 2000; Shimada et al., 2000; Kaneda et al., 1997). One unit of hydrolysis activity toward peptidyl-*p*NA was defined as the activity producing μkat (μmol of the products per s) under the stated conditions (pH 7.5, at 37°).

3.3. Enzyme purification

Melthoria peptidase was purified as follows. Unreipened fruits (100 g) of *Melthoria japonica* were homogenized with equal weights of buffer A (20 mM sodium, potassium-phosphate buffer, pH 7.5). After centrifugation (7000×*g*, 5 min), the supernatant was dialyzed against buffer A. After sitting over night at 7° the dialysate was placed on a column of DEAE-Sepharose (1.8×13 cm) equilibrated with buffer A. The enzyme was then eluted with 0.2 M sodium, potassium-phosphate buffer containing 0.4 M NaCl, pH 7.5. The active fractions were collected and concentrated with an Advantec-UHP-76 ultra filtering unit. The concentrated solution was put on a Sephacryl S-300 (1.8×46 cm) column equilibrated with 0.2 M sodium, potassium-phosphate buffer containing 0.1 M NaCl, pH 7.5. The active fraction was collected and kept at −20°.

3.4. Hydrolysis of angiotensin I

The peptide bonds of human angiotensin I cleaved by *Melothria* peptidase were determined by analyzing the newly formed N-terminal. Angiotensin I (10 nmol) was incubated at 37° with *Melthoria* peptidase (0.1 nmol) in buffer A, pH 7.5 (final volume, 20 μl). After 30 min, 0.1% TFA (10 μl) was added to the mixture and analyzed for the newly formed N-terminal using an Applied Biosystems Model 477A protein sequencer.

Acknowledgements

The authors thank Miss Y. Ouchida for her generous help in obtaining the fruits of *Melthoria japonica*.

References

Aducci, P., Ascenzi, P., Pierini, M., Ballio, A., 1986. Purification and characterization of Leu-proteinase, the leucine specific serine proteinase from spinach (*Spinacia oleracea* L.) leaves. Plant Physiology 81, 812–816.

Arima, K., Uchikoba, T., Yonezawa, H., Shimada, M., Kaneda, M., 2000. Cucumisin-like protease from the latex of *Euphorbia supina*. Phytochemistry 53, 639–644.

Kaneda, M., Tominaga, N., 1975. Isolation and characterization of a proteinase from the sacocarp of melon fruit. Journal of Biochemistry 78, 1287–1296.

Kaneda, M., Yonezawa, H., Uchikoba, T., 1997. Purification and characterization of a cysteine protease from corms of freesia, *Freesia reflacta*. Biosci. Biotechnol. Biochem. 61, 1554–1559.

Kobayashi, T., Kobayashi, E., Sato, S., Hotta, Y., Miyajima, N., Tanaka, A., Tabata, S., 1994. Characterization of cDNAs induced in meiotic prophase in lily microsporocytes. DNA Research 1, 15–26.

Laemmli, U.K., 1970. Cleavage of structural proteins during assembly of the head of bacteriophage T4. Nature 227, 680–685.

McDonald, J.K., 1998. Introduction: unsequenced serine peptidases. In: Barrett, A.J., Rawlings, N.D., Woessner, J.F. (Eds.), Handbook of proteolytic enzymes. Academic Press, London, pp. 536.

Neuteboom, L.W., Ng, J.M.Y., Kuyper, M., Clijdesdale, O.R., Hooykaas, P.J.J., van der Zaal, B.J., 1999. Isolation and characterization of cDNA clones corresponding with mRNAs that accumulate during auxin-induced lateral root formation. Plant Mol. Biol. 39, 273–287.

Ribeiro, A., Akkermans, A., Kammen, A., Bisseling, T., Pawlowski,

K., 1995. A nodule-specific gene encoding a subtilisin-like protease is expressed in early stages of actinorhizal nodule development. Plant Cell, 785–794.

Shimada, M., Uchikoba, T., Yonezawa, H., Arima, K., Kaneda, M., 2000. Isolation and characterization of a cucumisin-like serine protease from the latex of *Eurphorbia pseudochamaesyce* Fisch. J. Biochem. Mol. Biol and Biophys. 4, 223–231.

Taylor, A., Horsch, A., Rzepczyk, A., Hasenkampt, C., Riggs, D., 1998. Maturation and section of a serine proteinase is associated with events of late microsporogenesis. Plant J. 12, 1261–1271.

Tornero, P., Conejero, V., Vera, P., 1996. Primary structure and expression of a pathogen-induced protease (PR-P69) in tomato plants: similarity of functional domains to subtilisin-like endoproteases. Proc. Natl. Acad. Sci. USA 93, 6332–6337.

Tornero, P., Conejero, V., Vera, P., 1997. Identification of a new pathogen-induced member of the subtilisin-like processing protease family from plants. J. Biol. Chem. 272, 14412–14419.

Tsuru, D., 1998. Oligopeptidase B. In: Barrett, A.J., Rawlings, N.D., Woessner, J.F. (Eds.), Handbook of Proteolytic Enzymes. Academic Press, London, pp. 375–376.

Uchikoba, T., Yonezawa, H., Kaneda, M., 1995. Cleavage specificity of cucumisin, a plant serine protease. Journal of Biochemistry 117, 1126–1130.

Uchikoba, T., Yonezawa, H., Kaneda, M., 1998. Cucumisin like protease from the sarcocarp of *Benincasa hispida* var. *Ryukyu*. Phytochemistry 49, 2215–2219.

Uchikoba, T., Arima, K., Shimada, M., Yonezawa, H., Kaneda, M., 2000. Isolation and some properties of a serine protease from the fruits of *Cudrania cochinchinensis* (Lour.) Kudo et Masam. Biosci. Biotechnol. Biochem. 64, 623–624.

Yamagata, H., Masuzawa, T., Nagaoka, Y., Ohnishi, T., Iwasaki, T., 1994. Cucumisin, a serine protease from melon fruit, shares structural homology with subtilisin and is generated from a large precursor. J. Biol. Chem. 269, 32725–32731.

PERGAMON

Phytochemistry 57 (2001) 7–14

PHYTOCHEMISTRY

www.elsevier.com/locate/phytochem

Biosynthesis of the hemi- and monoterpene moieties of isoprenyl phenyl ethers from the liverwort *Trichocolea tomentella*☆

Anna J. Barlow [a], Hans Becker [b], Klaus Peter Adam [b,*]

[a] *Plant Extracts Research Unit, New Zealand Institute for Crop and Food Research Limited, Department of Chemistry, University of Otago, PO Box 56, Dunedin, New Zealand*

[b] *FR 8.7, Pharmakognosie und Analytische Phytochemie der Universität des Saarlandes, 66041 Saarbrücken, Germany*

Received in revised form 15 December 2000

Abstract

The incorporation of ^{13}C labelled glucose into trichocolein, deoxytomentellin, *trans*-phytol and stigmasterol has been studied in axenic cultures of the liverwort *Trichocolea tomentella*. Quantitative ^{13}C NMR spectroscopic analysis of the resulting labelling patterns showed that the isoprene units of the hemi- and monoterpenoid moieties and the diterpene phytol are derived from the methylerythritol phosphate pathway, whereas the isoprene units of stigmasterol are built up via the mevalonic acid pathway. These results indicate the involvement of both IPP biosynthetic pathways in different cellular compartments. A new, hydroperoxy geranyl phenyl ether derivative is also described. © 2001 Elsevier Science Ltd. All rights reserved.

Keywords: *Trichocolea tomentella*; Isopentenyl diphosphate; Mevalonic acid pathway; Methylerythritol phosphate pathway; Isoprenoids; Hemiterpene; Monoterpene; Phytol; Stigmasterol; ^{13}C-Labelling; Liverwort; Quantitative ^{13}C NMR spectroscopy

1. Introduction

Isoprenoids are the largest group of secondary metabolites with over 30,000 known compounds, including the steroids (Dictionary of Natural Products, 2000). Their common building block, the isoprene unit, is derived from isopentenyl diphosphate (IPP). In the past, the mevalonic acid (MVA) pathway has been accepted as the only biosynthetic route leading to IPP, which was believed to operate in all organisms. In contrast, the existence of the methylerythritol phosphate (MEP) pathway as an alternative route for IPP biosynthesis has only been known for a few years (Rohmer et al., 1993; Schwarz, 1994; for review, see Lichtenthaler et al., 1997a; Eisenreich et al., 1998; Lichtenthaler, 1999; Rohmer, 1999). So far, the reaction sequence of this pathway is established up to the formation of the cyclic diphosphate intermediate 2-*C*-methylerythritol 2,4-cyclodiphosphate (Rohmer et al., 1993; Sprenger et al., 1997; Lois et al., 1998; Takahashi et al., 1998; Rohdich et al., 1999; Herz et al., 2000; Lüttgen et al., 2000); the following steps to IPP are still uncharacterised.

The discovery of the methylerythritol phosphate (MEP) pathway has quite changed the general understanding of isoprenoid biosynthesis. Whereas vertebrates and archaebacteria appear to use only the mevalonate pathway to build isoprenoids, various eubacteria have been found to use either the mevalonate or the MEP pathway. Chlorophytes possess only the MEP pathway, whereas rhodophytes, chrysophytes, bryophytes and higher plants have been found to use the MVA pathway for the biosynthesis of steroids, and the MEP pathway for the formation of hemiterpenoids, monoterpenoids, carotenoids, phytol and other diterpenes (for review, see Lichtenthaler et al., 1997a; Eisenreich et al., 1998; Lichtenthaler 1999; Rohmer, 1999). The MVA pathway appears to be operative in the cytoplasm compartment of plant cells, whereas the MEP pathway seems to be located in the plastids. Segregation of the two pathways, however, is not necessarily complete, and exchange of metabolites between the two

☆ Publication No. 153 of "Arbeitskreis Chemie und Biologie der Moose".

* Corresponding author. Tel.: +49-681-302-2220; fax: +49-681-302-2476.

E-mail address: k.adam@rz.uni-sb.de (K.P. Adam).

0031-9422/01/$ - see front matter © 2001 Elsevier Science Ltd. All rights reserved.
PII: S0031-9422(01)00002-4

pools has been observed in plants and plant cell cultures (Schwarz, 1994; Nabeta et al., 1995; Arigoni et al., 1997; Adam and Zapp, 1998; Piel et al., 1998; Adam et al., 1999). Despite a significant amount of recent research in this area, our knowledge on the contribution of both pathways to the biosynthesis of the different plant terpenoid classes is still limited.

In continuation of our previous studies on IPP biosynthesis in bryophytes (Thiel et al., 1997; Adam et al., 1998; Eisenreich et al., 1999), we have chosen the liverwort *Trichocolea tomentella* to determine the origin of the prenyl moieties of its major constituents, a series of isoprenyl phenyl ethers. Our previous work has shown that trichocolein (**1**), which contains a hemiterpene moiety, and deoxytomentellin (**2**), with a monoterpene moiety, can both be easily isolated in significant amounts from axenic cultures of *T. tomentella* making this liverwort an ideal candidate for biosynthetic study (Helminger and Becker, 1992). Until now, no information on the biosynthesis of these types of compounds has been available. In particular, study of the biosynthesis of a hemiterpene moiety is of great interest as presently only four reports are known: isoprene in several higher plants (Zeidler et al., 1997), the hemiterpene units in the furanocoumarins of *Apium graveolens* (Stanjek et al., 1999), in the hops bitter acid humulone in *Humulus lupulus* (Goese et al., 1999) and the prenylated flavonoid glabrol in *Glycyrrhiza glabra* (Asada et al., 2000).

Axenic cultures of liverworts are useful experimental systems for such biosynthetic studies (Adam et al., 1996; Adam and Croteau, 1998; Adam et al., 1998). Due to their small size, these cultures can be grown fully differentiated in vitro. As has been shown previously, these differentiated cultures maintain their capability of synthesising in type and content the whole range of isoprenoids in vitro, similar to natural conditions (Becker, 1994). Furthermore, labelled precursors can be administered to the plants via the culture medium, similar to cell culture systems. The simple morphology of liverwort tissue cultures supports the uptake of the respective compounds under physiological conditions, in contrast to cell cultures where the dedifferentiated status of the cells might have a drastic impact on many biochemical processes. Therefore, ^{13}C labelling experiments should give a realistic impression of the biosynthetic origin of isoprenyl phenyl ethers (**1**, **2**) in *T. tomentella* and allow biosynthetic comparisons to be made between the various classes of isoprenoids.

In this paper we describe the incorporation of [1-^{13}C]glucose into the terpenoid moieties of two isoprenyl phenyl ethers. The resulting labelling patterns are compared to that of the steroid stigmasterol (**3**) as a reference for mevalonate derived isoprenoids of the cytoplasm, and the diterpene *trans*-phytol (**4**) as marker compound for the plastidial MEP pathway.

2. Results and discussion

[1-^{13}C]Glucose was administered to aseptic cultures of *T. tomentella*. After a 20-fold fr. wt increase the plant material was harvested and the compounds were isolated with standard chromatographic procedures. Assignments of ^{13}C NMR signals of the purified compounds were obtained from the literature (Goad, 1995; Perry et al., 1996). Labelling patterns and absolute ^{13}C enrichments of the compounds were determined by quantitative ^{13}C NMR spectroscopy using Cr(III)-acetylacetonate as a relaxation reagent (Braun et al., 1996). The acetyl derivative of compound **3** was synthesised (**3a**) in order to introduce an internal ^{13}C reference with the natural ^{13}C abundance of 1.11%. In the case of nonderivatised compounds (**1**, **2**, **4**) the absolute ^{13}C enrichment has been calculated from the integrals of ^{13}C NMR signals on the basis of ^{13}C satellite analysis of the well separated proton signals in the respective ^{1}H NMR spectra (see Tables 1 and 3).

Trichocolein (**1**) and deoxytomentellin (**2**) both show only two labelled carbons per isoprene unit, with an average ^{13}C abundance of 5.25 ± 0.17 and 5.36 ± 0.04% respectively (Table 1). The labelling positions correspond to the alternative methylerythritol phosphate pathway (Fig. 1). The remaining carbon atoms of both the hemiterpene part (compound **1**) and the monoterpene part (compound **2**) also display an increased ^{13}C abundance with 2.64 ± 0.26 and 2.29 ± 0.22% respectively, compared to the expected natural abundance of

Table 1
^{13}C Abundances of labelled trichocolein (**1**) and deoxytomentellin (**2**)

Carbon atom in IPP-units[d]	Carbon atom	%^{13}C[a] (**1**)	Carbon atom	%^{13}C[a] (**2**)
1^{I}	**1**	**5.36**[c]	**1**	**5.35**
2^{I}	2	2.31	2	1.99
3^{I}	3	2.61	3	2.57
4^{I}	4	2.79	4	2.11
5^{I}	**5**	**5.41**	**10**	**5.32**
1^{II}	–	–	**5**	**5.39**
2^{II}	–	–	6	2.04
3^{II}	–	–	7	2.37
4^{II}	–	–	8	2.42
5^{II}	–	–	**9**	**5.33**
[b]	1′	2.57	1′	2.02
[b]	**2′**	**5.33**	**2′**	**5.45**
[b]	3′	2.41	3′	2.33
[b]	4′	2.83	4′	2.46
[b]	5′	2.50	5′	2.26
[b]	**6′**	**5.29**	**6′**	**5.34**
[b]	7′	3.13	7′	2.62
[b]	**3′OMe**	**5.11**	**3′OMe**	**5.32**
[b]	**7′OMe**	**4.98**	**7′OMe**	**5.38**

[a] ^{13}C Abundances obtained from ^{13}C satellite analysis of H-1.
[b] From shikimic acid pathway.
[c] Bold type: labelled positions.
[d] I, II, Denote individual C_5 units.

1.11%. This general background labelling might be explained by complex metabolic turnover of [1-^{13}C]glucose during the growth period, resulting in a statistical distribution of the labelled carbon atoms in various positions of intermediates of the carbohydrate metabolism (e.g. metabolism of glucose to carbon dioxide and subsequent assimilation via the Calvin cycle). The labelling of the phenyl ring is in accordance with the biogenetic scheme of the shikimate pathway, with direct formation of the substituted aromatic ring via 5-dehydroshikimic acid as for gallic acid (see Fig. 2) (Luckner, 1990). This can be concluded from the fact that the carboxyl carbon in both trichocolein and deoxytomentellin is unlabelled. In the case of formation of the C6–C1 skeleton by a side chain reduction of a phenyl propane unit (C6–C3), the carboxyl group would also bear a label. Labelling of the methyl groups (methoxy and methyl ester) is in agreement with the formation of C_1-groups via methionine/methyl dehydrofolic acid (Fig. 2) (Luckner, 1990).

The quantitative ^{13}C NMR analysis of stigmasterol acetate (**3a**) showed an enrichment pattern typical for the mevalonic acid pathway, with an average ^{13}C abundance of 4.20±0.29% (Table 2). The isolated com-

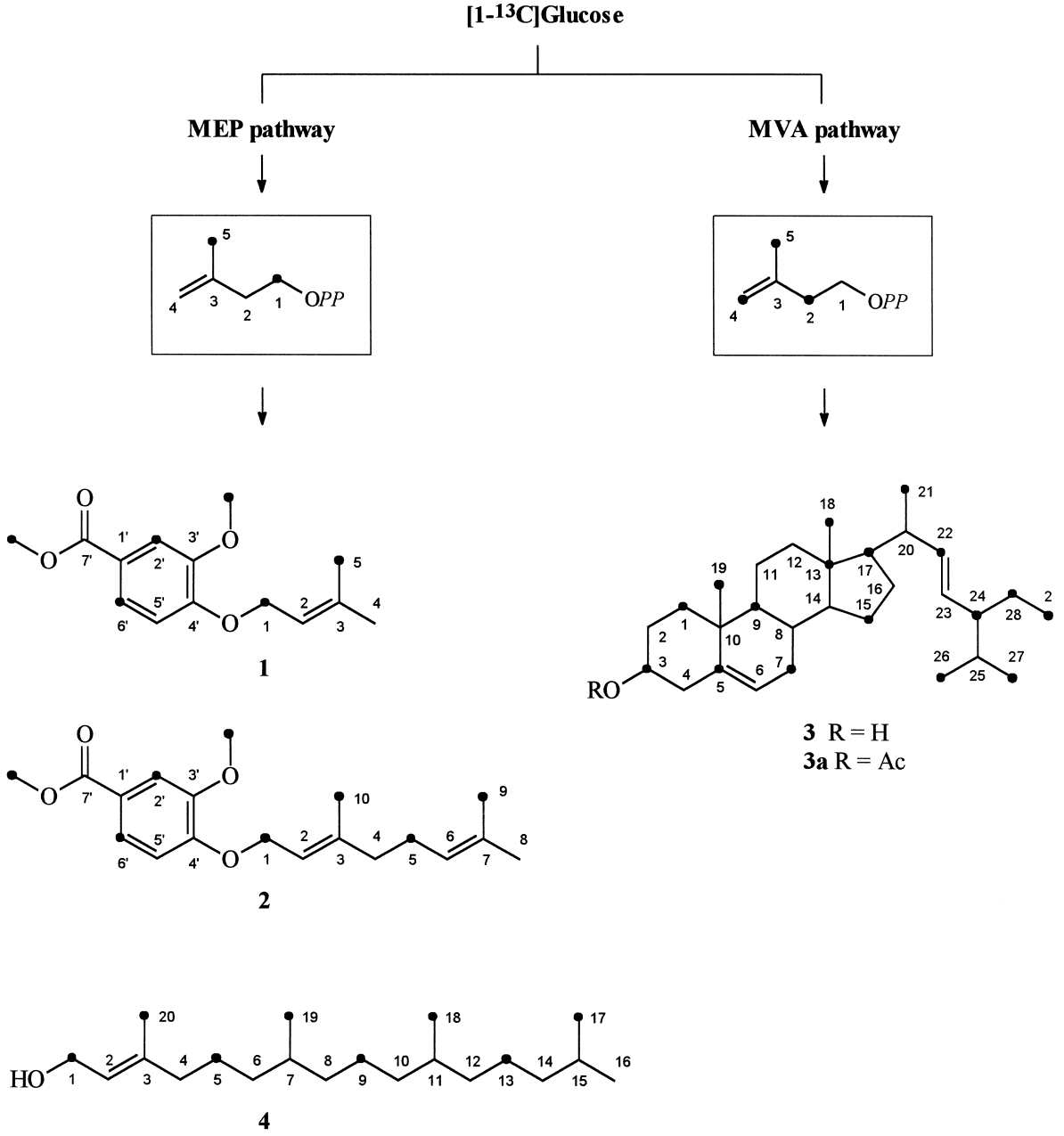

Fig. 1. Incorporation of [1-^{13}C]glucose into IPP via MVA pathway and MEP pathway and the resulting labelling patterns of compounds **1**, **2**, **3a** and **4**. *PP* = diphosphate residue, ● = ^{13}C labelled position.

pound also shows a ^{13}C enrichment (2.56±0.36%) of the unlabelled positions as already discussed for the hemi- and monoterpene moieties.

The labelling pattern of *trans*-phytol (**4**) from *T. tomentella* is in excellent agreement with that obtained from the liverworts *Ricciocarpos natans* and *Conocephalum conicum* (Adam et al., 1998), showing the formation of the isoprene units via the methylerythritol phosphate pathway (average ^{13}C abundance: 4.62±0.28%, Table 3). Again, an increased ^{13}C background labelling could be observed (2.86±0.04%, Table 3).

The average absolute ^{13}C abundances of all compounds are summarized in Table 4. These results demonstrate that both pathways of IPP biosynthesis

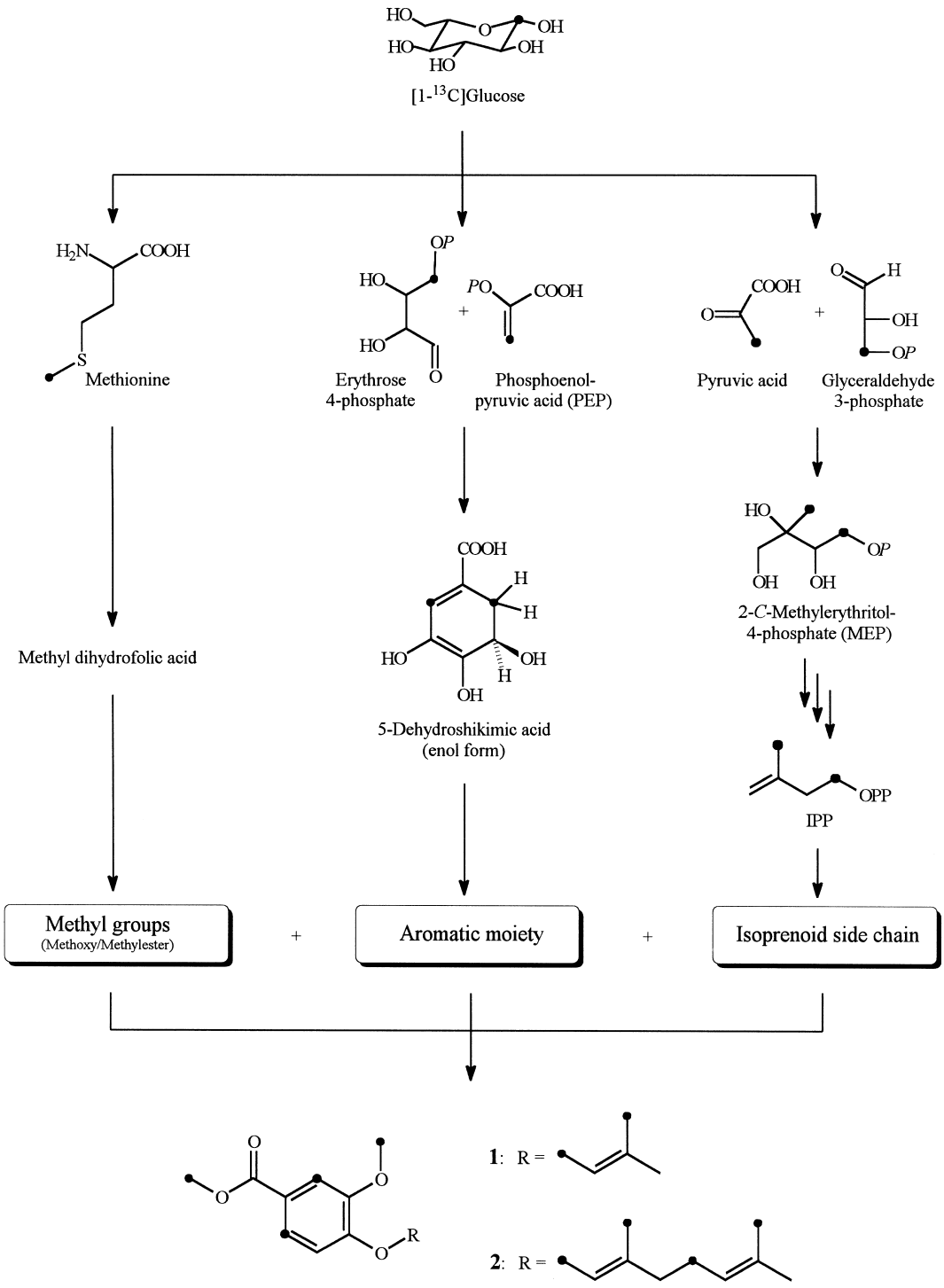

Fig. 2. Biosynthetic scheme for isoprenyl phenyl ethers showing incorporation of [1-^{13}C]glucose. Key: *P* = phosphate residue, *PP* = diphosphate residue, ● = ^{13}C labelled position.

operate in *T. tomentella*. The analysis of hemi-, mono- and diterpene units and sterols of *T. tomentella*, representing the basic terpenoid building blocks units C_5, C_{10} C_{15} (sterols = $2\times C_{15}$) and C_{20} gives a broad overview over the biosynthetic origin of isoprenoids of a single organism. The labelling patterns of all compounds investigated could be assigned to two groups formed independently from each other: firstly the sterols, formed via the mevalonic acid pathway, and secondly the hemi-, mono- and diterpenes, derived from the methylerythritol phosphate pathway.

In all compounds we observed a strict separation of the two pathway specific labelling patterns. A significant mixing of both IPP biosynthesis pathways in any of the isoprene units could not be deduced from the data. However, a minor incorporation of both IPP species in an isoprene unit could not be excluded, since the respective labelling could have been masked by the variation of the ^{13}C abundance data.

Table 2
^{13}C Abundances of acetylated stigmasterol (**3a**)

Carbon atom in IPP-units[e]	Carbon atom	% ^{13}C[a]
1^{I}	2	2.61
2^{I}	3	**4.61**[d]
3^{I}	4	2.33
1^{II}	6	3.13
2^{II}	5	**4.65**
3^{II}	10	2.51
4^{II}	1	**4.33**
5^{II}	19	**4.15**
1^{III}	11	2.54
2^{III}	9	**4.32**
3^{III}	8	2.56[b]
4^{III}	7	**4.20**[b]
1^{IV}	12	2.18
2^{IV}	13	**4.09**
3^{IV}	14	2.93
4^{IV}	15	**3.65**
5^{IV}	18	**4.03**
1^{V}	16	2.17
2^{V}	17	**4.22**
3^{V}	20	2.11
4^{V}	22	**4.63**
5^{V}	21	**3.88**
1^{VI}	23	3.07
2^{VI}	24	**4.01**
3^{VI}	25	2.56[b]
4^{VI}	26	**4.01**
5^{VI}	27	**4.16**
[c]	28	**4.03**
[c]	29	**4.00**
COO (acetyl)	30	1.11
CH_3 (acetyl)	31	0.98

[a] ^{13}C Abundances obtained from the ^{13}C signal of C-30 referenced to 1.11% (natural abundance of the acetate residue).
[b] Averaged values due to signal overlapping.
[c] Non terpenoid carbons.
[d] Bold type: labelled positions.
[e] I, II, III, IV, V: Denote individual C_5 units.

These facts agree with our earlier findings from the liverworts *R. natans* and *C. conicum* (Adam et al., 1998) and confirm that at least two well separated types of cellular compartments exist in liverworts, with different IPP biosynthesis machineries and prenyltransferase sets creating either C_{15} units, or C_5, C_{10} and C_{20} skeletons. These results are in agreement with the current hypothesis of the localization of the biosynthesis of the different terpenoid classes, assuming that mevalonic acid and sterol formation are located in the cytoplasm while the methylerythritol phosphate pathway and the biosynthesis of monoterpenes and diterpenes are segregated in plastids (Lichtenthaler, et al. 1997b; Rohdich et al., 1999).

Isohydroperoxytomentellin (**5**) (Fig. 3) is a previously unreported hydroperoxy compound which was isolated from unlabelled *T. tomentella* plant material during the course of this work. Mass spectrometry (DCIMS) showed a parent ion $[M+H]^+$ of 365.2, equating to a molecular formula of $C_{19}H_{24}O_7$. Both the ^1H and ^{13}C NMR spectra showed the substitution of the phenyl ring to be identical to that of the other isoprenyl ethers (**1**, and **2**), and very similar in structure to the related isoprenyl ether tomentellin (Perry et al., 1996). In contrast to tomentellin, the side chain differed in the position of one double bond (appearing as an exo-methylene group, δ_H 5.41, 5.19, both *s*), and the presence of an exchangeable proton signal at δ_H 10.75, suggesting either an alcoholic or peroxy proton. The structure of

Table 3
^{13}C Abundances of phytol (**4**)

Carbon atom in IPP-units[d]	Carbon atom	% ^{13}C[a]
1^{I}	13	**4.50**[c]
2^{I}	14	2.87
3^{I}	15	2.83
4^{I}	16	2.90
5^{I}	17	**4.51**
1^{II}	9	**4.48**
2^{II}	10	2.88b
3^{II}	11	2.84c
4^{II}	12	2.88b[b]
5^{II}	18	**5.06**d
1^{III}	5	**4.31**
2^{III}	6	2.82
3^{III}	7	2.84c
4^{III}	8	2.88b
5^{III}	19	**5.06**d
1^{IV}	1	**4.55**
2^{IV}	2	2.88
3^{IV}	3	2.76
4^{IV}	4	2.92
5^{IV}	20	**4.31**

[a] ^{13}C Abundances obtained from ^{13}C satellite analysis of H-1.
[b] b, c, d: Averaged values due to signal overlapping.
[c] Bold type: labelled positions.
[d] I, II, III, IV, denote individual C_5 units.

Table 4
Comparison of ^{13}C enrichments in isoprenoids from *T. tomentella*

Compound	% ^{13}C labelled carbons	% ^{13}C unlabelled carbons	Ratio labelled/unlabelled
Trichocolein (**1**)	5.25±0.17	2.64±0.26	1.99
Deoxytomentellin (**2**)	5.36±0.04	2.29±0.22	2.34
Ac-Stigmasterol (**3a**)	4.20±0.29	2.56±0.36	1.64
trans-Phytol (**4**)	4.62±0.28	2.86±0.04	1.61

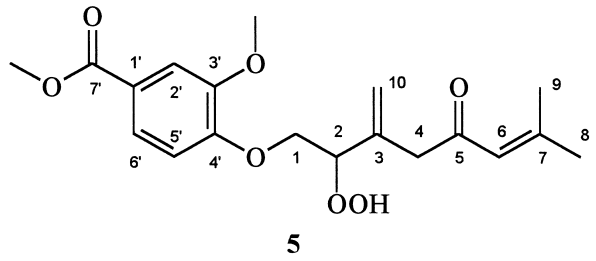

5

Fig. 3. Isohydroperoxytomentellin (**5**).

the prenyl side chain was established from DEPT, COSY, HSQC and HMBC NMR data. The assignment of the signal at δ_H 10.75 to a hydroperoxy group was supported by the literature data of a monoterpene with a similar substructure, kobusimin A, isolated from both *Magnolia kobus* (Iida et al., 1982) and *Schistostephium crataegifolium* (Bohlmann et al., 1983).

3. Experimental

3.1. Spectroscopy and spectrometry

NMR Spectra were recorded in $CDCl_3$ (^1H NMR (500 MHz), ^{13}C NMR (125 MHz)) relative to $CDCl_3$ at δ_H 7.24; δ_C 77.0. ^{13}C Multiplicities were determined using the DEPT pulse sequence. 2D Spectra were recorded as COSY, HSQC and HMBC experiments. Quantitative ^{13}C NMR measurements were recorded with the inverse gated decoupling pulse sequence in the presence of 0.1 M $Cr(acac)_3$ (Braun et al., 1996). For integration, the signal-to-noise ratio of the ^{13}C-signals was at least 40:1. Direct chemical ionisation mass spectra (DCIMS) were recorded at 120 eV, using methane as carrier gas.

3.2. Plant material

An axenic culture of *T. tomentella* was obtained from the Collection of Autotrophic Organisms, Department of Hydrobotany, Institute of Botany, Czech Academy of Sciences, Trebon, Czech Republic. Growth characteristics and chemical composition of this culture have been intensively studied (Helminger and Becker, 1992). The liverwort was grown in 250 ml Erlenmeyer flasks under continuous incandescent light (60 μmol photons m^{-2} s^{-1} photosynthetically active radiation) at 22°C in 75 ml of modified Gamborg B5 liquid medium (Gamborg et al., 1968) containing 10 g/l glucose.

3.3. Labelling procedure

In feeding experiments 20% of the glucose was substituted by [1-^{13}C]glucose. Cultures were grown for 3 months.

3.4. Extraction, isolation and derivatisation

The extraction and isolation scheme followed standard procedures of our group (Adam et al., 1998). All isoprenyl phenyl ethers, with the exception of compound **5**, were identified by previously published NMR data (Perry et al., 1996). Dried ^{13}C labelled plant material (24.71 g) was ground and extracted in a soxhlet apparatus using CH_2Cl_2 (1.5 l) After removal of the solvent, the crude extract (1.62 g) was chromatographed on silica gel (vacuum liquid chromatography, VLC) employing a *n*-hexane–EtOAc gradient. The VLC fraction containing crude trichocolein (**1**) and deoxytomentellin (**2**) (198.3 mg, 7–8% EtOAc) was further purified via HPLC (250×4 mm, Si 60 Lichrospher Merck, 5 μm, *n*-hexane–EtOAc, 93:7), yielding 143.5 mg of **1** and 21.0 mg of **2**. The sterol containing VLC fractions (28,4 mg, 10–12%EtOAc) were purified by HPLC (250×4 mm, Si 60 Lichrospher, Merck, *n*-hexane–EtOAc 90:10) yielding 7.8 mg of the sterol mixture (campesterol/sitosterol/stigmasterol, ratio 1:2:4) This was acetylated overnight at room temperature (acetic anhydride/pyridine/toluene, 1:1:2, by vol.) and further purified by HPLC using an Ag^+ coated ion exchange column (Van Beek and Subrtova, 1995) (200×4 mm, Nucleosil 5 SA, Macherey and Nagel, 5 μm, *n*-hexane–*tert*-butyl methyl ether, 92:8), yielding 2.5 mg of acetylated stigmasterol (**3a**). The chlorophyll-containing fractions were combined and saponified by reaction overnight at room temperature with 6% (*w*/*v*) KOH in methanol. Following hydrolysis, the mixture was extracted 5× with CH_2Cl_2. After removal of the solvent, the mixture was separated by VLC on silica gel *n*-hexane–EtOAc (3.8% EtOAc) yielding 23.6 mg of *trans*-phytol (**4**).

3.5. Isohydroperoxytomentellin (**5**)

Compound **5** was isolated from unlabelled plant material that was extracted by methods described above. Separation of a VLC fraction (9% EtOAc, 51.4 mg) of the crude extract via HPLC (250×4 mm, Si 60 Lichrospher, Merck, *n*-hexane–EtOAc, 80:20) yielded 4.3 mg of (**5**) as a colourless oil: TLC (*n*-hexane–EtOAc, 80:20), $R_f = 0.11$, UV, purple with anisaldehyde/H_2SO_4. ^{1}H NMR data: δ_H 1.91 (3H, *br s*, H-8); 2.16 (3H, *br s*, H-9); 3.32 (1H, *d*, $J = 17$ Hz, H-4); 3.51 (1H, *d*, $J = 17$ Hz, H-4); 3.86 (3H, *s*, 3′OCH_3); 3.86 (3H, *s*, 7′OCH_3); 4.20 (1H, *d*, $J = 4$ Hz, H-1), 4.20 (1H, *d*, $J = 6$ Hz, H-1); 4.80 (1H, br *t*, $J = 5.5$ Hz, H-2); 5.19 (1H, *s*, H-10); 5.41 (1H, *s*, H-10); 6.14 (1H, *m* (allylic), H-6); 6.88 (1H, *dd*, $J = 2$; 8 Hz, H-5′); 7.51 (1H, *d*, $J = 2$ Hz, H-2′); 7.61 (1H, *dd*, $J = 2$; 8 Hz, H-6′), 10.75 (1H, *s*, HOO-). ^{13}C NMR data: δ_C 21.2 (*q*, C-9), 28.0 (*q*, C-8), 47.8 (*t*, C-4), 52.0 (*q*, 3′OCH_3), 56.0 (*q*, 7′OCH_3), 68.9 (*t*, C-1), 86.6 (*d*, C-2), 112.5 (*d*, C-5′), 112.7 (*d*, C-2′), 121.6 (*t*, C-10), 123.1 (*d*, C-6), 123.4 (*d*, C-6′), 123.5 (*s*, C-1′), 8.9 (*s*, C-3), 149.1 (*s*, C-3′), 151.9 (*s*, C-4′), 159.0 (*s*, C-7), 166.8 (*s*, C-7′), 200.3 (*s*, C-5); DCIMS (methane, probe) 120 eV *m*/*z* (rel. int.) $[M+H]^+$ 365.2 (0.55).

Acknowledgements

We are grateful to the Deutscher Akademischer Austauschdienst (DAAD) and the New Zealand Federation of University Women (NZFUW) Harriet Jenkins Fund for providing financial support for A.J.B. For recording NMR spectra we thank Dr. Josef Zapp, from our group.

References

Adam, K.P., Crock, J., Croteau, R., 1996. Partial purification and characterization of a monoterpene cyclase, limonene synthase from the liverwort *Ricciocarpos natans*. Archives of Biochemistry and Biophysics 332, 352–356.

Adam, K.P., Croteau, R., 1998. Monoterpene biosynthesis in the liverwort *Conocephalum conicum*: Demonstration of sabinene synthase and bornyl diphosphate synthase. Phytochemistry 49, 475–480.

Adam, K.P., Thiel, R., Zapp, J., 1999. Incorporation of 1-[1-^{13}C]deoxy-D-xylulose in chamomile sesquiterpenes. Archives of Biochemistry and Biophysics 369, 127–132.

Adam, K.P., Thiel, R., Zapp, J., Becker, H., 1998. Involvement of the mevalonic acid pathway and the glyceraldehyde-pyruvate pathway in terpenoid biosynthesis of the liverworts *Conocephalum conicum* and *Ricciocarpos natans*. Archives of Biochemistry and Biophysics 354, 181–187.

Adam, K.P., Zapp, J., 1998. Biosynthesis of the isoprene units of chamomile sesquiterpenes. Phytochemistry 48, 953–959.

Arigoni, D., Sagner, S., Latzel, C., Eisenreich, W., Bacher, A., Zenk, M.H., 1997. Terpenoid biosynthesis from 1-deoxy-D-xylulose in higher plants by intramolecular skeletal rearrangement. Proceedings of the National Academy of Sciences of the USA 94, 10600–10605.

Asada, Y., Li, W., Yoshikawa, T., 2000. Biosynthesis of the dimethylallyl moiety of glabrol in *Glycyrrhiza glabra* hairy root cultures via a non-mevalonate pathway. Phytochemistry 55, 323–326.

Becker, H., 1994. Secondary metabolites from bryophytes in vitro cultures. Journal of the Hattori Botanical Laboratory 76, 283–291.

Bohlmann, F., Jakupovic, J., Ahmed, M., Schuster, A., 1983. Sesquiterpene lactones and other constituents form *Schistostephium species*. Phytochemistry 22, 1623–1636.

Braun, S., Kalinowski, H.O., Berger, S., 1996. 100 and more basic NMR experiments. VCH-Wiley, Weinheim, New York.

Dictionary of Natural Products on CD-ROM, 2000. Version 9.1, Chapman and Hall/CRC Press, London, New York.

Eisenreich, W., Rieder, C., Grammes, C., Heßler, G., Adam, K.-P., Becker, H., Arigoni, D., Bacher, A., 1999. Biosynthesis of a neo-*epi*-verrucosane diterpene in the liverwort *Fossombronia alaskana*. A retrobiosynthetic NMR study. Journal of Biological Chemistry 274, 36312–36320.

Eisenreich, W., Schwarz, M., Cartayrade, A., Arigoni, D., Zenk, M.H., Bacher, A., 1998. The deoxyxylulose phosphate pathway of terpenoid biosynthesis in plants and microorganisms. Chemistry and Biology 5, R221–R233.

Gamborg, O.L., Miller, R.A., Ojiama, K., 1968. Plant cell cultures. I. Nutrient requirements of suspension cultures of soybean root cells. Experimental Cell Research 50, 151–158.

Goad, L.J., 1995. Phytosterols. In: Charlwood, B.V., Banthorpe, D.V. (Eds.), Methods in Plant Biochemistry, Terpenoids, Vol. 7. Academic Press, London, pp. 369–434.

Goese, M., Kammhuber, K., Bacher, A., Zenk, M.H., Eisenreich, W., 1999. Biosynthesis of bitter acids in hops. A ^{13}C-NMR and ^{2}H-NMR study on the building blocks of humulone. European Journal of Biochemistry 263, 447–454.

Helminger, T., Becker, H., 1992. Aromatic esters from collected plants and in vitro-cultures of the liverwort *Trichocolea tomentella* (Erh.) Dum. Cryptogamic Botany 3, 74–76.

Herz, S., Wungsintaweekul, J., Schuhr, C.A., Hecht, S., Lüttgen, H., Sagner, S., Fellermeier, M., Eisenreich, W., Zenk, M.H., Bacher, A., Rohdich, F., 2000. Biosynthesis of terpenoids: YgbB protein of *Escherichia coli* phosphorylates the 2-hydroxy group of 4-diphosphocytidyl-2-C-methylerythritol. Proceedings of the National Academy of Sciences of the USA 97, 2486–2490.

Iida, T., Nakano, M., Ito, K., 1982. Hydroperoxysesquiterpene and lignan constituents of *Magnolia kobus*. Phytochemistry 21, 673–776.

Lichtenthaler, H.K., 1999. The 1-deoxy-D-xylulose-5-phosphate pathway of isoprenoid biosynthesis in plants. Annual Review of Plant Physiology and Plant Molecular Biology 50, 47–65.

Lichtenthaler, H.K., Rohmer, M., Schwender, J., 1997a. Two independent biochemical pathways for isopentenyl diphosphate and isoprenoid biosynthesis in higher plants. Physiologica Plantarum 101, 643–652.

Lichtenthaler, H.K., Schwender, J., Disch, A., Rohmer, M., 1997b. Biosynthesis of isoprenoids in higher plant chloroplasts proceeds via a mevalonate-independent pathway. FEBS Letters 400, 271–274.

Lois, L.M., Campos, N., Putra, S.R., Danielsen, K., Rohmer, M., Boronat, A., 1998. Cloning and characterization of a gene from *Escherichia coli* encoding a transketolase-like enzyme that catalyses the synthesis of D-1-deoxyxylulose-5-phosphate, a common precursor for isoprenoid, thiamin, and pyridoxol biosynthesis. Proceedings of the National Academy of Sciences of the USA 95, 2105–2110.

Luckner, M., 1990. Secondary Metabolism in Microorganisms, Plants and Animals. Springer Verlag, Berlin Heidelberg, New York.

Lüttgen, H., Rohdich, F., Herz, S., Wungsintaweekul, J., Hecht, S., Schuhr, C.A., Fellermeier, M., Sagner, S., Zenk, M.H., Bacher, A., Eisenreich, W., 2000. Biosynthesis of terpenoids: YgbB protein converts 4-diphosphocytidyl-2-C-methylerythritol 2-phosphate to 2-C-methylerythritol 2,4-cyclodiphosphate. Proceedings of the National Academy of Sciences of the USA 97, 1062–1067.

Nabeta, K., Ishikawa, T., Kawae, T., Okuyama, H., 1995. Biosynthesis of heteroscyphic acid A in cell cultures of *Heteroscyphus planus*: nonequivalent labelling of C-5 units in diterpene biosynthesis. Journal of the Chemical Society. Chemical Communications, 681.

Perry, N.B., Foster, L.M., Lorimer, S.D., May, B.C.H., Weavers, R.T., Toyota, M., Nakaishi, E., Asakawa, Y., 1996. Isoprenyl phenyl ethers from liverworts of the genus *Trichocolea*: cytotoxic activity, structural corrections, and synthesis. Journal of Natural Products 59, 729–733.

Piel, J., Donath, J., Bandemer, K., Boland, W., 1998. Mevalonate-independent biosynthesis of terpenoid volatiles in plants: induced and constitutive emission of volatiles. Angewandte Chemie 37, 2478–2481.

Rohdich, F., Wungsintaweekul, J., Fellermeier, M., Sagner, S., Herz, S., Kis, K., Eisenreich, W., Bacher, A., Zenk, M.H., 1999. Cytidine 5′-triphosphate-dependent biosynthesis of isoprenoids: YgbP protein of *Escherichia coli* catalyzes the formation of 4-diphosphocytidyl-2-C-methylerythritol. Proceedings of the National Academy of Sciences of the USA 96, 11758–11763.

Rohmer, M., 1999. The discovery of a mevalonate-independent pathway for isoprenoid biosynthesis in bacteria, algae and higher plants. Natural Product Reports 16, 565–574.

Rohmer, M., Knani, M., Simonin, P., Sutter, B., Sahm, H., 1993. Isoprenoid biosynthesis in bacteria: a novel pathway for the early steps leading to isopentenyl diphosphate. Biochemical Journal 295, 517–524.

Schwarz, M.K., 1994. Terpen-Biosynthese in *Ginkgo biloba*: Eine überraschende Geschichte. PhD thesis Nr. 10951, Eidgenössische Technische Hochschule, Zürich.

Sprenger, G.A., Schörgen, U., Wiegert, T., Grolle, S., De Graaf, A.A., Taylor, S.V., Begley, T.P., Bringer-Meyer, S., Sahm, H., 1997. Identification of a thiamin-dependent synthase in *Escherichia coli* required for the formation of the 1-deoxy-D-xylulose 5-phosphate precursor to isoprenoids, thiamin, and pyridoxol. Proceedings of the National Academy of Sciences of the USA 94, 12857–12862.

Stanjek, V., Piel, J., Boland, W., 1999. Biosynthesis of furanocoumarins: mevalonate independent prenylation of umbelliferone in *Apium graveolens* (Apiaceae). Phytochemistry 50, 1141–1145.

Takahashi, S., Kuzuyama, T., Watanabe, H., Seto, H., 1998. A 1-deoxy-D-xylulose 5-phosphate reductoisomerase catalyzing the formation of 2-C-methyl-D-erythritol 4-phosphate in an alternative nonmevalonate pathway for terpenoid biosynthesis. Proceedings of the National Academy of Sciences of the USA 95, 9879–9884.

Thiel R., Adam, K.P., Zapp, J., Becker, H., 1997. Isopentenyl diphosphate biosynthesis in liverworts. Pharmaceutical and Pharmacological Letters 7, 103–105.

Van Beek, T., Subrtova, D., 1995. Factors involved in the high pressure liquid chromatographic separation of alkenes by means of argentation chromatography on ion exchangers: overview of theory and new practical developments. Phytochemical Analysis 6, 1–19.

Zeidler, J.G., Lichtenthaler, H.K., May, H.U., Lichtenthaler, F.W., 1997. Is isoprene emitted by plants synthesized via the novel isopentenyl pyrophosphate pathway? Zeitschrift für Naturforschung 52c, 15–23.

PERGAMON

Phytochemistry 57 (2001) 15–22

PHYTOCHEMISTRY

www.elsevier.com/locate/phytochem

Seasonal variation in the content of hydrolysable tannins in leaves of *Betula pubescens*

Juha-Pekka Salminen [a,*], Vladimir Ossipov [a,b], Erkki Haukioja [b], Kalevi Pihlaja [a]

[a] *Laboratory of Physical Chemistry, Department of Chemistry, University of Turku, FIN-20014 Turku, Finland*
[b] *Section of Ecology, Department of Biology, University of Turku, FIN-20014 Turku, Finland*

Received 6 October 2000; received in revised form 1 December 2000

Abstract

The contents of 13 hydrolysable tannins in the leaves of white birch (*Betula pubescens* L.) trees were analysed at twelve stages throughout the growing season. All individual galloylglucoses, from 1-*O*-galloyl-β-D-glucopyranose to 1,2,3,4,6-penta-*O*-galloyl-β-D-glucopyranose, accumulated in young leaves, while ellagitannins showed significantly variable seasonal trends. The major ellagitannin during the whole growing season was pedunculagin, while 2,3-(*S*)-HHDP-glucopyranose, the end product of the proposed ellagitannin pathway, accumulated in mature leaves. Relationships between the characteristics of seasonal variation in the contents of individual ellagitannins and their chemical structures were used to unravel the biogenesis of ellagitannins in birch leaves. Evidence of degradation of ellagitannins through hydrolysis during leaf growth and development is presented and implications for herbivory are discussed. © 2001 Elsevier Science Ltd. All rights reserved.

Keywords: *Betula pubescens*; Betulaceae; Biosynthesis; Hydrolysable tannins; Gallotannins; Galloylglucoses; Ellagitannins; HPLC; ESI-MS

1. Introduction

Tannins form a large group of polyphenolic plant constituents that differ from most other natural phenolic compounds in their ability to precipitate proteins from solutions (Niehaus and Gross, 1997). The protein precipitation capacity of tannins has been suggested as an important factor reducing the suitability of plants for herbivores (Feeny, 1970; Hagerman and Robbins, 1987; Appel and Schultz, 1994). However, along with other measures of biological activities of tannins, this capacity varies depending on the chemical structure of the compound (Feldman and Sahasrabudhe, 1999; Feldman et al., 1999; Kilkowski and Gross, 1999). Thus the total content of tannins as such cannot serve as a measure of the biological activity of a plant sample. This holds true especially if seasonal variations in the contents of individual active and non-active tannins display different patterns even when their pooled content remains the same.

The tannins of terrestrial plants can be divided into two major structural groups: hydrolysable tannins (HTs) and proanthocyanidins (condensed tannins). HTs are characterised by a central polyol moiety (most often β-D-glucose) which is esterified with gallic acid (gallotannins, GTs) or hexahydroxydiphenic acid (ellagitannins, ETs). When the glucose core is esterified with five or fewer galloyl groups, the resulting compounds are defined as GT precursors or simple galloylglucoses (GGs), not GTs. The biogenesis of GGs has been shown to start with 1-*O*-galloyl-β-D-glucose as the first metabolite and to proceed by a series of consecutive and position-specific galloylation steps leading to 1,2,3,4,6-penta-*O*-galloyl-β-D-glucose (reviewed by Gross, 1999). In contrast to GGs, the biosynthetic pathway for the formation of ETs has not yet been determined, although it is generally assumed that all ETs are derived from 1,2,3,4,6-penta-*O*-galloyl-β-D-glucose by a stepwise, enzyme mediated oxidative coupling pathway (Helm et al., 1997).

Rapidly growing tree leaves display drastic seasonal changes in physical and biochemical characteristics, as has been shown in a number of studies (Feeny, 1970; Haukioja et al., 1978; Hatano et al., 1986; Baldwin et al., 1987; Makkar et al., 1991; Nurmi et al., 1996; Ossipov

* Corresponding author. Tel.: +358-2-333-6828; fax: +358-2-333-6700.
E-mail address: juhrau@utu.fi (J.-P. Salminen).

0031-9422/01/$ - see front matter © 2001 Elsevier Science Ltd. All rights reserved.
PII: S0031-9422(00)00502-1

et al., 1997; Kause et al., 1999). Most of these studies, however, measured the total contents of tannin groups, such as GTs or proanthocyanidins. Only in a few cases have individual HTs been quantified during the growing season (Hatano et al., 1986; Ossipov et al., 1997). Even then the numbers of individual HTs or sampling dates have been quite limited, thus preventing the determination, e.g. of ellagitannin pathways. Nevertheless, the high content of total GTs has been shown to reduce the suitability of birch leaves for larvae of the geometrid moth *Epirrita autumnata* (Kause et al., 1999; Ossipov et al., 2000).

Recently, using the sensitive and selective method of negative ion HPLC–ESI-MS, we have identified fourteen GGs and twenty ETs in birch (*Betula pubescens* L.) leaves (Salminen et al., 1999). In the present study the main HTs were isolated and purified, and the results of HPLC–ESI-MS identification were confirmed with ^{1}H and ^{13}C NMR spectroscopy. The contents of thirteen HTs were analysed 12 times during the growing season, using HPLC–ESI-MS with ion trace analysis. Relationships between the characteristics of seasonal variation in the contents of individual HTs and their chemical structures were used to unravel the biogenesis of ellagitannins in birch leaves. The results obtained will presumably contribute to an understanding of the great variability in the suitability of birch leaves for herbivores in different stages of leaf development (Kause et al., 1999).

2. Results

2.1. Identification of hydrolysable tannins

Birch leaf HTs have been earlier identified with chromatographic, UV spectral and mass spectrometric methods (Salminen et al., 1999). The structures of the main HTs were now confirmed by ^{1}H and ^{13}C NMR techniques as 1-*O*-galloyl-β-D-glucose (**1**) (Saijo et al., 1990), 1,6-di-*O*-galloyl-β-D-glucose (**2**) (Saijo et al., 1990), 1,2,6-tri-*O*-galloyl-β-D-glucose (**3**) (Haddock et al., 1982a), 1,2,3,6-tetra-*O*-galloyl-β-D-glucose (**4**) (Haddock et al., 1982a), 1,2,3,4,6-penta-*O*-galloyl-β-D-glucose (**5**) (Saijo et al., 1990; Haddock et al., 1982a), casuarictin (**6**) (Gupta et al., 1982), tellimagrandin I (**7**) (Wilkins and Bohm, 1976), pedunculagin (**8**) (Feldman and Smith, 1996; Lee et al., 1992) and 2,3-(*S*)-HHDP-glucose (**9**) (Lee et al., 1992). Tellimagrandin II (**10**) and isostrictinin (**11**) were identified on the basis of UV and mass spectra (Salminen et al., 1999) and retention times (Hatano et al., 1986; Okuda et al., 1982).

It has been proposed that the metabolic pathway of ETs includes, in addition to **6**, another galloyl-bis-HHDP-glucose isomer, namely potentillin (**12**) (Haddock et al., 1982b; Haslam, 1992). Haddock et al. (1982b) also reported the difficulty of separating **6** and **12** by chromatographic methods. We found birch leaves to contain two major isomers of galloyl-bis-HHDP-glucose that elute closely in HPLC (R_ts 19.8 and 20.2). The earlier eluted isomer was identified as **6** by NMR (see above), and thus the later one must have been **12**.

The identity of 1,2,3-tri-*O*-galloyl-4,6-(*S*)-HHDP-α-D-glucose (**13**) was proposed on the basis of UV and mass spectra (Salminen et al., 1999) and of seasonal changes in its content relative to its β-1-galloylated isomer, **10**. Likewise, the chirality of the HHDP moieties located at the 2,3- or 4,6-positions of the glucose core of natural ellagitannins has been reported to be invariably in the (*S*)-series (Feldman and Smith, 1996; Khanbabaee and Lötzerich, 1998).

2.2. Seasonal trends in the content of hydrolysable tannins

Seasonal variations in the contents of birch leaf galloylglucoses are shown in Fig. 1. The maximum level was found in the youngest leaves. During leaf maturation the contents of all individual GGs per unit leaf weight decreased rapidly. However, their amounts per leaf increased, with a maximum between 28 May (**1**) and 7 June (**5**) (data not shown). This implies that the synthesis of GGs continued during the time when their content per unit leaf weight decreased due to dilution of GGs into the increasing leaf mass (Koricheva, 1999). Interestingly, after the short shoot leaves had reached their final size (after 5 July), clear increases were observed in the contents of all GGs except **1** (see Fig. 1).

In contrast to GGs, the contents of individual ETs showed variable seasonal trends (see Fig. 2a–d). This was especially obvious after excluding the rapid increase in leaf biomass during May and early June from the data by calculating the amounts of ETs per leaf (see Fig. 2e–h). For instance, while the contents of **6** and **8** seemed to remain at almost stable levels between 20 May and 7 June (Fig. 2b and c), their actual amounts per leaf increased significantly (Fig. 2f and g).

The order of individual ETs within the proposed ET pathway (Fig. 3) was determined from the relationships between the seasonal variation in the contents of individual ETs and their chemical structures. Plotting pairs of structurally or biogenetically related ETs showed that in the early stages of the growing season the balance was in favour of the predecessor, while during leaf maturation the balance switched towards the successor metabolite (for examples see Fig. 2).

Such ETs as **6**, **10** and **12** disappeared totally from the leaves of four birch trees already at 6 September, while the main patterns of HT variation were the same in all experimental trees. There were, however, large differences in the levels of individual HTs between individual

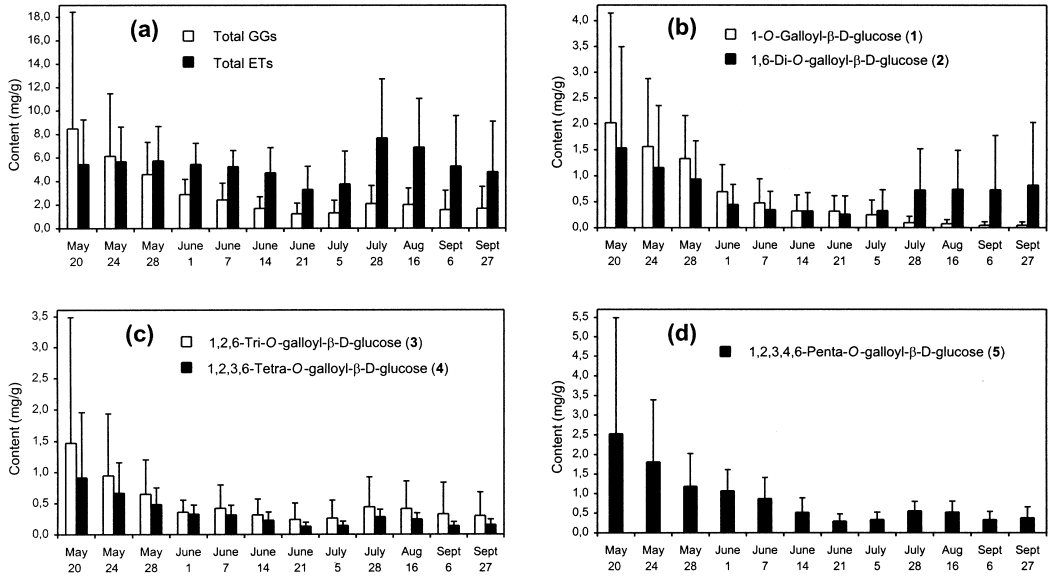

Fig. 1. Seasonal variation in the contents of hydrolysable tannins in leaves of white birch. (a) Total galloylglucoses and total ellagitannins; (b–d) individual galloylglucoses. Each bar on the graph represents the mean value of 10 trees. Vertical lines show standard deviations.

trees, as can be seen from the relatively large standard deviation bars in Figs. 1 and 2.

3. Discussion

Our results show that the contents of individual birch leaf HTs follow distinct seasonal patterns. This variation in the contents of individual GGs was consistent with previous studies (Nurmi et al., 1996; Ossipov et al., 1997); the patterns of variation of individual ETs, on the other hand, were now determined for the first time. These results allow us to describe the biosynthetic pathways of the main GGs, and in particular ETs, in birch leaves.

1-*O*-Galloyl-β-D-glucose has been shown to be the first metabolite in the biogenesis of GGs, being formed from UDP-glucose and gallic acid (Gross, 1982). This same phenomenon was confirmed in our birch data: **1** was one of the major GGs in young leaves, representing more than 24% of the total content of GGs. Several studies have also suggested that **1** acts as a principal galloyl donor for a series of consecutive and position-specific galloylation steps leading to **5**, the specificity of galloylations being usually 1-galloyl > 6-galloyl > 2-galloyl > 3-galloyl ⩾ 4-galloyl (reviewed by Gross, 1999). The biosynthesis of the second metabolite, **2**, requires two molecules of **1**. The first molecule acts as a galloyl donor and the second as an acceptor. Thus the increase in the content of **2** would mean a clear decrease in the content of **1**, especially if the rate of biosynthesis of **1** is simultaneously low. This was found to occur in mature leaves, after 5 July, as **2** became the major GG while **1** vanished almost totally (see Fig. 1b). The position-specificity of galloylations was proved to function in birch leaves as well; the other main GGs were identified as **3**, **4** and **5**.

In our study the final product of GG biosynthesis was **5**, as indicated by the absence of hexagalloylglucoses even in trace amounts. The metabolism of **5** in birch leaves thus mainly relates to the biosynthesis of ETs and not to transformation into hexagalloylglucose or other higher galloylated GTs. This specificity of birch leaves could be the result of the lack of enzymes that catalyse the formation of GTs from **5** (Hofmann and Gross, 1990; Niemetz and Gross, 1998, 1999).

Denzel and Gross (1991) found that **5** inhibited the activity of sumac leaf galloyltransferase, which in turn activated the transfer of 1-galloyl from **2** to the 2-position of the same compound. A similar feedback inhibition may take place in the transfer of 1-galloyl from **1** as well. Accordingly, when the content of **5** declines in birch leaves, for example in the process of its active utilisation, this inhibition would diminish. This would be followed by a simultaneous decrease in the content of **1** and by an increase in the content of **2** and all the biosynthetically subsequent HTs, as was found in our study (see Figs. 1 and 2, after 5 July). The function of **2** as a galloyl donor in birch leaves is unlikely, since it would also have meant an increase in the content of 6-*O*-galloyl-β-D-glucose as the deacylated by-product; this was not observed (data not shown).

According to Yoshida et al. (1992) there is a direct position-specific dependence on the ease of cleavability of different galloyl as well as HHDP groups through hydrolysis: 1-galloyl > 2-galloyl > 3-galloyl ⩾ 6- and 4-galloyl, 4,6-HHDP > 2,3-HHDP. The only galloyl group observed to be hydrolysed during this study was

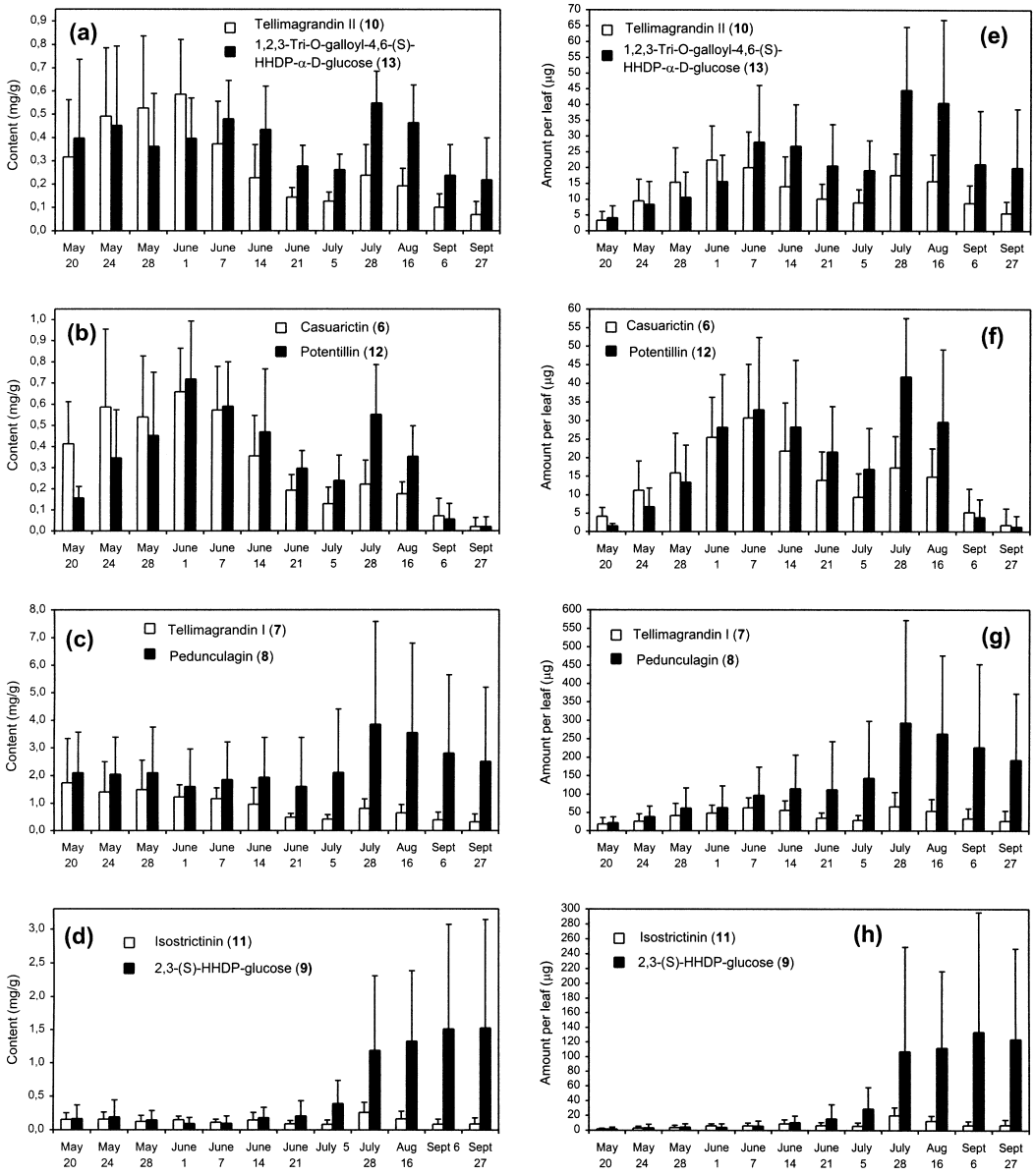

Fig. 2. Variation in contents (a–d) and amounts per leaf (e–h) of individual ellagitannins during leaf development. Each bar on the graph represents the mean value of 10 trees. Vertical lines show standard deviations.

the 1-galloyl of ETs. This indicates that for instance in **7** the oxidative coupling between 2- and 3-galloyls to yield **8** is preferred compared to the hydrolysis of 2-galloyl. This hydrolysis would have yielded 3-*O*-galloyl-4,6-HHDP-glucose, which has an ungalloylated anomeric centre, thus producing two peaks in HPLC; this, however, was not observed. The more rapid cleavability of 4,6-HHDP compared to 2,3-coupled was confirmed, since 8 h hydrolysis of **8** in 100°C water yielded **9** and ellagic acid. It is interesting that while the 2,3-HHDP group of **8** is less prone to hydrolysis than the 4,6-HHDP, it is also more difficult to incorporate into the glucose core than the 4,6-HHDP in chemical syntheses of **8** (Feldman and Smith, 1996). The delayed degradation of **8**, resulting in higher amounts of **9** in mature leaves only (see Fig. 2), could be due to the younger leaves having higher contents of certain GGs that inhibited the activity of ET degrading enzymes (Daniel et al., 1991).

In addition to hydrolysis, polymerisation and insolubilisation have also been suggested to decrease the content of ellagitannins (Scalbert et al., 1988; Peng et al., 1991; Klumpers et al., 1994; Viriot et al., 1994). According to Hatano et al. (1992), the intermolecular oxidative coupling producing oligomeric ETs in plants does not depend on a simple self-association of constituent monomeric tannins. Rather, it is controlled regiospecifically by enzymatic systems that vary among plant species. Presumably such enzymes were not present in our experimental trees, as polymerisation of

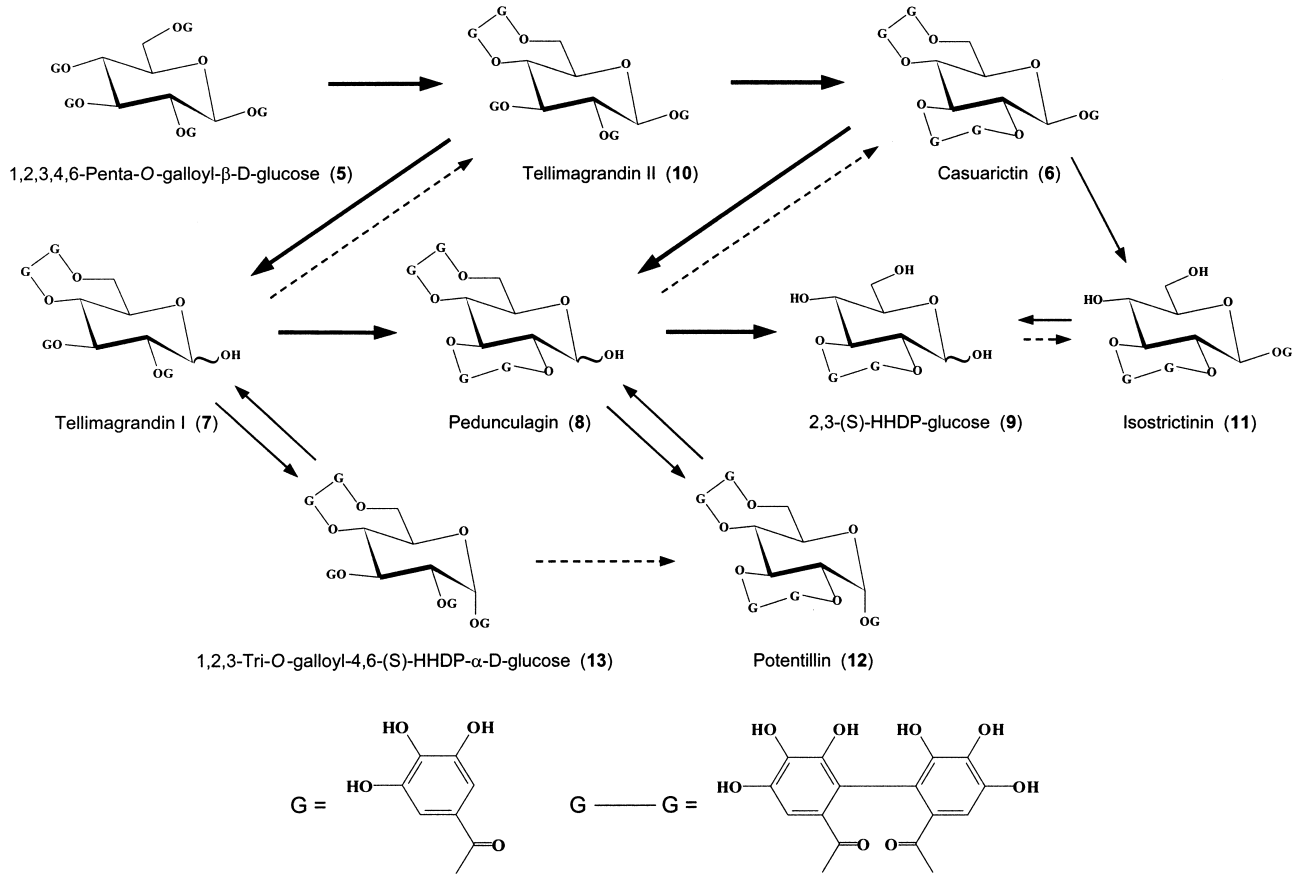

Fig. 3. Proposed biosynthetic pathway for formation of ellagitannins in the leaves of *Betula pubescens*.

birch leaf ellagitannins, for instance to dimers, was not observed. The amount of insoluble ETs, on the other hand, has been shown to increase during birch leaf growth and development (Salminen et al., unpublished work). One explanation for the almost total disappearance of **6** and **12** in autumn leaves could have been the opening of their glucose ring and the formation of C-glycosidic ETs such as vescalagin and castalagin, the main ETs for instance of oak wood (Helm et al., 1997; Puech et al., 1999). However, such ring opening is not characteristic of birch leaf ETs as neither vescalagin or castalagin, nor their degradation products vescalin or castalin were detected in any stage of leaf development.

In the ecological literature, foliar tannins are traditionally viewed as precipitators of leaf proteins, which by this means increase the herbivore resistance of plants (Feeny, 1970). The formation of only monomeric ETs from **5**, instead of highly galloylated GTs, suggests other functions for birch leaf hydrolysable tannins in addition to protein precipitation. Indeed, the accumulation of **9** in mature birch leaves is indirect proof of the existence and accumulation of ellagic acid, a proposed insect growth inhibitor (Klocke et al., 1986), in those same leaves as well. According to this view, HTs could play a dual role in plant-herbivore interactions, not only by a direct astringency-dependent deterrence of herbivorous insects, but also indirectly through their degradation products (Niehaus and Gross, 1997).

To sum up, we urge the need for studies in which individual HTs, including ETs, are considered as determinants of the changing suitabilities of birch leaves for herbivores (Kause et al., 1999). Such detailed studies will make it possible to determine whether these structurally diverse tannins, with possibly diverse biological activities, are truly effective defences against herbivores. In the words of Haslam (1988): "If tannins are so generalised in their action as supposed, it is very difficult to rationalise this generality with the very structural diversity found among the plethora of plant polyphenols — particularly those of the hydrolysable tannin class based on gallic acid and its derivatives."

4. Experimental

4.1. Plant material

Short shoot leaves of 10 29- to 33-year-old white birches (*Betula pubescens* L.) of known seed origin were sampled in the Botanical Garden of the University of Turku (SW Finland) 12 times during the growing season of 1999. All short shoot leaves in a tree are

produced in the spring flush; thus the age of sampled leaves grew monotonously with the season. The first samples were collected when the leaves had just opened from the bud, while the last leaves sampled were senescent and about to fall. Since the major changes in the content of birch leaf HTs have been reported to take place in young leaves (Baldwin et al., 1987; Nurmi et al., 1996; Ossipov et al., 1997) the sampling interval varied from four days in the early spring to three weeks in the autumn. Samples of 10–15 leaves per tree were collected between 9 and 10 a.m. haphazardly from branches located 2–5 m above the ground. The leaves were clipped from the petioles and placed in sealed plastic vials, which were enclosed in an insulated box filled with ice and transported immediately to a laboratory freezer. Voucher specimens have been deposited at TUR under the following accession codes: TUR 360093 and TUR 360103.

4.2. Sample preparation

The freeze-dried birch leaves (300 mg dry wt) were extracted three times with 70% aq. Me_2CO. After removal of Me_2CO at room temp., the aq. extract was freeze-dried and dissolved in 6 ml water. These aq. samples were filtered through 0.45 μm PTFE filters and kept frozen at −20°C until analysed with HPLC–ESI-MS.

4.3. Isolation and purification of hydrolysable tannins

A large number of freeze-dried white birch leaves (1.8 kg dry wt) were extracted with 70% aq. Me_2CO (containing 0.1% ascorbic acid to prevent oxidation) and fractionated on a Sephadex LH-20 column (40×2.5 cm i.d.) into seven fractions (fr 1–7), as previously described (Salminen et al., 1999). Individual HTs in the resulting fractions were purified further by chromatography on a Merck LiChroprep RP-18 column (44×3.7 cm i.d., 40–63 μm) using different gradients of CH_3CN in 1% aq. HCO_2H. This purification resulted in **1** (fr 1, 88 mg), **2** (fr 3, 48 mg), **3** (fr 5, 33 mg), **4** (fr 6, 39 mg), **5** (fr 7, 45 mg), **6** (frs 5 and 6, 23 mg), **7** (fr 5, 66 mg), **8** (fr 4, 35 mg) and **9** (fr 1, 19 mg).

4.4. Equipment and chromatographic conditions

4.4.1. HPLC–ESI-MS

HPLC–ESI-MS analysis of birch leaf extracts was performed using a Perkin-Elmer Sciex API 365 triple quadrupole mass spectrometer (Sciex, Toronto, Canada). This instrument is equipped with an ion-spray (pneumatically assisted electrospray) interface and a Macintosh data system. The HPLC system consists of two Perkin-Elmer Series 200 micro pumps (Perkin-Elmer, Norwalk, CT, USA) connected to a Series 200 autosampler. The eluate passes through a Merck Superspher 100 RP-18 column (75×4 mm i.d., 4 μm), and the UV trace is recorded with a 785A UV/VIS detector at 280 nm. After UV detection, part of the eluate was split off and introduced into the ESI-MS system.

Chromatographic and ESI-MS conditions were as described in a previous paper (Salminen et al., 1999).

4.4.2. ^1H and ^{13}C NMR

The ^1H and ^{13}C NMR spectra were recorded on a Jeol Lambda 400 MHz series spectrometer and a Brüker routine AM-200 NMR spectrometer, respectively. The spectra were run at ambient temperature in Me_2CO-d_6 (in some measurements a few drops of D_2O were added to enhance the solubility of the analyte). Chemical shifts were measured in relation to the solvent peak and converted to the TMS scale by adding 2.05 ppm (^1H NMR) and 29.92 ppm (^{13}C NMR).

4.5. Quantification of hydrolysable tannins

HTs of birch leaves were separated and quantified with HPLC–ESI-MS using ion trace analysis of deprotonated molecules ($[M–H]^-$) (Salminen et al., 1999). The mass selectivity of this method allows the quantitative analysis of HTs even though many of them are co-eluting in HPLC with other phenolic compounds present in birch leaf extracts. Calibration curves for quantification were prepared with known concentrations of **1**, **2**, **3**, **4**, **5** and **8**. The contents of **6**, **7**, **9** and **12** were calculated as **8** equivalents; **10** and **13** as **5** equivalents; and **11** as **3** equivalent mg/g in dry wt basis. Differences in the ionisation of HTs between individual runs were standardised by monitoring the ionisation of chlorogenic acid as an internal standard.

The R_ts and values of deprotonated molecules used for the quantification of tannins were as follows: **9**, 1.6 and 2.8 min (anomeric mixture), *m*/*z* 481; **1**, 5.0 min, *m*/*z* 331; **8**, 9.5 and 12.4 min (anomeric mixture), *m*/*z* 783; **7**, 14.0 and 16.8 min (anomeric mixture), *m*/*z* 785; **2**, 15.0 min, *m*/*z* 483; **11**, 15.6 min, *m*/*z* 633; **3**, 18.0 min, *m*/*z* 635; **6**, 19.8 min, *m*/*z* 935; **12**, 20.2 min, *m*/*z* 935; **10**, 21.1 min, *m*/*z* 937; **4**, 21.8 min, *m*/*z* 787; **13**, 23.6 min, *m*/*z* 937; **5**, 24.3 min, *m*/*z* 939.

Acknowledgements

The authors wish to acknowledge the help of Matti Yli-Rekola from the Botanical Garden of Turku University, Jaakko Hellman from the Instrument Centre of the Department of Chemistry, Kyösti Lempa from the Department of Biology, and Riitta Koivikko from the Department of Chemistry, all at the University of Turku. Ellen Valle kindly checked the language. The study was funded by the Emil Aaltonen Foundation (J.-P.S.) and the Academy of Finland.

References

Appel, H.M., Schultz, J.C., 1994. Oak tannins reduce effectiveness of thuricide (*Basillus thuringiensis*) in the gypsy moth (Lepidoptera: Lymantriidae). Plant Resistance 87, 1736–1742.

Baldwin, I.T., Schultz, J.C., Ward, D., 1987. Patterns and sources of leaf tannin variation in yellow birch (*Betula allegheniensis*) and sugar maple (*Acer Saccharum*). Journal of Chemical Ecology 13, 1069–1078.

Daniel, E.M., Ratnayake, S., Kinstle, T., Stoner, G.D., 1991. The effects of pH and rat intestinal contents on the liberation of ellagic acid from purified and crude ellagitannins. Journal of Natural Products 54, 946–952.

Denzel, K., Gross, G.G., 1991. Biosynthesis of gallotannins: enzymatic 'disproportionation' of 1,6-digalloylglucose to 1,2,6-trigalloylglucose and 6-galloylglucose by an acyltransferase from leaves of *Rhus typhina* L. Planta 184, 285–289.

Feeny, P., 1970. Seasonal changes in oak leaf tannins and nutrients as a cause of spring feeding by winter moth caterpillars. Ecology 51, 565–581.

Feldman, K.S., Smith, R.S., 1996. Ellagitannin chemistry. First total synthesis of the 2,3- and 4,6-coupled ellagitannin pedunculagin. Journal of Organic Chemistry 61, 2606–2612.

Feldman, K.S., Sahasrabudhe, K., 1999. Ellagitannin chemistry. Syntheses of tellimagrandin II and a dehydrodigalloyl ether-containing dimeric gallotannin analogue of coriariin A. Journal of Organic Chemistry 64, 209–216.

Feldman, K.S., Sambandam, A., Lemon, S.T., Nicewonger, R.B., Long, G.S., Battaglia, D.F., Ensel, S.M., Laci, M.A., 1999. Binding affinities of gallotannin analogs with bovine serum albumin, ramifications for polyphenol-protein molecular recognition. Phytochemistry 51, 867–872.

Gross, G.G., 1982. Synthesis of β-glucogallin from UDP-glucose and gallic acid by an enzyme preparation from oak leaves. FEBS Letters 148, 67–70.

Gross, G.G., 1999. Biosynthesis of hydrolyzable tannins. In: Pinto, B.M. (Ed.), Comprehensive Natural Products Chemistry, Vol. 3. Elsevier, Amsterdam, pp. 799–826.

Gupta, R.K., Al-Shafi, S.M.K., Layden, K., Haslam, E., 1982. The metabolism of gallic acid and hexahydroxydiphenic acid in plants. Part 2. Esters of (S)-hexahydroxydiphenic acid with D-glucopyranose ($^4C_1$). Journal of the Chemical Society Perkin Transactions I, 2525–2534.

Haddock, E.A., Gupta, R.K., Al-Shafi, S.M.K., Haslam, E., 1982a. The metabolism of gallic acid and hexahydroxydiphenic acid in plants. Part 1. Introduction. Naturally occurring galloyl esters. Journal of the Chemical Society Perkin Transactions I, 2515–2524.

Haddock, E.A., Gupta, R.K., Al-Shafi, S.M.K., Layden, K., Haslam, E., Magnolato, D., 1982b. The metabolism of gallic acid and hexahydroxydiphenic acid in plants: biogenetic and molecular taxonomic considerations. Phytochemistry 21, 1049–1062.

Hagerman, A.E., Robbins, C.T., 1987. Implications of soluble tannin-protein complexes for tannin analysis and plant defence mechanisms. Journal of Chemical Ecology 13, 1243–1259.

Haslam, E., 1988. Plant polyphenols (syn. vegetable tannins) and chemical defence — a reappraisal. Journal of Chemical Ecology 14, 1789–1805.

Haslam, E., 1992. Gallic acid and its metabolites. In: Hemingway, R.W., Laks, P.E. (Eds.), Plant Polyphenols. Plenum Press, New York, pp. 169–194.

Hatano, T., Kira, R., Yoshizaki, M., Okuda, T., 1986. Seasonal changes in the tannins of *Liquidambar formosana* reflecting their biogenesis. Phytochemistry 25, 2787–2789.

Hatano, T., Okonogi, A., Okuda, T., 1992. Oligomeric hydrolyzable tannins from *Liquidambar formosana* and spectral analysis of the orientation of valoneoyl groups in their molecules. In: Hemingway, R.W., Laks, P.E. (Eds.), Plant Polyphenols. Plenum Press, New York, pp. 195–207.

Haukioja, E., Niemelä, P., Iso-Iivari, L., Ojala, H. and Aro, E.M., 1978. Birch leaves as a resource for herbivores. I. Variation in the suitability of leaves. Reports of the Kevo Subarctic Research Station 14, 5-12.

Helm, R.F., Ranatunga, T.D., Chandra, M., 1997. Lignin-hydrolyzable tannin interactions in wood. Journal of Agricultural and Food Chemistry 45, 3100–3106.

Hofmann, A.S., Gross, G.G., 1990. Biosynthesis of gallotannins: formation of polygalloylglucoses by enzymatic acylation of 1,2,3,4,6-penta-*O*-galloylglucose. Archives of Biochemistry and Biophysics 283, 530–532.

Kause, A., Ossipov, V., Haukioja, E., Lempa, K., Hanhimäki, S., Ossipova, S., 1999. Multiplicity of biochemical factors determining quality of growing birch leaves. Oecologia 120, 102–112.

Khanbabaee, K., Lötzerich, K., 1998. Synthesis of enetiomerically pure unusual ellagitannins 1,4,6-tri-*O*-galloyl-2,3-(*R*)-hexahydroxydiphenoyl-β-D-glucopyranoside and 4,6,-di-*O*-galloyl-2,3-(R)-hexahydroxydiphenoyl-D-glucoside. The proposed chemical structures for cercidinin A and B must be revised. Journal of Organic Chemistry 63, 8723–8728.

Kilkowski, W.J., Gross, G.G., 1999. Color reaction of hydrolyzable tannins with Bradford reagent, Coomassie brilliant blue. Phytochemistry 51, 363–366.

Klocke, J.A., van Wagenen, B., Balandrin, M.F., 1986. The ellagitannin geranin and its hydrolysis products isolated as insect growth inhibitors from semi-arid land plants. Phytochemistry 25, 85–91.

Klumpers, J., Scalbert, A., Janin, G., 1994. Ellagitannins in european oak wood: polymerization during wood ageing. Phytochemistry 36, 1249–1252.

Koricheva, J., 1999. Interpreting phenotypic variation in plant allelochemistry: problems with the use of concentrations. Oecologia 119, 467–473.

Lee, M.-W., Tanaka, T., Nonaka, G.-I., Nishioka, I., 1992. Dimeric ellagitannins from *Alnus japonica*. Phytochemistry 31, 2835–2839.

Makkar, H.P.S., Dawra, R.K., Singh, B., 1991. Tannin levels in leaves of some oak species at different stages of maturity. Journal of the Science of Food and Agriculture 54, 513–519.

Niehaus, J.U., Gross, G.G., 1997. A gallotannin degrading esterase from leaves of pedunculate oak. Phytochemistry 45, 1555–1560.

Niemetz, R., Gross, G.G., 1998. Gallotannin biosynthesis: Purification of β-glucogallin: 1,2,3,4,6-pentagalloyl-β-D-glucose galloyltransterase from sumac leaves. Phytochemistry 49, 327–332.

Niemetz, R., Gross, G.G., 1999. Gallotannin biosynthesis: a new β-glucogallin-dependent galloyltransferase from sumac leaves acylating gallotannins at positions 2 and 4. Journal of Plant Physiology 155, 441–446.

Nurmi, K., Ossipov, V., Haukioja, E., Pihlaja, K., 1996. Variation of total phenolic content and individual low-molecular-weight phenolics in foliage of mountain birch trees. Journal of Chemical Ecology 22, 2023–2040.

Okuda, T., Yoshida, T., Hatano, T., Yazaki, K., Ashida, M., 1982. Ellagitannins of the casuarinaceae, stachyuraceae and myrtaceae. Phytochemistry 21, 2871–2874.

Ossipov, V., Loponen, J., Ossipova, S., Haukioja, E., Pihlaja, K., 1997. Gallotannins of birch *Betula pubescens* leaves: HPLC separation and quantification. Biochemical Systematics and Ecology 25, 493–504.

Ossipov, V., Haukioja, E., Ossipova, S., Hanhimäki, S. and Pihlaja, K. 2000. Phenolic and phenolic-related factors as determinants of suitability of mountain birch leaves to an herbivorous insect. Biochemical Systematics and Ecology, in press.

Peng, S., Scalbert, A., Monties, B., 1991. Insoluble ellagitannins in *Castanea Sativa* and *Quercus Petraea* woods. Phytochemistry 30, 775–778.

Puech, J.-L., Mertz, C., Michon, V., Le Guernevé, C., Doco, T., Hervé

du Penhoat, C., 1999. Evolution of castalagin and vescalagin in ethanol solutions. Identification of new derivatives. Journal of Agricultural and Food Chemistry 47, 2060–2066.

Saijo, R., Nonaka, G.-I., Nishioka, I., 1990. Gallic acid esters of bergenin and norbergenin from *Mallotus japonicus*. Phytochemistry 29, 267–270.

Salminen, J.-P., Ossipov, V., Loponen, J., Haukioja, E., Pihlaja, K., 1999. Characterisation of hydrolysable tannins from leaves of *Betula pubescens* by high-performance liquid chromatography–mass spectrometry. Journal of Chromatography A 864, 283–291.

Scalbert, A., Monties, B., Favre, J.-M., 1988. Polyphenols of *Quercus robur*: Adult tree and in vitro grown calli and shoots. Phytochemistry 27, 3483–3488.

Viriot, C., Scalbert, A., Hervé du Penhoat, C.L.M., Moutounet, M., 1994. Ellagitannins in woods of sessile oak and sweet chestnut dimerization and hydrolysis during wood ageing. Phytochemistry 36, 1253–1260.

Wilkins, C.K., Bohm, B.A., 1976. Ellagitannins from *Tellima grandiflora*. Phytochemistry 15, 211–214.

Yoshida, T., Hatano, T., Kuwajima, T., Okuda, T., 1992. Oligomeric hydrolyzable tannins — their ^{1}H NMR spectra and partial degradation. Heterocycles 33, 463–482.

PERGAMON

Phytochemistry 57 (2001) 23–32

PHYTOCHEMISTRY

www.elsevier.com/locate/phytochem

The biosynthesis of benzoic acid glucosinolate esters in *Arabidopsis thaliana*

Gerson Graser, Neil J. Oldham, Paul D. Brown [1], Ulrike Temp, Jonathan Gershenzon *

Max Planck Institute for Chemical Ecology, Carl-Zeiss-Promenade 10, D-07745 Jena, Germany

Received 18 September 2000; received in revised form 4 December 2000

Abstract

The siliques and seeds of *Arabidopsis thaliana* accumulate a series of glucosinolates containing an alkyl side chain of varying length with a terminal benzoate ester function. The biosynthesis of these unusual nitrogen- and sulfur-containing natural products was investigated by feeding isotopically-labeled precursors to detached flowering stems. Glucosinolates were extracted, purified and analyzed by tandem mass spectrometry. Phenylalanine and benzoic acid were incorporated into the benzoate ester function, and methionine and acetate were incorporated into the aliphatic portion of the side chain in a position-specific manner. The labeling patterns observed were consistent with the chain extension of methionine by a three-step elongation cycle which begins with the condensation of acetyl-CoA with a 2-oxo acid derived from methionine and ends with an oxidative decarboxylation forming a new 2-oxo acid with an additional methylene group. Incorporation of desulfo-4-methylthiobutyl glucosinolate into 4-benzoyloxybutyl glucosinolate suggested chain-extended methionine derivatives are first converted to their corresponding methylthioalkyl glucosinolates with further side chain modification occurring later. Transformation of the methylthiol function to a hydroxyl group is followed by esterification with benzoic acid. The siliques appear to possess the complete machinery for carrying out all of the reactions in the biosyntheis of these complex glucosinolates. © 2001 Elsevier Science Ltd. All rights reserved.

Keywords: *Arabidopsis thaliana*; Brassicaceae; Crucifers; Biosynthesis; Mass spectrometry; Glucosinolates; Benzoyloxy glucosinolates; Benzoic acid esters

1. Introduction

Glucosinolates are sulfur containing secondary metabolites found mainly in members of the Brassicaceae, the mustard family (Underhill, 1980; Poulton and Møller, 1993; Halkier, 1999), where they play an important role in plant–herbivore and plant–pathogen interactions (Van Etten and Tookey, 1979; Chew, 1988). Their biological activities are often due to hydrolysis products released by the action of myrosinase (a β-thioglucoside glucohydrolase, EC 3.2.3.1), an enzyme stored separately from glucosinolates in the intact plant. All glucosinolates share a basic skeleton comprised of a β-thioglucose moiety, a sulfonated oxime and a side chain (Halkier, 1999) (Fig. 1). The great structural diversity of this class results from their variable side-chains (Brown and Mora, 1997; Fahey et al., 2001), which are all believed to be derived from a small group of common amino acids and their chain elongated derivatives (Underhill, 1980; Wallsgrove and Bennett, 1995).

The biosynthesis of the common glucosinolate skeleton is in large part understood, and many of the enzymes involved have been well-characterized (Halkier and Du, 1997; Halkier, 1999). The parent amino acid is first oxidized to an aldoxime (Fig. 1), catalyzed in most if not all cases by cytochrome P450 monooxygenases (Hull et al., 2000; Wittstock and Halkier, 2000). Then, a thiol group is added, probably as a result of conjugation with cysteine (Halkier, unpublished results), followed by C–S cleavage (Kiddle et al., 1999) to produce a thiohydroximate. Finally, transfer of glucose and sulfate moieties completes the basic skeleton.

Abbreviations: 3-BZO, 3-benzoyloxypropyl glucosinolate; 4-BZO, 4-benzoyloxybutyl glucosinolate; 4-MTB, 4-methylthiobutyl glucosinolate; APCI-MS, atmospheric pressure chemical ionization mass spectrometry;

* Corresponding author. Tel.: +49-3641-643661; fax: +49-3641-643650.

E-mail address: gershenzon@ice.mpg.de (J. Gershenzon).

[1] Current adress: Department of Plant, Soil and Entomological Sciences, University of Idaho, Moscow, ID 83844, USA.

0031-9422/01/$ - see front matter © 2001 Elsevier Science Ltd. All rights reserved.
PII: S0031-9422(00)00501-X

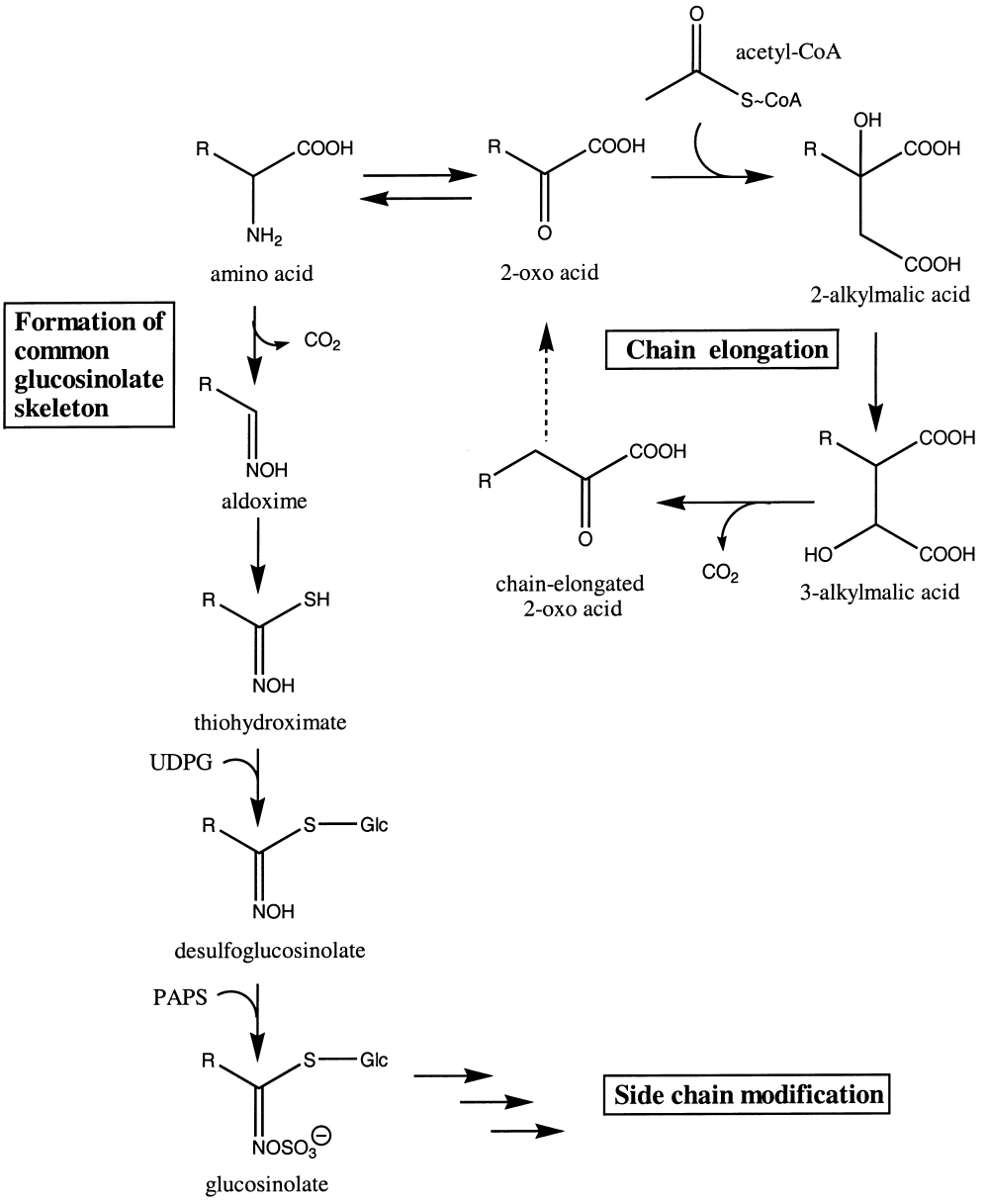

Fig. 1. Outline of glucosinolate biosynthesis showing the conversion of amino acids to the basic glucosinolate skeleton via a 4-step pathway. Prior to entering this pathway, amino acids such as methionine and phenylalanine can undergo one or more rounds of chain elongation. Additional side chain modifications can occur following the pathway. R indicates the variable side chain.

Much less is known about the biogenetic sequences responsible for side chain elongation and modification. In vivo metabolic studies, carried out in the 1960s using radio-labeled precursors (summarized in Underhill, 1980; Wallsgrove and Bennett, 1995), provided evidence for side chain elongation by deamination of the parent amino acid followed by a 3-step elongation cycle. Recent experiments with stable isotope labels have confirmed this pathway for the glucosinolates derived from elongated methionine derivatives in *Eruca sativa* (Graser et al., 2000). In the first step (Fig. 1), the 2-oxo acid formed by deamination condenses with acetyl CoA to form a 2-malic acid derivative which has been detected (Chapple et al., 1988). Then, isomerization to a 3-malic acid derivative followed by oxidative decarboxylation leads to the formation of a 2-oxo acid extended by one methylene group. Similar three-step elongations of 2-oxo acids are known in the citric acid cycle and in leucine biosynthesis (Bryan, 1980). Once extended, a 2-oxo acid can undergo additional cycles of chain elongation to form longer homologues with as many as six additional methylene groups in *Arabidopsis thaliana*, before being transaminated and entering the main pathway of glucosinolate biosynthesis. (Poulton and Møller, 1993; Wallsgrove and Bennett, 1995). In addition to elongation, the side chains of glucosinolates can be modified by thiol

oxidation, hydroxylation, esterification and other transformations. However, little information is available about the biosynthetic conversions involved.

The seeds and siliques of *A. thaliana* accumulate a series of benzoic acid glucosinolate esters of which 3-benzoyloxypropyl glucosinolate (3-BZO) and 4-benzoyloxybutyl glucosinolate (4-BZO) are the major compounds (Hogge et al., 1988). These unusual non-polar glucosinolates may be uniquely adapted for storage in the low-water environment of the seed. The benzoyloxy function may also have significance in altering susceptibility to cleavage by myrosinase. Given the co-occurrence of these substances with a series of methylthioalkyl and methylsulfinylalkyl glucosinolates, it may be postulated that the alkyl portion of the side chain is derived from the chain elongation of methionine, with one cycle of chain elongation required for 3-BZO and two cycles for 4-BZO. Following the loss of the methylthiol (or methylsulfinyl) function and its replacement by a hydroxyl function, ester formation can occur. The benzoic acid residue itself can be expected to arise from phenylalanine *via* cinnamic acid (Lee et al., 1995), but it is unclear if benzoylation and the other side chain modifications occur before or after formation of the common glucosinolate skeleton. Here we report the results of a series of experiments to study the formation of 3-BZO and 4-BZO in the siliques of *A. thaliana*. Isotopically-labeled precursors were fed in vivo, and the glucosinolate products isolated, purified and analyzed by tandem mass spectrometry. In addition to determining the precursors of each portion of the side chain, we investigated whether the steps in side chain modification precede or follow the other steps in the formation of glucosinolates.

2. Results and discussion

2.1. Incorporation of methionine, acetate, phenylalanine and benzoic acid

The biosynthesis of benzoic acid glucosinolate esters in *A. thaliana* siliques was investigated by feeding a variety of precursors to flowering stems. Glucosinolates were isolated in their desulfonated forms and analyzed by atmospheric pressure chemical ionization mass spectrometry from a 1:1 mixture of acetonitrile and water. Fig. 3 shows the molecular ion regions of the spectra of desulfo-4-benzoyloxybutyl glucosinolate (desulfo-4-BZO) isolated after feeding different precursors. The desulfo-4-BZO from an unfed control plant (Fig. 3a) gave a molecular species ($[M+H]^+$) at m/z 416 (100%) and two significant (>5% relative intensity) higher mass peaks at m/z 417 (30±0.3%, mean and standard error from five measurements) and 418 (8.5±0.1%). Administration with [2-^{13}C]acetate gave rise to desulfo-4-BZO with a mass spectrum (Fig. 3b) showing increases in the relative intensities of both m/z 417 (40.1±0.7%) and 418 (22.5±0.3%), demonstrating the incorporation of label from both one and two acetate units, respectively (Fig. 2). Fig. 3c shows the spectrum of desulfo-4-BZO following administration of [U-^{13}C]methionine. An intense ion at m/z 419 (42.8±0.8%) indicated the presence of three ^{13}C atoms and, therefore, the incorporation of only 3 of the 5 carbon atoms of methionine (Fig. 2). Application of either [$^2H_5$]phenylalanine or [$^2H_5$]benzoic acid to *A. thaliana* resulted in incorporation of all five ^{2}H atoms (m/z 421 = 6.4±0.1% from [$^2H_5$]Phe treatment, Fig. 3d; m/z 421 = 5.5±0.2% from [$^2H_5$]benzoic acid treatment). A similar pattern of results was observed for desulfo-3-BZO; however, only one acetate unit was incorporated after [2-^{13}C]acetate feeding (Fig.1).

To locate the sites of label within the molecule, tandem mass spectrometry, using low energy collision induced dissociation (CID), was carried out with the ions listed above. Fig. 4a shows the CID spectrum of m/z 416 ($[M+H]^+$) of unlabelled desulfo-4-BZO. Two major fragment ions are visible at m/z 254 and m/z 132, and their presence can be rationalized by the scheme shown in Fig. 5. First, loss of the glucopyran ring, by a proposed six-membered pericyclic mechanism can generate the ion at m/z 254, which can in turn undergo a second pericyclic fragmentation to give m/z 132 by loss of benzoic acid. Thus, the glucosinolate molecule fragmented conveniently into three parts: the sugar moiety, the benzoate group, and the aliphatic chain with N and S atoms attached. The CID spectrum of m/z 419 (Fig. 4b), from [$^{13}C_3$]-desulfo-4-BZO formed following [U-^{13}C]methionine treatment (see also Fig. 3c), showed ions at m/z 257 and 135, in contrast to m/z 254 and 132 in the native 4-BZO, unambiguously locating the three ^{13}C atoms on the aliphatic chain. On the other hand, fragmentation of $[M+H]^+$ from [$^2H_5$]-desulfo-4-BZO (m/z 421) formed following incorporation of either [$^2H_5$]phenylalanine or [$^2H_5$]benzoic acid gave product ions at m/z 259 and 132 (Fig. 4c). This result can only be explained by the presence of deuterium labeling on the benzoate group of the glucosinolate (Fig. 5). Therefore, it can be concluded that three of the five C atoms of 4-BZO arise from methionine, while the benzoate group is derived from phenylalanine (Fig. 2). Similar results were observed for 3-BZO.

From the mass spectrum of desulfo-4-BZO obtained following administration with [2-^{13}C]acetate (Fig. 3b), it appeared that the remaining two carbon atoms in the aliphatic chain of 4-BZO originated from the C-2 carbon atoms of two acetate residues (Fig. 2). Tandem MS experiments required to confirm this finding were less straightforward than those employed for the species obtained from the administration of methionine, phenylalanine or benzoic acid. The major difficulty was the small mass shift associated with incorporation of one or two ^{13}C atoms, and the consequent overlap of product

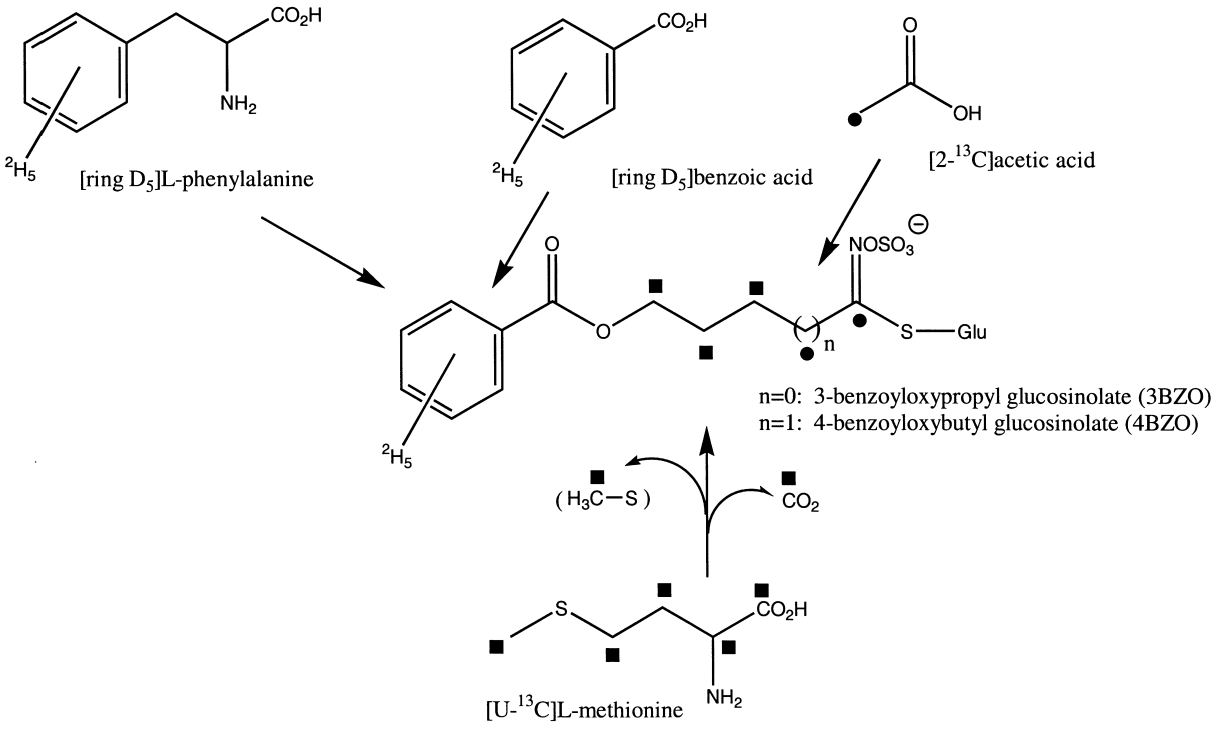

Fig. 2. In vivo labeling patterns of [$^2H_5$]L-phenylalanine, [$^2H_5$]benzoic acid, [U-^{13}C]L-methionine and [2-^{13}C]acetate incorporated into 3-benzoyloxypropyl- and 4-benzoyloxybutyl glucosinolate in siliques of *Arabidopsis thaliana*. Results show that phenylalanine and benzoic acid were incorporated into the benzoate ester function, while methionine and acetate were incorporated into the aliphatic portion of the glucosinolate side chain according to the chain elongation sequence proposed.

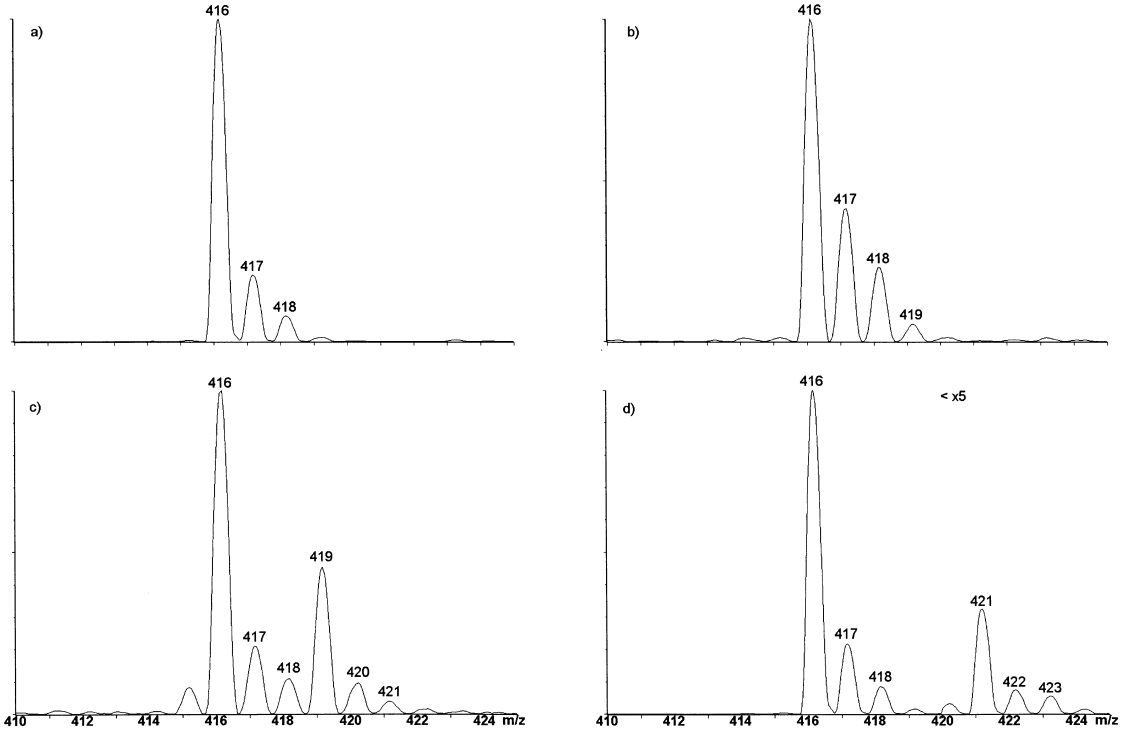

Fig. 3. The molecular ion region of the mass spectra of 4-BZO isolated from *Arabidopsis thaliana* siliques after administration of (b) [2-^{13}C]acetate, (c) [U-^{13}C]methionine, and (d) [$^2H_5$]phenylalanine or [$^2H_5$]benzoic acid. Panel (a) is the 4-BZO spectrum from unlabeled control plants. 'x5' in panel (d) indicates five-fold enhancement of signal intensity in the above region m/z 420.

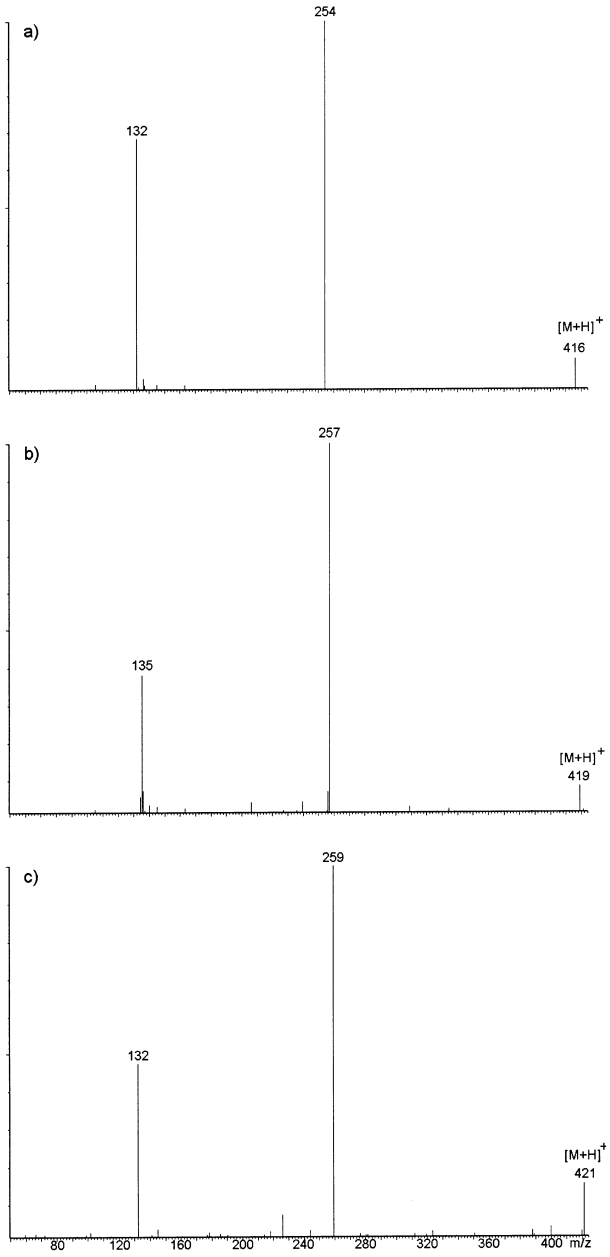

Fig. 4. Collision induced dissociation-product ion mass spectra for (a) $[M+H]^+$ of unlabeled 4-BZO, (b) $[M+H]^+$ of 4-BZO isolated from plants fed [U-^{13}C]methionine, and (c) $[M+H]^+$ of 4-BZO isolated from plants fed [$^2H_5$]phenylalanine or [$^2H_5$]benzoic acid.

$[M+H]^+$ ions (m/z 417 and 418) with those resulting from natural isotopic abundance in the unlabeled glucosinolate ($[M+H+1]^+ = m/z$ 417 and $[M+H+2]^+ = m/z$ 418). However, comparison of the CID spectra of m/z 417 and 418 from unlabeled desulfo-4-BZO with those obtained after [2-^{13}C]acetate incorporation did allow differentiation of natural isotopic abundance from specific precursor labeling. Fig. 6a shows the fragmentation pattern of $[M+H+1]^+$ (m/z 417) for the unlabelled glucosinolate, where 417 is largely due to the presence of a natural atom of ^{13}C somewhere in the molecule.

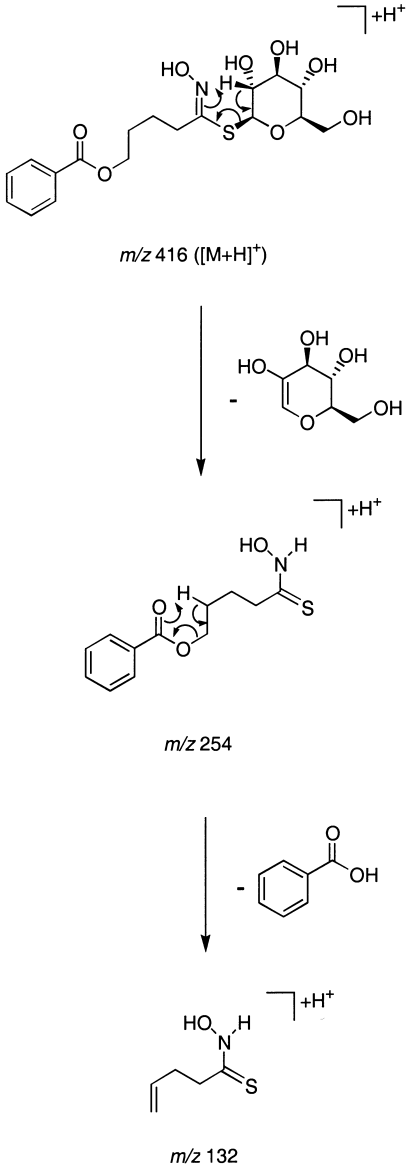

Fig. 5. Proposed mass spectral fragmentation of protonated 4-BZO under low energy CID conditions.

Fragmentation of m/z 417 gives m/z 255 and 254 with the ion at m/z 255 retaining ^{13}C, whereas m/z 254 arises from loss of the isotope during fragmentation (see Fig. 5). A similar effect is seen with m/z 132/133; however, here the ion retaining ^{13}C is relatively small — an observation consistent with the near random nature of isotope positioning caused by natural abundance. Fig. 6c shows the fragmentation pattern of $[M+H+1]^+$ (m/z 417) for desulfo-4-BZO labeled with ^{13}C from [2-^{13}C]acetate. In contrast to the spectrum obtained from the unlabeled compound, the m/z 133 ion is larger than that at m/z 132, indicating higher enrichment of one ^{13}C atom in the fragment. Since the m/z 132/133 ions originate from the glucosinolate aliphatic side-chain (Fig. 5), it is possible to conclude that the C-2 carbon of acetate is incorporated into this portion of the glucosinolate

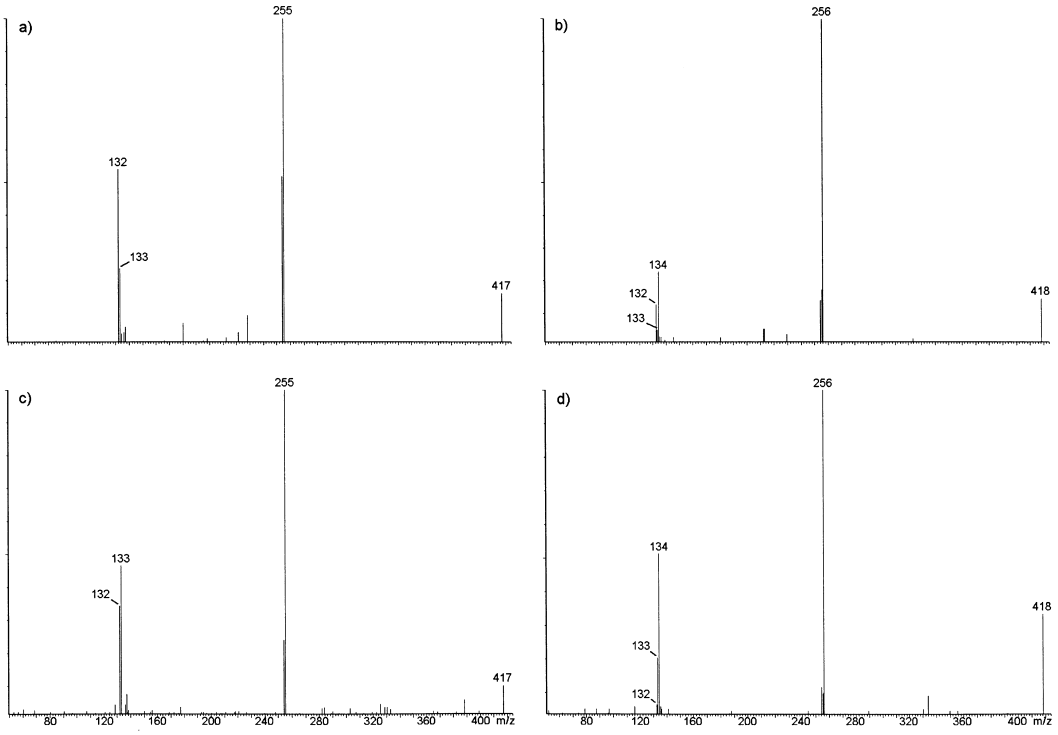

Fig. 6. Collision induced dissociation-product ion mass spectra of (a) $[M+H+1]^+$ from unlabeled 4-BZO, (b) $[M+H+2]^+$ from unlabeled 4-BZO, (c) $[M+H+1]^+$ from 4-BZO isolated from plants fed [2-^{13}C]acetate, and (d) $[M+H+2]^+$ from 4-BZO isolated from plants fed [2-^{13}C]acetate.

molecule. Examination of the CID spectrum of $[M+H+2]^+$ (m/z 418, Fig. 6b) for unlabeled desulfo-4-BZO shows that the +2 mass shift is largely retained in both major fragment ions (seen at m/z 256 and 134). This phenomenon results from the relatively high natural abundance of ^{34}S (4.4%), which contributes considerably to m/z 418, and from the fact that the sulfur atom is not lost during this fragmentation. However, Fig. 6d shows that the $[M+H+2]^+$ product ion spectrum from desulfo-4-BZO following [2-^{13}C]acetate treatment is different from the natural abundance spectrum. The ratio of m/z 134:132 in the spectrum from [2-^{13}C]acetate fed plants is 17:1, while the same ratio in the spectrum of unlabeled plants is only 2:1. Thus, there is a substantial enrichment of two ^{13}C atoms in the aliphatic side-chain fragment following treatment with labeled acetate, demonstrating that the aliphatic portion of the 4-BZO side-chain is formed from methionine elongated by two carbon atoms arising from the C-2 position of acetate. This result is consistent with the operation of the three-step chain elongation sequence proposed previously (Fig. 1) (Graser et al., 2000). During the biosynthesis of 4-BZO, an entire acetate residue is incorporated during each of the two rounds of chain elongation. However, the COOH group (C-1) of the first acetate residue is lost as CO_2 during the second round of elongation, and the COOH group of the second residue is lost during the conversion of the elongated methionine into the basic glucosinolate skeleton.

2.2. Incorporation of [1,2-^{14}C]desulfo-4-methylthiobutyl glucosinolate

The results described above account for the origin of all carbon atoms in the side-chains of 3-BZO and 4-BZO. However, they do not provide information about the sequence of biosynthetic steps in the formation of these benzoyloxyalkyl glucosinolates. In theory, many of the modifications of the side chain could occur either before or after the formation of the common skeleton. However, given the co-occurrence of 3-BZO and 4-BZO in *A. thaliana* siliques along with 3-OH-propyl- and 4-OH-butyl glucosinolates (Hogge et al., 1988), it is logical to assume that hydroxyalkyl glucosinolates are direct precursors of benzoyloxyalkyl glucosinolates, and that ester formation occurs after formation of the common skeleton (Kjaer and Christiansen, 1961). Related pairs of hydroxyalkyl- and benzoyloxyalkyl glucosinolates are also found in other plants (Daxenbichler et al., 1980).

To explore the sequence of side chain modifications in *A. thaliana*, a sample of [1,2-^{14}C]desulfo-4-methylthiobutyl glucosinolate was synthesized *in planta* by administering [2-^{14}C]acetate to detached *Eruca sativa* leaves. When this substance was administered to siliques of *A. thaliana*, radioactivity was detected in three other glucosinolates, 4-methylsufinyl-, 4-hydroxybutyl- and 4-benzoyloxybutyl glucosinolate with a specific incorporation of 2–3% (Table 1). All other glucosinolates in the tissue, including

Table 1
Incorporation of radioactivity into different glucosinolates of *A. thaliana* after siliques were fed with [1,2-^{14}C]desulfo-4-methylthiobutyl glucosinolate (4-MTB). All other glucosinolates including 3-benzoyloxypropyl (3-BZO), 7-methylthioheptyl, 7-methylsulfinyl, 8-methylthiooctyl, 8-methylsulfinyloctyl, indol-3-ylmethyl showed activities in the range of the background (0.48 Bq)

Glucosinolates	Radioactivity (Bq)	Spec. activity (GBq/mol)	Spec. incorporation (%)
4-Methylthiobutyl (4-MTB)	16.2	0.065	2.5
4-Methylsulfinylbutyl	2.35	0.07	2.7
4-Hydroxybutyl	1.6	0.08	3.3
4-Benzoyloxybutyl (4-BZO)	4.88	0.05	1.9

other chain elongated methionine derivatives were not labeled above the background. These results support a conversion of 4-methylthiobutyl glucosinolate (4-MTB) to 4-BZO via 4-methylsulfinylbutyl glucosinolate and 4-hydroxybutyl glucosinolate (Fig. 7). It has been previously suggested that 4-MTB is likely to be oxidized to 4-methylsulfinylbutyl glucosinolate, either enzymatically or spontaneously (Graham and Stanley, 1972). Next, loss of the sulfinylmethyl group and replacement by a terminal hydroxyl function (Haughn et al., 1991; McGrath et al., 1994) allows condensation with an activated benzoic acid intermediate (benzoyl-CoA, benzoyloxyglucose), to yield the benzoyloxyalkyl glucosinolates. Regardless of the exact sequence of intermediates, all of these transformations clearly occur after the formation of the common glucosinolate skeleton.

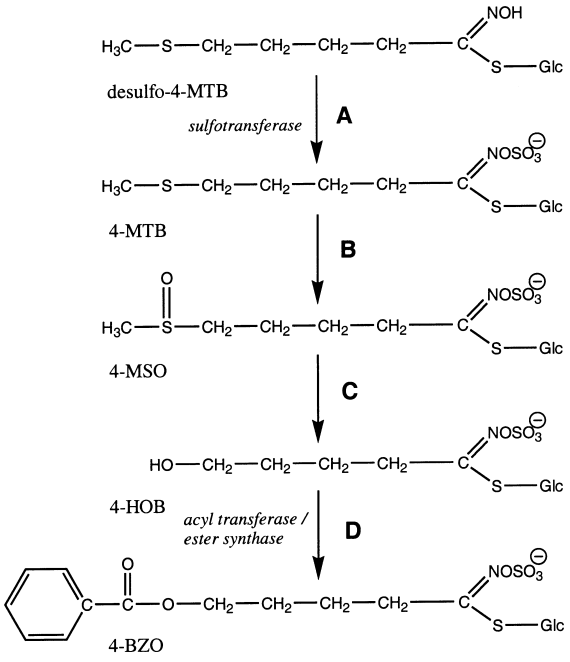

Fig. 7. Postulated intermediates in the final steps of 4-benzoyloxybutyl glucosinolate biosynthesis. The side chain of 4-methylthiobutyl glucosinolate (4-MTB) is modified by: (A) Oxidation of the thiol group to a sulfinyl, (B) replacement of the methylsulfinyl function by a hydroxyl group, and (C) condensation with activated benzoic acid to form 4-BZO.

The incorporation of desulfo-4-MTB into intact (sulfonated) glucosinolates suggests that *A. thaliana* possesses a sulfotransferase activity accessible to administered desulfonated glucosinolates. The sulfotransferases of glucosinolate biosynthesis have been previously characterized (Glendening and Poulton, 1988, 1990), and an incorporation of desulfoglucosinolates into intact glucosinolates has also been shown in other plant species (e.g. Chisholm and Matsuo, 1972). These findings raise the possibility that desulfoglucosinolates are a natural glucosinolate transport form in plants (Brudenell et al., 1999). When plants are damaged, intact glucosinolates are cleaved by myrosinase releasing toxic hydrolysis products. Hence, it may be advantageous for plants to transport glucosinolates in a form that is not susceptible to myrosinase activity (Lori et al., 1996).

2.3. Presence of biosynthetic pathway of 3 BZO and 4 BZO in A. thaliana siliques

Benzoyloxyalkyl glucosinolates in *A. thaliana* are only known to accumulate in the siliques and seeds (Hogge et al., 1988). To investigate the site of biosynthesis in this species, detached siliques were administered [U-^{14}C]phenylalanine and [2-^{14}C]acetate. For both precursors, analysis of the resulting 3-BZO and 4-BZO by liquid scintillation counting after HPLC separation showed substantial radioactivity in both glucosinolates after either precursor was administered (data not shown). Thus, the siliques themselves appear to contain the complete enzymatic apparatus for *de novo* biosynthesis of benzoyloxyalkyl glucosinolates. Indeed, previous workers have identified the silique walls as a major site for the formation of various types of glucosinolates (Lein, 1972; Du and Halkier, 1998). Nevertheless, at least part of the benzoyloxyalkyl pool in the seeds could arise from glucosinolates imported from other organs, whose side chains have been secondarily modified.

3. Conclusion

Our results have clarified the biosynthetic origin of the benzoyloxyalkyl glucosinolates of *A. thaliana*. Three discrete stages can be identified. First, methionine is extended by addition of 1,2 or more methylene residues via a three-step chain-elongation sequence involving the condensation of a 2-oxo acid with acetyl-CoA, as shown for the glucosinolates of *Eruca sativa* (Graser et al., 2000). Second, elongated amino acids derived from methionine

are converted into glucosinolates with methythioalkyl side chains. Third, the methylthioalkyl side chains are transformed to the corresponding hydroxylalkyl chains and then condensed with an activated benzoic acid species. While most of the reactions of the second stage (amino acids to glucosinolates) are now well understood (Halkier, 1999), much less is known about the enzymology or mechanism of the steps of the first and third stages (chain extension and modification). Detailed studies of some of these reactions are now in progress in our laboratory.

4. Experimental

4.1. Chemicals

[2-^{13}C]Acetic acid (>99%) and [ring-$^{2}H_5$]benzoic acid were purchased from Aldrich, [U-^{13}C]L-methionine (>97%) and [ring-$^{2}H_5$]L-phenylalanine (>98%) from Cambridge Isotope Laboratories, Inc. and [^{15}N]L-methionine (>99%) from Campro Scientific. All other reagents were from Sigma-Aldrich Chemical Co. unless otherwise stated.

4.2. Plant material

Seeds of *Arabidopsis thaliana* L. (ecotype Columbia), obtained from Lehle Seeds (Round Rock, Texas, USA), were sown in ordinary potting soil and raised in a controlled environment chamber with a day/night cycle of 16/8 h and 22°C/18°C. Illumination was with high-pressure sodium lamps (100% light intensity = 880 μmol m^{-2} s^{-1}) according to the following 16 h light program: 5 h with 50% illumination, 6 h with 75% illumination and 5 h with 50% illumination. Plants were watered every four days and fertilized once a week with 15:11:13, N:P:K (Osmocote, Scotts Europe).

4.3. Administration of basic precursors

Flowering stems of *A. thaliana* (12–20 cm long) were excised, by cutting just above the leaf rosette with a razor blade, and transferred into a 15 ml Falcon tube with 10 ml tracer solution. The incubations were performed for 5 days, under the growing conditions described above, using one of the following solutions: 5 mM [ring-$^{2}H_5$]phenylalanine with 3 mM L-methionine; 5 mM [ring-$^{2}H_5$]benzoic acid with 3 mM L-methionine; 5 mM [U-^{13}C]L-methionine; and 10 mM [2-^{13}C]acetic acid with 3 mM L-methionine and 3 mM L-phenylalanine. Unlabeled amino acids were fed together with labeled precursors to increase the rate of glucosinolate biosynthesis. All solutions were prepared in sterilized water containing sucrose (5%). Each precursor was fed to one tube containing 10–15 flowering stems. Additional tracer solution was added during the incubation as necessary. No microbial contamination of the incubation solutions were evident during the course of incubation.

4.4. Administration of desulfo-4-methylthiobutyl glucosinolate

[1,2-^{14}C]Desulfo-4-methylthiobutyl glucosinolate was prepared by feeding *Eruca sativa* with [2-^{14}C]acetate as described in Graser et al. (2000). [2-^{14}C]Acetate (8.8 TBq/mol) was administered to 120 expanding leaves of *E. sativa*. After leaves were incubated under standard growing conditions for 72 h, [1,2-^{14}C]4-MTB was isolated and purified as described below. One flowering stem was fed with [1,2-^{14}C]4-MTB (2.6 GBq/mol) in a volume of 12 ml water as described for the amino acid experiments. Siliques were harvested shortly before ripening.

4.5. Glucosinolate extraction

Extracts were made using methods adapted from previously published protocols (Thies, 1979; Graser et al., 2000). Fresh siliques were immersed in boiling, deionized water (5 ml per g sample) containing 100 μl 0.3 M $Pb(OAc)_2$–0.3 M $Ba(OAc)_2$ solution for 15 min. After 30 min gentle shaking at room temperature, samples were centrifuged at 4000 *g* for 10 min and the supernatant fraction loaded onto a small (100 mg) column of DEAE Sephadex A25. The column was rinsed with 67% (aqueous) MeOH and deionized water and, after capping, was treated with 50 μl sulfatase solution (prepared as described below) in 1 ml 20 mM NaOAc, pH 5.5, and left to stand overnight. The resulting desulfoglucosinolates were eluted from the column with 2×0.8 ml 60% (aqueous) MeOH, and the combined eluent was evaporated to dryness with nitrogen at 45°C. For HPLC analysis samples were redissolved in water. Unlabeled 3-BZO and 4-BZO were extracted from untreated siliques (5 g) of *A. thaliana* for use as standards.

Sulfatase for glucosinolate extraction (Thies, 1979) was prepared by dissolving 700 mg aryl sulfatase (Sigma type H-1 from *Helix pomatia*) in 30 ml deionized water and mixing with 30 ml absolute ethanol. After centrifugation at 5000 *g* for 20 min, the supernatant was mixed with 90 ml additional absolute ethanol and centrifuged again at 4000 *g* for 15 min. The pellet from this second centrifugation was dissolved in 25 ml deionized water and divided into 1 ml aliquots for storage at −20°C.

4.6. Desulfoglucosinolate purification and analysis

For APCI-MS analysis, desulfated 3-BZO and 4-BZO were purified by semi-preparative HPLC on a Hewlett Packard HP 1100 Series system with autosampler, column oven and diode-array detector. The procedure employed a C-18, fully-endcapped, reversed phase col-

umn (Hypersil ODS, 250×10 mm i.d., 5 μm particle size, Chrompack, Frankfurt, Germany) operated at 4.3 ml min^{-1} and 25°C, and eluted with a gradient (solvent A: H_2O, solvent B: MeCN) of 0–6% B (7 min), 6–24% B (30 min) and 24–32% B (8 min), followed by a cleaning cycle (32–92% B in 1 min, 5 min hold, 92–0% in 2 min, holding at 0 for 4 minutes to equilibrate). The eluent was monitored at 229 nm. Quantitation was achieved by addition of an internal standard (allyl glucosinolate, 0.5 μmol) during extraction with peak areas adjusted using response factors (Graser et al., 2000).

For radioactivity measurements, analytical HPLC was performed with a C-18 reversed phase column (LiChrospher RP-18, 250×4.6 mm i.d., 5 μm particle size, Chrompack) operated at 1 ml min^{-1} and 25°C. Elution was accomplished with a gradient (solvent A: H_2O, solvent B: MeCN) of 1.5–4% B (6 min), 4–18% B (7 min), 18–28% B (4 min), and 28–53% B (5 min), followed by a cleaning cycle (53–93% B in 2 min, 5 min hold, 93–1.5% B in 3 min, 2 min hold). Elution was monitored at 229 nm and the radioactivity of the collected fractions was quantified by liquid scintillation counting in 5 ml Lipoluma cocktail (Packard Bioscience, Groningen, The Netherlands) using a Packard Tricarb 2300TR liquid scintillation counter (^{14}C efficiency = 96.2%). Both analytical and semi-preparative HPLC systems were equipped with a C-18 LiChrospher (75×4.6 mm i.d., 5 μm particle size, Chrompack) reverse phase guard column.

4.7. APCI-MS analysis of 4-benzoyloxybutyl glucosinolate

Mass spectrometry was performed on a Quattro II (Micromass Ltd, Altrincham, UK) tandem quadrupole mass spectrometer (geometry quadrupole-hexapole-quadrupole) equipped with an atmospheric pressure chemical ionization (APCI) source. The corona pin was operated at 3.5 kV and the sample cone at 16 V. A mixture of acetonitrile and water (1:1) was used as the solvent, at a flow rate of 0.5 ml min^{-1}. Vaporization was achieved with a nitrogen sheath gas (300 l h^{-1}) and drying gas (150 l h^{-1}) at 400°C. Standard mass spectra were measured using the first quadrupole analyzer only, employing a narrow scan range of m/z 395–410 for 3-BZO and m/z 410–425 for 4-BZO and a scan time of 0.5 s. Product ion mass spectra were recorded by setting the first quadrupole to transmit the parent ion of interest and scanning the second quadrupole from m/z 50 to 425. Argon was used as the collision gas at 2×10^{-3} mbar, and a collision energy of 10 eV was employed to achieve fragmentation. Purified desulfoglucosinolates (typically 10–50 μg) were dissolved in water (0.3 ml) and aliquots (10 μl) injected directly into the APCI solvent flow using a loop injection valve (Rheodyne, CA, USA). If required, the solutions were diluted to ensure a similar detector response for each sample. For standard MS measurements, each sample was injected five times and average ion intensities calculated from peak areas.

Acknowledgements

We thank John L. Allen for assistance with the glucosinolate analysis and the Max-Planck-Gesellschaft for financial support.

References

Brown, P.D., Mora, R.R., 1997. Control of soil-borne plant pests using glucosinolate-containing plants. In: Sparks, D.L. (Ed.), Advances in Agronomy, Vol. 61. Academic Press, San Diego, pp. 167–231.

Brudenell, A.J., Griffiths, H., Rossiter, J.T., Baker, D.A., 1999. The phloem mobility of glucosinolates. Journal of Experimental Botany 50, 745–756.

Bryan, J.K., 1980. Synthesis of the aspartate family and branched-chain amino acids. In: Miflin, B.J. (Ed.), The Biochemistry of Plants Amino Acids and Derivatives, Vol. 5. Academic Press, New York, pp. 403–452.

Chapple, C.C.S., Decicco, C., Ellis, B.E., 1988. Biosynthesis of 2-(2′-methylthio)ethylmalate in *Brassica carinata*. Phytochemistry 27, 3461–3463.

Chew, F.S., 1988. Searching for defensive chemistry in the *Cruciferae*, or, do glucosinolates always control interaction of *Cruciferae* with their potential herbivores and symbionts? No! In: Spencer, K.C. (Ed.), Chemical Mediation of Coevolution. Academic Press, San Diego, pp. 81–112.

Chisholm, M.D., Matsuo, M., 1972. Biosynthesis of allylglucosinolates and 3-methylthiopropylglucosinolate in horseradish, *Armoracia lapathifolia*. Phytochemistry 11, 203–207.

Daxenbichler, M.E., Spencer, G.F., Schroeder, W.P., 1980. 3-Hydroxypropylglucosinolate, a new glucosinolate in seeds of *Erysimum hieracifolium* and *Malcolmia maritima*. Phytochemistry 19, 813–815.

Du, L., Halkier, B.A., 1998. Biosynthesis of glucosinolates in the developing silique walls and seeds of *Sinapis alba*. Phytochemistry 48, 1145–1150.

Fahey, J.W., Zalcmann, A.T., Talalay, P., 2001. The chemical diversity and distribution of glucosinolates and isothiocyanates among plants. Phytochemistry 56, 5–51.

Glendening, T.M., Poulton, J.E., 1988. Glucosinolate biosynthesis. Sulfation of desulfoglucosinolate by cell-free extracts of cress (*Lepidium sativum* L.) seedlings. Plant Physiology 86, 319–321.

Glendening, T.M., Poulton, J.E., 1990. Partial purification and characterization of a 3′-phosphoadenosine 5′- phosphosulfate — desulfoglucosinolate sulfotransferase from cress (*Lepidium sativum*). Plant Physiology 94, 811–818.

Graham, R., Stanley, W.M., 1972. An economical procedure for the preparation of L-[^{35}S]methionine of high specific activity. Analytical Biochemistry 47, 505–513.

Graser, G., Schneider, B., Oldham, N.J., Gershenzon, J., 2000. The methionine chain clongation pathway in the biosynthesis of glucosinolates in *Eruca sativa* (Brassicaceae). Archives of Biochemistry and Biophysics 378, 411–419.

Halkier, B.A., 1999. Glucosinolates. In: Ikan, R. (Ed.), Naturally Occurring Glycosides: Chemistry, Distribution and Biological Properties, pp. 193–223.

Halkier, B.A., Du, L., 1997. The biosynthesis of glucosinolates. Trends Plant Science 2, 425–431.

Haughn, G.W., Davin, L., Giblin, M., Underhill, E.W., 1991. Biochemical genetics of plant secondary metabolites in *Arabidopsis thaliana*. The glucosinolates. Plant Physiology 97, 217–226.

Hogge, L.R., Reed, D.W., Underhill, E.W., Haughn, G.W., 1988. HPLC separation of glucosinolates from leaves and seeds of *Arabidopsis thaliana* and their identification using thermospray liquid chromatography/mass spectrometry. J. Chromatogr. Sci. 26, 551–556.

Hull, A.K., Vij, R., Celenza, J.L., 2000. *Arabidopsis* cytochrome P450s that catalyze the first step of tryptophan-dependent indole-3-acetic acid biosynthesis. Proceedings of the National Academy of Science USA 97, 2379–2384.

Lori, R., Rollin, P., Streicher, H., Thiem, J., Palmieri, S., 1996. The myrosinase-glucosinolate interaction mechanism studied using some synthetic competitive inhibitors. FEBS Letters 385, 87–90.

Kiddle, G.A., Bennett, A.J., Wallsgrove, R.M., 1999. C-S lyase activities in leaves of crucifers and non-crucifers, and the characterization of three classes of C-S lyase activities from oilseed rape (*Brassica napus* L.). Plant, Cell and Environment 22, 433–445.

Kjaer, A., Christensen, B.W., 1961. Glucobenzosisymbrin, a new glucoside present in seeds of *Sisymbrium austriacum*. Jacq. Acta Chem. Scand. 15, 1477–1484.

Lee, H.J., León, J., Raskin, I., 1995. Biosynthesis and metabolism of salicylic acid. Proceedings of the National Academy of Science USA 92, 4076–4079.

Lein, K.A., 1972. Zur quantitativen Bestimmung des Glucosinolatgehaltes in *Brassica*-Samen. I. Gewinnung und Reinigung der Myrosinase. Angew. Bot. 46, 137–159.

McGrath, R., Bano, F., Morgner, M., Parkin, I., Sharpe, A., Lister, C., Dean, C., Turner, J., Lydiate, D., Mithen, R., 1994. Genetics of aliphatic glucosinolates. I. Side chain elongation in *Brassica napus* and *Arabidopsis thaliana*. Heredity 72, 290–299.

Poulton, J.E., Møller, B.L., 1993. Glucosinolates. In: Lea, P.J. (Ed.), Methods in Plant Biochemistry, Enzymes of Secondary Metabolism, Vol. 9. Academic Press, London, pp. 209–237.

Thies, W., 1979. Detection and utilization of a glucosinolate sulfohydrolase in the edible snail, *Helix pomatia*. Naturwissenschaften 66, 364–365.

Underhill, E.W., 1980. Glucosinolates. In: Bell, E.A., Charlwood, B.V. (Eds.), Encyclopedia of Plant Physiology, Vol. 8. Springer Verlag, Berlin, pp. 493–511.

Van Etten, C.H., Tookey, H.L., 1979. Chemistry and biological effects of glucosinolates. In: Rosenthal, G.A., Janzen, D.H. (Eds.), Herbivores Their Interaction with Secondary Plant Metabolites. Academic Press, New York, pp. 471–500.

Wallsgrove, R.M., Bennett, R.N., 1995. The biosynthesis of glucosinolates in *Brassicas*. In: Wallsgrove, R.M. (Ed.), Amino Acids and their Derivatives in Higher Plants. Cambridge University Press, Cambridge, pp. 243–259.

Wittstock, U., Halkier, B.A., 2000. Cytochrome P450 CYP79A2 from *Arabidopsis thaliana* L. catalyzes the conversion of L-phenylalanine to phenylacetaldoxime in the biosynthesis of benzylglucosinolates. J. Biol. Chem. 275, 14659–14666.

PERGAMON

Phytochemistry 57 (2001) 33–42

PHYTOCHEMISTRY

www.elsevier.com/locate/phytochem

Tracer studies with ^{13}C-labeled carbohydrates in cultured plant cells. Retrobiosynthetic analysis of chelidonic acid biosynthesis

Z.-W. Shen [a], U. Fisinger [a], A. Poulev [a], W. Eisenreich [b,*], I. Werner [b], E. Pleiner [b], A. Bacher [b], M.H. Zenk [a]

[a] *Biozentrum-Pharmazie, Universität Halle, Weinbergweg 22, D-06120 Halle/Saale, Germany*
[b] *Lehrstuhl für Organische Chemie und Biochemie, Technische Universität München, Lichtenbergstr. 4, D-85747 Garching, Germany*

Received 12 September 2000; received in revised form 23 November 2000

Abstract

The biosynthesis of chelidonic acid was studied in cell suspension cultures of *Leucojum aestivum*. Cell cultures were supplied with [U-$^{13}C_6$]glucose, [1-^{13}C]glucose or [U-$^{13}C_5$]ribose/ribulose in standard medium containing unlabeled glucose. ^{13}C labeling patterns of amino acids obtained by hydrolysis of biomass were determined by NMR spectroscopy and compared to the labeling pattern of chelidonic acid. The data document the incorporation of a contiguous 4-carbon fragment derived from the pentose phosphate pool into chelidonic acid. This suggests a biosynthetic pathway involving the condensation of phosphoenolpyruvate with a pentose phosphate followed by dehydration, dehydrogenation, ring closure and decarboxylation conducive to the loss of C-5 of the pentose precursor. © 2001 Elsevier Science Ltd. All rights reserved.

Keywords: *Leucojum aestivum*; Biosynthesis; NMR spectroscopy; Plant cell culture; Retrobiosynthetic analysis; Isotopes; Chelidonic acid

1. Introduction

The γ-pyrones, chelidonic acid (**1**) and meconic acid (**2**) (Fig. 1), are found in various alkaloid producing plants where they are supposed to serve as counterions for the storage of positively charged alkaloids in the vacuolar compartment (Ramstadt, 1953). Moreover, in *Cassia mimosoides* potassium chelidonate was claimed to serve as a leaf-closing factor (Ueda et al., 1998).

The biosynthesis of chelidonic acid is poorly understood. On the basis of radioisotope studies, a three-carbon unit and a four-carbon unit produced from the photosynthetic reduction cycle were proposed as building blocks of the γ-pyrone (Malcolm and Gear, 1971). More specifically, the shikimate precursor, 2-keto-3-deoxyarabinoheptulosonate 7-phosphate (DAHP, **5**) obtained by condensation of phosphoenolpyruvate (**3**) and erythrose 4-phosphate (**4**) has been suggested as an intermediate of chelidonic acid biosynthesis (Fig. 2).

We decided to perform incorporation experiments with *Leucojum aestivum* cultivated cells using mixtures of various ^{13}C-labeled carbohydrates with an excess of unlabeled glucose as precursors. The metabolic breakdown of ^{13}C-labeled carbohydrates yields labeled fragments which can be subsequently combined at random with fragments derived from unlabeled glucose by anabolic reactions of intermediary metabolism. ^{13}C-Labeled fragments from the precursor carbohydrate will be diverted to virtually all plant cell metabolites, and the individual metabolic products will be complex mixtures of different isotopomers reflecting their random assembly from ^{13}C-labeled and unlabeled glucose catabolites. In other words, the resulting metabolites derived from the glucose precursor are isotopomer mixtures reflecting their biosynthetic history.

The isotopomer composition of intermediary metabolites can be determined via analysis of biosynthetic amino acids which are easily obtained by hydrolysis of plant cell mass. The isotopomer composition of each biosynthetic amino acid can be determined quantitatively by NMR spectroscopy. By a systematic comparison

* Corresponding author at Technische Universität München, Lehrstuhl für Organische Chemie und Biochemie, Lichtenbergstr. 4, 85747 Garching, Germany. Tel.: +49-89-28913043; fax: +49-28913363.

E-mail address: wolfgang.eisenreich@ch.tum.de (W. Eisenreich).

0031-9422/01/$ - see front matter © 2001 Elsevier Science Ltd. All rights reserved.
PII: S0031-9422(00)00496-9

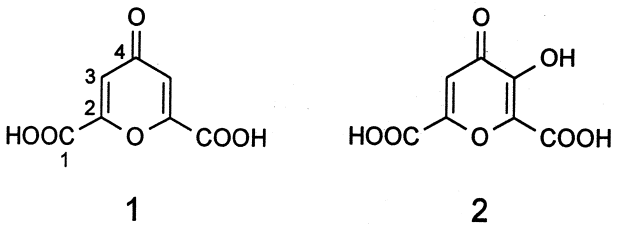

Fig. 1. Structure of chelidonic acid (**1**) and meconic acid (**2**).

between the labeling patterns of many primary metabolites with that of the secondary metabolite under study, the biosynthetic building blocks of the latter can be determined, even in the absence of a biosynthetic working hypothesis (for reviews, see Bacher et al., 1999; Eisenreich and Bacher, in press). Using this retrobiosynthetic approach, we here report that the carbon skeleton of chelidonic acid is assembled from one molecule each of a pentose and phosphoenolpyruvate.

2. Results

The analysis of chelidonic acid biosynthesis is complicated by the inherent symmetry of the molecule under study. The problem can be illustrated using the hypothetical pathway via DAHP as proposed by Malcolm and Gear (1971). In terms of this hypothesis, carbon atoms 1 and 7 of DAHP (**5**) would contribute isotope labels to the symmetry related carboxylic groups of chelidonic acid (**1**); since the NMR signals of the two carboxylic groups are degenerate due to the molecular symmetry, it would be impossible to discriminate between the label contributions by C-1 of phosphoenolpyruvate (**3**) and C-4 of erythrose 4-phosphate (**4**), respectively (Fig. 2).

These difficulties may be one of the reasons for the murky state of information on the biosynthesis of chelidonic acid. We decided to reanalyze this problem using the retrobiosynthetic method based on comparisons between labeling patterns of secondary and primary metabolites (for reviews, see Bacher et al., 1999; Eisenreich and Bacher, 2001). For this purpose, we performed incorporation experiments with various carbohydrates carrying single or multiple ^{13}C labels.

A cell culture of *L. aestivum* was incubated for 30 days in mineral salts medium containing 4 g of [U-$^{13}C_6$]glucose and 26 g of unlabeled glucose per litre (Table 1). The cell mass was harvested, and chelidonic acid was extracted and purified as described in Experimental. Subsequent to the extraction of chelidonic acid, the biomass was subjected to acid hydrolysis, and amino acids were isolated by chromatographic procedures. The ^{13}C labeling patterns of chelidonic acid and amino acids were then established by NMR spectroscopy as described under methods (Eisenreich and Bacher, 2001).

The catabolism of [U-$^{13}C_6$]glucose generates multiply ^{13}C-labeled fragments that can subsequently be combined in a stochastic manner with unlabeled fragments (derived from unlabeled glucose) by anabolic reactions. Further modification of the isotope distribution pattern is possible by passage through metabolic cycles such as the pentose phosphate cycle. Every specific metabolite is therefore a mixture of different isotopomers, and its NMR signals appear as complex multiplets resulting from the contributions of the ^{13}C–^{13}C coupling patterns of each respective isotopomer (Table 2). As an example, Fig. 3(a) shows the ^{13}C signature of C-3 of chelidonic acid. The central signal marked by b represents molecules carrying a single ^{13}C atom (isotopomer b, Fig. 4) that may have been formed from natural abundance glucose; alternatively, a single ^{13}C could have been contributed from the labeled glucose, but only after extensive fragmentation and reassembly.

The coupling satellites represent [1,2,3,4-$^{13}C_4$]-**1** (isotopomer k), [2,3,4-$^{13}C_3$]-**1** (isotopomer h), [2,3-$^{13}C_2$]-**1** (isotopomer f), and [3,4-$^{13}C_2$]-**1** (isotopomer e) (Fig. 4).

Table 1
Isotope incorporation experiments with cell cultures of *Leucojum aestivum*. The precursors were added as a bolus at the beginning of the growth phase

Experiment	^{13}C-Labeled precursor	Unlabeled carbohydrates
1	22 mM [U-$^{13}C_6$]glucose	145 mM glucose
2	55 mM [1-^{13}C]glucose	110 mM glucose
3	9 mM [U-$^{13}C_5$]ribose/ribulose	27 mM ribose, 156 mM glucose
4	0.2 mM [2-^{13}C]sedoheptulose	165 mM glucose

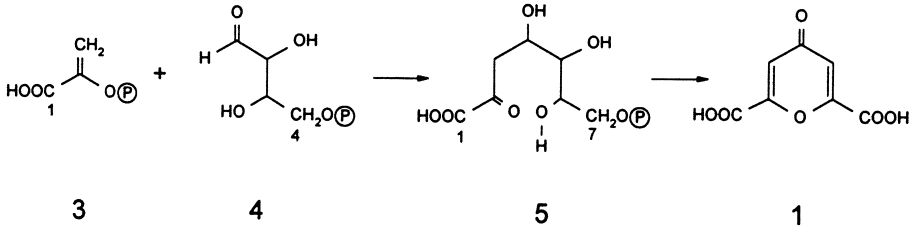

Fig. 2. Proposed biosynthesis of chelidonic acid (Malcolm and Gear, 1971).

Table 2
NMR data of chelidonic acid in D_2O

Position	Chemical shift [ppm]		^{13}C–^{13}C coupling constants[a]	Isotope shifts[b]
	^{1}H	^{13}C	Hz	ppb
1		163.62	79.8 (2), 3.5 (4), 5.0 (3)	+19 (2)
2		157.31	79.5 (1), 71.1 (3)	−32 (1), −20 (3)
3	6.99	117.34	54.8 (4), 71.2 (2), 5.1 (1)	−16 (4), −25 (2), +4 (1)
4		184.13	54.8 (3), 3.4 (1)	−7 (3)

[a] Coupled atoms are given in parentheses.
[b] ^{13}C atoms causing isotope shifts to the chemical shift of the respective index atom are given in parentheses.

Due to heavy isotope chemical shift effects (Table 2), the respective centers of the satellite signals are offset to high field.

The molar fraction of each respective isotopomer in the sample can be obtained from the signal integrals as described in Experimental (Table 3). The salient feature of the labeling pattern is the occurrence, albeit at low level, of [1,2,3,4-$^{13}C_4$]chelidonic acid (isotopomer k, Fig. 4) containing four contiguous ^{13}C atoms incorporated en bloc from the proffered glucose.

The labeling patterns of representative amino acids isolated from biomass are shown in Fig. 5. In order to save space, the different isotopomers observed are all superimposed in one respective structure. The bars indicate the groups of adjacent ^{13}C atoms of each respective multiple-labeled isotopomer. The abundance of each isotopomer is shown by the width of the bars as well as by the numerical subscripts.

The labeling patterns are qualitatively similar to those found with numerous other plant cell cultures supplied with a mixture of [U-$^{13}C_6$]glucose and natural abundance glucose (Eichinger et al., 1999a,b; Goese et al., 1999; Werner et al., 1997). However, it should be noted that fragments with four respectively five contiguous carbon atoms occur only in the ring systems of aromatic amino acids and in histidine. This reflects the origin of these respective amino acids from erythrose 4-phosphate respectively ribose 5-phosphate. In the other amino acids, no contiguous blocks exceeding three ^{13}C atoms were found (Fig. 5).

In summary, these observations support the hypothesis that the detected $^{13}C_4$-carbon block in chelidonic acid has been introduced via a carbohydrate precursor that remains to be identified more accurately.

As described in detail previously, the isotopomer compositions of central metabolites can be determined retrobiosynthetically from the observed labeling patterns in amino acids (Bacher et al., 1999). Thus, the labeling pattern of ribose 5-phosphate (**7**) can be reconstructed from that of histidine (**6**). Moreover, tyrosine (**8**) reflects the labeling patterns of phosphoenolpyruvate (**3**) and erythrose 4-phosphate (**4**, Fig. 6). Using the reconstructed labelling patterns of central metabolites it is now possible to predict the labelling pattern of biosynthetic chelidonic acid via hypothetical biosynthetic pathways.

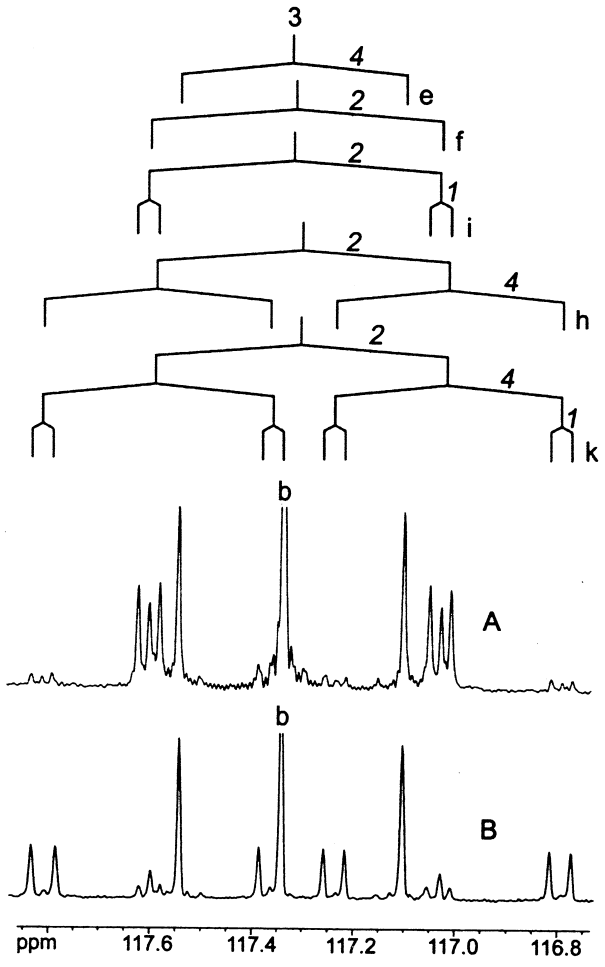

Fig. 3. ^{13}C NMR signal of C-3 of chelidonic acid obtained from the experiment with (a) [U-$^{13}C_6$]glucose and (b) [U-$^{13}C_5$]ribose/ribulose. ^{13}C coupling patterns are indicated. Numbers in italics indicate carbon atoms ^{13}C coupled to C-3. Letters denote isotopomers shown in Fig. 4.

Two hypothetical pathways for the assembly of chelidonic acid from carbohydrates are shown in Fig. 7. Pathway A involves a condensation of erythrose 4 phosphate (**4**) with phosphoenol-pyruvate (**3**) via the shikimate pathway intermediate, 2-keto-3-deoxyar-

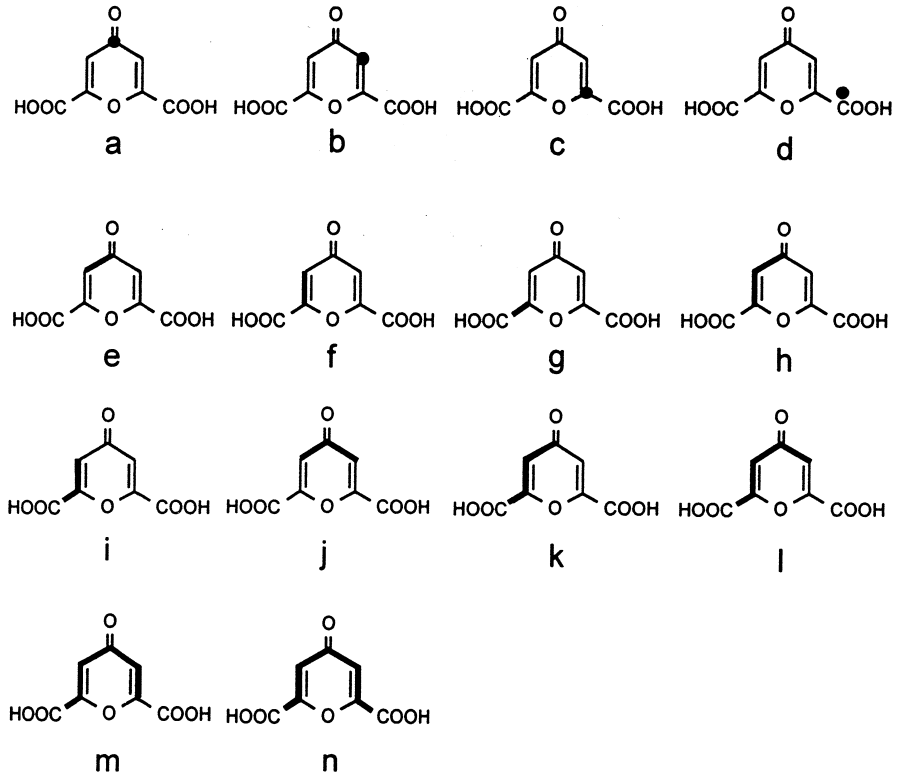

Fig. 4. ^{13}C Labelled isotopomers of chelidonic acid (a–n). Filled circles indicate ^{13}C atoms in single labelled isotopomers. Bold bars indicate adjacent ^{13}C atoms in multiple labelled isotopomers.

Table 3
Multiple ^{13}C-labeled isotopomers of chelidonic acid (**1**) from *Leucojum aestivum* supplemented with [U-$^{13}C_6$]glucose and [U-$^{13}C_5$]ribose/ribulose in mol%

	Experiment with	
	[U-$^{13}C_6$]glucose	[U-$^{13}C_5$]ribose/ribulose
[1,2-$^{13}C_2$]-**1**	4.4	1.0
[2,3-$^{13}C_2$]-**1**	1.8	1.0
[3,4-$^{13}C_2$]-**1**	3.4	6.2
[1,2,3-$^{13}C_3$]-**1**	4.4	0.9
[2,3,4-$^{13}C_3$]-**1**	< 0.2	< 0.3
[1,2,3,4-$^{13}C_4$]-**1**	0.8	8.4

abinoheptulosonate 7-phosphate (**5**, DAHP). Pathway B similarly involves the condensation of a pentose 5-phosphate (**7**) with phosphoenolpyruvate (**3**) and subsequent loss of one carbon atom. The hypothetical pathway A via DAHP has been proposed earlier by Malcolm and Gear (1971) (see Fig. 2).

The labeling patterns expected for the formation of chelidonic acid via pathways A and B can be predicted quantitatively from the labeling patterns for phosphoenolpyruvate, erythrose 4-phosphate and ribose 5-phosphate extracted from the experimentally observed labeling patterns of tyrosine and histidine (Fig. 6). Due to the inherent symmetry of chelidonic acid, pairs of carbon atoms are homotopic. As a result, the isotopomer pattern present in the homotopic parts of the molecule cannot be distinguished by NMR spectroscopy and the "folded" pattern shown in the box is detected. The highest degree of similarity is found between prediction B and the experimental labeling pattern [Fig. 7(c)] but the evidence is far from conclusive. Therefore, an additional experiment was performed with [1-^{13}C]glucose as precursor. The data were processed in the same way as in the previous experiment.

The prediction of chelidonic acid labeling from [1-^{13}C]glucose via pathways A and B is summarized in Fig. 8. The agreement between the prediction B and the observed labeling pattern of chelidonic acid [Fig. 8(c)] is excellent. On the other hand, the experimental data differ substantially from the prediction via pathway A.

The data suggested that a further confirmation might be obtained using a universally ^{13}C labeled pentose rather than a hexose as precursor. On the other hand, it was unknown whether cultured plant cells metabolize exogenous pentoses.

An experiment with a [U-$^{13}C_5$]ribose/ribulose mixture was performed as summarized in Table 1. Natural abundance glucose as well as ribose were added together with the ^{13}C-labeled pentose mixture. The NMR signal of C-3 of chelidonic acid is shown in Fig. 3(b). Qualitatively, the spectrum shows the same satellite pattern

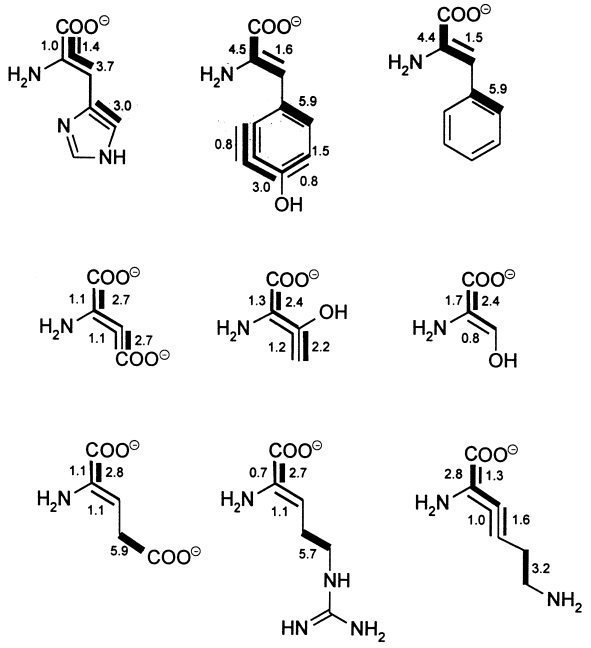

Fig. 5. Incorporation of [U-$^{13}C_6$]glucose diluted with unlabelled glucose into *Leucojum aestivum*. ^{13}C labelling patterns of amino acids obtained from cellular protein. Bold bars indicate multiple ^{13}C labelled isotopomers. The numbers indicate molar fractions of respective isotopomers.

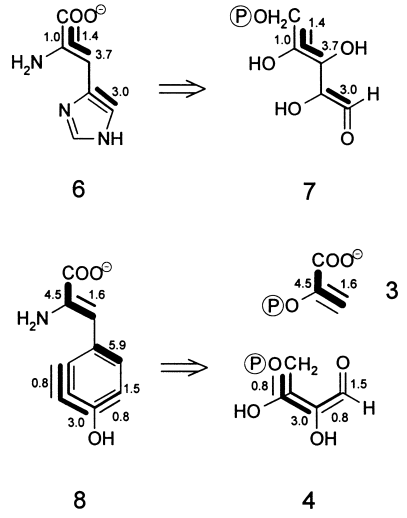

Fig. 6. Incorporation of [U-$^{13}C_6$]glucose diluted with unlabelled glucose into *Leucojum aestivum*. Reconstruction of the labelling patterns of ribose 5-phosphate (**7**), phosphoenolpyruvate (**3**), and erythrose 4-phosphate (**4**) from the detected labelling patterns of histidine (**6**) and tyrosine (**8**), respectively. For further details, see Fig. 5.

obtained from the experiment with [U-$^{13}C_6$]glucose. However, the relative intensity of the various satellite groups is different; most notably, the [$^{13}C_4$]-isotopomer has become the dominant species (Table 3). No [$^{13}C_5$]-isotopomer could be detected.

The data show that ribose and/or ribulose can serve as precursor in cultured plant cells with unexpected efficacy. Amino acid labelling patterns from the experiment with ribose/ribulose are shown in Fig. 9. As described above, the labelling pattern of ribose 5-phosphate and phosphoenolpyruvate was extracted from that of histidine and tyrosine/phenylalanine, respectively.

Starting from these data the labelling pattern of chelidonic acid was predicted again, as shown in Fig. 10. The isotopomers are correctly predicted by the hypothetical pathway via incorporation of an intact pentose with subsequent loss of the terminal carbon atom. However, the absolute abundance of isotopomers with multiple ^{13}C labels is not correct as predicted. The reason for this is at present not known. It could be caused by the localization of histidine biosynthesis and chelidonic acid biosynthesis in different compartments. It could also be influenced by the fact that a mixture of totally ^{13}C-labeled ribose and ribulose has been used as exogenous precursor. Nothing is known as yet about the metabolic utilization of ribulose. Thus, the quantitative outcome of the labeling experiment with the pentose/pentulose mixture could also be related to dynamic aspects of pentose vs. pentulose utilization.

3. Discussion

The elucidation of the biosynthesis of chelidonic acid is substantially hampered by the inherent symmetry of the molecule. The data reported in this paper confirm that, even in such a situation, biosynthetic hypotheses can be analysed by a retrobiosynthetic approach.

The use of cell cultures provides substantial advantages for biosynthetic experiments by comparison with whole plants or plant tissues, such as an unlimited time frame and the ease of application of nutrients and precursors. However, for a long time, plant cell cultures had been assumed to be very limited with regard to the set of compounds that could be used as isotope-labelled exogenous precursors. The general feeling was that very few, if any, exogenous compounds beside sucrose could be absorbed and utilized efficiently.

We have found that ribose is an excellent precursor for plant cell studies. By comparison with glucose as a precursor, ribose has the potential to contribute fragments containing more than three contiguous ^{13}C atoms via the pentose phosphate cycle. Glucose, on the other hand, is predominantly metabolized via glycolysis in plant cell cultures, thus generating primarily 3 carbon fragments.

On the basis of our results, DAHP can be ruled out as a precursor of chelidonic acid. Moreover, sedoheptulose also appears very unlikely as a precursor. The generation of sedoheptulose 7-phosphate specifically carrying a 4-carbon block supplied from [U-$^{13}C_5$]ribose/ribulose could be explained by the pentose phosphate cycle via the intermediate formation of [U-$^{13}C_4$]erythrose 4-phosphate.

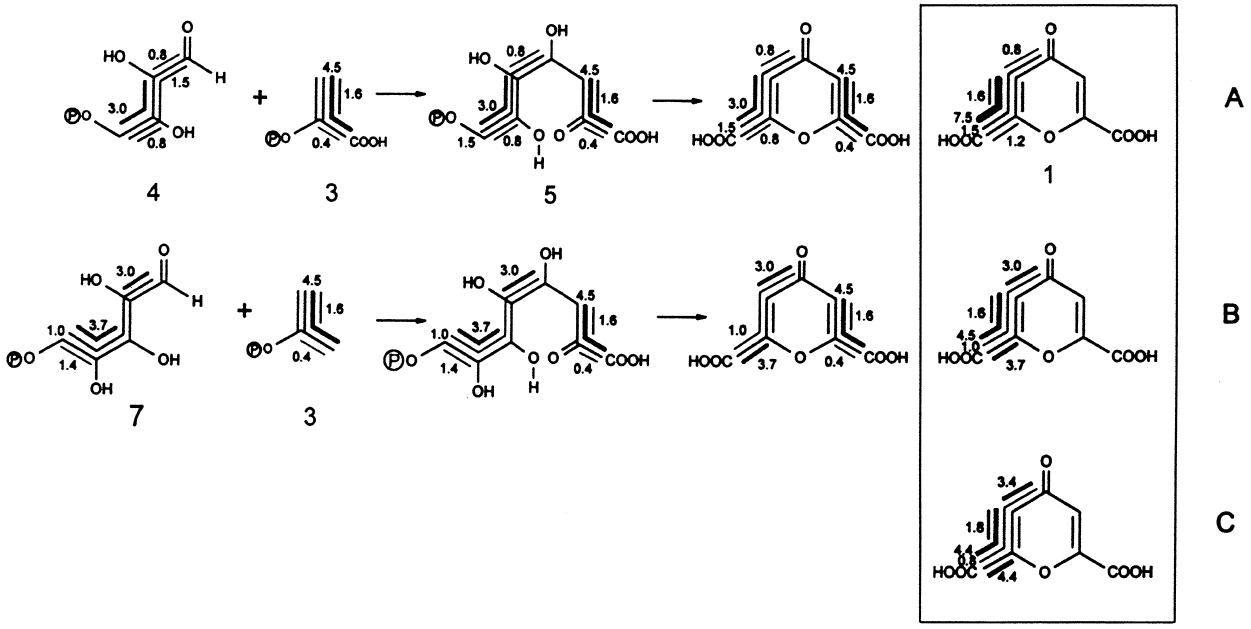

Fig. 7. ^{13}C Labelling patterns of chelidonic acid from the experiment with [U-$^{13}C_6$]glucose. (a) Prediction via a biosynthetic pathway starting from erythrose 4-phosphate (**4**) and phosphoenolpyruvate (**3**); (b) prediction via ribose 5-phosphate (**7**) and phosphoenolpyruvate (**3**); (c) observed. For further details, see Fig. 5 and text.

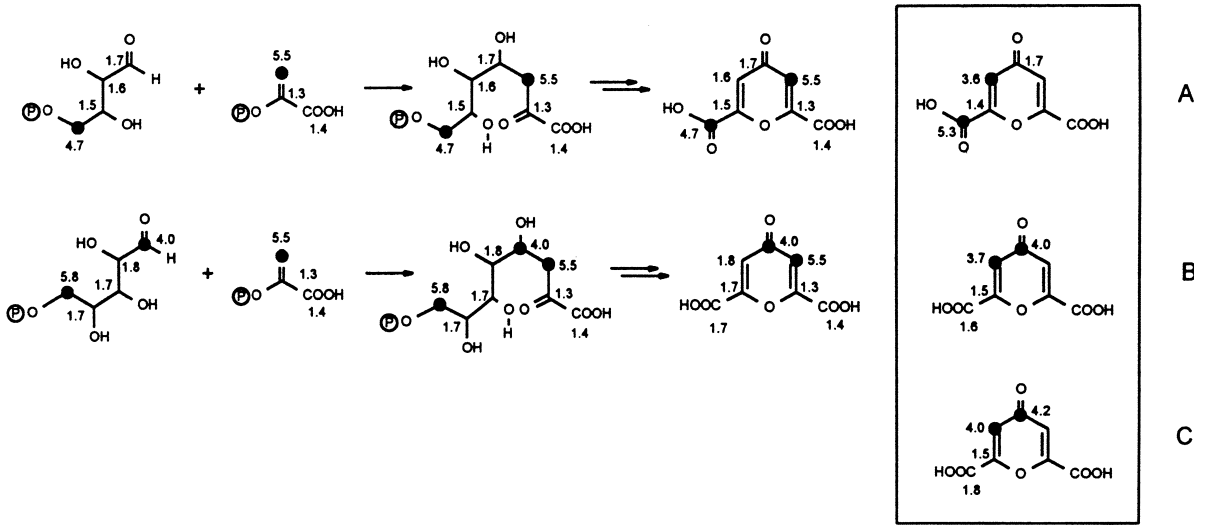

Fig. 8. ^{13}C Labelling patterns of chelidonic acid from the experiment with [1-^{13}C]glucose. (a) Prediction via erythrose 4-phosphate and phosphoenolpyruvate; (b) prediction via ribose 5-phosphate and phosphoenolpyruvate; (c) observed. Filled circles indicate significantly ^{13}C enriched atoms (> 3% ^{13}C abundance). Numbers indicate ^{13}C abundances. For more details, see Fig. 7 and text.

However, sedoheptulose could also be obtained directly from a pentose phosphate resulting in the formation of $^{13}C_5$-chelidonic acid. We have no evidence whatsoever for the presence of a chelidonic acid isotopomer with five contiguous ^{13}C atoms from either [U-$^{13}C_5$]ribose/ribulose or [U-$^{13}C_6$]glucose. Confirming this hypothesis, ^{13}C labelled sedoheptulose could not be incorporated into chelidonic acid (Table 4).

On the other hand, the data support the assembly of the chelidonic acid carbon skeleton from a pentose or pentose phosphate and phosphoenolpyruvate via a hypothetical mechanism summarized in Fig. 11. The proposed condensation between a pentose phosphate and phosphoenolpyruvate is analogous to the well-documented formation of DAHP from erythrose phosphate and phosphoenolpyruvate in the shikimate pathway of aromatic acid biosynthesis. The terminal carbon atom of the pentose precursor could then be removed via dephosphorylation, dehydrogenation and oxidative decarboxylation. Ring closure could occur by hemiacetal formation followed by two dehydrogenation steps. The order of events is hypothetical and additional

studies are necessary in order to elucidate the details of chelidonic acid biosynthesis.

4. Experimental

4.1. Materials

[U-$^{13}C_6$]glucose (99% ^{13}C) and [1-^{13}C]glucose (99% ^{13}C) were obtained from Omicron (South Bend, Indiana).

4.2. Synthesis of [U-$^{13}C_5$]ribose/ribulose

[U-$^{13}C_5$]ribose/ribulose was synthesized enzymatically from [U-$^{13}C_6$]glucose. The reaction mixture contained 100 mM Tris hydrochloride, pH 7.8, 6 mM dithiothreitol, 60 mM $MgCl_2$, 1 g of [U-$^{13}C_6$]glucose, 3 mM ATP, 75 mM phosphoenolpyruvate, 200 mM 2-oxoglutarate, 200 mM ammonium acetate, 5 mM $NADP^+$, 250 U of hexokinase, 250 U of glucose 6-phosphate dehydrogenase, 100 U of 6-phosphogluconate dehydrogenase, 250 U of pyruvate kinase and 250 U of glutamate dehydrogenase in a total volume of 90 ml. The mixture was incubated at 37°C. The pH of the solution was kept at 7.8 by addition of 3 M potassium hydroxide, and the progress of the reaction was monitored by ^{13}C NMR spectroscopy. After 5 h, the glucose had been completely converted into ribulose 5-phosphate. Thirty millilitres of 1 M barium chloride was added, and the white precipitate was removed by centrifugation. The supernatant was diluted with 600 ml of ethanol. The mixture was stirred overnight at 4°C. The white precipitate was collected by centrifugation and dried in vacuo over $CaCl_2$ at 4°C.

The white solid was dissolved in 150 ml of water. Ba^{++} was precipitated by the addition of 0.4 M Na_2SO_4 solution. The precipitate of $BaSO_4$ was removed by centrifugation. To the supernatant, $MgCl_2$ and $ZnSO_4$ were added to a final concentration of 10 and 1 mM, respectively. Phosphoriboisomerase (250 U) and alkaline phosphatase (1000 U) were added, and the mixture was incubated for 4 h at 37°C. The pH was kept at 7.8 by addition of 3 M potassium hydroxide. Aliquots of the mixture were monitored by ^{13}C NMR at intervals. The reaction was terminated after 4 h. Dowex 1X8 (OH^- form, 94 g) and Dowex 50WX8 (H^+ form, 70 g) was added, and the suspension was shaken for 15 h and then filtered. The filtrate was lyophilized.

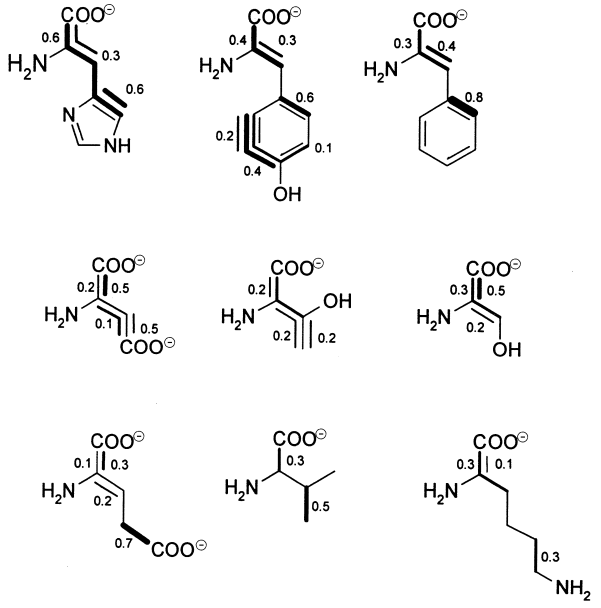

Fig. 9. Incorporation of [U-$^{13}C_5$]ribose/ribulose into *Leucojum aestivum*. ^{13}C labelling patterns of amino acids obtained from cellular protein. Bold bars indicate multiple ^{13}C labelled isotopomers. The numbers indicate molar fractions of respective isotopomers.

Table 4
^{13}C NMR abundances of chelidonic acid obtained from the experiment with [2-^{13}C]sedoheptulose

Position	^{13}C abundance in %
1	1.3
2	1.2
3	1.1
4	1.3

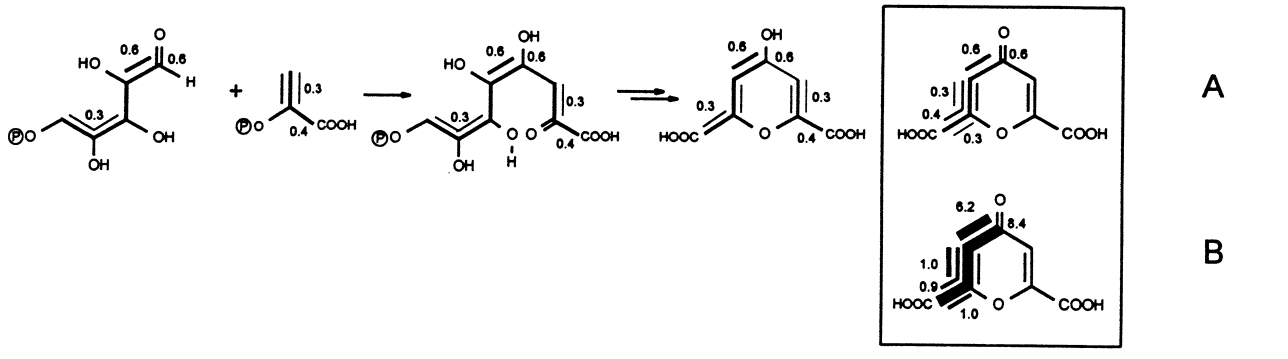

Fig. 10. ^{13}C Labelling patterns of chelidonic acid from the experiment with [U-$^{13}C_5$]ribose/ribulose. (a) Prediction via ribose 5-phosphate (**5**) and phosphoenolpyruvate (**3**); (b) observed. For further details, see Fig. 5 and text.

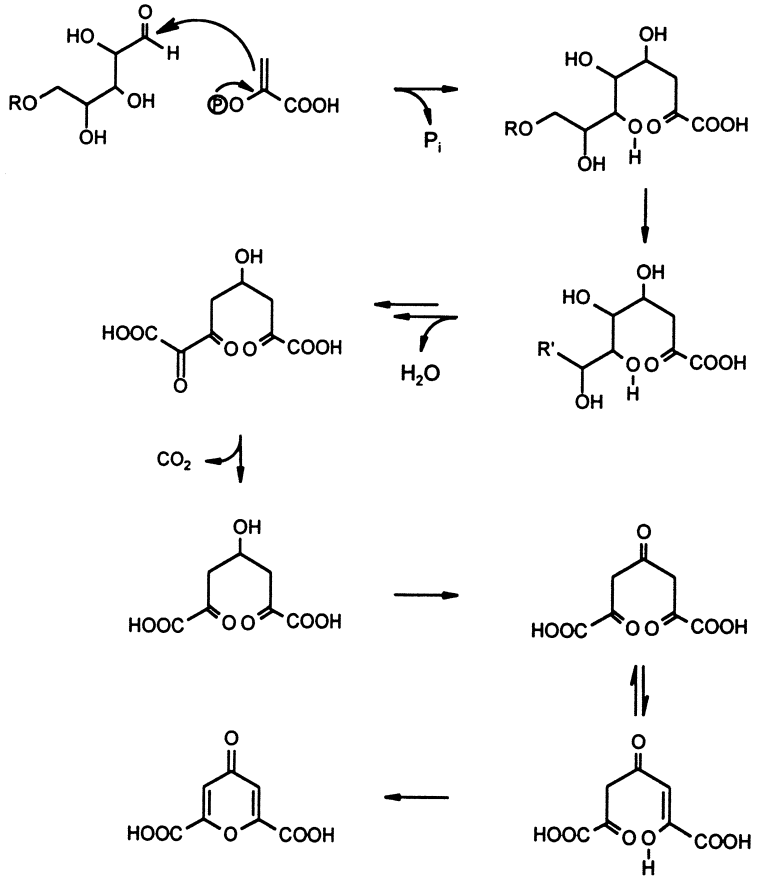

Fig. 11. Hypothetical mechanism of chelidonic acid biosynthesis. R = H or PO_3^{2-}, R′ = OH, or PO_4^{2-}, or COO^-.

4.3. Synthesis of [2-^{13}C]sedoheptulose (by a modified procedure from Wolfrom et al., 1952)

A solution containing 3 g of ribose in 10 ml of water was cooled to 4 °C. A cold solution of 1.31 g of K^{13}CN in 10 ml of distilled water was added, and the mixture was stirred at 4°C for 24 h. The reaction mixture was then boiled under reflux for 8 h. The solution was cooled, passed through a column of Amberlite IR-120 (Ca^{++}-form), and concentrated under reduced pressure. The solution (25 ml) was kept at 4°C for crystallization. Calcium[1-^{13}C]-D-altronate was collected as white crystals in 49% yield (1.8 g).

Calcium[1-^{13}C]altronate (1.6 g) was dissolved in 100 ml of hot water and applied to a column of Dowex 1X4 (Cd^{++}-form). The column was developed with 300 ml of water. The eluate was concentrated under reduced pressure. The residue was repeatedly suspended in 50 ml of benzene and concentrated under reduced pressure. Crystalline cadmium [1-^{13}C]D-altronate (1.6 g) was suspended in 30 ml of acetic acid anhydride. Dry HCl gas was passed slowly through the agitated slurry at 10°C for 15–20 min and at 50°C for 1 h. The reaction mixture was then stirred at room temperature for 16 h. The solution was concentrated under reduced pressure. Water (100 ml) was added, and the suspension was stirred at room temperature for 30 min. The mixture was extracted with CH_2Cl_2. The organic phase was washed with water and dried over Na_2SO_4. Removal of solvent under reduced pressure yielded [1-^{13}C]pentaacetyl-D-altronic acid as a colorless oil (2.6 g; 85%). ^{1}H NMR ($CDCl_3$, 360 MHz): δ, 5.69 (^{1}H, *d*, 2-H, $J = 8.0$ Hz), 5.36 (^{1}H, *dd*, $J1 = 8.0$ Hz, $J2 = 2.8$ Hz, 3-H), 5.22 (^{2}H, *dd*, $J1 = 8.0$ Hz, $J2 = 2.4$ Hz), 4.40 (^{1}H, *dd*, $J1 = 10.0$ Hz, $J2 = 2.8$ Hz), 4.20 (^{1}H, *dd*, $J1 = 8$ Hz, $J2 = 10$ Hz). ^{13}C NMR ($CDCl_3$, 96 MHz): δ, 172 (1-C*); 170.77; 170.20; 169.40; 168.10; 168.08; 70.03; 69.60; 69.10; 68.70; 61.61; 20.76; 20.51; 20.77

[1-^{13}C]Pentaacetyl-D-altronic acid (406 mg) was dissolved in 20 ml of toluene. Freshly distilled $SOCl_2$ (5 ml) was added, and the solution was heated under reflux for 2 h. The reaction mixture was concentrated under reduced pressure to yield [1-^{13}C]pentaacetyl-D-altronic chloride as a colorless oil which was dissolved in 50 ml of diethylether containing 500 mg of diazomethane. The solution was stirred at room temperature for 3 h. After removal of the solvent, the residue was dissolved in 10 ml of acetic acid containing 20 mg of Cu(II)acetate. The mixture was heated under reflux for 30 min. The acetic acid was then removed under vacuum, and the

oily residue was purified by chromatography (Silica gel; 200–300 mesh, gradient of ethyl acetate/hexane). Hexaacetyl-sedoheptulose (258 mg, 56%) was obtained as an oil. ^{1}H NMR ($CDCl_3$, 360 MHz) δ, 2.038 (3H, *s*); 2.031 (3H, 3); 2.060 (3H, *s*); 2.107 (3H, *s*); 2.118 (3H, *s*); 2.197 (3H, *s*); 4.210 (1H, *dd*, *J*1 = 12.24 Hz, *J*2 = 4.20 Hz), 4.340 (1H, *dd*, *J*1 = 12.24 Hz, *J*2 = 3.96 Hz), 4.670 (1H, *dd*, *J*1 = 3.96 Hz, *J*2 = 17 Hz), 4.920 (1H, *dd*, *J*1 = 3.96 Hz, *J*2 = 17.0 Hz), 5.226 (1H, *p*, *J* = 3.50 Hz), 5.365 (1H, *dd*, *J*1 = 3.50 Hz, *J*2 = 8.8 Hz); 5.460 (1H, *dd*, *J*1 = 2.00 Hz, *J*2 = 4.20 Hz); 5.645 (1H, *dd*, *J*1 = 8.80 Hz, *J*2 = 2.00 Hz). ^{13}C NMR ($CDCl_3$, 96 MHz): δ, 197.8 (2-C*); 170.5; 169.9; 169.6; 169.1; 168.2; 168.0; 74.25; 69.70; 68.57; 66.83; 66.33; 61.33; 20.29; 20.34; 20.47; 20.53; 20.63; 20.72.

[2-^{13}C]Hexaacetyl sedoheptulose (100 mg) was dissolved in 15 ml of methanol. Two-hundred milligrams of sodium methoxylate was added, and the solution was stirred at 4°C for 16 h. The reaction mixture was then kept at 4°C for 2 days. Methanol was removed under vacuum. The oily residue was dissolved in 4 ml of water. The solution was applied to a column of Dowex 1X4 (H^+-form). The elute was concentrated and purified by paper chromatography (Whatman paper No. 4) using pyridine–*n*-butanol–H_2O (2:5:1.8, v/v) as mobile phase. Sedoheptulose was visualized with $AgNO_3$/NaOH reagent and orcinol spray. [2-^{13}C]Sedoheptulose (28 mg, 62% yield) was obtained by elution with water.

4.4. Plant cell cultures

A cell suspension culture of *L. aestivum* cells growing in LS medium (pH 6.0) was gradually adapted to growth with glucose as carbon source over a period of 2 months. Cell suspensions were incubated on a gyratory shaker (130 rpm) at 22°C in continuous light. Doubling of cell mass required 4 weeks under these conditions.

4.5. Labeling experiments

Cells of *L. aestivum* (19 g) grown on D-glucose (natural ^{13}C abundance) as carbon source were transferred into a 250 ml Erlenmeyer flasks containing 75 ml of autoclaved LS medium (Linsmaier and Skoog, 1965) without sugar. ^{13}C-Labeled precursors were diluted with unlabeled nutrients in 6 ml of water, filter-sterilized and added (Table 1). After 1 month, the cell culture was transferred into 250 ml of the same medium (Table 1). The cell suspension was harvested by suction and was washed with a small amount of water.

4.6. Isolation of chelidonic acid

Wet *L. aestivum* cell mass (20 g) was macerated in 150 ml of hot water. The crude extract was centrifuged at 13,000 rpm for 30 min. The supernatant was applied to a column of Dowex 1X4 (12 × 1.1 cm, 200–400 mesh, H^+-form). The column was washed with 150 ml of water and developed with 150 ml of 2 M HCl. The eluate was concentrated under reduced pressure. The residue was purified by paper chromatography (Whatman paper No. 3) using 30% aqueous 2-propanol as mobile phase. Chelidonic acid was visualized with 5% aqueous KOH (R_f = 0.5, yellow band). The band of chelidonic acid was eluted with water. The eluate was concentrated under reduced pressure, and the crude product was recrystallized from ethanol. Typically, 10 mg of chelidonic acid were obtained from 20 g of *L. aestivum* cells (wet weight).

4.7. Isolation of amino acids

Amino acids were isolated from cell mass as described elsewhere (Eisenreich et al., 1991).

4.8. NMR spectroscopy

^{1}H and ^{13}C NMR spectra were recorded at 500.13 and 125.76 MHz, respectively, with a Bruker DRX500 spectrometer. Chelidonic acid was measured in D_2O; tyrosine, tryptophan and aspartic acid were measured in 0.1 M NaOD; other amino acids were measured in 0.1 M DCl.

4.9. Determination of ^{13}C enrichment

^{13}C Enrichments for all carbon atoms of biosynthetic me-tabolites were determined by quantitative NMR spectroscopy as described earlier (Eisenreich and Bacher, 2001). NMR signal assignments for chelidonic acid were based on two-dimensional HMQC, HMBC, and INADEQUATE experiments.

Acknowledgements

This work was supported by the Deutsche Forschungsgemeinschaft (through SFB 369) and the Fonds der Chemischen Industrie. Z.-W.S. would like to thank the Alexander-von-Humboldt foundation, Bonn, for financial supports. We thank Angelika Werner, Fritz Wendling, and Gabi Bergauer for expert help with the preparation of the manuscript.

References

Bacher, A., Rieder, C., Eichinger, D., Fuchs, G., Arigoni, D., Eisenreich, W., 1999. Elucidation of biosynthetic pathways and metabolic flux patterns via retrobiosynthetic NMR analysis. FEMS Microbiology Reviews 22, 567–598.

Eisenreich, W., Schwarzkopf, B., Bacher, A., 1991. Biosynthesis of nucleotides, flavins, and deazaflavins in *Methanobacterium thermoautotrophicum*. J. Biol. Chem. 266, 9622–9631.

Eisenreich, W., Bacher, A., 2001. Elucidation of biosynthetic pathways by retrodictive/predictive comparison of isotopomer patterns determined by NMR spectroscopy. In: Genetic Engineering, Principles and Methods, Vol. 22. Plenum Press, New York, in press.

Eichinger, D., Bacher, A., Zenk, M.H., Eisenreich, W., 1999a. Analysis of metabolic pathways via quantitative prediction of isotope labelling patterns: a retrobiosynthetic ^{13}C NMR study on the monoterpene loganin. Phytochemistry 51, 223–236.

Eichinger, D., Bacher, A., Zenk, M.H., Eisenreich, W., 1999b. Quantitative assessment of metabolic flux by ^{13}C NMR analysis. Biosynthesis of anthraquinones in *Rubia tinctorum*. J. Am. Chem. Soc. 121, 7469–7475.

Goese, M., Kammhuber, K., Bacher, A., Zenk, M.H., Eisenreich, W., 1999. Biosynthesis of bitter acid in hop. A ^{13}C NMR and ^{2}H NMR study on the building blocks of humulone. European Journal of Biochemistry 263, 447–454.

Linsmaier, E.M., Skoog, F., 1965. Organic growth factor requirements of tobacco tissue cultures. Physiol. Plantarum 18, 100–127.

Malcolm, M.J., Gear, J.R., 1971. The biosynthesis of chelidonic acid. Can. J. Biochem. 49, 412–416.

Ramstadt, E., 1953. The presence and distribution of chelidonic acid in some plant families. Pharm. Acta Helv. 28, 45–57.

Ueda, M., Ohnuki, T., Yamamura, S., 1998. Leaf-opening substance of a nyctinastic plant, *Cassia mimosoides*. Phytochemistry 49, 633–635.

Werner, I., Bacher, A., Eisenreich, W., 1997. Formation of gallic acid in plants and fungi: a retrobiosynthetic study with ^{13}C-labeled glucose. J. Biol. Chem. 272, 25474–25482.

Wolfrom, M.L., Berkebile, J.M., Thompson, A., 1952. Synthesis of sedoheptulose (D-altroheptulose). J. Am. Chem. Soc. 74, 2197–2198.

PERGAMON

Phytochemistry 57 (2001) 43–50

PHYTOCHEMISTRY

www.elsevier.com/locate/phytochem

Equilibrium between basic nitrogen compounds in lupin seeds with differentiated alkaloid content

Tadeusz Aniszewski [a,*], Danuta Ciesiołka [b], Krzysztof Gulewicz [b]

[a] *Laboratory of Applied Botany, Department of Biology, University of Joensuu, PO Box 111, 80101 Joensuu, Finland*
[b] *Laboratory of Phytochemistry, Institute of Bioorganic Chemistry, Polish Academy of Sciences, 61-704 Poznań, Poland*

Received 27 July 2000; received in revised form 4 December 2000

Abstract

The results of studies on the content of the nitrogen basic compounds, viz. quinolizidine alkaloids, biogenic polyamines and basic amino acids in lupin seeds are presented. The investigations concerned three lupin species (*Lupinus angustifolius* L., *Lupinus albus* L. and *Lupinus luteus* L.) and 10 bitter and sweet cultivated varieties. Content of quinolizidine alkaloids in *L. angustifolius* ranged from 11.4 to 19.6 μg mg^{-1} dw (bitter cultivars), from 0.18 to 0.47 μg mg^{-1} dw (sweet), in *L. albus* from 0.58 μg mg^{-1} dw (sweet) to 29.6 μg mg^{-1} dw (bitter) and in *L. luteus* from 0.59 (sweet) to 14.7 μg mg^{-1} dw (bitter). Total biogenic polyamine content ranged in *L. angustifolius* from 2773.9 to 3180.2 pmol mg^{-1} dw (bitter) and from 315.0 to 599.0 pmol mg^{-1} dw (sweet), in *L. albus* from 432.6 pmol mg^{-1} dw (sweet) to 1832.0 pmol mg^{-1} dw (bitter) and in *L. luteus* from 506.9 pmol mg^{-1} dw (sweet) to 2091.8 pmol mg^{-1} dw (bitter). Total basic amino acids varied in *L. angustifolius* from 1034.3 to 1704.6 pmol mg^{-1} dw (bitter) and from 1761.9 to 2101.9 pmol mg^{-1} dw (sweet), in *L. albus* from 696.9 pmol mg^{-1} dw (bitter) to 1269.2 pmol mg^{-1} dw (sweet) and in *L. luteus* from 927.6 pmol mg^{-1} dw (bitter) to 1598.3 pmol mg^{-1} dw (sweet). We found a close dependence between alkaloid content and level of biogenic polyamines and basic amino acids in all three lupin species tested. All bitter lupin seeds also contain high level of biogenic polyamines but a low content of basic amino acids. The reverse relationship in sweet lupin seeds was found. The findings demonstrate that lupin nitrogen basic compounds are in steady equilibrium and that change of content in one compound leads to corresponding change in the content of another. © 2001 Elsevier Science Ltd. All rights reserved.

Keywords: *Lupinus angustifolius*; *Lupinus albus*; *Lupinus luteus*; Leguminosae; Lupins; Basic nitrogen compounds; Basic amino acids; Biogenic polyamines; Quinolizidine alkaloids

1. Introduction

Nitrogen basic compounds constitute an integral part of all plants. They include protein amino acids, such as arg, lys, his, and non protein amino acids, such as orn, its homologues (α-,β-diaminopropylic acid, α-,γ-diaminobuturic acid), α-*N*- and δ-*N*-acyl derivatives and 5-hydroxyarginine, homoarginine and lathirine and 6-*N*-acyl lysine and 5-hydroxylysine derivatives. Most of the non protein amino acids occur in numerous genera of *Lathyrus*, *Vicia* and others. They are condensed nitrogen reserves and show strong lathyrogenic properties (Fowden, 1970, 1974). Nitrogen basic compounds also include metabolic products of amino acids, i.e. biogenic amines and alkaloids. Biogenic amines are positively charged cellular components, which makes it hard to elucidate their possible cellular functions besides a straight forward cation effect (Villanueva et al., 1978; Friedman and Oshima, 1989). Di- and polyamines — put, cad, spd and spm are metabolic products of basic amino acids and are characterized by an unpleasant smell and toxic properties. This toxicity is manifested as nephotoxicity, hypothermia and sedation (Janne et al., 1978). The quinolizidine alkaloids (QAs) occurring in lupins are lys metabolic products. One of the di-amines, cad, is also a precursor of QAs in the alkaloid biosynthesis pathway. Basic amino acids (BAAs), biogenic polyamines (BPAs) and QAs are nitrogen reserves in plants. These reserves also play a very important physiological role (Wink, 1993; Aniszewski, 1994, 1995; El Ghachtouli et al., 1995; Tarenghi and Martin-Tanguy, 1995; Wang et al., 2000).

Abbreviations: agm, agmatine; arg, arginine; BAAs, basic amino acids; BPAs, biogenic polyamines; cad, cadaverine; dw, dry weight; his, histidine; lup, lupanine; lys, lysine; put, putrescine; QAs, quinolizidine alkaloids; orn, ornithine; spd, spermidine; spm, spermine.

* Corresponding author. Tel.: +358-13-2513581; fax: +358-13-251 3590.

E-mail address: tadeusz.aniszewski@joensuu.fi (T. Aniszewski).

0031-9422/01/$ - see front matter © 2001 Elsevier Science Ltd. All rights reserved.
PII: S0031-9422(00)00498-2

Previous studies have been concerned with BAAs and QAs as these compounds have been considered as very important from the viewpoint of the potential use of lupins (Aniszewski, 1993a,b; Saito et al., 1993; Chango et al., 1993; Muzquiz et al., 1994; Aniszewski, 1998). In contrast, BPAs of lupins have not previously been studied although the effect of polyamines on animal cell growth, cell differentiation and their regulatory role in plants have been suggested (Bachrach et al., 1989; Hölttä and Sistonen, 1989; Galston and Sawhney, 1990). The question of the possible dependence of different nitrogen basic compounds in lupins has not been studied either, although it would seem to be very important from both the physiological and chemical points of view. The lack of empirical results on the relationship between nitrogen basic compounds in lupins was a strong motivation for us to set up the present experiments. The main aim of our work was to determine the correlation between the content of nitrogen basic compounds in 10 lupin cultivars from 3 lupin species (*Lupinus angustifolius* L., *Lupinus albus* L. and *Lupinus luteus* L.). The choice of the lupin as a test plant was not accidental. Lupin species are characterised by amounts of alkaloids ranging from 0.0000% to 4.0% of dry matter (Aniszewski, 1993a; Christiansen et al., 1999), various amino acids (Aniszewski, 1993b) and, probably varying amounts of polyamines. We addressed two basic questions in this study: (1) do changes in the amount of QAs affect changes in amount of BPAs and BAAs? and (2) what is the basic mechanism of this potential dependence between QAs, BPAs and BAAs in lupins?

2. Results

The compounds detected were products of the lys metabolic pathway and of the arg metabolic pathway. Cad and QAs are from the lys metabolic pathway and BPA from the arg metabolic pathway (Fig. 1).

The content of QAs clearly varied between and within species, according to the breeding quality of the cultivars. Table 1 shows the content of QAs in the three lupin species tested. *L. angustifolius* was represented by three bitter and three sweet cultivars. The content of QAs in these cultivars ranged from 0.18 in Emir to 19.6 μg mg^{-1} dw in Mirela. The mean total content of QAs in the bitter cultivars was about 40 times higher than in the sweet cultivars. *L. albus* and *L. luteus* was represented by one

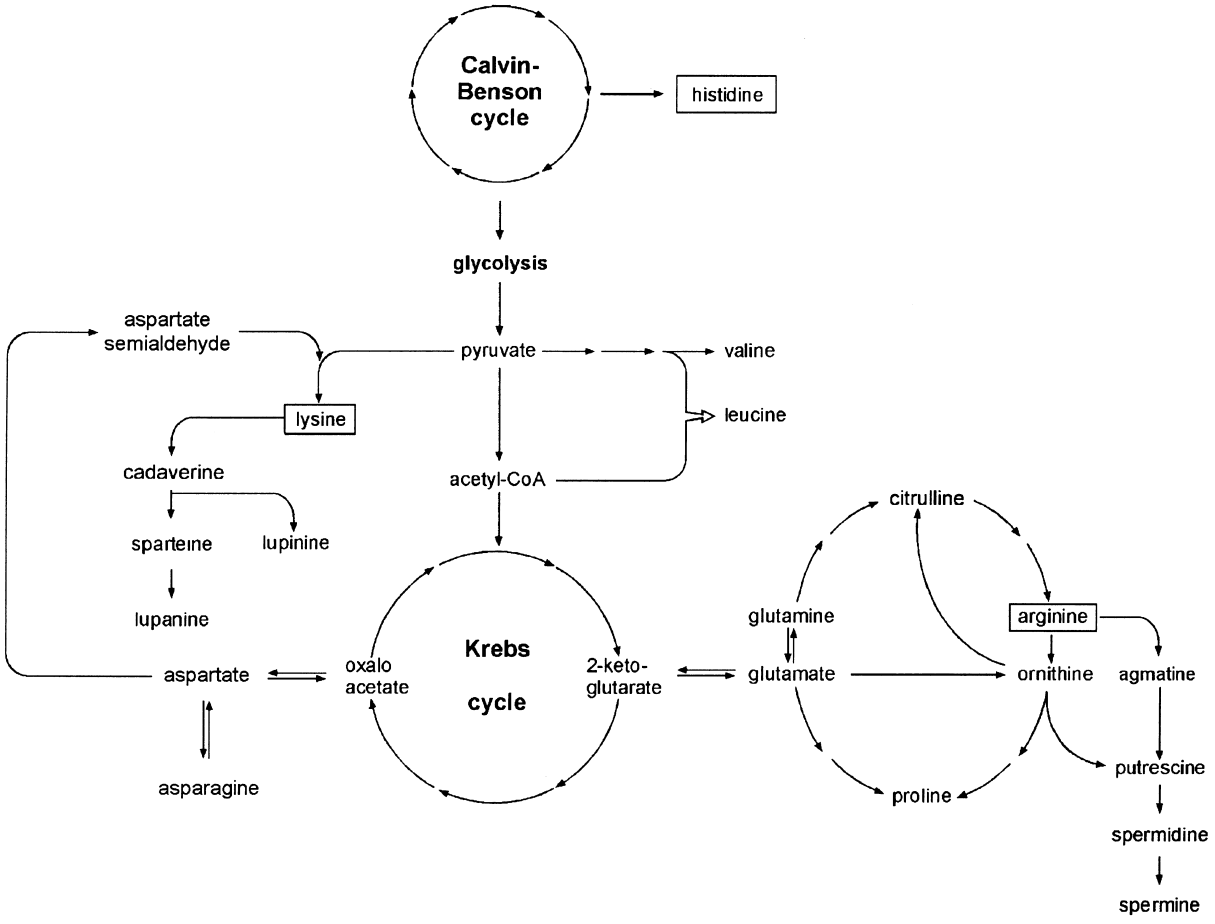

Fig. 1. Biosynthetic relationships of basic amino acids.

Table 1
Content of quinolizidine alkaloids (QAs) in lupin species tested

Species	Cultivars	Alkaloid content (μg mg^{-1} dw)	±S.D.	Mean total QA content in cultivar group (μg mg^{-1} dw)
Lupinus angustifolius	Mirela	19.6	0.29	
	Ernani	12.3	0.205	
	Trebatsch	11.4	0.205	
	Bitter cultivar (mean)			14.4
	Emir	0.18	0.0032	
	Ernani 1	0.43	0.00795	
	Topless	0.47	0.0067	
	Sweet cultivar (mean)			0.36
Lupinus albus	Bac	29.6	0.53	
	Bitter cultivar (mean)			29.6
	WTD	0.58	0.00105	
	Sweet cultivar (mean)			0.58
Lupinus luteus	Milfontes	14.7	0.24	
	Bitter cultivar (mean)			14.7
	Parys	0.59	0.009	
	Sweet cultivar			0.59

bitter and one sweet cultivar. In the case of *L. albus* the bitter cultivar contained about 50 times more QAs than the sweet one. The content of QAs in bitter *L. luteus* was about 25 times higher than in the sweet cultivar.

The content of BPAs clearly varied between and within species, according to the breeding quality of the cultivars (Table 2). As we can see, the bitter cultivars contained considerably more BPAs than the sweet varieties. The ratio of mean total BPAs in the three bitter cultivars tested to mean total BPAs in the three sweet ones was about 6.0 in the case of *L. angustifolius* L. For *L. albus* and *L. luteus* this ratio was about 4.2 and 4.1, respectively. It is noteworthy that agm and cad was not found in either the sweet or bitter cultivars tested: Bac (*L. albus*) and Milfontes (*L. luteus*). Also put was found only in 4 (2 bitter and 2 sweet) cultivars. In the case of *L. albus* we did not find put in either the bitter or sweet cultivar.

Content of BAAs varied between species and cultivars (Table 3). The results showed that the sweet lupin cultivars contained clearly higher amounts of BAAs in comparison to the bitter ones. For example, the ratio of mean total BAAs in sweet to bitter cultivars was 1.48, 1.83 and 1.72 in *L. angustifolius*, *L. albus* and *L. luteus*, respectively. Among the tested amino acids arg had its highest content in sweet cultivars, especially in the case of *L. angustifolius*.

The difference between bitter and sweet cultivars is very clear in the case of BPAs and BAAs (Tables 2 and 3). It is also evident that all the bitter cultivars of the three lupin species tested contained considerably more BPAs (average 2.4 times) than BAAs. Inversely, in the sweet varieties there were substantially more BAAs (average 3.3 times) than BPAs. The ratio of BPAs corresponding to 1 μg of QAs in sweet to bitter cultivars was 6.62; 12.50 and 6.29 for *L. angustifolius*, *L. albus* and *L. luteus*, respectively. In the case of BAAs this ratio is 59.21, 93.12 and 42.93, respectively.

3. Discussion

The results show that there is a different distribution of free BAAs, lys and arg, and their metabolites in lupin plants. All these compounds are a source of nitrogen and play a very important role in the primary (BAAs) and secondary metabolism (QAs, BPAs). Lys is a basic amino acid synthesed by pyruvate and aspartate (Azevedo et al., 1997). The biosynthesis of orn and arg involves glutamate transformation. Of course, the origin of 2-ketoglutarate for glutamate synthesis continues to be debated (Gálvez et al, 1999; Lancien et al., 2000). However, glutamine and glutamate are considered to be compounds of crucial importance, since they are donors for the biosynthesis of major N-containing compounds, including amino acids, nucleotides, chlorophylls, polyamines, and alkaloids (Ireland and Lea, 1999). Glutamate is a donor for the biosynthesis of both orn and arg. To understand the role of lys, orn and arg in lupin metabolism means taking into account these amino acids as resources for secondary metabolism. As presented in the results, lys is a source for QAs synthesis via cad, which is one of the

Table 2
Content of polyamines in lupin species tested[a]

Species/cultivars	Content of polyamines (pmol mg^{-1} dw)					Mean total PA (pmol mg^{-1} dw)
	spm	spd	put	agm	cad	
Lupinus angustifolius						
Mirela	1785.0 (101.9)	429.9 (25.9)	112.7 (5.2)	–[b]	5852.6 (125.7)	3180.2
Ernani	122.0 (6.3)	540.0 (34.1)	–	25.0 (1.2)	2086.9 (114.1)	2773.9
Trebatsch	127.7 (6.3)	718.8 (47.7)	–	355.7 (20.6)	1972.0 (91.3)	3174.2
Bitter cultivar (mean)						3042.8
Emir	169.0 (9.2)	350.0 (21.8)	73.2 (4.2)	–	–	592.2
Ernani 1	–	315.0 (19.8)	–	–	–	315.0
Topless	240.0 (13.0)	359.0 (22.4)	–	–	–	599.0
Sweet cultivar (mean)						502.1
Lupinus albus						
Bac	375.0 (20.6)	1457.0 (87.5)	–	–	–	1832.0
Bitter cultivar (mean)						1832.0
WTD	90.2 (5.4)	342.4 (20.6)	–	–	–	432.6
Sweet cultivar (mean)						432.6
Lupinus luteus						
Milfontes	1589.7 (92.9)	378.6 (21.5)	123.5 (6.6)	–	–	2091.8
Bitter cultivar (mean)						2091.8
Parys	155.0 (8.6)	242.6 (13.2)	109.3 (6.2)	–	–	506.9
Sweet cultivar (mean)						506.9

[a] Abbreviations: spm, spermine; spd, spermidine; put, putrescine; agm, agmatine; cad, cadaverine.
[b] Not detected.

BPAs, but from a different pathway than that of the other polyamines studied. Arg and orn are a source of BPA synthesis. QAs are compounds specific only to lupin species whereas BPAs are compounds generally found in plants and animals. Functionally, both these groups of compounds are similar. QAs have a defensive role in lupin and allelopathic functions in relation to biocenosis (Wink, 1993; Aniszewski, 1994, 1995; Wang et al., 2000). BPAs perform a significant control function in plant cell pH and in maintaining balance between anions and cations as well as allelopathic functions in relation to the abiotic and biotic environment (Altman and Levin, 1993; Walters and Mackintosh, 1997). The similarities in the functions of BPAs, QAs and BPAs in lupin plants suggest that the content of one compound is dependent on the content of the others.

The results show that QAs are present in considerable amounts in bitter lupins and small amounts in sweet lupins. Bitter lupins are more primitive and sweet lupins are bred to reduce alkaloid content. It is known that the synthesis of QAs occurs in chloroplasts, from which QAs are transported to the other organs (Wink and Hartmann, 1980). Suzuki et al. (1996) reported that two acyltransferases for QA biosynthesis were not located in chloroplasts, where de novo synthesis of QA skeleton is assumed to take place. The enzyme activity was associated with the mitochondrial fractions and localized in the matrix, as judged from the marker enzyme assay. However, the ECTase activity was not associated with the mitochondrial fractions (Suzuki et al., 1996). Nonetheless, the intracellular transport of QAs is a very important process. In this process ATP energy is used (Barłóg, 1999) and the transportation of assimilates and nitrogen compounds in the phloem takes place (Nalborczyk, 1993). Seed alkaloid content is a result of the balance between synthesis processes in the vegetative organs and the accumulation processes in the seeds (Barłóg, 1999). The synthesis of QAs and their transportation to the seeds is more effective in bitter than in sweet lupins. Rich-alkaloid lupins also contain a high level of free BPAs, which form in the metabolic pathways of arg. We found that the content of total BPAs in the bitter cultivars of three lupin species ranged from 1832.0 pmol mg^{-1}dw in cv. Bac (*L. albus*) to 3180.2 pmol mg^{-1}dw in cv. Mirela (*L. angustifolius* L.). It is known that intracellular polyamine concentrations vary throughout the cell cycle, and polyamine synthesis is a very early event in cell proliferation (Morgan, 1998). On the other hand, it is also known that adequate intracellular levels of BPAs are necessary for the optimal growth and replication of all living organisms, including plants. Bitter lupins grow in stress conditions generally better than sweet lupins (Aniszewski, 1993a). Possibly the high content of BPAs in bitter lupins influences this

Table 3
Content of basic amino acids (BAA) in lupin species tested[a]

Species/cultivars	Content of BAA (pmol mg^{-1} dw)			Mean total BAA (pmol mg^{-1} dw)
	ORN	LYS	ARG	
Lupinus angustifolius				
Mirela	6.6 (0.2)	726.0 (25.2)	522.0 (19.8)	1254.6
Ernani	25.6 (1.0)	506.7 (18.3)	502.0 (18.4)	1034.3
Trebatsch	138.0 (4.9)	653.8 (23.7)	212.8 (7.2)	1704.6
Bitter cultivar (mean)				1331.2
Emir	254.0 (9.6)	680.9 (23.2)	1167.0 (42.5)	2101.9
Ernani	132.3 (4.8)	450.6 (14.6)	1179.0 (48.0)	1761.9
Topless	112.0 (3.9)	503.0 (19.2)	1417.0 (54.2)	2032.0
Sweet cultivar (mean)				1965.3
Lupinus albus				
Bac	3.9 (0.1)	372.4(13.4)	318.6(11.6)	696.9
Bitter cultivar (mean)				696.9
WTD	260.5 (9.2)	571.9 (19.2)	436.8 (14.6)	1269.2
Sweet cultivar (mean)				1269.2
Lupinus luteus				
Milfontes	41.1 (1.2)	466.5 (16.0)	420.0 (16.3)	927.6
Bitter cultivar (mean)				927.6
Parys	157.8 (5.4)	570.0 (19.4)	870.5 (30.8)	1598.3
Sweet cultivar (mean)				1598.3

[a] Abbreviations: orn, ornithine; lys, lysine; arg, arginine.

better growth. BPAs influence the transcriptional and translational stages of protein synthesis, interact with nucleic acids, stabilize membranes and alter intracellular free calcium. Fruit-ripening and flower-setting processes in plants are modulated by polyamines (Morgan, 1998). On the other hand, the transport mechanisms of BPAs and the means by which polyamine uptake is induced are not clear. Our results show that a high content of QAs and BPAs accompanies a low content of free BAAs. The content of BAAs in bitter cultivars ranged from 696.9 pmol mg^{-1} dw in cv. Bac to 1704.6 pmol mg^{-1} dw in cv. Trebatsch. The low content of free BAAs in bitter cultivars is probably due to their incorporation into the synthesis of QAs (lys) and BPAs (arg and orn).

In contrast to bitter lupins, sweet cultivars show a reverse relationship between the nitrogen basic compounds. The breeding of sweet cultivars from bitter varieties results in a decrease in the content of QAs and BPAs, which is parallelled by an increase in the content of BAAs. This might suggest that the metabolism of lys and arg into QAs and BPAs respectively is very limited (Tables 1–3). This would eventually lead to the observed accumulation of BAAs in the pool of free amino acids in seeds. We are aware that Saito et al. (1993) suggested that the suppressed step for the formation of QAs in sweet plants is neither the various steps prior to the formation of cadaverine nor the specific reactions after the formation of cyclic QAs but is the ring closure reaction from cad to the initial bicyclic and tetracyclic QAs. The concentration of lys does not change in bitter and sweet plants, because protein-amino acid biosynthesis is strictly regulated in the plant cell (Saito et al., 1993). The content of BAAs in sweet cultivars tested by us ranged from 1267.2 pmol mg^{-1} dw in cv. WTD to 2101.9 pmol mg^{-1} dw in cv. Emir, while the content of BPAs was of the order 315–599 pmol mg^{-1} dw of seeds. On the other hand, the greater availability of BAAs might also result in facilitated biosynthesis of lys- and arg-containing proteins. Such a mechanism would explain the higher content of lys and arg in the population of seed protein in sweet cultivars of lupin.

It is worth noticing that the choice of lupin material used in this study was limited to the availability of different varieties of lupins, mainly bitter cultivars (in Poland the bitter variety of *L. luteus* is no longer cultivated and only 1 bitter variety Bac of *L. albus* is grown). Hence, in the case of these species, we tested only 1 bitter and 1 sweet cultivar. In spite of this, the results obtained for these two species shows a similar relationship and are highly compatible with those for *L. angustifolius*.

The data collected so far indicate that a decrease in the content of one group of compounds (QAs and PAs) is parallelled by an increase in the content of BAAs, and vice versa.

4. Experimental

4.1. Plant experimental material

The seeds of three lupin species (*Lupinus angustifolius* L., *Lupinus albus* L. and *Lupinus luteus* L.) were used in the determination of basic nitrogen compounds. These species were represented in the experimental study by two groups of cultivars. One group of cultivars was formed by low-alkaloid cultivars, also known in the literature as "sweet" cultivars and the second group by high-alkaloid cultivars, known as "bitter" cultivars (Aniszewski 1993b). Bitter cultivars are close to native varieties of lupins and sweet cultivars are bred varieties of lupins. Both *L. angustifolius* cv. Emir (sweet) and *L. albus* cv. Bac (bitter) were obtained for research by courtesy of Dr. Stanisław Stawiński of the Przebędowo Breeding Station of the Institute of Plant Breeding and Acclimatization located near Poznań. By courtesy of Dr. Jan Nijaki of the Plant Breeding Station in Wiatrowo near Poznań the following lupin cultivars were obtained for research: *L. angustifolius* cv. Ernani (bitter), *L. angustifolius* cv. Trebatsch (bitter), *L. angustifolius* cv. Topless (sweet), *L. angustifolius* cv. Ernani 1 (sweet), *L. albus* cv. WTD (sweet) and *L. luteus* cv. Parys (sweet). *L. luteus* cv. Milfontes (bitter) was obtained for research by courtesy of Dr Joao Neves Martins of the Agricultural University of Lisbon in Portugal. All seeds were harvested in 1998.

4.2. Analysis of metabolic pathways

The metabolic pathways of his, lys and arg were studied before the present experiments were set up (Nicholson, 1997). The pathways of QAs and BPAs were also analyzed, and on the basis of this analysis their route was constructed.

4.3. QAs analysis procedure

Two grams of lupin seed flour with 100 ml 80% methanol was sonicated by 30 min on a Sonorex Super AK 103H bath. Next, the mixture was filtrated on a Büchner funnel and the lupin flour was washed with methanol to an end volume of 100 ml. In the case of the analysis of bitter lupin varieties 10 ml water was added to 5 ml of extract. After removal of methanol the solution was also adjusted with water to 15 ml. In the case of the analysis of sweet lupin varieties 25 ml of extract was evaporated for removal of methanol and the solution was also adjusted with water to 15 ml.

Fifteen millilitres of alkaloid solution was applied on a column (2×0.8 cm) SCX (Strong Cation Exchanger), Alltech, USA. Before applying the alkaloids the column was activated by 5 ml of methanol and 5 ml of water. After applying the alkaloid sample the column was washed with 5 ml of water, 5 ml of methanol and 2.5 ml of water. The alkaloids were washed with 12 ml of 6% ammonia. The alkaloids were then extracted three times in 12 ml of chloroform. The chloroform was evaporated to dryness under a vacuum. Then 10 μl of caffeine (1 mg/ml) as an internal standard was added and dryed. After drying 40 μl methyl chloride was added to the sample. One microlitre of sample was applied on the GC–MS column.

GC–MS analyses were carried out with a Hewlett Packard gas chromatograph (Model 5890) with a mass selective detector (Model 5971A), equipped with DB-5 fused silica capilary column (30 m×0.25 mm i.d.; J&W, Folsom, CA, USA). The carrier gas was helium at a flow rate of 1 ml/min and the column temperature was programmed from 200°C (held for 2 min) at a rate of 5°C/min to 300°C, which was held for 12 min. The injector temperature was 250°C and the injections were performed in the split (1:20) mode (Stobiecki et al., 1997). Each analysis was done in four replications.

4.4. Free BAAs analysis

One gram of lupin fluor with 20 ml of 0.1% trifluoroacetic acid (TFA) was mixed and extracted for 3.5 h at room temperature. Then the sample was centrifuged at 3000 rpm 20 min on a Janetzky K70. The supernatant was evaporated to dryness. The residue was solved in 10 ml water and applied on a column (3×0.8 cm) with Dowex 50WX8 (H^+). The column was washed in 10 ml of metanol and then 5 ml of water. The amino acids were eluted with 15 ml 7 N of ammonia. The alkaline solution was shaken three times with 15 ml of chloroform to remove the alkaloids. The ammonia layer was than evaporated to dryness. To each sample 50 μl (3 mg/ml) DL-γ-amino-butyric acid (S.A.F. Hoffmann La Roche, Switzerland) was added as an internal standard. The samples were dried in a vacuum overnight. The dried amino acid samples were derivatized with isobutyl alcohol for esterification of carboxyl group. Esterification was performed in 3 N HCl solution in isobutanol at temperature of 100°C for 15 min. Acetylation of amino groups was done in a 300 μl mixture of methylene chloride and trifluoracetic acid anhydride 2:1 (v/v) at a temperature of 110°C for 5 min. After cooling, 1 μl of the reaction mixture was injected onto a GS-MS column. The carrier gas was helium at a flow rate of 1 ml/min and the column temperature was programmed from 100°C (held for 2 min) at a rate of 5°C/min, and at a rate 10°C/min, to 300°C which was held for 2 min. The injector temperature was 250° C and injections were done in the split mode. The analyses were performed in four replications.

4.5. Analysis of BPAs

The extraction of polyamines and their determination on the basis of TLC chromatography were adapted according to the method described by Flores and Galston

(1982), Friedman et al. (1986) as follows: lupin seeds were freezed in liquid nitrogen after which they were ground 2×15 s in a mill. Two hundred milligrams of lupin flour were scaled and mixed with 2 ml of 5% $HClO_4$ and extracted for 1 h in an ice bath. The sample was then centrifuged at 3000 rpm 20 min on a Janetzky K70. The supernatant was received and centrifuged again (supernatant is stable for about 6 months at −20°C). Dansylation of the polyamines obtained was done as follows: 200 μl of polyamine extract at $HClO_4$ was mixed with 400 μl of dansyl chloride (5 mg/ml) in acetone, prepared fresh. After that 200 μl of saturated Na_2CO_3 was added. The mixture was briefly vortexed and incubated in darkness overnight. Excess dansyl chloride was removed by reaction with 100 μl (100 mg/ml) of added proline and incubation in darkness for 30 min at room temperature. The dansylpolyamines were then extracted in 0.5 ml benzene for 1 min. Benzene fractions were stored in glass vials (stable for 1 month at −20°C). The standards (spm, spd, put, cad, agm) were dansylated in the same way. Twenty nanomol of standard were used for each reaction. Samples were put on DC-Plastikfolien Kieselgel (20×20 cm) plates in amounts of 30, 40, 50 and 60 μl. TLC was developed for about 1 h with either of two solvent systems: chloroform:triethylamine (25:2 v/v) or cyclohexane:ethylacetate (5:4 v/v). After TLC, the dansylpolyamine bands were scraped and eluted in 2 ml ethylacetate. The polyamines were quantified with a F-2000 Fluorescence Spectrometer, Hitachi (exitation at 350 nm and emission at 495 nm).

4.6. Reagents and standards

Reagents and standards used in the determination were DL-ornithine (Sigma), DL-citrulline (Sigma), agmatine (Sigma), spermine ×4 HCl (Sigma), spermidine ×3 HCl (Sigma), putrescine (Sigma), caffeine (Sigma), L-arginine (Aldrich), lysine (Aldrich), DL-γ-amino-butiric acid (S.A.F. Hoffmann La Roche, Switzerland). Four alkaloids used as standard were isolated and purificated from lupin seeds in the Institute of Bioorganic Chemistry of the Polish Academy of Sciences in Poznań. The purity of lupanine was 97.1%, 13-hydroxylupanine, 95.1%, angustifoline, 95.3% and sparteine, 96.4%.

4.7. Recovery tests

Recovery tests for QAs, BAAs and BPAs were done. Lup was used in recovery tests for QAs, lys for BAAs and put for BPAs. When the lup was passed thorough the experimental procedure, recovery was 96.0%. When the lup was mixed with seed flour and passed through the experimental procedure, recovery was 95.2%. The respective recoveries for lys were 95.1 and 94.7% and for put 93.7 and 93.2%. The recoveries were high and proved that analytical methods worked well.

Acknowledgements

This work was supported by the Academy of Finland and the Polish Academy of Sciences in the frame of the bilateral scientific cooperation.

References

Altman, A., Lewin, N., 1993. Interactions of polyamines and nitrogen nutrition in plants. Physiologia Plantarum 89, 653–658.

Aniszewski, T., 1993a. Lupine: a potential crop in Finland. Studies on the ecology, productivity and quality of *Lupinus* spp. PhD thesis. University of Joensuu, Joensuu.

Aniszewski, T., 1993b. Nutritive quality of the alkaloid-poor Washington lupin (*Lupinus polyphyllus* Lindl var SF/TA) as a potential protein crop. Journal of the Science of Food and Agriculture 61, 409–421.

Aniszewski, T., 1994. The biological basis of quinolizidine alkaloids. Science of Legumes 1, 1–24.

Aniszewski, T., 1995. Ecological role of lupin alkaloids. In: Frencel, I., Gulewicz, K. (Eds.), Progress in Lupin Research. Polish Lupin Association and Institute of Bioorganic Chemistry. Polish Academy of Sciences, Poznań, pp. 9–31.

Aniszewski, T., 1998. Perennial stability of total quinolizidine alkaloid content in alkaloid-poor Washington lupin (*Lupinus polyphyllus* Lindl). Journal of the Science of Food and Agriculture 76, 195–199.

Azevedo, R.A., Arruda, P., Turner, W.L., Lea, P.J., 1997. The biosynthesis and metabolism of the aspartate derived amino acids in higher plants. Phytochemistry 46, 395–419.

Bachrach, U., Katz, E., Shayovitz, A., Rajbabu, P., 1989. Polyamines and oncogenes. In: Goldemberg, S.I., Algranati, I.D. (Eds.), The Biology and Chemistry of Polyamines. ICSU Press and Oxford University Press, Oxford–New York–Tokyo, pp. 181–191.

Barłóg, P., 1999. Growth dynamics and accumulation of alkaloids and polyamines by narrow leafed lupin in different magnese and nitrogen conditions. Doctoral dissertation. Department of Agricultural Chemistry, Agricultural University of Poznań, Poznań.

Chango, A., Villaume, C., Bau, H.M., Nicolas, J.P., Mejean, L., 1993. Debittering of lupin (*Lupinus luteus* L.) protein by calcium alginate and nutritional-evaluation. Journal of the Science of Food and Agriculture 63, 195–200.

Christiansen, J.L., Raza, S., Ortiz, R., 1999. White lupin (*Lupinus albus* L.) germplasm collection and preliminary in situ diversity assessment in Egypt. Genetic Resources and Crop Evolution 46, 169–174.

Flores, H.E., Galston, A.W., 1982. Analysis of polyamines in higher plants by high performance liquid chromatography. Plant Physiology 69, 701–706.

Fowden, L., 1970. The non-protein amino acids of plants. Phytochemistry 2, 203–266.

Fowden, L., 1974. Non-protein amino acids from plant, distribution, biosynthesis and analog functions. Recent Advances in Phytochemistry 8, 95–122.

Friedman, R., Lewin, N., Altman, A., 1986. Presence and identification of polyamines in xylem and phloem exudates of plants. Plant Physiology 82, 1154–1157.

Friedman, S.M., Oshima, T., 1989. Polyamines of sulfur-dependent archaebacteria and their role in protein synthesis. Journal of Biochemistry 105, 1030–1033.

Galston, A.W., Sawhney, R.K., 1990. Polyamines in plant physiology. Review. Plant Physiology 94, 406–410.

Gálvez, S., Lancien, M., Hodges, M., 1999. Are isocitrate dehydrogenases and 2-oxoglutarate involved in the regulation of Glu synthesis? Trends in Plant Science 4, 484–490.

El Ghachtouli, N., Paynot, M., Morandi, D., Martin-Tanguy, J., Gianinazzi, S., 1995. The effect of polyamines on endomycorrhizal

infection of wild-type *Pisum sativum* cv. Frisson (nod^+myc^+) and two mutants (nod^-myc^+). Mycorrhiza 5, 189–192.

Hölttä, E., Sistonen, L., 1989. Ornithine decarboxylase gene expression in normal and transformed cells. In: Goldemberg, S.I., Algranati, I.D. (Eds.), The Biology and Chemistry of Polyamines. CSU Press and Oxford University Press, Oxford–New York–Tokyo, pp. 193–202.

Ireland, R.L., Lea, P.J., 1999. The enzymes of glutamine, glutamate, asparagine and aspartate metabolism. In: Singh, B.K. (Ed.), Plant Amino Acids: Biochemistry and Biotechnology. Marcel Dekker, New York, pp. 49–109.

Janne, J., Paso, H., Raina, A., 1978. Polyamines in rapid growth and cancer. Biochem. Biophys. Acta 473, 241–293.

Lancien, M., Gadal, P., Hodges, M., 2000. Enzyme redundancy and the importance of 2-oxoglutarate in higher plant ammonium assimilation. Plant Physiology 123, 817–824.

Morgan, D.M.L., 1998. Polyamines. An introduction. In: Morgan, D.M.L. (Ed.), Polyamine Protocols. Methods in Molecular Biology. Volume 79. Humana Press, Totowa, New Jersey, pp. 3–30.

Muzquiz, M., Cuadrado, C., Ayet, G., De la Cuadra, C., Burbano, C., Osagie, A., 1994. Variation of alkaloid components of lupin seeds in 49 genotypes of *Lupinus albus* L. from different countries and locations. Journal of Agricultural and Food Chemistry 42, 1447–1450.

Nalborczyk, E., 1993. Biological basis of legumes productivity. Fragmenta Agronomica 4, 147–150.

Nicholson, D.E., 1997. Metabolic Pathways. 20th Edition. Designed by Dr. Donald E. Nicholson, Department of Biochemistry and Molecular Biology, The University of Leeds, England, and Sigma. Product No. M 3907.

Saito, K., Koike, Y., Suzuki, H., Murakoshi, I., 1993. Biogenetic implication of lupin alkaloid biosynthesis in bitter and sweet forms of *Lupinus luteus* and *Lupinus albus*. Phytochemistry 34, 1041–1044.

Stobiecki, M., Wojtaszek, P., Gulewicz, K., 1997. Application of solid phase extraction for profiling quinolizidine alkaloids and phenolic compounds in *Lupinus albus*. Phytochemistry Analysis 8, 153–158.

Suzuki, H., Koike, Y., Murakoshi, I., Saito, K., 1996. Subcellular localization of acyltransferases for quinolizidine alkaloids biosynthesis in *Lupinus*. Phytochemistry 42, 1557–1562.

Tarenghi, E., Martin-Tanguy, J., 1995. Polyamines, floral induction and floral development of strawberry (*Fragaria ananasse* Duch.). Plant Growth Regulation 17, 157–165.

Villanueva, V.R., Adekha, R.C., Cantera-Soler, A.M., 1978. Changes in polyamine concentration during seed germination. Phytochemistry 17, 1245–1249.

Walters, D.R., Mackintosh, C.A., 1997. Control of plant disease by perturbation of fungal polyamine metabolism. Physiologia Plantarum 100, 689–695.

Wang, S.F., Liu, A.Y., Ridsdill-Smith, T.J., Ghisalberti, E.L., 2000. Role of alkaloids in resistance of yellow lupin to red-legged earth mite *Halotydeus destructor*. Journal of Chemical Ecology 26, 429–441.

Wink, M., 1993. Biological activities and potential application of lupin alkaloids. Proceed 7th International Lupin Conference Evora, Portugal, pp. 161–178.

Wink, M., Hartmann, T., 1980. Localization of the enzymes of quinolizidine alkaloids biosynthesis in leaf chloroplasts of *Lupinus polyphyllus*. Plant Physiology 70, 74–77.

PERGAMON

Phytochemistry 57 (2001) 51–56

PHYTOCHEMISTRY

www.elsevier.com/locate/phytochem

Transformation of naturally-occurring 1,9-*trans*-9,5-*cis* sweroside to all *trans* sweroside during acetylation of sweroside aglycone

Marion M. Horn [a], Siegfried E. Drewes [a,*], Nicola J. Brown [a], Orde Q. Munro [a], J.J. Marion Meyer [b], Abbey D.M. Mathekga [b]

[a] *School of Chemical and Physical Sciences, University of Natal, Pietermaritzburg, P. Bag X01, Scottsville, 3209, South Africa*
[b] *Department of Botany, University of Pretoria, Pretoria 0001, South Africa*

Received 26 April 2000; received in revised form 3 November 2000

Abstract

From the rootstock of *Scabiosa columbaria* L. loganin and sweroside were isolated. Sweroside showed moderate antibacterial activity. Pure sweroside was converted to the sweroside aglycone 1-acetoxy derivative (DABCO/Ac_2O) after hydrolysis of the glucose unit. X-ray crystallography of the monoacetate showed unambiguously that it had been transformed to a new seco-iridoid having the novel *trans* diaxial configuration for the protons on C-1, C-9 and C-5. The mechanism for the rearrangement is discussed. © 2001 Elsevier Science Ltd. All rights reserved.

Keywords: *Scabiosa columbaria*; Dipsaceae; Loganin; Sweroside; Rearrangement; Sweroside aglycone-1-acetate

1. Introduction

Scabiosa columbaria L. is a perennial herb, which grows to a meter in height, flowers in midsummer, and has a large woody rootstock in the form of a tuber. Traditionally root decoctions are used for sterility. Ointments made from the charred tubers are also applied to venereal sores (Hutchings, 1996). Chemically almost nothing is known about the plant although the glycoside scabiosin has been isolated from it (Watt and Breyer-Brandwijk, 1962).

We started investigating the plant because it grows profusely in many parts of South Africa, and, despite its frequent use by the Zulu people, the chemistry of its constituents is almost unknown (Van Wyk, 1997).

2. Results and discussion

2.1. Isolation of loganin and sweroside

It was immediately clear from the preliminary examination of the extracts ($CHCl_3$)/EtOH) that *Scabiosa columbaria* contained several iridoids, mostly in the form of their glycosides. Fractionation of the extract yielded pure loganin **1a**. This compound was first isolated from the fruits of *Strychnos nux vomica* (Dunstan and Short, 1883). The full structure, stereochemistry and biosynthesis was only elucidated some 86 years later (Battersby and Hall, 1969).

Also present in the extract we found the seco-iridoid sweroside **2a** (Inouye et al., 1970) and this is the first isolation from the family Dipsaceae. It was accompanied by a complex mixture of other iridoids, all possessing an aldehyde functionality. This latter mixture and sweroside, **2a**, showed only moderate antibacterial activity when tested against a selection of gram-positive and gram-negative bacteria.

2.2. Rearrangement of sweroside on acetylation and X-ray analysis of the resultant product

Iridoids and seco-iridoids all possess the labile acetal moiety and are frequently subjected to varying degrees of acid or base treatment during work-up or subsequent manipulation. In this connection Bianco (1994) has published a review article which deals specifically with acid hydrolysis and the subsequent rearrangements which can occur.

We report here on the rearrangement which sweroside aglycone **2b** undergoes during acetylation in the presence

* Corresponding author. Tel.: +27-33-260-5243; fax: +27-33-260-5009.
E-mail address: drewes@science.unp.ac.za (S.E. Drewes).

0031-9422/01/$ - see front matter © 2001 Elsevier Science Ltd. All rights reserved.
PII: S0031-9422(00)00460-X

of the base diazabicyclooctane (DABCO). (DABCO is easier to remove at the end of the reaction than pyridine). The reaction afforded the highly crystalline 1-acetoxy sweroside aglycone, a new compound with novel stereochemistry. This seco-iridoid **3**, has the protons at C-1, C-9 and C-5 in the axial orientation, giving rise to an all *trans*-configuration at these three carbon atoms. This stands in contrast to the "normal" 1,9-*trans*-9,5-*cis* arrangement found in iridoids and seco-iridoids in which the protons on C-1, C-9 and C-5 assume *eq.eq*. and *ax* orientations respectively. Since **3** was obtained as colourless orthorhombic crystals, amenable to X-ray analysis, the relative stereochemistry could be established with certainty (Fig. 1). Comparison with the extensive published NMR data (Ma et al., 1994) confirmed the view that "our" parent sweroside indeed had the accepted 1,9-*trans*-9,5-*cis* stereochemistry. Subsequent formation of **3**, with its 1,9-*trans*-9,5-*trans*-configuration was, therefore, attainable only if rearrangement had occurred during acetylation.

The seco-iridoid decentapicrin A, a compound for which X-ray data was available is shown in (**4**) (Van der Sluis and Labadie, 1981; Kojic-Prodic et al. 1985). This compound is identical in all respects to sweroside and differs only in the nature of the glycoside at C-1. A comparison of the magnitude of the coupling constants $J_{1,9}$ and $J_{5,9}$ respectively for **4** and **3** shows clearly a H-1/H-9 (*trans* di*equatorial*), H-5/H-9 (*cis axial*, *equatorial*) stereochemistry for **4**, compared with a *trans diaxial*, *trans diaxial*, arrangement for the same proton on **3**.

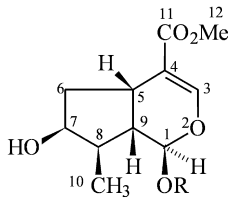

1a R = Glucose (Loganin)
1b R = H (aglucone)
1c R = $COCH_3$

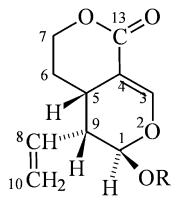

2a R = glucose (sweroside)
2b R = H (aglucone)

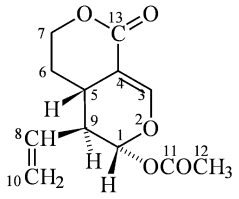

3

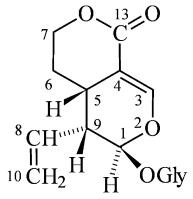

Decentapicrin **4**

We were reassured that the proposed rearrangement occurs *during* the acetylation procedure, and not earlier, by showing that the sweroside aglycone (**2b**) had a stereochemistry unchanged from that of the parent sweroside (**2a**). A comparison of ^{1}H NMR spectral data for sweroside (**2a**), sweroside aglycone (**2b**) (see Section 3), and the rearranged acetate (**3**) (Table 1) confirms the

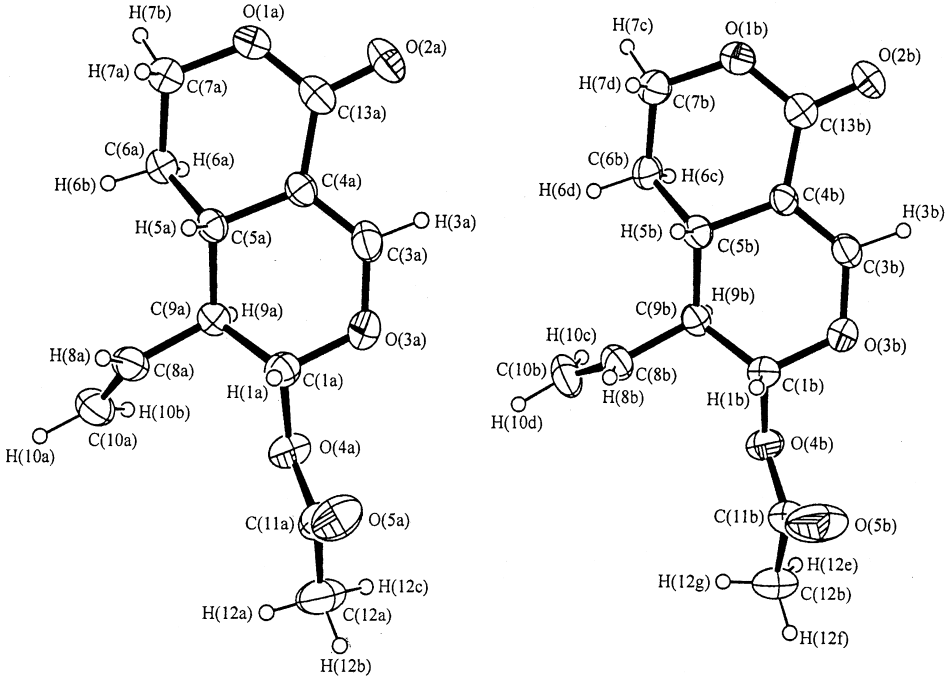

Molecule A **Molecule B**

Fig. 1. Two crystallographically-distinct conformations of sweroside aglycone-1-acetate **3**.

Table 1
NMR spectral data of rearranged acetate **3** ($CDCl_3$, δ ppm, J = Hz)

No.	^1H	^{13}C
1	6.11 (1H, *d*, 9.3)	93.1
3	7.64 (1H, *d*, 2.2)	154.1
4	–	104.4
5	2.56 (1H, *ddd*, 4.5,2.3)	34.0
6	6a 1.56 (1H, *m*)	
	6b 2.06 (1H, *m*)	27.2
7	7a 4.27 (1H, *ddd*, 24.1, 12.5, 2.4)	
	7b 4.48 (1H, *ddd*, 11.5, 4.5, 2.0)	68.1
8	5.52 (1H, *ddd*, 16.9, 10.3, 9.3)	132.6
9	2.21 (1H, *ddd*, 9.2, 7.4, 1.6)	46.2
10	10a 5.29 (1H, *ddd*, 16.9, 1.5, 0.7)	
	10b 5.33 (1H, *ddd*, 10.4, 1.4)	121.4
CO_2 lactone		169.1
Acetate CO		164.7
OCH_3	2.13 (*s*)	20.7

stereochemistry shown for (**2a**), (**2b**) and **3**. There is no doubt that the aglycone still retains the 1,9 *trans* d*ieq*. arrangement prior to acetylation. It is suggested that the rearrangement during acetylation proceeds as shown in Scheme 1.

1. The aglycone of sweroside, **2b**, under influence of the base (DABCO) ring opens to generate **2c**.
2. In a final step, prior to attachment of the acetyl moiety, **2c** loses an acidic proton at C-9, undergoes keto-enol tautomerism and ring-closes to **2d** (and also presumably the isomer of opposite configuration).

We suggest that a series of products, all in equilibrium with one another, are formed. On acetylation, and quite fortuitously, one of these products, **3**, crystallised out from the reaction mixture in reasonable yield. The product was amenable to X-ray and NMR analysis.

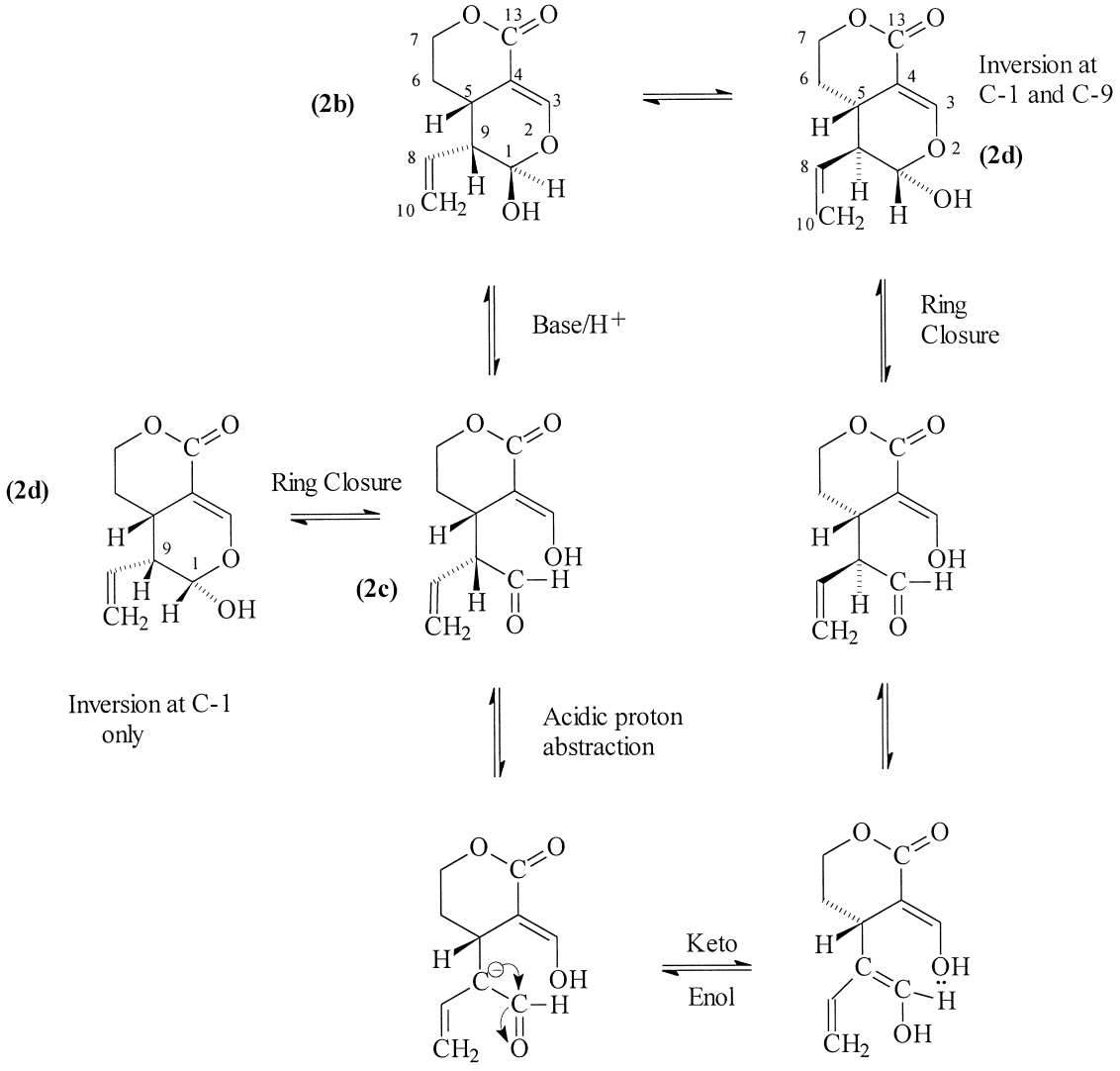

Scheme 1. Mechanism of inversion at C-1 and C-9.

Since acetylation usually occurs in the presence of pyridine (rather than DABCO/Ac_2O) the reaction on sweroside aglucone was also carried with this reagent. To our pleasant surprise the rearranged all *trans* sweroside **3** was obtained in 73% yield.

2.3. Rearrangement in the NMR tube

In order to study the effect of DABCO on sweroside aglycone **2b** (with intact stereochemistry at C-1, C-9 and C-5) the compound was dissolved in $CDCl_3$ in an NMR tube and DABCO only added. Progress of the reaction was monitored over 10 h. Small changes in the NMR spectrum were apparent within minutes. The H-1 signal disappeared rapidly, and after 40 min several new peaks appeared in the region δ 6.5–9.55. The most significant of these was a doublet at δ 9.4. ($J = 3.82$ Hz). This peak gradually increased in amplitude and after 4.5 h a further peak was visible at δ 9.87. Both peaks are presumed to be aldehyde peaks and their presence is regarded as evidence that ring opening occurs (Scheme 1). The effect is in line with earlier proposals (Bianco, 1994).

2.4. Iridoids with an *all*-trans ring fusion in nature

The first naturally-occurring iridoid of the above nature was reported by Foderaro et al. (1992). These iridoids are rare and the authors make the observation that "there are no known instances of epimerisation at C-5 among the hundreds of iridoid isolations". In a subsequent report Foderaro and Stermitz (1992) present detailed spectral data to support their finding. They record a $J_{1,9}$ coupling constant of 9.9 Hz for the compound (5dH)-6-*epi*dihydrocornin. The X-ray structure of a suitable derivative revealed clearly the all *trans* diaxial nature of the protons on C-1, C-9 and C-5.

The seco-iridoid **3**, produced synthetically, thus joins a small group of naturally-occurring iridoid compounds with distinctive stereochemical features and hopefully will alert other researchers to stereochemical changes which can occur during manipulation of iridoids.

2.5. Attempts to ring-open loganin with DABCO

Loganin aglycone **1b** (from β-glucosidase hydrolysis of loganin) was subjected to the same acetylation conditions of DABCO/acetic anhydride as described for sweroside aglycone. No rearrangement occurred and the 1-acetoxy derivative was isolated in good yield and high purity. The ^{1}H NMR spectrum differs very little from that of the parent aglucone apart from H-1 which showed the anticipated downfield shift from δ 4.98 to δ 6.07. The $J_{1,9}$ coupling constant is 3.5 Hz and in loganin itself it is 4.5 Hz (Boros and Stermitz, 1990). In this instance it is possible that the iridoid skeleton (as in loganin) is less susceptible to ring opening and subsequent rearrangement than the seco-iridoid system as in sweroside aglucone.

2.6. Biological activity tests

Since aq. root decoctions of Scabiosa columbaria find a traditional use in the treatment of venereal sores (Hutchings, 1996), some of the isolated components (sweroside, loganin and a semi-purified mixture) were tested for antibacterial activity. At concentrations of 0.001–0.50 mg/ml none of the compounds showed any activity. At a conc. of 1.0 mg/ml (minimum inhibitory concentration, MIC), sweroside and the "mixture" were active against *Bacillus cereus*, *B. pumulus*, *B. subtilis*, *Micrococcus kristinae*, *Staphylococcus aureus* (gram positive) and *Escherichia coli*, *Klebsiella pneumoniae*, *Pseudomonas aerugenosa*, *Enterobacter cloacae* (gram negative). Neither inhibited the growth of Serratia marcescence. These activities can be regarded as "moderate" only.

3. Experimental

3.1. General

^{1}H and ^{13}C NMR spectra were recorded on Varian-200 and Varian-500 spectrometers. High resolution mass spectra were recorded on a Kratos MS 80 RF double-focussing magnetic sector instrument at 70 eV. For optical rotations a Perkin Elmer 241 digital polarimeter was used.

3.2. Plant material

Scabiosa columbaria (rootstock) was collected in an open field in the Hayfields area of Pietermaritzburg during January 1999. It was identified by Dr Trevor Edwards, Curator of the Bews Herbarium at the University of Natal. A voucher specimen (SED No. 6) of the whole plant has been deposited in the Herbarium.

3.3. Extraction and isolation

Freshly-collected tubers (850 g) were milled and extracted with 95% EtOH–$CHCl_3$ (1:1) for 6 days at RT. The solution was filtered and the lower phase separated off and concentrated (16 g). A portion of this material (9 g) was fractionated on a dry silica gel (Merck Silica Gel 9385) column using CH_2Cl_2–MeOH (100: 0→85: 15) as eluent. Three fractions were collected: fraction (i) afforded loganin aglycone (**1b**) (35 mg) after purification on the chromatron [CH_2Cl_2–Et_2O(1: 1)]; fraction (ii) gave loganin (**1a**) (70 gm) following separation on the chromatotron [CH_2Cl_2–MeOH (93: 7)]; fraction (iii) gave a crude mixture

(726 mg) which on separation as above [CH_2Cl_2–MeOH (90:10→85:15)] afforded impure sweroside (**2a**) (140 mg) and a mixture of other compounds unidentified as yet (280 mg). Further separation on the chromatotron [CH_2Cl_2–MeOH (93:7→90:10)] gave pure sweroside (**2a**) (77 mg).

3.4. Studies on loganin

The properties of loganin (above, mp 220°C) were identical in all aspects (NMR, mass spectra) to values published in the literature (Boros and Stermitz, 1990). The optical rotation, $[\alpha]_D^{25} = -62.4°$ ($c = 0.0004$, MeOH), is somewhat lower than the literature value of −82.8°C (El-Naggar and Beal, 1980).

Loganin (**1a**) (230 mg) was suspended in water pH 6.8 (5 ml) and β-glucosidase (30 mg) added. The solution was stirred at 37°C for 5 h, then exhaustively extracted with ether to give impure loganin aglucone. The latter was purified on the chromatotron [(CH_2Cl_2–Et_2O (5:4)] to give pure loganin aglucone (**1b**) (98 mg), oil. ^{1}H NMR (200 MHz, $CDCl_3$): $\delta = 1.15$ (3H, *d*, $J = 6.6$ Hz, Me), 1.53 (1H, *m*, H-6a), 2.30 (1H, *m*, H-6b), 1.95 (1H, *m*, H-8), 1.95 (1H, *m*, H-9), 3.17 (1H, *m*, H-5), 3.72 (3H, s, CO_2Me), 4.13 (1H, *m*, H-7), 4.98 (1H, *d*, $J = 4.9$ Hz, H-1), 7.41 (1H, *d*, $J = 1.3$ Hz, H-3). ^{13}C NMR (50 MHz, $CDCl_3$): $\delta = 13.3$ (C-10), 31.5 (C-5), 41.4 (C-6), 42.0 (C-8), 46.2 (C-9), 51.4 (OMe), 74.5 (C-7), 95.6 (C-1), 115.5 (C-4), 151.7 (C-3), 168.2 (C-11).

Loganin aglycone-1-monoacetate **1(c)**. Loganin aglycone (43 mg) was treated with DABCO (6 mg) and shaken to dissolve in THF (2.5 ml). Ac_2O (0.2 ml) was added and the solution stirred at RT overnight. Removal of solvent, followed by separation on a small column (silica gel) eluted with $CHCl_3$, followed by CH_2Cl_2–Et_2O (7:3) gave a pure oil, (35.4 mg). EI–MS *m*/*z* (rel. int.): 270 (M^+, 2.1), 210 (M-OAc, 19), 192 (M–OAc–H_2O, 22), 150 (21), 139 (100), 125 (24), 97 (19). δ H NMR (200 MHz, $CDCl_3$): $\delta = 1.15$ (3H, *d*, $J = 6.8$ Hz, Me), 1.80 (1H, *m*, H-6a), 2.11 (3H, *s*, OCOMe), 2.20 (2H, *m*, H-8, H-9), 2.32 (1H, *m*, H-6b), 3.18 (1H, *m*, H-5), 3.73 (3H, *s*, CO_2Me), 4.14 (1H, *m*, H-7), 6.07 (1H, *d*, $J = 3.5$ Hz, H-1), 7.32 (1H, *d*, $J = 0.8$ Hz, H-3).

3.5. Studies on sweroside *2a* and its derivatives

Pure sweroside (**2a**) crystals softened at 82°C and melted (decomp.) at 120°C, (lit. Ma et al., 1994, 106–109°C), $[\alpha]_D^{25} = -164.6°$ ($c = 0.005$, MeOH), (lit. Ma et al., 1994, −157.6°). The ^{1}H NMR spectrum in CD_3OD was identical to that recorded by Ma et al. (1994).

Sweroside (**2a**) (280 mg) was hydrolysed as described for loganin and afforded the aglycone (**2b**) (after separation on a column) (73 mg) as an unstable oil. ^{1}H NMR (500 MHz, $CDCl_3$): $\delta = 1.52$ (1H, *m*, H-6a), 1.96 (1H, *m*, H-6b), 2.02–2.11 (1H, *m*, H-9), 2.70 (1H, sym. *m*, H-5), 4.32 (1H, *m*, H-7a), 4.48 (1H, *m*, H-7b), 5.21–5.28 (2H, *m*, H-10), 5.44 (1H, broadened s, H-1), 5.73 (1H, *ddd*, $J = 17.3$, 10.3, 9.2 Hz, H-8), 7.63 (1H, *d*, $J = 2.1$ Hz, H-3). ^{13}C NMR (125 Hz, $CDCl_3$): $\delta = 26.7$ (C-6), 28.5 (C-5), 46.9 (C-9), 68.5 (C-7), 94.4 (C-1), 104.8 (C-4), 119.8 (C-10), 134.7 (C-8), 153.6 (C-3), 166.3 (COO-). EI–MS *m*/*z* (rel int.): 120 (.5), 85 (62), 83 (100).

3.6. Sweroside aglucone-1-acetate (*3*)

Sweroside aglucone (**2b**) (above, 45 mg) was treated with DABCO (6.2 mg), THF (2.5 ml) and acetic anhydride as detailed for loganin aglycone to give the 1-acetory derivative (**3**) (31 mg), mp 112–113°C, (obtained only after several recrystallisations from 95% EtOH), $[\alpha]_D^{20} = +36.4°$ ($c = 0.112$, $CHCl_3$); IR (KBr): $\nu_{(mu)}$: 3160, 1765, 1701, 1618, 1404, 1284, 1201, 1189, 1060. EI–MS *m*/*z* (rel int.): 238 (M^+, 2.4), 196 (1.4). 178 (2.6), 160 (8.5), 127 (100), 112 (2.5), 97 (8.8). ^{1}H and ^{13}C NMR (500 and 125 MHz, $CDCl_3$) are collected in Table 1.

For the X-ray study on (**3**) diffraction data were collected on a Nonius CAD 4 diffractometer with graphite monochromated MoK radiation. The unit cell parameters were determined by a least squares fit. The structure was resolved by direct methods. Further details for 1-acetoxy sweroside aglucone (**3**) are: $C_{12}H_{14}O_5$. Final *R* value 0.0470, colourless orthorhombic crystals, cell parameters (A°) $a = 7.9637$ (7), $b = 10.2678$ (8), $c = 29.326$ (2), crystal dimensions (mm) $0.58 \times 0.46 \times 0.35$, space group $P2_12_12_1$, V(A°^{3}) 2398.0(3), $Z = 8$. (Fig. 1).

The dihedral angles H-1/C-1–C-9/H-9 and H-5/C-5–C-9/H-9 were 177.9 and 174.5° respectively, in good accord with the stereochemistry predicted by the ^{1}H NMR data.

Acknowledgements

We thank the National Research Foundation for financial support.

References

Battersby, A.R., Hall, E.S., Southgate, R., 1969. The structure, stereochemistry and biosynthesis of loganin. J. Chem. Soc. (C) 712–728.

Bianco, A., 1994. Recent developments in iridoids chemistry. Pure and Appl. Chem. 66, 2335–2338.

Boros, C.A., Stermitz, F.R., 1990. Iridoids. An updated review. J. Nat. Prod. 53, 1055–1147.

Dunstan, W.R., Short, F.W., 1883. Isolation of loganin from the fruit of *Strychnos nux-vomica*. Pharm. J. 14, 1025–1028.

El-Naggar, L.J., Beal, J.L., 1980. Iridoids. A review. J. Nat. Prod. 43, 649–707.

Foderaro, T.A., Stermitz, F.R., Hope, H., 1992. (5αH)-6-Epidihydrocornin, the first known iridoid glycoside with a *trans*-fused ring system. Tetrahedron Letters 33, 2953–2954.

Foderaro, T.A., Stermitz, F.R., 1992. Iridoid glycosides from Penstemon species: a C-5, C-9 *trans* iridoid and C-8 epimeric pairs. Phytochemistry 31, 4191–4195.

Hutchings, A., 1996. Zulu medicinal plants. University of Natal Press, Pietermaritzburg, South Africa.

Inouye, H., Ueda, S., Nakamura, Y., 1970. Secoiridoid-glucoside aus *Swertia japonica*. Isolierung von fünf secoiridoid glucosiden sowie die strukturaufklarung des swerosids, des swertiamarins und des gentiopicrosids. Chemical and Pharmaceutical Bulletin 18, 1856–1865.

Kojic-Prodic, B., Spek, A.L., Van der Sluis, W.G., Labadie, R.P., 1985. Structure of decentapicrin A. Acta Cryst. Sect. C-Cryst. Structure. Commun. C41, 379–383.

Ma, W.G., Fuggati, N., Wolfender, J.L., Hostettmann, K.H., Yang, C.R., 1994. Rhodentoside A, a new type of acylated secoiridoid glycoside from *Gentiana rhodentha*. Helv. Chim. Acta 77, 1660–1671.

Van der Sluis, W.G., Labadie, R.P., 1981. Secoiridoids and xanthones in the genus Centaurium. Planta Medica 41, 150–160.

Van Wyk, B.E., Van Oudshoorn, B., Gericke, N., 1997. Medicinal Plants of South Africa. Briza Publications, Pretoria, South Africa.

Watt, J.M., Breyer-Brandwijk, M.G., 1962. Medicinal and Poisonous Plants of Southern and East Africa. E and S Livingstone, London.

PERGAMON

Phytochemistry 57 (2001) 57–64

PHYTOCHEMISTRY

www.elsevier.com/locate/phytochem

Insecticidal flavaglines and other compounds from Fijian *Aglaia* species

Harald Greger [a,*], Thomas Pacher [a], Brigitte Brem [a], Markus Bacher [b], Otmar Hofer [b]

[a] *Comparative and Ecological Phytochemistry Department, Institute of Botany, University of Vienna, Rennweg 14, A-1030 Wien, Austria*
[b] *Institute of Organic Chemistry, University of Vienna, Währingerstrasse 38, A-1090 Wien, Austria*

Received 30 August 2000; received in revised form 13 November 2000

Abstract

Bioassays with lipophilic crude extracts of four Fijian *Aglaia* species against *Spodoptera littoralis* displayed strong insecticidal activity for *A. basiphylla* and *A. gracilis*, whereas *A. archboldiana* and *A. vitiensis* did not have any significant effects. The insect toxicity of *A. basiphylla* was caused by the well known benzofuran flavaglines rocaglamide, desmethylrocaglamide and aglafoline. In contrast, *A. gracilis* contained four related pyrimidinone derivatives in the root and stem bark, including two new congeners named marikarin and 3′-hydroxymarikarin. Moreover, two new putrescine bisamides, secoodorine and secopiriferine, a new benzopyran flavagline, desacetylaglain A, and a new norsesquiterpene were isolated from the leaves together with three known bisamides and 3-hydroxy-5,7,4′-trimethoxyflavone. The structures of the new compounds were elucidated by spectroscopic methods. Comparative feeding assays within the active pyrimidinone flavaglines showed that the free hydroxy group in aromatic ring A of marikarin diminishes insecticidal activity. © 2001 Elsevier Science Ltd. All rights reserved.

Keywords: *Aglaia archboldiana*; *A. basiphylla*; *A. gracilis*; *A. vitiensis*; Meliaceae; Cyclopenta[*b*]benzofurans; Cyclopenta[*bc*]benzopyrans; Flavaglines; Bisamides; Flavonol; Norsesquiterpene; Diterpene; Triterpene; Insect toxicity; *Spodoptera littoralis*

1. Introduction

In the last decade the genus *Aglaia* of the family Meliaceae has attracted considerable attention as a possible new source for unique natural products for integrated pest management. In contrast to other genera of the family the very high insecticidal activity of many different species cannot be attributed to the accumulation of nortriterpenoid limonoids, like e.g. azadirachtin, but to the formation of flavonol-cinnamate derived cyclopenta[*b*]benzofurans (Janprasert et al., 1993; Satasook et al., 1994; Nugroho et al., 1997, 1999; Brader et al., 1998). This has been confirmed in our laboratory by a preliminary survey of 30 different *Aglaia* species. Together with biogenetically related but less active cyclopenta[*bc*]benzopyrans and benzo[*b*]oxepines they represent a distinct class of natural compounds named flavaglines (Brader et al., 1998; Bacher et al., 1999). At present flavagline-producing species are known mainly from Indonesia, Sri Lanka, Thailand, and Vietnam, covering mainly the western range of the geographical extent of the genus (Pannell, 1992), whereas only one report is known from the eastern part, across the Wallace's line. In this case the well known flavagline rocaglaol (Ishibashi et al., 1993) was isolated from an Australian collection of *A. tomentosa* Teijsm. & Binn. (syn.: *A. ferruginea* C. T. White & Francis) (Mulholland and Naidoo, 1998), which is regarded as a complex species also widely distributed in the western range (Pannell, 1992; Hopkins et al., 1998).

In order to contribute to a better understanding of the different biogenetic capacities of *Aglaia* species as well as to provide an eco-geographical interpretation of the varying occurrence of the highly active flavaglines, we now compared different HPLC profiles and insecticidal activities of four Fijian *Aglaia* species, representing far eastern and endemic representatives of the genus. Using freshly hatched larvae of the polyphagous cotton leaf worm *Spodoptera littoralis* (Lepidoptera, Noctuidae), the lipophilic crude extracts of *A. gracilis* A. C. Smith and *A. basiphylla* A. Gray exhibited high insect toxicity, whereas those of *A. archboldiana* A. C. Smith and

* Corresponding author. Tel.: +43-1-4277-54070; fax: +43-1-4277-9541.
E-mail address: greger@s1.botanik.univie.ac.at (H. Greger).

0031-9422/01/$ - see front matter © 2001 Elsevier Science Ltd. All rights reserved.
PII: S0031-9422(00)00471-4

A. vitiensis A. C. Smith had no significant effects. Accordingly, an accumulation of flavaglines could only be detected in the first two species by HPLC–UV-diode array analyses. In *A. basiphylla* the insecticidal properties could be attributed to the well known flavaglines rocaglamide (**1**) (King et al., 1982), desmethylrocaglamide (**2**) (Ishibashi et al., 1993), and aglafoline (=methyl rocaglate) (**3**) (Ko et al., 1992; Ishibashi et al., 1993), whereas *A. gracilis* clearly deviated by a more complex chemical profile. Besides the known aglafoline (**3**), aglaiastatin (=aglaroxin D) (**4**) (Ohse et al., 1996; Molleyres and Kumar, 1996), and its dehydroderivative (**5**) (Kokpol et al., 1994), the root and stem bark additionally accumulate the two new cyclopenta[*b*]benzofurans **6** and **7**. Compared to the 43 already known benzofuran flavaglines, the two new compounds are characterized by a different substitution pattern in aromatic ring A, containing one methoxy and one hydroxy group in *meta*-position. Therefore, the new trivial names marikarin (**6**) and 3′-hydroxymarikarin (**7**) were introduced in appreciation of Mr. Marika Tuiwawa from the University of the South Pacific, Fiji, for all his help in collecting plants.

In accordance to our previous papers (Brader et al., 1998; Greger et al., 2000), the active cyclopenta[*b*]benzofurans (**3**–**7**) of *A. gracilis* mostly accumulate in the root and stem bark and are accompanied by large amounts of the secodammarane triterpene shoreic acid (**8**), previously described for other *Aglaia* species (Cui et al., 1997; Mohamad et al., 1999a,b). Moreover, from the roots the already known diterpene 13-hydroxy-7-oxolabda-8, 14-diene (**9**) (Wu and Lin, 1997) was also isolated and identified. In contrast, the HPLC profile of the leaves deviated by the dominating bisamides piriferine (**10**) (Saifah et al., 1988), odorine (**11**) (Shiengthong et al., 1979), and pyramidatine (**12**) (Saifah et al., 1993) together with the new putrescine derivatives secopiriferine (**13**) and secoodorine (**14**). Beyond that, the known 3-hydroxy-5,7,4′-trimethoxyflavon (**16**) and a series of cyclopenta[*bc*]benzopyrans also contribute to the characteristic HPLC profile of the leaves. However, from the latter series only the structure of the new desacetylaglain A (**15**) could unambiguously be identified in the present paper because of scarce plant material. In addition, small amounts of a new norsesquiterpene (**17**) could also be obtained for structure elucidation. In the present paper we report the isolation and structure elucidation of the new derivatives as well as the insecticidal activities of the new benzofuran flavaglines against *S. littoralis*.

2. Results and discussion

Methanolic crude extracts of leaves and root bark of three different individuals of *A. gracilis* (HG682-684) with nearly identical HPLC profiles were pooled together and the different organs separately analyzed by preparative MPLC linked with UV detection. Altogether fifteen compounds could be isolated, five of which were shown to be cyclopenta[*b*]benzofurans (**3**–**7**) accumulated in the root and stem bark. Based on their spectral

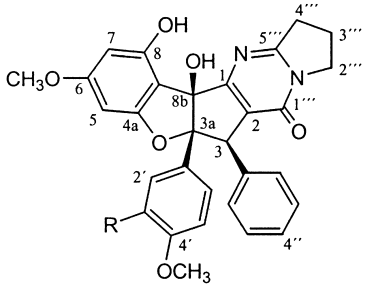

6 R = H marikarin
7 R = OH 3′-hydroxymarikarin

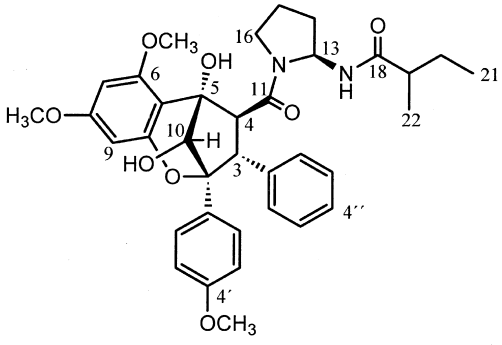

15 desacetylaglain A (H3-β, H-4α, 13*S*)

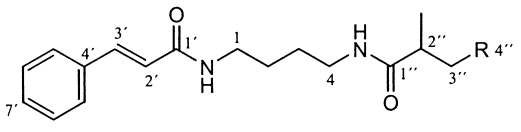

13 R = H secopiriferine
14 R = CH_3 secoodorine

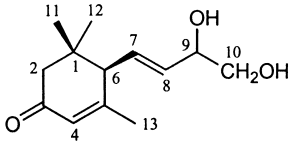

17 9,10-dihydroxy-4,7-megastigmadien-3-one

characteristics and on comparison with already published data, compounds **3**–**5** were readily identified as the well-known derivatives aglafoline (**3**), aglaiastatin (**4**), and its dehydroderivative (**5**).

The new compounds marikarin (**6**) and 3′-hydroxymarikarin (**7**) belong, like **4** and **5**, to a group of benzofuran flavaglines characterized by a pyrimidinone unit. Their inconspicuous UV spectra showed small maxima at 273 nm (MeOH) for **6**, and 279 nm for **7**, and their IR spectra were characterized by strong signals at 1600–1678 cm^{-1} and 1146 cm^{-1} ($CHCl_3$). High resolution MS data of **6** resulted in the molecular formula $C_{30}H_{26}N_2O_6$ and the ^1H and ^{13}C NMR spectra were very similar to a pyrimidinone flavagline which has previously been isolated from *A. odorata* (Kokpol et al., 1994; Ohse et al., 1996) and *A. duppereana* (Nugroho et al., 1997). However, in the NMR spectra of marikarin (**6**) one methoxy resonance was missing and the MS showed a mass which was less by one CH_2 unit. On the other hand, the ^{13}C NMR data, including the quaternary resonances, proved the same oxygenation pattern of the flavagline skeleton in comparison with the 6,8,4′-trimethoxylated derivative from the literature cited above. Obviously compound **6** carries a phenolic hydroxy group at one of the positions 6, 8, or 4′. The methoxy groups at C-6 and C-4′ were still present in compound **6** which was confirmed by differential NOE measurements showing the effects 6-OCH_3 ↔ 5-H, 6-OCH_3 ↔ 7-H, and 4′-OCH_3 ↔ 3′/5′-H. Thus, the unsubstituted hydroxy group is positioned at C-8. Extensive 2D NMR measurements, especially long range shift correlation (HMBC), supported the structure of **6** and allowed to assign all ^1H and ^{13}C NMR resonances. 3′-Hydroxymarikarin (**7**) differed from **6** by a different substitution pattern of the phenyl ring attached at position 3a. In the ^1H NMR spectrum of compound **6** this ring showed the typical pattern of a *para* substituted benzene. In compound **7** however, the symmetry of the ring substitution got lost due to a further substituent in *meta* position resulting in the typical ^1H NMR resonance system of three aromatic protons with their typical *ortho* and *meta* coupling constants. The high resolution MS derived molecular formula $C_{30}H_{26}N_2O_7$ showed that an additional oxygenation took place with respect to compound **6**. The ^1H coupling pattern allowed the conclusion that the newly introduced oxygen is attached at C-3′. This was also supported by the ^{13}C chemical shift changes as a consequence of the additional oxygenation of this ring. The positions 3′ for the OH substituent and 4′ for OCH_3 were finally confirmed by the strong differential NOE from 4′-OCH_3 to 5′-H. The assignments of the absolute configurations at C-3, C-3a, and C-8b were based on the optical rotation of $[\alpha]_D^{20} = -45^\circ$ for **6** and -53° for **7** ($CHCl_3$), which agreed perfectly with a value of -50.1° for the closely related dehydroaglaiastatin (**5**). The latter was correlated via CD measurements with synthetic (-)-rocaglamide (see Nugroho et al., 1997).

Besides the dominating bisamides piriferine (**10**), odorine (**11**), and pyramidatine (**12**), already known from different *Aglaia* species, the leaf extract of *A. gracilis* additionally accumulated two hitherto undescribed derivatives, secopiriferine (**13**) and secoodorine (**14**). The prominent and broad maxima at 274 nm (MeOH) in the UV-spectra as well as the typical IR bands at 3441–3443 cm^{-1} ($CHCl_3$) for >NH stretching and dominating signals at 1627–1665 and 1517–1518 cm^{-1} for the >N–C=O/C=C stretching region showed immediately that they belong to the group of bisamides characteristic for *Aglaia* species. This was also confirmed by two broad NH resonances in the ^1H and two characteristic CO singlets in the ^{13}C NMR spectra of both compounds (Brader et al., 1998; Greger et al., 2000). The acid parts of **13** were cinnamic acid and a simple aliphatic isobutyric acid as in piriferine (**10**), however, unlike to piriferine the bifunctional amine part was not a cyclic 2-aminopyrrolidine, but an open chain putrescine. The NMR data for the acid moieties were very similar to piriferine (Saifah et al., 1988, 1993), the amine moiety showed the characteristic resonances for the four methylene groups of putrescine (Saifah et al, 1993; Brader et al., 1998; Greger et al., 2000). Secoodorine (**14**) was very similar to secopiriferine (**13**) with the only difference, that there was a 2-methylbutanoic acid component instead of isobutyric acid. The corresponding bisamide with a cyclic amine component is the widespread odorine. The NMR data of secoodorine (**14**) could be assigned by comparison with Purushothaman et al. (1979) and Shiengthong et al. (1979) for the acid moieties, and Saifah et al. (1993), Brader et al. (1998), and Greger et al. (2000), for the putrescine part. High resolution MS agreed with the molecular formulas $C_{17}H_{24}N_2O_2$ for **13**, and $C_{18}H_{26}N_2O_2$ for **14**. The 100% peaks in the EI mass spectra of both compounds were at m/z = 131 which was characteristic for the very stable cinnamoyl ion (Shiengthong et al., 1979). The absolute configuration at C-2″ in secoodorine (**14**), $[\alpha]_D^{20} = +11^\circ$ ($CHCl_3$), was not determined. However, in epi-odorine (= roxburghilin) it was determined as (*S*) by hydrolysis to (+)-2-methylbutanoic acid (Purushothaman et al., 1979).

The ^1H and ^{13}C NMR data of the cyclopenta[*bc*] benzopyran flavagline **15** were almost identical with those of aglain A (Dumontet et al., 1996). The only difference is the lack of the 10-OAc group which is changed to an unsubstituted OH group in **15**, thus named desacetylaglain A. Based on comparative HPLC of the crude extract and the corresponding CC and TLC fractions it became evident that **15** seems to be at least partly the result of a conversion during TLC separation from a compound with higher retention time and the same UV spectrum. Most probably it represents the hydolysis

product of aglain A. The relative stereochemistries at C-3, C-4, C-10, and the stereochemically labile N-acetale center C-13 can be derived from NOESY data (Dumontet et al., 1996; Brader et al., 1998). The crosspeaks 3-H ↔ 10-H proved the H-3β position and an *endo* arrangement between 3-H and 10-H, the NOE contact 4-H → 2″/6″-H indicated a H-4α position, whereas the crosspeaks 4-H ↔ 13-H were only possible for the 13*S* configuration (Dumontet et al., 1996) (see Section 3 for the complete NOESY data). The absolute configuration of the 2-methylbutanoic acid moiety (C-19) was not determined (compare discussion of compound **14**). However, the stereochemical presentation of formula **15** followed biogenetic considerations linking the known cyclopenta[*b*]benzofurans with the closely related cyclopenta[*bc*]benzopyrans (Bacher et al., 1999; Nugroho et al., 1999).

According to MS and NMR data, compound **17** was a new norsesquiterpene of the 4,7-megastigmadien-3-one type with additional hydroxy groups at positions 9 and 10 in the side chain ($C_{13}H_{20}O_3$). An analoguous 9-hydroxy compound, lacking the terminal C-10 oxygenation, was described for *Nicotiana tabacum* L. (Solanaceae) (Aasen et al., 1973) and *Teucrium heterophyllum* L'Her. (Lamiaceae) (Fraga et al., 1995). Corresponding glycosides of the latter have also been isolated from raspberry fruit (*Rubus idaeus* L., Rosaceae) (Pabst et al., 1992) and from the seeds of *Trifolium alexandrinum* L. (Fabaceae) (Mohamed et al., 1999a,b). Comparison of ^1H and ^{13}C NMR spectra of **17** with the data of these related compounds and additional 2D NMR measurements proved clearly the postulated structure. The absolute configuration at C-6 followed from the positive sign of the optical rotation $[\alpha]_D^{20} = +145^\circ$, which is due to the cyclic enone chromophore dominating the chiroptical properties (CD and $[\alpha]_D$) in the long wave length region (compare Pabst et al., 1992; Mohamed et al., 1999a,b). The absolute configuration of the peripheric asymmetric center C-9 was not determined.

Based on the present data, the biogenetic capacity towards flavagline formation of *Aglaia* species from the eastern part of their geographical range (Pannell, 1992) did not show significant differences to those of the western part, across the Wallace's line: the biologically very active benzofuran derivatives also accumulated mainly in the stem and root bark, whereas the ineffective benzopyrans were preferably found in the leaves together with bisamides (see Brader et al., 1998; Greger et al., 2000). Moreover, the accumulation of the triterpene shoreic acid (**8**) represents a further common character of the roots (e.g. Cui et al., 1997; Mohamad et al., 1999a,b). Since there are only very few reports on the occurrence of sesquiterpenes and diterpenes in *Aglaia* species, nothing can be said about the chemosystematic significance of compound **9** and **17** in the roots or leaves, respectively. Of special biogenetic interest, however, was the isolation of 3-hydroxy-5,7,4′-trimethoxyflavon (**16**) from the leaves which showed the same substitution of aromatic rings A and B as the co-occurring flavaglines. Hence it is most likely, that the characteristic substitution patterns of flavaglines were already formed on the stage of the flavonol precursor, which was later linked to a cinnamic acid moiety (Dumontet et al., 1996; Bacher et al., 1999; Nugroho et al. 1999). This co-occurrence of the same substitution pattern of aromatic rings A and B in flavonols and flavaglines was also reported for other *Aglaia* species, e.g. in an Indonesian provenance of *A. odorata*, where a disubstituted B-ring could be observed in both types of compounds (Nugroho et al., 1999). Furthermore, the co-occurrence of the pyrrolidine derived bisamides piriferine (**10**) and odorine (**11**) together with the corresponding open-chain putrescine derivatives secopiriferine (**13**) and secoodorine (**14**) also suggested close biogenetic connections. Like in the recently reported sulphur containing bisamides of *A. leptantha* (Greger et al., 2000), the putrescine derivatives may be regarded as biosynthetic precursors of the corresponding pyrrolidine derived bisamides.

The well-known insect toxicity of benzofuran flavaglines was confirmed by chronic feeding bioassays with freshly hatched larvae of *S. littoralis*. Insufficient quantities of 3′-hydroxymarikarin (**7**) precluded a bioassay. As shown in Table 1, the free hydroxy group in aromatic ring A of the new pyrimidinone derivative marikarin (**6**) led to a decrease of insecticidal activity, compared to the co-occurring pyrimidinones **4** and **5**.

Table 1
Insecticidal and growth inhibitory activities of pyrimidinone-type flavaglines and azadirachtin against neonate larvae of *Spodoptera littoralis*[a]

Compound	LC_{50} (95% FL[b]) ppm	EC_{50} (95% FL[b]) ppm
Marikarin (**6**)	12.2 (9.8–15.4)	0.69 (0.37–0.99)
Aglaiastatin (**4**)	1.2 (0.7–2.3)	0.09 (0.07–0.11)
Dehydroaglaiastatin (**5**)	1.7 (1.6–1.9)	0.19 (0.15–0.23)
Azadirachtin[c]	8.2 (6.6–11.6)	0.04 (0.02–0.07)
Azadirachtin[d]	0.6 (0.3–1.7)	n.m.[e]

[a] Assays were conducted with neonate larvae of *S. littoralis* ($n = 20$ for each treatment) that were forced to feed on artificial diet spiked with 8 different concentrations of the test compounds (0.025–25 ppm). After 5 days, survival and weight of the surviving larvae were determined and compared to controls that had been exposed to diet treated with solvent (MeOH) only. From the dose-response curves LC_{50} and EC_{50} values were calculated by probit-log analysis. In the case of azadirachtin, the surviving larvae were weighed after 5 days of exposure to obtain the EC_{50} value and then transferred to fresh untreated diet and reassessed after another 6 days. The survival rate of larvae after 11 days was again recorded and the LC_{50} value determined.

[b] Fiducial limits.

[c] Results after 5-day exposure.

[d] Results after 11-day exposure.

[e] Not measured.

After 5 days of exposure, aglaiastatin (**4**), characterized by a N–H group, displayed the highest toxicity with a LC_{50} value of 1.2 ppm. This value was clearly lower than that of the positive control azadirachtin of 8.2 ppm. Whereas the LC_{50} and EC_{50} values of **4** and **5** were comparable with those already published, the LC_{50} value of azadirachtin, purchased from Roth (Karlsruhe, Germany), clearly deviated (Nugroho et al., 1997). In order to clarify these discrepancies a reinvestigation was carried out using different times of exposure. As already described previously, azadirachtin is a very potent, but at low concentrations a rather slowly acting toxin displaying the highest activity during the molting process of the larvae (Rembold, 1995). The rather high LC_{50} value of 6.1 ppm previously published by Brader et al. (1998), was determined after a 5-day exposure where strong growth retarding effects of azadirachtin towards the first instar larvae may have delayed the transition to the next larval stage. After a 11-day exposure, however, the toxic effects clearly increased with a LC_{50} value of 0.6 ppm, probably due to the fact that all larvae entered the next molting process (see Table 1). Hence, it appears obvious that the time of exposure plays a prominent role in the determination of insecticidal activities and might also explain the different values reported in the literature.

3. Experimental

3.1. General

NMR: Bruker, AM 400 WB and AC 250. MS: Finnigan MAT 900 S. IR: Perkin-Elmer 16PC FT-IR. UV: Hewlett-Packard, 8452A Diode Array Spectrophotometer. Optical rotation: Perkin Elmer Polarimeter 241. HPLC: Hewlett-Packard 1090 II, UV diode array detection at 230 nm, column 250 × 4 mm, Hypersil BDS C-18, 5 μm, mobile phase MeOH (gradient 60–100%) in aqueous buffer (0.015 M *o*-phosphoric acid, 0.0015 M tetrabutylammonium hydroxide, pH 3), flow rate 1 ml/mm.

3.2. Plant material

Leaves, stem, and root bark from different individuals of four Fijian *Aglaia* species were collected separately: (a) *A. gracilis* from northwest Viti Levu, Lautoka, Mt.Evans, near Abaca, three individuals (HG 682-684); (b) *A. basiphylla* from east Viti Levu, Wailoku, near Suva, three individuals (HG 673-674, HG 692); (c) *A. vitiensis* from south Viti Levu, near Narukunimbua, three individuals (HG 732-734), and from east Viti Levu, Wailoku, near Suva, one individual (HG 735); (d) *A. archboldiana* from south Viti Levu, near Narukunimbua, three individuals (HG 693-695), and from north Viti Levu, near Nandarivatu, two individuals (HG 696-697). Voucher specimens are deposited at the Herbarium of the Institute of Botany, University of Vienna (WU).

3.3. Extraction and isolation

Dried leaves, stem and root bark of *A. archboldiana*, *A. basiphylla*, *A. gracilis*, and *A. vitiensis* were ground separately and extracted with MeOH at room temp. for 3 days, filtered and conc. The aqueous residues were extracted with $CHCl_3$ and the concentrated $CHCl_3$ fractions were used as lipophilic crude extracts for comparative HPLC analyses and preliminary bioassays. From three individuals of A. *gracilis* (HG 682-684) the $CHCl_3$ fractions from dried leaves (72 g) and roots (17 g) were combined separately, evapd to dryness under reduced pressure, and roughly sepd by column chromatography (Merck silica gel 60, 35–70 mesh) with hexane, EtOAc and MeOH. From the leaf extract (2500 mg) the combined fractions eluted with 100% EtOAc (530 mg) were further sepd by prep MPLC (400 × 38 mm column, Merck LiChroprep Si 60, 25–40 μm, UV detection, 254 nm) starting with 50% EtOAc in hexane to yield a fraction (16 mg) which led to 4.5 mg pure flavonol **16** by crystallization in MeOH. MPLC fraction with 70% EtOAc in hexane afforded a mixture (260 mg) which was sepd by cyclic MPLC to give 70 mg odorine (**11**), 75 mg piriferine (**10**), 10 mg pyramidatine (**12**), 2 mg norsesquiterpene (**17**) and a mixture (8.5 mg) which was further sepd by prep TLC (Merck silica gel 60, F_{254};CH_2Cl_2:EtOAc:MeOH = 70:25:5) to give 4.5 mg desacetylaglain A (**15**). Another MPLC fraction with 70% EtOAc led (i) to another mixture (15 mg), from which 2.5 mg aglaiastatin (**4**) was sepd by prep TLC, and (ii) to secopiriferine (**13**) and secoodorine (**14**) which were also purified by prep TLC to give 10 mg **13** and 16 mg **14**. In addition to the CC fractions with 100% EtOAc, those with 50%EtOAc in MeOH (210 mg) gave again 24 mg odorine (**11**), 28 mg piriferine (**10**), 3 mg secopiriferine (**13**), 5 mg secoodorine (**14**) and 6 mg flavagline (**5**). From the root extract (1400 mg) the combined CC fractions with 30% EtOAc in hexane (200 mg) were further sepd by prep MPLC with 15% EtOAc in hexane to give the impure labdanoid diterpene **9** (30 mg), which was purified by prep TLC (CH_2Cl_2: EtOAc:MeOH = 70:29:1) to yield 13 mg pure compound. Combined CC fractions eluted with 50% EtOAc in hexane and 100% EtOAc (500 mg) were further sepd by prep. MPLC starting with 30% EtOAc in hexane to yield 120 mg shoreic acid (**8**), and 32 mg impure aglafoline (**3**). With 50% EtOAc in hexane 42 mg impure **6**, 7 mg impure **7**, and 8 mg impure **3** were obtained, which all were further sepd by prep TLC (CH_2Cl_2:EtOAc:MeOH = 70:25:5) to give pure compounds: 18 mg aglafoline (**3**), 5 mg dehydroaglaiastatin (**5**), 4.5 mg marikarin

(**6**), 3.5 mg aglaiastatin (**4**) and 1 mg 3′-hydroxymarikarin (**7**).

3.4. Marikarin {(−)-(6R,6aR, 11bS)-11,11b-dihydroxy-9-methoxy-6a-(4-methoxyphenyl)-6-phenyl-2,3,5,6,6a, 11b-hexahydro-1H-benzo[4″,5″]furo[2″,3″:4″,5″]cyclopenta [1′,2′-d]pyrrolo[1,2-a]pyrimidin-5-one} (*6*)

Colourless oil; $[\alpha]_D^{20} = -45°$ ($c = 0.3$, $CHCl_3$). UV λ^{MeOH} nm 273. IR ν^{CHC13} cm^{-1} 3528 w, 3316 br, 2932 *m*, 2850 *w*, 1678 *s*, 1636 *s*, 1604 *s*, 1550 *m*, 1512 *m*, 1496 *m*, 1462 *w*, 1454 *w*, 1410 *w*, 1378 *w*, 1346 *w*, 1298 *w*, 1178 *m*, 1146 *s*, 1088 *m*, 1050 *w*, 1030 *w*, 956 *w*. ^{1}H NMR ($CDCl_3$) δ = 7.00–7.20 (*m*, 3H, 3″-, 4″-, and 5″-H), 7.08 (*d*, 2H, J = 9.0 Hz, 2′- and 6′-H), 6.92 (*dd*, 2H, J = 8.7 and 2.0 Hz, 2″- and 6″-H), 6.56 (*d*, 2H, J = 9.0 Hz, 3′- and 5′-H), 6.20 (*d*, 1H, J = 1.8 Hz, 5-H), 6.08 (*d*, 1H, J = 1.8 Hz, 7-H), 4.75 (*s*, 1H, 3-H), 4.16 (*br.t*, 2H, J = ca. 7.5 Hz, 2‴-H), 3.78 (*s*, 3H, 6-OCH_3), 3.66 (*s*, 3H, 4′-OCH_3), 3.27 (2H, *m*, 4‴-H), 2.32 (*m*, 2H, 3‴-H). ^{13}C NMR ($CDCl_3$) δ = 167.6 *s* (C-5‴), 165.6 *s* (C-1‴), 164.4 *s* (C-6), 160.2 *s* (C-1), 158.7 *s* (C-4′), 158.7 *s* (C-4a), 155.2 *s* (C-8), 135.9 *s* (C-1″), 129.0 *d* (C-2″/6″), 128.6 *d* (C-2′/6′), 127.5 *d* (C-3″/5″), 126.63 *d* (C-4″), 126.58 *s* (C-1′), 120.6 *s* (C-2), 112.4 *d* (C-3′/5′), 106.7 *s* (C-8a), 104.8 *s* (C-3a), 96.1 *d* (C-7), 89.8 *d* (C-5), 89.5 *s* (C-8b), 59.0 *d* (C-3), 55.7 *q* (6-0CH_3), 55.1 *q* (4′-OCH_3), 47.2 *t* (C-2‴), 32.9 *t* (C-4‴), 18.0 *t* (C-3‴). HMBC crosspeaks (H → C): H-3 → 2, 3a, 8b, 1, 1″, 2″/6″, 1‴; H-5 → 4a, 6, 7, 8a; H-7 → 5,6, 8, 8a; H-2′/6′ → 4′; H-3′/5′ → 1′, 4′; H-2″/6″ → 4″; H-2‴ → 3‴, 5‴; H-3‴ → 4‴, 5‴; H-4‴ > 5‴; 6-OCH_3 → 6; 4′-OCH_3 → 4′. EI-HR-MS (70 eV, 250°C) *m/z*: 510.1792 (47%) M^+ (calc. for $C_{30}H_{26}N_2O_6$ 510.1791), 494 (37), 492 (53), 415 (63), 370 (100), 343 (24), 341 (30), 135 (31).

3.5. 3′-Hydroxymarikarin {(−)-(6R, 6aR, 11bS)-11,11b-dihydroxy-9-methoxy-6a-(3-hydroxy-4-methoxyphenyl)-6-phenyl-2, 3,5,6, 6a, 11b-hexahydro-1H-benzo[4″,5″] furo[2″,3″:4′,5′]cyclopenta[1′,2′-d]pyrrolo[1,2-a] pyrimidin-5-one} (*7*)

Colourless oil; $[\alpha]_D^{20} = -53°$ ($c = 0.1$, $CHCl_3$). UV λ^{MeOH} nm 279. IR ν^{CHC13} cm^{-1} 3540 *w*, 3290 *br*, 2926 *m*, 2850 *w*, 1678 *s*, 1634 *m*, 1600 *s*, 1552 *m*, 1512 *m*, 1496 *w*, 1462 *w*, 1456 *w*, 1418 *w*, 1350 *w*, 1290 *w*, 1172 *w*, 1146 *s*, 1006 *w*, 958 *w*, 926 *w*. ^{1}H NMR ($CDCl_3$) δ = 6.95–7.15 (*m*, 5H, 2″- 6″-H), 6.77 (*d*, 1H, J = 2.2 Hz, 2′-H), 6.67 (*dd*, 1H, J = 8.6 and 2.2 Hz, 6′-H), 6.52 (*d*, 1H, J = 8.6 Hz, 5′-H), 6.21 (*d*, 1H, J = 2.0 Hz, 5-H), 6.09 (*d*, 1H, J = 2.0 Hz, 7-H), 4.72 (*s*, 1H, 3-H), 4.16 (*br.t*, 2H, J = ca. 7.0 Hz, 2‴-H), 3.79 (*s*, 3H, 6-OCH_3), 3.74 (*s*, 3H, 4′-OCH_3), 3.27 (2H, *m*, 4‴-H), 2.33 (*m*, 2H, 3‴-H). ^{13}C NMR ($CDCl_3$) δ = 164.5 *s* (C-6), 145.9 *s* (C-4′), 128.9 *d* (C-2″/6″), 127.1 *d* (C-3″/5″), 126.5 *d* (C-4″), 119.2 *d* (C-6′), 113.6 *d* (C-2′), 109.1 *d* (C-5′), 95.8 *d* (C-7), 89.6 *d* (C-5), 58.8 *d* (C-3), 55.6 *q* (4′-OCH_3), 55.4 *q* (6-OCH_3), 47.1 *t* (C-2‴), 32.6 *t* (C-4‴), 19.3 *t* (C-3‴). EI–HR–MS (70 eV, 280 °C) *m/z*: 526.1740 (77%) M^+ (calc. for $C_{30}H_{26}N_2O_7$ 526.1740), 508 (75), 449 (27), 431 (100), 388 (28), 386 (58), 375 (26), 359 (21), 343 (22), 301 (26), 213 (20), 151 (68), 140 (35), 135 (24), 111 (24), 57 (47).

3.6. Secopiriferine {N-cinnamoyl-N-(isobutyryl)-putrescinebisamide} (*13*)

Colourless crystals from $CHCl_3$, mp 155–157°C. UVλ^{MeOH} nm 274, 218. IR ν^{CHC13} cm^{-1} 3441 *m*, 3290 *br*, 2923 *m*, 2853 *w*, 1665 *s*, 1627 *s*, 1578 *w*, 1517 *s*, 1468 *m*, 1332 *w*, 1284 *m*, 1140 *w*, 975 *m*. ^{1}H NMR ($CDCl_3$) δ = 7.64 (*d*, 1H, J = 15.7 Hz, 3′-H), 7.51 (*m*, 2H, 5′-/9′-H), 7.36 (*m*, 3H, 6′-8′-H), 6.44 (*d*, 1H, J = 15.7 Hz, 2′-H), 6.23 (*br.s*, 1H, NH), 5.84 (*br.s*, 1H, NH), 3.44 and 3.31 (2 × *m*, 2 × 2H, 1-H and 4-H), 2.39 (hept, 1H, J = 6.9 Hz, 2″-H), 1.61 (*m*, 4H, 2-H and 3-H), 1.17 (*d*, 6H, J = 6.9 Hz, 2 × 3″-H). ^{13}C NMR ($CDC1_3$) δ = 177.5 *s* (C-1″), 166.7 *s* (C-1′), 141.3 *d* (C-3′), 130.0 *d* (C-7′), 129.2 *d* and 128.2 *d* (C-5′/9′ and C-6′/8′), 121.1 *d* (C-2′), 39.7 t and 39.3 *t* (C-1 and C-4), 36.1 *d* (C-2″), 27.6 t and 27.0 *t* (C-2 and C-3), 20.1 *q* (2×C-3″); the quaternary *s* of C-4′ was too weak for detection. EI–HR–MS (70 eV, 160°C) *m/z*: 288.1837 (13%) M^+ (calc. for $C_{17}H_{24}N_2O_2$ 288.1838), 245 (5) M^+–C_3H_7, 201 (22) M^+–C_3H_7 $CONH_2$, 131 (100) C_6H_5–CH=CH–CO^+, 103 (37) 131-CO, 70 (66), 57 (18).

3.7. Secoodorine {(+)-N-cinnamoyl-N-(2-methyl-butanoyl)-putrescinebisamide} (*14*)

Colourless crystals from $CHCl_3$, mp 135–137°C; $[\alpha]_D^{20} = +11°$ ($c = 0.3$, $CHCl_3$). UV λ^{MeOH} nm 274, 218. IR ν^{CHC13} cm^{-1} 3443 *m*, 3318 *br*, 2927 *m*, 2852 *w*, 1665 *s*, 1627 *s*, 1578 *w*, 1518 *s*, 1461 *w*, 1451 *m*, 1379 *w*, 1334 *m*, 1228 *m*, 1126 *w*, 976 *m*. ^{1}H NMR ($CDCl_3$) δ = 7.64 (*d*, 1H, J = 15.7 Hz, 3′-H), 7.50 (*m*, 2H, 5′/9′-H), 7.36 (*m*, 3H, 6′-8′-H), 6.49 (*v.br.t*, 1H, NH), 6.48 (*d*, 1H, J = 15.7 Hz, 2′-H), 6.04 (*v.br.t*, 1H, NH), 3.44 and 3.32 (2 × *m*, 2 × 2H, 1-H and 4-H), 2.16 (hex, 1H, J = 6.9 Hz, 2″-H), 1.66 (*m*, 1H, 3a″-H), 1.62 (*m*, 4H, 2-H and 3-H), 1.43 (*m*, 1H, 3b″-H), 1.15 (*d*, 3H, J = 6.9 Hz, 5″-H), 0.90 (*t*, 3H, J = 7.5 Hz, 4″-H). ^{13}C NMR ($CDCl_3$) δ = 177.6 *s* (C-1″), 166.8 *s* (C-1′), 141.5 *d* (C-3′), 130.1 *d* (C-7′), 129.2 *d* and 128.2 *d* (C-5′/9′ and C-6′/8′), 121.0 *d* (C-2′), 43.5 *t* (C-2″), 39.7 *t* and 39.3 *t* (C-1 and C-4), 27.5 *t* and 27.0 *t* (C-2 and C-3), 27.7 *t* (C-3″), 17.9 *q* (C-5″), 12.3 *d* (C-4″); the quaternary *s* of C-4′ was too weak for detection. EI–HR–MS (70 eV, 160°C) *m/z*: 302.1996 (18%) M^+ (calc. for $C_{18}H_{26}N_2O_2$ 302.1994), 245 (5) M^+–C_4H_9, 201 (27) M^+–$C_4H_9CONH_2$, 131 (100) C_6H_5–CH=CH–CO^+, 103 (32) 131 - CO, 70 (76), 57 (30).

3.8. Desacetylaglain A {(+)-(2R,3R,4S,5R,10R,2′S)-1-[2,3,4,5-tetrahydro-5,10-dihydroxy-2-(4-methoxyphenyl)-6,8-dimethoxy-3-phenyl-2,5-methano-1-benzoxepin-4-carbonyl]-2-(2-methylbutanoylamino)-pyrrolidine} (**15**)

Colourless oil; $[\alpha]_D^{20} = -14^\circ$ ($c = 0.1$, $CHCl_3$). UV λ^{MeOH} nm 277sh, 271. ^{1}H NMR ($CDCl_3$) $\delta = 7.55$ (*d*, 2H, $J = 8.8$ Hz, 2′/6′-H), 7.08 (*dd*, 1H. $J = 7.3$ and 1.6 Hz, H-4″), 7.00 (*dd*, 2H, $J = 7.3$ and 7.3 Hz, 3″/5″-H), 6.90 (*d*, 2H, $J = 8.8$ Hz, 3′/5′-H), 6.49 (*br.d*, 2H, $J = 7.3$ Hz, 2″/6″-H), 6.25 (*d*, 1H, $J = 2.3$ Hz, 7-H), 6.14 (*br.d*, 1H, $J = 6.2$ Hz, 13-H), 6.04 (*d*, 1H, $J = 2.3$ Hz, 9-H), 5.81 (*s*, 1H. 5-OH), 5.40 (*d*, 1H, $J = 7$ Hz, NH), 5.07 (*s*, 1H, 10-H), 4.37 (*d*, 1H, $J = 4.9$ Hz, 3-H), 4.07 (*s*, 3H, 6-OCH_3), 3.84 (*d*, 1H, $J = 4.9$, 4-H), 3.82 (*s*, 3H, 4′-OCH_3), 3.75 (*s*, 3H, 8-OCH_3), 3.50–3.65 (*m*, 2H, 16-H), 2.15 and 2.05 (*m*, 2H, 14-H), 2.03 and 1.82 (*m*, 2H, 15-H), 2.00 (*s*, 1H, 10-OH), 1.72 (sept, 1H, $J = 7.0$ Hz, 19-H), 1.40 and 1.20 (*m*, 2H, 20-H), 0.84 (*d*, 3H, $J = 7.0$ Hz, 22-H), 0.72 (*t*, 3H, $J = 7.4$ Hz, 21-H). ^{13}C NMR ($CDCl_3$) $\delta = 175.2$ *s* (C-18), 170.1 *s* (C-11), 161.1 *s* (C-8), 160.9 *s* (C-4′), 159.1 *s* (C-6), 137.3 *s* (C-1″), 129.8 *s* (C-1′), 128.7 *d* (C-2″/6″), 128.0 *d* (C-3″/5″), 126.7 *d* (C-2′/6′), 126.5 *d* (C-4″), 113.2 *d* (C-3′15′), 108.3 *s* (C-5a), 92.6 *d* (C-9), 92.5 *d* (C-7), 79.8 *s* (C-5), 74.0 *d* (C-10), 64.5 *d* (C-13), 56.3 *d* (C-4), 56.1 *q* (6-OCH_3), 55.5 *q* (4′-OCH_3), 55.2 *q* (8-OCH_3), 55.1 *d* (C-3), 46.4 *t* (C-16), 42.4 *d* (C-19), 34.0 *t* (C-14), 26.8 *t* (C-20), 21.0 *t* (C-15), 16.5 *q* (C-22), 11.2 *q* (C-21). NOESY: 3-H (4, 10, 2′/6′, 2″/6″), 4-H (3, 13, 2″/6″), 7-H (6-OCH_3), 10-H (3, 2′/6′), 13-H (4, 14a/b, 2′/6′). EI–HR–MS (70 eV, 200°C) *m/z*: 630.2946 (10%) M^+, calc. for $C_{36}H_{42}N_2O_8$ 630.2941), 456 (100), 417 (40), 375 (58), 330 (48), 327 (91), 238 (40), 200 (54), 195 (38), 131 (45), 70 (62).

3.9. 9,10-Dihydroxy-4,7-megastigmadien-3-one {(+)-4-(3,4-dihydroxy-1-butenyl)-3,5,5-trimethyl-2-cyclohexenone} (**17**)

Colourless oil; $[\alpha]_D^{20} = +145^\circ$ ($c = 0.1$, $CHCl_3$). UV λ^{MeOH} nm 243. ^{1}H NMR ($CDCl_3$) $\delta = 5.91$ (*s*, 1H, 4-H), 5.71 (*dd*, 1H, $J = 15.2$ and 9.0 Hz, 7-H), 5.62 (*dd*, 1H, $J = 15.2$ and 5.5 Hz, 8-H), 4.30 (*m*, 1H, 9-H), 3.69 (*dd* 1H, $J = 11.0$ and 3.5 Hz, 10-Ha), 3.50 (*dd* 1H, $J = 11.0$ and 7.4 Hz, 10-Hb), 2.55 (*d*, 1H, $J = 9$ Hz, 6-H), 2.33 (*d*, 1H, $J = 16.4$ Hz, 2-Ha), 2.09 (*d*, 1H, $J = 16.4$ Hz, 2-Hb), 1.90 (*d*, 3H, $J = 1.6$ Hz, 13-H), 1.03 (*s*, 3H, 12-H), 0.96 (*s*, 3H, 11-H). ^{13}C NMR ($CDCl_3$) $\delta = 199.0$ *s* (C-3), 161.3 *s* (C-5), 132.8 *d* (C-8), 129.8 *d* (C-7), 126.1 *d* (C-4), 72.5 *d* (C-9), 66.6 *t* (C-10), 55.7 *d* (C-6), 47.5 *t* (C-2), 36.1 *s* (C-1), 27.9 *q* (C-12), 27.2 *q* (C-11), 23.5 *q* (C-13). HMBC crosspeaks (H → C): H-2 → 1, 3, 6, 12, 13; H-11 → 4, 5, 6; H-12 → 1, 2, 6, 12, 13; H-13 → 1, 2, 6, 12, 13. EI–MS (70 eV, 200°C) *m/z*: 193 (12%), 137 (57), 109 (100), 91 (50), 69 (97), 55 (26). FD–MS *m/z* = 225 (85) $M^+ + 1$ (calc. for $C_{13}H_{20}O_3$ 224.1412), 207 (26) 225 - H_2O, 193 (100).

3.10. Insect bioassays

Chronic feeding bioassays were carried out with freshly hatched larvae ($n = 20$) of the polyphagous pest insect *S. littoralis* (Noctuidae, Lepidoptera). The larvae were from a laboratory colony reared on artificial diet under controlled conditions at 26°C as described previously (Srivastava and Proksch, 1991). The test insects were kept on artificial diet spiked with 8 different concentrations of the test compounds (0.025–25 ppm) which were applicated with MeOH. After 5 days (moist chamber, darkness, 26°C) the survival rate and the larval growth of the surviving larvae were monitored in comparison to controls that had been exposed to diet treated with solvent only. LC_{50} and EC_{50} values were calculated by probit-log analysis (Table 1). Commercial azadirachtin (> 96%) purchased from Roth (Karlsruhe, Germany) was used as a positive control. In case of azadirachtin, the larvae were weighed after a 5-day exposure (for calculation of the EC_{50} value), transferred to an untreated fresh diet and reassessed after another 6 days. After 11 days the number of surviving larvae was recorded again and the LC_{50} value calculated.

Acknowledgements

The authors thank Mr. Marika Tuiwawa, curator from South Pacific Regional Herbarium, Institute of Applied Science, University of the South Pacific, Suva, Fiji, for his valuable help in collecting plants. Dr. Caroline M. Pannell from the Department of Plant Sciences, University of Oxford, gave valuable taxonomic advice. This work was supported by the Austrian National Committee for the Intergovernmental Program "Man and Biosphere" and the Fonds zur Förderung der wissenschaftlichen Forschung in Österreich (proj. no. 12385-CHE).

References

Aasen, A.J., Kimland, B., Enzell, C.R., 1973. Tobacco chemistry, 18. Absolute configuration of (9*R*)-9-hydroxy-4,7*E*-megastigmadiene-3-one (3-oxo-α-ionol). Acta Chimica Scandinavica 27, 2107–2114.

Bacher, M., Hofer, O., Brader, G., Vajrodaya, S., Greger, H., 1999. Thapsakins: possible biogenetic intermediates towards insecticidal cyclopenta[*b*]benzofurans from *Aglaia edulis*. Phytochemistry 52, 253–263.

Brader, G., Vajrodaya, S., Greger, H., Bacher, M., Kalchhauser, H., Hofer, O., 1998. Bisamides, lignans, triterpenes, and insecticidal cyclopenta[*b*]benzofurans from *Aglaia* species. Journal of Natural Products 61, 1482–1490.

Cui, B., Chai, H., Santisuk, T., Reutrakul, V., Farnsworth, N.R., Cordell, G.A., Pezzuto, J.M., Kinghorn, A.D., 1997. Novel cytotoxic 1*H*-cyclopenta[*b*]benzofuran lignans from *Aglaia elliptica*. Tetrahedron 53, 17625–17632.

Dumontet, V., Thoison, O., Omobuwajo, O.R., Martin, M.T., Perromat,

G., Chiaroni, A., Riche, C., Pais, M., Sévenet, T., 1996. New nitrogenous and aromatic derivatives from *Aglaia argentea* and *A. forbesii*. Tetrahedron 52, 6931–6942.

Fraga, B.M., Hernandez, M.G., Mestres, T., Terrero, D., Arteaga, J.M., 1995. Norsesquiterpenes from *Teucrium heterophyllum*. Phytochemistry 39, 617–619.

Greger, H., Pacher, T., Vajrodaya, S., Bacher, M., Hofer, O., 2000. Infraspecific variation of sulfur-containing bisamides from *Aglaia leptantha*. Journal of Natural Products 63, 616–620.

Hopkins, H.C.F., Huxley, C.R., Pannell, C.M., Prance, G.T., White, F., 1998. The Biological Monograph. The Importance of Field studies and Functional Syndromes for Taxonomy and Evolution of Tropical Plants. Royal Botanic Gardens, Kew, London.

Ishibashi, F., Satasook, C., Isman, M.B., Towers, G.H.N., 1993. Insecticidal 1H-cyclopentatetrahydro[b]benzofurans from *Aglaia odorata*. Phytochemistry 32, 307–310.

Janprasert, J., Satasook, C., Sukumalanand, P., Champagne, D.E., Isman, M.B., Wiriyachitra, P., Towers, G.H.N., 1993. Rocaglamide, a natural benzofuran insecticide from *Aglaia odorata*. Phytochemistry 32, 67–69.

King, M.L., Chiang, C.C., Ling, H.C., Fujita, E., Ochiai, M. and McPhail, A.T., 1982. X-Ray crystal structure of rocaglamide, a novel antileukemic 1*H*-cyclopenta[*b*]benzofuran from *Aglaia elliptifolia*. Journal of the Chemical Society, Chemical Communications 1150-1151.

Ko, F.N., Wu, T.S., Liou, M.J., Huang, T.F., Teng, C.M., 1992. PAF antagonism *in vitro* and *in vivo* by aglafoline from *Aglaia elliptifolia*. European Journal of Pharmacology 218, 129–135.

Kokpol, U., Venaskulchai, B., Simpson, J., Weavers, R. T., 1994. Isolation and X-ray structure determination of a novel pyrimidinone from *Aglaia odorata*. Journal of the Chemical Society, Chemical Communications 773-774.

Mohamad, K., Sévenet, T., Dumontet, V., Pais, M., Tri, M.V., Hadi, H., Awang, K., Martin, M.-T., 1999. Dammarane triterpenes and pregnane steroids from *Aglaia lawii* and *A. tomentosa*. Phytochemistry 51, 1032–1037.

Mohamed, K.M., Mohamed, M.H., Ohtani, K., Kasai, R., Yamasaki, K., 1999b. Megastigmane glycosides from seeds of *Trifolium alexandrinum*. Phytochemistry 50, 859–862.

Molleyres, L.P., Kumar, V., 1996. Insecticidal polycyclic compounds. PCT Int. Appl. WO 96/04284; CA 124, 335673.

Mulholland, D.A., Naidoo, N., 1998. A revision of the structure of ferrugin from *Aglaia ferruginaea*. Phytochemistry 47, 1163.

Nugroho, B.W., Edrada, R.A., Güssregen, B., Wray, V., Witte, L., Proksch, P., 1997. Insecticidal rocaglamide derivatives from *Aglaia duppereana*. Phytochemistry 44, 1455–1461.

Nugroho, B.W., Edrada, R.A., Wray, V., Witte, L., Bringmann, G., Gehling, M., Proksch, P., 1999. An insecticidal rocaglamide derivatives and related compounds from *Aglaia odorata* (Meliaceae). Phytochemistry 51, 367–376.

Ohse, T., Ohba, S., Yamamoto, T., Koyano, T., Umezawa, K., 1996. Cyclopentabenzofuran lignan protein synthesis inhibitors from *Aglaia odorata*. Journal of Natural Products 59, 650–652.

Pabst, A., Barron, D., Semon, E., Schreier, P., 1992. Two diastereomenic 3-oxo-α-ionol β-D-glucosides from raspberry fruit. Phytochemistry 31, 1649–1652.

Pannell, C.M., 1992. A Taxonomic Monograph of the Genus *Aglaia* Lour. (Meliaceae). Kew Bulletin Additional Series XVI. Royal Botanic Gardens, Kew, London.

Purushothaman, K.K., Sarada, A., Connolly, J.D., Akinniyi, J.A., 1979. The structure of roxburghilin, a bisamide of 2-aminopyrrolidine from the leaves of *Aglaia roxburghiana* (Meliaceae). Journal of the Chemical Society, Perkin Transaction I, 3171–3174.

Rembold, H., 1995. Growth and metamorphosis. In: Schmutterer, H. (Ed.), The Neem Tree. Source of Unique Natural Products for Integrated Pest Management, Medicine, Industry and Other Purposes. VCH Verlagsgesellschaft, Weinheim, pp. 177–194.

Saifah, E., Jongbunprasert, V., Kelley, C.J., 1988. Piriferine, a new pyrrolidine alkaloid from *Aglaia* pirifera leaves. Journal of Natural Products 51, 80–82.

Saifah, E., Puripattanavong, J., Likhitwitayawuid, K., Cordell, G.A., Chai, H., Pezzuto, J.M., 1993. Bisamides from *Aglaia* species: structure analysis and potential to reverse drug resistance with cultured cells. Journal of Natural Products 56, 473–477.

Satasook, C., Isman, M.B., Ishibashi, F., Medbury, S., Wiriyachitra, P., Towers, G.H.N., 1994. Insecticidal bioactivity of crude extracts of *Aglaia* species. Biochemical Systematics and Ecology 22, 121–127.

Shiengthong, D., Ungphakorn, A., Lewis, D.E., Massy-Westropp, R.A., 1979. Constituents of Thai medicinal plants — IV. New nitrogenous compounds — odorine and odorinol. Tetrahedron Letters, 2247–2250.

Srivastava, R.P., Proksch, P., 1991. Kontakttoxizität und Fraßhemmung von Chromenen aus Asteraceae gegenüber *Spodoptera littoralis* (Lepidoptera: Noctuidae). Entomologia Generalis 15, 265–274.

Wu, C.L., Lin, H.R., 1997. Labdanoids and bis(bibenzyls) from *Jungermannia* species. Phytochemistry 44, 101–105.

PERGAMON

Phytochemistry 57 (2001) 65–69

PHYTOCHEMISTRY

www.elsevier.com/locate/phytochem

The essential oil of *Origanum vulgare* L. ssp. *vulgare* growing wild in Vilnius district (Lithuania)

Danute Mockute, Genovaite Bernotiene, Asta Judzentiene *

Institute of Chemistry, A. Gostauto 9, LT-2600, Vilnius, Lithuania

Received 25 April 2000; received in revised form 14 November 2000

Abstract

The plants of wild *Origanum vulgare* L. ssp. *vulgare* were collected in 10 localities of Vilnius district (Lithuania) in 1995–1999. The main constituents of the essential oils from 8 localities were β-ocimene (14.9–21.6%), germacrene D (10.0–16.2), β-caryophyllene (10.8–15.7%) and sabinene (6.6–14.2%). The essential oils from two localities contained only three above compounds as major components: germacrene D, β-ocimene and sabinene or β-caryophyllene, β–ocimene and germacrene D. Three chemotypes of essential oils were identified. The main chemotype was β-ocimene–germacrene D–β-caryophyllene. The terpenic hydrocarbons made up 52.8–80.6% of the essential oils. The 42 identified components made up 85.6–98.0% of the essential oil. © 2001 Elsevier Science Ltd. All rights reserved.

Keywords: *Origanum vulgare* L. ssp. *vulgare*; *Labiatae*; Essential oils; Chemotypes; β-Ocimene–germacrene D–β-caryophyllene chemotype

1. Introduction

Origanum vulgare is the only species of the *Origanum* genus growing wild in Lithuania (Natkevicaite-Ivanauskiene, 1976). *Origanum vulgare* L. ssp. *vulgare* is widely spread in all the country. Another subspecies, *Origanum vulgare* L. ssp. *puberula* Beck, is rare and was found only in one locality near Trakai.

The composition of essential oils of *O. vulgare* L. ssp. *vulgare* was carefully analysed in Italy (Melegari et al., 1995) and France (Chalchat and Pasquier, 1998) (Table 1). The seeds from 4 localities were studied in Italy and four chemotypes of essential oils were identified. The seeds of 70 clones cultivated in France were collected from different sources in France and other European countries (Chalchat and Pasquier, 1998). Chalchat and Pasquier (1998) classified the essential oils into six groups: sabinene, germacrene D, germacrene D–β-caryophyllene, *cis*-sabinene hydrate, terpinen-4-ol and monoterpene hydrocarbons. Only one terpinen-4-ol chemotype was found in both countries (Table 1, No. 3 and 9). The major three constituents (terpinen-4-ol, β-caryophyllene and γ-terpinene) of the above essential oils were the same. Data in Table 1 demonstrate that *O. vulgare* L. ssp. *vulgare* plants may synthesize at least nine chemotypes of essential oil.

The other subspecies of *O. vulgare* L. form several different chemotypes based on essential oil. The thymol and carvacrol chemotypes were identified in *O. vulgare* L. ssp. *hirtum* (Melegari et al., 1995; Sivropoulou et al., 1996; Kokkini et al., 1997; Bocchini et al., 1998; Skoula et al., 1999). The composition of essential oil depended on collection season (Kokkini et al., 1997). Bocchini et al. (1998) showed that plants with white and pink flowers have different pathways of monoterpene biosynthesis.

The carvacrol chemotype of essential oil is characteristic for *O. vulgare* L. ssp. *glandulosum* (Melegari et al., 1995). The thymol (Melegari et al., 1995) and sabinene–germacrene D (Leto et al., 1994) chemotypes were synthesized by *O. vulgare* L. ssp. *gracile*.

The *O. vulgare* L. ssp. *virens* plants produced germacrene D–sabinene or γ-terpinene (Chalchat and Pasquier, 1999), linalool–δ-elemene (Alves-Pereira and Fernandes-Ferreira, 1998), linalool (–β-caryophyllene), linalool–α-terpineol, linalool–terpinen–4-ol, terpineol–linalool, terpineol (–carvacrol) (Melegari et al., 1995) chemotypes of essential oils.

The main constituents of the essential oil *O. vulgare* L. ssp. *viride* growing wild in Iran were linalyl acetate, β-caryophyllene and sabinene (Afsharypuor et al., 1997), but carvacrol, γ-terpinene, *p*-cymene were characteristic for plants cultivated in Kishenev botanical garden (Bodrug et al., 1990). The carvacrol and germacrene D chemotypes were found in cultivated *O. vulgare* L. (without subspecies characterization) from Finland (Nykanen

* Corresponding author. Fax: +370-2-617018.
E-mail address: judzent@ktl.mii.lt (A. Judzentiene).

0031-9422/01/$ - see front matter © 2001 Elsevier Science Ltd. All rights reserved.
PII: S0031-9422(00)00474-X

Table 1
The main chemotypes and their constituents of the known essential oil of *O. vulgare* L. ssp. *vulgare* identified in Italy (Melegari et al., 1995) and France (Chalchat and Pasquier, 1998)[a]

No.	Compound	Amount in percentage
1.	**β-Caryophyllene**	**17.2**
	β-Cubebene	14.1
	Carvacrol	7.6
2.	**Thymol**	**39.3**
	Linalool	28.3
	p-Cymene	10.9
	1.8-Cineole	10.6
3.	**Terpinen-4-ol**	**31.3**
	β-Caryophyllene	14.6
	γ-Terpinene	10.5
	Sabinene	10.2
4.	***p*-Cymene**	**18.9**
	β-Caryophyllene	**18.6**
	Terpinen-4-ol	13.8
	Sabinene	9.9
5.	**Sabinene**	**⩽40.1**
	Germacrene D	⩽33.1
	β-Caryophyllene	⩽21.9
	β-Bourbonene	⩽19.9
	(Z)- β-Ocimene	⩽18.9
	(E)- β-Ocimene	⩽18.4
6.	**Germacrene D**	⩽33.0
	(Z)- β-Ocimene	⩽36.5(?)
	(E)- β-Ocimene	⩽20.1
	γ-Terpinene	⩽20.8
7.	**Germacrene D**	**⩽28.3**
	β-Caryophyllene	**⩽26.2**
	Caryophyllene oxide	⩽20.5
	δ-Cadinene	⩽11.2
8.	***cis*-Sabinene hydrate**	**⩽41.2**
	Terpinen-4-ol	⩽16.1
	Sabinene	⩽10.7
	(Z)- β-Ocimene	⩽6.7
9.	**Terpinen-4-ol**	**⩽39.5**
	β-Caryophyllene	⩽21.1
	γ-Terpinene	⩽18.4
	Germacrene D	⩽16.3
10.	***(Z)*- β-Ocimene**	**⩽41.9**
	***(E)*- β-Ocimene**	**⩽21.1**
	p-Cymene	⩽17.2
	β-Caryophyllene	⩽11.0
	Germacrene D	⩽10.6
	Sabinene	⩽8.9

[a] Numbers 1–4 were cultivated in Italy; 5–10 were cloned in France. Origin of seeds: 1, USA; 2, Budakalasz; 3, Liegi; 4, Spagna; 5–10, France and other European countries.

and Lebensen, 1986). The thymol chemotype of essential oil of *O. vulgare* L. was determined in Sicily (Baratta et al., 1998). The major components of *O. vulgare* L. from north India were linalool and myrcene (Kaul et al., 1996).

The other subspecies *O. vulgare* L. synthesize some more chemotypes (carvacrol, linalool, α-terpineol, linalyl acetate–β-caryophyllene) in comparison with *O. vulgare* L. ssp. *vulgare* (Table 1) (Melegari et al., 1995; Chalchat and Pasquier, 1998).

The other species of the *Origanum* genus mainly formed the same chemotypes as *O. vulgare* L. The main constituents of the essential oil of *O. laevigatum* Boiss. were bicyclogermacrene, germacrene D and β-caryophyllene (Tucker and Maciarelle, 1992; Baser et al., 1996) and that of *O. husnucan-baserii*–borneol and *trans*-sabinene hydrate (Baser et al., 1998). The bicyclogermacrene type has not been found in investigated *O. vulgare* L. species.

This paper presents the composition of the essential oils of *O. vulgare* L. ssp. *vulgare* grown wild in various localities of Vilnius district (Lithuania).

2. Results and discussion

The essential oils from *Origanum vulgare* L. ssp. *vulgare* plants collected in 8 localities of Vilnius district contained β-ocimene as the main constituent (Table 2 and Table 4 (H)). β-Ocimene exists in two forms — *cis* (*Z*) and *trans* (*E*). The ratio of isomers depends on location. Higher quantities of *trans*- rather than *cis*-β-ocimene were found in 5 localities (B, C, D, F, G). The plants with a relative high percentage of β-ocimene in essential oil were collected in ecologically clean places (in the forests far from the town and industrial objects). The four major constituents (β-ocimene, germacrene D, β-caryophyllene, sabinene) of essential oils were the same in all 11 samples from 8 localities (Tables 2–4). The basic composition of the essential oils under study (Tables 2 and 4) was the same as that of the plants *O. vulgare* L. ssp. *vulgare* cultivated in France and attributed by the investigators Chalchat and Pasquier (1998), to terpene hydrocarbons group (Table 1, No. 10). The essential oils under study contained lower percentage of *p*-cymene (0–2.5%) (Tables 2 and 4), than in the plants cultivated in France (0.7–17.2%) (Table 1, No. 10) (Chalchat and Pasquier, 1998). The plants in Vilnius district showed higher percentages sabinene, germacrene D and β-caryophyllene than those in France (Tables 1, 2 and 4).

The quantities of β-ocimene, germacrene D and β-caryophyllene exceeded 10% in all essential oils presented in Table 2. The amount of sesquiterpene hydrocarbons, germacrene D and β-caryophyllene, depended on growing location (Table 2, compare samples of 1999) and seasonal conditions (A locality: samples A, A1, A2). The samples of plants with as main component germacrene D and β-caryophyllene of essential oils were collected in ecologically polluted places (near the city and roads). The composition of the essential oils in locality D is associated with the colour of flowers (Table 2) as it was earlier noticed for plants of *O. vulgare* L. ssp. *hirtum* (Bocchini et al., 1998). The essential oil of plants with violet-pink flowers contained more β-ocimene than germacrene D or β-caryophyllene, while plants with pink flowers contained approximately the same quantities of

Table 2
The composition of the essential oil of *Origanum vulgare* L. ssp. *vulgare* (%) growing wild in Vilnius district (Lithuania)[a]

No.	R_t	Compound	A	A1	A2	B	C	D1	D2	E	F	G	Interval
1.	6.29	α-Thujene	0.3	1.1	0.3	0.2	0.2	0.3	0.7	0.4	0.4		0.2–1.1
2.	6.48	α-Pinene	0.5	0.9	0.5	0.5	0.4	0.6	0.3	0.3	1.0	0.8	0.3–1.0
3.	6.68	Camphene		0.1	0.1	0.2	0.1	0.1	0.7	0.5	0.2		0–0.7
4.	7.81	**Sabinene**	**6.9**	**8.2**	**6.6**	**10.8**	**11.0**	**6.4**	**8.0**	**11.8**	**10.0**	**14.2**	**6.4–14.2**
5.	7.89	β-Pinene	0.9	1.2	0.5	0.7	0.6	0.9	1.2	0.8	1.1	0.9	0.5–1.2
6.	8.04	1-Octen-3-ol	0.7	0.7	0.9	0.3	0.3	0.4	0.3	0.4	0.5		0–0.9
7.	8.47	Myrcene	1.4	2.0	1.8	1.5	1.1	1.4	1.7	2.0	1.8	1.3	1.1–2.0
8.	9.40	α-Terpinene	0.8	1.6	0.7	0.9	0.9	0.8	1.2	0.8	1.4	0.6	0.6–1.6
9.	9.71	*p*-Cymene		0.4	0.3	0.1	0.2	0.8	0.8	0.7	0.9	0.7	0–0.9
10.	9.93	β-Phellandrene + 1.8-Cineole	4.7	5.0	6.8	7.1	6.7	5.7	6.9	4.8	7.9	6.6	4.7–7.9
11.	10.45	*(Z)*-β-Ocimene	8.6	9.1	10.3	6.2	7.0	7.2	7.2	11.0	7.9	7.3	6.2–11.0
12.	10.85	*(E)*-β-Ocimene	7.6	8.6	7.0	11.5	10.9	7.7	9.0	10.6	9.0	9.4	7.0–11.5
		$\sum$11 + 12	**16.2**	**17.7**	**17.3**	**17.7**	**17.9**	**14.9**	**16.2**	**21.6**	**17.0**	**16.7**	**14.9–21.6**
13.	11.20	γ-Terpinene	1.8	2.6	1.2	1.7	2.0	2.1	2.1	1.7	2.2		0–2.6
14	11.45	*cis*-Sabinene hydrate	0.4	0.3	0.3	0.3	0.1	0.2	0.4	0.3	0.2		0–0.4
15.	12.38	Terpinolene	0.3	0.6	0.3	0.3	0.3	0.2	0.4	0.2	0.4		0–0.6
16.	12.80	*trans*-Sabinene hydrate	0.8	0.8	0.4	0.2			0.7	0.2			0–0.8
17.	13.00	Linalool	1.2	2.9	1.3	0.9	0.6	1.5	0.6	1.1	1.0	4.7	0.6–2.9
18.	16.40	Terpinen-4-ol	1.6	3.0	1.2	1.3	1.4	0.8	1.7	1.6	1.5		0–3.0
19.	17.01	α-Terpineol	1.4	1.2	1.2	2.2	1.4	1.2	2.4	1.8	1.4	0.8	0.8–2.4
20.	25.70	β-Bourbonene	0.5	0.5	0.5	0.5	0.5	0.8	1.0	0.7	0.7	0.9	0.5–1.0
21.	26.08	β-Elemene	0.3	0.2	0.4	0.3	0.3	0.4	0.3	0.2	0.3		0–0.4
22.	27.33	**β-Caryophyllene**	**11.5**	**11.6**	**14.0**	**13.0**	**13.6**	**14.7**	**11.2**	**10.9**	**10.8**	**15.4**	**10.8–15.4**
23.	27.59	β-Gurjunene			0.2	0.2	0.2	0.2	0.2	0.1			0–0.2
24.	28.70	α-Humulene	2.0	1.9	2.4	2.6	2.6	2.5	1.5	2.2	1.8	1.8	1.5–2.6
25.	28.90	*allo*-Aromadendrene	0.6	0.5	0.4	0.5	0.6	0.6	0.4	0.3	0.5		0–0.6
26.	29.95	**Germacrene D**	**10.0**	**13.3**	**16.9**	**16.2**	**14.3**	**15.9**	**13.0**	**13.8**	**14.3**	**14.2**	**10.0–16.9**
27.	30.46	Bicyclogermacrene	4.5	3.0	3.1	3.3	2.4	2.6	1.5	1.4	2.8	1.5	1.4–4.5
28.	30.70	α-Muurolene	0.8	0.5	0.6	0.7	0.8	0.8	0.4	0.5	0.4		0–0.8
29.	31.20	α-Farnesene + β-Bisabolene	6.9	4.4	4.2	6.1	5.8	6.2	4.7	4.1	5.2	5.6	4.1–6.9
30.	31.65	δ-Cadinene	2.9	1.5	1.5	2.7	3.0	2.1	1.3	3.2	2.1	1.9	1.3–3.2
31.	33.67	Germacrene-D-4-ol[1] + Spathulenol[2]	3.2[1]	2.1	2.9[1]	2.9	2.2[1]	2.1[1]	2.5[1]	1.4	2.1[1]	2.1	1.4–3.2
32.	34.04	Caryophyllene oxide	1.8	2.2	3.9	0.9	1.7	3.7	7.1	1.1	3.3	6.6	0.9–7.1
33.	36.40	α-Cadinol	0.5	0.3	1.2	0.5			0.4	0.1		0.7	0–1.2
		Sum	85.6	92.3	94.2	97.1	93.2	90.9	91.8	91.0	93.2	98.0	85.6–98.0
		Hydrocarbons $C_{10}+C_{15}$	69.3	73.8	74.1	80.6	78.8	75.3	69.0	78.2	75.3	71.4	69.0–80.6

[a] The plants collected at full flowering except sample A1 (at the beginning of flowering) in the localities: Silenai vicinity (A, 1995; A1, 1999; A2, 1999; and B, C, 1999); Rastinenai vicinity in 1999 (D1, with pink flowers; D2, with violet-pink flowers, E, F, G).

Table 3
The main constituents (I, II, III, IV) of essential oil of *O. vulgare* L. ssp. *vulgare* growing wild in Vilnius district[a]

Compound	A	A1	A2	B	C	D1	D2	E	F	G	H
β-Ocimene	I	I	I	I	I	II	I	I	I	I	I
Germacrene D	III	II	II	II	II	I	II	II	II	III–IV	II–III
β-Caryophyllene	II	III	III	III	III	III	III	IV	III	II	II–III
Sabinene	IV	IV	IV	IV	IV	IV	IV	III	IV	III–IV	IV

[a] The growing localities as in Table 2.

all three main constituents (Table 2, samples D1 and D2). The quantities of the first and second major components of the essential oil in samples from A–H and K localities were similar (Tables 2 and 4).

The largest difference was found in plants from locality J collected in 1999 (Table 4, J3). The amount of the first major constituent germacrene D exceeded~ 2.5 fold that of the second major compound, β-ocimene. The third main constituent was sabinene. The plants from locality J showed low percentages of β-caryophyllene in comparison with plants presented in Table 2. The essential oils from the above localities may be attributed to germacrene D–β-ocimene–sabinene chemotype (Table 4, J1, J2 and J3). The plants from locality K accumulated proportionally higher amounts of β-caryophyllene, and lower amounts of sabinene. The essential oils of K was of β-caryophyllene–β-ocimene–germacrene D chemotype (Table 4, K1, K2). The composition of essential oils

Table 4
The composition of the essential oils (%) of plants[a] growing wild in Rokantiskes and Sapiegine (Vilnius district)

No.	R_t	Compound	H	J1	J2	J3	Interval J	Mean	K1	K2	K3	Interval K	Mean
1.	6.29	α-Thujene	0.6	0.2		tr.	0–0.20	<0.1	0.3	0.4	0.7	0.3–0.7	0.5
2.	6.48	α-Pinene		0.5	0.2	0.3	0.2–0.5	0.3	0.2	0.4	0.3	0.2–0.4	0.3
3.	7.81	**Sabinene**	**7.2**	**14.0**	**15.0**	**8.7**	**8.7–15.0**	**12.6**	2.1	4.7	3.7	2.1–4.7	3.5
4.	7.89	β-Pinene	1.3						0.4	0.8	0.6	0.4-0.8	0.6
5.	8.04	1-Octen-3-ol		1.2	0.5	0.9	0.5–1.2	0.9	0.5	1.2	0.9	0.5–1.2	0.9
6.	8.47	Myrcene	2.0	3.2	3.2	2.0	2.0–3.2	2.8	0.3	1.3	1.0	0.3–1.3	0.9
7.	9.40	α-Terpinene	0.4	0.7	0.2	0.3	0.2–0.7	0.4	0.7	0.9	0.9	0.7–0.9	0.8
8.	9.71	*p*-Cymene		0.2			0–0.2	<0.1	1.2	1.1	0.4	0.4–1.2	0.9
9.	9.93	β-Phellandrene + 1.8-Cineole		4.4	3.0	3.4	3.0–4.4	3.6	5.0	6.5	4.2	4.2–6.5	5.2
10.	10.45	*(Z)*-β-Ocimene	9.2	9.1	11.0	7.2	7.2–11.0	9.1	6.0	10.2	7.1	6.0–10.2	7.7
11.	10.85	*(E)*-β-Ocimene	7.4	5.6	5.1	4.9	4.9–5.6	5.2	4.8	5.2	5.9	4.8–5.9	5.3
		Σ 10 + 11	**16.6**	**14.7**	**16.1**	**12.1**	**12.1–16.1**	**14.3**	**10.8**	**15.4**	**13.0**	**10.8–15.4**	**13.1**
12.	11.20	γ-Terpinene	1.4	1.2	0.7	0.8	0.7–1.2	1.0	1.4	1.9	2.5	1.4-2.5	1.9
13.	11.45	*cis*-Sabinene hydrate							0.5	0.2	0.6	0.2–0.6	0.4
14.	12.38	Terpinolene	0.2	0.2			0–0.2	<0.1	0.4	0.4	0.4	0.4	0.4
15.	12.80	*trans*-Sabinene hydrate							1.4	0.6	1.8	0.6–1.8	1.3
16.	13.00	Linalool		0.6	0.6	0.9	0.6–0.9	0.7	0.9	1.2	1.2	0.9–1.2	1.0
17.	16.40	Terpinen-4-ol	0.8	0.9	1.4	0.9	0.9–1.4	1.1	2.5	2.1	2.6	2.1–2.6	2.4
18.	17.01	α-Terpineol		1.0	0.7	1.3	0.7–1.3	1.0	0.9	1.0	1.0	0.9–1.0	1.0
19.	21.99	Thymol			0.3	0.5	0–0.5	0.3		0.4		0–0.4	0.1
20.	22.38	Carvacrol			3.1	tr.	0–3.1	1.0					
21.	25.70	β-Bourbonene	0.7	0.9	1.0	0.7	0.7–1.0	0.2	0.9	0.7	0.6	0.6–0.9	0.7
22.	26.08	β-Elemene	0.4	0.5	0.5	0.4	0.4–0.5	0.5	0.3	0.3	0.3	0.3	0.3
23.	27.33	**β-Caryophyllene**	15.7	2.3	6.7	5.0	2.3–6.7	4.7	16.1	16.6	13.4	13.4–16.6	15.3
24.	27.59	β-Gurjunene	0.2	0.3	0.3		0–0.3	0.2	0.2	0.2	0.2	0.2	0.2
25.	28.70	α-Humulene	2.8	0.5	0.6	0.6	0.5–0.6	0.6	2.0	2.8	2.6	2.0–2.8	2.5
26.	28.90	allo-Aromadendrene	0.6	0.9	0.5	0.6	0.5-0.9	0.7	0.2	0.7	0.6	0.2–0.7	0.5
27.	29.95	**Germacrene D**	**15.7**	**27.2**	**21.6**	**29.4**	**21.6–29.4**	**26.1**	**7.5**	**10.4**	**19.3**	**7.5–19.3**	**12.4**
28.	30.46	Bicyclogermacrene	5.8	1.5	1.5	2.1	1.5–2.1	1.7	0.9	1.8	2.9	0.9–2.9	1.9
29.	30.70	α-Muurolene	0.8	1.0	0.7	0.7	0.7–1.0	0.8	0.1	0.5	0.7	0.1–0.7	0.4
30.	31.20	β-Bisabolene + α-Farnesene	5.5	4.8	6.6	3.1	3.1–6.6	4.8	4.2	4.3	6.0	4.2–6.0	4.8
31.	31.65	δ-Cadinene	2.7	2.0	1.7	9.0	1.7–9.0	4.2	2.6	1.9	2.1	1.9–2.6	2.2
32.	33.67	Germacrene-D-4-ol + Spathulenol	1.9	3.2	1.5	2.0	1.5–3.2	2.2	5.0	3.2	3.1	3.1–5.0	3.8
33.	34.04	Caryophyllene oxide	2.5	1.1	1.5	2.0	1.1–2.0	1.5	13.8	8.7	2.3	2.3–13.8	8.3
34.	36.40	α-Cadinol		1.3			0–1.3	0.4	2.1	1.2	0.1	0.1–2.1	1.1
		Sum	91.3	90.5	89.8	87.7	87.7–90.5	88.9	85.4	93.8	90.0	85.4–93.8	89.6
		Hydrocarbons $C_{10} + C_{15}$	80.6	76.8	77.2	75.8	75.8–77.2	76.2	52.8	67.5	72.3	52.8–72.3	64.1

[a] The plants collected at full flowering in the localities: Sapiegine II in 1999 (H); Rokantiskes vicinity (J1, 1997; J2, 1998; J3, 1999); Sapiegine I (K1, 1997; K2, 1998, K3, 1999).

of plants collected in 1999 different from those collected in 1997 and 1998 (Table 4). The increase of germacrene D relative amount in 1999 was noticed not only in localities K, but in A and J (Tables 2 and 4), too. This phenomenon may be caused by the very warm spring and summer of 1999. It is known that some plants in Italy that synthesize mainly monoterpenic compounds in spring, produce sesquiterpenes in summer (Giner et al., 1993).

Of the 42 compounds identified in the essential oils, 38 are given in Tables 2 and 4. Apart from the above components α-cadinene (0.1–0.2%) and 3-octanone (0.1–0.2%) were found in samples B, C and D1, and borneol — in C and F. 32 compounds from Tables 2 and 4 were earlier identified in *Origanum vulgare* L. ssp. *vulgare* in Italy (Melegari et al., 1995) and France (Chalchat and Rasquier, 1998). Borneol, β-gurjunene, *allo*-aromadendrene, β-bisabolene and α-cadinene (Tables 2 and 4) were found in the essential oils of other subspecies of *O. vulgare* L. (Leto et al., 1994; Sivropoulou et al., 1996; Baratta et al., 1998; Bocchini et al., 1998). Bicyclogermacrene (Tucker and Maciarelle, 1992; Baser et al., 1996) and β-elemene (Baser et al., 1998) were identified in the essential oils of other species of *Origanum* genus.

Myrcene, 1,8-cineole + β-phellandrene, γ-humulene, bicyclogermacrene, α-farnesene + β-bisabolene, δ-cadinene, germacrene-D-4-ol + spathulenol made up more than 1% in all 17 samples of essential oils and caryophyllene oxide in 16 samples. The relative quantity of some constituents varied in wide interval (Tables 2 and 4). The amount of 9 constituents did not exceed 1%.

Mono- and sesquiterpene hydrocarbons made up 52.8–80.6% of essential oils (Tables 2 and 4). The major constituents of all investigated essential oils were hydrocarbons. All essential oils under study according

to Ietswaart's classification (Skoula et al., 1999) may be attributed to acyclic- and sesquiterpene-rich subspecies of *Origanum vulgare* L. The essential oil of 8 localities from 10 may be named as β-ocimene–germacrene D–β-caryophyllene chemotype (Tables 2–4; A–H).

3. Experimental

The aerial parts (~35 cm) of plants (0.2–1.0 kg) growing wild in 10 localities of Vilnius district (indicated here by alphabetic symbols, A–K) were collected in August 1995 (A sample), 1997 (J, K samples), 1998 (J, K) and 1999. A, B, and C localities are near Silenai, D-G–in Rastinenai vicinity, H–in Sapiegine II, J–in Rokantiskes and K–in Sapiegine I.

Voucher specimens have been deposited in the Herbarium of the Institute of Botany, Vilnius, Lithuania (numbers: A-61114, B-61115, C-61116, D-61117, E-61118, F-61119, G-61120, K-61121, H-61122 and J-61123).

All samples were collected at full flowering except A1, which was collected at the beginning of flowering stage. The ration of stems/leaves/flowers is approximately the same in all samples. The plants were dried at room temperature (20–25°C). The essential oils were prepared by hydrodistilation of 20–100 g of air-dried plants.

The analyses of the essential oils were carried out by GC and GC–MS. The HP 5890II chromatograph equipped with FID and capillary column HP-FFAP (30 m × 0.25 mm) was used for quantitative analysis. The GC oven temperature was set at 70°C for 10 min and then programmed from 70 to 210°C at a rate of 3°C min^{-1}, using He as the carrier gas (0.7 ml min^{-1}). Injector and detector temperatures were 200 and 250°C, respectively. Analyses by GC–MS were performed, using a chromatograph interfaced to a HP 5971 mass spectrometer (ionization voltage 70 eV) and equipped with capillary column CP-Sil 8 CB (50 m×0.32 mm). The oven temperature was held at 50°C for 2 min, then programmed from 50 to 180°C at a rate 3°C min^{-1}, held for 1 min, then programmed from 180 to 250°C at rate 20 °C min^{-1}, and isothermal at 250°C for 2 min, using He as the carrier gas (2.0 ml min^{-1}). Injector and detector temperatures −250°C.

The percentage composition of the essential oils was computed from GC peak areas without correction factors. Qualitative analysis was based on a comparison of retention times and indexes on both columns and mass spectra with corresponding data in the literature (Adams, 1995; Chung et al., 1993) and computer mass spectra libraries (Wiley and NBS 54K).

References

Adams, R., 1995. Identification of Essential Oil Components by Gas Chromatography/Mass Spectrometry. Allured Publishing, Carol Stream, IL.

Afsharypuor, S., Sajjadi, E.S., Erfan-Manesh, M., 1997. Volatile constituents of *Origanum vulgare* ssp viride (syn. *O. heracleoticum*) from Iran. Planta Medica 63, 179–180.

Alves-Pereira, I.M.S., Fernandes-Ferreira, M., 1998. Essential oils and hydrocarbons from leaves and calli of *Origanum vulgare* ssp. *virens*. Phytochemistry 48, 795–799.

Baratta, T.M., Dorman, D.J.H., Deans, G.S., 1998. Chemical composition, antimicrobial and antioxidative activity of laurel, sage, rosemary, oregano and coriander essential oils. Journal of Essential Oil Research 10, 618–627.

Baser, K.H.C., Kurkcouglu, M., Duman, H., Aytac, Z., 1998. Composition of the essential oil of *Origanum husnucan-baserii* H. Duman, Z. Aytac et A. Duran, a new species from Turkey. Journal of Essential Oil Research 10, 419–421.

Baser, K.H.C., Ozek, T., Kurkcouglu, M., Tumen, G., 1996. Essential oil of *Origanum laevigatum* Boiss. Journal of Essential Oil Research 8, 185–186.

Bocchini, P., Russo, M., Galletti, G.C., 1998. Pyrolysis-gas chromatography/mass spectrometry used as a microanalytical technique for the characterization of *Origanum heracleoticum* from Calabria, Southern Italy. Rapid Communications in Mass Spectrometry 12, 1555–1563.

Bodrug, M.V., Dragalin, I.P., Vlad, P.F., 1990. Composition of essential oil of *Origanum heracleoticum* L. at vegetation phases (in Russian). Thesis of Simpheropol Conference, Ukraina, p. 161.

Chalchat, J.C., Pasquier, B., 1998. Morphological and chemical studies of origanum clones: *Origanum vulgare* L. ssp. *vulgare*. Journal of Essential Oil Research 10, 119–125.

Chalchat, J.C., Pasquier, B., 1999. Chemical Studies of *Origanum vulgare* L. ssp. *gracile* (Koch) letswaart and *Origanum vulgare* L. ssp. *virens* (Hoffm. et Link) letswaart. Journal of Essential Oil Research 11, 143–144.

Chung, T.Y., Eiserich, J.P., Shibamoto, T., 1993. Volatile compounds isolated from edible Korean Chamchwi (*Aster scaber* Thunb.). Journal of Agricultural and Food Chemistry 41, 1693–1697.

Giner, R.M., Maner, S., Rios, J.L., 1993. Seasonal variations in the essential oils of *Santolina chamaccyparissus*. Science of Pharmacology 61, 169–173.

Kaul, V.K., Singh, B., Sood, R.P., 1996. Essential oil of *Origanum vulgare* L. from North India. Journal of Essential Oil Research 8, 101–103.

Kokkini, S., Karousou, R., Dardioti, A., Krigas, N., Lanaras, T., 1997. Autumn essential oils of Greek oregano. Phytochemistry 44, 883–886.

Leto, C., Carrubba, A., Trapani, P., 1994. Taxonomy, ecology, properties and uses of genus *Origanum*. Atti del Convegno Internazionale. Coltivazione e miglioramento di piante officinali. Trento, Italy, pp. 343–355.

Melegari, M., Severi, F., Bertoldi, M., Benvenuti, S., Circetta, G., Fortunato, I.M. et al., 1995. Chemical characterization of essential oils of some *Origanum vulgare* L. sub-species of various origin. Rivista Italiana EPPOS 16, 21–29.

Natkevicaite-Ivanauskiene, M., 1976. Flora of Lithuania, Vol. 5. Mokslas, Vilnius pp. 305–307.

Nykanen, I., Lebensen, Z., 1986. Untersuch. und Forsch. 183, 267–272.

Sivropoulou, A., Papanikolaou, E., Nikolaou, C., Kokkini, S., Lanaras, T., Arsenakis, M., 1996. Antimicrobial cytotoxic activities of *Origanum* essential oils. Journal of Agricultural and Food Chemistry 44, 1202–1205.

Skoula, M., Gotsiou, P., Naxakis, G., Johnson, B.C., 1999. A chemosystematic investigation on the mono- and sesquiterpenoids in the genus *Origanum* (Labiatae). Phytochemistry 52, 649–657.

Tucker, O., Maciarelle, M., 1992. The Essential Oils of *Origanum laevigatum* Boiss (Labiatae). Journal of Essential Oil Research 4, 419–420.

PERGAMON

Phytochemistry 57 (2001) 71–76

PHYTOCHEMISTRY

www.elsevier.com/locate/phytochem

Variability of essential oils of *Satureja montana* L. and *Satureja kitaibelii* Wierzb. ex Heuff. from the central part of the Balkan peninsula

Violeta Slavkovska [a], Radisa Jancic [a], Srdjan Bojovic [b,*], Slobodan Milosavljevic [c], Dejan Djokovic [c]

[a] *Department of Botany, Faculty of Pharmacy, University of Belgrade, Vojvode Stepe 450, 11000 Belgrade, Yugoslavia*
[b] *Institute of Forestry, Kneza Viseslava 3, 11030 Belgrade, Yugoslavia*
[c] *Faculty of Chemistry, University of Belgrade, Studentski trg 16, 11001 Belgrade, Yugoslavia*

Received 21 March 2000; received in revised form 3 November 2000

Abstract

The results of the essential oil composition confirm that there are differences between populations within the same subspecies (*Satureja montana* ssp. *montana*), between the subspecies (*Satureja montana* ssp. *montana* and *Satureja montana* ssp. *pisidica*) and the species (*Satureja montana* and *S. kitaibelii*). The essential oil composition of *S. montana* ssp. *montana* is more related to the *Satureja montana* ssp. *pisidica* than *S. kitaibelii* which separates as a whole species. © 2001 Elsevier Science Ltd. All rights reserved.

Keywords: *Satureja montana* ssp. *montana*; *S. montana* ssp. *pisidica*; *S. kitaibelii*; *Lamiaceae*; Chemotaxonomy; Essential oils

1. Introduction

The genus *Satureja* L. embraces over 30 species whose center of distribution is located in the eastern part of the Mediterranean (Silic, 1979). These are annual or perennial semi-bushy aromatic plants that inhabit the arid, sunny, stony and rocky habitats.

The genus *Satureja* belongs to the family *Lamiaceae*, sub-family *Nepetoideae,* and the tribe *Mentheae* (Cantino et al., 1992). One of the diagnostic characteristics of the sub-family *Nepetoideae* is that its representatives contain more than 0.5% of essential oil (El-Gazzar and Watson, 1970). The essential oils have certain biological functions such as physiological function (in plant metabolism) and ecological function (in interactions of the plants with their environment) (Jancic et al., 1995). The essential oils are also significant for an explanation of phylogenetic relations.

The species *Satureja montana* L. is confusing from the taxonomic and, therefore, chorological point of view. Its high variability is evident, even within a single population polymorphism, and especially in populations coming from distant habitats. The variability is reflected in morphologic characteristics such as the form and size of the calyx and corolla, calycal dents, size, form and color of the nutlets, and particularly in the form, size and pubescence of the leaves and in a more or less pronounced pubescence of the stems (Silic, 1979). The taxa *S. montana* contains numerous subspecies.

Satureja kitaibelii Wierzb. ex Heuff. has been shown by the older authors as a member of one of the infraspecies systematic categories within an extremely polymorphic species *S. montana* (Briquet, 1893; Hayek, 1931; Stojanov and Stefanov, 1948; Ball and Getliffe, 1972; Diklic, 1974). Silic (1979) thinks that the pronounced morphologic differences and clearly separated area, in regard to the related taxons, confirm the view of those authors that consider *S. kitaibelii* as a separate species (Ravarut, 1961).

The essential oil composition of the species S. *montana* and *S. kitaibelii* is very variable. According to some authors the dominant components in the oil of *S. montana* are caryophyllene and geraniol (Sevarda et al., 1986), and according to others it is carvacrol (Palic and Gasic, 1993; Kustrak et al., 1996). The dominant components in the oil of *S. kitaibelii* are ρ-cymene, geraniol and β-elemene (Sevarda et al., 1989; Palic and Gasic, 1993; Chalchat et al., 1999).

The aim of the work is investigating the essential oil composition variability on different levels: within a

* Corresponding author. Fax: +381-11-545-969.
E-mail address: bojos@ptt.yu (S. Bojovic).

0031-9422/01/$ - see front matter © 2001 Elsevier Science Ltd. All rights reserved.
PII: S0031-9422(00)00458-1

population, between populations of the same subspecies (two populations of *S. montana* ssp. *montana*), between the subspecies (S. *montana* ssp. *montana* and *S. montana* ssp. *pisidica*) and between the species *S. montana* and *S. kitaibelii*. The results could aid in solving the position of these taxons whose place within the clasification system is unclear.

2. Results and discussion

The composition and content of essential oils in the aerial parts of the plants of the studied populations are given in Table 2. Monoterpene hydrocarbons and their derivatives dominate in the chemical composition of essential oils of the studied populations. The sesquiterpene compounds are present in small quantities.

In the population *S. montana* ssp. *montana* from Beli Rzav gorge in the essental oil of the 33% of plants the acyclic monoterpene alcohol linalool is found as the dominating component, while in 43% of individuals it was aromatic monoterpene, ρ-cymene. In 10% of plants the essential oil is dominated by bicyclic alcohol of bornan class, borneol, while in 13% of individuals dominates bicyclic alcohol of thujanic class, trans-sabinen hydrate.

The population of *S. montana* ssp. *montana* from the surroundings of Zvornik is characterized by the presence of the same components in essential oils, except β-caryophyllene, as the previous population (from the gorge of the river Beli Rzav). Linalool as a dominant component was detected in the essential oils of 23% of individuals, ρ-cimene also in 23%, *trans*-sabinen hydrate in 27% and borneole in 3% of individuals. In this population 23% of the plants are dominated by phenol of the menthane class (ρ-cymen-8-ol).

According to the presence and quantity of dominant compounds, the essential oil composition of the investigated populations of *S. montana* ssp. *montana* differs from the results published earlier (Sevarda et al., 1986; Kustrak et al., 1996).

In 33% of the plants of *S. montana* ssp. *pisidica* from the mountain Galicica dominates linalool, in 37% of individuals ρ-cymene, in 3% borneole and in 27% — monoterpene phenol of the menthane class — carvacrol. These results agree with those from previous investigations of *S. montana* ssp. *pisidica* (Palic and Gasic, 1993).

In the essential oils of the plants of population *S. kitaibelii* coming from the gorge of the river Jelasnica, 14 components were identified (Table 2). The compounds which are absent in the essential oils with regard to the essential oils from populations of the species *S. montana* are: β-pinene, α-terpinene, z-(β)-ocymene and carvacrol. In 27% of the plants the dominant component in essential oils is monoterpene of the menthane class — limonene, in 63% is ρ-cymene and in 10% the dominant component is *trans*-sabinene hydrate. ρ-Cymene as the dominant component of the essential oil of the species *S. kitaibelii* had been also determined in earlier investigations (Sevarda et al., 1989; Palic and Gasic, 1993; Chalchat et al., 1999).

The principal component analysis was done on the basis of the quantitative content of 19 analyzed compounds in 120 individuals (Fig. 2). The PCA revealed that the first three axes represent 47.5% of total information. The first axe explains the most variabilities (22.7%) and possesses the highest biological significance, since it is capable to clearly separates the species *S. montana* ssp. *pisidica* from the species *S. kitaibelii* according to the limonene, α-pinene and camphene percentages (Fig. 2). By comparing the studied populations (based on the qualitative and quantitative composition of essential oils) a conclusion could be made that the most similar populations are the ones of *S. montana* ssp. *montana*.

The essential oil of *S. montana* ssp. *pisidica* differs from the essential oil of *S. montana* ssp. *montana* from the gorge of the river Beli Rzav and the surroundings of Zvornik in domination of carvacrol which in other populations is found in irrelevant quantities (Table 2). The small quantity of *trans*-sabinene hydrate and domination of carvacrol in the essential oils of some individuals could be a "reason plus" to differentiate it from the subspecies *montana*.

In the plants of *S. kitaibelii,* linalool appears in small quantities, while in the essential oils of some individuals there is a clear domination of limonene (Fig. 2). The *S. kitaibelii* population is specific for not having some compounds such as z-(β)-ocymene, α-terpinene, β-pinene and carvacrol (Table 2). The qualitative difference in the composition of essential oils in *S. kitaibelii* (absence of some compounds) might be a result of a specific genetic

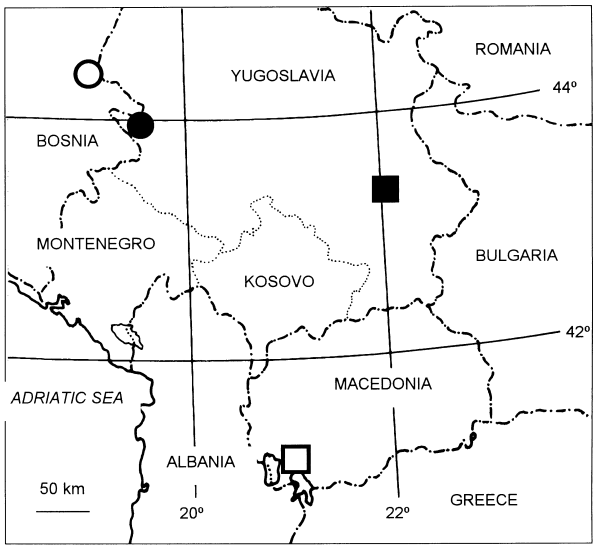

Fig. 1. Location of the analyzed populations. ○, *Satureja montana* ssp. *montana*; Beli Rzav; ●, *Satureja montana* ssp. *montana*; Zvornik; □, *Satureja montana* ssp. *pisidica*; Galicica; ■, *Satureja kitaibelii*, Jelasnica.

basis of this species. Since there are clear morphologic and chorologic differences, including even the pronounced chemical differences, it is to be accepted that the view of the authors that this taxon classify into a separate species *S. kitaibelii* (Ravarut, 1961; Silic, 1979).

The multivariate analysis reveals that *S. montana* ssp. *montana* represents a heterogeneous group while *S. montana* ssp. *pisidica* and *S. kitaibelii* are clearly separated between themselves. Cluster analysis using three methods (UPGMA, single linkage and complete linkage) revealed that essential oil composition of *S. montana* ssp. *montana* is more related to the one of *S. montana* ssp. *pisidica* than of *S. kitaibelii* (Fig. 3).

Our results contribute to the better knowledge of the chemotaxonomic structure of this polymorphic genus from the central part of the Balkan peninsula — and particularly the specificity of the species *S. kitaibelii*.

3. Experimental

3.1. Plant material

The plant material was collected from the following localities: *S. montana* ssp. *pisidica* (Wettst.) Silic from the

Table 1
Basic characteristic of localities

Locality	H[a] (m)	N[b] (°)	E[c] (°)	Exposition	Substrate	Climate	Studied species
Beli Rzav gorge	600	43.7	19.2	S	Limestone	Sub-mediterranean	*S. montana* ssp. *montana*
Zvornik area	200	44.2	19.0	SE	Limestone	Sub-mediterranean	*S. montana* ssp. *montana*
Galicica mountain	1800	40.9	20.9	E	Limestone	Sub-med. montane	*S. montana* ssp. *pisidica*
Jelasnica gorge	400	43.2	22.0	SW	Limestone	Sub-mediterranean	*S. kitaibelii*

[a] H = height above sea level.
[b] N = north geographical latitude.
[c] E = east geographical longitude.

Table 2
Composition of essential oils of studied populations of *Satureja montana* and *Satureja kitaibelii*

	Satureja montana ssp. *montana*		*Satureja montana* ssp. *pisidica*	*Satureja kitaibelii*
Compound	Beli Rzav gorge	Zvornik area	Galicica mountain	Jelasnica gorge
1. α-Pinene	**1.5** (0.9)[a]	**3.6** (2.7)	**0.9** (0.5)	**6.0** (2.5)
2. Camphene	**2.2** (1.3)	**1.9** (1.2)	**1.1** (0.9)	**3.7** (1.2)
3. β-Pinene	**0.8** (0.5)	**1.3** (1.1)	**1.1** (1.4)	–
4. Myrcene	**1.2** (0.6)	**1.9** (1.6)	**1.3** (0.6)	**1.0** (0.5)
5. α-Terpinene	**0.9** (0.5)	**2.5** (3.0)	**0.8** (0.4)	–
6. Limonene	**2.0** (1.7)	**4.5** (2.8)	**0.6** (0.5)	**16.0** (7.5)
7. (z)-β-Ocimene	**3.0** (2.6)	**2.8** (2.1)	**1.9** (1.6)	–
8. γ-Terpinene	**4.9** (3.6)	**5.0** (3.6)	**6.2** (3.3)	**2.0** (1.4)
9. ρ-Cymene	**18.8** (12.2)	**13.3** (12.2)	**29.3** (15.8)	**20.9** (8.2)
10. t-Sabinene hyd.	**7.2** (7.5)	**9.3** (9.7)	**1.6** (2.0)	**8.2** (8.7)
11. Linalool	**22.8** (23.8)	**8.1** (10.7)	**24.0** (17.7)	**1.6** (1.0)
12. Terpinen-4-ol	**2.6** (2.4)	**5.9** (4.3)	**2.4** (2.9)	**3.8** (3.0)
13. β-Caryophyllene	**0.1** (0.2)	–	**1.1** (0.9)	–
14. Borneol	**10.6** (7.5)	**7.1** (3.5)	**4.6** (8.3)	**9.8** (3.3)
15. ρ-Cymen-8-ol	**3.7** (5.7)	**8.6** (8.0)	**1.3** (2.3)	**0.7** (0.5)
16. $C_{15}H_{26}O$	**2.0** (0.9)	**3.0** (1.6)	**1.8** (0.8)	**3.9** (2.0)
17. $C_{15}H_{26}O$	**1.9** (0.9)	**1.3** (0.8)	**1.0** (0.7)	**2.4** (1.5)
18. Thymol	**0.7** (1.0)	**1.9** (3.0)	**1.5** (1.4)	**0.9** (0.6)
19. Carvacrol	**0.4** (0.2)	**1.1** (0.9)	**18.3** (16.1)	–
Monoterpene comp.	84.3	78.8	95.9	74.6
Monoter. hydrocarbons	35.3	36.8	42.2	49.6
Oxygenated monoterp.	49.0	42.0	53.7	25.0
Alcohols	43.2	30.4	32.6	23.4
Phenols	5.8	11.6	21.1	1.6
Sesquiterpene comp.	4.3	4.3	3.9	6.3
Sesquit. hydrocarbons	0.4	–	1.1	–
Oxygenated sesquit.	3.9	4.3	2.8	6.3
Total	88.6	83.1	99.8	80.9

[a] Average value in bold; standard deviation in parentheses.

mountain Galicica — the south-western Macedonia; *S. montana* ssp. *montana* from the surroundings of Zvornik and the gorge of the river Beli Rzav — western Serbia; *S. kitaibelii* Wierzb. ex Heuff. from the gorge of the river Jelasnica — eastern Serbia (Fig. 1). Basic characteristics of the mentioned localities are given in Table 1. From each locality 30 plants were collected, picked in the period of blooming.

3.2. Steam distillation

The dried aerial part of each individual was submitted to the steam distillation with simultaneous extraction of the distillate by methylene-chloride (CH_2Cl_2), which enabled the separation of the essential oil. For this procedure the Likens–Nickerson apparatus was used (Maarse and Belz, 1981).

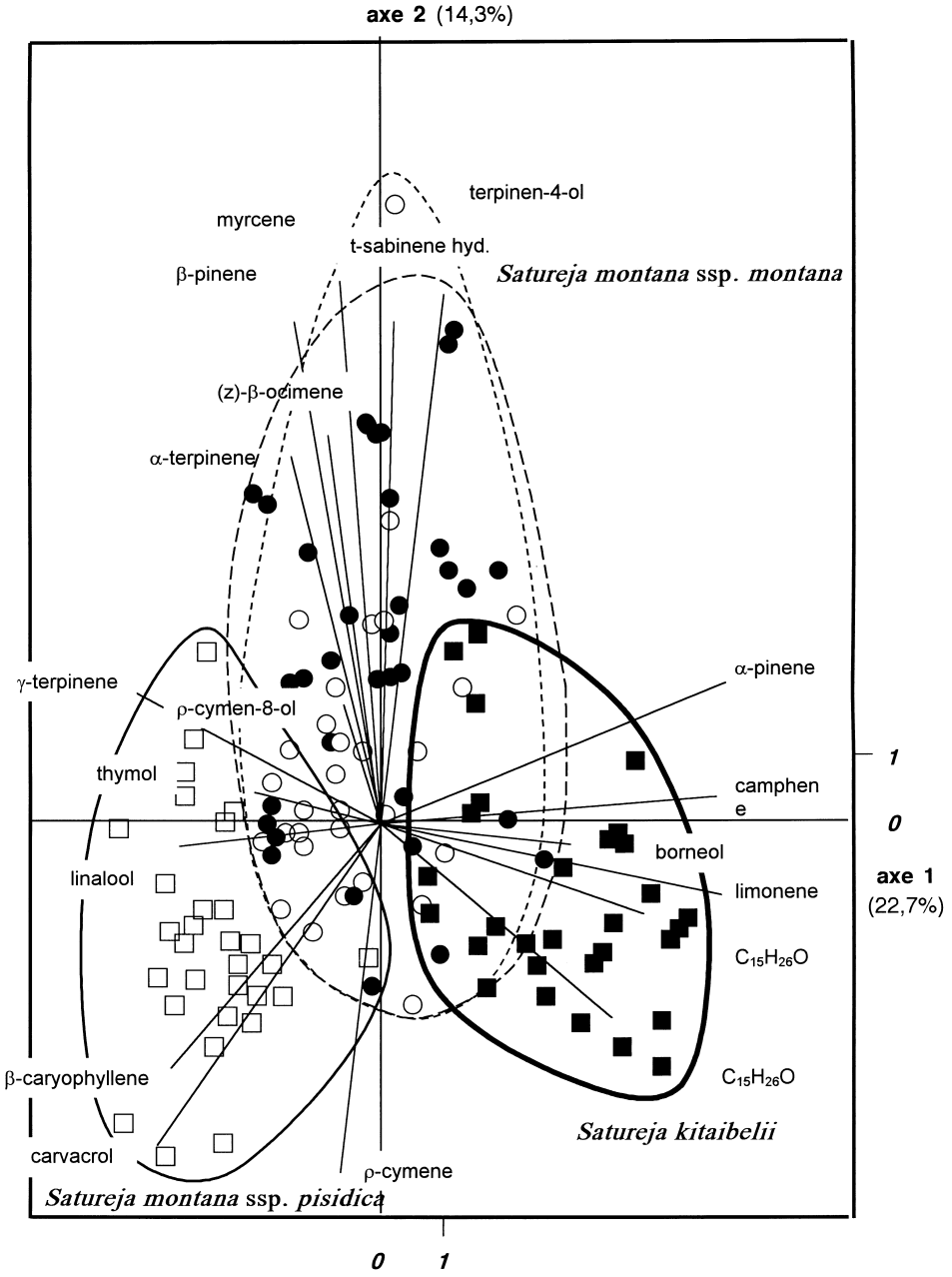

Fig. 2. PCA — graphical review of observations grouped in characters and individuals in the plan of the first two axes. ○, *Satureja montana* ssp. *montana*; Beli Rzav; ●, *Satureja montana* ssp. *montana*; Zvornik; □, *Satureja montana* ssp. *pisidica*; Galicica; ■, *Satureja kitaibelii*, Jelasnica. The space containing all the individuals of one populations is approximately bordered with a line.

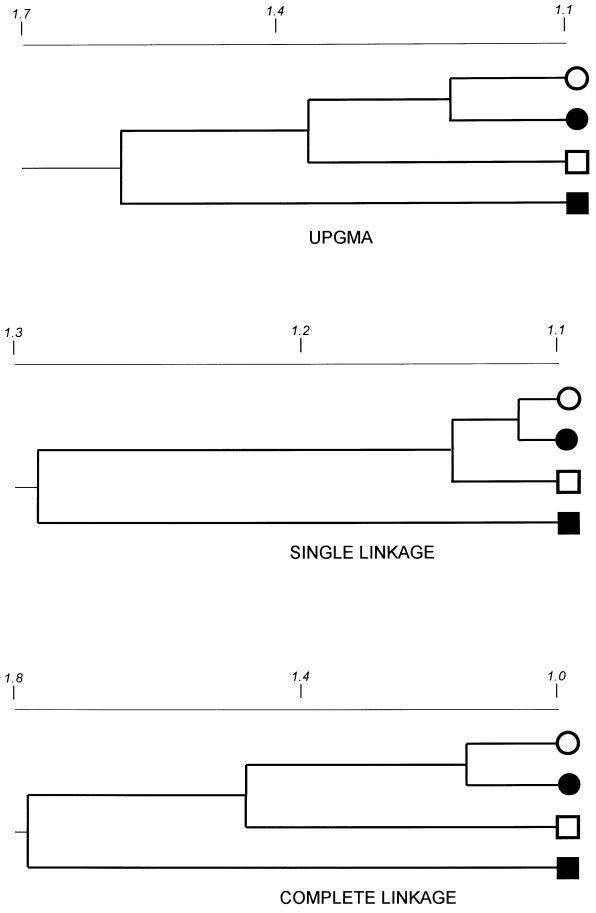

Fig. 3. Cluster analyses of *Satureja montana* and *Satureja kitaibelii* based on population means of essential oils. ○, *Satureja montana* ssp. *montana*; Beli Rzav; ●, *Satureja montana* ssp. *montana*; Zvornik; □, *Satureja montana* ssp. *pisidica*; Galicica; ■, *Satureja kitaibelii*, Jelasnica.

3.2.1. Combined GC–MS

The qualitative and quantitative analysis of the essential oils were done by GC and GC/MS under the following conditions: Analytical GC-A Varian model 3400 gas chromatograph equipped with a split/splitless injector (250°C), and a 30 m×0.32 mm DB-Wax silica capillary column and FID (300°C), were used for GC and GC/MS masurements. The column was temperature programmed from 50°C (3 min) to 200°C at 10°C/min; carrier gas 3 ml H_2/min. Peak areas were calculated electronically by a Varian DS-604 data station. GC/MS — the gas chromatograph was connected via an open split interface, and a fused silica capillary (at 250°C) to the ion source of a Finnigan MAT 8230 mass spectrometer, equipped with a PDP 11/74 computer. Working conditions: carrier gas 2 ml He/min; other GC conditions as above. MS: ion source (electron impact), 170°C, 70 eV. Constituents were identified by co-injection with authentic compounds, and by comparison of their mass spectra to those from the MS library (Wiley, 1984) taking into account the relative retention times.

3.3. Statistical analysis

In data processing, the multivariatiate statistic analysis was applied (De Lagarde, 1983). The principal component analysis (PCA) was used as a statistical method capable to suggest the structure of the set and analysis of the variables in relation to the studied characteristics. In total, 19 characteristics (chemical compounds) were analyzed in 120 individuals.

The program Statgraphics 5.0 (Statistical Graphics Corporation, USA, 1991) was used. Agglomerative cluster analyses on population means for all essential oils used the UPGMA (unweighted pair-group method, arithmetic average), single-link and complete-link clustering methods of the SAHN procedure of the NTSYS-pc computer program (Rohlf, 1990).

Acknowledgements

Our special thanks go to Dr. Bruno Fady for his useful comments and suggestions, and to Danica Bajic, Institute of Chemistry, Technology and Metallurgy from Belgrade for the GC analysis.

References

Ball, P.W., Getliffe, F.M., 1972. *Satureja* L. In: Tutin, G.T., Heywood, H.V., Burges, A.N., Moore, D.M., Valentine, H.D., Walters, M.S., Webb, A.D. (Eds.), Flora Europeae, Vol. 3. Cambridge University Press, Cambridge, pp. 163–165.

Briquet, I.J., 1893. Les *Labiées* des Alpes Maritimes. Genève & Bâle.

Cantino, P.D., Harley, R.M., Wagstaff, S.J., 1992. Genera of *Labiatae*: *s*tatus and classification. In: Harley, M.R., Reynolds, T. (Eds.), Advances in *Labiate s*cience. Royal Botanic Gardens, Kew, pp. 511–522.

Chalchat, J., Gorunovic, S.M., Maksimovic, A.Z., 1999. Essential oil of *Satureja kitaibelii* Wierzb. f. *aristata* (Vand.) Hayek, *Lamiaceae* from Eastern Serbia. Journal of Essential Oil Research 11, 691–692.

De Lagarde, J., 1983. Initiation à l'analyse des données. Dunod, Paris.

Diklic, N., 1974. *Satureja* L. In: Josifovic, M. (Ed.), Flore de la République Socialiste de Serbie, Vol. 6. Académie Serbe des Sciences et des Arts, Beograd, pp. 455–458.

El-Gazzar, A., Watson, L., 1970. A taxonomic study of *Labiatae* and related genera. New Phytologist 69, 451–486.

Hayek, A., 1931. Prodromus florea peninsulae balcanicae. 2. Band *Dicotyledonae Sympetalae*. Dahlem bei Berlin.

Jancic, R., Stosic, D., Mimica-Dukic, N., Lakusic, B., 1995. Aromatic plants of Serbia. NIP Decije novine, Beograd-Gornji Milanovac.

Kustrak, D., Kuftinec, J., Blazevic, N., Maffei, M., 1996. Comparison of the essential oil composition of two subspecies of *Satureja montana*. Journal of Essential Oil Research 8, 7–13.

Maarse, H., Belz, R., 1981. Isolation, sepration, and identification of volatile compounds in aroma research. Academie-Verlag, Berlin.

Palic, M.R., Gasic, J.M., 1993. Hemijski sastav etarskog ulja biljaka roda *Satureja* L. Farmaceutsko-hemijska industrija "Zdravlje", Leskovac.

Ravarut, M., 1961. *Calamintha* Adans., *Satureja* L. & *Micromeria* Benth. In: Savulescu, T. (Ed.), Flora R.P. Romine, Vol. 8. Bucuresti, pp. 279–297.

Rohlf, F.J., 1990. NTSYS-pc, Version 1.60. Exeter Software, New York.

Sevarda, L.A., Kuznjecova, A.G., Pavlovic, S., Zivanovic, P., Jancic, R., 1986. Quantity and composition of essential oil and anatomic structure *Satureja montana* L. (*Lamiaceae*). Archiv of Pharmacy 36 (4), 167–175.

Sevarda, L.A., Kuznjecova, A.G., Zivanovic, P., Pavlovic, S., Vujcic, S., 1989. Essential oil configuration of some population of the species *Satureja kitaibelii* Wierzb. et Heuf. Archiv of Pharmacy 39 (5), 159–162.

Silic, C., 1979. Monographie der Gattungen *Satureja* L., *Calamintha* Miller, *Micromeria* Bentham, *Acinos* Miller und *Clinopodium* L. in der Flora Jugoslawiens. Zemaljski Muzej BiH, Sarajevo.

Stojanov, N., Stefanov, B., 1948. Flora na Blgaria. Blgarskata Akademija na naukite, Sofija.

Wiley, J., 1984. NBS Library.

PERGAMON

Phytochemistry 57 (2001) 77–89

PHYTOCHEMISTRY

www.elsevier.com/locate/phytochem

Prenylated flavonoids from *Deguelia hatschbachii* and their systematic significance in *Deguelia*

Aderbal F. Magalhães [a,*], Ana Maria G.A. Tozzi [b], Eva G. Magalhães [a], Valéria Regina de Souza Moraes [a]

[a] *Departamento de Química Orgânica, Instituto de Química, UNICAMP, CP 6154, Campinas, 13083-970, São Paulo, Brazil*
[b] *Departamento de Botânica, Instituto de Biologia, UNICAMP CP 6154, Campinas, 13083-970, São Paulo, Brazil*

Received 30 December 1999; received in revised form 14 November 2000

Dedicated to Professor Otto Richard Gottlieb on the occasion of his 80th birthday

Abstract

Chemical investigation of dichloromethane and petrol extracts from the roots of *D. hatschbachii* A. M. G. Azevedo furnished thirteen compounds from which five are described for the first time and their structures were determined to be 3-(4′-hydroxyphenyl)-5-methoxy-6-(3,3-dimethylallyl)-2″,2″-dimethylchromene-(5″,6″:8,7)-3-(propyl-2-one)-4H-1-benzo-2,3-dihydropyran-2,4-dione; 6,4′-dihydroxy-3-(3,3-dimethylallyl)-2″,2″-dimethylchromene (5″,6″:5,4)-2-methoxy deoxybenzoin; 6,4′-dihydroxy-3-(3,3-dimethylallyl)-2″,2″-dimethylchromene (5″,6″:5,4)-2-methoxy-8-(propyl-2-one) deoxybenzoin; 6-(3,3-dimethylallyl)-2″,2″-dimethylchromene (5″,6″:4,5)-4′-hydroxy-3-methoxy stilbene and 3,5-dimethoxy-4′-hydroxy-4-(3,3-dimethylallyl) stilbene by spectral analysis (UV, IR, MS and 1D- and 2D- NMR experiments). The root extracts and some isolated compounds were bioactive, as revealed by bioautography and brine shrimp lethality assays. © 2001 Elsevier Science Ltd. All rights reserved.

Keywords: *Deguelia hatschbachii*; Leguminosae; Flavonoids; Stilbenes; Deoxybenzoins; 4-Hydroxy-3-phenylcoumarins; Flavanones; Isoflavones; Lupeol; Bioassays

1. Introduction

The genus *Deguelia* Aubl. belongs to the family Leguminosae, subfamily Papilionoideae, tribe Millettieae (Geesink, 1984; Tozzi, 1989, 1994, 1998). In this tribe are included some tropical trees and lianas, mainly of the genera *Lonchocarpus* Kunth, *Derris* Lour. and *Millettia* Wight. & Arn., in which the definition of natural groupings remains problematic. Since these genera were established, their circumscription and infrageneric classification have been modified by several authors. Geesink (1984), in his study of the Millettieae based on cladistic analyses, proposed many changes. Thus he elevated some sections to the generic level, as *Derris* sect. *Paraderris* Miq., and reinstated the genera *Brachypterum* (Wight & Arn.) Benth., *Deguelia* and *Philenoptera* A. Richard. In this sense, *Derris*, *Lonchocarpus* and *Millettia* received a more restricted treatment. This taxonomic analysis has been adopted with some modifications (Tozzi, 1989, 1992, 1994, 1995, 1998). Accordingly the generic delimitation of *Deguelia* now comprises those species previously belonging to *Lonchocarpus* subg. *Phacelanthus* Pittier (= *Lonchocarpus* ser. *Fasciculati* Benth.) and American *Derris* and *Millettia*. Analogously *Lonchocarpus* has been defined by Geesink's (1984) concept, enlarged by the inclusion of some species with panicles that should be classified in the genus *Philenoptera*. *Deguelia* and *Lonchocarpus* species can be recognized by the habit, the inflorescence structure and morphological characters of the flowers and fruits.

Deguelia comprises 20 species, which are found in tropical South America. Based on analysis of their morphological characters, two sections were recognized for *Deguelia*. *Deguelia* sect. *Multiovulis* A.M.G. Azevedo comprises five species and *Deguelia* Aubl. sect. *Deguelia* has the 15 remaining species. It has been suggested that flavonoid profiles might help to elucidate the problematic differentiation of the genera of the tribe Millettieae and their phylogenetic relationship (Gomes et al., 1981; Gottlieb et al., 1981; Gottlieb, 1982). The "potentiality of

* Corresponding author. Tel.: +55-197-883-064; fax: +55-197-883-023.
E-mail address: aderbal@iqm.unicamp.br (A.F. Magalhães).

0031-9422/01/$ - see front matter © 2001 Elsevier Science Ltd. All rights reserved.
PII: S0031-9422(00)00509-4

flavonoid characters to aid in taxonomic revision'' has been recently recognized (Harborne, 2000).

Chemical reports about flavonoid composition have been published for 35 species of *Derris* or *Lonchocarpus*, from which eight species are now included in *Deguelia*.

The flavonoid profiles furnished by some *Deguelia* species (Table 1) consist mainly of isoflavonoids. Among *Deguelia* isoflavonoids, a high incidence of rotenoids is found in *Deguelia* sect. *Deguelia* species while 4-hydroxy-3-phenylcoumarins predominate in *Deguelia* sect. *Multiovulis* species.

It is well known that many isoflavonoids have antimicrobial and insecticidal activities (Dewick, 1988), which can be respectively evaluated through bioautography (Saxena et al., 1995) and brine shrimp lethality assays (McLaughlin et al., 1995).

Deguelia hatschbachii A.M.G.Azevedo is a new species native to Brazil that was recently classified in *Deguelia* sect. *Multiovulis*.

We have undertaken a phytochemical study of roots extracts of *Deguelia hatschbachii* in order to evaluate whether its flavonoid profile can be used to complement morphological data in studies of taxonomy and phylogeny.

2. Results and discussion

Petrol and dichloromethane extracts of *D. hatschbachii* roots were submitted to chromatographic analysis (column, TLC and prep. TLC), allowing the isolation of ten flavonoids **(1, 2a–b, 3a–b, 4a–b, 5–7)**, two stilbenes **8,9** and lupeol **10**. Flavonoids **5–7** and stilbenes **8–9** are new compounds (Fig. 1).

Scandenin **(1)** (Garcia et al., 1986), robustic acid **(2a)** (Khalid and Waterman, 1983; Donnelly et al., 1995), robustic acid methyl ether **(2b)** (East et al., 1969; Olivares et al., 1982); 4′,5- dihydroxy-6-(3,3-dimethylallyl)-7-methoxy flavanone **(3a)** (Mahmoud and Waterman, 1985), lupinifolin **(3b)** (Mahidol et al., 1997), osajin **(4a)** (Delle Monache, et al., 1994), scandinone **(4b)** (Sekine et al., 1999) and lupeol **(10)** (Wenkert et al., 1978; Lehn and Ourisson, 1962; Budzikiewicz et al., 1963) were characterized by comparison of the respective spectral data with literature values.

Compound **5** was a new flavonoid. Its HREIMS showed a molecular ion $[M]^+$ of *m*/*z* 490.1989, corresponding to $C_{29}H_{30}O_7$ (required M^+ 490.1991). The ^1H and ^{13}C NMR spectral data indicated that A and B rings are similar to those in scandenin **1** (Tables 2 and 3). However, the ^1H NMR spectrum showed two sets of one-proton doublets at δ 3.87 ($J = 18.1$ Hz) and 3.53 ($J = 18.1$ Hz) assignable to diastereotopic methylene hydrogens, while a singlet at δ 2.20 (3H) was compatible with the expected resonance for an acetyl or acetate methyl group. It should be mentioned that the two sets of one-proton double doublets at δ 3.27 ($J = 13.9$ and 7.2 Hz) and 3.21 ($J = 13.9$ and 7.2 Hz) assignable to the methylene hydrogens of 3,3-dimethylallyl group is also evidence that **5** is chiral, which was further confirmed by optical rotation measurements. On the other hand, a signal corresponding to the hydrogen of the hydroxyl at C-4 of scandenin **1** was not observed, while the ^{13}C NMR spectrum showed typical carbonyl signals at δ 205.9, 187.6 and 169.1, respectively, corresponding to an alkyl ketone; an α,β- unsaturated ketone and a phenyl acetate groups, which was reinforced by the presence of strong absorptions at ν_{max} 1704, 1682 and 1770 cm^{-1} in the IR spectrum. The DEPT spectrum showed six CH_3, two CH_2, seven CH and fourteen quaternary carbons. The carbon signal at δ 61.4 was assigned to C-3. The EIMS showed a peak of *m*/*z* 300 (38%) corresponding to a fragment furnished by retro-Diels Alder cleavage of C-ring such as was previously observed for scandenin **1**. However, instead of a peak of *m*/*z* 134 representing the B-ring fragment, there was a fragment of *m*/*z* 190 (5%) suggesting that in compound **5** the corresponding fragment is 56 a.m.u. higher and must be attached to C-3. According to the NMR spectra discussed above, it is a propyl-2-one group and C-3 is chiral. These findings were further confirmed by extensive 2D- NMR experiments as well from the enhancements observed in the NOE difference spectrum (Fig. 2). In the HMBC spectrum, $^3J_{C\text{-}H}$ correlations between methylene hydrogens of propyl-2-one group with C-1′, C-2 and C-4 carbons as well as those observed between C-3 and H-2′, H-6′ hydrogens are especially illustrative concerning C-ring constitution. Based on MS/MS experiments selecting the ions of *m*/*z* 475 [285 (100%)], *m*/*z* 300 [285 (100%), 269 (5%), 257 (54%), 245 (25%)], *m*/*z* 257 [242 (20%)] and *m*/*z* 190 [147 (100%), 119 (48%)] we can suggest a fragmentation pathway for this compound (Fig. 3).

Compound **5** represents the first example of a 4-hydroxy-3-phenylcoumarin derivative where the corresponding β-keto ester tautomer is fixed by the presence of a substitute on C-3.

In the ^1H and ^{13}C NMR spectra of compound **6,** typical signals of a 3,3-dimethylallyl group, a dimethylchromene ring, an aromatic methoxyl group and a *para*-substituted aromatic ring were observed (Tables 2 and 3). In addition, singlets at δ 13.20 (1H) and 4.32 (2H), in the ^1H NMR spectrum, correspond to the absorptions of a hydrogen bonded hydroxyl and α-methylene hydrogens of a deoxybenzoin derivative (Kiuchi et al., 1990), which was confirmed by the presence of a carbonyl carbon signal at δ 203.6 and a methylene carbon signal at δ 47.6 in the ^{13}C NMR spectrum. Other signals in the ^{13}C NMR spectrum were compatible and DEPT (90° and 135°) experiments showed the presence of five CH_3, two CH_2, seven CH and eleven quaternary carbons. While these data lead to three structural possibilities [**6** (Fig. 1); **6a** and **6b** (Fig. 4)], the NOE difference spectral data

Table 1
Number and class of compounds furnished by *Deguelia* species

	Flavonoids			Isoflavonoids							
	Stilbene	Chalcone	Flavanone	Isoflavanone	3-Phenylcoumarin	Pterocarpan	Isoflavan	Isoflavone	Deoxybenzoin	Rotenoid	Ref.
Deguelia sect. *Deguelia* species											
D. rufescens var. urucu [a]	3	3	4	2	–	1	–	–	–	5	Gottlieb et al., 1981; Filho et al., 1975a; Fang and Casida, 1999
D. nitidula [b]	2	5	1	–	–	–	–	–	–	–	Gottlieb et al., 1981; Filho et al., 1975a
D. rariflora [c]	1	–	2	–	–	–	–	–	–	–	Filho et al., 1975b
D. negrensis [d]	–	–	–	–	–	–	–	–	–	6	Gottlieb et al., 1981; Vasconcelos and Maia, 1976
D. amazonica [e]	–	–	–	–	–	1	1	–	–	–	Filho et al., 1975a
D. utilis[f]	3	2	4	2	–	–	–	–	–	2	Fang and Casida, 1999
Deguelia sect. *Multiovulis* species											
D. spruceana [g]	1	–	–	–	3	–	–	1	–	–	Garcia et al., 1986
D. densiflora [h]	–	–	–	–	2	–	–	2	–	–	Delle Monache et al., 1977
D. hatschbachii	2	–	2	–	4	–	–	2	2	–	–

[a] Sinonimia: *Lonchocarpus urucu, Derris urucu* and *Lonchocarpus nicou* var. *urucu*.
[b] *Lonchocarpus floribundus, Derris floribunda* and *Lonchocarpus nitidulus*.
[c] *Derris rariflora* and *Lonchocarpus rariflorus*.
[d] *Lonchocarpus longifolius, Derris longifolia, Deguelia longifolia, Lonchocarpus killipii* and *Derris negrensis*.
[e] *Derris amazonica* and *Lonchocarpus negrensis*.
[f] *Lonchocarpus utilis*.
[g] *Derris spruceana* and *Lonchocarpus spruceanus*.
[h] *Derris glabrescens, Lonchocarpus glabrescens, Lonchocarpus boliviensis* and *Lonchocarpus densiflorus*.

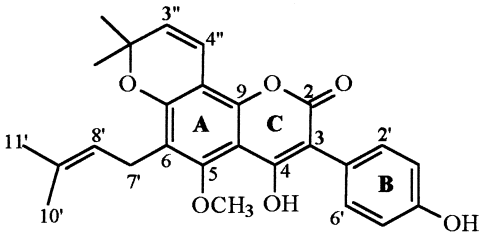

(1) *Scandenin*

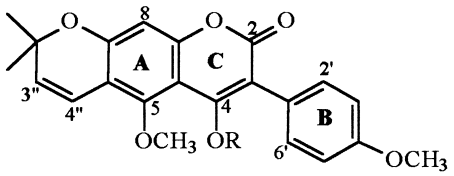

(2a) R= H, *Robustic acid*
(2b) R= CH_3, *Robustic acid methyl ether*

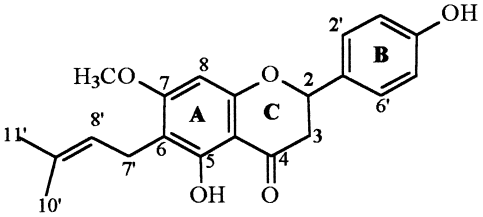

(3a)

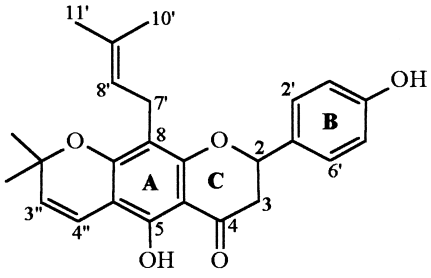

(3b) *Lupinifolin*

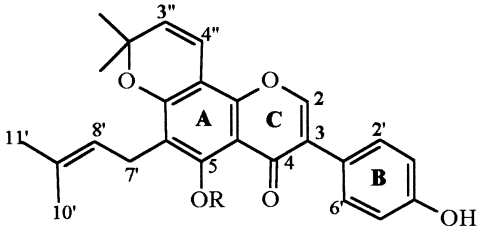

(4a) R= H, *Osajin*
(4b) R=CH_3, *Scandinone*

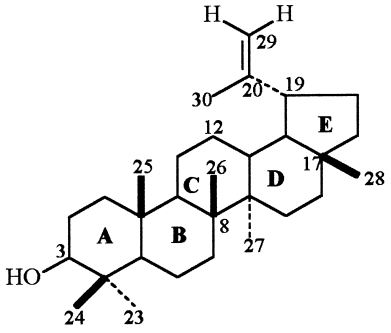

(10) *Lupeol*

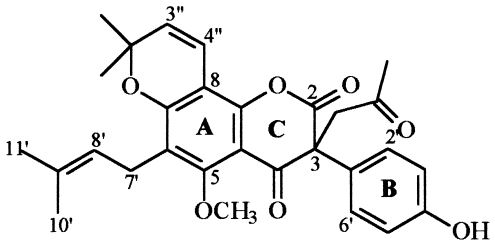

(5)*

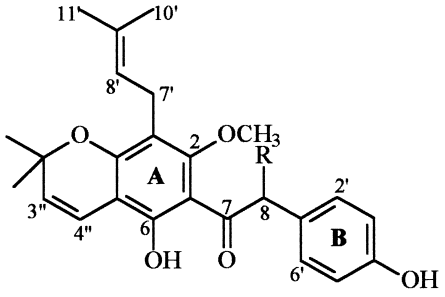

(6)* R=H
(7)* R= CH_2COCH_3

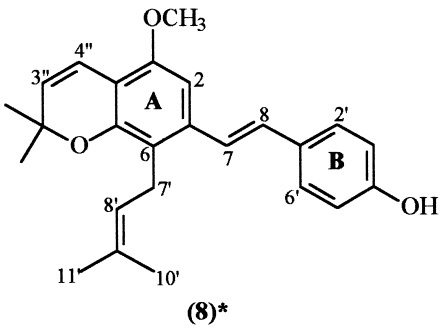

(8)*

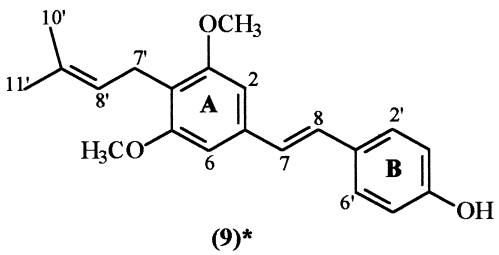

(9)*

Fig 1. Compounds isolated from *Deguelia hatschbachii*. (* New compounds.)

Table 2
^{1}H NMR spectroscopy values for compounds **5**, **6**, **7**, **8** and **9**

H	**5** (δ)[a]	**6** (δ)[b]	**7** (δ)[b]	**8** (δ)[b]	**9** (δ)[b]
CH_2COCH_3	3.87 (1H, *d*, *J* = 18.1 Hz)	–	3.50 (1H, *dd*, *J* = 17.8, 10.5 Hz)	–	–
	3.53 (1H, *d*, *J* = 18.1 Hz)	–	2.57 (1H, *dd*, *J* = 17.8, 4.0 Hz)	–	–
CH_2COCH_3	2.20 (3H, *s*)	–	2.12 (3H, *s*)	–	–
H-2	–	–	–	6.59 (1H, *s*)	6.67 (1H, *s*)
H-6	–	–	–	–	6.67 (1H, *s*)
H-7	–	–	–	6.84 (1H, *d*, *J* = 16.6 Hz)	6.90 (1H, *d*, *J* = 16.3 Hz)
H-8	–	4.32 (2H, *s*)	5.34 (1H, *dd*, *J* = 10.5, 4.0 Hz)	7.15 (1H, *d*, *J* = 16.6 Hz)	7.00 (1H, *d*, *J* = 16.3 Hz)
6-OH	–	13.20 (1H, *s*)	12.89 (1H, *s*)	–	–
2′ and 6′	7.10 (2H, *d*, *J* = 8.9 Hz)	7.12 (2H, *d*, *J* = 8.5 Hz)	7.05 (2H, *d*, *J* = 8.4 Hz)	7.32 (2H, *d*, *J* = 8.6 Hz)	7.40 (2H, *d*, *J* = 8.6 Hz)
3′ and 5′	6.70 (2H, *d*, *J* = 8.9 Hz)	6.80 (2H, *d*, *J* = 8.5 Hz)	6.61 (2H, *d*, *J* = 8.4 Hz)	6.75 (2H, *d*, *J* = 8.6 Hz)	6.80 (2H, *d*, *J* = 8.6 Hz)
7′	3.27(1H, *dd*, *J* = 13.9, 7.2 Hz)	3.25 (2H, *d*, *J* = 6.9 Hz)	3.16 (1H, *dd*, *J* = 14.5, 7.0 Hz)	3.34 (2H, *d*, *J* = 6.8 Hz)	3.34 (2H, *d*, *J* = 7.0 Hz)
	3.21 (1H, *dd*, *J* = 13.9, 7.2 Hz)		3.03 (1H, *dd*, *J* = 14.5, 7.0 Hz)		
8′	5.07 (1H, *td*, *J* = 7.2, 1.2 Hz)	5.17 (1H, *td*, *J* = 6.9 Hz)	5.02 (1H, *m*)	5.06 (1H, *m*)	5.18 (1H, *td*, *J* = 7.0, 1.3 Hz)
10′	1.75 (3H, *s*)	1.79 (3H, *s*)	1.66 (3H, *s*)	1.75 (3H, *s*)	1.77 (3H, *s*)
11′	1.64 (3H, *s*)	1.70 (3H, *s*)	1.58 (3H, *s*)	1.61 (3H, *s*)	1.66 (3H, *s*)
3″	5.65 (1H, *d*, *J* = 10.1 Hz)	5.51 (1H, *d*, *J* = 10.0 Hz)	5.37 (1H, *d*, *J* = 10.1 Hz)	5.50 (1H, *d*, *J* = 9.8 Hz)	–
4″	6.74 (1H, *d*, *J* = 10.1 Hz)	6.66 (1H, *d*, *J* = 10.0 Hz)	6.53 (1H, *d*, *J* = 10.1 Hz)	6.60 (1H, *d*, *J* = 9.8 Hz)	–
3-OCH_3	–	–	–	3.79 (3H, *s*)	3.86 (3H, *s*)
5-OCH_3	3.73 (3H, *s*)	–	–	–	3.86 (3H, *s*)
2-OCH_3	–	3.74 (3H, *s*)	3.69 (3H, *s*)	–	–
CH_3-2″	1.46(3H, *s*)	1.44 (3H, *s*)	1.34 (3H, *s*)	1.34 (3H, *s*)	–
CH_3-2″	1.45 (3H, *s*)	1.44 (3H, *s*)	1.29 (3H, *s*)	1.34 (3H, *s*)	–

[a] ^{1}H NMR (500 MHz).
[b] ^{1}H NMR (300 MHz).

Table 3
^{13}C NMR spectroscopy values (75 MHz, $CDCl_3$) for compounds **5**, **6**, **7**, **8** and **9**

C	**5** (δ)	**6** (δ)	**7** (δ)	**8** (δ)	**9** (δ)
$CH_2\underline{C}OCH_3$	205.9	–	207.6	–	–
$\underline{CH_2}COCH_3$	51.7	–	47.7	–	–
$\overline{CH_2}CO\underline{CH_3}$	28.9	–	30.0	–	–
1	–	131.2	131.1	136.7	136.4
2	169.1	160.6	160.4	99.6	102.1
3	61.4	108.5	108.0	155.1	158.1
4	187.6	154.4	154.7	120.6	117.9
5	159.3	115.0	115.1	153.2	158.1
6	106.4	158.8	158.6	110.2	102.1
7	158.3	203.6	204.4	124.9a[a]	127.4 b
8	120.8	47.6	49.7	128.6a	127.2 b
9	148.9	–	–	–	–
10	105.7	–	–	–	–
1′	126.0	106.0	105.8	130.4	130.3
2′ and 6′	127.8	130.9	129.3	127.8	127.8
4′	155.9	158.5	158.2	151.2	155.1
3′ and 5′	116.2	115.3	115.5	115.6	115.6
7′	22.0	22.3	22.3	24.3	22.3
8′	122.2	123.1	123.2	123.5	122.7
9′	131.6	127.5	130.9	130.7	131.1
10′	17.9	17.9	17.9	18.0	17.7
11′	25.7	25.7	25.7	25.7	25.8
2″	78.3	77.9	77.7	75.6	–
3″	115.3	116.0	116.0	117.1	–
4″	129.1	126.7	126.4	129.0	–
CH_3-2″	28.5	28.3	28.3	27.5	–
CH_3-2″	28.4	28.3	28.3	27.5	
2-O$\underline{CH_3}$	–	63.0	63.4	–	–
3-O$\underline{CH_3}$	–	–	–	55.6	55.8
5-O$\underline{CH_3}$	62.1	–	–	–	55.8

[a] a,b, Interchangeable values.

(Fig. 2) correspond to structure **6**. The EIMS displayed a molecular ion $[M]^+$ of m/z 408 (3%) suggesting the molecular formula $C_{25}H_{28}O_5$. The base peak of m/z 69 (100%) and those of m/z 301 (32%) and m/z 107 (15%), respectively, correspond to an isoprenyl cation as well as a fragment resulting from C_7-C_8 bond cleavage (Fig. 5). UV (λ_{max} 266 nm) and IR (ν_{max} 1700.1 cm^{-1}) spectral data were also in agreement with structure **6**.

Compound **6** was detected in the dichloromethane extract by HPLC, indicating that it is not an artifact produced from hydrolysis followed by decarboxylation of scandenin **1**, during the isolation process. Moreover we found that scandenin **1** remained unchanged after it was left in an alcoholic solution of potassium hydroxide under reflux (Uma Rani and Darbarwar, 1987). These results lead us to suggest that scandenin **1** is the biogenetic precursor of compound **6**.

Compound **7** showed a molecular ion $[M]^+$ of m/z 464 (16%), in the EIMS, suggesting the molecular formula $C_{28}H_{32}O_6$. This time, the base peak (m/z 301) corresponds to the fragment including ring A, originating from C_7–C_8 bond cleavage (Fig. 5). The presence of a 3,3-dimethylallyl group, a dimethylchromene ring, an aromatic methoxyl group and a *para*-substituted aromatic ring were deduced from their NMR spectral data (Tables 2 and 3), which were closely related to those of compound **6**. However, instead of a resonance for the hydrogens of a methylene group, three double doublets at δ 5.34 (J = 10.5, 4.0 Hz), 3.50 (J = 17.8, 10.5 Hz) and 2.57 (J = 17.8, 4.0 Hz) assignable to an ABX system were observed, while a singlet at δ 2.12 (3H) indicated the presence of an acetyl or acetate methyl group. In addition, the ^{13}C NMR spectrum showed two carbonyl signals at δ 207.6 and 204.4, respectively, corresponding to an alkyl ketone and an α,β-unsaturated ketone. In the ^1H NMR spectrum, the presence of the two sets of one-proton double doublets at δ 3.16 (J = 14.5, 7.0 Hz) and 3.03 (J = 14.5, 7.0 Hz), assignable to the methylene hydrogens of a 3,3-dimethylallyl group, also indicated that **7** is chiral. The ^{13}C NMR spectrum (Table 3) is totally compatible, showing signals for the presence of six CH_3, two CH_2, eight CH and twelve quaternary carbons, confirmed by DEPT (90° and 135°) experiments. These data are compatible with three structures [**7** (Fig. 1); **7a** and **7b** (Fig. 4)]; the CycleNOE experiments lead us to structure **7** (Fig. 2).

By analogy to compound **6**, we suggest that compound **7** is biogenetically derived from compound **5**; the natural occurrence of deoxybenzoin derivatives is rarely found.

The HREIMS for compound **8,** showed a molecular ion $[M]^+$ of m/z 376.2039 consistent with the molecular formula $C_{25}H_{28}O_3$ (376.2038). In the ^1H NMR spectrum, two one-proton doublets at δ 7.15 (J = 16.6 Hz) and 6.84 (J = 16.6 Hz) were observed, these being typical of olefinic hydrogens in *trans*-stilbenes; an AA′BB′ system at δ 7.32 (2H, *d*, J = 8.6 Hz) and 6.75 (2H, *d*, J = 8.6 Hz) was also noted this being ascribed to hydrogens of a *para*-substituted aromatic ring. The spectrum also showed signals corresponding to the presence of a 3,3-dimethylallyl group, a dimethylchromene ring, an aromatic methoxyl group and an aromatic hydrogen (Table 2). The ^{13}C NMR spectrum and DEPT (90° and 135°) experiments showed the presence of nine quaternary carbons, ten CH, one CH_2 and three CH_3 groups (Table 3). These data are compatible with four structural possibilities [**8** (Fig. 1); **8a**, **8b** and **8c** (Fig. 6)] by taking into account the oxidation pattern of A-ring originating from stilbene biosynthesis (Norin, 1989).

Structure **8b** can be eliminated because in the NOE difference spectrum, irradiation of methylene hydrogens at δ 3.34 (H-7′) caused an enhancement of H-3″ (δ 5.50; 0.9%), H-8′ (δ 5.06; 3.4%), H-10′ (δ 1.75; 5.1%) and H-7 (δ 6.84; 7.9%) signals. In the ^{13}C NMR spectrum, the signal for the methoxyl group was at δ55.6, and since that *ortho*-disubstituted methoxyl groups absorb around δ 60.0 (Agrawal, 1989), structure **8a** does not fit. In the ^1H NMR spectrum, the signal at δ 6.59 (1H) is not in agreement with H-4 such as in **8c**, because in lonchocarpene (Kaouadji, 1988; Kaouadji et al., 1986) the H-2

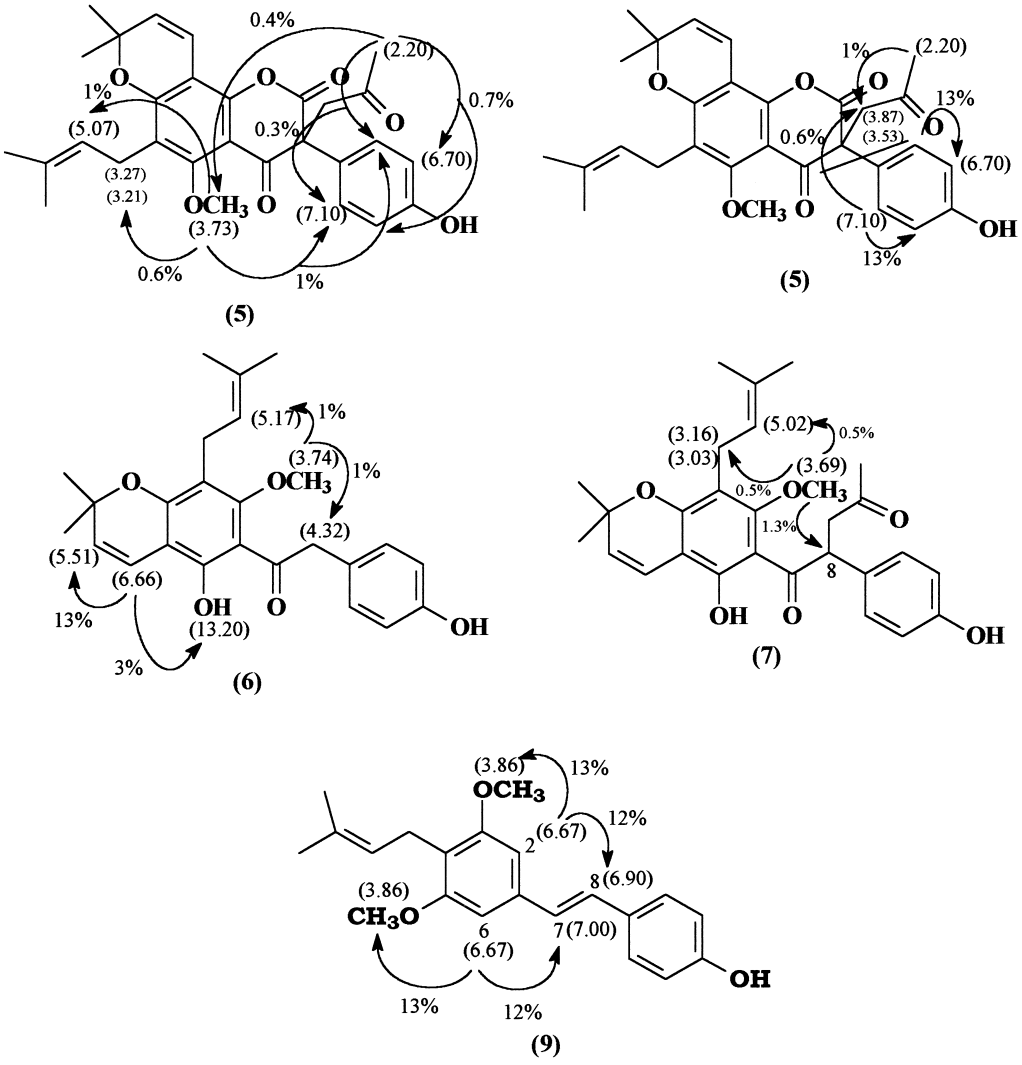

Fig. 2. NOE effects observed for some compounds isolated from *Deguelia hatschbachii*.

and H-4 signals resonate at δ 6.63 and 6.37, respectively. The main peaks observed in the EIMS represent the molecular ion $[M]^+$ of *m/z* 376 (21%) and loss of methyl radical of *m/z* 361 (100%). UV (λ_{max} 330 nm) and IR (ν_{max} 959.6 cm^{-1}) spectral data were also in agreement.

The HREIMS for compound **9,** showed a molecular ion $[M]^+$ of *m/z* 324.1725 consistent with the molecular formula $C_{21}H_{24}O_3$ (324.1725). The ^1H NMR spectrum (Table 2) showed a pair of doublets corresponding to a chain of a *trans*-stilbene derivative and an AA′BB′ system as observed for compound **8**. In addition, the spectrum showed typical resonances for a 3,3-dimethylallyl group and two singlets assigned to two equivalent aromatic hydrogens and two equivalent methoxyl groups. These findings indicate structure **9**, which was supported by NOE difference spectral data (Fig. 2). The ^{13}C NMR spectrum (Table 3) is also compatible with this proposition, where the presence of four CH_3, one CH_2 and nine CH groups, and seven quaternary carbons was confirmed by DEPT (90° and 135°) experiments. The EIMS showed a molecular ion $[M]^+$ of *m/z* 324 (100%) and the peaks of *m/z* 309 (93%) and *m/z* 269 (10%) presumably originated from the loss of -CH_3 and -C_4H_7 radicals, respectively. The UV (λ_{max} 325 nm) and IR (ν_{max} 958 cm^{-1}) spectral data were also compatible with this assignment.

Although eight flavonoids were identified by HPLC analysis in the dichloromethane extract, only five were quantified, because the peaks corresponding to compounds **2b** and **5** coeluted and compound **6** had decomposed. Quantitative analysis showed that lupinifolin **3b** and scandenin **1** are the most abundant compounds in petrol and dichloromethane extracts (Table 4).

Thus the flavonoids of *D. hatschbachii* mainly consist of isoflavonoids, as observed for the *Deguelia* species previously investigated.

The occurrence of 4-hydroxy-3-phenylcoumarins in *D. hatschbachii* reinforces its inclusion in *Deguelia* sect. *Multiovulis*. That is, these data support the use of flavonoid characters in studies of taxonomy.

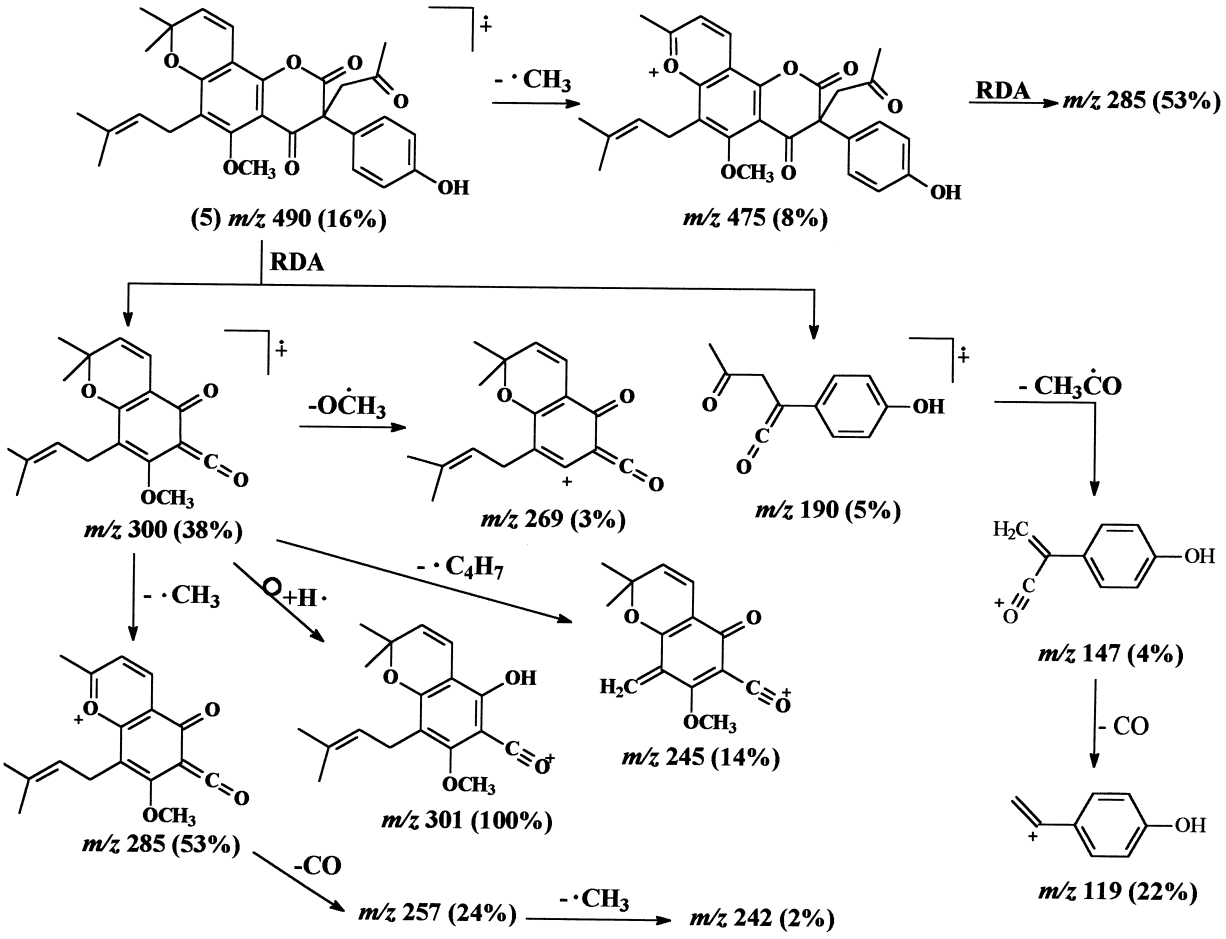

Fig. 3. Fragmentation pathway of compound **5**, based on MS/MS experiment.

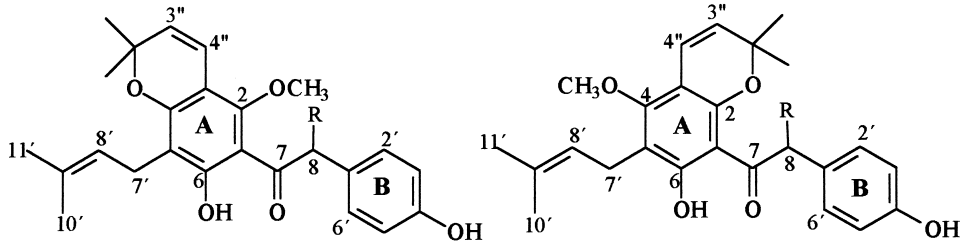

Fig. 4. Structural alternatives for compounds **6** and **7**.

Bioautography was performed according to Saxena et al. (1995) with some modification (Magalhães et al., 1998). Table 5 shows the results obtained with six *bacteria* and nine *fungi*. The dichloromethane extract and **1** showed activity against *Bacillus subtilis* and *Staphylococcus aureus* while **3a**, **3b** and **9** were active only against *Bacillus subtilis*. None of the flavonoids were active against the fungi, but the methanol extract showed activity against *Cladosporium cladosporioides*. A brine shrimp lethality assay was performed according to McLaughlin et al. (1995). As shown in Table 6, all tested samples displayed high toxicity with LC_{50} values

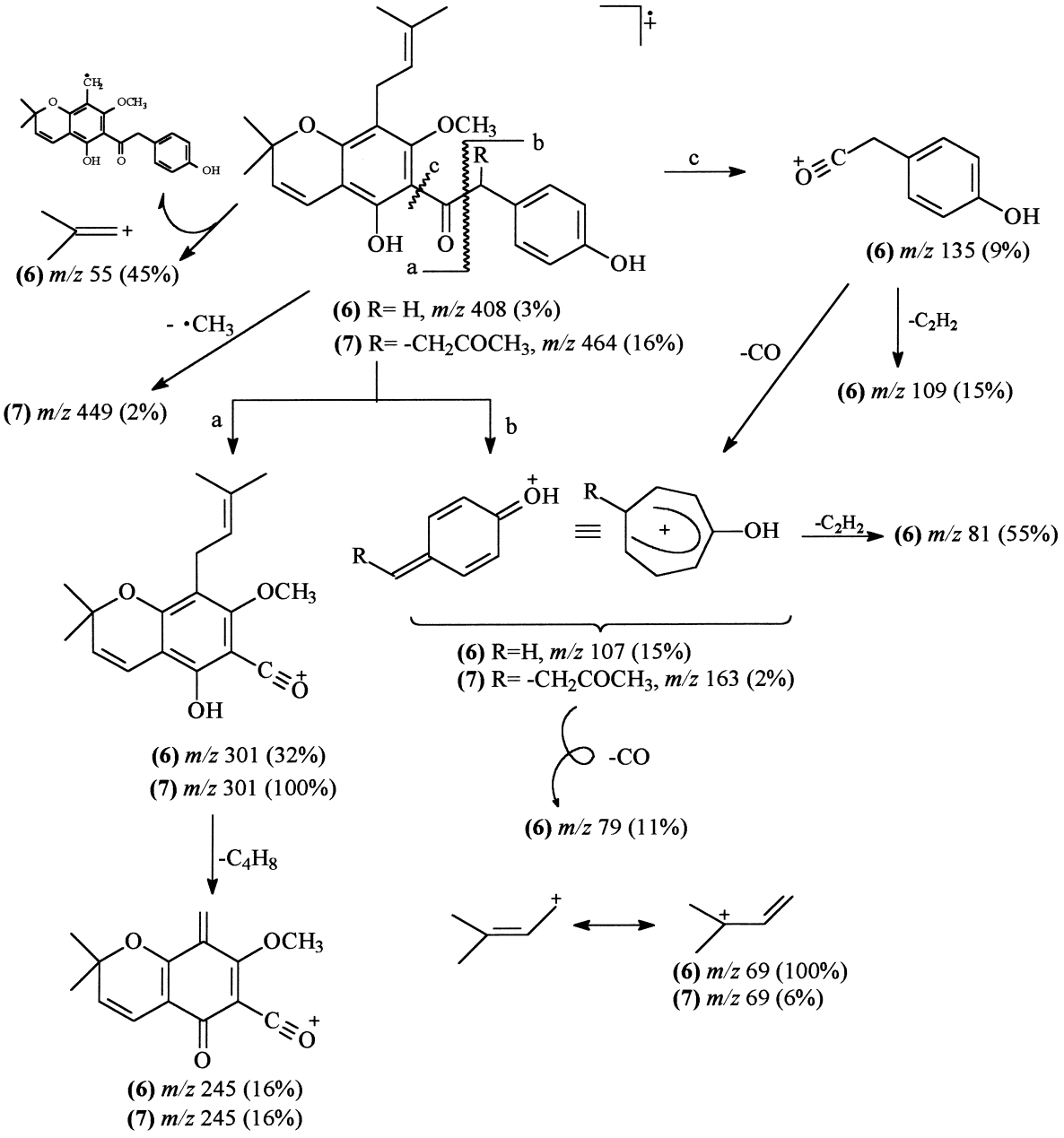

Fig. 5. Fragmentation pathway of compounds **6** and **7**.

being very low. It is important to bear in mind that even the known compounds (**1**, **2a**, **2b**, **3a**, **3b** and **4b**) have not been submitted to any biological assays before.

3. Experimental

UV: $CHCl_3$ or MeOH. IR: film or KBr. ^1H NMR in $CDCl_3$, at 7 or 11 tesla instruments with TMS as int. standard. EIMS 70 eV, direct probe. HREIMS and MS/MS experiments were performed using a VG Auto Spec-Fisions Instrument by using electron ionization technique at 70 eV (linked scan at 8 keV collisions with Helium). HPLC: Reversed-phase HPLC analyses were performed on a C-18 Nova Pak column, by using a variable wavelength UV and diode-array detection. Identification of the peaks in the chromatograms was carried out by co-injection with eight flavonoids previously isolated from the extracts of *D. hatschbachii* roots and further purified by preparative HPLC. Each standard compound was dissolved in acetonitrile and purified by semi-preparative HPLC (Waters) system, consisting of an universal liquid chromatograph injector, a model 484 variable-wavelength detector (adjusted to 240 nm), a model 740 data module and a model 600E system controller and pump, with a Regis ODS, 5 μm,

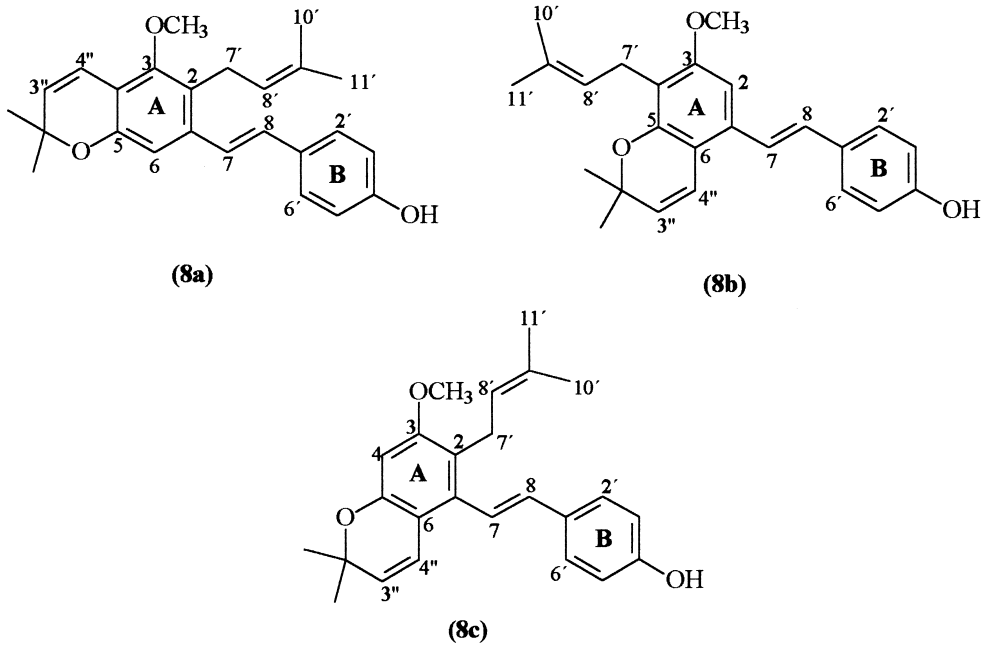

Fig. 6. Structural alternatives for compound **8**.

Table 4
Flavonoid content of extracts of *Deguelia hatschbachii* roots

Contents (mg/g of roots)		
Extract		
Flavonoids	Petrol	Dichloromethane
1	nd[b]	12.37
2a	nd	0.57
2b	nd	nq[a]
3a	0.64	2.90
3b	1.27	12.03
4b	nd	0.46
5	Nd	nq
6	nd	nq

[a] nq = not quantified.
[b] nd = not detected.

250×10 mm i.d. column, and a CH_3CN-H_2O gradient of 20–100% CH_3CN in 45 min at a flow rate of 2.0 ml min^{-1}.

3.1. Quantitative analysis

Light petroleum and dichloromethane root extracts from *D. hatschbachii* were dissolved in acetonitrile. An aliquot (2 μl) of each extract was analyzed by a Hewlett Packard model 1090, series II/M HPLC with a Waters Nova-pak 3 μm column, with a CH_3CN–H_2O gradient of 20–100% CH_3CN in 45 min at a flow rate of 0.8 ml min^{-1}, with the column at ambient temperature. Detection was with a HP photodiode array. The identification of each peak in the corresponding chromatograms was achieved by comparison of retention times, t_R, and UV spectra with those obtained for the standards, as well as by coinjection with the corresponding standard. The retention times are given in minutes as **1** scandenin (27.7), **2a** robustic acid (24.3), **2b** methyl robustate (28.2), **3a** (26.2), **3b** lupinifolin (31.3), **4b** scandinone (30.9), **5** (27.3) and **6** (32.5).

3.2. Calibration curves

Standard solutions were prepared by serial dilutions of the isolated compounds in acetonitrile. Calibration curves were obtained by plotting the integrated peak areas at the maximum UV absorption for each compound versus concentration by performing linear regression analysis. Quantification was made by external calibration with correlation coefficients of 0.999 for each analysed compound.

3.3. Plant material

Roots of *Deguelia hatschbachii* were collected at UNICAMP campus next to the Economy Institute, in March 1994. Voucher specimens have been deposited at the herbarium (uec 95-38) of Campinas State University, Campinas-SP, Brazil.

3.4. Extraction and isolation

Dried roots (97.7 g) of *D. hatschbachii* were successively extracted with petrol (30–60°C), CH_2Cl_2 and MeOH for 50 hr in a Soxhlet apparatus. After solvent evaporation, the petrol extract gave a viscous yellow oil (1.7 g), while the dichloromethane extract gave a brown

Table 5
Bioautography assay results of extracts and some isolated compounds (Fig. 1) from *Deguelia hatschbachii* roots

Tested micro-organism	EEP[b]	ED[c]	EM[d]	**1**	**5**	**6**	**3a**	**3b**[h]
Bacteria[g]								
**Staphylococcus aureus* TCC[a] 4295	–	+[e]	–[f]	+	–	–	–	–
***Escherichia coli* TCC 5050	–	–	–	–	–	–	–	–
***Rodococcus equi* TCC 0541	–	–	–	–	–	–	–	–
****Bacillus subtilis* TCC 0089	–	+	–	+	–	–	+	+
***Salmonella typhimurium* TCC 0528	–	–	–	–	–	–	–	–
***Micrococcus luteus* TCC 2720	–	–	–	–	–	–	–	–
Fungi								
***Candida albicans* TCC 0776	–	–	–	–	–	–	–	–
◆*Cladosporium cladosporioides* TCC 5039	–	–	+	–	–	–	–	–
◆◆*Aspergillus niger* TCC 1435	–	–	–	–	–	–	–	–
◆◆*Penicillium funiculosum* TCC 0490	–	–	–	–	–	–	–	–
◆◆*Fusarium oxysporium* TCC 3244	–	–	–	–	–	–	–	–
◆◆◆*Alternaria alternata* TCC 1250	–	–	–	–	–	–	–	–
◆◆◆*Rhizopus oryzae* TCC 4964	–	–	–	–	–	–	–	–
◆◆◆*Aspergillus fumigatus* TCC 01277	–	–	–	–	–	–	–	–
◆◆◆◆*Penicillium oxalicum* TCC 4815	–	–	–	–	–	–	–	–

[a] TCC: tropical culture collection — Fundação Tropical de Pesquisa e Tecnologia 'André Tosello'.
[b] EEP: petrol extract.
[c] ED: dichloromethane extract.
[d] EM: methanol extract.
[e] + positive test (visualization of an inhibition growth halo).
[f] – negative test (no inhibition growth halo).
[g] The amount of sample applied on TLC plates against tested microorganisms was respectively (from left to right):
(*) 24.0, 34.8, 66.4, 32.8, 83.6, 11.2, 20.0 and 20.0 μg,
(**) 40.0, 39.2, 39.7, 20.0, 19.5, 20.0, 20.3, 20.4 μg,
(***) 40.0, 39.2, 39.7, 112.5 (and 32.8), 13.5 (and 83.6), 14.0 (and 11.2), 20.3, 20.4 μg,
(◆) 30.0, 87.0, 166, 20.0, 19.5, 20.0, 20.3, 20.4 μg,
(◆◆) 12.0, 34.8, 66.4, 32.8, 83.6, 11.2, 20.0 and 20.0 μg,
(◆◆◆) 30.0, 87.0, 166, 82.0, 209, 28.0, 20.0 and 20.0 μg,
(◆◆◆◆) 30.0, 87.0, 166, 82.0, 19.5, 20.0, 20.0 and 20.0 μg.
[h] Obs: The compounds **2a**, **2b**, **4b**, **8** and **9** (Fig. 1) respectively 97.5, 71.3, 66.6, 56.6 and 24.0 μg were also tested against *Bacillus subtilis* TCC 0089, but only **9** gave positive test, while the compounds **8** and **9** respectively 34.0 and 48.0 μg were also tested against *Candida albicans* TCC 0776 and *Cladosporium cladosporioides* TCC 5039, but gave negative test. The inhibition growth halo was compared with those showed by the commercial antibiotics cloranfenicol (against bacteria) and ciclopirox olamina (against fungi) in a range 1–2 μl.

Table 6
Brine shrimp lethality test results of extracts from *Deguelia hatschbachii* roots and compounds **1**, **3a** and **3b** (Fig. 1)

Tested samples	LC_{50} (μg/ml)
Petrol extract	3.60
Dichloromethane extract	0.83
Methanol extract	79.98
Compound **1**	4.31
Compound **3a**	0.0004
Compound **3b**	13.01
Control (H_2O)	> 1000

solid (4.2 g) and the methanol extract (4.1 g) gave a brown gum. An aliquot of the dichloromethane extract (3.0 g) was applied to a silica gel column (120 g) eluted first with dichloromethane. The eluent polarity was gradually increased by addition of EtOAc and MeOH to furnish 342 fractions of 200 ml each which were reduced to 82 groups after TLC analysis. Most of the compounds were found in six groups ranging from fractions 4 to 66. A sample of each was further fractionated by successive prep. TLC (silica gel). Flavonoids were visualized under UV light ($\lambda = 254$ and 366 nm) and recovered from TLC plates by extraction with mixtures of CH_2Cl_2 and MeOH to furnish compounds **1** (12.4 mg), **2a** (4.1 mg), **2b** (5.7 mg), **3a** (20.0 mg), **3b** (20.1 mg), **4a** (2.0 mg), **4b** (4.0 mg), **5** (7.7 mg), **6** (2.9 mg), **7** (2.0 mg), **8** (21.4 mg) and **9** (4.8 mg). Analogously a part of the petrol extract (1.5 g) furnished compounds **3a** (3.2 mg), **3b** (8.2 mg), **8** (10.2 mg), **9** (5.0 mg) and **10** (7.4 mg),

3.5. 3-(4′-Hydroxyphenyl)-5-methoxy-6-(3,3-dimethylallyl)-2″,2″-dimethylchromene-(5″,6″:8,7)-3-(propyl-2-one)-4H-1-benzo-2,3-dihydropyran-2,4-dione **5**

Viscous yellowish oil. $[\alpha]_D^{20}$ +6.16° (CH_2Cl_2; *c* 0.0138). UV $\lambda_3^{CHCl}{}_{3max}$ nm (log ε): 257 (4.55), 305 (4.06). IR ν_{max} cm^{-1} (KBr): 3410, 1770, 1704, 1682. ^1H NMR spectral data (500 MHz, $CDCl_3$/TMS): Table 2. ^{13}C NMR spectral data (75 MHz, $CDCl_3$): Table 3. EIMS (probe) 70

eV, *m/z* (rel. int.): 490 $[M]^+$ (16), 475 $[M\text{-}Me]^+$ (8), 300 $[M\text{-}190]^+$ (38), 285 $[M\text{-}190\text{-}Me]^+$ (53), 269 $[M\text{-}221]^+$ (3), 257 $[M\text{-}190\text{-}Me\text{-}CO]^+$ (24), 245 $[M\text{-}245]^+$ (14), 242 $[M\text{-}190\text{-}Me\text{-}CO\text{-}Me]^+$ (2), 227 $[M\text{-}190\text{-}Me\text{-}CO\text{-}30]^+$ (4), 201 $[M\text{-}190\text{-}Me\text{-}CO\text{-}56]^+$ (4), 190 $[M\text{-}300]^+$ (5), 189 $[M\text{-}190\text{-}Me\text{-}CO\text{-}68]^+$ (3), 162 $[M\text{-}300\text{-}CO]^+$ (2), 159 $[M\text{-}190\text{-}Me\text{-}CO\text{-}98]^+$ (2), 147 $[M\text{-}343]^+$ (4), 135 $[M\text{-}300\text{-}CO + H\text{-}CO]^+$ (3), 119 $[M\text{-}343\text{-}CO]^+$ (22). HR-EIMS *m/z*: found 490.1989 $[M]^+$ ($C_{29}H_{30}O_7$ requires 490.1991).

*3.6. 6,4′-Dihydroxy-3-(3,3-dimethylallyl)-2″,2″-dimethylchromene (5″,6″:5,4)-2-methoxy deoxybenzoin (**6**)*

White powder. UV λ_{max}^{MeOH} nm (log ϵ): 266 (4.14), 316,5 (3,72). IR $\nu_2^{CH_2Cl_2}{}_{max}$ cm^{-1} (film): 3388, 1700. ^1H NMR spectral data (300 MHz, $CDCl_3$/TMS): Table 2. ^{13}C NMR spectral data (75 MHz, $CDCl_3$): Table 3. EIMS (probe) 70 eV, *m/z* (rel. int.): 408 $[M]^+$ (3), 301 $[M\text{-}107]^+$ (32), 245 $[M\text{-}163]^+$ (16), 135 $[M\text{-}273]^+$ (9), 109 $[M\text{-}299]^+$ (15), 107 $[M\text{-}301]^+$ (15), 81 $[M\text{-}327]^+$ (55), 79 $[M\text{-}301\text{-}CO]^+$ (11), 69 (100), 57 (44), 55 (45).

3.7. 6,4′-Dihydroxy-3-(3,3-dimethylallyl)-2″,2″-dimethylchromene (5″,6″:5,4)-2-methoxy-8-(propyl-2-one) deoxybenzoin (7)

Viscous yellowish oil. ^1H NMR spectral data (300 MHz, $CDCl_3$/TMS): Table 2. ^{13}C NMR spectral data (75 MHz, $CDCl_3$): Table 3. EIMS (probe) 70 eV, *m/z* (rel. int.): 464 $[M]^+$ (16), 449 $[M\text{-}Me]^+$ (2), 301 $[M\text{-}163]^+$ (100), 245 $[M\text{-}219]^+$ (16), 215 $[M\text{-}249]^+$ (2), 163 $[M\text{-}301]^+$ (2), 135 $[M\text{-}301\text{-}CO]^+$ (3), 69 (6).

*3.8. 2′-(3,3-Dimethylallyl)-2″,2″-dimethylchromene (5″,6″:4′,3′)-4-hydroxy-5′-methoxy stilbene (**8**)*

Yellow amorphous solid. UV λ_{max}^{MeOH} nm (log ϵ): 273 (3.96), 330 (4.23). IR $\nu_{2\ max}^{CH}$ cm^{-1} (film): 3404, 959. ^1H NMR spectral data (300 MHz, $CDCl_3$/TMS): Table 2. ^{13}C NMR spectral data (75 MHz, $CDCl_3$) Table 3 EIMS (probe) 70 eV, *m/z* (rel. int.): 376 $[M]^+$ (21), 361 $[M\text{-}Me]^+$ (100), 333 $[M\text{-}Me\text{-}CO]^+$ (6), 213 $[M\text{-}Me\text{-}CO\text{-}120]^+$ (35), 107 $[M\text{-}269]^+$ (17), 69 (3), 55 (3). HR-EIMS *m/z*: found 376.2039 $[M]^+$ ($C_{25}H_{28}O_3$ requires 376.2038).

*3.9. 3′,5′-Dimethoxy-4-hydroxy-4′-(3,3-dimethylallyl) stilbene (**9**)*

Yellowish oil. UV λ_{max}^{MeOH} nm (log ϵ): 313 (4.20), 325 (4.21). IR$\nu_2^{CH_2Cl_2}{}_{max}$ cm^{-1} (film): 3407, 958. ^1H NMR spectral data (300 MHz, $CDCl_3$/TMS): Table 2. ^{13}C NMR spectral data (75 MHz, $CDCl_3$): Table 3. EIMS (probe) 70 eV, *m/z* (rel. int.): 324 $[M]^+$ (100), 309 $[M\text{-}Me]^+$ (93), 281 $[M\text{-}Me\text{-}CO]^+$ (5), 256 $[M\text{-}68]^+$ (44), 255 $[M\text{-}69]^+$ (13), 269 $[M\text{-}55]^+$ (10), 241 $[M\text{-}55\text{-}CO]^+$ (2), 107 $[M\text{-}217]^+$ (20), 89 $[M\text{-}217\text{-}H_2O]^+$ (6), 81 $[M\text{-}243]^+$ (6), 69 (14), 55 (12). HR-EIMS *m/z*: found 324.1725 $[M]^+$ ($C_{21}H_{24}O_3$ r equires 324.1725).

Acknowledgements

The authors are grateful to CNPq and CAPES for scholarships awarded to V.R.S.M. and to FAPESP for financial support.

References

Agrawal, P.K., 1989. Carbon-13 NMR of flavonoids. Elsevier, Amsterdam.

Budzikiewicz, H., Wilson, J.M., Djerassi, C., 1963. Mass spectrometry in structural and stereochemical problems. XXXII. Pentacyclic triterpenes. Journal of American Chemical Society 85 (20), 3688–3699.

Delle Monache, F., Valera, G.C., Zapata, D.S., Marini-Bettolo, G.B., 1977. 3-Aryl-4-methoxycoumarins and isoflavones from *Derris glabrescens*. Gazzetta Chimica Italiana 107 (7-8), 403–407.

Delle Monache, G., Scurria, R., Vitali, A., Botta, B., Monacelli, B., Pasqua, G., Palocci, C., Cernia, E., 1994. Two isoflavones and a flavone from the fruits of Maclura pomifera. Phytochemistry 37 (3), 893–898.

Dewick, P.M., 1988. Isoflavonoids. In: Harbone, J.B. (Ed.), The Flavonoids: Advances in Research Since 1980. Chapman and Hall, London.

Donnelly, D.M.X., Molloy, D.J., Reilly, J.P., Finet, J.-P., 1995. Aryllead-mediated synthesis of linear 3-arylpyranocoumarins: synthesis of robustin and robustic acid. J. Chem. Soc. Perkin Trans 1, 20, 2531–2534.

East, A.J., Ollis, W.D., Wheeler, R.E., 1969. Natural occurrence of 3-aryl-4-hydroxycoumarins. Part I. Phytochemical examination of Derris robusta (Roxb.) Benth. J. Chem. Soc. C 3, 365–374.

Fang, N., Casida, J.E., 1999. New bioactive flavonoids and stilbenes in cube resin insecticide. J. Natl. Prod. 62 (2), 205–210.

Filho, R.B., Gottlieb, O.R., Mourão, A.P., Da Rocha, A.I., Oliveira, F.S., 1975. Chemistry of Brazilian Leguminosae. 51. Flavonoids from *Derris* species. Phytochemistry 14 (5-6), 1454–1456.

Filho, R.B., Gottlieb, O.R., Mourão, A.P., 1975b. Chemistry of Brazilian Leguminosae. 47. Stilbene and 2 flavanones from *Derris rariflora*. Phytochemistry 14 (1), 261–263.

Garcia, M., Kano, M.H.C., Vieira, D.M., do Nascimento, M.C., Mors, W.B., 1986. Isoflavonoids from *Derris spruceana*. Phytochemistry, 25 (10), 2425–2427.

Geesink, R., 1984. Scala Millettiearum. A survey of the genera of the tribe Millettieae (Legum.- Pap.) with methodological considerations. Leiden Botanical Series 8. Leiden, E.J. Brill and Leiden University Press, Leiden.

Gomes, C.M.R., Gottlieb, O.R., Gottlieb, R.G., Salatino, A., 1981. Phytochemistry in perspective: chemosystematics of the Papilionoideae. In: Polhill, R.M., Raven, P.H. (Eds.), Advances in Legume Systematics. Vol. 2, Royal Botanic Gardens, Kew, pp. 465–488.

Gottlieb, O.R., Gomes, C.M.R., Marini Bettolo, G.B., Delle Monache, F., Polhill, R.M., 1981. Systematic significance of flavonoids in *Derris* and *Lonchocarpus*. Biochem. Syst. and Ecol. 9 (2/3), 129–147.

Gottlieb, O.R., 1982. Evolution of flavonoids in Tephrosieae. In: Gottlieb, O.R. (Ed.), Micromolecular evolution, systematics and ecology. Springer-Verlag, Berlin, pp. 120–130.

Harborne, J.B., 2000. Arsenal for survival: secondary plant products. Taxon 49, 435–448.

Kaouadji, M., Agban, A., Mariotte, A.M., 1986. Lonchocarpene, a stilbene, and lonchocarpusone, an isoflavone- 2 new pyranopolyphenols from *Lonchocarpus nicou* roots. J. Nat. Prod. 49 (2), 281–285.

Kaouadji, M., 1988. 2 New C-prenylated derivatives of 2,4-dihydroxy benzoic-acid from *Lonchocarpus nicou* roots. Journal of Natural Products 51 (2), 376–378.

Khalid, S.A., Waterman, P.G., 1983. Thonningine-A and Thonningine-B: two 3-phenylcoumarins from the seeds of *Millettia thonningii*. Phytochemistry 22 (4), 1001–1003.

Kiuchi, F., Chen, X., Tsuda, Y., 1990. Four new phenolic constituents from licorice (root of *Glycyrrhiza* sp.). Heterocycles 31 (4), 629–636.

Lehn, J.-M., Ourisson, G., 1962. Résonance magnétique nucléaire de produits naturels. I.- Introduction générale. Triterpènes de la série du Lupane: les groupes méthyles. Mémoires Presentés a la Societé Chimique, 1137–1142.

Magalhães, A.F., Tozzi, A.M.G.A., Magalhães, E.G., Nogueira, M.A., Roncancio, V.J.F., 1998. Ensayos biológicos com extractos obtenidos de raíces de *Lonchocarpus latifolius* (WILLD.) D. C. Y. de un nuevo dibenzoilmetano aislado. Revista Ceres 45 (260), 351–358.

Mahidol, C., Prawat, H., Ruchirawat, S., Lihkitwitayawuid, K., Lin, L.-Z., Cordell, G.A., 1997. Prenylated flavanones from *Derris reticulata*. Phytochemistry 45 (4), 825–829.

Mahmoud, E.N., Waterman, P.G., 1985. Minimiflorin: a new 2′-hydroxyflavanone from *Lonchocarpus minimiflorus* seeds. J. Nat. Prod. 48 (4), 648–650.

McLaughlin, J.L., Saizarbitoria, T-C., Anderson, J.E., 1995. Tres bioensayos simples para quimicos de productos naturales.. Revista de la Sociedad Venezolana de Quimica 18 (4), 13–18.

Norin, T., 1989. In Rowe, J.W (Ed.), Natural Products of Woody Plants I. Springer-Verlag, Berlin, Heidelberg, pp. 512–517.

Olivares, E.M., Lwande, W., Delle Monache, F., Marini Bettolo, G.B., 1982. A pyrano-isoflavone from seeds of *Millettia thonningii*. Phytochemistry 21 (7), 1763–1765.

Saxena, G., Farner, S., Towers, G.H.N., Hancock, R.E.W., 1995. Use of specific dyes in the detection of antimicrobial compounds from crude plant extracts a thin layer chromatography agar overlay technique. Phytochemical Analysis 6 (3), 125–129.

Sekine, T., Inagaki, M., Ikegami, F., Fujii, Y., Ruangrungsi, N., 1999. Six diprenylisoflavones, derrisisoflavones A-F, from *Derris scandens*. Phytochemistry 52 (1), 87–94.

Tozzi, A.M.G. de A., 1989. Estudos taxonômicos dos gêneros *Lonchocarpus* Kunth e *Deguelia* Aubl. no Brasil. PhD thesis. Campinas-SP, Instituto de Biologia, Universidade Estadual de Campinas.

Tozzi, A.M.G. de A., 1992. *Lonchocarpus monilis* (L.). Az.-Tozzi, comb. nov. (Leguminosae- Papilionoideae): considerações nomenclaturais e taxonômicas. Revista Brasileira de Botânica 15 (2), 151–155.

Tozzi, A.M.G. de A., 1994. Espécies novas de *Deguelia* Aubl. (Leguminosae-Papilionoideae-Millettieae). Revista Brasileira de Botânica 17 (1), 45–52.

Tozzi, A.M.G. de A., 1995. New species of *Lonchocarpus* Kunth (Leguminosae-Papilionoideae-Millettieae) from Brazil. Kew Bulletin 50 (1), 173–177.

Tozzi, A.M.G., de, A., 1998. A identidade do timbó-verdadeiro: *Deguelia utilis* (A. C.Sm. emendavit A.M.G.Azevedo) A.M.G.Azevedo (Leguminosae-Papilionoideae). Revista Brasileira de Biologia 58 (3), 511–516.

Uma Rani, B.S., Darbarwar, M., 1987. Synthesis of oxygenated deoxybenzoins and isoflavones. J. Indian Chem. Soc. 64, 555–558.

Vasconcelos, M.N.L., Maia, J.G.S., 1976. Estudo químico de *Derris negrensis*. Acta Amazonica 6 (1), 59–61.

Wenkert, E., Baddeley, G.V., Burfitt, I.R., Moreno, L.N., 1978. Carbon-13 nuclear magnetic resonance spectroscopy of naturally-occurring substances. LVII. Triterpenes related to lupane and hopane. Org. Mag. Res. 11 (7), 337–343.

PERGAMON

Phytochemistry 57 (2001) 91–98

PHYTOCHEMISTRY

www.elsevier.com/locate/phytochem

Effect of (+)-pulegone and other oil components of *Mentha×piperita* on cucumber respiration

Marco Mucciarelli [b], Wanda Camusso [a], Cinzia M. Bertea [a], Simone Bossi [a], Massimo Maffei [a,*]

[a] *Department of Plant Biology, University of Turin, Viale P.A. Mattioli, 25 I-10125 Torino, Italy*
[b] *Department of Morphophysiology, University of Turin, Viale P.A. Mattioli, 25 I-10125 Torino, Italy*

Received 14 June 2000; received in revised form 28 August 2000

Abstract

Peppermint (*Mentha×piperita* L.) essential oil and main components were assessed for their ability to interfere with plant respiratory functions. Tests were conducted on both root segments and mitochondria isolated by etiolated seedlings of cucumber (*Cucumis sativus* L.). Total essential oil inhibited 50% of root and mitochondrial respiration (IC_{50}) when used at 324 and 593 ppm, respectively. (+)-Pulegone was the most toxic compound, with a 0.08 and 0.12 mM IC_{50} for root and mitochondrial respiration, respectively. (−)-Menthone, followed (+)-pulegone in its inhibitory action (IC_{50} values of 1.11 and 2.30 mM for root and mitochondrial respiration respectively), whereas (−)-menthol was the less inhibitory compound (IC_{50} values of 1.85 and 3.80 mM respectively). A positive correlation was found for (+)-pulegone, (−)-menthone and (−)-menthol between water solubility and respiratory inhibition. The uncoupling agent, carbonyl-cyanide-*m*-chlorophenyl-hydrazone (CCCP), lowered (−)-menthol and (−)-menthone inhibition and annulled (+)-pulegone inhibition of mitochondrial respiration, whereas salicyl-hydroxamic acid (SHAM) 2-hydroxybenzohydroxamic acid, the alternative oxidase (AO) inhibitor, increased (−)-menthone inhibition and annulled both (+)-pulegone and (−)-menthol inhibitory activity. The possible interaction of (+)-pulegone and (−)-menthol with AO and the mechanism of action of (+)-pulegone, (−)-menthone and (−)-menthol on mitochondrial respiration are discussed. © 2001 Elsevier Science Ltd. All rights reserved.

Keywords: *Mentha×piperita*; Labiatae; Peppermint; *Cucumis sativus*; Cucumber; Root respiration; Mitochondrial respiration; Allelochemicals; Essential oils; (+)-Pulegone

1. Introduction

Higher plants synthesize a great variety of terpenoids, which can be involved in allelophatic interactions. Monoterpenoids are the major components of some essential oils and have been recognized as main allelochemicals in higher plants: they have toxic effects on seed germination (Robinson, 1983; Rice, 1984), growth of some bacterial strains (Knobloch et al., 1989; Economou and Nahrstedt, 1991), development and growth of some insects (Lee et al., 1999), and growth of pathogenic fungi (Adam et al., 1998).

Plants from the genus *Mentha* are a natural and important source of monoterpenoids used in food, pharmaceutical, and cosmetic industries (Hendriks, 1998). Peppermint, along with cornmint (*Mentha arvensis* var. *piperascens*) and spearmint (*Mentha spicata*), is one of the most economically important essential oil crops, with a world production exceeding 2000 metric tons per year (Deans and Waterman, 1993). The main monoterpenes in peppermint are menthol and menthone, followed by good percentages of menthyl acetate, limonene, 1,8-cineole and low percentages of pulegone (Maffei and Sacco, 1987).

Several pharmacological and biological effects have been associated with these oil components. In particular: menthol is a known antifungal and antimicrobial agent (Morris et al., 1979) and larvae repellent (Kelsey et al., 1984). It has been found to interact at the cell level with cytosolic Ca^{2+}, probably through an intracellular Ca^{2+} store release (Takeuchi et al., 1994) and Ca^{2+} channel blocking (Taylor et al., 1985; Hills and

* Corresponding author. Tel.: +39-011-658387; fax: +39-011-6707-459.
E-mail address: maffeima@bioveg.unito.it (M. Maffei).

0031-9422/01/$ - see front matter © 2001 Elsevier Science Ltd. All rights reserved.
PII: S0031-9422(00)00393-9

Aaroson, 1992). Menthone is a growth inhibitor (Slama, 1978), whereas pulegone, a potent abortifacient, is metabolized by hepatic microsomal mono-oxygenases to a series of hepatotoxins that cause liver cancer (Nelson, 1995) and is involved in many reported cases of intoxication in humans and animals (Bakerink et al., 1996). Furthermore, pulegone is considered one of the most powerful allelochemicals and has been demonstrated to be about twice as toxic as HCN (Asplund, 1968,1969; Fisher, 1986,1991).

The effect of allelopathic compounds on mitochondrial respiration may be an important mechanism of action through which allelochemicals control growth of several weed species. Rasmussen and co-workers (1992) found that the hydroquinonic compound, sorgoleone, a major component in the exudate of grain *Sorghum bicolor* roots is a potent inhibitor of both soybean and corn mitochondrial respiration. Juglone (5-hydroxy-1,4-naphthoquinone), the main allelochemical isolated from the black walnut (*Juglans nigra* L.), exerts an opposite effect by stimulating oxygen uptake in mitochondria of *Glycine max* (Hejl et al., 1993). The inhibition of growth and spore formation of some plant pathogenic fungi by essential oil applications has been shown to be correlated with their respiration-inhibitory activity (Inouye et al., 1998).

Considering the extended application of mint oil and the possible future applications of natural compounds, such as essential oils in crop pest and weed control, we aimed to determine whether peppermint essential oil may affect oxygen uptake in plants. As a study system we used cucumber seedlings for their easiness of handling, uniform germination and growth and for the quick response they give to allelopathic agents (Maffei et al., 1999a).

2. Results and discussion

The oil chemical composition of peppermint plants used in this study was characterized by the presence of the monoterpene oxygenated compounds (−)-menthol (44.99%), (−)-menthone (20.78%), (+)-menthofuran (4.32%), (+)-menthyl acetate (4.07%) and (+)-pulegone (0.80%), along with good percentages of the monoterpene oxide 1,8-cineole (6.53%) and the olefin (−)-limonene (2.57%). Minor mono- and sesquiterpenes as reported earlier (Maffei and Sacco, 1987) made the remainder.

2.1. Root respiration

Peppermint essential oil prompted a significant inhibition of cucumber root respiration, for concentrations higher than 60 mg/l (Fig. 1). The amount of essential oil needed to obtain a 50% inhibition (IC_{50}) was 324 mg/l ($R=0.99$). This observation is in accordance with literature data on the inhibition of seed germination after exposure to volatile terpenes, which disrupt cell membranes and lead to cytological alterations with a reduction of biochemical activity of mitochondria and other organelles (Fisher, 1991).

A greater inhibitory effect was observed when roots were exposed to increasing concentrations of (−)-menthone [$IC_{50}=169.07$ mg/l, 1.11 mM, correlation coefficient (R) $=0.99$] and (−)-menthol ($IC_{50}=287.91$ mg/l, 1.85 mM, $R=0.96$). A slight stimulation of root oxygen uptake was registered for total essential oil, (−)-menthone and (−)-menthol concentrations ranging from 10 to 50 mg/l. On the contrary, (+)-pulegone inhibited oxygen uptake at all tested concentrations, with a 11.20 mg/l IC_{50} (0.075 mM, $R=0.99$). These results indicate that (+)-pulegone is a strong inhibitor of root respiration, being able to inhibit root respiration almost 29 times more than total essential oil, 15 times more than (−)-menthone and almost 26 times more than (−)-menthol. Usually, unsaturated monoterpene hydrocarbons require high concentrations (>2 mM) to cause 50% inhibition of germination (IC_{50}), whereas higher phytotoxic effects are observed from cyclic alcohols to cyclic ketones (<0.1 mM IC_{50}) (Reynolds, 1987). The greater toxicity of monoterpene ketones with respect to alcohols has been demonstrated in several cell systems (Reynolds, 1987; Fisher, 1991) and in rat liver tissues the exocyclic double bond of pulegone is responsible for its well known hepatotoxic effects (McClanahan et al., 1989). Inhibition of root respiration caused by (+)-pulegone is in accordance with the well known toxic properties already tested for this molecule (Thomassen et al., 1990; Nelson et al., 1992; Franzios et al., 1997) as well as its effect on plasma alkaline phosphatase (Molck et al., 1998).

Assuming that root respiratory rate inhibition (50%) by single peppermint oil components was additive and dependent on the relative percentage of each component in the total oil, from regression lines of Fig. 1 and considering the oil composition as stated above, it is possible to extrapolate that (−)-menthol contributed to the 43% of the overall oil inhibition, whereas (−)-menthone and (+)-pulegone to the 33 and 24% respectively.

2.2. Mitochondrial respiration

The effect of peppermint essential oil and oil components on mitochondrial respiration is shown in Fig. 2. The amount of total essential oil (595.03 mg/l, $R=0.99$) and (−)-menthol (592.91 mg/l, 3.80 mM, $R=0.95$) able to inhibit mitochondrial respiration by 50% were statistically the same. We still registered an increase in oxygen uptake for concentrations of total essential oil as high as 75 mg/l and for (−)-menthol applications up to 260 mg/l. Despite its lower IC_{50} (351.38 mg/l, 2.30 mM,

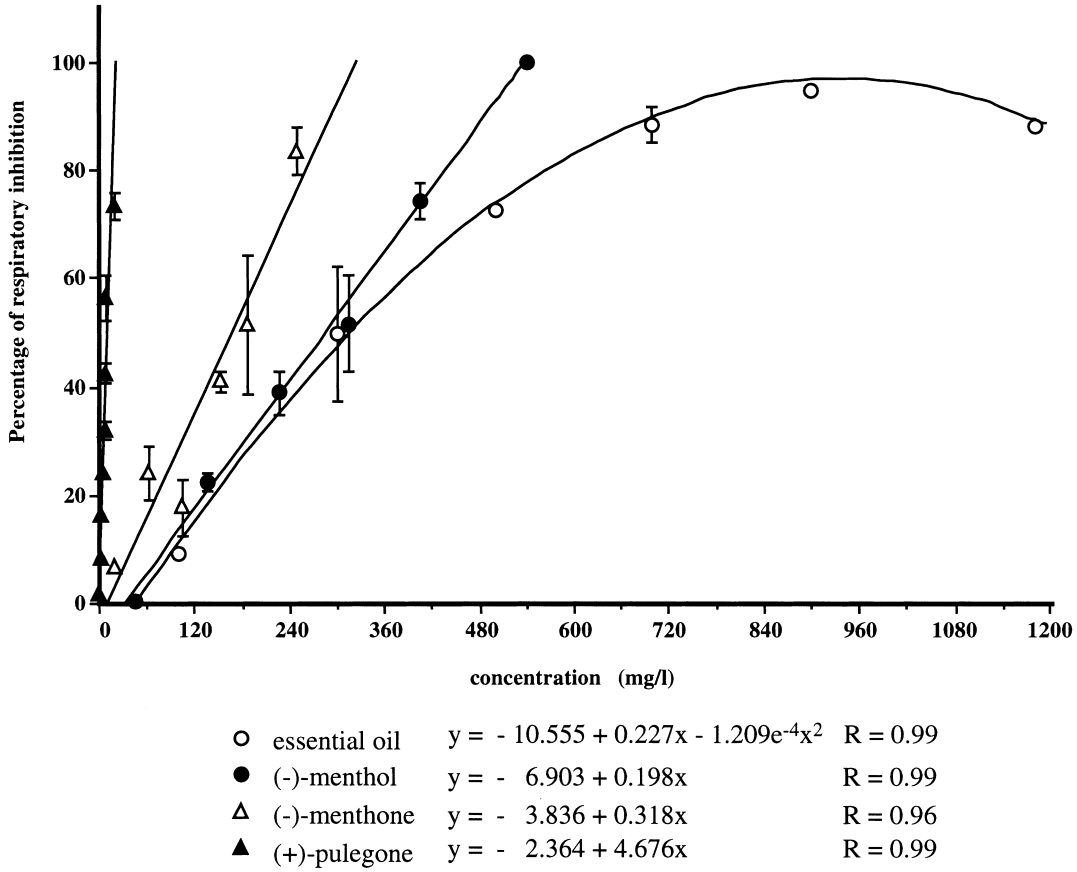

Fig. 1. Percentage of respiratory inhibition as a function of concentration of total essential oil, (−)-menthol, (−)-menthone and (+)-pulegone in cucumber (*Cucumis sativus*) roots. Bars indicate standard deviation.

$R=0.93$) also (−)-menthone resulted stimulatory at low concentrations. As in the root, (+)-pulegone IC_{50} (18.43 mg/l, 0.12 mM, $R=0.99$) was found to be the lowest. Washing of mitochondria in buffered solutions, with consequent recovery of full respiratory activity (data not shown) annulled the effect of total essential oil, (−)-menthol, (−)-menthone and (+)-pulegone applications. Our results showed that (+)-pulegone is a powerful inhibitor of mitochondria respiration, being effective in a range of concentrations equal or below other reported allelochemicals (Moreland and Novitzky, 1987). The complete recovery of respiration after washing of mitochondria indicates that membrane interactions could be the initial site of action of such molecules, as demonstrated in previous studies on ultrastructural alterations caused by several monoterpenes on plant cells and organelles (Muller, 1986). This could also explain why monoterpenes are usually sequestered in specialized glandular structures and kept away from cell membranes and living cytoplasm, in order to prevent plant tissues from autotoxicity.

The plot of IC_{50} against the water solubility (WS, expressed in ppm) (Fischer, 1991) of (−)-menthol, (−)-menthone and (+)-pulegone (Fig. 3) showed a negative significant correlation, with decreasing IC_{50} values with increasing water solubility, and a greater inhibition of roots with respect to purified mitochondria for (−)-menthone and (−)-menthol applications. In peppermint oil, there is an increasing trend in the inhibition of root and mitochondrial respiration that follows the order: alcohols [(−)-menthol], saturated ketones [(−)-menthone], unsaturated ketones [(+)-pulegone]. This trend parallels the capability of these compounds to solubilize in water. These data are in agreement with previous investigations done on antimicrobial activity (Knobloch et al.,1989), toxicity in plant cell cultures (Brown et al., 1987) and inhibition of tissue respiration (Fisher, 1986,1991).

Injection of the oxidative phosphorylation uncoupler CCCP (5 μM) in the purified mitochondrial fraction prompted a 26% (± 4.2) increase of the oxygen consumption rate (117 nmol O_2 h^{-1} μg $protein^{-1}$), which indicated the uncoupling of the electron transport system from ATP production. When CCCP was followed by total essential oil, a significant increase in the IC_{50} value (1032.33 mg/l) was observed with respect to CCCP untreated mitochondria and the same was for menthol (758.21 mg/l, 4.86 mM) and menthone (1558.47, 10.19 mM) (Fig. 4). (+)-Pulegone lost all its inhibitory action

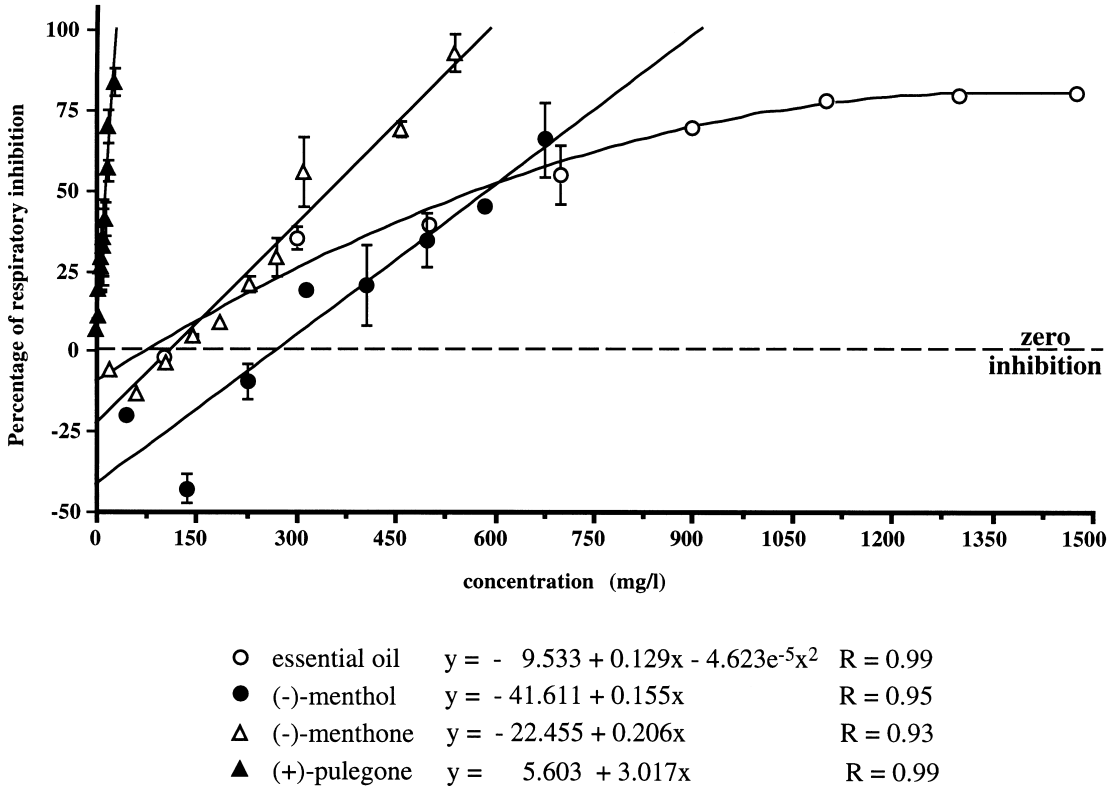

Fig. 2. Percentage of respiratory inhibition as a function of concentration of total essential oil, (−)-menthol, (−)-menthone and (+)-pulegone in cucumber (*Cucumis sativus*) mitochondria purified from root extracts. Bars indicate standard deviation.

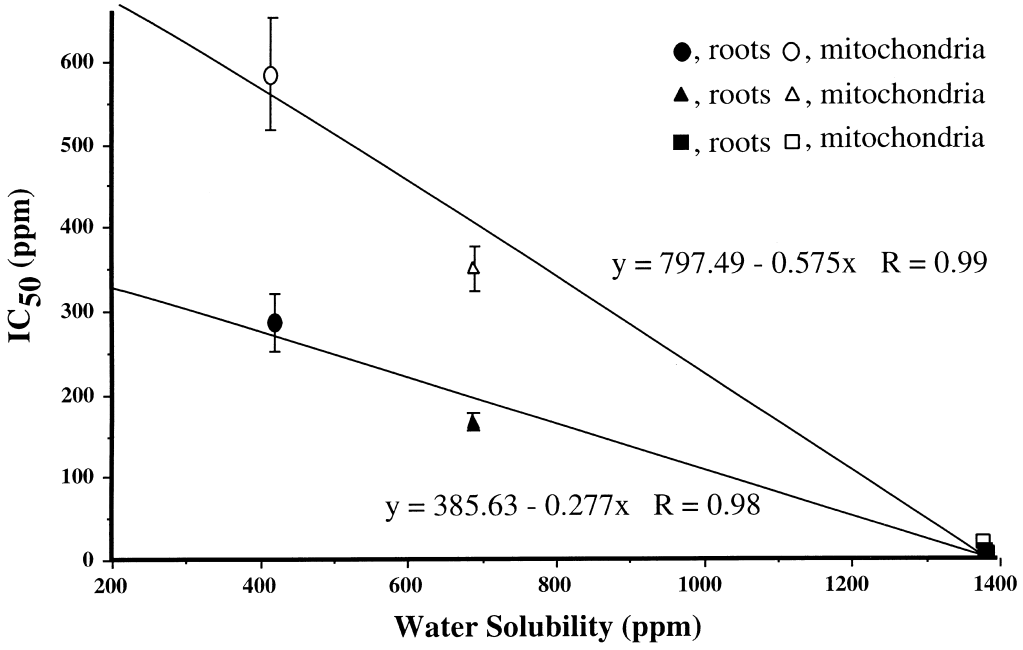

Fig. 3. Plot of the concentration of (−)-menthol, (−)-menthone and (+)-pulegone able to cause 50% of inhibition of respiration (IC_{50}) against their water solubility (Fisher, 1991). A positive correlation was found between respiratory inhibition and water solubility of compounds. Bars indicate standard deviation.

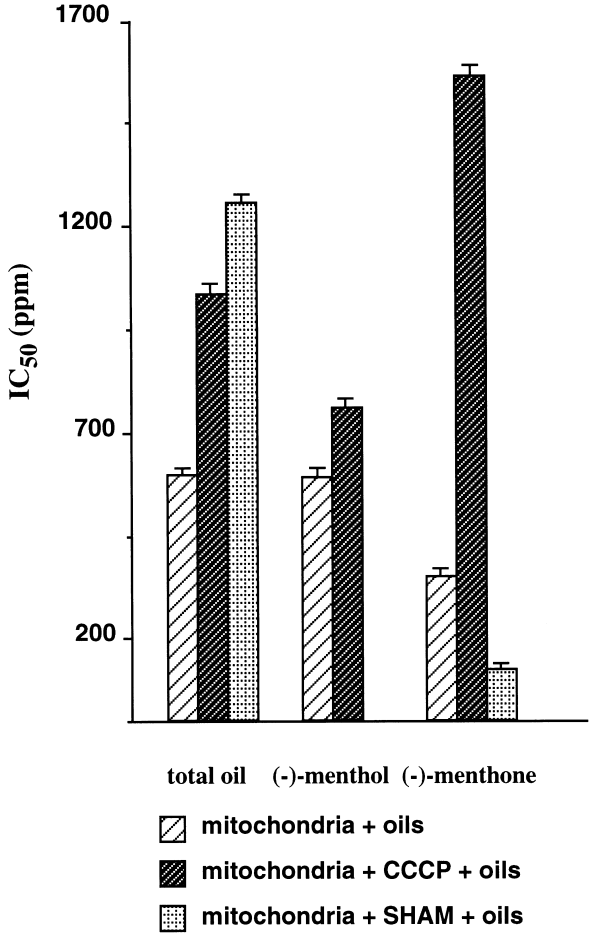

Fig. 4. Respiratory IC_{50} (ppm) in purified mitochondria preparations and after mitochondria incubation with the uncoupler CCCP (total essential oil, (−)-menthol and (−)-menthone) and the alternative oxidase (AO) inhibitor SHAM (total essential oil and (−)-menthone). Columns represent oil and components concentration (ppm) enough to inhibit mitochondrial respiration by 50%. Bars indicate standard deviation.

by dropping above zero inhibition at a concentration of 9.72 mg/l (Fig. 5). Spectrophotometric analyses indicated complete lack of interaction between CCCP and total essential oil and oil components (data not shown).

The protonophor CCCP, dissipating the membrane potential and catalyzing the movement of protons through the inner mitochondrial membrane (Daie et al., 1987; Felle, 1988), reduced the inhibitory action of peppermint oil, menthol and menthone. A CCCP-mediated pH increase in the intermembrane mitochondrial space could lower the ability of terpenoids to inhibit oxygen consumption, by rendering their possible site of action more polar. Meanwhile, the ability of CCCP to totally circumvent inhibition of state 3 rate by pulegone suggests a specific action of pulegone on cucumber mitochondrial functions.

Plant cells possess an alternative oxidation (AO) pathway that diverts the electron flow from ubiquinone to complex III. The electron flow is used to reduce oxygen to water with the production of heat. One of the specific inhibitors of the AO pathway is SHAM. The use of SHAM in control cucumber mitochondrial fractions caused a 24% (± 2.0) decrease in the oxygen uptake rate (99 nmol O_2 h^{-1} μg $protein^{-1}$). When peppermint essential oil was added to SHAM treated mitochondria, a consistent and significant IC_{50} increase was observed (1253.11 mg/l) (Fig. 4) with respect to inhibition observed in mitochondria without the use of SHAM. On the contrary, menthone showed a significantly decreased IC_{50} (125.39 mg/l, 0.82 mM) (Fig. 4) when compared to both SHAM untreated and treated mitochondria (351.38 mg/l) and significant lower IC_{50} values with respect to root respiration (169.07 mg/l, 1.11 mM) (Fig. 1). After treatment with SHAM, menthol and pulegone showed no inhibitory activity, by stimulating respiration for concentrations higher than 299.41 and 9.65 mg/l, respectively (Fig. 5). Even in this case spectrophotometric analyses indicate complete lack of interaction between SHAM and essential oil and oil components (data not shown).

When cucumber mitochondria are treated with SHAM (AO inhibitor), oxygen consumption by AO can be excluded (Vanlerberghe and McIntosh, 1997). The effect of SHAM on pulegone and menthol activity indicates that these two monoterpenes exert maximum inhibition of oxygen consumption when AO is active. The absence of interference between menthol, pulegone and SHAM supports these data. Partitioning of electrons through complex IV varies linearly with the degree of ubiquinone reduction and AO is not active until the level of reduced ubiquinone reaches a high threshold level (Dry et al., 1989). The increased menthone inhibition in the presence of SHAM could indicate a possible specific action on electron transfer chain from complex II (succinate dehydrogenase) to complex IV (cytochrome oxidase). On the other hand, the complete absence of inhibition by pulegone and menthol in the presence of SHAM indicates that these two monoterpenes might act on transfer of electrons from ubiquinone to complex III, thus triggering AO activity. Considering that AO accounts for 24% of cucumber respiration, an eventual diversion to AO would eventually reduce the total oxygen consumption by about 76%.

In conclusion, the mechanism by which peppermint essential oil and some of its oil components affect cucumber respiration is still unknown (Fisher, 1986, 1991). The greater inhibition shown when cucumber roots were exposed to terpenoids with respect to isolated mitochondria led us suggest that it is probably due to terpenoid interaction with cell walls and plasma membranes. This would trigger the initiation of a series of physiological responses via intracellular transduction pathways (Kombrink and Somssich, 1995). Besides, terpenes may interact by altering ion permeability and fluxes across the plasma membrane and possibly diverting oxygen toward

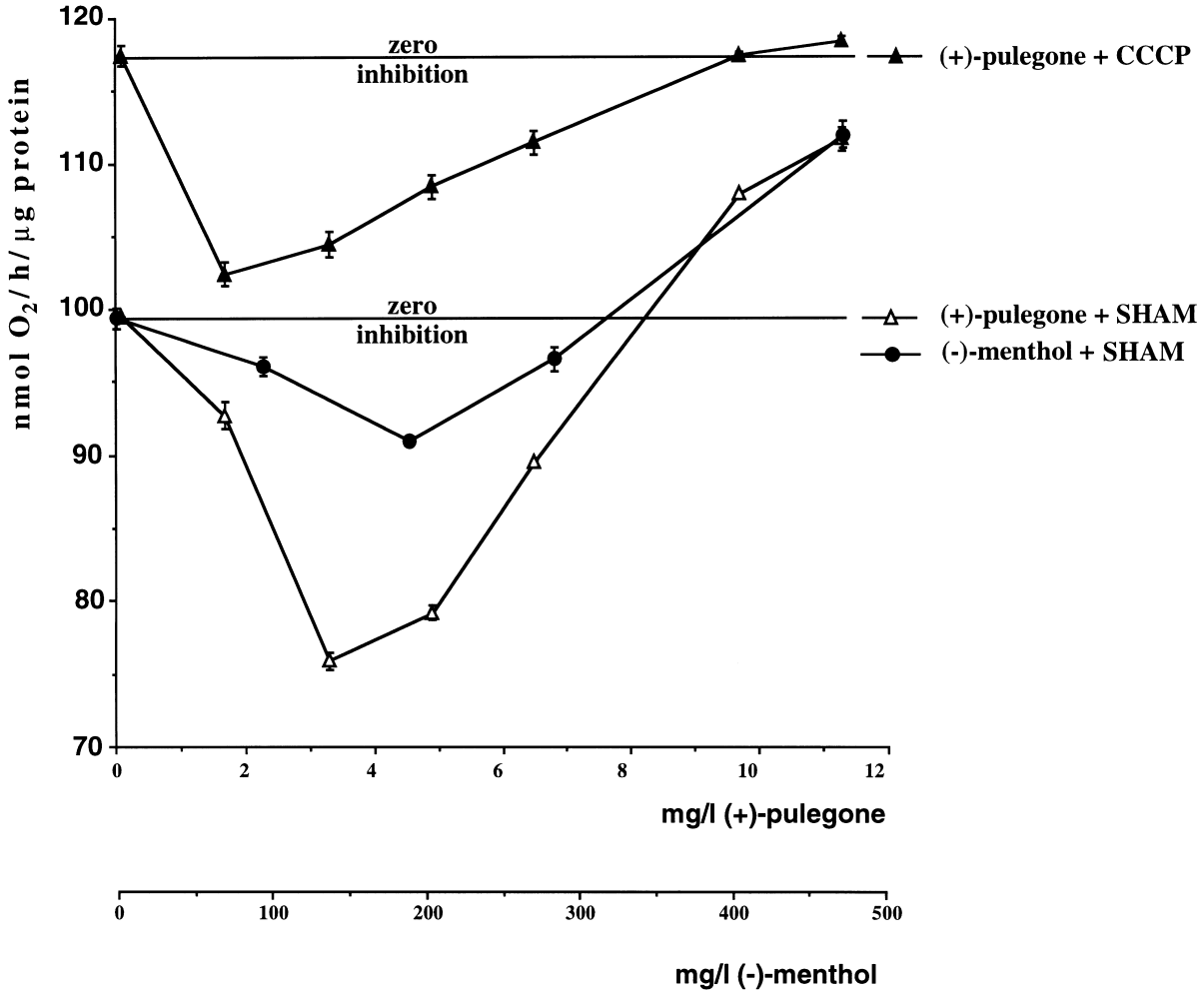

Fig. 5. Oxygen consumption in the presence of (+)-pulegone after treatment with CCCP and SHAM and in the presence of (−)-menthol after treatment with SHAM. Bars indicate standard deviation.

oxidative burst, as observed in some plant cell systems after elicitor treatments (Nürnberger et al., 1994).

3. Experimental

3.1. Plant material

Cucumber (*Cucumis sativus* L. var. "Piccolo di Parigi") seeds were grown as previously described (Maffei et al., 1999a). Peppermint (*Mentha×piperita* L.) plants are currently grown in experimental plots of the Botanical Garden of the University of Torino, and were distilled when in full bloom.

3.2. Essential oil distillation and chemicals

Peppermint oil was steam distilled by using a modified Clevenger apparatus. Distillation, GC analyses and compound identification were performed as reported elsewhere (Maffei et al., 1999b). (−)-Menthol, (−)-menthone and (+)-pulegone (purity >99%) were purchased from Sigma-Aldrich (Milan, Italy).

3.3. Mitochondria purification

Mitochondria isolation and purification were carried out at 4°C according to the protocol reported by Randall and Miernyk (1990) modified as follows. Roots from five day-old cucumber seedlings were harvested and homogenized in a solution (1:2 w/v) containing 0.3 M mannitol, 50 mM MOPS [3-(*N*-morpholino)-propanesulfonic acid] pH 7.2, 1 mM EDTA (ethylene diamine tetra acetic acid), 0.2% (w/v) defatted BSA (bovine serum albumine), 0.5% PVP-40 (polyvinylpyrrolidone), 2 mM L-cysteine and 10 mM 2-mercaptoethanol. The following procedures of mitochondria isolation, washing and purification were the same of Randall and

Miernyk (1990) with the exception for the use of 20 mM MOPS instead of TES in media in which mitochondria were resuspended and loaded on the Percoll density gradient, before centrifugation at 58.500×*g* (SW 41Ti rotor). All Percoll solutions contained 0.25 M sucrose, 10 mM MOPS pH 7.2, 0.1% defatted BSA (Randall and Miernyk, 1990).

Mitochondria, collected at the interface between 47 and 26% Percoll, were re-suspended and stored at 4°C overnight. Fixation and inclusion in resins for transmission electron microscopy were used for checking the purity of the mitochondrial fraction.

3.4. Oxygen consumption in root segments and mitochondrial preparations

Oxygen uptake was measured polarographically at 25°C with a Clark-type electrode (YSI Model 5300). A known amount of five-day-old root segments of 7 mm length were assayed in a 5 ml MES–NaOH 5 mM pH 6.00 solution. Mitochondrial respiration was measured in 2.5 ml respiration medium containing 0.25 M sucrose, 10 mM potassium phosphate buffer, 5 mM $MgCl_2$, 10 mM MOPS pH 7.4, with a known amount of mitochondrial protein. Protein content was measured according to Bradford (1976) and adjusted to 0.3–0.5 mg for each experiment. The integrity of mitochondria was verified using both HCN as respiratory chain inhibitor and the uncoupling agent CCCP (carbonyl-cyanide-*m*-chlorophenyl-hydrazone) (5 μM). Respiratory control and ADP:O ratios were calculated for each mitochondrial isolation as described by Estabrook (1967).

During mitochondrial experimentation, a constant state 3 respiratory rate, as defined by Chance and Williams (1955), with 10 mM succinate as respiration substrate was achieved before injection of the essential oils into the reaction chamber; the ADP:O ratio for succinate was 1.6. Total essential oil, (−)-menthol, (−)-menthone and (+)-pulegone, dissolved in methanol (= 0.4%), were tested in the range from 0 to 1500 ppm on both root segments and mitochondria. Methanol was present in both treated and control root/mitochondria preparations.

Essential oil effects on mitochondrial oxygen uptake was tested also after the treatment with the oxidative phosphorilation uncoupler CCCP (5 μM) and with the alternative oxidase inhibitor salicyl-hydroxamic acid (SHAM) supplied at 2 mM. Data are expressed as percentages of inhibition or stimulation of control respiration rate (state 3); IC_{50} values correspond to the concentration required to inhibit oxygen uptake by 50%.

3.5. Statistics

At least five replicates were performed for each experiment. The data obtained were analyzed by standard ANOVA using Systat 5.2 software for Macintosh. Significant differences are intended at $P < 0.05$. Linear and second-degree polynomial regressions were also calculated.

Acknowledgements

This work was supported by a M.U.R.S.T. grant (ex quota 60%). The authors are grateful to Jonathan Gershenzon for helpful discussion.

References

Adam, K., Sivropoulou, A., Kokkini, S., Lanaras, T., Arsenakis, M., 1998. Antifungal activities of *Origanum vulgare* subsp. Hirtum, *Mentha spicata*, *Lavandula angustifolia* and *Salvia fruticosa* essential oils against human pathogenic fungi. J. Agric. Food Chem. 46, 1739–1745.

Asplund, R.O., 1968. Monoterpenes: relationship between structure and inhibition of germination. Phytochemistry 7, 1995–1997.

Asplund, R.O., 1969. Some quantitative aspects of the phytotoxicity of monoterpenes. Weed Sci. 17, 454–455.

Bakerink, J.A., Gospe Jr., S.M., Dimand, R.J., Eldridge, M.W., 1996. Multiple organ failure after ingestion of pennyroyal oil from herbal tea in two infants. Pediatrics 98, 944–947.

Bradford, M.M., 1976. A rapid and sensitive method for the quantities of protein utilizing the principle of protein-dye binding. Anal. Biochem. 72, 248–254.

Brown, J.T., Hegaty, P.K., Charlwood, B.V., 1987. Mono- and sesquiterpene biosynthesis in plant cells in culture. Part 4. The toxicity of monoterpenes to plant cell cultures. Plant Sci. 48, 195–201.

Chance, B., Williams, G.R., 1955. Respiratory enzymes in oxydative phosphorylation III. The steady state. J. Biol. Chem. 217, 409–428.

Daie, J., Chin, C., Pitcher, L., 1987. Differential rates of sucrose and hexose transport by asparagus cell cultures. Plant Sci. 53, 101–107.

Deans, S.G., Waterman, P.G., 1993. Biological activity of volatile oils. In: Hay, R.K.M., Waterman, P.G. (Eds.), Volatile oil crops: their biology, biochemistry and production. Longman, Harlow, pp. 97–111.

Dry, I.B., Moore, A.L., Day, D.A., Wiskich, J.T., 1989. Regulation of alternative pathway activity in plant mitochondria: non linear relationship between electron flux and the redox poise of the quinone pool. Arch. Biochem. Biophys. 273, 148–157.

Economou, D., Nahrstedt, A., 1991. Chemical, physiological, and toxicological aspects of the essential oil of some species of the genus *Bystropogon*. Planta Med. 57, 347–351.

Estabrook, R.W., 1967. Mitochondrial respiratory control and the polarographic measurements of ADP:O ratios. Methods Enzymol. 10, 41–47.

Felle, H., 1988. Short-term pH regulation in plants. Physiol. Plant 74, 583–591.

Fischer, N.H., 1986. The function of mono and sesquiterpenes as plant germination and growth regulators. In: Putnam, A.R., Tang, C.-S. (Eds.), The science of allelopathy. Wiley-Interscience, New York, pp. 203–218.

Fischer, N.H., 1991. Plant terpenoids as allelopathic agents. In: Harborne, J.B., Tomas-Barberan, F.A. (Eds.), Ecological chemistry and biochemistry of plant terpenoids. Oxford Science Publications, Oxford, pp. 377–398.

Franzios, G., Mirotsou, M., Hatziapostolou, E., Kral, J., Scouras, Z.G., Mavragani-Tsipidou, P., 1997. Insecticidal and genotoxic activities of mint essential oils. J. Agric. Food Chem. 45, 2690–2694.

Hejl, A.M., Einhellig, F.A., Rasmussen, J.A., 1993. Effects of juglone on growth, photosynthesis and respiration. J. Chem. Ecol 19, 559–569.

Hendriks, H., 1998. Pharmaceutical aspects of some *Mentha* herbs and their essential oils. Perfum. Flav 23, 15–23.

Hills, J.M., Aaroson, P.I., 1992. The mechanism of action of peppermint oil on gastrointestinal smooth muscle. Gastroenterology 101, 55–65.

Inouye, S., Watanabe, M., Nishiyama, Y., Takeo, K., Akao, M., Yamaguchi, H., 1998. Antisporulating and respiration-inhibitory effects of essential oils on filamentous fungi. Mycoses 41, 403–410.

Kelsey, R.G., Reynolds, G.W., Rodriguez, E., 1984. The biologically active constituents secreted and stored in plant glandular hairs. In: Rodriguez, E.R., Healey, P.L., Mehta, I. (Eds.), Biology and Chemistry of Plant Trichomes. Plenum Press, New York, pp. 187–244.

Knobloch, K., Pauli, A., Iberl, B., Weigand, H., Weis, N., 1989. Antibacterial and antifungal properties of essential oil components. J. Essent. Oil Res. 1, 119–128.

Kombrink, E., Somssich, I.E., 1995. Defense responses of plants to pathogens. Adv. Bot. Res. 21, 1–34.

Lee, S., Tsao, R., Coats, J.R., 1999. Insecticidal activity of monoterpenoids to western corn rootworm (Coleoptera: Chrisomelidae), twospotted spider mite (Acari: Tetranychidae) and house fly (Diptera: Muscidae). J. Econ. Entomol 92 (1), 56–67.

Maffei, M., Sacco, T., 1987. Chemical and morphometrical comparison between two peppermint notomorphs. Planta Med. 2, 214–216.

Maffei, M., Bertea, C.M., Garneri, F., Scannerini, S., 1999a. Effect of benzoic acid hydroxy- and methoxy-ring substituents during cucumber (*Cucumis sativus* L.) germination. I. Isocitrate lyase and catalase activity. Plant Sci. 141, 139–147.

Maffei, M., Canova, D., Bertea, C.M., Scannerini, S., 1999b. UV-A effects on photomorphogenesis and essential-oil composition in *Mentha piperita*. J. Photochem. Photobiol 52, 105–110.

McClanahan, R.H., Thomassen, D., Slattery, J.T., Nelson, S.D., 1989. Metabolic activation of (R)-(+)-pulegone to reactive enonal that covalently binds to mouse liver proteins. Chem. Res. Toxicol 2, 349–355.

Molck, A.M., Poulsen, M., Tindgard Lauridsen, S., Olsen, P., 1998. Lack of histological cerebellar changes in Wistar rats given pulegone for 28 days. Comparison of immersion and perfusion tissue fixation. Toxicol. Lett. 31, 117–122.

Moreland, D.E., Novitzky, W.P., 1987. Effects of phenolic acids, coumarins and flavonoids on isolated chloroplasts and mitochondria. In: Allelochemicals: Role in Agriculture and Forestry. American Chemical Society, Washington, DC.

Morris, J.A., Khettry, A., Seitz, E.W., 1979. Antimicrobial activity of aroma chemicals and essential oils. J. Am. Oil Chem. Soc. 56, 595–599.

Muller, W.H., 1986. Allelochemical mechanisms in the inhibition of herbs by Chapparal shrubs. In: Putnam, A.R., Tang, C.-S. (Eds.), The science of allelopathy. Whiley-Interscience, New York, pp. 189–199.

Nelson, S.D., 1995. Mechanisms of the formation and disposition of reactive metabolites that can cause acute liver injury. Drug. Metab. Rev. 27, 147–177.

Nelson, S.D., McClanahan, R.H., Thomassen, D., Gordon, W.P., Knebel, N., 1992. Investigations of mechanisms of reactive metabolite formation from (R)-(+)-pulegone. Xenobiotica 22, 1157–1164.

Nürnberger, T., Nennstiel, D., Jabs, T., Sacks, W.R., Hahlbrock, K., Scheel, D., 1994. High affinity binding of a fungal oligopeptide elicitor to parsley plasma membranes triggers multiple defense responses. Cell 78, 449–460.

Randall, D.D., Miernyk, J.A., 1990. The mitochondrial pyruvate dehydrogenase complex. Methods Plant Biochem. 3, 182–183.

Rasmussen, J.A., Hejl, A.M., Einhellig, F.A., Thomas, J.A., 1992. Sorgoleone from root exudate inhibits mitochondrial functions. J. Chem. Ecol. 18 (2), 196–207.

Reynolds, T., 1987. Comparative effects of alicyclic compounds and quinones on inhibition of lettuce fruit germination. Ann. Bot 60, 215–223.

Rice, E.L., 1984. Allelopathy, 2nd Ed.. Academic Press, Orlando.

Robinson, T., 1983. The organic constituents of higher plants, 5th Ed.. Cordus Press, North Amherst, MA.

Slama, K., 1978. The principles of antihormone action in insects. Acta Entomol. Bohemoslov 75, 65–82.

Takeuchi, S., Tamaoki, L., Kondo, M., Konno, K., 1994. Effect of menthol on cytosolic Ca^{2+} levels in canine airway epithelium in culture. Biochem. Biophys. Res. Commun. 201, 1333–1338.

Taylor, B.A., Duthie, H.L., Luscombe, D.K., 1985. Calcium antagonist activity of menthol on gastrointestinal smooth muscle. Br. J. Clin. Pharm 20, 293–294.

Thomassen, D., Slattery, J.T., Nelson, S.D., 1990. Menthofuran-dependent and independent aspects of pulegone hepatotoxicity: roles of glutathione. J. Pharmacol. Exp. Ther. 253, 567–572.

Vanlerberghe, G.C., McIntosh, L., 1997. Alternative oxidase: from gene to function. Annu. Rev. Plant Physiol. Plant Mol. Biol. 48, 703–734.

PERGAMON

Phytochemistry 57 (2001) 99–102

PHYTOCHEMISTRY

www.elsevier.com/locate/phytochem

Antifungal activity of the essential oil of flowerheads of garland chrysanthemum (*Chrysanthemum coronarium*) against agricultural pathogens

Pino P. Alvarez-Castellanos [a], Chris D. Bishop [b], Maria J. Pascual-Villalobos [a,*]

[a] *Consejería de Agricultura, Agua y Medio Ambiente, Centro de Investigación y Desarrollo Agroalimentario, Estación Sericícola 30150 La Alberca, Murcia, Spain*

[b] *School of Biological and Earth Sciences, Liverpool John Moores University, Byrom Street, Liverpool L33AF, UK*

Received 14 June 2000; received in revised form 6 November 2000

Abstract

The antifungal activity of *Chrysanthemum coronarium* was evaluated against 12 agricultural pathogens. Flowerhead oil was active both in contact and headspace in vitro assays producing hyphal growth inhibition, although there was less activity on faster growing fungi. The main compounds identified in the oil were camphor (29.2%), α-pinene (14.8%), β-pinene (9.5%) and lyratyl acetate (9.8%). The blue color of the oil was due to the presence of chamazulene (0.5%). © 2001 Elsevier Science Ltd. All rights reserved.

Keywords: *Chrysanthemum coronarium*; Asteraceae; Garland chrysanthemum; Antifungal activity; Essential oil composition; Camphor; α-Pinene; β-Pinene; Lyratyl acetate

1. Introduction

The Anthemidae tribe of the family Asteraceae includes medicinal species of the genera *Artemisia, Achillea, Chamaemelum, Chamomilla* and *Tanacetum*. The volatile components of their essential oils exhibit strong odours and many of them have been used as flavourings. In addition, the oils of *Tanacetum* species are reported to possess antibacterial activity (Gören et al., 1990). Essential oils contain monoterpenoids, sesquiterpenoids and other non-terpenoid compounds. Some of them have been reported to exhibit a wide range of biological activities (Picman, 1986).

Many species within the genera *Pyrethrum* and *Chrysanthemum* have been transferred to the genus *Tanacetum*, including small pyrethrum [*T. cinerariifolium* (Trevir.) vis.] which is used for insecticide production. Only two species of *Chrysanthemum* (*C. coronarium* L. and *C. segetum* L.) are widely distributed in the Mediterranean, western Africa and Asia (Trehane, 1995). *C. coronarium* var. *coronarium* is an ornamental and can be found as a common weed, while *C. coronarium* var. *spatiosum*, is used as a Chinese vegetable (chop-suey). Green leaves and stems of *C. segetum* L. are also consumed as vegetables (Sánchez-Monge, 1991).

Flowerheads of *C. coronarium*, are typically bicolored white and yellow, or only yellow, and have been used as chamomile adulterants (Garg and Sastry, 1996). In Japan the leaves are used for suppression of fishy odours in prepared foods (Kasahara and Nishibori, 1995).

The chemical composition of *C. coronarium* leaves has been studied by other authors: polyacetylenic compounds have been isolated from the aerial parts and insect antijuvenile hormone activity has been detected for some of them (Bowers and Aregullin, 1987; Sanz et al., 1990). From flowerheads of *C. coronarium*, sesquiterpene lactones (cumambrin and dihydrocumambrin) have been isolated (El-Masry et al., 1984).

In recent years, there has been a clear tendency towards the utilization of alternative methods for pest and disease control in agriculture, that are less damaging to the environment and human health. Research on natural products including plant extracts which might substitute for agrochemicals or contribute to the development of new agents (Addor, 1995) for pest control is extremely important. Essential oils have properties as

* Corresponding author. Tel.: +34-68-366768; fax: +34-68-366792.
E-mail address: mjesus.pascual@carm.es (M.J. Pascual-Villalobos).

0031-9422/01/$ - see front matter © 2001 Elsevier Science Ltd. All rights reserved.
PII: S0031-9422(00)00461-1

fungicidal agents (Knobloch et al., 1987; Bishop and Thornton, 1996).

In this paper, we report the results of several bioassays to test activity of the essential oil of flowerheads of garland chrysanthemum (*C. coronarium*) by contact or by vapours against a panel of agricultural fungal pathogens. The chemical composition of this oil was also studied for the first time.

2. Results and discussion

The result of GC/MS analysis of the oil is summarized in Table 1. The main compounds identified were camphor (29.2%), α- and β-pinene (14.8 and 9.5%, respectively) and lyratyl acetate (9.8%). Significant amounts of camphene (5.2%), 2,7,7-trimethylbicyclo-[3.1.1]hept-2-en-6-ol acetate (3.8%), *p*-menthatriene (3.4%), germacrene D (2.7%) and α-phellandrene (2.6%) were also detected. Chamazulene, which gave the blue color to the oil, was present (0.5%).

To the best of our knowledge, this is the first report of the chemical composition of flowerheads of *C. coronarium*. Nevertheless, some compounds have been previously identified (Kameoka et al., 1975) from the leaf oil of *C. coronarium* L. var. *spatiosum*, although only α- and β-pinene and camphene were found in both cases.

The flowerhead oil of *C. coronarium* was active both in contact and on exposure to the headspace volatiles, since they both significantly reduced the growth of fungi in comparison with the control (although some exceptions are shown in Table 3). It should be mentioned, though, that results from the agar diffusion plate assay might also include some effects of the oil vapours besides the contact action.

Table 1
Chemical composition of the essential oil of flowerheads of *Chrysanthemum coronarium*

Component	Percentage (%)
α-Pinene	14.8
Camphene	5.2
α-Phellandrene	2.6
β-Pinene	9.5
4 Methylenecyclohexene	Trace
Limonene	0.7
β-Ocimene	0.3
Camphor	29.2
2,7,7-Trimethylbicyclo-[3.1.1]hept-2-en-6-ol acetate	3.8
Bornyl acetate	0.9
Lyratyl acetate	9.8
β-Caryophyllene	1.1
Germacrene D	2.7
p-Mentha-1,3,8-triene	3.4
Chamazulene	0.5
Total	84.5

In Table 2, the results indicate the growth of *Alternaria* sp., *Aspergillus flavus* and *Pythium ultimum* were highly reduced (>80%) when measured at the third day. Although no clear differences in activity could be observed for many fungi, the more resistant species were *Mycocentrospora acerina* and *Penicillium digitatum*.

In the volatile assay (Table 3), differences were obtained depending on species, e.g. *Fusarium moniliforme* was less affected than *P. ultimum*. The activity in the vapor phase was different for rapid growing species like *Botrytis cinerea* or *Sclerotinia sclerotiorum*, in which it changed from high inhibition (>70%) at day 3

Table 2
Growth inhibition of fungal species in agar diffusion plate assay by oil (20 μl/Petri dish) of *Chrysanthemum coronarium*

Species[a]	Day 3			Day 6		
	Treated (mm)	Control (mm)	Inhibition (%)[b]	Treated (mm)	Control (mm)	Inhibition (%)[b]
As	1	7	79.4***	2	16	84.0***
Ab	5	10	53.8***	7	17	57.3***
Af	2	11	82.6***	3	12	74.4***
Bc	13	32	60.1***	24	40	40.8***
Fm	6	12	51.2***	10	23	54.8***
Fs	6	8	25.9**	9	14	36.4***
Ma	8	8	4.7ns	13	16	20.0***
Pd	10	13	21.4*	17	20	13.0ns
Pu	0	11	95.5***	4	25	83.9***
Rs	8	13	38.1***	14	37	62.9***
Ss	27	36	24.2***	37	40	8.0*
Sl	5	19	74.6***	22	40	45.1***

[a] See Experimental for species tested.
[b] *t*-Test for comparison between treatment and control (ns = non-significant, $*P<0.05$, $**P<0.01$, $***P<0.001$).

Table 3
Growth inhibition of fungal species by volatile oil (10 μl/Petri dish) of *Chrysanthemum coronarium*

Species[a]	Day 3			Day 6		
	Treated (mm)	Control (mm)	Inhibition[b] (%)	Treated (mm)	Control (mm)	Inhibiton[b] (%)
As	1	4	84.2***	6	24	76.5***
Ab	2	10	82.4**	6	40	85.5***
Af	4	9	57.4**	13	34	62.2***
Bc	12	40	69.8***	77	77	0.0
Fm	6	9	36.4***	27	34	21.2***
Fs	6	6	−3.2ns	24	34	30.8***
Ma	7	9	22.2ns	35	34	−1.2ns
Pd	5	15	69.3***	29	43	32.4***
Pu	1	9	88.4***	5	38	87.8***
Rs	12	36	66.7***	54	68	20.5ns
Ss	3	52	93.5***	77	77	0.0
Sl	0	12	98.4***	28	70	60.5***

[a] See Experimental for species tested.
[b] *t*-Test for comparison between treatment and control (ns = non-significant, $*P<0.05$, $**P<0.01$, $***P<0.001$).

to covering all the dish at day 6, than for others like *Fusarium* sp. and *M. acerina* whose growth was further reduced over time (see Table 3). In general, growth inhibition percentages were high, with variations depending on the day of observation and the test species. The activity of *C. coronarium* oil is clear, Bishop and Thornton (1996) reported similar results for *Monarda citriodora* L. essential oil when using a dose ten times higher (100 μl).

In our experiments, the volatile activity found was significant but less persistent for fast growing species such as *S. sclerotiorum*, *R. solani* and *B. cinerea* (Table 3). An interesting observation from the bioassays was that *B. cinerea, P. digitatum* and *S. sclerotiorum* decreased spore production in the presence of oil (either by contact or from the headspace volatiles). Other authors have associated secondary metabolites with spore production (Dionigi et al., 1992); sporulation of *Streptomyces tendae* was inhibited by geosmin production (derived from a sesquiterpene precursor).

Tanacetum species contain similar compounds in their essential oils although α- and β-pinene are found in very low quantities in comparison with *C. coronarium*. *T. parthenium* (L.) Bernth is characterized by a high camphor (44%) and *trans*-chrysanthemyl acetate (23%) content. *T. vulgare* L. (Hendriks et al., 1990) contains also lyratyl acetate, thujone and germacrene (depending on chemotype). Mosquito repellent activity of these oils was proved but without identification of the active principles (De Pooter et al., 1989). Camphor and bornyl acetate (Schearer, 1984) were identified as some of the more active (repellent to potato beetles) of the mixture of products present in the oil of tansy (*T. vulgare*). Probably some of the compounds present in low amounts also contribute to these effects.

The blue color of the oils was attributed to the presence of chamazulene which is known to be produced during the steam distillation. Other members of Asteraceae such as *Chamomilla, Stevia, Artemisia* and *Achillea* also give azulenic compounds (Kaneko et al., 1971; Sacco et al., 1983; Acosta et al., 1989; Román et al., 1990; Abad et al., 1995). For example, chamazulene is being used in large quantities in the pharmaceutical and cosmetic industries.

3. Experimental

3.1. Fungal species

The fungi were obtained from the culture collection at Liverpool John Moores University (School of Biological and Earth Sciences). Cultures of each of the fungi were maintained on potato dextrose agar (PDA), slants stored at 5°C. The fungal species used in the experiments were: *Alternaria* sp. (As), *Alternaria brassicola* (Ab), *Aspergillus flavus* (Af), *Botrytis cinerea* (Bc), *Fusarium moniliforme* (Fm), *Fusarium solani* (Fs), *Mycocentrospora acerina* (Ma), *Penicillium digitatum* (Pd), *Pythium ultimum* (Pu), *Rhizoctonia solani* (Rs), *Sclerotinia sclerotiorum* (Ss) and *Serpula lacrymans* (Sl).

3.2. Essential oils

Essential oil of bicoloured flowerheads of *Chrysanthemum coronarium* L. was obtained by hydrodistillation using a Clevenger-type apparatus. Material was obtained from plants grown in an experimental plot (Torreblanca Exp. Stat., Campo de Cartagena) in Murcia (Spain). Plants were sown in autumn (26 October 1995) and samples were harvested in April. Voucher specimens (no. 207) were deposited in the Centro de Investigación y Desarrollo Agroalimentario (Murcia, Spain) Herbarium (CIDAHERB). Before distillation the flowerheads were freeze dried. The yield of oil was about 0.1%(v/w) and it had a blue color and a disagreeble smell.

3.3. Contact assay

PDA plates were prepared using 9 cm glass Petri dishes containing Twenty microlitres of PDA. A 1 cm disc of agar was removed from the centre of the Plates. Twenty microlitres of water (control) or undiluted oil was pipetted into the wells. Two 5 mm diam. discs of the test species were cut from the periphery of less than 1 week old cultures on PDA plates and placed mycelial surface down on opposite edges of the test plates against the sides of the dishes. The plates were incubated in the dark at 20°C. After 3 and 6 days of inoculation, extension of hyphae towards the central well was measured from the inner edge of the inoculum discs to the leading edges of colonies at a point nearest the well. Mean growth measurements were calculated from 10 replicates of each of the fungal species.

3.4. Volatile assay

PDA plates were prepared using 8.2 cm plastic Petri dishes containing 20 ml of PDA. A 5 mm diam. disc of the test species was cut from the periphery of the actively growing culture of the PDA plates and placed mycelial surface down on the centre of the dish. The Petri dishes were placed with the lid upside down. A 10 μl aliquot of water (control) or undiluted oil was pipetted on the lid without agar. The plates were incubated in the dark at 20°C. Mean growth measurements were calculated from 10 replicates of each fungal species.

3.5. Chemical analyses

The oil was analysed by GC/MS. Operating conditions were 240°C for the injection temperature and the

oven was initially at 70°C and was then gradually increased at a rate of 4°C/min up to 220°C and held for 120 s. The Supelcowax 10 capillary column (30 m × 0.25 mm) was used. For chamazulene identification, a SE-54 capillary column (25 m × 0.25 mm) was operated at similar conditions but the oven temperature was increased to 220°C and held for 1 h. Mass spectra were recorded with a 5970 HP Mass Selective detector, the electron impact source operating at 70 eV and 240°C. Identifications were made by retention indices and direct comparison with authentic standards.

3.6. Statistics

Growth inhibition of the treatment against the control was measured by percentage, using the formula (C-T/C) × 100 where C is hyphal extension (mm) of controls and T is hyphal extension (mm) of oil treated plates. A *t*-test was also computed for statistical significance of the results in the contact and volatile assays.

Acknowledgements

This research was funded by the National Institute for Agricultural Research in Spain with a PhD grant and the project SC98-022. We thank C. Armstrong and W. Harley, for their technical support in the bioassays. An special acknowledgement to M.V. Ruiz and M.C. Dobarganes of Instituto de la Grasa y sus Derivados (CSIC) in Sevilla for their help in the chemical analyses of the oil.

References

Abad, M.J., Bermejo, P., Villar, V., 1995. An approach to the genus *Tanacetum* L. (Compositae): Phytochemical and pharmacological review. Phytotherapy Research 9, 79–92.

Acosta, L., Granda, M., Sánchez, E., Martin, G., Rodriguez, E., 1989. Variation in the content of essential oil and (−)-α-bisabolol in camomile (*Matricaria recutita*) harvest of head flowers at different stages of development. Revista Plantas Medicinales 9, 25–32.

Addor, R.W., 1995. Insecticides. In: Godfrey, C.R.A. (Ed.), Agrochemicals from Natural Products. Marcel Dekker, New York, pp. 1–63.

Bishop, C.D., Thornton, I.B., 1996. Evaluation of the antifungal activity of the essential oils of *Monarda citriodora* var. *citriodora* and *Melaleuca alternifolia* on post harvest pathogens. Journal of Essential Oil Research 9, 77–82.

Bowers, W.S., Aregullin, M., 1987. Discovery and identification of an antijuvenile hormone from *Chrysanthemum coronarium*. In: Mem. Inst. Oswaldo Cruz (Intern. Symp. on Insects) Río de Janeiro 82 (Suppl. III), pp. 51–54.

De Pooter, H.L., Vermeesch, J., Schamp, N.M., 1989. The essential oil of *Tanacetum vulgare* L. and *Tanacetum parthenium* (L.) Schultz-Bip. Journal of Essential Oil Research 1, 9–13.

Dionigi, C.P., Millie, D.F., Spanier, A.M., Johnsen, P.B., 1992. Spore and geosmin production by *Streptemyces tendae* on several media. Journal of Agricultural and Food Chemistry 40, 122–125.

El-Masry, S., Abou-Dania, A.H.A., Darwish, F.A., Abou-Karum, M.A., Grenz, M., Bohlmann, F., 1984. Sesquiterpene lactones from *Chrysanthemum coronarium*. Phytochemistry 23, 2953–2954.

Garg, S., Sastry, T.C.S., 1996. Indian Compositae. foods and flavours, a review. In: Caligari, P.D.S., Hinds, D.J.N. (Eds.), Compositae: Biology and utilization, Proceedings of the International Compositae Conference, Vol 2, RBG Kew, UK, pp. 381–382.

Gören, N., Jakupovic, J., Topal, S., 1990. Sesquiterpene lactones with antibacterial activity from *Tanacetum argyrophyllum* var. *argyrophyllum*. Phytochemistry 29, 1467–1469.

Hendriks, H., Van der Elst, D.J.D., Van Putten, F.M.S., Bos, R., 1990. The essential oil of dutch tansy (*Tanacetum vulgare* L.). Journal of Essential Oil Research 2, 155–162.

Kameoka, H., Kitagawa, C., Husebe, Y., 1975. The constituents of the steam volatile oil from *Chrysanthemum coronarium* L. var *spatiosum*. Journal of Agricultural Chemical Society of Japan 49, 625–627.

Kaneko, H., Naruto, S., Takahashi, S., 1971. Sesquiterpenes of *Achillea subirica*. Phytochemistry 10, 3305–3306.

Kasahara, K., Nishibori, K., 1995. The suppressing effect of garland chrysanthemum on the odor of nishibori soup stock. Fisheries Sciences 61, 672–674.

Knobloch, K., Pauli, A., Iberi, B., Weis, N., Weigand, H., 1987. Mode of action of essential oil components on whole cells of bacteria and fungi in plate tests. In: Schreier, P. (Ed.), Bioflavor 87: Analysis, Biochemistry, Biotechnology (Proceedings of the International Conference, 29–30 September 1987), Würzburg, Germany, Walter de Gruyter, Berlin, pp. 287–299.

Picman, A.K., 1986. Biological activities of sesquiterpene lactones. Biochemical Systematics and Ecology 14, 255–285.

Román, L.U., Mora, Y., Hernández, J.D., 1990. *Stevia serrata*, a source of chamazulene. Fitoterapia 61, 84.

Sacco, T., Frattini, C., Bicchi, C., 1983. Constituents of essential oil of *Artemisia arborescens*. Planta Med. 47, 49–51.

Sánchez-Monge, E., 1991. Flora Agrícola, Tomo. I. MAPA, Madrid.

Sanz, J.F., Falco, E., Marco, J.A., 1990. New acetylenes from *Chrysanthemum coronarium* L. Liebigs Ann. Chem., 303–305.

Schearer, W.R., 1984. Components of oil of tansy (*Tanacetum vulgare*) that repel colorado potato beetles (*Leptinotarsa decemlineata*). Journal of Natural Products 47, 964–989.

Trehane, P., 1995. Proposal to conserve *Chrysanthemum* L. with a conserved type (Compositae). Taxon 44, 439–441.

PERGAMON

Phytochemistry 57 (2001) 103–107

PHYTOCHEMISTRY

www.elsevier.com/locate/phytochem

A sesquiterpene drimane with antinociceptive activity from *Drimys winteri* bark

Angela Malheiros [a], Valdir Cechinel Filho [b], Clarisse B. Schmitt [a], Adair R.S. Santos [b], Cristiano Scheidt [c], João B. Calixto [c], Franco Delle Monache [d], Rosendo A. Yunes [a,*]

[a] *Departamento de Química, Campus Universitário, Trindade, Universidade Federal de Santa Catarina (UFSC), 88040-900, Florianópolis, SC, Brazil*
[b] *Núcleo de Investigações Químico-Farmacêuticas (NIQFAR)/CCS, Universidade do Vale do Itajaí (UNIVALI), 88302-202, Itajaí, SC, Brazil*
[c] *Departamento de Farmacologia, Campus Universitário, Trindade, Universidade Federal de Santa Catarina (UFSC), 88040-900, Florianópolis, SC, Brazil*
[d] *Centro Chimica Recettori, CNR, Universitá Cattolica Del Sacro Cuore, Largo F. Vito 1, 00168, Rome, Italy*

Received 8 March 2000; received in revised form 20 November 2000

Abstract

Along with three known drimanes, polygodial, 1-β-(*p*-methoxycinnamoyl) polygodial and mukaadial, the sesquiterpene drimane named drimanial was isolated from the bark of *Drimys winteri* (Winteraceae). Its structure was elucidated based on spectroscopic evidence. Drimanial exhibited antinociceptive action against acetic acid induced pain, being about 3-fold less active than polygodial. © 2001 Elsevier Science Ltd. All rights reserved.

Keywords: *Drimys winteri*; Winteraceae; Antinociception; Sesquiterpene drimane; Drimanial

1. Introduction

Drimys winteri (J.R. Forst and G. Forst) is a plant used in the folk medicine of many countries, including Brazil, to treat several ailments, such as inflammatory and dolorous processes (Houghton and Manby, 1985). Phytochemical studies have demonstrated that this plant contains mainly sesquiterpenes of the drimane type (Cruz and Silva, 1973; Sierra et al., 1986; Brown, 1994; Cechinel Filho et al., 1998), and flavonoids (Cruz and Silva, 1973; Williams and Harvey, 1982; Reyes et al., 1990; Torres et al., 1992; Cechinel Filho et al., 1998). These drimanes have attracted particular interest because of their antifeedant, plant growth regulation, cytotoxic, antimicrobial and insecticidal properties (Jansen and Groot, 1991).

In previous studies, we showed that the hydroalcoholic extract obtained from *D. winteri* bark exhibits anti-asthmatic, anti-allergic, anti-inflammatory and antinociceptive effects (El Sayah et al., 1997; Tratsk et al., 1997; Mendes et al., 1998). These effects were related, at least partially, to the presence of polygodial (**1**), a sesquiterpene drimane, which is the main component of the plant (Cechinel Filho et al., 1998; El Sayah et al., 1998; Mendes et al., 1998; Andre et al., 1999; Mendes et al., 2000; El Sayah et al., 2000)

In the present study, we have investigated other components present in the *D. winteri* bark and isolated a new compound named drimanial (**2**), together with polygodial (**1**), 1-β-(*p*-methoxycinnamoyl) polygodial (**3**) and mukaadial (**4**). The preliminary antinociceptive effect of drimanial was analyzed against acetic acid induced pain in mice.

2. Results and discussion

Drimanial **2** ($C_{25}H_{30}O_6$) displays a ^{1}H NMR spectrum with signals for two aldehydes (δ 9.36, *s* and δ 9.78, *d*, $J = 3.3$ Hz), one olefinic proton (δ 7.04), three methyl singlets (δ 1.06, 1.17 and 1.23) and a *p*-methoxycinnamoyl residue (δ 3.86, *s*, OMe; δ 7.64 and 6.99, *d*, $J = 8.9$ Hz, 2 H each; δ 7.60 and 6.25, *d*, $J = 16$ Hz). The complete assignment of ^{1}H, ^{13}C NMR parameters for **2** are reported in Table 1 and are the result of one and two bond HETCOR experiments (Table 2). Comparison of

* Corresponding author. Tel.: +55-48-331-9219; fax: +55-48-331-9711.

E-mail address: ryunes@qmc.ufsc.br (R.A. Yunes).

0031-9422/01/$ - see front matter © 2001 Elsevier Science Ltd. All rights reserved.
PII: S0031-9422(00)00515-X

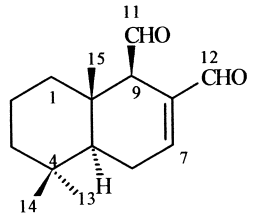

1

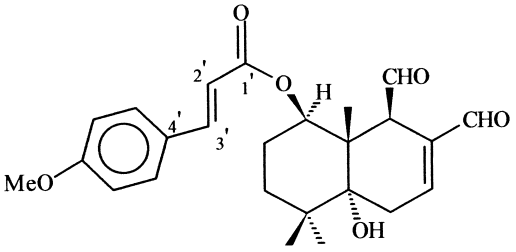

2

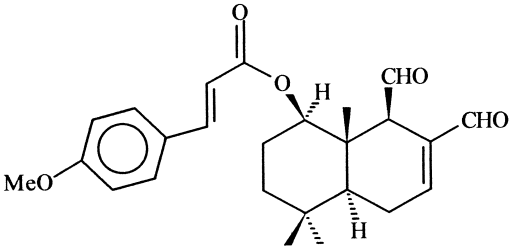

3

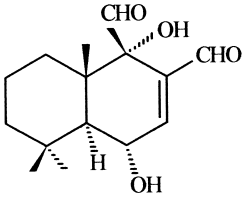

4

the ^{13}C NMR spectral data with those of 1-β-(*p*-methoxycinnamoyl) polygodial **3**, $C_{25}H_{30}O_5$ (Table 1), there was an additional oxygen present in drimanial in position 5. The paramagnetic shift of the signals due to C-4, C-6 and C-10 (α effect), and the diamagnetic shift observed for the signals to C-3, C-7 and C-9 (βeffect) support this assignment. The correctness of the assigned structure for drimanial (**2**) and of the NMR spectral parameters was further supported by the long-range connectivity reported in Table 2. In particular, in the long range NMR spectrum, the resonance at δ 78.1 assigned to C-5 shows a cross peak with Me-13; conversely, in the

Table 1
NMR spectral data for compounds **2** and **3** in acetone-d_6[a]

		2	**3**
Position	^1H	^{13}C	^{13}C
1	5.35 *dd*	77.6	81.5
2	1.82 *m*	25.0	24.9
3	2.04; 1.27 *m*	35.1	39.8
4		38.9	33.3
5		78.1	49.0
6	2.93 *dt*; 2.52 *dddd*	32.6	27.5
7	7.04 *q*	150.7	153.5
8		141.4	140.7
9	3.73 *br s*	56.3	60.2
10		47.4	42.8
11	9.78 *d*	201.2	200.3
12	9.36 *s*	193.2	193.2
13	1.06 *s*	27.7	32.7
14	1.23 *s*	25.6	22.2
15	1.17 *s*	13.5	10.9
1′		166.4	166.4
2′	6.35 *d*	116.7	116.6
3′	7.60 *d*	145.2	145.3
4′		127.9	127.9
5′, 9′	7.64 *d*	130.8	130.9
6′, 8′	6.99 *d*	115.2	115.2
7′		162.5	162.5
Ome	3.86 *s*	55.6	55.7
OH	3.80 *s*		

[a] *J* (Hz): J_{1-2}, 11.6 and 4.9; J_{6gem}, 20.0; J_{6-7}, 5.5 and 1.8; J_{11-9}, 3.3; $J_{2'-3'}$, 16.0; $J_{5'-6'}$, $J_{8'-9'}$, 8.9.

Table 2
Long-range connectivities for compound **2**

C-H[a]		H–C[b]	
C-3	1.06 (MeH-13)	H-1	166.4 (C-1′), 56.3 (C-9), 47.4 (C-10), 13.5 (Me-15)
C-4	1.06 (MeH-13)	H_2-6	150.7(C-7), 141.4 (C-8)
	1.23 (MeH-14)		47.4 (C-10), 78.1 (C-5)
C-5	1.06 (MeH-13)	H-11	141.4 (C-8)
C-10	1.17 (MeH-15)	H-12	56.3 (C-9)
C-7′	7.64 (H-5′/H-9′)	MeH-13	78.1(C-5), 38.9 (C-4) 35.1 (C-3)
C-4′	6.99 (H-6′/H-8′)	MeH-14	78.1(C-5), 38.9 (C-4) 35.1 (C-3)
		MeH-15	78.1(C-5), 77.6 (C1) 56.3 (C-9), 47.4 (C-10)

[a] Long range HETCOR.
[b] Selective INEPT experiments.

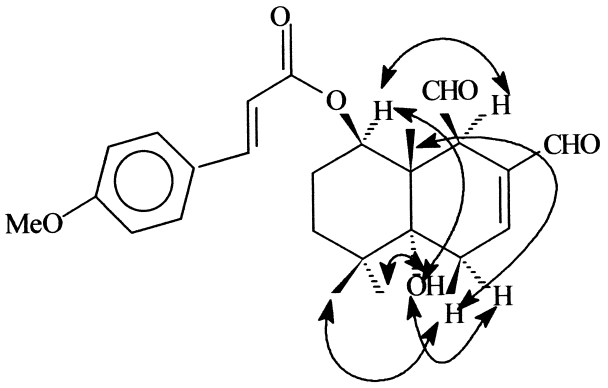

Fig. 1. DIF NOE compound **2**.

Table 3
Antinociceptive action of polygodial **1**, drimanial **2** and 1-β-(*p*-methoxycinnamoyl) polygodial **3** isolated from *Drimys winteri* bark against acetic acid induced abdominal constriction in mice

Compound	ID_{50} (μmol/kg, i.p.)[a]	MI (%)[b]
Polygodial **1**[c]	3.6 (2.6–5.0)	90±3
Drimanial **2**	11.0 (10.3–11.5)	92±3
1-β-(*p*-methoxycinnamoyl) polygodial **3**[c]	16.0 (12.0–21.0)	93±3
Aspirin[d]	133.1 (73.0–243.3)	83±2
Acetaminophen[d]	125.0 (104.0–250.0)	88±1

[a] With their respective 95% confidence limits.
[b] Maximal inhibition, MI.
[c] Data from Cechinel Filho et al., 1998.
[d] Data from Vaz et al., 1996.

INEPT experiments, the selective irradiation of each methyl signal (δ 1.23, δ 1.17 and δ 1.06) gave a response, inter alia, to the quaternary oxygenated carbon. Finally, the difference NOE spectra (Fig. 1) indicated that H-9, H-1, Me-13 and OH-5 are on the same side of the molecule, establishing the stereochemistry of **2** (Vichnewski et al., 1986).

Polygodial **1** and mukaadial **4** were identified by comparison of the spectral data with that reported in the literature (Brown, 1994; Mashimbye et al., 1999). However, mukaadial is reported for the first time in this genus. No reports were found on the ^{13}C NMR for 1-β-(*p*-methoxy cinnamoyl) polygodial **3** (Ferreto et al., 1988). Thus, the ^{13}C NMR spectral data for **3** are presented in Table 1 in this paper.

The in vivo pharmacological studies revealed that drimanial (**2**) produced a dose-related and almost complete inhibition of abdominal constrictions elicited by acetic acid. At the ID_{50} level, drimanial exhibited the same potency as 1-β-(*p*-methoxycinnamoyl) polygodial but it was about 3-fold less potent than polygodial in antagonizing acetic acid-induce nociception. However, drimanial was about 11- to 12-fold more potent than the positive control drugs aspirin and acetaminophen (Table 3).

In conclusion, results of the current study and those previously reported by our group indicated that a mixture of at least 3 sesquiterpenes, identified as being polygodial, 1-β-(*p*-methoxycinnamoyl) polygodial and drimanial, seem to be the main constituents present in the bark of the plant *Drymis winteri*, being responsible for the remarkable antinociceptive, anti-inflammatory and anti-allergic actions reported by the crude extract of this plant (Tratsk et al., 1997; Mendes et al., 1998, 2000). Considering the relatively higher concentrations of polygodial and to a lesser extenct, drimanial in the bark of *D. winteri*, it can be suggested that the 2 sesquiterpenes are the most relevant active compounds and responsible for the major pharmacological action of the plant.

3. Experimental

3.1. General experimental procedures

Optical rotations were recorded on a polarimeter Schmidt + Haensch Polartronic E Eloptron. IR spectra were recorded on FTIR 16 PC Perkin-Elmer aparatus (KBr film). ^1H (300 MHz) and ^{13}C (75.5 MHz) NMR were determined on a Varian Gemini 300 Spectrometer in acetone-d_6 with TMS as internal standard. MS were recorded on a Shimadzu-14 spectrometer in the electron impact mode (EI–MS) at 70 eV. Elemental analysis was determined in elemental CHN Perkin-Elmer 2400. CC: silica gel 60 (230–400 mesh); TLC: silica gel plates F_{254} (0.25 mm in thickness).

3.2. Plant material

Drimys winteri (Winteraceae) was collected in Bom Retiro (State of Santa Catarina, Brazil) in January 1994 and identified by Professor Leila da Graça Amaral (Department of Botany, Universidade Federal de Santa Catarina). A voucher specimen was deposited in the Herbarium Flor (UFSC) under number 26313.

3.3. Isolation

Air-dried powdered bark (1.5 kg) was extracted at room temperature with $CHCl_3$ for 7 days. Solvent was removed (in vacuo) to obtain the $CHCl_3$ extract (27 g). The extract was roughly fractionated by silica gel CC, eluting with *n*-hexane, EtOAc, MeOH mixtures of increasing polarity. Extended purification of the fraction eluted with hexane–EtOAc 9:1 yielded polygodial **1** (2.53 g). In a similar manner, the fraction eluted with hexane–EtOAc 8:2 gave mukaadial **4** (17 mg), hexane–EtOAc 6:3 gave 1-β-(*p*-methoxycinnamoyl) polygodial **3** (25 mg), and that eluted with hexane–EtOAc 1:1 afforded drimanial **2** (362 mg).

3.4. Acetic acid-induced abdominal constriction

Non-fasted male Swiss mice (25–35 g), housed at 22±2°C under a 12-h light/12 h-dark cycle and with access to food and water ad libitum, were acclimatised to the laboratory for at least 1 h before testing and were used throughout the experiments. The abdominal constrictions resulting from intraperitoneal injection of acetic acid (0.6%), consisting of a contraction of the abdominal muscle together with a stretching of hind limbs, was carried out according to the procedure described previously (Vaz et al. 1996; Mendes et al., 1998). Animals (6 to 8 per group) were treated with different doses of drimanial (2.3–23.5 μmol/kg, i.p.) or with vehicle (Tween 80 plus 0.9% NaCl solution) used to dilute the sesquiterpene (10 ml/kg, i.p.), 30 min prior to injection of acetic acid. Antinociceptive activity was expressed as the reduction in the number of abdominal constrictions, i.e. the difference between the control animals (vehicle pre-treated mice) and the mice pre-treated with drimanial.

3.5. Statistical analysis

Results are presented as mean±S.E.M., except the ID_{50} values (i.e. the dose of drugs reducing the nociceptive response by 50% relative to control value), which are reported as geometric means accompanied by their respective 95% confidence limits. The ID_{50} values were determined by linear regression from individual experiments using linear regression Graph Pad software (Graph Pad Software, San Diego, CA). The statistical significance between groups was performed by ANOVA followed by Dunnett's multiple comparison test. P values less than 0.05 ($P<0.05$) were considered as indicative of significance.

3.6. Drimanial 2

Amorphous powder. Mp 95–97°, $[\alpha]_D^{25}+43.2°$ ($CHCl_3$; c 0.926), IR ν_{max} cm^{-1}; 3482, 2928, 2854, 2732, 1710, 1682, 1632 and 1602. ^1H NMR (300 MHz, acetone-d_6) and ^{13}C NMR (75.5 MHz, acetone-d_6) in Table 1. IEMS: m/z (rel. int.) 426 [M^+] (1.2), 398 (0.5), 380 (0.5), 202 (7.6), 178 (25), 161 (100), 145 (12), 133 (13.6), 118 (7.6), 91 (6.5), 77 (7.6). Elemental analysis results, found: C, 70.25; H, 7.15. $C_{25}H_{30}O_6$ requires: C, 70.40; H, 7.09%.

3.6.1. 1-β-(p-Methoxycinnamoyl) polygodial **3**

^1H NMR (300 MHz, acetone-d_6) δ 9.71 (1H, *d*, $J=3.3$ Hz, H-11), 9.35 (1H, *s*, H-12), 7.65 (2H, *d*, $J=9.0$Hz, H-5′, H-9′), 7.60 (1H, *d*, $J=16.0$ Hz, H-3′), 7.22 (1H, *q*, H-7), 7.00 (2H, *d*, $J=9.0$ Hz, H-6′ and H-8′), 6.37 (1H, *d*, $J=16.0$ Hz, H-2′), 4.88 (1H, *dd*, $J=11.0$ and 4.0 Hz, H-1), 3.83 (3H, *s*, OMe), 3.30, (1H, *br s*, H-9), 2.52 (2H, *m*, H-6), 2.05 (H-3a, partially overlapped by the solvent) 1.80 (2H, *m*, H-2), 1.56 (2H, *m*, H-5), 1.28 (1H, *m*, H-3b) 1.09 (3H, *s*, Me 13), 1.03 (3H, *s*, Me 14), 0.98 (3H, *s*, Me 15). ^{13}C NMR (75.5 MHz, acetone-d_6) in Table 1. IEMS: m/z (rel. int.) 410 [M^+] (2), 328 (25), 178 (40), 161 (100), 43 (70). Elemental analysis results, found: C, 73.02; H, 7.46. Calc. for $C_{25}H_{30}O_5$: C, 73.14; H, 7.37%.

Acknowledgements

The authors are grateful to Dr. Leila da Graça Amaral (Department of Botany, UFSC, Florianópolis) for classification of the plant. The work was supported by grants from CNPq and FINEP, Brazil.

References

André, E., Malheiros, A., Cechinel Filho, V., Yunes, R.A., Calixto, J.B., 1999. Mechanisms underlying the endothelium-dependent and independent relaxation caused by the sesquiterpene polygodial in vessels from rabbit and guinea-pig in vitro. European Journal of Pharmacology 386, 47–53.

Brown, G.D., 1994. Drimenol, a sesquiterpene from *Drimys winteri*. Phytochemistry 35 (4), 975–977.

Cechinel Filho, V., Schlemper, V., Santos, A.R.S., Pinheiro, T.R., Yunes, R.A., Mendes, G.L., Calixto, J.B., Delle Monache, F., 1998. Isolation and identification of active compounds from *Drimys winteri* barks. J. Ethnopharmacol. 62, 223–227.

Cruz, A., Silva, M., 1973. Further terpenoids and phenolics of *Drimys winteri*. Phytochemistry 12, 2549–2550.

El Sayah, M., Cechinel Filho, V., Yunes, R.A., Calixto, J.B., 1997. Action of the extract of *Drimys winteri* on contraction induced by inflammatory mediators, compound 40/80 and ovalbumin of the guinea pig trachea in vitro. Gen. Pharmacol. 28, 699–704.

El Sayah, M., Cechinel Filho, V., Yunes, R.A., Pinheiro, T.R., Calixto, J.B., 1998. Action of polygodial, a sesquiterpene isolated from *Drimys winteri* in the guinea pig ileum and trachea in vitro. Eur. J. Pharmacol. 344, 215–221.

El Sayah, M., Cechinel Filho, V., Yunes, R.A., Malheiros, A., Calixto, J.B., 2000. Action of polygodial on agonist induced contraction of the rat portal vein in vitro. J. Cardiovas. Pharmacol. 35 (4), 670–675.

Ferreto, L., Ciccio, J.F., Castro, V., Andrade, R., 1988. Drimane derivates from *Drimys granadensis* L. F. (Winteraceae). Spectroscopy Int. J. 6, 133–136.

Houghton, P.J., Manby, J., 1985. Medicinal plants of the Mapuche. J. Ethnopharmacol. 13, 89–103.

Jansen, B.J.M., Groot, A., 1991. The occurrence and biological activity of drimane sesquiterpenoids. Nat. Prod. Rep. 8 (3), 309–318.

Mashimbye, M.J., Maumela, M.C., Drewes, S.E., 1999. A drimane sesquiterpenoid lactone from *Warburgia salutaris*. Phytochemistry 51, 435–438.

Mendes, G.L., Santos, A.R.S., Campos, M.M., Tratsk, K.S., Yunes, R.A., Cechinel-Filho, V., Calixto, J.B., 1998. Anti-hiperalgesic properties of the extract and the main sesquiterpene polygodial isolated from the barks *Drimys winteri*. Life Sciences 63 (5), 369–381.

Mendes, G.L., Santos, A.R.S., Malheiros, A., Cechinel Filho, V., Yunes, R.A., Calixto, J.B., 2000. Assessment of mechanisms involved in antinociception caused by sesquiterpene polygodial. J. Pharmacol. Exp. Ther. 292, 164–172.

Reyes, A., Reyes, M., Alveal, A., García, H., 1990. Compuestos fenolicos de *Drimys winteri* Forst variedad andina. Rev. Latinoamer. Quím 2 (1), 42.

Sierra, J.R., López, J.T., Cortés, M.J., 1986. (−)-3β-Acetoxydrimenin from the leaves of *Drimys winteri*. Phytochemistry 25 (1), 253–254.

Torres, R., Pardo, F., Velasco, M.V., 1992. Flavonoid from *Drimys winteri*. Fitoterapia 6, 553–558.

Tratsk, K.S., Campos, M.M., Vaz, Z.R., Cechinel Filho, V., Schlemper, V., Yunes, R.A., Calixto, J.B., 1997. Anti-allergic effects and oedema inhibition caused by the extract of *Drimys winteri*. Inflamm. Res. 46, 509–514.

Vaz, Z.R., Cechinel Filho, V., Yunes, R.A., Calixto, J.B., 1996. Antinociceptive action of 2-(4-bromobenzoyl)-3-methyl-4-6-dimethoxybenzofuran, a novel xanthoxyline derivative on chemical and thermal models of nociception in mice. J. Pharmacol. Exp. Ther. 278, 304–312.

Vichnewki, W., Kulanthaivel, P., Herz, W., 1986. Drimane derivates from *Drimys brasiliensis*. Phytochemistry 25 (6), 1476–1478.

Williams, C.A., Harvey, W.J., 1982. Leaf flavonoid patterns in the Winteraceae. Phytochemistry 21 (2), 329–337.

PERGAMON

Phytochemistry 57 (2001) 109–113

PHYTOCHEMISTRY

www.elsevier.com/locate/phytochem

Allelopathic sesquiterpenoids from rhizomes of *Petasites japonicus* ssp. *giganteus* Kitam

Yoko Goto [a], Yasuo Kojima [b,*], Tomoki Nakayama [b], Minoru Terazawa [b]

[a] *Forest Tree Breeding Center, Ishi 3809-1, Juo, Taga, Ibaraki 319-1301, Japan*
[b] *Department of Forest Science, Faculty of Agriculture, Hokkaido University, Sapporo 060-0809, Japan*

Received 5 March 1999; received in revised form 6 November 2000

Abstract

Four sesquiterpenoids were isolated from *Petasites japonicus* (Siebold and Zucc.) Maxim. ssp. *giganteus* (F. Schmidt ex Trautv.) Kitam. (Compositae, Japanese name: Akitabuki) as allelochemicals. Their structures were elucidated on the basis of spectroscopic methods and their allelopathic effects were assessed. © 2001 Elsevier Science Ltd. All rights reserved.

Keywords: *Petasites japonicus* ssp. *giganteus* Kitam; Compositae; Rhizomes; Eremophilane derivatives; Allelopathy

1. Introduction

Petasites japonicus (Siebold & Zucc.) Maxim. ssp. *giganteus* (F. Schmidt ex Trautv.) Kitam is mainly distributed in the eastern area of Hokkaido, Japan. *P. japonicus* ssp. *giganteus* appears early in secondary succession and extends by rapid vegetative propagation via rhizomes. It is sometimes observed in forests where *P. japonicus* ssp. *giganteus* dominates in a place where trees are lacking and the vegetation beneath the plant is poor. These observations suggest that *P. japonicus* ssp. *giganteus* is allelopathic. In this investigation, we isolated four sesquiterpenoids from rhizomes of *P. japonicus* ssp. *giganteus* and determined their allelopathic effects on seed germination and seedling growth of lettuce (*Lactuca sativa* L.). Two were novel nor-eremophilane derivatives (**1, 3**), one was a novel dinor-eremophilane derivative (**2**), and the other was eremophilenolide (**4**). Although many reports about isolation of eremophilane derivatives from *Compositae* species have been published (Novoton et al., 1963; Sugama et al., 1985; Yaoita et al., 1996; Tori et al., 1997; Zhao et al., 1997), only a few have reported either nor- (Yaoita et al., 1994) or dinor-eremophilane derivatives (Yaoita et al., 1996).

2. Results and discussion

2.1. Allelopathic effects of *P. japonicus* ssp. *giganteus* rhizomes

Allelopathic effects of *P. japonicus* ssp. *giganteus* rhizomes were determined by seed germination and seedling growth test of lettuce with milled powder of freeze-dried rhizomes of *P. japonicus* ssp. *giganteus*. The results showed that *P. japonicus* ssp. *giganteus* had an inhibitory effect on the seedling growth of lettuce (Fig. 1).

Extracts from freeze-dried rhizomes of *P. japonicus* ssp. *giganteus* were divided into four fractions based on their solubilities in organic solvents, i.e. *n*-hexane, ethyl acetate, ethyl alcohol and water extracts, respectively. The effects of each fraction were estimated at 67 ppm, using the same method as used for the rhizome powder (Fig. 1). It was found that all of fractions, except for ethyl alcohol soluble fraction, had a significant inhibitory effect on lettuce seedling growth ($P < 0.01$, *t*-test), and that the *n*-hexane and water soluble fractions had a higher inhibitory effect than ethyl acetate soluble fraction. The *n*-hexane fraction was selected for further study.

2.2. Isolation and elucidation of allelochemicals

The *n*-hexane extract of fresh rhizomes of *P. japonicus* ssp. *giganteus* was subjected to a combination of silica

* Corresponding author. Fax: +81-11-706-3634.
E-mail address: koji@for.agr.hokudai.ac.jp (Y. Kojima).

0031-9422/01/$ - see front matter © 2001 Elsevier Science Ltd. All rights reserved.
PII: S0031-9422(00)00506-9

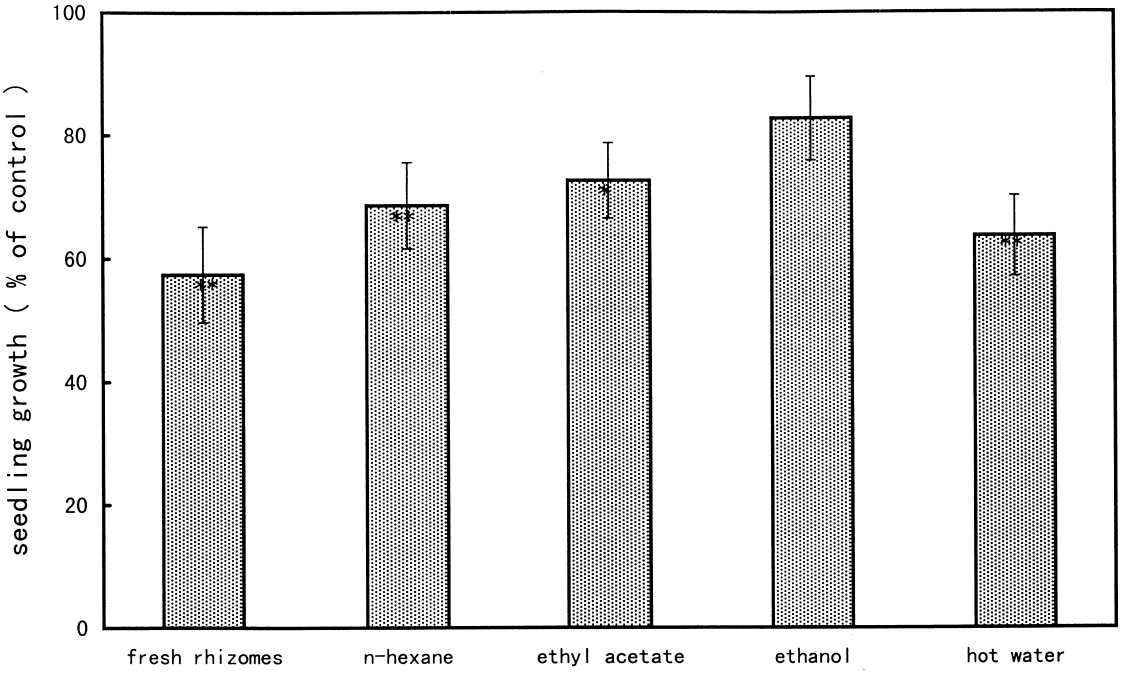

Fig. 1. Effects of *P. japonicus* ssp. *giganteus* rhizomes on seedling growth of lettuce. Vertical bars mean ±S.E. *,**; *t*-test significantly different from the control at 0.05 and 0.01 levels respectively.

gel CC, prep. TLC and prep.HPLC to afford compounds **1–4**. Their structures were shown in Fig. 2.

Compound **1**, $C_{14}H_{20}O_2$, was isolated as a yellow oil. The molecular formula was determined to be $C_{14}H_{20}O_2$ by FD and HRMS. The ^{1}H (Table 1) and ^{13}CNMR spectra (Table 2) showed signals due to a tertiary methyl group [δ_H1.19 (3H, *s*, H-13) δ_C20.1 (C-13)], a secondary methyl group [δ_H0.96 (3H, *d*, H-14) δ_C16.0 (C-14)], an olefin group [δ_H7.5 (1H, *s*, H-6) δ_C166.7 (C-6), 137.0 (C-7)], and two carbonyl groups [δ_C197.8 (C-8), 198.6 (C-11)]. In the ^{1}H–^{1}H COSY spectrum, correlations between H-1 and H-2, H-2 and H-3, H-3 and H-4, H-1 and H-10, H-10 and H-9, and H-4 and H-14 were observed. The HMBC correlations of H-1, H-6, H-9 and H-10 to C-5 supported the structure of A ring. The HMBC correlations between H-9 and C-8, H-6 and C-11, and H-6 and C-7 determined the structure of B ring, and the correlation between H-14 and C-5 established the position of the tertiary methyl group. Furthermore, the HMBC correlations of H-12, H-6 to C-11 and between H-12 and C-7 were observed, suggesting the presence of an acetyl group (H-12, C-11, C-12) at C-7. The stereostructure of **1** was determined by analysis of the NOESY spectrum. The NOEs between H-10 and H-13 indicated a *cis*-junction of the A/B rings. From the NOEs between H-9α and H-2α, H-9α and H-4, and H-6 and H-14, it was implied that rings A and B should be in the chair type.

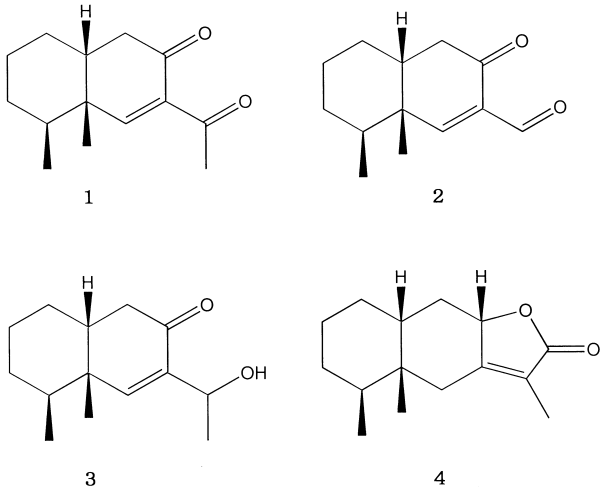

Fig. 2. Structures of compounds **1–4**.

Compound **2**, $C_{13}H_{18}O_2$, was isolated as a colorless oil. The molecular formula was determined to be $C_{13}H_{18}O_2$ by FD and HRMS, and by analysis of the DEPT spectrum. The molecular formula suggested that **2** had one less methyl group than **1**, which was also supported by the DEPT spectrum, in which the signals of only two methyl groups [δ_C20.9 (C-12), 16.1 (C-13) appeared. In the ^{1}H (Table 1) and ^{13}C NMR spectra (Table 2), signals due to a carbonyl group [δ_C199 (C-8)] and an aldehyde group [δ_H9.58 (1H, *s*, H-11), δ_C, 201.3 (C-11)] were observed. These facts suggested that the acetyl group at C-7 of **1** was replaced by an aldehyde group. The other signals in the ^{1}H and ^{13}C NMR spectra were very similar to those of **1**, indicating that both compounds had the same skeleton. This was supported by analysis of the ^{1}H–^{1}H COSY and HMBC spectra.

Table 1
^{1}H NMR spectral data for compounds **1**–**4**

	1	**2**	**3**	**4**
1 α	1.75 *m*	1.78 *m*	1.75 *m*	1.88 *m*
β	1.38 *m*	1.37 *m*	1.31 *m*	1.35 *m*
2 α	1.49 *m*	1.47 *m*	1.47 *m*	1.46 *m*
β	1.58 *m*	1.57 *m*	1.57 *m*	
3 α	1.36 *m*	1.31 *m*	1.31 *m*	1.25 *m*
β	1.46 *m*	1.49 *m*	1.47 *m*	1.44 *m*
4	1.85 *tq* (6.9,3.5)	1.81 *tq* (6.9,6.8)	1.80 *tq* 1.45 *m*	
6 α	7.50 *s*	6.59 *s*	6.72 *d* (7.4)	2.90 *d* (13.8)
β				1.84 *d* (14.3)
8				4.64 *dd* (7.9,6.9)
9 α	2.74 *dd* (17.0,4.4)	2.70 *dd* (17.2,2.0)	2.69 *dd* (17.2,2.8)	2.08 *ddd* (12.3,6.9,3.2)
β	2.32 *dd* (16.8,12.6)	2.32 *dd* (17.3,4.7)	2.24 *ddd* (17.2,4.2,4.2)	1.75 *dd* (13.4,10.8)
10	2.09 *dddd* (12.9,4.7,4.4,2.2)	2.09 *dddd* (16.6.10.4,4.7,1.5)	2.05 *dddd* (11.5,10.4,4.5,1.8)	1.68 *dddd* (12.1,11.1,6.5,3.7)
11		9.58 *s*	4.57 *dd* (12.0,6.4)	
12	2.47 *s*	1.13 *s*	1.34 *dd* (6.5,3.3)	
13	1.19 *s*	0.91 *d* (6.8)	1.13 *s*	1.83 *s*
14	0.96 *d* (6.9)		1.04 *d* (6.9)	1.04 *s*
15				0.79 *d* (6.7)

Table 2
^{13}C NMR spectral data for compounds **1**–**4**

	1	**2**	**3**	**4**
1	26.9	27.2	22.2	26.7
2	20.3	20.6	20.6	20.6
3	30.2	30.4	27.1	30.7
4	35.6	36.1	35.8	30.0
5	39.7	39.4	38.8	40.0
6	166.7	158.8	155.9	36.5
7	137.0	135.5	139.1	161.2
8	197.8	199.0	201.9	80.5
9	40.5	39.5	40.1	35.1
10	39.4	39.9	39.8	40.3
11	198.6	201.3	66.9	120.6
12	30.8	20.9	30.3	175.0
13	20.1	16.1	20.6	8.3
14	16.0		16.2	21.6
15				16.0

Compound **3**, $C_{14}H_{22}O_2$, was isolated as an yellow oil. The molecular formula was determined to be $C_{14}H_{22}O_2$ by FD and HRMS, and by analysis of the DEPT spectrum. The fragment ion peak at m/z 204 $[M\text{-}H_2O]^+$ in the EIMS spectrum indicated the presence of an alcohol OH group, supported by signals due to a hydroxyl-bearing methine group [δ_H 4.57 (1H, *dq*, H-11), δ_C66.9 (C-11)] in the ^{1}H (Table 1) and ^{13}C NMR spectra (Table 2). In the ^{1}H and ^{13}CNMR spectra, a signal due to just one carbonyl group [δ_C201.9 (C-8)] was observed. This fact indicated that one of the carbonyl groups of **2** (C-8 or C-11) was replaced by a secondary hydroxyl group. The presence of a hydroxyl group at C-11 was suggested by the ^{1}H–^{1}H correlation between H-11 and H-12. The ^{1}H and ^{13}CNMR, ^{1}H–^{1}H COSY and HMBC spectra suggested that **3** had the same skeleton as **1** and **2**.

Compound **4**, $C_{15}H_{24}O_2$, was identified as eremophilenolide by comparing the ^{1}H and ^{13}C NMR spectral data with those reported by Sugama et al (1985). The structure assignment was supported by ^{1}H–^{1}H COSY and HMBC spectra. In the report of Sugama et al. (1985), **4** was produced by converting 6β-hydroxyeremophilenolide isolated from the young flower stalks of *P.japonicus* according to the method of Naya et al. (1978), so it was not isolated from this species directly. However the isolation of eremophilenolide from *P. officinalis* Moench. was reported by Novotony et al. (1963), but this is the first report of its isolation from *P. japonicus* ssp. *giganteus*.

2.3. Allelopathic effects of isolated compounds

Allelopathic effects of isolated compounds were determined at 100, 300 and 500 ppm (Fig. 3). Although the inhibitory effects of all four compounds on hypocotyl growth increased with increasing concentration, the influence on radicle growth varied. Compounds **1** and **3,** to a lesser extent, promoted radicle growth (Fig. 3b), while partially inhibiting hypocotyl growth (Fig. 3a). Compound **1** significantly promoted radicle growth at each concentration, and the promotion rates did not differ among the concentrations examined ($P > 0.05$, *t*-test). Compounds **2** and **4** partially inhibited the growth of both the hypocotyl and radicle, and the inhibitory effects increased proportionally with their increased concentrations. Both compounds **2** and **4** inhibited the hypocotyl more strongly than that of the radicle at each concentration. Compound **2** showed the strongest

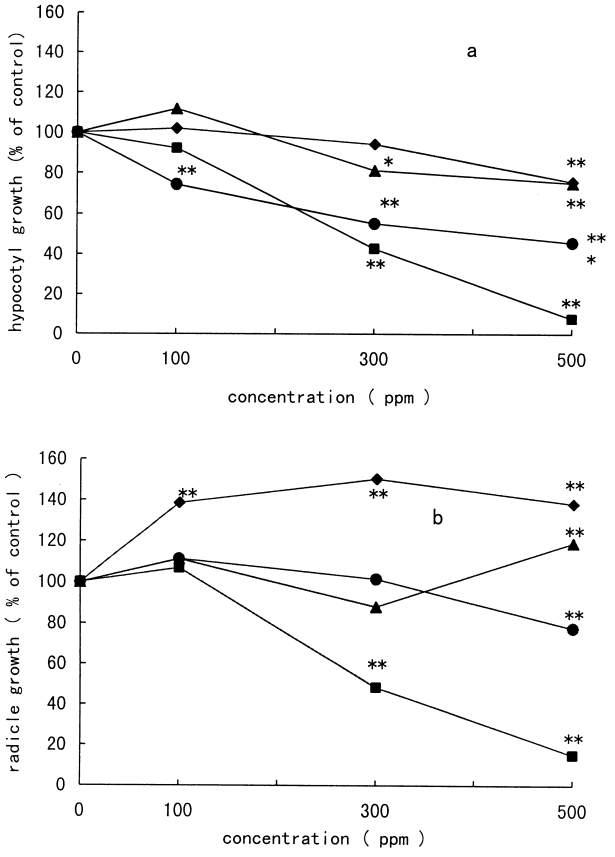

Fig. 3. Effects of isolated compounds on hypocotyl (a) and radicle (b) growth of lettuce. ◆; compound 1, ■; compound **2**, ▲; compound **3**, ●; compound **4**. *,**; *t*-test significantly different from the control at 0.05 and 0.01 level, respectively.

inhibition on both hypocotyl and radicle growth among the four compounds at 300 and 500 ppm. That is compound **2** had a much greater effect than compounds **1** or **3**, even though compounds **1–3** have similar, except for the functional group adapting to C-7. In order to examine any relationship between structure and activity, a more detailed study of this inhibition is required; this in turn add to our knowledge of the allelopathic effects of other eremophilane derivatives.

Compound **2** was the most potent inhibitor among the four compounds examined, but it did no account for the entire activity, *n*-hexane extented. This suggests the existence of other allelochemicals which are either even more effective than those compounds reported here, or the inhibitory effects are enhanced via interaction of allelochemicals. (Li et al., 1993). We thus investigated interactions of phenolic compounds as allelochemicals, and found that combinations of two phenolic compounds showed an additive inhibition effect on seed germination and seedling growth of lettuce. In the future, we will identify whether other allelochemicals are also present, and if their effects are enhanced when in combination with each other.

3. Experimental

3.1. General methods

^{1}H and ^{13}C NMR spectra were recorded on a Bruker AMX-500 FTNMR spectrometer. Chemical shifts are reported in δ units relative to TMS as an internal standard with $CDCl_3$ as solvent. EIMS were obtained at 70 eV with a direct inlet system. CC used Wakogel C-200, whereas prep. TLC utilized on Kieselgel 60 PF254. Prep. HPLC was carried out using a JASCO 880-PU (column, ODS, Wakosil-II 5C18HG, flow rate, 5.0 ml/min, temperature of column, 35°C, detector, JASCO 875-UV).

3.2. Plant material

Rhizomes of *P. japonicus* ssp. *giganteus* were collected in July 1997, in Ashoro-cho, Hokkaido, Japan.

3.3. Bioassay

Germination and seedling growth tests of lettuce (*Lactuca sativa* L.) were carried out on a silica gel support. For bioassays, rhizome powder (0.3 g) was added to a Petri dish containing silica gel (0.3 g) and distilled water (5 ml, containing 100 ppm (w/v) Tween 80). Lettuce seeds (50) were next placed onto the Petri dish and incubated at 20°C, 17 lux for 5 days.

To test either isolated compounds or fractions soluble in organic solvents, specified amounts of a sample were dissolved in either $CHCl_3$ (0.3 ml) or ethyl alcohol (0.3 ml) and the solution was added to silica gel (1.0 g). When isolated compounds were tested, the same amount of $CHCl_3$ was added as a control. The silica gel was left in a draft chamber for 24 h to remove organic solvents by volatilization and added to 5 cm Petri dish. Distilled water (2 ml) containing 100 ppm (w/v) Tween 80 was poured into the Petri dish and left overnight to allow the sample to dissolve completely. To test water soluble fraction, a sample was dissolved in distilled water (2 ml), and the solution was poured into a Petri dish containing silica gel (1 g). 30 seeds were placed in each dish and incubated under the same conditions as described above. The concentration of either compounds or fractions were calculated over the weight of distilled water plus silica gel (w/w).

Numbers of germinated seeds were counted every 24 h and the lengths of hypocotyls and radicles were measured on the 5th day and compared to those of the controls. Each test was repeated 3 times.

3.4. Extraction and isolation

Fresh rhizomes of *P. japonicus* ssp. *giganteus* (800 g) were extracted with *n*-hexane for 2 weeks at room temperature. The filtered extract was concentrated under

reduced pressure. The extract (4.2 g) was subjected to silica gel column chromatography using a *n*-hexane-EtOAc gradient to afford 19 fractions (Fr.1–19). Fr.13 (377 mg) was purified by prep.TLC (*n*-hexane:EtOAc = 4:1) and further by prep.HPLC using CH_3CN-H_2O gradient (1:1–3:1) to give 1 (13.6 mg). Fr.14 (676 mg) was applied to a silica gel column using an *n*-hexane-EtOAc (10:1), 9 fractions (14A–14I) were obtained. 14E (114 mg) was purified by prep. HPLC using CH_3CN-H_2O gradient (1:1–3:1) following CC using benzene-acetone (20:1) to give **2** (11.7 mg). 14I (99.4 mg) was pure **3**. Fr.17 (544 mg) was separated into 4 fractions (17A–17D) by prep.HPLC using a CH_3CN-H_2O gradient (1:1–3:1). 17A contained **1**. 17B mainly contained **4** and its further recrystallization with *n*-hexane-EtOAc gave pure crystalline **4** (10 mg).

1. IRν_{max} (film) cm^{-1} 1693,1597. UVλ_{max}^{EtOH} nm: 227. $[\alpha]_D$ −19.4° ($CHCl_3$, *c* 0.34) EIMS *m/z* (rel. int.): 220 $[M]^+$ (100) (HRMS found: *m/z* 220.1459 requires: 220.1464), 205 $[M\text{-}Me]^+$ (10), 177$[M\text{-}Me\text{-}CO]^+$ (9), 109 (99). For ^1H and ^{13}C NMR spectra: see Tables 1 and 2.
2. IRν_{max} (film) cm^{-1} 1733,1690,1594. UVλ_{max}^{EtOH} nm: 235. $[\alpha]_D$ + 5.05°($CHCl_3$, *c* 0.21). EIMS *m/z* (rel. int.): 206 [M]+ (100) (HRMS found: *m/z* 206.1303 requires: 220.1307), 205 [M-H]+ (23), 191 $[M\text{-}Me]^+$ (32), 177 $[M\text{-}HCO]^+$ (21), 149 (52). For ^1H and ^{13}C NMR spectra: see Tables 1 and 2.
3. IRν_{max} (film) cm^{-1} 3447,1670,1590. UVλ_{max}^{EtOH} nm: 230. $[\alpha]_D^{29}$ + 12.4° ($CHCl_3$, *c* 1.0). EIMS *m/z* (rel. int.): 222 $[M]^+$(65) (HRMS found: *m/z* 222.1619 requires: 220.1621), 207 $[M\text{-}Me]^+$(80), 204 $[M\text{-}H_2O]^+$(36), 151 (91), 109 (100). For ^1H and ^{13}C NMR spectra: see Tables 1 and 2.
4. (Eremophilenolide) IRν_{max} (film) cm^{-1}: 1757, 1693, 1591. UVλ_{max}^{EtOH} nm: 223° $[\alpha]_D$ + 146.1° ($CHCl_3$, *c* 0.20). EIMS *m/z* (rel. int.): 234 $[M]^+$(20), 123 (100), 109 (34). For ^1H and ^{13}C NMR spectra: See Tables 1 and 2.

Acknowledgements

The authors thank Dr. Fukushi for the measurements of mass spectra and NMR spectra.

References

Li, H.H., Inoue, M., Nishimura, H., Mizutani, J., Tsuzuki, E., 1993. Interactions of *trans*-cinnamic acid, its related phenolic allelochemicals, and abcisic acid in seedling growth and seed germination of lettuce. Journal of Chemical Ecology 19 (8), 1775–1787.

Naya, K., Matsumoto, T., Makiyama, M., Tsumura, M., 1978. The convertion of furanoerenophilanes to eremophilenolides. Heterocycles 10, 177–184.

Novotony, L., Jizba, J., Herout, V., Sorm, F., Zalkow, L.H., Hu, S., Djerassi, C., 1963. Constitution and absolute configuration of Eremophilenolide. Tetrahedron 19, 1101–1107.

Sugama, K., Hayashi, K., Mitsuhashi, H., 1985. Eremophilenolides from *Petasites japonicus*. Phytochemistry 24, 1531–1535.

Tori, M., Kawahara, M., Sono, M., 1997. Epoxyeremophilanolides, eremopetasitenins A1, A2, B1, and B2, from *Petasites japonicus*. Tetrahedron Letters 38, 1965–1968.

Yaoita, Y., Kikuchi, M., 1994. Structure of six new eremophilenolides from the rhizomes of *Petasites japonicus* Maxim. Phytochemistry 37, 1765–1766.

Yaoita, Y., Kikuchi, M., 1996. New eremophilanolides from the rhizomes of *Petasites japonicus* Maximum. Chemical Pharmacy Bulletin 44, 1731–1735 (and references cited therein).

Zhao, Y., Parsons, S., Smart, B.A., Tan, R., Jia, Z., Sun, H., Rankin, D.W.H., 1997. Eremophilane derivatives with a novel skeleton from *Liglaria veitchina*. Tetrahedron 53, 6195–6208.

PERGAMON

Phytochemistry 57 (2001) 115–123

PHYTOCHEMISTRY

www.elsevier.com/locate/phytochem

Cuticular waxes on *eceriferum* mutants of *Arabidopsis thaliana*

Aaron M. Rashotte [a,*], Matthew A. Jenks [b], Kenneth A. Feldmann [a,1]

[a] *Department of Plant Sciences University of Arizona, Tucson, AZ 85721, USA*
[b] *Department of Horticulture and Landscape Architecture, Purdue University, West Lafayette, IN 47907, USA*

Received 12 September 2000; received in revised form 27 November 2000

Abstract

We present cuticular wax chemical profiles for the leaves and stems of *Arabidopsis* wildtype Landsberg *erecta* and eleven isogenic *eceriferum* mutants: *cer5*, *cer10* to *cer15*, and *cer17* to *cer20*. These *cer* mutants have wax profiles that are different from those of wildtype in chemical chain length distribution, amount per chemical class, and/or total wax load. Analyses of detailed leaf and stem wax profiles for these *cer* mutants have allowed us to place some of these mutants at specific steps in wax production. The *cer13* gene is predicted to affect release of the 30 carbon fatty acid from the elongation complex or the reduction of C30 fatty acid to C30 aldehyde. The *CER19* gene product is predicted to be involved in C28 to C30 fatty acyl-CoA elongation. The *CER20* gene is predicted to affect the oxidation of C29 alkane to C29 secondary alcohol. Several predicted gene products affect only stem specific steps in the wax pathway. © 2001 Elsevier Science Ltd. All rights reserved.

Keywords: *Arabidopsis thaliana*; Cruciferae; Cuticular wax; *Eceriferum* mutants; *cer*

1. Introduction

Arabidopsis thaliana is a powerful model plant system for dissecting genetic components in cuticular wax production. In previous studies, 20 distinct wax loci of *A. thaliana*, designated *eceriferum* or *cer* were identified using a visual screen for altered stem surface glaucousness (Koornneef et al., 1989). Detailed wax chemical profiles of leaves and stems from nine of these *cer* mutant loci, *cer1* to *cer4*, *cer6* to *cer9*, and *cer16* were used to predict the role of *CER* gene function in the *A. thaliana* wax formation pathway (Jenks et al., 1995).

In this report, detailed analyses of leaf and stem cuticular wax of an additional 11 *cer* mutant loci are presented. Previous studies reported the amount of major wax classes on stems of these 11 *cer* mutants and some chemical chain length data for seven of these mutants (Hannoufa et al., 1993; McNevin et al., 1993; Lemieux et al., 1994). However, leaf wax, stem wax loads, and amount of stem wax constituents by chain length relative to plant area were not examined. Our detailed leaf and stem analyses of *cer5*, *cer10* to *cer15*, and *cer17* to *cer20* have allowed us to place some of these mutations at specific blocks in the *A. thaliana* wax enzymatic pathway, and for three loci to predict gene function. Detailed analysis of *cer* mutants is essential to the continued development of an accurate pathway for wax production.

2. Results and discussion

2.1. Cuticular wax load

The total wax load for the leaves and stems of wildtype, *cer5*, *cer10* to *cer15*, and *cer17* to *cer20* are presented in Table 1. Placement of these mutants on the genetic map confirms that each represents a distinct locus (Rashotte and Feldmann, unpublished results). The wax loads of the mutant tissues are significantly lower than the wildtype except for the stems of *cer15* and *cer17* and the leaves of *cer5, cer10*, and *cer11* (Table 1). While the total load is not significantly different for every mutant, the waxes of both the leaves and stems for all mutants are significantly altered in two

* Corresponding author at current address: Department of Biology, Wake Forest University, Winston-Salem, NC 27109, USA. Tel.: +1-336-758-4349; fax: +1-336-758-6008.

E-mail address: rashotam@wfu.edu (A.M. Rashotte).

[1] Current address: Ceres, Inc., 3007 Malibu Canyon Road, Malibu, CA 90265, USA.

0031-9422/01/$ - see front matter © 2001 Elsevier Science Ltd. All rights reserved.
PII: S0031-9422(00)00513-6

Table 1
Arabidopsis stem and leaf cuticular wax on 25 day old wild-type Landsberg *erecta* (Ler) and *eceriferum* (*cer*) mutants

Genotype		Total load[a]	Acids	Alde.	Alkane	Primary alcohols	Secondary alcohols	Ketone	Esters
Ler	Stem	2336±23.7	25.7	76.8	1051	116	323	690	53.4
	Leaf	100.7±10.1	3.4	2.2	70.0	19.7	0.6	1.3	3.5
cer5	Stem	950±112.1	15.4	8.5	128	107	211	428	52.5
	Leaf	83.6±20.2	3.3	2.7	66.0	8.9	0.1	0.9	1.7
cer10	Stem	831±105.5	16.4	41.7	354	79.1	89.8	207	42.8
	Leaf	81.9±11.9	3.1	2.4	48.4	22.5	0.4	0.7	4.4
cer11	Stem	1234±191	21.2	33.1	509	95.9	170	295	24.9
	Leaf	74.0±17.9	5.9	3.4	47.8	10.4	0.3	0.6	4.2
cer12	Stem	1741±95.7	18.0	48.3	590	166	270	602	46.7
	Leaf	64.3±6.8	3.1	3.0	46.9	7.9	0.2	0.8	2.4
cer13	Stem	1398±138	14.3	23.6	486	245	160	401	68.5
	Leaf	74.9±3.6	4.0	2.3	49.3	12.3	0.4	1.4	5.2
cer14	Stem	1645±389	18.3	46.9	657	148	237	489	49.4
	Leaf	49.5±1.5	3.4	1.5	35.7	6.5	0.1	0.4	1.9
cer15	Stem	2129±250	18.3	76.4	976	83.4	289	657	28.6
	Leaf	59.1±1.3	2.7	2.7	41.8	8.0	0.3	0.7	2.9
cer17	Stem	2210±182	16.2	88.4	1045	130	264	582	84.0
	Leaf	73.4±8.9	4.0	1.9	48.7	12.3	0.2	0.7	5.6
cer18	Stem	1897±268	14.5	48.1	685	190	252	635	72.1
	Leaf	70.9±8.9	4.3	2.0	49.6	10.7	0.1	0.5	3.7
cer19	Stem	712±36.2	13.9	33.1	184	128	65.4	187	100.4
	Leaf	68.4±6.2	4.0	2.9	43.1	14.3	0.1	0.4	3.6
cer20	Stem	1642±144	19.5	81.0	902	93.5	174	305	66.9
	Leaf	70.9±3.9	3.4	2.7	49.3	10.2	0.3	0.8	4.2

[a] All values are presented in μg dm^{-2} for three replicates: total load represents the average total amount of hexane soluble surface wax constituents (excluding triterpenoids and unknowns) in μg dm^{-2} for three replicate surface areas ± standard error.

or more chemical classes (Table 1). In general, the *cer* mutants displayed no correlation between reductions of wax load on the leaves vs. the stems, suggesting organ specific patterns.

2.2. *cer* Mutant cuticular waxes

The major chemical constituents of cuticular wax found in the leaf and stem of Arabidopsis are presented for all 11 *cer* mutants compared to their wildtype background in Figs. 1–4. These figures show detailed wax chemical profiles of these mutants as absolute values of μg dm^{-2} as has previously been presented for other Arabidopsis *cer* mutants and ecotypes (Jenks et al., 1995, 1996; Rashotte et al., 1997).

The wildtype background, Landsberg-erecta, has a leaf cuticular profile very similar to the previously examined Ws background (Jenks et al., 1996). Both wildtype backgrounds are almost entirely composed of alkanes and primary alcohols in the leaf, with C29 and C31 as the predominate alkanes and C26 and C28 as the predominate primary alcohols (Fig. 1). The differences in the 11 *cer* mutant leaf profiles in this paper in comparison to the wildtype appear mainly due to changes in the overall amounts or the chain-length distribution within the alkanes and primary alcohols (Figs. 1 and 2). Additionally, the stem cuticular profile of the wildtype is very similar to previously examined wildtype backgrounds (Jenks et al., 1996; Rashotte et al., 1997). Wildtype Arabidopsis stem profiles show a diversity of major chemical constituents as well as an increased overall load in comparison to leaf profiles. The most abundant wax chemical components in the stem are the C29 alkane, C29 ketone and C29 secondary alcohol, while the C28 fatty acid, the C30 aldehyde and the C28 primary alcohol are the most predominate components within their respective classes (Fig. 3). The change in the amount of these components or their predominance within a chemical class is found within each of the 11 *cer* mutants presented in Figs. 3 and 4.

The leaves of *cer5* have reduced primary alcohol and ester levels, 45 and 49% of wildtype levels, respectively (Fig. 1). The reduction in primary alcohols is mostly due to the greatly reduced levels of C26 and C28 constituents. In contrast to the leaf profile, the *cer5* stem profile has reduced levels in all chemical classes except primary alcohols and esters (Fig. 3). The C30 aldehyde and the C29 alkane levels are the most dramatically reduced. While the C29 ketone and C29 secondary alcohols levels are also reduced compared to wildtype levels, they are still at higher levels that the usually predominate C29 alkane (Fig. 1 and Table 1).

The leaves and stems of *cer10* show a slight skewing of chemical components toward longer chain lengths

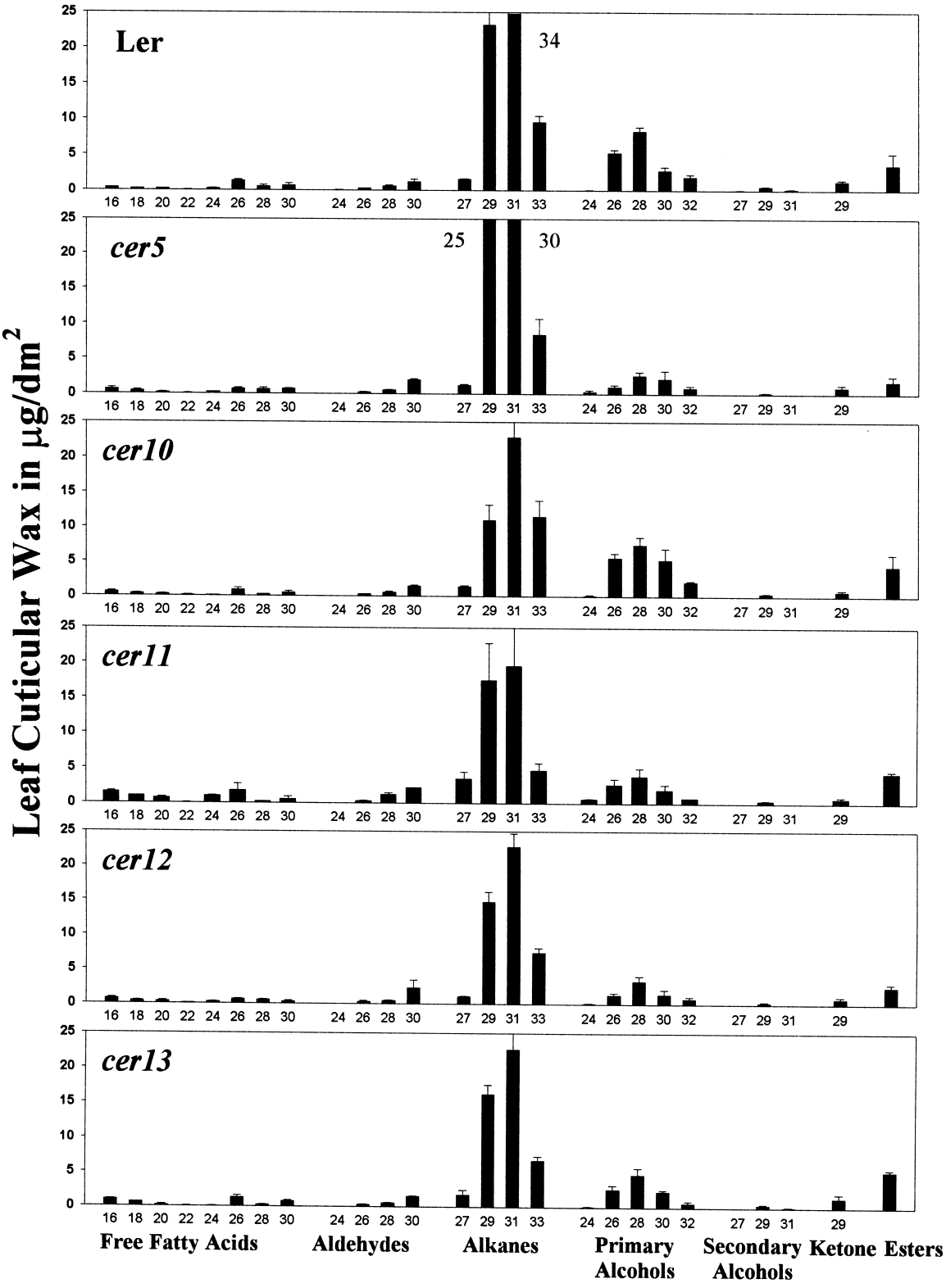

Fig. 1. Cuticular wax profiles of *A. thaliana* Wildtype and *cer* Mutants. Each bar shows the amount of a specific wax constituent, labeled on the X-axis by a wax class and a carbon unit length of that constituent. The ketone represents a 29 carbon length ketone. All measurements are in µg/dm^2 and are presented as and average of three replicates ± standard error. Bars that reach the top of the graph have additional numbers adjacent to them, indicating the actual wax amount, which is off the Y-axis. Fig. 1 shows leaf wax profiles of *cer5*, *10*, *11*, *12*, and *13* along with the wildtype Ler (Landsberg-erecta).

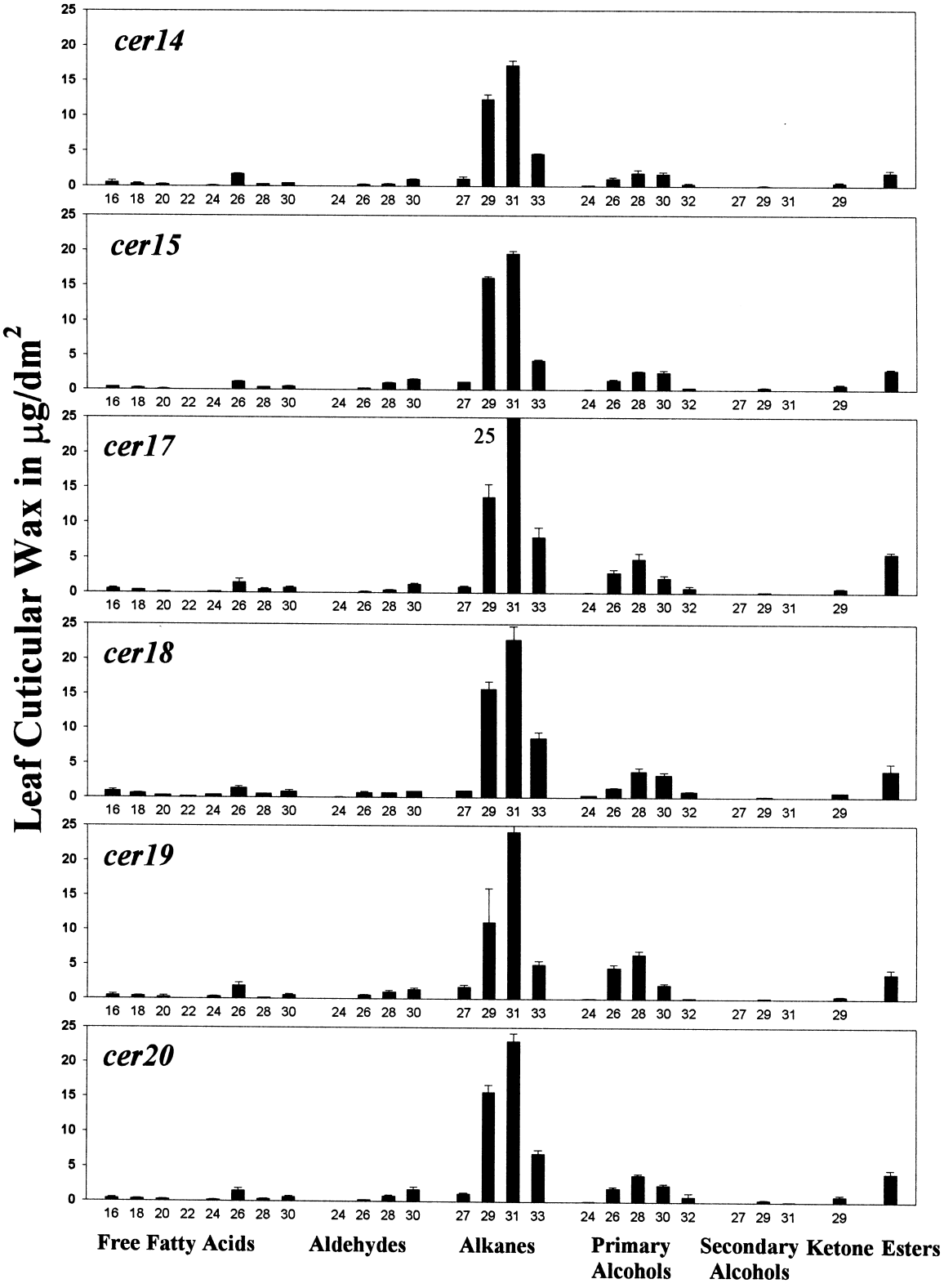

Fig. 2. Cuticular wax profiles of *A. thaliana* Wildtype and *cer* Mutants. Each bar shows the amount of a specific wax constituent, labeled on the X-axis by a wax class and a carbon unit length of that constituent. The ketone represents a 29 carbon length ketone. All measurements are in μg/dm^2 and are presented as and average of three replicates ± standard error. Bars that reach the top of the graph have additional numbers adjacent to them, indicating the actual wax amount, which is off the Y-axis. Fig. 2 shows leaf wax profiles of *cer14*, *15*, *17*, *18*, *19*, and *20*.

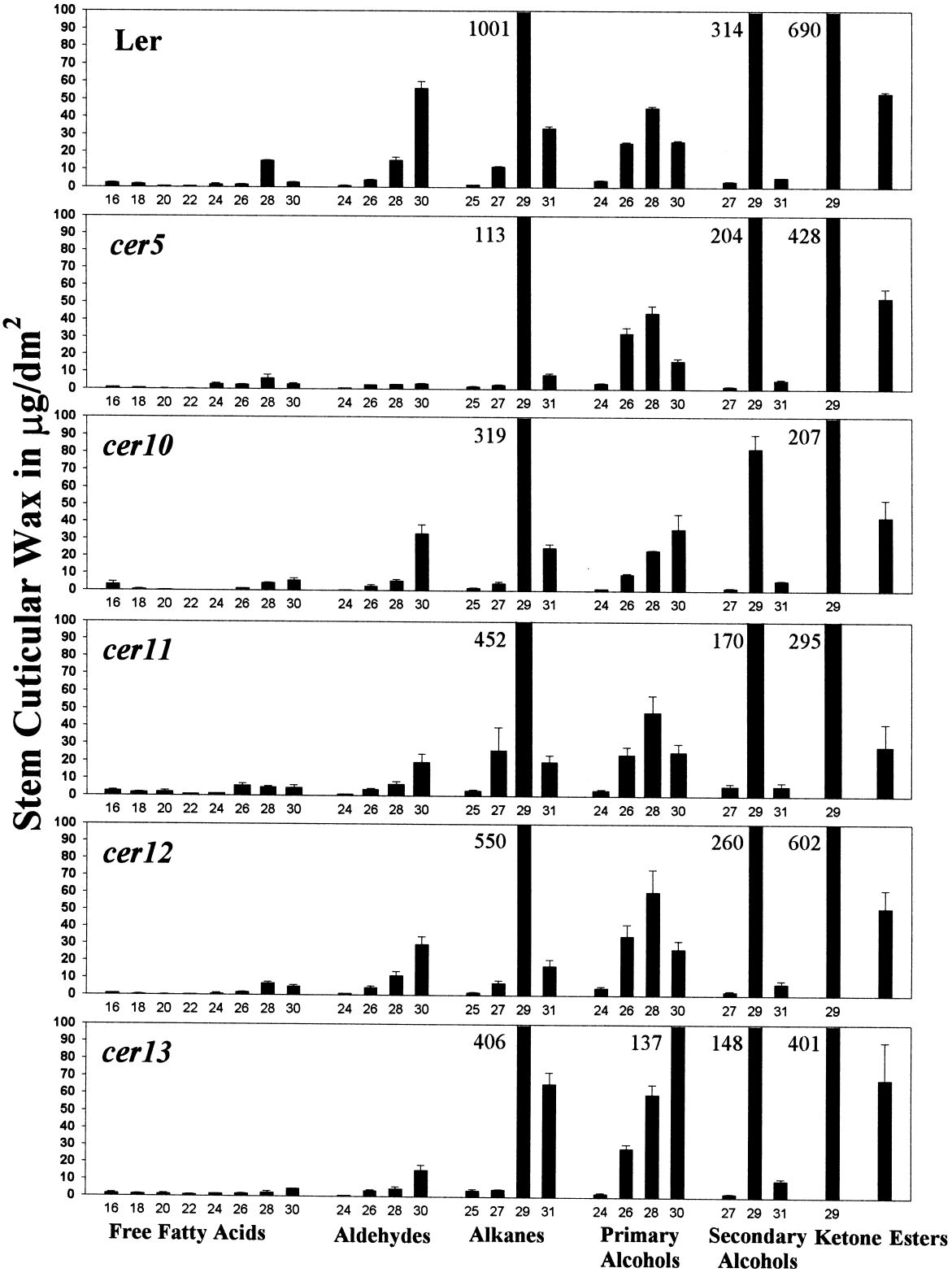

Fig. 3. Cuticular wax profiles of *A. thaliana* Wildtype and *cer* Mutants. Each bar shows the amount of a specific wax constituent, labeled on the X-axis by a wax class and a carbon unit length of that constituent. The ketone represents a 29 carbon length ketone. All measurements are in μg/dm^2 and are presented as and average of three replicates ± standard error. Bars that reach the top of the graph have additional numbers adjacent to them, indicating the actual wax amount, which is off the Y-axis. Fig. 3 shows stem wax profiles of the mutants *cer5*, *10*, *11*, *12*, and *13* along with Ler.

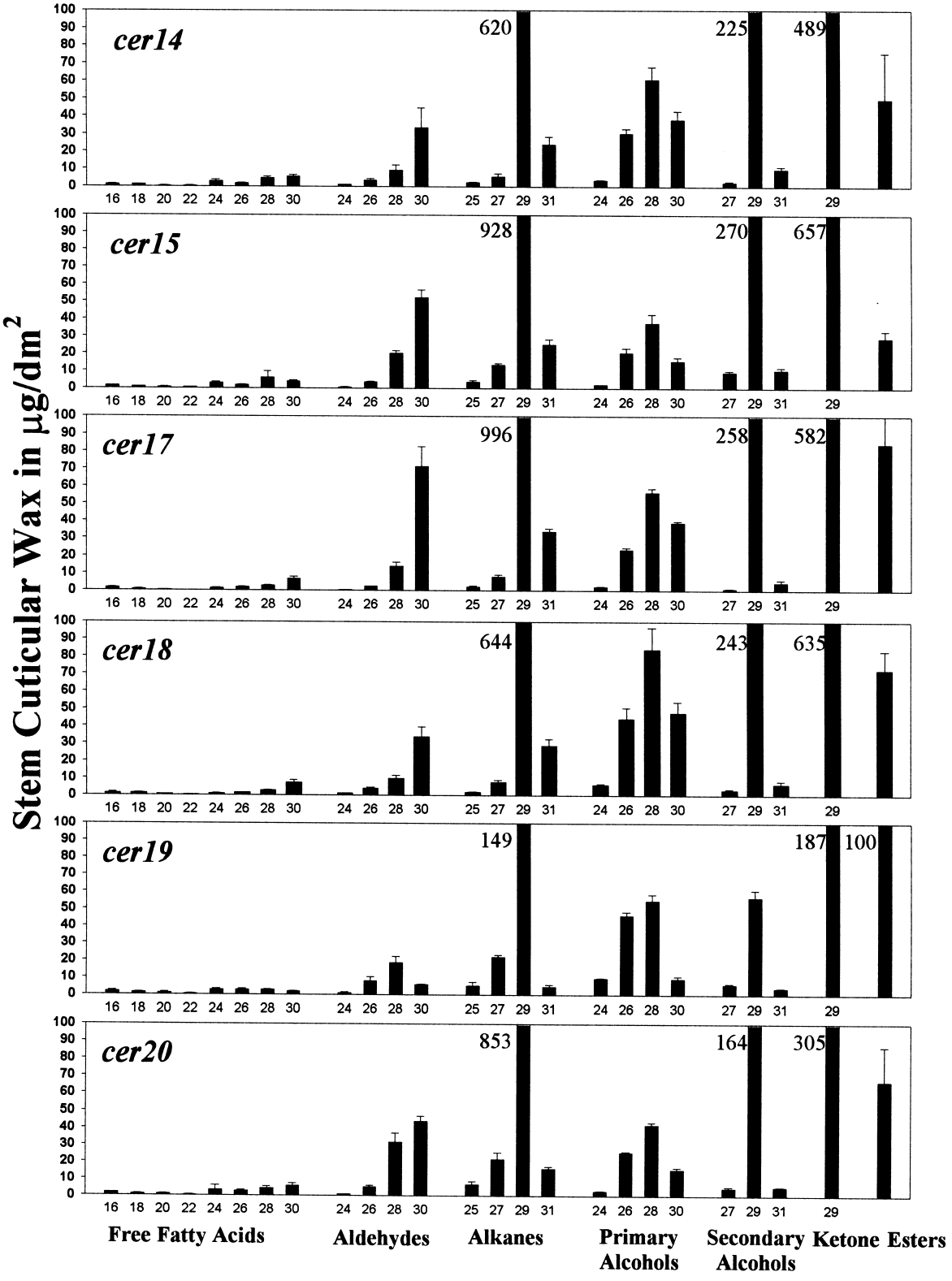

Fig. 4. Cuticular wax profiles of *A. thaliana* Wildtype and *cer* Mutants. Each bar shows the amount of a specific wax constituent, labeled on the X-axis by a wax class and a carbon unit length of that constituent. The ketone represents a 29 carbon length ketone. All measurements are in µg/dm^2 and are presented as and average of three replicates ± standard error. Bars that reach the top of the graph have additional numbers adjacent to them, indicating the actual wax amount, which is off the Y-axis. Fig. 4 shows stem wax profiles of *cer14*, *15*, *17*, *18*, *19*, and *20*.

(Figs. 1 and 3). In the leaves this skewing is due to the reduction of C29 alkane and the increase of C30 primary alcohol. The stems show a similar pattern having reduced C29 components and increased C30 primary alcohol levels.

The leaves of both *cer11* and *cer12* have a reduction in alkane and primary alcohol levels with little or no change in profile distribution (Fig. 1). The stems of *cer11* show about a 50% reduction in C29 components and C30 aldehyde with little to no reduction in primary alcohol levels or distribution. *cer12* also shows a major reduction in C29 alkane levels, although there is little change in other wax components (Fig. 3).

The leaves of *cer13* show a general reduction in wax load, with no change in wax profile (Fig. 1). In contrast, *cer13* stems show major reductions in all C29 components and major increases in the C31 alkane and C30 primary alcohol levels (Fig. 3). This has the effect of skewing the chain length distribution of *cer13* longer than wildtype.

The leaves of *cer14* and *cer15* have similar major reductions in alkane and primary alcohol levels that do not effect profile distribution (Fig. 2). The stems of *cer14* and *cer15*, however, are quite different. *cer14* stems show a reduction in C29 alkane, secondary alcohol and ketone levels, while other components are mostly unaffected (Fig. 4). In contrast, *cer15* stems have minor reductions in primary alcohol and esters.

The leaves of *cer17* leaves have reductions in C29 and C31 alkanes as well as C26 and C28 primary alcohols (Fig. 2). The stems of *cer17* have minor reductions in overall load with little effect on profile distribution (Fig. 4).

The leaves of *cer18* have a general load reduction, with little change from the wildtype wax profile (Fig. 2). The *cer18* stems have specific reductions in C29 alkane and C29 secondary alcohol levels, while primary alcohol levels show a general increase although maintaining the wildtype primary alcohol profile (Fig. 4).

The leaves of *cer19* have greatly reduced alkane levels, in addition to minor reductions in primary alcohol levels (Fig. 2). Stems show a different alteration in wax levels than leaves. All wax components greater than 29-carbon length are dramatically reduced compared to wildtype levels, while esters levels are greatly increased (Fig. 4).

The leaves of *cer20* have a general reduction in wax levels with little change in profile distribution (Fig. 2). *cer20* stem wax is primarily effected by reductions in C29 secondary alcohol and C29 ketone levels, with most other components remaining unaffected (Fig. 4).

2.3. Prediction of CER gene function

The detailed chemical analyses of leaf and stem wax chemistry of the *cer* mutants presented in Figs. 1–4 along with previous biochemical-genetic studies of *A. thaliana* have allowed us to make predictions about the altered gene functions in the mutants examined here (Hannoufa et al., 1993; McNevin et al., 1993; Lemieux et al., 1994; Jenks et al., 1995: and Rashotte and Feldmann, unpublished results). We have been able to predict the function of three *CER* genes and have placed blocks corresponding to the mutant genes on a wax enzymatic pathway (Fig. 5).

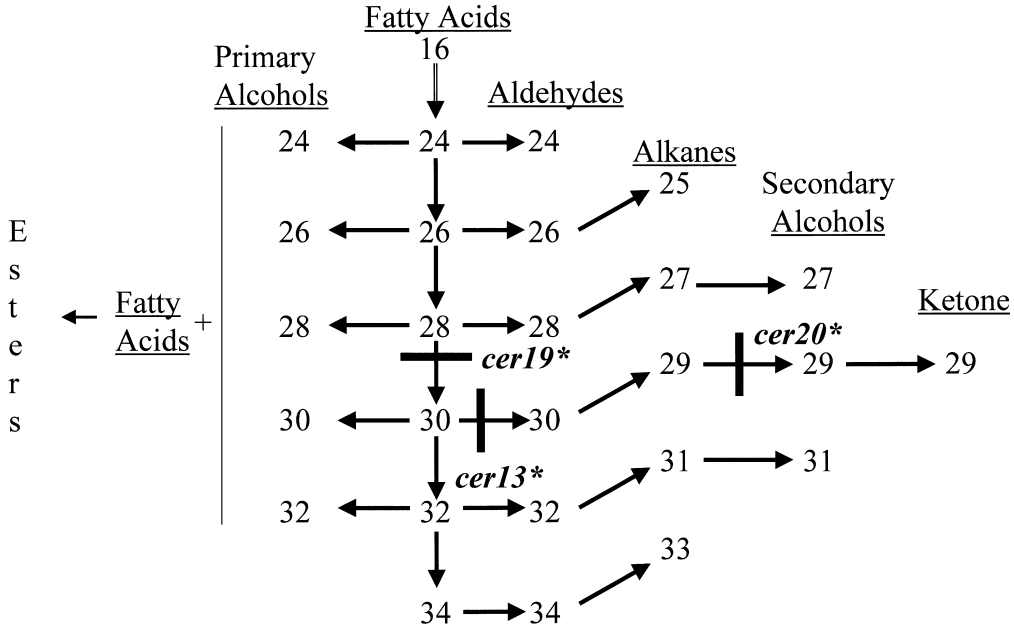

Fig. 5. Cuticular wax formation pathway in *A. thaliana*. A single lined arrow indicates single steps in this pathway, while a double lined arrow indicates multiple steps. Mutational blocks at specific steps of this pathway are indicated by a thick line across an arrow and are labeled by the mutation(s) that are proposed to block there. * Stem specific mutational block.

The *cer13* mutant stem has increased amounts of longer chain length components for both primary alcohols and alkanes compared to wildtype, and resembles the *cer3* and *cer7* mutants [Fig. 3 and Jenks et al. (1995)]. We propose that the *CER13* gene product is involved in C30 fatty acid to C30 aldehyde reduction. A block or mutation in the C30 fatty acid reductase should cause a build-up of C30 fatty acid, which could either be reduced directly to C30 primary alcohol or further elongated to C32 fatty acid. This C32 fatty acid would subsequently be reduced to C32 aldehyde and decarbonylated to C31 alkane (Fig. 5). In *cer13* stems there was a decrease of C30 aldehyde and subsequent C29 components, along with an increase of both C30 primary alcohol and C31 alkane components supporting this hypothesis (Fig. 1). However, we cannot rule out the possibility that this mutant could also have defects in a C30 fatty acid elongase release mechanism which only contributes fatty acids to the alkane flux of the pathway as had previously been suggested for *cer3* and *cer7* (Jenks et al., 1995). Additionally, because our pathway modification eliminates aldehydes as intermediates in the reduction of fatty acids to primary alcohols, the hypothesis of a fatty acid to aldehyde reduction block for *cer3* and *cer7* similar to that for *cer13* seems likely as well (Rashotte and Feldmann, unpublished results). It may be that more than one gene product is needed for the conversion of C30 fatty acid to C30 aldehyde in *A. thaliana*, since the *cer13* mutation does not cause a complete loss of C30 aldehyde or subsequently derived pathway products (Fig. 1). One possible candidate would be the *CER10* gene, since there is a similar trend of increased longer chain length components in the leaf and stem of the *cer10* mutant. These trends are, however, minor when examined as a percent of the total mutant wax load and thus the function of *CER10* must remain speculative.

Cer19 has dramatically reduced levels of wax constituents derived from any 30 carbon or longer acyl-CoA precursors in the stems, as observed in fatty acid, aldehyde, alkane, and primary alcohol classes (Fig. 4). Coenzyme A (CoA) activated fatty acyl chains, which are progressively elongated through condensation by two-carbon units, constitute the backbone of the wax enzymatic pathway from which all other wax components are formed (Lemieux et al., 1994). Thus, a defect in a specific step of fatty acid elongation should have greatly reduced levels of all wax components of chain lengths greater than the defective step. Therefore, *CER19* is predicted to be a gene directly involved in the C28 fatty acyl-CoA elongation step in the wax enzymatic pathway in the stem (Fig. 5). Although the leaves of *cer19* also have reduced amounts of components greater than C30, there is a reduction of components less than C30 with no obvious increase of C28 or C27 components as in the stem (Figs. 2 and 4). Thus, we hypothesize the *CER19* gene product is stem specific. Other mutants, such as the *gl3* mutation in *Z. mays* (Bianchi et al., 1985) and the *gl2* and *gl5* mutations of *Brassica oleracea* (Macey and Barber, 1970) have similar wax profiles.

Stem ester loads were higher on *cer19* than any other *cer* mutants [Jenks et al. (1995) and Figs. 3 and 4]. Interestingly, stem ester levels were also high on the *cer2* and *cer9* mutants of *Arabidopsis* that, like *cer19*, appear to have defects in fatty acid elongation (Jenks et al., 1995). It is possible that increased flow of C28 and shorter fatty acids to similar chain length primary alcohols allowed for greater amounts of esters to be produced. A putative transacylase with specificity for shorter chain length fatty acids and primary alcohols is thought to synthesize very long chain esters (Kolattukudy, 1967; 1996). The relative increase of primary alcohols in *cer19* and also in the *cer2* and *cer9* putative elongation mutants may result in increased ester levels, because the pools of short chain fatty acid and primary alcohol substrates for esterification were increased (Table 1 and Jenks et al., 1995).

The *cer20* stem appears to be blocked in the conversion of C29 alkane to C29 secondary alcohol (Fig. 4). The conversion of alkanes to secondary alcohols is putatively carried out by an oxidation of the 14th or 15th carbon in C29 alkane (Lemieux et al., 1994). A block in this specific oxidation step should result in higher C29 alkane levels, relative to the total load of the mutant, and reductions of C29 secondary alcohol and C29 ketone levels (Fig. 5). *cer20* is the only *cer* mutant that has increased levels of C29 alkane and reduced levels of both C29 secondary alcohol and C29 ketone, as a percent of its total wax load (Figs. 3 and 4 and Jenks et al., 1995). Interestingly, while the largest change in constituent levels relative to the total load of this mutant is between the levels of C29 alkane to C29 secondary alcohol (12.4% reduction), there is also a reduction between levels of C29 secondary alcohol to C29 ketone (Fig. 4). It is possible that the gene product of *CER20* is directly involved in the enzymatic oxidation of C29 alkane to C29 secondary alcohol or indirectly involved with oxidation events for both the oxidation of C29 alkane to C29 secondary alcohol and C29 secondary alcohol to C29 ketone.

The other *cer* mutants, *cer5, 10, 11, 12, 14, 15, 17,* and *18*, have distinct leaf and stem wax differences from the wildtype (Figs. 1–4). However, we were unable to place these mutants at specific steps in the wax pathway or predict their gene function. It is possible the gene products disrupted in these mutants are involved in wax functions other than biosynthesis, such as transport, regulation, or development. Cloning of the genes in the wax pathway as well as double mutant analyses may help confirm the role of each locus in cuticular wax formation.

3. Experimental

3.1. General experimental procedures

3.1.1. Cuticular wax analysis

The hexane soluble surface lipids (designated cuticular wax or wax) were bulk extracted from leaves and stems of 25 day old plants by immersing tissues in hexane for 30 s. Derivatization, gas chromatography, mass spectrometry, quantification of identified wax constituents, and measurement of surface area were performed according to (Jenks et al., 1995: Rashotte et al., 1997) as modified from McNevin et al. (1993). Three replicates were conducted for each wax profile and the data is presented as an average ± standard error in μg dm^{-2}.

3.1.2. Plant material

Arabidopsis thaliana ecotype Landsberg *erecta* (Ler) along with chemical- and radiation-induced *cer* mutants from (Koornneef et al., 1989) were used for wax analyses. Plants were grown in a controlled environmental chamber (CONVIRON, Winnipeg, Manitoba) at 22°C with a 16 hour photoperiod (~240 μmol min^{-2} s^{-1}; approximately 75% RH) and at 18°C in the dark. The *cer21* mutant was not used in our analyses because the uniqueness of the locus could not be confirmed (Hannoufa et al., 1993; Rashotte and Feldmann, unpublished results).

3.1.3. Chemicals identified as wax constituents on Arabidopsis

Hexadecanoic, octadecanoic, eicosanoic, docosanoic, tetracosanoic, hexacosanoic, octacosanoic, triacontanoic acids as C16, C18, C20, C22, C24, C26, C28, and C30 free fatty acids; *n*-pentacosane, *n*-heptacosane, *n*-nonacosane, *n*-hentriacosane, *n*-tritriacontane as C25, C27, C29, C31, and C33 alkanes; 1-tetracosanol, 1-hexacosanol, 1-octacosanol, 1-triacontanol, 1-dotriacontanol as C24, C26, C28, C30, and C32 primary alcohols; tetracosanal, hexacosanal, octacosanal, triacontanal as C24, C26, C28, and C30 aldehydes; 13- and 14-heptacosanol, 14- and 15-nonacosanol, 15- and 16-hentriacontanol as C27, C29, and C31 secondary alcohols; and 15-nonacosanone as C29 ketone.

Acknowledgements

We would like to acknowledge support from the NSF/DOE/USDA grant (BIR-9220332), NSF grants IBN-9419093 and BIR-9116247.

References

Bianchi, A., Bianchi, G., Avato, P., Salamini, F., 1985. Biosynthetic pathways of epicuticular wax of maize as assessed by mutation, light, plant age and inhibitor studies. Maydica 30, 179–198.

Hannoufa, A., McNevin, J.P., Lemieux, B., 1993. Epicuticular waxes of *eceriferum* mutants of *Arabidopsis thaliana*. Phytochemistry 33, 851–855.

Jenks, M.A., Tuttle, H.A., Eigenbrode, S.D., Feldmann, K.A., 1995. Leaf epicuticular waxes of the *eceriferum* mutants in *Arabidopsis* during development. Plant Physiology 108, 369–377.

Jenks, M.A., Rashotte, A.M., Tuttle, H.A., Feldmann, K.A., 1996. Mutants in *Arabidopsis thaliana* altered in epicuticular wax and leaf morphology. Plant Physiology 110, 377–385.

Kolattukudy, P.E., 1967. Mechanism of synthesis of waxy esters in broccoli (*Brassica oreracea*). Biochemistry 6, 2705–2717.

Kolattukudy, P.E., 1996. Biosynthetic pathways of cutin and waxes and their sensitivity to environmental stresses. In: Kersteins, G. (Ed.), Plant Cuticles. BIOS Scientific, Oxford, pp. 83–108.

Koornneef, M., Hanhart, C.J., Thiel, F., 1989. A genetic and phenotypic description of *eceriferum* (*cer*) mutants in *Arabidopsis thaliana*. Journal of Heredity 80, 118–122.

Lemieux, B., Koornneef, M., Feldmann, K.A., 1994. Epicuticular wax and *eceriferum* mutants. In: Meyerowitz, E., Somerville, C. (Eds.), Arabidopsis. Cold Springs Harbor Laboratory Press, New York, pp. 1031–1047.

Macey, M.J.K., Barber, H.N., 1970. Chemical genetics of wax formation on leaves of *Pisum sativum*. Phytochemistry 9, 13–23.

McNevin, J.P., Woodward, W., Hannoufa, A., Feldmann, K.A., Lemieux, B., 1993. Isolation and characterization of *eceriferum* (*cer*) mutants induced by T-DNA insertions in *Arabidopsis thaliana*. Genome 36, 610–618.

Rashotte, A.M., Jenks, M.A., Nguyen, T.D., Feldmann, K.A., 1997. Epicuticular wax variation in ecotypes of *Arabidopsis thaliana*. Phytochemistry 45, 251–255.

PERGAMON

Phytochemistry 57 (2001) 125–130

PHYTOCHEMISTRY

www.elsevier.com/locate/phytochem

Melampolides from *Enydra anagallis*

Alicia Bardón [a], Luz Cardona [b], Elena Cartagena [a], César A.N. Catalán [a], José R. Pedro [b,*]

[a] *Instituto de Química Orgánica, Facultad de Bioquímica,Química y Farmacia, Universidad Nacional de Tucumán, Ayacucho 491, S.M. de Tucumán 4000, Argentina*

[b] *Departamento de Química Orgánica, Facultad de Química, Universitat de València, 46100-Burjassot Valencia, Spain*

Received 16 June 2000; received in revised form 13 November 2000

Abstract

The investigation of an Argentine collection of *Enydra anagallis* afforded sesquiterpene lactones of the melampolide type two of which were previously known. Their structures were elucidated by spectroscopic methods. © 2001 Elsevier Science Ltd. All rights reserved.

Keywords: *Enydra*; Compositae; Heliantheae; Sesquiterpene lactones; Melampolides

1. Introduction

The genus *Enydra* (Asteraceae, tribe Heliantheae) was placed by Stuessy (1977) in the subtribe Ecliptinae and then by Robinson (1981) in the subtribe Enhydrinae. Karis sampled many genera of Heliantheae in his morphological cladistic analysis and placed *Enydra* in the subtribe Melampodiinae (Bremer, 1994). It is one of the few genera of wet or aquatic habitats in the Compositae. The genus was originally described by Loureiro (1790) as *Enydra* but later it was spelled as "*Enhydra*" (De Candolle, 1836) taking in account the etymology of the word (from Greek, enhydra: in water).

From numerous species of *Tetragonotheca*, *Sigesbeckia*, *Acanthospermum*, *Melampodium*, *Lecocarpus*, and *Smallanthus*, all included in the subtribe Melampodiinae (Bremer, 1994), many diterpenoids and melampolide type sesquiterpenoids were isolated (Quijano et al., 1979; Barua et al., 1980; Saleh et al., 1980; Bohlmann et al., 1981, 1984a; Castro et al., 1989; Zdero et al., 1991; Macías and Fischer, 1992; Macías et al., 1993; Inoue et al., 1995; Quijano et al., 1997). Phytochemical studies of *E. fluctuans*, the only species of the genus previously investigated, have led to the isolation of several sesquiterpene lactones of melampolide type (Ali et al., 1972; Bohlmann et al., 1982a,b; Krishnaswamy and Ramh, 1995). *E. fluctuans* is used in Indian medicine in treatment of nervous ailments, skin diseases and has been employed as laxative (Chopra, 1956), anti-inflammatory, anti-bilious and demulcent (Kirtikar and Basu, 1933; Sastri, 1952).

From *E. anagallis*, the only species of this genus growing in Argentina, we now report the isolation of eight melampolides (**1**–**8**). Compounds **2**, **3** and **5**–**8** are described for the first time in this paper, and their structures were elucidated by extensive highfield NMR studies, standard ^{1}H–^{1}H COSY, HMQC and NOE experiments.

2. Results and discussion

Compound **1** was a gum with IR absorptions at 1760, 1735 and 1710 cm^{-1} which accounts for an α-methylene γ-lactone, a saturated ester and an α,β-unsaturated ester respectively. ^{1}H NMR data (Table 1) strongly suggested the presence of a 6,12-melampolide skeleton with two acyloxy side chains located at C-8 and C-9. An extensive NMR study, including ^{1}H, ^{13}C and NOE experiments, allowed us to assigne compound 1 the structure of uvedalin previously isolated from *Polymnia uvedalia* (Herz and Bhat, 1970) and *Smallanthus sonchifolius* (Inoue et al., 1995). Relative stereochemistry was supported by NOE experiments.

Compounds **2**–**5** showed ^{1}H and ^{13}C NMR data almost identical to those of the previously described for the 6,12-melampolide skeleton of compound **1**, even the signals for the C-14 methyl ester group and the C-9

* Corresponding author Tel.: +34-09-638-64329; fax: +34-09-638-64328.

E-mail address: jose.r.pedro@uv.es (J.R. Pedro).

0031-9422/01/$ - see front matter © 2001 Elsevier Science Ltd. All rights reserved.
PII: S0031-9422(00)00500-8

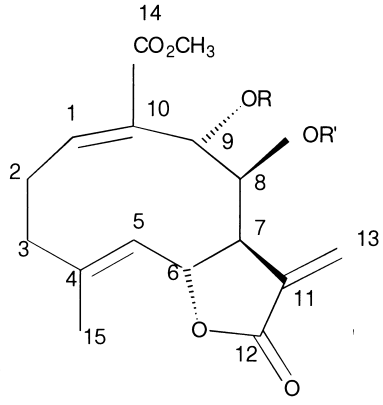

	R	R'
1	Ac	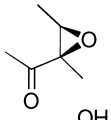
2	Ac	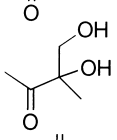
3	Ac	
4	Ac	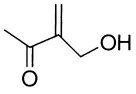
5	Ac	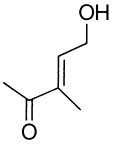
6	H	
7	H	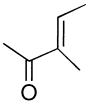
8	H	H

acetate group. Close similarity in chemical shifts, coupling patterns and coupling constants led us to assume identical skeletal features for all of them. Differences were found in the side chains located at C-8. The ^{1}H NMR spectrum of **2** showed a three-proton singlet at δ 1.37 and a two proton AB system centered at δ 3.60 (J = 11.2 Hz), while the ^{13}C NMR spectrum displayed two signals at δ 56.9 (*s*) and δ 50.5 (*t*) for tetra- and disubstituted carbons bearing oxygen. The mentioned signals suggested a 2,3-dihydroxy-2-methylpropanoyloxy side chain at C-8 (Abegaz et al., 1994). This was further confirmed by diagnostic MS peaks. The MS spectrum showed the base peak at m/z 272 [M-HOAc-HOCOC(-CH_3)(OH)CH_2 (OH)]$^+$, a strong peak at m/z 213 (60%) due to the loss of 2,3-dihydroxy-2-methylpropionic acid, acetic acid and -(CO)OCH_3 group from the molecular ion and a small peak at m/z 240 related to the loss of 2,3-dihydroxy-2-methylpropionic acid, acetic acid and methanol from the molecular ion.

Compound **3** had a molecular formula $C_{22}H_{26}O_8$ (molecular ion peak at m/z 418.1630) and the ^{1}H NMR spectral parameters were nearly identical to those of the 6,12-melampolide **1**. ^{1}H NMR signals associated with the side chain were one vinyl proton broad singlet at δ 6.02, one vinyl proton triplet at δ 5.57 (J = 1.6 Hz) and a three- proton broad singlet at δ 1.93 (vinyl methyl protons). These values as well as the ^{13}C NMR signals at δ 126.6 (CH_2), δ 135.4 (C) and δ 16.9 (CH_3) suggested the presence of a methacrylate side chain (Rustaiyan et al., 1991; Abegaz et al., 1994). The structure of compound **3** was further supported by the mass spectral pattern with peaks at m/z 272 [(M-HOAc–HOCOC(CH_3)=CH_2)]$^+$, m/z 213 due to the loss of methacrylic acid, acid acetic and -(CO)OCH_3 from the molecular ion and m/z 240 due to the loss of methacrylic acid, acetic acid and methanol from the molecular ion as well as by a base peak at m/z 69 [C_4H_5O]$^+$ (Walachy and Fischer, 1981).

Compound **4**, $C_{22}H_{26}O_9$ (molecular peak at m/z 434.1576) showed ^{1}H NMR spectral data nearly identical to those of compound **3** being the signals of the side chain the most noticeable difference. These ^{1}H NMR data, including coupling constants, were in good agreement with the compound named 19-hydroxy-15-desoxy-orientalide previously isolated from *Clibadium pittierii* (Tamayo-Castillo et al., 1988).

The mass spectrum of compound **5** showed the [M]$^+$ at m/z 448.1739 which agreed with the molecular formula $C_{23}H_{28}O_9$. The features of the ^{1}H and ^{13}C NMR spectra suggested, as in the previously described compounds a 6,12-melampolide skeleton bearing methyl ester at C-14 and an acetate group at C-9. The main differences were observed in the signals of the side chain located at C-8. The ^{1}H NMR spectrum showed a three- proton doublet at δ 1.79 (J=1.2 Hz); a two-proton doublet at δ 4.34 (J= 5.6 Hz) and a one-proton triple doublet at δ 6.79 (J=6.0 and 1.6 Hz). Both doublets at δ 1.79 and 4.34 collapsed into singlets when the signal at δ 6.79 was irradiated. The ^{13}C NMR spectrum exhibited signals for two olefinic carbons at δ 127.6 (*d*) and δ 141.6 (*s*) and a methylene group at δ 59.7 (*t*) linked to oxygen, probably a hydroxyl group (IR absorption at 3473 cm^{-1}). This results, together with the presence of peaks at m/z 272 [M-HOAc–HOCO–C(CH_3)=CH–CH_2OH]$^+$, 99 [C_5H_7 O_2]$^+$ and 71 [C_4H_7 O]$^+$ in the mass spectrum led us to the conclusion that the side chain group must be 4-hydroxy-3-methyl-2-butenoyl (Bohlmann et al., 1982a, 1984b; El-Masry et al., 1985; Hernández et al., 1994), 4-hydroxy-2-methyl-3-butenoyl

(Bohlmann et al., 1982b; Öksuz and Ayyildiz, 1986) or 2-hydroxymethyl-2-butenoyl (Herz et al., 1984; El-Masry et al., 1985; Rustaiyan et al., 1991). The stereochemistry of the side chain double bond was deduced by NOE experiments. Saturation of the H-4′ signal led to an increment in intensity of the H-5′ and H-3′ signals, however, saturating the H-3′ signal only caused an increment of the H-4′signal intensity. Therefore the side chain in 5 must be a 4′-hydroxytiglate and not a 4′-hydroxyangelate.

The ^{1}H NMR spectra of compounds **6** and **7** showed the spectral pattern observed in compounds described above (Tables 1 and 2). However, the signal corresponding to the C-9 acetate group was not present. Instead, a higher field signal assigned to H-9 was observed suggesting a hydroxyl group situated at this position. In compound **6** this signal appeared at δ 4.00 as a triplet ($J=10$ Hz) coupling with H-8 (δ 6.27) and with the signal at δ 2.75 which was assigned to the proton of hydroxyl group. The signals corresponding to the acyloxy side chain located at C-8 were very similar to that compound **3** (Tables 1 and 2) so compound **6** was the 9-deacyl-derivative of compound **3**. The exact mass measurement of the $[M]^+$ at m/z 376.1522, provides the molecular formula $C_{20}H_{24}O_7$ and confirms this assignment.

In compound **7** the H-9 signal at δ 4.00 (*t*, *J ca* 9.0 Hz) and a signal at δ 2.80 (*d*, $J=9.6$ Hz) ascribable to the hydroxyl proton suggested again the structure of a 9-deacyl derivative. The nature of the acyloxy side chain at C-8 was evident from the ^{1}H NMR data: a one-proton multiplet overlapped with the H-1 signal at δ 6.84, and two three-proton signals, a broad singlet at δ 1.83 and a broad doublet at δ 1.80 ($J=7.2$ Hz) typical of a tiglic ester moiety (Lazari et al., 1998; Spring et al., 1999). Tiglate was clear also by the signals at δ 166.9 (C), 127.8 (C), 138.8 (CH), 14.5 and 12.8 (two CH_3) in the ^{13}C NMR spectrum. The side chain double bond configuration was confirmed by NOE experiments. The exact mass measurement of the $[M]^+$ at m/z 390.1675 provides a molecular formula $C_{21}H_{26}O_7$ and the mass peaks at m/z 290 $[M\text{-}HOCO\text{–}C(CH_3)=CH(CH_3)]^+$ and m/z 83 confirmed the nature of the ester side chain.

The ^{1}H NMR spectrum of compound **8** showed all the signals corresponding to a 6,12-melampolide skeleton. However two characteristics in the spectrum of compound **8** with respect to all other compounds previously described were obvious: absence of signals due to the lack of any side chain and a dramatic highfield shift of the signal for H-8 from *ca* δ 6.30 to δ 4.69. The molecular peak of compound **8** at m/z 309.1354 $[M+H]^+$ indicative for a molecular formula $C_{16}H_{20}O_6$, together with a large OH band in the IR spectrum at 3425 cm^{-1} and the sixteen peaks present in the ^{13}C NMR spectrum allow us to propose the structure of compound **8**.

3. Experimental

3.1. General

NMR: 400 MHz (^{1}H) and 75.4 MHz (^{13}C) in $CDCl_3$. NOE measurements were carried out by the one-dimensional difference method. Optical rotations at 20°. Low

Table 1
^{1}H NMR chemical shifts of compounds **1–4** (400 MHz, $CDCl_3$, δ values)

H	1	2	3	4
1	7.00 *dd* (10.4, 7.6)[d]	7.01 *dd* (10.0, 7.2)	7.00 *dd* (10.0, 7.2)	7.01 *dd* (10.0, 7.6)
2a	2.66 *dddd* (12.8, 12.8, 10.8, 2.0)	2.64 *dddd* (12.8, 12.8, 10.4, 2.0)	2.65 *dddd* (12.4, 12.4, 10.4, 2.0)	2.62 *dddd* (12.8, 12.8, 10.8, 2.0)
2b	2.46 *dddd* (12.4, 7.6, 5.6, 1.6)	2.45 *dddd* (12.4, 8.0, 6.0, 2.0)	2.44 *dddd* (12.0, 8.0, 6.0, 2.0)	2.45 *dddd* (12.4, 8.0, 6.0, 2.0)
3a	2.39 *ddd* (12.4, 5.6, 2.0)	2.39 *ddd* (12.0, 6.0, 2.0)	2.39 *ddd* (12.0, 6.0, 2.0)	2.38 *ddd* (13.0, 6.0, 2.0)
3b	2.03 *brt* (*ca* 11.6)	2.03 *brt* (*ca* 12.0)	2.03 *brt* (*ca* 11.6)	2.04 *brt* (*ca* 11.8)
5	4.95 *brd* (10.8)	4.95 *brd* (10.8)	4.96 *brd* (10.4)	4.96 *brd* (11.2)
6	5.10 *t* (10.4)	5.08 *t* (10.0)	5.11 *t* (10.0)	5.12 *t* (10.0)
7	2.78 *dddd* (9.6, 3.2, 3.2, 1.2)	2.78 *dddd* (9.6, 3.2, 3.2, 1.2)	2.76 *dddd* (10.0, 3.2, 2.8, 1.2)	2.78 *dddd* (9.6, 3.6, 3.6, 1.2)
8	6.65 *dd* (8.4, 1.2)	6.64 *dd* (8.4, 1.2)	6.62 *dd* (8.8, 1.4)	6.64 *dd* (8.4, 1.4)
9	5.40 *d* (8.4)	5.41 *d* (8.4)	5.43 *d* (8.4)	5.46 *d* (8.4)
13a	6.25 *d* (3.2)	6.29 *d* (3.6)	6.26 *d* (3.2)	6.27 *d* (3.6)
13b	5.72 *d* (2.8)	5.77 *d* (2.8)	5.81 *d* (3.2)	5.80 *d* (3.2)
15[a]	1.99 *s*	1.99 *s*[c]	1.89 *s*[c]	1.94 *s*[c]
-OCH_3	3.80 *s*	3.80 *s*	3.79 *s*	3.80 *s*
-OAc	1.99 *s*	1.98 *s*[c]	2.03 *s*[c]	2.02 *s*[c]
-OH				
3′a	3.01 *q* (5.2)	3.67 *d* (11.2)	6.02 *brs*	6.17 *brs*
3′b		3.52 *d* (11.2)	5.57 *t* (1.6)	5.86 *d* (1.2)
4′	1.18 *d* (5.2)[a]	1.37 *s*[a]	1.93 *s*[a]	4.28 *brs*[b]
5′[a]	1.46 *s*			

[a] Three proton intensity.
[b] Two proton intensity.
[c] Assignments may be interchanged.
[d] Figures in parentheses are coupling constants in Hertz.

Table 2
^{1}H NMR chemical shifts of compounds **5–8** (400 MHz, $CDCl_3$, δ values)

H	5	6	7	8
1	7.00 *dd* (10.4, 7.6)[e]	6.84 *dd* (10.4, 7.2)	6.84 *dd* (10.0, 7.6)[d]	6.80 *dd* (10.4, 7.6)
2a	2.64 *dddd* (12.4, 12.4, 10.8, 2.0)	2.48 *dddd* (12.8, 7.2, 6.0, 2.0)	2.48 *dddd* (12.4, 7.2, 6.0, 2.0)	2.45 *m*
2b	2.45 *dddd* (12.4, 8.0, 6.0, 2.0)	2.24 *dddd* (12.8, 12.8, 10.4, 2.0)	2.24 *dddd* (12.4, 12.8, 10.8, 2.0)	2.22 *dddd* (12.4, 12.8, 12.8, 2.0)
3a	2.38 *ddd* (12.0, 5.6, 2.0)	2.35 *ddd* (12.0, 6.0, 2.0)	2.35 *ddd* (12.0, 6.0, 2.0)	2.33 *ddd* (12.0, 6.0, 2.0)
3b	2.03 *brt* (ca 11.8)	2.03 *ddd* (12.0, 12.0, 2.0)	2.03 *ddd* (12.8, 12.0, 2.0)	2.01 *ddd* (12.8, 12.8, 2.0)
5	4.96 *brd* (10.4)	4.94 *brd* (10.8)	4.95 *brd* (9.6)	4.90 *brd* (10.4)
6	5.12 *t* (10.0)	5.09 *t* (10.0)	5.10 *t* (10.0)	5.17 *t* (10.0)
7	2.78 *dddd* (9.6, 3.2, 3.2, 1.2)	2.64 *dddd* (9.6, 3.2, 3.2, 1.6)	2.64 *dddd* (9.6, 3.2, 2.8, 1.6)	2.45 *m*
8	6.64 *dd* (8.4, 1.4)	6.27*dd* (8.4, 1.6)	6.28 *dd* (8.0, 1.6)	4.69 *dd* (8.0, 1.4)
9	5.43 *d* (8.4)	4.00 *t* (*ca* 9.0)	4.00 *t* (*ca* 9.0)	3.82 *m*
13a	6.25 *d* (3.6)	6.23 *d* (3.2)	6.22 *d* (3.2)	6.31 *d* (3.6)
13b	5.79 *d* (2.8)	5.66 *d* (3.2)	5.66 *d* (3.2)	5.57 *d* (3.2)
15[a]	1.93 *s*[c]	1.89 *s*[c]	1.90 *brs*	1.85 *s*
-OCH_3	3.80 *s*	3.80 *s*	3.80 *s*	3.77 *s*
-OAc	2.01 *s*[c]			
-OH		2.75 *d* (10.0)	2.80 *d* (9.6)	
3′a	6.74 *td* (6.0, 1.6)	6.09 *brs*	6.84 [d]	
3′b		5.61 *t* (1.6)		
4′	4.34 *d* (5.6)[b]	1.94 *s* [a,c]	1.80 *d* (7.2)[a]	
5′[a]	1.79 *d* (1.2)		1.83 *brs*	

[a] Three proton intensity.
[b] Two proton intensity.
[c] Assignments may be interchanged.
[d] Signals overlapped.
[e] Figures in parentheses are coupling constants in Hertz.

and high-resolution MS measured with a Fisons Instruments VG Autospec, GC 8000 (70 eV). For separation of mixtures Waters and Konik equipments were used. Columns: (A) Beckman Ultrasphere C 8 (5 μm, 10 mm i.d.×250 mm) and (B) Phenomenex Ultemex C 18 (5 μm, 10 mm i.d.×250 mm). Retention times were measured from the solvent peak.

3.2. Plant material

Aerial parts and roots of *Enydra anagallis* Gadner were collected at the flowering stage in December 1993 in wet places of the riverside of Rio Romano, Monteros, Tucumán province, Argentine (a voucher specimen, LIL No 595793 is deposited in the herbarium de la Fundación Miguel Lillo, Tucumán, Argentina).

3.3. Extraction and isolation

Flowers, leaves and roots (350 g) were extracted with $CHCl_3$ (2×3 l) at rt for 4 days with shaking to give 11.5 g of residue (yield 3.2%) which was suspended in 100 ml of EtOH at 55°C, diluted with 75 ml of H_2O and extracted successively with hexane (2×150 ml) and $CHCl_3$ (2×150 ml). The second $CHCl_3$ extract was evapd under red. pres. to give 1.9 g of residue which was chromatographed on Si gel (57 g, 70–230 Mesh) with $CHCl_3$ and increasing amounts of EtOAc (0–100%) and finally MeOH; 82 fractions of 10 ml each being collected. Fractions containing sesquiterpene lactones (IR band at 1765 cm^{-1}) were further purified. Frs. 1-14 (383 mg) were eluted with $CHCl_3$ and increasing amounts of EtOAc (0–5%) and combined (383 mg). They were defatted with MeOH and, after filtration and evapn of solvent, the residue was processed by HPLC (Column B, MeOH–H_2O 2:1, 2 ml min^{-1}) to give compounds **6** (40 mg, R_t 6 min), **1** (78 mg, R_t 10 min) and **3** (52 mg, R_t 17 min). Frs. 15-29 (eluted with $CHCl_3$-EtOAc 95:5) were combined (509 mg) and processed by HPLC (Column B, MeOH–H_2O 4:3, 1.5 ml min^{-1}) to give four fractions which showed to be mixtures by TLC analysis. Rechromatography by HPLC (Column A, MeOH–H_2O 1:1, 1.7 ml min^{-1}) afforded compounds **6** (93 mg, R_t 19 min), **7** (8 mg, R_t 29 min) and **1** (5 mg, R_t 31 min). Fr 30-51 eluted with a $CHCl_3$-EtOAc gradient (9:1→8:2) and combined (375 mg). A portion (200 mg) was processed by HPLC (Column B, MeOH–H_2O 4:3,1.3 ml min^{-1}) to give compound **2** (22 mg, R_t 30 min). Frs 52-65 eluted with a $CHCl_3$–EtOAc gradient (3:1→1:2) and combined (183 mg). HPLC (Column B, MeOH–H_2O 6:5, 1.5 ml min^{-1}) gave compound **4** (37 mg, R_t 21 min) and a mixture (R_t 22-23 min) which was further processed by HPLC (Column A, MeOH–H_2O 6:5, 2 ml min^{-1}) to give a new portion of **4** (3 mg, R_t 22 min) and **5** (3 mg, R_t 27 min). Frs 66-82 were eluted with EtOAc and finally MeOH. They were combined (280 mg) and chromatographed by HPLC (Column B, MeOH–H_2O 1:1, 1.2 ml min^{-1}) to give compound **8** (46.8 mg, R_t 8 min).

*3.3.1. Compound **1***

Oil; $[\alpha]_D^{20}$ +20.9° ($CHCl_3$, *c* 0.004); UV λ_{max}(MeOH) nm: 219; IR ν_{max}(film) cm^{-1}: 1760, 1735, 1710; ^1H NMR and ^{13}C NMR: Tables 1 and 3; HREIMS (70 eV) *m/z* (rel. int.): 272.1064 $[M–R'OH–AcOH]^+$ (calc. for $C_{16}H_{16}O_4$ 272.1048), 240 (27), 213 (57), 71 (8).

*3.3.2. Compound **2***

Oil; $[\alpha]_D^{20}$ −13.6° ($CHCl_3$, *c* 0.006); IR ν_{max}(film) cm^{-1}: 3473, 1767, 1746, 1714; ^1H NMR and ^{13}C NMR: Tables 1 and 3; HREIMS (70 eV) *m/z* (rel. int.): 333.1345 $[M-R'O]^+$ (4.7) (calc. for $C_{18}H_{21}O_6$ 333.1338), 272 (100), 258 (21), 213 (60), 128 (13), 91 (26).

*3.3.3. Compound **3***

Oil; $[\alpha]_D^{20}$ +54.2° ($CHCl_3$, *c* 0.012); IR ν_{max} (film) cm^{-1}: 1765, 1730, 1715; ^1H NMR and ^{13}C NMR: Tables 1 and 3; HREIMS (70 eV) *m/z* (rel. int.): 418.1630 $[M]^+$ (2.1) (calc. for $C_{22}H_{26}O_8$ 418.1628), 272 (77), 240 (16), 213 (35), 69 (100).

*3.3.4. Compound **4***

Oil; $[\alpha]_D^{20}$ +50.7° ($CHCl_3$, *c* 0.002); UV λ_{max} (MeOH) nm: 218; IR ν_{max} (film) cm^{-1}: 3400, 1760, 1730, 1630; ^1H NMR and ^{13}C NMR: Tables 1 and 3; HREIMS (70 eV) *m/z* (rel. int.): 434.1576 $[M]^+$ (1) (calc. for $C_{22}H_{26}O_9$ 434.1577), 374 (8.9), 272 (100), 240 (15), 213 (53), 85 (53).

*3.3.5. Compound **5***

Oil; $[\alpha]_D^{20}$ +63.7° ($CHCl_3$, *c* 0.003); UV λ_{max} (MeOH) nm: 210; IR ν_{max} (film) cm^{-1}: 3473, 1767, 1738; ^1H NMR and ^{13}C NMR: Tables 2 and 3; HREIMS (70 eV) *m/z* (rel. int.): 448.1739 $[M]^+$ (2.6) (calc. for $C_{23}H_{28}O_9$ 448.1733), 350 (2.8), 272 (84), 240 (14), 213 (33), 99 (100), 71 (41).

*3.3.6. Compound **6***

Oil; $[\alpha]_D^{20}$ +60.5° ($CHCl_3$, *c* 0.013); UV λ_{max} (MeOH) nm: 221; IR ν_{max} (film) cm^{-1}: 3450, 1760, 1715, 1630; ^1H NMR and ^{13}C NMR: Tables 2 and 3; HREIMS (70 eV) *m/z* (rel. int.): 376.1522 $[M]^+$ (0.3) (calc. for $C_{20}H_{24}O_7$ 376.1522), 290 (9), 258 (22), 230 (10), 212 (16), 162 (15), 128 (9), 91 (9), 69 (100).

*3.3.7. Compound **7***

Oil; $[\alpha]_D^{20}$ +70.4° ($CHCl_3$, *c* 0.006); IR ν_{max} (film) cm^{-1}: 3465, 1765, 1714; ^1H NMR and ^{13}C NMR: Tables 2 and 3. HREIMS (70 eV) *m/z* (rel. int.): 390.1675 $[M]^+$ (0.5) (calc. for $C_{21}H_{26}O_7$ 390.1678), 359 (7), 290 (15), 258 (25), 240 (11), 2122 (13), 162 (12), 128 (5.8), 83 (100).

*3.3.8. Compound **8***

Oil; $[\alpha]_D^{20}$ −22.7° ($CHCl_3$, *c* 0.007); IR ν_{max} (film) cm^{-1}: 3452, 1761,1710; ^1H NMR and ^{13}C NMR: Tables 2 and 3; HRCIMS *m/z* (rel. int.): 309.1354 $[M+H]^+$ (36) (calc.

Table 3
^{13}C NMR chemical shifts of compounds **1**–**8** (75 MHz, $CDCl_3$, δ values)[b]

C	**1**[a]	**2**[a]	**3**[a]	**4**[a]	**5**[a]	**6**[a]	**7**[a]	**8**[a]
1	148.4	148.4	148.3	148.4	148.3	144.4	144.3	144.5
2	26.1	26.1	26.1	26.1	26.1	25.8	25.8	25.9
3	36.9	36.9	36.9	36.9	36.9	36.8	36.8	36.8
4	130.6	130.5	130.6	130.6	130.6	133.8	133.9	133.5
5	126.2	126.4	126.3	126.2	126.2	126.5	126.6	126.9
6	76.9	74.9	75.3	75.2	75.3	75.5	75.6	74.8
7	50.9	50.8	50.9	50.9	51.0	51.6	51.6	51.6
8	70.9	72.3	70.2	70.4	70.2	72.8	72.4	71.6
9	75.2	70.8	71.1	70.9	71.1	71.3	71.4	72.8
10	134.4	133.6	134.3c	134.2	134.3	134.7c	134.7	136.0
11	138.6	138.6	138.5	138.5b	138.5	137.6	137.6	137.6
12	169.1a	170.2a	170.2a	170.4a	170.2a	169.3a	169.4a	169.9a
13	121.5	122.1	121.8	119.9	121.8	121.3	121.3	120.1
14	168.4a	169.0a	170.2a	169.2a	169.4a	167.0a	167.8a	167.6a
15	16.9b	16.8b	16.9b	16.9	16.9	16.9b	16.9	
-OCH_3	53.3	52.3	52.3	52.1	52.3	52.3	52.3	52.1
-OAc	165.9	165.8	165.9	165.9	165.9			
	20.9	20.9	20.8	20.8	20.8			
1′	170.2a	172.7a	165.9a	164.9a	166.1a	166.9a	166.9a	
2′	59.3	56.9	135.4c	138.8b	127.6	135.5c	127.8	
3′	59.9	50.5	126.6	126.9	141.6	126.6	138.8	
4′	13.6	23.6	18.3b	62.3	59.7	18.3b	14.5	
5′	19.1b				12.8		12.2	

[a] Assignments a,b,c may be interchanged within each column.
[b] Signals of all compounds have been assigned by means of 2D NMR experiments.

for $C_{16}H_{21}O_6$ 306.1338), 291 (43), 273 (37), 259 (100), 241 (51), 231 (37), 213 (26), 128 (31).

Acknowledgements

Work in Argentina was supported by grants from Agencia Nacional de Promoción Científica y Tecnológica (ANPCyT), Consejo Nacional de Investigaciones Científicas y Técnicas de Argentina (CONICET) and Consejo de Investigaciones de la Universidad Nacional de Tucumán (CIUNT).

References

Abegaz, B.M., Keige, A.W., Diaz, J.D., Herz, W., 1994. Sesquiterpene lactones and other constituents of *Vernonia* species from Ethiopia. Phytochemistry 37, 191–196.

Ali, E., Ghosh-Dastidar, P.P., Pakarashi, S.C., Durham, L.J., Dufield, A.M., 1972. Studies on Indian medicinal plants-XXVIII: sesquiterpene lactones of *Enhydra fluctuans* Lour. Structures of enhydrin, fluctuanin and fluctuadin. Tetrahedron 28, 2285–2298.

Barua, R.N., Sharma, R.P., Thyagarajan, G., Herz, W., Govindan, S.V., 1980. New melampolides and darutigenol from *Sigesbeckia orientalis*. Phytochemistry 19, 323–325.

Bohlmann, F., Jakupovic, J., Dhar, A.K., King, R.M., Robinson, H., 1981. Two sesquiterpene and three diterpene lactones from *Acanthospermum australe*. Phytochemistry 20, 1081–1083.

Bohlmann, F., Ahmed, M., Robinson, H., King, M., 1982a. Melampolides from *Enhydra fluctuans var. Fluctuans*. Phytochemistry 21, 1675–1678.

Bohlmann, F., Singh, P., King, R.M., Robinson, H., 1982b. New guaianolides from *Pseudostifftia kingii*.. Phytochemistry 21, 1171–1172.

Bohlmann, F., Schmeda-Hirschmann, G., Jakupovic, J., 1984a. Neue Melampolide aus *Acanthospermum australe*. Planta Medica 50, 37–39.

Bohlmann, F., Schmeda-Hirschmann, G., Jakupovic, J., 1984b. Heliangolides and germacranolides from *Disynaphia multicrenulata*. Phytochemistry 23, 1435–1437.

Bremer, K., 1994. Asteraceae. Cladisticts Classification. Timber Press, Portland, Oregon.

Castro, V., Jakupovic, J., Dominguez, X.A., 1989. Melampolides from *Melampodium* and *Smallanthus* species. Phytochemistry 28, 2727–2729.

Chopra, N.R., 1956. Glossary of Indian Medicinal Plants. Publication and Information Directorate, New Delhi.

De Candolle, A.P., 1836. Compositae, Part I. Prodromus Systematis Naturalis Regni Vegetabilis 5.

El-Masry, S., Darwish, F.A., Abou-Donia, A., Abou-Karam, M.A., Grenz, M., 1985. Sesquiterpene lactones from *Centaurea glomerata*. Phytochemistry 24, 999–1001.

Hernández, L.R., Catalán, C.A.N., Cerda-García-Rojas, C.M., Nathan, P.J., 1994. Sesquiterpene lactones from *Stevia breviaristata*. Phytochemistry 37, 1331–1335.

Herz, W., Bhat, S.V., 1970. Isolation and structure of two new germacranolides from *Polymnia uvedalia* (L.) L. Journal of Organic Chemistry 35, 2605–2611.

Herz, W., Watanabe, K., Blount, J.F., 1984. Stereochemistry of chapliatrin and its congeners from *Liatris gracilis*. Phytochemistry 23, 373–382.

Inoue, A., Tamogami, S., Kato, H., Nakazato, Y., Akiyama, M., Kodama, O., Akatsuka, T., Hashidoto, Y., 1995. Antifungal melampolides from leaf extracts of *Smallanthus sonchifolius*. Phytochemistry 39, 845–848.

Kirtikar, K.R., Basu, B.D., 1933. Indian Medicinal Plants 2, 1360.

Krishnaswamy, N.R., Ramh, N., 1995. Sesquiterpene lactones from *Enhydra fluctuans*. Phytochemistry 38, 433–435.

Lazari, D., García, B., Skaltsa, H., Pedro, J.R., Harvala, C., 1998. Sesquiterpene lactones from *Onopordon laconicum* and *O. sibthorpianum*. Phytochemistry 47, 415–422.

Loureire, J de, 1970. Flora Cochinkinesis, 510.

Macías, F.A., Fischer, N.H., 1992. Melampolides from *Lecocarpus pinnatifidus*. Phytochemistry 31, 2747–2754.

Macías, F.A., Molinillo, J.M., Fischer, N.H., 1993. Melampolides and c*is*,*cis*-Germacranolides from *Lecocarpus lecocarpoides*. Phytochemistry 32, 127–131.

Öksuz, S., Ayyildiz, H., 1986. Sesquiterpene lactones from *Centaurea coronopifolia*. Phytochemistry 25, 535–537.

Quijano, L., Bloomenstiel, D., Fischer, N.H., 1979. Tetraludin A, B and C, three new melampolides from *Tetragonotheca ludoviciana*. Phytochemistry 18, 1529–1532.

Quijano, L., Núñez, I.S., Fronczek, F.R., Fischer, N.H., 1997. A guaianolide and four melampolides from *Melampodium leucanthum*. Phytochemistry 45, 769–775.

Robinson, H., 1981. A revision of the tribal and subtribal limits of the Heliantheae (Asteraceae). Smithsonian Contributions to Botany 51, 1.

Rustaiyan, A., Saberi, M., Habibi, Z., Jakupovic, J., 1991. Melampolides and other constituents from *Jurinea leptoloba*. Phytochemistry 30, 1929–1932.

Saleh, A.A., Cordell, G.A., Farnsworth, N.R., 1980. Potencial Anticancer Agents. Part 13. Cytotoxic constituents of *Acanthospermum glabratum*. J. Chem. Soc. Perkin 1, 1090–1097.

Sastri, B.N., 1952. Wealth of India, Raw Materials, Vol. 3. Council of Scientific and Industrial Research, New Delhi.

Spring, O., Zipper, R., Vogler, B., Callegari-Lopes, J.L., Vichnewski, W., Dias, D.A., Cunha, W.R., 1999. Sesquiterpene lactones in *Blainvillea rhomboidea*. Phytochemistry 52, 79–85.

Stuessy, T.F. In: Heywood, V.H., Harborne, J.B., Turner, B.L. (Eds.). The Biology and Chemistry of the Compositae. Academic Press, New York, pp. 621.

Tamayo-Castillo, G., Jakupovic, J., Bohlmann, F., Castro, V., 1988. Clibadiolide, a sesquiterpene lactone esterified with a homoditerpene from *Clibadium pittierii*. Phytochemistry 27, 1868–1870.

Walachy, J., Fischer, N.H., 1981. Four new *cis,cis*-germacranolides from cytotoxic fractions of *Melampodium cinereum*. Phytochemistry 20, 840–842.

Zdero, C., Bohlmann, F., King, R.M., Robinson, H., 1991. Sesquiterpene lactones and other constituents from *Sigesbechia orientalis* and *Guizotia scabra*. Phytochemistry 30, 1579–1584.

PERGAMON

Phytochemistry 57 (2001) 131–134

PHYTOCHEMISTRY

www.elsevier.com/locate/phytochem

ent-Pimarane derivatives from *Dysoxylum hainanense*

Xiao-Dong Luo *, Shao-Hua Wu, Yun-Bao Ma, Da-Gang Wu

Laboratory of Phytochemistry, Kunming Institute of Botany, The Chinese Academy of Sciences, Kunming 650204 Yunnan, People's Republic of China

Received 4 May 2000; received in revised form 2 October 2000

Abstract

Four *ent*-pimarene diterpenoids, *ent*-18-acetoxy-8(14)-pimarene-15*S*,16-diol, *ent*-18-acetoxy-16-hydroxy-8(14)-pimaren-15-one, *ent*-16,18-dihydroxy-8(14)-pimaren-15-one and *ent*-19-nor-4,16,18-trihydroxy-8(14)-pimaren-15-one, together with three known damarane triterpenoids, richenoic acid, eichlerianic acid and shoreic acid were isolated from the bark of *Dysoxylum hainanense* Merr. Their structures were elucidated on the basis of spectroscopic techniques. The absolute configurations of four diterpenoids were assigned as *ent*-pimarene type by chemical transformation and by co-occurrence in the plant as well as by negative optical rotations for four compounds. © 2001 Elsevier Science Ltd. All rights reserved.

Keywords: Dysoxylum hainanense; Meliaceae; *ent*-Pimarene diterpenoids

1. Introduction

The genus *Dysoxylum*, comprising about 200 species grows naturally in India and southeast Asia. Fourteen of them are distributed in China. About 10 species of this genus have been found in the Yunnan province and *D. hainanense* Merr. is distributed in the Guangxi, Hainan, and Xishuangbanna County, Yunnan provinces (Yunnan Institute of Botany, 1977). While diterpenoids have been isolated from this genus (Onan et al., 1985; Aladesanmi and Adewunmi, 1990), the chemical constituents of this species have not been reported previously. As a continuing study on chemical constituents from Meliaceae plants (Luo et al., 1999), we examined the EtOH extract of the bark of *D. hainanense*. Four new diterpenoids, together with three known damarane triterpenoids, richenoic acid, eichlerianic acid and shoreic acid (Aalbersberg and Singh, 1991) were obtained. This paper describes the isolation and structural elucidation of these compounds.

2. Results and discussion

Compound **1** was assigned the molecular formula of $C_{22}H_{36}O_4$ by negative-ion HRFABMS. The IR spectrum showed absorption bands at 3318 cm^{-1} (–OH), 1714 cm^{-1} (C=O) and 1622 cm^{-1} (olefinic linkage). The ^1H NMR spectrum exhibited signals for an olefinic proton (δ_H 5.19, s), three upfield tertiary (δ_H 0.94, 0.84, 0.77) and downfield (δ_H 2.03) methyl singlets. The EIMS spectrum exhibited a strong fragment peak at m/z 303 (the loss of $-CHOHCH_2OH$ from the molecular ion peak). In addition, the ^{13}C and DEPT NMR spectra displayed the presence of nine methylenes, two of which were oxymethylenes, three methines, one of which was oxygenated, three quaternary carbons, two olefinic carbons (δ_C 127.3, 139.7), and an acetate group. All these data suggested that **1** was either a pimarene or isopimarene diterpenoid having a 1,2-dihydroxyethyl side chain and a double bond between C-8 and C-14 (Cambie et al., 1975; Jakupovic et al., 1987; Tsichritzis and Jakupovic, 1990). This was confirmed by analysis of the HMBC spectrum, with long range coupling for H-14 (δ_H 5.19, *s*) to C-13 (δ_C 36.6, *s*), H-15 (δ_H 3.40, *dd*, $J = 9.1$, 2.1 Hz) to C-16 (δ_C 62.7, *t*), and H-15 to C-13.

The chemical shift value (δ_C 139.7) of the olefinic carbon (C-8) suggested a pimar-8(14)-ene skeleton and not its C-13 epimer (about 136 ppm) (Cambie et al., 1975) for compound **1**. The ^{13}C NMR spectrum of **1** showed a resonance at δ_C 79.4, almost identical with the value of 15*R* (i.e. *ent*-15*S*), but very different from that reported for the 15*S* epimer (Wenkert et al., 1979) which also provided proof of the stereochemistry at C-15. Comparison of the chemical shift of the other oxymethylene (δ_C 73.0)

* Corresponding author. Tel.: +86-0871-5150660; fax: +86-0871-5150227.

E-mail address: x_dluo@hotmail.com (X.-D. Luo).

0031-9422/01/$ - see front matter © 2001 Elsevier Science Ltd. All rights reserved.
PII: S0031-9422(00)00482-9

in **1** with that of 18-hydroxy (about 72 ppm) and 19-hydroxy (about 65ppm) diterpenic substances (Jakupovic et al., 1987) suggested that an acetoxyl or a hydroxyl group was connected at C-18 rather than at C-19 in compound **1**. The assumption was further supported by NOE interactions between H-18 [3.83 (1H, *d*, 10.9), 3.61 (1H, *d*, 10.9)] and H-5 [δ_H 1.30 (m)], and δ_H 0.77 (H-20) and 0.84 (H-19) in the ROESY spectrum. In the HMBC spectrum, cross-peaks between oxymethylene protons (H-18) to δ_C 17.9 (*q*, C-19), 37.9 (*s*, C-4), and 171.2 (*s*, OAc) confirmed an acetoxyl attached to C-18.

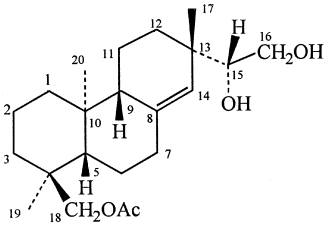

1

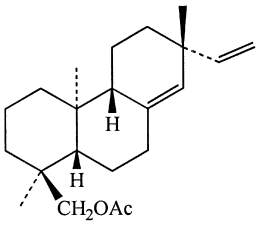

1a

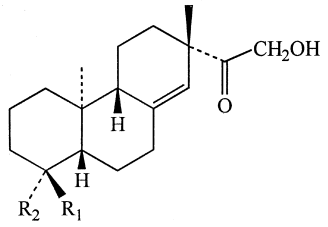

2. $R_1 = CH_2OAc$, $R_2 = CH_3$

3. $R_1 = CH_2OH$, $R_2 = CH_3$

4. $R_1 = CH_2OH$, $R_2 = OH$

In order to establish the absolute configuration of compound **1**, a chemical transformation was performed according to the literature (Hiyama and Nozaki, 1973). Compound **1** was converted to **1a** whose optical rotation {$[\alpha]_D^{23}$ −82.3° (*c* 0.15, $CHCl_3$)} was similar in magnitude, but of opposite sign to that of pimarinol ($[\alpha]_D^{22}$ −94°) (Erdtman and Westfelt, 1963). The optical rotation value of **1a** was the same sign and similar in magnitude to those of (−)-pimara-8(14),15-diene ($[\alpha]_D$ −90°) and its derivatives (Hanson and White, 1970). Hence **1a** was determined to be an *ent*-pimarene type rather than a pimarene type. Thus, **1** was elucidated as *ent*-18-acetoxy-8(14)-pimarene-15*S*,16-diol.

Because of the co-occurrence in the plant as well as the negative optical rotations for all four compounds, compounds **2**–**4** were also regarded as *ent*-pimarenes.

Compound **2** was analyzed for $C_{22}H_{34}O_4$ by negative-ion HRFABMS. The ^{13}C and ^1H NMR spectral data of **2** and **1** were similar. The main difference was that a ketonic carbonyl group was present in the ^{13}C NMR spectrum of **2**, instead of the oxymethine in **1**. The ketonic carbonyl group was assigned to be C-15 since the proton signal for the H-15 was missing in that of **2**. A singlet peak appearing at δ_H 4.30 (2H, s) in the ^1H NMR spectrum of **2** was attributed to H-16 which was free from coupling with the neighboring proton. Compound **2** was regarded as the 15-oxo derivative of **1**. Therefore, **2** was deduced to be *ent*-18-acetoxy-16-hydroxy-8(14)-pimaren-15-one.

Compound **3** possessed the molecular formula $C_{20}H_{32}O_3$ as revealed by negative-ion HRFABMS and analysis of its ^{13}C NMR spectra. The NMR spectral data of **3** were very similar to those of **2** except for the absence of the acetyl data in **3**, which was consistent with its molecular formula comprising twenty carbons. The chemical shift value of H-18 shifted upfield to δ_H 3.36, 3.07 (each 1H) in the ^1H NMR spectrum of **3**, which suggested that **3** was the 18-deacetylated derivative of **2**. Thus **3** was elucidated as *ent*-16,18-dihydroxy-8(14)-pimaren-15-one.

The high resolution negative-ion FABMS spectrum of compound **4** indicated a molecular formula of $C_{19}H_{30}O_4$. Comparison of the ^1H and ^{13}C NMR spectral data of **4** with those of **3** revealed that there were two tertiary methyl groups present in **4** instead of three in **3**. Taking the similar spectral data and molecular formula ($C_{19}H_{30}O_4$) into account, compound **4** was an *ent*-norpimaren-15-one bearing a double bond between C-8 and C-14.

The HMBC spectrum showed correlations from δ_H 3.40 (2H, *d*, 10.8, H-18) to δ_C 73.7 (*s*, C-4), and 35.8 (*t*, C-3), which suggested that the methyl group attached to C-4 (C-19) was lost and replaced by a hydroxyl in **4**. The remainder of the structure was identical to that of **3** based on comparing the ^1H and ^{13}C NMR spectral data of two compounds, and detailed analysis of the HMBC and ROESY spectra of **4**. So compound **4** was determined to be *ent*-19-nor-4,16,18-trihydroxy-8(14)-pimaren-15-one.

Three known damarane triterpenoids, richenoic acid, eichlerianic acid and shoreic acid were identified by direct comparison of their spectral data with authentic samples (Aalbersberg and Singh, 1991).

3. Experimental

3.1. General

Mps: uncorr.; IR: KBr; ^1H, ^{13}C and 2D NMR spectra were recorded on a Brüker AM-400 and a DRX-500 NMR spectrometer with TMS as an internal standard. Chemical shift values were reported in δ (ppm) and coupling constants in Hz; FAB and EIMS data were recorded on a VG Autospec-3000 spectrometer; EIMS: 70 eV

3.2. Plant material

The bark of *D. hainanense* Merr. was collected from Xishuangbanna, Yunnan province, PR China, in December 1996. The plant was identified by Professor Tao, G.-D., Xishuangbanna Botany Garden, Academia Sinica. A voucher specimen (No. 7188) was deposited in the herbarium of Taxonomy Department, Kunming Institute of Botany, Academia Sinica, Kunming, PR China.

3.3. Extraction and isolation

Dried and powdered bark (4.2 kg) of *D. hainanense* was extracted three times with EtOH under reflux conditions, the extracts were combined and solvent was evaporated in vacuo. The resulting residue was suspended in H_2O and partitioned with EtOAc. The EtOAc layer was concentrated in vacuo to give a residue (72 g), which was subjected to column chromatography (silica gel), using $CHCl_3$–Me_2CO (from $CHCl_3$ to $CHCl_3$–Me_2CO 1:1) as eluent. Fractions were combined on the basis of their TLC profiles. Fractions 1–6 were further purified on silica gel CC with petroleum ether-EtOAc (from 5:1 to 1:1) as eluent and finally on reversed-phase C_{18} silica gel CC, eluted with CH_3OH–H_2O (3:1-3:2) to yield **1** (118 mg), **2** (66 mg), **3** (106 mg), **4** (27 mg), and three known damarane triterpenoids, richenoic acid, eichlerianic acid and shoreic acid.

3.4. ent-18-Acetoxy-8(14)-pimarene-15S,16-diol (1)

Viscous oil; $[\alpha]_D^{26}$ −3.5° (*c* 0.50, CH_3OH); EIMS *m/z* (70 eV): 364 $[M]^+$ (1.4), 303 (88), 289 (37), 243 (73), 229 (25), 213 (8), 181 (10), 161 (21), 147 (29), 135 (95), 121 (100), 107 (81), 95 (86), 81 (84), 69 (45); negative-ion HRFABMS *m/z*: 363.2500 $[M\text{-}1]^-$ (calc. for $C_{22}H_{35}O_4$, 363.2535); IR (KBr) ν_{max} cm^{-1}: 3418, 2931, 2870, 1714, 1622, 1469, 1381, 1240, 1036, 947; ^1H NMR ($CDCl_3$, 400 MHz): δ 5.19 (1H, *s*, H-14), 3.83 (1H, *d*, *J* = 10.9 Hz, H-18a), 3.61 (1H, *d*, *J* = 10.9 Hz, H-18b), 3.70 (1H, *brd*, *J* = 10.6 Hz, H-16a), 3.48 (1H, *J* = 11.0, 9.1 Hz, H-16b), 3.40 (1H, *dd*, *J* = 9.1, 2.1 Hz, H-15), 2.03 (3H, *s*, OAc), 0.94 (3H, *s*, H-17), 0.84 (3H, *s*, H-19), 0.77 (3H, *s*, H-20); for ^{13}C NMR spectral data: see Table 1.

3.5. Preparation of ent-18-acetoxyl-pimara-8(14),15-diene (1a)

Compound **1** (22 mg), ethyl orthoformate (100 mg), and benzoic acid (3 mg) were mixed and heated at 90–100°C for 2 h. After concentration in vacuo, benzoic acid (5 mg) was added and the mixture was heated at 175–180°C for 1.5 h. After cooling, CH_2Cl_2 (2 ml) was added, and the solution was washed with saturated Na_2CO_3. The CH_2Cl_2 fraction was concentrated and purified by CC on silica gel with CH_2Cl_2 as eluent to give **1a** (5 mg) (yield 25). Viscous oil; $[\alpha]_D^{23}$ −82.3° (*c* 0.15, $CHCl_3$); EIMS *m/z* (70eV): 330 $[M]^+$ (78), 316 (64), 301 (45), 270 (32), 257 (87), 241 (33), 225 (66), 211 (34), 181 (44), 149 (61), 135 (91), 121 (100), 105 (78), 55 (87); ^1H NMR ($CDCl_3$, 400 MHz): δ 5.75 (1H, *dd*, *J* = 17.6, 10.5 Hz, H-15), 5.20 (1H, *s*, H-14), 4.89 (1H, *dd*, *J* = 17.6, 1.0 Hz, H-16a), 4.86 (*dd*, *J* = 10.5, 2.2 Hz, H-16b), 3.84 (1H, *d*, *J* = 10.9 Hz, H-18a), 3.63 (1H, *d*, *J* = 10.9 Hz, H-18b), 2.04 (3H, *s*, OAc), 1.02 (3H, *s*, H-17), 0.85 (3H, *s*, H-19), 0.81 (3H, *s*, H-20).

Table 1
^{13}C NMR spectral data for compounds **1–4** (in $CDCl_3$, 100 MHz)

C	1	2	3	4
1	38.8 *t*	38.8 *t*	38.8 *t*	38.5 *t*
2	18.1 *t*	18.1 *t*	18.2 *t*	18.6 *t*
3	35.5 *t*	35.6 *t*	35.3 *t*	35.8 *t*
4	37.9 *s*	38.3 *s*	37.7 *s*	73.7 *s*
5	48.5 *d*	48.5 *d*	47.5 *d*	55.2 *d*
6	22.3 *t*	22.3 *t*	22.1 *t*	21.2 *t*
7	35.9 *t*	36.7 *t*	35.6 *t*	36.1 *t*
8	139.7 *s*	140.8 *s*	141.0 *s*	140.4 *s*
9	51.0 *d*	50.2 *d*	50.1 *d*	49.7 *d*
10	38.0 *s*	38.3 *s*	38.2 *s*	39.0 *s*
11	18.3 *t*	18.4 *t*	18.4 *t*	19.6 *t*
12	29.1 *t*	31.2 *t*	31.2 *t*	31.1 *t*
13	36.6 *s*	46.7 *s*	46.6 *s*	46.6 *s*
14	127.3 *d*	123.0 *d*	122.6 *d*	123.3 *d*
15	79.4 *d*	214.3 *s*	214.4 *s*	214.2 *s*
16	62.7 *t*	64.8 *t*	64.7 *t*	64.6 *t*
17	22.9 *q*	23.5 *q*	23.5 *q*	23.6 *q*
18	73.0 *t*	72.9 *t*	71.9 *t*	62.8 *t*
19	17.9 *q*	17.8 *q*	17.9 *q*	
20	15.3 *q*	15.5 *q*	15.5 *q*	15.6 *q*
OAc	20.9 *q*	20.9 *q*		
	171.2 *s*	171.1 *s*		

3.6. ent-18-Acetoxy-16-hydroxy-8(14)-pimaren-15-one (2)

Viscous oil; $[\alpha]_D^{26}$ −0.4° (*c* 0.85, CH_3OH); EIMS *m/z* (70eV): 362 $[M]^+$ (2) 318 (5), 303 (55), 289 (56), 275 (10), 259 (7), 243 (51), 229 (49), 213 (16), 201 (10), 181 (29), 197 (24), 161 (39), 147 (43), 135 (65), 121 (100), 105 (63), 93 (57), 79 (64), 69 (40), 55 (45); negative-ion HRFABMS *m/z*: 361.2329 $[M\text{-}1]^-$ (calc. for $C_{22}H_{33}O_4$, 361.2379); IR (KBr) ν_{max} cm^{-1}: 3478, 2934, 2870, 1713, 1620, 1453, 1382, 1242, 1149, 1102, 1037, 1001, 946, 857, 756; ^1H NMR ($CDCl_3$, 400 MHz): δ 5.38 (1H, *s*, H-14), 4.30 (2H, *s*, H-16), 3.84 (1H, *d*, *J* = 10.9 Hz, H-18a), 3.62 (1H, *d*, *J* = 10.9 Hz, H-18b), 2.04 (3H, *s*, OAc), 1.17 (3H, *s*, H-17), 0.84 (3H, *s*, H-19), 0.79 (3H, *s*, H-20); for ^{13}C NMR spectral data: see Table 1.

3.7. ent-16,18-Dihydroxy-8(14)-pimaren-15-one (3)

Viscous oil; $[\alpha]_D^{25}$ −9.1° (*c* 0.55, CH_3OH); EIMS *m/z* (70eV): 320 $[M]^+$ (1.2), 261 (100), 243 (15), 229 (16), 187 (5), 175 (8), 159 (10), 153 (11), 135 (26), 121 (55), 109 (69), 95 (66), 81 (44), 67 (25), 59 (77); negative-ion HRFABMS *m/z*: 319.2235 $[M\text{-}1]^-$ (calcd. for $C_{20}H_{31}O_3$, 319.2273).IR (KBr) ν_{max} cm^{-1}: 3425, 2934, 2870, 1711, 1460, 1384, 1275, 1197, 1102, 1040, 1010, 886, 752; ^1H NMR ($CDCl_3$, 400 MHz): δ 5.36 (1H, *s*, H-14), 4.29 (2H, *d*, *J* = 1.7 Hz, H-16), 3.36 (1H, *d*, *J* = 10.9 Hz, H-18a), 3.07 (1H, *d*, *J* = 10.9 Hz, H-18b), 1.16 (3H, *s*, H-17), 0.79 (3H, *s*, H-19), 0.76 (3H, *s*, H-20); for ^{13}C NMR spectral data: see Table 1.

3.8. ent-19-Nor-4,16,18-trihydroxy-8(14)-pimaren-15-one (**4**)

Colorless needles (Me_2CO); mp 121–123°C; $[\alpha]_D^{19}$ −25.6° (*c* 0.31, CH_3OH); EIMS *m/z* (70eV): 322 $[M]^+$ (0.4), 291 (13), 273 (5), 263 (100), 245 (36), 227 (17), 217 (10), 189 (5), 171 (5), 159 (11), 145 (13), 133 (16), 121 (63), 107 (61), 95 (53), 81 (59), 67 (27), 55 (41); negative-ion HRFABMS *m/z*: 321.2079 $[M-1]^-$ (calc. for $C_{19}H_{29}O_4$, 321.2066); IR (KBr) ν_{max} cm^{-1} 3524, 3339, 2928, 2870, 1720, 1621, 1463, 1446, 1383, 1344, 1310, 1278, 1253, 1103, 1063, 1048; ^1H NMR ($CDCl_3$, 400 MHz): δ 5.38 (1H, *s*, H-14), 4.28 (2H, *d*, *J* = 1.3 Hz, H-16), 3.61 (1H, *d*, *J* = 10.8 Hz, H-18a), 3.40 (1H, *d*, *J* = 10.8 Hz, H-18b), 1.14 (3H, *s*, H-17), 0.64 (3H, *s*, H-20); for ^{13}C NMR spectral data: see Table 1.

Acknowledgements

The authors are grateful to the National Natural Science Foundation of China (Project No. C30000213) and Yunnan Committee of Science and Technology (Project No. 2000C0021Q,2000YP23) for financial support, and members of the analytical group in the Laboratory of Phytochemistry, Kunming Institute of Botany, for the spectral measurements.

References

Aalbersberg, W., Singh, Y., 1991. Dammarane triterpenoids from *Dysoxylum richii*. Phytochemistry 30, 921–926.

Aladesanmi, A.J., Adewunmi, C.O., 1990. Molluscicidal properties of the new constituents from the stem of the *Dysoxylum lenticellare* on *Biomphalaria glabrata*. Phytotherapy Research 4, 85.

Cambie, R.C., Burfitt, I.R., Goodwin, T.E., Wenkert, E., 1975. The structure of hallol. Journal of Organic Chemistry 40, 3789–3791.

Erdtman, H., Westfelt, L., 1963. The neutral diterpenes from pine wood resin. Acta Chemica Scandinavica 17, 1826–1827.

Hanson, J.R., White, A.F., 1970. Diterpenes of spikenard root. Phytochemistry 9, 1359–1361.

Hiyama, T., Nozaki, H., 1973. A facile, stereospecific preparation of olefins from pinacol. Bulletin of the Chemical Society of Japan 46, 2248–2249.

Jakupovic, J., Castro, V., Bohlmann, F., 1987. Millerenolides, sesquiterpene lactones from *Milleria quinqueflora*. Phytochemistry 26, 2011–2017.

Luo, X., Ma, Y., Wu, S., Wu, D., 1999. Two novel azadirachtin derivatives from *Azadirachta indica*. Journal of Natural Products 62, 1022–1024.

Onan, K.D., Kelley, C.J., Patarapanich, C., Leary, J.D., Aladesanmi, A.J., 1985. Ferrubietolide: X-ray crystal structure of a novel Bis-diterpene from *Dysoxylum lenticellare*. Journal of the Chemical Society, Chem. Commun, 121–122.

Tsichritzis, F., Jakupovic, J., 1990. Diterpenes and other constituents from *Relhania* species. Phytochemistry 29, 3173–3187.

Wenkert, E., Ceccherelli, P., Raju, M.S., Polonsky, J., Tingoli, M., 1979. The C(15) configuration of naturally occurring pimarane-15,16-diols. Journal of Organic Chemistry 44, 146–148.

Yunnan Institute of Botany, 1977. Meliaceae, *Flora Yunnanica*, Vol 1. Tomus, China, pp. 250–251.

PERGAMON

Phytochemistry 57 (2001) 135–141

PHYTOCHEMISTRY

www.elsevier.com/locate/phytochem

Terpenoids and γ-pyrone derivatives from *Prangos tschimganica*

Yasuhiro Shikishima [a], Yoshihisa Takaishi [a,*], Gisho Honda [b], Michiho Ito [b], Yoshio Takeda [c], Olimjon K. Kodzhimatov [d], Ozodbek Ashurmetov [d]

[a] *Faculty of Pharmaceutical Sciences, University of Tokushima, Shomachi 1-78, Tokushima 770-8505, Japan*
[b] *Faculty of Pharmaceutical Sciences, Kyoto University, Yoshida Sakyoku, Kyoto 606-8501, Japan*
[c] *Faculty of Integrated Arts and Sciences, University of Tokushima, Jyosanjima, Tokushima 770-8502, Japan*
[d] *Academy of Sciences, Uzbekistan Institute of Botany, F. Khodzhaev, St. 32, 700143 Tashkent, Uzbekistan*

Received 26 April 2000; received in revised form 20 September 2000

Abstract

The methanol extract of the dried aerial parts of *Prangos tschimganica* afforded seven monoterpenoids and four γ-pyrone derivatives. Their structures were established on the basis of chemical and spectroscopic evidence. © 2001 Elsevier Science Ltd. All rights reserved.

Keywords: *Prangos tschimganica*; Umbelliferae; Monoterpenoids; γ-Pyrone derivatives

1. Introduction

Prangos tschimganica, which belongs to the family of the Umbelliferae, is indigenous to Central Asia. This plant has been used in traditional drugs for treatment of leukoplakia in Uzbekistan. Earlier reports described that coumarins and monoterpenes were abundant in the Umbelliferae (Lemmich and Havelund, 1978; Harkar et al., 1984), and previous phytochemical investigations of this plant led to the identification of several coumarins (Kuznetsova and Belenovskaya, 1966; Abyshev, 1980). Recently, coumarin derivatives isolated from the seeds of *Ammi majus* Linn (umbelliferae) have been used in the clinical treatment of various leukoplakic disorders in Japan (Takashima et al., 1988). The precise mechanism of the therapeutic effect of *P. tschimganica*, however, was not completely understood. In order to determine which of the components present in this plant were responsible for such diverse activites, we started work on the isolation of the constituents of *P. tschimganica*. We report here on the isolation and structural elucidation of 20 compounds (**1**–**20**), including seven new monoterpenoids (**1**–**7**) and four γ-pyrone derivatives (**10**–**13**) from the aerial parts of this plant collected in Uzbekistan.

2. Results and discussion

The ethyl acetate and *n*-BuOH soluble parts of the methanol extract of *P. tschimganica* were separated by a combination of silica gel and Toyo pearl column chromatographies as well as by normal and reversed-phase HPLC, to give 20 compounds.

Compound **1** had the molecular formula $C_{16}H_{24}O_6$ as established from its HR FABMS (*m*/*z* 311.1515), and its IR spectrum showed the presence of hydroxy groups (3360 cm^{-1}) and an aromatic ring (1643, 1618 cm^{-1}). The UV spectrum also showed the presence of an aromatic moiety with maxima at 220 nm. The ^1H NMR spectrum of **1** suggested the presence of three methyl groups [δ_H 2.29, 2.26, 2.19 (each 3H, *s*)] connected to an aromatic ring, two AB type aromatic protons [δ_H 7.09, 6.93 (each 1H, *d*, $J = 7.5$ Hz)] and a pair of methylene protons [δ_H 4.93, 4.63 (each 1H, *d*, $J = 11.3$ Hz)] bearing an oxygen function and a sugar moiety (Table 1 and Experimental section). The ^{13}C NMR spectrum of **1** showed 16 carbon signals which could be resolved by DEPT experiment into three methyls, two methines and four quaternary carbons, as well as an additional two methylenes and five methines attached to an oxygen

* Corresponding author. Tel.: +81-88-633-7275; fax: +81-88-633-501.
E-mail address: takaishi@ph.tokushima-u.ac.jp (Y. Takaishi).

0031-9422/01/$ - see front matter © 2001 Elsevier Science Ltd. All rights reserved.
PII: S0031-9422(00)00407-6

function, respectively (Table 2). Additionally, the hexose was identified as β-glucopyranose from the chemical shifts. From this information, compound **1** was assumed to be a 1, 2, 3, 4-tetrasubstitude benzene derivative. In the HMBC spectrum of **1**, the proton signal at δ_H 4.93 (H-7a) was correlated with the carbon signals at δ_C 134.5 (C-1), 137.3 (C-2) and 128.6 (C-6) (Fig. 2). From this observation, a connection of C-7 the methylene carbon to C-1 was inferred. The proton signals at δ_H 4.93 (H-7a) and 4.63 (H-7b) were correlated with the carbon signal at δ_C 103.3 (C-1 of glc), detected in the HMBC spectrum. Furthermore, an NOESY experiment showed a correlation of H-7 with H-6 and H-8, H-5 with H-10 (Fig. 2). From these observations, the structure of **1** was deduced as 2, 3, 4-trimethylbenzylalcohol-*O*-β-D-glucopyranoside.

The HR FABMS spectrum of **2** showed a peak due to $[M+H]^+$ at *m/z* 329.1608, which agreed with the molecular formula of **2** as $C_{16}H_{25}O_7$. The UV and IR spectra of **2** indicated the existence of a conjugated carbonyl carbon (240 nm and 1731 cm^{-1}). The ^1H NMR spectrum of **2** revealed the presence of three methyls [δ_H

Table 1
^1H NMR spectral data for compounds **1**, **2**, **5** and **6**[a]

Aglycone	**1**[b]	**2**[b]	**5**[c]	**6**[b]
H-1	–	–	–	2.79 (*t*, *J* = 5.6)
H-2	–	–	2.39 (*t*, *J* = 4.7)	–
H-3	–	6.54 (*s*)	2.99 (*t*, *J* = 5.0)	5.75 (*s*)
H-5	6.93 (*d*, *J* = 7.5)	–	–	2.69 (*t*, *J* = 5.7)
H-6	7.09 (*d*, *J* = 7.5)	6.75 (*s*)	6.49 (*s*)	–
H-7	–	–	5.32 (*d*, *J* = 4.7)	–
H-7a	4.93 (*d*, *J* = 11.3)	4.72 (*d*, *J* = 15.9)	–	2.12 (*m*)
H-7b	4.63 (*d*, *J* = 11.3)	4.44 (*d*, *J* = 15.9)	–	2.92 (*m*)
H-8	2.29 (3H, *s*)	1.28 (3H, *s*)	1.25 (3H, *s*)	–
H-8a	–	–	–	4.29 (1H, *d*, *J* = 9.9)
H-8b	–	–	–	3.87 (1H, *d*, *J* = 9.9)
H-9	2.19 (3H, *s*)	1.29 (3H, *s*)	1.26 (3H, *s*)	1.10 (3H, *s*)
H-10	2.26 (3H, *s*)	1.89 (3H, *s*)	1.77 (3H, *s*)	2.09 (3H, *s*)
H-11a	–	–	4.37 (*d*, *J* = 8.3)	–
H-11b	–	–	4.11 (*dd*, *J* = 5.0, 8.3)	–

[a] Signal assignments were based on HSQC and DEPT experiments.
[b] Measured in CD_3OD.
[c] Measured in $CDCl_3$.

Table 2
^{13}C NMR spectral data for compounds **1**–**6** and **7**[a]

	1[b]	**2**[b]	**3**[c]	**4**[b]	**5**[c]	**6**[b]	**7**[b]
Aglycone							
C-1	134.5	40.3	38.9	36.6	32.5	55.2	53.9
C-2	137.3	166.8	167.5	45.6	57.4	206.3	205.5
C-3	136.6	121.6	112.6	38.9	48.6	122.2	121.6
C-4	137.8	189.6	187.8	203.7	198.5	174.0	177.2
C-5	128.2	133.6	132.8	133.6	134.2	47.5	84.6
C-6	128.6	156.7	154.3	158.6	153.9	58.4	61.8
C-7	71.4	67.7	60.9	72.0	100.5	42.2	44.8
C-8	16.1	26.6	26.5	21.6	26.9	75.2	44.8
C-9	16.1	26.6	26.5	29.2	31.1	18.6	23.7
C-10	21.3	15.9	15.6	16.0	16.2	24.5	23.9
C-11	–	–	–	–	71.4	–	–
β-D-Glucose							
C-1	103.3	104.0	–	105.3	–	104.4	100.3
C-2	75.5	75.2	–	75.5	–	75.2	75.2
C-3	78.5	78.2	–	78.5	–	78.2	79.9
C-4	71.4	71.6	–	71.7	–	71.8	71.7
C-5	78.2	78.1	–	78.3	–	78.1	78.2
C-6	63.3	62.9	–	63.1	–	62.9	62.8

[a] Signal assignments were based on HSQC and DEPT experiments.
[b] Measured in CD_3OD.
[c] Measured in $CDCl_3$.

1.89, 1.29, 1.28 (each 3H, *s*)], two methines [δ_H 6.75, 6.54 (each 1H, *s*)], a methylene [δ_H 4.72, 4.44 (each 1H, *d*, $J=15.9$ Hz)] bearing an oxygen function and sugar moiety. The ^{13}C NMR spectrum of **2** showed conjugated diene carbonyl carbon signals at δ_C 189.6 (C-4), 166.8 (C-2), 156.7 (C-6), 133.6 (C-5) and 121.6 (C-3), in addition to three methyls, a quaternary carbon, as well as an additional methylene attached to an oxygen atom and β-glucose carbons (Table 2). From the above results, **2** was assumed to be monoterpene glucoside from the carbon number and the presence of three methyl groups. The ^1H NMR spectral data (Table 1) of **2** was similar to that of compound **3** (Bohlmann and Zdero, 1969), except for the presence of an additional β-glucopyranosyl moiety. This linkage of methylene (C-7) and anomeric carbon (C-1 of glc) was established by HMBC spectrum, in which a cross peak between the signal at δ_H 4.38 (1H, *d*, $J=7.7$ Hz, H-1 of glc) and the carbon signal at δ_C 67.7 (C-7) was observed. Therefore, **2** was determined to be 1,1,5-trimethyl-2-hydroxymethyl-(2,5)-cyclohexadien-(4)-one-*O*-β-D-glucopyranoside. The aglycone of **3** was synthesized from the 1,1,5-trimethyl-2-hydroxymethyl-(2,5)-cyclohexadiene-(4)-one by treatment with sodium borohydride (Bohlmann and Zdero, 1969). This is the first time that **3** has been isolated from a natural source.

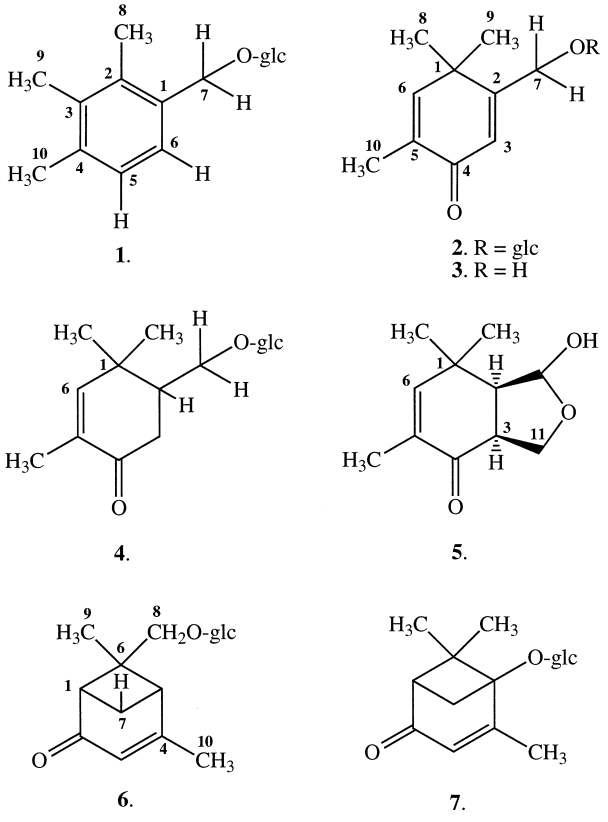

Fig. 1. Structures of compounds isolated from *P. tschimganica*.

Compound **4**, $C_{16}H_{26}O_7$, showed the presence of hydroxyl and ketone groups (3393 and 1732 cm^{-1}) in the IR spectrum and the conjugated ketone group (235 nm) in the UV spectrum. The ^1H NMR spectrum revealed the presence of three methyls [δ_H 1.71, 1.22, 1.04 (each 3H, *s*)], a pair of methylene [δ_H 2.69, 2.41 (each 1H, *dd*, $J=4.4$, 16.0 and 12.5, 16.0 Hz)], a methine [δ_H 6.46 (1H, *s*)] attached to a double bond, a methine [δ_H 2.21 (1H, *m*)] and a pair of methylene [δ_H 4.15, 3.42 (each 1H, *dd* and *t*, $J=4.1$, 9.6 and 9.6 Hz)] groups bearing an oxygen function. The ^{13}C NMR spectrum of **4** was similar to that of **2** expect for the signal at δ_C 203.7 (C-4), 45.6 (C-2) and 38.9 (C-3) (Table 2). From the $^1H^1H$ COSY experiment, the presence of a partial structure [$-CH_2(3)-CH(2)-CH_2(7)-$] was suggested. In the HMBC spectrum of **4**, correlations of δ_H 1.22 (H_3-9) and 1.04 (H_3-8) with δ_C 45.6 (C-2) and 158.6 (C-6); δ_H 2.21 (H-2) with δ_C 203.7 (C-4); δ_H 1.71 (H_3-10) with δ_C 158.6 (C-6) and 203.7 (C-4); δ_H 4.24 (H-1 of glc) with δ_C 72.0 (C-7) were detected. From these observations, the structure of **4** was deduced to be a 2,3 dihydro derivative of **2**. The relative stereochemistry of **4** was determined from the NOESY spectrum. The proton signal at δ_H 2.21 (Hb-2) was correlated with the proton signal at δ_H 1.22 (H_3-9), whereas that the proton signal at δ_H 2.41 (Ha-3) was correlated with the proton signal at δ_H 1.04 (H_3-8). From these correlations, the hydroxymethyl group could be assignment to be equatorial. The coupling constants ($J=4.4$ and 16.0 Hz) of the

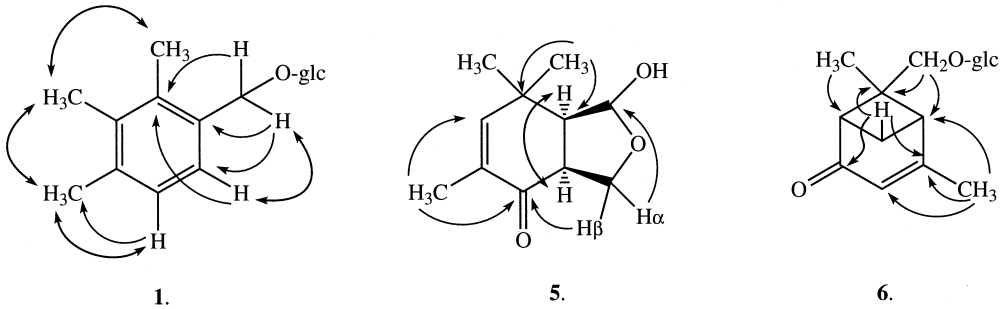

Fig. 2. Long range ^1H, ^{13}C NMR correlations and NOE calculations observed by HMBC, NOESY for **1**, **5** and **6**. ^1H, ^{13}C long correlation →; NOESY correlation ↔.

proton signal at δ_H 2.69 (Hb-3) also supported the above conclusion. Therefore, the structure of **4** was elucidated to be 1,1,5-trimethyl-2-hydroxymethyl-5-cyclohexene-4-one-7-*O*-β-D-glucopyranoside.

Compound **5**, showed the presence of an hydroxyl (3464 cm^{-1}) functionality in the IR spectrum and an α, β-unsaturated carbonyl carbon in the UV spectrum (234 nm). The EI mass spectrum gave a peak at *m/z* 196.1086 ($C_{11}H_{16}O_3$), suggesting that the degree of unsaturation in **5** was 4. The ^1H NMR spectrum of **5** displayed the presence of three methyl protons [δ_H 1.77, 1.26 and 1.25 (each 3H, *s*)], a pair of methylene protons [δ_H 4.37 and 4.11 (each 1H, *d*, $J=8.3$ and *dd*, $J=5.0$, 8.3 Hz)] bearing an oxygen function, two methine proton [δ_H 2.99 and 2.39, each 1H, *t*, $J=5.0$ and 4.7 Hz)], a methine proton (δ_H 5.32 1H, *d*, $J=4.7$ Hz) attached to the oxygen function, and one aromatic proton (δ_H 6.49, 1H, *s*) (Table 1). The ^{13}C NMR spectrum of **5** revealed that the 11 carbon signals included three methyl, three methine and three quaternary carbons, as well as an additional methine carbon (δ_C 100.5) and a methylene carbon (δ_C 71.4) connected to the oxygen function, respectively. From the ^1H ^1H COSY spectrum of **5**, the presence of partial structure [−CH(O−)−CH−CH−CH_2(O−)] was deduced. On the basis of correlations of the HMBC spectrum of **5**, the proton signals at δ_H 4.37 (H-11) was correlated with the carbon signal at δ_C 100.5 (C-7); δ_H 1.25 (H_3-8) with δ_C 57.4 (C-2); δ_H 2.99 (H-3) and 4.11 (Hb-11) with δ_C 198.5 (C-4); δ_H 1.77 (H_3-10) with δ_C 198.5 (C-4). These facts clearly indicated that **5** had the same basic skeleton as **4**. The correlation of δ_H 2.39 (H-2) with 2.99 (H-3) (Fig. 2) in the NOESY spectrum confirmed that the relative configuration of C-2 and C-3 was in a *cis* orientation. Hence, the structure of tschimganical A (**5**) was determined as shown (Fig. 1).

The molecular formula of **6** was determined to be $C_{16}H_{24}O_7$ on the basis of the FABMS and ^{13}C NMR spectral data (Table 2). Its IR spectrum showed absorption bands due to hydroxyl (3422 cm^{-1}) groups, and the UV spectrum suggested the presence of an α, β-unsaturated carbonyl carbon with a maxima at 252 nm. The ^1H NMR spectrum of **6** (Table 1) exhibited two tertiary methyl groups, two methine and methylene groups, as well as a methine attached to a double bond and a methylene bearing oxygen functionality, signals due to a sugar moiety was also noted. From the $^1H^1H$ COSY spectrum, the partial structure [−CH(1)−CH_2(C-7)−CH(C-5)−] was deduced. The structure of **6** was assumed to be a verbenone type tricyclic monoterpene, which was supported by HMBC correlations between; the proton signal at δ_H 2.92 (H-7b) with the quaternary carbon δ_C 174.0 (C-4), the carbonyl carbon δ_C 206.3 (C-2) and the carbon δ_C 58.4 (C-6); the proton signal at δ_H 4.29 (H-8a) with the carbon signals at δ_C 58.4 (C-6), 55.2 (C-1) and 47.5 (C-5); the proton signal at δ_H 2.09 (H_3-10) with δ_C 122.2 (C-3) and 47.5 (C-5) (Fig. 2). The location of the β-D-glucopyranose was also determined as follows; the proton signal at δ_H 4.29 (H-8a) was correlated with δ_C 104.4 (C-1 of glc). Thus, the structure of **6** was assigned as shown (Fig. 1).

The HR FABMS of **7** gave same molecular formula of $C_{16}H_{24}O_7$ as that of **6**. Its ^1H and ^{13}C NMR spectral data were very similar to that for **6**, except for the presence of two methyls and a methylene and a methine in **6** and three methyls and one quaternary carbon in **7**. Its 2D NMR spectra suggested that both compounds **6** and **7** have same skeleton, except for the connecting position of the glucose moiety. In the HMBC spectrum of **7**, the correlation of δ_H 4.56 (H-1 of glc) with δ_C 84.6 (C-5), suggested the structure of **7** as shown (Fig. 1).

Compound **10** exhibited a quasi-molecular ion peak at *m/z* 463 in the negative FAB MS giving the molecular formula as $C_{22}H_{24}O_{11}$ in combination with ^{13}C NMR spectral analysis. The UV and IR spectra of **10** indicated the presence of hydroxyl groups (3382 cm^{-1}) and a conjugated double bond (326 and 246 nm). The ^1H and ^{13}C NMR spectral data of **10** were very similar to that of **9** except for the presence of signals assignable to the feruloyl moiety. In the HMBC spectrum of **10**, the correlations of δ_H 4.81 (H-1 of glc) and 4.43 (H_2-6 of glc) with δ_C 143.4 (C-3) and 168.9 (C-1 of feruloyl) (Table 3). From these results, the connectivities of the glucose and feruloyl groups were determined as shown

Table 3
^{13}C NMR spectral data for compounds **8**–**12** amd **13**

	8[b]	**9**[a]	**10**[a,c]	**11**[a,d]	**12**[a,e]	**13**[a,f]
Aglycone						
C-2	149.4	164.7	164.7	164.9	164.9	164.7
C-3	143.4	143.7	143.6	143.8	142.8	143.3
C-4	154.3	157.3	157.2	157.5	157.6	157.2
C-5	173.2	177.7	177.1	177.4	177.4	177.1
C-6	113.3	117.4	117.4	117.6	117.9	117.4
C-7	14.4	15.9	15.9	16.1	16.1	15.9
β-D-Glucose						
C-1	–	105.5	105.5	105.4	105.1	104.9
C-2	–	75.4	75.5	74.9	75.7	75.5
C-3	–	78.1	77.9	78.2	78.1	77.9
C-4	–	71.1	71.6	71.9	71.7	71.7
C-5	–	78.0	76.1	76.3	76.3	76.0
C-6	–	62.5	64.3	64.4	64.5	64.3

[a] Measured in CD_3OD.
[b] Measured in $CDCl_3$.
[c] Additional signals: 168.9 (C-1′), 115.3 (C-2′), 147.1 (C-3′), 127.1 (C-4′), 111.8 (C-5′), 149.5 (C-6′), 150.8 (C-7′), 116.6 (C-8′), 124.6 (C-9′), 56.9 (OCH_3).
[d] Additional signals: 168.2 (C-1′), 116.5 (C-2′), 146.1 (C-3′), 128.4 (C-4′), 116.1 (C-5′), 148.7 (C-6′), 150.6 (C-7′), 117.6 (C-8′), 127.4 (C-9′), 56.8 (OCH_3).
[e] Additional signals: 174.8 (C-1′), 44.6 (C-2′), 27.3 (C-3′), 23.1 (C-4′ and C-5′).
[f] Additional signals: 168.9 (C-1′), 115.3 (C-2′), 147.2 (C-3′), 128.2 (C-4′), 116.6 (C-5′), 146.9 (C-6′), 149.7 (C-7′), 114.9 (C-8′), 123.6 (C-9′).

(Fig. 3). Hence, **10** was determined to be 3-hydroxyl-2-methyl-4-*H*-pyran-4-one-3-*O*-(6-)-β-D-glucopyranoside.

The NMR spectral data of **11** were similar to those of **10**, and its HR FABMS gave the same molecular formula of $C_{22}H_{24}O_{11}$ as that of **10**. In the ^{1}H NMR spectral data for **11** and **10**, the evident differences between them were the signals due to the double bond [**11**: δ_H 6.85 and 5.76 (each 1H, *d*, $J=12.9$ Hz), **10**: δ_H 7.56 and 6.30 (each 1H, *d*, $J=15.0$ Hz)] of the feruloyl group. From the coupling constant of the double bond protons, its geometry of **11** was determined to be *cis*. That evidence was supported by the NOESY spectrum, in which a cross-peak between δ_H 6.85 and 5.76 was observed. From these results, the structure of **11** was determined to be 3-hydroxyl-2-methyl-4-*H*-pyran-4-one-3-*O*-(6-*O*-*cis*-feruloyl)-β-D-glucopyranoside (Fig. 3).

The ^{1}H and ^{13}C NMR spectral data of **12** and **13** were very similar to those of **9** except for the appearance of the signals due to the isovaleryl and caffeoyl moieties, respectively, suggesting that **12** and **13** have the same γ-pyrone glucoside moiety. The positions of both functions were established by correlations of the HMBC spectrum between the carbonyl carbon and proton signal of H_2-6 in the glucose moiety. Thus, **12** and **13** were shown to be 3-hydroxyl-2-methyl-4-*H*-pyran-4-one-3-*O*-(6-*O*-isovaleryl)-β-D-glucopyranoside and 3-hydroxyl-2-methyl-4-*H*-pyran-4-one-3-*O*-(6-*O*-caffeoyl)-β-D-glucopyranoside respectively (Fig. 3).

The following known compounds were identified by comparison with the literature data: 1,1,5-trimethyl-2-formyl-4-methoxyl-(2,5)-cyclohexadiene (**14**) and 1,1,5-trimethyl-2-formyl-6-methoxyl-(2,4)-cyclohexadiene (**15**) (Lemmich and Pedersen, 1971), (+)-spathulenol (**16**) and globulol (**17**) (Bohlmann and Robinson, 1983a,b), 1β, 6α-dihydroxyeudesm-4(15)-ene (**18**) (Bohlmann and Robinson, 1983a,b), (−)-caryophyllene β-oxide (**19**) (Fukuyama and Kodama, 1992), maltol (**8**) and maltol-β-D-glucopyranoside (**9**) (Tanaka et al., 1986), xanthotoxin (**20**) (Grande et al., 1986). The trade name of xanthotoxin was called methoxalen, which has been used in clinical treatment of various leukoplakic diseases in Japan (Takashima et al., 1988).

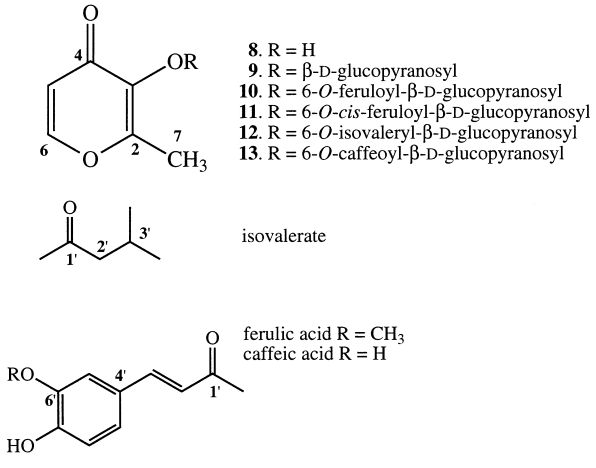

Fig. 3. Structures of compounds isolated from *P. tschimganica*.

3. Experimental

3.1. General

^{1}H NMR: 400 MHz with TMS as int. stand; ^{13}C NMR: 100 MHz; CC: silica gel 60 (Merck), Sephadex LH-20 (Pharmacia) and Toyo pearl HW-40 (TOSOH); HPLC: GPC H-2002 (SHODEX), ODS: D-ODS-5 (YMC).

3.2. Plant material

The aerial parts of *Prangos tschimganica* were collected in June 1998 from Uzbekistan. Herbarium specimens were deposited in the herbarium of Institute of Botany, Academy of Sciences, Uzbekistan. This plant was identified by Dr. Olimjon K. Kodzhimatov.

3.3. Extraction and fractionation

The MeOH extracts (357 g) of the dried aerial parts of *P. tschimganica* (1.9 kg) were partitioned between EtOAc and H_2O. The EtOAc layer was concentrated to give a residue (80 g), which was subjected to silica gel column chromatography, this being eluted with solvents of increasing polarity (*n*-hexane-AcOEt) to give 21 frs (frs 1–21). Fr. 12 (1.2 g) was applied to a Toyo pearl column, eluted with $CHCl_3$–MeOH (2:1) to give 7 frs (12.1–12.7). Fr. 12. 4 (345 mg) was purified by GPC (MeOH) to give compound **5** (1 mg). Fr. 15 (3.2 g) was subjected to on Toyo pearl chromatography, with $CHCl_3$–MeOH (2:1) as eluted to give 7 frs (15.1–15.7). Fr. 15. 4 (824 mg) was separated by using GPC ($CHCl_3$) to yield compound **3** (48 mg). Fr. 20 (8.8 g) was applied to a silica gel column, this being eluted with $CHCl_3$–MeOH (9:1 to 7:3), to give 10 frs (fr. 20.1–20.10). Then, fr. 20. 6 was isolated by HPLC (ODS, MeOH–H_2O, 9:1), giving compound **12** (3 mg). The water layer was partittioned between *n*-BuOH and H_2O to give the *n*-BuOH soluble part (44 g). The *n*-BuOH layer was applied to a silica gel column, eluted with $CHCl_3$–MeOH (8:2 to 1:1). Twelve fractions were obtained. Fr. 2 (2.2 g) was subjected to silica gel column chromatography and eluted with $CHCl_3$–MeOH (9:1), to give 7 frs (fr. 2.1–2.7). Fr. 2.4 and 2.5 were purified by GPC (MeOH), and gave compounds **1** (18 mg), and a mixture (74 mg) of compounds **10** and **11**; this mixture was again purified by HPLC (ODS, MeOH–H_2O, 8:2), and gave pure compounds **10** (63 mg) and **11** (10 mg). Fr. 3 (3.8 g) was subjected to silica gel column chromatography, and eluted with $CHCl_3$–MeOH (8:2), to afford 4

fractions (3.1–3.4). The mixture of fr. 3.3 and fr. 3.4 was separated by GPC (MeOH), and gave a further 10 frs (fr. 3.3.1–3.3.10), compounds **2** (54 mg), **4** (7 mg), **6** (6 mg) and **7** (6 mg) were obtained after the purification of fr. 3.3.3 (226 mg) using HPLC (ODS, MeOH–H_2O, 4:6). Fr. 4 (3.4 g) was applied to a Toyo pearl column, eluted with $CHCl_3$–MeOH (2:1), to gave 4 frs (fr. 4.1–4.4). The mixture of fr. 4.2 and 4.3 was subjected to silica gel column chromatography and eluted with $CHCl_3$–MeOH (8:2), to give 6 frs (fr. 4.2.1–4.2.6).compound **13** (15 mg) was obtained after the purification of fr. 4.2.1 using GPC (MeOH).

*3.3.1. 2,3,4-Trimethylbenzyl alcohol-O-β-D-glucopyrano-side (**1**)*

White amorphous powder, $[\alpha]_D^{25}$ −35.6 (*c* 1.1, MeOH); IR ν_{max}^{KBr} cm^{-1}: 3360, 2951, 1643, 1618, 1476, 1089, 1063; UV λ_{max}^{MeOH} nm (log ε): 220 (4.2); HR FABMS: *m/z* 311.1515 $[M\text{-}H]^-$, calcd. for $C_{16}H_{23}O_6$, 311.1495; ^1H NMR spectral data (CD_3OD) δ: 4.30 (1H, *d, J* = 7.7 Hz, H-1 of glc), 3.90 (1H, *dd, J* = 1.9, 11.9 Hz, H-6 of glc), 3.68 (1H, *dd, J* = 5.6, 11.9 Hz, H-6 of glc), 3.40–3.30 (3H, *m*, H-3∼5 of glc), 3.25 (1H, *t, J* = 7.7 Hz, H-2 of glc); ^{13}C NMR spectral data: Table 2.

*3.3.2. 1,1,5-Trimethyl-2-hydroxymethyl-(2,5)-cyclohexadien-(4)-one-O-β-D-glucopyranoside (**2**)*

Clear oil, $[\alpha]_D^{25}$ −45.6 (*c* 1.0, MeOH); IR ν_{max}^{KBr} cm^{-1}: 3387, 1731, 1668, 1624, 1450, 1373, 1165, 1077; UV λ_{max}^{MeOH} nm (log ε): 240 (4.3); HR FABMS: *m/z* 329.1608 $[M+H]^+$, calcd. for $C_{16}H_{25}O_7$, 329.1600; ^1H NMR spectral data (CD_3OD) δ: 4.38 (1H, *d, J* = 7.7 Hz), 3.89 (1H, *d, J* = 11.8 Hz, H-6 of glc), 3.68 (1H, *br d, J* = 11.8 Hz, H-6 of glc), 3.35–3.27 (4H, *m*, H-2∼5 of glc); ^{13}C NMR spectral data: Table 2.

*3.3.3. 1,1,5-Trimethyl-2-hydroxymethyl-(2,5)-cyclohexadien-(4)-one (**3**)*

Pale yellow oil, IR ν_{max}^{KBr} cm^{-1}: 3416, 1730, 1669, 1625, 1452, 1373, 1100; UV λ_{max}^{MeOH} nm (log ε): 234 (4.2); EI MS: *m*/z 166.0968 $[M]^+$, calcd. for $C_{10}H_{14}O_2$, 166.0994; ^1H NMR spectral data ($CDCl_3$) δ: 6.52 (1H, *s*, H-6), 6.45 (1H, *s*, H-3), 4.40 (2H, *s*, H-7), 1.87 (3H, *s*, H-10), 1.24 (6H, *s*, H-8 and H-9); ^{13}C NMR spectral data: Table 2.

*3.3.4. 1,1,5-Trimethyl-2-hydroxymethyl-(5)-cyclohexene-(4)-one-O-β-D-glucopyranoside (**4**)*

Clear oil, $[\alpha]_D^{25}$ −24.6 (*c* 0.7, MeOH); IR ν_{max}^{KBr} cm^{-1}: 3393, 1732, 1668, 1450, 1368, 1163, 1078; UV λ_{max}^{MeOH} nm (log ε): 235 (4.2); HR FABMS: *m/z* 353.1544 $[M+Na]^+$, calcd. for $C_{16}H_{26}O_7Na$, 353.1576; ^1H NMR spectral data (CD_3OD) δ: 6.46 (1H, *s*, H-6), 4.24 (1H, *d, J* = 7.8 Hz, H-1 of glc), 4.15 (1H, *dd, J* = 4.1, 9.6 Hz, H-7), 3.87 (1H, *d, J* = 10.7 Hz, H-6 of glc), 3.67 (1H, *dd, J* = 4.8, 10.7 Hz), 3.42 (1H, *t, J* = 9.6 Hz, H-7), 3.37–3.26 (3H, *m*, H-3, 4 and 5 of glc), 3.18 (1H, *t, J* = 7.8 Hz, H-2 of glc), 2.69 (1H, *dd, J* = 4.4, 16.0 Hz, H-3), 2.41 (1H, *dd, J* = 12.5, 16.0 Hz, H-3), 2.21 (1H, *m*, H-2), 1.71 (3H, *s*, H-10), 1.22 (3H, *s*, H_3-9), 1.04 (3H, *s*, H_3-8); ^{13}C NMR spectral data: Table 2.

*3.3.5. Tschimganical A (**5**)*

Clear oil, $[\alpha]_D^{25}$ +4.0 (*c* 0.1, $CHCl_3$); IR ν_{max}^{KBr} cm^{-1}: 3464, 1667, 1601, 1521, 1473, 1213, 1016; UV λ_{max}^{MeOH} nm (log ε): 234 (4.3); EI MS: *m/z* 196.1086 $[M]^+$, calcd. for $C_{11}H_{16}O_3$, 196.1099; ^1H and ^{13}C NMR spectral data: Tables 1 and 2.

*3.3.6. Vervenone-8-O-β-D-glucopyranoside (**6**)*

Clear oil, $[\alpha]_D^{25}$ +3.5 (*c* 0.6, MeOH); IR ν_{max}^{KBr} cm^{-1}: 3422, 1673, 1653,1077; UV λ_{max}^{MeOH} nm (log ε): 252 (4.2). HR FABMS: *m/z* 351.1435 $[M+Na]^+$, calcd. for $C_{16}H_{24}O_7Na$, 351.1420; ^1H NMR spectral data (CD_3OD) δ: 4.33 (1H, *d, J* = 7.7 Hz, H-1 of glc), 3.85 (1H, *d, J* = 11.5 Hz, H-6 of glc), 3.68 (1H, *dd, J* = 3.7, 11.5 Hz, H-6 of glc), 3.35–3.27 (3H, *m*, H-3, 4 and 5 of glc), 3.21 (1H, *t, J* = 7.6 Hz, H-2 of glc); ^{13}C NMR spectral data: Table 2.

3.3.7. Vervenone-5-O-β-D-glucopyranoside (7)

Clear oil, $[\alpha]_D^{25}$ +1.8 (*c* 0.5, MeOH); IR ν_{max}^{KBr} cm^{-1}: 3421, 1670, 1650,1078; UV λ_{max}^{MeOH} nm (log ε): 253 (4.2); HR FABMS: *m/z* 351.1426 $[M+Na]^+$, calcd. for $C_{16}H_{24}O_7Na$, 351.1420; ^1H NMR (CD_3OD) δ: 5.67 (1H, *s*, H-3), 4.56 (1H, *d, J* = 7.5 Hz, H-1 of glc), 3.85 (1H, *d, J* = 11.9 Hz, H-6 of glc), 3.68 (1H, *dd, J* = 5.3, 11.9 Hz, H-6 of glc), 3.35–3.27 (3H, *m*, H-3, 4 and 5 of glc), 3.21 (1H, *t, J* = 7.6 Hz, H-2 of glc), 3.16 (1H, *dd, J* = 2.3, 9.3 Hz, H-7), 2.55 (1H, *dd, J* = 2.3, 6.8 Hz, H-1), 2.47 (1H, *d, J* = 9.3 Hz, H-7), 2.06 (3H, *s*, H_3-10), 1.46 (3H, *s*, H_3-8), 1.04 (3H, *s*, H_3-9). ^{13}C NMR: Table 2.

*3.3.8. 3-Hydroxyl-2-methyl-4-H-pyran-4-one-3-O-(6-O-feruloyl)-β-D-glucopyranoside (**10**)*

Pale yellow oil, $[\alpha]_D^{25}$−75.0 (*c* 1.2, MeOH); IR ν_{max}^{KBr} cm^{-1}: 3382, 1706, 1644, 1515, 1430, 1255, 1176, 1065; UV λ_{max}^{MeOH} nm (log ε): 326 (4.6), 300 (4.5), 246 (4.6); HR FABMS: *m/z* 463.1238 $[M\text{-}H]^-$, calcd. for $C_{22}H_{23}O_{11}$, 463.1240; ^1H NMR spectral data (CD_3OD) δ: 7.81 (1H, *d, J* = 4.9 Hz, H-6), 7.56 (1H, *d, J* = 15.0 Hz, H-3′), 7.15 (1H, *br s*, H-5′), 7.03 (1H, *d, J* = 7.2 Hz, H-9′), 6.80 (1H, *d, J* = 7.2 Hz, H-8′), 6.35 (1H, *d, J* = 4.9 Hz, H-5), 6.30 (1H, *d, J* = 15.0 Hz, H-2′), 4.81 (1H, *d, J* = 7.6 Hz, H-1 of glc), 4.43 (2H, *m*, H_2-6 of glc), 3.89 (3H, *s*, OCH_3), 3.49–3.38 (4H, *m*, H2∼5 of glc), 2.34 (3H, *s*, H_3-7); ^{13}C NMR spectral data: Table 3.

*3.3.9. 3-Hydroxyl-2-methyl-4-H-pyran-4-one-3-O-(6-O-cis-feruloyl)-β-D-glucopyranoside (**11**)*

Pale yellow oil, $[\alpha]_D^{25}$ −62.0 (*c* 0.7, MeOH); IR ν_{max}^{KBr} cm^{-1}: 3406, 1723, 1644, 1515, 1431, 1254, 1196, 1068;

UV λ_{max}^{MeOH} nm (log ε): 326 (4.6), 299 (4.5), 247 (4.6); HR FABMS: *m/z* 463.1243 [M-H]$^-$, calcd. for $C_{22}H_{23}O_{11}$, 463.1240; ^{1}H NMR spectral data (CD_3OD) δ: 7.92 (1H, *d, J* = 5.5 Hz, H-6), 6.89 (1H, *br s*, H-5′), 7.13 (1H, *d, J* = 7.9 Hz, H-9′), 6.85 (1H, *d, J* = 12.9 Hz, H-3′), 6.82 (1H, *d, J* = 7.9 Hz, H-5′), 6.76 (1H, *d, J* = 7.9 Hz, H-8′), 6.41 (1H, *d, J* = 5.5 Hz, H-5), 5.76 (1H, *d, J* = 12.9 Hz, H-2′), 4.80 (1H, *d, J* = 7.6 Hz, H-1 of glc), 4.48 (1H, *d, J* = 10 Hz, H_2-6 of glc), 4.36 (1H, *dd, J* = 6.0 and 10.0 Hz, H_2-6 of glc), 3.89 (3H, *s*, OCH_3), 3.45–3.35 (4H, *m*, H2∼5 of glc), 2.34 (3H, *s*, H_3-7); ^{13}C NMR spectral data: Table 3.

*3.3.10. 3-Hydroxyl-2-methyl-4-H-pyran-4-one-3-O-(6-O-isovaleryl)-β-D-glucopyranoside (**12**)*

Clear oil, $[\alpha]_D^{25}$ −19.2 (*c* 0.5, MeOH); IR ν_{max}^{KBr} cm^{-1}: 3397, 1733, 1648, 1436, 1254, 1195, 1067; UV λ_{max}^{MeOH} nm (log ε): 256 (4.7); HR FABMS: *m/z* 395.1342 [M + Na]$^+$, calcd. for $C_{17}H_{24}O_7Na$, 395.1318; ^{1}H NMR spectral data (CD_3OD) δ: 8.00 (1H, *d, J* = 5.6 Hz, H-6), 6.43 (1H, *d, J* = 5.6 Hz, H-5), 4.85 (1H, *d, J* = 7.7 Hz, H-1 of glc), 4.42 (1H, *d, J* = 12.0 Hz, H_2-6 of glc), 4.17 (1H, *dd, J* = 6.1, 12.0 Hz, H_2-6 of glc), 3.30–3.22 (4H, *m*, H-2∼5 of glc), 2.38 (3H, *s*, H_3-7), 2.16 (2H, *d*, *J* = 7.5 Hz, H-2′), 2.04 (1H, *m*, H-3′), 0.93 (6H, *d*, *J* = 7.3 Hz, H_3-4′ and -5′); ^{13}C NMR spectral data: Table 3.

*3.3.11. 3-Hydroxyl-2-methyl-4-H-pyran-4-one-3-O-(6-O-caffeoyl)-β-D-glucopyranoside (**13**)*

Pale yellow oil, $[\alpha]_D^{25}$−57.0 (*c* 1.0, MeOH); IR ν_{max}^{KBr} cm^{-1}: 3266, 1723, 1644, 1515, 1455, 1254, 1196, 1066; UV λ_{max}^{MeOH} nm (log ε): 329 (4.6), 301 (4.5), 250 (4.6); HR FABMS: *m/z* 449.1075 [M-H]$^-$, calcd. for $C_{21}H_{21}O_{11}$, 449.1084; ^{1}H NMR spectral data (CD_3OD) δ: 7.91 (1H, *d, J* = 4.9 Hz, H-6), 7.49 (1H, *d, J* = 15.8 Hz, H-3′), 7.08 (1H, *s*, H-5′), 6.92 (1H, *d, J* = 7.3 Hz, H-8′), 6.79 (1H, *d, J* = 7.3 Hz, H-9′), 6.37 (1H, *d, J* = 4.9 Hz, H-5), 6.21 (1H, *d, J* = 15.8 Hz, H-2′), 4.81 (1H, *d, J* = 7.6 Hz, H-1 of glc), 4.43 (2H, *m*, H_2-6 of glc), 3.49–3.38 (4H, *m*, H2∼5 of glc), 2.34 (3H, *s*, H_3-7); ^{13}C NMR spectral data: Table 3.

References

Abyshev, A.Z., 1980. Coumarin composition of *Prangos tschimganica*. Khim. Prir. Soedin. 6, 830–831.

Bohlmann, F., Zdero, C., 1969. Uber terpenderivate aus *Ferula hispanica*. Chem. Ber. 102, 2211–2215.

Bohlmann, F., Robinson, H., 1983a. Two sesquiterpenes from *Senecio* species. Phytochemistry 22, 1675–1677.

Bohlmann, F., Robinson, H., 1983b. Four heliangolides and other sesquiterpenes from *Brasilia sickii*. Phytochemistry 22, 1213–1218.

Fukuyama, Y., Kodama, M., 1992. Neurotrophic sesquterpene-neolignans from *Magnolia obovata*: structure and neurotrophic activity. Tetrahedron 48, 377–392.

Grande, M., Aguado, T.M., Piera, F., 1986. Coumarins and ferulol esters from *Cachrys sicula*. Phytochemistry 25, 505–507.

Harkar, S., Razdan, K.T., Waight, S., 1984. Steroids, chromone and coumarins from *Angelica officinalis*. Phytochemistry 23, 419–426.

Kuznetsova, G.A., Belenovskaya, L.M., 1966. Prantschimgin-a new coumarin from the roots of *Prangos tschimganica*. Khim. Prir. Soedin. Akad. Nauk Uz. 2 (4), 235–239.

Lemmich, J., Pedersen, A.P., 1971. Constituents of umbelliferous plants. Acta Chem. Scand. 25, 995–999.

Lemmich, J., Havelund, S., 1978. Coumarin glycosides of *Seseli montanun*. Phytochemistry 17, 139–141.

Tanaka, N., Sakai, H., Murakami, T., 1986. Chemische und chemotaxonomische Untersuchungen der Pterophyten. LXII. Chemische untersuchungen der inhaltsstoffe von arachniodes maximowiczii OHWI. Chem. Pharm. Bull. 34, 1015–1022.

Takashima, A., Sunohara, A., Matsunami, E., 1988. Comparison of therapeutic efficacy of topical PUVA, oral etretinat, and combined PUVA and etretinate for the treatment of psoriasis and development of PUVA lentigines and antinuclear antibodies. J. Dermat. 15, 473–479.

PERGAMON

Phytochemistry 57 (2001) 143–144

PHYTOCHEMISTRY

www.elsevier.com/locate/phytochem

Book reviews

Root Methods: A Handbook
Edited By A. L. Smit, A. G. Bengough, C. Engels, M. van Noordwijk, S. Pellerin and S. C. van de Geijn, Springer Press, Berlin Heidelberg, 2000, 587 pp. 108 figs., DM 198. ISBN 3-540-66728-8

Roots play a vital role in plant architecture as well as in water and nutrient supply for plant growth. Yet our understanding on root physiology and biochemistry is still poor. This is primarily due to methodological reasons. Work on roots is tedious and time-consuming and there is a need for new methods. The most recent developments in root research has particularly been supported by new developments in computing hardware and software. Thus it seems timely to publish a modern handbook on root methods such as the present one. *Root Methods* is a comprehensive review on modern and revised older methods for plant root research, describing methods used in the field and in the laboratory. The book covers various interactions of plant roots with soil emphasizing root dynamics and distribution. Besides methods of root observations, a survey of the application of isotope techniques in root physiology is given.

In the preface of the book A. L. Smit emphasizes that "not only sophisticated methods (image analysis, CT scans etc.) are described, but also time-saving quick and (hopefully not too) dirty tricks to quantify root growth and root distribution in the soil profile". The following chapters of the book were written by leading experts on the respective subjects. The first chapter on "Root Characteristics: Why and What to Measure", written by D. Atkinson, explains the importance of roots in ecology and crop production. The questions are asked "Why do particular plant species grow in the places they do?" "What root parameters need to be measured?" and "What is the functional, physiological, or ecological significance of a particular morphological assessment?" This introductory chapter provides a background to the later chapters discussing methods of the different aspects of root research. These chapters are on "Anatomy and Histology of Roots and Root-Soil Boundary" (E. de Neergarrd et al.), "Control and Measurement of the Physical Environment" (W.R. Whalley et al.), "Modelling Root System Growth and Architecture" (L. Pagès et al.), "Sampling Strategies, Scaling and Statistics" (A.G. Bengough et al.), "Auger Sampling, Ingrowth Cores and Pinboard Methods" (M. do Rosário G. Oliveira et al.), "Trench Profile Techniques and Core Break Methods" (M. van Noordwijk et al.), "Root Observations and Measurements at (Transparent) Interfaces with Soil" (A.L. Smit et al.), "The Measurement and Analysis of Fine Root Longevity" (J.E. Hooker et al.), "Root Image Analysis and Interpretation" (R. Richner et al.), "Computer-Assisted Tomography" (S. Asseng et al.), "Isotope Techniques" (I.J. Bingham et al.), "Assessing the Ability of Roots for Nutrient Acquisition" (Ch. Engels et al.), "Water Uptake" (J.E. Fernández et al.), "Modelling Water and Nutrient Uptake" (P. de Willigen et al.) and finally a chapter entitled "Plant Anchorage" (A.R. Ennos and S. Pellerin). The book ends with a list of suppliers (companies, addresses, items) and a extensive subject index.

Root Methods gives a broad overview of available methods of root-specific research, emphasizing root interactions with their physicochemical environment and it is indeed a Handbook for direct use in laboratories and in the field. The reader will miss, however, comprehensive coverage of methods of studying biotic (pathogenic and symbiotic) interactions, especially associations that occur between roots and soil microorganisms. Some short paragraphs on mycorrhizas are insufficient for readers interested in mutualistic root-fungus interactions. Nevertheless the book should be available in libraries of institutes and universities. It can be recommended to any scientist interested in plant metabolism, physiologists and biochemists as well as agricultural engineers. It should also attract graduate students in plant biology and will be of great help for those starting their scientific work in root metabolism.

Dieter Strack
Leibniz-Institut für Pflanzenbiochemie,
Abt. Sekundärstoffwechsel,
Weinberg 3,
Halle (Saale), Germany
E-mail address: dstrack@ipb-halle.de

PII: S0031-9422(00)00495-7

ChemOffice Ultra 2000
CambridgeSoft, c/o CHEM Research GmbH, Frankfurt, DM 3,290

ChemOffice is the most popular chemical software package containing three applications: *ChemDraw Ultra* (chemical structure drawing), *Chem3D Ultra* (molecular modeling and analysis) and *ChemFinder Ultra* (searching and information integration). The program has been sold and installed more than 100,000 times. Each of the *ChemOffice* applications can be used as a single program, however, an automatic data exchange is possible.

ChemDraw is a well-known standard program for drawing chemical structures. It creates high quality chemical publishing materials and has also become the preferred drawing tool for chemical information querying. It is probably the most powerful chemical software on the market. After a long development over many years, this software is now easy to learn and comfortable in daily use. Chemists can search by structure and substructure, using automatic reaction mapping and specifying atom and bond properties. Using structure cleanup and chemical intelligence gives accurate drawings, chemically correct structures and reaction diagrams from rough drawings where bond angles and length might be wrong. (Some problems, however, can arise by correcting complex structures.)

ChemDraw Ultra adds *ChemNMR* that predicts ^{13}C and ^{1}H NMR shifts and displays their line spectra from *ChemDraw* structures. The line spectra are inserted as graphical objects which are moveable within the *ChemDraw* document. And *Name = Struct* generates a *ChemDraw* structure by typing in systematic chemical names — and vice versa — for most substances. It also allows to automatically insert the name of a structure. Beilstein's AutoNom 2.1 program is included to generate IUPAC-standard names from *ChemDraw* structures.

The *Chem3D Ultra* software converts *ChemDraw* structures into 3D models. It uses molecular mechanics to find low energy conformations to visualize molecular surface properties and calculate partial charges. Besides small molecules, there are basic functions to depict also proteins and other macromolecular structures. The *MOPAC Pro* component adds advanced functionality such as computing properties and advanced energy minimizations.

The third software, *Chemfinder Ultra*, is a chemically intelligent database search engine, giving access to chemical information for tens of thousand of compounds using the *ChemDraw Plugin*. You are able to create structure query to search on-line databases. You can search by names, CAS numbers, formulas, molecular weights or boiling and melting points. The program enables you to integrate *ChemDraw* documents in the Web or to visualize 3D molecules in the Web.

I can strongly recommend *ChemOffice Ultra 2000* to researchers and students giving them an invaluable tool to solve their problems in the field of chemistry. The program is easy to use and reliable. (The handbooks are also useful!)

Dieter Strack
Leibniz-Institut für Pflanzenbiochemie
Weinberg 3, D-06120 Halle (Saale), Germany
E-mail address: dstrack@ipb-halle.de

PII: S0031-9422(00)00503-3

PERGAMON

Phytochemistry 57 (2001) 145–148

PHYTOCHEMISTRY

www.elsevier.com/locate/phytochem

Editorial comment

Phytochemistry in the genomics and post-genomics eras☆,[1]

In this guest editorial we interview Dr Richard A Dixon, President of the Phytochemical Society of North America (2000–2001), on his thoughts about the future of phytochemistry now that whole plant genomes are becoming available. Rick is Director of the Plant Biology Division at the Samuel Roberts Noble Foundation in Ardmore, Oklahoma, and is a member of the Editorial Board. He has already aired these views on the future of phytochemistry in two thought-provoking articles in the PSNA Newsletter, which we felt, with permission, deserved to reach a wider audience through *Phytochemistry*. We have taken the liberty to re-edit these in the form of an interview, but acknowledge that the contents are more or less an abridged version of the articles in the PSNA Newsletter. We reproduce his views.

How do you feel phytochemistry as a discipline stands at the present time and where will it go in the future?

Before starting to think about where phytochemistry is going in the future, let us first consider the past achievements of some scientists who can clearly be classified as phytochemists based on the dedication to them of special issues of the journal Phytochemistry. These include some of the founding members of the society and the journal. Eric Conn, Tom Mabry, Neil Towers, Jeffrey Harborne and Clarence Ryan have all made major contributions to phytochemistry, and have trained many of the new generation of phytochemists. The important point is that, together, their work encompasses a variety of subdisciplines, including chemotaxonomy, ethnobotany, pharmacognosy, ecological biochemistry, enzymology, metabolic biochemistry, and molecular biology. Each has taken an individual approach to understanding the chemical processes that make plants such a rich source of molecular diversity. Understanding this chemical diversity at the level of simply cataloging molecules was never the be all and end all of phytochemistry, but a first step towards utilizing plant natural products to benefit humankind by exploitation of their activities as, for example, medicines or plant protectants.

However, the discipline of phytochemistry is entering a new era with the coming of the third millennium. During the last 30 years or more, phytochemistry has taken something of a back seat to other branches of plant science, such as developmental biology and physiology, that have somehow appeared to be more glamorous. Over the last 10 years, the rapidly developing "discipline" of plant molecular biology, with its associated "spinning off" of the field of agricultural biotechnology, has tended to further obscure the purpose and potential impact of phytochemistry. This is particularly so for young scientists who have been attracted by the demonstrable power of molecular biology away from more traditional chemical training. It is, therefore, somewhat ironic that the new developments in molecular biology are now driving renewed interest in phytochemistry.

If that is so, how can phytochemistry be integrated with these other disciplines?

In the past, successful molecular biology labs working on plant natural product pathways would require at least one lab member to be familiar with the chemistry of the favorite class of compound worked on by that particular group. Few molecular labs would have the chemical expertise to work on a broad range of natural product classes, or indeed feel a need to do so. That is now changing. Genomics has fundamentally altered the way in which we view plant biology. The pre-genomics reductionist view ("I work on this pathway") is being superceded by a new ability to take a global view of cellular processes. The complete genome sequence of *Arabidopsis* is now available, to be soon followed by that of rice. Large-scale sequencing programs are rapidly documenting the expressed genes in many other species, including wheat, soybean, *Medicago truncatula* (as a model for alfalfa, Fig. 1) and banana. The big question is what all these genes do, and the science that addresses this

☆ The views expressed in Editorial comment articles are the sole opinion of the authors and publication shall not imply the concurrence of the Editors or Publisher.

[1] Largely reproduced from the Phytochemical Society of North America Newsletter published July 2000.

0031-9422/01/$ - see front matter © 2001 Elsevier Science Ltd. All rights reserved.
PII: S0031-9422(01)00073-5

question has been termed functional genomics. Many companies and institutes engaged in large scale functional genomics programs are beginning to see the relative paucity of graduates trained in chemistry and biochemistry (read phytochemistry in the case of plant genomics programs) as a major limitation to future progress.

There are several ways of addressing plant gene function on a large scale, but, for most genes, these approaches ultimately lead to some kind of biochemical analysis. In one approach, an attempt is made to sequence all expressed genes, from a range of developmentally or environmentally selected cDNA libraries (Newman et al., 1994). Expressed sequence tags (ESTs) are compared to sequences in existing gene databases, from which function can sometimes be inferred (but always with caution!). If the function is not apparent, analysis of gene expression profiles using microarray technology (''DNA chips'') might give clues as to function based on the developmental or environmental control pattern of the candidate genes (Kehoe et al., 1999). However, if a gene becomes a candidate for a particular function, it is usually necessary to confirm that function by expressing the gene in some heterologous expression system, such as *E. coli*, yeast, or insect cells. Plants themselves are also becoming vehicles for rapid functional identification of cloned genes, since the development of high throughput transformation systems for some species. Availability of substrates (possibly labeled, and with the correct stereochemistry, of course!) and a specific assay method are then essential. They always were, but the point now is that the speed with which EST programs may lead to candidate genes for plant natural product biosynthesis makes the biochemical assay of enzyme activities the potential rate limiting step.

How can we accelerate the rate at which we can understand biosynthesis and modification of natural products?

Alternative approaches to functional genomics further expand the scale of experiments. Thus, several strategies now exist for creating DNA-tagged mutants in which genes may be randomly up-regulated or down-regulated (Azpiroz-Leehan and Feldmann, 1997; Weigel et al., 2000), and the independent transgenic lines may then be directly screened for biochemical phenotype by phytochemical analysis. Such an approach, that has been termed ''phytochemical biopanning'' in cases where genes are up-regulated, requires the establishment of high throughput metabolic profiling for analysis of gene function, since many thousands of lines may have to be screened before establishing a ''hit'' on a particular gene or pathway of interest. Phytochemical analysis therefore becomes an essential analytical tool for gene discovery. The only difference from classical metabolite analyses carried out in labs throughout the world is one of scale (tens of thousands of samples rather than hundreds) with the need for an attendant increase in speed via automation. The currently applied techniques for metabolic profiling are well familiar to phytochemists- liquid or gas chromatography coupled to light absorption, fluorescence or mass detection. Significant opportunities exist for developing improved techniques for metabolic profiling, particularly in the area of nanoscale separations and their automation, and in more efficient mass detection methods, such as Fourier transformation ion cyclotron MS.

For phytochemists with an interest in computer science, a major challenge will be to assemble databases of metabolic profiles that will be able to communicate with gene sequence, protein profile and gene expression databases. This new field of ''metabolomics'' or ''metanomics'' will facilitate a far greater understanding of how gene expression regulates the metabolic phenotype of the cell than has been hitherto possible (Trethewey et al., 1999).

Can you, therefore, foresee the acquisition of this knowledge giving rise to new and innovative science?

The term ''structural genomics'' was initially applied to large-scale studies of genome structure and organization, but is now also used to describe how the primary sequence of amino acids in a protein relates to the function of that protein. Currently, the core of structural genomics is protein structure determination, primarily by X-ray crystallography, and the design of computer programs to predict protein fold structures for new proteins based on their amino acid sequences and structural principles derived from those proteins whose 3-dimensional structures have been determined (Skolnick and Fetrow, 2000). Plant natural product pathways are a unique source of information for the structural biologist in view of the almost endless catalytic diversity encountered in the various pathway enzymes, but based on a finite number of reaction types. Plants are combinatorial chemists par excellence, and understanding the principles that relate enzyme structure to function will speed up the gene discovery process for enzymes of plant natural product pathways. It will also open up possibilities for the rational design of new enzymes to generate novel biologically active natural products (Ferrer et al., 1999). The chemical diversity that is currently explored by analyzing natural products from new plants collected in diverse habitats throughout the world may soon be generated in vitro by site-directed mutagenesis or shuffling of gene sequences derived from well understood classes of plant natural product biosynthetic enzymes. Phytochemistry will have the same goals as before, but a different source of chemical diversity with which to work.

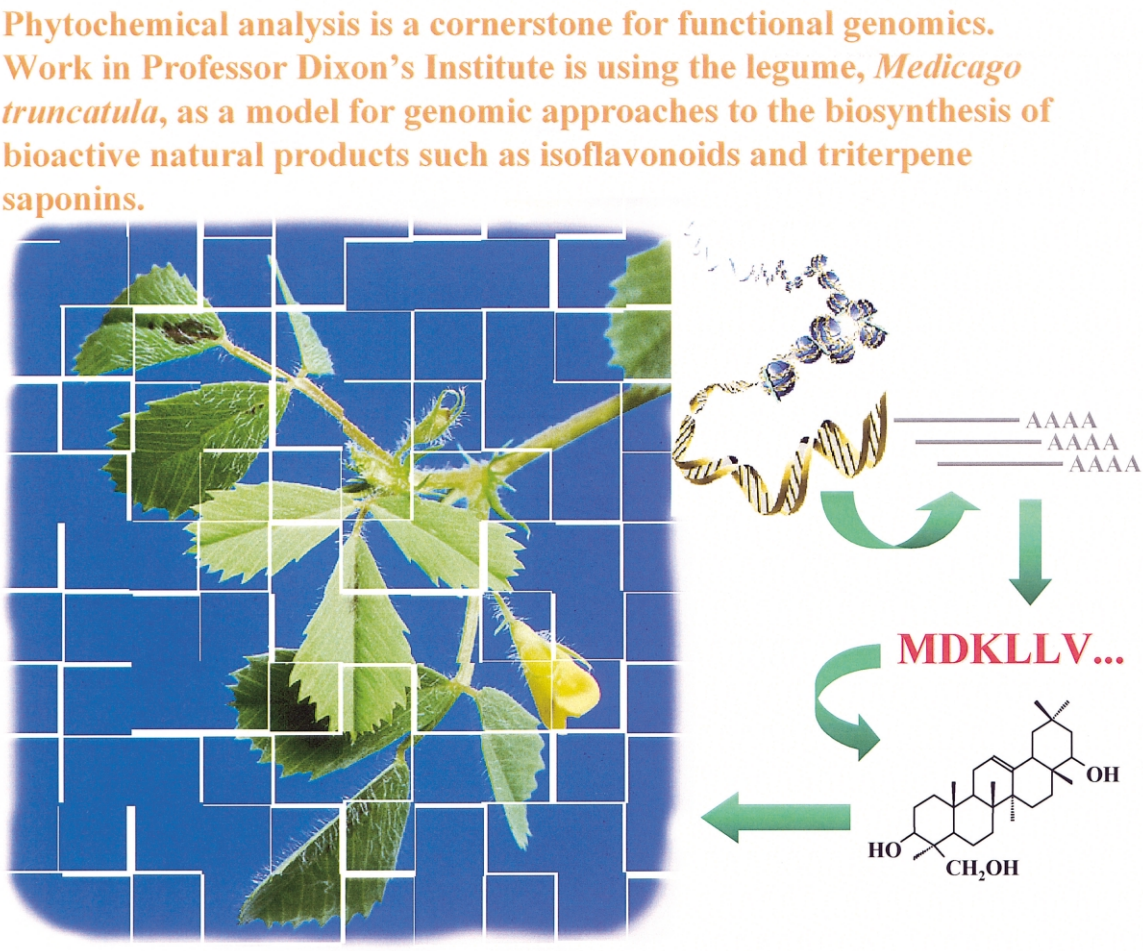

Fig. 1. Professor Dixon's Institute is using the legume, *Medicago truncatula*, as a model for genomic approaches to the biosynthesis of bioactive natural products such as isoflavonoids and triterpene saponins,

Do you see any new radical alterations in our perceptions and basic understanding of natural products biosynthesis arising as a result?

Structural biology will play an increasing role in the "post-genomics era" after the completion of the major plant genome sequencing initiatives. However, even when the biochemical functions of all the genes in the plant are known, there is still a major challenge, namely understanding how metabolic networks function within the cell (Huang, 2000). This understanding is necessary for full realization of the potential of metabolic pathway engineering. It is becoming increasingly clear that the enzymes of primary and secondary metabolic pathways, and signal transduction components such as protein kinase cascades, are somehow localized in loosely associated complexes, even if operationally soluble according to classical biochemical criteria. Understanding the subcellular organization of plant metabolism will require the development of new technologies, at the interface of phytochemistry and cell biology, to localize metabolites and their enzymes within the cell, and integration with computational methods for modeling of pathway flux through organized enzyme complexes.

In a recent *Phytochemistry* editorial comment by Mark Plotkin, who posed the ethnobotanist view, he considered the lack of trained phytochemists to be real in the west. How do you view the situation and how do we move forward?

I hope I will not offend any of my colleagues by stating that it is usually easier to train a chemist or biochemist to become a molecular biologist than it is to train someone whose background is in molecular biology or genetics to become a good biochemist or phytochemist. Those enzymes and small molecules all seem to have different properties, and there don't seem to be any expensive kits to help solve the problems! Phytochemists should therefore be in increasing demand as we move into the genomics and post-genomics eras. It is therefore of critical importance for our field that young scientists with an interest in plant chemistry become familiar with

the new fields of functional and structural genomics. They should not, however, forego a rigorous training in all aspects of plant chemistry. The older ones among us should also be looking for new opportunities to apply our knowledge of plant chemistry and biochemistry in the context of the new advances in plant science. I hope the readership of *Phytochemistry* will realize the enormous opportunity we all now face, and become increasingly involved in multidisciplinary studies that will ultimately tell us exactly how plants elaborate the fascinating chemical structures that many have spent their careers elucidating.

References

Azpiroz-Leehan, R., Feldmann, K.A., 1997. T-DNA insertion mutagenesis in *Arabidopsis*: going back and forth. Trends in Genetics 13, 152–156.

Ferrer, J.-L., Jez, J.M., Bowman, M.E., Dixon, R.A., Noel, J.P., 1999. Structure of chalcone synthase and the molecular basis of plant polyketide biosynthesis. Nature Structural Biology 6, 775–784.

Huang, S., 2000. The practical problems of post-genomic biology. Nature Biotechnology 8, 471–472.

Kehoe, D.M., Villand, P., Somerville, S., 1999. DNA microarrays for studies of higher plants and other photosynthetic organisms. Trends Plant Science 4, 38–41.

Newman, T., de Bruijn, F.J., Green, P., Keegstra, K., Kende, H., McIntosh, L., Ohlrogge, J., Raikhel, N., Somerville, S., Thomashow, M., Retzel, E., Somerville, C., 1994. Genes galore: a summary of methods for accessing results from large-scale partial sequencing of anonymous *Arabidopsis* cDNA clones. Plant Physiology 106, 1241–1255.

Skolnick, J., Fetrow, J.S., 2000. From genes to protein structure and function: novel applications of computational approaches in the genomic era. Trends in Biotechnology 18, 34–39.

Trethewey, R.N., Krotzky, A.J., Willmitzer, L., 1999. Metabolic profiling: a Rosetta Stone for genomics? Current Opinion in Plant Biology 2, 83–85.

Weigel, D., Ahn, J.H., Blázquez, M.A., Borevitz, J., Christensen, S.K., Fankhauser, C., Ferrándiz, C., Kardailsky, I., Neff, M.N., Nguyen, J.T., Sato, S., Wang, Z., Xia, Y., Dixon, R.A., Harrison, M.J., Lamb, C.J., Yanofsky, M.F., Chory, J., 2000. Activation tagging in *Arabidopsis*. Plant Physiology 122, 1003–1013.

Dr. Richard A. Dixon
Plant Biology Division
Samuel Roberts Noble Foundation
Ardmore, OK, USA
E-mail address: radixon@noble.org

PERGAMON

Phytochemistry 57 (2001) 149–156

PHYTOCHEMISTRY

www.elsevier.com/locate/phytochem

Inhibition of polygalacturonase from *Verticillium dahliae* by a polygalacturonase inhibiting protein from cotton

Jacinda T. James, Ian A. Dubery *

Department of Chemistry and Biochemistry, Rand Afrikaans University, PO Box 524, Auckland Park, 2006, South Africa

Received 26 April 2000; received in revised form 20 July 2000

Abstract

An extracellular endo-polygalacturonase (PGase) [E.C. 3.2.1.15] was isolated from 18-day-old culture filtrates of *Verticillium dahliae* and partially purified using gel permeation chromatography. The band responsible for PGase activity was electrophoretically characterized as having a molecular mass of approximately 29 500 and an isoelectric point of 5.4. Kinetic studies indicate a K_m of 3.3 mg ml^{-1} and V_{max} of 0.85 μmol reducing units min^{-1} ml^{-1} with polygalacturonic acid as substrate. Polygalacturonase inhibitor protein (PGIP) in cotton seedlings was induced by 5 mM salicylic acid and immunochemical analysis indicated high levels in the hypocotyl tissues. PGIP was purified from roots and stems using affinity chromatography with endo-PGase from *Aspergillus niger* as an immobilised ligand. The purified PGIP contained monomeric and dimeric molecules with molecular masses of 34 and 66 kDa respectively. Purified cotton PGIP inhibited endo-polygalacturonase from *A. niger* in a non-competitive or mixed manner with an inhibition constant, K_I of 15 nM. The isolated *V. dahliae* PGase was, however, inhibited in a positive cooperative manner, indicative of allosteric interactions between the enzyme and the inhibitor protein. In addition to reducing the reaction rate, decreased substrate affinity may contribute to the accumulation of elicitor-active oligouronides. © 2001 Elsevier Science Ltd. All rights reserved.

Keywords: *Gossypium hirsutum*; Malvaceae; Cotton; *Verticillium dahliae*; Polygalacturonase; Polygalacturonase inhibiting protein

1. Introduction

Verticillium dahliae is a destructive soil-borne fungal pathogen that causes vascular wilt diseases on more than 160 plant species including important crop plants such as cotton, tomatoes and potatoes. *V. dahliae* penetrates the host through the roots and spreads systemically through the xylem, leading to the appearance of wilt symptoms (Daayf et al., 1995).

The plant cell wall plays a complex role in resistance by presenting a physical barrier to the infecting pathogen. Polysaccharides capable of regulating gene expression and defense responses, as well as enzymes and proteins involved in host defense mechanisms, are localized in the cell wall (Karr and Albersheim, 1970). The importance of polygalacturonases (PGases) in fungal pathogenesis is now well established for certain plants (Karr and Albersheim, 1970; Jones et al., 1972). Research on fungal endopolygalacturonases has demonstrated that these enzymes release elicitor-active oligogalacturonide fragments from the plant cell wall rather than being elicitors of defense themselves.

Polygalacturonase inhibiting proteins (PGIPs) have been found to be present in the cell wall of most dicotyledonous plants, and are specific, reversible, saturable, high-affinity ''receptors'' for fungal, but not plant endopolygalacturonases (Cervone et al., 1989, 1990). PGIPs are structurally related to several resistance gene products and belong to a super-family of leucine-rich repeat proteins specialized for recognition of non-self molecules and rejection of pathogens (Jones and Jones, 1997). The receptor-like leucine-rich molecular structure of the PGIP protein provides a molecular basis for the proposed role of PGIP as a secreted receptor component of the cell-surface signaling system involved in recognition events between plant and fungi (De Lorenzo et al., 1993; Jones and Jones, 1997). Although PGIPs, which have a broad specificity against fungal endo-PGase (Cervone et al., 1990), can reduce the activity of

* Corresponding author. Tel./fax: +27-11-489-2401.
E-mail address: iad@na.rau.ac.za (I.A. Dubery).

0031-9422/01/$ - see front matter © 2001 Elsevier Science Ltd. All rights reserved.
PII: S0031-9422(01)00024-3

these enzymes in vitro (Cervone et al., 1987); PGIPs from different plants inhibit PGase from a single fungal species to different extents (Yao et al., 1995). Furthermore, the inhibition of PGases by PGIPs can be highly specific (Leckie et al., 1999). Different isoforms of PGIP from a single plant source can differentially inhibit PGases from several fungal species or PGase isozymes from a single fungal pathogen. The possibility exists that different PGIP members encode PGIPs with distinct regulation and specificity (Desiderio et al., 1997).

Formation of the endo-PGase-PGIP complex in vitro results in an alteration of the balance between the release of elicitor-active oligosaccharides and the depolymerisation of the active oligogalacturonides into inactive molecules, thus favouring the accumulation of elicitor active molecules at the site of infection and the resulting activation of the defense responses of the host (Cervone et al., 1989; Bergmann et al., 1994). This intriguing concept of plant-derived elicitors for activating pathogen defense is very likely to function in many plant-pathogen interactions. In this cotton:*V. dahliae* study we have characterized PGIP from the host and extracellular PGase from the pathogen and report on the kinetics of interaction between the inhibitor protein and its ligand.

2. Results and discussion

2.1. Polygalacturonase purification and characterization

PGase (E.C. 3.2.1.15) was isolated from 18-day-old cultures. The maximum PGase levels were determined by the agarose diffusion assay (Dingle et al., 1953) and correlated to a growth curve. Mycelial growth peaked at days 14–15, decreasing thereafter. Maximum PGase production was obtained from day 17 to 20 when the glucose in the medium was consumed and growth conditions became limiting.

The main fraction of *V. dahliae* PGase activity was partially purified by means of $(NH_4)_2SO_4$ precipitation and chromatography on a Sepharose Cl-6B gel filtration column (Fig. 1) with a yield of 4.1%. In addition to the main peak of PGase activity, several smaller activity peaks of higher molecular mass, possible aggregates, were observed. The purification procedure is summarized in Table 1. The final specific activity of the preparation varied between 100 and 200 U mg^{-1}.

Although it is known that PGase play a central role in pathogenesis (Cervone et al., 1986), the amount of information on it's structure and function is minimal, due to the technical difficulties in preparing suitable quantities of homogenous PGase. Most of the physiological studies involving PGase have been performed with preparations containing contaminating proteins or enzymes.

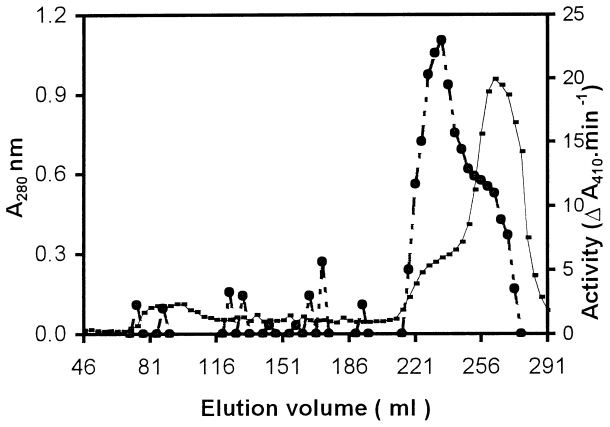

Fig. 1. Elution profile of a Sepharose Cl-6B gel filtration column to purify PGase from *Verticillium dahliae*. The $(NH_4)_2SO_4$ precipitate fraction was loaded onto the column (60×2.5 cm) at a flow rate of 20 ml h^{-1}, eluted with dH_2O and 3.5 ml samples were collected. The fractions were monitored spectrophotometrically at 280 nm (■). PGase activity (-●-), is expressed as $\Delta A_{410}.10^{-4}$ min^{-1} ml^{-1}.

Table 1
Purification of extracellular endo-polygalacturonase from *Verticillium dahliae* culture filtrates

Purification step	Protein concentration (μg ml^{-1})	Vol. (ml)	Total protein (mg)	Yield (%)
Culture filtrate[a]	57.1	1350	77.1	100
$(NH_4)_2SO_4$ precipitation[a]	3020	10	30.2	39.2
Sepharose Cl-6B column	104.8	43	4.5	5.8
Post-column concentration	145.6	23	3.4	4.1

[a] Final specific activity varied between 100 and 200 U mg^{-1}. Activity could not be reproducibly assayed in crude extracts.

The apparent molecular mass determined by means of SDS–PAGE (Fig. 2) for *V. dahliae* PGase was approximately 29.5 kDa which correlated with the value of 31 kDa calculated by gel filtration. Molecular mass values, ranging from 32 to 37 kDa seems to be a characteristic property among endo-PGases from different fungi (Cervone et al., 1986). Using native IEF-gels, the pI value determined for partially purified PGase from *V. dahliae* was 5.4 (Fig. 3). Polygalacturonases from different fungal sources exhibit a great variability of isozymatic forms, distinguishable by their isoelectric points. Apart from structural and functional differences more information is needed on the regulation of PGases to fully understand their biological significance.

2.2. PGIP induction and purification

A variation in the distribution of PGIP throughout the plant has been reported (Salvi et al., 1990), and a study was done to determine the occurrence of PGIP in the different plant organs of cotton seedlings.

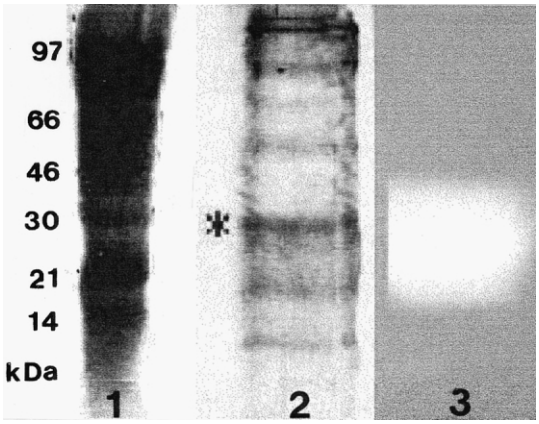

Fig. 2. SDS–PAGE analysis of the Sepharose Cl-6B-purified PGase from *Verticillium dahliae*. Proteins, stained with silver, are indicated in lane 2. Activity staining of the renatured enzyme, indicated with an asterix, on an agarose overlay gel is shown in lane 3. Standard M_r markers are indicated in lane 1.

Immunochemical detection of PGIP levels in crude *Gossypium hirsutum* L. homogenates by Western blot analyses, using a primary antibody against a conserved, surface exposed peptide from bean PGIP, indicated that the highest amount of PGIP was induced in the hypocotyls and to a lesser extend in the first leaves (Fig. 4). The prominent band detected by the antibody in hypocotyls had a M_r of 34 kDa that corresponds with the value reported for deglycosylated PGIP (Stotz et al., 1994, Yao et al., 1995). The results also show a reaction with other proteins present in the crude extract. Bergmann et al. (1994) reported the same for *Phaseolus vulgaris* L. homogenates and attributed the cross-reaction to antibodies interacting with carbohydrate moieties.

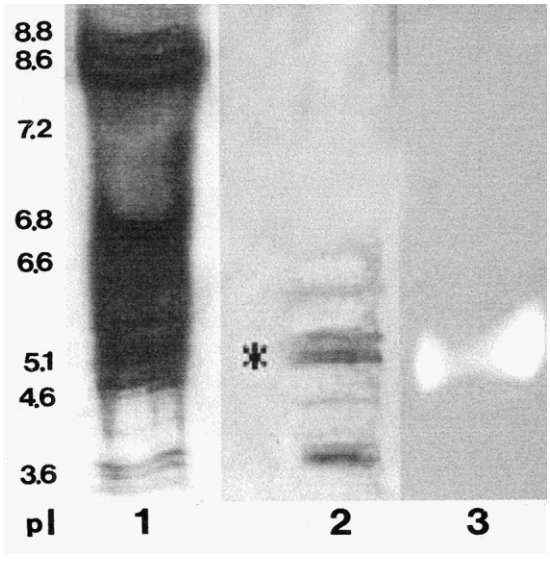

Fig. 3. PAGIEF analysis of the Sepharose Cl-6B–purified PGase from *Verticillium dahliae*. Proteins were stained with silver (lane 2). Activity staining of the enzyme, indicated with an asterix, on an agarose overlay gel is shown in lane 3. Standard pI markers are indicated in lane 1.

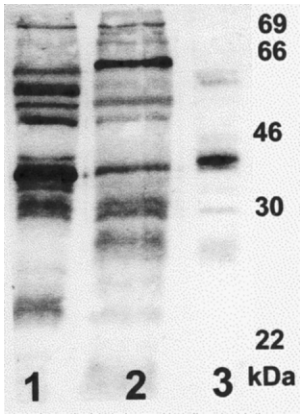

Fig. 4. Tissue specific distribution of PGIP in cotton seedlings. Western blot analysis of immunoreactive proteins present in crude extracts of the hypocotyls (roots and stems, lane 1) and first leaves (lane 2) of cotton seedlings following separation by 12.5% PAGE. Shown in lane 3 is affinity purified PGIP from bean pods, used as a positive control. Molecular mass markers are indicated at right.

The root and stem tissues of infected plants play an important role in the defense mechanisms to *Verticillium* wilt (Lahkim and Nachmias, 1995). PGIP was isolated from cotton hypocotyls by means of $(NH_4)_2SO_4$ precipitation and affinity chromatography on an *Aspergillus niger* endo-PGase-Sepharose column as indicated in Fig. 5 (Cervone et al., 1987). PGIP is an inducible protein and mRNA transcripts accumulate in response to wounding, elicitors and fungal infection (Devoto et al., 1997). It is known that endogenous levels of salicylic acid increase both locally and systematically as a consequence of pathogen attack and that the application of salicylic acid can induce defense responses and resistance towards pathogens (Yalpani et al., 1991). Following the procedure of Bergmann et al. (1994), who reported that the treatment of bean seedlings with salicylic acid resulted in an increase in steady-state levels of PGIP, cotton seedlings were sprayed with 5 mM salicylic acid at 24 h intervals over a time period of 72 h in order to induce maximal amounts of PGIP. The kinetics of induction of PGIP in cotton was not investigated; however, the yield of salicylic acid induced PGIP was approximately 1.0 μg protein per g tissue (Table 2)

Table 2
Purification of polygalacturonase inhibitor protein, PGIP, from hypocotyls of cotton, *Gossypium hirsutum,* cv, OR_{19} seedlings

Purification step	Protein concentration (μg ml^{-1})	Vol. (ml)	Total protein (mg)	Yield (%)
Crude preparation[a]	180.9	233	42.3	100
$(NH_4)_2SO_4$ precipitation[a]	335.6	6	2	4.8
Dialysis	238.1	10	2.38	5.6
Endo-PGase affinity column	9.52	21	0.2	0.5

[a] Activity could not be determined in the crude extracts.

compared to barely detectable levels in noninduced seedlings. PGIP purified from bean hypocotyls was used as a control and produced the same elution pattern as for cotton PGIP (Fig. 5).

2.3. Electrophoretic analyses of cotton PGIP

Purified cotton PGIP was characterized by means of SDS–PAGE and Western blot analyses. One prominent band was detected by SDS–PAGE analysis corresponding to apparent molecular masses of 66 kDa (Fig. 6A).

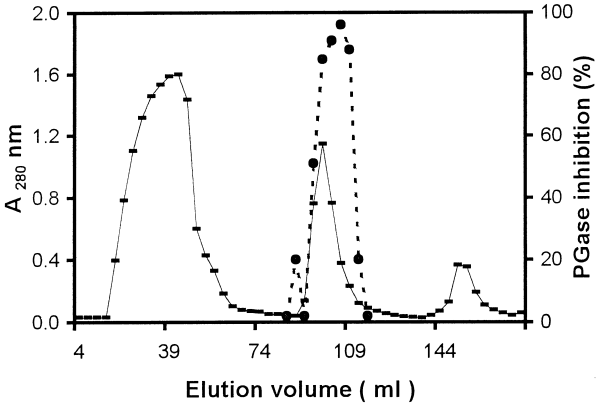

Fig. 5. Elution profile of extracts from cotton roots and stems, induced with 5 mM salicylic acid, on an endo-PGase affinity column (13×1.5 cm). The post-dialysis PGIP fraction (13 ml) was applied to the column with 20 mM NaOAc pH 5.0 and the PGIP fraction was desorbed at 60 ml h^{-1} with phosphate buffered saline, pH 7.3. Fractions were monitored spectrophotometrically at A_{280} (-■-). The PGIP peak (-●-) was identified by the inhibition of *A. niger* polygalacturonase, using the reducing sugar assay. The third peak was obtained with 0.1 M sodium borate buffer, pH 8.0, used to wash and desorb bound phenolics from the column.

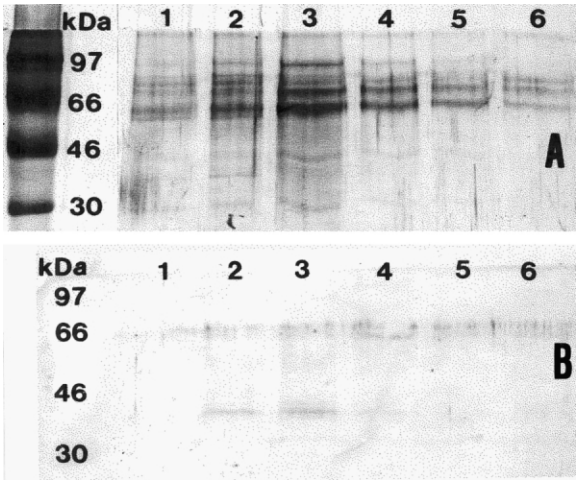

Fig. 6. Electrophoretic and immuno-blot analysis of the protein fractions desorbed from the endo-PGase affinity column. SDS–PAGE followed by silver staining, was performed on 12.5% gels on the PGIP fractions eluted from the colum (part A, lanes 1–6) with subsequent Western blot analysis of these fractions (part B of the figure). The M_rs are indicated on the left.

This band was also observed in the Western blot (Fig. 6B), together with the 34 kDa band observed in crude extracts. Yao et al. (1995) reported a 34 kDa polypeptide for apple PGIP and suggested that differential glycosylation accounted for the observed heterogeneity in molecular mass. Molecular masses of 34–45 kDa have been reported for PGIPs from several sources (Cervone et al., 1987; Bergmann et al., 1994; Stotz et al., 1994) as well as higher molecular weight forms (91 kDa, Abu-Goukh et al., 1983). It is possible that cotton PGIP exists as a dimer, binding covalently to negatively charged pectin in the cell wall or to each other through non-specific interactions. Cross-linking during the purification procedure due to reaction with bifunctional terpene aldehydes such as gossypol, could also lead to dimerization (Mahoney and Chan, 1985).

2.4. Inhibition of the PGase from Verticillium dahliae by cotton PGIP

An agarose diffusion assay showed that purified cotton PGIP inhibited the PGase purified from *V. dahliae* culture filtrates to various degrees when added in different ratios to the reaction mixture (results not shown). A molar ratio of 1(PGase) : 4(PGIP) reduced the activity to near zero but since the inhibition is reversible, a high concentration of PGIP would be needed to completely inhibit the PGase. The inhibition was confirmed with native-PAGE gels and subsequent overlays in the absence and presence of cotton PGIP (overlay gels not shown).

2.5. Kinetic analysis of inhibition

PGase from *V. dahliae,* diluted to a concentration of 30 ng ml^{-1} in a 400 μl reaction volume, producing a linear response over 30 mins ($\Delta A_{410} = 9.3\times10^{-3}$ min^{-1}), was used for kinetic studies. The ΔA_{410} min^{-1} was calculated for the inhibited and uninhibited assay and the percentage of inhibition was determined. An inhibition value of 50% was obtained with 7.5 ng ml^{-1} of purified cotton PGIP, and the activity was reduced to 30% at 9.5 ng ml^{-1}, indicating that cotton PGIP is an effective inhibitor of PGase from *V. dahliae*. The inhibition of reaction rate by increasing concentrations of purified cotton PGIP was measured at different concentrations of polygalacturonic acid (PGA). Increasing concentrations of PGIP lead to the progressive inhibition of PGase activity (Fig. 7A).

Kinetic studies of PGIPs revealed that some inhibit fungal PGases by a competitive type of inhibition whereas others are non-competitive, however this difference might depend on the source of the PGase rather than the source of the PGIP (Jones and Jones, 1997). Mixed or non-competitive inhibition was displayed between cotton PGIP and PGase from *A. niger*, with a K_m of 3.3 mg ml^{-1}, a V_{max} of 1.07 μm reducing sugar

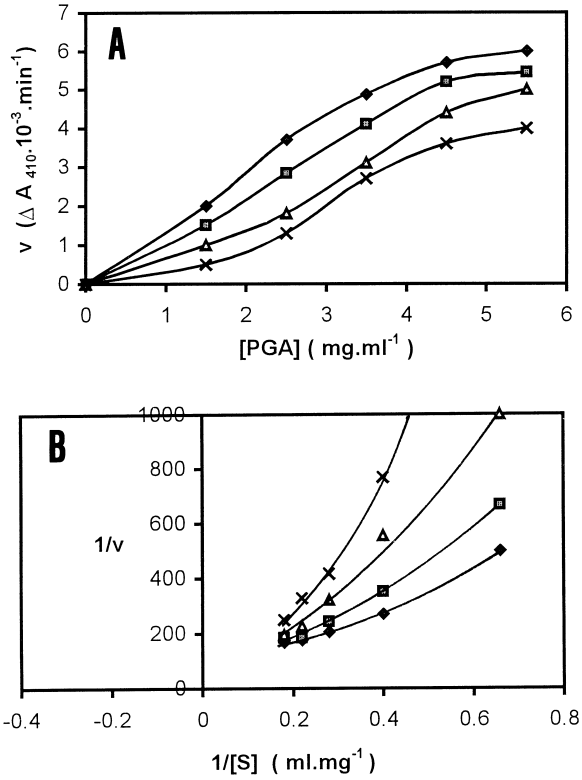

Fig. 7. Inhibition of purified PGase from *V. dahliae* by cotton PGIP at fixed enzyme concentration (30 ng ml^{-1}) and varying inhibitor concentrations: ◆, the uninhibited assay; assay with 2.4 ng ml^{-1} PGIP ■; 4.8 ng ml^{-1} PGIP ▲, and 7.2 ng ml^{-1} PGIP, X. A: Michaelis–Menten plot of PGase activity with different concentrations of PGA together with three different concentrations of PGIP. B: Lineweaver–Burk plot showing the positive allosteric inhibition with several inhibitor concentrations. v = Enzyme activity; S = substrate concentration.

equivalents produced min^{-1} ml^{-1} and a K_i of 15 nM (Fig. 8). Non-competitive inhibition is an indication of the inhibitor binding to a site on the PGase molecule different from the active site. Using a mutagenesis approach, Caprari et al. (1996), was able to confirm that the PGIP does not bind to the active site of the PGase from *Fusarium moniliforme*.

Lineweaver–Burk analysis of the data was performed to determine the type of inhibition displayed between PGase from *V. dahliae* and PGIP from cotton (Fig. 7A and B). V_{max} for the uninhibited treatment was estimated as 0.85 μmol reducing sugar equivalents produced min^{-1} ml^{-1} with a K_m of 3.3 mg ml^{-1}. The graphs obtained are not typical Michaelis–Menten curves and the sigmoidal pattern obtained indicates a positive allosteric interaction between PGase, PGIP and the PGA substrate, suggesting that the reaction rate is reduced at low substrate concentrations but not necessarily at others. Co-operative allosteric interactions occur when the binding of one ligand at a specific site is influenced by the binding of another ligand, modulator or effector at a different (allosteric) site on the protein (Palmer, 1995). Previously, no allosteric inhibition of a fungal PGase by a PGIP have been reported in the few cases where the kinetics of inhibition have been described.

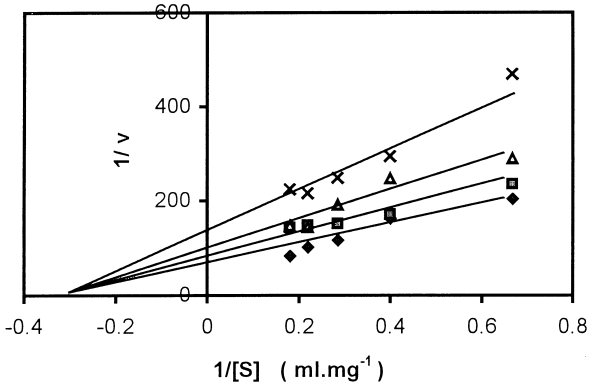

Fig. 8. Inhibition of PGase from *Aspergillus niger* by cotton PGIP at fixed enzyme concentration (100 ng ml^{-1}) and varying inhibitor concentrations (0–7.2 ng ml^{-1}). The Lineweaver–Burk plot shows the non-competitive inhibition with several inhibitor concentrations: 2.4 ng ml^{-1} (■), 4.8 ng ml^{-1} (▲) and 7.2 ng ml^{-1} (X). The uninhibited assay is denoted by ◆. v = Enzyme activity; S = substrate concentration.

The results obtained indicate that the PGase from *V. dahliae* is a "K"-series enzyme, where the presence of the modifier (in this case PGIP), results in a change in K_m but not in the apparent V_{max} for the substrate. If the binding characteristics alone are affected, V_{max} will usually remain unchanged, so the inhibition pattern could be regarded as non-competitive or mixed inhibition. As PGIP does not bind directly to the active site of the enzyme, it could be possible that binding induces a conformational change in the enzyme, resulting in a lower substrate affinity. The sigmoidal binding of a modifier or inhibitor can amplify the regulatory effect (Palmer, 1995), thus reducing the activity of the PGase. This would delay the rapid degradation of PGA to inactive monomers and result in the generation of elicitor-active oligogalacturonides with a higher degree of polymerization. These results are in support of the model proposed for the PGIP:endo PGase interaction (De Lorenzo et al., 1993) where the formation of the enzyme-inhibitor complex in vitro, results in an alteration of the balance between the release of elicitor-active oligosaccharides and the depolymerisation of the active oligogalacturonides into inactive molecules, thereby favouring the accumulation of elicitor active molecules at the site of infection and the resulting activation of the defense responses of the host.

3. Experimental

3.1. Plant material and fungal isolate

Seeds of *Verticillium* resistant cotton cultivar OR_{19} (obtained from the Agriculture Research Council's Institute for Tobacco and Cotton, Rustenburg, South

Africa) were germinated and maintained at 30°C. Roots and stems of 3-week-old plants were used in all experiments. A pathogenic isolate of *V. dahliae* was obtained from infected *Acala*$_{1517/70}$ cotton stems (Meyer et al., 1994).

3.2. Polygalacturonase purification and characterization

Fungal mycelia were cultivated in liquid culture in the dark at 25°C for 18 days, in 1 l flasks, containing 500 ml of medium (Nachmias et al., 1982). A growth curve was determined over a period of 21 days. The extracts were screened by means of an agarose diffusion assay (Dingle et al., 1953) to determine maximum PGase production (Section 3.8).

Culture filtrates harvested on day 18 were used for purification of PGase. Following centrifugation at 15 000×*g*, proteins present in the the clear supernatant (1350 ml) was precipitated at 90% $(NH_4)_2SO_4$ saturation for a minimum of 1 h. The precipitate was collected by centrifugation at 15 000×*g* for 20 min and dissolved in dH_2O. The sample was fractionated using gel permeation chromatography on Sepharose CL-6B (2.5×60 cm) with dH_2O as eluant (Meyer et al., 1994) at a flow rate of 20 ml h^{-1}. The fractions obtained after gel filtration that exhibited PGase activity were combined and concentrated in a dialysis bag against glycerol to stabilize the enzyme for storage at 4°C.

PGase from *V. dahliae* was characterized by native PAGE, agarose overlay gels (Kanellis et al., 1991), SDS–PAGE (Laemmli, 1970) and IEF gels (Robertson et al., 1987). The M_r was determined using analytical gel filtration with a Sepharose CL-6B column (2.5×60 cm) using 0.1 M NaPi buffer, pH 8.0 as eluting buffer (Andrews, 1970). V_0 and V_t were determined with blue dextran and DNP-alanine respectively to calibrate the column, together with a set of calibration proteins from 14 to 158 kDa.

3.3. Enzyme staining in gels

Enzyme activity of endo-PGases present in the culture filtrates and crude extract were screened by means of an agarose diffusion assay (Dingle et al., 1953).

Following PAGE, the gels were incubated in 0.1 M NaOAc, pH 5.0 for 10 min. Agarose gels (2×85×100 mm) were poured onto Gelbond® film (FMC Bioproducts). The agarose soln. contained 0.8% agarose (w/v), 100 mM HOAc (pH 5.0) and 1 mg ml^{-1} PGA (w/v). Following incubation, the overlay gels were stained in 0.005% ruthenium red for 2 h and destained in dH_2O until clear bands were evident (Kanellis et al., 1991).

In order to determine activity following SDS–PAGE, gels were washed twice for 15 min in 0.1 M NaOAc, pH 4.5 containing 0.05 mg ml^{-1} BSA and 0.1% Triton-X100 at room temperature. The enzyme was allowed to renature at 4°C overnight in 0.1 mM NaOAc, pH 4.5 containing 0.05 mg ml^{-1} BSA and 0.02% β-mercaptoethanol. Gels were then washed for 10 min in 20 mM NaOAc, pH 4.5 and enzyme activity localized as described above. The band of activity was compared to the SDS-gel to determine the molecular weight of PGase from *V. dahliae*.

3.4. Enzyme activity determinations

A reducing sugar assay for the determination of released galacturonic oligomers was used with the colour reagent p-hydroxybenzoic acid hydrazide (Kombrink et al., 1988). PGase, either the positive control *Aspergillus niger* PGase, 100 ng ml^{-1}, or purified PGase from *Verticillium dahliae,* 30 ng ml^{-1}, was added as a 200 μl aliquot to 200 μl autoclaved PGA (2.5 mg ml^{-1}) in 20 mM NaOAc buffer, pH 5.0. PGase activity was assessed over time (0–60 min) to determine the linear range. Duplicate samples were taken at 4 different time intervals (0, 10, 20 and 30 min). Activity was expressed as ΔA_{410} min^{-1} ml^{-1} or converted to arbitrary units, one unit being equivalent to the release of 1.0 μmol galacturonic acid units min^{-1} ml^{-1} at pH 5.0.

3.5. Induction and purification of PGIP

PGIP in cotton seedlings was chemically induced with salicylic acid. Seedlings were sprayed with 5 mM sodium salicylate, pH 7.0 for 72 h. Distilled water was used as a control. The extraction procedure of Salvi et al. (1990) was carried out at 4°C with slight modifications. Plant material (hypocotyls, 200 g) was homogenized for 2 min in cold 20 mM NaOAc, pH 5.0 containing 500 mM NaCl (1:2 m/v). Proteinase inhibitor, PMSF (0.1%), was added prior to homogenization. The suspension was vacuum filtered through a number 1 sinter glass funnel and the filtrate centrifuged at 12 000×*g* for 20 min. The proteins in the supernatant were precipitated for 1 h with $(NH_4)_2SO_4$ at a final saturation of 90%, followed by centrifugation 12 000×*g* for 20 min to collect the precipitate. The precipitate was resuspended in a small volume of 20 mM NaOAc, pH 5.5 and dialyzed with at least 4 changes of the same buffer in a dialysis membrane with a molecular cut-off value of 12–14 kDa. The suspension was centrifuged at 12 000×*g* for 20 min and the PGIP purified further by affinity chromatography on an endo-PGase affinity column as described by Cervone et al. (1987). PGIP activity was measured using the PGase assay described above. One unit was defined as the amount of inhibitor required to reduce the activity of one unit of enzyme by 50%

3.6. Electrophoretic analyses

Protein concentration was determined according to Bradford (1976) or the bicinchoninic acid protein assay from Pierce (Rockford, IL). Purified preparations were

analysed by native PAGE, agarose overlay gels (Kanellis et al., 1991) and IEF gels (Robertson et al., 1987). SDS-electrophoresis was carried out according to Laemmli (1970); gels were stained with either Coomassie R250 or silver (Bristow, 1990).

3.7. Western blot analyses

Blotting was performed overnight at 4°C and 36 V using PVDF-Plus membranes and 25 mM Tris (pH 8.2), 192 mM glycine, 20% (v/v) methanol and 0.1% (w/v) SDS as transfer buffer. The primary antibody was raised in rabbits against a synthetic peptide, A-L-L-Q-I-K-K-D-L-G-N-P-Y, located near the N-terminus of bean PGIP and coupled to Keyhole Limpet Haemocyanin (Bergmann et al., 1994). Goat anti-rabbit IgG, conjugated to alkaline phosphatase was used as secondary antibody at a dilution of 1:1000 with nitro blue tetrazolium chloride/5-bromo-4-chloro-3-indolyl phosphate as substrate (Berger et al., 2000).

3.8. Inhibition studies

The agarose diffusion assay (Dingle et al., 1953) for PGase activity was performed to test for the presence of PGIP. The assay medium consisted of 100 mM citrate and 200 mM NaPi (pH 5.3) to which final concentrations of 1% agarose, 0.5% ammonium oxalate and 0.1 mg l^{-1} PGA were added. The assay was carried out with the addition of 50 μl culture medium supernatant into each well and overnight incubation at 30°C. Activity zones were visualized by staining the background with 0.05% ruthenium red.

For enzyme assays and kinetic studies the reducing sugar assay as described in Section 3.4 was used. Enzyme was added to different concentrations of cotton PGIP (0–7.2 ng ml^{-1}) to determine the degree of inhibition. PGIP preparations were mixed with PGase and incubated for 10 min prior to the addition of the PGA substrate. Substrate concentrations were varied between 1.5 and 5.5 mg ml^{-1} to determine the type of inhibition. Duplicate samples were taken at 0, 10, 20 and 30 min and analyzed for galacturonic acid.

Acknowledgements

We wish to acknowledge Dr. D. Berger (ARC, Agricultural Research Council) for cooperation and the gift of the anti-PGIP antibody, and the National Research Foundation (NRF) for research funding.

References

Abu-Goukh, A.A., Greve, L.C., Labavitch, J.M., 1983. Purification and partial characterization of "Bartlett" pear fruit polygalacturonase inhibitors. Physiological Plant Pathology 23, 111–122.

Andrews, P., 1970. Estimation of molecular size and molecular weights of biological compounds by gel filtration. Methods in Biochemical Analysis 18, 1–53.

Berger, D.K., Oelofse, D., Arendse, M.S., du Plessis, E., Dubery, I.A., 2000. Bean polygalacturonase inhibitor protein-1 (PGIP-1) inhibits polygalacturonases from Stenocarpella maydis. Physiological and Molecular Plant Pathology 57, 5–14.

Bergmann, C.W., Ito, Y., Singer, D., Albersheim, P., Darvill, A.G., 2000. Polygalacturonase-inhibiting protein accumulates in *Phaseolus vulgaris* L. in response to wounding, elicitors and fungal infection. The Plant Journal 5, 625–634.

Bradford, M.M., 1976. A rapid and sensitive method for the quantititation of microgram quantities of dye utilizing the principle of protein-dye binding. Analytical Biochemistry 72, 248–254.

Bristow, A.F., 1990. Purification of proteins for therapeutic use. In: Harris, E.L.V., Angal, S. (Eds.), Protein Purification and Applications. Information Press Ltd, Oxford, pp. 29–44.

Caprari, C., Mattei, B., Basile, M.L., Salvi, G., Crescenzi, V., De Lorenzo, G., Cervone, F., 1996. Mutagenesis of endopolygalacturonase from *Fusarium moniliforme*: histidine residue 234 is critical for enzymatic and macerating activities and not for binding to polygalacturonase-inhibiting protein (PGIP). Molecular Plant Microbe Interactions 9, 617–624.

Cervone, F., De Lorenzo, G., Camardella, L., 1986. Molecular evolution of fungal polygalacturonase. In: Bailey, J. (Ed.), Biology and Molecular Biology of Plant-Pathogen interactions. Springer-Verlag, Berlin, pp. 385–392.

Cervone, F., De Lorenzo, G., Degrá, L., Salvi, G., Bergami, M., 1987. Purification and characterization of a polygalacturonase-inhibiting protein from *Phaseolus vulgaris* L. Plant Physiology 85, 631–637.

Cervone, F., De Lorenzo, G., Pressey, R., Darvill, A.G., Albersheim, P., 1990. Can *Phaseolus* PGIP inhibit pectic enzymes from microbes and plants? Phytochemistry 29, 447–449.

Cervone, F., Hahn, M.G., De Lorenzo, G., Darvill, A., Albersheim, P., 1989. Host plant interactions. XXXIII. A plant protein converts a fungal pathogenesis factor of plant defense responses. Plant Physiology 85, 631–637.

Daayf, F., Nicole, M., Geiger, J.P., 1995. Differentiation of *Verticillium dahliae* populations on the basis of vegetative compatibility and pathogenicity on cotton. European Journal of Plant Pathology 101, 69–79.

De Lorenzo, G., Cervone, F., Bellincampi, D., Capari, C., Clark, A.J., Desiderio, A., Devoto, A., Forrest, R., Leckie, F., Nuss, L., Salvi, G., 1993. Polygalacturonase, PGIP and oligogalacturonides in cell-cell communication. Biochemical Society Transactions 22, 394–398.

Desiderio, A., Aracri, B., Leckie, F., Mattei, B., Salvi, G., Tigelaar, H., Van Roekel, J.S., Baulcombe, D.C., Melchers, L.S., DeLorenzo, G., Cervone, F., 1993. Polygalacturonase-inhibiting proteins (PGIPs) with different specificities are expressed in *Phaseolus vulgaris*. Molecular Plant Microbe Interactions 10, 852–860.

Devoto, A., Clark, A.J., Nuss, L., Cervone, F., De Lorenzo, G., 1997. Developmental and pathogen-induced accumulation of transcripts of polygalacturonase-inhibiting protein in *Phaseolus vulgaris* L. Planta 202, 284–292. .

Dingle, J., Reid, W.W., Solomons, G.L., 1953. The enzymatic degradation of pectin and other polysaccharides. Journal of the Science of Food and Agriculture 4, 149–153.

Jones, D.A., Jones, J.D.G., 1997. The role of leucine-rich repeat proteins in plant defenses. Advances in Botanical Research incorporating Advances in Plant Pathology 24, 120–127.

Jones, T.O., Anderson, A.J., Albersheim, P., 1972. Host pathogen interactions IV. Studies on the polysaccharide-degrading enzymes secreted by *Fusarium oxysporum* f. sp. *Lycopersci*. Physiological Plant Pathology 2, 153–166.

Kannellis, A.K., Solomons, T., Roubelakis-Angelakis, K.A., 1991.

Suppression of cellulase and polygalacturonase and induction of alcohol dehydrogenase isozymes in avocado fruit mesocarp subjected to low oxygen stress. Plant Physiology 98, 269–274.

Karr, A.L., Albersheim, P., 1970. Polysaccharide-degrading enzymes are unable to attack plant cells without prior action by a "wall-modifying" enzyme. Plant Physiology 46, 69–80.

Kombrink, E., Schröder, M., Halbrock, K., 1988. Several "pathogenesis-related" proteins in potato are 1,3-β-glucanases and chitinases. Proceedings of the National Academy of Sciences of the United States of America 85, 782–786.

Leckie, F., Mattei, B., Capodicasa, C., Hemmings, A., Nuss, L., Aracri, B., De Lorenzo, G., Cervone, F., 1999. The specificity of polygalacturonase-inhibiting protein (PGIP): a single amino acid substitution in the solvent-exposed beta-strand/beta-turn region of the leucine-rich repeats (LRRs) confers a new recognition capability. EMBO Journal 18, 2352–2363.

Laemmli, U.K., 1970. Cleavage of structural proteins during the assembly of the head of Bacteriophage T4. Nature 227, 680–685.

Lahkim, L.T., Nachmias, A., 1995. Significance of the root system in Verticillium wilt tolerance in potato and resistance in tomato. Israel Journal of Plant Sciences 43, 315–323.

Mahoney, N.E., Chan, B.G., 1985. High-performance liquid chromatographic analysis of terpene aldehydes in cotton. Journal of Chromatography 329, 91–98.

Meyer, R., Slater, V., Dubery, I.A., 1994. A phytotoxic protein-lipopolysaccharide complex produced by *Verticillium dahliae*. Phytochemistry 35, 1449–1453.

Nachmias, A., Buchner, V., Krikun, J., 1982. Comparison of protein-lipopolysaccharide complexes produced by pathogenic and non-pathogenic strains of *Verticillium dahliae* Kleb. from potato. Physiological Plant Pathology 20, 213–221.

Palmer, T., 1995. Understanding Enzymes, 4th Edition. Prentice Hall, Ellis Horwood, pp. 148–151, 243–245, 262–263.

Robertson, E.F., Dannelly, H.K., Malloy, P.J., Reeves, H.C., 1987. Rapid isoelectric focusing in a vertical polyacrylamide minigel system. Analytical Biochemistry 167, 290–294.

Salvi, G., Giarrizzo, F., De Lorenzo, G., Cervone, F., 1990. A polygalacturonase-inhibiting protein in the flowers of *Phaseolus vulgaris* L. Plant Physiology 136, 513–518.

Stotz, H.U., Contos, J.J.A., Powell, A.L.T., Bennet, A.B., Labavitch, J.M., 1994. Structure and expression of an inhibitor of polygalacturonases from tomato. Plant Molecular Biology 25, 607–617.

Yalpani, N., Silverman, P., Wilson, T.M.A., Kleier, D.A., Raskin, I., 1991. Salicylic acid is a systemic signal an inducer of pathogenesis-related proteins in virus-infected tobacco. The Plant Cell 3, 809–818.

Yao, C., Conway, W.S., Sams, C.E., 1995. Purification and characterization of a polygalacturonase-inhibiting protein from apple fruit. Phytopathology 85, 373–1377.

PERGAMON

Phytochemistry 57 (2001) 157–163

PHYTOCHEMISTRY

www.elsevier.com/locate/phytochem

Cell-wall proteins from Sitka spruce xylem are selectively insolubilised during formation of dehydrogenation polymers of coniferyl alcohol

Gordon J. McDougall *

Unit of Plant Biochemistry, Biochemistry and Cell Biology Division, Scottish Crop Research Institute, Invergowrie, Dundee DD2 5DA, Scotland, UK

Received 13 September 2000; received in revised form 5 January 2001

Abstract

Extracts from the lignifying xylem of Sitka spruce that were enriched in cell-wall-associated glycoproteins contained peroxidase and oxidase activity and readily formed lignin-like water-insoluble dehydrogenation polymers (DHPs) from coniferyl alcohol (CA) when supplied with H_2O_2. During the formation of DHPs, the abundance of a number of polypeptides in the extracts was diminished. However, these polypeptides were also diminished in control reactions that contained H_2O_2 but lacked CA. Polypeptides could be recovered from the DHPs by heating in SDS-PAGE sample buffer but no insolubilised polypeptides could be recovered from the $+H_2O_2$ reactions. Although most of the DHP-bound polypeptides were easily removed by pre-washing the DHPs, two polypeptides at 125 and 52 kDa remained tightly bound to the DHPs. The abundance of the two DHP-bound polypeptides mirrored the diminution of 120 and 46 kDa polypeptides in the extracts. The N-terminal protein sequences of the 125 and 52 kDa DHP-bound polypeptides were essentially identical to the sequences obtained from the 120 and 46 kDa polypeptides from the extracts, which confirmed that the DHP-bound polypeptides were derived from these soluble polypeptides. The 125-kDa DHP-bound polypeptide yielded an N-terminal protein sequence that was identical to a laccase-type oxidase previously identified in similar extracts from lignifying Sitka xylem. The N-terminal protein sequence of the 46-kDa polypeptide was homologous with a subset of plant peroxidases. The DHPs had tightly bound peroxidase and oxidase activity, which suggested that these polypeptides were active in their insolubilised state. The mechanism and selectivity of insolubilisation of these enzymes is discussed. © 2001 Elsevier Science Ltd. All rights reserved.

Keywords: *Picea sitchensis*; *Pinus*; Sitka spruce; Xylem; Lignin; coniferyl alcohol; Laccase; Peroxidase; Dehydrogenation polymers

1. Introduction

Insoluble dehydrogenation polymers (DHPs) produced from monolignols by the action of peroxidase and H_2O_2 are, in effect, synthetic lignins (Monties, 1989) and have been used to predict the structure (Freudenberg and Neish, 1968) and model the behaviour (Adler, 1977) of natural lignins.

It has been noted that peroxidases used to catalyse the formation of DHPs in vitro become tightly associated with the DHPs and retain activity (Evans and Himmelsbach, 1991). The nature of this association is not understood. In this paper, I describe the selective insolubilisation of cell-wall-associated glycoproteins from the lignifying xylem of Sitka spruce during the peroxidase-catalysed dehydrogenation of coniferyl alcohol.

2. Results and discussion

As noted in previous studies (McDougall, 1997; Richardson et al., 1997; Deighton and McDougall, 1998), high salt and ConA bound extracts from the lignifying xylem of Sitka spruce had appreciable oxidase and peroxidase activity (Table 1). The ConA bound extract, which was enriched in cell-wall-associated glycoproteins (McDougall, 1997), represented a 5.8-fold and 3.7-fold enrichment in oxidase and peroxidase activity over the

* Fax: +44-1382-562426.
E-mail address: gmcdou@scri.sari.ac.uk

0031-9422/01/$ - see front matter © 2001 Elsevier Science Ltd. All rights reserved.
PII: S0031-9422(01)00027-9

Table 1
Oxidase and peroxidase activities in cell-wall extracts from lignifying xylem of Sitka spruce

	Oxidase		Peroxidase	
Extract	Specific[a]	Total[b]	Specific	Total
High salt	0.43±0.01	0.032±0.001 (13.65)[c]	1004±25	69.3±1.9 (29099)
ConA bound	2.50±0.02	0.133±0.002 (7.96)	3749±59	198.7±3.11 (11920)

[a] nkat mg^{-1} protein.
[b] nkat ml^{-1} extract.
[c] Figures in parentheses represent the total activity applied to the ConA column and recovered. All assays are averages of quadruplicate assays±S.E.

high salt extract with recoveries of 58 and 41%, respectively. The ConA bound extract readily formed insoluble dehydrogenation polymers (DHPs) from coniferyl alcohol when supplied with H_2O_2.

Four polypeptides (of apparent Mrs of 120, 69, 62 and 46 kDa) were consistently diminished in abundance after the formation of DHPs from CA and H_2O_2 (see Fig. 1, compare lanes a and c). The same polypeptides were also diminished by the addition of H_2O_2 alone (Fig. 1, lane b). These polypeptides may have been oxidatively cross-linked in a manner similar to the proline-rich and extensin-like polypeptides secreted from chickpea (Otte and Barz, 2000) and French bean cultures (Wojtaszek et al., 1997). These polypeptides were not diminished unless the H_2O_2 concentration was greater than 35 mM (Fig. 2) which is much higher than the conditions noted in these papers. This suggests that the diminution of these proteins occurred by a different mechanism. However, it is should be noted that the same polypeptides were diminished when DHPs were produced over longer (2–3 days) reaction times with lower H_2O_2 concentrations (results not shown). No insoluble polypeptides could be recovered in pellets from the + H_2O_2 control samples (Fig. 3, lane d), even if insoluble polymers, such as cellulose or pre-formed DHPs, were added as carriers after the reactions were completed.

Although other polypeptides were carried into the DHPs, they were removed by pre-washing in water. Only two polypeptides (of apparent Mrs of 125 and 52 kDa) were consistently recovered from the DHPs by boiling in SDS-sample buffer (Fig. 1, lane d; Fig. 3, lane e) after the stringent pre-washing procedure. The 125 and 52 kDa polypeptides remained bound to the DHPs after successive extractions in 250 mM sodium acetate pH 5.0, 250 mM Tris pH 8.5 and 1 M NaCl. Therefore, it is unlikely that these polypeptides were bound to charged groups, which, in any case, are rare in DHPs (Monties, 1989). As they were not extracted by 1 M NaCl containing 0.5% Triton X-100, it is unlikely that hydrophobic interactions were involved. On this point, it was also noted that the addition of pre-formed DHPs to incubations did not cause the diminution of any polypeptide (Fig. 4, lane d). These observations indicate that the diminished polypeptides did not adsorb to the surfaces of the insoluble polymers.

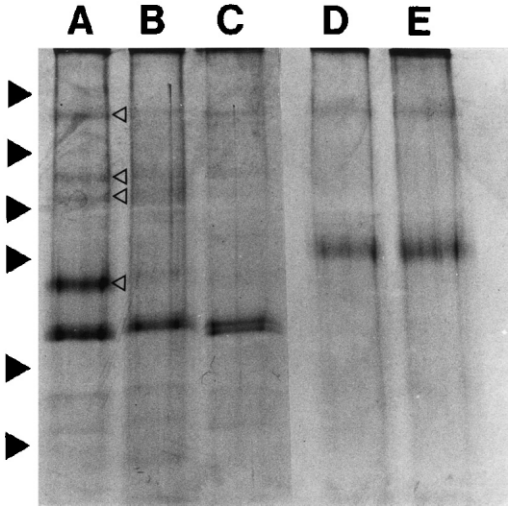

Fig. 1. Insolubilisation of xylem proteins and DHP formation. Lanes a–c contain the equivalent of 2 μg protein (based on the protein content of the original extracts) of the supernatants from the control reaction (a), + H_2O_2 reaction (b) and the + H_2O_2 + CA reaction. Lanes d and e are replicates and represent one-fifth of the DHP-bound sample. Closed triangles denote the migration of the molecular mass marker proteins at 175, 83, 62, 47.5, 32.5 and 25 kDa respectively. Open triangles mark the polypeptide bands discussed in the text.

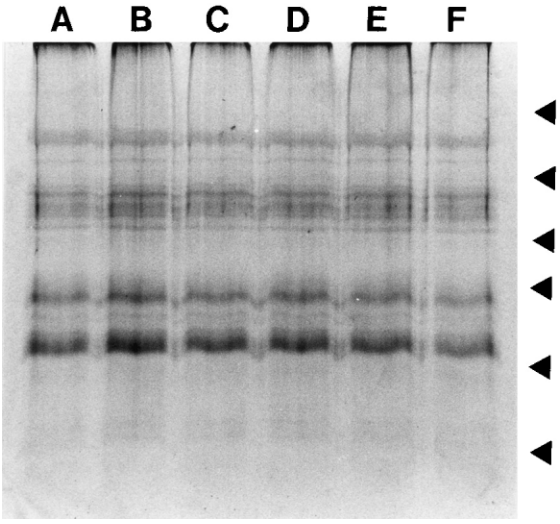

Fig. 2. Effect of H_2O_2 concentration on insolubilisation of xylem proteins. All lanes contain the equivalent of 2 μg protein (based on the protein content of the original extracts) of the supernatants from the various reactions. Lane a = control, lane b = 1 mM H_2O_2, lane c = 5 mM H_2O_2, lane d = 10 mM H_2O_2, lane e = 25 mM H_2O_2 and lane f = 35 mM H_2O_2. Closed triangles denote the migration of the molecular mass marker proteins at 175, 83, 62, 47.5, 32.5 and 25 kDa respectively.

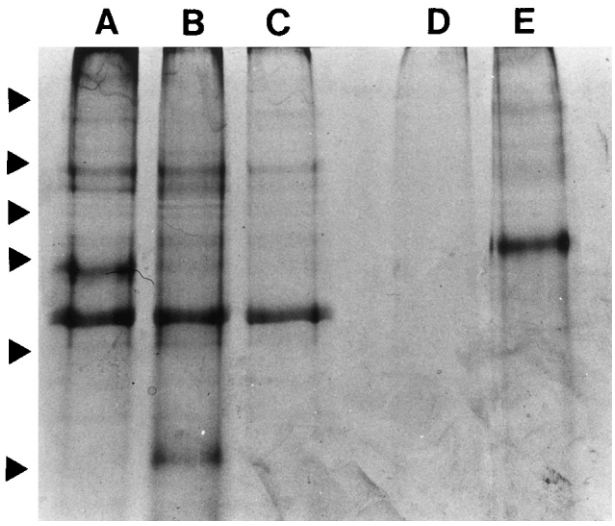

Fig. 3. Insolubilisation of xylem proteins and DHP formation. Lanes a–c contain the equivalent of 2.5 μg protein (based on the protein content of the original extracts) of the supernatants from the control reaction (a), $+H_2O_2$ reaction (b) and the $+H_2O_2+$CA reaction (c). Lane d contains half of the $+H_2O_2$ pellet sample and lane e contains one-fifth of the DHP-bound sample from the $+H_2O_2+$CA reaction. Closed triangles denote the migration of the molecular mass marker proteins at 175, 83, 62, 47.5, 32.5 and 25 kDa respectively.

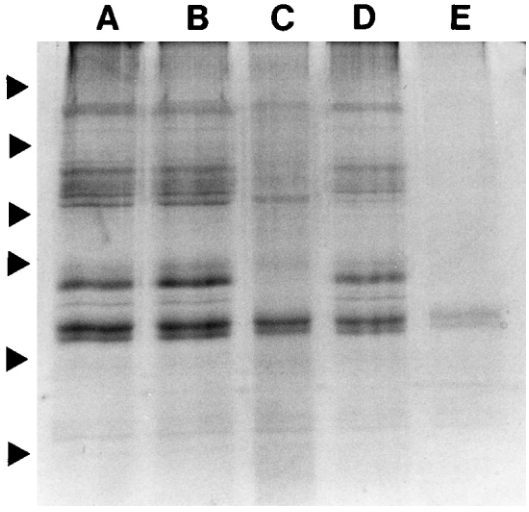

Fig. 4. Insolubilisation of xylem proteins and DHP formation. Lanes a–e contain the equivalent of 2.5 μg protein (based on the protein content of the original extracts) of the supernatants from the control reaction (a), the +CA reaction (b), $+H_2O_2$ reaction (c), the reaction containing pre-formed CA-DHPs (d) and the $+H_2O_2$ +CA reaction (e). Closed triangles denote the migration of the molecular mass marker proteins at 175, 83, 62, 47.5, 32.5 and 25 kDa respectively.

The abundance of the 125 and 52 kDa DHP-bound polypeptides with the DHPs appeared to mirror the diminution of the 120 and 46 kDa bands from the ConA bound extract (see Figs. 1 and 3). The 125 and 52 kDa DHP-bound polypeptides yielded N-terminal protein sequences that were essentially identical to the sequences obtained from the 120 and 46 kDa polypeptides (respectively) from the ConA bound extract (Table 2). This strongly suggests that the DHP-bound polypeptides were derived from these polypeptides. The sequence of the 125/120 kDa polypeptides was identical to a polypeptide previously identified in a study of cell-wall-associated glycoproteins that were more abundant in the developing xylem of compression wood than non-compression wood of Sitka spruce (McDougall, 2000). This sequence was identified as a laccase-type polyphenol oxidase (EC. 1.10.3.3) by its homology with a number of plant laccases (Table 2). The sequence had greatest homology with one of the four laccase genes from the developing xylem of *Liriodendron tulipifera*, Laccase 2–4 (65% identity and 85% similarity) (Lafayette et al., 1999) but it also had considerable homology to an *Arabidopsis* EST for a putative laccase (T9I4.21) and a laccase (Poplar-110) from poplar xylem (Ranocha et al., 1999). In addition, the amino-terminal sequence of the Sitka protein could be aligned exactly with the amino-terminal residues predicted (Nielsen et al., 1997) or observed for these proteins. Moreover, the 125/120-kDa polypeptide had homology (53% identity) with an EST sequence from the developing xylem of Loblolly pine (*Pinus taeda*) which, in turn, had considerable homology to other plant laccase genes over its full sequence (Allona et al., 1998).

The 52/46kDa polypeptide was homologous, particularly in the residues 6 to 15, with the amino-terminal sequences of peroxidases (EC. 1. 11.1.7) from *Arabidopsis*, *Vigna angularis*, *Glycine max*, *Oryza sativa* and an EST clone from *Pinus taeda* (Table 1). This sequence was also similar to a polypeptide of apparent M_r 48 kDa (QDDEPPXXKE) that was more abundant in extracts of cell-wall-associated glycoproteins from the developing xylem of compression wood of Sitka spruce than non-compression wood (McDougall, 2000).

After the multi-step washing procedure, the insoluble DHPs retained oxidase and peroxidase activity at approximately 10 and 3% respectively of the total activities of the extract (results not shown). It was not possible to judge whether the peroxidase or oxidase activities of the supernatants were reduced after the formation of the DHPs. CA (and its oxidation products) remained in the supernatants even after desalting on PD-10 columns (results not shown) and were oxidised in preference to ABTS (Richardson et al., 1997). However, peroxidase activity was readily detected in the supernatant samples after non-denaturing SDS-PAGE and staining with *o*-dianisidine/H_2O_2 (Fig. 5). The predominant peroxidase activity in all samples was centred on 36 kDa (Fig. 5, lanes a–d).

The mechanism of insolubilisation of the laccase and peroxidase enzymes is unclear but it is possible that the enzymes became attached to the DHPs as they catalysed their formation. The insolubilisation of peroxidases that catalyse the formation of DHPs has been reported

Table 2
Comparison of the amino-terminal protein sequences of DHP-bound polypeptides with database sequences[e]

Sequence[a]	1				5					10					15					20	ID[b]	s[c]	N[d]
SITKA 120 kDa	K	H	W	Q	T	T	R	N	Y	K	F	N	V	R	L	K	X	V	T	R			
SITKA 125 kDa	K	H	W	Q	T	T	R	N	Y	K	F	N	V	R	L	K	X	V	T	R	100	100	20
Liriodendron 2–4	K	H	A	G	I	T	R	H	Y	K	F	N	I	R	L	Q	N	V	T	R	65	80	20
A. thaliana (T9I4.21)	A	S	A	G	I	T	R	H	Y	Q	F	D	I	Q	L	K	N	I	T	R	40	70	20
Pinus taeda (1C6D)				K	M	T	R	H	Y	S	F	H	V	R	M	X	N	V	T	R	53	70	17
Populus-110						T	R	Q	Y	T	F	N	I	T	H	K	N	F	T	R	53	73	15
SITKA 46 kDa						X	D	E	P	P	L	V	K	G	L	X	W	X	F	Y			
SITKA 52 kDa						X	D	E	P	P	L	V	K	G	L	S	X	X	F	Y	73	73	15
A. thaliana PRX6			K	K	R	S	R	D	A	P	I	V	K	G	L	S	W	N	F	Y	53	73	15
Glycine max			S	Q	V	E	A	K	P	P	V	V	K	G	L	S	Y	S	F	Y	53	66	15
Vigna angularis						Q	A	R	P	P	T	V	R	G	L	S	Y	T	F	Y	53	66	15
Oryza sativa				V	V	T	T	G	E	P	V	V	A	G	L	S	W	G	F	Y	47	53	15
Pinus taeda (7C5H)	I	R	X	N	V	L	T	L	N	A	D	P	P	L	A	N	G	L	S	W	T	F	Y	60	73	15

[a] Each sequence begins at the predicted or observed N-terminal residue. Codes for ESTs are given in parentheses. Potential N-glycosylation sequons are underlined.

[b] ID denotes identity.

[c] S denotes similarity.

[d] N denotes number of residues compared.

[e] The blank cycle at residue 17 of the 120/5-kDa polypeptide was preceded and followed by good quality cycle peaks and coincides with an asparagine residue in a potential *N*-glycosylation consensus sequon (i.e. N-X-S/T where X can be any amino acid residue except P; see Hubbard and Ivatt, 1981) in all the other sequences. Therefore, this blank cycle was most likely to be due to a glycosylated asparagine residue as the hydrophilic glycosylated-Asn-anilinothiazolinone (ATZ) derivative formed during Edmann degradation is not recovered.

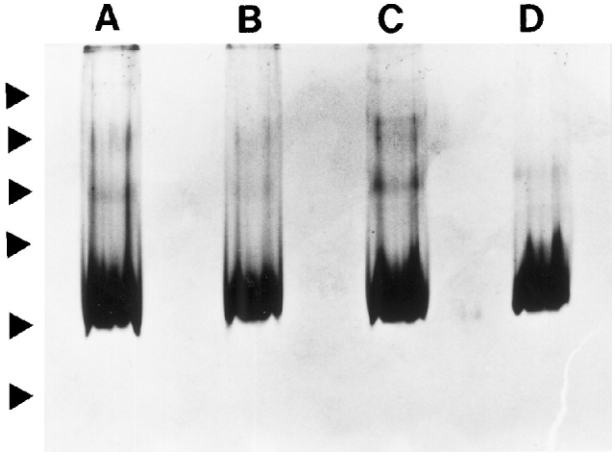

Fig. 5. Peroxidase activities of supernatant samples after separation by ND SDS–PAGE. Equivalent volumes of supernatants were separated by ND SDS–PAGE then stained for peroxidase activity using *o*-dianisidine/H_2O_2. Lane a = control reaction, lane b = + CA reaction, lane c = + H_2O_2 reaction and lane d = + H_2O_2 + CA reaction. Closed triangles denote the migration of the molecular mass marker proteins at 175, 83, 62, 47.5, 32.5 and 25 kDa respectively.

(Evans and Himmelsbach, 1991) and oxidase activity in similar extracts of Sitka xylem can oxidise and polymerise CA to water-insoluble DHPs (Deighton et al., 1999). Considering that the DHP-bound polypeptides have higher apparent M_rs than their putative precursors (125 and 52 kDa versus 120 and 46 kDa), these polypeptides may have been covalently modified during the formation of DHPs, presumably by the addition of CA groups. Testing this hypothesis would require the purification and comparison of the soluble and DHP-bound polypeptides. It has been suggested that peroxidases become covalently attached to lignin, whilst catalysing its polymerisation, through linkages between tyrosine residues and the growing lignin polymer (Evans and Himmelsbach, 1991; McDougall, 1993a). Indeed, there is evidence that tyrosine residues enhance the incorporation of synthetic proteins into DHPs during the peroxidase-catalysed polymerisation of CA (McDougall, 1996). It has also been suggested that the near-invariant tyrosine residue, found close to the N-terminal of plant peroxidases, was particularly well situated to be involved in such a linkage (McDougall, 1993b). However, the N-terminal protein sequences of both the DHP-bound peroxidase and laccase-type oxidase contained tyrosine residues in their expected positions. This suggests that these tyrosine residues were available to the sequencing reactions and were not involved in cross-links.

The selective insolubilisation of the 46 kDa peroxidase into the DHPs is intriguing, as it was a minor component of the peroxidase profile of the supernatants as judged by ND SDS-PAGE (Fig. 5). However, the 46 kDa peroxidase may have a low affinity for the oxidation of *o*-dianisidine but a particular affinity for the oxidation and polymerisation of CA. It may have been predominantly responsible for the formation of the DHPs and, indeed, Zimmerlin et al. (1994) reported that a 46 kDa cationic cell-wall-associated peroxidase from French bean had high specificity for the oxidation of ferulic acid.

On the other hand, the 46 kDa peroxidase and the 120 kDa laccase may have structural motifs that lead to

their insolubilisation. Welinder et al. (1996) aligned the available N-terminal sequences of *Arabidopsis* peroxidases and identified 28 sub-groups. The peroxidases with the greatest homology to the Sitka 46 kDa sequence belong to a sub-group that has a longer N-terminal sequence before the near-invariant FY motif than other peroxidases. A cysteine-rich peptide motif has been identified that mediates the insolubilisation of proteins into cell walls (Domingo et al., 1999) and a novel peroxidase with structural protein-like properties from *Scutellaria* (Morimoto et al., 1999), which rapidly became insolubilised to the cell wall in the presence of H_2O_2, has been discovered. However, the sequences that are most homologous to the 46 kDa Sitka peroxidase and the 120 kDa Sitka laccase do not contain similar structural motifs.

Although the conditions for the formation of the DHPs (70 mM H_2O_2 and 10 mM CA) are unlikely to exist in vivo, the selective insolubilisation of oxidases and peroxidases into DHPs in vitro may have parallels in lignifying tissues. If peroxidases and oxidases became cross-linked to lignin whilst catalysing its deposition, this could explain the accumulation of tightly bound peroxidase (e.g. Fukuda and Komamine, 1982; Abeles and Biles, 1991; McDougall, 1992) and oxidase activities (McDougall et al., 1994; McDougall and Morrison, 1996; Richardson et al., 1997) in the cell walls of lignifying tissues. The attachment of these enzymes to lignin during its formation would immobilise these enzymes and may limit the extent of lignification in the wall (McDougall, 1993a,b).

3. Experimental

3.1. Plant material

Branches of Sitka spruce (*Picea sitchensis* (Bong) Carr.) were obtained from the Forest Research clone bank at Ledmore, Perth and Kinross, Scotland, in late May 1998. In the laboratory, the developing xylem was carefully scraped from the old wood then frozen. The scraped tissue contained only enlarging and differentiating xylem cells, which were confirmed as lignifying cells by acid phloroglucinol staining (Kneebone, 1962).

3.2. Extraction procedure

Tissue was thawed then placed in an excess of ice-cold homogenisation buffer [25 mM MOPS pH 7.0 containing 0.5% v/v polyvinylpolypyrrolidine (PVPP) and 0.5 mM phenylmethylsulphonyl fluoride (PMSF)], homogenised in a Waring blender then in an Ultra-Turrax disintegrator (Deighton and McDougall, 1998). The insoluble residue was re-homogenised in buffer that lacked PVP and PMSF. These filtrates were discarded and the entire procedure was repeated ×3. The insoluble crude cell walls were extracted with 25 mM MOPS pH 7.0 containing 200 mM $CaCl_2$ (ConA buffer) for 1 h on ice with stirring. The high salt extracts were applied to Concanavalin-A (ConA) Sepharose columns (8 ml bed volume) and the eluate discarded. After a five-column volume wash of ConA buffer, the ConA-bound extract, enriched in cell-wall-associated glycoproteins (McDougall, 1997), was eluted with ConA buffer containing 100 mM α-methyl mannoside.

3.3. Assays for protein content and oxidase activity

Protein content was measured by the dye-binding method (Bradford, 1976). Peroxidase activity was determined by measuring the oxidation of 2, 2′-azinobis (3-ethylbenzothiazoline-6-sulphonic acid) (ABTS) at A_{420} (Sterjiades et al., 1992). Oxidase activity was determined by measuring the increase in A_{420} due to the formation of the oxidised chromophore of ABTS in 1 h (Deighton and McDougall, 1998).

3.4. Production of dehydrogenation polymers (DHPs) of coniferyl alcohol

Assays were based on the method of Tsutsumi et al. (1998) and contained the Sitka ConA-bound extract and final concentrations of 10 mM coniferyl alcohol (CA) in 100 mM NaOAc pH 5.0. Reactions were started by the addition of an aliquot of 0.882 M (1/10 stock) H_2O_2 (equivalent to 36 mM) then a further aliquot of H_2O_2 was added after 30 min to a final concentration of 70 mM. After 60 min incubation at 30°C, insoluble DHPs were precipitated by centrifugation (15 000 rpm, 5 min, 8°C) and the supernatants carefully removed. Equivalent aliquots of the supernatants were precipitated using 2.5-fold excess of cold (−20°C) acetone. Control assays that lacked CA, H_2O_2 or the ConA-bound extract were also run. No DHPs were formed in these controls but putative insoluble material was put through the same washing procedures.

The DHPs were resuspended in an excess of washing solution, mixed well then recovered by re-centrifugation. The multi-step washing procedure consisted of successive 3×2 ml washes of H_2O, 250 mM sodium acetate buffer pH 4.0, 250 mM Tris-HCl pH 8.5, 1 M NaCl, 1 M NaCl containing 0.5% Triton X-100 then H_2O. The washed DHPs were resuspended in SDS–PAGE sample buffer, boiled for 5 min then centrifuged prior to analysis by SDS–PAGE. Twenty-fold larger incubations were used to obtain sufficient material for the sequencing experiments.

Insoluble DHPs, formed under the same conditions from horseradish peroxidase (SIGMA product P-8250) and coniferyl alcohol, were dissolved in 1, 4-dioxane then re-precipitated by the addition of excess water. These purified DHPs contained no bound peroxidase or other proteins (apparent by SDS–PAGE and silver staining)

and they were used to judge the effect of added preformed DHPs on the supernatant proteins.

3.5. Sodium dodecyl sulphate polyacrylamide gel electrophoresis (SDS–PAGE)

Extracts were precipitated with acetone and separated on 10% acrylamide gels as described before (Richardson et al., 1997). Gels were stained using the Bio-Rad silver-stain method.

3.6. N-terminal protein sequencing

This procedure has been described before (McDougall, 2000). Sequence similarities were determined by the "BLITZ" method against the non-redundant protein and DNA databases maintained by the European Bioinformatics Institute (at http://www2.ebi.ac.uk/bic_sw). The loblolly pine cDNA sequence analysis project jointly run by the University of Minnesota and North Carolina State University (at http://www.cbc.umn.edu.researchprojects) was also searched. Where required, the positions of N-terminal residues of protein sequences derived from DNA sequences were predicted using the SignalP programme (at http://www.cbs.dtu.dk/services/SignalP). The sequence retrieval system at ExPASy Geneva (at http://www.expasy.ch/srs5) was also used.

Acknowledgements

I thank Julie Duncan for technical help, Dr. Heather Ross for expert guidance on protein sequencing and Professor Howard Davies for his support. I thank Dr. Steve Lee of Forest Research for access to the Sitka spruce clone bank. SCRI receives Grant-in-Aid from the Scottish Executive Rural Affairs Department.

References

Abeles, F.B., Biles, C.L., 1991. Characterisation of peroxidases in lignifying peach fruit endocarp. Plant Physiology 95, 269–273.

Adler, E., 1977. Lignin chemistry — past, present and future. Wood Science and Technology 11, 169–218.

Allona, I., Quinn, M., Shoop, E., Swope, K., St. Cyr, S., Carlis, J., Riedl, J., Retzl, E., Campbell, M.M., Sederoff, R.R., Whetten, R.W., 1998. Analysis of xylem formation in pine by cDNA sequencing. Proceedings of the National Academy of Sciences, USA 95, 9693–9698.

Bradford, M.M., 1976. A rapid and sensitive method for the detection of microgram amounts of protein utilising the principle of dye-binding. Analytical Biochemistry 7, 248–526.

Deighton, N., McDougall, G.J., 1998. Coniferyl alcohol oxidase operates via a free radical intermediate. Phytochemistry 48, 601–606.

Deighton, N., Richardson, A., Stewart, D., McDougall, G.J., 1999. Cell-wall-associated oxidases from the lignifying xylem of angiosperms and gymnosperms: Monolignol oxidation. Holzforschung 53, 503–510.

Domingo, C., Sauri, A., Mansila, E., Conjero, V., Vera, P., 1999. Identification of a novel peptide motif that mediates cross-linking of proteins to cell walls. The Plant Journal 20, 563–570.

Evans, J.J., Himmelsbach, D.S., 1991. Incorporation of peroxidase into synthetic lignin. Journal of Agricultural and Food Chemistry 39, 830–832.

Freudenberg, K., Neish, A.C., 1968. The Constitution and biosynthesis of lignin. Springer-Verlag, Berlin, Germany.

Fukuda, H., Komamine, A., 1982. Lignin synthesis and its related enzymes as markers of tracheary element differentiation in single cells isolated from the mesophyll of *Zinnia elegans*. Planta 155, 423–430.

Hubbard, S.C., Ivatt, R.J., 1981. Synthesis and processing of asparagine-linked oligosaccharides. Annual Review of Biochemistry 50, 555–583.

Kneebone, W., 1962. A rapid staining procedure for lignin. Crop Science 2, 268–271.

Lafayette, P.R., Eriksson, K.-E.L., Dean, J.F.D., 1999. Characterisation and heterologous expression of laccase cDNAs from xylem tissues of yellow-poplar (*Liriodendron tulipifera*). Plant Molecular Biology 40, 23–35.

McDougall, G.J., 1992. Changes in cell-wall-associated peroxidases during the lignification of flax fibres. Phytochemistry 31, 3385–3389.

McDougall, G.J., 1993a. Covalently bound peroxidases and lignification. In: Welinder, K.G., Rasmussen, S.K., Penel, C., Greppin, H. (Eds.), Plant Peroxidases: Biochemistry and Physiology. University of Geneva, Geneva, Switzerland, pp. 277–282.

McDougall, G.J., 1993b. Solubilisation of wall-bound peroxidase by limited proteolysis. Phytochemistry 33, 765–767.

McDougall, G.J., 1996. Tyrosine residues enhance the cross-linking of synthtetic proteins into lignin-like dehydrogenation products. Phytochemistry 41, 43–47.

McDougall, G.J., 1997. Procedure for selection of cell wall-associated glycoproteins. Phytochemistry 45, 633–636.

McDougall, G.J., 2000. A comparison of proteins from the developing xylem of compression and non-compression wood of branches of Sitka spruce (*Picea sitchensis*) reveals a differentially expressed laccase. Journal of Experimental Botany 51, 1395–1401.

McDougall, G.J., Morrison, I.M., 1996. Extraction and partial purification of a cell-wall-associated coniferyl alcohol oxidase from developing xylem of Sitka spruce. Holzforschung 50, 549–553.

McDougall, G.J., Stewart, D., Morrison, I.M., 1994. Cell-wall-bound oxidases from tobacco (*Nicotiana tabacum*) xylem participate in lignin formation. Planta 194, 9–14.

Monties, B., 1989. Lignins. In: Harborne, J.B. (Ed.), Methods in plant biochemistry Vol. 1. Academic Press, London, pp. 113–157.

Morimoto, S., Tateishi, N., Inuyama, M., Taura, F., Tanaka, H., Shoyoma, Y., 1999. Identification and molecular characterisation of novel peroxidase with structural protein-like properties. Journal of Biological Chemistry 274, 26192–26198.

Nielsen, H., Engelbrecht, J., Brunak, S., von Heijne, G., 1997. Identification of prokaryotic and eukaryotic signal peptides and prediction of their cleavage sites. Protein Engineering 10, 1–6.

Otte, O., Barz, W., 2000. Characterisation and oxidative in vitro cross-linking of an extensin-like protein and a proline-rich protein from chick-pea cell walls. Phytochemistry 53, 1–5.

Ranocha, P., McDougall, G.J., Hawkins, S., Sterjiades, R., Borderies, G., Stewart, D., Cabanes-Macheteau, M., Boudet, A.M., Goffner, D., 1999. Biochemical characterization, molecular cloning and expression of laccases — a divergent gene family in poplar. European Journal of Biochemistry 259, 485–495.

Richardson, A., Stewart, D., McDougall, G.J., 1997. Identification and partial characterisation of a coniferyl alcohol oxidase from lignifying xylem of Sitka spruce (*Picea sitchensis*). Planta 203, 35–43.

Sterjiades, R., Dean, J.F.D., Eriksson, K.-E.L., 1992. Laccase from Sycamore maple (*Acer pseudoplatanus*) oxidises monolignols. Plant Physiology 99, 1162–1168.

Tsutsumi, Y., Matsui, M., Sakai, K., 1998. Substrate-specific peroxidases in woody angiosperms and gymnosperms participate in regulating

the dehydrogenative polymerisation of syringyl and guaiacyl type lignins. Holzforschung 52, 275–281.

Welinder, K.G., Jespersen, H.M., Kjaersgard, I.V.H., Ostergard, L., Abelskov, A.K., Hansen, L.N., Rasmussen, S.K., 1996. What can we learn from *Arabidopsis* peroxidases? In: Obinger, C., Burner, U., Ebermann, R., Penel, C., Greppin, H. (Eds.), Plant Peroxidases: Biochemistry and physiology. University of Geneva, Geneva, Switzerland, pp. 173–178.

Wojtaszek, P., Trethowan, J., Bolwell, G.P., 1997. Reconstitution in vitro of the conditions required for the oxidative cross-linking of extracellular proteins in French bean (*Phaselous vulgaris* L.). FEBS Letters 405, 95–98.

Zimmerlin, A., Wojtaszek, P., Bolwell, G.P., 1994. Synthesis of dehydrogenation polymers of ferulic acid with high specificity by a purified cell-wall peroxidase from French bean (*Phaselous vulgaris* L.). Biochemical Journal 299, 747–753.

PERGAMON

Phytochemistry 57 (2001) 165–169

PHYTOCHEMISTRY

www.elsevier.com/locate/phytochem

Biosynthesis of diaporthin and orthosporin by *Aspergillus ochraceus*

Jonathan P. Harris, Peter G. Mantle *

Biochemistry Department, Imperial College of Science, Technology and Medicine, London SW7 2AY, UK

Received 26 July 2000; received in revised form 19 December 2000

Abstract

Diaporthin and orthosporin were characterised from the fungus *Aspergillus ochraceus* D2306. Diaporthin was identified by high-resolution electron impact mass spectrometry and ^{1}H and ^{13}C NMR spectroscopy, from which new spectroscopic assignments were made. Orthosporin was also identified by mass spectrometry and both fungal metabolites are reported for the first time as co-metabolites and also as products of *A. ochraceus*. The methylation inhibitor ethionine affected production of both diaporthin and orthosporin in spite of no obvious methylation step in the biosynthesis of orthosporin, implying that extracellular orthosporin may arise by de-*O*-methylation of diaporthin. The biosynthetic origin of diaporthin was demonstrated by incorporation of [1-^{14}C]acetate and [methyl-^{14}C]methionine administered in early idiophase. © 2001 Elsevier Science Ltd. All rights reserved.

Keywords: Aspergillus ochraceus; Polyketides; Biosynthesis; Diaporthin; Orthosporin

1. Introduction

Diaporthin (Fig. 1, **1**) was first described by Bazzigher (1953), who showed that it could reproduce symptoms of the canker of Chestnut trees caused by *Endothia parasitica* (Murr.) And. Epidemics of this disease had almost destroyed Chestnut forests in North America. Diaporthin from *E. parasitica* was further characterised and was shown to inhibit the growth of several bacteria and yeasts (Boller et al., 1957). Diaporthin structure was further explored by Hardegger et al. (1966) by ^{1}H NMR spectroscopy of diaporthinic acid (both as a product of anaerobic hydrolysis of diaporthin and of chemical synthesis) and diaporthinic acid derivatives.

Independently, orthosporin (de-*O*-methyldiaporthin; Fig. 1, **2**) was isolated from the plant pathogenic fungus *Drechslera siccans*, which causes irregular brown spots on leaves of oats, and of both perennial and Italian ryegrass (Hallock et al., 1988); limited physico-chemical data was obtained. Orthosporin caused necrosis when applied in solution to leaves of maize, crabgrass, soya bean, barnyard grass and spiny amaranth, but not to leaves of perennial ryegrass. Ichihara et al. (1989) isolated orthosporin from cultures of *Rhynchosporium orthosporum*, which causes leaf scald on orchard grass and, by treatment with diazomethane, obtained diaporthin and extended assignment of its NMR spectroscopic data.

No biosynthetic studies have previously been performed on diaporthin and it has only been reported as a metabolite of plant pathogens. The present study arose from finding several polyketide metabolites other than the important mycotoxin ochratoxin A (Fig. 2, **3**) in fermentations of the saprophytic fungus *Aspergillus ochraceus* (Harris, 1996). This study was, therefore, in the context of competing demands on acetate by pathways of secondary metabolism.

2. Results and discussion

In submerged fermentation, the production of diaporthin closely followed biomass accumulation by *A. ochraceus* D2306 (Fig. 3), both reaching a maximum value at approximately 100 h. Thereafter, the concentration of diaporthin declined, possibly by metabolic recycling analogous to that for the pentaketide citrinin (Barber et al., 1988). In the fermentation broth, orthosporin was a minor component, typically about half of the concentration of diaporthin; data are not shown since the purity of the HPLC peak could not always be assured in samples taken later in the fermentation.

* Corresponding author. Tel.: +44-207-594-5245; fax: +44-207-225-0960.

E-mail address: p.mantle@ic.ac.uk (P.G. Mantle).

0031-9422/01/$ - see front matter © 2001 Elsevier Science Ltd. All rights reserved.
PII: S0031-9422(01)00004-8

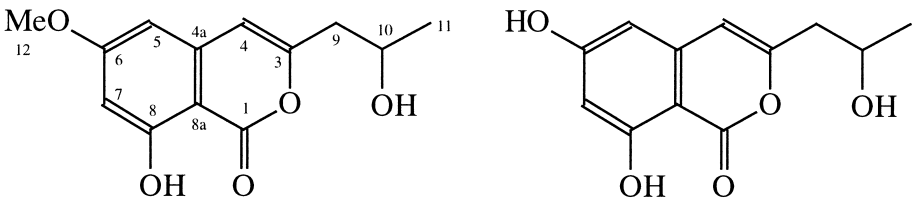

1 **2**

Fig. 1. Structures of diaporthin (**1**) and orthosporin (**2**).

The first biosynthetic experiment explored a range of precursor feeding times for [1-^{14}C]acetate and [methyl-^{14}C] methionine (Table 1) during the early stage of diaporthin accumulation and the consequent specific radioactivities of the diaporthin isolated at 168 h. Although measured during a phase of diaporthin decline, the highest specific activity from acetate was evident from feeding during mid-accumulation of diaporthin when most of the cellular replication had occurred. Measured radioactivity above background was in the range 120–730 dpm. This was more clearly evident concerning demonstration of

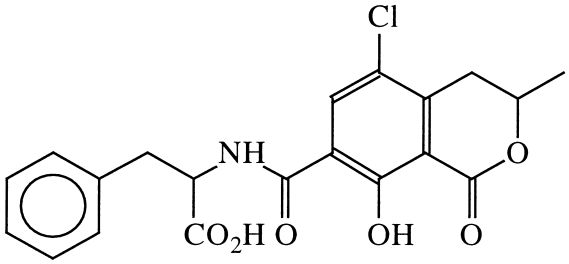

3

Fig. 2. Structure of ochratoxin A (**3**).

Table 1
The amount (μg) and specific radioactivity (dpm/μg) of [^{14}C]diaporthin recovered from *A. ochraceus* D2306 potato dextrose broth fermentations fed either [1-^{14}C]acetate (3.7 or 5 μCi) or [methyl-^{14}C]-methionine (2 μCi) at specified times

Experiment	Time (h)	Diaporthin amount (μg)	Specific radioactivity (dpm/μg)
1st [1-^{14}C]acetate feed	32	4	37
	50	9	60
	72	10	73
2nd [1-^{14}C]acetate feed	8	155	3
	22.5	63	35
	32	113	70
	50	52	93
[Methyl-^{14}C]methionine feed	32	6	20
	72	4	152

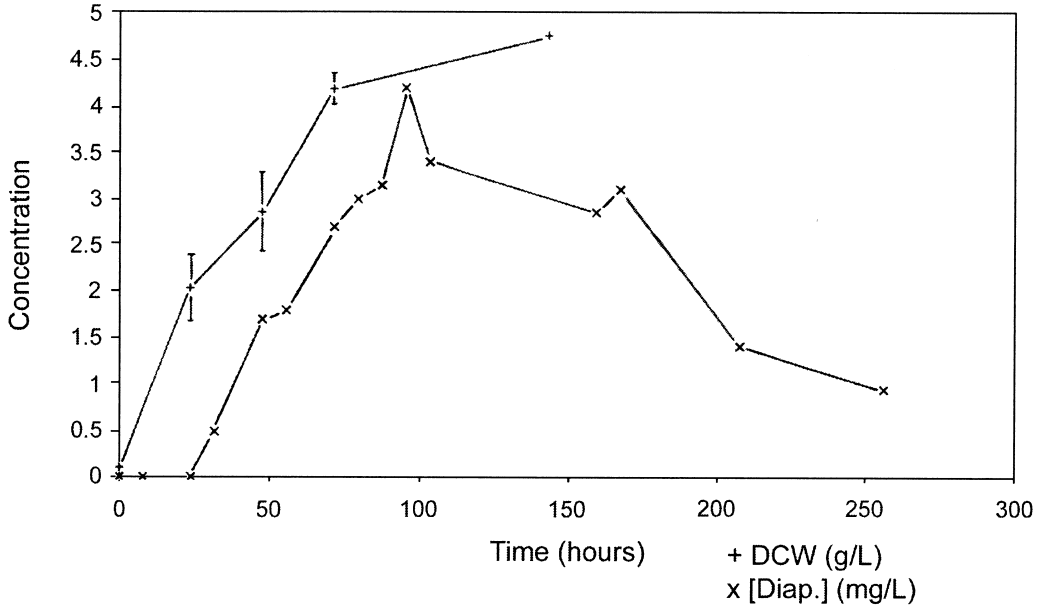

Fig. 3. Dry cell weight (DCW) and diaporthin concentration (Diap.) versus time for an *A. ochraceus* potato dextrose broth fermentation.

O-methylation of orthosporin (classified as a hexaketide by Turner, 1971) from [methyl-^{14}C]methionine, consistent with this probably being the last step in the biosynthesis of diaporthin.

A second experiment, using rather more radiolabelled acetate given over a wider range of early stages of fermentation and assessed with greater confidence (numerical values 465–7910 dpm) in the diaporthin isolated at 80 h, more clearly focused on the 50 h stage in giving the strongest evidence of acetate origin. This was in the context of the competing demands of primary and secondary metabolism on acetate.

Autoradiography of the TLC resolution of the diaporthin from these experiments showed a single radioactive area in each case, and combined eluates from these areas gave a typical mass spectrum for diaporthin.

Table 2
The concentration of orthosporin and diaporthin 80 h post inoculation in *A. ochraceus* D2306 potato dextrose broth fermentations fed with 50 mg ethionine at specified times

Addition time (h)	Orthosporin (mg/l)	Diaporthin (mg/l)
32	0.3	0.5
50	0.9	1.4
56	0.9	1.8
72	1.4	2.9
Control	1.2	2.3

The methylation inhibitor ethionine had a marked effect on the yield of both diaporthin and orthosporin measured at 80 h, especially when added to fermentations at early stages in the accumulation of diaporthin (Table 2). In the assumption that diaporthin arises intracellularly by methylation of orthosporin, the influence of ethionine on the concentration of orthosporin in the fermentation broth might only occur if extracellular orthosporin arises through demethylation of diaporthin, analogous to the demethylation steps in the biosynthesis of opiate alkaloids (Mann, 1987).

Notably, neither orthosporin nor diaporthin were detected in similar fermentations of the five other *A. ochraceus* isolates tested.

New MS fragmentation data for diaporthin (Scheme 1) formed the basis for interpretation also of analogous HREIMS data for orthosporin to refine the schematic predictions of Hallock et al. (1988). The fully assigned ^{1}H NMR data for diaporthin was assisted by DEPT experiments, 500 MHz resolution of the signals for C9 protons, ^{1}H/^{1}H decoupling experiments and evidence that the aromatic protons at C5 and C7 are meta coupled. MS data for orthosporin conformed closely to that of Hallock et al. (1988).

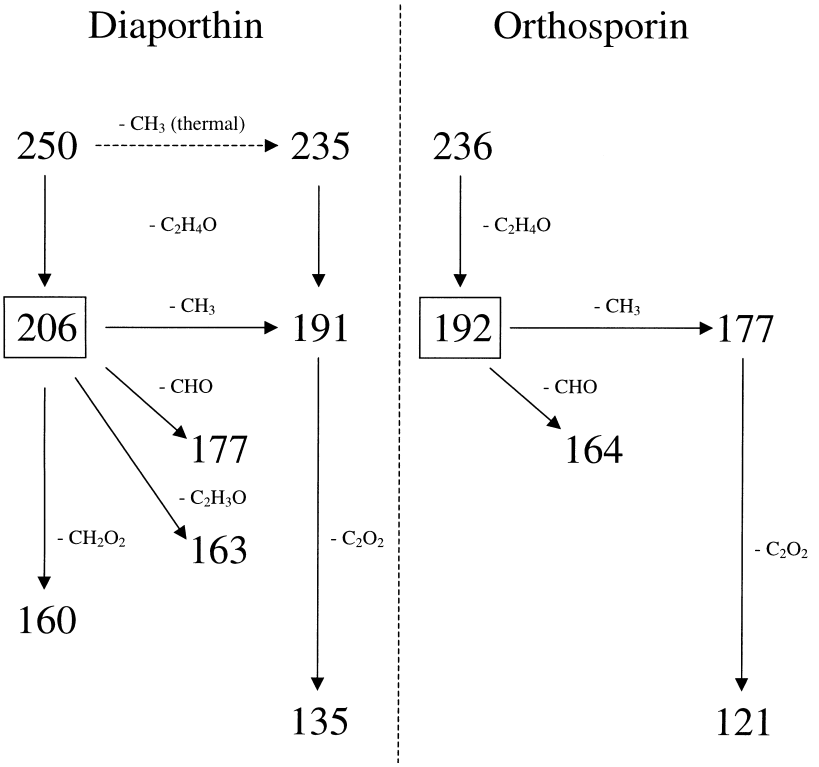

Scheme 1. Interpretation of MS fragmentation of diaporthin according to linked scan (B/E) experiments and HREIMS data. Analogous fragmentations for orthosporin are matched according to HREIMS data.

3. Experimental

3.1. Aspergillus ochraceus isolates

The main study used an Australian isolate D2306 (Connole et al., 1981), also used in biochemical and toxicological studies (Tapia and Seawright, 1984; Mantle and Chow, 2000; Stander et al., 2000; Stoev et al., 2000) on account of its high ability to produce ochratoxin A. Occurrence of diaporthin was also tested in the classic ochratoxin-producing isolate NRRL 3174 (=ATCC 22947 as used by Madhyastha et al. (1990). Also three isolates from USA red and white beans marketed for food in the UK and which did not produce ochratoxin A were tested, as was one from Bulgarian wheat which produced only a trace of ochratoxin A (Mantle and McHugh, 1993).

3.2. Fungal culture

Isolates were grown to sporulate profusely on 20 g shredded wheat moistened with water (8 ml) in 500 ml Erlenmeyer flasks at 28 C for 3 weeks. The material was homogenised (Sorvall Omni-Mixer) in water to give spore inoculum for potato dextrose broth (Difco, 100 ml in 500 ml flasks, $2–4\times10^6$ spores ml^{-1}). Flasks were incubated at 28°C on a rotary shaker (200 rpm and 10 cm eccentric throw).

3.3. Measurement of fermentation dynamics

3.3.1. Biomass

At intervals 10 ml samples were taken from triplicate flasks for dry cell weight analysis. The broth was filtered through a pre-weighed sintered 10 ml syringe which was then freeze-dried to constant weight.

3.3.2. Diaporthin and orthosporin

The amounts of diaporthin and orthosporin were measured by extracting (as below) the broth of whole flasks at intervals. Solvent extract residues were dissolved in a standard volume of MeOH and 20 μl analysed by HPLC. The system used an isocratic mobile phase (H_2O: HOAc: acetonitrile, 59.5: 1: 39.5, v:v:v) at 1 ml min^{-1} through a Separon SGX C-18 column (150×5 mm, Kolona Chromatografika, Czechoslovakia) into a Hewlett Packard 1040 M diode array detector (monitoring wavelength 239 nm, Rt 3.5 min for diaporthin and 1.8 min for orthosporin) controlled by ChemStation software on an IBM 486 PC, calibrated for diaporthin quantification.

3.4. Isolation and characterisation of diaporthin and orthosporin

Twenty flasks of potato dextrose broth, incubated with *A. ochraceus* D2306 for 5 days, were filtered through sintered glass, the pH value adjusted to 3 (conc. HCl) and extracted with an equal volume of EtOAc. The organic phase was partitioned against 3% $NaHCO_3$ to remove acidic metabolites such as the ochratoxins, evaporated to dryness and the residue of neutral metabolites dissolved in MeOH for preparative HPLC. The first of two systems used an isocratic mobile phase of H_2O: HOAc: acetonitrile (59.5:1:39.5, v:v:v) at 5.6 ml min^{-1} through a Dynamax Macro C-18 column (30×2.5 cm) with UV absorbance detection at 239 nm (Pye Unicam PU4020). Fractions of enriched diaporthin (Rt 23 min) were concentrated and re-injected into the second system which differed only in the mobile phase (MeOH: H_2O, 70:30, v:v, Rt 15 mm). HREIMS of the isolated diaporthin (Micromass autospec Q, source temp. 210–220°C, electron energy 70 eV) was made, and linked scans (B/E) were performed on the four most abundant ions (m/z 250, 235, 206 and 191) using He as the collision gas in the first field-free region. NMR spectra of diaporthin in acetone-d_6 were obtained on a Bruker 500 MHz instrument.

A further 20 flask cultures incubated for 3 days were extracted for orthosporin, which was isolated for EIMS analysis by the protocol for diaporthin (Rt for orthosporin 14 and 13 min in the first and second HPLC systems, respectively).

The other *A. ochraceus* isolates described above were cultured similarly to determine whether they produced diaporthin and/or orthosporin.

3.5. Biosynthetic experiments

3.5.1. Experiment 1

[1-^{14}C] Sodium acetate (3.7 μCi) was added to a flask culture at 32, 50 or 72 h post-inoculation, whilst [methyl-^{14}C]methionine (2 μCi) was added to another flask at 32 or 72 h post-inoculation. Cultures were incubated until 168 h post-inoculation and then extracted.

3.5.2. Experiment 2

[1-^{14}C] Sodium acetate (5 μCi) was added to a flask at 8, 22.5, 32, or 50 h post-inoculation. Cultures were incubated until 80 h post-inoculation and then extracted.

A portion (10–25%) of each culture extract was analysed by HPLC, quantifying the diaporthin (peak purity indicated from diode array data) and collecting the corresponding eluate for scintillation counting. Ecolume scintillant (8 ml, ICN Biomedicals, California, USA) was mixed with the eluate, refrigerated overnight and counted three times for 1 min in an Intertechnique SL 30 liquid scintillation counter, when reproducible values were obtained. Specific radioactivities of the [^{14}C]diaporthin were calculated. Confirmation that radioactivity resided specifically in diaporthin was obtained by autoradiography (Fuji RX film for 4 weeks at −70°C) of 2-dimensional chromatograms (Polygram SW G/UV254

plates, 10×10 cm) developed first in xylene: MeOH: HOAc (90:5:5, v:v:v, R_f 0.33) and then in toluene: EtOAc: HCO_2H (5:4:1, v:v:v, R_f 0.64). Silica corresponding to the radiolabelled diaporthin was eluted with propan-2-ol and the eluate analysed by EIMS.

3.6. Methylation inhibition with ethionine

The methylation inhibitor ethionine (10 ml of a 5 mg ml^{-1} sterile solution) was added to a flask culture at 32, 50, 56 or 72 h post-inoculation. Sterile H_2O was added similarly to a control culture. Cultures were incubated until 80 h, when the broth was extracted and diaporthin and orthosporin quantified.

3.7. Diaporthin

^1H NMR (500 MHz, acetone-d_6): δ; 1.23 (3H, *d*, $J=6.3$ Hz, H-11), 2.57 (H, *dd*, $J=14.3$, 7.8 Hz, H_A-9), 2.62 (H, *dd*, $J=14.3$, 4.9 Hz, H_B-9), 3.90 (H, *s*, H-12), 4.16 (H, *m*, H-10), 6.45 (H, *d*, $J=2.3$ Hz, H-5), 6.48 (H, *s*, H-4), 6.53 (H, *d*, $J=2.4$ Hz, H-7). ^{13}C NMR (125.8 MHz, acetone-d_6): δ; 23.6 (C-11), 43.9 (C-9), 56.2 (C-12), 65.5 (C-10), 100.6 (C-8a), 100.9 (C-7), 101.9 (C-5), 106.5 (C-4), 140.8 (C-4a), 156.7 (C-3), 164.2 (C-8), 167.1 (C-6), 167.9 (C-1).

HREIMS *m/z* (rel. int.): 250.0868 (26), $C_{13}H_{14}O_5$, calc. 250.0841; 235.0621 (3), $C_{12}H_{11}O_5$, calc. 235.0606; 206.0640 (100), $C_{11}H_{10}O_4$, calc. 206.0579; 191.0352 (4), $C_{10}H_7O_4$, calc. 191.0344; 177.0543 (7), $C_{10}H_9O_3$, calc. 177.0552; 163.0401 (5), $C_9H_7O_3$, calc. 163.0395; 160.0534 (10), $C_{10}H_8O_2$, calc. 160.0524; 135.0442 (6), $C_8H_7O_2$, calc. 135.0446.

Acknowledgements

The authors wish to thank R.N. Sheppard and J. Barton, Chemistry Department, Imperial College for obtaining NMR spectroscopy and mass spectrometry data. J.P.H. acknowledges a Research Studentship from the BBSRC (UK).

References

Barber, J., Chapman, A.C., Howard, T.D., Tebb, G., 1988. Recycling of polyketides by fungi: the degradation of citrinin by *Penicillium citrinum*. Applied Microbiology and Biotechnology 29, 387–391.

Bazzigher, G., 1953. Beitrag zur Kenntnis der *Endothia parasitica* (Murr.) And. dem Erreger des Kastaniensterbens. Phytopathologische Zeitschrift 21, 105–132.

Boller, A., Gaumann, E., Hardegger, E., Kugler, F., Naef-Roth, St., Rosner, M., 1957. Diaporthin, ein Welketoxin aus Kulturen von *Endothia parasitica* (Murr.) And. Helvetica Chimica Acta 40, 875–880.

Connole, M.D., Blaney, B.J., McEwan, T., 1981. Mycotoxins in animal feeds and toxic fungi in Queensland 1971–80. Australian Veterinary Journal 57, 314–318.

Hallock, Y.F., Clardy, J., Kenfield, D.S., Strobel, G., 1988. De-*O*-methyldiaporthin, a phytotoxin from *Drechslera siccans*. Phytochemistry 27, 3123–3125.

Hardegger, E., Rieder, W., Walser, A., Kugler, F., 1966. Konstitution des Diaporthins und Synthese der Diaporthinsäure. Helvetica Chimica Acta 49, 1283–1290.

Harris, J.P., 1996. The biosynthesis of ochratoxin A and other structurally related polyketides by *Aspergillus ochraceus*. PhD thesis, University of London.

Ichihara, A., Hashimoto, M., Hirai, T., Takeda, I., Sasamura, Y., Sakamura, S., Sato, R., Tajimi, A., 1989. Structure, synthesis, and stereochemistry of (+)-orthosporin, a phytotoxic metabolite of *Rhynchosporium orthosporum*. Chemistry Letters, 1495–1498.

Madhyastha, S.M., Marquardt, R.R., Fröhlich, A.A., Platford, G., Abramson, D., 1990. Effects of different cereal and oilseed substrates on the growth and production of toxins by *Aspergillus alutaceus* and *Penicillium verrucosum*. Journal of Agricultural and Food Chemistry 38, 1506–1510.

Mann, J., 1987. Secondary metabolites. Oxford University Press, Oxford.

Mantle, P.G., McHugh, K.M., 1993. Nephrotoxic fungi in foods from nephropathy households in Bulgaria. Mycological Research 97, 205–212.

Mantle, P.G., Chow, A.M., 2000. Ochratoxin formation in *Aspergillus ochraceus* with particular reference to spoilage of coffee. International Journal of Food Microbiology 56, 105–109.

Stander, M.A., Steyn, P.S., Lubben, A., Miljkovic, A., Mantle, P.G., Marais, G., 2000. Influence of halogen salts on the production of the ochratoxins by Aspergillus ochraceus Wilh. Journal of Agricultural and Food Chemistry 48, 1865–1871.

Stoev, S.D., Goundasheva, D., Mirtcheva, T., Mantle, P.G., 2000. Susceptibility to bacterial infections in growing pigs as an early response in ochratoxicosis. Experimental and Toxicologic Pathology 52, 287–296.

Tapia, M.O., Seawright, A.A., 1984. Experimental ochratoxicosis A in pigs. Australian Veterinary Journal 61, 219–222.

Turner, W.B., 1971. Fungal metabolites. Academic Press, London.

PERGAMON

Phytochemistry 57 (2001) 171–178

PHYTOCHEMISTRY

www.elsevier.com/locate/phytochem

Accumulation of 6-deoxocathasterone and 6-deoxocastasterone in *Arabidopsis*, pea and tomato is suggestive of common rate-limiting steps in brassinosteroid biosynthesis

Takahito Nomura [a], Tatsuro Sato [b], Gerard J. Bishop [c], Yuji Kamiya [d], Suguru Takatsuto [e], Takao Yokota [a,*]

[a] *Department of Biosciences, Teikyo University, Utsunomiya 320-8551, Japan*
[b] *Center for Research on Wild Plants, Utsunomiya University, Utsunomiya 321-8505, Japan*
[c] *Institute of Biological Sciences, University of Wales Aberystwyth, Aberystwyth SY23 3DD, UK*
[d] *The Institute of Physical and Chemical Research (RIKEN), Wako-shi, Saitama 351-0198, Japan*
[e] *Department of Chemistry, Joetsu University of Education, Joetsu-shi, Niigata 943-8512, Japan*

Received 31 July 2000; received in revised form 16 October 2000

Abstract

To gain a better understanding of brassinosteroid biosynthesis, the levels of brassinosteroids and sterols related to brassinolide biosynthesis in *Arabidopsis*, pea, and tomato plants were quantified by gas chromatography-selected ion monitoring. In these plants, the late C-6 oxidation pathway was found to be the predominant pathway in the synthesis of castasterone. Furthermore, all these plant species had similar BR profiles, suggesting the presence of common biosynthetic control mechanisms. The especially high levels of 6-deoxocathasterone and 6-deoxocastasterone may indicate that their respective conversions to 6-deoxoteasterone and castasterone are regulated in planta and hence are important rate-limiting steps in brassinosteroid biosynthesis. Other possible rate-limiting reactions, including the conversion of campestanol to 6-deoxocathasteonre, are also discussed. Tomato differs from *Arabidopsis* and pea in that tomato contains 28-norcastasterone as a biologically active brassinosteroid, and that its putative precursors, cholesterol and its relatives are the major sterols. © 2001 Elsevier Science Ltd. All rights reserved.

Keywords: *Arabidopsis thaliana*; Cruciferae; *Pisum sativum*; Leguminosae; Garden pea; *Lycopersicon esculentum*; Solanaccae; Tomato; Brassinosteroid; Biosynthesis

1. Introduction

Brassinosteroids (BRs) are steroidal hormones that regulate plant growth. Brassinolide is the most bioactive of all the naturally occurring BRs and is derived from castasterone, which, in turn, is synthesized via either the early C-6 oxidation or late C-6 oxidation pathways, as shown in Fig. 1 (Choi et al., 1997; Fujioka and Sakurai, 1997; Sakurai, 1999; Fujioka et al., 2000). Mutants defective in either BR biosynthesis or sensitivity were isolated from *Arabidopsis thaliana* L., garden pea (*Pisum sativum* L.) and tomato (*Lycopersicon esculentum* M.). These mutants have a characteristic dwarf phenotype (for reviews, see Yokota, 1997; Clouse and Feldmann, 1999) and have provided proof that BRs play a hormonal role in the growth and development of plants.

It is essential that the concentration of plant hormones is regulated to sustain normal plant growth. To maintain this hormone homeostasis there needs to be a balance of biosynthesis and metabolism or inactivation (Yokota, 1999). The aim of this work was to examine how BR biosynthesis is controlled in planta. To this end all BRs and sterols related to brassinolide biosynthesis in *Arabidopsis*, pea, and tomato were quantified by GC–SIM and the data obtained are discussed in the context of defining the possible control points on an assumption that the levels of intermediates should be elevated prior to the control biosynthetic steps. Furthermore, it is demonstrated that tomato shoots are rich in cholesterol and related 28-norsterols, which are the likely precursors

* Corresponding author. Tel.: +81-28-6277209; fax: 81-28-6277187.
E-mail address: yokota@nasu.bio.teikyo-u.ac.jp (T. Yokota).

0031-9422/01/$ - see front matter © 2001 Elsevier Science Ltd. All rights reserved.
PII: S0031-9422(00)00440-4

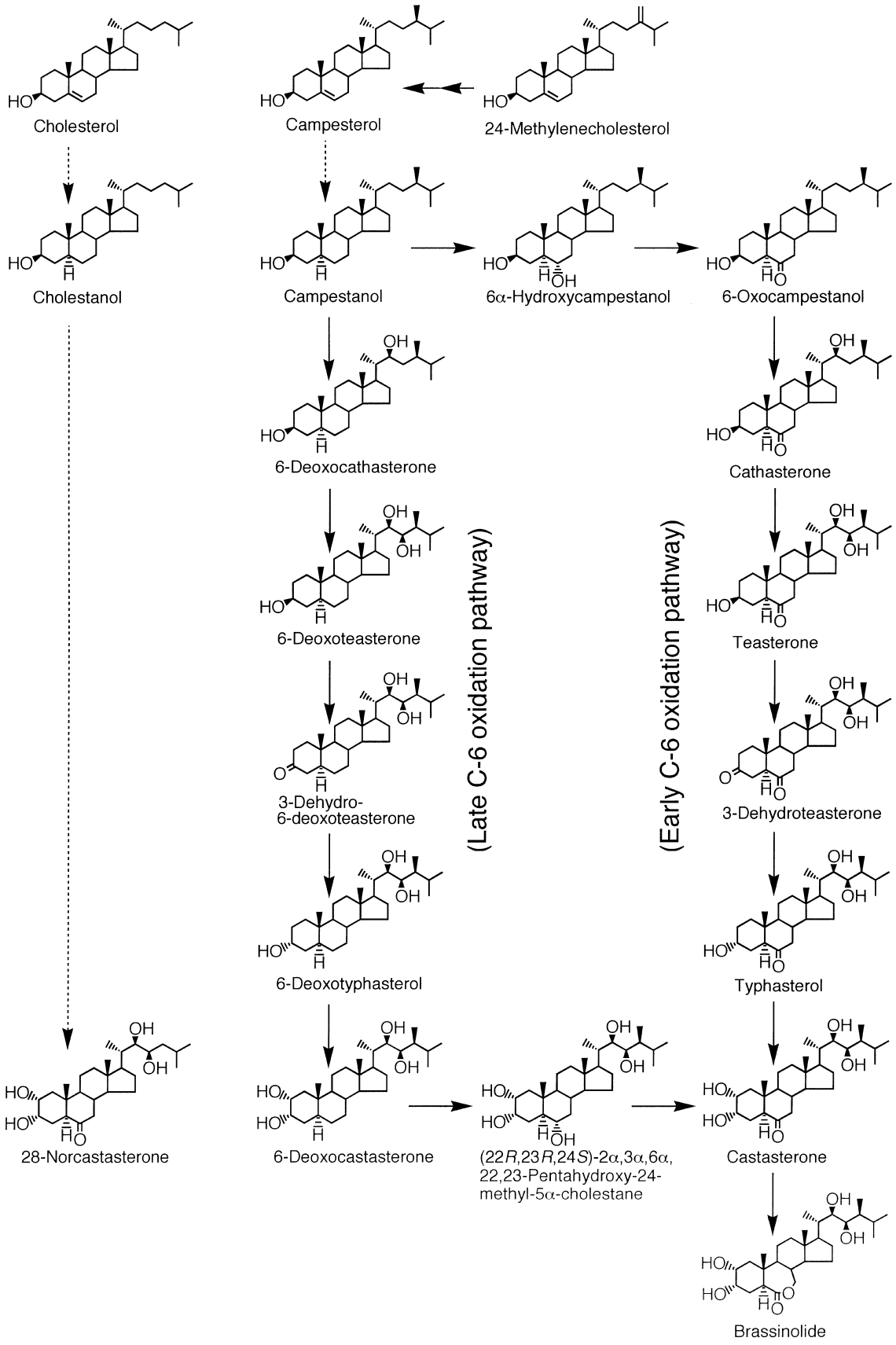

Fig. 1. Biosynthetic pathways of brassinosteroids. Broken arrows indicate multiple steps. The pathway from cholesterol to 28-norcastasterone via cholestanol is hypothetical.

of 28-norcastasterone that has been identified as a bioactive BR by Yokota et al. (1997).

2. Results and discussion

In order to quantify all the biosynthetic precursors of brassinolide, it is necessary to know their precise chromatographic properties when using procedures such as charcoal chromatography, Sephadex LH-20 chromatography, silica gel chromatography, reversed-phase HPLC, and gas chromatography. We found that charcoal and Sephadex LH-20 can separate various BRs as a group (see Section 4). Elution profiles of BRs on silica gel column chromatography are shown in Table 1 and use of ethanol-free chloroform was found appropriate, as elution profiles were altered when commercial chloroform was used. Table 1 also summarizes the elution profiles of BRs in reversed-phase HPLC using water-acetonitrile gradients. Table 2 shows the retention times of BRs in GC, as well as mass spectrometric data obtained by GC–SIM. The levels of BRs in *Arabidopsis* seedlings, pea and tomato shoots are shown in Table 3. The quantitative data of campestanol and unsaponifiable bulk sterols in *Arabidopsis*, pea and tomato are shown in Table 4. The relevant GC–MS data are listed in Table 5.

Table 1
Elution profiles of BRs in silica gel chromatography and reversed phase HPLC

BR	Silica gel chromatography		Reversed phase HPLC[c]
	MeOH% in commercial $CHCl_3$[a]	MeOH% in EtOH-free $CHCl_3$[b]	Fraction no.
6-Oxocampestanol	–	1	–
6-Deoxocathasterone	–	1	50/51
3-Dehydro-6-deoxoteasterone	0	1	45
6-Deoxoteasterone	0	1	43[d]/44
6α-Hydroxycampestanol	–	3	–
Cathasterone	–	3	40[d]/41
3-Dehydroteasterone	0/0.5	3	36[d]/37
6-Deoxotyphasterol	0.5	3	47
Teasterone	1/2.5	5	31[d]/32
Typhasterol	1/2.5	5	36[d]/37
6-Deoxocastasterone	2.5	5	39[d]/40
Castasterone	2.5/5	5	21[d]/22
Brassinolide	5	7	15
6α-Hydroxy-6-deoxocastasterone	–	10	19
28-Norcastasterone	–	–	14

[a] Samples were subjected to silica gel column chromatography (0.5 g) using 0, 0.5, 1, 2.5, 5, 7, and 10% of MeOH in $CHCl_3$ (20 ml each). –, not examined.
[b] Samples were subjected to silica gel column chromatography (0.5 g) using 0, 0.5, 1, 3, 5, 7, and 10% of MeOH in $CHCl_3$ (20 ml each).
[c] For HPLC conditions, see Section 4.
[d] Major fraction.

Table 2
GC-SIM[a] data of BRs obtained from *Arabidopsis*, pea, and tomato

BR	Derivative	R_t (min)	Characteristic ions m/z (relative intensity, %)
Cathasterone	TMSi	12.08	561 (M^+-15, 6), 462 (100), 187 (61)
Teasterone	MB-TMSi	12.62	544 (M^+, 51), 529 (100), 515 (92)
3-Dehydroteasterone	MB	11.92	470 (M^+, 49), 316 (20), 155 (100)
Typhasterol	MB-TMSi	11.23	544 (M^+, 100), 529 (46), 515 (92)
6-Deoxocathasterone	TMSi	9.52	547 (M^+-15, 2), 297 (4), 187 (100)
6-Deoxoteasterone	MB-TMSi	9.85	530 (M^+, 100), 515 (48), 440 (41)
3-Dehydro-6-deoxoteasterone	MB	9.67	456 (M^+, 97), 231 (100), 155 (38)
6-Deoxotyphasterol	MB-TMSi	9.00	530 (M^+, 74), 515 (12), 440 (100)
6-Deoxocastasterone	BMB	9.92	498 (M^+, 77), 273 (100), 155 (26)
Castasterone	BMB	12.12	512 (M^+, 81), 358 (37), 155 (100)
28-Norcastasterone	BMB	11.08	498 (M^+, 100), 287 (38), 141 (45)
Brassinolide	BMB	13.58	528 (M^+, 11), 374 (47), 155 (100)

[a] For GC–MS conditions, see Section 4. BMB, bismethaneboronate. MB, monomethaneboronate.

The present work revealed that a higher concentration of the late C-6 oxidation pathway metabolites exist in all plants (Table 3). In contrast to the high levels of 6-deoxocathasterone in these tissues, no trace of cathasterone, a key intermediate in the early C-6 oxidation pathway could be detected. Some of the early C-6 oxidation pathway metabolites were detected at quite low levels in *Arabidopsis* and pea, but no trace was found in tomato. Thus, the late C-6 oxidation pathway is most likely the major biosynthetic route to castasterone in *Arabidopsis* and pea, while it is an exclusive route in tomato. Many higher plants including shoots of *Castanea crenata* (Arima et al., 1984), cultured cells of *Catharanthus roseus* (Choi et al., 1996) and pollen of *Cupressus arizonica* (Griffiths et al., 1995) contain 6-deoxoBRs at higher levels than 6-oxoBRs (for review, see Fujioka, 1999). Recently, Koka et al. (2000) revealed that 6-deoxoBRs are far more active than 6-oxoBRs in restoring the growth of the BR-deficient tomato mutant *dumpy*. Thus, it may be assumed that the late C-6 oxidation pathway is more prevalent and more important than the early C-6 oxidation pathway in many plants. Furthermore, the profiles of the late C-6 oxidation pathway metabolites were quite similar in *Arabidopsis*, pea and tomato (Table 3), suggesting the presence of common biosynthetic control mechanisms in each species. Tissues of the three species examined were all of different ages, suggesting that such biosynthetic control mechanisms is not transient but persistent through a considerably long growth period.

In these plant tissues, the most abundant BR is 6-deoxocastasterone (Table 3). The level of 6-deoxocastasterone is at least one order of magnitude higher than that of its metabolite castasterone, suggesting the conversion of 6-deoxocastasterone to castasterone is an important rate-limiting step. This reaction is catalyzed by the DWARF enzyme (Bishop et al., 1999). Thus, it is likely that the level or activity of DWARF protein is

Table 3
Endogenous BR levels in *Arabidopsis*, pea, and tomato

BR	BR level (ng kg-1 fr. wt)		
	26-day-old *Arabidopsis* plants	19-day-old pea shoots	60-day-old tomato shoots[a]
Cathasterone	ND	ND	ND
Teasterone	25	ND	ND
3-Dehydroteasterone	ND	ND	ND
Typhasterol	54	23	ND
6-Deoxocathasterone	1960	3750	1060
6-Deoxoteasterone	100	47	44
3-Dehydro-6-deoxoteasterone	127	74	31
6-Deoxotyphasterol	884	800	466
6-Deoxocastasterone	3390	5180	5250
Castasterone	406	362	217
28-Norcastasterone	–	–	234
Brassinolide	40	28	ND

[a] Taken from Bishop et al. (1999). ND, not detected. –, not analyzed.

Table 4
Endogenous sterol levels in *Arabidopsis*, pea, and tomato

Sterol	Concentration (μg g^{-1} fr. wt)[a]		
	20-day-old *Arabidopsis* shoots	11-day-old pea shoots	60-day-old tomato shoots
24-Methylenecholesterol	6.0 (2)	ND	ND
Campesterol/24-epicampesterol	46.7 (12)	24.4 (14)	2.8 (4)
Campestanol/24-epicampestanol	0.9 (0.2)	1.9 (1)	0.1 (0.1)
Isofucosterol	44.6 (20)	9.2 (5)	11.4 (16)
Sitosterol	232.0 (62)	58.1 (33)	11.9 (16)
Sitostanol	4.7 (1)	3.7 (2)	ND
Stigmasterol	3.6 (1)	75.7 (43)	2.9 (4)
Lophenol	–	–	6.8 (9)
Lathosterol	–	–	6.1 (8)
Cholesterol	18.1 (5)	2.2 (1)	14.7 (20)
Cholestanol	–	–	0.3 (0.4)
Unknown 1	–	–	5.9 (8)
Unknown 2	–	–	10.3 (14)

[a] Figures in parentheses denote relative amounts (total sterol = 100). ND, not detected. –, not analyzed because of scarcity.

Table 5
GC–MS data of sterols obtained from *Arabidopsis*, pea, and tomato

Sterol[a]	R_t (min)[b]	Characteristic ions m/z (relative intensity, %)
24-Methylenecholesterol	8.75	470 (M^+,74), 455 (35), 386 (100), 380 (90), 341 (71), 296 (63), 129 (88)
Campesterol/24-epicampesterol	8.80	472 (M^+,73), 457 (39), 382 (100), 367 (40), 343 (94), 129 (82)
Campestanol/24-epicampestanol	8.92	474 (M^+,100), 459 (73), 384 (50), 369 (39), 306 (16), 305 (19), 215 (85)
Isofucosterol	9.78	484 (M^+,22), 469 (11), 394 (21), 386 (100), 296 (66), 281 (21), 129 (27)
Sitosterol	9.63	486 (M^+,45), 471 (12), 396 (100), 381 (39), 357 (71), 129 (49)
Sitostanol	9.73	488 (M^+,100), 473 (73), 398 (35), 383 (39), 306 (27), 305 (30), 215 (74)
Stigmasterol	9.03	484 (M^+,85), 469 (14), 394 (100), 379 (21), 351 (39), 255 (57), 129 (45)
Lophenol[c]	9.18	472 (M^+,100), 457 (20), 382 (29), 367 (24), 269 (48), 227 (19)
Lathosterol	8.43	458 (M^+,100), 443 (24), 368 (24), 353 (27), 255 (63), 229 (22)
Cholesterol	7.93	458 (M^+,54), 443 (14), 368 (100), 353 (43), 329 (83), 129 (50)
Cholestanol	8.03	460 (M^+,100), 445 (71), 370 (54), 355 (44), 306 (42), 305 (35), 215 (81)
Unknown 1	8.72	486 (M^+,35), 471 (86), 429 (7), 396 (6), 381 (100), 355 (6)
Unknown 2	9.10	484 (M^+,74), 469 (79), 394 (13), 379 (100), 297 (6), 227 (15)

[a] Sterols analyzed after trimethylsilylation.
[b] For GC–MS conditions, see Section 4.
[c] Identified based on the spectral data of Goad and Akihisa (1997).

strictly regulated. Over-expressing the tomato *Dwarf* gene reduces the level of 6-deoxocastasterone 50-fold suggesting that the *Dwarf* gene is transcriptionally regulated (Bishop et al., 1999). However, in mutants which have a defect in the perception or signaling of BRs, the level of castasterone is dramatically increased, as seen in the pea mutant *lka* (Nomura et al., 1997, 1999), the *Arabidopsis* mutant *bri1-4* (Noguchi et al., 1999a) and the tomato mutant *curl-3* (T. Yokota, T. Nomura and G.J. Bishop, unpublished results, 1999). Thus, suppression of the DWARF protein activity or level in normal plants may be ascribed to feedback control by a repressor that is regulated through perception or signaling of BRs. Similar mechanisms have been proposed for the biosynthesis of the plant hormone gibberellin A1 by analyzing gibberellin insensitive mutants of *Zea mays, Arabidopsis* and wheat which accumulate gibberellins (Hedden and Kamiya, 1997).

The second most abundant BR after 6-deoxocastasterone was 6-deoxocathasterone in all the plant tissues examined. The levels of its product, 6-deoxoteasterone is two to three orders of magnitude lower. Thus, C-23 hydroxylation of 6-deoxocathasterone to 6-deoxoteasterone appears also to be a rate-limiting step. In *Arabidopsis*, C-23 hydroxylation in both the late and early C-6 oxidation pathways may be catalyzed by a CPD protein named CYP 90A (Szekeres et al., 1996, Altmann, 1998; Clouse and Feldmann, 1999). Recently the tomato *DUMPY* gene was demonstrated to be likely involved in C-23 hydroxylation (Koka et al., 2000). The transcription of the *CPD* gene has been found to be suppressed by active BRs through a feedback mechanism (Mathur et al., 1998). This indicates that the synthesis of 6-deoxoteasterone is also an important control point in BR biosynthesis.

It was postulated that C-22 hydroxylation of 6-oxocampestanol to cathasterone serves as the rate-limiting reaction in Madagascar periwinkle (*Catharanthus roseus*) cells because the level of the latter is extremely low as compared with the former (Fujioka et al., 1995). Such a proposition was also applied to *Arabidopsis* in which the C-22 hydroxylation is catalyzed by DWF4 protein designated CYP90B (Choe et al., 1998). Our data showed that the levels of 6-deoxocathasterone are ca. one to five hundredths as compared with its precursor campestanol in *Arabidopsis* and pea and one hundredth in tomato (Tables 3 and 4). This indicates that C-22 hydroxylation may also be a reaction that controls the BR biosynthesis in the late C-6 oxidation pathway. No molecular evidence to confirm this proposition, however, has yet been obtained.

The synthesis of campestanol from campesterol comprises four reactions in which 5α-reduction is included (Fujioka et al., 1997; Noguchi et al., 1999b). All of the three intermediates seem to have a short lifetime because their abundance is generally quite low in plants (Takatsuto et al., 1999). Irrespectively, the ratios of campestanol relative to campesterol were found to be small, namely 1:52 in *Arabidopsis*, 1:13 in pea and 1:20 in tomato, suggesting that this pathway may also be the control point of BR synthesis. However, this seems not to be always the case, because the level of campestanol is often comparable to that of campesterol in higher plant tissue such as *M. periwinkle* cells (Fujioka et al., 1995) and wheat seeds (Takatsuto et al., 1999).

Although campesterol is a precursor of C_{28} BRs, it is not a major sterol in *Arabidopsis*, pea and tomato compared to many other plants (Yokota, 1999). Conversely, major sterols like sitosterol are usually not preferred precursors of BRs (Yokota, 1997, 1999; Takatsuto et al., 1999). However, tomato is unique in that 28-norcastasterone, a C_{27} BR, is a major biologically active BR (Table 3) and, in accord with this, the sum of cholesterol and related C_{27} precursors account for about 60% of the total sterol amount (Table 4). Such C_{27} precursors

detected include lathosterol (5α-cholest-7-en-3β-ol) and, tentatively, lophenol (4α-methyl-5α-cholest-7-en-3β-ol) together with two unknown sterols 1 and 2, the mass spectra of which are reminiscent of those being early precursors of cholesterol (Table 5). It should be noted that these sterols were undetectable by total ion current monitoring in *Arabidopsis* and pea. 28-Norcastasterone may be synthesized from cholestanol derived from cholesterol similarly to the biosynthesis of castasterone from campestanol (Fujioka and Sakurai, 1997; Sakurai, 1999). Although cholestanol was identified from tomato in this study (Table 4), other putative downstream intermediates have not yet been analyzed. Synthesis of authentic BRs to assist in the identification of the intermediates is now in progress.

3. Concluding remarks

The relative levels of BR intermediates provide some indication as to likely control points in the biosynthesis of BRs. Especially three reactions in the late C-6 oxidation pathway, from campestanol to 6-deoxocathasterone, from 6-deoxocathasterone to 6-teasterone and from 6-deoxocastasterone to castasterone seem to be universally controlled at least in dicotyledonous plant species. It is also intriguing to investigate on why there appear to be multiple rate-limiting steps in the BR biosynthesis pathway. To this end, metabolic studies will be required using radioactive labeled intermediates. In addition the cloned biosynthetic genes will enable the transcriptional regulation of the biosynthetic pathway to be studied and provide further information as to the potential control points.

4. Experimental

4.1. Plant materials

The following plant tissues were used for BR analysis: (1) whole plants ($n = 271{,}191$ g fr. wt) of 26-day-old *Arabidopsis* (cv. Landsberg) grown in a growth room at 23°C under continuous light; (2) shoots ($n = 204$, 427 g fr. wt) of 19-day-old pea (cv. Torsdag) grown in a greenhouse at 20°C under natural photoperiod; and (3) apical shoots ($n = 35$, 192 g fr. wt) of 60-day-old tomato (cv. Ailsa Craig) grown in cabinets as described by Bishop et al. (1999). For sterol analysis, 20-day-old *Arabidopsis* plants, 11-day-old pea shoots, and 60-day-old tomato apical shoots were harvested.

4.2. Bioassay

To monitor the biological activity of BRs, sample aliquots were assayed by the rice lamina inclination test (Yokota et al., 1996).

4.3. Extraction and purification of BRs

The MeOH extract of the harvested materials was spiked with $^2H_6$-labelled BRs as internal standards before reduction to an aq. residue. The aq. residue was partitioned between EtOAc and 0.5 M K_2HPO_4. The EtOAc phase was evaporated to dryness and partitioned between hexane and 80% MeOH. The 80% MeOH phase was evaporated to dryness and the residual solid was purified on a silica gel column (Wakogel C-300; Wako Pure Chemicals, Osaka, Japan) eluted with $CHCl_3$ containing 0, 8, and 10% MeOH in the case of *Arabidopsis*, with $CHCl_3$ containing 0, 1, 7, and 10% MeOH in the case of pea, and with $CHCl_3$ containing 0, 10, and 20% MeOH in the case of tomato. Immediately before use, $CHCl_3$ was washed with H_2O to remove EtOH used as a stabilizer, washed with saturated NaCl, dried over anhydrous Na_2SO_4 and distilled. Based on the biological activity of the eluates and the elution profiles of authentic BRs (Table 1), the 8% MeOH fraction of *Arabidopsis*, and the combined 1 and 7% MeOH fractions of pea were applied to a charcoal column (chromatography grade; Wako Pure Chemicals) which was eluted with MeOH–H_2O (6:4 and 8:2, v/v), MeOH, MeOH–$CHCl_3$ (9:1, 7:3, 5:5, 3:7, and 1:9, v/v) and $CHCl_3$. The MeOH–$CHCl_3$ (9:1–3:7) fractions from charcoal column chromatography of *Arabidopsis* and pea, and the 10% MeOH fraction of silica column chromatography of tomato were then applied to a Sephadex LH-20 column (bed volume, 500 ml; Pharmacia) using MeOH–$CHCl_3$ (4:1) as a mobile phase. Successive 10-ml fractions were collected. Fractions 36–40 were combined, dissolved in MeOH and passed through columns of diethylaminopropyl silica (Bondesil; Varian, Palo Alto, CA) and octadecyl silica (ODS-SS-1020-T; Senshu Science, Tokyo, Japan). Reversed-phase HPLC was carried out on a Senshu Pak ODS-3251-D column (250×8 mm i.d.; Senshu Science) eluted with the following acetonitrile-H_2O gradient at a flow rate of 2.5 ml min^{-1}: 0–20 min, 45% acetonitrile; 20–40 min, 45–100% acetonitrile; 40–60 min, 100% acetonitrile. Fractions were collected every min. The column oven temp. was maintained at 40°C. Based on bioassay and the HPLC R_ts of authentic BRs (Table 1), BR fractions were collected for analysis by GC–MS/SIM.

4.4. Extraction and purification of sterols

Plant materials were extracted with MeOH–$CHCl_3$ (4:1), evaporated to dryness and partitioned between EtOAc and 0.5 M K_2HPO_4. A portion equivalent to 100 mg fr. wt of the EtOAc-soluble phase was spiked with [$^2H_6$]campestanol as an internal standard, evaporated to dryness and saponified with 1 N KOH in MeOH at 90°C for 1.5 h. The hydrolysate was diluted with H_2O and extracted with hexane. The hexane phase

was washed with H_2O, evaporated to dryness, dissolved in $CHCl_3$ and passed through a short silica gel column. The eluate was subjected to GC–MS/SIM analysis.

4.5. GC–MS/SIM analysis of BRs

BRs except cathasterone and 6-deoxocathasterone were converted to monomethaneboronate (MB) or bismethaneboronate (BMB) by heating at 70°C for 30 min with pyridine that contains 2 mg ml^{-1} methaneboronic acid. Typhasterol, teasterone, 6-deoxotyphasterol, and 6-deoxoteasterone were further treated with *N*-methyl-*N*-trimethylsilyl-trifluoroacetamide (MSTFA) at room temp. for 5 min to give MB-TMSi derivatives. Cathasterone and 6-deoxocathasterone were converted to TMSi derivatives with MSTFA-pyridine (1:4) at 70°C for 30 min. GC-EI MS/SIM (70 eV) was carried out on a JMS AX 505W instrument (JEOL, Tokyo, Japan) fitted with a DB-1 column (0.25 mm i.d.×15 m; 0.25-μm film thickness; J & W Scientific, Folsom, CA). The carrier gas was He at a flow rate of 1 ml min^{-1}, the injection port temp. was 280°C, and samples were introduced by splitless injection. The column oven temp. was programmed at 170°C for 1.5 min, before being elevated to 280°C at 37°C min^{-1}, and then to 300°C at 1.5°C min^{-1}. Identification of BRs was verified when the relative intensities of the M^+ ion and two daughter ions for each molecule were consistent with those of the corresponding deuterated internal standards (Table 2). The contents of BRs were calculated from the peak area ratios of $^2H_6$ and $^2H_0$ M^+ ions or $^2H_6$ and $^2H_0$ fragment ions. No internal standard was available for 28-norcastasterone, so that its level was determined from a calibration curve constructed from the peak area ratios of the M^+ ions of 28-norcastasterone and [$^2H_6$]brassinolide BMB derivatives.

4.6. GC–MS/SIM analysis of sterols

Sterol samples were trimethylsilylated with MSTFA at room temperature for 5 min, and then subjected to GC–MS/SIM using the same conditions used for BR analysis except that the column was a HP-5 Trace Analysis (0.2 mm i.d.×12 m; 0.33-μm film thickness; Hewlett Packard, Palo Alto, CA). Identification of sterols was conducted by comparing their full-scan mass spectra with those of authentic specimens (Table 5). In case of lophenol, the mass spectral data published by Goad and Akihisa (1997) were used as reference. The levels of sterols were determined by GC–SIM using calibration curves constructed from the ratios of the M^+ peak areas of [$^2H_6$]campestanol–TMSi to those of authentic respective sterols. The levels of lophenol, lathosterol, unknown sterol 1, and unknown sterol 2 were calculated from their total ion current trace areas, relative to that of [$^2H_6$]campestanol–TMSi.

Acknowledgements

This work was supported by a Grand-in-Aid for Scientific Research (11460057) to T.Y. from the Ministry of Education, Science, Sports and Culture of Japan. T.N. is a Research Fellow of the Japan Society for the Promotion of Science for Young Scientists since 1998. We thank Takashi Shinozaki and Kazuyuki Hoshino for technical assistance. T.Y., G.J.B. and T.N. would also like to acknowledge the support of the British Council and the Royal Society.

References

Altmann, T., 1998. Recent advances in brassinosteroid molecular genetics. Curr. Opin. Plant Biol. 1, 378–383.

Arima, M., Yokota, T., Takahashi, N., 1984. Identification and quantification of brassinolide-related steroids in the insect gall and healthy tissues of the chestnut plant. Phytochemistry 23, 1587–1591.

Bishop, G.J., Nomura, T., Yokota, T., Harrison, K., Noguchi, T., Fujioka, S., Takatsuto, S., Jones, J.D.G., Kamiya, Y., 1999. The tomato DWARF enzyme catalyses C-6 oxidation in brassinosteroid biosynthesis. Proc. Natl Acad. Sci. USA 96, 1761–1766.

Choe, S., Dilkes, B.P., Fujioka, S., Takatsuto, S., Sakurai, A., Feldmann, K.A., 1998. The *DWF4* gene of *Arabidopsis* encodes a cytochrome P450 that mediates multiple 22a-hydroxylation steps in brassinosteroid biosynthesis. Plant Cell 10, 231–243.

Choi, Y.-H., Fujioka, S., Harada, A., Yokota, T., Takatsuto, S., Sakurai, A., 1996. A brassinolide biosynthetic pathway via 6-deoxocastasterone. Phytochemistry 43, 593–596.

Choi, Y.-H., Fujioka, S., Nomura, T., Harada, A., Yokota, T., Takatsuto, S., Sakurai, A., 1997. An alternative brassinolide biosynthetic pathway via late C-6 oxidation. Phytochemistry 44, 609–613.

Clouse, S.D., Feldmann, K.A., 1999. Molecular genetics of brassinosteroid action. In: Sakurai, A., Yokota, T., Clouse, S.D. (Eds.), Brassinosteroids, Steroidal Plant Hormones. Springer Verlag, Tokyo, pp. 163–190.

Fujioka, S., 1999. Natural occurrence of brassinosteroids in the plant kingdom. In: Sakurai, A., Yokota, T., Clouse, S.D. (Eds.), Brassinosteroids, Steroidal Plant Hormones. Springer Verlag, Tokyo, pp. 21–45.

Fujioka, S., Sakurai, A., 1997. Biosynthesis and metabolism of brassinosteroids. Physiol. Plant 100, 710–715.

Fujioka, S., Inoue, T., Takatsuto, S., Yanagisawa, T., Yokota, T., Sakurai, A., 1995. Identification of a new brassinosteroid, cathasterone, in cultured cells of *Catharanthus roseus* as a biosynthetic precursor of teasterone. Biosci. Biotech. Biochem. 59, 1543–1547.

Fujioka, S., Li, J., Choi, Y.-H., Seto, H., Takatsuto, S., Noguchi, T., Watanabe, T., Kuriyama, H., Yokota, T., Chory, J., Sakurai, A., 1997. The Arabidopsis *deetiolated 2* mutant is blocked early in brassinosteroid biosynthesis. Plant Cell 9, 1951–1962.

Fujioka, S., Noguchi, T., Watanabe, T., Takatsuto, S., Yoshida, S., 2000. Biosynthesis of brassinosteroids in cultured cells of *Catharanthus roseus*. Phytochemistry 53, 549–553.

Goad, L.J., Akihisa, T. 1997. Analysis of Sterols. Blackie, London.

Griffiths, P.G., Sasse, J.M., Yokota, T., Cameron, D.W., 1995. 6-Deoxotyphasterol and 3-dehydro-6-deoxocastasterone, possible precursors to brassinosteroids in the pollen of *Cupressus arizonica*. Biosci. Biotech. Biochem. 59, 956–959.

Hedden, P., Kamiya, Y., 1997. Gibberellin biosynthesis, enzymes, genes and their regulation. Annu. Rev. Plant Physiol. Plant Molec. Biol. 48, 431–460.

Koka, C.V., Cerny, R.E., Gardner, R.G., Noguchi, T., Fujioka, S., Takatsuto, S., Yoshida, S., Clouse, S.D., 2000. A putative role for

the tomato genes *DUMPY* and *CURL-3* in brassinosteroid biosynthesis and response. Plant Physiol. 122, 85–98.

Mathur, J., Molnár, G., Fujioka, S., Takatsuto, S., Sakurai, A., Yokota, T., Adam, G., Voigt, B., Nagy, F., Maas, C., Schell, J., Koncz, C., Szekeres, M., 1998. Transcription of the *Arabidopsis* CPD gene, encoding a steroidogenic cytochrome P450, is negatively controlled by brassinosteroids. Plant J. 14, 593–602.

Noguchi, T., Fujioka, S., Choe, S., Takatsuto, S., Yoshida, S., Yuan, H., Feldmann, K.A., Tax, F.E., 1999a. Brassinosteroid-insensitive dwarf mutants of *Arabidopsis* accumulate brassinosteroids. Plant Physiol. 121, 743–752.

Noguchi, T., Fujioka, S., Takatsuto, S., Sakurai, A., Yoshida, Li, J., Chory, J., 1999b. *Arabidopsis det2* is defective in the conversion of (24*R*)-24-methylcholest-4-en-3-one to (24*R*)-24-methyl-5α-cholestan-3-one in brassinosteroid biosynthesis. Plant Physiol. 120, 833–839.

Nomura, T., Nakayama, M., Reid, J.B., Takeuchi, Y., Yokota, T., 1997. Blockage of brassinosteroid biosynthesis and sensitivity causes dwarfism in garden pea. Plant Physiol. 113, 31–37.

Nomura, T., Kitasaka, Y., Takatsuto, S., Reid, J.B., Fukami, M., Yokota, T., 1999. Brassinosteroid/sterol synthesis and plant growth as affected by *lka* and *lkb* mutations of pea. Plant Physiol. 119, 1517–1526.

Sakurai, A., 1999. Biosynthesis. In: Sakurai, A., Yokota, T., Clouse, S.D. (Eds.), Brassinosteroids, Steroidal Plant Hormones. Springer Verlag, Tokyo, pp. 91–111.

Szekeres, M., Németh, K., Koncz-Kálmán, Z., Mathur, J., Kauschmann, A., Altmann, T., Rédei, G.P., Nagy, F., Schell, J., Koncz, C., 1996. Brassinosteroids rescue the deficiency of CYP90, a cytochrome P450, controlling cell elongation and de-etiolation in *Arabidopsis*. Cell 85, 171–182.

Takatsuto, S., Kosuga, N., Abe, B., Noguchi, T., Fujioka, S., Yokota, T., 1999. Occurrence of potential brassinosteroid precursor steroids in seed of wheat and foxtail millet. J. Plant Res. 112, 27–33.

Yokota, T., 1997. The structure, biosynthesis and function of brassinosteroids. Trends Plant Sci. 2, 137–143.

Yokota, T., 1999. Brassinosteroids. In: Hooykaas, P.J.J., Hall, M.A., Libbenga, K.R. (Eds.), Biochemistry and Molecular Biology of Plant Hormones. Elsevier, Amsterdam, pp. 277–293.

Yokota, T., Matsuoka, T., Koarai, T., Nakayama, M., 1996. 2-Deoxybrassinolide, a brassinosteroid from *Pisum sativum* seed. Phytochemistry 42, 509–511.

Yokota, T., Nomura, T., Nakayama, M., 1997. Identification of brassinosteroids that appear to be derived from campesterol and cholesterol in tomato shoots. Plant Cell Physiol. 38, 1291–1294.

PERGAMON

Phytochemistry 57 (2001) 179–187

PHYTOCHEMISTRY

www.elsevier.com/locate/phytochem

Metabolism of indole-3-acetic acid by orange (*Citrus sinensis*) flavedo tissue during fruit development

Jesús Chamarro [a,*], Anders Östin [b,1], Göran Sandberg [b]

[a] *Instituto de Biología Molecular y Celular de Plantas, UPV-CSIC, Avda. de los Naranjos, s/n, 46022, Valencia, Spain*
[b] *Department of Forest Genetics and Plant Physiology, The Swedish University of Agricultural Sciences, S901 83, Umeå, Sweden*

Received 1 August 2000; received in revised form 8 January 2001

Abstract

[5-^{3}H, 1′-^{14}C, $^{13}C_6$, ^{12}C] Indole-3-acetic acid (IAA), was applied to the flavedo (epicarp) of intact orange fruits at different stages of development. After incubation in the dark, at 25°C, the tissue was extracted with MeOH and the partially purified extracts were analyzed by reversed phase HPLC-RC. Six major metabolite peaks were detected and subsequently analyzed by combined HPLC-frit-FAB–MS. The metabolite peak 6 contained oxindole-3-acetic acid (OxIAA), indole-3-acetyl-*N*-aspartic acid (IAAsp) and also indole-3-acetyl-*N*-glutamic acid (IAGlu). The nature of metabolite 5 remains unknown. Metabolites 3 and 4 were diastereomers of oxindole-3-acetyl-*N*-aspartic acid (OxIAAsp). Metabolite 2 was identified as dioxindole-3-acetic acid and metabolite 1 as a DiOxIAA linked in position three to a hexose, which is suggested to be 3-(-*O*-β-glucosyl) dioxindole-3-acetic acid (DiOxIAGlc). Identification work as well as feeding experiments with the [5-^{3}H]IAA labeled metabolites suggest that IAA is metabolized in flavedo tissue mainly through two pathways, namely IAA–OxIAA–DiOxIAA–DiOxIAGlc and IAA–IAAsp–OxIAAsp. The flavedo of citrus fruit has a high capacity for IAA catabolism until the beginning of fruit senescence, with the major route having DiOxIAGlc as end product. This capacity is operative even at high IAA concentrations and is accelerated by pretreatment with the synthetic auxins 2,4-D, NAA and the gibberellin GA_3. © 2001 Elsevier Science Ltd. All rights reserved.

Keywords: *Citrus sinensis*; Aurantoideae; cv. Washington Navel; Orange fruit; Flavedo; Indole-3-acetic acid metabolism; High performance liquid chromatography; Gas chromatography–mass spectrometry

1. Introduction

The flavedo of citrus fruit (epicarp) is the outer colored part of the fruit ca 1 mm thick. In addition to the pigments that provide the characteristic color to the fruit, this tissue is rich in essential oils and constitutes the first barrier of defense against pathogens. Plant growth regulators (PGRs) have an important influence on the flavedo during fruit development, and the effect of endogenous and applied PGRs have attracted considerable attention of basic and applied research (Baldwin, 1993).

Several experimental evidences suggest that auxins are ripening inhibitors, which have to be inactivated for the advancement of the maturation process (Frenkel, 1975; Given et al., 1988; Cohen, 1996). The concentration of IAA, the most important natural auxin in plants, is very low in *Citrus unshiu* during growth, except 2–3 weeks after full bloom (Takahashi et al., 1975) and exogenous IAA application has not been reported to have major effects on citrus peel coloration (Goldshmidt, 1988). By contrast, application of synthetic auxins such as 2,4-D, 2,4,5-T and NAA, which are not as easily metabolized as IAA by plant tissues, delay aging and the loss of green color, reduce external decay and improve keeping quality in citrus fruit (Dezakos, 1983). Consequently, caution should be exercised when analyzing these observations. In fact, it has been demonstrated that most of the IAA applied to tomato pericarp is inactivated in less than 10 h (Catalá et al., 1992), which could not be enough time to cause the expected responses. In this line of evidence, the effect of exogenous IAA application has been controversial; for example, the role of IAA in promoting cell elongation in intact plants could not be demonstrated

* Corresponding author. Tel.: +34-9-6-387-7874; fax: +34-9-6-387-7859.
E-mail address: chamarro@ibmcp.upv.es (J. Chamarro).
[1] Present address: National Institute of Working Life, S-907 13 Umeå, Sweden.

0031-9422/01/$ - see front matter © 2001 Elsevier Science Ltd. All rights reserved.
PII: S0031-9422(01)00023-1

until a continuous auxin infusion system was used (Romano et al., 1995).

How a plant controls its hormonal metabolism to regulate its developmental events continues to be of interest. This is particularly important in the case of IAA, where the levels of the hormone seem to be very strictly regulated (Kawaguchi and Syono, 1996). The level of IAA in plant tissue is the balance of the biosynthesis, transport and inactivation pathways. Indoleacetic acid is metabolized by conjugation to sugars and amino acids and by hydroxylation and/or oxidation at various positions of the indole ring (Normanly, 1997; Normanly and Bartel, 1999). Deactivation of the hormone through such mechanisms is likely to be an integral part of the homeostatic control of IAA levels. Hence, structural as well as quantitative analysis of IAA metabolites is crucial for the elucidation of regulatory points in the catabolism of the hormone. In the present study, we analyze the chemical structure and metabolism of the major metabolite compounds and propose the main routes for IAA inactivation in the flavedo of orange fruits.

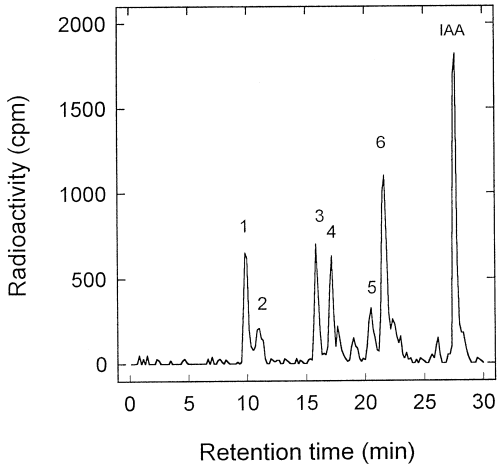

Fig. 1. Gradient elution reversed-phase HPLC-RC of an aliquot of a MeOH extract from orange flavedo tissue following application of 12.3 kBq [5-^{3}H]IAA (999 GBq mmol^{-1}) and incubation in the dark, at 25°C for 6 h. The identity of the metabolite peaks is: 1, DiOxIAGlc; 2, DiOxIAA; 3 and 4, diastereomers of OxIAAsp; 5, unidentified; 6, OxIAA and IAAsp.

2. Results

2.1. Decarboxylative/nondecarboxylative IAA metabolism

In a preliminary experiment we observed that crude extracts and excised discs of orange flavedo tissue had a high capacity to decarboxylate [1′-^{14}C]IAA but, when the labeled IAA was applied to the flavedo of intact fruits, decarboxylation could not be detected. These results suggest that IAA decarboxylation may be an artifact attributable to a wound induced increase in extracellular peroxidase activity and that the IAA fed to the flavedo is deactivated by nondecarboxylative mechanisms, in concordance with previous observations with tomato pericarp discs (Catalá et al., 1992, 1994). Gradient elution reversed phase HPLC-RC analysis of partially purified MeOH extracts of mature green orange flavedo tissue, fed with [5-^{3}H]IAA, showed 6 main metabolite peaks, all of which eluted before IAA and were designated in order of decreasing polarity from 1 to 6 (Fig. 1).

2.2. Identification of metabolite peak 1

The FAB spectrum of methylated metabolite 1 (Table 1a) contained $[M+H]^+$, m/z 384/390 (endogenous/[$^{13}C_6$] fragment), which corresponded to a methylated DiOxIAA-*O*-glucoside (3-(*O*-β-glucosyl)-2-indolone-3-HOAc). The fragment m/z 222/228 $[M+H\text{-}162]^+$

Table 1
Tabulated mass spectra of identified IAA metabolites[a]

Metabolite peak	Compound	$[MH]^+$	Other ions
(a) FAB spectra of methylated IAA metabolites			
1	DiOxIAGlc	384/390 (43/70)	222/228 (73/Bp), 206/212 (29/50), 205/211 (13/57), 204/210 (50/83), 146/152 (9/11)
2	DiOxIAA	228 (Bp)	212 (38), 211 (29), 210 (46), 152 (15)
3–4	OxIAAsp	341 (25)	204 (7), 180 (7), 162 (11), 152 (16), 102 (7)
6	IAAsp	325 (Bp)	162 (24), 136 (90), 102 (8)
6	IAGlu	339 (Bp)	136 (54)
(b) FAB spectra of methylated and acetylated IAA metabolites			
1	DiOXIAGlc	594/600 (11/7)	437/441 (7/13), 331 (Bp), 247/253 (9/13), 246/252 (10/19), 211 (4), 204/210 (6/12), 169 (21), 109 (12), 43 (9),
2	DiOxIAA	312 (80)	252 (Bp), 211 (19), 210 (28)
(c) Electron impact spectra of methylated and silylated IAA metabolites			
6	IAAAsp	396 (28)	208 (Bp), 136 (4), 73 (23)
6	IAGlu	410 (27)	208 (Bp), 135 (5), 73 (15)

[a] The intensity of non-labeled versus labeled peaks are presented in parentheses. Bp, base peak with relative intensity 100%.

corresponded to the loss of a Glc, leaving a protonated methylated DiOxIAA with further loss of H_2O from the methylated DiOxIAA, *m/z* 204/210 $[M\text{-}162\text{-}H_2O]^+$. Further, the oxidized indole appeared as a quinolonium ion, *m/z* 146/152. The loss of *m/z* 222/228 to *m/z* 204/210 $[m/z\ 222/228\text{-}H_2O]^+$, and not to $[m/z\ 222/228\text{-}O]^+$, was diagnostic for loss of an O in position 3 from a hydroxylated OxIAA. This was also confirmed by a quinolonium observed at *m/z* 146/152 since a OH, positioned elsewhere in the benzene ring, would have been retained in the quinolonium structure giving *m/z* 162/168, which was not present in the spectrum (Östin et al., 1995). Since the molecule was methylated in the carboxyl group and lacked specific fragments for N-linked sugars, the glucosylation must have occurred through the 3-positioned OH group (Östin et al., 1995).

The methylated and acetylated metabolite 1 (Table 1b) contained a $[M+H]^+$ at *m/z* 594/600, which corresponded to the incorporation of five acetyl groups. Four of these acetyl groups were incorporated into the Glc showing up in the fragment series *m/z* 331, 169, 109, 43. No double labeling of endogenous/fed [$^{13}C_6$]IAA was visible in these fragments, since the label was situated in the benzene ring of the oxidized indole. The relative intensities of this series of acetylated hexose peaks at *m/z* 169 > *m/z* 109 and the absence of a dominant *m/z* 211 excluded fructose and pointed at Glc, as deduced from spectra of acetylated sugars; however, galactose, lactose and mannose could not be excluded. The fifth acetyl group was linked to the N in the oxidized indole and the loss of Glc produced methylated/acetylated DiOxIAA with *m/z* 246/252; the quinolonium ion was present as *m/z* 146/152.

2.3. Identification of metabolite peak 2

The FAB spectrum of methylated metabolite 2 only contained peaks from the fed [$^{13}C_6$]IAA with a $[M+H]^+$ at *m/z* 228, corresponding to the methylated DiOxIAA characteristic fragmentation, $[M\text{–}H_2O]^+$, *m/z* 210, and the quinolonium ion, *m/z* 152 (Table 1a).

The protonated methylated/acetylated molecule of DiOxIAA was present as $[M+H]^+$, *m/z* 312. This corresponded to the incorporation of two acetyl groups, which were then sequentially lost as $[M\text{–}CH_3COOH]$, *m/z* 252 and $[MH\text{–}CH_3COO\text{–}CH_3CO]$, *m/z* 210 (Table 1b). The acetylation occurred through the OH groups in the 3 and N positions.

2.4. Identification of metabolite peaks 3 and 4

The metabolite peaks 3 and 4 were identified as stereoisomers of OxIAAsp as their methylated derivatives by LC–MS (Table 1a). The protonated molecule $[M+H]^+$, *m/z* 341, corresponded to the $^{13}C_6$-labeled compounds and no endogenous compounds were detected. The side chain with the methylated Asp gave the fragments *m/z* 204, *m/z* 162 and *m/z* 102. Loss of Asp retained the $^{13}C_6$ fragment *m/z* 180, with further quinolonium formation at *m/z* 152. The formation of the two stereoisomers, which rapidly isomerized into each other, were diagnostic of the oxindole (Plüss et al., 1989; Tuominen et al., 1994).

2.5. Identification of metabolite peaks 5 and 6

Metabolite 5 (Fig. 1) could not be identified in these experiments. The putative OxIAA and IAAsp comigrated in peak 6. In our study they were separated by TLC, after methylation, into two radiolabeled fractions corresponding to the retention time of the methylated OxIAA and IAAsp, respectively. The proportion of the two metabolites was 1:14 (OxIAA:IAAsp). However, the amount OxIAA obtained in this experiment was not enough to facilitate a complete identification. The identity of OxIAA was based on retention time in the two chromatographic systems, combined with the presence of DiOxIAA and DiOxIAGlc as products of the putative OxIAA in the feeding experiments (Table 2). The IAAsp peak was also found to contain IAGlu. IAAsp was identified in GC–MS as its methylated silylated derivative with its $^{13}C_6$-labeled molecular ion $[M]^+$, *m/z* 396, and formation of the silylated quinolinium ion, *m/z* 208, and quinolinium ion, *m/z* 136. The TMSi group was represented by *m/z* 73 (Table 1c). The LC–MS spectrum of the methylated IAAsp contained a $[M+H]^+$ at *m/z* 325 and a quinolinium ion at *m/z* 136, as well as the fragment *m/z* 162 and its immonium fragment 102 (Table 1a). IAGlu was identified by GC–MS as its methylated silylated derivative with its $^{13}C_6$-labeled molecular ion $[M]^+$, *m/z* 410, and formation of the silylated quinolinium ion, *m/z* 208, the TMSi group was represented by *m/z* 73 (Table 1c). The LC-MS spectrum of the methylated IAGlu contained a protonated molecule $[M+H]^+$ at *m/z* 339 and a quinolinium ion at *m/z* 136 (Table 1a).

2.6. Metabolism of the main IAA metabolites by orange flavedo

The results of these experiments are depicted in Table 2. When putative OxIAA was fed to the flavedo, two metabolite peaks with the same retention time as DiOxIAA and DiOxIAGlc, respectively, were obtained. Application of DiOxIAA to the tissue produced one metabolite peak with the same retention time as DiOxIAGlc, while feeding with the putative DiOxIAAGlc did not result in any further conversions. These results suggest the following metabolic sequence IAA–OxIAA–DiOxIAA–DiOxIAGlc. Metabolism of IAA has been reviewed by Bandurski et al. (1995), Normanly (1997) and Normanly and Bartel (1999). IAAsp and/or OxIAA appear to be the first committed step of non-decarboxylative

Table 2
Metabolism of the main orange flavedo IAA metabolites[a]

Metabolite fed	Incubation time. (h)	Percentage of radioativity in the extract						
		DiOxIAGlc	DiOxIAA	OxIAAsp[b]	OxIAAsp[c]	Peak 5	OxIAA	IAAsp
DiOxIA Glc	5	**93.2±11.0**						
	10	**99.4±0.7**						
	20	**90.9±4.7**						
DiOxIAA	10	30.0	**49.6**					
	20	62.8	**30.7**					
OxIAAsp[b]	5			**46.1±1.4**	43.4±0.4			
	10			**46.6±0.7**	43.3±0.3			
	20			**46.1±1.4**	41.8±1.2			
OxIAAsp[c]	5			46.2±3.0	**43.2±0.8**			
	10			46.3±1.2	**44.3±1.9**			
	20			47.3±1.2	**45.6±2.2**			
5	5					**86.5±4.5**		
	10					**79.9±2.1**		
	20					**81.2±1.2**		
OxIAA	5	22.2±8.5	2.9±1.1				**67.7±0.4**	
	10	39.5±11.7	4.7±4.2				**51.7±4.6**	
	20	53.8±12.8	7.8±2.0				**34.6±9.0**	
IAAsp	5			5.2±3.5	7.0±2.0			**81.2±9.2**
	10			11.2±3.0	12.4±2.5			**66.7±5.9**
	20			17.5±3.2	18.5±2.2			**44.8±9.8**

[a] Ten microlitres of a soln containing ca 12.5 kBq of the purified [5-^{3}H]IAA metabolite indicated in each case (figures in bold) were applied to the surface of the equatorial part of the peel. After incubation, the flavedo MeOH extracts were analyzed by HPLC-RC. Radioactivity associated with IAA metabolites expressed as % of total radioactivity in the extract ±S.D. ($n=3$).
[b] and [c] Are diastereomers of OxIAAsp, corresponding to metabolite peaks 3 and 4 (Fig. 1), respectively.

oxidation of IAA. The OxIAA/DiOxIAA oxidation pathway has been observed in several plant species including rice, corn, broad bean and *Arabidopsis*. One of the most established catabolic pathway has been described for *Zea mays*, where IAA is converted to OxIAA as the first step in a route leading to 7-Glc–OxIAA, which has been hypothesized to accumulate in the vacuoles. (Nonhebel et al., 1985). In the flavedo, we have shown that OxIAA is converted to DiOxIAGlc, following a novel catabolic pathway. The presence of a Glc in the indole ring as a major "end product" of the OxIAA pathway had only been reported previously in *Zea mays* by Nonhebel et al., 1985.

We have also shown that application of IAAsp to the flavedo produced two peaks identified as the two diastereomers of OxIAAsp and, when these diastereomers were fed separately, a similar profile was obtained showing both isomers, but no further metabolism could be detected, suggesting the metabolic sequence IAA–IAAsp–OxIAAsp. Metabolism of IAAsp to OxIAAsp has also been described in several plant species such as in cuttings (Plüss et al., 1989) and shoots (Tuominen et al., 1994) from *Populus*; in this latter case, OxIAAsp was converted to OxIAA and subsequently hydroxylated in the benzene ring. In *Dalbergia dolichopetala* (Östin et al., 1992) IAAsp has been proposed as an intermediate giving rise to both DiOxIAAsp and ring hydroxylated OxIAAsp derivative. Another pathway having IAAsp as an intermediate has been described in *Vicia faba* cotyledons (Tsurumi and Wada, 1985, 1986a,b) through the formation of DiOxIAAsp, having probably OxIAAsp as an intermediate which, in turn, is transformed into Glc–DiOxIAAsp and then transported to the roots. In tomato fruit the IAAsp pathway leads to OxIAAsp, linked to a diglucoside in the N position (Östin et al., 1995).

When the unidentified metabolite peak 5 was fed to the flavedo, only one major peak, with the same retention time as the metabolite fed, was obtained, suggesting that this is a catabolic end product or a non utilised storage form.

2.7. Effect of incubation time and maturity on [5-^{3}H]IAA metabolism

Table 3 shows the results of three representative moments in the study i.e. green, turning (start of change

Table 3
Effect of incubation time and maturity on the metabolism of [5-H]IAA by orange flavedo tissue[a]

Fruit maturity	Incubation time (h)	Percentage of radioativity in the extract						
		DiOxIA-Glc	DiOxIAA	OxIAAsp	OxIAAsp	Unidentified peak 5	IAAsp + OxIAA	IAA
Immature green	3		1.5±1.3	10.9±2.6	9.9±2.2	8.8±1.9	34.5±5.3	27.4±11.6
	6		3.7±0.6	12.4±0.9	12.0±0.3	10.7±1.6	27.0±4.6	18.1±6.9
	12	13.7±1.8	4.4±0.4	12.2±2.3	12.5±2.1	10.2±2.4	22.6±5.8	14.6±7.9
	24	28.4±5.6	6.3±1.8	14.9±1.1	17.6±1.3	9.7±4.0	9.2±4.4	5.2±0.8
	48	44.4±6.0	6.1±0.7	10.1±2.0	13.4±1.6	6.3±0.7	9.5±2.6	3.9±1.4
Turning	3	2.3±1.5	1.3±0.2	4.3±1.1	3.4±0.9	2.7±9.8	9.8±2.3	71.7±9.2
	6	9.4±1.8	3.3±0.6	11.1±1.7	10.1±1.5	7.1±1.2	22.5±4.8	31.6±5.2
	12	25.1±7.1	4.2±0.3	10.1±1.9	10.3±1.2	6.2±1.5	16.9±2.8	25.4±4.5
	24	34.4±5.3	4.9±0.6	9.5±1.5	13.8±1.7	6.2±1.5	11.6±1.5	13.8±4.5
	48	56.3±2.9	4.3±0.6	6.4±0.5	10.3±1.1	4.0±1.8	8.7±2.8	7.7±1.7
Orange	3					0.5±0.8	23.9±8.8	72.5±8.8
	6			3.6±1.6	3.2±1.1	4.3±0.3	27.3±20.8	59.3±25.7
	12	3.1±1.1		8.9±1.6	8.8±1.6	9.9±2.7	30.6±7.9	35.2±2.2
	24	4.7±1.9	1.0±0.1	11.2±0.5	10.5±2.2	10.1±2.0	29.9±14.9	28.6±13.1
	48	10.8±4.1	0.9±0.2	10.1±2.4	9.8±2.6	9.9±2.4	21.2±4.5	30.9±10.8

[a] Ten microlitres of a soln containing 12.3 kBq [5-^{3}H]IAA, 999 GBq mmol^{-1} were applied. After incubation, the flavedo MeOH extracts were analyzed by HPLC-RC. Radioactivity associated with IAA metabolites expressed as % of radioactivity in the extract ±S.D. ($n=3$).

in peel color), and fully colored senescent fruit. In green and turning fruits, most of the [5-^{3}H]IAA taken up by the tissue was metabolized in less than 24 h, while, in orange colored senescent tissue, the metabolism was considerably slower. DiOxIAGlc accumulated to the greatest extent at the end of the incubation period, DiOxIAA accumulated from the beginning, but at a lower extent and peaked at 24 h of incubation. The two diastereomers of OxIAAsp soon reached maximum and equivalent concentrations, thereafter decreasing slowly. Metabolite 5, which was not identified, accumulated after 6–12 h incubation. Metabolite peak 6, identified as a mixture of IAAsp and OxIAA, accumulated rapidly during the first hours of incubation and then decreased, as they were further metabolised. In orange senescent fruit the degradation of IAA was much slower and higher levels of the metabolite peak 6 could be observed. This could probably be attributed to the accumulation of OxIAA, as a result of the decline of its metabolism to DiOxIAA and DiOxIAGlc. In green tissue, the most abundant metabolite after 48 h incubation was DiOxIAGlc. An estimation about the relative abundance of the metabolites formed in these experiments indicated that the route branching from OxIAA, in green and turning tissue, would account for 50–60% of IAA metabolism; the IAAsp route would take 15–25%, while metabolite 5 would account for 5–10% of total IAA metabolism. In senescent tissue the metabolism of IAA was strongly reduced and, after 48 h of incubation, 30% of the [5-^{3}H]IAA remained unmetabolized.

2.8. Effect of IAA concentration

When applying growth substances to plant tissues, the question always arises as to whether apparent metabolism actually represents detoxification of an abnormally large amount of exogenous compounds. Increasing IAA concentrations from 1.23 to 12.3 μM scarcely affected the pattern of IAA metabolism, while increasing the concentration to 123 μM resulted in an increase of unmetabolized IAA, a decrease in metabolites OxIAAsp, DiOxIAA, DiOxIAGlc, and a progressive accumulation of unidentified metabolite 5, OxIAA and IAAsp (Table 4). *Arabidopsis* fed with low concentrations of tritiated IAA (Östin et al., 1998) produced mainly OxIAA and much smaller proportions of the conjugates IAAsp and IAGlu. Increasing the concentration of the IAA fed induced a larger proportion of the amino acid conjugates formed. A similar shift in metabolism seems to be valid even for the orange flavedo tissue with DiOxIAGlc as the final product in the OxIAA pathway and OxIAAsp in the IAAsp pathway.

2.9. Effect of treatment with plant growth regulators

The effect of PGRs in plant tissues depends on a complex network of interactions. It has been speculated that one hormone may influence the stability and metabolism of a second one (Palni et al., 1988). In Table 5, it can be observed that pre-treatment with the synthetic auxins, 2,4-D, NAA and the giberellin GA_3 increased

Table 4
Effect of substrate concentration on [5-^{3}H]IAA metabolism of orange flavedo tissue[a]

Applied IAA (μM)	Incubation time (h)	Percentage of radioativity in the extract						
		DiOxIA-Glc	DiOxIAA	OxIAAsp	OxIAAsp	Unidentified peak 5	IAAsp + OxIAA	IAA
1.23	5	11.6±4.2	2.0±1.7	15.0±8.1	12.3±5.7	10.7±1.6	25.2±3.5	18.4±10.6
	10	22.9±1.7	4.1±0.8	15.4±0.9	16.6±0.6	8.7±0.7	21.0±0.7	6.7±1.2
	20	22.3±10.5	2.4±1.2	13.6±0.7	14.4±0.1	5.9±5.4	17.8±7.1	11.8±2.5
12.3	5	6.7±3.3	1.1±0.1	13.6±2.1	10.3±2.1	12.4±2.2	31.6±1.7	14.4±5.5
	10	14.3±1.8	3.3±0.9	13.9±0.4	13.1±1.3	16.7±3.1	22.7±2.7	5.5±1.3
	20	23.1±4.0	5.5±1.2	13.3±2.1	14.5±2.5	10.0±2.6	16.4±2.4	5.8±0.7
123	5	1.0±1.0		2.9±1.2	1.9±0.3	5.0±0.8	25.0±6.6	58.1±7.2
	10	4.2±1.1	0.6±1.0	5.6±1.6	4.6±1.7	14.6±1.8	47.4±11.7	9.5±5.8
	20	5.0±2.8	2.0±1.3	8.6±0.8	8.6±0.3	19.1±6.9	27.8±5.3	13.2±7.4

[a] Ten microlitres of a soln containing 12.3 kBq [5-^{3}H]IAA (999 GBq mmol^{-1}), made up to 1.23, 12.3, and 123 μm with [^{12}C]IAA, were applied. After incubation, the flavedo MeOH extracts were analyzed by HPLC-RC. Radioactivity associated with IAA metabolites expressed as % of total radioactivity in the extract ±S.D. ($n=3$).

Table 5
Effect of treatment with PGRs on IAA metabolism by orange flavedo tissue[a]

Incubation time (h)	Treatment	Percentage of radioativity in the extract						
		DiOxIA-Glc	DiOxIAA	OxIAAsp	OxIAAsp	Peak 5	IAAsp + OxIAA	IAA
5	Control	7.5±0.9	1.9±1.2	14.6±5.5	12.7±2.8	9.0±4.6	21.9±3.2	23.6±14.5
	2,4-D	9.6±5.8	3.8±1.0	17.9±1.7	17.8±0.7	10.9±1.2	20.3±5.5	7.1±4.9
	NAA	12.7±2.3	4.5±1.5	16.5±4.7	15.1±4.0	9.1±0.8	23.3±3.9	8.8±1.0
	GA_3	15.9±3.0	3.6±0.6	16.5±2.5	16.4±1.8	11.6±3.3	18.5±1.3	10.7±6.7
10	Control	19.8+3.0	7.4+1.7	13.4+3.6	15.1+4.5	10.4+2.3	18.7+3.8	3.6+2.5
	2,4-D	20.7+3.6	6.0+2.3	16.5+3.3	17.5+1.7	9.0+1.9	16.8+0.4	1.6+0.5
	NAA	–	–	–	–	–	–	–
	GA_3	19.8+6.9	6.1+2.5	13.6+3.2	14.7+4.5	9.2+2.7	16.6+4.4	3.6+1.9
20	Control	27.6±2.0	4.0±2.0	13.9±2.0	17.3±1.5	7.4±2.0	14.8±3.6	4.1±2.0
	2,4-D	31.2±2.2	8.1±2.5	16.0±0.3	17.9±2.5	12.0±6.6	11.3±1.0	1.7±0.2
	NAA	30.1±9.4	5.8±2.0	15.3±2.7	17.7±1.9	9.2±1.8	11.7±1.6	2.5±1.2
	GA_3	24.8±2.3	4.1±1.7	16.6±3.6	19.2±1.5	9.7±1.3	14.5±1.7	1.6±0.6

[a] Fruits were submerged 30 min in a 1 mM soln of the hormone. Then, 10 μl of a soln containing 12.3 kBq [5-^{3}H]IAA (99 GBq mmol^{-1}) were applied. After incubation, the flavedo MeOH extracts were analyzed by HPLC-RC. Radioactivity associated to IAA metabolites expressed as % of total radioactivity in the extract ±S.D. ($n=3$).

IAA metabolism during the first 5 h of incubation. For longer periods, no changes could be observed because of the low levels of unmetabolized IAA remaining in the tissue.

3. Conclusions

Despite a number of papers dealing with IAA metabolism in different plant systems, only in a few cases a more comprehensive overview, particularly for non-decarboxylative catabolism, has been found in the last years (Kleczkowski and Schell 1995; Normanly, 1997). It is still of interest to extend these studies to a representative number of plant systems to know what is common and what is different among them. In fruits, only the tomato, a climacteric fruit characterized by an upsurge of respiration and ethylene production associated to ripening, catabolism has been comprehensively approached; in this case the IAAsp pathway leads to OxIAAsp, linked to a diglucoside in the N position (Östin et al., 1995). In our studies with oranges, first of this nature in non-climacteric fruits, the OxIAA pathway is predominant for IAA inactivation, leading to DiOxIAGlc according to a novel pathway. The presence of a Glc in the indole ring as a major "end product" of the OxIAA pathway has only been reported previously in *Zea mays* by Nonhebel et al. (1985), with formation of 7-Glc-OxIAA. Glucosylation of

the indole ring is also a quite common "end product" of the OxIAAsp pathway in several plant systems, but only in *Vicia* seedlings has been shown that GlcDiOxIAAsp formed in the cotyledons is transported to the roots (Tsurumi and Wada, 1986b). By analogy, it could be suggested that these metabolites could be transported to other parts of the plant or engulfed by the vacuoles.

Despite their utility, feeding experiments are limited in several aspects, such as the difficulty to detect high turnover metabolites or the short timing of the experiments in relation to many physiological processes, which could conceal the fate of the so called "end products". The multiplicity and redundancy of reactions involved in the regulation of IAA levels are serious obstacles to the knowledge of the mechanisms involved in IAA homeostasis. Identification of the enzymes involved in IAA metabolism, and isolation of the corresponding genes, coupled to the introduction of *Arabidopsis*, a model system with outstanding possibilities, has improved considerably, in the last years, our knowledge of auxin biology (Leyser, 1997; Normanly and Bartel, 1999). While biosynthesis, transport and conjugation have received extensive attention, degradation has been largely ignored. Recently, Östin et al., 1998, have studied several aspects of IAA metabolism, in *Arabidopsis*, in order to devise novel and relevant screens with which to identify mutants of IAA metabolism. Hopefully, in a near future, application of biochemical and genetic approaches to *Arabidopsis* defective mutants in IAA catabolism will allow a more comprehensive understanding of IAA homeostasis and the extension of this knowledge to other plant systems.

4. Experimental

4.1. Plant material

Orange fruits (*Citrus sinensis* L., cv. Washington Navel), grown in an orchard close to Valencia (Spain) were picked at different stages of development as indicated in the text.

4.2. Isotopically labeled substrates

[5-^{3}H]IAA, 999 GBq mmol^{-1}; [1′-^{14}C]IAA, 2.04 GBq mmol^{-1} and [$^{13}C_6$]IAA, or a mixture of them, were used. When required, the concentration was adjusted with [^{12}C]IAA.

4.3. Incubation conditions

Orange fruits were washed with H_2O, surface sterilized with a 0.2% NaOCl soln and rinsed with sterile H_2O. Ten microlitres of [5-^{3}H, 1′-^{14}C, $^{13}C_6$, ^{12}C]IAA, or a mixture of them, dissolved in citrate Pi buffer 50 mM, pH 4.5, were placed on the equatorial part of the fruit in a circle of 10 mm diameter. Fruits were incubated in the dark, at 25°C, in a 25 l vacuum desiccator through which 300 ml min^{-1} of air was circulated. At specified intervals, peel discs of 15 mm diameter were taken out with a cork borer and the flavedo was excised with a razor blade and frozen at −80°C until analysis. For metabolic studies, except when otherwise indicated, 10 μl of a soln containing 12.3 kBq [5-^{3}H]IAA (999 GBq mmol^{-1}) was applied. To obtain [$^{13}C_6$ and 5-^{3}H]IAA metabolites for identification by mass spectrometry and for re-application studies, respectively, large scale incubations were carried out with mature green fruits. Ten microlitres of 40 μM [$^{13}C_6$]IAA containing 24.5 kBq of [5-^{3}H]IAA as a tracer in the first case and 10 μl of a soln 37 μM IAA containing 377 kBq [5-^{3}H]IAA, in the second, were applied to each fruit.

4.4. Extraction and purification

For metabolic studies, flavedo discs were homogenized in 80% MeOH, 100 mg l^{-1} BHT, (4 ml g^{-1} fr. wt) and extracted for 1 h, in the dark, at 4°C, with constant shaking, centrifuged 10 min at 3000 *g* and the pellet re-extracted with MeOH (2 ml g^{-1}). The combined supernatants were reduced to the aq. phase, adjusted to pH 3 with 1 M HCl, and passed through a C_{18} cartridge. IAA metabolites were then eluted with 5 ml of MeOH, 0.1 M HOAc. The dried eluate was dissolved in 10% MeOH, 0.1 M HOAc, and filtered through a 45 μm membrane before HPLC-RC.

To obtain IAA metabolites for feeding experiments and MS identification, the extraction was performed in groups of 20 discs, as described previously. The MeOH extracts were reduced to the aq. phase, in a rotary evaporator under vacuum. Ten millilitres of 50 mM Pi buffer, pH 8, were added, and the extract was run through a 30×10 mm i.d. PVP column and then eluted with 12 ml of the same buffer. The eluent, adjusted to pH 3 with 1 M HCl, was run through a C_{18} cartridge, which was eluted with 5 ml of MeOH, 0.1 M HOAc. The MeOH eluate was reduced to dryness in vacuum and dissolved in 10% MeOH, 0.1 M HOAc, before reversed phase HPLC.

4.5. Elution by HPLC

For metabolic studies reversed-phase HPLC was carried out using a 150 x 3.9 mm i.d. 5 μm C_{18} column. The column was eluted at a flow rate of 1 ml min^{-1} with a 30 min linear gradient of 10–50% MeOH in 0.1 M HOAc. The eluate was directed to a radioactivity monitor, fitted with a 500 μl flow cell operating in homogenous mode. The scintillant to eluate ratio was 3:1 (v/v).

To obtain IAA labeled metabolites for mass spectrometric identification and for feeding experiments the same HPLC conditions were used, except that a fraction collector substituted the radioactivity monitor. Aliquots

of the fractions were analyzed for radioactivity by liquid scintillation counting, and those corresponding to individual metabolite peaks were combined and reduced to dryness in Speed Vac. In order to improve the purity of the metabolite peaks and to avoid cross contamination, for feeding experiments with [5-^{3}H]IAA metabolites, a second purification step by reversed phase HPLC in isocratic mode was performed. Each fraction was resuspended in 10% MeOH, 0.1 M HOAc and resolved, in 12.5% MeOH (fractions 1 and 2), 15%, (fractions 3, 4 and 5) and 20% (fraction 6).

4.6. Derivatisation and further purification for mass spectrometric identification

To improve separation and sensitivity in the LC–MS, free carboxylic acids were methylated in the HPLC-purified fractions. The samples were soulibilized with a droplet of 1% HOAc and diluted with 100 μl MeOH. Thereafter 900 μl of Et_2O and 100 μl TMSi–CH_2N_2 were added and the mixture was incubated at room temp. overnight. The methylated fractions were further purified by TLC (Kieselgel 60 F_{254}, 10×5 cm; Merck), and the plates were eluted with butanone-EtOAc–EtOH–H_2O (3:5:1:1). Transversal 1 cm sections were scraped, suspended in MeOH, and the radioactive fractions were further purified by HPLC, in a system consisting of two Beckman 110B solvent delivery modules with a Beckman Model 420 controller. The column, 100×80 mm (i.d.), was packed with 4 μm C18 ODS. The radioactivity detector was an heterogeneous flow cell packed with Ce-activated Li glass scintillant. Radioactive fractions were collected, divided into two aliquots for GC–MS and for LC–MS, respectively and dried in Speed Vac. The aliquot analyzed by GC–MS was previously dissolved in 25 μl acetonitrile and silylated by adding 25 μl of bis (TMSi)-trifluoroacetamide with 1% (v/v) trimethylchlorosilane, heated in a sealed vial at 70°C for 15 min and, finally, reduced to dryness and re-dissolved in acetonitrile. The other aliquot was dissolved in LC–MS eluent, prior to analysis by LC–MS.

4.7. Analysis by GC–MS and LC–MS

GC-MS was performed using a Hewlett-Packard 5890 gas chromatograph linked to a Jeol JMS SX 102 mass spectrometer. Samples were injected, splitless, at 280°C, onto a 25 m×0.25 mm methyl silicone fused silica column with a film thickness of 0.25 μm. The carrier gas was He. The column temp. was programmed to rise 20°C min^{-1} from 70 to 280°C and then held at this temp. until elution of the sample. Ions were generated with 70 eV, with an ionisation current of 300 μA, the acceleration voltage being 10 kV, and positive ion mass spectra were obtained at a rate of 1 s per scan for a mass range of m/z 25–800.

The capillary HPLC frit-FAB MS system used for the identification of the metabolites has been described (Östin et al., 1992). For the initial HPLC separation a 300×0.32 mm capillary column packed with ODS, 5 μm was used. The ion source temp. was 50°C and ions were generated with a beam of 5 kV Xe atoms at an emission current of 20 mA. The acceleration voltage was 10 kV. Positive ion mass spectra were obtained at a rate of 5 s per scan for m/z 50–800. The spectra were background subtracted and the data were processed by a JEOL-MD7000 data system.

4.8. Metabolism of the main IAA metabolites by orange flavedo

The main [5-^{3}H] metabolites, purified as indicated previously, were applied individually (ca 12.5 kBq each) to mature-green orange fruits and, after incubation, the tissue was extracted and analyzed by HPLC-RC.

4.9. Effect of incubation time and maturity on [5-^{3}H]IAA metabolism

A time course study of the metabolism of [5-^{3}H]IAA by orange flavedo tissue was conducted from the end of September, with young small immature green fruits, until the end of December, with fully colored senescent oranges, at one or two week intervals. Ten microlitres of a 50 mM citrate buffer pH 4.5, containing 12.3 kBq [5-^{3}H]IAA, were applied to the fruit. After incubation, flavedo discs were excised, extracted with MeOH, and the partially purified extracts were analyzed by HPLC-RC, as indicated previously.

4.10. Effect of treatment with plant growth regulators

Fruits were submerged for 1/2 h in 1 mM 2,4-D, NAA and GA_3 respectively. Then, fruits were blotted dry and 10 μl of a 50 mM citrate buffer pH 4.5, containing 12.3 kBq [5-^{3}H]IAA, were applied to the fruit. After incubation, flavedo discs were excised, extracted with MeOH, and the partially purified extracts were analyzed by HPLC-RC, as indicated previously.

Acknowledgements

This work was supported by the Spanish DGICYT, grants ALI94-0738 and ALI1997-0587-C01, the Swedish Council of Forestry and Agricultural Research (SJFR) and The Foundation for Strategic Research (SSF).

References

Baldwin, E.A., 1993. Citrus fruit. In: Seymour, G., Taylor, J., Tucker, G. (Eds.), Biochemistry of Fruit Ripening. Chapman & Hall, London, pp. 107–151.

Bandurski, R.S., Cohen, J.D., Pernise, J., Slovin, J.P., Reinecke, D.M., 1995. Auxin Biosynthesis and Metabolism. In: Davies, P.J. (Ed.), Plant Hormones: Physiology, Biochemistry and Molecular Biology. Kluwer Academic Publishers, Dordrecht, Netherlands, pp. 39–65.

Catalá, C., Crozier, A., Chamarro, J., 1994. Decarboxylative metabolism of [1′-^{14}C]indole-3-acetic acid by tomato pericarp discs during ripening. Planta 193, 508–513.

Catalá, C., Östin, A., Chamarro, J., Sandberg, G., Crozier, A., 1992. Metabolism of indole-3-acetic acid by pericarp discs from immature and mature tomato (*Lycopersicon esculentum* Mill.). Plant Physiology 100, 1457–1463.

Cohen, J.D., 1996. In vitro tomato fruit cultures demonstrate a role for indole-3-acetic acid in regulating fruit ripening. Journal of the American Society for Horticultural Sciences 12, 520–524.

Dezakos, E.D., 1983. Effect of post harvest treatments of growth and bioregulators on quality and longevity of fruits and vegetables. In: Lieberman, M. (Ed.), Postharvest Physiology and Crop Preservation. Plenum Press, London, pp. 355–381.

Frenkel, C., 1975. Oxidative turnover of auxins in relation to the onset of ripening in Barlett pear. Plant Physiology 55, 480–484.

Given, N.K., Venis, M.A., Grierson, D., 1988. Hormonal regulation of ripening in the strawberry, a non-climacteric fruit. Planta 174, 402–406.

Goldshmidt, E.E., 1988. Regulatory aspects of chloro-chromoplast interconversions in senescing citrus fruit peel. Israel Journal of Botany 37, 123–130.

Kawaguchi, M., Syono, K., 1996. The excessive production of indole-3-acetic acid and its significance in studies of the biosynthesis of this regulator of plant growth and development. Plant Cell Physiology 37, 1043–1048.

Kleczkowski, K., Schell, J., 1995. Phytohormone conjugates: nature and function. Critical Reviews in Plant Sciences 14, 283–298.

Leyser, O., 1997. Auxin: lessons from a mutant weed. Physiologia Plantarum 100, 407–414.

Nonhebel, H.M., Kruse, L.I., Bandurski, R.S., 1985. Indole-3-acetic acid catabolism in *Zea mays* seeds. Metabolic conversion of indole-3-acetic acid to 7-hydroxy-2-oxindole-3-acetic acid-7′-*O*-β-D-glucopyranoside. Journal of Biological Chemistry 260, 12685–12689.

Normanly, J., 1997. Auxin metabolism. Physiologia Plantarum 100, 431–442.

Normanly, J., Bartel, B., 1999. Redundancy as a way of life- IAA metabolism. Current Opinion in Plant Biology 2, 207–213.

Östin, A., Catalá, C., Chamarro, J., Sandberg, G., 1995. Identification of glucopyranosyl-β-1,4-glucopyranosyl-β-1-*N*-oxindole-3-acetyl-*N*-aspartic acid, a new IAA catabolite, by liquid chromatography/tandem mass spectrometry. Journal of Mass Spectrometry 30, 1007–1017.

Östin, A., Kowalyczk, M., Bhalerao, R.P., Sandberg, G., 1998. Metabolism of indole-3-acetic acid in *Arabidopsis*. Plant Physiology 118, 285–296.

Östin, A., Moritz, T., Sandberg, G., 1992. Liquid chromatography/mass spectrometry of conjugates and oxidative metabolites of indole-3-acetic acid. Biological Mass Spectrometry 21, 292–298.

Palni, L.M., Burch, L., Horgan, R., 1988. The effect of auxin concentration on cytokinin stability and metabolism. Planta 174, 231–234.

Plüss, R., Titus, J., Meier, H., 1989. IAA-induced adventitious root formation in greenwood cuttings of *Populus tremula* and formation of 2-indolone-3-acetyl aspartic acid, a new metabolite of exogenously applied indole-3-acetic acid. Physiologia Plantarum 75, 89–96.

Romano, C.P., Hobson, P.R.H., Smith, H., Estelle, M., 1995. Transgene-mediated auxin overproduction in *Arabidopsis*: hypocotyl elongation phenotype and interactions with the hy6-1 hypocotyl elongation and axr1 auxin-resistant mutants. Plant Molecular Biology 27, 1071–1083.

Takahashi, N., Yamaguchi, I., Kôno, T., Igoshi, M., Hirose, K., Suzuki, K., 1975. Characterization of plant growth substances in *Citrus unshiu* and their change in fruit development. Plant Cell Physiology 16, 1101–1111.

Tsurumi, S., Wada, S., 1985. Identification of 3-(*O*-β-glucosyl)-2-indolone-3-aspartic acid as a new indole-3-acetic acid metabolite in *Vicia* seedlings. Plant Physiology 79, 667–671.

Tsurumi, S., Wada, S., 1986. Identification of 3-hydroxy-2-indolone-3-acetylaspartic acid as a new indole-3-acetic acid metabolite in *Vicia* roots. Plant Cell Physiology 27, 559–562.

Tsurumi, S., Wada, S., 1986. Dioxindole-3-acetic acid conjugates formation from indole-3-aspartic acid in *Vicia* seedlings. Plant Cell Physiology 27, 1513–1522.

Tuominen, H., Östin, A., Sundberg, B., Sandberg, G., 1994. A novel metabolic pathway for indole-3-acetic acid in apical shoots of *Populus tremula* (L.) x *Populus tremuloides* (Michx.). Plant Physiology 106, 1–10.

PERGAMON

Phytochemistry 57 (2001) 189–198

PHYTOCHEMISTRY

www.elsevier.com/locate/phytochem

The uptake and speciation of various Al species in the *Brassica rapa pekinensis*

Tjaša Bantan Polak [a], Radmila Milačič [a,*], Boris Pihlar [b], Bojan Mitrović [c]

[a] *Department of Environmental Sciences, Jožef Stefan Institute, Jamova 39, 1000 Ljubljana, Slovenia*
[b] *Faculty of Chemistry and Chemical Technology, University of Ljubljana, Aškerčeva 5, 1000 Ljubljana, Slovenia*
[c] *Lek Pharmaceutical and Chemical Company d.d., Celovška 135, 1000 Ljubljana, Slovenia*

Received 28 August 2000; received in revised form 30 January 2001

Abstract

An investigation was carried out on the uptake and speciation of Al species in Al tolerant Chinese cabbage (*Brassica rapa* L. ssp. *pekinensis*). Plants were exposed to 10 μg cm^{-3} of Al in the chemical forms of Al^{3+}, Al-citrate and Al-malate in a time span from 1 up to 24 h. In each experiment the nutrient solution and stem sap were analysed by a combination of FPLC–ICP–AES and ES–MS–MS techniques. Speciation analysis enabled determination of particular chemical forms of Al present in the nutrient solution or in stem sap. The results indicate that Al^{3+} added to the nutrient solution remained as Al^{3+} in the solution during the experiments, but in the roots transformation to Al-malate occurred. Al was transported from roots to the upper parts of the plant as Al-malate (70%) and Al^{3+} (30%). Al-citrate or Al-malate added to the nutrient solution were transferred to the upper parts of the plant without transformation of their chemical forms. © 2001 Elsevier Science Ltd. All rights reserved.

Keywords: Chinese cabbage; *Brassica rapa* L. ssp. *pekinensis*; Brassicaceae; Uptake of aluminium; Al tolerance; Al speciation

1. Introduction

Al toxicity is a well-known limiting factor in plants growing in acid soils. However, some plants are able to tolerate even phytotoxic concentrations of Al. They have evolved special tolerance mechanisms, among which external and internal tolerance mechanisms (Taylor, 1988, 1991) are mostly reported. It was presumed that low molecular weight organic acids are involved in both tolerance mechanisms (Bartlett and Riego, 1972; Hue et al., 1986; Jones, 1998). The detoxification of Al proceeds through complexation reactions either outside or inside the roots. Numerous studies of these mechanisms were based on the determination of low molecular weight organic acids. Pellet et al. (1995) demonstrated that Al exposure triggered a stimulation of citrate release in Al-tolerant maize. Citric acid exudation into the rhizosphere also appears to be one of the mechanisms of Al-tolerance in snapbeans (Miyasaka et al., 1991), in *Cassia tora* L. (Ma et al., 1997b) and in tropical maize (Jorge and Arruda, 1997). The study of Ma et al. (1997a) indicated that the formation of an Al-citrate complex in the cells of *Hydrangea macrophylla* leaves is responsible for the internal detoxification of Al. Zheng et al. (1998) and Ma et al. (1997c, 1998) proved that internal and external Al-detoxification mechanisms contribute to high Al resistance in buckwheat, since excretion of oxalic acid from the roots and accumulation of Al in the form of Al-oxalate in the leaves appears as a response to Al stress. Similarly Ma and Miyasaka (1998) demonstrated that the roots of Taro exuded oxalic acid under elevated concentrations of Al. Delhaize et al. (1993b) and Ryan et al. (1995) reported that addition of Al to the nutrient solution stimulated excretion of malic and succinic acid from roots of wheat seedlings. de la Fuente et al. (1997) reduced the Al inhibition of root growth by over-expression of the bacterial citrate synthase gene in transgenic tobacco. In addition, a supplement of organic acids to the nutrient solution containing Al has been shown to protect root growth and reduce Al toxicity in many crops (Ownby and Popham, 1989; Delhaize et al., 1993b; Ginting et al., 1998). In order to explain Al-tolerance mechanisms, the uptake, the kinetics of Al uptake and the spatial distribution of Al in Al-tolerant and Al-sensitive plants were investigated (Zhang and Taylor, 1989; Ryan et al., 1993; Delhaize et al., 1993a; Lazof et al.,

* Corresponding author. Tel.: +386-1-477-3900; fax: +386-1-2519-385.

E-mail address: radmila.milacic@ijs.si (R. Milačič).

0031-9422/01/$ - see front matter © 2001 Elsevier Science Ltd. All rights reserved.
PII: S0031-9422(01)00055-3

1994). These studies were based on the determination of total Al.

Al toxicity greatly depends on the chemical species of the element. For better understanding of Al uptake and its translocation into the upper parts of plants, it is essential to identify the Al species formed in the nutrient solution after exposure, and in the stem sap. There are only a few analytical methods available for identification and quantification of monomeric aqua- and hydroxy- Al species (Mitrovič et al., 1996) and low molecular weight Al (LMW-Al) complexes (Michalas et al., 1992; van Hees et al., 1996; Ma et al., 1997a, 1998; Bantan et al., 1998a,b, 1999a,b). Fast protein liquid chromatography (FPLC) in combination with optical atomic spectrometric methods and electrospray tandem mass spectrometry (ES–MS–MS), provides a powerful tool for the speciation of LMW-Al species in plants (Bantan et al., 1999a,b). By combining the proposed analytical techniques the quantitative determination of various LMW-Al species is possible.

In the present study the uptake and speciation of different Al species in the Chinese cabbage (*Brassica rapa* L. ssp. *pekinensis*) was examined, focusing on the identification and quantification of Al forms present in the nutrient solution and stem sap.

2. Results

2.1. Determination of various Al species in synthetic solutions

In order to examine the behaviour of different positively and negatively charged Al species at pH 4.2, synthetic working solutions of Al^{3+}, Al-citrate, Al-malate (10 μg Al cm^{-3}) were injected on the Mono Q or Mono S columns. Typical chromatograms are presented in Fig. 1. These data indicate that the positively charged Al^{3+} was quantitatively eluted on the Mono S column from 3.5 to 4.5 min (Mitrovič et al., 1996). On the Mono Q column Al^{3+} was strongly adsorbed and did not disturb further separations (Bantan et al., 1998b). Negatively charged Al-citrate was quantitatively eluted from 2.5 to 3.0 min on the Mono Q column. On the Mono S column it was eluted with the solvent front (Bantan et al., 1998a). At pH 4.2 Al-malate exists as a mixture of positively and negatively charged complexes. The portion of Al-malate that corresponds to negatively charged complexes (65%) was separated on the Mono Q column from 2.0 to 3.0 min, and the remaining positively charged species were strongly adsorbed on the column. On the Mono S column 65% of negatively charged Al-malate was eluted with the solvent front, while positively charged Al species (35%) were separated from 3.0 to 4.0 min (Bantan et al., 1999a). Speciation of Al-phosphate was also investigated on the Mono Q or Mono S columns. This species is difficult to study because of precipitation of Al-phosphate. At ppm concentration levels the colloidal solution of Al-phosphate above the precipitate was strongly adsorbed on the Mono S and Mono Q columns (Bantan et al., 1999b).

The fractions that contained Al were also identified by ES–MS–MS. The corresponding spectra are presented in Fig. 2. In the mass spectrum of separated Al-citrate synthetic solution (A) a peak with m/z 191 corresponded to deprotonated citric acid. The other peaks with masses m/z 124, 125, 142, 147 and 188 resulted from the eluent of the chromatographic run (NH_4NO_3). The peak m/z 191 was selected for chemically induced dissociation (CID) and after the fragmentation, daughter ions with masses m/z 111, 87 and 85 resulted. In the mass spectrum of separated Al-malate synthetic solution (B), the peak with m/z 133 represented deprotonated malic acid. It was selected as a parent ion for CID and in the MS/MS spectrum peaks with m/z 114.6, 70.3, 72.3 and 88.5 appeared.

2.2. Determination of various Al species in the nutrient solution

In order to test the stability and to determine the chemical forms of Al added to the nutrient solution, speciation of the growth media was performed by FPLC–ICP–AES and ES–MS–MS techniques immediately after the addition of particular Al species, and after 24 h. It is evident from Fig. 3, that in the nutrient solution at pH of 4.2, the Al species added were not transformed. Al^{3+} added to the nutrient solution was separated quantitatively on a Mono S column from 3.5 to 5 min [Fig. 3(A)]. Al-citrate added to the nutrient solution was eluted quantitatively from 2.5 to 3.0 min on a Mono Q column [Fig. 3(B)]. Al-malate added to the nutrient media was eluted as negatively charged complex on a Mono Q column (65%) and a positively charged complex on a Mono S column (35%) [Fig. 3(C) and (D)]. ES–MS–MS analyses of fractions after the chromatographic separations, which contained Al, confirmed the presence of Al^{3+}, Al-citrate or Al-malate. The same results were obtained immediately after the addition of Al species to the nutrient solution, and after 24 h.

2.3. The uptake of Al^{3+}

Aluminium concentrations applied in the experiments did not result in the appearance of phytotoxicity symptoms in the cabbage. When the plants were transferred to the nutrient solution with or without Al, no significant difference in the root growth was observed during one month of the exposure.

For determination of Al species initially present in the stem sap (control), plants were transferred to fresh nutrient solution without Al. After that stem sap was collected and analysed for total Al and its species. The

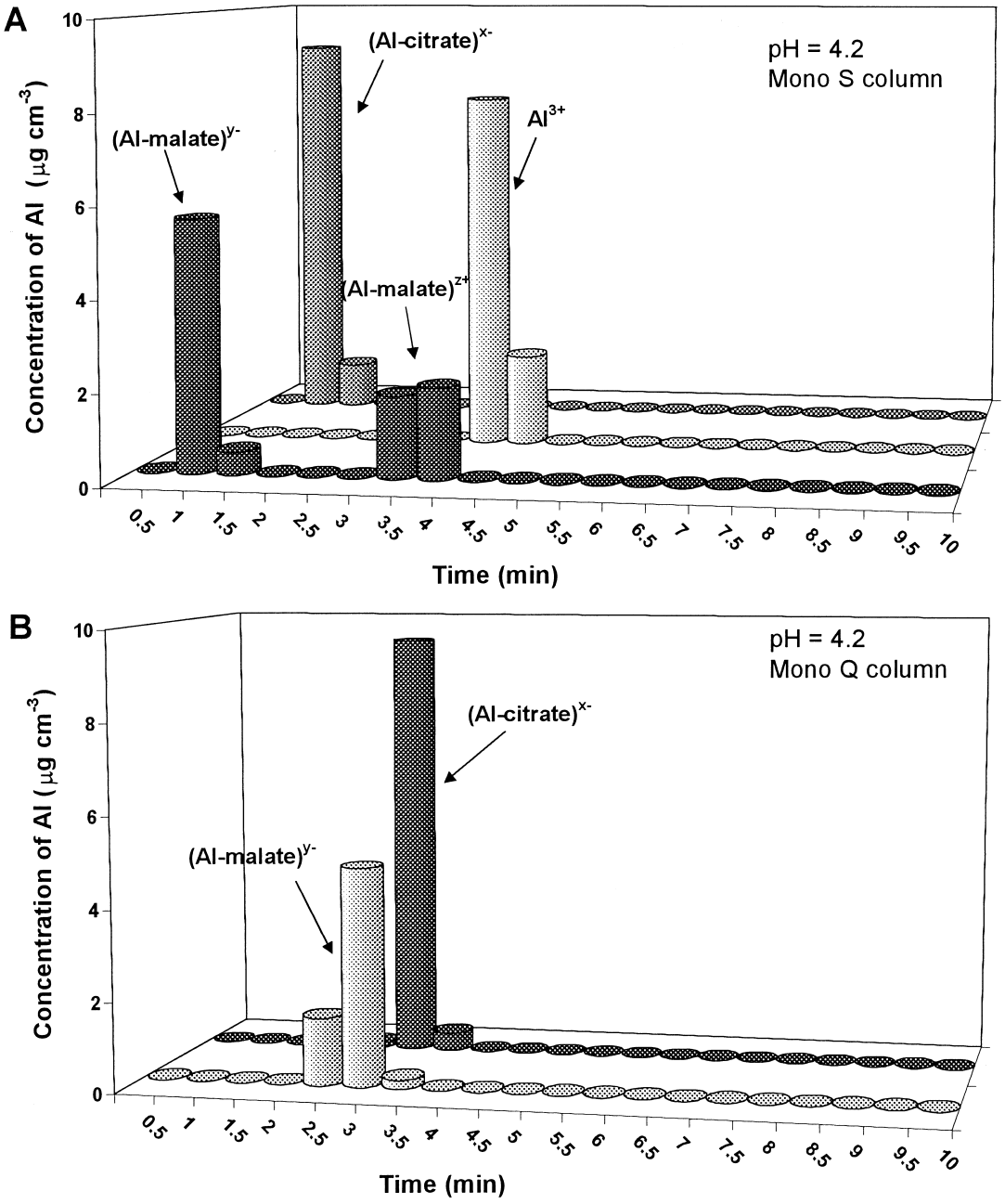

Fig. 1. Typical distribution of Al^{3+}, Al-citrate and Al-malate at pH 4.2 on a cation exchange Mono S column (A) and on an anion exchange Mono Q column (B) using ICP–AES detection. Data represent a mean of three samples with the relative standard deviation of ±5%.

total Al concentration was found to be 0.048±0.002 μg cm^{-3}. Speciation on a Mono Q column with ICP–AES and ES–MS detection indicated that Al was eluted from 2.0 to 3.0 min at the retention time typical for Al-malate. ES–MS spectra confirmed the presence of a peak with m/z 133. These data demonstrated that the Al species initially present in stem sap corresponded quantitatively to Al-malate. The concentration of this Al species was negligible in comparison to the 10 μg cm^{-3} (0.37 mM) Al used in the plant experiments.

In order to study the uptake and speciation of Al^{3+}, the plants were kept in the nutrient solution containing 10 μg cm^{-3} Al^{3+} for various time periods. The nutrient solution and the stem sap were analysed in each experiment. The results are given in Tables 1 and 2 and represent the average of two successive determinations per sample. It can be seen from Table 1 that the total concentration of Al in the nutrient solution decreased with time. It was 50% lower after 1 h of the exposure and at the limit of detection after 7 h. Analysis by FPLC–ICP–

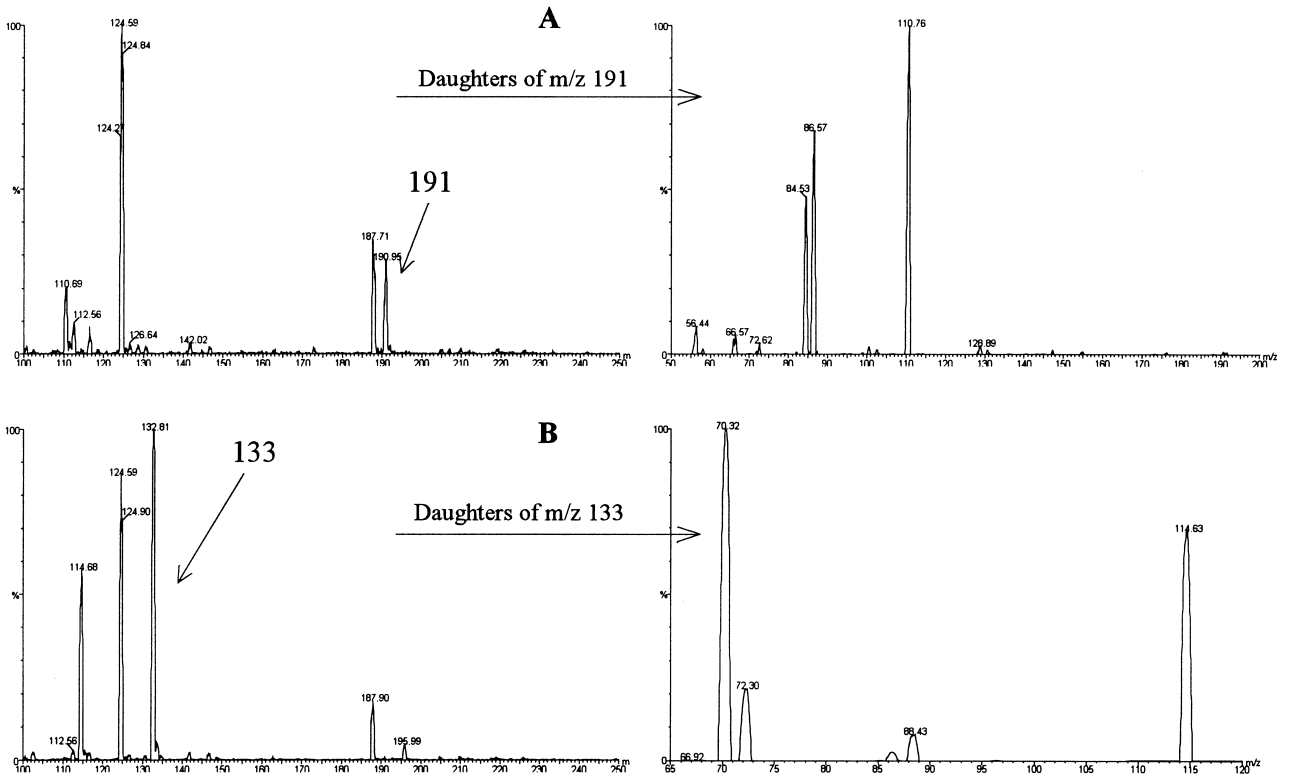

Fig. 2. ES–MS spectra and corresponding daughter ion mass spectra for synthetic solutions of Al-citrate (A) and Al-malate (B) separated on a Mono Q column.

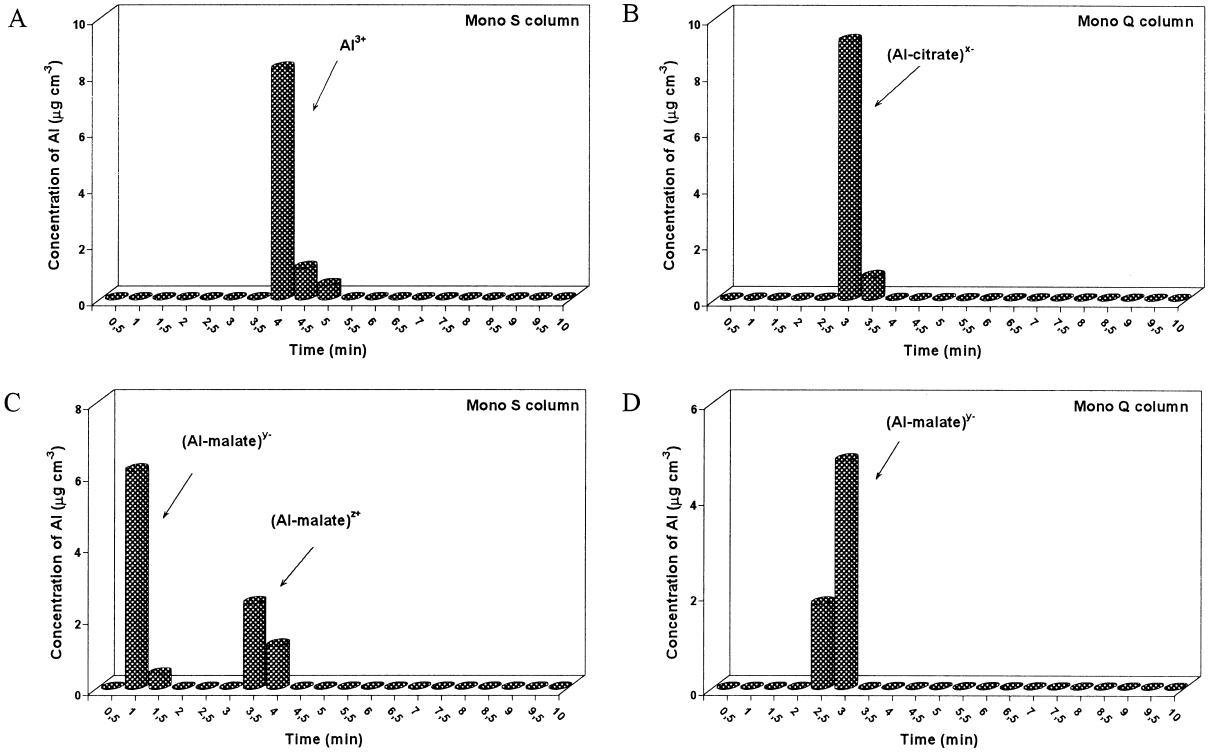

Fig. 3. Distribution of Al^{3+} (A), Al-citrate (B) and Al-malate (C, D) by FPLC–ICP–AES 24 h after the addition of particular Al species to the nutrient solution at pH 4.2. Data represent a mean of three samples with the relative standard deviation of ±5%.

Table 1
Separation of Al species present in the nutrient solution by the FPLC–ICP–AES method. Samples were taken after different periods of exposure of the cabbage plant to 10 μg of Al^{3+} cm^{-3} in a half strength Hoagland nutrient solution

Time of exposure (h)	Total conc. of A1 (μg cm^{-3})	Concentration of Al (μg cm^{-3})								
		FPLC Mono Q separation time (min)	FPLC Mono S separation time (min)							
		0→10	0–0.5	0.5–1	1→3.5	3.5–4	4-4.5	4.5–5	5-5.5	5.5→10
1	5.3±0.2	*[a]	*	*	*	3.5	1.0	0.5	0.3	*
4	2.8±0.2	*	*	*	*	1.7	0.45	0.25	*	*
7	0.25±0.1	*	*	*	*	0.2	*	*	*	*
14	0.4±0.2	*	*	*	*	0.25	0.1	*	*	*
24	0.3±0.1	*	*	*	*	0.25	*	*	*	*

[a] *Below LOD 0.1 μg cm^{-3}.

Table 2
Separation of Al species present in stem sap by the FPLC–ICP–AES method. Samples were taken after different periods of exposure of the cabbage plant to 10 μg of Al^{3+} cm^{-3} in a half strength Hoagland nutrient solution

Time of exposure (h)	Total conc. of Al (μg cm^{-3})	Concentration of Al (μg cm^{-3})												
		FPLC Mono Q separation time (min)					FPLC Mono S separation time (min)							
		0→2	2–2.5	2.5–3	3–3.5	3.5→10	0–0.5	0.5–1	1–1.5	1.5→3.5	3.5–4	4–4.5	4.5–5	5→10
1	1.75±0.2	*[a]	0.35	0.6	0.1	*	*	1.0	*	*	0.2	0.35	*	*
4	1.20±0.2	*	0.30	0.45	0.2	*	*	0.85	*	*	*	0.2	*	*
7	0.3±0.05	*	*	0.15	*	*	*	0.15	*	*	0.2	*	*	*
14	0.5±0.05	*	*	0.25	*	*	*	0.25	*	*	0.02	0.01	*	*
24	0.2±0.1	*	*	*	*	*	*	*	*	*	*	*	*	*

[a] *Below LOD 0.1 μg cm^{-3}.

AES indicated (Table 1) that Al^{3+} in the nutrient solution did not change its chemical form in the course of the experiment. It was quantitatively eluted as Al^{3+} on the Mono S column from 3.5 to 4.5 min, while on the Mono Q column it was strongly retained by the resin. Additional mass spectrometric analysis (Fig. 4) demonstrated that the concentration of known LMW organic acids in the nutrient solution was below the limit of detection, since characteristic peaks with m/z 191 (citrate), 173 (aconitate), 149 (tartrate), 133 (malate), 195 (gluconate) were not present in the mass spectrum. Two intensive peaks with m/z 210 and 226 appeared in the mass spectrum of the nutrient solution (Fig. 4), but we were not able to identify them.

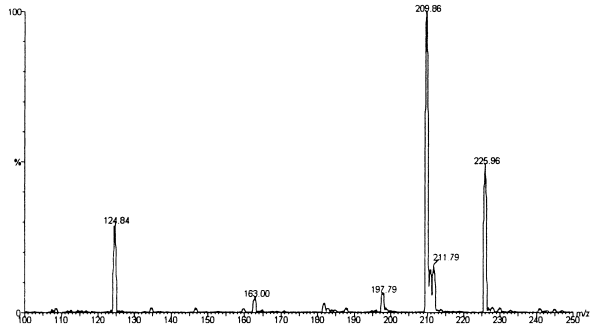

Fig. 4. ES–MS spectra of nutrient solution sampled after 1 h of exposure of cabbage to Al^{3+}.

Analysis of stem sap indicated (Table 2) that after 1 h of exposure only 1.75 μg cm^{-3} of Al was present in the sap, and that its concentration decreased with time to 0.2 μg cm^{-3} of Al after 24 h. The FPLC separations indicated that on a Mono Q column Al was eluted from 2.0 to 3.0 min. The same portion of Al was eluted with the solvent front on a Mono S column. On the basis of the retention times on the two columns it could be presumed that this species corresponds to Al-malate. The mass spectra resulted in a small peak with m/z 133, which in MS–MS analysis was fragmented to peaks with m/z 114.6, 70.3, 72.3 and 88.5 (Fig. 5). Additional peaks present in the Fig. 5 (m/z 142 and 147) corresponded to the eluent of the chromatographic run. This confirmed the presence of Al-malate. The remaining 30% of the total Al in stem sap (Table 2) was separated from 3.5 to 4.5 min on a Mono S column and corresponded to unchanged Al^{3+}. These experiments demonstrated that Al^{3+}, which was added to the nutrient solution, was mainly transformed to Al-malate.

In order to examine Al accumulation in the plant, root and leaf saps were analysed after 4 h of exposure. It

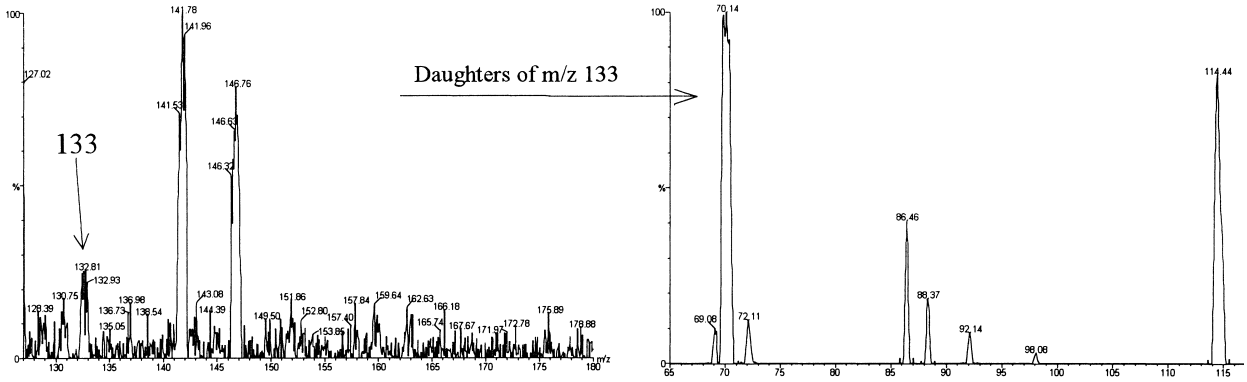

Fig. 5. ES–MS spectrum and corresponding MS–MS spectrum of m/z 133 for eluted fraction from 2 to 2.5 min on a Mono Q column for stem sap sampled after 1 h of exposure to Al^{3+}.

was found that 27 μg cm^{-3} of Al was present in the roots and 0.6 μg cm^{-3} was present in the leaves.

2.4. Uptake of Al-malate and Al-citrate

In order to test the response of Chinese cabbage to other Al species, Al-citrate or Al-malate were added to the nutrient solution. The nutrient solution and the stem sap were analysed by FPLC–ICP–AES and ES–MS–MS techniques 4 h after exposure. The results are presented in Table 3. In both experiments the total concentration of Al in the stem sap was approximately 8 μg cm^{-3}. Al-Citrate present in the nutrient solution was transferred to the stem sap and was quantitatively eluted from 2.5 to 3.5 min on a Mono Q column. On the Mono S column it was eluted with the solvent front (Table 3). In the mass spectra a peak with a m/z 191 was observed and MS–MS analysis confirmed that it corresponded to Al-citrate. Similarly, Al-malate that was transferred to the stem sap did not change its form. It was eluted as negatively charged species from 2.0 to 3.0 min on the Mono Q column (60%). The same portion was eluted with the solvent front on the Mono S column and the residual 40% as a positively charged species from 3.0–4.0 min (Table 3). The MS and MS/MS analysis confirmed the presence of Al-malate. The experimental data proved that neither Al-citrate nor Al-malate changed their chemical forms in the stem sap.

Analysis of the nutrient solution indicated that in both experiments the total concentration of Al 4 h after exposure was approximately 12 μg cm^{-3}. FPLC–ICP–AES (Table 3) in combination with ES–MS–MS analysis demonstrated that Al-citrate or Al-malate, which were added to the nutrient solution, were the only species present at the end of the experiments. Mass analysis confirmed that no other LMW acids were exuded in the course of the experiments.

The same experiments were carried out employing 1 and 7 h of exposure to Al-citrate or Al-malate. At the end of these experiments the total concentration of Al was found to be 12 μg cm^{-3} in the nutrient solution and 8 μg cm^{-3} in stem sap. FPLC–ICP–AES and ES–MS–MS confirmed the presence of the same Al species as in the 4 h exposure experiments.

Table 3
Separation of Al species in the stem sap or in the nutrient solution by FPLC–ICP–AES method after 4 h of exposure of the cabbage plant to 10 μg cm^{-3} Al-citrate or Al-malate in a half stength Hoagland nutrient solution

Al species added to the nutrient	Time of exposure (h)	Total conc. of Al (μg cm^{-3})	Concentration of Al (μg cm^{-3})											
			FPLC Mono Q separation time (min)					FPLC Mono S separation time (min)						
			0→2	2–2.5	2.5–3	3–3.5	3.5→10	0–0.5	0.5–1	1→3	3–3.5	3.5–4	4–4.5	4.5→10
Al-citrate	4-sap[b]	7.9±0.2	*[a]	0.2	6.2	1.2	*	0.2	7.5	*	*	*	*	*
	4-nut[c]	12.0±0.4	*	0.35	10.5	1.45	*	0.2	11.8	*	*	*	*	*
Al-malate	4-sap	8.8±0.3	*	1.2	3.3	0.95	*	0.15	5.0	*	2.5	1.5	*	*
	4-nut	11.8±1	*	2.1	4.5	0.4	*	0.15	6.75	*	2.8	5.5	*	*

[a] *Below LOD 0.1 μg cm^{-3}.
[b] Stem sap.
[c] Nutrient solution.

2.5. Discussion

Nutrient solution contains various ions that are possible chelators of Al. To minimize problems related with Al speciation, precipitation and polymerization, many authors (Ryan et al., 1995; Pellet et al., 1995; Ma et al., 1997b; Zheng et al., 1998) used a simple $CaCl_2$ solution treated with or without Al. Such experiments may lead to plant stress due to the lack of essential nutrients. Lazof et al. (1994) added Al to a nutrient solution and calculated the activity of free Al^{3+} by a computer program. Regarding speciation calculations on Al distribution the reliability of the calculations is a direct function of the thermodynamic data used (Berthon, 1996). A rigorous selection, or, better determination under appropriate conditions (pH, ionic strength) of stability and solubility product constants is thus required for all the complexes possibly formed between the reactants included in the model (Berthon, 1996). The latter aspect is particularly important in the case of Al, because of the difficulties in studying its complexes. In the computer speciation of Al the complexity of the nutrient solution (other cations present and their stability constants with ligands available, ionic strength of the nutrient solution) is usually not taken into consideration. Additionally, cations that are present in the nutrient solution are already in the equilibrium with available ligands. Therefore, the kinetic parameters should be taken into consideration in the calculations as well. Keeping all this difficulties in mind may help in understanding how speciation data may sometimes be so controversial.

In our investigation the concentrations of different Al species added to the nutrient solution were measured experimentally. It was evidently proven that Al was not complexed by phosphate or EDTA present in the nutrient solution, although they are strong chelators of Al^{3+}. If Al was complexed, these species would be identified and quantified with the analytical techniques applied. Al-phosphate would precipitate and the colloidal particles would be adsorbed on the resin of both columns (Bantan et al., 1999b). If the negatively charged Al-EDTA complex was formed, it would be eluted from 1.0 to 2.0 min on the Mono Q column (Bantan et al., 1998b) and with a solvent front on a Mono S column. The formation of $Al(SO_4)^+$ complex is not favourable, because the pH of the nutrient solution was 4.2 (Mitrovič et al., 1996). These observations can be explained by the fact that other cations present in the nutrient solution (Fe, Ca and Mg) compete for the available ligands. So, the concentrations of free phosphate and EDTA were not sufficient for complexation of Al. Besides, the pH of the nutrient solution was very low (4.2) and the formation of Al complexes at this pH is not favourable.

When Al-citrate or Al-malate were added to the nutrient solution their chemical forms did not change, since citrate and malate are strong chelators of Al. These observations enabled us to use the same nutrient solution for plant growth and for the Al treatment experiments, so that the possibility of plant stress caused by lack of essential nutrients was eliminated.

Most researchers studied the response of plants to Al stress by measuring the exudation of organic acids into the nutrient solution or its synthesis in the roots. However, Ma et al. (1997a, 1998) recently focussed on the identification of the form of Al present in Al accumulator plants by NMR spectroscopy. They suggested that internal detoxification of Al was achieved by formation of Al-citrate (Ma et al., 1997a) or Al-oxalate (Ma et al., 1998) in plant leaves. In our investigation the species, which were transported from roots to the leaves were identified and quantified. It is evident from the speciation analysis of the stem sap that 70% of Al was in the form of Al-malate and 30% in the form of Al^{3+}. The determination of total concentration of Al in root sap and in leaves sap confirmed that Al was partially accumulated in the roots. It was presumed that 30% of Al was immobilised in the apoplasts of roots and did not enter the cytoplasm. This presumption was based also on the data of total concentrations of Al in stem sap Al, which decreased with the time of exposure. If Al entered the cytoplasm it would be probably transformed to the Al-malate complex and transported in the upper parts of the plant. The total concentration of Al species in the stem sap would be consequently much higher during the course of the experiments. Additionally, the concentration of Al^{3+} in the nutrient solution (Table 1) was rapidly decreased. Eight hours after the exposure the concentration of Al in the nutrient solution was almost negligible. According to these data the rate of Al uptake was much higher than the rate of water uptake. Al was most likely immobilised in the root cell wall, rather than taken up in the cytoplasm. Nevertheless, further experiments are necessary to confirm this prediction.

In order to test the response of the cabbage to other Al species, Al-citrate or Al-malate were added to the nutrient solution. These experiments were performed in order to determine if the form of Al in the nutrient solution is important in the uptake patterns. The total concentration of Al in the nutrient solution 1 up to 7 h after the exposure was slightly higher than at the beginning of the experiment. It could be therefore concluded that both Al species were taken up into the plant roots at a slightly slower rate than water/nutrient solution. Since the volume of the nutrient solution was reduced, the Al species in the nutrient solution was concentrated. The total concentration of Al in the stem sap was constant (8 $\mu g\ cm^{-3}$) during the course of the experiments and was much higher than in the stem sap of the cabbage exposed to Al^{3+}. Speciation analysis of the stem sap indicated that Al-citrate or Al-malate did not change their chemical forms.

The results presented in this work demonstrated that the form of Al species has an important role in the uptake and transport mechanisms in Chinese cabbage. Al-citrate and Al-malate were taken up without being transformed. Al^{3+} was probably immobilised on the root cell wall. Only a small portion of Al entered the cells, where it was partially transformed to Al-malate and transported to the upper parts of the plant.

2.6. Experimental

2.6.1. Plant cultivation

Seeds of Chinese cabbage (*Brassica rapa* L. ssp. *pekinensis* (Lour.) Hanelt) were sown in the soil in pots. When the plantlets were about 10 cm tall, with an average of four leaves, they were carefully removed from the soil and the roots and stem were washed with water. The plants were transferred to one-half strength aerated Hoagland nutrient solution (pH 4.8) containing 2.6 mM KNO_3, 2.5 mM $Ca(NO_3)_2{\cdot}4H_2O$, 1 mM $MgSO_4{\cdot}7H_2O$, 0.5 mM KH_2PO_4, 0.054 mM $FeCl_3{\cdot}4H_2O + 0.06$ mM EDTA, 0.023 mM H_3BO_3, 4.57 μM $MnCl_2{\cdot}4H_2O$, 0.366 μM $ZnCl_2$, 0.146 μM $CuCl_2{\cdot}2H_2O$, 0.042 μM $H_2MoO_4{\cdot}4H_2O$. The cabbage was grown at 23°C, with 13-h/11-h day/night cycles and at 40 Wm^{-2} light intensity for 3 weeks. After that period the height of the plants was about 15 cm with an average of seven leaves, while the roots were approximately 10 cm long. These plants were used during the course of the experiments.

2.6.2. Preparation of Al solutions

A stock Al^{3+} solution (500 μg Al cm^{-3}) was prepared in a 100 cm^3 calibration flask by dissolving 0.694 g of $Al(NO_3)_3{\cdot}9H_2O$ (Riedel-de Haën) in doubly distilled water.

Stock Al-citrate and Al-malate solutions (500 μg Al cm^{-3}) were prepared in 100 cm^3 calibration flasks by dissolving 0.694 g of $Al(NO_3)_3{\cdot}9H_2O$ in water, followed by addition of either 3.5 g of citric acid or 2.5 g of malic acid. The Al:ligand molar ratio was 1:10, which was adequate for the formation of LMW-Al complexes (Bantan et al., 1999a).

Synthetic working solutions of Al^{3+}, Al-citrate and Al-malate (10 μg Al cm^{-3}) were prepared from Al stock solutions in imidazole-HCl buffer adjusted to pH 4.2, and were used for the study of the behaviour of these Al species on both FPLC columns. A synthetic working solution of Al-phosphate (pH = 4.2, 10 μg cm^{-3}) was made by mixing appropriate amounts of stock Al^{3+} solution and 2 mol dm^{-3} H_3PO_4 in an imidazole-HCl buffer (10:1 PO_4^{3-} to Al molar ratio).

2.6.3. Preparation of nutrient solutions containing various Al species

An appropriate amount of Al^{3+}, Al-citrate or Al-malate stock solution (500 μg Al cm^{-3}) was added to the nutrient solution, so that the final concentration of Al was 10 μg cm^{-3}. The pH of the nutrient solution after addition of the Al^{3+} stock solution was reduced from 4.8 to 4.2. When the stock solutions of Al-citrate or Al-malate were added to the nutrient media, the pH dropped to 2.5 and was adjusted to 4.2 by careful addition of 0.5 mol dm^{-3} NaOH.

In order to determine the Al chemical species present in the nutrient solution at pH 4.2 and to test their stability, analysis of the growth media by FPLC–ICP–AES technique were carried out immediately after the addition of Al^{3+}, Al-citrate or Al-malate, and after 1 day.

2.6.4. Treatment of plants with various Al species

In order to investigate the uptake and speciation of various Al species, each plant was placed in aerated growth vessel and exposed to the 50 cm^3 of half strength Hoagland nutrient solution containing Al^{3+}, Al-citrate or Al-malate (10 μg cm^{-3} Al). Plants were kept in the growth media containing particular Al species for 1, 4, 7, 14 and 24 h. At the end of each experiment the plant was taken from the nutrient solution, the stem washed with doubly distilled water and cut with stainless steel knife. The roots with the remaining stem were then returned to the same nutrient solution and the plant stem was held above the surface of the nutrient media. 0.5 to 1 cm^3 of the stem sap was collected with a plastic syringe from the stem cutting. It took about 30 min to collect approximately 1 cm^3 of stem sap. In the stem sap the total Al and Al species were determined. The nutrient solution used in the course of the experiments was analysed as well. Each experiment was performed with three replicate plants.

2.6.5. Determination of Al

The total Al in nutrient solution and in the fractions after chromatographic separation was determined by inductively coupled plasma-atomic emission spectrometry (ICP–AES) on a Perkin-Elmer (Norwalk, CT, USA) Plasma 40 emission spectrometer at 396.152 nm (Bantan et al., 1998b). Total Al in stem sap was determined by electrothermal atomic absorption spectrometry (ETAAS) on a Hitachi (Hitachi, Tokyo, Japan) Z-8270 polarised Zeeman atomic absorption spectrophotometer at 309.3 nm. Prior to analysis the stem sap was diluted 1:100 with water and analysed under the optimal measurement conditions (Bantan et al., 1998a).

In order to determine the total concentration of Al in roots or in plant leaves, the biological specimens were carefully washed with doubly distilled water and dried at room temperature. The samples were cut into small pieces with a stainless steal knife and frozen with liquid nitrogen. Then the samples were equilibrated to room temperature and squeezed with a stainless steal squeezer. The plant sap from roots or leaves was collected in polyethylene cups and analysed by ETAAS under the optimal measurement conditions (Bantan et al., 1998a).

2.6.6. Determination of Al species in nutrient solution and stem sap

A Merck-Hitachi (Darmstadt, Germany) 6200 gradient high-pressure pump, equipped with a Rheodyne (Cotati, CA, USA) Model 7161 injector was used in the chromatographic separations. Separation of negatively charged LMW organic Al complexes was performed on a Mono Q strong anion exchange fast protein liquid chromatography (FPLC) column (Pharmacia, Uppsala, Sweden). Stem sap or nutrient solution (0.2 cm^3) was injected onto the column and an aqueous-(0–100% 4 mol dm^{-3} NH_4NO_3) linear gradient elution was applied for 10 min at a flow rate of 1 cm^3 min^{-1}. Eluate was collected in 0.5 cm^3 fractions and diluted with 0.5 cm^3 of yttrium (Y) standard solution, so that the internal standard concentration was 10.0 μg Y cm^{-3}. The concentration of Al was determined "off line" by the ICP–AES technique at optimum measurement conditions (Mitrovič et al., 1996; Bantan et al., 1999a). Positively charged monomeric aqua- and hydroxy-Al species (Mitroviæ et al., 1996) and positively charged LMW-Al organic complexes (Bantan et al., 1999a) were separated on a Mono S strong cation exchange FPLC column (Pharmacia, Uppsala, Sweden) applying aqueous-(0–100% 8 mol dm^{-3} NH_4NO_3) linear gradient elution for 10 min. All other chromatographic parameters and the detection of separated Al species were the same as for the Mono Q FPLC column.

For the identification of the LMW Al binding ligands, the fractions were diluted 1:10 with water and analysed by the electrospray tandem mass spectrometry (ES–MS–MS, Micromass Quatro LC tandem quadrupole mass spectrometer UK Ltd. Manchester, UK) technique, employing a Z spray ion source as described previously (Bantan et al., 1999b).

Acknowledgements

This work was financially supported by the Ministry of Science and Technology of Slovenia.

References

Bantan, T., Milačič, R., Mitrović, B., Pihlar, B., 1999a. Combination of various analytical techniques for speciation of low molecular weight aluminium complexes in plant sap. Fresenius J. Anal. Chem. 365, 545–552.

Bantan, T., Milačič, R., Mitrović, B., Pihlar, B., 1999b. Investigation of low molecular weight Al complexes in human serum by fast protein liquid chromatography (FPLC)–ETAAS and electrospray (ES)–MS–MS techniques. J. Anal. Atom. Spectrom. 14, 1743–1748.

Bantan, T., Milačič, R., Pihlar, B., 1998a. Quantitative determination of trace amounts of Al-citrate by anion-exchange FPLC–ETAAS. Talanta 47, 929–941.

Bantan, T., Milačič, R., Pihlar, B., 1998b. Possibilities for speciation of Al-citrate and other negatively charged Al complexes by anion-exchange FPLC–ICP–AES. Talanta 46, 227–235.

Bartlett, R.J., Riego, D.C., 1972. Effect of chelation on the toxicity of aluminum. Plant and Soil 37, 419–423.

Berthon, G., 1996. Chemical speciation studies in relation to aluminium metabolism and toxicity. Coord. Chem. Rev. 149, 241–280.

de la Fuente, J.M., Ramirez-Rodriguez, V., Cabrera-Ponce, J.L., Herrera-Estrella, L., 1997. Aluminium tolerance in transgenic plants by alternation of citrate synthesis. Science 276, 1566–1568.

Delhaize, E., Craig, S., Beaton, C.D., Bennet, R.J., Jagadish, V.C., Randall, P.J., 1993a. Aluminium tolerance in wheat (*Triticum aestivum* L.). I. Uptake and distribution of aluminum in root apices. Plant Physiol. 103, 685–693.

Delhaize, E., Ryan, P.R., Randall, P.J., 1993b. Aluminum tolerance in wheat (*Triticum aestivum* L.). II. Aluminum-stimulated excretion of malic acid from root apices. Plant Physiol. 103, 695–702.

Ginting, S., Johnson, B.B., Wilkens, S., 1998. Alleviation of aluminium phytotoxicity on soybean growth by organic anions in nutrient solutions. Aust. J. Plant Physiol. 25, 901–908.

Hue, N.V., Craddock, G.R., Adams, F., 1986. Effect of organic acids on aluminum toxicity in subsoils. Soil Sci. Soc. Am. J. 50, 28–34.

Jones, D.L., 1998. Organic acid in the rhizosphere — a critical review. Plant and Soil 205, 25–44.

Jorge, R.A., Arruda, P., 1997. Aluminum-induced organic acid exudation by roots of an aluminum-tolerant tropical maize. Phytochemistry 45, 675–681.

Lazof, D.B., Goldsmith, J.G., Rufty, T.W., Linton, R.W., 1994. Rapid uptake of aluminum into cells of intact soybean root tips. Plant Physiol. 106, 1107–1114.

Ma, J.F., Hiradate, S., Matsumoto, H., 1998. High aluminum resistance in buckwheat. II. Oxalic acid detoxifies aluminum internally. Plant Physiol. 117, 753–759.

Ma, J.F., Hiradate, S., Namoto, K., Iwashita, T., Matsumoto, H., 1997a. Internal detoxification mechanism of Al in *Hydrangea*. Identification of Al form in the leaves. Plant Physiol. 113, 1033–1039.

Ma, J.F., Zheng, S.J., Matsumoto, H., 1997b. Specific secretion of citric acid induced by Al stress in *Cassia tora* L. Plant Cell Physiol. 38, 1019–1025.

Ma, J.F., Zheng, S.J., Matsumoto, H., Hiradate, S., 1997c. Detoxifying aluminium with buckwheat. Nature 390, 569–570.

Ma, Z., Miyasaka, S.C., 1998. Oxalate exudation by Taro in response to Al. Plant Physiol. 118, 861–865.

Michalas, F., Glavac, V., Parlar, H., 1992. The detection of aluminium complexes in forest soil solutions and beech xylem saps. Fresenius J. Anal. Chem. 343, 308–312.

Mitrovič, B., Milačič, R., Pihlar, B., 1996. Speciation of aluminium in soil extracts by employing cation-exchange fast protein liquid chromatography-inductively coupled plasma atomic emission spectrometry. Analyst 121, 627–634.

Miyasaka, S.C., Buta, J.G., Howell, R.K., Foy, C.D., 1991. Mechanism of aluminum tolerance in snapbeans. Root exudation of citric acid. Plant Physiol 96, 737–743.

Ownby, J.D., Popham, H.R., 1989. Citrate reverses the inhibition of wheat root growth caused by aluminum. J. Plant Physiol. 135, 588–591.

Pellett, D.M., Grunes, D.L., Kochian, L.V., 1995. Organic acid exudation as an aluminum-tolerance mechanism in maize (*Zea mays* L.). Plant 196, 788–795.

Ryan, P.R., Delhaize, E., Randall, P.J., 1995. Charactertisation of Al-stimulated efflux of malate from the apices of Al-tolerant wheat roots. Plant 196, 103–110.

Ryan, P.R., Ditomaso, J.M., Kochian, L.V., 1993. Aluminum toxicity in roots: an investigation of spatial sensitivity and the role of the root cap. J. Exp. Bot. 44, 437–446.

Taylor, G.Y., 1988. The physiology of aluminum tolerance. In: Sigel, H. (Ed.), Metal Ions in Biological Systems. Aluminum and Its Role in Biology, Vol. 24. Marcel Dekker, New York, pp. 165–198.

Taylor, G.Y., 1991. Current views of the aluminum stress response; the physiological basis of tolerance. Current Top Plant Biochem. Physiol. 10, 57–93.

van Hees, P.A.W., Andersson, A.M.T., Lundström, U.S., 1996. Separation of organic low molecular weight aluminium complexes in soil solution by liquid chromatography. Chemosphere 33, 1951–1996.

Zhang, G., Taylor, G.J., 1989. Kinetics of aluminum uptake by excised roots of aluminum-tolerant and aluminum-sensitive cultivars of *Triticum aestivum* L.. Plant Physiol. 91, 1094–1099.

Zheng, S.J., Ma, J.F., Matsumoto, H., 1998. High aluminum resistance in buckwheat I. Al-induced specific secretion of oxalic acid from root tips. Plant Physiol. 117, 745–751.

PERGAMON

Phytochemistry 57 (2001) 199–208

PHYTOCHEMISTRY

www.elsevier.com/locate/phytochem

Biotransformation of (*R*)-(+)- and (*S*)-(−)-limonene by fungi and the use of solid phase microextraction for screening

Jan C.R. Demyttenaere *, Kristof Van Belleghem, Norbert De Kimpe

Department of Organic Chemistry, Faculty of Agricultural and Applied Biological Sciences, Ghent University, Coupure Links 653, B-9000 Ghent, Belgium

Received 29 September 2000; received in revised form 1 December 2000

Abstract

The biotransformation of (*R*)-(+)- and (*S*)-(−)-limonene by fungi was investigated. More than 60 fungal cultures were screened for their ability to bioconvert the substrate, using solid phase microextraction as the monitoring technique. After screening, the best fungal strains were selected for further study and were grown as sporulated surface cultures in conical flasks and as submerged liquid cultures. It was found that (+)- and (−)-limonene were converted by *Penicillium digitatum* to α-terpineol (main metabolite), *cis*- and *trans*-*p*-menth-2-en-1-ol, neodihydrocarveol and limonene oxide (minor metabolites) using liquid cultures. The bioconversion of (*R*)-(+)- and (*S*)-(−)-limonene by *Corynespora cassiicola* yielded (1*S*,2*S*,4*R*)- and (1*R*,2*R*,4*S*)-limonene-1,2-diol respectively. The bioconversions by liquid cultures were also monitored by solid phase microextraction as a function of time. The optimum conversion of limonene to α-terpineol by *Penicillium digitatum* was obtained after 8 hours (yield up to 100%). Since an important pH-decrease was noticed in some liquid broths, the stability of limonene under acidic conditions was investigated. No acid catalysed conversion products were recovered after 8 days from control flasks at pH 3.5 containing limonene. © 2001 Elsevier Science Ltd. All rights reserved.

Keywords: *Penicillium digitatum*; *Corynespora cassiicola*; Fungi; Fungal spores; Biotransformation; Bioconversion; Limonene; α-Terpineol; (1*S*,2*S*,4*R*)-Limonene-1,2-diol; (1*R*,2*R*,4*S*)-Limonene-1,2-diol; SPME

1. Introduction

Much work has been done on the biotransformation of the inexpensive hydrocarbon monoterpene limonene (Bowen, 1975), which is, besides α-pinene, the most widely distributed terpene in nature (Krasnobajew, 1984). The (+)-isomer is present in citrus peel oils at a concentration of over 90%; a low concentration of the (−)-isomer is found in oils from the *Mentha* species and conifers (Bauer et al., 1990). The microbial conversion of limonene is very well documented, the first data date back to the sixties. A soil pseudomonad was isolated by an enrichment culture technique on limonene as the sole source of carbon (Dhavalikar and Bhattacharyya, 1966) and was able to convert the substrate to a large number of neutral and acidic products. Another group isolated a *Pseudomonas incognita* by an enrichment technique on the monoterpene alcohol linalool (Madyastha et al., 1977). The metabolism of limonene by this bacterium was investigated (Rama Devi and Bhattacharyya, 1977). After fermentation the medium yielded as the main product a crystallic acid, perillic acid, together with unmetabolised limonene and some oxygenated compounds, such as dihydrocarvone, carvone and carveol. The biotransformation of limonene by another *Pseudomonas* strain, *P. gladioli* was also reported (Cadwallader et al., 1989; Cadwallader and Braddock, 1992). Major conversion products from (+)-limonene were (+)-α-terpineol and (+)-perillic acid. This was the first time that the microbial conversion of limonene to α-terpineol was reported. α-Terpineol is widely distributed in nature and is one of the most commonly used perfume chemicals (Fenaroli, 1975). The first data on fungal bioconversion of limonene date back to the late sixties. A *Cladosporium* sp. designated as T_7 was isolated on limonene and was able to convert the substrate to *trans*-limonene-1,2-diol (Mukherjee et al., 1973). Another

* Corresponding author. Tel.: +32-9-264-549-64; fax: +32-9-264-62-43.

E-mail address: jan.demyttenaere@rug.ac.be (J.C.R. Demyttenaere).

0031-9422/01/$ - see front matter © 2001 Elsevier Science Ltd. All rights reserved.
PII: S0031-9422(00)00499-4

Cladosporium, designated T_{12}, converted limonene into α-terpineol (Kraidman et al., 1969).

Fungi, isolated from rotting orange rind, were also found to be able to convert limonene to α-terpineol (Mattison et al., 1971). Bowen (1975) isolated two common citrus moulds, *Penicillium italicum* and *P. digitatum*, responsible for the postharvest diseases of citrus fruits. Fermentation of *P. italicum* on limonene yielded *cis*- and *trans*-carveol (26%) as main products, together with (+)-carvone (6%) and minor metabolites. Conversion by *P. digitatum* yielded the same products in lower yields. The bioconversion of limonene by *Aspergillus niger* has also been described (Rama Devi and Bhattacharyya, 1978). This fungus was able to carry out three types of oxygenative rearrangements. More recently, a Japanese group studied the biotransformation of limonene and related compounds (1-methylcyclohexene and cyclohexene) by *Aspergillus cellulosae* M-77 (Noma et al., 1992). (+)-Limonene was mainly converted to (+)-isopiperitenone (19%), (+)-limonene-1,2-*trans*-diol (21%), (+)-*cis*-carveol (5%) and (+)-perillyl alcohol (12%). The production of isopiperitenone from limonene was published for the first time.

The production of glycols from limonene and other terpenes with a 1-menthene skeleton was reported (Abraham et al., 1984). The most appropriate strains were *Corynespora cassiicola* and *Diplodia gossypina*. The same group (Abraham et al., 1985) also investigated the biotransformation of (*R*)-limonene to (*R*)-α-terpineol by the fungus *Penicillium digitatum*. An extensive overview on the microbial transformations of terpenoids with a 1-*p*-menthene skeleton was published by this group (Abraham et al., 1986). One of the most recent publications in this area reported the bioconversion of limonene to α-terpineol by immobilised *P. digitatum* (Tan and Day, 1998a) and studied the effect of organic cosolvents on the bioconversion of (*R*)-(+)-limonene to (*R*)-(+)-α-terpineol (Tan and Day, 1998b). In all these examples submerged liquid cultures were used. The bioconversion of limonene by fungal spores has not been published to date.

This paper reports the biotransformation of (*R*)-(+)-(**1**) and (*S*)-(−)-limonene (**19**) by sporulated surface cultures and liquid cultures of fungi and the use of solid phase microextraction (SPME) for fast screening.

2. Results and discussion

2.1. Screening of sporulated surface cultures by fungi by SPME

More than 60 fungal strains, grown as sporulated surface cultures, were screened for their ability to bioconvert the substrate (*R*)-(+)-limonene (**1**), using solid phase microextraction (SPME) as the monitoring technique. Therefore, a method was developed to cultivate sporulated surface cultures of the fungi in small vials, and the SPME-parameters were optimised. Different SPME-fibers, extraction times and temperatures were compared. Extraction of volatiles (limonene and metabolites) was done by headspace SPME. It was found that the best SPME fiber for extraction of limonene and its metabolites was 50/30 μm divinylbenzene/carboxen on polydimethylsiloxane. The optimum adsorption time was 30 min. The best extraction temperature was room temperature, but because of temperature fluctuation, a constant adsorption temperature of 25°C was chosen as optimum. A desorption temperature of 250°C and desorption time of 2 min was sufficient to desorb all volatiles into the gaschromatographic inlet.

The most interesting conversion of (*R*)-(+)-limonene (**1**) was the formation of (*R*)-(+)-α-terpineol (**2**) by various *Penicillium* species. Other metabolites recovered were γ-terpinene (**3**), terpinolene (**4**), α-phellandrene (**5**), *endo*-fenchol (**11**), menth-3-en-1-ol (**6**), *p*-cymene (**9**), *neo*-dihydrocarveol (**12**), *cis*-limonene oxide (**7**), *trans*-limonene oxide (**8**) and perillyl alcohol (**10**) (see Scheme 1). The most interesting strains were *P. digitatum* (both isolated (CMC) and obtained, DSM 62840) and *Corynespora cassiicola* DSM 62475.

2.2. Biotransformation of (R)-(+)-limonene by sporulated surface cultures

After screening, the best fungal strains were selected for further study and were grown as sporulated surface cultures in conical flasks. The biotransformation was monitored by dynamic headspace, steam distillation solvent extraction and liquid/liquid extraction.

In a first experiment, the bioconversion of (*R*)-(+)-limonene (**1**) by two strains was compared, namely *Penicillium digitatum* (CMC), selected as interesting strain, based on the SPME screening results, and *Aspergillus niger* (AND), since *A. niger* has been used successfully in many bioconversion reactions (Rama Devi and Bhattacharrya, 1978; Arfmann et al., 1987, 1988; Demyttenaere and Willemen, 1998; Demyttenaere and De Kimpe, 2000; Demyttenaere et al., 2000). To 10-day old sporulated surface cultures, 100 μl of a 20% limonene in EtOH solution was sprayed. Two more substrate additions took place after 15 and 17 days respectively. It was found that *Aspergillus niger* was not able to convert limonene, whereas *Penicillium digitatum* produced (*R*)-(+)-α-terpineol (**2**) from limonene with low yields (0.7–1.4%). In a second experiment, the bioconversion of (*R*)-(+)-limonene (**1**) by two strains of *Penicillium digitatum*, namely strain CLE and strain PDD was compared in duplicate. The first substrate addition (125 μl of a 20% limonene in EtOH solution) was performed after 7 days. Two more substrate

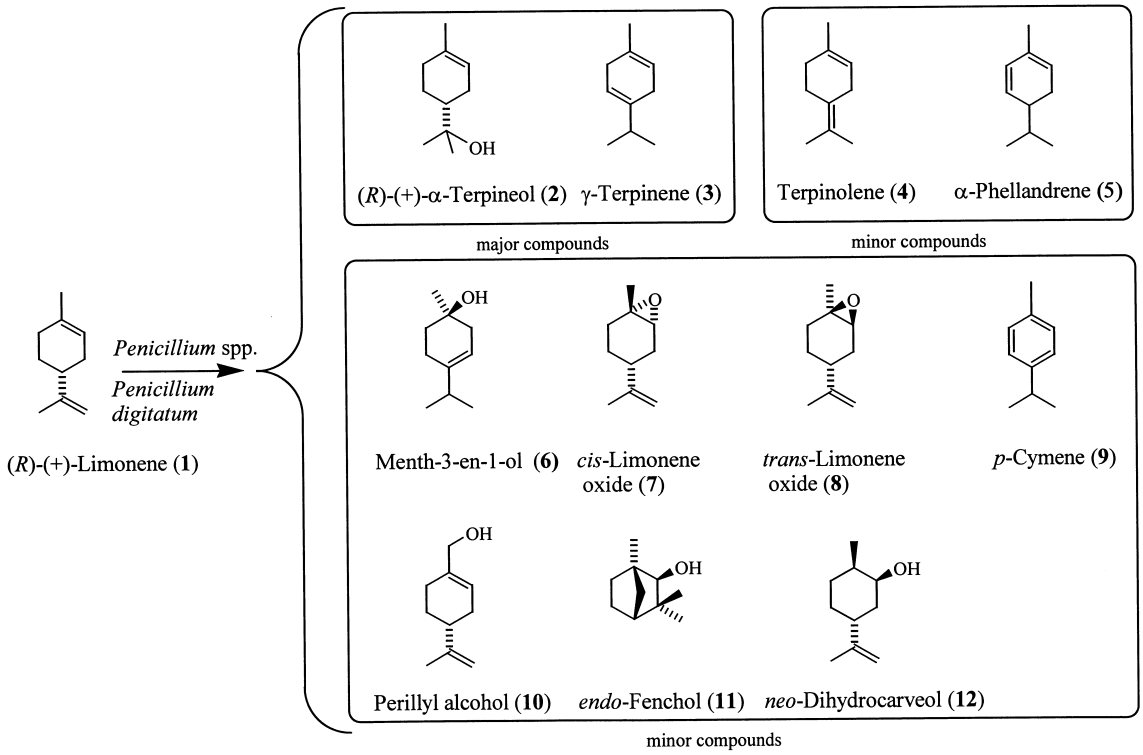

Scheme 1. Biotransformation of (*R*)-(+)-limonene by sporulated surface cultures of fungi — monitoring by SPME.

additions took place after 12 and 14 days resp. From the headspace extracts of the surface cultures, it could be seen that up to 44% of the substrate (*R*)-limonene (**1**) was recovered unchanged. The yield of conversion to (*R*)-α-terpineol (**2**) was 1.1 and 1.3% for the two *P. digitatum* cultures of strain CLE resp. and 2.7 and 2.9% for the two cultures of strain PDD resp. Minor metabolites were 1,3,5-*p*-menthatriene (**13**) (0.2–0.6%), *cis*-limonene oxide (**7**) (0.1–0.2%) and *exo*-2-hydroxycineol (**14**) (0.1–0.2%) (see Scheme 2).

It is important to note that the pH of the surface cultures dropped to pH 3 after the cultures were subjected to steam distillation/solvent extraction. Therefore, a control experiment was run to check the degradation of limonene in sterile agar medium and MEA-medium, acidified to pH 3.5 (at lower pH, the agar did not solidify), during headspace sampling and steam distillation/solvent extraction. The substrate (*R*)-limonene happened to be very stable: only small traces (0.14%) of β-myrcene were recovered from the steam distillate. No acid catalysed conversion products from limonene were recovered from the headspace extracts.

It can be concluded that sporulated surface cultures of *P. digitatum* are able to convert the substrate (*R*)-(+)-limonene (**1**) to (*R*)-α-terpineol (**2**). Since the very high volatility of the substrate, limonene, a high amount of substrate loss due to evaporation during headspace extraction was noticed, resulting in high substrate recovery. Therefore, when dynamic headspace sampling is compared with headspace SPME-sampling, the latter

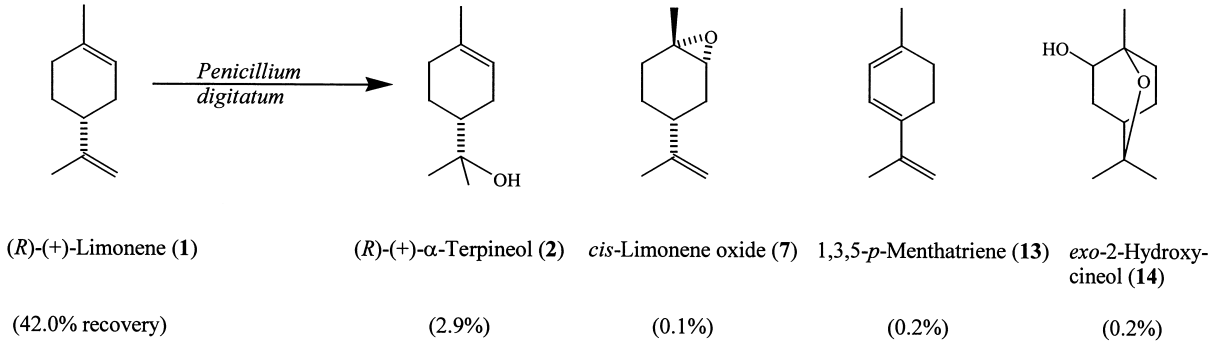

Scheme 2. Bioconversion of (*R*)-(+)-limonene by sporulated surface cultures of *Penicillium digitatum*.

method is more sensitive and efficient for fast screening.

2.3. Bioconversion of (R)-(+)- and (S)-(−)-limonene by liquid cultures

In a first experiment the bioconversion of (*R*)-(+)-limonene by submerged liquid cultures was studied, comparing five fungal strains, namely *Corynespora cassiicola* (marked COC), *Aspergillus niger* (marked AND) and three different strains of *Penicillium digitatum* (marked CLE, CMC and PDD respectively). All strains were cultivated in duplicate, except strain CLE. As a control, the stability of the precursor was checked in acidified broth (pH 3.5) that was not inoculated but kept under sterile conditions.

Over a period of 8 days, 3×25 μl of (*R*)-(+)-limonene (each time 125 μl of a 20% solution of limonene in EtOH) was added to cultures of 50 ml each. The first substrate addition was performed after 46 h of cultivation, the second after 5 days and the third after 7 days. Samples were taken 24 h after the first substrate addition, and 22.5 h after the second and third substrate addition, respectively. *Corynespora cassiicola* was able to transform the substrate to (1*S*,2*S*,4*R*)-limonene-1,2-diol (**15**) with a final yield of 46.9–60.6%. This biotransformation confirms previously published literature data (Abraham et al., 1986). All *P. digitatum* cultures converted (*R*)-(+)-limonene (**1**) to (*R*)-(+)-α-terpineol (**2**) with an initial yield up to 45.7% (after 24 h). These results are in agreement with literature data (Abraham et al., 1985). *Aspergillus niger*, however, was not able to convert the substrate. The substrate recovery was very low, namely 0.0% from the two *C. cassiicola* cultures and 0.11–0.14% from the *A. niger* cultures. From the control flasks, no acid catalysed conversion products were recovered. This means that all products recovered from the culture media are bioconversion metabolites and that all the substrate was either metabolised or evaporated.

The substrate recovery and yields of biotransformation products obtained from limonene by the *Penicillium digitatum* cultures are displayed in Table 1.

It is important to note that the conversion of (*R*)-(+)-limonene to (*R*)-(+)-α-terpineol by *P. digitatum* took place during the first part of the experiment (first 24-h period). The conversion of (*R*)-limonene (**1**) to (1*S*,2*S*,4*R*)-limonene-1,2-diol (**15**) by *C. cassiicola* on the other hand was slow. The highest yield was obtained at the end of the experiment (after 5 days of conversion). The final pH of the *C. cassiicola* culture media was neutral, whilst the culture media of *P. digitatum* were slightly basic (pH 8.5) at the end of the experiment.

In a second experiment the bioconversion of (*R*)-(+)-limonene (**1**) and (*S*)-(−)-limonene (**19**) by submerged liquid cultures was studied, comparing two fungal strains, namely *Corynespora cassiicola* (COC) and *Penicillium digitatum* (PDD). Also the difference between high (3×50 μl limonene per 50-ml culture) and low (3×25 μl limonene per 50-ml culture) precursor addition was compared (only for the conversion of (*R*)-limonene to limonene-1,2-diol by *C. cassiicola*). The first substrate addition took place after 42 h of cultivation, the second after 50 h cultivation and the third after 66 h cultivation. Samples were taken 8 h after the first substrate addition, 16 h after the second substrate addition and 8 and 24 h, respectively, after the third substrate addition.

The percentage of substrate recovery and the yields of the bioconversion products are listed in Table 2 (bioconversion of (*R*)-limonene) and Table 3 (bioconversion of (*S*)-limonene).

Again it was noticed that the bioconversion of both (*R*)-(+)- and (*S*)-(−)-limonene to (*R*)-(+)- and (*S*)-(−)-α-terpineol, respectively, by *P. digitatum* was fast (67.2% yield of (+)-α-terpineol after 8 h when 50 μl substrate was administered to a 50-ml culture), whilst the conversion to limonene-1,2-diol by *C. cassiicola* was a slow process (max. yield only obtained after 3 substrate additions, i.e. at the end of the experiment (5 days)). No difference was observed between high (3×50 μl) and low (3×25 μl) substrate addition in the conversion of limonene to limonene-1,2-diol by *C. cassiicola*. Substrate recovery was very low, especially for the cultures of *C. cassiicola* (< 1%). When control experiments were run with 50 μl of (*R*)-limonene dissolved in 50 ml of sterile culture broth in the presence of 0.5% EtOH, it was shown that the concentration of limonene dropped to half of its original concentration after less than one hour and that all limonene was evaporated after six hours.

The bioconversion of (*R*)-(+)- and (*S*)-(−)-limonene by *C. cassiicola* and *P. digitatum* is given schematically in Schemes 3 and 4.

2.4. Monitoring of the bioconversion of limonene by liquid cultures during time course

2.4.1. Monitoring of the bioconversion by liquid cultures in conical flasks by liquid extraction

The bioconversion of (*R*)-(+)-limonene by two *Penicillium digitatum* (CMC and PDD) strains and one *Corynespora cassiicola* strain grown as liquid cultures in conical flasks was monitored during time course by liquid extraction with Et_2O. To the pregrown cultures of 50 ml, one substrate addition of 250 μl of a 20%-solution of (*R*)-limonene in EtOH (i.e. 50 μl limonene) was performed. At time $t = 0$ min, 30 min and consequently every 90 min until 480 min, a 5-ml sample was taken from each culture and extracted with E_2O. From the results displayed in Fig. 1 it can be seen that the maximum yield for the bioconversion of (*R*)-limonene to (*R*)-α-terpineol was obtained after 8 hours (almost

Table 1
Substrate recovery (%) and yield (%) of bioconversion products of *R*-(+)-limonene by fungi (experiment 1 with liquid cultures of *Penicillium digitatum*)

Substrate and metabolites		CMC 1[a]	CMC 2	PDD 1[b]	PDD 2	CLE[c]
(*R*)-(+)-Limoneen (**1**)	Recovery (%)	0.63	0.57	0.00	0.07	0.00
(*R*)-(+)-α-Terpineol (**2**)	Initial yield (%)	45.65	25.43	11.35	12.16	7.34
Unknown 1	Final yield (%)	0.48	0.47	0.03	0.55	0.37
exo-2-Hydroxycineol (**14**)	Final yield (%)	1.08	0.83	6.76	0.93	0.47
Unknown 2	Final yield (%)	0.52	0.59	0.00	1.15	1.09

[a] CMC = *Penicillium digitatum* isolated from spoiled mandarin.
[b] PDD = *Penicillium digitatum* DSM 62840.
[c] CLE = *Penicillium digitatum* ATCC 201167 isolated from spoiled tangerin.

Table 2
Substrate recovery (%) and yield (%) of bioconversion products after bioconversion of (*R*)-(+)-limonene by fungi (experiment 2 with liquid cultures)

Substrate and metabolites		COC[a] low[c]	COC high[d]	PDD[b] high
(*R*)-(+)-Limonene (**1**)	Recovery (%)	0.85	0.07	3.16
(1*S*,2S,4*R*)-Limonene-1,2-diol (**15**)	Final yield (%)	46.7	48.6	0.00
(*R*)-(+)-α-Terpineol (**2**)	Initial yield (%)	0.00	0.00	67.2
cis-p-Menth-2-en-1-ol (**17**)	Final yield (%)	0.35	0.35	1.27
trans-p-Menth-2-en-1-ol (**18**)	Final yield (%)	0.00	0.10	0.68
neo-Dihydrocarveol (**12**)	Initial yield (%)	1.70	1.04	1.70
cis-Limonene oxide (**7**)	Final yield (%)	0.00	0.14	0.29
Piperitone (**16**)	Final yield (%)	0.27	0.27	0.00

[a] COC = *Corynespora cassiicola*.
[b] PDD = *Penicillium digitatum*.
[c] Low = 3×25 μl substrate addition.
[d] High = 3×50 μl substrate addition/50 ml.

Table 3
Substrate recovery (%) and yield (%) of bioconversion products after bioconversion of (*S*)-(−)-limonene by fungi (experiment 2 with liquid cultures)

Substrate and metabolites		COC[a] low[c]	COC high[d]	PDD[b] low
(*S*)-(−)-Limonene (**19**)	Recovery (%)	0.00	0.23	5.05
(1*R*,2*R*,4*S*)-Limonene-1,2-diol (**20**)	Final yield (%)	50.49	49.11	0.00
(*S*)-(−)-α-Terpineol (**22**)	Initial yield (%)	0.00	0.00	16.97
cis-p-Menth-2-en-1-ol (**21**)	Final yield (%)	1.18	0.00	1.47
trans-p-Menth-2-en-1-ol (**23**)	Final yield (%)	0.00	0.35	0.50
trans-Dihydrocarvone (**24**)	Final yield (%)	0.00	0.00	0.10

[a] COC = *Corynespora cassiicola*.
[b] PDD = *Penicillium digitatum*.
[c] Low = 3×25 μl substrate addition.
[d] High = 3×50 μl substrate addition/50 ml.

100% yield for strain CMC and approx. 75% yield for strain PDD). The conversion of (*R*)-limonene to limonene-1,2-diol by *C. cassiicola* however was only approx. 12% after 8 h, suggesting that this conversion is very slow.

2.4.2. Monitoring of the bioconversion by liquid cultures in SPME-vials by SPME

The bioconversion of (*R*)-(+)-limonene by two strains of *Penicillium digitatum* (CMC and PDD), grown as liquid cultures in small SPME-vials, was monitored by SPME. From 50-ml pregrown cultures of 48 h, 15 ml culture was transferred into 40-ml SPME vials and stirred (800 rpm). To each culture 10 μl of a 10%-solution of (*R*)-limonene in EtOH (i.e. 1 μl of limonene) was added. At time $t = 0$ min and consequently every 90 min until 540 min, the cultures were sampled by liquid SPME. The conversion was monitored by plotting the peak area of (*R*)-limonene and (*R*)-α-terpineol of the chromatograms as a function of time (see Fig. 2). From this graph, it can be concluded that SPME is a very powerful technique to monitor the

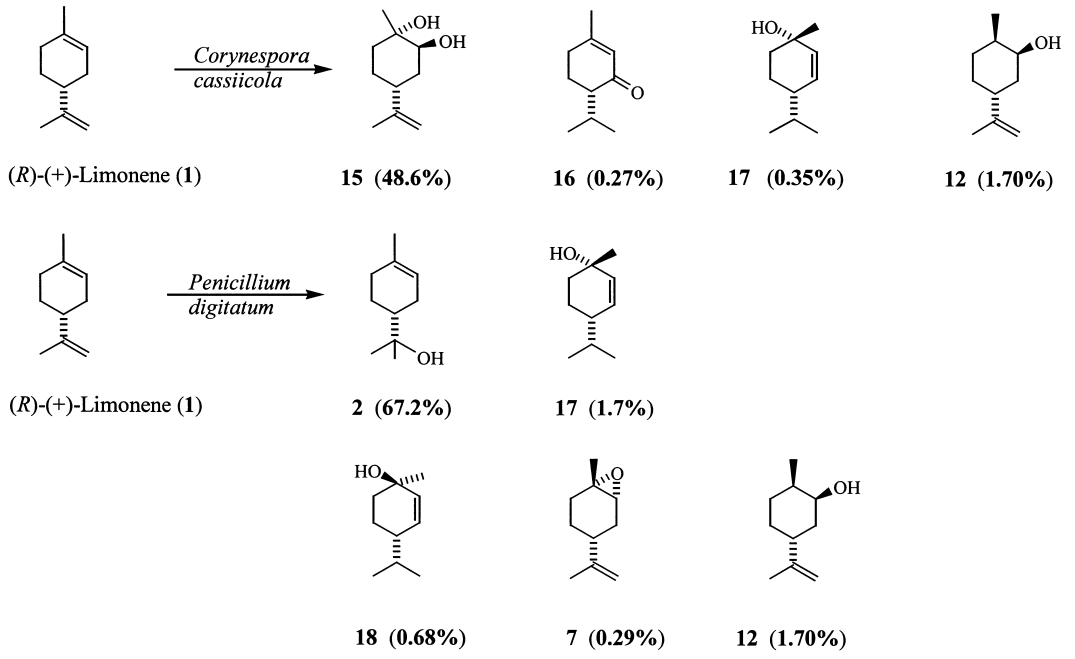

Scheme 3. Biotransformation of (*R*)-(+)-limonene by liquid cultures of *Penicillium digitatum* and *Corynespora cassiicola* — for the names of the molecular structures, see Table 2.

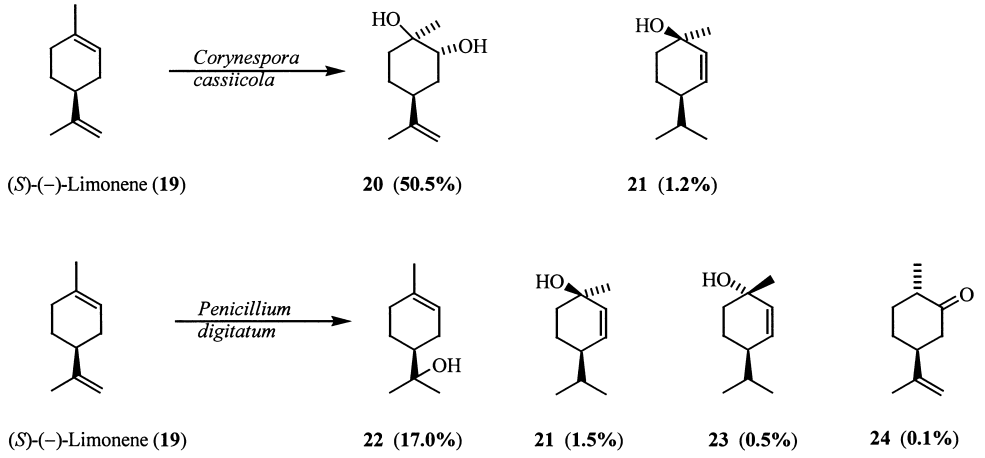

Scheme 4. Biotransformation of (*S*)-(−)-limonene by liquid cultures of *Penicillium digitatum* and *Corynespora cassiicola* — for the names of the molecular structures, see Table 3.

bioconversion of limonene by fungi as a function of time. However, since peak areas and not concentrations are plotted, no conversion yields can be calculated from SPME-extractions. It is clear that all (*R*)-limonene is either consumed or evaporated after 300 min and a maximum conversion is obtained after 360 min.

2.4.3. Monitoring of the bioconversion by spore suspensions in SPME-vials by SPME

The bioconversion of (*R*)-(+)-limonene by spore suspensions in the course of time was monitored by SPME. Two strains of *Penicillium digitatum* were compared (CMC and PDD). For this experiment, spore suspensions were prepared by harvesting spores from Petri dish cultures with a physiological solution (0.85% NaCl) containing 0.5% Tween 80. The spore suspensions thus obtained contained approx. 1×10^8 spores/ml. A control experiment was also run, consisting of pure water. To each spore suspension and to the water control, 10 μl of a 10%-solution of (*R*)-limonene in EtOH (i.e. 1 μl of limonene) was added. At time $t=0$ min and consequently every 90 min until 450 min, the suspensions were sampled by liquid SPME. The conversion was monitored by plotting the peak area of (*R*)-limonene and (*R*)-α-terpineol of the chromatograms as a function of time (see Fig. 3). It can be concluded that

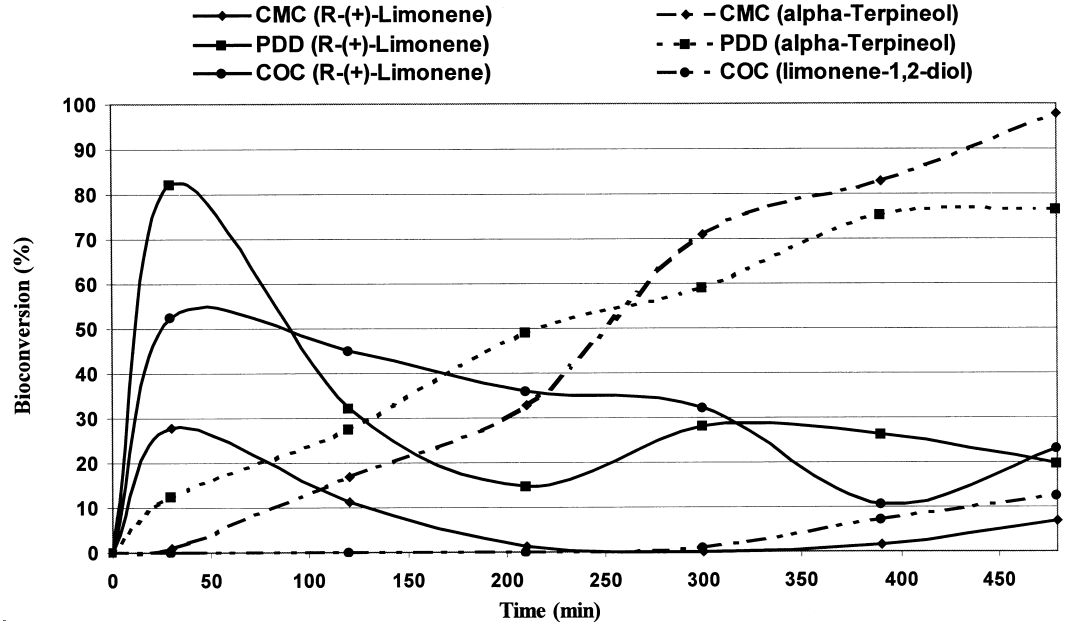

CMC = *Penicillium digitatum* isolated from spoiled mandarin – PDD = *Penicillium digitatum* DSM 62840
COC = *Corynespora cassiicola* DSM 62475

Fig. 1. Monitoring bioconversion of (*R*)-limonene by liquid fungal cultures in conical flasks by liquid extraction.

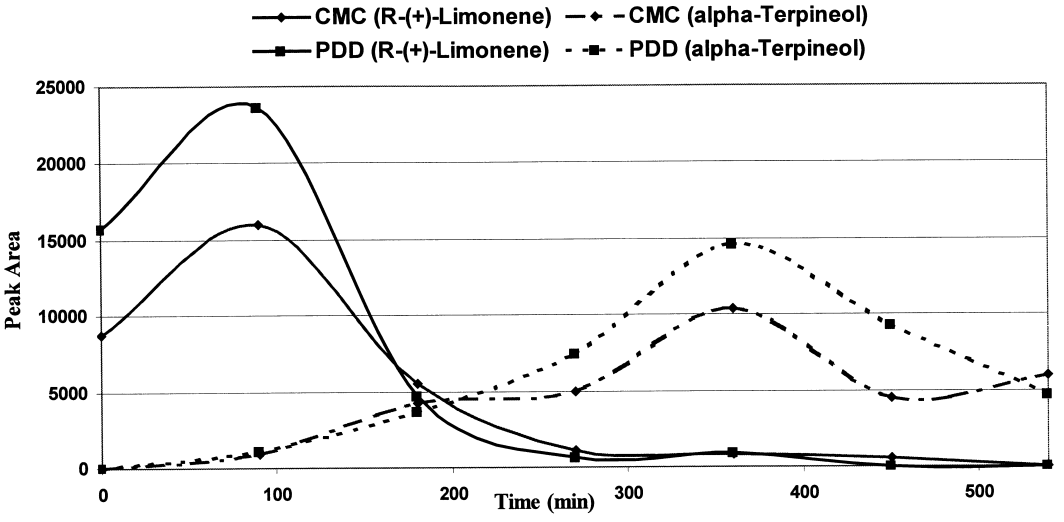

CMC = *Penicillium digitatum* isolated from spoiled mandarin – PDD = *Penicillium digitatum* DSM 62840

Fig. 2. Monitoring bioconversion of (*R*)-limonene by liquid cultures in small SPME vials by SPME.

the optimum conversion yield of spores of strain PDD was higher and appeared earlier (after 270 min) than the strain CMC (optimum later than 450 min). Since no conversion products were noticed in the control, it can be concluded that spores of *Penicillium digitatum* were able to convert (*R*)-(+)-limonene to (*R*)-(+)-α-terpineol and that SPME is a suitable screening technique for monitoring the biotranformation capacity of fungal spores.

3. Experimental

3.1. Microorganisms and cultivation

More than 60 fungal strains were used in this study. They belonged to the following species: *Penicillium digitatum*, *P. italicum*, *P. roquefortii*, *P. chrysogenum*, *P. lividum*, *Aspergillus niger*, *Aspergillus versicolor*, *Botryodiplodia malorum*, *Rhizopus oryzae*, *Beauveria*

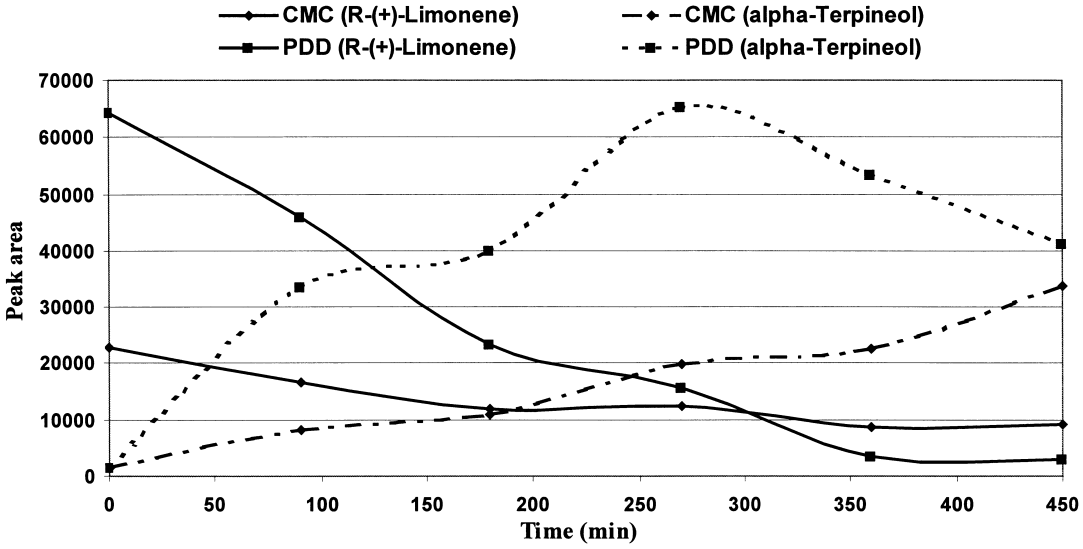

CMC = *Penicillium digitatum* isolated from spoiled mandarin – PDD = *Penicillium digitatum* DSM 62840

Fig. 3. Monitoring bioconversion of (*R*)-limonene by spore suspensions in small SPME vials by SPME.

bassiana, *Cunninghamella elegans*, *C. blakesleeana*, *Hyphozima roseoniger*, *Corynespora cassiicola*, *Chaetomium cochliodes* and *Mortierella* sp. The fungi were either isolated from spoiled fruit or contaminated media, or obtained from DSM (Deutsche Sammlung von Mikroorganismen). After screening experiments, some fungal strains were selected for further study and marked as follows: CMC (*Penicillium digitatum* isolated from spoiled mandarin), CLE (*Penicillium digitatum* Saccardo isolated from spoiled tangerine and assigned ATCC 201167), PDD (*Penicillium digitatum* DSM 62840), COC (*Corynespora cassiicola* DSM 62475), AND (*Aspergillus niger* DSM 821). The cultures were cultivated and conserved by periodic replications (every 2 weeks) on malt extract agar (MEA: malt extract 2%, bacteriological peptone 0.1%, glucose 2% and agar 2%–pH 5.4).

3.2. Screening of sporulated surface cultures by fungi by SPME

The fungi were cultivated as small sporulated surface cultures in 40-ml SPME-vials (Supelco Inc., Bellafonte, USA) (Demyttenaere and De Kimpe, 2000; Demyttenaere et al., 2000). Therefore, the vials were filled with 10 ml medium (MEA), autoclaved, and inoculated with fresh spores. The vials were covered with cotton wool and the cultures were incubated at 30°C during 24 h and at room temp during 48 h, after which complete sporulation had taken place. To each sporulated surface culture, 5 μl of a solution of (*R*)-(+)-limonene (puriss., >99%, FLUKA) in EtOH (10%) was sprayed. The vials were covered with PTFE-Silicone Septa and Open Top Phenolic Closures (Supelco) and stored at room temperature until the start of the headspace SPME-extraction. During extraction, the SPME fibers were exposed to the headspace of the cultures for 5, 15 or 30 min at 25°C.

To select the best sampling parameters, 40-ml SPME-vials were filled with 10 ml agar medium (2% agar/water) to which 5 μl of the same solution of limonene in EtOH (10%) or solutions containing limonene and α-terpineol in different ratios were sprayed. Different SPME fibers were used, namely 100 μm polydimethylsiloxane (PDMS), 50/30 μm divinylbenzene/carboxen on polydimethylsiloxane, 65 μm carbowax/divinylbenzene (CWDB) and 85 μm polyacrylate (PA) (Supelco Inc., Bellafonte, USA). Different sampling times (5, 15, 30 and 60 min) and temperatures (10, 20, 30, 40, 50°C and room temperature) were compared.

3.3. Biotransformation of (*R*)-(+)-limonene by sporulated surface cultures

For the experiments with sporulated surface cultures, 500-ml conical flasks were used, filled with 100 ml MEA-medium and inoculated with 0.5 ml of freshly obtained spore suspensions. For the first experiment, spore suspensions of *Penicillium digitatum* (CMC) containing 1.8×10^8 spores/ml and *Aspergillus niger* (AND) containing 4.5×10^8 spores/ml were used as inoculum. For the second experiment with sporulated surface cultures, spore suspensions of *Penicillium digitatum* (CLE) containing 1.5×10^8 spores/ml and *P. digitatum* (PDD) containing 9.9×10^7 spores/ml (as counted with a Malassez cell) were used to inoculate the medium. After inoculation, the cultures were incubated at 30°C for 24 h and at room temp during the rest of the experiment. Substrate addition was carried out by spraying a

solution of (*R*)-(+)-limonene in EtOH (20%) onto the sporulated surface cultures. The biotransformation was monitored by dynamic headspace, steam distillation solvent extraction and liquid/liquid extraction as described earlier (Demyttenaere and Willemen, 1998). Control experiments with acidified (pH 3.5) sterile agar medium and MEA-medium without fungi were also performed as described previously (Demyttenaere and De Pooter, 1998).

3.4. Bioconversion by liquid cultures

The biotransformation by submerged liquid cultures was run during 5–8 days with various strains of *Penicillium digitatum*, *Aspergillus niger* and *Corynespora cassiicola*. The fungi were cultivated in 250-ml conical flasks, filled with 50 ml liquid medium (YMPG: yeast extract 0.5%, malt extract 1%, bacteriological peptone 0.5%, glucose 1%–pH 6.1) as described earlier (Demyttenaere and Willemen, 1998). Inoculation was done with 0.5 ml of freshly obtained spore suspensions containing 1.7×10^8 spores/ml (AND), 9.7×10^7 spores/ml (CMC), 9.9×10^7 spores/ml (PDD) and 1.5×10^8 spores/ml (CLE) as counted with a Malassez cell. The test substrate ((*R*)-(+)- or (*S*)-(−)-limonene) was added as a 20% (v/v) solution in absolute EtOH (125 or 250 μl of this solution were added to the cultures). At different time intervals, 5-ml samples were taken and extracted with Et_2O. This experiment was also run with control flasks, which contained sterile YMPG-broth which was acidified to pH 3.5 by addition of acetic acid but no inoculation was executed.

3.5. Chemical compounds

The substrates used for the biotransformation experiments were (*R*)-(+)- and (*S*)-(−)-limonene (puriss. ⩾ 99%, Fluka, Belgium). As reference compounds α-terpineol (98%, Janssen Chimica, Belgium) and (1*S*,2*S*,4*R*)-limonene-1,2-diol (kindly supplied by Dr. Mariët van der Werf, TNO-Voeding, Department of Applied Microbiology and Gene Technology, Zeist, The Netherlands) were used.

3.6. Preparative separation and identification of metabolites

For the isolation of the bioconversion product (1*S*,2*S*,4*R*)-limonene-1,2-diol, combined extracts were concentrated under a gentle N_2-flow and injected in a Delsi Intersmat IGC 120 ML gas chromatograph equipped with a 3 m packed column (5% SE-30, Chromosorb W-AW 60–80, 6 mm o.d.) and a Thermal Conductivity Detector (TCD). The carrier gas was H_2 (1 bar). The fraction was collected and the metabolite was identified by ^1H and ^{13}C NMR (JEOL JNM-EX270, 270 MHz). The melting point was measured by a Büchi 535 apparatus and the IR-spectrum was obtained with a Nicolet Impact 410 spectrometer.

3.7. Analysis of the samples with GC and GC–MS

GC- and GC–MS-analyses were performed as described earlier (Demyttenaere and Willemen, 1998). For the analysis of the SPME-extracts, a HP 6890 GC Plus coupled with a HP 5973 MSD (Mass Selective Detector-Quadrupole type), equipped with a CIS-4 PTV (Programmed Temperature Vaporisation) Injector (Gerstel), and a HP5-MS capillary column (30 m×0.25 mm i.d.; coating thickness 0.25 μm) was used. Working conditions were: injector 250°, transfer line to MSD 250°, oven temperature: start 40°C, hold 2 min; programmed from 40 to 150°C at 5°C min^{-1}, from 150 to 170°C at 10°C min^{-1} and from 170 to 250°C at 30°C min^{-1}, hold 2 min; carrier gas (He) 1.2 ml min^{-1}; split 1/10; ionisation: EI 70 eV; acquisition parameters: scanned *m*/*z*: 40–180 (5–20 min), 40–250 (> 20 min).

Substances were identified by comparison of their mass spectra and retention indexes (Kováts Indexes) with those of reference substances (where possible) and by comparison with the NIST Mass Spectral Library (Version 1.6d, 1998).

For elucidation of the chirality of the metabolite limonene-1,2-diol, the sample was analysed by chiral GC using a 25 m column (0.33 mm i.d.) with a permethylated CYDEX-B stationary phase (SGE) (coating thickness 0.25 μm) and it was co-injected with an authentic sample of (1*S*,2*S*,4*R*)-limonene-1,2-diol.

3.8. (1S,2S,4R)-Limonene-1,2-diol

Yellow solid. Mp 53.9°C. ^1H NMR (270 MHz, $CDCl_3$): δ 1.18–1.97 (7H, *m*); 1.27 (3H, *s*); 1.73 (3H, *s*); 2.22–2.27 (1H, *m*); 3.50 (2H, *s*); 4.73 (2H, *s*). ^{13}C NMR (68 MHz, $CDCl_3$): δ 21.0 (*q*); 26.1 (*t*); 26.6 (*q*); 33.6 (*t*); 33.9 (*t*); 37.4 (*d*); 71.3 (*s*); 73.8 (*d*); 108.9 (*t*); 149.3 (*s*). IR (NaCl, cm^{-1}): ν_{OH} = 3458. Kováts Retention Index: 1343. EIMS 70 eV *m*/*z*: (rel. int.): 152 (33), 109 (32), 108 (42), 93 (29), 82 (29), 71 (100), 69 (34), 67 (49), 43 (59), 41 (25).

Acknowledgements

Part of this work was supported by a grant form the European Community (FAIR-CT98-3559). The authors wish to express their gratitude to Dr. Mariët van der Werf, for supplying the reference compound.

References

Abraham, W.-R., Hoffmann, H.M.R., Kieslich, K., Reng, G., Stumpf, B., 1985. Microbial transformation of some monoterpenoids and

sesquiterpenoids. In: Porter, R., Clark, S. (Eds.), Enzymes Org. Synth. Ciba Found. Symp. 1985, Vol. 111. Pitman Press, London, pp. 146–160.

Abraham, W.-R., Kieslich, K., Reng, H., Stumpf, B. 1984. Formation and production of 1,2-*trans*-glycols from various monoterpenes with 1-menthen-skeleton by microbial transformation with *Diplodia gossypina* In: Eur. Congr. Biotechnol., 3rd, Vol. 1. Verlag Chemie, Weinheim, Germany, pp. 245-248.

Abraham, W.-R., Stumpf, B., Kieslich, K., 1986. Microbial transformations of terpenoids with 1-*p*-menthene skeleton. Applied Microbiology and Biotechnology 24, 24–30.

Arfmann, H.-A., Abraham, W.-R., Kieslich, K., 1987. Microbial ω-hydroxylation of terpenoids. In: Neijssel et al. (Eds.), Proceedings 4th European Congress on Biotechnology, Vol. 2. Elsevier, Amsterdam, pp. 212–215.

Arfmann, H.-A., Abraham, W.-R., Kieslich, K., 1988. Microbial ω-hydroxylation of *trans*-nerolidol and structurally related sesquiterpenoids. Biocatalysis 2, 59–67.

Bauer, K., Garbe, D., Surburg, H. (Eds.), 1990. Common Fragrance and Flavor Materials. Preparation, Properties and Uses. 2nd Edition. VCH Publishers, New York.

Bowen, E.R., 1975. Potential by-products from microbial transformation of D-limonene. In: Proceedings of the Florida State Horticultural Society, Miami Beach, pp. 304-308.

Cadwallader, K.R., Braddock, R.J., 1992. Enzymatic hydration of (4*R*)-(+)-limonene to (4*R*)-(+)-α-terpineol. Dev. Food Sci. 29, 571-584.

Cadwallader, K.R., Braddock, R.J., Parish, M.E., Higgins, D.P., 1989. Bioconversion of (+)-limonene by *Pseudomonas gladioli*. Journal of Food Science 54, 1241–1245.

Demyttenaere, J., De Kimpe, N., 2000. Biotransformation of geraniol and nerol by sporulated surface cultures of *Aspergillus niger*. In: Schieberle, P., Engel, K.-H. (Eds.), Frontiers of Flavour Science, Proceedings of the Ninth Weurman Flavour Research Symposium 22–25 June 1999, Freising, Germany, pp. 400-404.

Demyttenaere, J.C.R., De Pooter, H.L., 1998. Biotransformation of citral and nerol by spores of *Penicillium digitatum*. Flavour Fragr. J. 13, 173–176.

Demyttenaere, J.C.R., Herrera, M., del, C., De Kimpe, N., 2000. Biotransformation of geraniol, nerol and citral by sporulated surface cultures of *Aspergillus niger* and *Penicillium* sp. Phytochemistry 55, 363–373.

Demyttenaere, J.C.R., Willemen, H.M., 1998. Biotransformation of linalool to furanoid and pyranoid linalool oxides by *Aspergillus niger*. Phytochemistry 47, 1029–1036.

Dhavalikar, R.S., Bhattacharyya, P.K., 1966. Microbiological transformations of terpenes: part VIII — fermentation of limonene by a soil pseudomonad. Indian Journal of Biochemistry 3, 144–157.

Fenaroli, G., 1975. In: Furia, T.E., Bellanca, N. (Eds.), Handbook of Flavor Ingredients, 2nd Ed. CRC Press, Cleveland, Ohio.

Kraidman, G., Mukherjee, B.B., Hill, I.D., 1969. Conversion of D-limonene into an optically active isomer of α-terpineol by a *Cladosporium* species. Bacteriological Proceedings, 63.

Krasnobajew, V., 1984. Terpenoids. In: Rehm, H.-J., Reed, G. (Eds.), Biotechnology, Vol. 6a. Verlag Chemie, Weinheim, pp. 97-125.

Madyastha, K.M., Bhattacharyya, P.K., Vaidyanathan, C.S., 1977. Metabolism of a monoterpene alcohol, linalool, by a soil pseudomonad. Canadian Journal of Microbiology 23, 230–239.

Mattison, J.E., McDowell, L.L., Baum, R.H., 1971. Cometabolism of selected monoterpenoids by fungi associated with monoterpenoid-containing plants. Bacteriological Proceedings, 141.

Mukherjee, B.B., Kraidman, G., Hill, I.D., 1973. Synthesis of glycols by microbial transformation of some monocyclic terpenes. Applied Microbiology 25, 447–453.

Noma, Y., Yamasaki, S., Asakawa, Y., 1992. Biotransformation of limonene and related compounds by *Aspergillus cellulosae*. Phytochemistry 31, 2725–2727.

Rama Devi, J., Bhattacharyya, P.K., 1977. Microbiological transformations of terpenes: part xxiii — fermentation of geraniol, nerol and limonene by a soil pseudomonad, *Pseudomonas incognita* (linalool strain). Indian Journal of Biochemistry and Biophysics 14, 288–291.

Rama Devi, J., Bhattacharyya, P.K., 1978. Molecular rearrangements in the microbiological transformations of terpenes and the chemical logic of microbial processes. Journal of the Indian Chemistry Society 55, 1131–1137.

Tan, Q., Day, D.F., 1998a. Organic co-solvent effects on the bioconversion of (*R*)-(+)-limonene to (*R*)-(+)-α-terpineol. Process Biochemistry 33, 755–761.

Tan, Q., Day, D.F., 1998b. Bioconversion of limonene to α-terpineol by immobilized *Penicillium digitatum*. Applied Microbiology and Biotechnology 49, 96–101.

PERGAMON

Phytochemistry 57 (2001) 209–221

PHYTOCHEMISTRY

www.elsevier.com/locate/phytochem

Comprehensive chemical profiling of gramineous plant root exudates using high-resolution NMR and MS

Teresa W.-M. Fan [a,*], Andrew N. Lane [b], Moshe Shenker [c], John P. Bartley [d], David Crowley [e], Richard M. Higashi [f]

[a] *Department of Land, Air and Water Resources, University of California, One Shields Avenue, Davis, CA 95616, USA*
[b] *Division of Molecular Structure, National Institute for Medical Research, Mill Hill, London NW71AA, UK*
[c] *Department of Soil and Water Sciences, Faculty of Agricultural, Food and Environmental Quality Sciences, The Hebrew University of Jerusalem, Rehovot 76-100, Israel*
[d] *School of Physical Sciences, Queensland University of Technology, GPO Box 2434, Brisbane 4001, Queensland, Australia*
[e] *Department of Soil and Environmental Sciences, University of California, Riverside, CA 92521-0424, USA*
[f] *Crocker Nuclear Laboratory, University of California, One Shields Avenue, Davis, CA 95616, USA*

Received 9 August 2000; received in revised form 11 December 2000

Abstract

Root exudates released into soil have important functions in mobilizing metal micronutrients and for causing selective enrichment of plant beneficial soil micro-organisms that colonize the rhizosphere. Analysis of plant root exudates typically has involved chromatographic methods that rely on a priori knowledge of which compounds might be present. In the research reported here, the combination of multinuclear and 2-D NMR with GC–MS and high-resolution MS provided de novo identification of a number of components directly in crude root exudates of different plant types. This approach was applied to examine the role of exudate metal ion ligands (MIL) in the acquisition of Cd and transition metals by barley and wheat. The exudation of mugineic acids and malate was enhanced by Fe deficiency, which in turn led to an increase in the tissue content of Cu, Mn, and Zn. The presence of elevated Cd maintained at a free activity pCd of 8.8 ($10^{-8.8}$ M), resulted in reduced phytosiderophore production by Fe deficient plants. The buffer morpholinoethane sulfonate (MES), which is commonly used in chelator-buffering nutrient solutions, was detected in the root exudate mixture, suggesting uptake and re-secretion of this compound by the roots. The ability to detect this compound in complex mixtures containing organic acids, amino acids, and other substances suggests that the analytical methods used here provide an unbiased method for simultaneous detection of all major components contained in root exudates. © 2001 Elsevier Science Ltd. All rights reserved.

Keywords: *Hordeum vulgare*; *Triticum aestivum*; Gramineae; Multinuclear and 2-D NMR spectroscopy; High-resolution MS; Fe deficiency; Metal sequestration; Metal ion ligands; Cadmium; Phytosiderophores; Mugineic acids

1. Introduction

Plant root exudates can constitute up to 30–40% of the plant's photosynthetic productivity (Samtsevich, 1965; Oades, 1978; Sauerbeck et al., 1981; Whipps, 1990). They are known to play important roles in a number of rhizospheric processes, including nutrient (e.g. Fe and Zn) acquisition (Romheld, 1991; Zhang et al., 1991; Hopkins et al., 1998), plant-microbe associations (e.g. *Rhizobium* symbiosis with leguminous roots) (Janczarek et al., 1997; Scheidemann and Wetzel, 1997), regulation of plant growth (Einhellig et al., 1993), and determination of microbial community structure in the plant rhizosphere (Grayston et al., 1995; Yang and Crowley, 2000). It is also expected that root exudate components interact with both organic and inorganic contaminants to regulate their bioavailability and transport in the soil environment. Moreover, root exudation may be an important mediator in altering the species composition of the rhizosphere microflora that function in nutrient transformations, decomposition

* Corresponding author. Tel.: +1-530-752-1450; fax: +1-530-752-1552.
E-mail address: twfan@ucdavis.edu (T.W.-M. Fan).

0031-9422/01/$ - see front matter © 2001 Elsevier Science Ltd. All rights reserved.
PII: S0031-9422(01)00007-3

and mineralization of organic substances, and formation of soil organic matter, all of which are related to soil quality (Hodge and Millard, 1998). This latter aspect is particularly in need of clarification, in view of the ever-increasing threat of global environmental change and soil pollution caused by anthropogenic activity. However, the relationship between changes in exudate composition and microbial community structure and function in soils is poorly understood. The lack of comprehensive knowledge of exudate chemistry has been a major barrier to such mechanistic understanding.

The slow progress in exudate characterization can be largely attributed to the lack of analytical approaches that are comprehensive, require neither sample fractionation nor a priori knowledge, and that are capable of rigorous structure identification. Using a combination

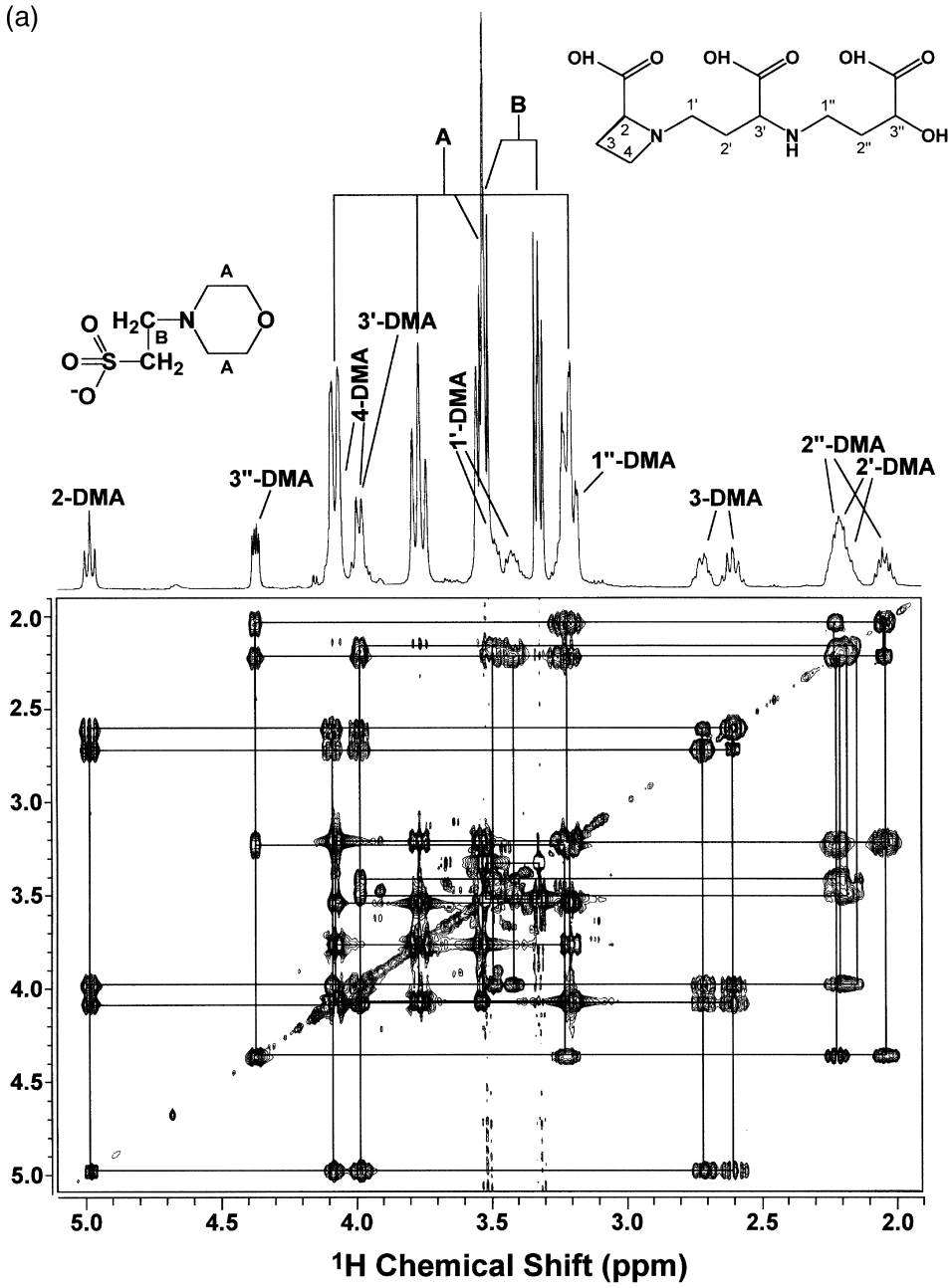

Fig. 1. (a) 2-D ^{1}H TOCSY, (b) ^{1}H–^{13}C HSQC, and (c) ^{1}H–^{13}C HMBC spectra of crude AgCS wheat exudate. The TOCSY spectrum was acquired with 2.5 s interpulse delay, 5 kHz spectral width in both dimensions, 8.2 kHz B1 field strength, 47.3 ms mixing time, and 0.41 and 0.072 s acquisition time in F2 and F1, respectively. The HSQC spectrum was obtained with 2.5 s interpulse delay, 5 kHz spectral width in F2 and 25 kHz in F1, and 0.147 and 0.022 s acquisition time in F2 and F1, respectively. The HMBC spectrum was recorded with the same parameters as the HSQC spectrum except for 0.499 s acquisition time in F2. DMA: 2′-deoxymugineic acid (right structure); C_A, C_B: A and B carbons of morpholinoethane sulfonate (MES, left structure), respectively. The pH of the exudate sample was 2.5.

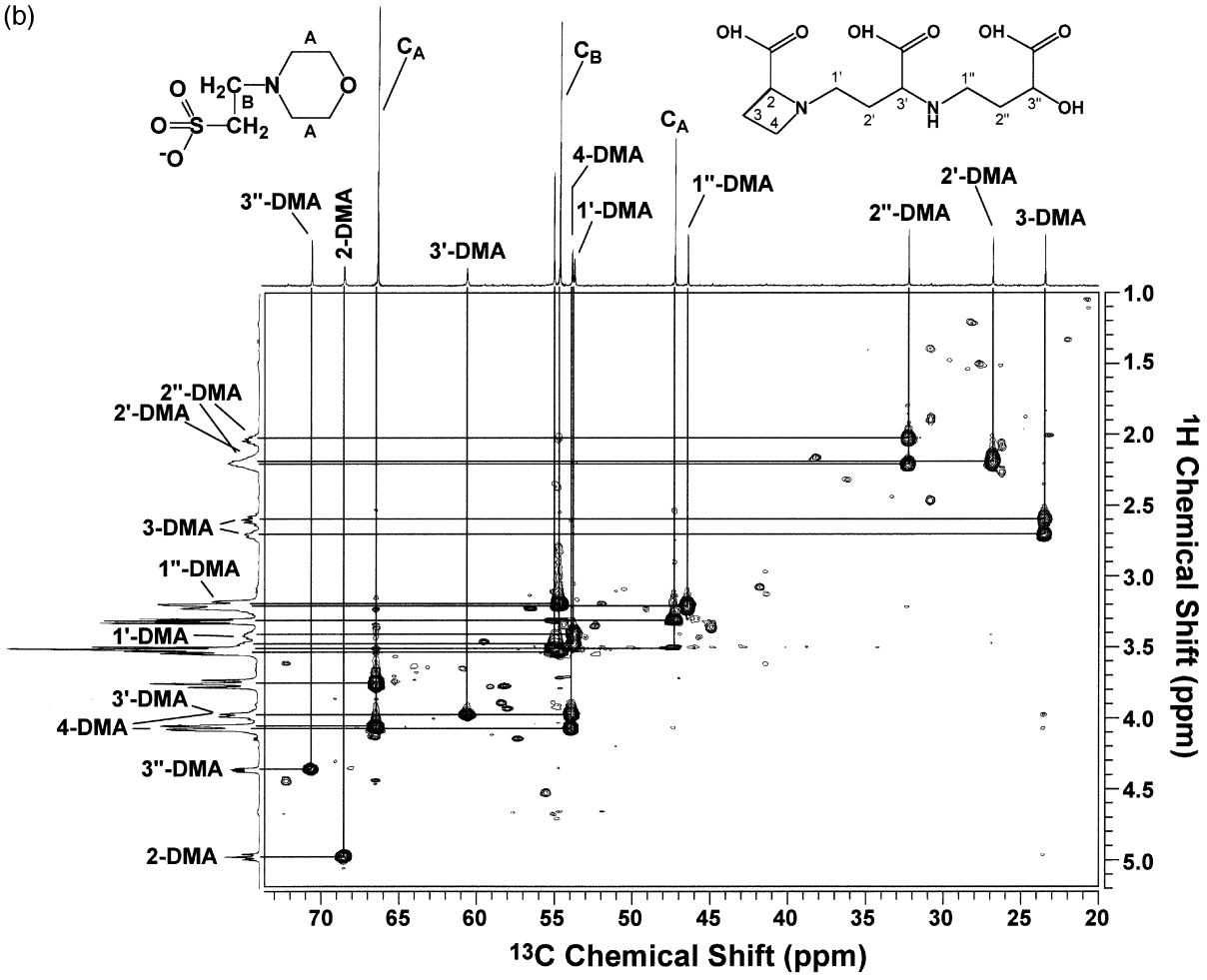

Fig. 1 (*continued*).

of multi-nuclear and 2-D NMR with GC–MS, we have previously demonstrated a comprehensive determination of barley root exudates (Fan et al., 1997b) based on known spectroscopic databases (Fan, 1996) and literature information on phytosiderophores (Ma and Nomoto, 1993).

However, for totally unknown compounds or those not represented in the databases, the above approach is not always sufficient to deduce the complete structure(s). To supply the necessary information, we have now added high-resolution mass spectrometry to the previous methods to obtain molecular formula information. This greatly facilitated the determination of the complete structures of various exudate components not in the databases. We also demonstrated that root exudate profiles were highly dependent on plant species and genotypes of the same species as well as growth conditions. Moreover, we observed a significant attenuating effect of Cd treatment on root exudate profiles and yet an enhancement of transition metal uptake for both barley and wheat plants.

2. Results and discussion

2.1. Exudate analysis

Roots exudates of wheat, barley, and rice plants were analyzed by a combination of NMR and GC–MS methods as described previously (Fan et al., 1997b). Using this approach, comprehensive profiles of the components were obtained directly from crude exudates without sample fractionation. Illustrated in Fig. 1 are results of 2-D ^{1}H total correlation spectroscopy (TOCSY), ^{1}H–^{13}C heteronuclear single quantum coherence spectroscopy (HSQC), and ^{1}H–^{13}C heteronuclear multiple bond correlation spectroscopy (HMBC) for the root exudate of the wheat amphiploid (AgCS) under the low Fe-high Cd (↓Fe-↑Cd) treatment. From ^{1}H TOCSY analysis, covalent correlations between pairs of protons that are up to 4 bonds apart were traced, while the HSQC and HMBC experiments revealed carbon coupling to its directly attached protons and to protons 2-4 bonds away, respectively. Two dominant components

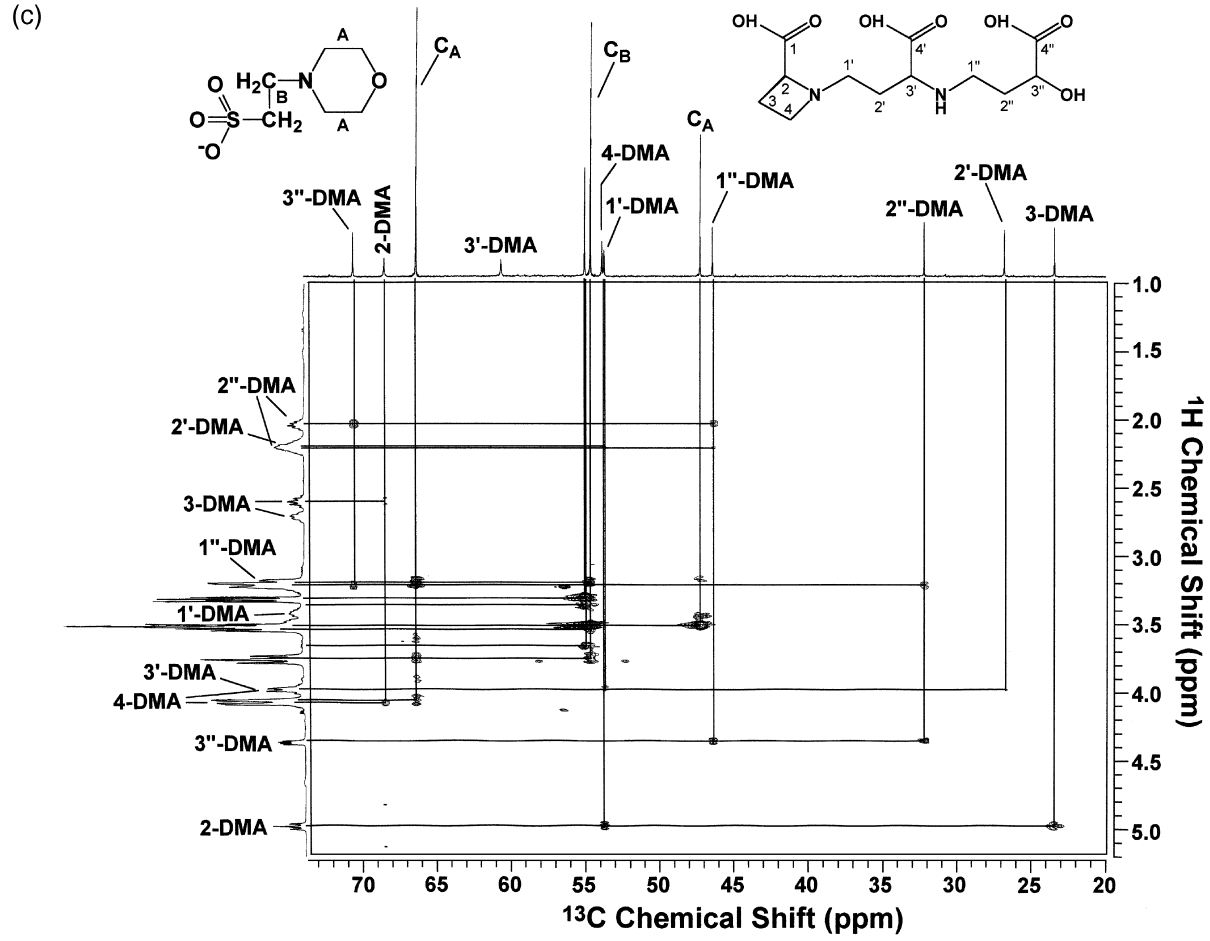

Fig. 1 (*continued*).

of the AgCS exudate were identified from these spectra, i.e. 2′-deoxymugineic acid (2′-DMA) and MES (the buffer included in the plant growth medium but not during exudate collection). The phytosiderophore, 2′-DMA, has been reported in common wheat (*Triticum aestivum* L.) root exudates (Murakami et al., 1989), but its exudation by the AgCS hybrid has not been characterized previously. As for MES, it is thought to be an impermeant buffer (but see below) and is not expected to be present in root exudates.

2′-DMA was assigned based on the ^{1}H and ^{13}C chemical shifts, proton covalent (scalar) connectivity acquired from the TOCSY spectrum (Fig. 1A), the proton to carbon covalent connectivity obtained from the HSQC (Fig. 1B) and HMBC spectra (Fig. 1C), as well as molecular ion data acquired from electrospray MS (ES–MS). All proton connectivities expected for 2′-DMA (H-2 to H-3 to H-4, H-1′ to H-2′ to H-3′, and H-1″ to H-2″ to H-3″) were present in Fig. 1A, so were the one-bond carbon to proton correlations in Fig. 1B. In addition, scalar correlations were evident in the HMBC spectrum (Fig. 1C) for the three carboxylate carbons to their closest protons (C-1 to H-2, C-4′ to H-3′, and C-4″ to H-3″) and between protonated carbons and their neighboring protons that are 2 (e.g. C-2″ to H-3″), 3 (e.g. C-1″ to H-3″), and 4 bonds (e.g. C-1′ to H-4) apart. Moreover, two mass ions (m/z 304 and 326) were evident in the full scan ES-MS spectrum (Fig. 2) of the same exudate, which corresponded to the molecular ion (M) and M + Na of 2′-DMA. Taken together, these NMR and MS data provided unequivocal identification of 2′-DMA in crude AgCS root exudates.

The presence of MES was deduced from the NMR [Fig. 1(a)–(c)], ES-MS (Fig. 2), and high-resolution fast atom bombardment (FAB) mass spectral data (data not shown). As shown in Fig. 2, the ES-MS spectrum of the crude AgCS exudate was abundant in the mass ions of 196, 218, and 413, in addition to 304 and 326. The *m*/*z* 218 and 413 ions were related to the *m*/*z* 196 ion based on their daughter ion patterns (data not shown), and could correspond to the Na adduct of the 196 monomer and dimer, respectively. From the FAB data of *m*/*z* 196, a molecular formula of $C_6H_{14}O_4NS$ was inferred with a mass error of 5.8 ppm. This information greatly assisted NMR in deducing the MES structure as described below.

The ^{1}H TOCSY data [Fig. 1(a)] revealed two sets of –CH_2–CH_2– groups with one set (A) having nonequivalent and the other (B) equivalent geminal protons. The integrated area of set A resonances was roughly twice that of set B resonances. In accordance with the molecular formula, set A protons should have originated from two chemically equivalent –CH_2–CH_2– groups while set B protons were derived from one –CH_2–CH_2– group. These three –CH_2–CH_2– groups accounted for all six of the carbons allowed in the molecular formula. In addition, the chemical shifts of both set A and B protons indicated that they were neighboring to heteroatoms such as N, O, or S. No other carbons including those from the carboxylates were present in the structure based on the analysis of 1-D ^{13}C NMR and 2-D HMBC [Fig. 1(c) and data not shown], which is consistent with the molecular formula. Moreover, no exchangeable (primary or secondary) amines were present based on the ^{1}H TOCSY spectrum recorded in H_2O instead of D_2O (data not shown), suggesting that the N is in a tertiary amine. A quarternary amine was ruled out based on the required number (14) of protons in the molecular formula. Altogether, the above structural clues allowed the MES structure to be deduced ab initio. Further proof for this assignment was obtained from the ^{1}H NMR analysis of the MES standard (data not shown), which matched exactly with that acquired from the AgCS exudate. Thus, using the combined NMR and MS approach, molecular structures of exudate components were identified from crude exudates without the need for a priori knowledge or any sample fractionation.

Using a similar approach, the exudate profile for the Chinese spring wheat (CS, a parent of AgCS) was examined. An example analysis of the CS exudates by TOCSY is shown in Fig. 3. Assigned components included Ile, Leu, Val, lactate (lac), Ala, acetate, 2′-DMA (peaks 1–9), malate, citrate, glycinebetaine (GB), Gly, α- and β-glucose (Glc), and α-trehalose (see Fan, 1996 for NMR parameters for these compounds). Except for the sugars, these assignments were verified by the ^{1}H–^{13}C HSQC analysis (data not shown) and in part by the GC–MS analysis of the same exudate (see below). In addition to components yielding sharp resonances, there were those whose cross-peaks were relatively broad (indicated by arrows). The identities of these components are currently unknown, although they are likely to be of macromolecular origin (e.g. proteins), as indicated by their chemical shifts and broad peak widths. A polypeptide that appears to be related to Al resistance has been reported in wheat root exudates (Basu et al., 1999)

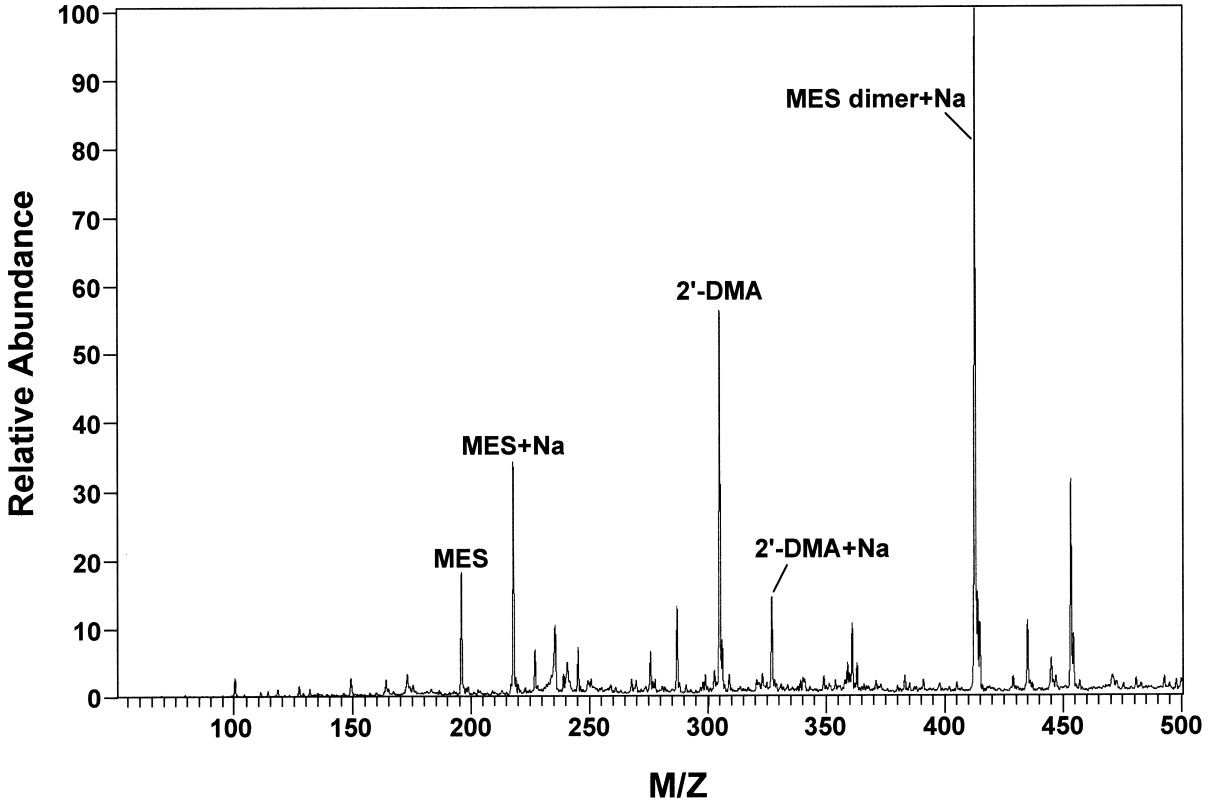

Fig. 2. Full scan electrospray mass spectrum of crude AgCS wheat exudate. The ES–MS spectrum was acquired in 50% methanol plus 1% formic acid from a LC-Q mass spectrometer.

2.2. Comparison of root exudate profiles from different plant species, genotypes, and growth conditions

Altogether, the above NMR spectroscopic analysis provided comprehensive profiles of exudate components (both known and unknown to our database) excreted by barley, wheat, and rice plants, as illustrated in Fig. 4. By comparing these ^{1}H NMR spectra, it is clear that exudate profiles varied with plant species and genotypes as well as treatment conditions. For example, the barley exudate differed from wheat exudates (CS and AgCS), most notably in the dominant mugineic acids present (3-*epi*-OHMA + MA for barley and 2′-DMA for wheat). A significant difference in the relative quantity of GB, Ala, γ-aminobutyrate (GAB), Gly, Glu, and acetate was also noted, although the difference in acetate may be complicated by a differential loss through volatilization during the freeze-drying process. The rice exudate profile was different again from those of barley and wheat, in that except for Gly, the amino acids and mugineic

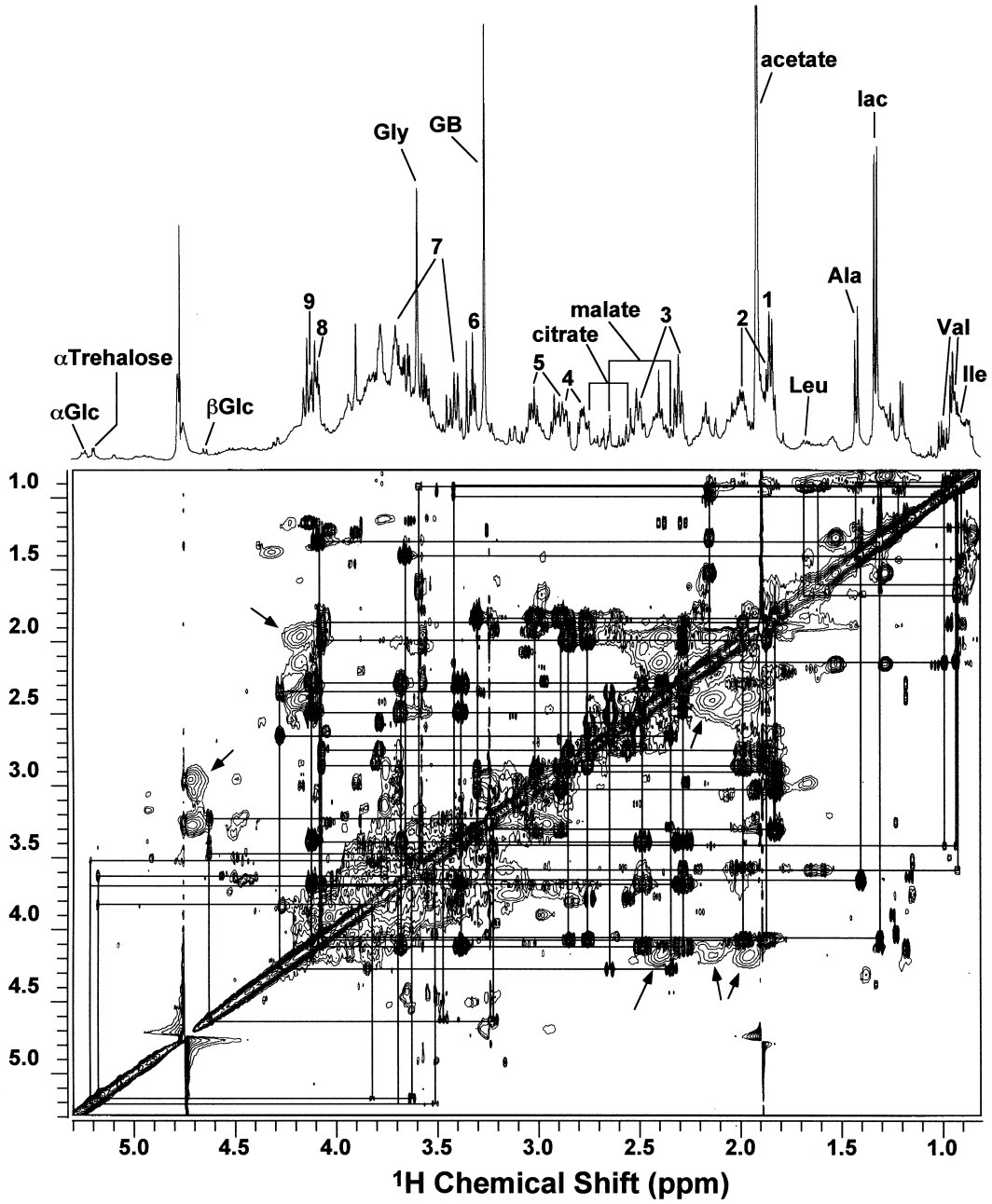

Fig. 3. 2-D ^{1}H TOCSY spectrum of Chinese Spring wheat root exudate. The TOCSY spectrum was acquired using 1.5 s interpulse delay, 5 KHz spectral width in both dimensions, 8.54 kHz B1 field strength, 47.3 ms mixing time, and 0.41 s and 0.051 s acquisition time in F2 and F1, respectively. Peaks 1-9: H-2′, H-2″, H-3, H-1″, H-1′, H-3′, H-4, H-3″, and H-2 of 2′-DMA, respectively; lac: lactate, GB: glycinebetaine, α,β-Glc: α,β-glucose. The pH of the exudate sample was 7.5.

acids were present only at very low concentration. In addition, an unknown polyol component was abundant in the rice exudate but absent in barley or wheat exudates.

Except for the exudation of 2′-DMA, the two wheat genotypes (CS vs. AgCS) exhibited rather different exudate profiles (Fig. 4). The AgCS exudate was dominated by the medium buffer MES and contained relatively little amino and organic acids, while the CS exudate was abundant in both amino and organic acids. In addition, unknown component(s) represented by a group of resonances from 1.1 to 1.6 ppm in the AgCS exudate were absent in the CS exudate. The difference in the MES content was presumably a result of the different treatment conditions, with MES included in the AgCS but absent in CS growth media. However, it is unlikely that the abundance of MES in the AgCS exudate was purely a result of contamination from the growth medium. This is because extensive rinsing of roots was performed before exudate collection. Moreover, an identical MES treatment was used to culture barley, yet MES was much less abundant in the barley exudate (Fig. 4). Instead, it is plausible that MES was taken up by AgCS roots and then excreted along with other exudate components. The possible effects of MES on the physiology of plants grown in buffered hydroponic media are unknown, but this finding suggests that this question should be studied in more detail for experimental protocols that use MES and other buffers to maintain the pH of plant growth media.

The same exudates from Fig. 4 were also analyzed by GC–MS and the results are shown in Table 1, along with those from the NMR spectroscopic analysis. The GC–MS analysis not only confirmed many of the NMR assigned components described above, but also provided absolute quantification of these components plus those that were below NMR detection limits. At the same time, the NMR analysis (with the aid of GC–MS analysis) provided absolute quantification for components (e.g. mugineic acids) that were not readily analyzed by GC–MS. Thus, the two approaches complemented each other in providing richer information than that achievable by each method alone.

In terms of total amounts of identified exudate components on a per gram root weight basis, the wheat hybrid AgCS ranked the highest (although a major portion was attributed to MES), followed by barley, wheat CS, and rice. It is also notable that many quantitative

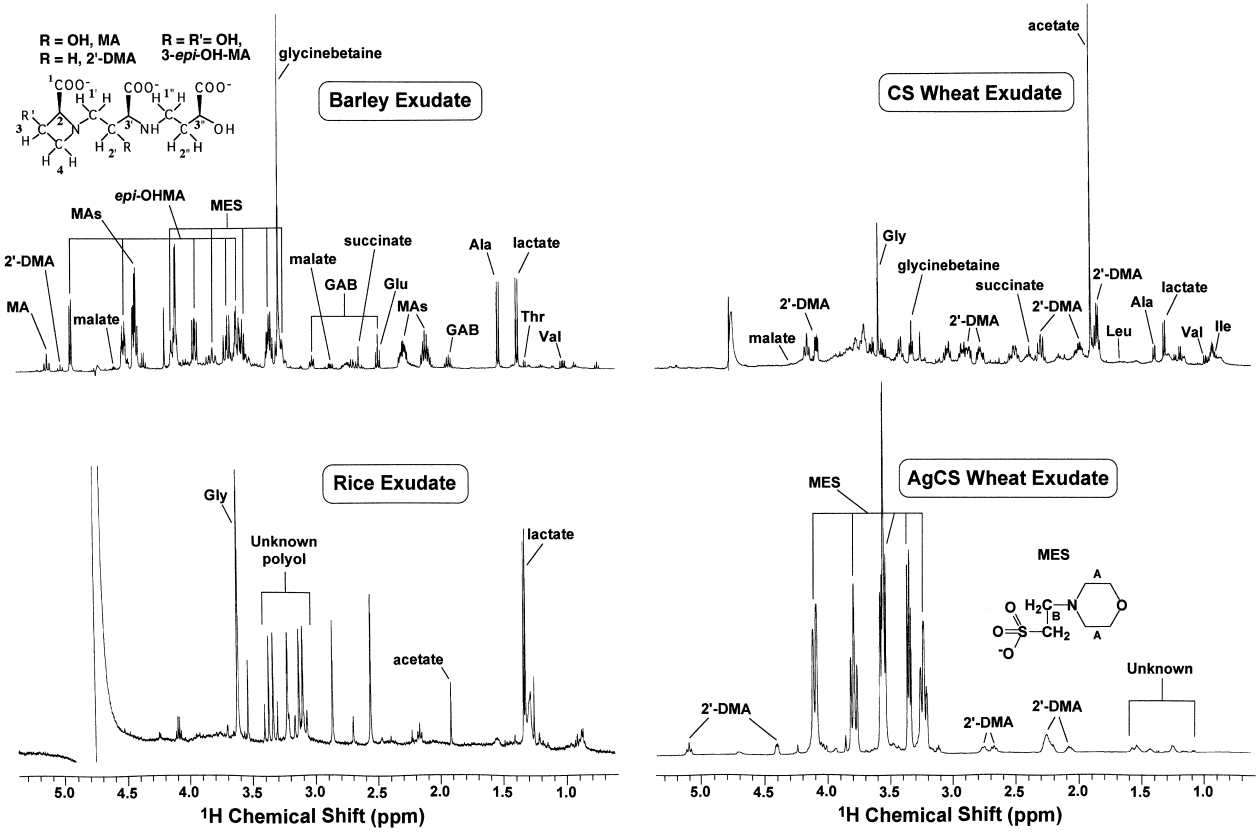

Fig. 4. 1-D ^{1}H NMR spectra of barley, wheat (CS and AgCS), and rice root exudates. The 1-D spectra were acquired using 2 s acquisition time, 2 (rice) or 5 s (the rest) interpulse delay, 5000 Hz spectral width, and 512 (rice) or 128 (the rest) transients. The abbreviations are as those in Figs. 1 and 5. The pH values of barley and AgCS root exudates were 2.2 and 2.5, respectively while those of rice and CS root exudates were 7.5.

differences in the exudate components of the four plant types were evident from the GC–MS profiles, which is consistent with the NMR characterization. Moreover, the abundance of the mugineic acid phytosiderophores in barley and wheat exudates was noted. In contrast, the exudation of these phytosiderophores by Fe-deficient rice roots was not apparent, which may be related to the NMR detection limit plus a much lower capacity of rice roots in excreting these compounds (Kawai et al., 1988). This lower capacity for mugineic acid exudation by rice roots has been correlated with their reduced ability to tolerate Fe deficiency (Marschner et al., 1986; Kawai et al., 1988; Mori et al., 1991).

2.3. Effect of combined Cd and Fe deficiency treatment on root exudate profiles of barley and wheat plants

Utilizing the above approach, we examined the chemical profiles of both barley and AgCS wheat exudates collected under a combination of Cd and Fe deficiency treatments. The effects of these treatments on plant growth, metal uptake, total Fe-mobilizing capacity, and other physiological parameters have been reported elsewhere (Shenker et al., submitted to Journal of Environmental Quality, JEQ). Here, we compared the effect of these treatments on root metal content with that on exudate composition, as shown in Figs. 5 and 6, for barley and wheat, respectively. Although many more exudate components have been analyzed (see Fig. 4), the comparison is illustrated for abundant metal ion ligands (MIL), since they are more likely to influence metal mobilization and uptake by plant roots. The stability constants of these MIL with different metal ions vary considerably, and their actual ability to mobilize various metal ions will depend on the pH and ionic composition of the soil solution, as well as kinetic factors involved in the dissolution of soil minerals.

Table 1
GC–MS and NMR quantification of wheat and barley root exudates under low Fe plus Cd treatment

	μmol/g root dry wt.			
Component	Barley[a]	Wheat CS[a]	Wheat AgCs[b]	Rice[a]
Lactate	3.51	1.70	–[c]	3.23
Pyruvate	6.95	ND[c]	–	ND
Ala	2.08	0.13	–	0.01
Gly	0.28	0.07	–	0.52
Val	0.32	0.07	–	ND
Leu	0.16	0.07	–	ND
Ile	0.08	0.05	–	ND
Succinate	0.26	0.03	–	ND
GAB	1.22	ND	–	ND
Pro	0.17	0.01	–	ND
Fumarate	0.23	0.02	–	ND
PO_4-containing	0.10	0.02	–	1.24
Ser	0.38	0.05	–	0.06
Thr	0.36	ND	–	ND
Malate	0.46	0.49	–	0.38
Phe	0.06	0.01	–	ND
Asp	0.22	0.02	–	0.01
Glu	0.25	ND	–	ND
Asn	0.21	ND	–	ND
Gln	0.17	ND	–	ND
3-*epi*-OHMA	8.19	ND	–	ND
2′-DMA	0.87	5.64	25.37	ND
MA	2.13	ND	ND	ND
GB	1.54	0.22	ND	ND
MES	2.43	ND	209.18	ND
Acetate	ND	11.60	ND	ND
Total	32.63	20.19	234.55	5.46

[a] Quantified by GC–MS except for 3-*epi*-OHMA, 2′-DMA. MA, GB, MES, and acetate, which were analyzed by NMR using existing lactate as an internal standard.

[b] AgCs quantified by NMR with the addition of 1 mM Ala as an internal standard.

[c] ND, not detected; –, not determined.

Under Fe deficient conditions (↓Fe-↓Cd and ↓Fe-↑Cd), the increased exudation of the 3-*epi*-OHMA, MA, 2′-DMA, and malate in barley (Fig. 5 and Table 2) and 2′-DMA in wheat exudates (Fig. 6) was evident, as compared to Fe sufficient conditions (↑Fe-↑Cd and ↑Fe-↓Cd). This increase was in turn related to the elevated production of Fe mobilizing substances (FeMS) by barley (data not shown) and wheat (Fig. 6) under Fe deficiency. These results are consistent with the role of these MIL in Fe acquisition. The exudation of other abundant MIL (i.e. lactate, Ala, GAB, and GB for barley; MES for wheat) did not exhibit a clear response to Fe deficiency (Figs. 5, 6 and Table 2), which suggests that they are not specifically involved in Fe acquisition. However, these MIL may still function generally in chelating Fe for uptake.

Accompanying the increased exudation of the phytosiderophores was the elevated content of Zn and Cu in barley roots (Fig. 5), Cu in wheat roots (Fig. 6) as well as Zn, Cu, and Mn in both shoots (Shenker et al., 2000). This finding suggests that the MAs may be important in the acquisition of Zn, Cu, and Mn, in addition to Fe. It is also noteworthy that the exudation pattern of malate was similar to that of the MAs by barley roots (Fig. 5). This result could be accounted by the exudation of malate and MAs via a common anion channel. However, other abundant anions in root tissues including citrate and malate (unpublished results) did not exhibit such exudation pattern, which argues against a systemic leakage through such a channel. In fact, citrate was not exuded by barley or wheat roots to any significant extent (data not shown). Regardless of the exudation mechanism(s), it is possible that the exuded malate could serve a similar role as MAs in mediating the observed accumulation of transition metals in barley and wheat tissues.

As for Cd acquisition, there was no statistically significant correlation of the above MIL to the Cd content

of roots (Figs. 5 and 6) or shoots (data not shown) of barley and wheat. This result suggests that Cd acquisition may involve a mechanism different from that of transition metal acquisition. It is also interesting to note that there appeared to be a weak correlation between MES concentration in wheat exudates and root Cd content (Fig. 6). It is possible that the presence of MES may interact with Cd to affect the latter uptake into wheat. Cd accumulation could weaken membrane integrity or increase membrane permeability via lipid peroxidation (Stohs and Bagchi, 1995; Goyer, 1997), which allows Cd-bound MES to enter into root cells

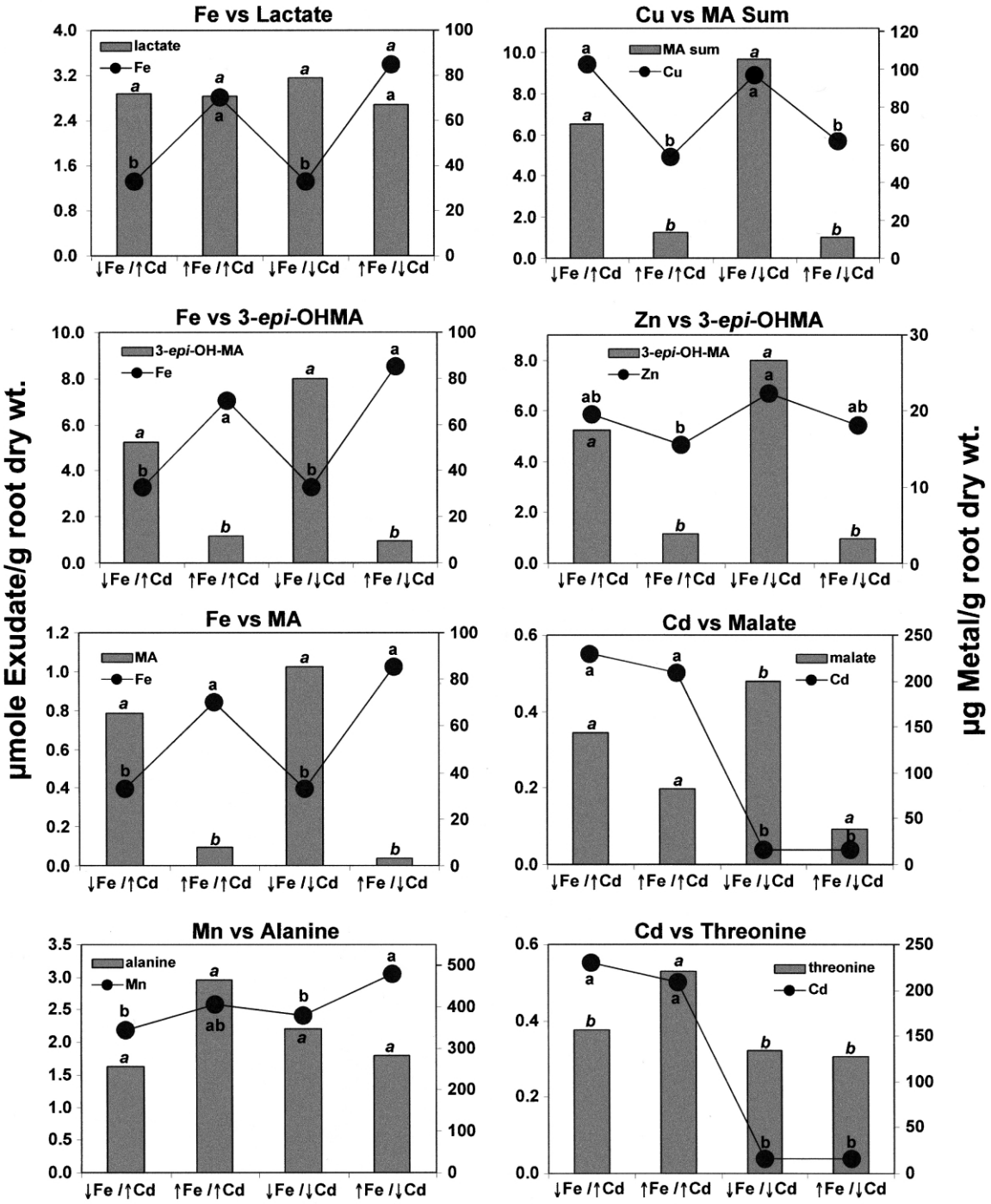

Fig. 5. Relation of barley root exudate components to root metal contents. The root exudate components were analyzed as described in Materials and Methods while the root metal content was acquired from Shenker et al. (2000). 3-*epi*-OHMA, 3-*epi*-hydroxymugineic acid; 2′-DMA, 2′-deoxymugineic acid; MA Sum, 3-*epi*-OHMA + 2′-DMA + MA. Two-way ANOVA test or Duncan's multiple range analysis of variance from the GLM statistical package of SAS was performed on the data. Different letters (italicized letters for exudate components and normal letters for root metal content) indicate statistical difference at a $P < 0.05$ significance level.

and later to be released to the collection solution down the concentration gradient. This hypothesis is consistent with the higher Cd uptake and MES release by AgCS wheat roots than by barley roots (cf. Figs. 5 and 6; Table 1). For barley, the exudation of Ser, Thr, and Glu appeared to be related to the high Cd treatment under Fe sufficient conditions (Fig. 5 and Table 2). It is possible that these MIL may be involved in Cd acquisition.

In conclusion, the combination of multinuclear and 2-D NMR with GC–MS and high-resolution MS provided de novo identification of a number of components directly in crude root exudates of different plant types. This approach was applied to examine the role of exudate MIL in the acquisition of Cd and transition metals by barley and wheat. The results suggest that enhanced exudation of mugineic acids and malate may be involved in transition metal but not Cd acquisition. Therefore, the acquisition mechanism appears to differ between the essential and toxic pollutant metals.

3. Experimental

3.1. Plant growth

The plant varieties used were Barley (*Hordeum vulgare* L., cv. CM-72), wheat (*Triticum aestivum* L., cv. AgCS, a hybrid of Chinese spring wheat and *Lophopyrum*. sp) supplied by Dr. J. Dvorak (Rommel and Jenkins, 1959), Chinese spring wheat (CS, a parent of AgCS), and rice (*Oryza sativa*, L., cv M201). Barley and AgCS wheat seedlings (eight per treatment) were grown for 22 days in nutrient solutions containing $CdCl_2$ buffered by an excess of EDTA and HEDTA (Fan et al., 1997b; Shenker et al., 2000) to produce Fe-sufficient (pFe = 17.2) and deficient (pFe = 18.2–18.4) conditions in combination with free Cd activity (pCd) of 8.8 or 10.0. Other free metal activities were pZn = 10.1, pCu = 13.5; and pMn = 7.3 (for complete plant growth protocol refer to Shenker et al., 2000). The four treatments

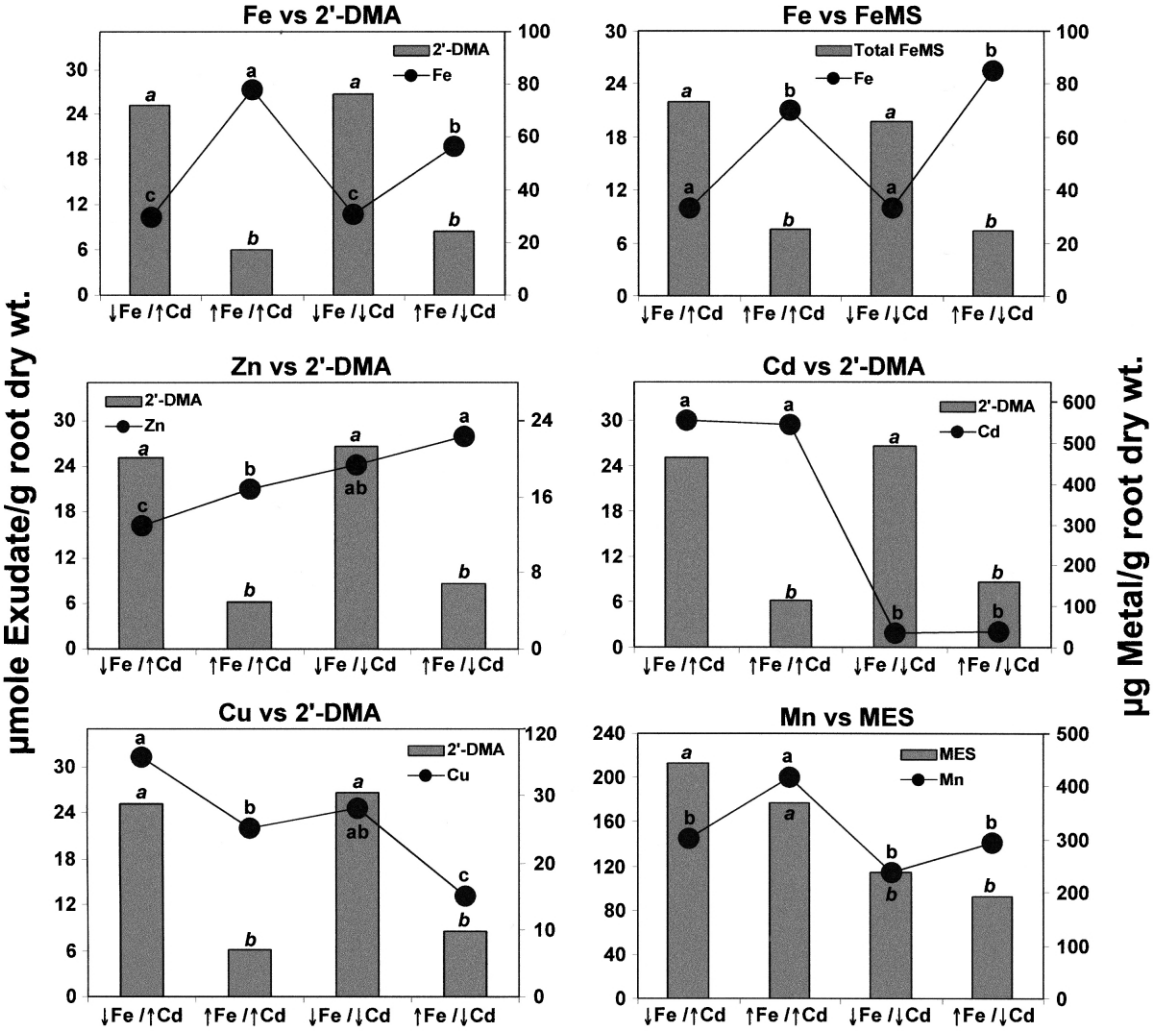

Fig. 6. Relation of wheat root exudate components to root metal contents. The root exudate components were analyzed as described in Materials and Methods while the root metal content and concentration of Fe mobilizing substance (FeMS) were acquired from Shenker et al. (2000). 2′-DMA, 2′-deoxymugineic acid; MES, morpholinoethane sulfonate. Statistical analysis was performed as in Fig. 5.

are designated as: (1) low Fe/high Cd (↓Fe-↑Cd); (2) high Fe/high Cd (↑Fe-↑Cd); (3) low Fe/low Cd (↓Fe-↓Cd); and (4) high Fe/low Cd (↑Fe-↓Cd). Morpholinoethane sulfonate (MES) at 2 mM was also included to buffer the pH of the nutrient solution at 6.2±0.2. Chinese spring (CS) wheat and rice (cv. M201) seedlings (four per treatment) were grown similarly for a month except that the nutrient solution employed was half-strength modified Hoagland solution (Epstein, 1972) containing full-strength (50 μM) Fe(III)-EDTA, 25 μM EDTA, and 10 μM $CdSO_4$ in the absence of MES (Fan et al., 2000). The calculated pMs in this nutrient solution were pFe = 17.6, pMn = 7.3, pCu = 12.8, pZn = 9.9, pNi = 12.1, and pCd = 8.9 (Shenker et al., 2000). The pH of the growth media was maintained at 6.0±0.3 by daily titration with 0.1 M HCl or KOH while the nutrient solution was renewed frequently to avoid nutrient depletion.

3.2. Root exudate collection

Roots were soaked in 1 mM $Ca(NO_3)_2$ for 10–20 min and rinsed extensively with doubly deionized (DD) H_2O to remove organic and inorganic constituents of the nutrient solution, including metabolites, exudates, chelates, mineral elements, and buffer ions before exudate collection. Root exudates were collected 2–3 times each in 150–200 ml DDH_2O during peak diurnal release of phytosiderophores (2–4 h after light onset) of the last 3–6 growth days. The collected solutions were immediately filtered through glass microfiber filters (GF/C, Whatman, Maidstone, England) to exclude root fragments and much of the microbial population, pooled, and lyophilized for storage. Prior to NMR studies, the exudates were resuspended in sterile water, filter sterilized, and passed through Chelex 100 resin (BioRad, Hercules, CA) to remove paramagnetic ions, as described previously (Fan et al., 1997b).

3.3. NMR analysis

The Chelex 100-treated exudates of barley and AgCS were acidified to pH 2, lyophilized, and redissolved in D_2O, whereas the CS and rice exudates were not acidified (pH values ranging from 7.0 to 7.8). NMR spectra were recorded at 25°C on a Varian (Palo Alto, CA) 11.75 Tesla UnityPlus (all ^1H experiments) and a Bruker AM-400 spectrometer (1-D ^{13}C analysis). The following 2-D ^1H experiments were conducted: ^1H total correlation (TOCSY), double-quantum filtered correlation (DQF-COSY), ^1H–^{13}C heteronuclear single quantum coherence (HSQC), and ^1H-^{13}C heteronuclear multiple bond correlation (HMBC). Selected samples were dissolved in DD H_2O containing 10% D_2O + 0.9 M HCl

Table 2
Interactive effect of Cd and Fe deficiency on barley exudate profiles[a]

Compound	↓Fe-↑Cd	S.D.	↑Fe-↑Cd	S.D.	↓Fe-↓Cd	S.D.	↑Fe-↓Cd	S.D.
Lactate	2.88	0.48	2.83	1.07	3.15	1.13	2.69	0.10
Pyruvate	7.59	1.74	5.72	0.69	6.06	0.91	5.98	1.70
Alanine	1.63	0.45	2.95	0.98	2.20	1.44	1.80	0.62
Glycine	0.24	0.07	0.38	0.12	0.27	0.14	0.23	0.08
Valine	0.28	0.06	0.30	0.11	0.33	0.14	0.21	0.06
Leucine	0.15	0.02	0.17	0.04	0.16	0.05	0.12	0.03
Succinate	0.28	0.06	0.21	0.06	0.29	0.13	0.15	0.04
GAB	1.03	0.19	1.35	0.36	1.16	0.61	0.74	0.19
Fumarate	0.27	0.08	0.28	0.05	0.27	0.13	0.24	0.02
Serine	0.36	0.03	0.49	0.14	0.35	0.16	0.31	0.09
Threonine	0.38	0.09	0.53	0.07	0.32	0.15	0.31	0.10
Malate	0.34	0.08	0.20	0.08	0.48	0.53	0.09	0.05
Aspartate	0.19	0.05	0.27	0.11	0.14	0.05	0.11	0.05
Glutamate	0.19	0.05	0.35	0.16	0.22	0.10	0.19	0.08
Asparagine	0.17	0.03	0.19	0.06	0.15	0.08	0.13	0.05
Glutamine	0.11	0.09	0.14	0.05	0.23	0.16	0.16	0.05
α-Glycerol-3-P	0.20	0.05	0.16	0.02	0.17	0.07	0.12	0.05
3-*epi*-OH-MA	5.25	2.14	1.15	0.77	7.97	4.06	0.96	0.22
2′-DMA	0.49	0.29	0.00	0.01	0.62	0.36	0.01	0.01
MA	0.79	0.92	0.09	0.16	1.02	0.35	0.04	0.07
GB	1.14	0.32	1.56	0.56	1.52	1.00	0.82	0.34
MES	1.28	0.77	1.44	1.04	2.28	1.44	3.24	2.04
Total	25.94		21.45		30.36		19.13	

[a] Units in μmol/g root dry wt.

for Watergate TOCSY measurement (Piotto et al., 1992) at 5°C which optimized the detection of exchangeable protons (Fan et al., 1997a). Detailed acquisition parameters are described in respective figure legends. The 1-D NMR spectra were apodized using an exponential function yielding 0.5-2 Hz line broadening, and zerofilled to 64 or 128 K points before Fourier transformation. The 2-D NMR data were zerofilled or linear-predicted to 8×2 K points and apodized with a mild Gaussian function before 2-D Fourier transformation.

3.4. Mass spectrometry

Nanospray mass spectra were acquired on an LCQ "classic" quadrupole ion trap mass spectrometer (ThermoQuest, Austin, TX) equipped with a nanospray source (Protana, Odense, Denmark) operated at a spray voltage of 800 V and a capillary temperature of 150°C. Lyophilized root exudates were dissolved in 50% methanol, 1% formic acid and 2 μl transferred to an Econo12 nanospray needle (New Objective Inc, Cambridge, MA). MS^2 and MS^3 analyses were performed at a collision energy of 30% and an isolation width of 4 Da.

Accurate mass of exudate components were measured on a Finnigan 2001 Newstar FT/MS system (ThermoQuest, Madison WI) at 3 .0 Tesla. The spectrometer was externally calibrated with PMMA 640. The lyophilized sample was delivered to the mass spectrometer by flow injection at 5 ml / min using a syringe pump (Cole Palmer, Vernon Hills, IL) to an Analytica, API external source operating at a capillary voltage of 5.5 kV.

3.5. GC–MS analysis

All exudates were acidified in 0.1 N HCl before an aliquot was lyophilized and derivatized with *N*-methyl-*N*-[*tert*-butyldimethylsilyl]trifluoroacetamide (MTBSTFA) before analysis on a Varian 3300 gas chromatograph interfaced to a Finnegan ITD 806 mass spectrometer (Fan et al., 1997b).

3.6. Exudate quantification

All components of exudate collection solutions were quantified by their GC–MS response as compared to that of the standard with known concentration, except for the mugineic acids (MAs), glycinebetaine (GB), acetate, and MES (see Fig. 4). The latter were quantified from their ^1H NMR responses by comparison with the methyl resonance of alanine at 1.47 ppm (either endogenous or added) after corrected for signal saturation and number of protons. The concentration of the endogenous Ala was determined from GC–MS analysis (Fan et al., 1997b). In addition, the FeMS data were adapted from Shenker et al. (2000), which were acquired using the Cu–CAS (chrome azurol S) colorimetric assay (Shenker et al., 1995). This assay measured the total capacity of Fe mobilization in crude exudates.

Acknowledgements

This work was supported by US Department of Energy grant numbers DE-FG07-96ER20255, US EPA grant No. R825960010, and US EPA funded (No. R819658) Center for Ecological Health Research at University of California at Davis. We thank Dr. Steven Howell of NIMR for recording the nanospray ES-MS spectra. NMR spectra were recorded at the MRC Biomedical NMR Centre, Mill Hill.

References

Basu, U., Good, A.G., Aung, T., Slaski, J.J., Basu, A., Briggs, K.G., Taylor, G.J., 1999. A 23-kDa, root exudate polypeptide co-segregates with aluminum resistance in *Triticum aestivum*. Physiologia Plantarum 106, 53–61.

Einhellig, F.A., Rasmussen, J.A., Hejl, A.M., Souza, I.F., 1993. Effects of root exudate sorgoleone on photosynthesis. Journal of Chemical Ecology 19, 369–375.

Epstein, E., 1972. Mineral nutrition of plants: principles and perspectives. John Wiley & Sons, New York.

Fan, T.W.-M., 1996. Metabolite profiling by one- and two-dimensional NMR analysis of complex mixtures. Progress in Nuclear Magnetic Resonance Spectroscopy 28, 161–219.

Fan, T.W.-M., Higashi, R.M., Frenkiel, T.A., Lane, A.N., 1997a. Anaerobic nitrate and ammonium metabolism in flood-tolerant rice coleoptiles. Journal of Experimental Botany 48, 1655–1666.

Fan, T.W.-M., Pedler, J., Lane, A.N., Crowley, D., Higashi, R.M., 1997b. Comprehensive analysis of organic ligands in whole root exudates using nuclear magnetic resonance and gas chromatography–mass spectrometry. Analytical Biochemistry 251, 57–68.

Fan, T.W.-M., Baraud, F., Higashi, R.M., (Eds.), Eller, P.G., Heinemann, W.R., 2000. Genotypic influence on metal ion mobilization and sequestration via metal ion ligand production by wheat. In: Nuclear Site Remediation. American Chemical Society Symposium Series, vol. 778, pp. 417–431, Washington, DC.

Grayston, S.J., Campbell, C.D., Vaughan, D., Jones, D., 1995. Influence of root exudate heterogeneity on microbial diversity in the rhizosphere. Journal of Experimental Botany 46, 27.

Goyer, R.A., 1997. Toxic and essential metal interactions. Annual Review of Nutrition 17, 37–50.

Hodge, A., Millard, P., 1998. Effect of elevated CO_2 on carbon partitioning and exudate release from *Plantago lanceolata* seedlings. Physiologia Plantarum 103, 280–286.

Hopkins, B.G., Whitney, D.A., Lamond, R.E., Jolley, V.D., 1998. Phytosiderophore release by sorghum, wheat, and corn under zinc deficiency. Journal of Plant Nutrition 21, 2623–2637.

Janczarek, M., Urbanik-Sypniewska, T., Skorupska, A., 1997. Effect of authentic flavonoids and the exudate of clover roots on growth rate and inducing ability of nod genes of *Rhizobium leguminosarum bv. trifolii*. Microbiological Research 152, 93–98.

Kawai, S., Takagi, S., Sato, Y., 1988. Mugineic acid-family phytosiderophores in root-secretions of barley, corn and sorghum varieties. Journal of Plant Nutrition 11, 633–642.

Ma, J.F., Nomoto, K., 1993. Two related biosynthetic pathways of mugineic acid in gramineous plants. Plant Physiology (Rockville) 102, 373–378.

Marschner, H., Römheld, V., Kissel, M., 1986. Journal of Plant Nutrition 9, 695–713.

Mori, S., Nishizawa, N., Hayashi, H., Chino, M., Yoshimura, E., Ishihara, J., 1991. Why are young rice plants highly susceptible to iron-deficiency? Plant and Soil 130, 143–156.

Murakami, T., Ise, K., Hayakawa, M., Kamei, S., Takagi, S., 1989. Chemical Letters 1989, 2137–2140.

Oades, J.M., 1978. Mucilages at the root surface. Journal of Soil Science 29, 1–16.

Piotto, M., Saudek, V., Sklenar, V., 1992. Gradient-tailored excitation for single-quantum NMR spectroscopy of aqueous solutions. Journal of Biomolecular NMR 2, 661–665.

Rommel, R., Jenkins, B.C., 1959. Amphiploids in *Triticeae* produced at the University of Manitoba from March 1958 to December 1959. Wheat Information Service 9-10, 23.

Römheld, V., 1991. The role of phytosiderophores in acquisition of iron and other micronutrients in graminaceous species — an ecological approach. Plant and Soil 130, 127–134.

Samtsevich, S.A., 1965. Active excretion of plant roots and their significance. Soviet Plant Physiology 12, 731–740.

Sauerbeck, D., Nonnen, S., Allard, J.L., 1981. Consumption and turnover of photosynthates in the rhizosphere depending on plant species and growth conditions. Landw. Forschung Sonderheft 37, 207–216.

Scheidemann, P., Wetzel, A., 1997. Identification and characterization of flavonoids in the root exudate of *Robinia pseudoacacia*. Trees (Berlin) 11, 316–321.

Shenker, M., Hadar, Y., Chen, Y., 1995. Rapid method for accurate determination of colorless siderophores and synthetic chelates. Soil Science Society of American Journal 59, 1612–1618.

Shenker, M., Fan, T.W.M., Crowley, D. E. 2000. Phytosiderophores influence on cadmium uptake by wheat and barley plants. Journal of Environmental Quality, submitted.

Stohs, S.J., Bagchi, D., 1995. Oxidative mechanisms in the toxicity of metal ions. Free Radical Biology in Medicine 18, 321–336.

Whipps, J.M., 1990. Carbon economy. In: Lynch, J.M. (Ed.), The Rhizosphere. John Wiley & Sons, Chichester, UK, pp. 59–97.

Zhang, F., Römheld, V., Marschner, H., 1991. Diurnal rhythm of release of phytosiderophores and uptake rate of zinc in iron-deficient wheat. Soil Science and Plant Nutrition 37, 671–678.

PERGAMON

Phytochemistry 57 (2001) 223–228

PHYTOCHEMISTRY

www.elsevier.com/locate/phytochem

Phytoalexins from *Pinus strobus* bark infected with pinewood nematode, *Bursaphelenchus xylophilus*

Fujinori Hanawa *, Toshihiro Yamada, Tadakazu Nakashima

Forestry and Forest Products Research Institute (FFPRI), PO Box 16, Tsukuba, Ibaraki 305-8687, Japan

Received 11 August 2000; received in revised form 4 December 2000

Abstract

From the bark of *Pinus strobus* infected with pinewood nematode, *Bursaphelenchus xylophilus,* a stilbenoid 3-*O*-methyldihydropinosylvin and a flavanone (2*S*)-pinocembrin were isolated as active principles of inducibly produced antifungal compounds. The structures of the compounds were determined on the basis of spectroscopic analyses. Close investigations of spectroscopic analyses led to the complete assignment of ^{13}C NMR and ^{1}H NMR chemical shifts for the former compound and to the determination of the stereochemistry of the latter compound from *P. strobus* to be 2*S*. Furthermore, the distribution and time course accumulation of the identified compounds were investigated. The former compound was demonstrated to be nematocidal and the concentrations of the compound in the inoculated branches were sufficient enough to inactivate the pinewood nematode within one week after inoculation. © 2001 Elsevier Science Ltd. All rights reserved.

Keywords: Pinus strobus; Pinaceae; Stilbenoid; Flavonoid; Phytoalexin; Nematocide; Fungicide; Nematode; *Bursaphelenchus xylophilus*

1. Introduction

When plants are challenged by microbial invasion, many of them produce phytoalexins (Harborne, 1999) to ward off microbes. Phytoalexins are defined (Paxton, 1981) as "low molecular weight, antimicrobial compounds that are both synthesized and accumulated in plants after exposure to microorganisms". During our survey of chemical defense responses of pine species which are resistant to the pinewood nematode *Bursaphelenchus xylophilus,* which causes pine wilt disease (Kiyohara and Tokushige, 1971), *Pinus strobus* was demonstrated to accumulate antifungal compounds against *Cladosporium herbarum* in its xylem and those compounds were identified as pinosylvin, pinosylvin monomethylether, pinobanksin, and pinocembrin (Yamada and Ito, 1993a). However, there were two unidentified compounds in the pine bark after infection by the nematode. Here we report the isolation and structural determination of the unidentified compounds based on spectroscopic analyses. We also report the distribution and time course accumulation of isolated antifungal compounds in the bark and wood of nematode-infected *P. strobus* together with the inhibitory effects of one of the isolated compounds on the nematode. The possible roles of these compounds in the defense mechanisms of pine are also discussed.

2. Results and discussion

An antifungal compound **1** in the bark of *P. strobus* was isolated as a clear oil. A comparison of UV, EIMS, HREIMS, and ^{1}H NMR spectra with previously reported spectra (Takasugi et al., 1987; Suga et al., 1993) showed that the structure of compound **1** could be a 3-*O*-methyldihydropinosylvin. This compound was previously reported as a heartwood constituent of *P. armandii* (Fang et al., 1988) without any data and as that of *P. albicaulis* (Lindström and Westfelt, 1967) with only the melting point. Lindstedt and Misiorny (1951) used paper chromatography to determine the presence of compound **1** together with pinosylvin and 3-*O*-methylpinosylvin in the heartwood of *P. strobus*. However, they did not detect compound **1** in the bark of the plant. These results suggest that compound **1** is inducibly produced in the bark or transferred to the bark from the

* Corresponding author.
E-mail address: fujinori@ffpri.affrc.go.jp (F. Hanawa).

0031-9422/01/$ - see front matter © 2001 Elsevier Science Ltd. All rights reserved.
PII: S0031-9422(00)00514-8

xylem as a response to nematode infection. As there had not yet been a complete assignment of ^{1}H NMR and ^{13}C NMR spectral data for this compound, close investigation using 2D NMR (COSY, HSQC, HMBC, and NOESY) and DEPT analyses on the compound were conducted. Fifteen carbon signals which were assigned to 12 aromatic carbons (8 methines, 4 quaternary carbons), 2 methylene carbons, and a methoxyl carbon were obtained by DEPT analysis. Diagnostically significant C–H long-range correlations found in HMBC and NOESY are given in Fig. 1. A proton at δ 6.20 ppm which showed a C–H long-range correlation with an aliphatic methine at δ 2.76 ppm were assignable to H–2 or H–6. Moreover, because this proton showed an NOE with a methoxyl group at δ 3.68 ppm, it was assigned to H-2. This key assignment allowed us to complete the remaining assignments. Finally, the complete assignment of ^{1}H NMR and ^{13}C NMR chemical shifts was determined as shown in the experimental section.

The second antifungal compound, **2**, in the bark was obtained as a clear oil. The ^{1}H NMR spectrum of **2** was identical with pinocembrin (Kuroyanagi et al., 1983), and the assignment of ^{13}C NMR chemical shifts based on 2D NMR (COSY, HSQC, and HMBC) of **2** was identical with that based on the 1D long-range C–H coupling and deuterium isotope effects from hydroxyl groups to ^{13}C chemical shifts (Jung and McLaughlin, 1990). In a EIMS of pinocembrin-3-*d* (**3**), a base ion *m/z* 258 $[M]^{+}$ (100) and fragment ions *m/z* 181 (60) and *m/z* 152 (52), which were assigned as an A–C ring fragment and an A ring fragment, respectively, were observed. The CD spectra of this compound showed a positive absorption around 310–325 nm and a negative absorption around 285 nm. These findings indicate for the first time that the absolute configuration at C-2 of pinocembrin from *P. strobus* to be *S* (Miyaichi et al., 1987). Although the presence of compound **2** in the heartwood and sapwood of *P. strobus* had been shown, the presence of compound **2** in the bark of the plant had not yet been detected using paper chromatography (Lindstedt and Misiorny, 1951) and may be inducibly produced in the bark or transferred to the bark from the xylem as a response to nematode infection.

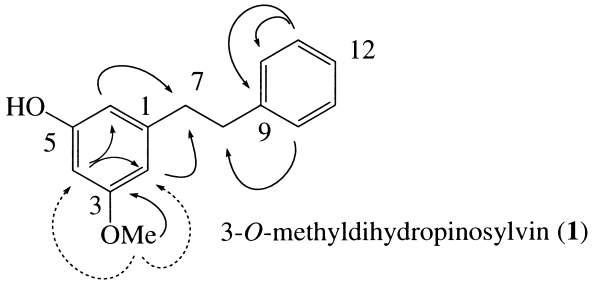

3-*O*-methyldihydropinosylvin (**1**)

Fig. 1. Arrows show the diagnostically significant C–H correlation found in HMBC (⟶) and NOE (⇢).

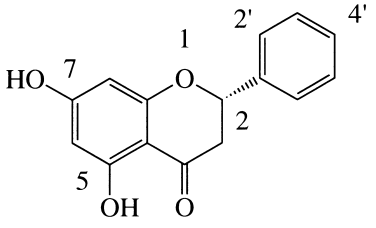

pinocembrin (**2**)

We also investigated the distribution and time course accumulation of these compounds in the bark and the wood of nematode-infected *P. strobus* using GC. Branches of the *P. strobus* were divided into three portions based on distance from the site of infection to determine the distribution of the compounds. Fig. 2 shows the time course accumulation of compound **1** in the bark and the wood and that of compound **2** in the bark of inoculated and non-inoculated branches. Compound **1** accumulated in the bark of all portions (A, B, and C) one week after infection. However, no accumulation of compound **1** was found in the bark of the non-inoculated control. In the case of the wood, which was found to consist only of sapwood by microscopic analysis, compound **1** accumulated in portion C of the inoculated branches. However, the amount was only about one-third of that found in bark one week after inoculation. In portions A and B of the wood of inoculated branches, only a trace accumulation of compound **1** was detected. On the other hand, no accumulation of compound **1** was found in the wood of any portions of the non-inoculated branches. These findings concerning the accumulation of compound **1** in the wood were similar to those regarding the accumulation of 3-*O*-methylpinosylvin, pinobanksin, and pinocembrin in wood of nematode-infected *P. strobus* branches (Yamada and Ito, 1993a). These compounds also accumulated only in portion C of the inoculated branches. When the nematode *B. xylophilus* was inoculated to the branches of susceptible pine trees *P. thunbergii,* most of them were located in the resin canals of cortex and were hardly found in the xylem three days after inoculation (Mamiya, 1985). Therefore, the difference in the accumulation pattern of compound (**1**) in the bark and the wood of *P. strobus* might be related to the amounts of nematodes which might locate in those tissues of the plant in the same manner as in *P. thunbergii*. It is often considered that there is a close association between the age of sapwood and the formation of heartwood, which contains a high amount of secondary metabolites (Hillis, 1987). The age of portion C, which was adjacent to a stem, could be sufficient to produce secondary metabolites in relatively higher amounts than that accumulated

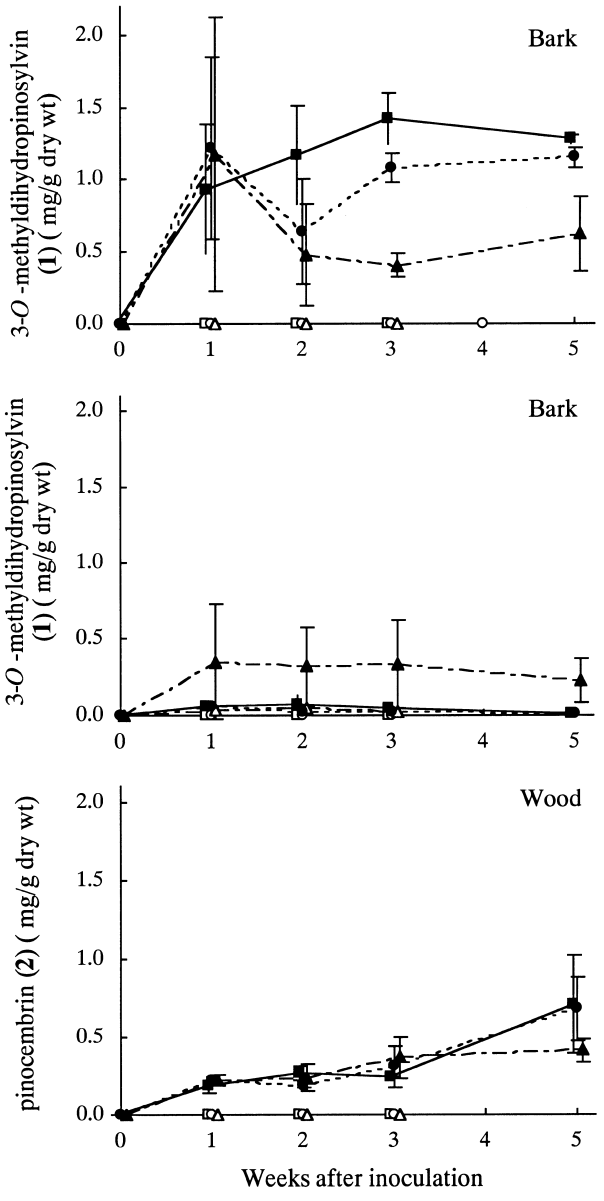

Fig. 2. Distribution and time course accumulation of inducibly produced compounds in the bark and in the wood of *Pinus strobus* branches after inoculation with *Bursaphelenchus xylophilus*. Inoculated and control branches were divided into three portions based on distance from the infection site (A: 6–11 cm, B: 16–21 cm and C: 26–31 cm). The infection site is 31 cm away from the stem and portion C is adjacent to the stem. 3-*O*-methyldihydropinosylvin (**1**) in the bark (upper) and in the wood (middle) and pinocembrin (**2**) in the bark (lower). Vertical bars show standard deviations of three replicates. ——□——, portion A in noninoculated branches; – – ○ – –, portion B in non-inoculated branches; —— △ ——, portion C in non-inoculated branches; ——■——, portion A in inoculated branches; – – ● – – portion B in inoculated branches; —— ▲ —— portion C in inoculated branches.

in portions A and B. The accumulation pattern of compound **2** in the bark of inoculated branches was different from that found for compound **1** in the bark and wood and also different from that found for compound **2** in the wood (Yamada and Ito, 1993a). Compound **2** gradually accumulated in all portions of the bark of nematode-inoculated branches. However, it did not accumulate in any portions of non-inoculated branches. It is supposed that these secondary metabolites in heartwoods and in plants tissues under certain stresses such as mechanical injury or fungal infection are produced in situ from transport and/or storage metabolites, such as carbohydrates and/or lipids by living parenchyma cells (Hart, 1981; Hillis, 1987). 3-*O*-Methyldihydropinosylvin (**1**) and pinocembrin (**2**) could also be produced in situ at portions A, B and C of the bark and the wood of inoculated branches. In addition, it is difficult to hypothesize that these compounds were transferred to the bark from the wood where the accumulation level of these compounds was lower than that in the bark (compound **1** was almost absent in portions A and B of the wood). Therefore, it could be concluded that the biosynthetic pathway of *3-O*-methyldihydropinosylvin (**1**) and pinocembrin (**2**) in both bark and wood were activated in the respective portions by the infection stress of *B. xylophilus,* which can move in tissues of *P. strobus* (Tamura et al., 1988; Yamada and Ito, 1993b). It may be possible that these compounds were derived from glucosides of respective compounds by the hydrolyzing activity of β-glucosidase which was released from invading microbes into infected tissue, as in the case of Sitka spruce (Woodward and Pearce, 1988). This possibility could be unlikely, since the glucosides of 3-*O*-methyldihydropinosylvin (**1**) and pinocembrin (**2**) have not been reported from *P. strobus* thus far.

Compound **1**, which was obtained by catalytic hydrogenation of 3-*O*-methylpinosylvin, was reported to have strong nematocidal activity (Ali et al., 1992; Suga et al., 1993). This fact helps us to understand the chemical defense mechanisms of *P. strobus* against microbial invasion. Because compound **1** accumulated in the bark and the wood of nematode infected branches was not only antifungal but also nematocidal against *B. xylophilus,* it is possible to assume that, as a phytoalexin, compound **1** can protect *P. strobus* from invasion of those organisms. However, the role of the induced compound **1** in nature remains unclear. The nematocidal and nematode-immobilizing activities of compound **1** are not distinguishable in the present study from those of previous reports. Hence, we investigated the nematocidal and nematode-immobilizing activity of compound **1** on *B. xylophilus*. These activities were measured by comparing the ratio of nematodes, which did not move in medium containing compound **1**, with the ratio of nematodes, which were not recovered from an immobilized state within one or three days after transferring then into compound **1**-free medium (see experimental). Nematodes were completely killed in 250 ppm soin. of compound **1** (Table 1). About half of the nematodes were immobilized in a 100 ppm soln. of compound **1** (0 days). Among the

Table 1
Effects of 3-*O*-methyldihydropinosylvin (**1**) on the mobility of pine wood nematodes[a]

Dose (ppm)	Immobilized nematode (%)					
	One-day-treatment[b]			Two-day-treatment[b]		
	Days after transfer			Days after transfer		
	0	1	3	0	1	3
250	100±0	100±0	100±0	100±0	100±0	100±0
100	54±1	27±8	25±6	46±7	22±10	18±6
50	7±2	4±1	12±2	7±3	7±0	13±6
25	2±1	6±2	12±5	4±1	4±2	8±3
0	2±1	3±2	11±2	4±2	5±1	8±2

[a] Data are shown as average±S.D. of 3 replicates.
[b] Nematodes were incubated with 3-*O*-methyldihydropinosylvin for one day and two days respectively.

immobilized nematodes, ca. half did not recover by 1 and 3 days after transferring them into compound **1**-free medium; they were considered to have been killed by the nematocidal activity of compound **1**. Soln. with conc. of less than 50 ppm did not affect the mobility of the nematodes. A significant difference was not observed between one-day- and two-day-treatments with compound **1** before transferring nematodes into compound **1**-free medium. These results indicate that within one week after nematode infection, the conc. of 3-*O*-methyldihydropinosylvin was sufficient (ca. 1000 ppm in the bark and ca. 400 ppm in the wood) to completely inhibit nematode activity in the bark of inoculated branches and in the wood adjacent to the stems of the inoculated branches. In our previous studies, a rapid dispersion of nematode was not inhibited in *P. strobus* branches within one week after infection (Yamada and Ito, 1993b; Tamura et al., 1988). However, the reproduction of the nematode was thereafter inhibited. This phenomenon can be explained by the time delay of the accumulation of inhibitory compounds that occurs after the infection. In addition to the above results, nematocidal compounds pinosylvin and pinosylvin monomethylether (Suga et al., 1993) also accumulated in the wood of inoculated branches (Yamada and Ito, 1993a). The amount of the latter compound was also sufficient to completely inhibit nematode activity. These inhibitory compounds found in the bark and wood from *B. xylophilus-infected* branches of *P. strobus* play important roles in the chemical resistance of the plant against pine wood nematodes. Some phytoalexins which were initially found as antibiotic principles in plant–microbe interactions were known to be also induced by nematodes and showed nematostatic and nematocidal activities (Veech, 1982). Therefore, nematodes could be included among the "microorganisms" referred to in the definition of phytoalexins in the report of by Paxton (1981).

3. Experimental

3.1. General

Analytical TLC was carried out using Merck pre-coated silica gel 60 plates (F254; layer thickness, 0.25 mm). Compounds on the TLC plates were detected under UV light (wavelength, 365 and 254 nm) and by visualization with Gibbs reagent (Tahara et al., 1984). ElMS spectrometry was conducted on a JEOL JMS-DX303 HF instrument (direct inlet system, 70 eV ionization potential). ^{1}H NMR (500 MHz) and ^{13}C NMR (125 MHz) spectra were determined on a JEOL alpha 500; TMS was used as an internal standard. Data are described in δ ppm. Capillary GC was carried out on a CBP-1 (1: 25 m, i.d.: 0.22 mm, film thickness: 0.25 μm; carrier gas: N_2 1 ml/mm; column temp. prog.: 150–270° C at 4°C/min; injector temp.: 270°C) coupled to a Shimadzu GC-9AM using an FID detector set at 270°C. Low resolution GC–MS were recorded by an HP5790 coupled to an HP5890 equipped with an HP-i fused silica capillary column (1: 25 m, i.d.: 0.2 mm, film thickness: 0.11 μm; carrier gas: He 1 ml/min; column temp. prog.,: 120–210°C at 3°C/min; injector temp.: 260°C.

3.2. Plant material and inoculation of nematode

These procedures have been described previously (Yamada and Ito, 1993a,b). Briefly, the procedure progressed as follows: five thousand *B. xylophilus* were inoculated to cut-wound sites on branches on seven-year-old *P. strobus* trees. The branches were at 120–140 cm height from the ground and the age of them at portion C, which was adjacent to a stem, was 3–4 years old. The inoculation sites were 31 cm away from the stems. Sterile water was used for the control experiment. After a set number of weeks, bark and wood in three portions A–C (A, 6–11 cm; B, 16–21 cm and C, 26–31 cm from the inoculation site) of the branches were separated.

The bark and wood were both extracted with EtOH and the extracts were used as samples for the GC analysis. The entire procedure was replicated three times. A portion of the bark extract was used as the source of the antifungal compounds.

3.3. Extraction and isolation

EtOH extraction of *B. xylophilus-infected* bark tissue of *P. strobus* (9.7 g) afforded 1.53 g of crude extract (Yamada and Ito, l993a) which was subjected to silica gel chromatography and fractionated into 31 fractions (10 ml each) using *n*-hexane-Me_2CO (10:1) as an eluting solvent. A spot showing quenching and navy blue against Gibbs reagent on TLC (R_f 0.33; *n*-hexane Me_2CO 7:3) in fractions 12–15 exhibited antifungal activity against *C. herbarum* (isolate OCh-1) on TLC

bioautography (Oku et al., 1979). The active principle in these fractions was isolated by HPLC [R_t 18.59 mm, column: Prepsil ODS 10×250 mm with a guard column 10×50 mm (GL science Co.), solvent: 50% aq. soln. of CH_3CN, flow rate 5 ml/min, detection: UV 254 nm]. Finally 6.3 mg of a clear paste of compound **1** was obtained. A spot showing quenching, being dark under 365 nm UV light, and appeared sky blue against Gibbs reagent on TLC (R_f 0.31; hexane–acetone 7:3) was detected in fractions 21–30. This spot also exhibited antifungal activity against *C. herbarum*. The active principle in these fractions was isolated by HPLC (R_t 11.87 mm, in the same conditions applied for compound **1**). Finally, 1.2 mg of clear paste of compound **2** was obtained.

3.4. GC analysis

EtOH extract from each tissue samples was analyzed by GC after trimethylsilylation as follows: 20 μl from 4 ml of EtOH soln. of the bark (1 g dry wt) extract and 20 μl of 1-naphthol (1 mg/ml in Me_2CO) as the internal standard were mixed and concd. under red. press. then TMSI-H (GL Sciences Inc.) and BSA (GL Sciences Inc.) — 20 μl each — were added and heated at 109°C for ca. 10 s. One microlitre of the sample was used for the capillary GC analysis. The R_t of the TMSi derivative of compound **1** was 18.1 mm. The peak of the TMSi derivative of compound **1** in crude extract was confirmed by a comparison of the fragmentation pattern with those of an TMSi-derivative of isolated compound **1**. The analytical conditions used for compound **2** have been reported previously (Yamada and Ito, 1993a,b).

3.5. Physicochemical properties

3.5.1. 3-O-Methyldihydropinosylvin (*1*)

Gibbs test: (+), navy blue. UV, HREIMS, ElMS, and ^{1}H NMR spectral data were in good agreement with literature values (Takasugi et al., 1987; Suga et al., 1993). The following data are presented for the assignment of chemical shift values. ^{1}H NMR (500 MHz, CD_3OD): δ2.76 (2H, *dd, J*=9.3, 6.0 Hz, H-7), 2.85 (2H, *dd, J*=9.3, 6.0 Hz, H-8), 3.68 (3H, *s,* OMe), 6.16 (1H, *t, J*=2.1 Hz, H-4), 6.20 (1H, *br.t, J*=1.8 Hz, H-2), 6.22 (1H, *br.t, J*=2.0 Hz, H-6), 7.14 (3H, *m,* H-10, H-12, H-14), 7.22 (2H, t, *J*=7.5 Hz, H-11, H-13). ^{13}C NMR 6(125 MHz, CD_3OD): 38.9 (C-8, -CH_2-), 39.3 (C-7, -CH_2-), *55.5* (OMe), 99.9 (C-4), 106.5 (C-2), 109.0 (C-6), 126.8 (C-12), 129.3 (C-11, C-13), 129.5 (C-10, C-14), 143.1 (C-9), 145.1 (C-1), 159.4 (C-5), 162.2 (C-3).

3.5.2. (2S)-Pinocembrin (*2*)

Gibbs test: (+), sky blue. ^{1}H NMR and ^{13}C NMR data were in good agreement with literature values (Kuroyanagi et al., 1983; Jung and McLaughlin, 1990).

3.5.3. (2S)-Pinocembrin-3-d_2

This (ca. 0.5 mg) was obtained by dissolving compound **2** in MeOH-d_6 for one month. UVλ_{max}^{MeOH} nm: 321 sh 290. CD (in MeOH, rel. int.): $[\theta]_{326}$ +0.25, $[\theta]_{3llsh}$ +0.20 $[\theta]_{286}$ −1.00, $[\theta]_{220}$ +1.47. EIMS *m/z* (rel. int.): 259 $[MH]^+$ (41), 258 $[M]^+$ (100), 257 (59), 256 (16), 182 (23), 181 (60), 180 (17), 154 (17), 153 (37), 152 (52), 149 (12), 124 (21), 106 (14), 105 (12). HREIMS: $[M]^+$ 258.0921 ($C_{15}H_{10}D_2O_4$ requires 258.0861).^{1}H NMR (500 MHz, Me_2CO-d_6): δ 5.57 (1H, *s,* H-2), 5.97 (1H, *br. s,* H-6), 6.00 (1H, *br. s,* H-8), 7.40 (1H, *dd*-like, *J*=7.5, 1.5 Hz, H-4′), 7.45 (2H, *dd*-like, *J*=*7.5,* 7.2 Hz, H-3′ and H-5′), 7.57 (2H, *dd*-like, *J*=7.6, 1.5 Hz, H-2′ and H-6′). 9.66 (*s,* C-7-OH), 12.16 (*s,* C-5-OH).

3.6. Bioassay

Sterilized pine wood nematodes (Tamura and Mamiya, 1973) [isolate: S-10 (Kiyohara, 1989)] were incubated on a mycelial mat of *Botrytis cinerea* on potato dextrose agar, and were extracted with a Baerman funnel apparatus (Southey, 1986). EtOH-H_2O (1:49) soln. (0.5 ml) of 3-*O*-methyldihydropinosylvin in conc. ranging from 0 to 500 ppm was added to 4 ml glass vials. A soln. without 3-*O*-methyldihydropinosylvin was used as a control. Incubated nematodes (ca. 1000 nematodes of all stages in 0.5 ml of H_2O) were then added to each vial (final conc. ranged from 0 to 250 ppm). All test vials were maintained in the dark at 25°C. After 1 or 2 days of the exposure to the compound soln., moving and immobilized nematodes were counted under a microscope and the ratio of them (R_1) against entire nematodes was calculated. Then the entire nematodes were transferred into H_2O in vials. One and 3 days after transfer, immobilized nematodes were counted again and the ratio of the immobilized nematodes (R_2) was calculated. The immobilized nematodes at this stage were judged as dead. The difference of the two ratios (R_1-R_2) shows the ratio of nematodes which were recovered from immobilized state by the effect of the compound.

Acknowledgements

We thank Dr Tomoya Kiyohara, Forestry and Forest Products Research Institute, for providing *B. xylophilus* isolate.

References

Ali, M.A., Kondo, K., Tsuda, Y., 1992. Synthesis and nematocidal activity of hydroxystilbenes. Chemical and Pharmaceutical Bulletin 45, 1992, 1130-1136.

Fang, J.M., Su, W.C., Cheng, Y., 1988. Flavonoids and stilbenes from armand pine. Phytochemistry 27, 1395–1398.

Harborne, J.B., 1999. The comparative biochemistry of phytoalexin induction in plants. Biochemical Systematics and Ecology 27, 335–367.

Hart, J.H., 1981. Role of phytostilbenes in decay and disease resistance. Annual Review of Phytopathology 19, 1981, 437–458.

Hillis, W.E., 1987. Heartwood and tree exudates. Springer-Verlag, Berlin.

Jung, J.H., McLaughlin, J.L., 1990. ^{13}C-^{1}H NMR long-range coupling and deuterium isotope effects of flavanones. Phytochemistry 29, 1271–1275.

Kiyohara, T., 1989. Etiological study of pine wilt disease. Bulletin of the Forestry and Forest Products Research Institute 353, 127–176.

Kiyohara, T., Tokushige, Y., 1971. Inoculation experiments of a nematode, *Bursaphelenchus* sp., onto pine trees. Journal of the Japanese Forestry Society 53, 210.

Kuroyanagi, M., Noro, T., Fukushima, S., Aiyama, R., Ikuta, A., Itokawa, H., Morita, M., 1983. Studies on the constituents of the seed of *Alpinia katsumadai* HAYATA. Chemical and Pharmaceutical Bulletin 31, 1544–1550.

Lindstedt, G., Misiorny, A., 1951. Constituents of pine heartwood XXV. Investigation of forty-eight *Pinus* species by paper partition chromatography. Acta Chemica Scandinavia 5, 121–128.

Lindström, J.-O., Westfelt, L., 1967. Sesqui- and diterpenes from the wood of *Pinus albicaulis* Engelm. Arkiv. för Kemi 26, 539–543.

Mamiya, Y., 1985. Initial pathological changes and disease development in pine trees induced by the pine wood nematode, *Bursaphelenchus xylophilus*. Annals of the Phytopathological Society of Japan 51, 546–555.

Miyaichi, Y., Imoto, Y., Tomimori, T., Lin, C.-C., 1987. Studies on the constituents of Scutellaria Species. IX. On the flavonoid constituents of the root of *Scutellaria indica* L. Chemical Pharmaceutical Bulletin 35, 3720–3725.

Oku, H., Shiraishi, T., Kurozumi, S., 1979. Participation of toxin in wilting of Japanese pines caused by a nematode. Naturwissenschaften 66, 210.

Paxton, J.D., 1981. Phytoalexins — a working redefinition. Phytopathologische Zeitschrift 101, 106–109.

Southey, J.F. (Ed.), 1986. Laboratory Methods for Work with Plant and Soil Nematodes. Ministry of Agriculture, Fisheries and Food, Reference Book, Her Majesty's Stationery Office, London, pp. 202.

Suga, T., Ohta, S., Munesada, K.I.N., Kurokawa, M., Shimizu, M., Ohta, E., 1993. Endogenous pine wood nematicidal substances in pines, *Pinus massoniana*. *P. strobus* and *P. palustris*. Phytochemistry 33, 1395–1401.

Tahara, S., Ingham, J.L., Nakahara, S., Mizutani, J., Harborne, J.B., 1984. Fungitoxic dihydrofuranoisoflavones and related compounds in white lupin *Lupinus albus*. Phytochemistry 23, 1889–1900.

Takasugi, M., Kawashima, S., Monde, K., Katsui, N., Masamune, T., Shirata, A., 1987. Antifungal compounds from *Dioscorea batatas* inoculated with *Pseudomonas cichorii*. Phytochemistry 26, 371–375.

Tamura, H., Mamiya, Y., 1973. A method for disinfection of *Bursaphelenchus lignicolus*. Japanese Journal of Nematology 3, 30–32.

Tamura, H., Yamada, T., Mineo, K., 1988. Host responses and nematode distribution in *Pinus strobus* and *P. densiflora* infected with the pine wood nematode, *Bursaphelenchus xylophilus*. Annals of the Phytopathological Society of Japan 54, 327–331.

Veech, J.A., 1982. Phytoalexins and their role in the resistance of plants to nematodes. Journal of Nematology 14, 2–9.

Woodward, S., Pearce, R.B., 1988. The role of stilbenes in the resistance of Sitka spruce (*Picea sitchensis* (Bong.) Carr.) to entry of decay fungi. Physiological and Molecular Plant Pathology 33, 127–149.

Yamada, T., Ito, S., 1993a. Chemical defence responses of wilt-resistant pine species, *Pinus strobus* and *P. taeda*, against *Bursaphelenchus xylophilus* infection. Annals of the Phytopathological Society of Japan 59, 666–672.

Yamada, T., Ito, S., 1993b. Histological observations on the responses of pine species, *Pinus strobus* and *P. taeda*, resistant to *Bursaphelenchus xylophilus* infection. Annals of the Phytopathological Society of Japan 59, 659–665.

PERGAMON

Phytochemistry 57 (2001) 229–234

PHYTOCHEMISTRY

www.elsevier.com/locate/phytochem

Synergism between the potato glycoalkaloids α-chaconine and α-solanine in inhibition of snail feeding

David B. Smith [a], James G. Roddick [a,*], J. Leighton Jones [b]

[a] *School of Biological Sciences, University of Exeter, Washington Singer Laboratories, Perry Road, Exeter EX4 4QG, UK*
[b] *Campden and Chorleywood Food Research Association, Chipping Campden, GL55 6LD, UK*

Received 16 November 2000; received in revised form 29 December 2000

Abstract

Snails (*Helix aspersa* L.) were fed filter paper treated with the potato glycoalkaloids, α-solanine and α-chaconine, singly or together. In pure form, both glycoalkaloids deterred feeding, with chaconine being the more active compound. In combination, authentic solanine and chaconine interacted synergistically in their inhibition of feeding. The antifeedant activities of methanolic extracts of tuber peel of the potato varieties Majestic and Sharpe's Express presented via filter paper discs did not differ significantly from those of authentic glycoalkaloid solutions of comparable concentration and ratio. In contrast, feeding inhibition by diluted tuber peel extracts of the variety Homeguard was greater than that elicited by comparable authentic glycoalkaloid solutions suggesting additional inhibitory compound(s) in the peel of this variety. Comparison of data from peel extracts of all three potato varieties and authentic glycoalkaloids indicated that the level of feeding inhibition by the extracts was, at least in part, a consequence of a synergism between solanine and chaconine. © 2001 Elsevier Science Ltd. All rights reserved.

Keywords: Snail; *Helix aspersa*; Potato; *Solanum tuberosum*; Solanaceae; Glycoalkaloids; α-Chaconine; α-Solanine; Antifeedants; Synergism

1. Introduction

The principal potato glycoalkaloids α-solanine and α-chaconine are biologically interesting and economically important compounds (Friedman and McDonald, 1997). They are toxic to a wide range of organisms and are generally considered to be defensive allelochemicals (Roddick, 1996; Friedman and McDonald, 1997). Membrane disruption is arguably the most important mechanism by which glycoalkaloids compromise the structural and functional integrity of cells/tissues of other organisms and, in this respect, chaconine is invariably more damaging than solanine. In addition, it is now well established that synergism between these two glycoalkaloids significantly enhances the membrane-disruptive activity of potato glycoalkaloid mixtures. This interaction was first conclusively demonstrated using synthetic lipid membrane vesicles (liposomes) (Roddick and Rijnenberg, 1987), but has subsequently been confirmed in various membrane/living systems (Table 1). Synergisms also occur between other similarly 'paired' glycoalkaloids of other *Solanum* species with a common aglycone and a solatriose or chacotriose carbohydrate moiety (Roddick et al., 1990, 2001). In contrast, solanine and chaconine are equally effective in inhibiting the neurotransmission enzyme acetylcholinesterase and do not synergise in this action (Roddick, 1989).

One of the main ways in which plant allelochemical action is manifest is through feeding deterrence. Preingestive antifeedant effects of glycoalkaloids are probably due to the bitter/burning taste sensations they impart (Sinden et al., 1976; Zitnak and Filadelfi, 1985). Both taste tests with pure glycoalkaloids (Zitnak and Filadelfi, 1985) and electrophysiological studies of insect galeal and tarsal chemosensilla (Mitchell and Harrison, 1985) showed chaconine to be the more potent of the potato glycoalkaloids, but whether a synergism occurs between solanine and chaconine in antifeedant activity is not known. This question acquires added interest from the facts that (i) taste perception, an integral component of feeding, relies on both membrane integrity and neurotransmitory enzymes, and (ii) potato glycoalkaloids synergise in disruption of membranes but not in inhibition of acetylcholinesterase.

* Corresponding author. Tel.: +44-1392-264606; fax: +44-1392-264668.
E-mail address: j.g.roddick@exeter.ac.uk (J.G. Roddick).

0031-9422/01/$ - see front matter © 2001 Elsevier Science Ltd. All rights reserved.
PII: S0031-9422(01)00034-6

Table 1
Test systems in which solanine and chaconine individually show differential activity and in combination synergise

System	Example	Effect	Reference
Membranes	Liposomes	Lysis	Roddick and Rijnenberg (1987)
Protoplasts	*Penicillium notatum*	Lysis	Roddick et al. (1988)
Cells	Rabbit erythrocytes	Lysis	Roddick et al. (1988)
	Human erythrocytes	Lysis	Smith (1997)
	Drosophila blood	Lysis	Smith (1997)
Tissues	Red beet root	Lysis	Roddick et al. (1988)
	Rat jejunum	Depolarisation	Gee et al. (1996)
Fungi	*Rhizoctonia solani*	Growth inhibition	Fewell and Roddick (1993)
	Ascobolus crenulatus	Growth inhibition	Fewell and Roddick (1993)
	Phoma medicaginis	Growth inhibition	Fewell and Roddick (1993)
	Alternaria brassicicola	Growth inhibition	Fewell and Roddick (1993)
Amphibian	*Xenopus* embryos	Mortality/malformation	Rayburn et al. (1995)

The aim of this study was to determine whether solanine and chaconine, singly and in combination, are capable of deterring feeding activity, using as the test organism the snail, *Helix aspersa*. In contrast to slugs such as *Deroceras reticulatum* which is a serious pest of potato and apparently shows some tolerance of potato glycoalkaloids (Johnston et al., 1989; Johnston and Pearce, 1994), snails are highly susceptible to *Solanum* glycoalkaloids (Alzérreca and Hart, 1982; Marston and Hostettmann, 1984). However, no major investigation of the effects of potato glycoalkaloids on snails has been conducted; a single report exists of solanine lacking molluscicidal activity (see Marston and Hostettmann, 1984). The present study also compared the antifeedant activity of potato peel extracts from three potato varieties and equivalent (in concentration) authentic glycoalkaloid solutions to determine whether compounds in peel other than glycoalkaloids also influence feeding and/or modulate the effects of glycoalkaloids.

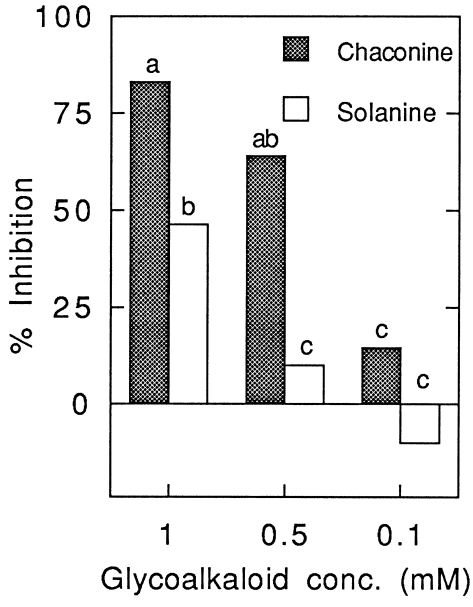

Fig. 1. Effects of authentic solanine and chaconine on feeding by *Helix aspersa*. Snails were presented with two filter paper discs presoaked with methanolic solutions of authentic solanine or chaconine. Control discs were treated with methanol only. After evaporation of the alcohol, snails were left to eat for 48 h at 15°C. Feeding was assessed by measuring the dry weight of the remaining discs. Values are means of six replicates. Treatments marked with different letters (a, b or c) are significantly different from each another at $P \leqslant 0.05$.

2. Results

Both solanine and chaconine caused appreciable feeding inhibition at 1.0 mM (Fig. 1), although solanine was only about half as effective as chaconine. At 0.5 mM chaconine still caused 65% inhibition, but solanine was inactive. Neither compound caused significant inhibition of feeding at 0.1 mM.

To assess the antifeedant effects of solanine/chaconine mixtures, snails were presented with filter paper treated with either authentic solanine or chaconine or a combination of the two compounds, at a range of concentrations (and ratios) determined by the data in Fig. 1. The highest concentration of glycoalkaloid used was 0.4 mM, at which feeding inhibition was unlikely to be greater than 65% thus making it possible to observe any interactive effects between solanine and chaconine, whether antagonistic, additive or synergistic. As shown in Fig. 2, chaconine caused significant inhibition of feeding at 0.2 mM and above and values were consistent with those in Fig. 1 but, unexpectedly, solanine was inhibitory at 0.4 mM, but not below this.

The combinations of solanine and chaconine tested all had a total glycoalkaloid strength of 0.4 mM (Fig. 2). Each of the three combinations containing both glycoalkaloids produced a synergistic inhibition of snail feeding (Fig. 2). Individually, neither 0.3 mM solanine nor 0.1 mM chaconine altered feeding significantly,

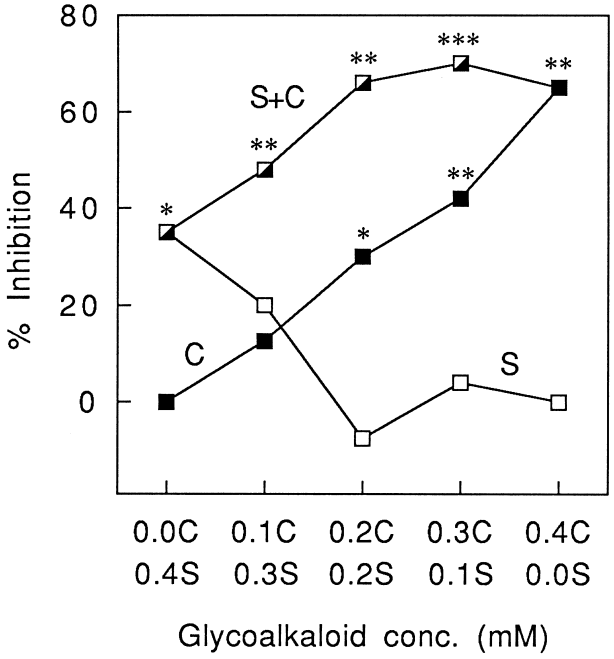

Fig. 2. Antifeedant effects of authentic solanine and chaconine in *Helix aspersa* when supplied singly and in combination. Snails were presented with two filter paper discs pre-soaked with methanolic solutions of authentic solanine or chaconine. Control discs were treated with methanol only. After evaporation of the alcohol, snails were left to eat for 48 h at 15°C. Feeding was assessed by measuring the dry weight of the remaining discs. Values are means of six replicates. *, **, *** = significantly different from control at $P \leqslant 0.05$, 0.01 and 0.001 respectively. S = solanine; C = chaconine.

whereas in combination feeding was reduced by ca 50%. The combination of 0.2 mM chaconine and 0.2 mM solanine (which individually elicited ca 30 and 0% inhibition respectively), produced more than 60% inhibition. Similarly, inhibition by the combination of 0.3 mM chaconine (ca 40% inhibition) and 0.1 mM solanine (zero inhibition) was nearly 70%.

Following glycoalkaloid analyses of methanol extracts of peel of three potato varieties, Majestic, Sharpe's Express and Homeguard (Table 2), equivalent methanolic solutions of authentic solanine and chaconine (in terms of concentration and ratio) were prepared for comparison of antifeedant activity. Majestic and Sharpe's Express peel contained roughly comparable levels of chaconine and solanine, but those in Homeguard were approximately 25% less. In Majestic and Sharpe's Express, all peel extracts and authentic mixtures produced virtually identical inhibition (Fig. 3). Dilution by one-half did not alter the level of inhibition in any treatment whereas dilution to one-tenth strength essentially eliminated inhibition in both authentic mixtures and peel extract (Fig. 3). In Homeguard, there was not the same consistency between the effects of peel extracts and authentic glycoalkaloid mixtures. The full-strength extract and the authentic mixture again produced virtually identical inhibition (Fig. 3), but at one-half dilution the activity of the authentic mixture was substantially less whereas that of the peel extract was not significantly different from the full-strength extract (Fig. 3). Dilution to one-tenth nullified inhibition by the authentic glycoalkaloid mixture, but did not affect the peel extract activity (Fig. 3).

Table 2
Glycoalkaloid concentrations in methanolic tuber peel extracts of the three potato varieties tested for antifeedant activity on *Helix aspersa*[b]

Variety	Glycoalkaloid conc. (mM)		C:S ratio
	Chaconine[a]	Solanine	
Sharpe's Express	0.44	0.18	2.44
Majestic	0.39	0.13	3.00
Homeguard	0.30	0.10	3.00

[a] Values are means of six replicates.
[b] Authentic glycoalkaloid solutions were prepared with identical strengths of solanine and chaconine.

3. Discussion

The finding that chaconine is a more powerful inhibitor of feeding by *H. aspersa* than solanine concurs with comparisons of the activity of these glycoalkaloids in many other test systems from synthetic and cell membranes (Roddick et al., 1988; Roddick and Rijnenberg, 1986; Tschesche and Wulff, 1964), through micro-organisms and simple animals (McKee, 1959; Allen and Feldmesser, 1971; Sinden et al., 1973; Thorne et al., 1985; Fewell and Roddick, 1993), to insects (Mitchell and Harrison, 1985) and mammals (Sharma et al., 1979). The synergism demonstrated here in antifeedant activity also extends the range of test systems/activities that exhibit this interaction (Table 1) to those which have behavioural implications. It is thus probable that a synergistic interaction between solanine and chaconine contributes to many of the other adverse effects elicited by potato glycoalkaloids (including illness/toxicity in humans), although the experimental evidence is still awaited.

The differential antifeedant activity of solanine and chaconine and the synergism between them suggest that their inhibition of feeding by *H. aspersa* is more likely mediated through effects on the membranes of chemoreceptor cells than via impairment of enzymes involved in nervous signal transduction. Sensory cell function can be impaired by changing membrane potential/trans-membrane ion transport and glycoalkaloids are indeed known to alter these parameters (Blankemeyer et al., 1992, 1995) and to synergise in this action (Gee et al., 1996).

Alternatively, it is possible that membrane damage per se does not occur, but that the synergism between solanine and chaconine extends to their organoleptic properties. Consistent with this possibility is that chaconine is more bitter/burning (by 4× and 2× respectively) than solanine (Zitnak and Filadelfi, 1985). On

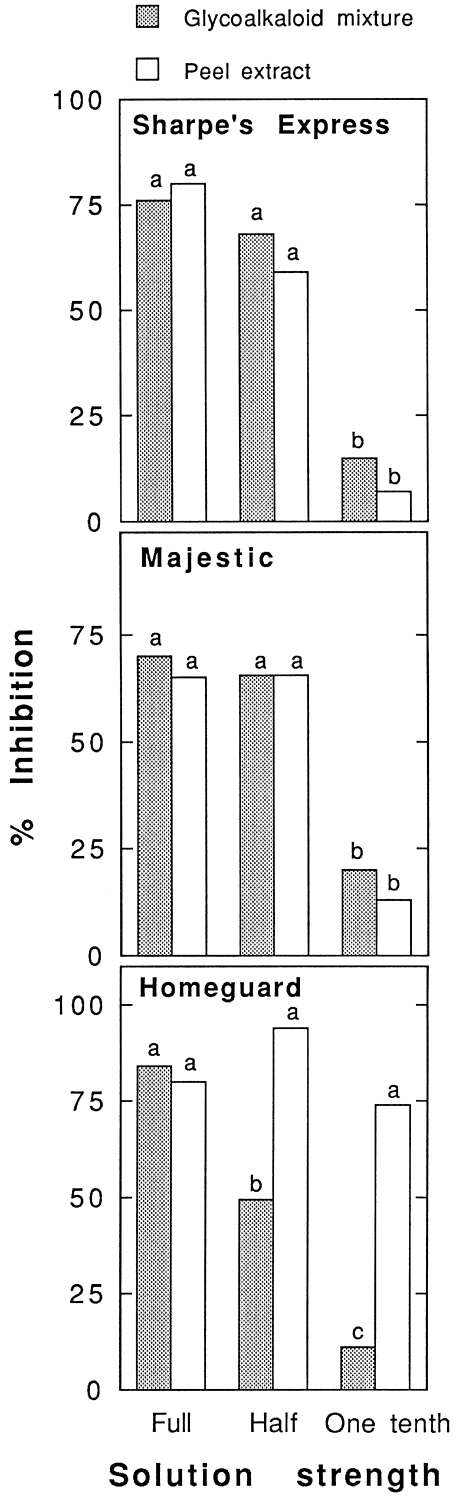

Fig. 3. Comparison of the antifeedant effects in *Helix aspersa* of methanolic extracts of tuber peel from three potato varieties and equivalent strength mixtures of authentic solanine and chaconine. Snails were presented with two filter paper discs pre-soaked with methanolic solutions of solanine or chaconine, or methanolic extracts of peel. Control discs were treated with methanol only. After evaporation of the alcohol, snails were left to eat for 48 h at 15°C. Feeding was assessed by measuring the dry weight of the remaining discs. Values are means of six replicates. Treatments marked with different letters (a, b or c) are significantly different from each another at $P \leqslant 0.05$.

the other hand, comparative taste tests (by humans) on bland potato tissue enhanced with solanine and with an equal concentration of a 3:1 mixture of chaconine:solanine yielded no evidence of a synergism between the glycoalkaloids (Sinden et al., 1976). However, comparison of the levels of glycoalkaloids that inhibit feeding in snails with those causing adverse taste sensations in humans is not only hindered by the use of different experimental systems, but of questionable validity in view of the taxonomic distance between humans and snails, compounded by the biochemical/physiological/behavioural distance between taste and feeding activity. The possibility has not escaped us that feeding activity in the snails may also have been adversely influenced by the blandness of the filter paper diet and the lack of choice/variety in the diet (Speiser and Rowell-Rahier, 1993).

The finding that feeding inhibition caused by full-strength peel extracts of Sharpe's Express and Majestic and equivalent authentic glycoalkaloid mixtures (Fig. 3) was of a similar order to that by chaconine alone (Fig. 2) at approximately the same strength (0.4 mM — Table 2, solanine is inactive at all concentrations in extracts) may have been due to deterrence by 0.4 mM chaconine alone being nearly maximal, thus masking any synergism. The declining apparency of a synergism with the increasing strength of the glycoalkaloid solution is well known from other studies (Roddick et al., 1990; Fewell and Roddick, 1993). That it may explain this observation is supported by the half-strength peel extracts and authentic mixtures causing about twice the effect of 0.2 mM chaconine alone (i.e. demonstrating the synergism). The observation that the full-strength peel extract of Homeguard (and the equivalent authentic glycoalkaloid mixture) caused similar inhibiton to full-strength Sharpe's Express and Majestic peel extracts (and authentic mixtures) even though glycoalkaloid levels were ~25% lower could be attributed to manifestation of the synergism at the lower chaconine concentration. Although in Homeguard, inhibition by the half-strength authentic mixture is less than by the full-strength mixture, this still represents a marked synergism when compared with inhibition by 0.15 mM chaconine (Fig. 2).

Of considerable interest is that Homeguard peel extracts diluted to one-half or one-tenth strength showed no reduction in feeding inhibiton and were more inhibitory than could be explained by their glycoalkaloid content alone. This could suggest that a factor(s) other than glycoalkaloids contributes to feeding inhibition by this variety of potato. Sinden et al. (1976) found that authentic potato glycoalkaloids did not produce as intense taste sensations as equivalent levels in natural tissues, although the differences were not as marked as reported here. Potatoes are known to elaborate other secondary compounds which affect feeding, e.g phenolics, terpenoids and protease inhibitors (Johnston and Pearce, 1994) and a number of inorganic and organic

compounds are known to be able to suppress or enhance glycoalkaloid activity (see Roddick and Leonard, 1999). In addition, the presence of small, unidentified late-eluting peaks in the glycoalkaloid extracts raises the question of whether glycoalkaloids other than solanine and chaconine may have been present which were inhibitory in their own right and/or capable of synergising with each other and/or with solanine and chaconine. Knowledge of the anti-feedant activity (and indeed the biological activity) of glycoalkaloids is restricted to only a few (~5) major compounds found in important food plants; for all other glycoalkaloids, including the minor compounds, no such information exists.

4. Experimental

4.1. Potato material

Certified seed tubers of the maincrop potato variety Majestic and the two early varieties, Homeguard and Sharpe's Express, were planted 30 cm apart in single rows in the experimental plot of the School of Biological Sciences, University of Exeter. Each trench was 15–20 cm wide and deep and was partially filled with manure before planting. Plants were watered twice weekly. Tubers were harvested by hand and stored in paper sacks at 15° and 40% relative humidity.

4.2. Glycoalkaloids

Pure (98%) solanine and chaconine used in feeding studies were prepared and supplied by Dr. A. Fewell (Fewell, 1993). Analysis of tuber peel glycoalkaloids was as described by Smith (1997). This involved extraction into MeOH and clean-up using a C18 SPE column (Anachem, UK) according to the method of Carman et al. (1986). Qualitative and quantitative analyses of glycoalkaloids were based on the HPLC method of Bushway and Storch (1982). The column was a carbohydrate analysis column (Waters Associates, USA) with an amino pre-column; mobile phase was tetrahydrofuran:water:acetonitrile (53:17:30); flow rate 1 ml/min; detector wavelength 215 nm. The identity of extracted glycoalkaloids was confirmed by their retention times on HPLC relative to authentic samples, and by electrospray MS.

4.3. Source and maintenance of snails

Snails (*Helix aspersa* L.) were gathered locally and housed in a lidded glass tank (40×60×40 cm) the bottom of which was lined with gravel. The tank was moistened periodically by sprinkling with distilled water and a constant supply of fresh lettuce leaves provided as food. Tanks were kept in a room at an ambient temperature of approximately 15°C with natural illumination.

4.4. Feeding experiments

Feeding experiments were conducted in lidded plastic propagating trays (22×17×20 cm) the base of which was lined with moist paper towelling. Perforated cling-film was placed over the towelling to prevent the snails from feeding on the towelling. Preliminary experiments established that snails will readily consume dry filter paper discs. Glycoalkaloids were applied to Whatman GP1 5.5 cm diameter filter papers in 0.25 ml MeOH (the minimum volume required to wet the entire surface). The MeOH was allowed to evaporate (ca 5 min) before the snails were introduced into the propagating tray. For experiments involving tuber extracts, MeOH peel extracts were prepared from single tubers of each of the three varieties and their solanine and chaconine content measured (Smith, 1997). The MeOH extracts were then applied to filter papers, as above. MeOH extracts were employed in preference to expressed sap since the latter would contain enzymes that would (a) produce polyphenolic compounds that may have adversely effected snail feeding behaviour, and (b) hydrolyse the glycoalkaloids (Bergenstråhle et al., 1992). MeOH extracts were, therefore, considered to provide a closer approximation of the state in which glycoalkaloids and other intracellular components exist in vivo, although it was appreciated that other factors such as pH would not operate in such extracts.

Snails were starved at 18°C for 24 h prior to each experiment, after which three were placed centrally in each of 6 propagating trays together with 2 discs of control or treated filter paper and left to feed under natural illumination at 15°C for 48 h. Only snails weighing between 6 and 8 g were used in experiments. Feeding activity was quantified by determining the amount of filter paper (dried to constant weight) remaining in control and glycoalkaloid treatments.

4.5. Replication and statistical analysis

All treatments in all experiments were replicated six times. Experiments involving glycoalkaloid-containing peel extracts and equivalent authentic solutions were carried out on two separate occasions. All data were analysed by ANOVA and *t*-tests, where appropriate after sin transformation.

Acknowledgements

We thank Dr. Alison Fewell for a supply of pure solanine and chaconine, Mr. James Kingdon and Mrs Anna Leonard (School of Biological Sciences, University of Exeter) for growing the potatoes and technical assistance, respectively, and Dr. Stephen Lock (Campden and Chorleywood Food Research Association) for electrospray

MS analyses of glycoalkaloids. DBS gratefully acknowledges receipt of a BBSRC CASE studentship in conjunction with the Campden and Chorleywood Food Research Association.

References

Allen, E.H., Feldmesser, J., 1971. Nematicidal activity of α-chaconine: effect of hydrogen-ion concentration. Journal of Nematology 3, 58–61.

Alzérreca, A., Hart, G., 1982. Molluscicidal steroid glycoalkaloids possessing stereoisomeric spirosolane structures. Toxicology Letters 12, 151–155.

Bergenstråhle, A., Tillberg, E., Jonsson, L., 1992. Characterization of UDP-glucose:solanidine glucosyltransferase and UDP-galactose:solanidine galactosyltransferase from potato tuber. Plant Science 84, 35–44.

Blankemeyer, J.T., Stringer, B.K., Rayburn, J.R., Bantle, J.A., Friedman, M., 1992. Effect of potato alkaloids, α-chaconine and α-solanine, on membrane potential of frog embryos. Journal of Agricultural and Food Chemistry 40, 2022–2025.

Blankemeyer, J.T., Atherton, R., Friedman, M., 1995. Effect of potato glycoalkaloids α-chaconine and α-solanine on sodium active transport in frog skin. Journal of Agricultural and Food Chemistry 43, 636–639.

Bushway, R.J., Storch, R.H., 1982. Semi-preparative high-performance liquid chromatographic separation of potato glycoalkaloids. Journal of Liquid Chromatography 5, 731–742.

Carman, A.S., Kuan, S.S., Ware, G.M., Francis, O.J., Kirschenheuter, G.P., 1986. Rapid high-performance liquid chromatographic determination of the potato glycoalkaloids α-solanine and α-chaconine. Journal of Agricultural and Food Chemistry 34, 279–282.

Fewell, A.M., 1993. Interactive Antifungal Activity Between Co-occurring *Solanum* Glycoalkaloids. PhD thesis, University of Exeter, Exeter, UK.

Fewell, A.M., Roddick, J.G., 1993. Interactive antifungal activity of the glycoalkaloids α-solanine and α-chaconine. Phytochemistry 33, 323–328.

Friedman, M., McDonald, G.M., 1997. Potato glycoalkaloids: chemistry, analysis, safety, and plant physiology. Critical Reviews in Plant Science 16, 55–132.

Gee, J.M., Wortley, G.M., Johnson, I.T., Price, K.R., Rutten, A.A.J.J.L., Houben, G.F., Penninks, A.H., 1996. Effects of saponins and glycoalkaloids on the permeability and viability of mammalian intestinal cells and on the integrity of tissue preparations in vitro. Toxicology In Vitro 10, 117–128.

Johnston, K.A., Kershaw, W.J.S., Pearce, R.S. 1989. Biochemical mechanisms of resistance of potato cultivars to slug attack. British Crop Protection Council Monograph No. 41, pp. 281–288.

Johnston, K.A., Pearce, R.S., 1994. Biochemical and bioassay analysis of resistance of potato (*Solanum tuberosum* L.) cultivars to attack by the slug *Deroceras reticulatum* (Muller). Annals of Applied Biology 124, 109–131.

Marston, A., Hostettmann, K., 1984. Plant molluscicides. Phytochemistry 24, 639–652.

McKee, R.K., 1959. Factors affecting the toxicity of solanine and related alkaloids to *Fusarium caeruleum*. Journal of General Microbiology 20, 686–696.

Mitchell, B.K., Harrison, G.D., 1985. Characterization of galeal chemosensilla in the adult Colorado potato beetle. Physiological Entomology 9, 49–56.

Rayburn, J.R., Friedman, M., Bantle, J.A., 1995. Synergistic interaction of glycoalkaloids α-chaconine and α-solanine on developmental toxicity in *Xenopus* embryos. Food Chemistry and Toxicology 33, 1013–1019.

Roddick, J.G., 1989. The acetylcholinesterase-inhibitory activity of steroidal glycoalkaloids and their aglycones. Phytochemistry 28, 2631–2634.

Roddick, J.G., 1996. Steroidal glycoalkaloids: nature and consequences of bioactivity. In: Waller, G.R., Yamasaki, K., (Eds.), Saponins used in traditional and modern medicine. Plenum Press, New York, pp. 277–295.

Roddick, J.G., Leonard, A.L., 1999. Amelioration by glucose-6-phosphate and NADP of potato glycoalkaloid inhibition in cell, enzyme and liposome assays. Phytochemistry 51, 23–27.

Roddick, J.G., Rijnenberg, A.L., 1986. Effect of steroidal glycoalkaloids of the potato on the permeability of liposome membranes. Physiologia Plantarum 68, 436–440.

Roddick, J.G., Rijnenberg, A.L., 1987. Synergistic interaction between the potato glycoalkaloids α-solanine and α-chaconine in relation to lysis of phospholipid/sterol liposomes. Phytochemistry 26, 1325–1328.

Roddick, J.G., Rijnenberg, A.L., Osman, S.F., 1988. Synergistic interaction between potato glycoalkaloids α-solanine and α-chaconine in relation to destabilization of cell membranes: ecological implications. Journal of Chemical Ecology 14, 889–902.

Roddick, J.G., Rijnenberg, A.L., Weissenberg, M., 1990. Membrane-disrupting properties of the steroidal glycoalkaloids solasonine and solamargine. Phytochemistry 29, 1513–1518.

Roddick, J.G., Weissenberg, M., Leonard, A.L., 2001. Membrane disruption and enzyme inhibition by naturally-occurring and modified chacotriose-containing *Solanum* steroidal glycoalkaloids. Phytochemistry 56, 603–610.

Sharma, R.P., Willhite, C.C., Shupe, J.L., Salunkhe, D.K., 1979. Acute toxicity and histopathological effects of certain glycoalkaloids and extracts of *Alternaria solani* or *Phytophthora infestans* in mice. Toxicology Letters 3, 349–355.

Sinden, S.L., Goth, R.W., O'Brien, M.J., 1973. Effect of potato alkaloids on the growth of *Alternaria solani* and their possible role as resistance factors. Phytopathology 63, 303–307.

Sinden, S.L., Deahl, K.L., Aulenbach, B.B., 1976. Effect of glycoalkaloids and phenolics on potato flavor. Journal of Food Science 41, 520–523.

Smith, D.B., 1997. Profiles and Biological Activity of Potato Glycoalkaloids. PhD thesis, University of Exeter, Exeter, UK.

Speiser, B., Rowell-Rahier, M., 1993. Does the land snail *Arianta arbutorum* prefer sequentially mixed over pure diets? Functional Ecology 7, 403–410.

Thorne, H.V., Clarke, G.F., Skuce, R., 1985. The inactivation of herpes simplex virus by some solanaceous glycoalkaloids. Antiviral Research 5, 335–343.

Tschesche, R., Wulff, G., 1964. Konstitution und Eigenschaften der Saponine. Planta Medica 12, 272–292.

Zitnak, A., Filadelfi, M.A., 1985. Estimation of taste thresholds of three potato glycoalkaloids. Canadian Institute of Food Science and Technology Journal 18, 337–339.

PERGAMON

Phytochemistry 57 (2001) 235–244

PHYTOCHEMISTRY

www.elsevier.com/locate/phytochem

A chemotaxonomic investigation of volatile constituents in *Stachys* subsect. Swainsonianeae (Labiatae)

Helen D. Skaltsa [a,*], Anna Mavrommati [a], Theophanis Constantinidis [b]

[a] *Division of Pharmacognosy, School of Pharmacy, University of Athens, Panepistimiopolis, Zografou, GR-157 71, Athens, Greece*
[b] *Botanical Institute, Department of Biology, University of Patras, GR-265 00, Patras, Greece*

Received 29 May 2000; received in revised form 28 November 2000

Abstract

The composition of the previously unknown essential oils of *Stachys* subsect. Swainsonianeae (Labiatae) are investigated by GC–MS analyses. The group includes the taxa *Stachys ionica*, *St. spruneri*, *St. swainsonii* ssp. *swainsonii*, *St. swainsonii* ssp. *argolica*, *St. swainsonii* ssp. *melangavica* and *St. swainsonii* ssp. *scyronica*, all endemic to Greece. Eighteen populations were analyzed, and more than two hundred components were identified. Statistical analyses of oil components separated *St. ionica*, due to its high amount of (*E*)-nerolidol, high amount of α-cadinol and low amount of (+)-(*E*)-caryophyllene. The rest of the taxa forms a coherent group where (+)-(*E*)-caryophyllene, δ-cadinene and partly β-elemene, (+)-caryophyllene oxide and (+)-limonene predominate but each of them never exceeds 20% of the total. Essential oil composition reflects current taxonomy and phytogeography of the group with a somewhat isolated position for *St. ionica*. Similarities in morphology and essential oil composition of the *St. swainsonii* group and *St. spruneri* may be the result of extensive gene flow in the past. Evidence from volatile oil compounds that may attribute to *St. swainsonii* ssp. *melangavica* a hybrid origin from crosses between *St. spruneri* and *St. swainsonii* ssp. *swainsonii*/*scyronica* group is scarce. © 2001 Elsevier Science Ltd. All rights reserved.

Keywords: *Stachys* subsect. Swainsonianeae; *Stachys ionica*; *Stachys spruneri*; *Stachys swainsonii*; Labiatae; Chemotaxonomy; Volatile constituents; Intraspecific variability; Hybridization; Statistics

1. Introduction

The subcosmopolitan genus *Stachys* L. comprises more than 270 species (Mabberley, 1997) and is justifiably considered as one of the largest genera of the Labiatae. In the Old World area there are two main centres of diversity for the genus, as assessed by the number and distribution of the species. One is confined to S and E Anatolia, Caucasia, NW Iran and N Iraq, and the other to the Balkan Peninsula (Bhattacharjee, 1980). Greece is certainly an area particularly rich in taxa. More than 50 species and subspecies are distributed in the mainland and/or the islands (Greuter et al., 1986); a significant proportion of them are considered endemic. *Stachys* sect. Swainsoniana Bhattacharjee subsect. Swainsonianeae Bhattacharjee is confined to Greece and includes seven perennial, suffruticose taxa of narrow distribution, particular habitat preference, and the same chromosome number of $2n=34$. Among them, the vulnerable *St. euboica* Rech. fil. is localized to the SE part of Evvia island (Constantinidis, 1995), and its subsectional placement appears problematic: although originally described as an ally of *St. mollisima* Willd., it was not placed together with it in subsect. Decumbentes by Bhattacharjee (1980) but in subsect. Swainsonianeae. Because of its taxonomic uncertainty, this species will be studied together with members of subsect. Decumbentes in a forthcoming paper. *St. ionica* Halácsy, wholly confined to the islands of the Ionian sea, is a good example of insular differentiantion; its populations do not reach adjacent west Greek mainland. *St. spruneri* Boiss. is distributed in SE Sterea Ellas, mostly in Attiki. Its populations in certain areas grow sympatrically or parapatrically with the last and more diverse species, *St. swainsonii* Bentham. This last species has been further divided into four subspecies (Phitos and Damboldt, 1969; Persson, 1981) all narrow endemic chasmophytes which, according to morphological and palaeogeographical evidence, presumably represent relicts of formally more widespread species complexes.

* Corresponding author. Tel.: +30-1-7274593; fax: +30-1-8613965.
E-mail address: skaltsa@pharm.uoa.gr (H.D. Skaltsa).

0031-9422/01/$ - see front matter © 2001 Elsevier Science Ltd. All rights reserved.
PII: S0031-9422(01)00003-6

In spite of the large size of *Stachys*, the composition of volatile compounds is known in only a small number of species. These include *St. balansae* Boiss. (Cakir et al., 1997) and *St. obliqua* Waldst. and Kit. (Harmandar et al., 1997), two species of sect. *Eriostomum*; *St. palustris* L. (Maly, 1985) and *St. sylvatica* L. (Maly, 1985; Lawrence, 1992) of sect. *Stachys*; *St. candida* Bory and Chaub. and *St. chrysantha* Boiss. (Skaltsa et al., 1999) of sect. *Candida*; *St. annua* L. (Maly, 1988) and *St. recta* L. (Maly, 1985; Cakir et al., 1997) of sect. *Olisia*; *St. corsica* Pers. (Pélissier et al., 1999) of sect. *Corsica*; *St. glutinosa* L. (Mariotti et al., 1997) of sect. *Aucheriana*; *St. lavandulifolia* Vahl (Sezik and Basaran, 1986; Ghannadi and Alemdoost, 1996) of sect. *Zietenia*; *St. aegyptiaca* Pers. (Halim et al., 1991) and *St. inflata* (Sajjadi, 1996) of sect. *Ambleia*; and *St. betonica* Benth. [= *St. officinalis* (L.) Trevisan] (Maly, 1985) of sect. *Betonica*.

The present study aims at investigating the volatile compounds, previously unknown, of all members of *Stachys* subsect. Swainsonianeae, with the exception of *St. euboica* (see above). Intraspecific variability is also examined by processing more than one population per taxon (Table 1). The results are compared with the biology and taxonomy of the taxa, to extract evidence of possible chemotaxonomic significance. Eighteen populations of the following six taxa were examined: *Stachys ionica*, *St. spruneri*, *St. swainsonii* ssp. *argolica* (Boiss.) Phitos and Damboldt, *St. swainsonii* ssp. *melangavica* D. Persson, *St. swainsonii* ssp. *scyronica* (Boiss.) Phitos and Damboldt and *St. swainsonii* ssp. *swainsonii*.

2. Results and discussion

All the investigated *Stachys* taxa contain essential oils that range from 0.16 to 0.38% based on dry wt (Table 2). The highest oil contents were found in *St. ionica* (0.36–0.38%) and *St. spruneri* (0.29–0.31%). In the other four taxa, the oil content was between 0.16 and 0.23%. As it is shown in the analytical Table 2, all the essential oils are complex mixtures of more than one hundred constituents in each investigated case, with contributions of main products never exceeding 20% of the total. Among them the sesquiterpenes consist the main portion in all studied taxa, while a population of *St. spruneri* (spr-1) has a high content in monoterpene hydrocarbons (41.4%) as well. Apart from a population of *St. swainsonii* ssp. *argolica* (arg-2) which has a significant aldehyde fraction (15.9%), and relatively high terpene esters content (7.3%), all other populations have a much lower level of such compounds ($<4.1\%$). Generally, all taxa have rather low amounts of phenylpropanoids, and fatty acids and aliphatic esters, with the exception of swa-2. The use of a chiral column allowed the determination of enantiomers in several main

Table 1
List of the *Stachys* subsect. Swainsonianeae taxa investigated with provenance, abbreviations used and voucher specimens

Name	Abbreviation	Locality	Coordinates	Voucher specimen (UPA)
Stachys spruneri	spr-1	Attiki, Mt. Gerania, NW Panorama, 400–420 m.	37°59′ N, 23°12′ E	Const. 7684
	spr-2	Viotia, Mt. Kitheron, c. 6 km from Vilia, 850 m.	38°10′ N, 23°17′ E	Const. & Lazari 7896
	spr-3	Attiki, Mt. Pateras, around the low summit of Kandili, 380–440 m.	38°03′ N, 23°24′ E	Const. 7897
	spr-4	Attiki, Mt. Pateras, W of Paleokoundoura, 400 m.	38°07′ N, 23°23′ E	Const. 619
Stachys swainsonii subsp. *melangavica*	mel-1	Korinthia, close to Ireon ancient temple, 5–70 m.	38°01′ N, 22°51′ E	Const. 7444
	mel-2	Viotia, c. 2.7 km NNE Paralia Sarandi, 250–280 m.	38°15′ N, 22°52′ E	Const. 7503
	mel-3	Korinthia, c. 5.8 km from Pisia to Schinos, 400 m.	38°02′ N, 23°00′ E	Const. 7681
Stachys swainsonii subsp. *argolica*	arg-1	Korinthia, c. 8.1–8.9 km after turn-off to Korfos, 50–80 m.	37°44′ N, 23°06′ E	Const. 7640
	arg-2	Argolida, c. 4.4 km ESE Vivarion, 70–90 m.	37°32′ N, 22°57′ E	Const. 7893
	arg-3	Attiki, c. 3.7 km NW Kalloni, 120 m.	37°33′ N, 23°16′ E	Const. 7894
Stachys swainsonii subsp. *swainsonii*	swa-1	Fokida, c. 7.5–8.0 km after Itea along road to Galaxidi, 10–20 m.	38°25′ N, 22°24′ E	Const. 7598
	swa-2	Fokida, c. 2.0 km NW Itea, 30–40 m.	38°27′ N, 22°25′ E	Const. 7599
	swa-3	Fokida, N of Lidorikion, 600–650 m.	38°33′ N, 22°11′ E	Const. 7913
Stachys swainsonii subsp. *scyronica*	scy-1	Attiki, c. 5.5–6.5 km ENE Kineta, 130–160 m.	37°58′ N, 23°17′ E	Const. 7438
	scy-2	Attiki, Mt. Gerania, NW Panorama, 360–380 m.	37°58′ N, 23°12′ E	Const. 7685
Stachys ionica	ion-1	Zakinthos island, locality known as Faros Keriou, 250–280 m.	37°39′ N, 20°48′ E	Phitos et al. 25924
	ion-2	Kefallinia island, c. 4.1 km NNW Farsa, 180 m.	38°15′ N, 20°28′ E	Const. 7911
	ion-3	Kefallinia island, c. 1.1 km N Anomeria, 320 m.	38°20′ N, 20°32′ E	Const. 7912

Table 2
Qualitative and quantitative composition (% v/v) of volatile compounds in *Stachys* subsect. *Swainsonianeae*

	Compounds	RI[a]	spr-1	spr-2	spr-3	spr-4	mel-1	mel-2	mel-3	arg-1	arg-2	arg-3	swa-1	swa-2	swa-3	scy-1	scy-2	ion-1	ion-2	ion-3
1	Hexanal	800	–	–	–	–	–	–	–	–	–	–	tr	–	–	–	–	–	–	–
2	(*E*)-2-Hexenal	854	–	–	–	–	0.5	–	0.1	–	–	–	0.7	tr	–	–	–	–	–	–
3	(*Z*)-3-Hexenol	857	–	–	–	–	–	–	–	–	–	–	–	tr	–	–	–	–	–	–
4	Heptanal	899	–	–	–	–	0.1	–	tr	–	–	–	tr	–	–	–	–	–	–	–
5	**α-Thujene**	929	3.3	0.6	0.7	tr	2.3	–	1.5	–	tr	2.5	0.6	–	–	1.9	0.7	–	0.1	0.1
6	(*E*)-Heptenal	951	–	–	–	–	tr	–	–	–	–	–	–	–	–	–	–	–	–	–
7	**(+)-α-Pinene**	936	8.0	0.3	2.0	0.2	2.7	–	1.1	tr	–	2.2	1.8	–	–	1.0	0.3	tr	0.4	0.3
8	Camphene	952	0.1	tr	tr	–	tr	–	tr	–	–	–	tr	–	–	tr	tr	–	–	–
9	Benzaldeyde	959	–	–	–	–	–	–	–	tr	–	tr	–	–	–	–	–	–	–	–
10	**Sabinene**	972	4.1	0.7	1.3	0.3	1.5	tr	1.4	tr	0.1	1.4	0.5	tr	0.1	1.3	0.7	tr	0.2	0.2
11	**1-Octen-3-ol**	977	0.2	2.4	0.1	0.1	1.0	0.5	1.9	2.1	0.9	0.2	4.3	0.6	0.5	1.7	2.1	–	0.1	0.1
12	**(+)-β-Pinene**	978	1.3	0.2	0.3	tr	1.9	0.1	0.8	0.1	tr	0.5	1.7	–	0.1	0.3	0.2	–	tr	tr
13	6-Methyl-5-hepten-2-one	985	–	–	–	–	–	–	–	tr	–	–	–	–	–	–	–	–	–	–
14	3-Octanone	986	–	–	–	–	–	–	–	–	–	–	tr	–	tr	–	–	–	–	–
15	**β-Myrcene**	988	0.7	0.3	0.2	0.1	0.6	tr	0.5	0.1	0.2	1.1	–	tr	–	0.5	0.4	–	–	–
16	3-Octanol	993	tr	0.2	tr	–	tr	–	0.1	–	0.2	–	tr	tr	tr	0.2	0.2	tr	0.1	0.1
17	Octanal	1001	–	–	–	–	–	–	–	0.1	0.5	–	–	–	–	–	–	tr	tr	tr
18	α-Phellandrene	1003	0.2	0.2	tr	tr	0.3	–	0.4	–	–	0.2	tr	tr	0.2	0.3	0.2	–	–	–
19	δ-3-Carene	1011	–	0.1	–	–	0.1	–	–	–	–	0.4	–	–	–	0.1	0.1	–	–	–
20	**α-Terpinene**	1018	1.3	0.2	0.2	0.1	0.3	–	0.4	tr	0.1	–	tr	tr	–	0.5	0.2	–	–	–
21	*p*-Cymene	1024	0.3	0.3	–	tr	0.3	tr	0.3	0.1	0.2	0.3	tr	tr	0.2	tr	0.3	–	0.1	tr
22	**(+)-Limonene**	1027	17.3	1.4	8.6	3.9	4.4	0.4	2.4	0.5	–	4.0	0.9	0.2	0.2	–	1.4	0.6	1.2	1.1
23	**β-Phellandrene**	1028	–	–	–	–	–	–	–	–	0.6	–	–	–	0.2	1.4	–	–	–	–
24	1,8-Cineole	1031	–	0.3	–	–	–	–	–	0.2	0.5	–	0.2	tr	0.1	–	0.3	–	0.1	tr
25	***cis*-Ocimene**	1038	0.2	0.4	0.1	0.1	–	tr	tr	0.3	0.1	4.1	4.7	0.8	1.3	tr	0.4	–	0.1	–
26	Phenylacetaldehyde	1041	0.1	0.1	0.1	–	tr	tr	tr	0.1	0.1	–	0.1	tr	tr	tr	0.1	–	–	tr
27	***trans*-Ocimene**	1048	1.3	0.1	0.1	tr	1.0	tr	0.9	0.2	0.3	1.0	0.6	0.1	0.1	tr	0.1	–	0.7	tr
28	**γ-Terpinene**	1059	2.3	0.8	0.4	0.3	–	–	–	0.2	0.7	0.9	0.3	0.1	0.2	1.1	0.8	–	tr	tr
29	***cis*-Sabinene hydrate**	1064	0.5	1.5	0.1	–	0.7	0.2	1.5	0.5	0.3	0.4	0.5	0.1	0.5	0.6	1.4	–	–	–
30	***n*-Octanol**	1068	tr	0.2	tr	–	0.1	0.1	0.3	0.6	1.2	0.1	tr	tr	0.1	tr	0.2	–	0.3	0.3
31	**Terpinolene**	1085	1.0	0.2	0.2	0.8	1.2	tr	1.7	1.4	0.4	3.1	tr	tr	–	0.3	0.2	–	tr	tr
32	2-Nonanone	1091	–	–	–	–	–	–	–	–	tr	–	–	–	–	–	–	–	–	–
33	*trans*-Sabinene hydrate	1095	0.2	0.5	0.1	–	0.2	–	0.4	0.2	–	0.2	–	–	–	0.3	0.5	–	tr	tr
34	**(+)-β-Linalool**	1098	0.2	0.1	0.2	0.5	0.1	0.2	0.3	0.9	8.2	3.5	0.4	0.2	0.4	tr	0.2	tr	0.4	0.4
35	(−)-β-Linalool	1098	0.2	0.1	0.4	–	–	–	–	–	–	–	–	–	–	–	–	–	–	–
36	***n*-Nonanal**	1102	0.2	0.5	0.1	–	0.6	0.2	0.6	0.8	8.5	0.9	0.2	0.1	0.2	tr	0.5	tr	0.2	0.3
37	*p*-Mentha-1,3,8-triene	1108	–	–	–	–	–	–	–	–	–	0.1	–	tr	–	–	–	–	–	–
38	*trans*-Thujone	1115	–	tr	–	–	–	–	tr	tr	–	–	–	–	–	–	tr	–	–	–
39	*cis-p*-2-Menthen-1-ol	1117	0.3	0.4	0.1	–	0.1	–	0.3	0.2	0.3	0.1	–	–	–	tr	0.3	–	–	–
40	3-Acetoxy octane	1124	–	–	–	–	tr	–	-	–	–	–	–	–	–	tr	–	–	–	–
41	α-Campholenal	1125	tr	tr	tr	–	–	tr	–	0.1	–	–	–	tr	tr	–	tr	–	–	–
42	*allo*-Ocimene	1128	0.1	–	–	–	–	–	–	–	–	–	tr	tr	0.1	–	–	–	–	–
43	*trans*-Pinocarveol	1134	–	–	tr	–	–	–	–	0.2	–	–	tr	–	0.1	–	–	–	–	–
44	*trans-p*-2-Menthen-1-ol	1140	–	–	–	–	–	–	–	0.1	0.1	–	–	–	–	0.1	0.1	–	–	–
45	Camphor	1143	–	–	–	–	tr	–	tr	–	tr	–	–	–	–	–	–	–	–	–
46	2,6-Nonadienal	1151	–	–	–	–	0.1	tr	tr	0.1	–	–	tr	tr	–	–	–	–	–	–
47	2-Nonenal	1158	–	–	–	–	0.2	tr	0.1	0.3	0.3	0.1	tr	tr	–	–	–	–	–	–
48	Borneol	1165	–	–	–	–	–	–	–	–	–	–	tr	tr	–	tr	0.1	–	–	–
49	*p*-Mentha-1,5-dien-8-ol	1166	–	–	–	–	–	–	–	–	–	–	–	–	tr	–	–	–	–	–
50	Nonanol	1171	–	–	–	–	–	tr	tr	0.1	0.1	–	–	–	–	tr	–	–	–	–
51	**(+)-Terpinen-4-ol**	1175	3.1	3.3	0.5	1.5	1.6	0.2	3.5	1.6	3.6	2.2	0.3	0.2	2.1	1.8	3.2	–	tr	tr
53	(−)-Terpinen-4-ol	1175	0.5	–	0.5	–	–	–	–	–	–	–	–	0.2	–	–	–	–	–	–
54	*p*-Cymen-8-ol	1182	–	–	–	0.1	–	–	–	0.1	–	–	–	tr	–	–	–	–	–	–
55	**(+)-α-Terpineol**	1187	0.1	0.4	0.1	0.2	0.1	tr	0.3	0.8	1.6	0.6	tr	0.1	0.3	–	0.4	–	0.2	0.2
56	(−)-α-Terpineol	1187	0.1	–	–	0.2	–	–	–	–	0.9	0.5	–	–	–	–	–	–	–	–
57	Methyl salicylate	1190	0.1	tr	–	tr	tr	–	tr	–	0.2	–	tr	tr	–	–	tr	–	–	–
58	*cis*-Piperitol	1191	–	0.1	–	–	–	–	0.1	–	–	–	–	–	–	tr	0.1	–	–	–
59	Myrtenal	1193	–	–	–	–	–	–	–	–	–	–	tr	–	–	–	–	–	–	–
60	Myrtenol	1194	–	–	–	–	–	–	–	0.3	–	–	tr	–	0.1	–	–	–	–	–
61	Decanal	1203	0.1	0.1	0.1	tr	0.1	0.1	0.2	0.2	0.5	0.1	0.1	0.1	0.1	0.1	0.1	–	tr	tr
62	*trans*-Carveol	1217	–	–	–	–	–	–	–	0.2	–	–	0.2	0.1	–	–	–	–	–	–
63	β-Cyclocitral	1218	tr	0.1	0.1	0.1	0.1	0.1	0.1	–	–	–	0.2	0.1	–	0.2	0.1	–	–	–
64	Nerol	1225	–	–	–	–	–	–	–	–	0.5	0.2	–	–	–	–	–	–	–	–

(*continued on next page*)

Table 2 (*continued*)

	Compounds	RI[a]	spr-1	spr-2	spr-3	spr-4	mel-1	mel-2	mel-3	arg-1	arg-2	arg-3	swa-1	swa-2	swa-3	scy-1	scy-2	ion-1	ion-2	ion-3
65	*cis*-Carveol	1228	–	–	–	tr	–	–	–	–	–	–	–	–	–	–	–	–	–	–
66	Myrtenyl acetate	1234	–	–	–	–	–	–	–	–	–	–	0.2	–	–	–	–	–	–	–
67	Pulegone	1237	–	–	–	–	–	–	–	–	–	–	–	–	tr	–	–	–	–	–
68	Neral	1240	tr	tr	–	tr	–	–	–	–	–	–	tr	tr	–	tr	tr	–	–	–
69	Carvone	1241	–	tr	tr	tr	–	–	–	0.1	–	–	–	–	tr	–	tr	–	–	–
70	**(+)-Linalyl acetate**	1258	0.1	–	0.1	0.1	tr	–	–	–	5.1	2.5	–	–	–	–	–	–	–	–
71	**(*E*)-2-Decenal**	1260	tr	0.1	tr	0.2	0.1	–	0.1	0.3	2.5	0.2	tr	0.1	–	tr	0.1	–	tr	–
72	Dec-9-en-1-ol	1262	–	0.2	–	–	–	–	–	–	–	–	–	–	–	–	0.2	–	–	0.1
73	Geranial	1270	–	tr	–	–	–	–	tr	–	–	–	tr	tr	–	–	tr	–	–	–
74	*n*-Decanol	1272	–	–	–	–	tr	tr	tr	–	tr	–	–	tr	tr	–	tr	–	–	–
75	Bornyl acetate	1284	–	tr	tr	tr	–	tr	tr	0.1	–	–	tr	–	–	tr	tr	–	–	–
76	(2*E*, 4*Z*)-2,4-Decadienal	1291	–	0.1	–	tr	–	–	–	0.1	0.1	–	0.2	0.1	–	tr	tr	–	–	–
77	Thymol	1294	–	–	–	–	–	–	–	–	–	–	tr	–	–	–	–	–	–	–
78	*trans*-Pinocarvyl acetate	1297	–	–	–	–	–	–	–	0.1	–	–	0.1	–	–	–	–	–	–	–
79	**Tridecane**	1298	–	–	–	–	–	–	–	–	1.5	–	–	0.1	–	–	–	–	–	–
80	**Carvacrol**	1299	0.1	–	–	0.1	–	0.1	–	1.4	–	0.2	–	–	–	0.1	–	–	0.3	tr
81	Dihydrocarveol acetate	1304	–	–	–	–	–	–	–	–	–	–	–	–	–	–	–	–	–	–
82	Undecanal	1305	–	0.1	tr	–	–	tr	0.1	–	0.2	–	tr	0.2	0.3	tr	0.1	–	–	–
83	*cis*-Pinocarvyl acetate	1308	0.1	tr	–	–	–	–	–	–	–	–	tr	tr	–	–	–	–	–	–
84	(2*E*,4*E*)-2,4-Decadienal	1312	–	0.1	0.2	–	0.1	tr	0.1	0.3	–	–	tr	tr	–	tr	0.1	–	tr	–
85	*iso*-Dihydrocarvyl acetate	1323	–	–	tr	–	–	0.2	–	–	–	–	–	–	–	–	–	–	–	–
86	*trans*-Carvyl acetate	1337	tr	–	0.1	–	–	–	–	–	–	–	tr	tr	–	–	–	–	–	–
87	δ-Elemene	1339	0.8	–	–	–	–	–	–	–	–	–	0.2	–	0.1	–	–	–	–	–
88	**α-Cubebene**	1348	–	–	–	–	0.3	0.7	–	–	1.9	0.6	tr	0.2	–	–	–	–	0.1	0.1
89	**α–Terpinyl acetate**	1347	–	0.7	1.2	1.4	–	–	0.2	0.6	–	–	tr	–	–	tr	0.7	–	–	–
90	2-Phenyl ethyl propanoate	1350	–	–	–	–	–	–	–	0.1	–	–	–	–	–	–	–	–	–	–
91	Eugenol	1353	–	–	–	0.5	–	tr	0.1	tr	–	–	tr	0.1	–	tr	0.1	–	0.1	0.1
92	**(*E*)-2-Undecenal**	1358	–	0.1	0.1	–	–	–	0.2	0.5	3.1	–	–	–	–	–	–	–	–	–
93	*cis*-Carvyl acetate	1362	0.2	–	–	–	–	–	–	–	–	–	–	–	–	–	–	–	–	–
94	**Cyclosativene**	1364	–	1.1	0.4	0.4	–	1.5	–	–	–	1.7	tr	0.6	–	tr	1.1	–	tr	0.1
95	α-Ylangene	1368	–	–	–	–	–	–	–	–	–	–	–	tr	–	–	–	–	–	–
96	Undecanol	1370	–	–	–	–	–	–	–	–	–	–	–	–	0.4	–	–	–	–	–
97	**α-Copaene**	1375	3.9	4.7	2.6	2.5	1.5	9.4	0.6	1.3	1.3	4.4	0.6	2.8	–	0.8	4.6	0.3	0.4	0.4
98	**Geranyl acetate**	1380	–	–	–	–	–	–	–	–	2.2	1.1	–	–	–	–	–	–	–	–
99	**β-Bourbonene**	1382	0.5	0.4	1.0	0.6	tr	0.3	1.0	1.6	–	–	0.4	0.4	0.4	–	–	–	–	-
100	**β-Cubebene**	1388	0.1	–	–	–	1.4	0.5	–	0.3	0.4	0.3	0.3	–	–	–	0.4	–	0.1	0.1
101	**β-Elemene**	1391	1.8	5.1	3.9	1.2	18.8	0.7	10.8	0.9	2.4	1.2	0.5	2.2	0.3	8.4	5.0	–	0.2	0.2
102	β-Longipinene	1398	–	–	–	–	–	–	–	–	–	–	tr	0.1	–	–	–	–	–	–
103	Cyperene	1399	–	–	tr	–	–	–	–	–	–	–	–	–	–	–	–	–	–	–
104	(*Z*)-Caryophyllene	1404	0.1	–	0.1	0.6	–	–	–	–	0.2	0.1	–	0.1	–	–	–	–	–	–
105	**Dodecanal**	1407	–	0.3	tr	–	–	–	0.3	–	–	–	–	1.0	3.4	–	0.3	–	–	–
106	α-Cedrene	1408	0.1	–	–	–	–	–	–	–	–	–	tr	–	–	–	–	–	–	–
107	α-Gurjunene	1409	–	0.5	0.1	0.3	–	1.0	–	0.2	–	0.4	0.4	tr	–	–	0.5	0.4	0.4	0.4
108	α-*cis*-Bergamotene	1414	–	–	–	–	0.1	–	–	–	–	–	–	–	–	–	–	–	–	–
109	(−)-(*E*)-Caryophyllene	1418	1.0	–	1.0	1.0	–	–	–	–	–	–	–	–	–	–	–	–	–	–
110	**(+)-(*E*)-Caryophyllene**	1418	8.7	8.7	8.5	15.0	5.4	7.3	4.8	7.8	16.3	10.7	7.8	7.9	12.8	1.1	8.4	0.3	1.1	1.1
111	*cis*-Thujopsene	1426	–	–	–	–	–	–	–	–	–	–	tr	–	–	–	–	–	–	–
112	Calarene	1428	0.1	0.1	0.2	0.1	–	0.5	0.1	0.5	–	–	tr	0.2	0.1	–	0.1	–	0.1	0.1
113	**α-*trans*-Bergamotene**	1434	tr	1.1	0.3	–	–	–	–	0.2	tr	–	tr	0.2	0.6	–	1.1	–	–	–
114	**Aromadendrene**	1438	–	tr	1.0	–	–	0.5	0.2	0.2	–	–	–	0.2	–	tr	tr	–	–	–
115	α-Guaiene	1439	–	–	–	–	–	–	–	–	–	–	–	0.1	–	–	–	–	–	–
116	α-Neo-clovene	1451	–	–	–	–	–	–	–	–	–	0.1	–	–	–	–	–	–	–	–
117	**α-Humulene**	1452	0.8	1.1	1.3	2.1	0.8	0.8	0.7	1.2	1.5	0.9	0.9	1.1	1.4	0.5	1.1	–	0.3	0.3
118	**(*E*)-β-Farnesene**	1457	–	1.7	1.0	1.7	–	–	–	2.6	1.1	–	0.2	–	0.1	–	1.6	–	–	–
119	**Alloaromadendrene**	1458	0.3	0.1	–	–	1.0	0.5	0.9	–	0.7	0.3	–	0.4	0.1	1.2	0.2	–	–	1.2
120	β-Acoradiene	1462	–	–	–	–	–	–	–	–	–	0.1	tr	–	0.2	–	–	–	–	–
121	**γ-Selinene**	1469	1.0	0.1	0.2	0.2	0.5	–	1.5	–	–	–	0.2	0.3	0.1	–	–	–	–	–
122	**γ-Muurolene**	1477	–	0.4	0.5	0.4	1.1	1.3	–	7.4	1.8	1.9	tr	0.4	–	0.9	0.7	0.4	0.6	0.7
123	***epi*-Bicyclo-sesquiphellandrene**	1478	0.9	0.4	2.2	1.8	2.0	1.2	1.7	–	–	–	4.7	2.6	5.6	2.0	0.4	0.3	0.3	0.4
124	**Ar-Curcumene**	1479	–	–	–	–	–	–	–	–	1.8	0.8	1.7	0.7	3.6	–	–	–	–	–
125	**Germacrene D**	1480	–	–	0.2	–	–	5.4	–	–	–	–	–	–	–	–	–	–	–	–
126	(*E*)-β-Ionone	1484	–	–	–	0.3	–	0.2	–	0.7	–	–	–	0.5	0.2	–	–	–	–	–
127	**β-Selinene**	1485	1.0	0.7	0.3	–	1.8	0.6	1.5	–	–	6.1	–	–	–	0.6	0.7	–	0.3	0.3

(*continued on next page*)

Table 2 (*continued*)

	Compounds	RI[a]	spr-1	spr-2	spr-3	spr-4	mel-1	mel-2	mel-3	arg-1	arg-2	arg-3	swa-1	swa-2	swa-3	scy-1	scy-2	ion-1	ion-2	ion-3
128	1-Pentadecene	1489	–	–	–	–	–	–	–	–	–	–	0.2	–	–	–	–	–	–	–
129	***cis*-β-Guaiene**	1491	–	–	1.5	–	–	–	–	–	–	–	–	–	–	–	3.4	–	–	–
130	**Valencene**	1491	–	–	–	–	–	–	–	–	–	–	–	–	–	–	–	–	2.4	2.5
131	**Viridiflorene**	1493	–	–	–	–	4.6	4.8	10.6	5.8	–	–	3.7	4.7	–	7.3	–	–	–	–
132	**α-Selinene**	1494	11.0	3.5	–	–	–	–	–	–	4.1	–	–	0.2	5.4	–	–	–	–	–
133	**Bicyclogermacrene**	1494	–	–	–	4.5	5.0	–	4.7	3.2	–	–	–	0.9	–	1.9	–	–	–	–
134	***trans*-β-Guaiene**	1499	–	–	–	0.3	–	–	–	–	–	–	–	–	–	–	–	1.3	–	–
135	β-Himachalene	1499	–	–	–	–	–	–	–	–	–	–	–	–	–			0.7	–	-
136	**α-Muurolene**	1499	0.8	0.7	1.2	0.3	1.1	1.1	0.7	–	–	0.6	0.3	0.4	–	1.9	2.3	1.4	1.9	2.0
137	**Eremophilene**	1502	–	1.6	–	–	8.1	0.2	–	0.2	–	–	0.2	0.8	–	2.8	1.6	–	–	–
138	Cuparene	1502	–	–	–	–	–	–	–	–	–	–	–	–	0.1	–	–	–	0.1	0.1
139	Germacrene A	1503	0.5	–	1.0	–	–	–	–	–	–	0.4	–	–	–	–	–	–	–	–
140	**(*E*,*E*)-α-Farnesene**	1508	0.4	–	0.2	0.2	0.3	0.9	4.2	1.5	0.2	0.7	0.6	1.2	0.8	tr	1.2	–	0.1	tr
141	α-Dehydro-himachalene	1509	–	–	–	–	–	–	–	–	–	0.5	–	–	–	–	–	–	–	–
142	**γ-Cadinene**	1513	0.7	1.2	1.6	0.7	1.6	2.9	1.6	0.8	0.3	0.7	0.4	0.3	1.0	2.8	–	1.6	2.3	2.3
143	**7-*epi*-α-Selinene**	1515	–	–	1.0	–	–	–	–	–	–	–	–	–	–	1.4	–	–	1.5	1.6
144	**δ-Cadinene**	1524	4.5	5.8	5.5	4.2	3.7	13.7	4.0	2.1	1.3	6.5	0.8	3.6	0.7	8.5	5.7	4.7	6.2	6.3
145	Cadina-1,4-diene	1531	0.1	0.2	0.4	0.2	0.1	0.5	0.2	0.1	–	0.1	tr	0.2	–	0.7	0.2	–	0.6	0.6
146	**α-Cadinene**	1537	–	tr	0.2	0.1	tr	0.3	0.2	–	–	–	tr	0.1	–	0.5	0.3	2.8	0.5	0.5
147	β-Cedranoxide	1540	–	–	–	–	–	–	–	0.3	–	–	–	–	–	–	–	–	–	–
148	α-Calacorene	1540	0.1	–	0.2	0.2	–	0.3	–	–	–	0.1	–	0.2	–	–	–	–	0.1	tr
149	**Selina-3,7-diene**	1542	–	–	–	–	–	–	–	–	–	–	–	–	–	–	–	1.7	–	0.2
150	**Elemol**	1550	–	–	–	0.6	–	–	–	0.3	tr	–	–	0.2	–	–	–	5.5	4.6	1.2
151	Germacrene B	1554	–	–	–	–	–	–	–	–	–	–	–	–	–	–	–	–	–	–
152	**(*E*)-Nerolidol**	1564	–	–	–	–	–	0.2	–	0.4	–	0.7	tr	–	0.5	0.3	0.4	14.3	14.9	14.7
153	Ledol	1565	–	0.4	–	–	–	–	–	–	–	0.2	–	–	–	–	–	–	–	–
154	Dodecanoic acid	1566	–	–	–	–	–	–	–	–	–	–	–	0.1	–	–	–	–	–	–
155	Caryophyllene alcohol	1568	–	–	0.6	–	–	–	–	0.2	–	–	–	–	–	–	–	–	–	–
156	(Z)-Hexenyl benzoate	1569	0.1	–	–	0.3	–	–	0.2	0.3	–	0.1	0.4	0.5	0.3	–	–	–	–	–
157	Germacrene-D-4-ol	1574	–	–	–	–	–	–	3.4	–	–	–	–	–	–	–	–	–	–	–
158	*n*-Tridecanol	1575	–	–	–	–	–	–	–	–	–	–	–	0.2	0.2	–	–	–	–	–
159	**Spathulenol**	1577	–	4.9	3.9	7.4	4.1	6.2	1.4	4.4	1.3	2.0	–	6.3	7.8	tr	2.6	7.2	7.6	8.0
160	β-Copaen-4-α-ol	1579	0.7	–	–	–	–	–	–	–	–	–	–	–	–	–	–	–	–	–
161	**(−)-Caryophyllene oxide**	1581	0.4	0.6	0.3	–	–	–	–	–	–	tr	1.2	tr	3.4	tr	tr	–	–	–
162	**(+)-Caryophyllene oxide**	1581	3.0	1.2	2.9	–	1.0	2.6	–	2.6	7.1	2.8	12.5	6.5	15.4	16.3	2.4	–	–	–
163	**Globulol**	1585	–	–	–	–	–	–	–	–	–	–	–	–	–	0.6	1.8	–	–	–
164	**Viridiflorol**	1589	0.1	0.5	0.3	2.9	–	–	0.2	–	–	0.3	11.4	8.9	–	0.2	0.5	–	0.5	–
165	**α-Cedrol**	1599	–	1.8	0.4	–	–	–	–	0.5	–	1.8	–	–	–	–	1.8	–	–	–
166	***epi*-Globulol**	1608	–	0.7	–	–	–	–	–	–	–	–	–	–	–	–	–	3.6	2.4	1.8
167	1-*epi*-Cubenol	1625	–	–	–	–	–	–	–	–	–	–	–	–	–	–	1.0	1.0	–	0.1
168	**γ-Eudesmol**	1631	–	–	–	–	–	–	–	–	–	–	–	–	–	–	–	0.9	–	1.1
169	**T-Cadinol**	1635	–	1.0	0.7	–	–	–	–	–	–	–	–	–	–	–	–	1.3	4.6	0.9
170	***epi*-α-Muurolol = T-muurolol**	1641	–	2.2	2.9	0.5	–	3.7	1.5	–	–	1.1	0.5	1.1	–	7.4	2.1	4.4	–	–
171	**Torreyol**	1643	–	0.2	0.6	0.8	0.3	0.4	0.5	1.7	–	1.6	–	0.2	–	1.1	0.2	0.9	7.6	7.9
172	**β-Eudesmol**	1650	–	–	–	–	3.1	0.2	–	–	–	–	0.2	0.3	0.4	–	–	0.6	0.5	1.5
173	**α-Eudesmol**	1652	–	–	–	1.2	–	–	5.4	–	–	–	0.5	0.8	–	–	–	–	–	0.3
174	**α-Cadinol**	1656	1.4	1.0	3.5	0.2	–	–	0.1	1.5	0.8	–	0.2	0.7	–	9.9	1.0	8.8	13.1	10.5
175	β-Bisabolol	1671	–	–	–	–	–	–	0.5	–	–	–	0.6	–	–	–	–	–	–	–
176	**Valeranone**	1672	–	–	–	–	–	–	–	–	–	–	–	–	–	–	–	–	1.0	0.5
177	**Cadalene**	1674	0.2	–	–	1.6	–	4.0	–	–	–	–	–	–	–	–	–	–	–	–
178	**(*Z*)-Nerolidol acetate**	1675	–	2.7	0.8	–	–	–	–	–	–	–	–	–	–	–	–	–	–	–
179	**Tetradecanol**	1676	–	–	0.7	–	–	–	–	0.3	0.6	0.6	–	–	–	–	2.7	–	–	–
180	(*Z*)-α-Santalol	1678	–	–	–	0.1	–	–	–	–	–	–	0.2	–	–	–	–	–	–	–
181	Heptadecene	1692	–	–	–	–	–	–	0.1	–	–	–	0.6	0.3	0.3	–	–	–	–	0.1
182	**(*Z*, *E*)-Farnesol**	1699	–	–	–	0.1	–	–	–	–	–	–	–	0.1	2.9	–	–	–	–	–
183	Heptadecane	1700	–	–	–	–	–	–	–	0.1	–	–	0.2	0.2	–	–	–	–	–	–
184	Pentadecanal	1714	–	–	–	–	–	0.1	0.1	0.1	0.3	0.1	0.2	0.3	tr	–	–	–	–	–
185	**(*E*, *E*)-Farnesol**	1722	–	–	–	–	–	–	–	–	–	–	–	–	–	–	–	8.0	1.0	5.0
186	(*E*, *Z*)-Farnesol	1740	–	–	–	–	–	–	–	–	–	–	–	–	–	–	–	2.5	–	–
187	**α-Sinensal**	1752	–	–	–	–	–	–	–	–	–	–	–	–	–	–	–	10.5	2.1	2.1
188	Benzyl benzoate	1764	–	0.2	0.1	0.1	–	0.4	0.2	0.7	–	–	0.9	1.1	0.7	0.3	0.2	–	–	–
189	Tetradecanoic acid	1769	–	–	–	0.2	–	–	–	–	–	–	–	–	–	–	–	–	–	–
190	1-Octadecene	1793	–	–	–	–	–	–	–	–	–	–	0.1	0.1	–	–	–	–	–	–

(*continued on next page*)

Table 2 (*continued*)

	Compounds	RI[a]	spr-1	spr-2	spr-3	spr-4	mel-1	mel-2	mel-3	arg-1	arg-2	arg-3	swa-1	swa-2	swa-3	scy-1	scy-2	ion-1	ion-2	ion-3
191	**(*Z,E*)-Farnesyl acetate**	1818	–	–	–	–	–	–	–	–	–	–	3.0	4.0	1.1	–	–	–	–	–
192	Isopropyl myristate	1827	–	0.1	tr	–	–	–	0.1	0.2	–	0.2	–	–	–	–	0.1	–	–	–
193	**6,10,14-Trimethyl pentadecan-2-one**	1845	–	0.6	0.1	0.2	0.2	1.3	0.2	0.7	0.5	0.2	0.6	0.9	–	0.1	0.6	–	–	–
194	Hexadecanol	1882	–	0.1	0.2	–	–	–	tr	0.2	–	–	–	0.3	–	–	0.1	–	–	–
195	***iso*-Pimar-9(11),15-diene**	1899	–	–	–	–	–	–	–	–	–	–	0.3	0.2	0.8	–	–	–	–	–
196	(*E, E*)-Farnesyl acetone	1918	–	–	–	–	–	0.1	tr	0.2	–	–	0.2	0.2	–	tr	–	–	–	–
197	Methyl hexadecanoate	1926	–	–	–	–	–	–	–	tr	–	–	–	tr	–	–	–	–	–	–
198	Cembrene	1941	–	–	–	–	–	–	–	0.2	–	–	–	–	–	–	–	–	–	–
199	Pimaradiene	1942	–	–	–	–	–	–	–	–	0.3	–	–	–	–	–	–	–	–	–
200	(*E*)-Phytol	1950	–	–	–	–	–	tr	–	–	–	–	–	–	–	–	–	–	–	–
201	Neocembrene	1960	–	–	–	–	–	–	–	–	–	0.2	–	–	–	–	–	–	–	–
202	**Sandaracopimara-8(14), 15-diene**	1961	–	5.8	–	0.9	–	–	–	–	–	0.2	–	–	–	–	–	–	–	–
203	**Sclarene**	1964	–	–	–	–	–	–	–	–	–	–	–	–	–	–	5.7	–	6.0	7.0
204	**Hexadecanoic acid**	1972	–	0.5	0.1	0.8	–	0.6	–	1.1	0.3	0.1	1.6	5.9	–	–	0.5	–	–	–
205	Isokaurene	1988	–	–	–	1.0	–	–	–	–	–	–	–	–	–	–	–	–	–	–
206	**Manoyl oxide**	1991	–	0.5	0.4	–	0.9	–	0.5	0.8	0.2	0.6	0.7	2.3	7.7	0.1	0.5	–	2.0	1.2
207	**13-*epi*-Manoyl oxide**	2011	–	–	–	1.6	–	0.2	0.7	1.6	–	1.3	0.9	0.9	–	–	–	–	0.3	0.4
208	**Cembra-2,7,11-trien-4-ol**	2057	–	–	–	–	–	–	–	2.6	–	–	–	–	–	–	–	–	–	-
209	**Abietatriene**	2058	1.3	2.4	6.9	7.6	0.4	1.0	0.4	1.4	1.9	3.4	1.4	1.5	2.1	0.2	2.4	–	0.1	0.1
210	**Octadecanol**	2082	–	–	–	–	0.1	1.6	–	1.0	0.2	0.4	1.4	0.9	0.6	0.5	0.2	–	–	–
211	**Abietadiene**	2082	–	1.3	–	1.3	–	–	–	–	–	–	–	–	–	–	–	–	–	–
212	*trans*-Phytol	2114	–	–	–	–	–	–	–	0.5	0.1	–	–	–	–	–	0.6	–	–	–
213	Methyl Octadecanoate	2135	–	–	–	–	–	–	–	–	–	–	0.2	0.2	–	–	–	–	–	–
214	**(*Z*)-9-Octadecanoic acid**	2152	–	–	–	–	–	–	–	–	–	–	–	2.8	–	–	–	–	–	–
215	Octadecanoic acid	2178	–	–	–	–	–	–	–	–	–	–	–	0.5	0.3	–	–	–	–	–
216	Ethyl octadecanoate	2194	–	–	–	–	–	–	–	–	–	–	–	–	–	–	0.7	–	–	–
217	Sclareol	2228	–	–	–	–	–	–	–	–	–	–	–	–	–	tr	0.1	tr	0.1	tr
218	**Dehydroabietal**	2268	0.1	1.4	2.1	3.2	0.2	–	0.5	0.5	–	0.2	–	–	–	0.1	1.4	–	–	–
219	Tricosane	2300	–	–	–	–	–	–	–	–	–	–	0.3	0.3	0.2	–	–	–	–	–
220	**Abieta-7,13-diene-3-one**	2302	–	–	–	1.3	–	–	–	–	–	–	–	–	–	–	–	–	–	–
221	***trans*-Ferruginol**	2325	–	–	tr	1.0	–	–	–	–	0.5	–	–	–	–	–	–	–	–	–
222	**4-*epi*-Dehydroabietol**	2332	–	0.4	1.7	2.1	0.2	0.2	0.3	0.2	–	0.1	–	–	–	0.1	0.7	–	–	–
223	Neoabietic acid	2335	–	–	–	–	–	–	–	0.2	–	–	0.4	0.3	0.3	–	–	–	–	–
Total			94.4	87.5	85.1	86.5	92.1	82.3	88.6	79.6	94.9	92.3	83.6	87.3	89.9	94.3	88.4	86.0	92.6	89.0
Yield (%v/dry wt)			0.30	0.29	0.29	0.31	0.23	0.24	0.23	0.26	0.22	0.21	0.16	0.17	0.20	0.21	0.21	0.36	0.38	0.38
Aliphatics																				
Alkanes, alkenes			–	–	–	–	–	–	–	0.1	1.5	–	1.1	0.9	0.4	–	–	–	–	0.1
Alcohols			0.3	3.1	0.9	0.1	1.3	2.1	2.4	4.2	3.2	1.4	5.8	2.1	4.7	2.3	5.8	tr	0.4	0.5
Aldehydes			0.5	1.3	0.5	0.7	1.7	0.5	2.0	2.8	15.9	1.5	1.6	2.0	4.1	0.2	1.0	tr	0.3	0.3
Ketones			–	0.6	0.1	0.2	0.2	1.4	0.2	0.8	0.6	0.1	0.8	1.1	tr	0.2	0.5	–	–	–
Fatty acids and aliphatic esters			0.0	0.5	0.1	1.0	tr	0.6	0.1	1.3	0.3	0.2	1.8	9.6	0.3	tr	1.2	–	–	–
Terpenoids																				
Monoterpene hydrocarbons			41.4	5.6	14.0	5.9	17.5	0.8	13.3	3.5	3.0	22.6	11.4	1.6	3.1	9.5	7.7	0.6	2.7	1.7
Oxygenated monoterpenes			5.3	6.8	2.1	2.6	2.0	0.6	4.4	6.1	15.6	7.3	1.5	0.9	3.1	2.3	4.9	tr	1.1	0.8
Sesquiterpene hydrocarbons			39.4	39.5	37.7	40.0	59.1	60.7	50.2	44.6	35.0	39.1	23.8	33.3	33.7	43.1	40.9	15.9	19.4	21.5
Oxygenated sesquiterpenes			5.5	14.5	16.0	13.8	8.7	13.4	13.0	11.7	9.3	10.5	27.4	25.0	27.5	36.0	14.1	69.5	60.1	55.4
Diterpenoids			1.3	11.8	11.2	20.1	1.6	1.4	2.3	7.5	2.9	5.9	3.7	5.1	10.9	0.4	10.7	tr	8.5	8.6
Miscellaneous terpenoids			–	–	–	–	–	tr	–	0.5	0.1	–	–	–	–	–	0.6	–	–	–
Terpene esters			0.3	3.5	2.3	1.6	tr	0.2	0.3	0.8	7.3	3.6	3.4	4.1	1.1	0.3	0.9	–	–	–
Aromatics			0.1	0.3	0.2	0.5	tr	0.4	0.4	1.1	0.2	0.1	1.3	1.6	1.0	tr	0.1	–	0.1	0.1

[a] Kovats index on HP-5 column.

compounds. In most cases only one isomer is present in the essential oil, the other being absent or present in trace amounts.

The main constituents of the essential oils in *Stachys* subsect. Swainsonianeae are (+)-α-pinene (8.0% in spr-1), (+)-limonene (17.3% in spr-1 and 8.6% in spr-3), (+)-β-linalool (8.2% in arg-2), α-copaene (9.4% in mel-2), (+)-(*E*)-caryophyllene (relatively high values in several populations), α-cadinol (high percentages in *St. ionica*), (*E*)-nerolidol (high amounts in *St. ionica*) and α-sinensal (10.5% in ion-1). A quick glance at the other investigated representatives of various *Stachys* sections

reveals two significant indications. First, that there is a wide range of principal compounds in the oils of *Stachys* species studied so far, as, e.g. germacrene D in *St. obliqua* (Harmandar et al., 1997), a member of section *Eriostomum* and carvacryl acetate in *St. corsica* (Pélissier et al., 1999), a member of section *Corsica*. Both constituents are unknown, or present in small quantities in the members of *Stachys* subsect. Swainsonianeae. Thus, chemical variation of volatile compounds may be promising as chemotaxonomically important for the whole genus. Second, two investigated members of *St.* sect. *Candida* (*St. candida* and *St. chrysantha*; Skaltsa et al., 1999), most closely related to sect. *Swainsoniana,* share relatively high values of (*E*)-caryophyllene and α-cadinol with the studied taxa. To what extent composition of volatile oils reflects taxonomic or phylogenetic relationships in *Stachys* is unknown at present, since many of its ca 270 members remain to be investigated. However, chemistry of volatile compounds has been proved particularly helpful in assessing taxonomic relationships of several genera in Labiatae (Stahl-Biskup, 1991; Kokkini, 1992; Skoula et al., 1999; Sanz et al., 2000).

To evaluate whether the identified constituents may be useful in reflecting taxonomic relationships in *Stachys* subsect. Swainsonianeae all the components of Table 2 that exceed 1% of total oil contribution in at least one *Stachys* population (marked in bold in Table 2) were subject to principal component analysis (PCA) and cluster analysis (CA). In the absence of information about shape of the groupings and/or statistical distribution of values, Euclidean distance combined with unweighted pair group average linking were used for CA (Dunlop et al., 1997). The resulted dendrogram appears in Fig. 2. In PCA (Fig. 1), horizontal axis accounts for ca. 38% of the variation while vertical axis for a further 15%.

As it is evident from both statistical analyses, the three populations of *St. ionica* clearly stand out forming a separate group in PCA or a deep dichotomy in CA. Thus, chemically speaking, *St. ionica* appears to be the most differentiated species, with metabolic pathways leading to compounds in its essential oil not significantly shared with the rest of the species. Indeed, useful chemotaxonomic markers for *St. ionica* include its high content in (*E*)-nerolidol (>14% in all populations, <0.7% in all other taxa), relatively high amounts of α-cadinol (>8.8%, generally <3.5% in other taxa except an anomalous high value in scy-1), and low amounts of (+)-(*E*)-caryophyllene (<1.2%, usually >4.7% in other taxa except scy-1). Thus, compared to the rest of the species in the subsection, *St. ionica* appears to have the most distinguishable chemotype. Chemical differentiation is correlated to the distribution of the species, which is confined to the Ionian islands and is, therefore, well-isolated from the rest of the group. Such a pattern of distribution does not currently permit gene exchange between *St. ionica* and the rest of the taxa in subsect. Swainsonianeae. Further, chemical differentiation of essential oil appears to be the result of genetic differentiation enhanced by spatial isolation. Crossing experiments between all taxa of subsection Swainsonianeae performed by Persson (1981) and subsequent estimation of pollen stainability in F_1 generation indicated mean percentages of functional

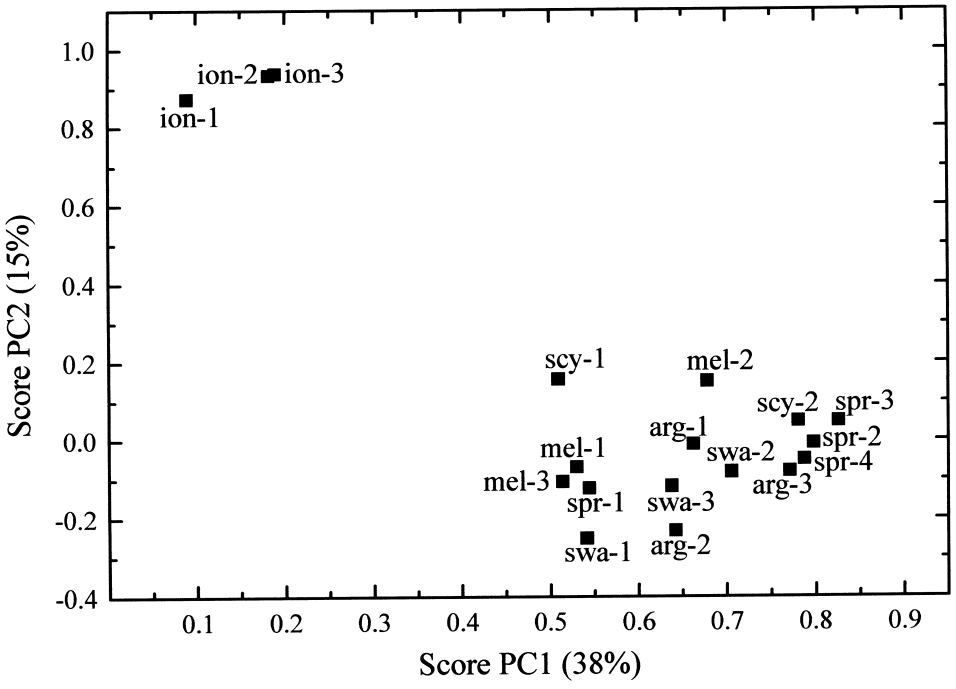

Fig. 1. Principal component analysis (PCA) of main volatile constituents in *Stachys* subsect. Swainsonianeae. For abbreviations of taxa see Table 1.

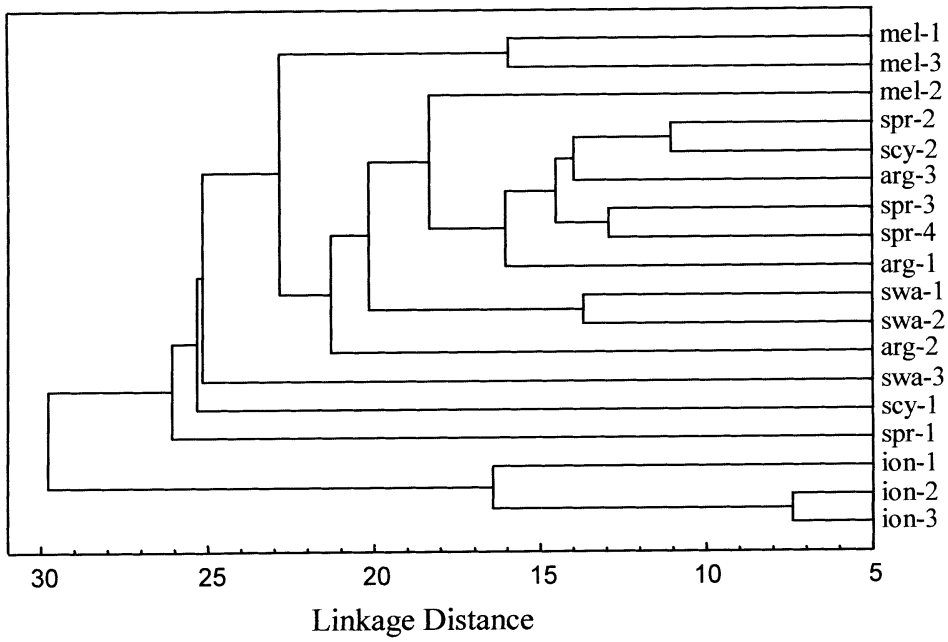

Fig. 2. Dendogram resulted from cluster analysis (CA) of main volatile constituents in *Stachys* subsect. Swainsonianeae. For abbreviations of taxa see Table 1.

pollen between 40 and 59% in all crossings between *St. ionica* and any of the *St. swainsonii* subspecies as opposite to functional pollen between 60 and 79% in all crossings among *St. swainsonii* subspecies.

The role that distance may play in the composition of essential oils within *St. ionica* is effectively presented in populations ion-2 and ion-3. These populations share a great resemblance in essential oil constituents and are grouped together in both PCA and CA. The populations originate from the same island, and are separated from each other by a few kilometers distance. Their pronounced chemical similarity can be attributed to either free gene flow (all members of *St.* sect. Swainsonianeae are pollinated by insects but are capable of inbreeding) or comparatively recent fragmentation of a previously more continuous population. Essential oil of ion-1 from Zakinthos is weakly differentiated, mainly by the relatively low amount of torreyol, lack of sclarene and relatively high levels of α-sinensal.

For the rest of the taxa, resolution provided by both statistical analyses is rather low. All four populations of *St. spruneri* are characterized by the high amounts of (+)-(*E*)-caryophyllene (>8.5%). Spr-1 deviates somewhat by the presence of relatively high amounts of (+)-α-pinene, (+)-limonene and α-selinene but its position is not highlighted by either PCA or CA. This particular population grows in the vicinity of two subspecies of *St. swainsonii* (ssp. *melangavica* and ssp. *scyronica*) but shows no morphological evidence of hybridization. The two populations of *St. spruneri* collected on the same mountain (spr-3 and spr-4) are not grouped together, as in the case of ion-2 and ion-3.

For the four subspecies of *St. swainsonii* main chemical constituents vary. Like *St. spruneri,* all share high proportions of (+)-(*E*)-caryophyllene (but this compound is unusually low in scy-1). Arg-2 is characterized by quite high levels of (+)-β-linalool and n-nonanal, while rather high levels of manoyl oxide are found in swa-3. The sesquiterpene β-elemene is higher than 8.3% in scy-1, mel-1 and mel-3. However, none of these populations is given any particular position in PCA or CA.

Lack or resolution in statistical processing within *St. spruneri* and *St. swainsonii* essential oils may be attributed to two important reasons. Firstly, all five taxa are taxonomically closely related and occasionally grow intermixed or parapatrically to each other. They can be experimentally crossed, and pollen stainability of F_1 generation ranges at quite high levels, mostly between 60 and 79% (Persson, 1981). Some populations of the Mt. Gerania area may even be attributed to hybrid swarms but have not been included in the present study to avoid masking chemical results of 'pure' taxa. Secondly, *St. spruneri* and all *St. swainsonii* members have probably been evolved rather recently, and speciation processes are still in progress. Facilitated by climatic fluctuations, extensive gene flow that occurred in the past (Persson, 1981) may have significantly contributed towards a shading of distinct secondary products that would characterize each taxon.

Based on morphological and experimental evidence, *St. swainsonii* ssp. *melangavica* was given an unusual origin by Persson (1981). This taxon may represent the stabilized hybridogenous result of ancient crossings between *St. spruneri, St. swainsonii* ssp. *swainsonii* and

St. swainsonii ssp. *scyronica*. This being true, the formation and establishment of ssp. *melangavica* may be attributed to homoploid hybridization coupled with spatial isolation and disappearance of certain ancestor populations. The composition of the essential oil of the three *St. swainsonii* ssp. *melangavica* populations examined compared to those of the three presumably parental taxa gives us, however, rather sparse data of intermediacy.

Mean values of caryophyllene oxide (both isomers) of *St. swainsonii* ssp. *melangavica* ($\bar{a}_1 = 1.2$) come closer to *St. spruneri* ($\bar{a}_2 = 2.1$) than to ssp. *swainsonii*/*scyronica* group ($\bar{a}_3 = 11.5$). The same happens to the mean limonene amounts. Viridiflorene seems to be absent in *St. spruneri*, while it exists in considerable amounts in ssp. *melangavica* ($\bar{a}_4 = 6.6$) and lower values in the ssp. *swainsonii*/*scyronica* group ($\bar{a}_5 = 3.1$). The percentage of β-elemene in mel-1 and mel-3 is high (18.8 and 10.8, respectively) compared to its presumed parental taxa, but the low percentage of mel-2 (0.7) is contrasting. Finally, the related germacrene D and germacrene-D-4-ol appear in mel-2 and mel-3 respectively, but not in any other examined population except a low amount of germacrene D in spr-2. In other compounds differentiation is either weak or random, and mostly provides no information. These results are less spectacular than those reported in e.g. hybrids of *Origanum* (Skoula et al., 1999), where the volatile fraction of *O. x intercedes* Rech. fil. was found intermediate between the parents, while *O. x minoanum* P.H. Davis had some constituents higher than in both parents; or in *Mentha x villoso-nervata* Opiz, with percentages of main compounds resembling one parent or the other, while the amount of germacrene D was considerably higher than in both parents (Gavalas et al., 1998). The reasons for rather weak indications of intermediacy in *St. swainsonii* ssp. *melangavica* volatile compounds should be attributed to the high similarity in composition of all essential oils of the *St. spruneri*/*swainsonii* group, and the rather pronounced interspecific variation observed.

3. Experimental

3.1. Plant material

All 18 members of *Stachys* subsect. Swainsonianeae were collected from natural populations growing on calcareous rocks or stony slopes. In *St. ionica* and *St. swainsonii* (less so in *St. spruneri*) it was observed that basal parts of stem may follow rock fissures and root, often in quite a distance from the parental plant. This vegetative propagation imposes the threat of collecting ramets in case that neighbouring populations are carelessly sampled. To avoid this, the distance that separates each of the populations in the present study was assured to be never less than 2 km. As intraspecific rather than intrapopulational variation was our concern, flowering shoots of at least 10 different individuals of each population were merged to constitute each sample. Details of the collection localities are presented in Table 1. To make our results comparable, only plants in similar stages of development were analyzed. Voucher specimens of each population were determined by Th. C. and deposited in the Herbarium of the Institute of Botany, University of Patras (UPA).

3.2. Analysis of volatile compounds

Fifty grams of air-dried plant material from each population were cut in small pieces, and the essential oils were obtained by steam distillation in 500 ml H_2O for 3 h (Hellenic Pharmacopoeia IV, 1989), in a modified Clevenger apparatus with a water-cooled oil receiver to reduce hydrodistillation over-heating artifacts. Although steam distillation is a rather harsh method to obtain oil samples, and presumably responsible for the production of artifacts, the same method was followed by several previous workers with *Stachys* (see introduction) and was adopted here to obtain comparative results. The oils taken in 2 ml of capillary GC grade *n*-pentane and dried over anhydrous sodium sulphate, were subsequently analyzed by GC–MS and stored at −20°C. The composition of the volatile constituents was established by GC–MS analyses. GC–MS analyses were performed on a Hewlett-Packard 5973-6890 system operating in EI mode (70 eV) equipped with a split/splitless injector (220°C), a split ratio 1/10, using three different columns: a fused silica HP-5 MS capillary column (30 m×0.25 mm (i.d.), film thickness: 0.25 μm); a HP-Innowax capillary column (30 m×0.25 mm (i.d.), film thickness: 0.50 μm) and a chiral Cydex B capillary column (50 m×0.22 mm (i.d.), film thickness: 0.25 μm). The temperature program for HP-5 MS column was from 60°C (5 min) to 280°C at a rate of 4°C/min; for HP-Innowax column from 60°C to 260°C at a rate of 3°C/min and for Cydex B column from 50 to 130°C (2 min) at a rate of 2°C/min and from 130 to 250°C at a rate of 4°C/min. Helium was used as a carrier gas at a flow rate of 0.8 ml/min. Injection volume of each sample was 2 μl. Retention indices for all compounds were determined according to the Van der Dool approach (Van den Dool and Kratz, 1963), using *n*-alkanes as standards. The identification of the components was based on comparison of their mass spectra with those of Wiley and NBS Libraries (Massada, 1976) and those described by Adams (1995), as well as by comparison of their retention indices with literature data (Davies, 1990; Adams, 1995; Bisio et al., 1998). In many cases, the essential oils were subject to co-chromatography with authentic compounds (Fluka, Sigma). The recognition of the optical isomers was made by comparison with authentic

samples and according to reported elution order for the particular column (Ravid et al., 1994, 1995; SGE Scientific Ltd data).

Acknowledgements

We thank E. Vardaka (Aristotelian University of Thessaloniki) for her kind assistance with the statistical analyses.

References

Adams, R., 1995. Identification of Essential Oil Components by Gas Chromatography/Mass Spectroscopy. Allured Publishing, Carol Stream, Il.

Bhattacharjee, R., 1980. Taxonomic studies in *Stachys*: II. A new infrageneric classification of *Stachys* L. Notes from the Royal Botanic Garden Edinburgh 38, 65–96.

Bisio, A., Ciarallo, G., Romussi, G., Fontana, N., Mascolo, N., Capasso, R., Biscardi, D., 1998. Chemical composition of essential oils from some *Salvia* species. Phytotherapy Research 12, S117–S120.

Cakir, A., Duru, M.E., Harmandar, M., Izumi, S., Hirata, T., 1997. The volatile constituents of *Stachys recta* L. and *Stachys balansae* L. from Turkey. Flavour and Fragrance Journal 12, 215–218.

Constantinidis, T., 1995. *Stachys euboica* Rech. fil. In: The Red Data Book of Rare and Threatened Plants of Greece. Athens, pp. 478–479.

Davies, N.N., 1990. Gas chromatographic retention indices of monoterpenes and sesquiterpenes on methyl silicone and Carbowax 20M phases. Journal of Chromatography 503, 1–24.

Dunlop, P.J., Bignell, C.M., Hibbert, D.B., 1997. Use of gas chromatograms of the essential leaf oils of the genus *Eucalyptus* for taxonomic purposes. Australian Journal of Botany 45, 1–13.

Gavalas, N., Bosabalidis, A., Kokkini, S., 1998. Comparative study of leaf anatomy and essential oils of the hybrid *Mentha* × *villosonervata* and its parental species *M. longifolia* and *M. spicata*. Israel Journal of Plant Sciences 46, 27–33.

Ghannadi, A.R., Alemdoost, G., 1996. Composition of the essential oil of *Stachys lavandulifolia*. 44th Annual Congress on Medicinal Plant Research, Prague, 3–7 September, p. 206.

Greuter, W., Burdet, H.M. and Long, G., 1986. Med-Checklist, Vol. 3. Editions des Conservatoire et Jardin botaniques de la Ville de Genève, Genève.

Halim, A.F., Mashaly, M.M., Zaghouli, A.M., Abd El-Fattah, H., De Pooter, H.L., 1991. Chemical constituents of the essential oils of *Origanum syriacum* and *Stachys aegyptiaca*. International Journal of Pharmacognosy 29, 183–187.

Harmandar, M., Duru, M.E., Cakir, A., Hirata, T., Izumi, S., 1997. Volatile constituents of *Stachys obliqua* L. (Lamiaceae) from Turkey. Flavour and Fragrance Journal 12, 211–213.

Hellenic Pharmacopoeia IV, 1989. Vol. 1, Atlantis-Pechlyvanides, Athens, p. 191.

Kokkini, S., 1992. Essential oils as taxonomic markers in *Mentha*. In: Advances in Labiatae Science. Kew Royal Botanic Gardens, Kew, pp. 325–334.

Lawrence, M., 1992. Chemical components of Labiatae oils and their exploitation. In: Advances in Labiatae Science. Kew Royal Botanic Gardens, Kew, pp. 399–436.

Mabberley, D.J. 1997. The Plant-Book. Cambridge University Press, Cambridge, New York, Melbourne

Maly, E., 1985. Paper chromatography of the essential oils occurring in the genus *Stachys*. Journal of Chromatography 333, 288–289.

Maly, E., 1988. A sesquiterpene enol and hydrocarbon from *Stachys annua* L. Herba Hungarica 27, 107–116.

Mariotti, J.P., Costa, J., Bianchini, A., Bernardini, A.F., Casanova, J., 1997. Composition and variability of the essential oil of *Stachys glutinosa* L. from Corsica (France). Flavour and Fragrance Journal 12, 205–209.

Massada, Y., 1976. Analysis of Essential Oil by Gas Chromatography and Spectrometry. John Wiley & Sons, New York.

Pélissier, Y., Marion, C., Rapior, S., 1999. Volatile components of *Stachys corsica* Pers. (Lamiaceae). Journal of Essential Oil Research 11, 63–64.

Persson, D., 1981. Biosystematics of *Stachys swainsonii* Benth. (Lamiaceae) and its Relations to Some Other Chasmophytic *Stachys* species. PhD thesis, University of Lund, Lund.

Phitos, D., Damboldt, J., 1969. Beiträge zur Flora Ionica, I. Die *Stachys swainsonii*-Gruppe (Labiatae). Berichte der Deutschen Botanischen Gesellschaft 82, 595–601.

Ravid, U., Putievsky, E., Katzir, I., 1994. Chiral GC analysis of enantiomerically pure (R)(−)-linalyl acetate in some Lamiaceae, myrtle and petigrain oils. Flavour and Fragrance Journal 9, 275–276.

Ravid, U., Putievsky, E., Katzir, I., 1995. Determination of the enantiomeric composition of α-terpineol in essential oils. Flavour and Fragrance Journal 10, 281–284.

Sanz, J., Mus, M., Rosselló, J., 2000. Volatile components variation in the *Teucrium marum* complex (Lamiaceae) from the Balearic Islands. Botanical Journal of the Linnean Society 132, 253–261.

Sajjadi, S.E., 1996. Essential oil composition of aerial parts from *Stachys inflata*. 44th Annual Congress on Medicinal Plant Research, Prague, 3–7 September, p. 216.

Sezik, E., Basaran, A., 1986. Phytochemical investigations on the plants used as folk medicine and herbal tea in Turkey II. Essential oil of *Stachys lavandulifolia* var. *lavandulifolia*. Istanbul Universitesi Eczacilik Fakultesi Mecmuasi 21, 98–107.

SGE Scientific Ltd. Data; available at http://www.sge.com.au/capillary.

Skoula, M., Gotsiou, P., Naxakis, G., Johnson, C.B., 1999. A chemosystematic investigation on the mono- and sesquiterpenoids in the genus *Origanum* (Labiatae). Phytochemistry 52, 649–657.

Skaltsa, H.D., Lazari, D.M., Chinou, I.B., Loukis, A.E., 1999. Composition and antimicrobial activity of the essential oils of *Stachys candida* and *S. chrysantha* from southern Greece. Planta Medica 65, 255–256.

Stahl-Biskup, E., 1991. The chemical composition of *Thymus* oils: a review of the literature 1960–1989. Journal of Essential Oil Research 3, 61–82.

Van den Dool, H., Kratz, P.D., 1963. A generalization of the retention index system including linear temperature programmed gas-liquid partition chromatography. Journal of Chromatography 11, 463–471.

PERGAMON

Phytochemistry 57 (2001) 245–250

PHYTOCHEMISTRY

www.elsevier.com/locate/phytochem

Essential oils from Azorean *Laurus azorica*

Luis G. Pedro [a,*], Pedro A.G. Santos [a], Jaime A. da Silva [a], A. Cristina Figueiredo [a], José G. Barroso [a], Stanley G. Deans [b], Anja Looman [c], Johannes J.C. Scheffer [c]

[a] *Centro de Biotecnologia Vegetal, Departamento de Biologia Vegetal, Faculdade de Ciências de Lisboa, Bloco C2, Campo Grande, 1749-016 Lisbon, Portugal*

[b] *Department of Food Science and Technology, SAC, Auchincruive, Ayr KA6 5HW, Scotland, UK*

[c] *Division of Pharmacognosy, LACDR, Leiden University, Gorlaeus Laboratories, PO Box 9502, 2300 RA Leiden, The Netherlands*

Received 13 June 2000; received in revised form 28 November 2000

Abstract

The essential oils isolated from leaves of ten and from unripe berries of eight populations of *Laurus azorica* (Seub.) Franco, collected on five islands of the Azorean archipelago, were analysed by GC and GC–MS. All oil samples were dominated by their monoterpene fraction (60–94%), α-pinene (15–37%) and 1,8-cineole (12–31%) being the main components of the leaf oils, while *trans*-β-ocimene (27–45%) and α-pinene (12–22%) were the main components of the oils from the berries. The sesquiterpene fractions of the oils ranged from 3 to 17% and the main components were β-caryophyllene (traces — 8%) and β-elemene (traces—3%) both in the leaf and berry oils. Some phenylpropanoid components were also present, in total amounting to 17%, *trans*-cinnamyl acetate (215% of the leaf oils) being the main component of this fraction. Cluster analysis of the enantiomeric composition of α- and β-pinene in the oils from the leaves clearly showed two groups, one constituted by the two populations growing on the island S. Jorge, and the other constituted by the remaining populations. © 2001 Elsevier Science Ltd. All rights reserved.

Keywords: *Laurus azorica*; Lauraceae; Essential oil; α-Pinene; 1,8-Cineole; *trans*-β-Ocimene; Enantiomeric composition; Azores

1. Introduction

Laurus azorica (Seub.) Franco (= *L. canariensis* Webb & Berth., non Willd.), most commonly known as ''loireiro'', ''loureiro'', or ''louro'', is an endemic species of the Azores, Madeira and the Canary islands. The tree is an important constituent of the laurel-juniper forest (cloud-zone forest) that, according to Sjögren (1984), occurs on all islands of the Azorean archipelago except on Graciosa, generally above 500 m, but occasionally down to 175 m and, on Pico, rarely above 1400 m. Pena and Cabral (1997) reported the presence of this species at Feiteira, Graciosa, which we confirmed recently (June 1999). The berries and the fixed oil extracted from them are used as an anti-infective skin preparation; the oil is applied externally as an anti-rheumatic and for wound-healing, and is taken orally for treatment of apoplexy; the fixed oil is also used for treating boils, as a hemostatic and for troubles of the respiratory system (Neves and Valente, 1992; Rivera and Obón, 1995). Recently, Candeias et al. (1999) suggested that the leaf essential oil has a moderate hepatoprotectant activity.

As part of a screening programme of the aromatic flora of Macaronesia, the present study deals with the analysis of the essential oils from *L. azorica* collected on five Azorean islands.

2. Results and discussion

2.1. Essential oil composition

2.1.1. Essential oil from the leaves

The essential oil samples isolated from the leaves were obtained in yields ranging from 0.3 to 0.7% (v/w). Fifty to fifty-five components were identified in each oil sample, amounting to 83–95% of the total oils (Table 1). The total percentages of the fraction of sesquiterpene hydrocarbons in the oils from the leaves collected in 1996 and 1997 (at Cabrito and Pico Rachado on Terceira and

* Corresponding author. Tel.: +351-21-7500069; fax: +351-21-7500 048.

E-mail address: luis.pedro@fc.ul.pt (L.G. Pedro).

0031-9422/01/$ - see front matter © 2001 Elsevier Science Ltd. All rights reserved.
PII: S0031-9422(00)00497-0

Table 1
Composition of the essential oils isolated from leaves of ten Azorean populations of *Laurus azorica* (Seub.) Franco

Components	RI[a]	Mean percentage	Percentage limits	Components	RI[a]	Mean percentage	Percentage limits
Tricyclene	921	0.1	t–0.1[b]	α-Cubebene	1345	t	nd–0.1
α-Thujene	924	0.1	0.1–0.2	*cis*-Cinnamyl acetate	1360	t	nd–0.1
α-Pinene	930	25.5	15.0–36.9	Geranyl acetate	1370	0.5	0.1–0.9
Camphene	938	1.0	0.5–2.7	Methyleugenol	1377	t	nd–0.1
Sabinene	958	1.7	1.0–2.6	β-Bourbonene	1379	t	nd–0.1
β-Pinene	963	13.3	9.0–18.4	β-Elemene	1388	0.9	t–3.3
β-Myrcene	975	0.5	0.2–0.8	β-Caryophyllene	1414	3.0	t–8.1
α-Phellandrene	995	0.1	0.1–0.2	*trans*-Cinnamyl acetate	1414	7.6	2.2–14.6
α-Terpinene	1002	0.3	0.2–0.6	*trans*-Isoeugenol	1422	0.3	0.1–0.7
p-Cymene	1003	0.2	0.1–0.4	α-Humulene	1447	0.2	t–0.5
1,8-Cineole	1005	17.8	12.1–31.1	*allo*-Aromadendrene	1454	0.3	0.1–1.1
Limonene	1009	0.8	0.6–1.1	*trans*-Methylisoeugenol	1471	0.1	nd–0.3
cis-β-Ocimene	1017	0.3	t–0.7	Germacrene-D	1474	t	nd–0.2
trans-β-Ocimene	1027	0.5	t–1.2	β-Selinene	1476	0.3	0.1–0.6
γ-Terpinene	1035	0.5	0.3–1.0	Valencene	1477	t	nd–0.1
trans-Sabinene hydrate	1037	0.1	0.1–0.2	α-Selinene	1486	0.1	nd–0.3
cis-Linalool oxide	1045	t	nd–0.2[c]	Bicyclogermacrene	1487	0.8	nd–2.2
2-Nonanone	1058	0.1	nd–0.2	γ-Cadinene	1496	0.2	0.1–0.2
Terpinolene	1064	0.4	0.1–0.7	δ-Cadinene	1505	0.1	nd–0.2
cis-Sabinene hydrate	1066	0.1	0.1–0.1	Spathulenol	1549	0.7	0.1–1.4
Linalool	1074	1.7	0.4–5.0	*trans*-Nerolidol	1551	0.1	nd–1.0
α-Campholenal	1088	0.2	t–0.5	β-Caryophyllene epoxide	1561	1.5	0.8–2.9
trans-Pinocarveol	1106	0.6	0.1–1.8	Viridiflorol	1569	t	nd–0.5
cis-Verbenol	1110	t	nd–0.2	Ledol	1580	t	nd–0.3
trans-Verbenol	1114	0.2	t–0.9	T-Cadinol	1616	t	nd–0.3
Pinocarvone	1121	0.5	0.2–1.4	α-Cadinol	1626	0.1	nd–0.5
δ-Terpineol	1134	0.3	0.2–0.6	% Identified		91.2	83.4–94.7
Terpinen-4-ol	1148	1.0	0.7–1.6				
Myrtenal	1153	0.2	0.1–0.8	Grouped components			
α-Terpineol	1159	1.6	0.7–4.2	Monoterpene hydrocarbons		45.4	30.2–63.1
Verbenone	1164	0.1	t–0.6	Oxygen-containing monoterpenes		28.6	20.5–41.9
Myrtenol	1168	0.3	0.1–0.6	Sesquiterpene hydrocarbons		6.0	0.9–12.9
trans-Carveol	1189	0.1	nd–0.2	Oxygen-containing sesquiterpenes		2.5	1.4–4.3
Bornyl acetate	1265	0.9	0.3–3.4	Phenylpropane derivatives		8.7	2.5–16.6
Sabinyl acetate	1277	0.2	t–0.3	Others		0.1	nd–0.2
α-Terpinyl acetate	1334	2.0	0.2–3.1				
Hydrocinnamyl acetate	1341	0.5	t–1.3	Oil yield		0.5	0.3–0.7

[a] Retention index relative to C_9–C_{17} *n*-alkanes on the DB-1 column.
[b] t = Trace (< 0.05%).
[c] nd = Not detected.

at Santo António on S. Jorge) seem to show marked differences, as these values were 5–10 times higher for the leaves of July 1997 than for those of April 1996. The question whether these differences are due to seasonal variations or to the different year of collection cannot be answered at this moment.

All the oil samples were dominated by their monoterpene fraction (60–86%). α-Pinene (15–37%), 1,8-cineole (12–31%) and β-pinene (9–18%) were the main components. The oxygen-containing monoterpenes represented 21–42% of the total oils. The sesquiterpene fraction occurred in smaller amounts (3–17%), β-carbophyllene (traces — 8%) and β-elemene (traces — 3%) being the only sesquiterpenes that attained relative amounts larger than 3%. The essential oils contained also a phenylpropanoid fraction, amounting to 17%, *trans*-cinnamyl acetate (2–15%) being the main component. It may be noteworthy that in the oils isolated from the leaves collected in April 1996 at Cabrito (Terceira) and at S. António (S. Jorge), *trans*-cinnamyl acetate was the third major component of the total oil.

2.1.2. Essential oil from the berries

The essential oil samples isolated from the berries were obtained in yields ranging from 0.4 to 0.9% (v/w). Fifty to fifty-four components were identified in each oil sample, amounting to 89–98% of the total oils (Table 2). The composition of the essential oils showed almost no marked qualitative or quantitative differences.

All the oil samples were dominated by their monoterpene fraction (84–94%). *trans*-β-Ocimene (27–45%), α-pinene (12–22%), *cis*-β-ocimene (9–16%) and β-pinene

Table 2
Composition of the essential oils isolated from unripe berries of eight Azorean populations of *Laurus azorica* (Seub.) Franco.

Components	RI[a]	Mean percentage	Percentage limits	Components	RI[a]	Mean percentage	Percentage limits
Tricyclene	921	t[b]	t–0.1	Sabinyl acetate	1277	0.3	0.2–0.5
α-Thujene	924	t	t–0.1	α-Terpinyl acetate	1334	0.2	0.1–0.6
α-Pinene	930	17.4	12.0–21.7	α-Cubebene	1345	t	nd–t
Camphene	938	0.6	0.4–1.1	Geranyl acetate	1370	0.4	0.2–0.6
Sabinene	958	0.3	0.2–0.4	β-Elemene	1388	0.9	0.5–2.1
β-Pinene	963	9.8	7.0–12.5	β-Caryophyllene	1414	1.1	0.3–2.2
β-Myrcene	975	0.9	0.8–1.0	*trans*-Cinnamyl acetate	1414	0.5	t–1.7
α-Phellandrene	995	t	t–0.1	α-Humulene	1447	0.1	0.1–0.4
α-Terpinene	1002	0.1	0.1–0.2	*allo*-Aromadendrene	1454	0.7	0.3–1.2
p-Cymene	1003	t	t–0.1	Germacrene-D	1474	0.2	t–0.4
1,8-Cineole	1005	2.9	1.7–4.2	β-Selinene	1476	0.1	t–0.4
Limonene	1009	0.4	0.3–0.4	Bicyclogermacrene	1487	0.5	0.3–1.1
cis-β-Ocimene	1017	13.3	9.2–15.8	γ-Cadinene	1496	0.1	t–0.2
trans-β-Ocimene	1027	37.7	26.6–44.7	δ-Cadinene	1505	0.2	0.1–0.4
γ-Terpinene	1035	0.1	t–0.2	Spathulenol	1549	0.1	nd–0.2
trans-Sabinene hydrate	1037	0.1	t–0.1	*trans*-Nerolidol	1551	0.1	nd–0.4
2-Nonanone	1058	0.1	t–0.2	β-Caryophyllene epoxide	1561	0.3	0.1–0.4
Terpinolene	1064	0.1	0.1–0.2	Ledol	1580	t	nd–0.1
cis-Sabinene hydrate	1066	t	nd[c]–t	T-Cadinol	1616	0.1	nd–0.2
Linalool	1074	1.1	0.3–3.5	δ-Cadinol	1618	t	nd–0.1
α-Campholenal	1088	0.1	t–0.2	α-Cadinol	1626	0.2	0.1–0.3
allo-Ocimene	1110	0.6	0.5–0.6				
cis-Verbenol	1110	0.2	0.1–0.3	% Identified		94.7	89.0–97.5
trans-Verbenol	1114	0.6	0.3–0.8				
Pinocarvone	1121	0.2	0.1–0.2	Grouped components			
δ-Terpineol	1134	0.3	0.1–0.5	Monoterpene Hydrocarbons		81.3	70.8–87.9
Terpinen-4-ol	1148	0.2	0.1–0.4	Oxygen-containing monoterpenes		8.0	5.1–9.3
Myrtenal	1153	0.1	t–0.3	Sesquiterpene hydrocarbons		4.1	2.1–7.5
α-Terpineol	1159	0.6	0.3–1.0	Oxygen-containing sesquiterpenes		0.8	0.4–1.2
Verbenone	1164	0.1	t–0.2	Phenylpropane derivatives		0.5	t–1.7
Myrtenol	1168	0.1	t–0.2	Others		0.1	nd–0.2
trans-Carveol	1189	0.1	t–0.1				
Bornyl acetate	1265	0.5	0.3–1.2	Oil yield		0.6	0.4–0.9

[a] Retention index relative to C_9–C_{17} *n*-alkanes on the DB-1 column.
[b] t = Trace (< 0.05%).
[c] nd = Not detected.

(7–13%) were the major components. The oxygen-containing monoterpenes represented only 5–9% of the oils. The sesquiterpene fraction occurred in smaller amounts (3–8%) and all sesquiterpenes occurred in concentrations lower than 2%, except for β-carbophyllene (0.3–2%) and β-elemene (0.5–2%). The phenylpropanoid fraction, consisting only of *trans*-cinnamyl acetate, ranged from traces to 2%.

A literature search provided only one reference to a paper on the composition of the essential oil from the leaves of *L. azorica* (Hokwerda et al., 1982). No data were found on the oil from the berries of this species. In the steam distilled leaf oil of *L. azorica* grown in the Hortus Botanicus of the University of Groningen, Hokwerda et al. (1982) also found α-pinene (13%), 1,8-cineole (10%) and β-pinene (7%) as main components, but in smaller amounts than those found in the present study. Although the exact amounts for the components of the other fractions were not reported in that work, *allo*-aromadendrene (5–10%) was the main component among the sesquiterpenes, and cinnamyl acetate and elemicin (both 1–5%) were the major constituents of the phenylpropanoid group.

The well-known laurel oil is obtained from the leaves of *L. nobilis*, the only other species of this genus. Considering some of the more recent publications on the composition of the leaf oil of *L. nobilis* (Kutubidze and Kharebava, 1990; Kharebava, 1991; Baghdadi et al., 1992; Borges et al., 1992; Tucker et al., 1992; Biondi et al., 1993; Pino et al., 1993; Fiorini et al., 1997; Baratta et al., 1998), there are some noteworthy quantitative differences, regarding the main components, in comparison with the leaf oil of *L. azorica*. 1,8-Cineole, the major compound in laurel oil is the second main component in *L. azorica* leaf oil, whereas α- and β-pinene, two main components in *L. azorica* leaf oil, are present in smaller amounts in laurel oil; other main components in laurel oil, namely linalool, α-terpinyl acetate and

sabinene, are minor components of the leaf oils from *L. azorica* we analysed.

2.2. Enantiomeric composition of α- and β-pinene

Of the chiral compounds present in the monoterpene fraction of the essential oils, only α- and β-pinene were investigated for their enantiomeric ratio, due to the low concentrations of the other chiral monoterpenes in the oils, in most cases below 2%. In all oil samples (+)-α-pinene (74–91% in the leaf oils, 86–93% in the berry oils) and (−)-β-pinene (64–88% in the leaf oils, 83–94% in the berry oils) were the predominant enantiomers. The cluster analysis of the enantiomeric composition of α- and β-pinene in the oil samples isolated from the leaves and berries yielded one marked result: a clear separation of the leaf oils of the two populations of S. Jorge from the leaf oils of the rest of the populations collected at the other four islands (Fig. 1). The samples isolated from the leaves collected on the island S. Jorge (SAJ and EsJ) showed concentrations of (−)-α-pinene above 20% and of (+)-β-pinene above 29%, and those isolated from the leaves collected on the other four islands showed concentrations of (−)-α-pinene and (+)-β-pinene less than 14 and 20%, respectively.

Although the enantiomeric ratios of α- and β-pinene in the oils from the berries showed some variation, we did not observe a certain trend, *e.g.* related to location or island.

According to Kreis et al. (1990), the enantiomeric ratios of α- and β-pinene in the leaf oil of *L. nobilis* were 61% of (+)-α-pinene and 56% of (+)-β-pinene. These values are considerably different from those we observed for the leaf oil of *L. azorica*.

Our results suggest that there is a considerable homogeneity in the populations of *L. azorica* grown in the Azorean archipelago, at least in relation to their essential oils, despite of some differences concerning the enantiomeric composition.

3. Experimental

3.1. Plant material

Collective samples of leaves and of unripe berries from *L. azorica* (Seub.) Franco were collected, in April 1996 and/or in July 1997, at Cabrito (530 m) and Pico Rachado (830 m) on Terceira, at Santo António (500 m) and Espigão (580 m) on S. Jorge, at Cabeço do Gato on Pico (300 m), at Pico Bartolomeu (890 m) and Pico Longo (500 m) on S. Miguel, and at Arrochela (700 m), Cabeço dos Trinta (800 m) and Areeiro (200 m) on Faial. A voucher specimen of the plant has been deposited in the Herbarium of the Museu, Laboratório e Jardim Botânico de Lisboa (no. LISU 165930).

3.2. Isolation procedure

The essential oil samples were isolated from deep-frozen (−20°C) material by distillation-extraction for 3

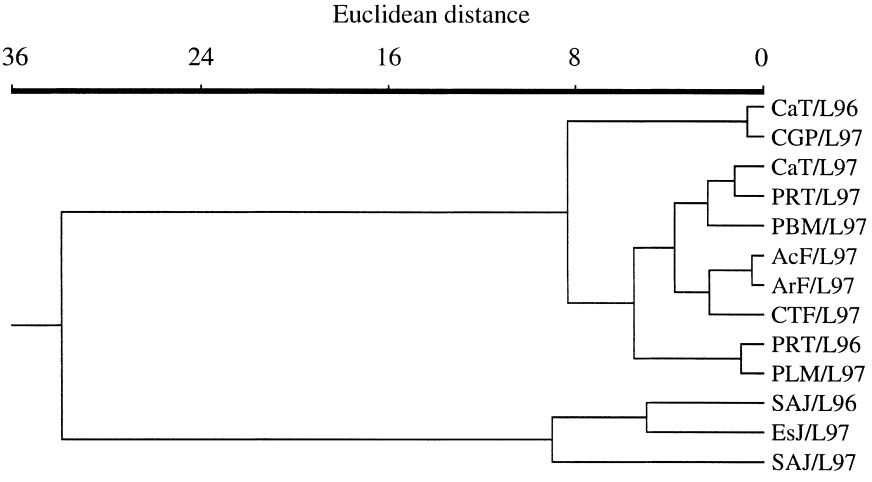

CaT – Cabrito, Terceira; CGP - Cabeço do Gato, Pico; PRT – Pico Rachado, Terceira; PBM – Pico Bartolomeu, S. Miguel; AcF - Arrochela, Faial; ArF - Areeiro, Faial; CTF – Cabeço dos Trinta, Faial; PLM - Pico Longo, S. Miguel; SAJ – Santo António, S. Jorge; EsJ - Espigão, S. Jorge.

L96 – Leaves collected in April 1996; L97 - Leaves collected in July 1997.

Fig.1. Dendrogram obtained by cluster analysis of the enantiomeric composition of α- and β-pinene in the essential oils from leaves of ten Azorean populations of *Laurus azorica*, based on Euclidean distance and using the unweighed pair-group method with arithmetic average (UPGMA).

h, using a Likens-Nickerson-type apparatus (Likens and Nickerson, 1964) with *n*-pentane as organic solvent, or by hydrodistillation for 3 h, using a Clevenger-type apparatus (Anonymous, 1996). The samples isolated by hydrodistillation were used to estimate the oil yields, and those isolated by distillation-extraction to determine their percentage composition, since the chance of artifact formation must be considered smaller when the latter isolation method is used.

3.3. Gas chromatography

GC analyses were performed using a twin FID instrument, a data handling system and a vapourizing injector port into which two columns of different polarities were installed: a DB-1 fused-silica column (30 m×0.25 mm i.d., film thickness 0.25 μm; J & W Scientific Inc.) and a DB-17HT fused-silica column (30 m×0.25 mm i.d., film thickness 0.15 μm; J & W Scientific Inc.). The oven temp. was programmed, 45–175°C, at 3°C min^{-1}, subsequently at 15°C min^{-1} up to 300°C, and then held isothermally for 10 min; injector and detector temps were 280 and 300°C, respectively; carrier gas, H_2 at 30 cm s^{-1}.

GC chiral analyses were performed using an FID instrument, a data handling system and a Cyclodex-B fused-silica column (30 m×0.25 mm i.d., film thickness 0.25 μm; J & W Scientific Inc.). The oven temp. was 75°C isothermal; injector and detector temps were 230 and 240°C, respectively; carrier gas, H_2 at 42 cm s^{-1}.

In the chiral analyses, authentic samples of α- and β-pinene enantiomers were used for comparison.

Samples were injected using the split-sampling technique with a ratio of 1:50. Percentage composition of the oils was computed using the normalization method from the GC peak areas without correction factors. Percentage data shown are mean values of two injections of each oil sample.

3.4. Gas chromatography-mass spectrometry

The GC–MS unit was equipped with a DB-1 fused-silica column (30 m×0.25 mm i.d., film thickness 0.25μm; J & W Scientific Inc.), and interfaced with an ion trap detector (ITD, software version 4.1). Oven temp. was as described above; transfer line temp., 280°C; ion trap temp., 220°C; carrier gas, He at 30 cm s^{-1}; split ratio, 1:40; ionization energy, 70 eV; ionization current, 60 μA; scan range, 40–300 μm; scan time, 1 s.

The identity of the components was assigned by comparison of their RIs, relative to C9–C17 *n*-alkanes, and MS with corresponding data of components of reference oils.

3.5. Cluster analysis

The percentage composition of the essential oil samples and the enantiomeric composition of α- and β-pinene in the oils were used to determine the relationship between the different populations of *L. azorica* by cluster analysis using the NTSYS software (Rohlf, 1992). Euclidean distance was selected as the measure of similarity, and the unweighed pair-group method with arithmetic average (UPGMA) was used for cluster definition.

Acknowledgements

This study was funded by the Fundação para a Ciência e a Tecnologia (FCT), Lisbon, under research contract PBIC/C/BIA/2070/95. The authors are grateful to the FCT for scholarships to P.A.G. Santos and J.A. da Silva.

References

Anonymous, 1996. European Pharmacopoeia, 3rd Edn. Council of Europe, Strasbourg, pp. 121–122.

Baghdadi, H.H., Ahmad, S.S., Fournier, G., Refaat, A.M., 1992. On the essential oil of *Laurus nobilis* grown in Egypt. Egyptian Journal of Horticulture 19, 93–97.

Baratta, M.T., Dorman, H.J., Deans, S.G., Biondi, D.M., Ruberto, G., 1998. Chemical composition, antimicrobial and antioxidative activity of laurel, sage, rosemary, oregano and coriander essential oils. Journal of Essential Oil Research 10, 618–627.

Biondi, D., Cianci, P., Geraci, C., Ruberto, G., Piattelli, M., 1993. Antimicrobial activity and chemical composition of essential oils from Sicilian aromatic plants. Flavour and Fragrance Journal 8, 331–337.

Borges, P., Pino, J., Sanchez, E., 1992. Isolation and chemical characterization of laurel leaf oil. Nahrung 36, 494–496.

Candeias, F., Tinoco, M.T., Morais, J.C., 1999. Actividade hepatoprotectora do óleo essencial de *Laurus azorica* (Seub.) J. Franco. I Congresso das Plantas Aromáticas e Medicinais dos Países de Língua Oficial Portuguesa, Ansião, Portugal, p. 58 (abstract).

Fiorini, C., Fourasté, I., David, B., Bessière, J.M., 1997. Composition of the flower, leaf and stem essential oils from *Laurus nobilis* L. Flavour and Fragrance Journal 12, 91–93.

Hokwerda, H., Bos, R., Tattje, D.H.E., 1982. Malingré, Th. M., Composition of the essential oils of *Laurus nobilis*, L. *nobilis* var. *angustifolia* and *Laurus azorica*. Planta Medica 44, 116–119.

Kharebava, L.G., 1991. Composition of leaf essential oils of different cultivars of bay laurel growing in identical conditions. Subtropicheskie Kul'tury 1991, 143–147.

Kreis, P., Hener, U., Mosandl, A., 1990. Chirale Inhaltsstoffe ätherischer Öle. III. Stereodifferenzierung von α-Pinen, β-Pinen und Limonen in ätherischen Ölen, Drogen und Fertigarzneimitteln. Deutsche Apotheker Zeitung 30, 985–988.

Kutubidze, V.V., Kharebava, L.G., 1990. Studies on the essential oils of some laurel plants growing in the nursery of the Chakvskii field station. Subtropicheskie Kul'tury 1990, 111–116.

Likens, S.T., Nickerson, G.B., 1964. Detection of certain hop oil constituents in brewing products. American Society of Brewing Chemists, Proceedings, 5–13.

Neves, H.C., Valente, A.V., 1992. Conheça o Parque Natural da Madeira. Parque Natural da Madeira, Funchal.

Pena, A., Cabral, J., 1997. Roteiros da Natureza – Região Autónoma dos Açores. Temas e Debates, Lisbon.

Pino, J., Borges, P., Roncal, E., 1993. The chemical composition of laurel leaf oil from various origins. Nahrung 37, 592–595.

Rivera, D., Obón, C., 1995. The ethnopharmacology of Madeira and Porto Santo Islands, a review. Journal of Ethnopharmacology 46, 73–93.

Rohlf, J.F., 1992. NTSYS-pc, Numerical Taxonomy and Multivariate Analysis System. Applied Biostatistics, New York.

Sjögren, E., 1984. Azores Flowers, No. 52. Direcção Regional de Turismo. Horta, Faial.

Tucker, A.O., Maciarello, M.J., Hill, M., 1992. *Litsea glaucescens* Humb., Bonpl. and Kunth var. glaucescens (*Lauraceae*): a Mexican bay. Economic Botany 46, 21–24.

PERGAMON

Phytochemistry 57 (2001) 251–260

PHYTOCHEMISTRY

www.elsevier.com/locate/phytochem

Cyclolinopeptides F–I, cyclic peptides from linseed

Teruki Matsumoto, Akira Shishido, Hiroshi Morita, Hideji Itokawa, Koichi Takeya *

School of Pharmacy, Tokyo University of Pharmacy and Life Science, 1432-1 Horinouchi, Hachioji, Tokyo 192-0392, Japan

Received 5 July 2000; received in revised form 23 October 2000

Abstract

Four cyclic peptides, cyclolinopeptides F–I, were isolated from seeds of *Linum usitatissimum*. Their structures were elucidated by extensive 2D NMR spectroscopic methods and by chemical degradation. Further, their immunosuppressive activity is examined.
© 2001 Elsevier Science Ltd. All rights reserved.

Keywords: *Linum usitatissimum*; Linaceae; Cyclolinopeptide; Cyclic peptide; Immunosuppresive activity

1. Introduction

Cyclolinopeptide A (CLA), a cyclic nonapeptide, which exhibits various biological activities (Wieczorek et al., 1991; Naider et al., 1971; Brewster and Bovey, 1971; Tonelli, 1971; Blasio et al., 1989) has been isolated from linseed oil as one of the first isolated natural cyclic peptides (Kaufmann and Tobschirbel, 1959). In a previous paper, we reported on the separation, purification and structure elucidation of cyclolinopeptides B–E having cyclic nona- or octapetides, from the seeds of *Linum usitatissimum* (Morita et al., 1997, 1999). As part of our investigation on new biologically active cyclic peptides from higher plants (Itokawa et al., 1997), we focused our attention on the isolation of additional cyclic peptides from linseed. In this report, we describe both the isolation and structural elucidation of four new cyclic peptides, cyclolinopeptides F (**1**)–I (**4**) by extensive 2D NMR spectroscopic methods and their immunosuppressive activities against mouse splenocytes.

2. Results and discussion

Purification of the methanolic extract prepared from the linseed involving Diaion HP-20 column chromatography, using a H_2O–MeOH gradient system. The MeOH eluate was next applied to a silica gel column, this being followed by HPLC [ODS] to yield the four new cyclic peptides, cyclolinopetides F–I (CLF–CLI) in yields of 0.0008%, 0.0024%, 0.0002% and 0.00007%, respectively.

Cyclolinopeptides F (CLF) and G (CLG) were obtained as white powders. Their molecular formulae were shown to be $C_{55}H_{74}N_9O_{10}S_2$ and $C_{56}H_{76}N_9O_{10}S_2$, respectively by the quasi-molecular ion peak at m/z 1084.5018 $[M+H]^+$ and at m/z 1098.5138 $[M+H]^+$ in the HR-FABMS. Both IR spectra had absorption peaks which were attributed to amine, amide carbonyl and sulfoxide groups. Since the UV absorption maximum in the neighborhood of 280 nm suggested the presence of a tryptophan residue, the compounds were hydrolyzed with 6 N HCl containing 4% thioglycolic acid. HPLC analysis of each hydrolysate showed that CLF was a cyclic octapeptide consisting of two phenylalanines (Phe), two methionines (Met), proline (Pro), leucine (Leu), valine (Val) and tryptophan (Trp) per mol and CLG was a cyclic octapeptide consisting of two phenylalanines (Phe), two methionines (Met), proline (Pro), leucine (Leu), isoleucine (Ile) and tryptophan (Trp) per mol. However, both methionines in CLF and CLG were present as methionine sulfoxides, because each molecular formula had an additional two oxygen atoms, compared with the cyclic octapeptide presumed from above amino acid degradation and both had IR absorption bands (CLF: 1016 and CLG: 1015 cm^{-1}) indicating sulfoxide groups.

In the ^1H and ^{13}C NMR spectra (Tables 1 and 2), CLF and CLG had seven amide protons and eight amide carbonyl carbons, respectively, and thus were

* Corresponding author. Tel.: +81-426-763007; fax: +81-426-771436.

E-mail address: takeyak@ps.toyaku.ac.jp (K. Takeya).

0031-9422/01/$ - see front matter © 2001 Elsevier Science Ltd. All rights reserved.
PII: S0031-9422(00)00442-8

Table 1
^{1}H and ^{13}C NMR signal assignments for cyclolinopeptide F (**1**) in DMSO-d_6 at 320 K

	^{1}H NMR assignment δ_H [int, mult, J(Hz)]	^{13}C NMR δ_C		δ_H [int, mult, J(Hz)]	δ_C
Pro[1]			Val[5]		
α	4.21 (1H, *t*, 7.8)	62.04	α	4.50 (1H, *m*)	56.88
β	2.11 (1H, *m*)	29.04	β	2.20 (1H, *m*)	30.92
	1.59 (1H, *m*)		γ_{CH3}	0.94 (3H, *d*, 6.7)	19.20
γ	1.85 (2H, *m*)	24.17		0.85 (3H, *d*, 6.7)	17.39
δ	3.58 (1H, *m*)	46.89	NH	7.27 (1H, *d*, 6.3)	
	3.48 (1H, *m*)		C=O		172.52[a]
C=O		173.55	Mso[6]		
Phe[2]			α	3.98 (1H, *m*)	54.57
α	4.10 (1H, *dt*, 6.4, 7.6)	56.60	β	2.08 (1H, *m*)	23.23
β	2.80 (2H, *m*)	35.10		1.97 (1H, *m*)	
γ		137.68	γ	2.74 (2H, *m*)	49.48
δ	7.21 (2H, *m*)	127.87	ε_{CH3}	2.49 (3H, *s*)	38.00
ε	7.01 (2H, *d*, 6.6)	128.39	NH	8.31 (1H, *br.s*)	
ζ	7.19 (1H, *m*)	125.88	C=O		170.74[a]
NH	8.39 (1H, *d*, 6.4)		Leu[7]		
C=O		170.35	α	3.88 (1H, *m*)	52.41
Phe[3]			β	1.84 (1H, *m*)	37.85
α	4.67 (1H, *m*)	52.73		1.61 (1H, *m*)	
β	3.44 (1H, *m*)	36.22	γ	1.62 (1H, *m*)	24.30
	2.82 (1H, *m*)		δ_{CH3}	0.91 (3H, *d*, 8.4)	22.78
γ		138.09		0.85 (3H, *d*, 8.4)	20.77
δ	7.21 (2H, *m*)	127.95	NH	8.05 (1H, *d*, 6.5)	
ε	7.20 (2H, *m*)	128.39	C=O		171.07[a]
ζ	7.19 (1H, *m*)	126.06	Mso[8]		
NH	7.92 (1H, *d*, 8.1)		α	4.70 (1H, *dt*, 6.9, 14.0)	50.35
C=O		171.16	β	2.39 (1H, *m*)	25.60
Trp[4]				1.93 (1H, *m*)	
α	3.99 (1H, *m*)	55.61	γ	2.78 (2H, *m*)	50.35
β	3.38 (2H, *m*)	23.42	ε_{CH3}	2.44 (3H, *s*)	37.85
1_{NH}	10.62 (1H, *s*)		NH	7.36 (1H, *br.s*)	
2	7.15 (1H, *d*, 7.5)	122.55	C=O		170.35[a]
3		110.71			
4	7.45 (1H, *d*, 7.8)	117.63			
5	7.04 (1H, *t*, 7.8)	120.58			
6	6.95 (1H, *t*, 7.8)	117.95			
7	7.31 (1H, *d*, 7.8)	111.04			
8		135.82			
9		127.21			
NH	8.06 (1H, *d*, 6.3)				
C=O		170.74[a]			

[a] Assignments may be interchanged.

obviously octapeptides. However, analysis of the NOE data and $2J_{H–C}$ and $3J_{H–C}$ correlations by HMBC did not permit elucidation of their amino acid sequences as shown in Figs. 1 and 3. Hence, CLF and CLG were chemically transformed to their corresponding linear derivatives (CLF′ and CLG′), i.e. by reduction of their methionine sulfoxide using thioglycolic acid and subsequent decomposition with cyanogen bromide. This gave the linear peptides, which displayed an absorption IR bands at 1775 cm^{-1} attributed to an homoserine lactone. Sequential analyses due to the HMBC correlations indicated by arrows in Figs. 2 and 4 showed that CLF′ and CLG′ were, respectively, the linear peptides Pro–Phe–Phe–Trp–Val–HomoSer Lactone and as Pro-Phe–Phe–Trp–Ile–HomoSer Lactone each additional dipeptide was assumed to be Leu[7] HomoSer lactone. ROE correlations of CLF were observed between the Mso[6] α-proton and the Leu[7] amide proton, and between the Mso[8] α-proton and the Pro[1] δ-proton, respectively. Also, ROE correlations of CLG were noted between the Mso[8] α-proton and Pro[1] δ-proton, and between the Ile[5] α-proton and the Mso[6] amide proton. Consequently, the structure of CLF was identified as *cyclo* (-Pro–Phe–Phe–Trp–Val–Mso–Leu–Mso-) and CLG as *cyclo* (-Pro–Phe–Phe–Trp–Ile–Mso–Leu–Mso-). The absolute stereochemistries of the component amino acids was

Table 2
^{1}H and ^{13}C NMR signal assignments for cyclolinopeptide G (**2**) in DMSO-d_6 at 320 K

	^{1}H NMR assignment δ_H [int, mult, J(Hz)]	^{13}C NMR δ_C		δ_H [int, mult, J(Hz)]	δ_C
Pro[1]			Ile[5]		
α	4.21 (1H, *t*, 7.8)	62.03	α	4.49 (1H, *br.s*)	56.81
β	2.09 (1H, *m*)	29.01	β	1.91 (1H, *m*)	37.14
	1.57 (1H, *m*)		γ	1.39 (1H, *m*)	23.84
γ	1.85 (2H, *t*, 6.6)	24.17		1.12 (1H, *m*)	
δ	3.58 (1H, *m*)	46.90	γ_{CH3}	0.92 (3H, *d*, 6.6)	15.30
	3.51 (1H, *m*)		δ_{CH3}	0.88 (3H, *t*, 9.2)	11.06
C=O		173.42	NH	7.32 (1H, *m*)	
Phe[2]			C=O		172.30[a]
α	4.11 (1H, *dt*, 6.4, 7.5)	56.59	Mso[6]		
β	2.84 (2H, *m*)	35.07	α	4.01 (1H, *m*)	54.36
γ		137.76	β	2.16 (1H, *m*)	23.13
δ	7.22 (2H, *m*)	127.84		1.97 (1H, *m*)	
ε	7.02 (2H, *m*)	128.35	γ	2.73 (1H, *m*)	49.54
ζ	7.27 (1H, *m*)	125.85		2.65 (1H, *m*)	
NH	8.40 (1H, *d*, 6.4)		ε_{CH3}	2.49 (3H, *s*)	37.83
C=O		170.36	NH	8.27 (1H, *br.s*)	
Phe[3]			C=O		170.29
α	4.69 (1H, *m*)	52.66	Leu[7]		
β	3.44 (1H, *m*)	36.19	α	3.84 (1H, *m*)	52.49
	2.79 (1H, *m*)		β	1.79 (1H, *m*)	37.83
γ		138.09		1.62 (1H, *m*)	
δ	7.22 (2H, *m*)	127.95	γ	1.61 (1H, *m*)	24.27
ε	7.02 (2H, *m*)	128.42	δ_{CH3}	0.89 (3H, *d*, 6.1)	22.76
ζ	7.06 (1H, *m*)	126.01		0.84 (3H, *d*, 6.1)	20.83
NH	7.93 (1H, *d*, 6.3)		NH	8.01 (1H, *m*)	
C=O		170.85[a]	C=O		170.92[a]
Trp[4]			Mso[8]		
α	6.95 (1H, *m*)	55.65	α	4.70 (1H, *m*)	50.35
β	3.36 (2H, *m*)	23.38	β	2.39 (1H, *m*)	25.63
1_{NH}	10.61 (1H, *s*)			1.95 (1H, *m*)	
2	7.18 (1H, *d*, 6.8)	122.58	γ	2.75 (2H, *m*)	50.35
3		110.65	ε_{CH3}	2.45 (3H, *s*)	38.05
4	7.45 (1H, *d*, 7.8)	117.62	NH	7.36 (1H, *m*)	
5	7.05 (1H, *t*, 7.8)	120.57	C=O		171.03[a]
6	6.95 (1H, *t*, 7.8)	117.94			
7	7.31 (1H, *d*, 7.8)	111.03			
8		135.82			
9		127.20			
NH	8.11 (1H, *br.s*)				
C=O		173.17[a]			

[a] Assignments may be interchanged.

determined to be entirely in the L-configurations as evidenced by derivatization of the acid hydrolysate with Marfey's reagent (Marfey, 1984), followed by HPLC analyses.

Cyclolinopeptides H (CLH) and I (CLI) were isolated as white powders, and their molecular formulae were determined to be $C_{56}H_{76}N_9O_9S_2$ for CLH by HR-FABMS m/z 1082.5201 $[M+H]^+$ and $C_{55}H_{74}N_9O_9S_2$ for CLI by HR-FABMS m/z 1068.5110 $[M+H]^+$. HPLC of their acid hydrolysates showed that CLH was an octapeptide consisting of two Phe, two Met, Pro, Leu, Ile, Trp per mole and CLI was an octapeptide consisting of two Phe, two Met, Pro, Leu, Val, Trp per mole. Each amino acid was confirmed to be in the L-configuration using Marfey's method. The amino acid components of CLH and CLI were similar to those of CLG and CLF. However, the FAB mass spectra are 16 amu less than those of CLG and CLF. The facts suggested the presence of one methionine and one methionine sulfoxide in CLH and CLI instead of two methionine sulfoxides in CLG and CLF, respectively. According to the above speculation, reductive transformations of methionine sulfoxide in CLG and CLF by thioglycolic acid are demonstrated to give three compounds, respectively. One of them in CLG (or CLF) agreed completely with CLH (or CLI) in comparison of

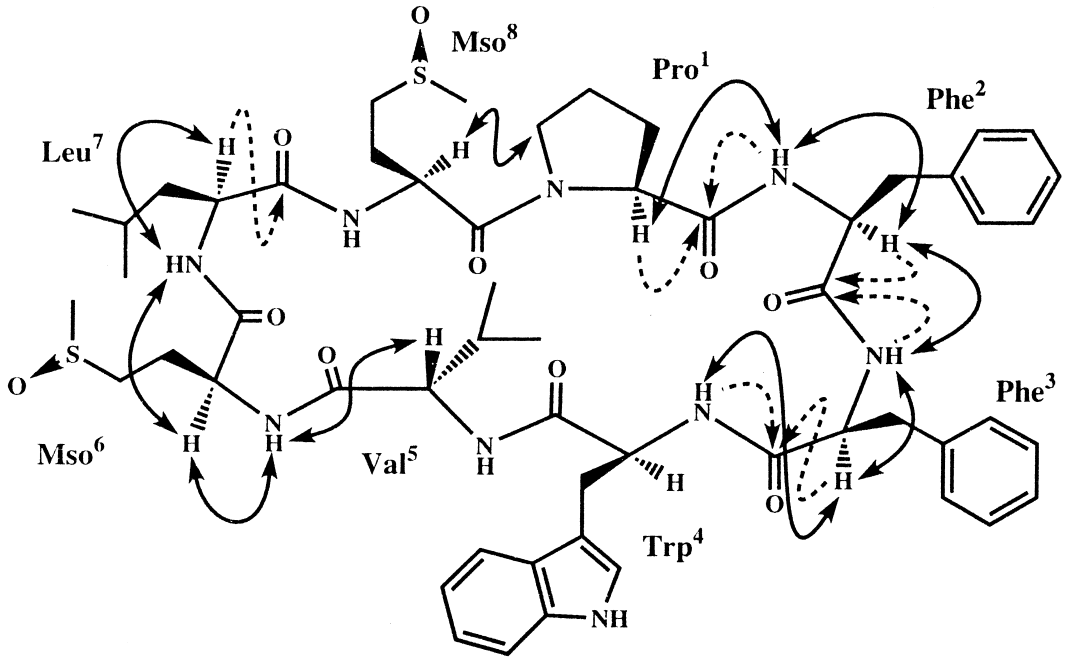

Fig. 1. Cyclolinopeptide F (**1**): dashed arrows show selected HMBC correlations and arrows show some selected NOE relationship.

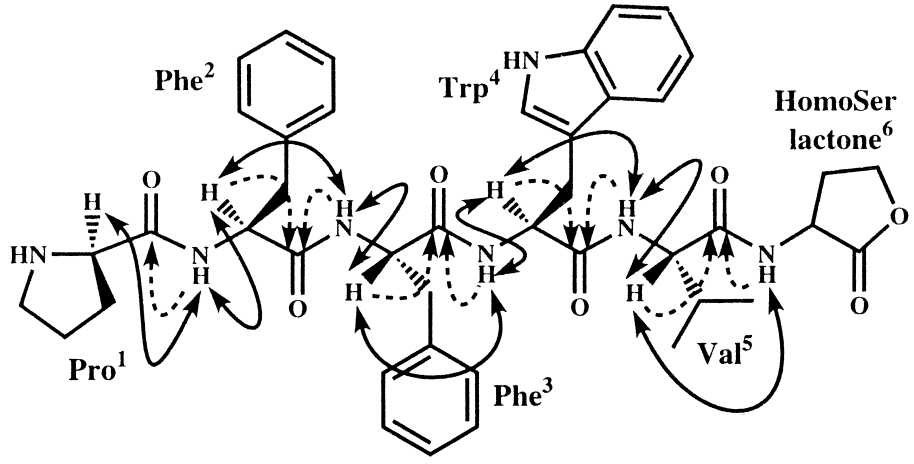

Fig. 2. Cyclolinopeptide F′: dashed arrows show HMBC correlations and arrows show some selected NOE relationship.

various physical and spectral data. Consequently, the sequence of amino acids in CLH (or CLI) is basically same to that in CLG (or CLF). The amino acid sequences of CLH and CLI were determined from ROE correlations as shown in Figs. 5 and 6. Consequently, the structures of CLH were identified as *cyclo* (-Pro–Phe–Phe–Trp–Ile-Mso–Leu–Met-) and CLI as *cyclo* (-Pro–Phe–Phe–Trp-Val–Met–Leu–Mso-).

CLB (*cyclo* (-Pro–Pro–Phe–Phe–Val–Ile–Met–Leu-Ile-)) showed an inhibitory effect on mitogen (concanavalin A) induced response of human peripheral-blood lymphocytes (IC_{50}: 44 ng/ml), which is comparable to that of cyclosporin A (Morita et al., 1997). Furthermore, CLA (*cyclo* (-Pro–Pro–Phe–Phe–Leu–Ile–Ile–Leu–Val-)), CLB and CLE (*cyclo* (-Pro–Leu–Phe–Ile–Mso–Leu–Val-Phe-)) possessing different amino acid sequences showed a moderate inhibitory effect of about the same potency on the mouse lymphocyte proliferation induced by Con. A (IC_{50}: CLA 2.5 μg/ml; CLB 39 μg/ml; CLE 43 μg/ml) (Morita et al., 1999). However, CLC (*cyclo* (-Pro–Pro–Phe–Phe-Val–Ile–Mso–Leu–Ile-)), CLD (*cyclo* (-Pro–Phe-Phe–Trp–Ile–Mso–Leu–Leu-)) and CLF–CLI (IC_{50}: >100 μg/ml, respectively) did not show any of the above activities. It is known that the biological activity of CLA is critically dependent on the sequence and conformation (Kessler et al., 1988). The conformational analyses and further conformation–biological activity relationship of CLA–CLI, are currently being investigated in our laboratories.

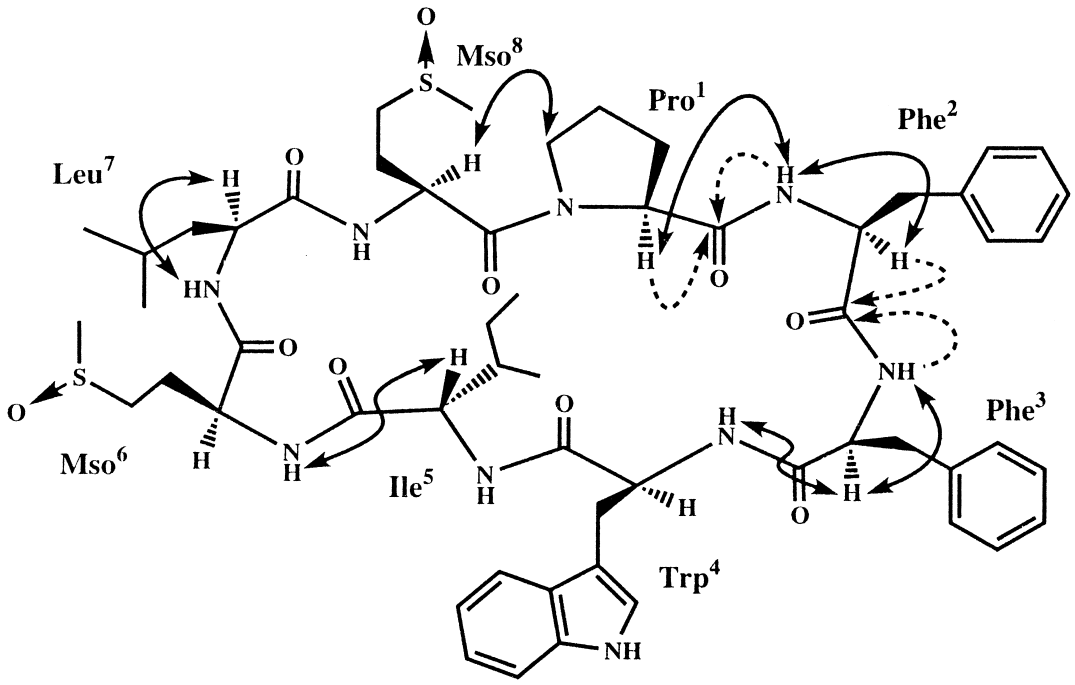

Fig. 3. Cyclolinopeptide G (**2**): dashed arrows show selected HMBC correlations and arrows show some selected NOE relationship.

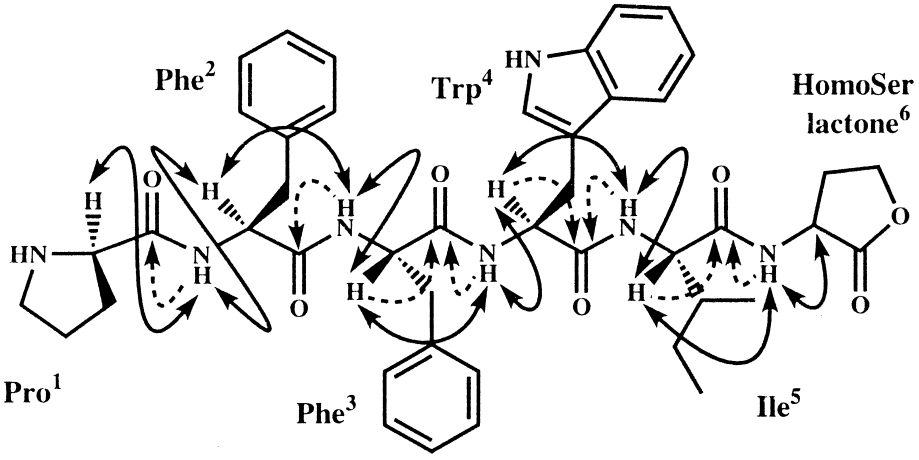

Fig. 4. Cyclolinopeptide G′: dashed arrows show HMBC correlations and arrows show some selected NOE relationship.

3. Experimental

3.1. General

Optical rotations were measured on a JASCO DIP-4 spectrometer and $[\alpha]_D$ values are given in 10^{-1} deg cm^2 g^{-1}. The IR and UV spectra were taken on JASCO FT/IR 620 and Hitachi 557 spectrometers, respectively, and the ^{1}H and ^{13}C NMR spectra were recorded on Brüker AM-500 spectrometers, with chemical shifts (δ) reported in ppm, the spectra were recorded at 320°. FABMS were taken with a VG Autospec spectrometer. HPLC was carried out using an Inertsil PREP-ODS column (20 mm i.d.×250 mm and 30 mm i.d.×250 mm, GL Science Inc.) packed with 10 μm ODS. TLC was conducted on precoated Kieselgel 60 F254 (Art. 5715; Merck) with spots detected by use of the Dragendorff reagent.

3.2. Plant material

Seeds (*Linum usitatissium*, Linaceae) were purchased from Nikka Oil Co., Japan and the oil was removed by manual pressing. The plant was identified by Professor Yutaka Sashida, director of the medicinal garden in Tokyo University of Pharmacy and Life Science. A voucher specimen is deposited in our Laboratory.

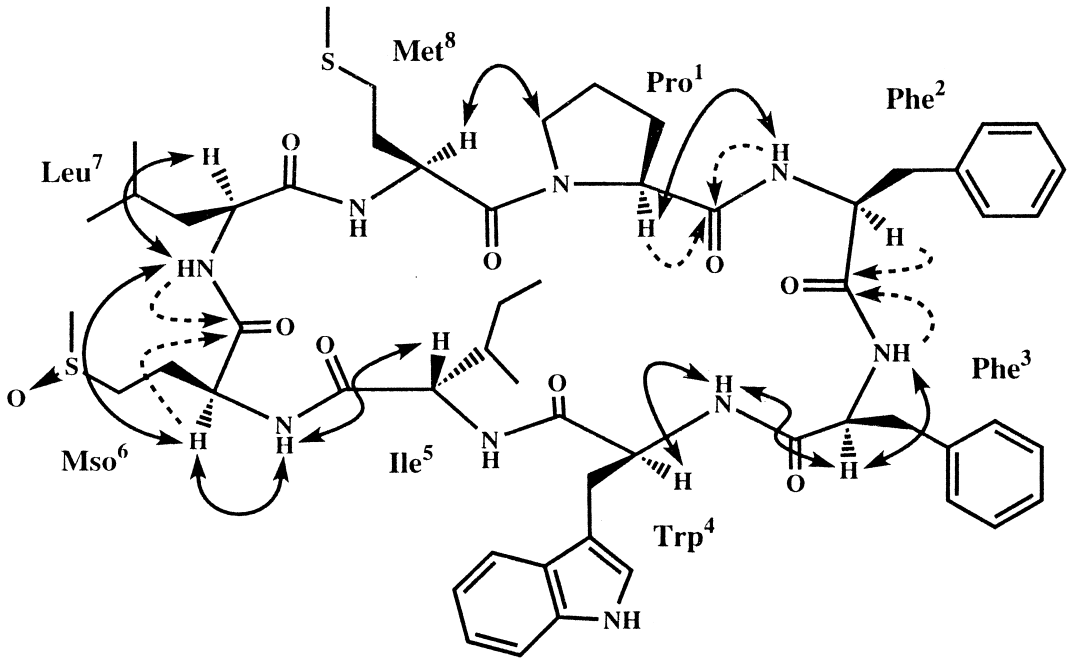

Fig. 5. Cyclolinopeptide H (**3**): dashed arrows show selected HMBC correlations and arrows show some selected NOE relationship.

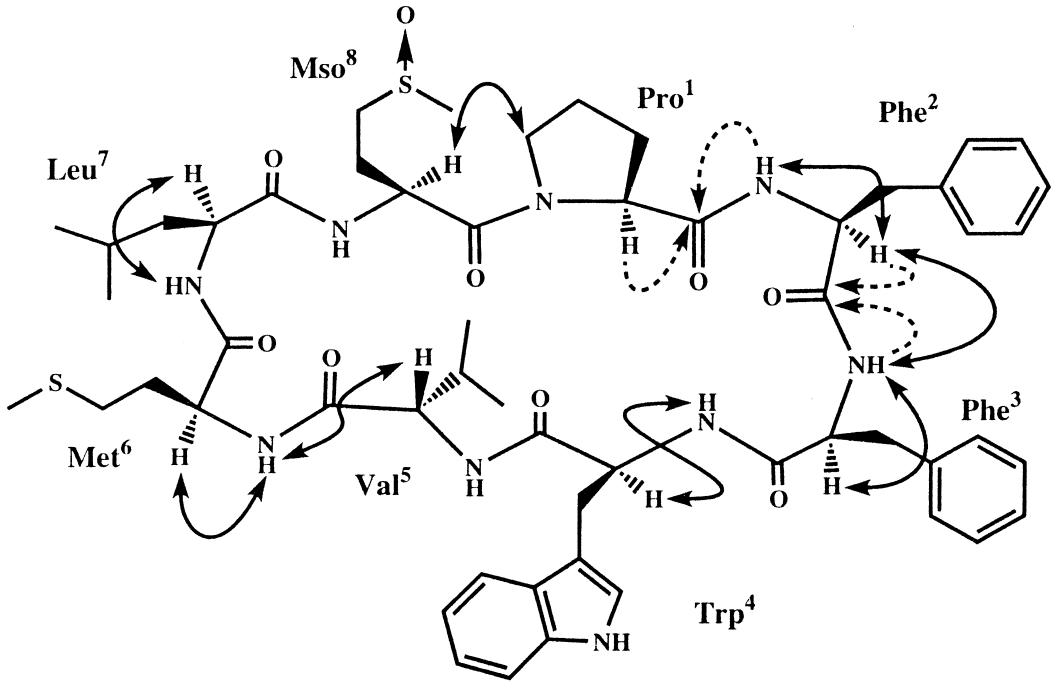

Fig. 6. Cyclolinopeptide I (**4**): dashed arrows show selected HMBC correlations and arrows show some selected NOE relationship.

3.3. Extraction and separation

Seeds (*L. usitatissium*, 30 kg) were manually pressed to remove oil by squeezing, these being extracted with hot MeOH three times to give a MeOH extract (4 kg). The latter was subjected to Diaion HP-20 column chromatography using a H_2O–MeOH gradient system (0:1–1:0), and the fraction eluted with 100% MeOH was further subjected to silica gel column chromatography using a $CHCl_3$–MeOH gradient system (1:0–0:1). A 15% MeOH fraction was subjected to ODS HPLC with 40–60% CH_3CN solvent system to give CLF (0.0008%), CLG (0.0024%), CLH (0.0002%) and CLI (0.00007%).

Table 3
^{1}H and ^{13}C NMR signal assignments for cyclolinopeptide H (**3**) in DMSO-d_6 at 320 K

	^{1}H NMR assignment δ_H [int, mult, J(Hz)]	^{13}C NMR δ_C		δ_H [int, mult, J(Hz)]	δ_C
Pro[1]			Ile[5]		
α	4.16 (1H, *t*, 7.8)	61.89	α	4.34 (1H, *m*)	57.20
β	2.09 (1H, *m*)	28.75	β	1.85 (1H, *m*)	37.01
	1.66 (1H, *m*)		γ	1.26 (1H, *m*)	24.21
γ	1.91 (2H, *m*)	24.39		1.11 (1H, *m*)	
δ	3.61 (1H, *m*)	46.94	γ_{CH3}	0.90 (3H, *d*, 7.6)	15.24
	3.56 (1H, *m*)		δ_{CH3}	0.85 (3H, *t*, 6.1)	11.05
C=O		173.17	NH	7.45 (1H, *d*, 7.7)	
Phe[2]			C=O		171.41[a]
α	4.05 (1H, *m*)	56.33	Mso[6]		
β	2.96 (1H, *t*, 10.3)	35.14	α	4.03 (1H, *m*)	54.14
	2.83 (1H, *m*)		β	2.17 (1H, *m*)	23.20
γ		137.78		1.96 (1H, *m*)	
δ	7.18 (2H, *m*)	127.86	γ	2.69 (1H, *m*)	49.71
ε	6.98 (2H, *m*)	128.42	ε_{CH3}	2.47 (3H, *s*)	37.86
ζ	7.22 (1H, *m*)	126.00	NH	8.18 (1H, *d*, 7.5)	
NH	8.20 (1H, *d*, 6.2)		C=O		170.76
C=O		170.06	Leu[7]		
Phe[3]			α	3.78 (1H, *m*)	52.83
α	4.58 (1H, *m*)	53.39	β	1.84 (1H, *m*)	37.92
β	3.33 (1H, *m*)	36.47		1.61 (1H, *m*)	
	2.77 (1H, *m*)		γ	1.58 (1H, *m*)	24.31
γ		138.13	δ_{CH3}	0.87 (3H, *d*, 6.1)	22.76
δ	7.18 (2H, *m*)	127.86		0.83 (3H, *d*, 6.0)	20.88
ε	7.28 (2H, *m*)	128.60	NH	8.06 (1H, *d*, 6.1)	
ζ	7.22 (1H, *m*)	126.00	C=O		170.06[a]
NH	7.88 (1H, *d*, 8.8)		Met[8]		
C=O		170.76[a]	α	4.78 (1H, *dt*, 3.9, 8.8)	49.57
Trp[4]			β	2.05 (1H, *m*)	31.69
α	4.08 (1H, *m*)	55.63		1.87 (1H, *m*)	
β	3.33 (2H, *m*)	24.31	γ	2.48 (2H, *m*)	29.52
1_{NH}	10.59 (1H, *s*)		ε_{CH3}	2.00 (3H, *s*)	14.75
2	7.18 (1H, *d*, 7.6)	122.76	NH	7.31 (1H, *d*, 8.8)	
3		110.37	C=O		170.91[a]
4	7.45 (1H, *d*, 7.7)	117.65			
5	7.04 (1H, *t*, 7.7)	120.59			
6	6.97 (1H, *t*, 7.7)	117.97			
7	7.31 (1H, *d*, 7.7)	111.04			
8		135.81			
9		127.19			
NH	8.18 (1H, *d*, 7.5)				
C=O		171.80[a]			

[a] Assignments may be interchanged.

3.4. Cyclolinopeptide F (CLF)

Colorless powder, $[\alpha]_D$ −71.4° (*c* 0.21, MeOH); FABMS *m/z* 1084.6 $[M+H]^+$; HR-FABMS *m/z* 1084.5018 $[M+H]^+$, calcd for $C_{55}H_{74}N_9O_{10}S_2$, 1084.5000; IR ν_{max} (KBr) cm^{-1}: 3375, 1657 and 1016; UV λ_{max} (MeOH) nm (log ε): 280 (3.65) and 228 (4.02). ^{1}H and ^{13}C spectra are listed in Table 1.

3.5. Cyclolinopeptide G (CLG)

Colorless powder, $[\alpha]_D$ −66.6° (*c* 0.20, MeOH); FABMS *m/z* 1098.6 $[M+H]^+$; HR-FABMS *m/z* 1098.5138 $[M+H]^+$, calcd for $C_{56_H}76N_9O_{10}S_2$, 1098.5157; IR ν_{max} (KBr) cm^{-1}: 3364, 1657 and 1015; UV λ_{max} (MeOH) nm (log ε): 281 (3.65) and 219 (3.96). ^{1}H and ^{13}C spectra are listed in Table 2.

3.6. Cyclolinopeptide H (CLH)

Colorless powder, $[\alpha]_D$ −87.7° (*c* 0.15, MeOH); FABMS *m/z* 1081.6 $[M+H]^+$; HR-FABMS *m/z* 1082.5201 $[M+H]^+$, calcd for $C_{56}H_{76}N_9O_9S_2$, 1082.5207; IR ν_{max} (KBr) cm^{-1}: 3422, 1653 and 1029; UV λ_{max} (MeOH) nm (log ε): 281 (3.62) and 229 (3.94). ^{1}H and ^{13}C spectra are listed in Table 3.

3.7. Cyclolinopeptide I (CLI)

Colorless powder, $[\alpha]_D$ −60.6° (*c* 0.20, MeOH); FABMS *m/z* 1068.2 $[M+H]^+$; HR-FABMS *m/z* 1068.5110 $[M+H]^+$, calcd for $C_{55}H_{74}N_9O_9S_2$, 1068.5051; IR ν_{max} (KBr) cm^{-1}: 3383, 1657 and 1027; UV λ_{max} (MeOH) nm (log ε): 281 (3.65) and 228 (4.00). ^{1}H and ^{13}C spectra are listed in Table 4.

Table 4
^{1}H and ^{13}C NMR signal assignments for cyclolinopeptide I (**4**) in DMSO-d_6 at 320 K

	^{1}H NMR assignment δ_H [int, mult, J(Hz)]	^{13}C NMR δ_C		δ_H [int, mult, J(Hz)]	δ_C
Pro[1]			Val[5]		
α	4.20 (1H, *m*)	62.02	α	4.43 (1H, *m*)	57.25
β	2.09 (1H, *m*)	28.97	β	2.14 (1H, *m*)	30.64
	1.61 (1H, *m*)		γ_{CH3}	0.93 (3H, *d*, 6.4)	19.08
γ	1.88 (2H, *m*)	24.19		0.84 (3H, *d*, 6.4)	17.53
δ	3.63 (1H, *m*)	46.93	NH	7.34 (1H, *d*, 7.1)	
	3.52 (1H, *m*)		C=O		170.74[a]
C=O		173.38	Met[6]		
Phe[2]			α	4.03 (1H, *m*)	54.05
α	4.12 (1H, *m*)	56.49	β	2.49 (1H, *m*)	29.46
β	2.86 (2H, *m*)	35.09		2.39 (1H, *m*)	
γ		137.76	γ	2.01 (1H, *m*)	30.01
δ	7.22 (2H, *m*)	127.85		1.85 (1H, *m*)	
ε	7.04 (2H, *m*)	128.41	ε_{CH3}	2.02 (3H, *s*)	14.30
ζ	7.19 (1H, *m*)	125.87	NH	8.15 (1H, *br.s*)	
NH	8.38 (1H, *d*, 7.0)		C=O		170.94
C=O		170.34	Leu[7]		
Phe[3]			α	3.83 (1H, *m*)	52.38
α	4.67 (1H, *m*)	52.78	β	1.85 (1H, *m*)	37.57
β	3.41 (1H, *m*)	36.97		1.61 (1H, *m*)	
	2.76 (1H, *m*)		γ	1.55 (1H, *m*)	24.32
γ		138.05	δ_{CH3}	0.90 (3H, *d*, 6.2)	22.77
δ	7.22 (2H, *m*)	127.93		0.86 (3H, *d*, 6.2)	20.73
ε	7.26 (2H, *m*)	128.41	NH	8.07 (1H, *d*, 6.2)	
ζ	7.19 (1H, *m*)	126.02	C=O		171.03
NH	7.90 (1H, *d*, 8.3)		Mso[8]		
C=O		171.26[a]	α	4.71 (1H, *m*)	50.29
Trp[4]			β	2.39 (1H, *m*)	25.61
α	4.06 (1H, *m*)	55.73		1.94 (1H, *m*)	
β	3.36 (2H, *m*)	24.19	γ	2.82 (1H, *m*)	50.29
1_{NH}	10.60 (1H, *s*)			2.71 (1H, *m*)	
2	7.04 (1H, *d*, 7.3)	120.58	ε_{CH3}	2.46 (3H, *s*)	37.89
3		110.55	NH	7.35 (1H, *br.s*)	
4	7.45 (1H, *d*, 7.7)	117.62	C=O		170.43
5	7.18 (1H, *m*)	122.63			
6	6.95 (1H, *t*, 7.7)	117.95			
7	7.32 (1H, *d*, 7.7)	111.04			
8		135.83			
9		127.20			
NH	8.25 (1H, *d*, 5.5)				
C=O		172.27[a]			

[a] Assignments may be interchanged.

3.8. Absolute configuration of amino acid

A solution of each peptide (1 mg) in 6 N HCl was heated at 110°C for 24 h in a sealed tube. After removal of HCl by repeated evaporation in vacuo, the hydrolysate was dissolved in water and treated with 1-fluoro-2,4-dinitrophenyl-5-L-alanine amide (Marfey's reagent) and 1 M $NaHCO_3$ at 35°C for 1 h. After cooling, it was treated with 2 M HCl and then concentrated to dryness. This residue was subjected to HPLC, flow rate 1 ml/min, detection at 340 nm, solvent: 10–80% MeOH (80 min gradient added on 10 min to be eluted with 100% MeOH)/50 mM triethylamine phosphate (TEAP) buffer (pH 3.2). Retention time (min) of authentic amino acids were as follows: L-Pro (54.8), D-Pro (60.6), L-Met (63.9), D-Met (76.8), L-Val (66.8), D-Val (79.7), L-Trp (67.4), D-Trp (75.8), L-Phe (71.9), D-Phe (84.6), L-Ile (74.0), D-Ile (86.4), L-Leu (75.5), D-Leu (87.4), L-Msn (46.7), D-Msn (51.2), L-Mso (45.4), D-Mso (47.4).

3.9. Reaction of CLF and CLG with thioglycolic acid and cyanogen bromide

Solutions of CLF (18.9 mg) and CLG (21.1 mg) in 40% thioglycolic acid (1.0 ml) were individually heated at 50°C for 24 h, respectively. Each reaction mixture

was subjected to HP-20 column chromatography, then further purified by HPLC, to give two cyclic octapeptides consisting of one methionine sulfoxide and one methionine, and one cyclic octapeptide containing two methionine. The latter was treated with 100 M cyanogen bromide and 70% formic acid (1.0 ml) for 24 h at room temperature. The reaction mixture from CLF (or CLG) was lyophilized and purified by HPLC to give an acyclic homoserine lactonic product CLF′ (3.0 mg) (or CLG′ (5.5 mg)).

3.9.1. CLF′

Colorless powder; MS m/z 778.4 $[M+H]^+$; IR ν_{max} (KBr) cm^{-1}: 3427, 3293 (NH), 1775 (γ-lactone) and 1641 (amide carbonyl). ^1H NMR (DMSO-d_6, 300 K): Pro[1] 4.02 (1H, *t*, 7.4, α), 2.02 (1H, *m*, β), 1.71 (1H, *m*, β), 1.79 (2H, *m*, γ), 3.16 (2H, *m*, δ), 9.31 (1H, br.s, NH); Phe[2] 4.54 (1H, *m*, α), 2.98 (1H, *m*, β), 2.68 (1H, *dd*, 10.3, 14.0, β), 7.21 (2H, *m*, δ), 7.19 (2H, *m*, ε), 7.16 (1H, *m*, ζ), 8.63 (1H, *d*, 8.5, NH); Phe[3] 4.55 (1H, *m*, α), 3.00 (1H, *m*, β), 2.78 (1H, *dd*, 9.5, 13.9, β), 7.20 (2H, *m*, δ), 7.18 (2H, *m*, ε), 7.15 (1H, *m*, ζ), 8.25 (1H, *d*, 8.2, NH); Trp[4] 4.68 (1H, *dt*, 5.4, 7.8, α), 3.15 (1H, *m*, β), 3.03 (1H, *m*, β), 10.80 (1H, *s*, NH), 7.17 (1H, *d*, 6.6), 7.60 (1H, *d*, 7.9), 7.05 (1H, *t*, 7.9), 6.97 (1H, *t*, 7.9), 7.31 (1H, *d*, 7.9), 8.22 (1H, *d*, 7.8); Val[5] 4.18 (1H, *dd*, 6.8, 8.9, α), 1.98 (1H, *m*, β), 0.89 (3H, *d*, 6.8, γ), 0.87 (3H, *d*, 6.8, γ), 7.98 (1H, *d*, 8.9, NH); HomoSer lactone[6] 4.60 (1H, *m*, α), 2.40 (1H, *m*, β), 2.15 (1H, *m*, β), 4.35 (1H, *m*, γ), 4.23 (1H, *m*, γ), 8.41 (1H, *d*, 8.1, NH). ^{13}C NMR Pro[1] 58.57 (α), 29.47 (β), 23.27 (γ), 45.59 (δ), 167.73 (CO); Phe[2] 53.79 (α), 37.36 (β), 137.48 (γ), 127.88 (δ), 129.19 (ε), 126.09 (ζ), 170.28 (CO); Phe[3] 54.15 (α), 37.54 (β), 137.56 (γ), 127.99 (δ), 129.19 (ε), 126.25 (ζ), 170.71 (CO); Trp[4] 53.22 (α), 27.53 (β), 123.55, 109.77, 118.44, 120.73, 118.14, 111.16, 135.98, 127.38, 171.05 (CO); Val[5] 57.47 (α), 30.82 (β), 19.00 (γ), 18.04 (γ), 170.68 (CO); HomoSer lactone[6] 47.72 (α), 27.91 β), 65.22 (γ), 174.95 (CO).

3.9.2. CLG′

Colorless powder; MS m/z 814.7 $[M+H]^+$; IR ν_{max} (KBr) cm^{-1}: 3423 (NH), 1775 (γ-lactone) and 1640 (amide carbonyl). ^1H NMR (DMSO-d_6, 300 K): Pro[1] 4.02 (1H, *t*, 7.4, α), 2.18 (1H, *m*, β), 1.68 (1H, *m*, β), 1.80 (2H, *m*, γ), 3.15 (2H, *m*, δ); Phe[2] 4.56 (1H, *m*, α), 2.68 (1H, d*d*, 10.0, 14.2, β), 2.18 (1H, *m*, β), 7.21 (2H, *m*, δ), 7.19 (2H, *m*, ε), 7.16 (1H, *m*, ζ), 8.61 (1H, *d*, 8.7, NH); Phe[3] 4.54 (1H, *m*, α), 2.96 (1H, *m*, β), 2.77 (1H, d*d*, 9.9, 14.0, β), 7.20 (2H, *m*, δ), 7.18 (2H, *m*, ε), 7.15 (1H, *m*, ζ), 8.25 (1H, *d*, 8.3, NH); Trp[4] 4.67 (1H, α), 3.17 (1H, *m*, β), 3.03 (1H, *m*, β), 10.79 (1H, *s*, NH), 7.18 (1H, *d*, 7.3), 7.59 (1H, *d*, 7.8), 7.05 (1H, *t*, 7.8), 6.97 (1H, *t*, 7.8), 7.31 (1H, *d*, 7.8), 8.20 (1H, *d*, 7.8); Ile[5] 4.20 (1H, *t*, 8.8, α), 1.72 (1H, *m*, β), 1.46 (1H, *m*, γ), 1.11 (1H, *m*, γ), 0.86 (3H, *d*, 6.9, γ), 0.82 (3H, *t*, 7.4, γ), 8.00 (1H, *d*, 8.8, NH); HomoSer lactone[6] 4.60 (1H, *m*, α), 2.38 (1H, *m*, β), 2.15 (1H, *m*, β), 4.35 (1H, *m*, γ), 4.22 (1H, *m*, γ), 8.40 (1H, *d*, 8.0, NH). ^{13}C NMR Pro[1] 58.59 (α), 29.46 (β), 23.28 (γ), 45.61 (δ), 167.79 (CO); Phe[2] 54.13 (α), 37.59 (β), 137.59 (γ), 127.98 (δ), 129.17 (ε), 126.25 (ζ), 167.79 (CO); Phe[3] 53.77 (α), 37.36 (β), 137.47 (γ), 127.88 (δ), 129.05 (ε), 126.09 (ζ), 170.66 (CO); Trp[4] 53.17 (α), 27.88 (β), 123.54, 109.76, 118.44, 120.73, 118.13, 111.16, 135.97, 127.39, 170.91 (CO); Ile[5] 56.63 (α), 36.90 (β), 24.28 (γ), 15.13 (γ), 10.98 (δ), 170.77 (CO); HomoSer lactone[6] 47.71 (α), 28.63 (β), 65.24 (γ), 174.93 (CO).

3.10. Biological assay

The bio-assay method using mouse lymphocytes was as follows. After dislocation of cervical vertebrae of ICR mice aged 5–8 week*s*, the spleen was removed and mashed. Then, the cells were suspended in RPMI 1640 medium and passed through a stainless steel mesh. The single cell suspension was washed twice with the medium and finally suspended in RPMI 1640 medium containing 10% fetal calf serum, and 10 mg/ml kanamycin to give 3.5×10^6 cells/ml. 200 μl of this suspension was placed in each well of a microtiter plate with 96 flatbottom wells. Concanavalin A was added to each well to a final concentration of 2.5 μg/ml. Subsequently, 4 μl of serially diluted EtOH solution of test compound was added to a final concentration of 10–100 000 ng/ml. The plate was incubated for 3 days in 5% CO_2/95% air at 37°C. After termination of cell culture, 20 μl of 5 mM 1-methoxy PMS and 0.2 mM WST-1 (DOJINDO Laboratories) in phosphate buffered saline was added to every well and the plate was incubated again at 37°C in 5% CO_2/air for a 4 h. The plate was read on a microplate reader (Corona MT P-32, Corona Co., Japan) at 415 nm. A dose–response curve was plotted for each drug, and the concentration which gave 50% inhibition of cell growth (IC_{50}) was recorded.

Acknowledgements

The authors thank the Ministry of Education, Science and Culture, Japan, for financial support through Grant-in-Aid for General Scientific Research.

References

Blasio, B.D., Rossi, F., Benedetti, E., Pavone, C., Temussi, P.A., Zanotti, G., Tancredi, T., 1989. Bioactive peptide: solid-state and solution conformation of cyclolinopeptide A. J. Am. Chem. Soc. 111, 9089–9098.

Brewster, A.I., Bovey, F.A., 1971. Conformation of cyclolinopeptide A observed by nuclear magnetic resonance spectroscopy. Proc. Natl. Acad. Sci. USA 68, 1199–1202.

Itokawa, H., Takeya, K., Hitotsuyanagi, Y., Morita, H., 1997. Macrocyclic peptide alkaloids from plants. The Alkaloids, Vol. 49. Academic Press, New York, pp. 301–387.

Kaufmann, H.P., Tobschirbel, A., 1959. An oligopeptide from linseed. Chemische Berichte 92, 2805–2809.

Kessler, H., Bats, J.W., Griesinger, C., Koll, S., Will, M., Wagner, K., 1988. Peptide conformations. 46. Conformational analysis of a superpotent cytoprotective cyclic somatostatin analog. J. Am. Chem. Soc. 110, 1033–1049.

Marfey, P., 1984. Determination of D-amino acids. II. Use of a bifunctional reagent, 1,5-difluoro-2,4-dinitrobenzene. Carlsberg Res. Commun. 49, 591–596.

Morita, H., Shishido, A., Matsumoto, T., Takeya, K., Itokawa, H., Hirano, T., Oka, K., 1997. Cyclic peptides from higher plants. 42. A new immunosuppressive cyclic nonapeptide B from *Linum usitatissium*. Bioorganic and Medicinal Chemistry Letters 7, 1269–1272.

Morita, H., Shishido, A., Matsumoto, T., Itokawa, H., Takeya, K., 1999. Cyclic peptides from higher plants. 45. Cyclolinopeptides B–E, new cyclic peptides from *Linum usitatissium*. Tetrahedron 55, 967–976.

Naider, F., Benedetti, E., Goodman, M., 1971. Conformation of cyclolinopeptide A by circular dichroism. Proc. Natl Acad. Sci. USA 68, 1195–1198.

Tonelli, A.E., 1971. Approximate treatment of the conformational characteristics of a cyclic nonapeptide, cyclolinopeptide A. Proc. Natl. Acad. Sci. USA 68, 1203–1207.

Wieczorek, Z., Bengtsson, B., Trojnar, J., Siemion, I.Z., 1991. Immunosuppressive activity of cyclolinopeptide A. Peptide Res. 4, 275–283.

PERGAMON

Phytochemistry 57 (2001) 261–265

PHYTOCHEMISTRY

www.elsevier.com/locate/phytochem

Jesterone and hydroxy-jesterone antioomycete cyclohexenone epoxides from the endophytic fungus *Pestalotiopsis jesteri*

Jia Yao Li, Gary A. Strobel *

Department of Plant Sciences, Montana State University, Bozeman, MI, 59717, USA

Received 16 October 2000; received in revised form 8 December 2000

Abstract

Jesterone and hydroxy-jesterone are novel highly functionalized cyclohexenone epoxides isolated from a newly described endophytic fungal species — *Pestalotiopsis jesteri*. They were purified from cultures of the fungus by bioassay guided fractionation using *Pythium ultimum* as the indicator organism. Jesterone, in particular, displays selective antimycotic activity against the oomycetous fungi which are some of the most plant pathogenic of all disease causing fungi. The possible importance of these cyclohexenones to the biology of the endophytic fungus–host plant relationship is also discussed. © 2001 Elsevier Science Ltd. All rights reserved.

Keywords: Rainforest; Endophyte; Oomycete; Cyclohexenone; Plant pathogen; Antimycotic

1. Introduction

Pestalotiopsis jesteri is a new endophytic fungus recently described from the Southern Highland Province of Papua New Guinea (Strobel et al., 2000). The fungus was isolated from the inner bark of small limbs of a *Fragraea bodenii* (locally termed an oak tree but belonging to the family, Gentianaceae) located at the singsing grounds of the Aluakambe village. Limbs from the top, middle and lower crown of the tree each yielded this peculiar fungal endophyte. This particular plant species is common to the forests of the tropical New Guinea Highlands. This region of the world was selected for study since nearly 70% of Papua New Guinea is covered with virtually undisturbed rainforests. Specifically, the Southern Highlands province receives between 80 and 100 cm of rainfall per year and this region of the world is virtually unexplored microbiologically. Under these moist conditions various plant pathogenic microorganisms (especially the oomycetes) normally thrive. Yet the forest seems to remain relatively healthy suggesting the presence of substances that are suppressive or lethal to oomycetes. Thus, our rationale to find novel antioomycetous compounds focuses on tropical regions of the world such as Papua New Guinea. In particular, we commonly search for unusual endophytic or epiphytic fungi or other microbes found associated with normally healthy appearing plants. These plants may survive the onslaught of plant pathogens in such environments because of the antimicrobial compounds being produced by endophytic or epiphytic microbes associated with them (Strobel et al., 1999). Thus, the focus of this report is to describe the isolation, and structural elucidation of two novel cyclohexenone epoxides being produced by two of the three isolates of the newly described endophytic fungus — *Pestalotiopsis jesteri*. In addition, we report that one of these cyclohexenone epoxides possesses impressive antimycotic activity against a suite of plant pathogenic oomycetes.

2. Results and discussion

Each of the isolates of *P. jesteri* used in this study was obtained from the top, middle and lower crown areas of a 20 m high oak tree (*Fragraea bodenii*) in the Southern Highlands provience of Papua New Guinea. These fungal isolates were obtained as endophytes from representative small limbs (0.5–1.0 cm in dia.) from one tree in the Aluakambe village. They were cultured and initially examined for activity against *P. ultimum* (a plant pathogenic oomycete). Only isolates from the lower and

* Corresponding author. Tel.: +1-406-994-5148; fax: +1-406-994-7600.

E-mail address: uplgs@montana.edu (G.A. Strobel).

0031-9422/01/$ - see front matter © 2001 Elsevier Science Ltd. All rights reserved.
PII: S0031-9422(01)00021-8

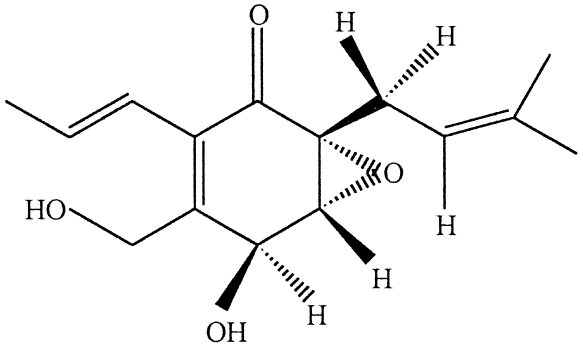

Jesterone (1)

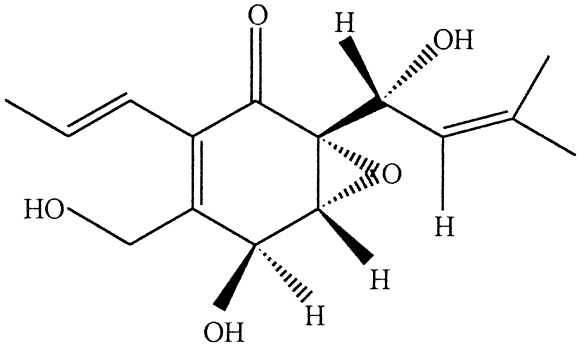

Hydroxy-jesterone (2)

middle crown locations in the tree were biologically active. These isolates were selected for further study. After culturing, extracting and purification, the yield of a biologically active product was 20 mg/l. This product was ultimately shown to be homogeneous by TLC in solvents A and B and was termed — "**jesterone (1)".** The various fractions obtained during the purification procedures were consistently subjected to an agar plate bioassay system employing *P. ultimum* as the test organism. While some other fractions had some bioactivity, **(1)**, the primary fermentation product, obtained using the processes described, had the greatest bioactivity against the test organism.

However, in the process of purifying **(1)**, another fermentation product appeared. This compound also possessed antifungal activity, but to a lesser extent than **(1)**. The yield of this compound was about 120 mg/l. This compound was purified and also shown to be homogeneous by TLC and was structually related to **(1)**, it was termed — "**hydroxy-jesterone (2)".**

The names jesterone **(1)** and hydroxy-jesterone **(2)** have been selected for these compounds in reference to the biological source from which they arise, namely *Pestalotiopsis jesteri*. We originally named the source organism *P. jesteri* because the 3–4 appendages on each spore bear terminal spheroid structures making the spore appear as a jester's hat (Strobel et al., 2000).

Both **(1)** and **(2)** are liquids at room temperature possessing a slightly yellowish tinge. Electrospray mass spectrometry of **(1)** revealed an M + M (dimer) + Na^+ at 551 *m*/*z* yielding a mass of 264 for this compound. On the other hand, **(2)** showed an M + H^+ at 281 *m*/*z*, thus, a M_r of 280. By high resolution mass spectroscopy **(1)** yielded an observed molecular ion at 264.135338 (calculated M_r = 264.136572) with an empirical formula of $C_{15}H_{20}O_4$. In HRMS **(2)** yielded a M_r = 280.130447 (calculated M_r = 280.131074). Thus, the empirical formula of **(2)** is $C_{15}H_{20}O_5$.

The ^1H NMR spectrum of **(1)** showed 18 non-exchangeable protons including 3 olefinic protons and those with 3 methyl groups. Analyses of the ^{13}C NMR, DEPT and HSQC spectra of **(1)** allowed for the identification of 2 methylene carbons including 1 hydroxymethylene functionality, 2 methine carbons possessing oxygen substituents, 5 quaternary carbons including 3 olefinic, 1 carbonyl and 1 bearing an oxygen substituent. The IR spectrum showed a strong -OH absorption band at 3426 cm^{-1} and an α-β- unsaturated ketone band at 1678 cm^{-1}. The carbon skeleton of **(1)** was constructed from the COSY and HMBC spectra (Table 1, Fig. 1). The coupling constant of protons on carbons 2 and 3 (J = 16.11 Hz) indicated a *trans*-olefinic bond. On the other hand, The NOESY spectrum showed no NOE between individual protons on carbons 6, 9 and 10 indicating that the -OH on carbon 6 and the epoxy on carbons 7 and 8 are in a transconfiguration. This structural assignment was confirmed by observing NOE interactions between protons on carbons 7 and 9 and 10.

The NMR spectra of **(2)** were similar to **(1),** and they revealed that carbon 9 possesses a hydroxyl group. The structure of **(2)** was constructed from COSY, HMBC and NOESY experiments (Table 2). Based on all of the data

Table 1
NMR spectra and HMBC spectral correlations for jesterone **(1)**

No.[a]	^{13}C	^1H	HMBC
1	19.16	1.81(*dd*, J = 6.17, J = 1.23)	C2, C3
2	134.89	5.85 (*dt*, J = 6.45, J = 16.11)	C1, C3, C4
3	122.14	6.06 (*d*, J = 16.11)	C1, C2, C4, C5, C13
4	131.52		
5	145.75		
6	65.28	4.89 (*s*)	C4, C5, C7, C8, C12
7	59.59	3.64 (*d*, J = 1.61)	C5, C6, C8, C9
8	60.13		
9	26.60	9a, 2.75 (*dd*, J = 7.89, J = 15.30)	C7, C8, C10, C11, C13
		9b, 2.53 (*dd*, J = 6.82, J = 15.23)	C7, C8, C10, C11, C13
10	116.52	5.04 (*m*)	C9, C14, C15
11	136.06		
12	62.97	12a, 4.70 (*dd*, J = 14.29, J = 2.34)	C4, C5
		12b, 4.44 (*d*, J = 14.26)	C4, C5
13	195.21		
14	18.02	1.63 (*s*)	C10, C11
15	25.83	1.69 (*s*)	C10, C11

[a] Refers to the assigned position of each carbon atom as shown in Fig. 1 for jesterone.

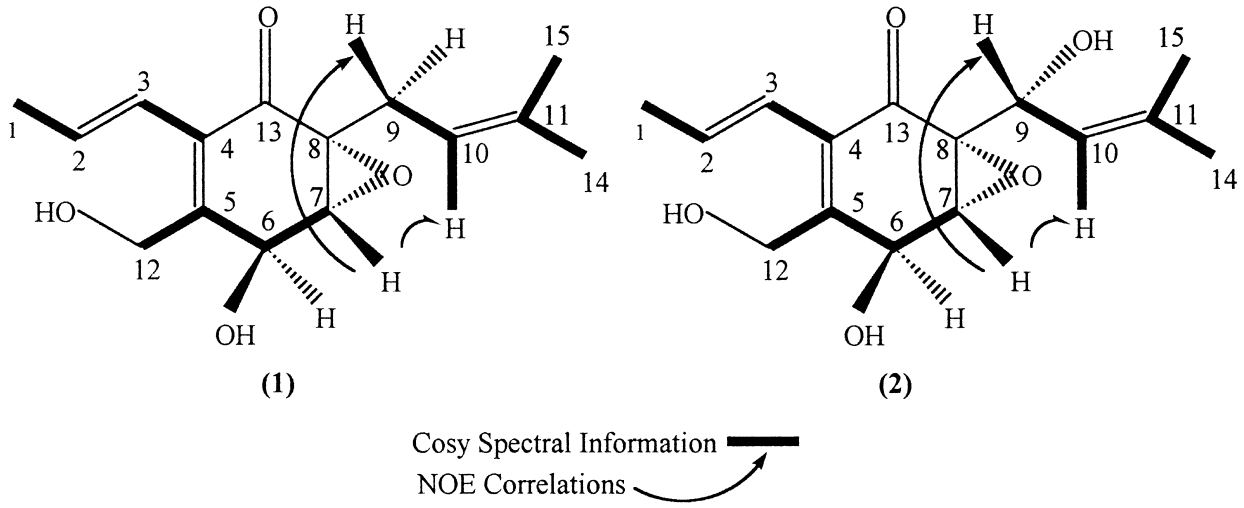

Fig. 1. COSY and NOE correlations aiding in the structural determination of both jesterone and hydroxy-jesterone (left and right, respectively).

Table 2
NMR spectra and HMBC spectral correlations for hydroxy-jesterone **(2)**

No.[a]	^{13}C	^{1}H	HMBC
1	19.23	1.8 (*d*, *J* = 6.1)	C2, C3
2	134.9	5.8 (*dt*, *J* = 6.28, *J* = 15.91)	C1, C3, C4
3	121.7	6.0 (*d*, *J* = 16.2)	C1, C2, C4, C5, C13
4	131.2		
5	145.8		
6	63.9	4.8 (*s*)	C4, C5, C7, C8
7	57.87	3.80 (*s*)	C5, C6, C8
8	60.70		
9	65.1	4.9 (*d*, *J* = 8.6)	C7, C8, C10, C11, C13
10	120.2	5.1 (*d*, *J* = 8.5)	C8, C9, C11, C14, C15
11	139.2		
12	61.6	12a, 4.62 (*d*, *J* = 14.6)	
		12b, 4.39 (*d*, *J* = 14.6)	C4, C5, C6
13	195.53		
14	18.73	1.7 (*s*)	C10, C11
15	25.89	1.73 (*s*)	C10, C11

[a] Refers to the assigned position of each carbon atom as shown in Fig. 1 for hydroxy-jesterone.

available the structures of both **(1)** and **(2)** can be assigned with some relative stereochemistry in place.

The newly isolated cyclohexenones **(1)** and **(2)** belong to a relatively rare class of oxygenated cyclohexanoids which occur in microbes as well as in higher plants (Muhlenfeld and Achenbach, 1988). These substances have a range of activities from antifungal, antitumor, phytotoxic, to enzyme inhibitory and phytotoxic. The latter case is illustrated by the discovery of the PT toxin from the fungus *Pestalotiopsis longiseta* and *P. theae,* which are pathogens of tea (Nagata et al., 1992). The PT toxin and its related compound, epipoxydon are cyclohexenone epoxides with structures markedly different than either **(1)** or **(2)**, but still have the cyclohexenone ring system. In addition, other phytotoxins in this same group of oxygenated cyclohexenones are phyllostine and phyllosinol (Sakamura et al., 1971). Although a number of cyclohexenones related to **(1)** and **(2)** have been reported in the chemical literature, until now, with the exception of ambuic acid, none have any indication of anti-oomycete activity (Li et al., 2001). However, activities against other fungi have been noted. For instance, eupenoxide is an antimycotic from *Eupenicillum* sp. (Duke and Rickards, 1984). It possesses a hydroxylated cyclohexene ring system with both an alkene (7-carbon) and hydroxy methylene side chain. On the other hand, panepoxydone, with a core epoxycyclohexenone structure comparable to jesterone/hydroxy-jesterone is an impressive inhibitor of NF-κB mediated signal transduction in COS-7 cells (Erkel et al., 1996).

Recently, ambuic acid has been isolated and its structure determined from many isolates of *Pestalotiopsis* spp. worldwide (Li et al., in press). It turns out that *Pestalotiopsis* spp. are some of the most commmon inhabitants, as endophytes, of many higher plants in the world's rainforests. Ambuic acid is also a highly functionalized cyclohexenone epoxide possessing some biological activity against certain plant pathogenic fungi including *P. ultimum* (Li et al., 2001). Because ambuic acid bears many structural features with **(1)** and **(2)**, it appears that they have a metabolic pathway in common. In addition, because such a wide variety of metabolites have been recently isolated from *Pestalotiopsis* spp., it would also appear that this group of fungi represents a potential "factory" of previously undiscovered, as well as important secondary fungal products including taxol (Strobel et al., 1996). Presently, the role of these compounds to the biology of the fungus, as it exists within plant tissues, is only a matter of conjecture. However, given the impressive biological activity of some of these molecules, especially as antifungal agents, their role may be to protect the very plants that they inhabit.

Both **(1)** and **(2)** are antimycotics. The minimum inhibitory concentrations (MIC) required to produce total inhibition of fungal growth after exposure to given concentrations of these compounds is reported (Table 3). These compounds have no inhibitory effect against the ascomycetous fungus *Sclerotina sclerotiorum* and the imperfect fungus *Geotrichum candidum*. However, the basidiomycetous fungus *Rhizoctonia solani* and the ascomycetous fungus *Pyricularia oryzae* were both sensitive to **(1)** but not **(2)** (Table 3). However, the most noticeable biological activty of either of these compounds was that of **(1)** on the oomyceteous fungi *Pythium ultimum, Aphanomyces* sp., *Phytophthora citrophthora, P. citrophthora* and *P. cinnamomi* (Table 3). These, relatively low MIC values for **(1)** against these important plant pathogenic fungi suggests that it may have commercial potential. On the other hand, (2) while having some activity against a few of the test fungi (some of the oomycetes), was relatively inactive against the majority of the fungi tested (Table 3).

We also note that *P. jesteri* behaves as many other fungi relative to secondary product formation. That is, after several serial transfers on the PDA (potato dextrose agar) medium and then placement into the MID medium the fungus did not produce **(1)**, however, **(2)** was still produced. Commonly, as has been shown with other fungi, this phenomenon may be related to the absence of critical plant metabolites that can affect the metabolism of a plant inhabiting fungus (Pinkerton and Strobel, 1975; Li et al., 1998). Usually, after one or more of these plant compounds are restored to the medium used to grow the fungus, the production of the fungal metabolite resumes. While this problem has been solved in other microbe-plant cases we have not solved it yet in the case of *P. jesteri*.

Representatives of the fungal genus *Pestalotiopsis* sp. are some the most commonly isolated endophytes of the higher plants of the world's rainforests (Li et al., 2001). The novel fungus *P. jesteri* was originally obtained from an oak species native to the Southern Highlands of Papua New Guinea. Although we had made vast collections of other plants in this area, the fungus was only obtained from this one tree species. It maybe that *P. jesteri* is host-selective. Another interesting biological aspect of *P jesteri* is that only certain isolates of it make **(1)** and **(2)**. Thus, while the association of these secondary products with this particular fungus does not always occur we can only speculate that they may play some role in the microbe-host plant relationship.

Table 3
Minimum inhibitory concentrations of jesterone and hydroxy-jesterone for a representative group of plant pathogenic fungi[a]

Test fungus (genus and species)	Jesterone μg/ml	Hydroxy-jesterone μg/ml
Pythium ultimum	25	> 500
Aphanomyces sp.	6.5	125
Phytophthora citrophthora	25	250
Phytophthora cinnamomi	6.5	62.5
Sclerotinia sclerotiorum	100	> 500
Rhizoctonia solani	25	> 500
Geotrichum candidum	> 100	> 500
Pyricularia oryzae	25	> 500

[a] Details of the testing procedures are given (see Experimental).

3. Experimental

3.1. General spectroscopic procedures

All NMR data were collected in a Bruker DRX-500 NMR with the sample dissolved in 0.5 ml of $CDCl_3$. Specific details and results on each NMR experiment performed are available from the authors.

Electrospray mass spectra of **1** and **2** were obtained on a home built instrument with the sample dissolved in methanol/water/acetic acid 50:50:1 by vol. Each sample was injected into the instrument with a flow rate of 2 μl per min. with a spray voltage of 2.2 kV via the loop injection method. High resolution EI mass spectrometry was performed on a VG 70E-HF double focusing mass spectrometer operating at a mass resolution of 1500.

The ultraviolet absorption spectra of **1** and **2** were obtained in a Beckman DU 50 spectrometer with the compounds dissolved in methanol.

3.2. Thin layer chromatography

Thin layer chromatography of fungal fermentation products was performed on Merck silica gel plates (0.25 mm thick) using solvent systems A = chloroform: methanol 10:1 v/v: and solvent system B = hexane: ethyl acetate 1:1 v/v. compounds were detected with the anisaldehyde/sulfuric acid reagent (Cardellina, 1991).

3.3. Jesterone **(1)** and hydroxy-jesterone **(2)** isolation

Jesterone was isolated from 3-week old still cultures of *P. jesteri* grown at 23°C in two 2 l flasks each containing 500 ml of MID medium (Strobel et al., 1996). After removal of the mycelium by filtration, the culture fluid was successively extracted twice with equal volumes of methylene chloride. After flash evaporation of the solvent, approximately 450–500 mg of residue remained. This residue was dissolved in 2 ml of methylene chloride and applied to a 3×30 cm column of silica gel. On to the column was placed 400 ml of a mixture of chloroform/methanol 10:1 v/v. Fractions of 10 ml were collected and nearly mid-way in the elution profile, a compound with an $R_F = 0.44$ in solvent A appeared. Each of the tubes containing this compound were pooled with a final yield of 50–60 mg of material. This residue was

again subjected to flash column silica chromatography on a comparable sized silica column on to which was placed a 400 ml mixture of hexane /ethyl acetate 2:1 v/v until a compound having the appropriate migration pattern in solvent A appeared.

Furthermore, another compound appeared in the elution profile of the first silica gel column. It, however, possessed a greater retention time on the flash column than jesterone and also had weaker activity against *P. ultimum*. The R_F of this compound in solvent A was 0.34 and in solvent B the R_F was 0.15. About 150 mg of this impure compound was collected and subjected to additional flash chromatograpy on a new silica column. On to it was placed 400 ml of a hexane and ethyl acetate mixture but at a ratio of 1:1 v/v, which allowed its elution at about 200 ml. The yield of this compound was about 120 mg/l. It was biologically active against the test fungus, but to a lesser extent. This compound was also shown to be homogeneous by TLC and was structually related to **(1)**.

3.4. Agar plate bioassay test

The agar plate bioassay test consisted of the placement of an aliquot (20 μl) of each column fraction on a potato dextrose agar (PD) plate. The solution was allowed to evaporate to dryness on the surface in a decontaminated (alcohol sprayed) laminar flow hood for 15–20 min. Subsequently, 1 mm plugs of PD agar containing a rapidly growing culture of *Pythium ultimum* were placed within 1 cm of the test residue previously deposited on the plate. After 2 days of incubation at 23°C, fungal colony inhibition could be assessed by virtue of its uneven growth, with little or no growth developing toward the dried residue possessing active antifungal compounds.

3.5. Minimum inhibitory concentration (MICs) tests

MIC (minimum inhibitory concentration) values for **1** and **2** were obtained using a standard plate bioassay test method that employs a microtitre plate containing various concentrations of the test compound and the fungus to be tested in PD broth. The test fungus to be observed is placed in the wells as a 1 mm dia agar plug obtained from a rapidly growing PDA plate supporting the growth of the test fungus. Each well, after 48 h at 23°C, was examined and the well showing no growth next to well having some growth was taken as the MIC value.

3.6. Jesterone (*1*)

Liquid (yellowish) at room temperature. UV λ max (methanol) (log ε): 216, 240 and 265 (3,193, 3,252 respectively) HRMS: found 264.135338 (M^+): calc. for $C_{15}H_{10}O_4 = 264.136572$. For ^1H and ^{13}C NMR spectral analysis, see Table 1.

3.7. Hydroxy-jesterone (*2*)

Liquid (yellowish) at room temperature. UV λ max (methanol) (log ε): 216, 240 and 265 (3.193, 3.252, and 3.243 respectively); HRMS: found 280.130447 (M^+); calc. for $C_{15}H_{20}O_5 = 280.131074$. For ^1H and ^{13}C NMR spectral analysis, see Table 2.

Acknowledgements

This work was supported by the Montana Agricultural Experiment Station. Help in acquiring the NMR spectroscopic data was provided by Dr. Scott Busse, and all mass spectral data were acquired by Dr. Joe Sears, both at the MSU Department of Chemistry.

References

Cardellina, J.H., 1991. HPLC separation of taxol and cephalomannine. Journal of Liquid Chromatography 14, 659–665.

Duke, R.K., Rickards, R.W., 1984. Stereospecific toatl synthesis of the cyclohexene oxide antibiotic eupenoxide. Journal of Organic Chemistry 49, 1898–1904.

Erkel, G., Anke, T., Sterner, O., 1996. Inhibition of NF-κB activation factor by panepoxydone. Biochemical and Biophysical Research Communications 226, 214–221.

Li, J.Y., Harper, J.K., Grant, D.M., Tombe, B.O., Bashyal, B., Hess, W.M., Strobel, G.A., 2001. Ambuic acid, a highly functionalized cyclohexenone with antifungal activity from *Pestalotiopsis* spp. and *Monochaetia* sp. Phytochemistry 56, 463–468.

Li, J.Y., Sidhu, R.S., Ford, E.J., Long, D.M., Hess, W.M., Strobel, G.A., 1998. The induction of taxol production in the endophytic fungus — *Periconia* sp. from *Torreya grandifolia*. Journal of Indian Microbiology 20, 259–264.

Muhlenfeld, A., Achenbach, H., 1988. Asperpentyn, a novel acetylenic cyclohexene epoxide from *Aspergillus duricaulus*. Phytochemistry 27, 3853–3855.

Nagata, T., Ando, Y., Hirota, A., 1992. Phytotoxins from tea gray blight fungi, *Pestalotiopsis longiseta* and *Pestalotiopsis theae*. Bioscience, Biotechnology and Biochemistry 56, 810–811.

Pinkerton, R., Strobel, G.A., 1975. Serinol as an activator of toxin production in attenuated cultures of *Helminthosporium sacchari*. Proceedings of the National Academy of Sciences 73, 4007–4011.

Sakamura, S., Ito, J., Sakai, R., 1971. Phytotoxic metabolites of *Phyllosticta* sp. Agriculture and Biological Chemistry 35, 105–110.

Strobel, G., Li, J.Y., Sugawana, F., Koshino, H., Harper, J., Hess, W.M., 1999. Oocydin A, a chlorinated macrocyclic lactone with potent anti-oomycete activity from *Serratia marcesens*. Microbiology 145, 3557–3564.

Strobel, G., Li, J.Y., Worapong, J., Baird, G., Hess, W.M., 2000. *Pestalotiopsis jesteri*, sp. nov. an endophyte from *Fragraea bodenii* from the Southern Highlands of Papua New Guinea. Mycotaxon. 76, 257–266.

Strobel, G., Yang, X., Sears, J., Kramer, R., Sidhu, R.S., Hess, W.M., 1996. Taxol from *Pestalotiopsis microspora*, an endophytic fungus of *Taxus wallachiana*. Microbiology 142, 435–440.

PERGAMON

Phytochemistry 57 (2001) 267–272

PHYTOCHEMISTRY

www.elsevier.com/locate/phytochem

Sesquiterpene lactones and a myoinositol from glandular trichomes of *Viguiera quinqueremis* (Heliantheae; Asteraceae)

Otmar Spring [a,*], Reinhard Zipper [a], Sabine Reeb [b], Bernhard Vogler [b], Fernando B. Da Costa [c]

[a] *Institut für Botanik, Universität Hohenheim, D-70599 Stuttgart, Germany*
[b] *Institut für Chemie, Universität Hohenheim, D-70599 Stuttgart, Germany*
[c] *Faculdade de Ciências Farmacêuticas de Ribeirão Preto, Universidade de São Paulo, Av. do Café s/n°, 14040-903, Ribeirão Preto, SP, Brazil*

Received 17 July 2000; received in revised form 17 November 2000

This paper is dedicated to Professor W. Kraus on the occasion of his 70th birthday

Abstract

The extract of the floral parts of *Viguiera quinqueremis* afforded, in addition to known compounds, six new sesquiterpene lactones as well as a new myoinositol derivative. All compounds were detected in glandular trichomes which were collected micromechanically from the anther appendages and were analyzed by HPLC. Structure identification was performed by ^{1}H NMR measurements including LC NMR and LC MS experiments. © 2001 Elsevier Science Ltd. All rights reserved.

Keywords: *Viguiera quinqueremis*; Heliantheae; Asteraceae; Chemotaxonomy; Sesquiterpene lactones; Myoinositols

1. Introduction

Viguiera quinqueremis Blake is part of a group of approximately 14 species that Blake (1918) merged in the series *Bracteatae* of section *Paradosa*, the South American branch of the large and polyphyletic genus *Viguiera*. The taxa of *Bracteatae* are endemic to Brazil and Paraguay and so far relatively few attempts were made to establish their phytochemical patterns. Up to now, four heliangolides of the 1-keto-2,3-unsaturated-3,10-epoxy-type were identified from *V. oblongifolia* (Bohlmann et al., 1984; Tamayo-Castillo et al., 1990) and *V. robusta* (Da Costa et al., 1996), respectively, while *V. nervosa* was reported to lack sesquiterpene lactones (Tamayo-Castillo et al., 1990). *V. quinqueremis* is a perennial herb with sessile, mostly alternate and linear-oblong leaves. Microscopic studies of vegetative plant parts revealed the absence of glandular trichomes that are typical for the sequestration of sesquiterpene lactones, while numerous such glands were present on the anther appendages. It was the aim of the current study to identify the chemical constituents of these trichomes.

2. Results and discussion

HPLC analyses of extracts from glandular trichomes of anther appendages of *V. quinqueremis* plants from a population collected near Diamantina, State of Minas Gerais, Brazil, showed the presence of at least 15 peaks with UV-spectra and chromatographic behavior typical for sesquiterpene lactones. Comparison with retention times of reference compounds from our previous chemotaxonomic studies on Helianthinae (Spring and Buschmann, 1996) together with spectral data obtained by LC ^{1}H NMR and LC MS measurements led to the identification of the known heliangolides **1**–**6** (De Vivar et al., 1976; Ohno and Mabry, 1980; Delgado et al., 1982; Gao and Mabry, 1986) and **11**–**13** (Buschmann and Spring, 1995; Spring et al., 1982, 1989) (Fig. 1). Preparative HPLC was used to purify the remaining unidentified compounds for detailed spectroscopic measurements. The structures were elucidated by extensive MS and NMR studies, including ^{1}H–^{1}H COSY, HSQC and 2D-NOESY experiments. Low sample amounts prohibited the determination of the absolute configuration of the discussed compounds and the chemical formulae are given in analogy to known compounds.

^{1}H NMR and COSY spectra of compounds **7** and **8** (Table 1) were mostly similar to those of the niveusin A

* Corresponding author. Tel.: +49-711-459-3811; fax: +49-711-579-3355.
E-mail address: spring@uni-hohenheim.de (O. Spring).

0031-9422/01/$ - see front matter © 2001 Elsevier Science Ltd. All rights reserved.
PII: S0031-9422(01)00019-X

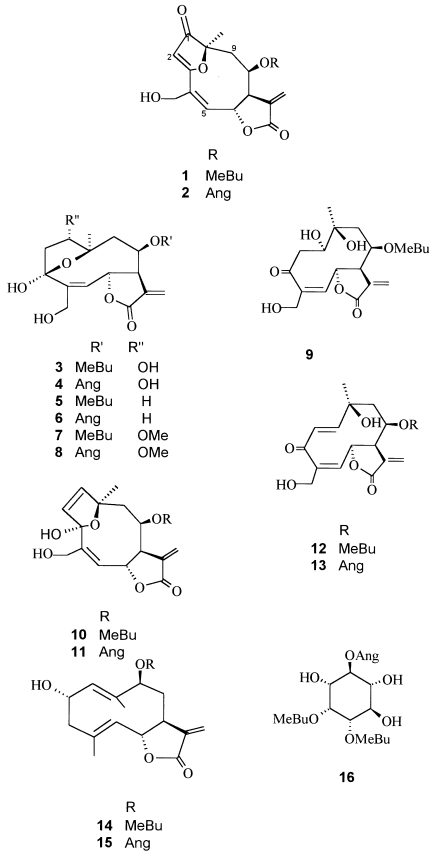

Fig. 1. Compounds isolated from *Viguiera quinqueremis*. The absolute configuration of the discussed compounds was not determined and the chemical formulae are given in analogy to known compounds.

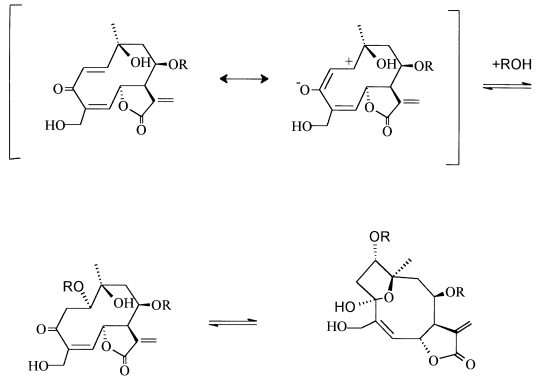

Scheme 1. Possible reaction of 1,2-unsaturated tifruticin type sesquiterpene lactones (e.g. **12**) with nucleophiles leading to 1-*O*-substitued derivatives (e.g. **9**) and to 3,10-epoxy-isomers (e.g. **3** and **7**) after spontaneous reaction from the keto alcohol to the hemiketal form.

derivatives **3** and **4**, respectively. However, the signal of the hydroxyl function at C-1 (e.g. δ 2.97 *d*, $J = 7.6$ Hz in **3**) was missing in the spectra of **7** and **8**. Instead, a signal at δ 3.42 (*s*, 3H), suggested the presence of a methoxy group at this position in both compounds. This was confirmed by APCI MS data of **7** and **8** which showed $m/z = 411$ $[M+H]^+$, indicative of $C_{21}H_{30}O_8$, and 409 $[M+H]^+$, indicative of $C_{21}H_{28}O_8$, respectively. The substitution of a hydroxyl by a methoxy group also explained the more lipophilic migration behavior of the two compounds in HPLC separations when compared with the hydroxylated derivatives **3** and **4**. This raised questions about their occurrence as natural constituents or as artifacts arising from addition of MeOH to the tifruticin precursors **12** and **13** when MeOH was used in the purification process (Scheme 1). Attempts were made to clarify this by extracting glandular trichomes and performing the subsequent HPLC separation using solvents with and without MeOH. CH_3CN extracts separated in 30% CH_3CN and in 50% MeOH, respectively, led to HPLC diagrams that clearly showed minor peaks with retention times and UV spectra typical of **7** and **8**. The same peaks in similar amounts appeared in samples extracted with MeOH. These results support the natural occurrence of the methoxy derivatives. On the other hand, current experiments (data not shown) with the tifruticins **12** and **13** purified from *Helianthus annuus* indicate that in these instances spontaneous methoxylation at C-1 occurs upon storage in MeOH over several weeks. It therefore cannot be ruled out that both ways of origin contributed to the existence of **7** and **8**.

The ^{1}H NMR and COSY spectra of compound **9** (Table 1) showed the characteristic signals of a 1,15-dihydroxy-4, 11(13)-unsaturated heliangolide with a methylbutyrate side chain. Since the protons at C-2 showed coupling with only one neighboring hydrogen (H-1), C-3 was assumed to be quaternary. A 3,10-epoxy-substitution was excluded due to the chemical shift of H-7 (δ 3.41 instead of ca. δ 4.1 as in niveusin-type compounds). This led to the assumption of a keto form at C-3, similar as in compound **12** and **13**. MS data (APCI) showed $m/z =$ 397 $[M+H]^+$ indicative of $C_{20}H_{28}O_8$, thus confirming the proposed structure of **9**. The relative stereochemistry of the substituents was deduced from 2D-NOESY experiments which showed effects between H-7/H-8, H-7/H-2b, H-6/H-9a and H15a,b/H-1. This indicated the β-orientation of the ester at C-8 and the α-position of the hydroxyl at C-1. Compound **9** therefore has to be regarded as the keto derivative of niveusin A methylbutyrate (**3**). The purification of this isomer in a stable form was unexpected to us, since similar changes in the constitution of niveusin B (**6**) and of niveusin C derivatives, previously observed during HPLC separation, led to NMR spectra (measured in $CDCl_3$) of only the hemiketal form which appears to be stabilized in aprotic solvents (Spring et al., 1991).

The ^{1}H NMR spectrum of compound **10** (Table 1) was identical with that of 1,2-anhydridoniveusin A (**11**) (Spring et al., 1989), except for the side chain signals which indicated the presence of a methylbutyrate instead of an angelate. The β-orientation of the side chain at C-8 was deduced from the NOE between H-7 and H-8. MS data (APCI) showed $m/z = 379$ $[M+H]^+$ indicative of $C_{20}H_{26}O_7$, thus confirming the suggested structure. The

Table 1
^{1}H NMR spectral data of compounds **7**–**10**, **14** and **15** from *Viguiera quinqueremis* (300 MHz, $CDCl_3$, δ $CDCl_3$ = 7.27 ppm)[a]

H	7	8	9	10	14	15
1	4.07 *dd* (6.7, 10.4)	4.05 *m*	4.52 *m*	5.79 *d* (5.6)	5.03 *m*	5.03 *m*
2a	2.62 *dd* (6.7, 14)	2.62 *dd*	2.02 *m*	6.35 *d* (5.6)	4.81 *dt* (6, 9.7)	4.78 *dt* (5.8, 10.2)
2b	2.08 *dd* (10.4, 14)	2.07 *dd*	1.78 *m*			
3a					2.79 *dd* (6, 11)	2.76 *dd* (5.8, 11)
3b					2.35 *dd* (9.7, 11)	2.14 *dd* (10.2, 11)
5	5.89 *t* (4.8)	5.93 *bt* (3.9)	5.72 *d* (9.4)	5.88 *bd* (6.7)	5.00 *bd* (9.5)	5.08 *bd* (9.5)
6	5.46 *bd* (4.8)	5.49 *bt* (3.9)	6.04 *dd* (3.2, 9.4)	5.95 *ddd* (1.0,3.2,6.7)	5.11 *t* (9.5)	5.11 *t* (9.5)
7	4.13 *bs*	4.16 *bs*	3.40 *bs*	3.51 *dddd* (1.0,2.1,2.3,3.2)	2.98 *m*	2.97 *m*
8a	5.60 *m*	5.62 *m*	5.43 *ddd* (3.7, 5.2, 10)	5.12 *ddd* (1.0,3.2, 4)	2.83 *ddd* (2, 5.2, 14)	2.90 *ddd* (2, 5.2, 14.1)
8b					2.40 *m* (1.5, 14)	2.38 *m* (1.6, 14.1)
9a	2.18 *dd* (10.2, 15)	[b]	2.52 *dd* (10, 15.1)	2.41 *dd* (4, 15)	5.82 *m*	5.82 *m*
9b	1.75 *dd* (5.2, 15)	[b]	1.91 *dd* (5.2, 15.1)	2.30 *dd* (3.2, 15)		
13a	6.27 *d* (2.1)	6.31 *d* (2.1)	6.35 *d* (2.1)	6.32 *d* (2.3)	6.38 *d* (3.5)	6.34 *d* (3.4)
13b	5.63 *d* (1.8)	5.67 *d* (1.8)	5.80 *d* (1.8)	5.72 *d* (2.1)	5.64 *d* (3)	5.63 *d* (3)
14	1.55 *s*	1.58 *s*	1.34 *s*	1.41 *s*	1.56 *bs*	1.55 *bs*
15a	4.22 *bd* (11.7)	4.25 *bd*	4.12 *m*	4.43 *bd* (12.2)	1.81 *bs*	1.83 *bs*
15b	4.12 *bd* (11.7)	4.15 *bd*	4.12 *m*	4.17 *bd* (12.2)		
2′	2.26 *m*		2.31 *m*	2.32 *m*	2.38 *m*	
3′a	1.60 *m*	6.12 *qq* (1.5, 7.3)	1.63 *m*	1.61 *m*	1.65 *m*	6.14 *qq* (1.5, 7.3)
3′b	1.44 *m*		1.45 *m*	1.45 *m*	1.50 *m*	
4′	0.86 *dd* (7)	1.98 *dq* (1.5, 7.3)	0.90 *dd* (7)	0.86 *dd* (7)	0.92 *dd* (7)	1.99 *dq* (1.5, 7.3)
5′	1.04 *d* (7)	1.79 *dq* (1.5)	1.09 *d* (7)	1.10 *d* (7)[†]	1.15 *d* (7)	1.84 *dq* (1.5)
OMe	3.42 *s*	3.45 *s*				

[a] Calculated coupling constants (*J* [Hz]) for stereochemical considerations: comp. **7**, **8**: 1α-OMe→1,2a = 7; 1,2b = 10; 1β-OMe→1,2a = 2; 1,2b = 4; comp. **10**: 5,6 = 4.5; 6,7 = 3; 7,8 = 2.3; 8,9a = 4; 8,9b = 5; comp. **14**, **15**: 2β-OH→2,3a = 2.7; 2,3b = 3.8; 2α-OH→2,3a = 4.6; 2,3b = 11.5.
[b] Signal obscured.

signal of H-7 (δ 3.51 *m*) was upfield by ca. 0.5 ppm compared with the niveusin-type compounds **3**–**8**. According to the lowest conformation found by searching the conformational space with the GMMX option of PCMODEL, this is most likely due to inverse shift effects of the 3, 10-epoxy group and the 1,2-double bond with respect to H-7. These force field calculations (see Experimental) also support the ß-orientation of the side chain when comparing theoretical coupling constants with those experimentally determined (Table 1).

Coupling constants for H-7/13 (*J* = 3 and 3.5 Hz) of **14** (Table 1) indicated the presence of a 1(10), 4-*E*,*E*-germacradienolide. COSY experiments revealed the sequence of H-7 to H-9 and H-7 to H-5. The methylbutyrate side chain had to be attached to H-9 due to its chemical shift. H-1 (δ 5.03) was coupled to the H-14 methyl (δ 1.56 *bs*) and to a complex signal at δ 4.81 (*ddd*) which was consistent with the presence of a hydroxyl group at H-2. The suggested structure was confirmed by MS data (APCI) which showed $m/z = 349$ $[M+H]^+$ indicative of $C_{20}H_{28}O_5$. The relative stereochemistry at C-9 and C-2 was deduced from an NOE between H-7 and H-9 which indicated ß-orientation of the ester at C-9. On the other hand, NOEs between H-2 and both methyl groups (H-14 and H-15), and the absence of NOEs between H-2, H-7 and H-9 indicated that the C-2 hydroxyl was α-oriented. This was substantiated by force field calculations in the following manner: For either orientation (α or β hydroxyl) four principal conformational options exist with respect to the orientation of the methyl groups at C-4 and C-10 (Scheme 2). However, only the two conformations are likely to explain the observed NOEs of H-2, where both methyl groups are oriented opposite to the hydroxyl (Scheme 2: conformation A for α-hydroxyl and conformation D for β-hydroxyl). Considering the energetic

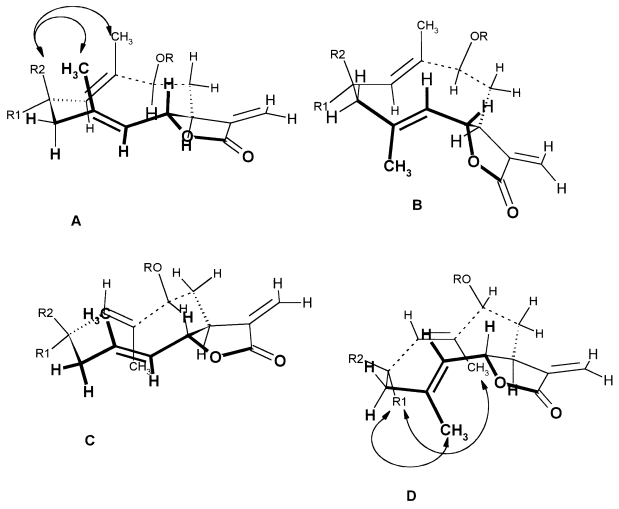

Scheme 2. Possible conformations of **14** with respect to the orientation of C-2 hydroxyl and the methyl groups at C-4 and C-10. 2α–OH: R1 = OH, R2 = H, R = methylbutyrate; 2β-OH: R1 = H, R2 = OH, R = methylbutyrate.

status (see Experimental) of the 8β-O-methylbutyrate derivative, the assumption of a 2β-hydroxyl leads to an equilibrium between all four previously described conformations (A–D). This would cause more NOEs than observed. On the other hand, for the 2α-hydroxyl, only one (A) out of these conformations has to be considered which fully explains the measured NOEs. Finally, the theoretically derived coupling constants of the 2α-hydroxyl form are in best agreement with those experimentally determined (see Table 1).

The ^{1}H NMR spectrum of **15** (Table 1) was identical with that of **14** in all parts, except for the side chain which showed the typical signals of an angelate. The proposed structure was confirmed by MS data (APCI) which showed $m/z = 347$ $[M+H]^+$ (consistent for $C_{20}H_{26}O_5$). HSQC spectra of compound **9**, **10** and **14** allowed the assignment of the proton bearing carbon signals (Table 2).

Compound **16** was isolated from the less polar fractions. The ^{1}H NMR data (Table 3) showed the presence of three side chains, one angelate and two methylbutyrates, but no signals typical of a sesquiterpene lactone skeleton. Instead, six protons with signals between δ 3.65 and 5.61 indicated the pattern of an inositol. The positions of the side chains were deduced from HMBC in combination with COSY spectra. The carbonyl carbon of the angelate residue showed coupling to a triplet at δ 5.18 (H-6) which was further coupled to the signals at δ 3.65 *t* (H-5) and δ 3.91 *dd* (H-1). The sequence of the remaining protons followed from COSY experiments and HMBC measurements indicated the connection of the two methylbutyrate residues through coupling with the protons at δ 5.61 *t* (H-2) and δ 4.88 *dd* (H-3), respectively. The relative stereochemistry of the substituents was deduced from coupling constants and supported by force field calculations (Table 3) leading to the suggested structure which was finally confirmed by MS data (APCI) which showed $m/z = 431$ $[M+H]^+$ indicative of $C_{21}H_{34}O_9$.

Table 2
Carbon data (HSQC NMR) of compounds **9, 10** and **14** from *Viguiera quinqueremis* [500 MHz, $CDCl_3$, δ $CDCl_3 = 7.27$ ppm (^{1}H)/77.0 ppm (^{13}C)]

C	**9**	**10**	**14**
1	72.2	126.8	133.6
2	35.4	139.8	69.2
3	n.o.[a]	n.o.	48.4
4	n.o	n.o.	n.o.
5	128.1	134.7	129.1
6	73.7	73.5	74.9
7	46.0	47.7	52.8
8	73.2	76.4	44.0
9	38.8	43.8	70.6
10	n.o.	n.o	n.o.
11	n.o.	n.o	n.o.
12	n.o.	n.o	n.o.
13	123.1	124.6	121.0
14	31.8	31.2	20.1
15	67.3	66.5	18.4
1′	n.o.	n.o.	n.o.
2′	41.3	41.2	41.2
3′	26.3	26.2	26.1
4′	11.5	11.5	11.4
5′	16.4	16.4	16.8

[a] n.o., signals not observed due to HSQC; sample amounts were insufficient for HMBC.

2.1. Chemotaxonomic aspects

Comparison of the sesquiterpene lactone pattern of *V. quinqueremis* with that of other members of its section revealed similarity in the overall dominance of heliangolides. However, the 1-keto-2,4-unsaturated budlein derivatives which were the exclusive constituents of *V. oblongifolia* (Bohlmann et al., 1984) and *V. robusta* (Da Costa et al., 1996) are only present to a minor extent in *V. quinqueremis*. The lack of sesquiterpene lactones reported from *V. nervosa* (Tamayo-Castillo et al., 1990) is most likely due to the low amount of glandular trichomes present in plant samples which were dominated by vegetative plant parts. Reexamination of the flowering parts of this species appears to be necessary. The isolation of a myoinisitol from glandular trichomes of *V. quinqueremis* is so far a unique feature of this taxon within the whole

Table 3
^{1}H NMR (500 MHz, $CDCl_3$) and ^{13}C NMR (75 MHz, $CDCl_3$) data of compound **16** from *Viguiera quinqueremis*[a]

Position	δ_C (carbon signal)	δ_H (proton signal)
1	69.5	3.91 *dd* (3, 10)
2	70.6	5.61 *t* (3)
3	70.7	4.88 *dd* (3, 10)
4	71.7	3.98 *t* (10)
5	73.0	3.65 *t* (10)
6	74.8	5.18 *t* (10)
OAng		
1′	169.2	
2′	127.1	
3′	140.3	6.18 *qq* (1.5, 7)
4′	20.5	2.02 *dq* (1.5, 7)
5′	16.0	1.93 *bs*
OMebut		
1″	175.7	
2″	41.2	2.49 *tq* (7, 7, 7)
3″	26.4	1.73 *ddq* (7, 7, 14)
		1.54 *ddq*
4″	11.4	0.97 *t* (7)
5″	16.4	1.22 *d* (7)
OMebut		
1‴	176.0	
2‴	41.0	2.37 *tq*
3‴	26.7	1.67 *ddq*
		1.45 *ddq*
4‴	11.5	0.90 *t*
5‴	16.9	1.14 *d*

[a] Calculated coupling constants (J [Hz]) for stereochemical considerations: **16**: 1,2 = 3.4; 2,3 = 3.1; 3,4 = 9.2; 4,5 = 9.6; 5,6 = 8.9; 1,6 = 9.6.

genus. Within the Heliantheae, inositols have only been reported from *Hymenoxys texana* and *H. biennis* (Gao et al., 1990a,b; Spring et al.; 1994).

3. Experimental

3.1. Extraction of plant material

V. quinqueremis Blake was collected near Diamantina, along km 473–475 on BR-259 highway (S 18°25′, W 43°43′, altitude 1370 m), State of Minas Gerais, Brazil, in April 1998 by F.B. Da Costa and determined by J.N. Nakajima and E.E. Schilling (voucher specimens are deposited at the herbarium SPFR, Ribeirão Preto, SP under the collection number FBC No. 64). For HPLC (Hypersil ODS, 5 mμm; 4×250 mm; 30% MeCN, 1.3 ml/min or 50% MeOH, 1 ml/min; UV detection simultaneously at 225 and 265 nm or with diode array detection; dimethylphenol as int. standard). For screening of compounds and for solvent experiments with respect to the natural occurrence of compound **7** and **8**, glandular trichomes were collected mechanically from the anther appendages as previously described (Spring, 1991).

For isolation of compounds, air-dried flower heads (84 g) were extracted with CH_2Cl_2. The solvent was evaporated, the residue was redissolved in MeOH, diluted with water (1:1 v/v) and centrifuged in order to remove insoluble parts. The clear supernatant was applied to HPLC (conditions as given above) and compounds were separated in a gradient of aqueous MeOH (40–60% in 20 min, 1 ml/min). When necessary, 30% MeCN (1.3/per min) was used for repurification of fractions on the same type of column. Prior to preparative separation of specific compounds, an aliquot of the crude extract (equivalent to ca. 2 g plant material) was used for LC ^{1}H NMR and LC MS analysis which were carried out under identical HPLC conditions (MeOH gradient) in order to allow direct correlation of the obtained data. LC ^{1}H NMR spectra were measured on a Varian Unity *Inova*; 500 MHz, detector type 9050 equipped with a NMR flow cell of 60 μl detectable volume. Routine NMR experiments were carried out on 300 MHz Varian Unity *Inova*. LC MS experiments were performed on a Finnigan TSQ 700 under atmosphere pressure chemical ionization (APCI), positive mode. Calculations were done with PCMODEL, Ver. 7, Serena Software, Bloomington using the MMX force field. Conformational search was done with the GMMX option. Conformations are considered within a 3 Kcal limit from the lowest energy. Coupling constants are derived from the Altona equations which are implemented in the program. They are averaged over the Boltzmann distribution of their corresponding conformer.

HPLC retention times of compounds from *V. quinqueremis* in 50% MeOH (RRT_1) and in 30% MeCN (RRT_2) relative to dimethylphenol (retention time ca. 13 min in both solvents): **1**, 0.56/0.59; **2**, 0.53/0.56; **3**, 0.62/0.46; **4**, 0.57/0.42; **5**, 1.17/0.82; **6**, 1.12/0.79; **7**, 1.37/0.95; **8**, 1.25/0.90; **9**, 0.46/0.31; **10**, 0.60/0.54; **11**, 0.59/0.53; **12**, 0.72/0.60; **13**, 0.68/0.51; **14**, 1.96/1.63; **15**, 1.86/1.60; **16**, 1.60/1.48 (RRT_1/RRT_2).

3.1.1. 1α-Methoxy-3α,15-dihydroxy-3,10-epoxy-8β-O-methylbutanoyl-4,11(13)-germacradien, 6α,12-olide (7)

$C_{21}H_{30}O_8$, APCI +; grad. 40–60% MeOH in 20 min: 411 $[M+H]^+$, 379 $[411-MeOH]^+$, 361 $[379-H_2O]^+$, 259 [361−methylbutyrate]$^+$, 85 $[C_5H_9O]^+$.

3.1.2. 1α-Methoxy-3α,15-dihydroxy-3,10-epoxy-8β-O-angeloyl-4,11(13)-germacradien, 6α,12-olide (**8**)

$C_{21}H_{28}O_8$, APCI +; grad. 40–60% MeOH in 20 min: 409 $[M+H]^+$, 377 $[411-MeOH]^+$, 359 $[377-H_2O]^+$, 259 [359−angelate]$^+$, 83 $[C_5H_7O]^+$.

3.1.3. 1α, 10β,15-Trihydroxy-3-oxo-8β-O-methylbutanoyl-4,11(13)-germacradien, 6α,12-olide (**9**)

$C_{20}H_{28}O_8$, APCI +; grad. 40–60% MeOH in 20 min: 397 $[M+H]^+$, 379 $[M+H-H_2O]^+$, 277 [379−methylbutyrate]$^+$.

3.1.4. 3α,15-Dihydroxy-3,10-epoxy-8β-O-methylbutanoyl-1,4,11(13)-germacratrien, 6α,12-olide (**10**)

$C_{20}H_{26}O_7$, APCI +; grad. 40–60% MeOH in 20 min: 379 $[M+H]^+$, 361 $[M+H-H_2O]^+$, 259 [361−methylbutyrate]$^+$, 85 $[C_5H_9O]^+$.

3.1.5. 2α-Hydroxy-9β-O-methylbutanoyl-1(10),4,11(13)-germacratrien, 6α,12-olide (**14**)

$C_{20}H_{28}O_5$, APCI +; grad. 40–60% MeOH in 20 min: 349 $[M+H]^+$, 247 [M + H−methylbutyrate]$^+$, 229 $[247-H_2O]^+$, 85 $[C_5H_9O]^+$. Force field calculations: 2α–OH: lowest energy calculated: 41.6 Kcal/mol; 23 conformations including side chain conformations within 3 Kcal/mol. 2β-OH: 44.53 Kcal/mol, 76 conformations including side chain conformations within 3 Kcal/mol.

3.1.6. 2α-Hydroxy-9β-O-angeloyl-1(10),4,11(13)-germacratrien, 6α,12-olide (**15**)

$C_{20}H_{26}O_5$, APCI +; grad. 40–60% MeOH in 20 min: 347 $[M+H]^+$, 247 [M + H−angelate]$^+$, 229 $[247-H_2O]^+$, 83 $[C_5H_7O]^+$.

3.1.7. 6-Angeloyl-2,3-dimethylbutanoyl-myoinositol (**16**)

$C_{21}H_{34}O_9$, APCI +; grad. 40–60% MeOH in 20 min: 431 $[M+H]^+$, 413 $[431-H_2O]^+$, 331 [431−angelate]$^+$, 85 $[C_5H_9O]^+$, 83 $[C_5H_7O]^+$.

Acknowledgements

We wish to thank Dr. J.N. Nakajima, Universidade Federal de Uberlândia, Brazil, and Dr. E.E. Schilling,

University of Tennessee, Knoxville, USA, for determination of plant material and I. Klaiber, University of Hohenheim for MS-measurements. This work was partly supported by a grant of FAPESP for F.B. da Costa (process number 97/05729-4).

References

Blake, S.F., 1918. A revision of the genus *Viguiera*. Contr. Gray Herb. 54, 1–205.

Bohlmann, F., Gerke, T., Jakupovic, J., King, R.M., Robinson, H., 1984. Cadina-4,11-diene from *Viguiera oblongifolia*. Phytochemistry 23, 1183–1184.

Buschmann, H., Spring, O., 1995. Sesquiterpene lactones as a result of interspecific hybridization in *Helianthus* species. Phytochemistry 39, 367–371.

Da Costa, F.B., Vichnewski, W., Herz, W., 1996. Constituents of *Viguiera aspillioides* and *V. robusta*. Biochem. Syst. Ecol. 24, 585–587.

Delgado, G., de Vivar, A.R., Herz, W., 1982. Sesquiterpene lactones from *Viguiera* species. Phytochemistry 21, 1305–1308.

De Vivar, A.R., Guerrero, C., Diaz, E., Bratoeff, E.A., Jiminez, L., 1976. The germacranolides of *Viguiera buddleiaeformis*. Structures of budlein-A and -B. Phytochemistry 15, 525–527.

Gao, F., Mabry, T.J., 1986. Sesquiterpene lactones from *Viguiera deltoidea*. Phytochemistry 25, 137–140.

Gao, F., Wang, H., Mabry, T.J., 1990. Inositol derivatives and pseudoguaianolides from *Hymenoxys texana*. Phytochemistry 29, 2273–2276.

Gao, F., Wang, H., Mabry, T.J., 1990. Sesquiterpene lactone aglycones and glycosides and inositol derivatives from *Hymenoxys biennis*. Phytochemistry 29, 3875–3880.

Ohno, N., Mabry, T.J., 1980. Sesquiterpene lactones and diterpene carboxylic acids in *Helianthus niveus* subspecies *nieveus*. Phytochemistry 19, 609–614.

Spring, O., 1991. Trichome microsampling of sesquiterpene lactones for the use of systematic studies. In: Fischer, N.H., Isman, M.B., Stafford, A.H. (Eds.), Modern Phytochemical Methods. Plenum Press, New York, pp. 319–345.

Spring, O., Buschmann, H., 1996. A chemotaxonomic survey of sesquiterpene lactones in the Helianthinae. In: Hind, D.J.N., Beentje, H.J. (Eds.), Compositae: Systematics. Proc. Intern. Compositae Conf., Vol. 1, Kew 1994, pp. 307–316.

Spring, O., Albert, K., Hager, A., 1982. Three biologically active heliangolides from *Helianthus annuus*. Phytochemistry 21, 2551–2553.

Spring, O., Benz, T., Ilg, M., 1989. Sesquiterpene lactones of the capitate glandular trichomes of *Helianthus annuus*. Phytochemistry 28, 745–749.

Spring, O., Vargas, D., Fischer, N.H., 1991. Sesquiterpene lactones and benzofurans in glandular trichomes of three *Pappobolus* species. Phytochemistry 30, 1861–1867.

Spring, O., Zitterell-Haid, B., Bierner, M.W., Mabry, T.J., 1994. Chemistry of glandular Trichomes in *Hymenoxys* and related genera. Biochem. Sys. Ecol. 22, 171–195.

Tamayo-Castillo, Jakupovic, J., Bohlmann, F., King, R.M., Boldt, P.E., 1990. Germacranolides and diterpenes from *Viguiera* species. Rev. Latinoamer. Quim. 21/2, 67–69.

PERGAMON

Phytochemistry 57 (2001) 273–278

PHYTOCHEMISTRY

www.elsevier.com/locate/phytochem

Benzopyran derivatives from *Mallotus apelta*

Tian-Ying An, Li-Hong Hu *, Xiao-Fang Cheng, Zhong-Liang Chen

National Center for Drug Screening, Shanghai Institute of Materia Medica, Shanghai Institutes for Biological Sciences, Chinese Academy of Sciences, Shanghai, 200031, People's Republic of China

Received 17 July 2000; received in revised form 20 November 2000

Abstract

From the leaves of *Mallotus apelta*, seven benzopyran compounds were obtained and their structures were determined using spectroscopic methods. One showed moderate antibiotic activity against *Micrococcus lutens*. © 2001 Elsevier Science Ltd. All rights reserved.

Keywords: *Mallotus apelta*; Euphorbiaceae; Benzopyran; *Micrococcus lutens*

1. Introduction

Mallotus apelta Muell. Arg. (Euphorbiaceae), widely distributed plant in the south of China, is used in Chinese medicine for the treatment of chronic hepatitis (Jiangsu New Medical College, 1977). Some antibiotic triterpenoids and steroids have been reported to be isolated from its root (Shan and Feng, 1985). Our previous study on the root of this plant has shown the presence of five new diterpenoids (Cheng and Chen, 1999; Cheng et al., 1999) and one new alkaloid (Cheng et al., 1998), and further investigation of its leaves has resulted in the isolation of seven new benzopyran derivatives **1**–**7**. Compound **1** showed moderate inhibitory activity against *Micrococcus lutens*.

2. Results and discussion

Compound **1**, obtained as a yellow oil, showed an $[M]^+$ at *m*/*z* 3412.2609 in the HREIMS, which corresponded to $C_{22}H_{30}O_4$ (*calc*. 412.2614). The IR spectrum suggested the presence of an hydroxyl group (3434 cm^{-1}) and conjugated carbonyl groups (1716, 1602 cm^{-1}). The ^1H NMR and ^{13}C NMR spectral data (Table 1) revealed **1** had the same 4-hydroxy-2H-1-benzopyran-5,7(3H,6H)-dione skeleton as hariganetin, which was previously isolated from the fronds of *Wagneriopteris japonica* Loeve et Loeve (Wada et al., 1988). The ^1H NMR, ^{13}C NMR, ^1H–^1H COSY and HMQC spectra further revealed the presence of a chelated hydroxyl group (δ 15.99, *s*, OH-4), two methyls (δ 1.45, *d*, $J = 6.3$ Hz, H_3-11; δ 1.37, *s*, H_3-22), an isoprenyl side chain (δ 3.11, *m*, H_2-23; δ 5.08, *m*, H-24; δ 1.64, *s*, H_3-26 and δ 1.72, *s*, H_3-27) and a geranyl side chain (δ 2.64, *m*, H_2-12; δ 4.83, *m*, H-13; δ 1.84, *m*, H_2-15; δ 1.91, *m*, H_2-16; δ 5.00, *m*, H-17; δ 1.64, *s*, H_3-19; δ 1.56, *s*, H_3-20 and δ 1.53, *s*, H_3-21).

HMBC correlations (Fig. 1) between the methylene protons at δ 2.64 (H_2-12) and two carbonyl carbons at δ 201.2 (C-5) and δ 196.9 (C-7) and a quaternary carbon at δ 56.3 (C-6) established the geranyl side chain was at C-6. The observed HMBC crosspeaks between the methylene protons at δ 3.11 (H_2-23) and two olefinic carbons at δ 112.4 (C-8), δ 161.6 (C-9) and C-7 allowed the assignment of isoprenyl group at C-8. Correlations between the doublet methyl protons at δ 1.45 (H_3-11) and the oxygenated methine carbon at δ 71.4 (C-2) and the methylene carbon at δ 38.0 (C-3); the methyl protons at δ 1.37 (H_3-22) and C-5, C-6, and C-7, showed that the two methyl groups were connected with C-2 and C-6, respectively. The axial orientation of H-2 was deduced from its *J* coupling constant values with H_2-3 ($J_{2,3} = 4.3$, 9.6 Hz) (Lambert et al., 1987). The stereochemistry of the substitutents at C-6 and C-2 were not assigned. So compound **1** was determined to be 4-hydroxy-2,6-dimethyl-6-(3,7-dimethyl-2,6-octadienyl)-8-(3-methyl-2-butenyl)-2H-1-benzopyran-5,7(3H,6H)-

* Corresponding author. Tel.: +86-21-64311833, ext. 332; fax: +86-21-64370269.

E-mail address: simmhulh@mail.shcnc.ac.cn (L. Hu).

0031-9422/01/$ - see front matter © 2001 Elsevier Science Ltd. All rights reserved.
PII: S0031-9422(00)00512-4

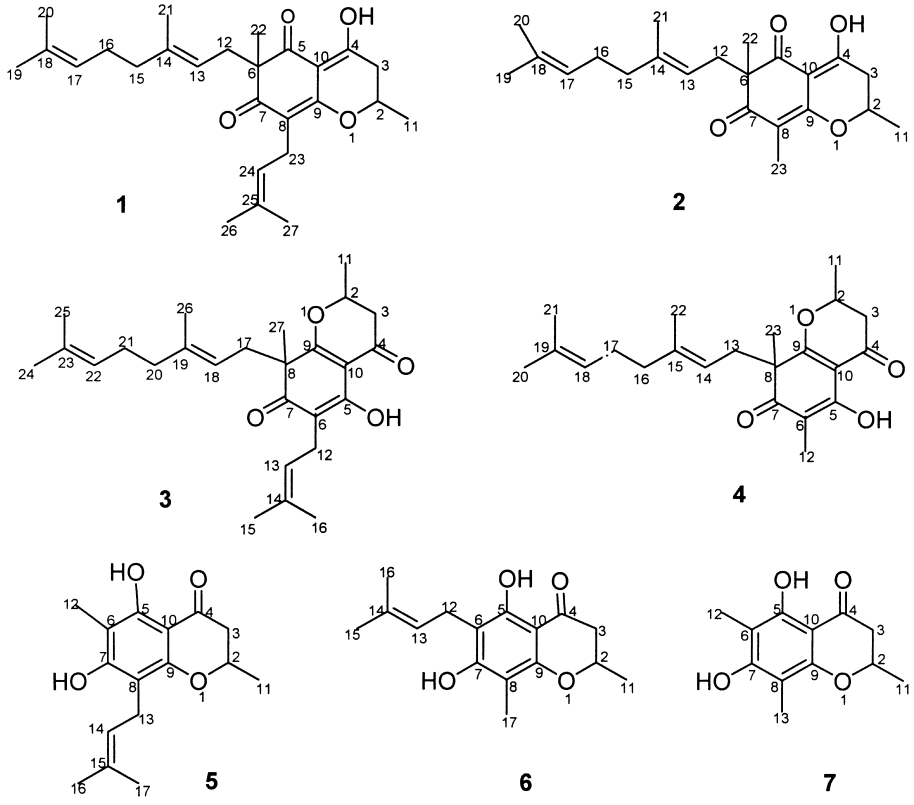

Table 1
^{1}H NMR($CDCl_3$, 400 Hz) and ^{13}C NMR ($CDCl_3$, 100 Hz) spectral data for compounds **1** and **2**

Position	Compound **1**			Compound **2**	
	δ_H	δ_C	HMBC[a]	δ_H	δ_C
2	4.37 *m*	71.4		4.37 *m*	71.2
3	2.66 *dd* (17.8, 4.3) 2.60 *dd* (17.8, 9.6)	38.0	4, 10, 11	2.63 *dd* (17.6, 4.0) 2.60 *dd* (17.6, 9.4)	38.1
4		183.5			183.4
5		201.2			201.1
6		56.3			56.3
7		196.9			197.5
8		112.4			108.1
9		161.6			161.6
10		102.6			102.4
11	1.45 *d* (6.3)	20.7	2, 3	1.47 *d* (6.6)	20.8
12	2.64 *m*	39.1	5, 6, 7, 13, 14, 22	2.62 *m*	38.5
13	4.83 *m*	118.0	6, 15, 21	4.73 *m*	118.1
14		138.7			138.7
15	1.84 *m*	39.8	13, 14, 17,21	1.83 *m*	39.7
16	1.91 *m*	26.8	14, 17, 18	1.88 *m*	26.7
17	5.00 *m*	124.1	15, 19, 20.	4.95 *m*	123.9
18		131.2			131.3
19	1.64 *s*	25.7	17, 20	1.61 *s*	25.6
20	1.56 *s*	17.6	17, 19	1.53 *s*	17.6
21	1.53 *s*	16.1	13, 15	1.51 *s*	16.1
22	1.37 *s*	23.1	5, 6, 7, 12	1.35 *s*	23.5
23	3.11 *m*	21.6	7, 8, 9, 24, 25	1.78 *s*	7.6
24	5.08 *m*	122.4	26, 27		
25		131.0			
26	1.64 *s*	25.6	24, 25, 27		
27	1.72 *s*	17.7	24, 25, 26		
4-OH	15.99 *s*			15.96 *s*	

[a] Carbons that correlate with the proton resonance.

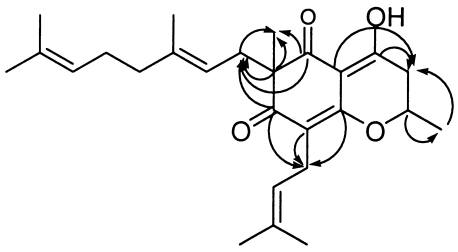

Fig. 1. Important HMBC interactions in compound **1**.

dione. These compounds which have the structure of β-hydroxyl carbonyl showed a pair of signals of two tautomers in acetone-d_6 in their ^{1}H NMR spectra (Anthonsen et al., 1971), while they only showed one tautomer signal in $CDCl_3$ (Wada et al., 1988).

Compound **2**, a yellow oil, has the molecular formula $C_{22}H_{30}O_4$, which was established by HREIMS (found. 358.2145; calc. 358.2144). Its UV and IR spectra were very similar to those of **1**. A comparison of the ^{1}H NMR and ^{13}C NMR spectra of **2** with those of **1** revealed that the only difference was that the isoprenyl side chain at C-8 in **1** was replaced by a methyl in **2**. Therefore, the structure of **2** was determined to be 4-hydroxy-2,6,8-trimethyl-6-(3,7-dimethyl-2,6-octadienyl)-2H-1-benzopyran-5,7(3H,6H)-dione, which was confirmed by analysis of its 2 D NMR spectra.

Compound **3**, *m*/*z* 412.2598, $C_{26}H_{36}O_4$, was obtained as a yellow oil. Its UV and IR spectra indicated it was also a benzopyran derivative. The NMR spectra data (Table 2) revealed that it had the same side chains as those in **1**, namely, a geranyl, an isoprenyl group and two methyls. The structure of **3** was determined by tracing the connectivities shown in the HMBC spectrum. Crosspeaks (Fig. 2) were observed between the methylene protons at δ 3.04 (H_2-12) and the oxygenated olefinic carbon at δ 164.7 (C-5), the quaternary olefinic carbon at δ 110.6 (C-6) and the carbonyl carbon at δ 195.6 (C-7). The chelated hydroxyl proton at δ 11.68 (5-OH) was correlated with C-10 (δ 104.4), C-9 (δ 186.3), C-6 and C-5. Moreover, the methyl at δ 1.40 (H_3-27) was correlated with C-7 and C-9; the methylene protons at δ 2.65 (H_2-17) were correlated with C-9 and the quarternary carbon at δ 53.0 (C-8). Thus, compound **3** was determined to be 5-hydroxy-2,8-dimethyl-6-(3-methyl-2-butenyl)-8-(3,7-dimethyl-2,6-octadienyl)-2H-1-benzopyran-4,7(3H, 8H)-dione.

Table 2
^{1}H NMR ($CDCl_3$, 400 Hz) and ^{13}C NMR ($CDCl_3$, 100 Hz) spectral data for compounds **3** and **4**

Position	Compound **3**			Compound **4**	
	δ_H	δ_C	HMBC[a]	δ_H	δ_C
2	4.58 *m*	76.5	4, 11	4.53 *m*	76.3
3	2.66 *dd* (17.2, 12.7) 2.60 *dd* (17.2, 4.3)	41.9	2, 4, 11	2.65 *dd* (17.3, 12.7) 2.60 *dd* (17.3, 4.0)	41.8
4		194.6			194.5
5		164.7			164.7
6		110.6			106.4
7		195.6			196.1
8		53.0			52.9
9		186.3			186.2
10		104.4			104.3
11	1.56 *d* (6.3)	20.1	3, 4	1.52 *d* (6.8)	20.1
12	3.04 *m*	20.6	5, 6, 7, 13 14	1.75 *s*	6.5
13	5.10 *m*	122.4	6, 15, 16	2.68 *m*	38.6
14		131.2		4.72 *m*	118.3
15	1.64 *s*	25.6	13, 14, 16		138.1
16	1.73 *s*	17.7	13, 14, 15	1.85 *m*	39.5
17	2.65 *m*	39.0	8, 9, 18, 19	1.93 *m*	26.5
18	4.78 *m*	118.2	8, 20, 26	4.92 *m*	123.7
19		138.2			131.5
20	1.87 *m*	39.6	19, 22, 26	1.60 *s*	25.6
21	1.95 *m*	26.5	19, 20, 23	1.55 *s*	17.6
22	4.98 *m*	123.9	20, 24, 25	1.52 *s*	16.1
23		131.5		1.37 *s*	24.5
24	1.64 *s*	25.7	22, 25		
25	1.55 *s*	17.6	22, 24		
26	1.58 *s*	16.1	19, 20		
27	1.40 *s*	24.3	7, 9, 17		
5-OH	11.68 *s*		5, 6, 9, 10	11.69 *s*	

[a] Carbons that correlate with the proton resonance.

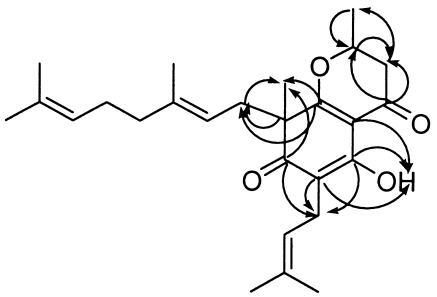

Fig. 2. Important HMBC interactions in compound **3**.

The HREIMS of **4** gave a m/z at 358.2151 for $[M]^+$, which was consistent with the molecular formula $C_{22}H_{30}O_4$. The UV, ^1H NMR and ^{13}C NMR spectra (Table 2) were very similar to those of **3**. A comparison of the ^1H NMR and ^{13}C NMR of **4** with those of **3** revealed that the isoprenyl side chain at C-6 in **3** was replaced by a methyl in **4**. So the structure of **4** was determined to be 5-hydroxy-2,8,6-trimethyl-8-(3,7-dimethyl-2,6-octadienyl)-2H-1-benzopyran-4,7(3H,8H)-dione.

Compound **5** was isolated as optically active pale yellow needles, $[\alpha]_D^{25}$ −92.8° (c 0.13, $CHCl_3$), mp 122–124°C, whose molecular formula $C_{16}H_{20}O_4$ was established from analysis of the HREIMS. The IR spectrum suggested the presence of hydroxyl groups (3240 cm^{-1}) and a conjugated carbonyl group (1635 cm^{-1}) and the UV spectrum gave λ_{max} at 244, 294, 350 nm. Its ^1H NMR and ^{13}C NMR spectra were closely similar to lespedezaflavanone G, isolated from *Lespedeza formosa* (Li et al., 1992), except that the 4-methoxyl-3-(3-methyl-2-butenyl) phenyl at C-2 was replaced by a methyl in compound **5**. So compound **5** was determined to be 2,3-dihydro-5,7-dihydroxy-2,6-dimethyl-8-(3-methyl-2-butenyl)-4H-1-benzopyran-4-one, which was confirmed by its HMBC spectrum.

Compound **6** was isolated as optically active pale yellow needles. Its HREIMS indicated a molecular formula of $C_{16}H_{20}O_4$ (m/z 276.1427). Comparison of the NMR spectral data of **6** with those of **5** revealed that they had the same skeleton and side chains. HMBC showed correlations between the methylene protons at δ 3.35 (H_2-12) and the carbons at δ 159.6 (C-5), δ 105.6 (C-6) and δ 161.9 (C-7); and the correlations between the methyl protons at δ 1.98 (H_3-17) and C-7, C-8 (δ 102.8) and C-9 (δ 158.3). So the isoprenyl group at C-6 and the methyl at C-8 were established. Therefore **6** was established to be 2,3-dihydro-5,7-dihydroxy-2,8-dimethyl-6-(3-methyl-2-butenyl)-4H-1-benzopyran-4-one.

The molecular formula of $C_{12}H_{14}O_4$ for **7** was established from its HREIMS. Its ^1H NMR and ^{13}C NMR spectra were closely similar to compound **5** except that the 3-methyl-2-butenyl side chain at C-8 was replaced by a methyl in compound **7**. So the structure of **7** was assigned to be 2,3-dihydro-5,7-dihydroxy-2,6,8-trimethyl-4H-1-benzopyran-4-one.

All compounds were tested for their antibiotic activity against *Staphylococcus aureus*, *Micrococcus lutens*, *Pseudomonas aeruginosa* and *Escherichia coli* (see Table 4). Only compound **1** showed moderate activity against *M. lutens* with a minimum inhibitory concentration (MIC) of 7.34 μg/ml. (Reference: Triclosan).

Table 3
^1H NMR ($CDCl_3$, 400 Hz) and ^{13}C NMR ($CDCl_3$, 100 Hz) spectral data for compounds **5**–**7**

Position	Compound **5**		Compound **6**		Compound **7**[a]	
	δ_H	δ_C	δ_H	δ_C	δ_H	δ_C
2	4.46 *m*	73.7	4.53 *m*	73.5	4.52 *m*	74.5
3	2.66 *dd* (17.0, 11.8)	43.3	2.65 *dd* (17.3, 12.7)	43.3	2.67 *dd* (17.0, 11.8)	43.6
	2.60 *dd* (17.0, 3.6)		2.60 *dd* (17.3, 4.0)		2.62 *dd* (17.0, 3.6)	
4		196.8		196.8		197.6
5		159.6		159.6		159.5
6		103.8		105.6		103.8
7		161.6		161.9		162.9
8		104.8		102.8		103.0
9		157.3		158.3		157.7
10		102.6		102.5		102.6
11	1.47 *d* (6.2)	20.9	1.48 *d* (6.2)	20.9	1.47 *d* (6.2)	20.9
12	2.00 *s*	6.8	3.35 *d* (7.1)	21.2	2.00 *s*	8.0
13	3.32 *d* (7.2)	21.8	5.21 *m*	121.5	2.00 *s*	7.4
14	5.19 *m*	121.7		135.8		
15		135.3	1.75 *s*	25.8		
16	1.74 *s*	25.8	1.81 *s*	17.8		
17	1.80 *s*	17.8	1.98 *s*	7.3		
5-OH	12.31 *s*		12.37 *s*		12.31 *s*	
7-OH	6.03 *s*		6.21 *s*		6.03 *s*	

[a] In actone-d_6.

Table 4
Antibacterial activities of compounds **1**–**7**

Compounds	Minimum inhibitory concentration (MIC) in broth (in μg/ml)			
	S. aureus	*M. lutens*	*P. aeruginosa*	*E. coli*
1	>25	7.34	>25	>25
2	>25	>25	>25	>25
3	>25	>25	>25	>25
4	>25	>25	>25	>25
5	>25	>25	>25	>25
6	>25	>25	>25	>25
7	>25	>25	>25	>25
Triclosan	0.10	3.12	>200	0.125

3. Experimental

3.1. General experimental procedures

The melting points were determined on a Yanaco melting point apparatus and were uncorrected. Optical rotations were recorded on a Perkin-Elmer 241 polarimeter using $CHCl_3$ as solvent. IR spectra were recorded on a Perkin-Elmer 599B spectrophotometer. UV spectra were measured on a Shimadzu UV-250 spectrophotometer. NMR spectra were recorded on a Brüker AM-400 and DRX-400 spectrophotometer. Mass spectra (EIMS and HREIMS) were taken on a MAT-711 instrument.

3.2. Plant material

The leaves of *M. apelta* were collected from Guilin, Guangxi of China, in August 1997. The plant was identified by comparing with voucher specimens, which were already deposited in the herbarium of the Guilin Institute of Medicinal Control. Guangxi, PR China (NO: 90007).

3.3. Extraction and isolation

The leaves of *M. apelta*. (2.0 kg) were extracted with petroleum ether (8 l × 3) at 20°C. Removal of the solvent under reduced pressure left an oily extract (32 g). Into this extract, 200 ml acetone was added, and, after the insoluble solid was filtered, the mother liquid was concentrated to a residue (25 g), which was subjected to Si gel chromatography, eluted with petroleum ether containing increasing amounts of EtOAc to yield 8 fractions. Fraction 2 (500 mg, eluted with petroleum ether-EtOAc, 10:1) was further purified on Si gel and eluted with petroleum ether-$CHCl_3$ (2:3) to afford two subfractions I and II. Subfraction I was then subjected to RP-18 column chromatography, eluted with Me_2CO–H_2O (3:1) to afford compound **1** (29.0 mg). Subfraction II was also subjected to RP-18 column chromatography, eluted with Me_2CO–H_2O (3:1) to afford compound **2** (21.0 mg). Fraction 4 (367 mg, eluted with petroleum ether–EtOAc, 10:1) was further purified using Si gel chromatography and eluted with petroleum ether–$CHCl_3$ (1:2) to give compounds **3** (14.0 mg) and **4** (20.0 mg). Fraction 5 (320 mg, eluted with petroleum ether–EtOAc, 5:1) was further purified on Si gel (petroleum ether-$CHCl_3$–Me_2CO, 5:1:1) to give a mixture which was finally purified on preparative TLC plates (petroleum ether-$CHCl_3$–Me_2CO, 5:1:1) to give compound **5** (6.4 mg) and **6** (5.6 mg). Fraction 6 (76 mg, eluted with petroleum ether–EtOAc, 5:1) was further purified on Sephadex LH-20 eluted with EtOH to obtained compound **7** (6.8 mg).

3.4. 4-Hydroxy-2,6-dimethyl-6-(3,7-dimethyl-2,6-octadienyl)-8-(3-methyl-2-butenyl)-2H-1-benzopyran-5,7(3H,6H)-dione (*1*)

Yellow oil; $[\alpha]_D^{25}$ −1.31° (*c* 0.57, $CHCl_3$); UV ($CHCl_3$) λ_{max} (log ε): 305 (3.92), 248 (3.64) nm; IR (film) ν_{max} : 3434, 1716, 1602, 1452 cm^{-1}; ^1H NMR and ^{13}C NMR spectral data see Table 1; EIMS *m*/*z* (rel. Int): 412 $[M]^+$ (7), 275 (94), 69 (92), 41 (100); HREIMS *m*/*z* 412.2609 (calc. for $C_{26}H_{36}O_4$, 412.2614).

3.5. 4-Hydroxy-2,6,8-trimethyl-6-(3,7-dimethyl-2,6-octadienyl)-2H-1-benzopyran-5,7(3H,6H)-dione (*2*)

Yellow oil; $[\alpha]_D^{25}$ +0.71° (*c* 0.42, $CHCl_3$); UV ($CHCl_3$) λ_{max} (log ε): 305 (3.89), 248 (3.74) nm; IR (film) ν_{max}:3419, 1728, 1606, 1454 cm^{-1}; ^1H NMR and ^{13}C NMR spectral data see Table 1; EIMS *m*/*z* (rel. Int): 358 $[M]^+$ (2), 289 (16), 222 (94), 69 (14); HREIMS *m*/*z* 358.2145 (calc. for $C_{22}H_{30}O_4$, 358.2144).

3.6. 5-Hydroxy-2,8-dimethyl-6-(3-methyl-2-butenyl)-8-(3,7-dimethyl-2,6-octadienyl)-2H-1-benzopyran-4,7(3H,8H)-dione (*3*)

Yellow oil; $[\alpha]_D^{25}$ −22.0° (*c* 0.29, $CHCl_3$); UV ($CHCl_3$) ε_{max} (log ε): 298 (3.78), 245 (3.67) nm; IR (film) ν_{max}: 3408, 1707, 1666, 1620, 1552 cm^{-1}; ^1H NMR and ^{13}C NMR spectral data see Table 2; EIMS *m*/*z* (rel. Int): 412 $[M]^+$ (1), 275 (100), 221 (21), 69 (13), HREIMS *m*/*z* 412.2598 (calc. for $C_{26}H_{36}O_4$, 412.2614).

3.7. 5-Hydroxy-2,8,6-trimethyl-8-(3,7-dimethyl-2,6-octadienyl)-2H-1-benzopyran-4,7(3H,8H)-dione (*4*)

Yellow oil; $[\alpha]_D^{25}$ −152.0° (*c* 0.59, $CHCl_3$); UV ($CHCl_3$) λ_{max} (log ε): 298(3.71), 245(3.54) nm; IR (film) ν_{max}: 3234, 1713, 1670, 1623, 1413 cm^{-1}; ^1H NMR and ^{13}C NMR spectral data see Table 2; EIMS *m*/*z* (rel. int): 358 $[M]^+$ (2), 289 (10), 222 (100), 149 (45), HREIMS *m*/*z* 358.2151 (calc. for $C_{22}H_{30}O_4$, 358.2144).

3.8. 2,3-Dihydro-5,7-dihydroxy-2,6-dimethyl-8-(3-methyl-2-butenyl)-4H-1-benzopyran-4-one (**5**)

Pale-yellow needles; mp 122–124°C; $[\alpha]_D^{25}$ −92.8° (*c* 0.13, $CHCl_3$); UV ($CHCl_3$) ε_{max} (log ε): 244 (3.21), 294 (3.90), 350 (3.09) nm; IR (KBr) ν_{max}: 3240, 1635, 1606, 1595 cm^{-1}; ^1H NMR and ^{13}C NMR spectral data see Table 3; EIMS *m*/*z* (rel. int): 276 $[M]^+$ (87), 261 (100), 221 (53), 219 (70), 208 (47),179 (38), 149 (23), 83 (38); HREIMS *m*/*z* 276.1362 (calcd. for $C_{16}H_{20}O_4$ 276.1362).

3.9. 2,3-Dihydro-5,7-dihydroxy-2,8-dimethyl-6-(3-methyl-2-butenyl)-4H-1-benzopyran-4-one (**6**)

Pale-yellow needles; mp 160–162°C; $[\alpha]_D^{25}$ −45.4° (*c* 0.11, $CHCl_3$); UV ($CHCl_3$) λ_{max} (log ε): 244 (3.44), 294 (4.10), 350 (3.39) nm; IR (KBr) ν_{max}: 3245, 1645, 1622, 1577 cm^{-1}; ^1H NMR and ^{13}C NMR spectral data see Table 3; EIMS *m*/*z* (rel. int): 276 $[M]^+$ (66), 261 (85), 221 (100), 208 (24), 179 (48),; HREIMS *m*/*z* 276.1427 (calc. for $C_{16}H_{20}O_4$ 276.1362)

3.10. 2,3-Dihydro-5,7-dihydroxy-2,6,8-trimethyl-4H-1-benzopyran-4-one (**7**)

Pale-yellow needles; mp 200–202°C $[\alpha]_D^{25}$ -44.1° (*c* 0.14, $CHCl_3$); UV ($CHCl_3$) ε_{max} (log ε): 244 (3.31), 294 (4.11), 350 (3.53) nm; IR (KBr) ν_{max}: 3340, 1631, 1606, 1591 cm^{-1}; ^1H NMR and ^{13}C NMR spectral data see Table 3; EIMS, *m*/*z* (rel. int): 222 $[M]^+$ (100), 207 (58),181 (44), 152 (80) 124 (19); HREIMS *m*/*z* 222.0888 (calc. for $C_{12}H_{14}O_4$ 222.0892)

3.11. Biological activity

Antibiotic testings were performed against *Staphylococcus aureus*, *Micrococcus lutens*, *Pseudomonas aeruginosa* and *Escherichia coli* using microtitre plate broth dilution method (Hammer et al., 1996).

References

Anthonsen, T., Falkenberg, I., Laake, M., Midelfart, A., Mortensen, T., 1971. Unusual flavonoids from *Myrica gale*. Acta Chemica Scandinavica 25, 1929–1930.

Cheng, X.F., Chen, Z.L., 1999. Three new diterpenoids from *Malltus apelta*. Journal of Asian Natural Products Research 1, 319–325.

Cheng, X.F., Chen, Z.L., Meng, Z.M., 1999. Two new diterpenoids from *Malltus apelta*. Journal of Asian Natural Products Research 1, 163–168.

Cheng, X.F., Meng, Z.M., Chen, Z.L., 1998. A pyridine-type alkaloid from *Malltus apelta*. Phytochemistry 49, 2193–2194.

Hammer, K.A., Carson, C.F., Riley, T.V., 1996. Broth microdilution method for determining the susceptibility of *Escherichia coli* and *Staphylococcus aureus* to the *Melaleuca alternifolia*. American Journal of Infection Control 24, 186–189.

Jiangsu New Medical College (Ed.), 1977. Dictionary of Chinese Crude Drugs. Shanghai Scientific Technologic Publisher, Shanghai, (p. 731).

Lambert, J.B., Shurvell, H.F., Lighter, D.A., Cooks, R.G., 1987. Introduction to Organic Spectroscopy. Collier Macmillan Publisher, London (pp. 67–80).

Li, J.R., Yuan, H.M., Wang, M.S., 1992. Two flavanones from the root bark of *Lespedeza Formosa*. Phytochemistry 31, 3664–3665.

Shan, X.Q., Feng, L.B., 1985. Chemical constituents of the roots of *Mallatus apelta* (Lour.) Muell-Arg. Zhiwu Xuebao 27, 192–195.

Wada, H., Tanaka, N., Murakaml, T., Uchida, T, Kozawa, K., Saki, Y., Chen, C.M., 1988. Chemical and chemotaxonomical studies of Fillices LXXVI. An unusual flavanone derivative from *Wagneriopterts jiponica a* Loeve et Loeve. Yakugaku Zasshi 108, 740–744.

PERGAMON

Phytochemistry 57 (2001) 279–283

PHYTOCHEMISTRY

www.elsevier.com/locate/phytochem

Nemorosone, the major constituent of floral resins of *Clusia rosea*☆

Osmany Cuesta-Rubio [a], Herman Velez-Castro [b], Bernardo A. Frontana-Uribe [c], Jorge Cárdenas [c,*]

[a] *Instituto de Farmacia y Alimentos, Universidad de la Habana, Ave. 23 No. 21425, Lisa, C. Habana, 13600, Cuba*
[b] *Centro de Química Farmacéutica, Calle 200 esq. 21, C. Habana, 13600, Cuba*
[c] *Instituto de Química, Universidad Nacional Autónoma de México, Circuito Exterior, Ciudad Universitaria, Coyoacán C.P. 04510, México DF*

Received 25 July 2000; received in revised form 8 December 2000

Abstract

Nemorosone, the major constituent of the floral resin of *Clusia rosea* was isolated after exhaustive chromatography. This compound was fully characterized as it is in the nature, without methylation as reported before. A keto–enol equilibrium was observed and both isomers were totally characterized by NMR spectroscopic techniques. The previously announced structure for methyl-nemorosone was corrected on the basis of application of chemical methylation, high field 2D NMR techniques and NOE difference spectroscopy experiments on the natural product. Our studies concluded that an interchange occurred in the assignment of the benzoyl moiety position with an isoprenyl group in that structure. © 2001 Elsevier Science Ltd. All rights reserved.

Keywords: *Clusia rosea*; Guttiferae; Copey; Polyisoprenylated benzophenone; Nemorosone

1. Introduction

Polyisoprenylated benzophenones with a bicyclo 3.3.1-nonane-2,4,9-trione system have been isolated from the Guttiferae family. Plukenetione E acetate **1** (Henry et al., 1999) (benzophenone type A),[1] clusianone **2** (Delle Monache et al., 1991) (benzophenone type B) and methyl-nemorosone **3** (De Oliveira et al., 1996) (benzophenone type C) show this bicyclic structure, but the relative position of the benzoyl group is different for these compounds (Fig. 1). Methyl-nemorosone **3**, 16-hydroxy-methyl-nemorosone and 7-epi-methyl-nemorosone were isolated from the methylated floral resins of *Clusia* species (including *Clusia rosea*) and they are the sole type C prenylated benzophenone described (De Oliveira et al., 1996, 1999). It is common to use diazomethane during the study of these floral resins to obtain the methylated derivatives of the natural products (De Oliveira et al., 1996, 1999). In this study without any previous treatment of the resin, we have examined the major constituent of the floral resin of *Clusia rosea*, a polyisoprenylated benzophenone, nemorosone **4** exists in its keto–enol equilibrium. The NMR spectroscopic studies of the tautomeric forms of nemorosone and the methyl derivatives obtained, revealed data which are inconsistent with the described structure of methyl-nemorosone **3**. This prompted us to reinvestigate the chemical structure.

2. Results and discussion

Floral resins of *Clusia rosea* were extracted with ethanol and a major compound was obtained using a combined method of crystallization and VLC (see Experimental). The molecular formula $C_{33}H_{42}O_4$, identical to clusianone, was deduced using MS, ^{13}C NMR and DEPT analyses. In the EIMS spectrum, peaks at m/z 105 and 69 showed the presence of an unsubstituted benzoyl group and isopentenyl moieties, respectively. Two tautomers were observed in the NMR spectroscopic experiments and their ^{13}C and ^{1}H NMR spectral data are given in Table 1.

The ^{1}H NMR spectrum indicated the presence of three isopentenyl groups and one enolic proton for each isomer. A bicyclo 3.3.1 nonane-2,4,9-trione system could be recognized by the ^{13}C NMR chemical shifts of C-1 (δ

☆ Contribution No. 1725 from Instituto de Química, UNAM.

* Corresonding author. Fax: +52-56162217.
E-mail address: rjcp@servidor.unam.mx (J. Cárdenas).

[1] We propose to group the polyisoprenylated benzophenones in accord with the benzoyl moiety position: type A if it is on C-1, type B if it is on C-3 and finally type C if it is on C-5.

0031-9422/01/$ - see front matter © 2001 Elsevier Science Ltd. All rights reserved.
PII: S0031-9422(00)00510-0

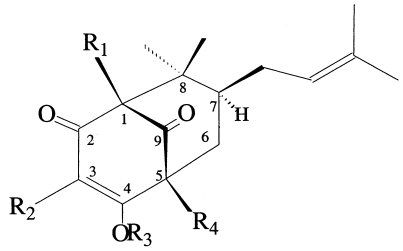

1. 7-epi, R_1= C_6H_5CO, R_2=R_4=C_5H_9, R_3= $COCH_3$ (Type A)

2. R_1=R_4=C_5H_9, R_2 = C_6H_5CO, R_3= H (Type B)

3. R_1=R_2= C_5H_9, R_3=CH_3, R_4= C_6H_5CO (Type C)

C_5H_9= 3-methyl-2-butenyl, C_6H_5CO=Benzoyl

Fig. 1. Related polyisoprenylated benzophenones with a [3.3.1] nonane-2,4,9-trione system.

78.0 and 71.4), C-5 (δ 57.1 and 64.8), C-8 (δ 48.2 and 47.3), three conjugated ketonic carbonyls C-2, C-4 (δ 192.2, 195.0) and C-10 (193.2 and 193.1), two enolic carbons C-2 and C-4 (δ 168.2 and 170.9) and a carbonyl group at C-9 (δ 207.3 and 207.6). The bicyclo and isopentenyl groups were also identified by the HMBC experiments. HMBC connectivities enabled differentiation between the two isomers, (see Table 1).

The presence of the enolizable 1,3-diketone system for nemorosone generates a tautomeric pair **4a** and **4b** in a ratio ca. 2:1 in the NMR spectra (Fig. 2). The analysis of the tautomeric pair was essential to define the correct structure of nemorosone. In order to observe if the signals simplified, NMR spectra were obtained at $-55°$, but the ratio of the tautomeric mixture did not change, although the signals were better defined. After the analysis of the NMR spectra, only the methyl groups of the 3-methyl-2-butenyl substituents could not be assigned due to the splitting of the signals.

The presence of allylic methylenes at δ 3.14–3.38 indicated a 3-methyl-2-butenyl group on C-3 as is described for plukenetione D acetate, plukenetione E acetate **1** and methyl nemorosone **3** (De Oliveira et al., 1996; Henry et al., 1999; Grossman and Jacobs, 2000). The chemical shift of these protons can only be justified in that position, which led us to eliminate the possibility of a type B benzophenone for the analyzed compound. A benzoyl group at C-1 was suggested by the high chemical shift of this carbon (δ 78.0 and 71.4) in the observed tautomers. This characteristic was similar to plukenetiones and propolone A (De Oliveira et al., 1996; Cuesta-Rubio et al., 1999; Henry et al., 1999).

In order to define between a structure type A or C for the isolated benzophenone, nOe difference spectroscopy experiments were performed. Saturation at the frequency of the Me-33 gave positive increment at the aromatic protons signals (H-12 and H-16) of the benzoyl group and the protons of methylene-27. In the same way, irradiation of H-$6_{eq.}$ showed an interaction with methylene protons at C-22 and when the latter protons were irradiated, interactions with methylene protons at C-6 and Me-25 were observed. These results confirmed unequivocally structure **4** for nemorosone, a type A benzophenone.

The basic bicyclic ring system in **4** requires the phenyl ketone at C-1 and the isopentenyl chain at C-5 to be in an equatorial orientation. The ^{13}C chemical shift of Me-$33_{ax.}$ (δ 15.6) suggested an equatorial position for the isopentenyl group at C-7. The upfield shift of the C-$33_{ax.}$ signal results from steric compression of a gauche interaction between this carbon and the CH_2-22 of the equatorial isopentenyl group on C-7 (Wehrli et al., 1988; Günther, 1998). The coupling constant between H-$6_{ax.}$ and H-7 confirmed this observation and it was deduced by selective irradiation at the frequency of H-$6_{eq.}$ This decoupling simplified the H-$6_{ax.}$ signal to a doublet J = 12.6 Hz, which must be a diaxial H-$6_{ax.}$ and H-7 coupling constant. The coupling constants observed are similar to those reported for propolone A and guttiferone B in which the side chain on C-1, C-5 and C-7 have an equatorial orientation and a coupling constant

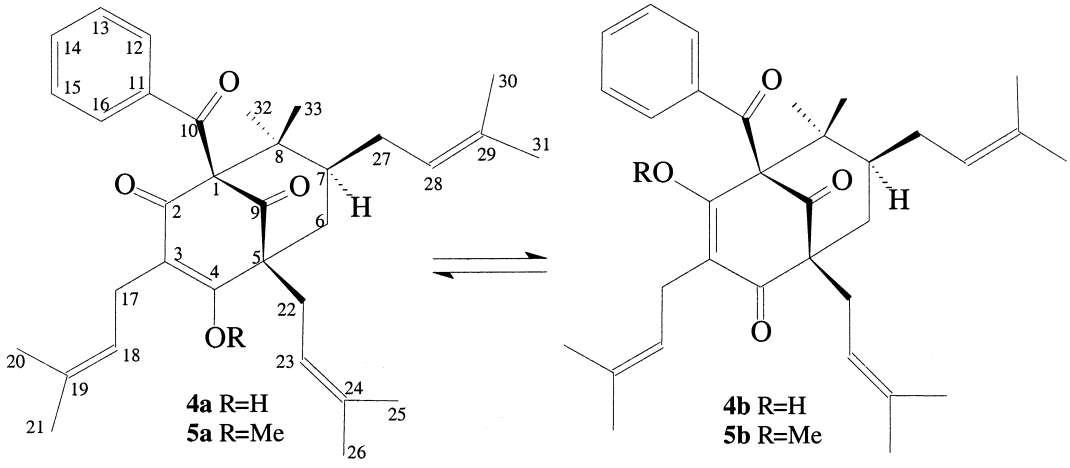

Fig. 2. Keto–enol equilibrium isomers for nemorosone (**4**).

Table 1
NMR spectral data for both tautomers of nemorosone **4** (500 MHz for ^{1}H NMR and 125 MHz for ^{13}C NMR, $CDCl_3$, −55° TMS)

Position	**4a**			**4b**		
	δ C	δ H (*J* Hz)	HMBC (H→C)	δ C	δ H (*J* Hz)	HMBC (H→C)
1	78.0 *s*	–		71.4 *s*	–	
2	192.2 *s*	–		168.2 *s*	–	
3	117.6 *s*	–		117.2 *s*	–	
4	170.9 *s*	–		195.0 *s*	–	
5	57.1 *s*	–		64.8 *s*	–	
$6_{ec.}$	39.4 *t*	2.09, *dd* (13.5, 4)	C-4, 5, 7, 8, 9	42.1 *t*	1.97, *dd* (13.5, 4)	C-4, 5, 7, 8, 9
$6_{ax.}$	–	1.47, *t* (13.3)	C-5		1.42, *t* (13.3)	
7	42.9 *d*	1.68, overlapped		42.1 *d*	1.70, overlapped	
8	48.2 *s*	–		47.3 *s*	–	
9	207.3 *s*	–		207.6 *s*	–	
10	193.2 *s*	–		193.1 *s*	–	
11	136.6 *s*	–		135.9 *s*	–	
12 and 16	128.1 *d*	7.53, *dd* (7.5, 1)	C-10, 13, 14, 15	128.0 *d*	7.67, *dd* (7.5, 1.5)	C-10, 13, 14, 15
13 and 15	127.9 *d*	7.31, *t* (7.5)	C-11,12, 14, 16	127.9 *d*	7.35, *t* (7.5)	C-11,12, 14, 16
14	132.4 *d*	7.47, *t* (7.5)	C-13, 15	132.6 *d*	7.51, *t* (7.5)	C-13, 15
17	21.6 *t*	3.14, *dd* (16, 7)	C-2, 3, 4, 18, 19	21.7 *t*	3.20, *dd* (16.5, 7)	C-2, 3, 4, 18, 19
		3.20, *dd* (16, 7)	C-2, 3, 4, 18, 19		3.28, *dd* (16.5, 7)	C-2, 3, 4, 18, 19
18	119.6 *d*	4.89, *m*		119.1 *d*	5.23, *m*	
19	138.2 *s*	–		139.5 *s*	–	
20	17.9 *q*†[a]	1.56–1.76, *s*		17.9 *q*†	1.56–1.76, *s*	
21	25.9 *q**	1.66–1.8, *s*		25.9 *q**	1.66–1.8, *s*	
22	28.9 *t*	2.47, *dd* (15, 7.5)	C-4, 5, 6, 9, 23, 24	29.2 *t*	2.47, *dd* (14, 7)	C-4, 5, 9, 23, 24
		2.65, *dd* (15, 7.5)	C-4, 5, 6, 9, 23, 24		2.56, *dd* (14, 7)	C-5, 9, 23, 24
23	118.4 *d*	5.11, *m*		119.3 *d*	5.13, *m*	
24	135.2 *s*	–		134.7 *s*	–	
25	18.0 *q*†	1.56–1.76, *s*		18.0 *q*†	1.56–1.76, *s*	
26	26.0 *q**	1.66–1.8, *s*		26.0 *q**	1.66–1.8, *s*	
27	26.4 *t*	1.80, overlapped		27.3 *t*	1.71, overlapped	
		2.16, *dd* (13, 4)	C-6, 28, 29		2.11, *dd* (13.5, 4)	C-6, 28, 29
28	122.1 *d*	4.94, *m*		122.1 *d*	4.98, *m*	
29	133.6 *s*	–		133.6 *s*	–	
30	18.2 *q*†	1.56–1.76, *s*		18.2 *q*†	1.56–1.76, *s*	
31	26.3*	1.66–1.8, *s*		26.3*	1.66–1.8, *s*	
32	23.2 *q*	1.35, *s*	C-1, 7, 8, 33	24.1 *q*	1.40, *s*	C-1, 7, 8, 33
33	15.6 *q*	1.13, *s*	C-1, 7, 8, 32	15.6 *q*	1.17, *s*	C-1, 7, 8, 32
−OH enolic[‡]		7.15, *s*	C-3, 4, 5		6.83, *s*	C-1, C2

[a] * and †, these methyl groups could be interchanged between them. [‡] The chemical shift changes with the concentration.

of ca. 10 Hz was observed between H-7 and H-$6_{ax.}$ (Gustafson et al., 1992; Cuesta-Rubio et al., 1999). Therefore, the non-enolic part of the bicyclo structure must have a *pseudo*-chair conformation, with H-7 in an α-axial orientation and the isopentenyl group on C-7 in a β-equatorial orientation. All bicyclo 3.3.1 nonane derivatives with axial isopentenyl groups on C-7 that have been analyzed by HMBC experiments showed a higher ^{13}C chemical shift for C-33 (δ 22–23) than at observed for nemorosone, i.e.: plukenetiones D and E, guttiferone E, guttiferone F, 30-epi-cambogin and isoxanthochymol (Gustafson et al., 1992; Fuller et al., 1999; Henry et al., 1999; Grossman and Jacobs, 2000). In the case of the xanthochymol and cambogin structures which have an isopentenyl group in axial position at C-7 as confirmed by X-ray crystallography, we think that the NMR spectral assignment of the axially oriented methyl of the *gem*-dimethyl group, has been interchanged with that of a methyl belonging to an isopentenyl moiety.

Initially, the presence of nemorosone **4** in floral resins of *Clusia rosea* was deduced by mean of a derivative, methyl-nemorosone and structure **3** was proposed for this compound. The NOE and the HMBC experiments described by De Oliveira et al., (1996), are consistent with both their proposed structure for methyl-nemorosone **3** and with the methyl derivative **5b** generated from the methylation of tautomer **4b** of our proposal. In order to confirm this hypothesis, we proceeded to treat nemorosone with an ethereal solution of diazomethane. After usual workup, we isolated a product whose NMR spectrum showed that both methylated isomers **5a** and **5b** were present in a ratio 1:3. After comparison of the ^{1}H and ^{13}C NMR chemical shifts of the natural product and the methyl derivatives with other similar compounds previously

described, we propose that the correct structure for methyl-nemorosone must be **5b**. The NMR spectral data observed for one of the methylated isomers, produced after treatment of nemorosone with diazomethane, are exactly the same reported for the previously described methyl-nemorosone structure **3** (De Oliveira et al., 1996). Recently, the methyl derivative corresponding to the methylation of the tautomer **4a** has been isolated from the same floral resins (De Oliveira et al., 1999). The NMR spectral data of this product called nemorosone II, are in complete agreement with the NMR data observed for the other methyl isomer **5a** produced after treatment of the natural product nemorosone **4** with diazomethane.

The results lead us to postulate that all prenylated benzophenones with a bicyclo 3.3.1 nonane-2,4,9-trione system isolated heretofore, are derivatives of type A or B. Propolone A, isolated from propolis, is a derivative of nemorosone and plukenetiones are stereoisomers of Nemorosone (Cuesta-Rubio et al., 1999; Henry et al., 1999; Grossman and Jacobs, 2000). The reported structures for methyl-nemorosone **3** and 14-hydroxy-methyl nemorosone, the only described type C benzophenones, are not correct due to an interchange in the assignment of the benzoyl moiety position with an isoprenyl group (De Oliveira et al., 1996, 1999). The proposed structure for 7-epi-nemorosone is probably also incorrect, but further NMR measurements would be needed to confirm this.

From a biogenetic point of view, type A or B polyisoprenylated benzophenones could be biosynthesized from a common precursor **6**, by an opposite mechanism of cyclization over an activated moiety (i.e.: pyrophosphate) from the aromatic ring, could generate both types of benzophenones. This fact can also explain the absence of type C polyisoprenylated benzophenones (Fig. 3).

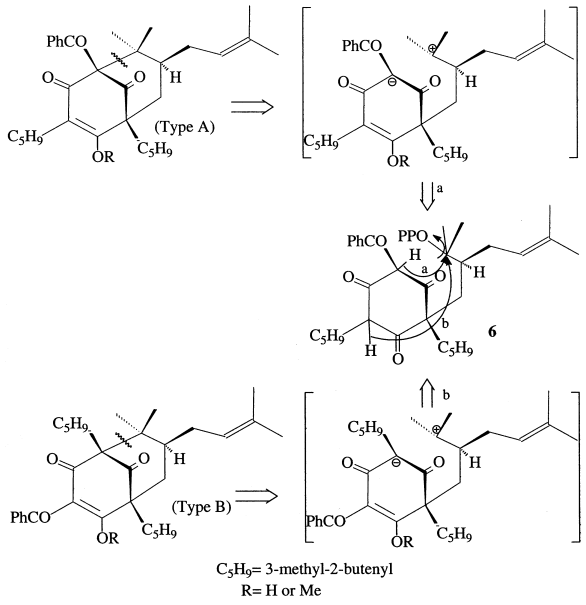

Fig. 3. Proposed biogenetic pathway for type A and B polyisoprenylated benzophenones.

3. Experimental

Flowers of *Clusia rosea* were collected in Habana (Cuba) in October 1999 and a voucher specimen (No. 705) was deposited in the Herbarium of the Instituto de Investigaciones Fundamentales de la Agricultura, Habana, Cuba. Melting points were uncorrected and determined using a Fisher-Johns apparatus. Optical rotation was measured in a Jacob DIP-360 polarimeter equipped with a sodium lamp (589 nm) and a 10 cm microcell. UV spectra was obtained with a Shimadzu U-160 spectrophotometer and IR spectra with a Nicolet Magna 750 spectrophotometer. EI–MS was obtained at 70 eV by direct inlet with a Jeol JMS-AX505HA. ^{1}H NMR (500 MHz) and ^{13}C NMR (125 MHz) spectra were recorded with a Varian Unity Plus 500 using TMS as internal standard, at a temperature of −55°. nOe difference spectroscopy experiments were measured in a sealed deoxygenated tube.

The floral resin of *Clusia rosea* (3.5 g) was removed with a palette knife and extracted immediately with ethanol. Nemorosone was crystallized from a mixture of EtOH–H_2O, yielding 510 mg of impure compound. The product was subject to a VLC (Targett et al., 1979) on silica gel with C_6H_{12}–EtOAc (3:1) in order to purify it to homogeneity.

Nemorosone **4**: $C_{33}H_{42}O_4$ mixture of tautomers **4a** (1-benzoyl-3,5,7-tri-(3-methyl-2-butenyl)-4-hydroxy-8-dimethyl-biciclo[3.3.1]-3-nonene-2,9-dione) and **4b** (1-benzoyl-3,5,7-tri-(3-methyl-2-butenyl)-2-hydroxy-8-dimethyl-biciclo[3.3.1]-2-nonene-4,9-dione). White crystals (EtOH/H_2O); mp 66–68° (became yellow in solution on exposure to light and air); α_D^{23} +112.8 ($CHCl_3$; *c* 0.101); UV: λ_{max}^{MeOH} [1.3×10^{-4} M] nm (logε): 208.5 (4.19), 246 (4.15), 278 (4.04); IR: ν_{max}^{KBr} cm^{-1}: 3541 *m*, 3431 *m*, 2969 *m*, 2919 *m*, 1708 (C=O) *s*, 1590 (C=C) *vs*; EIMS (probe) 70 eV, *m*/*z* (rel. int.): 502 M^+ (25), 433 M–$C_5H_9^+$ (40), 309 M–C_5H_9–$C_9H_{16}^+$ (100), 105 $C_7H_5O^+$ (38), 69 $C_5H_9^+$; FAB–MS HR: $C_{33}H_{42}O_4$ requires [M^+] at *m*/*z* 502.3083, observed 502.3067; ^{1}H and ^{13}C NMR spectra see Table 1.

Acknowledgements

We are very grateful to Messrs. Isabel Chávez, Luis Velazco, Javier Pérez, Rocío Patiño for their technical assistance and to Dr. Victor Fuentes Fiallo for botanical classification of the plant material. O.C.-R. thanks DGIA–UNAM for the grant received.

References

Cuesta-Rubio, O., Cuellar Cuellar, A., Rojas, N., VelezCastro, H., Rastrelli, L., Aquino, R., 1999. A polyisoprenylated benzophenone from cuban propolis. Journal of Natural Products 62, 1013–1015.

Delle Monache, F., Delle Monache, G., Gacs-Baitz, E., 1991. Prenylated benzophenones from *Clusia sandiensis*. Phytochemistry 30, 2003–2005.

De Oliveira, C.M.A., Porto, A.M., Bittrich, V., Vencanto, I., Marsaioli, A.J., 1996. Floral Resins of *Clusia* spp.: chemical composition and biological function. Tetrahedron Letters 37, 6427–6430.

De Oliveira, C.M.A., Porto, A.M., Bittrich, V., Marsaioli, A.J., 1999. Two polyisoprenylated benzophenones from the floral resins of the Clusia species. Phytochemistry 50, 1073–1079.

Fuller, R.W., Blunt, J.W., Boswell, J.L., Cardellina II, J.H., Boyd, M.R., 1999. Guttiferone F, the first prenylated benzophenone from *Allanblackia stuhlmannii*. Journal of Natural Products 62, 130–132.

Grossman, R.B., Jacobs, H., 2000. On the structures of plukenetiones b, d and e and their relationships to other polycyclic polyprenylated acylphloroglucinols. Tetrahedron Letters 41, 5165–5169.

Günther, H., 1998. NMR spectroscopy: basic principles, concepts and applications in chemistry, 2nd Edition. John Wiley & Sons, London.

Gustafson, K.R., Blunt, J.W., Munro, M.H.G., Fuller, R.W., Mc Kee, T.C., Cardellina II, J.H., McMahom, J.B., Gragg, G.M., Boyd, M.R., 1992. The guttiferones, HIV-inhibitory benzophenones from *Symphonia globulifera, Garcinia livingstonei, Garcinia ovalofolia* and *Clusia rosea*. Tetrahedron 48, 10093–10102.

Henry, G.E., Jacobs, H., Sean-Carrington, C.M., McLean, S., Reynolds, W.F., 1999. Prenylated benzophenone derivatives from caribean *Clusia* species (*Guttiferae*). Plukenetiones B-G and xerophenone A. Tetrahedron 55, 1581–1596.

Targett, N.M., Kilcoyne, J.P., Green, B., 1979. Vaccum liquid chromatography: an alternative to common chromatographic methods. Journal of Organic Chemistry 44, 4962–4964.

Wehrli, F.W., Marchand, A.P., Wehrli, S., 1988. Interpretation of ^{13}C NMR spectra, 2nd Edition. John Wiley and Sons, London, p. 40.

PERGAMON

Phytochemistry 57 (2001) 285–296

PHYTOCHEMISTRY

www.elsevier.com/locate/phytochem

Minor constituents of *Spigelia anthelmia* and their cardiac activities☆

Harald Hübner [a,*], Wolfgang Vierling [b], Wolfgang Brandt [b], Melchior Reiter [b], Hans Achenbach [a]

[a] *Department of Pharmaceutical Chemistry, University of Erlangen, D-91052 Erlangen, Germany*
[b] *Institute of Pharmacology and Toxicology, Technical University, D-80802 München, Germany*

Received 16 August 2000; received in revised form 21 December 2000

Abstract

A more detailed phytochemical analysis of extracts of the aerial parts of *Spigelia anthelmia L.* (Loganiaceae) yielded 20 structurally related new compounds besides spiganthine and ryanodine. Structure elucidation was achieved mainly by spectroscopic methods. The compounds were tested on their cardiac and on their insect antifeedant activities. © 2001 Elsevier Science Ltd. All rights reserved.

Keywords: *Spigelia anthelmia*; Loganiaceae; Spiganthine; 20-Deoxyspiganthine; 8α-Hydroxyspiganthine; 20-Norspiganthine-5-carboxylic acid; Ryanodine; 10-*epi*-Ryanodine; 8,9-Dehydro-10-*epi*-ryanodine; 20-Hydroxyryanodine; Cardioactivity; Insect antifeedant activity

1. Introduction

Stimulated by the bioassay-monitored isolation of the cardioactive spiganthine from extracts of *Spigelia anthelmia* (Achenbach et al., 1995), we were interested in a more detailed phytochemical analysis of the plant. Major target of this investigation was the isolation of minor constituents, their structure elucidation and biological tests in order to gain structure–activity correlations.

2. Results and discussion

An extract from 2 kg dried aerial parts of *S. anthelmia* (''Urtinktur'' prepared with EtOH/water according to the prescription of the German Homoeopathic Pharmacopoeia) was diluted with water and repeatedly extracted with chloroform and then EtOAc followed by chromatography of the dried extracts on Sephadex LH 20® and silica gel, respectively. The separation procedures were monitored by the characteristic colour reaction of the spiganthine- and ryanodine-type compounds with anisaldehyde on TLC plates.

Further separation and isolation of pure constituents was achieved by HPLC on reversed phase silica gel. These procedures yielded constituents **1–17** from the $CHCl_3$-extracts and the more polar constituents **18–22** from the EtOAc-extracts (Table 1).

The spectroscopic investigations, and particularly FAB–MS (negative ions) revealed a number of differently oxygenated but structurally related C_{20}-structures with the common feature of a pentacyclic $C_{14}O$-skeleton carrying a pyrrolecarboxylic ester group, which is typical for spiganthine (Achenbach et al., 1995) and ryanodine (Wiesner et al., 1967).

In the ^1H NMR and ^{13}C NMR, all signals appeared well separated and — supported by the results of our earlier studies (Achenbach et al., 1995) — could easily be assigned to the individual positions. Correlation spectroscopy and NOE-measurements corroborated the assignments (Tables 2 and 3).

The structures of the spiganthine-type compounds **1–3** and **18** are easily recognized by a double doublet in the range of δ 3.23–3.86, which belongs to H-4 and causes a splitting of the typical low-field signal of H-3 at δ 5.6–5.8 (see Table 2).

☆ Part 91 in the series 'Constituents of Tropical Medicinal Plants'. For part 90 see Nkunya et al., 2000.

* Corresponding author. Fax: +49-9131-8522585.

E-mail addresses: Huebner@pharmazie.uni-erlangen.de (H. Hübner), achenbach@pharmazie.uni-erlangen.de (H. Achenbach).

0031-9422/01/$ - see front matter © 2001 Elsevier Science Ltd. All rights reserved.
PII: S0031-9422(01)00020-6

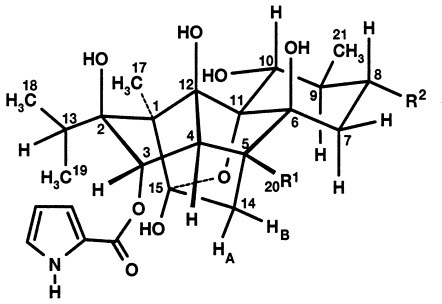

1 Spiganthine: $R^1 = CH_2OH$, $R^2 = H$
2 20-Deoxyspiganthine: $R^1 = CH_3$, $R^2 = H$
3 8α-Hydroxyspiganthine: $R^1 = CH_2OH$, $R^2 = OH$
18 20-Norspiganthine-5-carboxylic acid: $R^1 = CO_2H$, $R^2 = H$

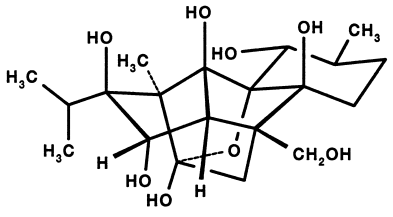

23

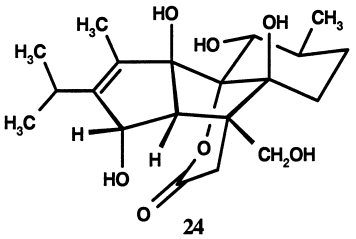

24

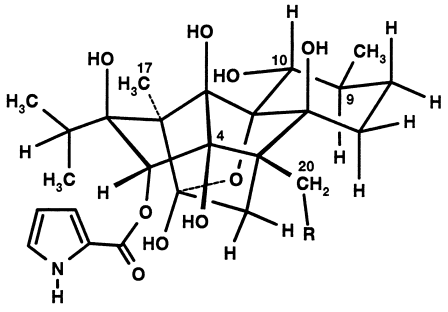

4 Ryanodine: R = H
19 20-Hydroxyryanodine: R = OH

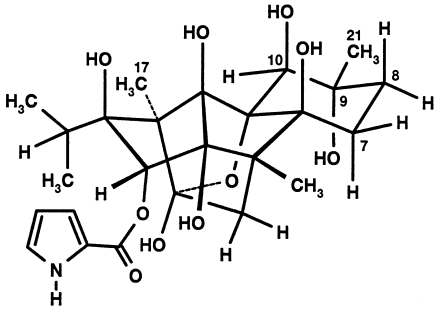

5 9-Hydroxy-10-*epi*-ryanodine

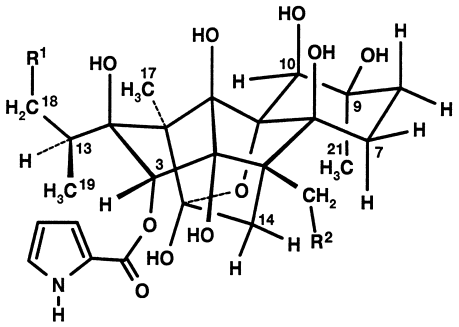

6 9-Hydroxy-9-*epi*-10-*epi*-ryanodine: $R^1 = R^2 = H$
7 9,18-Dihydroxy-9-*epi*-10-*epi*-ryanodine: $R^1 = OH$, $R^2 = H$
20 9,20-Dihydroxy-9-*epi*-10-*epi*-ryanodine: $R^1 = H$, $R^2 = OH$

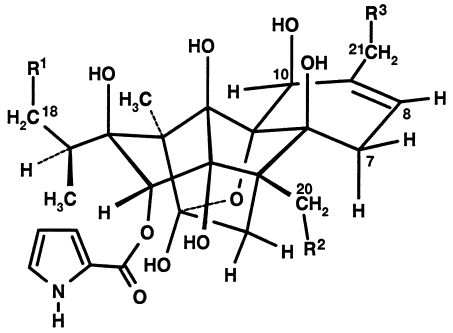

8 $\Delta^{8,9}$-10-*epi*-Ryanodine: $R^1 = R^2 = R^3 = H$
9 18-Hydroxy-$\Delta^{8,9}$-10-*epi*-ryanodine: $R^1 = OH$, $R^2 = R^3 = H$
10 20-Hydroxy-$\Delta^{8,9}$-10-*epi*-ryanodine: $R^1 = R^3 = H$, $R^2 = OH$
11 21-Hydroxy-$\Delta^{8,9}$-10-epi-ryanodine: $R^1 = R^2 = H$, $R^3 = OH$
21 18,21-Dihydroxy-$\Delta^{8,9}$-10-*epi*-ryanodine: $R^1 = R^3 = OH$, $R^2 = H$
22 20,21-Dihydroxy-$\Delta^{8,9}$-10-*epi*-ryanodine: $R^1 = H$, $R^2 = R^3 = OH$

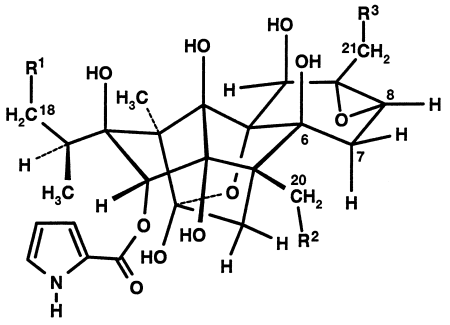

12 8α,9α-Epoxy-10-*epi*-Ryanodine: $R^1 = R^2 = R^3 = H$
14 18-Hydroxy-8,9-epoxy-10-*epi*-ryanodine: $R^1 = OH$, $R^2 = R^3 = H$
16 20-Hydroxy-8,9-epoxy-10-*epi*-ryanodine: $R^1 = R^3 = H$, $R^2 = OH$
17 21-Hydroxy-8,9-epoxy-10-epi-ryanodine: $R^1 = R^2 = H$, $R^3 = OH$

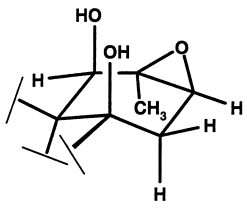

13 8β,9β-Epoxy-10-epi-Ryanodine: R1 = R2 = H

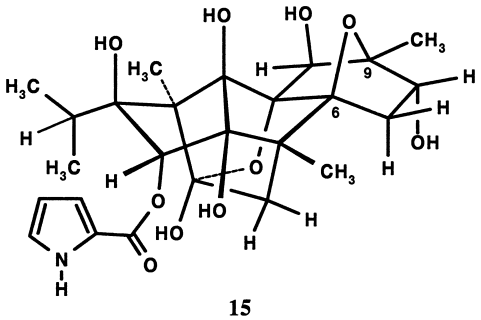

15

The less polar compound **2** carried the methyl group CH_3-20 at C-5 instead of the hydroxymethyl in spiganthine (**1**). In comparison to **1**, the more polar **3** was additionally hydroxylated at C-8. The equatorial configuration of this hydroxyl resulted from the coupling constants of the neighbouring protons and from NOE studies. Within the spiganthine-group, **18** with a free carboxyl at C-5 represented the most polar compound. On treatment with diazomethane, **18** promptly formed the methyl ester.

Under hydrolytic conditions, **1** underwent saponification giving spiganthol (**23**) and 2-pyrrolecarboxylic acid; in addition, anhydrospiganthol (**24**) was formed.

These results were in accordance with the reaction of ryanodine under aqueous acidic conditions (Kelly et al., 1951).

In contrast to the spiganthines, constituents **4–17** and **19–22** exhibited "only" a singulet signal for H-3 at considerably lower field (δ 5.60–5.70 ppm), which indicated a hydroxy-substituted quarternary C-4. Further NMR-studies revealed **4** as ryanodine (Wiesner et al., 1967) and **19** as its 20-hydroxy derivative.

The remaining isolated constituents were mainly characterized by typical differences of the resonance signal of H-10: whereas this signal in **1–4**, **18** and **19** always appeared in the δ 3.69–3.80 ppm range as a doublet ($J\sim10$ Hz) indicating a *trans*-diaxial relationship, it was observed in all other compounds as a singulet, "broad" singulet or a doublet with only a small coupling constant of 1 Hz at δ 3.66–4.66 ppm. These spectral features suggested "loss" of the neighbouring H-9 and/or an equatorial position of H-10 (=10-*epi*-configuration). Consequently, NOE measurements were performed and corroborated an equatorial H-10 by the significant interaction observed between H-10 and CH_3-17 for constituents **5–17** and **20–22**. The results gave evidence that these compounds belong to the rare 10-*epi*-ryanodine series.

Table 1
Compounds isolated from the "Urtinktur" of *Spigelia anthelmia*

Compound class	Compound	Fraction	Content[a] ($\%\times10^{-3}$)
Spiganthines			
	Spiganthine (**1**)	$CHCl_3$	7.7
	20-Deoxyspiganthine (**2**)	$CHCl_3$	0.5
	8α-Hydroxyspiganthine (**3**)	$CHCl_3$	0.3
	20-Norspiganthine-5-carboxylic acid (**18**)	EtOAc	6.7
Ryanodines			
(a) Ryanodine-type			
	Ryanodine (**4**)	$CHCl_3$	2.7
	20-Hydroxyryanodine (**19**)	EtOAc	6.3
(b) 10-epi-Ryanodines with a 9-OH group			
	9-Hydroxy-10-*epi*-ryanodine (**5**)	$CHCl_3$	1.2
	9-Hydroxy-9-*epi*-10-*epi*-ryanodine (**6**)	$CHCl_3$	13.3
	(13*S*)-9,18-Dihydroxy-9-*epi*-10-*epi*-ryanodine (**7**)	$CHCl_3$	1.0
	9,20-Dihydroxy-9-*epi*-10-*epi*-ryanodine (**20**)	EtOAc	1.0
(c) 10-epi-Ryanodines with a $\Delta^{8,9}$-double bond			
	8,9-Dehydro-10-*epi*-ryanodine (**8**)	$CHCl_3$	2.0
	(13*S*)-8,9-Dehydro-18-hydroxy-10-*epi*-ryanodine (**9**)	$CHCl_3$	2.0
	8,9-Dehydro-20-hydroxy-10-*epi*-ryanodine (**10**)	$CHCl_3$	1.5
	8,9-Dehydro-21-hydroxy-10-*epi*-ryanodine (**11**)	$CHCl_3$	5.0
	(13*S*)-8,9-Dehydro-18,21-dihydroxy-10-*epi*-ryanodine (**21**)	EtOAc	0.5
	8,9-Dehydro-20,21-dihydroxy-10-*epi*-ryanodine (**22**)	EtOAc	1.5
(d) 10-epi-Ryanodines with an epoxy group			
	8α,9α-Epoxy-10-*epi*-ryanodine (**12**)	$CHCl_3$	4.5
	8β,9β-Epoxy-10-*epi*-ryanodine (**13**)	$CHCl_3$	1.3
	(13*S*)-8α,9α-Epoxy-18-hydroxy-10-*epi*-ryanodine (**14**)	$CHCl_3$	1.2
	6-Deoxy-6β,9β-epoxy-8β-hydroxy-10-*epi*-ryanodine (**15**)	$CHCl_3$	1.2
	8α,9α-Epoxy-20-hydroxy-10-*epi*-ryanodine (**16**)	$CHCl_3$	0.7
	8α,9α-Epoxy-21-hydroxy-10-*epi*-ryanodine (**17**)	$CHCl_3$	1.3

[a] Amount of residue after evaporation of the "Urtinktur"=100%.

Table 2
^{1}H NMR data of the isolated natural compounds **1–22** and their derivatives **23** and **24** [δ (ppm), multiplicity and J (Hz); solvent CD_3OD]

Proton	1	2	3	4	5	6	7	8	9	10	11	12	13	14	15	16	17	18	19	20	21	22	23	24
H-3	5.78 *d* 8.5	5.65 *d* 8.5	5.76 *d* 8.5	5.63 *s*	5.67 *s*	5.67 *s*	5.63 *s*	5.69 *s*	5.65 *s*	5.69 *s*	5.69 *s*	5.65 *s*	5.62 *s*	5.60 *s*	5.68 *s*	5.66 *s*	5.65 *s*	5.78 *d* 8.5	5.67 *s*	5.67 *s*	5.65 *s*	5.70 *s*	4.46 *d* 8	5.14 *dq* 8, 2
H-4	3.55 *dd* 8.5, 2	3.23 *dd* 8.5, 2	3.53 *dd* 8.5, 2	–	–	–	–	–	–	–	–	–	–	–	–	–	–	3.86 *dd* 8.5, 2	–	–	–	–	3.31–3.36 *m*	3.04 *dd* 8, 2
H-7α	2.10 *ddd* 12, 12, 6	2.04 *ddd* 13.5, 12, 6	2.06 *dd* 12, 11	2.10 *ddd* 12.5, 12, 5	2.20 *ddd* 13, 13, 4.5	2.08 *ddd* 12, 12, 4	2.08 *ddd* 13, 12.5, 5	2.58 *brd* 17	2.58 *brd* 17	2.77 *brd* 17	2.64 *brd* 17	2.40 *d* 15	2.44 *dd*15, 2	2.40 *d* 14.5	1.81 *dd* 13, 4.5	2.59 *d* 15	2.43 *d* 15	2.15–2.25 *m*	2.08–2.30 *m*	2.20–2.30 *m*	2.64 *brd* 18	2.83 *brd* 18	2.07–2.16 *m*	1.50–1.60 *m*
H-7β	1.35–1.41 *m*	1.22 *ddd* 13.5, 4.5, 4	1.82 *dd* 12, 5	1.26 *ddd* 12.5, 5, 2.5	1.35-1.42 *m*	1.39 *ddd* 12, 4, 4	1.37–1.43 *m*	1.92 *brdd* 17, 5.5	1.92 *brdd* 17, 5.5	2.22–2.30 *m*	2.00 *brdd* 17, 5	1.82 *dd* 15, 6	1.93 *dd* 15, 2	1.83 *dd* 14.5, 6	2.04 *dd* 13, 10	2.20 *dd* 15, 6	1.82 *dd* 15, 6	1.21 *brd* 12	1.65 *ddd* 13, 4 ,3	1.81 *ddd* 14, 5, 4	2.00 *dd* 18, 5	2.34 *brdd* 18, 5	1.28–1.36 *m*	1.64–1.70 *m*
H-8α	1.50–1.64 *m*	1.45–1.58 *m*	–	1.40–1.57 *m*	1.54 *ddd* 14, 4.5, 2.5	1.59 *ddd* 13, 4, 4	1.59 *ddd* 12.5, 5, 4.5	5.47 *brd* 5.5	5.47 *brd* 5.5	5.46 *brd* 5	5.77 *brd* 5	–	3.36 *dd* 2, 2	–	–	–	–	1.49–1.61 *m*	1.43–4.55 *m*	1.57 *ddd* 14, 4, 4	5.77 *brd* 5	5.76 *brd* 5	1.49–1.60 *m*	1.54–1.64 *m*
H-8β	1.50–1.64 *m*	1.45–1.58 *m*	3.68 *ddd* 11, 10, 5	1.40–1.57 *m*	2.00 *ddd* 14, 13, 4.5	1.95 *ddd* 13, 12, 4	1.95 *ddd* 13, 12.5, 5	–	–	–	–	3.08 *dd* 6, 1	–	3.09 *dd* 6, 1	3.84 *dd* 10, 4.5	3.05 *dd* 6, 1	3.23 *dd* 6, 1	1.49–1.61 *m*	1.43–4.55 *m*	1.96 *ddd* 14, 14, 5	–	–	1.49–1.60 *m*	1.54–1.64 *m*
H-9	1.76–1.86 *m*	1.77-1.87 *m*	1.70–1.80 *m*	1.79–1.89 *m*	–	–	–	–	–	–	–	–	–	–	–	–	–	1.73–1.87 *m*	1.78–1.86 *m*	–	–	–	1.77–1.85 *m*	1.74–1.83 *m*
H-10	3.69 *d* 10	3.75 *d* 10	3.73 *d* 10.5	3.79 *d* 10	3.66 *s*	3.67 *s*	3.67 *s*	3.93 *brs*	3.94 *brs*	3.92 *brs*	4.21 *brs*	4.00 *d* 1	4.14 *s*	4.02 *d* 1	4.66 *s*	4.00 *d* 1	4.30 *d* 1	3.73 *d* 10	3.80 *d* 10	3.68 *brs*	4.22 *brs*	4.21 *brs*	3.69 *d* 10	3.92 *d* 10
H-13	2.36 *qq* 6.5, 6.5	2.41 *qq* 6.5, 6.5	2.36 *qq* 7, 7	2.27 *qq* 6.5, 6.5	2.19–2.29 *m*	2.24 *qq* 6.5, 6.5	2.15–2.23 *m*	2.26 *qq* 6.5, 6.5	2.17–2.26 *m*	2.21–2.29 *m*	2.27 *qq* 7, 7	2.23 *qq* 6.5, 6.5	2.23 *qq* 6.5, 6.5	2.14–2.24 *m*	2.21 *qq* 7, 7	2.18–2.28 *m*	2.24 *qq* 7, 7	2.31 *qq* 6.5, 6.5	2.20–2.30 *m*	2.18–2.27 *m*	2.18–2.26 *m*	2.21–2.31 *m*	2.15–2.25 *m*	2.70–2.80 *m*
H-14$_A$	2.21 *d* 13	2.35 *d* 13.5	2.23 *d* 13.5	2.56 *d* 13.5	2.63 *d* 14	2.60 *d* 13.5	2.54 *d* 14	2.66 *d* 14	2.60 *d* 14	2.58 *d* 14	2.68 *d* 14	2.58 *d* 14	2.64 *d* 14	2.52 *d* 14	2.51 *d* 14	2.50 *d* 14	2.59 *d* 14	2.66 *d* 14	2.50 *d* 14	2.53 *d* 14	2.62 *d* 14	2.59 *d* 14	2.21 *d* 13	3.35 *d* 19.5
H-14$_B$	1.73 *dd* 13, 2	1.77 *dd* 13.5, 2	1.73 *dd* 13.5, 2	1.93 *d* 13.5	1.96 *d* 14	1.87 *d* 13.5	1.88 *d* 14	1.94 *d* 14	1.95 *d* 14	2.30 *d* 14	1.95 *d* 14	1.86 *d* 14	1.91 *d* 14	1.87 *d* 14	1.61 *d* 14	2.21 *d* 14	1.87 *d* 14	2.24 *dd* 14, 2	2.24 *d* 14	2.22 *d* 14	1.96 *d* 14	2.31 *d* 14	1.60 *dd* 13, 2	2.39 *dd* 19.5, 2
CH_3-17	1.38 *s*	1.36 *s*	1.39 *s*	1.39 *s*	1.36 *s*	1.35 *s*	1.37 *s*	1.37 *s*	1.41 *s*	1.38 *s*	1.39 *s*	1.34 *s*	1.36 *s*	1.38 *s*	1.41 *s*	1.34 *s*	1.35 *s*	1.36 *s*	1.39 *s*	1.35 *s*	1.42 *s*	1.39 *s*	1.32 *s*	1.77 *d* 2
CH_3-18	1.16 *d* 6.5	1.16 *d* 6.5	1.16 *d* 7	1.11 *d* 6.5	1.09 *d* 6.5	1.09 *d* 6.5	–	1.10 *d* 6.5	–	1.10 *d* 6.5	1.10 *d* 7	1.08 *d* 6.5	1.09 *d* 6.5	–	1.09 *d* 7	1.09 *d* 7	1.09 *d* 7	1.14 *d* 6.5	1.12 *d* 6.5	1.10 *d* 6.5	–	1.11 *d* 6.5	1.12 *d* 6.5	1.12 *d* 7
or																								
CH_2-18	–	–	–	–	–	–	3.93 *dd* 10.5, 5 3.84 *dd* 10.5, 4	–	3.96 *dd* 10.5, 4 3.83 *dd* 10.5, 4.5	–	–	–	–	3.97 *dd* 10.5, 5 3.81 *dd* 10.5, 4	–	–	–	–	–	–	3.97 *dd* 10.5, 5.5 3.83 *dd* 10.5, 4	–	–	–
CH_3-19	0.81 *d* 6.5	0.84 *d* 6.5	0.81 *d* 7	0.76 *d* 6.5	0.75 *d* 6.5	0.75 *d* 6.5	0.90 *d* 7	0.75 *d* 6.5	0.92 *d* 6.5	0.75 *d* 6.5	0.76 *d* 7	0.74 *d* 6.5	0.73 *d* 6.5	0.91 *d* 6.5	0.73 *d* 7	0.73 *d* 7	0.74 *d* 7	0.77 *d* 6.5	0.75 *d* 6.5	0.73 *d* 6.5	0.93 *d* 7	0.75 *d* 6.5	1.02 *d* 6.5	1.18 *d* 7
CH_3-20	–	0.77 *s*	–	0.89 *s*	0.93 *s*	0.91 *s*	0.91 *s*	0.94 *s*	0.95 *s*	–	0.96 *s*	0.90 *s*	0.92 *s*	0.91 *s*	0.94 *s*	–	0.91 *s*	–	–	–	0.97 *s*	–	–	–
or																								

(*continued on next page*)

Table 2 (*continued*)

Proton	1	2	3	4	5	6	7	8	9	10	11	12	13	14	15	16	17	18	19	20	21	22	23	24
CH_3-20	3.58 *d*	–	3.59 *d*	–	–	–	–	–	–	3.99 *d*	–	–	–	–	–	3.95 *d* 11.5	–	–	3.93	3.96 *d*	–	4.00 *d*	3.69 *d*	3.78 *s*
	11 3.48		11 3.50							11.5						3.66			*d* 11.5	11.5 3.65		11.5 3.69	10 3.74	3.78 *s*
	d 11		*d* 11							3.68						*d* 11.5			3.69	*d* 11.5		*d* 11.5	*d* 10	
										d 11.5									*d* 11.5					
CH_3-21	1.01	1.01	1.14	1.01	1.22 *s*	1.38 *s*	1.38 *s*	1.81 *brs*	1.82 *brs*	1.81 *brs*	–	1.41 *s*	1.45 *s*	1.41 *s*	1.30 *s*	1.41 *s*	–	1.01	1.01	1.38 *brs*	–	–	1.00	1.00
	d 6.5	*d* 6.5	*d* 7	*d* 6.5														*d* 6.5	*d* 6.5				*d* 6.5	*d* 6.5
or																								
CH_2-21	–	–	–	–	–	–	–	–	–	–	4.17 *brd*	–	–	–	–	–	4.13 *d*	–	–	–	4.17 *brd*	4.17 *brd*	–	–
											13 4.11						12.5 3.51				13 4.11	13 4.09		
											brd 13						*d* 12.5				*brd* 13	*brd* 13		
H-24	6.85 *dd*	6.85 *dd*	6.85 *dd*	6.87 *dd*	6.87 *dd*	6.87 *dd*	6.88 *dd*	6.88 *dd*	6.89 *dd*	6.95 *dd*	6.88 *dd*	6.87 *dd*	6.86 *dd*	6.88 *dd*	6.85 *dd*	6.94 *dd*	6.87 *dd*	6.82 *dd*	6.95 *dd*	6.95 *dd*	6.89 *dd*	6.96 *dd*	–	–
	4, 1.5	4, 1.5	4, 1.5	4, 1.5	4, 1.5	4, 1.5	4, 1.5	4, 1.5	4, 1.5	4, 1.5	4, 1.5	4, 1.5	4, 1.5	4, 1.5	4, 1.5	4, 1.5	4, 1.5	4, 1.5	4, 1.5	4, 1.5	4, 1.5	4, 1.5		
H-25	6.22 *dd*	4.22 *dd*	6.23 *dd*	6.24 *dd*	6.24 *dd*	6.24 *dd*	6.24 *dd*	6.24 *dd*	6.25 *dd*	6.25 *dd*	6.25 *dd*	6.24 *dd*	6.23 *dd*	6.24 *dd*	6.23 *dd*	6.25 *dd*	6.24 *dd*	6.17 *dd*	6.24 *dd*	6.25 *dd*	6.25 *dd*	6.26 *dd*	–	–
	4, 2.5	4, 2.5	4, 2.5	4, 2.5	4, 2.5	4, 2.5	4, 2.5	4, 2.5	4, 2.5	4, 2.5	4, 2.5	4, 2.5	4, 2.5	4, 2.5	4, 2.5	4, 2.5	4, 2.5	4, 2.5	4, 2.5	4, 2.5	4, 2.5	4, 2.5		
H-26	7.02 *dd*	7.01 *dd*	7.02 *dd*	7.03 *dd*	7.04 *dd*	7.04 *dd*	7.04 *dd*	7.04 *dd*	7.05 *dd*	7.05 *dd*	7.04 *dd*	7.03 *dd*	7.03 *dd*	7.04 *dd*	7.03 *dd*	7.04 *dd*	7.04 *dd*	6.96 *dd*	7.04 *dd*	7.04 *dd*	7.05 *dd*	7.05 *dd*	–	–
	2.5, 1.5	2.5, 1.5	2.5, 1.5	2.5, 1.5	2.5, 1.5	2.5, 1.5	2.5, 1.5	2.5, 1.5	2.5, 1.5	2.5, 1.5	2.5, 1.5	2.5, 1.5	2.5, 1.5	2.5, 1.5	2.5, 1.5	2.5, 1.5	2.5, 1.5	2.5, 1.5	2.5, 1.5	2.5, 1.5	2.5, 1.5	2.5, 1.5		

Further ^{1}H and ^{13}C NMR-studies revealed the structure of 9-hydroxy-10-*epi*-ryanodine (**5**) (NOE between CH_3-21 and H_{ax}-8) and of the hydroxylated 9-*epi*-10-*epi*-ryanodines **6, 7** and **20**, which carried the CH_3-21 methyl group in the axial position. Major argument for this configuration at C-9 comes from the observed NOE between CH_3-21 and H_{ax}-7.

The depicted stereochemistry at C-13 in **7** is also based on NOE-studies, which revealed strong effects from CH_3-17 to CH_2-18, from CH_3-19 to H-3, and from H-13 to H-14. With regard to the established absolute configuration of ryanodine, these NMR-observations confirmed the 13*S*-configuration for **7**.

Among the 10-*epi*-ryanodines, the common structural feature of constituents **8–11**, **21** and **22** was an unsaturation within the cyclohexane ring system. ^{1}H and ^{13}C NMR easily determined its $\Delta^{8,9}$-position and also recognized the presence and positions of additional hydroxyl groups. The configuration at the steric center C-13 in **9** and **21** was established as in **7**.

Catalytic hydrogenation of **11** saturated the double bond and simultaneously deoxygenated the allylic OH-group at C-21 to give 9-*epi*-10-*epi*-ryanodine in about 70% yield.

Treatment of **11** with 3-chloroperoxybenzoic acid (Waterhouse et al., 1987) produced, among others, the two expected stereoisomeric epoxides, one of which proved to be identical with the isolated constituent **17.** Assignment of structure **17** and its corresponding stereoisomer was deduced from characteristic coupling differences in the H-7/H-8 spin-system of their ^{1}H NMR: in **17**, H-8 appears as a doublet ($J_{7eq,8}\sim$6 Hz) with $J_{7ax,8}\sim$0 Hz, whereas in the stereoisomeric epoxide obtained only by epoxidation of **11** coupling constants of $J_{7ax,8}\sim J_{7eq,8}\sim$2 Hz were observed for H-8. On the basis of these data, the structure with the α-orientation of the oxirane ring has to be attributed to **17**.

This result was valuable for the structure elucidation of constituents **12–14** and **16**, which belonged to the α-series of epoxides with the only exemption of **13**.

A small amount of the epoxide **12** was subjected to a hydrolytic ring-opening reaction using oxalic acid. This reaction resulted in the —almost quantitative—conversion of **12** to an isomeric product identical with the isolated constituent **15**.

A very characteristic feature in the ^{13}C NMR of **15** was a pronounced downfield-shift of the resonance of the C-6 from δ 84.3 ppm (in **12** and all other hitherto mentioned constituents) to δ 96 ppm in **15**. Extensive NMR-studies established structure **15** and rationalized the in vitro conversion of **12** to **15**: protonation of the oxirane oxygen facilitates the nucleophilic attack of C-9 by the axial hydroxyl at C-6. This process might occur as a concerted reaction and brings about **15**.

The colour reaction with anisaldehyde/sulfuric acid was used as a spot test on TLC plates in the course of

Table 3
^{13}C NMR data of the isolated compounds **1**–**22** and their derivatives **23** and **24** [δ (ppm); solvent CD_3OD]

Carbon	**1**	**2**	**3**	**4**	**5**	**6**	**7**	**8**	**9**	**10**	**11**	**13**	**14**	**15**	**16**	**17**	**18**	**19**	**20**	**21**	**22**	**23**	**24**
1	65.3	64.7	65.5	65.9	66.3	66.2	66.4	66.4	66.6	66.5	66.5	66.6	66.1	66.2	66.0	66.0	65.1	66.0	66.3	66.6	66.6	65.1	151.5[a]
2	86.1	86.6	86.8	84.4	84.0	84.1	84.7	84.4	85.0	84.3	84.4	84.4	84.9	84.5	84.2	84.3	87.0	84.3	84.0	85.0	84.3	87.2	134.4[a]
3	85.0	85.2	84.8	91.0	90.5	90.3	90.3	90.6	90.4	90.3	90.6	89.9	90.4	89.9	90.4	90.7	83.2	90.7	90.3	90.4	90.4	83.3	75.1
4	52.6	57.7	52.6	92.4	92.4	92.5	92.5	92.3	92.2	92.7	92.3	92.5	92.1	90.6	92.6	92.2	57.7	92.8	93.0	92.2	92.8	57.3	58.1
5	51.3	48.3	51.1	49.5	49.5	49.1	49.0	49.1	49.6	54.0	49.2	49.0	49.0	46.7	53.3	49.0	56.8	54.0	53.7	49.3	54.1	52.3	50.9
6	84.9	84.3	84.0	86.6	85.7	85.5	85.4	84.0	83.8	83.6	84.4	84.4	83.8	96.0	83.8	84.3	83.6	86.5	85.3	84.2	84.0	84.4	83.5
7	28.0	26.4	37.4	26.8	24.2	25.8	25.9	31.5	31.5	34.4	31.4	28.5	29.7	32.1	32.5	29.4	28.1	29.5	28.6	31.5	34.4	27.6	27.5
8	29.8	29.9	73.1	29.3	31.6	32.3	32.3	122.7	122.7	123.7	124.0	63.4	59.0	75.9	59.2	55.3	30.0	29.6	32.4	124.0	125.2	29.9	29.4
9	35.3	35.4	43.4	35.4	74.9	73.1	73.1	134.6	134.5	133.7	138.5	61.4	61.2	92.2	60.8	63.4	35.2	35.2	72.8	138.5	137.7	35.3	35.2
10	72.5	72.9	70.6	72.8	76.8	78.8	78.9	74.6	74.2	74.0	70.4	75.1	73.8	77.9	73.6	70.8	72.8	72.8	78.8	70.4	70.2	72.7	72.7
11	86.8	86.8	86.2	87.4	83.3	82.6	82.8	81.5	81.7	81.7	81.2	81.0	81.2	88.2	81.2	80.7	87.7	87.5	82.8	81.4	81.4	86.7	96.0[a]
12	97.9	97.8	97.5	96.7	96.8	96.9	96.9	97.1	97.0	96.9	97.0	96.6	98.2	101.0	98.2	98.3	97.1	96.7	96.9	96.9	96.8	97.4	93.0[a]
13	31.1	31.1	31.1	30.9	30.8	30.8	37.1	30.8	37.1	30.8	30.8	30.8	37.0	30.9	30.8	30.8	30.8	30.9	30.8	37.1	30.9	30.9	28.8
14	37.1	41.5	37.1	41.8	41.2	41.2	41.6	41.6	41.9	36.9	41.6	41.3	42.0	40.9	37.1	41.8	37.4	37.2	36.5	41.9	37.0	40.0	35.6
15	103.6	103.6	103.6	102.9	104.6	103.2	103.2	103.3	103.2	103.5	103.3	103.9	103.9	104.6	104.1	104.0	103.4	103.1	103.4	103.2	103.5	103.9	173.5
17	9.7	9.6	9.8	10.2	11.1	11.2	10.9	11.2	10.9	11.3	11.2	11.2	11.0	11.0	11.3	11.3	9.6	10.3	11.2	10.9	11.2	9.8	11.8
18	19.6	19.5	19.6	19.5	19.3	19.4	65.8	19.4	65.8	19.5	19.4	19.3	65.8	19.3	19.5	19.3	19.5	19.7	19.6	65.8	19.5	19.7[a]	19.5[a]
19	19.0	19.1	19.0	18.9	18.7	18.7	13.5	18.7	13.5	18.7	18.7	18.6	13.5	18.6	18.7	18.7	18.8	18.9	18.7	13.5	18.7	19.5[a]	22.0[a]
20	64.0	16.7	64.0	12.6	11.9	12.1	12.2	12.1	12.1	59.8	12.1	12.0	12.0	13.1	59.5	12.0	176.6	60.4	59.5	12.1	59.8	64.3	64.9
21	18.9	18.9	15.2	19.0	26.5	27.7	27.7	21.0	20.9	20.9	64.3	22.5	19.8	14.7	19.8	63.4	18.8	19.0	27.6	64.3	64.3	18.9	18.7
22	161.8	162.0	161.7	161.9	161.6	161.7	161.5	161.7	161.5	161.5	161.7	161.4	161.5	161.4	161.5	161.7	161.8	161.7	161.6	161.5	161.5	–	–
23	123.1	123.6	123.4	123.4	123.3	123.3	123.3	123.4	123.3	123.3	123.4	123.4	123.2	123.4	123.2	123.3	123.5	123.3	123.3	123.3	123.3	–	–
24	116.9	116.8	116.9	117.0	117.0	116.9	117.0	116.9	117.0	117.2	116.9	116.8	117.1	116.9	117.3	117.0	117.0	117.3	117.3	117.0	117.2	–	–
25	110.9	110.9	111.0	111.0	111.0	110.9	111.0	110.9	111.0	111.1	110.9	110.9	111.0	111.9	111.1	111.0	110.7	111.0	111.1	111.0	111.1	–	–
26	125.2	125.3	125.5	125.6	125.7	125.6	125.6	125.6	125.6	125.7	125.6	125.5	125.7	125.5	125.7	125.6	124.9	125.6	125.7	125.7	125.7	–	–

[a] Similar values might be interchanged.

our isolation work: all isolated compounds gave this rather sensitive reaction, which, in addition, permitted a general distinction between ryanodines/*epi*-ryanodines and spiganthines, respectively. In contrast to the ryanodines/*epi*-ryanodines, which produced a yellow-ochre colour, the spiganthines gave a red-purple spot. Obviously, the colour reaction did not depend on the presence of the 2-pyrrolecarboxylic ester group, since compounds **23** and **24** also reacted positively.

Despite all the precautions taken during our isolation and structure elucidation work (avoidance of higher temperatures, storage under nitrogen at low temperatures, absence of acidic or alkaline media, no excessive light etc.) some of the isolated compounds might be artefacts or partly artefacts: 9-hydroxylated compounds might have been transferred into the corresponding 8,9-dehydro compounds (e.g. **5** or **6**→**8**; **7**→**9**). Proton catalyzed rearrangement during work-up might have converted **12** to **15**. Oxygenating enzymes might be responsible for the generation of some of the epoxides.

However, considering the amounts isolated of the individual constituents and the various distinct grades of hydroxylation we regard most of the described compounds original natural products.

Among these, only spiganthine, ryanodine and 9-hydroxy-10-*epi*-ryanodine (**5**) (Jefferies et al., 1992) are already known compounds, whereas the others represent new natural products.

3. Biological activities

Ryanodine and spiganthine are known for their cardiac (Jenden and Fairhurst, 1969; Penefsky, 1974; Vierling, 1988; Achenbach et al., 1995; Sutko et al., 1997) and insecticidal (Jefferies et al., 1992; González-Coloma et al., 1996, 1999) activities. The availability of quite a number of new substances with structural variations arouse the interest to start structure–activity studies.

3.1. Cardiac activity

These tests were carried out as described earlier (Achenbach et al., 1995). Each of the tested compounds induced a delay in the development of cardiac contractions in a similar way as spiganthine (**1**) and ryanodine (**4**) but with divergent potencies. Fig. 1 shows a representative experiment using **8**, a substance about equally potent as **1** and **4**.

The concentration-versus-activity relationships of 12 of the most effective compounds are presented in Fig. 2, and the corresponding EC_{50} values are compiled in Table 4, where they have been divided in roughly three groups: strong, medium and weak activity. The EC_{50} values of the other tested compounds (**3, 5, 14–18** and **20–22**) were 100–1000 times higher than the value of ryanodine (**4**).

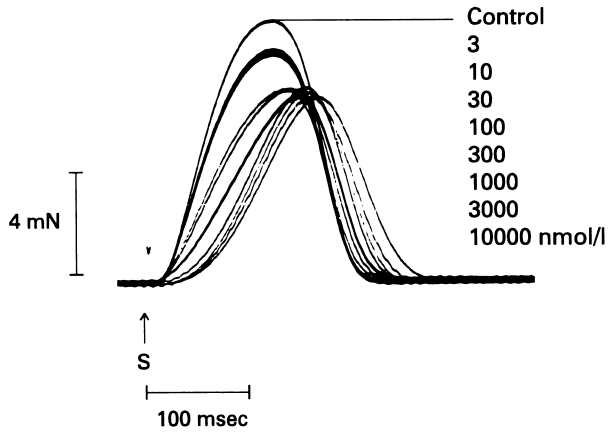

Fig. 1. Effect of 8,9-dehydro-10-*epi*-ryanodine (**8**) on the contraction of the guinea-pig papillary muscle. Increasing concentrations (nmol/l) of **8** caused a remarkable prolongation of the latency time between the stimulus (S) and the beginning of the contraction; additionally, the force of contraction (mN) decreases. (Stimulation frequency: 1 Hz). Ordinate: force in mN; abscissa: time in msec.

For the most active substances **1, 2, 4** and **8**, the following structure–activity relationships were revealed: omission of the hydroxy group from position C-4 (**4**→**2**) or C-20 (**1**→**2**) with an otherwise unchanged structure caused only slight attenuation of the biological activity; and transfer of the hydroxyl from C-4 to C-20 (**4**→**1**) did also not significantly influence the activity. Furthermore, compound **8**, which represents the least hydroxylated substance in the 8,9-dehydro-series, is similarly active as **4**, from which it structurally differs by unsaturation ($\Delta^{8,9}$) and epimerisation at C-10. But 10-epimerisation combined with 8,9-epoxidation (**4**→**12**, **13**) reduced the cardiac activity considerably to less than 10%, and the presence of the two hydroxy groups at C-4 and C-20 (**1**→**19** or **4**→**19**) led to an even more dramatic reduction of activity. These results suggested an essential influence of the polarity of ryanodine/spiganthine-type compounds for their cardiac activity.

As a general guide line we summarize our results: the already known compounds spiganthine (**1**) and ryanodine (**4**) exhibit highest cardiac activity, which is not much influenced by neither removal of their hydroxy group at C-4 or C-20 nor by introduction of an 8,9-double bond together with 10-epimerization. In contrast, 8,9-epoxidation and, particularly, introduction of additional hydroxy groups causes loss of cardiac activity.

3.2. Insect antifeedant and insecticidal activity

Major efforts have been invested to study the antifeedant and insecticidal potential of ryanodine (**4**) and structurally related compounds (Wiesner et al., 1967;

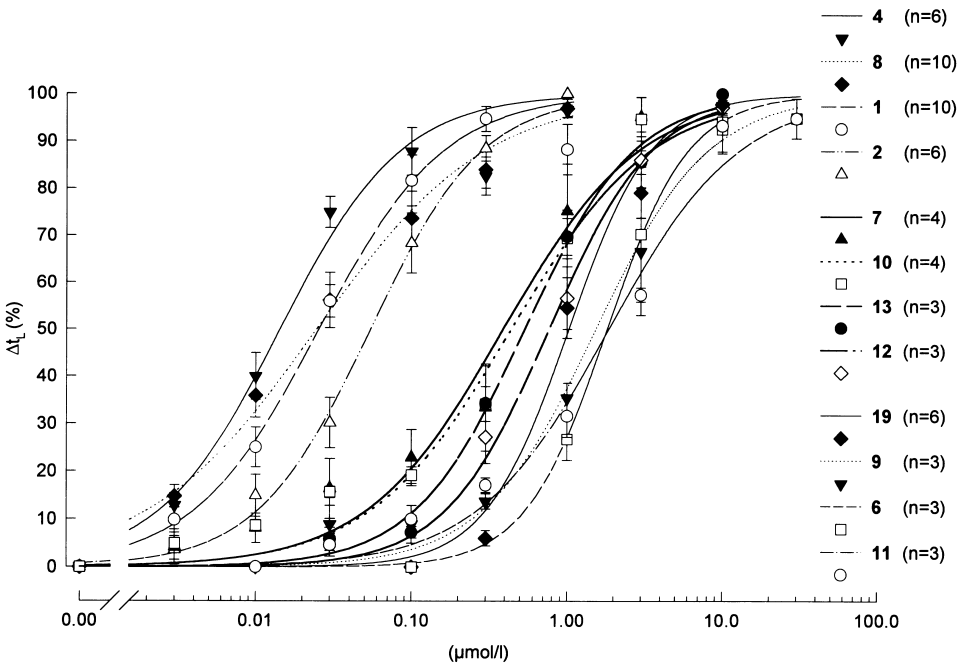

Fig. 2. Concentration–activity relationship of the 12 most active compounds isolated from *Spigelia anthelmia*. Ordinate: prolongation of the latency time (Δt_L) in % of the maximal prolongation of each muscle group. (Shown are mean values ± S.E.M.) Abscissa: concentration of the test compounds in μmol/l (logarithmic scale). The depicted curves were fitted to the mean values using a logistic function.

Table 4
EC_{50} values (nmol/l) of the most active compounds isolated from *Spigelia anthelmia* determined by fitting a logistic function to the mean values of the concentration–activity curves presented in Fig. 2

Substance	Number of experiments (*n*)	EC_{50} (nmol/l)
4	5	14
8	9	17
1	8	25
2	6	54
7	4	390
10	4	440
13	3	540
12	3	770
19	6	1100
9	3	1500
6	6	1800
11	3	1900

Waterhouse et al., 1987; Jefferies et al., 1992; González-Coloma et al., 1996). A newer investigation also included spiganthine (**1**) and a number of our isolated ryanodine derivatives in these studies. The results have been published very recently (González-Coloma et al., 1999) and demonstrated significant antifeedant activity against some test beetles for spiganthine, ryanodine, the β-epoxide **13** and, particularly, 9-hydroxy-10-*epi*-ryanodine (**5**). In addition, considerable insecticidal activities were observed for spiganthine, ryanodine, and the α-epoxide **12**. These effects were especially remarkable for **12** in the presence of piperonyl butoxide, an agent known as a synergist for the insecticidal action of ryanodine (Waterhouse et al., 1987), which might inhibit the biological decomposition of **12** (González-Coloma et al., 1999).

4. Experimental

4.1. General

TLC was done on ready-made plates using S-1 = $CHCl_3$:MeOH:H_2O (80:20:1). Detection: UV and anisaldehyde reagent (Stahl and Kaltenbach, 1961). Unless stated otherwise, IR were run as dry films on NaCl; [α]D, UV, and CD measurements in MeOH at 20°. ^1H NMR at 360 MHz and ^{13}C NMR at 90 MHz in CD_3OD with TMS as int. standard. MS were recorded by FABMS (negative ions) in glycerol (xenon, 8 kV). Sephadex® LH 20 was used for CC, Si gel 60 for MPLC (at ca 3 bar); HPLC was done on Nucleosil® RP18 with the solvent systems S-2 = MeOH:H_2O (43:57), S-3 = MeOH:H_2O (30:70) or S-4 = MeOH:H_2O (20:80).

4.2. Extraction and chromatography

The exctract of 2 kg dried aerial parts of *Spigelia anthelmia* (purchased from Müggenburg, Hamburg, Germany, batch-no. 2917) was prepared with 20 l EtOH:H_2O (86:14) according to the German Homoeopathic Pharmacopoeia. Evapn. yielded 260 g residue, which was diluted in 6 l MeOH:H_2O (1:3) and subsequently extracted with $CHCl_3$ (3×5 l) and EtOAc (3×3

l). Evapn of the solvents afforded 75 g $CHCl_3$-I, 1.8 g $CHCl_3$-II, 1.2 g $CHCl_3$-III, 8.2 g EtOAc-I, 2.3 g EtOAc-II and 1.2 g EtOAc-III. Repeated CC of $CHCl_3$-II, $CHCl_3$-III, and EtOAc-I was done on Sephadex LH 20 with MeOH followed by MPLC on Si gel using the solvent system $CHCl_3$:MeOH (from 95:5 to 8:2). Finally, HPLC with S-2 or S-3 yielded pure spiganthines/ryanodines as described in Table 1. The separation procedures were monitored by the characteristic colour reaction of these compounds with anisaldehyde reagent.

4.3. Spiganthine (*1*)

Crystals from $CHCl_3$:Me_2CO (3:1) (23 mg), mp 159°. TLC: R_f 0.46; anisaldehyde: red-purple. HPLC: R_t 35.0 min (S-2). [α]D +35° (*c* 0.5). CD λ_{max} nm (Θ): 205 (+5875), 225 (−4000), 245 (+570), 265 (−95), 280 (+275). ^{1}H NMR: Table 2. ^{13}C NMR: Table 3. FABMS *m/z* (rel. int.): 492 $[M-H]^-$ (100), 381 $[M-111-H]^-$ (40). All other physicochemical properties were also identical with an authentic sample (Achenbach et al., 1995).

4.4. Hydrolysis of spiganthine (*1*)

A solution of 7.5 mg of **1** in 5 ml aqueous KOH (1%) was stirred for 90 min at 60°C. After neutralization with 2 n H_2SO_4, the aqueous phase was extracted with EtOAc, the organic extract evapd and the residue purified by CC on silica gel using S-1. This yielded compounds **23** (2.5 mg), **24** (2.5 mg) and 2-pyrrolecarboxylic acid (1 mg).

4.5. Spiganthol (*23*)

Amorphous. TLC: R_f 0.31; anisaldehyde: pink. ^{1}H NMR: Table 2. ^{13}C NMR: Table 3. FABMS *m/z* (rel. int.): 399 $[M-H]^-$ (80), 367 $[M-32-H]^-$ (90), 281 (100).

4.6. Anhydrospiganthol (*24*)

Amorphous. TLC: R_f 0.44; anisaldehyde: pink. ^{1}H NMR: Table 2. ^{13}C NMR: Table 3. FABMS *m/z* (rel. int.): 381 $[M-H]^-$ (100).

4.7. 2-Pyrrolecarboxylic acid

Amorphous. TLC: R_f 0.27; anisaldehyde: yellow. UV λ_{max} nm (log ε): 260 (3.54). ^{1}H NMR: δ 6.12 (1H, *dd*, J_1 = 4, J_2 = 2.5 Hz, H-4), 6.76 (1H, *dd*, J_1 = 4, J_2 = 1.5 Hz, H-3), 6.85 (1H, *dd*, J_1 = 2.5, J_2 = 1.5 Hz, H-5).

4.8. 20-Deoxyspiganthine (*2*)

Crystals from $CHCl_3$:Me_2CO (1:1) (1.5 mg), mp 144–147°. TLC: R_f 0.48; anisaldehyde: red-purple. HPLC: R_t 57.5 min (S-2). [α]D +12° (*c* 0.1). IR ν_{max} cm^{-1}: 3400, 2925, 1695. UV λ_{max} nm (log ε): 265 (3.88). CD λ_{max} nm (Θ): 205 (+2165), 225 (−2801), 295 (−515). ^{1}H NMR: Table 2. ^{13}C NMR: Table 3. FABMS *m/z* (rel. int.): 476 $[M-H]^-$ (50), 365 $[M-111-H]^-$ (60), 281 (100).

4.9. 8α-Hydroxyspiganthine (*3*)

Crystals from $CHCl_3$:Me_2CO (3:1) (1 mg), mp 255–257°. TLC: R_f 0.24; anisaldehyde: red-purple. HPLC: R_t 17.5 min (S-2). [α]D +26° (*c* 0.1). IR ν_{max} cm^{-1}: 3410, 2930, 1700. UV λ_{max} nm (log ε): 265 (4.18). CD λ_{max} nm (Θ): 205 (+4170), 225 (−3650), 244 (+390), 265 (−576). ^{1}H NMR: Table 2. ^{13}C NMR: Table 3. FABMS *m/z* (rel. int.): 508 $[M-H]^-$ (80), 397 $[M-111-H]^-$ (50), 281 (100).

4.10. 20-Norspiganthine-5-carboxylic acid (*18*)

Crystals from $CHCl_3$:MeOH (1:1) (20 mg), mp >300°. TLC: R_f 0.09; anisaldehyde: red-purple. HPLC: R_t 5.0 min (S-2), R_t 7.5 min (S-4). [α]D +15° (*c* 0.4). IR ν_{max}^{KBr} cm^{-1}: 3400, 2970, 1680. UV λ_{max} nm (log ε): 265 (4.11). CD λ_{max} nm (Θ): 205 (+55), 230 (−3170), 265 (+1995). ^{1}H NMR: Table 2. ^{13}C NMR: Table 3. FABMS *m/z* (rel. int.): 506 $[M-H]^-$ (100).

4.11. Methyl ester of *18*

Compound **18** (7 mg) was dissolved in 1 ml MeOH and treated with 3 ml diazomethane/Et_2O at room temp. for 5 h. After evapn the residue was purified by HPLC on RP-18 using S-2 to obtain 1 mg of the methyl ester of **18** (amorphous). TLC: R_f 0.51; anisaldehyde: red-purple. HPLC: R_t 34.0 min (S-2). [α]D +18° (*c* 0.1). ^{1}H NMR: δ 0.78 (3H, *d*, *J* = 6.5 Hz, Me-19), 1.00 (3H, *d*, *J* = 6.5 Hz, Me-21), 1.14 (3H, *d*, *J* = 6.5 Hz, Me-18), 1.15–1.22 (1 H, *m*, H-7β), 1.36 (3H, *s*, Me-17), 1.45–1.56 2H, *m*, H-8β, H-8α), 1.74–1.87 (1H, *m*, H-9), 2.23 (1H, *ddd*, J_1 = 13, J_2 = 11, J_3 = 6 Hz, H-7α), 2.26–2.36 (1H, *m* , H-13) overlapped by 2.32 (1H, *d*, *J* = 13 Hz, H-14_B), 2.61 (1H, *d*, *J* = 14Hz, H-14_A), 3.10 (3H, *s*, CO_2Me), 3.75 (1H, *d*, *J* = 10, H-10), 3.94 (1H, *dd*, J_1 = 8,5 J_2 = 2 Hz, H-4), 5.76 (1H, *d*, *J* = 8.5 Hz, H-3), 6.19 (1H, *dd*, J_1 = 4, J_2 = 2.5 Hz, H-25), 6.72 (1H, *dd*, J_1 = 4, J_2 = 1.5 Hz, H-24), 6.99 (1H, *dd*, J_1 = 2.5, J_2 = 1.5 Hz, H-26). FABMS *m/z* (rel. int.): 520 $[M-H]^-$ (100).

4.12. Ryanodine (*4*)

Crystals from $CHCl_3$:Me_2CO (3:1) (8 mg), mp 180°. TLC: R_f 0.46; anisaldehyde: yellow-ochre. HPLC: R_t 57.5 min (S-2). [α]D +9° (c 0.7). IR ν_{max} cm^{-1}: 3305, 2930, 1695. UV λ_{max} nm (log ε): 265 (4.15). CD λ_{max} nm (Θ): 205 (+4495), 230 (−4915), 245 (−510), 260

(−2095). ^{1}H NMR: Table 2. ^{13}C NMR: Table 3. FABMS *m/z* (rel. int.): 492 [M-H]$^-$ (100), 381 [M-111-H]$^-$ (70). All other physicochemical properties were also identical with an authentic sample purchased from Calbiochem® Biochemicals.

4.13. 20-Hydroxyryanodine (**19**)

Crystals from $CHCl_3$:MeOH (3:1) (19 mg), mp 188°. TLC: R_f 0.33; anisaldehyde: yellow-ochre. HPLC: R_t 18.5 min (S-2). [α]D +8° (*c* 1.0). IR ν_{max} cm^{-1}: 3305, 2955, 1695. UV λ_{max} nm (log ε): 265 (4.32). CD λ_{max} nm (Θ): 205 (+5815), 230 (−5040), 245 (−765), 265 (−2565). ^{1}H NMR: Table 2. ^{13}C NMR: Table 3. FABMS *m/z* (rel. int.): 508 [M-H]$^-$ (100), 397 [M-111-H]$^-$ (40).

4.14. 9-Hydroxy-10-epi-ryanodine (**5**)

Crystals from $CHCl_3$:Me_2CO (3:1) (3.5 mg), mp 169°. TLC: R_f 0.51; anisaldehyde: yellow-ochre. HPLC: R_t 71.0 min (S-2). [α]D +2° (*c* 0.1). IR ν_{max} cm^{-1}: 3305, 2930, 1695. UV λ_{max} nm (log ε): 265 (4.06). CD λ_{max} nm (Θ): 205 (+6435), 230 (−7670), 245 (−460), 265 (−3200). ^{1}H NMR: Table 2. ^{13}C NMR: Table 3. FABMS *m/z* (rel. int.): 508 [M-H]$^-$ (100), 397 [M-111-H]$^-$ (40).

4.15. 9-Hydroxy-9-epi-10-epi-ryanodine (**6**)

Crystals from $CHCl_3$:Me_2CO (3:1) (40 mg), mp 178°. TLC: R_f 0.40; anisaldehyde: yellow-ochre. HPLC: R_t 60.0 min (S-2). [α]D +11° (*c* 1.0). IR ν_{max}^{KBr} cm^{-1}: 3340, 2935, 1690. UV λ_{max} nm (log ε): 265 (4.33). CD λ_{max} nm (Θ): 205 (+4915), 230 (−5465), 245 (−325), 265 (−2415). ^{1}H NMR: Table 2. ^{13}C NMR: Table 3. FABMS *m/z* (rel. int.): 508 [M-H]$^-$ (100), 397 [M-111-H]$^-$ (50).

4.16. (13S)-9,18-Dihydroxy-9-epi-10-epi-ryanodine (7)

Crystals from $CHCl_3$:Me_2CO (3:1) (3 mg), mp 190°. TLC: R_f 0.28; anisaldehyde: yellow-ochre. HPLC: R_t 24.0 min (S-2). [α]D +10° (*c* 0.35). IR ν_{max} cm^{-1}: 3305, 2925, 1695. UV λ_{max} nm (log ε): 265 (4.17). CD λ_{max} nm (Θ): 210 (+2025), 230 (−3940), 245 (−470), 270 (−4720). ^{1}H NMR: Table 2. ^{13}C NMR: Table 3. FABMS *m/z* (rel. int.): 524 [M-H]$^-$ (100), 413 [M-111-H]$^-$ (90).

4.17. 9,20-Dihydroxy-9-epi-10-epi-ryanodine (**20**)

Crystals from $CHCl_3$:MeOH (3:1) (3 mg), mp 178°. TLC: R_f 0.28; anisaldehyde: yellow-ochre. HPLC: R_t 20.0 min (S-2). [α]D +4° (*c* 0.1). IR ν_{max} cm^{-1}: 3390, 2930, 1695. UV λ_{max} nm (log ε): 265 (4.26). CD λ_{max} nm (Θ): 205 (+5030), 230 (−3730), 245 (−410), 265 (−2350). ^{1}H NMR: Table 2. ^{13}C NMR: Table 3. FABMS *m/z* (rel. int.): 524 [M-H]$^-$ (100), 413 [M-111-H]$^-$ (20).

4.18. 8,9-Dehydro-10-epi-ryanodine (**8**)

Crystals from $CHCl_3$:Me_2CO (1:1) (6 mg), mp 165. TLC: R_f 0.56; anisaldehyde: yellow-ochre. HPLC: R_t 62.0 min (S-2). [α]D +20 (*c* 0.1). IR ν_{max} cm^{-1}: 3365, 2930, 1700. UV λ_{max} nm (log ε): 265 (4.15). CD λ_{max} nm (Θ): 210 (+2205), 230 (−4370), 245 (−385), 265 (−1920). ^{1}H NMR: Table 2. ^{13}C NMR: Table 3. FABMS *m/z* (rel. int.): 490 [M-H]$^-$ (100), 379 [M-111-H]$^-$ (40).

4.19. (13S)-8,9-Dehydro-18-hydroxy-10-epi-ryanodine (**9**)

Crystals from $CHCl_3$:Me_2CO (3:1) (6 mg), mp 168°. TLC: R_f 0.46; anisaldehyde: yellow-ochre. HPLC: R_t 26.0 min (S-2). [α]D +11° (*c* 0.2). IR ν_{max} cm^{-1}: 3390, 2920, 1695. UV λ_{max} nm (log ε): 265 (4.07). CD λ_{max} nm (Θ): 210 (−355), 230 (−3730), 245 (−445), 265 (−2375). ^{1}NMR: Table 2. ^{13}C NMR: Table 3. FABMS *m/z* (rel. int.): 506 [M-H]$^-$ (60), 395 [M-111-H]$^-$ (60), 281 (100).

4.20. 8,9-Dehydro-20-hydroxy-10-epi-ryanodine (**10**)

Crystals from $CHCl_3$:Me_2CO (3:1) (4.5 mg), mp 148°. TLC: R_f 0.40; anisaldehyde: yellow-ochre. HPLC: R_t 23.0 min (S-2). [α]D +14° (*c* 0.2). IR ν_{max} cm^{-1}: 3350, 2920, 1700. UV λ_{max} nm (log ε): 265 (4.18). CD λ_{max} nm (Θ): 210 (+1615), 230 (−2355), 245 (−355), 265 (−1680). ^{1}H NMR: Table 2. ^{13}C NMR: Table 3. FABMS *m/z* (rel. int.): 506 [M-H]$^-$ (100), 395 [M-111-H]$^-$ (60).

4.21. 8,9-Dehydro-21-hydroxy-10-epi-ryanodine (**11**)

Crystals from $CHCl_3$:Me_2CO (3:1) (15 mg), mp 178°. TLC: R_f 0.35; anisaldehyde: yellow-ochre. HPLC: R_t 33.0 min (S-2). [α]D +25° (*c* 1.0). IR ν_{max} cm^{-1}: 3365, 2935, 1700. UV λ_{max} nm (log ε): 265 (4.71). CD λ_{max} nm (Θ): 205 (+3070), 230 (−4175), 245 (−165), 265 (−1565). ^{1}H NMR: Table 2. ^{13}C NMR: Table 3. FABMS *m/z* (rel. int.): 506 [M-H]$^-$ (100), 395 [M-111-H]$^-$ (50).

4.22. 9-Epi-10-epi-ryanodine from **11**

The solution of 4.5 mg **11** in 4 ml EtOH was stirred in the presence of palladium (10% on carbon) (25 mg) under hydrogen for 6 h at room temp. The reaction mixture was evapd and the residue purified by CC on silica gel using S-1 to obtain 3 mg of 9-*epi*-10-*epi*-ryanodine (amorphous). TLC: R_f 0.56; anisaldehyde:

yellow-ochre. [α]D +14° (*c* 0.3). UV λ_{max} nm (log ε): 265 (4.25). CD λ_{max} nm (Θ): 200 (+4760), 230 (−4040), 245 (−180), 255 (−595), 265 (+890). ^{1}H NMR: δ 0.74 (3H, *d*, *J* = 6.5 Hz, Me-19), 0.90 (3H, *s*, Me-20), 1.08 (3H, *d*, *J* = 6.5 Hz, Me-18), 1.14 (3H, *s*, Me-21), 1.27–1.43 (5H, *m*, H-7β, H-8α) including 1.34 (3H, *s*, Me-17), 1.89 (1H, *d*, *J* = 14 Hz, H-14$_B$), 1.95–2.08 (2H, *m*, H-9, H-8β), 2.11–2.28 (2H, *m*, H-7α, H-13), 2.58 (1H, *d*, *J* = 14 Hz, H-14$_A$), 3.78 (1H, *d*, *J* = 2.5 Hz, H-10), 5.65 (1H, *s*, H-3), 6.24 (1H, *dd*, J_1 = 4, J_2 = 2.5 Hz, H-25), 6.87 (1H, *dd*, J_1 = 4, J_2 = 1.5 Hz, H-24), 7.03 (1H, *dd*, J_1 = 2.5, J_2 = 1.5 Hz, H-26). FABMS *m*/*z* (rel. int.): 492 [M-H]$^-$ (100), 381 [M-111-H]$^-$ (90).

4.23. Epoxydation of **11**

Compound **11** (7 mg) was epoxydized with 3-chloroperoxybenzoic acid (20 mg) according to Waterhouse et al. (1987). Purification of the reaction mixture by CC on silica gel using S-1 and subsequent HPLC on RP-18 (S-2) yielded the two epoxydation products EP-1 (**17**) and EP-2 (*iso*-**17**).

4.24. EP-1

Amorphous (0.8 mg). TLC: R_f 0.30; anisaldehyde: yellow-ochre. [α]D +10° (*c* 0.05). All other physicochemical properties were also identical with the isolated natural compound **17**.

4.24.1. 8α,9α-Epoxy-21-hydroxy-10-epi-ryanodine (**17**) (=EP-1)

Crystals from $CHCl_3$:Me_2CO (3:1) (4 mg), mp 193°. TLC: R_f 0.30; anisaldehyde: yellow-ochre. HPLC: R_t 30.0 min (S-2). [α]D +13° (*c* 0.2). IR ν_{max} cm^{-1}: 3365, 2935, 1700. UV λ_{max} nm (log ε): 265 (4.14). CD λ_{max} nm (Θ): 205 (+4160), 230 (−4780), 245 (−290), 265 (−2060). ^{1}H NMR: Table 2. ^{13}C NMR: Table 3. FABMS *m*/*z* (rel. int.): 522 [M-H]$^-$ (100), 411 [M-111-H]$^-$ (50).

4.25. EP-2 (=8β,9β-Epoxy-21-hydroxy-10-epi-ryanodine)

Amorphous (1 mg). TLC: R_f 0.30; anisaldehyde: yellow-ochre. HPLC: R_t 36.0 min (S-2). [α]D +20° (*c* 0.05). ^{1}H NMR: δ 0.73 (3H, *d*, *J* = 6.5 Hz, Me-19), 0.93 (3H, *s*, Me-20), 1.09 (3H, *d*, *J* = 6.5 Hz, Me-18), 1.37 (3H, *s*, Me-17), 1.91 (1H, *d*, *J* = 14 Hz, H-14$_B$), 1.98 (1H, *dd*, J_1 = 15, J_2 = 2 Hz, H-7β), 2.17–2.28 (1H, *m*, H-13), 2.42 (1H, *dd*, J_1 = 15, J_2 = 2 Hz, H-7α), 2.64 (1H, *d*, *J* = 14 Hz, H-14$_A$), 3.55 (1H, *dd*, J_1 = J_2 = 2 Hz, H-8), 3.71 (2H, *s*, H-21$_A$, H-21$_B$), 4.29 (1H, *s*, H-10), 5.63 (1H, *s*, H-3), 6.24 (1H, *dd*, J_1 = 4, J_2 = 2.5 Hz, H-25), 6.86 (1H, *dd*, J_1 = 4, J_2 = 1.5 Hz, H-24), 7.03 (1H, *dd*, J_1 = 2.5, J_2 = 1.5 Hz, H-26). FABMS *m*/*z* (rel. int.): 522 [M-H]$^-$ (100), 411 [M-111-H]$^-$ (20).

4.26. (13S)-8,9-Dehydro-18,21-dihydroxy-10-epi-ryanodine (**21**)

Crystals from $CHCl_3$:MeOH (1:1) (1.5 mg), mp 162°. TLC: R_f 0.26; anisaldehyde: yellow-ochre. HPLC: R_t 14.5 min (S-2). [α]D +7° (*c* 0.2). IR ν_{max} cm^{-1}: 3390, 2930, 1695. UV λ_{max} nm (log ε): 265 (4.56). CD λ_{max} nm (Θ): 210 (+1450), 230 (−2580), 245 (±0), 265 (−1185). ^{1}H NMR: Table 2. ^{13}C NMR: Table 3. FABMS *m*/*z* (rel. int.): 522 [M-H]$^-$ (100), 411 [M-111-H]$^-$ (50).

4.27. 8,9-Dehydro-20,21-dihydroxy-10-epi-ryanodine (**22**)

Crystals from $CHCl_3$:MeOH (1:1) (4.5 mg), mp 173°. TLC: R_f 0.20; anisaldehyde: yellow-ochre. HPLC: R_t 16.0 min (S-2). [α]D +6° (*c* 0.2). IR ν_{max} cm^{-1}: 3365, 2930, 1695. UV λ_{max} nm (log ε): 265 (4.08). CD λ_{max} nm (Θ): 205 (+2275), 230 (−3630), 245 (−300), 265 (−1730). ^{1}H NMR: Table 2. ^{13}C NMR: Table 3. FABMS *m*/*z* (rel. int.): 522 [M-H]$^-$ (100), 411 [M-111-H]$^-$ (20).

4.28. 8α,9α-Epoxy-10-epi-ryanodine (**12**)

Crystals from $CHCl_3$:Me_2CO (3:1) (13.5 mg), mp 196°. TLC: R_f 0.54; anisaldehyde: yellow-ochre. HPLC: R_t 42.0 min (S-2). [α]D +13° (*c* 0.4). IR ν_{max} cm^{-1}: 3305, 2935, 1705. UV λ_{max} nm (log ε): 265 (4.11). CD λ_{max} nm (Θ): 205 (+5035), 230 (−4520), 245 (−410), 265 (−2455). ^{1}H NMR: Table 2. ^{13}C NMR: Table 3. FABMS *m*/*z* (rel. int.): 506 [M-H]$^-$ (100), 395 [M-H-111]$^-$ (30).

4.29. Acid-catalyzed isomerization of **12**

Aqueous oxalic acid (1%) (3 ml) was added to a solution of **12** (4 mg) in Me_2CO (3 ml) and stirred for 60 h at room temp. After evapn of the organic solvent, the aqueous residue was diluted with 5 ml H_2O and extracted with 3×10 ml EtOAc. Evapn and CC of the extract on silica gel using S-1 yielded 3.5 mg of the pure product. Crystals from $CHCl_3$:Me_2CO (3:1), mp 172°. TLC: R_f 0.38; anisaldehyde: yellow-ochre. HPLC: R_t 41.5 min (S-2). [α]D −10° (*c* 0.2). All spectroscopic data were also identical with those of genuine **15**.

4.30. 6-Deoxy-6β,9β-epoxy-8α-hydroxy-10-epi-ryanodine (**15**)

Crystals from $CHCl_3$:Me_2CO (3:1) (6 mg), mp 172°. TLC: R_f 0.38; anisaldehyde: yellow-ochre. HPLC: R_t 41.5 min (S-2). [α]D −8° (*c* 0.2). IR ν_{max} cm^{-1}: 3400, 2930, 1695. UV λ_{max} nm (log ε): 265 (3.93). CD λ_{max} nm (Θ): 205 (+1685), 230 (−3265), 245 (−400), 265 (−2400), 295 (+230). ^{1}H NMR: Table 2. ^{13}C NMR:

Table 3. FABMS m/z (rel. int.): 506 $[M\text{-}H]^-$ (80), 395 $[M\text{-}111\text{-}H]^-$ (60), 275 (100).

4.31. 8β,9β-Epoxy-10-epi-ryanodine (**13**)

Crystals from $CHCl_3$:Me_2CO (3:1) (4 mg), mp 212°. TLC: R_f 0.51; anisaldehyde: yellow-ochre. HPLC: R_t 50.0 min (S-2). $[\alpha]_D$ +7° (c 0.2). IR ν_{max} cm^{-1}: 3390, 2915, 1595. UV λ_{max} nm (log ε): 265 (4.03). CD λ_{max} nm (Θ): 205 (+1705), 230 (−3015), 245 (±0), 265 (−1245). ^1H NMR: Table 2. ^{13}C NMR: Table 3. FABMS m/z (rel. int.): 506 $[M\text{-}H]^-$ (100), 395 $[M\text{-}111\text{-}H]^-$ (10).

4.32. (13S)-8α,9α-Epoxy-18-hydroxy-10-epi-ryanodine (**14**)

Crystals from $CHCl_3$:Me_2CO (3:1) (3.5 mg), mp 200°. TLC: R_f 0.39; anisaldehyde: yellow-ochre. HPLC: R_t 17.0 min (S-2). $[\alpha]_D$ +7° (c 0.2). IR ν_{max} cm^{-1}: 3370, 2930, 1695. UV λ_{max} nm (log ε): 265 3.87). CD λ_{max} nm (Θ): 205 (+1015), 230 (−2365), 245 (−360), 265 (−1210). ^1H NMR: Table 2. ^{13}C NMR: Table 3. FABMS m/z (rel. int.): 522 $[M\text{-}H]^-$ (100), 411 $[M\text{-}111\text{-}H]^-$ (30).

4.33. 8α,9α-Epoxy-20-hydroxy-10-epi-ryanodine (**16**)

Crystals from $CHCl_3$:Me_2CO (3:1) (2 mg), mp 208°. TLC: R_f 0.37; anisaldehyde: yellow-ochre. HPLC: R_t 19.0 min (S-2). $[\alpha]_D$ +8° (c 0.1). IR ν_{max} cm^{-1}: 3365, 2930, 1700. UV λ_{max} nm (log ε): 265 (4.12). CD λ_{max} nm (Θ): 205 (+3730), 230 (−3530), 245 (−480), 265 (−2030).

4.34. Pharmacological experiments

Pharmacological tests were performed as described previously (Achenbach et al., 1995).

Acknowledgements

Thanks are due to the Deutsche Forschungsgemeinschaft and to the Fonds der Chemischen Industrie for financial support.

References

Achenbach, H., Hübner, H., Vierling, W., Brandt, W., Reiter, M., 1995. Spiganthine, the cardioactive principle of *Spigelia anthelmia*. Journal of Natural Products 58, 1092–1096.

González-Coloma, A., Gutiérrez, C., Hübner, H., Achenbach, H., Terrero, D., Fraga, B.M., 1999. Selective insect antifeedant and toxic action of ryanoid diterpenes. Journal of Agricultural and Food Chemistry 47, 4419–4424.

González-Coloma, A., Terrero, D., Perales, A., Escoubas, P., Fraga, B.M., 1996. Insect antifeedant ryanodane diterpenes from *Persea indica*. Journal of Agricultural and Food Chemistry 44, 296–300.

Jenden, D.J., Fairhurst, A.S., 1969. The pharmacology of ryanodine. Pharmacological Reviews 21, 1–25.

Jefferies, P.R., Toia, R.F., Brannigan, B., Pessah, I.N., Casida, J.E., 1992. Ryania insecticide: analysis and biological activity of 10 natural ryanoids. Journal of Agricultural and Food Chemistry 40, 142–146.

Kelly, R.B., Whittigham, D.J., Wiesner, K., 1951. The structure of ryanodine. Canadian Journal of Chemistry 29, 905–910.

Nkunya, M.H.H., Jonker, S.A., Makangara, J.J., Waibel, R., Achenbach, H., 2000. Aporphinoid alkaloids and other constituents from *Lettowianthus stellatus*. Phytochemistry 53, 1067–1073.

Penefsky, Z.J., 1974. Studies on mechanism of inhibition of cardiac muscle contractile tension by ryanodine. Mechanical response. Pflügers Archiv 347, 173–184.

Stahl, E., Kaltenbach, U., 1961. Thin-layer chromatography. VI. Trace analysis of sugar mixtures on layers of Kieselgur G. Journal of Chromatography 5, 351–355.

Sutko, J.L., Airey, J.A., Welch, W., Ruest, L., 1997. The pharmacology of ryanodine and related compounds. Pharmacological Reviews 49, 53–98.

Vierling, W., 1988. Ryanodine in mammalian heart ventricular muscle: indication for the induction of calcium leakage from the sarcoplasmic reticulum. European Journal of Pharmacology 145, 329–334.

Waterhouse, A.L., Pessah, I.N., Francini, A.O., Casida, J.E., 1987. Structural aspects of ryanodine action and selectivity. Journal of Medicinal Chemistry 30, 710–716.

Wiesner, K., Valenta, Z., Findlay, J.A., 1967. The structure of ryanodine. Tetrahedron Letters, 221–225.

PERGAMON

Phytochemistry 57 (2001) 297–301

PHYTOCHEMISTRY

www.elsevier.com/locate/phytochem

Flavonoid glucuronides from *Helicteres isora*☆

Kohei Kamiya [a,b], Yasuhisa Saiki [a], Takao Hama [a], Yasuo Fujimoto [c], Hanani Endang [d], Mansur Umar [d], Toshiko Satake [a,b,*]

[a] *Faculty of Pharmaceutical Sciences, Kobe Gakuin University, Nishi-ku, Kobe 651-2180, Japan*
[b] *High Technology Research Center, Kobe Gakuin University, Nishi-ku, Kobe 651-2180, Japan*
[c] *College of Pharmacy, Nihon University, 7-7-1, Narashinodai, Funabashi, Chiba 274-8555, Japan*
[d] *Department of Pharmacy, Faculty of Mathematics and Natural Sciences, University of Indonesia, Depok-Jawa Barat, Indonesia*

Received 11 September 2000; received in revised form 11 December 2000

Abstract

Five flavonoid glucuronides were obtained from the fruit of *Helicteres isora*, three of which were previously unknown compounds: isoscutellarein 4′-methyl ether 8-*O*-β-D-glucuronide 6″-*n*-butyl ester, isoscutellarein 4′-methyl ether 8-*O*-β-D-glucuronide 2″, 4″-disulfate and isoscutellarein 8-*O*-β-D-glucuronide 2″,4″-disulfate. The structures were determined on the basis of spectroscopy and hydrolysis experiments. © 2001 Elsevier Science Ltd. All rights reserved.

Keywords: *Helicteres isora*; Sterculiaceae; Jamu; Flavonoid glucuronide; Sulfate; Structural elucidation

1. Introduction

Helicteres isora L. (Sterculiaceae) is widely distributed from southern China, to India, Southeast Asia and Australia. The roots are used in the treatment of chronic nephritis and gastric ulcers in China. In Indonesia, the fruit of *H. isora* is referred to as "Ulet-Ulet" on Java island and is a raw material for production of "Jamu". It is used as an anthelmintic against tapeworm and in the treatment of gastrospasm. Chemical analyses of *H. isora* have detected the presence of cucurbitacins (Bean et al., 1985), flavonoids (Romesh and Yuvarajan, 1995), neolignans (Tezuka et al., 1999) and rosmarinic acid derivatives (Satake et al., 1999). In the present paper, we discuss the isolation and structural elucidation of five flavonoids including three new compounds (Fig. 1).

2. Results and discussion

A 70% methanol extract of the fruit of *H. isora* was fractionated by combination of MCI gel, SiO_2 gel, Sephadex LH-20 and RP-18 column chromatography to afford a series of flavonoids (**1**–**5**). Compounds **1**–**5**, positive on Mg–HCl and anthrone tests, were obtained as yellow amorphous powders, indicating them to be flavonoid glycosides.

Compound **1** was identical to isoscutellarein 4′-methyl ether 8-*O*-β-D-glucuronide. Its structure was confirmed by NMR and UV spectrum in addition to acid hydrolysis and enzymic hydrolysis. This compound was previously isolated from *Takakia lepidoziodes* (Markham and Porter, 1979) (Tables 1 and 2).

Compound **2** gave an $[M–H]^-$ at m/z 531.1581, which corresponded with the molecular formula of $C_{26}H_{28}O_{12}$ from the HR-negative-FAB-MS spectrum. The IR spectrum showed absorption bands assignable to an ester group (1738 cm^{-1}) and an alkyl group (2970 cm^{-1}). The ^{13}C NMR spectrum of **2** showed 24 carbon signals; 4 carbon units more than that of **1**. The ^1H NMR spectrum of **2** indicated a similar pattern to that of **1**, except for the signals corresponding to an *n*-butyl moiety. In the HMBC spectrum (Fig. 2), the methylene signals at δ 3.95 and 3.96 in the *n*-butyl moiety correlated with the carboxyl carbon signal at δ 168.94. Based on the above observation, the *n*-butyl group must be attached to glucuronic acid at the 6″-position as an ester linkage. Furthermore, the location of the glycosyl linkage was determined to be at C-8 from the HMBC spectrum; the

☆ Part 2 in the series "The chemical constituents from the fruit of *Helicterse isora*".

* Corresponding author. Tel.: +81-78-974-1551; fax: +81-78-974-5689.

E-mail address: satake@pharm.kobegakuin.ac.jp (T. Satake).

0031-9422/01/$ - see front matter © 2001 Elsevier Science Ltd. All rights reserved.
PII: S0031-9422(01)00005-X

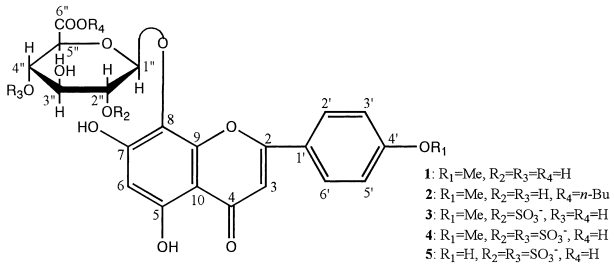

Fig. 1. Structures of compounds **1**–**5**.

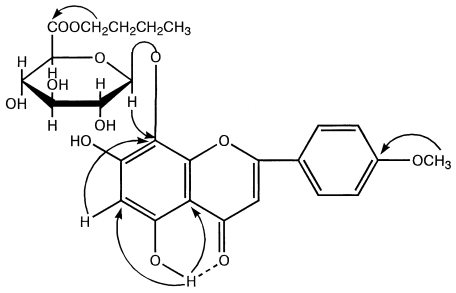

Fig. 2. Long range (HMBC) correlations of **2**.

Table 1
^{13}C NMR spectral data for compounds **1**–**5** in DMSO-d_6

^{13}C	1	2	3	4	5
2	162.94	162.59	163.11	163.13	163.46
3	102.82	102.76	102.72	102.75	101.81
4	181.38	181.31	181.47	181.73	181.60
5	157.27	157.40	157.01	157.24	157.06
6	99.88	99.68	100.05	99.55	99.37
7	162.13	162.08	162.09	161.47	160.95
8	125.88	125.69	124.54	123.66	123.45
9	149.35	149.32	149.32	149.30	149.16
10	102.82	101.87	102.72	102.75	102.49
1′	122.90	122.99	122.80	122.64	120.89
2′	128.81	128.48	129.07	129.05	129.07
3′	114.46	114.34	114.66	114.90	116.36
4′	162.13	162.08	162.09	162.22	160.95
5′	114.46	114.34	114.66	114.90	116.36
6′	128.81	128.48	129.07	129.05	129.07
1″	106.68	106.73	101.34	101.17	100.67
2″	73.20	73.81	78.05	75.87	76.20
3″	75.74	75.36	75.86	73.90	74.36
4″	72.21	71.40	72.56	81.70	81.31
5″	76.53	75.68	76.52	77.82	77.59
6″	171.15	168.94	173.42	172.92	172.59
4′-OCH3	55.42	55.44	55.37	55.44	
n-Butyl moiety					
1		64.20			
2		29.35			
3		18.34			
4		13.34			

anomeric proton signal at δ 4.69 showed a long range correlation with an oxygenated quaternary carbon at δ 124.88, assignable to C-8 on the basis of the long rang correlation with 6-H (δ 6.11). Further correlation was observed between the methoxyl proton signal at δ 3.84 and oxygenated carbon signal at δ 162.08 assignable to C-4″. From these results, **2** was determined to be isoscutellarein 4′-methyl ether 8-*O*-β-D-glucuronide 6″-*n*-butyl ester. Compound **2** is not considered to be an artifact of isolation, as compound **1** could not be converted into compound **2** after stirring in an *n*-BuOH for 12 h at 70°C.

HR-negative-FAB-MS spectrum of **3** showed a molecular ion at m/z 555.0485 corresponding with the molecular formula of $C_{22}H_{19}O_{15}S$. The ^{1}H and ^{13}C NMR spectra of **3** were similar to those of **1**, except for the proton and carbon signals due to C-1″ and C-2″ of the glucuronic acid moiety. Acid hydrolysis of **3** yielded isoscutellarein 4′-methyl ether and D-glucuronic acid {$[\alpha]_D = +21.0^\circ$ (H_2O, $c = 0.58$)}, in addition to sulfate. The sulfate ion can be precipitated with barium chloride. However, **3** was not hydrolyzed with β-glucuronidase. This result confirmed that the sulfate group must be linked to the glucuronic acid moiety. The position of the sulfate group was determined by comparison of the ^{1}H and ^{13}C NMR spectra of **1** and **3**. In the NMR spectrum

Table 2
^{1}H NMR spectral data for compounds **1**–**5** in DMSO-d_6

No.	1		2		3		4		5	
H-3	6.80 *s*		6.81 *s*		6.81 *s*		6.85 *s*		6.74 *s*	
H-6	6.11 *s*		6.11 *s*		6.15 *s*		6.10 *s*		6.06 *s*	
H-2′, 6′	8.23 *d*	(8.9)	8.10 *d*	(8.9)	8.27 *d*	(9.0)	8.26 *d*	(9.0)	8.14 *d*	(8.8)
H-3′, 5′	7.06 *d*	(8.9)	7.02 *d*	(8.9)	7.09 *d*	(9.0)	7.11 *d*	(9.0)	6.96 *d*	(8.8)
H-1″	4.69 *d*	(7.8)	4.73 *d*	(7.8)	4.96 *d*	(7.4)	5.02 *d*	(7.3)	4.99 *d*	(7.5)
H-2″	3.44 *dd*	(9.0, 7.8)	3.46 *brt*	(9.2)	4.44 *dd*	(8.6. 7.4)	4.56 *dd*	(9.8, 7.3)	4.57 *dd*	(9.8, 7.5)
H-3″	3.27 *brt*	(9.0)	3.41 *brt*	(8.0)	3.47 *dd*	(8.6, 7.8)	3.58 *dd*	(9.8, 3.5)	3.55 *dd*	(9.8, 3.0)
H-4″	3.55 *brt*	(8.5)	3.55 *brt*	(9.2)	3.67 *brt*	(7.9)	5.02 *brd*	(3.5)	4.99 *brd*	(3.0)
H-5″	3.67 *d*	(8.5)	3.86 *d*	(9.5)	3.56 *d*	(8.2)	4.49 *brs*		4.47 *brs*	
4′-OCH3	3.84 *s*		3.84 *s*		3.84 *s*		3.83 *s*			
5-OH	12.71 *s*		12.70 *s*		12.71 *s*		12.71 *s*		12.74 *s*	
n-Butyl moiety										
1			3.96, 3.95 *t*	(6.9)						
2			1.36, 1.35 *quint*	(6.9)						
3			1.14 *brhex*	(6.9)						
4			0.72 *t*	(6.9)						

of **3**, sulfation shifts (Gudej, 1991) were observed for 2″-H (+1.00 ppm) in ^{1}H resonance and for C-1″ (−5.34 ppm) and C-2″ (+4.85 ppm) in ^{13}C resonances as compared with those of **1**. These data indicated that the sulfate group must be linked to the C-2″ hydroxyl of the glucuronic acid unit. Furthermore, the location of the glycosyl linkage was determined to be at C-8 from the HMBC spectrum. Thus, the structure of **3** was characterized as isoscutellarein 4′-methyl ether 8-*O*-β-D-glucuronide 2″-sulfate. This compound was already isolated from the same genus plant, *Helicteres angustifolia* (Chen et al., 1994).

The UV spectrum of **4** resembled that of **1**, also indicating it to be the same aglycone. The ^{1}H- and ^{13}C NMR spectral data of **4** were almost identical to those of **3**, except for the signals in the aliphatic region. Acid hydrolysis of **4** yielded isoscutellarein 4′-methyl ether and D-glucuronic acid, in addition to sulfate ($BaCl_2$, ppt), whereas **4** was not hydrolyzed with β-glucuronidase. In the ^{13}C NMR spectrum of the sugar region, it was observed that the carbon signal at C-4″ appeared at a much lower magnetic field than that in **3**. Furthermore, in the ^{1}H NMR, the proton signals due to H-4″ and H-5″ appeared at δ 5.02 (*brd*, $J = 3.5$ Hz) and 4.49 (*brs*), respectively. From the downfield shifted signal at C-4″, the C-4″ position was assumed to be substituted with the second sulfate group. However, under these solvent conditions (DMSO-d_6), $J_{3'',4''}$ (3.5 Hz) and $J_{4'',5''}$ (< 1.0 Hz) based on equatorial coupling were observed, without indicating di-axial coupling [*J* value (7–10 Hz)] due to the chair form of glucuronic acid. This observation can be explained as follows (Fig. 3): the carboxyl and sulfate groups are less solvated in DMSO and exist in a free state. Thus, the preferred conformation is believed to be one in which both the carboxyl group and the sulfate group are axial because of a dipolar interaction between the two groups (Djerassi, 1960). This phenomenon was further suggested by the observation whereby the sugar ring was converted from a twist boat to a chair form when the solvent was changed to the polar protic solvent D_2O (data not shown). These data demonstrated that **4** was isoscutellarein 4′-methyl ether 8-*O*-β-D-glucuronide 2″,4″-disulfate.

The NMR spectra of **5** exhibited the same diagnostic signals for 8-*O*-β-D-glucuronide 2″,4″-disulfate as did **4**. Based on both the ^{13}C and ^{1}H NMR spectral data, the absence of the signal due to the methoxyl group was demonstrated. Furthermore, the UV spectrum of **5** in H_2O upon addition of NaOMe indicated the isoscutellarein-skeleton with a free 4′-hydroxyl. Therefore, **5** was concluded to be isoscutellarein 8-*O*-β-D-glucuronide 2″,4″-disulfate.

3. Experimental

3.1. General procedures and plant material

Optical rotations were measured using a Jasco DIP-1000 digital polarimeter. HR-FAB-MS were recorded on a JEOL JMS-BU 20 spectrometer. IR and UV spectra were measured on a Shimadzu FT-IR 8300 infrared spectrometer and a Hitachi U-3000 spectrometer, respectively. The NMR spectra were recorded in DMSO-d_6, on a

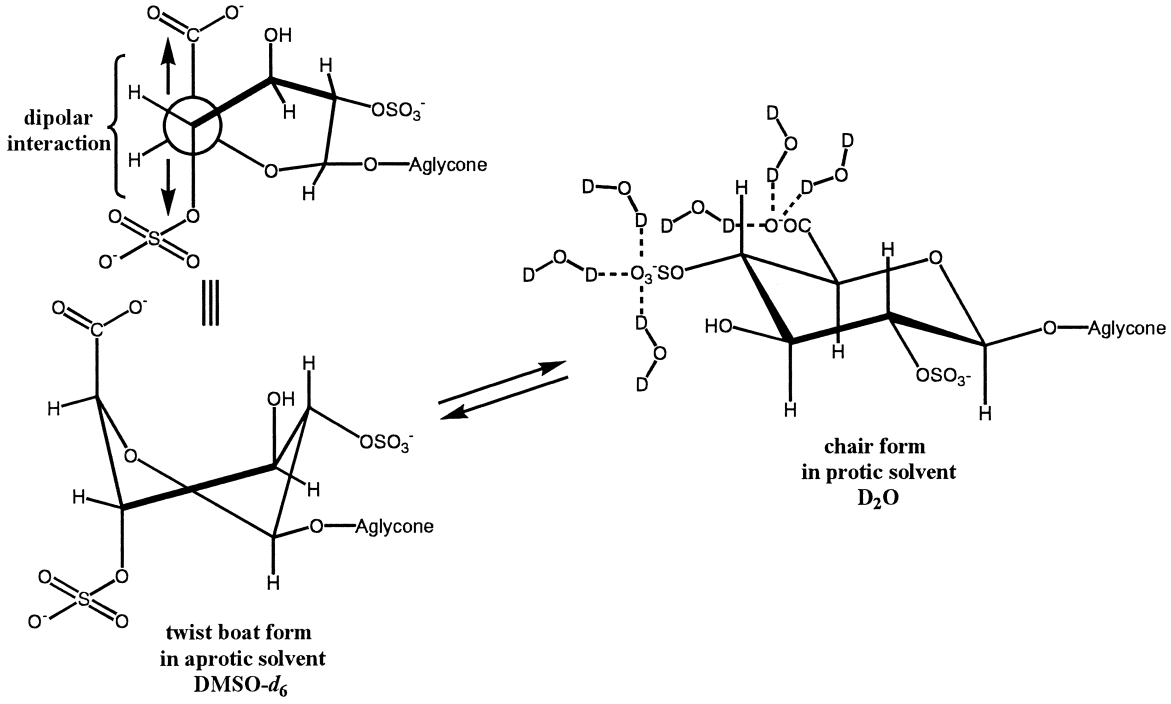

Fig. 3. Solvent effects in compounds **4** and **5**.

Bruker DPX-400 instrument. GC used a Shimadzu gas chromatograph model GC-17A (capillary column: DB-17, 30 m×0.32 mm, carrier gas: He, 1.73 ml/min, column temp.: 170°C). The fruit of *H. isora* was purchased from JAMU factory in Jakarta and the plant was identified by Dr. Asmanizar, University of Indonesia. The herbarium specimen has been deposited at the Botanical Museum of Kobe Gakuin University.

3.2. Extraction and isolation

The fruit of *H. isora* (4 kg) was initially extracted using hot MeOH (7 hr, 12 l×5) and further extracted using hot 70% MeOH (7 h, 12 l×3). Each solvent was removed under reduced pressure to yield a MeOH and a 70% MeOH extract. The 70% MeOH extract was suspended in a MeOH–H_2O (400:1200 ml) mixture and further extracted in successive steps using $CHCl_3$, AcOEt and *n*-BuOH (each 1600 ml×3). The *n*-BuOH extract was subjected to silica gel chromatography using a gradient of AcOEt, MeOH and H_2O system to give flavonoid-containing fractions. These fractions were subjected repeatedly to RP-18 column chromatography using MeOH–H_2O (1:7) and finally were purified by CC on Sephadex LH-20 using MeOH–H_2O (4:1) to give compounds **1** (15 mg) and **2** (10 mg). The H_2O extract was applied to MCI-gel using a gradient of MeOH and H_2O (1:4–4:1) to give flavonoid-containing fractions. These fractions were subjected repeatedly to RP-18 column chromatography using H_2O and finally were purified by CC on Sephadex LH-20 using MeOH–H_2O (1:1) to give compounds **3** (30 mg), **4** (100 mg) and **5** (10 mg).

3.3. Acid hydrolysis

Refluxing each compound (5 mg) for 4 h in 5% HCl yielded aglycone, D-glucuronic acid (identified by comparison with authentic sample, GC and $[\alpha]_D$) and sulfate (ppt. with $BaCl_2$).

3.4. Isoscutellarein 4′-methyl ether 8-O-β-D-glucuronide (*1*)

Yellow amorphous powder. $[\alpha]_D^{21}$ +10.5°(c = 0.4, H_2O). IR ν_{max}^{KBr} cm^{-1}: 3421 (OH), 1658 (C=O), 1609, 1578, 1508 (aromatic ring); UV $\lambda_{max}^{H_2O}$ (log ε): 272 (4.13), 301 (4.00), 331 (4.04); +NaOMe: 279, 306 *sh*, 363; +$AlCl_3$: 277, 303, 339, 392; +$AlCl_3$+HCl: 275, 302, 339, 393; +NaOAc: 278, 301, 367; +NaOAc+H_3BO_3: 278, 301, 353; ^1H and ^{13}C NMR (400 MHz, DMSO-d_6): Tables 2 and 1, respectively.

3.5. Isoscutellarein 4′-methyl ether 8-O-β-D-glucuronide 6″-n-butyl ester (*2*)

Yellow amorphous powder. $[\alpha]_D^{21}$ +73.2°(c = 0.13, MeOH). IR ν_{max}^{KBr} cm^{-1}: 3435 (OH), 2970 (alkyl), 1738 (ester), 1655 (C=O), 1605, 1558, 1508 (aromatic ring); UV λ_{max}^{MeOH} (log ε): 275 (4.28), 301 (4.20), 314 (4.19), 334 (4.14); +NaOMe: 281, 299, 368; +$AlCl_3$: 281, 308, 347, 387; +$AlCl_3$+HCl: 282, 307, 342, 385; +NaOAc: 282, 299, 368; +NaOAc+H_3BO_3: 281, 299, 368; ^1H and ^{13}C NMR (400 MHz, DMSO-d_6): Tables 2 and 1, respectively.

3.6. Isoscutellarein 4′-methyl ether 8-O-β-D-glucuronide 2″-sulfate (*3*)

Yellow amorphous powder. $[\alpha]_D^{21}$ −38.4°(c = 1.09 H_2O). HR-FAB-MS m/z: $[M–H]^-$ 555.0485 (calc. for 555.0444). IR ν_{max}^{KBr} cm^{-1}: 3420 (OH), 1657 (C=O), 1607, 1581, 1510 (aromatic ring), 1028 (sulfate); UV $\lambda_{max}^{H_2O}$ (log ε): 271 (4.06), 298 (3.95), 331 (4.06); +NaOMe: 281, 300 *sh*, 374; +$AlCl_3$: 278, 303, 339, 393; +$AlCl_3$+HCl: 276, 303, 339, 392; +NaOAc: 280, 302, 370; +NaOAc+H_3BO_3: 280, 301, 371; ^1H and ^{13}C NMR (400 MHz, DMSO-d_6): Tables 2 and 1, respectively.

3.7. Isoscutellarein 4′-methyl ether 8-O-β-D-glucuronide 2″,4″-disulfate (*4*)

Yellow amorphous powder. $[\alpha]_D^{21}$ −98.4°(c = 1.22 H_2O). HR-FAB-MS m/z: $[M–Na]^-$ 656.9832 [calc. for 656.9832, $C_{22}H_{18}O_{18}S_2Na$ (detected as sodium salt)]. IR ν_{max}^{KBr} cm^{-1}: 3431(OH), 1657 (C=O), 1607, 1582, 1508 (aromatic ring), 1026 (sulfate); UV $\lambda_{max}^{H_2O}$ (log ε): 271 (4.04), 301 (3.93), 332 (4.04); +NaOMe: 281, 298 *sh*, 376; +$AlCl_3$: 277, 303, 339, 382; +$AlCl_3$+HCl: 275, 303, 339, 382; +NaOAc: 280, 300, 372; +NaOAc+H_3BO_3: 280, 301, 372; ^1H and ^{13}C NMR (400 MHz, DMSO-d_6): Tables 2 and 1, respectively.

3.8. Isoscutellarein 8-O-β-D-glucuronide 2″,4″-disulfate (*5*)

Yellow amorphous powder. $[\alpha]_D^{21}$ −82.4°(c = 0.43 H_2O). IR ν_{max}^{KBr} cm^{-1}: 3420 (OH), 1661 (C=O), 1628, 1576, 1506 (aromatic ring), 1026 (sulfate); UV $\lambda_{max}^{H_2O}$ (log ε): 270 (4.10), 298 (3.94), 333 (4.06); +NaOMe: 280, 327, 399; +$AlCl_3$: 277, 303, 340, 381; +$AlCl_3$+HCl: 274, 302, 340, 378; +NaOAc: 279, 317, 395; +NaOAc+H_3BO_3: 272, 318, 338; ^1H and ^{13}C NMR (400 MHz, DMSO-d_6): Tables 2 and 1, respectively.

Acknowledgements

The authors are grateful to Dr. K. Hori, Akita Research Institute of Food and Brewing, for measurements of HR-FAB-MS and Miss T. Takahaya, Y. Yamamoto and Miss. M. Teraoka, Kobe Gakuin University, for their cooperation in experiments.

References

Bean, M.F., Antoun, M., Abramson, D., Chang, C.J., Mclaughlin, J.L., Cassady, J.M., 1985. Cucurbitacin B and isocucurbitacin B: cytotoxic components of *Helicteres isora*. Journal of Natural Products 48, 500.

Chen, Z.T., Lee, S.W., Chen, C.M., 1994. New flavonoid glycosides of *Helicteres angustifolia*. Heterocycles 38, 1399–1406.

Djerassi, C., 1960. Optical Rotatory Dispersion. McGraw-Hill, New York, pp. 125–126.

Gudej, J., 1991. Flavonoids, phenolic acids and coumarins from the roots of *Althaea officinalis*. Planta Medica 57, 284–285.

Markham, K.R., Porter, L.J., 1979. Flavonoids of the primitive liverwort *Takakia* and their taxonomic and phylogenetic significance. Phytochemistry 18, 611–615.

Romesh, P., Yuvarajan, C.R., 1995. A new flavone methyl ether from *Helicteres isora*. Journal of Natural Products 58, 1242–1243.

Satake, T., Kamiya, K., Saiki, Y., Hama, T., Fujimoto, Y., Kitanaka, S., Kimura, Y., Uzawa, J., Endang, H., Umar, M., 1999. Studies on the constituents of fruits of *Helicteres isora*. Chemical and Pharmaceutical Bulletin 47, 1444–1447.

Tezuka, Y., Terazono, M., Kusumoto, T.I., Kawashima, Y., Hatanaka, Y., Kadota, S., Hattori, M., Namba, T., Kikuchi, T., 1999. Helisterculins A and B, two new (7. 5′, 8. 2′)-neolignans, and herisorin, the first (6. 4′, 7. 5′, 8. 2′)-neolignan, from the Indonesian medicinal plant *Helicteres isora*. Helvetica Chemica Acta 82, 408–417.

PERGAMON

Phytochemistry 57 (2001) 303–306

PHYTOCHEMISTRY

www.elsevier.com/locate/phytochem

Rapid detection of chlorinated bisbibenzyls in *Bazzania trilobata* using MALDI-TOF mass spectrometry

Andreas Speicher [a,*], Klaus Hollemeyer [b], Elmar Heinzle [b]

[a] *Institut für Organische Chemie, Universität des Saarlandes, PO Box 151150, 66041 Saarbrücken, Germany*
[b] *Institut für Technische Biochemie, Universität des Saarlandes, PO Box 151150, 66041 Saarbrücken, Germany*

Received 26 September 2000; received in revised form 20 December 2000

Abstract

Chlorinated bisbibenzyls of the bazzanin type are detected in crude bryophyte plant extracts of *Bazzania trilobata* from different locations using MALDI-TOF mass spectrometry. These results show that these chlorinated compounds are not artefacts of an incidental occurrence or of the sample preparation but are genuine and produced by the liverwort or an endosymbiotic metabolism. Further experiments were performed concerning the in vitro chlorination of the halogen free basic unit isoplagiochin C. © 2001 Elsevier Science Ltd. All rights reserved.

Keywords: Liverworts; *Bazzania trilobata*; Chlorometabolites; MALDI-TOF-MS; Halogenation

1. Introduction

The number of halogenated natural products isolated from different living organisms has strongly increased during the last years (Naumann, 1993). Most of these metabolites with a broad structural diversity are found in marine organisms like algae and invertebrates (sponges, molluscs, worms) (Faulkner, 1992). Halometabolites from bacteria (e. g. chloramphenicol, chlortetracyclin) (van Pée, 1996) and fungi (e. g. griseofulvin) (Turner and Aldridge, 1983) exhibit high therapeutic significance. Halogenated compounds from higher plants are less numerous although they were detected in all plant divisions (ferns, lichen, flowering plants) (Neidleman and Geigert, 1986). Recently, chlorinated metabolites named bazzanin A **1** to bazzanin K **11** were isolated for the first time from mosses (bryophytes), in particular from the liverwort *Bazzania trilobata* (Martini et al., 1998). With the exception of the modified structure of **11** these compounds are obviously derived from isoplagiochin C **12** or isoplagiochin D **13**, two known bryophyte constituents (Hashimoto et al., 1996). Similar chlorometabolites were detected nearly at the same time in *Plagiochila sp*. (Anton et al., 1997) and *Lepidozia incurvata* (Schmidt, 1996) and very recently in *Herbertus sakuraii* and *Mastigophora diclados* (Hashimoto et al., 2000).

The bazzanins originally were isolated from crude moss extracts of *Bazzania trilobata* through multiple chromatographic separation steps in quantities of 2–23 mg; their structures have been elucidated based on extensive NMR spectral evidence and by usual mass spectrometry (EI–MS, CI–MS, DCI–MS) (Martini et al., 1998). It is always a point of discussion whether halometabolites detected in any living organisms are genuine (Neidleman and Geigert, 1986). So it is well accepted that the halogenated compounds isolated from marine invertebrates in many cases originate from incorporation of algae food. For plant materials exo- or even endosymbiontic fungi could be producers of halometabolites — especially when very small amounts are detected (Sakai et al., 1988). Halogen containing compounds even may be an artefact of isolation procedures especially in the case of halohydrins (Hashimoto et al., 1989). We searched for a rapid screening method for bazzanins in *Bazzania trilobata* from different locations with minimal sample pre-treatment to exclude artificial formation of these chlorometabolites.

2. Results and discussion

MALDI mass spectrometry has been shown to be a robust technique tolerating considerable salt loads and permitting the analysis of even complex mixtures because of the soft ionisation (Goheen et al., 1997). Its use for the analysis of low molecular weight compounds

* Corresponding author. Fax: +49-681-302-2409.
E-mail address: anspeich@mx.uni.saarland.de (A. Speicher).

0031-9422/01/$ - see front matter © 2001 Elsevier Science Ltd. All rights reserved.
PII: S0031-9422(01)00010-3

is quite rare because of possible matrix interferences (Krishnamurthy et al., 1996). The analysis of chlorinated organic compounds in a complex biological matrix has not been reported before to our knowledge. Chlorinated compounds and their degree of chlorination can be identified because of the characteristic isotope patterns.

The plant material from the original detection of chlorinated compounds was collected in Weißkirchen, Saarland, Germany. The plant samples analysed in this paper originate from Rinnthal, Rheinland-Pfalz, Germany and Lautzkirchen, Saarland, Germany. The air-dried and powdered plant material was extracted with methanol and subjected directly to MALDI mass spectroscopy. A pre-extraction with ether to remove the non-polar fraction proved to be not necessary. To achieve a further purification the methanol extract was distributed between ethyl acetate and water and the ethyl acetate soluble fraction was chromatographed on Sephadex LH-20. The last fraction was finally obtained as a powder and gave the best results in the MALDI-TOF detection. Because of their polar and aromatic structures the bazzanins absorb laser light directly and their detection does not need any additional matrix.

Containing one to six halogen atoms the bazzanins should give very specific molecular-weight distributions in mass spectra according to the isotope pattern calculation. The MALDI-MS spectra of all analysed fractions of both plant samples resulted in peak patterns being in significant accordance to the molecular formulas of bazzanins (Table 1 and Fig. 3) showing the characteristic intensity distribution (for an example see Fig. 4). We found no substantial differences between the plant samples from Rinnthal and Lautzkirchen. The chlorinated bisbibenzyls were detected in purified samples as well as in the crude methanolic extract.

These results show that the bazzanins are genuine substances from *Bazzania trilobata* which are not produced during the sample preparation and do not occur incidentally. This novel detection of chlorinated organic compounds in the complex biological matrix of a crude plant extract should be a suitable instrument for further phytochemical studies.

The biogenesis of the bazzanins is a point of discussion. Haloperoxidases are enzymes which catalyse the incorporation of halogen atoms into organic molecules in the presence of a halide and hydrogen peroxide and

Table 1
Bazzanins detected in the plant extracts of *Bazzania trilobata* using MALDI-TOF MS

Peak pattern (maximum peak) *m/z*	In accordance with formula	Corresponding bazzanins (see Fig. 1)
456–460 (456)	$C_{28}H_{21}ClO_4$	Bazzanin A **1**
490–495 (490)	$C_{28}H_{20}Cl_2O_4$	Bazzanin B **2**
524–529 (524, 526)	$C_{28}H_{19}Cl_3O_4$	Bazzanins C, D, **3**,**4**
558–564 (560)	$C_{28}H_{18}Cl_4O_4$	Bazzanins E,F **5**,**6**
592–598 (594)	$C_{28}H_{17}Cl_5O_4$	Bazzanins G,H **7**,**8**
626–636 (628)	$C_{28}H_{16}Cl_6O_4$	Bazzanin I **9**
492–497 (492)	$C_{28}H_{22}Cl_2O_4$	Bazzanin J **10**
502–508 (502)	$C_{29}H_{20}Cl_2O_4$	Bazzanin K **11**

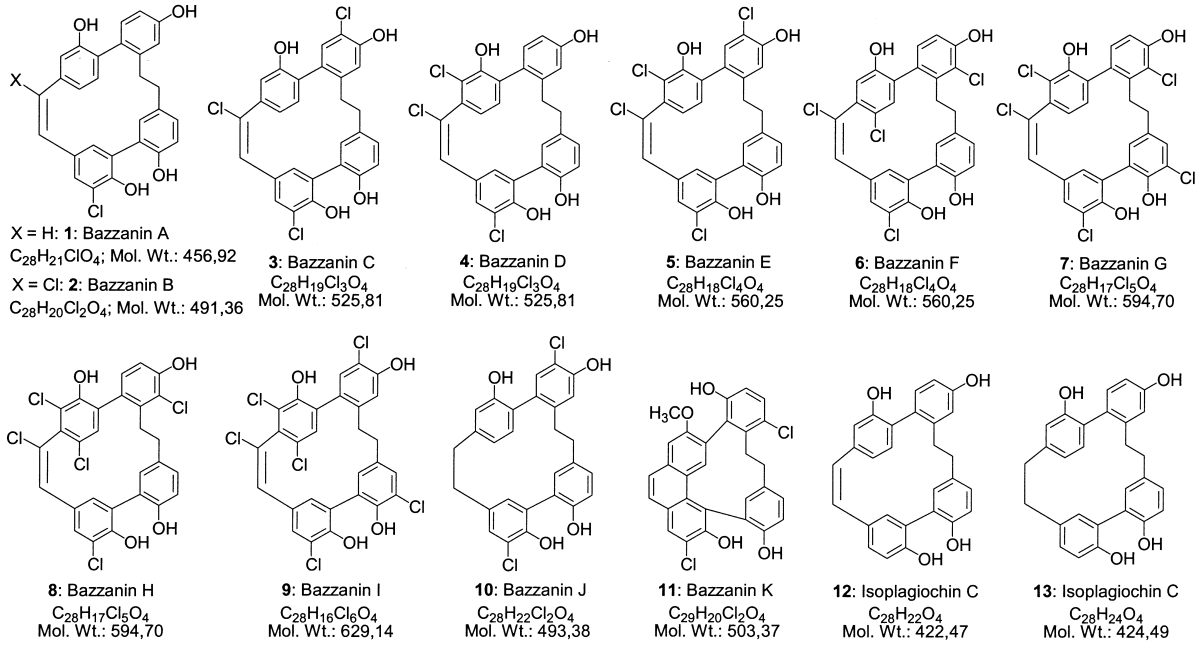

Fig. 1. Structures of bazzanins A-K **1**–**11** and the parent compounds **12**, **13** (the formulas and molecular weights are given with respect to the MALDI detection).

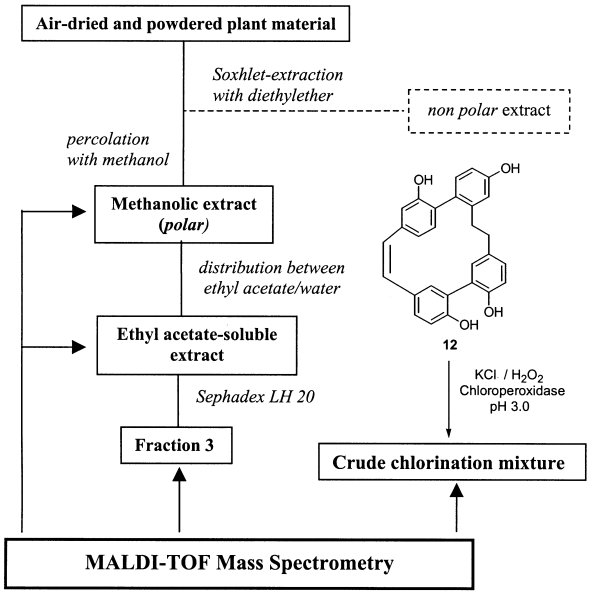

Fig. 2. Samples subjected to MALDI-MS: Preparation of extracts from plant materials and in vitro chlorination of **12**.

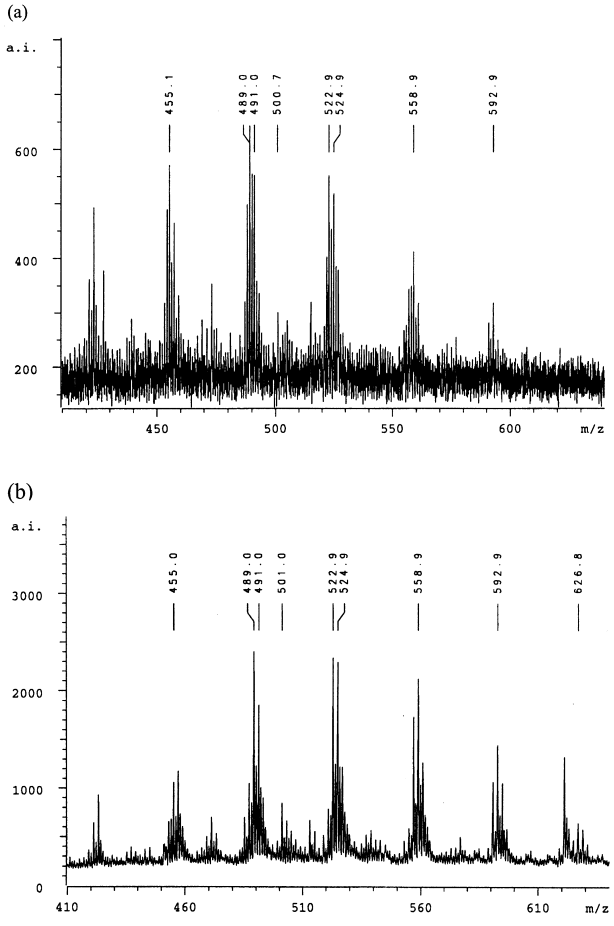

Fig. 3. (a) MALDI-MS of the crude methanol extract of *Bazzania trilobata*, location Rinnthal; (b) MALDI-MS of the same probe after purification on Sephadex LH 20 (in negative mode as $(M\text{-}H)^-$ions).

which are thought to be involved in the biosynthesis of most halometabolites (Neidleman and Geigert, 1986; Hohaus et al., 1997). Numerous in vitro reactions are described for the commercially available chloroperoxidase (CPO, EC 1.11.1.10) from *Caldariomyces fumago* (Franssen, 1994). We subjected a synthetic sample of isoplagiochin C **12** (Eicher et al., 1998) to a chemoenzymatic transformation with KCl/H_2O_2 in the presence of CPO in a buffered aqueous medium (Speicher, 2000) and the crude reaction mixture was also analysed using MALDI-MS (see Fig. 2). The in vitro chlorination of isoplagiochin C **12** resulted in the incorporation of 1–5 chlorine atoms. The MALDI mass spectra of the crude reaction mixture were in good agreement with the spectra from the natural sources. In this experiment the addition of an enzyme solution is essential to achieve chlorination.

3. Experimental

3.1. Plant material

The plant materials of the liverwort *Bazzania trilobata* (L.) S. F. Gray (family: Lepidoziaceae) were collected in Weißkirchen, Saarland, Germany in March 1994 (Martini et al., 1998), Rinnthal, Rheinland-Pfalz, Germany during June 1999 and Lautzkirchen, Saarland, Germany

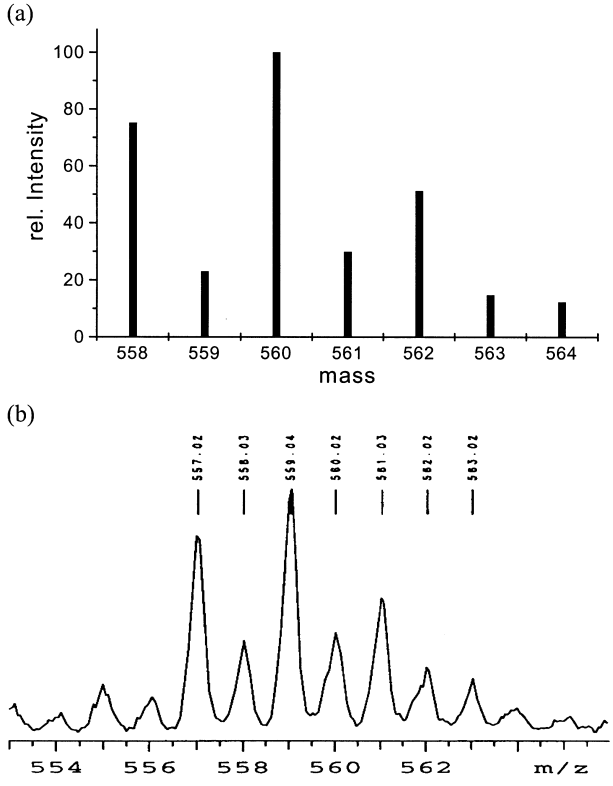

Fig. 4. (a) Calculated (Sheffield ChemPuter: http://www.shef.ac.uk/chemistry/chemputer) and (b) measured (in negative mode as $(M\text{-}H)^-$ions) peak pattern of bazzanins E, F **5**,**6** ($C_{28}H_{18}Cl_4O_4$).

during December 1999 and identified by Prof. Dr. R. Mues (Institut für Botanik der Universität des Saarlandes, Saarbrücken, Germany). Voucher specimens are deposited in the herbarium SAAR, Saarbrücken.

3.2. Extraction and analysis

Air dried and powdered plant materials (60 g) were extracted with diethyl ether (250 ml) in a Soxhlet apparatus to remove the non polar compounds (this part was omitted in a control experiment), followed by an exhaustive percolation with methanol (1000 ml) in a glass column (8×50 cm). The evaporated methanolic extract was distributed between ethyl acetate (250 ml) and water (250 ml). The organic layer was evaporated in vacuo and the resulting ethyl acetate phase (ca. 0.60 g) chromatographed on Sephadex LH-20 (4×60 cm, Amersham Pharmacia Biotech, Uppsala) using methanol–diethylether (4:1) as eluent to yield three main fractions. After solvent removal fractions 1 (0.35 g) and 2 (0.10 g) were green-brown viscous oils whereas fraction 3 (0.10 g) was obtained as an ochreous powder. Solvents with a high grade purity were used for isolation and purification procedures.

3.3. In vitro halogenation of isoplagiochin C **12**

126.6 mg (0.30 mmol) of isoplagiochin C **12** (pre-dissolved in 1 ml ethanol) were added to a solution of 3.00 mmol potassium chloride in 120 ml 0.1 M potassium phosphate buffer (pH 3.0). The temperature of the mixture was kept constant to 30–35°C and 6.0 mmol H_2O_2 (30% in H_2O) as well as 1000 units of the chloroperoxidase (EC 1.11.1.10 from *Caldariomyces fumago* obtained from Fluka as suspension in 0.1 M sodium phosphate pH 4.0, 1717 U/mg, 8 mg protein/ml) were added in ten portions each during 10 h. After five portions an additional amount of the halide (3.00 mmol) was added. The mixture was extracted with ethyl acetate, dried ($MgSO_4$) and concentrated.

3.4. Mass spectrometry

The MALDI-TOF measurements were performed using a Bruker Reflex III MALDI-TOF mass spectrometer equipped with a delayed extraction system facility using a N_2-Laser (337 nm) with a single pulse duration of 3 ns and 10^7–10^8 W/cm^2 irradiation.

The sample preparation for MALDI-TOF analysis was performed by dissolving the oily or powdered samples in methanol at concentrations of about 1 mg/ml. One microliter of the solutions were spotted on the metal target plate and dried at room temperature. MALDI-TOF mass spectra were recorded in reflectron mode with negative acceleration voltage without matrix.

Acknowledgements

A.S. thanks Prof. Dr. T. Eicher for generous support and H. Roeser for technical assistance.

References

Anton, H., Kraut, L., Mues, R., Morales, M.I., 1997. Phenanthrenes and bibenzyls from a *Plagiochila* species. Phytochemistry 46, 1069–1075.

Eicher, T., Fey, S., Puhl, W., Büchel, E., Speicher, A., 1998. Bryophyte constituents 9: syntheses of cyclic bisbibenzyl systems. European Journal of Organic Chemistry, 877–888.

Faulkner, D.J., 1992. Marine natural products. Natural Products Report 9, 323–364.

Franssen, M.C.R., 1994. Halogenation and oxidation reactions with haloperoxidases. Biocatalysis 10, 87–111.

Goheen, S.C., Wahl, K.L., Campbell, J.A., Hess, W.P., 1997. Mass spectrometry of low molecular mass solids by matrix-assisted laser desorption/ionization. Journal of Mass Spectrometry 32, 820–828.

Hashimoto, T., Tori, M., Asakawa, Y., 1989. Drimane-type sesquiterpenoids from the liverwort *Makinoa crispata*. Phytochemistry 28, 3377–3381.

Hashimoto, T., Kanayama, S., Kann, Y., Tori, M., Asakawa, Y., 1996. Isoplagiochins C and D, new type of macrocyclic bis(bibenzyls) having two biphenyl linkages from the liverwort *Plagiochila fruticosa*. Chemistry Letters 741–742.

Hashimoto, T., Irita, H., Takaoka, S., Tanaka, M., Asakawa, Y., 2000. New chlorinated cyclic bis(bibenzyls) from the liverworts *Herbertus sakuraii* and *Mastigophora diclados*. Tetrahedron 56, 3153–3159.

Hohaus, K., Altmann, A., Burd, W., Fischer, I., Hammer, P. E., Hill, D. S., Ligon, J. M., van Pée, K.-H., 1997. NADH-abhängige Halogenasen sind wahrscheinlich eher an der Biosynthese von Halogenmetaboliten beteiligt als Haloperoxidasen. Angewandte Chemie 109, 2102–2104; Angewandte Chemie, International Edition English 36, 2012–2014.

Krishnamurthy, T., Ross, P.L., Rajamani, U., 1996. Detection of pathogenic and non-pathogenic bacteria by matrix-assisted laser desorption/ ionization time-of-flight mass spectrometry. Rapid Communications in Mass Spectrometry 10, 883–888.

Martini, U., Zapp, J., Becker, H., 1998. Chlorinated macrocyclic bisbibenzyls from the liverwort *Bazzania trilobata*. Phytochemistry 47, 89–96.

Naumann, K., 1993. Chlorchemie der Natur. Chemie unserer Zeit 27, 33–41.

Neidleman, S.L., Geigert, J., 1986. Biohalogenation: principles, basic roles and applications. Ellis Horwood, Chichester.

Sakai, K., Ichikawa, T., Yamada, K., Yamashita, M., Tanimoto, M., Hikita, A., Ijuin, Y., Kondo, K., 1988. Antitumor principles in mosses: The first isolation and identification of maytansinoids, including a novel 15-methoxyansamitocin P3. Journal of Natural Products 51, 845–850.

Schmidt, A., 1996. Phytochemische Untersuchung des Lebermooses *Lepidozia incurvata* Lindenberg. Dissertation thesis, Universität des Saarlandes, Germany.

Speicher, A., 2000. Chemical and in vitro syntheses of brominated and chlorinated 3,4′-dihydroxybibenzyls (halogenated lunularins). Journal für praktische Chemie 342, 162–168.

Turner, W.B., Aldridge, D.C., 1983. Fungal metabolites II. Academic Press, New York.

van Pée, K.-H., 1996. Biosynthesis of halogenated metabolites by bacteria. Annual Review of Microbiology 50, 375–399.

PERGAMON

Phytochemistry 57 (2001) 307–313

PHYTOCHEMISTRY

www.elsevier.com/locate/phytochem

Pacifigorgianes and tamariscene as constituents of *Frullania tamarisci* and *Valeriana officinalis*

Claudia Paul [a], Wilfried A. König [a,*], Hermann Muhle [b]

[a] *Institut für Organische Chemie, Universität Hamburg, Martin-Luther-King-Platz 6, D-20146 Hamburg, Germany*
[b] *Abteilung Spezielle Botanik, Universität Ulm, D-89091 Ulm, Germany*

Received 13 November 2000; received in revised form 2 January 2001

Abstract

The sesquiterpenoid constituents of the essential oils from the liverworts *Frullania tamarisci*, *Frullania fragilifolia* and of the angiosperm *Valeriana officinalis* were investigated. Tamariscene, a compound with a new sesquiterpene skeleton, valerena-4,7(11)-diene and five new pacifigorgiadienes, namely pacifigorgia-1,10-diene, pacifigorgia-1(6),10-diene, pacifigorgia-1(9),10-diene, pacifigorgia-2,10-diene, and pacifigorgia-2(10),11-diene were isolated and identified. Structure elucidation was carried out by NMR spectroscopy and chemical correlations to establish absolute configurations. Compounds present in both the essential oils of the *Frullania species* and *Valeriana officinalis* were enantiomeric to each other. A plausible biogenetic relationship between the pacifigorgiane, valerenane and tamariscane skeletons is postulated. Pacifigorgia-6,11-diene, not yet detected in nature, was generated by dehydration and rearrangement of natural (−)-tamariscol. © 2001 Elsevier Science Ltd. All rights reserved.

Keywords: *Frullania tamarisci*; *F. fragilifolia*; *Valeriana officinalis*; Hepaticae; Essential oil; Structure elucidation; Pacifigorgiane; Tamariscane; Valerenane; Sesquiterpene

1. Introduction

The leafy liverworts *Frullania tamarisci* and *F. fragilifolia* (Tayl.) of the order Jungermanniales and the medicinal plant *Valeriana officinalis* L. were investigated and showed a striking chemical relationship concerning their volatile constituents. Essential oil samples were obtained by hydrodistillation and analysed by gas chromatography–mass spectrometry (GC–MS). Individual components, including a number of new sesquiterpene hydrocarbons, were isolated by liquid chromatography and preparative GC and investigated by NMR (^{1}H, ^{13}C, ^{1}H–^{1}H–COSY, HMQC, HMBC, NOESY). The absolute configuration of the new compounds was derived by dehydration of the related natural alcohols, polarimetric measurements, total hydrogenation and enantioselective gas chromatography using cyclodextrin as stationary phases.

2. Results and discussion

The following sesquiterpenoids in the order of their elution from a capillary column with polydimethylsiloxane were identified as constituents of the essential oil of *F. fragilifolia*: (−)-tamariscene (**1**), α-copaene, (−)-pacifigorgia-1(9),10-diene (**2**), β-elemene, (−)-pacifigorgia-1,10-diene (**3**), (−)-pacifigorgia-1(6),10-diene (**4**), (−)-pacifigorgia-2,10-diene (**5**), 11-bourbonene (Warmers et al., 1998), (+)-pacifigorgia-2(10),11-diene (**6**), selina-5,11-diene, α-humulene, γ-muurolene, bicyclogermacrene and (+)-germacrene A.

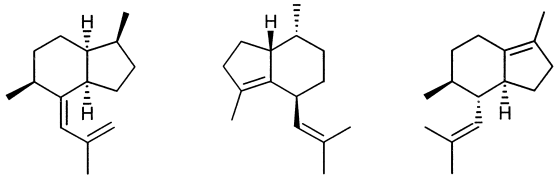

6 **7** **8**

In the essential oil of *F. tamarisci* in addition to **1–4** and **6** the following sesquiterpenoids were identified: α-copaene, (−)-β-elemene, 11-bourbonene, γ-gurjunene, selina-4,11-diene, eremophilene, (+)-germacrene A, β-

* Corresponding author Tel.: +49-40-42838-2824; fax: +49-40-42838-2893.

E-mail address: wkoenig@chemie.uni-hamburg.de (W.A. König).

0031-9422/01/$ - see front matter © 2001 Elsevier Science Ltd. All rights reserved.
PII: S0031-9422(01)00018-8

bazzanene, (−)-tamariscol (**9**) (Connolly et al., 1984; Tori et al., 1991), globulol, rosifoliol, ledol and T-cadinol.

In the essential oil of *Valeriana officinalis* (Valerianaceae) the following sesquiterpenoids were identified: (+/−)-δ-elemene, (+)-**1**, α-ylangene, α-copaene, (+)-**2**, β-elemene, (+)-**4**, β-caryophyllene, γ-elemene, (−)-valerena-4,7(11)-diene (**7**), alloaromadendrene, 2-*epi*-*trans*-β-caryophyllene, germacrene D, bicyclogermacrene, δ-cadinene, (−)-pacifigorgiol (**10**) (Bos et al., 1986), germacrene B, spathulenol, alismol and valerianol.

All known compounds were identified by mass spectrometry in conjunction with their gas chromatographic retention indices by comparison with a spectral library established under identical experimental conditions (Joulain and König, 1998). Main components of the sesquiterpenoids present in the essential oils were **1** in *F. fragilifolia* with 11% relative to all compounds detected in the essential oil, **9** with 56% in *F. tamarisci*, and γ-elemene with 11% in *V. officinalis*. All other components ranged between trace amounts and 3% of all constituents of the essential oil.

The new sesquiterpene hydrocarbon tamariscene (**1**) was the major constituent of *F. fragilifolia*. The mass spectrum exhibits a molecular ion signal at *m/z* 204 and an elemental composition of $C_{15}H_{24}$. The proton NMR spectrum shows the presence of two doublets for methyl groups ($\delta = 1.01$, 1.03) and one methyl singlet with a downfield shift ($\delta = 1.74$) indicating that the methyl group is attached to a double bond. An exocyclic methylene group must be present due to two singlets at $\delta = 4.71$ and 4.89. As the ^{13}C NMR reveals only one downfield shifted quaternary carbon ($\delta = 144.66$) the methyl group must be attached to the same carbon as the exocyclic methylene group. Thus, an isopropylidene group is established and therefore the main structure must be postulated to be tricyclic with one double bond. In the ^{13}C NMR three primary carbon atoms ($\delta = 19.16$, 21.29, 24.37), five secondary carbons ($\delta = 29.04$, 30.32, 30.41, 35.53, 109.50), five tertiary ($\delta = 28.93$, 30.06, 33.55, 44.64, 50.19) and two quaternary carbons ($\delta = 34.15$, 144.66) are found. It is remarkable that the two protons appearing at $\delta = 0.54$ (H-4a) and 0.72 (H-5a), respectively, belong to methylene groups (C-4: $\delta = 29.04$; C-5: $\delta = 30.32$) as derived from the ^1H-^{13}C-COSY spectrum. The connectivity of the different groups was established through ^1H–^1H–COSY and HMBC experiments: The methyl group H-15 ($\delta = 1.03$; 19.16) couples to one proton of the multiplet at $\delta = 1.44$–1.55 (H-7, H-9a) in the COSY spectrum and to the multiplet at $\delta = 1.13$–1.26 (H-6/H-8a) in the HMBC spectrum. Proton H-5a couples to the multiplets $\delta = 1.66$–1.76 (H-5b/H-8b), 1.33–1.41 (H-4b) and 1.13–1.26 (H-6/H-8a), which indicates that the methylene groups are located between the tertiary carbons C-3 ($\delta = 28.93$) and C-6 ($\delta = 50.19$). As the methyl group H-14 ($\delta = 1.01$; 21.29) exclusively couples to the methine proton H-3, this connection is established also. The doublet signal with the integral of one proton at $\delta = 0.95$ is assigned to the methine proton H-10 because its carbon ($\delta = 33.55$) couples to the doublet of doublets at $\delta = 1.07$ (H-2), as well as to the signals at $\delta = 1.76$–1.86 (H-3), 1.74 (H-13) and 1.44–1.55 (H-7/H-9a) and to the signal at $\delta = 1.58$–1.66 (H-9b) in the HMBC. In the ^1H–^1H–COSY spectrum only couplings from H-10 to the signals at $\delta = 4.71$ (H-12a) and to H-13 are observed. The quaternary carbon C-1 ($\delta = 34.15$) couples to H-10, H-6/H-8a, H-7/H-9a, H-9b, H-12a ($\delta = 4.71$) in the HMBC experiment. As proton H-9b shows cross peaks with H-7/H-9a and H-6/H-8a and the other proton of this methylene group H-9a (located in the multiplet with H-7) couples with H-5b/H-8b, H-9b and H-6/H-8a the methylene groups H-8a,b and H-9a,b must be adjacent. As C-7 couples not only to H-15, as known from the ^1H–^1H–COSY spectrum, but also to H-6/H-8a, H-7/H-9a, H-5a, H-9b and H-5b/H-8b, the HMBC spectrum proves that this molecule has a tricyclo[5.3.0.$0^{1,3}$]decane backbone.

The relative configuration was derived from the NOE experiment: H-10 shows a correlation with H-4_{ax} and H-6 as well as with the methylene group H-13. Proton H-6 itself interacts with methylene group H-15. H-4_{ax} gives a NOE signal indicating the proximity of methylene group H-14. From this, a *cis*-configuration for all substituents and *exo*-orientation of the isopropylidene group can be concluded.

The mass spectrum of pacifigorgia-1(6),10-diene (**4**) shows a molecular ion signal at *m/z* 204. From this the elemental composition of $C_{15}H_{24}$ is derived. In the ^1H-NMR spectrum four methyl groups can be detected. Two of the methyl groups represented by singlets at $\delta = 1.65$ and 1.71 (H-12, H-13) are attached to a quaternary olefinic carbon and the other two (H-14 and H-15) exhibit doublet signals in the aliphatic region ($\delta = 0.83$, 0.95) and are thus bonded to tertiary carbons. As the ^{13}C NMR spectrum shows four downfield shifted signals two double bonds must be present in this bicyclic compound. Four primary carbon atoms ($\delta = 18.15$, 18.35, 19.55, 26.04), four secondary carbons ($\delta = 23.56$, 27.51, 31.77, 33.02), four tertiary ($\delta = 32.92$, 39.86, 41.74, 124.40) and three quaternary carbons ($\delta = 131.50$, 137.23, 137.71) are found in the ^{13}C NMR. As both downfield shifted methyl groups (H-12 and H-13) show cross peaks in the ^1H–^1H–COSY spectrum with the olefinic proton H-10 at $\delta = 4.88$, an isobutylene group is evident. H-10 couples to H-2 ($\delta = 2.82$) which in turn couples to H-3/H-5a ($\delta = 1.73$–1.87), the proton next to the methyl group H-14, which is indicated through a cross peak in the ^1H–^1H–COSY spectrum. The methylene groups H-4 ($\delta = 1.36$–1.52; 27.51) and H-5 (5a: 1 H absorbing in the multiplet $\delta = 1.73$–1.87; 5b: 1 H in multiplet $\delta = 1.93$–2.10; 23.56) must follow in that order because H-4 couples to H-3/H5a ($\delta = 1.73$–1.87) and H-5b/H-8b/H-9a ($\delta = 1.93$-2.10). Furthermore, the

coupling between the proton H-7 ($\delta = 2.47$–2.57) to the methyl group H-15 ($\delta = 0.95$) and to the methylene group H-8a,b is indicated by cross peaks with the multiplets of H-8a ($\delta = 1.23$–1.31) and H-5b/H-8b/H-9a ($\delta = 1.93$–2.10). The methylene group H-8a,b in turn couples to the multiplets at $\delta = 1.93$–2.10 (H-5b, H-8b, H-9a) and 2.16–2.25 (H-9b), thus establishing the second ring separated by a double bond from the six-membered ring. From the HMBC it becomes clear that C-6 ($\delta = 137.7$) is bonded to C-7 ($\delta = 41.74$) and C-5 ($\delta = 23.56$) because it shows a coupling to H-15, H-8a and H-4a,b as well as to the multiplet H-5b/H-8b/H-9a. In the six-membered ring the connectivity is established through the couplings of C-2 ($\delta = 39.86$) to H-14, H-12, H-13 and H-4a,b on one hand and of C-4 ($\delta = 27.51$) to H-14, H-3/H-5a on the other hand. Carbon C-1 ($\delta = 137.23$) gives only poor couplings to H-8a and to the multiplet H-5b/H-8b/H-9a. With these data the pacifigorgiane skeleton is evident with the double bonds in 1(6) and 10 position. The observed NOE shows close correlation between H-10 and H-14, but not with H-3, which is only possible when the olefinic proton H-10 is turned towards the ring and the isobutylene group is *cis* to the methyl group H-14. As dehydration of the alcohol (−)-pacifigorgiol (**10**) with known absolute configuration (Martin, 1983) yielded the identical compound **4** in the product mixture, it was evident that all substituents are in *cis*-orientation.

The same techniques were applied to identify the structures of the pacifigorgiadienes **2**, **3**, **5**, **6** and the rearrangement product pacifigorgia-6,11-diene (**8**). The data of the 2-dimensional NMR experiments for **2**, **6** and **8** are given in Tables 1–3.

The absolute configuration of (+)-tamariscene (**1**) was established through the dehydration reaction of (−)-pacifigorgiol (**10**), which was isolated from the essential oil of *V. officinalis*. As illustrated in Fig. 1, path b, (+)-**2** and (+)-**4** were obtained in ca. 1:10 ratio. The same products, this time in ca. 1:1 ratio, were formed in the rearrangement reaction (Fig. 1, path a) of (+)-tamariscene by storage of a sample of this compound in chloroform at 8° C for 21 days. The identity of the products was proved by enantioselective GC and by GC–MS.

It is remarkable that in the dehydration reaction (Fig. 1, path b) the *cis* elimination, which would lead to (+)-**3** does not occur even though the conjugated, disubstituted diene should be thermodynamically favoured. When (−)-tamariscol (**9**) is submitted to dehydration with prolonged reaction time (Fig. 2) the elimination reaction leading to (−)-pacifigorgia-1,10-diene (**3**) and (−)-pacifigorgia-2,10-diene (**5**) is indeed taking place. Comparison of the dehydration products (−)-**3** and (−)-**5** and the earlier isolated authentic compounds by enantioselective GC led to the absolute configuration.

The structure of (−)-valerena-4(7),11-diene (**7**) was established by NMR investigation (Table 4). The relative configuration was assigned from the results of NOE experiments, the absolute configuration is assumed to be

Table 1
NMR coupling correlations of pacifigorgia-1(9)10-diene (**2**)

Proton	^{1}H–^{1}H–COSY-couplings	NOESY-couplings
H-2	H-10	H-3, H-12, H-14
H-3	H-4a,b, H-14	H-2
H-4a,b	H-3, H-5a, H-5b	H-14, H-5a, H-5b, H-6, H-10
H-5a	H-4a,b, H-5b, H-6	H-4a,b, H-5b, H-6
H-5b	H-4a,b, H-5a	H-4a,b, H-5a
H-6	H-5a	H-4a,b, H-5a, H-10, H-15
H-7/H-8a	H-8b, H-15	–
H-8b	H-7/H-8a, H-9	H-9
H-9	H-8b	H-8b, H-12
H-10	H-2, H-12, H-13	H-4a,b, H-6, H13, H-14
H-12	H-10	H-2, H-9
H-13	H-10	H-10
H-14	H-3	H-2, H-4a,b, H-10
H-15	H-7/H-8a	H-6

Table 2
NMR coupling correlations of pacifigorgia-2,10(11)-diene (**6**)

Proton	^{1}H–^{1}H–COSY-couplings	NOESY-Couplings
H-1/H-3/H-5b/H-8b	H-5a/H-9a, H-6, H-8a, H-9b	H-6, H-7, H-12a, H-15
H-4a,b	H-1/H-3/H-5b/H-8b, H-5a/H-9a	H-5a/H-9a
H-5a/H-9a	H-4a,b	H-1/H-3/H-5b/H-8b, H-4a,b, H-6
H-6	H-1/H-3/H-5b/H-8b	H-1/H-3/H-5b/H-8b, H-5a/H-9a, H-7
H-7	H-15	H-1/H-3/H-5b/H-8b, H-6
H-8a	H-1/H-3/H-5b/H-8b	H-15
H-9b	H-1/H-3/H-5b/H-8b	H-12a
H-10	H-12a, H-12b, H-13	H-13, H-14
H-12a	H-10, H-13	H-1/H-3/H-5b/H-8b, H-9b
H-12b	H-10, H-13	H-13
H-13	H-10, H-12a, H-12b	H-10, H-12b
H-14	H-1/H-3/H-5b/H-8b, H-8a	H-10
H-15	H-7	H-1/H-3/H-5b/H-8b, H-8a

Table 3
NMR coupling correlations of pacifigorgia-6,10-diene (**8**)

Proton	^{1}H–^{1}H–COSY-Couplings	NOESY-Couplings
H-1/H-8a,b	H-2, H-3/H-9a, H-9b, H-13/H-15	H-10, H-13/H-15
H-2	H-1/H-8a,b, H-3/H-9a, H-10	H-4a, H-14
H-3/H-9a	H-1/H-8a,b, H-2, H-4a, H-4b/H-5a, H-9b, H-14	H-4b/H-5a, H-10
H-4a	H-3/H-9a, H-4b/H-5a, H-5b	H-2, H-5b, H-14
H-4b/H-5a	H-4a, H-5b	H-3/H-9a, H-5b, H-13/H-15, H-14
H-5b	H-4a, H-4b/H-5a	H-4a, H-4b/H-5a, H-13/H-15
H-9b	H-1/H-8a,b, H-3/H-9a	H-12, H-13/H-15
H-10	H-2, H-12, H-13/H-15	H-1/H-8a,b, H-3/H-9a, H-14
H-12	H-10, H-13/H-15	H-9b
H-13/H-15	H-1/H-8a,b, H-12	H-1/H-8a,b, H-4b/H-5a, H-5b, H-9b
H-14	H-3/H-9a	H-2, H-4a, H-4b/H-5a, H-10

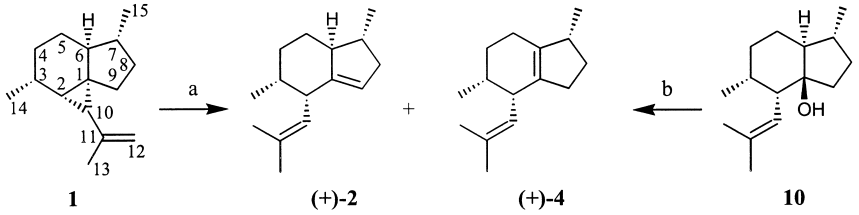

Fig. 1. Correlation reactions between tamariscene (**1**) and pacifigorgiol (**10**). Rearrangement conditions: (a) $CHCl_3$, 8°C, 21 days dehydration conditions: (b) pyridine, $SOCl_2$, 0°C, 3 min.

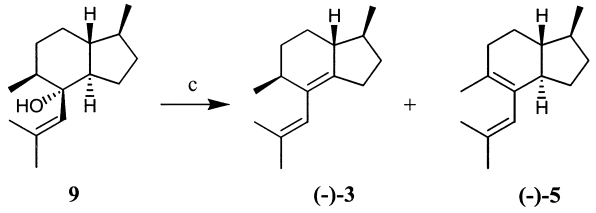

Fig. 2. Correlation reaction between tamariscol (**9**) and the pacifigorgiadienes (**3**) and (**5**). Dehydratisation conditions: (c) pyridine, $SOCl_2$, 0°C, 3 h.

identical to known oxygenated constituents of *V. officinalis*, with the same skeleton. The same applies to **6**, where the relative configuration was established through NOE experiments, but hydrogenation reactions could not reveal the absolute configuration by comparison with other pacifigorgianes as the rings are *cis*-fused.

For the rearrangement product (+)-pacifigorgia-6,10-diene (**8**) as obtained from (−)-tamariscol (**9**), only the relative configuration can be assigned (NOE) as the chiral centre at C-7 is eliminated and it is not known if the other two chiral centres at C-2 and C-3 are affected by the rearrangement reaction.

Table 4
NMR coupling correlations of valerena-4,7(11)-diene (**7**)

Proton	^{1}H–^{1}H–COSY-Couplings	NOESY-Couplings
H-1	–	H-7, H-10
H-2	H-2b/H-9b, H-3a,b	H-10, H-14
H-2b/H-9b	H-2a, H-3a, H-8a/H-9a, H-8b	H-7, H-8a/H-9a, H-14
H-3a,b	H-2a, H-2b/H-9b, H-15	H-10, H-14, H-15
H-6	H-7, H-8b	H-8a/H-9a, H-8b, H-15
H-7	H-6, H-12, H-13	H-1, H-2b/H-9b, H-8a/H-9a, H-13
H-8a/H-9a	H-2b/H-9b, H-8b	H-2b/H-9b, H-6, H-7, H-10, H-14
H-8b	H-2b/H-9b, H-6, H-8a/H-9a	H-6
H-10	H-14	H-1, H-2a, H-3a,b, H-8a/H-9a
H-12	H-7	–
H-13	H-7	H-7
H-14	H-10	H-2a, H-2b/H-9b, H-3a,b, H-8a/H-9a
H-15	H-3a,b	H-3a,b, H-6

The co-occurrence of valerenanes and pacifigorgianes in *Valeriana officinalis* and the presence of tamariscene led to the assumption, that tamariscanes may be a common precursor for both valerenanes and pacifigorgianes. This is schematically rationalized in Fig. 3.

3. Experimental

3.1. General experimental procedures

GC: Orion Micromat 412 double column instrument with 25 m fused silica capillaries with polysiloxane CPSil-5 and polysiloxane CPSil-19 (Chrompack); Carlo Erba Fractovap 2150, 4160 gas chromatographs with 25 m fused silica capillaries with heptakis(2,6-di-*O*-methyl-3-*O*-pentyl)-β-cyclodextrin or heptakis(6-*O*-*tert*-butyldimethylsilyl-2,3-di-*O*-methyl)-β-cyclodextrin in OV 1701 (50%, w/w), split injection; split ratio approx. 1:30; FID; carrier gas 0.5 bar H_2; injector and detector temperatures were 200 and 250°C, respectively. Preparative GC (Hard and König, 1994): Modified Varian 1400 and 2800 instruments, equipped with a stainless steel column (1.85 m×4.3 mm) with 10% polydimethylsiloxane SE-30 on Chromosorb W-HP; and Silcosteel® (Amchro) column (1.95 m×5.3 mm) with heptakis(6-*O*-*tert*-butyldimethylsilyl-2,3-di-*O*-methyl)-β-cyclodextrin dissolved in polysiloxane SE-52 (1:1, w/w) on Chromosorb W-HP; FID; helium as carrier gas at a flow rate of 240 ml/min; injector and detector temperatures were 200 and 250°C, respectively. GC–MS measurements (EI, 70 eV) were carried out with a Hewlett Packard HP 5890 gas chromatograph coupled to a VG Analytical 70-250S mass spectrometer. Ion source temperature: 200°C. NMR-spectroscopy: NMR measurements were carried out with a Bruker WM 400 or a Bruker WM 500 instrument using TMS as internal standard. Polarimetry: measurements were carried out with a polarimeter 341 (Perkin Elmer) at 589 nm at 20°C. Due to very small amounts of isolated compounds only the sense of optical rotation is given to avoid inaccuracies. Dehydration of **9** was carried out by addition of thionylchloride to a solution of the

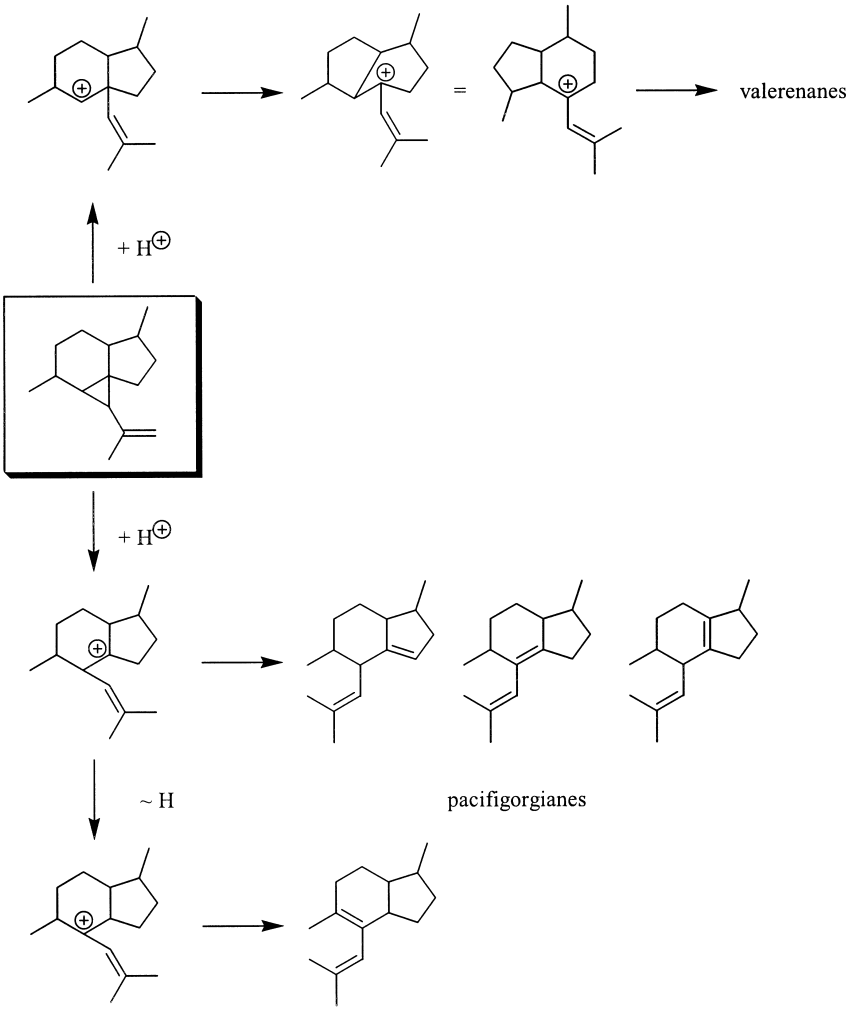

Fig. 3. Possible biogenetic relationship between tamariscene, pacifigorgianes and valerenanes.

alcohol in pyridine at 0°C. After 3 h of stirring water was added and the workup was performed with aq. $NaHCO_3$ solution and hexane extraction. For the dehydration of **10** the reaction was quenched after 3 min.

Hydrogenation was executed by bubbling hydrogen gas through the sample dissolved in hexane and addition of palladium/charcoal for 1 min and additional stirring of the reaction mixture under slight positive hydrogen pressure for 30 min.

Rearrangement reaction of (+)-**1** was performed in chloroform over a period of 21 days at 8°C.

3.2. Plant material and essential oils

Frullania fragilifolia (Tayl.) was collected at the Hinanger Wasserfall (Sonthofen, Allgäu, Germany) in November 1997 at 850 m alt. *Frullania tamarisci* was collected in Wintergreen (Virginia, USA) in May 1997 and at Loekeberg, Sweden, in September 1995. The essential oils of the liverworts were obtained by hydrodistillation (2 h) of aqueous homogenates of the fresh and green liverworts using ca. 1 ml of *n*-hexane as collection solvent. The oil of *Valeriana officinalis* (Europäisches Baldrianöl, Ref.: 971651, 14.08.97) was obtained from Paul Kaders GmbH, Hamburg, Germany.

3.3. Isolation of single constituents of essential oils

The isolation was carried out using column chromatography (silica gel 60 (Merck), eluent: *n*-pentane, −20°C) and preparative GC.

3.4. Tamariscene (*1*)

(−)-(1*R*,2*S*,3*R*,4*S*,7*R*,8*S*)-4,8-dimethyl-2-(1′-methylethylene)-tricyclo[5.3.0.0^{1,3}]decane, colourless oil; RI_{CPSil5}: 1355; sense of optical rotation (benzene): negative for enantiomer isolated from *Frullania fragilifolia* and *F. tamarisci*; positive for enantiomer isolated from *Valeriana officinalis*; ^{1}H NMR (400.1 MHz, C_6D_6): δ 0.54 (1H, *m*, H-4a), 0.72 (1H, *m*, H-5a), 0.95 (1H, *d*, H-10, $J=6.1$ Hz), 1.01 (3H, *d*, CH_3-3, $J=6.6$ Hz), 1.03 (3H, *d*, CH_3-7, $J=6.6$ Hz), 1.07 (1H, *dd*, H-2, $J=5.6$; 5,6 Hz), 1.13–1.26 (2H, *m*, H-6, H-8a), 1.33–1.41 (1H, *m*, H-4b), 1.44–1.55 (2H, *m*, H-7, H-9a), 1.58–1.66 (1H, *m*, H-9b), 1.66–1.76 (2H, *m*, H-5b, H-8b), 1.74 (3H, *s*, CH_3-11), 1.76–1.86 (1H, *m*, H-3), 4.71 (1H, *s*, H-12a), 4.89 (1H, *s*, H-12b); ^{13}C NMR (100.6 MHz, C_6D_6): $\delta=19.16$ (*q*, C-15), 21.29 (*q*, C-14), 24.37 (*q*, C-13), 28.93 (*d*, C-3), 29.04 (*t*, C-4), 30.06 (*d*, C-2), 30.32 (*t*, C-5), 30.41 (*t*, C-9), 33.55 (*d*, C-10), 34.15 (*s*, C-1), 35.53 (*t*, C-8), 44.64 (*d*, C-7), 50.19 (*d*, C-6), 109.50 (*t*, C-12), 144.66 (*s*, C-11); MS (EI, 70 eV), *m*/*z* (rel. int.): 204 $[M]^+$(26), 162 (23), 161 (21), 147 (48), 133 (30), 119 (24), 109 (25), 108 (40), 107 (38), 105 (55), 95 (30), 94 (36), 93 (85), 91 (55), 81 (40), 79 (53), 77 (35), 67 (36), 55(56), 53 (32), 43 (16), 42 (22), 41 (100), 39 (50).

3.5. Pacifigorgia-1(9),10-diene (*2*)

(−)-(1*S*,4*R*,5*S*,7a*R*)-2,4,5,6,7,7a-hexahydro-1,5-dimethyl-4-(2-methyl-1-propenyl)-1*H*-indene, colourless oil; RI_{CPSil5}: 1384; sense of optical rotation (chloroform): positive for enantiomer isolated from *V. officinalis*; negative for enantiomer present in *F. tamarisci*; ^{1}H NMR (400.1 MHz, $CDCl_3$): δ 0.80 (3H, *d*, CH_3-3, $J=6.6$ Hz), 1.07 (3H, *d*, CH_3-7, $J=6.6$ Hz), 0.92-1.04 (1H, *m*, H-5a), 1.31–1.40 (2H, *m*, H-4a,b), 1.55–1.61 (1H, *m*, H-3), 1.64 (3H, *s*, *trans* CH_3-11), 1.71 (3H, *s*, *cis* CH_3-11), 1.74–1.93 (2H, *m*, H-7, H-8a), 1.95–2.03 (1H, *m*, H-5b), 2.05–2.15 (1H, *m*, H-6), 2.39-2.48 (1H, *m*, H-8b), 3.24 (1H, *dd*, H-2, $J=4.6$; 10.2 Hz), 5.18 (1H, *s*, H-9), 5.19 (1H, *d*, H-10, $J=11.7$ Hz); ^{13}C NMR (100.6 MHz, $CDCl_3$): δ 18.07 (*q*, C-13), 19.35 (*q*, C-14), 20.24 (*q*, C-15), 26.31 (*q*, C-12), 29.55 (*t*, C-4), 34.64 (*t*, C-5), 37.25 (*d*, C-3), 40.05 (*t*, C-8), 40.44 (*d*, C-7), 42.57 (*d*, C-2), 49.27 (*d*, C-6), 118.91 (*d*, C-9), 122.09 (*d*, C-10), 130.77, 133.50 (both *s*, C-1, C-11); MS (EI, 70 eV), *m*/*z* (rel. int.): 204 $[M]^+$(53), 147 (54), 107 (41), 105 (58), 93 (56), 91 (54), 55 (50), 41 (100), 39 (45).

3.6. Pacifigorgia-1,10-diene (*3*)

(−)-(1*S*,5*S*,7a*R*)-2,3,5,6,7,7a-hexahydro-1,5-dimethyl-4-(2-methyl-1-propenyl)-1*H*-indene, colourless oil; RI_{CPSil5}: 1400; sense of optical rotation (chloroform): negative for enantiomer isolated from *F. tamarisci*; ^{1}H NMR (400.1 MHz, $CDCl_3$): δ 0.93-0.99 (1H, *m*), 0.89 (3H, *d*, $J=7.1$ Hz), 1.01 (3H, *d*, $J=6.1$ Hz), 1.08–1.33 (4H, *m*), 1.55 (3H, *s*), 1.74 (3H, *s*), 1.63-1.82 (2H, *m*), 1.88-2.02 (2H, *m*), 2.05–2.15 (2H, *m*), 5.46 (1H, *s*); MS (EI, 70 eV), *m*/*z* (rel. int.): 204 $[M]^+$(52), 189 (22), 162 (63), 161 (16), 147 (100), 119 (32), 105 (72), 91 (34), 79 (16), 77 (19), 55 (18), 41 (32), 39 (15).

3.7. Pacifigorgia-1(6),10-diene (*4*)

(−)-(1*S*,4*R*,5*S*-2,3,4,5,6,7)-hexahydro-1,5-dimethyl-4-(2-methyl-1-propenyl)-1*H*-indene, colourless oil; RI_{CPSil5}: 1414; sense of optical rotation (chloroform): positive for enantiomer isolated from *V. officinalis*; negative for enantiomer present in *F. tamarisci*; ^{1}H NMR (400.1 MHz, $CDCl_3$): δ 0.83 (3H, *d*, CH_3-3; $J=7.1$ Hz), 0.95 (3H, *d*, CH_3-7; $J=6.6$ Hz), 1.23–1.31 (1H, *m*, H-8a), 1.36–1.52 (2H, *m*, H-4a,b), 1.65 (3H, *s*, *cis* CH_3-11), 1.71 (3H, *s*, *trans* CH_3-11), 1.73–1.87 (2H, *m*, H-3, H-5a), 1.93-2.10 (3H, *m*, H-5b, H-8b, H-9a), 2.16–2.25 (1H, *m*, H-9b), 2.47–2.57 (1H, *m*, H-7), 2.82 (1H, *br s*, H-2), 4.88 (1H, *d*, H-10, $J=10.2$ Hz); ^{13}C NMR (125.8 MHz, $CDCl_3$): δ 18.15 (*q*, C-13), 18.35 (*q*, C-14), 19.55 (*q*, C-15), 23.56 (*t*, C-5), 26.04 (*q*, C-12), 27.51 (*t*, C-4), 31.77 (*t*, C-8), 32.92 (*d*, C-3), 33.02 (*t*, C-9), 39.86 (*d*, C-2), 41.74 (*d*, C-7), 124.40 (*d*, C-10), 131.50 (*s*, C-11), 137.23 (*s*, C-1), 137.71 (*s*, C-6); MS (EI, 70 eV), *m*/*z* (rel. int.):

204 $[M]^+$(48), 189 (19), 162 (61), 161 (17), 147 (100), 119 (30), 105 (70), 91 (28), 77 (17), 55 (17), 41 (32).

3.8. Pacifigorgia-2,10-diene (**5**)

(−)-(1*S*,3a*R*,7a*R*)-2,3,3a,6,7,7a-hexahydro-1,5-dimethyl-4-(2-methyl-1-propenyl)-1*H*-indene, colourless oil; RI_{CPSil5}: 1422; sense of optical rotation (chloroform): negative for enantiomer isolated from *F. tamarisci*; ^1H NMR (400.1 MHz, $CDCl_3$): δ 0.97 (3H, *d*, $J=6.6$ Hz), 0.88–1.02 (1H, *m*), 1.09–1.29 (4H, *m*), 1.49 (3H, *s*), 1.51 (3H, *s*), 1.74 (3H, *s*), 1.64–1.79 (1H, *m*), 1.85-1.97 (3H, *m*,), 2.11-2.18 (2H, *m*), 5.55 (1H, *s*); MS (EI, 70 eV), *m*/*z* (rel. int.): 204 $[M]^+$(56), 189 (25), 162 (62), 161 (16), 147 (100), 133 (16), 120 (17), 119 (33), 107 (17), 105 (74), 93 (15), 91 (35), 79 (16), 55 (19), 41 (36), 39 (16).

3.9. Pacifigorgia-2(10),11-diene (**6**)

(+)-(1*S*,3a*R*,5*S*,7a*S*)-2,3,3a,5,6,7,7a-octahydro-1,5-dimethyl-4-(2-methyl-2-propenyl)-1*H*-indene, colourless oil; RI_{CPSil5}: 1435; sense of optical rotation (benzene): positive for enantiomer isolated from *F. tamarisci*; ^1H NMR (400.1 MHz, C_6D_6): δ 0.81–0.92 (1H, *m*, H-6), 0.95 (3H, *d*, CH_3-7, $J=6.6$ Hz), 0.97-1.15 (2H, *m*, H-5a, H-9a), 1.05 (3H, *d*, CH_3-3, $J=6.6$ Hz), 1.15–1.27 (1H, *m*, H-8a), 1.35–1.45 (1H, *m*, H-7), 1.69–1.78 (2H, *m*, H-4a,b), 1.81 (3H, *s*, CH_3-11), 1.82-1.92 (4H, *m*, H-1, H-3, H-5b, H-8b), 1.96–2.06 (1H, *m*, H-9b), 4.84 (1H, *s*, H-12a *cis*), 4.92 (1H, *s*, H-12b *trans*), 5.68 (1H, *s*, H-10); ^{13}C NMR (100.6 MHz, C_6D_6): δ 19.38 (*q*, C-14), 19.76 (*q*, C-15), 24.99 (*q*, C-13), 29.83 (*t*, C-9), 31.22 (*t*, C-5), 32.57 (*t*, C-8), 37.84 (*t*, C-4), 39.43 (*d*, C-7), 39.57 (*d*, C-3), 52.62 (*d*, C-1), 56.55 (*d*, C-6), 113.71 (*t*, C-12), 121.62 (*d*, C-10), 144.37 (*s*, C-11), 145.66 (*s*, C-2); MS (EI, 70 eV), *m*/*z* (rel. Int.): 204 $[M]^+$(31), 162 (35), 147 (62), 133 (32), 119 (32), 109 (31), 108 (44), 107 (45), 105 (67), 95 (36), 94 (37), 93 (100), 91 (62), 81 (42), 79 (50), 77 (40), 67 (41), 55 (49), 41 (83), 39 (40).

3.10. Valerena-4,7(11)-diene (**7**)

3,3a,4,5,6,7-hexahydro-1,4-dimethyl-7-(2-methyl-1-propenyl)-2*H*-indene, colourless oil; RI_{CPSil5} 1456; sense of optical rotation (chloroform): negative; ^1H NMR (400.1 MHz, $CDCl_3$): δ 0.75 (3H, *d*, CH_3-10, $J=7.1$ Hz), 1.27–1.38 (2H, *m*, H-8a, H-9a), 1.48–1.57 (1H, *m*, H-2a), 1.61–1.63 (1H, *m*, H-8b), 1.63 (3H, *s*, CH_3-4), 1.66 (3H, *s*, *cis* CH_3-11), 1.69 (3H, *s*, *trans* CH_3-11), 1.76–1.89 (2H, *m*, H-2b, H-9b), 1.90–2.00 (1H, *m*, H-10), 2.11–2.25 (2H, *m*, H-3a,b), 2.93 (1H, *br s*, H-1), 3.36–3.42 (1H, *m*, H-6), 5.46 (1H, *d*, H-7, $J=9.4$ Hz); ^{13}C NMR (125.8 MHz, $CDCl_3$): δ 12.07 (*q*, C-14), 13.39 (*q*, C-15), 17.78 (*q*, C-12), 24.60 (*t*, C-2), 26.11 (*q*, C-13), 26.56 (*t*, C-8), 28.69 (*t*, C-9), 33.57 (*d*, C-10), 33.65 (*d*, C-6), 37.55 (*t*, C-3), 47.40 (*d*, C-1), 126.21 (*d*, C-7), 128.38 (*s*, C-4), 129.77 (*s*, C-11), 136.04 (*s*, C-5); MS (EI, 70 eV), *m*/*z* (rel. Int.): 204 $[M]^+$(77), 189 (56), 161 (50), 147 (62), 133 (51), 119 (53), 109 (57), 107 (58), 105 (74), 93 (70), 91 (74), 55 (51), 41 (100).

3.11. Pacifigorgia-6,10-diene (**8**)

Rel. config.: (3a*S**,4*R**,5*S**)-3,3a,4,5,6,7-hexahydro-1,5-dimethyl-4-(2-methyl-1-propenyl)-2*H*-indene, colourless oil; RI_{CPSil5}: 1427; sense of optical rotation (chloroform): positive for enantiomer isolated from rearrangement of (−)-tamariscol (**9**); ^1H NMR (500.1 MHz, $CDCl_3$): δ 0.79 (3H, *d*, CH_3-3, $J=6.6$ Hz), 0.88-0.98 (1H, *m*, H-4a), 1.19–1.30 (2H, *m*, H-3, H-9a), 1.49–1.56 (1H, *m*, H-2), 1.60 (3H, *d*, CH_3-11, $J=1.3$ Hz), 1.61 (3H, *s*, CH_3-7), 1.72 (3H, *d*, CH_3-11, $J=0.9$ Hz), 1.74–1.80 (2H, *m*, H-4b, H-5a), 1.85-1.92 (1H, *m*, H-9b), 2.17–2.21 (3H, *m*, H-1, H-8a,b), 2.44–2.48 (1H, *m*, H-5b), 4.81 (1H, *br d*, H-10, $J=10.1$ Hz); ^{13}C NMR (125.8 MHz, $CDCl_3$): δ 13.53 (*q*, C-15), 18.76 (*q*, C-12/13, 20.01 (*q*, C-14), 25.58 (*t*, C-5), 25.93 (*q*, C-13/12), 27.96 (*t*, C-9), 35.06 (*t*, C-4), 36.96 (*t*, C-8), 37.10 (*d*, C-3), 52.54 (*d*, C-2), 52.71 (*d*, C-1), 128.20 (*s*, C-6/7), 129.19 (*d*, C-10), 130.88 (*s*, C-11), 136.35 (*s*, C-7/6); MS (EI, 70 eV), *m*/*z* (rel. Int.): 204 $[M]^+$ (15), 148 (9), 147 (8), 109 (100), 95 (14), 93 (8), 91 (8), 79 (13), 67 (22), 55 (10), 41 (13), 39 (4).

Acknowledgements

Compound **8** was isolated by undergraduate student Tina Even (University of Hamburg). The financial support of the Fonds der Chemischen Industrie is gratefully acknowledged.

References

Bos, R., Hendriks, H., Kloosterman, J., Sipma, G., 1986. Isolation of the sesquiterpene alcohol (−)-pacifigorgiol from *Valeriana officinalis*. Phytochemistry 25, 1234–1235.

Connolly, J.D., Harrison, L.J., Rycroft, D.S., 1984. The structure of tamariscol, a new pacifigorgiane sesquiterpenoid alcohol from the liverwort *Frullania tamarisci*. Tetrahedron Lett. 25, 1401–1402.

Hard, I., König, W.A., 1994. Preparative enantiomer separation with modified cyclodextrins as chiral stationary phases. Journal of Chromatography A 666, 611–615.

Joulain, D., König, W.A., 1998. The Atlas of Spectral Data of Sesquiterpene Hydrocarbons. E.B.-Verlag, Hamburg.

Martin, M. G., 1983. Total Synthesis of Pacifigorgiol. PhD thesis, Cornell University.

Tori, M., Sono, M., Nishigaki, Y., Nakashima, K., Asakawa, Y., 1991. Studies on the liverwort alcohol tamariscol. Synthesis and absolute configuration. Journal of Chemical Society Perkin Trans 1, 1435–1445.

Warmers, U., Wihstutz, K., Bülow, N., Fricke, C., König, W.A., 1998. Sesquiterpene constituents of the liverwort *Calypogeia muelleriana*. Phytochemistry 49, 1723–1731.

PERGAMON

Phytochemistry 57 (2001) 315–316

PHYTOCHEMISTRY

www.elsevier.com/locate/phytochem

Book reviews

The Wealth of India, First Supplement, Volume 1: A–Ci
Edited by R. Kochhar, National Institute of Science Communication, CSIR, New Delhi, India, 2000. 283 pp. ISBN 81-7236-208-0.

Historically, the first comprehensive dictionary of the economic products of the Indian subcontinent was prepared by a Scotsman, George Watt (1851–1931) and was published between 1889 and 1893. This was eventually superceded by the *Wealth of India* produced by the Indian Commonwealth Service, which appeared in 11 volumes from 1948 to 1976. What is presented here is the first of five volumes, which are intended to update the major work and to cover the literature from 1985 to 1992. The main plant entries in this first supplement include *Acacia*, *Arachis*, *Artemisia*, *Brassica*, *Camellia*, *Catharanthus* and *Citrus*. There are, of course, animal entries as well on bees, camels and civet cats. In general, older botanical names are retained, so that the pyrethrum plant, now properly referred to as *Tanacetum cinerariifolium*, appears in this volume as *Chrysanthemum*.

Since the agricultural, medicinal and industrial exploitation of the Indian flora depends on their phytochemistry, phytochemical information is very much to the fore. Results published in *Phytochemistry* appear on almost every page. There is a useful listing of the acetogenins isolated from *Annona* spp. with details of m.p., molecular formulae, source and biological activity. The medicinal uses of plants dominate in many entries. I was surprised that *Atropa acuminata*, a plant I have worked on myself, is treated here as being synonymous with *A. belladonna*, when our published work on the alkaloids and phenolics favour recognition as a distinct species in its own right. Incidentally, it is interesting to see that the product atropine which was formerly imported into India, is now harvested from *A. acuminata* plantations and exported to several countries.

I was concerned generally that the various entries failed to alert the reader to the toxic effects of some of the plant products. Thus, abrin, the protein of *Abrus precatorius* seed, is well known to be extremely poisonous. And yet it is stated that the seeds may be utilised for human consumption after (unspecified) processing and may also be used to treat prostate and breast cancer. I suspect that any medicinal uses applied to *Abrus* seed extracts have to be carefully monitored. The article on Neem (*Azadirachta*) was interesting in that in India the medicinal and cosmetic uses seem to be more important than the pesticidal value.

This volume is attractively produced and contains a workmanlike index. Although principally intended as a contribution to economic botany and the medicinal plant literature, it will be of interest and value to a wide audience of scientists.

Jeffrey B. Harborne
Department of Botany
School of Plant Sciences
The University of Reading Whiteknights
PO Box 221, Reading RG6 6AS, UK

PII: S0031-9422(00)00508-2

African Traditional Medicine
H.D Neuwinger, Medpharm Scientific Publishers, Stuttgart, 589 pp., + 46 pp. supplement, hardcover. ISBN 3-88763-086-6. Price DM/sFr 198.

The African flora provides a rich source of drugs that have been used in traditional medicine. Reports on this use have been published in several books, some reviewed journals and quite often in quite unknown and obscure publications. Therefore, it had been quite difficult for scientists interested in a particular African plant to find out whether this plant had been used in traditional African medicine. As traditional medical application can give a hint to the active principles present in a plant, this information can be quite valuable.

Hans Dieter Neuwinger, who has already written important scholarly works on "African ethnobotany: Poisons and drugs" (1996) and "Afrikanische Arznei-

pflanzen und Jagdgifte'' (1994, 1998), has again drawn our attention to African medicinal plants. He has screened the available literature (books, journal articles in English, French, German) for papers on African traditional medicine. The result is a reference source covering 5400 African plant species and 16,300 medicinal applications.

The book is organised in short monographs of the 5400 plant species which have been ordered alphabetically. Each monograph lists particular medicinal applications such as ''headache, cough, narcotic effects, cardiac pains, anthelmintic, aphrodisiac or purgative'' followed by the plant organ used and a reference. These monographs are a treasure trove for information on African medicines which could lead to more detailed studies on ingredients and active principles. A supplement provides a key to plants used for particular medical applications.

The author is certainly right in his warning: ''Let's say it right away: this book is purely a reference book, not one to be read for entertainment. It documents in the form of a dictionary our knowledge of African plants with their immeasurable richness in variety of species and their use in traditional medicine.'' For a non-botanists it might be difficult to identify a particular plant (whose scientific name can be ambiguous because of synonyms) as no family names are provided. Also, the list of references appears to be small in comparison to the wealth of information provided. In addition, no information is given on active ingredients or mode of actions. However, more expanded information can be found in ''African ethnobotany'' or ''Afrikanische Arzneipflanzen und Jagdgifte 1994, 1998), of the same author.

In conclusion, *African Traditional Medicine* is a true reference book which should not me missed by phytochemists, pharmacologists or ethnopharmacologists interested in African ethnobotany.

Michael Wink
Institut für Pharmazeutische Biologie,
Universität Heidelberg Im Neuenheimer Feld 364,
69120 Heidelberg, Germany
E-mail address: wink@uni-hd.de

PII: S0031-9422(01)00008-5

PERGAMON

Phytochemistry 57 (2001) 315–316

PHYTOCHEMISTRY

www.elsevier.com/locate/phytochem

Book reviews

The Wealth of India, First Supplement, Volume 1: A–Ci
Edited by R. Kochhar, National Institute of Science Communication, CSIR, New Delhi, India, 2000. 283 pp. ISBN 81-7236-208-0.

Historically, the first comprehensive dictionary of the economic products of the Indian subcontinent was prepared by a Scotsman, George Watt (1851–1931) and was published between 1889 and 1893. This was eventually superceded by the *Wealth of India* produced by the Indian Commonwealth Service, which appeared in 11 volumes from 1948 to 1976. What is presented here is the first of five volumes, which are intended to update the major work and to cover the literature from 1985 to 1992. The main plant entries in this first supplement include *Acacia*, *Arachis*, *Artemisia*, *Brassica*, *Camellia*, *Catharanthus* and *Citrus*. There are, of course, animal entries as well on bees, camels and civet cats. In general, older botanical names are retained, so that the pyrethrum plant, now properly referred to as *Tanacetum cinerariifolium*, appears in this volume as *Chrysanthemum*.

Since the agricultural, medicinal and industrial exploitation of the Indian flora depends on their phytochemistry, phytochemical information is very much to the fore. Results published in *Phytochemistry* appear on almost every page. There is a useful listing of the acetogenins isolated from *Annona* spp. with details of m.p., molecular formulae, source and biological activity. The medicinal uses of plants dominate in many entries. I was surprised that *Atropa acuminata*, a plant I have worked on myself, is treated here as being synonymous with *A. belladonna*, when our published work on the alkaloids and phenolics favour recognition as a distinct species in its own right. Incidentally, it is interesting to see that the product atropine which was formerly imported into India, is now harvested from *A. acuminata* plantations and exported to several countries.

I was concerned generally that the various entries failed to alert the reader to the toxic effects of some of the plant products. Thus, abrin, the protein of *Abrus precatorius* seed, is well known to be extremely poisonous. And yet it is stated that the seeds may be utilised for human consumption after (unspecified) processing and may also be used to treat prostate and breast cancer. I suspect that any medicinal uses applied to *Abrus* seed extracts have to be carefully monitored. The article on Neem (*Azadirachta*) was interesting in that in India the medicinal and cosmetic uses seem to be more important than the pesticidal value.

This volume is attractively produced and contains a workmanlike index. Although principally intended as a contribution to economic botany and the medicinal plant literature, it will be of interest and value to a wide audience of scientists.

Jeffrey B. Harborne
Department of Botany
School of Plant Sciences
The University of Reading Whiteknights
PO Box 221, Reading RG6 6AS, UK

PII: S0031-9422(00)00508-2

African Traditional Medicine
H.D Neuwinger, Medpharm Scientific Publishers, Stuttgart, 589 pp., + 46 pp. supplement, hardcover. ISBN 3-88763-086-6. Price DM/sFr 198.

The African flora provides a rich source of drugs that have been used in traditional medicine. Reports on this use have been published in several books, some reviewed journals and quite often in quite unknown and obscure publications. Therefore, it had been quite difficult for scientists interested in a particular African plant to find out whether this plant had been used in traditional African medicine. As traditional medical application can give a hint to the active principles present in a plant, this information can be quite valuable.

Hans Dieter Neuwinger, who has already written important scholarly works on "African ethnobotany: Poisons and drugs" (1996) and "Afrikanische Arznei-

PERGAMON

Phytochemistry 57 (2001) 317

PHYTOCHEMISTRY

www.elsevier.com/locate/phytochem

Corrigendum

Corrigendum to "Pyrrolizidine alkaloids from *Cynoglossum creticum*" [Phytochemistry 42 (1996) 1217–1221]☆

A. El-Shazly [a], T. Sarg [a], L. Witte [b], M. Wink [c]

[a] *Department of Pharmacognosy, Faculty of Pharmacy, Zagazig University, Zagazig, Egypt*
[b] *Institut für Pharmazeutische Biologie der Technischen Universität, Mendelssohnstrasse 1, D-38106 Braunschweig, Germany*
[c] *Institut für Pharmazeutische Biologie der Universität, Im Neuenheimer Feld 364, D-69120 Heidelberg, Germany*

The authors regret the following error in the second line of Table 4, page 1221; "undetermined PA" should be replaced with "3′-acetylechinatine".

☆ SSDI of original article: S0031-9422(96)00112-4

0031-9422/01/$ - see front matter © 2001 Elsevier Science Ltd. All rights reserved.
PII: S0031-9422(00)00457-X

PERGAMON

Phytochemistry 57 (2001) 319–323

PHYTOCHEMISTRY

www.elsevier.com/locate/phytochem

Molecules of Interest

The latest hype on Hyp-*O*-glycosylation codes

Marcia Jane Kieliszewski *

Department of Chemistry and Biochemistry, Ohio University, Athens, OH 45701, USA

Received 30 November 2000; received in revised form 13 January 2001

Abstract

Contemporary glycobiology reflects the intense interest in glycoproteins and their biological roles. Addition of saccharides by *N*- or *O*-glycosylation is precise rather than random and forms a uniquely interactive molecular surface. We designate these well conserved glycomotifs as glycomodules to emphasize their functional significance. Thus, elucidation of the glycosylation codes that determine saccharide addition is a significant goal. The focus here is on the Hyp *O*-glycosylation of cell wall proteins. This involves two consecutive posttranslational modifications, proline hydroxylation and glycosylation. Peptide sequence rather than conformation seems to determine these modifications. Hyp glycosylation occurs in two distinct modes: Hyp arabinosylation and Hyp galactosylation. The Hyp contiguity hypothesis predicts arabinosylation of contiguous Hyp residues and galactosylation of clustered non-contiguous Hyp. Elucidation of Hyp glycosylation codes involves the design and expression of putative glycomotifs as simple repetitive peptides. Thus, repetitive $(Ser\text{-}Hyp)_n$ directed Hyp galactosylation resulting in the exclusive addition of arabinogalactan polysaccharide to all the non-contiguous Hyp residues, and a new AGP. Another repetitive peptide from gum arabic glycoprotein, containing both contiguous and non-contiguous Hyp, directed both modes of Hyp glycosylation. Furthermore, expression of the $(Ser\text{-}Hyp_x)_n$ series confirmed the arabinosylation of contiguous Hyp. Thus, the Hyp contiguity hypothesis is a useful predictive tool in the functional genomics toolbox. © 2001 Elsevier Science Ltd. All rights reserved.

Keywords: Hydroxyproline-rich glycoprotein; Arabinogalactan-protein; Extensin; Glycosylation; Cell walls

1. Introduction

Glycobiology is currently of intense interest because biologists now know that carbohydrate is much more than a dietary filler. Carbohydrate addition to proteins confers new properties that contribute to biological function. This glycosylation is not random. It is not uniform. It is not readily deduced from genome readouts. It is the most common posttranslational modification and involves more than 50% of eukaryotic proteins (Apweiler et al., 1999). As a multipurpose tool, it yields a dazzling array of designer products to suit the function planned. So, what determines it?

Protein glycosylation involves the enzymic transfer of specific sugars to specific amino acid residues of a protein. While Table 1 shows that a surprising number of amino acids are potential sugar acceptors, they fall into two major categories: *N*- and *O*-glycosylation. Thus asparagine residues are involved in *N*-glycosylation while *O*-glycosylation involves the hydroxyamino acids, mainly serine and threonine, occasionally tyrosine, and, specific to plants, hydroxyproline. Recent advances in identifying Hyp glycosylation motifs and the elucidation of Hyp glycosylation codes are the focus of this review.

2. *N*- And *O*-glycosylation motifs

N- and *O*-glycosylation differ in virtually all aspects: biosynthetic strategy, donor sugars, glycosylation site sequence motifs and chemical stability of the sugar-amino acid "glycopeptide" linkage. Although both types of glycosylation construct complex sugar sequences (oligosaccharides or repetitive polysaccharides) by "strict order" stepwise addition (Staudacher and Marz, 1998), the sugars and linkages differ. *N*-glycosylation involves mannose addition to a chitobiose core followed by the block transfer of a preformed oligosaccharide from its dolichol lipid carrier to the polypeptide (Sturm, 1995). In contrast *O*-glycosylation is generally viewed as

* Tel.: +1-740-593-9466; fax: +1-740-593-0148.
E-mail address: kielisze@helios.phy.ohiou.edu

0031-9422/01/$ - see front matter © 2001 Elsevier Science Ltd. All rights reserved.
PII: S0031-9422(01)00029-2

Table 1
Occurrence of glycopeptide linkages [updated from (a)][a]

		Eukaryotes			
Linkage	Prokaryotes	Protists	Fungi	Plants	Animals
N-Glycosidic					
GlcNAc-Asn	(a)	(a)	(a)	(a, b)	(a)
Rha-Asn	(c)	–	–	–	–
O-Glycosidic					
Gal-Hyl	–	–	–	–	(a)
Ara-Hyp	–	(a)	–	(a)	–
Gal-Hyp	–	(a)	–	(a)	–
GlcNAc-Hyp	–	–	(d)	–	–
Glc-Hyp	–	–	–	(a)	–
Fuc-Ser	–	–	–	–	(e)
Gal-Ser	–	–	–	(a)	(a)
GalNAc-Ser	–	–	–	–	(f)
Glc-Ser	–	–	–	–	(g)
GlcNAc-Ser	–	–	–	–	(h)
Man-Ser	–	–	(a)	–	–
Xyl-Ser	–	(a)	–	–	(i)
Fuc-Thr	–	–	–	–	(e)
Gal-Thr	(c)	–	–	–	(a)
GalNAc-Thr	–	–	–	(a, f)	
GlcNAc-Thr	–	–	–	–	(h)
Man-Thr	(c)	–	(a)	–	–
Xyl-Thr	–	(a)	–	(a)	–
Gal-Tyr	(c)	–	–	–	–
Glc-Tyr	(c)	–	–	–	–
C-Glycosidic					
Man-Trp	–	–	–	–	(e)

[a] (a) Lamport, 1980; (b) Sturm, 1995; (c) Moens and Vanderleyden, 1997; (d) Teng-Umnuay et al., 1999; (e) Vliegenthart and Casset, 1998; (f) Clausen and Bennett, 1996; (g) Nishimura et al., 1992; (h) Hart et al., 1995; (i) Kresse, 1997.

sequential transfer of single sugar residues from their sugar nucleotides to the polypeptide. This includes neutral sugars, amino sugars and uronic acids, but not mannose. However, there are exceptions: Yeast transfers dolichol-activated mannose to Ser or Thr residues of secretory proteins in the ER (Strahl-Bolsinger et al., 1999). In plants lipid-linked acidic arabinosyl oligosaccharides are transferred to HRGP acceptors (Bolwell, 1986). One intermediate contained about 15 sugar residues and a galactose reducing end (Hayashi and Maclachlan, 1984). This implies the block transfer of lipid-linked oligosaccharide modules as building blocks of AGP polysaccharides and a possible paradigm for pre-assembly of other complex modular polysaccharides.

The genome does not explicitly encode glycosylation sites as ''glycocodons'' but implicitly as codes within a code. These glycosylation codes include the classic *N*-glycosylation motif Asn-Xaa-Thr/Ser, the clustered Ser/Thr *O*-glycosylation sites of animal mucins and the serine consensus sequences that act as substrate for the xylosyltransferase that initiates the attachment of glycosaminoglycans to the core proteins of animal proteoglycans (Brinkmann et al., 1997).

3. Localization of hydroxylation and glycosylation

Glycosylation codes depend on another code, the N-terminal signal sequence, to target the polypeptide to the ER/Golgi for posttranslational processing. Additional codes, or targeting signals determine final destinations. These include retention by the ER/Golgi, or further transfer to protein storage bodies, central vacuole, or plasma membrane. The major ''default'' secretory pathway exiles HRGPs to the exterior, where they appear as components of sticky stigma adhesives, root-cap slime lubricants and wound-induced gummosis exudates. HRGPs also participate in the extracellular matrix as major components of the plasma membrane glycocalyx (GPI-anchored AGPs; Serpe and Nothnagel, 1999) and crosslinked cell wall networks (extensins) while the role of the repetitive proline-rich proteins (PRPs) is less clear (Frueauf et al., 2000).

As Hyp-glycosylation forms the interactive molecular surface of most HRGPs, carbohydrate must be a major determinant of function. It is therefore of considerable interest to elucidate the rules that direct the addition of saccharide sidechains to the extended Hyp-rich polypeptide template that determines their spatial orientation.

The glycosylation profile of an HRGP results from two consecutive posttranslational modifications: The first occurs in the ER (Wojtaszek et al., 1999) and involves hydroxylation of some, but not all proline residues by prolyl hydroxylases. The second occurs in the Golgi and involves glycosylation of some, but not all hydroxyproline residues by glycosyltransferases. Thus prolyl hydroxylases, glycosyltransferases and the HRGP polypeptide itself are the primary determinants of HRGP glycosylation.

If prolyl hydroxylases and glycosyltransferases are the primary enzymic determinants of HRGP glycosylation patterns what features of the macromolecular substrate do these enzymes recognize?

4. The Hyp contiguity hypothesis

Plant prolyl hydroxylase hydroxylates peptidyl proline but the substrate specificity is not well defined, although poly-L-proline is an excellent substrate (Tanaka et al, 1980). In aqueous solution this occurs as a characteristic three-residue per turn extended helix, designated polyproline II. Initially this suggested recognition of conformation rather than sequence. However, subsequent work, including CD spectroscopy, shows that Hyp residues and glycosylated Hyp occur in sequences lacking a

polyproline II conformation (Kieliszewski and Lamport, 1994). This implies that plant prolyl hydroxylase, like animal prolyl hydroxylase, is primarily directed by the amino acid sequence of the substrate. However, peptide motifs hydroxylated by plants differ from those hydroxylated by animals (Myllyharju and Kivirikko, 1999); for example, plants do not hydroxylate transgenic collagen (Ruggiero et al., 2000).

Two modes of Hyp glycosylation characterize the HRGPs, namely, arabinosylation and galactosylation. Arabinosylation predominates in the extensins and PRPs; on alkaline hydrolysis they yield Hyp-arabinosides. Galactosylation gives rise to the arabinogalactan polysaccharides of arabinogalactan-proteins; on alkaline hydrolysis AGPs yield Hyp-polysaccharides. What structural differences might account for this difference in glycosylation? A preponderance of highly conserved peptide motifs containing contiguous Hyp residues in the extensins and clustered non-contiguous Hyp residues in the arabinogalactan proteins suggested a simple glycosylation code and the concept of functional glycomodules (Table 2). Thus, the Hyp contiguity hypothesis, as originally formulated (Kieliszewski and Lamport, 1994), predicted arabinosylation of contiguous Hyp residues and galactosylation of clustered, non-contiguous Hyp residues. We designate these evolutionarily conserved glycomotifs as glycomodules to emphasize their likely functional significance (Shpak et al., 1999) although it remains to be fully elucidated. Thus, further refinement and verification of the Hyp contiguity hypothesis will help to identify glycomodules from HRGP gene sequences and thus contribute to the functional and structural modeling of the plant extracellular matrix.

5. Experimental testing of the Hyp contiguity hypothesis

Rigorous testing of the Hyp contiguity hypothesis demands an initial identification of glycosylated Hyp-rich motifs by direct methods. There are two approaches, degradative and biosynthetic. The first depends on degrading an isolated HRGP to yield identifiable glycopeptides; the second depends on the biosynthesis of identifiable glycopeptides through the genetic engineering of endogenous test substrates. Both approaches depend on characterizing the products based on the very different chemical reactivities of peptide bonds and glycosidic linkages towards aqueous acid, aqueous alkali, and anhydrous hydrogen fluoride. The following summarizes the salient points:

Both peptides and glycosides are acid-labile, especially arabinofuranosides which cleave at pH 1. However, peptides and glycosides exhibit markedly different labilities to alkali. While peptides undergo base-catalyzed hydrolysis, glycosidic linkages are stable with the significant exception of *O*-seryl- or *O*-threonyl-linked sugars that are cleaved in mild alkali due to elimination (not hydrolysis) of the sugar from the β-carbon. Thus, glycosylated serine and threonine cannot be directly isolated and quantified, but must be inferred indirectly. On the other hand the Hyp-*O*-glycosidic linkage is to the γ-carbon and is base-stable. Complete alkaline hydrolysis of the polypeptide releases intact Hyp glycosides: Hyp arabinosides from extensins, Hyp arabinosides and Hyp polysaccharides from AGPs, and Hyp hetero-oligosaccharides from cell walls of the Chlorophycean algae (Lamport, 1980). Further chromatographic separation yields a quantitative Hyp glycoside profile that indicates the number of Hyp glycosylation sites in an HRGP and the relative abundance of each species, but not their position.

Finally, there is the stability of the peptide bond in anhydrous hydrogen fluoride (HF) in contrast to the rapid HF-solvolysis of glycosidic linkages (Mort and Lamport, 1977). Removal of the *O*-glycosides from various HRGP polypeptides enabled both direct and indirect peptide sequence analysis, hence identification of putative Hyp glycosylation motifs whose number should tally with the Hyp glycoside profile. But assigning the appropriate Hyp arabinoside or Hyp polysaccharide to each glycomotif based on the Hyp contiguity hypothesis requires independent verification.

Defining the position of each Hyp-glycoside in an isolated HRGP is difficult. In theory a "brute force" approach based on enzymic or partial alkaline hydrolysis of the glycoprotein should yield unique glycopeptides that define the glycosylation motifs. However, there are limitations to that approach when dealing with highly glycosylated macromolecules that are difficult to purify and not available in bulk (i.e. tens to hundreds of milligrams). While this degradative approach is feasible for the PRPs (Kieliszewski et al., 1995), it is difficult for extensins and extremely difficult for AGPs.

An alternative strategy uses a biosynthetic approach that exploits the highly repetitive character of HRGPs. Indeed, the PRPs and extensins frequently contain only two major repeat motifs while AGPs exhibit a more cryptic periodicity consisting of simple motifs largely defined by carefully spaced Hyp residues. Therefore, we considered the possibility of presenting the cells with a range of simple repetitive test motifs as candidates for hydroxylation and glycosylation.

Table 2
HRGP glycomodules

Repetitive peptide motif	Hydroxyproline oligosaccharide
$(Xaa^{a})_{1–3}$-Hyp-$(Xaa)_{1–3}$-Hyp	Arabinogalactan polysaccharide
Xaa-Hyp-Hyp	Ara_{1-3} addition mainly to first Hyp
Xaa-Hyp-Hyp-Hyp-Hyp	Ara_{3-4} addition to Hyp residues

[a] Xaa is commonly Ser, Ala, Thr, but not Hyp.

Earlier work had demonstrated the feasibility of a genetic engineering approach based on ligation of small overlapping oligonucleotides for the construction of synthetic genes and the expression of repetitive proteins in bacteria (McGrath et al., 1990). Therefore, we explored the extension of this technique to the elucidation of posttranslational codes in plants. This meant designing simple repetitive polypeptides to encode putative glycosylation motifs, generally only one or two of a kind in each construct to avoid ambiguity. Addition of an appropriate N-terminal signal peptide targeted these polypeptides into the ER/Golgi secretory pathway. Further addition of a C-terminal green fluorescent protein (GFP) reporter facilitated separation of these new HRGPs from others lacking GFP, and in amounts sufficient for biochemical characterization: Hyp-glycoside profiles, sugar and amino acid analyses, circular dichroism, NMR, and so on.

Our first designs tested the hypothesis that clustered non-contiguous Hyp motifs direct the addition of arabinogalactan-polysaccharide to AGPs. Thus a synthetic gene encoding (Ser-Pro) repeats gave rise to a fusion glycoprotein which was an arabinogalactan-protein (Shpak et al., 1999). Repetitive Ser-Pro was an excellent substrate for tobacco prolyl hydroxylase, and the non-contiguous Hyp directed polysaccharide addition exclusively to all the Hyp residues, creating a new AGP.

Another synthetic gene encoding a variant of the *Acacia senegal* 19-residue gum arabic glycoprotein consensus sequence contained motifs for polysaccharide addition to Hyp (Ser-Hyp-Ser-Hyp-Thr-Hyp) and for Hyp arabinosylation (contiguous Hyp blocks). Thus, expression of the repetitive gum arabic glycoprotein consensus sequence in *Nicotiana tabacum* directed arabinosides to some Hyp residues and polysaccharide to others consistent with known Hyp glycoside profiles for native gum arabic glycoprotein (Shpak et al., 1999).

These results established the feasibility of the approach and make it possible to move on and ask more detailed questions about the glycosylation and molecular design of HRGPs. For example, what defines "clusters of non-contiguous Hyp"- how much separation is required to confer non-glycosylated status on a lone Hyp residue? Which intervening amino acids confer non-glycosylated status? Does that explain the absence of Hyp-polysaccharide from the non-contiguous Hyp motif, Tyr-Thr-Hyp-Ser-Hyp-Lys-Pro-Hyp, of the moncocot extensin THRGP? Do flanking residues modify the glycosylation code? Does the polysaccharide vary according to the motif? Does it vary from species to species or even within a species, for example by undergoing processing in different tissues?

To date we know that in tobacco cultures repetitive $(SP)_n$ and $(AP)_n$ give very similar glycosylated products (L. Tan and M. Kieliszewski, unpublished data), indicating that within a species and particular tissue type, arabinogalactan polysaccharide attached to non-contiguous Hyp is probably identical both in size, composition, and frequency of attachment. Comparison between species is instructive. The similarity between the compositions of Hyp-polysaccharides isolated from *Acacia senegal* GAGP and transgenic *Nicotiana tabacum* "GAGP" confirms Akiyama's observation: "The structure and the sugar compositions of the carbohydrate portions of the tobacco AGP are quite similar to the *A. senegal* gum, suggesting that they are closely related to each other" (Akiyama and Kato, 1981). Such similarity in polysaccharide structure between two widely separated families, *Leguminosae* and *Solanaceae*, argues for a global Hyp glycosylation code, at least in higher plants. It also implies a certain elegant simplicity where an AGP peptide template directs the number and arrangement of identical polysaccharide substituents, which are tailored to the tissue by the expression of respective glycosyl transferases, and which might undergo further modification or processing of the polysaccharide sidechains (Cheung et al., 1995).

Most recently we tested the contiguous Hyp, $(SP_x)_n$ series of expression products: $(Ser\text{-}Hyp_2)_n$, $(Ser\text{-}Hyp_3)_n$ and $(Ser\text{-}Hyp_4)_n$ (Shpak and Kieliszewski, unpublished data). They confirm that arabinosylation of contiguous Hyp begins with dipeptidyl Hyp, at least in tobacco. However, increasing the Hyp contiguity increased both the number of Hyp residues arabinosylated in the glycomotif and the size of the added arabinooligosaccharide. Surprisingly however, the putative $(Ser\text{-}Hyp_3)_n$ product contained a mixture of Hyp-glycosides including Hyp-polysaccharide, rather than the expected uniform arabinosylation. This apparently anomalous addition of polysaccharide was due to incomplete hydroxylation of $(Ser\text{-}Pro_3)_n$ resulting in a mixture of contiguous and non-contiguous Hyp residues. The virtual absence of $Ser\text{-}Pro_3$ motifs in *Nicotiana* (compared with other species like *Acacia* and *Arabidopsis*) suggests that tobacco prolyl hydroxylase has a low affinity for an unusual substrate. This emphasizes that the specificity of multiple prolyl hydroxylases underpins the glycosylation framework of HRGPs.

These results with synthetic genes were consistent with the Hyp contiguity hypothesis and encouraged us to extend the genetic engineering approach to naturally occurring HRGPs, particularly the "difficult-to-purify" AGPs notoriously present as mixtures (Serpe and Nothnagel, 1999). Could we isolate a pure GFP-AGP fusion glycoprotein free from other AGPs? And would its glycosylation profile conform to that predicted by the Hyp contiguity hypothesis? We chose LeAGP1 in view of its outstanding interest as the major AGP of tomato, the likely occurrence of a homolog in tobacco, and the availability of the LeAGP1 gene (Gao et al., 1999). As predicted, LeAGP1 containing EGFP was significantly more hydrophobic than other endogenous AGPs thus permitting purification of LeAGP1, the first AGP purified to homogeneity. The experimentally determined

Hyp glycoside profile agreed with that predicted from the Hyp contiguity hypothesis (Z.D. Zhao, A. Showalter and M. Kieliszewski, unpublished data).

6. Conclusion

To conclude we suggest that relating the structure and function of extracellular matrix macromolecules is not as difficult as once feared. It is now possible to make cautious predictions about HRGP structure starting from the primary sequence, and perhaps even genomic sequences. The clear distinction between Hyp arabinoside motifs of extensins and Hyp polysaccharide motifs of AGPs suggests a molecular architecture built of small functional units or glycomodules. In "mix and match" mode an appropriate blend of glycomodules results in HRGPs tailored to the tissue. Thus, in the cell wall the rigidity and tensile properties of extensin depend on stabilization of the HRGP polypeptide by the arabinosylated Ser-Hyp_4 glycomodule. On the other hand, at the surface of the plasma membrane the Hyp-arabinogalactan polysaccharides of GPI-anchored AGPs act as a hydrophilic buffer retaining water through the mobility of their 1,6-linked oligosaccharide sidechains.

Acknowledgements

This work was supported by grants from the National Science Foundation (MCB-9874744 and IBN-9727757) and the United States Department of Agriculture National Research Initiative Competitive Grants Program (97-01299). I thank Drs. Linda Schnabelrauch and Derek Lamport for comments regarding this manuscript.

References

Akiyama, Y., Kato, K., 1981. An extracellular arabinogalactan-protein from *Nicotiana tabacum*. Phytochemistry 20, 2507–2510.

Apweiler, R., Hermjakob, H., Sharon, N., 1999. On the frequency of protein glycosylation, as deduced from analysis of the SWISS-PROT database. Biochimica Biophysica Acta 1473, 4–8.

Bolwell, G.P., 1986. Microsomal arabinosylation of polysaccharide and elicitor-induced carbohydrate-binding glycoprotein in french bean. Phytochemistry 25, 1807–1813.

Brinkmann, T., Weilke, C., Kleesiek, K., 1997. Recognition of acceptor proteins by UDP-D-xylose proteoglycan core protein β-D-xylosyltransferase. Journal of Biological Chemistry 272, 11171–11175.

Cheung, A.Y., Wang, H., Wu, H., 1995. A floral transmitting tissue-specific (TTS) glycoprotein attracts pollen tubes and stimulates their growth. Cell 82, 383–393.

Clausen, H., Bennett, E.P., 1996. A family of UDP-GalNAc: polypeptide *N*-acetylgalactosaminyl-transferases control the inititation of mucin-type *O*-linked glycosylation. Glycobiology 6, 635–646.

Frueauf, J.B., Dolata, M., Leykam, J.F., Lloyd, E.A., Gonzales, M., VandenBosch, K., Kieliszewski, M.J., in press. Peptides isolated from cell walls of *Medicago truncatula* nodules and uninfected root. Phytochemistry 55, 429–438.

Gao, M., Kieliszewksi, M.J., Lamport, D.T.A., Showalter, A.M., 1999. Isolation, characterization and immunolocalization of a novel modular tomato arabinogalactan-protein corresponding to the *LeAGP-1* gene. Plant Journal 18, 43–55.

Hart, G.W., Greis, K.D., Dong, L.-Y.D. et al., 1995. *O*-linked *N*-acetylglucosamine: The "Yin-Yang" of Ser/Thr phosphorylation Nuclear and cytoplasmic glycosylation? Advances in Experimental Medical Biology 376, 115–123.

Hayashi, T., Maclachlan, G., 1984. Biosynthesis of pentosyl lipids by pea membranes. Biochemical Journal 217, 719–803.

Kieliszewski, M.J., Lamport, D.T.A., 1994. Extensin: repetitive motifs, functional sites, posttranslational codes and phylogeny. Plant Journal 5, 157–172.

Kieliszewski, M.J., O'Neill, M., Leykam, J., Orlando, R., 1995. Tandem mass spectrometry and structural elucidation of glycopeptides from a hydroxyproline-rich plant cell wall glycoprotein indicate that contiguous hydroxyproline residues are the major sites of hydroxyproline-*O*-arabinosylation. Journal of Biological Chemistry 270, 2541–2549.

Kresse, H., 1997. Proteoglycans — structure and functions. In: Gabius, H.-J., Gabius, S. (Eds.), Glycosciences. Chapman & Hall, Weinheim, Germany, pp. 201–222.

Lamport, D.T.A., 1980. Structure and function of plant glycoproteins. In: Preiss, J. (Ed.), The Biochemistry of Plants (Vol. 3). Academic Press, New York, pp. 501–541.

McGrath, K.P., Tirrell, D.A., Kawai, M., Mason, T.L., Fournier, M.J., 1990. Chemical and biosynthetic approaches to the production of novel polypeptide materials. Biotechnology Progress 6, 186–192.

Moens, S., Vanderleyden, J., 1997. Glycoproteins in prokaryotes. Archives of Microbiology 168, 169–175.

Mort, A.J., Lamport, D.T.A., 1977. Anhydrous hydrogen fluoride deglycosylates glycoproteins. Analytical Biochemistry 82, 289–309.

Myllyharju, J., Kivirikko, K.I., 1999. Identification of a novel proline-rich peptide-binding domain in prolyl 4-hydroxylase. EMBO Journal 18, 306–312.

Nishimura, H., Yamashita, S., Zeng, Z., Iz, D.A., Iwanaga, S., 1992. Evidence for the existence of *O*-linked sugar chains consisting of glucose and xylose in bovine thrombospondin. Journal of Biochemistry 111, 460–464.

Ruggiero, F., Exposito, J.Y., Bournat, P., Gruber, V., Perret, S., Comte, J., Olagnier, B., Garrone, R., Theissen, M., 2000. Triple helix assembly and processing of human collagen produced in transgenic tobacco plants. FEBS Lett. 469, 132–136.

Serpe, M.D., Nothnagel, E.A., 1999. Arabinogalactan-proteins in the multiple domains of the plant cell surface. Advances in Botanical Research 30, 207–289.

Shpak, E., Leykam, J.F., Kieliszewski, M.J., 1999. Synthetic genes for glycoprotein design and the elucidation of hydroxyproline-*O*-glycosylation codes. Proceedings of the National Academy of Sciences, USA 96, 14736–14741.

Staudacher, E., Marz, L., 1998. Strict order of (Fuc to Asn-linked GlcNAc) fucosyltransferases forming core-difucosylated structures. Glycoconjugate Journal 15, 355–360.

Strahl-Bolsinger, S., Gentzsch, M., Tanner, W., 1999. Protein *O*-mannosylation. Biochimica Biophysical Acta 1426, 297–307.

Sturm, A., 1995. *N*-Glycosylation of plant proteins. New Comprehensive Biochemistrya 29a, 521–541.

Tanaka, M., Shibata, H., Uchida, T., 1980. A new prolyl hydroxylase acting on poly-L-proline from suspension cultured cells of *Vincea rosea*. Biochimica Biophysica Acta 616, 188–198.

Teng-Umnuay, P., Van der Wel, H., West, C.M., 1999. Identification of a UDP-GlcNAc:Skp1-hydroxyproline GlcNAc-transferase in the cytoplasm of Dictyostelium. Journal of Biological Chemistry 274, 36392–36402.

Vliegenthart, J.F.G., Casset, F., 1998. Novel forms of protein glycosylation. Current Opinions Structural Biology 8, 565–571.

Wojtaszek, P., Smith, C.G., Bolwell, G.P., 1999. Ultrastructural localization and further biochemical characterization of prolyl 4-hydroxylase from Phaseolus vulgaris: comparative analysis. International Journal of Biochemistry and Cell Biology 31, 463–477.

PERGAMON

Phytochemistry 57 (2001) 325–339

PHYTOCHEMISTRY

www.elsevier.com/locate/phytochem

Review

Phytoecdysteroids: biological aspects

Laurence Dinan*

Department of Biological Sciences, University of Exeter, Hatherly Laboratories, Prince of Wales Road, Exeter, Devon, EX4 4PS, UK

Received 30 November 2000; received in revised form 8 February 2001

Abstract

Phytoecdysteroids are a family of about 200 plant steroids related in structure to the invertebrate steroid hormone 20-hydroxyecdysone. Typically, they are C_{27}, C_{28} or C_{29} compounds possessing a 14α-hydroxy-7-en-6-one chromophore and A/B-*cis* ring fusion (5β-H). In the present review, the distribution, biosynthesis, biological significance and potential applications of phytoecdysteroids are summarised. © 2001 Elsevier Science Ltd. All rights reserved.

Keywords: Phytoecdysteroid; Distribution; Biological activity; Biosynthesis; 20-Hydroxyecdysone

Contents

1. Introduction 326

2. Distribution of ecdysteroids in the plant world 326

3. Structural diversity 327

4. Phytoecdysteroid production in vitro 329

5. Biosynthesis 329

6. Biological significance of phytoecdysteroids to plants 330

7. Structure–activity studies 331

8. Applications of phytoecdysteroids 332
   8.1. Agricultural applications 332
      8.1.1. Improvement of silk yields 332
      8.1.2. Design of more specific invertebrate pest control agents 333
      8.1.3. Modification of ecdysteroid levels in crop species 333

Abbreviations: CoMFA, comparative molecular field analysis; E, ecdysone; EcR, ecdysteroid receptor; GM, genetically-modified; 20E, 20-hydroxyecdysone; PE, phytoecdysteroid; ponA, ponasterone A; RXR, retinoid X receptor; USP, Ultraspiracle

* Tel.: +44-1392-264605; fax: +44-1392-263700.
E-mail address: l.n.dinan@exeter.ac.uk

0031-9422/01/$ - see front matter © 2001 Elsevier Science Ltd. All rights reserved.
PII: S0031-9422(01)00078-4

8.2. Biomedical applications 333
8.2.1. Effects of ecdysteroids on vertebrates 333
8.2.2. Gene switches 334
8.2.3. Antimicrobial agents 334

9. Concluding remarks 334

Acknowledgements 334

References 334

1. Introduction

Ecdysteroids were first recognised as steroidal hormones controlling moulting and metamorphosis in insects. Today, it is realised that these steroids are present at all stages of insect development, regulating many biochemical and physiological processes: in newly-laid eggs, during embryonic and postembryonic developments and in adult insects, regulating aspects of development, metamorphosis, reproduction and diapause. Ecdysteroids are the steroid hormones of all classes of arthropods and probably of other invertebrates too (see Koolman, 1989, for reviews). Analogues of ecdysteroids (phytoecdysteroids) also occur in a certain proportion of plant species. Their function in plants is still conjectural, but it is believed that they provide some degree of protection against non-adapted phytophagous insects and/or soil nematodes (Bergamasco and Horn, 1983; Kubo and Hanke, 1986). The first ecdysteroid, ecdysone (E), was isolated by Butenandt and Karlson (1954) from silkworm pupae and its structure was finally elucidated in 1965 by means of X-ray crystallography (Huber and Hoppe, 1965). Subsequently, 20-hydroxyecdysone (Fig. 1; 20E; see Lafont et al., 1993, for standardised abbreviations for ecdysteroids) was identified from a number of arthropod sources and this compound is now generally recognised as the major biologically active ecdysteroid in most invertebrate systems, although this

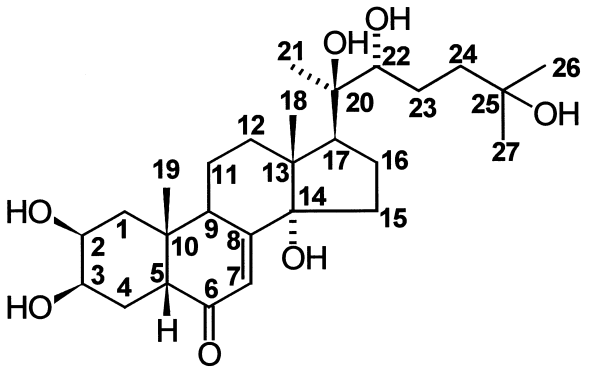

Fig. 1. Structure of a typical ecdysteroid (20-hydroxyecdysone), showing the numbering of the carbon atoms.

does not exclude the possibility that other ecdysteroids may be active in certain types of invertebrate or at specific stages of development. The first isolations of ecdysteroids from plant sources were a rather remarkable coincidence. While investigating the chemical constituents of the leaves of *Podocarpus nakaii* for antitumour agents, Nakanishi et al. (1966) isolated three polyhydroxylated steroids (ponasterones A, B and C). At almost the same time, Takemoto's group isolated 20E and inokosterone from the roots of *Achyranthes fauriei* (Takemoto et al., 1967). Likewise, 20E was found in the wood of *Podocarpus elatus* (Galbraith and Horn, 1966), the rhizomes of *Polypodium vulgare* (Heinrich and Hoffmeister, 1967) and in dry pinnae of *Pteridinium aquilinum* (Kaplanis et al., 1967). These early reports stimulated further research and it soon became apparent that ecdysteroids were rather widespread in plants (reviewed in Hikino and Hikino, 1970; Horn, 1971; Nakanishi, 1971, 1992; Prakash and Ghosal, 1979; Hetru and Horn, 1980; Abubakirov, 1982; Bergamasco and Horn, 1983; Horn and Bergamasco, 1985; Kubo and Hanke, 1986; Lafont and Horn, 1989; Camps, 1991; Lafont and Wilson, 1996). Since the discovery of ecdysteroid analogues in plants, it has been convenient to designate these as phytoecdysteroids to differentiate them from those isolated from insects, crustaceans and other animal sources (zooecdysteroids). However, this division must be regarded as non-exclusive, since many ecdysteroids (e.g. E, 20E, makisterone A, ajugasterone C) are present in both animals and plants. This review will consider the distribution of ecdysteroids in the plant world, their structural diversity, biosynthesis, possible functions and also their potential agrochemical and medicinal applications. Emphasis will be placed on the more recent literature. The reader is referred to the excellent reviews listed above for earlier literature.

2. Distribution of ecdysteroids in the plant world

Phytoecdysteroids (PEs) have been reported to occur in over 100 terrestrial plant families representing ferns, gymnosperms and angiosperms. They are found in both

annuals and perennials. The ecdysteroid-like compound 14α-hydroxypinnasterol (like 20E, but having unsaturation at C-4 and a 3α-hydroxyl function, yet lacking a 25-hydroxyl group) and related compounds have been also characterized from the red marine alga *Laurencia pinnata* (Fukuzawa et al., 1986). In both an early survey of Japanese plants (Imai et al., 1969) and a recent survey of more widely-distributed plant species (Dinan, 1995a), it was found that 5–6% of the tested species were positive for ecdysteroids. The occurrence of PEs in plants does not seem, at first sight, to reflect any precise evolutionary trend, but appears rather random. However, recent studies focussing on significant numbers of species in specific families indicate that the occurrence of ecdysteroids can be related to phylogenetic position (Dinan et al., 1998; Savchenko et al., 1998; Zibareva, 2000). For example, within the genus *Chenopodium*, ecdysteroids appear to be absent from all members of the subgenus *Ambrosia* and present in most (but not all) members of the subgenus *Chenopodium* (Dinan et al., 1998). This study focussing on the Chenopodiaceae revealed the need to study a significant number of related species before the taxonomic patterns became discernable. Since less than 2% of the world's flora has been investigated for the presence of ecdysteroids, it is not surprising that the distribution of ecdysteroid-containing species has appeared random to most investigators. However, it can be stated with some certainty that even in families which have been previously regarded as devoid of phytoecdysteroids, representatives can be found which are ecdysteroid-positive provided that enough species are screened (e.g. Gramineae and Solanaceae; Dinan, 1995a; Savchenko et al., 2000). There does not appear to be a correlation between the frequency of positive species in a family and the levels of ecdysteroids found. For example, certain species in the genera *Leuzea* (*Rhaponticum*) and *Serratula* contain large amounts of ecdysteroids (Volodin et al., 1993), but overall the frequency of ecdysteroid-containing species in the Compositae is rather low (Sarker et al., 1997; Dinan et al., unpublished). In most ecdysteroid-containing species, levels are typically 0.1% or less of the dry weight. However, as indicated above, levels attain much higher levels in certain organs of particular species: e.g. 3.2% in the stem of *Diploclisia glaucescens* (Bandara et al., 1989). Ecdysteroid patterns may be complex. 20E seems to be the most abundant PE. It is usually accompanied by one or two other major ecdysteroids (e.g. *Rhagodia baccata*; Dinan et al., 1999b) and a plethora of other minor PEs (e.g. *Silene otites*; Báthori et al., 1999). The other major PEs are normally related to 20E by one biochemical change (e.g. 5β-hydroxylation generating polypodine B or 24β-methyl substitution generating makisterone A). The composition of the main and minor constituents of a species is often changed during the course of development (summarised in Lafont et al., 1991), and, moreover, their contents vary in the different parts, or even between plants at the same stage of development (e.g. *Limnanthes douglasii*: Sarker et al., 1997). There seems to be no general rule as to where the largest concentrations of PEs are located: fruits, flowers, bark, rhizomes, roots or seeds. Indeed, the concentration and chemical nature of the PEs may vary, and often changes, with the plant part, according to season, the habitat, vegetation period, and developmental stage (Dinan, 1992a,b; Grebenok and Adler, 1991). However, evidence is gradually accumulating that ecdysteroid concentrations are highest in tissues which are most important for the survival of the plant or, in the case of annuals, of the species into the next generation. Although it is by no means conclusive, these variations in ecdysteroid levels and profiles during development and between organs/plants can be most readily reconciled with a role in phytophagous predator deterrence, rather than the other suggested functions for PEs (see below). In theory, the profile of ecdysteroids (especially the cocktail of minor ecdysteroids) could be used as a chemical fingerprint for chemotaxonomic purposes. The variations in levels and profiles of ecdysteroids during development complicate this application of PEs. However, seed extracts do appear to have value in this regard (Zibareva, 1997; Dinan et al., 1998, 2000). Various chromatographic procedures applicable for the separation of PEs were recently reviewed (Lafont et al., 1994).

3. Structural diversity

A compilation of known ecdysteroid structures up to 1995 has been published (Lafont and Wilson, 1996). Structural diversity among (phyto)ecdysteroids has been previously reviewed (Hetru and Horn, 1980; Lafont and Horn, 1989; Lafont et al., 1991; Lafont, 1997,1998). In the following discussion, references are cited for PEs which appeared in the literature after 1995; for compounds first published prior to this, the reader is referred to The Ecdysone Handbook (Lafont and Wilson, 1996). Most PEs possess a cholest-7-en-6-one carbon skeleton (C_{27}), derived biosynthetically from cholesterol. Some phytoecdysteroids are derived from phytosterols and thus possess a C_{28} or C_{29} skeleton, with an alkyl group at C-24. In all naturally occurring PEs, the methyl groups at C-10 and C-13 have a β-configuration. The B/C- and C/D-ring junctions are always *trans*. The A/B-ring junction is normally *cis* (5β-H), and only rarely *trans* (5α-H). Most ecdysteroids possess a hydroxyl group in the 14α-position. The 14α-hydroxy-7-en-6-one chromophore results in a characteristic ultra-violet absorption with λ_{max} at 242 nm in methanol. Although variation in the steroid ring structure is not substantial, significant variation lies in the number, position and

orientation of the hydroxyl groups and the conjugating moieties linked through these. The commonly hydroxylated sites are the 2β-, 3β-, 14α-, 20*R*- and 22*R*- positions, which together give rise to the highly biologically active ponasterone A (25-deoxy-20-hydroxyecdysone). Hydroxyl groups may be present at the 1α- (e.g. integristerone A), 1β- (e.g. 1-*epi*-integristerone A; Sarker et al., 1998a), 2α- (e.g. paristerone), 3α- (e.g. 3-*epi*-2-deoxyecdysone), 5α- (e.g. 5α-polypodine B), 5β- (e.g. polypodine B), 9- (e.g. viperidinone), 11α- (e.g. turkesterone), 12β- (e.g. 22-dehydro-12-hydroxycyasterone; Calcagno et al., 1995) 19- (e.g. sogdisterone), 21- (e.g. 22-deoxy-20,21-dihydroxyecdysone; Dinan et al., 1999b), 22*S*- (e.g. 22-*epi*-20-hydroxyecdysone) 24*S*- (e.g. pteroserone), 24*R*- (e.g. 24-*epi*-pterosterone), 25- (e.g. 20-hydroxyecdysone), 26*R*/*S*- (e.g. inokosterone), 28- (e.g. makisterone D) and/or 29- (e.g. amarasterone B) positions, but rarely at C-23 (gerardiasterone [Báthori et al., 1998], 23-hydroxycyasterone, rapisterone). 21-Hydroxyecdysteroids have only recently been detected (Báthori et al., 1999; Dinan et al., 1999a,b). The hydroxyl group(s) may also be involved in glycosidic (galactoside [e.g. Baltayev, 1998; Sadikov et al., 2000], glucoside, xyloside), ester [acetate, benzoate, cinnamate, 3-*p*-coumarate, crotonate [2-deoxy-20-hydroxyecdysone 3-crotonate; Báthori et al., 1997] 3-hydroxybutanoate [venustone], pyrrole 2-carboxylate [canescensterone], sulphate), ether (methoxy; e.g. polypodoaurein) and/or isopropylidene (2,3- or 20,22-monoacetonide) bond formation resulting in a wide variety of ecdysteroid conjugates.

In keto-ecdysteroids, an oxo-group may be located at the 2- (e.g. 2-dehydro-3-*epi*-20-hydroxyecdysone; Sarker et al., 1998b), 3- (e.g. silenosterone), 12- (e.g. ajugalactone), 17- (e.g. rubrosterone), 20- (e.g. poststerone) or 22- (e.g. 22-oxo-cyasterone) position, in addition to the characteristic one at C-6. The ecdysteroid-related compound calonysterone has an unusual structure to ring-B (6-hydroxy-5,8-dien-7-one; Canonica et al., 1973) and its chemical formation from 20E has been reported (Suksamrarn et al., 1994). Olefinic bonds have been so far reported at 4- (e.g. 14α-hydroxypinnasterol), 8- (e.g. praemixisterone), 9(11)- (e.g. kaladasterone), 12- (e.g. stachysterone A), 14- (e.g. podecdysone B), 24- (e.g. stachysterone C), 25- (e.g. ajugasterone B or decumbesterone A [Takasaki et al., 1999]) and/or the 24(28)- (e.g. 24(28)-dehydromakisterone A) positions in unsaturated PEs. In some of these compounds the conjugated system of the chromophoric group is extended with the result that, in the UV-spectrum, the λ_{max} is shifted to longer wavelength (e.g dacryhainansterone, which is a 7,9-dien-6-one, absorbs maximally at 298 nm in methanol). A few ecdysteroid analogues have been isolated which lack unsaturation at C-7 (cheilanthones A and B, 7,8-dihydroajugasterone C and tenuifoliosides A and B).

When a one- or two-carbon alkyl group is present at C-24, resulting in a C_{28} (e.g. makisterone A [24*R*] or 24-*epi*-makisterone A [24*S*]) or a C_{29} (e.g. makisterone C) carbon skeleton, such extention of the C_{27} skeleton provides a basis for the classification of these compounds into C_{28}, C_{29} or C_{30} (if a 4-methyl group is also present; e.g carpesterol) PEs. The alkyl group may be unsaturated (methenyl [e.g. 24(28)-dehydromakisterone A] or ethenyl) or hydroxylated at C-24[1] (e.g. makisterone D) or C-24[2] (e.g. amarasterone B), or a combination of these (e.g. 24(24[1])[*Z*]-dehydroamarasterone B; Baltayev et al., 1997). Rapisterone C is currently unique in possessing a 23-alkyl (ethyl) group (Baltaev, 1992). Carpesterol and 14α-hydroxycarpesterol possess a 4-methyl group (Kusano et al., 1975) and, in stachysterone A, the methyl group usually located at C-13 is translocated to C-14 (Imai et al., 1970). Further oxidation of a primary hydroxyl group, resulting in a carboxylic acid, has been detected in ecdysteroids isolated from invertebrate sources (e.g. at C-26 to yield ecdysonoic acid). Ecdysteroids with free carboxyl groups have not yet been isolated from plant sources. However, several PEs possess a lactone ring in the side-chain, where a carboxyl at C-24 (sidisterone), C-26 (e.g. [29-nor]cyasterone), or C-29 (carthamosterone) forms an internal ester with a hydroxyl at C-20 (sidisterone), C-22 (e.g. ajugalactone), C-25 (carthamosterone), C-28 (e.g. [29-nor]cyasterone) or C-29 (e.g. repansterone; Calcagno et al., 1996). A furan ring may be generated in some cases by cyclization of a parent C_{27} skeletal side-chain through dehydration of C-22 and C-25 hydroxyls (e.g. ajugasterone D and stachysterone D). PEs lacking either a complete or a partial side-chain, possessing a C_{19} (e.g. rubrosterone), C_{21} (e.g. poststerone) or C_{24} (e.g. sidisterone) parent skeleton, have been characterized from several plants and are regarded as ecdysteroid metabolites because of their low biological activities (in insect systems: e.g. Dinan et al., 1999a).

If one considers combinations of the known individual structural modifications of PEs, this suggests that there are over 1000 possible structures which might occur in nature, of which ca. 250 permutations have been identified so far, leaving many more which could be detected in the future. It should be mentioned that most of the structural modifications are found only in minor ecdysteroids and the available biological evidence suggests that most of these modifications result in compounds which are less active than 20E (Dinan et al., 1999a). Many of the modifications found in PEs are also found in other classes of plant triterpenoids (brassinosteroids, cucurbitacins, withanolides etc.). This raises the possibility that enzymes of the later stages of the biosynthetic pathways may lack specificity and be common to plants producing these different classes of secondary compounds; if each pathway has a distinct early intermediate, this would permit the generation of many diverse analogues in each class without massive genetic redundancy of hydroxylases etc.

A number of ecdysteroids (mycoecdysteroids) with unusual structural features (16-hydroxy, 24-hydroxy or 22,23-epoxide) have been isolated from the mushrooms *Paxillus atrotomentosus* and *Tapinella panuoides* (Vokác et al., 1998a,b). Several unusual ecdysteroids have been isolated from *Polyporus umbellatus* (polyporusterones A–G; Ohsawa et al., 1992) and *Polyporus versicolor* (Valisolalao et al., 1983). Further, 3β,14α,17α,20,24,25-hexahydroxy-5α-ergosta-7,22-dien-6-one has been isolated from *Lasiosphaera nipponica* (Takaishi et al., 1992). However, it is currently unclear if the ecdysteroids are biosynthesised by the fungi themselves or taken up from the substratum and modified.

4. Phytoecdysteroid production in vitro

The occurrence of ecdysteroids in callus cultures was first described for seedling callus tissues from several *Achyranthes* species (Hikino et al., 1971) and *Trianthema portulacastrum* (Ravishankar and Metha, 1979). PEs have also been isolated from the culture filtrates of *Ajuga turkestanica* (Lev et al., 1990), *A. reptans* var. *atropurpurea* (Matsumoto and Tanaka, 1991), *Pteridium aquilinum* (McMorris and Voeller, 1971) and *Serratula tinctoria* (Corio-Costet et al., 1996). 20E was produced at a two- to six-fold higher level by cell and callus cultures of *Ajuga turkestanica* than the level found in root and aerial parts (Camps et al., 1990). Similarly, suspension cultures of *Pteridium aquilinum* produced higher concentrations of ecdysteroids (especially ponA) than found in the wild plant. Unfortunately, the growth rate of the cultures was very slow (Vanek et al., 1990), but a strategy could be developed for the culture to be used as a source of these compounds (Svatoš and Macek, 1994). Hairy root cultures of *A. reptans* var. *atropurpurea* transformed with *Agrobacterium rhizogens* produced four phytoecdysteroids (20E, 29-norcyasterone, cyasterone and isocyasterone), which were present in the methanol extract of the roots (Matsumoto and Tanaka, 1991). In vitro culture studies of root and shoot tissue of *A. reptans* revealed that the roots produced PEs when cultured isolated from the rest of the plant, whereas the PEs were not detected in shoots cultured in the absence of root tissue. These results reveal that the ecdysteroids in *A. reptans* are biosynthesised in the roots (Tomás et al., 1992; 1993). Ecdysteroid concentrations were higher in cultures supplemented with hormone than in basal medium and increased during the growing period. The C_{28}/C_{29} ecdysteroid ratio was very high and different from those observed in in vivo and in vitro whole plant cultures. A comparison of sterol and ecdysteroid profiles of plant and cell culture of *Serratula tinctoria* suggested that roots are the organs containing the highest quantities of PEs (Corio-Costet et al., 1993). Callus cultures of *S. coronata* produce 20E, inokosterone and E together with unidentified ecdysteroids in variable proportions and at levels which are lower than those in wild plants but higher than those in plants grown in vitro (Anufrieva et al., 1998).

5. Biosynthesis

Our understanding of the biosynthetic pathway(s) for ecdysteroids in plants is limited. In part, this was a consequence of the lack of convenient study systems, a situation which is beginning to change with the application of amenable in vitro systems, such as hairy root cultures or cell suspension cultures. In view of the potential applications of PEs in crop protection (see below) it is surprising that more emphasis has not been placed on the elucidation of the biosynthetic pathway(s) for PEs, since modification of PE levels/profiles through genetic engineering is heavily dependent on prior knowledge of the biosynthetic pathway(s) and their regulation. Current knowledge of the biosynthetic pathways for ecdysteroids has been recently reviewed (Warren and Hetru, 1990; Grieneisen, 1994; Rees, 1995; Lafont, 1997), but the emphasis has inevitably been on synthesis in invertebrates, for which somewhat more is known. Only the review by Adler and Grebenok (1995) deals specifically with the biosynthesis of PEs. The presence of PEs in various plant parts at very different concentrations does not allow any conclusion to be drawn about the tissue or organ in which these compounds are primarily produced (rather than accumulated). Recent studies have demonstrated that active biosynthesis of PEs takes place in developing tissues (Grebenok and Adler, 1991,1993), and these compounds are transported to other organs (Ripa et al., 1990; Grebenok and Adler, 1991; Tomás et al., 1993). Plants (unlike insects) are capable of biosynthesising PEs from mevalonic acid. In many cases, the biosynthesis of PEs has been demonstrated to proceed *via* cholesterol and/or lathosterol (Adler and Grebenok, 1995). In insects, it has been suggested that 7-dehydrocholesterol is an intermediate in the ecdysteroid pathway (Grieneisen et al., 1991). In relation to this in plants, it has been shown by application of [4-^{14}C, 7α-$^{3}H_1$] and [4-^{14}C, 7β-$^{3}H_1$] cholesterols to *Taxus baccata* and *Polypodium vulgare* that the *cis* 7β- and 8β-hydrogens of cholesterol are removed during the biosynthesis of E and 20E (Cook et al., 1973). From other studies involving specifically-labelled cholesterols, the location of the radiolabel in biosynthesised 20E indicated that hydrogen migration occurred from the 3α- and 4β-positions to C-4 and C-5, respectively, whereas the 4α-hydrogen was retained at C-4. According to these results, the formation of the A/B *cis*-ring junction might be best explained by concomitant 1,2-Wagner–Meerwein hydride migrations from the 4β- to the 5β- and from the 3α- to the 4α-position with the implicit displacement of the 4α-hydrogen of cholesterol

to the 4β-position in the ecdysteroid (Davies et al., 1980). Despite these studies, the early stages in the biosynthesis of PEs from cholesterol still remained to be fully understood (Adler and Grebenok, 1995). Incubation of radiolabelled [2-^{14}C]mevalonic acid, [4-^{14}C]cholesterol and [23,24-^{3}H]ecdysone in *Zea mays* led to the formation of radiolabelled E and 20E conjugates, which were hydrolysable with an acid phosphatase preparation (Devarenne et al., 1995). A recent report indicates that (poly)phosphorylated ecdysteroid conjugates are also formed in spinach, where they may be involved in the down-regulation of ecdysteroid biosynthesis (Grebenok et al., 1994). In the only study on the enzymology of ecdysteroid synthesis in plants, it was shown that hydroxylation of ecdysone at the C-20 position to form 20E is a cytochrome P_{450}-dependent reaction occurring predominantly in the microsomal fraction in spinach leaves (Grebenok et al., 1996).

As mentioned above, several new experimental systems have been identified which show considerable promise for the elucidation of the biosynthetic pathway for ecdysteroids. In vitro cultures of *Polypodium vulgare* prothalli revealed that labelled mevalonate and cholesterol were incorporated into all identified PEs (Reixach et al., 1996). In hairy root cultures of *Serratula tinctoria*, radiolabelled [^{3}H]cholesterol and [^{14}C]mevalonic acid provide an efficient incorporation into PEs (Delbecque et al., 1995).

As far as the biosynthesis of PEs in *Ajuga reptans* is concerned, recent studies have concerned in vitro cultures of non-transformed (Tomás et al., 1993) and transformed (Matsumoto and Tanaka, 1991) roots. In non-transformed root cultures, 6 phytoecdysteroids (20E, ajugalactone, 29-norcyasterone, 29-norsengosterone, cyasterone and sengosterone) were found to accumulate in the root cultures in proportions which varied with the culture conditions and which were different to the proportions found in whole plants from the wild or in vitro whole plant cultures. The authors conclude that two major biosynthetic pathways, side-chain dealkylation ($C_{29}\rightarrow C_{28}$, but not $C_{29}\rightarrow C_{27}$) and 5β-hydroxylation, are operating leading to two series of related $C_{29}/C_{28}/C_{27}$ compounds, namely cyasterone/29-norcyasterone/20-hydroxyecdysone (5β-H) and sengosterone/ 29-norsengosterone/5,20-dihydroxyecdysone (5β-OH), although the levels of the C_{27} ecdysteroids were very low ($< 5\%$), such that 5,20-dihydroxyecdysone could not be quantified in the in vitro root cultures. Ajugalactone was viewed as a dead-end product in the biosynthesis. The extent to which both 5β-hydroxylation and dealkylation are operational is very dependent on the culture conditions, and this goes a long way to explaining the highly variable ecdysteroid profiles found in *A. reptans* samples.

In an elegant series of papers (summarised in Fujimoto et al., 2000), ^{13}C- and deuterium-labelled precursors have been fed to ecdysteroid-producing hairy roots of *A. reptans* var. *atropurpurea* and ^{13}C and ^{2}H NMR was used to identify the enriched positions in the biosynthesised ecdysteroids. In these hairy-root cultures, a much simpler ecdysteroid profile was found (mainly 20E, with lesser amounts of 29-norcyasterone and cyasterone). 20E could be labelled from both [^{13}C]cholesterol and [^{13}C]acetate, whereas 29-norcyasterone (C_{28}) and cyasterone (C_{29}) were only labelled from [^{13}C]acetate (Nagakari et al., 1994a), indicating that the last two are generated from an appropriate phytosterol (also supported by the lack of labelling at C-28 and C-29 after application of [^{13}C]acetate, indicating that C-28 and C-29 derive from S-adenosyl methionine; Yagi et al., 1996). Recently, clerosterol has been shown to be a precursor phytosterol of the C_{28} and C_{29} ecdysteroids (Nomura et al., 2000). The conversion of cholesterol to 20E in this system has been more closely studied; the retention of label, without migration, from [3α-^{2}H]-, [4α-^{2}H]- and [4β-^{2}H]-cholesterols and [3α-^{2}H]- and [5-^{2}H]3β-hydroxy-5β-cholest-7-en-6-ones are all compatible with 3β-hydroxy-5β-cholest-7-en-6-one being an intermediate in the biosynthesis of 20E. Further [5-^{2}H]3β-hydroxy-5α-cholest-7-en-6-one was not converted to 20E (Nagakari et al., 1994b). These results are in contrast to those described above for *Polypodium vulgare* (Davies et al., 1980), which demonstrated migration of the hydrogens at C-3 and C-4 and indicated the involvement of a 3-oxo-4-ene intermediate. Application of [6-^{2}H]cholesterol to *A. reptans* hairy roots revealed that 6-H largely migrates to become the 5β-H (compatible with the intermediacy of a 5α,6α-epoxide), but one-third of the 5β-H derives from another source, indicating that the route(s) to the A/B *cis*-ring junction are more complex (Fujimoto et al., 1997). This hairy root system has also been used to investigate the stereochemistry of hydroxylation at C-25 during 20E formation, which was found to proceed with a mixture of retention and inversion of configuration (Nakagawa et al., 1997). Hydroxylation at C-2 proceeds with retention of configuration (Nomura and Fujimoto, 2000), as had previously been found in the insect *Schistocerca gregaria* (Greenwood et al., 1984). *Ajuga* hairy roots convert 3β-hydroxy-5β-cholestan-6-one and 2β,3β-dihydroxy-5β-cholestan-6-one to 20E, demonstrating that the 7-ene can be introduced at a later stage in the biosynthetic pathway and that 7-dehydrocholesterol is not an obligatory intermediate (Hyodo and Fujimoto, 2000). This finding is compatible with the detection of 7,8-dihydroecdysteroids in other plant species (e.g. Pomilio et al., 1996).

6. Biological significance of phytoecdysteroids to plants

The importance of the ecdysteroids in the life-cycle of plants has not been fully elucidated. There are two main

hypotheses. The first is that PEs have a hormonal role within the plant, but there is very little hard evidence in support of this hypothesis and quite a lot against it (reviewed in Dinan, 1998). Alternatively, it has long been recognised that PEs possess insect moulting hormone activity and they could participate in the defence of plants against non-adapted phytophagous invertebrates. This is supported by the fact that the major PE present in most ecdysteroid-containing plants is 20E, which is also the major ecdysteroid in insects. Deterrent effects of 20E on non-adapted insect species are observed at 2–25 ppm (Blackford and Dinan, 1997b, and references cited therein), which is well within the concentration range found in ecdysteroid-containing plants. The biological activity of some PEs has been tested in a wide variety of insect bioassays (reviewed in Bergamasco and Horn, 1980; Cymborowski, 1989; Dinan, 1989). Almost all PEs demonstrate quantifiable ecdysteroid activity (Dinan et al., 1999a). They have also been shown to affect insect growth and reproduction when added to natural or artificial diets, which would otherwise support optimum growth and reproduction (Melé et al., 1992; Sláma et al., 1993; Tanaka and Takeda, 1993; Blackford and Dinan, 1997b; Mondy et al., 1997). Investigation of the consequences of ingestion of dietary PEs is appropriate for an understanding of the ecological or physiological phenomena involved in plant–insect interactions. The activity of a PE depends on its affinity for, and the effective concentration at, the target site (normally assumed to be the ecdysteroid receptor complex), and, if it is ingested, its potency depends also on the amount ingested, the ability to cross the gut wall and the consequences of the metabolism. A number of researchers have suggested the possibility of allelochemical properties of PEs as hormonal disruptors and toxins for insects and other invertebrates (Robbins et al., 1970; Kubo et al., 1983; Arnault and Sláma, 1986; Camps and Coll, 1993; Savolainen et al., 1995; Mondy et al., 1997). It has also been demonstrated that ecdysteroids possess antifeedant activity against certain species of insects and that some species possess taste receptors which respond to ecdysteroids (Ma, 1969; Tanaka et al., 1994; Descoins and Marion-Poll, 1999). However, there are several highly polyphagous insect species which develop normally on diets containing very high concentrations (400 ppm) of 20E (Robbins et al., 1968; Kubo et al, 1987; Robinson et al., 1987; Tanaka and Naya, 1995; Blackford et al., 1996; Blackford and Dinan, 1997a,c). Hence, PEs can be considered as a chemical defence against certain, but not all, herbivorous insects (Lafont and Horn, 1989).

As already mentioned, 20E is generally accompanied in plants by one or two other major ecdysteroids and several other minor ecdysteroids. The relative contribution of the various major and minor ecdysteroids to a potential defensive role of PE is a moot point at present. It has been suggested that the minor PEs provide evolutionary flexibility to respond to predation if and when the major compounds are no longer effective; mutation results in plants with altered ecdysteroid profiles and new major ecdysteroids which are effective in deterring the predators (Jones and Firn, 1991; Alison et al., 1997).

Recently, it has been demonstrated that ecdysteroid accumulation in spinach is inducible by mechanical (Schmelz et al., 1998) or insect (Schmelz et al., 1999) damage to roots. Evidence was further provided for the involvement of jasmonates in the induction of de novo ecdysteroid synthesis. Also, short- and long-term labelling of 20E from [2-^{14}C]mevalonic acid in spinach demonstrate that ecdysteroids are metabolically stable in this species, which fits much better with a role in plant defence, rather than a phytohormonal role (Schmelz et al., 2000).

Definitive assessment of the contribution of PEs to the deterrence of invertebrate predators must await the comparison of the susceptibility of genetic lines of the same plant species which differ in their ecdysteroid levels and/or profiles (Dinan, 1998).

7. Structure–activity studies

It is often presumed that most, if not all, ecdysteroid responses are mediated by intracellular ecdysteroid receptor complexes, of which the two main components (the *EcR* and *USP* proteins) belong to the nuclear receptor superfamily (Yao et al., 1993), and which modify the activity of specific gene sets. However, it should be mentioned that evidence is accumulating that ecdysteroids may also have non-genomic effects (reviewed in Tomaschko, 1999). Consequently, SAR studies can be strongly influenced by the invertebrate species used, its stage of development and the format of the bioassay in addition to the more usual problems common to all bioassays (purity of the test compound, penetration, sequestration, metabolism etc.). PEs have been tested in a variety of insect bioassays, and found to exhibit moulting hormone activity. From both in vitro (Cherbas et al., 1980) and a variety of in vivo assays (mainly the dipteran *Calliphora* and *Musca* pupariation bioassays; Cymborowski, 1989; Dinan, 1989) the following structural requirements for high activity were deduced (Bergamasco and Horn, 1980): (a) a *cis* A/B ring junction; (b) a 7-en-6-one group; (c) a complete sterol side-chain having a 22*R* oxygen function, and containing, in some cases, additional alkyl groups at the 24α-position; (d) an oxygen function generally in the form of a 3β-OH group; and (e) additional OH groups at C-14α and C-2β, and, in many cases, also at C-20 and C-25. More recently, a systematic study on 20E conjugates (fatty acid/benzoic acid mono, di- and tri-esters, glucoside and glucosidic esters) for ecdysteroid activity in common assays on *Sarcophaga* (Diptera) and *Galleria*

(Lepidoptera) revealed that the 2-acetyl derivative and the 25-benzoate derivatives of 20E retain a significant amount of activity, but di- and tri-esters, as well as all glucosidic derivatives of 20E, were much less or virtually inactive relative to 20E (Píš et al., 1991; Sláma et al., 1993). PEs having an 11α-OH group bind with about the same affinity to the *Chironomus tentans* (Diptera) ecdysteroid receptor as the corresponding compound lacking this OH group. For these compounds, the potency to elicit a hormonal response corresponds with the affinity for the ecdysteroid receptor, as detected by induction of acetycholinesterase enzyme for cell differentiation (Spindler-Barth et al., 1997). However, the results of in vivo studies reveal that there may be a wide variation in the susceptibility of different insects to a particular ecdysteroid analogue, and an equally wide variation in the response of a single insect species to different molecular structures (Robbins et al., 1970; Sláma et al., 1993). In view of this, an extensive study involving the quantitative assessment of a large number of HPLC-purified ecdysteroids in a uniform assay system (the *Drosophila melanogaster* B_{II} bioassay; Clément et al., 1993) has recently been undertaken (Harmatha and Dinan, 1997; Dinan et al., 1999a). Structure-activity relationships were analysed by Comparative Molecular Field Analysis (CoMFA) to generate two models with good predictive capabilities. Further, it was possible to propose a pharmacophore hypothesis for ligand interaction with the ecdysteroid receptor (Fig. 2), in which binding is the result of incremental contributions of a number of molecular features (heteroatoms at C-2, C-3, C-20 and C-22, a large dipole at C-6 and a moderately bulky hydrophobic group, located beyond C-22) at the angles and distances approximating to those present in 20E. Each of these features contributes to the binding affinity, but there is no absolute requirement for any one of them. In comparison to the previous empirically derived SAR conclusions (summarised above), it is now clear that the *cis*-A/B-ring junction, the Δ^7-double bond, the 6-keto group, the full 8-carbon side-chain and each of the hydroxyls listed above is not essential for activity, although absence of both parts of the 7-en-6-one moiety do seem to remove all activity. Also, it is clear that the consequences of the addition/removal of individual structural features is not always additive; e.g. the consequences of presence/absence of hydroxyl groups at C-5 or C-25 depend on the structural features present in other parts of the molecule. It remains to be seen if a completely different structural scaffold bearing several or all of the six pharmacophore elements would retain activity, but the models from which the pharmacophore hypothesis was derived are being successfully used to predict the activity of novel ecdysteroids prior to their chemical synthesis (Hormann et al., unpublished results). Biological activity data obtained for phytoecdysteroids have also contributed significantly to two other modelling studies of ligand binding to the ecdysteroid receptor. Wurtz et al. (2000) have used homology modelling and docking to generate virtual models for 20E and bisacylhydrazine interaction with the ligand binding domain. Ravi et al. (unpublished) have applied 4D-QSAR techniques to the same dataset which was used for CoMFA modelling (Dinan et al., 1999a,b). There is generally good agreement between the CoMFA and 4D-QSAR models, but the 4D-QSAR additionally permits the prediction of which functional groups on the ecdysteroid are involved in hydrogen-bonding to the receptor.

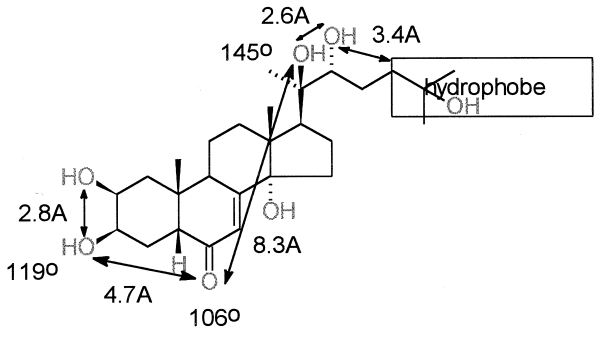

Fig. 2. Pharmacophore hypothesis for ecdysteroid binding to the *Drosophila melanogaster* ecdysteroid receptor (redrawn from Dinan et al., 1999a,b).

8. Applications of phytoecdysteroids

Since the discovery of large amounts of ecdysteroids in plants (relative to the much lower concentrations found in most animal sources), PEs have been purified for use in biochemical and physiological experiments in invertebrate systems. In fact, it is fair to say that our knowledge of the role of ecdysteroids in insect endocrinology would be much poorer if it had not been for the availability of ecdysteroids (especially 20E, E and ponA) from plant sources. In recent years, however, new areas of potential applications have been identified. These fall into two broad categories; agricultural and biomedical. Of necessity, the discussion which follows is more speculative than in the preceeding sections.

8.1. Agricultural applications

8.1.1. Improvement of silk yields

Feeding of exogenous ecdysteroids to larvae of the silkworm, *Bombyx mori*, at certain stages of development has been shown to enhance synchronous development of the larvae and, when co-administered with a juvenile hormone analogue, to elevate significantly the yield of silk obtainable from the cocoon (Chou and Lu, 1980; Ninagi and Maruyama, 1996). Such treatments have considerable potential to improve the efficiency of

silkworm rearing by Asian farmers, especially since the hormonal treatments could be based on extracts of appropriate indigenous plant species.

8.1.2. Design of more specific invertebrate pest control agents

Identification of compounds which specifically interfere with the mode of action of ecdysteroids in invertebrates is a very attractive and promising way of controlling pest species while reducing the effects on other animal groups and lowering the environmental burden. The effectiveness of such a strategy has recently been demonstrated by the identification of non-steroidal bisacylhydrazines as agonists of the ecdysteroid receptor complex and the development of two of the compounds as selective and successful insect control agents (Dhadialla et al., 1998). The ecdysteroids themselves have very limited application in the control of pests, since they do not possess the required properties for successful pesticides; they are too polar, too chemically complicated and too metabolically and environmentally unstable (Dinan, 1989). However, they can contribute significantly as lead compounds. In this sense, the vast diversity of ecdysteroid analogues found in plants provides a natural resource for structure-activity studies (see previous section). This was realised some time ago (Cherbas et al., 1980), but the more restricted availability of ecdysteroid analogues in very pure form, the requirement for larger amounts of each analogue and, most importantly, the complexity of the available bioassay systems then available, restricted the possibilities of this approach at that time. However, the methodological and technical advances of recent years, permitting rapid purification and identification of analogues, extensive QSAR and computerised molecular modelling, will ultimately permit the recognition of further simple, non-steroidal molecules which fit the pharmacophore hypothesis and may lead to novel insecticides. Such approaches can be extended to the taste receptors of insects to identify ecdysteroid analogues (steroidal or non-steroidal) which are potent antifeedants.

8.1.3. Modification of ecdysteroid levels in crop species

An alternative approach to crop protection based on ecdysteroids is to modify ecdysteroid levels and/or profiles in crop plants (most of which do not contain ecdysteroids) to enhance protection against invertebrate predators. This is based on the assumption that ecdysteroids contribute significantly to the protection of the plants which contain them, at least against non-adapted predators. There is increasing evidence that this is true, but the situation is complicated by the knowledge that there are certain polyphagous insect pests which are unaffected by diets containing very high concentrations of ecdysteroids (reviewed in Dinan, 1998). However, these tolerant species appear to detoxify the ingested ecdysteroids in specific ways (commonly by acylation with long-chain fatty acids at C-22; Robinson et al., 1987; Kubo et al., 1987; Blackford et al., 1997; Blackford and Dinan, 1997a) and it seems feasible that plants could be generated which contain ecdysteroid analogues which do not permit the ready biochemical detoxification by predators (e.g. by generating high levels of 22-deoxy ecdysteroids which retain activity on ingestion because they are not a substrate for the detoxification enzymes; Connat et al., 1983). The very broad, but uneven, distribution of ecdysteroid-containing species in the plant world leads most researchers in this area to believe that most, if not all, plants retain the genetic capacity to produce ecdysteroids, but that the biosynthetic pathway is not expressed in most species. If this is true, modification of the activity of genes which regulate ecdysteroid biosynthesis (either through a traditional selection approach, genetic modification or application of appropriate elicitors) could generate crop plants with elevated ecdysteroid levels. Thus, ecdysteroids have potential for the GM or non-GM protection of crop species. The apparent non-toxicity of ecdysteroids to mammals (see below) makes this potentially very attractive, as it may not be necessary to incorporate tissue- or temporally-specific accumulation of ecdysteroids into the system.

8.2. Biomedical applications

8.2.1. Effects of ecdysteroids on vertebrates

The reader is referred to two excellent reviews (Simon and Koolman, 1989; Sláma and Lafont, 1995) which summarise the disparate literature on this aspect. The wide-spread occurrence of ecdysteroids in invertebrates and plants suggests that man's consumption of these steroidal compounds may not be insignificant. Spinach, for example, contains ca. 50 μg/g f.w. (Dinan, 1995b). Although no thorough toxicological study appears to have been performed for any ecdysteroid, there is evidence that the acute toxicity of these compounds to mammals is extremely low (Ogawa et al., 1974; Kosar et al., 1997). On the contrary, there is some evidence that they may even be beneficial under certain circumstances (Hikino and Takemoto, 1972; Kuzmenko et al., 1997; Wu et al., 1998; Trenin and Volodin, 1999). They appear to be mildly anabolic (Koudela et al., 1995; Sláma et al., 1996), supposedly without the adverse side-effects associated with vertebrate steroids or their analogues (Syrov, 1984); rumour suggests that some athletes and sportsmen of various nations have taken advantage of this since the mid-1980s. 20E has significant spermicidal activity (Bandara et al., 1989) and influences the sexual activity of male rats (Mirzaev and Syrov, 1992). Other pharmacological effects have also been ascribed to ecdysteroids or to extracts of ecdysteroid-containing plants. A number of preparations and tonics with reported roborant, adaptogenic and antidepressive

effects are based on the plant *Leuzea carthamoides* which possesses very high levels of ecdysteroids, mainly 20E (Sláma and Lafont, 1995). A number of reports suggest that ecdysteroids may be effective in the control of diabetes (Yoshida et al., 1971; Uchiyama and Yoshida, 1974; Najmutdinova and Saatov, 1999). Recent studies (Badal'yants et al., 1996; Prymak et al., 1996) have shown that derivatives of PEs exhibit a hepatoprotective action which was related to their effect on liver chromatin and their ability to prevent negative shifts of phospholipid metabolism. Three ecdysteroids from *Ajuga decumbens* (cyasterone, polypodine B and decumbesterone A) have been reported to be potential cancer chemopreventative agents (Takasaki et al., 1999). Thorough clinical trials are required to substantiate and confirm all the above findings.

8.2.2. Gene switches

There is considerable interest in gene replacement therapies to correct inborn errors. However, such introduced genes require the correct temporal expression to be fully effective. Thus, systems are being sought which allow these genes to be switched on and off by the availability of an appropriate elicitor. One transgenic system which is receiving attention is the ecdysteroid/ecdysteroid receptor complex (Sawicki et al., 1998; Morgan et al., 1999; Albanese et al., 2000; Lüers et al., 2000), since the ecdysteroid receptor is not a natural component of vertebrate cells, ecdysteroids are believed to be non-toxic to vertebrates and ecdysteroids do not appear to activate vertebrate steroid hormone receptors, even at very high concentrations. A number of permutations using either all of the *EcR* protein or the ligand-binding part fused to the DNA-binding domain of another member of the nuclear receptor superfamily are being considered. In insects, *EcR* naturally forms a heterodimer with *USP*. The homologue of *USP* in verbrates is the retinoid X receptor, *RXR*. When expressed in vertebrate systems, *EcR* will partner *RXR*. However, the ecdysteroid binding specificity is considerably altered, such that 20E is largely ineffective at inducing reporter gene activity, while the rare phytoecdysteroid muristerone A is much more effective, but only at high concentrations (1–10 μM, whereas 100-fold lower concentrations are effective with *EcR*/*USP* heterodimers). Ponasterone A is also effective, but concentrations (1–10 μM) are required which are 1000-fold greater than those required in insect systems. The non-steroidal bisacylhydrazines (which also have very low mammalian toxicity) are being considered as alternative ligands (Suhr et al., 1998). Gene switches based on ecdysteroid systems are also being developed for plants (Jepson et al., 1998; Martinez et al., 1999a,b). While these developments are highly interesting, it is clear that they will have to undergo considerable refinement before commercially or medically viable systems are available.

8.2.3. Antimicrobial agents

The antimicrobial activity of *Asparagus dumosus* against several fungal and bacterial species was ascribed to the presence of 20E (Ahmad et al., 1996).

9. Concluding remarks

PEs are attracting renewed attention because of their specific effects on invertebrate development (potential in invertebrate pest control) and their varied benign pharmacological actions on mammals (biomedical applications and gene switches). In the past three decades, several thousand species of plants have been surveyed for the presence of PEs and the structures of over 200 PEs have been deduced. The most frequently encountered PE is 20E, the principal physiological inducer of moulting and metamorphosis in arthropods. It is currently not clear what the biological significance of this extensive structural variety among PEs is, but the numerous structural analogues provide an excellent natural resource for biochemical and physiological structure-activity studies. Studies on the distribution of PEs within the plant kingdom are still fragmentary, but it is becoming apparent that ecdysteroid-containing species are to be found grouped together in particular genera or tribes within families. Continuation of the search for new plant sources of PEs will provide a better understanding about their distribution in plants, their possible chemotaxonomic and ecological implications, and furnish further analogues for structure-activity relationship studies. Potential medical, pharmacological and agricultural applications of PEs are beginning to be recognised and implemented and these will provide further impetus to investigate the fundamental aspects of PE research, such as elucidation of the biosynthetic pathway, which have been rather neglected.

Acknowledgements

Research in Exeter was supported by the Biotechnology and Biological Sciences Research Council of the UK, EU-INTAS (Contract 96-1291) and Rohm & Haas Co. (Spring House, PA, USA). I thank Pauline Bourne for reading and commenting on the manuscript.

References

Abubakirov, N.K., 1982. Ecdysteroids of flowering plants (Angiospermae). Proceedings of Indian National Science Academy 48A (Suppl. 1), 122–138.

Adler, J.H., Grebenok, R.J., 1995. Biosynthesis and distribution of insect-molting hormones in plants — a review. Lipids 30, 257–262.

Ahmad, V.U., Khaliq, S.M., Ali, M.S., Perveen, S., Ahmad, W., 1996. An antimicrobial ecdysone from *Asparagus dumosus*. Fitoterapia 67, 88–91.

Albanese, C., Reutens, A.T., Bouzahzah, B., Fu, M., D'Amico, M., Link, T., Nicholson, R., Depinho, R.A., Pestell, R.G., 2000. Sustained mammary gland-directed, ponasterone A-inducible expression in transgenic mice. FASEB Journal 14, 877–884.

Alison, B., Whiting, P., Sarker, S.D., Dinan, L., Underwood, E., Šik, V., Rees, H.H., 1997. 20-Hydroxyecdysone-2β-*D*-glucopyranoside from the seeds of *Xerophyllum tenax*. Biochemical Systematics and Ecology 25, 255–261.

Anufrieva, E.N., Volodin, V.V., Nosov, A.M., Garcia, M., Lafont, R., 1998. The content and composition of ecdysteroids in plants and tissue cultures of *Serratula coronata*. Russian Journal of Plant Physiology 45, 326–332.

Arnault, C., Sláma, K., 1986. Dietary effects of phytoecdysones in the leek-moth, *Acrolepiopsis assectella* Zell. (Lepidoptera: Acrolepiidae). Journal of Chemical Ecology 12, 1979–1986.

Badal'yants, K.L., Nabiev, A.N., Khushbaktova, Z.A., Syrov, V.N., 1996. Mechanism of hepatoprotective action of ecdystene in acute heliotrine intoxication. Doklady Akademii Nauk Respublinki Uzbekistan, 46–48.

Baltayev, U.A., 1992. Phytoecdysteroids of *Rhaponticum carthamoides*. III. Rapisterone C. Khimiya Prirodnykh Soedinenii, 231–233.

Baltayev, U.A., 1998. Ecdysteroside, a phytoecdysteroid from *Silene tatarica*. Phytochemistry 47, 1233–1235.

Baltayev, U.A., Dinan, L., Girault, J.-P., Lafont, R., 1997. 24(24^1)[Z]-Dehydroamarasterone B, a phytoecdysteroid from seeds of *Leuzea carthamoides*. Phytochemistry 46, 103–105.

Bandara, B.M.R., Jayasinghe, L., Karunaratne, V., Wannigama, G.P., Bokel, M., Kraus, W., Sotheeswaran, S., 1989. Ecdysterone from stem of *Diploclisia glaucescens*. Phytochemistry 28, 1073–1075.

Báthori, M., Girault, J.-P., Kalasz, H., Mathé, I., Lafont, R., 1997. New minor ecdysteroids from *Silene otites* (L.) Wib. Journal of Pharmaceutical and Biomedical Analysis 16, 327–336.

Báthori, M., Girault, J.-P., Kalasz, H., Mathé, I., Dinan, L.N., Lafont, R., 1999. Complex phytoecdysteroid cocktail of *Silene otites* (Caryophyllaceae). Archives of Insect Biochemistry and Physiology 41, 1–8.

Báthori, M., Mathé, I., Girault, J.-P., Kalasz, H., Lafont, R., 1998. Isolation and structural elucidation of two ecdysteroids, gerardiasterone and 22-*epi*-20-hydroxyecdysone. Journal of Natural Products 61, 415–417.

Bergamasco, R., Horn, D.H.S., 1980. The biological activities of ecdysteroids and ecdysteroid analogs. In: Hoffmann, J.A. (Ed.), Developments in Endocrinology, 7, (Progress in Ecdysone Research). Elsevier/North Holland, Amsterdam, pp. 299–324.

Bergamasco, R., Horn, D.H.S., 1983. Distribution and role of insect hormones in plants. In: Endocrinology of Insects, A.R. Liss Inc., New York, pp. 627–654.

Blackford, M., Clarke, B., Dinan, L., 1996. Tolerance of *Spodoptera littoralis* (Lepidoptera: Noctuidae) to ingested phytoecdysteroids. Journal of Insect Physiology 42, 931–936.

Blackford, M.J.P., Clarke, B.S., Dinan, L., 1997. Distribution and metabolism of exogenous ecdysteroids in the Egyptian Cotton Leafworm *Spodoptera littoralis* (Lepidoptera: Noctuidae). Archives of Insect Biochemistry and Physiology 34, 329–346.

Blackford, M., Dinan, L., 1997a. The tomato moth *Lacanobia oleracea* (Lepidoptera: Noctuidae) detoxifies ingested 20-hydroxyecdysone, but is susceptible to the ecdysteroid agonists RH-5849 and RH-5992. Insect Biochemistry and Molecular Biology 27, 167–177.

Blackford, M.J.P., Dinan, L., 1997b. The effects of ingested 20-hydroxyecdysone on the larvae of *Aglais urticae*, *Inachis io*, *Cynthia cardui* (Lepidoptera: Nymphalidae) and *Tyria jacobaeae* (Lepidoptera: Arctiidae). Journal of Insect Physiology 43, 315–327.

Blackford, M., Dinan, L., 1997c. The effects of ingested ecdysteroid agonists (20-hydroxyecdysone, RH5849 and RH5992) and an ecdysteroid antagonist (cucurbitacin B) on larval development of two polyphagous lepidopterans (*Acherontia atropos* and *Lacanobia oleracea*). Entomologia Experimentalis et Applicata 83, 263–276.

Butenandt, A., Karlson, P., 1954. Über die Isolierung eines Metamorphose-hormons der Insekten in kristallisierter Form. Zeitschrift für Naturforschung 9B, 389–391.

Calcagno, M.-P., Camps, F., Coll, J., Melé, E., Sánchez-Baeza, F., 1995. A new family of phytoecdysteroids isolated from aerial part of *Ajuga reptans* var *atropurpurea*. Tetrahedron 51, 12119–12126.

Calcagno, M.-P., Camps, F., Coll, J., Melé, E., Sánchez-Baeza, F., 1996. New phytoecdysteroids from roots of *Ajuga reptans* varieties. Tetrahedron 52, 10137–10146.

Camps, F., 1991. Plant ecdysteroids and their interactions with insects. In: Harborne, J.B., Thomas Barberan, F.A. (Eds.), Ecological Chemistry and Biochemistry of Plant Terpenoids. Claredon Press, Oxford, pp. 331–376.

Camps, F., Claveria, E., Coll, J., Marco, M.P., Messeguer, J., Melé, E., 1990. Ecdysteroid production in tissue cultures of *Polypodium vulgare*. Phytochemistry 29, 3819–3821.

Camps, F., Coll, J., 1993. Insect allelochemicals from *Ajuga* plants. Phytochemistry 32, 1361–1370.

Canonica, L., Danieli, B., Ferrari, G., Krepinsky, J., Rainoldi, G., 1973. Structure of calonysterone, an unusually modified phytoecdysone. Journal of the Chemical Society Chemical Communications, 737–738.

Cherbas, L., Yonge, C.D., Cherbas, P., Williams, C.M., 1980. The morphological response of Kc-H cells to ecdysteroids: hormonal specificity. Wilhelm Roux's Archives Developmental Biology 189, 1–15.

Chou, W.S., Lu, M.S., 1980. Growth regulation and silk production in *Bombyx mori* L. from phytogenous ecdysteroids. In: Hoffmann, J.A. (Ed.), Developments in Endocrinology, 7 (Progress in Ecdysone Research). Elsevier/North-Holland Biomedical Press, Amsterdam, pp. 281–297.

Clément, C.Y., Bradbrook, D.A., Lafont, R., Dinan, L., 1993. Assessment of a microplate-based bioassay for the detection of ecdysteroid-like or antiecdysteroid activities. Insect Biochemistry and Molecular Biology 23, 187–193.

Connat, J.-L., Diehl, P.A., Dumont, N., Carminati, S., Thompson, M.J., 1983. Effects of exogenous ecdysteroids on the female tick *Ornithodorus moubata*: induction of supermolting and influence on oogenesis. Zeitschrift für angewandte Entomologie 96, 520–530.

Cook, I.F., Lloyd-Jones, J.G., Rees, H.H., Goodwin, T.W., 1973. Stereochemistry of hydrogen elimination from C-7 during biosynthesis of ecdysones in insects and plants. Biochemical Journal 136, 135–145.

Corio-Costet, M.-F., Chapuis, L., Delbecque, J.-P., 1996. XXIII *Serratula tinctoria* L. (Dyer's savory): in vitro culture and the production of ecdysteroids and other secondary metabolites. In: Bajaj, Y.P.S. (Ed.), Biotechnology in Agriculture and Forestry 37: Medicinal and Aromatic Plants X. Springer-Verlag, pp. 384–401.

Corio-Costet, M.F., Chapuis, L., Mouillet, J.F., Delbecque, J.P., 1993. Sterol and ecdysteroid profiles of *Serratula tinctoria* (L.): plant and cell cultures producing steroids. Insect Biochemistry and Molecular Biology 23, 175–180.

Cymborowski, B., 1989. Bioassays for ecdysteroids. In: Koolman, J. (Ed.), Ecdysone: From Chemistry to Mode of Action. Georg Thieme Verlag, Stuttgart, pp. 144–149.

Davies, T.G., Lockley, W.J.S., Boid, R., Rees, H.H., Goodwin, T.W., 1980. Mechanism of formation of the A/B *cis*-ring junction of ecdysteroids in *Polypodium vulgare*. Biochemical Journal 190, 537–544.

Delbecque, J.-P., Beydon, P., Chapuis, L., Corio-Costet, M.F., 1995. In vitro incorporation of radiolabelled cholesterol and mevalonic acid into ecdysteroids by hairy root cultures of a plant, *Serratula tinctoria*. European Journal of Entomology 92, 301–307.

Descoins Jr., C., Marion-Poll, F., 1999. Electrophysiological responses of gustatory sensilla of *Mamestra brassicae* (Lepidoptera, Noctuidae)

larvae to three ecdysteroids: ecdysone, 20-hydroxyecdysone and ponasterone A. Journal of Insect Physiology 45, 871–876.
Devarenne, T.P., Sen-Michael, B., Adler, J.H., 1995. Biosynthesis of ecdysteroids in *Zea mays*. Phytochemistry 40, 1125–1131.
Dhadialla, T.S., Carlson, G.R., Le, D.P., 1998. New insecticides with ecdysteroidal and juvenile hormone activity. Annual Review of Entomology 43, 545–569.
Dinan, L., 1989. Ecdysteroid structure and hormonal activity. In: Koolman, J. (Ed.), Ecdysone: From Chemistry to Mode of Action. Georg Thieme Verlag, Stuttgart, pp. 345–354.
Dinan, L., 1992a. The analysis of phytoecdysteroids in single (preflowering stage) specimens of fat hen, *Chenopodium album*. Phytochemical Analysis 3, 132–138.
Dinan, L., 1992b. The association of phytoecdysteroids with flowering in fat hen, *Chenopodium album*, and other members of the Chenopodiaceae. Experientia 48, 305–308.
Dinan, L., 1995a. A strategy for the identification of ecdysteroid receptor agonists and antagonists from plants. European Journal of Entomology 92, 271–283.
Dinan, L., 1995b. Distribution and levels of phytoecdysteroids within individual plants of species of the Chenopodiaceae. European Journal of Entomology 92, 295–300.
Dinan, L., 1998. A strategy towards the elucidation of the contribution made by phytoecdysteroids to the deterrence of invertebrate predators on plants. Russian Journal of Plant Physiology 45, 296–305.
Dinan, L., Bourne, P. Whiting, P., 2000. Phytoecdysteroid profiles in seeds of *Sida* spp. (Malvaceae). Phytochemical Analysis (in press).
Dinan, L., Hormann, R.E., Fujimoto, T., 1999a. An extensive ecdysteroid CoMFA. Journal of Computer-Aided Molecular Design 13, 185–207.
Dinan, L., Sarker, S.D., Bourne, P., Whiting, P., Šik, V., Rees, H.H., 1999b. Phytoecdysteroids in seeds and plants of *Rhagodia baccata* (Labill.) Moq. (Chenopodiaceae). Archives of Insect Biochemistry and Physiology 41, 18–23.
Dinan, L., Whiting, P., Scott, A.J., 1998. Taxonomic distribution of phytoecdysteroids in seeds of members of the Chenopodiaceae. Biochemical Systematics and Ecology 26, 553–576.
Fujimoto, Y., Kushiro, T., Nakamura, K., 1997. Biosynthesis of 20-hydroxyecdysone in *Ajuga* hairy roots: hydrogen migration from C-6 to C-5 during cis-A/B ring formation. Tetrahedron Letters 38, 2697–2700.
Fujimoto, Y., Ohyama, K., Nomura, K., Hyodo, R., Takahashi, K., Yamada, J., Morisaki, M., 2000. Biosynthesis of sterols and ecdysteroids in *Ajuga* hairy roots. Lipids 35, 279–288.
Fukuzawa, A., Miyamoto, M., Kumagai, Y., Masamune, T., 1986. Ecdysone-like metabolites, 14α-hydroxypinnasterols, from the red alga *Laurencia pinnata*. Phytochemistry 25, 1305–1307.
Galbraith, M.N., Horn, D.H.S., 1966. An insect-moulting hormone from a plant. Journal of Chemical Society, Chemical Communications 905–906.
Grebenok, R.J., Adler, J.H., 1991. Ecdysteroid distribution during development of spinach. Phytochemistry 30, 2905–2910.
Grebenok, R.J., Adler, J.H., 1993. Ecdysteroid biosynthesis during ontogeny of spinach leaves. Phytochemistry 33, 341–347.
Grebenok, R.J., Galbraith, D.W., Benveniste, I., Feyereisen, R., 1996. Ecdysone 20-monooxygenase, a cytochrome P450 enzymes from spinach, *Spinacia oleracea*. Phytochemistry 42, 927–933.
Grebenok, R.J., Venkatachari, S., Adler, J.H., 1994. Biosynthesis of ecdysone and ecdysone phosphates in spinach. Phytochemistry 36, 1399–1408.
Greenwood, D.R., Dinan, L.N., Rees, H.H., 1984. Mechanism of hydroxylation at C-2 during the biosynthesis of ecdysone in ovaries of the locust, *Schistocerca gregaria*. Biochemical Journal 217, 783–789.
Grieneisen, M.L., 1994. Recent advances in our knowledge of ecdysteroid biosynthesis in insects and crustaceans. Insect Biochemistry and Molecular Biology 24, 115–132.
Grieneisen, M.L., Warren, J.T., Sakurai, S., Gilbert, L.I., 1991. A putative route to ecdysteroids: metabolism of cholesterol in vitro by mildly disrupted prothoracic glands of *Manduca sexta*. Insect Biochemistry 21, 41–51.
Harmatha, J., Dinan, L., 1997. Biological activity of natural and synthetic ecdysteroids in the B_{II} bioassay. Archives of Insect Biochemistry and Physiology 35, 219–225.
Heinrich, G., Hoffmeister, H., 1967. Ecdyson als Begleitsubstanz des Ecdysterons in *Polypodium vulgare* L. Experientia 23, 995.
Hetru, C., Horn, D.H.S., 1980. Phytoecdysteroids and zooecdysteroids. In: Hoffmann, J.A. (Ed.), Developments in Endocrinology, 7 (Progress in Ecdysone Research). Elsevier North Holland Biomedical Press, Amsterdam, pp. 13–28.
Hikino, H., Hikino, Y., 1970. Anthropod molting hormones. In: Herz, W., Grisebach, H., Scott, A.I. (Eds.), Progress in the Chemistry of Organic Natural Products, 28. Springer-Verlag, Vienna, pp. 256–312.
Hikino, H., Jin, H., Takemoto, T., 1971. Occurrence of insect-moulting substance ecdysterone and inokosterone in callus tissue of *Achyranthes*. Chemical and Pharmaceutical Bulletin 19, 438–439.
Hikino, H., Takemoto, T., 1972. Arthropod moulting hormones from plants, *Achyranthes* and *Cyathula*. Die Naturwissenschaften 59, 91–98.
Horn, D.H.S., 1971. Ecdysones. In: Jacobson, M., Crosby, D.G. (Eds.), Naturally Occurring Insecticides. Marcel Dekker, New York, pp. 333–459.
Horn, D.H.S., Bergamasco, R., 1985. Chemistry of ecdysteroids. In: Kerkut, G.A., Gilbert, L.I. (Eds.), Comprehensive Insect Physiology Biochemistry and Pharmacology, Vol. 7. Pergamon Press, Oxford, pp. 185–248.
Huber, R., Hoppe, W., 1965. Die Kristall- und Molekülstrukturanalyse des Insektenverpuppungshormons Ecdyson mit der automatisierten Faltmolekülmethode. Chemische Berichte 98, 2403–2404.
Hyodo, R., Fujimoto, Y., 2000. Biosynthesis of 20-hydroxyecdysone in *Ajuga* hairy roots: the possibility of 7-ene introduction at a late stage. Phytochemistry 53, 733–737.
Imai, S., Murata, E., Fujioka, S., Matsuoka, T., Koreeda, M., Nakanishi, K., 1970. Structures of stachysterone A, the first natural 27-carbon steroid with a rearranged methyl group and stachysterone B. Journal of the American Chemical Society 92, 7510–7512.
Imai, S., Toyosata, T., Sakai, M., Sato, Y., Fujioka, S., Murata, E., Goto, M., 1969. Screening results of plants for phytoecdysones. Chemical and Pharmaceutical Bulletin 17, 335–339.
Jepson, I., Martinez, A., Sweetman, J.P., 1998. Chemical-inducible gene expression systems for plants — a review. Pesticide Science 54, 360–367.
Jones, C.G., Firn, R.D., 1991. On the evolution of plant secondary chemical diversity. Philosophical Transactions of the Royal Society, London, B 333, 273–280.
Kaplanis, J.N., Thompson, M.J., Robbins, W.E., Bryce, M., 1967. Insect hormones: alpha ecdysone and 20-hydroxyecdysone in bracken fern. Science 157, 1436–1438.
Koolman, J. (Ed.), 1989. Ecdysone: From Chemistry to Mode of Action. Georg Thieme Verlag, Stuttgart, pp. 482.
Kosar, K., Opletal, L., Vokác, K., Harmatha, J., Sovová, M., Cerovský, J., Krátký, F., Dvorák, J., 1997. Embryotoxicity of 20-hydroxyecdysone and polypodine B from *Leuzea carthamoides* DC. Pharmazie 52, 406–407.
Koudela, K., Tenora, J., Bajer, J., Mathova, A., Sláma, K., 1995. Stimulation of growth and development in Japanese quails after oral administration of ecdysteroid-containing diet. European Journal of Entomology 92, 349–354.
Kubo, I., Hanke, F.J., 1986. Chemical methods for isolating and identifying phytochemicals biologically active in insects. In: Miller, J.R., Miller, T.A. (Eds.), Insect Plant Interactions. Springer Verlag, New York, pp. 225–249.

Kubo, I., Klocke, J.A., Asano, S., 1983. Effects of ingested phytoecdysteroids on the growth and development of two lepidopterous larvae. Journal of Insect Physiology 29, 307–316.

Kubo, I., Komatsu, S., Asaka, Y., de Boer, G., 1987. Isolation and identification of apolar metabolites of ingested 20-hydroxyecdysone in frass of *Heliothis virescens* larvae. Journal of Chemical Ecology 13, 785–794.

Kusano, G., Takemoto, T., Beisler, J.A., Sato, Y., 1975. Steroidal constituents of *Solanum xanthocarpum*. Phytochemistry 14, 529–532.

Kuzmenko, A.I., Morozova, R.P., Nikolenko, I.A., Korniets, G.V., Kholodova, Y.D., 1997. Effects of vitamin D_3 and ecdysterone on free-radical lipid peroxidation. Biochemistry (Moscow) 62, 609–612.

Lafont, R., 1997. Ecdysteroids and related molecules in animals and plants. Archives of Insect Biochemistry and Physiology 35, 3–20.

Lafont, R., 1998. Phytoecdysteroids in the world flora: diversity, distribution, biosynthesis and evolution. Russian Journal of Plant Physiology 45, 276–295.

Lafont, R., Bouthier, A., Wilson, I.D., 1991. Phytoecdysteroids: structures, occurrence, biosyntheis and possible ecological signficance. In: Hrdy, I. (Ed.), Insect Chemical Ecology. Academia Prague, pp. 197–214.

Lafont, R., Horn, D.H.S., 1989. Phytoecdysteroids: structures and occurrence. In: Koolman, J. (Ed.), Ecdysone: From Chemistry to Mode of Action. George Thieme Verlag, Stuttgart, pp. 39–64.

Lafont, R., Koolman, J., Rees, H.H., 1993. Standardized abbreviations for common ecdysteroids. Insect Biochemistry and Molecular Biology 23, 207–209.

Lafont, R., Morgan, E.D., Wilson, I.D., 1994. Chromatographic procedures for phytoecdysteroids. Journal of Chromatgraphy 658, 31–53.

Lafont, R., Wilson, I.D., 1996. The Ecdysone Handbook, 2nd Edition. The Chromatographic Society, Nottingham, UK, p. 525.

Lev, S.V., Zakirova, R.P., Saatov, Z., Gorovits, M.B., Abubakirov, N.K., 1990. Ecdysteroids from tissue and cell cultures of *Ajuga turkestanica*. Khimiya Prirodnykh Soedinenii, 51–52.

Lüers, G.H., Jess, N., Franz, T., 2000. Reporter-linked monitoring of transgene expression in living cells using the ecdysone-inducible promoter system. European Journal of Cell Biology 79, 653–657.

Ma, W.-C., 1969. Some properties of gustation in the larva of *Pieris brassicae*. Entomologia Experimentalis et Applicata 12, 584–590.

Martinez, A., Sparks, C., Drayton, P., Thompson, J., Greenland, A., Jepson, I., 1999aa. Creation of ecdysone receptor chimeras in plants for controlled regulation of gene expression. Molecular and General Genetics 261, 546–552.

Martinez, A., Sparks, C., Hart, C.A., Thompson, J., Jepson, I., 1999bb. Ecdysone agonist inducible transcription in transgenic tobacco plants. The Plant Journal 19, 97–106.

Matsumoto, T., Tanaka, N., 1991. Production of phytoecdysteroids by hairy root cultures of *Aguga reptans* var. *atropurpurea*. Agricultural and Biological Chemistry 55, 1019–1025.

McMorris, T.C., Voeller, B., 1971. Ecdysones from gametophytic tissues of a fern. Phytochemistry 10, 3253–3254.

Melé, E., Messeguer, J., Gabarra, R., Tomás, J., Coll, J., Camps, F., 1992. In vitro bioassay for the effect of *Ajuga reptans* phytoecdysteroids on *Trialeuroides vaporariorum* larval development. Entomologia Experimentalis et Applicata 62, 163–168.

Mirzaev, Y.R., Syrov, V.N., 1992. Effect of phytoecdysteroids on the sexual activity of male rats. Doklady Academii Nauk Respublinki Uzbekistan 3, 47–49.

Mondy, N., Caïssa, C., Pitoizet, N., Delbecque, J.-P., Corio-Costet, M.-F., 1997. Effects of the ingestion of *Serratula tinctoria* extracts, a plant containing phytoecdysteroids, on the development of the vineyard pest *Lobesia botrana* (Lepidoptera. Tortricidae). Archives of Insect Biochemistry and Physiology 35, 227–235.

Morgan, W.W., Richardson, A., Sharp, Z.D., Walter, C.A., 1999. Application of exogenously regulatable promoter systems to transgenic models for the study of aging. Journal of Gerontology 54A, B30–B40.

Nagakari, M., Kushiro, T., Matsumoto, T., Tanaka, N., Kakinuma, K., Fujimoto, Y., 1994a. Incorporation of acetate and cholesterol in to 20-hydroxyecdysone by hairy root clone of *Ajuga reptans* var. *atropurpurea*. Phytochemistry 36, 907–910.

Nagakari, M., Kushiro, T., Yagi, T., Tanaka, N., Matsumoto, T., Kakinuma, K., Fujimoto, Y., 1994b. 3β-Hydroxy-5β-cholest-7-en-6-one as an intermediate of 20-hydroxyecdysone biosynthesis in a hairy root culture of *Ajuga reptans* var. *atropurpurea*. Journal of the Chemical Society, Chemical Communications, 1761–1762.

Najmutdinova, D.K., Saatov, Z., 1999. Lung local defense in experimental *Diabetes mellitus* and the effect of 11,20-dihydroxyecdysone in combination with maninil. Archives of Insect Biochemistry and Physiology 41, 144–147.

Nakagawa, T., Hara, N., Fujimoto, Y., 1997. Biosynthesis of 20-hydroxyecdysone in *Ajuga* hairy roots: stereochemistry of C-25 hydroxylation. Tetrahedron Letters 38, 2701–2704.

Nakanishi, K., 1971. Ecdysones. Pure and Applied Chemistry 25, 167–195.

Nakanishi, K., 1992. Past and present studies with ponasterones, the first insect molting hormones from plants. Steroids 57, 649–657.

Nakanishi, K., Koreeda, M., Sasaki, L., Chang, M.L., Hsu, H.Y., 1966. Insect hormones I. the structure of ponasterone A, an insect molting hormone from the leaves of *Podocarpus nakaii* H. Journal of Chemical Society, Chemical Communications, 915–917.

Ninagi, O., Maruyama, M., 1996. Utilization of 20-hydroxyecdysone extracted from a plant in sericulture. Japan Agricultural Research Quarterly 30, 123–128.

Nomura, K., Fujimoto, Y., 2000. Mechanism of C-2 hydroxylation during the biosynthesis of 20-hydroxyecdysone in *Ajuga* hairy roots. Chemical and Pharmaceutical Bulletin 48, 344–348.

Nomura, K., Nakamura, A., Fujimoto, Y., Yamada, J., Takahashi, K., Morisaki, M., 2000. Clerosterol as a common precursor of cyasterone and related ecdysteroids in *Ajuga* hairy roots. 2000 International Chemical Congress of Pacific Basin Societies (Pacifichem 2000), Bioscience and Technology Section, Abstract 377.

Ogawa, S., Nishimoto, N., Matsuda, H., 1974. Pharmacology of ecdysones in vertebrates. In: Burdette, W.J. (Ed.), Invertebrate Endocrinology and Hormonal Heterophylly. Springer Verlag, pp. 341–344.

Ohsawa, T., Yukawa, M., Takao, C., Muruyama, M., Bando, H., 1992. Studies on constituents of fruit body of *Polyporus umbellatus* and their cytotoxic activity. Chemical and Pharmaceutical Bulletin 40, 143–147.

Píš, J., Harmatha, J., Sláma, K., 1991. Action of some new synthetic derivatives of phytoecdysones on insects. In: Hrdy, I. (Ed.), Insect Chemical Ecology, Proceedings of the Conference on Insect Chemical Ecology, Tabor, August 1990. SPB Academic Publishing, The Hague, pp. 227–234.

Pomilio, A.B., González, M.D., Eceizabarrena, C.C., 1996. 7,8-Dihydroajugasterone C, norhygrine and other constituents of *Nierembergia hippomanica*. Phytochemistry 41, 1393–1398.

Prakash, A., Ghosal, S., 1979. Phytoecdysones. Journal of Scientific and Industrial Research (India) 38, 632–647.

Prymak, R.G., Levitsky, E.L., Gubsky, Yu. I., Goryushko, H.K., Kholodova, Yu., D., Vistunova, I.E., 1996. Effects of the phytoecdysteroid composition BTK-8L on fractionated intact rat liver chromatin. Ukrainskii Biokhimichnii Zhurnal 68, 84–89.

Ravishankar, G.A., Mehta, A.R., 1979. Control of ecdysterone biogenesis and tissue cultures of *Trianthema postulacastrum*. Journal of Natural Products 42, 152–158.

Rees, H.H., 1995. Ecdysteroid biosynthesis and inactivation in relation to function. European Journal of Entomology 92, 9–39.

Reixach, N., Irurre-Santilari, J., Casas, J., Melé, E., Messeguer, J., Camps, F., 1996. Biosynthesis of ecdysteroids in in vitro prothalli cultures of *Polypodium vulgare*. Phytochemistry 43, 597–602.

Ripa, P.V., Martin, E.A., Cocciolone, S.M., Adler, J.H., 1990. Fluctuation of phytoecdysteroids in developing shoots of *Taxus cuspidata*. Phytochemistry 29, 425–427.

Robbins, W.E., Kaplanis, J.N., Thompson, M.J., Shotino, T.J., Cohen, C.F., Joyner, S.C., 1968. Ecdysone analogs: effects on development and reproduction in insects. Science 161, 1158–1160.

Robbins, W.E., Kaplanis, J.N., Thompson, M.J., Shortino, T.J., Joyner, S.C., 1970. Ecdysones and synthetic analogs: molting hormone activity and inhibitive effects on insect growth, metamorphosis, and reproduction. Steroids 16, 105–125.

Robinson, P.D., Morgan, E.D., Wilson, I.D., Lafont, R., 1987. The metabolism of ingested and injected [^{3}H]ecdysone by final instar larvae of *Heliothis armigera*. Physiological Entomology 12, 321–330.

Sadikov, Z.T., Saatov, Z., Girault, J.-P., Lafont, R., 2000. Sileneoside H, a new phytoecdysteroid from *Silene brahuica*. Journal of Natural Products 63, 987–968.

Sarker, S.D., Girault, J.-P., Lafont, R., Dinan, L.N., 1997. Ecdysteroid xylosides from *Limnanthes douglasii*. Phytochemistry 44, 513–521.

Sarker, S.D., Savchenko, T., Whiting, P., Šik, V., Lafont, R., Dinan, L., 1997. Occurrence of ecdysteroids in the genus *Centaurea* (Compositae): 20-hydroxyecdysone from *Centaurea moschata*. Biochemical Systematics and Ecology 25, 367–368.

Sarker, S.D., Šik, V., Rees, H.H., Dinan, L., 1998a. 1α,20R-Dihydroxyecdysone from *Axyris amaranthoides* (Chenopodiaceae). Phytochemistry 49, 2305–2310.

Sarker, S.D., Šik, V., Rees, H.H., Dinan, L., 1998b. 2-Dehydro-3-*epi*-20-hydroxyecdysone from *Froelichia floridana* (Amaranthaceae). Phytochemistry 49, 2311–2314.

Savchenko, T., Whiting, P., Germade, A., Dinan, L., 2000. Ecdysteroid agonist and antagonist activities in species of the Solanaceae. Biochemical Systematics and Ecology 28, 403–419.

Savchenko, T., Whiting, P., Šik, V., Underwood, E., Sarker, S.D., Dinan, L., 1998. Distribution and identities of phytoecdysteroids in the genus *Briza* (Gramineae). Biochemical Systematics and Ecology 26, 781–791.

Savolainen, V., Wuest, J., Lafont, R., Connat, J.-L., 1995. Effects of ingested phytoecdysteroids in the female soft tick *Ornithodorus moubata*. Experientia 51, 596–600.

Sawicki, J.A., Monks, B., Morris, R.J., 1998. Cell-specific ecdysone-inducible expression of FLP recombinase in mammalian cells. BioTechniques 25, 868–875.

Schmelz, E.A., Grebenok, R.J., Galbraith, D.W., Bowers, W.S., 1998. Damage-induced accumulation of phytoecdysteroids in spinach: a rapid root response involving the octadecanoic acid pathway. Journal of Chemical Ecology 24, 339–360.

Schmelz, E.A., Grebenok, R.J., Galbraith, D.W., Bowers, W.S., 1999. Insect-induced synthesis of phytoecdysteroids in spinach, *Spinacia oleracea*. Journal of Chemical Ecology 25, 1739–1757.

Schmelz, E.A., Grebenok, R.J., Ohnmeiss, T.E., Bowers, W.S., 2000. Phytoecdysteroid turnover in spinach: long-term stability supports a plant defense hypothesis. Journal of Chemical Ecology 26, 2883–2896.

Simon, P., Koolman, J., 1989. Ecdysteroids in vertebrates: pharmacological aspects. In: Koolman, J. (Ed.), Ecdysone: From Chemistry to Mode of Action. George Thieme-Verlag, Stuttgart, pp. 254–259.

Sláma, K., Abubakirov, N.K., Gorovits, M.B., Baltaev, U.A., Saatov, Z., 1993. Hormonal activity of ecdysteroids from certain Asiatic plants. Insect Biochemistry and Molecular Biology 23, 181–185.

Sláma, K., Koudela, K., Tenora, J., Mathová, A., 1996. Insect hormones in vertebrates: anabolic effects of 20-hydroxyecdysone in Japanese quail. Experientia 52, 702–706.

Sláma, K., Lafont, R., 1995. Insect hormones — ecdysteroids: their presence and actions in vertebrates. European Journal of Entomology 92, 355–377.

Spindler-Barth, M., Quack, S., Rauch, P., Spindler, K., 1997. Biological effects of muristerone A and turkesterone on the epithelial cell line from *Chironomus tentans* (Diptera: Chironomidae) and correlation with binding affinity to the ecdysteroid receptor. European Journal of Entomology 94, 161–166.

Suhr, S.T., Gil, E.B., Senut, M.-C., Gage, F.H., 1998. High level transactivation by a modified *Bombyx* ecdysone receptor in mammalian cells without exogenous retinoid X receptor. Proceedings of the National Academy of Sciences, USA 95, 7999–8004.

Suksamrarn, A., Ganpinyo, P., Sommechai, C., 1994. Base-catalyzed autoxidation of 20-hydroxyecdysone: synthesis of calonysterone and 9,20-dihydroxyecdysone. Tetrahedron Letters 35, 4445–4448.

Svatoš, A., Macek, T., 1994. The rate of ecdysteroid production in suspension cultured cells of the fern *Pteridium aquilinum*. Phytochemistry 35, 651–654.

Syrov, V.N., 1984. Mechanism of anabolic action of phytoecdysteroids in mammals. Biol. Nauki (Moscow) 11, 16–20.

Takaishi, Y., Adachi, R., Murakami, Y., Ohashi, T., Nakano, K., Tomimatsu, T., 1992. A polyoxygenated steroid from *Lasiosphaera nipponica*. Phytochemistry 31, 243–246.

Takasaki, M., Tokuda, H., Nishino, H., Konoshima, T., 1999. Cancer chemopreventative agents (antitumor-promoters) from *Ajuga decumbens*. Journal of Natural Products 62, 972–975.

Takemoto, T., Ogawa, S., Nishimoto, N., 1967. Studies on the constituents of Achyranthis radix. I. Yakugaku Zasshi 87, 1463–1468.

Tanaka, Y., Asaoka, K., Takeda, S., 1994. Different feeding and gustatory responses to ecdysone and 20-hydroxyecdysone by larvae of the silkworm, *Bombyx mori*. Journal of Chemical Ecology 20, 125–133.

Tanaka, Y., Naya, S.-I., 1995. Dietary effect of ecdysone and 20-hydroxyecdysone on larval development of two lepidopteran species. Applied Entomology and Zoology 30, 285–294.

Tanaka, Y., Takeda, S., 1993. Ecdysone and 20-hydroxyecdysone supplements to the diet affect larval development in the silkworm, *Bombyx mori*, differently. Journal of Insect Physiology 20, 805–809.

Tomás, J., Camps, F., Coll, J., Melé, E., Messeguer, J., 1993. Phytoecdysteroid production in *Ajuga reptans* tissue cultures. Phytochemistry 32, 317–324.

Tomás, J., Camps, F., Claveria, E., Coll, J., Melé, E., Messeguer, J., 1992. Composition and location of phytoecdysteroids in *Ajuga reptans* in vivo and in vitro cultures. Phytochemistry 31, 1585–1591.

Tomaschko, K.-H., 1999. Nongenomic effects of ecdysteroids. Archives of Insect Biochemistry and Physiology 41, 89–98.

Trenin, D.S., Volodin, V.V., 1999. 20-Hydroxyecdysone as a human lymphocyte and neutrophil modulator: in vitro evaluation. Archives of Insect Biochemistry and Physiology 41, 156–161.

Uchiyama, M., Yoshida, T., 1974. Effect of ecdysterone on carbohydrate and lipid metabolism. In: Burdette, W.J. (Ed.), Invertebrate Endocrinology and Hormonal Heterophylly. Springer Verlag, pp. 401–416.

Vanek, T., Macek, T., Vaisar, T., Breznovits, A., 1990. Production of ecdysteroids by plant cell culture of *Pteridium aquilinum*. Biotechnology Letters 12, 727–730.

Valisolalao, J., Luu, B., Ourisson, G., 1983. Stéroïdes cytotoxiques de *Polyporus versicolor*. Tetrahedron 39, 2779–2785.

Vokác, K., Budešínský, M., Harmatha, J., Kohoutová, J., 1998a. Ecdysteroid constituents of the mushroom *Tapinella panuoides*. Phytochemistry 49, 2109–2114.

Vokác, K., Budešínský, M., Harmatha, J., Píš, J., 1998b. New ergostane type ecdysteroids from fungi. Ecdysteroid constituents of mushroom *Paxillus atrotomentosus*. Tetrahedron 54, 1657–1666.

Volodin, V.V., Mishurov, V.P., Kolegova, N.A., Tiukavin, Y.A., Portiagina, N.V., Postnikov, B.A., 1993. The ecdysteroids of plants of the Asteraceae family. Scientific Reports of the Komi Science Centre, Ural Division, Academy of Sciences of Russia, Issue 319, 1–17.

Warren, J.T., Hetru, C., 1990. Ecdysone biosynthesis: pathways, enzymes, and the early steps problem. Invertebrate Reproduction and Development 18, 91–99.

Wu, X., Jiang, Y.-G., Fan, S.-Z., Wang, R.-W., Xiang, M.-Z., Niu, H.-J., Li, T.-X., 1998. The effect of ecdysterone on rat lung reperfusion injury. Chinese Pharmacological Bulletin 14, 256–258.

Wurtz, J.-M., Guillot, B., Fagart, J., Moras, D., Tietjen, K., Schindler, M., 2000. A new model for 20-hydroxyecdysone and dibenzoylhydrazine binding: a homology modeling and docking approach. Protein Science 9, 1073–1084.

Yagi, T., Morisaki, M., Kushiro, T., Yoshida, H., Fujimoto, Y., 1996. Biosynthesis of 24β-alkyl-Δ^{25}-sterols in hairy roots of *Ajuga reptans* var. *atropurpurea*. Phytochemistry 41, 1057–1064.

Yao, T.P., Forman, B.M., Jiang, Z.Y., Cherbas, L., Chen, J.D., McKeown, M., Cherbas, P., Evans, R.M., 1993. Functional ecdysone receptor is the product of EcR and Ultraspiracle genes. Nature 366, 476–479.

Yoshida, T., Otaka, T., Uchiyama, M., Ogawa, S., 1971. Effect of ecdysterone on hyperglycemia in experimental animals. Biochemical Pharmacology 20, 3263–3268.

Zibareva, L.N., 1997. The prognosis of the presence of ecdysteroids among the species *Silene* L. and *Chenopodium* L. to their contents in the seeds. Rastitelny Resursy 33, 89–92.

Zibareva, L., 2000. Distribution and levels of phytoecdysteroids in plants of the genus *Silene* during development. Archives of Insect Biochemistry and Physiology 43, 1–8.

PERGAMON

Phytochemistry 57 (2001) 341–347

PHYTOCHEMISTRY

www.elsevier.com/locate/phytochem

Enzymatic halogenation of flavanones and flavones

Panadda Yaipakdee[a,*], Larry W. Robertson[b]

[a]*Department of Pharmaceutical Chemistry, Faculty of Pharmacy, Silpakorn University, Sanam Chan Palace Campus, Mueng, Nakorn Pathom, 73000, Thailand*

[b]*Department of Medicinal Chemistry and Pharmacognosy, College of Pharmacy, The Ohio State University, Columbus, OH, 43210, USA*

Received 26 October 2000; received in revised form 3 January 2001

Abstract

The whole cells and the chloroperoxidase enzyme of *Caldariomyces fumago* were capable of halogenating the flavanones, naringenin and hesperetin, at C-6 and C-8 in the presence of either Cl^- or Br^-. However, they did not act on other test flavones. The biohalogenated products of naringenin and hesperetin were isolated and found to be identical to those obtained from chemical reactions using molecular halogen and hypohalous acid. © 2001 Elsevier Science Ltd. All rights reserved.

Keywords: *Caldariomyces fumago*; Chloroperoxidase; Enzymatic halogenation; Flavanones; Flavones

1. Introduction

The use of microbial enzymes for the transformation of organic compounds has been employed as a powerful method in metabolism studies and in modern synthetic organic chemistry for decades (Smith and Rosazza, 1975; Faber, 1992). One of the enzymatic reactions that has been widely studied is a chloroperoxidase-catalyzed halogenation (Franssen, 1994). Chloroperoxidase from *Caldariomyces fumago* (CPO; EC 1.11.1.10) is a well-known enzyme, capable of halogenating a great variety of organic compounds such as β-ketoacids (Shaw and Hager, 1959), cyclic β-diketones (Hager et al., 1966), steroids (Levine et al., 1968), alkenes (Yamada et al., 1985), activated aromatic compounds (Wannstedt et al., 1990), and heterocylcic compounds (Franssen et al., 1987). The reaction mechanism of CPO involves the formation of a halogenium ion (X^+) or hypohalous acid (HOX) as an intermediate which can effect electrophilic substitution with electron-rich substrates (Yamada et al., 1985; Libby et al., 1992).

The enzymatic halogenation of several flavanones and flavones having electron-donating groups was investigated in this study. Flavonoids are very common as secondary metabolites found in nature with a great variety of structural forms and biological activities (Harborne, 1988). The vast literature related to flavonoid biotransformations is primarily concerned with oxidation, methylation and glucosidation (Ibrahim and Abul-Hajj, 1990a,b; Ibrahim et al., 1997). One study was found on the microbial chlorination of the isoflavone genistein by *Streptomyces griseus* and *S. plicatus* (Anyanwutaku et al., 1992). There are no previous reports on the chloroperoxidase-catalyzed halogenation of flavonoid compounds. Therefore, we examined the use of whole cells and CPO of *C. fumago* to brominate and chlorinate various flavanones and flavones. The enzymatic study was also compared with chemical halogenation using molecular halogen and hypohalous acid.

2. Results and discussion

The enzymatic bromination and chlorination of flavanones and flavones using *C. fumago* whole cells and CPO gave the results shown in Table 1. With Br^- and Cl^- present as halides, both *C. fumago* and CPO catalyzed the halogenation of the flavanones, naringenin and hesperetin, but were inactive toward the test flavones. The metabolic products were isolated and identified on the basis of NMR and mass spectral analyses. Mass spectra of halogenated compounds showed typical characteristics of isotope peak, suggesting a number of halogen atoms present in each metabolite.

* Corresponding author. Tel.: +66-34-255800; fax: +66-34-255801.
E-mail address: ypanadda@su.ac.th (P. Yaipakdee).

0031-9422/01/$ - see front matter © 2001 Elsevier Science Ltd. All rights reserved.
PII: S0031-9422(01)00075-9

Table 1
Reaction products from various flavanones and flavones by chloroperoxidase-catalyzed reaction

Substrate	Halide	Product	Yield (%)	
			C. fumago whole cells	$CPO/H_2O_2/X^-$
Flavone, flavonol,	Br^-	–	–	–
7-Hydroxyflavone,	Cl^-	–	–	–
5,7-Dihydroxyflavone,		–	–	–
Quercetin, 6-chloroflavone		–	–	–
Naringenin	Br^-	6,8-Dibromonaringenin (**1**)	2.4	9.3
		8-Bromonaringenin (**2**)	1.8	7.8
	Cl^-	6,8-Dichloronaringenin (**3**)	21	2.8
		6-Chloronaringenin (**4**)	7.6	1.9
Hesperetin	Br^-	6,8-Dibromohesperetin (**5**)	Not tested	8.3
		8-Bromohesperetin (**6**)	Not tested	2.2
	Cl^-	6,8-Dichlorohesperetin (**7**)	3.0	Trace
		6-Chlorohesperetin (**8**)	1.7	1.0

The biobrominations of naringenin and hesperetin gave 6,8-dibromonaringenin (**1**), 8-bromonaringenin (**2**), 6,8-dibromohesperetin (**5**), and 8-bromohesperetin (**6**), respectively. The mass spectral analysis indicated the presence of two bromine atoms in **1** and **5** and one bromine atom in **2** and **6**. The ^1H NMR spectra of brominated compounds were similar to those of naringenin and hesperetin, except for the disappearance of two proton signals in **1** and **5** and one proton signal in **2** and **6** at the H-6 and/or H-8 regions (Tables 2 and 3). These data clearly supported that **1** and **5** were dibrominated products having two bromine atoms at positions 6 and 8. The position of the bromine atoms in **2** and **6** were identified by analysis of the ^{13}C NMR spectra. Relative to naringenin and hesperetin, the ^{13}C NMR spectra of **2** and **6** showed a new quaternary carbon signal around 88 ppm, while one of the two methine carbon peaks in the 96 ppm region disappeared (Table 4). This suggested that the bromine atom might be at either C-6 or C-8. HMBC data of **2** showed that the hydroxyl proton at 12.15 ppm (OH-5) had long range couplings to the methine carbon at 96.30 ppm, and two quaternary carbons at 102.97 and 162.97 ppm corresponding to C-6, C-4a, and C-5, respectively. The methine proton at 6.14 ppm (H-6) showed long range couplings with signals at 88.41 (C-8), 102.97 (C-4a), and 162.97 (C-5 and C-7) ppm. In addition, compounds **2** and **6** gave similar ^{13}C NMR spectral patterns and the carbon signals at C-7 and C-8a of **2** and **6** were shifted upfield by 4.5 ppm compared to those of naringenin and hesperetin. These results indicated that the bromine atom in **2** and **6** must be at C-8.

The enzymatic chlorinations of naringenin and hesperetin also gave four metabolic products, 6,8-dichloronaringenin (**3**), 6-chloronaringenin (**4**), 6,8-dichlorohesperetin (**7**) and 6-chlorohesperetin (**8**). The mass and ^1H NMR spectral analyses of **3** and **7** established the presence of two chlorine atoms at positions 6 and 8. The mass and ^1H NMR spectra of **4** and **8** indicated one chlorine atom at either position 6 or 8 (Tables 2 and 3). The ^{13}C NMR

Table 2
^1H NMR spectral data of naringenin and compounds **1–4** in $(CD_3)_2CO$

Position	Naringenin[a]	**1**[b]	**2**[b]	**3**[b]	**4**[a]
H-2	5.43, *dd* (3.0, 13.0)[c]	5.67, *dd* (3.1, 12.5)	5.58, *dd* (3.4, 12.5)	5.64, *dd* (2.8, 12.8)	5.45, *dd* (3.0, 12.9)
H-3ax	3.16, *dd* (13.1, 17.0)	3.32, *dd* (12.5, 17.1)	3.21, *dd* (12.5, 17.1)	3.31, *dd* (12.7, 17.2)	3.21, *dd* (12.9, 17.2)
H-3eq	2.71, *dd* (3.1, 17.3)	2.95, *dd* (3.1, 17.1)	2.85, *dd* (3.4, 17.1)	2.90, *dd* (3.1, 17.1)	2.74, *dd* (3.0, 17.4)
OH-5	12.17, *s*	12.92, *s*	12.15, *s*	12.81, *s*	12.74, *s*
H-6	5.94, *s*	–	6.14, *s*	–	–
H-8	5.94, *s*	–	–	–	6.13, *s*
H-2′	7.37, *d* (8.4)	7.43, *d* (8.2)	7.39, *d* (8.2)	7.43, *d* (8.9)	7.35, *d* (8.5)
H-3′	6.88, *d* (8.7)	6.92, *d* (8.6)	6.87, *d* (8.6)	6.91, *d* (8.9)	6.85, *d* (8.7)
H-5′	6.88, *d* (8.7)	6.92, *d* (8.6)	6.87, *d* (8.2)	6.91, *d* (8.9)	6.85, *d* (8.7)
H-6′	7.37, *d* (8.4)	7.43, *d* (8.2)	7.39, *d* (8.2)	7.43, *d* (8.9)	7.35, *d* (8.5)

[a] ^1H NMR spectrum taken at 270 MHz.
[b] ^1H NMR spectrum taken at 500 MHz.
[c] Coupling constants (Hz) in parentheses.

Table 3
^{1}H NMR spectal data of hesperetin and compounds **5–8** in $(CD_3)_2CO$

Position	Hesperetin[a]	**5**[b]	**6**[b]	**7**[a]	**8**[b]
H-2	5.43, *dd* (3.1, 12.6)[c]	5.65, *dd* (3.4, 12.2)	5.60, *dd* (3.2, 11.9)	5.63, *dd* (3.3, 12.2)	5.60, *dd* (3.1, 12.2)
H-3ax	3.15, *dd* (12.6, 17.2)	3.29, *dd* (12.1, 17.2)	3.22, *dd* (11.9, 17.1)	3.28, *dd* (12.5, 17.0)	3.24, *dd* (12.2, 17.1)
H-3eq	2.74, *dd* (3.0, 17.0)	2.97, *dd* (3.2, 17.2)	2.90, *dd* (3.4, 17.1)	2.92, *dd* (3.3, 17.1)	2.89, *dd* (3.4, 17.1)
OH-5	12.17, *s*	12.98, *s*	12.17, *s*	12.80, *s*	12.12, *s*
H-6	5.94, *d* (2.0)	–	6.16, *s*	–	–
H-8	5.96, *d* (2.1)	–	–	–	6.15, *s*
H-2′	7.04, *m*	7.09, *m*	7.09, *m*	7.08, *m*	7.09, *m*
OMe-4′	3.85, *s*	3.86, *s*	3.86, *s*	3.85, *s*	3.86, *s*
H-5′	6.97, *m*	7.00, *m*	6.99, *m*	6.97, *m*	7.00, *m*
H-6′	6.97, *m*	7.00, *m*	6.99, *m*	6.97, *m*	7.00, *m*

[a] ^{1}H NMR spectrum taken at 270 MHz.
[b] ^{1}H NMR spectrum taken at 500 MHz.
[c] Coupling constants (Hz) in parentheses.

Table 4
^{13}C NMR spectral data of naringenin, hesperetin and compounds **2**, **4, 6** and **8** in $(CD_3)_2CO$

Position	Naringenin[a]	**2**[b]	**4**[a]	Hesperetin[a]	**6**[b]	**8**[b]
C-2	79.86 *d*	79.50 *d*	80.22 *d*	79.79 *d*	79.35 *d*	79.98 *d*
C-3	43.43 *t*	42.01 *t*	43.25 *t*	43.52 *t*	41.97 *t*	43.23 *t*
C-4	197.15 *s*	196.37 *s*	197.70 *s*	197.09 *s*	196.31 *s*	197.34 *s*
C-5	165.23 *s*	162.97 *s*	160.33 *s*	165.29 *s*	163.27 *s*[c]	160.27 *s*
C-6	96.81 *d*	96.30 *d*	101.02 *s*	96.87 *d*	96.46 *d*	101.10 *s*
C-7	167.30 *s*	162.97 *s*	162.20 *s*[c]	167.36 *s*	163.20 *s*[c]	162.03 *s*[c]
C-8	95.83 *d*	88.41 *s*	96.26 *d*	95.91 *d*	88.51 *s*	96.37 *d*
C-4a	103.19 *s*	102.97 *s*	103.52 *s*	103.28 *s*	103.02 *s*	103.25 *s*
C-8a	164.31 *s*	159.51 *s*	162.46 *s*[c]	164.28 *s*	159.39 *s*	163.10 *s*[c]
C-1′	130.73 *s*	129.48 *s*	130.48 *s*	132.84 *s*	131.49 *s*	132.51 *s*
C-2′	128.94 *d*	127.99 *d*	129.09 *d*	114.38 *d*	113.50 *d*	114.37 *d*
C-3′	116.15 *d*	115.35 *d*	116.25 *d*	147.61 *s*	146.59 *s*	147.58 *s*
C-4′	158.62 *s*	157.85 *s*	158.83 *s*	148.69 *s*	147.94 *s*	148.74 *s*
C-5′	116.15 *d*	115.35 *d*	116.25 *d*	112.38 *d*	111.54 *d*	112.30 *d*
C-6′	128.94 *d*	127.99 *d*	129.09 *d*	118.78 *d*	117.81 *d*	118.82 *d*
OMe-4′				56.37 *q*	55.98 *q*	56.31 *q*

[a] ^{13}C NMR spectrum taken at 67.9 MHz.
[b] ^{13}C NMR spectrum taken at 125 MHz.
[c] Assignments could be reversed.

spectra of **4** and **8** showed a quaternary carbon and a methine carbon signals in the C-6 and C-8 regions at lower field compared to those of their precursors (Table 4). The structural assignment of **4** as 6-chloronaringenin was supported by a COLOC experiment. The hydroxy proton at δ 12.74 (OH-5) had long range couplings to the quaternary signals at 101.02, 103.52, and 160.33 ppm thus corresponding to C-6, C-4a, and C-5, respectively. Since the ^{13}C NMR spectral pattern of **8** was similar to that of **4,** the chlorine atom in **8** was placed at C-6. This was supported by the appearance of carbon signals at C-5 and C-7 of **4** and **8** at higher field by about 5 ppm compared to those of naringenin and hesperetin.

It was noted that, when the CPO enzyme was employed to halogenate naringenin and hesperetin, brominated products were obtained in better yields than chlorinated ones (Table 1). This was explainable since the halogenation of CPO is electrophilic and the reactivity of halogenium ions increases in the following order: Cl^+, Br^+ and I^+ (Yamada et al., 1985). However, when *C. fumago* whole cells were used, yields of chlorinated metabolites were higher. This might be due to the weak growth of *C. fumago* in the medium containing KBr. Overall, the halogenated products were obtained in low yields together with starting material. The halogenation of the substrates may proceed in competition with the halogenation of CPO itself at tyrosine residues until the enzyme is no longer active (Wannstedt et al., 1990). Furthermore, since the enzymatic reactions were carried out in suspension, the uptake of the substrates for biotransformation may be poor.

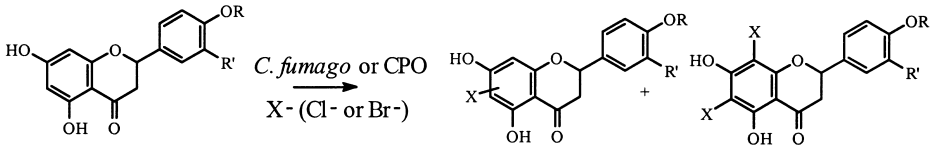

naringenin; R = R' = H
hesperetin; R = Me, R' = OH

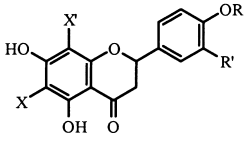

6,8-dibromonaringenin (**1**); R = R' = H, X = X' = Br
8-bromonaringenin (**2**); R = R' = H, X = H, X' = Br
6,8-dichloronaringenin (**3**); R = R' = H, X = X' = Cl
6-chloronaringenin (**4**); R = R' = H, X = Cl, X' = H
6,8-dibromohesperetin (**5**); R = Me, R' = OH, X = X' = Br
8-bromohesperetin (**6**); R = Me, R' = OH, X = H, X' = Br
6,8-dichlorohesperetin (**7**); R = Me, R' = OH, X = X' = Cl
6-chlorohesperetin (**8**); R = Me, R' = OH, X = Cl, X' = H

The flavone-type compounds, flavone, flavonol, 7-hydroxyflavone, 5,7-dihydroxyflavone, quercetin, and 6-chloroflavone, were not suitable as substrates of CPO. The aromatic rings of these compounds possessing a strongly conjugated system were quite stable, and were thus inert to the enzymatic reaction. The relevant flavanones were reactive since the conjugation in the flavanone system was disrupted by removing the 2,3-double bond. The biomimetic reactions of naringenin and hesperetin with chemical halogenating agents were examined. Their reaction products were identical to those obtained from the enzymatic reactions. The halogenations of naringenin and hesperetin are electrophilic and occurred at the C-6 and C-8 positions on the A-rings. With the two hydroxy groups at C-5 and C-7, the A-rings of naringenin and hesperetin are considerably more nucleophilic and hence reactive towards electrophilic halogenating species than their B-rings.

3. Experimental

3.1. General experimental procedures

^{1}H NMR spectra were recorded on an IBM AF-270 and a JNM-A500 spectrometer. ^{13}C NMR spectra were recorded on an IBM AF-270 at 67.9 MHz, a JNM-A500 and a Bruker AM-500 at 125 MHz. $(CD_3)_2CO$ was used as solvent. MS was performed using a VG 70 250S mass spectrometer and HP 5989B MS engine at 70 eV. FTIR spectra were obtained using a Magna-IR^{TM} spectrometer 750, using KBr plates. Optical rotations were measured with a Perkin Elmer 241 photoelectric polarimeter.

Chemicals, all test samples, flavone, flavonol, 7-hydroxyflavone, 5,7-dihydroxyflavone, quercetin, 6-chloroflavone, naringenin, and hesperetin, were obtained from Sigma. Bromine and CPO were also purchased from Sigma. Sodium hypochlorite was obtained from Carlo. Other chemicals used were reagent grade.

3.2. Micro-organism

Caldariomyces fumago ATCC 11925 was obtained from the American Type Culture Collection. Live cultures were maintained by subculturing on suitable slants at room temperature or storage at 4°C in tightly capped culture tubes.

3.3. Enzymatic halogenation of flavanones and flavones by C. fumago whole cells

A two-stage fermentation technique was employed. Stage I and stage II cultures were prepared by the following method. The surface growth from *C. fumago* slants on mycophil agar (BBL) was suspended in 5 ml volumes of normal saline solution. One milliliter of the suspension was transferred into 100 ml of stage I medium in 500 ml erlenmeyer flasks. The stage I cultures were incubated at ambient temperature (20°C) on a rotary shaker at 250 rpm for 48–72 h. Approximately 10 ml volumes of the actively growing stage I cultures were transferred to 100 ml of fresh medium in 500 ml erlenmeyer flasks. All fermentation experiments were carried out in a Czapek-yeast- KCl or Czapek-yeast-KBr medium, consisting of glucose, 30 g; $NaNO_3$, 3.0 g; K_2SO_4, 1.0 g; $MgSO_4$, 0.5 g; KCl or KBr, 0.5 g; $(Fe)_2(SO_4)_3$, 0.01 g; yeast extract, 3.3 g in 1 l H_2O. Media were sterilized by autoclaving at 121°C, 15 lb/in^2 for 15 min.

For initial screening experiments, 10 mg of each sample as a solution in DMF (50 mg/ml) was added and suspended into each flask of 24 h stage II cultures. The culture was further incubated and monitored. Ten milliliters of the cultures were sampled daily and extracted

with 10 ml of $CHCl_3$, twice. The extracts were concentrated to dryness and redissolved in 0.25 ml of 95% EtOH. The solutions were subjected to silica gel TLC and developed with toluene-Me_2CO (10:1) and/or CH_3Cl-MeOH (40:1). TLC plates exposed to UV light and Fast Blue BB spray reagent were analyzed. Control cultures of organism without substrate and controls consisting of substrate in medium without organism were performed along with sample cultures.

Preparative scale fermentations were conducted on 150–190 mg of substrates, using a two-stage shaken culture fermentation as described above. The stage II cultures with substrate were incubated for 24–48 h before being harvested. The whole culture broths were exhaustively extracted twice with an equal volume of $CHCl_3$. The $CHCl_3$ extracts were dried over Na_2SO_4, evaporated and purified.

3.4. Enzymatic halogenation of flavanones and flavones by CPO (Sigma)

The reaction conditions were modified from the method described by Yamada et al. (1985). For initial screening, the enzymatic reaction mixture contained 10 ml of 0.1 M potassium phosphate buffer (pH 2.75), 100 μmol of KBr or KCl, 25–50 units of CPO, and 20 μmol of a substrate. All substrates were insoluble in water, and had to be first dissolved in 70 μl of warm EtOH, then poured and suspended in the reaction mixture. The reaction was initiated by slowly adding 100 μmol of H_2O_2 and continued for 60 min at room temperature with constant stirring. The control test was performed without the enzyme. The reaction was monitored by TLC as above.

Preparative scale halogenation was conducted on 0.8 mmol of substrates. Each substrate was dissolved in 3 ml of warm EtOH, then poured into the reaction mixture. The reaction mixture consisted of 400 ml of 0.1 M potassium phosphate buffer (pH 2.75), 4 mmol of KBr or KCl, and 1000 units of CPO. H_2O_2 (4 mmol) was then slowly added. After 60 min, the reaction mixture was extracted with $CHCl_3$ (200 ml×3). The extracts were concentrated to dryness and followed by a series of chromatographic methods for the isolation of the halogenated products.

3.5. Isolation procedures

3.5.1. Halogenated products 1–4 of naringenin formed by C. fumago whole cells

From the microbial bromination of naringenin (180 mg) with *C. fumago* in Czapek-yeast-KBr, the dried $CHCl_3$ extract was subjected to silica gel PF_{254} chromatography using toluene–Me_2CO (10:1) as eluant. Naringenin (58 mg) was recovered. Flavonoid-containing fractions (18 mg) were subjected to prep. TLC using a silica gel 60 F_{254} plate at 0.25 mm thickness. The chromatogram was developed three times, using toluene–Me_2CO (10:1) for the first development, then, $CHCl_3$–MeOH (40:1) for the last two. The plate was visualized under UV light at 254 nm. Two major bands were observed. The compound from each band was extracted from silica gel using Me_2CO. 6,8-Dibromonaringenin (**1**) (4.3 mg) and 8-bromonaringenin (**2**) (3.2 mg) were isolated.

The microbial chlorination of naringenin (190 mg) was performed with *C. fumago* in Czapek-yeast-KCl. The dried $CHCl_3$ extract was applied to a silica gel PF_{254} column with toluene–Me_2CO (12:1) giving 6,8-dichloronaringenin (**3**) (40 mg) and 6-chloronaringenin (**4**) (14.5 mg).

3.5.2. Halogenated products 1–4 of naringenin formed by CPO (Sigma)

Each preparative scale bromination and chlorination was conducted on 217 mg of naringenin according to the method described above. The dried extract of each reaction mixture was subjected to silica gel 60 GF_{254} column chromatography with toluene–Me_2CO (12:1) as eluant. 6,8-Dibromonaringenin (**1**) (20.2 mg), 8-bromonaringenin (**2**) (16.9 mg), and naringenin (126 mg) were isolated from the dried extract of the enzymatic bromination. 6,8-Dichloronaringenin (**3**) (6 mg), 6-chloronaringenin (**4**) (4.2 mg), and naringenin (135 mg) were isolated from the dried extract of the enzymatic chlorination mixture.

*3.5.2.1. 6,8-Dibromonaringenin (**1**).* An amorphous powder; $[\alpha]_D^{20}$ 0° (MeOH; *c* 0.1); λ_{max}^{MeOH} nm (log ε): 224 (4.1), 331 (4.1); ν_{max} (KBr) cm^{-1}: 3350 (OH), 1625 (>C=O); ^1H NMR cf. Table 2; EIMS *m/z* (rel. int.): 432 $[M+4]^+$ (7), 430 $[M+2]^+$ (18), 428 $[M]^+$ (9), 311 $[(M+2)\text{-}120+H]^+$ (29), 120 [M-308]$^+$ (100).

*3.5.2.2. 8-Bromonaringenin (**2**).* An amorphous powder; $[\alpha]_D^{20}$ 0° (MeOH; *c* 0.1); λ_{max}^{MeOH} nm (log ε): 224 (4.3), 291 (4.0), 329 (4.0); ν_{max} (KBr) cm^{-1}: 3325 (OH), 1635 (>C=O); ^1H NMR cf. Table 2; ^{13}C NMR cf. Table 4; EIMS *m/z* (rel. int.): 352 $[M+2]^+$ (69), 350 $[M]^+$ (71), 233 $[(M+2)\text{-}120+H]^+$ (15), 231 $[M\text{-}120+H]^+$ (11), 120 [M-230]$^+$ (100).

*3.5.2.3. 6,8-Dichloronaringenin (**3**).* An amorphous powder; $[\alpha]_D^{20}$ 0° (MeOH; *c* 0.1); λ_{max}^{MeOH} nm (log ε): 223 (3.7), 253 (3.3), 331 (3.7); ν_{max} (KBr) cm^{-1}: 3350 (OH), 1619 (>C=O); ^1H NMR cf. Table 2; EIMS *m/z* (rel. int.): 344 $[M+4]^+$ (4), 342 $[M+2]^+$ (19), 340 $[M]^+$ (35), 221 $[M\text{-}120+H]^+$ (43), 120 [M-220]$^+$ (100).

*3.5.2.4. 6-Chloronaringenin (**4**).* An amorphous powder; $[\alpha]_D^{20}$ 0° (MeOH; *c* 0.1); λ_{max}^{MeOH} nm (log ε): 223 (3.6), 247 (3.1), 325 (3.5); ν_{max} (KBr) cm^{-1}: 3340 (OH), 1637 (>C=O); ^1H NMR cf. Table 2; ^{13}C NMR cf. Table 4; EIMS *m/z* (rel. int.): 308 $[M+2]^+$ (22), 306 $[M]^+$ (68), 189 $[(M+2)\text{-}120+H]^+$ (26), 187 $[M\text{-}120+H]^+$ (81), 120 [M-186]$^+$ (100).

*3.5.3. Halogenated products **5**–**8** of hesperetin formed by CPO (Sigma)*

Preparative scale bromination and chlorination were performed on 240 mg and 120 mg of hesperetin, respectively, according to the method described above. The dried extract of each reaction mixture was chromatographed over silica gel 60 GF_{254} with toluene–Me_2CO (15:1). 6,8-Dibromohesperetin (**5**) (20 mg), 8-bromohesperetin (**6**) (5.1 mg), and hesperetin (120.8 mg) were isolated from the dried extract of the enzymatic bromination mixture. 6-Chlorohesperetin (**8**) (1.2 mg) and hesperetin (82 mg) were isolated from the dried extract of the enzymatic chlorination mixture. Trace amounts of 6,8-dichlorohesperetin (**7**) were observed on a silica gel TLC plate.

*3.5.4. Chlorinated products **7** and **8** of hesperetin formed by C. fumago whole cells*

One hundred and ninety milligrams of hesperetin were biotransformed with *C. fumago* in Czapek-yeast-KCl. The dried $CHCl_3$ extract was chromatographed over silica gel 60 (230–400 mesh) with toluene–Me_2CO (12:1). Hesperetin (64 mg) was recovered. Prep. TLC of flavonoid-containing fractions (23 mg) was performed on a silica gel 60 F_{254} plate at 0.25 mm thickness using $CHCl_3$:MeOH (40:1). Two metabolic products, 6,8-dichlorohesperetin (**7**) (5.7 mg) and 6-chlorohesperetin (**8**) (3.2 mg), were isolated.

*3.5.4.1. 6,8-Dibromohesperetin (**5**).* An amorphous powder; $[\alpha]_D^{20}$ 0° (MeOH; c 0.1); λ_{max}^{MeOH} nm (log ε): 230 (4.1), 332 (4.0); ν_{max} (KBr) cm^{-1}: 3410 (OH), 1635 (>C=O); ^1H NMR cf. Table 3; EIMS *m/z* (rel. int.): 462 $[M+4]^+$ (28), 460 $[M+2]^+$ (51), 458 $[M]^+$ (27), 150 $[M\text{-}308]^+$ (100).

*3.5.4.2. 8-Bromohesperetin (**6**).* An amorphous powder; $[\alpha]_D^{20}$ 0° (MeOH; c 0.1); λ_{max}^{MeOH} nm (log ε): 230 (4.1), 294 (4.0), 330 (4.0); ν_{max} (KBr) cm^{-1}: 3400 (OH), 1635 (>C=O); ^1H NMR cf. Table 3; ^{13}C NMR cf. Table 4; EIMS *m/z* (rel. int.): 382 $[M+2]^+$ (84), 380 $[M]^+$ (86), 233 $[(M+2)\text{-}150+H]^+$ (13), 150 $[M\text{-}230]^+$ (84).

*3.5.4.3. 6,8-Dichlorohesperetin (**7**).* An amorphous powder; $[\alpha]_D^{20}$ 0° (MeOH; c 0.1); λ_{max}^{MeOH} nm (log ε): 231 (4.1), 287 (3.5), 332 (4.2); ν_{max} (KBr) cm^{-1}: 3400 (OH), 1635 (>C=O); ^1H NMR cf. Table 3; EIMS *m/z* (rel. int.): 374 $[M+4]^+$ (2), 372 $[M+2]^+$ (12), 370 $[M]^+$ (21), 220 $[M\text{-}150]^+$ (7), 150 $[M\text{-}220]^+$ (100).

*3.5.4.4. 6-Chlorohesperetin (**8**).* An amorphous powder; $[\alpha]_D^{20}$ 0° (MeOH; *c* 0.1); λ_{max}^{MeOH} nm (log ε): 231 (4.3), 287 (4.0), 329 (4.2); ν_{max} (KBr) cm^{-1}: 3400 (OH), 1635 (>C=O); ^1H NMR cf. Table 3; ^{13}C NMR cf. Table 4; EIMS *m/z* (rel. int.): 338 $[M+2]^+$ (12), 336 $[M]^+$ (38), 187 $[M\text{-}150+H]^+$ (7), 150 $[M\text{-}186]^+$ (100).

3.6. Chemical reaction with molecular halogen and hypohalous acid

3.6.1. Chemical bromination of naringenin

The biomimetic reaction of naringenin with bromine was examined under conditions similar to the chloroperoxidase reaction. The reaction mixture consisted of 7.8 ml of 1 M phosphate buffer (pH 2.75), 1.5 mmol of H_2O_2, 0.76 mmol of KBr, 20 ml of H_2O, and 10 ml of EtOH–Me_2CO (1:1). Naringenin (100 mg; 0.37 mmol) dissolved in 4.0 ml of EtOH–Me_2CO (1:1) was added to the reaction mixture and thoroughly mixed. Bromine solution (0.76 mmol of Br_2 in 400 μl of EtOH) was then slowly added at room temperature with mild stirring. After 45 min, the reaction mixture was extracted with $CHCl_3$ (25 ml×2). The combined extract was dried over Na_2SO_4 and evaporated to dryness. The residue was subjected to silica gel GF_{254} chromatography with toluene–Me_2CO (12:1) as eluant to give 6,8-dibromonaringenin (**1**) (26 mg) and 8-bromonaringenin (**2**) (17.0 mg).

3.6.2. Chemical bromination of hesperetin

Hesperetin (200 mg; 0.66 mmol) was dissolved in 8.0 ml of EtOH–Me_2CO (1:1), then poured into the reaction mixture. The reaction mixture contained 14 ml of 1 M phosphate buffer (pH 2.75), 2.6 mmol of H_2O_2, 1.3 mmol of KBr, 40 ml of H_2O, and 20 ml of EtOH-Me_2CO (1:1). The reaction was started by slowly adding bromine solution (1.3 mmol of Br_2 in 700 μl of EtOH). After 45 min, the reaction mixture was extracted with $CHCl_3$ (45 ml×2). The combined extract was dried over Na_2SO_4 and evaporated to dryness. The residue was applied to silica gel GF_{254} with toluene–Me_2CO (15:1) as eluant to afford 6,8-dibromohesperetin (**5**) (23.8 mg) and 8-bromonaringenin (**6**) (26.0 mg).

3.6.3. Chemical chlorination of naringenin

The reaction mixture consisted of 14 ml of 1 M phosphate buffer (pH 2.75), 40 ml of H_2O, 20 ml of EtOH–Me_2CO (1:1), and 200 mg of naringenin dissolved in 8.0 ml of EtOH–Me_2CO (1:1). To the reaction mixture was added dropwise 3.75 ml of sodium hypochlorite solution, then, 3.75 ml of HOAc. After stirring the mixture for 1 h at room temperature, the mixture was extracted with $CHCl_3$ (45 ml×2). The combined extract was dried over Na_2SO_4 and evaporated to dryness. The residue was subjected to silica gel GF_{254} chromatography with toluene–Me_2CO (12:1) as eluant. 6-Chloronaringenin (**4**) (6 mg) was isolated. Trace amounts of 6,8-dichloronaringenin (**3**) were observed by silica gel TLC plate.

3.6.4. Chemical chlorination of hesperetin

The biomimetic chlorination of hesperetin (200 mg) was performed under similar conditions as above. The dried residue was applied to silica gel GF_{254} with toluene-

Me_2CO (15:1) as eluant, yielding 6-chlorohesperetin (**8**) (9 mg). Trace amounts of 6,8-dichlorohesperetin (**7**) were observed by silica gel TLC plate.

Acknowledgements

This work was supported by grants from Graduate School Research Alumni, The Ohio State University, and National Science and Technology Development Agency, Thailand. We wish to thank Dr. Raymond W. Doskotch, College of Pharmacy, The Ohio State University, for his helpful suggestions and for the help with HMBC and COLOC experiments. Thanks are also given to Dr. David Chang, the Ohio State University chemical instrumentation, Miss Panit Wedkanjana and Mr. Witoon Ngow, Faculty of Science, Silpakorn University, for providing MS analysis.

References

Anyanwutaku, I.O., Zirbes, E., Rosazza, J.P.N., 1992. Isoflavonoids from streptomycetes: origins of genistein, 8-chlorogenistein, and 6,8-dichlorogenistein. Journal of Natural Products 55, 1498–1504.

Faber, K., 1992. Biotransformation in organic chemistry. Springer-Verlag, Germany.

Franssen, M.C.R., 1994. Halogenation and oxidation reactions with haloperoxidases. Biocatalysis 10, 87–111.

Franssen, M.C.R., van Boven, H.G., van der Plas, H.C., 1987. Enzymatic halogenation of pyrazoles and pyridine derivatives. Journal of Heterocyclic Chemistry 24, 1313–1316.

Hager, L.P., Morris, D.R., Brown, F.S., Eberwein, H., 1966. Chloroperoxidase II. Utilization of halogen anions. Journal of Biological Chemistry 241, 1769–1777.

Harborne, J.B., 1988. The Flavonoids advances in research since 1980. Chapman and Hall, London.

Ibrahim, A.R., Abul-Hajj, Y.J., 1990a. Microbiological transformation of chromone, chromanone, and ring A hydroxyflavones. Journal of Natural Products 53, 1471–1478.

Ibrahim, A.R., Abul-Hajj, Y.J., 1990b. Microbiological transformation of flavone and isoflavone. Xenobiotica 20, 363–373.

Ibrahim, A.R., Gatal, A.M., Mossa, J.S., El-Feraly, F.S., 1997. Glucose-conjugation of the flavones of *Psiadia arabica* by *Cunninghamella elegans*. Phytochemistry 46, 1193–1195.

Levine, S.D., Neidleman, S.L., Oberc, M., 1968. An enzymatic route to α-bromo steroidal ketones. Tetrahedron 24, 2979–2984.

Libby, R.D., Shedd, A.L., Phipps, A.K., Beachy, T.M., Gerstberger, S.M., 1992. Defining the involvement of HOCl or Cl_2 as enzyme-generated intermediates in chloroperoxidase-catalyzed reactions. The Journal of Bilological Chemistry 267, 1769–1775.

Smith, R.V., Rosazza, J.P., 1975. Microbial models of mammalian metabolism. Journal of Pharmaceutical Science, 1737–1759.

Shaw, P.D., Hager, L.P., 1959. Biological chlorination III. β-Ketoadipate chlorinase: a soluble enzyme system. Journal of Biological Chemistry 234, 2565–2569.

Wannstedt, C., Rotella, D., Siuda, J.F., 1990. Chloroperoxidase mediated halogenation of phenols. Bulletin of Environmental Contamination and Toxicology 44, 282–287.

Yamada, H., Itoh, N., Izumi, Y., 1985. Chloroperoxidase-catalyzed halogenation of *trans*-cinnamic acid and its derivatives. Journal of Biological Chemistry 260, 11962–11969.

PERGAMON

Phytochemistry 57 (2001) 349–359

PHYTOCHEMISTRY

www.elsevier.com/locate/phytochem

Purification and characterization of isoforms of β-galactosidases in mung bean seedlings

Sing-Chung Li [a], Jiahn-Wern Han [a], Kuan-Chung Chen [a], Ching-San Chen [a,b,*]

[a] *Graduate Institute of Agricultural Chemistry, National Taiwan University, Taipei 106, Taiwan*
[b] *Institute of Botany, Academia Sinica, Nankang, Taipei 115, Taiwan*

Received 17 April 2000; received in revised form 14 December 2000

Abstract

Five isoforms of β-galactosidase (EC 3.2.1.23), designated as β-galactosidases I–V, were isolated from five-day-old mung bean (*Vigna radiata*) seedlings. β-Galactosidases II and III were purified to electrophoretic homogeneity by a procedure involving acid precipitation, ammonium sulfate fractionation, chromatography on diethylaminoethyl-cellulose (DEAE-Cellulose) and con A-Sepharose, and chromatofocusing. β-Galactosidases I, II and III have the same molecular mass of 87 kDa, comprising two non-identical subunits with molecular masses of 38 and 48 kDa, while β-galactosidases IV and V have molecular masses of 45 and 73 kDa, respectively. All the enzymes were active against *p*-nitrophenyl-β-D-galactoside, and to a lesser extent, *p*-nitrophenyl-α-L-arabinoside and *p*-nitrophenyl-β-D-fucoside. The enzymes were inhibited by D-galactono-1,4-lactone, D-galactose, Hg^{2+}, Ag^{+} and sodium dodecyl sulfate (SDS). β-Galactosidases I, II and III were shown to be competitively inhibited by either D-galactono-1, 4-lactone or D-galactose. Isoforms I, II and III have a common optimal pH of 3.6, while isoforms IV and V have pH optima at 3.8 and 4.0, respectively. Isoelectric points of isoforms I, II and III were 7.7, 7.5 and 7.3, respectively. Double immunodiffusion analysis indicated that β-galactosidases I, II, III and V are immunologically similar to each other, while β-galactosidase IV shares partially identical antigenic determinants with the other four isoforms. The purified β-galactosidases II and III were capable of releasing D-galactose residue from the hemicellulose fraction isolated from mung bean seeds. © 2001 Elsevier Science Ltd. All rights reserved.

Keywords: *Vigna radiata*; Leguminosae; β-Galactosidase; Enzyme purification; Natural substrates

1. Introduction

β-Galactosidase (EC 3.2.1.23) is widely distributed in plant tissues. The enzyme has been implicated in a number of biological processes including plant growth and fruit ripening. One characteristic of fruit ripening and softening is the mobilization of cell wall components. The release of monomeric galactose from cell walls of ripening fruits has been described with apple, tomato, melon, avocado, kiwifruit and mango (Bartley, 1976; Pressey, 1983; Ranwala et al., 1992; Deveau et al., 1993; Ross et al., 1993; Ali et al., 1995). Molecular approaches were also used to unravel the role of β-galactosidases in fruit development and ripening. Ross et al. (1994) isolated a cDNA clone encoding an apple β-galactosidase. Northern blot analysis showed accumulation of a transcript homologous to the cDNA clone during fruit ripening. A cDNA clone, a member of the β-galactosidase gene family, was isolated from a cDNA library of tomato fruit. This cDNA showed ripening-related gene expression in normal fruits, with lower levels apparent in the non-softening mutants (Carey et al., 1995). Another cDNA, corresponding to β-galactosidase II of tomato, was also cloned. Northern blot analysis revealed that the β-galactosidase II gene transcript was detectable at the breaker stage of ripeness, maximum at the turning stage, and present at decreasing levels during the later stages of normal tomato fruit ripening (Smith et al., 1998).

The correlation of β-galactosidases with plant growth and development has also been investigated. This included the isolation and characterization of β-galactosidases from cowpea, nasturtium, radish, mung bean, barley, carrot, rice shoots and lupins (Biswas, 1987; Edwards et al., 1985, 1988; Sekimata et al., 1989; Kundu et al., 1990; Giannakouros et al., 1991; Konno and Katoh, 1992; Konno and Tsumuki, 1993; Buckeridge and Reid, 1994).

* Corresponding author. Tel.: +886-2-2789-9590, ext. 222, 251; fax: +886-2-2785-8936.
E-mail address: bocschen@ccvax.sinica.edu.tw (C.-S. Chen).

0031-9422/01/$ - see front matter © 2001 Elsevier Science Ltd. All rights reserved.
PII: S0031-9422(01)00022-X

We have found that the activities of some glycosidases in germinating mung bean seeds increased to a high level between days 4–6. β-*N*-Acetylglucosaminidase, β-galactosidase and α-mannosidase showed the highest specific activity. The increase of β-galactosidase activity during seed germination was also reported in plants such as pinto beans (Agrawal and Bahl, 1968), castor beans (Harley and Beevers, 1985), nasturtium (Edwards et al., 1988), barley (Giannakouros et al., 1991) and lupin (Buckeridge and Reid, 1994). The increase of β-galactosidase activity during the germination of barley seeds seems to be very moderate when compared with the many-fold increase in the activity of the same enzyme observed in the seeds of dicotyledon plants (Giannakouros et al., 1991). Thus, the developmental regulation of plant β-galactosidase during germination and growth has become evident. However, much less is known about the mechanism underlying this regulation. We investigated the structure and function of mung bean β-galactosidase as a first step towards studying its gene expression and regulation. This paper deals with the purification and characterization of five isoforms of β-galactosidase, and the activity of the two purified isoforms, II and III, of the enzyme towards cell wall polysaccharides of mung bean seeds. Separation by two-dimensional electrophoresis, followed by Western blot analysis of the two purified isoforms, II and III, as well as the immunological relationship of the five isoforms are also described.

2. Results

2.1. Purification

Acid precipitation removed a large portion of the contaminating proteins (about 65% of total proteins) in the cell-free extract, resulting in a 2.6-fold purification (Table 1). With the purification procedure shown in Scheme 1, five β-galactosidases, I–V, were isolated as summarized in Table 1 and Fig. 1. β-Galactosidases I, II and III, which did not bind to either DEAE-cellulose or Con A-Sepharose, were purified by chromatofocusing. β-Galactosidases II and III were purified to electrophoretic homogeneity after repeating chromatofocusing twice, and whereas a faint contaminating band ran ahead of β-galactosidase I in a non-denaturing gel (Fig. 2), it did not indicate the actual molecular weights. The β-galactosidase IV, retained on the DEAE-cellulose (Fig. 1A) and Con A-Sepharose columns (Fig. 1C), was eluted in sequence from the columns. The eluted β-galactosidase IV was shown to be still contaminated with many proteins in a non-denaturing gel (data not shown). Thus, β-galactosidase V, which bound to Con A-Sepharose (Fig. 1B), was purified with this column. The purified isoform V contained approximately equal amounts of a contaminating protein that moved slightly faster than the enzyme in a non-denaturing gel (data not shown). The overall recovery of the five β-galactosidase isoforms was about 34%.

2.2. Characteristics of β-galactosidases

The molecular masses of β-galactosidases I, II, III, IV and V, estimated from their elution volumes from Sephacryl S-200, were 87, 87, 87, 73 and 45 kDa, respectively (data not shown). However, β-galactosidases I, II and III showed mobilities corresponding to 300–400 kDa in a non-denaturing gel (Fig. 2). A possible explanation for this discrepancy is that, firstly, the enzyme with isoelectric points in the range 7.3–7.7 might form aggregates during their concentration in the stacking gel (pH 6.8). Secondly, these isoforms are likely to be glycoproteins in nature, because they bound to a Con A column when NaCl was eliminated from the elution buffer. SDS–PAGE of β-galactosidases I, II and III showed that each form consisted of two non-identical subunits

Table 1
Purification of β-galactosidases from five-day-old mung bean seedlings[a]

Step	Total protein (mg)	Total activity (units)	Specific activity (units/mg protein)	Purification (fold)	Yield (%)
Cell-free extract	11,206.0	645.5	0.0576	1.0	100
Acid precipitation	3946.3	580.2	0.15	2.6	89.9
Ammonium sulfate precipitation	2106.1	502.8	0.24	4.1	77.9
DE52 non-adsorbed	86.3	241.2	2.79	48.5	37.4
DE52 adsorbed	283.3	163.4	0.58	10.1	25.3
Con A non-adsorbed	5.4	139.1	25.76	447	21.5
Con A adsorbed (V)	12.9	45.9	3.65	63.4	7.1
Con A adsorbed (IV) (DE52 adsorbed)	33.2	51.8	1.56	27.1	8.1
Chromatofocusing					
I	0.48	19.1	39.79	691	2.96
II	0.51	48.7	95.49	1657	7.54
III	0.58	55.5	95.69	1661	8.59

[a] A total of 4.1 kg of mung bean seedlings was used for the purification. Roman numerals I–V stand for β-galactosidases I–V, respectively.

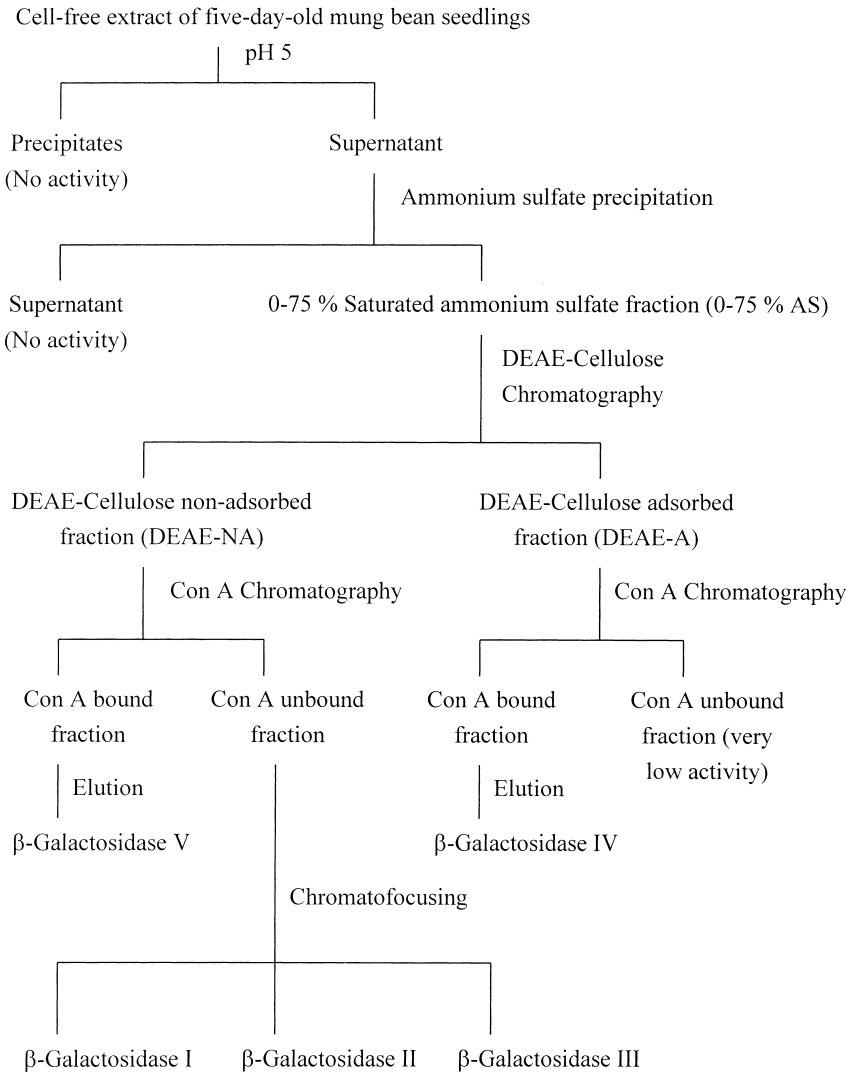

Scheme 1.

with molecular masses of 38 and 48 kDa (Fig. 3). Since the SDS–PAGE provided only a rough estimation of molecular mass, these two figures (38 and 48 kDa) were more accurately determined by running these two subunits through 0.1% SDS polyacrylamide gradient gel (10–20%) along with molecular weight standard proteins (data not shown). Two proteins bands, approximately 22 and 30 kDa, were also observed in β-galactosidase I and were probably due to contaminating proteins in the enzyme preparation (Fig. 3).

Effects of sugars and sugar derivatives on β-galactosidases I, II and III are shown in Table 2. D-Galacto-1,4-lactone was the most potent inhibitor followed by D-galactose and lactose. D-Galacto-1, 4-lactone at 12.5 mM almost completely inhibited the three isoforms (97.7–98.3% inhibition). The three isoforms were 71–72% inhibited by 50 mM D-Galactose, 26–28% inhibited by 50 mM lactose and slightly inhibited by 12.5 mM D-glucono-δ-lactone. D-Arabinose and D-fucose at 50 mM had no effect on the three enzymes. A kinetic analysis indicated that D-galactono-1, 4-lactone and D-galactose acted as competitive inhibitors. K_i values for these two competitive inhibitors were determined by replots of data taken from double reciprocal plots. D-Galacto-1, 4-lactone has K_i values of 0.13, 0.085 and 0.17 mM for isoforms I, II and III, respectively, while D-galactose has K_i values of 11.4, 15 and 13 mM for I, II and III, respectively. The three isoforms have a common optimal pH of 3.6. Isoforms IV and V have pH optima at 4.0 and 3.8, respectively (Fig. 4). Isoforms I, II and III have temperature optima around 50–53°C (Fig. 5) and isoelectric points of 7.7, 7.5 and 7.3, respectively. All of the isoforms were stable from pH 4.0 to 8.0. Effects of metallic ions, EDTA, and SDS on β-galactosidase activities are shown in Table 3. Ag^+, Hg^{2+} and SDS at 1 mM strongly inhibited the activities of isoforms I, II and III. The cell-free extract was active against 12 *p*-nitrophenyl glycosides tested. After purification, isoforms II and III retained the activities of β-galactosidase, β-D-fucosidase and α-L-arabinosidase, but were essentially devoid of activity

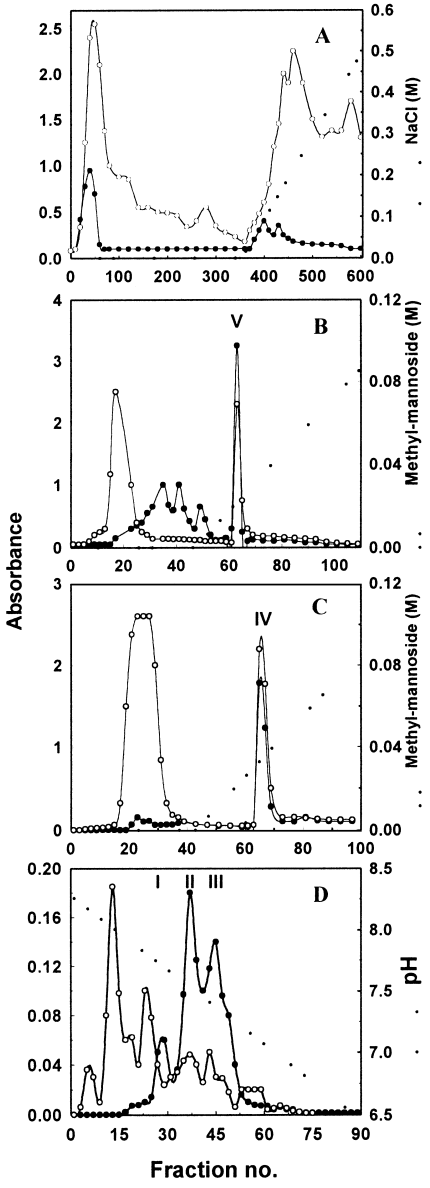

Fig. 1. Elution profiles of β-galactosidases on DEAE-cellulose columns (A), Con A-Sepharose columns (B, C) and chromatofocusing (D). The ammonium sulfate precipitated enzyme sample was applied to a DEAE-cellulose column (A). The DEAE-cellulose non-adsorbed fraction containing β-galactosidases I, II, III and V, and the adsorbed fraction (β-galactosidase IV), were then purified by Con A-Sepharose chromatography (B, C). The Con A-Sepharose adsorbed fraction is called β-galactosidase V. The non-adsorbed fraction containing β-galactosidases I, II and III was further purified by chromatofocusing. Experimental details are given in the Experimental section. Protein is expressed as absorbance at 280 nm (○) and β-galactosidase activity as absorbance at 420 nm (●).

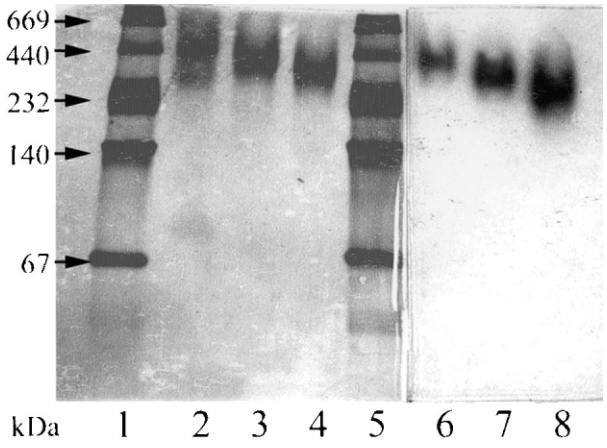

Fig. 2. The electrophoretic pattern of purified β-galactosidases I, II and III. After electrophoresis of the native enzymes (ca 5 μg protein each), the left half of the gel (lanes 1–5) was stained with silver nitrate, and the right half (lanes 6–8), with activity staining. Lanes 1 and 5, molecular mass markers from top: thyroglobulin (669 kDa), ferritin (440 kDa), catalase (232 kDa), lactate dehydrogenase (140 kDa) and bovine serum albumin (67 kDa); lanes 2 and 6, β-galactosidase I; lanes 3 and 7, β-galactosidase II; lanes 4 and 8, β-galactosidase III.

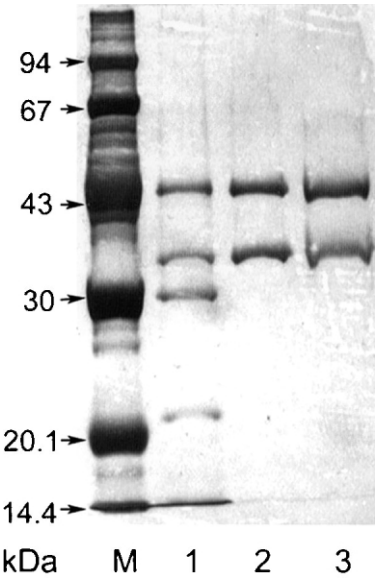

Fig. 3. SDS–PAGE of purified β-galactosidases I, II and III. Molecular mass markers from top: phosphorylase b (94 kDa), bovine serum albumin (67 kDa), ovalbumin (43 kDa), carbonic anhydrase (30 kDa), trypsin inhibitor (20.1 kDa) and α-lactalbumin (14,4 kDa). The numbers 1, 2 and 3 stand for β-galactosidases I, II and III, respectively. The gel was stained with silver nitrate.

towards the nine other *p*-nitrophenyl glycosides (less than 5%) (Table 4). Ratios of the activities of β-D-galactosidase, β-D-fucosidase and α-L-arabinosidase exhibited by isoforms II and III are 100, 35.7, 32.7% and 100, 31.2, 24.6%, respectively. Plant β-galactosidases with multiple glycosidase activities have been described (Conchie et al., 1968; Kiss et al., 1981; Simos and Georgatsos, 1988). Since β-galactosidases II and III were purified to apparent homogeneity, cross-contamination from other glycosidases seems unlikely. Therefore, it is reasonable to suggest that the three glycosidase activities mentioned above reside in a single molecular species of β-galactosidases II and III.

Table 2
Effects of sugars and sugar derivatives on β-galactosidase activities[a]

	β-Galase activity (nkatals)		
	I	II	III
No inhibitor	3.76×10^{-2} (100%)	3.87×10^{-2} (100%)	4.41×10^{-2} (100%)
D-Galactono-1,4-lactone (12.5 mM)	8.35×10^{-4} (2.2%)	6.68×10^{-4} (1.7%)	1.0×10^{-3} (2.3%)
D-Glucono-δ-lactone (12.5 mM)	3.46×10^{-2} (92%)	3.44×10^{-2} (89%)	3.74×10^{-2} (85%)
D (+) Arabinose (50 mM)	3.72×10^{-2} (99%)	3.67×10^{-2} (95%)	4.28×10^{-2} (97%)
D (+) Fucose (50 mM)	3.64×10^{-2} (97%)	3.64×10^{-2} (94%)	4.19×10^{-2} (95%)
D (+) Galactose (50 mM)	1.05×10^{-2} (28%)	1.12×10^{-2} (29%)	1.24×10^{-2} (28%)
Lactose (50 mM)	2.71×10^{-2} (72%)	2.87×10^{-2} (74%)	3.22×10^{-2} (73%)

[a] Sugars and sugar derivatives at a final concentration of 12.5 or 50 mM were pre-incubated with appropriate amount of enzyme in 50 mM sodium citrate buffer (pH 3.6) at 37°C for 10 min. PNP-β-D-galactopyranoside was then added to the mixture to assay the enzyme activity.

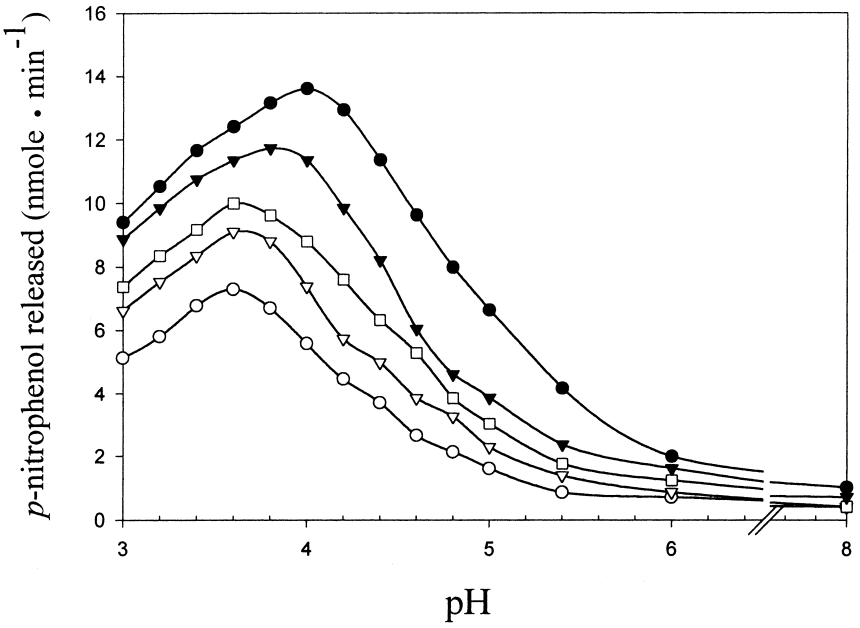

Fig. 4. Effect of pH on the purified β-galactosidases. McIIValine buffer (pH 3–6) and Na-phosphate buffer (pH 7–8) were used. The purified β-galactosidases I (○), II (▽), III (□), IV (●) and V (▼) were assayed at various pH by the method given in Experimental.

2.3. Immunochemical study

In order to investigate immunological relationships of the five isoforms of mung bean β-galactosidase, antisera were raised against the purified β-galactosidases II and III. Ouchterlony double immunodiffusion analysis indicated that all five β-galactosidase isoforms cross-reacted with anti β-galactosidase II antiserum (antiserum II) (Fig. 6A). The same result was obtained when anti β-galactosidase III antiserum (antiserum III), instead of antiserum II, was used (Fig. 6B). A spur was shown between the purified β-galactosidase IV and either β-galactosidase III or V. These results suggest that β-galactosidases I, II, III and V are immunologically similar to each other, while β-galactosidase IV shares partially identical antigenic determinants with the other four isoforms. In the purification of these β-galactosidases, isoform IV was the only β-galactosidase bound to the DEAE-cellulose column equilibrated at a pH of 7.2 (Fig. 1A). The charge difference on the surface of isoform IV may in part account for its different immunological properties as compared with the other four isoforms.

Purified isoforms II and III were separated with two-dimensional electrophoresis using the method of O'Farrell (1975) and probed with antiserum II or III. The 2-D electrophoresis gel of isoform II is shown in Fig. 5. Similar results were obtained with isoform III. The results indicated that both isoforms II and III consisted of two groups of polypeptides with molecular masses of 38 and 48 kDa, the former containing at least six polypeptides and the latter four. The results are in accord with the finding that β-galactosidases II and III consist of two non-identical subunits (Fig. 3). The results also suggest that β-galactosidases in mung bean may be encoded by a multiple gene family. The β-galactosidases purified from cotyledons of mung bean

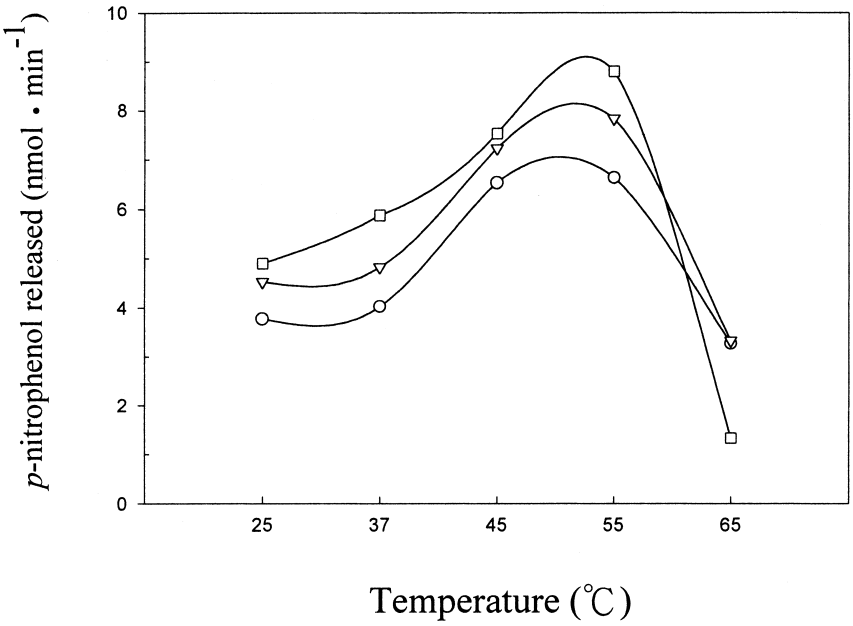

Fig. 5. Temperature optima of β-galactosidases I, II and III. Enzyme activities of the purified β-galactosidases I (○), II (▽) and III (□) were assayed at various temperatures by the method given in the Experimental.

Table 3
Effect of metal ions, EDTA and SDS on β-galactosidase activities

	β-Galase activity (nkatals)		
	I	II	III
Control	4.43×10^{-2} (100%)	3.17×10^{-2} (100%)	4.81×10^{-2} (100%)
Fe^{2+}	3.76×10^{-2} (84.9%)	2.79×10^{-2} (87.9%)	4.19×10^{-2} (87.2%)
Ag^{2+}	3.67×10^{-3} (8.3%)	4.01×10^{-3} (12.6%)	2.34×10^{-3} (4.9%)
Hg^{2+}	2.17×10^{-3} (4.9%)	1.67×10^{-3} (5.3%)	4.34×10^{-3} (9%)
Ca^{2+}	3.76×10^{-2} (84.9%)	2.79×10^{-2} (87.9%)	4.19×10^{-2} (87.2%)
Cu^{2+}	3.39×10^{-2} (76.6%)	3.06×10^{-2} (96.3%)	4.04×10^{-2} (84%)
Mn^{2+}	3.49×10^{-2} (78.9%)	3.14×10^{-2} (98.9%)	4.79×10^{-2} (99.7%)
Mg^{2+}	3.74×10^{-2} (84.5%)	3.26×10^{-2} (102.6%)	4.73×10^{-2} (98.3%)
Zn^{2+}	4.46×10^{-2} (100.8%)	2.94×10^{-2} (92.6%)	4.86×10^{-2} (101%)
SDS	6.68×10^{-4} (1.5%)	8.35×10^{-4} (2.6%)	3.17×10^{-3} (6.6%)
EDTA	4.02×10^{-2} (90.9%)	3.06×10^{-2} (96.3%)	4.86×10^{-2} (101%)

Table 4
Enzyme activities of the purified β-galactosidases towards various *p*-nitrophenyl glycoside substrates

	β-Galase activity (nkatals)				
Substrate	I	II	III	IV	V
PNP-β-D-galactopyranoside	9.87×10^{-2} (100%)	1.22×10^{-1} (100%)	1.31×10^{-3} (100%)	1.65×10^{-1} (100%)	1.54×10^{-1} (100%)
PNP-α-L-arabinopyranoside	1.99×10^{-2} (20.1%)	4.01×10^{-2} (32.7%)	3.21×10^{-2} (24.6%)	2.07×10^{-2} (12.5%)	2.86×10^{-2} (18.5%)
PNP-β-D-fucopyranoside	2.72×10^{-2} (27.6%)	4.38×10^{-2} (35.7%)	4.07×10^{-2} (31.2%)	2.45×10^{-2} (14.8%)	4.04×10^{-2} (26.2%)
PNP-α-D-mannopyranoside	6.68×10^{-4} (0.70%)	1.67×10^{-3} (1.4%)	5.01×10^{-4} (0.4%)	8.18×10^{-2} (49.4%)	8.35×10^{-4} (0.5%)
PNP-β-D-mannopyranoside	6.68×10^{-4} (0.7%)	1.0×10^{-3} (0.8%)	8.35×10^{-4} (0.6%)	7.01×10^{-3} (4.2%)	8.35×10^{-4} (0.5%)
PNP-α-D-glucopyranoside	1.12×10^{-2} (11.3%)	6.01×10^{-3} (4.9%)	2.67×10^{-3} (2.0%)	1.34×10^{-2} (8.1%)	1.05×10^{-2} (6.8%)
PNP-β-D-glucopyranoside	1.34×10^{-3} (1.4%)	1.17×10^{-3} (1.0%)	4.68×10^{-3} (3.6%)	7.35×10^{-3} (4.4%)	2.51×10^{-3} (1.6%)
PNP-*N*-acetyl-β-D-glucosaminide	2.0×10^{-3} (2.0%)	5.85×10^{-3} (4.8%)	1.84×10^{-3} (1.4%)	1.72×10^{-2} (10.4%)	2.17×10^{-3} (1.4%)
PNP-β-D-xylopyranoside	1.5×10^{-3} (1.5%)	2.67×10^{-3} (2.2%)	2.17×10^{-3} (1.7%)	7.85×10^{-3} (4.7%)	3.51×10^{-3} (2.3%)
PNP-α-D-galactopyranoside	2.0×10^{-3} (2.0%)	3.67×10^{-3} (3.0%)	1.0×10^{-3} (0.8%)	6.51×10^{-3} (3.9%)	2.17×10^{-3} (1.4%)
PNP-α-L-fucopyranoside	1.34×10^{-3} (1.4%)	1.34×10^{-3} (1.1%)	1.5×10^{-3} (1.2%)	7.68×10^{-3} (4.6%)	2.51×10^{-3} (1.6%)
PNP-β-D-glucuronide	4.68×10^{-3} (4.7%)	4.68×10^{-3} (3.8%)	1.0×10^{-3} (0.8%)	2.59×10^{-3} (15.6%)	9.85×10^{-3} (64.0%)

Table 5
Activity of the purified β-galactosidases II and III toward cell wall polysaccharides of mung bean seeds[a]

Substrate	Enzyme activity (mkatals/kg)		
	Cell-free extract	Galase II	Galase III
Hot water soluble pectin	23.5±0.67	7114.2±2120.9	4024.7±317.3
Oxalate soluble pectin	18.2±1.0	7732.1±3406.8	1553.1±33.4
4% KOH soluble hemicellulose	71.0±9.0	16,082.1±3089.5	14,228.4±935.2
24% KOH soluble hemicellulose	74.5±9.0	24,114.8±2872.4	22,261.1±2471.6
Xyloglucan	18.2±0.3	12,057.4±1553.1	12,675.3±935.2
Lactose	103.7±9.0	92,785.2±8032.7	159,585.2±3089.5

[a] Experimental conditions are given in Experimental. Enzyme activity is expressed as μmol of D-galactose liberated per min per mg protein. The data are expressed as mean ± S.D. from three determinations.

were previously shown to be homodimers (Kundu et al., 1990). A question arises whether the 38 kDa subunit is the degradation product of the 48 kDa subunit. To clarify this point, cell-free extracts of the 5-day-old germinated mung bean seeds, the supernatant fraction of acid (pH 5.0) precipitated fraction and 0–70% saturated ammonium sulfate of the cell-free extract were separated by SDS–PAGE and subjected to Western blot analysis. The results showed that all three samples exhibited two polypeptides with molecular masses corresponding to 38 and 48 kDa, which cross-reacted with antiserum II (data not shown).

2.4. Degradation of cell wall polysaccharides by β-galactosidases II and III

β-Galactosidase activity was determined during the course of mung bean germination. The enzyme activity increased from day 1 after imbibition in the dark, approached a high level around day 5 and remained about the same until day 9 (data not shown). To understand whether β-galactosidases II and III potentially participate in the mobilization of cell wall polysaccharides, the two purified enzymes and cell-free extract were examined for their hydrolytic activity towards cell wall polysaccharides isolated from mung bean seeds.

The results indicated that both β-galactosidases II and III were capable of releasing monomeric galactose from the cell wall polysaccharides in vitro (Table 5). Rates of galactose liberation by β-galactosidase II were high with 4 and 24% KOH soluble hemicellulose as substrates, and moderate with xyloglucan, hot water soluble and oxalate soluble pectins. While exhibiting high activity towards 24 and 4% KOH soluble hemicellulose and xyloglucan similar to β-galactosidase II, β-galactosidase III showed relatively lower activity on hot water soluble and oxalate soluble pectin. The cell-free extract exhibited higher activity on 24 and 4% KOH soluble hemicellulose than the other cell wall polysaccharides. The release of monomeric D-galactose from 4 or 24% KOH soluble hemicellulose by purified β-galactosidase II amounted to 2.5–2.6 μg after prolonged incubation for more than 6 h. This is approximately equivalent to 3.3–3.5% of total polysaccharides (75 μg) in the reaction mixture. Purified β-galactosidase III gave similar results (data not shown). Both enzymes also have high activity against lactose (Table 5). Thus, purified β-galactosidases II and III were capable of efficiently releasing D-galactose residue from the hemicellulose fraction in vitro.

3. Discussion

In this report, we have isolated and characterized five isoforms of β-galactosidase from etiolated mung bean seedlings. β-Galactosidases II and III were purified to electrophoretic homogeneity, while I, IV and V were partially purified. Optimal pH (3.6–4.0) and temperature (50–53°C), isoelectric points (7.3–7.7) and molecular mass (87, 87, 87, 73, 45 kDa) of these enzymes were comparable with those of other plant β-galactosidases previously described (Li et al., 1975; Biswas, 1987; Edwards et al., 1988; Kundu et al., 1990), with the exception that the β-galactosidase isolated from mature seeds of mung bean had molecular masses of 162 kDa (Dey, 1984).

The results of SDS–PAGE (Fig. 3) and two-dimensional electrophoresis (Fig. 5) indicate that β-galactosidases II and III are composed of two non-identical subunits (38 and 48 kDa). Fig. 7 also shows that the 38 and 48 kDa

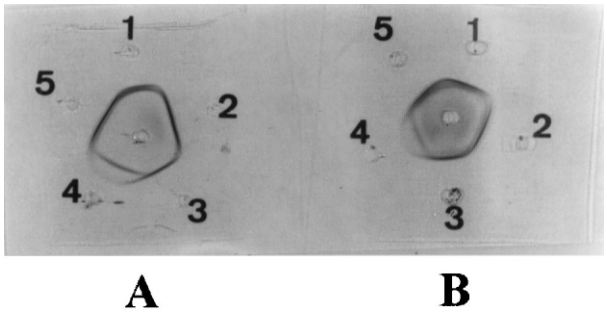

Fig. 6. Double immunodiffusion analysis of β-galactosidases I–V. Panel A: centre well, anti β-galactosidase II antiserum; wells 1–5, the purified β-galactosidases I–V, respectively. Panel B: centre well, anti β-galactosidase III antiserum; wells 1–5, the same as panel A.

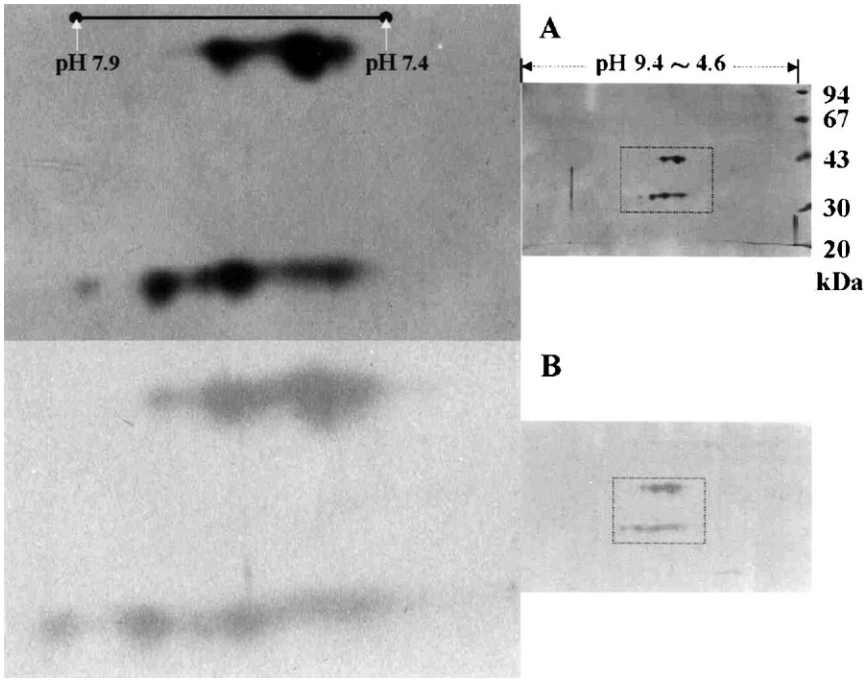

Fig. 7. Two-dimensional gel electrophoresis of β-galactosidase II. A, silver staining; B, Western blotting. The areas marked with dotted lines are enlarged at left.

subunits were further separated into six and four polypeptides, respectively, which differed only in isoelectric point values. These results, together with the previous reports (Simos et al., 1989; Giannakouros et al., 1991), suggest that the multiplicity of plant β-galactosidases was at least in part due to different isoelectric point values.

It has been suggested that β-galactosidases play a vital role in plant growth and development, the β-galactosidases described here, which are capable of efficiently hydrolysing the hemicellulose fractions of mung bean seeds (Table 5), are apparently similar to a number of broad specificity β-galactosidases found in cotyledons and germinated seeds. The mung bean β-galactosidases are developmentally regulated as suggested by the finding that the activity of the β-galactosidases rapidly increased to a high level between day 4 and day 6 of germination. Our results, together with the previous findings (Edwards et al., 1985; Konno and Tsumuki, 1993), suggest that a number of β-galactosidases differing in substrate specificities are synthesized or activated to mobilize, or modify cell wall components during seed germination and plant growth, and that the temporal expression of the β-galactosidase genes are subjected to developmental regulation.

4. Experimental

4.1. Plant material and enzyme source

Mung bean seeds (*Vigna radiata* VC 3890 Sel No. 5) were submerged in distilled water at 25°C for 2 h and surface-sterilized with 0.5% hydrogen peroxide, thoroughly washed with H_2O and germinated in the dark at 28°C. Five-day-old germinated seeds were thoroughly washed with ice-cold H_2O and homogenized with Polytron (Kinematica) in 50 mM Tris–HCl (pH 7.2) containing 10 mM 2-mercaptoethanol and 1 mM EDTA. Unless otherwise indicated, all steps and the purification procedure were conducted at 5°C. The resultant slurry was squeezed through three layers of cheesecloth, phenyl methylsulphonyl fluoride (PMSF) was added at a final concentration of 1 mM, and centrifuged at 12,800×*g* for 30 min. The supernatant was dialysed against the same buffer solution containing 1 mM PMSF. The dialysed enzyme solution was referred to as cell-free extract.

4.2. Enzyme purification

The overall procedure for the purification of mung bean β-galactosidases is shown in Scheme 1. The cell-free extract was adjusted to a pH of 5.0 to precipitate large amounts of contaminating proteins, while retaining most of the β-galactosidase activity in the supernatant. Solid ammonium sulfate was added to the supernatant to obtain a 0–75% saturated ammonium sulfate fraction, which contained most of the β-galactosidase activity. The 0–75% saturated ammonium sulfate fraction was applied to a DE-52 column. Both DEAE-cellulose adsorbed (DEAE-A) and non-adsorbed (DEAE-NA) fractions were shown to contain β-galactosidase activity. These two fractions, therefore, were further subjected to Con A affinity column chromatography. After

Con A chromatography, almost all of the β-galactosidase activity in the DEAE-A was recovered in the Con A bound fraction. The β-galactosidase eluted from this column is named β-galactosidase IV. On the other hand, β-galactosidase activity in the DEAE-NA was separated into Con A bound and Con A unbound fractions. The former was eluted as a single protein peak that is called β-galactosidase. The latter was further separated into three activity peaks by chromatofocusing. These three isoforms were called β-galactosidases I, II and III, based on the order of their emergence from the column. β-Galactosidases II and III were purified to apparent homogeneity by repeated chromatofocusing on the same column. The experimental conditions for each purification step are described as follows.

The cell-free extract was adjusted to pH 5.0 with 3.5 M acetic acid, allowed to stand at 5°C for 2 h, and the precipitates were removed by centrifugation. Solid ammonium sulfate was added to the supernatant until 75% saturation was reached. The sample obtained from 75% saturated ammonium sulfate precipitation was redissolved in a small volume of 10 mM Tris–HCl (pH 7.2) containing 10 mM 2-mercaptoethanol (Buffer A), dialysed overnight against the same buffer solution and applied to a DEAE-cellulose (DE-52, Whatman) column (4.4×15 cm) previously equilibrated with Buffer A. The column was washed with 10 volume of Buffer A and eluted with a linear gradient (2 l total volume) of 0–0.5 M NaCl in 10 mM Tris–HCl (pH 7.2) containing 10 mM 2-mercaptoethanol. Fractions of 8 ml each were collected at a flow rate of 2 ml/min. Active fractions were pooled and concentrated using an Amicon ultrafiltration device (Ya 1000 membrane). This sample was called the DEAE-cellulose adsorbed fraction (DEAE-A). The column washing solution that still had β-galactosidase activity was concentrated and referred to as the DEAE-cellulose non-adsorbed fraction (DEAE-NA).

For purification of the DEAE-NA, Con A-Sepharose column (2.6×10 cm) was equilibrated with 20 mM Tris–HCl buffer (pH 7.2) containing 0.3 M NaCl, 1 mM $CaCl_2$ and 1 mM $MnCl_2$ (Con A affinity buffer). The DEAE-NA were pooled, concentrated with the Amicon ultrafiltration device, and dialysed against the Con A affinity buffer. The non-dialysable solution was placed on the Con A-Sepharose column. After washing with the Con A affinity buffer, the column was eluted with a linear gradient (250 ml total volume) of 0–0.2 M α-methylmannoside in 20 mM Tris–HCl (pH 7.2) containing 0.3 M NaCl. Fractions of 6 ml were collected. It was found that the effluent and washing showed β-galactosidase activity that had not bound to Con A-Sepharose under the chromatographic conditions used. The fractions exhibiting β-galactosidase activity in the effluent and washing were pooled and designated as a Con A-Sepharose non-adsorbed fraction that was shown to contain β-galactosidases I, II and III. β-Galactosidase V bound on Con A-Sepharose was eluted from the column.

The DEAE-A was also purified with the Con A-Sepharose column. The procedure was essentially as described above except that the column was equilibrated with 20 mM Tris–HCl (pH 7.2) containing 1 M NaCl. There was no detectable β-galactosidase activity in the washing solution and effluent. The protein peak that coincidentally came off the column with β-galactosidase activity after elution was referred to as β-galactosidase IV.

The Con A-Sepharose non-adsorbed fraction containing β-galactosidases I, II and III was concentrated to 3–4 ml and purified by chromatofocusing according to the instruction manual of Pharmacia. Polybuffer Exchanger PBE 94 (Pharmacia) column (1.0×15 cm) was equilibrated with 25 mM Tris–HCl (pH 8.3). Polybuffer 96 (Pharmacia) was diluted 13-fold with deionized water and adjusted to pH 6.8 with 6 M HCl (eluent). Eighteen milliliters of the eluent was introduced to the column to create a pH gradient from 6.8 (top) to 8.3 (bottom). The concentrated enzyme solution was dialysed against the eluent and placed on the column. β-Galactosidases I, II and III were eluted in this order from the column with 90 ml of the eluent. In order to obtain homogeneous enzyme, chromatofocusing was conducted twice more for each β-galactosidase peak.

4.3. Enzyme assays

β-Galactosidase activity was determined by measuring the release of *p*-nitrophenol from *p*-nitrophenyl (PNP)-β-D-galactopyranoside according to the method of Agrawal and Bahl (1968). The reaction mixture contained, in a final volume of 0.5 ml, 50 mM sodium citrate buffer (pH 3.6), 5 mM substrate, and varying amounts of enzyme. The reactions were carried out at 37°C for 10 min. Liberated *p*-nitrophenol was measured spectrophotometrically at 420 nm after stopping the reaction with the addition of 0.7 ml of 0.2 M sodium carbonate. Absorbance (A_{420}) was proportional to the amount of enzyme in the reaction mixture under the assay conditions. The absorbance, A_{420}, was also linear with time within the amounts of enzyme used. One unit of β-galactosidase is defined as the amount that hydrolyses 1 μmol of PNP-β-D-galactopyranoside per min at pH 3.6 and 37°C. One katal is defined as the amount of β-galactosidase that hydrolyses 1 mol of PNP-β-D-galactopyranoside per second under the same condition. Other glycosidase activities were determined by the use of the respective PNP-glycoside. The reaction conditions were essentially the same as those described above.

Release of D-galactose from cell wall polysaccharides was determined using β-D-galactose dehydrogenase (Sigma) (Kurz and Wallenfels, 1974). Protein concentration was determined by the methods of Bradford (1976) using bovine serum albumin as a standard.

4.4. Preparation of cell walls

Cell walls of mung bean seeds were prepared according to the method described by Jarvis et al. (1981). Mung bean seeds were homogenized in ice-cold H_2O (5 l/kg) containing 5 g/l sodium deoxycholate and 10 g/l *n*-octanol in a Waring blender. The homogenate was filtered through three layers of cheesecloth and washed on a 120-mesh sieve with ice-cold H_2O (4 l/kg). The crude cell walls were suspended in distilled water (650 ml/kg), homogenized for 2 min with Polytron (Kinematica) and washed with distilled water (8 l/kg). The homogenization and sieving was repeated until no more starch grains were released. Lipids were removed by stirring with 800 ml/kg chloroform–methanol (1:1/v:v), and the cell walls removed by filtration and freeze-dried.

4.5. Cell wall fractionation

The dry cell walls were sequentially extracted with hot water, 0.25% ammonium oxalate-oxalic acid, 4% KOH and 24% KOH by the method of Kato and Matsuda (1976). Xyloglucan was prepared from mung bean seeds according to the procedure previously described (Edwards et al., 1985).

4.6. Degradation of cell wall polysaccharides

Each of the two pectic fractions (hot water and oxalate soluble fractions), the two hemicellulosic fractions (4% KOH and 24% KOH soluble fractions), and xyloglucan obtained above was dissolved in 0.2 M sodium citrate buffer (pH 3.6) at a final concentration of 1.5 mg/ml and used as substrate for purified β-galactosidases II and III, and the cell-free extract. The reaction mixture contained, in a final volume of 0.83 ml, 75 μg substrate and an appropriate amount of enzyme or cell-free extract. The reaction mixture was incubated at 37°C and aliquots were taken at various intervals for determination of D-galactose with galactose dehydrogenase (Kurz and Wallenfels, 1974).

4.7. Preparation of antisera

Purified β-galactosidases II and III, which are homogeneous on disc polyacrylamide gel electrophoresis, were used as the antigens. Two rabbits were injected subcutaneously four times with 150–180 μg each of β-galactosidases II and III emulsified with Freund's complete adjuvant. Intervals between injections were 2–3 weeks. The rabbits were killed one month after the final injection. The blood clots were centrifuged and the clear serum lyophilized and stored at −70°C.

4.8. Immunological methods

Ouchterlony double immunodiffusion was performed at room temperature in a 2% agarose gel as previously described (Ouchterlony and Nilsson 1973). Western blot analysis was performed according to the method of Burnette (1981) with some modification.

4.9. Electrophoresis

Purified β-galactosidases were analysed by electrophoresis in non-denaturing conditions using 4% acrylamide stacking gel and 5–20% acrylamide gradient separating gel (Hames, 1981), SDS–PAGE (Laemmli, 1970) and two-dimensional electrophoresis (O'Farrell, 1975). Proteins were stained with 0.2% (w/v) Coomassie Brilliant Blue R-250 or silver nitrate (Blum et al., 1987). Activity staining of β-galactosidase was performed according to the method described by Spielman and Mowshowitz (1982) using 6-bromo-2-naphthy-β-D-galactoside (Sigma) as a substrate.

4.10. Enzyme characterization

The molecular mass of the native β-galactosidases were determined by gel filtration on a Sephacryl S-200 column (1.6×90 cm). The column was calibrated with Blue Dextran and standard proteins (ribonuclease A, chymotrypsinogen A, ovalbumin, albumin, aldolase, catalase, ferritin, and thyroglobulin) (Sigma). The molecular mass of the denatured enzymes was estimated by SDS–PAGE. The pH optima of the purified enzymes against PNP-β-D-galactopyranoside was determined in McII-Valine buffer covering a pH range of 3–6 and Na-phosphate buffer covering a pH range of 7–8. The isoelectric point of the purified enzyme was estimated from the elution profile of chromatofocusing. In the inhibition study of β-galactosidase activity by sugars, sugar derivatives, metallic ions and SDS, β-galactosidase was preincubated for 10 min at 37°C with each compound or metallic ion at a concentration of 1 mM (for metallic ion and SDS) or 12.5 mM (for sugar and sugar derivatives), then assayed as normal. In order to understand the mechanism of inhibition of β-galactosidase, either by D-galactono-(1→4)-lactone or by D-galactose, β-galactosidase activity was assayed in the presence of varying concentrations of the inhibitor. The data were analysed with a double reciprocal plot.

Acknowledgements

This work was financially supported by the National Science Council, ROC, under the grant NSC 84-2311-B-001-044.

References

Agrawal, K.M., Bahl, O.P., 1968. Glycosidases of *Phaseolus vulgaris*. II. Isolation and general properties. Journal of Biological Chemistry 243, 103–111.

Ali, Z.M., Armugam, S., Lazan, H., 1995. β-Galactosidase and its significance in ripening mango fruit. Phytochemistry 38, 1109–1114.

Bartley, I.M., 1976. Changes in the glucans of ripening apples. Phytochemistry 15, 625–626.

Biswas, T.K., 1987. Characterization of β-galactosidase from the germinating seeds of *Vigna sinensis*. Phytochemistry 26, 359–364.

Blum, H., Beier, H., Gross, H.J., 1987. Improved silver staining of plant proteins, RNA and DNA in polyacrylamide gels. Electrophoresis 8, 93–99.

Bradford, M.M., 1976. A rapid and sensitive method for the quantification of microgram quantities of protein utilizing the principles of protein-dye binding. Analytical Biochemistry 72, 248–254.

Buckeridge, M.S., Reid, J.S.G., 1994. Purification and properties of a novel β-galactosidase or exo-(1→4)-β-D-galactanase from the cotyledons of germinated *Lupinus angustifolius* L. seeds. Planta 192, 502–511.

Burnette, W.N., 1981. "Western Blotting": electrophoretic transfer of protein from sodium dodecyl sulfate polyacrylamide gels to unmodified nitrocellulose and radiographic detection with antibody and radioiodinated protein A. Analytical Biochemistry 112, 195–203.

Carey, A.T., Holt, K., Picard, S., Wilde, R., Tucker, G.A., Bird, C.R., Schuch, W., Seymour, G.B., 1995. Tomato exo-(1→4)-β-D-galactanase. Plant Physiology 108, 1099–1107.

Conchie, J., Gelman, A.L., Levvy, G.A., 1968. Inhibition of glycosidases by aldonalactones of corresponding configuration. Biochemical Journal 106, 135–140.

Deveau, E.J.I., Gross, K.C., Huber, D.J., Watada, A.E., 1993. Degradation and solubilization of pectin by β-galactosidase purified from avocado mesocarp. Physiologia Plantarum 87, 279–285.

Dey, P.M., 1984. Occurrence of glycoprotein glycosidases in mature seeds of mung bean (*Vigna radiata*). Phytochemistry 23, 257–260.

Edwards, M., Bowman, Y.J.L., Dea, I.C.M., Reid, J.S.G., 1988. A β-D-galactosidase from nasturtium (*Tropaeolum majus* L.) cotyledons. Journal of Biological Chemistry 22, 4333–4337.

Edwards, M., Dea, I.C.M., Bulpin, P.V., Reid, J.S.G., 1985. Xyloglucan (amyloid) mobilization in the cotyledons of *Tropaeolum majus* L. seeds following germination. Planta 163, 133–140.

Giannakouros, T., Karagiorgos, A., Simos, G., 1991. Expression of β-galactosidase multiple forms during barley (*Hordeum vulgare*) seed germination. Separation and characterization of enzyme isoforms. Physiologia Plantarum 82, 413–418.

Hames, B.D., 1981. An introduction to polyacrylamide gel electrophoresis. In: Gel Electrophoresis of Proteins. A Practical Approach. pp. 1–86.

Harley, S.M., Beevers, H., 1985. Characterization and partial purification of three galactosidases from castor bean endosperm. Phytochemistry 24, 1459–1464.

Jarvis, M.C., Hall, M.A., Threlfall, D.R., Friend, J., 1981. The polysaccharide structure of potato cell walls: chemical fractionation. Planta 152, 93–100.

Kato, Y., Matsuda, K., 1976. Prescence of a xyloglucan in the cell wall of *Phaseolus aureus* hypocotyls. Plant and Cell Physiology 17, 1185–1198.

Kiss, L., Berki, L.K., Nanasi, P., 1981. Evidence for a single catalytic and two binding sites in the almond emulsin β-D-glucosidase molecule. Biochemical and Biophysical Research Communicator 98, 792–799.

Konno, H., Katoh, K., 1992. An extracellular β-galactosidase secreted from cell suspension cultures of carrot. Its purification and involvement in cell wall polysaccharide hydrolysis. Physiologia Plantarum 85, 507–514.

Konno, H., Tsumuki, H., 1993. Purification of a β-galactosidase from rice shoots and its involvement in hydrolysis of the natural substrate in cell walls. Physiologia Plantarum 89, 40–47.

Kundu, R.K., Dekundu, P., Banerjee, A.C., 1990. Multiple forms of β-galactosidase from the germinating seeds of *Vigna radiata*. Phytochemistry 29, 2079–2082.

Kurz, G., Wallenfels, K., 1974. D-Galactose. U.V. Assay with galactose dehydrogenase. In: Methods of Enzymatic Analysis. pp. 1279–1282.

Laemmli, U.K., 1970. Cleavage of structural proteins during the assembly of the head of bacteriophage T4. Nature 227, 680–685.

Li, S.C., Mazzotta, M.Y., Chien, S.F., Li, Y.T., 1975. Isolation and characterization of jack bean β-galactosidase. Journal of Biological Chemistry 250, 6786–6791.

O'Farrell, P.H., 1975. High resolution two-dimensional electrophoresis of proteins. Journal of Biological Chemistry 250, 4007–4021.

Ouchterlony, O., Nilsson, L.A., 1973. Immunodiffusion and immunoelectrophoresis. In: Weir, D.W. (Ed.), Handbook of Experimental Immunology. Blackwell, Oxford and Edinburgh, pp. 39–40.

Pressey, R., 1983. β-Galactosidase in ripening tomatoes. Plant Physiology 71, 132–135.

Ranwala, A.P., Suematsu, C., Masuda, H., 1992. The role of β-galactosidases in the modification of cell wall components during muskmelon fruit ripening. Plant Physiology 100, 1318–1325.

Ross, G.S., Redgwell, R.J., MacRae, E.A., 1993. Kiwifruit β-galactosidase: isolation and activity against specific fruit cell-wall polysaccharides. Planta 189, 499–506.

Ross, G.S., Wegrzyn, T., Macrae, E.A., Redgwell, R.J., 1994. Apple β-galactosidase activity against cell wall polysaccharides and characterization of a related cDNA clone. Plant Physiology 106, 521–528.

Sekimata, M., Ogura, K., Tsumuraya, Y., Hashimoto, Y., Yamamoto, S., 1989. A β-galactosidase from radish (*Raphanus sativus* L.) seeds. Plant Physiology 90, 567–574.

Simos, G., Georgatsos, J.G., 1988. Lactose hydrolyzing β-glycosidase of barley meal. Biochimica Biophysica Acta 967, 17–24.

Simos, G., Giannakouros, T., Georgatsos, J.G., 1989. Plant β-galactosidase: purification by affinity chromatography and properties. Phytochemistry 28, 2587–2592.

Smith, D.L., Starrett, D.A., Gross, K.C., 1998. A gene coding for tomato fruit beta-galactosidase II is expressed during fruit ripening. Cloning, characterization, and expression pattern. Plant Physiology 117, 417–423.

Spielman, L.L., Mowshowitz, D.B., 1982. A specific stain for α-glucosidase in isoelectric focusing gels. Analytical Biochemistry 120, 66–70.

PERGAMON

Phytochemistry 57 (2001) 361–363

PHYTOCHEMISTRY

www.elsevier.com/locate/phytochem

Biosynthesis of 2-aminobenzaldehyde in flowers of *Robinia pseudoacacia* and *Philadelphus coronarius*

Peter Spiteller, Wolfgang Steglich *

Department Chemie der Ludwig-Maximilians-Universität, Butenandtstraße 5-13 (Hauß F), D-81377 München, Germany

Received 29 November 2000; received in revised form 18 January 2001

Abstract

Feeding experiments with ^{13}C- and fluorine-labelled precursors were performed to reveal the biosynthesis of 2-aminobenzaldehyde in flowers of *Robinia pseudoacacia* and *Philadelphus coronarius*. The results are in agreement with the transformation of anthranilic acid to indole followed by oxidative ring opening and hydrolysis of the resulting *N*-formyl-2-aminobenzaldehyde. This route differs from that observed in *Hebeloma saccharioliens* (Basidiomycetes) in which anthranilic acid is directly reduced to 2-aminobenzaldehyde. © 2001 Elsevier Science Ltd. All rights reserved.

Keywords: *Robinia pseudoacacia*; Fabaceae; *Philadelphus coronarius*; Saxifragaceae; Biosynthesis; Feeding experiments; Flavour components; 2-Aminobenzaldehyde

1. Introduction

2-Aminobenzaldehyde is an essential flavour component of many flowers (Joulain, 1987; Tollsten and Bergström, 1988; Surburg et al., 1990; Brunke et al., 1997; Kaiser, 1997) and has been detected in honey (Ichimura, 1994). 2-Aminobenzaldehyde is also present in the mushroom *Hebeloma saccharioliens* (Wood et al., 1992) where it is formed by reduction of anthranilic acid (von Nussbaum et al., 1997).

In bacteria (Uchida et al., 1953) and plants (Nair and Vaidyanathan, 1964; Divakar et al., 1979; Pundir et al., 1984; Kunapuli and Vaidyanathan, 1991) 2-aminobenzaldehyde (**3**) is considered to be derived from indole (**1**) by a dioxygenase-catalyzed cleavage of the pyrrole ring and hydrolysis of the resulting *N*-formyl-2-aminobenzaldehyde (**2**) (Scheme 1). This pathway, however, has not yet been confirmed by labelling experiments.

2-Aminobenzaldehyde is also responsible for the sweet fragrance of blossoms from *Robinia pseudoacacia* L. and *Philadelphus coronarius* L. (Joulain, 1987). In order to study the biosynthesis of this compound we applied several ^{13}C- and fluorine-labelled precursors to flowers of both species and followed their metabolism. Fluorine labels can be detected by mass spectrometry with high sensitivity as was demonstrated in our studies with *Hebeloma saccharioliens* (von Nussbaum et al., 1997).

2. Results and discussion

R. pseudoacacia and *P. coronarius* were harvested by cutting flowering twigs at their lower end. Feeding experiments were performed by dipping the stems into a water/DMSO solution of the labelled compound. After 2 days the flowers were extracted with diethyl ether. The extract was carefully concentrated and then distilled into a vial cooled to −78°C. The distillate was diluted with diethyl ether and injected into the GC–MS combination. The results of the feeding experiments are given in Table 1.

2-Amino-4-fluorobenzaldehyde, 2-amino-5-fluorobenzaldehyde and 2-amino-6-fluoro-benzaldehyde were obtained in good yield after feeding flowers of *P. coronarius* with 4-, 5- or 6-fluoroanthranilic acid, respectively. Importantly, no incorporation of ^{13}C was detectable in 2-aminobenzaldehyde after application of 2-amino[*carboxy*-^{13}C]benzoic acid. These results exclude a direct conversion of anthranilic acid into 2-aminobenzaldehyde and

* Corresponding author. Tel.: +49-89-21807757; fax: +49-89-21807756.

E-mail address: wos@cup.uni-muenchen.de (W. Steglich).

0031-9422/01/$ - see front matter © 2001 Elsevier Science Ltd. All rights reserved.
PII: S0031-9422(01)00036-X

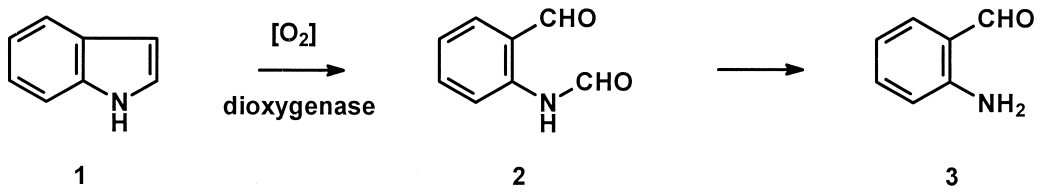

Scheme 1. Biosynthesis of 2-aminobenzaldehyde in plants.

Table 1
Feeding experiments with *Philadelphus coronarius*[a]

Precursor fed to *P. coronarius*	Product	R_i (product)	Incorporation rate in%[b]
2-Amino-4-fluorobenzoic acid	6-Fluoroindole	1331	14
	2-Amino-4-fluorobenzaldehyde	1218	12
2-Amino-5-fluorobenzoic acid	5-Fluoroindole	1344	35
	2-Amino-5-fluorobenzaldehyde	1224	6
2-Amino-6-fluorobenzoic acid	4-Fluoroindole	1365	5
	2-Amino-6-fluorobenzaldehyde	1218	8
5-Fluoroindole	2-Amino-5-fluorobenzaldehyde	1224	27
6-Fluoroindole	2-Amino-4-fluorobenzaldehyde	1218	32
5-Chloroindole	2-Amino-5-chlorobenzaldehyde	–	0

[a] Nearly identical incorporation rates were obtained by feeding 2-amino-5-fluorobenzoic acid, 2-amino-[*carboxy*-^{13}C]benzoic acid, and 5-fluoroindole to *Robinia pseudoacacia*.

[b] In the GC–MS experiments the ratio of the ion current of the molecular ion $m/z = 139$ (labelled compound) is given in % in relation to the sum of the ion current of the molecular ions $m/z = 121$ and 139 (unlabelled and labelled compounds).

are in accordance with the well known indole (tryptophan) pathway (Umbarger, 1978; Miles, 1991; Stryer, 1999), whereby the ^{13}C-carboxyl group of anthranilic acid is lost as $^{13}CO_2$ (Scheme 2).

The role of indole as an intermediate was confirmed by feeding flowers of *P. coronarius* with 5-, respectively 6-fluoroindole. As expected 2-amino-5-fluorobenzaldehyde, respectively 2-amino-4-fluorobenzaldehyde were formed in good yields (Table 1).

This proves that in flowers of *P. coronarius* 2-aminobenzaldehyde is generated by conversion of anthranilic acid to indole followed by oxidative cleavage of the pyrrole ring and not by direct reduction of anthranilic acid as in the fungus *Hebeloma sacchariolens*. Remarkably, each of the six enzymes involved in the "indole pathway" tolerates a fluorine label at least in position 4, 5 or 6 of 2-aminobenzoic acid. On the other hand, 5-chloroindole is not incorporated, showing the limits of halogen labelling. When 2-amino-6-fluoroanthranilic acid was fed to flowers of *P. coronarius*, the production of 2-amino-6-fluorobenzaldehyde was higher than that of the intermediate 4-fluoroindole. Probably, 4-fluoroindole is a better substrate for the dioxygenase than indole itself.

Comparable incorporation rates were obtained by applying 2-amino-4-fluorobenzoic acid, 2-amino-5-fluorobenzoic acid, 2-amino[*carboxy*-^{13}C]benzoic acid and 5-fluoroindole to flowers of *Robinia pseudoacacia*.

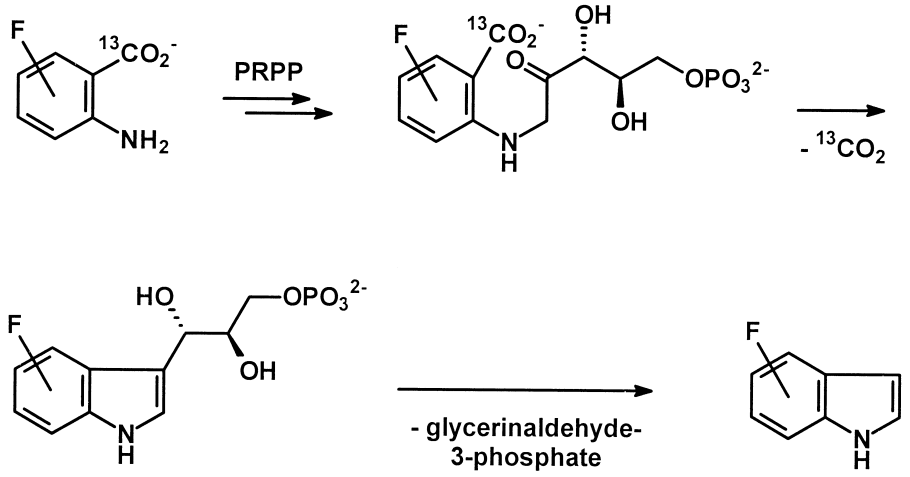

Scheme 2. Conversion of 2-aminobenzoic acids to indoles in plants (PRPP = 5′-phosphoribosyl-1-pyrophosphate).

3. Experimental

3.1. General

Gas chromatography–mass spectrometry (GC–MS) was performed on a Finnigan MAT 90 double focussing mass spectrometer, equipped with an EI ion source operating at 70 eV. For GC–MS, a Varian GC 3400 gas chromatograph with a fused silica DB-5ms capillary column (30 m×0.25 mm, coated with a 0.25 μm layer of liquid phase) and helium as a carrier gas (flow rate: 1.5 ml/min; split ratio: 1:30) was used for sample separation. The injector temperature was kept at 300°C, injection volumes were 0.2–0.4 μl of a 1–2% (m/v) solution. Temperature programme: 2 min isothermal at 50°C, then 10 K/min up to 300°C, finally 10 min isothermal at 300°C. Retention indices R_i (Kováts, 1958) were determined by co-injection of a 0.2 μl sample of a standard mixture of saturated straight chain alkanes (C_{10}–C_{36}).

3.2. Plant material

Flowers of *R. pseudoacacia* and *P. coronarius* were collected in München in May 1998, 1999 and 2000.

3.3. Feeding experiments

Two hundred and fifty milligrams of the precursor were dissolved in 200 ml water containing 1 ml DMSO. In the case of 2-amino[*carboxy*-^{13}C]benzoic acid only 100 mg were used. Flowering twigs (200–400 g) from *P. coronarius* or *R. pseudoacacia* were dipped with their stems into these solutions. Two days later, the flowers were collected and kept at −20°C until processing.

3.4. Preparation of GC–MS-samples

The flowers were extracted twice with 150 ml diethyl ether and the combined extracts dried over Na_2SO_4. After careful removal of the solvent, the residue (~ 0.1 ml) was distilled at 50°C (0.01 mbar) into a vial cooled to −78°C. The distillate was then diluted with 50 μl diethyl ether and injected in 1–3 μl portions into the GC–MS.

3.5. Mass spectral data and retention indices

2-Aminobenzaldehyde: $R_i = 1221$; GC–MS: *m*/*z* (rel. int.): 121 (67), 93 (100), 92 (28), 76 (12), 66 (44), 65 (37). 2-Amino-4-fluorobenzaldehyde: $R_i = 1218$; GC–MS: *m*/*z* (rel. int.): 139 (59), 124 (11), 111 (100), 84 (39), 83 (38). 2-Amino-5-fluorobenzaldehyde: $R_i = 1224$. 2-Amino-6-fluorobenzaldehyde: $R_i = 1218$. Indole: $R_i = 1303$; GC–MS: *m*/*z* (rel. int.): 117 (100), 90 (49), 89 (30). 4-Fluoroindole: $R_i = 1365$; GC–MS: *m*/*z* (rel. int.): 135 (100), 108 (51), 107 (38). 5-Fluoroindole: $R_i = 1344$. 6-Fluoroindole: $R_i = 1331$.

Acknowledgements

We are grateful to the Deutsche Forschungsgemeinschaft (SFB 369) for financial support.

References

Brunke, E.-J., Hammerschmidt, F.-J., Rittler, F., Schmaus, G., 1997. Scents of nature: analytical and sensory information as a tool for creativity. Riv. Ital. EPPOS, 338–354.

Divakar, N.G., Subramanian, V., Sugumaran, M., Vaidyanathan, C.S., 1979. Indole oxygenase from the leaves of *Jasminum grandiflorum*. Plant Sci. Lett. 15, 177–181.

Ichimura, N., 1994. Volatile flavor components in Longan honey. Koryo 182, 133–138.

Joulain, D., 1987. The composition of the headspace from fragrant flowers: further results. Flavour Fragrance J. 2, 149–155.

Kaiser, R., 1997. New or uncommon volatile components in the most diverse natural scents. Riv. Ital. EPPOS, 17–47.

Kováts, E., 1958. Gas-chromatographische Charakterisierung organischer Verbindungen. Teil 1: Retentionsindizes aliphatischer Halogenide, Alkohole, Aldehyde und Ketone. Helv. Chimi. Acta 41, 1915–1932.

Kunapuli, S.P., Vaidyanathan, C.S., 1991. New indole oxygenase from the leaves of *Tecoma stans* L. Part II: Immunological characterization. J. Indian Inst. Sci. 71, 515–522.

Miles, E.W., 1991. Structural basis for catalysis by tryptophan synthase. Adv. Enzymol. Relat. Areas Mol. Biol. 64, 93–172.

Nair, P.M., Vaidyanathan, C.S., 1964. An indole oxidase isolated from the leaves of *Tecoma stans*. Biochem. Biophys. Acta 81, 496–506.

von Nussbaum, F., Spahl, W., Steglich, W., 1997. Reduction of anthranilic acid and related amino acids in fruit-bodies of *Hebeloma sacchariolens*. Phytochemistry 46, 261–264.

Pundir, C.S., Garg, G.K., Rathore, V.S., 1984. Purification and properties of indole 2,3-dioxygenase from maize leaves. Phytochemistry 23, 2423–2427.

Stryer, L., 1999. Biochemie, 4th Edition. Spektrum Akad. Verlag, Heidelberg, pp. 762–764.

Surburg, H., Guentert, M., Schwarze, B., 1990. Volatile constituents of European bird cherry flowers (*Padus avium* Mill.). J. Essent. Oil Res. 2, 307–316.

Tollsten, L., Bergström, G., 1988. Headspace volatiles of whole plants and macerated plant parts of *Brassica* and *Sinapis*. Phytochemistry 27, 2073–2077, Erratum: Phytochemistry 27, 4013–4018.

Uchida, M., Sakamoto, Y., Ichihara, K., 1953. The bacterial decomposition of indole. Medical Journal of Osaka University 3, 487–495.

Umbarger, H.E., 1978. Amino acid biosynthesis and its regulation. Annu. Rev. Biochem. 47, 533–606.

Wood, W.F., Brownson, M., Smudde, R.A., Largent, D.L., 1992. 2-Aminobenzaldehyde: the source of the "sweet odor" of *Hebeloma sacchariolens*. Mycologia 84, 935–936.

PERGAMON

Phytochemistry 57 (2001) 365–371

PHYTOCHEMISTRY

www.elsevier.com/locate/phytochem

Ginsenoside production in different phenotypes of *Panax ginseng* transformed roots

Anna Mallol, Rosa M. Cusidó, Javier Palazón, Merce Bonfill, Carmen Morales, M. Teresa Piñol*

Sección de Fisiología Vegetal, Facultad de Farmacia, Universidad de Barcelona, AVD/ Diagonal 643, 08028 Barcelona, Spain

Received 13 November 2000; received in revised form 5 February 2001

Abstract

Transformed roots were obtained after the inoculation of sterile root discs of *Panax ginseng* C.A. Meyer with *Agrobacterium rhizogenes* A4. The established hairy root lines displayed three morphological phenotypes when cultured on hormone-free liquid Schenk and Hildebrandt medium. Most of the cultures showed the characteristic traits of hairy roots (HR-M), while others were either callus-like (C-M) or thin (T-M) without branching. The growth rate of the transformed root lines was always higher than that of untransformed roots, showing that the genetic changes caused by the *A. rhizogenes* transformation conditioned a higher biomass formation. When considering the different transformed root phenotypes, we can observe that the highest ginsenoside production was achieved by HR-M root lines, closely followed by C-M ones, whereas the lowest yield was reached by T-M root phenotype. The study of the integration of the TL-DNA and TR-DNA fragments of the pRiA4 in the root genome showed that the *aux1* gene was always detected in HR-M and C-M root phenotypes which presented the highest biomass and ginsenoside productions. This fact suggests a significant role of *aux* genes in the morphology of *Panax ginseng* transformed roots. The ginsenoside pattern of transformed roots varied according to their morphology, although the ginsenoside contents of the Rg group was always higher than that of the Rb group. From our results, we can infer the potential of some root phenotypes of *Panax ginseng* hairy root cultures for an improved ginsenoside production. © 2001 Published by Elsevier Science Ltd. All rights reserved.

Keywords: *Panax ginseng* C.A. Meyer; *Araliaceae*; Ginseng; Hairy root cultures; *rol* Genes; *aux* Genes; Opines; Ginsenosides

1. Introduction

Panax ginseng roots have been widely used in Chinese traditional medicine since ancient times owing to their stimulating and tonic properties. The pharmacological activities of ginseng or its crude extracts are based on the presence of a mixture of triterpenic saponins referred to as ginsenosides. The two major groups of ginsenosides are the Rb and Rg groups, which have 20 (S) protopanaxadiol and 20 (S) protopanaxatriol, respectively, as the sapogenines. Rb group includes the ginsenosides Rb1, Rb2, Rc and Rd, while Rg group includes the Re, Rf and Rg1 ones as the main compounds. Among all these ginsenosides, Rb1 and Rg1 are the most effective compounds (Tanaka and Kasai, 1984).

Ginsenosides accumulate in the root of the plant, but the agricultural production of roots is expensive. Therefore, the production of ginsenosides, by means of different biotechnological alternatives has been extensively studied by a number of researchers, using callus tissues (Furuya et al., 1983a; Odnevall et al., 1989; Asaka et al., 1993; Mathur et al., 1994), cell suspensions (Furuya et al., 1983b; Mathur et al., 1994) and root cultures (Yoshikawa and Furuya, 1987); nevertheless, the productivity obtained so far has been low because of the low growth rates of cultures. The induction and establishment of hairy roots after the infection of *Panax ginseng* rhizomes with *Agrobacterium rhizogenes* has been successfully performed (Yoshikawa and Furuya, 1987; Ko et al., 1989; Inomata et al., 1993; Bulgakov et al., 1998; Washida et al., 1998). These roots grow more rapidly and produce higher levels of saponins than the ordinary cultured roots obtained by hormonal control.

Hairy root formation is a consequence of the integration of the T-DNA of Ri-plasmid of *Agrobacterium*

* Corresponding author. Tel.: +34-93-402-4493; fax: +34-93-402-9043.

E-mail address: pinyol@farmacia.far.ub.es (M.T. Piñol).

0031-9422/01/$ - see front matter © 2001 Published by Elsevier Science Ltd. All rights reserved.
PII: S0031-9422(01)00062-0

rhizogenes A4 into the plant genome. In the case of agropine type strains (such as *A. rhizogenes* A4), two T-DNA fragments (TL-DNA and TR-DNA) are separately transferred into the plant material (Huffmann et al., 1984; Jouanin, 1984). The integration of the TL-DNA into the plant genome is essential for developing transformed roots; three genes of this fragment, known as *rol*A, *rol*B and *rol*C are responsible for the full hairy root syndrome (Carderelli et al., 1987; Palazón et al., 1997, 1998a). Although the TR-DNA is not essential for hairy root formation, it has been shown that the *aux1* genes harboured in this T-DNA segment provide to the transformed cells with an additional source of auxin. Recently, we have found that *aux* genes play a significant role in the morphology and alkaloid production of transformed roots of *Datura metel* and *Duboisia hybrid* (Moyano et al., 1999).

In this work, we report the establishment of three different phenotypes of *Panax ginseng* C.V. Meyer transformed roots in which the role of the TL-DNA and TR-DNA fragments of the pRiA4 on the root morphology is considered. At the same time, the relationship between the different root phenotypes and their capacity to produce biomass and ginsenosides is also studied.

2. Results

2.1. Study of growth and ginsenoside productivity

Root discs developed both callus tissues and roots 4–8 weeks after infection with *A. rhizogenes* A4. At the same time, numerous roots began to emerge from the surface of these callus pieces. Sixty five per cent of the inoculated root discs developed roots either directly from them or through callus formation.

These hairy root lines showed 3 different morphologycal phenotypes: 50% presented the characteristic traits of hairy roots described by Carderelli et al. (1987) with primary roots with extensive lateral branching and a profusion of root hairs (HR-M); 35% showed callus-like appearance with very thick primary roots and several secondary roots (C-M), and 15% were rather long and thin without branching points, tending to become brown except for newly developing yellowish parts (T-M) (Fig. 1). These three root phenotypes were maintained stable over successive subcultures for 2 years.

Hairy root lines started to grow without any lag phase (data not shown) and growth pattern varied according to observed phenotypes. When considering the growth rate

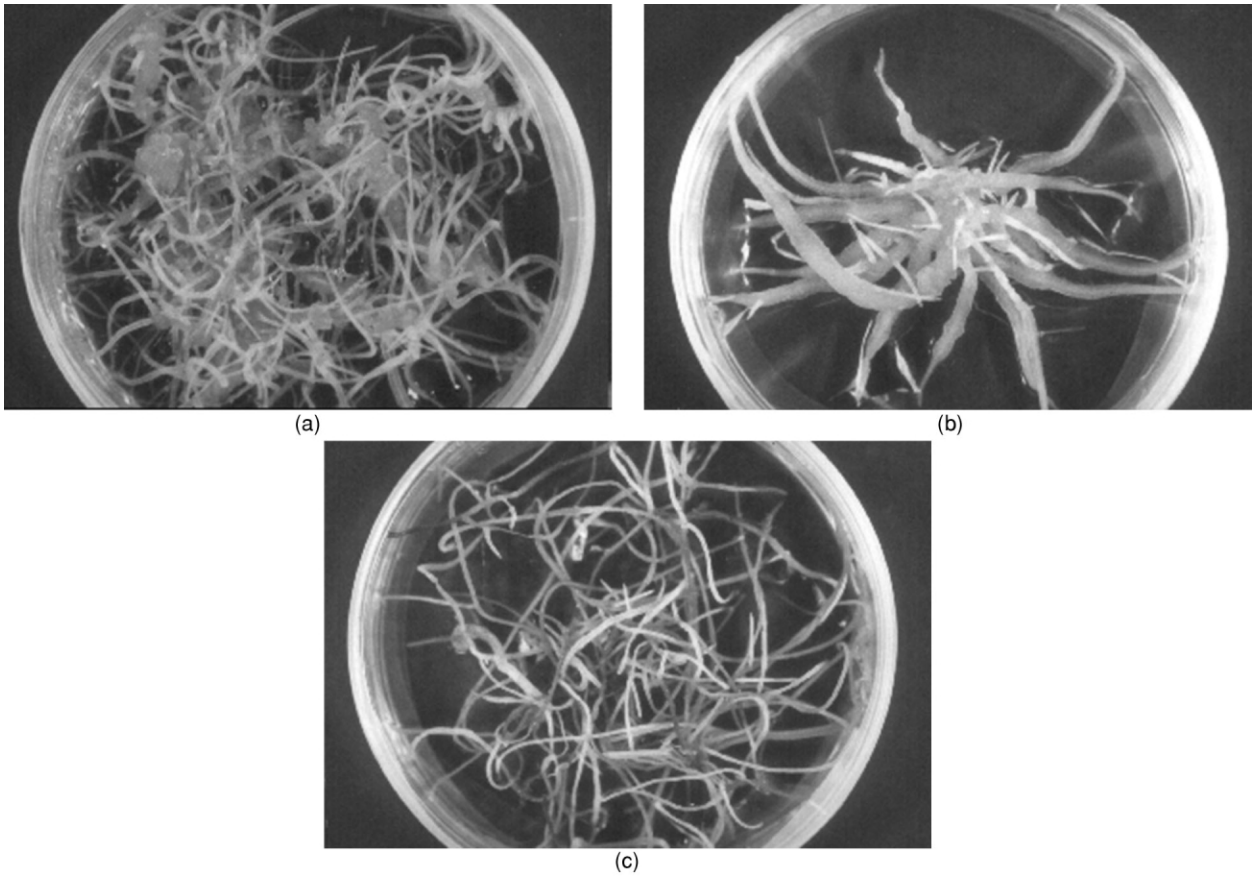

Fig. 1. Four week old *Panax* ginseng hairy root cultures on SH solid medium, showing three different phenotypes. (a) Roots with the characteristic traits of hairy roots (HR-M). (b) Roots with callus-like morphology (C-M). (c) Roots with thin morphology (T-M).

average of the transformed root lines studied (Fig. 2), it was possible to observe that the C-M and HR-M root lines achieved the highest values; the growth rate (final fresh weight/fresh inoculum weight) obtained after 4 weeks of culture, by C-M, HR-M and T-M roots was 7.9, 7.1 and 3.2, respectilvely, while in control roots it was 1.5. From these results we can infer that the genetic changes caused by the *A. rhizogenes* transformation conditioned a higher capacity for the biomass formation affecting branching, as shown in cucumber (Amselem and Tepfer, 1992), *Catharanthus roseus* (Palazón et al., 1998b) and in *Duboisia*, *Datura* and tobacco transformed root cultures (Moyano et al., 1999). At the same time, as described by Rhodes et al. (1990), the growth rate of transformed roots depends, to a large extent, on linear extension, on the formation of a large number of new growing points as lateral branches and on a secondary increase in root diameter as the root cells undergo cell expansion and differentiation.

Four ginsenosides (Rb1, Rb2, Rc, Rd) of Rb group and three (Re, Rf and Rg1) of Rg group were extracted and quantified from the root lines studied. HR-M root lines achieved the highest total ginsenoside level (5.4 mg/gDW) followed by C-M (4.8 mg/gDW) and control roots (4.5 mg/gDW). Roots with thin morphology produced less than half of the ginsenoside production achieved by the HR phenotype (Table 1 and Fig. 2).

In the three root phenotypes considered, as well as in the untransformed roots, the RbT/RgT ratio was lower than 1, indicating that the production of Rg group ginsenosides was always higher than that of the Rb group (Table 1). Similar results were obtained by Bulgakov et al. (1998) with *P. ginseng* transgenic roots for the *rol*C gene of *A. rhizogenes*. As indicated by Ko et al. (1989) and Inomata et al. (1993), the maximum production of the different ginsenosides occurs at different growth stages. Maximum levels of Rb1 are usually found in the early growth stages, while maximum amounts of Rg1 appear later; these facts could explain the ginsenoside patterns of transformed root cultures after 4 weeks of growth.

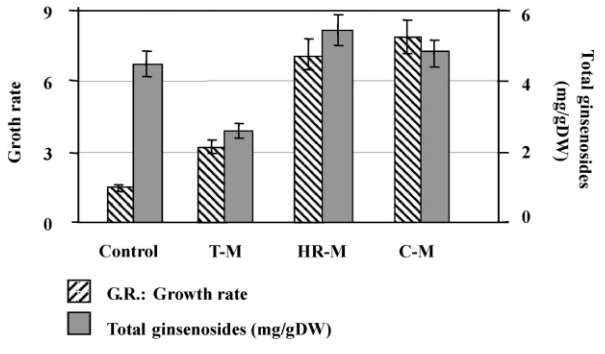

Fig. 2. Growth rate (final fresh weight/inoculum fresh weight) and ginsenoside contents (mg/g DW) of the different root phenotypes. Roots were cultured for 4 weeks in hormone-free SH liquid medium. In all cases the inoculum fresh weight was 0.5±0.05 g. Each value was the mean of five replicates of each one of the 15 root lines considered, belonging to each respective phenotype studied.

Table 1
Ginsenoside contents (expressed as percentage of DW) of the different hairy root phenotypes studied. Roots were cultured for 4 weeks in hormone-free SH liquid medium. In all cases the inoculum fresh weight was 0.5±0.05 g. Each value is the mean of five replicates of each one of the 15 root lines considered, belonging to each respective phenotype studied. Total ginsenoside contents is expressed as mg ginsenosides/gDW

Ginsenosides	Control	T-M	HR-M	C-M
Rb1	11.3	8.0	14.8	21.2
Rb2	2.8	5.3	4.8	3.5
Rc	0.5	4.1	4.5	3.7
Rd	0.1	2.6	7.6	3.6
Re	68.3	57.7	40.1	38.1
Rf	2.0	5.6	2.1	2.0
Rg1	15.0	16.8	28.5	27.9
RbT	14.7	20.0	29.1	31.9
RgT	85.3	80.0	70.8	68.1
Total (mg/gDW)	4.55	2.58	5.44	4.84
RbT/RgT	0.17	0.25	0.41	0.47

The ginsenoside pattern also varied depending on the root phenotypes. The main ginsenoside found in T-M, HR-M and C-M root lines was the Re ginsenoside followed by the Rg1 one (Table 1). Whereas in T-M roots the Re and Rg1 represented 57.7 and 16.8%, respectively, of the total ginsenoside contents, in HR-M and C-M root lines, the Re constituted 40.1 and 38.1%, and the ginsenoside Rg1, represented 28.5 and 27.9%, respectively of the total. As it is known (Gubar et al., 1997), the Re ginsenoside is formed after the addition of two rhamnose residues to the Rg1. These results suggest a higher activity of enzymes involved in the incorporation of rhamnose to the Rg1 compound in the T-M root phenotype than on the other phenotypes studied. The main ginsenoside of the Rb group in T-M, HR-M and C-M root lines was the Rb1, which represented 8, 14.8 and 21.2% of the total ginsenosides determined. Because the Rd ginsenoside represented at most 2.6% of the total, and from it Rb1, Rb2 and Rc are formed by the action of different enzymes involved in the addition of sugar residues, our results suggest that the activity of these enzymes was high and dependent on the root phenotypes studied. But in order to clarify the ginsenoside metabolism, further assays are requested.

The control roots presented a different ginsenoside pattern from that achieved by HR-M and C-M roots, but more similar to that of T-M roots. The Re, Rg1 and Rb1 constituted 68, 15 and 11.3% of the total ginsenoside contents.

When considering the ginsenoside yield of the *P. ginseng* transformed root cultures after 4 weeks of growth (Fig. 3), we can observe that the highest yield was achieved by HR-M root lines (72.9 mg/l), followed by

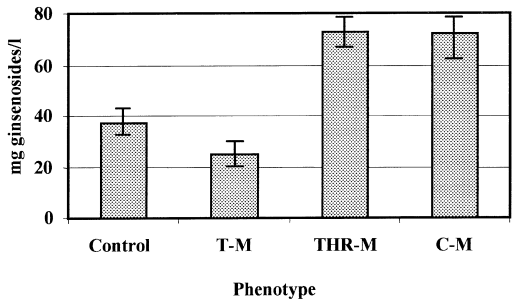

Fig. 3. Ginsenoside yield, expressed as mg total ginsenosides/l, in the different *Panax ginseng* hairy root phenotypes studied. Roots were cultured for 4 weeks in hormone-free SH liquid medium. In all cases the inoculum fresh weight was 0.5±0.05 g. Each value is the mean of five replicates of each one of the 15 root lines considered, belonging to each respective phenotype studied.

the C-M ones (71.6 mg/l). The lowest ginsenoside yield of the transformed root phenotypes studied corresponded to the T-M roots (24.8 mg/l), which also presented low ginsenoside contents and a limited growth. The ginsenoside production of untransformed roots (36.8 mg/l), was always lower than that obtained by HR-M and C-M root lines studied.

As it is known, the ginsenoside yield of the cultures not only depends on the accumulation of these compounds but also on the biomass formation. In our case, although the ginsenoside contents of HR and C root phenotypes were only 1.2 and 1.1 times higher than that achieved by control, in both cases their productivity was twice as high as that of the controls. These results show that in our *P. ginseng* transformed root cultures, the capacity to produce and accumulate ginsenosides is associated with biomass formation because the highest productivity was achieved by the root phenotypes with the highest growth rate.

From our results we can infer that the transformed nature of *P. ginseng* roots conditioned an important increase of biomass and productivity, especially in roots displaying the full hairy root morphology, corroborating the suitability of transformed root cultures for an improved secondary metabolite production.

2.2. Study of the fragments of Agrobacterium T-DNA integrated into the transformed root genome

The presence of the *rolC* gene of the TL-DNA of the pRiA4 as well as that of the *aux1*, *ags* and *mas1* genes of the TR-DNA has been studied in the three different transformed root phenotypes established. The transformed nature of the all selected root lines of each morphology was confirmed by the presence of the *rolC* gene in the plant genome. The products of *aux* genes are involved in the additional route for indole acetic acid in transformed cells (Nilsson and Olsson, 1997), whereas *ags* and *mas1* genes code the enzymes responsible for agropine and manopine biosyntheses, respectively. 100% of the root lines displaying callus-like (C-M) or hairy root morphology (HR-M) but only 25–45% of root lines showing a thin structure (T-M) presented this gene in their genome. Previously, we reported that in *D. metel*, *Duboisia* and tobacco transformed roots, the presence of *aux1* gene in the plant genome conditioned the callus-like morphology (Moyano et al., 1999). We could observe that 100% of roots displaying this structure included this gene in their genome, whereas only 25–60% of roots with typical hairy root morphology presented this gene in their cells. From our results obtained in *P. ginseng* transformed roots, we can infer that the *aux1* gene is related to root morphology, especially to lateral branching development, since thin roots did not form secondary root, whereas C-M and HR-M roots presented a very high degree of secondary root formation. In our case, the additional source of auxin induced by *aux1* gene in the root genomes, was not the only factor responsible for the disorganization of root tissues (Jung et al., 1995), since roots displaying the full hairy root morphology also harboured the *aux1* gene in their genome.

The presence of the opines agropine and manopine and the genes which codify for enzymes involved in their formation, *ags* and *mas1* genes in the root genomes was also studied (Table 2). The results obtained show that 25% of thin root lines, 75% of hairy roots and 100% of callus-like ones included the *ags* gene in their genome whereas *mas1* gene was present in 100% of HR and C roots but only in 50% of thin root lines. When considering the presence of both opines, agropine and manopine, in the selected root lines it can be seen that the root lines with thin morphology did not include these compounds in their cells, but that they were present in all root lines with callus-like structure. On the other hand in the HR-M root lines studied, it was possible to observe that roots which lacked the *ags* gene did not include agropine in their composition and manopine was hardly detected. When studying the relationship between the presence of opines in the transformed root phenotypes established with their ginsenoside production it is possible to

Table 2
PCR study of the presence of different fragments of *Agrobacterium rhizogenes* T-DNA inserted in the genome of the transformed root phenotypes. Percentage of transformed root lines of each phenotype studied in which the presence of opines was detected

Root morphology	Genes				Opines	
	rolC	*aux1*	*ags*	*mas1*	Agropine	Manopine
HR-M	100%	100%	75%	100%	75%	100%
C-M	100%	100%	100%	100%	100%	100%
T-M	100%	25–45%	25%	50%	0%	50%

observe that the less productive root lines (T-M ones) also lacked the *ags* and *mas1* genes and consequently the capacity to produce opines. Nevertheless, further studies are needed in order to know the effect of the presence of the genes responsible for the opine biosynthesis in ginsenoside production.

Taking all these results together, we can observe that the transformed root phenotypes, which presented the highest growth rate (HR-M and C-M phenotypes) were also those with the highest ginsenoside production. At the same time, together with the *rol* genes of the TL-DNA segment of *A. rhizogenes*, 100% of root lines belonging to these two phenotypes harboured the *aux1* gene of the TR-DNA fragment. On the contrary, the phenotype with very slow growth and ginsenoside production (T-M) never included this gene in its genome, although the *rol* genes were always present. From these results we can infer that *aux1* gene, although not essential for the root formation, plays an important role in the root morphology by increasing lateral branching resulting in higher biomass and ginsenoside production. Our results also show that in *P. ginseng*, the capacity of transformed roots to produce opines does not interfere with the ginsenoside production. To our knowledge, this is the first report that a relationship between growth and ginsenoside production, and the presence of different genes of the TL-DNA and TR-DNA of the Ri plasmid of *A. rhizogenes* has been shown in *P. ginseng* hairy root cultures.

3. Materials and methods

3.1. Induction and culture of hairy roots

Transformed roots of *Panax ginseng* C.A. Meyer were induced from 4-year-old rhizomes after infection with *Agrobacterium rhizogenes* A4 strain. Sterilized root discs were wounded with a sterile needle loaded with *A.rhizogenes* suspension grown in liquid YEB medium (Vervliet et al., 1975) for 24 h at 28±2°C on a rotary shaker at 100 rpm. The inoculated root discs were placed on Schenk-Hildebrandt's medium (SH) (Schenk and Hildebrandt, 1972) containing 3% (w/v) sucrose, 0.1% (w/v) myo-inositol and 0.27% (w/v) Phytagel (Sigma) at 26°C. The medium was adjusted to pH 7.0 before autoclaving. After 2 days of cocultivation the explants were transferred to the fresh medium containing cefotaxime (500 mg/l) in order to eliminate the bacteria. After cultivation for one or two months, roots started to appear at the infection sites and, in order to obtain the root lines, single roots were picked off and placed onto new media together with cefotaxime, until the bacteria were eliminated. Hairy roots with no bacterial contamination were cultured on hormone-free SH solid medium, already described, in the dark at 26°C. After 6 months of subculturing the roots every two weeks on fresh solid medium, the root lines were transferred to SH liquid medium and kept in a rotary shaker at 100 rpm, 26°C in the dark. Subcultures were performed every two weeks in fresh medium. Untransformed roots (control roots) were obtained from sterile rhizome discs cultured in Murashige and Skoog (MS) medium (Murashige and Skoog, 1962) supplemented with 3% (w/v) sucrose, 0.01% (w/v) myo-inositol, 2 mg/l indole butyric acid, 0.1 mg/l kinetin and 0.27% (w/v) Phytagel (Sigma) at 26°C in darkness. Roots 2–3 cm long were transferred separately to the same medium used for hairy roots and subcultured every 2–3 weeks.

In order to study the capacity of hairy roots to produce biomass and ginsenosides, from 80 hairy root lines established, 15 relatively quickly growing root lines showing each phenotype considered were selected and cultured for 4 weeks in the above mentioned medium and conditions. Biomass formation was expressed as growth rate (final fresh weight/inoculum fresh weight); the inocula fresh weight (0.5±0.05 g) were cultured in 100 ml Erlenmeyer flasks containing 10 ml of SH liquid medium.

3.2. PCR analysis

Total DNA was isolated from hairy roots by using "genomic Prep ™ Cells and Tissue DNA isolation Kit" (Pharmacia Biotech). PCR analyses were performed using the pre-formulated, predispensed single dose reaction beads "Ready to Go™" (Pharmacia Biotech). The complete mixture contained 200 ng of total DNA, 12.5 pmol/μl of each oligonucleotide primer, 200 μM dNTPs, 1.5 units Taq polymerase, and buffer supplied by the enzyme manufacturer (1/10 V) in a total volume of 25 μl. The oligonucleotide primers used that would anneal to *rol*C gene of the TL-DNA of pRi of *A. rhizogenes* A4, produced a DNA fragment of 534 bp.

3.3. Opine analyses

Opine analyses were performed by High Voltage Paper Electrophoresis according to a modification of the method indicated by Petit et al. (1983), as described in Moyano et al. (1999).

3.4. Extraction and analysis of ginsenosides

Extraction of ginsenosides was based on the method described by Samukawa et al. (1995). Freeze-dried powdered samples (50 mg) were washed in petroleum ether (3×8 ml) and centrifuged at 33,520 *g* for 10 min. The pellet was extracted and sonicated for 15 min with 15 ml of 70% methanol and centrifuged again at 33,520 *g* for 10 min. After evaporating the methanolic extract to dryness and dissolving it in 10 ml of acetonitrile: water (80:20), 20 μl of the ginsenoside extract was loaded onto a Hewlett-Packard Lichrospher® 100 Diol (5 μm) column

(250×4 mm) connected to a Pharmacia LKB HPLC system. The solvent mixture of acetonitrile-water (4.5:1 v/v, pH 2.5 with H_3PO_4) was eluted at a flow rate of 0.8 ml/min and ginsenosides were detected at 202 nm. The peak areas corresponding to ginsenosides from the samples, with the same retention time as authentic ginsenosides (Rf, Rg1, Rd, Re, Rc, Rb2, Rb1), were integrated by comparison with an external standard calibration curve. Ginsenosides Rb1, Rb2, Rc, Rd, Re, Rf and Rg1 (99.8%) were purchased from Karl Roth (Germany).

Ginsenoside contents of the analyzed samples were expressed as mg ginsenosides/g DW (dry weight). The total ginsenoside productivity, after 4 weeks of culture, of transformed roots was indicated as mg of total ginsenosides per liter of culture medium as described by Jouhikainen et al. (1999).

Acknowledgements

This work has been partially supported by a grant from the Boehringer Ingelheim Industry and the Spanish CICYT (PB98-1243). The authors are very grateful to Dr. Hiroko Murata from the Setsunan University, Osaka, Japan, for supplying *Panax ginseng* rhizomes. A.M. is also grateful for her research grant from the University of Barcelona.

References

Amselem, J., Tepfer, M., 1992. Molecular basis for novel root phenotypes induced by *Agrobacterium rhizogenes* A4 on cucumber. Plant Mol. Biol. 19, 421–432.

Asaka, I., Ii, I., Hirotani, M., Asada, Y., Furuya, T., 1993. Production of ginsenoside saponins by culturing ginseng (*Panax ginseng*) embryogenic tissues in bioreactors. Biotech. Lett. 15, 1259–1264.

Bulgakov, V.P., Khodakovskaya, M.V., Labetskaya, N.V., Chernoded, G.K., Zhuravlev, Y.N., 1998. The impact of plant *rol*C oncogene on ginsenoside production by ginseng hairy root cultures. Phytochemistry 49, 1929–1934.

Carderelli, M., Mariotti, D., Pomponi, M., Spanò, L., Capone, I., Constantino, P., 1987. *Agrobacterium rhizogenes* T-DNA genes capable of inducing hairy root phenotype. Mol. Gen. Genet. 209, 475–480.

Furuya, T., Yoshikawa, T., Ishii, T., Kajii, K, 1983a. Regulation of saponin production in callus cultures of *Panax ginseng*. Planta Med. 47, 200–204.

Furuya, T., Yoshikawa, T., Orihara, Y., Oda, H., 1983b. Saponin production in cell suspension cultures of *Panax ginseng*. Planta Med. 48, 83–87.

Gubar, S.I., Gulko, T.P. Kunakh, V.A., 1997. Growth and glycoside accumulation in Ginseng callus tissue culture under a long-term action of exogenous phytohormones. Russ. J. Plant Physiol. 44, 83–89.

Huffmann, G.A., White, F.F., Gordon, M.P., Nester, G.W., 1984. Hairy root inducing plasmid: physical map and homology to tumor-inducing plasmids. J. Bacteriol. 152, 269–276.

Inomata, S., Yokoyama, M., Gozu, Y., Shimizu, T., Yanagi, M., 1993. Growth pattern and ginsenoside production of *Agrobacterium*-transformed *Panax ginseng* roots. Plant Cell Rep. 12, 681–686.

Jouanin, L., 1984. Restriction map of an agropine-type Ri plasmid and its homologies with Ti plasmids. Plasmid 12, 91–102.

Jouhikainen, K., Lindgren, L., Jokelainen, T., Hiltunen, R., Teeri, T.H., Oksman-Caldentey, K.M., 1999. Enhancement of scopolamine production on *Hyoscyamus muticus* L. Hairy root cultures by genetic engineering. Planta 208, 545–551.

Jung, K.H., Kawah, S.S., Choi, C.Y., Liu, J.R., 1995. An interchangeable system of hairy root and cell suspension cultures of *Catharanthus roseus* for indole alkaloid production. Plant Cell Rep. 15, 51–54.

Ko, K.S., Noguchi, H., Ebizuka, Y., Sankawa, U., 1989. Oligoside production by hairy root cultures transformed by Ri plasmids. Chem. Pharm. Bull. 37, 245–248.

Mathur, A., Shukla, Y.N., Pal, M., Ahuja, P.S., Uniyal, G.C., 1994. Saponin production in callus and cell suspension cultures of *Panax quinquefolium*. Phytochemistry 35, 1221–1225.

Moyano, E., Fornalé, S., Palazón, J., Cusidó, R.M., Bonfill, M., Morales, C., Piñol, M.T., 1999. Effect of *Agrobacterium rhizogenes* T-DNA on alkaloid production in *Solanaceae* plants. Phytochemistry 52, 1287–1292.

Murashige, T., Skoog, F., 1962. A revised medium for rapid growth and bioassays with tobacco tissue cultures. Physiol. Plant. 15, 473–497.

Nilsson, O., Olsson, O., 1997. Getting to the root: the role of the *Agrobacterium rhizogenes* rol genes in the formation of hairy roots. Physiol. Plant. 100, 463–473.

Odnevall, A., Björk, L., Berglund, T., 1989. Rapid establishment of tissue cultures from seeds of *Panax ginseng* and *Panax pseudoginseng*. Biochem. Physiol. Pflanzen 185, 131–134.

Palazón, J., Cusidó, R.M., Gonzalo, J., Bonfill, M., Morales, C., Piñol, M.T., 1998. Relation between the amount of *rol*C gene product and indole alkaloid accumulation in *Catharanthus* transformed root cultures. J. Plant Physiol. 153, 712–718.

Palazón, J., Cusidó, R.M., Roig, C., Piñol, M.T., 1997. Effect of *rol* genes from *Agrobacterium rhizogenes* TL-DNA on nicotine production in tobacco root cultures. Plant Physiol. Biochem. 35, 155–162.

Palazón, J., Cusidó, R.M., Roig, C., Piñol, M.T., 1998b. Expression of the *rol*C gene and nicotine production in transgenic roots and their regenerated plants. Plant Cell Rep. 17, 384–390.

Petit, A., David, C., Dahl, G.A., Ellis, J.G., Guyon, P., Casse-Delbart, F., Tempé, J., 1983. Further extension of the concept: plasmids in Agrobacterium thizogenes cooperate for opine degradation. Mol. Gen. Genet. 190, 204–214.

Rhodes, M.L.C., Robins, R.J., Hamill, J.D., Parr, A.J., Hilton, M.G., Walton, N.J., 1990. Properties of transformed root cultures. In: Charlwood, B.V., Rhodes, M.J.C. (Eds.), Secondary Products from Plant Tissue Culture: Proceedings of the Phytochemical Society of europe, vol. 30. Oxford University Press, Oxford, pp. 201–225.

Samukawa, K., Yamashita, H., Matsuda, H., Kubo, M., 1995. Simultaneous analysis of saponins in *Ginseng radix* by high performance liquid chromatography. Chem. Pharm. Bull. 43, 137–141.

Schenk, R.U., Hildebrandt, A.C., 1972. Medium and techniques for induction and growth of monocotyledonous and dicotyledonous plant cell cultures. Can. J. Bot. 50, 199–204.

Tanaka, O., Kasai, R., 1984. Saponins of ginseng and related plants. In: Herz, W., Grisebach, H., Kirby, G.W., Tamm, Ch. (Eds.), Progress in the Chemistry of Organic Natural Products, Vol. 46. Springer-Verlag, Berlin, pp. 1–76.

Vervliet, G., Holsters, M., Teuchy, H., Van Montagu, M., Schell, J., 1975. Characterization of different plaque-forming and defective temperate phages in *Agrobacterium* strains. J. Gen. Virol. 26, 33–48.

Washida, D., Shimomura, K., Nakajima, Y., Takido, M., Kitanaka, S., 1998. Ginsenosides in hairy roots of a *Panax hybrid*. Phytochemistry 49, 2331–2335.

Yoshikawa, T., Furuya, T., 1987. Saponin production by cultures of *Panax ginseng* transformed with *Agrobacterium rhizogenes*. Plant Cell Rep. 6, 449–453.

PERGAMON

Phytochemistry 57 (2001) 373–376

PHYTOCHEMISTRY

www.elsevier.com/locate/phytochem

Studies on the biosynthesis of 2-hydroxy-1,4-benzoxazin-3-one (HBOA) from 3-hydroxyindolin-2-one in *Zea mays*

Peter Spiteller [a], Erich Glawischnig [a], Alfons Gierl [b], Wolfgang Steglich [a,*]

[a] *Department Chemie der Ludwig-Maximilians-Universität, Butenandtstraße 5-13 (Hauß F), D-81377 München, Germany*
[b] *Institut und Lehrstuhl für Genetik, Technische Universität München, Lichtenbergstraße 4, D-85747 Garching, Germany*

Received 13 November 2000; received in revised form 18 January 2001

Abstract

The ring expansion of 3-hydroxyindolin-2-one to 2-hydroxy-1,4-benzoxazin-3-one (HBOA) was investigated by labelling experiments. Action of the cytochrome P450 enzyme BX4 from maize on 3-hydroxyindolin-2-one under an $^{18}O_2$ atmosphere induced production of 2-hydroxy-1,4-benzoxazin-3-one in which the ring oxygen — but not the 2-hydroxy group of HBOA — is labelled. A mechanism for this transformation is proposed. © 2001 Elsevier Science Ltd. All rights reserved.

Keywords: *Zea mays*; Gramineae; Biosynthesis; Ring expansion; Mono-oxygenase; P450; HBOA; BX4

1. Introduction

The cyclic hydroxamic acids DIBOA (2,4-dihydroxy-1,4-benzoxazin-3-one) and DIMBOA (2,4-dihydroxy-7-methoxy-1,4-benzoxazin-3-one) are important enhancers of the sustainability of grasses (Gramineae) against insects and micro-organisms (Niemeyer, 1988; Sicker et al., 2000).

Investigations on the biosynthesis of DIBOA and DIMBOA in maize revealed the involvement of several P450 enzymes (Frey et al., 1997). Their corresponding genes have been cloned (Frey et al., 1995) and heterologously expressed in yeast. The general course of the biosynthesis from indole has been established (Frey et al., 1997) and the kinetic parameters for each reaction step have been determined (Glawischnig et al., 1999). BX4, an enzyme of the CYP71C subfamily, catalyses the oxidative ring expansion of 3-hydroxy-indolin-2-one to 2-hydroxy-1,4-benzoxazin-3-one (HBOA), a reaction, whose mechanism remained obscure (Frey et al., 1997). In this paper we demonstrate that the action of $^{18}O_2$ on 3-hydroxyindolin-2-one (**1**) in the presence of BX4 leads to labelling of the ring oxygen atom in HBOA in accordance with the mechanism proposed in Scheme 2.

2. Results and discussion

BX4 was expressed heterologously in the yeast strain WAT11 (Frey et al., 1997; Glawischnig et al., 1999). Microsomes were isolated from galactose induced yeast cells (Pompon et al., 1996). 3-Hydroxyindolin-2-one (**2**) was incubated with these microsomes under an atmosphere of $^{18}O_2$, and the reaction product HBOA was isolated. The labelled HBOA and the unlabelled HBOA, respectively, were subjected to trimethylsilylation in order to allow further purification by GC and identification by MS (Woodward et al., 1979). The GC of the unlabelled compound exhibits two main peaks. One with a molecular ion at m/z 237 corresponds to *O*-trimethylsilyl-HBOA, the second at m/z 309 to the *O,N*-bistrimethylsilyl derivative (Woodward et al., 1979). The spectra of the products prepared under an $^{18}O_2$ atmosphere indicated the incorporation of one labelled oxygen atom by a shift of two mass units for the corresponding molecular ions. The position of the label can be deduced from the fragmentation pattern of *O*-trimethylsilyl-HBOA (m/z 239) given in Scheme 1. Most indicative are two fragment ions at m/z 210 and 121 that are formed from the molecular ion by loss of $H^{16}CO$ or

* Corresponding author. Tel.: +49-89-21807757; fax: +49-89-2180 7756.
E-mail address: wos@cup.uni-muenchen.de (W. Steglich).

0031-9422/01/$ - see front matter © 2001 Elsevier Science Ltd. All rights reserved.
PII: S0031-9422(01)00037-1

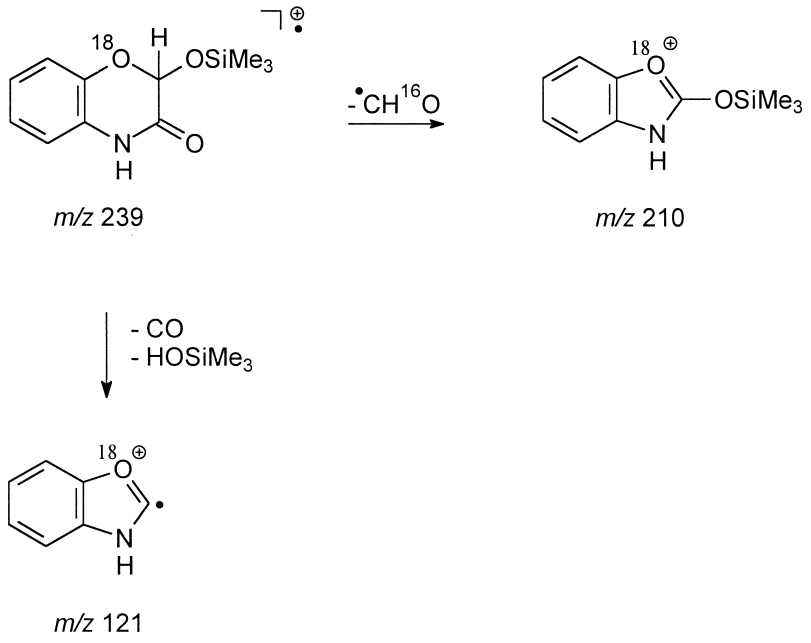

Scheme 1. Generation of the ions *m/z* 210 and 121 in the MS of ^{18}O-labelled *O*-trimethylsilyl-HBOA (*m/z* 239).

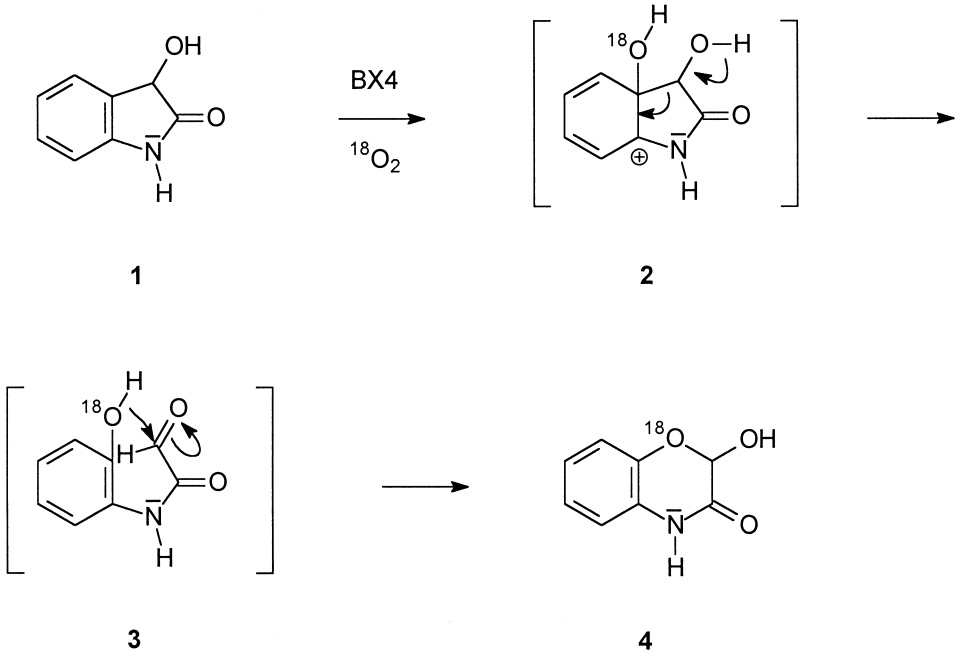

Scheme 2. Ring expansion of 3-hydroxyindolin-2-one (**1**) catalyzed by BX4 under an $^{18}O_2$-atmosphere.

$C^{16}O$ and $H^{16}OSiMe_3$, respectively. Since the ion *m/z* 121 still retains the ^{18}O-label, the labelled oxygen in HBOA has to be placed at ring position 1.

Cytochrome P450 enzymes (Sono et al., 1996) are known to catalyze arene epoxidation and aromatic hydroxylation by molecular oxygen. These biochemical transformations are involved in a great variety of oxidative biosynthetic pathways in plants (Halkier, 1996; Schuler, 1996). In the case of 3-hydroxyindolin-2-one (**1**) the oxidative ring expansion to 2-hydroxy-1,4-benzoxazinone (**4**) by BX4 and molecular oxygen can be explained by the mechanism given in Scheme 2. Attack of an electrophilic oxygen species at C-3a of the indole system should lead to a delocalized cation **2** (Newcomb and

Toy, 2000) or its protonated epoxide equivalent, which then fragments under rearomatization to yield the phenolic aldehyde **3**. In the last step, 2-hydroxy-1,4-benzoxazin-3-one (**4**) is formed by intramolecular addition of the phenolic ^{18}OH group to the aldehyde function. This mechanism is in accordance with the outcome of the labelling experiment.

3. Experimental

3.1. General

Gas chromatography/mass spectrometry (GC–MS) was performed on a Finnigan MAT 90 double focussing mass spectrometer, equipped with an EI ion source operating at 70 eV. For GC–MS, a Varian GC 3400 gas chromatograph with a fused silica DB-5ms capillary column (30 m × 0.25 mm, coated with a 0.25 μm layer of liquid phase) and helium as carrier gas was used for sample separation (flow rate: 1.5 ml/min; split ratio: 1:30). The injector temperature was kept at 300°C, injection volumes were 0.2–0.4 μl of a 1–2% (m/v) solution. Temperature programme: 2 min isothermal at 50°C, then 10 K/min up to 300°C, finally 10 min isothermal at 300°C. Retention indices R_i (Kováts, 1958) were determined by co-injection of a 0.2 μl sample of a standard mixture of saturated straight chain alkanes (C_{10}–C_{36}).

3.2. Labelling experiment

3-Hydroxyindolin-2-one was synthesized from isatin by reduction in a yeast cell culture (Frey et al., 1997). BX4 was expressed heterologously in the yeast strain WAT11 as described (Frey et al., 1997). Microsomes were isolated from galactose induced yeast cells (Pompon et al., 1996) and the concentration of microsomal protein was determined. Microsomes (18 mg microsomal protein) were suspended in 5 ml of sodium phosphate buffer (40 mM, pH 7.5), containing dithiothreitol (1.4 mM) and glycerol (6%) and kept at 0°C. NADPH and 3-hydroxyindolin-2-one were added (0.7 and 0.19 mM final concentration, respectively). The reaction vessel was flushed with nitrogen before $^{18}O_2$ (Cambridge Isotope) was applied. After 2 h at 25°C, the reaction was stopped by addition of MeOH (1.5 ml) and acidified to pH 2 with HOAc (1 M, 0.4 ml). The suspension was centrifuged (15 min, 4800 rpm) and the supernatant was extracted (3×) with EtOAc (3 ml). After evaporation of the solvent, the residue was dissolved in MeOH. The labelled HBOA was purified by HPLC [90% H_2O, 10% HOAc, 6 ml/min, detection at 254 nm using a Merck Lichrosphere RP-18 column (10 × 250 mm), R_t: 15 min]. HBOA was trimethylsilylated with 10 μl BSTFA [bis(trimethylsilyl)trifluoroacetamide] (65°C, 30 min) (Stalling et al., 1968). Unlabelled HBOA as reference compound was also subjected to trimethylsilylation prior to the GC–MS investigation.

3.3. Mass spectral data

Unlabelled *O*-trimethylsilyl-HBOA: R_i 1741; GC–MS *m/z* (rel. int.): 237 $[M]^+$ (76), 222 (58), 209 $[M\text{-}CO]^+$ (19), 208 (59), 194 (60), 166 (41), 150 (20), 135 (12), 119 (45), 75 (78), 73 (100), 65 (8), 45 (18); unlabelled *N,O*-bistrimethylsilyl-HBOA: R_i 1634; GC–MS *m/z* (rel. int.): 309 $[M]^+$ (45), 294 (19), 280 (6), 266 (18), 250 (2), 237 (8), 220 (10), 208 (13), 192 (20), 179 (9), 176 (15), 165 (16), 164 (15), 147 (50), 119 (5), 103 (11), 91 (3), 75 (25), 73 (100), 59 (4), 45 (13); ^{18}O-labelled *O*-trimethylsilyl-HBOA: R_i 1741; GC–MS *m/z* (rel. int.): 239 $[M]^+$ (65), 224 (59), 211 $[M\text{-}CO]^+$ (25), 210 (78), 196 (47), 183 (3), 180 (4), 178 (3), 168 (38), 152 (21), 137 (9), 135 (6), 121 (42), 97 (3), 91 (4), 75 (98), 73 (100), 65 (6), 45 (15);^{18}O-labelled *N,O*-bistrimethylsilyl-HBOA: R_i 1634; GC–MS *m/z* (rel. int.): 311 $[M]^+$ (100), 296 (27), 282 (12), 268 (23), 252 (2), 239 (8), 222 (16), 210 (19), 194 (22), 191 (18), 181 (8), 178 (9), 167 (13), 166 (11), 147 (65), 121 (3), 103 (5), 91 (2), 77 (3), 75 (21), 73 (100), 59 (2), 45 (13).

Acknowledgements

We thank Dr. Monika Frey, Garching, for suggestions and helpful discussions and Sebastian Grün for preparation of the induced yeast cell culture. This work was supported by SFB 369 of the Deutsche Forschungsgemeinschaft.

References

Frey, M., Chomet, P., Glawischnig, E., Stettner, C., Grün, S., Winklmair, A., Eisenreich, W., Bacher, A., Meeley, R.B., Briggs, S.P., Simcox, K., Gierl, A., 1997. Analysis of a chemical plant defence mechanism in grasses. Science 277, 696–699.

Frey, M., Kliem, R., Saedler, H., Gierl, A., 1995. Expression of a cytochrome P450 gene family in maize. Mol. Gen. Genet. 246, 100–109.

Glawischnig, E., Grün, S., Frey, M., Gierl, A., 1999. Cytochrome P450 monooxygenases of DIBOA biosynthesis: specificity and conservation among grasses. Phytochemistry 50, 925–930.

Halkier, B.A., 1996. Catalytic reactivities and structure/function relationships of cytochrome P450 enzymes. Phytochemistry 43, 1–21.

Kováts, E., 1958. Gas-chromatographische Charakterisierung organischer Verbindungen. Teil 1: Retentionsindizes aliphatischer Halogenide, Alkohole, Aldehyde und Ketone. Helv. Chimi. Acta 41, 1915–1932.

Newcomb, M., Toy, P.H., 2000. Hypersensitive radical probes and the mechanisms of cytochrome P450-catalyzed hydroxylation reactions. Acc. Chem. Res. 33, 449–455.

Niemeyer, H.M., 1988. Hydroxamic acids (4-hydroxy-1,4-benzoxazin-3-ones), defense chemicals in the Gramineae. Phytochemistry 27, 3349–3358.

Pompon, D., Louerat, B., Bronine, A., Urban, P., 1996. Yeast expression of animal and plant P450s in optimized redox enviroments. Methods in Enzymology 2, 51–64.

Schuler, M.A., 1996. Plant cytochrome P450 monooxygenases. Crit. Rev. Plant. Sci. 15, 235–284.

Sicker, D., Frey, M., Schulz, M., Gierl, A., 2000. Role of natural benzoxazinones in the survival strategy of plants. Int. Rev. Cytol. 198, 319–346.

Sono, M., Roach, M.P., Coulter, E.D., Dawson, J.H., 1996. Heme-containing oxygenases. Chem. Rev. 96, 2841–2887.

Stalling, D.L., Gehrke, Ch.W., Zumwalt, R.W., 1968. A new silylation reagent for amino acids: *N*,*N*-bis(trimethylsilyl)trifluoroacetamide (BSTFA). Biochem. Biophys. Res. Commun. 31, 616–622.

Woodward, M.D., Corcuera, L.J., Schnoes, H.K., Helgeson, J.P., Upper, C.D., 1979. Identification of 1,4-benzoxazin-3-ones in maize extracts by gas-liquid chromatography and mass spectrometry. Plant Physiol. 63, 9–13.

PERGAMON

Phytochemistry 57 (2001) 377–383

PHYTOCHEMISTRY

www.elsevier.com/locate/phytochem

Biotransformation of squamulosone by *Curvularia lunata* ATCC 12017

Dwight O. Collins [a], Greg O. Buchanan [a], William F. Reynolds [b], Paul B. Reese [a,*]

[a] *Department of Chemistry, University of the West Indies, Mona, Kingston 7, Jamaica*
[b] *Department of Chemistry, University of Toronto, Toronto, Ontario, Canada M5S 3H6*

Received 28 September 2000; received in revised form 26 January 2001

Dedicated to Dr. Earle V. Roberts in celebration of his service of over 30 years to the Chemistry Department, University of the West Indies, Mona Campus

Abstract

Squamulosone (aromadendr-1(10)-en-9-one), isolated in large quantity from the plant *Hyptis verticillata* Jacq. (Labiatae), was incubated with the fungus *Curvularia lunata* ATCC 12017 in two different growth media. Six metabolites were isolated from each medium, with five of the products being common to both fermentations. All seven metabolites are novel. The insecticidal activity of these aromadendranes was evaluated against the sweet potato weevil *Cylas formicarius elegantulus*. © 2001 Elsevier Science Ltd. All rights reserved.

Keywords: *Curvularia lunata* ATCC 12017; Squamulosone; Biotransformation; Hydroxylation; *Hyptis verticillata*; Aromadendrane; Cadinane; Sesquiterpene

1. Introduction

Hyptis verticillata Jacq., a member of the Labiatae family of plants, has been traditionally used in the treatment of eczema, psoriasis, scabies, athlete's foot, rheumatoid arthritis and cold-related problems (Stanley, 1928; Ayensu, 1981; Morton, 1981). Previous investigations of this plant have led to the isolation of several compounds including lignans, flavonoids, triterpenes and a sesquiterpene (cadina-4,10(15)-dien-3-one), some of which possess interesting biological activities (German, 1971; Okuda et al., 1982, 1984; Tsuchiya et al., 1985; Klopman and Buyukbingol, 1988; Wang et al., 1989; Yasukawa et al., 1989; Broomhead and Dewick, 1990; Novelo et al., 1993; Kuhnt et al., 1994, 1995; Porter et al., 1995).

We now report the isolation of two further sesquiterpenes: squamulosone (aromadendr-1(10)-en-9-one) (**1**) and cadin-4-en-1β-ol (**9**). Squamulosone (**1**), first isolated from *Phebalium squamulosum* Vent. (Rutacaceae), was rigorously characterised by chemical means (Batey et al., 1971). Its enantiomer, millecrone B, was later isolated from the South African nudibranch *Leminda millecra* (Pika and Faulkner, 1994). Cadin-4-en-1β-ol (**9**) was first identified from a *Streptomyces* sp. (Gerber, 1971). This is, however, the first reported isolation of these compounds from *H. verticillata*.

In our ongoing programme to examine the metabolism of terpenes by fungi (Hanson et al., 1994b; Buchanan and Reese, 2000), compound **1** was fed to *Curvularia lunata* ATCC 12017 (synonyms: IMI 61535, CBS 215.54, NRRL 2380) using two different media: potato dextrose broth (PDB) and a beef extract medium (BEM). Six metabolites were isolated from each fermentation with five of the products being common to both fermentations. All analogues produced were novel. *C. lunata* is well known for its efficient 11β-hydroxylation of steroids (Lin and Smith, 1970a, 1970b; Ohlson et al., 1980; Sonomoto et al., 1983; Holland and Riemland, 1985; Mazumder et al., 1985; Chen and Wey, 1990), but it has also been used to transform a number of terpenes (Azerad, 2000) including *R*-(+)-pulegone (Ismaili-Alaoui et al., 1992), (*R*)-hydrophenanthrenone (Hammoumi et al., 1993), a number of 1,6-difunctionalised eudesmanes (Garcia-Granados et al., 1991), and an

* Corresponding author. Tel.: +876-927-1910; fax: +876-977-1835.

E-mail address: pbreese@uwimona.edu.jm (P.B. Reese).

0031-9422/01/$ - see front matter © 2001 Elsevier Science Ltd. All rights reserved.
PII: S0031-9422(01)00060-7

aromadendrane (de Lima et al., 1999). Previously, a number of aromadendranes have been incubated with fungi including *Cephalosporium aphidicola* (Hanson et al., 1994a), *Glomerella cingulata* (Miyazawa et al., 1994, 1995), *Mucor plumbeus* (Guillermo et al., 1997), *Beauveria densa* and *B. bassiana* (de Lima et al., 1999), and also with a limited number of bacteria (Abraham et al., 1992). However, this is the first report of the incubation of squamulosone with a microorganism and also the first record of hydroxylation on the cyclopentane ring of the aromadendrane skeleton by any microorganism.

2. Results and discussion

Reinvestigation of the dichloromethane extract of *H. verticillata* has led to the isolation of the aromadendrane **1** in a significant (0.06%) yield. The IR and UV spectra of **1** revealed the presence of an α,β-unsaturated carbonyl, while the ^{13}C and DEPT NMR spectra indicated a molecular formula of $C_{15}H_{22}O$. The compound was thus a tricyclic terpene. The ^{1}H NMR spectrum contained two highly shielded protons resonating at 0.71 and 0.82 ppm, that were indicative of a cyclopropane ring. A comparison of the ^{1}H and ^{13}C NMR data with the literature (Batey et al., 1971; Pika and Faulkner, 1994) indicated that **1** was aromadendr-1(10)-en-9-one: either squamulosone or its enantiomer millecrone B. The laevorotatory nature of **1**, however, confirmed the structure of this compound as that of squamulosone.

The second sesquiterpene isolated was obtained as a mixture with cadina-4,10(15)-dien-3-one, a major compound of the dichloromethane extract (Porter et al., 1995). The mixture was subjected to reduction using lithium aluminium hydride in the presence of lanthanum chloride. This produced the more polar 3α-hydroxycadina-4,10(15)-diene (Neef et al., 1982) and thus enabled the isolation of cadin-4-en-1β-ol (epicubenol) (**9**) as an oil that was identified by spectral studies and comparative analyses with literature values (Gerber, 1971).

Squamulosone (aromadendr-1(10)-en-9-one) (**1**) was incubated with *C. lunata* to yield seven analogues that were identified as 2α-hydroxyaromadendr-1(10)-en-9-one (**2**), 2β-hydroxyaromadendr-1(10)-en-9-one (**3**), 13-hydroxyaromadendr-1(10)-en-9-one (**4**), 14-hydroxyaroma dendr-1(10)-en-9-one (**5**), 2β,13-dihydroxyaromadendr-1(10)-en-9-one (**6**), 13,14-dihydroxyaromadendr-1(10)-en -9-one (**7**) and 10α-hydroxy-1,2-epoxyaromadendran-9-one (**8**).

The IR spectrum of **2** highlighted the presence of a hydroxyl group and this was seen to be borne by a methine resonating at 74.8 ppm in the ^{13}C NMR spectrum. The downfield shift of ~10 ppm for C-3 and the the upfield shift of 5.1 ppm for C-4 justified the placement of the new hydroxyl at C-2. Additionally, data from the HR(EI)MS confirmed the molecular formula to be $C_{15}H_{22}O_2$ (*m*/*z* 234.1610). This formula was also applicable to **3**, ($[M]^+ = 234.1617$), which was found to be a C-2 epimer of **2**. The stereochemistry of the new function in **2** followed from the large coupling constant of 14.6 Hz for H-2. Analogue **3**, having a much reduced coupling constant ($J = 5.1$ Hz) and a slightly higher resonance value (δ 4.92) when compared with **2**, therefore, possessed a β stereochemistry for the hydroxyl.

In isomer **4**, the disappearance of the methyl singlet at δ 1.07 in the ^{1}H NMR spectrum of the substrate occurred simultaneously with the appearance of two doublets at δ 3.33 and 3.42 ($J = 11.1$ Hz). These signals were assigned to the diastereotopic protons on the now hydroxylated C-13. This was supported by the appearance of a methylene resonance at δ 72.0 in the ^{13}C NMR spectrum and was confirmed by the HR(EI)MS data (*m*/*z* 234.1615, $C_{15}H_{22}O_2$).

Similar observations were made for analogue **5** where a large downfield shift of the vinylic methyl protons of the substrate from 1.78 to 4.31 ppm was seen. The relatively low value of the oxygen-bearing methylene at δ 61.1, which was a direct result of the anisotropic effect of the carbon–carbon double bond on the primary alcohol, reinforced the positioning of the new hydroxyl function on C-14.

Data from the HR(EI)MS of **6** suggested a molecular formula of $C_{15}H_{22}O_3$ ($[M]^+ = 250.1569$) and this indicated the presence of two additional hydroxyl groups. The two new oxygen-bearing carbons observed in the ^{13}C NMR were present as a methine (δ 74.2) and a methylene (δ 71.9) and were assigned to C-2 and C-13, respectively. Comparison of the chemical shifts within the cyclopentane and cyclopropane rings with those observed for **3** and **4** supported hydroxyl insertion at the sites proposed. Again, the low value for the coupling constant of the H-2 proton (d, $J = 4.7$) proved useful in fixing the stereochemistry of the C-2 hydroxyl as β.

The second dihydroxylated product, **7**, lacked the H-13 and H-14 methyl singlets (δ 1.07 and 1.78) present in the ^{1}H NMR spectrum of the fed substrate. A comparison of the carbon resonance values of this metabolite with both **4** and **5** verified **7** as 13,14-dihydroxyaromadendr-1(10)-en-9-one.

Derivative **8** possessed a molecular formula of $C_{15}H_{22}O_3$ ($[M]^+ = 250.1561$) and inherently had five degrees of unsaturation. With the carbonyl remaining intact (δ 208.3), the additional ring was evidently derived from an epoxide function (1107 cm^{-1}) within the structure. 2D NMR data aided correct placement of the groups on the skeleton and were particularly useful in assigning stereochemistries. Analogue **8** is thought to proceed firstly through the 1,10-epoxy derivative which is then hydroxylated at C-2. This epoxide then rearranges to relieve the increased strain induced by the rigid ring

systems and the sp^2 hybridised carbon of the carbonyl. The more stable 10α-hydroxy-1,2-epoxide is thus formed. As in previous studies, where methyl groups on the cyclopropane ring of aromadendranes were hydroxylated by fungal mono-oxygenases, it was observed that the cyclopropane ring remained intact (Azerad, 2000).

Squamulosone (**1**) was found to possess insecticidal activity against *Cylas formicarius elegantulus* (the sweet potato weevil), a major pest of the sweet potato, *Ipomoea* sp. (Buchanan and Reese, 2000). Thus we were prompted to compare the toxicity of **1** with that of its biotransformed analogues (Table 2). Epoxide **8** was not isolated in quantities sufficient for bioassay. Squamulosone (**1**) was an effective insecticide after 48 h at a concentration of 60 μg per insect, surpassed only by its 13-hydroxy derivative (**4**). All metabolites effected high mortalities after 72 h. It would appear that the insertion of a hydroxyl group at C-13 increases the toxicity of the terpene, however, the opposite is seen when this substituent is placed at C-2 or-14.

In summary sesquiterpenes **1** and **9** have been isolated for the first time from aerial parts of *H. verticillata*. Terpene **1** has been transformed by *C. lunata* to seven novel metabolites. Hydroxylation occurred on the C-13 methyl group and at the C-2 and-14 allylic positions. The aromadendranes **1**–**7** were found to possess insecticidal activity.

3. Experimental

^1H and ^{13}C NMR spectra were generated in deuterated chloroform at 200 and 50 MHz, respectively, using a Bruker AC200 instrument. 2D NMR data were also generated in deuterated chloroform at 500 and 125 MHz, respectively, using a Varian Unity 500 NMR spectrometer. Tetramethylsilane (TMS) was used as the internal standard. ^{13}C NMR assignments for the aromadendranes are listed in Table 1. Melting points were determined on a Thomas–Hoover capillary melting point apparatus. Infrared data were acquired on a Perkin Elmer FTIR Paragon 1000 instrument using KBr disks. The UV spectra were determined on a Hewlett Packard HP 8452A spectrophotometer. Optical rotations were acquired on a Perkin Elmer 241 polarimeter. High-resolution electron impact mass spectrometry (HREIMS) was performed on a VG 70-250S instrument at an ionising voltage of 70 eV. Column chromatography was performed with Kieselgel silica (40–63 μm). Compounds on TLC plates were visualised by the use of the ammonium phosphomolybdate/sulfuric acid spray reagent followed by heating at 120°C. *Curvularia lunata* ATCC 12047 was obtained from the American Type Culture Collection, Rockville, MD, USA. Petrol refers to the petroleum fraction boiling between 60 and 80°C.

Table 1
C-13 NMR chemical shifts for aromadendranes **1**–**8**

	Compound							
	1	**2**	**3**	**4**	**5**	**6**	**7**	**8**
C-1	166.4	164.7	163.7	166.0	170.6	163.2	170.2	73.6
C-2	34.1	74.8	74.2	34.0	33.2	74.2	33.1	61.7
C-3	32.2	42.3	41.5	32.2	32.3	41.5	32.3	32.8
C-4	37.2	32.1	33.6	37.3	36.7	33.8	36.9	31.1
C-5	45.2	45.1	43.5	44.2	45.5	42.5	44.5	39.1
C-6	31.3	31.6	31.9	27.7	31.3	28.2	27.7	21.1
C-7	22.8	22.7	22.4	19.7	22.5	19.2	19.4	21.1
C-8	41.9	42.1	41.9	41.2	42.2	41.3	41.6	33.8
C-9	201.0	201.6	202.0	200.4	203.0	201.2	202.8	208.3
C-10	130.3	133.6	133.8	130.5	133.6	134.1	133.7	77.5
C-11	25.7	25.8	25.8	31.6	25.9	31.6	31.7	19.5
C-12	16.0	16.2	16.0	11.8	16.0	11.6	11.6	27.7
C-13	28.2	28.1	28.1	72.0	28.1	71.9	71.7	15.4
C-14	14.9	14.3	14.6	14.9	61.1	14.7	61.1	24.4
C-15	15.4	15.6	15.1	15.4	15.3	15.2	15.3	13.9

Table 2
Insecticidal activity of the aromadendranes against adult *Cylas formicarius elegantulus*. Values are means of duplicate assays

Compounds	Dosage per insect (mg)	Mortality (%)		
		24 h	48 h	72 h
	0.02	0	50	70
1	0.04	10	60	100
	0.06	10	80	100
	0.02	0	0	0
2	0.04	0	30	80
	0.06	0	30	80
	0.02	0	30	70
3	0.04	0	30	100
	0.06	0	30	100
	0.02	0	40	80
4	0.04	10	40	100
	0.06	10	100	100
	0.02	0	0	70
5	0.04	0	30	80
	0.06	0	30	90
	0.02	0	10	60
6	0.04	0	20	70
	0.06	10	30	80
	0.02	10	30	80
7[a]	0.04	10	40	80
	0.06	*	*	*
Control	0.00	0	0	0

[a] *Compound **7** was not present in sufficient quantities for evaluation at 0.06 mg/insect.

4. Extraction and isolation

Hyptis verticillata plant material was collected in St Andrew, Jamaica. A voucher specimen was deposited in

the Botany Herbarium, UWI (accession number No. 33483). The green leaves and stems (17.61 kg) were chopped and extracted twice with CH_2Cl_2 (47 l) at room temperature. The extracts were pooled and concentrated in vacuo to produce a dark green gum (145.5 g). The crude gum was chromatographed on silica gel using 3% EtOAc in petrol to give eight major fractions (A–H). The moderately non-polar fraction B (42.3 g) was subjected to further purification by column chromatography using 1% EtOAc in petrol. This led to the isolation of a (99:1) (w/w) mixture of cadina-4,10(15)-dien-3-one and cadin-4-en-1β-ol (**9**) (6.3 g) and aromadendr-1(10)-en-9-one (**1**) (10.3 g).

4.1. Aromadendr-1(10)-en-9-one (*1*)

Needles from acetone, mp 50–51°C, $[\alpha]_D^{25}$:−202° ($c=1.43$, $CHCl_3$) [lit. mp 45–46°C, $[\alpha]_D$:−234° ($c=1.2$, $CHCl_3$) (Batey et al., 1971)]; IR ν_{max} 2954, 2871, 1639 (C=O), 1468, 1315 cm^{-1}; UV (MeOH) λ_{max} (log ε) 254 (3.81); ^1H NMR: δ 0.71 (1H, *ddd*, $J=5.2$, 9.5, 11.8 Hz, H-7), 0.82 (1H, *dd*, $J=9.5$, 11.1 Hz, H-6), 1.04 (3H, *d*, $J=6.5$ Hz, H-15), 1.07 (3H, *s*, H-13), 1.18 (3H, *s*, H-12), 1.42 (1H, *m*, $\frac{w}{2}=26.7$ Hz, H-3), 1.78 (3H, *bs*, H-14), 1.87 (1H, *m*, $\frac{w}{2}=18.7$ Hz, H-3), 2.21 (1H, *m*, $\frac{w}{2}=24.0$ Hz, H-4), 2.34 (1H, *m*, $\frac{w}{2}=22.3$ Hz, H-2), 2.35 (1H, *dd*, $J=11.8$, 14.8 Hz, H-8), 2.62 (1H, *bt*, $J=11.0$ Hz, H-5), 2.67 (1H, *bdd*, $J=8.2$, 18.0 Hz, H-2), 2.81 (1H, *dd*, $J=5.2$, 14.8 Hz, H-8).

4.2. Cadin-4-en-1β-ol (*9*)

A mixture of cadina-4,10(15)-dien-3-one and cadin-4-en-1β-ol (**9**) (2.00 g) was dissolved in dry THF (50 ml). Lanthanum chloride (2.22 g, 9.13 mmol) was added and the suspension was stirred at room temperature (15 min). Lithium aluminium hydride (1.39 g, 36.52 mmol) was added and the mixture was stirred for another 10 min (until effervescence ceased). The mixture was neutralised with dilute hydrochloric acid and extracted with Et_2O (100 ml×3). The organic layer was dried with magnesium sulfate and concentrated in vacuo to afford a solid which was chromatographed on silica gel with 3% EtOAc in petrol. This gave 3α-hydroxycadina-4,10(15)-diene (1.35 g, 6.14 mmol) as needles from petrol-acetone, mp 115–117°C, $[\alpha]_D^{25}$ −107° ($CHCl_3$ 0.15) [lit. mp 116–117°C, $[\alpha]_D^{25}$ −107° ($CHCl_3$ 0.15) (Buchanan and Reese, 2000)]; IR (KBr) ν_{max} cm^{-1} 3402 (OH), 1652 (C=C); ^1H NMR δ 0.74 (3H, *d*, $J=7.60$ Hz, H-14), 0.90 (3H, *d*, $J=7.60$ Hz, H-13), 1.78 (3H, *d*, $J=0.80$ Hz, H-11), 4.25 (1H, *bm*, $\frac{w}{2}=19.10$ Hz, H-3), 4.57 (1H, *d*, $J=0.85$ Hz, H-15), 4.70 (1H, *d*, $J=0.85$ Hz, H-15), 5.60 (1H, *d*, $J=0.85$ Hz, H-5); ^{13}C NMR δ 15.0 (C-13), 19.3 (C-11), 21.4 (C-14), 26.3 (C-12), 26.4 (C-8), 35.9 (C-9), 36.2 (C-2), 43.6 (C-6), 45.4 (C-7), 46.3 (C-1), 71.0 (C-3), 103.7 (C-15),125.7 (C-5), 136.8 (C-4), 151.6 (C-10).

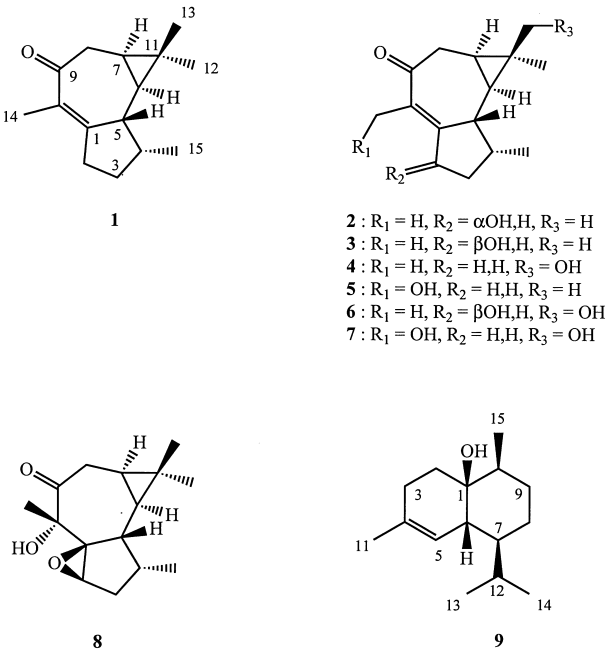

Fig. 1. Aromadendrane and cadinane sesquiterpenes.

Also eluting in 3% EtOAc in petrol was cadin-4-en-1β-ol (**9**) (23 mg), as a gum, $[\alpha]_D^{25}$: 100° ($c=0.3$, $CHCl_3$) [lit. oil, $[\alpha]_D^{25}$: −96° ($CHCl_3$) (Gerber, 1971)]; IR (KBr) ν_{max} cm^{-1} 3425, 1456, 1386, 1074, 1026; ^1H NMR δ 0.84 (3H, *s*, H-14), 0.90 (3H, *s*, H-13), 1.02 (3H, *d*, $J=7.5$ Hz, H-15), 1.14 (1H, *septet*, $J=4.8$ Hz, H-7), 1.32 (2H, *t*, $J=4.7$ Hz, H-8), 1.38 (1H, *m*, $\frac{w}{2}=17.7$ Hz, H-2α), 1.52 (2H, *m*, $\frac{w}{2}=17.5$ Hz, H-9), 1.69 (3H, *s*, H-11), 1.80 (1H, *m*, $\frac{w}{2}=16.7$ Hz, H-10), 1.99 (1H, *d*, $J=2.5$ Hz, H-3β), 2.01 (1H, *m*, $\frac{w}{2}=5.4$ Hz, H-12), 2.07 (1H, *m*, $\frac{w}{2}=15.0$ Hz, H-6), 2.13 (1H, *s*, H-2β), 2.15 (1H, *s*, H-3α), 5.37 (1H, *d*, $J=5.0$ Hz, H-5); ^{13}C NMR: δ 14.0 (C-15), 16.8 (C-14), 18.9 (C-8), 21.8 (C-13), 23.4 (C-11), 27.2 (C-12), 27.8 (C-3), 28.5 (C-9), 31.3 (C-2), 37.2 (C-10), 41.8 (C-6), 49.1 (C-7), 72.3 (C-1), 123.4 (C-5), 133.4 (C-4).

5. Feeding protocol

The fungus was maintained on potato dextrose agar (PDA) slants. PDB was comprised of potato dextrose broth (24 g l^{-1}) (Chen and Wey, 1990). BEM was composed of peptone (1 g l^{-1}), yeast extract (1 g l^{-1}), beef extract (1 g l^{-1}) and glucose (5 g l^{-1}) (Garcia-Granados et al., 1991). One 14 day old slant was used to inoculate four 500 ml conical flasks each containing 125 ml of liquid medium. The flasks were incubated at 200 rpm at 27°C. An EtOAc solution (2 ml) containing 10% of the total mass of the substrate was fed 24 h after inoculation. The remaining 20, 30 and 40% portions of the substrate were fed at 36, 48 and 60 h after inoculation, respectively. The fermentation was allowed to proceed for a further 10 days. The pH was measured and the

mycelium was filtered from the broth. Broth extraction utilised EtOAc (3×500 ml). The mycelium was homogenised in EtOAc. The extracts were dried with sodium sulfate, concentrated in vacuo, and analysed by thin-layer chromatography.

6. Incubation of aromadendr-1(10)-en-9-one (1)

Squamulosone (**1**) (1 g) was fed to *C. lunata* in 20 flasks of each medium as outlined above. The fungus was harvested 10 days after the final feed to give broth extracts (0.578 and 0.683 g) and mycelial extracts (0.922 and 0.762 g) from PDB and BEM, respectively. The pH at the end of each fermentation was 6.5. Analysis of both extracts by TLC indicated the presence of biotransformed compounds. The broth and mycelial extracts of each fermentation were combined and subjected to column chromatography using increasing concentrations of EtOAc in petrol.

6.1. 2α-Hydroxyaromadendr-1(10)-en-9-one (2)

(PDB, 71 mg; BEM, 88 mg) cubes from acetone; mp 72–74°C; $[\alpha]_D^{25}$: −91° ($c=18.6$, $CHCl_3$); IR ν_{max} cm^{-1} 3348 (OH), 1628 (C=O); UV ($CHCl_3$) λ_{max} (log ε) 257 (2.69); EIMS *m/z* (rel. int.) 234.1610 (93) ($[M]^+$, $C_{15}H_{22}O_2$, 234.1620), 219 (57), 173 (63), 165 (48), 163 (45), 149 (100), 147 (54), 121 (42), 119 (78), 107 (84), 91 (46); ^1H NMR: δ 0.77 (1H, *ddd*, *J* = 5.4, 9.5, 11.7 Hz, H-7), 1.00 (1H, *dd*, *J* = 9.5, 11.4 Hz, H-6), 1.08 (3H, *s*, H-13), 1.10 (3H, *d*, *J* = 6.6 Hz, H-15), 1.18 (3H, *s*, H-12), 1.62 (1H, *ddd*, *J* = 7.6, 9.5, 12.3 Hz, H-3), 1.95 (3H, *t*, *J* = 2.9 Hz, H-14), 2.08 (1H, *ddt*, *J* = 2.9, 6.6, 14.6 Hz, H-3), 2.24 (1H, *dd*, *J* = 1.0, 6.6 Hz, H-4), 2.37 (1H, *d*, *J* = 11.7 Hz, H-8), 2.62 (1H, *m*, $\frac{w}{2}$ = 15.2 Hz, H-5), 2.87 (1H, *dd*, *J* = 5.4, 15.2 Hz, H-8), 4.81 (1H, *t*, *J* = 14.6 Hz, H-2).

6.2. 2β-Hydroxyaromadendr-1(10)-en-9-one (3)

(PDB, 24 mg; BEM, 37 mg) cubes from acetone; mp 85–86°C; $[\alpha]_D^{25}$: −186° ($c=6.3$, $CHCl_3$); IR ν_{max} cm^{-1} 3423 (OH), 2933, 1652 (C=O); UV ($CHCl_3$) λ_{max} (log ε) 256 (3.00); EIMS *m/z* (rel. int.) 234.1617 (38) ($[M]^+$, $C_{15}H_{22}O_2$, 234.1620), 219 (59), 149 (100), 147 (44), 121 (41), 119 (73), 102 (96), 91 (39); ^1H NMR: δ 0.66 (H, *m*, $\frac{w}{2}$ = 9.2 Hz, H-7), 0.78 (1H, *dd*, *J* = 9.2, 19.6 Hz, H-6), 1.05 (3H, *d*, *J* = 6.6 Hz, H-15), 1.07 (3H, *s*, H-13), 1.19 (3H, *s*, H-12), 1.56 (1H, *ddd*, *J* = 4.7, 12.3, 13.3 Hz, H-3), 1.93 (3H, *d*, *J* = 1.6 Hz, H-14), 2.37 (1H, *dd*, *J* = 11.7, 14.9 Hz, H-8), 2.84 (1H, *dd*, *J* = 5.1, 14.9 Hz, H-8), 4.92 (1H, *d*, *J* = 5.1 Hz, H-2).

6.3. 13-Hydroxyaromadendr-1(10)-en-9-one (4)

(PDB, 5 mg; BEM, 6 mg) Oil; $[\alpha]_D^{25}$: −118° ($c=4.4$, $CHCl_3$); IR ν_{max} cm^{-1} 3488 (OH), 2953, 1630 (C=O); UV ($CHCl_3$) λ_{max} (log ε) 256 (3.12); EIMS *m/z* (rel. int.) 234.1615 (8) ($[M]^+$, $C_{15}H_{22}O_2$, 234.1620), 179 (83), 159 (44), 149 (100), 91 (55); ^1H NMR: δ 0.87 (1H, *m*, $\frac{w}{2}$ = 14.9 Hz, H-7), 0.99 (1H, *m*, $\frac{w}{2}$ = 8.5 Hz, H-6), 1.06 (3H, *d*, *J* = 7.0 Hz, H-15), 1.29 (3H, *s*, H-12), 1.78 (3H, *dd*, *J* = 1.6, 2.9 Hz, H-14), 1.88 (1H, *m*, $\frac{w}{2}$ = 19.0 Hz, H-3), 2.41 (1H, *m*, $\frac{w}{2}$ = 14.9 Hz, H-8), 2.82 (1H, *dd*, *J* = 5.1, 14.9 Hz, H-8), 3.33 (1H, *d*, *J* = 11.1 Hz, H-13), 3.42 (1H, *d*, *J* = 11.1 Hz, H-13).

6.4. 14-Hydroxyaromadendr-1(10)-en-9-one (5)

(PDB, 29 mg; BEM, 20 mg) cubes from EtOH; m.p. 61–62°C, $[\alpha]_D^{25}$: −98° ($c=3.9$, $CHCl_3$); IR ν_{max} cm^{-1} 3488 (OH), 2955, 1647 (C=O); UV ($CHCl_3$) λ_{max} (log ε) 255 (2.54); EIMS *m/z* (rel. int.) 234.1606 (13) ($[M]^+$, $C_{15}H_{22}O_2$, 234.1620), 216 (22), 173 (22), 163 (30), 161 (27), 152 (32), 149 (100), 137 (79), 119 (28), 91 (45); ^1H NMR: δ 0.72 (1H, *m*, $\frac{w}{2}$ = 9.5 Hz, H-7), 0.85 (1H, *dd*, *J* = 9.5, 19.6 Hz, H-6), 1.05 (3H, *d*, *J* = 7.0 Hz, H-15), 1.09 (3H, *s*, H-13), 1.19 (3H, *s*, H-12), 1.43 (1H, *ddd*, *J* = 7.0, 11.4, 22.5 Hz, H-3), 1.89 (1H, *m*, $\frac{w}{2}$ = 19.9 Hz, H-3), 2.22 (1H, *m*, $\frac{w}{2}$ = 12.7 Hz, H-4), 2.46 (1H, *m*, $\frac{w}{2}$ = 19.9 Hz, H-2), 2.62 (1H, *dd*, *J* = 10.1, 19.6 Hz, H-5), 4.31 (2H, *s*, H-14).

6.5. 2β,13-Dihydroxyaromadendr-1(10)-en-9-one (6)

(PDB, 12 mg) needles from acetone, mp 145–146°C; $[\alpha]_D^{25}$: −128° ($c=0.6$, $CHCl_3$); IR ν_{max} cm^{-1} 3424 (OH), 2933, 1651 (C=O); UV ($CHCl_3$) λ_{max} (log ε) 232 (2.15); EIMS *m/z* (rel. int.) 250.1569 (1) ($[M]^+$, $C_{15}H_{22}O_3$, 250.1569), 159 (41), 149 (46), 147 (55), 145 (50), 119 (51), 107 (100), 105 (44), 91 (50); ^1H NMR: δ 1.08 (3H, *d*, *J* = 6.6 Hz, H-15), 1.30 (3H, *d*, *J* = 1.3 Hz, H-12), 1.95 (3H, *t*, *J* = 1.3 Hz, H-14), 2.43 (1H, *dd*, *J* = 12.0, 15.5 Hz, H-8), 2.86 (1H, *dd*, *J* = 4.7, 14.9 Hz, H-8), 3.33 (1H, *d*, *J* = 11.0 Hz, H-13), 3.42 (1H, *d*, *J* = 11.0 Hz, H-13), 4.94 (1H, *d*, *J* = 4.7, H-2);

6.6. 13,14-Dihydroxyaromadendr-1(10)-en-9-one (7)

(PDB, 9 mg; BEM, 23 mg) oil; $[\alpha]_D$: −160° ($c=1.0$, $CHCl_3$); IR ν_{max} cm^{-1} 3438 (OH), 2935, 1621 (C=O); UV ($CHCl_3$) λ_{max} (log ε) 234 (3.07); EIMS *m/z* (rel. int.) 250.1580 (6) ($[M]^+$, $C_{15}H_{22}O_3$, 250.1569), 179 (100), 161 (55), 159 (40), 152 (52), 149 (51), 137 (99), 91 (54); ^1H NMR: δ 1.08 (3H, *d*, *J* = 6.6 Hz, H-15), 1.30 (3H, s, H-12), 2.83 (1H, *dd*, *J* = 5.1, 15.2 Hz, H-8), 3.35 (1H, *d*, *J* = 11.1 Hz, H-13), 3.44 (1H, *d*, *J* = 11.1 Hz, H-13), 4.31 (2H, bs, H-14).

6.7. 10α-Hydroxy-1,2-epoxyaromadendran-9-one (8)

(BEM, 3 mg) oil; $[\alpha]_D^{25}$: −12° ($c=0.85$, $CHCl_3$); IR ν_{max} cm^{-1} 3442 (OH), 2362, 1643 (C=O), 1107 (C–O–

C); EIMS m/z (rel. int.) 250.1561 (6) ($[M]^+$, $C_{15}H_{22}O_3$, 250.1569), 219 (13), 155 (34), 128 (36); ^{1}H NMR: δ 0.62 (1H, *dd*, $J=6.0$, 8.9 Hz, H-6), 0.68 (1H, *dd*, $J=5.6$, 8.9 Hz, H-7), 0.96 (3H, *d*, $J=7.0$ Hz, H-15), 1.08 (3H, *s*, H-13), 1.13 (3H, *s*, H-12), 1.32 (1H, *m*, $\frac{w}{2}=4.5$ Hz, H-3), 1.48 (3H, *s*, H-14), 1.90 (1H, *m*, $\frac{w}{2}=15.5$ Hz, H-5), 2.02 (1H, *d*, $J=1.3$ Hz, H-3), 2.22 (1H, *m*, $\frac{w}{2}=7.0$ Hz, H-4), 2.40 (1H, *bt*, $J=23.4$ Hz, H-8), 2.74 (1H, *dd*, $J=5.7$, 12.0 Hz, H-8), 3.77 (1H, *s*, H-2), 4.13 (1H, *s*, OH).

7. Insecticidal activity

The assays were conducted according to the method described previously (Porter et al., 1995). Briefly, adult *Cylas formicarius elegantulus* (Summer) were reared in the laboratory in glass aquaria on sweet potato tubers, *Ipomoea* sp., and were then used for insecticidal screening four weeks after adult emergence. Ten insects were transferred to each petri dish where the compounds in acetone were applied to the insects' abdomens using a Hamilton microapplicator. Applications of 2, 4 or 6 μl were done from stock solutions of 1.0% (w/v, 2.0 mg in 0.2 ml acetone) prepared for each compound. Each assay was performed in duplicate. The controls received only 2, 4 and 6 μl of acetone. The number of dead insects was recorded at 24, 48 and 72 h.

Acknowledgements

This work was supported in part by funds secured under the University of the West Indies/Interamerican Development Bank (UWI/IDB) Programme and the granting of a UWI Postgraduate Scholarship to DOC. The authors are grateful to Professor D. John Faulkner (Scripps Institute of Oceanography) for providing NMR spectra for millecrone B and, more recently to Professor Michael Davies-Coleman (Rhodes University, South Africa) for the generous gift of a sample of the compound. The authors acknowledge Professor Herbert L. Holland (Brock University) and Dr. Lawrence A. D. Williams (UWI) for helpful discussions. Optical rotations were measured at the Bureau of Standards, Kingston. Fermentations were carried out in the Biotechnology Centre, UWI.

References

Abraham, W., Kieslich, K., Stumpf, B., Ernst, L., 1992. Microbial oxidation of tricyclic sesquiterpenoids containing a dimethylcyclopropane ring. Phytochemistry 31, 3749–3755.

Ayensu, E.S., 1981. Medicinal Plants of the West Indies. Reference Publications, Algonac, MI.

Azerad, R., 2000. Regio- and stereoselective microbial hydroxylation of terpenoid compounds. In: Patel, R.N. (Ed.), Stereoselective Biocatalysis. Marcel Dekker, New York, pp. 153–180.

Batey, I.L., Hellyer, R.O., Pinhey, J.T., 1971. The structure of squamulosone, a new sesquiterpene ketone from *Phebalium squamulosum*. Aust. J. Chem. 24, 2173–2177.

Broomhead, A.J., Dewick, P., 1990. Tumour-inhibitory aryltetralin lignans in *Podophyllum versipelle*, *Diphylleia cymosa* and *Diphylleia grayi*. Phytochemistry 29, 3831–3837.

Buchanan, G.O., Reese, P.B., 2000. Biotransformation of cadinane sesquiterpenes by *Beauveria bassiana* ATCC 7159. Phytochemistry 54, 39–45.

Chen, K., Wey, H., 1990. Dissolution enzyme kinetics of 11β-hydroxylation of cortexolone by *Curvularia lunata*. Enzyme Microb. Technol. 12, 616–621.

de Lima, D.P., Carnell, A.J., Roberts, S. M., 1999. Microbial transformation of (+)-10β,14-dihydroxy-*allo*-aromadendrane and (−)-*allo*-aromadendrone. J. Chem. Res. (S) 396–397.

Garcia-Granados, A., Martinez, A., Onorato, M.E., Rivas, F., Arias, J.M., 1991. Chemical-microbial synthesis of 6β-eudesmanolides by *Curvularia lunata* cultures from eudesmanes with functions at C-1 and C-6. Tetrahedron 47, 91–102.

Gerber, N.N., 1971. Sesquiterpenoids from actinomycetes: cadin-4-ene-1-ol. Phytochemistry 10, 185–189.

German, V.F., 1971. Isolation and characterization of cytotoxic principles of *Hyptis verticillata* Jacq. J. Pharm. Sci. 60, 649–654.

Guillermo, R., Hanson, J.R., Truneh, A., 1997. Hydroxylation of aromadendrane derivatives by *Mucor plumbeus*. J. Chem. Res. (S), 28–29.

Hammoumi, A., Girault, J., Azerad, R., 1993. Microbial hydroxylation and functionalization of synthetic polycyclic enones. Tetrahedron Asymmetry 4, 1295–1306.

Hanson, J.R., Hitchcock, P.B., Manickavasagar, R., 1994a. The hydroxylation of globulol and 7-epiglobulol by *Cephalosporium aphidicola*. Phytochemistry 37, 1023–1025.

Hanson, J.R., Reese, P.B., Takahashi, J.A., Wilson, M.R., 1994b. Biotransformation of some stemodane diterpenoids by *Cephalosporium aphidicola*. Phytochemistry 36, 1391–1393.

Holland, H.L., Reimland, E., 1985. Microbial hydroxylation of steroids. Rearrangement during epoxidation and hydroxylation, and the stepwise nature of these enzyme reactions. Can. J. Chem. 63, 1121–1126.

Ismaili-Alaoui, M., Bemjilali, B., Buisson, D., Azerad, R., 1992. Biotransformation of terpenic compounds by fungi. I. Metabolism of *R*-(+)-pulegone. Tetrahedron Lett. 33, 2349–2352.

Klopman, G., Buyukbingol, E., 1988. An artificial intelligence approach to the study of the structural moieties relevant to drug-receptor interactions in aldose reductase inhibitors. Mol. Pharmacol. 34, 852–862.

Kuhnt, M., Proebstle, A., Bauer, R., Heinrich, M., 1995. Biological and pharmacological activities and further constituents of *Hyptis verticillata*. Planta Med. 61, 227–232.

Kuhnt, M., Rimpler, H., Heinrich, M., 1994. Lignans and other compounds from the Mixe Indian medicinal plant *Hyptis verticillata*. Phytochemistry 36, 485–489.

Lin, Y.Y., Smith, L.L., 1970. Microbial hydroxylations VII. Kinetic studies on the hydroxylation of 19-norsteroids by *Curvularia lunata*. Biochim. Biophys. Acta 515–525.

Lin, Y.Y., Smith, L.L., 1970. Microbial hydroxylations VIII. Induction of steroid hydroxylases of *Curvularia lunata* by 19-nortestosterone analogs. Biochim. Biophys. Acta 526–531.

Mazumder, T.K., Sonomoto, K., Tanaka, A., Sukui, S., 1985. Sequential conversion of cortexolone to prednisolone by immobilized mycelia of *Curvularia lunata* and immobilized cells of *Arthrobacter simplex*. Appl. Microbiol. Biotechnol. 21, 154–161.

Miyazawa, M., Uemura, T., Kameoka, H., 1994. Biotransformation of sesquiterpenoids, (−)-globulol and (+)-ledol by *Glomerella cingulata*. Phytochemistry 37, 1027–1030.

Miyazawa, M., Uemura, T., Kameoka, H., 1995. Biotransformation of sesquiterpenoids (+)-aromadendrene and (−)-alloaromadendrene by *Glomerella cingulata*. Phytochemistry 40, 793–796.

Morton, J.F., 1981. Atlas of Medicinal Plants of Middle America: Bahamas to Yucatan. Charles Thomas, Springfield, IL.

Neef, G., Eder, U., Petzoldt, K., Seeger, A., Wieglepp, H., 1982. Microbial hydroxylation on β-carboline derivatives. J. Chem. Soc. Chem. Comm. 366–367.

Novelo, M., Cruz, J.G., Hernandez, L., Pereda-Miranda, R., Chai, H., Mar, W., Pezzuto, J.N., 1993. Cytotoxic constituents from *Hyptis verticillata*. J. Nat. Prod. 56, 1728–1736.

Ohlson, S., Slygare, S., Larsson, P., Mosbach, K., 1980. Steroid hydroxylation using immobilized spores of *Curvularia lunata* germinated in situ. Eur. J. Appl. Microbiol. Biotechnol. 10, 1–9.

Okuda, J., Miwa, I., Inagaki, K., Horie, T., Nakayama, M., 1982. Inhibition of aldose reductases from rat and bovine lenses by flavonoids. Biochem. Pharmacol. 31, 3807–3822. Chem. Abstr. 98: 83231y.

Okuda, J., Miwa, I., Inagaki, K., Horie, T., Nakayama, M., 1984. Inhibition of aldose reductase by 3′,4′-dihydroxyflavones. Chem. Pharm. Bull. (Japan), 32, 767–772. Chem. Abstr. 101: 103606k.

Pika, J., Faulkner, D.J., 1994. Four sesquiterpenes from the South African nudibranch *Leminda millecra*. Tetrahedron 50, 3065–3070.

Porter, R.B.R., Reese, P.B., Williams, L.A.D., Williams, D.J., 1995. Acaricidal and insecticidal activities of cadina-4,10(15)-dien-3-one. Phytochemistry 40, 735–738.

Sonomoto, K., Hoq, M.M., Tanaka, A., Sukui, S., 1983. 11β-Hydroxylation of cortexolone (Reichstein compound S) to hydrocortisone by *Curvularia lunata* entrapped in photo-cross-linked resin gels. Appl. Environ. Microbiol. 45, 436–443.

Stanley, P.C., 1928. Flora of the Panama Canal Zone. United States Government Printing Office, Washington, DC, p. 326.

Tsuchiya, Y., Shimizu, M., Hiyama, Y., Itoh, K., Hashimoto, Y., Nakayama, M., Horie, T., Morita, N., 1985. Antiviral activity of natural occurring flavonoids in vitro. Chem. Pharm. Bull. (Japan) 33, 3881–3886. Chem. Abstr. 104: 14552j.

Wang, Y., Hamburger, M.O., Gaeho, J., Hostettmann, K., 1989. Antimicrobial flavonoids from *Psiadia trinervia* and their methylated and acetylated derivatives. Phytochemistry 28, 2323–2327.

Yasukawa, K., Takeuchi, M., Nakagawa, S., 1989. Effect of chemical constituents from plants on 12-*O*-tetradecanoylphorbol-13-acetate-induced inflammation in mice. Chem. Pharm. Bull. (Japan) 37, 1071–1073. Chem. Abstr. 111: 49912y.

PERGAMON

Phytochemistry 57 (2001) 385–391

PHYTOCHEMISTRY

www.elsevier.com/locate/phytochem

Blend effects in the toxicity of the essential oil constituents of *Ocimum kilimandscharicum* and *Ocimum kenyense* (Labiateae) on two post-harvest insect pests

Jembere Bekele[1], Ahmed Hassanali*

International Centre of Insect Physiology and Ecology (ICIPE), PO Box 30772, Nairobi, Kenya

Received 12 October 2000; received in revised form 12 January 2001

Abstract

The lethal toxicity of major components of the essential oils of *Ocimum kilimandscharicum* and *O. kenyense* and of selected blends of these against *Sitophilus zeamais* and *Rhyzopertha dominica* were compared with those of the full blends of the essential oils. The compounds were assayed in amounts and proportions present in the minimum 100% lethal dose of the oils. Whereas a major component of *O. kilimandscharicum* was found to be largely responsible for the toxic action of its essential oil against *R. dominica,* the results with the other treatments indicated that the toxic action of the essential oils were due to the combined effects of different components, either with or without significant individual toxic action of their own against the insects. The significance of the results and their implication in screening and using plants and their phytochemicals for pest and microbial control are highlighted. © 2001 Elsevier Science Ltd. All rights reserved.

Keywords: *Ocimum kilimandscharicum*; *O. kenyense*; Labiateae; *Sitophilus zeamais*; *Rhyzopertha dominica*; Essential oils; Blend effects; Synergism

1. Introduction

Ethnobotany has played a very important role in traditional methods of protection against storage pests in Africa and Asia (Hassanali et al., 1990; Tierto Niber, 1994; Tiwari, 1994; Talukder and Howse, 1995). In view of the potential of plant products in small-scale farm holdings typical of the bulk of grain production in Africa, there has been growing interest in evaluating their efficacies and in elucidating the basis of their protective action (Weaver et al., 1991, 1994a,b; Schmidt and Streloke, 1994; Tierto Niber, 1994; Jembere et al., 1995; Bekele et al., 1996, 1997; Obeng-Ofori et al., 1997). Previously, we evaluated crude products prepared from three species of the genus *Ocimum* against three serious post-harvest pests in Africa (the maize weevil, *Sitophilus zeamais* Mots, the lesser grain borer, *Rhyzopertha dominica* (F.) and the angoumois grain moth, *Sitotroga cerealella*), and found varying degrees of repellent, toxic and protective effects against the pests (Jembere et al., 1995; Bekele et al., 1996, 1997). The effects of two specific constituents of the plants on the insects have also been reported (Obeng-Ofori and Reichmuth, 1997; Obeng-Ofori et al., 1997). The aim of the present study was to compare the toxicity of the essential oils of *O. kilimandscharicum* and *O. kenyense* with those of their major constituents, individually and in selected blends, with the purpose of identifying the constituents important in conferring the biological activities of the two plants against the stored product pests. It was envisaged that this information would help guide the selection and use of appropriate varieties of such plants in traditional post-harvest practices.

2. Results

2.1. Essential oil compositions

The GC profiles of the oil samples of *O. kilimandscharicum* and *O. kenyense* which were tested for insect activity are shown in Fig. 1A and B, respectively.

* Corresponding author. Tel.: +254-2-861-6804; fax: +254-2-860110/803360.

E-mail addresses: biology.aau@telecom.net.et (J. Bekele), ahassanali@icipe.org (A. Hassanali).

[1] Present address: Addis Ababa University, Biology Department, PO Box 1176, 33244, Addis Ababa, Ethiopia.

0031-9422/01/$ - see front matter © 2001 Elsevier Science Ltd. All rights reserved.
PII: S0031-9422(01)00067-X

Constituents present in >0.45% were identified by GC–MS and co-injections with standards (Table 1). The relative amounts of compounds of oils of *O. kilimandscharicum* collected from different locations varied sharply, e.g. the proportion of camphor in the oil from plants collected at Siaya district was higher (>70%) than that collected from Ngong (Nairobi) area (~40%). The former was used as a basis of toxicity tests described in this study.

2.2. Toxicity of individual and blends of constituent compounds of the essential oils in Petri dish assays

2.2.1. Ocimum kilimandscharicum

In a minimum dose of 1.44 mg per cm^2 of filter paper, *O. kilimandscharicum* essential oil caused 100% mortality of *S. zeamais* with LC_{50} of 0.76 mg per cm^2. None of the six major compounds of the essential oil (camphor, limonene, 4-terpeneol, 1,8-cineole, camphene and *trans*-caryophyllene) in amounts present at that dose of the oil (1.44 mg per cm^2), was toxic to the insect (Table 2). However, 100% mortality of the insect was obtained when all the six compounds were present. In subtraction assays (Table 2, Treatments 8–14), absence of camphor caused the largest drop in the activity of the resulting 5-component blend, showing that this component contributes most to the activity of the essential oil. Subtraction of any of the other five components, except 1, 8-cineole, did not cause any significant drop in the toxicity of the resulting blends. A binary blend of camphor and 1,8-cineole (Treatment 16) was moderately active (47±2.4%). The activity of the tertiary blend of the three most abundant components, camphor, limonene and 1,8-cineole (Treatment 17) was high (82±2.0%) but not 100%, showing that the other components also contribute to the activity of the essential oil. All combinations of the compounds tested in the absence of camphor did not cause any mortality of the weevil (data not shown) indicating that the presence of this compound was essential for the toxicity of the oil.

For *R. dominica*, a minimum dose of 0.8 mg per cm^2 caused 100% mortality, with LC_{50} at 0.7 mg per cm^2 (Table 2). Toxicity of the oil against *R. dominica* appears to be largely due to camphor (Treatment 2). No mortality of the insect was obtained in the absence of this constituent (Treatments 3–7, 9, 11). The presence of

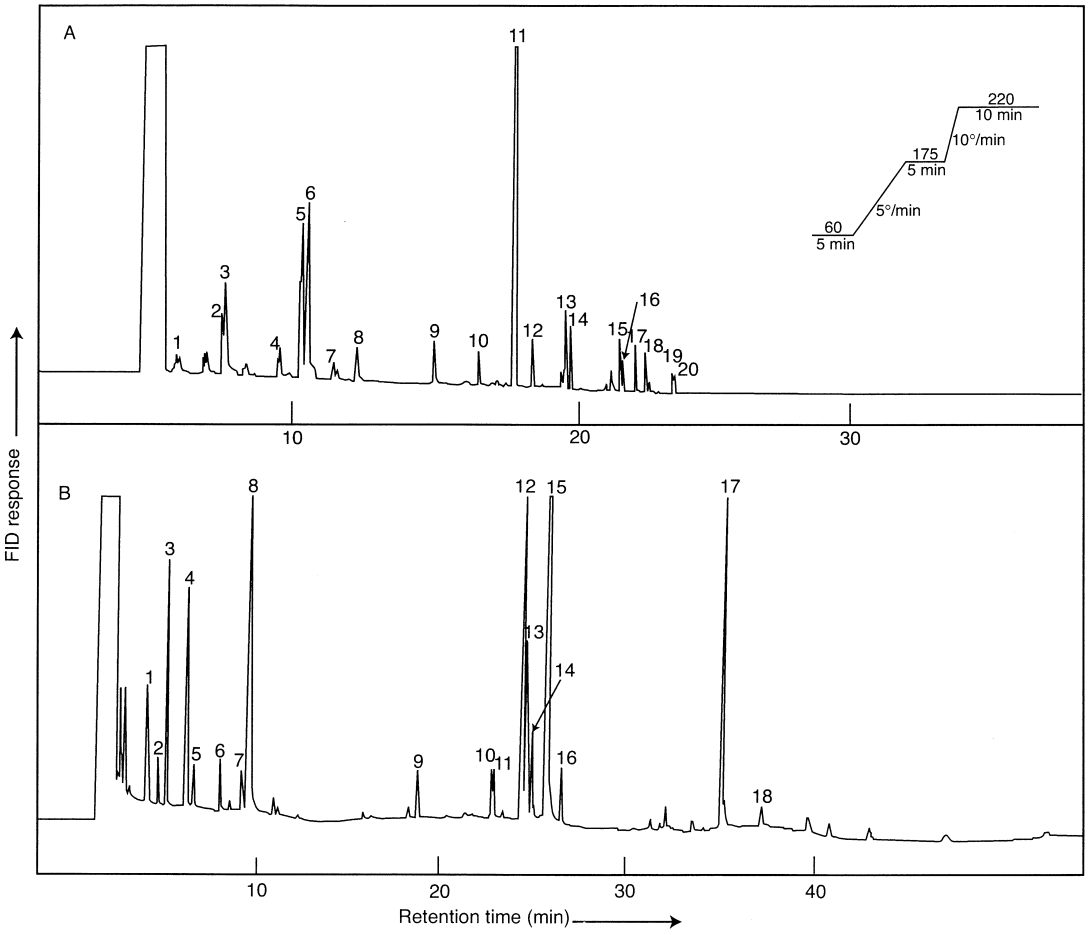

Fig. 1. Gas chromatograms of essential oils of (A) *Ocimum kilimandscharicum* (collected in the Siaya district, Kenya), and (B) *O. Kenyese* (collected from Nairobi): 50 m fused silica capillary column, 0.22 μm i.d., coated with carbowax (0.32 μm) on Hewlett Packard 5890A GC.

any of the other components with camphor had no antagonistic effect on the toxic effect of this compound (Treatments 8, 10, 12–17).

2.2.2. Ocimum kenyense

A minimum dose of 2 mg per cm^2 of the filter paper was needed to effect 100% mortality of *S. zeamais* with LC_{50} at 0.85 mg per cm^2. Among constituents of the essential oil of *O. kenyense* tested, 1,8-cineole and *iso*-eugenol showed significant toxic effects against *S. zeamais* at levels present in the lethal dose of the essential oil (Table 3, Treatments 5 and 6). The presence of the two compounds in other blends (Treatments 7–10, 14, 16) caused high (100%) mortality of the insect. In subtraction assays, absence of 1,8-cineole (Treatment 5) caused a significant drop in the activity of resulting blend; however, that of *iso*-eugenol (Treatment 12) had no significant effect.

For *R. dominica,* 100% mortality was obtained with a minimum dose of 0.6 mg per cm^2 of *O. kenyense* essential oil, with its LC_{50} at 0.36 mg per cm^2 (Table 3). None of the compounds of *O. kenyense* essential oil tested individually, with the exception of *iso*-eugenol (which was weakly active), caused any mortality of *R. dominica* in amounts present in the minimum lethal dose of the oil (Table 3, Treatments 2–6). On the other hand, a combination of the 5 major constituents in the same relative amounts resulted in 100% mortality of the insect (Treatment 7). Subtraction of any of the five components (Treatments 8–12), had either no or only a small effect on the toxicity of the resulting four-component blends.

3. Discussion

Previously, we showed that products derived from *Ocimum* spp. provide varying degrees of protection against three major stored product insect pests (Jembere et al., 1995; Bekele et al., 1996, 1997). In the present study, we compared the toxic effects of major constituents of the oils of *O. kilimandscharicum* and *O. kenyense* and various blends of these with those of the full blends of the essential oils against *S. zeamais* and *R.*

Table 1
Major identified constituents of *Ocimum kilimandscharicum* and *O. kenyense* essential oils and their relative proportion in the oils

Ocimum kilmandscharicum			*Ocimum kenyense*		
GC peak number	Component (%)		GC peak number	Component (%)	
3	Camphene	(5.07)	3	Ethyl isovalerate	(2.99)
5	Limonene	(6.23)	4	β-Pinene	(2.86)
6	1,8-Cineole	(7.20)	7	α-Terpineol	(0.55)
11	Camphor	(70.43)	8	1,8-Cineole	(36.93)
12	Linalool	(0.47)	10	*trans*-Caryophyllene	(0.66)
13	4-Terpineol	(1.44)	11	4-Terpineol	(0.79)
14	*trans*-Caryophyllene	(2.80)	12	Methyl chavicol	(12.86)
15	α-Terpineol	(0.60)	13	α-Humulene	(2.78)
16	Endo-borneol	(0.60)	15	β-Selinene	(23.57)
20	Myrtenol	(1.30)	16	γ-Cardinene	(0.78)
			17	*iso*-Eugenol	(8.23)

dominica, respectively. Our aim was two-fold: to elucidate the roles and relative importance of the major constituents of the oils in conferring some of the observed biological effects of the plants, and to use this information to guide effective deployment of such plants by small-scale farmers in post-harvest grain protection.

Of the essential oils, that of *O. kilimandscharicum* was more toxic to both insects consistent with the relative performance of products derived from these plants (Jembere et al., 1995; Bekele et al., 1997). On filter papers in Petri dish assays, the minimum lethal dose (giving 100% mortality) of this oil was found to be 1.4 mg cm^{-2} for *S. zeamais* and 0.8 mg cm^{-2} for *R. dominica*, confirming the greater sensitivity of the latter to the oil. Of special interest is the contrasting ways in which the major components of the oil contribute to its toxicity to the two test insects (Table 2). In amounts present in the minimum lethal dose of the oil, none of the six individual components (camphor, limonene, 4-terpeneol, 1,8-cineole, camphene and *t*-caryophyllene) that were tested, had significant toxic effect against *S. zeamais*. However, the mixture of these six components and that minus *t*-caryophyllene, were as effective as the essential oil, showing clearly that the toxic action of the oil results from the combined action of five of its major constituents. Subtraction assays provided an additional insight into the relative contribution of these components. Absence of camphor in the blend resulted in the largest drop in the toxic action of the resulting blend, identifying it as the most important component of the active blend. On the other hand, a single component, camphor, in the amount present in the lethal dose of the oil, was found to be responsible for the toxic action of the oil against *R. dominica*. The blend of the other five components was non-toxic to this insect. Their presence in the blends with camphor had no deleterious or antagonistic effect on the toxicity of this compound.

The minimum 100% lethal dose of the oil of *O. kenyense* against *S. zeamais* and *R. dominica* (2.0 and 0.8 mg cm^{-2}, respectively) showed that the latter was also the more sensitive insect to this oil. Of the individual major constituents tested (methyl chavicol, ethyl isovalerate, α-humulene, 1,8-cineole and *iso*-eugenol), only 1,8-cineole and *iso*-eugenol were significantly toxic to *S. zeamais*. On the other hand, except for the weak toxic action of *iso*-eugenol, none of the components was active against *R. dominica*. Subtraction assays and tests involving different combinations of the constituents against *S. zeamais* and *R. dominica* also indicated the special potency of some of the mixtures (Table 3). Three variants of blend effects may be noted from these results: production of an active blend from inactive constituents; enhancement of the activity of an active compound by an inactive constituent; and synergism between moderately active compounds to give a mixture that is more active than a linear summation of the individual activities

Table 2
Percent mortality of *Sitophilus zeamais* and *Rhyzopertha dominica* adults exposed to *Ocimum kilimandscharicum* constituents individually and in blends at doses equivalent to the relative proportion of each compound in the 100% lethal dose of the essential oil

Treatment[a]		Mean % mortality	
Compounds		*S. zeamais*	*R. dominica*
1.	Essential oil[b]	100±0.0a	100±0.0a
2.	Camphor	0±0.0e	100±0.0a
3.	Limonene	0±0.0e	0±0.0b
4.	4-Terpineol	0±0.0e	0±0.0b
5.	1,8-Cineole	0±0.0e	0±0.0b
6.	Camphene	0±0.0e	0±0.0b
7.	*t*-Caryophyllene	0±0.0e	0±0.0b
8.	2-7 combined	100±0.0a	100±0.0a
9.	3-7 combined	22±2.9d	0±0.0b
10.	2-7 without 3	97±2.1a	100±0.0a
11.	2-7 without 4	94±2.4ab	100±0.0b
12.	2-7 without 5	84±2.1b	100±0.0a
13.	2-7 without 6	100±0.0a	100±0.0a
14.	2-6	100±0.0a	100±0.0a
15.	2+3	23±2.9d	100±0.0a
16.	2+5	47±2.4c	100±0.0a
17.	2+3+7	82±2.0b	100±0.0a
18.	Acetone	0±0.0e	0±0.0b

[a] Treatment means (average of six replicates) followed by the same letter are not significantly different from each other (SNK, $P < 0.05$).
[b] Minimum lethal dose of 1.44 mg cm^{-2} for *S. zeamias* and 0.8 mg cm^{-2} for *R. dominica*.

Table 3
Percent mortality of *Sitophilus zeamais* and *Rhyzopertha dominica* adults exposed to *Ocimum kenyense* constituents, individually and in blends, at doses equivalent to the proportion of each compound in the 100% lethal dose of essential oil

Treatment[a]		Mean % mortality	
Compounds		*S. zeamais*	*R. dominica*
1.	Essential oil[b]	100±0.0a	100±0.0a
2.	Methyl chavicol	0±0.0e	0±0.0f
3.	Ethyl isovalerate	0±0.0e	0±0.0f
4.	α-Humulene	0±0.0e	0±0.0f
5.	1,8-Cineole	44±3.0c	0±0.0f
6.	*iso*-Eugenol	39±2.4d	5±1.3e
7.	2-6 combined	100±0.0a	100±0.0a
8.	3-6 combined	100±0.0a	100±0.0a
9.	2-6 without 3	100±0.0a	100±0.0a
10.	2-6 without 4	100±0.0a	100±0.0a
11.	2-6 without 5	85±3.0b	97±3.3a
12.	2-5	97±2.1a	82±1.5ab
13.	2+5	100±0.0a	10±2.1d
14.	5+6	100±0.0a	18±2.1d
15.	2+6	82±2.9b	22±3.3c
16.	2+5+6	100±0.0a	72±3.8b
17.	2+3+4	39±2.4d	19±3.0cd
18.	Acetone	0±0.0e	0±0.0f

[a] Treatment means (average of six replicates) followed by the same letter are not significantly different from each other (SNK, $P < 0.05$).
[b] Minimum lethal dose of 2.0 mg cm^{-2} for *S. zeamais* and 0.85 mg cm^{-2} for *R. dominica*.

of the constituents. The first variant is illustrated by the high lethal activity of the quaternary mixture of methyl chavicol, ethyl isovalerate, α-humulene and 1,8-cineole against *R. dominica*. As in the case of the five major components of *O. kilimandscharicum* with respect to *S. zeamais,* none of the components of the quaternary mixture were individually toxic to *R. dominica*. The second variant is illustrated by significant enhancement of the activities of 1,8-cineole and *iso*-eugenol against *S. zeamais* from 44 to 100% and from 39 to 82%, respectively, in blends with methyl chavicol. The third, probably the most frequently reported in the past, is illustrated by 100% mortality of *S. zeamais* exposed to the binary mixture of 1,8-cineole and *iso*-eugenol, which individually caused 44 ± 3.0% and 39 ± 2.4% mortality, respectively.

These results stress the importance of evaluating plant components in blends to elucidate their full potency in a given bioactivity. A number of previous studies on the effects of essential oils on post-harvest and other pests focused on the identification of active components rather than mixtures (e.g. Klocke et al., 1989; Kurowska et al., 1991; Shaaya and Vladmir, 1991; Shaaya et al., 1991; Weaver et al., 1991; Regnault-Roger et al., 1993; Seck et al., 1993). In the present study, the result obtained with camphor (the major component of the oil of *O. kilimandscharicum*) against *R. dominica*, where it appears to be largely responsible for the toxicity of the oil, may be less common. Blend effects in the bioactivity of plant products may well be the norm. Indeed, there is accumulating evidence of adaptive value of phytochemical diversity in ecological interactions among plants and their associated herbivores and pathogens (Berenbaum and Zangerl, 1996; Cates, 1996). This has an important practical implication in the strategy adopted in the search for and use of plants and their phytochemicals for pest and microbial control.

4. Experimental

4.1. Mass rearing of the test insects

Mass rearing of the test insects was carried out following the method of Santhoy and Rejesus (1975) and Jembere et al. (1995). The two insect pests (*S. zeamais* and *R. dominica*) were obtained from stocks maintained at the International Centre of Insect Physiology and Ecology (ICIPE) and the Kenya Agricultural Research Institute (KARI) laboratories. Maize and sorghum seeds (local varieties) were obtained from farmers in Kisii, Ugunja and Kitale districts of Kenya. Prior to the experiments, the seeds were disinfested by keeping them in an oven at 40°C for 4 h (Santhoy and Rejesus, 1975). Twenty pairs of each test insects, sexed following the methods of Halstead (1963) and Stenley and Wilbur (1966), were introduced into glass jars (1l) containing disinfested maize and sorghum seeds, respectively. The jars were covered with nylon mesh and held with rubber bands and kept in a room maintained at 60±5% relative humidity and 26±1°C using heaters and water troughs. The adults of *S. zeamais* and *R. dominca* were allowed to stay in the glass jars for 30 and 15 days (optimum oviposition time), respectively, after which they were removed and discarded. The seeds were kept in the room until the emergence of the first progeny. On days 35–65 and 27–42, respectively, after the first introduction of the two insects, the new progenies that emerged daily were transferred into their respective disinfested grains in the glass jars. A sieve of mesh number 10 (sieve size 2 mm, Endecotts LTD, London) was used to sieve out the insects. The ages of the insects in each jar were recorded.

4.2. Plant materials and isolation of their essential oils

Fresh aerial parts of *O. kilimandscharicum* collected from the Siaya district and *O. kenyense* collected from around Nairobi (Kenya) were brought to the laboratory and stored at 4°C. Voucher specimens are kept at the University of Nairobi herbarium in the Botany Department. The fresh plant materials comprising leaves, inflorescence and succulent stems were subjected to steam distillation to obtain the essential oils. The distillation process was carried out using a clavenger type of apparatus (Gunter, 1946). The condensing oil was collected in hexane (Aldrich, HPLC grade). The hexane solution was filtered through a filter paper containing anhydrous sodium sulphate to remove traces of moisture. Hexane was then removed by distillation at 60°C, the residual oil collected and weighed.

4.3. Analysis of the essential oils

The chemical components of the essential oils were initially identified on a VG Masslab 12–250 mass spectrometer (GC–MS) equipped with data system linked to Hewlett Packard 5790 gas chromatograph (GC). The identity of each component was confirmed by co-injection with authentic compounds on a Hewlett Packard 5890A gas chromatograph equipped with a splitless injector and a flame ionization detector. Helium and nitrogen gases were used as carrier gases for GC–MS and GC, respectively. In both GC–MS and GC analyses, a fused silica capillary column (Hewlett Packard 50 m long, 0.22 mm id) coated with carbowax (0.32 μm film) was used. The column temperature programme in both analyses comprised of an initial temperature of 60°C (5 min), a rise to 175°C at 5 min, a hold at 175°C (5 min), another rise to 220°C at 10°C/min and final hold at 220°C for 10 min.

4.4. Comparative toxicity tests of essential oil and its constituents

These were conducted in Pyrex glass Petri dishes, 10 cm dia. (Weaver et al., 1991). A sample of each essential oil was weighed, dissolved in 1 ml of acetone (Merck 95–97%) and delivered to a Whatman No 1 filter paper (9 cm dia.) in the petridishes. Various doses of the essential oils (2.5–0.5 mg cm^{-2}) were used to identify the minimum doses which gave 100% mortality of the two insects. The minimum doses of *O. kilimandscharicum* essential oil used against *S. zeamais* and *R. dominica* were 1.44 and 0.8 mg cm^{-2}), while that of *O. kenyese* oil against both insects were 2.0 and 0.64 mg cm^{-2}, respectively. Acetone was allowed to evaporate off (20 min) prior to the introduction of the insects. Acetone treated filter papers were used as controls. 10 pairs of *S. zeamais* or *R. dominica* were introduced and the Petri dishes were kept for 24 h in the laboratory maintained at $26 \pm 1^{\circ}C$ and $60 \pm 5\%$ relative humidity.

The number of dead insects was counted after 24 h. Insects were considered dead if they were immobile and did not react to three probings with a blunt dissecting probe. The experiment was repeated with commercially available constituents (Aldrich) of the essential oils and blends of these at their natural proportions (GC) in the oils and in amounts present in the minimum 100% lethal dose of the oils, with each component absent (subtracted) from the blend in turn to determine its relative contribution to the overall toxicity of the natural oil (Owaga et al., 1988).

4.5. Data analysis

The mortality data obtained in the different treatments were analyzed using analysis of variance following the method of Gomez and Gomez (1984). Appropriate data transformation methods (arc sine and square root) were applied where necessary. Probit analysis for the determination of LC_{50} was based on the methods of Busvine (1971) and Finney (1978).

Acknowledgements

The first author is grateful to the German Academic Exchange Program (DAAD) and the African Regional Post-graduate Program in Insect Science (ARPPIS) for the grants they provided him with to undertake this work. We thank the Biostatistics Unit of ICIPE for advice in statistical analysis.

References

Bekele, A.J., Obeng-Ofori, D., Hassanali, A., 1996. Evaluation of *Ocimum suave* (Willd.) as a source of repellents, toxicants and protectants in storage against three stored product insect pests. International Journal of Pest Management 42, 139–142.

Bekele, A.J., Obeng-Ofori, D., Hassanali, A., 1997. Evaluation of *Ocimum kenyense* (Ayobangira) as a source of repellents, toxicants and protectants in storage against three stored product insect pest. Journal of Applied Entomology 121, 169–173.

Berenbaum, M.R., Zangerl, A.R.1996. Phytochemical diversity: adaptation or random variation? In: Romeo, J.T., Saunders, J.A., Barbosa, P. (Eds.), Phytochemical Diversity and Redundancy in Ecological Interactions. Plenum Press, New York, pp. 1–24.

Busvine, J.R., 1971. A Critical Review of the Techniques for Testing Insecticides. Commonwealth Agricultural Bureaux (CAB).

Cates, R.G., 1996. The role of mixtures and variation in the products of terpenoids in conifer-insect-pathogen interactions. In: Romeo, J.T., Saunders, J.A., Barbosa, P. (Eds.), Phytochemical Diversity and Redundancy in Ecological Interactions. Plenum Press, New York, pp. 179–216.

Finney, D.J., 1978. Statistical Methods in Biological Assay, 3rd Edition. Charles Griffin and Company, London.

Gomez, K.A., Gomez, A.A., 1984. Statistical Procedures for Agricultural Research, 2nd Edition. John Wiley and Sons.

Gunter, E., 1946. The Essential Oils. Vol. III. Toronto, Van Nostrand.

Halstead, D.G.H., 1963. External sex difference in stored products Coleoptera. Bulletin of Entomological Research 54, 119–134.

Hassanali, A., Lwande, W., Sitayo, O., Moreka, L., Nokoe, S., Chayapa, A., 1990. Weevil repellent constituents of *Ocimum suave* leaves and *Eugenia caryophyllata* cloves used as grain protectant in parts of East Africa. Discovery and Innovation 2, 91–95.

Jembere, B., Obeng-Ofori, D., Hassanali, A., Nyamasyo, G.H.N., 1995. Products derived from the leaves of *Ocimum kilimandscharicum* (Labiatae) as post harvest protectant against the infestation of three major stored product insect pests. Bulletin of Entomological Research 85, 361–367.

Klocke, J.A., Balandrin, M.F., Barnby, M.A., Bryan, N.R., 1989. Limonoids, phenolics and furanocoumarins as insect antifeedants, repellents and growth inhibitary compounds. In: Arnason, J.T., Philogene, R.J.R., Mornad, P. (Eds.), Insecticides of Plant Origin. ACS Symposium Series 387, Washington, DC, pp. 136–149.

Kurowska, A., Kalemba, D., Gora, J., Madia, T., 1991. Analysis of essential oils: influence on insects. Part IV: essential oil of garden thyme (*Thymus vulgaris* L.). Pestycydy (Warsaw) 2, 25– 29.

Obeng-Ofori, D., Reichmuth, C., 1997. Biological activity of eugenol, a major component of *Ocimum suave* (Wild.) against four species of stored product coleoptera. International Journal of Pest Management 43, 89–94.

Obeng-Ofori, D., Reichmuth, C., Bekele, J., Hassanali, A., 1997. Biological activity of 1,8-cineole, a major component of essential oil of *Ocimum kenyense* (Ayobangira) against stored product beetles. Journal of Applied Entomology 121, 237–243.

Owaga, M.L., Hassanali, A., McDowell, P.G., 1988. The role of 4-cresol and 3-*n*-propylphenol in the attraction of tsetse flies to buffalo urine. Insect Science and Application 9, 95–100.

Regnault-Roger, C., Hamraoul, A., Holeman, M., Theron, E., Pionel, R., 1993. Insecticidal effects of essential oils from Mediterranean plant up on *Acanthoscelides obtectus* (Sat.) (Coleoptera: Bruchidae) a pest of kidney bean *Phaseolus vulgaris* (L.). Journal of Chemical Ecology 19, 1233–1244..

Santhoy, G., Rejesus, B.M., 1975. The development rate, body weight and reproduction capacity of *Sitophilus zeamais* (Motschulsky) reared on three natural hosts. Philippines Entomology 2, 311–321.

Schmidt, G.H., Streloke, M., 1994. Effects of *Acorus calamus* (L.) (Araceae) oil and its main component β-asarone on *Prostephanus trancatus* (Horn) (Coleoptera: Bostrichidae). Journal of Stored Product Research 31, 55–61.

Seck, D., Lognay, G., Haubruge, E., Wathelet, J.P., Marlier, M., Gaspar, C., Severin, M., 1993. Biological activity of the shrub

Bosica senegalensis (Pers.) (Capparaceae) on stored grain insects. Journal of Chemical Ecology 19, 377–390.

Shaaya, E., Vladmir, P., 1991. Toxicity of plant oils and their main constituents against stored product insects. Journal of Agriculture and Food Chemistry 27, 629–638.

Shaaya, E., Ravid, U., Paster, N., Juven, B., Zisman, U., Pissarev, V., 1991. Fumigant toxicity of essential oils against four major stored products insects. Journal of Chemical Ecology 17, 499–504.

Stenley, P.G., Wilbur, D.A., 1966. Color characteristics for sexing live adults of lesser grain borer. Journal of Economic Entomology 59, 760–761.

Talukder, F.A., Howse, P.E., 1995. Evaluation of *Aphanamaxis polystachya* as a source of repellents, antifeedants, toxicants and protectantds in storage against *Tribolium castaneum* (Herbst). Journal of Stored Product Research 31, 55–61.

Tierto Niber, B., 1994. The ability of powders and slurries from ten plant species to protect stored grain from attack by *Prostephnus trancatus* (Horn) (Coleoptera: Bostrichidae) and *Sitophilus oryzae* (Coleoptera: Curculeonidae). Journal of Stored Product Research 30, 297–301.

Tiwari, S.N., 1994. Efficacy of some plant products as grain protectants against *Rhyzoperta dominica* (F.). (Coleoptera: Bostrichidae). International Journal of Pest Management 40, 94–97.

Weaver, D.K., Dunkel, F.V., Ntezurubanza, L., Jackson, L.L., Stock, D.T., 1991. The efficacy of linalool, a major component of freshly milled *Ocimum canum* Sims (Lamiaceae), for protection against post-harvest damage by certain stored product Coleoptera. Journal of Stored Products Research 27, 213–220.

Weaver, D.K., Wells, C.D., Dunkel, F.V., Bertsch, W., Sing, S.E., Sriharan, S.C., 1994a. Insecticidal activity of floral, foliar, and root extracts of *Tagetes minuta* (Asterales: Asteraceae) against Mexican bean weevils (Coleoptera: Bruchidae). Journal of Economic Entomology 87, 1718–1725.

Weaver, D.K., Dunkel, F.V., VanPuyvelde, L., Richards, D.C., Fitzgerald, G.W., 1994b. Toxicity and protectant ability potential of the essential oils of *Tetradenia riparia* (Lamiales: Lamiaceae) against *Zobratus subfasciatus* (Coleoptra: Bruchidae) infesting dried pinto beans (Fabales: Leguminosae). Journal of Applied Entomology 118, 179–196.

PERGAMON

Phytochemistry 57 (2001) 393–400

PHYTOCHEMISTRY

www.elsevier.com/locate/phytochem

Identification and ecdysteroid antagonist activity of three oligostilbenes from the seeds of *Carex pendula* (Cyperaceae)

Yanhui Meng [a,1], Pauline C. Bourne [a], Pensri Whiting [a], Vladimir Šik [b], Laurence Dinan [a,*]

[a] *Department of Biological Sciences, University of Exeter, Hatherly Laboratories, Prince of Wales Road, Exeter, Devon, EX4 4PS, UK*
[b] *Department of Chemistry, University of Exeter, Stocker Road, Exeter, Devon, EX4 4QD, UK*

Received 28 September 2000; received in revised form 7 February 2001

Abstract

Methanolic extracts of seeds of several *Carex* species were found to antagonise the action of 20-hydroxyecdysone in the *Drosophila melanogaster* microplate-based B_{II} cell bioassay. Bioassay-guided HPLC analysis of seeds of *Carex pendula* (drooping sedge) provided one previously unknown tetrastilbene (*cis*-miyabenol A) and two known oligostilbenes (kobophenol B and *cis*-miyabenol C) as the biologically active compounds (EC_{50} values were 31, 37 and 19 μM, respectively, vs. 5×10^{-8} M 20-hydroxyecdysone). The structures and relative stereochemistries of these compounds were deduced by comprehensive 1D- and 2D-NMR experiments. These compounds are isolated from *Carex pendula* for the first time. In vitro experiments with dipteran and lepidopteran ecdysteroid receptor proteins demonstrate that the oligostilbenes are able to compete with radiolabelled ecdysteroid ([^{3}H]ponasterone A) for occupancy of the ligand binding site. IC_{50}/K_i values are similar to the EC_{50} values obtained in the B_{II} bioassay. © 2001 Elsevier Science Ltd. All rights reserved.

Keywords: Cyperaceae; *Carex*; Antagonist; Ecdysteroid; Steroid hormone receptor; Stilbenoid

1. Introduction

Carex species (family: Cyperaceae) are rich in oligostilbenes (Kawabata et al., 1989) and a number of oligostilbenes have been isolated and identified (Suzuki et al., 1987; Kurihara et al., 1990, 1991; Kawabata et al., 1991). Oligostilbenes are resveratrol-type oligomeric phenols and most of them show antimicrobial activity (Sotheeswaran and Pasupathy, 1993) and other interesting biological activities. We are searching for plant natural products which act as agonists or antagonists of the insect steroid hormone (ecdysteroid) receptor (Dinan et al., 1999). Ecdysteroids are important regulators of development, metamorphosis and reproduction in arthropods and probably other invertebrates too (Koolman, 1989). Consequently, the intracellular ecdysteroid receptor is an attractive target for new invertebrate pest control agents. Plant natural products should be a good source of lead compounds for such control agents. We now report the isolation, structural elucidation and biological activity of one previously unknown tetrastilbene, *cis*-miyabenol A (**1**), together with the known tetrastilbene, kobophenol B (**2**) and the known tristilbene, *cis*-miyabenol C (**3**), from the seeds of *Carex pendula* (drooping sedge). These oligostilbenes are isolated as constituents from *C. pendula* for the first time and they exhibit ecdysteroid antagonist activity. Antagonists of ecdysteroid action in invertebrate systems will be useful as biochemical probes for the investigation of the control of gene expression by ecdysteroids as well as lead compounds for the development of new insect pest control agents (Dinan, 1995; Keckeis et al., 2000).

2. Results and discussion

2.1. Ecdysteroid antagonist activity in Carex spp

Initial studies revealed that methanolic seed extracts of several species in the genus *Carex* (including *C. pendula*) antagonise the activity of 20-hydroxyecdysone on

* Corresponding author. Tel.: +44-1392-264605; fax: +44-1392-263700.

E-mail address: l.n.dinan@exeter.ac.uk (L. Dinan).

[1] Supported by Royal China Fellowship to Yanhui Meng. Permanent address: Department of Applied Chemistry, Zhongshan College, Zhongshan 528403, PR China.

0031-9422/01/$ - see front matter © 2001 Elsevier Science Ltd. All rights reserved.
PII: S0031-9422(01)00061-9

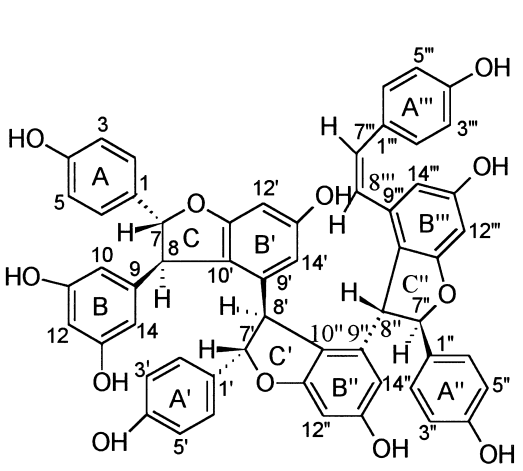

1

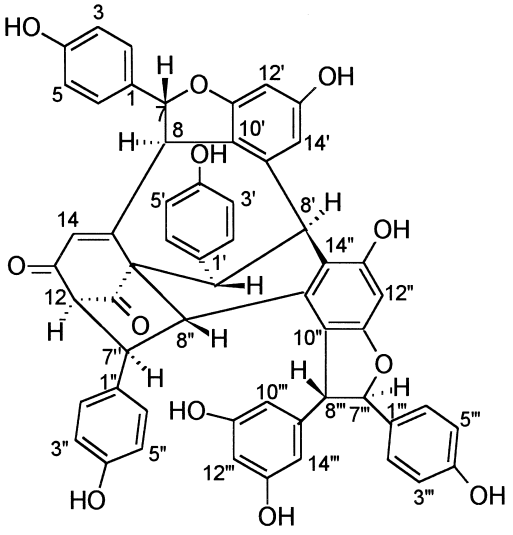

2

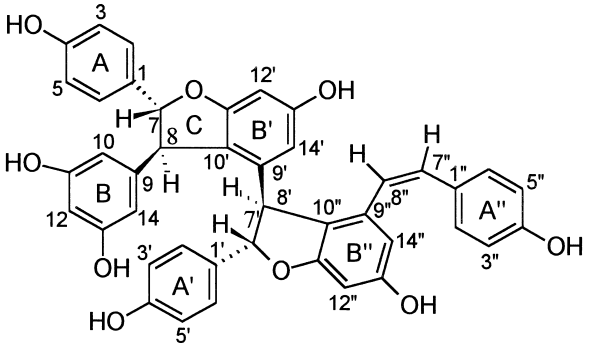

3

the *Drosophila melanogaster* B_{II} cell line (Table 1). We also examined extracts of leaves and roots of four of the *Carex* species, but activity appears to be highest in seeds. Consequently, the identities of the active principle(s) from this source were pursued.

2.2. Isolation and structural elucidation

Bioassay-guided HPLC analysis of the active fractions from solid-phase extraction (SPE) on C_{18}-cartridges of a MeOH extract (defatted with hexane) of the seeds of *C. pendula* resulted in the isolation of a previously unknown tetrastilbene *cis*-miyabenol A (**1**) and two known oligostilbenes, kobophenol B (**2**) (Kawabata et al., 1991) and *cis*-miyabenol C (**3**) (Ono et al., 1995). The compounds were identified on the basis of comprehensive analysis of their 1D- and 2 D-NMR spectra and, in the case of the known compounds, by comparison of their UV, MS, ^{1}H NMR and ^{13}C NMR and NOESY data with published data (Kawabata et al., 1991; Ono et al., 1995).

Compound **1** is a colourless glassy solid. LSIMS (+ve ion-mode) gave an $[M+H]^+$ ion at m/z 907 and an $[M+Na]^+$ ion at 929 compatible with the molecular formula $C_{56}H_{42}O_{12}$, which was supported by the ^{13}C and ^{1}H NMR spectra (Table 2) and was compatible with a tetrastilbene (Kurihara et al., 1991). The UV spectrum with an absorption maximum (λ_{max}) at 286 nm was similar to those of other *Carex* oligostilbenes (Ono et al., 1995). The ^{1}H NMR spectrum (Table 2) showed eight sets of ortho-coupled aromatic hydrogens, assignable to four 4-hydroxylphenol groups ("A"-rings of **1**), and signals from four other 3,5-dihydroxyphenol systems ("B"-rings of **1**), characteristic for four resveratrol units. In addition, three sets of coupled methines (each set containing a deshielded oxymethine; δ 3.88 [d, $J=2.7$ Hz]/δ 5.40 [*d*, $J=2.7$ Hz], δ 3.99 [*d*, $J=6.3$ Hz]/δ 5.02 [*d*, $J=6.3$ Hz] and δ 4.40 [1H, $J=2.0$]/δ 5.12 [*d*,

Table 1
Ecdysteroid agonist and antagonist activities in seed extracts of *Carex* species

Species[a]	Bioassay response[b]	
	Agonist	Antagonist
Carex baccans[1]	- - -	+ - -
leaves	C- -	C- -
roots	- - -	- - -
Carex berggrenii[1]	- - -	- - -
leaves	C- -	C- -
roots	- - -	- - -
Carex bohemica[2]	- - -	+ - -
Carex buchananii[3]	- - -	- - -
Carex comans[4]	- - -	- - -
Carex dallii[3]	- - -	(+)- -
Carex demissa[2]	C- -	+(+)-
Carex duriuscula[2]	- - -	(+)- -
Carex flagellifera[1]	- - -	- - -
leaves	C- -	C- -
roots	- - -	- - -
Carex grayi[5]	- - -	(+)- -
Carex hirta[6]	- - -	(+)- -
Carex hordeistichos[2]	- - -	+ - -
Carex lasiocarpa[2]	- - -	- - -
Carex licerica[5]	- - -	+(+)-
Carex limosa[2]	- - -	(+)- -
Carex muricata[7]	C- -	C- -
Carex muskingumensis[2]	- - -	+ - -
Carex nigra[6]	- - -	+(+)-
Carex otrubae[6]	- - -	+(+)-
Carex pallescens[2]	- - -	(+)- -
Carex pendula[4]	- - -	+ - -
Carex pendula[8]	- - -	+ - -
Carex plantaginea[7]	- - -	- - -
Carex pseudocyperus[5]	- - -	(+)- -
Carex pseudocyperus[9]	- - -	(+)- -
Carex pseudocyperus[6]	- - -	(+)- -
Carex rostrata[2]	- - -	+ - -
Carex secta[3]	- - -	(+)- -
leaves	- - -	- - -
roots	- - -	- - -
Carex sylvatica[2]	- - -	+ - -
Carex trifida[3]	- - -	(+)- -

[a] Source; 1: The Seed Guild, Lanark, UK; 2: Botanischer Garten der Universität Halle, Germany; 3: Ness Gardens, Wirral, UK; 4: Chiltern Seeds, Ulverston, UK; 5: Humboldt Universität zu Berlin, Germany; 6: Botanischer Garten der Universität Osnabrück, Germany; 7: Bundesgarten Wien, Austria; 8: B&T World Seeds, Olonzac, France; 9: Gruga Park, Essen, Germany.

[b] 25 mg samples were extracted 3×1 ml with methanol at 55°C, the pooled extracts were mixed with 1.3 ml H_2O and partitioned against 2 ml hexane to give 4.3 ml methanolic extract. Aliquots (10 μl) of 1-, 10- and 100-fold dilutions were assessed in the agonist and antagonist versions of the B_{II} bioassay; - - -, inactive; + - -, active as neat extract; +(+)-, active as 10-fold dilution; + + +, active as 100-fold dilution; C- -, cytotoxic as neat extract; (+), weak activity.

$J = 2.0$ Hz]) and pair of coupled olefinic protons at δ5.85 (*d*, $J = 12$ Hz) and δ 5.90 (*d*, $J = 12$ Hz) in the ^{1}H NMR spectrum, revealed that this tetrastilbene contains three dihydrofuran rings and a double bond in a structure which was similar to another known *Carex* tetrastilbene, miyabenol A (Suzuki et al., 1987). However, some differences in the ^{1}H and ^{13}C NMR signals between **1** and miyabenol A, especially the comparatively smaller chemical shifts of the hydrogens on the double bond of **1** (δ 5.85 *d* and 5.90 *d* compared to δ 6.63 *d* and δ 6.87 *d* in miyabenol A) and lower coupling constants between the two olefinic protons in **1** ($J = 12$ Hz compared to $J = 16.2$ Hz in miyabenol A; Kawabata et al., 1995) indicated that the double bond in **1** is *cis*, not *trans*. ^{1}H–^{1}H COSY experiments confirmed the coupling patterns between the three sets of methine protons (H-7–H-8, H-7′–H-8′and H-7″–H-8″) in the three dihydrofuran rings, between the four sets of ortho-coupled aromatic hydrogens in the four 4-hydroxyphenol groups (H-2,6–H-3,5, H-2′,6′–H-3′,5′, H-2″,6″–H-3″,5″ and H-2‴,6‴–H-3‴,5‴) and the two protons on the double bonds (H-7‴–H-8‴) as mentioned above. A ^{1}H–^{13}C HMQC spectrum (Table 3) identified all ^{1}H–^{13}C direct ^1J correlations and thus confirmed the assignment of all methine carbons. The other connections of the molecule were determined unambiguously by HMBC spectra (Table 3). Among the correlation peaks observed in the HMBC spectra, the most important were: from H-7 to C2, 6, H-8 to C-9, H-8 to C10, 14, H-8 to C10′, H-8 to C11′, H-7′ to C-2′,6′, H-8′ to C-9′, H-8′ to C-10″, H-8′ to C-11″, H-8″ to C-9″, H-8″ to C-10‴ and C-11‴, H-7″ to C-2″,6″, H-8‴ to C-9‴ and H-7‴ to C-2‴, 6‴. Thus, **1** was deduced to be *cis*-miyabenol A, a previously undescribed isomer of miyabenol A.

The relative stereochemistry of **1** was assigned from NOESY experiments (Table 4). On ring C, NOE interactions were clearly observed between H-7/ H-10 (14), H-8 /H2 (6), which indicates a *trans*-2, 3-diaryl substitution on ring C. In a similar manner, NOEs between H-7′/H-14′, H-8′/H-2′ (6′) and H-7″/H-14″, H-8″/H-2″(6″) support the trans-diaryl substitution on rings C' and C″. The relative stereochemical relationship among rings C, C′ and C″ is more difficult and the NOESY experiments are again informative to determine it. Strong NOEs between H-8, H-8′ and H-8″ showed the three hydrogens H-8, H-8′ and H-8″ are located in spatial vicinity of each other, and the NOEs between H-8 to H-7‴ and H-8‴, H-8′ to H-7‴ and H-8‴, H-8″ to H-7‴ and H-8‴ showed the three hydrogens (H-8, H-8′ and H-8″) are also spatially close to the double bond. The NOEs between H-2′/H-6′ and H-7‴, H-8‴ showed the *cis*-double bond is in spatial vicinity with ring-A' as well. Molecular modelling suggested that the stereochemical relationship among rings C, C' and C'' in **1** is as shown in order to meet the requirement of the vicinity of the double bond with ring-A′ and the three hydrogens (H-8, H-8′ and H-8''). Thus, the relative stereochemistry of **1** was concluded to be *rel*-(7*R*, 8*R*, 7′*S*, 8′*S*, 7″*R*, 8″*R*).

Compound **2** was isolated as a yellowish powder. LSIMS (+ve ion-mode) showed an $[M+H]^+$ ion at *m*/*z*

Table 2
^{1}H NMR and ^{13}C NMR (DEPT) (400 MHz, CD_3OD) data (δ values; J in Hz) for **1**, **2** and **3**

C/H	δ H			δ C		
	1	**2**	**3**	**1**	**2**	**3**
1				131.4	128.8	133.9
2,6	6.61 *d* (2H, 8.6)	6.79 *d* (2H, 8.8)	7.05 *d* (2H, 8.5)	127.2	128.7	126.1
3,5	6.51*d* (2H, .6)	6.66 *d* (2H, 8.8)	6.77 *d* (2H, 8.5)	114.9	115.2	114.9
4				156.8	157.8	157.2
7	5.02 *d* (1H, 6.3)	5.17 *d* (1H, 10.5)	5.23 *d* (1H, 2.8)	95.2	87.6	92.9
8	3.99 *d* (1H, 6.3)	3.87 *dd* (1H,10.5, 1.9)	4.15 *d* (1H, 2.8)	55.9	51.3	56.1
9				146.4	169.5	147.3
10	5.78 *brs* (1H)		5.84 *d* (1H, 2.2)	105.7	62.5	105.5
11				158.9	202.6	158.7
12	5.92 *t* (1H, 2.0)	3.36 *d* (1H, 7.9)	6.07 *d* (1H, 2.2)	101.1	69.3	100.9
13				158.9	195.5	158.7
14	5.78 *brs* (1H)	5.63 *s* (1H)	5.84 *d* (1H, 2.2)	105.7	124.9	105.5
1′				132.5	131.2	132.6
2′,6′	6.44 *d* (2H, 8.6)	7.12 *d* (2H, 8.8)	6.36 *d* (2H, 8.5)	126.8	128.5	125.8
3′,5′	6.40 *d* (2H, 8.6)	6.72 *d* (2H, 8.8)	6.48 *d* (2H, 8.5)	114.3	115.2	114.5
4′				156.1	155.8	156.2
7′	5.12 *d* (1H, 2.0)	3.84 *brs* (1H)	5.23 *d* (1H, 2.8)	92.0	39.0	91.7
8′	4.40 *d* (1H, 2.0)	5.80 *brs* (1H)	3.82 *d* (1H, 2.8)	50.0	37.9	51.6
9′				142.6	139.6	142.6
10′				118.4	115.1	118.7
11′				161.5	158.8	160.8
12′	6.27 *d* (1H, 2.1)	6.10 *d* (1H, 2.2)	6.21 *d* (1H, 2.0)	95.4	95.5	94.6
13′				159.3	158.5	159.2
14′	6.06 *d* (1H, 2.1)	6.96 *d* (1H, 2.2)	6.09 *d* (1H, 2.0)	106.7	109.0	106.1
1”				132.8	128.3	127.8
2”,6”	6.49 *d* (2H, 8.6)	6.74 *d* (2H, 8.8)	6.63 *d* (2H, 8.5)	125.2	128.7	129.8
3”,5”	6.60 *d* (2H, 8.6)	6.68 *d* (2H, 8.8)	6.42 *d* (2H, 8.5)	115.1	115.2	114.5
4”				156.2	156.1	156.6
7”	5.40 *d* (1H, 2.7)	4.28 *dd* (1H, 7.9,6,9)	5.73 *d* (1H, 12.1)	92.5	39.0	130.4
8”	3.88 *d* (1H, 2.7)	3.85 *d* (1H, 6.9)	5.81 *d* (1H, 12.1)	52.3	46.2	124.5
9”				142.1	132.9	136.5
10”				120.3	115.6	121.5
11”				160.5	160.7	160.7
12”	6.17 *d* (1H, 2.1)	6.59 *s* (1H)	6.25 *d* (1H, 2.0)	94.5	96.5	95.3
13”				159.2	153.8	158.3
14”	6.25 *d* (1H, 2.1)		6.06 *d* (1H, 2.0)	105.7	124.5	107.5
1”’				127.8	132.3	
2”’,6”’	6.72 *d* (2H, 8.6)	6.80 *d* (2H, 8.8)		130.0	126.1	
3”’,5”’	6.45 *d* (2H, 8.6)	6.58 *d* (2H, 8.8)		114.4	114.7	
4”’				156.3	156.5	
7”’	5.90 *d* (1H, 12.0)	5.12 *s* (1H)		131.3	91.2	
8”’	5.85 *d* (1H, 12.0)	3.90 *s* (1H)		124.8	54.7	
9”’				136.3	148.0	
10”’		5.80 *brs* (1H)		120.5	104.7	
11”’				160.7	158.8	
12”’	6.30 *d* (1H, 2.1)	6.23 *t* (1H, 2.0)		95.5	101.0	
13”’				157.9	158.8	
14”’	6.00 *d* (1H, 2.1)	5.80 *brs* (1H)		107.6	104.7	

905, suggesting the molecular formula $C_{56}H_{40}O_{12}$, compatible with a tetrastilbene. By analysis of its ^{1}H NMR, ^{13}C NMR, HMQC, HMBC, NOESY spectra and comparison with published data (Kawabata et al., 1991), it was confirmed as kobophenol B.

Compound **3** was white and amorphous. LSIMS (+ ve ion-mode) showed an $[M+H]^+$ ion at m/z 681, suggesting the molecular formula $C_{42}H_{32}O_9$, compatible with a tristilbene. By analysis of its ^{1}H NMR, ^{13}C NMR, HMQC, HMBC, NOESY spectra and comparison with published data (Ono et al., 1995), it was confirmed as *cis*-miyabenol C. It would appear that **3** is the biogenetic precursor of **1**, since the A/B, A′/B′ and A″/B″ portions of the molecules have the same stereochemistries and **1**

Table 3
^1H–^{13}C correlations in **1** obtained from HMQC (^1J) and HMBC (^2J and ^3J)[a]

H	C		
	^1J	^2J	^3J
H-2	C-2		C-4, C-6, C-7
H-3	C-3	C-4	C-1, C-5
H-5	C-5	C-4	C-1, C-3
H-6	C-6		C-2, C-4, C-7
H-7	C-7	C-8	C-2, C-6, C-9, C-10′, C-11′
H-8	C-8	C-7, C-9, C-10′	C-1, C-10, C-14, C-11′
H-10	C-10		C-8, C-14, C-12
H-12	C-12	C-11, C-13	C-10, C-14
H-14	C-14		C-8, C-10, C-12
H-2′	C-2′	C-3′	C-4′, C-6′
H-3′	C-3′	C-4′	C-1′, C-5′
H-5′	C-5′	C-4′	C-1′, C-3′
H-6′	C-6′	C-5′	C-4′, C-2′
H-7′	C-7′		C-2′, C-6′, C-9′, C-10″, C-11''
H-8′	C-8′	C-9′, C-10''	C-1′, C-10′, C-11'', C-14′
H-12′	C-12′	C-11′, C-13′	C-10′, C-14′
H-14′	C-14′	C-13′	C-12′, C-10′
H-2″	C-2″		C-7″, C-4″
H-3″	C-3″	C-4″	C-1″, C-5″
H-5″	C-5″	C-4″	C-1″, C-3″
H-6″	C-6″		C-7″, C-4″
H-7″	C-7″		C-2″, C-6″, C-9″, C-10''', C-11'''
H-8″	C-8″	C-9″, C-10‴	C-1″, C-10″, C-14″, C-11‴
H-12″	C-12″	C-11″, C-13″	C-10″, C-14″
H-14″	C-14″		C-10″, C-12″
H-2‴	C-2‴	C-3‴	C-6‴, C-7‴, C-4‴
H-3‴	C-3‴	C-2‴, C-4‴	C-1‴
H-5‴	C-5‴	C-4‴, C-6‴	C-1‴
H-6‴	C-6‴	C-5‴	C-2‴, C-7‴, C-4‴
H-7‴	C-7‴	C-1‴	C-2‴, C-6‴, C-9‴
H-8‴	C-8‴	C-7‴, C-9‴	C-1‴, C-10‴, C-14‴
H-12‴	C-12‴	C-11‴, C-13‴	C-10‴, C-14‴
H-14‴	C-14‴		C-8‴, C-10‴, C-12‴

[a] Spectra obtained in CD_3OD.

can be formed by the addition of a further resveratrol unit to the 7″/8″ double bond of **3**.

It is worth mentioning that *cis*-miyabenol A and *cis*-miyabenol C are not fully stable. When exposed to light, they readily isomerise to the *trans*-isomers. So although NMR experiments and bioassay tests were performed immediately after the compounds were purified by HPLC, there were still minor amounts of the *trans*-isomers present (5 to 10% according to ^1H NMR areas) together with their *cis*-isomers.

Compounds **1**, **2** and **3** are isolated for the first time from *C. pendula*, and *cis*-miyabenol A and *cis*-miyabenol C are the first oligostilbenes with *cis*-double bonds isolated from *Carex* species. Among the three oligostilbenes, kobophenol B is the most prominent component (1.27% of the seed weight), as has been found for other *Carex* species (Kawabata et al., 1991), while *cis*-miyabenol A and *cis*-miyabenol C are present in much smaller amounts.

Table 4
Key NOE interactions found in ^1H–^1H NOESY spectra of **1**[a]

From	To
H-2/H-6	H-8, H-7
H-7	H-8, H-2/ H-6, H-10/H-14,
H-8	H-8′ H-8″, H-7, H-8‴,H-7‴, H-2/H-6, H-2‴/H-6‴(w)
H-2′/ H-6′	H-8′, H-7′, H-7‴, H-8‴, H-12 (w)
H-7′	H-8′, H-10/H-14, H-7(w), H-2′/H-6′, H-14′
H-8′	H-8, H-8″, H-7′, H-10/H-14 (w), H-7‴, H-8‴, H-2′/H-6′
H-2″/H-6″	H-8″, H-7″, H-12‴ (w), H-2‴/H-6‴
H-7″	H-8″, H-14″, H-14′, H-2″/H-6″
H-8″	H-2″/H-6″, H-8, H-8′, H-7″, H-7‴, H-8‴, H-14′(w), H-14″(w), H-2‴/H-6‴
H-2‴/H-6‴	H-8″, H-8(w), H-7‴, H-8‴, H-14‴, H-2″/H-6″
H-7‴	H-8″, H-8′, H-8, H-2′/H-6′, H-2‴/H-6‴
H-8‴	H-8″, H-8′, H-8, H-2′/H-6′, H-2‴/H-6‴

[a] Spectra obtained in CD_3OD; w = weak.

2.3. Biological activity

Purified compounds **1**, **2** and **3** were found to be active as ecdysteroid antagonists. In the *Drosophila melanogaster* B_{II} cell bioassay (Clément et al., 1993), compounds **1** (95% purity according to ^1H NMR peak areas, containing a minor amount of the *trans*-isomer), **2** (100% purity) and **3** (90% purity, containing a minor amount of the *trans*-isomer according to ^1H NMR peak areas) antagonised the action of 20-hydroxyecdysone (5×10^{-8} M) with 50% responses at 3.1×10^{-5} M, 3.7×10^{-5} M and 1.9×10^{-5} M, respectively. Their antagonist activities in this bioassay are similar to those of other stilbenoids previously isolated from *Paeonia suffruticosa* (Sarker et al., 1999) and *Iris clarkei* (Keckeis et al., 2000). The EC_{50} values of all these compounds are within the range of 1×10^{-5} M to 5.3×10^{-5} M and, at high concentration, all of them are cytotoxic. Prior to the identification of the three oligostilbenes from *C. pendula*, we had found the monomeric (resveratrol), dimeric (ampelopsin B) and trimeric (α-viniferin and suffruticosols) resveratrol-type stilbenes are antagonistic. *cis*-Miyabenol A and kobophenol B add tetrameric resveratrol-type stilbenes to the active stilbenoids and provide more data to consider the interesting question of the steric interaction of molecules of such differing size with the binding site, which will be useful for deducing the relationship between steroid hormone receptors and non-steroidal ligands and, thus, designing new chemicals for invertebrate pest control (Keckeis et al., 2000).

2.4. Interaction with the ligand-binding site of ecdysteroid receptors

There are many possible sites of action for steroid hormone antagonists. In order to clarify the mode of

action of these stilbenoids, we tested the ability of the compounds isolated from *C. pendula* to compete with radiolabelled ecdysteroid for the ligand-binding site of dipteran and lepidopteran ecdysteroid receptor complexes. Fig. 1 shows the results of competition experiments involving bacterially-expressed *Drosophila melanogaster* EcR/USP complexes. It is apparent that all three of the stilbenoids are able to compete with specifically-bound [^{3}H]ponasterone A. The IC_{50} values (kobophenol B, 13 μM [$K_i = 5.6$ μM]; *cis*-miyabenol A, 33 μM [$K_i = 14.2$ μM]; *cis*-miyabenol C, 100 μM [$K_i = 42.9$ μM]) are similar to the EC_{50} values presented above. These values compare to an IC_{50} value of 0.12 μM for 20-hydroxyecdysone ($K_i = 5.2\times10^{-8}$M; cf. EC_{50} for 20-hydroxyecdysone in the B_{II} bioassay $= 7.5\times10^{-9}$ M; Clément et al., 1993). Since the stilbenoids are antagonists, their activities in the B_{II} assay will depend on their relative potencies and concentrations in relation to the added 20-hydroxyecdysone (5×10^{-8} M), so EC_{50} values in the bioassay and IC_{50} values in the cell-free receptor assays cannot be directly compared. However, these results demonstrate that the affinity of the stilbenoids for the ligand binding site on the receptor is probably adequate to account for their activity as antagonists in the B_{II} assay. Also included in Fig. 1 are data for *trans*-resveratrol. We have previously shown that *cis*-resveratrol is an antagonist in the B_{II} bioassay ($EC_{50} = 1.2\times10^{-5}$ M; Sarker et al., 1999), while *trans*-resveratrol is inactive

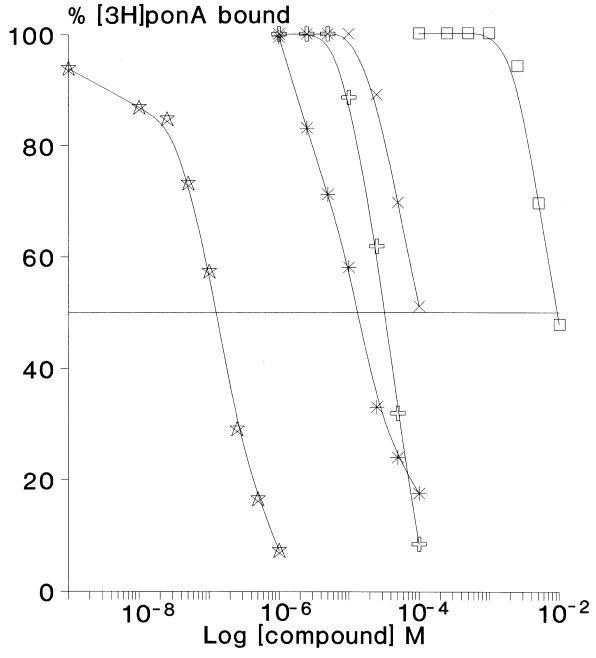

Fig. 1. Competition of test compounds with radiolabelled ecdysteroid for the ligand binding site of the *Drosophila melanogaster* ecdysteroid receptor complex. The ability of 20-hydroxyecdysone (☆), kobophenol B (*), *cis*-miyabenol A (✠), *cis*-miyabenol C (×) and *trans*-resveratrol (□) to compete with [^{3}H]ponasterone A (0.2 nM) for specific binding to DmEcR/DmUSP. Unbound material was removed by the addition of dextran-coated charcoal.

(Dinan et al., 2001). The competition experiments with DmEcR/DmUSP demonstrate clearly that *trans*-resveratrol has a very poor affinity for the ligand-binding site ($IC_{50} = 10^{-2}$ M), thus explaining the lack of activity of this compound in the bioassay.

Similar experiments with CfEcR/CfUSP (data not shown) demonstrate that kobophenol B (**2**) and *cis*-miyabenol A (**1**) also compete with [^{3}H]ponasterone A with this receptor (IC_{50}/K_i values are 25/20 and 40/32 μM, respectively). It was not possible to assess *cis*-miyabenol C (**3**) in this assay owing to the paucity of the amount isolated.

3. Experimental

3.1. General experimental procedures

UV spectra were obtained in MeOH. NMR spectra were performed in CD_3OD or acetone-d_6 on a Brüker AVANCE DRX400 instrument using Bruker microprograms. LSIMS (+ve ion-mode); glycerol matrix using a Cs^+ primary beam on a VG Quattro triple quadruple mass spectrometer (VG Biotech, Altrincham, UK); SPE; Sep-Pak Vac 35cc (10 g) C_{18} cartridge (Waters/Millipore, Watford, Herts., UK) was used for pre-HPLC fractionation; HPLC: (a) preparative/semipreparative; Gilson Model 806 HPLC coupled with a Gilson UV-visible detector, (b) analytical; Gilson model 811 HPLC coupled with a Gilson 160 diode-array detector and using Gilson Unipoint computer program (Anachem, Luton, Beds., UK); RP-semiprep. HPLC columns: Spherisorb analytical and semipreparative C_{18} and C_6 reversed-phase columns (Waters/Millipore) and Apex II semiprep. Diol normal-phase column (Jones Chromatography, Hengoed, Mid-Glamorgan, U.K.). Chromatographic separations were monitored at 223 and 283 nm.

3.2. Plant material

Seeds of *C. pendula* were purchased from B&T World Seeds. A voucher specimen has been retained at the Department of Biological Sciences, University of Exeter. The sources of other seed samples are given in Table 1.

3.3. Bioassay

Ecdysteroid antagonist activities of the seed extracts, SPE fractions, HPLC fractions and the pure compounds were assessed with a microplate-based bioassay using the *Drosophila melanogaster* B_{II} cell line (Clément et al., 1993). All samples were tested in quadruplicate. Pure compounds were tested at concentrations ranging from 10^{-7} to 10^{-3} M. 20-Hydroxyecdysone at 5×10^{-8} M was used in the antagonist version of the bioassay.

3.4. Extraction and isolation

Ground seeds (19 g) were extracted three times (3×24 h) with 3×400 ml MeOH at 55°C with stirring using a magnetic stirrer. Extracts were pooled and reduced by evaporation to 210 ml. This was made to a 70% aq. methanolic solution by adding 90 ml water. After being defatted with *n*-hexane (4×150 ml), the extract was concentrated by rotary evaporation at a maximum temperature of 45°C. The defatted extract was subjected to SPE fractionation (using MeOH/H_2O step-gradient) which afforded seven fractions. Two fractions (eluted with 30 and 50% aq. MeOH) showed ecdysteroid antagonist activity. The two fractions were pooled and subjected to RP-semiprep. HPLC (eluted at 2 ml/min with a linear gradient from 30% MeOH in H_2O to 70% MeOH in H_2O over 30 min, followed by elution with MeOH for another 10 min) which afforded three fractions (P-1, P-2 and P-3). P-2 showed ecdysteroid antagonist activity. The further isolation of P-2 proceeded by C_6-semiprep. HPLC, eluted with 45% MeOH in H_2O at a flow rate of 2 ml/min, affording **2** (240.4 mg) and another two bioactive fractions (P-2-2 and P-2-4). P-2-2 was subjected to NP-HPLC on a semiprep. diol column, eluted with 8% MeOH in dichloromethane and then to RP-HPLC on an analytical C_{18} column, eluted with 40% MeOH in H_2O, and **1** (3.93 mg) was obtained. P-2-4 was further purified, using both a semiprep. C_{18} column and an analytical C_6 column, eluted with 40% MeOH in H_2O and 38% MeOH in H_2O, respectively, yielding **3** (0.94 mg).

cis-Miyabenol A (**1**), white amorphous, UVλ_{max}^{MeOH} nm (log ε) = 286 (4.46); LSIMS (+ve ion-mode): *m*/*z* 907 $[M+H]^+$. ^1H NMR and ^{13}C NMR (in CD_3OD) see Table 1.

Kobophenol B (**2**), pale-yellow needles, UV λ_{max}^{MeOH} nm (log ε) = 285 (4.05), LSIMS (+ve ion-mode): *m*/*z* 905 $[M+H]^+$. ^1H NMR and ^{13}C NMR (in CD_3OD) see Table 1. ^1H NMR (in acetone-d_6), as published data (Kawabata et al., 1991).

cis-Miyabenol C (**3**), white amorphous, UVλ_{max}^{MeOH} (log ε) = 286 (4.40), LSIMS (+ve ion mode): *m*/*z* 681 $[M+H]^+$. ^1H NMR and ^{13}C NMR data (in CD_3OD) see Table 1. ^1H NMR (in acetone-d_6), as published data (Ono et al., 1995).

3.5. Receptor assay

Bacterially-expressed DmEcR, DmUSP, CfEcR and CfUSP were generously provided by Dr. Tarlochan Dhadialla (Rohm & Haas Co.). EcR protein (15 μl) and USP (1 μl) were incubated with 84 μl 10 mM Tris/HCl (pH 7.2, containing 1 mM DTT and 0.4 mg fatty acid free BSA), [24,25,26,27-^{3}H]ponasterone A (0.2 nM; 150 Ci/mmol; ARC Inc., St Louis, MO, USA) and known concentrations of 20-hydroxyecdysone, **1**, **2**, **3** or *trans*-resveratrol. Non-specific binding was determined by the inclusion of a 500-fold excess of unlabelled ponasterone A. Assays were incubated for 16 h (DmEcR + DmUSP) or 3 h (CfEcR + CfUSP) at 7°C. Dextran-coated charcoal (25 μl: 500 mg acid-washed charcoal + 50 mg T70 dextran in 20 ml 10 mM Tris/HCl buffer, pH 7.2) was added to each tube and incubated for 5 min at 7°C before centrifuging at 13,000 × *g* for 5 min. Aliquots of the supernatants (100 μl) were radioassayed after the addition of 1 ml scintillation cocktail (Emulsifier-Safe; Packard Bioscience, Groningen, The Netherlands). IC_{50} values for compounds were converted to K_i values according to the formula $K_i = IC_{50}/(1 + [ponA]/Kd)$, where [ponA] is the concentration of [^{3}H]ponasterone A used (0.2 nM) and Kd is the equilibrium dissociation constant for the interaction of the receptor complex with [^{3}H]ponasterone A (determined by Scatchard analysis; 0.15 nM for DmEcR/DmUSP and 0.8 nM for CfEcR/CfUSP; Bourne, unpublished).

Acknowledgements

Y.M. was supported by a Royal Society Royal China Fellowship. The research was also funded by EU-INTAS (Contract No. 96-1291). We thank Professor Huw H. Rees (University of Liverpool) for mass spectra, Dr. Satyajit D. Sarker (Robert Gordon University, Aberdeen) for his assistance with the interpretation of NMR spectra and Dr. Tarlochan S. Dhadialla (Rohm & Haas Co., Springhouse, PA, USA) for the provision of ecdysteroid receptor proteins.

References

Clément, C.Y., Bradbrook, D.A., Lafont, R., Dinan, L., 1993. Assessment of a microplate-based bioassay for the detection of ecdysteroid-like or antiecdysteroid activities. Insect Biochem. Mol. Biol. 23, 187–190.

Dinan, L., 1995. A strategy for the identification of ecdysteroid receptor agonists and antagonists from plants. Eur. J. Entomol. 92, 271–283.

Dinan, L., Savchenko, T., Whiting, P., Sarker, S.D., 1999. Plant natural products as insect steroid receptor agonists and antagonists. Pest. Sci. 55, 331–335.

Dinan, L., Bourne, P., Whiting, P., Hutchinson, T.H., 2001. Screening environmental contaminants for ecdysteroid agonist and antagonist activity using the *Drosophila melanogaster* B_{II} cell in vitro assay. Environ. Toxicol. Chem.

Kawabata, J., Ichikawa, S., Kurihara, H., Mizutani, J., 1989. Kobophenol A, a unique tetrastilbene from *Carex kobomugi* Ohwi (Cyperaceae). Tetrahedron Lett. 30, 3785–3788.

Kawabata, J., Mishima, M., Kurihara, H., Mizutani, J., 1991. Kobophenol B, a tetrastilbene from *Carex pumila*. Phytochemistry 30, 645–647.

Kawabata, J., Mishima, M., Kurihara, H., Mizutani, J., 1995. Stereochemistry of two tetrastilbenes from *Carex* species. Phytochemistry 40, 1057–1510.

Keckeis, K., Sarker, S.D., Dinan, L., 2000. Resveratrol-type oligostilbenes from *Iris clarkei* antagonise 20-hydroxyecdysone action in a *Drosophila melanogaster* cell line. Cell. Mol. Life Sci. 57, 333–336.

Koolman, J., 1989. Ecdysone. Thieme Verlag, Stuttgart.

Kurihara, H., Kawabata, J., Ichikawa, S., Mishima, M., Mizutani, J., 1991. Oligostilbenes from *Carex kobomugi*. Phytochemistry 30, 649–653.

Kurihara, H., Kawabata, J., Ichikawa, S., Mizutani, J., 1990. (−)-ε-Viniferin and related oligostilbenes from *Carex pumila* Thunb. (Cyperaceae). Agric. Biol. Chem. 54, 1097–1099.

Ono, M., Ito, Y., Kinjo, J., Yahara, S., Nohara, T., Niiho, Y., 1995. Four new glycosides of stilbene trimer from foeniculi fructus (fruit of *Foeniculum vulgare* Miller). Chem. Pharm. Bull. 43, 868–871.

Sarker, S.D., Whiting, P., Dinan, L., Šik, V., Rees, H.H., 1999. Identification and ecdysteroid antagonist activity of three resveratrol trimers (suffruticosols A, B and C) from *Paeonia suffruticosa*. Tetrahedron 55, 513–524.

Sotheeswaran, S., Pasupathy, V., 1993. Distribution of resveratrol oligomers in plants. Phytochemistry 32, 1083–1092.

Suzuki, K., Shimizu, T., Kawabata, J., Mizutani, J., 1987. New 3,5,4′-trihydroxystilbene (resveratrol) oligomers from *Carex fedia* Nees var. *miyabei* (Franchet) T. Koyama (Cyperaceae). Agric. Biol. Chem. 51, 1003–1008.

PERGAMON

Phytochemistry 57 (2001) 401–407

PHYTOCHEMISTRY

www.elsevier.com/locate/phytochem

Ecdysteroids and bufadienolides from *Helleborus torquatus* (Ranunculaceae)

Yanhui Meng[a,1], Pensri Whiting[a], Vladimir Šik[b], Huw H. Rees[c], Laurence Dinan[a,*]

[a]*Department of Biological Sciences, University of Exeter, Hatherly Laboratories, Prince of Wales Road, Exeter, Devon, EX4 4PS, UK*
[b]*Department of Chemistry, University of Exeter, Stocker Road, Exeter, Devon, EX4 4QD, UK*
[c]*School of Biological Sciences, University of Liverpool, Life Sciences Building, Crown Street, Liverpool, L69 7ZB, UK*

Received 28 September 2000; received in revised form 12 February 2001

Abstract

Three bufadienolides, hellebortin A (5-[β-D-glucopyranosyloxy]-10,14,16-trihydroxy-19-nor-{5β,10β,14β,16β}-bufa-3,20,22-trienolide [**1**]), hellebortin B (5-[β-D-glucopyranosyloxy]-3,4-epoxy-14-hydroxy-19-oxo-bufa-20,22-dienolide [**2**]) and hellebortin C (5-[β-D-glucopyranosyloxy]-3,4-epoxy-10,14-dihydroxy-19-nor-bufa-20,22-dienolide [**3**]), together with 20-hydroxyecdysone 3-*O*-β-D-glucoside (**4**) and 20-hydroxyecdysone (**5**) have been isolated by bioassay- and RIA-directed HPLC analyses of a methanol extract of the seeds of *Helleborus torquatus*. The structure and relative stereochemistry of the novel bufadienolide hellebortin A (**1**) and the structures of hellebortin B (**2**) and hellebortin C (**3**) were determined unambiguously by comprehensive analyses of their 1D and 2D NMR data. These five compounds are isolated from *Helleborus torquatus* for the first time. The biological activities of compound **1**, **4** and **5** as ecdysteroid agonists and antagonists have been assessed. © 2001 Elsevier Science Ltd. All rights reserved.

Keywords: Ranunculaceae; Ecdysteroid; Bufadienolides; *Helleborus torquatus*; Hellebortin *A* (5-[β-D-glucopyranosyloxy]-10, 14, 16-trihydroxy-19-nor-{5β, 10β, 14β, 16β}-bufa-3, 20, 22-trienolide [**1**]); Hellebortin B (5-[β-D-glucopyranosyloxy]-3, 4-epoxy-14-hydroxy-19-oxo-bufa-20, 22-dienolide [**2**]); Hellebortin C (5-[β-D-glucopyranosyloxy]-3, 4-epoxy-10, 14-dihydroxy-19-nor-bufa-20, 22-dienolide [**3**]); Bioassay

1. Introduction

Helleborus species are evergreen, rhizomatous plants belonging to the family Ranunculaceae. Some plants from this genus have important biological activities and medicinal effects. For example, *H. foetidus* shows anti-insect activity (Pascual-Villalobos and Robledo, 1998) and poisonous activity towards cattle (Holliman and Milton, 1990), *H. niger* is used in homeopathy and as an adjuvant therapy in the treatment of tumour patients in anthroposophical medicine in Germany (Bussing and Schweitzer, 1998) and a transcutaneous implantation of the root of *H. purpurascens* is used to provoke leucocytosis and neutrophils for better healing of chronic diseases in Romanian traditional medicine (Bogdan et al., 1990). With regard to the chemical constituents of the genus of *Helleborus*, many kinds of compounds have been isolated, including lipids and fatty acids (Aitzetmüller et al., 1999; Colombo et al., 1991), a steroidal sapogenin (Vladimirov et al., 1991) and phytoecdysteroids (Kissmer and Wichtl, 1987; Liedtke et al., 1997). The bufadienolide helleborin (**6**), a cardiac glycoside which was formerly used in therapy for heart rhythm irregularities, was isolated from *Helleborus* spp. (Muhr et al., 1995). The co-occurrence of ecdysteroids and bufadienolides in *Helleborus* spp. has been investigated (Hardman and Benjamin, 1976). However, no previous studies on the chemical constituents of *H. torquatus* Archer-Hind (syn. *H. serbicus* Adamovic) have been reported. Here we report the isolation, structural elucidation and biological assessment of three new bufadienolides (hellebortin A [**1**], hellebortin B [**2**] and hellebortin C [**3**]) and two phytoecdysteroids (**4** and **5**) from the seeds of this species.

Phytoecdysteroids are analogues of insect steroid hormones and are believed to contribute to the deterrence of invertebrate predators by acting as antifeedants

* Corresponding author. Tel.: +44-1392-264605; fax: +44-1392-263700.
E-mail address: l.n.dinan@exeter.ac.uk (L. Dinan).

[1] Supported by Royal China Fellowship. Permanent address: Department of Applied Chemistry, Zhongshan College, Zhongshan 528403, People's Republic of China.

0031-9422/01/$ - see front matter © 2001 Elsevier Science Ltd. All rights reserved.
PII: S0031-9422(01)00070-X

or by disrupting hormone balance on ingestion. Phytoecdysteroids are detectable in 5–6% of plant species, sometimes in very high concentrations. Differences in the presence and profiles of phytoecdysteroids in related species may have chemotaxonomic value (Dinan, 1995; Dinan et al., 1999b).

Bufadienolides are important cardiac glycosides which increase the contractile force of the heart by inhibiting the enzyme Na^+, K^+–ATPase (Akizawa et al., 1994). They also show toxic activities to livestock (Steyn and van Heerden, 1998). Some bufadienolides have antineoplastic and cell growth inhibitory properties (Yamagishi et al., 1988). A number of bufadienolides have been isolated from both plant and animal sources (Steyn and van Heerden, 1998), but only six families of plants have been studied for their bufadienolide components. Within the Ranunculaceae, *Helleborus* is the only genus known to contain these compounds; three bufadienolides (all derivatives of hellebrigenin, the steroid aglycone of hellebrin) had previously been isolated from *Helleborus* spp. (Steyn and van Heerden, 1998). The discovery of two new 19-nor-bufadienolides (hellebortins A and C) in *H. torquatus* is the first detection of 19-nor-bufadienolides from any source.

2. Results and discussion

Initial bioassay/RIA assessment of a seed extract of *Helleborus torquatus* revealed the presence of ecdysteroid agonist activity and considerable amounts of RIA-positive material (72.6 μg ecdysone equivalents/g with the ecdysteroid-specific DBL-1 antiserum), strongly indicating the presence of phytoecdysteroids. On hydrolysis with a mixture of hydrolases from *Helix pomatia*, the RIA-response increased considerably, demonstrating the additional presence of conjugated ecdysteroids. No antagonist activity was detected.

Reversed-phase chromatographic analysis of the seed extract of *H. torquatus* by RP–HPLC revealed the presence of two major UV-absorbing peaks, one of which co-chromatographed with 20-hydroxyecdysone and the other, eluting slightly earlier, was RIA- and bioassay-positive only after hydrolysis with *Helix* enzymes. Following fractionation of the extract by C_{18} SPE cartridge, RP– and NP–HPLC chromatography of the 60% MeOH in H_2O fraction guided by bioassay/RIA resulted in the isolation of 20-hydroxyecdysone 3-*O*-β-D-glucoside (**4**), 20-hydroxyecdysone (**5**) and two novel bufadienolides hellebortin B (5-[β-D-glucopyranosyloxy]-3,4-epoxy-14-hydroxy-19-oxo-bufa-20,22-dienolide [**2**]) and hellebortin C (5-[β-D-glucopyranosyloxy]-3,4-epoxy-10,14-dihydroxy-19-nor-bufa-20,22-dienolide [**3**]). Further chromatographic analyses of the non-RIA-positive components of the 60% MeOH in H_2O SPE fraction afforded another new bufadienolide, hellebortin A (5-[β-D-glucopyranosyloxy]-10,14,16-trihydroxy-19-nor-{5β,10β,14β,16β}-bufa-3,20,22-trienolide [**1**]). The structures of the two known compounds (**4** and **5**) were readily identified by comparing their retention times with those of reference compounds and comparing their ^1H and ^{13}C NMR spectra with those published (Lafont and Wilson, 1996). The structure and relative stereochemistry of **1** were unambiguously determined by extensive analysis of its 1D and 2D NMR experiments. The structures of compounds **2** and **3** were also determined by analyses of their 1D and 2D NMR spectra.

Compound **1** was a colourless glassy solid. LSIMS (-ve ion-mode) gave a $[M–H]^+$ ion at m/z 563 compatible with the molecular formula $C_{29}H_{40}O_{11}$, which was supported by the ^{13}C NMR (DEPT) spectra (Table 2). The ^1H NMR (Table 1) and ^{13}C NMR spectra of **1** showed very similar features to hellebrin which was isolated from *H. niger* (Muhr et al., 1995), suggesting that **1** was also a bufadienolide. Compound **1** had only one sugar unit attached to the genin, which was confirmed by the presence of only one anomeric carbon signal (δ 97.0) in the ^{13}C NMR spectrum. The identity of the sugar unit in **1** was readily established as a β-D-pyranoglucose by comparing the chemical shifts and coupling constants of the characteristic anomeric proton (δ 4.64 [1H, *d*, 7.7 Hz]) and five other oxymethine protons at δ 3.19 (*t*, 7.7), 3.34 (*dd*, 8.5, 7.7), 3.28 (*t*, 8.5), 3.22 (*ddd*, 8.5, 5.5, 2.2), 3.64 (*dd*, 12, 5.5) and 3.80 (*dd*, 12, 2.2) with those published (Agrawal, 1992). The ^{13}C NMR data of the genin part of **1** were very similar to those of the genin of hellebrin except for some differences in rings A and D (Table 2). Compared with that of hellebrin, the ^{13}C NMR spectrum of **1** showed no 19-aldehyde signal, but showed four oxygenated carbon signals in its genin instead of the three oxygenated carbons (δ 74.8 [*d*], 75.0 [*s*] and 84.1 [*s*]) for hellebrin. In addition to the signals associated with the two double bonds of a α-pyrone ring (δ_C 111.5 [*d*], 151.4 [*d*], 119.0 [*s*] and 150.3 [*d*]), there were two other olefinic carbon signals (δ_C 131.4 [*d*] and 131.1 [*d*]). The ^1H–^1H COSY spectrum of **1** confirmed all connections of protons to adjacent carbons and that the two olefinic carbons were associated with a double bond connected to C-2. Additionally, one oxygenated carbon signal (δ 72.1 [*d*]) could be assigned to C-16. The structure of **1** was determined as 5-[β-D-glucopyranosyloxy]-10,14,16-trihydroxy-19-nor-{5β,10β,14β,16β}-bufa-3,20,22-trienolide [**1**] (hellebortin A). This was fully supported by HMQC and HMBC spectra which identified all ^1H–^{13}C direct ^1J and ^2J, ^3J correlations, especially all connections to quaternary carbons, such as attachment of the glucose unit to C-5 (δ 77.8 [*s*]), the double bond situated between C-3 and C-4, the α-pyrone ring linked to C-17, and the two other hydroxyl groups situated at C-10 (δ 73.5 [*s*]) and C-14 (84.1 [*s*]).

The relative stereochemistry of **1** has been assigned from NOESY experiments (Fig. 1). On ring B and ring

C, strong NOE interactions observed between H-8/H-6a, H-8/H-11a, H-8/H-18, H-9/H-7a and H-9/H-12a were typical 1,3-diaxial correlations on a six-membered ring in the chair conformation, indicating that ring B and ring C existed in chair conformations and are *trans*-fused. On ring C and ring D, the NOEs observed clearly between H-17/H12a (H-12e), H-15a/H-9 and H-18/H-22 not only suggested ring C and ring D are *cis*-fused, but also supported that the 18-methyl group and H-17 are *trans* on ring D. That H-16 and H-17 were *cis* on ring D was readily confirmed by NOEs between H-16 and H-17. Similarly, NOEs between H-9/H-2a, H-11e/H-1e, H-1′/H-6a (H-6e) and H-4/H-6e demonstrated that H-9 and the 10-hydroxyl group are *trans* on ring B, and also confirmed the *cis*-connection of rings A and B. Therefore, the relative stereochemistry of hellebortin A was unambiguously determined as shown in Fig. 1.

Compound **2** was a white glassy solid. LSIMS (-ve ion-mode) showed $[M–H]^+$ ion at *m*/*z* 575 compatible with the molecular formula $C_{30}H_{40}O_{11}$. ^1H NMR (Table 1) and ^{13}C NMR (Table 2) showed similar features to those of hellebortin A (**1**) and hellebrin (**6**), indicating that **2** was also a bufadienolide. The sugar unit of **2** was identified as β-D-pyranoglucose by comparing the chemical shifts and coupling constants of the characteristic anomeric proton (δ 4.64 [1H, *d*, 7.5 Hz])

Table 1
^1H NMR data of hellebortin A (**1**), hellebortin B (**2**), hellebortin C (**3**) and hellebrin (**6**)[a] (Muhr et al., 1995) (400 MHz, MeOH-d_4, constant *J*, Hz, in parentheses)

H	1	2	3	6
1ax[d]	2.10 *m*	2.03/1.83	2.01/1.85	2.71/2.42
1eq[e]	1.68 *m*			
2ax	2.02 *m*	2.03/1.63	1.85/1.28	2.48/2.37
2eq	2.17 *m*			
3	5.85 *brd* (9.9)	3.38[b]	3.26[b]	4.80
4	5.59 *brd* (9.9)	3.09 *d* (3.4)	3.10 *d* (3.4)	2.87/2.29
6ax	1.98 *td* (12.5, 3.0)	2.40/2.32	2.09/2.01	2.81/2.36
6eq	1.85*dt* (12.5, 3.0)			
7ax	2.03 *qd* (12.5, 3.0)	2.35/1.23	2.15/1.12	2.87/2.04
7eq	1.03 *dq*(12.5, 3.0)			
8	1.69 *td* (12.5, 3.0)	1.89	1.72	2.61
9	1.42 *td* (12.5, 3.5)	1.54	1.49	2.38
11ax	1.61 *qd* (12.5, 3.5)	1.46/1.11	1.60/1.43	2.20/1.79
11eq	1.48 *dq* (12.5, 3.5)			
12ax	1.59 *td* (12.5, 3.5)	1.52/1.42	1.48/1.43	2.18/2.10
12eq	1.33 *dt* (12.5, 3.5)			
15ax	2.32 *dd* (14.5, 7.5)	2.03/1.63	2.01/1.65	2.76/2.35
15eq	1.68 *d* (14.5)			
16	4.45 *dd* (7.7,7.5)	2.23/1.76	2.18/1.76	2.86/2.45
17	2.75 *d* (7.7)	2.54 *dd* (10, 7.0)	2.54 *dd* (10, 6.8)	3.22
18	0.82 *s*	0.68 *s*	0.74 *s*	1.36
19		9.88 *s*		10.8
21	7.44 *dd* (2.2, 0.9)	7.43 *dd* (2.5,0.9)	7.43 *dd* (2.5,0.9)	8.14
22	8.11 *dd* (9.5, 2.2)	7.98 *dd* (9.5,2.2)	8.01 *dd* (9.3, 2.5)	8.66
23	6.19 *dd* (9.5, 0.9)	6.28 (9.5,0.9)	6.28 *dd* (9.3, 0.9)	6.96
1′ax	4.64 *d* (7.7)	4.64 *d* (7.5)[c]	4.70 *d* (7.5)	5.23
2′ax	3.19 *t* (7.7)	3.20 *dd* (7.8, 7.5)	3.38 *dd* (7.8, 7.5)	3.86
3′ax	3.34 *dd* (8.5, 7.7)[b]	3.37 *dd* (8.5,7.8)[b]	3.37 *dd* (8.0,7.8)	4.02
4′ax	3.28 *t* (8.5)	3.36 *t* (8.5)[b]	3.36 *t* (8.0)	3.97
5′ax	3.22 *ddd* (8.5, 5.5, 2.2)	3.32 *ddd* (8.5,5.5,2.2)	3.25 *ddd* (8.0,5.0, 2.2)	3.95
6′a	3.64 *dd* (12, 5.5)	3.65 *dd* (12.5, 5.5)	3.67 *dd* (12.0,5.0)	4.49/4.34
6′b	3.80 *dd* (12, 2.2)	3.84 *dd* (12.5,2.2)	3.84 *dd* (12.0, 2.2)	
1″eq				5.52
2″eq				4.47
3″ax				4.50
4″ax				4.31
5″ax				4.34
6″				2.03

[a] 500 MHz, MeOH-d_4, MeOH signal was used as internal standard (δ_H 3.3).
[b] Signals obscured by MeOH peaks, but could be observed by HMQC and ^1H–^1H COSY.
[c] Signals shielded by H_2O peaks, but could be observed by HMQC and ^1H–^1H COSY.
[d] ax = Axial.
[e] eq = Equatorial.

Table 2
^{13}C NMR (DEPT) data of hellebortin A (**1**), hellebortin B (**2**), hellebortin C (**3**) and hellebrin (**6**)[a] (Muhr et al., 1995) (100 MHz, MeOH-d_4)

C	1	2	3	6
1	26.4 *t*	19.8 *t*	22.7 *t*	19.1
2	24.6 *t*	30.9 *t*	21.9 *t*	26.0
3	131.4 *d*	53.2 *d*	53.8 *d*	74.8
4	131.1 *d*	57.1 *d*	58.3 *d*	36.6
5	77.8 *s*	75.0 *s*	75.4 *s*	75.0
6	30.8 *t*	31.7 *t*	29.8 *t*	37.5
7	23.3 *t*	23.5 *t*	23.1 *t*	25.3
8	40.2 *d*	41.2 *d*	39.4 *d*	43.0
9	40.0 *d*	40.0 *d*	40.1 *d*	40.4
10	73.5 *s*	52.0 *s*	72.7 *s*	56.1
11	21.1 *t*	23.1 *t*	19.8 *t*	23.7
12	40.6 *t*	40.1 *t*	40.2 *t*	41.3
13	48.8 *s*	48.5[b]	48.5[b]	48.5[b]
14	84.1 *s*	84.0 *s*	83.9 *s*	85.1
15	41.4 *t*	31.5 *t*	31.7 *t*	32.5
16	72.1 *d*	28.4 *t*	28.4 *t*	29.7
17	57.9 *d*	50.6 *d*	50.5 *d*	51.9
18	15.8 *q*	15.6 *q*	15.7 *q*	17.4
19		206.2 *s*		209.6
20	119.0 *s*	123.6 *s*	123.4 *s*	124.4
21	150.3 *d*	147.9 *d*	148.0 *d*	150.6
22	151.4 *d*	149.2 *d*	149.7 *d*	148.9
23	111.5 *d*	114.1 *d*	114.0 *d*	115.5
24	163.7 *s*	163.4 *s*	163.4 *s*	163.6
1′	97.0 *d*	96.6 *d*	96.5 *d*	105.9
2′	74.0 *d*	73.6 *d*	73.5 *d*	76.0
3′	76.9 *d*	76.8 *d*	76.5 *d*	78.1
4′	70.3 *d*	70.0 *d*	70.0 *d*	71.5
5′	76.2 *d*	76.5 *d*	76.6 *d*	78.2
6′	61.4 *t*	61.4 *t*	61.4 *t*	62.8
1″				100.9
2″				72.2
3″				72.3
4″				83.4
5″				69.3
6″				18.5

[a] 500 MHz, MeOH-d_4, MeOH signal was used as internal standard (δ_C 49.0).
[b] Signals obscured by H_2O peaks, but could be observed by HMBC.

and five other oxymethine protons at δ 3.20 (*dd*, 7.8, 7.5), 3.37 (*dd*, 8.5, 7.8), 3.36 (*t*, 8.5), 3.32 (*ddd*, 8.5, 5.5, 2.2), 3.65 (*dd*, 12, 5.5) and 3.84 (*dd*, 12, 2.2) with those published (Agrawal, 1992). The ^{13}C NMR data of the genin part of **2** were very similar to those of the genin part of hellebrin except there were some differences in ring A. Besides the oxymethine protons from the glucose unit, the presence of two other oxygen-bearing methine groups at δ 3.38 and 3.09 (*d*, 3.4) in the ^{1}H NMR spectrum and two corresponding oxygenated carbon at δ 53.2 and 57.1 in the ^{13}C NMR spectrum of **2** could be explained by an epoxide ring, which would agree with the calculated degree of unsaturation ($n=11$) of **2**. ^{1}H–^{1}H COSY, HMQC and HMBC spectra of **2** (as a mixture with **3**) located this epoxide ring at C-3 and C-4, and confirmed that the glucose unit was linked to C-5, as in hellebortin A. Thus, the structure of **2** was unambiguously deduced as 5-[β-D-glucopyranosyloxy]-3,4-epoxy-14-hydroxy-19-oxo-bufa-20,22-dienolide (hellebortin B).

Compound **3** was a white glassy solid. LSIMS (-ve ion-mode) showed an $[M\text{-}H]^+$ ion at m/z 563 compatible with the molecular formula $C_{29}H_{40}O_{11}$, one carbon less than compound **2**. ^{1}H NMR (Table 1) and ^{13}C NMR (Table 2) of **3** were in good agreement with those of **2** except that there were no signals corresponding to 19-aldehyde group, and the chemical shift of C-10 was at lower field (δ 72.2) compared with that of **2** (δ 52.0). This indicated that a hydroxyl group was attached to C-10. ^{1}H–^{1}H COSY, HMQC, HMBC spectra of **3** (as a mixture with **2**) confirmed all connections in the molecule. Therefore, the structure of **3** was unambiguously deduced as (5-[β-D-glucopyranosyloxy]-3,4-epoxy-10,14-dihydroxy-19-nor-bufa-20,22-dienolide (hellebortin C).

After final purification, the amounts of compounds **2** and **3** isolated were too low to be able to determine their relative stereochemistries through NOESY experiments.

The biological activities of compound **1**, **4** and **5** as ecdysteroid agonists and antagonists were assessed. 20-hydroxyecdysone 3-*O*-β-D-glucoside (**4**) and 20-hydro-

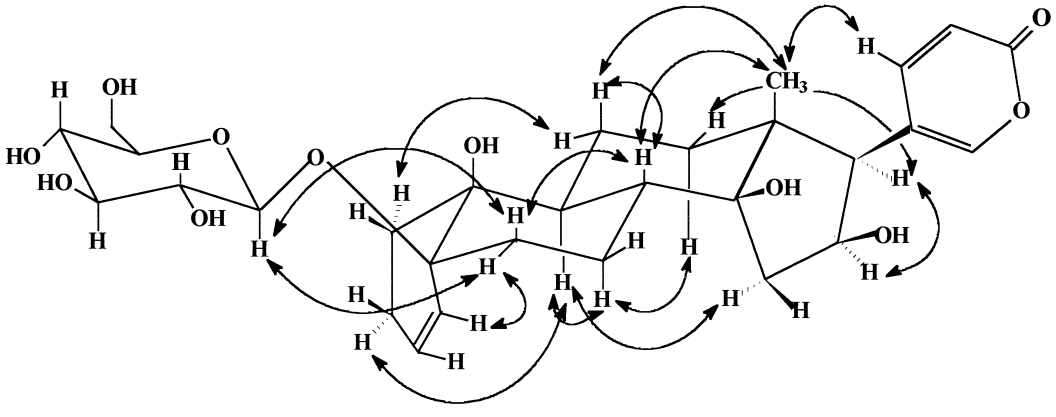

Fig. 1. The key NOEs in Hellebortin A (**1**).

xyecdysone (**5**) possess agonist activities with EC_{50} values of 1.3×10^{-5} M and 7.5×10^{-9} M, respectively (Dinan et al., 1999a), but hellebortin A (**1**) showed no agonist or antagonist activity within the concentration range of 10^{-6} M to 10^{-3} M in the B_{II} cell line assay. The activities of hellebortins B (**2**) and C (**3**) could not be tested because of their limited availability.

3. Experimental

3.1. General experimental procedures

UV spectra were obtained in MeOH. NMR spectra were performed in CD_3OD on a Brüker AVANCE DRX400 instrument using Brüker microprograms. LSIMS (-ve ion-mode); glycerol matrix using a Cs^+ primary beam on a VG Quattro triple quadrupole mass spectrometer (VG Biotech, Altrincham, UK); Sep-Pak Vac 35 cc (10 g) C_{18} solid-phase extraction (SPE) cartridge (Waters/Millipore, Watford, Herts., UK) was used for pre-HPLC fractionation; HPLC: (a) preparative/semipreparative; Gilson Model 806 HPLC coupled with a Gilson UV-visible detector; (b) analytical; Gilson model 811 HPLC coupled with a Gilson 160 diode-array detector and using Gilson Unipoint computer program (Anachem, Luton, Beds., UK); RP and NP stand for reversed-phase and normal-phase, respectively. Spherisorb semipreparative C_{18} and C_6 columns, an Apex II semiprep. Diol column and Spherisorb 5 ODS(2) analytical C_{18} and C_6 columns (Jones Chromatography, Hengoed, Mid-Glamorgan, UK) were used. Chromatographic separations were monitored at 242 and 300 nm.

3.2. Radioimmunoassay and bioassay

RIA was performed according to the procedure described previously (Dinan, 1992) using the ecdysteroid-specific antiserum DBL-1, which was generously donated by Professor Jan Koolman (University of Marburg, Germany). The cross-reactivities of this antiserum with a range of phytoecdysteroids are given elsewhere (Dinan, 1995). Ecdysteroid agonist activities of the extract, SPE fractions, HPLC fractions and purified compounds were assessed with a microplate-based bioassay using the *Drosophila melanogaster* B_{II} cell line (Clément et al., 1993).

3.3. Extraction

Seeds of *H. torquatus* were purchased from B&T World Seeds. A voucher specimen has been retained at the Department of Biological Sciences, University of Exeter. Seeds (9.7 g) were ground and extracted four times (4×24 h) with 3×200 ml of MeOH at 55°C with constant stirring using a magnetic stirrer. Extracts were pooled and evaporated to 210 ml and this was made to a 70% aq. methanolic solution by adding 90 ml H_2O. After being defatted with *n*-hexane (4×150 ml), the extract was concentrated using a rotary evaporator at a maximum temperature of 45°C to give 0.84 g residue.

3.4. Isolation of the compounds

The residue was subjected to SPE fractionation (using a MeOH/H_2O step-gradient) which afforded five fractions. According to the results of bioassay and RIA, Fraction 3 (eluted with 60% MeOH in H_2O) contained most of RIA-positive material. Fraction 3 was subjected to RP(C_6)-semiprep. HPLC (with a linear gradient from 30% MeOH in H_2O to 70% MeOH in H_2O over 45 min, followed by elution with MeOH for another 10 min), which afforded four fractions (P-1, P-2, P-3 and P-4). P-2 and P-3 showed ecdysteroid agonist activity. The further isolation of P-2 and P-3 proceeded by C_6-semiprep. HPLC, eluted with 40% MeOH in H_2O at a flow rate of 2 ml/min, and then by diol-semiprep. HPLC, eluted with 6% MeOH in CH_2Cl_2 at a flow rate 2 ml/min, affording **4** (460 μg) and 5 (1.1 mg). Calculations based on the peak areas of the original chromatogram of the extract indicated that the true amounts of **4** and **5** were 385 μg/g seeds and 250 μg/g seeds, respectively. The further isolation of P-1 proceeded by C_6-semiprep. HPLC, eluted with 35% MeOH in H_2O at a flow rate of 2 ml/min, and then by NP–HPLC with a semiprep. diol column, eluting with 6% MeOH in CH_2Cl_2, afforded **1** (5.47 mg). Bioassay data also showed that P-4 contained some RIA-positive material. The further isolation of P-4 using the same procedure as that of P-1 afforded **2** (490 μg) and **3** (510 μg).

Hellebortin A (5-[β-D-glucopyranosyloxy]-10,14,16-trihydroxy-19-nor-{5β,10β,14β,16β}-bufa-3,20,22-trienolide [**1**]). A colourless, glassy solid. UV λ_{max}^{MeOH} nm (log ε) 296 nm (3.84). LSIMS (-ve ion-mode) m/z 563[M–H]$^+$. ^{1}H NMR see Table 1, ^{13}C NMR see Table 2.

Hellebortin B (5-[β-D-glucopyranosyloxy]-3,4-epoxy-14-hydroxy-19-oxo-bufa-20,22-dienolide [**2**]). A white glassy solid. UV λ_{max}^{MeOH} nm (log ε) 299 nm (3.06). LSIMS (-ve ion-mode) m/z 575[M–H]$^+$. ^{1}H NMR see Table 1, ^{13}C NMR see Table 2.

Hellebortin C (5-[β-D-glucopyranosyloxy]-3,4-epoxy-10,14-dihydroxy-19-nor-bufa-20,22-dienolide [**3**]). A colourless glassy solid. UV λ_{max}^{MeOH} nm (log ε) 299 nm (3.64). LSIMS (-ve ion-mode) m/z 563[M–H]$^+$. ^{1}H NMR see Table 1, ^{13}C NMR see Table 2.

20-Hydroxyecdysone 3-*O*-β-D-glucoside (**4**), amorphous. UV, ^{1}H NMR and ^{13}C NMR data as reported (Lafont and Wilson, 1996).

20-Hydroxyecdysone (**5**), amorphous. UV, ^{1}H NMR and ^{13}C NMR data as reported (Lafont and Wilson, 1996).

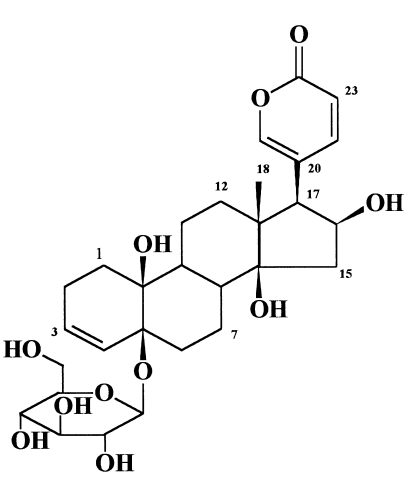

1

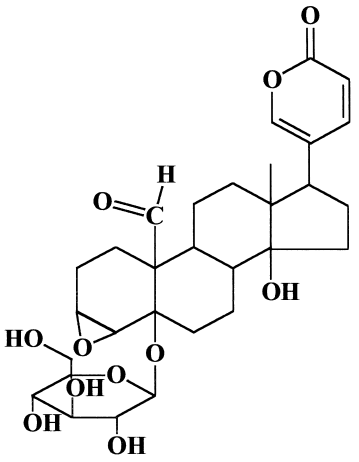

2

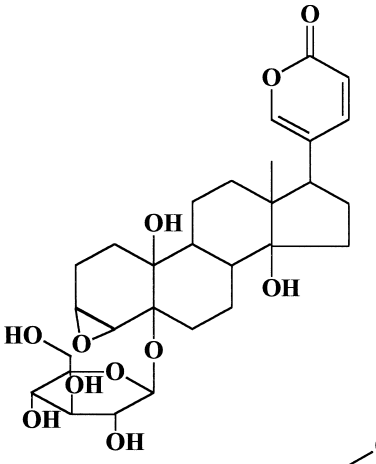

3

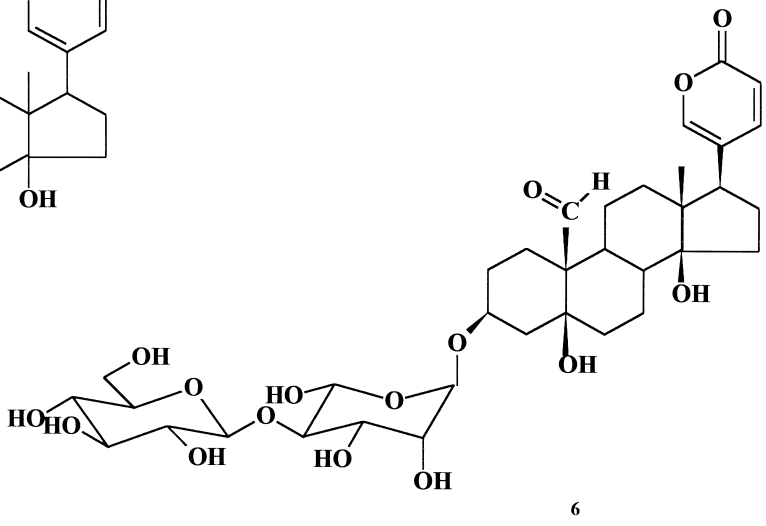

6

Acknowledgements

We thank the Royal Society for a Royal China Fellowship to Y.M. The research was also funded by EU-INTAS (Contract No. 96-1291). We thank Professor Jan Koolman (University of Marburg, Germany) for antisera and Dr. Juraj Harmatha (IOCB, Prague, Czech Republic) for the reference sample of 20-hydroxyecdysone 3-glucoside.

References

Agrawal, P.K., 1992. NMR spectroscopy in the structural elucidation of oligosaccharides and glycosides. Phytochemistry 31, 3307–3330.

Akizawa, T., Mukai, T., Matsukawa, M., Yoshioka, M., Morris, J.F., Butler, V.P., 1994. Structures of novel bufadienolides in the eggs of toad, *Bufo marinus*. Chem. Pharm. Bull. 42, 745–756.

Aitzetmüller, K., Tseveguren, N., Werner, G., 1999. Seed oil fatty acid patterns of the *Aconitum–Delphinium–Helleborus* complex (Ranunculaceae). Plant System. Evol. 215, 37–47.

Bogdan, I., Nechifor, A., Basea, I., Hruban, E., 1990. From the Romanian traditional medicine — unspecific irratating therapy by transcutaneous implantation of *Helleborus purpurascens*, fam Ranunculaceae, in farm-animals. Deutsche Tierärztliche Wochenschrift 97, 525–529.

Bussing, A., Schweizer, K., 1998. Effects of a phytopreparation from *Helleborus niger* on immunocompetent cells in vitro. J. Ethnopharm. 59, 139–146.

Colombo, M.L., Tomè, F., Bugatti, C., 1991. Lipid-content and fatty-acid composition in hypogeous organs of *Helleborus* species (Ranunculaceae). Plant System. Evol. 178, 55–63.

Clément, C.Y., Bradbrook, D.A., Lafont, R., Dinan, L., 1993. Assessment of a microplate-based bioassay for the detection of ecdysteroid-like or antiecdysteroid activities. Insect. Biochem. Mol. Biol. 23, 187–190.

Dinan, L., 1992. The analysis of phytoecdysteroids in single (pre-flowering stage) specimens of fat hen, *Chenopodium album*. Phytochem. Anal. 3, 132–138.

Dinan, L., 1995. A strategy for the identification of ecdysteroid receptor agonists and antagonists from plants. Eur. J. Entomol. 92, 271–283.

Dinan, L., Hormann, R.E., Fujimoto, T., 1999a. A extensive ecdysteroid CoMFA. J. Computer-aided Mol. Design 13, 185–207.

Dinan, L., Savchenko, T., Whiting, P., Sarker, S.D., 1999b. Plant natural products as insect steroid receptor agonists and antagonists. Pestic. Sci. 55, 331–335.

Hardman, R., Benjamin, T.V., 1976. The co-occurrence of ecdysones with bufadienolides and steroidal saponins in the genus Helleborus. Phytochemistry 15, 1515–1516.

Holliman, A., Milton, D., 1990. *Helleborus foetidus* poisoning of cattle. Veterinary Record 127, 339–340.

Kissmer, B., Wichtl, M., 1987. Ecdysteroids from roots and seeds of *Helleborus* species. Archiv. Pharm. 320, 541–546.

Lafont, R., Wilson, I., 1996. The Ecdysone Handbook, 2nd Edition. The Chromatographic Society, Nottingham.

Liedtke, S., Lorch, E., Goedings, P., Wichtl, M., 1997. Isolation of beta-ecdysone and macranthoside I from roots of *Helleborus niger* subsp. *niger* (Ranunculaceae). Pharmazie 52, 964–965.

Muhr, P., Kerek, F., Dreveny, D., Likussar, W., Schubertzsilavecz, M., 1995. The structure of hellebrin. Liebigs Annalen Organ. Bioorgan. Chem. 2, 443–444.

Pascual-Villalobos, M.J., Robledo, A., 1998. Screening for anti-insect activity in Mediterranean plants. Indust. Crops Prod. 8, 183–194.

Steyn, P.S., Van Heerden, F.R., 1998. Bufadienolides of plant and animal origin. Nat. Prod. Reports 15, 397–413.

Vladimirov, S.M., Zivanovstakic, D.S., Ribar, B.J., 1991. A steroidal sapogenin from *Helleborus multifidus* subsp. *serbicus*. Phytochemistry 30, 1724–1725.

Yamagishi, T., Yan, X.-Z., Wu, R.-Y., McPhail, A.R., McPhail, A.T., Lee, K.-H., 1988. Structure and stereochemistry of bryophyllin-A, a novel potent cytotoxic bufadienolide orthoacetate from *Bryophyllum pinnatum*. Chem. Pharm. Bull. 36, 1615–1617.

PERGAMON

Phytochemistry 57 (2001) 409–416

PHYTOCHEMISTRY

www.elsevier.com/locate/phytochem

Induced emissions of apple fruit volatiles by the codling moth: changing patterns with different time periods after infestation and different larval instars

Alan Hern, Silvia Dorn *

Institute of Plant Sciences, Applied Entomology, Swiss Federal Institute of Technology (ETH), CH 8092 Zurich, Switzerland

Received 28 August 2000; received in revised form 5 February 2001

Abstract

The changes in the emission of volatiles from mature apple fruits in response to larval feeding by the codling moth (*Cydia pomonella*) under laboratory conditions are reported. A time course experiment investigated the emission of volatiles throughout the period of larval development following infestation. The volatiles consisted mainly of esters, a few aldehydes, and the terpene α-farnesene. Infested apples emitted the same compounds as healthy apples. The quantities of volatiles released were much higher for infested as compared to healthy fruits for an initial three day period. Following this period there was a decrease in volatile emissions (days 6–9), eventually declining back to the levels emitted from healthy apples or below by 9–21 days after infestation. In a separate experiment, the volatile emissions from healthy and artificially damaged fruits were compared to those from herbivore damaged fruits for each of the five larval instars of *C. pomonella*. The results from the discriminant analysis indicate that the most effective induction of volatiles occurred when fruits were infested with first instar larvae. Induction by first instar larvae was generally higher than after infestation by later instars, and for most compounds it also exceeded the emission from artificially damaged fruits.
© 2001 Elsevier Science Ltd. All rights reserved.

Keywords: *Malus domestica*; Rosaceae; Apple volatiles; Induced response; *Cydia pomonella*; Larval instars; Solid phase microextraction; Linear discriminant analysis

1. Introduction

Herbivore feeding often induces volatile emissions from plants, and such emissions have been well documented (reviewed by Karban and Baldwin, 1997; Baldwin and Preston, 1999; Vet, 1999). In a tri-trophic context, volatile chemicals emitted by plants may potentially act as semiochemicals to both insect herbivores and their natural antagonists (Vet and Dicke, 1992; Vet, 1999). Most of these studies have been carried out under standardised laboratory conditions and only a few deal with field situations (for example, Bernasconi et al., 1998, for herbivores, and De Moraes et al., 1998, for natural antagonists). The plant's role in these interactions is an active one, due to the signalling of its status of health or infestation via changes in the emission of volatile semiochemicals (for example, Dicke and Sabelis, 1988, 1989; Turlings et al., 1990; Turlings and Tumlinson, 1991; Tumlinson et al., 1992, 1993; Vet and Dicke, 1992; Dicke, 1994).

The majority of herbivore induced plant volatiles studies deal with phyllophagous herbivores i.e. those which feed on leaves. In contrast, studies upon the chemical effects triggered by insects which feed on the fruit, i.e. carpophagous insects, are scarce. A previous study in which apple fruitlets (*Malus domestica* Borkh. (Rosaceae)) were freshly picked or still attached to the tree was used to investigate herbivore induced emissions from apple fruits (Boevé et al., 1996). This study demonstrated that apple fruitlets respond to the feeding of the European apple sawfly, *Hoplocampa testudinea*, by emitting volatile chemicals in greater amounts than undamaged fruits. Picked apple fruitlets released significantly higher amounts of *E,E*-α-farnesene, β-ocimene and an unidentified terpenoid. The methodology employed, however, imposed limitations upon the number of samples

* Corresponding author. Tel.: +41-1-632-3921; fax: +41-1-632-1171.
E-mail address: silvia.dorn@ipw.agrl.ethz.ch (S. Dorn).

0031-9422/01/$ - see front matter © 2001 Elsevier Science Ltd. All rights reserved.
PII: S0031-9422(01)00058-9

which could be evaluated, with the consequence that statistical analysis of the field derived data was not feasible.

In this study, our goal was to elucidate the temporal pattern of volatile emissions from fruit in response to herbivory, and to gain an insight into the effect of each larval instar on volatile emissions. This contrasts with the study by Boevé et al. (1996), not only with respect to the herbivore used, but as the response of apple fruits was characterised from the beginning to the end of the period of larval development of the herbivore. In addition, the response of apple fruits to the different larval instars has been analysed.

Laboratory conditions offer a number of advantages for this purpose. Environmental variables which affect volatile sampling can be held constant, such as temperature. In addition, the number of replicates with fruits of the same age and degree of maturation can be high enough to allow statistical evaluation of the data. For the purpose of these experiments fruit standardisation is crucial as apple fruits can show a large variation in their volatile emissions in the course of maturation (Sutherland et al., 1977; Carle, et al., 1987).

Thus we have chosen to model this system using mature apple fruits and in conjunction with a key pest of fruit orchards, the codling moth, *Cydia pomonella* L. (Lepidoptera: Tortricidae). The codling moth larva has five instars all of which feed inside the fruit. The larvae bore into the centre of the fruit and consume the seeds. The objectives of this study were to (1) characterise changes in the emission of induced apple volatiles over the period from initial infestation with newly emerged larvae until their maturation to final instar larvae within the apple and (2) to compare the effect of the individual herbivore instars on the volatile emissions from fruits.

2. Results and discussion

2.1. Time course of volatile emissions

Apples infested by *C. pomonella* emitted the same compounds as healthy apples. Both of the volatile blends consist mainly of esters, with a few aldehydes and the terpene α-farnesene (both the *Z,E* and *E,E* isomers). The temporal pattern of the emissions for the individual compounds was relatively uniform (Table 1). In general, for the first 3 days after infestation the amount of each compound collected from the infested fruits was higher than those collected from the healthy fruits. Following this period (9–21 days), the amount of each compound collected from infested fruits generally decreased to levels equivalent or lower than those collected from healthy fruits (Table 1).

In order to test the hypothesis that the blend of volatiles from infested and non-infested apples were different, we have used linear discriminant analysis. This statistical method evaluates differences or similarities between groups using a multivariate data set. The results of these analyses clearly demonstrate differences between the volatile blends emitted by healthy and infested fruits at eight of the nine sampling periods (except day 15) (Table 2). Therefore, we conclude that the effect of infestation goes beyond an induction of volatiles which is typically measured in the initial phase of infestation, and that it is pervasive for virtually the complete period of herbivore development. In the later phases of the experiment a marked decrease, or even the absence of some compounds from infested as compared to healthy fruits is noted (Table 1).

Infestation of apple fruits with first instar *C. pomonella* larvae caused marked changes in the volatile emissions of the fruits. Although these increases in the emissions of volatiles were of a relatively short duration (ca 3–6 days), even towards the end of the larval development within the fruit, i.e. at 21 days, the volatile blends from the healthy and infested fruits were still different as shown by the linear discriminant analysis.

Boevé (1996) suggested that differences in volatile emissions after fruit infestation by *H. testudinea* may represent an induced defence in fruits. Under this scenario the volatile chemicals induced by herbivory act as synomones to natural enemies which negatively affect the herbivore and have a positive effect on the plant (for example, Dicke and Sabelis, 1989; Turlings et al., 1990; Turlings and Tumlinson, 1991; Dicke, 1994 see Dick and van Loon (2000) for a recent review). In the present tritrophic system, there is evidence that the herbivore induced plant volatiles may act as synomones for a parasitoid. For example, using an experimental system fully comparable to that used in the present study, an insect parasitic wasp of *C. pomonella* preferentially discriminates in favour of infested fruits. *Hyssopus pallidus* spent more time searching on an infested apple than either an artificially damaged or on an healthy apple (Mattiacci et al., 1999). The authors postulated that the cues responsible are probably chemical, our data demonstrates that such chemical differences between the two types of fruit exist (Tables 1 and 2). *H. pallidus* prefers to parasitise fourth or fifth instar *C. pomonella* larvae (Zaviezo and Mills, 1999) and the oviposition of the parasitoid is greatly enhanced in the presence of cues related to apple fruits (Mattiacci et al., 2000). However, to gain a comprehensive understanding of the ecological ramifications of herbivore induced plant volatiles in this particular perennial system will require more investigations.

Defensive mechanisms of the plant are considered to be metabolically costly (Karban and Baldwin, 1997; Baldwin and Preston, 1999, and references therein). Using apples which are removed from sources of further nutrient supplies we found that the initial induction of volatile emissions was short lived which may be related to the high metabolic cost of this induced process (Table 1).

Table 1
Effect of time (days) since infestation with first instar larvae of *Cydia pomonella* on the volatile emissions from apple fruits of *Malus domestica* cv Bohnäpfel (expressed as ratio of areas infested:healthy)[a]

	Time (days) after infestation with instar I larvae																	
Compound	1		2		3		6		9		12		15		18		21	
Butyl acetate	3.5 (3.3–3.8)[c]	***[b]	1.2 (1.0–1.3)	ns[b]	1.1 (1.0–1.1)	ns	1.4 (1.4–1.4)	ns	1.3 (1.3–1.3)	ns	0.9 (0.9–0.9)	ns	0.6 (0.5–0.6)	ns	0.7 (0.7–0.8)	ns	0.2 (0.1–0.3)	*
2-Methylbutyl acetate	2.4 (2.2–2.6)	***	1.3 (1.2–1.5)	ns	1.5 (1.5–1.5)	ns	1.1 (1.1–1.1)	ns	0.8 (0.8–0.8)	ns	0.7 (0.6–0.7)	ns	0.4 (0.4–0.4)	*	0.6 (0.5–0.7)	ns	0.3 (0.3–0.3)	**
Hexyl acetate	2.4 (2.3–2.5)	***	1.3 (1.1–1.4)	ns	2.1 (2.0–2.2)	*[b]	1.7 (1.7–1.8)	*	1.3 (1.3–1.3)	ns	1.0 (1.0–1.2)	ns	0.6 (0.6–0.7)	ns	0.8 (0.8–0.8)	ns	0.5 (0.4–0.5)	*
Butyl butanoate	2.8 (2.5–3.2)	**[b]	1.2 (1.1–1.3)	ns	1.9 (1.8–1.9)	ns	1.5 (1.4–1.5)	ns	1.0 (1.0–1.0)	ns	1.0 (1.0–1.1)	ns	0.5 (0.5–0.5)	ns	0.8 (0.8–0.9)	ns	0.4 (0.4–0.5)	*
Butyl 2-methylbutanoate	2.9 (2.8–3.2)	***	1.5 (1.3–1.7)	ns	2.6 (2.4–2.6)	ns	2.1 (1.9–2.2)	ns	1.2 (1.2–1.3)	ns	1.3 (1.2–1.4)	ns	0.8 (0.8–0.8)	ns	1.4 (1.3–1.4)	ns	0.6 (0.5–0.6)	ns
Hexyl butyrate	2.1 (2.0–2.1)	ns	1.0 (0.9–1.1)	ns	3.5 (3.4–3.5)	*	2.2 (1.9–2.4)	ns	0.7 (0.7–0.7)	ns	1.2 (1.0–1.5)	ns	0.6 (0.5–0.6)	ns	0.7 (0.7–0.8)	ns	0.5 (0.4–0.6)	ns
Propyl hexanoate	2.8 (2.6–3.1)	**	1.3 (1.1–1.3)	ns	2.6 (2.2–3.5)	ns	1.4 (1.4–1.4)	ns	0.8 (0.8–0.8)	ns	0.7 (0.7–0.8)	ns	0.5 (0.4–0.5)	*	0.7 (0.7–0.7)	ns	0.4 (0.4–0.4)	ns
Butyl hexanoate	2.3 (2.2–2.3)	**	1.1 (0.9–1.2)	ns	3.2 (3.1–3.4)	ns	1.7 (1.5–1.8)	ns	0.6 (0.6–0.6)	ns	1.2 (1.1–1.4)	ns	0.7 (0.7–0.7)	ns	1.0 (0.9–1.1)	ns	0.7 (0.6–0.8)	ns
Hexyl hexanoate	2.0 (1.9–2.0)	ns	0.9 (0.8–1.0)	ns	53.2 (44.9–105.6)	**	a	ns	b[d]	ns	14.5 (12.3–25.3)	ns	b	ns	0.2 (0.2–0.3)	ns	(0.6–0.6) (0.6–0.8)	ns
Butyl propanoate	3.1 (3.0–3.4)	**	1.1 (0.9–1.2)	ns	0.9 (0.9–1.0)	ns	1.4 (1.4–1.4)	ns	1.0 (1.0–1.1)	ns	0.5 (0.3–0.7)	ns	0.2 (0.0–0.3)	ns	b	ns	b	ns
Hexyl propanoate	2.3 (2.2–2.4)	*	1.0 (0.8–1.1)	ns	1.9 (1.9–2.0)	*	1.6 (1.6–1.7)	ns	0.9 (0.9–1.0)	ns	1.0 (1.0–1.1)	ns	0.5 (0.5–0.5)	ns	0.6 (0.6–0.7)	ns	0.4 (0.3–0.4)	ns
Z,E-α-farnesene	2.0 (1.7–2.4)	**	1.8 (1.5–2.0)	ns	1.9 (1.8–2.0)	*	1.6 (1.5–1.6)	ns	0.5 (0.4–0.5)	ns	1.1 (1.1–1.2)	ns	0.7 (0.7–0.7)	ns	1.3 (1.2–1.6)	ns	0.5 (0.5–0.6)	ns
E,E-α-farnesene	1.7 (1.4–2.1)	*	2.0 (1.9–2.1)	ns	2.1 (2.1–2.2)	**	1.8 (1.6–2.0)	ns	0.4 (0.3–0.4)	ns	0.7 (0.7–0.7)	ns	0.6 (0.5–0.6)	ns	0.9 (0.9–0.9)	ns	0.6 (0.5–0.8)	ns
Hexanol	2.9 (2.7–3.3)	***	1.2 (1.0–1.4)	ns	4.8 (3.8–9.6)	ns	29.4 (−8.3–8.3)	ns	0.6 (−1.1–0.9)	ns	3.1 (2.2–9.6)	ns	1.1 (1.1–1.1)	ns	1.3 (1.2–1.6)	ns	0.9 (0.7–13.4)	ns
Nonanal	14.3 (−41.7–6.3)	***	0.6 (0.4–0.7)	ns	2.3 (2.2–2.5)	*	14.6 (−15.7–6.2)	*	8.6 (−29.6–4.4)	*	6.5 (4.3–17.9)	**	0.7 (0.4–0.8	ns	1.1 (1.1–1.2)	ns	1.1 (1.0–1.1)	ns
Decanal	1.9 (1.8–2.1)	***	0.8 (0.8–0.8)	ns	3.2 (2.8–3.4)	**	1.9 (1.9–2.0)	*	1.7 (1.6–1.8)	*	0.1 (−0.1–0.2)	**	0.8 (0.7–0.9)	ns	0.7 (0.7–0.8)	ns	0.8 (0.8–0.8)	ns
Dodecanal	11.6 (11.1–12.8)	**	a[d]	***	a	***	30.5 (−18.9–9.7)	***	1.1 (1.0–1.3)	ns	100.0 (−8.2–8.1)	**	1.8 (1.4–3.5)	ns	1.2 (1.1–1.2)	ns	0.2 (0.1–0.2)	***

[a] $N = 10$ for each time and treatment.
[b] ns = $P > 0.05$; * = $P < 0.05$; ** = $P < 0.01$; *** = $P < 0.001$, Mann–Whitney test on untransformed data.
[c] Figures in parentheses refer to the ratio calculated using the mean ± 1 S.E. to illustrate variability.
[d] a = Compound not detected in infested fruits, b = compound not detected in healthy fruits.

Table 2
Summary of linear discriminant analysis for each time interval since infestation[a]

Time (days)	*F*-approximation of Wilks' lambda	DF	*P*	Number of cases misclassified [b]
1	16.2	4,15	0.0001	Healthy 0 Infested 0
2	6.05	2,17	0.01	Healthy 0 Infested 2
3	9.77	3,16	0.001	Healthy 1 Infested 2
6	19.59	1,18	0.001	Healthy 1 Infested 2
9	9.79	2,17	0.01	Healthy 2 Infested 2
12	23.76	3,16	0.001	Healthy 1 Infested 0
18	8.73	2,17	0.01	Healthy 2 Infested 1
21	29.95	3,16	0.0001	Healthy 0 Infested 0

[a] Note that for time 15 no statistically significant ($P > 0.05$ for the *F*-approx. of Wilk's lambda) model could be found and no results for this time period are reported.
[b] Based on Mahalanobis distance square from group means and posterior probabilities of group membership being 0.5 in each case.

2.2. Effect of different herbivore instars on volatile emissions

The majority of the compounds showed significant quantitative differences between the treatments (Examples are given in Fig. 1a and b). For example, *E,E*-α-farnesene was found in higher amounts in the samples from the herbivore infested and artificially damaged fruits than from the healthy fruits (*F*-value 11.4, DF = 6,98; $P < 0.001$) (Fig. 1a). Perusal of Fig. 1a and b indicates that the different larval instars had quite different effects on the amount of each compound collected. In general terms, the highest degree of volatile induction occurred when fruits were infested with first instar larvae, whilst second instar larvae were less effective in eliciting an induced response.

In order to more completely understand the data, we have used linear discriminant analysis to highlight differences between treatments applied to the fruits (summarised in Table 3). Wilk's Lambda indicates that there are highly significant differences between the treatments (*F*-approx. 19.02; DF = 18, 272; $P < 0.001$). By comparing the *F*-matrix it is apparent that the largest differences between the infested treatments are between first instar infested fruits and the other instars (second to fifth inclusive). Differences between the second to fifth instar infested fruits were much smaller (*F*-values are in the range 0.14–3.23). In addition, there are large differences

Table 3
Summary of linear discriminant analysis for the data from treated apples either *Cydia pomonella* larvae infested, instar I–V inclusive, artificially damaged or healthy apple fruits, *Malus domestica* cv. Bohnäpfel[a]

	Between groups F-matrix DF3,96						Number of cases misclassified[b]
	I	II	III	IV	V	AD	
I							3
II	22.90						8
III	32.37	3.23					9
IV	31.15	2.88	1.70				12
V	29.00	2.97	2.60	0.14			11
AD	9.10	20.73	26.47	32.50	32.40		4
H	59.35	19.80	31.59	21.80	20.40	71.14	2

[a] Wilks' lambda: lambda = 0.0998; DF = 3,6,98; approx. $F = 19.02$; DF = 18,272, $P < 0.001$.
[b] Based on Mahalanobis distance square from group means and posterior probabilities of group membership being 0.143 in each case.

between all the types of infested fruits as compared to the artificially damaged fruits, although the *F*-value for the first instar larvae is ca. 2–3×smaller than the other instar treatments. Our analysis also indicates large differences between the healthy fruits and all of the other treatments (*F*-values range from 19.8 for second instar infested fruits to 71.14 for artificially damaged fruits) (Table 3). It is clear form the classification matrix within Table 3 that the most easily separated groups are first instar infested fruits, artificially damaged fruits and healthy fruits. The other types of infested fruits are most difficult to separate and tend to be miss-classified as either second to fifth instar inclusive.

There is a substantial induction of volatiles from the apple fruits during *C. pomonella* infestation. The amounts of volatiles are clearly different from those produced by the artificially damaged or healthy fruits. Previous studies with potato plants have demonstrated that the biochemical response can be considered specific for herbivore damage as compared to the response which occurs to a general wound (Korth and Dixon, 1997).

All larval instars of *C. pomonella* were capable of inducing volatile emissions. Therefore, the effects observed in the time-course study may not solely be related to the development of larvae as induced volatile emissions were not observed in the later phases of the experiment. In a phyllophagous herbivore of *Zea mais* L., *Pseudaletia seperata*, young instar larvae induced a much greater change in volatile emissions than sixth instar larvae. Only leaves infested with young larvae were attractive to the parasitic wasp *Cotesia kariyai*. This effect could be mimicked by the application of regurgitant from larvae onto artificially damaged leaves. This would suggest that the saliva or buccal secretions of the larvae differ in composition and that the plant responds differently to these secretions (Takabayashi et al., 1995).

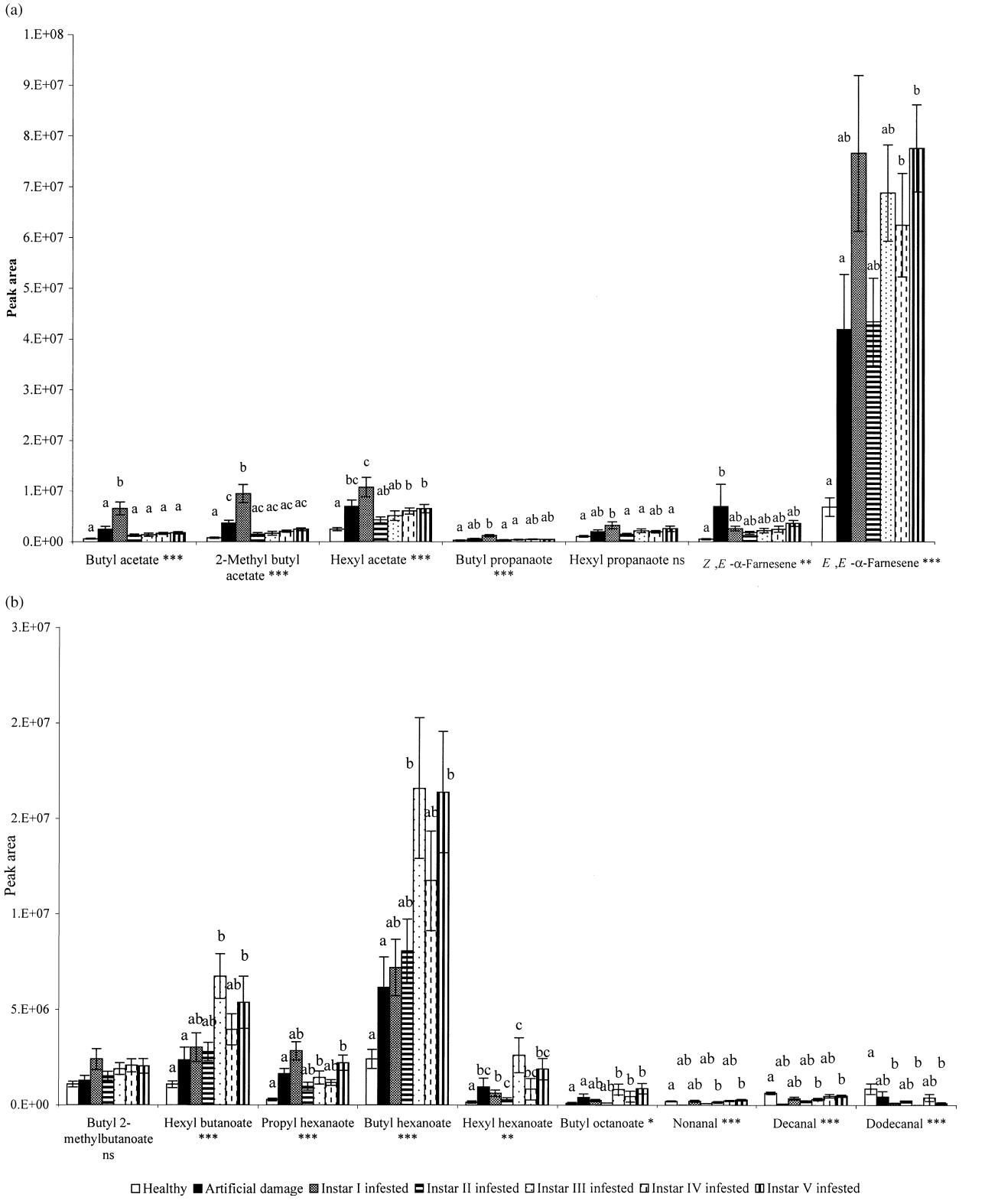

Fig. 1. (a) and (b) Mean ± S.E. peak area from treated apples either *Cydia pomonella* larvae infested, instar I–V inclusive, artificially damaged or healthy apple fruits, *Malus domestica* cv. Bohnäpfel. Columns with different letters indicate the result of Tukey pairwise multiple comparisons ($P < 0.05$). $N = 15$ for each treatment. Following the compound name the result of an ANOVA analysis for overall treatment effect is illustrated, ns = $P > 0.05$; * = $P < 0.05$; ** = $P < 0.01$; *** = $P < 0.001$.

In contrast, volatiles induced in *Brassica oleracea* L. var. *gemmifera* by different larval instars of *Pieris brassicae* could not be discriminated amongst by *Cotesia glomerata* (Mattiacci and Dicke, 1995a). After landing on the infested plant, however, the duration of searching by the parasitic wasp was affected differently by cues related to the presence of the herbivore of different age classes (Mattiacci and Dicke, 1995b).

For *C. pomonella* the elicitor of induced volatiles emitted by *M. domestica* is unknown, but in the systems analysed so far the elicitor is present in the oral secretion of the larva (Mattiacci et al., 1994; Turlings et al., 1993). The enzyme β-glucosidase in *P. brassicae* oral secretions elicits volatile synomone production in cabbage plants (Mattiacci et al., 1995). A different compound, volicitin (*N*-(17-hydroxylinolenoyl)-L-glutamine), accounts for the total activity of beet army worm (*Spodoptera exigua*) oral secretions in eliciting volatile induction in corn seedlings (Alborn et al., 1997).

Our results are consistent with the hypothesis that an elicitor from *C. pomonella* larvae induces the emission of volatiles from apple fruits. Either quantitative or qualitative differences in the elicitor(s) exist depending upon the instar of *C. pomonella* larva.

3. Experimental

3.1. Apple fruits

Mature apple fruits Malus domestica Borkh. (Rosaceae) cv. Bohnäpfel were obtained from an organic commercial farm and stored at 4°C for up to 6 months.

3.2. Cydia pomonella

Larvae were reared from adults purchased from a commercial breeding station within Switzerland. First instar larvae were obtained from eggs and used to infest apples on the first day following emergence. Other instars were reared on an artificial diet (Huber et al., 1972) at 25°C; RH 70% and a light dark photoperiod of 18:6. Larval development was assessed by means of head capsule widths: first instar 0.33 mm (mean duration 4 days); second instar 0.5 mm (mean duration 2 days); third instar 0.8 mm (mean duration 3 days); fourth instar 1.15 (mean duration 4 days) and fifth instar 1.52 mm (mean duration 11 days) (Ashby et al., 1985).

3.3. Time-course experiment

Infested apples were obtained by placing two larvae on each fruit. Volatile sampling (as described below) was carried out every day for the first three days following infestation and then at three day intervals until 21 days after infestation.

Healthy apples were treated in an identical manner to the infested fruits but left uninfested. Therefore, a total of 10 volatile samples were taken over the 21 day period for each fruit used. Experiments were conducted in an insectary at 23±2°C, 60±10% RH and 18:6 LD.

A Mann–Whitney test was used to test for significant differences between healthy and infested fruits at each sampling time; as the data are not statistically independent, no comparisons between sampling times were made. In addition, linear discriminant analysis of the data was conducted. Huberty (1994) discusses this statistical technique and Robertson et al. (1991) give an example of the application of this analysis in the context of insect chemical ecology. Such multivariate methods as discriminant analysis offer advantages over univariate methods for analysing data. For example, Hunter et al. (1997) suggest that many attributes in a multivariate dataset may be highly correlated. These correlations can complicate data interpretation as it is tempting to assume that each attribute, or in the present case each compound, supplies an independent element of information.

The linear discriminant analysis was carried out in a backward stepwise fashion, to eliminate variables which contributed least to the model. This was evaluated by the *P*-value associated with the *F*- value of each variable in the model, a *P*-value of 0.05 was used to eliminate variables from the model. This conservative value was used to reduce the problem of correlations between variables affecting the overall analysis.

3.4. Effect of the individual larval instars on volatile emission

Artificially damaged apples were obtained by piercing a fruit twice near the calyx with a needle (1 mm in diameter) to a depth of 2.5 cm. Infested apples were obtained by placing two larva of a given instar, first to fifth, on a healthy fruit. Three days later the volatiles from the fruit were collected and analysed as described below. Healthy apples were treated in an identical manner to the other fruits but were left undamaged. Environmental conditions were as described above. The volatiles of 15 apple fruits were analysed for each treatment.

Transformed data (squareroot datum + 0.5) were analysed using ANOVA. In order to compare which treatments differed, a Tukey test was employed. A linear discriminant analysis of the data as described above was also performed.

3.5. Volatile collection system

In all experiments volatiles were collected using solid phase microextraction (SPME). The fibre used was a 100 μm poly dimethyl siloxane (PDMS) fibre. Volatile collections were made from the apples placed in a dilated glass tube (length 35 cm; diameter 6 cm). The dilated

glass tube was sealed with a PTFE or glass stopper with a PTFE/silicon septa. The SPME fibre was exposed to the headspace of the apple through this septa and sampling was carried out for one hour. Volatile collections were carried out between 15.00±2 h (CET) which corresponds with the middle of the photophase under the light conditions of this experiment.

3.6. Chemical analysis

The samples were analysed using a Hewlett Packard GC–MS instrument (GC 6890 mass selective detector 5973). The analysis details were as follows: injector operated in splitless mode, purge valve on @ 2.00 min; flow 50 ml/min; injection temperature 250°C; helium flow rate 1.0 ml min (constant flow); column HP-1 (poly dimethyl siloxane) 30 M in length; 250 μm diameter; 1.00 μm film thickness; oven temperature 50°C for 2 min then ramped to 300 at 8°C per min; MS transfer line 280°C MS source 230°C MS Quad 150°C; MS operated in scan mode low mass 25, high mass 800; threshold 50. Prior to sampling the SPME fibre was thermally conditioned at 250°C for 1 h in the injection port of a GC (Hewlett Packard 5890 series II+). Both of these instruments were fitted with a SPME inlet liner (0.75 mm id; Supelco).

The sample spectra were compared to library spectra, both a commercial database (NIST98) and a user created library of authentic standards and the retention time of the standard was also matched with the sample in all cases. Standards for this process were either purchased from chemical suppliers or samples were obtained from other laboratories.

Acknowledgements

We would like to offer our sincere thanks to Dr. R. Kaiser (Givaudan-Roure, Dubendorf, Switzerland) who has provided us with many chemical standards for use in compound identification. In addition we thank Dr. A. Dutly (ETH Technical Chemistry) and D. Tunnah (Scottish Agricultural Science Agency) for advice on the chromatographic methods employed and Dr. L. Mattiacci for advice on aspects of the experimental design and for commenting on an earlier version of this manuscript.

References

Alborn, H.T., Turlings, T.C.J., Jones, T.H., Stenhagen, G., Loughrin, J.H., Tumlinson, J.H., 1997. An elicitor of plant volatiles from beet armyworm oral secretion. Science 276, 945–949.

Ashby, M.D., Singh, P., Clare, K., 1985. *Cydia pomonella*. In: Singh, P., Moore, R.F. (Eds.), Handbook of Insect Rearing, Vol. II. Elsevier, Oxford, pp. 237–248.

Baldwin, I.T., Preston, C.A., 1999. The eco-physiological complexity of plant responses to insect herbivores. Planta 208, 137–145.

Bernasconi, M.L., Turlings, T.C.J., Ambrosetti, L., Bassetti, P., Dorn, S., 1998. Herbivore-induced emissions of maize volatiles repel the corn leaf aphid, *Rhopalosiphum maidis*. Entomologia Experimentalis et Applicata 87, 133–142.

Boevé, J.L., 1996. Chemoecology of larvae of the European apple sawfly. Entomologia Experimentalis et Applicata 80, 286–288.

Boevé, J.L., Lengwiler, U., Tollsten, L., Dorn, S., Turlings, T.C.J., 1996. Volatiles emitted by apple fruitlets infested by larvae of the European apple sawfly. Phytochemistry 42, 373–381.

Carle, S.A., Averill, A.L., Rule, G.S., Reissig, W.H., Roelofs, W.L., 1987. Variation in host fruit volatiles attractive to apple maggot fly, *Rhagoletis pomonella*. Journal of Chemical Ecology 13, 795–805.

De Moraes, C.M., Lewis, W.J., Pare, P.W., Alborn, H.T., Tumlinson, J.H., 1998. Herbivore-infested plants selectively attract parasitoids. Nature 393, 570–573.

Dicke, M., 1994. Local and systemic production of volatile herbivore-induced terpenoids: their role in plant-carnivore mutualism. Journal of Plant Physiology 143, 465–472.

Dicke, M., van Loon, J.J.A., 2000. Multitrophic effects of herbivore-induced plant volatiles in an evolutionary context. Entomologia Experimentalis et Applicata 97, 237–249.

Dicke, M., Sabelis, M.W., 1988. Infochemical terminology: Should it be based on cost-benefit analysis rather than origin of compound? Functional Ecology 2, 131–139.

Dicke, M., Sabelis, M.W., 1989. Does it pay plants to advertise for bodyguards ? Towards a cost-benefit analysis of induced synomone production. In: Lambers, H., Cambridge, M.L., Konings, H., Pons, T.L. (Eds.), Causes and Consequences of Variation in Growth Rate and Productivity of Higher Plants. SPB Academic Publishing, The Hague, pp. 341–358.

Huber, J., Benz, G., Schmidt, K., 1972. Zuchtmethode und semi-synthetische Nährmedien für Apfelwickler. Experientia 28, 1260–1261.

Huberty, C.J., 1994. Applied Discriminant Analysis. John Wiley and Sons, Chichester.

Hunter, E.A., McNulty, D.A., Banks, J.M., 1997. Statistical design and analysis of experiments in cheese technology. Lebensmittel-Wissenschaft und Technologie 30, 121–128.

Karban, R., Baldwin, I.T., 1997. Induced responses to herbivory. The University of Chicago Press, Chicago.

Korth, K.L., Dixon, R. A., 1997. Evidence of chewing insect-specific molecular events distinct from a general wound response in leaves. Plant Physiology 115, 1299–1305.

Mattiacci, L., Dicke, M., 1995a. Host-age discrimination during host location by *Cotesia glomerata*, a larval parasitoid of *Pieris brassicae*. Entomologia Experimentalis et Applicata 76, 37–48.

Mattiacci, L., Dicke, M., 1995b. The parasitoid *Cotesia glomerata* (Hymenoptera: Braconidae) discriminates between first and fifth larval instars of its host *Pieris brassicae*, on the basis of contact cues from frass, silk, and herbivore-damaged leaf tissue. Journal of Insect Behavior 8, 485–498.

Mattiacci, L., Dicke, M., Posthumus, M.A., 1994. Induction of parasitoid attracting synomone in brussel sprouts plants by feeding of *Pieris brassicae* larvae: role of mechanical damage and herbivore elicitor. Journal of Chemical Ecology 20, 2229–2247.

Mattiacci, L., Dicke, M., Posthumus, M.A., 1995. β-Glucosidase: an elicitor of herbivore-induced plant odor that attracts host-searching parasitic wasps. Proceedings of the National Academy of Science of the United States of America 92, 2036–2040.

Mattiacci, L., Hütter, E., Dorn, S., 1999. Host location of *Hyssopus pallidus*, a larval parasitoid of the codling moth, *Cydia pomonella*. Biological Control 15, 241–251.

Mattiacci, L., Hütter, E., Schoch, D., Scascighini, N., Dorn, S., 2000. Plant-odour mediates parasitoid host handling and oviposition in an endophytic tritrophic system. Chemoecology 10, 185–192.

Robertson, G.W., Griffiths, D.W., Birch, A.N.E., Jones, A. T., McNicol, J. W., Hall, J. E., 1991. Further evidence that resistance in raspberry to the virus vector aphid, *Amphorophora idaei*, is related to the chemical composition of the leaf surface. Annals of Applied Biology 119, 443–449.

Sutherland, O.R.W., Wearing, C.H., Hutchins, R.F.N., 1977. Production of α-farnesene, an attractant and oviposition stimulant for codling moth, by developing fruit of ten varieties of apple. Journal of Chemical Ecology 3, 625–631.

Takabayashi, J., Takahashi, S., Dicke, M., Posthumus, M.A., 1995. Developmental stage of herbivore *Pseudaletia seperata* affects production of herbivore induced synomone by corn plants. Journal of Chemical Ecology 21, 273–287.

Tumlinson, J.H., Turlings, T.C.J., Lewis, W.J., 1992. The semiochemical complexes that mediate insect parasitoid foraging. Agricultural Zoology Reviews 5, 221–252.

Tumlinson, J.H., Turlings, T.C.J., Lewis, W.J., 1993. Semiochemically mediated foraging behaviour in beneficial parasitic insects. Archives of Insect Biochemistry and Physiology 22, 385–391.

Turlings, T.C.J., McCall, P.J., Alborn, H.T., Tumlinson, J.H., 1993. An elicitor in caterpillar oral secretions that induces corn seedlings to emit chemical signals attractive to parasitic wasps. Journal of Chemical Ecology 19, 411–425.

Turlings, T.C.J., Tumlinson, J.H., 1991. Do parasitoids use herbivore-induced plant chemical defenses to locate hosts? Florida Entomologist 74, 42–50.

Turlings, T.C.J., Tumlinson, J.H., Lewis, W. J., 1990. Exploitation of herbivore-induced plant odours by host-seeking parasitic wasps. Science 250, 1251–1253.

Vet, L.E.M., 1999. From chemical to population ecology: infochemical use in an evolutionary context. Journal of Chemical Ecology 25, 31–49.

Vet, L.E.M., Dicke, M., 1992. Ecology of infochemical use by natural enemies in a tritrophic context. Annual Review of Entomology 37, 141–172.

Zaviezo, T., Mills, N., 1999. Aspects of the biology of *Hyssopus pallidus* (Hymenoptera: Eulophidae), a parasitoid of the codling moth (Lepidoptera: Olethreutidae). Environmental Entomology 28, 748–754.

PERGAMON

Phytochemistry 57 (2001) 417–420

PHYTOCHEMISTRY

www.elsevier.com/locate/phytochem

Methyl jasmonate increases reported alkamides and ketoalkene/ynes in *Echinacea pallida* (Asteraceae)

Shannon E. Binns [a], Iniyal Inparajah [a], Bernard R. Baum [b], John T. Arnason [a,*]

[a] *Biology Department, University of Ottawa, 30 Marie Curie St., Ottawa, Ont, Canada, K1N 6N5*
[b] *Eastern Cereal and Oilseed Research Centre, Agriculture and Agri-Food Canada, Ottawa, Ont, Canada, K1A 0C6*

Received 4 April 2000; received in revised form 19 October 2000

Abstract

Methyl jasmonate (MJ), a naturally-occurring plant cellular signal molecule, was found to induce production of lipophilic secondary metabolites in *Echinacea pallida* seedlings. Seedling aerial parts were sprayed with 100 ppm MJ, and roots were harvested and extracted 24 h later. Lipophilic root extracts, separated by HPLC, revealed significant increases ($P < 0.05$) in six alkamides or related ketoalkene/ynes produced by 34 day-old plants and in seven compounds produced by 58 day-old plants. © 2001 Published by Elsevier Science Ltd. All rights reserved.

Keywords: *Echinacea pallida*; Asteraceae; Secondary metabolite induction; Alkamides; Ketoalkene/ynes; Methyl jasmonate

1. Introduction

Jasmonic acid (JA) and methyl jasmonate (MJ) are widely distributed regulatory signal molecules derived from linolenic acid in plants in a pathway first described by Vick and Zimmerman (1984). Farmer and Ryan (1990) described the effects of jasmonates on growth, senescence and as a predominant signal in wound-induced defense. MJ induces resistance towards insect herbivory in both tobacco and cabbage crops (Avdiushko et al., 1997).

Echinacea, endemic to North America, is a plant genus known for its traditional medicinal qualities (Hobbs, 1989). The secondary chemistry of commercial *Echinacea* species (*E. purpurea, E. pallida* and *E. angustifolia*) has been well-characterized (Bauer et al., 1988; Bauer and Remiger, 1989; Cheminat et al., 1988; Bohlmann and Hoffmann, 1983; reviewed in Bauer and Wagner, 1991; Bauer, 1998) and remains the primary method of botanical identification for marketed *Echinacea* plant materials.

Echinacea possesses a high level of constitutive diversity within each of its numerous classes of defense compounds, particularly the family of alkamides, polyacetylenes and ketoalkene/ynes, some of which are known insecticides (Jacobson, 1967). Diversity within phytochemical classes is a common defensive strategy against herbivory (Karban et al., 1997). Another strategy is a rapid increase in quantity and/or variability of phytochemical defenses in response to wounding or fungal infection, which can be simulated by application of the signal molecule MJ. The induction of *Echinacea* phytochemicals whether naturally or by MJ is important for increased efficacy and efforts to standardize *Echinacea* phytomedicines.

Identified alkamides and polyacetylenes in *Echinacea* spp exhibit other biological activities in vitro, including fungicidal (Binns et al., 2000) and immunostimulatory activities (Bauer and Wagner, 1991). Here we report that the volatile chemical signal MJ induces alkamide and ketoalkene/yne biosynthesis in *Echinacea pallida*.

2. Results and discussion

The alkamide composition of *Echinacea* is known to vary quantitatively and qualitatively throughout growth and development (Letchamo et al., 1998) and in our experiments, alkamide levels tended to decline naturally between 34 days and 58 days in *E. pallida* roots of control plants (Figs. 1 and 2). The only qualitative difference observed was the formation of the ketoalkyne **1*** as the roots aged (compounds denoted by an asterisk are ketoalkene/ynes, while the others are alkamides).

* Corresponding author. Tel.: +1-613-5625262; fax: +1-613-5625765.
E-mail address: jarnason@science.uottawa.ca (J.T. Arnason).

0031-9422/01/$ - see front matter © 2001 Published by Elsevier Science Ltd. All rights reserved.
PII: S0031-9422(00)00444-1

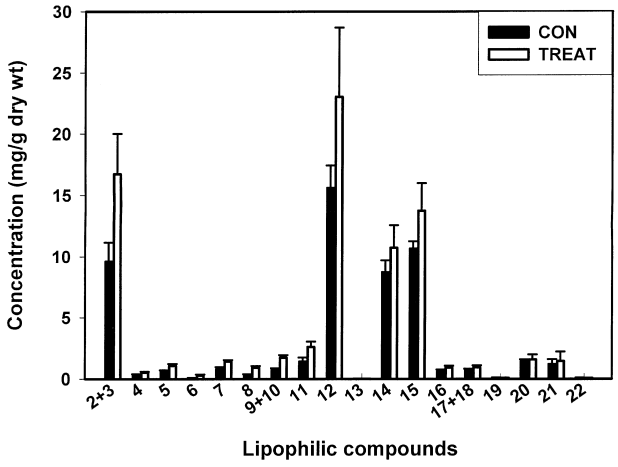

Fig. 1. Lipophilic compounds (mean + SE) in *Echinacea pallida* roots aged 34 days ($n = 10$) from methyl jasmonate-treated (TREAT) and control plants (CON).

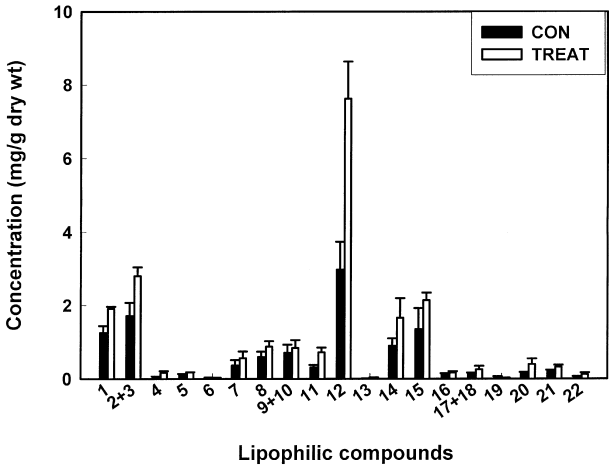

Fig. 2. Lipophilic compounds (mean + SE) in *Echinacea pallida* roots aged 58 days ($n = 10$) from methyl jasmonate-treated (TREAT) and control plants (CON).

Compound **1*** is used in the marketplace to distinguish older *E. pallida* roots from *E. angustifolia*, which has the isomers **2** + **3** as its major constituents, but lacks **1*** (Bauer and Remiger, 1989). In our trials with very young (34 day old) roots, the formation of **2** + **3** in high concentrations (control and treated) occurs early in development (Fig. 1), followed by a remarkable decrease later (58 day old) when **1*** begins to appear (Fig. 2).

After treatment with 100 ppm MJ, the majority of compounds identified showed an increase in concentration in the MJ-treated plants over the concentrations in control roots (Figs. 1 and 2) at both plant ages. Statistically significant increases were observed with a number of compounds and ranged from 54 to 353% (mg/g dry wt) (Table 1). MJ treated *E. pallida* plants aged 34 days contained significantly higher levels ($P < 0.05$) of compounds **4**, **5**, **6**, **7**, **8** and **9** + **10*** compared to control plants of the same age (Fig. 1, Table 1). MJ treated *E. pallida* plants aged 58 days contained significantly higher levels of compounds **2** + **3**, **4**, **11**, **12**, **13*** and **1*** compared to

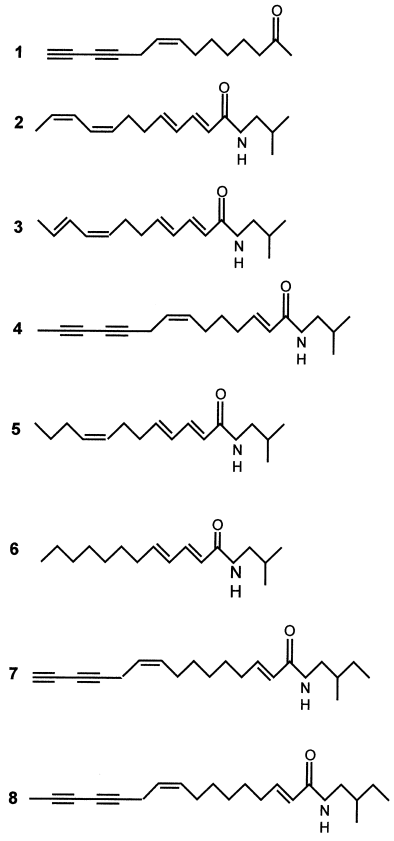

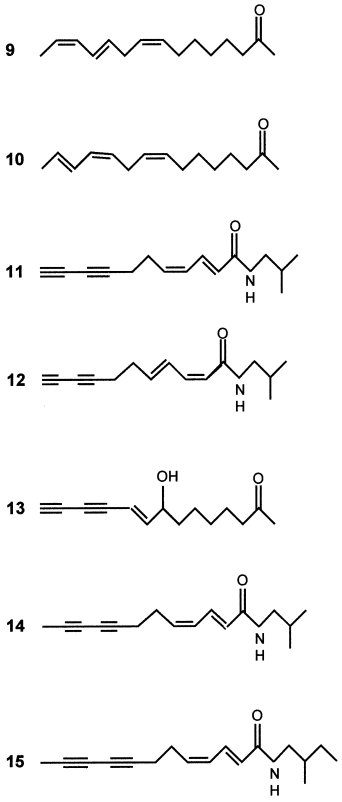

Table 1
Alkamides and ketoalkene/ynes in *E. pallida* roots of two age classes (34 days and 58 days) that showed a statistically significant increase by methyl jasmonate treatment

Compound induced		% increase[a]			
		34 days	$P=$	58 days	$P=$
1	Tetradeca-8*Z*-ene-11,13-diyn-2-one[c]	–	–	**151**	0.016[b]
2+3	Dodeca-2*E*,4*E*,8*Z*,10*E*/*Z*-tetraenoic AIBA	+	0.090	**63**	0.046[b]
4	Trideca-2*E*,7*Z*-dien-10,12-diynoic AIBA	**54**	0.031	**227**	0.035[b]
5	Dodeca-2*E*,4*E*,8*Z*-trienoic AIBA	**84**	0.030	+	0.128[b]
6	Dodeca-2*E*,4*E*-dienoic AIBA	**251**	0.003[b]	+	0.539[b]
7	Pentadeca-2*E*,9*Z*-dien-12,14-diynoic AIBA	**78**	0.019[b]	+	0.098
8	Hexadeca-2*E*,4*E*-dienoic AIBA	**238**	0.035[b]	+	0.170[b]
9+10	Pentadeca-8*Z*,11*Z*/*E*-13*E*/*Z*-trien-2-one[c]	**151**	0.006[b]	+	0.33
11	Undeca-2*E*,4*Z*-dien-8,10-diynoic AIBA	+	0.058	**134**	0.021
12	Undeca-2*Z*,4*E*-dien-8,10-diynoic AIBA	+	0.270	**156**	0.007
13	8-Hydroxytetradeca-9*E*-ene-11,13-diyn-2-one[c]	+	0.269[b]	**353**	0.001[b]

Notes: Significantly different means were determined at $\alpha = 0.05$ by a two-tailed *t*-test using SYSTAT software and original quantitative data for MJ treated and control plants. + Denotes an increasing trend that was not statistically significant.

[a] % increase = treatment mean/control mean ×100.

[b] Original data transformed by Log_{10} to meet assumptions for statistical analyses.

[c] Denotes ketoalkene/ynes without amide group. AIBA = acid isobutylamide. $n = 10$ each age class.

control plants of the same age (Fig. 2, Table 1). The compounds found in treated and control *E. pallida* roots common to both ages were **2+3**, **12**, **14** and **15**. Younger roots contained approximately five times more of these common constituents than did the older roots (Figs. 1 and 2).

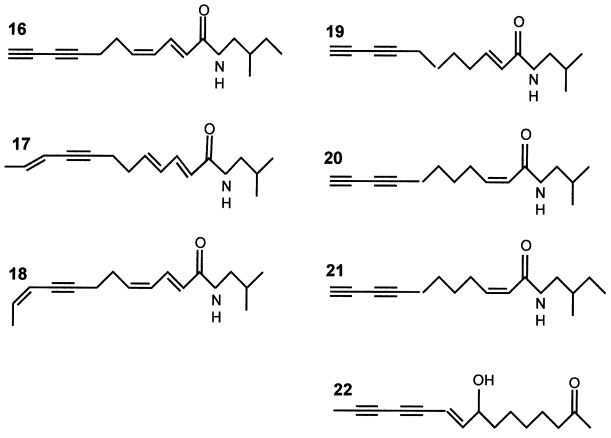

The statistically significant increases presented here suggest that alkamides and ketoalken/ynes are inducible defense compounds in *Echinacea* plants. In-depth investigation of this phenomenon and possible species variation is currently being studied in our laboratory.

3. Experimental

3.1. Plant material

E. pallida achenes from a wild population (DAO #EPA013, coll. S. Binns, Arkansas, 1998) were germinated and grown to 34 days and 58 days in 2:1 soil: vermiculite in a controlled environment chamber at 25°C under a 16:8 light to dark regime. Voucher specimens are deposited in the National Herbarium of Canada—Department of Agriculture, Ottawa, Canada.

3.2. Treatment

Initial trials at 10, 100 and 1000 ppm MJ showed the best induction at 100 ppm and this concentration was used in trials reported here. Half of the individuals at each life stage were designated control plants ($n = 10$). Treated plants were sprayed with MJ solution and control plants were sprayed with dH_2O and DMSO. MJ (100 ppm) was prepared in aqueous solution of 19 μl MJ, 19 μl DMSO and 200 ml distilled water. Treated plants were isolated from control plants in different growth chambers, under identical conditions, to avoid inter-plant communication through airborne MJ (Farmer and Ryan, 1990).

3.3. Extraction and isolation

Twenty-four hours after MJ treatment, entire roots of all plants were harvested, cleaned, weighed and extracted using 95% aqueous ethanol for another 24 h under moderate mechanical agitation (70 rpm). Extraction time after MJ treatment was based on time-course experiments (2–72 h) with dill (*Anethum graveolens*), which showed maximum phytochemical induction by MJ after 24 h (Belzile, 1998). Filtered extracts (No. 1 Whatman, Buchner funnel) were concentrated in vacuo (not to dryness) and root tissue residues dried (50°C). The dry weight of root residues was used to calculate the volume of solvent required to adjust each extract to a standard concentration of 0.01 g extracted dried root/ml 95% ethanol.

Extracts were then filtered with 0.2 μm nylon membranes prior to separation of lipophilic constituents using HPLC. Chromatography was achieved using a solvent system of acetonitrile:water (6:4) at 1 ml/min and 5 μl injection on a 7.5 cm reversed phase C-18 column (3 mm particle size). Lipophilic compounds were detected at 210 and 260 nm and identified by comparison with reference standards. Reference standards **2** + **3**, **6**, **7** and **11** were isolated previously in our laboratory by column chromatography on silica gel (Bergeron et al., 2000). Spectra obtained for these by ^{1}H, ^{13}C NMR, EI–MS conformed with reported values (Perry et al., 1997; Yasuda et al., 1981). Other compounds were identified based on relative retention time and online UV spectra (Bauer and Remiger 1989). The standard **2** + **3** was used to calculate a response factor for the HPLC detector. Quantitation of each previously reported compound (μg/per ml injected) was achieved using peak area multiplied by the response factor. This figure was then divided by the original concentration of 0.01 g extracted dried root/ ml sample and multiplied by 10^3 to reach mg/g dry wt of whole root.

Acknowledgements

This work was supported by the Trout Lake Farm Co. and Agriculture and Agri-Food Canada's Matching Investment Initiative Program.

References

Avdiushko, S.A., Brown, G.C., Dahlman, D.L., Hildebrand, D.F., 1997. Methyl jasmonate exposure induces insect resistance in cabbage and tobacco. Physiological and Chemical Ecology 26 (3), 642–654.

Bauer, R., 1998. Phytomedicines of Europe: Chemistry and Biological Activity. In: Lawson, L.D., Bauer, R. (Eds.), American Chemical Society Symposium Series 691. ACS, Washington, DC, pp. 140–157.

Bauer, R., Remiger, P., 1989. TLC and HPLC analysis of alkamides in *Echinacea* drugs. Planta Medica 55, 367–371.

Bauer, R., Wagner, H., 1991. *Echinacea* species as potential immunostimulatory drugs. In: Wagner, H., Farnsworth, N. (Eds.), Economic and Medicinal Plant Research, 5 ed. Academic Press, London. pp. 253–321.

Bauer, R., Khan, I.A., Wagner, H., 1988. TLC and HPLC analysis of *Echinacea pallida* and *Echinacea angustifolia* roots. Planta Medica 54, 426–430.

Bergeron, C., Livesey, J.F., Awang, D.V.C., Arnason, J.T., Rana, J., Baum, B.R., Letchamo, W., 2000. A quantitative method for identity and quality assurance of *Echinacea* products on the North American market. Phytochemical Analysis 11, 1–9.

Belzile, A.S., 1998. Synergistic activity of the monolignol dillapiol and variation of its production in two plants, *Anethum graveolens* and *Piper aduncum*. MSc Thesis, University of Ottawa, Ont., Canada, 78 pp.

Binns, S.E., Purgina, B., Bergeron, C., Smith, M.L., Ball, L., Baum, B.R., Arnason, J.T., 2000. Light-mediated antifungal activity of *Echinacea* extracts. Planta Medica 66, 241–244.

Bohlmann, F., Hoffmann, H., 1983. Further amides from *Echinacea purpurea*. Phytochemistry 22 (5), 1173–1175.

Cheminat, A., Zawatzky, R., Becker, H., Brouillard, R., 1988. Caffeoyl conjugates from *Echinacea* species: structures and biological activity. Phytochemistry 27 (9), 2787–2794.

Farmer, E.E., Ryan, C.A., 1990. Interplant communication: airborne methyl jasmonate induces sysnthesis of proteinase inhibitors in plant leaves. Proceedings of the National Academy of Science, USA 87, 7713–7716.

Hobbs, C., 1989. The Echinacea Handbook. Eclectic Medical Publications, Portland, Oregon.

Jacobson, M., 1967. The structure of Echinacein, the insecticidal component of American coneflower roots. Journal of Organic Chemistry 32, 1646–1647.

Karban, R., Agrawal, A.A., Mangel, M., 1997. The benefits of induced defenses against herbivores. Ecology 78 (5), 1351–1355.

Letchamo, W., Livesey, J., Arnason, J.T., Bergeron, C., Krutilina, V.S., 1998. Cichoric acid and isobutylamide content in *Echinacea purpurea* as influenced by flower developmental stages. New Crops and New Uses Biodiversity and Agricultural Sustainability, AAIC-Phoenix, AZ, November 8–11.

Perry, N., van Klink, J.W., Burgess, E.J., Parmenter, G.A., 1997. Alkamide levels in *Echinacea purpurea*: a rapid analytical method revealing differences among roots, rhizomes, stems, leaves and flowers. Planta Medica 63, 58–62.

Vick, B.A., Zimmerman, D.C., 1984. Biosynthesis of jasmonic acid by several plant species. Plant Physiology 75, 458–461.

Yasuda, I., Takeya, K., Itokawa, H., 1981. Structures of amides from *Asiasarum heterotropoides* var. *mandshuricum* Maek. Chem. Pharm. Bull. 29, 564–566.

PERGAMON

Phytochemistry 57 (2001) 421–425

PHYTOCHEMISTRY

www.elsevier.com/locate/phytochem

Antiplatelet activity of *N*-methoxycarbonyl aporphines from *Rollinia mucosa*

Reen-Yen Kuo[a], Fang-Rong Chang[a], Chung-Yi Chen[a,b], Che-Ming Teng[c], Hsin-Fu Yen[d], Yang-Chang Wu[a,*]

[a]*Graduate Institute of Natural Products, Kaohsiung Medical University, Kaohsiung 807, Taiwan*
[b]*Fooyin Institute of Technology, Kaohsiung County 831, Taiwan*
[c]*Pharmacological Institute, College of Medicine, National Taiwan University, Taipei 100, Taiwan*
[d]*Division of Science Education, National Museum of Natural Science, Tai-Chung 300, Taiwan*

Received 8 August 2000; received in revised form 11 January 2001

Abstract

Bioassay-directed fractionation of the stems of *Rollinia mucosa* led to the isolation of new *N*-methoxycarbonyl aporphine alkaloids, romucosine A (**1**), romucosine B (**2**), romucosine C (**3**), and romucosine D (**4**), along with the known alkaloid, *N*-methoxylcarbonyl-nornuciferine (**5**). Alkaloids **1** and **4** exhibited significant inhibition of collagen, arachidonic acid, and platelet activating factor-induced platelet aggregation, and alkaloid **3** also showed an inhibitory effect on arachidonic acid induced platelet aggregation. © 2001 Elsevier Science Ltd. All rights reserved.

Keywords: *Rollinia mucosa*; Annonaceae; *N*-Methoxycarbonyl aporphines; Antiplatelet activity

1. Introduction

The genus *Rollinia* (Annonaceae) is comprised of 65 species (Leboeuf et al., 1982), some of which were investigated previously for their chemical composition and pharmacological activities (Hartwell, 1982; Caetano and Dabun, 1987; Chen et al., 1996b,c; 1996; Paulo et al., 1991; Liaw et al., 1999). Within the genus, *Rollinia mucosa* Baill. has been used as a traditional medicine for the treatment of tumors in the West Indies and Indonesia (Hartwell, 1982). In further biological evaluation, alkaloidal extracts were shown to exhibit antimicrobial and antifungal activities (Caetano and Dabun, 1987). In Brazil and Peru, the lignans isolated from this species were reported to be active against a wide variety of insects (Paulo et al., 1991). In previous studies, numerous aporphine alkaloids and acetogenins were isolated from this plant (Chen et al., 1996a,c; Zafra-Polo et al., 1996, 1998; Alali et al., 1999; Liaw et al., 1999). In the course of our studies on bioactive natural substances, the alkaloid fraction of the stems of *R. mucosa* was found to exhibit a significant inhibitory effect on antiplatelet aggregation induced by several aggregating agents. Bioassay-directed fractionation led to the isolation of four new *N*-methoxycarbonyl aporphine alkaloids, romucosine A–D (**1**–**4**), and a known alkaloid, *N*-methoxylcarbonyl-nornuciferine (**5**) (Tschesche et al., 1964). Their isolation, structural elucidation and biological activity are reported herein.

2. Results and discussion

Romucosine A (**1**) was obtained as a brown amorphous powder. The HREIMS revealed a $[M]^+$ at m/z 325.1309 (calc. 325.1314) corresponding to the molecular formula $C_{19}H_{19}O_4N$. The base peak at m/z 237 $[M–H–(NCOOCH_3)]^+$ (M-88) in EIMS, derived from a retro-Diels–Alder fragmentation, and the UV absorptions at 237, 285, and 307 nm, revealed **1** as a 1,2-disubstituted *N*-methoxycarbonyl aporphine (Shamma, 1972; Chen et al., 1996b). The IR spectrum of **1** showed absorption bands at 3400 and 1690 cm^{-1}, indicating the presence of phenolic hydroxyl and carbonyl groups,

* Corresponding author. Tel.: +886-7-3121101, ext. 2197; fax: +886-7-3114773.
E-mail address: yachwu@cc.kmu.edu.tw (Y.-C. Wu).

0031-9422/01/$ - see front matter © 2001 Elsevier Science Ltd. All rights reserved.
PII: S0031-9422(01)00076-0

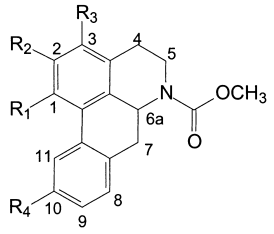

	R_1	R_2	R_3	R_4	6a
1	OCH_3	OH	H	H	*R*
2	OCH_3	OH	Cl	H	*S*
3	OCH_3	OCH_3	H	OH	*S*
4	OCH_3	OCH_3	H	OCH_3	*S*
5	OCH_3	OCH_3	H	H	*S*

respectively. The ^{1}H NMR spectrum showed a doublet at δ 8.30 (1H, *d*, $J=8.0$ Hz) and multiplets for three protons in the range δ 7.28–7.32 which demonstrated the presence of an unsubstituted D-ring. The aromatic proton at δ 6.75 (1H, *s*) was assigned to H-3 (Chen et al., 1996b). Two signals due to methoxy groups at δ 3.56 and 3.76 (each 3H, *s*) were evident. Based on the ring current of twisted A/D rings and the correlation from the NOESY spectrum, the methoxyl at δ 3.56 which correlated to H-11 was unambiguously assigned to C-1 (Shamma, 1972). The methoxyl at δ 3.76 was assigned to the methoxyl on the *N*-methoxycarbonyl group (Chen et al., 1996b). In the aliphatic region of the ^{1}H NMR spectrum resonances were observed at δ 4.22 (1H, *d*) for H-5a and at δ 4.66 (1H, *dd*) for H-6a. These spectral data were similar to those of romucosine (Chen et al., 1996b), but with a different substitution. The stereochemistry at C-6a was elucidated as the *R* configuration by the $[\alpha]_D^{25}$ -105° (Shamma, 1972). Based on the results mentioned above, the structure was determined as **1**, and named as romucosine A.

Romucosine B (**2**) was obtained as a white amorphous powder. The HREIMS revealed a $[M]^+$ at *m/z* 359.0915 (calc. 359.0924) corresponding to the molecular formula $C_{19}H_{18}O_4NCl$. The fragment ion at *m/z* 271 (M-88) and the UV absorption maximas at 245 and 285 nm revealed the typical pattern of a 1,2,3-trisubstituted *N*-methoxycarbonyl aporphine (Shamma, 1972; Chen et al., 1996b). MS fragments at *m/z* 359 $[M]^+$, 361 $[M+2]^+$ (3:1), and 323 $[M–Cl]^+$ suggested the presence of one chlorine atom. The IR and ^{1}H NMR spectra of **2** were similar to those of **1**, except for the disappearance of H-3. Thus, it was apparent that H-3 was replaced by chlorine. The configuration of C-6a was deduced to be *S* by the $[\alpha]_D^{25}$ $+153^\circ$ (Shamma, 1972). Therefore, the structure was elucidated as **2**, and named as romucosine B.

Romucosine C (**3**) was obtained as a brown amorphous powder. The HREIMS revealed a $[M]^+$ at *m/z* 355.1419 (calc. 355.1419) corresponding to the molecular formula $C_{20}H_{21}O_5N$. The fragment ion at *m/z* 267 (M-88) and the UV absorption maximas at 265, 280, and 305 nm revealed **3** as a 1,2,10-trisubstituted *N*-methoxycarbonyl aporphine (Shamma, 1972; Chen et al., 1996b). The IR absorption bands at 3350 and 1698 cm^{-1} of **3** indicated the presence of hydroxyl and carbonyl groups, respectively. In the ^{1}H NMR spectrum, the aromatic region presented an ABX pattern, which matched the observed UV absorptions. Furthermore, the appearance of a methoxyl group at δ 3.76 and the downfield shifted aliphatic protons at δ 4.29 (H-5a) and 4.69 (H-6a) demonstrated the presence of a *N*-methoxycarbonyl group. In the NOESY spectrum, correlations between H-3/H-4/H-5, H-8/H-9 and H-11/1-OMe were observed (Fig. 1). Therefore, the hydroxyl group was located at C-10. The configuration of C-6a was determined by the $[\alpha]_D^{25}$ $+140^\circ$, which indicated it as *S* (Shamma, 1972). From the above indications, the structure was determined as romucosine C (**3**).

Romucosine D (**4**) was isolated as a brown amorphous powder. The HREIMS revealed a $[M]^+$ at *m/z* 369.1575 (calc. 369.1576) corresponding to the molecular formula $C_{21}H_{23}O_5N$. A characteristic fragment ion at *m/z* 281 (M-88) was also observed. The UV, IR, and ^{1}H NMR spectra were similar to those of **3**, except for the appearance of one more methoxyl group (δ 3.84). In the NOESY spectrum, the methoxyl group was correlated to H-11 and H-9. In contrast to **3**, compound **4** therefore possessed a methoxyl group at C-10. The configuration of C-6a was deduced to be *S* by $[\alpha]_D^{25}$ $+145^\circ$ (Shamma, 1972). The structure was determined as romucosine D (**4**).

N-Methoxylcarbonyl-nornuciferine (**5**) was isolated as a white amorphous powder. The HREIMS revealed a $[M]^+$ at *m/z* 339.1474 (calc. 339.1471) corresponding to

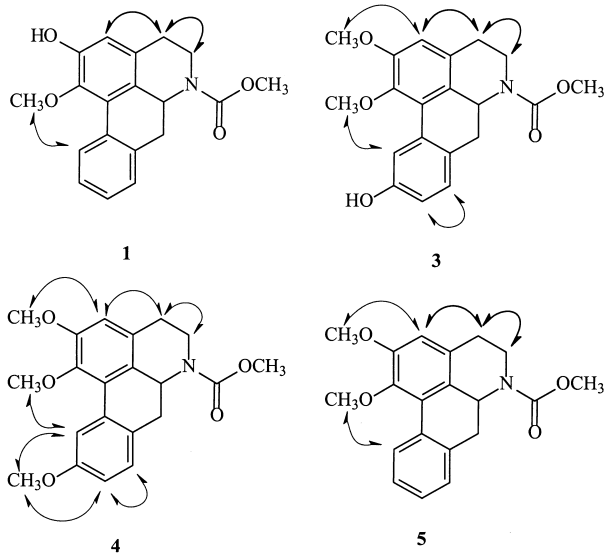

Fig. 1. NOESY correlations of compounds **1**, **3**, **4** and **5**.

the molecular formula $C_{20}H_{21}O_4N$. The UV and ^1H NMR spectra **5** were similar to those of **1**, except for the appearance of methoxyl signal at δ 3.95 in ^1H NMR. This methoxy resonance was correlated to H-3 in the NOESY spectrum (Fig. 1), and was assigned to C-2. The configuration of C-6a was also considered as *S* from the $[\alpha]_D^{25}$ +165° (Shamma, 1972). Therefore, the structure of **5** was determined as illustrated. Because the parent aporphine, nornuciferine, was easily obtained from annonaceous plants, *N*-methoxycarbonyl-nornuciferine was prepared using the established method (Chen et al., 1996b). The spectral data of the reaction product matched those of **5**, and established **5** to be *N*-methoxycarbonyl-nornuciferine. Alkaloid **5** is described here from natural sources and its spectral assignments are revealed for the first time.

Alkaloids **1**–**5** were evaluated for antiplatelet aggregation induced by thrombin, arachidonic acid (AA), collagen, and platelet-activating factor (PAF). As indicated in Table 1, alkaloid **4** was more active in AA-, collagen-, and PAF-induced platelet aggregation among these isolates. From the data presented in Table 1, the results were implied as follows: (i) alkaloids **1** and **4** displayed significant inhibition of the platelet aggregation induced by AA; (ii) methoxyl substitution of C-10 enhanced the activity more than hydroxyl substitution (among alkaloids **3**, **4**, and **5**); (iii) *N*-methoxycarbonyl aporphines, a new class of aporphines, presented a higher selectivity to AA-induced platelet aggregation than the parent aporphines (Chen et al., 1996a).

3. Experimental

3.1. General experimental procedures

The UV spectra were obtained on a Hitachi 200-20 spectrophotometer, IR spectra were measured on a Mattson Genesis II spectrometer. NMR spectra were obtained on Varian NMR spectrometers (Unity Plus 400 MHz and Gemini 200 MHz) using $CDCl_3$ as solvent. Low-resolution EIMS were collected on a Jeol JMS-SX/SX 102A mass spectrometer or Quattro GC/MS spectrometer having a direct inlet system. High-resolution EIMS were measured on a Jeol JMS-HX 110 mass spectrometer. Silica gel 60 (Merck, 230–400 mesh) was used for column chromatography. Semi-preparative columns (LichroCART, Licrosphere 250-10, Merck) were used for HPLC analysis (Shimadzu LC-10AT), and the fractions were recorded using a UV detector (Shimadzu SPD-10A). TLC spots were detected by spraying with 50% H_2SO_4 and heating.

3.2. Plant material

Fresh stems of *Rollinia mucosa* (11.5 kg) were collected from Chia-Yi, Taiwan in August 1997. A voucher specimen was identified by Dr. Hsin-Fu Yen and is deposited in the Graduate Institute of Natural Products, Kaohsiung Medical University, Kaohsiung, Taiwan.

3.3. Extraction and isolation

Fresh stems of *R. mucosa* (11.5 kg) were extracted repeatedly with MeOH at room temperature. The combined MeOH extracts were evaporated under reduced pressure to yield a dark-brown syrup (305.5 g). The syrup was partitioned between $CHCl_3$ and H_2O to give two layers. The $CHCl_3$ layer was then extracted with 3% HCl to give a $CHCl_3$ solution (Fraction A) (108.7 g) and an acidic aq. layer. The latter aq. layer was basified with NH_4OH and extracted with $CHCl_3$ to give Fraction B (3.1 g). Fraction B gave a positive alkaloidal test with Dragendorff's reagent. The crude alkaloid portion (Fraction B) was subjected to silica gel chromatography and eluted with increasingly polar mixtures of $CHCl_3$–MeOH to afford 21 Fractions. Romucosine B (**2**) (1.4 mg, $CHCl_3$–*n*-hexane 3:1 $R_f = 0.6$) was isolated as an insoluble powder from acetone in Fraction 5. Fraction 14 was separated by silica gel CC with increasingly polar mixtures of $CHCl_3$–MeOH to give 5 Fractions. Further separation of Fraction 14-1 by reverse phase

Table 1
Effects of tested alkaloids **1**–**5** on the platelet aggregation induced by thrombine, arachidonic acid (AA), collagen and platelet activating factor (PAF) in washed rabbit platelets[a]

Agent (100 μg)	Thrombin (0.1 U/ml)[b]	AA (10 μM)	Collagen (10 μg/ml)	PAF (2 ng/ml)
Control	92.5±0.4 (3)	84.9±1.1 (3)	88.2±0.5 (4)	91.3±0.3 (3)
1	89.0±0.3 (3) ***[c]	0.0±0.0 (3) ***	15.7±5.2 (4) ***	37.0±11.7 (3) ***
2	89.0±0.3 (3) ***	75.2±3.2 (3)*	87.2±0.7 (4)**	88.3±0.9 (3)*
3	90.4±0.4 (3) **	21.1± 2.7 (3) ***	62.5±7.9 (4)*	87.4±0.3 (3) ***
4	87.2±1.1 (3) ***	0.0±0.0 (3) ***	0.0±0.0 (3) ***	6.1±5.0 (3)***
5	88.7±0.6 (3) ***	58.3±6.1 (3) ***	56.5±13.9 (3) *	83.8±2.5 (3) *

[a] Platelets were preincubated with DMSO (0.5%, control), aspirin or tested compounds at 37°C for 3 min, then Thr (0.1 U/ml), AA (10 μM), collagen (10 μg/ml) or PAF (2 ng/ml) was added. Percentage of aggregation are presented as means ±S.E. ($n = 3$ or 4).

[b] U (thrombin unit) is expressed in NIH unit.

[c] *$P < 0.05$, ** $P < 0.01$,*** $P < 0.001$ as compared with the respective control.

HPLC (MeOH–H_2O 80:20, flow rate = 2.0 ml/min) yielded romucosine C (**3**) (1.5 mg, t_R = 23.5 min) and romucosine D (**4**) (2.6 mg, t_R = 21.0 min). Fraction 15 (0.4 g) was subjected to CC ($CHCl_3$–*n*-hexane 1:3) to give romucosine A (**1**) (2.5 mg, $CHCl_3$–*n*-hexane 1:2, R_f = 0.47) and *N*-methoxycarbony-nornuciferine (**5**) (3.0 mg, $CHCl_3$-*n*-hexane 3:2, R_f = 0.56), respectively.

3.4. Platelet aggregation assay

The platelet aggregation assays were carried out according to established protocols (Chen et al., 1996a).

3.4.1. Romucosine A (*1*)

[2-Hydroxy-1-methoxy-4,5,6a,7-tetrahydro-dibenzo[*de,g*]quinoline-6-carboxylic acid methyl ester]. Brown amorphous powder; $[\alpha]_D^{25}$ −105° ($CHCl_3$; *c* 0.1,); UV λ_{max}^{MeOH}nm (log ε): 237 (4.40), 285 (4.22), 307 (4.05); IR ν_{max}^{KBr} cm^{-1}: 3400 (−OH) and 1690 (>C=O) ^1H NMR ($CDCl_3$, 400 MHz): δ 8.30 (1H, *d*, *J* = 8.0 Hz, H-11),7.28–7.32 (3H, *m*, H-8, 9 and 10), 6.75 (1H, *s*, H-3), 4.66 (1H, *dd*, *J* = 15.2, 3.6 Hz, H-6a), 4.22 (1H, *d*, *J* = 11.2 Hz, H-5a), 3.76 (3H, *s*, *N*-COOCH_3), 3.56 (3H, *s*, C1–OCH_3) and 2.65–2.98 (5H, *m*, H-4a, 4b, 5b and 7); EIMS (70 eV) *m*/*z* 325 $[M]^+$ (71), 310 (43), 294 (4), 237 (100); HREIMS *m*/*z* $[M]^+$ 325.1309 (calc. $C_{19}H_{19}O_4N$ 325.1314).

3.4.2. Romucosine B (*2*)

[3-Chloro-2-hydroxy-4,5,6a,7-tetrahydro-dibenzo[*de,g*]quinoline-6-carboxylic acid methyl ester]. White amorphous powder; $[\alpha]_D^{25}$ +153° ($CHCl_3$, *c* 0.05); UV λ_{max}^{MeOH} nm (log ε): 245 (4.43) and 285 (4.25); IR $\nu_{max}^{KBr}cm^{-1}$: 3400 (−OH) and 1700 (>C=O); ^1H NMR ($CDCl_3$, 400 MHz): δ 8.34 (1H, *d*, *J* = 8.0 Hz, H-11), 7.20–7.38 (3H m, H-8, 9 and 10), 4.72 (1H, *dd*, *J* = 13.2, 3.6 Hz, H-6a), 4.48 (1H, *d*, *J* = 10.8 Hz, H-5a), 3.76 (3H, *s*, *N*-COOCH_3), 3.62 (3H, *s*, C1–OCH_3) and 2.63–3.06 (5H, *m*, H-4a, 4b, 5b and 7); EIMS (70 eV) *m*/*z* 361 (15), 359 (46), 346 (7), 344 (21), 323 (12), 271 (63); HREIMS *m*/*z* $[M]^+$ 359.0915 (calc. $C_{19}H_{18}O_4NCl$ 359.0924).

3.4.3. Romucosine C (*3*)

[10-Hydroxy-1,2-dimethoxy-4,5,6a,7-tetrahydro-dibenzo[*de,g*]quinoline-6-carboxylic acid methyl ester]. White amorphous powder; $[\alpha]_D^{25}$ +140° ($CHCl_3$, *c* 0.05); UV λ_{max}^{MeOH} nm (log ε): 265 (4.25), 280 (4.02), 305 (4.35); IR $\nu_{max}^{KBr}cm^{-1}$: 3350 (−OH) and 1698 (>C=O); ^1H NMR ($CDCl_3$, 400 MHz): δ 7.98 (1H, *d*, *J* = 2.8 Hz, H-11), 7.15, (1H, *d*, *J* = 8.4 Hz, H-8), 6.77 (1H, *dd*, *J* = 8.4, 2.8 Hz, H-9), 6.68 (1H, *s*, H-3), 4.69 (1H, *br d*, *J* = 17.2 Hz, H-6a), 4.29 (1H, *br s*, H-5a), 3.90 (3H, *s*, C2-OCH_3), 3.76 (3H, *s*, NCOOCH_3), 3.68 (3H, *s*, C1–OCH_3) and 2.60–3.03 (5H, *m*, H-4a, 4b, 5b and 7); EIMS (70 eV) *m*/*z* 355 $[M]^+$ (70), 340 (13) and 267 (100); HREIMS *m*/*z* $[M]^+$ 355.1419 (calc. $C_{20}H_{21}O_5N$ 355.1419).

3.4.4. Romucosine D (*4*)

White amorphous powder; $[\alpha]_D^{25}$ +145° ($CHCl_3$, *c* 0.05); UV λ_{max}^{MeOH} nm (log ε): 263 (4.33), 275 (4.22), 307 (3.75); IR ν_{max}^{KBr} cm^{-1}: 3350 (−OH); ^1H NMR ($CDCl_3$, 400 MHz): δ 8.11 (1H, *d*, *J* = 2.8 Hz, H-11), 7.19 (1H, *d*, *J* = 8.4 Hz, H-8), 6.83 (1H, *dd*, *J* = 8.4, 2.7 Hz, H-9), 6.68 (1H, *s*, H-3), 4.70 (1H, *dd*, *J* = 13.4, 4.7 Hz, H-6a), 4.45 (1H, *d*, *J* = 10.8, H-5a), 3.90 (3H, *s*, C2-OCH_3), 3.84 (3H, *s*, C10–OCH_3), 3.75 (3H, *s*, NCOOCH_3), 3.68 (3H, *s*, C1–OCH_3) and 2.61–3.05 (5H, *m*, H-4a, 4b, 5b and 7); EIMS (70 eV) *m*/*z* (rel. int.) 369 $[M]^+$ (60), 354 (10), 281 (100); HREIMS *m*/*z* $[M]^+$ 369.1575 (calc. $C_{21}H_{23}O_5N$ 369.1576).

3.4.5. N-Methoxylcarbonyl-nornuciferine (*5*)

White amorphous powder; $[\alpha]_D^{25}$ +165° ($CHCl_3$, *c* 0.05); UV λ_{max}^{MeOH} nm (log ε): 235 (4.23), 285 (4.20), 307 (3.36); IR $\nu_{max}^{KBr}cm^{-1}$: 1690 (>C=O); ^1H NMR ($CDCl_3$, 400 MHz): δ 8.38 (1H, *d*, *J* = 8.0 Hz, H-11), 7.25–7.34 (3H, m, H-8, 9 and 10), 6.94 (1H, *s*, H-3), 4.77 (1H, *dd*, *J* = 13.2, 4.0 Hz, H-6a), 4.44 (1H, *br d*, *J* = 11.2 Hz, H-5a), 3.76 (3H, *s*, *N*-COOCH_3), 3.56 (3H, *s*, C1–OCH_3), 3.61 (3H, *s*, C2-OCH_3) and 2.65–3.02 (5H, *m*, H-4a, 4b, 5b and 7); EIMS (70 eV) *m*/*z* (rel. int.) *m*/*z* 339 $[M]^+$ (33), 324 (23), 309 (6), and 251 (100); HREIMS *m*/*z* $[M]^+$ 339.1474 (calc. $C_{20}H_{21}O_4N$ 339.1471).

3.4.6. Preparation of N-methoxylcarbonyl-nornuciferine (*5*)

(+)-Nornuciferine (10 mg) in dry CH_2Cl_2 (10 ml) was dissolved in triethylamine (5 μl) with stirring at 0°C for 10 min, and then methyl chloroformate (2 ml) was added dropwise. The reaction mixture was stirred for 10 min, and H_2O was added to quench the excess reagent. The mixture was partitioned with $CHCl_3$ and then passed through a disposable pipette (0.6×6 cm) containing silica gel (230–400 mesh) and eluted with $CHCl_3$ repeatedly to afford a white amorphous powder (10.2 mg, 84%) which was identical with **5** (mixed mp, co-TLC, UV, IR, and ^1H NMR).

Acknowledgements

This investigation was supported by a grant from the National Science Council of the Republic of China.

References

Alali, F.Q., Liu, X.X., McLaughlin, J.L., 1999. Annonaceous acetogenins: recent progress. Journal of Natural Products 62 (3), 504–540.

Caetano, L.C., Dadoun, H., 1987. Pallidine and aporphinoid alkaloids from *Rollinia mucosa*. Journal of Natural Products 50 (2), 330.

Chen, K.S., Ko, F.N., Teng, C.M., Wu, Y.C., 1996. Antiplatelet and vasorelaxing action of some aporphinoids. Planta Medica 62 (2), 133–136.

Chen, Y.Y., Chang, F.R., Wu, Y.C., 1996. Isoquinoline alkaloids and lignans from *Rollinia mucosa*. Journal of Natural Products 59 (9), 904–906.

Chen, Y.Y., Chang, F.R., Yen, S.F., Wu, Y.C., 1996. Epomusenins A and B, two acetogenins from fruits of *Rollinia mucosa*. Phytochemistry 42 (4), 1081–1093.

Hartwell, J.L., 1982. Plants Used Against Cancer. Quarterman Publications Inc, Lawrence, MA, p 379.

Liaw, C.C., Chang, F.R., Chen, Y.Y., Chiu, F.F., Wu, M.J., Wu, Y.C., 1999. New annonaceous acetogenins from *Rollinia mucosa* Baill. Journal of Natural Products 62 (12), 1613–1617.

Leboeuf, M., Cave, A., Bhaumik, P.K., Mukherjee, B., Mukherjee, R., 1982. The phytochemistry of annonaceae. Phytochemistry 21 (12), 2783–2813.

Paulo, M.D.Q., Kaplan, M.A.C., Laprevote, O., Roblot, F., Hocquemiller, R., Cave, A., 1991. Lignans and other non-alkalodial constituents from *Rollinia mucosa*. Fitoterapia 62 (2), 150–152.

Shamma, M., 1972. The Isoquinoline Alkaloids. Academic Press, New York, pp. 195–228.

Tschesche, R., Welzel, P., Moll, R., Legler, G., 1964. über 2 Alkaloide aus der Rinde von *Symplocos celastrinea* Mart. Tetrahedron 20, 1435–1447.

Zafra-Polo, M.C., González, M.C., Sahpaz, S., Cortes, D., 1996. Acetogenins from annonaceae, inhibitors of mitochondrial complex I. Phytochemistry 42 (2), 253–271.

Zafra-Polo, M.C., Figadère, B., Gallardo, T., Tormo, J.R., Cortes, D., 1998. Natural acetogenins from annonaceae, synthesis and mechanisms of action. Phytochemistry 48 (7), 1087–1117.

PERGAMON

Phytochemistry 57 (2001) 427–435

PHYTOCHEMISTRY

www.elsevier.com/locate/phytochem

Benzyl isothiocyanate is the chief or sole anthelmintic in papaya seed extracts

Rohan Kermanshai[a,1], Brian E. McCarry[b], Jack Rosenfeld[c], Peter S. Summers[a], Elizabeth A. Weretilnyk[a], George J. Sorger[a,*]

[a]*Department of Biology McMaster University, Hamilton, Ontario, Canada L8S 4K1*
[b]*Department of Chemistry, McMaster University, Hamilton, Ontario, Canada, L8S 4K1*
[c]*Department of Pathology, McMaster University, Hamilton, Ontario, Canada, L8S 4K1*

Received 3 February 2000; received in revised form 22 December 2000

Abstract

Papaya (*Carica papaya*) seeds were extracted in an aqueous buffer or in organic solvents, fractionated by chromatography on silica and aliquots tested for anthelmintic activity by viability assays using *Caenorhabditis elegans*. For all preparations and fractions tested, anthelmintic activity and benzyl isothiocyanate content correlated positively. Aqueous extracts prepared from heat-treated seeds had no anthelmintic activity or benzyl isothiocyanate content although both appeared when these extracts were incubated with a myrosinase-containing fraction prepared from papaya seeds. A 10 h incubation of crude seed extracts at room temperature led to a decrease in anthelmintic activity and fractionated samples showed a lower benzyl isothiocyanate content relative to non-incubated controls. Benzyl thiocyanate, benzyl cyanide, and benzonitrile were not detected in any preparations and cyanogenic glucosides, which were present, could not account for the anthelmintic activity detected. Thus, our results are best explained if benzyl isothiocyanate is the predominant or sole anthelmintic agent in papaya seed extracts regardless of how seeds are extracted. © 2001 Published by Elsevier Science Ltd. All rights reserved.

Keywords: *Carica papaya*; Caricaceae; Anthelmintic; Benzyl isothiocyanate; *Caenorhabditis elegans*; Myrosinase; Nematode

1. Introduction

Papaya seeds have been used for centuries as a vermifuge in India (Lal et al., 1976), Central and South America (Roig y Mesa,1974) and throughout the world (Werner, 1992). Clinical trials with humans have led to seemingly contradictory results with Robinson (1958) claiming that papaya seeds are effective and Fernando (1959) claiming they are not. However, laboratory studies have confirmed that various preparations of papaya seeds can kill helminths effectively in vitro and in infected animals (Krishnakumari and Majumder, 1960; Dar et al., 1965; Lal et al.,1976).

The number and identity of anthelmintic compounds present in papaya seeds has not yet been established. Previous work has shown that seeds ground and extracted with either water or organic solvents, including alcohol, all produce crude extracts with anthelmintic activity and contain bioactive compounds such as benzyl isothiocyanate (BITC) (Dar et al., 1965; Ettlinger and Hodgkins, 1956; Krishnakumari and Majumder, 1960; Tang, 1971; Tang et al., 1972). In some cases, diethyl ether could be used to concentrate the bioactive principle(s) from water soluble seed extracts but, while the material that partitioned to the diethyl ether or organic solvent layer was shown to have anthelmintic activity and contain BITC, fractions that were produced by the initial extraction of the seeds with water or which partitioned to the water layer were apparently never tested for anthelmintic activity (Ettlinger and Hodgkins, 1956; Tang, 1971, 1973). Steam distillates using water-soluble extracts of papaya seeds also yielded BITC and the activity of this fraction against helminths was demonstrated (quoted in Ettlinger and Hodgkins, 1956). Since BITC is volatile and relatively insoluble in water, distillation of this compound from an aqueous solution

* Corresponding author. Tel.: +1-905-525-9140, ext. 24376; fax: +1-905-522-6066.
E-mail address: sorger@mcmaster.ca (G.J. Sorger).
[1] Permanent address: Department of Biology, Faculty of Sciences, Esfahan University, Esfahan, Iran.

0031-9422/01/$ - see front matter © 2001 Published by Elsevier Science Ltd. All rights reserved.
PII: S0031-9422(01)00077-2

at a relatively low temperature is not surprising. However, the steam distillation carried out by these researchers would not have identified any other putative bioactive compounds that may have been heat-labile. Given the variety of solvents and extraction conditions that can produce extracts with bioactive properties against helminths, there is little compelling evidence that BITC is the only anthelmintic principle that can be extracted from papaya seeds.

The anthelmintic effect of papaya seeds has been variously ascribed to carpaine (an alkaloid) and carpasemine (later identified as benzyl thiourea by Panse and Paranjpe, 1943), and BITC (Krishnakumari and Majumder, 1960; Tang, 1971). Benzyl thiourea is reported to be an artifact that arose during purification of the bioactive principle due to a reaction between ammonia and BITC (Ettlinger and Hodgkins, 1956) and it was present in preparations from seeds at a concentration of one-tenth that of BITC. Subsequently, Dar et al. (1965) tested BITC and benzyl thiourea individually for bioactivity and showed BITC to be about 20 times more toxic to *Ascaris lumbricoides* than benzyl thiourea. Since this study only tested compounds already known to be present in papaya seed extracts it falls short of proving that BITC is the only active anthelmintic principle in these seeds.

In addition to anthelmintic properties, papaya seed extracts also contain antimicrobial activity (Ettlinger and Hodgkins, 1956; Emeruna, 1982) due, at least in part, to BITC (Das et al., 1954). Again, however, it is not clear whether all the antibiotic activities are due to one or more compounds present in these seed preparations.

In papaya seeds, BITC is formed from benzyl glucosinolate (Gmelin and Kjær, 1970; Tang, 1973; Bennett et al., 1997), the major or perhaps only glucosinolate present. Glucosinolates in the seeds of many plants are metabolized to yield isothiocyanates by the action of enzymes commonly called myrosinases (thio-glucoside hydrolases, EC 3.2.3.1) (Ettlinger and Hodgkins, 1956; Palmieri et al., 1982), enzymes that are brought into contact with their substrate(s) upon damage to seeds in which they are found. The myrosinase and glucosinolates are in different compartments of the papaya seed (the endosperm and sarcotesta of the seed, respectively), although a small fraction of substrate and enzyme reside together in the embryo (Tang, 1973). It follows that papaya seeds must be crushed or otherwise damaged to produce substantial amounts of the antibiotic BITC.

Different myrosinase/glucosinolate combinations give rise to different products, with some producing a combination of thiocyanates and isothiocyanates, others a mix of nitriles, thiocyanates and isothiocyanates and still others isothiocyanates alone (Saarivirta and Virtanen, 1963; Virtanen, 1965). It remains to be determined whether the myrosinase/benzyl glucosinolate combination of papaya seed gives rise to all the possible products listed above or only BITC.

More recently, Bennett et al. (1997) found that papaya leaves and stems contain cyanogenic glucosides. This finding was unanticipated because plants that contain glucosinolates do not, as a rule, contain cyanogenic glucosides (Bennett et al., 1997; Conn, 1980). However, cyanogenic glucosides offer a potential source of highly toxic cyanide if they are also present in seeds. The prospect of cyanide contributing to the antibiotic properties of papaya seed preparations is difficult to address since seeds were not tested for these glucosides in the earlier study (Bennett et al., 1997) and so we felt it necessary to test for the presence of cyanogenic glucosides in papaya seeds.

In this study we elected to use *C. elegans* as an endpoint to measure anthelmintic activity. While *C. elegans* is a free living nematode and not a parasite, it is considered to be a good nematode model with important genetic similarities to parasitic nematodes (Blaxter, 1998). Furthermore, parasitic nematodes have yet to be propagated outside of their hosts. Our findings show that anthelmintic activity is present or recovered from either water-soluble (''aqueous'') or non-polar organic solvent (''nonaqueous'') extracts prepared from papaya seeds and that BITC is present in both extracts. We propose that BITC is the major and probably only source of anthelmintic activity present in papaya seeds and that it is produced in preparations of these seeds primarily, and probably exclusively, as the result of the action of resident myrosinase(s).

2. Results

Commercial BITC (98% pure) was toxic to *C. elegans,* as expected (Table 1). Extracts of fresh papaya seeds prepared with water were also toxic to *C. elegans* and were shown to contain BITC (Table 1). A volume of 10–20 μl of these aqueous extracts, when freshly prepared, representing the contents of about 1.2–2.4 mg of seed, was sufficient to kill *C. elegans* in our 0.5 ml assay. BITC was also found in oil concentrates prepared from seeds that were Soxhlet extracted with pentane and between 0.04 and 0.1 μl of this oil, representing the contents of 4–10 mg of seed, killed the nematodes in our assay (Table 1). If one considers the measure of toxicity as the LC90 or the concentration of the compound needed to kill $>90\%$ of the nematodes within 4–5 h, this value is roughly equivalent regardless of the source of BITC (Table 1).

Exposures for periods exceeding 12 h were generally lethal to all the nematodes in the assay when the concentration of BITC was at the LC90, irrespective of the source of BITC. Fig. 1 shows the log of the concentration of BITC in commercial BITC and in the aqueous and oil extracts of papaya seeds plotted against the log of the minimum volume of these preparations needed to kill 90% of the nematodes. A highly significant constant

Table 1
BITC and papaya seed extracts decrease the viability of *Caenorhabditis elegans*[a]

Preparation		Dose to kill > 90% nematodes		BITC	
		Volume (μl)	Seed number[c]	Concentration (M)	LC90[d] (μM)
BITC standard[b]		0.001–0.002	–	7.46	15.30
Seed extract	Crude aqueous	10–20	0.03–0.06	0.0006	12–24
	Crude oil	0.04–0.1	0.1–0.25	0.196	16.39

[a] Representative results shown, experiment was repeated three times.
[b] Commercially available, 98% pure.
[c] One seed weighs approximately 40 mg after the mucilaginous coat has been removed.
[d] Concentration of BITC in the 0.5 ml nematode viability assay required to kill >90% of the *C. elegans* in 4–5 h.

relationship is found with an r^2 of 0.989, an outcome that is best explained if BITC is the active anthelmintic principle in each of these preparations.

When the seed residue, after having been thoroughly extracted with pentane to remove BITC, is re-extracted with water, the resulting extract is still a potent anthelmintic (100 μl of this extract kills >90% of *C. elegans*). This could be explained if one or more of the active principles present is soluble in water and not in pentane, or if a water-soluble precursor of the active principle is converted to the active principle, that is only then soluble in pentane. Since benzyl glucosinolate is water soluble, is known to be present in papaya seeds (Tang, 1973; Bennett et al., 1997) and is a precursor of BITC that, in turn, is soluble in pentane, the latter hypothesis is plausible and could explain why both extractions yield BITC (Table 1).

Myrosinase, an enzyme that catalyzes the conversion of glucosinolates to isothiocyanates (Tang, 1973; Palmieri et al., 1982), was present in water extracts of ground papaya seeds and was found to elute in the void volume of a Sephadex G-50 column, as expected, because of the high molecular weight of myrosinases (Botti et al., 1995). Anthelmintic activity eluted much later from the column and was absent from the void volume (results not shown). The results in Table 2 show that aqueous extracts of seeds ground after heat-treatment of the seed exhibit no apparent nematode killing activity relative to extracts of untreated seeds at the volumes tested. Also, subjecting the extract of heat-treated seeds to a cyclocondensation reaction with benzene dithiol (Zhang et al., 1992) produced an absorption spectrum with no symmetrical peak at 365 nm thus giving no evidence for the presence of BITC (Fig. 2A). However, when extracts from these heat-treated seeds were incubated with an aliquot of the void volume obtained from a Sephadex G-50 column loaded with an extract prepared from fresh seeds, the nematode killing potential of the mixture increased markedly (Table 2). When this preparation was subjected to the cyclocondensation reaction described above, the absorbance spectrum produced (Fig. 2B) is typical of that published for pure isothiocyanates processed in the

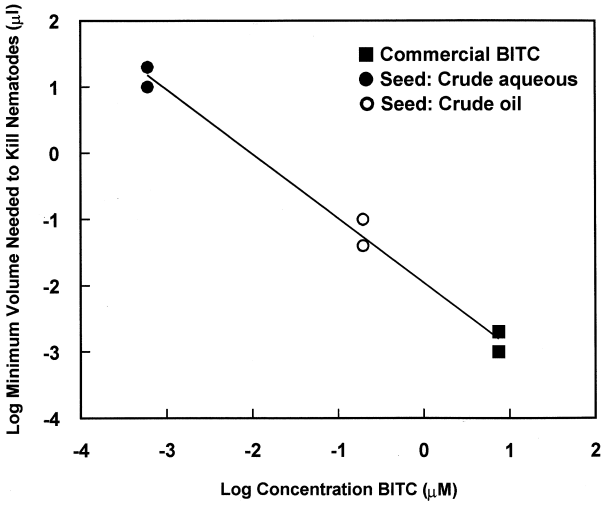

Fig. 1. Regression plot showing the relationship between BITC concentration of various preparations and dose required to kill >90% of *Caenorhabditis elegans* in a nematode killing assay.

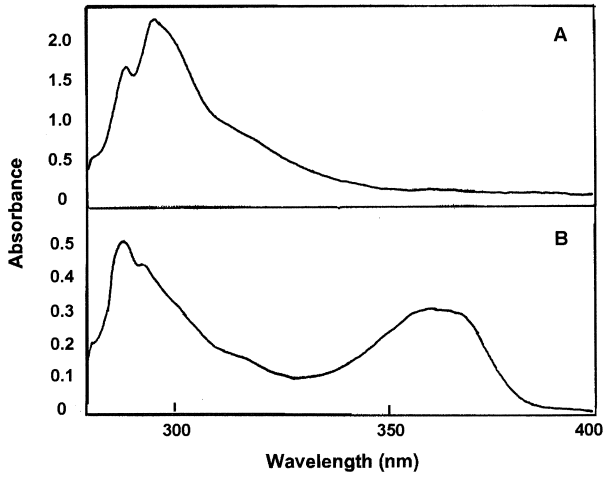

Fig. 2. Absorption spectra of an extract of heat-treated seed before (A) and after (B) incubation of the extract with a VoG50 fraction containing myrosinase activity. For panel B, the sample was incubated for 30 min and diluted eight fold with 10 mM potassium phosphate (pH 6) buffer before measurement.

same fashion (Zhang et al., 1992). No nematode killing activity was found in samples where the fresh seed extract obtained from the void volume of a Sephadex G-50 column was boiled for 10 mm prior to incubation with the heat-treated seed extract (Table 2). In a comparable experiment the LC90 of BITC for the sample subjected to activation conditions was determined to be 20 μM. This LC90 is similar to that listed for all the preparations used in Table 1, again suggesting that BITC is the active nematode killing principle here.

An oil fraction of papaya seed, prepared by Soxhlet extraction with pentane, was applied to a silica column and compounds present were separated by elution from the column with increasingly polar organic solvents. The BITC content and the *C. elegans* killing activity eluted in the same fraction (Table 3). In preliminary experiments, 40–60% of the nematode killing activity eluted in a 90% hexane (H)/10% dichloromethane (DCM) mixture with the balance of the killing activity eluting in a 75% H/25% DCM mixture. The 90% H/10% DCM fraction was examined by GC and found to contain a single prominent peak that upon subsequent examination by mass spectroscopy and infrared spectroscopy, was found to correspond to BITC (analysed by the Center for Mass Spectrometry, McMaster University). The 75% H/25% DCM fraction was examined by TLC, and upon exposure to iodine vapour, was found to contain a number of spots, so no further tests were performed with this fraction (results not shown). In subsequent fractionations, all the BITC and all the anthelmintic activity co-eluted from the column in a mixture of 85% H/15% DCM (Table 3). Despite the presence of other compounds as shown by TLC and a recovery of BITC that was less than 100% of the crude, this fraction yields an LC90 estimate which is similar to that determined for the crude oil from which it was produced and one that lies within the range of values quoted in Table 1.

We noted that the nematode killing power of aqueous extracts of papaya seeds incubated at room temperature for 10 h decreased to 30–50% of a freshly prepared extract (Table 4). Aqueous extracts of papaya seeds were either extracted immediately with diethyl ether or following a 10 h incubation at room temperature. Both diethyl ether extracts were then fractionated on a silica column and the *C. elegans* killing activity and BITC content of each solvent fraction were determined. For both the unincubated and incubated samples, the nematode killing activity and BITC co-eluted in the 85% H/15% DCM fraction (Table 4). In the case of the sample that had first been incubated for 10 h, the BITC content of the 85% H/15% DCM fraction was only half that found in the same fraction of the unincubated

Table 2
Loss of toxicity in aqueous papaya seed extracts due to heat treatment can be restored upon incubation with a protein fraction prepared from fresh papaya seeds[a]

Incubation mixture		Dosage tested in nematode viability test	
Main component[b]	Addition[c]	Volume (μl)	Nematodes killed (%)
Buffer	VoG50[d]	100	0
Extract of heat-treated seed in buffer	Buffer[e]	100	0
	VoG50	50	100
		100	100
	Boiled VoG50	100	0

[a] Representative results shown, experiment was repeated five times.
[b] 0.5 ml Volume with buffer comprised of 10 mM potassium phosphate (pH 6.0) and 1 mM ascorbic acid.
[c] Volume of addition was 0.2 ml.
[d] VoG50 is the void volume fraction from a Sephadex G-50 column (see Experimental). No nematode killing activity was detected in this fraction.
[e] 10 mM potassium phosphate (pH 6.0) and 1 mM ascorbic acid.

Table 3
BITC content and toxicity of silica column fractions of papaya seed extracts[b]

Solvent for elution of fraction	BITC	
	Concentration (mM)[a]	LC90 (μM)
Crude oil	196	39
100% Hexane	0	0
85% Hexane/15% dichloromethane	130	29
100% Dichloromethane	0	0
100% Methanol	0	0

[a] The volume of each fraction was reduced by evaporation and, where necessary, volumes were made equivalent by the addition of hexane.
[b] Representative data shown. The experiment was completed twice with identical results.

Table 4
Incubating crude seed extracts of papaya for 10 h reduces their BITC content and toxicity to nematodes

Seed extract incubation[a]	Fraction	BITC (mM)	Minimum volume required for 100% nematode kill (μl)[c]
None	Crude	n.d.[b]	30–50
	85% Hexane/15% dichloromethane	504	16
10 h	Crude	n.d.	100
	85% Hexane/15% dichloromethane	240	50

[a] Incubation at room temperature prior to chromatographic separation of crude extract on silica and the subsequent testing for BITC content and toxicity to nematodes.
[b] n.d. Means not determined.
[c] Volumes were corrected for differences in resuspension volume of the chromatographic fractions (see Experimental for silica chromatography and GC quantification of BITC).

sample (Table 4). In separate experiments aliquots of the aqueous extract were incubated for up to 9 h at room temperature before extraction with diethyl ether. The diethyl ether layer was then assayed for anthelmintic activity and BITC content. After six hours of incubation, only 75% of the anthelmintic activity and 70% of BITC remained relative to those measured for the non-incubated sample. After nine hours of incubation, these values decreased to 50 and 39% for anthelmintic activity and BITC level, respectively. Thus, the same conclusion was reached, *C. elegans* killing activity and BITC content decreased with the length of incubation.

In an effort to identify other putative anthelmintic compounds in papaya seed extracts we attempted to obtain carpaine from the papaya seeds following the procedure of Govindachari et al. (1965) but all our attempts were unsuccessful. Seed extracts *of Lepidium sativum* have been found by colorimetric methods to contain BC (benzyl cyanide) and BTC (benzyl thiocyanate) as well as BITC, their proportions varying with extraction conditions (Virtanen, 1962; Saarivirta and Virtanen, 1963, 1965; Gil and MacLeod, 1980). Preparations from *Tropaeolum* and *Sinapsis alba* seeds, on the other hand, contained only BITC (Saarivirta and Virtanen, 1963).

Papaya seeds have not been examined specifically for their content of BTC, BC and benzonitrile (BN). An aqueous preparation of seeds was extracted twice with diethyl ether, the diethyl ether layer was evaporated in vacuuo and the resulting oil resuspended in hexane. This sample, which contained all the anthelmintic activity from the extracted seeds, was applied to a silica column and the anthelmintic activity containing fraction (85% H/15% DCM), was subjected to GC under conditions that separate BITC, BTC and BC (Fig. 3, inset). BITC was found as was an unknown compound tentatively identified as butylated hydroxytoluene (BHT is introduced as the stabilizing additive for the diethyl ether) but no BTC or BC was detected in this preparation (Fig. 3). By an in vitro assay, BITC was more potent as an anthelmintic than BTC and far more potent than BC (Table 5). Taken together, these observations indicate that BTC and BC do not appear to contribute significantly towards the anthelmintic power of papaya seed extracts. A commercial source of benzonitrile (BN) was also examined for its toxicity towards *C. elegans* and was found to have a very high LC90 of >19 mM (Table 5). Also, BN has a retention time of 2.98 min when subjected to the same GC elution conditions as used to separate BITC, BTC and BC (data not shown) and no such peak was noted on the chromatograph shown in Fig. 3.

Therefore, insufficient BN is present in the biologically active fraction for BN to be considered responsible for killing *C. elegans*.

Bennett et al. (1997) reported that leaves and stems of papaya seedlings contained cyanogenic glucosides with the highest concentration found in leaves (extracts showing 8 μM cyanide) but seeds were not tested. We found that the *C. elegans* LC90 for KCN exceeded 100 μM in our killing assay (Table 5) and while cyanide at this concentration caused nematodes to move more slowly relative to the assay without cyanide, they recovered completely within 5 h. The cyanide content of aqueous extracts of papaya seeds was always less than 28 μM even after the extracts had been incubated with β-glucosidase at room temperature for two hours. When these extracts are used in a nematode killing assay, the final concentration of cyanide present in the assay at which 90% of the nematodes are killed is less than 5 μM, a concentration well below the 100 μM KCN found to be non-lethal to nematodes. Processing a papaya seed sample with KCN added to a final concentration of 20 μM yielded a sample whose concentration was equivalent to that of the original sample plus

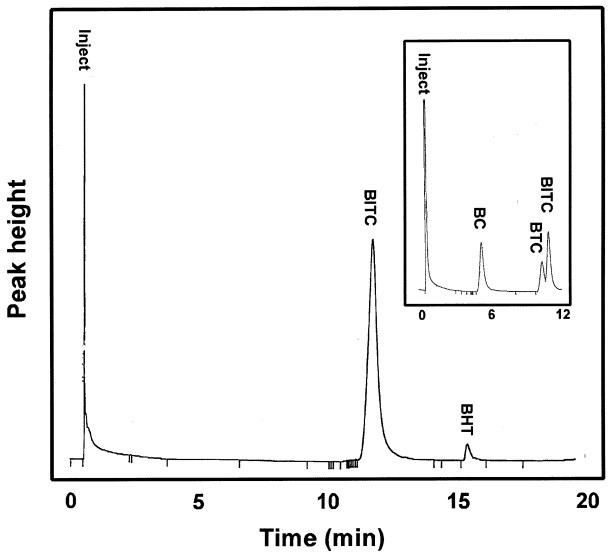

Fig. 3. GC analysis of papaya seed preparations with anthelmintic activity shows that BITC is present but BC and BTC are absent. An aqueous papaya seed extract was extracted with diethyl ether, concentrated and dissolved in hexane and this was fractionated on a silica column. The 85% H/15% DCM fraction containing anthehnintic activity was evaporated to dryness and dissolved in CS_2 for GC analysis (see Experimental). This experiment was performed twice with similar results. The inset shows a GC separation of commercially available BC, BTC and BITC.

Table 5
Toxicity of various compounds to *Caenorhabditis elegans*

Compound[a]	LC90 (μM)
BITC	15–45
Benzyl thiocyanate	200
Benzyl cyanide	5000
BN	>19,000
KCN	>100

[a] Commerically available compounds were dissolved in DMSO. DMSO controls had no negative effect on nematodes.

the added KCN, demonstrating that cyanide was not disappearing from the extract during the extraction procedure. BITC added to extracts and to the cyanide assay mixture did not give rise to cyanide, hence there was no complication from endogenous glucosinolates or BITC. It follows from the above that the cyanide/cyanogenic glucoside contents of the papaya seed extracts do not contribute to their anthelmintic power.

3. Discussion

3.1. BITC is the active compound in papaya seed preparations

Our results show that the anthelmintic activity of papaya seed extracts prepared using water or pentane co-purifies with BITC during column chromatography. Further, re-extraction of aqueous extracts with diethyl ether leads to a complete recovery of both bioactivity and BITC in the diethyl ether fraction. We noted that changes in nematode killing activity of preparations were paralleled by changes in their BITC content. For example, the increase in anthelmintic activity obtained by incubating extracts of heat-treated seeds with a soluble protein fraction containing myrosinase activity is accompanied by an increase in BITC concentration. Also, when extracts are left for 10 h at room temperature, there is a decrease in killing activity of the extract that coincides with a decrease in BITC concentration. Aqueous extracts of papaya seeds do not appear to contain enough cyanogenic glucosides to be toxic to nematodes nor is there any detectable BTC, BC or BN in the fraction containing the anthelmintic activity. Taken together with the previous literature, all these results indicate that the main and perhaps the only effective anthelmintic in the papaya seed preparations we investigated is BITC. This conclusion supports the earlier proposal by Dar et al. (1965), but provides a more thorough investigation of possible candidate bioactive compounds naturally occurring in the papaya seed extract.

3.2. Toxicity of papaya seed preparations

According to our measurements it takes the equivalent of 1.2–2.4 mg of seed to kill >90% of the *C. elegans* in our 500 μl assay within 4–5 h and completely rid the assay mixture of live nematodes within 12 h. Given these in vitro viability results and assuming that the volume of the small intestine of an adult human is approximately 1.3 l (Masoro, 1973), then a dose of 3.1–6.2 g of papaya seeds would be equivalent to that which is effective against *C. elegans* in our assay. However, this dosage is likely to be an underestimate given that it does not consider factors that would reduce the intestinal BITC concentration over time including the movement of contents through the gut [with the residence time of a bolus being very short for the stomach and 3–7 h for the small intestine, (Osterwald, 1990; Fleisher et al., 1999)], and the likelihood that BITC is absorbed by the intestinal epithelium. Our calculated dose approaches the published daily dose recommended for the medicinal use of papaya seeds in Cuba (1–1.5 g three times a day, Roig y Mesa, 1974). If one gives the equivalent of 3.1–6.2 g of seeds to a 55 kg human, this amounts to a dose of 56–112 mg/kg. Despite the speculative nature of this dosage, this value was shown to be non-lethal to mice and rats (Chinoy et al., 1994) and a 5–10-fold lower dose was shown to be effective against *Ascaris* in children (Robinson, 1958).

A consideration relevant to the medicinal use of papaya seeds, is that BITC must be released from benzyl glucosinolate by a papaya myrosinase. It follows that factors that could inhibit myrosinase or inactivate BITC could compromise the concentration of BITC in the small intestine. One such factor might be exposure to acid (pH 2) in the stomach (Magee, 1973). We tested the effect of acid exposure on the potency of papaya seed extracts by deliberately acidifying aqueous seed extracts to pH 2.6 with HCl and then neutralized the extract to pH 6.5 with 2 M Na_2CO_3 either immediately or after one hour. Comparison of the in vitro anthelmintic activity of these acidified and neutralized extracts relative to that of an untreated control seed extract showed that all the preparations were of equivalent potency. An additional consideration that was not evaluated in this study is that there may be variability among papayas with respect to myrosinase or glucosinolate content. Such variation or indeed any factor that could affect BITC content of seed extracts would, in turn, lead to differences in nematode killing potency between preparations.

The BITC content of papaya seeds could be lethal to some beneficial as well as harmful intestinal microorganisms (Emeruna, 1982). Thus while treatment with papaya seeds might eliminate intestinal bacteria, this treatment would not lead to an infection of the intestine by eukaryotic parasites, such as *Candida,* since they would also be killed by the BITC (Stoll and Seebeek, 1948).

In addition to nematode killing activity, BITC appears to elicit several biological effects. BITC inhibits chemically induced carcinogenesis in animal models and cell cultures (reviewed in Wattenberg, 1977; Zhang and Talalay, 1994) but is potentially toxic at therapeutic dosages since it is reported to be goitrogenic, carcinogenic and mutagenic (Yamaguchi, 1980; Fenwick et al., 1983). Thus a concern in any therapeutic application of BITC must address how different are the therapeutic and toxic/lethal doses of the vermifuge.

Fenwick et al. (1983) analysed data that suggests that BITC is goitrogenic and proposed that the goitrogenic effect is probably more associated with iodine deficiency

than to a direct effect of BITC alone. If such is the case, any adverse effects of BITC might be averted by an iodine supplement.

Lohiya et al. (1994) showed that papaya seed extracts administered to male rats for 30–60 days (at a dose equivalent to 67–333 mg/kg/day) can result in temporary but completely reversible sterility. This daily dose is comparable to our speculative dosage (see above), but the comparatively short duration for therapy to kill nematodes in humans should pose no threat in this regard.

Yamaguchi (1980) found that BITC at 50 μM (roughly equivalent to 7.5 mg of papaya seed/l) doubled the spontaneous reversion rate of *Salmonella typhimurium* strain TA100 and that activation by rat liver extract S-9 had no effect on this reversion rate. TA100 is much more sensitive than the wild type strain to mutagens and a petri dish assay is very different from the inside of a mammalian intestine, but the 7.5 mg seed/l is only slightly greater than that used to kill *C. elegans* in our assay (2.4–4.8 mg of seed/l) and could be, therefore, a source of concern. In contrast, at much higher concentrations in experimental animals, BITC seems to act as an anticarcinogen that seems to be due to the antagonistic effect of BITC on the enzymatic activation of mutagens (Wattenberg, 1977; Zhang and Talalay, 1994; Talalay and Zhang, 1996; Fahey et al. 1997). Isothiocyanates, formed from their respective glucosinolates, have been found in a number of different plants (notably in members of the Cruciferae) where they have been shown to have anticarcinogenic properties (Wattenberg, 1977; Zhang and Talalay, 1994; Talalay and Zhang, 1996).

With respect to cyanide/cyanogenic glucosides in papaya seeds, a fatal dose of KCN for humans, according to Merck (1989), is between 1.85 and 2.22 mM and the fatal blood level of CN is reported as 115 μM (Henry, 1979). These levels are obviously well above those found by us in the seeds, let alone the levels expected after dilution by the digestive tract, the bloodstream and inter- plus intrastitial water.

It would appear from the foregoing discussion and from many generations of traditional use of papaya seeds as an anthelmintic that this work, based upon chemical and biological analysis of papaya seed extracts, supports existing practices and provides insight into how they may be improved.

4. Experimental

4.1. Strains and materials

Caenorhabditis elegans strain N2 was obtained from Dr. J. Culotti, Hospital for Sick Children, Toronto, ON, Canada. BITC, 1,2 benzenedithiol, BTC, BC, BN, *N*-chlorosuccinimide, succinimide, pyridine and barbituric acid were from Aldrich. Papaya (*Carica papaya*) was purchased locally.

4.2. Growth and maintenance of C. elegans and toxicity assay

C. elegans was maintained on solid NGM medium (Sulston and Hodgkin, 1988). Between 20 and 50 nematodes were placed in 500 μ1 of S medium (Sulston and Hodgkin, 1988) in microtitre wells (Falcon No 3047, Becton Dickinson) containing 30 μl of a 5 times concentrated overnight culture of *E. coli* WP2 *(uvrA trp malB,* Witkin, 1975) resuspended in S medium. Aliquots (5–100 μl) of aqueous extracts (in water or 10 mM potassium phosphate, pH 6) were added directly to the wells while concentrated oils, fractions in non-aqueous solvents and commercial BITC were diluted with dimethyl sulfoxide (DMSO) prior to being added to the wells as 10 μl volumes. Dilute extracts prepared in non-aqueous solvents were concentrated first by evaporation under N_2, the residue resuspended with 1 ml of hexane, dried with air and the final residue was dissolved in 10 μl of DMSO which was then added to the test wells. Controls with the equivalent volumes of DMSO alone were negative. Nematode survival was measured 4–5 h after addition of the extracts and again 12–13 h later.

4.3. Preparation of seed extracts

Seeds harvested from papaya fruit had their mucilaginous coating removed prior to extract preparation. "Aqueous extracts" were prepared by grinding seeds with a mortar and pestle using distilled water (1 g seeds to 10 ml water), at room temperature and removing the debris by centrifugation at 16,000 *g* at 4°C for 30 min. "Oils" were prepared by grinding seeds in a mortar and pestle, with no added solvent and then adding the ground material to a thimble and extracting by refluxing 10 times in 8 volumes of pentane, in a Soxhlet extractor. The final extract in pentane was concentrated in vacuuo at 38°C. A typical extraction of 14 g of seeds yielded approximately 0.9 ml of crude oil following Soxhlet extraction.

4.4. Fractionation of extracts

Aqueous extracts (10 ml), prepared as described above, were extracted with 10 ml of diethyl ether and the aqueous phase was recovered and re-extracted two more times with 10 ml of diethyl ether each time. The three diethyl ether fractions were pooled and evaporated in vacuuo. The resulting residue was dissolved in 1 ml of hexane and 0.45 ml was loaded onto a 10 g silica (Silica gel, 63–200 μm mesh, BDH) column (23×1.3 cm). Oil prepared from seeds (described above) was also

fractionated by a comparable silica column. In this case, oil (0.45 ml) was loaded without further preparation onto the matrix. For fractionation of either aqueous or oil extracts, samples were eluted from the column at a rate of 0.7 ml min^{-1} with successive 100 ml volumes of 100% hexane, 85% hexane/15% dichloromethane, 100% dichloromethane and 100% methanol. The resulting eluates were evaporated in vacuuo at 42°C and the residues were made to a final volume of 500 μl with hexane and stored at −18°C. Aliquots (10–100 μl) of each fraction were evaporated to dryness, the residue dissolved in 10 μl DMSO which was then used in the nematode killing bioassay to titre the potency of the fraction.

4.5. Activation of heated seed extracts with myrosinase

Seeds (with their mucilaginous coats removed) were either left unheated or were heat-treated by immersing a tube containing seeds in boiling water for 10–20 mm or by autoclaving the seeds at 18 psi for 20 mm. Aqueous extracts were then prepared from the unheated and heat-treated seeds by grinding 1 g seeds with 10 ml of 10 mM potassium phosphate (pH 6) buffer. One milliliter of extract from unheated seeds was loaded onto a Sephadex G-50 column (10 ml bed volume). The fraction eluting in the 3.5 ml void volume (VoG50) contained the myrosinase activity (1.25 μmol sinigrin disappearing min^{-1} ml^{-1}, using the assay of Palmieri et al., 1982). Heat-treated seed extracts (0.5 ml) were incubated with 0.2 ml of the above VoG50 fraction for 30 mm at room temperature and then placed on ice. L-Ascorbic acid was included at a final concentration of 1 mM in the activation incubations. Aliquots of the activated extract were removed and used to measure killing of *C. elegans* as described above (5–100 μl per assay) and measure BITC concentration (10–100 μl for colorimetric determinations or 1–5 μl of 10–50-fold diluted preparation for GC measurements).

4.6. Measurement and detection of compounds

TLC was used as an initial method for determining purity of extracts. Samples were spotted onto silica Gel-G plates, developed in methanol–*n*-butanol–conc. HCl–H_2O (10:10:1:1; v/v/v/v), and plates were then exposed to iodine vapours to visualize organic compounds

Colorimetric measurement of BITC was made following a procedure modified from that described by Zhang et al. (1992). Two aliquots of a sample to be measured were each made to a final volume of 500 μl with 10 mM Tris–HCl (pH 7.5). To one aliquot, 500 μl of 13 mM benzene dithiol in methanol was added while to the second aliquot 500 μl of methanol (control) was added. A blank reaction with buffer and benzene dithiol was also prepared. All of the reactions were incubated at 65°C for 60 min in a microfuge tube and then microfuged for 5 min. Absorbance of the supernatant was taken at 365 nm with a Uvikon 930 spectrophotometer and compared to those of a standard curve prepared using commercial BITC.

For BITC determinations, measurement using GC was found to have greater specificity. GC was performed on a Hewlett Packard 5790A equipped with a flame ionization detector. The column was a Megabore DBI column with a 30 m length, 0.52 mm inner diameter and 0.24 μm film thickness. The carrier gas was H_2 maintained at a flow rate of 12 ml min^{-1}. Injector port and flame ionization detector were set at 250 and 300°C, respectively. Hydrogen and compressed air were delivered to the detector at flow rates of 120 and 300 ml min^{-1}, respectively. Typical injection size was 1–3 μl of sample dissolved in CS_2 or diethyl ether. At injection, the oven temperature was 65°C and was maintained at that temperature for 4 min and then increased at a rate of 5°C per min to a final temperature of 160°C. The output signals from the detector were recorded and integrated with a Shimadzu CR3A Chromatopac Integrator. Calibration using a dilution series of standards with known concentrations was analysed prior to each set of sample measurements. Concentrations were determined by comparing the responses from samples with those of the standards for injections of the same volume. For GC analysis, papaya oil samples were diluted directly in CS_2 or diethyl ether. Aqueous samples were extracted into diethyl ether and either injected directly into the GC or evaporated under N_2 gas, the residue dissolved in CS_2 and then injected as above.

Measurement of cyanogenic glucosides and cyanide followed the procedure of Halkier and Møller (1989). Papaya seeds were ground with 50 mM Mes-NaOH (pH 6.5) and extracts incubated at room temperature with almond β-glucosidase at 1 mg ml^{-1} (Sigma G-0395) for 2 h. Reaction mixtures were adjusted to 0.83 M NaOH and incubated for 1 h to liberate free CN. A 50 μl aliquot of glacial acetic acid was then added to each reaction mixture and the whole mixture was assayed for CN content (Halkier and Møller, 1989). The absorbance of the coloured complex formed was read at 585 and 650 mm and the difference in absorbance values were used to quantify CN levels by comparison to a standard curve prepared with KCN.

Acknowledgements

We gratefully acknowledge K. Green, McMaster Regional Centre for Mass Spectrometry for mass spectrometry analysis. This research was supported in part by a research grant to E.A.W. by the Natural Sciences and Engineering Research Council of Canada.

References

Bennett, R.N., Kiddle, G., Wallsgrove, R.M., 1997. Biosynthesis of benzylglucosinolate, cyanogenic glucosides and phenylpropanoids in *Carica papaya*. Phytochemistry 45, 59–66.

Blaxter, M., 1998. *C. elegans* is a nematode. Science 282, 2041–2046.

Botti, M.G., Taylor, M.G., Botting, N.P., 1995. Studies on the mechanism of myrosinase. Journal of Biological Chemistry 270, 20530–20535.

Chinoy, N.J., D'Souza, D.M., Padman, P., 1994. Effects of crude aqueous extract of *Carica papaya* seeds in male albino mice. Reproductive Technology 8, 75–79.

Conn, E.E., 1980. Cyanogenic compounds. Annual Review of Plant Physiology 31, 433–451.

Dar, R.N., Garg, L.C., Pathak, R.D., 1965. Anthelmintic activity of *Carica papaya* seeds. Indian Journal of Pharmacy 27, 335–336.

Das, B.R., Kurup, P.A., Rao, P.L.N., 1954. Antibiotic principle from *Moringa pterygosperma*. Naturwissenschaften 41, 66.

Emeruna, A.C., 1982. Antibacterial substance from *Carica papaya* fruit extract. Journal of Natural Products 45, 123–127.

Ettlinger, M.G., Hodgkins, J.E., 1956. The mustard oil of papaya seed. Journal of Organic Chemistry 21, 204–205.

Fahey, J.W., Zhang, Y., Talalay, P., 1997. Broccoli sprouts: an exceptionally rich source of inducers of enzymes that protect against chemical carcinogens. Proceedings of the National Academy of Science of USA 94, 10367–10372.

Fenwick, G.R., Heaney, R.K., Mullin, W.J., 1983. Glucosinolates and their breakdown products in food and food plants. CRC Critical Review of Food Science and Nutrition 18, 123–201.

Fernando, P.V.D., 1959. Preliminary investigation of *Carica papaya* seeds as a vermifuge. Indian Journal of Child Health 8, 96–100.

Fleisher, D., Li, C., Zhou, Y., Pao, L.H., Karim, A., 1999. Drug, meal and formulation interactions influencing drug absorption after oral administration. Pharmacokinetics 36, 233–254.

Gil, V., MacLeod, A.J., 1980. Studies on glucosinolate degradation in *Lepidium sativum* seed extracts. Phytochemistry 19, 1369–1374.

Gmelin, R., Kjær, A., 1970. Glucosinolates in the Caricaceae. Phytochemistry 9, 591–593.

Govindachari, T.R., Nagarajan, K., Viswanathan, N., 1965. Carpaine and pseudocarpaine. Tetrahedron Letters 24, 1907–1916.

Halkier, B.A., Møller, B.L., 1989. Biosynthesis of the cyanogenic glucoside dhurrin in seedlings of *Sorghum bicolor* (L.) Moench and partial purification of the enzyme system involved. Plant Physiology 90, 1552–1559.

Henry, J.B., (Ed.), 1979. Todd-Sanford-Davidsohn Clinical Diagnosis and Management by Laboratory Methods, Vol. 1, 16th Edition. W.B. Saunders, Philadelphia.

Krishnakumari, M.K., Majumder, S.K., 1960. Studies on anthelmintic activities of seeds of *Carica papaya* Linn. Annals of Biochemistry and Experimental Medicine 20, 551–556.

Lal, J., Chandra, S., Raviprakash, V., Sabir, M., 1976. In vitro anthelmintic action of some indigenous medicinal plants on *Ascaridia gali* worms. Indian Journal of Physiology and Pharmacology 20, 64–68.

Lohiya, N.K., Goyal, R.B., Jayaprakash, D., Ansari, S., Sharma, S, 1994. Antifertility effects of aqueous extracts of papaya seeds in male rats. Planta Medica 60, 400–404.

Magee, D.F., 1973. Secretions of the digestive tract. In: Ruch, T.C., Patton, H.D. (Eds.), Howell Fulton Physiology and Biophysics, 20th Edition. W.B. Saunders, Philadelphia, pp. 40–64.

Masoro, E.J., 1973. Absorption from the gastrointestinal tract. In: Ruch, T.C., Patton, H.D. (Eds.), Howell Fulton Physiology and Biophysics, 20th edition. W.B. Saunders, Philadelphia, pp. 65–78.

Merck and Co., 1989. The Merck Index, 11th Edition. Merck and Co.

Osterwald, H.P., 1990. Pharmaceutical development. Scandavian Journal of Gastroenterology 72, 43–46.

Palmieri, S., Leoni, O., Iori, R., 1982. A steady state kinetics study of myrosinase with direct UV spectrophotometric assay. Analytical Biochemistry 123, 320–324.

Panse, T.B., Paranjpe, A.S., 1943. Isolation of carpasemine from papaya seeds. Proceedings of the Indian Academy of Science 18A, 140.

Robinson, P., 1958. Seeds *of Carica papaya* for mass treatment against *Ascariasis*. Indian Journal of Child Health 7, 815–817.

Roig y Mesa, J.T., 1974. Plantas Medicinales Aromaticas o Venenosas de Cuba. Ciencia y Tecnica. Instituto del Libro, La Habana.

Saarivirta, M., Virtanen, A.I., 1963. A method for estimating benzyl isothiocyanate, benzyl thiocyanate and benzyl nitrile in crushed moistened seeds of *Lepidiurn sativum*. Acta Chemica Scandinavica 17, S74–S78.

Stoll, A., Seebeck, E., 1948. Die Isolierung von Sinigrin als Genuine, kristallisierte Muttersubstanz des Meerrettichöls. Helvetica Chimica Acta 31, 1432–1434.

Sulston, J., Hodgkin, J., 1988. Methods. In: Wood, W.B. (Ed.), The Nematode *Caenorhabditis elegans*. Cold Spring Harbor Laboratory Press, pp. 587–606.

Talalay, P., Zhang, Y., 1996. Chemoprotection against cancer by isothiocyanates and glucosinolates. Biochemical Society Transactions 24, 806–810.

Tang, C.S., 1971. Benzyl isothiocyanate of papaya fruit. Phytochemistry 10, 117–121.

Tang, C.S., Syed, M.M., Hamilton, R.A., 1972. Benzyl isothiocyanate in the Caricaceae. Phytochemistry 11, 2531–2535.

Tang, C.S., 1973. Localization of benzyl glucosimolate and thioglucosidase in *Carica papaya* fruit. Phytochemistry 12, 769–733.

Virtanen, A.I., 1962. On enzymatic and chemical reactions in crushed plants. Archives of Biochemistry and Biophysics (Suppl. 1), 200–208.

Virtanen, A.I., 1965. Studies on organic sulphur compounds and other labile substances in plants. Phytochemistry 4, 207–228.

Wattenberg, W., 1977. Inhibition of carcinogenic effects of polycyclic hydrocarbons by benzyl isothiocyanate and related compounds. Journal of the National Cancer Institute 58, 395–397.

Werner, D., 1992. Where There Is No Doctor. Hesperian Foundation, Palo Alto, CA.

Witkin, E., 1975. Elevated mutability of polA and uvrA polA derivatives of *Escherichia coli* B/r at sublethal doses of ultraviolet light: evidence for an inducible error-prone repair system ("SOS repair") and its anomalous expression of these strains. Genetics 79, 199–213.

Yamaguchi, T., 1980. Mutagenicity of isothiocyanates, isocyanates and thioureas on *Salmonella typhimurium*. Agricultural and Biological Chemistry 44, 3017–3018.

Zhang, Y., Cho, C.G., Posner, G.H., Talalay, P., 1992. Spectroscopic quantitation of organic isothiocyanates by cyclocondensation with vicinal dithiols. Analytical Biochemistry 205, 100–107.

Zhang, Y., Talalay, P., 1994. Anticarcinogenic activities of organic isothiocyanates: chemistry and mechanisms. Cancer Research 54, 1976–1981.

PERGAMON

Phytochemistry 57 (2001) 437–442

PHYTOCHEMISTRY

www.elsevier.com/locate/phytochem

Lipophyllic antioxidants from *Iryanthera juruensis* fruits

Dulce H.S. Silva [a,*], Francisco C. Pereira [a], Maria V.B. Zanoni [a], Massayoshi Yoshida [a,b]

[a] *Instituto de Química, Universidade Estadual Paulista, CP 355, CEP 14800-900, Araraquara-SP, Brazil*
[b] *Instituto de Química, Universidade de São Paulo, CP 26077, CEP 05599-970, São Paulo-SP, Brazil*

Received 7 January 2000; received in revised form 9 October 2000

Dedicated to Professor Otto Richard Gottlieb on the occasion of his 80th birthday

Abstract

The phytochemical investigation of the hexane extract of *Iryanthera juruensis* (Myristicaceae) fruits led to the isolation of two tocotrienols and four lignans which exhibited antioxidant activity towards β-carotene on TLC autographic assay. Two inactive quinones and three ω-arylalkanoic acids were also isolated. The isolates were investigated for their redox properties using cyclic voltammetry. The structure elucidation of the new compounds (one tocotrienol, one quinone and three ω-arylalkanoic acids) was based on analysis of spectroscopic data. © 2001 Elsevier Science Ltd. All rights reserved.

Keywords: *Iryanthera juruensis*; Myristicaceae; Tocotrienol; Plastoquinone; ω-Arylalkanoic acid; Lignan; Antioxidant

1. Introduction

Iryanthera juruensis is a widespread Amazonian species known as ucu-úba, which means fat-producing tree, this being a general designation given to myristicaceous species. Their seeds are valued in Brazil for their high yields of fatty acids, mainly myristic acid (C-14), which is extensively used in pharmaceutical and cosmetic industries. Other *Iryanthera* species were reported to have their crushed leaves used by Amazon indians for healing seriously infected wounds and cuts and to have their latex from the barks mixed with warm water for treating stomache infections (Schultes and Holmstedt, 1971). In the course of our systematic studies on *Iryanthera*, we have demonstrated the presence of tocotrienols with higher antioxidant activity than α-tocopherol in fruits of *I. grandis* and *I. lancifolia,* evaluated through malondialdehyde (MDA) and chemiluminescence (CL) assays (Barros et al., 1993) and of antioxidant dihydrochalcones and flavonolignans in *I. lancifolia* (Silva et al., 1999). Studies on tocotrienol biological activities revealed the ability of α- and γ-tocotrienol in inhibiting solid tumour growth of sarcoma 180 and also the highly metastic Lewis lung carcinoma cells (Komiyama et al., 1992). Moreover, these tocotrienols are effective against vascular smooth muscle cell proliferation, which plays a central role in atherosclerosis (Azzi et al., 1992). Oxidative damage to cell components is the initial event in several human disease processes including cancer and atherosclerosis (Gordon, 1996), and this has intensified the search for natural antioxidants. The antioxidant activity of a compound depends ultimately on its ease of oxidation and, for a variety of natural or synthetic compounds, good correlations have been observed between antioxidant activities and low oxidation potentials (Born et al., 1996). In this work we report on the isolation of antioxidant compounds of *I. juruensis* fruits guided by the β-carotene TLC assay (Pratt and Miller, 1984) and the evaluation of their oxidation potentials through cyclic voltammetry. Further examination of the lipophyllic constituents led to isolation of inactive compounds, which were also investigated electrochemically.

2. Results and discussion

Dried and powdered fruits were extracted with hexane. Fractionation of the crude extract guided by the antioxidant TLC assay afforded **1**, **2** and **6**–**9**. In addition, inactive metabolites **3**, **4** and **5a**–**c** were isolated (see Experimental).

The structural determination of compounds **1** and **2** was based on analysis of their NMR and MS spectra as well as on comparison with literature data for similar

* Corresponding author. Tel.: +55-16-232-2022; fax: +55-16-222-7932.
E-mail address: dhsilva@iq.unesp.br (D.H.S. Silva).

0031-9422/01/$ - see front matter © 2001 Elsevier Science Ltd. All rights reserved.
PII: S0031-9422(00)00477-5

compounds (Vieira et al., 1983a). The ^{1}H NMR spectra of compounds **1** and **2** showed two doublets at δ 5.47±0.02 (*d*, J = 9.7±0.1 Hz) and δ 6.17±0.02 (*d*, J = 9.7±0.1 Hz) assigned to H-3 and H-4, respectively, typical of the chromene ring of C-3 unsaturated tocotrienols, which had only been found previously in brown seaweeds from genera *Sargassum* and *Stypopodium* (Kusumi et al., 1979; Gerwick and Fenical, 1981). The other spectral features are similar to those of C-3 saturated tocotrienols; therefore, ^{1}H and ^{13}C NMR data could be assigned by comparison with δ-tocotrienol and 17-carboxy-δ-tocotrienol, previously isolated from pericarps of *I. lancifolia* and fruits of *I. grandis* (Vieira et al., 1983b; Lopes et al., 1998). Tocotrienol **2** was identified as sargachromenol, originally isolated from *Sargassum serratifolium* (Kusumi et al., 1979). The new tocotrienol **1** differs from **2** by one additional methyl group on the chromene ring (C-7); its only aromatic proton was placed at C-5 after observation of NOE interactions between H-5 and H-4. Further NOE observations, COSY and DEPT as well as ESMS data led to elucidation of **1** as 2,7,8-trimethyl-2-[(*3E,7Z*)-4,12-dimethyl-8-carboxyl-3,7,11-tridecatrienyl]-3-chromen-6-ol for which we propose the name 7-methyl-sargachromenol.

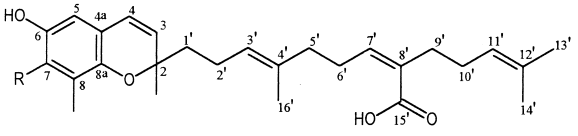

1 R=Me

2 R=H

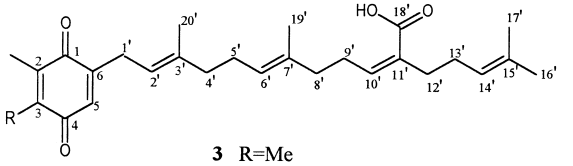

3 R=Me

4 R=H

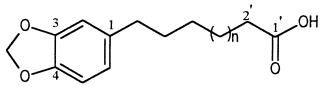

5a n=10

5b n=12

5c n=14

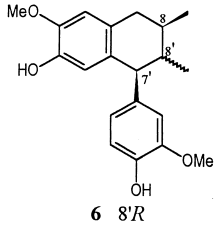

6 8′*R*

7 8′*S*

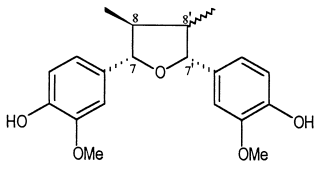

8 8′*S*

9 8′*R*

The ^{13}C NMR spectra of **3** and **4** showed two signals at δ 187.7 ± 0.2 and δ 187.9 ± 0.1 for two ketone groups conjugated to sp^2 carbons, which were assigned, respectively, to C-1 and C-4 of the quinone ring. DEPT 135° experiments indicated the presence of six methyl groups in compound **3** and five methyl groups in **4**. The ^{1}H NMR spectra of **3** and **4** showed one doublet at δ 3.05 (J = 7.1 Hz) integrating for two hydrogens on a sp^3 carbon linked to two sp^2 carbons. The ^{1}H–^{1}H NMR spectrum showed the correlation of this signal with the multiplet centered at δ 5 and the signal at δ 6.39, assigned to H-2′ and H-3, respectively, and confirms the placement of the only quinone ring hydrogen of compound **3** on C-3. The additional methyl group of compound **3** was then placed at C-5. The remaining spectral data were consistent with the proposed structures, including the placement of a carboxyl group on the isoprenic chain, determined through MS data (Fig. 1). The structure of this new quinone, named as 3-methyl-sargaquinoic acid, was established as 2,3-dimethyl-6-[(2*E*,6*E*,10*Z*)-3,7,15-trimethyl-11-carboxyl-2,6,10,14-hexadecatetraenyl]-2,5-cyclohexadiene-1,4-dione. Compound **4**, which was identified as sargaquinoic acid after comparison of its NMR spectrum and MS profile with literature data, was originally isolated from the brown algae *Sargassum serratifolium* (Kusumi et al., 1979) and differs from **3** only concerning the quinone ring substitution pattern. The new compounds **1** and **3** follow the γ-tocotrienol pattern, while the known **2** and **4** follow the δ-tocotrienol substitution pattern.

Compounds **5a–c** were identified as ω-arylalkanoic acids based on a broad singlet at δ 1.18 of a methylene chain and the absence of a terminal methyl group, (ca. δ 0.8, *t*) in the ^{1}H NMR spectrum, associated to the signal at δ 179.4 on the ^{13}C NMR spectrum and the presence of an aromatic ring. The substitution pattern of this ring, linked to the methylene chain, was defined through observation of two doublets at δ 6.61 (J = 1.6 Hz) and δ 6.66 (J = 7.7 Hz) and one doublet of doublets at δ 6.55 (J = 1.6 and 7.7 Hz) in the ^{1}H NMR spectrum. The presence of a methylenedioxy group was inferred through observation of signals at δ 5.85 and δ 100.6 in the ^{1}H and ^{13}C NMR spectra, respectively. The LC–UV–MS analysis of the mixture of **5a–c** evidenced the presence of three substances (R_T 15.0, 16.1 and 17.1 min.), which absorbed at λ_{max} 284 nm. The ESMS analysis indicated a molecular weight of 362, 390 and 418 for compounds **5a–c**, inferred from base peaks at m/z 385, 413 and 441 ($[M+Na]^+$), respectively. The on-line analysis showed additional peaks at 363, 391 and 419 ($[M+1]^+$) which confirmed the length of the methylene chains of these compounds. The ω-arylalkanoic acids **5a–c** result biogenetically from condensation of substituted dihydrocinnamic acid and lauric, myristic and palmitic acids, respectively. As these ω-arylalkanoic acids proved to be new natural products, their isolation was subsequently undertaken. Their EIMS spectra showed base

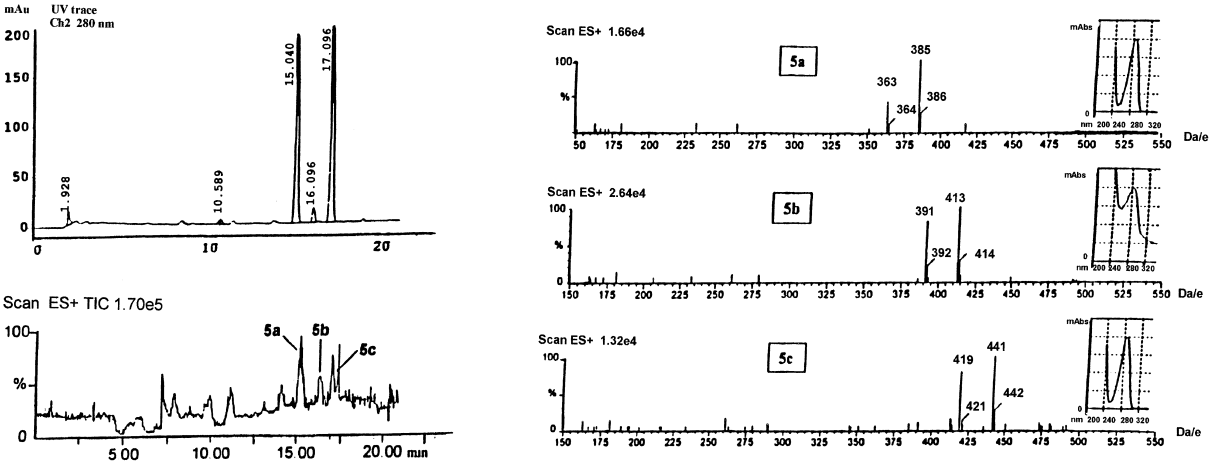

Fig. 1. LC/UV/ESMS analysis of fraction 5 from hexane extract of *Iryanthera grandis* fruits, containing ω-arylalkanoic acids **5a**–**c**.

peaks at m/z 135 $[C_7H_5.CH_2O_2]^+$, which confirmed the proposed structures for these compounds. These ω-arylalkanoic acids had not been isolated from natural sources yet and are probably the biosynthetic precursors of juruenolides, ω-arylalkanoic acids condensed with pyruvic acid followed by γ-lactonization, found in the trunk wood of *Iryanthera juruensis* (Vieira et al., 1983b) and pericarps of *Virola surinamensis* (Lopes et al., 1998).

Lignans **6**–**9** were identified as *epi*-guaiacin, guaiacin, verrucosin and nectandrin B, respectively, from their spectroscopic data and comparison with literature (Majunder et al., 1972; Gottlieb et al., 1976; Joshi et al., 1979; Moro et al., 1987; Ward, 1997).

Antioxidative properties of compounds **1**–**9** were evaluated against β-carotene (Pratt and Miller, 1984). By using β-carotene as a TLC spray reagent, tocotrienols **1** and **2** and lignans **6**–**9** (10 μg) appeared as yellow spots against a white background, meaning these compounds inhibited the bleaching of β-carotene. The same amounts of quinones **3** and **4** and ω-arylalkanoic acids **5a**–**c** were completely inactive.

The evaluation of the redox properties of tocotrienols **1** and **2** was carried out electrochemically in order to compare their voltammetric behaviour and to correlate the corresponding oxidation potentials with antioxidant properties of these compounds (Born et al., 1996). Firstly, the electrochemical behaviour was investigated with α-tocopherol being used as reference compound. In addition, taking into consideration that oxidation products of tocopherols and tocotrienols can be electrochemically reduced, the reduction of the oxidized products of tocotrienols **1** and **2**, previously generated on the electrode surface after oxidation step were also studied and compared to the voltammetric behaviour of plastoquinones **3** and **4**. The cyclic voltammograms of α-tocopherol and tocotrienols **1** and **2** showed oxidation peaks at +0.28, +0.23 and +0.32 V (Table 1) respectively, suggesting a higher antioxidant capacity for tocotrienol **1**, when compared to α-tocopherol. The comparison among oxidation potentials of tocotrienols **1** and **2** and α-tocopherol shows that **1** is the most easily oxidizable compound. Alkyl groups *meta* to the aromatic hydroxyl have little effect on the oxidation ability of phenolic compounds, but inductive effects from either *ortho* or *para* alkyl groups may lower the oxidation potential and make the molecule even easier oxidized than the phenol itself (Marcus and Hawley, 1970). This could explain the lower oxidation potential of **1** when compared to **2**, as they possess the aromatic substitution pattern of γ- and δ-tocotrienol, respectively. The lower oxidation potential of **1** when compared to α-tocopherol might be due to its C-3 double bond, which is conjugated with the aromatic ring and stabilizes the intermediate cation previous to completion of oxidation steps.

The structure–activity relationship indicates, in this case, that the stabilizing effect of the C-3 double bond on the intermediate cation due to the presence of one aromatic methyl group *ortho* to the hydroxyl (e.g. compound

Table 1
Voltammetric parameters for isolates **1**–**9** and reference compound α-tocopherol in TFBTBA/dichloromethane on glass carbon electrode, at $\nu = 50$ mV/s

Substance	$Ep_{oxid.}$ (V)	$Ep_{red.}$ (V)
α-Tocoferol[a]	+0.28	−0.90[a]
1[a]	+0.23	−0.43[a]; −1.00[a]
2[a]	+0.32	−0.38[a]; −0.93[a]
3	–	−0.50; −0.90
4	–	−0.38; −0.88
5a–**c**	+1.51	–
6	+0.80	–
7	+0.81	–
8	+0.81	–
9	+0.81	–

[a] Reduction potentials of the oxidized products of α-tocopherol and tocotrienols **1** and **2**, generated on the electrode surface.

1) overcomes, although slightly, the stabilizing effect of two aromatic methyl groups *ortho* to the hydroxyl, if the C-3 double bond is absent (e.g. α-tocopherol). The contribution of this double bond is, however, not enough to keep up the intermediate cation stability if no methyl group *ortho* to the hydroxyl group is present in the molecule, as in compound **2**. The electrochemical behaviour of quinones **3** and **4** was compared to those of the oxidized products of tocotrienols **1** and **2**, respectively. The great similarity observed for the reduction potentials of these oxidation products and tocotrienols **1** and **2** suggests that the products generated after oxidation of tocotrienols **1** and **2** are structurally closely related to quinones **3** and **4**, respectively.

The high oxidation potential of the ω-arylalkanoic acids **5a**–**c** is probably a result of the lack of aromatic hydroxyl groups in these molecules. The absence of oxidation peak in the cyclic voltammograms of **3** and **4** as well as the high value (+1.52) for **5a**–**c** are in agreement with the inactivity observed on the β-carotene assay for these compounds.

The cyclic voltammograms of lignans **6**–**9** showed oxidation potentials in the range 0.8–0.9 V, suggesting that they should act as rather less effective antioxidants than tocotrienols **1** and **2**. The structure–activity correlations of these results can not be promptly inferred, as electron donor groups *ortho* to a hydroxyl should enhance the stabilization capacity of the molecule after hydrogen radical loss (Rice-Evans et al., 1996). The lower oxidation potential of tocotrienols might nonetheless be explained by the stabilization of the molecule conferred by the C-3 double bond conjugated with the aromatic ring, which might enhance the ease of oxidation of tocotrienols more efficiently than the methoxyl group *ortho* to the hydroxyl group in lignans **6**–**9**. Nevertheless, the qualitative analyses of the antioxidative properties of tocotrienols **1**, **2** and lignans **6**–**9** through the β-carotene assay showed all these compounds were active, as previously referred.

3. Experimental

3.1. General experimental procedures

The UV and IR spectra were recorded on a Perkin-Elmer Lambda 3B and a Perkin-Elmer FT-IR 1750 spectrophotometer, respectively. NMR spectra (^1H, ^{13}C, COSY and NOE experiments) were measured on a Brüker DPX-300 spectrometer (300 MHz for ^1H and 75 MHz for ^{13}C) in $CDCl_3$ for all compounds; the chemical shifts are reported in ppm with TMS as internal standard, and coupling constants (*J*) are given in Hz. EIMS spectra were measured at 70 eV on a HP 5988-A. Elemental analyses were performed on a Perkin-Elmer CHN Elemental Analyzer 2400.

3.2. Plant material

Fruits were collected in Reserva do Mocambo, in the Amazon Forest, in the rainy season and identified as *Iryanthera juruensis* Warburg by Botanist Nelson Rosa. A voucher specimen was deposited at the Herbarium João Murça Pires at Museu Paraense Emílio Goeldi.

3.3. Extraction and isolation

The dried fruits were grounded and extracted with hexane. The extract was dried under reduced pressure and partitioned between hexane and 90% methanol. The hydroalcoholic fraction (7.6 g) was submitted to vacuum column chromatography over silica gel, which was eluted with hexane/EtOAc mixtures of increasing polarity to yielded 8 fractions (A–H). Flash column chromatography over silica gel of fraction B eluted with gradient of hexane/EtOAc afforded **2** (31 mg), **4** (53 mg) and other 13 pooled fractions. Purification of fractions B-5 and B-11 through prep. TLC (hexane/EtOAc 8:2) gave **3** (15 mg) and **1** (12 mg), respectively. Purification of fraction B-8 through prep. TLC (hexane/EtOAc 8:2) gave the mixture of the ω-arylalkanoic acids **5a**–**c**, which was further purified by HPLC (RP-18, MeOH/H_2O 85:15) to afford **5a** (5 mg) and **5c** (6 mg). Compound **5b** was not isolated as the HPLC analysis indicated it was a minor compound (~ 5% of the mixture of **5a**–**c**). Flash column chromatography over silica gel of fraction E eluted with a gradient of hexane/EtOAc gave 6 pooled fractions (A′–F′). Purification of fraction C′ through prep. TLC (hexane/EtOAc 1:1) and HPLC (RP-18, MeOH/H_2O 86:14) gave **6** (8 mg). Partial dissolution of fraction D′ in $CHCl_3$ gave a precipitate which was further washed with MeOH to give **7** (60 mg). Purification of fraction E′ through prep. TLC ($CHCl_3$/MeOH 95:5) and HPLC (RP-18, MeOH/H_2O 78:22) gave **8** (6 mg) and **9** (4 mg).

3.4. LC/UV/MS

The separation of compounds **5a**–**c** was achieved by using MeOH:H_2O in the isocratic mode (85:15, 1 ml/min.). UV spectra were recorded from 200 to 400 nm. For MS, the temperature of the electrospray (ES) source block was set to 75°C. The cone voltage was 70 V and ionization was achieved in the positive mode at an ionization voltage of 4.5 kV. Nitrogen was used as a nebulizing and curtain gas. Nebulizer gas was set to 0.5 l/min, curtain gas to 5.0 l/min. Full-scan spectra from *m*/*z* 150 to 550 were recorded every 1.2 s.

3.5. 2,7,8-Trimethyl-2-[(3E,7Z)-4,12-dimethyl-8-carboxyl-3,7,11-tridecatrienyl]-3-chromen-6-ol (1)

Brown oil. Found: C, 76.62; H, 8.76. $C_{28}H_{38}O_4$ requires: C, 76.71; H, 8.68%. UV λ_{max}^{MeOH} nm (ε): 326 (3800). IR

ν_{max}^{film} cm^{-1}: 3408, 2923, 1686, 1634. ^{1}H NMR (300 MHz, $CDCl_3$): δ 1.27 (3H, *s*, H-7), 1.50 (6H, *s*, H-14′, H-16′), 1.59 (3H, *s*, H-13′), 1.9–2.2 (8H, *m*, H-1′, H-2′, H-5′, H-10′), 2.04 (3H, *s*, H-2), 2.05 (3H, *s*, H-8), 2.2–2.3 (2H, *m*, H-9′), 2.50 (2H, *dd*, J = 14.4, 7.3 Hz, H6′), 5.45 (1H, *d*, J = 9.6 Hz, H-3), 6.14 (1H, *d*, J = 9.6 Hz, H-4), 6.22 (1H, *s*, H-5); ^{13}C NMR (75 MHz, $CDCl_3$): δ 11.5 (*q*, Me-8), 11.9 (*q*, Me-7), 15.7 (*q*, C-16′),17.5 (*q*, C-14′), 22.6 (*t*, C-2′), 25.4 (*q*, Me-2), 25.8 (*q*, C-13′), 27.8 (*t*, C-6′), 28.1 (*t*, C-10′), 34.4 (*t*, C-1′), 39.0 (*t*, C-5′), 40.9 (*t*, C-9′), 77.7 (*s*, C-2), 109.9 (*d*, C-5), 118.7 (*s*, C-4a), 122.8 (*d*, C-4), 123.5 (*d*, C-3′), 123.6 (*s*, C-8), 125.1 (*d*, C-11′), 125.1 (*s*, C-7), 129.6 (*d*, C-3), 130.6 (*s*, C-12′), 132.1 (*s*, C-4′), 134.2 (*s*, C-8′), 144.7 (*s*, C-8a), 144.8 (*d*, C-7′), 146.9 (*s*, C-6), 171.6 (*s*, C-15′). EIMS (70 eV): Scheme 1; additional data: *m*/*z* (rel. int.) 175 [189-Me]$^+$ (20).

3.6. 2,3-Dimethyl-6-[(2E,6E,10Z)-3,7,15-trimethyl-11-carboxyl-2,6,10,14-hexadecatetraenyl]-2,5-cyclohexadiene-1,4-dione (**3**)

Brown oil. Found: C, 76.89; H, 8.66. $C_{28}H_{38}O_4$ requires: C, 76.71; H, 8.68%). UV λ_{max}^{MeOH}.nm (ε): 257 (4400). IR ν_{max}^{film} cm^{-1}: 2923, 1666, 1634. ^{1}H NMR (300 MHz, $CDCl_3$): δ 1.51 (3H, *s*, H-17′), 1.53 (3H, *s*, H-19′), 1.54 (3H, *s*, H-20′), 1.60 (3H, *s*, H-16′), 1.93 (3H, *s*, Me-3), 1.95 (3H, *s*, Me-2), 2.0–2.1 (8H, *m*, H-4′, H-5′, H-8′, H-13′), 2.19 (2H, *t*, J = 6.6 Hz, H-12′), 2.52 (2H, *dd*, J = 14.8, 7.3 Hz, H-9′), 3.05 (2H, *d*, J = 7.1 Hz, H-1′), 4.9-5.1 (2H, *m*, H-6′, H-14′), 5.93 (1H, *t*, J = 7.1 Hz, H-10′), 6.39 (1H, *s*, H-5); ^{13}C NMR (75 MHz, $CDCl_3$): δ 12.0 (*q*, Me-2), 12.4 (*q*, Me-3), 15.9 (*q*, C-20′), 16.1 (*q*, C-19′), 17.7 (*q*, C-17α), 25.6 (*q*, C-16′), 26.3 (*t*, C-1′), 27.4 (*t*, C-5′), 27.9 (*t*, C-9′), 28.2 (*t*, C-13′), 39.0 (*t*, C-8′), 39.6 (*t*, C-12′), 34.5 (*t*, C-4′), 118.2 (*d*, C-2′), 123.5 (*d*, C-6′), 124.6 (*d*, C-14′), 130.6 (*s*, C-15′), 132.0 (*d*, C-5), 134.6 (*s*, C-7′), 134.6 (*s*, C-11′), 139.6 (*s*, C-3′), 140.6 (*s*, C-2), 141.0 (*s*, C-3), 145.5 (*d*, C-10′), 148.0 (*s*, C-6), 172.9 (*s*, C-18′), 187.6 (*s*, C-1), 187.9 (*s*, C-4). EIMS (70 eV): Scheme 1; additional data: *m*/*z* (rel. int.) 379 [M-COOH-Me]$^+$ (1), 175 [189-Me]$^+$ (24).

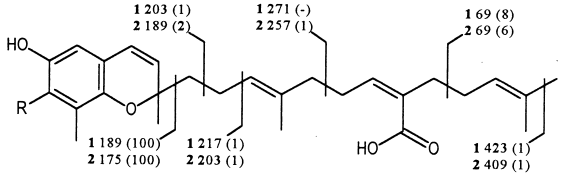

1 R = Me $M^{+\cdot}$ 438 (2)

2 R = H $M^{+\cdot}$ 424 (3)

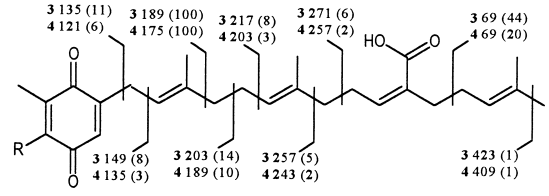

3 R = Me $M^{+\cdot}$ 438 (6)

4 R = H $M^{+\cdot}$ 424 (3)

Scheme 1. EIMS selected fragments of *m*/*z* (rel. int.) for compounds **1**–**4**.

3.7. 15′-(3,4-Methylenedioxyphenyl)-pentadecanoic acid (**5a**)

Colorless oil. Found: C, 72.98; H, 9.69. $C_{22}H_{34}O_4$ requires: C, 72.93; H, 9.39%). UV λ_{max}^{MeOH} nm (ε): 284 (7710). IR ν_{max}^{film} cm^{-1}: 3320, 1721, 1600, 1504. ^{1}H NMR (300 MHz, $CDCl_3$): δ 1.18 (26H, *s*, H-4′- H-16′), 1.50 (2H, *m*, H-3′), 2.28 (2H, *t*, J = 7.6 Hz, H-2′), 2.45 (2H, *t*, J = 7.9 Hz, H-17′), 5.85 (2H, *s*, CH_2O_2), 6.55 (1H, *dd*, J = 1.6, 7.7 Hz, H-6), 6.61 (1H, *d*, J = 1.6 Hz, H-2), 6.66 (1H, *d*, J = 7.7 Hz, H-5). ^{13}C NMR: (75 MHz, $CDCl_3$): δ 179.4 (*s*, C-1′), 33.9 (*t*, C-2′), 24.7 (*t*, C-3′), 28.6–29.0 (*t*, C-4′- C-12′), 29.0 (*t*, C-15′), 31.8 (*t*, C-16′), 35.7 (*t*, C-17′), 136.8 (*s*, C-1), 107.9 (*d*, C-2), 145.3 (*s*, C-3), 147.4 (*s*, C-4′), 108.8 (*d*, C-5′), 120.9 (*d*, C-6′), 100.6 (*t*, CH_2O_2). EIMS (70 eV): *m*/*z* (rel. int.) 362 $[M]^{+\cdot}$ (10); 135 $[C_7H_5.CH_2O_2]^+$ (100). ESMS: *m*/*z* (rel. int.) 385 $[M + Na]^+$ (100), 363 $[M + 1]^+$ (45).

3.8. 17′-(3,4-Methylenedioxyphenyl)-heptadecanoic acid (**5b**)

ESMS: *m*/*z* (rel. int.) 413 $[M + Na]^+$ (100), 391 $[M + 1]^+$ (82).

3.9. 19′-(3,4-Methylenedioxyphenyl)-nonadecanoic acid (**5c**)

Colorless oil. Found: C, 74.39; H, 10.10. $C_{26}H_{42}O_4$ requires: C, 74.64; H, 10.05%. UV λ_{max}^{MeOH} nm (ε): 285 (7710). IR ν_{max}^{film} cm^{-1}: 3328, 1720, 1605,1510. ^{1}H NMR (300 MHz, $CDCl_3$): δ 1.18 (32H, *s*, H-4′- H-20′), 1.50 (2H, *m*, H-3′), 2.28 (2H, *t*, J = 7.6 Hz, H-2′), 2.45 (2H, *t*, J = 7.9 Hz, H-21′), 5.85 (2H, *s*, CH_2O_2), 6.55 (1H, *dd*, J = 1.6, 7.7 Hz, H-6), 6.61 (1H, *d*, J = 1.6 Hz, H-2), 6.66 (1H, *d*, J = 7.7 Hz, H-5). ^{13}C NMR: (75 MHz, $CDCl_3$): δ 179.4 (*s*, C-1′), 33.9 (*t*, C-2′), 24.7 (*t*, C-3′), 28.6–29.0 (*t*, C-4′- C-16′), 29.0 (*t*, C-17′), 31.8 (*t*, C-18′), 35.7 (*t*, C-19′), 136.8 (*s*, C-1), 107.9 (*d*, C-2), 145.3 (*s*, C-3), 147.4 (*s*, C-4), 108.8 (*d*, C-5), 120.9 (*s*, C-6), 100.6 (*t*, CH_2O_2). EIMS (70 eV): *m*/*z* (rel. int.) 135 $[C_7H_5.CH_2O_2]^+$ (29). ESMS *m*/*z* (rel. int.) 441 $[M + Na]^+$ (100), 419 $[M + 1]^+$ (78).

3.10. Bleaching experiment on β-carotene

The test was carried out on TLC plates. After developing and drying, plates were sprayed with a 0.02% solution of β-carotene (Aldrich) in CH_2Cl_2. Plates were

placed under natural light until discoloration of background. The yellow spots remaining indicated the presence of antioxidant substances.

3.11. Electrochemical assay

The cyclic voltammograms were carried out with a Polarecord E-506 (Metrohm) potentiostat. A three electrode system (663 VA, Metrohm) with a working electrode of glassy carbon (GC), a Ag/AgCl reference electrode and a carbon auxiliary electrode was used. Dichoromethane (Merck) was used as solvent and tetra-*n*-butyl ammonium tetrafluorborate (Merck), as the supporting electrolyte. Vitamin E (Aldrich) was used as reference compound. The working electrode was polished with aluminium oxide 0.3 μm (Buehler) and special polishing cloth (Buehler) prior to each measurement, because formation of a polymeric film inactivated the electrode after each scan. The electrode was then washed thoroughly with water, dried and cycled several times in the range −1.6 to +0.6 V in order to reassure the absence of voltammetric signal due to the supporting electrolyte. Each compound was dissolved to concentrations of 10–20 mM in dichloromethane and added to a 15 ml aliquot of the supporting electrolyte. The solns. were then deoxygenated with nitrogen for 10 min. and the cyclic voltammograms were carried out at scan rate of 50 mV/s.

Acknowledgements

The authors thank to FAPESP, FUNDUNESP, CNPq and CAPES for financial support.

References

Azzi, A., Boscoboinik, D.O., Chatelain, E., 1992. Modulation of cell proliferation by tocopherols and tocotrienols: role in arteriosclerosis. In: Ong, A.S.H., Parker, L. (Eds.), Lipid-soluble Antioxidants: Biochemistry and Clinical Applications. Birkhaeuser, Basel, pp. 123–133.

Barros, S.M.B., Ishii, I., Silva, D.H.S., Yoshida, M., 1993. Antioxidant properties of tocotrienols isolated from *Iryanthera grandis*. In: IV International Symposium on Orthomolecular Medicine, São Paulo, p. 34.

Born, M., Carrupt, P.-A., Zini, R., Brée, F., Tillemnt, J.-P., Hostettman, K., Testa, B., 1996. Electrochemical behaviour and antioxidant activity of some natural polyphenols. Helvetica Chimica Acta 79, 1147–1158.

Gerwick, W.H., Fenical, W., 1981. Ichthyotoxic and cytotoxic metabolites of the tropical brown alga *Stypopodium zonale* (Lamouroux) Papenfuss. Journal of Organic Chemistry 46, 22–27.

Gordon, M.H., 1996. Dietary antioxidants in disease prevention. Nat. Prod. Rep. 13, 265–273.

Gottlieb, O.R., Maia, J.G.S., Ribeiro, M.N.deS., 1976. Neolignans from *Virola carinata*. Phytochemistry 15, 773–774.

Joshi, B.S., Viswanatha, N., Balakrishnan, V., Gawad, D.H., Ravindranath, K.R., 1979. Attenuol — structure, stereochemistry and synthesis. Tetrahedron 35, 1665–1671.

Komiyama, K., Hayashi, M., Cha, S., Yamaoka, M., 1992. Antitumour and antioxidant activity of tocotrienols. In: Ong, A.S.H., Parker, L. (Eds.), Lipid-soluble Antioxidants: Biochemistry and Clinical Applications. Birkhaeuser, Basel, pp. 152–159.

Kusumi, T., Shibata, Y., Ishitsuka, M., Kinoshita, T., Kakisawa, H., 1979. Structures of new plastoquinones from the brown alga *Sargassum serratifolium*. Chemistry Letters 277-278, .

Lopes, N.P., Silva, D.H.S., Kato, M.J., Yoshida, M., 1998. Butanolides as a common feature of *Iryanthera lancifolia* and *Virola surinamensis*. Phytochemistry 49, 1405–1410.

Majunder, P.L., Chaterjee, A., Sengupta, G.C., 1972. Lignans from *Machilus edulis*. Phytochemistry 11, 811–814.

Marcus, M.F., Hawley, M.D., 1970. Eletrochemical studies of the redox behavior of α-tocopherol. Biochimica et Biophysica Acta 201, 1–8.

Moro, J.C., Fernandes, J.B., Vieira, P.C., Yoshida, M., Gottlieb, O.R., Gottlieb, H.E., 1987. Neolignans from *Nectandra puberula*. Phytochemistry 26, 269–272.

Pratt, D.E., Miller, E.E., 1984. A flavonoid antioxidant in Spanish peanuts (*Arachia hypogea*). Journal of the American Oil Chemists Society 61, 1064–1067.

Rice-Evans, C.A., Miller, N.J., Paganga, G., 1996. Structure-antioxidant activity relationships of flavonoids and phenolic acids. Free Radical Biology and Medicine 20, 933–956.

Schultes, R.E., Holmstedt, B., 1971. Miscellaneous notes on Myristicaceous plants of South America. Lloydia 34, 61–78.

Silva, D.H.S., Davino, S.C., Barros, S.M.B., Yoshida, M., 1999. Antioxidant activity of flavonolignoids from *Iryanthera lancifolia*. Journal of Natural Products 62 (11), 1475–1478.

Vieira, P.C., Gottlieb, O.R., Gottlieb, H.E., 1983a. Tocotrienols from *Iryanthera grandis*. Phytochemistry 22, 2281–2286.

Vieira, P.C., Yoshida, M., Gottlieb, O.R., Paulino Filho, H., Nagem, T.J., Braz-Filho, R., 1983b. γ-Lactones from *Iryanthera* species. Phytochemistry 22, 711–713.

Ward, R.S., 1997. Lignans, neolignans and related compounds. Nat. Prod. Rep. 14, 43–74.

PERGAMON

Phytochemistry 57 (2001) 443–457

PHYTOCHEMISTRY

www.elsevier.com/locate/phytochem

Volatile constituents in mosses (Musci)

Yücel Saritas[a], Mesmin Mekem Sonwa[a], Hassan Iznaguen[a], Wilfried A. König[a,*], Hermann Muhle[b], Rüdiger Mues[c]

[a]*Institut für Organische Chemie, Universität Hamburg, Martin-Luther-King-Platz 6, D-20146 Hamburg, Germany*
[b]*Abteilung Systematische Botanik und Ökologie, Universität Ulm, D-89091 Ulm, Germany*
[c]*Fachrichtung 8.1 Botanik, Universität des Saarlandes, D-66041 Saarbrücken, Germany*

Received 13 December 2000; received in revised form 8 February 2001

Abstract

The essential oils of mosses of the genera *Mnium, Plagiomnium*, *Homalia, Plagiothecium* and *Taxiphyllum* (Musci) have been investigated by gas chromatography and mass spectrometry. The new sesquiterpenes (+)-10-*epi*-muurola-4,11-diene and 10,11-dihydro-α-cuparenone were isolated by preparative gas chromatography and identified as major constituents of the hydrodistillation products of *Mnium hornum* (Hedw.) using NMR and mass spectrometry. In addition, (+)-dauca-8,11-diene and two new butenolides, 3,4,5-trimethyl-5-pentyl-5*H*-furan-2-one and 3,4-dimethyl-5-pentyl-5*H*-furan-2-one were identified as constituents in *Plagiomnium undulatum* (Hedw.) T. Kop. Although the amounts of volatiles present in the investigated mosses are generally smaller than in liverworts, the spectrum of terpenoid compounds is similar. The investigated mosses also generate aliphatic compounds of greater abundance and structural variety. © 2001 Elsevier Science Ltd. All rights reserved.

Keywords: *Mnium hornum*; *Plagiomnium undulatum*; Musci; Terpenoid compounds; Butenolides; Sesquiterpene hydrocarbons; 10-*epi*-Muurola-4, 11-diene; Dauca-8, 11-diene; 10, 11-Dihydro-α-cuparenone

1. Introduction

The chemistry of liverworts (Hepaticae) has been subject to intensive investigations over the last decades mainly because of the abundance of terpenoid and aromatic compounds in this plant family (Asakawa, 1995; Mues, 2000). Much less interest was devoted to the mosses (Musci) which are represented by approximately 10,000 species worldwide and which differ by the lack of oil bodies which are common in the cells of most liverworts. On the contrary, most review articles on the chemistry of bryophytes (Huneck, 1983; Zinsmeister et al., 1991; Asakawa, 1995; Mues, 2000) emphasized the absence or only scattered occurrence of terpenoid compounds, particularly of sesquiterpenes, in mosses. The first proof of the presence of a sesquiterpene hydrocarbon, *ent*-β-cedrene, together with a diterpene alcohol, dolabella-3,7-dien-18-ol, in a Japanese moss was reported by Toyota et al. (1998). After submission of this paper we became aware of a recent publication (Suire et al., 2000) reporting on the chemical constituents of 13 moss species, including some of the *Mnium* and *Plagiomnium* family. Among other compounds the occurrence of several sesquiterpenes and higher terpenoid constituents was described. A kaurane type diterpene alcohol was identified in *Saelania glaucescens* (Nilsson and Mårtensson, 1971).

Led by the observation that some mosses generate a distinct, sometimes pleasant, odour in the fresh state we have collected the volatile constituents of mosses by hydrodistillation of fresh or air-dried plant material and analyzed them by gas chromatography–mass spectrometry (GC–MS) and by comparison of the mass spectra and retention indices with a spectral library which was established under standardized experimental conditions (Joulain and König, 1998). Some unknown compounds were isolated by preparative GC and investigated by 1- and 2-dimensional NMR techniques. In some cases absolute configurations were determined by chemical correlations with known compounds and by enantioselective GC with cyclodextrin stationary phases. Although numerous mosses were investigated, only the results of a few selected

* Corresponding author. Tel.: +49-40-42838-2824; fax: +49-40-42838-2893.
E-mail address: wkoenig@chemie.uni-hamburg.de (W.A. König).

0031-9422/01/$ - see front matter © 2001 Elsevier Science Ltd. All rights reserved.
PII: S0031-9422(01)00069-3

species are discussed in this report on the terpenoid chemistry of Musci.

2. Results and discussion

The plant material was collected at different locations in Europe all over the year. No large variations in the pattern of constituents according to seasonal or local changes were observed. Before hydrodistillation the plant material was carefully inspected for contaminations. Conifer needles, other plant material and soil were completely removed. The possibility of contamination was also reduced by investigating the same plant growing in different locations and plant communities. The volatiles of most mosses were abundant in aliphatic and aromatic aldehydes (*n*-heptanal, *n*-nonanal, *E,E*-2,4-decadienal, benzaldehyde, phenylacetaldehyde), aliphatic alcohols (*n*-octanol, 1-octen-3-ol, etc.) and acids (C-12–C-18, saturated, mono- and di-unsaturated, arachidonic acid). It can be assumed that *E,E*-2,4-decadienal is a metabolite formed by oxidation of linolic acid (Spiteller and Spiteller, 2000), an abundant constituent in many of the investigated mosses. Another aliphatic compound, heneicosa-6,9,12,15-tetraene, which was described as a constituent of the moss *Polytrichum commune* before (Karunen, 1974), was also present in most samples. In addition, a great variety of terpenoid compounds was detected. Some of them could be readily identified by their characteristic mass spectra and seem to be almost ubiquitous in mosses such as β-cyclocitral (**1**), α- (**2**) and β-ionone (**3**) and geosmin (**4**) (Fig. 1). **1** was before reported as a constituent of the genus *Microcystis* (Cyanobacteria) (Jüttner, 1976), while **4** was observed in the cyanobacteria *Symploca muscorum* (Safferman et al., 1967) and *Oscillatoria tenuis* (Medsker et al., 1968). Very common constituents of the essential oils of musci are furthermore the monoterpene hydrocarbons α- and β-pinene, camphene, sabinene, myrcene, limonene, *p*-cymene, α-terpinene and γ-terpinene as well as camphor, borneol, bornylacetate, terpinen-4-ol, α-terpineol and α-terpinylacetate. Occasionally also Δ-3-carene (in *Plagiomnium undulatum* and *Plagiothecium undulatum*), *trans*-pinocarveol (in *Homalia trichomanoides*), pinocarvone (in *Plagiomnium undulatum*), myrtenal and carvone (in *Plagiothecium undulatum*) and myrtenol (in *H. trichomanoides*) were detected.

Surprising was the high abundance and variability of sesquiterpene hydrocarbons, which could be identified by comparison of their mass spectra and retention indices with a data bank (Joulain and König, 1998). Particularly β-barbatene (**5**) is a common constituent of mosses and was found in all investigated species. Table 1 lists the identified compounds in mosses. Many of these compounds have also been found previously as constituents of liverworts. Thus, 4,8a-dimethyl-1,2,3,4,6,7,8,8a-octalin (**6**) (Wu et al., 1991; Rieck et al., 1995), (+)-(4*S*,4a*S*,5*R*,8a*S*)-4a,5-epoxydecalin (**7**) (Rieck et al., 1995), 10,11-dihydro-α-cuparenone (**8**) (Mekem Sonwa et al., in preparation) and α-cuparenone (**9**) (Benesova, 1976), found before in *Lophocolea bidentata*, were now identified in *Plagiothecium undulatum* and *M. hornum,* respectively. A sesquiterpene, peculiaroxide (**10**), which was earlier identified in the Taiwanese liverwort *Plagiochila peculiaris* (Wu et al., 1993), was detected in *H. trichomanoides*. In the same species the sesquiterpene hydrocarbons pentalenene (**11**) and maali-1,3-diene (**12**), which were earlier found as constituents of the liverworts *Porella obtusata* (Joulain and König, 1998; Fricke, 1999) and *Calypogeia muelleriana*, respectively (Warmers et al., 1999), and the sesquiterpene spirolactone fukinanolide (bakkenolide A) (**13**), earlier identified as a constituent of *Petasites japonicus* (Abe and Onoda, 1968) and *P. albus* (Brunke et al., 1992), were identified. Remarkable is also the occurrence of maalin-5-ol (**14**) in *Mnium marginatum* and *M. stellare*, which was already identified as a constituent of *Plagiochila ovalifolia* (Matsuo et al., 1979), and mintsulfide (**15**) (Yoshida et al., 1979) in *M. marginatum*. As also shown in Table 1, the sesquiterpene alcohols α-cadinol and T-cadinol are common, while diterpenes as 16-kaurene, rosa-5,15-diene, 8(14), 15-isopimaradiene and manool were occasionally present in the investigated species.

Some mosses predominantly generate one specific sesquiterpene hydrocarbon. This is apparent in *M. hornum*, which produces relatively large amounts of (+)-10-*epi*-muurola-4,11-diene (**16**) (Fig. 2). The epimer (−)-muurola-4,11-diene (**17**) was recently described as a constituent of the essential oil of *Amyris balsamifera* (König et al., 1999). The NMR data of both compounds are listed in Table 2. (−)-β-Caryophyllene is a major constituent of *Mnium spinulosum* and (+)-dauca-8,11-diene (**18**) is the main constituent of the essential oil of *Plagiomnium undulatum* (Fig. 3). (−)-Amorpha-4,11-diene (**19**), which was found before as a constituent of *Viguiera oblongifolia* (erroneously named cadina-4,11-diene) (Bohlmann et al., 1984) and *Artemisia annua*, where it functions as an intermediate in artemisinin biosynthesis (Bouwmeester et al., 1999) and the unusual (−)-enantiomer of β-cedrene are also present in *Plagiomnium undulatum* as minor constituents. All these identifications are based on comparisons of mass spectra (Joulain and König, 1998) in connection with retention indices on different polysiloxane and cyclodextrin derived chiral stationary phases with reference compounds of known absolute configuration and, in the case of new compounds, by NMR investigations after micro-preparative isolation.

Finally, the structures of two new butenolides, 3,4,5-trimethyl-5-pentyl-5*H*-furan-2-one (**22**) and 3,4-dimethyl-5-pentyl-5*H*-furan-2-one (**23**), could be elaborated by mass spectrometric and NMR spectroscopic investigations.

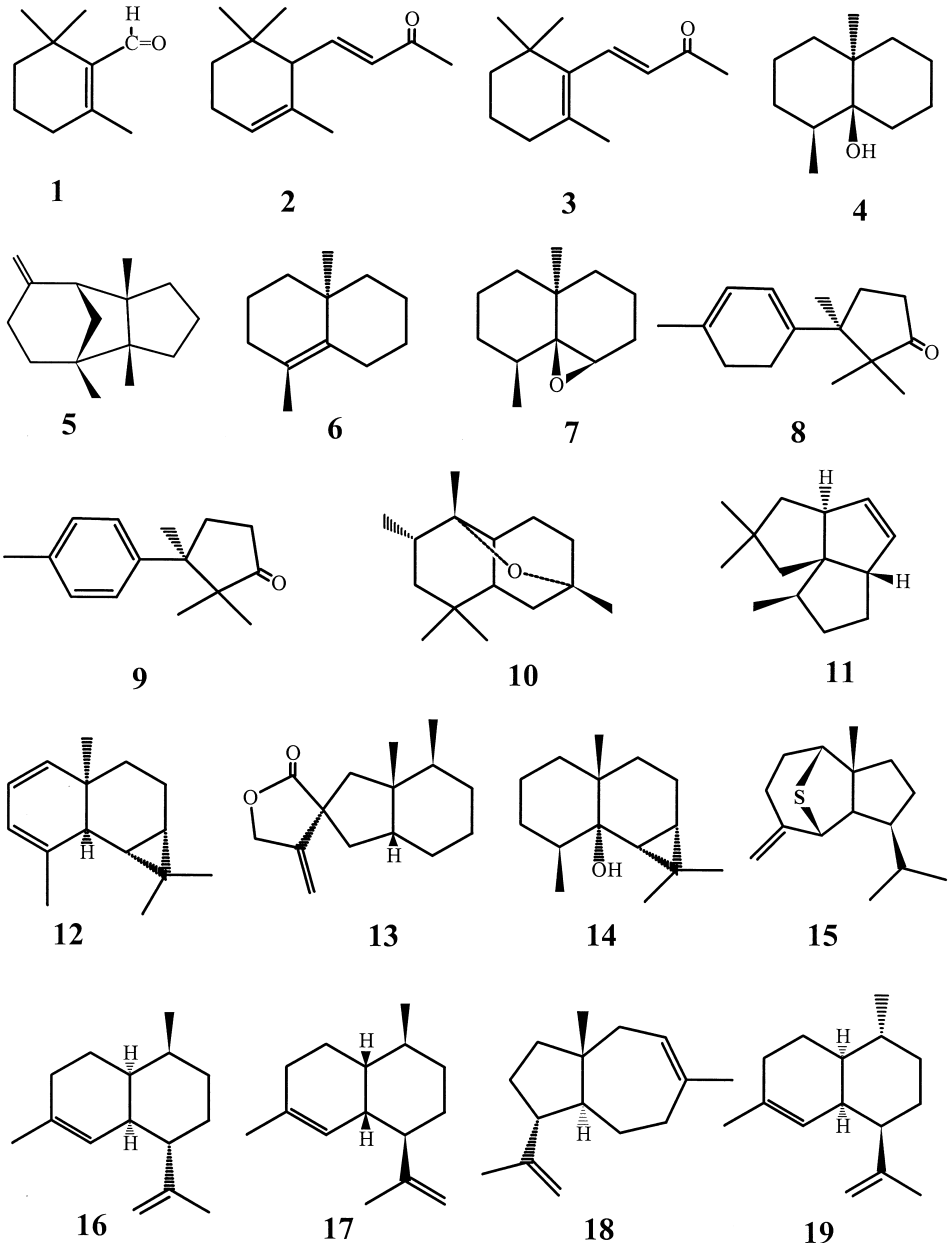

Fig. 1. Structures identified as constituents of mosses.

Hydrocarbon **16**, the main sesquiterpene constituent of *M. hornum*, was isolated by preparative GC and gave a molecular ion signal at *m/z* 204 corresponding to the elemental composition of $C_{15}H_{24}$. It is not distinguishable from muurola-4,11-diene (**17**) by capillary gas chromatography on several polysiloxane and cyclodextrin derived chiral stationary phases with only one exception [octakis(2,6-di-*O*-methyl-3-*O*-pentyl)-β-cyclodextrin]. Moreover, the mass spectra are absolutely identical. In this case the epimers **16** and **17** could only be discriminated by NMR.

The ^{13}C NMR spectrum (Table 2) showed signals of 15 carbon atoms, four of which absorbed in the olefinic region at δ 148.6, 133.2, 126.0 and 110.9 corresponding to two double bonds and a bicyclic structure. Inspection of the ^{1}H NMR data (Table 2) confirmed the presence of an exocyclic olefinic methylene group by a broad singlet at δ 4.87 and a multiplet at δ 4.86, corresponding to 2 protons. One additional olefinic proton absorbs at δ 5.57. In the absorption range of methyl groups 2 singlets are found at δ 1.63 and 1.69 indicating bonding of the methyl groups to olefinic double bonds. An additional methyl doublet is found at δ 0.91. From the DEPT spectrum the presence of 3 primary, 5 secondary, 5 tertiary and 2 quaternary carbons can be concluded. The ^{1}H- and ^{13}C data of **16** and **17** show only small differences (Table 2). More detailed structural information with respect to coupling correlations can be derived from the

Table 1
Compounds identified in Musci

Compound	Species						
	Homal. trich	*M. hornum*	*M. marginat.*	*M. stellare*	*Plagiom. und.*	*Plagioth. und.*	*Taxiph. wisgr.*
2-Heptanone	+						
n-Heptanal	+	+	+	+	+	+	+
Benzaldehyde	+		+				+
α-Pinene	+	+	+		+	+	
Camphene	+	+	+		+	+	
3-Octanone	+		+	+	+		+
β-Pinene	+				+	+	
2-Pentylfuran					+		
3-Octanol				+			
Myrcene						+	
Phenylacetaldehyde	+			+			
Δ-3-Carene					+	+	
Limonene	+	+	+		+	+	
E-2-Octenal	+				+		+
1-Octen-3-ol					+		+
1-Octanol					+		
2-Nonanone						+	
n-Nonanal	+		+	+	+		
trans-Pinocarveol	+						
E-2-Nonenal						+	
m-Dimethoxybenzene	+			+			
n-Nonanol				+			+
Pinocarvone					+		
Camphor	+	+				+	
Borneol	+				+		
Terpinen-4-ol	+						
Myrtenal						+	
Myrtenol	+						
n-Decanal			+				
E,E-2,4-Nonadienal						+	
α-Terpineol							+
β-Cyclocitral	+	+		+	+	+	+
Carvone						+	
4,8a-Dimethyloctalin						+	
Bornylacetate	+	+	+		+	+	
2E,4E-Decadienal	+	+			+	+	+
Pentalenene	+						
α-Terpinylacetate		+			+	+	
Maali-1,3-diene	+		+				
Epoxydecalin		+				+	
1-*epi*-α-Pinguisene			+				
α-Longipinene						+	
Anastreptene	+		+				
α-Copaene	+	+	+	+			
Longicyclene						+	
β-Bourbonene						+	
β-Funebrene			+				
Geosmin	+	+	+		+		
Sativene						+	
α-Ionone	+						
β-Longipinene						+	
Longifolene	+	+				+	
α-Barbatene	+		+				
Peculiaroxide	+						
α-Cedrene	+	+				+	
β-Caryophyllene						+	+
Aristolene	+		+				
β-Cedrene			+		+		
γ-Maaliene			+				
trans-α-Bergamotene	+					+	

(*continued on next page*)

Table 1 (*continued*)

Compound	Species						
	Homal. trich	*M. hornum*	*M. marginat.*	*M. stellare*	*Plagiom. und.*	*Plagioth. und.*	*Taxiph. wisgr.*
Aromadendrene	+						
epi-β-Santalene	+						
Isobazzanene			+				
Sesquisabinene						+	
β-Barbatene	+	+	+	+		+	+
E-β-Farnesene	+						
α-Humulene	+		+	+		+	+
10-*epi*-Muurola-4,11-diene		+					
β-Santalene	+						
β-Acoradiene	+		+	+			+
Amphora-4,11-diene					+		
β-Ionone	+				+	+	
ar-Curcumene		+				+	
γ-Curcumene		+					
γ-Muurolene						+	
β-Chamigrene				+			+
Z,E-α-Farnesene							+
Germacrene D	+		+			+	
β-Selinene		+					
α-Selinene		+					
α-Muurolene						+	
Bicyclogermacrene	+		+	+			+
α-Cuprenene				+			
Cuparene			+	+			
2-Tridecanone	+						
β-Bisabolene			+	+	+		+
α-Chamigrene			+				
β-Curcumene		+				+	
Z-γ-Bisabolene							
γ-Cadinene	+					+	
cis/*trans*-Calamenen	+					+	
δ-Cadinene		+					
β-Sesquiphellandrene	+				+	+	
β-Bazzanene		+		+			+
α-Cadinene				+			+
Zonarene	+						
γ-Cuprene		+					
trans-α-Bisabolene		+	+			+	
α-Calacorene		+					
δ-Cuprenene	+						
Deoxopinguisone		+					+
Palustrol			+				
Germacrene-D-4-ol			+				
1-*epi*-Cubenol	+				+		
Maalian-5-ol		+					
T-Cadinol			+	+			
α-Cadinol	+	+	+		+		
3-Methoxybibenzyl	+	+	+		+	+	
Mintsulfide	+						
α-Cuparenone			+				
10,11-Dihydro-α-cuparenone		+					
Fukinanolide		+					
Isopimara-8(14),15-diene	+						
Diplophyllolide			+				
Heneicosa-6,9,12,15-tetraene	+		+				
Abietatriene	+	+			+	+	
16-Kaurene	+						
Manool			+		+		
Arachidonic acid	+					+	

Table 2
^1H and ^{13}C NMR spectral data of the compounds **16** and **17** in C_6D_6

16			**17**				**16**	**17**
δ (ppm)	Protons	J (Hz)	δ (ppm)	Protons	J (Hz)	^{13}C	δ (ppm)	δ (ppm)
0.91	Me-15	*d*, 3H, (6.9)	1.00	Me-15	*d*, 3H, (7.2)	C-1	38.8 (*d*)	39.4 (*d*)
1.08–1.19	H-8	*m*, 1H	1.23–1.31	H-5, H-9	*m*, 2H	C-2	17.6 (*t*)	26.0 (*t*)
1.24–1.36	H-8, H-9	*m*, 2H	1.34–1.42	H-8	*m*, 1H	C-3	31.7 (*t*)	30.8 (*t*)
1.36–1.52	H-10, H-2	*m*, 2H	1.49–1.57	H-1	*m*, 1H	C-4	133.2 (*s*)	133.2 (*s*)
1.52–1.65	H-2, H-9	*m*, 2H	1.57–1.61	H-8, H-9, H-10	*m*, 3H	C-5	126.0 (*d*)	126.2 (*d*)
1.65–1.71	H-1	*m*, 1H				C-6	40.5 (*d*)	34.9 (*d*)
1.63	Me-14	*s*, 3H	1.63	Me-14	*s*, 3H	C-7	48.4 (*d*)	48.6 (*d*)
1.69	Me-13	*s*, 3H	1.68	Me-13	*s*, 3H	C-8	29.7 (*t*)	26.5 (*t*)
1.86–1.92	H-3	*m*, 2H	1.77–1.95	H-2, 2H-3	*m*, 3H	C-9	33.3 (*t*)	28.8 (*t*)
1.94–2.01	H-6	*m*, 1H	2.06	H-7	*m*, 1H	C-10	35.6 (*d*)	33.3 (*d*)
2.05	H-7	*m*, 1H	2.28–2.34	H-6	*m*, 1H	C-11	148.6 (*s*)	148.5 (*s*)
4.86	H-12	*m*, 1H	4.88	2H-12	*m*, 2H	C-12	110.9 (*t*)	110.9 (*t*)
4.87	H-12	*br. s*, 1H				C-13	19.9 (*q*)	20.4 (*q*)
5.57	H-5	*m*, 1H	5.48	H-5	*m*, 1H	C-14	23.8 (*q*)	23.8 (*q*)
						C-15	19.8 (*q*)	19.6 (*q*)

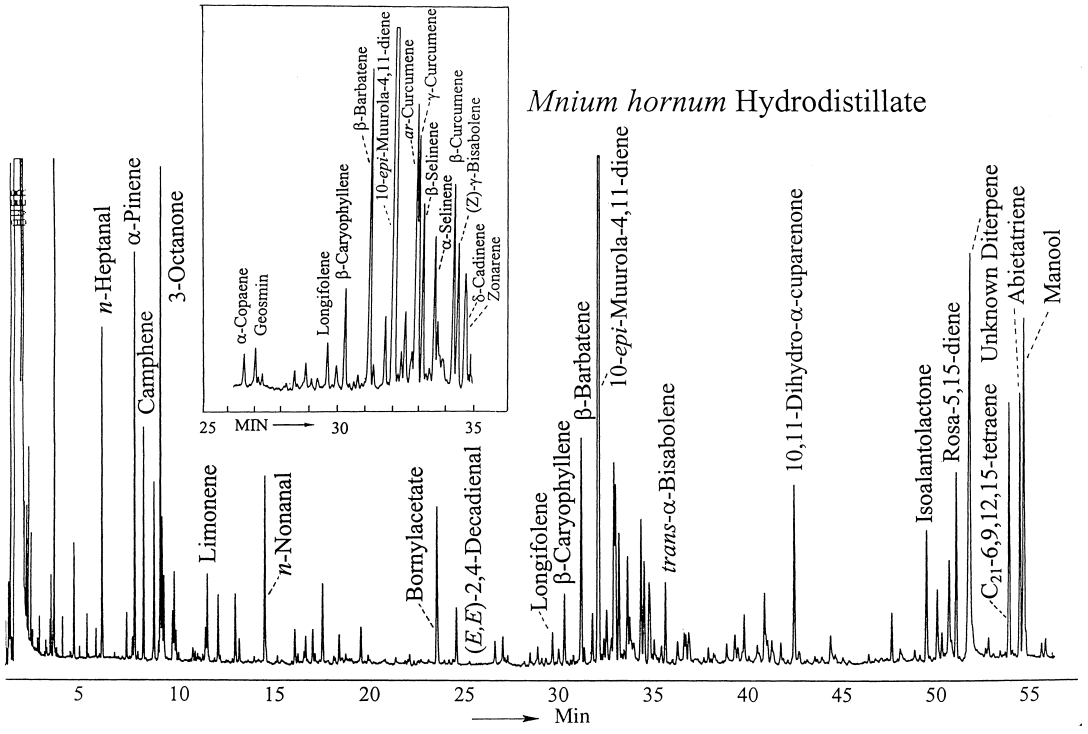

Fig. 2. Gas chromatogram of the hydrodistillate of *Mnium hornum*. 25 m Fused silica capillary column, CPSil 5, column temp. 50°C, temp. progr. 3°C/min to 230°C.

two-dimensional NMR spectra. ^1H–^{13}C-COSY, HMQC and ^1H–^1H-COSY allow the assignment of partial structures A, B and C (Fig. 4). Information about the connection of the partial structures is obtained from the HMBC correlations as shown in Fig. 5. With all these informations a bicyclic sesquiterpene of the type 1,2,3,4,4a,5,6,8a-octahydro-4,7-dimethyl-1-(methylethenyl)-naphthalin (D in Fig. 4) can be derived. The relative configuration, particularly the presence of a *cis*-fused ring system of **16**, was derived from a NOESY spectrum. NOE correlations were observed between the C-14 methyl protons and the protons at C-1 and C-6 (Fig. 5). The absolute configuration was deduced by a chemical correlation with both enantiomers of γ-muurolene with an excess of the (−)-enantiomer (Fig. 6) after partial hydrogenation of the exocyclic double bonds of the γ-muurolene enantiomers and **16**, in correspondence to a published procedure (König et al., 1999).

The molecular formula of 10,11-dihydro-α-cuparenone (**8**) was calculated as $C_{15}H_{22}O$ by mass spectrometry

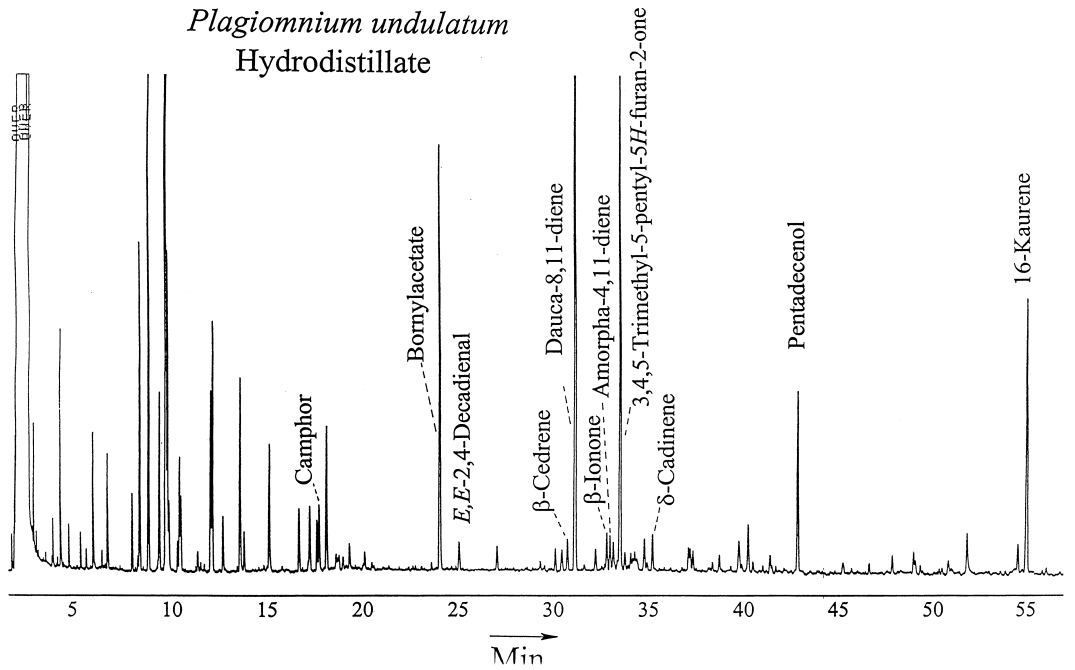

Fig. 3. Gas chromatogram of the hydrodistillate of *Plagiomnium undulatum*. 25 m Fused silica capillary column, CPSil 5, column temp. 50°C, temp. progr. 3°C/min to 230°C.

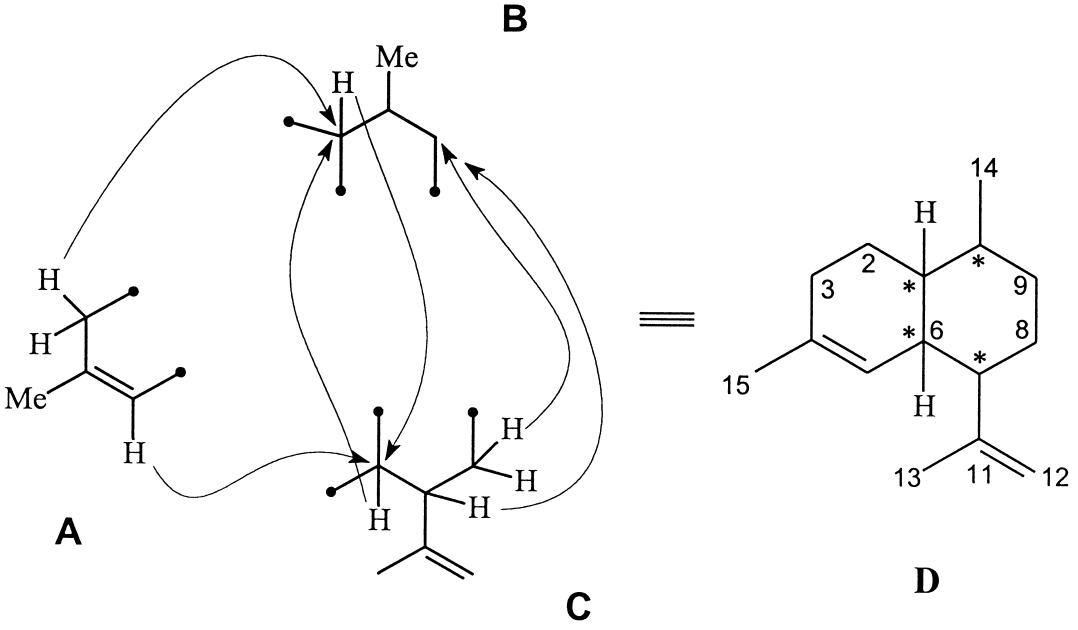

Fig. 4. Partial structures and HMBC correlations for 10-*epi*-muurola-4,11-diene (**16**).

([M]$^+$ = 218). The ^{13}C NMR and DEPT spectra of the compound showed 15 carbon atoms with four methyl groups, two methylene groups, two olefinic methine carbons, four quaternary carbon atoms, two being olefinic, and one carbonyl carbon. The two methyl groups CH_3-14 (δ 0.72) and CH_3-15 (δ 1.07) show strong coupling correlations to each other in the ^{1}H–^{1}H COSY spectrum which are indicative of geminal methyl groups. This assumption is confirmed by the HMBC diagram of the compound: protons of the methyl group CH_3-14 show long-range correlation to the quaternary carbons C-1 and C-5, the carbonyl carbon C-2 and carbon C-15 while the protons of the methyl group CH_3-15 show connectivities to the carbons C-1, C-5, C-2 and C-14 leading to the partial structure C–C$(CH_3)_2$–CO–. The methyl group CH_3-13 (δ 0.75) has a long-range coupling correlation (W coupling) with the proton $H_{8\alpha}$ (δ 1.86) which also couples with the proton $H_{8\beta}$ (δ 1.25). These

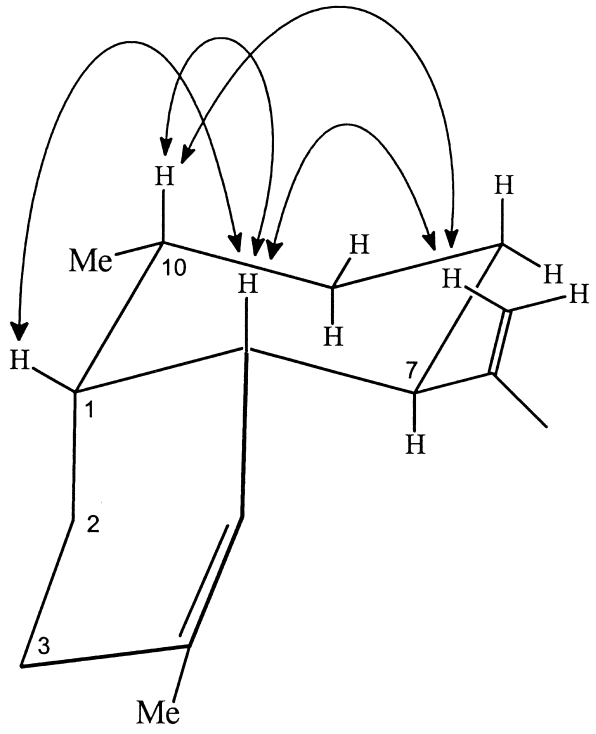

Fig. 5. NOE correlations for 10-*epi*-muurola-4,11-diene (**16**).

two protons couple further with the C-3 methylene-group (δ 1.98; δ 2.08) to give the substructure CH_3–C–CH_2–CH2–. In the HMBC spectrum protons of CH_2-4 are long-range correlated to carbons C-3, C-2, C-5, C-1 and C-13. Those of CH_2-3 show correlations to carbons C-4, C-2, C-1 and C-5 while protons of the methyl group CH_3-13 are correlated to C-4, C-1, C-5 and C-6. All these informations give the partial structure consisting of the five membered ring A (Fig. 6). The methylene group CH_2-11 (δ 2.50; δ 2.58) couples with the methylene group CH_2-10 (δ 2.51; δ 2.50) leading to the partial structure CH_2–CH_2. The two olefinic methine protons CH-8 (δ 5.37) and CH-7 (δ 5.36) couple to each other resulting in substructure C=CH–CH=C. In the HMBC spectrum the methyl group CH_3–12 is long-range correleted to carbons C-10, C-9, C-8. Methylene group CH_2-11 shows connectivities to carbons C-6, C-10, C-9 C-7 and C-5. The observed correlations can be rationalized to form a six-membered ring B (Fig. 7) and allow the assumption of a cuparane skeleton and the structure of 10,11-dihydro-α-cuparenone (**8**) for the molecule. The 8,11-dihydro-isomer of **8** is a constituent of the liverwort *Reboulia hemisphaerica* and was described by Morais et al. (1988).

The main sesquiterpene hydrocarbon (**18**) of the hydrodistillate of *Plagiomnium undulatum* showed the elemental composition of $C_{15}H_{24}$ ($M^+ = 204$) and was isolated by preparative GC. From the ^{1}H NMR, ^{1}H–^{1}H COSY, HMBC and HMQC data a daucane skeleton with 2 olefinic double bonds in positions 8 and 11 was identified. The ^{1}H NMR spectrum of **18** (Table 3) contains one quaternary methyl group (δ 0.90, *s*), two olefinic methyl groups (δ 1.73, *s*, and 1.84, *br. s*), two methylene protons of an exocyclic olefinic double bond (δ 4.92, *br. s*, and 4.94, *m*) and an olefinic proton (δ 5.58, *m*). The ^{13}C NMR and DEPT spectra showed 15 carbon signals: three methyl (δ 18.7, 19.2, 27.7), six methylene (δ 24.4, 27.1, 34.7, 41.3, 41.7, 111.3), three methine (δ 52.3, 57.4, 123.4) and three quaternary carbons (δ 42.4, 139.7, 147.9). The inspection of the ^{1}H–^{1}H COSY and HMQC spectra allowed to derive partial structures **A–C**. The connection of these partial structures was deduced from the HMBC spectrum (Fig. 8). The combination of the total NMR information allowed to assign the structure of dauca-8,11-diene to compound **18**.

The NOESY spectrum clearly indicated a strong correlation signal between H-4 and the CH_3-15 protons, indicating a *trans* correlation of methyl group C-15 and the isopropenyl group in position 4. The reported literature data for dauca-8,11-diene are quite intriguing. In the ^{13}C NMR spectrum of our compound **18** signals

Table 3
^{1}H and ^{13}C NMR spectral data of dauca-8,11-diene (**18**) in C_6D_6

δ (ppm)	Protons	*J* (Hz)	Carbons	δ (ppm)
0.90	Me-15	*s*, 3H	C-1	42.4 (*s*)
1.19	H-6	*dddd*, (14.4, 12.0, 2.5,12.0), 1H	C-2	41.3 (*t*)
1.40–1.54	H-5, H-2, H-10	*m*, 3H	C-3	27.1 (*t*)
1.55-1.68	H-3, H-6	*m*, 2H	C-4	52.3 (*d*)
1.73	Me-14	*s*, 3H	C-5	57.4 (*d*)
1.84	Me-12	*br. s*, 3H	C-6	24.4 (*t*)
1.92	H-3	*dddd*, (9.1, 13.5, 9.4, 9.4), 1H	C-7	34.7 (*t*)
2.02–2.21	2H-7, 1H-2, 1H-10	*m*, 4H	C-8	139.7 (*s*)
2.45	H-4	*ddd*, (11.0, 6.9, 2.5, 11.0), 1H	C-9	123.4 (*d*)
4.92	H-12	*br. s*, 1H	C-10	41.7 (*t*)
4.94	H-12	*m*, 1H	C-11	147.9 (*s*)
5.58	H-9	*m*, 1H	C-12	111.3 (*t*)
			C-13	19.2 (*q*)
			C-14	27.7 (*q*)
			C-15	18.7 (*q*)

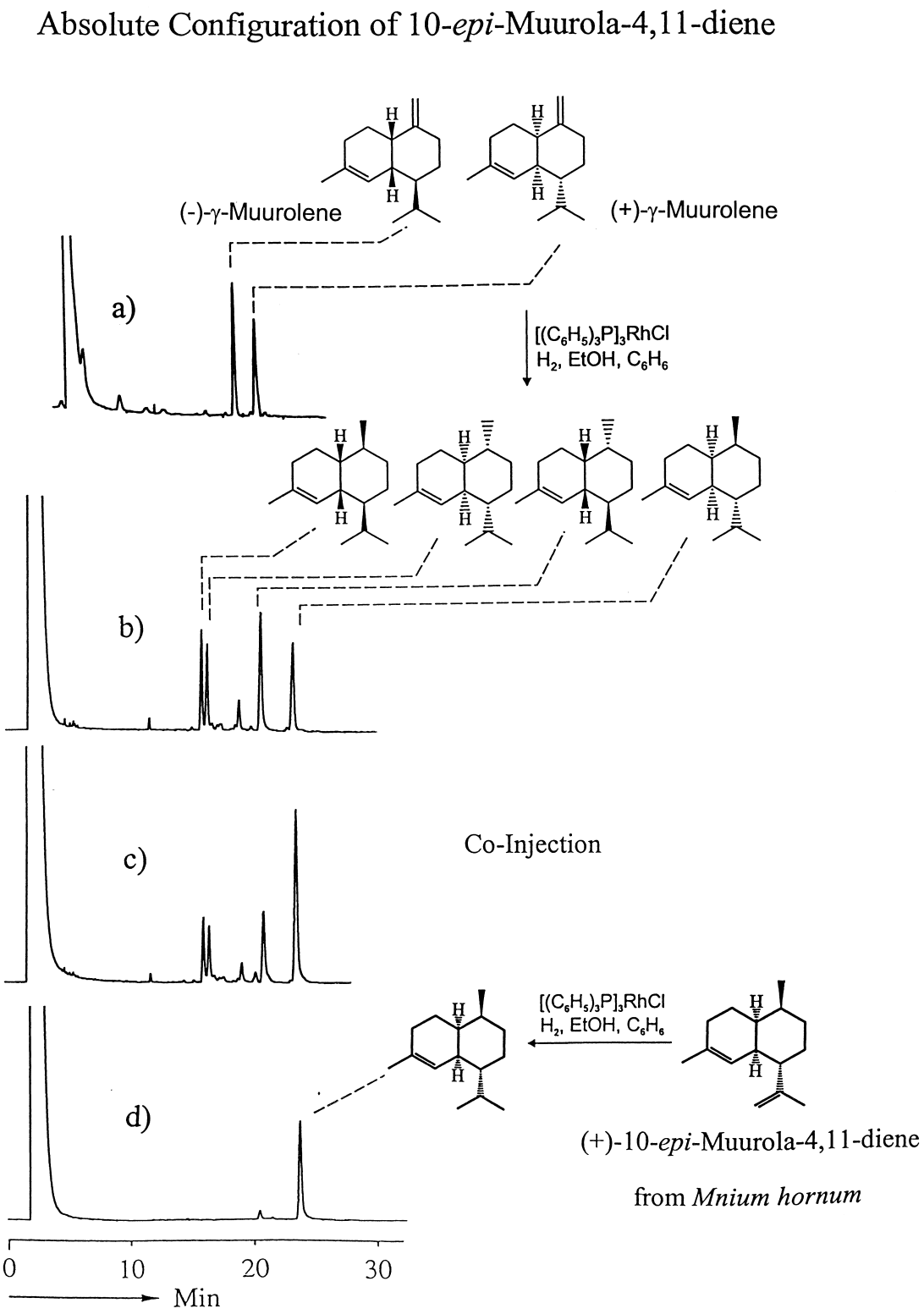

Fig. 6. Investigation of the absolute configuration of 10-*epi*-muurola-4,11-diene (**16**) by comparing products of partial hydrogenation of both enantiomers of γ-muurolene with those of 16 by enantioselective gas chromatography. 25 m Fused silica capillary column with heptakis(2,6-di-*O*-methyl-3-*O*-pentyl-)-β-cyclodextrin (50% in polysiloxane OV1701, w/w) at 110°C. (a) enantiomer separation of γ-muurolene [excess of (−)-enantiomer]; (b) separation of 2 enantiomeric pairs of diastereomeric dihydro derivatives of γ-muurolene; (c) co-injection with product obtained by partial hydrogenation of 10-*epi*-muurola-4,11-diene (**16**); (d) partial hydrogenation product of 10-*epi*-muurola-4,11-diene (**16**).

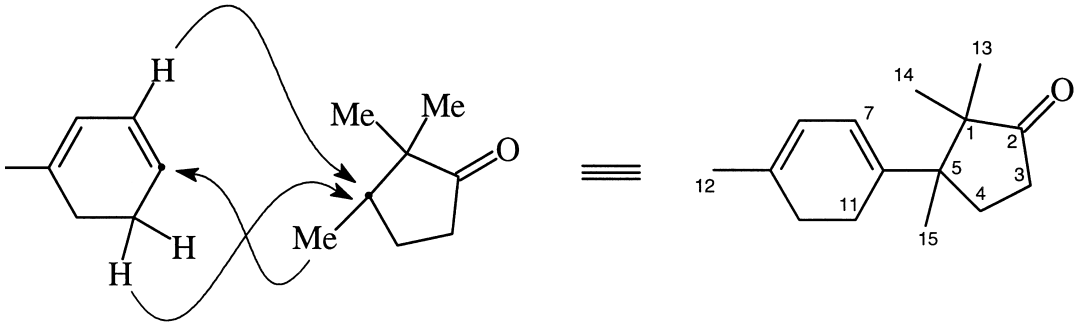

Fig. 7. Partial structures and HMBC correlations for 10,11-dihydro-α-cuparenone (**8**).

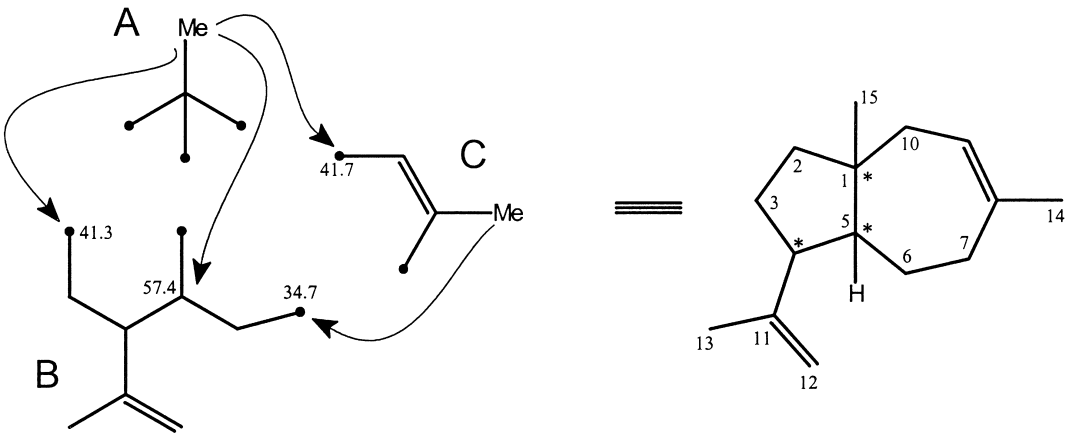

Fig. 8. Partial structures and HMBC correlations for dauca-8,11-diene (**18**).

were observed in excellent agreement with chemical shift values reported by Cassidy and Ghisalberti (1993), who isolated dauca-8,11-diene from a marine sponge and assigned a structure with *trans* ring junction and *trans* correlation of methyl C-15 and the isopropenyl group. However, for the same compound isolated from *Rosa rugosa* leaves a set of different ^{13}C data was reported by Hashidoko et al. (1992) and again, differing from these data, for a compound of structure **18** isolated from the composite *Vernonia galpinii* by Bohlmann and Zdero (1982). We have, therefore, carried out a chemical correlation by comparing the fully hydrogenated products of **18**, (+)-daucene (**20**) and dauca-3,8-diene (**21**) by enantioselective GC. **20** and **21** were isolated from the product mixture which is obtained by dehydration of carotol, as reported by Bülow and König (2000). Carotol was isolated from commercial carrot seed oil by preparative GC. As expected, 4 fully hydrogenated products were obtained from dauca-3,8-diene (**21**) (Fig. 9). Also 4 out of 8 possible products were obtained from (+)-daucene (**20**) and 2 products from compound **18**. Comparison by capillary GC with several different cyclodextrin derived chiral stationary phases revealed that the retention times of the 2 hydrogenated products originating from **18** were identical with 2 out of 4 products from hydrogenated (+)-daucene (**20**), thus proving the identity of the absolute configuration of **18** and **20** at carbon 1. The identity of 2 out of 4 products originating from hydrogenated dauca-3,8-diene (**21**) with hydrogenated **18**, proved the identity of the absolute configuration at carbon atoms 1 and 5, as illustrated in Fig. 9. In contrast to the isomer identified by Cassidy and Ghisalberti (1993), our compound **18** shows a positive optical rotation. Thus, the absolute configuration of **18** is correlated with (+)-daucene and (1*S*,5*R*)-dauca-3,8-diene as obtained from carotol (with known absolute configuration).

The isolation of the butenolide **22** was achieved by preparative gas chromatography. It has the molecular formula $C_{12}H_{22}O_2$ ([M^+], m/z = 196), while its homologue

Table 4
^1H and ^{13}C NMR spectral data of butenolide **22** in C_6D_6

δ (ppm)	Protons	*J* (Hz)	Carbons	δ (ppm)
0.81	Me-9	*t*, (7.25), 3H	C-1	172.7 (*s*)
0.97	Me-12	*s*, 3H	C-2	123.4 (*s*)
0.86–0.94	2H-6	*m*, 2H	C-3	160.9 (*s*)
1.09–1.14	2H-8	*m*, 2H	C-4	86.7 (*s*)
1.03	2H-7	*m*, 2H	C-5	37.1 (*t*)
1.15	H-5	*m*, 1H	C-6	22.9 (*t*)
1.17	Me-11	*s*, 3H	C-7	32.0 (*t*)
1.45	H-5	*m*, 1H	C-8	22.7 (*t*)
1.59	Me-2	*s*, 3H	C-9	14.2 (*q*)
			C-10	8.5 (*q*)
			C-11	10.3 (*q*)
			C-12	23.7 (*q*)

23, which is always present as a minor component, has the elemental composition $C_{11}H_{19}O_2$ ([M^+], $m/z = 182$), according to high resolution MS. The presence of a pentyl group was concluded from the loss of a C_5H_{11} radical from the molecular ion to $m/z = 125$ in **22** and $m/z = 111$ in **23.** The ^{13}C- and DEPT spectra (Table 4) permitted the identification of 2 olefinic carbons, 1 carbonyl carbon, 1 quaternary carbon, 4 methylene groups and 4 methyl groups. The presence of a carbonyl group (δ 172.72) and an oxygenated quaternary carbon (δ 86.74) suggested an ester function. The DEPT spectra also indicated that the olefinic carbons (δ 160.93 and 123.43) are quaternary. Further, the ^1H NMR spectrum (Table 4) showed the presence of 3 tertiary methyl groups

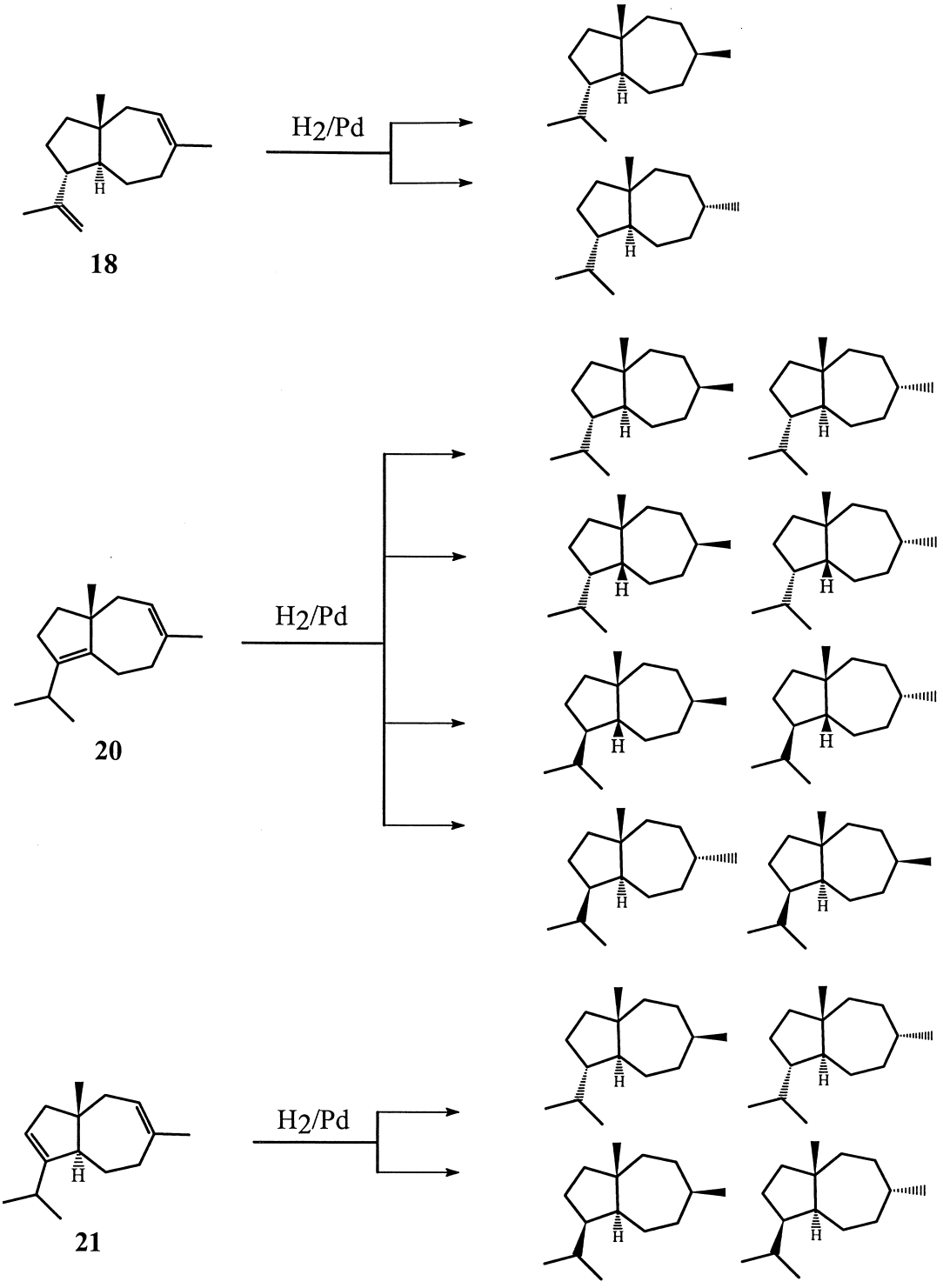

Fig. 9. Possible hydrogenation products of (+)-dauca-8,11-diene (**18**), (+)-daucene (**20**) and dauca-3,8-diene (**21**).

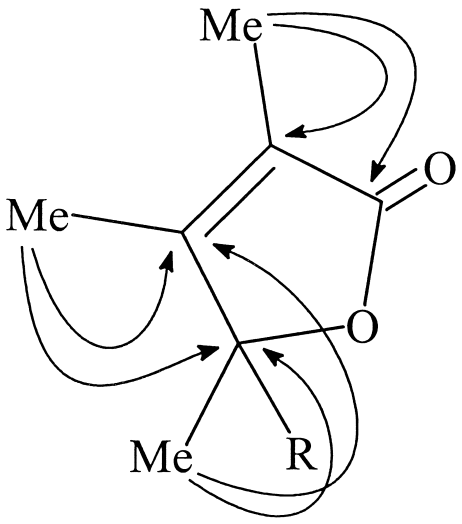

Fig. 10. HMBC correlations for 3,4,5-trimethyl-5-pentyl-5*H*-furan-2-one (**22**).

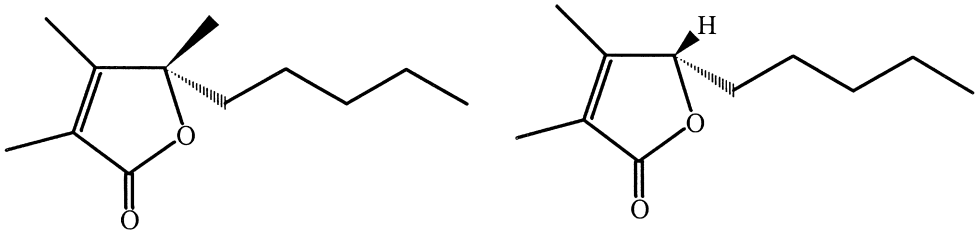

22 **23**

Fig. 11. Structures of butenolides **22** and **23** from *Plagiomnium undulatum*.

at δ 0.97, 1.17 and 1.59. A secondary methyl group was detected at δ 0.81 as a doublet. The HMBC spectrum showed a characteristic pattern of correlation peaks in the region between δ 80 and 172 for the methyl groups at δ 1.59, 1.17 and 0.97. From different correlations of the methyl protons to the olefinic carbons (δ 160.92, 123.44), carbonyl carbon (δ 172.72) and the quaternary carbon (δ 86.73) the partial structure of the butenolide **21** was derived (Fig. 10). From the HSQC spectrum it was concluded that the multiplet signal at δ 1.45 is part of the resonance of a methylene group (δ 37.11) which in the HMBC spectrum shows a correlation to the quaternary carbon at δ 86.73 and to the olefinic carbon at δ 160.92. The second proton of the methylene group is detected at δ 1.15 as part of overlapping signals in the ^{1}H NMR at δ 1.09–1.16. Further analysis of the ^{1}H–^{1}H COSY, HSQC and HMBC spectra led to the identification of three additional methylene groups of the pentyl chain. The absolute configuration of the butenolides **22** and **23** (Fig. 11) was not determined, but compound **21** is optically active and has a positive optical rotation. The structural assignment of **22** is only based on the homology of the mass spectra of **22** and **23** and on exact mass measurements by high resolution MS.

The identified butenolides seem to be quite common as constituents of mosses. **22** was also found in the hydrodistillation products of *Hylocomium splendens* and *H. brevirostre*.

3. Conclusion

Mosses produce a great variety of volatile metabolites, which can be isolated from their essential oils after hydrodistillation and identified by spectroscopic methods. Like liverworts, mosses generate a great variety of mono-, sesqui- and diterpenes and, in addition, many aliphatic metabolites.

4. Experimental

4.1. Plant material

Mosses were collected in various forests in Germany, Austria, France and Italy and identified by the authors (H. Muhle, R. Mues):

Mnium hornum: near Hamburg; Ilsetal (Harz mountains); Gräfinthal (Saarland).

M. marginatum: Sonthofen, Altmühl valley (Bavaria), Blaustein (Baden-Württemberg).

M. stellare: Altmühl valley (Bavaria)

Homalia trichomanoides: Lonsee, Beuron (Baden-Württemberg); Irsee (Bavaria), Gräfinthal (Saarland).

Plagiomnium undulatum: near Hamburg, Irsee, Neu-Ulm (Bavaria), Zachersmühle (Baden-Württemberg), Chamonix (France), Sicily (Italy).

Plagiothecium undulatum: near Hamburg, Niederwürzbach (Saarland), Pitztal (Austria).

Taxiphyllum wisgrillii: Immenstadt (Bavaria).

Plant samples are deposited in the Abteilung Allgemeine Botanik, University of Ulm and Fachrichtung 8.1 Botanik, University of Saarbrücken.

4.2. Hydrodistillation

The essential oil was prepared by hydrodistillation (2 h) of aq. homogenates of fresh and green or air-dried plants using *n*-hexane as collection solvent. Because of the greatly differing weight the fresh material was not weighed.

4.3. Capillary GC

Orion Micromat 412 double column instrument with 25 m fused silica capillaries with polysiloxane CPSil 5 and CPSil 19 (Chrompack); Carlo Erba Fractovap 2150, 4160 instruments with 25 m fused silica capillaries with heptakis(2,6-di-*O*-methyl-3-*O*-pentyl)-β- and-γ-cyclo dextrin, respectively, and heptakis(6-*O*-t.butyldimethyl silyl-2,3-di-*O*-methyl)-β-cyclodextrin, all in polysiloxane OV1701 (50 wt.%); split injection, flame ionization detection; carrier gas 0.5 bar hydrogen.

4.4. Preparative GC

Isolation of compounds **8**, **16**–**18** and **20**–**22** was performed by prep. GC on a modified Varian 1400 instrument, equipped with a stainless steel columns with 2.5% heptakis(6-*O*-t.hexyldimethylsilyl-2,3-di-*O*-methyl)-β-cyclodextrin/SE30 (1:1, w/w;) on Chromosorb G-HP (2.00 m×4.3 mm) or with 6.4% polydimethylsiloxane SE30 on Chromosorb W-HP (1.85 m×4.3 mm); flame ionization detection; helium as carrier gas at a flow rate of 240 ml/min (Hardt and König, 1994).

4.5. Partial hydrogenation of *16*

This was carried out by adding approx. 1 mg of Wilkinson catalyst $[(C_6H_5)_3P]_3RhCl$. **18** was fully hydrogenated by adding 0.5 mg Pd/C to a solution of approx. 1 mg of sample in 500 μl *n*-hexane. In both cases the suspension was treated with H_2 and stirred under H_2 at room temp. for 4 hours and 1 hour, respectively. After that the reaction mixture was filtered and the reaction products were analysed by GC–MS and GC on capillary columns with conventional polysiloxane stationary phases and cyclodextrin derivatives.

4.6. Dehydration of carotol

To a solution of approx. 1 mg of carotol from carrot seed oil in 1 ml of pyridine 0.1 ml of $SOCl_2$ was added and left for 20 min at 0° C. To the reaction mixture 10% $NaHCO_3$-solution was added and the products extracted with *n*-hexane. From the organic extract (+)-daucene (**2**) and dauca-3,8-diene (**21**) were isolated by prep. GC.

4.7. NMR spectroscopy

NMR measurements were carried out with Bruker WM 500 or WM 400 instruments using TMS as internal standard.

4.8. Polarimetry

Only the sense of the optical rotation was determined, since the isolated sample amounts were too small for an accurate determination of the *specific* optical rotation.

4.9. Mass spectrometry

GC–MS measurements (EI, 70 eV) were carried out with a Hewlett Packard HP 5890 gas chromatograph coupled to a VG Analytical 70-250S mass spectrometer. Exact mass measurements were performed at a resolution of 5000 with PFK masses as reference.

4.10. (+)-10-epi-Muurola-4,11-diene (*16*)

^{1}H NMR (500 MHz, C_6D_6) and ^{13}C NMR (125 MHz, C_6D_6): see Table 2.

MS (EI, 70 eV): *m*/*z* (rel. int.): 204 (34) [M^+], 189 (29), 175 (8), 162 (20), 149 (14), 147 (14), 133 (25), 121 (100), 119 (89), 107 (25), 105 (34), 93 (75), 81 (44), 79 (65), 67 (30), 55 (34), 41 (53).

4.11. (−)-Muurola-4,11-diene (*17*)

^{1}H NMR (500 MHz, C_6D_6) and ^{13}C NMR (125 MHz, C_6D_6): see Table 2.

MS (EI, 70 eV): *m*/*z* (rel. int.) 204 (34) [M^+], 189 (40), 175 (8), 162 (20), 149 (16), 147 (16), 133 (20), 121 (100), 119 (89), 107 (30), 105 (37), 93 (75), 81 (44), 79 (65), 67 (30), 55 (34), 41 (53).

4.12. (+)-Dauca-8,11-diene (*18*)

^{1}H NMR (400 MHz, C_6D_6) and ^{13}C NMR (125 MHz, C_6D_6): see Table 3.

MS (EI, 70 eV): *m/z* (rel. int.): 204 (34) [M^+], 189 (32), 175 (10), 161 (24), 147 (24), 133 (22), 121 (100), 94 (35), 93 (97), 91 (35), 81 (40), 79 (50), 68 (76), 55 (38), 53 (38), 41 (68).

4.13. (+)-3,4,5-Trimethyl-5-pentyl-5H-furan-2-one (**22**)

^{1}H NMR (400 MHz, C_6D_6) and ^{13}C NMR (125 MHz, C_6D_6): see Table 4.

MS (EI, 70 eV): *m/z* (rel. int.) 196 [M^+] (2), 181 [M-CH_3]$^+$ (1), 153 [M-CH_3-CO]$^+$ (14), 125 [M-C_5H_{11}]$^+$ (100), 58 (17), 43 (59). MS (high resolution): 181.1238 ($C_{11}H_{17}O_2$), 153.1288 ($C_{10}H_{17}O$), 125.0623 ($C_7H_9O_2$).

4.14. 4,5-Dimethyl-5-pentyl-5H-furan-2-one (**23**)

MS (EI, 70 eV): *m/z* (rel. int.) 182 [M]$^+$ (8), 153 [M-C_2H_5]$^+$ (4), 111 [M-C_5H_{11}]$^+$ (38), 83 [M-C_5H_{11}-CO]$^+$ (100), 55 (53), 43 (19), 41 (22), 39 (18). MS (high resolution): 182.1318 ($C_{11}H_{18}O_2$), 111.0462 ($C_6H_7O_2$), 83.0502 (C_5H_7O).

4.15. (−)-10,11-Dihydro-α-cuparenone (**8**)

^{1}H NMR (400 MHz, C_6D_6): 0.72 (3H, *s*), 0.75 (3H, *s*), 1.07 (3H, *s*), 1.25 (1H, *ddd*, $J_1 = 12.61$ Hz, $J_2 = 8.82$ Hz, $J_3 = 2.21$ Hz), 1.60 (3H, *s*), 1.86 (1H, *ddd*, $J_1 = 12.61$ Hz, $J_2 = 10.50$ Hz, $J_3 = 9.70$ Hz), 1.98 (1H, *ddd*, $J_1 = 19.23$ Hz, $J_2 = 10.50$ Hz, $J_3 = 8.80$ Hz), 2.08 (1 H, *ddd*, $J_1 = 19.23$ HZ, $J_2 = 9.70$ Hz, $J_3 = 2.21$ Hz), 2.50-2.58 (4H, *m*), 5.36 (1H, *m*), 5.37 (1H, *m*). ^{13}C NMR (C_6D_6): 20.21 (*q*), 21.74 (*q*), 23.20 (*q*), 23.25 (*q*), 28.79 (*t*), 30.46 (*t*), 32.44 (*t*), 32.44 (*t*), 33.98 (*t*), 49.45 (*s*), 52.47 (*s*), 119.58 (*d*), 119.87 (*d*), 130.89 (*s*), 139.45 (*d*), 220.45 (*s*). MS (EI, 70 eV): *m/z* (rel. int.): 218 [M]$^+$ (17), 203 (2), 185 (1), 175 (4), 157 (5), 147 (41), 132 (100), 119 (21), 105 (30), 91 (27), 83 (12), 77 (18), 71 (7), 67 (8), 65 (8), 55 (22), 41 (36).

Acknowledgements

We are grateful to Dr. V. Sinnwell, University of Hamburg, for his help in NMR spectroscopy and to Mrs. A. Meiners and Mr. M. Preusse, University of Hamburg, for their assistence in obtaining the mass spectral data. The financial support of the Fonds der Chemischen Industrie is acknowledged.

References

Abe, N., Onoda, R., 1968. The structure of bakkenolide-A. Tetrahedron Letters 3, 369–373.

Asakawa, Y., 1995. Chemical constituents of the bryophytes. In: Herz, W., Kirby, G.W., Moore, R.E., Steglich, W., Tamm, C. (Eds.), Progress in the Chemistry of Organic Natural Compounds, Vol. 65. Springer Verlag, Vienna, New York.

Benesova, V., 1976. Terpenes. CCXLII. (R)-(−)-α-cuparenone from *Mannia fragrans*. Collection of Czechoslovak Chemical Communications 41, 3812–3814.

Bohlmann, F., Gerke, T., Jakupovic, J., King, R.M., Robinson, H., 1984. Cadina-4,11-diene from *Viguiera oblongifolia*. Phytochemistry 23, 1183–1184.

Bohlmann, F., Zdero, C., 1982. Glaucolides and other constituents from south African *Vernoia* species. Phytochemistry 21, 2263–2267.

Bouwmeester, H.J., Wallaart, T.E., Janssen, M.H.A., van Loo, B., Posthumus, M.A., Schmidt, C.O., De Kraker, J.-W., König, W.A., Fransen, C.R., 1999. Amorpha-4,11- diene synthesis catalyses the first probable step in artemisinin biosynthesis. Phytochemistry 52, 843–854.

Brunke, E.-J., Hammerschmidt, F.-J., Schmaus, G., 1992. In: Woidich, H., Buchbauer, G. (Eds.), Headspace Analysis of Selected European Medicinal Plants. Proceedings of the 12th International Congress of Flavours, Fragrances and Essential Oils, Vienna, pp. 105–124.

Bülow, N., König, W.A., 2000. The role of germacrene D as a precursor in sesquiterpene biosynthesis: investigations of acid catalyzed, photochemically and thermally induced rearrangements. Phytochemistry 55, 141–168.

Cassidy, M.P., Ghisalberti, E.L., 1993. New terpene hydrocarbons from the sponge *Higginsia* sp. Journal of Natural Products 56, 1190–1193.

Fricke, C., 1999. Terpenoide Inhaltsstoffe von Lebermoosen und Heilpflanzen. Doctoral thesis, University of Hamburg, Hamburg.

Hardt, I., König, W.A., 1995. Preparative enantiomer separation with modified cyclodextrins as chiral stationary phases. Journal of Chromatography A 666, 611–615.

Hashidoko, Y., Tahara, S., Mizutani, J., 1992. Sesquiterpene hydrocarbons in glandular trichome exudate of *Rosa rugosa* leaves. Zeitschrift für Naturforschung 47c, 353–359.

Huneck, S., 1983. Chemistry and biochemistry of bryophytes. In: Schuster, R.M. (Ed.), New manual of Bryology, vol. 1. The Hattori Botanical Laboratory, Nichinan, Miyazaki, Japan, pp. 1–116.

Joulain, D., König, W.A., 1998. The atlas of spectral data of sesquiterpene hydrocarbons. E.B.-Verlag, Hamburg . (now also available as an electronic version *MassFinder 1.5* developed by D.H. Hochmuth, University of Hamburg).

Jüttner, F., 1976. β-Cyclocitral and alkanes in *Microcystis* (Cyanophyceae). Zeitschriff für Naturforsch. 31c, 491–495.

Karunen, P., 1974. Polyunsaturated hydrocarbons from *Polytrichum commune* spores. Phytochemistry 13, 2209–2213.

König, W.A., Saritas, Y., Bülow, N., 1999. Identification of sesquiterpene hydrocarbons by gas-phase analytical methods. Flavour and Fragrance Journal 14, 367–378.

Matsuo, Nozaki, H., Nakayama, M., Hayashi, S., 1979. (−)-Maalian-5-ol, a new enantiomeric sesquiterpenoid form the liverwort *Plagiochila ovalifolia*. Experientia 35, 1279–1280.

Medsker, L.L., Jenkins, D., Thomas, F.J., 1968. Odorous compounds in natural waters. An earthy-smelling compound associated with blue-green algae and Actinomycetes. Environmental Science and Technology 2, 461–464.

Mekem Sonwa, M., Rieck, A., König, W.A., (manuscript in preparation).

Morais, R.M.S.C., Harrison, L. J., Becker, H., 1988. (+)-Gymnomitr-8(12)-en-9α-ol and (*R*)-(−)-8,11-dihydro-α-cuparenone. Two novel sesquiterpenoids from the liverwort *Reboulia hemisphaerica*. Journal of Chemistry Research, S380–S381.

Mues, R., 2000. Chemical constituents and biochemistry. In: Shaw, A.J., Goffinet, B. (Eds.), Bryophyte Biology. Cambridge University Press, Cambridge, pp. 150–181.

Nilsson, E., Mårtensson, O., 1971. Chemical studies on bryophytes. 11. (−)-16α-Hydroxykaurane from *Saelania glaucescens* (Hedw.). Acta Chem. Scand. 25, 1486–1487.

Rieck, A., Bülow, N., König, W.A., 1995. An epoxy-trinoreudesmane sesquiterpene from the liverwort *Lophocolea bidentata*. Phytochemistry 40, 847–851.

Safferman, R.S., Rosen, A.A., Mashni, C.J., Morris, M.E., 1967. Earthy-smelling substance from a blue-green alga. Environmental Science and Technology 1, 25–26.

Spiteller, D., Spiteller, G., 2000. Direkter Nachweis von toxischem 2,4-Decadienal in oxydiertem Low-Density-Lipoprotein durch Festphasenextraktion. Angew. Chem. 112, 595–597.

Suire, C., Bourgeois, G., Koponen, T., 2000. Some chemical constituents of thirteen mosses from the traditional Mniaceae family. J. Hattori Bot. Lab. 89, 233–246.

Toyota, M., Kimura, K., Asakawa, Y., 1998. Occurrence of *ent*-sesquiterpene in the Japanese moss *Plagiomnium acutum*: first isolation of the *ent*-sequi- and dolabellane-type diterpenoids from the Musci. Chemical and Pharmaceautical Bulletin 46, 1488–1489.

Warmers, U., Wihstutz, K., Bülow, N., Fricke, C., König, W.A., 1999. Sesquiterpene constituents of the liverwort *Calypogeia muelleriana*. Phytochemistry 49, 1723–1731.

Wu et al., 1991 Wu, C.-L., Lin, S.-C., Chen, J. A., 1991. (+)-*trans*-1,4-Dimethyl-1,2,3,4,4a,5,6,7- octahydronaphthalene, a trinoreudesmene from Taiwanese liverwort *Bazzania fauriana*. Journal of Chemical Research, S50–S51.

Wu, C.-L., Huang, C.-H., Shih, T.-L., 1993. A sesquiterpene oxide of a novel skeleton from the liverwort *Plagiochila peculiaris*. Tetrahedron Letters 34, 4855–4856.

Yoshida, T., Muraki, S., Takahashi, K., 1979. Isolation and X-ray crystal structure of mintsulfide, a novel sulfur containing sesquiterpene. J. Chem. Soc. Chem. Commun., 512–513.

Zinsmeister, H.D., Becker, H., Eicher, T., 1991. Moose, eine Quelle biologisch aktiver Naturstoffe? Angew. Chem. 103, 134–151.

PERGAMON

Phytochemistry 57 (2001) 459–467

PHYTOCHEMISTRY

www.elsevier.com/locate/phytochem

High molecular weight lipids from the trilaminar outer wall (TLS)-containing microalgae *Chlorella emersonii*, *Scenedesmus communis* and *Tetraedron minimum*

B. Allard*, J. Templier

Laboratoire de Chimie Bioorganique et Organique Physique, UMR CNRS 7573, E.N.S.C.P., 11 rue Pierre et Marie Curie, 75231 Paris Cedex 05, France

Received 11 December 2000; received in revised form 12 February 2001

Abstract

High molecular weight lipids were isolated from *Chlorella emersonii*, *Scenedesmus communis* and *Tetraedron minimum*, thin trilaminar outer wall (TLS)-containing freshwater microalgae producing an insoluble non-hydrolysable biopolymer (i.e. algaenan). Molecular weight determination by gel permeation chromatography indicated that their molecular weights range from ca. 400 to 2000 Da. Flash pyrolysis with in situ methylation using tetramethylammonium hydroxide (TMAH) and alkaline hydrolysis showed that the high molecular weight lipids isolated from *C. emersonii* and *S. communis* are mainly composed of saturated *n*-C26 and *n*-C28 fatty acids and alcohols and of saturated *n*-C30 and *n*-C32 α,ω-diols and ω-hydroxy acids. In contrast the high molecular weight lipids isolated from *T. minimum* are predominantly composed of long-chain fatty acids and ω-hydroxy acids. Aromatic moieties were also identified in small amounts in the thermochemolysate and in the hydrolysate. Chemical structural models containing long-chain mono- and polyesters were proposed for the high molecular weight lipids isolated from the three microalgae in agreement with analytical and spectroscopic data. Structural similarity between the outer cell wall of these microalgae and the cuticular membrane of higher plants is suggested. © 2001 Elsevier Science Ltd. All rights reserved.

Keywords: *Chlorella emersonii*; *Scenedesmus communis*; *Tetraedron minimum*; Long-chain esters; Polyesters; Tetramethylammonium hydroxide (TMAH) thermochemolysis; Trilaminar outer walls (TLS); Algaenan

1. Introduction

A number of recent studies of green freshwater and marine microalgae from the class of Chlorophyceae, Dinophyceae and Eustigmatophyceae indicated the existence of microalgae exhibiting a characteristic membrane-like trilaminar cell wall structure (TLS) (Derenne et al., 1992; Gelin et al., 1999; Allard and Templier, 2000). It has also been shown that in most cases such outer walls are predominantly composed of a biopolymer (so-called algaenan) exhibiting a high resistance to drastic non-oxidative chemical treatments (de Leeuw and Largeau, 1993). However, the absence of a one-to-one relationship between the presence of a TLS and the occurrence of algaenan has been noted (Brunner and Honegger, 1985; Allard and Templier, 2000). Through recent pyrolysis and chemical degradation studies it has been suggested that these biopolymers consist mainly of linear polyester chains cross-linked by ether bridges (Blokker et al., 1998a,b). Our continued phytochemical investigations of TLS-containing microalgae have resulted in the isolation of high molecular weight lipids from the three TLS- and algaenan-containing microalgae *Chlorella emersonii*, *Scenedesmus communis* and *Tetraedron minimum*. We now report the isolation and the tentative identification of these new high molecular weight lipids using pyrolysis in the presence of tetramethylammonium hydroxide (TMAH) and alkaline hydrolysis techniques.

2. Results

The dry biomass was extracted with chloroform. After concentration of the solvent, addition of acetone to the crude neutral lipid extract yielded a precipitate

* Corresponding author. Tel.: +33-1-44-27-67-16; fax: +33-1-43-25-79-75.

E-mail address: allard@ext.jussieu.fr (B. Allard).

0031-9422/01/$ - see front matter © 2001 Elsevier Science Ltd. All rights reserved.
PII: S0031-9422(01)00071-1

(NL-2). The yield of NL-2 depends on the age of the culture and was higher for cultures harvested in the stationary phase of growth. This precipitated material accounts for ca. 10–30% of the total extract for the microalgae harvested at the end of linear phase of growth and has been isolated as level up to 70% of the total neutral lipid extract for some aged cultures of *T. minimum*. However, once dried, these precipitates became insoluble in usual organic solvents. The supernatants (NL-1) contained the same lipids as previously identified in neutral lipids of the three microalgae (Allard and Templier, 2000).

2.1. Spectroscopic features

FTIR spectra of the NL-2 samples are shown in Fig. 1. All NL-2 samples show absorption bands at ca. 3400 cm^{-1} (OH stretching vibrations), 2920 and 2850 cm^{-1} (symmetric and asymmetric stretching of methylene groups), 1470 cm^{-1} (methylene deformation mode), 720 cm^{-1} (methylene rocking mode) and 1735 cm^{-1} (carbonyl stretching vibrations) suggesting the presence of long-chain esters in these samples. The band progression caused by methylene wagging modes between ca. 1380 and 1170 cm^{-1} is clearly observed in spectra of the NL-2 samples from *C. emersonii* and *S. communis* (see inset of Fig. 1) and is consistent with the presence of long-chain *n*-alkyl compounds (Jones et al., 1952; Holland and Nielsen, 1962). The low intensity of the absorption band at ca. 1375 cm^{-1} due to symmetric methyl deformation mode is indicative of the low degree of branching in these lipids.

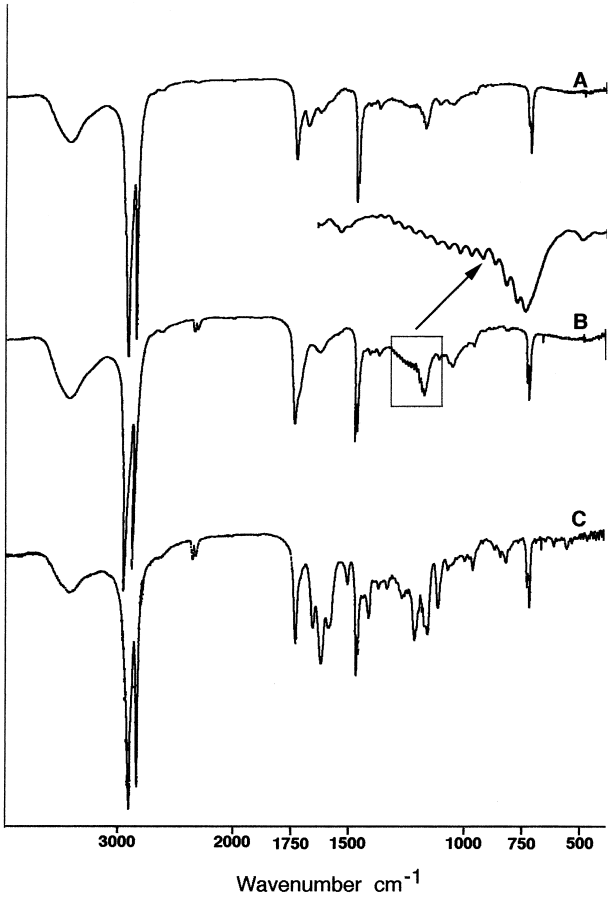

Fig. 1. FTIR spectra of NL-2 samples isolated from (**A**) *Chlorella emersonii*, (**B**) *Scenedesmus communis*, (**C**) *Tetraedron minimum*.

In the region 1500–1750 cm^{-1} several differences are observed between the FTIR spectra of the NL-2 samples isolated from the microalgae studied. A shoulder at ca. 1710 cm^{-1} which can be assigned to carboxyl groups is present in the FTIR spectrum of the NL-2 sample from *S. communis*. In this region the FTIR spectrum of the NL-2 sample originated from *T. minimum* shows strong absorption bands at ca. 1660, 1625 and 1595 cm^{-1}. These bands were not shifted by pH changes. If we consider (i) the strong intensity of these bands, (ii) the low intensity of the absorption band near 3400 cm^{-1} and (iii) the low nitrogen content of the sample (0.7% as determined by elemental analysis) it seems unlikely that these bands arise from amide groups. Additionally, these latter bands seem to be associated with the presence of several bands in the region 1100–1250 cm^{-1} corresponding to C–O stretching vibrations. Therefore, it can be suggested that these three absorption bands could represent different populations of C=O groups, likely ester groups, with different intermolecular and/or intramolecular hydrogen bonding. Nevertheless if we consider the presence of absorption bands between 750 and 1000 cm^{-1} the contribution of unsaturated and/or aromatic groups to these absorption bands cannot be ruled out.

2.2. Molecular weight determination

The NL-2 samples isolated from the different microalgae became soluble in 2-methyl-1-propanol at temperatures higher than 90°C. Therefore, when immediately handled, these samples can be assayed for molecular weight determination by gel permeation chromatography (GPC). The GPC traces of the NL-2 samples were given in Fig. 2. The total observed molecular weight range was between ca. 400 and 2000 Da for all samples. Calibrated GPC revealed prominent peaks at M_r ca. 430, 860 and 1530 Da, 430 and 630 Da and 640, 1150 and 1920 Da for the NL-2 samples isolated respectively from *C. emersonii*, *S. communis* and *T. minimum*.

2.3. Tetramethylammonium hydroxide (TMAH) thermochemolysis

Pyrolysis with in situ methylation using tetramethylammonium hydroxide (TMAH) has been introduced by Challinor (1989, 1994) for the characterisation of polar macromolecules. This technique has been

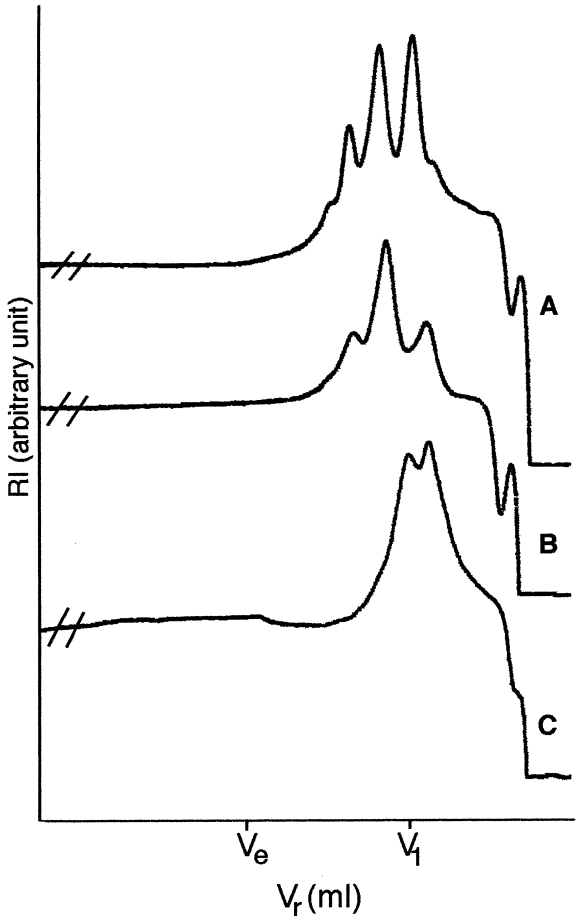

Fig. 2. GPC traces of NL-2 samples isolated from (**A**) *Tetraedron minimum*, (**B**) *Chlorella emersonii*, (**C**) *Scenedermus communis*. Styragel HR-2 column, eluent: THF, flow rate: 1 ml min^{-1}, RI detection. V_e: exclusion volume, V_1: retention volume of docosanyl docosanoate.

applied to characterise geo- and biopolymers (de Leeuw and Baas, 1993; Martin et al., 1994; McKinney et al., 1995; del Rio et al., 1994, 1998; Challinor, 1995; Clifford et al., 1995; Mckinney and Hatcher, 1996) and humic materials (Hatcher and Clifford, 1994; del Rio et al., 1995, 1996; del Rio and Hatcher, 1996). This technique yields methyl esters of carboxylic acids and methylates compounds containing hydroxyl groups, yielding products volatile enough for GC analyses. It has been shown that TMAH thermochemolysis is effective for the transesterification of fatty acids associated with humic substances (Hatcher and Clifford, 1994) and cleaves activated alkyl aryl labile ether bonds, such as ether bond activated by an α-hydroxy group in lignin, but does not chemically attack non activated ether linkages (McKinney et al., 1996).

Fig. 3 shows the total ion current (TIC) traces of the TMAH thermochemolysis products obtained from the NL-2 samples isolated from the three species of microalgae. The major peaks, identified by their MS fragmentation (see experimental) are shown in Table 1. The reported relative percentages of thermochemolysis products (Table 1) were based on integrated area of the GC–MS peaks.

Under thermochemolysis conditions the NL-2 samples from *C. emersonii* yielded saturated fatty acid methyl esters (FAMEs) from *n*-C16 to *n*-C30, with *n*-C28 as the major component, alcohol methyl ethers from *n*-C26 to *n*-C30, with *n*-C26 and *n*-C28 as the predominant components, saturated α,ω-diol di-methyl ethers and ω-methyl ether fatty acid methyl esters from *n*-C30 to *n*-C32. Significant amounts of *n*-alkane/*n*-alk-1-ene doublets were identified in the chromatogram. This homologous series probably results from conventional flash-pyrolysis and may be due to one of two possibilities (1) the too high flash pyrolysis temperature (650°C) leading to the thermal degradation of the esters and/or ethers produced by TMAH thermochemolysis or (2) the presence of non-hydrolysable bonds in the NL-2 sample isolated from *C. emersonii*. The presence of non-hydrolysable ether linkages seems unlikely. Indeed in the FTIR spectrum of this NL-2 sample no strong absorption was observed in the range expected (1150–1050 cm^{-1}) for C–O–C stretching vibrations of ether groups (Fig. 1). Moreover, the pyrolysis of alkyl ether-linked moieties should give mid-chain ketones in addition to the series of *n*-alkane/*n*-alk-1-ene doublets. However, no ketone, even in trace amount, was detected in the thermochemolysis chromatogram of the NL-2 sample from *C. emersonii*. The type of functionalities identified in the chromatogram together with the absence of tri-functional moieties indicate the presence of linear ester type bonds in this sample in agreement with the FTIR data.

Under thermochemolysis conditions the NL-2 sample from *S. communis* yielded saturated and mono-unsaturated alcohol methyl ethers from *n*-C22 to *n*-C30, saturated and to a lesser extent mono-unsaturated FAMEs with saturated *n*-C28 as the predominant component, α,ω-diol di-methyl ethers and ω-methyl ether fatty acid methyl esters with saturated *n*-C32 as the major components. In contrast to the thermochemolysis products of the NL-2 sample from *C. emersonii* only very low amounts of *n*-alkane/*n*-alk-1-ene doublets was observed in this chromatogram (Fig. 2). As in the case of *C. emersonii* the nature of compounds released during TMAH thermochemolysis of this NL-2 sample and the absence of tri-functional moieties indicate the occurrence of linear ester type linkages in these lipids.

In sharp contrast, no straight-chain alcohol methyl ethers were present in the thermochemolysis products of the NL-2 sample isolated from *T. minimum* and only very small amounts of α,ω-diol di-methyl ethers and ω-methoxy FAMEs were detected. Under thermochemolysis conditions this sample yielded predominantly saturated *n*-C24, *n*-C26 and *n*-C28 FAMEs. In addition to FAMEs, methoxy phytol and methoxylated benzene structures were identified. The major aromatic compounds identified were 1,3,5-tri-methoxybenzene (P1) and tetra-methoxybenzene (P3). Other minor aromatic compounds were identified as 1,2-di-methoxybenzyl methyl ether, 3,4,5-tri-

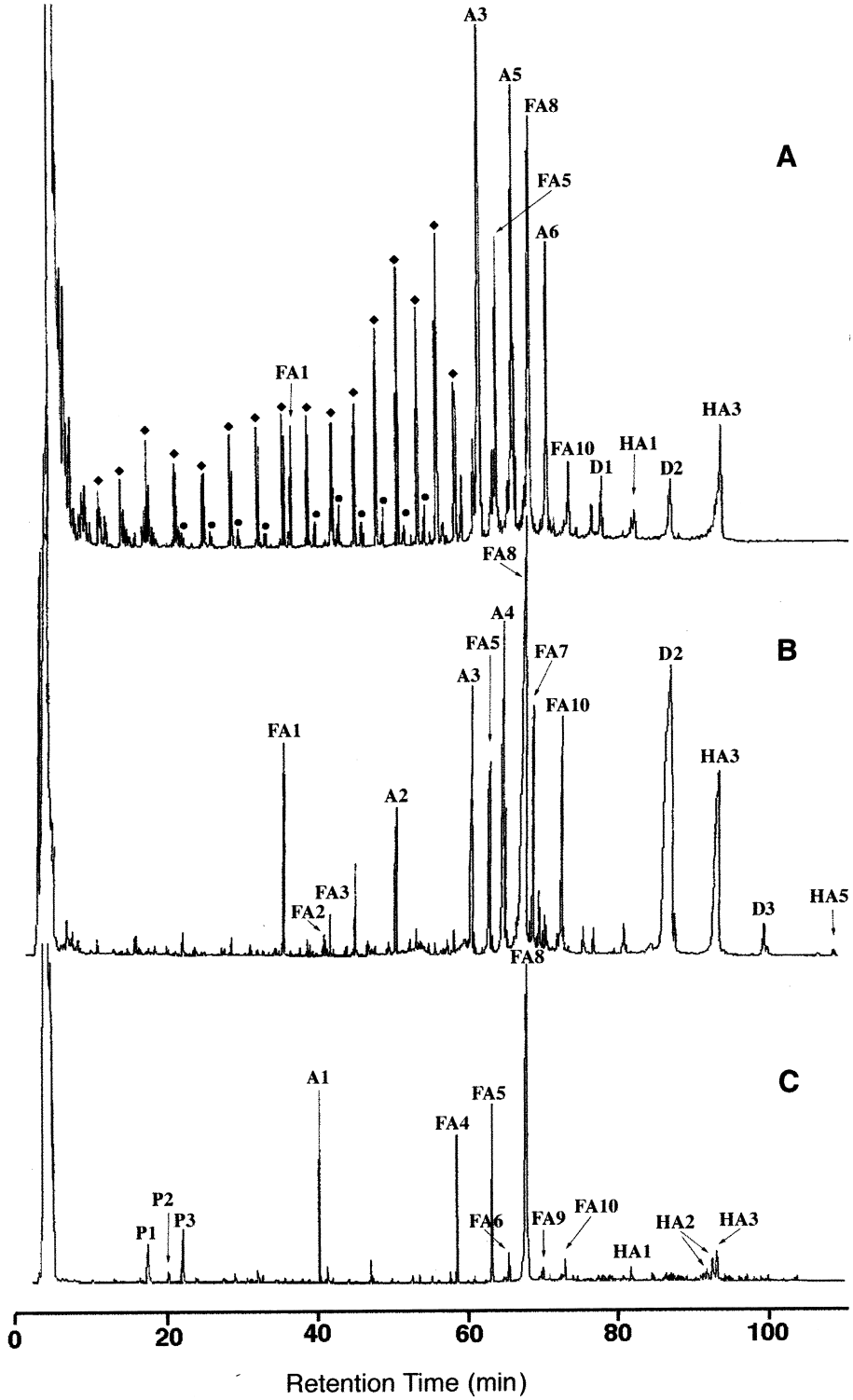

Fig. 3. Total ion current (TIC) traces for the TMAH thermochemolysis (Curie temperature 650°C) of the NL-2 samples isolated from (**A**) *Chlorella emersonii*, (**B**) *Scenedesmus communis* and (**C**) *Tetraedron minimum*. ◆ *n*-alkane/*n*-alk-1-ene doublets ● mono-unsaturated/saturated FAME doublets.

methoxybenzyl methyl ether, 1,3-benzenedicarboxylic acid di-methyl ester, di-methoxybenzoic acid methyl ester and tri-methoxyacetophenone. However, at this point, there is no evidence that all methoxy groups of aromatic rings derive from the alcohol counterparts of an ester structure and some of them could be present as such in the original sample. In the same way, it is not possible to ensure that methoxy phytol identified in the thermochemolysate derives from an ester structure or originates from free phytol precipitated with the high molecular weight lipids.

Table 1
Peak identification for Fig. 3 and quantitative estimate of the TMAH thermochemolysis products of NL-2 samples isolated from *Chlorella emersonii*, *Scenedesmus communis* and *Tetraedron. minimum*

Peak identification	Peak	*Chlorella emersonii*	*Scenedesmus communis*	*Tetraedron minimum*
Aromatic methyl ethers				
tri-Hydroxybenzene	P1			2
di-Hydroxybenzyl alcohol	P2			tr
tetra-Hydroxybenzene	P3			3
Alcohol methyl ether				
Phytol	A1			11
n-C22:0	A2		2	
n-C26:0	A3	30	4	
n-C28:1	A4		6	
n-C28:0	A5	19	2	
n-C30:0	A6	8	tr	
Fatty acid methyl ester				
n-C16:0	FA1	tr	4	
n-C18:1	FA2			tr
n-C18:0	FA3		tr	
n-C24:0	FA4		tr	8
n-C26:0	FA5	8	3	10
n-C27:0	FA6			2
n-C28:1	FA7		4	
n-C28:0	FA8	23	27	59
n-C29:0	FA9		tr	tr
n-C30:0	FA10	2	5	1
α,ω-Diol di-methyl ether				
n-C30:0	D1	2	tr	
n-C32:0	D2	2	32	
n-C34:0	D3		tr	
ω-Methyl ether fatty acid methyl ester				
n-C30:0	HA1	tr	tr	tr
n-C32:1	HA2			2
n-C32:0	HA3	7	10	2
n-C33:0	HA4		tr	
n-C34:0	HA5		tr	

Table 2
Composition (%) of the alkaline hydrolysis products of the NL-2 samples isolated from *Chlorella emersonii*, *Scenedesmus communis* and *Tetraedron minimum*[a]

	Chlorella emersonii[b]	*Scenedesmus communis*[b]	*Tetraedron minimum*[c]
Alcohol			
n-C22:0		2	
n-C26:0	24	9	
n-C28:1		2	
n-C28:0	15	6	
n-C30:0	5	4	
n-C32:0		2	
Fatty acid			
n-C16:0	7	4	tr
n-C18:1	tr		tr
n-C18:0	tr	1	tr
n-C22:0			tr
n-C24:0	tr	tr	5
n-C26:0	10	4	25
n-C27:0			1
n-C28:1		9	
n-C28:0	16	44	46
n-C29:0			1
n-C30:1			tr
n-C30:0	2	5	1
α,ω-Diol			
n-C28:0	tr		
n-C30:0	3		
n-C32:0	2	5	
ω-Hydroxy acid			
n-C28:1			tr
n-C28:0	tr		tr
n-C30:1			1
n-C30:0	4		2
n-C32:1			4
n-C32:0	11	2	3
n-C34:1			2
n-C34:0			5
n-C36:1			1
n-C36:0			tr

[a] The composition was estimated from the GC chromatograms of acetoxy and 2-methyl-1-propyl ester derivatives.
[b] Identified as acetoxy 2-methyl-1- propyl ester.
[c] Identified as acetoxy 2-methyl-1-propyl ester and 2-methyl-1-propyl ester TMSi ether.

2.4. Hydrolysis of the NL-2 samples

The NL-2 samples isolated from the different microalgae were saponified in 2-methoxyethanol/H_2O (Daffé et al., 1983). Upon extraction, very low amounts of products were recovered in the organic phase and an interfacial material containing the hydrolysis products developed between the organic and aqueous phases whatever the solvent used. The esterification of gathered organic phase and interfacial material with HCl/2-methyl-1-propanol allowed the solubilisation of all products released during hydrolysis. These latter were identified by GC–MS of their 2-methyl-1-propyl ester TMSi ethers and acetoxy 2-methyl-1-propyl esters (see experimental). The composition of hydrolysis products of each NL-2 sample is shown in Table 2.

Upon hydrolysis the NL-2 sample from *C. emersonii* yielded saturated *n*-C26, *n*-C28 and *n*-C30 fatty alcohols and fatty acids with saturated *n*-C26 and *n*-C28 as major components and saturated α,ω-diols and ω-hydroxy acids with *n*-C32 ω-hydroxy acid as the pre dominant constituent. The structure of the hydrolysis products and the absence of tri-functional moieties are in good agreement with the TMAH thermochemolysis data and corroborate the linear ester type structure for this NL-2 sample.

Saponification of the NL-2 sample isolated from *S. communis* yielded saturated and mono-unsaturated alcohols from *n*-C22 to *n*-C32, fatty acids from *n*-C16 to *n*-C30 with saturated *n*-C28 acid as predominant constituent. In contrast to the thermochemolysis products only low amounts of saturated *n*-C32 α,ω-diol and ω-hydroxy acid were detected in the hydrolysis products.

This discrepancy may be due to the fact that thermochemolysis and hydrolysis have been carried out with NL-2 samples isolated from two different cultures.

The hydrolysis products of the NL-2 sample originated from *T. minimum* consist of saturated and mono-unsaturated fatty acids from *n*-C16 to *n*-C30 with saturated *n*-C26 and *n*-C28 as major constituents and ω-hydroxy acids from *n*-C28 to *n*-C36. As in the case of thermochemolysis no alcohol and α,ω-diol was present in the hydrolysis products of this NL-2 sample. In contrast to the TMAH thermochemolysis products phytol has not been detected in the hydrolysis products. The random presence of phytol suggests that phytol identified in the thermochemolysate is likely present as free phytol which has been co-precipitated with the NL-2 sample. In addition to the acids and ω-hydroxy acids aromatic compounds have been identified in trace amount in the GC–MS chromatogram of the hydrolysate of this NL-2 sample. The major aromatic compounds identified were 3,5-di-methoxy tri-methyl silyloxy benzene (corresponding to the peak P1 of TMAH thermochemolysis), 3-methoxy-2-tri-methylsilyloxy benzyl tri-methylsilyl ether (corresponding to the peak P2 of TMAH thermochemolysis) and 2-methoxy-3-tri-methylsilyloxy benzoic acid 2-methyl-1-propyl ester. The nature of the substitutents on the aromatic rings identified in the hydrolysis products, methoxy or tri-methylsilyloxy, indicates that some methoxy groups identified in the TMAH thermochemolysis chromatogram do not derive from free hydroxyl groups. The very low amounts of the aromatic structures in the hydrolysis products and the content of ω-hydroxy acids which accounts for ca. 18% of the hydrolysate suggest that in this NL-2 sample linear ester-type structures likely predominate over alkyl-aryl ester-type structures.

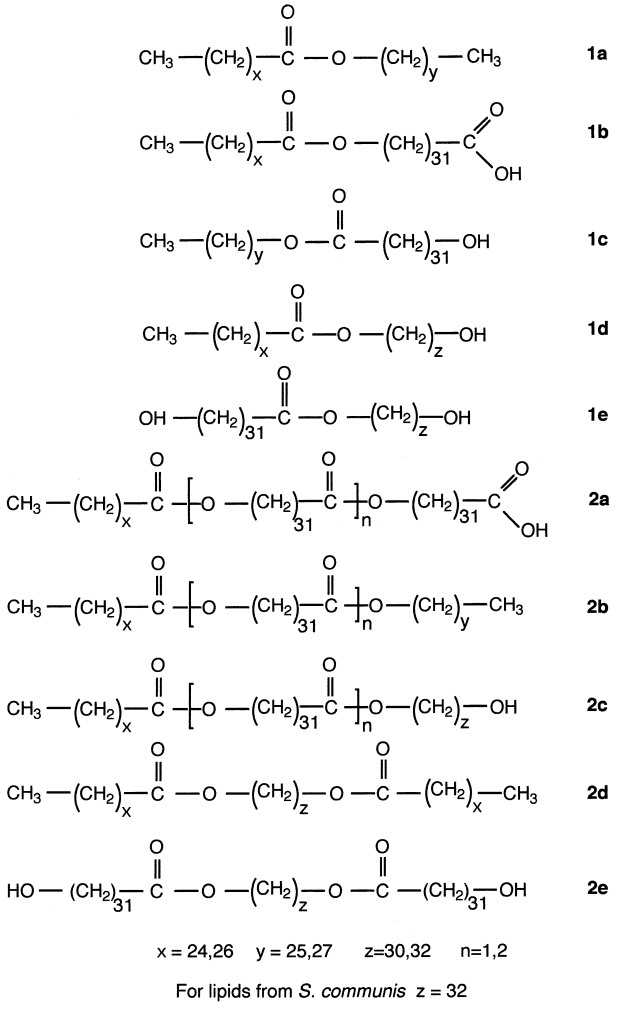

Fig. 4. Proposed chemical structures for the constituents of the high molecular weight lipids isolated from *Chlorella emersonii* and *Scenedesmus communis*.

3. Discussion

High molecular weight lipids with M_r ranging from ca. 400 to 2000 Da have been isolated from the neutral lipids of three TLS-containing freshwater microalgae and have been analysed by thermochemolysis in the presence of TMAH and alkaline hydrolysis.

From the data collected in this study we can devise structural models for the high molecular weight lipids biosynthesised by these algae which takes into account spectroscopic, GPC, TMAH thermochemolysis and hydrolysis results. The results obtained about *C. emersonii* suggest that these lipids are probably constituted of (i) long-chain saturated alcohols, acids, ω-hydroxy acids and/or α,ω-diols monomers corresponding to the peak at M_r ca. 430 Da in the GPC chromatogram, (ii) long-chain saturated monoester(s) corresponding to the GPC peak at M_r ca. 860 Da. Their possible structures depicted in Fig. 4 (compounds **1a**–**d**) are consistent with TMAH thermochemolysis and hydrolysis data, (iii) higher molecular weight ester(s) with M_r at ca. 1530 Da which could be constituted of polyester(s) having two or three ester groups per chain. Taking into account the products identified in the thermochemolysate and/or in the hydrolysate, the number of possible structures for this type of polyesters becomes very large. Possible structures of these polyesters represented by compounds **2a**–**e** are shown in Fig. 4.

The high molecular lipids isolated from *S. communis* have lower molecular weight than those isolated from *C. emersonii* and are likely constituted of long-chain saturated and, to a smaller extent, mono-unsaturated monomers (alcohols, acids, ω-hydroxy acids and/or α,ω-diols) and of monoester(s). From the analytical data obtained about these lipids, similar structural models than those depicted for monoesters isolated from *C. emersonii* (compounds **1a**–**e** in Fig. 4) can be proposed for these latter. However, considering the large amounts of diols and hydroxy acids identified in the thermochemolysate

the possibility of biosynthesis of higher polyesters by this microalga cannot be ruled out.

In contrast to the two other microalgae, the high molecular weight lipids isolated from *T. minimum* do not yield any alcohol and α,ω-diol upon TMAH thermochemolysis and hydrolysis. Moreover, this microalga is the only one which biosynthesises high molecular weight lipids yielding aromatic moieties upon thermochemolysis and hydrolysis although in small quantities. This indicates the possibility of ester linkages between long chain fatty acids and aromatic alcohols in these lipids. Similar aromatic compounds have been identified in the TMAH thermochemolysate of the cutan biopolymer derived from the leaf cuticles of *Agave americana* (McKinney et al., 1996), and these authors proposed a new chemical structure containing long chain *n*-alkyl units linked to aromatic rings by ester linkages for the cutan biopolymer. However, the quantitative analysis of the thermochemolysate and the hydrolysate which consist predominantly of saturated *n*-C26 and *n*-C28 acids is difficult to correlate with the GPC data (Fig. 2). Indeed, the contribution of mono- and polyester(s) is relatively large in comparison with that of monomers, in this case fatty acids and ω-hydroxy acids, and therefore greater amounts of ω-hydroxy acids were expected in the thermochemolysate. Some of the possible structures of mono- and polyesters which can account for both GPC and qualitative analytical data are shown in Fig. 5.

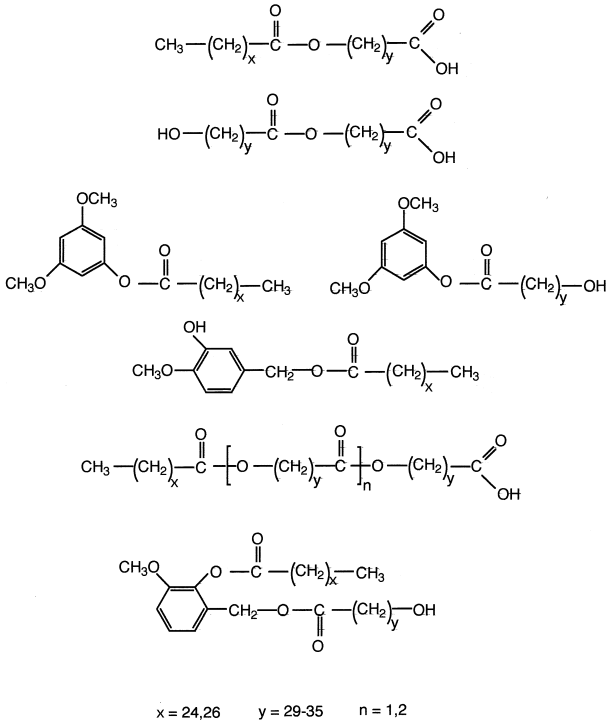

Fig. 5. Proposed chemical structures for the constituents of the high molecular weight lipids isolated from *Tetraedron minimum*.

Monoesters from C24 to C50 have already been detected, although in trace amount, in microalgae belonging to the genus *Chlorella* and *Scenedesmus* (Rezanka and Podojil, 1986; Allard and Templier, 2000). However, to our knowledge, polyesters have never been identified in microalgae probably because of their high molecular weight and their insolubility in the usual solvents. However, this type of polymeric esters, the estolides, formed from a series of ω-hydroxy acids either by interesterification or by esterification with long-chain diols are well known as constituents of higher plant epicuticular waxes (Bianchi, 1995). Moreover, rather unusual monoesters formed by esterification of benzoic acid with C22 to C26 fatty alcohols or by esterification of C22 to C28 fatty acids with benzyl alcohol and 2-phenyl ethanol have been found as well in epicuticular waxes of several plants (Gültz and Marner, 1986; Prasad and Gültz, 1990a,b). Therefore we can suggest that at least some TLS-containing microalgae are able to biosynthesise wax lipids which may have the same protective role against environmental factors and pathogenic infections as higher plants epicuticular waxes.

The microalgae studied show a membrane-like trilaminar outer wall (TLS) which contains algaenan, an insoluble biopolymer resistant to drastic non-oxidative chemical treatments (Derenne et al., 1991; Afi et al., 1996; Allard and Templier, 2000). It is noteworthy that no such high molecular weight lipids were found in neutral lipids of *Chlorella vulgaris* a TLS- and algaenan-devoid microalga (Afi et al., 1996) and of *Chlorella marina* and *Chlorella minutissima marina* TLS-containing microalgae which do not produce algaenan (Allard and Templier, 2000). Therefore, a relationship between the presence of high molecular weight lipids in the microalga and its ability to produce algaenan can be suggested. These high molecular weight lipids could be involved in the formation of the outer cell walls of the TLS- and algaenan-containing microalgae. They could be a less condensed form of the algaenan. Such a similarity of chemical structure between insoluble algaenan and soluble high molecular weight aliphatic lipids has been already demonstrated for the colonial Chlorophycea *Botryococcus braunii* (Metzger and Largeau, 1999). If this hypothesis is confirmed the outer cell wall of TLS- and algaenan-containing microalgae could be described as an insoluble biopolymer (i.e. algaenan) embedded in a complex mixture of highly aliphatic lipid classes (i.e. monomers and esters constituting the high molecular weight lipids). The structure of the outer cell walls of these microalgae would thus display great similarities with the cuticular membrane of higher plants. Such similarities would be consistent with the evolutionary lineage that led to land plants. Similarities of some of the biological functions of cutin and algaenan have been already suggested (Blokker et al., 1998a).

4. Materials and methods

4.1. General

FTIR spectra were recorded on a single-beam Bruker 45 spectrometer. The discs were prepared by mixing 1% (w/w) of the sample with KBr.

Analytical GC was performed on a fused silica RSL-300 capillary column (25 m × 0.25 mm i.d., 0.2 μm film thickness) programmed from 100 to 300°C at 4°C min^{-1}. GC–MS analyses were carried out using a HP5890 gas chromatograph equipped with a fused silica CPSil5CB capillary column (25 m × 0.22 mm i.d., 0,4 μm film thickness) programmed from 100 to 300°C at 3°C min^{-1} coupled to a HP5989 mass spectrometer operated at 70 eV.

Axenic strains of *C. emersonii* (CCAP 211/8P), *S. communis* (CCAP 276/4b) and *T. minimum* were cultured under air-lift conditions and continuous illumination as previously described (Allard and Templier, 2000). Neutral lipids were extracted as previously described (Allard and Templier, 2000).

4.2. NL-2 Sample isolation

Neutral lipid extracts were dissolved in $CHCl_3$ at room temperature. Acetone was added until the formation of a precipitate and the resulting mixture was kept at 4°C for 2–4 days. The precipitate was filtered trough a millipore FH 0.5 μm filter, washed with acetone and dried.

4.3. Gel permeation chromatography

Analyses were performed on a HPLC instrument (Waters) fitted with a differential refractometer thermostated at 30°C, using a Styragel HR-2 column (Waters, 7.8 × 300 mm; effective molecular weight range 500–20000) thermostated at 25°C. The samples were eluted with THF at a flow rate of 1 ml min-[1]. Calibration of the column was performed with standards of polyethylene glycols (Polymer Laboratories).

4.4. Flash pyrolysis with in situ methylation using tetramethylammonium hydroxide (TMAH)

NL-2 Samples (0.5–2 mg) were loaded in tubular ferromagnetic wires (Curie temperature 650°C). Five microliters of 25% TMAH in methanol were added four times in 2 h. The wires were placed into the pyrolysis unit (Fisher 0316M) connected to a high frequency generator which heated them inductively in 0.15 s to the Curie temperature. This temperature was maintained for 10 s. The pyrolysis unit was directly coupled to a HP5890 gas chromatograph equipped with a fused silica CPSil5CB capillary column (25 m × 0.22 mm i.d., 0.4 μm film thickness) programmed from 80 to 300°C at 3°C min^{-1} coupled to a HP5989 mass spectrometer operated at 70 eV.

4.5. Alkaline hydrolysis

NL-2 Samples (10–20 mg) were saponified by refluxing for 1 h with 5% KOH in 2-methoxy ethanol/H_2O, 88/12 (v/v) (Daffé et al. 1983). The reaction mixture was neutralised with 6 N HCl and extracted with $CHCl_3$. The organic phase and the interfacial material developed between aqueous and organic phases were combined, dried and subjected to further derivatisation.

The mixture was treated with 2-methyl-1-propanol/HCl for 1 h at 90°C to convert acids into their 2-methyl-1-propyl esters. After evaporation of the solvent the residue was dissolved in 2-methyl-1-propanol and reduced to dryness once more to completely remove HCl.

For conversion of hydroxyl groups into *O*-trimethylsilyl groups the esterified mixture was treated with a mixture of anhydrous pyridine/1,1,1,3,3,3-hexamethyldisilazane/chlorotrimethylsilane (20/2/1 v/v/v). The mixture was centrifuged and the supernatant analysed.

For conversion of hydroxyl groups into acetoxy groups the esterified mixture was acetylated with a mixture of acetic anhydride/pyridine (1/1 v/v). After addition of H_2O the solvents were evaporated and the residue dissolved in CH_2Cl_2.

4.6. GC–MS identification, characteristic fragmentation ions

4.6.1. Alcohol

TMSi ether: *m/z* 75 (base peak); $M^+ - CH_3$. Acetoxy: *m/z* 61 $[CH_3CO_2H_2]^+$; $M^+ - CH_3$; $M^+ - CH_3CO_2H$.

4.6.2. Acid

2-Methyl-1-propyl ester: *m/z* 56 $[(CH_3)_2CHCH_2 - 1]^+$; *m/z* 57 (base peak); M^+; $M^+ - 56$; $M^+ - OCH_2CH(CH_3)_2$.

4.6.3. α,ω-Diol

TMSi ether: *m/z* 75 (base peak); *m/z* 149 $[(CH_3)_2Si(O)Si(OH)(CH_3)_2]^+$; $M^+ - (CH_3)_3SiOH$; $M^+ - 2 \times (CH_3)_3SiOH$. Acetoxy: *m/z* 61 $[CH_3CO_2H_2]^+$; $M^+ - CH_3CO_2H$; $M^+ - 2 \times CH_3CO_2H$. di-Methyl ether: *m/z* 45; $M^+ - CH_3$; $M^+ - CH_3OH$; $M^+ - 2 \times CH_3OH$.

4.6.4. ω-Hydroxy acid 2-methyl-1-propyl ester

TMSi ether: *m/z* 75; $M^+ - CH_3$; $M^+ - [(CH_3)_2CHCH_2 - 1]^+$; $M^+ - OCH_2CH(CH_3)_2$; $M^+ - OSi(CH_3)_3$. Acetoxy: *m/z* 61 $[CH_3CO_2H_2]^+$; $M^+ - CH_3CO_2H$; $M^+ - HOCH_2CH(CH_3)_2$; $M^+ - [CH_3CO_2H + HOCH_2CH(CH_3)_2]$.

4.6.5. ω-Hydroxy acid methyl ester

Methyl ether: *m/z* 45; *m/z* 74; $M^+ - CH_3$; $M^+ - CH_3OH$; $M^+ - 2 \times CH_3OH$.

References

Afi, L., Metzger, P., Largeau, C., Connan, J., Berkaloff, C., Rousseau, B., 1996. Bacterial degradation of green microalgae: incubation of *C. emersonii* and *C. vulgaris* with *Pseudomonas olevorans* and *Flavobacterium aquatile*. Organic Geochemistry 25, 117–130.

Allard, B., Templier, J., 2000. Comparison of neutral lipid profile of various trilaminar outer cell wall (TLS)-containing microalgae with emphasis on algaenan occurrence. Phytochemistry 54, 369–380.

Bianchi, G., 1995. Plant waxes. In: Hamilton, R.J. (Ed.), Waxes: chemistry, molecular biology and functions. The Oily Press, pp. 175–222.

Blokker, P., Schouten, S., van den Ende, H., de Leeuw, J.W., Sinninghe Damsté, J.S., 1998a. Cell wall-specific ω-hydroxy fatty acids in some freshwater green microalgae. Phytochemistry 49, 691–695.

Blokker, P., Schouten, S., van den Ende, H., de Leeuw, J.W., Hatcher, P.G., Sinninghe Damsté, J.S., 1998b. Chemical structure of algaenan from the freshwater *Tetraedron minimum*, *Scenedesmus communis* and *Pediastrum boryanum*. Organic Geochemistry 29, 1453–1468.

Brunner, U., Honegger, R., 1985. Chemical and ultrastructural studies on the distribution of sporopolleninlike biopolymers in six genera of lichen phycobionts. Canadian Journal of Botany 63, 2221–2230.

Challinor, J.M., 1989. A pyrolysis-derivatization- gas chromatograph technique for the elucidation of some synthetic polymers. Journal of Analytical and Applied Pyrolysis 16, 323–333.

Challinor, J.M., 1994. On the mechanism of high temperature reactions of quaternary ammonium hydroxides with polymers. Journal of Analytical and Applied Pyrolysis 29, 223–224.

Challinor, J.M., 1995. Characterisation of wood by pyrolysis derivatisation-gas chromatography/mass spectrometry. Journal of Analytical and Applied Pyrolysis 35, 93–107.

Clifford, D.J., Carson, D.M., McKinney, D.E., Bortiatynski, J.M., Hatcher, P.G., 1995. A new rapid technique for the characterization of lignin in vascular plants: thermochemolysis with tetramethylammonium hydroxide (TMAH). Organic Geochemistry 23, 169–175.

Daffé, M., Lanéelle, M.A., Asselineau, C., Levy-Frebault, V., David, H., 1983. Interêt taxonomique des acides gras des mycobactéries: Proposition d'une méthode d'analyse. Annales de Microbiologie (Institut Pasteur) 134B, 241–256.

Derenne, S., Largeau, C., Berkaloff, C., Rousseau, B., Wilhem, C., Hatcher, P.G., 1992. Non-hydrolysable macromolecular constituents from outer walls of *Chlorella fusca* and *Nanochlorum eucaryotum*. Phytochemisry 31, 1923–1929.

Derenne, S., Largeau, C., Casadevall, E., Berkaloff, C., Rousseau, B., 1991. Chemical evidence of kerogen formation in source rocks and oil shales via selective preservation of thin resistant outer walls of microalgae: origin of Ultralaminae. Geochimica Cosmochimica Acta 55, 1041–1050.

Gelin, F., Volkman, J.K., Largeau, C., Derenne, S., Sinninghe Damsté, J.S., de Leeuw, J.W., 1999. Distribution of aliphatic nonhydrolysable biopolymers in marine microalgae. Organic Geochemistry 30, 147–159.

Gültz, P.G., Marner, F.J., 1986. Esters of benzyl alcohol and 2-phenyl-ethanol-1 in epcuticular waxes from Jojoba leaves. Zeitschrift für Naturforschung 41c, 673–676.

Hatcher, P.G., Clifford, D.J., 1994. Flash pyrolysis and in situ methylation of humic acids from soil. Organic Geochemistry 21, 1081–1092.

Holland, R.F., Nielsen, J.R., 1962. Infrared spectra of single crystals II. Four forms of octadecanoic acid. Journal of Molecular Spectroscopy 9, 436–460.

Jones, R.N., McKay, A.F., Sinclair, R.G., 1952. Band progressions in the infrared spectra of fatty acids and related compounds. Journal of the American Chemical Society 74, 2575–2578.

de Leeuw, J.W., Baas, M., 1993. The behaviour of esters in the presence of tetramethylammonium salts at elevated temperatures; flash pyrolysis or flash chemolysis? Journal of Analytical and Applied Pyrolysis 26, 175–184.

de Leeuw, J.W., Largeau, C., 1993. A review of macromolecular organic compounds that comprise living organisms and their role in kerogen, coal and petroleum formation. In: Engel, M. (Ed.), Organic Geochemistry Principles and Applications. Plenum Press, New York, pp. 23–72.

Martin, F., Gonzalez-Vila, F.J., del Rio, J.C., Verdejo, T., 1994. Pyrolysis derivatization of humic substances. 1. Pyrolysis of fulvic acids in the presence of tetramethylammonium hydroxide. Journal of Analytical and Applied Pyrolysis 28, 71–80.

McKinney, D.E., Bortiatynski, J.M., Carson, D.M., Clifford, D.J., de Leeuw, J.W., Hatcher, P.G., 1996. Tetramethylammonium hydroxide (TMAH) thermochemolysis of the aliphatic biopolymer cutan: insights into chemical structure. Organic Geochemistry 24, 641–650.

McKinney, D.E., Carson, D.M., Clifford, D.J., Minard, R.D., Hatcher, P.G., 1995. Off-line thermochemolysis versus flash pyrolysis for the in situ methylation of lignins: is pyrolysis necessary? Journal of Analytical and Applied Pyrolysis 34, 41–56.

McKinney, D.E., Hatcher, P.G., 1996. Characterization of peatified and coalified wood by tetramethylammonium hydroxide (TMAH) thermochemolysis. International Journal of Coal Geology 32, 217–228.

Metzger, P., Largeau, C., 1999. Chemicals of *Botryococcus braunii*. In: Cohen, Z. (Ed.), Chemicals from microalgae. Taylor & Francis.

Prasad, R.B.N., Gültz, P.G., 1990a. Developmental and seasonal variations in the epcuticular waxes of beech leaves (*Fagus sylvatica* L.). Zeitschrift für Naturforschung 45c, 805–812.

Prasad, R.B.N., Gültz, P.G., 1990b. Epicuticular waxes from leaves of maple (*Acer pseudoplatanus* L.). Zeitschrift für Naturforschung 45c, 599–601.

Rezanka, T., Podojil, M., 1986. Identification of wax esters of the fresh-water green alga *Chlorella kessleri* by gas chromatography-mass spectrometry. Journal of Chromatography 362, 399–406.

del Rio, J.C. Hatcher, P.G., 1996. Structural characterization of humic substances using thermochemolysis with tetramethylammonium hydroxide. In humic and fulvic acids: isolation, structure and environmental role. In: Gaffney, J.S., Marley, N.A., Clarck, S.B. (Eds.), ACS Symposium Series, 651. American Society, Washington DC, pp. 78-95.

del Rio, J.C., Gonzalez-Vila, F.J., Martin, F., 1996. Thermally assisted hydrolysis and alkylation as a novel pyrolytic approach for the structural characterization of natural biopolymers and geomacromolecules. Trends in Analytical Chemistry 15, 70–79.

del Rio, J.C., Gonzalez-Vila, F.J., Martin, F., Verdejo, T., 1994. Characterization of humic acids from law rank coals by ^{13}C-NMR and pyrolysis-methylation. Formation of benzenecarboxylic moieties during coalification process. Organic Geochemistry 22, 885–891.

del Rio, J.C., Gonzalez-Vila, F.J., Martin, F., Verdejo, T., 1995. Chemical structural investigation of asphaltenes and kerogens by pyrolysis-methylation. Organic Geochemistry 23, 1009–1022.

del Rio, J.C., McKinney, D.E., Knicker, H., Nanny, M.A., Minard, R.D., Hatcher, P.G., 1998. Structural characterization of bio- and geo-macromolecules by off-line thermochemolysis with tetramethylammonium hydroxide. Journal of Chromatography A 823, 433–448.

PERGAMON

Phytochemistry 57 (2001) 469–478

PHYTOCHEMISTRY

www.elsevier.com/locate/phytochem

Triterpenoid saponins from the stem bark of *Elattostachys apetala*

Catherine Lavaud [a,*], Marie-Laure Crublet [a], Isabelle Pouny [b], Marc Litaudon [c], Thierry Sévenet [d]

[a] *Laboratoire de Pharmacognosie, UMR CNRS 6013, Bâtiment 18, BP 1039, 51687 Reims cedex 2, France*
[b] *Laboratoires Pierre Fabre, CRSN, UMR CNRS 1973, 3 rue Ariane, Parc Technologique du Canal, 31527 Ramonville, France*
[c] *Laboratoire des Plantes médicinales, CNRS, Parc Forestier Montravel, BP 643, Nouméa, New Caledonia*
[d] *ICSN, UPR 2031 CNRS, avenue de la Terrasse, 91198 Gif-sur-Yvette cedex, France*

Received 27 November 2000; received in revised form 5 February 2001

Abstract

Six new triterpenoid saponins have been isolated from the stem bark of *Elattostachys apetala* together with four known triterpenoid saponins. Three of these new compounds are glycosides of a newly described genin, 29-hydroxyhederagenin (**1**). On the basis of spectral evidence, the structures of the new saponins were concluded to be α-hederin 28-*O*-[α-L-rhamnopyranosyl-(1→2)-β-D-glucopyranosyl] ester (**2**), sapindoside B 28-*O*-[α-L-rhamnopyranosyl-(1→2)-β-D-glucopyranosyl] ester (**3**), 3-*O*-β-D-xylopyranosyl astrantiasaponin VII (**4**), 3-*O*-[α-L-rhamnopyranosyl-(1→2)-α-L-arabinopyranosyl]-28-*O*-[β-D-glucopyranosyl-(1→2)-{β-D-glucopyranosyl-(1→6)}-β-D-glucopyranosyl]-29-hydroxyhederagenin (**5**), 3-*O*-[α-L-arabinopyranosyl-(1→3)-α-L-rhamnopyranosyl-(1→2)-α-L- arabinopyranosyl]-28-*O*-[β-D-glucopyranosyl(1→2)-{β-D-glucopyranosyl(1→6)}-β-D-glucopyranosyl]-29-hydroxyhederagenin (**6**), and 3-*O*-[β-D-xylopyranosyl-(1→3)-α-L-rhamnopyranosyl-(1→2)-α-L-arabinopyranosyl]-28-*O*-[β-D-glucopyranosyl-(1→2)-{β-D-glucopyranosyl-(1→6)}-β-D-glucopyranosyl]-29-hydroxyhederagenin (**7**). © 2001 Elsevier Science Ltd. All rights reserved.

Keywords: *Elattostachys apetala*; Sapindaceae; Stem bark; Triterpenoid saponins; 29-Hydroxyhederagenin

1. Introduction

The genus *Elattostachys* (Blume) Radlk. (Sapindaceae) comprises fourteen species which are distributed in Malaysia, Australia and Polynesia (Delaude, 1993). *E. apetala* (Labill.) Radlk. (syn. *E. falcata* (A. Gray) Radlk.) is a shrub growing in secondary forests of New Caledonia and named Mako in traditional medicine (Adema, 1993a,b). Its stem bark has been traditionally used as an abortive which is considered dangerous since it may induce female or male sterility (Rageau, 1973). We report here the isolation and structural elucidation of four known saponins: α-hederin, astrantiasaponin VII, clemontanoside-C and sapindoside B, and of six new triterpenoid saponins isolated from the stem bark of this plant.

2. Results and discussion

Ground stem bark of *E. apetala* was extracted with 80% methanol and the methanolic extract was concentrated. The residue was dissolved in pure methanol and poured into acetone to form a precipitate which was finally dialysed against pure water. This extract was then purified using a combination of silica gel column chromatography, preparative TLC and reversed-phase C-18 column chromatography to give ten saponins.

Acid hydrolysis of the crude extract yielded two aglycones identified as hederagenin and 29-hydroxyheder agenin **1**, a new olean-12-ene triterpenoid. The major differences between the ^{1}H and ^{13}C NMR spectra of **1** and hederagenin were due to the replacement of a methyl group by a hydroxymethyl in ring E (Table 1). The ^{1}H NMR spectrum of **1** showed a supplementary two-proton singlet at δ_H 3.2 which correlated with a hydroxymethyl at δ_C 73.4 in an HSQC experiment. The observation of HMBC cross peaks between these protons and four carbons at δ_C 18.6 (CH_3), 28.7 (CH_2), 35.6

* Corresponding author. Tel.: +33-32-69-13-548; fax: +33-32-69-13-596.
E-mail address: catherine.lavaud@univ-reims.fr (C. Lavaud).

0031-9422/01/$ - see front matter © 2001 Elsevier Science Ltd. All rights reserved.
PII: S0031-9422(01)00063-2

Table 1
^{1}H and ^{13}C NMR spectral data (500 MHz) of the aglycon moieties of compounds **1**–**7** and **11**

	1[a]		**2**[b]		**3**[b]		**4**[b]		**5**[b]		**6**[b] and **7**[b]		**11**[b]	
	C	H	C	H	C	H	C	H	C	H	C	H	C	H
1	38.0		39.9	1.00, 1.64	40.6		39.3	0.95, 1.62	39.7	0.98, 1.63	39.7	0.98, 1.63	39.7	
2	25.8	1.54 – 1.65	26.7	1.78, 1.88	26.8	1.82, 1.91	26.6	1.76, 1.86	26.6	1.75, 1.98	26.6	1.76, 1.90	26.6	1.79, 1.86
3	75.2	3.58 (*dd*, 12.2, 4.6)	82.4	3.64 (*dd*, 11.8, 4.6)	82.4	3.64 (*dd*, 11.7, 4.3)	82.3	3.61 (*dd*, 12, 4)	82.3	3.64 (*dd*, 12, 4.7)	82	3.62	82.3	3.64 (*dd*, 12.1, 4.3)
4	41.5		44.1		44.1		44.0		44.0		44		44	
5	49.3		nd[c]	1.65	nd[c]		48.1	1.26	48.2	1.28	48.2	1.28	nd[c]	
6	18.6		19.0	1.38, 1.51	nd[c]		18.8	1.37, 1.47	18.9	1.41, 1.52	18.8	1.42, 1.52	18.9	
7	32.2		33.5	1.40, 1.62	nd[c]		33.5	1.29, 1.36	33.5	1.33, 1.62	33.5	1.33, 1.63	33.4	
8	39.1		40.9		40.9		40.7		40.8		40.8		40.8	
9	47.5		48.2	1.28 (*d*)	48.2	1.62	nd[c]	1.62	nd[c]	1.65	nd[c]	1.65	48.2	
10	36.7		37.8		37.9		37.7		37.6		37.7		37.7	
11	22.8	1.88	24.7	1.92	24.8	1.93	24.6		24.6	1.90	24.6	1.92	24.6	1.92
12	122.3	5.27 (*br t*, 3)	123.8	5.29 (*t*, 3)	123.8	5.29 (*t*, 3.5)	123.3	5.26 (*t*, 3.5)	123.8	5.28 (*t*, 3.4)	123.8	5.28 (*t*, 3.2)	123.6	5.29 (*br t*, 3)
13	143.0		145.0		145.6		145.0		145.1		145.1		145.0	
14	41.5		43.3		43.3		43.1		42.9		42.9		43.2	
15	27.4		29.3		29.5		29.2	1.18, 1.58	29.8	1.06, 1.79	29.8	1.07, 1.80	29.3	
16	23.2		24.2		nd[c]		23.7	1.65, 2.06	23.6	1.88, 2.02	23.6	1.88, 2.03	24.2	
17	nd[c]		48.2		nd[c]		48.1		48.4		48.3		48.2	
18	40.7	2.86 (*dd*, 13.5, 3.5)	43.0	2.84 (*dd*, 13.7, 4.1)	42.8	2.84 (*dd*, 13.3, 4.1)	42.8	2.82 (*dd*, 11.8, 3.8)	41.8	2.89 (*dd*, 13.2, 3.9)	41.3	2.80 (*dd*, 13.6, 4.3)	42.8	2.85 (*dd*, 13.6, 4)
19	40.7	1.08 (*dm*, 14)	47.5	1.16	47.5	1.17	47.5	1.13	41.4	1.11	40.8	1.12 (*dm*, 13.5)	47.4	1.16 (*dm*, 13)
		1.71 (*t*, 13.5)		1.75		1.75		1.72 (*t*, 13)		1.85		1.83 (*t*, 14)		1.75 (*t*, 13.8)
20	35.6		31.6		31.7		31.5		36.8		36.8		31.6	
21	28.7		35	1.25, 1.42	34.7		34.9	1.22, 1.39	29.3	1.18, 1.53	29.3	1.18, 1.52	34.9	
22	31.8		33.1		nd[c]		33.1	1.56, 1.77	32.4	1.71 - 1.76	32.4	1.70 - 1.76	33.1	
23	69.6	3.33	64.7	3.36	64.7	3.36 (*d*, 12)	64.8	3.34 (*d*, 13)	64.6	3.36 (*d*, 11.5)	64.7	3.36 (*d*, 11)	64.6	3.36 (*d*, 12)
		3.59 (*d*, 11)		3.51		3.53 (*d*, 12)		3.52 (*d*, 13)		3.50 (*d*, 11.4)		3.54		3.51 (*d*, 12)
24	11.4	0.80 (*s*)	13.9	0.72 (*s*)	14.0	0.73 (*s*)	13.8	0.70 (*s*)	13.8	0.72 (*s*)	13.9	0.73 (*s*)	13.8	0.72 (*s*)
25	15.4	0.95 (*s*)	16.6	1.05 (*s*)	16.7	1.01 (*s*)	16.6	0.98 (*s*)	16.6	1.00 (*s*)	16.6	1.00 (*s*)	16.7	1.01 (*s*)
26	16.6	0.79 (*s*)	17.9	0.83 (*s*)	18.3	0.83 (*s*)	18.0	0.80 (*s*)	17.9	0.82 (*s*)	17.9	0.82 (*s*)	18.0	0.83 (*s*)
27	25.5	1.14 (*s*)	26.4	1.19 (*s*)	26.4	1.20 (*s*)	26.2	1.16 (*s*)	26.6	1.20 (*s*)	26.5	1.20 (*s*)	26.3	1.19 (*s*)
28	183.0		178.1		nd[c]		178.1		178.2		178.1		178.1	
29	73.4	3.20 (*s*)	33.6	0.93 (*s*)	33.2	0.93 (*s*)	33.5	0.89 (*s*)	74.4	3.21 (*s*)	74.4	3.21 (*s*)	33.5	0.93 (*s*)
30	18.6	0.93 (*s*)	24.2	0.97 (*s*)	23.8	0.96 (*s*)	24.3	0.93 (*s*)	19.8	0.95 (*s*)	19.8	0.95 (*s*)	24.3	0.97 (*s*)

[a] Measured in $CDCl_3$.
[b] Measured in CD_3OD.
[c] Not determinated.

(C) and 40.7 (CH_2) suggested that position C-29 or C-30 was oxygenated. The EI MS of **1** lacked a molecular ion but showed fragment ion peaks arising from the characteristic retro Diels–Alder cleavage of ring C at *m/z* 264, 233 (264-CH_2OH), 219 (264-COOH) and 201 (219-H_2O). In the ROESY spectrum, the Overhauser interactions of the β-axial H-18 (δ_H 2.86, *dd*, $J = 13.5$, 3.5 Hz) with the ethylenic proton H-12 (δ_H 5.27) and with the methyl group at δ_H 0.93, therefore, CH_3-30 indicated that the hydroxymethyl group (CH_2OH) was C-29, in an α-equatorial position (Fig. 1). This was confirmed by the observation of an ROE between H-29 and the α-axial H-19 (δ_H 1.71, *t*, $J = 13.5$ Hz). The assignments of other proton and carbon signals of **1** were deduced from analysis of the usual 2D NMR experiments: COSY, HSQC and HMBC (Table 1). The ^{13}C NMR values of the B/C/D/E ring moieties are in good agreement with those reported for dianic acid which possesses a carboxylic acid function instead of a hydroxymethyl group at C-23 (Oshima et al., 1984; Elgamal et al., 1996). Thus sapogenin **1** is 29-hydroxyhederagenin, i.e. the 3β-hydroxy isomer of the previously described aglycone, spinogenin C_5, of *Acanthopanax spinosus* (Miyakoshi et al., 1993).

Three of the new saponins, compounds **2**, **3** and **4**, are bisdesmosides of hederagenin, while three others, saponins **5**, **6** and **7**, have 29-hydroxyhederagenin as the aglycone. Their structures were established as follows.

In the ESI–MS positive mode, pseudomolecular ions $[M+Na]^+$ were detected at *m/z* 1081, $C_{53}H_{86}O_{21}Na$ for saponin **2**, at *m/z* 1213, $C_{58}H_{94}O_{25}Na$ for saponin **3** and at *m/z* 1375, $C_{64}H_{104}O_{30}Na$ for saponin **4**. The molecular formulae were confirmed by the observation of the corresponding $[M-H]^-$ pseudomolecular ions in the negative mode (at *m/z* 1057 for **2**, 1189 for **3** and 1351 for **4**). The common positive fragment ion at *m/z* 773 and negative fragment at *m/z* 749 were attributed to the formation of an α-hederin type substructure (**8**) that was present in the three new compounds. The ^{13}C NMR spectra demonstrated that these three saponins were all glycosides of an α-hederin unit [3-*O*-α-L-rhamnopyranosyl-(1→2)-α-L-arabinopyranosyl hederagenin, **8**] (Table 1) (Encarnación et al., 1981; Kimata et al., 1983; Lavaud et al., 1994). The presence of this structural unit was corroborated by analysis of heteronuclear correlations in the HSQC and HMBC spectra of the three compounds. The ^1H and ^{13}C NMR data for compound **2** displayed signals for four anomeric protons at δ_H 5.45 (*d*, $J = 7.3$ Hz), 5.38 (*d*, $J = 1.2$ Hz), 5.18 (*d*, $J = 1.2$ Hz) and 4.57 (*d*, $J = 5.1$ Hz), and carbons at δ_C 95.2, 101.8, 102 and 104.5, respectively. The last two pairs of signals were attributed to the diglycosidic chain [α-L-rhamnopyranosyl-(1→2)-α-L-arabinopyranosyl] of α-hederin on the basis of COSY and HSQC connectivities. By comparison with α-hederin, a supplementary methyl carbon at δ_C 18.4 was assigned to a 6-deoxyhexose, and a hydroxymethyl at δ_C 62.5 to a hexose. COSY and HOHAHA experiments allowed full identification of two spin systems: one for a β-D-glucose starting from the deshielded anomeric proton whose chemical shift corresponded to an ester chain, and one for an α-L-rhamnose starting from the anomeric doublet at δ_H 5.38. Sequencing of the diglycosidic ester chain in saponin **2** was achieved by analysis of the HMBC spectrum which showed correlations between C-28 of α-hederin (δ_C 178.1) and H-1 of the glucose ester, and between C-2 of this glucose (δ_C 77.4) and H-1 of the second terminal rhamnose. Thus the structure of the new saponin **2** is 3-*O*-[α-L-rhamnopyranosyl-(1→2)-α-L-arabinopyranosyl]-3β, 23-dihydroxyolean-12-en-28-oic acid 28-*O*-[α-L-rhamnopyranosyl-(1→2)-β-D-glucopyranosyl] ester.

Comparison of the NMR spectra of saponin **2** and compounds **3** and **4** indicated that **3** and **4** possessed one and two supplementary sugar units, respectively. The tandem mass spectrum (ESI–MS/MS) of their pseudomolecular ion $[M+Na]^+$ yielded the same intense fragment ion at *m/z* 905 corresponding to the loss of their ester glycosidic chain. A similar result was obtained in the negative mode starting from $[M-H]^-$ with a fragment ion at *m/z* 881 [M-ester chain]$^-$. This indicated that saponin **4** only differed from **3** by the presence of an additional hexose in its ester chain. The MS/MS fragmentation of the product ion yielded intense ions at *m/z* 773 (positive mode) and 749 (negative mode), suggesting that **3** and **4** possessed a supplementary pentose in the glycosidic chain of the α-hederin moiety. Identification of this pentose as a β-D-xylose, was achieved by analysis of COSY, HOHAHA and HSQC spectra. The ROE interactions observed between H-1 [δ_H 4.50 (**3**), 4.47 (**4**)] and H-3 [δ_H 3.35 (**3**), 3.34 (**4**)] and the axial H-5 [δ_H 3.24 (**3**), 3.21 (**4**)], confirmed the α-axial orientation of these three protons and the β-anomeric configuration of this sugar. In the ROESY spectrum of **3**, the anomeric proton of the xylose revealed an intense ROE with

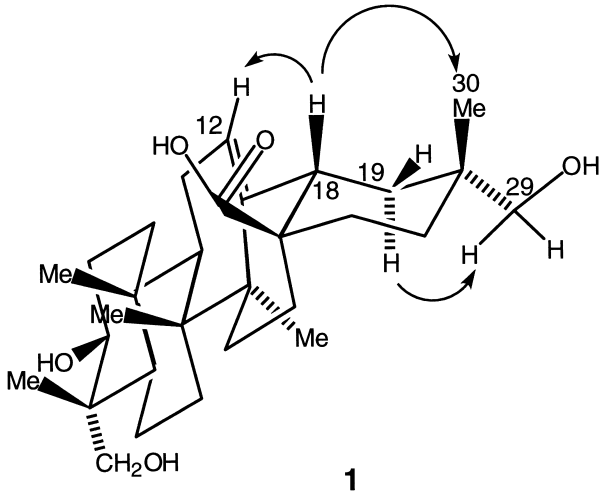

Fig. 1. Significant ROE correlations in ROESY experiment of **1**.

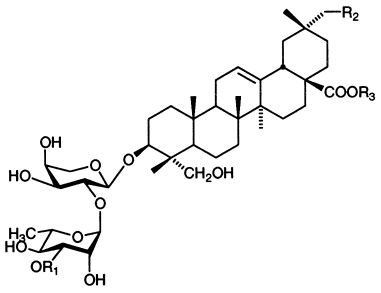

	R_1	R_2	R_3
2	H	H	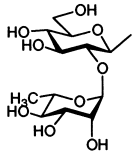
3		H	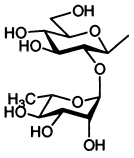
4	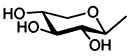	H	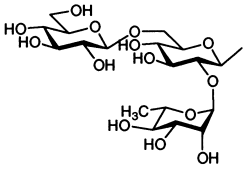
5	H	OH	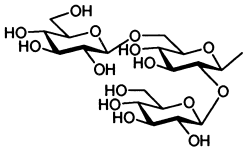
6	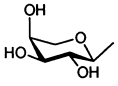	OH	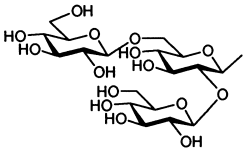
7		OH	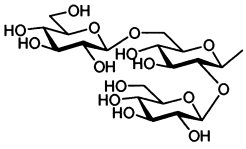
8	H	H	H
9		H	H
10	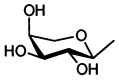	H	H
11	H	H	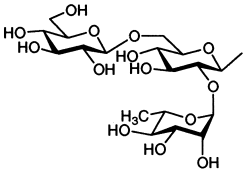

H-3 of the rhamnose of the α-hederin part. Thus, the new saponin **3** corresponds to 3-*O*-[β-D-xylopyranosyl-(1→3)-α-L-rhamnopyranosyl-(1→2)-α-L-arabinopyranosyl]-3β,23-dihydroxyolean-12-en-28-oic acid 28-*O*-[α-L-rhamnopyranosyl-(1→2)-β-D-glucopyranosyl] ester.

The supplementary hexose in the ester chain of saponin **4** was identified as a β-D-glucose by analysis of its proton multiplicities and of COSY and HOHAHA correlations (Table 2). Despite the use of a 500 MHz NMR spectrometer, the presence of six sugar units in **4** resulted in considerable overlap of the glycosidic protons. A relayed COSY experiment was carried out to disentangle the spin systems and obtain unequivocal assignments. This experiment was found particularly useful for the assignments of the glucose H-3 and H-4 protons, which all resonated as large triplets in the same area. The glucose ester (H-1 at δ_H 5.40, C-1 at δ_C 95.2) had its C-6 deshielded (δ_C 69.6) as a consequence of substitution by another sugar unit. The two glycosidic chains of **4** were sequenced by the observation of ROE interactions and HMBC correlations. In the ester triglycosidic chain, ROEs were found between H-1 of the terminal glucose (δ_H 4.33) and the glucose ester H-6 (δ_H 3.74), and between H-1 of the terminal rhamnose (δ_H 5.34) and H-2 and H-3 of the glucose ester. In the triosidic chain at C-3, effects were observed between arabinose H-1 and H-3 of hederagenin, between xylose H-1 and rhamnose H-3, and between rhamnose H-1 and arabinose

Table 2
^{1}H and ^{13}C NMR spectral data (500 MHz) of the glycosidic part of saponins **2**–**4** and **11** in CD_3OD

	2		**3**		**4**		**11**	
	C	H	C	H	C	H	C	H
α-L-Arabinose								
(C-3)								
1	104.5	4.57 (*d*, 5.1)	104.6	4.53 (*d*, 5.7)	104.7	4.51	104.4	4.57 (*d*, 5)
2	76.8	3.73 (*t*, 6)	76.3	3.72	76.2	3.69	76.7	3.72
3	73.9	3.71	74.4	3.71	73.7	3.69	73.7	3.72
4	69.3	3.79	69.9	3.77	69.5	3.75	69.2	3.79
5	65.0	3.52 (*dd*, 12.1, 2.4)	65.6	3.54 (*dd*, 12.7, 3.2)	65.3	3.51 (*dd*, 10, 2)	64.9	3.52 (*dd*, 11.6, 2.3)
		3.85 (*br d*, 12.3)		3.86 (*dd*, 12.8, 4)		3.83 (*dd*, 10, 4)		3.86 (*dd*, 11.3, 4.9)
α-L-Rhamnose								
1	102.0	5.18 (*d*, 1.2)	101.6	5.26 (*d*, 1.6)	101.2		101.9	5.18 (*br s*)
2	72.2	3.93 (*dd*, 3.2, 1.5)	71.8	4.11 (*dd*, 3, 1.8)	71.6		72.0	3.93 (*dd*, 3.2, 1.6)
3	72.3	3.74 (*dd*, 9.5, 3.5)	82.3	3.87 (*dd*, 9.2, 3)	82.1		72.2	3.74 (*dd*, 9.9, 3.2)
4	74.1	3.40 (*t*, 9.4)	73.1	3.58 (*t*, 9.5)	72.8		74.0	3.40 (*t*, 9.5)
5	70.3	3.87 (*dq*, 10, 6)	70.1	3.96	69.9		70.2	3.86
6	18.1	1.26 (*d*, 6.2)	18.1	1.27 (*d*, 6.2)	18.2		18.0	1.26 (*d*, 6.2)
β-D-Xylose								
1			106.6	4.50 (*d*, 7.2)	106.5	4.47 (*d*, 7.2)		
2			75.4	3.31 (*t*, 9.1)	75.2	3.28 (*t*, 8.7)		
3			77.8	3.35 (*t*, 8.8)	77.6	3.34 (*t*, 7)		
4			71.2	3.51	71.1	3.49		
5			69.3	3.24 (*dd*, 11.3, 10.6)	67.0	3.21 (*dd*, 11, 9)		
				3.89 (*dd*, 11.2, 5.4)		3.86 (*dd*, 11, 5)		
β-D-Glucose (ester)								
1	95.2	5.46 (*d*, 7.3)	95.2	5.46 (*d*, 7.4)	95.2	5.40 (*d*, 7.4)	95.2	5.43 (*d*, 7.4)
2	77.4	3.60 (*t*, 8.5)	77.4	3.60 (*t*, 8.6)	77.3	3.58 (*t*, 8.5)	77.3	3.61 (*t*, 8.5)
3	79.3	3.57 (*t*, 8.7)	79.3	3.57 (*t*, 10)	78.9	3.55 (*t*, 7)	78.9	3.58 (*t*, 8.4)
4	71.5	3.42 (*t*, 10)	71.5	3.42 (*t*, 9.9)	71.2	3.48	71.2	3.48 (*brt*, 8.2)
5	78.5	3.36	78.5	3.36	77.6	3.49	77.6	3.52
6	62.5	3.69 (*dd*, 12.3, 3.9)	62.6	3.69 (*dd*, 12.5, 6)	69.6	3.74 (*dd*, 10)	69.6	3.77 (*dd*, 11.5, 4.8)
		3.81 (*dd*, 12.1, 2.3)		3.82 (*dd*, 12, 2.2)		4.09 (*dd*, 10, 4)		4.12 (*dd*, 11.5, 1.5)
α-L-Rhamnose								
1	101.8	5.38 (*d*, 1.2)	101.8	5.38 (*d*, 1.6)	101.7	5.34 (*d*, 1.8)	101.7	5.34 (*br s*)
2	72.0	3.96 (*dd*, 3.2, 1.7)	72.1	3.96 (*dd*, 3.3, 1.9)	71.9	3.93 (*dd*, 3.3, 1.8)	71.9	3.96 (*dd*, 3.1, 1.6)
3	72.3	3.69	72.3	3.68 (*dd*, 9.2, 3)	72.2	3.66 (*dd*, 9, 4)	72.2	3.69 (*dd*, 9.5, 3.2)
4	73.9	3.40 (*t*, 9.4)	73.8	3.40 (*t*, 9.4)	73.2	3.37 (*t*, 9.3)	74.0	3.40 (*t*, 9.5)
5	70.4	3.78	70.4	3.77	70.3	3.74	70.4	3.77
6	18.4	1.26 (*d*, 6.2)	18.1	1.27 (*d*, 6.2)	18.2	1.23 (*d*, 6)	18.3	1.27 (*d*, 6)
β-D-Glucose								
1					104.7	4.33 (*d*, 7.8)	104.7	4.36 (*d*, 7.8)
2					75.2	3.19 (*dd*, 9, 8)	75.2	3.23 (*dd*, 9, 7.5)
3					78.0	3.35 (*t*, 8.9)	78.0	3.37 (*t*, 8.8)
4					71.3	3.28 (*t*, 8.7)	71.5	3.32 (*t*, 8.7)
5					78.0	3.23	78.0	3.26
6					62.7	3.66 (*dd*, 11, 5.3)	62.8	3.69 (*dd*, 11.8, 5.3)
						3.83 (*dd*, 11, 4)		3.87 (*dd*, 12, 1.5)

H-2 and H-3. HMBC cross-peaks confirmed these results, although they did not permit the definitive assignment of the positions of the rhamnoses in these chains. The comparison of ^{1}H and ^{13}C NMR data of **4** with those found for saponin **3** and sapindoside B (**9**) suggested that these three glycosides possessed the same triglycosidic chain attached at C-3 of hederagenin. Finally, comparison of the carbon chemical shifts of the ester glucose moities with those reported in the literature for the lonicerosides from *Lonicera japonica* (Son et al., 1994), showed coherent values with small differences due to solvent effects ($\Delta\delta$ from -0.2 to $+1.2$ ppm). The structure of saponin **4** was thus deduced as 3-*O*-[β-D-xylopyranosyl-(1→3)-α-L-rhamnopyranosyl-(1→2)-α-L-arabinopyranosyl]-3β,23-dihydroxyolean-12-en-28-oic acid 28-*O*-[α-L-rhamnopyranosyl-(1→2)-{β-D-glucopyranosyl-(1→6)}-β-D-glucopyranosyl] ester.

The presence of 29-hydroxyhederagenin as the aglycone in the structure of saponins **5**–**7** was deduced from analysis of their proton and carbon NMR spectra

(Tables 1 and 3) and in particular, by the HSQC experiment which showed only five angular methyls. Two hydroxymethyls were detected in the COSY and HSQC experiments: one formed an AB system at δ_H 3.36 and 3.54 (two *d*, $J=11$ Hz) for the CH_2OH-23 (δ_C 64.7), and the second a singlet at δ_H 3.21 for the two accidentally equivalent protons of the CH_2OH-29 (δ_C 74.4). The HMBC correlations of the methyl and hydroxymethyl protons confirmed the presence of 29-hydroxyhederagenin in the three saponins. Analysis of MS/MS fragmentation revealed common intense product ions at *m/z* 789 (positive mode) and 765 (negative mode), suggesting that the same diglycosidic chain rhamnose-arabinose, was attached at C-3 of the aglycone, as in compounds **2**–**4** with α-hederin. The MS/MS of pseudomolecular ions of saponins **6** and **7** differed

Table 3
^1H and ^{13}C NMR spectral data (500 MHz) of the glycosidic part of saponins **5**–**7** in CD_3OD

	5		**6**		**7**	
	C	H	C	H	C	H
α-L-Arabinose (C-3)						
1	104.4	4.57 (*m*, $W_{1/2}$ 5.7)	104.6	4.59 (*br d*, 5.5)	104.6	4.56 (*d*, 5.5)
2	76.8	3.72	76.2	3.72	76.2	
3	73.7	3.72	74.2	3.74	74.2	
4	69.2	3.79	69.8	3.78 (*m*, $W_{1/2}$ 7.5)	69.8	
5	64.9	3.52 (*dd*, 12, 2.2) 3.86 (*dd*, 11.4, 4.6)	65.6	3.53 (*dd*, 10.8, 3) 3.86 (*dd*, 11, 5)	65.6	
α-L-Rhamnose						
1	102.0	5.17 (*d*, 1.6)	101.3	5.27 (*d*, 1.5)	101.3	5.26 (*d*, 1.5)
2	72.0	3.94 (*dd*, 3.4, 1.6)	71.7	4.15 (*dd*, 3.3, 1.4)	71.7	
3	72.2	3.74 (*dd*, 9.6, 3.4)	82.1	3.86 (*dd*, 9, 3)	82.1	
4	73.9	3.40 (*t*, 9.4)	72.8	3.58 (*t*, 9.4)	72.8	
5	70.2	3.87	69.9	3.95 (*dq*, 9.5, 6.5)	69.9	
6	18.0	1.26 (*d*, 6.2)	18.1	1.26 (*d*, 6.2)	18.1	
β-D-Xylose			*α-L-arabinose*		*β-D-xylose*	
1			106.5	4.51 (*d*, 7.1)	106.5	4.47 (*d*, 7.2)
2			73.0	3.67 (*t*, 9)	75.3	3.31 (*br t*, 9)
3			74.1	3.56 (*dd*, 9, 3.5)	77.7	3.35 (*t*, 9)
4			69.7	3.84 (*br s*)	70.7	3.52
5			67.2	3.59 (*dd*, 10, 2.5) 3.89 (*dd*, 10, 1)	67.1	3.24 (*dd*, 13, 9) 3.89 (*br d*, 12)
β-D-Glucose (ester)						
1	94.0	5.45 (*d*, 8)	93.9	5.46 (*d*, 8)	93.9	
2	78.0	3.87 (*br t*, 8.8)	78.2	3.88 (*t*, 8)	78.2	
3	78.7	3.68 (*t*, 8.8)	78.7	3.68 (*dd*, 9.5, 8)	78.7	
4	70.7	3.51 (*br t*, 8.6)	70.7	3.51 (*t*, 9.5)	70.7	
5	77.8	3.53	77.9	3.53	77.9	
6	69.5	3.80 (*dd*, 11.5, 4.6) 4.13 (*dd*, 11.6, 1.5)	69.5	3.80 (*dd*, 12, 4.6) 4.13 (*dd*, 11, 1.8)	69.5	
β-D-Glucose						
1	103.7	4.82 (*d*, 7.8)	103.7	4.82 (*d*, 7.8)	103.7	
2	75.8	3.23 (*dd*, 9.2, 7.7)	75.8	3.24 (*t*, 8)	75.8	
3	78.0	3.38 (t, 9)	78.0	3.38 (*t*, 9)	78.0	
4	72.6	3.15 (*dd*, 9.5, 9.2)	72.6	3.15 (*t*, 9.4)	72.6	
5	78.2	3.31	78.0	3.31	78.0	
6	63.7	3.65 (*dd*, 11.3, 7) 3.92 (*dd*, 11.6, 2.5)	63.7	3.65 (*dd*, 11.4, 7.2) 3.92 (*dd*, 11.5, 2.4)	63.7	
β-D-Glucose						
1	104.7	4.36 (*d*, 7.8)	104.5	4.36 (*d*, 7.8)	104.5	
2	75.2	3.22 (*dd*, 9, 7.8)	75.2	3.22 (*dd*, 8.9, 7.6)	75.2	
3	78.0	3.37 (*t*, 8.7)	78.0	3.37 (*t*, 8.8)	78.0	
4	71.6	3.30 (*t*, 8.5)	71.6	3.30 (*t*, 8.4)	71.6	
5	78.0	3.26	78.0	3.27	78.0	
6	62.8	3.68 (*dd*, 12, 5.6) 3.87 (*dd*, 12, 2.5)	62.8	3.68 (*dd*, 12.3, 5.9) 3.87 (*dd*, 12, 2)	62.8	

from that obtained for **5** by the presence of a product ion at *m/z* 921 in the positive mode displaced to *m/z* 897 in the negative mode. This proved that an additional terminal pentose was present in the osidic chain of **6** and **7** relative to **5**. Comparison of the NMR data of reference saponins **2**–**4** and clemontanoside-C (**10**), and those of **5**, **6** and **7** enabled us to propose the part-structures 3-*O*-α-L-rhamnopyranosyl-(1→2)-α-L-arabinopyranosyl-29-hydroxyhederagenin for **5**, 3-*O*-α-L-arabinopyranosyl-(1→3)-α-L-rhamnopyranosyl-(1→2)-α-L-arabinopyranosyl -29-hydroxyhederagenin for **6** and 3-*O*-β-D-xylopyranosyl-(1→3)-α-L-rhamnopyranosyl-(1→2)-α-L-arabino pyranosyl-29-hydroxyhederagenin for **7** (Tables 1 and 3). The mass spectra indicated that saponins **5**–**7** contained the same ester glycosidic chain, which was composed of three hexoses. This was confirmed in the ^{13}C NMR by the detection of three hydroxymethyls at δ_C 62.8, 63.7 and 69.5 (Table 3). As above, the identification of these hexoses as three β-D-glucoses was achieved by analysis of COSY and HOHAHA correlations and from the multiplicities and coupling constants of the osidic protons. The glucose ester [anomeric signals at δ_H 5.45 (*d*, $J=8$ Hz) and δ_C 94] was substituted on positions 2 and 6 as shown by the deshielding of C-2, C-6 and H-6. ROE cross-peaks were detected between H-1 of the two other terminal glucoses (δ_H 4.82 and 4.36) and ester glucose H-2 (δ_H 4.82) and H-6 (δ_H 3.80), respectively. The localisation of the ester chain on the carboxylic function C-28 of 29-hydroxyhederagenin was established by its HMBC correlation with H-1 of the ester glucose. Sequencing of the two glycosidic chains was also confirmed by the observation of $^3J_{H\text{-}C}$ correlations through the glycosidic linkages (HC–O–C) in the HMBC spectrum of saponins **5**–**7**. From all these data, the structure of saponin **5** was assigned as 3-*O*-[α-L-rhamnopyranosyl-(1→2)-α-L-arabinopyranosyl]-3β,23,29-trihydroxyolean-12-en-28-oic acid 28-*O*-[β-D-glucopyranosyl-(1→2)-{β-D-glucopyranosyl-(1→6)}-β-D-gluco pyranosyl] ester, that of saponin **6** 3-*O*-[α-L-arabinopyranosyl-(1→3)-α-L-rhamnopyranosyl-(1→2)-α-L-arabino pyranosyl]-3β,23,29-trihydroxyolean-12-en-28-oic acid 28-*O*-[β-D-glucopyranosyl-(1→2)-{β-D-glucopyranosyl-(1→6)}-β-D-glucopyranosyl] ester, and that of saponin **7** 3-*O*-[β-D-xylopyranosyl-(1→3)-α-L-rhamnopyranosyl-(1→2)-α-L-arabinopyranosyl]-3β,23,29-trihydroxyolean-12-en-28-oic acid 28-*O*-[β-D-glucopyranosyl-(1→2)-{β-D-glucopyranosyl-(1→6)}-β-D-glucopyranosyl] ester. Saponins **6** and **7** were obtained as a mixture which was not amenable to separation by silica gel chromatography.

Compounds **8**, **9**, **10** and **11** were identified as known saponins by analysis of their spectral data (ESI–MS, ^1H and ^{13}C NMR) and by comparison with literature values. Saponin **8** corresponded to α-hederin (Encarnación et al., 1981; Lavaud et al., 1994), and saponins **9** and **10** sapindoside B and clemontanoside-C (= saponin A from *Sapindus mukurossi*), respectively (Encarnación et al., 1981; Kimata et al., 1983; Thapliyal and Bahuguna, 1993; Lavaud et al., 1994). Saponin **11** was concluded to be astrantiasaponin VII previously isolated from *Astrantia major* (Hiller et al., 1990). Analysis of ESI–MS and 2D NMR spectra permitted full characterisation of this compound for the first time.

These results are a part of our ongoing study on the saponins of species belonging to the family of Sapindaceae. The isolation and structure elucidation of bisdesmosides of hederagenin and of 29-hydroxyhederagenin from the stem bark of *E. apetala* support the chemotaxonomical proposals of Delaude (1993), namely that species of the subfamily Sapindoideae contain saponins with hederagenin as aglycone, while the genins of saponins from species of the subfamily Dodonaeoideae are most often polyhydroxylated triterpenoids.

3. Experimental

3.1. General

^1H and ^{13}C NMR spectra were recorded on a Bruker DRX-500 spectrometer in CD_3OD or $CDCl_3$ at 500 and 125 MHz, respectively. Two dimensional NMR experiments were performed using standard Bruker microprograms (XWIN-NMR version 2.6 software). ESI mass spectra and MS–MS experiments were performed using a Bruker Esquire LC–MS instrument. Optical rotations were measured on a Perkin-Elmer 241 polarimeter.

3.2. Plant material

The leaves and stem bark of *Elattostachys apetala* were collected in Dumbéa, New-Caledonia by J.P. Cosson and identified by one of us (M.L.). The herbarium sample (CORE 1358) is deposited in the herbarium of the botany laboratory at the IRD centre of Nouméa (New Caledonia).

3.3. Extraction and isolation

Powdered stem bark (720 g) was boiled in 20% aq. MeOH (600 ml) for 3 h. After cooling and filtration, the hydromethanolic extract was evaporated to provide a residue (107.5 g) which was dissolved in MeOH (400 ml). The solution was added to 2 l of Me_2CO and the ppt. was filtered and dried over KOH in vacuo. This ppt. was dissolved in H_2O (360 ml) and dialysed in cellulose tubing against H_2O during 48 h. After freeze-drying of the content of the tubes, 13 g of a saponin mixt. was obtained (yield 1.8%).

A part of the dialysed saponin mixt. (4 g) was purified by silica gel CC (160 g) using a gradient of $CHCl_3$–MeOH–H_2O (95:5:0, 8:2:0, 80:20:1, 80:20:2, 70:30:2, 60:40:5). Frs. eluted with 8:2:0 contained saponin **9** (frs.

[18–22]), a mixt. of saponins **8** and **9** (frs. [32–34]) and saponin **10** (frs [35–45]). Frs. [71–84] eluted with 80:20:1 contained saponins **2** and **3**. Frs. eluted with 70:30:2 contained saponin **11** (frs. [130–143]) and saponin **4** (frs. [144–169]). Frs. [180–195] eluted with 60:40:5 contained saponins **5**, **6** and **7**.

Saponins **2** (14.1 mg) and **3** (6.2 mg) were purified by reversed-phase CC eluted with a gradient of MeOH–H_2O (from 5:5 to 65:35) as eluent and then by prep. TLC in $CHCl_3$–MeOH–H_2O (60:40:5). Saponin **4** (4.1 mg) was purified by reversed-phase CC (C-18) eluted with a gradient of MeOH–H_2O (from 3:7 to 6:4) as eluent and then prep. TLC in $CHCl_3$–MeOH–H_2O (60:40:7). Frs. containing saponin **5** (24 mg), and mixt. of saponins **6** and **7** (26.3 mg) were subjected to ion exchange chromatography by using an Amberlite IRN 77 (H^+) resin column before purification by silica gel CC eluted with $CHCl_3$–MeOH–H_2O (from 9:1:0 to 70:30:4); pure compounds were then obtained by prep. TLC in $CHCl_3$–MeOH–H_2O (60:40:5) using two migrations. Saponins **8** (6.7 mg) and **9** (33.4 mg) were obtained by flash CC eluted with a gradient of $CHCl_3$–MeOH (from 100:0 to 8:2) and then purified by prep. TLC in $CHCl_3$–MeOH (8:2). Saponin **10** (3.8 mg) was purified by silica gel CC with of $CHCl_3$–MeOH (from 100:0 to 8:2) as eluent, followed by reversed-phase CC (MeOH–H_2O; from 5:5 to 8:2); frs. eluted with 7:3 were then purified by prep. TLC in $CHCl_3$–MeOH (7:3). Saponin **11** was purified by prep. TLC in $CHCl_3$–MeOH–H_2O (60:40:7; two migrations) of frs. obtained from reversed-phase CC (MeOH–H_2O; from 5:5 to 6:4).

3.4. Acid hydrolysis of saponins

The crude saponin (300 mg) was dissolved in 20 ml of a mixture (1:1) of H_2SO_4 0.02 N and 6.5% $HClO_4$, and heated at 140°C in a sealed tube for 2 h. After cooling, the sapogenin ppt. was filtered, rinsed with H_2O until pH 7 and dried in vacuo over P_2O_5. The acid aq. layer was neutralized with KOH 0.5 M and freeze-dried. Five sugars were identified with authentic samples by TLC [MeCOEt–Me_2CH_2OH–Me_2CO–H_2O (20:10:7:6)] as glucose, rhamnose, arabinose, xylose and galactose. The sapogenin mixt. (255 mg) was purified by CC on silica gel eluted with a gradient of $CHCl_3$–MeOH. Hederagenin (8.5 mg) was in frs. eluted with $CHCl_3$ and was finally purified by prep-TLC in $CHCl_3$–MeOH [97:3]. The polar frs. were purified by silica gel CC eluting with mixts. of $CHCl_3$–MeOH [100:0, 98:2, 95:5]. Frs. 15–32 contained hederagenin (3.2 mg) and frs. 47–77 eluted with $CHCl_3$–MeOH [95:5] contained 29-hydroxyhederagenin **1** (3.7 mg).

3.5. 29-Hydroxyhederagenin (*1*)

$[\alpha]_D^{20}$ +26° (MeOH, *c* 0.09); EI–MS *m/z* (rel. int.): 264 $[RDA]^+$ (67), 248 (47), 233 $[264\text{-}CH_2OH]^+$ (100), 219 $[264\text{-}COOH]^+$ (34), 201 $[264\text{-}COOH\text{–}H]_2O^+$ (68); ^1H NMR and ^{13}C NMR: see Tables 1 and 2.

3.6. Saponin (*2*)

$[\alpha]_D^{20}$ −14°3 (MeOH, *c* 0.53); ESI–MS (positive) *m/z*: 1081.8 $[M+Na]^+$; ESI–MS–MS (1081) *m/z*: 773.5 $[M+Na\text{-(Rha-glc)}+H]^+$, 729.5 $[M+Na\text{-(Rha-glc-COO)}+H]^+$, 627.5 $[M+Na\text{-(Rha-glc)-Rha}+2H]^+$; ESI–MS–MS (774) *m/z*: 729.5, 627.5, 583.5 $[M+Na\text{-(Rha-glc-COO)-Rha}+2H]^+$, 451.4 $[M+Na\text{-(Rha-glc-COO)-(Rha-ara)}+2H]^+$; ESI–MS (negative) *m/z*: 1057.8 $[M\text{-}H]^-$; ESI–MS–MS (1058) *m/z*: 749.5 $[M\text{-}H\text{-(Rha-glc)}]^-$; ^1H NMR and ^{13}C NMR: see Tables 1 and 2.

3.7. Saponin (*3*)

$[\alpha]_D^{20}$ −14°1 (MeOH, *c* 0.28); ESI–MS (positive) *m/z*: 1213.9 $[M+Na]^+$, 1081.7 $[M+Na\text{-Xyl}+H]^+$; ESI–MS–MS (1214) *m/z*: 905.7 $[M+Na\text{-(Rha-glc)}+H]^+$, 861.8 $[M+Na\text{-(Rha-glc-COO)}+H]^+$, 627.5 $[M+Na\text{-(Rha-glc)-(Xyl-rha)}+2H]^+$; ESI–MS–MS (905) *m/z*: 861.7, 773.5 $[M+Na\text{-(Rha-glc)-Xyl}+2H]^+$, 729.7 $[M+Na\text{-(Rha-glc-COO)-Xyl}+2H]^+$, 627.5, 583.5 $[M+Na\text{-(Rha-glc-COO)-(Xyl-rha)}+2H]^+$;. ESI–MS (negative) *m/z*: 1189.7 $[M\text{-}H]^-$, 1057.7 $[M\text{-}H\text{-Xyl}]^-$, 881.5 $[M\text{-(Rha-glc)}]^-$, 837.5 $[M\text{-}H\text{-(Rha-glc-COOH)}]^-$, 749.5 $[M\text{-(Rha-glc)-Xyl}+H]^-$; ^1H NMR and ^{13}C NMR: see Tables 1 and 2.

3.8. Saponin (*4*)

$[\alpha]_D^{20}$ −12°6 (MeOH, *c* 0.32); ESI–MS (positive) *m/z*: 1375.8 $[M+Na]^+$; ESI–MS–MS (1375.8) *m/z*: 905.7 $[M+Na\text{-(Glc-rha-glc)}+H]^+$, 861.6 $[M+Na\text{-(Glc-rha-glc-COO)}+H]^+$, 773.8 $[M+Na\text{-(Glc-rha-glc)-Xyl}+2H]^+$, 627.7 $[M+Na\text{-(Glc-rha-glc)-(Xyl-rha)}+2H]^+$; ESI–MS (negative) *m/z*: 1351.6 $[M\text{-}H]^-$; ESI–MS–MS (1351.7) *m/z*: 1219.5 $[M\text{-Xyl}]^-$, 1189.5 $[M\text{-Glc}]^-$, 1069.3 $[M\text{-Xyl-Rha-4H}]^-$, 881.4 $[M\text{-(Glc-rha-glc)}]^-$, 749.4 $[M\text{-(Glc-rha-glc)-Xyl}+H]^-$, 603.4 $[M\text{-(Glc-rha-glc)-(Xyl-rha)}+H]^-$; ESI–MS–MS (1219) *m/z*: 1054.4 $[M\text{-Xyl-Glc-2H}]^-$, 937.2 $[M\text{-(Xyl-rha-ara)-4H}]^-$, 791.5 $[M\text{-(Xyl-rha-ara)-Rha-3H}]^-$, 749.3 $[M\text{-(Glc-rha-glc-)-Xyl}+H]^-$; ESI–MS–MS (1189.3) *m/z*: 1069.3, 923.2 $[M\text{-(Xyl-rha-)-Rha-3H}]^-$, 881.3, 791.2 $[M\text{-}H\text{-(Xyl-rha-ara)-Rha-2H}]^-$; ESI–MS–MS (1069.3) *m/z*: 937.2, 881.2; ESI–MS–MS (937.2) *m/z*: 791.4, 749.3; ^1H NMR and ^{13}C NMR: see Tables 1 and 2.

3.9. Saponin (*5*)

$[\alpha]_D^{20}$ −15° (MeOH, *c* 0.32); ESI–MS (positive) *m/z*: 1275.8 $[M+Na]^+$; ESI–MS–MS (1276) *m/z*: 789.5 $[M+Na\text{-(Glc-glc-glc)}+H]^+$, 745.7 $[M+Na\text{-(Glc-glc-}$

glc-COO) + H]$^+$, 509.6 [M + Na-(Glc-glc-glc)-(Rha-ara)]$^+$; ESI–MS–MS (789) *m/z*: 745.7, 643.5 [M + Na-(Glc-glc-glc)-Rha + 2H]$^+$, 599.7 [M + Na-(Glc-glc-glc-COO)-Rha + 2H]$^+$; ESI–MS (negative) *m/z*: 1251.8 [M-H]$^-$, 1287.7 [M + Cl]$^-$. ESI–MS–MS (1251) *m/z*: 970.5 [M-H-(Rha-ara)-2H]$^-$, 927.3 [M-H-Glc-Glc-2H]$^-$, 807.5 [M-H-(Rha-ara)-Glc-2H]$^-$, 765.5 [M-Glc-Glc-glc)]$^-$; ^{1}H NMR and ^{13}C NMR: see Tables 1 and 3.

3.10. Saponins (**6**) and (**7**)

ESI–MS (positive) *m/z*: 1407.9 [M + Na]$^+$, 1275.7 [M + Na-Xyl or Ara]$^+$; ESI–MS–MS (1407) *m/z*: 921.5 [M + Na-(Glc-Glc-glc) + H]$^+$, 509.3 [M + Na-(Glc-Glc-glc)-(Xyl (or Ara)-rha-ara)]$^+$; ESI–MS–MS (921) *m/z*: 877.5 [M + Na-(Glc-Glc-glc-COO) + H]$^+$, 789.7 [M + Na-(Glc-Glc-glc)-Xyl (or Ara) + 2H]$^+$, 599.3 [M + Na-(Glc-Glc-glc-COO)-(Xyl (or Ara)-rha) + 2H]$^+$; ESI–MS (negative) *m/z*: 1419.8 [M + Cl]$^-$, 1383.9 [M-H]$^-$, 1251.7 [M-Xyl]$^-$, 897.5 [M-(Glc-Glc-glc)]$^-$; ESI–MS–MS (1383) *m/z*: 897.5 [M-(Glc-Glc-glc)]$^-$, 765.5 [M-(Glc-Glc-glc)-Xyl or Ara + H]$^-$, 619.3 [M-(Glc-Glc-glc)-(Xyl (or Ara)-rha) + H]$^-$, 487.4 [M-(Glc-Glc-glc)-(Xyl (or Ara)-rha-ara) + H]$^-$; ^{1}H NMR and ^{13}C NMR: see Tables 1 and 3.

3.11. α-Hederin (**8**)

^{1}H NMR spectral data (CD_3OD): δ 0.71 (3H, *s*, Me-24), 0.89 (3H, *s*, Me-26), 0.90 (3H, *s*, Me-29), 0.97 (3H, *s*, Me-30), 0.99 (3H, *s*, Me-25), 1.10 (*m*, H-19), 1.17 (3H, *s*, Me-27), 1.26 (3H, *d*, $J = 6.2$ Hz, Rha-6), 1.68 (*t*, $J = 13.7$ Hz, H-19′), 1.75 (2H, *m*, H-2), 1.90 (2H, *m*, H-11), 2.92 (*dd*, $J = 13.7$, 3.9 Hz, H-18), 3.37 (*d*, $J = 11.2$ Hz, H-23), 3.40 (*t*, $J = 9.5$ Hz, Rha-4), 3.49 (*d*, $J = 11.2$ Hz, H-23′), 3.52 (*dd*, $J = 12.1$, 2.6 Hz, Ara-5), 3.64 (*dd*, $J = 12$, 4.8 Hz, H-3), 3.72 (*m*, Ara-3), 3.73 (*m*, Ara-2), 3.74 (*dd*, $J = 9.4$, 3.3 Hz, Rha-3), 3.78 (*dt*, $J = 5$, 2.7 Hz, Ara-4), 3.86 (*dd*, $J = 12.3$, 5 Hz, Ara-5), 3.87 (*m*, Rha-5), 3.92 (*dd*, $J = 3.4$, 1.7 Hz, Rha-2), 4.58 (*d*, $J = 5.1$ Hz, Ara-1), 5.18 (*d*, $J = 1.6$ Hz, Rha-1), 5.22 (*t*, $J = 3.4$ Hz, H-12); ^{13}C NMR spectral data (CD_3OD): δ 13.6 (C-24), 16.3 (C-25), 17.9 (C-26), 18.1 (Rha-6), 18.8 (C-6), 24.2 (C-30), 24.4 (C-16), 24.5 (C-11), 26.5 (C-27), 26.6 (C-2), 29.2 (C-15), 31.7 (C-20), 33.5 (C-22), 33.8 (C-29), 34.3 (C-7), 35.4 (C-21), 37.6 (C-10), 39.6 (C-1), 40.4 (C-8), 43.0 (C-14), 43.3 (C-18), 43.9 (C-4), 48.0 (C-19), 48.1 (C-9), 64.5 (C-23), 64.5 (Ara-5), 69.1 (Ara-4), 70.1 (Rha-5), 72.0 (Rha-2), 72.1 (Rha-3), 73.6 (Ara-3), 73.9 (Rha-4), 72.8 (Rha-4), 76.5 (Ara-2), 82.3 (C-3), 101.8 (Rha-1), 104.2 (Ara-1), 122.5 (C-12), 146.5 (C-13), 185.8 (C-28).

3.12. Sapindoside B (**9**)

^{1}H NMR spectral data (CD_3OD): δ 0.72 (3H, *s*, Me-24), 0.89 (3H, *s*, Me-26), 0.90 (3H, *s*, Me-29), 0.97 (3H, *s*, Me-30), 0.99 (3H, *s*, Me-25), 1.11 (*dd*, $J = 12$ Hz, H-19), 1.17 (3H, *s*, Me-27), 1.27 (3H, *d*, $J = 6.1$ Hz, Rha-6), 1.64 (*m*, H-19′), 1.76 (*m*, H-2), 1.85 (*m*, H-2), 1.85-1.98 (2H, *m*, H-11), 2.93 (*dd*, $J = 13$, 3.5 Hz, H-18), 3.24 (*t*, $J = 11.3$ Hz, Xyl-5ax), 3.31 (*dd*, $J = 9$, 7.5 Hz, Xyl-2), 3.35 (*t*, $J = 8.6$ Hz, Xyl-3), 3.51 (*m*, Xyl-4), 3.54 (*dd*, $J = 11.8$, 2.2 Hz, Ara-5), 3.58 (*t*, $J = 9.6$ Hz, Rha-4), 3.63 (*dd*, $J = 12$, 5.6 Hz, H-3), 3.72 (*m*, Ara-2), 3.72 (*m*, Ara-3), 3.77 (*m*, $W_{1/2} = 10$ Hz, Ara-4), 3.86 (*dd*, $J = 11.5$, 3.9 Hz, Ara-5), 3.87 (*dd*, $J = 9$, 3.5 Hz, Rha-3), 3.88 (*dd*, $J = 11.5$, 5.3 Hz, Xyl-5eq), 3.94 (*dq*, $J = 9.5$, 6.1 Hz, Rha-5), 4.11 (*dd*, $J = 3$, 1.7 Hz, Rha-2), 4.51 (*d*, $J = 7.3$ Hz, Xyl-1), 4.54 (*d*, $J = 5.4$ Hz, Ara-1), 5.23 (*t*, $J = 3.3$ Hz, H-12), 5.27 (*d*, $J = 1.5$ Hz, Rha-1); ^{13}C NMR spectral data (CD_3OD): δ 13.7 (C-24), 16.3 (C-25), 17.9 (C-26), 18.1 (Rha-6), 18.9 (C-6), 24.3 (C-30), 24.5 (C-11), 24.5 (C-16), 26.4 (C-27), 26.5 (C-2), 29.2 (C-15), 31.7 (C-20), 33.5 (C-22), 33.5 (C-29), 34.3 (C-7), 35.4 (C-21), 37.6 (C-10), 39.6 (C-1), 40.4 (C-8), 43.1 (C-14), 43.4 (C-18), 43.9 (C-4), 48.1 (C-17), 48.1 (C-9), 64.5 (C-23), 65.4 (Ara-5), 66.9 (Xyl-5), 69.6 (Ara-4), 69.9 (Rha-5), 71.0 (Xyl-4), 71.6 (Rha-2), 72.7 (Rha-4), 74.1 (Ara-3), 75.2 (Xyl-2), 76.0 (Ara-2), 77.5 (Xyl-3), 82.1 (Rha-3), 82.3 (C-3), 101.2 (Rha-1), 104.6 (Ara-1), 106.5 (Xyl-1), 122.3 (C-12), 146.7 (C-13).

3.13. Clemontoside-C (**10**)

ESI–MS (positive) *m/z*: 905.6 M + Na$^+$; ESI–MS (negative) *m/z*: 881.5 M-H$^-$; ^{1}H NMR spectral data (CD_3OD): δ 0.72 (3H, *s*, Me-24), 0.89 (3H, *s*, Me-29), 0.90 (3H, *s*, Me-26), 0.97 (3H, *s*, Me-30), 0.99 (3H, *s*, Me-25), 0.99 (*m*, H-1), 1.01 (*m*, H-15),1.10 (*dm*, $J = 13$ Hz, H-19), 1.14 (*m*, H-21), 1.17 (3H, *s*, Me-27), 1.27 (3H, *d*, $J = 6.2$ Hz, Rha-6), 1.28 (*m*, H-5), 1.31 (*m*, H-7), 1.31 (*m*, H-22), 1.35 (*m*, H-21), 1.39 (*m*, H-6), 1.50 (*m*, H-6), 1.62 (*m*, H-7), 1.63 (2H, *m*, H-16), 1.65 (*m*, H-9), 1.66 (*t*, $J = 13$ Hz, H-19′), 1.73 (*m*, H-22), 1.75 (*td*, $J = 12.4$ Hz, H-2), 1.88 (*m*, H-11), 1.89 (*m*, H-2),1.92 (*m*, H-15), 2.93 (*dd*, $J = 13.4$, 3.6 Hz, H-18), 3.24 (*t*, $J = 11.3$ Hz, Xyl-5 eq), 3.31 (*dd*, $J = 9$, 7.5 Hz, Xyl-2), 3.35 (*t*, $J = 8.6$ Hz, Xyl-3), 3.51 (*m*, Xyl-4), 3.38 (*d*, $J = 11.2$ Hz, H-23), 3.52 (*d*, $J = 11.1$ Hz, H-23), 3.54 (*dd*, $J = 12.2$, 2.5 Hz, Ara-5), 3.57 (*d*, $J = 9$ Hz, Ara′-3), 3.58 (*t*, $J = 9.6$ Hz, Rha-4), 3.59 (*dd*, $J = 12$,1.9 Hz, Ara′-5), 3.64 (*dd*, $J = 12$, 4.6 Hz, H-3), 3.66 (*dd*, $J = 9.1$, 7.1 Hz, Ara′-2), 3.72 (*m*, Ara-3), 3.74 (*t*, $J = 7.6$ Hz, Ara-2), 3.78 (*dt*, $J = 5$, 2.7 Hz, Ara-4), 3.83 (*m*, $W_{1/2} = 8$ Hz, Ara′-4), 3.86 (*dd*, $J = 12$, 4 Hz, Ara-5), 3.86 (*dd*, $J = 9.5$, 3 Hz, Rha-3), 3.89 (*dd*, $J = 12.4$, 2.7 Hz, Ara′-5), 3.94 (*dq*, $J = 9$, 6.4 Hz, Rha-5), 4.14 (*dd*, $J = 3$, 1.8 Hz, Rha-2), 4.48 (*d*, $J = 7.1$ Hz, Ara′-1), 4.56 (*d*, $J = 5.5$ Hz, Ara-1), 5.23 (*t*, $J = 3.5$ Hz, H-12), 5.25 (*d*, $J = 1.4$ Hz, Rha-1); ^{13}C NMR spectral data (CD_3OD): δ 13.8 (C-24), 16.4 (C-25), 18.0 (Rha-6), 18.6 (C-26), 18.9 (C-6), 24.4 (C-30), 24.6 (C-11), 24.6 (C-16), 26.5 (C-27), 26.6 (C-2), 29.3 (C-15), 31.8 (C-20), 33.6 (C-7), 34.0 (C-29), 34.4 (C-22), 35.6 (C-

21), 37.7 (C-10), 39.7 (C-1), 40.5 (C-14), 43.1 (C-8), 43.5 (C-18), 44.0 (C-4), 48.5 (C-5), 48.5 (C-19), 49.3 (C-9), 64.7 (C-23), 65.2 (Ara-5), 67.1 (Ara′-5), 69.5 (Ara-4), 69.7 (Ara′-4), 69.9 (Rha-5), 71.7 (Rha-2), 72.7 (Ara′-2), 72.8 (Rha-4), 74.1 (Ara′-3), 74.1 (Ara-3), 76.1 (Ara-2), 82.3 (Rha-3), 82.5 (C-3), 101.3 (Rha-1), 104.6 (Ara-1), 106.5 (Ara′-1), 122.3 (C-12), 146.8 (C-13), 186.1 (C-28).

3.14. Astrantiasaponin VII (**11**)

$[\alpha]_D^{20}$ −16°7 (MeOH, *c* 0.30); ESI–MS (positive) *m*/*z*: 1243.8 $[M+Na]^+$; ESI–MS–MS (1243) *m*/*z*: 1097.8 $[M+Na\text{-}Rha+H]^+$, 773.5 $[M+Na\text{-}(Rha\text{-}Glc\text{-}glc)+H]^+$, 729.5 $[M+Na\text{-}(Rha\text{-}Glc\text{-}glc\text{-}COO)+H]^+$; ESI–MS (negative) *m*/*z*: 1255.8 $[M+Cl]^-$, 1219.8 $[M\text{-}H]^-$, 937.5 $[M\text{-}H\text{-}Rha\text{-}ara\text{-}2H]^-$, 791.5 $[M\text{-}Rha\text{-}(Rha\text{-}ara)\text{-}3H]^-$, 749.5 $M\text{-}(Glc\text{-}Rha\text{-}glc)^-$; ESI–MS–MS (1219) *m*/*z*: 937.5, 791.5, 749.5; ^1H NMR and ^{13}C NMR: see Tables 1 and 2.

Acknowledgements

The authors are grateful to Dr. Georges Massiot of Laboratoires Pierre Fabre, France, for arranging mass spectral analysis and for revising the manuscript.

References

Adema, F., 1993a. *Elattostachys* (Blume) Radlk. (Sapindaceae) in New Caledonia. Bulletin du Museum national d'Histoire naturelle, Paris 15 (4e sér.), 147–151.

Adema, F., 1993b. *Elattostachys* (Blume) Radlk. (Sapindaceae) in Fidji. Pacific Science 47, 295–297.

Delaude, C., 1993. Les Sapindaceae et leurs saponines. Bulletin de la Société des Sciences de Liège 62, 93–120.

Elgamal, M.H.A., Soliman, H.S.M., Tóth, G., Halász, J., Duddeck, H., 1996. Structure of a novel triterpene saponin from *Gypsophila capillaris* (Forssk.). Magnetic Resonance in Chemistry 34, 697–702.

Encarnación, R., Kenne, L., Samuelsson, G., Sandberg, F., 1981. Structural studies on some saponins from *Lecaniodiscus cupanioides*. Phytochemistry 20, 1939–1942.

Hiller, K., Leska, M., Gründemann, E., Dube, G., Karwatzki, A., Franke, P., 1990. Zur Struktur der bidesmosidischen Saponine von *Astrantia major* L. Pharmazie 45, 615–617.

Kimata, H., Nakashima, T., Kokubun, S., Nakayama, K., Mitoma, Y., Kitahara, T., Yata, N., Tanaka, O., 1983. Saponins from pericarps of *Sapindus mukurossi* GAERTN. and solubilization of monodesmosides by bidesmosides. Chemical Pharmaceutical Bulletin 31, 1998–2005.

Lavaud, C., Voutquenne, L., Massiot, G., Le Men-Olivier, L., Delaude, C., 1994. Saponines triterpeniques de *Smelophyllum capense* (Sapindaceae). Bulletin de la Société Royale des Sciences de Liège 63, 455–463.

Miyakoshi, M., Ida, Y., Isoda, S., Shoji, J., 1993. 3α-Hydroxy-oleanane-type triterpene glycosyl esters from leaves of *Acanthopanax spinosus*. Phytochemistry 34, 1599–1602.

Oshima, Y., Ohsawa, T., Hikino, H., 1984. Structure of dianosides C, D, E and F, triterpenoid saponins of *Dianthus superbus* var. *longicalycinus* herb. Planta Medica, 42–47.

Rageau, J., 1973. Les Plantes Médicinales de la Nouvelle-Calédonie. Travaux et Documents de l'O.R.S.T.O.M., p. 63.

Son, K.H., Jung, K.Y., Chang, H.W., Kim, H.P., Kang, S.S., 1994. Triterpenoid saponins from the aerial parts of *Lonicera japonica*. Phytochemistry 35, 1005–1008.

Thapliyal, R.P., Bahuguna, R.P., 1993. Clemontanoside-C, a saponin from *Clematis Montana*. Phytochemistry 33, 671–673.

PERGAMON

Phytochemistry 57 (2001) 479–488

PHYTOCHEMISTRY

www.elsevier.com/locate/phytochem

Hydroquinone derivatives and monoterpenoids from the Neotropical liverwort *Plagiochila rutilans*☆

David S. Rycroft *, W. John Cole

Department of Chemistry, University of Glasgow, Glasgow G12 8QQ, Scotland, UK

Received 15 November 2000; accepted 26 January 2001

Abstract

The structure of a prenylbenzene derivative isolated previously from a Cuban specimen of the liverwort *Plagiochila rutilans* is revised to 2-methoxy-6-prenylhydroquinone. The hydroquinone was observed as a prominent component of the NMR and GC–MS fingerprints of five recent specimens of the liverwort from Bolivia, Brazil and Costa Rica. The corresponding quinone was observed as a minor component. Two new methylated derivatives of the hydroquinone were observed as prominent components in one specimen from Bolivia; these were isolated, characterized, and their structures elucidated as 2-methoxy-1-*O*-methyl-6-prenylhydroquinone and 2-methoxy-4-*O*-methyl-6-prenylhydroquinone using ^{1}H NMR spectroscopy. The liverwort has a strong peppermint-like odour that is caused by the presence of several menthane monoterpenoids, including notably pulegone, menthone, isomenthone, terpinolene and limonene. One of the Costa Rican specimens contained considerable amounts of the new lactone 3,7-dimethyl-2,6-octadien-1,6-olide as the principal monoterpenoid in place of pulegone. Two Costa Rican specimens distinguished morphologically as *Plagiochila standleyi* (a taxon closely related to *P. rutilans* and reduced elsewhere to a variety of that species) are characterized by large amounts of 3-hydroxy-4′-methoxybibenzyl. *P. standleyi* was also reported to have a peppermint-like odour in the field. Menthane monoterpenoids were again responsible but in this case the major components were limonene, β-phellandrene, α-terpinene and the endoperoxide ascaridole. © 2001 Elsevier Science Ltd. All rights reserved.

Keywords: *Plagiochila rutilans*; *Plagiochila standleyi*; Hepaticae; NMR spectroscopy; Structural revision; Chemosystematics; Menthane monoterpenoids; Prenylbenzenes; 3-Methoxy-5-(3-methylbut-2-enyl)-benzene-1,2-diol; 2-Methoxy-6-(3-methylbut-2-enyl)-benzene-1,4-diol; 7-Isopropylidene-4-methyl-6,7-dihydro-5*H*-oxepin-2-one

1. Introduction

Plagiochila (Dumort.) Dumort. is the most numerous hepatic genus: a compilation of names up to the end of 1973 includes around 2500 taxa (Inoue, 1989). Revision of Neotropical *Plagiochilae* is establishing extensive synonymy (Heinrichs et al., 1998), and cooperative morphological and phytochemical studies are helping to improve our understanding of this difficult genus (Heinrichs et al., 2000). We have recently been involved in a taxonomic investigation of *Plagiochila rutilans* Lindenb. (Heinrichs et al., 2001), a species that is poorly known despite a notable peppermint-like odour. A previous chemical study by Huneck et al. (1984) resulted in isolation of an oil with a peppermint-like odour (that was not investigated further) and of a dihydroxymethoxyprenylbenzene that was assigned structure **1** on the basis of NMR data and confirmation by synthesis. A second synthesis of the dimethyl ether of **1** was reported very recently (Brunner et al., 2000). Using NMR and GC–MS fingerprinting (Rycroft, 1996, 1998) we have observed a compound that apparently corresponded to **1** and, in addition, two isomeric hydroxydimethoxyprenylbenzenes, both giving NMR spectra with non-equivalent, *meta*-coupled protons. These two isomers could not both have the same oxygenation pattern as **1**. We have elucidated the structures of this pair of isomers independently, using NOE experiments and by comparison of ^{1}H NMR parameters, and discovered that both have 1,2,4-trioxy-substitution (and are new compounds). NOE experiments also established that the dihydroxymethoxyprenylbenzene reported previously by Huneck et al. (1984) has the same oxygenation pattern and that the correct structure is 2-methoxy-6-prenylhydroquinone (**2**). This paper reports details of the characterization and structural elucidation of these compounds and of a new lactone based on the menthane skeleton, identifies several of the monoterpenoids

☆ Part 11 in the series 'NMR Fingerprinting of Liverworts'. For Part 10 see Rycroft et al. (2001).

* Corresponding author. Fax: +44-141-330-4888.

E-mail address: d.rycroft@chem.gla.ac.uk (D.S. Rycroft).

0031-9422/01/$ - see front matter © 2001 Elsevier Science Ltd. All rights reserved.
PII: S0031-9422(01)00056-5

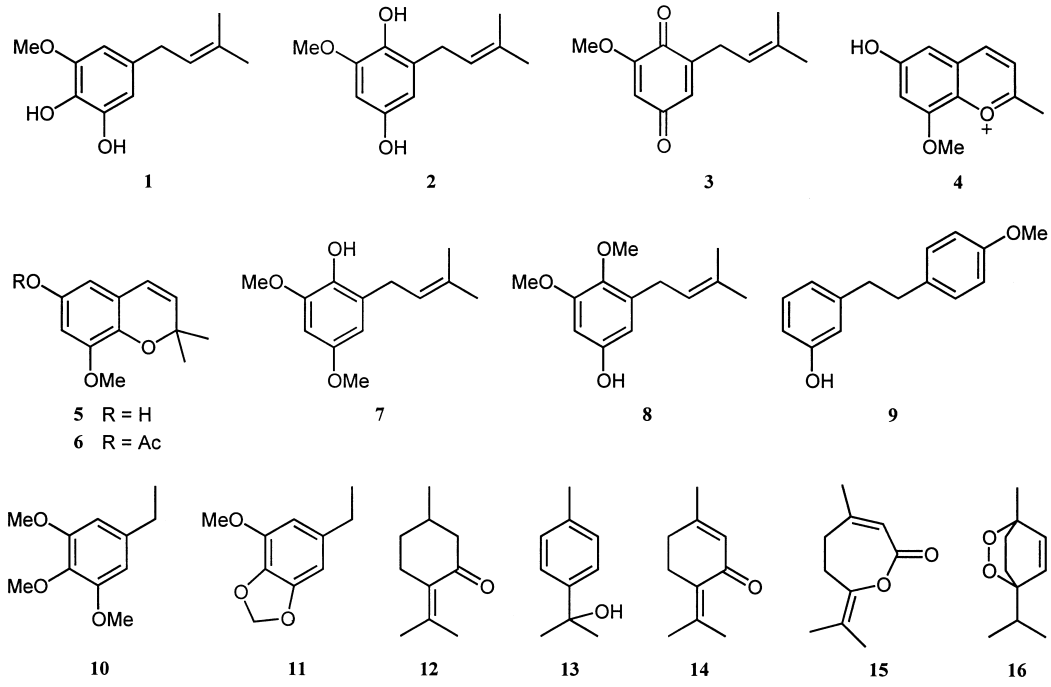

responsible for the odour of *P. rutilans*, and in addition reports details of the composition of the extracts of nine specimens of *P. rutilans* and two of *P. standleyi* Herzog ex Carl, a closely related taxon that is reduced in another publication to a variety of *P. rutilans* (Heinrichs et al., 2001).

2. Results and discussion

2.1. NMR and GC–MS fingerprinting

Six specimens, (i)–(vi) in Table 1, of *Plagiochila rutilans* and two, (vii)–(viii), of *P. standleyi* collected recently from Bolivia, Brazil and Costa Rica were investigated together with three older specimens, (ix)–(xi), from Ecuador and Cuba, including a voucher from the previous work on *P. rutilans* (Huneck et al., 1984). Data for 26 components identified using NMR and GC–MS fingerprinting are summarized in Table 1. Extracts (i)–(viii) from the eight recent specimens gave good NMR fingerprints whereas extracts (ix)–(xi) from the oldest three specimens were poorer and were discounted when trends in the presence of secondary metabolites were assessed in order to delineate chemical races.

2.2.1. Hydroquinone derivatives

NMR fingerprints of the $CDCl_3$ extracts of specimens (ii)–(vi) were dominated in the aromatic and methoxyl regions by proton signals from a pair of *meta*-coupled protons and one methoxyl group. Comparison within the set of spectra showed that one of the Brazilian specimens, (iv), was particularly rich in the compound responsible and a set of signals was observed that was consistent with that reported for compound **1** (Huneck et al., 1984). GC–MS confirmed that the predominant component of the extract had M_r 208. One-dimensional NOE experiments involving pulsed field gradients (PFGs, cf. Stott et al., 1997) produced NOEs between the allylic methylene protons and only one of the aromatic protons, and between the methoxyl protons and the other aromatic proton. The base peak in the mass spectrum has m/z 152 $[M–C_4H_8]^+$, indicative of a hydroxyl group *ortho* to the prenyl group, whereby the hydroxyl proton can undergo intramolecular transfer to a departing C_4H_7 fragment (Ritchie et al., 1964). This evidence leads to the conclusion that structure **1** should be revised to **2**, namely 2-methoxy-6-prenylhydroquinone. Differences between *ortho*- and *para*-shielding effects in an aromatic ring are rather subtle, so that ^{13}C NMR spectra cannot readily be used to assign structures **1** and **2** a priori. The ^{13}C chemical shifts assigned previously (Huneck et al., 1984) to the oxygenated aromatic carbons are in fact very similar to values reported for an oligoprenyl homologue of **2** (Bonny and Capon, 1994).

GC–MS of the extracts containing **2** always indicated the presence of a component with M_r 206 that was assigned to the corresponding quinone, 2-methoxy-6-prenyl-1,4-benzoquinone (**3**). A set of aromatic, methoxyl and allylic methylene ^1H NMR peaks was observed to correlate with the proportions of this component. and had chemical shifts very close to those of an oligoprenyl homologue (Bonny and Capon, 1994). The proportion of **3** increased slowly as an extract was stored and the proportion derived from GC–MS, performed after the NMR fingerprinting, was often greater than the minor

amount observed in the initial NMR spectrum (Table 1). It is possible that some of the quinone observed was formed by oxidation of **2** during extraction. The base peak in the mass spectrum of **3** has m/z 191 $[M–CH_3]^+$ and is assigned to the chromenium ion **4**, formed following the characteristic intramolecular cyclization of 1,4-benzoquinones prenylated in the *ortho* position (Das et al., 1965). GC–MS of extract (vi) showed a minor peak (24% of **3**) that eluted just before **3** ($\Delta R_i = 4$) and that produced a very similar mass spectrum, the main differences being that the base peak was relatively more intense and the three peaks with m/z 159, 121 and 69 were much less intense. As m/z 69 arises from cleavage producing a prenyl fragment $C_5H_9^+$, the minor component is assigned to the chromenol **5**, the cyclized isomer that is unlikely to eliminate $C_5H_9^+$. The mass spectrum we observed is similar to that obtained for the synthetic compound **5** (Garcías et al., 1991; Saá, personal communication). Reduction of the temperature of the injection port from 250 to 200°C did not affect the ratio of **5** to **3** and provided evidence that **5** was present in the solution before injection. GC–MS of the acetylated extracts showed that **3** could be acetylated along with the hydroxyl-containing compounds; the main product showed an increase in mass of 42 Da and is presumably the monoacetate **6**, formed from both **3** and **5**.

^{1}H NMR spectra indicated that the $CDCl_3$ extracts of the oldest three specimens of *P. rutilans* were weak and few peaks were identifiable in the NMR fingerprints. GC–MS of these extracts nevertheless gave useful information about the phenolic compounds and demonstrated that **2** and **3** were present in both Cuban specimens, (ix) and (x), whereas only the quinone **3** was present in the Ecuadorian specimen (xi). Specimen (i) (Bolivia, 1997) gave a weaker extract than the more recent specimens but the NMR fingerprint was very useful. A dominant pair of methoxyl signals as well as a pair of *meta*-coupled aromatic protons indicated a methylated derivative of **2** and an additional set of analogous minor signals (also observable in the more recent specimens) suggested the presence of a second isomer. GC–MS of the extract confirmed the presence of two components with M_r 222.

The extract of a larger amount of the 1997 Bolivian collection was chromatographed, using $CDCl_3$ as eluent, through a short plug of silica gel in a Pasteur pipette and fractions were collected in NMR tubes. The first fraction contained the less polar, minor hydroxydimethoxy-isomer (0.2 mg). GC–MS high resolution mass measurement confirmed the formula $C_{13}H_{18}O_3$. A hydroxyl group *ortho* to a prenyl group, analogous to **2**, was indicated by the base peak m/z 166 arising from $[M–C_4H_8]^+$. NOE experiments using PFG selective excitation produced an NOE from the allylic methylene protons to the more shielded aromatic doublet. Selective excitation of the latter signal enhanced the more shielded methoxyl signal, whereas selective excitation of the less shielded aromatic doublet enhanced both methoxyl signals. These observations lead to the conclusion that the less polar isomer is 2-methoxy-4-*O*-methyl-6-prenylhydroquinone (**7**). Apart from the side-chain, the chemical shifts are extremely similar to those reported for analogous compounds with straight chain alkenyl and alkyl groups such as belamcandol A (Fukuyama et al., 1991), hierridin (González et al., 1992b) and belamcandaphenol P (Seki et al., 1995).

The fourth fraction from the mini-column contained the more polar, major hydroxydimethoxy-isomer (0.4 mg). GC–MS high resolution mass measurement again confirmed the formula $C_{13}H_{18}O_3$. Attempts to measure NOEs were frustrated by decomposition of the compound in dilute $CDCl_3$ solutions during long experiments, even when an amber tube was used. There are four possible structures remaining with a pair of non-equivalent *meta*-coupled protons. The more polar isomer was assigned structure **8**, 2-methoxy-1-*O*-methyl-6-prenylhydroquinone, on three grounds. First, the chemical shifts are extremely similar to those reported for analogues with a straight chain alkenyl or alkyl group instead of a prenyl group; comparators are a synthetic isomer of hierridin (González et al., 1992a), the (*Z*)-heptadec-10-enyl compound (Marner and Horper, 1992) and irisphenol (Seki et al., 1995). Secondly, the chemical shift, δ4.6, and breadth of the NMR signal of the remaining hydroxyl proton indicate that it is not hydrogen-bonded to an adjacent methoxyl group; in contrast, in **7** the hydroxyl group at C-1 can hydrogen-bond to the methoxyl group at C-2 and the hydroxyl proton is observed as a relatively sharp singlet at δ5.27. Thirdly, the compound elutes more slowly than its isomer **7** both on silica gel and on GC, and structure **8** has the hydroxyl group in the most accessible position. Decomposition presumably occurs via phenolic oxidation and the presence of aromatic protons *ortho* to the hydroxyl group in **8** also accounts for the greater tendency of **8**, compared to **7**, to decompose.

2.1.2. Bibenzyls and ethylbenzenes

The *P. standleyi* specimens, (vii) and (viii), stand apart from the others in containing very large amounts (5% w/w) of 3-hydroxy-4′-methoxybibenzyl (**9**). This bibenzyl, unknown in Nature until it was reported recently from *Plagiochila* sect. *Glaucescentes* Carl (Heinrichs et al., 2000), was generally detectable in only trace amounts in the other extracts.

Although the ^{1}H NMR spectra of the three oldest specimens were generally less informative, extract (ix), from the 1978 Cuban specimen, did show three methoxyl signals and three aromatic signals with relative intensities 12:6:3:4(s):1(d):1(m), respectively, as well as a singlet with relative intensity 2 at an intermediate chemical shift. GC–MS showed two substantial unassigned peaks with M_r 196 and 180 in the ratio 2:1. Although

Table 1
Compounds in $CDCl_3$ extracts of *Plagiochila rutilans* Lindenb., (i)–(vi) and (ix)–(xi), and *Plagiochila standleyi* Herzog ex Carl, (vii)–(viii), in order of elution on GC. Minor components observed only using GC–MS are included if they were >5% in at least of three extracts (i)–(viii), except that some additional peaks with R_i <1200 are included so that the monoterpenoid picture is more complete

		Specimen and extract number										
		(i)	(ii)	(iii)	(iv)	(v)	(vi)	(vii)	(viii)	(ix)	(x)	(xi)
		Country, year of collection and collection number										
		Bolivia		Brazil		Costa Rica				Cuba		Ecuador
		1997 Heinr. et al. 4181	2000 Groth 101	2000 Co. and Gr. 3868	2000 Co. and Gr. 3776	1999 Heinr. et al. 4195	2000 Holz CR 00-0654	1999 Heinr. et al. 4191	1999 Heinr. et al 4302	1978 Pócs and R. 9046/E	1980 Pócs 9200/M	1991 Arts Ec. 18/036
		Weight of liverwort extracted (mg)										
		45	6	34	51	17	17	35	17	20	28	20
Compound name (R_i)[a]	Structure number	GC–MS TIC ratio expressed as % of the most abundant compound in each extract; '*t*' indicates <1% (in parentheses: % w/w extracted from the liverwort, derived from concentrations measured in the NMR spectra)										
Sabinene (964)		1	1	2	1	2	2	–	–	*t*	*t*	–
β-Pinene (983)		–	2	3	1	3	1	–	–	–	–	–
α-Terpinene (1006)		–	*t*	*t*	*t*	–	–	6 (0.5)	*t* (0.5)	–	–	–
p-Cymene (1010)		1	*t*	*t*	*t*	1	–	1	2	3	2	–
β-Phellandrene[b] (1017)		+ (0.01)	–	+	+	+ (0.1)	–	+ (0.5)	+ (0.6)	–	*t*	*t*
Limonene[b]		23 (0.02)	5 (0.2)	9 (0.3)	5 (0.2)	30 (0.2)	4	25 (1.2)	36 (1.8)	6	8	*t*
p-Isopropenyltoluene (1067)		*t*	*t*	*t*	*t*	1	–	–	*t*	6	4	–
Terpinolene (1073)		–	49 (1.2)	45 (1.5)	27 (0.4)	3 (0.3)	22	–	–	–	–	–
1-Octen-3-yl acetate (1093)		12	3	4	2	4	2	1	*t*	*t*	2	*t*
Menthone (1127)		6	3	1 (0.3)	25 (0.1)	33	–	–	–	48	18	1
Isomenthone (1137)		*t*	*t*	2	6	2	–	–	–	15	7	*t*
8-*p*-Cymenol (1157)	**13**	25 (0.02)	*t*	1	*t*	4	3	–	–	100 (0.1)	30 (0.04)	*t*
Ascaridole (1205)	**16**	–	–	–	–	–	–	6[c] (0.5)	16[c] (0.8)	–	–	–
Pulegone (1208)	**12**	81 (0.1)	100 (2.3)	100 (2.9)	34 (0.5)	100 (0.7)	–	–	–	3	2	8 (0.02)
3,7-Dimethyl-2,6-octadien-1,6-olide	**15**	–	–	–	–	–	100 (0.5)	–	–	–	–	–

(*continued on next page*)

Table 1 (*continued*)

Compound name (R_i)[a]	Structure number	Specimen and extract number										
		(i)	(ii)	(iii)	(iv)	(v)	(vi)	(vii)	(viii)	(ix)	(x)	(xi)
		Country, year of collection and collection number										
		Bolivia		Brazil		Costa Rica				Cuba		Ecuador
		1997 Heinr. et al. 4181	2000 Groth 101	2000 Co. and Gr. 3868	2000 Co. and Gr. 3776	1999 Heinr. et al. 4195	2000 Holz CR 00-0654	1999 Heinr. et al. 4191	1999 Heinr. et al 4302	1978 Pócs and R. 9046/E	1980 Pócs 9200/M	1991 Arts Ec. 18/036
		Weight of liverwort extracted (mg)										
		45	6	34	51	17	17	35	17	20	28	20
		GC–MS TIC ratio expressed as % of the most abundant compound in each extract; '*t*' indicates <1% (in parentheses: % w/w extracted from the liverwort, derived from concentrations measured in the NMR spectra)										
Peculiaroxide (1391)		100 (0.1)	7 (0.2)	7 (0.2)	14 (0.2)	24 (0.2)	51 (0.2)	–	*t* (0.1)	–	–	10 (0.03)
5-Ethyl-1-methoxy-2,3-methylenedioxybenzene	**11**	–	–	–	–	–	–	–	–	34 (0.05)	*t*	–
5-Ethyl-1,2,3-trimethoxybenzene	**10**	–	–	–	–	–	–	–	–	78 (0.1)	2	–
Bicyclogermacrene (1475)		–	12 (0.2)	12 (0.3)	16 (0.2)	9 (0.2)	2	*t* (0.1)	*t* (0.1)	–	–	–
Spathulenol (1544)		30 (0.04)	*t*	2 (0.05)	2 (0.02)	17 (0.1)	*t*	–	*t*	–	25 (0.04)	32 (0.1)
2-Methoxy-6-prenyl-1,4-benzoquinone	**3**	8	10 (0.1)	8 (0.04)	15 (0.1)	52 (0.1)	34 (0.03)	–	–	4	24	1
2-Methoxy-4-*O*-methyl-6-prenylhydroquinone	**7**	5 (0.02)	*t*	*t* (0.02)	4 (0.02)	8 (0.1)	*t*	–	–	–	1	–
2-Methoxy-1-*O*-methyl-6-prenylhydroquinone	**8**	31 (0.06)	–	–	–	–	–	–	–	–	–	–
2-Methoxy-6-prenylhydroquinone	**2**	–	34 (1.0)	17 (0.8)	100 (1.4)	14 (0.6)	4 (0.2)	–	–	2	*t*	–
Fusicoccadiene (1962)		7	3	2	5	10	17	–	–	61	80	16
3-Hydroxy-4′-methoxybibenzyl	**9**	1	–	*t*	*t*	*t*	–	100 (5.2)	100 (5.2)	*t*	2	*t*

[a] The Kováts retention index is in Section 3 (Experimental) if it is not in this column.

[b] Limonene and β-phellandrene are almost coincident under our elution conditions but the mass spectra are distinguishable; the TIC ratios shown against limonene are for the sum of both compounds and '+' indicates that β-phellandrene was also present.

[c] Sum of the TIC ratios of ascaridole and its isomeric thermal transformation product.

the compounds were not isolated, consideration of the signals and ratios observed led to the proposal that the compounds are a pair of ethylbenzene derivatives with structures **10** and **11** respectively; appropriate ethyl NMR signals could also be identified. The published ^{1}H NMR and GC–MS data for compound **10** (Pincock and Wedge, 1994) are extremely similar to those observed in extract (ix). The assignment of structure **11** relies on the close analogy of the data to those of compound **10**.

Ironically, the oxygenation pattern of **10** and **11** is the same as that of **1**, the structure published originally for the prenylhydroquinone derivative **2**. Structures **10** and **11** were in fact assigned before it was realised that the published structure was incorrect. Nevertheless, although the biogenesis of compounds **10** and **11** is unknown, bibenzyls with the same arrangement of oxygen substituents as **10** and **11** have in fact been reported from liverworts (Asakawa, 1995). The NMR signals observed militate in favour of the symmetry of structure **10** rather than the pattern of oxygen substituents in structure **2** and we can find no direct evidence pointing to structures other than **10** and **11**.

Compounds **10** and **11** were also detectable in the extract of the second Cuban specimen, (x), but not in any of the others.

2.1.3. Monoterpenoids

GC–MS of the extracts used for NMR fingerprinting showed the presence of several monoterpenoids (Table 1). In the recent specimens there could be large amounts, e.g. pulegone (**12**) was 3% w/w of specimen (iii). There were still significant amounts of pulegone in the oldest specimen, (ix); here, however, there were much larger amounts of other monoterpenoid ketones, namely menthone and isomenthone, and the most abundant component was 8-*p*-cymenol (**13**). The first report from a liverwort (*Riella helicophylla*) of this compound was made only recently by Becker and Martini (1999). In the present case, the presence in the older specimens of greater amounts than in the newer raises the suspicion that **13** may be formed during storage by oxidation of other monoterpenoids.

Extract (vi) differed significantly from (i)–(v) in that pulegone was absent. However, there were large NMR signals rather similar, but not identical, to those of piperitenone (**14**) (Baeckström et al., 1985) and a COSY experiment showed that the proton connectivity was the same as in **14**. A fraction in which the compound responsible was the major component (0.08 mg) was obtained by evaporating the extract and passing it through a short plug of silica gel using $CDCl_3$ as eluent. The NMR spectrum of the fraction confirmed the set of signals assigned to the compound and high resolution GC–MS gave the molecular formula $C_{10}H_{14}O_2$. Modification of structure **14** by addition of one oxygen so that the ^{1}H NMR spectrum changes minimally can only be achieved by inserting the oxygen between C-3 and C-4 of piperitenone. The alternative, epoxidation of the 4(8) double bond, would not only create a chiral centre that could render the C-5 methylene protons non-equivalent but also shift the methyl groups on C-8 to more shielded positions. The compound is, therefore, the new lactone 3,7-dimethyl-2,6-octadien-1,6-olide (**15**).

The *P. standleyi* extracts, (vii) and (viii), already distinct from the others by virtue of the absence of hydroquinone derivatives and the presence of large amounts of the bibenzyl **9**, are also distinct with respect to the monoterpenoid content. Here there are large amounts of limonene (1–2% w/w of the liverwort) and at least 0.5% w/w each of β-phellandrene, α-terpinene and the endoperoxide ascaridole (**16**), identified from signals in the ^{1}H NMR spectrum (Tokuyama and Nakamura, 1994) and comparison with an authentic sample (as *Oleum Chenopodii anthelminthici*). Ascaridole rearranges thermally to *cis*-1,2:3,4-diepoxy-*p*-menthane (Boche and Runquist, 1968), partially even in the injection port of the GC (Nitz et al., 1989). We could largely avert rearrangement by reducing the injection port temperature to 75°C. The mass spectrum we observed for the rearrangement product was very similar to that reported by Nitz et al. (1989) and to that presented by Adams (1995) as arising from *trans*-ascaridole (sic). The mass spectrum we observed for ascaridole itself with a base peak m/z 121 (Section 3.4.10) was very different and also substantially different from those in the literature for ascaridole, e.g. Nitz et al. (1989), Ogawa et al. (1996) and as *cis*-ascaridole (sic), Adams (1995), where the base peak is m/z 43. These spectra were all obtained from GC–MS and we believe the discrepancy is because rearrangement can occur to different extents in the short section of column in the heated transfer tube between the GC and the MS, depending on the characteristics of the column. We consider that our mass spectrum of ascaridole (after GC on a non-polar column) more closely represents that truly arising from fragmentation of structure **16** in the mass spectrometer. Published mass spectra show only small differences between ascaridole and its rearrangement product whereas our spectra show gross differences. Indeed our mass spectrum of ascaridole, with a large m/z 136 peak, is similar to that of α-terpinene, suggesting that loss of dioxygen is the most important primary fragmentation.

Extract (viii) was stored in a freezer over a weekend after the NMR fingerprint was taken. Despite this precaution, a check of the NMR spectrum before the GC–MS measurements were performed revealed no signals for α-terpinene and an increase in the intensity of the ascaridole signals. This observation raises the question of whether or not ascaridole is present in the liverwort originally. Ascaridole can indeed be produced by chlorophyll-sensitized photooxygenation of α-terpinene (Gollnick, 1968). However, our experience with *P. retrorsa* Gottsche

(Rycroft et al., 2001) using the same working methods was that no ascaridole was ever observed in extracts that contained α-terpinene. We conclude that the ascaridole observed in the extract when first prepared was present in the plant originally.

The present work is the first report of ascaridole from liverworts, although two derivatives are known (Becker and Martini, 1999). A putative degradation product was found in *Jungermannia obovata* (Connolly, 1990), although two menthanoid hydroperoxides have also been isolated (Buchanan et al., 1998) and it is possible that ascaridole is not involved.

It is clear that the compounds principally responsible for the peppermint-like odour of *P. rutilans* are pulegone, menthone, isomenthone, terpinolene and limonene. The *P. standleyi* specimens, (vii) and (viii), were also noticed to have a peppermint-like odour in the field; in this case limonene, β-phellandrene and α-terpinene combine to produce the odour.

2.1.4. Sesquiterpenoids

The extracts contain relatively few sesquiterpenoids. Along with peculiaroxide (Wu et al., 1993), the tricyclic compound now known from several *Plagiochilae* (Rycroft et al., 2001), there are the almost ubiquitous bicyclogermacrene and/or the bicyclogermacrene-derived spathulenol (Toyota et al., 1996).

2.2. Chemosystematics

Some of the secondary metabolite data have been incorporated as characters in the redescription of *P. rutilans* (Heinrichs et al., 2001). The phytochemical basis of this chemotaxonomic application of the data is considered here along with the chemosystematic relationships of *P. rutilans*.

2.2.1. Phytochemical variation

The lipophilic secondary metabolite profiles indicated by the data in Table 1 show a related pattern for specimens (i)–(vi). This group of specimens, representing *P. rutilans*, is characterized by substantial amounts of menthane derivatives (especially with a carbonyl group at C-3) and hydroquinone derivatives. The profiles of specimens (vii) and (viii) clearly represent a chemically distinct taxon. Specimens (vii) and (viii) were collected from the same locality but several metres apart and have been assigned to *P. standleyi*. This taxon currently has species status but is differentiated morphologically only weakly from *P. rutilans*. With the support of the present results, its status is being reduced to that of a variety within *P. rutilans* (Heinrichs et al., submitted).

There is chemical variation even within *P. rutilans* as currently circumscribed. In specimens (ii)–(v) the principal monoterpenoid is pulegone (**12**) and the principal hydroquinone is compound **2**. The profiles of specimens (ix)-(xi) are less well defined, but pulegone and the quinone **3** are always present and these older specimens can be placed with specimens (ii)-(v) to form one group. Specimen (i) is differentiated by the presence of compound **8** as the principal hydroquinone, with **2** absent. Specimen (vi) is differentiated by the presence of lactone **15** as the principal monoterpenoid, with pulegone absent.

2.2.2. Phytochemical relationships

Pulegone (together with the lactone **15**) and the hydroquinone derivatives are good chemical markers for characterizing *P. rutilans*, but, as they are unknown elsewhere in *Plagiochila*, they cannot indicate possible phylogenetic relationships of *P. rutilans*. The large amounts of bibenzyl **9** distinguish *P. standleyi* very effectively in the present case, but *P.* sect. *Rutilantes* Carl (the section containing *P. rutilans* and *P. standleyi*) shows no special affinity to *P.* sect. *Glaucescentes*, the only other section where bibenzyl **9** is known (Heinrichs et al., 2000). Bibenzyls occur rather commonly in liverworts (Asakawa, 1995) and, therefore, they cannot serve as clues to close relationships; the unique presence of ascaridole is equally uninformative. The discovery that *P. rutilans* contains small and *P. standleyi* large amounts of the bibenzyl **9** nevertheless indicates that the chemosystematic position of *P. rutilans* (together with *P. standleyi*) is not as isolated as was indicated (Asakawa, 1995) by the results of the original chemical investigation (Huneck et al., 1984). The factor common to hydroquinones and bibenzyls, namely that they are benzene derivatives, may have chemosystematic significance in being able to differentiate *P. rutilans* from the large group of *Plagiochilae* that produces plagiochilines (2,3-secoaromadendranes) (Asakawa, 1995; Söderström et al., 1999). There appears to be a major divide of chemotypes in *Plagiochila* between species that produce 2,3-secoaromadendranes and those that produce benzene derivatives, and the phylogenetic basis of this division is of interest. There is already some evidence that the two groups are not completely mutually exclusive, as riccardin D, a cyclic bisbibenzyl ether, has been isolated together with several 2,3-secoaromadendranes from *P. cristata* (Sw.) Lindenb. (Valcic et al., 1997). However, the question of the relationships of *P.* sect. *Rutilantes* remains unresolved.

2.2.3. Biosynthetic implications

One of the stereogenic centres in menthone and isomenthone is *alpha* to the carbonyl group and might be equilibrated easily. It is clear, however, that the system is not at thermodynamic equilibrium as the menthone/isomenthone ratio varies between ca 20:1 and 1:2 in different extracts. Recent work has suggested that the reaction mechanisms and enzymes of monoterpenoid biosynthesis are very similar in both liverworts and higher plants (Adam and Croteau, 1998). The variable menthone/isomenthone ratio in *P. rutilans* is consistent

with the possibility that, as in *Mentha piperita* L., different enzymes are involved in the production of the two compounds from the co-occurring pulegone (Burbott and Loomis, 1980; Croteau et al., 1991). Alternatively, or in addition, catabolic processes (Croteau, 1991) may operate with different relative selectivities in different populations.

Few metabolites of presumed mixed terpenoid (mevalonate and/or glyceraldehyde-pyruvate) and shikimate biosynthetic origin are known in liverworts (Asakawa, 1995). Compounds **2**, **7** and **8** are the simplest examples known of such liverwort metabolites and indicate possible relationships with biosynthetic pathways leading to similar compounds in organisms where they have been reported, such as algae and sponges (Bonny and Capon, 1994).

2.3. Epilogue

Correction of the structure of the prenylhydroquinone derivative **2** has highlighted two pertinent points concerning structural elucidation. First, it is possible, with appropriate analytical methods and strategies, to establish structures of components of mixtures in situ. Secondly, it is possible for the classical approach of confirmation of structure by synthesis to be fallible. In the case of the synthetic material **1**, it is evident (with the benefit of hindsight) that comparison with the natural product **2** was too cursory.

3. Experimental

3.1. General experimental procedures

GC, GC–MS, GC–EI–HRMS mass measurements (all 70 eV) and ^{1}H NMR (400 MHz, $CDCl_3$ soln., int. ref. TMS) were generally performed as described previously (Rycroft et al., 1999).

3.2. Plant material

The specimens used (Table 1) were duplicates of material deposited recently in hb. GOET and vouchers of the Cuban material from JE (hb. Huneck) and U. Further details of the specimens can be found elsewhere (Heinrichs et al., 2001). Plant identities were determined or confirmed by Jochen Heinrichs (Department of Systematic Botany, Albrecht von Haller Institute of Plant Sciences, University of Göttingen). For preparation of extracts, shoots of *Plagiochila rutilans* and *P. standleyi* were selected from the specimens, with care taken that all shoots of any other hepatics were removed.

3.3. Extraction and NMR and GC–MS fingerprinting

Extracts were prepared by triturating dried plant material with sufficient $CDCl_3$ to produce 0.6–0.7 ml of a filtered solution. NMR fingerprints (Rycroft, 1996, 1998) were obtained by measuring ^{1}H NMR spectra of the solutions. The weight of liverwort extracted and percentage w/w of compounds in the specimens (calculated from concentrations derived from comparison of NMR integrals with the residual $CHCl_3$ signal integration) are shown in Table 1. Compounds in the extracts and acetylation derivatives were also characterized in situ using GC and GC–MS. The GC column (CP Sil 5 CB) was calibrated with a mixture of *n*-alkanes so that the Kováts retention indices shown in Table 1 could be determined. TIC ratios are also shown in Table 1. Data for the acetylated extracts were compared with data for the untreated extracts in order to identify compounds containing hydroxyl groups that could be acetylated. Known compounds were identified by comparison with authentic samples or data available from previous studies.

3.4. Compound isolation and characterization

Specimen (i) (1.3 g) was ground, extracted ($CDCl_3$), chromatographed (eluent $CDCl_3$) through a short plug of silica gel in a Pasteur pipette and six ca 0.7 ml aliquots were collected in 5 mm o.d. NMR tubes. The first fraction contained the minor hydroxydimethoxy-isomer **7** (0.2 mg). The fourth fraction contained the major hydroxydimethoxy-isomer **8** (0.4 mg). The third fraction contained a similar amount of **8** but was less pure; the fifth and sixth fractions contained much smaller amounts.

3.4.1. 2-Methoxy-6-prenylhydroquinone (*2*)

Observed as a major component in the NMR fingerprints of the liverwort extracts. GC–MS: R_i 1824; *m*/*z* (rel. int.): 208 $[M]^+$ (84), 161 (10), 153 (49), 152 (100), 151 (14), 125 (11), 123 (20), 69 (19). ^{1}H NMR: δ 1.71 (3H, *s*), 1.74 (3H, *s*), 3.30 (2H, *d*, $J=7.4$ Hz, 2H-1′), 3.84 (3H, *s*, 2-OMe), 4.4 (1H, *br*. *s*, 4-OH), 5.25 (1H, *s*, 1-OH), 5.30 (1H, *m*, H-2′), 6.21 (1H, *d*, $J=2.8$ Hz, H-5), 6.31 (1H, *d*, $J=2.8$ Hz, H-3). Acetylation product: GC R_i 1957.

3.4.2. 2-Methoxy-6-prenyl-1,4-benzoquinone (*3*)

Observed as a minor component in the NMR fingerprints of the liverwort extracts. GC–MS: R_i 1674; *m*/*z* (rel. int.): 206 $[M]^+$ (44), 191 (100), 159 (55), 121 (65), 93 (33), 91 (41), 77 (37), 69 (84), 53 (31). ^{1}H NMR: δ 1.64 (3H, *s*), 1.75 (3H, *s*), 3.12 (2H, *d*, $J=7.2$ Hz, 2H-1′), 3.82 (3H, *s*, 2-OMe), 5.14 (1H, *m*, H-2′), 5.87 (1H, *d*, $J=2.4$ Hz, H-3), 6.46 (1H, *dt*, $J=2.4$, 1.7 Hz, H-5). Acetylation product: GC R_i 1745.

3.4.3. 8-Methoxy-2,2-dimethyl-2H-chromen-6-ol (*5*)

Observed as a minor component in extract (vi). GC–MS: R_i 1670; *m*/*z* (rel. int.): 206 $[M]^+$ (25), 191 (100), 176 (19), 148 (7), 119 (4), 91 (9), 77 (4), 69 (9).

*3.4.4. 2-Methoxy-4-O-methyl-6-prenylhydroquinone (**7**)*

GC–EI–HRMS: *m/z* 222.1257 $[M]^+$ ($C_{13}H_{18}O_3$ requires 222.1256), 166.0629 $[M–C_4H_8]^+$ ($C_9H_{10}O_3$ requires 166.0630). GC–MS: R_i 1746; *m/z* (rel. int.): 222 $[M]^+$ (83), 175 (7), 167 (36), 166 (100), 151 (8), 139 (10), 137 (10), 123 (10). ^{1}H NMR: δ 1.73 (3H, *s*), 1.74 (3H, *s*), 3.33 (2H, *d*, $J=7.3$ Hz, 2H-1′), 3.75 (3H, *s*, 4-OMe), 3.85 (3H, *s*, 2-OMe), 5.27 (1H, *s*, 1-OH), 5.31 (1H, *m*, H-2́), 6.30 (1H, *d*, $J=2.8$ Hz, H-5), 6.36 (1H, *d*, $J=2.8$ Hz, H-3). Acetylation product: GC R_i 1846.

*3.4.5. 2-Methoxy-1-O-methyl-6-prenylhydroquinone (**8**)*

GC–EI–HRMS: *m/z* 222.1256 $[M]^+$ ($C_{13}H_{18}O_3$ requires 222.1256). GC–MS: R_i 1792; *m/z* (rel. int.): 222 $[M]^+$ (100), 207 (17), 191 (14), 175 (17), 165 (42), 152 (11), 150 (16), 147 (12), 137(11), 69 (12). ^{1}H NMR: δ 1.72 (3H, *s*), 1.73 (3H, *s*), 3.30 (2H, *d*, $J=7.2$ Hz, 2H-1′), 3.74 (3H, *s*, 1-OMe), 3.82 (3H, *s*, 2-OMe), 4.6 (1H, *br. s*, 4-OH), 5.25 (1H, *m*, H-2′), 6.20 (1H, *d*, $J=2.9$ Hz, H-5), 6.30 (1H, *d*, $J=2.9$ Hz, H-3). Acetylation product: GC R_i 1836.

*3.4.6. 3-Hydroxy-4′-methoxybibenzyl (**9**)*

Observed in extracts (vii) and (viii). GC–MS: R_i 2016; *m/z* (rel. int.): 228 $[M]^+$ (20), 165 (1), 152 (1), 121 (100), 106 (1), 91 (2), 78 (3), 77 (5). Acetylation product: GC R_i 2073.

*3.4.7. 5-Ethyl-1,2,3-trimethoxybenzene (**10**)*

Observed in extract (ix). GC–MS: R_i 1446; *m/z* (rel. int.): 196 $[M]^+$ (87), 181 (100), 153 (14), 138 (16), 121 (12), 77 (12), 69 (18), 41 (11). ^{1}H NMR: δ 1.24 (3H, *t*, $J=7.5$ Hz, CH_3CH_2) 2.60 (2H, *q*, $J=7.5$ Hz, CH_3CH_2), 3.83 (3H, *s*, 2-OMe), 3.86 (6H, *s*, 1- and 3-OMe), 6.42 (2H, *s*, 2H-4,6).

*3.4.8. 5-Ethyl-1-methoxy-2,3-methylenedioxybenzene (**11**)*

Observed in extract (ix). GC–MS: R_i 1396; *m/z* (rel. int.): 180 $[M]^+$ (48), 166 (9), 165 (100), 135 (4), 120 (3), 79 (6), 78 (3), 77 (13), 53 (3), 51 (3). ^{1}H NMR: δ 1.22 (3H, *t*, $J=7.5$ Hz, CH_3CH_2) 2.56 (2H, *q*, $J=7.5$ Hz, CH_3CH_2), 3.90 (3H, *s*, 1-OMe), 5.92 (2H, *s*, 2,3-O_2CH_2), 6.36 (1H, *br. s*, H-6), 6.40 (1H, *d*, $J=1.5$ Hz, H-4).

*3.4.9. 3,7-Dimethyl-2,6-octadien-1,6-olide (**15**)*

Major component (0.08 mg) in fraction 1 from mini-columning of extract (vi) through silica gel with $CDCl_3$ as eluent. GC–EI-HRMS: *m/z* 166.0997 $[M]^+$ ($C_{10}H_{14}O_2$ requires 166.0994), 123.0815 $[M–CH_3–CO]^+$ ($C_8H_{11}O$ requires 123.0810). GC–MS: R_i 1384; *m/z* (rel. int.): 166 $[M]^+$ (32), 123 (100), 96 (57), 95 (93), 82 (28), 70 (62), 67 (48), 41 (45), 39(50). ^{1}H NMR: δ 1.67 (3H, *s*), 1.70 (3H, *s*), 1.92 (3H, *s*, 3-Me), 2.39 (2H, *t*, $J=6.4$ Hz, 2H-4), 2.61 (2H, *t*, $J=6.4$ Hz, 2H-5), 5.83 (1H, *q*, $J=1.3$ Hz, H-2).

*3.4.10. Ascaridole (**16**)*

Observed in extracts (vii) and (viii), and as *Oleum Chenopodium anthelminthici*. GC–MS: R_i 1205; *m/z* (rel. int.): 136 $[M–O_2]^+$ (93), 121 (100), 107 (12), 93 (61), 92 (10), 91 (12), 79 (11), 43 (35), 41 (14).

Acknowledgements

This work has emerged from interdisciplinary collaboration with groups in Göttingen and Saarbrücken. We are grateful to Jochen Heinrichs (Göttingen) for sending plant material and for productive e-mail exchanges, Hermann Anton (Saarbrücken) for sending plant material and reference compounds, Dr. José M. Saá (Palma de Mallorca) for sending spectra of compound **5**, Tony Ritchie (Glasgow) for high resolution GC-MS measurements, and Professor Joe Connolly and Dr Bob Hill (Glasgow) for discussions.

References

Adam, K.-P., Croteau, R., 1998. Monoterpenoid biosynthesis in the liverwort *Conocephalum conicum*: demonstration of sabinene synthase and bornyl diphosphate synthase. Phytochemistry 49, 475–480.

Adams, R.P., 1995. Identification of Essential Oil Components by Gas Chromatography/Mass Spectroscopy. Allured Publishing Corporation, Carol Stream, IL.

Asakawa, Y., 1995. Chemical constituents of the bryophytes. In: Herz, W., Kirby, G.W., Moore, R.E., Steglich, W., Tamm, Ch. (Eds.), Progress in the Chemistry of Organic Natural Products, Vol. 65. Springer, Wien, pp. 1–618.

Baeckström, P., Jacobsson, U., Koutek, B., Norin, T., 1985. Photochemical transformations of protonated phenols. A one-step synthesis of umbellulone from thymol. J. Org. Chem. 50, 3728–3732.

Becker, H., Martini, U., 1999. Terpenoids from the in vitro cultured liverwort *Riella helicophylla*. Z. Naturforsch. 54c, 997–1004.

Boche, J., Runquist, O., 1968. Kinetics of the thermal rearrangement of ascaridole. J. Org. Chem. 33, 4285–4286.

Bonny, M.L., Capon, R.J., 1994. A sesquiterpene quinone and hydroquinone from the southern Australian marine sponge, *Thorecta choanoides*. J. Nat. Prod. 57, 539–540.

Brunner, H., Le Cousturier de Courcy, N., Genêt, J.-P., 2000. Heck reactions using aryldiazonium salts towards phosphonic derivatives. Synlett 201–204.

Buchanan, M.S., Connolly, J.D., Rycroft, D.S., 1998. Two new monoterpenoid hydroperoxides from the liverwort *Jungermannia obovata*. J. Indian Chem. Soc. 75, 613–615.

Burbott, A.J., Loomis, W.D., 1980. Monoterpene interconversions by cell-free enzymes from peppermint (*Mentha piperita*). Plant Physiology 65 (Suppl.), 96.

Connolly, J.D., 1990. Monoterpenoids and sesquiterpenoids from the Hepaticae. In: Zinsmeister, H.D., Mues, R. (Eds.), Bryophytes: Their Chemistry and Chemical Taxonomy. Proceedings of the Phytochemical Society of Europe, Vol. 29. Clarendon Press, Oxford, pp. 40–58.

Croteau, R., 1991. Metabolism of monoterpenes in mint (*Mentha*) species. Planta Medica 57 (Suppl. 1), S10–S14.

Croteau, R., Carp, F., Wagschal, K.C., Satterwhite, D.M., Hyatt, D.C., Skotland, C.B., 1991. Biochemical characterization of a spearmint mutant that resembles peppermint in monoterpene content. Plant Physiology 96, 744–752.

Das, B.C., Lounasmaa, M., Tendille, C., Lederer, E., 1965. Mass spectrometry of plastoquinones: the structure of plastoquinones B, C and D. Biochem. Biophys. Res. Commun. 21, 318–322.

Fukuyama, Y., Okino, J., Kodama, M., 1991. Structures of belamcandols A and B isolated from the seed of *Belamcanda chinensis*. Chem. Pharm. Bull. 39, 1877–1879.

Garcías, X., Ballester, P., Saá, J.M., 1991. Palladium catalyzed synthesis of chromenes and chromenols. Tetrahedron Lett. 32, 7739–7742.

Gollnick, K., 1968. Type II photooxidation reactions in solution. Adv. Photochem. 6, 1–122.

González, A.G., Bermejo, B., J., Rodríguez, P.E.M., 1992a. Synthesis of hierridin, a phenol from the lichen *Ramalina hierrensis*. Phytochemistry 31, 1436–1439.

González, A.G., Bermejo, B., J., Rodríguez, P.E.M., Hernández, P., C.E., Chemical constituents of the lichen *Ramalina hierrensis*. Planta Med., 58, 214–218.

Heinrichs, J., Anton, H., Gradstein, S.R., Mues, R., 2000. Systematics of *Plagiochila* sect. *Glaucescentes* Carl (Hepaticae) from tropical America: a morphological and chemotaxonomical approach. Plant Syst. Evol. 220, 115–138.

Heinrichs, J., Gradstein, S.R., Grolle, R., 1998. A revision of the Neotropical species of *Plagiochila* (Dumort.) Dumort. (Hepaticae) described by Olof Swartz. J. Hattori Bot. Lab. 85, 1–32.

Heinrichs, J., Groth, H., Gradstein, S.R., Rycroft, D.S., Cole, W.J., Anton, H., 2001. *Plagiochila rutilans* Lindenb. (Hepaticae): a poorly known species from tropical America. The Bryologist 104(3).

Huneck, S., Connolly, J.D., Harrison, L.J., Joseph, R.S.I., Pócs, T., 1984. 1-(3,4-Dihydroxy-5-methoxyphenyl)-3-methylbut-2-ene from the liverwort *Plagiochila rutilans*. Phytochemistry 23, 2396–2397.

Inoue, H. 1989. Plagiochila. In: Geissler, P., Bischler, H. (Eds.), Index Hepaticarum, Vol. 11. J. Cramer, Berlin, Stuttgart, pp. 106–273.

Marner, F.-J., Horper, W., 1992. Phenols and quinones from seeds of different *Iris* species. Helv. Chim. Acta 75, 1557–1562.

Nitz, S., Kollmannsberger, H., Spraul, M.H., Drawert, F., 1989. Oxygenated derivatives of menthatriene in parsley leaves. Phytochemistry 28, 3051–3054.

Ogawa, S., Shimazaki, R., Soejima, A., Takamure, E., Hanasaki, Y., Fukui, S., 1996. Diurnal changes of singlet oxygen like oxidants concentration in polluted ambient air. Chemosphere 32, 1823–1832.

Pincock, J.A., Wedge, P.J., 1994. The photochemistry of methoxy-substituted benzyl acetates and benzyl pivalates: homolytic vs heterolytic cleavage. J. Org. Chem. 59, 5587–5595.

Ritchie, E., Taylor, W.C., Shannon, J.S., 1964. The mass spectra of quinonoid pigments: characteristic cleavage processes of $\gamma\gamma$-dimethylallyl and other side-chains. Tetrahedron Lett. 1437–1442.

Rycroft, D.S., 1996. Fingerprinting of plant extracts using NMR spectroscopy: application to small samples of liverworts. Chem. Commun. 2187–2188.

Rycroft, D.S., 1998. Chemical comparison of liverworts using NMR spectroscopy. J. Hattori Bot. Lab. 84, 105–111.

Rycroft, D.S., Cole, W.J., Lamont, Y.M., 1999. Plagiochilines T and U, 2,3-secoaromadendranes from the liverwort *Plagiochila carringtonii* from Scotland. Phytochemistry 51, 663–667.

Rycroft, D.S., Heinrichs, J., Cole, W.J., Anton, H., 2001. A phytochemical and morphological study of the liverwort *Plagiochila retrorsa* Gottsche, new to Europe. J. Bryol. 23, 23–24.

Seki, K., Haga, K., Kaneko, R., 1995. Phenols and a dioxotetrahydrodibenzofuran from seeds of *Iris pallasii*. Phytochemistry 38, 965–973.

Söderström, L., Rycroft, D.S., Cole, W.J., Wei, S., 1999. *Plagiochila porelloides* (Plagiochilaceae, Hepaticae) from Changbai Mountain, new to China, with chemical characterization and chromosome measurements. Bryobrothera 5, 195–201.

Stott, K., Keeler, J., Van, Q.N., Shaka, A.J., 1997. One-dimensional NOE experiments using pulsed field gradients. J. Magn. Reson. 125, 302–324.

Toyota, M., Koyama, H., Mizutani, M., Asakawa, Y., 1996. (−)-*ent*-Spathulenol isolated from liverworts is an artefact. Phytochemistry 41, 1347–1350.

Tokuyama, H., Nakamura, E., 1994. Synthetic chemistry with fullerenes. Photooxygenation of olefins. J. Org. Chem. 59, 1135–1138.

Valcic, S., Zaap, J., Becker, H., 1997. Plagiochilines and other sesquiterpenoids from *Plagiochila* (Hepaticae). Phytochemistry 44, 89–99.

Wu, C.-L., Huang, C.-D., Shih, T.-L., 1993. A sesquiterpene oxide of a novel skeleton from the liverwort *Plagiochila peculiaris*. Tetrahedron Lett. 34, 4855–4856.

PERGAMON

Phytochemistry 57 (2001) 489–496

PHYTOCHEMISTRY

www.elsevier.com/locate/phytochem

Application of MS and NMR to the structure elucidation of complex sugar moieties of natural products: exemplified by the steroidal saponin from *Yucca filamentosa* L.

Annick Plock [a], Gabriele Beyer [a], Karl Hiller [a], Egon Gründemann [b], Eberhard Krause [c], Manfred Nimtz [d], Victor Wray [d,*]

[a] *Institut für Pharmazie, Humboldt-Universität zu Berlin, Goethestr. 54, 13086 Berlin, Germany*
[b] *Institut für Angewandte Chemie Berlin Adlershof e.V., Richard-Willstätter-Str. 12, 12489 Berlin, Germany*
[c] *Forschungsinstitut für Molekulare Pharmakologie, Alfred-Kowalke-Str. 4, 10315 Berlin, Germany*
[d] *GBF, Gesellschaft für Biotechnologische Forschung mbH, Mascheroder Weg 1, 38124 Braunschweig, Germany*

Received 18 September 2000; received in revised form 18 January 2001

Abstract

An approach, using well characterized procedures, is presented that should be of general applicability for the structural elucidation of complex sugar moieties of natural products. The methods used are exemplified by the structure elucidation of a new gitogenin-based steroidal saponin that has a strong leishmanicidal activity similar to preparations used in clinical practice and has been isolated by bioactivity-guided fractionation of the ethanolic extract of *Yucca filamentosa* L. leaves. The saponin has been characterized as 3-*O*-((ß-D-glucopyranosyl-(1→3)- ß-D-glucopyranosy-(1→2))(α-L-rhamnopyranosyl-(1→4)-ß-D-glucopyranosyl-(1→3))-ß-D-glucopyranosyl-(1→4)-ß-D-galactopyranosyl)-25R,5α-spirostan-2α,3ß-diol. © 2001 Published by Elsevier Science Ltd. All rights reserved.

Keywords: *Yucca filamentosa* L.; Agavaceae; Steroidal saponin; Gitogenin; Leishmaniasis; Sugar analysis

1. Introduction

The complexity of many bioactive natural products containing sugar residues dictates the use of a combination of modern techniques dominated by those involving mass spectrometry (MS) and nuclear magnetic resonance (NMR) spectroscopy for structure elucidation. In more and more cases the use of a single technique precludes a satisfactory unambiguous determination. In the majority of cases the approach to the complete unambiguous structure can best be categorized as the elucidation of the sugar unit(s) and the aglycone. Here we outline a general approach shown in Scheme 1 and apply it to the structure elucidation of a complex steroidal saponin isolated from *Yucca filamentosa* L. as example. It should be emphasized here that the aim of the application of these techniques is to obtain an unambiguous structure making the most efficient use of modern instrumental techniques. As such the complete assignment of the NMR data is not a prerequisite and, as the molecules become more complex, often not feasible in a reasonable time span even using the highest field NMR spectrometers.

Y. filamentosa L. belongs to the Agavaceae family which has more than 580 species which are widely distributed in tropic and subtropic dry climate regions throughout the world. It is indigenous to northern and middle America, and in Europe it is cultivated as an ornamental plant. The plant is rich in steroidal saponins (Mahato et al., 1982; Voigt and Hiller, 1987). Our interest in these plants arose from their potential in the treatment of leishmaniasis, an increasing major global public-health problem. The pentavalent antimonials are the preferred drugs for the treatment of most forms of leishmaniasis, although treatment with these agents is not consistently effective and has serious toxic side effects. It is known that natural products have potential in the search for new and selective agents (Akendengue

* Corresponding author. Tel.: +531-6181-362; fax: +531-6181-355.
E-mail address: vwr@gbf.de (V. Wray).

0031-9422/01/$ - see front matter © 2001 Published by Elsevier Science Ltd. All rights reserved.
PII: S0031-9422(01)00035-8

Sugar identification	**Aglycone identification**
a) Component monosaccharide identification and, when necessary, absolute configuration determination by chromatographic comparisons after acid hydrolysis	a) Molecular weight from MS data
b) Sugar-linkage analysis by GC-MS of partially methylated alditol acetates	b) 1D ^{1}H and ^{13}C data comparison with literature data for known aglycones
c) Sugar unit sequence from fragmentation ion identification in the MS-MS mode of ESI-MS of the native and permethylated molecule	c) Analysis of HMBC spectrum to confirm b) or to elucidate new structure. Most profitable approach involves the elucidation of correlations of the ^{1}H signals with neighbouring carbons two and three bonds removed in the order: i) Correlations from methyl groups ii) Correlations to and from substituents iii) Correlations from hydrogens bonded to heteroatom bonded carbons iv) Correlations to other hydrogens showing well defined ^{1}H signals assigned in the COSY spectrum
Combined data from a) to c) affords the partial identity of sugar units and sugar sequence	
d) Anomeric configuration and sugar conformation from NMR coupling constant ($^{3}J(HH)$ and $^{1}J(CH)$) data	d) Configuration analysis from "through-space" correlations in 1D NOE, and/or 2D NOESY/ROESY
e) Identity and sequence confirmation from correlations in HMBC spectrum	

Scheme 1. Steps required in the structure elucidation of sugar containing natural products.

et al., 1999). In a preliminary screening the ethanolic extract of *Y. filamentosa* L. showed a strong leishmanicidal activity against *Leishmania mexicana amazonensis*, and the bioactivity-guided fractionation of this extract led to the isolation of a new gitogenin-based steroidal saponin, 1. This activity has been studied by extracellular and intracellular assays with promastigote and amastigote forms of *Leishmania* spp. using microscopical and flow cytometric methods (Plock et al., 2001). Its extra cellular effect on promastigote cultures of *L. mexicana amazonensis* is as high as that of pentamidine which is a drug used in clinical practice. In an intracellular assay using macrophages infected with GFP-transfected *Leishmania major*, 1 showed a dose-related decline of the infection rate and of the number of parasites per cell. This leishmanicidal activity was shown to be at least partially due to the action on the parasite membrane. Clearly for a detailed understanding of such effects an unambiguous structure determination of this compound was desirable.

2. Results and discussion

As more and more modern NMR facilities become available it has become routine to use through-bond correlations, such as homonuclear ^{1}H–^{1}H COSY and TOCSY and inverse ^{1}H-detected heteronuclear ^{13}C–^{1}H HMQC and HMBC, for structure elucidation of sugar-containing molecules. Numerous publications report such determinations and in these a full assignment of the ^{1}H and ^{13}C data are usually attempted. However, as structures become more complex, particularly as the number of sugar units increases, this approach has its limitations and additional information from alternative sources is required. In particular information regarding the nature and linkage of the sugar can now be supplied from MS techniques that require only small amounts of material. We have already reported on the power of these techniques for the rapid, comparative analysis of saponin mixtures (Schöpke et al., 1996a). As an extension of this, here we show that a combination of MS and NMR techniques, in which MS data are initially used and are then supplemented with NMR data, afford an unambiguous structure elucidation without necessarily having recourse to a full, and often extremely time-consuming, complete assignment of the NMR data. Thus the step-by-step approach outlined in Scheme 1, and discussed in more detail below for a specific novel compound from *Y. filamentosa* L., has been used to afford structural information about the saponin in which the nature, position of attachment, and sequence of the sugar constituents as well as details of the aglycone have been umambiguously identified.

2.1. Component sugar identification

Initially a bioactivity-guided fractionation of the ethanolic extract of *Y. filamentosa* L. leaves by repeated column chromatography on silica gel and on reversed phase silica gel gave the leishmanicidal steroidal saponin **1**. Acidic hydrolysis yielded the aglycone and the sugars moieties, which by TLC comparison with authentic samples indicated the presence of galactose (Gal), glucose (Glc) and rhamnose (Rha). Although we have not determined the absolute configuration of the sugar units here they can be analysed using methods described by us previously (Schöpke et al., 1996b).

2.2. Sugar-linkage analysis

The sugar substitution pattern can be established after derivatization (methylation analysis) using micro-amounts of material (ca. 1 nmol) by methods originally developed by us for the oligosaccharide mapping of recombinant and natural glycoproteins (Grabenhorst et al., 1995). Thus the GC–MS of the partially methylated alditol acetates derived from **1** showed the presence of six partially methylated alditol acetates representing terminal rhamnose, terminal glucose, 3-substituted glucose, 4-substituted galactose, 4-substituted glucose and 2, 3-disubstituted glucose residues (Table 1). An aliquot of the intact permethylated compound was reserved for a MS–MS analysis reported below.

2.3. Sugar sequence analysis

Electrospray ionization in the positive as well as the negative ion mode, especially in combination with MS–MS techniques, has quickly become the method of choice for sugar sequence analysis. The methodology has the advantage of requiring only minute amounts of substance (<1 μg), and affords a direct analysis of both purified materials and mixtures without the necessity of derivatization. We have used this method previously for comparative analysis of saponin mixtures and have shown that the introduction of sodium salts has the advantage of producing sodium-adduct molecular ions, which resolves ambiguities arising in protonated molecular-ion spectra and afford readily interpretable spectra (Schöpke et al., 1996a). Thus the positive ion mode ESI-mass spectrum of **1** afforded a molecular ion at *m/z* 1412 $[M+Na]^+$. This parent ion was selected using the quadrupole mass analyser and collision-induced decomposition gave daughter ions that were separated in the time-of-flight mass analyser. The resulting MS–MS spectrum showed fragment ions at *m/z* 979 [hex + hex + hex + hex + hex + dhex + Na]$^+$, *m/z* 817 [hex + hex + hex + hex + hex + dhex + Na]$^+$, *m/z* 671 [hex + hex + hex + hex + Na]$^+$, *m/z* 655 [hex + hex + hex + dhex + Na]$^+$, *m/z* 509 [hex + hex + hex + Na]$^+$ and at *m/z* 347 [hex + hex + Na]$^+$. Peaks at *m/z* 1266 [M-dhex + Na]$^+$, *m/z* 1250 [M-hex + Na]$^+$, *m/z* 1104 [M-dhex-hex + Na]$^+$, *m/z* 1088 [M-hex-hex + Na]$^+$, *m/z* 942 [M-dhex-hex-hex + Na]$^+$, *m/z* 780 [M-dhex-hex-hex-hex + Na]$^+$ and at *m/z* 618 [M-dhex-hex-hex-hex-hex + Na]$^+$ were generated through loss of the respective saccharides. The appearance of a peak at *m/z* 979 which is generated by a hexasaccharide + Na-fragment and the presence of two terminal sugar units in the GS–MS analysis above indicates **1** is a monodesmoside with a branched sugar chain.

Table 1
Methylation analyses of **1** (derivatives are listed in the order of elution)

Per-*O*-acetylated derivatives with *O*-Me in position	Type	Interpretation
2,3,4	Rhamnitol	Terminal rhamnose
2,3,4,6	Glucitol	Terminal glucose
2,4,6	Glucitol	3-Substituted glucose
2,3,6	Galacitol	4-Substituted galactose
2,3,6	Glucitol	4-Substituted glucose
4,6	Glucitol	2,3-Disubstituted glucose

The above MS–MS analysis can of course be applied to the permethylated sample, which has to be produced during the sugar-linkage analysis. Such an analysis has the advantage of avoiding ambiguities in the fragmentation pattern of the native molecule. Thus in the present example the sequential elimination of two terminal monosaccharide units yields the same fragment ion mass as the loss of a single disaccharide unit from the native molecular ion, whereas from the permethylated sample these two fragments differ by one methyl group and therefore can be unequivocally distinguished. In addition the number of acidic protons in the aglycone, which are also permethylated, can be determined. The MS–MS analysis of the permethylated derivative of **1** is summarized in Fig. 1.

Thus the combined data indicated that the sugar sequence in 1 is {Glc-hex}{Rha-hex}-Glc-hex-R and are compatible with a molecular formula of $C_{63}H_{104}O_{33}$, Scheme 2.

At this stage in the analysis the combined methods afford information on the number, the nature and linkage positions, but not of the anomeric configuration or the exact sequence, of the constituent monosaccharides in the glycoside. The molecular weight of the agylcone is evident by default. NMR data are now necessary to afford the remaining stereochemical details of the sugars and identification of the aglycone.

In contrast to MS analyses considerably more material is required for NMR analyses. Thus in reality satisfactory 1D and 2D ^{1}H homonuclear spectra can be recorded of amounts >100–500 μg, while the less sensitive 2D inverse ^{1}H-dectected heteronuclear ^{13}C–^{1}H correlations require >1–2 mg of homogeneous material.

2.4. Anomeric configuration and sugar conformation

The anomeric configurations of the various sugar moieties followed from the magnitudes of the vicinal ^{1}H–^{1}H and one-bond ^{13}C–^{1}H coupling constants shown in Tables 2 and 3, respectively. All glucoses and galactose had a ß-configuration and the α-configuration of the rhamnose was unambiguously established from the ^{1}J(CH) of 169.6 Hz (Hansen, 1981). The latter is the most reliable coupling for establishing the rhamnose configuration as the similarity of the gauche dihedral angle for both α and ß anomers leads to similar small vicinal ^{1}H–^{1}H coupling constants. The linkage position of the sugar chain to the aglycone follows from either a

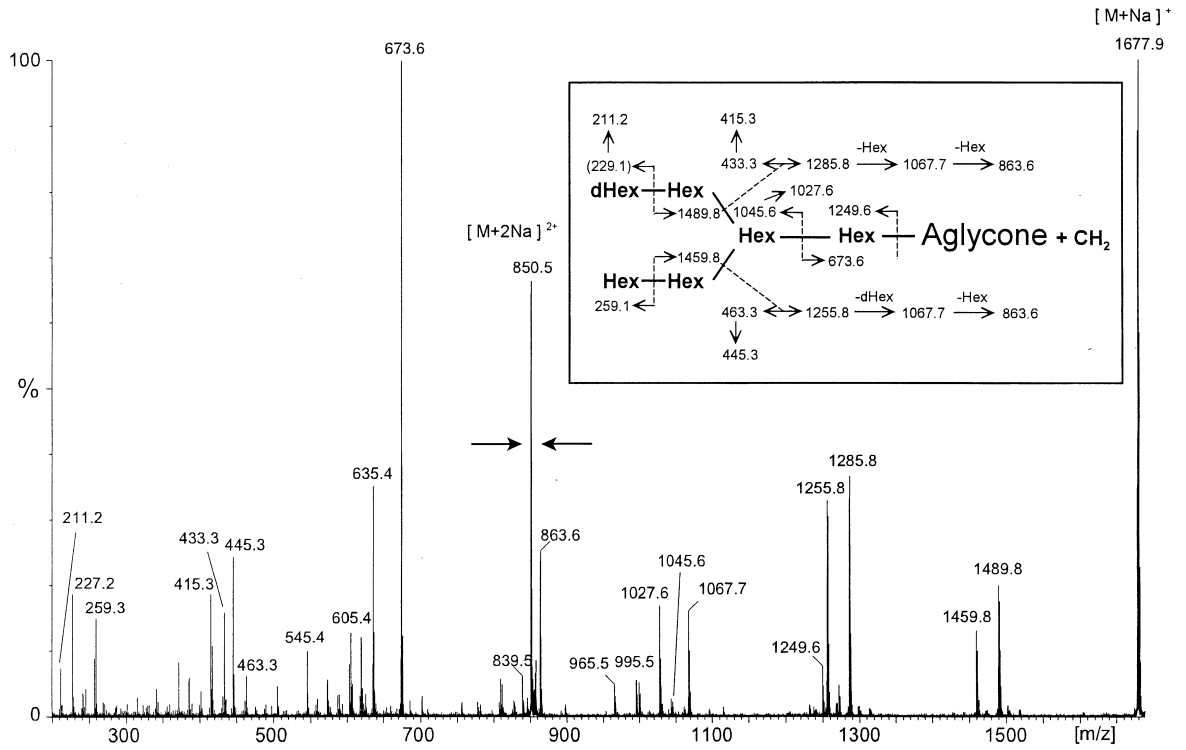

Fig. 1. ESI daughter ion spectrum of the doubly charged $[M+2Na]^{2+}$ permethylated molecular ion of the saponin isolated from *Yucca filamentosa* L. with inserted fragmentation scheme. The fragmentation pattern indicates a branched hexasaccharide glucan structure consisting of five hexose and one deoxyhexose residues.The aglycone has one acidic proton, as is indicated by its derivatisation with one methyl group upon permethylation. Hex = hexose, dHex = deoxyhexose.

a) Component identification: D-galactose (Gal), D-glucose (Glu), L-rhamnose (Rha)

b) Sugar-linkage analysis: 4-Gal, 3-Glu, 4-Glu, 2,3-Glu, terminal Glu, and terminal Rha in a ratio of ca. 1:1:1:1:1:1

c) Sugar sequence:

deoxyhexose(Rha) - hexose - hexose(Glu) - hexose
|
hexose(Glu) - hexose

d) NMR coupling data:

1α-deoxyhexose (Rha) - 1ß-hexose - 1ß-hexose(Glu) - 1ß-hexose
|
1ß-hexose(Glu) - 1ß-hexose

e) 2D NMR data:

Rha- (1α-4) -Glu- (1ß-3) -Glu- (1ß-4) -Gal- 1ß -Aglycone
|
Glu- (1ß-3) -Glu- (1ß-2)

Scheme 2. Structure elucidation of sugar chain in **1**.

comparison of ^{13}C data with that of the unsubstituted aglycone or more explicitly from vicinal ^{13}C–^{1}H correlations in the HMBC spectrum (see below, Table 4 and Scheme 2).

2.5. Exact sugar sequence

The identity and exact sugar sequence may already be apparent from the data accumulated above. If this is not the case, as here, then a partial interpretation of the 2D homonuclear and heteronuclear NMR correlations is necessary. The extent of such an analysis depends on the molecule under investigation, but in general will be of the form used for **1**.

The observation of a correlation of the anomeric proton of Gal (Table 2) to a low field carbon (C-3) of the aglycone, evident from further long-range correlations to aliphatic, non-sugar protons, identified the chain linkage to the aglycone. The H1–H4 spin system of the galactose unit was readily identified from the 2D COSY

Table 2
^{1}H NMR data for the sugar and aglycone moieties of **1**

	Sugar moiety		
	^{1}H shift, *J* in Hz		^{1}H shift, *J* in Hz
3-*O*-Gal		Glc (C)	
H-1	4.39, *J*(1–2) 7.8	H-1	4.61, *J*(1–2) 7.8
H-2	3.74, *J*(2–3) 9.7	H-2	3.34, *J*(2–3) 9.1
H-3	3.58, *J*(3–4) 3.2	H-3	3.44, *J*(3–4) 9.1
H-4	4.08, *J*(4–5) < 2	H-4	#[c]
H-5	3.59, *J*(5–6a) 7.2	H-5	*
H-6a	3.90	H-6a	*
H-6b	3.71, *J*(6a–6b) 11.2	H-6b	*
Glc (A)		Glc (D)	
H-1	4.66, *J*(1–2) 7.7	H-1	4.81, *J*(1–2) 8.0
H-2	3.80	H-2	3.35, *J*(2–3) 8.9
H-3	3.81	H-3	3.53, *J*(3–4) 9.0
H-4	3.39	H-4	3.58, *J*(4–5) 9.2
H-5	*[b]	H-5	3.47
H-6a	*	H-6a	3.87
H-6b	*	H-6b	3.69
Glc (B)		Rha	
H-1	5.07, *J*(1–2) 8.0	H-1	4.84[a] *J*(1–2) small
H-2	3.45, *J*(2–3) 9.0	H-2	3.87, *J*(2–3) small
H-3	3.63, *J*(3–4) 9.0	H-3	3.66, *J*(3–4) 9.6
H-4	3.49	H-4	3.45, *J*(4–5) 9.6
H-5	3.42, *J*(5–6a) 2.3	H-5	4.02, *J*(5–6) 6.2
H-6a	3.95	H-6	1.31
H-6b	3.87, *J*(6a–6b) 12.2		
Aglycone (only unambiguous assignments are shown)			
H-1a	2.03, (1a–1b) 12.6, (1a–2) 4.9		
H-1b	0.98, (1b–2) 12.4		
H-2	3.70		
H-3	3.52		
H-4a	1.77		
H-4b	1.45		
H-14	1.20		
H-15a	2.01		
H-15b	1.29		
H-17	1.78, (17–20) 6.9, (17–16) 6.7		
Me-18	0.93		
Me-19	0.83		
H-20	1.94, (20–21) 7.0		
Me-21	0.99		
H-23a	1.74, (23a–23b) 13.4, (23a–24) 4.7		
H-23b	1.60		
H-25	1.63		
Me-27	0.83, (25–27) 6.4		

[a] Under residual water signal.
[b] *There are two interchangeable sets of signals for Glc(A) and Glc(C) for H-6a/H-6b/H-5 at 3.96/3.64/3.39 and 3.93/3.68/3.38 with *J*(6a–6b)/*J*(6a–5) of ~12/~2 and 11.9/2.5 respectively.
[c] # Not assignable.

Table 3
^{13}C NMR chemical shifts and ^1J(CH)[a] of compound **1** (CD_3OD)

	Sugar moiety		
	^{13}C shift (^1J(CH))		^{13}C shift (^1J(CH))
3-0-Gal 1	102.9 (160.2)	Glc (C) 1	105.3 (163.0)
2	72.9	2	$
3	$[c]	3	#[d]
4	79.8	4	70.3
5	$	5	#
6	61.4	6	§[b]
Glc (A) 1	104.3 (163.6)	Glc (D) 1	103.9 (163.3)
2	81.0	2	$
3	87.5	3	76.9
4	71.6	4	79.5
5	#	5	#
6	§	6	61.8
Glc (B) 1	103.8 (166.4)	Rha 1	102.9 (169.6)
2	75.0	2	72.5
3	87.6	3	72.2
4	70.7 or 72.5	5	73.8
5	#	5	70.7
6	62.9	6	17.9
Aglycone			
	^{13}C shift		^{13}C shift
1	45.8	15	32.4
2	71.0	16	82.2
3	85.0	17	63.9
4	35.8	18	16.9
5	45.8	19	13.7
6	28.8	20	42.9
7	32.8	21	14.8
8	34.0	22	110.5
9	55.7	23	33.5
10	37.9	24	29.8
11	22.3	25	31.4
12	41.1	26	67.8
13	41.7	27	17.4
14	57.4		

[a] The magnitude of ^1J(CH) of the anomeric carbons of the sugar moieties, given in parentheses, were determined from the residual cross peaks in the inverse long-range ^{13}C–^{1}H correlation (HMBC).
[b] § The C-6 shifts at 62.7 and 63.1 ppm correspond to ^{1}H shifts at 3.93/3.68 and 3.96/3.64 ppm, respectively (see footnote of Table 2).
[c] $ Shifts at 75.5, 75.6, 75.6, 75.7 ppm.
[d] # Shifts at 77.1, 77.5, 77.8, 78.0, 78.1 ppm.

correlations in which H-4 was to low field and had two small vicinal ^{1}H–^{1}H couplings that are characteristic of this system. These observations implied the galactose unit was adjacent to the aglycone and the other four hexose units were glucose. The anomeric proton of the terminal rhamnose correlated with a sugar carbon at 79.5 ppm, which from the chemical shift must be that of a 4-substituted glucose unit, Glc (D) in Table 3 (C-3 of a 3-substituted glucose unit would be at ca. 87 ppm). Consequently these data and the linkage analysis above indicates the terminal glucose must be bound to the 3-substituted glucose, Glc (B) in Table 3, by default. The only question that now remains is the relative position of these two dissaccharides (glucose 4-1α rhamnose and glucose 3-1ß glucose) on the branching trisubstituted glucose unit, Glc (A) (Scheme 2). Again a partial analysis of the COSY spectrum and the considerable differences in

Table 4
Characteristic long-range correlations in the HMBC spectrum of the aglycone of **1**

Hydrogen	Carbons
Correlations from methyl groups	
Me-18	C-12, C-13, C-14, C-17
Me-19	C-1, C-5, C-10, C-9
Me-21	C-17, C-20, C-22
Me-27	C-24, C-25, C-26
Correlation from sugar substituent	
H-1 Gal	C-3
Correlations from hydrogens bonded to heteroatom carrying carbons[a]	
H-26A/B	C-22, C-24, C-25, C-27
Correlations from selective well defined ^1H signals assigned from COSY spectrum	
H-1A[b]	C-2, C-3, C-5, C-10, C-19
H-1B[b]	C-2, C-3, C-9, C-10, C-19
H-15A	C-13, C-14, C-16, C-17
H-20	C-13, C-17, C-21, C-22, C-23
H-17	C-12, C-13, C-16, C-18, C-20, C-21

[a] In the present case there are no long-range correlations apparent from H-2 and H-3.

[b] There are some differences in the carbons showing correlations due to the stereochemical dependence of the appropriate long-range coupling constants.

chemical shifts of C-2 and C-3 of Glc (A) together with the observation of the respective long-range correlations in the HMBC spectrum from the anomeric protons of Glc (B) and Glc (D), respectively, to these carbons established the relative chain orientations shown in Scheme 2 (e).

Again we emphasize that the unambiguous structure of the sugar unit was established without a complete assignment of the NMR data. Even on close inspection of the 2D correlations a number of assignments both in the ^1H and ^{13}C spectra (Tables 2 and 3, respectively) could not be unambiguously establish even at the high magnetic fields employed here (14 Tesla, 600 MHz: ^1H; 150 MHz: ^{13}C) because of signal overlap. As the complexity of the sugar chains increases full assignments will be even more difficult although it can be anticipated that correlations to the low-field carbons, i.e. those carrying the substituents and hence the information regarding the exact linkage, will still be determinable.

2.6. Aglycone identification

In many cases the aglycone can be readily identified from its molecular weight deduced from the MS data and from careful comparison of the ^1H and ^{13}C data with known literature data. In the present case the aglycone gitogenin was unambiguously identified (Agrawal et al., 1985; Nakano et al., 1988). When this is not possible then a detailed analysis of the heteronuclear and homonuclear "through-bond" NMR correlations is the most rigorous approach, followed by "through-space" data from 1D NOE and/or 2D/NOESY/ROESY spectra to determine the relative configurations of asymmetric centres.

In the present case a systematic inspection of the HMBC data detailed in Scheme 1 (right, c) for **1** yields the sets of correlations given in Table 4. The strongest correlations are from the methyl groups and provide correlations to all adjacent carbons two and three bonds from the respective protons. Additional correlations from the galactose (above) defines the sugar chain position while the correlations from H-26A/B and from a number of the well defined protons identified in the COSY spectrum are sufficient in combination to define the molecular fragments incorporating C-9/C-10(C-19)/C-1→C-5 and C-12/C-13(C-18)/C-14→C-27 of Fig. 2. These data provide unambiguous confirmation of the structure of the known aglycone. They would not, however, be sufficient to unambiguously define an unknown aglycone as the central section C-6/C-7/C-8 and C-11 together with their attached protons remain undefined. In such cases further 2D spectra would be necessary, in particular HMQC and "through-space" correlations.

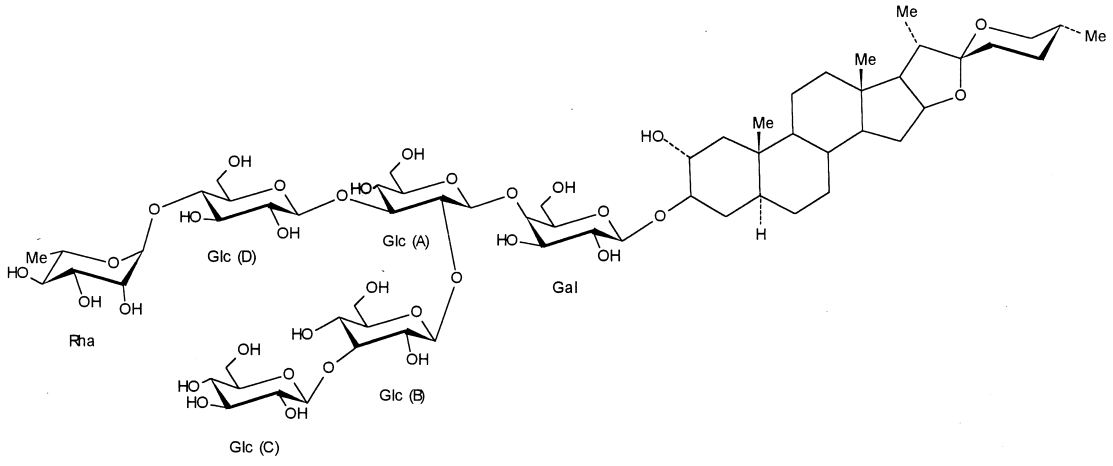

Fig. 2. Structure of **1** from *Yucca filamentosa* L.

3. Conclusion

Adherence to the procedures outlined in Scheme 1 affords an unambiguous identification of complex sugar moieties without recourse to full signal assignments. Similarly known aglycone structures can be readily identified and their structures confirmed with data already present in spectra recorded for the sugar analysis. In those cases where a novel aglycone is present additional NMR data will probably be necessary. In the present case the combined chemical and spectroscopic data, together with reasonable assumptions for the absolute stereochemistries of the sugar moieties, afforded unambiguous evidence for the novel structure for **1** of 3-*O*-((ß-D-glucopyranosyl-(1→3)-ß-D-glucopyranosyl-(1→2)) (α-L-rhamnopyranosyl-(1→4)-ß-D-glucopyranosyl-(1→3))-ß-D-glucopyranosyl-(1→4)-ß-D-galactopyranosyl)-25*R* 5α-spirostan-2α, 3ß-diol, Fig. 2.

4. Experimental

4.1. General experimental procedures

1D (^{1}H, ^{13}C and DEPT-135) and 2D (COSY and HMBC) NMR spectra of compound **1** were recorded in CD_3OD at 300 K on a Bruker AVANCE DMX-600 NMR spectrometer (^{1}H: 600.13 MHz, ^{13}C: 150.92 MHz) using standard Bruker software. Chemical shifts are reported in ppm relative to TMS but were recorded relative to the residual signal of the solvent (^{1}H: 3.35 ppm, ^{13}C: 49.00 ppm) and coupling constants in Hz. The NMR spectra of the aglycone of **1** were recorded in $CDCl_3$ on a Varian 500 MHz spectrometer. A Micromass QTOF2 mass spectrometer equipped with a nonspray ion source was used for ESI–MS and MS–MS. TLC was performed on silica gel 60 F_{254} or on reversed phase 18 silica gel plates or foils (Merck); solvent system A: $CHCl_3$–MeOH–H_2O (6:4:1) and B: MeOH–H_2O (8.5:1.5). The spots of the TLC were detected by 10% H_2SO_4 followed by heating for saponin and sapogenin, and with thymol/H_2SO_4 for sugars.

4.2. Plant material

The leaves of *Y. filamentosa* L. were provided by Dr. Paul Brueckner, Arboretum, Institute of Biology, Humboldt-University of Berlin, Germany, in July 1996. A plant specimen is on file in the Institut für Pharmazie, Humboldt-Unversität, Berlin.

4.3. Extraction and isolation

The air-dried pulverized leaves (500 g) were first macerated with petroleum ether, then with ethyl acetate, each for 90 min. Finally the dried material was extracted with ethanol/water 7:1 in a Soxhlet apparatus for 120 min. After filtration, the solvent was evaporated under reduced pressure to yield 31 g of extract. The isolation of the active component of this extract was performed by bioactivity-guided fractionation. The extract was chromatographed on 2000 g silica gel 60, 0.063–0.2 μm (Merck) with solvent system A as eluent to give 150 fractions. These fractions were combined into pools A–D according to their similar TLC patterns (silica gel, solvent system A). Pool A (6.5 g) showed high leishmanicidal activity and was chromatographed on 600 g reversed phase 18 silica gel material (Merck) with solvent system B as eluent to give pools Aa–Ad. The chromatography of Ac (1.3 g) on 100 g silica gel 60 with $CHCl_3$–MeOH–H_2O (10:3:1, lower phase) led to pure **1** (25.7 mg), (TLC solvent system A; R_f 0,4). **1**: Colorless needles (from MeOH), mp 292–293°C; ESI–MS positive mode *m*/*z*: 1412 $[M+Na]^+$, 1266, 1250, 1104, 1088, 942, 780, 618 (see text for peak assignments). ^{1}H and ^{13}C NMR data are given in Tables 2–4.

4.4. Acidic hydrolysis and aglycone identification

1 was hydrolysed with 1N HCl by refluxing for 90 min on a water bath. The reaction mixture was neutralized with 1 N NaOH and submitted to liquid-liquid partition with diethyl ether. The ether phase was evaporated to dryness under reduced pressure. From the residue gitogenin was identified: colorless needles (from $CHCl_3$), mp 268–270°C; ms 432 $[M]^+$, 417, 318, 289, 139; ^{1}H NMR ($CDCl_3$): $\delta = 0.76$ (3H, *s*), 0.78 (3H, *d*, $J = 6.3$ Hz), 0.86 (3H, *s*), 0.95 (3H, *d*, $J = 6.8$ Hz), 3.30–3.63 (4H, *m*), 4.36 *m* (1H, *m*); ^{13}C NMR ($CDCl_3$, C-1–C-27): 45.0, 73.0, 76.4, 35.6, 44.8, 27.8, 31.8, 34.4, 54.3, 37.6, 21.2, 39.9, 40.6, 56.1, 31.4, 80.8, 62.1, 16.5, 13.6, 41.5, 14.5, 109.2, 32.0, 28.8, 30.3, 66.8, 17.1

4.5. Component monosaccharide identification

1 was hydrolysed at 100°C for 1 h on TLC silica gel plates in a chamber filled with conc. HCl. After separation with solvent system A, galactose (R_f 0.36), glucose (R_f 0.39) and rhamnose (R_f 0.57) were identified by comparison with authentic samples.

4.6. Methylation analysis of the sugar constituents

For linkage analysis, the sample was permethylated as described (Anumula and Taylor, 1992). Purification of the permethylated sample, hydrolysis, reduction and acetylation were performed as described previously (Nimtz et al., 1990). The resulting partially methylated alditol acetates were analysed on a ThermoQuest GCQ ion trap GC/MS system (MS: EI mode, GC: 30 m DB 5 column).

Acknowledgements

We gratefully acknowledge the technical assistance of B. Jaschok-Kentner, C. Kakoschke, E. Surges and A. Tiepold (all GBF), and a grant from the Deutsche Forschungsgemeinschaft (Hi 505/3-2).

References

Agrawal, P.K., Jain, D.C., Gupta, R.K., Thakur, R.S., 1985. Carbon-13 NMR spectroscopy of steroidal sapogenins and steroidal saponins. Phytochemistry 24, 2479–2496.

Akendengue, B., Ngou-Milama, E., Laurens, A., Hocquemiller, R., 1999. Recent advances in the fight against leishmaniasis with natural products. Parasite 6, 3–8.

Anumula, K.R., Taylor, P.B., 1992. A comprehensive procedure for preparation of partially methylated alditol acetates from glycoprotein carbohydrates. Anal. Biochem. 203, 101–108.

Grabenhorst, E., Hoffmann, A., Nimtz, M., Zettlmeissl, G., Conradt, H., 1995. Construction of stable BHK-21 cells coexpressing human secretory glycoproteins and human Gal(ß1-4)GlcNAc-R α2,6-sialyltranferase. Eur. J. Biochem. 232, 718–725.

Hansen, P.O., 1981. Carbon-hydrogen spin-spin coupling constants. Prog. NMR Spectrosc. 14, 175–296.

Mahato, S.B., Ganguly, A.N., Sahu, N.P., 1982. Steroid saponins. Phytochemistry 21, 959–978.

Nakano, K., Matsuda, E., Tsurumi, K., Yamasaki, T., Murakami, K., Takaishi, Y., Tomimatsu, T., 1988. The steroidal glycosides of the flowers of *Yucca gloriosa*. Phytochemistry 27, 3235–3239.

Nimtz, M., Noll, G., Pâques, E.-P., Conradt, H.S., 1990. Carbohydrate structures of a human tissue plasminogen activator variant expressed in recombinant Chinese hamster ovary cells. FEBS 271, 14–18.

Plock, A., Sokolowska-Köhler W., Presber W., 2001. Application of flow cytometry and microscopical methods to characterize the effect of herbal drugs on *Leishmania* spp. Exp. Parasitol., in press.

Schöpke, T., Hiller, K., Wray, V., Nimtz, M., 1996a. Application of MS–MS for the rapid, comparative analysis of saponin mixtures as exemplified by the deacylated and partially deacylated triterpenoid saponins of *Bellis annua*. Planta Med. 62, 336–340.

Schöpke, T., Wray, V., Nimtz, M., Hiller, K., 1996b. Triterpenoid saponins from *Bellium bellidioides*. Structure of the minor deacylsaponins. Phytochemistry 41, 1399–1403.

Voigt, G., Hiller, K., 1987. Neuere Ergebnisse zur Chemie und Biologie der Steroidsaponine. Scientia Pharmaceutica 55, 201–227.

PERGAMON

Phytochemistry 57 (2001) 497–498

PHYTOCHEMISTRY

www.elsevier.com/locate/phytochem

Book reviews

Soil Biochemistry Volume 10
J.-M. Bollag and G. Stotzky (Eds.). Marcel Dekker, New York, $195.00, 519 pp., ISBN 0-8247-8834-6

This is only the 10th volume of *Soil Biochemistry* in over three decades and devotees have learned to wait patiently for the next shot of their favourite review series. The good news is that they won't be disappointed because this time 12 chapters and more than 500 pages contain topics of interest, not only to the soil biochemists but also to microbiologists, microbial and molecular ecologists, and agricultural and environmental scientists.

The chapters range from the obviously topical (environmental remediation, rhizobia genetics, enteric pathogens in soil) to the more esoteric (soil archaeology). All are written (and carefully edited) by experts in their respective fields and, for the most part, present a mixture of fact and thoughtful speculation.

I was particularly drawn to a nice up-to-date review of fungal bioremediation (Paszcznski and Crawford), organised according to various potential substrates (dyes, PAHs, explosives, plastics, etc.), and reasserting the potential of lignocellulose degraders for the removal of environmental pollutants. Another chapter, this time on enzyme activities in soil (Quiquampoix), caught my attention because it presents a succinct (and overdue) theoretical review of the relationships of proteins with clay surfaces and the consequences of these for activity. One particularly intriguing chapter (Hattori and Hattori) revisits (and, at least for me, resuscitates) some of the much maligned traditional plate counting procedures. Other chapters, on the anaerobic dehalogenation of pesticides (Haggblom and Milligan) — now recognised as an important process in anoxic microenvironments and sub-soils — and the genetics and ecology of soybean bradyrhizobia (Minamisawa and Mitsui), are both concise and well-researched.

Two methodology chapters, one on the use of silylation for the extraction of humic matter (Haider et al.) and the other on isoprenoid quinones as microbial biomarkers (Katayama and Fujie) will prove invaluable to the practitioners. Other very detailed chapters on the microbiology of rice fields (Kimura) and the relationships between biomolecules and clays (Violante and Gianfreda) will have their fans.

The final two chapters are, in turn, important (human pathogens in soil by Toranzos and Marcos) and intriguing (interactions of microbes with archaeological materials by Hopkins) and are full of signposts to future research.

Overall, the range of subjects expertly reviewed in this latest volume of *Soil Biochemistry* are a welcome addition to the bookshelf and I am sure that the founding father, Douglas McLaren, would be well pleased with the continued high quality of the series.

Richard G. Burns
Department of Biosciences
University of Kent at Canterbury
Canterbury, Kent CT2 7NJ, UK
E-mail address: r.g.burns@ukc.ac.uk

PII: S0031-9422(01)00014-0

Studies in Natural Products Chemistry, Vol. 21: Bioactive Natural Products (Part B)
Atta-ur-Rahman (Ed.). Elsevier Science, Amsterdam, The Netherlands, 2000, 812 pages, ISBN 0-444-50469-9, $ 432.00

This volume, in the extensive series of books initiated by the editor, Professor Atta-ur-Rahman of the H.E.J. Research Institute of Chemistry, University of Karachi, Pakistan, comprises 14 different chapters written by specialists in their respective fields of expertise.

Most chapters deal with bioactive plant constituents. Of particular interest are the contributions which include plant chemistry, modes of action and structure-activity relationships, e.g. the interference of alkaloids with neuroreceptors and ion channels by M. Wink, the chemistry and biological activity of chromone alkaloids by P.J. Houghton, the distribution and potential of polyene

amide derivatives of plant and fungal origin by C. Najara and M. Yus, the potential of plants as anti *Diabetes mellitus* drugs by Lamba et al., the update on bioactive saponins from plants by M.A. Lacaille-Dubois and H. Wagner and the excellent review on biologically active diterpenoids from *Scoparia dulcis* L. by T. Hayashi.

All these chapters are very useful and comprehensive reviews. Also of great interest is the chapter of G.E. Rohr et al. on the various analytical procedures for procyanidins. Another technical but well-written chapter deals with the extraction, identification and biological properties of various essential oils. Three chapters of the book are related to marine natural products. These reviews are nicely presented and accurate and will be of great help for all scientists working in the field of natural products. Finally, the book contains an interesting chapter by S. Michel et al. on prodrugs of natural anthracyclines suited for antibody directed enzyme prodrug therapy and prodrug monotherapy. There is no doubt that the approach presented in this chapter is highly innovative but it is questionable if such a chapter has a place in the present book. It would probably be more useful in a book on medicinal chemistry as it lies somewhat outside the general scope of this volume which has unfortunately one negative aspect — its high price. If the editor could reduce the size of future books in the series, this would also lower the price. Despite this, the present book provides a multitude of useful, accurate and practical information which will be of great help to every natural products chemist. It should be made available in every library, either in academia or in industry. Individual scientists will unfortunately not be able to afford this volume.

Kurt Hostettmann
Institute of Pharmacognosy and Phytochemistry
University of Lausanne,
CH-1015 Lausanne, Switzerland
E-mail address: kurt.hostettmann@ipp.unil.ch

PII: S0031-9422(01)00031-0

PERGAMON

Phytochemistry 57 (2001) 497–498

PHYTOCHEMISTRY

www.elsevier.com/locate/phytochem

Book reviews

Soil Biochemistry Volume 10
J.-M. Bollag and G. Stotzky (Eds.). Marcel Dekker, New York, $195.00, 519 pp., ISBN 0-8247-8834-6

This is only the 10th volume of *Soil Biochemistry* in over three decades and devotees have learned to wait patiently for the next shot of their favourite review series. The good news is that they won't be disappointed because this time 12 chapters and more than 500 pages contain topics of interest, not only to the soil biochemists but also to microbiologists, microbial and molecular ecologists, and agricultural and environmental scientists.

The chapters range from the obviously topical (environmental remediation, rhizobia genetics, enteric pathogens in soil) to the more esoteric (soil archaeology). All are written (and carefully edited) by experts in their respective fields and, for the most part, present a mixture of fact and thoughtful speculation.

I was particularly drawn to a nice up-to-date review of fungal bioremediation (Paszcznski and Crawford), organised according to various potential substrates (dyes, PAHs, explosives, plastics, etc.), and reasserting the potential of lignocellulose degraders for the removal of environmental pollutants. Another chapter, this time on enzyme activities in soil (Quiquampoix), caught my attention because it presents a succinct (and overdue) theoretical review of the relationships of proteins with clay surfaces and the consequences of these for activity. One particularly intriguing chapter (Hattori and Hattori) revisits (and, at least for me, resuscitates) some of the much maligned traditional plate counting procedures. Other chapters, on the anaerobic dehalogenation of pesticides (Haggblom and Milligan) — now recognised as an important process in anoxic microenvironments and sub-soils — and the genetics and ecology of soybean bradyrhizobia (Minamisawa and Mitsui), are both concise and well-researched.

Two methodology chapters, one on the use of silylation for the extraction of humic matter (Haider et al.) and the other on isoprenoid quinones as microbial biomarkers (Katayama and Fujie) will prove invaluable to the practitioners. Other very detailed chapters on the microbiology of rice fields (Kimura) and the relationships between biomolecules and clays (Violante and Gianfreda) will have their fans.

The final two chapters are, in turn, important (human pathogens in soil by Toranzos and Marcos) and intriguing (interactions of microbes with archaeological materials by Hopkins) and are full of signposts to future research.

Overall, the range of subjects expertly reviewed in this latest volume of *Soil Biochemistry* are a welcome addition to the bookshelf and I am sure that the founding father, Douglas McLaren, would be well pleased with the continued high quality of the series.

Richard G. Burns
Department of Biosciences
University of Kent at Canterbury
Canterbury, Kent CT2 7NJ, UK
E-mail address: r.g.burns@ukc.ac.uk

PII: S0031-9422(01)00014-0

Studies in Natural Products Chemistry, Vol. 21: Bioactive Natural Products (Part B)
Atta-ur-Rahman (Ed.). Elsevier Science, Amsterdam, The Netherlands, 2000, 812 pages, ISBN 0-444-50469-9, $ 432.00

This volume, in the extensive series of books initiated by the editor, Professor Atta-ur-Rahman of the H.E.J. Research Institute of Chemistry, University of Karachi, Pakistan, comprises 14 different chapters written by specialists in their respective fields of expertise.

Most chapters deal with bioactive plant constituents. Of particular interest are the contributions which include plant chemistry, modes of action and structure-activity relationships, e.g. the interference of alkaloids with neuroreceptors and ion channels by M. Wink, the chemistry and biological activity of chromone alkaloids by P.J. Houghton, the distribution and potential of polyene

PERGAMON

Phytochemistry 57 (2001) 499–506

PHYTOCHEMISTRY

www.elsevier.com/locate/phytochem

Sesquiterpene hydrocarbons with trifarane backbone in the liverwort *Trocholejeunea sandvicensis*

Mesmin Mekem Sonwa[a], Wilfried A. König[a,*], El Hassane Lahlou[b], Yoshinori Asakawa[b]

[a]*Institut für Organische Chemie, Universität Hamburg, D-20146 Hamburg, Germany*
[b]*Faculty of Pharmaceutical Sciences, Tokushima Bunri University, Tokushima, Japan*

Received 18 January 2001; received in revised form 28 February 2001

Abstract

The hydrocarbon fraction of the liverwort *Trocholejeunea sandvicensis* was investigated. Four new sesquiterpene hydrocarbons including the trifaranes (−)-trifara-9,14-diene (**6**) and (−)-3,7-di-*epi*-3,7-trifara-9,14-diene (**7**), as well as (+)-sandvicene (**8**), a sesquiterpene with uncommon skeleton, and the rearranged trifarane sesquiterpene (+)-neotrifaradiene (**9**) were isolated and their structure elucidated. A biogenetic pathway for the four compounds is proposed, with nerolidol as their common precursor. © 2001 Elsevier Science Ltd. All rights reserved.

Keywords: *Trocholejeunea sandvicensis*; *Lejeuneaceae*; Liverwort; Sesquiterpenes; (−)-Trifara-9,14-diene; (−)-3,7-di-*epi*-Trifara-9,14-diene; (+)-Sandvicene; (+)-Neotrifaradiene

1. Introduction

Previous work on the liverwort *Trocholejeunea sandvicensis* focussed on the polar fractions of this plant and resulted in the isolation of pinguisane- and lepidozane-type sesquiterpenes, kaurane-type diterpenoids, aromatic compounds, and flavonoids (Tori et al., 1993; Asakawa, 1995; Lahlou et al., 2000). Trifarienols A–E (**1**–**5**) (Fig. 8), sesquiterpenes with the rare trifarane skeleton, were identified as constituents of the Malaysian liverwort *Cheilolejeunea trifaria*, a member of the taxonomically related Lejeuneaceae family by Hashimoto et al. (1995). Here we report on the investigation of the hydrocarbon fraction of *Trocholejeunea sandvicensis*. Preliminary investigations of the ether extract by GC and GC–MS revealed the presence of more than 30 sesquiterpenes. Four compounds in the hydrocarbon fraction of *T. sandvicensis*, which had also formerly been observed as minor constituents in many *Porella* and *Ptilidium* species, had to be classified as unknown by comparison of their mass spectra with a data bank containing over 300 entries (Joulain and König, 1998). Isolation and structural investigations of these compounds lead to the identification of four new sesquiterpenes. Two of them, **6** and **7**, possess the unusual bicyclo[3.3.1]nonane (trifarane) skeleton. Compound **8** has a previously unknown carbon skeleton, while compound **9** is a rearranged trifarane sesquiterpene. Their structures were determined by spectrocopic methods. All four new compounds **6**–**9** possess a vinyl side chain as encountered in trifarane type sesquiterpenes **1**–**5** which are present in *C. trifaria* (Tori et al., 1993).

2. Results and discussion

The hydrocarbon fraction of *T. sandvicensis* was fractionated by preparative GC. By using a combination of columns with a polydimethylsiloxane and modified cyclodextrin stationary phase four new sesquiter pene hydrocarbons (−)-trifara-9,14-diene (**6**), (−)-3,7-di-*epi*-trifara-9,14-diene (**7**), (+)-sandvicene (**8**) and (+)-neotrifaradiene (**9**) were isolated (Fig. 1). On the base of mass spectrometric evidence several known sesquiterpenes including α-cedrene, β-ylangene, β-duprezianene (Barrero et al., 1996), selina-4(15),5-diene (Bülow and König, 2000), thujopsene, α-pinguisene (Asakawa,

* Corresponding author. Tel.: +49-404-28382824; fax: +49-404-2838-28293.

E-mail addresses: wkoenig@chemie.uni-hamburg.de (W.A. König), asakawa@ph.bunri-u.ac.jp (Y. Asakawa).

0031-9422/01/$ - see front matter © 2001 Elsevier Science Ltd. All rights reserved.
PII: S0031-9422(01)00123-6

1995), β-barbatene, β-acoradiene, di-*epi*-aristolochene (Joulain and König, 1998), eremophilene and eremophila-1(10),8,11-triene (Rieck et al., 1997) were identified.

2.1. Trifara-9,14-diene (**6**)

The molecular formula of **6** was deduced as $C_{15}H_{24}$ from its mass spectrum ($[M]^+ = 204$). The ^1H and ^{13}C NMR spectra revealed the presence of two tertiary methyl groups, one secondary methyl group, six methylene groups, two of which being olefinic, two quaternary sp^3 carbon atoms and one quaternary sp^2 carbon atom. Four substructures were obtained by combination of the results of ^1H–^1H COSY and the HSQC spectra. The presence of a vinyl group is attested by the methine proton CH-14 (δ 5.78) coupling with the two methylene protons CH_2-15 (δ 4.99). Long-range (^4J) coupling correlations in the ^1H–^1H COSY spectrum, which are observed between the methine proton CH-4 (δ 1.88) and the olefinic methylene group CH_2-10 (δ 4.69 and 4.85), give rise to substructure *a*: CH_2=C–CH–. This substructure is confirmed by the HMBC spectrum where correlations are found between the methylene group CH_2-10 and carbons C-9, C-4 and C-8 (Fig. 2). The methyl doublet CH_3-12 (δ 0.90) correlates with the methine proton CH-7 (δ 1.58), itself coupled to the methylene group CH_2-6 (δ 1.13 and 2.16), which further couples with another methylene group CH_2-5 (δ 1.67 and 1.83). CH_2-5 also couples with the methine proton CH-4 (δ 1.88), leading to partial structure *b*: CH_3–CH–CH_2–CH_2–CH–. The methylene group CH_2-1 (δ 1.54 and 1.56) couples with the methylene group CH_2-2 (δ 1.25 and 2.18) to give substructure *c*: –CH_2–CH_2–. With substructures *a* and *b* having methine group CH-4 in common, a new partial structure CH_2=C–CH–CH_2–CH_2–CH–CH_3 can be derived. The connectivities of the partial structures were deduced from the HMBC experiment (Fig. 2). The methylene protons CH_2-10 showed correlations to C-4, C-8 and C-9. The methyl group CH_3-12 correlated with carbons C-6, C-7 and C-8, while methyl group CH_3-11 (δ 0.92) is correlated with C-7, C-8, C-9 and C-1. Correlations are also observed between the methyl group CH_3-13 (δ 1.01) and C-2, C-3, C-4 and C-14. The vinylic methine proton CH-14 showed long-range correlation to C-3, while the methylenic protons CH_2-15 are correlated to C-3 and C-14. All these observations lead to a trifarane skeleton for the molecule. Its stereostructure was obtained from the NOESY spectrum as illustrated in Fig. 3. NOE's are observed between the methyl group CH_3-13 and the axial proton H_a-1 indicating also an axial orientation for CH_3-13, and thus an equatorial orientation for the vinyl group at C-3. This is confirmed by NOEs between the vinylic methine proton H-14 and the equatorial proton H_e-5 (δ 1.83, *dddd*, *J*: 13.9, 4.1, 4.1, 2.0, 1.0 Hz). A further proof of the equatorial orientation of the vinyl group is the deshielding anisotropic effect exerted on the two axial protons H_a-2 (δ 2.16) and H_a-6 (δ 2.18) (compare their chemical shifts with those of the corresponding protons in compound **7** where the vinyl group is axial; see Table 1). The NOE correlation between methyl group CH_3-12 and the axial proton H_a-5 (δ 1.67, *ddd*, *J*: 13.9, 13.6, 5.7 Hz) indicates that CH_3-12 also is axial. Therefore, compound **7** has the relative configuration as drawn in Fig. 3.

2.2. 3,7-Di-epi-trifara-9,14-diene (**7**)

The second compound has the molecular formula $C_{15}H_{24}$ in agreement with its mass spectrum ($[M]^+ = 204$). The analysis of the NMR spectra of **7** established the same planar structure as in **6** (Fig. 2). The relative

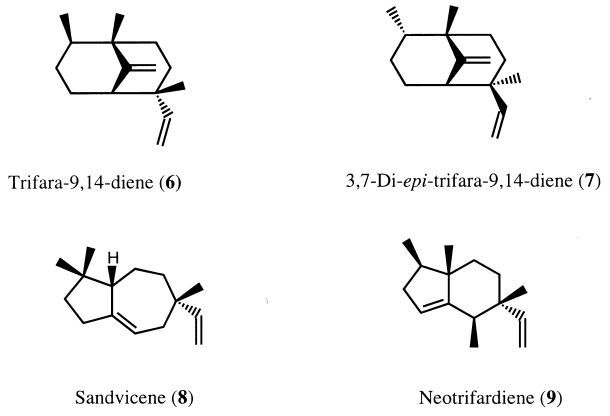

Fig. 1. Sesquiterpene hydrocarbons identified in *Trocholejeunea sandvicensis*.

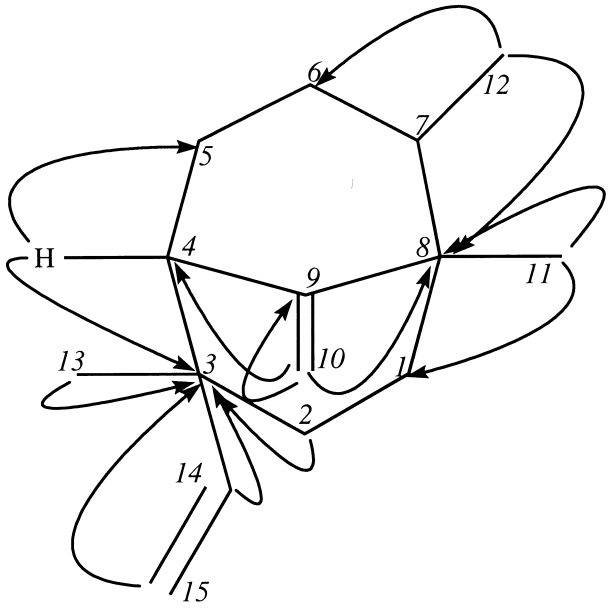

Fig. 2. Proton-carbon long-range correlations in the HMBC spectrum of trifara-9,14-diene (**6**).

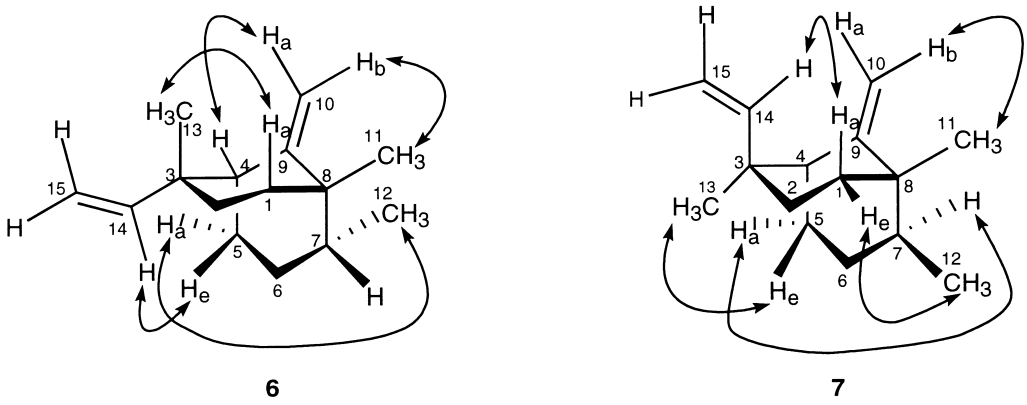

Fig. 3. Important NOESY correlations and relative configuration of trifara-9,14-diene (**6**) and 3,7-di-*epi*-trifara-9,14-diene (**7**).

Table 1
^{1}H NMR spectral data for compounds **6** and **7**[a]

H	**6**	**7**
1	1.54, *m*	1.34, *dddd* (13.9, 13.9, 6.3, 1.3)
	1.56, *m*	1.65, *dd* (13.9, 6.0)
2	1.25, *dddd* (14.2, 6.6, 2.0, 2.0)	1.45, *dd* (13.9, 6.3)
	2.18, *ddd* (14.2, 11.6, 8.3)	1.75, *ddd* (13.9, 13.9, 6.0)
4	1.88, *d* (5.7)	2.07, *d* (4.4)
5	1.67, *ddd* (13.9, 13.6, 5.7)	1.61, *m*
	1.83, *ddddd* (13.9, 4.1, 4.1, 2.0, 1.0)	2.03, *d* (12.7)
6	1.13, *dddd* (14.5, 6.3, 2.0, 2.0)	1.37, *dd* (12.7, 6.3)
	2.16, *dddd* (14.5, 13.6, 6.6, 6.6)	1.53, *ddd* (12.7, 12.7, 5.4)
7	1.58, *m*	1.44, *m*
10	4.69, *d* (2.2)	4.73, *d* (2.0)
	4.85, *d* (2.2)	4.76, *d* (2.0)
11	0.93, *s*	1.01, *s*
12	0.90, *d* (7.3)	0.90, *d* (7.3)
13	1.01, *d* (0.9)	1.04, *s*
14	5.78, *dd* (17.3, 11.0)	6.04, *dd* (17.3, 11.0)
15	4.99, *dd* (17.3, 1.3)	4.94, *dd* (11.0, 1.3)
	5.03, *dd* (11.0, 1.3)	4.98, *dd* (17.3, 1.3)

[a] All the measurements were done in C_6D_6. The assignments were established by ^{13}C–^{1}H HMBC and HSQC.

configuration of the compound was derived from the NOESY spectrum and the interpretation of relevant coupling constants. The methyl group CH_3-11 (δ 1.01) correlates with proton H_b-10 (δ 4.76) while methine proton H-4 (δ 2.05) correlates with proton H_a-10 (δ 4.73). The proton at δ 1.34, belonging to CH_2-1 exhibits four scalar coupling constants, $J_1 = 13.9$ Hz (geminal coupling), $J_2 = 13.9$ Hz (axial-axial coupling with H_a-2), $J_3 = 6.3$ Hz (axial-equatorial coupling with H_e-2) and $J_4 = 1.3$ Hz (^4J W-coupling with H-7). Therefore, this proton is axial (H_a-1) and the corresponding geminal proton is H_e-1 (δ 1.65, *dd*, $J_1 = 13.9$ Hz, $J_2 = 6.0$Hz). In the NOESY spectrum correlations are observed between the axial proton H_a-1 and the vinylic proton H-14, showing that the vinyl group at C-3 is in equatorial position. Thus the methyl group CH_3-13 is equatorial. This is confirmed by a correlation between CH_3-13 and the proton H_e-5 (δ 2.03). NOEs are observed between CH_3-12 and the proton H_e-1 (δ 1.65, *dd*, J: 13.9, 6.0), indicating that the methyl group CH_3-12 is equatorial. This is confirmed by the correlations of H_a-7 with H_a-5. The relative configuration of the compound was, therefore, established as **7** (Fig. 3). **7** is a diastereoisomer of **6** with opposite configuration at positions 3 and 7 and therefore the name 3,7-di-*epi*-trifara-9,14-diene is proposed for **7**.

2.3. Sandvicene (*8*)

From the mass spectrum of **8** ($[M]^+ = 204$), it was deduced that it has the molecular formula $C_{15}H_{24}$ and hence four unsaturations. The ^{13}C NMR spectrum suggested the presence of two double bonds (δ 112.30, 120.80, 137.50 and 147.50) in the molecule. The compound was, therefore, assumed to be bicyclic as a consequence of the two remaining unsaturations. Three methyl groups, six methylene and three methine groups were identified as well as three quaternary carbon atoms, one being olefinic. Evidence for a vinyl group was derived from the methine proton CH-14 (δ 5.95) which couples with the olefinic methylene group CH_2-15 (δ 5.15 and 5.16). Three other substructures were extracted from the ^{1}H–^{1}H COSY spectrum. The methylene group CH_2-9 (δ 1.37 and 1.75) couples with methylene group CH_2-10 (δ 1.40 and 1.62) which further couples with the methine proton CH-1 (δ 1.66) to give substructure –CH_2–CH_2–CH–. The methylene group CH_2-7 (δ 2.03 and 2.35) couples with the olefinic proton CH-6 (δ 5.48) yielding the partial structure –CH_2–CH=C–. The methylene group CH_2-3 (δ 1.35 and 1.42) couples to the methylene group CH_2-4 (δ 2.05 and 2.12), giving the partial structure –CH_2–CH_2–. The connectivities of the partial structures were established by the HMBC spectrum. The protons of the methyl group CH_3-11 and CH_3-12 show correlations to carbons C-1, C-2, C-3. The methyl groups CH_3-11 and CH_3-12 show a long-range (W-coupling) correlation to each other in the ^{1}H–^{1}H-COSY spectrum, suggesting a geminal dimethyl group. This is confirmed by ^{1}H–^{13}C long-range correlations

between CH_3-11 and C-12 as well as CH_3-12 and C-11. Protons of the methylene group CH_2-7 show correlations to carbons C-5, C-6, C-9 and C-14 and those of methyl group CH_3-13 are connected to C-7, C-8, C-9 and C-14. The protons of CH_2-15 correlate with C-8 and C-14. The methine proton H-1 correlates with the carbons C-2, C-5, C-10 and C-4. All these observations indicate the skeleton of the molecule as shown in Fig. 4.

The relative configuration of the compound was determined by the NOESY technique. The skeleton of the molecule can take a pseudo-chair conformation as represented in Fig. 4. In the NOESY spectrum of the molecule, the proton H_a-7 correlates with the methyl group CH_3-13 and with the proton H_a-9 which itself correlates with the methine proton H-1. These observations indicate that the methyl group CH_3-13 and the methine proton H-1 are on the same side of the molecule. This is confirmed by the correlation observed between the vinylic proton H-14 and the proton H_a-10 showing that the vinyl group at C-8 is axial. Thus, compound **8** has the relative configuration as shown in Fig. 5 and was called sandvicene.

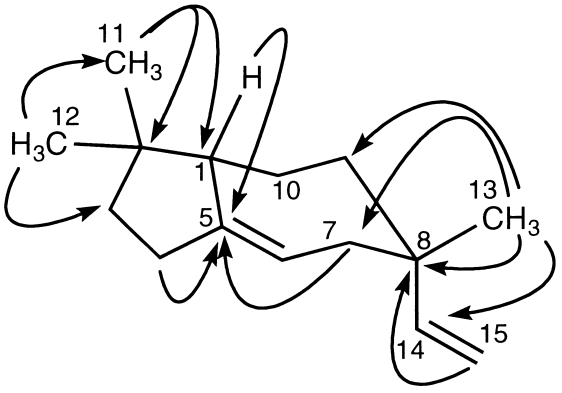

Fig. 4. Long-range correlations observed in the HMBC spectrum of sandvicene (**8**).

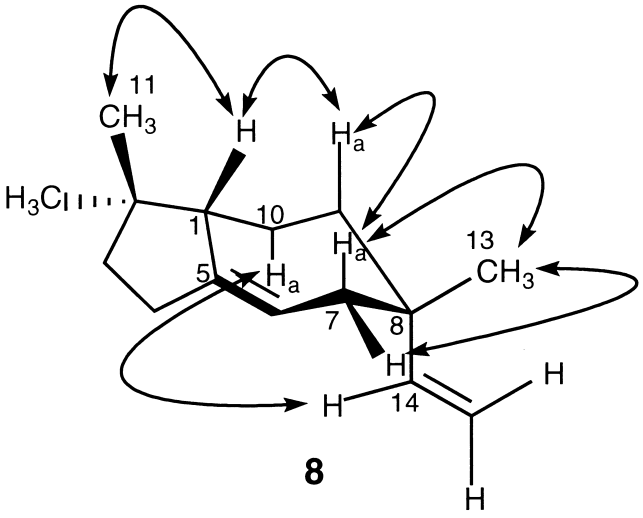

Fig. 5. Spatial correlations derived from the NOESY spectrum of sandvicene (**8**).

2.4. Neotrifaradiene (*9*)

The molecular formula of **9**, $C_{15}H_{24}$, was deduced from its mass spectrum ($[M]^+ = 204$). The ^1H and ^{13}C NMR spectra indicated two tertiary methyl and two secondary methyl groups, four methylene groups, one of which is olefinic, four methine groups, one being olefinic, and two sp^3 and one sp^2 quaternary carbon atoms. Evidence of a vinyl group in the molecule was given by the methine proton CH-10 (δ 5.98) which couples with the olefinic methylene group CH_2-11 (δ 5.13) in the ^1H–^1H-COSY spectrum. Further substructures were obtained from the ^1H–^1H COSY and HSQC experiments. Methyl group CH_3-14 (δ 1.03) correlates with the proton CH-1 (δ 1.98), itself coupled to the methylene group CH_2-2 (δ 2.03 and 2.30), which further couples to the methine proton CH-3 (δ 5.41), resulting in substructure CH_3–CH–CH_2–CH=C–. The methylene group CH_2-6 (δ 1.29 and 1.80) couples with the methylene group CH_2-7 (δ 1.52 and 1.53) giving the substructure –CH_2–CH_2–. The connectivities of the partial structures were determined by HMBC. The methyl group CH_3-15 (δ 1.16) which couples with proton CH-4 (δ 2.55) shows long-range correlations with carbons C-4, C-5 and C-9. The methyl group CH_3-14 correlates with C-1, C-2 and C-8. Methyl group CH_3-12 (δ 1.00) shows correlations with C-1, C-7, C-8 and C-9. Methyl group CH_3-13 (δ 1.05) has long-range correlation to C-4, C-5, C-6 and C-10. The vinyl proton H-10 shows long-range correlations to C-4, C-5, C-6 and C-13. Furthermore, methine proton H-4 shows long-range correlations to C-3, C-5, C-6, C-9 and C-15. These observations lead to the planar structure of **9** as given in Fig. 6.

The relative configuration of the molecule was deduced from the NOESY spectrum. Crosspeaks observed between the axial proton H_a-6 (δ 1.80, *ddd*, $J_{aa} = 11.03$ Hz, $J_{ae} = 6.62$ Hz, $J_{gem} = 13.56$ Hz) and the

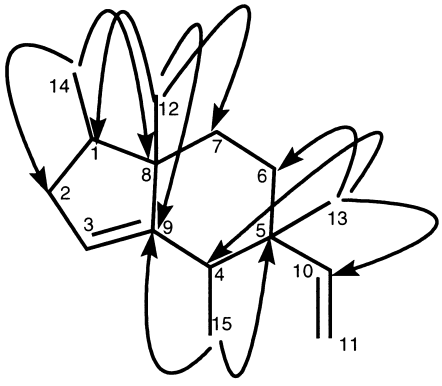

Fig. 6. Long-range correlations derived from the HMBC spectrum of neotrifaradiene (**9**).

two methyl groups CH_3-12 and CH_3-15 indicate that H_a-6 and the two methyl group are on the same side of the molecule. Due to the proximity of the signal of CH_3-12 and CH_3-14 no conclusion could be deduced from the NOESY. However, another set of correlations between the proton H_a-7 (δ 1.52, *dd*, $J_{aa}=11.03$ Hz, $J_{ae}=3.47$ Hz) and the two protons H-1 and H-10 show that the vinyl group at C-5 is in axial position and that the protons H-1, H_a-7 and H-10 are on the same side of the molecule. The methyl group CH_3-14 is thus on the same side of the molecule as CH_3-12. Therefore, the compound has the relative configuration as shown in Fig. 7.

Although the absolute configuration of the new sesquiterpene hydrocarbons **6**–**9** was not determined, biogenetic considerations suggest that it is identical to that of the trifarienols, which was derived by single crystal X-ray diffraction analysis (Hashimoto et al., 1995).

2.5. Biogenesis of trifarane sesquiterpenoids

The first natural trifarane to be reported was upial, a sesquiterpene aldehyde isolated from the marine sponge *Dysidea fragilis* (Schulte et al., 1980). Later, the alcohols trifarienols A–E (**1**–**5**) were isolated from the Malaysian liverwort *Cheilolejeunea trifaria* (Hashimoto et al., 1995). Two biogenetic pathways have been suggested considering striatane-type and pinguisane-type sesquiterpenes, respectively, as precursors of the trifarane system (Tori et al., 1993; Hashimoto et al., 1995). The four new sesquiterpenes **6**–**9** may be biogenetically related with nerolidol as their common precusor. Indeed trifara-9,14-diene (**6**) and 3,7-di-*epi*-trifara-9,14-diene (**7**) which might be biosynthesized from nerolidol (Hashimoto et al., 1995) are precursors for trifarienols **1**–**5** as shown in Fig. 8. Sandvicene (**8**) and neotrifaradiene might also be formed from nerolidol via monocyclonerolidol and striatol respectively (Fig. 8).

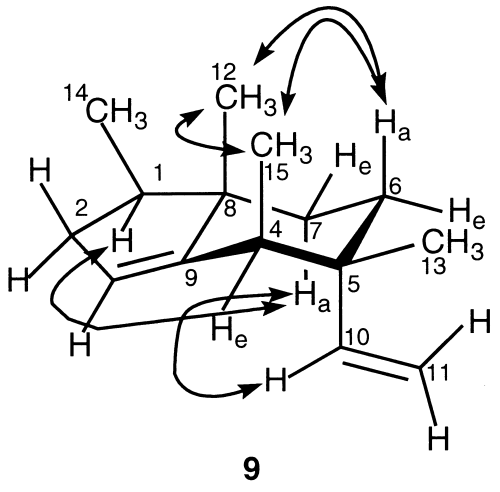

9

Fig. 7. NOE correlations and relative configuration of neotrifaradiene (**9**).

3. Experimental

3.1. NMR spectroscopy

NMR spectra were recorded using a Bruker WM 500 (500 MHz) instrument. The signal of benzene (δ 7.27 in ^{1}H NMR, 500 MHz and δ 128.40 in ^{13}C NMR, 125 MHz) was used as reference.

3.2. GC–MS

GC–MS (EI, 70 eV) measurements were carried on a Hewlett Packard 5890 gas chromatograph with a 25 m fused silica capillary column with polydimethylsiloxane CPSil 5 (Chrompack) coupled to a VG Analytical 70-250S mass spectrometer. Split injection (200°C); carrier gas He, 1 bar head pressure; ion source temp. 200°C.

3.3. Capillary GC

Orion Micromat 412 double column instrument with 25 m fused silica capillaries with polysiloxane CPSil 5 and CPSil 19 (Chrompack); Carlo Erba Fractovap 2150, 4160 instruments with 25 m fused silica capillaries with heptakis(2,6-di-*O*-methyl-3-*O*-pentyl)-β- and-γ-cyclo dextrin, respectively, and heptakis(6-*O*-t.butyldimethyl silyl-2,3-di-*O*-methyl)-β-cyclodextrin, all in polysiloxane OV1701 (50 wt.%); split injection (200°C), flame ionization detection (250°C); carrier gas hydrogen, 0.5 bar head pressure.

3.4. Polarimetry

For polarimetric measurements a Perkin-Elmer 241 polarimeter ($l=1$ dm; $\lambda=589$ nm) was used. Only the sense of the optical rotation was determined, since the isolated sample amounts were too small for an accurate determination of the *specific* optical rotation.

3.5. Plant material

The liverwort *Trocholejeunea sandvicensis* was collected in May 1999 near Tokushima, Japan. A voucher specimen has been deposited at the Institute of Pharmacognosy, Tokushima Bunri University.

3.6. Extraction and isolation

Dried plants of *T. sandvicensis* (1405 g) were extracted at room temp. with 2 l of Et_2O for 1 month. After filtration and evaporation of the solvent a slightly yellow oil (20.51 g) was obtained. The material was chromatographed on

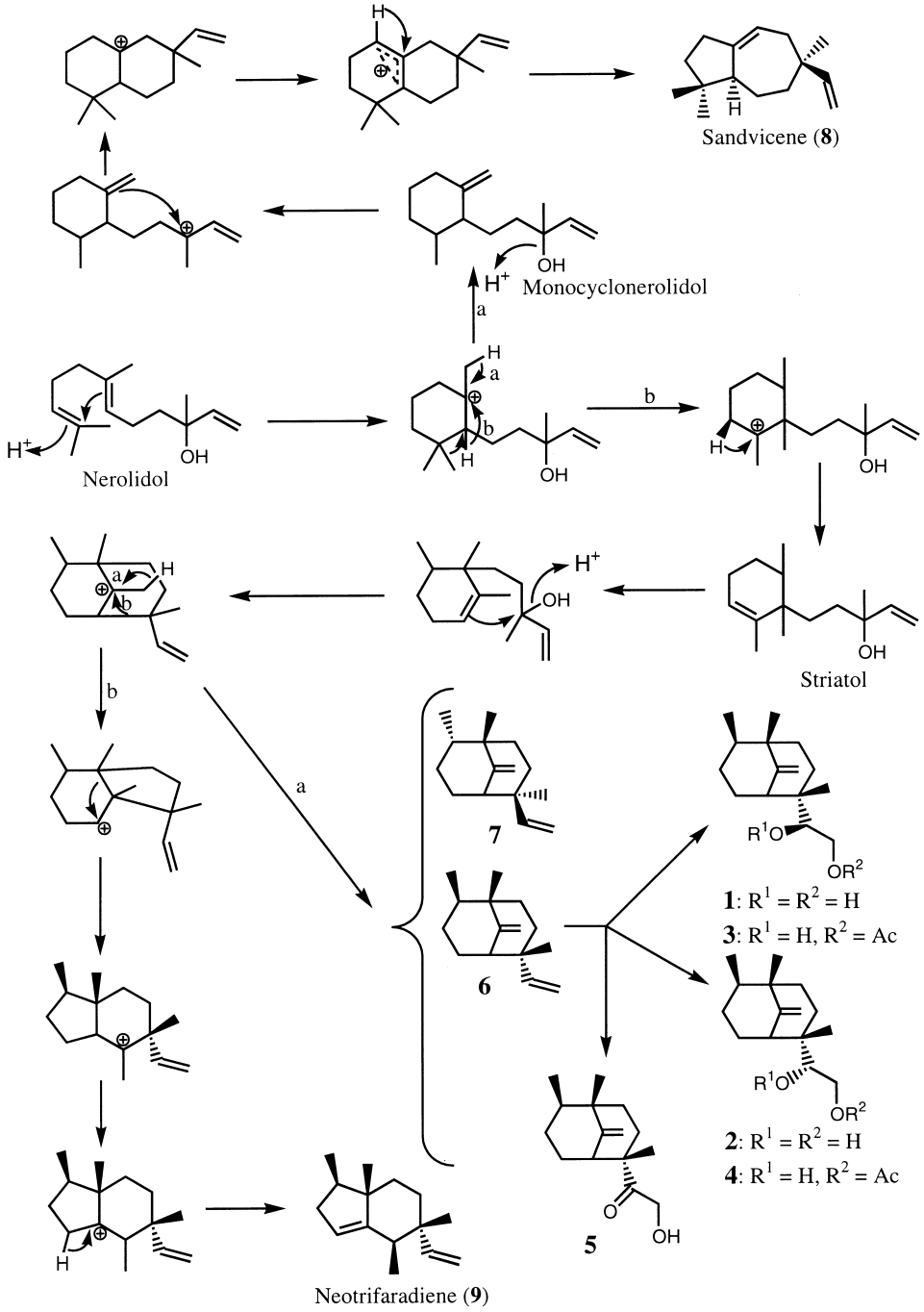

Fig. 8. Proposed biogenetic pathway for the four new sesquiterpenes **6**–**9**.

silica gel (70–230 mesh) column (300 g), using a *n*-hexane–EtOAc gradient to give 12 fractions. Fractions 1–5 (obtained with 100% *n*-hexane as eluting solvent) was subjected to GC–MS and revealed the presence of more than thirty sesquiterpenes. In order to isolate the unknown compounds of the hydrocarbon fraction, it was submitted to preparative GC using a Varian 2800 instrument, equipped with a stainless steel column (1.85 m × 4.3 mm) with 10% polydimethylsiloxane SE 30 on Chromosorb W-HP. Helium was used as carrier gas at a flow rate of 240 ml/min. The sample was injected at 90°C and after 10 min the temperature was allowed to rise at a rate of 2°/min to 180°C. Eleven fractions were collected and analysed by GC and GC–MS. GC–MS analysis of the third fraction showed the presence of three unknown compounds which were separated by preparative GC, using the same instrument, equipped with a stainless steel column (2.00×4.3 mm) containing 2.5% of a modified cyclodextrin heptakis(6-*O*-*t* butyldimethyl silyl-2,3-di-*O*-methyl)-β-cyclodextrin and polydimethyl siloxane SE 30 (1:1, w/w) on Chromosorb G-HP. A three ramp temperature program was used. The

temperature was held constant at 90°C for 15 min and then allowed to rise to 100°C at a rate of 1°/min. At 110°C the rate was changed to 2°/min. Three fractions were collected. The first fraction (TS31) eluting at 39 min contained trifara-9,14-diene (**6**) (1.5 mg), the second one (TS32) eluting at 42 min contained compound **7** (2 mg) and the third one eluting at 48 min contained sandvicene (**8**) (1.5 mg).

3.7. (−)-Trifara-9,4-diene (*6*)

^{1}H NMR see Table 1. ^{13}C NMR (125 MHz, C_6D_6): δ 18.42 (*q*, C-12), 26.34 (*q*, C-11), 26.46 (*t*, C-5), 27.78 (*q*, C-13), 30.22 (*t*, C-6), 32.92 (*t*, C-2), 39.39 (*t*, C-1), 40.59 (*s*, C-8), 41.94 (*d*, C-7), 42.53 (*s*, C-3) 51.82 (*d*, C-4), 107.16 (*t*, C-10), 111.32 (*t*, C-15), 149.62 (*d*, C-14), 152.68 (*s*, C-9). MS (EI, 70 eV), *m*/*z* (rel. int.): 204 (8) $[M]^+$, 189 (25), 175 (18), 161 (38), 147 (20), 134 (21), 133 (24), 123 (100), 122 (29), 121 (40), 119 (30), 107 (60), 105 (37), 95 (30), 93 (44), 91 (43), 81 (55), 79 (45), 77 (24), 67 (25), 55 (30), 41 (48).

3.8. (−)-3,7-Di-epi-trifara-9,14-diene (*7*)

^{1}H NMR see Table 1. ^{13}C NMR (125 MHz, C_6D_6): δ 17.08 (*q*, C-12), 26.33 (*q*, C-13), 26.44 (*q*, C-11), 30.74 (*t*, C-5), 31.69 (*t*, C-1), 31.85 (*t*, C-6), 34.75 (*t*, C-2), 39.71 (*s*, C-8), 41.74 (*s*, C-3), 44.21 (*d*, C-7), 51.56 (*d*, C-4), 104.50 (*t*, C-10), 110.08 (*t*, C-15), 148.77 (*d*, C-14), 158.90 (*s*, C-9). MS (EI, 70 eV), *m*/*z* (rel. int.): 204 (33) $[M]^+$, 189 (88), 175 (81), 161 (57), 147 (50), 135 (38), 133 (48), 123 (100), 121 (60), 119 (49), 107 (76), 105 (65), 95 (39), 93 (64), 91 (59), 81 (69), 79 (64), 77 (36), 67 (40), 55 (47), 41 (79).

Table 2
^{1}H NMR spectral data for the compounds **8** and **9**[a]

H	**8**	**9**
1	1.66, *m*	1.98, *m*
2	–	2.03, *m*
	–	2.30, *ddd* (13.6, 6.3, 3.2)
3	1.35, *m*	5.41, *m*
	1.42, *m*	–
4	2.05, *m*	2.55, *q* (7.3)
	2.12, *m*	–
6	5.48, *s*	1.29, *dddd* (13.6, 3.5, 3.5, 1.3)
	–	1.80, *ddd* (13.6, 11.0, 6.6)
7	2.03, *m*	1.52, *dd* (11.0, 3.5)
	2.35, *dd* (13.3, 2.5)	1.53, *dd* (6.6, 3.5)
9	1.37, *m*	–
	1.75, *dq* (12.3, 2.5)	–
10	1.40, *m*	5.98, *dd* (18.0, 10.7)
	1.62, *m*	–
11	1.04, *s*	5.13, *dd* (18.0, 1.3)
	–	5.13, *dd* (10.7, 1.3)
12	0.94, *s*	1.00, *m*
13	1.10, *s*	1.05, *m*
14	5.95, *dd* (17.3, 11.7)	1.03, *d* (7.0)
15	5.15, *dd* (17.3, 1.6)	1.16, *d* (7.3)
	5.16, *dd* (11.7, 1.6)	–

[a] All the measurements were done in C_6D_6. The assignments were established by ^{13}C–^{1}H HMBC and HSQC.

3.9. (+)-Sandvicene (*8*)

^{1}H NMR see Table 2. ^{13}C NMR (125 MHz, C_6D_6): δ 24.80 (*q*, C-11), 24.81 (*t*, C-4), 24.85 (*t*, C-10), 29.80 (*q*, C-12), 31.50 (*q*, C-13), 32.10 (*s*, C-2), 36.50 (*t*, C-3), 38.50 (*s*, C-8), 39.50 (*t*, C-9), 47.50 (*d*, C-1), 48.50(*t*, C-7), 112.30 (*t*, C-15), 120.80 (*d*, C-6), 137.50 (*s*, C-5), 147.50 (*d*, C-14). MS (EI, 70 eV), *m*/*z* (rel. int.): 204 (18) $[M]^+$, 189 (36), 175 (7), 162 (24), 161 (21), 148 (86), 133 (69), 119 (65), 105 (100), 106 (80), 93 (64), 91 (73), 79 (77), 67 (34), 55 (34), 41 (87).

3.10. Isolation of neotrifaradiene (*9*)

GC–MS analysis of the first fraction of the above described prep. GC separation showed that it contained only one major unknown product. The sample was purified by preparative GC on a dimethylpolysiloxane phase (SE 30). The sample was injected at a column temperature of 80°C. The temperature was then raised to 105°C at a rate of 2°C/min. Neotrifaradiene (**9**) eluted at 22 min as a pure compound (1.5 mg).

3.11. (+)-Neotrifaradiene (*9*)

^{1}H NMR see Table 2. ^{13}C NMR (125 MHz, C_6D_6): δ 14.17 (*q*, C-14), 19.42 (*q*, C-15), 19.91 (*q*, C-12), 26.64 (*q*, C-13), 31.09 (*t*, C-6), 36.24 (*t*, C-7), 38.28 (*t*, C-2), 40.01 (*s*, C-5), 41.20 (*d*, C-4), 45.95 (*s*, C-8), 49.22 (*d*, C-1), 112.25 (*t*, C-11), 123.01 (*d*, C-3), 148.45 (*d*, C-10), 155.37 (*s*, C-9). MS (EI, 70 eV): 204 (27) $[M]^+$, 189 (22), 175 (20), 161 (16), 147 (23), 134 (21), 123 (100), 121 (44), 107 (36), 105 (25), 91 (28), 81 (33), 79 (16), 77 (16), 67 (17), 55 (18), 41 (35).

Acknowledgements

We are indebted to Dr. V. Sinnwell, University of Hamburg, for his support in obtaining the NMR spectra and to Mrs. A. Meiners and Mr. M. Preusse, University of Hamburg, for their assistance in recording the mass spectra. The financial support of the Fonds der Chemischen Industrie is gratefully acknowledged.

References

Asakawa, Y., 1995. Chemical constituents of the bryophytes. In: Herz, W., Kirby, G.W., Moore, R.E., Steglich, W., Tamm, C. (Eds.), Progress in the Chemistry of Organic Natural Compounds, Vol. 65. Springer, Vienna, New York.

Barrero, A.J., Alvarez-Manzerreda, E., Lara, A., 1996. Novel tricyclic sesquiterpenes from *Juniperus thurifera* L.: chemical confirmation of the duprezianane skeleton. Tetrahedron Lett. 37, 3757–3760.

Bülow, N., König, W.A., 2000. The role of germacrene D as a precursor in sesquiterpene biosynthesis: investigation of acid catalyzed, photochemically and thermally induced rearrangements. Phytochemistry 55, 141–168.

Hashimoto, T., Koyama, H., Takaoka, S., Tori, M., Asakawa, Y., 1995. Trifarienols A–E, trifarane-type sesquiterpenoids from the Malaysian liverwort *Cheilolejeuna trifaria*. Phytochemistry 40, 171–176.

Joulain, D., König, W.A., 1998. The Atlas of Spectral Data of Sesquiterpene Hydrocarbons. E.B., Hamburg.

Lahlou, E.H., Hashimoto, T., Asakawa, Y., 2000. Highly oxygenated sesquiterpenes from the liverwort *Trocholejeunea sandvicensis*. Phytochemistry 53, 271–276.

Rieck, A., Bülow, N., Fricke, C., Saritas, Y., König, W.A., 1997. (-)-1(10),11-Eremophiladien-9β-ol from the liverwort *Marchantia polymorpha* ssp. *aquatica*. Phytochemistry 45, 195–197.

Schulte, G., Scheuer, J.P., McConnell, J.O., 1980. Upial, a sesquiterpenoid bicyclo[3.3.1]nonane aldehyde lactone from the marine sponge *Dysidea fragilis*. J. Org. Chem. 45, 552–554.

Tori, M., Arbiyanti, H., Taira, Z., Asakawa, Y., 1993. Terpenoids of the liverwort *Frullanoides densifolia* and *Trocholejeunea sandvicencis*. Phytochemistry 32, 335–348.

PERGAMON

Phytochemistry 57 (2001) 507–511

PHYTOCHEMISTRY

www.elsevier.com/locate/phytochem

Pregnene derivatives from *Solenostemma argel* leaves

Hanaa A. Hassan[a], Arafa I. Hamed[a], Nasr A. El-Emary[b,*], Irina V. Springuel[a], Hidemichi Mitome[c], Hiroaki Miyaoka[c]

[a]*Faculty of Science, South Valley University, Aswan 81528, Egypt*
[b]*Faculty of Pharmacy, Assiut University, Assiut 71526, Egypt*
[c]*Tokyo University of Pharmacy and Life Science, 1432-1 Horinouchi, Hachioji, Tokyo 192-03, Japan*

Received in revised form 14 December 2000; accepted 8 March 2001

Abstract

Two new pregnene derivatives 14β-15α-dihydroxy-Δ^4pregnene-3,20 dione and 3β-14β, 15α-16α hydroxy-20-oxo- Δ^5pregnene-tetra-ol, in addition to α- and β-amyrin and β-sitosterol, were isolated from *Solenostemma argel* leaves. The structures were established by extensive spectral analysis as well as comparison with reference materials. © 2001 Elsevier Science Ltd. All rights reserved.

Keywords: *Solenostemma argel*; Asclepiadaceae; Hydroxypregnene derivatives

1. Introduction

Solenostemma in the Asclepiadaceae, is a monotypic genus distributed widely in the Arabian desert, North Africa and Palestine (Jafri et al., 1977). *Solenostemma argel* (Hayne), is the only species found in Egypt (El-Hadidi et al., 1994) It is an erect shrub 60–100 cm high, with profuse branching especially in favoured places. It is commonly used in folk medicine for the treatment of coughs and as a purgative (Mahran and Saber, 1964).

So far the phytochemistry of *Solenostemma argel* (Hayne), has been attempted by many authors, with differing results. Mahran et al. (1967), in their study on the leaves, stems, flowers and fruits of *Solenostemma argel*, reported the presence of α and β-amyrins, β-sitosterol, 7-methoxy-3,22-dihydrostigmastene, ethoxy-vangurolic acid in addition to an unknown steroid. In another study (Mahran et al., 1969), using chromatographic examination of the alcoholic extract of *Solenostemma argel* leaves, they reported the presence of two crystalline substances named argelin and argeloside with no detailed spectral analysis or structure determination. The study performed in Hungary (Khaled et al., 1974), on *Solenostemma argel*, showed that the light petroleum and chloroform extracts do not contain steroids or alkaloids and flavonoids, while the methanolic extract was found to be rich in both flavonoids and steroids. The only quaternary base found in considerable amounts was choline. The chemical screening determined in Romania (Younis, 1988), on *Solenostemma argel* leaves, proved the existence of lipids, flavones, antocinan-oxides, mucilages, tannins, amino acids, polyholosides, polyphenolics, phytosterols and carotenoids. The biosynthetic study (Amariei et al., 1991), on the callus and shoots of *Solenostemma argel,* revealed the presence of rutoside, catchin, β-carotene and β-sitosterol.

In a recent study by (Michael, 1998), on the chemical constituents of *Solenostemma argel* leaves, she identified the new natural flavonol glycoside: kaempferol 3,4′-di-*O*-β-D-glucoside beside its 3-glucuronide, 3-rutinoside, 7,4′-diglucoside and the aglycone kaempferol.

In the present study to reach an understanding for the diversity of natural compounds isolated from *Solenostemma argel* by different investigators, we have isolated some known compounds, in addition to two new pregnene derivatives.

2. Results and discussion

Compound **1**, was found to have the molecular formula $C_{21}H_{30}O_4$ based on high resolution mass measurement *m*/*z*, $[M]^+$346. The IR spectrum of compound **1**, showed absorptions at 3405 cm^{-1} due to the hydroxyl group(s), 1706 cm^{-1} due to the carbonyl group, 1375 cm^{-1} due to the methyl ketone and 810 cm^{-1} for

* Corresponding author. Tel.: +20-88-333196; fax: +20-88-332776.
E-mail address: nemary@yahoo.com (N.A. El-Emary).

0031-9422/01/$ - see front matter © 2001 Elsevier Science Ltd. All rights reserved.
PII: S0031-9422(01)00121-2

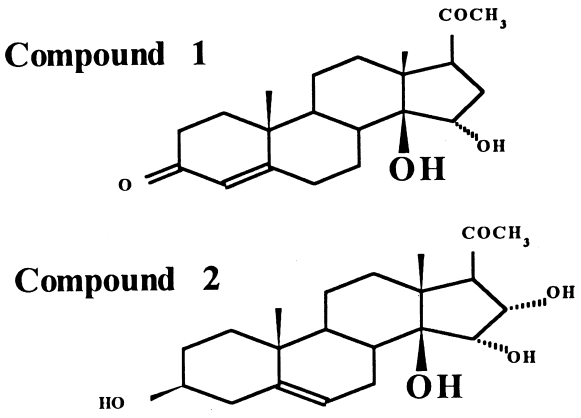

trisubstituted double bond. The UV absorption maxima at 238.4 nm, suggesting an unsaturated ketone chromophore. All 21 carbons appeared in the ^{13}C NMR spectrum of compound **1**, and examination of the DEPT spectrum disclosed the presence of 3 methyls, seven sp^3 methylenes, 5 sp^3 methines, 4 sp^3 quaternary carbons and 2 sp^2 quaternary carbons.

The calculated double bond equivalent value of 7 and the violet colour with the Libermann–Burchard test is indicative for a highly oxygenated steroid.

The ^1H NMR spectrum of compound **1**, displayed two singlets at δ 1.09 and δ 1.22 (3H, each) for the two angular methyl groups in the steroid nucleus at C-18 and C-19, in addition to a sharp three proton singlet at δ 2.27 for the methyl ketone group. Also there is a sharp singlet at δ 5.72 for one olefinic proton.

On the basis of the ubiquitous occurrence of the β-configuration of the C-14 hydroxyl group in natural pregnanes (Brandt et al., 1966) the C-14 hydroxyl group in compound **1** was also assigned as β-configuration, which showed the shift for the C-14 at δ 81.94 in the ^{13}C NMR spectrum, in good agreement with published data for natural pregnenes with C-14 hydroxyl group (Yamagishi et al., 1973). From the ^1H NMR spectrum, the second hydroxyl group must, therefore, be in ring D at the C-15 or C-16 position in order to be secondary in nature. The presence of a hydroxyl group at C-15 was derived from the one proton doublet of doublet at δ 4.38 (J= 6.3 and 9.3), suggesting an α-configuration of the C-15 hydroxyl group (Kapur et al., 1967; Sonia et al., 1998) and the correlation was demonstrated from the HMQC and HMBC spectra, where the proton at δ 4.38 correlated with C-15 at δ 73.71 and with C-17 at δ 59.91and C-8 at δ 39.89.

Also the presence of a secondary alcohol group at C-15 was confirmed by ^1H–^1H COSY experiment, which showed coupling with CH_2 at δ 2.60 (1H, *ddd*, J= 9.4,14.9,4.04 Hz) and at δ 1.43 (1H, overlapped with others) and this CH_2 was coupled with the proton at C-17 at δ 2.80 (1H, *dd*, J= 4.04, 10.38 Hz). Also there is a cross signal in NOESY experiment, between the proton at C-8 and the protons of both CH_3-18 and CH_3-19. The HMBC spectrum showed cross peaks between the proton H-4 at δ 5.71 and C-2 (at δ 33.06), C-6 (at δ 33.86) and C-10 (at δ 38.66).

Since some of the oxygen atoms in the suggested Δ^4 pregnene-20-one molecule for compound **1**, is present as hydroxyl group(s), this was demonstrated in the mass spectrum, where the molecular ion peak which appeared at m/z 346 $[M]^+$(45), was observed to lose the expected water molecule, yielding ion peak at m/z 328 $[M–H_2O]^+$ (30). The mass spectrum also displayed fragments representing the loss of acetyl functions at m/z 302 $[M–H–COMe-]^+$ (100); m/z 287 $[M–H–COMe-CH_3]^+$ (30) and 244 $[M–H–2COMe–CH_3]^+$ (23). Acetylation of compound **1** with acetic anhydride in dry pyridine by the customary method, revealed an acetate derivative. Its ^1H NMR spectrum showed signals at δ 2.08 (3H, *s*, $CO.CH_3$), and another signal at δ 2.25 for a methyl ketone group (3H, *s*, $CO.CH_3$), in addition to one proton signal at δ 5.30 for H-15. Its MS spectrum showed a molecular ion peak at m/z 389 $[M+H]^+$ (64), m/z 302 $[M–H–\ 2\ CO.CH_3]^+$ (100). From the above mentioned discussion of the spectral data presented, Compound **1** was suggested to be 14β-15α-dihydroxy-Δ^4pregnene-3, 20 dione (14β-15α-dihydroxyprogesterone), a compound which to our knowledge is not reported before from *Solenostemma argel* or from family Asclepiadaceae or from any other natural source.

Compound **2**, was isolated as colourless crystals, mp 232°C, analysed for $C_{21}H_{31}O_5$. Its IR spectrum displayed absorption bands at 3470, 1375 and 812 cm^{-1}, assigned to hydroxyl, methyl deformations of a methyl ketone and trisubstituted double bond respectively. The nature of the carbonyl function in compound **2**, was established by a positive nitroprusside test (Feigl, 1956), the presence of a three proton singlet at δ 2.27 in the ^1H NMR spectrum and the loss of COMe group from different fragments in the mass spectrum.

The calculated double bond equivalent value of 6 for compound **2**, and the violet colour in the Liebermann–Burchard test, is indicative for the steroidal nature of this compound, which is a C_{21} molecule expected to contain methyl ketone group, hydroxyl group(s) and a double bond(s).

The ^1H NMR spectrum of compound **2**, displayed signals at δ 0.94 (3H, *s*) and δ 1.03 (3H, *s*) indicative of C-18 and C-1angular methyl groups of a normal steroid ring system with Δ^5 double bond, in addition to a 3 proton sharp singlet at δ 2.27 for a methyl ketone group (CH_3–CO). A multiplet centered at δ 3.42, was associated with the α-hydrogen adjacent to the β-hydroxyl group at C-3 commonly reported in natural steroids (Kapur et al., 1967), and the coupling constants of the carbinyl proton (H-3, *dddd*, J= 4.8, 10.9,4.8 and 10.9 Hz) also supported the α- configuration (equatorial) of the hydroxyl group. Also there is a signal integrated for one vinyl proton at δ 5.40 (*d*, J=2.5 Hz) characterised for C-6 (at δ 121.86).

On the basis of the ubiquitous occurrence of the β-configuration of the C-14 hydroxyl group in natural pregnanes (Brandt et al., 1966), the C-14 hydroxyl group in compound **2** was also assigned as β-configuration, which showed the shift for the C-14 at δ 81.94 in the ^{13}C NMR spectrum, in good agreement with published data for natural pregnenes with C-14 β-hydroxyl group. From the ^{1}H NMR spectrum, the rest of hydroxyl groups must, therefore, be in ring D at the C-15 and C-16 position in order to be secondary in nature, since positions C-11 and C-12 are ruled out because of the clear coupling between H-15/H-16 and H-16/H-17 in the ^{1}H–^{1}H COSY spectrum. The configuration of the C-15 hydroxyl group could be extracted from the coupling constant of the 15β-methine proton, which appeared as a doublet at δ 4.05 (1H, *d*, $J=$ 6.8 Hz), suggesting an α-configuration for the C-15 hydroxyl group (Brandt et al., 1966; Sonia et al., 1998). The configuration of C-16 hydroxy group could be assigned from the 16β-methine proton appearing as double doublet at 4.21 ($J=$ 5.5 and 5.7 Hz) with a coupling constant value near to that of proton 15 and so, having the same α-configuration, like C-15 hydroxyl group. The ^{13}C NMR spectrum of compound **2** displayed the 21 carbons expected. Examination of the DEPT spectrum disclosed the presence of 3 methyls, 7 sp^3 methylenes, 6 sp^3 methines, 4 sp^3 quaternary carbons and one sp^2 quaternary carbon. The HMQC and HMBC spectra showed cross peaks between H-16 and C-20 (δ 2.60/ δ214.03), H-16 and C-13 (at δ 46.09), H-16 and C-14 (at δ 81.23), H-16 and C-15 (at δ 80.23), H-17 and C-12 (at δ 38.28), H-17 and C-21 (at δ 30.87), H-9 at δ 2.10 and C-14 (at δ 81.23), H-6 at δ 5.4 and C-8 (at δ 45.69) and C-10 (at δ 31.33), H-19 at δ 1.03 and C-5 (at δ 139.04) and H-3 at δ 3.42 and C-5 (at δ 139.04). Also there are cross signals in the NOESY spectrum between the proton of C-15 and both protons of C-8 and C-17. There is also cross peaks between proton at C-8 and the protons at C-6, C-18 and C-19. Since the oxygen atoms in the suggested Δ^5 pregnene molecule for compound **2**, are present as hydroxyl groups. This was demonstrated from its mass spectrum, which further helped in fixing the positions of these groups. The molecular ion peak $[M]^+$ which appears at *m/z* 365 $[M+H]^+$, was observed to lose the expected 4 water molecules yielding ion peaks at *m/z* 347 $[M–H–H_2O]^+$ (100), 329 $[347- H_2O]^+$ (19), 314 $[329\text{-}CH_3]^+$ (23) and 296 $[314- H_2O]^+$ (19). In addition the loss of the methyl ketone group at C-20, was represented by the fragment ions at *m/z* 304 $[M–H–H_2O–COMe]^+$ (7), 286 $[M–H–2H_2O–COMe]^+$ (10) and 271 $[M–H–2H_2O–CH_3–COMe]^+$ (16).

Acetylation of compound **2** in the same manner as compound **1**, revealed an acetate derivative. The ^{1}H NMR spectrum of the acetate showed the following signals: at δ 4.59 (1H, m, H-3), δ 5.78 (1H, *d*, $J=$ 6.08 Hz, H-15), δ 5.03 (1H, *dd*, $J=$ 3.33 and 6.08 Hz, H-16), δ 2.67 (1H, *d*, $J=3.33$ Hz, H-17), δ 1.00 (3H, *s*), δ 1.01 (3H, *s*), 2.34 (3H, *s*, CH_3-21), three acetate signals at δ 2.07 (3H, *s*), 2.07 (3H, *s*) and 2.12 (3H, *s*).

From the above given discussion, compound **2** is suggested to be 3β-14β,15α-16α-hydroxy-20-oxo-Δ^5pregnene-tetra-ol. A polyhydroxy pregn-ene ketone compound isolated for the first time from *Solenostemma argel* leaves and from family Asclepiadaceae.

3. Experimental

Melting points were measured on an Electrothermal Melting Point Instrument without correction. Optical rotations were measured with a JASCO DIP-360 automatic polarimeter. Infra red (IR) spectra were recorded on Shimadzu IR-470 spectrometer. UV spectra were recorded with a JASCO V-550 spectrometer. ID-NMR spectra were recorded with a Bruker DPX-400 and 2D-NMR spectra were recorded with a Bruker DRX-500 instrument. Chemical shifts were expressed on a δ (ppm) scale with tetramethylsilane (TMS) as the internal standard (*s*, singlet; *d*, doublet; *dd*, double doublet; *m*, multiplet; *t*, triplet). High resolution mass spectra were obtained with VG ZAB sperctrometer. Elemental analysis was conducted using a Perkin-Elmer 240 B instrument. Silica gel (0.063–0.200 mm, E-Merck), was used for column chromatography and silica gel GF_{254} was used for TLC and preparative PTLC purposes.

3.1. Extraction and isolation

Commercial sample (4 kg) of *Solenostemma argel* leaves, purchased from Aswan market, was cleaned from foreign materials, powdered and exhaustively extracted with alcohol 70% in a Soxhlet apparatus. The alcohol extract was condensed under reduced pressure to a syrupy consistency, then diluted with 200 ml distilled water and transfered into a separatory funnel. The extract was shaken with chloroform till exhaustion. The chloroform extract was collected, dried over anhydrous sodium sulphate and condensed under reduced pressure to give 53 g of chloroform soluble material. About 15 g of the chloroform soluble material was slurried with 50 g silica gel and placed on the top of a column packed with 600 g silica gel and elution started with hexane then gradiently with increasing proportions of ethyl acetate. Fractions eluted with hexane–ethyl acetate 9:1 and 8:2 and 7:3 were joined together and separated on preparative thick layers of silica gel GF_{254} and developing solvent composed of benzene–ethyl acetate 8:2, where 3 crystalline compounds were isolated and designated A,B and C. Fractions eluted with hexane–ethyl acetate 1:1, gave a crystalline compound **1**, mp 181°C. Fractions eluted with hexane–ethyl acetate 3:7, gave a crystalline compound **2**, mp 232°C.

Table 1
^{1}H NMR and ^{13}C NMR shifts for compounds **1** and **2**

	Compound **1**		Compound **2**	
	^{1}H NMR (400 MHz, $CDCl_3$)	^{13}C	^{1}H NMR (400 MHz, CD_3OD)	^{13}C
1	1.54 (1H, *m*), 2.20 (1H, *m*)	26.63	1.53 (1H, *m*), 1.50 (1H, *m*)	37.13
2	2.23 (2H, *m*)	33.06	2.23 (2H, *m*)	37.32
3	–	199.18	3.42 (1H, *m*)	71.08
4	5.71 (1H, *s*)	123.63	2.25 (2H, *m*)	36.95
5	–	170.49	–	139.04
6	2.4 (2H, *m*)	33.86	5.4 (1H, *dd*, *J*= 2.1, 2.7 Hz)	121.86
7	2.05 (1H, *m*), 1.7 (1H, *m*)	35.86	2.43 (1H, *m*), 2.25 (1H, *m*)	25.40
8	1.80 (1H, *m*)	39.89	2.15 (1H, *m*)	45.69
9	1.30 (1H, *m*)	48.53	2.10 (1H, *m*)	41.48
10	–	38.66	–	31.33
11	1.55 (1H, *m*), 1.45 (1H, *m*)	20.23	1.50 (1H, *m*), 1.40 (1H, *m*)	20.02
12	1.55 (1H, *m*), 1.37 (1H, *m*)	37.54	1.50 (1H, *m*), 1.11 (1H, *m*)	38.28
13	–	47.37	–	46.09
14	–	81.58	–	81.23
15	4.33 (1H, *dd*, *J*= 6.3, 9.3 Hz)	73.71	4.05 (1H, *d*, *J*= 6.8 Hz)	80.23
16	2.60 (1H, *ddd*, *J*=9.4,14.9,4.o4m), 1.43 (1H, *m*)[a]	36.29	4.21 (1H, *dd*, *J*= 5.5, 5.7 Hz)	80.23
17	2.80 (1H, *dd*, *J*= 4.04, 10. 38 Hz)	59.91	2.68 (1H, *d*, *J*= 5.4 Hz)	67.70
18	1.04 (3H, *s*)	15.69	0.94 (3H, *s*)	15.77
19	1.18 (3H, *s*)	17.74	1.03 (3H, *s*)	18.57
20	–	217.51	–	214.03
21	2.25 (3H, *s*)	32.87	2.27 (3H, *s*)	30.87

[a] Overlapped with others, coupling constant in parentheses.

3.2. Compound *A*

Obtained as colourless crystals, mp 201–203°C, gave rose red to pink colour on spraying with 40% H_2SO_4 on TLC (R_f 0.86) and subsequent heating at 100°C for few minutes. This compound has been identified as β-amyrin by comparison with reference sample.

Anal. calc. for $C_{30}H_{50}O$: C, 84.44; H, 11.81. Found: C, 84.73; H, 11.84. Mass spectrum *m/z* 426 $[M]^+$, 218, 203, 189. ^{1}H NMR (CCl_4) ppm: 0.74 (3H, *s*), 0.81 (3H, *s*), 0.87 (6H, *s*), 0.95 (9H, *s*), 1.11 (3H, *s*), 3.12 (1H, *dd*, *J*= 9, 6 Hz), 5.15 (1H, *t*, *J*= 3 Hz).

3.3. Compound *B*

This was similarly obtained from the preparative PTLC (R_f 0.84), and rerystallized from alcohol to give crystalline deposite, mp 185–187°C. Comparison with reference sample and the data presented in the literature, proved this compound to be α-amyrin.

3.4. Compound *C*

This was obtained as colourless plates from ethanol, mp 137–140°C. IR (Kbr) cm^{-1}: 3440 (OH). Although the TLC chromatogram of this compound showed only one spot R_f 0.66 in benzene–ethyl acetate 8:2, its mass spectrum gave parent peaks at *m/z*: 414, 412 and 400 suggesting the presence of a mixture of stigmasterol, campesterol and β-sitosterol.

3.5. Compound *1* (*14β-15α-dihydroxyprogesterone*)

Colourless crystals, mp 181°C; $[\alpha]_D$ +62.6° (*c*=1.31, $CHCl_3$); UV (nm): 238.4 (unsaturated ketone chromophore); IR spectrum cm^{-1}: 3405 (OH), 1706 (C=O), 1375 (CH_3–C=O) and 810 (trisubstituted double bond); mass spectrum *m/z*: 346 $[M]^+$(45). Anal. found 346. 213224 for $C_{21}H_{30}O_4$, C: 72.787514, H: 8.665180; requires 346.214410; C: 72.787264, H: 8.665150, MS *m/z* 328 $[M–H_2O]^+$ (30), 302 $[M–COMe–H]^+$ (100); *m/z* 287 $[M–COMe–CH_3]^+$ (30) and 244 $[M–2COMe–CH_3]^+$ (23). ^{1}H NMR and ^{13}C NMR spectra (Table 1). The acetate derivative, Anal. found 388.224669 for $C_{23}H_{32}O_5$, C: 71.092854, H: 8.242698; requires 388.224974; C: 71.092798, H: 8.242643.

3.6. Compound *2* (*3β-14β,15α-16α hydroxy-20-oxo-Δ^{5}pregnene-tetraol*)

Colourless crystals, mp 232°C; $[\alpha]_D$ −61.1° (c=0.31, $CHCl_3$); UV (nm): 204.4; IR spectrum^{-1}: 3470 (OH), 1706 (C=O), 1375 (CH_3–C=O) and 810 (trisubstituted double bond); mass spectrum *m/z* 365 $[M+H]^+$(5). Anal. found 364.214728 for $C_{21}H_{31}O_5$, C: 69.189953, H: 8.511462; requires 364.214410, C: 69.190013, H:

8.511469. MS, *m/z* 347 $[M–H–H_2O]^+$ (100), 329 $[347\text{-}H_2O]^+$ (14), 314 $[329\text{-}CH_3]^+$ (23) and 296 $[314\text{-}H_2O]^+$ (19), 304 $[M–H–H_2O–COMe]^+$ (7), 286 $[M–H–2H_2O–COMe]^+$ (10) and 271 $[M–H–2H_2O–CH_3–COMe]^+$ (16). ^1H NMR and ^{13}C NMR spectra (Table 1). The acetate derivative, Anal. found 490.257462 for $C_{27}H_{38}O_8$, C: 66.087724, H, 7.751029; requires 490.256669, C: 66.087831, H, 7.751041.

References

Amariei, D., Stanescu, U., Gille, E., Onisei, T., 1991. The biosynthetic capacity of the active principles of "in vitro" regenerated *Solenostema argel* (SEL). Hayne. callus and shoots. Rev. Roum. Biol. Veget., Bucharest 38 (1–2), 71.

Brandt, R., Stocklin, W., Reichstein, T., 1966. Structure determination of alloglaucotoxigenin. Helv. Chim. Acta 49, 1662.

El-Hadidi, M.N., Abdel-Aziz, F., 1994. *Tackholmia,* materials for Excursion Flora of Egypt (EFE), Vol. 15. El-Manar El-Arabi Printhouse, Cairo, 118.

Feigl, F., 1956. Spot Tests in Organic Analysis, 5th Edition. Elsevier, Amsterdam, p. 233.

Jafri, S.M.H., El-Gadi, A. (Eds.), 1977. Flora of Libya. Asclepiadaceae, Vol. 9. Al-Fateh University, Tripoli.

Kapur, B.M., Allegeier, H., Reichstein, T., 1967. Glycosides from *Kanahia laniflora* root. 1. Isolation. Helv. Chim. Acta 50, 2147.

Khaled, S.A., Kalman, S., Istvan, N., 1974. Studies on sudanese plants. 1 — *Solenostemma arghel* Hayne. Herba Hungarica 18 (3), 33.

Mahran, G.H., Saber, A.H., 1964. A contribution to the pharmacognostical study of leaves and stems of *Solenostemma argel* "Hayne" growing in Egypt. Bull. Fac. Pharm. Cairo University 3, 147.

Mahran, G.H., Wahba, S.K., Saber, A.H., 1967. Phytochemical study of *Solenostemma argel* "Hayne" leaves. Part 1 — isolation of two crytalline substances. Bull. Fac. Pharm. Cairo University 6 (1), 191.

Mahran, G.H., Ahmed, M.S., El-Fishawy, A.M., 1969. A phytochemical study of *Solenostemma argel* Hayne. Growing in Egypt. Bull. Fac. Pharm. Cairo University 8 (1), 1.

Michael, H.N., 1998. Chemical investigations on the leaves of *Solenostemma argel* [Del.] Hayne. Asian J. Chem. 10 (4), 1038.

Sonia, P., Maria, A.B., Helda, D.C., Cosimo, P., Vincenzo, D.F., 1998. *Croton ruizianus*: platelet preaggregating activity of two pregnane glycosides. J. Nat. Prod. 61, 318.

Yamagishi, T., Hayashi, K., Mitsuhashi, H., Imanari, M., Matsushita, K., 1973. Carbon-13 Nuclear magnetic resonance spectroscopy of C/D-CIS polyoxypregnanes. Tetrahedron Lett. 37, 3527.

Younis, G. M. A., PhD thesis, Bucharest, Romania, 1988.

PERGAMON

Phytochemistry 57 (2001) 513–515

PHYTOCHEMISTRY

www.elsevier.com/locate/phytochem

An eudesmanolide and a carotane from *Ferula sinaica*

Ahmed A. Ahmed[a,*], Mohamed H. Abdel-Razek[b], Mahmoud I. Nassar[c], Shunsuke Izumi[b], Sinji Ohta[d], Toshifumi Hirata[b]

[a]*Department of Chemistry, Faculty of Science, El-Minia University, El-Minia, Egypt*
[b]*Department of Mathematical and Life Sciences, Graduate School of Science, Hiroshima University, 1-3-1 Kagamiyama, Higashi-Hiroshima 739-8526, Japan*
[c]*Natural Products Chemistry Department, National Research Centre, Dokki, Cairo, Egypt*
[d]*Instrumental Center for Chemical Analysis, Hiroshima University, 1-3-1 Kagamiyama, Higashi-Hiroshima 739-8526, Japan*

Received in revised form 8 November 2000; accepted 6 March 2001

Abstract

Re-examination of the chemical constituents of the leaves of *Ferula sinaica* afforded a new eudesmanolide and a new carotane. The structures were elucidated by spectroscopic methods. © 2001 Elsevier Science Ltd. All rights reserved.

Keywords: *Ferula sinaica*; Apiaceae; Sesquiterpenes; Eudesmanolide; Carotane

1. Introduction

Ferula sinaica L. (Apiaceae) is widespread on Sinai peninsula, Egypt and its resin has been used in folk medicine for treatment of various diseases (Boulos, 1983). Chemically, the resin of the species is characterized by the presence of sesquiterpenes, sesquiterpene coumarins and monoterpenes (Al-Hazimi, 1986; Ahmed, 1990, 1991, 1999). A previous investigation of the leaves of *F. sinaica* has revealed the presence of a glucose derivative and 2-*C*-methyl-D-erythritol (Ahmed et al., 1996). We report here the isolation and characterization of a new carotane and a rare eudesmanolide constituent from the leaves of *F. sinaica*. Few eudesmanolides have been reported from the genus *Ferula* (Gonzalez and Barrera, 1995).

2. Results and discussion

Fractionation of the dichloromethane–methanol (1:1) extracts of the leaves of *F. sinaica* by column chromatography on silica gel and on Sephadex LH-20 gave a new eudesmanolide **1** and a new carotane **2**.

The spectral data of compound **1** suggested a different skeleton type than those which are common in the genus *Ferula*. ^{1}H NMR spectrum of **1**, in pyridine-d_5, displayed three methyl signals at δ 1.13, 1.15 and 1.47, two being due to two tertiary methyls and two protons geminal to hydroxyl groups were observed at δ 4.90 (J= 6.5, 9.5 Hz) and 3.60 (J=4, 11 Hz). The downfield shift of the signal at δ 4.90 suggested the oxygen function at C-6 could be acylated or lactonized. This proton showed a correlation with a narrow doublet at δ 1.86 and a multiplet at δ 2.58 in the ^{1}H–^{1}H COSY. Additionally, a methyl doublet at δ 1.15 was correlated with a multiplet signal at δ 2.82 which itself correlated with the multiplet at δ 2.58. These data could be assigned to a α-methyl-γ-lactone moiety. The double doublet at δ 3.60 (J= 4, 11 Hz) was characteristic for a proton geminal to equatorial hydroxyl group at C-3. The ^{13}C NMR spectrum of compound **1**, in $CDCl_3$, exhibited 15 nonequivalent carbon atoms. The assignment of the carbon signals was established from DEPT and HMQC experiments. This data suggested the presence of an eudesmanolide structure, a rare constituents in the genus *Ferula* (Gonzalez and Barrera, 1995). Although, the coupling constant suggested the stereochemistry of H-3, H-5 and H-6, NOESY experiment, in pyridine-d_5, supported the proposed stereochemistry. H-6 showed a cross-peak with H-7, H-14 and H-15. While, H-7 exhibited a cross-peak with H-14 and H-11; H-5 showed a correlation

* Corresponding author. Tel.: +20-86-345-267; fax: 20-86-342-601.
E-mail address: abdellaahmed@hotmail.com (A.A. Ahmed).

0031-9422/01/$ - see front matter © 2001 Elsevier Science Ltd. All rights reserved.
PII: S0031-9422(01)00115-7

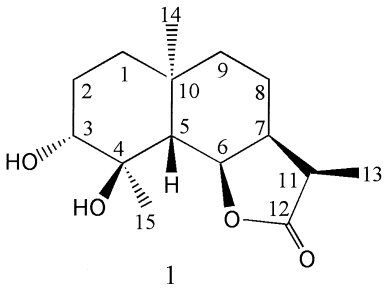

1

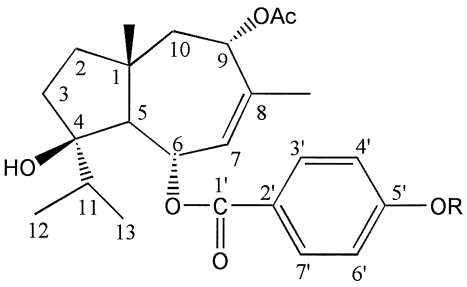

2 R = H

2a R = Ac

with H-3. HREI mass spectrum afforded a molecular ion peak at m/z 268.1660, $C_{15}H_{24}O_4$. Therefore, compound **1** has the structure of a 3α,4β-dihydroxy-5βH, 11α H-eudesman-6,12-olide. Of similar structure related compounds, one has been synthesized and showed cell growth inhibitory activity against lymphocytic leukemia (P-388) in vitro (Ando et al., 1991), the second was a biotransformation products (Amate et al., 1991).

The structure of compound **2** could be easily established by comparison of its spectral data with those of lancerotriol derivatives (Fraga et al., 1985, 1986; Garg et al., 1987; El-Sayed, 1990; Miski and Jakupovic, 1990). An additional sharp singlet signal, integrated for three protons appeared at δ 2.05 and could be assigned to an acetyl group. The chemical shift of H-9 as a multiplet at downfield (δ 5.57), compare to H-9 of lancerotriol 6-vanillate (δ 4.30) indicated the presence of an acetyl group at C-9. The second acyl group was established as p-hydroxybenzoate from the ^{1}H and ^{13}C NMR (Tables 1 and 2). The other ^{1}H and ^{13}C signals were very close to those of lancerotriol derivatives. The HRCI mass spectrum afforded a molecular ion at m/z 417.2251 (calc. 417.2277, $C_{24}H_{32}O_6$). Acetylation of **2** gave the acetyl product **2a**. Its ^{1}H and ^{13}C NMR data are reported in Tables 1 and 2. Moreover, the configuration at C-9 was supported from NOE experiment. Irradiation of H-14 of **2a** enhanced H-6 and H-9.

Table 1
^{1}H NMR of compounds **1**, **2** and **2a** (400 MHz, $CDCl_3$)

Protons	**1**[b]		**1**[c]	**2**	**2a**
H-1$_a$	1.55 *m*		1.24		
H-1$_b$	1.55 *m*		1.45		
H-2$_a$	1.50 *m*		1.80		1.30
H-2$_b$	1.65				1.60
H-3$_a$	3.45 *dd* (4.0, 11.0)[a]		3.60		1.80
H-3$_b$	–				
H-5	1.60 *d* (9.5)		1.86	2.20 *d* (10.0)	2.22
H-6	4.85 *dd* (6.5, 9.5)		4.90	5.87 *d* (10.0)	5.91
H-7	2.75 *m*		2.58	5.40 *br s*	5.40
H-8$_a$	1.50 *m*		1.23		
H-8$_b$	1.65 *m*		1.44		
H-9$_a$	1.60 *m*		1.95	5.57 *m*	5.50
H-9$_b$	1.75 *m*		1.85		
H-10$_a$	–	–			2.00
H-10$_b$	–	–			1.60
H-11	2.80 *m*		2.82	1.88 *qq* (7,7)	1.72
H-12	–	–		0.90 *d* (7.0)	0.98
H-13	1.25 *d* (7.0)		1.15	0.80 *d* (7.0)	0.82
H-14	0.90 *s*		1.13	1.73 *s*	1.75
H-15	1.35 *s*		1.47	1.22 *s*	1.23
3′, 7′				7.85 *d* (8.5)	8.07
4′, 6′				6.82 *d* (8.5)	7.19
AcO				2.05 *s*	2.08
					2.33

[a] *J* values (Hz) are given in parentheses.
[b] Assigned by ^{1}H and ^{1}H–^{13}C COSY.
[c] In pyridine-d_5.

Table 2
^{13}C NMR of compounds **1**, **2** and **2a** (100 MHz, $CDCl_3$, δ values)

Carbons	**1**	**2**	**2a**
C-1	37.3 *t*	42.1 *s*	42.0
C-2	18.4 *t*	41.6 *t*	41.6
C-3	79.9 *d*	31.5 *t*	31.6
C-4	71.6 *s*	86.5 *s*	86.2
C-5	51.8 *d*	54.6 *d*	54.5
C-6	79.0 *d*	72.4 *d*	71.8
C-7	36.2 *d*	127.7 *d*	127.4
C-8	28.3 *t*	135.6 *s*	135.8
C-9	39.1 *t*	72.0 *d*	72.9
C-10	37.9 *s*	46.3 *t*	46.2
C-11	37.2 *d*	36.7 *d*	36.8
C-12	178.4 *s*	17.3 *q*	17.2
C-13	11.4 *q*	18.2 *q*	18.2
C-14	16.3 *q*	23.5 *q*	23.5
C-15	24.4 *q*	18.7 *q*	18.7
C-1′		166.4 *s*	166.1
C-2′		121.7 *s*	127.6
C-3′, 7′		131.9 *d*	131.2
C-4′, 6′		115.3 *d*	121.6
C-5′		161.0 *s*	154.3
AcO		170.2 *s*	170.3, 168.7
		21.0 *q*	21.0, 21.0

3. Experimental

3.1. Plant material

Leaves of *F. sinaica* were collected from North Sinai peninsula, El-Arish, Egypt, in March 1997 by one of us (AAA). A voucher specimen (AAA 110) is deposited in the department of Botany, El-Minia University, Egypt.

3.2. Extraction

Air-dried leaves of *F. sinaica* (500 g) were extracted with MeOH–CH_2Cl_2 (1:1). The extract was defatted and chromatographed on Si gel column packed into petroleum ether (bp 40–60°C) and eluted with a petroleum ether–Et_2O step gradient. The fractions eluted with petroleum ether–Et_2O (1:1 and 1:2) were combined and further chromatographed on a Sephadex LH-20 column with an initial solvent of Et_2O–CH_2Cl_2–MeOH (7:4:0.5) to give 9 mg of **1**, and 11 mg of **2**.

3.3. Physical and spectral data

3.3.1. 3α,4β-Dihydroxy-5βH, 11α H-eudesman-6,12-olide (1)

IR ν_{max} $CHCl_3$ cm^{-1}: 3510, 3425, 1785. HREIMS *m/z* (rel. int): 268.1660 $[M]^+$ (45) (calc. 268.1675); molecular formula: $C_{15}H_{24}O_4$.

3.3.2. Lancerotriol 9-acetate-6-p-hydroxybenzoate (2)

IR ν_{max} $CHCl_3$ cm^{-1}: 3445, 2975, 2885, 1700, 1690. HRCIMS *m/z* (rel. int.): 417.2251 $[M+H]^+$ (calc. 417.2277, $C_{24}H_{32}O_6$), 399.2170 $[M+H–H_2O]^+$ (100) (Calc. 399.2171); molecular formula: $C_{24}H_{30}O_5$.

Acetylation of **2**: 8 mg of **2** was heated with Ac_2O in pyridine, at 70°C for 1 h. The mixture was decomposed by distilled water and was extracted with CH_2Cl_2. The organic layer was concentrated and purified by Sephadex LH-20 column (*n*-hexane–CH_2Cl_2–MeOH, 8:3:0.5) to give 6 mg of **2a**. IR ν_{max} $CHCl_3$ cm^{-1}: 2890, 2885, 1695, 1690. HRCIMS *m/z* (rel. int.): 459.2367 $[M+H]^+$ (11) (calc. 459.2383, $C_{26}H_{34}O_7$), 441.2275 $[M+H–H_2O]^+$ (100) (calc. 441.2278); molecular formula: $C_{26}H_{32}O_6$.

References

Ahmed, A.A., 1990. New sesquiterpenes from *Ferula sinaica*. Journal of Natural Products 53, 483–486.

Ahmed, A.A., 1991. Daucanes and other constituents from *Ferula sinaica*. Phytochemistry 30, 1207–1210.

Ahmed, A.A., 1999. Sesquiterpene coumarins and sesquiterpenes from *Ferula sinaica*. Phytochemistry 50, 109–112.

Ahmed, A.A., Abdel-Razek, M.H., Abu-Mustafa, E.A., Williams, H.J., Scott, A.I., Reibenspies, J.H., Mabry, T.J., 1996. A new derivative of glucose and 2-C-methyl-D-erythritol from *Ferula sinaica*. Journal of Natural Products 59, 1171–1173.

Al-Hazimi, H.M., 1986. Terpenoids and a coumarin from *Ferula sinaica*. Phytochemistry 25, 2417–2419.

Amate, Y., Granados, A.G., Martínez, A., Buruaga, A.S., Bretón, J.L., Onorato, M.E., Arias, J.M., 1991. Biotransformation of 6β-eudesmanolides functionolized at C-3 with *Curvularia lunata* and *Rhizoupus nigricans* cultures. Tetrahedron 47, 5811–5818.

Ando, M., Isogal, K., Azami, H., Hirata, N., Yanagi, Y., 1991. Studies on the synthesis of sesquiterpene lactones, 12. Synthesis of (+)-colartin, (+)-arbasculin A and their C-4 epimers and their biological activities. Journal Natural Products 54, 1017–1024.

Boulos, L., 1983. Medicinal Plants of North Africa. Algonac, MI.

El-Sayed, N.H., 1990. Carotane sesquiterpene from *Ferula sinaica*. Pharmazie 45, 538.

Fraga, B.M., Hernandez, M.G., Diaz, J.G., Gonzalez, A.G., Gonzalez, P., 1986. Carotane sesquiterpene from *Ferula linkii*. Phytochemistry 25, 2883–2886.

Fraga, B.M., Gonzâlez, A.G., Gonzâlez, P., Hernandez, M.G., Larruga, C.L., 1985. Carotane sesquiterpene from *Ferula lancerottensis*. Phytochemistry 29, 501–504.

Garg, S.N., Agarwal, S.K., Mahajan, V.P., Rastogi, S.N., 1987. Feruginidin and ferugin, two new sesquiterpenoids based on the carotane skeleton from *Ferula jaeschkeana*. Journal of Natural Products 50, 253–255.

Gonzalez, A.G., Barrera, B., 1995. Chemistry and sources of mono- and bicyclic sesquiterpenes from *Ferula* species. Progress in Chemistry of Organic Natural Products 64, 1–92.

Miski, M., Jakupovic, J., 1990. Daucane esters from *Ferula rigidula*. Phytochemistry 29, 173–178.

PERGAMON

Phytochemistry 57 (2001) 517–521

PHYTOCHEMISTRY

www.elsevier.com/locate/phytochem

Furanoditerpenoid lactones from the seeds of *Caesalpinia minax* Hance

Ren-Wang Jiang[a], Paul P.H. But[b], Shuang-Cheng Ma[b], Thomas C.W. Mak[a,*]

[a]*Department of Chemistry, The Chinese University of Hong Kong, Hong Kong SAR, PR China*
[b]*Department of Biology & Institute of Chinese Medicine, The Chinese University of Hong Kong, Hong Kong SAR, PR China*

Received 17 October 2000; received in revised form 11 January 2001

Dedicated to the memory of Dr. Hson-Mou Chang (1923–2000)

Abstract

Two furanoditerpenoid lactones, were isolated from the seeds of *Caesalpinia minax* Hance. Their structures and stereochemistry have been established by spectral data and single crystal X-ray analysis. © 2001 Elsevier Science Ltd. All rights reserved.

Keywords: *Caesalpinia minax*; Leguminosae; Furanoditerpenoid lactone; Caesalmin A and B; X-ray analysis

1. Introduction

Plants belonging to the genus *Caesalpinia* have proven to be a rich source of cassane furanoditerpenes (Balmain et al., 1967, 1970; Pascoe et al., 1986; Ogawa et al., 1992; Kinoshita et al., 1996; Kitagawa et al., 1996; Peter et al., 1997, 1998; Lyder et al., 1998). The molecular skeleton of this kind of diterpenoid is constructed from the fusion of three cyclohexane rings and a furan ring. In most cases structural determination was based on spectroscopic methods. However, the absolute configuration of ε-caesalpin (Birnbaum and Ferguson, 1969) and caesaldekarin A (Kitagawa et al., 1994), as shown in Fig. 1, were confirmed by X-ray analyses using the anomalous dispersion method.

Some of the extracts of plants of the genus *Caesalpinia* display interesting biological activities (Hikino et al., 1977; Sharma et al., 1997; Datte et al., 1998). *Caesalpinia minax* Hance, a member of this genus, is a prickly scandent shrub growing in the tropics and subtropics. The seeds of this plant, which is called 'kushilian', have long been used as Chinese folk medicine for the treatment of common cold, fever and dysentery (Jiangsu New Medical College, 1977). We report herein the isolation of two new furanoditerpenoid lactones, designated caesalmin A and caesalmin B, from the chloroform partition of the ethanol (95%) extract of this plant. Their structures were established by spectroscopic methods and single crystal X-ray analysis (Fig. 1).

2. Results and discussion

A 95% EtOH extract of the seeds of *Caesalpinia minax* Hance was suspended in distilled water and extracted successively with hexane, chloroform, ethyl acetate and *n*-butanol. The chloroform extract was subjected to silica gel column chromatography to yield caesalmin A and caesalmin B.

Caesalmin A was obtained as colorless block-like crystals of its 1:1 methanol solvate, $C_{22}H_{28}O_8{\cdot}CH_3OH$, mp 179–180°C, $[\alpha]_D^{20}$ −6.5° (*c* 0.1 in CH_3OH). Assignment of the molecular formula $C_{22}H_{28}O_8$ was based on HRLSIMS (*m*/*z* $[MH]^+$ 421.1847, calculated 421.1854). The ESI mass spectrum showed a $[M\text{-}1]^-$ ion peak at *m*/*z* 419. Its IR (KBr) showed bands at 3422 (hydroxyl), 1803 (saturated γ-lactone) and 1743 cm^{-1} (acetoxyl). The ultraviolet (UV) spectrum of caesalmin A showed a maximum at 219 nm (logε 3.84) which suggested the presence of a furan ring.

The ^1H NMR spectrum (Table 1) indicated the presence of three tertiary methyl group at δ_H 1.18 (6H, *s*, H-18 and H-19) and 1.15 (3H, *s*, H-20), one acetoxyl

* Corresponding author. Tel.: +852-2609-6279; fax: +852-2603-5057.
E-mail address: tcwmak@cuhk.edu.hk (T.C.W. Mak).

0031-9422/01/$ - see front matter © 2001 Elsevier Science Ltd. All rights reserved.
PII: S0031-9422(01)00134-0

group at δ_H 2.11 (3H, *s*, H-22), four low-field protons attached to carbon atoms bearing an oxygen function at δ_H 3.61 (1H, *d*, $J=2.6$ Hz, H-1), δ_H 4.03 (1H, *ddd*, $J=2.6$, 4.5, 12.5 Hz, H-2), δ_H 4.81 (1H, *dd*, $J=9.3$, 11.3 Hz, H-7) and δ_H 5.50 (1H, *d*, $J=9.3$ Hz, H-6), and two adjacent α and β double-bond protons at δ_H 6.54 (1H, *d*, $J=2.0$ Hz, H-15) and δ_H 7.38 (1H *d*, $J=2.0$ Hz, H-16) on a furan ring. Except for one acetoxyl group (δ_C 170.79 and 20.67), the ^{13}C NMR and DEPT spectrum of caesalmin A showed 20 carbon atoms: one lactonic carbonyl atom (δ_C 175.13), four olefinic carbon atoms of the furan ring (δ_C 152.74, 114.18, 107.69 and 142.10), five carbon atoms bearing oxygen (δ_C 73.70, 64.92, 83.91, 75.46 and 83.49), two methylene groups (δ_C 41.07 and 21.15), three methyl groups (δ_C 30.60, 24.86 and 15.53), three methine carbons (δ_C 44.69, 32.94 and 41.44) and two quaternary carbon atoms (δ_C 41.34, 44.78), which suggested that caesalmin A possesses a cassane furanoditerpene lactone structure (Peter et al., 1997) as shown in Fig. 1. The full assignments and connectivities were determined by ^1H–^1H COSY, HMQC and HMBC spectrum. The HMQC spectrum revealed a signal at δ_H 4.81 (1H, dd, $J=9.3$, 11.3, H-7) attached to a carbon at δ_C 83.49, and the HMBC spectrum showed that H-7 was correlated to C-6, C-8, C-14 and C-17, suggesting that the γ-lactone was formed by ring closure involving the oxygen atoms bridged to C-7 and C-17.

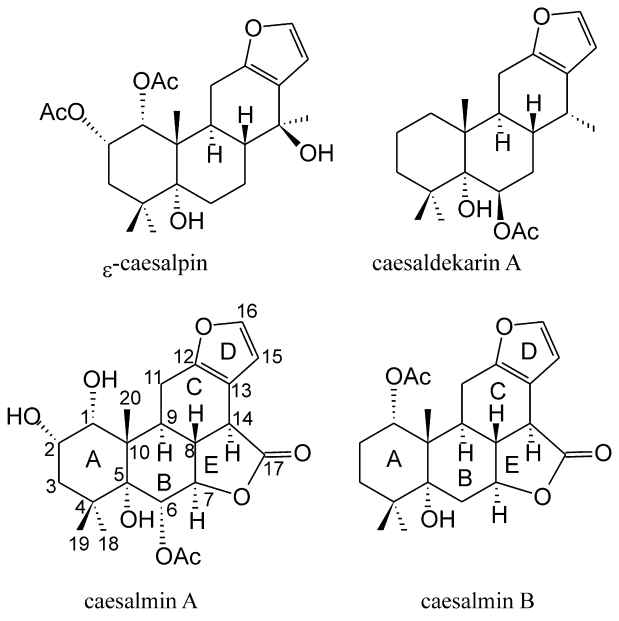

Fig. 1. Chemical formulae of some cassane furanoditerpenoids.

The molecular structure and stereochemistry of caesalmin A were established unequivocally by X-ray crystallographic analysis. The asymmetric unit consists of one independent caesalmin A and one methanol molecule connected by hydrogen bonds O-9 − O-7 (3.035 Å)

Table 1
^{13}C NMR (75 MHz, CD_3OD) and ^1H NMR (300 MHz, CD_3OD) spectral data[a]

Position	Caesalmin A		Caesalmin B	
	δ_c DEPT	δ_H (mult., *J* in Hz)	δ_c DEPT	δ_H (mult., *J* in Hz)
1	73.70 *d*	3.61 (1H, *d*, 2.6)	75.11 *d*	4.88 (1H, *br s*)
2	64.92 *d*	4.03 (1H, *ddd*, 2.6, 4.5, 12.5)	30.66 *t*	1.65 (1H, *m*, 2-H$^{\alpha}$)
				1.92 (1H, *m*, 2-H$^{\beta}$)
3	41.07 *t*	1.28 (1H, *dd*, 4.5, 13.4 3-H$^{\alpha}$)	30.91 *t*	1.28 (1H, *m*,3-H$^{\alpha}$)
		1.97 (1H, *dd*, 12.5, 13.4, 3-H$^{\beta}$)		1.96 (1H, *m*, 3-H$^{\beta}$)
4	41.34 *s*		39.66 *s*	
5	83.91 *s*		82.56 *s*	
6	75.46 *d*	5.50 (1H, *d*, 9.3)	23.04 *t*	1.84(2H, *dd*, 10.7, 11.1)
7	83.49 *d*	4.81 (1H, *dd*, 9.3, 11.3)	82.03 *d*	4.71 (1H, *ddd*, 10.7, 11.1, 5.4)
8	44.69 *d*	2.17 (1H, *m*)	45.51 d	2.31 (1H, *dd*, 5.4, 13.1)
9	32.94 *d*	3.18 (1H, *ddd*, 8.0, 8.8, 13.5)	34.03 *d*	2.90 (1H, *ddd*, 8.3, 8.8, 13.1)
10	44.78 *s*		47.30 *s*	
11	21.15 *t*	2.62 (1H, *dd*, 8.8, 16, 11- H$^{\alpha}$)	21.65 *t*	2.41 (1H, *dd*, 8.8, 17.6, 11- H$^{\alpha}$)
		2.75 (1H, *dd,* 8.0, 16, 11- H$^{\beta}$)		2.58 (1H, *dd*, 8.3, 17.6, 11- H$^{\beta}$)
12	152.74 *s*		152.79 *s*	
13	114.18 *s*		114.75 *s*	
14	41.44 *d*	3.48 (1H, *br d*, 13.2)	41.74 *d*	3.36 (1H, *br d*, 13.1)
15	107.69 *d*	6.54 (1H, *d*, 2.0)	107.99 *d*	6.52 (1H, *d*, 1.8)
16	142.10 *d*	7.38 (1H, *d*, 2.0)	142.28 *d*	7.34 (1H, *d*, 1.8)
17	175.13 *s*		176.64 *s*	
18	30.60 *q*	1.18 (3H, *s*)	28.08 *q*	1.12 (3H, *s*)
19	24.86 *q*	1.18 (3H, *s*)	24.41 *q*	1.15 (3H, *s*)
20	15.53 *q*	1.15 (3H, *s*)	17.35 *q*	1.06 (3H, *s*)
21	170.79 *s*		170.65 *s*	
22	20.67 *q*	2.11 (3H, *s*)	20.61 *q*	2.11 (3H, *s*)

[a] ^1H and ^{13}C data were assigned based on DEPT, ^1H–^1H COSY, HMQC and HMBC spectra.

and O-2–O-9 (2.867 Å, -x-1/2, -y, z+1/2). A view of the molecular structure is presented in Fig. 2. Bond lengths and angles are in generally close to normal values. The A and B rings adopt a normal chair conformation with mean torsion angles of 53.6 and 58.3° (the torsion angle of cyclohexane is 56°). The C ring exists in a twist chair conformation due to fusion with the furan ring, which is planar with a maximum deviation of 0.0035 Å. The lactone ring E exists in an envelope conformation with C-8 displaced by 0.722 Å from the least-squares plane of the remaining four atoms.

Caesalmin B was isolated as colorless crystals of its 2:1 acetone solvate. $2(C_{22}H_{28}O_6)\cdot CH_3COCH_3$, mp 148–149°C, $[\alpha]_D^{20}$ +52.5° (c 0.4 in CH_3OH). The molecular formula $C_{22}H_{28}O_6$ was based on HRLSIMS (m/z $[MH]^+$ 389.1951, calculated 389.1956). The IR and UV spectra were nearly the same as those of caesalmin A. The ^1H and ^{13}C NMR spectra of caesalmin B were similar to those of caesalmin A; however, two methine groups in caesalmin A (δ_C 64.92 and 75.46) were replaced by two methylene groups at δ_C 30.66 and 23.04 in caesalmin B (Table 1). ^1H–^1H COSY and HMQC spectra showed that the two methylene groups can be assigned to the 2 and 6 positions. The correlation between the acetate carbonyl signal at δ_C170.65 and the oxymethine proton H-1 (δ_H4.88) in the HMBC spectrum showed that the acetoxyl group is attached at C-1.

The structure of caesalmin B was verified by X-ray analysis. The asymmetric unit consists of two independent, nearly identical caesalmin B molecules and one acetone molecule connected by hydrogen bonds O-3′–O-5 (3.045 Å, x-1, y, z) and a weak C–H interaction C-16–O-7 (3.468 Å). A view of the molecular structure is presented in Fig. 3. The conformation of caesalmin B is similar to that of caesalmin A. The A, B, C, D and E rings adopt chair, chair, twist chair, planar and envelope conformations, respectively.

Both caesalmin A and caesalmin B have the same ring junctions, i.e. A/B *trans*, B/C *trans*, B/E *trans* and C/E *trans*. All furanoditerpenoids from *Caesalpinia* related species have an beta-oriented methyl group at C-10. Since the absolute configuration of both ε-caesalpin (Birnbaum and Ferguson, 1969) and caesaldekarin A (Kitagawa et al., 1994) are well established, the absolute configuration of caesalmin A and caesalmin B can be assigned by analogy as shown in Fig. 1.

3. Experimental

3.1. General

ORD were recorded on a Perkin-Elmer 341 Polarimeter in MeOH solution. Mps were determined using a Fisher Scientific instrument and are uncorrected. The UV spectra were obtained on a Beckman DU650 spectrophotometer in MeOH. IR spectra were recorded on a Nicolet Impact 420 FT–IR spectrometer. The NMR spectra were obtained on a Bruker 300 spectrometer with chemical shifts reported in δ (ppm) using TMS as an internal standard. HRLSIMS measurements were made on an APEX 47e FTMS spectrometer. ESIMS were recorded on a Finnigan MAT TSQ 7000 instrument. X-ray intensities of caesalmins A and B were measured on a Bruker SMART 1000 CCD diffractometer.

3.2. Plant material

The seeds of *Caesalpinia minax* Hance were collected in Guangxi Province, China in September, 1999. The seeds were identified at the Institute of Chinese Medicine,

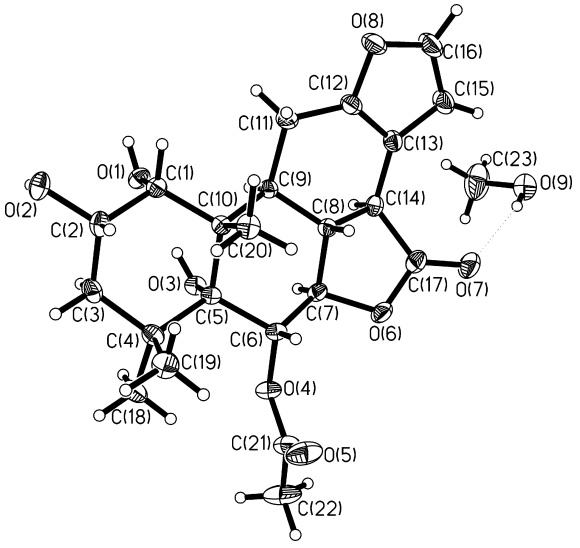

Fig. 2. Molecular structure of caesalmin A, showing the asymmetric unit of its 1:1 solvate with methanol and the atom labeling scheme.

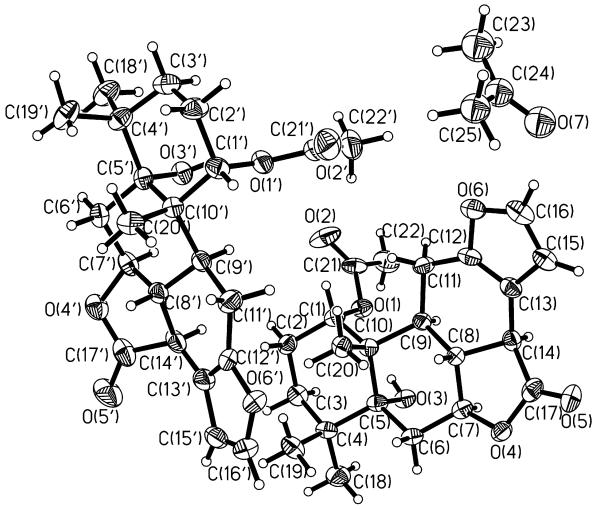

Fig. 3. Molecular structure of caesalmin B, showing the asymmetric unit of its 2:1 solvate with acetone and the atom labeling scheme.

The Chinese University of Hong Kong, where a voucher specimen (No. cm-99) is kept.

3.3. Isolation of caesalmin A and B

The seeds of *Caesalpinia minax* Hance (10 kg) were ground and refluxed with 95% ethanol but reflux temperature. The solubles were then evaporated in vacuo to yield an ethanol extract (892 g) which was then suspended in distilled water and extracted successively with hexane, chloroform, ethyl acetate and *n*-butanol. The chloroform extract (50 g) was subjected to silica gel column chromatography and eluted with hexane/acetone (10:1). Fractions of 150 ml each were taken and 32 fractions collected, and caesalmin A (16 mg) was obtained as a white powder from fractions 24 and 25, and recrystallized from methanol at room temperature. Similarly caesalmin B (50 mg) was obtained as a white powder from fractions 9, 10 and 11, and recrystallized from hexane/acetone (8:1) at room temperature.

3.4. Caesalmin A

Colorless blocks from methanol, $[\alpha]_D^{20}$ −6.5° (c 0.1 in CH_3OH); UV λ_{max}^{MeOH} nm (logε): 219 (3.84); IR (KBr) 3422 cm^{-1}, 1803 cm^{-1}, 1743 cm^{-1}; HRLSIMS *m*/*z* $[MH]^+$ 421.1847, calculated 421.1854. ESIMS 10 eV, *m*/*z* (rel. int.) 419 $[M\text{-}1]^-$ (60), 479 $[M+OAc]^-$ (100). ^1H and ^{13}C spectral data, see Table 1.

3.5. Caesalmin B

Colorless blocks from hexane–acetone mixture, $[\alpha]_D^{20}$ + 52.5° (*c* 0.4 in CH_3OH). UV λ_{max}^{MeOH} nm (log ε): 217 (3.82); IR 3590 cm^{-1}, 1790 cm^{-1}, 1743 cm^{-1}; HRLSIMS (*m*/*z* $[MH]^+$ 389.1951, calculated 389.1956. ESIMS 30 eV, *m*/*z* (rel. int.) 387 $[M\text{-}1]^-$ (5), 59 $[OAc]^-$ (69), 447 $[M+OAc]^-$ (100). ^1H and ^{13}C spectral data, see Table 1.

3.6. X-ray crystallography of caesalmin A — methanol (1/1)

$C_{22}H_{28}O_8{\cdot}CH_3OH$, colorless blocks, mp 179-180°C, M_r = 452.49, orthorhombic, $P2_12_12_1$, a = 7.465 (1), b = 16.806 (3), c = 17.955 (4) Å, V = 2252.6 (8) $Å^3$, Z = 4, d_x = 1.334 gcm^{-3}, $F(000)$ = 968, μ(Mo-K_α) = 0.102 mm^{-1}. Data collection was performed on a SMART CCD using graphite monochromated radiation (λ = 0.71073 Å); 5420 unique reflections were collected to θ_{max} = 28.01°, in which 4593 reflections were observed [$F^2 > 4\sigma(F^2)$]. The crystal structure was resolved by direct methods using SHELXS-97 and refined by full-matrix least-squares method on F^2 using SHELXS-97. Non-hydrogen atoms were refined with anisotropic temperature factors. Hydrogen atoms bonded to carbons were placed at their geometrically ideal positions. Hydrogen atoms bonded to oxygens were located on difference fourier maps and included in the calculation of structure factors with isotropic temperature factors. In the final stage, R = 0.0455, Rw = 0.0567 and S = 1.028.

3.7. X-ray crystallography of caesalmin B — acetone (2/1)

$2C_{22}H_{28}O_6{\cdot}CH_3COCH_3$, colorless blocks, mp 148–149°C, M_r = 834.97, triclinic, $P1$, a = 8.9126 (19), b = 10.586 (2), c = 12.623 (3) Å, α = 96.834 (5), β = 99.642 (5), γ = 107.439 (4), V = 1101.9 (4) $Å^3$, Z = 1, d_x = 1.258 gcm^{-3}, $F(000)$ = 448, μ(Mo-K_α) = 0.091 mm^{-1}. Data collection was performed on a SMART CCD using graphite monochromated radiation (λ = 0.71073 Å); 4848 unique reflections were collected to θ_{max} = 25.21°, in which 3333 reflections were observed [$F^2 > 4\sigma(F^2)$]. The crystal structure was resolved and refined using the same methods as for caesalmin A to R = 0.0561, Rw = 0.0867 and S = 0.996.

Complete lists of refined atomic coordinates and relevant information in standard CIF format for caesalmin A — methanol (1/1) and caesalmin B — acetone (2/1) have been deposited at the Cambridge Crystallographic Data Centre as CCDC Ref. No. 150454 and 150455, respectively.

Acknowledgements

This work is partially supported by Hong Kong Research Grant Council Earmarked Grant CUHK 4206/99P.

References

Balmain, A., Bjamer, K., Connolly, J.D., Ferguson, G., 1967. The constitution and stereochemistry of ε-caesalpin. Tetrahedron Lett. 49, 5027–5031.

Balmain, A., Connolly, J.D., Ferrari, M., Ghisalberti, E.L., Pagnoni, U.M., Pelizzoni, F. 1970. The stereochemistry of the furanoditerpenoids α-, β, and δ-caesalpin. Chem. Comm. 1244–1245.

Birnbaum, K.B., Ferguson, G., 1969. The crystal and molecular structure of a *p*-bromobenzoyl derivatives of ε-caesalpin. Acta Cryst. B 25, 720–730.

Datte, J.Y., Traore, A., Offoumou, A.M., Ziegler, A., 1998. Effects of leaf extract of *Caesalpinia bonduc* (Caesalpiniaceace) on the contractile activity of uterine smooth muscle of pregnant rats. J. Ethnopharm. 60, 149–155.

Hikino, H., Taguchi, T., Fujimura, H., Hiramatsu, Y., 1977. Antiinflammatory principles of *Caesalpinia sappan* wood and of *Haematoxylon campechianum* wood. Planta Medica 31, 214–220.

Jiangsu New Medical College, 1977. *Dictionary of Chinese Traditional Medicine*. Shanghai People's Publishing House, pp. 1289.

Kinoshita, T., Kaneko, M., Noguchi, H., Kitagawa, I., 1996. New cassane diterpenes from *caesalpinia bonduc*. Heterocycles 43, 409–414.

Kitagawa, I., Simanjuntak, P., Mahmud, T., Kobayashi, M., Fujii, S., Uji, T., Shibuya, H., 1996. Indonesian medicinal plants. XIII. Chemical structures of caesaldekarins c, d, and e, three additional cassane-type furanoditerpenes from the roots of *Caesalpinia major* (Fabaceace). Several interesting reaction products of caesaldekarin a provided by *N*-bromosuccinimide treatment. Chem. Pharm. Bull. 44, 1157–1161.

Kitagawa, I., Simanjuntak, P., Watano, T., Shibuya, H., Fujii, S., Yamagata, Y., Kobayashi, M., 1994. Indonesian medicinal plants. XI. Chemical structures of caesaldekarins a and b, two new cassane-type furanoditerpenes from the roots of *Caesalpinia major* (Fabaceace). Chem. Pharm. Bull. 42, 1798–1802.

Lyder, D.L., Peter, S.R., Tinto, W.F., Bissada, S.M., McLean, S., Reynolds, W.F., 1998. Minor cassane diterpenoids of *Caesalpinia bonduc*. J. Nat. Prod. 61, 1462–1465.

Ogawa, K., Aoki, I., Sashida, Y., 1992. Caesaljapin, a cassane diterpenoid from *Caesalpinia decapetala* var. *japonica*. Phytochemistry 31, 2897–2898.

Pascoe, K.O., Burke, B.A., Chan, W.R., 1986. Caesalpin F: new furanoditerpene from *Caesalpinia bonducella*. J. Nat. Prod. 49, 913–915.

Peter, S.P., Tinto, W.F., McLean, S., Reynolds, W.F., Tay, L.L., 1997. Caesalpinin, a rearranged cassane furanoditerpene of *Caesalpinia bonducella*. Tetrahedron Lett. 38, 5767–5770.

Peter, S.R., Tinto, W.F., McLean, S., Reynolds, W.F., Yu, M., 1997. Bonducellpins A-D, new cassane furanoditerpenes of *Caesalpinia bonduc*. J. Nat. Prod. 60, 1219–1221.

Peter, S., Tinto, W.F., Mclean, S., Reynolds, W.F., Yu, M., 1998. Cassane diterpenes from *Caesalpinia bonducella*. Phytochemistry 47, 1153–1155.

Sharma, S.R., Dwivedi, S.K., Swarup, D., 1997. Hypoglycaemic, antihyperglycaemic and hypolipidemic activities of *Caesalpinia bonducella* seeds in rats. J. Ethnopharm. 58, 39–44.

PERGAMON

Phytochemistry 57 (2001) 523–527

PHYTOCHEMISTRY

www.elsevier.com/locate/phytochem

Guaianolides from *Cichorium intybus* and structure revision of *Cichorium* sesquiterpene lactones

Wanda Kisiel*, Klaudia Zielińska

Department of Phytochemistry, Institute of Pharmacology, Polish Academy of Sciences, Pl-31-343 Kraków, Poland

Received 6 October 2000; received in revised form 12 February 2001

Abstract

The isolation and structure elucidation of a new lactucopicrin derivative from *Cichorium intybus* is described, together with the revised structures of several sesquiterpene lactones previously isolated from *Cichorium* species. The known eudesmanolide magnolialide and the known guaianolide ixerisoside D, reported for the first time from the plant material, along with the previously known chicory sesquiterpene lactones have been also isolated and identified. © 2001 Elsevier Science Ltd. All rights reserved.

Keywords: *Cichorium intybus*; Asteraceae; Lactuceae; Sesquiterpene lactones; Glycosides; Structure revision

1. Introduction

Leaves and roots of chicory (*Cichorium intybus* L., Asteraceae, tribe Lactuceae) produce bitter sesquiterpene lactones which promote appetite and digestion. A great deal of information exists on the guaianolide aglycone, lactucin (**1**) and its derivatives, in different tissues of the plant (Pyrek, 1985; van Beek et al., 1990; Blaschek et al., 1998). Only one report (Seto et al., 1988) shows the co-occurrence of germacranolides, eudesmanolides and lactucin-like guaianolides, accumulated mainly as glycosides, in chicory roots.

We now report isolation of lactucin (**1**) and structurally related compounds **2**–**10** (Glc = β-glucopyranosyl), the guaianolide **11**, the germacranolide **12**, the eudesmanolide **13**, as well as methyl and ethyl esters of *p*-hydroxyphenylacetic acid and loliolide. Compound **10** is a new natural product and compounds **11** and **13** are described for the first time from *Cichorium intybus*. Structures of *Cichorium* sesquiterpene lactones previously ascribed formulae **17**, **19**, **20**, **21** and **22**, and the eudesmanolide **18** have been revised.

2. Results and discussion

A combination of column and thin layer chromatographies on silica gel followed by semipreparative HPLC of ethanol extracts from root and leaf samples of *C. intybus* yielded sesquiterpenoid aglycones and glycosides. The compounds were then subjected to analytical HPLC for direct comparison with authentic standards wherever possible.

The leaves afforded 11β, 13-dihydrolactucin (**4**), jacquinelin (**5**), a mixture of lactucin (**1**) and **4**, a mixture of 8-desoxylactucin (**2**) and **5**, a mixture of lactucopicrin (**3**) and its derivatives **6** and **9**, crepidiaside B (**7**), compound **10** and loliolide. Of these, compounds **1**–**3** and **9** were previously known as constituents of chicory aerial parts (Pyrek, 1985).

The roots yielded, in addition to a mixture of methyl and ethyl esters of *p*-hydroxyphenylacetic acid, compounds **2** and **7**, mixtures of **3**, **9** and **3**, **6** and **9**, cichorioside B (**8**) and sonchuside A (**12**), previously obtained from chicory roots (Pyrek, 1985; Seto et al., 1988; van Beek et al., 1990). Moreover, compound **10**, ixerisoside D (**11**) (Warashina et al., 1990) and magnolialide (**13**) (El-Feraly et al., 1979) were isolated. The known compounds, except for **9** and **13**, were identified by direct comparison (HPLC, ^{1}H NMR, EIMS or ESIMS) with compounds from our collection isolated from other members of the tribe Lactuceae. The identity

* Corresponding author. Tel.: +48-12-6386087; fax: +48-12-6374500.

E-mail address: kisielw@if-pan.krakow.pl (W. Kisiel).

0031-9422/01/$ - see front matter © 2001 Elsevier Science Ltd. All rights reserved.
PII: S0031-9422(01)00072-3

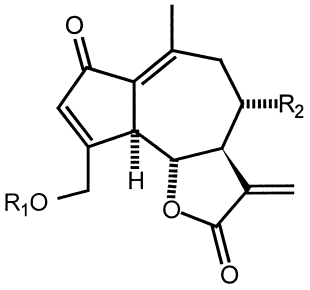

1 R_1 = H, R_2 = OH

2 R_1 = H, R_2 = H

3 R_1 = H, R_2 = A

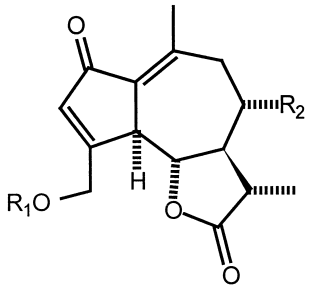

4 R_1 = H, R_2 = OH

5 R_1 = H, R_2 = H

6 R_1 = H, R_2 = A

7 R_1 = Glc, R_2 = H

8 R_1 = Glc, R_2 = OH

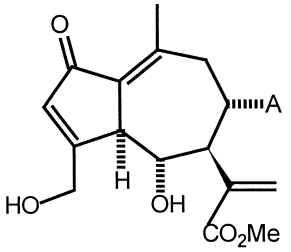

9

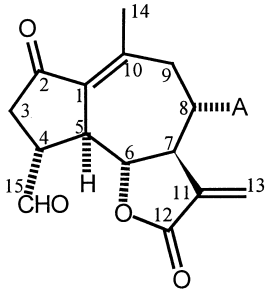

10

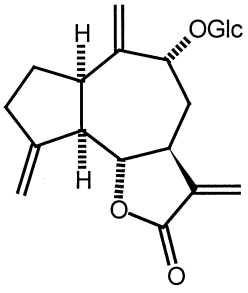

11

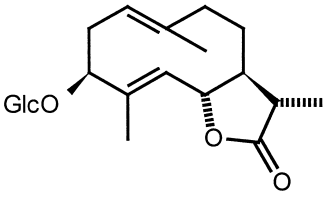

12

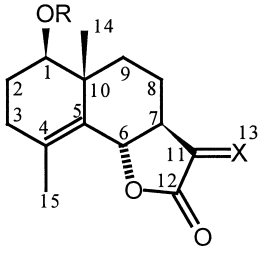

13 R = H, X = CH_2

14 R = H, X = H, α-Me

15 R = Glc, X = CH_2

16 R = Glc, X = H, α-Me

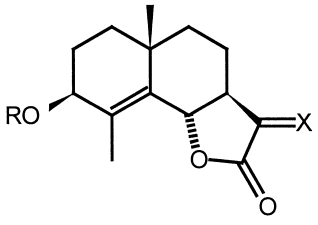

17 R = H, X = CH_2

18 R = H, X = H, α-Me

19 R = Glc, X = CH_2

20 R = Glc, X = H, α-Me

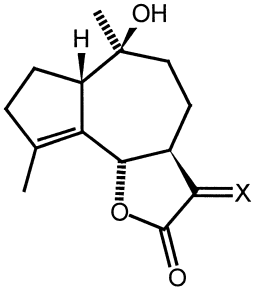

21 X = CH_2

22 X = H, α-Me

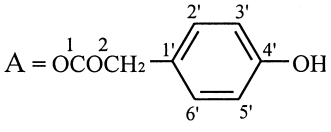

of the methyl ester **9** was established by comparison of its spectral data with those in the literature (Pyrek, 1985; Marco et al., 1992). Compounds **9** and **11** were first reported from *C. intybus* (Pyrek, 1985) and *Ixeris repens* (Warashina et al., 1990), respectively.

Compound **10** was unstable and proved difficult to separate from its mixture with two further compounds (as shown by HPLC), in view of the small amount available. Its structure was established by mass, 1D and 2D ^{1}H NMR spectral analyses, as well as by direct comparison with the spectra of lactucopicrin (**3**). The EI mass spectrum of **10** was in agreement with the molecular formula $C_{23}H_{22}O_7$. The most evident differences between the ^{1}H NMR spectra of **3** and **10** were due to the cyclopentanone ring protons. The spectrum of **10** (Table 1) lacked the downfield signal of the olefinic proton at C-3 and instead three proton resonances were observed upfield at δ 2.60, 2.67 and 3.34. Moreover, the signals for the C-4 hydroxymethylene group (H-15a and H-15b) were replaced by an aldehyde function (δ 9.94, br *d*, $J = 0.8$ Hz). Thus, we tentatively assigned structure **10** for the compound and turned to the ^{1}H–^{1}H COSY spectrum for further proof. The methine signal at δ 3.49 (H-5) was coupled with the signals at δ 3.73 (H-6), δ 2.37 (Me-14) and δ 3.34 (H-4). The latter was coupled with the signals at δ 2.60 and 2.67 assigned to the two methylene protons at C-3 which showed no further couplings. The relative stereochemistry at the carbon centres C-5 to C-8 of **10** was based on a comparison of the coupling constants for H-6 to H-8 with those of **3**, which were in very good agreement. The *trans*-disposition of H-4 and H-5 was deduced from the half bond width ($W_{1/2} = 22.7$ Hz) of H-5 and coupling values of H-4. We possess no firm evidence for absolute stereochemistry of **10**. However, the clear structural similarities between **10** and **3**, isolated from the same plant material, support the structure depicted in the formula. Thus, compound **10** was proved to be 3,4β-dihydro-15-dehydrolactucopicrin, a new natural product. In the plant extract **10** formed a mixture with two further structurally closely related compounds. The ^{1}H NMR spectrum of the mixture showed, in addition to the proton signals of **10**, two further aldehyde proton doublets at δ 9.92 ($J = 1.0$ Hz) and δ 9.81 ($J = 1.3$ Hz) due to H-15, two further olefinic methyl proton doublets at δ 2.36 ($J = 2.2$ Hz) and δ 2.28 ($J = 1.8$ Hz) due to H-14, as well as a secondary methyl proton doublet at δ 1.19 ($J = 6.9$ Hz) and two singlets at δ 5.61 and 6.22 due to H-13, respectively, suggesting the presence of three analogous guaiane derivatives with those of **3**, **6**, and **9**. Similar compounds, derivatives of 15-dehydrolactucin, were reported from *Hypochoeris* and *Lactuca* species (Bohlmann et al., 1981).

Compound **13**, $C_{15}H_{20}O_3$ (by EIMS), revealed ^{1}H NMR spectral features (Table 1) characteristic of an eudesman-12,6-olide with a Δ^4-double bond. The spec-

Table 1
^{1}H NMR (500.13 MHz) data of **10** and **13** and ^{13}C NMR (125.76 MHz) data of **13** in $CDCl_3$

Position	**10**, δ_H, *J* (Hz)	**13**, δ_H, *J* (Hz)	**13**, δ_C
1α	–	3.55 *br dd* (11.5, 4.2)	77.72
2α	–	1.73 *m*	27.04
2β	–	1.73 *m*	
3α	2.67 *dd* (18.2, 9.5)	2.20 *m*	33.16
3β	2.60 *m*	2.03 *br ddd* (17.7, 5.0, 2.5)	
4β	3.34 *dddd* (9.5, 9.5, 7.0, 0.8)	–	126.34[a]
5α	3.49 *t*-like *m* ($W_{1/2} = 22.7$ Hz)	–	128.87[a]
6β	3.73 *dd* (10.4, 10.2)	4.56 *br d* (11.6)	83.10
7α	3.20 *dddd* (10.4, 10.4, 3.1, 2.9)	2.58 *ddddd* (11.6, 11.6, 3.2, 3.0, 3.0)	49.57
8α	–	2.10 *m*	23.00
8β	4.88 *ddd* (10.4, 10.4, 2.5)	1.61 *dddd* (13.0, 13.0, 11.6, 4.0)	
9α	2.60 *m*	1.35 *ddd* (13.5, 13.0, 4.7)	38.08
9β	2.53 *dd* (13.7, 2.5)	2.10 *ddd* (13.5, 4.0, 2.4)	
10	–	–	41.95
11	–	–	138.96
12	–	–	170.41
13a	6.04 *d* (3.1)	6.15 *d* (3.2)	118.59
13b	5.23 *d* (2.9)	5.47 *d* (3.0)	
14	2.37 *d* (2.2)	1.10 *s*	18.40
15	9.94 *d* (0.8)	1.86 *br s*	19.57
Ester moiety			
2a	3.64 *d* (14.8)		
2b	3.59 *d* (14.8)		
2′, 6′	7.16 *d* (8.6)		
3′, 5′	6.81 *d* (8.6)		

[a] The assignments may by reversed.

trum of **13** showed a sharp singlet for the angular methyl group at δ 1.10, a broad singlet for the olefinic methyl group at δ 1.86, a proton under the lactone oxygen as a broad doublet at δ 4.56 ($J=11.6$ Hz), the exocyclic methylene proton doublets at δ 6.15 ($J=3.2$ Hz) and δ 5.47 ($J=3.0$ Hz) and a methine proton *dd* at δ 3.55 ($J=11.5$ and 4.2 Hz). Examination of the literature revealed that two eudesmanolides and one guaianolide with almost identical chemical shift values of the key protons have been described, i.e. magnolialide (**13**), cichoriolide (**17**) and cichopumilide (**21**). Magnolialide (**13**) was isolated from *Magnolia grandiflora* 20 years ago, the structure being confirmed by comparison with synthetic product obtained by cyclization of costunolide-1,10-epoxide (El-Feraly et al., 1979). Cichoriolide (**17**) was reported from *Cichorium intybus* and *C. endivia* (Seto et al., 1988), while cichopumilide (**21**) was found in *C. pumilum* (a subsp. of *C. endivia*) (El-Masry et al., 1984). In the reported ^{1}H NMR spectra of the three compounds the signals at δ 3.55 were ascribed to the methine protons at the C-1 and C-3 positions of the eudesmanolides magnolialide and cichoriolide, respectively, and at the C-1 position of the guaianolide cichopumilide. This unexpected similarity of the ^{1}H NMR spectral data of compound **13** to those of the above mentioned sesquiterpene lactones necessitated its detailed structural analysis. The proton and carbon assignments of **13** (Table 1) were made by ^{1}H–^{13}C correlation (HETCOR) method in combination with COSY and NOESY experiments, as well as by comparison with the complete spectral data of the closely related eudesmanolide artesin (**14**) (Marco, 1989). In the NOESY spectrum Me-14 correlated with H-6β, H-8β, H-9β and H-2α/2β; H-1α correlated with H-2α/2β, H-3α and H-9α, while H-7α with H-8α, H-9α and H-13a. On the basis of the above findings, the identity of compound **13** with magnolialide was considered. This consideration was supported by positive sign of optical rotations of both compounds and by comparison of their ^{13}C NMR data which were in good agreement. The carbon resonances of **13** were also indistinguishable from those of cichoriolide (**17**), after reassignments of the signals from C-1, C-2 and C-3 according to the structure of **13**, giving evidence in favour of the identity of **13** and **17**.

Additional support for the above, as well as for the identity of **13** and **21** was obtained from a comparison of physical and spectral data reported for their 11β, 13-dihydroderivatives, i.e. **14** (mp 172°C or 177°C cited by Marco, 1989), **18** (mp 173–175°C) (Miyase and Fukushima, 1987), and **22** (mp 176°C) (El-Masry et al., 1984). Again, the chemical shift values of ^{13}C NMR signals of **14** were identical with those of **18** when reassigned in accord with the structure of **14**. The ^{1}H NMR spectral properties of the three dihydroderivatives were also very similar, in particular when more complete data of **22** were compared with those of **14**. Accordingly, compounds **17**, **18** and **21**, **22** have been reassigned the revised structures **13** and **14**, respectively. This, in turn, give rise to the revision of the previously assigned structures of *Cichorium* glycosides **19** and **20**, now correctly represented by **15** and **16**, respectively. Cichorioside (**19**) was isolated from *C. endivia* (Seto et al., 1988), while sonchuside C (**20**) was obtained from *C. intybus* (Seto et al., 1988) following previous isolation from *Sonchus oleraceus* (Miyase and Fukushima, 1987). Cichopumilide (**21**) and its 11β, 13-dihydroderivative (**22**) first reported from *C. pumilum* (El-Masry et al., 1984) were then identified in *Sonchus macrocarpus* (Mahmoud et al., 1984).

The sesquiterpene lactone chemistry of *Cichorium* species is dominated by lactucin-like guaianolides and their glycosides, present in roots and aerial parts. Moreover, roots of the plants produce a small number of germacrane- and eudesmane-type sesquiterpene lactones and their glycosides. All eudesmanolides isolated to date possess Δ^4-double bonds and hydroxyl groups at the C-1 positions. These compounds have also been reported from *Sonchus* species of the tribe Lactuceae, along with biogenetically related derivatives of reynosin (Mahmoud et al., 1984; Miyase and Fukushima, 1987; Shimizu et al., 1989).

3. Experimental

3.1. General

CC: silica gel Merck Art. 7733 and Art. 7754; TLC: silica gel Merck Art. 5553; semiprep. and analytical HPLC: Delta-Pak C 18 cartridge column (particle size 15 μm, 25 mm×100 mm, flow rate of 3 ml min^{-1}) and μ-Bondapack C 18 column (particle size 10 μm, 2 mm×300 mm, flow rate of 0.5 ml min^{-1}), respectively, using MeOH–H_2O systems as mobile phase and monitoring with a UV photodiode-array detector.

3.2. Plant material

Leaves and roots of *C. intybus* were collected on 31 July 1998 from plants in the first year of their vegetation period, growing in the Garden of Medicinal Plants of the Institute of Pharmacology, Polish Academy of Sciences, Kraków, where a voucher specimen was deposited.

3.3. Extraction and isolation of compounds

Dried and powdered leaves (500 g) were exhaustively extracted with EtOH at room temperature with shaking and the residue (33 g), obtained by removal of the solvent under vacuum, was coarsely prefractionated on a silica gel column using successively hexane, hexane–

EtOAc (1:1), EtOAc and EtOAc–MeOH (1:1) to give four fractions, 2 l each. Fractions containing lactone constituents, eluted with hexane–EtOAc (1:1) and EtOAc, were combined and the solvent was removed giving 15 g of residue which was chromatographed on a silica gel column using hexane–EtOAc (up to 100% EtOAc) followed by EtOAc–MeOH (up to 10% MeOH) gradient solvent systems. The relevant fractions were further separated and purified by prep. TLC using $CHCl_3$–MeOH (19:1 and 9:1) mixtures as mobile phases. Fractions from hexane–EtOAc (1:1) elution afforded loliolide (11.5 mg), **5** (2.6 mg), a mixture of **2** and **5** (ca. 1:6, 18.6 mg), a mixture of three sesquiterpene aldehydes (ca. 1:1:0.2, 7.5 mg) described below and a mixture of **3**, **6** and **9** (ca. 1:3:0.3, 15.9 mg). More polar fractions, eluted with EtOAc, yielded **4** (21.2 mg), a mixture of **1** and **4** (ca. 1:7, 24.2 mg) and **7** (17.2 mg).

Fresh roots (1.5 kg) were cut into small pieces and transferred into boiling EtOH, and left to stand in a cold room. The solvent was evaporated under reduced pressure and the residue (108 g) was prefractionated on silica gel as described above to give fraction (7.5 g) eluted with hexane–EtOAc (1:1) and EtOAc. The fraction was chromatographed on a silica gel column using the above mentioned gradient solvent system. Elution of the column with hexane–EtOAc (7:3) yielded **13** (15.5 mg). Further elution with hexane–EtOAc (6:4 and 1:1) afforded a mixture of methyl and ethyl esters of *p*-hydroxyphenylacetic acid (ca. 9:1, 10.1 mg), **2** (85.6 mg), a mixture of three sesquiterpene aldehydes (ca. 2:1:0.3, 6.4 mg), containing **10** as a major constituent, a mixture of **3**, **6** and **9** (ca. 2.4:2:1, 16.2 mg) and a mixture of **3** and **9** (ca. 3:1, 7.9 mg), in that order, after separation by prep. TLC ($CHCl_3$–MeOH, 19:1). Sesquiterpene lactone glycosides, eluted with EtOAc and EtOAc–MeOH (19:1), were separated from crude fractions by repeated prep. TLC ($CHCl_3$-MeOH, 17 : 3) to give **12** (18.6 mg), **11** (2.7 mg), **7** (13.4 mg) and **8** (36.8 mg). The leaf and root sesquiterpene aldehyde mixtures (13.9 mg) were further separated by repeated semiprep. HPLC using MeOH–H_2O (1:1) to give almost pure **10** (3.2 mg). Other mixtures, indicated by ^{1}H NMR, were not separated further as the ^{1}H NMR signals could be readily assigned to the respective compounds on the basis of their relative amounts.

*3.4. 3,4β-Dihydro-15-dehydrolactucopicrin (**10**)*

Solid. EIMS *m*/*z* (rel. int.): 410 $[M]^+$ (1.5), 257 $[M–RCO_2H–H]^+$ (10.0), 229 (8.4), 135 (47.5), 107 (100); ^{1}H NMR: Table 1.

Acknowledgements

The authors acknowledge the State Committee for Scientific Research (KBN) of Poland for the research grant No. 4P05F00417 (1999-2001).

References

van Beek, T.A., Maas, P., King, B.M., Leclercq, E., Voragen, A.G.J., de Groot, A., 1990. Bitter sesquiterpene lactones from chicory roots. J. Agric. Food. Chem. 38, 1035–1038.

Blaschek, W., Hänsel, R., Keller, K., Reichling, J., Rimpler, H., Schneider, G., 1998. Hagers Handbuch der Pharmazeutischen Praxis, Bd 1. Springer Verlag, Berlin–Heidelberg–New York, pp. 865–871.

Bohlmann, F., Jakupovic, J., Abraham, W.-R., Zdero, Ch., 1981. The first sesquiterpene lactones esterified with a sesquiterpenic acid. Phytochemistry 20, 2371–2374.

El-Feraly, F.S., Chan, Y.M., Benigni, D.A., 1979. Magnolialide, a novel eudesmanolide from the root bark of *Magnolia grandiflora*. Phytochemistry 18, 881–882.

El-Masry, S., Ghazy, N.M., Zdero, Ch., Bohlmann, F., 1984. Two guaianolides from *Cichorium pumilum*. Phytochemistry 23, 183–185.

Mahmoud, Z., El-Masry, S., Amer, M., Ziesche, J., Grenz, M., 1984. Sesquiterpene lactones from *Sonchus macrocarpus*. Phytochemistry 23, 1105–1107.

Marco, J.A., 1989. Sesquiterpene lactones from *Artemisia herba-alba* subsp. *herba-alba*. Phytochemistry 28, 3121–3126.

Marco, J.A., Sanz, J.F., Albiach, R., 1992. A sesquiterpene ester from *Lactuca serriola*. Phytochemistry 31, 2539–2540.

Miyase, T., Fukushima, S., 1987. Studies on sesquiterpene glycosides from *Sonchus oleraceus* L. Chem. Pharm. Bull. 35, 2869–2874.

Pyrek, J.S., 1985. Sesquiterpene lactones of *Cichorium intybus* and *Leontodon autumnalis*. Phytochemistry 24, 186–188.

Seto, M., Miyase, T., Umehara, K., Ueno, A., Hirano, Y., Otani, N., 1988. Sesquiterpene lactones from *Cichorium endivia* L. and *C. intybus* L. and cytotoxic activity. Chem. Pharm. Bull. 36, 2423–2429.

Shimizu, S., Miyase, T., Ueno, A., Usmanghani, K., 1989. Sesquiterpene lactone glycosides and ionone derivative glycosides from *Sonchus asper*. Phytochemistry 28, 3399–3402.

Warashina, T., Ishino, M., Miyase, T., Ueno, A., 1990. Sesquiterpene glycosides from *Ixeris debilis* and *Ixeris repens*. Phytochemistry 29, 3217–3224.

PERGAMON

Phytochemistry 57 (2001) 529–535

PHYTOCHEMISTRY

www.elsevier.com/locate/phytochem

(*S*)-12-Hydroxygeranylgeraniol-derived diterpenes from the brown alga *Bifurcaria bifurcata*

Gérald Culioli [a], Mohammed Daoudi [b], Annick Ortalo-Magné [a], Robert Valls [c], Louis Piovetti [a,*]

[a] *Laboratoire de Recherche en Chimie Marine des Organométalliques (RCMO), Université de Toulon et du Var, BP 132, F-83957 La Garde cedex, France*
[b] *Laboratoire de Chimie Organique et Bioorganique, Faculté des Sciences Chouaïb Doukkali, El Jadida, Morocco*
[c] *Laboratoire des Organo-Phosphorés (LOP), Université d'Aix-Marseille III, BP 552, F-13397 Marseille cedex 13, France*

Received 28 September 2000; received in revised form 29 January 2001

Abstract

Four novel diterpenes were isolated from the brown alga *Bifurcaria bifurcata* collected off the Atlantic coast from Morocco, and their structures established by spectral and chemical methods. These compounds are acyclic diterpenes derived from (*S*)-12-hydroxygeranylgeraniol. One of them is its dehydration product at C-12, while the others are its oxidation derivatives : the methyl ester of the acid at C-1 and two stereoisomers (*Z* and *E*) of the aldehyde at C-1. These results are discussed from a chemotaxonomic point of view. © 2001 Elsevier Science Ltd. All rights reserved.

Keywords: *Bifurcaria bifurcata*; Cystoseiraceae; Brown alga; Acyclic diterpenes; (*S*)-12-Hydroxygeranylgeraniol derivatives; Chemotaxonomy

1. Introduction

As part of a phytochemical study of the Atlantic brown alga *Bifurcaria bifurcata* (Phaeophyceae) (Combaut and Piovetti, 1983; Valls et al., 1986, 1993a, 1995; Semmak et al., 1988; Culioli et al., 1999a,b, 2000), we describe the isolation and structure elucidation of four novel diterpenes. They were isolated from a specimen collected at Oualidia (Morocco) together with previous diterpenes described in this alga: **1** (Valls et al., 1986), **2a** (Semmak et al., 1988) and geranylgeraniol (Culioli et al., 1999a). It must be specified that these compounds are (*S*)-12-hydroxygeranylgeraniol derivatives instead of (*S*)-13-hydroxygeranylgeraniol ones, as for the secondary metabolites isolated from the same alga collected at Quiberon and Roscoff (France) (Culioli et al., 1999b).

2. Results and discussion

The ether extract of dried *B. bifurcata* collected at Oualidia was fractionated by liquid chromatography using silica gel. The fraction eluted with EtOAc–isooctane (3:7) was further purified by HPLC on normal phase silica. From this separation, we obtained the sterols and pure geranylgeraniol, as well as a small amount of two new compounds (**2b**, **3**). In the same way, fraction eluted with EtOAc-isooctane (1:1) led to (*S*)-12-hydroxygeranylgeranic acid (**2a**) and a mixture of two new compounds (**4**, **5**) which were subsequently separated and purified by analytical HPLC on normal phase silica [eluant EtOAc–isooctane (1:1)]. The more polar fraction eluted with EtOAc-isooctane (7:3) led to the known diterpene: (*S*)-12-hydroxygeranylgeraniol (**1**).

Diterpene **2b**, $C_{21}H_{34}O_3$ (HRMS), was an optically active oil, the identity of which was readily established by comparison of its spectral properties with those of the acid (**2a**) (Semmak et al., 1988). It showed hydroxyl absorption ($\nu_{OH} = 3400$ cm^{-1}) in its IR spectrum. This functionality corresponded to a secondary hydroxyl group localized at C-12, as was revealed by: (i) the ^{13}C NMR signals at δ 77.2 (C-12) and δ 11.5 (C-18), instead of δ 65.6 and δ 16.3, respectively, when the hydroxyl group is fixed at C-13 (Culioli et al., 1999b); (ii) the ^{1}H NMR signals at δ 3.97 (*t*, $J = 7$ Hz, H-12) and δ 5.36 (*t*, $J = 7$ Hz, H-10), instead of δ 4.37 (*ddd*, $J = 8.2$, 8.2, 5.3 Hz, H-13) and δ 5.18 (*t*, $J = 6.7$ Hz, H-10), when the hydroxyl group is fixed at C-13 (Culioli et al., 1999b).

* Corresponding author. Tel.: +33-4-94-14-23-46; fax: +33-4-94-14-21-68.
E-mail address: piovetti@univ-tln.fr (L. Piovetti).

0031-9422/01/$ - see front matter © 2001 Elsevier Science Ltd. All rights reserved.
PII: S0031-9422(01)00042-5

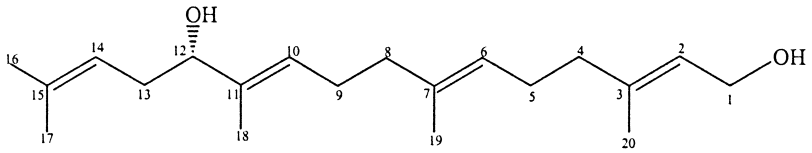

1 (*S*)-12-hydroxygeranylgeraniol

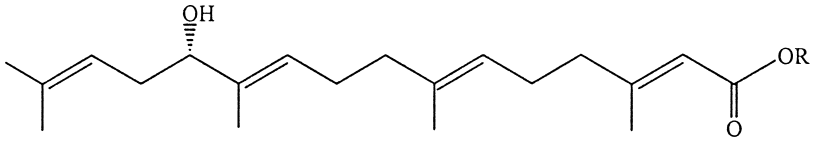

2a R = H (*S*)-12-hydroxygeranylgeranic acid
2b R = CH_3

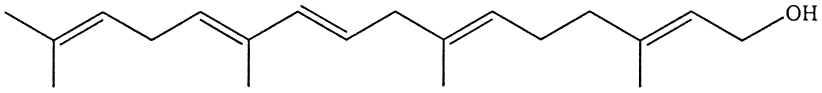

3

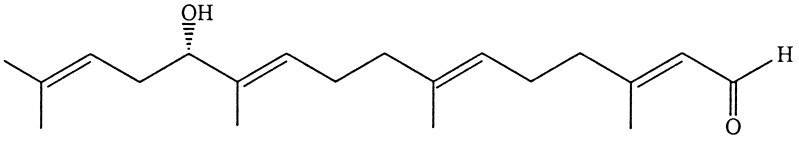

4

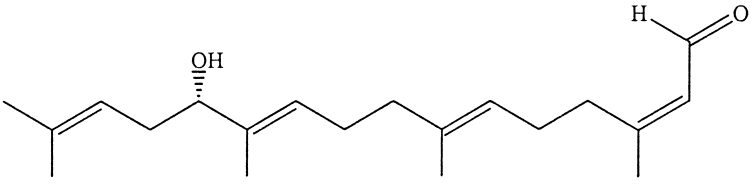

5

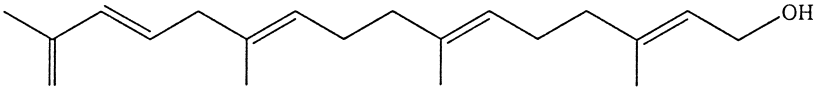

6

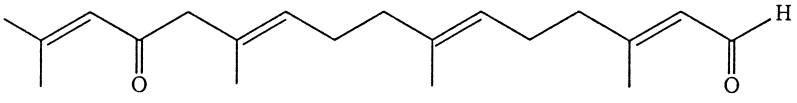

7 Eleganonal

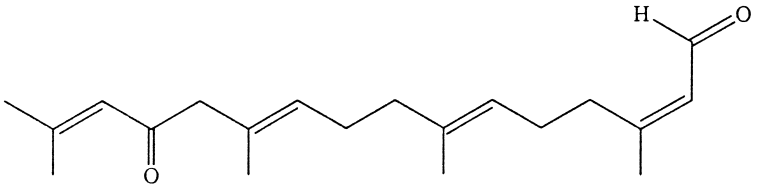

8 Isoeleganonal

The all *E* configuration of the double bonds of the isoprenoid chain was verified with the position of the C-18, C-19 and C-20 methyl signals observed above δ 20 in the ^{13}C NMR spectrum (Couperus et al., 1976; Coates et al., 1978).

The main difference with compound **2a** was the presence of a methyl ester function (δ 167.2 and δ 50.7 in its ^{13}C NMR spectrum; δ 3.68 (3H, *s*) of a methyl group in its ^{1}H NMR spectrum) instead of the acidic group (δ 171.3 in the ^{13}C NMR spectrum of **2a**). The assignment of proton and carbon signals (Tables 1 and 2 respectively) was confirmed by means of homonuclear (COSY) and heteronuclear (XHCORR) experiments. Moreover, the structure of **2b** was totally confirmed by : (i) the methylation with diazomethane of **2a** which led to the same methyl ester as **2b**; (ii) the reduction of **2b** with lithium aluminium hydride to give **1** as the end product of the reaction, with the same absolute configuration at C-12 [Horeau determination (Horeau and Nouaille, 1971)].

The second novel compound (**3**) had the molecular formula $C_{20}H_{32}O$ (HRMS). It was isolated as an optically inactive oil. This compound showed several spectral features in common with other geranylgeraniol-derived diterpenes, particularly with **6**. The main difference with geranylgeraniol was the presence of a –CH=C(CH_3)–CH=CH– unit as indicated by the inspection of UV (λ 245 nm, log ε 4.18), ^{1}H and ^{13}C NMR data (Tables 1 and 2). In particular the ^{1}H and ^{13}C signals at δ 6.05 (1H, *d*, H-10), δ 5.51 (1H, *dt*, H-9), δ 5.35 (1H, *t*, H-12) and δ 2.81 (2H, *t*, H-13) showed that the C-10 double bond of geranylgeraniol was replaced in **3** by a system of two conjugated double bonds at C-9 and C-11, respectively. The *E* configuration of the double bond at C-9 was revealed by the value of the coupling constant between H-9 and H-10 ($^{3}J_{\text{H-H}} = 15$ Hz). The assignment of proton and carbon signals (Tables 1 and 2 respectively) was confirmed by means of homonuclear (COSY) and heteronuclear (XHCORR) experiments. In particular, the location of the double bond at C-9 was precisely determined with the $^{3}J_{\text{H-H}}$ correlations between H-9/H-10 and H-9/H-8, as well as the location of the double bond at C-11 with the H-12/H-13 and H-12/H-18 correlations.

The third novel compound (**4**) had the molecular formula $C_{20}H_{32}O_2$ (HRMS). It was isolated as an optically active oil. This compound showed several spectral features in common with other acyclic diterpenes, particularly with **7** for the first isoprenic unit and with **2a** for the other three. It showed hydroxyl absorption ($\nu_{OH} = 3430$ cm^{-1}) in its IR spectrum. This functionality corresponded to a secondary hydroxyl group localized at C-12, as that was indicated by ^{1}H, ^{13}C NMR data (Tables 3 and 4) and comparison with those of **1**, **2a** and **2b**. This location showed that **4** was also a (*S*)-12-geranylgeraniol- derived diterpenoid. As for **2a** and **2b**, the all *E* configuration of the double bonds of the isoprenoid chain was verified with the position of the C-18, C-19 and C-20 methyl signals observed above δ 20 in the ^{13}C NMR spectrum. The only one difference with the compounds **1**, **2a** and **2b** resulted from the spectral data corresponding to the first isoprenic unit. A

Table 1
^{1}H NMR spectral data of compounds **2a**, **2b**, **3** and **6** (TMS as int. standard)[a]

	2a	**2b**	**3**	**6**
H	$CDCl_3$ (360 MHz)[b]	$CDCl_3$ (200 MHz)	$CDCl_3$ (200 MHz)	$CDCl_3$ (360 MHz)[b]
1	–	–	4.15 *d* (7.0)	4.10 *d* (6.8)
2	5.66 *s*	5.66 *s*	5.42 *t* (7.0)	5.37 *t* (6.8)
4	2.17 *m*	2.15 *m*	2.00-2.20 *m*	2.00 *m*
5	2.16 *d* (4.5)	2.12 *m*	2.00-2.20 *m*	2.07 *m*
6	5.06 *t* (4.5)	5.09 *t* (7.0)	5.15 *t* (7.0)	5.09 *t* (6.8)
8	2.00 *m*	2.00 *m*	2.75 *d* (7.0)	2.00 *m*
9	2.10 *m*	2.10 *m*	5.51 *dt* (15.0,7.0)	2.07 *m*
10	5.34 *t* (6.8)	5.36 *t* (7.0)	6.05 *d* (15.0)	5.13 *t* (6.8)
12	3.96 *dd* (6.0, 7.0)	3.97 *t* (7.0)	5.35 *t* (7.0)	2.72 *d* (7.2)
13	2.22 *ddd* (6.0,7.0,7.0)	2.20 *m*	2.81 *t* (7.0)	5.58 *dt* (15.6;7.2)
14	5.06 *t* (7.0)	5.09 *t* (7.0)	5.11 *t* (7.0)	6.10 *d* (15.6)
16	1.70 *s*	1.71 *s*	1.68 *s*	1.81 *s*
17	1.59 *s*	1.60 *s*	1.64 *s*	4.84 *s*
18	1.60 *s*	1.61 *s*	1.75 *s*	1.57 *s*
19	1.62 *s*	1.63 *s*	1.59 *s*	1.58 *s*
20	2.14 *s*	2.16 *s*	1.68 *s*	1.65 *s*
21	–	3.68 *s*	–	–

[a] Chemical shifts are δ values, coupling constants (*J* in parentheses) are given in Hz; assignments were confirmed by decoupling and 2D NMR experiments (COSY ^{1}H–^{1}H, XHCORR and HMBC).
[b] ^{1}H NMR data of Semmak et al., 1988, added for comparison.

Table 2
^{13}C NMR spectral data of compounds **2a**, **2b**, **3** and **6** (TMS as int. standard)[a]

	2a		**2b**		**3**		**6**	
C	$CDCl_3$ (90 MHz)[b]	DEPT	$CDCl_3$ (50 MHz)	DEPT	$CDCl_3$ (50 MHz)	DEPT	$CDCl_3$ (90 MHz)[b]	DEPT
1	171.3	C	167.2	C	59.4	CH_2	59.0	CH_2
2	115.2	CH	115.3	CH	123.4	CH	123.4	CH
3	162.4	C	159.9	C	139.6	C	139.1	C
4	41.1	CH_2	40.8	CH_2	39.5	CH_2	39.4	CH_2
5	26.1	CH_2	26.1	CH_2	26.4	CH_2	26.5	CH_2
6	122.9	CH	123.0	CH	124.5	CH	123.8	CH
7	136.0	C	135.9	C	134.6	C	135.0	C
8	39.2	CH_2	39.2	CH_2	43.1	CH_2	39.4	CH_2
9	25.9	CH_2	25.9	CH_2	125.6	CH	26.2	CH_2
10	125.9	CH	125.8	CH	135.9	CH	125.1	CH
11	136.7	C	136.9	C	131.8	C	133.5	C
12	77.3	CH	77.2	CH	129.4	CH	42.7	CH_2
13	34.2	CH_2	34.2	CH_2	27.2	CH_2	128.7	CH
14	120.2	CH	120.3	CH	122.5	CH	133.7	CH
15	134.4	C	134.1	C	133.3	C	141.9	C
16	25.8	CH_3	25.8	CH_3	25.7	CH_3	18.5	CH_3
17	17.9	CH_3	17.9	CH_3	17.7	CH_3	114.3	CH_2
18	19.1[c]	CH_3	11.5	CH_3	12.5	CH_3	15.9	CH_3
19	16.0	CH_3	15.9	CH_3	16.1	CH_3	15.8	CH_3
20	11.6[c]	CH_3	18.7	CH_3	16.2	CH_3	16.1	CH_3
21	–	–	50.7	CH_3	–	–	–	–

[a] Multiplicities were obtained with DEPT sequences.
[b] ^{13}C NMR data of Semmak et al., 1988, added for comparison.
[c] Assignments may be reversed.

Table 3
^1H NMR spectral data of compounds **4**, **5**, **7** and **8** (TMS as int. standard)[a]

	4	**5**	**7**	**8**
H	$CDCl_3$ (200 MHz)	$CDCl_3$ (200 MHz)	$CDCl_3$ (300 MHz)[b]	$CDCl_3$ (300 MHz)[b]
1	9.88 *d* (8.0)	9.82 *d* (8.0)	9.98 *d* (8.0)	9.88 *d* (8.0)
2	5.78 *d* (8.0)	5.82 *d* (8.0)	5.86 *d* (8.0)	5.86 *d* (8.0)
4	2.15 *m*	2.55 *t* (7.3)	~ 2.00 *m*	2.57 *t* (7.5)
5	2.15 *m*	2.11 *m*	~ 2.00 *m*	~ 2.00 *m*
6	4.99 *t* (4.0)	5.05 *t* (7.3)	5.09 *t* (6.0)	5.08 *t* (6.0)
8	1.95 *m*	1.98 *m*	~ 2.00 *m*	~ 2.00 *m*
9	1.95 *m*	2.07 *m*	~ 2.00 *m*	~ 2.00 *m*
10	5.26 *t* (6.3)	5.28 *t* (6.8)	5.22 *t* (6.5)	5.22 *t* (6.5)
12	3.87 *t* (6.6)	3.90 *t* (6.8)	3.02 *s*	3.02 *s*
13	2.19 *m*	2.18 *m*	–	–
14	4.99 *t* (6.9)	5.05 *t* (7.0)	6.11 *s*	6.11 *s*
16	1.61 *s*	1.65 *s*	1.86 *s*	1.86 *s*
17	1.52 *s*	1.55 *s*	2.17 *s*	2.12 *s*
18	1.52 *s*	1.55 *s*	1.60 *s*	1.60 *s*
19	1.53 *s*	1.57 *s*	1.60 *s*	1.60 *s*
20	2.08 *s*	1.93 *s*	2.17 *s*	1.96 *s*

[a] Chemical shifts are δ values, coupling constants (J in parentheses) are given in Hz; assignments were confirmed by decoupling and 2D NMR experiments (COSY ^1H–^1H, XHCORR and HMBC).
[b] ^1H NMR data of Amico et al., 1987, added for comparison.

conjugated carbonyl absorption was revealed in its IR spectrum ($\nu_{C=O}=1688$ cm^{-1}). From the ^1H NMR spectrum (Table 3) it was apparent that this functionality is embodied in a formyl group: δ 9.88 (1H, *d*, H-1), which was established by ^1H–^1H COSY experiment to be adjacent to an olefin proton, which was in turn allylically coupled with the methyl group resonating at δ 2.08 (3H, *s*, H-20). These data suggest the novel meta-

Table 4
^{13}C NMR spectral data of compounds **4**, **5**, **7** and **8** (TMS as int. standard)[a]

	4		**5**		**7**		**8**	
C	$CDCl_3$ (50 MHz)	DEPT	$CDCl_3$ (50 MHz)	DEPT	$CDCl_3$ (75.5 MHz)[b]	DEPT	$CDCl_3$ (75.5 MHz)[b]	DEPT
1	191.3	CH	190.9	CH	191.2	CH	190.2	CH
2	127.4	CH	128.6	CH	127.4	CH	128.8	CH
3	163.9	C	164.0	C	163.6	C	163.6	C
4	40.5	CH_2	34.1	CH_2	40.0	CH_2	32.6	CH_2
5	26.0	CH_2	26.8	CH_2	25.5	CH_2	26.7	CH_2
6	122.6	CH	122.2	CH	122.6	CH	122.6	CH
7	136.3	C	137.0	C	136.2	C	136.2	C
8	39.2	CH_2	39.1	CH_2	39.2	CH_2	40.0	CH_2
9	25.8	CH_2	25.8	CH_2	26.6	CH_2	26.5	CH_2
10	125.6	CH	125.5	CH	122.8	CH	122.6	CH
11	136.9	C	137.0	C	129.8	C	129.8	C
12	77.1	CH	77.1	CH	55.4	CH_2	55.4	CH_2
13	34.2	CH_2	32.3	CH_2	199.4	C	199.4	C
14	120.3	CH	120.4	CH	128.8	CH	127.4	CH
15	134.3	C	134.1	C	155.4	C	155.4	C
16	25.6	CH_3	25.0	CH_3	27.6	CH_3	27.6	CH_3
17	17.5	CH_3	17.9	CH_3	20.8	CH_3	20.8	CH_3
18	11.6	CH_3	11.6	CH_3	16.4	CH_3	17.7	CH_3
19	16.0	CH_3	16.0	CH_3	16.0	CH_3	16.0	CH_3
20	17.9	CH_3	25.8	CH_3	17.7	CH_3	25.2	CH_3

[a] Multiplicities were obtained with DEPT sequences.
[b] ^{13}C NMR data of Amico et al., 1987, added for comparison.

bolite is an oxidation product of the known (*S*)-12-hydroxygeranylgeraniol (**1**). The assignment of proton and carbon signals (Tables 3 and 4 respectively) was confirmed by means of homonuclear (COSY) and heteronuclear (XHCORR) experiments. This inference was supported by the comparison of both ^1H and ^{13}C NMR spectra with those of **1**, **2a**, **2b** and **7**, and definitely proved by the partial oxidation of **1** which gave two geometric isomers, one of which was indistinguishable from **4**. Moreover, the *E* configuration of the double bond at C-2 was confirmed by a ^1H–^1H NOESY experiment which showed a spatial correlation between H-1 and H-20.

The last novel metabolite isolated (**5**) is an isomer of **4**, to which it resembles closely in the mass fragmentation. Also the ^1H NMR spectrum of **5** is very similar to that of **4** (Table 3), a single characteristic difference being the downfield shift of the methylene protons at C-4 from δ 2.15 in **4** to δ 2.55 in **5** and the concurrent upfield shift of the C-20 vinyl methyl group from δ 2.08 in **4** to δ 1.93 in **5**. That is in agreement with a change of the geometry of the C-2 double bond from *E* in **4** to *Z* in **5**. As expected, the ^{13}C NMR spectrum of **5** (Table 4) differs from that of **4** mainly in the chemical shifts of C-4 (δ 34.1 in **5** as compared to δ 40.5 in **4**) and C-20 (δ 25.8 against δ 17.9). The same spectral features (^1H and ^{13}C NMR) were found in the first isoprenic unit of **8**, a stereoisomer of **7** previously described from *Cystoseira balearica* (Amico et al., 1987). This hypothesis was definitely proved by the partial oxidation of **1** from which the second compound obtained (*Z* isomer of **4**) was indistinguishable from **5**. It must be specified that the aldehyde **5** is a labile compound that, at room temperature, slowly converts into its more stable isomer **4**.

2.1. Chemotaxonomic relationships

Our previous studies of the geographical variations in the diterpenoid composition of *B. bifurcata* (Valls et al., 1993a,b, 1995) had revealed that the lipid extract of this species collected off the Moroccan coast, in the Oualidia zone (between El Jadida and Oualidia), was clearly distinguishable from the extracts obtained from the other zones of collection, with the presence as main constituents of (*S*)-12-hydroxygeranylgeraniol (**1**) and derivatives. The re-investigation of the lipid extract from *B. bifurcata* collected in the Oualidia zone led us to show : (i) the presence of four other derivatives from **1** ; (ii) the presence for the first time of geranylgeraniol; (iii) the absence of both (*S*)-13-hydroxygeranylgeraniol and 13-ketogeranylgeraniol, and their derivatives. This work showed that the only diterpene present in all the lipid extracts of *B. bifurcata* studied was geranylgeraniol (precursor of the acyclic diterpenes). On the other hand, 13-ketogeranylgeraniol which was present in all the lipid extracts from the other zones of collection (Culioli et al., 1999a,b) could not be identified. This chemical particularity led us to think that *B.*

bifurcata collected in the Oualidia zone (Morocco) could be regarded as a ≪ chemical variety ≫ of this species.

3. Experimental

3.1. General

MS: direct inlet, 70 eV; ^{1}H NMR: 200 MHz; ^{13}C NMR: 50 MHz. Chemical shifts are quoted in ppm (δ) relative to TMS and coupling constants are in Hz. Optical rotations were determined using a Perkin Elmer 341 polarimeter. Final purification of all metabolites was achieved by HPLC on silica gel (Lichrosorb Si-60, 5 μm) with RI monitoring.

3.2. Plant material

Bifurcaria bifurcata Ross was collected near Oualidia (32°49′N, 8°57′W), Morocco, in December 1998. A voucher specimen of this species was deposited in the Herbarium of Dr Pellegrini, Laboratoire de Biologie Marine Fondamentale et Appliquée, University of Marseille II, France.

3.3. Extraction and purification

The shade-dried material collected from Oualidia (340 g) was ground and extracted with Et_2O at room temperature. After filtration, the filtrate was evaporated to yield 10 g of a crude extract which was subjected to CC on silica gel eluted with a solvent gradient from isooctane to EtOAc. The two first new compounds (**2b** and **3**), with sterols and geranylgeraniol, were eluted with EtOAc-isooctane (3:7) and subsequently purified by analytical normal phase HPLC (EtOAc–isooctane, 3:7) to give **2b** (275 mg), geranylgeraniol (420 mg) and **3** (220 mg). The two other new compounds (**4** and **5**), with **2a**, were eluted with EtOAc–isooctane (1:1) and subsequently purified by semi-preparative normal phase HPLC (EtOAc–isooctane, 1:1) to give **4** (30 mg), **5** (15 mg) and **2a** (95 mg). The more polar fraction eluted with EtOAc–isooctane (7:3) led to **1** (2.42 g), after purification by semi-preparative normal phase HPLC (EtOAc-isooctane, 7:3).

3.4. Compound *2b*

Oil; $[\alpha]_D^{25}$ −7.7° (CH_2Cl_2; c 5.5); IR ν_{max}^{film} cm^{-1}: 3417, 2924, 2856, 1720, 1649, 1436, 1383, 1358, 1225, 1148, 1049, 864; HRMS: 334.2506 $[M]^+$ (calc. for $C_{21}H_{34}O_3$, 334.2508); EIMS (70 eV) *m/z* (rel. int.): 334 $[M]^+$(0.1), 316 $[M\text{-}H_2O]^+$(0.2), 265(20), 233(100), 215(0.4), 187(0.7), 137(21), 123(60), 107(19), 93(65), 81(40), 69(58), 55(53) ; ^{1}H and ^{13}C NMR: Tables 1 and 2.

3.5. Compound *3*

Oil; IR ν_{max}^{film} cm^{-1}: 3393, 3022, 2966, 2923, 2857, 1716, 1669, 1443, 1381, 1229, 1152, 1102, 1006, 965; UV λ_{max}^{EtOH} nm (log ε): 245 (4.18); HRMS: 288.2450 $[M]^+$ (calc. for $C_{20}H_{32}O$, 288.2453); EIMS (70 eV) *m/z* (rel. int.): 288 $[M]^+$(0.1), 270 $[M\text{-}H_2O]^+$ (0.4), 255(0.2), 201(10), 187(4), 175(9), 159(12), 148(19), 135(55), 119(32), 107(60), 93(100), 81(35), 69(70), 55(41); ^{1}H and ^{13}C NMR: Tables 1 and 2.

3.6. Compound *4*

Oil; $[\alpha]_D^{25}$ −3° (CH_2Cl_2; c1.0); IR ν_{max}^{film} cm^{-1}: 3410, 2965, 2904, 2852, 1688, 1649, 1438, 1383, 1272, 1079, 882, 803; HRMS: 304.2408 $[M]^+$ (calc. for $C_{20}H_{32}O_2$, 304.2402); EIMS (70 eV) *m/z* (rel. int.): 304 $[M]^+$(0.02), 286 $[M\text{-}H_2O]^+$(0.90), 235 (6), 217(7), 199 (6), 189 (3), 159 (14), 149 (7), 147 (9), 135 (18), 133 (16), 123 (20), 109 (24), 107 (30), 95 (100), 93 (71), 81(86), 69 (68), 55 (83); ^{1}H and ^{13}C NMR: Tables 3 and 4.

3.7. Compound *5*

Oil; IR ν_{max}^{film} cm^{-1}: 3415, 3067, 2968, 2915, 2868, 1690, 1656, 1436, 1380, 1268, 1140, 1078, 885; HRMS: 304.2410 $[M]^+$ (calc. for $C_{20}H_{32}O_2$, 304.2402); EIMS (70 eV) *m/z* (rel. int.): 304 $[M]^+$(0.05), 286 $[M\text{-}H_2O]^+$(0.16), 235 (34), 217 (4), 199 (4), 189 (3), 159(11), 149 (10), 147 (8), 135 (9), 133 (14), 123 (20), 109 (24), 107 (23), 95 (55), 93 (91), 81 (87), 69 (72), 55 (100); ^{1}H and ^{13}C NMR: Tables 3 and 4.

3.8. Reduction of *2b* with *LiAlH$_4$*

A cold solution of **2b** (20 mg) in dry Et_2O (1 ml) containing $LiAlH_4$ (30 mg) was stirred at 0°C for 1.3 h. Excess reagent was destroyed by slow addition of EtOAc. Addition of saturated $MgSO_4$ solution and extraction with Et_2O yielded 15 mg of an oil. After purification by semi-preparative normal phase HPLC (EtOAc–isooctane, 7:3), the corresponding reduction product (10 mg) was found to be identical to **1** by comparison of spectral data, and with the same absolute configuration of C-12 (Horeau determination: see Valls et al., 1986 for details).

3.9. Partial oxidation of *1*

One hundred milligrams of **1** were added to a solution of pyridinium dichromate (156 mg in 50 ml of dry CH_2Cl_2) and the mixture was stirred at room temperature for 12 h. The solution was then diluted with Et_2O, filtered on celite, dried on $MgSO_4$ and subsequently subjected to CC on silica gel eluted with Et_2O. After evaporation, the residue was purified by semi-preparative

normal phase HPLC (EtOAc–isooctane, 1:1) to give **4** (43 mg) and **5** (22 mg).

References

Amico, V., Neri, P., Piattelli, M., Ruberto, G., 1987. Linear diterpenoids from *Cystoseira balearica*. Phytochemistry 26, 2637–2639.

Coates, R.M., Ley, D.A., Cavender, P.L., 1978. Synthesis and carbon-13 nuclear magnetic resonance spectra of all-*trans*-geranylgeraniol and its nor analogues. J. Org. Chem. 43, 4915–4922.

Combaut, G., Piovetti, L., 1983. A novel acyclic diterpene from the brown alga *Bifurcaria bifurcata*. Phytochemistry 22, 1787–1789.

Couperus, P.A., Clague, A.D.H., Van Dongen, J.P.C.M., 1976. ^{13}C Chemical shifts of some model olefins. Org. Magn. Reson. 8, 426–431.

Culioli, G., Mesguiche, V., Piovetti, L., Valls, R., 1999a. Geranylgeraniol and geranylgeraniol-derived diterpenes from the brown alga *Bifurcaria bifurcata* (Cystoseiraceae). Biochem. Syst. Ecol. 27, 665–668.

Culioli, G., Daoudi, M., Mesguiche, V., Valls, R., Piovetti, L., 1999b. Geranylgeraniol-derived diterpenoids from the brown alga *Bifurcaria bifurcata*. Phytochemistry 52, 1447–1454.

Culioli, G., Di Guardia, S., Valls, R., Piovetti, L., 2000. Geranylgeraniol-derived diterpenes from the brown alga *Bifurcaria bifurcata*: Comparison with two other Cystoseiraceae species. Biochem. Syst. Ecol. 28, 185–187.

Horeau, A., Nouaille, A., 1971. Extension et simplification de la méthode de détermination de la configuration des alcools secondaires par ''dédoublement partiel''. Part VIII: Application à la génépine. Tetrahedron Lett. 22, 1939–1942.

Semmak, L., Zerzouf, A., Valls, R., Banaigs, B., Jeanty, G., Francisco, C., 1988. Acyclic diterpenes from *Bifurcaria bifurcata*. Phytochemistry 27, 2347–2349.

Valls, R., Banaigs, B., Francisco, C., Codomier, L., Cave, A., 1986. An acyclic diterpene from the brown alga *Bifurcaria bifurcata*. Phytochemistry 25, 751–752.

Valls, R., Banaigs, B., Piovetti, L., Archavlis, A., Artaud, J., 1993a. Linear diterpene with antimitotic activity from the brown alga *Bifurcaria bifurcata*. Phytochemistry 34, 1585–1588.

Valls, R., Banaigs, B., Piovetti, L., Zerzouf, A., 1993b. Variations géographiques de la composition en diterpènes de *Bifurcaria bifurcata* des côtes atlantiques marocaines. Ann. Inst. Ocean 63, 215–223.

Valls, R., Piovetti, L., Banaigs, B., Archavlis, A., Pellegrini, M., 1995. (S)-13-Hydroxygeranylgeraniol-derived furanoditerpenes from *Bifurcaria bifurcata*. Phytochemistry 39, 145–149.

PERGAMON

Phytochemistry 57 (2001) 537–541

PHYTOCHEMISTRY

www.elsevier.com/locate/phytochem

Diterpenes from the bark and seeds of *Colophospermum mopane*

Paul P. Mebe*

Department of Chemistry, University of Zimbabwe, PO Box MP 167, Mount Pleasant, Harare, Zimbabwe

Received 13 September 2000; received in revised form 12 January 2001

Abstract

The $CHCl_3$ extract of the bark and seeds of *Colophospermum mopane* gave three new diterpenes, dihydrogrindelic acid and dihydrogrindelaldehyde and methyl labd-13E-en-15-oate. The structures were assigned on the basis of detailed spectroscopic data analyses. The aldehyde showed significant cytotoxic activity against a human breast cancer cell line. © 2001 Elsevier Science Ltd. All rights reserved.

Keywords: *Colophospermum mopane*; Leguminosae; Diterpenes; Dihydrogrindelic acid; Dihydrogrindelaldehyde; Methyl labd-13*E*-en-15-oate

1. Introduction

Colophospermum mopane Kirk ex J. Leonard is a tree widespread in the dry regions of Southern Africa. It is used in traditional medicine as a remedy for syphilis and sore eyes (Watt and Breyer-Brandwijk, 1962). The $CHCl_3$ extract of the bark and seeds of *C. mopane* led to the isolation of three new labdane diterpenes: dihydrogrindelic acid, dihydrogrindelaldehyde and methyl labd-13-en-15-oate. Dihydrogrindelic acid has only been reported in the literature as a synthetic derivative of grindelic acid (Mangoni and Belardin, 1963; Adinolfi et al., 1988). To our knowledge, this is the first report of hydrogrindelic acid as a natural product. Grindelic acid has been isolated from a number of species of Grindelia, Solidaco and Chrysothamnus (Pannizi et al., 1961, 1962; Mangoni and Belardini, 1962; Anthonsen et al., 1969). The crude $CHCl_3$ extract showed significant cytotoxic activity against a human breast cancer cell line. We report herein the isolation and identification the new diterpenes and evaluations of their cytotoxicity.

2. Results and discussion

The bark and seeds of *C. mopane* were separately extracted with $CHCl_3$. The crude extracts appeared similar on TLC and were combined, and partitioned with *n*-hexane and MeOH. The *n*-hexane fraction was successively purified by silica gel CC and prep. TLC to give two new derivatives of grindelic acid **1** and **2** and a new diterpenoid labdane **3**. The crude $CHCl_3$ extract showed significant cytotoxic activity ($ED_{50} = 2.0$ μg/ml) in vitro against MCF7 (human breast cancer) cell line.

Compound **1** was obtained in large quantities as a colourless gum, and had a molecular formula of $C_{20}H_{34}O_3$ as deduced from the EIMS which displayed two major peaks at m/z 322 $[M]^+$ and 183 $[M-C_{10}H_{15}O_3]^+$. The molecular formula was supported by the ^{13}C NMR and DEPT spectra which showed 20 carbon signals which consisted of five methyl carbon signals, eight methylene carbon ones, two methine carbon ones and five quaternary carbon ones. The ^1H NMR spectrum showed signals of four methyl groups attached to quaternary centres at δ 0.79, 0.85, 0.94 and 1.37, and methyl adjacent to a methine at δ 1.05. Closer inspection of the above spectral data suggested that the structure of **1** was a labdane diterpene. The methyl signal at δ 1.37 indicated the presence of a methyl on a carbon bearing an oxygen and this was supported by the ^{13}C NMR spectrum which showed two peaks for carbons bearing oxygen at δ 81.29 and 96.75. These exceptionally downfield signals suggested that these carbons were quaternary and were bridged by an ether linkage, since the spectral data did not show the presence of an alcoholic hydroxyl group. The IR spectrum showed bands at 1705 ($>C=O$) and 2500–3400 cm^{-1} (−OH), both assignable to a carboxylic group and this was corroborated by the

* Tel.: +263-4-303211; fax: +263-4-333407.
E-mail address: mebe@compcentre.uz.ac.zw

0031-9422/01/$ - see front matter © 2001 Elsevier Science Ltd. All rights reserved.
PII: S0031-9422(01)00068-1

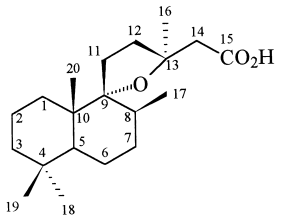

1

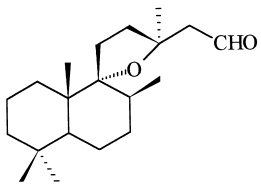

2

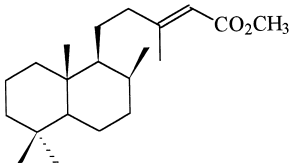

3

singlet signal in the ^{13}C NMR spectrum at δ 172.60 and a broad signal at δ 10.74 in the ^{1}H NMR spectrum. All the three oxygens in the formula of **1** were thus accounted for.

The presence of isolated two proton signals at δ 2.46 (*d*, $J=15$ Hz) and 2.68 (*d*, $J=15$ Hz) was consistent with the placement of the methylene at C-14, α to the carboxylic group and adjacent to a fully substituted carbon at C-13. The presence of a methyl doublet signal at δ 1.05 ($J=7$ Hz) was assignable to the C-17 methyl because it is consistent with a labdane diterpene structure.

A combination of NMR experiments (COSY, HETCOR, NOE and DEPT), allowed the assignments (Table 1) of all the proton and carbon signals in the ^{1}H and ^{13}C NMR spectra. The ^{1}H–^{1}H COSY contour map which showed two strong correlations between the

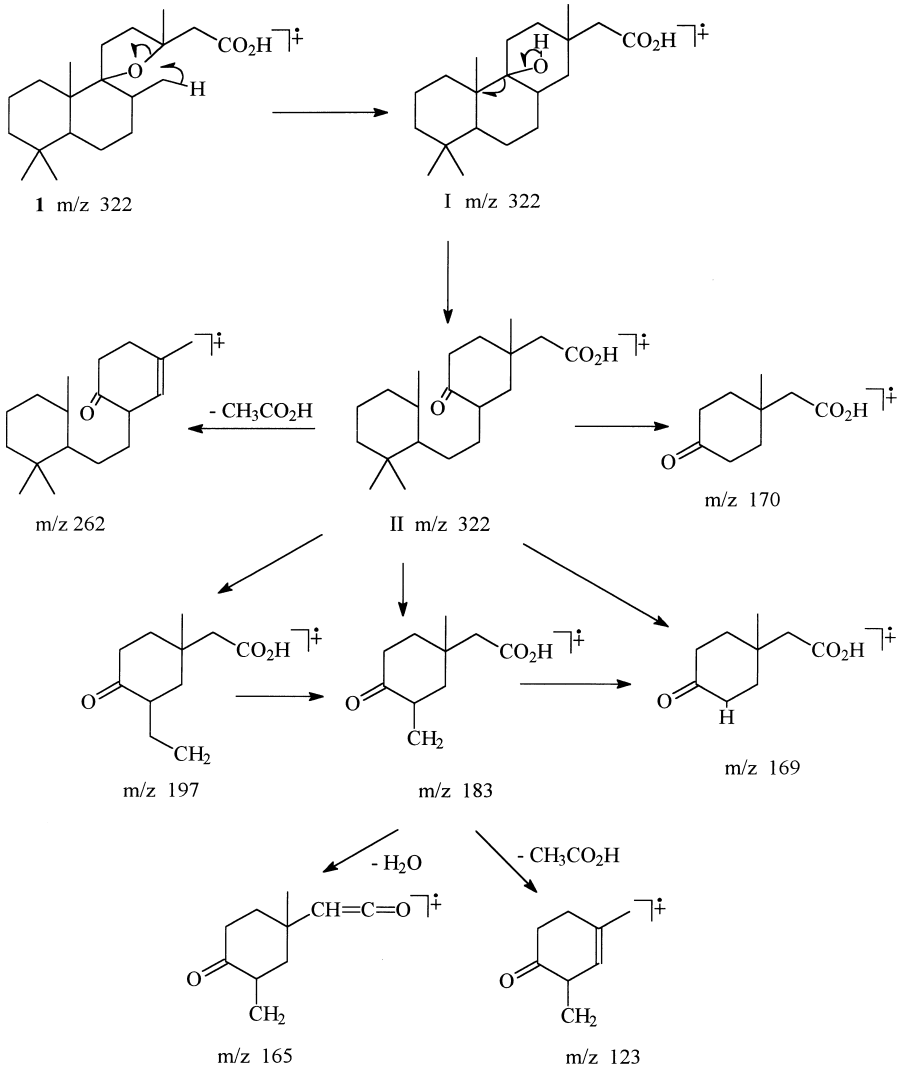

Scheme 1. Diagnostic ions and suggested fragmentations in mass spectrum of compound **1**.

Table 1
^{13}C NMR ($CDCl_3$, 75 MHz) assignments of compounds **1**–**3** and ^{1}H NMR ($CDCl_3$, 400 MHz) assignments of compound **1**

C/H	**1** (δC)	**2** (δC)	**3** (δC)	**1** (δH)[a]
1	34.03	34.21	34.64	1.57α, 1.90β, *m*
2	17.60	18.10	18.17	1.36β, 1.42α, *m*
3	30.03	29.43	30.11	1.44α, 1.52β, *m*
4	30.27	31.30	29.95	–
5	49.58	49.72	48.83	1.31, *m*
6	42.24	41.23	41.64	1.29α, 1.08β, *m*
7	18.62	18.45	18.01	1.54α, 1.39β, *m*
8	39.56	39.34	38.97	1.82, *m*
9	96.70	95.98	55.32	–
10	42.50	41.66	42.70	–
11	29.09	29.02	25.51	1.73β, 1.89α, *m*
12	38.72	38.20	32.52	1.98α, 1.89β, *m*
13	81.30	81.01	147.64	–
14	47.07	47.22	115.03	2.46, *d* (15) 2.68, *d* (15)
15	172.60	206.31	183.67	–
16	28.01	28.14	27.84	1.37, *s*
17	18.86	18.34	21.03	1.05, *d* (7)
18	34.07	34.11	33.21	0.79, *s*
19	22.16	21.68	20.47	0.85, *s*
20	18.70	18.74	17.42	0.94, *s*
OH	–	–	–	10.74, *s*
OCH_3	–	–	50.79	–

[a] Each multiplet signal overlapping with other signals.

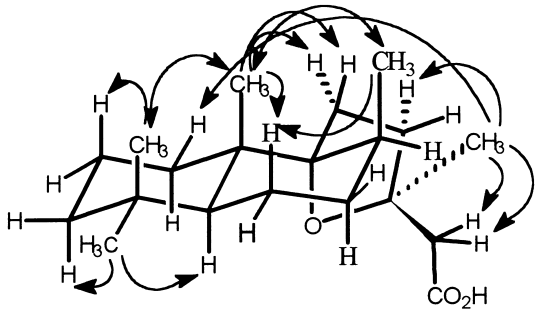

Fig. 1. Significant NOEs observed for compound **1** in the NOE difference spectra.

methylene signals at δ 2.46 and 2.68, and also between the C-17 methyl and the H-8 signals at δ 1.05 and 1.82, respectively. The methylene signals also showed long range corrolations with the C-16 methyl signal at δ 1.37, confirming the placement of these groups in **1**. With the C-17 methyl observed as a doublet, the ether linkage must therefore be restricted to C-9 and C-13 and therefore the C-16 methyl resonating at δ 1.37 was paced at C-13. The relative stereochemistry of **1** was deduced from studies of the difference NOE experiments whose correlations are shown in Fig. 1. The NOE spectra revealed the fact that H-19, H-20, H-11 and H-17 were on the β-side of the molecule, while the H-18, H-5 and H-8 were on the α-side. This follows from irradiations of the H-18, H-19 and H-20 methyl signals. Furthermore, it was noted that irradiation of the C-16 methyl signal had NOE effects on the H-12α, H-1α and the H-14 signals, but not on the H-8 signal. The latter observations indicated that the C-16 methyl was on the α-side of the tetrahydrofuran ring.

The mass spectrum showed significant and diagnostic fragmentation ions that are rationalized in Scheme 1. Structure **1** rearranged via intermediate **I** to structure **II** before any fragmentation occurred. Structure **II** then became the main structure from which most of the observed characteristic fragments were derived. McLafferty rearrangement of II produced fragment ions at *m*/*z* 262 and 170 due to the loss of acetic acid. This rearrangement also accounted for the ion at *m*/*z* 123 derived from fragment ion at *m*/*z* 183, the base peak. The ion at *m*/*z* 165 was due to the elimination of H_2O from fragment ion at *m*/*z* 183. The rest of the observed fragment ions at *m*/*z* 197, 183 and 169 were due to simple carbon–carbon cleavages. On the basis of the above spectral data analysis and the survey of spectral data of related grindelic derivatives (Rose, 1980; Rose et al., 1981; Jakupovic et al., 1986), structure **1** was elucidated as dihydrogrindelic acid.

Compound **2**, $C_{20}H_{34}O_2$ showed a molecular ion at *m*/*z* 306 and a peak at *m*/*z* 263 $[M-CH_2CHO]^+$ and the IR spectrum showed a strong peak at 1730 cm^{-1}. The spectral (^{1}H and ^{13}C NMR) characteristics of compound **2** were very similar to those of **1** suggesting that **2** is a derivative of **1**. Differences in the ^{1}H NMR spectra of the two compounds were apparent at the region about δ 2.50 where compound **1** had two doublets at δ 2.46 and 2.68, and compound **2** had instead two doublet of doublets ($J=6$, 15 Hz) at δ 2.43 and 2.67 ascribed to the C-14 methylene protons. The other noted difference in compound **2**, was a triplet signal at δ 9.84 ($J=6$ Hz) ascribed to the H-15, aldehyde proton. The coupling constant ($J=6$ Hz) clearly indicated the adjacent positions of the above groups. This assignment was confirmed by the ^{1}H–^{1}H COSY spectrum of **2** which showed the latter signals correlated. The presence of the C-15 aldehyde carbonyl group was further confirmed by the ^{13}C NMR and DEPT spectra of **2** which had a doublet signal at δ 206.31. Comparison of this spectral data of compound **1** and **2**, led to the elucidation of the structure of compound **2** as dihydrogridelaldehyde.

Compound **3** possessed a molecular formula of $C_{21}H_{36}O_2$ and a molecular ion *m*/*z* 320 as indicated by the EIMS. The IR indicated a strong carbonyl band at 1698 cm^{-1} suggesting that it has an α, β-unsaturated carbonyl group. The ^{1}H NMR spectrum showed three singlets which were absent in **1** and **2**, at δ 2.16 (vinyl C-13 methyl), δ 3.67 (methoxyl) and δ 5.68 (vinyl proton). In addition, the spectrum showed three tertiary methyl signals at δ 0.83, 0.88 and 0.92, and a secondary methyl signal at δ 1.04 ($J=7$ Hz) assignable to the C-17 methyl.

The upfield multiplet signals for **2** were similar to the signals observed in ^{1}H NMR spectrum of **1**. The ^{13}C NMR spectrum confirmed the presence of a methyl ester functionality by the presence of signals at δ 183.67 (C=O) and 50.79 (CH_3O). The presence of only two olefinic carbon signals at δ 147.64 and 115.03 in the ^{13}C NMR spectrum and an IR band at 1698 cm^{-1} confirmed the existence of the α,β-unsaturated ester group. The ^{1}H NMR spectrum of **3** was similar to that of methyl hydroxy-labd-13E-en-15-oate (Ates et al., 1982; Zdero et al., 1990). The relative stereochemistry was determined by the NOE experiment. The NOE effects of substituents on rings A and B were similar to those of compound **1** (Fig. 1), indicating that compound **3** was a normal labdane. Irradiation of the olefinic proton signal at δ 5.68 showed enhancement of signal at δ 2.25 attributed to the H-12, but no enhancement of the H-16 signal at δ 2.17 (*s*, 3H) was observed. Thus, the stereochemistry of the double bond was deduced to be 13E. On the basis of the above spectral data analysis **3** was identified as methyl labd-13E-en-15-oate.

The isolates were evaluated for their cytotoxic activity (ED_{50} <20 μg/ml) against a cancer cell line, MCF7 (breast adenocarcinoma). Only compound **2** showed a significant activity at 3.5 μg/ml level, accounting for some, but maybe not all, of the activity of the crude extract. The other compounds showed no cytotoxic activity.

3. Experimental

3.1. Plant material

The bark and seeds were collected from Matebeleland South, in Zimbabwe. A voucher specimen has been deposited at National Herbarium, Harare.

3.2. Extraction and isolation

The air dried and finely powdered stem bark and seeds of *C. mopane* (80 g, bark) and (60 g, seeds) were separately extracted with $CHCl_3$ and MeOH consecutively using a Soxhlet apparatus. The $CHCl_3$ and MeOH extracts of each plant material were separately concentrated using a rotary evaporator at a maximum temp. of 45°C to yield 7.1 and 6.4 g of bark residue and 8.2 and 3.02 g of seed residue, respectively.

The $CHCl_3$ extracts were combined and fractionated in *n*-hexane and 90% MeOH mixture and the *n*-hexane residue (1.9 g) was then fractionated by silica gel 60 CC eluting with a step-gradient of *n*-hexane-EtOAc mixture of increasing polarity. Further purification of the resulting fractions using CC and eluting with *n*-hexane–EtOAc (8.5:1.5), led to the isolation of **1** (857 mg), **2** (48 mg) and **3** (26 mg).

3.2.1. Dihydrogrindelic acid *1*

Colourless gum, IR (KBr) cm^{-1}: 3400–2500 (OH), 1705 (>C=O); MS *m/z* (rel. int.): 322.2541 M^+ (14) for, $C_{20}H_{34}O_3$, requires 322.2541, 262 $[M-CH_3CO_2H]^+$, (0.5%), 209 (8) 197 (12), 183 (100), 170 (11), 169 (3), 165 (13), 123 (17); ^{1}H and ^{13}C NMR, see Table 1.

3.2.2. Dihydrogrindelaldehyde *2*

Colourless gum, IR (KBr) cm^{-1}: 2945, 1730 cm^{-1}; MS *m/z* (rel. int) : 306.257 $[M]^+$ (8), $C_{20}H_{34}O_2$ requires 306.258, 263 $[M^+-CH_2CHO]^+$ (4), 167 $[C_{10}H_{15}O_2]^+$ (16); ^{1}H NMR (400 MHz, $CDCl_3$): δ 0.77 (3H, *s*, H-18), 0.84 (3H, *s*, H-19), 0.90 (3H, *s,* H-20), 1.03 (3H, *d,* *J*=7.8 Hz, H-17), 1.32 (3H, *s,* H-16), 2.43 (1H, *dd*, *J*=6,15 Hz, H-14a), 2.67 (1H, *dd,* *J*=6,15 Hz, H-14b), 9.84 (1H, *t*, *J*=6 Hz, H-15); ^{13} C NMR, see Table 1.

3.2.3. Methyl labd-13E-en-15-oate *3*

Colourless gum, IR (KBr) cm^{-1}: 2930, 1698 (>C=O); MS *m/z* (ret. int.): 320.246 $[M]^+$ (4), $C_{21}H_{36}O_2$, requires 320.248, 305 $[M\text{-}CH_3]^+$ (3), 289 $[M\text{-}OCH_3]^+$ (1), 205 $[C_{15}H_{25}]^+$ (37), 19 1 (26), 114 (27); FABMS *m/z* 319 (M+1); ^{1}H NMR (300 MHz, $CDCl_3$): δ 0.83 (3H, *s*, H-18), 0.88 (3H, *s*, H-19), 0.99 (3H, *s*, H-20), 1.04 (3H, *d*, J=7 Hz, H-17), 2.17 (3H, *s*, H-16), 3.67 (3H, *s,* OCH_3), 5.68 (1H, *brs,* H-14); ^{13}C NMR, see Table 1.

4. Bioassay

Cytoxicity evaluations of crude and pure samples against human breast tumour cell line, MCF7, were carried out at the Cancer Research Laboratory, Medical School, Ohio State University.

Acknowledgements

This work was supported by grants from the Fulbright Fellowship, the Elsa U. Pardee Foundation (USA), and the Research Board of the University of Zimbabwe. The author is also grateful to Dr. J.M. Cassady for assisting with the measurements of cytotoxic activities.

References

Adinolfi, M., Greca, M.D., Mangoni, L., 1988. Absolute configuration of grindelic acid. Phytochemistry 27, 1878–1881.

Anthonsen, T., McCabe, P.H., McCrindle, R., Murray, R.D., 1969. Constituents of *Solidaco* species. Tetrahedron 25, 2233–2239.

Ates, N., Ulubelen, A., Clark, W.D., Brown, G.K., Mabry, T.J., 1982. Flavonoids from *Haplopappus foliosus*. Journal of Natural Products 45, 189–191.

Jakupovic, J., Baruah, R.N., Zdero, C., Eid, F., Pathak, V.P., Chau-Thi, T.V., Bohlmann, F., King, R.M., Robinson, H., 1986. Further

diterpenes from plants of the compositae, subtribe solidagininae. Phytochemistry 25, 1873–1881.
Mangoni, L., Belardin, M., 1963. Determination of stereochemistry of grindelic acid and configuration at C-9. Gazzeta Chimica Italiana 93, 455–464.
Mangoni, L., Belardini, M., 1962. Components of *Grindelia robusta* – 6-oxo-grindelic acid. Gazzeta Chimica Italiana 92, 983–994.
Panizzi, L., Mangoni, L., Belardini, M., 1961. The structure of grindelic acid, a new diterpene acid. Tetrahedron Letters 12, 376–381.
Panizzi, L., Mangoni, L., Belardini, M., 1962. Components of *Grindelia robusta — grindelic acid*. Gazzeta Chimica Italiana 92, 522–538.
Rose, A.F., 1980. Grindelane diterpenoids from *Chrysothamnus nauscosus*. Phytochemistry 19, 2698–2693.
Rose, A.F., Jones, K.C., Haddon, W.F., Dreyer, D.L., 1981. Grindelane diterpenoid acids from *Grindelia humilis*. Phytochemistry 20, 2249–2252.
Watt, J.M., Breyer-Brandwijk, M.G., 1962. The Medicinal and Poisonous Plants of Southern and Eastern Africa, 2nd Edition. Livingstone, Edinburgh, pp. 577–580.
Zdero, C., Bohlmann, F., Niemeyer, H.M., 1990. Diterpenes and umbelliferone derivatives from *Haplopappus deserticopla*. Phytochemistry 29, 326–329.

PERGAMON

Phytochemistry 57 (2001) 543–546

PHYTOCHEMISTRY

www.elsevier.com/locate/phytochem

Flavonoids from *Aconitum napellus* subsp. *neomontanum*

Gelsomina Fico[a], Alessandra Braca[a,*], Nunziatina De Tommasi[b], Franca Tomè[c], Ivano Morelli[a]

[a]*Dipartimento di Chimica Bioorganica e Biofarmacia, Università di Pisa, Via Bonanno 33, 56126 Pisa, Italy*
[b]*Dipartimento di Scienze Farmaceutiche, Università di Salerno, Via Ponte Don Melillo, Invariante 11C, 84084 Fisciano, Salerno, Italy*
[c]*Dipartimento di Biologia, Università di Milano, Via Celoria 26, 20133 Milano, Italy*

Received 18 December 2000; received in revised form 21 February 2001

Abstract

Three flavonol glycosides quercetin 7-*O*-(6-*trans*-caffeoyl)-β-glucopyranosyl-(1→3)-α-rhamnopyranoside-3-*O*-β-glucopyranoside (**1**), kaempferol 7-*O*-(6-*trans*-caffeoyl)-β-glucopyranosyl-(1→3)-α-rhamnopyranoside-3-*O*-β-glucopyranoside (**2**), and kaempferol 7-*O*-(6-*trans*-*p*-coumaroyl)-β-glucopyranosyl-(1→3)-α-rhamnopyranoside-3-*O*-β-glucopyranoside (**3**), together with the known β-3,4-dihydroxyphenethyl β-glucopyranoside, were isolated from the flowers of *Aconitum napellus* subsp. *neomontanum*. Their structures were elucidated by spectroscopic methods, including 2D NMR spectral techniques. © 2001 Elsevier Science Ltd. All rights reserved.

Keywords: *Aconitum napellus* subsp. *neomontanum*; Ranunculaceae; Flavonoids

1. Introduction

The *Aconitum* genus is mainly characterized by the presence of diterpene alkaloids that being highly toxic, have been used in the past in China as source of arrow poison (Bisset, 1981). The alkaloid composition of different species of European *Aconitum* was analysed by Katz and Staehelin (1980); particularly qualitative and quantitative variations in diterpenoid alkaloids of the *A. napellus* subsp. *neomontanum* (Wulfen) Gáyer have been studied during its onthogenetic cycle (Colombo et al., 1988). Subsequent investigations of the seeds of the same subspecies showed the presence of norditerpenoid and diterpenoid alkaloids (Fuente et al., 1988; Liu and Katz, 1996). In the last years the study of *Aconitum* genus was directed to the other secondary metabolites such as flavonoids. The flavonol composition of the aerial parts of *A. jaluense* (Wang et al., 1994), A. *pseudolaeve* (Kim, et al., 1996), and *A. chiisanense* (Jeong et al., 1997) have been reported. Recently the flavonoids of five Korean species in the *A. jaluense* complex have been studied for recognising the relationships and levels of differentiation (Lim et al., 1999). Regarding the European species, the flowers of *A. paniculatum* have shown the presence of three new flavonol glycosides (Fico et al., 2000). In this paper we describe the isolation and structure elucidation of three new flavonol glycosides, compounds **1**–**3**, and the known, but new for the entity under study, β-3,4-dihydroxyphenethyl β-glucopyranoside, from the flowers of *A. napellus* subsp. *neomontanum*.

2. Results and discussion

The *n*-butanol fraction of the methanol extract from the flowers of *A. napellus* subsp. *neomontanum* was chromatographed successively on Sephadex LH-20 and RP-HPLC (C-18) to give pure compounds **1**–**3**, and β-3,4-dihydroxyphenethyl β-glucopyranoside.

Compound **1**, a yellow amorphous solid, showed molecular formula $C_{42}H_{46}O_{24}$ that was determined from its HPLC-MS, ^{13}C NMR (Table 2), and ^{13}C-DEPT data. The mass spectrum showed a $M+H^+$ peak at *m*/*z* 935 and fragment ions at *m*/*z* 773, 465, and 303. The UV spectrum of **1** showed two absorption maxima at 333 and 265 nm, indicating the presence of substituted aromatic rings and α,β unsaturated ketone in the molecule (Agrawal, 1989). The 600 MHz ^1H NMR spectrum of compound **1** (Table 1) showed a typical pattern of a

* Corresponding author. Tel.: +39-050-44074; fax: +39-050-43321.
E-mail address: braca@farm.unipi.it (A. Braca).

0031-9422/01/$ - see front matter © 2001 Elsevier Science Ltd. All rights reserved.
PII: S0031-9422(01)00102-9

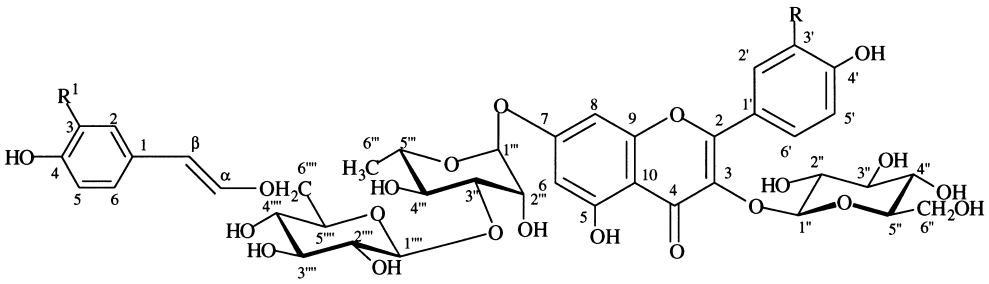

1 R = R^1 = OH

2 R = H R^1 = OH

3 R = R^1 = H

flavonol with a quercetin aglycon together with signals ascribable to sugar moieties and acyl residue. The three anomeric protons arising from the sugar moieties appeared at δ 5.41 (1H, *d*, *J*= 1.8 Hz), 5.38 (1H, *d*, *J*= 7.8 Hz), and 4.54 (1H, *d*, *J*= 7.8 Hz), which correlated respectively with signals at 99.2, 104.3 and 106.4 ppm in the HSQC spectrum. The ^{1}H NMR spectrum showed also the presence of a caffeoyl residue (Table 1). All the ^{1}H and ^{13}C NMR signals of **1** were assigned using ^{1}H–^{1}H COSY, HOHAHA, HSQC, and HMBC experi-

Table 1
^{1}H NMR (600 MHz) spectral data for compounds **1**–**3**

	Compound (δ, CD_3OD)[a]		
No. of atom	**1**	**2**	**3**
6	6.29 (1H, *d*, 1.8)	6.29 (1H, *d*, 1.8)	6.31 (1H, *d*, 1.8)
7			
8	6.36 (1H, *d*, 1.8)	6.35 (1H, *d*, 1.8)	6.33 (1H, *d*, 1.8)
2′	6.93 (1H, *d*, 2.0)	8.11 (2H, *d*, 8.0)	8.07 (2H, *d*, 8.0)
3′		6.93 (2H, *d*, 8.0)	6.91 (2H, *d*, 8.0)
5′	6.92 (1H, *d*, 8.0)	6.93 (2H, *d*, 8.0)	6.91 (2H, *d*, 8.0)
6′	7.65 (1H, *dd*, 8.0, 2.0)	8.11 (2H, *d*, 8.0)	8.07 (2H, *d*, 8.0)
3-*O*-glc-1″	5.38 (1H, *d*, 7.8)	5.35 (1H, *d*, 7.8)	5.30 (1H, *d*, 7.8)
2″	3.49 (1H, *br t*, 9.0)	3.47 (1H, *br t*, 9.0)	3.48 (1H, *br t*, 9.0)
3″	3.52 (1H, *t*, 9.0)	3.54 (1H, *t*, 9.0)	3.54 (1H, *t*, 9.0)
4″	3.33 (1H, *t*, 9.0)	3.32 (1H, *t*, 9.0)	3.34 (1H, *t*, 9.0)
5″	3.38 (1H, *m*)	3.40 (1H, *m*)	3.41 (1H, *m*)
6″a	3.78 (1H, *dd*, 12.0, 2.0)	3.79 (1H, *dd*, 12.0, 2.0)	3.77 (1H, *dd*, 12.0, 2.0)
6″b	3.57 (1H, *dd*, 12.0, 5.0)	3.55 (1H, *dd*, 12.0, 5.0)	3.56 (1H, *dd*, 12.0, 5.0)
7-*O*-rha-1‴	5.41 (1H, *d*, 1.8)	5.41 (1H, *d*, 1.8)	5.40 (1H, *d*, 1.8)
2‴	4.33 (1H, *m*)	4.35 (1H, *m*)	4.33 (1H, *m*)
3‴	3.82 (1H, *dd*, 8.5, 3.5)	3.84 (1H, *dd*, 8.5, 3.5)	3.81 (1H, *dd*, 8.5, 3.5)
4‴	3.62 (1H, *t*, 8.5)	3.65 (1H, *t*, 8.5)	3.64 (1H, *t*, 8.5)
5‴	3.58 (1H, *m*)	3.57 (1H, *m*)	3.56 (1H, *m*)
6‴	1.24 (3H, *d*, 6.0)	1.23 (3H, *d*, 6.0)	1.22 (3H, *d*, 6.0)
glc-1⁗	4.54 (1H, *d*, 7.8)	4.55 (1H, *d*, 7.8)	4.55 (1H, *d*, 7.8)
2⁗	3.42 (1H, *br t*, 9.0)	3.44 (1H, *br t*, 9.0)	3.43 (1H, *br t*, 9.0)
3⁗	3.31 (1H, *t*, 9.0)	3.33 (1H, *t*, 9.0)	3.33 (1H, *t*, 9.0)
4⁗	3.46 (1H, *t*, 9.0)	3.48 (1H, *t*, 9.0)	3.50 (1H, *t*, 9.0)
5⁗	3.70 (1H, *m*)	3.71 (1H, *m*)	3.72 (1H, *m*)
6⁗a	4.54 (1H, *dd*, 12.2, 2.0)	4.55 (1H, *dd*, 12.2, 2.0)	4.56 (1H, *dd*, 12.2, 2.0)
6⁗b	4.53 (1H, *dd*, 12.2, 5.2)	4.53 (1H, *dd*, 12.2, 5.2)	4.54 (1H, *dd*, 12.2, 5.2)
α	6.20 (1H, *d*, 16.1)	6.21 (1H, *d*, 16.0)	6.24 (1H, *d*, 16.0)
β	7.50 (1H, *d*, 16.1)	7.50 (1H, *d*, 16.0)	7.54 (1H, *d*, 16.0)
2	6.70 (1H, *d*, 2.0)	6.71 (1H, *d*, 2.0)	7.10 (2H, *d*, 8.0)
3			6.43 (2H, *d*, 8.0)
5	6.46 (1H, *d*, 7.8)	6.45 (1H, *d*, 8.0)	6.43 (2H, *d*, 8.0)
6	6.68 (1H, *dd*, 7.8, 2.0)	6.67 (1H, *dd*, 8.0, 2.0)	7.10 (2H, *d*, 8.0)

[a] Coupling constants (*J* in Hz) are given in parentheses.

Table 2
^{13}C NMR (600 MHz) spectral data for compounds **1**–**3**

	Compound (δ, CD_3OD)[a]		
No. of atom	**1**	**2**	**3**
2	157.7	157.9	157.8
3	136.1	136.0	135.9
4	179.6	179.5	179.7
5	162.7	162.5	162.7
6	100.1	100.1	100.0
7	163.0	163.0	163.1
8	95.6	95.6	95.7
9	157.7	157.3	157.8
10	107.5	107.7	107.5
1′	123.2	123.0	122.9
2′	117.8	132.6	132.5
3′	146.4	116.1	116.1
4′	145.9	161.4	161.7
5′	116.0	116.1	116.1
6′	123.5	132.6	132.5
3-*O*-glc-1″	104.3	104.0	104.2
2″	75.7	75.8	75.8
3″	77.8	77.8	77.8
4″	71.4	71.5	71.5
5″	78.3	78.3	78.3
6″	62.7	62.8	62.8
7-*O*-rha-1‴	99.2	99.1	99.3
2‴	72.0	71.9	72.0
3‴	83.6	83.6	83.5
4‴	72.7	72.7	72.7
5‴	71.4	71.4	71.5
6‴	18.2	18.2	18.3
glc-1⁗	106.4	106.4	106.3
2⁗	75.8	75.8	75.8
3⁗	78.2	78.2	78.2
4⁗	75.3	75.2	75.2
5⁗	75.8	75.8	75.1
6⁗	64.8	64.8	64.9
COO	169.0	169.0	169.0
α	114.6	114.6	114.7
β	147.3	147.3	146.9
1	127.3	127.2	126.7
2	114.6	114.6	130.9
3	149.9	149.6	116.4
4	146.4	145.6	161.0
5	122.9	122.9	116.4
6	123.5	123.8	130.9

[a] Coupling constants (J in Hz) are given in parentheses.

ments. Particularly ^{1}H–^{1}H COSY spectra together with a HOHAHA experiment allowed to identify the spin systems of each sugar residues. In particular the lower field shifts of H-6‴ (δ 4.53, 4.54) of one glucosyl unit together with the lower field shifts of C-3″ (83.6 ppm) and C-6‴ (δ 64.8) signals suggested the substitution pattern of glycosyl and acyl moieties. Unequivocal information could be obtained by 2D NMR spectra; the HMBC experiment indicated connections between δ 5.38 (H-1″) and 136.1 (C-3); δ 5.41 (H-1‴) and 83.6 (C-3‴); δ 4.53 and 4.54 (H-6⁗) and 169.0 (COO); δ 5.41 (H-1‴) and 163.0 (C-7) and 72.0 (C-2‴); δ 4.54 (H-1⁗) and 83.6 (C-3‴). Chemical shifts, multiplicity of the signal, absolute values of the coupling constant and the magnitude in the ^{1}H NMR, ^{1}H–^{1}H COSY, and 1D-TOCSY spectra as well as ^{13}C NMR data indicated the presence of two glucopyranosyl moieties with β-configuration at the anomeric carbon and one rhamnopyranosyl residue with α-configuration. On the basis of all this results the structure of compound **1** was established as quercetin 7-*O*-(6-*trans*-caffeoyl)-β-glucopyranosyl-(1→3)-α-rhamnopyranoside-3-*O*-β-glucopyranoside.

To compound **2** was assigned the molecular formula $C_{42}H_{46}O_{23}$ by HPLC–MS, ^{13}C NMR (Table 2), and ^{13}C-DEPT data. The UV spectrum of **2** showed absorptions at 341 and 255 nm (Agrawal, 1989). The ^{1}H NMR spectrum of **2** (Table 1) was very similar to **1** except for signals of ring B of the aglycon moiety that in **2** were typical of a kaempferol. The ^{1}H NMR and ^{13}C NMR exhibited signals which can be ascribed to the kaempferol and caffeoyl moieties along with those of three anomeric protons identified with the help of ^{1}H–^{1}H COSY and HOHAHA experiments as two glucose (δ 5.35 and 4.55, J = 7.8 Hz) and one rhamnose (δ 5.41, J = 1.8 Hz). The assignments of all protonated carbons were accomplished by interpretation of the HSQC NMR spectrum while HMBC experiment correlations were similar to those of compound **1** (H-1″-C-3; H-1‴-C-3‴, H-1‴-C-7, H-1‴-C-2‴; H-6⁗-COO; H-1⁗-C-3‴). From these results, the structure of **2** was concluded to be kaempferol 7-*O*-(6-*trans*-caffeoyl)-β-glucopyranosyl-(1→3)-α-rhamnopyranoside-3-*O*-β-glucopyranoside.

Finally the molecular formula of compound **3** was determined as $C_{42}H_{46}O_{22}$ from the HPLC–MS. NMR and other spectroscopic data were nearly identical with those of **2**; the only difference was that a *trans-p*-coumaroyl ester group appeared instead of the caffeoyl of **2**. In conclusion, the structure of the new compound **3** was determined to be kaempferol 7-*O*-(6-*trans-p*-coumaroyl)-β-glucopyranosyl-(1→3)-α-rhamnopyranoside-3-*O*-β-glucopyranoside.

The known compound, β-3,4-dihydroxyphenethyl β-glucopyranoside, was identified by comparison of its spectral and physical data with those reported in the literature (Shimomura et al., 1987).

3. Experimental

3.1. General

Melting points (uncorrected) were determined with a Kofler apparatus. Optical rotations were measured on a Perkin-Elmer 241 polarimeter equipped with a sodium lamp (589 nm) and a 1 dm microcell. The mass and UV-vis spectra (HPLC–MS) were performed on a HP 1090L instrument with a Diode Array Detector, managed by a HP 9000 workstation interfaced with a HP 1100 MSD

API-electrospray. A Bruker DRX-600 NMR spectrometer, operating at 599.19 MHz for ^1H and 150.86 MHz for ^{13}C, using the UXNMR software package was used for NMR experiments; chemical shifts are expressed in δ (ppm) referring to the solvent peaks, δ_H 3.34 and δ_C 49.0 for CD_3OD. ^{13}C-DEPT NMR experiments were performed using a transfer pulse of 135° to obtain positive signals for CH and CH_3 and negative ones for CH_2. Polarization transfer delays were adjusted to an average CH coupling of 135 Hz. ^1H–^1H DQF–COSY, ^1H–^{13}C HSQC, and HMBC experiments were carried out using the conventional pulse sequences as described in the literature. HOHAHA spectra were acquired using a waveform generator-based GAUSS shaped pulse, at mixing times ranging from 80 to 100 ms and a MLEV-17 spin-lock field of 10 kHz preceded by a 2.5 ms trim pulse. HPLC separations were performed on a Shimadzu LC-8A series pumping system equipped with a Waters R401 refractive index detector and with a Waters μ-Bondapak C_{18} column and Shimadzu injector. TLC was conducting on silica 60 F_{254} gel-coated aluminium sheets (Merck).

3.2. Plant material

The flowers of *A. napellus* subsp. *neomontanum* were collected in Val di Peio (Trento, Italy), 1200 m above sea level, during the late summer of 1998. A voucher specimen (no. An-201/2) has been deposited in Dipartimento di Biologia, Università di Milano.

3.3. Extraction and isolation

The air-dried powdered flowers (90 g) of *A. napellus* subsp. *neomontanum* were defatted with *n*-hexane and successively extracted with $CHCl_3$, $CHCl_3$–MeOH (9:1) and MeOH, each solvent for three times to give 1.6, 1.2, 2.0 and 17.0 g of residues, respectively. The methanol extract was chromatographed on Sephadex LH-20, using MeOH as eluent, to obtain one-hundred fractions of 12 ml, combined together into twenty-one groups according to TLC separations [Silica 60F_{254} gel-coated aluminium sheets; eluent: *n*-BuOH–CH_3COOH–H_2O (60:15:25)]. Group 12 was submitted to RP-HPLC on a C_{18} μ-Bondapak column (300 × 7.8 mm, flow rate 2.5 ml min^{-1}) with MeOH–H_2O (40:60) to yield respectively β-3,4-dihydroxyphenethyl β-glucopyranoside (7 mg) (t_R = 5 min), **1** (17 mg) (t_R = 10.8 min), **2** (25 mg) (t_R = 15.3 min), and **3** (19 mg) (t_R = 22.5 min).

3.4. Quercetin 7-O-(6-trans-caffeoyl)-β-glucopyranosyl-(1→3)-α-rhamnopyranoside-3-O-β-glucopyranoside (*1*)

Amorphous orange-yellow powder, mp 185–187°C; $[\alpha]_D^{25}$: −38.3° (*c* 0.1, MeOH); UV: λ_{max} (MeOH) 265, 333 nm; ^1H and ^{13}C NMR spectral data (CD_3OD): Tables 1 and 2; HPLC–MS *m/z*: 935 $[M+H]^+$, 773 [M-(glc) + H]$^+$, 465 [M-(rha + glc + caffeoyl) + H]$^+$, 303 [M-(glc + rha + glc + caffeoyl) + H]$^+$; Found: C, 53.89; H, 4.98; O, 41.13. $C_{42}H_{46}O_{24}$ requires: C, 53.96; H, 4.96; O, 41.08%.

3.5. Kaempferol 7-O-(6-trans-caffeoyl)-β-glucopyranosyl-(1→3)-α-rhamnopyranoside-3-O-β-glucopyranoside (*2*)

Amorphous yellow powder, mp 180–182°C; $[\alpha]_D^{25}$: −84.7° (*c* 0.1, MeOH); UV: λ_{max} (MeOH) 255, 341 nm; ^1H and ^{13}C NMR spectral data (CD_3OD): Tables 1 and 2; HPLC–MS: *m/z* 919 $[M+H]^+$, 757 [M-(glc) + H]$^+$, 449 [M-(rha + glc + caffeoyl) + H]$^+$, 287 [M-(glc + rha + glc + caffeoyl) + H]$^+$; Found: C, 54.84; H, 5.08; O, 40.08. $C_{42}H_{46}O_{23}$ requires: C, 54.90; H, 5.05; O, 40.05%.

3.6. Kaempferol 7-O-(6-trans-p-coumaroyl)-β-glucopyranosyl-(1→3)-α-rhamnopyranoside-3-O-β-glucopyranoside (*3*)

Amorphous yellow powder, mp 175–177°C; $[\alpha]_D^{25}$: −52.0° (*c* 0.1, MeOH); UV: λ_{max} (MeOH) 268, 321 nm; ^1H and ^{13}C NMR spectral data (CD_3OD): Tables 1 and 2; HPLC–MS: *m/z* 903 $[M+H]^+$, 741 [M-(glc) + H]$^+$, 449 [M-(rha + glc + *p*-coumaroyl) + H]$^+$, 287 [M-(glc + rha + glc + *p*-coumaroyl) + H]$^+$; Found: C, 55.82; H, 5.16; O, 39.02. $C_{42}H_{46}O_{22}$ requires: C, 55.88; H, 5.14; O, 38.99%.

References

Agrawal P.K., 1989. Carbon-13 NMR of Flavonoids. Elsevier Science Publishers, Amsterdam, p. 5.

Bisset, N.G., 1981. Arrow poisons in China. Part II. *Aconitum*-botany, chemistry, and pharmacology. J. Ethnopharmacol. 4, 247–336.

Colombo, M.L., Bravin, M., Tomè, F., 1988. A study of the diterpene alkaloids of *Aconitum napellus* ssp. *neomontanum* during its onthogenetic cycle. Pharm. Res. Comm. 20, 123–128.

Fico, G., Braca, A., Bilia, A.R., Tomè, F., Morelli, I., 2000. Flavonol glycosides from the flowers of *Aconitum paniculatum*. J. Nat. Prod. 63, 1563–1565.

Fuente, G., De La Reina, M., Valencia, E., Ojeda, A.R., 1988. The diterpenoid alkaloids from *Aconitum napellus*. Heterocycles 27, 1109–1113.

Jeong, H.J., Whang, W.K., Kim, I.H., 1997. New flavonoids from the aerial parts of *A. chiisanense*. Planta Medica 63, 329–334.

Katz, A., Staehelin, E., 1980. Further investigations pertaining to European Aconites. Planta Medica 39, 209–210.

Kim, D.K., Kwak, J.H., Song, K.W., Kwon, H.C., Zee, O.P., Lee, K.R., 1996. Phytochemical constituens from *A. pseudolaeve* var. *erectum*. Saengyak Hakhoechi 27, 75–79.

Lim, C.E., Park, J.H., Park, C.W., 1999. Flavonoid variation of the *Aconitum jaluense* complex (*Ranunculaceae*) in Korea. Plant Syst. Evol. 218, 125–131.

Liu, H.M., Katz, A., 1996. Norditerpenoid alkaloids from *Aconitum napellus* ssp. *neomontanum*. Planta Medica 62, 190–191.

Shimomura, H., Sashida, Y., Adachi, T., 1987. Phenolic glucosides from *Prunus grayana*. Phytochemistry 26, 249–251.

Wang, W.K., Oh, I.S., Lee, M.T., Kim, I.H., 1994. Flavonoids from the aerial parts of *A. jaluense* for album. Saengyak Hakhoechi 25, 336–341.

PERGAMON

Phytochemistry 57 (2001) 547–551

PHYTOCHEMISTRY

www.elsevier.com/locate/phytochem

Quercetin 3,3′,4′-tri-*O*-β-D-glucopyranosides from leaves of *Eruca sativa* (Mill.)

Bernhard Weckerle [a], Karin Michel [a], Barbara Balázs [b], Peter Schreier [a,*], Gábor Tóth [b]

[a] *Lehrstuhl für Lebensmittelchemie, Universität Würzburg, Am Hubland, D-97074 Würzburg, Germany*
[b] *Technical Analytical Research Group of the Hungarian Academy of Sciences, Institute for General and Analytical Chemistry, Budapest University of Technology and Economics, Szent Gellért tér 4, H-1111 Budapest, Hungary*

Received 4 December 2000; received in revised form 25 January 2001

Dedicated to Professor Dr. Gerhard Eisenbrand's 60th anniversary

Abstract

Three new quercetin 3,3′,4′-tri-*O*-β-D-glucopyranosides isolated from leaves of *Eruca sativa* (Mill.) were identified as quercetin 3,3′,4′-tri-*O*-β-D-glucopyranoside, quercetin 3′-(6-sinapoyl-*O*-β-D-glucopyranosyl)-3,4′-di-*O*-β-D-glucopyranoside, and quercetin 3-(2-sinapoyl-*O*-β-D-glucopyranosyl)-3′-(6-sinapoyl-*O*-β-D-glucopyranosyl)-4′-*O*-β-D-glucopyranoside. The structures were established by one- and two-dimensional ^{1}H and ^{13}C NMR spectra as well as by ESI MS/MS spectra 3 © 2001 Elsevier Science Ltd. All rights reserved.

Keywords: *Eruca sativa* (Mill.); Cruciferae; Rocket salad; Quercetin 3,3′,4′-tri-*O*-β-D-glucopyranosides; Acylated quercetin 3,3′,4′-tri-*O*-β-D-glucopyranosides; Sinapic acid; HPLC-ESI MS; ^{1} H NMR; ^{13}C NMR

1. Introduction

Nowadays the leaves of *Eruca sativa* (Mill.) are widely used as salad or food ingredients. Information about their constituents is surprisingly scarce. Most attention has been focused on seeds of *E. sativ*a, in which thiocyanates, isothiocyanates and their precursors, the glucosinolates, have been extensively studied (Hamence and Taylor, 1978; Adhikari et al., 1989; Mahran et al., 1992). In this paper, we describe the isolation and identification of three novel tri-*O*-β-D-glucosides of quercetin from *E. sativa* (Mill.) leaves. In the last decade, quercetin, which is ubiquitously present in plants in various glycosidically bound forms (Harborne, 1999), has attracted interdisciplinary research activities owing to its potential bioactivity. A number of its activities including cell cycle regulation, interaction with type II estrogen binding sites, and tyrosine kinase inhibition make it a potential anti-cancer agent (Lamson and Brignall, 2000). Its antioxidant properties are also well documented (Duthie et al., 2000; Madsen et al., 2000; O'Reilly et al., 2000). In spite of their β-glycosidic sugar conjugation, quercetin glycosides have been found to be absorbed in humans (Hollman et al., 1999). Interestingly, the sugar moiety affects their bioavailability. According to recent data of Olthof et al. (Olthof et al., 2000), the glucosides are more rapidly absorbed than glycosides. Thus, plants containing glucosidically bound quercetin might be of particular interest in the diet of man.

2. Results and discussion

From a water–methanol extract of leaves of *E. sativa* (Mill.) a glycosidic fraction was obtained by chromatography on Amberlite XAD. The screening for glycosides in the methanolic fraction after Amberlite XAD chromatography was done by HPLC coupled with an evaporative light scattering detector (ELSD) using a RP-18 column. Three major peaks (compounds **1–3**) were obtained at retention times between 12 and 15 min. In addition, the extract was analyzed by HPLC–DAD to check the peaks detected by ELSD for UV activity. This second profile was nearly identical to that achieved by HPLC–ELSD analysis. The UV spectra of compounds **2** and **3** were quite similar: for **1–3** λ_{max}^{MeOH} at 214, 248, 266 and 338 nm, 212, 241, 272 and 330 nm, as well as

* Corresponding author. Tel.: +49-931-888-5481; fax: +49-931-888-5484.
E-mail addresses: schreier@pzlc.uni-wuerzburg.de (P. Schreier), g-toth@chem.bme.hu (G. Tóth).

0031-9422/01/$ - see front matter © 2001 Elsevier Science Ltd. All rights reserved.
PII: S0031-9422(01)00059-0

224, 242, 273 and 330 nm, respectively, were observed. Purification was achieved by reversed phase preparative liquid chromatography yielding **1–3** in pure forms.

The fraction obtained by chromatography on Amberlite XAD as well as the purified compounds **1–3** were then analysed by HPLC–ESI–MS/MS (positive mode) to get structural information. The spectral data are outlined in Table 1. The data reveal that compound **1** is a triglycoside (loss of three hexose residues) of an aglycone with a molecular mass of 302 and that compounds **2** and **3** contain the same aglycone as well as at least two hexose substructures. In addition, the ESI–MS/MS spectra of **2** and **3** showed an intense fragment with m/z 207, indicating a further substructural unit. Moreover, the spectra exhibited quasimolecular ions $[M+H]^+$ at m/z 789, 995 and 1201 for compounds **1–3**, respectively.

The IR spectra gave additional information about the substructures of compounds **2** and **3**. The three isolated glycosides showed intense IR signals at 3400 cm^{-1} (O–H) and at 1645 cm^{-1} (α,β-unsaturated C=O), indicating a flavonol-like structure such as quercetin (Li et al., 1998). The additional signals at 1700 cm^{-1} for compound **2** as well as at 1680 and 1700 cm^{-1} for compound **3** indicated the presence of conjugated ester moieties in the molecules.

Finally, structural evaluation was performed by a number of NMR experiments. The structures of **1–3** (Fig. 1) were determined by 1D and 2D NMR studies using DEPT, sel-COSY, sel-TOCSY (Stott et al., 1995), HSQC and HMBC techniques including gradient selection and linear prediction. Due to severe signal overlap even at 600 MHz, we achieved a complete assignment not only for the carbon but also for the proton signals.

The ^1H and ^{13}C chemical shifts and characteristic HMBC connectivities of compounds **1–3** are summarized in Table 2. In the low-field part of the ^1H NMR spectrum of **1** two different spin systems were identified, one pair of doublets at 6.44 (1H, *d*, $J_{meta}=2.0$ Hz) and 6.21 (1H, *d*, $J_{meta}=2.0$ Hz), respectively, indicating one 1,2,3,5-tetra-substituted (mainly with oxygen functions) aromatic ring. The signal at 8.08 (1H, *d*, $J_{meta}=2.2$ Hz), 7.89 (1H, *dd*) and 7.37 (1H, *d*, $J_{ortho}=8.6$ Hz), respectively, form a separate spin system indicating the presence of an 1,2,4-tri-substituted aromatic ring. The upfield part of the spectrum exhibits three separated doublets 5.28 (1H, *d*, 7.6 Hz), 5.02 (1H, *d*, 7.6 Hz) and 4.99 (1H, *d*, 7.3 Hz), respectively, and further signals in the range 3.95–3.15 (18H, *m*) in strong overlapping. For assignment of these signals the selective 1D TOCSY (Stott et al., 1995) measurements proved to be the method of choice allowing the complete analysis of the sugar signals and identification of three β-glucose moieties. The ^{13}C NMR signals of the aglycone (180–94 ppm) consist of 15 peaks, corresponding to 5 sp^2 methines, 9 quaternary sp^2 C atoms and 1 conjugated C=O group (179.6), respectively. A comparison of the ^{13}C chemical shift of **1** (Table 2) with literature data of flavonol glycosides (Breitmaier and Voelter, 1987) strongly supports the presence of quercetin as aglycone.

The connectivities of the monosaccharide units were established on the basis of HMBC cross peaks (Table 2) indicating long-range ^{13}C–^1H couplings. The anomeric proton with the largest chemical shift (C1: $\delta=5.28$) correlates with C-3 (136.2). The B1 anomeric proton ($\delta=5.02$) gives a strong cross-peak with C-4′ signal (151.8), whereas the HMBC response between A1 (4.99)

Table 1
Main fragments of ESI mass spectra (achieved in MS/MS positive ion mode with Argon as collision gas) of **1–3**

m/z	Compound **1** exact mass 788.20	Compound **2** exact mass 994.26	Compound **3** exact mass 1200.32
1201	ø	ø	$[M^a+H]^+$
1039	ø	ø	$[M^a\text{-}G^b+H]^+$
995	ø	$[M^a+H]^+$	–
789	$[M^a+H]^+$	–	–
671	–	$[M^a-2\times G^b+H]^+$	$[M^a-2\times G^b-S^d+H]^+$
627	$[M^a-1\times G^b+H]^+$	–	–
465	$[M^a-2\times G^b+H]^+$ –	–	–
369	–	–	$[G^b+S^d+H]^+$
303	$[A^c+H]^+$	$[A^c+H]^+$	$[A^c+H]^+$
207	–	$[S^d+H]^+$	$[S^d+H]^+$
163	$[G^b+H]^+$	$[G^b+H]^+$	$[G^b+H]^+$

[a] M = total molecule.
[b] G = glucose less H_2O.
[c] A = aglycone (quercetin).
[d] S = sinapic acid less H_2O.

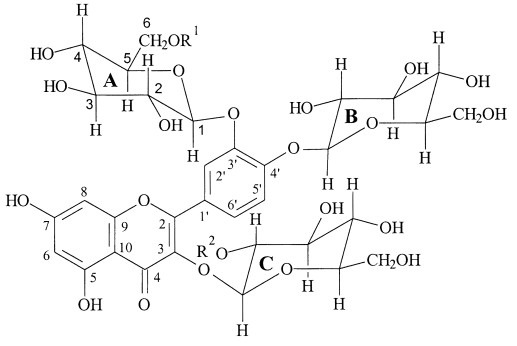

	1	2	3
R^1	H	Q	Q
R^2	H	H	Q*

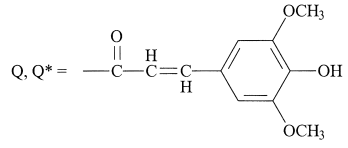

Fig. 1. Structures of compounds **1–3**.

Table 2
^{1}H and ^{13}C NMR chemical shifts and characteristic HMBC connectivities of **1–3**

	1			**2**			**3**		
	^{1}H	^{13}C	HMBC	^{1}H	^{13}C	HMBC	^{1}H	^{13}C	HMBC
2		157.8			156.7			155.6	
3		136.2			136.4			136.2	
4		179.6			179.2			178.6	
5		158.6			158.0			157.7	
6	6.44	94.9	C-5, C-8, C-10	6.28	94.8	C-5, C-7, C-8	6.09	94.6	C-5, C-8, C-10
7		166.1			166.0			165.6	
8	6.21	100.0	C-6, C-7, C-9, C-10	6.10	100.0	C-6, C-9	5.96	99.8	C-6, C-9, C-10
9		163.1			162.8			162.7	
10		105.9			106.3			105.9	
1′		126.9			126.5			126.7	
2′	8.08	122.5	C-2, C-3′, C-4′, C-6′	8.11	122.9	C-2, C-3′, C-4′, C-6′	8.08	120.8	C-2, C-3′, C-4′, C-6′
3′		148.3			147.6			148.3	
4′		151.8			151.8			150.9	
5′	7.37	119.0	C-1′, C-3′, C-4′	7.33	118.6	C-1′, C-3′,C-4′	7.31	119.1	C-1′, C-3′,C-4′
6′	7.89	126.8	C-4′	7.94	126.7	C-2, C-2′,C-4′	7.73	125.8	C-2, C-2′,C-4′
A1	4.99	104.6	C-3′	4.91	103.8	C-3′	4.98	103.4	C-3′
A2	3.55	75.2		3.58	74.9		3.60	75.0	
A3	3.52	77.7		3.53	77.9		3.58	77.9	
A4	3.41	71.3		3.39	72.2		3.38	72.4	
A5	3.41	78.4		3.68	75.9		3.86	75.9	
A6a	3.90	62.5		4.51	64.8	Q-CO	4.79	64.7	Q-CO
A6b	3.74			4.43		Q-CO	4.18		A5
B1	5.02	103.3	C-4′	5.03	102.9	C-4′	5.04	103.1	C-4′
B2	3.56	75.0		3.56	74.9	B1	3.57	74.9	
B3	3.50	77.0		3.50	77.7	B2, B4	3.50	77.8	
B4	3.42	71.3		3.41	71.3		3.44	71.3	
B5	3.45	78.4		3.47	78.4		3.44	78.4	
B6a	3.91	62.5		3.90	62.5		3.90	62.5	
B6b	3.72			3.72				3.73	
C1	5.28	104.0	C-3	5.17	104.3	C-3	5.72	100.2	C-3
C2	3.48	75.6		3.47	75.8		4.85	76.5	C1, Q*-CO
C3	3.41	78.0		3.40	77.7		3.54	76.5	
C4	3.32	71.3		3.32	71.3		3.42	71.5	
C5	3.19	78.4		3.17	78.4		3.38	79.1	
C6a	3.67	62.5		3.66	62.5		3.85	62.5	
C6b	3.52			3.52			3.71		
Q-CO				169.0				168.7	
Q-α				6.07	115.4	126.1	6.10	115.6	Q-1
Q-β				7.31	147.1	Q-α, Q-2,6, Q-CO	7.29	146.7	Q-α, Q-2,6,Q-CO
Q-1					126.1			126.1	
Q-2,6				6.47	106.3	Q-1; Q-4; Q-β;Q-3,5	6.42	106.2	Q-β, Q-1,Q-2,6, Q-3,5,Q-4
Q-3,5								148.9	
Q-4					139.4			139.2	
Q-3,5-OMe				3.72	56.6		3.72	56.5	Q-3,5
Q*-CO								167.7	
Q*-α							6.08	115.3	Q*-1
Q*-β							7.38	147.3	Q*-α, Q*-2,6, Q*-CO
Q*-1								126.5	
Q*-2,6							6.72	106.8	Q*-β; Q*-1; Q*-2,6; Q*-3,5,Q*-4;
Q*-3,5								149.3	
Q*-4								139.5	
Q*-3,5-OMe							3.85	56.8	Q*-3,5

and C-3′ (148.3) proves the position of the attached sugar unit.

In the ^{1}H and ^{13}C NMR spectra of **2** and **3** similar chemical shifts were observed accompanied with additional signals corresponding to one and two sinapoyl substituents, respectively. The high value of the coupling constants ($J_{H\text{-}\alpha,H\text{-}\beta} = 15.9$ Hz) proves the E-configuration of the double bond of sinapoyl substituents. The chemical shifts of the carbohydrate protons exhibit a strong deshielding where the sinapoyl moieties are attached. In this respect the straightforward assignment and differentiation of the three sugar units is also very important. The series of selective 1D TOCSY spectra of **2** measured with different mixing times prove that the above mentioned downfield-shift appeared at the methylene protons A6a and A6b. Strong HMBC cross-peaks were observed between these protons and the ester C=O carbon atom unambiguously proving the site of the sinapoyl substituents.

In conclusion, three new quercetin 3,3′,4′-tri-*O*-β-D-glycopyranosides were isolated from leaves of *E. sativa* (Mill.), i.e. quercetin 3,3′,4′-tri-*O*-β-D-glucopyranoside (**1**), quercetin 3′-(6-sinapoyl-*O*-β-D-glucopyranosyl)-3,4′-di-*O*-β-D-glucopyranoside (**2**) and quercetin 3-(2-sinapoyl-*O*-β-D-glucopyranosyl)-3′-(6-sinapoyl-*O*-β-D-glucopyranosyl)-4′-*O*-β-D-glucopyranoside. The flavonol tri-*O*-β-glucosides **1–3** show an uncommon sugar substitution pattern; a flavonol glycoside with this substitution pattern (rhamnetin 3,3′,4′-tri-*O*-glucoside) has been reported previously from *Pyrola chlazantha* and *P. vizeus* (Pyrolaceae) (Averett and Bohm, 1986). Also acylation at position 2 of glucose in compound **3** is uncommon; mainly, acylated flavonol glycosides show a linkage between the acid and the sugar at position 6 of the sugar moiety (Ferreres et al., 1995).

3. Experimental

3.1. Extraction and isolation

Fresh leaves of *E. sativa* (Mill.) (500 g; origin Italy, cultivar not specified; obtained by a local wholesaler) were homogenized in a Waring blender with 1250 ml of a methanol-water mixture (7:3 v/v). After maceration for 24 h at room temperature, the homogenate was filtered, the filtrate concentrated under reduced pressure to approximately 50 ml, and rediluted with water to approximately 500 ml. The aqueous extract was applied onto a glass column (8×75 cm) filled with Amberlite® XAD-2 (Supelco, Bellefonte, USA). After washing with water (1 l) and subsequently with diethyl ether (1 l) the glycosides were eluted with methanol (1.5 l). The glycosidic eluate was concentrated under reduced pressure and the residue lyophilized to yield 1.1 g dry powder. The lyophilsate was redissolved in 5 ml of water. Fractionation was done by LC on a RP-18 column (2.5× 20 cm; LiChrospher®, Merck, Darmstadt, Germany) using a methanol-water gradient starting with 100% water (100 ml) and increasing the proportion of methanol in steps of 10% (each step 100 ml) to end up with 100% methanol. Seven ml-fractions were collected and analysed by HPLC-ELSD. Fractions of the same composition were combined, concentrated under reduced pressure and lyophilized. In fractions 48–52, 61–62 and 67–68 pure compounds **1–3** were obtained in yields of 25, 15, and 12 mg, respectively.

3.2. NMR spectroscopy

NMR spectra were recorded in CD_3OD using a Bruker Avance DRX-600 spectrometer. Chemical shifts are given on the δ-scale and were referenced to TMS. In the 1D and 2D NMR experiments pulse programs were taken from the Bruker software library.

3.3. IR spectroscopy

IR spectra (KBr) were recorded on a Perkin Elmer IR spectrophotometer (model 1310).

3.4. HPLC–DAD

HPLC–DAD analysis was performed with a Hewlett Packard gradient pump (series 1100) and a Hewlett Packard photodiode array detector (series 1100) including Hewlett Packard software. UV spectra were monitored from 190 to 480 nm in steps of 1 nm. HPLC was carried out on an Eurospher 100 C-18 column (250×4.6 mm I.D., 5 μm) (Knauer) with a water (0.05% TFA)-acetonitrile linear gradient at a flow rate of 1.0 ml min^{-1} from 5 to 100% acetonitrile in 30 min.

3.5. HPLC–ELSD

HPLC–ELSD analysis was performed with a Knauer HPLC Maxi Star including Eurochrom 2000 software and a Sedere Evaporative Light Scattering Detector (ELSD, model Sedex 55). The temperature of the detector was set to 40°C and compressed air was used at a pressure of 240 kPa. HPLC was carried out as described above.

3.6. HPLC–ESI MS

Mass spectrometry was performed on a Finnigan triple-stage quadrupole TSQ 7000 HPLC-MS/MS system (Finnigan MAT, Bremen, Germany) with electrospray ionization (ESI) as interface in positive mode. For HPLC, an Applied Biosystems (Foster City, CA, USA) Model 140B pump was used. For ESI in the positive ion mode the spray capillary voltage was set to 4 kV and the

temperature of the heated inlet capillary was set to 230°C. Nitrogen served both as sheath gas (482 MPa) and as auxiliary gas. HPLC was carried out on an Eurospher 100 C-18 column (100×2 mm I.D., 5 μm) (Knauer) with a water (0.05% TFA) — acetonitrile linear gradient at a flow rate of 0.2 ml min^{-1} from 5 to 100% acetonitrile in 30 min. Positive ions were detected scanning from m/z 200 to 1500 with a total scan duration of 1.0 s. The MS/MS experiments were performed at a collision energy of −15 to −25 eV with Argon (0.24 Pa) serving as collision gas, scanning a mass range from m/z 20 to 1250.

3.7. Elemental analysis

The data for compounds **1**, **2** and **3** are as follows: compound **1** (found: C, 50.4; H, 5.2. $C_{33}H_{40}O_{22}$ requires: C, 50.3; H, 5.1%). Compound **2** (found: C, 53.3; H 5.1. $C_{44}H_{50}O_{26}$ requires: C, 53.1; H, 5.1%). Compound **3** (found: C, 55.2; H, 5.1. $C_{55}H_{60}O_{30}$ requires: C, 55.0; H, 5.0%).

Acknowledgements

G.T. thanks the Hungarian Scientific Research Foundation (OTKA No. T026264) for financial support and the A. v. Humboldt Foundation for a visiting grant (July 2000, University of Würzburg). The Fonds der Chemischen Industrie, Frankfurt, is thanked for financial support.

References

Adhikari, J., Adhikari, S., Achaya, A.T., 1989. Glucosinolates in the seeds of Indian brassicas and *Eruca sativa*. J. Oil Technol. Assoc. India 21, 13–14.

Averett, S.E., Bohm, B.A., 1986. Eight flavonol glycosides in *Pyrola* (Pyrolaceae). Phytochemistry 25, 1995–1996.

Breitmaier, E., Voelter, W., 1987. Carbon-13 NMR Spectroscopy. VCH Verlag, Weinheim pp. 452–453.

Duthie, G.G., Duthie, S.J., Kyle, J.A.M., 2000. Plant polyphenols in cancer and heart disease: implications as nutritional antioxidants. Nutrition Res. Rev. 13, 79–106.

Ferreres, F., Esteban, E., Carpena-Ruiz, R., Jimenez, M.A., Tomás-Barberán, F.A., 1995. Acylated flavonol sophorotriosides from pea shoots. Phytochemistry 39, 1443–1446.

Hamence, J.H., Taylor, D., 1978. The composition of rapeseed meals, part I: the determination of the isothiocyanate present in *Eruca sativa*, a cruciferous seed, present in some rapeseed meals. J. Assoc. Publ. Anal. 16, 49–57.

Harborne, J.B., 1999. Handbook of Natural Flavonoids. Wiley, Summerset, New York.

Hollman, P.C.H., Bijsman, M., van Gemeren, Y., Cnossen, E., de Vries, J.H.M., Katan, M.B., 1999. The sugar moiety is a major determinant of the absorption of dietary flavanoid glycosides in man. Free Radical Res. 31, 569–573.

Lamson, D.W., Brignall, M.S., 2000. Antioxidants and cancer, part 3: quercetin. Altern. Med. Rev. 5, 196–208.

Li, W., Chan, C., Leung, H., Yeung, H., Xiao, P., 1998. Xanthones and flavonoids of *Polygala caudate*. Pharm. Pharmacol. Commun. 4, 415–417.

Madsen, H.L., Anderson, C.M., Jorgensen, L.V., Skibsted, L.H., 2000. Radical scavenging by dietary flavonoids. A kinetic study of antioxidant efficiencies. Eur. Food Res. Technol. 211, 240–246.

Mahran, G.H., Kadry, H.A., Thabet, C.K., Olemy, M.M., Al-Azizi, M.M., Schiff, P.L., Wong, L.K., 1992. GC/MS Analysis of volatile oil from *Eruca sativa* seeds. Int. J. Pharmacognoscy 30, 135–137.

Olthof, M.R., Hollman, P.C.H., Vree, T.B., Katan, M.B., 2000. Bioavailabilities of quercetin-3-glucoside and quercetin-4′-glucoside do not differ in humans. J. Nutrition 130, 1200–1203.

O'Reilly, J.D., Sanders, T.A.B., Wiseman, H., 2000. Flavonoids protect against oxidative damage to LDL in vitro: use in selection of a flavanoid rich diet and relevance to LDL oxidation resistance ex vivo? Free Radical Res. 33, 419–426.

Stott, K., Stonehouse, J., Keeler, J., Hwang, T.L., Shaka, A.J., 1995. Excitation sculpting in high-resolution nuclear magnetic resonance spectroscopy: application to selective NOE experiments. J. Am. Chem. Soc. 117, 4199–4200.

PERGAMON

Phytochemistry 57 (2001) 553–557

PHYTOCHEMISTRY

www.elsevier.com/locate/phytochem

Natural and synthetic benzophenones: interaction with the cytosolic binding domain of P-glycoprotein

Sandrine Rancon[a], Annie Chaboud[a,b], Nicole Darbour[a,b], Gilles Comte[b], Christine Bayet[b], Pierre-Noël Simon[a,b], Jean Raynaud[a], Attilio Di Pietro[c], Pierre Cabalion[d], Denis Barron[b,*]

[a]*Laboratory of Pharmacognosy, Faculty of Pharmacy, 8 Avenue Rockefeller, 69373 Lyon Cedex 08, France*
[b]*Natural Products Laboratory, Claude Bernard University of Lyon, 43 Boulevard du 11 novembre 1918, 69622 Villeurbanne Cedex, France*
[c]*Institut de Biologie et Chimie des Protéines, CNRS-UMR 5086, 7 Passage du Vercors, 69367 Lyon Cedex 07, France*
[d]*ORSTOM, UR 4G, Département Santé, 213 rue Lafayette, 75010 Paris, France*

Received 24 November 2000; received in revised form 5 March 2001

Abstract

A benzophenone glycoside has been isolated from *Davallia solida*. Its structure was elucidated by chemical and spectral means as 4-*O*-β-D-glucopyranosyl-2,6,4′-trihydroxybenzophenone. It bound with moderate affinity to the purified C-terminal cytosolic domain of P-glycoprotein, but the binding affinity was 6- to 10-fold increased for its aglycone derivative and other related benzophenones. © 2001 Elsevier Science Ltd. All rights reserved.

Keywords: *Davallia solida*; Davalliaceae; Benzophenones; P-Glycoprotein; Drug resistance

1. Introduction

Resistance of neoplasic cells towards chemotherapeutic agents is a major obstacle in clinical cancer treatment. A large number of cancer cells are intrinsically resistant to chemotherapy, while others initially respond to treatment but progressively acquire resistance to the drugs used as well as to other drugs. The best studied mechanism of drug resistance is the overexpression of the *MDR*1 gene product P-glycoprotein (P-gp) that rejects chemotherapeutic drugs out of the cell, using ATP hydrolysis as an energetic source. (Gottesman et al., 1993; Gros and Buschmann, 1993). P-gp is composed of two homologous halves, each comprising a membrane domain, and a cytosolic domain. The site of ATP binding is present on the cytosolic domain. Among the various classes of plant secondary metabolites, flavonoid compounds have been reported as modulators of P-gp (Critchfield et al., 1994; Shapiro and Ling, 1997; Comte et al., 2001). They are able to interact with P-gp cytosolic moiety through binding to both steroid- and ATP-binding sites within NBD2, the C-terminal cytoplasmic domain of mouse P-glycoprotein (Conseil et al., 1998). On a structural point of view, the presence of the 4-carbonyl and of the 3- and/or the 5-hydroxyl groups are required for ATP mimicry. Xanthones, which are structurally related to flavonoids through the presence of a 9-carbonyl and of 1- and 8-hydroxyls, have been demonstrated to interact with NBD2 as well (Noungoué-Tchamo et al., 2000). In a previous work, mangiferin and a *C*-pentosyl xanthone have been found in *Davallia solida* (Rancon et al., 1999). The present study is oriented to the isolation of benzophenones, which are biosynthetic precursors of xanthones (Bennett and Lee, 1989), from the same plant species. In addition, most naturally occurring benzophenones possess the structural requirement (7-carbonyl plus 2-hydroxyl) for interaction with ATP-binding sites. Therefore benzophenones can be regarded as potential P-gp modulators. In this paper the isolation and the identification from *Davallia solida* of a new *O*-glucosyl benzophenone **1** is described. The results of the NBD2 interactions with compound **1**, its corresponding aglycone **2**, and three

* Corresponding author. Tel.: +33-472-431-421; fax: +33-472-431-557.
E-mail address: denis.barron@univ-lyon1.fr (D. Barron).

0031-9422/01/$ - see front matter © 2001 Elsevier Science Ltd. All rights reserved.
PII: S0031-9422(01)00120-0

other related benzophenones **3–5** are presented for the first time and discussed.

2. Results and discussion

Air dried rhizomes were sequentially extracted with solvents of increasing polarities as previously described (Rancon et al., 1999). The butanolic extract was submitted to a combination of chromatography techniques (gel filtration on Sephadex® LH-20, preparative TLC on cellulose, and finally column chromatography on RP-18) leading to the isolation of 4-*O*-β-D-glucopyranosyl-2,6,4′-trihydroxybenzophenone **1**.

The FAB–MS spectrum showed quasi-molecular ion peaks at $m/z = 431$ $[M+Na]^+$ and $m/z = 409$ $[M+H]^+$. The molecular formula $C_{19}H_{20}O_{10}$ was established on the basis of both NMR and MS data and confirmed by HR–MS experiments on the ion peak at m/z 431 $[M+Na]^+$ (see Experimental).

The presence of a sugar moiety was shown on the positive FAB–MS spectrum by the ion peak at m/z 247 $[M–Glc+H]^+$ and confirmed in the NMR data by signals noted in the ranges 3.00–5.00 ppm and 60.0–80.0 ppm in ^1H and ^{13}C NMR spectra, respectively. β-D-Gluco pyranose was identified on the basis of its ^1H and ^{13}C NMR data (Agraval, 1989, 1992; Breitmaier and Voelter, 1989) and after acidic hydrolysis. The glycosidic chaining was furthermore unambiguously confirmed by 2D NMR COSY, HSQC and HMBC experiments. Chemical shifts of both C-1″ at δ 100.7 and H-1″ at δ 4.87 showed the *O*-linkage between the sugar moiety and the aglycone part.

The ^{13}C NMR spectrum also indicated shielded aromatic methines at δ 95.9 (C-3), δ 98.1 (C-5), δ 133.2 (C-2′ and C-6′) and δ 115.2 (C-3′ and C-5′) typical of phenolic natural compounds. Among the quaternary carbon atom signals, 4 corresponded to *O*-linked aromatic carbons (145–165 ppm), while the signal noted at δ 197.7 showed the presence of a carbonyl group (Breitmaier and Voelter, 1989).

Moreover, the use of 1D NMR spectra together with 2D NMR correlation maps showed the presence of a *para*-disubstituted aromatic ring together with a phloroglucinol-type one.

The linkage between the glucosyl moiety and the genine was unambiguously demonstrated by the correlation noted between H-1″ (δ 4.87) and C-4 (δ 159.7) in the 2D NMR ^1H–^{13}C HMBC experiment. UV spectra in methanol and classical reagents, which were characteristic of a phenolic compound substituted by hydroxyl with neighbouring ketone and free hydroxyl groups, corroborate the product to be a benzophenone. Finally, acidic hydrolysis of **1** yielded, besides glucose, an aglycone the chromatographic behaviour of which was identical to that of synthetic 2,4,6,4′-tetrahydroxybenzophenone **2**. Compound **1** was thus identified to 4-*O*-β-D-glucopyranosyl-2,6,4′-trihydroxybenzophenone, a new natural product.

Table 1
NMR data for the benzophenone **1** at 75.48 MHz (^{13}C) and 300.13 MHz (^1H) in D_2O

Position	^1H	^{13}C/HSQC	HMBC
1		110.2	
2		156.3	
3	6.27 *br s*	95.9	C-1; C-3; C-4; C-5
4		159.7	
5	6.14 *br s*	98.1	
6		156.5	
7		197.7	
1′		130.5	
2′/6′	7.66 *d* (6.7)	133.2	C-2′/6′; C-4′; C-7
3′/5′	6.82 *d* (6.7)	115.8	
4′		162.0	
1″	4.87 *d* (7.7)	100.7	C-4
2″	3.11 *dd* (7.7; 9.4)	73.0	C-1″; C-3″
3″	3.41 *t* (9.4)	75.8	C-2″; C-4″
4″	3.28 *t* (9.2)	69.6	C-3″; C-5″; C-6″
5″	ca 3.45 *m*	76.4	
6″	3.61 *dd* (4.8; 12.0) 3.77 *br d* (12.0)	60.9	C-5″

The naturally occurring benzophenone glucoside **1**, its acidic-hydrolysis product **2** and commercial or synthetic benzophenone aglycones **3–5**, were later assayed for their affinity towards P-gp. Our study, however, was not carried out on the whole transporter for three main reasons: (1) the low availability of purified whole transporter; (2) the difficulty to get the fully-active transporter after using denaturating detergent; and (3) the lack of efficient overexpressing system. Alternatively, interaction of ligands can be studied with recombinant cytosolic domains containing the ATP binding sites, after overexpression in bacteria and purification. The recombinant protein is highly soluble and can be easily purified by affinity chromatography when fused to a hexahistidine tag. Our work was carried out on nucleotide binding domain 2 (NBD2), one of the two cytosolic domains from mouse P-gp. The domain contains a tryptophan residue and is appropriate for monitoring interactions by recording changes in intrinsic fluorescence, from the analysis of which apparent K_D values can be derived, as described previously for flavonoids (Conseil et al., 1998). Table 2 shows that glycosylated derivative **1** bound 6-fold less strongly ($K_D = 12.75 \pm 1.72$) than its aglycone **2** ($K_D = 2.19 \pm 0.72$). Methylation of the 4′-hydroxyl group as in synthetic benzophenone **3** further slightly increased the apparent affinity for quenching ($K_D = 1.27 \pm 0.59$ μM) as compared with **2** ($K_D = 2.19 \pm 0.72$ μM). The similar affinities displayed by compounds **3** and **4** suggest that the 6-hydroxyl group plays a minor, if any, role in the interaction, and that the absence of B-ring substitution is still more

Table 2
Role of benzophenone substituents on the affinity for NBD2

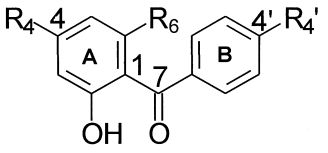

Benzophenones	Substituents				
	R_6	R_4	$R_{4'}$	ΔF_{max} (%)	Apparent K_D (μM)
1	OH	O-glc	OH	32.27±1.88	12.75±1.72
2	OH	OH	OH	30.30±3.41	2.19±0.72
3	OH	OH	OCH_3	19.57±2.53	1.27±0.59
4	H	OH	H	17.12±1.44	1.15±0.36
5	H	OCH_3	H	35.0±2.70	3.12±0.61

advantageous than the presence of a polar 4′-hydroxyl. Finally, methylation of the 4-hydroxyl in **5** produced a rather negative effect as compared to benzophenone **4**. Similar effects have been obtained in the past with flavonoid series (Conseil et al., 1998), i.e. increased affinity with compounds having non polar B-ring (either unsubstituted or 4′-methoxy-substituted, such as galangin or kaempferide compared to kaempferol), and decreased affinity in the case of glycosides (such as rutin compared to quercetin). However, the affinities obtained here for benzophenones were higher than those of flavonoids. On the contrary, the maximal fluorescence quenching values, ΔF_{max}, were rather small as compared to flavonoids, indicating a different modification of the tryptophan environment. This might reflect a different positioning within, or overlapping of, the binding site when comparing benzophenones and flavonoids.

Benzophenone derivatives are of common use in photolabelling of proteins (Andrus et al., 2000; Dorman and Prestwich, 1994; Fleming, 1995). Upon UV irradiation, they are able to couple with a wide range of protein regions, including hydrophobic ones, through a radical mechanism. Taking into account the fact that (i) information is lacking about the structures of the binding sites of P-gp, (ii) the NBD2 domain indeed contains a hydrophobic interacting region, and (iii) our previous labelling attempts using radioactive azido flavones have failed (De Wet et al., 2001), the possibility to use benzophenone derivatives directly as photolabelling probes for P-gp is open now.

3. Experimental

3.1. General

Prep. TLC was carried out on cellulose Macherey Nagel 301 plates. Gel filtration was performed on Sephadex® LH-20 (850×75 mm). LPLC was carried out on a Lobar® (310×250 mm) Lichrosorb RP 18 40-63 μm column.

NMR spectra were recorded using a 300.13 MHz (^{1}H) or a 75.48 MHz (^{13}C) apparatus. The solvent signal was used as internal reference. Complete proton and carbon assignments were based on 1D ^{1}H and ^{13}C, 2D ^{1}H–^{1}H COSY, ^{1}H–^{13}C HSQC and ^{1}H–^{13}C HMBC experiments. Anhydrous phloroglucinol, 2,4-dihydroxy- and 2-hydroxy-4-methoxybenzophenones were purchased from Lancaster (Strasbourg, France). 4-Hydroxy- and 4-methoxybenzonitriles were from Aldrich (St Quentin Fallavier, France).

3.2. Plant material

Davallia solida (Forst.) Swartz was collected and identified by Dr. Pierre Cabalion. A specimen is deposited at the Pharmacognosy department (Laboratory of Pharmacognosy, Faculty of Pharmacy, 8 Avenue Rockfeller, 69373 Lyon Cedex 08, France).

3.3. Extraction and isolation

The extraction and fractionation have been described (Rancon et al., 1999). The *n*-BuOH layer was chromatographed on Sephadex LH-20 using MeOH as mobile phase: 5 fractions (85 ml) were collected. The first one was purified by prep. cellulose TLC using aq. AcOH 15% as solvent (R_f 0,93). Final separation was carried out on a reverse phase LOBAR column using aq. MeOH (linear gradient) as solvent. The fraction eluted with 30% aq. MeOH afforded 27 mg of pure benzophenone **1**.

3.3.1. 4-O-β-D-Glucopyranosyl-2,6,4′-trihydroxybenzophenone *1*

UV λ MeOH nm: 221, 288; +$AlCl_3$: 248, 305, 365; +$AlCl_3$+HCl: 221, 296, 345; +NaOH: 245, 328, 361; +NaOAc: 225, 291, 339; FAB$^+$MS (thioglycerol) (*m*/*z*): 431 $[M+Na]^+$, 409 $[M+H]^+$, 247 $[M–Glc+H]^+$; HRMS (FAB): Calculated for $C_{19}H_{20}O_{10}$•Na^+: 431.0954. Found: 431.0954; NMR data : see Table 1.

3.3.2. Synthesis of 2,4,6,4′-tetrahydroxybenzophenone *2*

Nine grams (71 mmol) of anhydrous phloroglucinol were dissolved in dry Et_2O. To this solution were added 2.0 g (14.7 mmol; 0.2 eq.) of powdered fused $ZnCl_2$, followed by 10.0 g (83.9 mmol; 1.2 eq.) of 4-hydroxybenzonitrile. The medium was cooled to 4°C (ice bath) and saturated with HCl gas (prepared by the addition of 200 ml conc. hydrochloric acid to 200 ml conc. H_2SO_4). After 24 h at 4°C, the ether supernatant was decanted from the oily residue which deposited at the bottom of the flask. The oil was dissolved in 150 ml

H_2O (warm) and the solution was refluxed for 24 h. Filtration and cooling of the aqueous solution led to the crystallisation of 0.92 g of 2,4,6,4′-trihydroxybenzo phenone as white crystals. ^{1}H NMR (300 MHz, acetone-d_6): δ 5.99 (2H, *s*, H-3/5), 6.86 (2H, *d*, $J=8.7$ Hz, H-3′/5′), 7.62 (2H, *d*, $J=8.7$ Hz, H-2′/6′), 9.14 (2H, *brs*, OH-4/4′), 10.22 (2H, *brs*, OH-2/6). ^{13}C NMR (75.5 MHz, acetone-d_6): δ 96.9 (C-3/5), 106.6 (C-1), 116.1 (C-3′/5′), 133.4 (C-2′/6′), 134.4 (C-1′), 162.8 (C-4′), 164.0 (C-2/6), 164.6 (C-4), 198.9 (C-7).

3.3.3. Synthesis of 2,4,6-trihydroxy-4′-methoxybenzophenone **3**

Similar reaction of 4.0 g (31.7 mmol) of anhydrous phloroglucinol, 0.8 g (5.9 mmol; 0.2 eq.) of powdered fused $ZnCl_2$ and 5.0 g (37.6 mmol; 1.2 eq.) of 4-methoxybenzonitrile in dry Et_2O yielded 1.5 g of 2,4,6-trihydroxy-4′-methoxybenzophenone as white crystals. ^{1}H NMR (300 MHz, acetone-d_6): δ 3.88 (3H, *s*, OMe-4′), 5.99 (2H, *s*, H-3/5), 6.96 (2H, *d*, $J=8.9$ Hz, H-3′/5′), 7.68 (2H, *d*, $J=8.9$ Hz, H-2′/6′), 9.20 (1H, *s*, OH-4), 10.29 (2H, *s*, OH-2/6). ^{13}C NMR (75.5 MHz, acetone-d_6): δ 56.8 (OMe-4′), 96.9 (C-3/5), 106.5 (C-1), 114.6 (C-3′/5′), 133.0 (C-2′/6′), 135.5 (C-1′), 164.2 (C-2/6), 164.5 (C-4′), 165.8 (C-4), 199.1 (C-7).

3.4. Biological assays

The recombinant C-terminal cytosolic domain of P-pg, H_6–NBD2 was overexpressed and purified as described previously (Conseil et al., 1998). Fluorescence experiments were performed at 25.0 ± 0.1°C using a SLM-Aminco 8000C spectrofluorimeter with spectral bandwidths of 2 and 4 nm, respectively, for excitation and emission. H_6–NBD2 was diluted in 1.2 ml of dialysis buffer at pH 6.8, containing 20 mM potassium phosphate, 0.5 M NaCl, 20% glycerol, and 0.01% methyl-6-*O*-(*N*-heptylcarbamoyl)-α-D-glycopyranoside, in the presence of increasing concentrations of dimethyl sulfoxide solutions of the products. Tryptophan-intrinsic fluorescence of H_6–NBD2 was studied by scanning emission in the 310–360 nm range upon excitation at 295 nm, and integrating the spectrum area. The binding of the product was monitored by quenching of emission fluorescence produced by addition of increasing ligand concentrations. Corrections for inner-filter effect and dimethyl sulfoxide were determined under the same conditions by using *N*-acetyltryptophanamide. Curve fitting of ligand binding related to fluorescence decrease was performed with the Grafit program (Erithacus software) as previously described (Divita et al.,1993). Two main parameters of the binding were determined from the fitting: the maximal quenching of fluorescence (as the difference between starting maximal fluorescence and final minimal fluorescence), and the apparent dissociation constant, $K_D \pm$ S.D.

Acknowledgements

The Ligue Nationale contre le Cancer, Comité Départemental du Rhône and Dr. Florence Baltassat are acknowledged for financial support.

References

Agraval, P.K., 1989. Carbon-13 NMR of Flavonoids. Elsevier, Amsterdam.

Agraval, P.K., 1992. NMR spectroscopy in the structural elucidation of oligosaccharides and glycosides. Phytochemistry 31, 3307–3330.

Andrus, M.B., Turner, T.M., Sauna, Z.E., Ambudkar, S.V., 2000. Synthesis and preliminary analysis of a P-glycoprotein-specific [3H]-benzophenone photoaffinity label based on (−)-stipiamide. Bioorganic and Medicinal Chemistry Letters 10, 2275–2278.

Bennett, G.J., Lee, H.H., 1989. Xanthones from Guttiferae. Phytochemistry 28, 967–998.

Breitmayer, E., Voelter, W., 1989. Carbon-13 NMR Spectroscopy. VCH, Weinheim.

Comte, G., Daskiewicz, J.B., Bayet, C., Conseil, G., Viornery-Vanier, A.,Dumontet, C., Di Pietro, A., Barron, D., 2001. *C*-Isoprenylation of flavonoids enhances binding affinity towards P-glycoprotein and modulation of cancer cells chemoresistance. Journal of Medicinal Chemistry 44, 763–768.

Conseil, G., Baubichon-Cottay, H., Dayan, G., Jault, J.M., Barron, D., Di Pietro, A., 1998. Flavonoids: a class of modulators with bifunctional interactions at vicinal ATP — and steroid binding sites on mouse P-glycoprotein. Proceedings of the National Academy of Sciences of the USA 95, 9831–9836.

Critchfield, J.W., Welsh, C.J., Phang, J.M., Yeh, G.C., 1994. Modulation of adriamycin in accumulation and efflux by flavonoid in HCT-15 colon cells. Activation of P-glycoprotein as a putative mechanism. Biochemical Pharmacology 48, 1437–1445.

De Wet, H., McIntosh, D.V., Conseil, G., Baubichon-Cortay, H., Krell, T., Jault, J.M., Daskiewicz, J.B., Barron, D., Di Pietro, A., 2001. Interaction of nucleotides and flavonoids with recombinant C-terminal nucleotide binding domain of mouse multidrug resistance P-glycoprotein. Biochemistry, submitted.

Divita, G., Goody, R.S., Gautheron, D.C., Di Pietro, A., 1993. Structural mapping of catalytic site with respect to alpha-subunit and noncatalytic site in yeast mitochondria F1-ATPase using fluorescence resonance energy transfer. Journal of Biological Chemistry 268, 13178–13186.

Dorman, G., Prestwich, G.D., 1994. Benzophenone photophores in biochemistry. Biochemistry 33, 5661–5673.

Fleming, S.A., 1995. Chemical reagents in photoaffinity labelling. Tetrahedron 51, 12479–12520.

Gottesman, M.M., Hrycyna, C.A., Schoenlein, P.V., German, U.A., Pastan, L., 1993. Genetic analysis of the multidrug transporter. Annual Revue of Genetics 29, 607–649.

Gros, P., Buschmann, E., 1993. The mouse multidrug resistance gene family structural and functional analysis. International Revue of Cytology 137, 169–197.

Noungoué-Tchamo, D., Dijoux-Franca, M.J., Mariotte, A.M., Tsamo, E., Daskiewicz, J.B., Bayet, C., Barron, D., Conseil, G., Di Pietro, A., 2000. Prenylated xanthones as potential P-glycoprotein modulators. Bioorganic and Medicinal Chemistry Letters 10, 1343–1345.

Rancon, S., Chaboud, A., Darbour, N., Comte, G., Barron, D., Raynaud, J., Cabalion, P., 1999. A new *C*-glycosyl xanthone isolated from *Davallia solida*. Phytochemistry 52, 1677–1679.

Shapiro, A.B., Ling, V., 1997. Effect of quercetin on Hoechst 33342 transport by purified and reconstituted P-glycoprotein. Biochemical Pharmacology 53, 587–596.

PERGAMON

Phytochemistry 57 (2001) 559–564

PHYTOCHEMISTRY

www.elsevier.com/locate/phytochem

Two flavonoids and other compounds from the aerial parts of *Centaurea bracteata* from Italy

Guido Flamini*, Elena Antognoli, Ivano Morelli

Dipartimento di Chimica Bioorganica e Biofarmacia, Università degli Studi di Pisa, Via Bonanno 33, 56126 Pisa, Italy

Received 15 November 2000; received in revised form 8 February 2001

Abstract

The flowering aerial parts of *Centaurea bracteata* Scop. (Asteraceae) have been studied for the first time. Nineteen compounds were isolated and identified, namely a sterol glucoside, two phenolic acids, three quinic acid derivatives, and 13 flavonoids, two of which, are new natural products. Structural elucidation was performed mainly by mean of FABMS, 1D and 2D NMR spectroscopy. © 2001 Elsevier Science Ltd. All rights reserved.

Keywords: *Centaurea bracteata*; Asteraceae; Fiordaliso bratteato; Flavonoids; Quercetin 3-*O*-β-D-Glucopyranoside-3′-sulphate; Centabractein; Isokaempferide 7-*O*-β-D-glucopyranouronide; Bracteoside

1. Introduction

Centaurea bracteata Scop. (Asteraceae), known in Italy as "fiordaliso bratteato" is a herbaceous plant placed by Pignatti (1982) in the *Centaurea jacea* group, together with 10 other species. The plant is not used in the Italian folk medicine, although other species of the same genus (i.e. *Centaurea cyanus* and *Centaurea scabiosa*) are used against coughs and as ophthalmic drugs (Poletti, 1978). The studies on this genus deal mainly with sesquiterpene lactones, while flavonoids are less investigated; the species *C. bracteata* has never been studied at all.

This paper deals with the isolation and characterisation of 19 substances belonging to various classes of compounds, in particular three quinic acid derivatives, a sterol glucoside, two phenolic acids, and 13 flavonoids, two of which are new natural products.

2. Results and discussion

From the *n*-hexane residue (R_H), by repeated flash chromatographies, two compounds were isolated, namely β-sitosterol 3-*O*-β-D-glucopyranoside and jaceidin, which were identified by comparison of their physical and spectroscopic properties with literature reports (Roitman and James, 1985; Reher and Budensisky, 1992).

Fractionation of the $CHCl_3$–MeOH (9:1) extract (R_{CM}) by size-exclusion chromatography, Lobar RP-8 and preparative TLC, led to the isolation of 10 pure compounds. These were luteolin, axillarin, nepetin, 6-methoxy apigenin, isokaempferide, centaureidin, jacein, axillarin 7-glucoside, 5-caffeoylquinic acid and protocatechuic acid, all identified by ^1H and ^{13}C NMR spectroscopy (Collado et al., 1985; Iwahashi et al., 1985; Barbera et al., 1986; Berghöfer and Hölzl, 1987; Wada et al., 1987).

The EtOAc and BuOH residues, after size-exclusion chromatography and repeated Lobar RP-8 flash and preparative TLC chromatographies, gave 3,4-dicaffeoylquinic and caffeic acids, 6-hydroxyluteolin 6,4′-dimethyl ether, apigenin 7-glucoside, 3-caffeoylquinic acid methyl ester and two new flavonoid glycosides, which we named centabractein (**1**) and bracteoside (**2**). Known isolates were identified by comparison with literature data (Radaelli et al., 1980; Iwahashi et al., 1985; Kubo et al., 1986; Nishizawa et al., 1988).

Centabractein (**1**) was obtained as a yellowish amorphous powder that appears on TLC as a yellow-orange arrow-shaped spot after treatment with Naturstoffreagenz A-PEG. The negative FABMS spectrum gave a quasimolecular peak $[M–H]^-$ at 543 m/z, corresponding to the molecular formula $C_{21}H_{20}O_{15}S$, supported

* Corresponding author. Tel.: +39-05044074; fax: +39-05043321.
E-mail address: flamini@farm.unipi.it (G. Flamini).

0031-9422/01/$ - see front matter © 2001 Elsevier Science Ltd. All rights reserved.
PII: S0031-9422(01)00066-8

also by elemental analysis (see Experimental Section); another significant ion at m/z 565 ($[M+Na\text{-}H]^-$) showed the presence of sodium in the sample. The ^{13}C NMR spectrum showed 21 resonances, sorted by DEPT experiments into 10 CH, one CH_2 and 10 quaternary C. In the ^1H NMR spectrum obtained in DMSO-d_6 two broad singlets (δ 6.13 and 6.38) were present, really two coupled doublets with a very small J value, as shown by the COSY experiment, typical of the two *meta*-related H-6 and H-8 protons of ring A of a flavonoid unit. Ring B showed an ABM system (δ 7.96, *d*, $J=2.0$ Hz; 7.84, *dd*, $J=8.3$, 2.0 Hz; 6.91, *d*, $J=8.3$ Hz). Moreover, a one-proton doublet ($J=7.3$ Hz) was present at δ 5.40. This suggested the presence of a sugar having a β-configuration because of the J value due to a *trans*-diaxial interaction. The situation was very close to that of a quercetin glycoside, apart from the signals of ring B that resulted deshielded. This circumstance was more evident in the ^1H NMR spectrum recorded in CD_3OD, where the resonances of the ring B protons appeared at very low fields (8.31, *d*, $J=1.9$ Hz; 7.87, *dd*, $J=8.1$, 1.9 Hz; 7.00, *d*, $J=8.1$ Hz). Analysis of the ^{13}C NMR spectrum permitted the identification of the sugar moiety as β-D-glucose and confirmed the 'anomalous' situation of ring B with respect to quercetin. Resonances of ring B carbons showed the typical shifts due to the presence of a sulphate group (Barron et al., 1988): ca. 4.5 ppm upfield for the *ipso* carbon (C-3′) and ca. 7.0, 3.5, 1.5 and 5.0 ppm downfield for C-2′, C-4′, C-5′ and C-6′, respectively. The values are also in good agreement with those from an analogous compound (Seabra and Correia Alves, 1988). Placement of the glucose moiety at C-3 was determined on the basis of the typical glycosilation shifts that occurred with respect to quercetin (Flamini et al., 2000): downfield shifts of C-2 and C-4 (ca. 9.0 and 3.0 ppm, respectively) and an upfield shift of C-3 (ca. 2.0 ppm). Therefore, **1** is quercetin 3-*O*-β-D-glucopyranoside 3′-sulphate sodium salt, which we named centabractein. This structure is supported by its negative FABMS spectrum where, besides the quasimolecular peak at m/z 543, $[M\text{-}H]^-$, and at m/z 565, $[M+Na\text{-}H]^-$, there were peaks due to loss of a sulphate group at m/z 463, $[M\text{-}H\text{-}80]^-$, and of a glucose unit at m/z 301, $[M\text{-}H\text{-}162]^-$. Finally, the presence of sodium was confirmed by the yellow colour obtained by the flame assay; total acid hydrolysis of **1** liberated quercetin, glucose and sulphate, identified by TLC with authentic samples and precipitation with barium chloride, respectively.

Bracteoside (**2**) was obtained as a pale yellow powder that appears on TLC as a green-yellowish spot after treatment with Naturstoffreagenz A-PEG. The negative FABMS spectrum gave a quasimolecular peak $[M-H]^-$ at 475 m/z, corresponding to the molecular formula $C_{22}H_{20}O_{12}$, supported also by elemental analysis (see Experimental Section). The ^{13}C NMR spectrum showed 20 signals, sorted by DEPT experiments into one CH_3, 9 CH, and 10 quaternary C. In the ^1H NMR spectrum obtained in CD_3OD an AA′BB′ system constituted by two two-proton doublets ($J=8.8$ Hz) at δ 8.02 and 6.92, typical of a *para*-substituted B ring of a flavonoid. Two further coupled doublets ($J=1.9$ Hz) at δ 6.78 and 6.48 indicated the presence of the *meta*-related H-6 and H-8 ring A protons. The presence of a methoxyl group was evidenced by the three-protons singlet at δ 3.79. Moreover, a one-proton doublet ($J=7.3$ Hz) was present at δ 5.15, together with a not resolved area between 3 and 4 δ indicating the presence of a sugar having a β-configuration because of the J value due to a *trans*-diaxial interaction. Consequently, we can hypothesise the presence of a methoxykaempferol glycoside. The high resonance value of the methoxyl group (δ 59.7) suggested that both the *ortho* positions should be substituted, so it must be placed at the 3 position (Agrawal et al., 1989). This situation is corroborated by the characteristic downfield shifts observed for C-2, C-3 and C-4 (ca. 10.5, 4.0 and 2.5, respectively) with respect to kaempferol. Moreover, a cross peak was evidenced in the NOESY spectrum between the methoxyl and H-2′/H-6′ resonances. The sugar moiety was easily identified as glucuronic acid and its linkage to the 7-OH was established on the basis of the typical glycosilation shifts experienced by the aglycone, particularly the C-7 upfield shift (ca. 1.5 ppm) and the downfield shifts of the *ortho* (ca. 1.0 ppm) and *para* (ca. 2.5 ppm) carbons. This structure is also supported by its negative FABMS spectrum where, besides the quasimolecular peak at m/z 475, $[M-H]^-$, the peak due to the loss of glucuronic acid $[M-H-176]^-$ at 299 m/z was evident. Therefore, **2** was identified as isokaempferide 7-*O*-β-D-glucopyranouronide, which we have named bracteoside.

Summarising, the aerial parts of *C. bracteata* yielded 19 compounds, among which 13 were flavonoids, 4 caffeoylquinic derivatives, 1 phenolic acid and 1 sterol glucoside. Most of the flavonoids, according to the pattern of this genus, were polymethoxylated and two compounds have been obtained in great amounts (jacein 3650 mg, and jaceidin 750 mg; 0.31 and 0.06% with respect to the dry plant material). The other isolated compounds gave the following yields: β-sitosterol 3-glucoside and axillarin 7-glucoside 0.002%; luteolin, protocatechuic acid, 6-hydroxyluteolin 6,4′-dimethyl ether, caffeic acid and centaureidin 0.0004%; axillarin, nepetin, 6-methoxyapigenin, 3,4-dicaffeoylquinic acid and 5-caffeoylquinic acid 0.0009%; isokaempferide, centabractein (**1**) and bracteoside (**2**) 0.001%, One of the flavonoids, centabractein (**1**) was a sulphate conjugate; these compounds are relatively rare in nature (Williams and Harborne, 1994) and, among the Asteraceae, they are produced only by 4 tribes: Inuleae, Eupatorieae, Senecioneae and Heliantheae (Barron et al., 1988). This is the first report of a flavonoid sulphate ester in the genus *Centaurea* and this finding

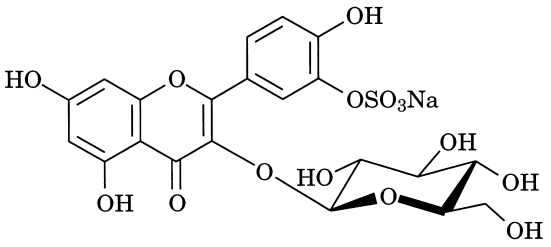

1

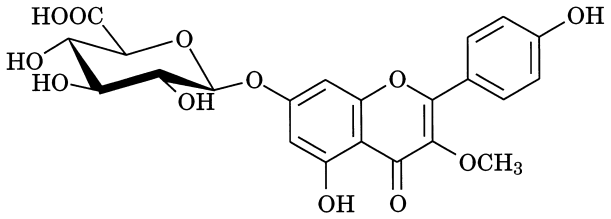

2

lead to 5 the producing tribes, comprising now also the Centaureinae.

The large diffusion of flavonoid sulphates in water or hydrophyte plants (Tomas-Barberan et al., 1987; Barron et al., 1988; Seabra and Correia Alves, 1988; De Beck et al., 1998) seems to support the view that this conjugation could represent an ecological adaptation to the aquatic habitat. However, *C. bracteata* has been collected in a very arid environment, the normal habitat according to Pignatti (1982), that describes this species as a xerophytic one. Further studies are in progress on the roots of this plant to confirm our findings.

Flavonoids sulphates showed many biological activities, useful both to human health and plant physiology. They are enzymes inhibitors (Haraguchi et al., 1996), allergens (Sallusto et al., 2000), antioxidants (Yagi et al., 1994), regulators of auxin transport (Faulkner and Rubery, 1992). Moreover, rutine sulfate was demonstrated to be not carcinogenic (Habs et al., 1984).

Sesquiterpene lactones, typical compounds of this genus, are not produced at all by *C. bracteata*.

3. Experimental

3.1. General

Melting points (uncorrected) were determined with a Kofler apparatus; optical rotations were measured on a Perkin-Elmer 241 polarimeter; FABMS were recorded, in the negative mode, with a VG ZAB instrument; ^1H and ^{13}C NMR spectra were obtained with a Bruker AC200 spectrometer in CD_3OD, DMSO-d_6, and $CDCl_3$, using TMS as internal standard. All 1D and 2D NMR experiments were performed using the standard Bruker library of microprograms.

The following adsorbents were used for purification: flash chromatography, Merck Kieselgel 60 (230–410 mesh); low-pressure chromatography, Merck Lobar Lichroprep RP-8 (31×2.5 cm); size-exclusion chromatography, Pharmacia Fine Chemicals Sephadex LH-20; analytical TLC, Merck Kieselgel 60 F_{254} precoated plates; chromatograms were visualised under UV light at 254 and 366 nm and/or sprayed with Komarowsky or Cerium Sulphate or Naturstoffreagenz A-PEG reagents.

3.2. Plant material

The flowered aerial parts were collected at Montelaterone, Amiata Mount, South Tuscany, Italy, at 600 m above the sea level, in July 1998. A voucher specimen is deposited in PI (Herbarium of the University of Pisa).

3.3. Extraction and isolation

The dried and ground aerial parts (1160 g) were extracted, successively, in a Soxhlet apparatus with *n*-hexane, $CHCl_3$, $CHCl_3$–MeOH (9:1) (4.5 l×30 h) and, at room temperature, with MeOH (3.5 l×7 days×3 times). After removal of solvents, in vacuo at up to 40°C, the following residues were obtained: R_H (26.1 g), R_C (9.9 g), R_{CM} (46.0 g), and R_M (49.8 g).

R_M was suspended in MeOH-H_2O (7:3) and extracted, in turn, with EtOAc and *n*-BuOH obtaining, after removal of the solvents, the residues R_{MAc} and R_{MBu}.

The R_H residue, after repeated SiO_2 flash chromatographies, gave β-sitosterol 3-*O*-β-D-glucopyranoside (18 mg) and jaceidin (750 mg).

The R_{CM} residue was submitted to Sephadex LH-20 size-exclusion chromatography with MeOH–$CHCl_3$ (4:1) as eluent and the fractions were submitted to Lobar RP-8 and SiO_2 p-TLC chromatographies, obtaining 10 pure compounds: luteolin (4 mg), axillarin (11 mg), nepetin (11 mg), 6-methoxy apigenin (10 mg), isokaempferide (15 mg), centaureidin (8 mg), jacein (3650 mg), axillarin 7-glucoside (22 mg), 5-caffeoylquinic acid (10 mg) and protocatechuic acid (5 mg).

R_{MAc} was chromatographed over Sephadex LH-20 column with MeOH as eluent, obtaining 10 main fractions (A–J). From fractions B,D and F–H, after gravity and flash column chromatography, and SiO_2 p-TLC, axillarin 7-glucoside (18 mg), 6-hydroxyluteolin 6,4′-dimethyl ether (6 mg), caffeic (6 mg), 3,4-dicaffeoylquinic (15 mg) and protocatechuic (4 mg) acids were obtained. Fraction J was filtered over a RP-8 column, using MeOH–H_2O (6:4) as eluent, obtaining pure centabractein (**1**) (12 mg).

The Sephadex LH-20 chromatography (eluent MeOH) yielded 8 main fractions (A′–H′). From fraction D′ a precipitate constituted by pure apigenin 7-glucoside

(10 mg) was separated. Fraction G′ gave, after SiO_2 column chromatography, pure 3-caffeoylquinic acid methyl ester. Bracteoside (**2**) (11 mg) was obtained by precipitation from fraction C′.

3.4. Centabractein (*1*)

Yellowish amorphous solid; $[\alpha]_D^{20}$ −60.0° (MeOH, $c = 0.13$); UV λ_{max} nm MeOH (log ε) 346 (3.90), 267 (4.18); (MeOH + $AlCl_3$) 398 (4.34), 350 (4.62), 267 (4.75); (MeOH + $AlCl_3$ + HCl) 396 (4.50), 341 (4.28), 302 (3.63), 274 (4.55); ^{1}H NMR spectral data (DMSO-d_6, 200 MHz) δ 5.40 (1H, *d*, $J = 7.3$ Hz, H-1″), 6.13 (1H, *br s*, H-6), 6.38 (1H, *br. s*, H-8), 6.91 (1H, *d*, $J = 8.3$ Hz, H-5′), 7.84 (1H, *dd*, $J = 8.3$, 2.0 Hz, H-6′), 7.96 (1H, *d*, $J = 2.0$ Hz, H-2′); ^{1}H NMR (CD_3OD, 200 MHz) δ 3.55 (1H, *m*, H-5″), 3.59 (1H, *m*, H-3″), 3.64 (1H, *m*, H-6″a), 3.72 (1H, *m*, H-2″), 3.77 (1H, *m*, H-6″b), 3.90 (1H, *m*, H-4″), 5.25 (1H, *d*, $J = 7.3$ Hz, H-1″), 6.24 (1H, *br. s*, H-6); 6.45 (1H, *br s*, H-8), 7.00 (1H, *d*, $J = 8.1$ Hz, H-5′), 7.87 (1H, *dd*, $J = 8.1$, 1.9 Hz, H-6′), 8.31 (1H, *d*, $J = 1.9$ Hz, H-2′); ^{13}C NMR data see Table 1; FABMS (negative mode) *m/z* 565 $[M + Na–H]^-$, 543 $[M–H]^-$, 463 [M–H–80]$^-$, 301 [M–H–162]$^-$; Elemental analysis: Found: C 46.19% H 3.79% S 5.96%, requires: C 46.33 H 3.70 S 5.89.

3.5. Bracteoside (*2*)

Pale yellow solid; $[\alpha]_D^{20}$ −42.3° (MeOH, $c = 0.10$); UV λ_{max} nm MeOH (log ε) 248 (*sh*, 3.65), 263 (4.24), 317 (*sh*, 3.22), 352 (3.74); (MeOH + $AlCl_3$) 265 (4.44), 298 (*sh*, 3.08), 354 (3.70), 398 (4.10); (MeOH + $AlCl_3$ + HCl) 266 (4.56), 298 (*sh*, 3.28), 352 (3.92), 398 (4.08); ^{1}H NMR spectral data (CD_3OD, 200 MHz) δ 3.35 (1H, *m*, H-2″), 3.40 (1H, *m*, H-3″), 3.46 (1H, *m*, H-4″), 3.68 (1H, *m*, H-5″), 3.79 (3H, *s*, 3-OCH_3) 5.15 (1H, *d*, $J = 7.2$ Hz, H-1″), 6.48 (1H, *d*, $J = 1.9$ Hz, H-6), 6.78 (1H, *d*, $J = 1.9$ Hz, H-8), 6.92 (2H, *d*, $J = 8.8$ Hz, H-2′, H-6′), 8.02 (2H, *d*, $J = 8.8$ Hz, H-3′, H-5′); ^{13}C NMR data see Table 1; FABMS (negative mode) *m/z* 475 $[M–H]^-$, 299 M–H–176]$^-$; Elemental analysis: Found: C 55.62%, H 4.11%, requires: C 55.47, H 4.23.

3.6. Known compounds

3.6.1. β-Sitosterol-3-glucoside

^{13}C NMR data (py-d_5, 50 MHz) δ 140.6 (C-5), 123.8 (C-6), 102.5 (C-1′), 78.5 (C-3′, C-5′), 78.1 (C-3), 75.3 (C-2′), 71.7 (C-4′), 62.8 (C-6′), 56.8 (C-14), 56.2 (C-17), 50.3 (C-9), 46.0 (C-24), 42.4 (C-13), 39.9 (C-12), 39.3 (C-4), 37.5 (C-1), 36.9 (C-10), 36.4 (C-20), 34.2 (C-22), 32.2 (C-8), 32.0 (C-7), 30.0 (C-2), 29.4 (C-25), 28.5 (C-16), 26.3 (C-23), 24.5 (C-15), 23.4 (C-28), 21.3 (C-11), 20.0 (C-27), 19.4 (C-19), 19.2 (C-26), 19.0 (C-21), 12.2 (C-29), 12.0 (C-18).

3.6.2. Jacein

^{13}C NMR data (DMSO-d_6, 50 MHz) δ 178.4 (C-4), 156.5 (C-2), 156.1 (C-7), 152.1 (C-9), 151.3 (C-5), 150.0 (C-4′), 147.6 (C-3′), 137.8 (C-3), 132.2 (C-6), 122.4 (C-6′), 120.8 (C-1′), 115.7 (C-5′), 112.1 (C-2′), 106.3 (C-10), 100.3 (C-1″), 94.5 (C-8), 77.5 (C-2″), 76.8 (C-3″), 73.3 (C-4″), 69.7 (C-5″), 60.7 (C-6″), 60.4 (6-OMe), 59.8 (3-OMe), 55.8 (3′-OMe).

3.6.3. Jaceidin

^{13}C NMR data (DMSO-d_6, 50 MHz) δ 178.2 (C-4), 157.4 (C-7), 155.5 (C-2), 152.3 (C-5), 151.6 (C-9), 149.8 (C-4′), 147.5 (C-3′), 137.4 (C-3), 131.2 (C-6), 122.2 (C-6′), 120.8 (C-1′), 115.6 (C-5′), 112.0 (C-2′), 104.6 (C-10), 94.1 (C-8), 60.0 (6-OMe), 59.7 (3-OMe), 55.7 (3′-OMe).

3.6.4. Luteolin

^{13}C NMR data (DMSO-d_6, 50 MHz) δ 181.7 (C-4), 164.2 (C-7), 163.9 (C-2), 161.5 (C-5), 157.3 (C-9), 149.7 (C-4′), 145.8 (C-3′), 121.5 (C-1′), 119.0 (C-6′), 116.0 (C-5′), 113.4 (C-2′), 103.7 (C-10), 102.9 (C-3), 98.8 (C-6), 93.8 (C-8).

3.6.5. 5-Caffeoylquinic acid

^{1}H NMR spectral data (DMSO-d_6, 200 MHz) δ 1.86 (4H, *m*, H-2, H-6), 3.86 (1H, *m*, H-4), 5.13 (1H, *m*, H-5), 6.21 (1H, *d*, $J = 15.6$ Hz, H-α), 6.72 (1H, *d*, $J = 8.3$ Hz, H-5′), 6.98 (1H, *m*, H-6′), 7.03 (1H, *br s*, H-2′), 7.43 (1H, *d*, $J = 15.6$ Hz, H-β).

Table 1
^{13}C NMR data for compounds **1** and **2** (50 MHz, in DMSO-d_6)[a]

Carbon	**1**	**2**
2	155.0 *s*	157.0 *s*
3	133.2 *s*	137.9 *s*
4	176.9 *s*	178.2 *s*
5	161.0 *s*	160.4 *s*
6	99.5 *d*	99.2 *d*
7	162.4 *s*	162.6 *s*
8	93.9 *d*	94.5 *d*
9	156.5 *s*	156.0 *s*
10	102.8 *s*	105.4 *s*
1′	121.2 *s*	121.0 *s*
2′	132.3 *d*	130.0 *d*
3′	140.5 *s*	116.1 *d*
4′	151.9 *s*	160.9 *s*
5′	116.6 *d*	116.1 *d*
6′	126.3 *d*	130.0 *d*
1″	101.1 *d*	99.4 *d*
2″	73.9 *d*	72.9 *d*
3″	77.3 *d*	75.1 *d*
4″	69.7 *d*	71.5 *d*
5″	76.4 *d*	75.8 *d*
6″	60.8 *d*	170.9 *s*
–OMe	–	59.7 *q*

[a] Multiplicities deduced by DEPT experiments.

3.6.6. Protocatechuic acid

^{13}C NMR data (CD_3OD, 50 MHz) δ 170.3 (-COOH), 151.5 (C-4), 146.0 (C-3), 123.9 (C-6), 123.0 (C-1), 117.7 (C-5), 115.8 (C-2).

3.6.7. Axillarin 7-glucoside

^{13}C NMR data (DMSO-d_6, 50 MHz) δ 178.3 (C-4), 156.4 (C-7), 152.1 (C-5), 151.3 (C-2), 148.9 (C-4′), 145.2 (C-3′), 137.6 (C-3), 132.2 (C-6), 120.7 (C-1′), 120.6 (C-6′), 115.7 (C-2′, C-5′), 106.2 (C-10), 100.1 (C-1″), 94.1 (C-8), 77.2 (C-5″), 76.7 (C-3″), 73.2 (C-2″), 69.6 (C-4″), 60.7 (C-6″), 60.3 (6-OMe), 59.7 (3-OMe).

3.6.8. Axillarin

^{13}C NMR data (CD_3OD, 50 MHz) δ 180.3 (C-4), 158.7 (C-7), 158.1 (C-2), 153.8 (C-5), 150.0 (C-4′), 146.5 (C-3′), 139.2 (C-3), 132.6 (C-6), 122.9 (C-1′), 122.4 (C-6′), 116.5 (C-5′), 105.3 (C-10), 95.0 (C-8), 61.0 (6-OMe), 60.5 (3-OMe).

3.6.9. Nepetin

^{13}C NMR data (CD_3OD, 50 MHz) δ 3.88 (3H, *s*, 6-OMe), 6.56 (1H, *s*, H-8)), 6.90 (1H, *d*, J = 8.3 Hz, H-5′), 7.38 (1H, *s*, H-3), 7.40 (1H, *br dd*, J = 8.3 Hz, H), 7.63 (1H, *d*, J = 1.9 Hz).

3.6.10. Centaureidin

^{13}C NMR data (CD_3OD, 50 MHz) δ 180.3 (C-4), 158.9 (C-7), 157.6 (C-2), 153.8 (C-9), 153.7 (C-5), 151.7 (C-4′), 147.6 (C-3′), 139.5 (C-3), 132.6 (C-6), 124.2 (C-1′), 122.1 (C-6′), 116.2 (C-2′), 112.3 (C-5′), 106.3 (C-10), 95.0 (C-8), 61.0 (6-OMe), 60.6 (3-OMe), 56.4 (4′-OMe).

3.6.11. Isokaempferide

^{1}H NMR spectral data (CD_3OD, 200 MHz) δ 3.78 (3H, *s*, 3-OMe), 6.21 (1H, *d*, J = 2.2 Hz, H-6), 6.42 (1 H, *d*, J = 2.2 Hz, H-8), 6.93 (2H, *d*, J = 8.8 Hz, H-3′ and H5′), 8.00 (2H, *d*, J = 8.8 Hz, H-2′ and H6′).

3.6.12. Hispidulin

^{13}C NMR data (CD_3OD, 50 MHz) δ 184.2 (C-4), 166.4 (C-2), 162.7 (C-7 and C4′), 160.0 (C-9), 153.8 (C-5), 132.4 (C-6), 129.5 (C-2′ and C-6′), 123.3 (C-1′), 117.1 (C-3′ and C-5′), 105.3 (C-10), 103.3 (C-3), 95.7 (C-8), 61.0 (6-OMe).

3.6.13. Caffeic acid

^{1}H NMR spectral data (CD_3OD, 200 MHz) δ 6.22 (1H, *d*, J = 15.6, H-8), 6.77 (1H, *d*, J = 8.2 Hz, H-5), 6.94 (1H, *dd*, J = 8.2 and 2.0Hz, H-6), 7.03 (1H, *d*, J = 2.0 Hz, H-2), 7.51 (1H, *d*, J = 15.6 Hz, H-7).

3.6.14. 6-Hydroxyluteolin-6,4′-dimethylether

^{1}H NMR spectral data (CD_3OD, 200 MHz) δ 3.89 (3H, *s*, 6-OMe), 3.97 (3H, *s*, 4′-OMe), 6.59 (1H, *s*, H-8), 6.65 (1H, *s*, H-3), 6.94 (1H, *d*, J = 7.8 Hz, H-5′), 7.50 (2H, *m*, 6′ and H2′).

3.6.15. Apigenin 7-glucuronide

^{13}C NMR data (DMSO-d_6, 50 MHz) δ 182.0 (C-4), 171.1 (C-6″), 164.3 (C-2), 162.7 (C-7 and C-4′), 161.4 (C-5), 156.9 (C-9), 128.6 (C-2′ and C6′), 120.9 (C-1′), 116.0 (C-3′ and C5′), 105.4 (C-10), 103.1 (C-3), 99.4 (C-6), 94.7 (C-8), 75.9 (C-5″), 75.0 (C-3″), 73.2 (C-2″), 71.5 (C-4″).

3.6.16. 3,4-Dicaffeoylquinic acid

^{1}H NMR spectral data (DMSO-d_6, 200 MHz) δ 2.28 (2H, *m*, H-2 and H-6), 4.02 (1H, *m*, H-5), 5.25 (2H, *m*, H-3 and H-4), 6.15 (1H, *d*, J = 15.1 Hz, H-α′), 6.54 (1H, d, J = 15.1 Hz, H-α″), 6.73 (2H, *d*, J = 7.8 Hz, H-5′), 6.93 (2H, *m*, H-6′ and H-6″), 7.02 (1H, *br s*, H-2′), 7.09 (1H, *br s*, H-2″), 7.38 (1H, *d*, J = 15.1 Hz, H-β′), 7.46 (1H, *d*, J = 15.1 Hz, H-β″).

3.6.17. 3-Caffeoylquinic acid methyl ester

^{13}C NMR data (DMSO-d_6, 50 MHz) δ 173.7 (COO), 165.7 (COO), 149.1 (C-4′), 146.0 (C-3′), 145.4 (C-β), 125.3 (C-1′), 116.1 (C-5′), 114.7 (C-2′ and C-6′), 113.8 (C-α), 73.3 (C-1), 71.1 (C-3), 69.6 (C-4), 67.1 (C-5), 51.9 (Me), 37.3 (C-2), 35.3 (C-6).

References

Agrawal, P.K., Takur, R.S., Bansal, M.C., 1986. Flavonoids. In: Agrawal, P.K. (Ed.), Carbon-13 NMR of Flavonoids. Elsevier, Amsterdam, pp. 159.

Barbera, O., Marco, J.A., Sanz, J.F., Sanchez-Parareda, J., 1986. 3-Methoxyflavones and coumarins from *Artemisia incanescens*. Phytochemistry 25, 2357–2360.

Barron, D., Varin, L., Ibrahim, R.K., Harborne, J.B., Williams, C.A., 1988. Sulphated flavonoids—an update. Phytochemistry 27, 2375–2395.

Berghöfer, B., Hölzl, J., 1987. Biflavonoids in *Hypericum perforatum*; part I. Isolation of I3,II8-biapigenin. Planta Med. 53, 216–218..

Collado, I.G., Macias, F.A., Massanet, G.M., Luis, F.R., 1985. Flavonoids from *Centaurea clementei*. J. Nat. Prod. 48, 819–822.

De Beck, P.O., Dijoux, M.-G., Cartier, G., Mariotte, A.-M., 1998. Quercitrin-3′-sulfate from leaves of *Leea guinensis*. Phytochemistry 47, 1171–1173.

Faulkner, I.J., Rubery, P.H., 1992. Flavonoids and flavonoid sulphates as probes of auxin-transport regulation in *Cucurbita pepo* hypocotyl segments and vesicles. Planta 186, 618–625.

Flamini, G., Bulleri, C, Morelli, I., Manunta, A., 2000. A new flavonoid glycoside from *Centaurea horrida*. J. Nat. Prod. 63, 662–663.

Habs, M., Habs, H., Berger, M.R., Schmahl, D., 1984. Negative dose–response study for carcinogenicity of orally administered rutin sulfate in Sprague–Dawley rats. Cancer Lett. 23, 103–108.

Haraguchi, H., Ohmi, I., Sakai, S., Fukuda, A., Toihara, Y., Fujimoto, T., Okamura, N., Yagi, A., 1996. Effect of *Polygonum hydropiper* sulfated flavonoids on lens aldose reductase and related enzymes. J. Nat. Prod. 59, 443–445.

Iwahashi, H., Morishita, H., Osaka, N., Kido, R., 1985. 3-*O*-Feruloyl-4-*O*-caffeoylquinic acid from coffee beans. Phytochemistry 24, 630–632.

Kubo, M., Sasaki, H., Endo, T., Taguchi, H., Yoshioka, I., 1986. The constituents of *Schizonepeta tenuifolia* Briq. Structure of a new monoterpene glucoside, schizonepetoside C. Chem. Pharm. Bull. 34, 3097–3101.

Nishizawa, M., Izuhara, R., Kaneko, K., Koshihara, Y., Fujimoto, Y., 1988. 5-Lipoxygenase inhibitors isoalted from Gardeniae fructus. Chem. Pharm. Bull. 36, 87–95.

Pignatti, S., 1982. Flora d'Italia. Edagricole, Bologna.

Poletti, A., 1978. Fiori e Piante Medicinali. Musumeci Editore, Milano.

Redaelli, C., Formentini, L., Santaniello, E., 1980. Apigenin 7-glucoside and its 2″- and 6″-acetates from ligulate flowers of *Matricaria chamomilla*. Phytochemistry 19, 985–986.

Reher, G., Budensisky, M., 1992. Triterpenoids from plants of the Sanguisorbeae. Phytochemistry 31, 3909–3914.

Roitman, J.N., James, L.F., 1985. Chemistry of toxic range plants. Highly oxygenated flavonol methyl ethers from *Gutierrezia microcephala*. Phytochemistry 24, 835–848.

Sallusto, F., Poupot, R., Clergue, M., DePalma, R., Fournie, J.J., 2000. A flavonoid sulfate antigen activates human alphabeta CD8 + Th2 lymphocytes in pollen allergy. Eur. J. Immunol. 30, 964–968.

Seabra, R.M., Correia Alves, A., 1988. Quercetin 3-glucuronide-3′-sulphate from *Hypericum elodes*. Phytochemistry 27, 3019–3020.

Tomas-Barberan, F.A., Harborne, J.B., Self, R., 1987. Twelve 6-oxygenated flavone sulfates from *Lippia nodiflora* and *L. canescens*. Phytochemistry 26, 2281–2284.

Wada, H., Fujita, M., Murakami, T., Saikai, Y., Chen, C.M., 1987. Chemical and chemotaxonomical studies of ferns. LXXIII. New flavonoids with modified B-ring from the genus *Pseudophegopteris* (Thelypteridaceae). Chem. Pharm. Bull. 35, 4757–4762.

Williams, C.A., Harborne, J.B., 1994. Flavone and flavonol glycosides. In: Harborne, J.B. (Ed.), The Flavonoids. Advances in research since 1986. Chapmann & Hall, Cambridge, pp. 344.

Yagi, A., Uemura, T., Okamura, N., Haraguchi, H., Imoto, T., Hashimoto, K., 1994. Antioxidative sulphated flavonoids in leaves of *Polygonum hydropiper*. Phytochemistry 35, 885–887.

PERGAMON

Phytochemistry 57 (2001) 565–569

PHYTOCHEMISTRY

www.elsevier.com/locate/phytochem

The flavonoids of leek, *Allium porrum*☆

Ernesto Fattorusso [a], Virginia Lanzotti [b,*], Orazio Taglialatela-Scafati [a], Carla Cicala [c]

[a] *Dipartimento di Chimica delle Sostanze Naturali, Università di Napoli "Federico II", Via D. Montesano 49, 80131 Napoli, Italy*
[b] *Dipartimento di Scienze e Tecnologie Agroalimentari, Ambientali e Microbiologiche, Università del Molise, Via F. De Sanctis, 86100 Campobasso, Italy*
[c] *Dipartimento di Farmacologia Sperimentale, Università di Napoli "Federico II", Via D. Montesano 49, 80131 Napoli, Italy*

Received 13 November 2000; received in revised form 24 January 2001

Abstract

A phytochemical investigation of the extracts obtained from bulbs of leek, *Allium porrum* L. has led to the isolation of five flavonoid glycosides based on the kaempferol aglycone. Two of them are new compounds and have been identified as kaempferol 3-*O*-[2-*O*-(*trans*-3-methoxy-4-hydroxycinnamoyl)-β-D-galactopyranosyl]-(1→4)-*O*-β-D-glucopyranoside, and kaempferol 3-*O*-[2-*O*-(*trans*-3-methoxy-4-hydroxycinnamoyl)-β-D-glucopyranosyl]-(1→6)-*O*-β-D-glucopyranoside, on the basis of spectroscopic methods, including 2D NMR. The isolated compounds have been evaluated for their human platelet anti-aggregation activity. © 2001 Elsevier Science Ltd. All rights reserved.

Keywords: *Allium porrum*; Alliaceae; Leek; Flavonoids; Kaempferol glycosides; NMR spectroscopy

1. Introduction

Plants of the genus *Allium* have been recognized as rich sources of secondary metabolites endowed with interesting biological activities (Augusti, 1990; Block, 1992). As a part of a systematic phytochemical study on Mediterranean *Allium* species, we have recently obtained a number of new kaempferol glycosides from the wild garlic, *A. ursinum* L. (Carotenuto et al., 1996), and from the ornamental garlic, *A. neapolitanum* Cyr (Carotenuto et al., 1997), this latter plant also contained some quercetin and isorhamnetin glycosides. We have now continued this investigation by examining the flavonoid glycosides of leek, *A. porrum* L. (Alliaceae). Although this plant is widely distributed and commonly used as a food, no systematic evaluation of its flavonoid composition has been reported yet. Herein we describe the isolation from bulbs of leek of five flavonol glycosides, two of which, based on a kaempferol aglycone and acylated with a 3-methoxy-4-hydroxycinnamoyl moiety, are new products.

All the isolated compounds have been evaluated for their inhibitory activity on human platelet aggregation, an action already evidenced for kaempferol (Landolfi et al., 1984). In particular, kaempferol has been reported to inhibit markedly (IC_{50} 20 μM) platelet aggregation and ATP release of platelets induced by arachidonic acid or collagen. In addition, kaempferol also acts as a thromboxane receptor antagonist, and it has been claimed as an active agent in the prevention of atherosclerosis and acute platelet thrombus formation (Tzeng et al., 1991).

2. Results and discussion

Plants of *Allium porrum* L. were collected near Benevento (Campania, Italy), during September 1999. The fresh bulbs (988 g) were extracted at room temperature with *n*-hexane, $CHCl_3$, $CHCl_3$/MeOH 9:1, and then MeOH, in sequence. The *n*-butanol soluble material of the methanol extract was subjected to repeated chromatographic separations on reverse-phase silica gel to yield the flavonol glycosides **1**–**5** in the pure state. The structures of the known compounds **1**–**3** have been assigned on the basis of their mass, UV and ^1H NMR

☆ Part 8 in the series "Chemistry of the genus *Allium*". Part 7: Fattorusso, E., Lanzotti, V., Taglialatela-Scafati, O., Di Rosa, M., Ianaro, A., 2000. J. Agric. Food. Chem. 48, 3455–3462.

* Corresponding author. Tel.: +39-0874-404649; fax: +39-0874-404652.

E-mail address: lanzotti@unimol.it (V. Lanzotti).

0031-9422/01/$ - see front matter © 2001 Elsevier Science Ltd. All rights reserved.
PII: S0031-9422(01)00039-5

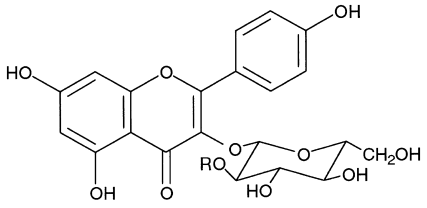

1 R = H
2 R = α-L-rhamnopyranose
3 R = *trans*-p-coumaroyl

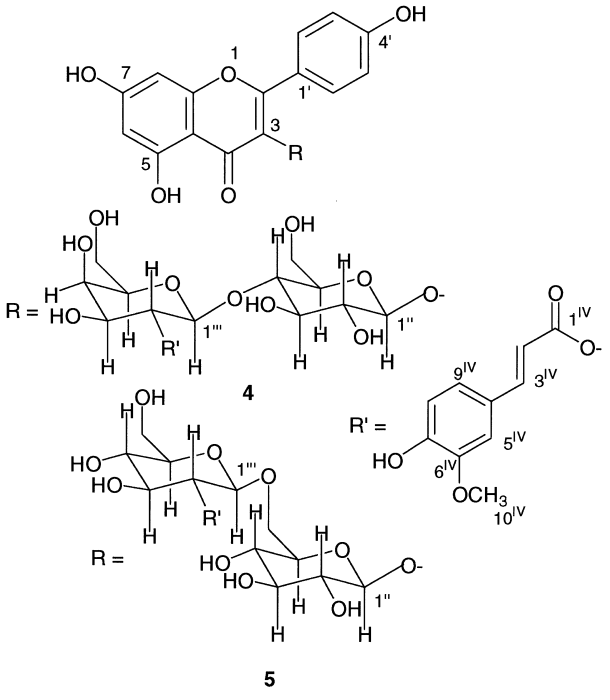

4

5

Table 1
UV spectral absorptions (λ_{max} in nm) of compounds **4** and **5**

	MeOH	NaOMe	$AlCl_3$	$AlCl_3$/HCl	NaOAc	NaOAc/H_3BO_3
4	355	400	400	400	387	344
	300 *sh*	324	353	353	313	285
	266	270	301	306	277	256
			273	272		
5	356	400	398	397	388	340
	295 *sh*	320	350	351	314	281
	264	274	302	306	274	256
			270	274		

spectral data in comparison with data reported in the literature. In particular, astragaline (**1**) and kaempferol-3-*O*-neohesperidoside (**2**) have been isolated from several sources comprising also some species of Alliaceae (Nakano et al., 1981), whereas compound **3** has been reported only as constituent of *Quercus suber* (Cupuliferae) (Romussi et al., 1991) and *Eryngium campestre* (Saniculoideae) (Hohmann et al., 1997).

The new compound **4**, a yellow powder with $[\alpha]_D^{25} = -9°$ (MeOH; *c* 0.02), gave a deprotonated molecule at *m/z* 785.2015 $(M-H)^-$ in the negative-ion high-resolution FAB mass spectrum consistent with the molecular formula $C_{37}H_{38}O_{19}$ (calcd. *m/z* 785.2007). The UV spectrum of **4** (Table 1) showed the characteristic absorptions of a kaempferol substituted at position 3, as indicated by the bathochromic shifts after addition of diagnostic reagents (Mabry et al., 1970). The ^1H and ^{13}C NMR spectra confirmed this structural hypothesis (Table 2) and also revealed that two sugar residues and a cinnamoyl-like subunit should account for the remaining atoms implied from the molecular formula. The combined analysis of these spectra was greatly aided by interpretation of 2D HMQC and HMBC data, allowing $^1J_{C\text{-}H}$ and $^{2,3}J_{C\text{-}H}$ connections, respectively.

In particular, the ^1H NMR signals of a *trans* olefinic double bond (δ 7.67 and 6.39, $J = 15.8$ Hz) conjugated with an aromatic ring system (two coupled doublets at δ 7.09 and 6.81, one singlet at δ 7.19), a methoxy singlet at δ 3.90, and the relevant ^{13}C NMR signals (Table 2) well fitted with data reported in the literature (Carotenuto et al., 1996) for a 3-methoxy-4-hydroxy-*trans*-cinnamoyl (feruloyl) moiety. The location of the methoxy group at position 6^{IV} was secured by the ROESY coupling between H_3-10^{IV} and H-5^{IV} (δ 7.19).

Going on, two anomeric proton signals at δ 4.69 and 5.17 were identified in the ^1H NMR spectrum, and associated with the relevant anomeric carbons (δ 102.8 and 104.3, respectively) through the 2D HMQC spectrum. The large coupling constants of the above protons (Table 2) indicated a β-configuration for both monosaccharides.

When the anomeric proton at δ 5.17 (H-1″) was used as a starting point, analysis of COSY and HOHAHA spectra allowed the identification, in sequence, of four oxymethine and one oxymethylene group (see Table 2). The sugar was identified as β-glucopyranose on the basis of the large coupling constants observed for all the oxymethine protons, implying their axial-axial relationship. In addition, the ROESY couplings of H-1″ with H-3″ and H-5″ and of H-2″ with H-4″ further supported this conclusion. Starting from the anomeric signal at δ 4.69 (H-1‴) we could identify, on the basis of COSY and HOHAHA data, the sequence of another hexose unit extending up to an oxymethylene residue via four oxymethine protons. The relative stereochemistry of this monosaccharide unit was elucidated by the analysis of coupling constants in the ^1H NMR spectrum. In particular, this sugar unit was characterized by large axial-axial couplings H-1‴/H-2‴, H-2‴/H-3‴, while the axial-equatorial relations H-3‴/H-4‴, H-4‴/H-5‴ were deduced by the small coupling constants between these protons. These data and the ROESY correlation peak between H-3‴ and H-5‴ were in accordance with the β-galactopyranose nature of this sugar. Finally, the relative

downfield shift of H-2‴ (δ 4.88) appeared in accordance with an acylation at this position, thus suggesting the *trans*-feruloyl linkage site.

In order to confirm the nature of the sugar residue, compound **4** (2 mg) was subjected to acid methanolysis followed by silylation with trisil-Z. The GC analysis of the released saccharides revealed the presence of glucose and galactose in the ratio 1:1.

The HMBC spectrum was used in order to unambiguously interconnect the above determined four substructures. It showed a correlation between the proton at δ 5.17 (H-1″) and C-3 (δ 134.5), indicating the linkage site of β-glucose to the aglycone. In addition, the HMBC correlation between the proton at δ 4.69 (H-1‴) and C-4″ (δ 80.0), and the ROESY coupling of H-1‴ with H-4″ both indicated C-4″ as the interglycosidic linkage position. Finally, the HMBC cross peak between H-2‴ and C-1^{IV} (δ 162.2) unambiguously confirmed that the feruloyl moiety is linked to the position 2 of the galactose. If we assume that both sugars belong to the commonly found D-series, the chemical structure of **4** is defined as kaempferol 3-*O*-[2-*O*-(*trans*-3-methoxy-4-hydroxycinnamoyl)-β-D-galactopyranosyl]-(1→4)-*O*-β-D-glucopyranoside.

Compound **5**, yellow powder $[\alpha]_D^{25} = -13^\circ$ (MeOH; *c* 0.02), gave a deprotonated molecule at *m*/*z* 785.2000 $(M-H)^-$ in the negative-ion high-resolution FAB mass spectrum, consistent with the same molecular formula of **4** ($C_{37}H_{38}O_{19}$). The close structural relationship of these two compounds was also evident by their ^1H and ^{13}C NMR spectra, showing virtually identical resonances for both the aglycone and the 3-methoxy-4-hydroxy cinnamoyl moiety. The UV spectrum of **5** (Table 1), that

Table 2
^{13}C and ^1H NMR data of compounds **4** and **5** in CD_3OD

Pos.	**4**		**5**	
	δ_C (mult.)	δ_H (mult., *J* in Hz)	δ_C (mult.)	δ_H (mult., *J* in Hz)
2	158.8 (C)		158.8 (C)	
3	134.5 (C)		134.0 (C)	
4	179.2 (C)		179.1 (C)	
5	161.5 (C)		161.5 (C)	
6	100.5 (CH)	6.11 (*d*, 1.8)	101.0 (CH)	6.18 (*d*, 1.8)
7	163.1 (C)		163.2 (C)	
8	96.1 (CH)	6.28 (*d*, 1.8)	96.4 (CH)	6.37 (*d*, 1.8)
9	158.0 (C)		158.0 (C)	
10	105.5 (C)		105.2 (C)	
1′	123.2 (C)		123.2 (C)	
2′-6′	132.0 (CH)	8.03 (*d*, 8.8)	132.1 (CH)	8.01 (*d*, 9.0)
3′-5′	116.5 (CH)	6.88 (*d*, 8.8)	116.4 (CH)	6.89 (*d*, 9.0)
4′	161.4 (C)		161.0 (C)	
1″	104.3 (CH)	5.17 (*d*, 7.5)	104.5 (CH)	5.14 (*d*, 7.1)
2″	75.5 (CH)	3.54 (*t*, 7.5)	75.7 (CH)	3.53 (*t*, 7.1)
3″	76.5 (CH)	3.64 (*dd*, 7.5, 9.5)	77.4 (CH)	3.59 (*dd*, 7.1, 9.1)
4″	80.0 (CH)	3.68[a]	73.3 (CH)	3.73[a]
5″	76.6 (CH)	3.24 (*ddd*, 9.5, 5.5, 3.5)	76.3 (CH)	3.44 (*m*)
6″	61.8 (CH_2)	3.68[a]	68.9 (CH_2)	4.25 (*br.d*, 11.6)
		3.60[a]		3.92[a]
1‴	102.8 (CH)	4.69 (*d*, 7.0)	102.8 (CH)	4.75 (*d*, 8.4)
2‴	75.0 (CH)	4.88 (*t*, 7.0)	75.5 (CH)	4.82 (*t*, 8.4)
3‴	76.0 (CH)	3.62[a]	76.5 (CH)	3.73[a]
4‴	71.5 (CH)	3.44 (*br.s*)	71.3 (CH)	3.55[a]
5‴	75.5 (CH)	3.73 (*dd*, 6.5, 1.5)	79.0 (CH)	3.62 (*br. dd*, 8.5, 6.5)
6‴	62.2 (CH_2)	3.97 (*br.d*, 6.5)	62.5 (CH_2)	3.98 (*br.d*, 8.5)
		3.91[a]		3.72[a]
1^{IV}	162.2 (C)		163.1 (C)	
2^{IV}	115.1 (CH)	6.39 (*d*, 15.8)	115.1 (CH)	6.45 (*d*, 16.1)
3^{IV}	147.4 (CH)	7.67 (*d*, 15.8)	148.2 (CH)	7.69 (*d*, 16.1)
4^{IV}	123.1 (C)		124.0 (C)	
5^{IV}	112.0 (CH)	7.19 (*s*)	113.2 (CH)	7.31 (*s*)
6^{IV}	150.7 (C)		150.7 (C)	
7^{IV}	151.7 (C)		152.0 (C)	
8^{IV}	116.7 (CH)	6.81 (*d*, 8.0)	116.8 (CH)	6.80 (*d*, 8.1)
9^{IV}	124.5 (CH)	7.09 (*d*, 8.0)	124.6 (CH)	7.10 (*d*, 8.1)
10^{IV}	56.1 (CH_3)	3.90 (*s*)	56.5 (CH_3)	3.91 (*s*)

[a] Overlapped with other signals.

showed characteristic absorption bands for a kaempferol substituted at position 3, confirmed this similarity.

Also in the case of **5** two monosaccharide units constitute the sugar portion, as indicated by two anomeric proton signals at δ 4.75 and 5.14 in the ^{1}H NMR spectrum, correlated with the relevant anomeric carbons (δ 102.8 and 104.5, respectively) through the HMQC spectrum. In particular, the ^{1}H and ^{13}C NMR data (Table 2) indicated that the inner sugar was unchanged. The second one, whose anomeric proton signal resonates at δ 4.75, was identified as a further β-glucopyranose due to the large value of the vicinal coupling constants interrelating all the oxymethine protons, arranged in sequence through COSY and HOHAHA experiments. Also in this case, the chemical shift of H-2‴ at relatively low field (δ 4.82) clearly pointed to the acylation site at this position.

As for compound **4**, the nature of the sugar portion of **5** was confirmed by GC analysis of the persilyl methylsaccharides obtained by methanolysis followed by treatment with trisil Z.

The HMBC spectrum, showing cross-peaks of H-1″ with C-3 (δ 134.0), and of H-2‴ with C-1^{IV} (δ 163.1), allowed an unambiguous connection among the deduced substructures. Furthermore, the key HMBC cross peak of C-1‴ (δ 102.8) with H_2-6″ (δ 4.25 and 3.92) defined the interglycosydic linkage site, which was also confirmed by the ROESY coupling of H-1‴ with H_2-6″. Compound **5** was therefore defined as kaempferol 3-*O*-[2-*O*-(*trans*-3-methoxy-4-hydroxycinnamoyl)-β-D-glucopyranosyl]-(1→6)-*O*-β-D-glucopyranoside.

The isolated compounds (**1**–**5**) were evaluated for their inhibitory activity on platelet aggregation induced by ADP. Compounds **1** and **2**, at a concentration of 10^{-3} M, were the only active inhibitors of platelet response to collagen (percentage of aggregation: control, 45.13 + 1.56%; reference compound kaempferol, 10.12 + 0.63%; compound **1**, 12.54 + 1.56%; compound **2** 20.35 + 0.83%). Compounds **3**–**5**, in the same conditions, showed no significant activity. This result is in agreement with our previous finding (Carotenuto et al., 1996) that the presence of a cinnamoyl esterification consistently lowers the in vitro anti-aggregating activity of the flavonoid glycosides. However, it should be noted that these results could be not strictly related to the in vivo activity, since this is greatly affected by absorption and metabolism. In particular, some metabolic reactions (hydrolysis, deacylation, etc.) could improve the anti-aggregating activity of the isolated kaempferol glycosides and acylated glycosides.

3. Experimental section

3.1. General experimental procedure

FABMS (recorded in glycerol matrix) were measured on a VG Prospec (FISONS) mass spectrometer (CsI ions). Optical rotations were determined on a Perkin-Elmer 192 polarimeter equipped with a sodium lamp (589 nm) and a 10-cm microcell. ^{1}H and ^{13}C NMR spectra were recorded at 500 and 125 MHz, respectively, on a Bruker AMX-500 spectrometer. Chemical shifts were referenced to the residual solvent signal (CD_3OD: $\delta_H = 3.34$, $\delta_C = 49.0$). The multiplicities of ^{13}C resonances were determined by DEPT experiments. ^{1}H connectivities were determined by using COSY and HOHAHA experiments. The 2D HOHAHA experiments were performed in the phase-sensitive mode (TPPI) using the MLEV-17 (mixing time 125 ms) sequence for mixing. One-bond heteronuclear ^{1}H-^{13}C connectivities were determined with 2D HMQC experiments with a BIRD pulse sequence followed by a delay of 0.5 s before each scan to suppress the signal from proton not directly bonded to ^{13}C. The interpulse delays were adjusted for an average ($^1J_{CH}$ of 125 Hz). Two- and three-bond heteronuclear ^{1}H–^{13}C connectivities were determined with 2D HMBC experiments optimized for a $^{2,3}J_{CH}$ of 8 Hz. Nuclear Overhauser effect (NOE) measurements were performed by 2D ROESY experiments. MPLC purification was performed on a Büchi 861 apparatus. HPLC in isocratic mode was performed on a Varian apparatus equipped with RI-3 refractive index detector and μ-Bondapack C18 columns.

3.2. Extraction and isolation

Plants of *Allium porrum* L. (1.6 kg) were collected near Benevento (Italy) in September 1999. The sample was sown about 6 months before its collection. Reference specimens have been deposited at the Dipartimento di Chimica delle Sostanze Naturali, Università di Napoli Federico II, Italy, with the voucher number 2025. The fresh bulbs (988 g) were air-dried immediately after collection, under controlled temperature (22°C) and without exposure to the light. They were chopped and then exhaustively extracted (79 g, dry weight after extraction) at room temperature with the following solvents: *n*-hexane, $CHCl_3$,$CHCl_3$/MeOH (9:1), and MeOH. Each extraction was repeated four times using 500 ml of solvent, under stirring. The *n*-butanol soluble material of the MeOH extract was concentrated in vacuo to afford a crude extract (5.5 g) which was subjected to silica RP-18 MPLC (gradient solvent system from H_2O to MeOH). Fractions eluted with H_2O/MeOH 3:7 (181 mg) were separated by preparative RP HPLC [μ-Bondapack C18 (7.8 × 300 mm) column, H_2O/MeOH 1:1] to obtain pure astragaline (**1**, 15.1 mg) and kaempferol-3-*O*-neohesperidoside (**2,** 8.8 mg). Fractions eluted with H_2O/MeOH 2:8 (147 mg) were separated by preparative RP HPLC [eluent H_2O/MeOH 6:4] thus obtaining pure compound **3** (5.5 mg) and crude compounds **4** and **5**. Consequently, the former was isolated carefully by analytical RP HPLC [μ-Bondapack C18 (3.9×300 mm) column, H_2O/MeOH 6:4] to yield pure compound **4** (8.1

mg). The latter was subjected to the same purification procedure which afforded 6.5 mg of pure compound **5**.

3.3. Kaempferol 3-O-[2-O-(trans-3-methoxy-4-hydroxy cinnamoyl)]-β-D-galactopyranosyl-(1→4)-O-β-D-glucopyranoside (**4**)

Yellow amorphous solid. $[\alpha]_D^{25} = -9°$ (MeOH; *c* 0.02); UV spectra: see Table 1; ^{1}H NMR and ^{13}C NMR spectra: see Table 2; FABMS (negative ion): *m/z* 785 (100), 285 (30) [M-H]$^-$. HR-FABMS (negative ion): *m/z* 785.2015 [M-H]$^-$, calcd. for $C_{37}H_{37}O_{19}$ *m/z* 785.2007.

3.4. Kaempferol 3-O-[2-O-(trans-3-methoxy-4-hydroxy-cinnamoyl)]-β-D-glucopyranosyl-(1→6)-O-β-D-glucopyranoside (**5**)

Yellow amorphous solid. $[\alpha]_D^{25} = -13°$ (MeOH; *c* 0.02); UV spectra: see Table 1; ^{1}H NMR and ^{13}C NMR spectra: see Table 2; FABMS (negative ion): *m/z* 785 (100), 285 (26) [M-H]$^-$. HR-FABMS (negative ion) *m/z* 785.2000 [M-H]$^-$, calcd. for $C_{37}H_{37}O_{19}$ *m/z* 785.2007.

3.5. Methanolysis and sugar analysis

A solution of **4** (2 mg) in anhydrous 2 M HCl–MeOH (0.5 ml) was heated at 80°C in a stoppered reaction vial for 8 h. Once cooled, the reaction mixture was neutralized with Ag_2CO_3, centrifuged and the supernatant evaporated to dryness. The residue was treated with TRISIL Z for 15 min at room temp. GLC analysis (Hewlett-Packard 5890, 25 m, SBB-I; column temp. 140°C, injector temp. 200°C; helium carrier flow 10 ml/min) gave peaks that co-eluted with those of authentic methyltrisilglucoside [R_t (min): 37.6 and 42.8 (1 mol)] and methyltrisilgalactoside [R_t (min): 28.2 and 33.4 (1 mol)]. By repeating the same analysis for compound **5** (2 mg), only the peaks of methyltrisilglucoside were obtained.

3.6. Platelet anti-aggregation test

Blood (20 ml) was withdrawn by cardiac puncture from rats into plastic syringes containing 1/10 vol. of 3.8% sodium citrate and mixed immediately. Platelet-rich plasma (PRP) was prepared by centrifugation of the anti coagulated blood at 250 × *g* for 10 min. Platelet-poor plasma (PPP) was obtained from centrifugation of the residue at 650 × *g* for 10 min. All procedures were performed at room temperature. Platelet aggregation was monitored in an Elvi Pyton (Born) light transmission aggregometer. PPP was used to adjust to 100% transmittance. For all experiments 250 μl of PRP and 5 μl of the aqueous test samples solutions, or vehicle, were left in contact at room temp., for 10 min. Then, they were incubated at 37°C for 1 min with stirring and ADP (10 μg/ml) was added as aggregating agent. Results obtained were analyzed by ANOVA one-way followed by Dunnett's test for multiple comparison; a value of $P < 0.05$ was taken as significant.

Acknowledgements

Financial support by MURST and by Università del Molise (ex quota 60%) is gratefully acknowledged. We also thank Mr. Raffaele Troiano for skilful technical assistance.

References

Augusti, K.T., 1990. Therapeutic and medicinal values of onions and garlic. In: Brewster, J.L., Rabinowitch, H.D. (Eds.), Onions and Allied Crops, Vol. 3. CRC Press, Boca Raton, pp. 93–104.

Block, E., 1992. The organosulfur chemistry of the genus *Allium*. Implications for organic sulfur chemistry. Angewande Chemie, Int. Ed. Engl. 31, 1135–1178.

Carotenuto, A., De Feo, V., Fattorusso, E., Lanzotti, V., Magno, S., Cicala, C., 1996. The flavonoids of *Allium ursinum*. Phytochemistry 41, 531–536.

Carotenuto, A., Fattorusso, E., Lanzotti, V., Magno, S., De Feo, V., Cicala, C., 1997. The flavonoids of *Allium neapolitanum*. Phytochemistry 44, 949–957.

Hohmann, J., Pall, Z., Guenther, G., Mathe, I., 1997. Flavonolacyl glycosides of the aerial parts of *Eryngium campestre*. Planta Medica 63, 96.

Landolfi, R., Mower, R., Steiner, M., 1984. Modification of platelet function and arachidonic acid metabolism by bioflavonoids. Structure-activity relations. Biochemical Pharmacology 33, 1525–1530.

Mabry, T.J., Markham, K.R., Thomas, M.B., 1970. The Systematic Identification of Flavonoids. Springer Verlag, New York.

Nakano, K., Murakami, K., Nohara, T., Tomimatsu, T., Kawasaki, T., 1981. The constituents of *Paris verticillata* M. *v.* Bieb. Chemical & Pharmacological Bulletin 29, 1445–1451.

Romussi, G., Bignardi, G., Pizza, C., De Tommasi, N., 1991. Constituents of Cupuliferae. XIII. New and revised structures of acylated flavonoids from *Quercus suber* L. Archives Pharmacology 324, 519–524.

Tzeng, S.H., Ko, W.C., Ko, F.N., Teng, C.M., 1991. Inhibition of platelet aggregation by some flavonoids. Thrombosis Research 64, 91–100.

PERGAMON

Phytochemistry 57 (2001) 571–574

PHYTOCHEMISTRY

www.elsevier.com/locate/phytochem

Flavones and phenylpropenoids in the surface exudate of *Psiadia punctulata*

Benard F. Juma[a], Abiy Yenesew[a], Jacob O. Midiwo[a,*], Peter G. Waterman[b]

[a]*Department of Chemistry, University of Nairobi, PO Box 30197, Nairobi, Kenya*
[b]*Centre for Phytochemistry, Southern Cross University, PO Box 157, Lismore, NSW 2480, Australia*

Received 7 November 2000; received in revised form 12 March 2001

Abstract

Three flavones, 5,7-dihydroxy-2′,3′,4′,5′-tetramethoxyflavone, 5,4′-dihydroxy-7,2′,3′,5′-tetramethoxyflavone, and 5,7,4′-trihydroxy-2′,3′,5′ -trimethoxyflavone were isolated from the leaf exudate of *Psiadia punctulata*, together with the previously reported 5-hydroxy-7,2′,3′,4′,5′-pentamethoxyflavone and 5,7,3′-trihydroxy-2′,4′,5′-trimethoxyflavone. The two phenylpropenoids, *Z*-docosyl-*p*-coumarate and *E*-docosyl-*p*-coumarate were also isolated. The structures were determined on the basis of spectroscopic evidence.
© 2001 Elsevier Science Ltd. All rights reserved.

Keywords: *Psiadia punctulata*; Compositae; Surface exudates; Flavones; Phenylpropenoids; 5,7-Dihydroxy-2′,3′,4′,5′-tetramethoxyflavone; 5,4′-Dihydroxy-7,2′,3′,5′-tetramethoxyflavone; 5,7,4′-Trihydroxy-2′,3′,5′-trimethoxyflavone; *Z*-Docosyl-*p*-coumarate

1. Introduction

The leaves of *Psiadia punctulata* (DC) Vatke are extensively covered by an exudate, especially when young. The exudate is most likely responsible for the unpalatability (to herbivores) and drought resistance (as we have observed) which is exhibited by this shrub, in a manner comparable to that described for *Larrea* spp. (Rhoades, 1977). The chemistry of the exudate could also explain the use of the species for relief of fever and abdominal pains (Kokwaro, 1976) as well as its use for expunging ectoparasites from cattle (Beentje, 1994).

In an earlier communication we described the presence of kaurene and trachyloban diterpenes in the exudate (Midiwo et al., 1997). We compared these metabolites with the diterpenes reported from *P. arabica* Jaub and Spach, with which *P. punctulata* is sometimes confused (Abou-Zaid et al., 1991), and suggested that there were differences which could be used to delineate them as distinct taxa.

Plant leaf exudates are known to most often contain mixtures of terpenoids and non-polar flavonoids (Wollenweber, 1988). In this paper we report on the isolation and characterisation of five flavones, three of which are new, along with two geometrically isomeric phenylpropenoid docosyl esters, one of which has not been reported before.

2. Results and discussion

Fresh leaves of *P. punctulata* were dipped in ethyl acetate for short periods (ca. 20 s) providing a gummy extract on removal of solvent. We have established (see Experimental) that the average exudate to dry leaf weight is about 1:4. TLC analysis of the extract revealed seven major spots of phenolic nature (254 nm UV light, ferric chloride spray reagent). Silica gel chromatography led to the successful isolation and characterization of five flavones and two phenylpropenoids.

The first compound (**1**) characterised was a flavone. The presence of the flavone moiety was deduced from the UV (λ_{max} 270 and 362 nm), ^{1}H NMR (δ 7.10 for H-3) and ^{13}C NMR (δ 162.7 for C-2, 110.6 for C-3 and 183.3 for C-4) spectra. The ^{1}H NMR spectrum also indicated the presence of a chelated hydroxyl, a free hydroxyl, meta-coupled H-6 and H-8 protons, a single B-ring proton and four methoxyl substituents. In the EIMS, the molecular ion was established as 374 ($C_{19}H_{18}O_8$), and a fragment ion appearing at m/z 153 derived from retro-Diels–Alder fragmentation (Mossa et al., 1992), suggested the presence of two hydroxy groups in ring A, at C-5 and C-7. The four methoxyl

* Corresponding author. Tel.: +254-2-440436; fax +254-2-446138.
E-mail address: jmidiwo@uonbi.ac.ke (J.O. Midiwo).

0031-9422/01/$ - see front matter © 2001 Elsevier Science Ltd. All rights reserved.
PII: S0031-9422(01)00147-9

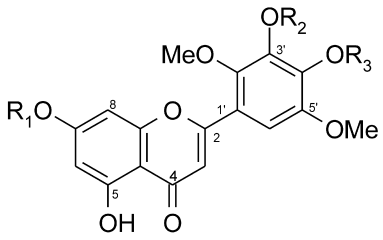

1 $R_1 = H, R_2 = R_3 = Me$
2 $R_1 = R_2 = R_3 = Me$
3 $R_1 = R_2 = Me, R_3 = H$
4 $R_1 = R_3 = H, R_2 = Me$
5 $R_1 = R_2 = H, R_3 = Me$

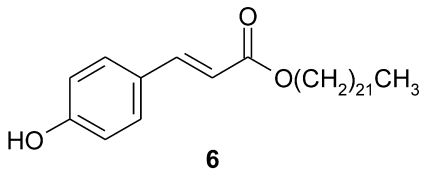

6

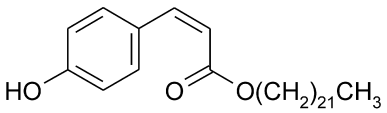

7

groups must therefore be placed in ring B, at positions C-2′,-3′,-4′, and -5′. The ^{13}C NMR resonances for the methoxyl carbons (Table 1) confirmed that three were di-*ortho* substituted (resonances > 59.5 ppm) while one had a free *ortho* position (resonance < 58.5 ppm) (Panichpol and Waterman, 1978). In a NOESY experiment the singlet at δ 7.22 (H-6′) was observed to interact with the methoxyl resonance at δ 3.84. On these grounds and comparison with data for 5-hydroxy-7,2′,3′,4′,5′-pentamethoxyflavone (**2**) (Mossa et al., 1992), compound **1** was identified as 5,7-dihydroxy-2′,3′,4′,5′-tetramethoxyflavone.

A second flavone (**3**) was similar to compound **1**, the NMR spectra indicating a tetramethoxyflavone with the same substitution pattern and with EIMS showing M^+ again at 374. However, the EIMS of this compound revealed that it had a methoxyl and a hydroxyl group in ring-A due to the presence of a fragment ion at *m/z* 167, with the hydroxyl group being placed at C-5 (chelated proton at δ 12.78 in the ^1H NMR spectrum). The ^{13}C NMR spectrum indicated the same B-ring oxygenation pattern as in **1** with the chemical shift for the ring-B methoxyls (δ 61.4, 61.3, 56.3 and 56.0) indicating that two of them were di-*ortho* substituted. Thus it was concluded the C-5′ was methoxylated with C-2′, C-3′ and C-4′ bearing two methoxyls and one hydroxyl. This hydroxyl group was deduced to be at the 4′-position because of the 40 nm shift in band I in the UV spectrum on addition of NaOH (Markham, 1982). This requires that compound **3** was 5,4′-dihydroxy-7,2′,3′,5′-tetramethoxyflavone. This assertion was confirmed by NOE interactions between the 4′-hydroxyl proton and two methoxy methyls (δ 3.86 and 4.02) and between one methoxyl (δ 3.89) and H-6 and H-8 and one methoxyl (δ 3.86) and H-6′.

The third flavone (**4**) showed the same oxygenation pattern but with only three methoxyl substituents. The EIMS indicated M^+ at 360 ($C_{18}H_{16}O_8$), with a fragment at *m/z* 153 which places two hydroxyl groups on ring A. The presence of hydroxyl groups at C-5 and C-7 were established by observation of bathochromic shifts for band I at 326 nm on addition of $AlCl_3$ (no change with HCl) and a NaOAc shift of bands II, respectively. This leaves three methoxyls and a further hydroxy group in ring B. The spectroscopic evidence (Experimental and Table 1) indicated that its ring B was identical to that of compound **3**. Compound **4** was therefore designated as 5,7,4′-trihydroxy-2′,3′,5′-trimethoxyflavone.

The other flavones isolated from this exudate were shown to be 5-hydroxy-7,2′,3′,4′,5′-pentamethoxyflavone (**2**) and 5,7,3′-trihydroxy-2′,4′,5′-trimethoxyflavone (**5**) which had previously been isolated from *P. arabica* (El-Feraly et al., 1990; Mossa et al., 1992).

The complexity of the non-polar flavone profile in the *P. punctulata* exudate is much less than that in *P. arabica*. Furthermore the *P. punctulata* flavones appear to be exclusively B-ring tetra-oxygenated while for *P. arabica*

Table 1
^{13}C NMR (125 MHz) chemical shift position for flavones **1**–**5**[a]

C	1	2	3	4	5
2	162.7	161.9	161.9	163.4	163.2
3	110.6	110.3	110.1	110.4	109.5
4	183.3	182.9	182.9	183.4	183.5
4a	105.6	105.8	102.9	105.6	105.5
5	163.7	162.5	162.4	163.7	163.7
6	100.6	98.1	98.2	100.5	100.5
7	166.7	165.7	165.8	166.6	166.4
8	95.5	92.2	92.8	95.5	95.4
8a	159.3	158.1	158.1	159.4	159.3
1′	121.0	120.0	119.8	121.0	115.3
2′	147.9[b]	147.9[b]	141.4[b]	144.0	149.0
3′	147.1[b]	146.8[b]	143.6[b]	146.8	143.5
4′	148.6[b]	147.6[b]	149.0[b]	142.0	146.7
5′	150.7[b]	149.7[b]	139.6[b]	150.6	146.6
6′	107.9	106.5	105.9	103.0	107.6
C-2′-OCH_3	61.6[c]	61.6[c]	61.3[c]	61.2	61.8
C-3′-OCH_3	61.9[c]	61.6[c]	61.4[c]	61.1	
C-4′-OCH_3	61.8[c]	61.5[c]			61.1
C-5′-OCH_3	56.9	56.7[d]	56.3[d]	56.8	57.0
C-7- OCH_3		56.0[d]	56.0[d]		

[a] Compounds **1**, **4** and **5** run in pyridine-d_5; **2** and **3** in $CDCl_3$.
[b,c,d] Values in the same column are interchangeable.

examples are observed of mono-, di-, tri- and tetra-oxygenation in this ring (Abou-Zaid et al., 1991). The differences in flavonoid composition sets the two taxa apart in the same manner as the diterpenoid disparities already noted. Therefore their proposed synonymy (Abou-Zaid et al., 1991) may not be correct.

Together with the flavones two isomeric *p*-coumarate esters were isolated. Compound **6** was identified as E-docosyl *p*-coumarate which is already known from the stems of *Bauhinia manca* (Achenbach et al., 1986). Compound **7** had similar characteristics to **6** and was shown to be its *Z*-isomer, which seems to be reported here for the first time. While the main components of aerial exudates are non-polar flavonoids and terpenes these two non-polar esters indicate that they are sometimes other minor components of the hydrophobic external exudate.

3. Experimental

3.1. General

Mps: uncorr. Analytical TLC: Merck pre-coated silica gel 60 F_{254} plates. CC on silica gel 60 (70–230 mesh). EIMS: direct inlet, 70 eV. ^{1}H NMR (500 MHz) and ^{13}C NMR (125 MHz) were run on a DRX-500 (Brüker) spectrometer using solvent resonances to calibrate the spectra.

3.2. Plant material

The material used and vouchers have been described previously (Midiwo et al., 1997).

3.3. Extraction

Extraction with ethyl acetate was done as previously described (Midiwo et. al., 1997) to give 494 g of exudate from aerial parts which when dried weighed 1700 g. The crude extract (100 g) was adsorbed onto silica gel (100 g) and added to a silica gel (500 g) column under *n*-hexane. Elution was achieved with *n*-hexane/CH_2Cl_2/MeOH mixtures of increasing polarity to give **1** (2.2 g), **2** (2.0 g), **3** (58 mg), **4** (10 mg), **5** (130 mg), **6** (267 mg), **7** (60 mg).

3.4. Physical and spectral data of isolated compounds

3.4.1. 5,7-Dihydroxy-2′,3′,4′,5′-tetramethoxyflavone (*1*)

Yellow needles (*n*-hexane/CH_2Cl_2). Mp 226–227°. UV λ_{max} (MeOH) nm: 216, 270, 362; NaOMe: 218, 285, 325; NaOAc: 222, 272, 362; NaOAc/H_3BO_3: 222, 272, 362; $AlCl_3$: 216, 285, 363; $AlCl_3$/HCl: 218, 279, 368. ^{1}H NMR (pyridine-d_5): δ 3.84 (OMe-5′), 3.88 (OMe-4′), 3.95 (OM-2′), 3.99 (OMe-3′), 6.79 (1H, *d*, J=2.0 Hz, H-6), 6.85 (1H, *d*, J=2.0 Hz, H-8), 7.10 (1H, *s*, H-3), 7.22 (1H, *s*, H-6′), 13.63 (1H, *s*, 5-OH). ^{13}C NMR: see Table 1. EIMS *m*/*z* (rel. int.): 374 (54, $[M]^+$), 359 (5), 333 (6), 301 (4), 257 (7), 153 (8), 149 (14), 129 (12), 115 (64), 69 (64), 61 (100).

3.4.2. 5-Hydroxy-7,2′,3′,4′,5′-pentamethoxyflavone (*2*)

Yellow needles (*n*-hexane/CH_2Cl_2). Mp 127–128° (lit. 124–125° Mossa et al. 1992). UV λ_{max} (MeOH) nm: 216, 268, 330; NaOMe: 220, 281, 364; NaOAc: 221, 270, 330; NaOAc/H_3BO_3: 221, 270, 330; $AlCl_3$: 218, 280, 364; $AlCl_3$/HCl: 220, 280, 362. ^{1}H NMR ($CDCl_3$): δ 3.88 (OMe-4′), 3.89 (OMe-7), 3.92 (OMe-2′), 3.97 (Me-5′), 3.99 (Me-3′), 6.38 (1H, *d*, J=2.2 Hz, H-6), 6.45 (1H, *d*, J=2.2 Hz, H-8) 6.88 (1H, *s*, H-3) 7.03 (1H, *s*, H-6′), 12.81 (1H, *s*, H-5). ^{13}C NMR: see Table 1. EIMS *m*/*z* (rel. int.): 388 (100, $[M]^+$), 373 (9), 342 (10), 7 (6).

3.4.3. 5,4′-Dihydroxy-7,2′,3′,5′-tetramethoxyflavone (*3*)

Yellow needles (*n*-hexane/CH_2Cl_2). Mp 164–166°. UV λ_{max} (MeOH) nm: 218, 267, 324; NaOMe: 220, 266, 364; NaOAc: 225, 260, 336; NaOAc/H_3BO_3: 225, 265, 323; $AlCl_3$: 220, 276, 362; $AlCl_3$/HCl: 220, 276, 362. ^{1}H NMR ($CDCl_3$): δ 3.86 (OMe-5′), 3.89 (OMe-7), 3.93 (OMe-2′), 4.02 (OMe-3′), 6.12 (1H, *s*, 4′-OH), 6.39 (1H, *d*, J=2.0 Hz, H-6), 6.46 (1H, *d*, J=2.0 Hz, H-8) 6.85 (1H, *s*, H-3), 6.93 (1H, *s*, H-6′), 12.78 (1H, *s*, 5-OH). ^{13}C NMR: see Table 1. EIMS *m*/*z* (rel. int.): 374 (100, $[M]^+$), 359 (8). 167 (6), 57 (8).

3.4.4. 5,7,4′-Trihydroxy-2′,3′,5′-trimethoxyflavone (*4*)

Yellow needles (*n*-hexane/EtOAc). Mp 231–233°.UV λ_{max} (MeOH) nm: 228, 269, 326; NaOMe: 230, 272, 368; NaOAc: 226, 272, 360; NaOAc/H_3BO_3: 226, 266, 368; $AlCl_3$: 228, 274, 360; $AlCl_3$/HCl: 228, 274, 334. ^{1}H NMR (acetone-d_6): δ 3.84(OMe-5′), 3.87(OMe-4′), 3.91 (OMe-2′), 6.27 (1H, *d*, J=2.0 Hz, H-6) 6.49 (1H, *d*, J=2.0 Hz, H-8), 6.49 (1H, *d*, J =2.0, H-8), 6.76 (1H, *s*, H-3), 6.97 (1H, *s*, H-6′) 13.68 (1H, *s*, 5-OH). ^{13}C NMR: see Table 1. EIMS *m*/*z* (rel. int.): 360 (100, $[M]^+$), 345 (8), 243 (11), 165 (6), 153 (9).

3.4.5. 5,7,3′-Trihydroxy-2′,4′,5′-trimethoxyflavone (*5*)

Yellow needles (*n*-hexane/EtOAc). Mp 254–255° (lit. 232–233° Mossa et al. 1992) UV λ_{max} (MeOH) nm: 216, 270, 362; NaOMe: 220, 280, 408; NaOAc: 220, 278, 365; NaOAc/H_3BO_3: 220, 268, 362; $AlCl_3$: 216, 276, 408; $AlCl_3$/HCl: 216, 276, 408. ^{1}H NMR (CD_3OD): δ 3.85 (OMe-5′), 3.92 (OMe-3′), 3.98 (OMe-2′), 6.78 (1H, *d*, J=2.1 Hz, H-6), 6.85 (1H, *d*, J=2.1 Hz, H-8), 7.04 (1H, *s*, H-3), 7.18 (1H, *s*, H-6′) 13.78 (1H, *s*, 5-OH). ^{13}C NMR: see Table 1. EIMS *m*/*z* (rel. int.): 360 (100, $[M]^+$), 345 (8).

3.4.6. E-Docosyl-p-coumarate (*6*)

White flakes (*n*-hexane/EtOAc). Mp 84–86°. UV λ_{max} (MeOH) nm: 214, 230, 300, 310, 360. ^{1}H NMR ($CDCl_3$): δ 7.63 (1H, *d*, J=16.0 Hz, H-β) 7.44 (2H, *d*, J=8.7 Hz, H-2/6), 6.82 (2H, *d*, J=8.7 Hz, H-3/5), 6.31 (1H, *d*, J=16.0 Hz, H-α), 4.20 (2H, *t*, OCH_2), 1.27–1.70

(37H, *m*, aliphatic chain), 0.89 (3H, *t*, Me). ^{13}C NMR ($CDCl_3$): δ 173.0 (C=O), 159.0 (C-4), 144.5 (C-α), 131.4 (C-2/6), 127.5 (C-5), 116.1 (C-3/5) 110.1 (C-β), 64.9 (OCH_2), 22.1–33.3 (aliphatic chain), 15.5 (Me).

3.4.7. Z-Docosyl-p-coumarate (7)

White flakes (*n*-hexane/EtOAc). Mp 61–63°. UV λ_{max} (MeOH) nm: 214, 230, 300, 360. ^{1}H NMR ($CDCl_3$): δ 7.64 (2H, *d*, $J=8.6$ Hz, H-2/6), 6.87 (2H, *d*, $J=8.6$ Hz, H-3/5), 6.82 (1H, *d*, $J=12.8$ Hz, H-α), 5.86 (1H, *d*, $J=12.8$ Hz, H-β), 4.15 (2H, *t*, OCH_2), 1.27–1.31 (37H, *m*, aliphatic chain), 0.89 (3H, *t*, Me). ^{13}C NMR ($CDCl_3$): δ 167.1 (C=O), 156.0 (C-4), 143.6 (α-C), 132.0 (C-2/6), 127.7 (C-1) 117.4 (C-3/5), 115.2 (C-β), 64.8 (OCH_2), 22.9–32.2 (aliphatic chain), 14.3 (Me). EIMS *m*/*z* (rel. int.): 472 (6, $[M]^+$), 444 (5), 416 (24), 164 (100), 147 (41), 120 (18), 69 (17), 59 (17).

References

Abou-Zaid, M.M., El-Karemy, Z., El-Negoumy, S.I., Altosaar, I., Saleh, N.A.M., 1991. The flavones of *Psiadia punctulata*. Bulletin of the Chemical Society of Ethiopia 5, 37–39.

Achenbach, H., Stocker, M., Constenla, M.A., 1986. Chemical investigation of tropical medicinal plants XXI. Long chain alkyl esters of ferulic and *p*-coumaric acids from *Bauhinia manca*. Z. Naturforsch Ser. C 41, 164–168.

Beentje, H.J., 1994. Kenya Trees, Shrubs and Lianas. National Museums of Kenya, Nairobi. p. 560.

El-Feraly, F.S., Mossa, J.S., Al-Yahya, M.A., Hifnawy, M.S., Hafez, M.M., Hufford, C.D., 1990. Two flavones from *Psiadia arabica*. Phytochemistry 29, 3372–3373.

Kokwaro, J.O., 1976. Medicinal Plants of East Africa. East African Literature Bureau, Nairobi. p. 69.

Markham, K.R., 1982. Techniques of Flavonoid Identification. Academic Press. 36.

Midiwo, J.O., Owuor, F.A.O., Juma, B.F., Waterman, P.G., 1997. Diterpenes from the leaf exudate of *Psiadia punctulata*. Phytochemistry 45, 117–120.

Mossa, J.S., El-Domiaty, M.M., Al-Meshal, I.A., Hufford, C.D., McPhail, D.R., McPhail, A.T., 1992. A flavone and diterpene from *Psiadia arabica*. Phytochemistry 31, 2863–2868.

Panichpol, K., Waterman, P.G., 1978. Novel flavonoids from the stem of *Popowia cauliflora*. Phytochemistry 17, 1363–1367.

Rhoades, D.F., 1977. Integrated anti-herbivore, anti-desiccant and ultraviolet screening of Creosote bush resin. Biochemical Systematics and Ecology 5, 281–290.

Wollenweber, E., 1988. Occurrence of flavonoid aglycones in medicinal plants. In: Plant Flavonoids, in Biology and Medicine II: Biochemical Cellular and Medicinal Properties. Allan, J. Riss Inc, pp. 45–55.

PERGAMON

Phytochemistry 57 (2001) 575–578

PHYTOCHEMISTRY

www.elsevier.com/locate/phytochem

Kaempferol triosides from *Reseda muricata*

Nabil H. El-Sayed [a], Nehad M. Omara [b], Adel K. Yousef [b], Ahmed M. Farag [c], Tom J. Mabry [d,*]

[a] *National Research Centre, El-Tahrir St., Dokki Cairo, Egypt*
[b] *Desert Research Centre, Cairo, Egypt*
[c] *Faculty of Science, Cairo University, Cairo, Egypt*
[d] *School of Biological Sciences, Molecular Cell and Developmental Biology, The University of Texas at Austin, Austin, TX 78712, USA*

Received 4 August 2000; received in revised form 24 October 2000

Abstract

A flavonoid trioside and its coumaryl ester together with seven known flavonoids and five phenolic acids were isolated from the leaves of *Reseda muricata*. Their structures were elucidated by spectroscopic methods including UV, FAB MS, ^{1}H, ^{13}C and 2D-NMR, DEPT, HMBC and HMQC experiments. The two compounds were identified as kaempferol 3-*O*-β-D-glucopyranosyl-(1‴ → 2″)-*O*-α-L-rhamnopyranoside 7-*O*-β-D-glucopyranoside and kaempferol 3-*O*-β-D-glucopyranosyl-(1‴ → 2″)-*O*-α-L rhamnopyranoside 7-*O*-β-D-(6‴-*O*-*E*-coumarylglucopyranoside), respectively. © 2001 Elsevier Science Ltd. All rights reserved.

Keywords: *Reseda muricata*; Resedaceae; Kaempferol trioside; Kaempferol coumaryltrioside; Flavones; Phenolic acids

1. Introduction

Reseda muricata C. Presl., a herb distributed in southeast Egypt, represents one of 6 genera and is one of some 75 species that comprise the family Resedaceae (Täckholm, 1974). The Resedaceae is a part of the phyletic group which also contains the Crucifereae and Capparidaceae (Rizk, 1986). Although very little information about *R. muricata* is reported (Rizk, 1986), earlier chemical screening of related *Reseda* species detected flavonoids and phenolic acids (Goris et al., 1961; Jacquin-Dubreuil, 1972; Pagani, 1983; Rizk, 1986), non-protein amino acids (Meier et al., 1979), glucosinolates (Olsen and Soerenson, 1979) and alkaloids (Nakhatov et al., 1977). Pharmacological studies of extracts of various *Reseda* species showed anti-inflammatory (Susplugas-Taillade et al., 1988; Susplugas et al., 1993) and antimicrobial (Watt and Breyer, 1962) activities. In traditional medicine, extracts of *R. muricata* are being used in external treatments of hemorrhoids and for stomach aches and diarrhea (Boulos, 1983). We here report the isolation and identification of two new compounds, the kaempferol trioside **1** and its *p*-coumaryl ester **2** together with twelve other known flavonoids and phenolic acids.

2. Results and discussion

The known compounds apigenin, luteolin, kaempferol and its 7-*O*-glucoside and 3-*O*-rhamnoside, quercetin and its 7-*O*- glucoside, as well as chlorogenic, ferulic, caffeic, coumaric and *p*-hydroxybenzoic acids were identified by comparison of their ^{1}H and ^{13}C NMR spectra with literature data. The UV spectra in methanol and with diagnostic reagents of the new compounds **1** and **2** were both in accord with 3,7-di-*O*-substituted flavonols (Mabry et al., 1970); for **2** an additional peak, which was observed at 315 nm in MeOH, is consistent with the presence of a coumaryl group (Markham, 1982). These findings were confirmed by acid hydrolysis; both compounds afforded kaempferol, glucose and rhamnose; in addition, **2** gave coumaric acid. The presence of the coumaryl group in **2** was also supported by ^{13}C DEPT experiments, which showed two methylene, one methyl, 27 methine and 12 quarternary carbons which, together with FAB MS, established a molecular formula for **2** of $C_{42}H_{46}O_{22}$. Compound **1** was subjected to mild hydrolysis and the intermediate known compound kaempferol

* Corresponding author. Tel.: +202-366-9927; fax: +202-337-0931.
E-mail addresses: mabry@mail.utexas.edu (T.J. Mabry), nabil_17@yahoo.com (N.H. El-Sayed),

0031-9422/01/$ - see front matter © 2001 Elsevier Science Ltd. All rights reserved.
PII: S0031-9422(00)00479-9

3-*O*-rhamnoside 7-*O*-glucoside was detected; this compound was also isolated from the plant. Attempts to obtain the intermediate diglycoside from **2** were unsuccessful.

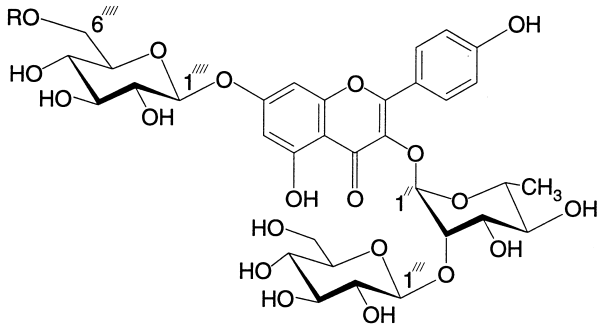

1, R = H

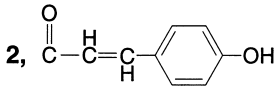

2,

The ^{1}H NMR spectra of both new compounds **1** and **2** exhibited A and B ring signals typical for a kaempferol 3,7-diglycoside (Mabry et al., 1970), and signals for three anomeric protons of three sugar moieties were detected for both compounds: one for a 3-*O*-rhamnosyl at δ 5.58 for **1** and δ 5.6 for **2** both *d*, $J = 1.1$ Hz, a signal for the anomeric proton of a 7-*O*-glucosyl at δ 5.05 for **1** and δ 5.06 for **2**, both *d*, $J = 7.5$ Hz and a third signal typical for a glucosyl unit linked to one of the other sugars at δ 4.25 for **1** and δ 4.33 for **2**, both *d*, $J = 7.8$ Hz. In addition, **2** exhibited doublets at δ 6.18 and δ 7.43, both $J = 15.85$ Hz plus signals for four protons at δ 6.69 and δ 7.35 *d*, both $J = 8.7$ Hz, indicative of a *trans p*-coumaryl group (Nasr et al., 1986; Schaufelberger et al., 1987).

The remaining structural questions for both **1** and **2** concerned the position of attachment of the terminal glucosyl moiety and, for **2**, the position of attachment of the coumaryl group. For both **1** and **2** the second glucosyl was assigned to the 2″-position of the 3-*O*-rhamnosyl moiety since the rhamnosyl H-2″ signal was shifted downfield to δ 4.11 for **1** and δ 4.13 for **2** (*t*, $J = 3.29$, 1.28 Hz). This assignment was confirmed by ^{13}C NMR spectroscopic analyses which showed the C-2″ downfield at δ 81.8 for **1** and δ 81.43 for **2**. HMQC and HMBC experiments for both **1** and **2** established correlations between C-1″ at δ 100.39 with H-1″ at δ 5.60, C-1″ with H-2″ at δ 4.13, C-3 at 134.28 with H-1″, C-2″ with H-1‴ at δ 4.33, thus confirming for both **1** and **2** assignment of the terminal glucosyl to the C-2 position of the rhamnosyl moiety.

The coumaryl group in **2** was established by NMR and FAB MS. The ^{1}H NMR spectrum of **2** showed the two protons for one C-6 methylene glucosyl shifted downfield to δ 4.23 m, and δ 4.14 *dd* ($J = 12$, 2.5 Hz) confirming acylation at the C-6 position (Yoshida et al., 1987; Kim, 1998; Zahir et al., 1999; Liu et al., 1999). The ^{13}C NMR spectrum also showed that the carbons of one of the C-6 methylenes was shifted downfield to δ62.81 further confirming acylation at the 6-position of a glucosyl moiety (Bloor and Falshaw, 2000). The assignment of the coumaryl group to C-6 of the 7-*O*-glucosyl was confirmed by an HMBC experiment which showed a correlation between the C=O of the coumaryl ester and H-6 of the 7-*O*-glucosyl at δ 4.14; significantly, the C-1‴″ carbon is also correlated to the same H-6 (Bloor, 1999). In the FAB MS of **2** a molecular ion peak $[M-H]^{-1}$ was observed at *m*/*z* 901; in addition an ion for the loss of the terminal glucosyl but without loss of the coumaryl group appeared at *m*/*z* 739 [M-H- 162]$^-$, thus establishing that the coumaryl moiety must be attached to the 7-*O*-glucosyl substituent.

Based on all these data the structure of **1** was assigned as kaempferol 3-*O*-β-D-glucopyranosyl-(1‴ → 2″)-*O*-α-L-rhamnopyranoside 7-*O*-β-D-glucopyranoside and **2** as kaempferol 3-*O*-β-D-glucopyranosyl-(1‴ → 2″)-*O*-α-L-rhamnopyranoside 7-*O*-β-D-(6‴″-*O*-*E*-coumarylglucopyranoside). Both **1** and **2** are new compounds.

3. Experimental

3.1. Spectral data

^{1}H and ^{13}C NMR spectra were recorded on a 500 MHz Bruker AMX and/or a Varian Unity Inova with TMS as an internal standard and DMSO-d_6 as solvent. FAB mass spectra were obtained using a Finigan MAT TSQ 700 spectrometer while UV in MeOH were recorded using a Shimadzu UV 240 spectrophotometer.

3.2. Plant material

Aerial parts of *Reseda muricata* were collected in 1999 in the Wadi Valley on the Dahb-Sharm El-Shaikh Road 140 Km from Sharm in the South of Sinai. A voucher specimen has been deposited in the Desert Research Centre Herbarium, Cairo, Egypt.

3.3. Extraction and isolation of flavonoids and phenolic acids

The dried aerial parts of *Reseda muricata* (500 g) were extracted with 70% EtOH (2.5 l×3). The EtOH extract was evaporated under reduced pressure affording (120 g) of crude extract. The latter was extracted with $CHCl_3$ and the residue (80 g) was examined by two dimensional PPC using benzene:acetone:water BAW and 15% HOAc as developing systems. A part of the latter extract was subjected to successive PPC using Whatmann No. 3MM paper and BAW and 15% HOAc for elution. Final purification was effected with a Sephadex LH-20 column using MeOH–H_2O (1:1) as eluant.

3.4. Hydrolysis experiments

Mild acid hydrolysis was carried out by treating 2–3 mg with 0.1 N HCl at 100° C for 1 h. Aliquots were removed after 5, 10, 15 and 20 min and immediately examined by paper chromatography using BAW as the developing solvent and with authentic samples. The final aqueous acidic mixture was treated with EtOAc then the residue was neutralized for determination of the released sugar moieties. Complete acid hydrolysis was carried out using 2 N HCl in aqueous MeOH for 2 h at 100°C. The final hydrolysate was treated as in the mild hydrolysis procedure.

3.5. Kaempferol 3-O-β-D-glucopyranosyl-(1‴ → 2″)-O-α-L-rhamnopyranoside 7-O-β-D-glucopyranoside) (1)

Yellow amorphous powder (12 mg), soluble in H_2O and 70% EtOH. $R_f \times 100 = 22$ and 77 in BAW and 15% HOAc, respectively. It gave a brown color which changed to yellowish brown with ammonia vapor under UV light; it gave a dirty green color with $FeCl_3$. UV λ max MeOH: 269, 350+ $AlCl_3$, 274, 305sh, 359sh, 407; +HCl 265, 302sh; 356, 405; NaOMe 275, 304, 365; NaOAc 269, 395, 397; NaOAc+ H_3BO_3 267, 305sh, 352. FAB MS *m/z* 755 $[M-H]^-$, 593 $[M-H-162]^-$.

^{1}H NMR of **1** (DMSO-d_6): δ 7.8 (2H, *d*, $J = 8.8$ Hz, H-2′, 6′), 6.9 (2H, *d*, $J = 8.7$ Hz, H-3′, 5′). 6.7(*d*, $J = 2$ Hz, H-8), 6.4 (*d*, $J = 2$ Hz H-6), 5.58 (*d*, $J = 1.1$ Hz, rham–3 H-1‴), 5.05 (*d*, $J = 7.5$ Hz, *glc*-7 H-1⁗), 4.25 (*d*, $J = 7.8$ Hz, *glc* terminal H-1‴), 4.11 (*t*, $J = 3.29$, 1.28 Hz, rham-3 H-2″), 3.7 (2H, *dd*, $J = 10.7$, 2 Hz *glc*-7 H-6 *a,b*), 3.55 (2H *m*, *glc*-3 terminal H-6 *a,b*), 3-3.5 (*m*, sugar protons), 0.88 (^{1}H, *d*, $J = 6$ Hz, rham- 3 CH_3). ^{13}C NMR; δ 176.58 (C-4), 162.7 (C-7), 159.6 (C-5), 157.6 (C-4′), 152.7 (C-2,9) 134 (C-3), 162.7 (C-7), 159.6 (C-5), 157.6 (C-4′), 105.6 (C-1‴), 105.4 (C-10), 100.3 (C-1″), 99.8 (C-1⁗), 99 (C-6), 94.4 (C-8), 81.8 (C-2″), 77.3 (C-3‴,3⁗), 75.4 (C-5‴,5⁗), 73 (C-2‴,2⁗), 70.9 (C-4″), 69.9 (C-3″), 69.6 (C-5″), 68.7 (C-4⁗), 68.3 (C-4‴), 62.8 (C-6⁗), 60 (C-6‴), 17.9 (CH_3 rham).

3.6. Kaempferol 3-O-β-D-glucopyranosyl-(1‴ → 2″)-O-α-L-rhamnopyranoside 7-O-β-D-(6⁗-O-E-coumaryl-glucopyranoside) (2)

Yellowish brown amorphous powder (15 mg), soluble in H_2O and 70% EtOH, $R_f \times 100 = 38$ and 62 in BAW and 15% HOAc, respectively. It gave the same color changes as **1**. UV λ max MeOH: 269, 315, 350;+$AlCl_3$ 274, 301 sh, 320, 360, 400 +HCl, 266, 300, 318, 395; +NaOAc 267, 320, 360, 390, +H_3BO_3 266, 302, 352. FAB MS *m/z*: 901 $[M-H]^-$, 739 $[M-162-H]^-$, 593 $[M-162-146-H]^-$, 447 $[M-162-146-146-H]^-$.

^{1}H NMR (DMSO-d_6): δ 7.74 (2H, *d*, $J = 8.8$ Hz, H-2′,6′), 7.43 (*d*, $J = 15.85$ Hz, *p*-coum H-7), 7.35 (2H, *d*, $J = 8.7$ Hz, *p*-coum H-2,6), 6.89 (2H, *d*, $J = 8.8$ Hz, H-3′5′), 6.69 (2H, *d*, $J = 8.7$ Hz, *p*-coum H-3,5), 6.66 (*d*, $J = 2.1$ Hz, H-8), 6.4 (*d*, $J = 2.1$ Hz, H-6), 6.18 (*d*, $J = 15.85$ Hz, *p*-coum H-8), 5.6 (*d*, $J = 1$ Hz rham-3 H-1″), 5.06 (*d*, $J = 7.5$ Hz, *glc*-7 H-1⁗), 4.33 (*d*, $J = 7.8$ Hz, terminal *glc* H-1‴), 4.23 (2H, *m* *glc*-7-H-6a), 4.14 (*dd*. 12.0, 2.5 Hz, *glc*-7 H-6_b), 4.13 (*t*, $J = 3.29$, 1.28 Hz, rham-3 H-2″), 3–4 (*m*, sugar protons), 0.91 (3H, *d*, $J = 6$ Hz, rham-3 CH_3).

^{13}C NMR (DMSO-d_6) δ 177.6 (C-4), 166.3 (CO *p*-coum), 162.71 (C-7), 155.84 (C-2,9), 160.8 (C-5), 160.04 (C-4 *p*-coum), 157.25 (C-4′), 144.64 (C-7 *p*-coum), 134.28 (C-3), 130.52 (C-2′,6′), 129.96 (C-2,6 *p*-coum), 124.53 (C-1 *p*-coum), 119.33 (C-1′), 115.67 (C-3′.5′), 115.56 (C-3,5 *p*-coum), 113.46 (C-8 *p*-coum), 105.89 (C-1‴), 105.59 (C-10), 100.39 (C-1″), 99.8 C-1⁗), 99.1 (C-6), 94.4 (C-8), 81.43 (C-2″), 77 (C-3⁗, 5⁗), 76.22 (C-3‴), 75.89 (C-5‴), 73.55 (C-2‴), 73 (C-2⁗), 71.51 (C-4″), 70.37 (C-3″), 69.98 (C-5″), 69.66 (C-4‴), 69.43 (C-4⁗), 62.81 (C-6⁗), 60.48 (C-6‴), 17.27 (CH_3 rham).

Acknowledgements

The research was supported at The University of Texas by a grant from The Robert A. Welch Foundation (F-130) to T.J.M.

References

Bloor, S.J., Falshaw, R., 2000. Covalently linked anthocyanin-flavonol pigments from blue *Agapanthus* flowers. Phytochemistry 53, 575–579.

Bloor, S.J., 1999. Novel pigments and copigmentation in the blue marguerite daisy. Phytochemistry 50, 1395–1399.

Boulos, L., 1983. Medicinal Plants of North Africa. Reference Publications, Algonac, MI.

Goris, A., Dubreuil, A., Moniez, R., 1961. Dyer's weld, *Reseda luteda* L. Distribution of flavones between the various parts of the plant. Annales Pharmaceutiques Francaisesanc. 19, 648–650.

Jacquin-Dubreuil, A., 1972. Direct densitometric determination by absorption of flavonoids of the yellow-weld (*Reseda luteda L.*). Journal of Chromatography 71, 487–498.

Kim, H.J., Woo, E-R., Shin, C-G., Park, H., 1998. A new flavonol glycoside gallate ester from *Acer okamotoanum* and its inhibitory activity against Human Immunodeficiency Virus-1 (HIV-1) integrase. Journal of Natural Products 61, 145–148.

Liu, H., Orjala, J., Sticher, O., Rali, T., 1999. Acetylated flavonol gylcosides from leaves of *Stenochlaena palustris*. Journal of Natural Products 62, 70–75.

Mabry, T.J., Markham, K.R., Thomas, M.B., 1970. The Systematic Identification of Flavonoids. Springer–Verlag, New York, Heidelberg, Berlin.

Markham, K.R., 1982. Techniques of Flavonoid Identification. Academic Press, London.

Meier, L.K., Olsen, O., Soerenson, H., 1979. Acidic amino acids in *Reseda luteola*. Phytochemistry 18, 1505–1509.

Nakhotov, I.K., Tadzhibaev, M., 1977. M, Malikov, V. M. Yunusov, S.Yu., Alkaloids of *Reseda lutea*. Khim. Prir. Soedin 3, 424–425.

Nasr, C., Haag-Berrurier, M., Lobstein-Guth, A., Anton, R., 1986. Kaempferol coumaroyl glucorhamnoside from *Ginko biloba*. Phytochemistry 25, 770–771.

Olsen, O., Soerenson, H., 1980. Glucosinolates and amines in *Reseda media*. Phytochemistry 19, 1783–1787.

Pagani, F., 1983. Caffeic acid choline ester: a new plant constituent from *Reseda luteola*. Planta Medica 48, 128.

Rizk, A.M., 1986. The Phytochemistry of the Flora of Qatar. Kingprint of Richmond, Great Britain.

Schaufelberger, D., Gupta, M.P., Hostettmann, K., 1987. Flavonol and secoiridoid glycosides from *Coutoubea spicata*. Phytochemistry 26, 2377–2379.

Susplugas, P., Mongold, J.J., Taillade, C., Serrano, J.J., 1993. Anti-inflammatory and analgesic activity of *Reseda phytenma*. Plant. Med. Phytother. 26, 375–382.

Susplugas-Taillade, C., Susplugas, P., Michel, F., 1988. Anti-inflammatory activity of an ether extract of *Reseda phytenma* L.: its effect on arachidonic acid metabolism. Pharmaceutica Acta Helvetiae 63, 59–63.

Täckholm, V., 1974. Student's Flora of Egypt, Cairo University. Cooperative Printing Company, Beirut.

Yoshida, T., Siato, T., Kadoya, S., 1987. New acylated flavonol glucosides in *Allium tuberosum*. Chemical and Pharmaceutical Bulletin 35, 97–107.

Watt, J.M., Breyer, M.G., 1962. The Medicinal and Poisonous Plants of Southern and Eastern Africa, 2nd Edition. Livingstone, E.S., Edinburgh and London.

Zahir, A., Jossang, A., Bodo, B., Provost, J., Cosson, J-P., Sévenet, T., 1999. Five new flavone 5-O-glycosides from *Lethedon tannaensis*: lethedosides and lethediosides. Journal of Natural Products 62, 241–243.

PERGAMON

Phytochemistry 57 (2001) 579–582

PHYTOCHEMISTRY

www.elsevier.com/locate/phytochem

Biflavonoids from *Ochna afzelii*

Dieudonné Emmanuel Pegnyemb[a], Raphael Ghogomu Tih[a], Beibam Lucas Sondengam[a,*], Alain Blond[b], Bernard Bodo[b]

[a]*Department of Organic Chemistry, Faculty of Science, University of Yaounde I, PO Box 812, Yaounde, Cameroon*
[b]*Laboratoire de Chimie des Substances Naturelles-ESA 8041 CNRS, Muséum National d'Histoire Naturelle, 63 rue Buffon 75005 Paris, France*

Received 19 July 2000; received in revised form 22 January 2001

Dedicated to the memory of Dr. P. Agendia

Abstract

The stem bark of *Ochna afzelii* furnished three biflavonoids among which two are new. Their structures were established from spectroscopic and chemical evidences. © 2001 Elsevier Science Ltd. All rights reserved.

Keywords: *Ochna afzelii*; Ochnaceae; Stem bark; Biflavonoids; Chalcone dimers; Lophirones

1. Introduction

In the continuation of our search for flavonoids in Cameroonian medicinal plants (Pegnyemb et al., 1998) we examined the MeOH extract of the stem bark of *Ochna afzelii* Oliv. (Ochnaceae), a small tree of the Ochnaceae family, found in groups on rocky peaks in forest areas in tropical Africa. Prominent medical uses include treatment of jaundice, toothache, female sterility, menstrual complaints, lumbago and dysentery. Recent phytochemical studies on related members of the Ochnaceae family led to the isolation of some bi-and tetraflavonoids (Bouquet, 1969; Ghogomu et al., 1989; Tih et al., 1992; Pegnyemb et al., 1994, 1998). No previous phytochemical studies on *O. afzelii* have been reported. In this paper, we report the isolation and the structural elucidation of two novel biflavonoids: isolophirone C, **2** and dihydrolophirone C, **3** obtained alongside with the known lophirone C, **1**.

2. Results and discussion

The methanol extract of the air-dried stem bark is a dark brown. Constituents were first separated by repeated column chromatography over silica gel with different eluting systems and then followed purified by gel chromatography on sephadex LH20 affording lophirone C, isolophirone C and dihydrolophirone C.

When analysed by CIMS, compound **1** gave a pseudomolecular ion $[M+H]^+$ at m/z 511, with the molecular formula $C_{30}H_{22}O_8$. It was identified as lophirone C after the comparison of its IR, ^1H and ^{13}C NMR spectra with those of an authentic sample (Ghogomu et al.,1989) from *L. lanceolata* (Table 1).

The IR spectrum of **2** was very similar to that of **1** and showed absorption bands at 3302 cm^{-1} (phenolic hydroxyl), 1635 cm^{-1} (conjugated carbonyl), 1625 cm^{-1} (conjugated double bonds) and at 1510 cm^{-1} (aromatic rings). Mass spectrometric studies revealed a molecular formula of $C_{30}H_{22}O_8$ suggesting that **2** is an isomer of **1** with the $[M+H]^+$ ion at m/z 511 in its chemical ionisation spectrum.

Peracetylation of **2** (Ac_2O/Py) afforded a pentaacetate derivative **4,** with no residual OH absorption in its IR . CIMS of **4** gave a $[M+H]^+$ ion at m/z 721 leading to a molecular mass of 720 for the pentaacetate derivative, confirmed by the appearance of five sharp singlet signals on its NMR spectrum. Hence **2** had five hydroxyl groups.

The ^{13}C NMR spectrum of **2** displayed signals for 30 carbon atoms which indicated two methylenes, 28 sp^2 carbons among which two were carbonyls, 13 sp^2 methine protons and seven quarternary carbons of which six are oxygenated.

The ^1H NMR spectrum displayed signals for two vicinal methylenes and 13 aromatic protons (Table 1).

* Corresponding author. Fax: +237-23-53-86.
E-mail address: epegny@uycdc.uninet.cm (B.L. Sondengam).

0031-9422/01/$ - see front matter © 2001 Elsevier Science Ltd. All rights reserved.
PII: S0031-9422(01)00101-7

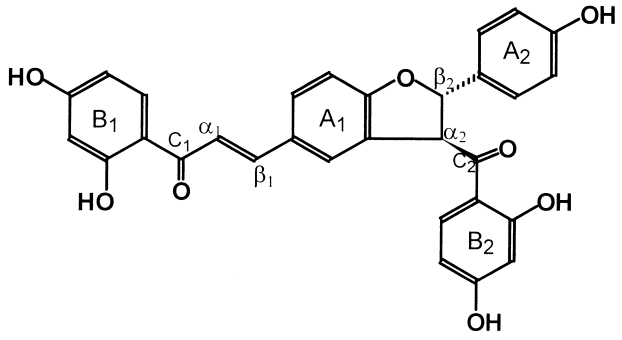

1 : Lophirone C.

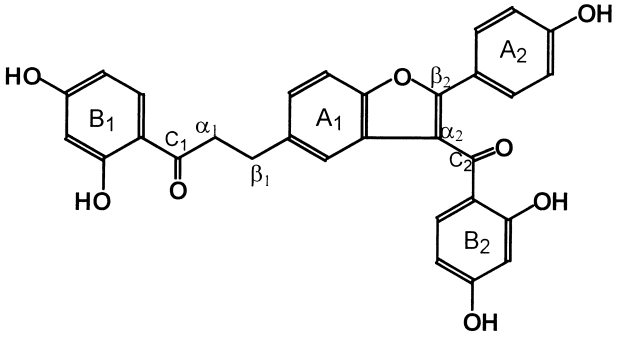

2 : Isolophirone C.

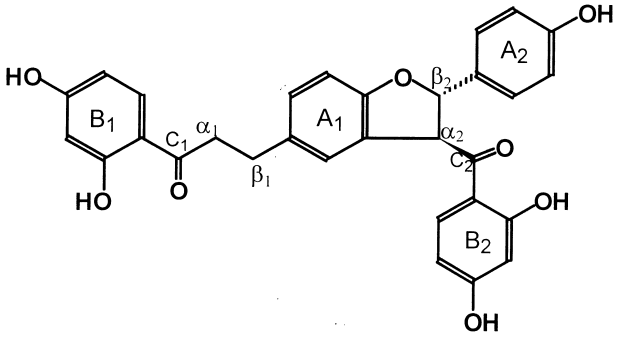

3 : Dihydrolophirone C.

From the analysis of the ^1H–^1H COSY spectrum, it was deduced that the aromatic protons were distributed into three 1, 2,4-trisubstituted (A_1, B_1 and B_2) and one para-disubstituted (A_2) aromatic rings. From the HMBC spectrum of compound **2**, correlations were noticed between the carbonyl carbon signal at 204.8 (C_1) and the aromatic proton at δ_H 7.79 (H-6 on the B_1-ring). The methylene carbon at δ_C 30.9 (β_1) was further correlated to the protons of the 1, 2, 4-trisubstituted aromatic A_1-ring. These results suggested a dihydrochalcone moiety. The upfield carbonyl carbon atom at δ_C 196.1 (C_2) showed long-range correlation with the H-6 proton (7.38 ppm) of the aromatic B_2-ring and the carbon at 156.5 (β_2) was correlated to the aromatic protons H-2′,H-6′ (7.61 ppm) of the para-disubstituted aromatic A_2-ring. Above evidence leads to structure **2** for which the name isolophirone C has been proposed.

Compound **3** also had an IR absorption very similar to **1** but its EI mass spectrum had the $[M]^+$ ion at m/z 512 which was resolved for $C_{30}H_{24}O_8$, hence having two hydrogens more than lophirone C **1**. The ^1H and ^{13}C NMR spectra of both compounds were similar suggesting a close relation between their structures. The presence of two carbonyl carbon atoms (δ_C 201.5 and 204.7), as well as one 1,4-disubstituted and three 1,2,4-trisubstituted aromatic rings, was evident in the spectrum of **3** as in the structure of **1**. Major differences in the ^{13}C NMR spectra of the two compounds, arise from the presence of another two sp^3 type carbon atoms at δ_C 40.2 and 29.5 in the spectrum of **3**, instead of two sp^2 methine carbon signals at δ_C 119.3 and 144.8 in the spectrum of **1**. The ^1H NMR spectrum of **3** differed from that of **1** mainly in the replacement of the AB system at δ_H 7.69 and 7.78 by an aliphatic A_2X_2 system at δ_H 3.17 (2H) and 2.88 (2H). Evidence that **3** had five phenolic hydroxyl groups was established when its complete acetylation furnished a penta-acetate derivative, (CIMS: $[M+H]^+$ at m/z 723). Chemical shift assignments were enabled through 2D NMR, HMBC data (Table 1). Higher NOE values were observed between H-α_2 and H-6 (B_2-ring) (24%) and between H-β_2 and H-(2′ + 6′, A_2-ring) (6%). While weaker NOE values were observed between H-α_2 and H-β_2 (2%), H-(2′ + 6′, A_2-ring) and H-2′ (A1-ring). This suggested a *trans* configuration of H-α_2 and H-β_2 and led to structure **3** for dihydrolophirone C.

3. Experimental

3.1. General

IR spectra were obtained using KBr discs. NMR ^1H, 300 MHz and ^{13}C, 75 MHz spectra were performed in Me_2CO-d_6 solution on a Bruker WM 300 instrument using TMS as internal standard. For the HMBC spectra, the delay was 70 ms ($J_{CH} \approx 7$ Hz).

3.2. Plant material

The stem bark of *Ochna afzelii*, Oliv. was harvested in Yaounde, Center Province of Cameroon in April 1997. A voucher specimen (No. 23456 /SRF/CAM) is on deposit at the National Herbarium in Yaounde, Cameroon.

3.3. Extraction and isolation

Ochna afzelii stem bark was chopped into small pieces, air-dried and finally reduced to a fine powder (7 kg)

Table 1
^{1}H NMR data for compounds **1–3** (acetone-d_6, TMS, 300 MHz)

	Compound no.								
	1			**2**			**3**		
	δH (ppm)	*m*	*J* (Hz)	δH (ppm)	*m*	*J* (Hz)	δH (ppm)	*m*	*J* (Hz)
2′-A_1	7.62	*brs*		7.42	*d*	1.8	7.00	*brs*	
5′-A_1	6.98	*d*	8.4	7.53	*d*	8.5	6.79	*d*	8.2
6′-A_1	7.80	*dd*	8.4, 1.7	7.36	*dd*	8.5, 1.8	7.15	*dd*	8.2, 1.4
α_1	7.69	*d*	15.4	3.33	*t*	7.5, 7.5	3.17	*t*	7.5, 7.5
β_1	7.78	*d*	15.4	3.09	*t*	7.5, 7.5	2.88	*t*	7.5, 7.5
3-B_1	6.34	*d*	2.3	6.30	*d*	2.3	6.31	*d*	2.4
5-B_1	6.44	*dd*	9.0, 2.3	6.39	*dd*	8.9, 2.3	6.38	*dd*	8.8, 2.4
6-B_1	7.97	*d*	9.0	7.79	*d*	8.9	7.70	*d*	8.8
2′-A_2	7.31	*m*		7.61	*m*		7.27	*m*	
3′-A_2	6.86	*m*		6.88	*m*		6.83	*m*	
5′-A_2	6.86	*m*		6.88	*m*		6.83	*m*	
6′-A_2	7.31	*m*		7.61	*m*		7.27	*m*	
α_2	5.47	*d*	6.8	–			5.32	*d*	7.2
β_2	6.19	*d*	6.8	–			6.14	*d*	7.2
3-B_2	6.39	*d*	2.3	6.49	*d*	2.3	6.39	*d*	2.4
5-B_2	6.54	*dd*	9.0, 2.3	6.23	*dd*	8.8, 2.3	6.51	*dd*	9.0, 2.4
6-B_2	7.95	*d*	9.0	7.38	*d*	8.8	7.92	*d*	9.0
OH	13.58	*s*		12.76	*s*		12.73	*s*	
OH	12.54	s		12.76	s		12.64	*s*	

which was extracted at room temperature with cold MeOH for 24 h in an iron tank equipped with a mechanical stirrer. Evaporation of the solvent yielded a dark brown gummy residue (400 g) which was fractionated by cc on silica gel using a CH_2Cl_2/MeOH gradient mixture starting from proportion 1/1 to pure MeOH, giving 11 fractions (OA_1 to OA_{11}). Fraction OA4 was a mixture of biflavonoids which was first chromatographed over silica gel (CH_2Cl_2/MeOH:20/1) to give crude fractions OA_4D and OA_4F which were further purified using sephadex LH20 (MeOH) to yield pure Lophirone C (18 mg), isolophirone C (17 mg) and dihydrolophirone C (12 mg).

3.4. Lophirone C, **1**, $C_{30}H_{22}O_8$

Yellow crystals, mp 190–191° (Me_2CO), lit: 191–193 °C [2]. $[\alpha]_D^{25} = -16.4°$ (Me_2CO; *c*, 0.5), CIMS (NH_3) *m/z* 511 $[M+H]^+$, 493 $[M-H_2O+H]^+$, EIMS (110°, 70 eV) *m/z* (%): 510 (0.4, M^+), 508 (2), 493 (24), 461 (1), 400 (13), 388 (11), 374 (10), 355 (13), 328 (2), 263 (17), 250 (9), 238 (7), 207 (6), 178 (7), 137 (75), 110 (80), 94 (58), 81 (47), 55 (65), ^{1}H and ^{13}C NMR: Tables 1 and 2.

3.5. Isolophirone C, **2**, $C_{30}H_{22}O_8$

Yellow crystals, mp 194–195° (Me_2CO) CIMS(NH_3) *m/z*: 528 $[M+NH_4]^+$, 511$[M+H]^+$ EIMS, (110°, 70eV), *m/z* (%): 510 (0.3, M^+), 498 (7), 467 (2), 418 (24), 359 (74), 343 (41), 327 (5), 309 (32), 297 (8), 273 (13), 267 (37), 249 (10), 217 (7), 203 (6), 177 (4), 137 (100), 110 (54), 94 (12).^{1}H and ^{13}C NMR: Tables 1 and 2.

3.6. Isolophirone C penta-acetate **4**

Compound **2** (10 mg) was dissolved in a mixture of pyridine (2 ml) and Ac_2O (2 ml). The reaction mixture was maintained at 50°C in a H_2O bath for 6 h after which it was concentrated to dryness under vacuum. The resulting crude acetate was first purified by prep. tlc followed by gel permeation cc over sephadex LH20 using MeOH as eluent yielding **4** (5 mg). CIMS (NH_3) *m/z*: 738 $[M+NH_4]^+$ 721 $[M+H]^+$. EIMS (110°, 70 eV) *m/z* (%): 720 (13, M^+), 660 (22.4), 636 (12.7), 618 (18.3), 576 (22.2), 533 (7.6), 457 (8.2), 442 (8.4), 441 (7.6), 400 (6.1), 373 (5.6), 355 (9.7), 261 (4.1), 236 (8.6), 179 (40.8), 163 (6.7), 137 (100), 121 (37.2). RMN ^{1}H (300 MHz) δ (ppm): 7.26 (1H, *d*, *J* = 2,4 Hz, H-2′A_1), 7,63 (1H, *d*, *J* = 8,1 Hz, H-5′A_1), 7.36 (1H, *dd*, *J* = 8,1; 2,4 Hz, H-6′A_1); 2.87 (2H, *t*, *J* = 7.6 Hz, H-α_1); 2.79 (2H, *t*, *J* = 7.6 Hz, H-β_1); 6.98 (1H, *d*, *J* = 2.5 Hz, H-3B_1); 7.07 (1H, *dd*, *J* = 8.9; 2,5 Hz, H-5B_1); 7.62 (1H, *d*, *J* = 8.9 Hz, H-6B_1), 7.76 (2H, *m*, *J* = 8.9 Hz, H-2′,6′A_2); 7.19 (2H, *m*, *J* = 8.9 Hz, H-3′, 5′A_2); 7.06 (1H, *d*, J = 2, 3Hz, H-2′,6′A_2); 6.86 (1H, *dd*, *J* = 8.6; 2.3 Hz, H-5B_2); 7.78 (1H, *d*, *J* = 8.6 Hz, H-6B_2); 2.18 (3H, *s*, OAc), 2.19 (3H, *s*, OAc), 2.22 (3H, *s*, OAc), 2.25 (3H, *s*, OAc) and 2.27 (3H, *s*, OAc).

3.7. Dihydrolophirone C, **3**, $C_{30}H_{24}O_8$

Yellow crystals, mp 187–188° (Me_2CO), $[\alpha]_D^{25} = -18°$ (Me_2CO; *c* 0.6), EIMS (110°, 70 eV) *m/z* (%): 512 (0.5, M +), 495 (13), 420 (41), 391 (11), 377 (8), 299 (3), 259 (0.8), 223 (6), 194 (0.5), 180 (0.9), 153 (3), 137 (100), 110 (84), 94 (12). ^{1}H and ^{13}C NMR: Tables 1 and 2.

Table 2
^{13}C NMR data and HMBC correlations for compounds **1–3** (Acetone-d_6, TMS, 75 MHz)

	Compound no.							
	1		**2**			**3**		
	δC (ppm)	*m*	δC (ppm)	*m*	HMBC (protons)	δC (ppm)	*m*	HMBC (protons)
1′-A_1	129.3	*s*	137.9	*s*	α_1, β_1, 5′A_1	134.4	*s*	α_1, β_1, 5′A_1
2′-A_1	126.9	*d*	120.7	*d*	β_1, 6′A_1	125.7	*d*	β_1, 6′A_1
3′-A_1	132.1	*s*	129.7	*s*	5′A_1	127.2	*s*	α_2, 5′A_1
4′-A_1	158.9	*s*	153.0	*s*	2′A_1, 6A_1	159.1	*s*	α_1, 2′6′A_1
5′-A_1	111.0	*d*	111.6	*d*	–	110.0	*d*	–
6′-A_1	132.1	*d*	126.6	*d*	β_1, 2′A_1	130.2	*d*	β_1, 2′A_1
α_1	119.3	*d*	40.5	*t*	β_1	40.2	*t*	β_1
β_1	144.8	*d*	30.9	*t*	α_1, 2′6′A_1	29.5	*t*	α_1, 2′6′A_1
C_1	192.8	*s*	204.8	*s*	α_1, β_1, 6B_1	204.7	*s*	α_1, β_1, 6B_1
1-B_1	114.7	*s*	113.8	*s*	3B_1, 5B_1	113.8	*s*	3B_1, 5B_1
2-B_1	167.7	*s*	165.5	*s*	3B_1, 6B_1	165.1	*s*	3B_1, 6B_1
3-B_1	103.9	*d*	103.5	*d*	5B_1	103.5	*d*	5B_1, OH
4-B_1	166.7	*s*	165.5	*s*	3B_1, 6B_1	166.4	*s*	3B_1, 6B_1
5-B_1	108.8	*d*	108.7	*d*	3B_1	108.7	*d*	3B_1
6-B_1	133.2	*d*	133.6	*d*	–	133.5	*d*	–
1′-A_2	129.3	*s*	121.7	*s*	3′A_2, 5′A_2	132.5	*s*	α_2, 3′, 5′A_2
2′-A_2	128.7	*d*	130.1	*d*	6′A_2	128.4	*d*	β_2,6′A_2
3′-A_2	116.5	*d*	116.5	*d*	5′A_2	116.2	*d*	5′A_2
4′-A_2	158.9	*s*	159.9	*s*	2′,6′A_2; 3′, 5′A_2	158.4	*s*	2′A_2, 6′A_2
5′-A_2	116.5	*d*	116.5	*d*	3′A_2	116.2	*d*	3′A_2
6′-A_2	128.7	*d*	130.1	*d*	2′A_2	128.4	*d*	β_2′, 2′A_2
α_2	57.6	*d*	114.4	*s*	2′A_1	57.8	*d*	β_2′, 2′A_1
β_2	88.6	*d*	156.5	*s*	2′,6′A_2	87.0	*d*	α_2, 2′, 6′A_2
c_2	201.4	*s*	196.1	*s*	6B_2	201.5	*s*	α_2, β_2, 6B_2
1-B_2	113.8	*s*	114.4	*s*	3B_2, 5B_2	113.6	*s*	3B_2, 5B_2
2-B_2	165.6	*s*	166.5	*s*	3B_2, 6B_2	166.1	*s*	3B_2, 6B_2
3-B_2	104.0	*d*	103.5	*d*	–	103.8	*d*	5B_2, OH
4-B_2	163.2	*s*	166.5	*s*	3B_2, 6B_2	167.2	*s*	3B_2, 6B_2
5-B_2	109.7	*d*	109.1	*d*	3B_2	109.5	*d*	3B_2
6-B_2	134.7	*d*	136.5	*d*	–	134.6	*d*	–

3.8. Dihydrolophirone C penta acetate **5**

The same procedure as for **2** was applied to **3** (6 mg) and its pentaacetate **5** (3 mg) was obtained. CIMS (NH_3) *m/z* 740 $(M+NH_4)^+$, 723 (M + H). RMN^{1}H (300 MHz) δ ppm 6.84 (1H, brs, H-2′A_1), 6.89 (1H, *d*, *J* = 7.9Hz, H-5′A_1); 7.15 (1H, *dd*, *J* = 7.9; 2,0 Hz, H-6′A_1); 2.79 (2H, *t*, *J* = 7.7 Hz, H-α_1); 2.58 (2H, *t*, *J* = 7.7 Hz, H-β_1); 6.99 (1H, *d*, *J* = 2.6 Hz,H-3B_1); 7.53 (1H, *d*, *J* = 8.8 Hz,H-6B_1); 7.4 (2H, *m*, *J* = 8.8 Hz,H-2′,6′A_2); 7.13 (2H, *m*, *J* = 8.8 Hz,H-3′,5′A_2); 5.39 (1H, *d*, *J* = 7.2 Hz,H-α_2); 6.25 (1H, *d*, *J* = 7.2 Hz,H-β_2); 6.95 (1H, *d*, *J* = 2.4 Hz, H-3B_2); 7.15 (1H, *dd*, *J* = 8.9, 2.4 Hz, H-5B_2); 8.32 (1H, *d*, *J* = 8.9 Hz,H-6B_2); 2.14 (3H, *s*, OAc); 2.22 (3H, *s*, OAc); 2.25 (3H, *s*, OAc); 2.27 (3H, *s*, OAc); 2.31 (3H, *s*, OAc).

Acknowledgements

We thank the botanist M. Nole (Centre d'Etudes des Plantes Médicinales, Yaoundé) for the identification of plant material and J.P. Brouard (Laboratoire de Chimie du Muséum-CNRS, France) for mass spectra. We are also indebted to the University of Yaounde I Grants committee, the International Foundation for Science (Grant F/1398-2) and French Ministère de l'Education Nationale (DAGIC) for financial assistance.

References

Bouquet, A., 1969. Féticheurs et Médecines Traditionnelles du Congo Brazzaville, ORSTOM; Paris, pp. 178–179.

Ghogomu Tih, R., Sondengam, B.L., Martin, M.T., Bodo, B., 1989. Structure of lophirones B and C, biflavonoids from the stem of *Lophira lanceolata*. Phytochemistry 28, 1557–1559.

Pegnyemb, D.E., Ghogomu Tih, R., Sondengam, B.L., Martin, M.T., Bodo, B., 1994. Minor biflavonoids of *Lophira lanceolata*. Journal of Natural Products 57, 1275–1278.

Pegnyemb, D.E., Messanga, B.B., Ghogomu Tih, R., Sondengam, B.L., Martin, M.T., Bodo, B., 1998. A new benzoylglucoside and a new prenylated isoflavone from *Lophira lanceolata*. Journal of Natural Products 61, 801–803.

Tih, A.E, Ghogomu Tih, R., Sondengam, B.L., Martin, M.T., Bodo, B., 1992. Tetraflavonoids of *Lophira alata*. Phytochemistry 31, 981–984.

PERGAMON

Phytochemistry 57 (2001) 583–585

PHYTOCHEMISTRY

www.elsevier.com/locate/phytochem

Oxanthrone esters from the aerial parts of *Cassia kleinii*

S.J. Anu[a], J. Madhusudana Rao[b,*]

[a]*Organic Chemistry Division, Regional Research Laboratory, Trivandrum-695 019, India*
[b]*Natural Products Laboratory, Indian Institute of Chemical Technology (CSIR), Hyderabad-500 007, India*

Received 12 July 2000; received in revised form 12 January 2001

Abstract

From the aerial parts of *Cassia kleinii* two new oxanthrone esters, kleinioxanthrone-1 and kleinioxanthrone-2 have been isolated. Their structures were established as 1,8-dihydroxy-3-methyl-6-methoxy-9(10H)-anthracenone-10-oxydecanoate **1** and 1,8-dihydroxy-3-methyl-9(10H)-anthracenone-10-oxytetradecanoate **2** respectively based on degradative and spectroscopic evidence. © 2001 Elsevier Science Ltd. All rights reserved.

Keywords: *Cassia kleinii*; Leguminosae; Kleinioxanthrone-1; Kleinioxanthrone-2

1. Introduction

Cassia kleinii W&A (Leguminosae family) is a rather diffuse undershrub distributed in southern India (Hooker, 1978) and is a member of the predominantly tropical genus *Cassia*. *Cassia* species are known to be rich in anthraquinones, anthrones, flavonoids and triterpenes. *Cassia* leaves and pods have long been used widely as purgatives and laxatives. The anthraquinone derivatives; anthronic, dianthronic and anthraquinone glycosides present in *Cassia* are responsible for their purgative action (Muffat et al., 1986; Muller et al., 1989). 1,8-Dihydroxy anthraquinone derivatives particularly their glycosides are shown to have purgative activity (Selvaraj and Chander Subhas, 1978). A lot of herbal preparations for liver diseases contain hydroxy anthraquinones whose medicinal property has been attributed to their laxative activity only. Cascarosides A, B and aloe emodin which are hydroxy anthraquinone derivatives isolated from *Rhamnus purshianus* bark a well known cathartic drug (Mannito et al., 1990, 1993) was found to show significant hepatoprotective effect on primary cultured hepatocytes against galactosamine cytotoxicity. Chrysophanol glycoside isolated from *Cassia tora* also showed hepatoprotective activity (Wong et al., 1989). Hydroxy anthraquinone derivatives, which have been known for their purgative, laxative and cathartic activities are now considered to be potent hepatoprotective drugs.

C. kleinii which is used for its antihepatotoxic activity in traditional medicine has remained an uninvestigated species till now. So far, only the occurrence of saponins has been reported from *C. kleinii* (Rao and Subhashini, 1986). This is the first report of a systematic phytochemical investigation on this plant. Herein, we report the isolation and structure elucidation of two new oxanthrone esters from the aerial parts of *C. kleinii*. The name kleinioxanthrone-1 and kleinioxanthrone-2 are proposed for the new compounds **1** and **2**. Three known compounds *n*-triacontanol, hentriacontanoic acid and β-sitosterol were also isolated from the aerial parts.

2. Results and discussion

Compound **1**, klenioxanthrone-1, was isolated as yellow needles from hexane, mp 196–197°C. The molecular formula $C_{26}H_{32}O_6$ was deduced from the positive ion FABMS $(M+H)^+$ 441. The UV spectrum displayed bands at 445 and 290 nm assignable to an anthrone system. The IR spectrum showed absorption bands at 3500 cm^{-1} (−OH), 1629 cm^{-1} (chelated−C=O) and 1735 cm^{-1} (ester, –C=O).

The 300 MHz ^1H NMR ($CDCl_3$) spectrum showed two broad one proton singlets at δ 12.1 and 12.3 which are characteristic of two chelated hydroxyl groups. It also showed two doublets at δ 6.69 (J 3 Hz) and δ 7.37

* Corresponding author. Tel.: +91-40-717-3874-77; fax: +91-40-717-0512.

E-mail address: janaswamy@iict.ap.nic.in (J.M. Rao).

0031-9422/01/$ - see front matter © 2001 Elsevier Science Ltd. All rights reserved.
PII: S0031-9422(01)00114-5

(J 3 Hz) which are assigned to H-4 and H-2 and two broad singlets at δ 7.09 and 7.63 assigned to H-5 and H-7 of 1. The occurrence of a three proton singlet at δ 3.94 is typical of an aromatic methoxyl group and the one proton multiplet at δ 3.5–3.9 is assigned to the oxymethine proton at C-10 of an oxanthrone system. The three proton singlet at δ 2.45 is characteristic of an aromatic methyl group. The triplet at δ 2.28 accounts for a $-OCO\underline{CH_2}-$ group. The broad singlet at δ 1.25 which integrates to 14 H, is characteristic of methylene groups belonging to an aliphatic straight chain. The triplet at δ 0.85 is typical of a terminal $-CH_3$ group. This data except for the one proton multiplet at δ 3.90 and the peaks due to the aliphatic ester side chain at δ 0.85–2.28 conform to that of physcion-9-anthrone (Tamano and Koketsu, 1982). So **1** was identified tentatively as a derivative of physcion-9-anthrone with an aliphatic side chain at C-10 position.

The EI MS of **1** gave the molecular weight of the corresponding anthraquinone, physcion, M^+ 284 due to cleavage of the side chain to form the oxonium ion (Monache et al., 1987) and hence the anthraquinone. The loss of fragments with mass 28 and 43 which is characteristic of fatty acid esters and formation of the oxonium ion (m/z 285) by loss of m/z 127 helps to identify the side chain ester as decanoic acid ester. The structure was further confirmed by alkaline hydrolysis which yielded decanoic acid. Decanoic acid was methylated and compared by co-TLC with authentic sample of methyldecanoate. Thus **1** was identified as 1,8-dihydroxy-3-methyl-6-methoxy-9(10H)-anthracenone-10-oxydecanoate.

Compound **2**, kleinioxanthrone-2, obtained as yellow needles, mp 188–189°C gave a $(M+H)^+$ at m/z 467 in the positive ion FAB MS attributable to the molecular formula $C_{29}H_{38}O_5$. Absorption bands at 440 and 229 nm were observed in the UV spectrum. The IR spectrum showed absorption bands at 3500 cm^{-1} (−OH), 1626 cm^{-1} (chelated –C=O) and 1749 cm^{-1} (ester −C=O).

The 300 MHz ^1H NMR ($CDCl_3$) spectrum showed two broad one proton singlets at δ 12.1 and 12.0 which is characteristic of two chelated hydroxyl groups. It also showed an ABC pattern of multiplets at δ 7.8 (J 9Hz), δ 7.7 (J 9Hz), δ 7.3 (J 9Hz) assigned to H-7, H-6 and H-5 of **2**. Two broad singlets were present at δ 7.6 and 7.1 in the aromatic region and were assigned to H-2 and H-4. The one proton multiplet at δ 3.9 was assigned to the oxymethine proton at C-10 of an oxanthrone. The three proton singlet at δ 2.47 was characteristic of an aromatic methyl group. The triplet at δ 0.85 was typical of a terminal aliphatic methyl group. This data except for the one proton multiplet at δ 3.90 and the peaks due to the aliphatic ester side chain at δ 0.85–2.31 conform to that of chrysophanol-9-anthrone (Tamano and Koketsu, 1982). So the compound was tentatively identified as a derivative of chrysophanol-9-anthrone with an aliphatic side chain.

From the EI MS (M^+ 254) and the FABMS of **2** the side chain was deduced as tetradecanoic acid ester. The structure was confirmed by degradation as in the case of **1**. Thus **2** was identified as 1,8-dihydroxy-3-methyl-9(10H)-anthracenone-10-oxytetradecanoate.

This is the first report of the natural occurrence of oxanthrone esters. Oxanthrones can be easily converted to their corresponding anthraquinones and their derivatives. Compounds **1** and **2** could serve as valuable intermediates in the development of hepatoprotective drugs.

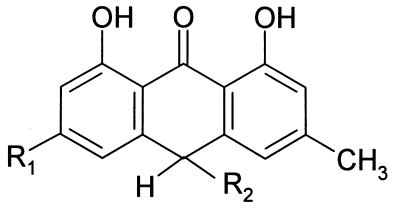

1 $R_1 = OCH_3$ $R_2 = OCO(CH_2)_8CH_3$

2 $R_1 = H$ $R_2 = OCO(CH_2)_{12}CH_3$

3. Experimental

3.1. Plant material

Cassia kleinii W&A was collected from Neyyatinkara, Thiruvananthapuram and identified by Dr. N. Sasidharan, Scientist, Kerala Forest Research Institute (KFRI), Peechi, Kerala and was deposited at the Herbarium of the KFRI and the voucher number is 7564.

3.2. Extraction and isolation

Dried and finely powdered aerial parts of the plant were extracted (Soxhlet) with petrol (60–80°C), and subsequently with chloroform for 48 h. The petrol extract and the chloroform extract were evaporated and the residues were chromatographed separately over silicagel (60–120 mesh) using hexane and hexane:EtOAc (98:2, 95:5) as eluents. **1** and **2** were crystallized from the hexane:EtOAc (98:2) fractions of the hexane extract and the chloroform extract respectively.

3.3. Kleinioxanthrone-1

$[\alpha]_D^{25}$ −5.6° ($CHCl_3$, c 1.04) UV: λ_{max} 445, 290 nm. IR KBr ν_{max} cm^{-1} 3500 (OH), 1629 (chelated−CO), 1735 (ester−CO), FAB MS (M+1) 441, M^+ 440 EI MS 284 (100), 254 (23), 241 (14), 226 (12), 213 (21), 198 (14), 185 (19), 152 (10), 139 (32), 128 (38), 115 (29), 89 (12), 77 (34). ^{13}C NMR (75 MHz $CDCl_3$) δ 162.5 (C-1), 106.8 (C-2),

165.2 (C-3), 108.2 (C-4), 124.5 (C-5), 148.4 (C-6), 121.3 (C-7), 166.5 (C-8), 190.8 (C-9), 69.2 (C-10), 133.2 (C-11), 113.7 (C-12), 110.2 (C-13), 135.3 (C-14), 22.1 (-CH_3), 56.1 (-OCH_3), 182.0 (C-1′), 30.6 (C-2′), 19.3–21.4 (C-3′-9′), 12.4 (C–10′).

3.4. Kleinioxanthrone-2

$[\alpha]_D^{25}$ −16° ($CHCl_3$, *c* 1.40) UV: λ_{max} 440, 229 nm. IR KBr ν_{max} cm^{-1} 3500 (OH), 1626 (chelated−CO), 1749 (ester−CO), FAB MS (M + H) 467 M^+ 466 EI MS 254 (100), 226 (16), 198 (10), 152 (10), 115 (10), 77 (21), 39 (24). ^{13}C NMR (75 MHz $CDCl_3$) δ 162.5 (C-1), 115.7 (C-2), 149.2 (C-3), 124.4 (C-4), 124.2 (C-5), 136.8 (C-6), 119.7 (C-7), 162.2 (C-8), 192.4 (C-9), 68.0 (C-10), 133.1 (C-11), 123.1 (C-12), 121.2 (C-13), 133.5 (C-14), 22.5 (-CH_3), 181.8 (C-1′), 31.7 (C-2′), 22.1–29.5 (C-3′-13′), 13.9 (C-14′).

3.5. Hydrolysis of kleinioxanthrone-1 and kleinioxanthrone-2

Kleinioxanthrone-1 (8 mg) and kleinioxanthrone-2 (6 mg) were taken separately in 2.5% alcoholic KOH (5 ml) refluxed for 1 h until an aliquot showed the disappearance of the original compound on TLC. It was then cooled and treated with water. The aqueous layer was neutralized with dil. HCl and extracted with ether and dried with Na_2SO_4. The acids **3** and **4** were obtained from **1** and **2** respectively.

3.6. Methylation of *3* and *4*

Compounds **3** (2 mg) and **4** (2.5 mg) were separately dissolved in methanol and 0.5 ml, 2% H_2SO_4 in methanol was added. The reaction mixture was refluxed for 30 min. It was then cooled, treated with water, extracted with hexane and washed with saturated sodium bicarbonate and water. The methyl esters obtained were identified by co-TLC with methyldecanoate and methyltetradecanoate respectively.

Acknowledgements

The authors are grateful to CSIR for financial help and to the Director, RRL, Trivandrum for providing facilities for this work.

References

Hooker, J.D., 1978. Flora of British India 2, 266.

Mannito, P., Monti, D., Speranza, G., 1990. Studies on aloe. Part 6. Conformation and absolute configuration of aloins A and B and related 10-C-glucosyl-9-anthrones. Journal of the Chemical Society Perkin Transactions 1, 1297.

Mannito, P., Monti, D., Speranza, G., Mulinacci, N., Vincieri, F.F., Griffini, A., Pifferi, G., 1993. Conformational studies of natural products. Part 4. Conformation and absolute configuration of cascarosides A, B, C, D.. Journal of the Chemical Society Perkin Transactions 1, 1577.

Monache, G.D., Monache, F.D., Benedetto, R.D., Ogukwa, J.U., 1987. New metabolites from *Psorospermum Tenuifolium*. Phytochemistry 26 (9), 2611.

Muffat, F., Bernard, Ph., Sabot, J.F., 1986. Determination of sennosides A and B in senna extracts by high- performance liquid chromatography. Journal of Chromatography 369, 261.

Muller, B.M., Kraus, J., Fraz, G., 1989. Chemical structure and biological activity of water-soluble polysaccharides from *Cassia angustifolia* leaves. Planta Medica 55, 536.

Rao, C.K., Subhashini, G., 1986. Saponins and leucoanthocyanins in *Cassia* L. Current Science 55 (6), 320.

Selvaraj, Y., Chander Subhas, M., 1978. Senna- it's chemistry, distribution and pharmaceutical value. Journal of Indian Institute of Science 60 (8), 179.

Tamano, M., Koketsu, J., 1982. Isolation of hydroxyanthrones from the roots of *Rumex acetosa* Linn. Agricultural and Biological Chemistry 46 (7), 1913.

Wong, S.M., Wong, M.M, Seligmann, O., Wagner, H., 1989. Anthraquinone glycosides from the seeds of *Cassia tora*. Phytochemistry 28 (1), 211.

PERGAMON

Phytochemistry 57 (2001) 587–591

PHYTOCHEMISTRY

www.elsevier.com/locate/phytochem

Ellagic acid rhamnosides from the stem bark of *Eucalyptus globulus*

Jong-Pyung Kim[a], In-Kyoung Lee[a], Bong-Sik Yun[a], Sung-Hyun Chung[b], Gyu-Seop Shim[b], Hiroyuki Koshino[c], Ick-Dong Yoo[a,*]

[a]*Korea Research Institute of Bioscience and Biotechnology, PO Box 115, Yusong, Taejon 305-600, South Korea*
[b]*Hansol Institute of Science and Technology, San 56-1, Oeibang-Ri, Sudong-Myun, Namyangju-Si, Kyungki-Do 472-850, South Korea*
[c]*RIKEN (The Institute of Physical and Chemical Research), Hirosawa 2-1, Wako, Saitama 351-0198, Japan*

Received in revised form 23 May 2000

Abstract

Four ellagic acid rhamnosides were isolated from the stem bark of *Eucalyptus globulus*. Their structures have been established on the basis of the analysis of their ^{1}H NMR, ^{13}C NMR, HMBC, IR and MS spectral data. The HMBC data of these compounds were most useful for their structure determinations, with these bring determined to be 3-*O*-methylellagic acid 3′-*O*-α-rhamnopyranoside, 3-*O*-methylellagic acid 3′-*O*-α-3″-*O*-acetylrhamnopyranoside, 3-*O*-methylellagic acid 3′-*O*-α-2″-*O*-acetylrhamnopyranoside, 3-*O*-methylellagic acid 3′-*O*-*a*-4″-*O*-acetylrhamnopyranoside, respectively. Their antioxidant activities were evaluated by measuring the inhibition of lipid peroxidation using rat liver microsomes, with IC_{50} values of 10.0–14.0 μg/ml. © 2001 Elsevier Science Ltd. All rights reserved.

Keywords: *Eucalyptus globulus*; Myrtaceae; Stem bark; Ellagic acid rhamnosides; Antioxidant activity

1. Introduction

Eucalyptus globulus Labill (Myrtaceae) grows under a wide range of climatic conditions and is widely distributed throughout Australia. Moreover *Eucalyptus* species have been utilized for medicinal purposes; for example, their barks and leaves have been used to treat colds, influenza, toothaches, snakebites, fevers, diarrhea and other complaints (Elliot and Jones, 1984; Lassak and McCarthy, 1983; Barr, 1993). Because of its fast growth and good quality, *E. globulus* is being established in plantations in many countries, mainly for pulp and paper production. Up to now, the bark is a waste material from the pulp industry, and the purpose of this study was to recover potentially useful compounds from the bark as by-products. Additionally, several biologically active compounds were isolated mainly from the leaves of *Eucalyptus*; Euglobals, isolated from the buds and leaves of *E. globulus,* show potent granulation inhibiting activity (Sawada et al., 1980; Amano et al., 1981; Kozuka et al., 1982a,b). Grandinol also was isolated from adult tissue of *E. grandis* as a rooting inhibitor (Crow et al., 1977), and robustadials are antimalarial compounds isolated from *E. robusta* (Xu et al., 1984). Lastly, the sesquiterpene aromadendrene, the main component of a commercially available distillation tail of the oil of *E. globulus*, has been exploited as a chiral pool synthon for the synthesis of several sesquiterpene derivatives (Gijsen et al., 1990, 1991, 1992, 1994).

We are interested in antioxidant substances from natural products and have reported several new natural antioxidants (Kim et al., 1996, 1997, 1999; Lee et al., 1996, 1999). We present here the isolation and structural elucidation of four antioxidants (**1**–**4**) from the stem bark of *E. globulus* and their antioxidant activities.

2. Results and discussion

The 80% aqueous methanolic extract of the stem bark of *E. globulus* was successively partitioned with $CHCl_3$ and EtOAc. Successive column chromatography of the EtOAc extract on silica gel, Sephadex LH-20 and C-18, followed by preparative HPLC on a C-18 column yielded an ellagic acid rhamnoside (**1**) and three ellagic acid acetylrhamnosides (**2**–**4**).

* Corresponding author. Tel.: +82-42-860-4330; fax: +82-42-860-4595.
E-mail address: idyoo@mail.kribb.re.kr (I.-D. Yoo).

0031-9422/01/$ - see front matter © 2001 Elsevier Science Ltd. All rights reserved.
PII: S0031-9422(01)00146-7

The physico-chemical properties of **1**–**4** were very similar to each other. The IR absorptions suggested the presence of α,β-unsaturated lactones (around 1725 cm^{-1}) and hydroxyl groups (around 3400 cm^{-1}). The UV spectra of these compounds in methanol were almost the same, which indicated the presence of similar chromophores.

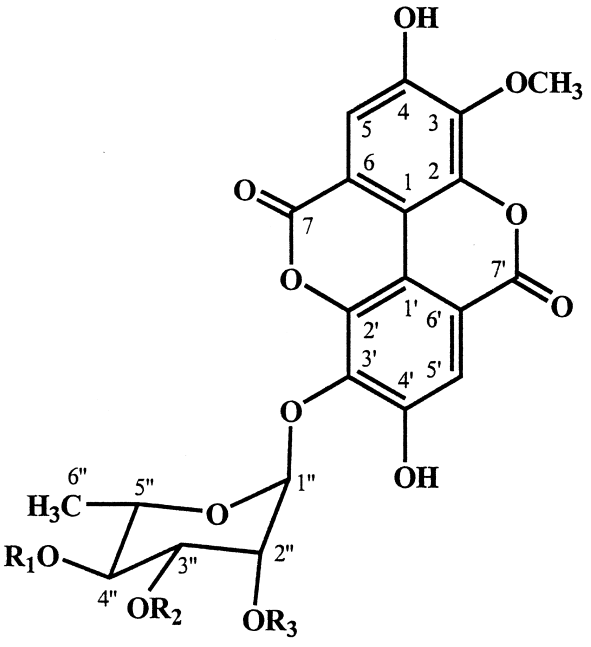

	R_1	R_2	R_3
1	H	H	H
2	H	CH_3CO	H
3	H	H	CH_3CO
4	CH_3CO	H	H

Compound **1** was obtained as a yellow powder. The HRFAB-MS measured with negative ion mode gave a parent ion peak at *m/z* 461.0727 ($[M-H]^-$ calc. for $C_{21}H_{17}O_{12}$ requires 461.0720). These results together with ^{13}C NMR spectroscopic analysis proposed the molecular formula $C_{21}H_{18}O_{12}$ for **1.** The IR spectrum displayed characteristic absorptions for hydroxyl groups (3411 cm^{-1}), α, β-unsaturated lactone functions (1727 cm^{-1}) and aromatic rings (1606 cm^{-1}). In its ^1H NMR spectrum, nine proton signals including two aromatic singlets (δ 7.46 and 7.47), a singlet methoxyl signal (δ 4.12), and five oxygenated methine protons were observed, along with a doublet methyl signal (δ 1.21, $J = 6.2$ Hz) indicating the existence of one 6-deoxysugar.

The glycoside was easily determined as rhamnose through analysis of the chemical shifts and coupling patterns of its proton signals, which were connected by a ^1H–^1H COSY spectrum. The anomeric proton signal appeared as a doublet at δ 5.73, attributed from the small coupling constant of 1.6 Hz to an α-configurated anomeric proton. The ^{13}C NMR spectrum of **1** exhibited 21 signals (Table 2), with two overlapped ester carbons (–COOR) at δ 161.8 due to α,β-unsaturated lactones, six oxygenated aromatic carbons, four aromatic quaternary carbons (=C<), two isolated aromatic methine carbons (=CH–) at δ 114.0 and 115.2, a methoxyl carbon at δ 61.6, and a methyl carbon at δ 17.9 and five oxygenated methine carbons due to rhamnose. These results, and the UV-visible spectrum measured in MeOH (246, 260, 285, 360, 375 nm), suggested the structure as *O*-methylellagic acid with rhamnose. The mass spectrum of **1** was dominated by two fragment ion peaks at *m/z* 315 and 145 due to the aglycone and the rhamnose moiety, respectively. Compound **1** was very similar to 3-*O*-methylellagic acid 4′-rhamnoside (Yazaki and Hillis, 1976) in its UV, IR and ^1H spectral data. However, the attachment position of sugar moiety to aglycone was different. The rhamnose attachment position and the structure of **1** were established through the interpretation of pulse field gradient (PFG)-HMQC and HMBC spectral data. From the HMQC spectrum, aromatic carbons (δ 114.0 and 115.2) bearing singlet methine protons (δ 7.46 and 7.47, respectively) were correlated (C-5 and C-5′, respectively).

In the HMBC spectral data (Fig. 1), ^1H–^{13}C long-range correlations were observed between the methoxyl protons (δ 4.12) to C-3 (δ 143.5), from the aromatic proton at δ 7.46 (H-5) to the lactone carbonyl carbon at δ 161.8 (C-7), and two quaternary carbons at δ 112.3 (C-1) and δ 143.5 (C-3). Long-range correlations from the other aromatic proton at δ 7.47 (H-5′) to another lactone carbonyl carbon at δ 161.8 (C-7′), the quaternary carbon at δ 110.6 (C-1′) and an oxygenated aromatic carbon at δ 140.3 (C-3′) were also observed in the aglycone of **1**. In the sugar moiety, the ^1H–^{13}C long-range correlation from the anomeric proton at δ 5.73 to C-3′ ascertained that the sugar was attached to C-3′-*O* at the aglycone. The other ^1H–^{13}C long-range correlations observed in the sugar moiety indicated that the sugar was rhamnose. All of the ^1H NMR and most of the ^{13}C NMR chemical shifts were assigned unambiguously from the data obtained from HMQC and HMBC, except that a few quaternary carbons (C-2, C-4, C-6, C-2′, C-4′ and C-6′) could not be unambiguously assigned. All of the NMR assignments were in good agreements with those of ellagic acid derivatives reported by Li et al. (1999). Accordingly, **1** was established as 3-*O*-methylellagic acid 3′-*O*-α-rhamnopyranoside.

During the structural elucidation, it was revealed that **2** and **3** were obtained as a mixture of regioisomers with the same molecular weight. Because of the small amount and difficulty of separation of these compounds, the

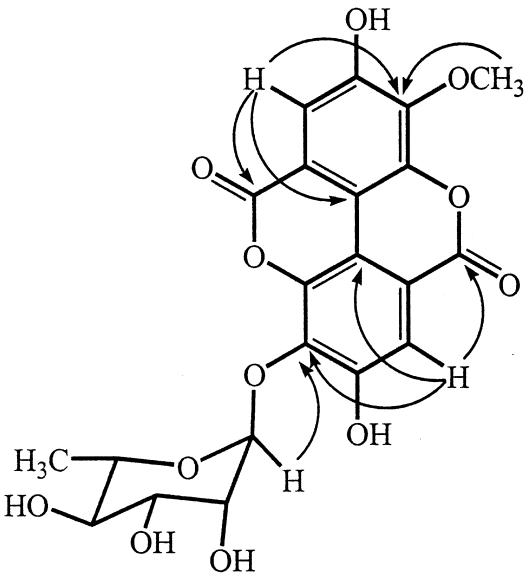

Fig. 1. ^{1}H–^{13}C long-range correlations of **1** in the PFG-HMBC spectrum.

structure determination of **2** and **3** was conducted in the mixture state. The physico-chemical properties of mixture of **2** and **3** were very similar to those of compound **1** except for the larger molecular weight. The UV and IR spectral data was almost the same with those of compound **1,** suggesting the 3-*O*-methylellagic acid structure. The molecular formulae of **2** and **3** were deduced to be $C_{23}H_{20}O_{13}$ from the parent ion peak at *m/z* 503.0835 ([M-H]$^{-}$, calc. for $C_{23}H_{19}O_{13}$, 503.0825) in the negative HRFAB–MS spectrum measured as mixture state. The integration of the proton signals of **2** and **3** in the ^{1}H NMR suggested that the ratio of these compounds in the mixture was 3:2. The ^{1}H, ^{13}C NMR and PFG-HMBC spectral data of these two compounds were almost the same as those of **1** in the aglycone regions, indicating that the aglycones of **2** and **3** were 3-*O*-methylellagic acid. However, the spectral data of the sugar moieties of these three compounds were different. The ^{1}H NMR data of **2** and **3** in the sugar regions exhibited each of six signals due to four methine protons, a methyl group and an acetyl group. The position of acetyl groups in **2** (δ 2.12) and **3** (δ 2.09) were determined carefully by the analysis of chemical shift values of methine protons and mostly by the ^{1}H–^{13}C long-range correlations in the HMBC spectra (Fig. 1). The long-range correlations from the down-field shifted methine proton at δ 5.24 (H-3″) to the carbonyl carbon of acetyl group at δ 172.7 and other long-range correlations in the sugar confirmed that the sugar moiety of **2** was 3″-*O*-acetylrhamnopyranoside. The ^{1}H–^{13}C long-range correlation from the anomeric proton at δ 5.64 to C-3′ (δ 138.6) confirmed the structure of **2** as 3-*O*-methylellagic acid 3′-*O*-α-3″-*O*-acetylrhamnopyranoside.

In the same manner, the structure of **3** was established. From the ^{1}H–^{13}C long-range correlations of the down-field shifted methine proton at δ 5.49 (H-2″) with the carbonyl carbon of acetyl group at δ 172.0 and other correlations in the sugar, the structure of **3** was determined as 3-*O*-methylellagic acid 3′-*O*-α-2″-*O*-acetylrhamnopyranoside.

The spectral data of **4** obtained from the negative HRFAB-MS (*m/z* 503.0828, [M-H]$^{-}$, calcd for $C_{23}H_{19}O_{13}$, 503.0838) and NMR experiments were almost the same as those of **2** and **3** except for the position of the acetyl group on the rhamnose-moiety, which suggested that **4** was a regioisomer of **2** and **3** with 3-*O*-methylellagic acid structure as the aglycone. By the ^{1}H–^{13}C long-range correlations from the down-field shifted methine proton at δ 5.04 (H-4″) to the carbonyl carbon of acetyl group at δ 172.6 and other correlations in the sugar moiety of **3** (Fig. 1), the complete structure of **3** was determined to be 3-*O*-methylellagic acid 3′-*O*-α-4″-*O*-acetylrhamnopyranoside. It was considered that one or two of compounds **2**, **3** and **4** might be an artifact(s) formed by acyl migration during the extraction and/or isolation procedure.

This is the first report of compounds **1**–**4** from a natural source, although the methyl or dimethyl ellagic acid derivatives which contain rhamnose as a sugar, 3-*O*-methylellagic acid 4′-rhamnoside (Yazaki and Hullis, 1976) and 3,3′-di-*O*-methylellagic acid 4′-O-α-L-rhamnoside (Malhotra and Misra, 1981) from *Eucalyptus* and 4-(α-rhamnopyranosyl)ellagic acid (Yang et al., 1998) has been reported previously.

The antioxidant activities of the compounds were evaluated by a thiobarbituric acid method using rat liver microsomes. Fig. 2 shows that the concentration effects of **1**, mixture of **2** and **3**, and **4** on the inhibition of lipid peroxidation in rat liver microsomes. The IC_{50} values of

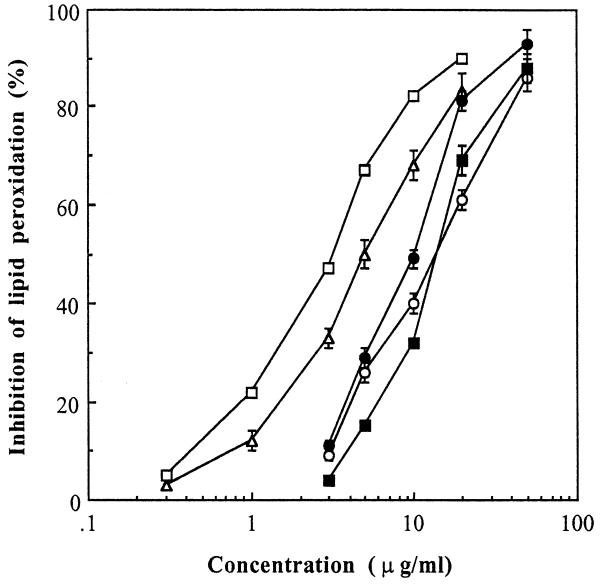

Fig. 2. Concentration effects of antioxidative activity of **1** (○), 3:2 mixture of **2** and **3** (●), **4** (■), BHA (□) and α-tocopherol (△). The values are mean ±S.E. of three independent test tubes.

them were 13.0, 10.0 and 14.0 mg/ml respectively, which were slightly weaker than those of α-tocopherol (IC_{50} 4.8 μg/ml) and butylated hydroxyanisole (BHA, IC_{50} 3.0 μg/ml).

3. Experimental

3.1. General

CC: silica gel 60 (Merck, 70–230 mesh), C_{18} gel (60–230 mesh) and Sephadex LH-20, the eluents were $CHCl_3$–MeOH (100:1–1:1), MeOH–H_2O (50:1–95:5), and MeOH, respectively. UV-visible: MeOH soln. IR: KBr discs. Negative HRFAB–MS spectra were measured on a Jeol HX-110 spectrometer using glycerol as a matrix. NMR: 400 MHz for ^1H, and 100 MHz for ^{13}C in CD_3OD with TMS as int. standard. Chemical shifts are given in δ from TMS. The 2D-NMR spectroscopy experiments were carried out on a Jeol JNM-A α-600 NMR spectrometer operating at 600/150 MHz for ^1H and 150 MHz for ^{13}C. For HMQC and HMBC experiments, duration time was optimized for $^1J_{CH} = 145$ Hz and $^nJ_{CH} = 8.3$ Hz, respectively. Prep. HPLC was performed on a C_{18} column (20×250 mm) using a MeOH–H_2O gradient, and by monitoring with a photodiode-array detector (200–650 nm).

3.2. Plant material

The stem bark of an eight-year old *G. globulus* tree was provided by Hansol Forem Co, and the voucher specimen is deposited at Korea Research Institute of Bioscience and Biotechnology.

3.3. Extraction and isolation

The dried stem bark (4 kg) was extracted with 80% aq. MeOH at room temp. for 5 days. The extract was filtered and concd under red. pressure. The residue was distributed between $CHCl_3$ and H_2O. The active aqueous phase was further partitioned between EtOAc and H_2O. The EtOAc layer was conc. in vacuro, and the residue (71.2 g) was applied to CC on a silica gel column eluted with a $CHCl_3$–MeOH gradient from (100:1–1:1). The fractions of interest were collected and subjected to further silica gel column chromatography with the same condition and the Sephadex LH-20 chromatography with MeOH as eluant, followed by C_{18} CC eluted with a MeOH–H_2O gradient (50:1–95:5). Further purification of the fractions of interest by prep. HPLC (C_{18}, MeOH–H_2O = 1:1) gave **1** (18.0 mg), mixture of **2** and **3** (20.0 mg) and **4** (8.2 mg). The ratio of **2** and **3** was 3:2 in the mixture.

3.4. Compound *1*

Yellow powder, UV-visible λ_{max} nm (log ε) in MeOH: 246 (4.6), 260 (*sh*, 4.5), 285 (*sh*, 4.0), 360 (*sh*, 3.9), 375 (4.0). IR λ_{max} (KBr) cm^{-1}: 3411, 2934, 1727, 1606, 1492, 1421, 1366, 1106, 1069. HRFAB-MS *m/z* 461.0727 $[M–H]^-$ ($C_{21}H_{17}O_{12}$ requires 461.0720). ^1H NMR: Table 1, ^{13}C NMR: Table 2.

3.5. Compounds *2* and *3*

Yellow powder, UV-visible max nm (log ε) in MeOH: 246 (4.9), 260 (*sh*, 4.8), 285 (*sh*, 4.3), 360 (*sh*, 4.2), 375 (4.3). IR λ_{max} (KBr) cm^{-1}: 3433, 2925, 1726, 1608, 1492, 1420, 1366, 1107, 1070. HRFAB-MS measured in the mixture *m/z* 503.0835 $[M–H]^-$ ($C_{23}H_{19}O_{13}$ requires 503.0825). ^1H NMR: Table 1. ^{13}C NMR: Table 2.

3.6. Compound *4*

Yellow powder, UV-visible λ_{max} nm (log ε) in MeOH: 246 (4.6), 260 (*sh*, 4.5), 285 (*sh*, 4.0), 360 (*sh*, 4.0), 375 (4.0). IR λ_{max} (KBr) cm^{-1}: 3423, 2934, 1726, 1608, 1490, 1421, 1366, 1104, 1069. HRFAB-MS *m/z* 503.0828 $[M–H]^-$ ($C_{23}H_{19}O_{13}$ requires 503.0825). ^1H NMR: Table 1. ^{13}C NMR: Table 2.

Table 1
^1H NMR spectral data of compounds **1, 2, 3** and **4**[a]

C	1	2	3	4
5	7.46 (IH, *s*)	7.47 (1H, *s*)	7.46 (IH, *s*)	7.47 (IH, *s*)
5′	7.47 (IH, *s*)	7.51 (IH, *s*)	7.48 (IH, *s*)	7.48 (IH, *s*)
OCH_3	4.12 (3H, *s*)	4.12 (3H, *s*)	4.12 (3H, *s*)	4.14 (3H, *s*)
1″	5.73 (IH, *d*, 1.6)	5.64 (IH, *d*, 1.6)	5.67 (1H, *d*, 1.6)	5.68 (IH, *d*, 1.6)
2″	4.34 (1H, *dd*, 1.6, 3.4)	4.44 (1H, *dd*, 1.6, 3.4)	5.49 (1H, *dd*, 1.6, 3.4)	4.38 (IH, *dd*, 1.6, 3.4)
3″	4.05 (IH, *dd*, 3.4,9.6)	5.24 (1H, *dd*, 3.4, 9.6)	4.18 (IH, *dd*, 3.4, 9.6)	4.19 (IH, *dd*, 3.4, 9.6)
4″	3.46 (IH, *t*, 9.6)	3.65 (IH, *t*, 9.6)	3.40 (IH, *t*, 9.6)	5.04 (1H, *t*, 9.6)
5″	4.46 (IH, *dq*, 9.6, 6.2)	4.50 (IH, *dq*, 9.6, 6.2)	4.32 (IH, *dq*, 9.6, 6.2)	4.60 (IH, *dq*, 9.6, 6.2)
6″	1.21 (3H, *d*, 6.2)	1.21 (3H, *d*, 6.2)	1.17 (3H, *d*, 6.2)	1.09 (3H, *d*, 6.2)
CH_3-C=O		2.12 (3H, *s*)	2.09 (3H, *s*)	2.14 (3H, *s*)

[a] Recorded in CD_3OD, chemical shifts values are reported as δ from TMS at 400 MHz, number of protons, signal multiplicity and coupling constants (Hz) are shown in parentheses.

Table 2
^{13}C chemical shift data for compounds **1**, **2**, **3** and **4** (chemical shifts in δ values from TMS)

C	1	2	3	4
1	112.3	113.2	113.2	113.5
2[a]	142.3	142.2	142.3	143.2
3	143.5	142.0	142.0	142.0
4[b]	154.4	154.4	154.3	154.8
5	114.0	114.4	114.0	113.0
6[c]	113.3	113.5	113.4	113.2
7[d]	161.8	160.4	160.4	160.3
1′	110.6	113.0	112.9	112.7
2[a]	143.6	143.6	143.6	143.6
3′	140.3	138.6	138.6	138.6
4′[b]	153.7	153.7	153.8	153.9
5′	115.2	113.0	113.4	113.0
6′[c]	114.6	114.6	114.4	114.6
7′[d]	161.8	160.4	160.4	160.3
OCH_3	61.6	62.0	62.0	62.0
1″	102.9	103.8	100.0	103.6
2″	72.0	70.9	75.4	71.8
3″	72.2	75.4	73.6	70.1
4″	73.9	71.9	71.9	75.1
5″	71.7	69.6	70.4	69.6
6″	17.9	17.8	20.5	17.7
COO		172.7	172.0	172.6
CH_3		21.1	20.9	21.0

[a,b,c] Assignments may be interchangeable within each column.
[d] Overlapped signals.

3.7. Antioxidant activity

Antioxidant activity was evaluated by the inhibitory activity of compounds against lipid peroxidation in rat liver microsomes according to the thiobarbituric acid method (Ohkawa et al., 1979) with minor modifications. The reaction was initiated by the addition of 100 μM $FeSO_4$ $7H_2O$ into a mixture of ascorbic acid (0.2 mM), a microsomal suspension (0.5 μg protein ml^{-1}) and each concentration of the samples dissolved in methanol. Lipid peroxidation was assessed by measuring the thiobarbituric acid reaction products at 532 nm.

References

Amano, T., Komiya, T., Hori, M., Goto, M., Kozuka, M., Sawada, T., 1981. Isolation and characterization of euglobal from *Eucalyptus globulus* Labill. by preparative reversed-phase liquid chromatography. Journal of Chromatography 208, 347–355.

Barr, A., 1993. Traditional Aboriginal Medicines in the Northern territory of Australia. Conservation Commission of the Northern Territory of Australia, Darwin.

Crow, W.D., Osawa, T., Paton, D.M., Willing, R.R., 1977. Structure of grandinol: A novel root inhibitor from *Eucalyptus grandis*. Tetrahedon Letters, 1073–1074.

Elliot, W.R., Jones, D.L., 1984. Encyclopaedia of Australian Plants Suitable for Cultivation, Vol. 4. Lothian, Melbourne.

Gijsen, H.J.M., Kanai, K., Stork, G.A., Wijnberg, J.B.P.A., Orru, R.V.A., Seelen, C.G.J.M., van der Kerk, S.M., de Groot, A., 1990. The conversion of natural (+)-aromadendrene into chiral synthons — I. Tetrahedron 46, 7237–7246.

Gijsen, H.J.M., Wijnberg, J.B.P.A., Stork, G.A., de Groot, A., 1991. The synthesis of (−)-kessane, starting from natural (+)-aromadendrene — II. Tetrahedron 47, 4409–4416.

Gijsen, H.J.M., Wijnberg, J.B.P.A., Stork, G.A., de Groot, A., 1992. The synthesis of mono- and dihydroxy aromadendrene sesquiterpenes, starting from natural (+)-aromadendrene — III. Tetrahedron 48, 2465–2476.

Gijsen, H.J.M., Wijnberg, J.B.P.A., Stork, G.A., de Groot, A., 1994. Rearrangement reactions of aromadendrene derivatives. The synthesis of (+)-maaliol, starting from natural (+)-aromadendrene — IV. Tetrahedron 50, 4733–4744.

Kim, J.P., Kim, W.G., Koshino, H., Jung, J., Yoo, I.D., 1996. Sesquiterpene *o*-naphthoquinones from the root bark of *Ulmus davidiana*. Phytochemistry 43, 425–430.

Kim, W.G., Lee, I.K., Kim, J.P., Ryoo, I.J., Koshino, H., Yoo, I.D., 1997. New indole derivatives with free radical scavenging activity from *Agrocybe cylindracea*. Journal of Natural Products 60, 721–723.

Kim, J.P., Yun, B.S., Shim, Y.K., Yoo, I.D., 1999. Inoscavin A, a new free radical scavenger from the mushroom *Inonotus xeranticus*. Tetrahedron Letters 40, 6643–6644.

Kozuka, M., Sawada, T., Kasahara, F., Mizuta, E., Amano, T., Komiya, T., Goto, M., 1982a. The granulation-inhibiting principles from *Eucalyptus globulus* Labill. II. The structures of euglobal-Ia_1, Ia_2,-Ib,-Ic,-IIa, IIb and-Iic. Chemical and Pharmacutical Bulletin 30, 1952–1963.

Kozuka, M., Sawada, T., Mizuta, E., Kasahara, F., Amano, T., Komiya, T., Goto, M., 1992b. The granulation-inhibiting principles from *Eucalyptus globulus* Labill. III. The structures of euglobal-III,-IVb, and-VII. Chemical and Pharmacutical Bulletin 30, 1964–1973.

Lassak, E.V., McCarthy, T., 1983. Australian Medicinal Plants. Methuen, Australia.

Lee, I.K., Yun, B.S., Cho, S.M., Kim, W.G., Kim, J.P., Ryoo, I.J., Koshino, H., Yoo, I.D., 1996. Betulinans A and B, two benzoquinone compounds from *Lenzites betulina*. Journal of Natural Products 59, 1090–1092.

Lee, S.J., Yun, Y.S., Lee, I.K., Ryoo, I.J., Yun, B.S., Yoo, I.D., 1999. An antioxidant lignan and other constituents from the root bark of *Hibiscus syriacus*. Planta Medica 65, 658–660.

Li, X.-C., Elsohly, H.N., Hufford, C.D., Clark, A.M., 1999. NMR assignments of ellagic acid derivatives. Magnetic Resonaniein Chemistry 37, 856–859.

Malhotra, S., Misra, K., 1981. 3,3′-di-*O*-methylellagic acid 4-O-rhamnoside from the roots of *Prosopis juliflora*. Phytochemistry 20, 2043–2044.

Ohkawa, H., Ohishi, N., Yagi, K., 1979. Assay for lipid peroxides in animal tissues by thiobarbituric acid reaction. Analytical Biochemistry 95, 351–358.

Sawada, T., Kozuka, M., Komiya, T., Amano, T., Goto, M., 1980. Euglobal-III, a novel granulation inhibiting agent from *Eucalyptus globulus* Labill. Chemical and Pharmaceutical Bulletin 28, 2546–2548.

Xu, R.-S., Snyder, J.K., Nakanishi, K., 1984. Robustadials A and B from *Eucalyptus robusta*. Journal of American Chemical Society 106, 734–736.

Yang, S.-W., Zhou, B.-N., Wisse, J.H., Evans, R., van der Werff, H., Miller, J.S., Kingston, D.G.I., 1998. Three new ellagic acid derivatives from the bark of *Eschweilera coricea* from the Suriname rainforest. Journal of Natural Products 61, 901–906.

Yazaki, Y., Hillis, W.E., 1976. Polyphenols of *Eucalyptus globulus*, *E. regnans* and *E. deglupta*. Phytochemistry 15, 1180–1182.

PERGAMON

Phytochemistry 57 (2001) 593–596

PHYTOCHEMISTRY

www.elsevier.com/locate/phytochem

Furomegistines I and II, two furanopyridine alkaloids from the bark of *Sarcomelicope megistophylla*

Nikolas Fokialakis[a], Prokopios Magiatis[a], Nektarios Aligiannis[a], Sofia Mitaku[a,*], François Tillequin[b], Thierry Sévenet[c]

[a]*Laboratory of Pharmacognosy, Department of Pharmacy, University of Athens Panepistimiopolis Zografou, GR-15771 Athens, Greece*

[b]*Laboratoire de Pharmacognosie de l' Université René Descartes, UMR au CNRS No 8638, Faculté de Pharmacie, 4 Avenue de l' Observatoire, F-75006 Paris, France*

[c]*ICSN du CNRS, F-91190 Gif-sur-Yvette, France*

Received 27 November 2000; received in revised form 8 February 2001

Abstract

Two alkaloids, furomegistine I (**1**) and furomegistine II (**2**), were isolated from the bark of *Sarcomelicope megistophylla*. Their structures have been elucidated on the basis of MS and NMR data. Both belong to the category of furanopyridine alkaloids and should be considered as oxidation products of a furo[2,3-*b*]quinoline precursor. The two alkaloids exhibited moderate cytotoxic activity. © 2001 Elsevier Science Ltd. All rights reserved.

Keywords: *Sarcomelicope megistophylla*; Rutaceae; Furanopyridine; Alkaloids; Furomegistine I; Furomegistine II

1. Introduction

Sarcomelicope megistophylla Hartley (Rutaceae) is a small to medium sized tree, 8–12 m high, easily recognized by its pubescent leaves, exceptionally large for the genus (up to 35 cm long). This species is endemic to the region of Néaoua, New Caledonia (Hartley, 1986). Recently, we described the chemical constituents of its leaves (Skaltsounis et al., 1995; Fokialakis et al., 1999) and the major alkaloids of the bark (Fokialakis et al., 2000; Papageorgiou et al., 2000). In a continuation of our studies of the genus *Sarcomelicope*, (Mitaku et al., 1986, 1987, 1989, 1995; Tillequin, 1997) we report here the isolation and structure determination of two new alkaloids, furomegistine I (**1**) and furomegistine II (**2**) from the bark of *Sarcomelicope megistophylla*. Both of them derive from a furanopyridine basic core and should be considered as *seco*-furoquinolines.

2. Results and discussion

Furomegistine I (**1**) was obtained as a yellow amorphous compound, and its molecular formula was determined by HRMS as $C_{15}H_{15}NO_7$. The ^1H NMR spectrum indicated two protons associated with a bisubstituted furano ring, four OCH_3 groups (two belonging to methyl ester functional groups and two placed on sp^2 carbons), and one deshielded olefinic proton (δ 5.28). The ^{13}C NMR spectrum confirmed the above observations and showed the presence of two carbonyl groups which correspond to $COOCH_3$ groups (δ 167.3, 165.4) and also the presence of six quaternary aromatic or olefinic carbons. Based on the HMBC spectrum (Fig. 1) it was clear that five of them constitute a penta-substituted pyridine ring and the sixth takes part in a double bond attached as a side chain to the pyridine ring. This side chain additionally includes a protonated olefinic carbon (δ 94.8), one $COOCH_3$ group (δ 3.54) and a OCH_3 group (δ 3.88) attached to the quaternary olefinic carbon. The chemical shift of the protonated olefinic carbon, which is highly shielded, is in good agreement with the theoretical value of the specific trisubstituted double bond (Pretsch et al., 1989).

* Corresponding author. Tel./fax: +301-7274594.
E-mail address: mitakou@pharm.uoa.gr (S. Mitaku).

0031-9422/01/$ - see front matter © 2001 Elsevier Science Ltd. All rights reserved.
PII: S0031-9422(01)00065-6

.

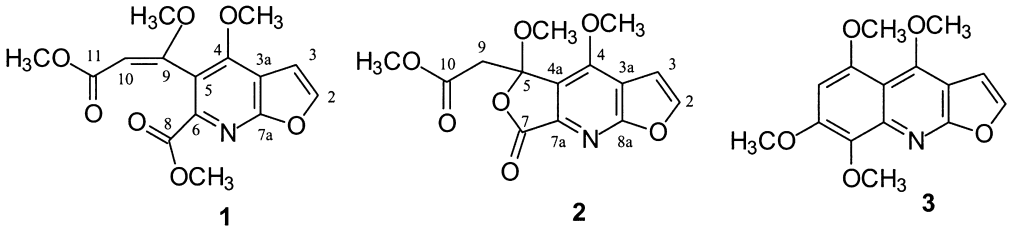

The type of fusion between the pyridine and the furano ring was found to be [2,3-*b*] based on the chemical shift of carbon 7a (163.5) which was identified by its J_3 correlation with the furano protons H-2 and H-3. This chemical shift indicates that this carbon is simultaneously attached to the nitrogen and oxygen atom. The OCH_3 group at 4.26 ppm was correlated with an aromatic carbon at 159.7 ppm, which was identified as C-4 by its J_3 correlation with the furano proton H-3. This arrangement was also confirmed by the NOE correlation of H-3 with the OCH_3 group. The side chain was attached on C-5 (δ 119.9), which was identified by its J_3 correlation with the olefinic proton H-10. The chemical shift of this carbon excluded the possibility that the site of attachment was C-6. Consequently C-6 was bearing the resting $COOCH_3$ group. Finally the stereochemistry of the 9, 10 double bond was investigated with NOESY experiments. The observed strong correlation between H-10 and OCH_3-9 was compatible only with the *cis*-isomer.

Furomegistine II (**2**) was obtained as a yellow amorphous compound, and its molecular formula was determined by HRMS as $C_{14}H_{13}NO_7$. From the IR spectrum ($\nu = 1789$) it was obvious that this molecule contained in its structure a five-membered lactone ring. As in the case of **1**, the ^1H NMR spectrum indicated two protons associated with a bisubstituted furano ring, and also three OCH_3 groups (one belonging to a methyl ester functional group, one placed on sp^2 carbon and one placed on a doubly oxygenated sp^3 carbon), and two equivalent aliphatic protons (δ 3.33). The ^{13}C NMR spectrum confirmed the above observations and showed the presence of two carbonyl groups, one corresponding to a $COOCH_3$ group (165.4) and one corresponding to a lactone (168.1). It also showed the presence of five quaternary aromatic carbons, of one doubly oxygenated aliphatic quaternary carbon and of one methylene carbon. As in **1** the five quaternary aromatic carbons constituted a pyridine ring fused with a furano ring with the same type of fusion.

From the HMBC spectrum (Fig. 1) it was clear that the methylene (H-9) was bearing the $COOCH_3$ group and it was attached to the doubly oxygenated carbon. This carbon (C-5) was included in the lactone ring and was also bearing an OCH_3 group. As in **1** the other OCH_3 group was attached on C-4 of the pyridine ring. The lactone ring was fused with the other two pyridine carbons C-4a and C-7a. The type of fusion was assigned by the chemical shift of C-4a which was identified by its J_3 correlation with the methylene protons H-9. This chemical shift (δ 121.9) is not consistent with the α-position of a pyridine nucleus and thus the opposite type of fusion is excluded. Furomegistine II (**2**) was optically inactive although a chiral center is included in its structure, indicating that the isolated compound was a racemate mixture.

From a biogenetic point of view, furomegistine I (**1**) and furomegistine II (**2**) most probably arise from the oxidation of the benzene aromatic ring of a furo[2,3-*b*]quinoline precursor, such as acronycidine (**3**), which is one of the major alkaloids isolated from the bark (Papageorgiou et al., 2000). The presence of three electron-donating groups on the A ring of this furoquinoline should greatly facilitate the oxidative cleavage of the C-7, C-8 double-bond, to give the furanopyridine skeleton of furomegistine I (**1**). Further recyclization of a *seco*-furoquinoline of this type, through C-5 and the

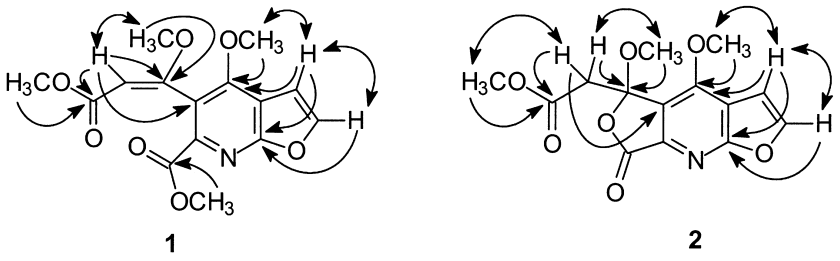

Fig. 1. HMBC (→) and NOESY (↔) correlations for furomegistine I (**1**) and furomegistine II (**2**).

carboxylic function at C-8, is a possible route to the formation of the fused furanolactone system of furomegistine II (**2**). It is interesting to note that a similar biogenetic origin, involving the oxidative ring opening of the aromatic ring, had been postulated, in the acridone series, for 1-methyl-4-quinolone-2,3-dicarboxylic acid dimethylester isolated from *Sarcomelicope dogniensis* (Mitaku et al., 1995) and for fareanine obtained from *Medicosma fareana* (Habtemariam et al., 1996). To the best of our knowledge, only one *seco*-furoquinoline (furanopyridine) alkaloid, dimethylrhoifolinate from *Zanthoxylum rhoifolium* (Arruda et al., 1992) and *Metrodorea nigra* (Müller et al., 1995), has been previously described.

It is interesting to point out that compound **2** possesses the heterocyclic ring system of furano[3,2-*b*]furano[3,4-*b*]pyridine that has never been described either from natural or synthetic origin.

The two new alkaloids **1** and **2** were tested for their cytotoxicity against A549 and HT-29 cells and exhibited a moderate activity with IC_{50} = 90 and 100 μM, respectively.

3. Experimental

3.1. General experimental procedures

UV spectra were recorded on a Shimadzu-160A spectrophotometer. The IR spectrum was obtained on a Perkin-Elmer Paragon 500 instrument. NMR spectra were recorded on Bruker DRX 400 and Bruker AC 200 spectrometers [^{1}H (400 and 200 MHz) and ^{13}C (50 MHz)]; chemical shifts are expressed in ppm downfield to TMS. The 2D NMR experiments were performed using standard Bruker microprograms. EIMS and HRMS were determined on HP-6890 and AEI MS-902 spectrometers, respectively.

3.2. Plant material

The plant material was collected at Nouméa (New Caledonia) in May 1984. A voucher sample (Pusset-Chauvière 261) is kept in the herbarium of the Centre ORSTOM at Néaoua (New Caledonia).

3.3. Extraction and isolation

Extraction of alkaloids was as described (Papageorgiou et al., 2000). The crude alkaloid mixture was chromatographed over a column containing Si gel (Merck 0.04–0.06 mm; flash), using a cyclohexane/EtOAc gradient to give 7 fractions. Fraction 6 was submitted to flash chromatography on silica gel with CH_2Cl_2 to afford furomegistine I (5 mg) and furomegistine II (12 mg).

3.4. Furomegistine I (*1*)

UV λ^{MeOH} nm (log ε): 298 (*sh*), 345 (2.64). ^{1}H NMR ($CDCl_3$, 400 MHz): δ 7.76 (1H, *d*, J = 2.6 Hz, H-2), 7.06 (1H, *d*, J = 2.6 Hz, H-3), 5.46 (1H, *s*, H-10), 4.26 (3H, *s*, OMe-C4), 3.95 (3H, *s*, OMe-C8), 3.88 (3H, *s*, OMe-C9), 3.54 (3H, *s*, OMe-C11). ^{13}CNMR ($CDCl_3$, 50 MHz): δ 167.3 (C-11), 166.7 (C-9), 165.4 (C-8), 163.5 (C-7a), 159.7 (C-4), 148.3 (C-6), 145.7 (C-2), 119.9 (C-5), 109.8 (C-3a), 105.9 (C-3), 94.8 (C-10), 59.9 (OMe-C4), 57.1 (OMe-C9), 53.1 (OMe-C8), 51.2 (OMe-C11). MS-DCI m/z: 322 $[M+H]^+$. EI m/z (rel. int.): 321 (5), 290 (10), 262 (100). HRMS m/z: 321.0844; found for $C_{15}H_{15}O_7N$; required m/z: 321.0848.

3.5. Furomegistine II (*2*)

$[\alpha]_D$ 0° (CH_2Cl_2, *c* 0.1). UV λ^{MeOH} nm (log ε): 278 (2.66), 307 (*sh*). IR ν_{max} (CH_2Cl_2) cm^{-1}: 2928, 1789, 1739, 1603. ^{1}H NMR ($CDCl_3$, 400 MHz): δ 7.85 (1H, *d*, J = 2.6 Hz, H-2), 7.15 (1H, *d*, J = 2.6 Hz, H-3), 4.42 (3H, *s*, OMe-C4), 3.55 (3H, *s*, OMe-C10), 3.33 (2H, *s*, H-9), 3.13 (3H, *s*, OMe-C5). ^{13}CNMR ($CDCl_3$, 50 MHz): δ 168.1 (C-7), 165.4 (C-10), 163.8 (C-8a), 156.3 (C-4), 146.1 (C-2), 143.6 (C-7a), 121.9 (C-4a), 110.6 (C-3a), 105.6 (C-3), 105.0 (C-5), 59.4 (OMe-C4), 52.0 (OMe-C10), 51.1 (OMe-C5), 40.9 (C-9). MS-DCI m/z: 308 $[M+H]^+$. EI m/z (rel. int.): 307 (10), 276 (15), 262 (10), 248 (10), 234 (100), 191 (20). HRMS m/z: 307.0697; found for $C_{14}H_{15}O_6N$; required m/z: 307.0692.

3.6. Cytotoxicity assay

Compounds **1** and **2** were tested for their cytotoxic activity on the following solid tumour cell lines: human lung carcinoma A549 and human colon adenocarcinoma HT29 (European Collection of Cell Cultures, Salisbury, UK). All cell lines were cultured in Dulbecco's minimal essential medium supplemented with penicillin (100 U/ml), streptomycin (100 μg/ml) and 10% fetal bovine serum (media and antibiotics from Biochrom KG, Berlin, Germany) in an environment of 5% CO_2, 85% humidity, 37°C. Cells were routinely subcultured using a trypsin 0.25%– EDTA 0.02% solution. The cytotoxicity assay was performed by a modification of the MTT-method (Denizot and Lang, 1986).

References

Arruda, M.S.P., Fernandes, J.B., Vieira, P.C., Das, M.F., Da Silva, G.F., Pirani, J.R., 1992. Chemistry of *Zanthoxylum rhoifolium*: a new secofuroquinoline alkaloid. Biochem. Syst. Ecol. 20, 173–178.

Denizot, F., Lang, R., 1986. Rapid colorimetric assay for cell growth and survival. Modifications to the tetrazolium dye procedure giving improved sensitivity and reliability. J. Immunol. Meth. 89, 271–277.

Fokialakis, N., Mitaku, S., Mikros, E., Skaltsounis, A.L., Tillequin, F., Sévenet, T., 1999. Megistosarcimine and megistosarconine, two

alkaloids from *Sarcomelicope megistophylla*. Phytochemistry 52, 1745–1748.

Fokialakis, N., Magiatis, P., Skaltsounis, A.L., Tillequin, F., Sévenet, T., 2000. The structure of sarcomejine: an application of long-range ^{1}H–^{15}N correlation at natural abundance. J. Nat. Prod. 63, 1004–1005.

Habtemariam, S., Waterman, P.G., Hartley, T.G., 1996. Fareanine and fareanol from leaves of *Medicosma fareana*. Phytochemistry 43, 291–294.

Hartley, T.G., 1986. Three new species of *Sarcomelicope* (Rutaceae) from New Caledonia (with a new key to the species of the genus). Adansonia 8, 183–189.

Mitaku, S., Skaltsounis, A.L., Tillequin, F., Koch, M., Pusset, J., Chauvière, G., 1986. Plantes de Nouvelle-Calédonie CVI. Alcaloids de *Sarcomelicope glauca*. J. Nat. Prod. 49, 1091–1095.

Mitaku, S., Skaltsounis, A.L., Tillequin, F., Koch, M., Pusset, J., Chauvière, G., 1987. Four new acridone alkaloids from *Sarcomelicope dogniensis* Hartley (Rutaceae). Heterocycles 26, 2057–2063.

Mitaku, S., Skaltsounis, A.L., Tillequin, F., Koch, M., Pusset, J., 1989. Alkaloids des écorces de *Sarcomelicope dogniensis*. Ann. Pharm. Fr. 47, 149–156.

Mitaku, S., Skaltsounis, A.L., Tillequin, F., Koch, M., Pusset, J., Sévenet, T., 1995. New alkaloids from *Sarcomelicope dogniensis*. Nat. Prod. Lett. 7, 219–225.

Müller, A.H., Vieira, P.C., Das, M.F., Da Silva, G.F., Fernandes, J.B., 1995. Dihydrochalcones, coumarins and alkaloids from *Metrodorea nigra*. Phytochemistry 40, 1797–1800.

Papageorgiou, M., Fokialakis, N., Mitaku, S., Skaltsounis, A.L., Tillequin, F., Sévenet, T., 2000. Two new alkaloids from the bark of *Sarcomelicope megistophylla*. J. Nat. Prod. 63, 385–386.

Pretsch, E., Simon, W., Seibl, J., Clerc, T., 1989. Tables of spectral data for structure determination of organic compounds, 2nd Edition. Springer Verlag, Berlin.

Skaltsounis, A.L., Seddrati, L., Tillequin, F., Koch, M., Pusset, J., Sévenet, T., 1995. Sarcomegistine, a new dihydrofuroquinoline alkaloid from *Sarcomelicope megistophylla*. Nat. Prod. Lett. 5, 281–287.

Tillequin, F., 1997. Alkaloids in the genus *Sarcomelicope* Engl. (Rutaceae). Recent Res. Devel. Phytochem. 1, 675–687.

PERGAMON

Phytochemistry 57 (2001) 597–602

PHYTOCHEMISTRY

www.elsevier.com/locate/phytochem

Alkaloids from *Haplophyllum tuberculatum*

Adnan J. Al-Rehaily [a,*], Tawfeq A. Al-Howiriny [a], Mohammad S. Ahmad [a], Mohammad A. Al-Yahya [a], Farouk S. El-Feraly [a], Charles D. Hufford [b], Andrew T. McPhail [c]

[a] *Department of Pharmacognosy, College of Pharmacy, King Saud University, Riyadh 11451, Saudi Arabia*
[b] *Department of Pharmacognosy and National Center for Natural Products Research, Research Institute of Pharmaceutical Sciences, School of Pharmacy, University of Mississippi, Mississippi, MS 38677, USA*
[c] *Department of Chemistry, PM. Gross Chemical Laboratory, Duke University, Durham, NC 27708, USA*

Received 24 October 2000; received in revised form 4 December 2000

Abstract

Two new alkaloids, haplotubinone (**3**) and haplotubine (**4**), were isolated from the aerial parts of *Haplophyllum tuberculatum* together with the known lignan diphyllin. The structures of the new alkaloids were established by spectroscopic methods in conjunction with X-ray crystallographic analysis of **3**. In addition, the amide *N*-(2-phenylethyl)-benzamide has been identified in this source for the first time. © 2001 Elsevier Science Ltd. All rights reserved.

Keywords: *Haplophyllum tuberculatum*; Rutaceae; Alkaloids; Haplotubinone; Haplotubine; *N*-(2-Phenylethyl)benzamide; X-ray crystallography

1. Introduction

Previous phytochemical work on *Haplophyllum tuberculatum* (Forssk.) A. Juss. (Rutaceae) collected in Saudi Arabia described the isolation of (+)-dihydroperfamine (Al-Yahya et al., 1991), tuberine (McPhail et al., 1990), tubacetine, tubasenecine and 7-hydroxy-8-(3-methyl-2-butenyl)-4-methoxyfuro[2,3b]quinoline (Al-Yahya et al., 1992). In addition, a number of known alkaloids were also isolated from this source, including buchapine, 3-dimethylallyl-4-dimethylallyloxy-2-quinolone, γ-fagarine and flindersine (Al-Rehaily, 1992). The present paper reports on the isolation and characterization of the new alkaloids haplotubinone (**3**) and haplotubine (**4**) from the aerial parts of *H. tuberculatum*, together with the known amide *N*-(2-phenylethyl)benzamide (**1**) (Batsuren et al., 1992) and the lignan dyphyllin (**2**) (Gozler et al., 1984).

2. Results and discussion

The methylene chloride extract of the aerial parts of *H. tuberculatum* was partitioned between *n*-hexane and acetonitrile. The acetonitrile extract was fractionated by flash column chromatography using mixtures of toluene and increasing concentrations of acetone. Compound **3** eluted first and yielded colorless crystals from ether, mp 177.0–178.0°C. Its molecular formula was established as $C_{19}H_{23}NO_4$ by FAB (*m*/*z* 352 for $[M+Na]^+$), ^{13}C and ^1H NMR spectral data. The UV spectrum exhibited absorption bands at λ_{max} 237, 262(sh), 352 nm, indicating the presence of a 2,4-quinoldione chromophore (Sheriha et al., 1987). The IR spectrum displayed absorption bands at ν_{max} 3450 (OH group), 1702 (C=O), 1673 (HN–CO) and 1611 cm^{-1} (C=C). The PND ^{13}C NMR (Table 1) and DEPT spectra revealed the presence of four methyls, one methylene, seven methines and seven quaternary carbons. On the other hand, the ^1H NMR spectrum of compound **3** (Table 1) showed resonances for four aromatic protons at δ 7.89 (*d*, *J* = 7.4 Hz, H-5), 7.22 (*t*, *J* = 7.6, H-6), 7.63 (*dd*, *J* = 6.9, 7.2 Hz, H-7) and 7.16 (*d*, *J* = 8.1 Hz, H-8). The relative deshielding of H-5 and H-7 was attributed to the 4-carbonyl function. In addition, there was one oxygenated methine proton resonating at δ 3.42 (*d*, *J* = 9.5 Hz, H-1′), one methine proton at δ 1.82 (*ddd*, *J* = 11.1, 3.4, 3.4 Hz, H-2′), two methyls as part of a dimethylallyl unit, and two methyls attached to an oxygenated quaternary carbon. The dimethylallyl unit was defined by the three proton ABX system comprising the nonequivalent AB methylene protons (H-3′) at δ_A 2.22 as a doublet and δ_B

* Corresponding author. Tel.: +11-966-467-7258; fax: +11-966-467-7245.
E-mail address: ajalreha@ksu.edu.sa (A.J. Al-Rehaily).

0031-9422/01/$ - see front matter © 2001 Elsevier Science Ltd. All rights reserved.
PII: S0031-9422(01)00041-3

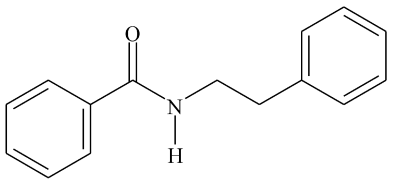

1

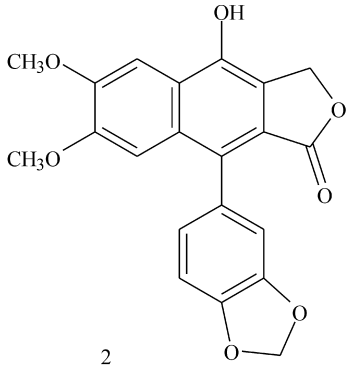

2

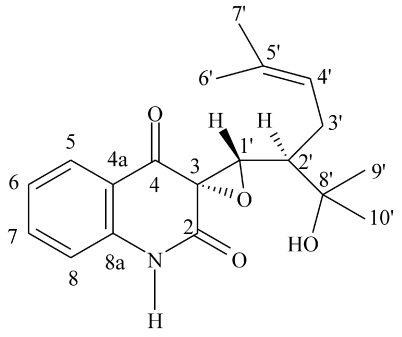

3

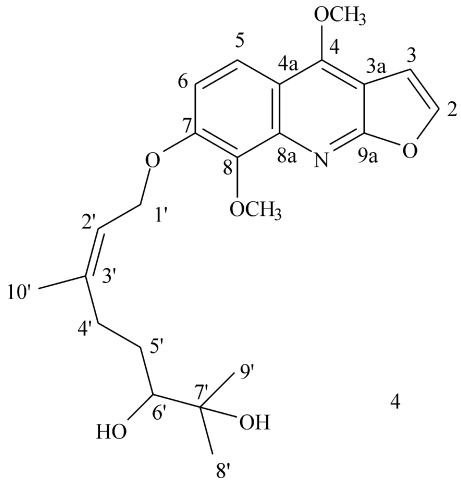

4

2.14–2.07 as a multiplet, the X vinylic proton at δ_X 4.52 (H-4′) as a doublet, and the nonequivalent vinylic geminal dimethyl singlets at δ 1.42 and 0.85.

Based on these data, it was clear that compound **3** was a C-3 substituted 4-ketoquinolone. The C-3 substituent contained a dimethylallyl function, an epoxide, and two methyls on an oxygenated quaternary carbon. In an effort to try to establish these bonding patterns, a 2D-inadequate experiment was conducted. All of the aliphatic connectivities were observed, except for those between δ_C 74.2 and 62.3. The 2D-inadequate was not conclusive, however, and there was an unusually upfield olefinic methyl signal (δ_H 0.85).

A single-crystal X-ray analysis established unequivocally the complete structure and relative stereochemistry of compound **3**. A view of the solid-state conformation is illustrated in Fig. 1. Bond lengths are all in accord with expectations (Allen et al., 1987). The hydroxy group is intramolecularly hydrogen-bonded to the epoxide oxygen atom [O(11′)...O(11) = 2.835(5) Å]. Pairs of enantiomers of **3** are associated by N–H...O hydrogen bonds [N(1)...O(9) = 2.877(6) Å] about crystallographic centers of symmetry.

Full assignments of the ^{1}H and ^{13}C signals of compound **3** were secured by the ^{1}H–^{1}H COSY, HMQC and HMBC spectra (Table 1). The HMBC spectrum of **3** showed ^{1}H–^{13}C long-range correlations between methine proton at δ 3.42 (H-1′) and δ 45.6 (C-2′), 62.3 (C-3) and 170.3 (C-2), and between the methine proton at δ 1.82 (H-2′) and δ 74.2 (C-1′), 73.8 (C-8′), 27.5 (C-9′ / C-10′), 29.8 (C-10′/C-9′) and 123.0 (C-4′). There were also long-range correlations between H-9′ and H-10′ and the carbons resonating at δ 45.6 (C-2′) and 73.8 (C-8′). It is interesting to note that X-ray-crystallography indicated that the C-6′ methyl was hovering right above the benzene ring of the quinoldione system. This perhaps explains the abnormally shielded chemical shift value of this vinylic methyl group at δ 0.85. This is the first reported isolation of this alkaloid from nature and it was given the trivial name haplotubinone.

Compound **4** was obtained as an amorphous yellow powder. Its UV spectrum exhibited absorption bands at λ_{max} 250, 320, 332 nm, characteristic of a furoquinoline alkaloid (Sangster and Stuart, 1965) and the spectrum remained unaffected by the addition of alkali. The IR spectrum showed a strong band at ν_{max} 3430 cm^{-1}

Table 1
^{13}C and ^{1}H NMR assignments and ^{1}H–^{13}C long-range correlations of compound **3** by HMQC and HMBC in CD_3OD

C	δ_C	δ_H	Cross peaks (δ_C) in HMBC spectrum
2	170.3 C		
3	62.3 C		
4	190.4 C		
4_a	122.9 C		
5	128.4 CH	7.89 (*d*, 7.4)	190.4 (4), 143.3 (8_a), 137.8 (7)
6	124.9 CH	7.22 (*t*, 7.6)	122.9 (4_a), 118.4 (8)
7	137.8 CH	7.63 (*dd*, 6.9, 7.2)	143.3 (8_a), 128.4 (5)
8	118.4 CH	7.16 (*d*, 8.1)	124.9 (6) 122.9 (4_a)
8_a	143.3 C		
1′	74.2 CH	3.42 (*d*, 9.5)	45.6 (2′), 62.3 (3), 170.3 (2)
2′	45.6 CH	1.82 (*ddd*, 11.1, 3.4, 3.4)	74.2 (1′), 73.8 (8′), 27.5 (9′/10′), 29.8 (10′/9′), 123.0 (4′)
3′	27.2 CH_a	2.22 (*d*, 15.5)	74.2 (1′), 45.6 (2′), 123.0 (4′), 135.7 (5′)
	27.2 CH_b	2.14–2.07 (m)	74.2 (1′), 45.6 (2′), 123.0 (4′), 135.7 (5′)
4′	123.0 CH	4.52 (*d*, 7.3)	17.9 (7′), 25.7 (6′)
5′	135.7 C		
6′	25.7 CH_3	0.85 (*s*)	123.0 (4′),135.7 ((5′)), 17.9 (7′)
7′	17.9 CH_3	1.42 (*s*)	123.0 (4′), 135.7 (5′), 25.7 (6′)
8′	73.8 C		
9′/10′	27.5/29.8 CH_3	1.39/1.38 (*s*)	45.6 (2′), 73.8 (8′)
10′/9′	29.8/27.5 CH_3	1.38/1.39 (*s*)	45.6 (2′), 73.8 (8′)

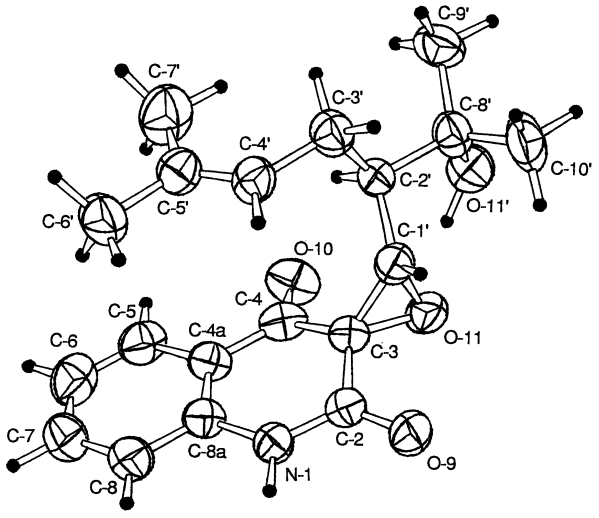

Fig. 1. ORTEP diagram (50% probability ellipsoids) showing the crystallographic atom numbering scheme and solid-state conformation of one enantiomer of haplotubinone (**3**); small filled circles represent hydrogen atoms.

supporting the presence of a hydroxyl absorption. The mass spectrum of compound **4** disclosed, in addition to the molecular ion $[M]^+$ at *m/z* 415 ($C_{23}H_{29}NO_6$), significant fragments at *m/z* 400 $[M-15]^+$, 356 $[M-59]^+$, 245 $[M-170]^+$ (100%) and 227 $[M-188]^+$. The ^{13}C NMR spectrum (Table 2) of **4** exhibited 23 carbon signals manifested via DEPT spectrum as five methyls, three methylene, six methines, and nine quaternary carbons. The ^{1}H NMR spectrum of compound **4** (Table 2) confirmed its furoquinoline nature and displayed signals for two methoxy groups at δ 4.11 and 4.42; the latter signal is indicative of a methoxy group at C-4, based on the proton chemical shift data characteristic of 4-methoxyfuro-quinoline alkaloids (Ayafor and Okogun, 1982). On the other hand, the second methoxy group could be safely positioned at C-8 owing to its deshielded carbon resonance (δ 61.6) (Panichpol and Waterman, 1978) leaving position C-7 for the side chain moiety. A pair of AB doublets at δ 7.04 and 7.58 ($J = 2.8$ Hz) corresponded to the two furan protons, while the other two aromatic protons appeared as doublets at δ 7.21 ($J = 9.2$ Hz) and 7.97 ($J = 9.6$ Hz), suggesting their positions at H-6 and H-5, respectively (Robertson, 1963).

In addition, the ^{1}H NMR spectrum (see Table 2) showed the presence of three tertiary methyl groups at δ 1.13, 1.15, and 1.75, with that at δ 1.75 deshielded enough to be on an olefinic functional group, three methylene groups, one olefinic methine proton (δ 5.61, *ddd*, $J = 1.2$, 6.6, 6.6 Hz), and one methine proton (δ 3.31, *dd*, $J = 1.6$, 10.6 Hz) on an oxygen-bearing group. These assignments, along with the loss of a fragment of *m/z* 170, pointed to the presence of a 6′,7′ - dihydroxygeranyloxyl moiety (Ulubelen et al., 1995), confirmation of which was derived from the correlations observed in ^{1}H–^{1}H COSY, HMQC and HMBC spectra (Table 2). In the HMBC spectrum of **4** the H-1′ (δ 4.79, *d*) signal showed $^{2}J_{C-H}$ and $^{3}J_{C-H}$ correlations with the ^{13}C signals at δ 120.4 (CH, C-2′), 141.6 (C, C-3′) and 151.3 (C, C-7), while H-2′ (δ 5.61, *ddd*) showed three-bond correlations with the signals at δ 36.5 (CH_2, C-4′) and 16.6 (CH_3, C-10′). Similarly, H-4′ (δ 2.20–2.12 and 2.32–2.29, m) exhibited two- and three-bond correlations with the carbon signals at δ 29.3 (CH_2, C-5′), 141.6 (C, C-3′), 120.4 (CH, C-2′) and 77.7 (CH, C-6′). The H-5′ signals (1.48–1.43 and 1.62–1.58, m) displayed correlations with the carbons signals at δ

Table 2
^{13}C and ^{1}H NMR assignments and ^{1}H–^{13}C long-range correlations of compound **4** by HMQC and HMBC in $CDCl_3$

C	δ_C	δ_H	Cross peaks (δ_C) in HMBC spectrum
2	143.0 CH	7.58 (*d*, 2.8)	164.2 (9_a), 102.1 (3_a), 104.6 (3)
3	104.6 CH	7.04 (*d*, 2.8)	164.2 (9_a), 102.1 (3_a), 143.0 (2)
3_a	102.1 C		
4	157.1 C		
4_a	115.1 C		
5	117.8 CH	7.97 (*d*, 9.6)	157.1 (4), 151.3 (7), 141.1 (8_a)
6	114.8 CH	7.21 (*d*, 9.2)	143.1 (8), 115.1 (4_a)
7	151.3 C		
8	143.1 C		
8_a	141.1 C		
9_a	164.2 C		
1′	66.9 CH_2	4.79 (*d*, 6.8)	151.3 (7), 141.6 (3′), 120.4 (2′)
2′	120.4 CH	5.61 (*ddd*, 1.2, 6.6, 6.6)	36.5 (4′), 16.6 (10′)
3′	141.6 C		
$4_a'$	36.5 CH_2	2.32–2.29 (*m*)	141.6 (3′), 120.4 (2′), 77.7 (6′), 29.3 (5′)
$4_b'$	36.5 CH_2	2.20–2.12 (*m*)	141.6 (3′), 120.4 (2′), 29.3 (5′)
$5_a'$	29.3 CH_2	1.62–1.58 (*m*)	36.5 (4′)
$5_b'$	29.3 CH_2	1.48–1.43 (*m*)	141.6 (3′), 77.7 (6′), 36.5 (4′)
6′	77.7 CH	3.31 (*dd*, 1.6, 10.6)	72.9 (7′), 36.5 (4′), 23.1 (9′)
7′	72.9 C		
8′	26.4 CH_3	1.15 (*s*)	77.7 (6′), 72.9 (7′), 23.1 (9′)
9′	23.1 CH_3	1.13 (*s*)	77.7 (6′), 72.9 (7′), 26.4 (8′)
10′	16.6 CH_3	1.75 (*s*)	141.6 (3′), 120.4 (2′)
4-OCH_3	59.0	4.42 (*s*)	157.1 (4)
8-OCH_3	61.6	4.11 (*s*)	143.1 (8)

36.5 (CH_2, C-4′), 77.7 (CH, C-6′) and 141.6 (C, C-3′). On the other hand, the H-6′ signal (δ 3.31) showed long-range correlations with δ 36.5 (CH_2, C-4′), 23.1 (CH_3, C-9′) and 72.9 (C, C-7′), which in turn was coupled to δ 1.15 and 1.13 (H-8′ and H-9′, respectively). These findings established the structure of **4** and it was given the trivial name haplotubine.

Haplophyllum tuberculatum also yielded compounds **1** and **2** which proved to be known compounds. Compound **1** was identified as *N*-(2-phenylethyl)benzamide which was previously found to occur in *Oxytropis muriceta and Oxytropis pseudoglandulosa*, members of the Fabaceae family (Batsurens et al., 1992). The present work is the first reported isolation of this compound from the genus *Haplophyllum* and the family Rutaceae. In contrast, compound **2** was identified as the lignan diphyllin which was previously isolated from *Haplophyllum tuberculatum* and other *Haplophyllum* species (Sheriha and Abou Amer, 1984).

3. Experimental

3.1. General

Melting points were determined in capillary tubes using an Electrothermal 9100 capillary melting-point apparatus and are uncorr. The UV spectra were recorded on a Hewlett-Packard HP-845 UV-vis spectrophotometer, while the FTIR spectra were determined on a Nicolet Impact 410 spectrophotometer. Specific rotations were measured as solutions in methylene chloride on a Perkin-Elmer 242 MC polarimeter. The ^{1}H and ^{13}C NMR spectra were obtained in $CDCl_3$ using either Varian INOVA-400 or a Bruker DRX-500 NMR spectrometers operating at 400 and 100 or 500 and 125 MHz, respectively, and using standard pulse sequences. The chemical shift values are reported as ppm using tetramethylsilane (TMS) as internal standard and coupling constants *J* are expressed in Hz. Low resolution MS were recorded on a Fison VG Autospec Spectrometer, while the high resolution spectra were taken in sodium m-nitrobenzyl alcohol, using a Bioapex FTMS with electrospray ionization. Thin layer chromatographic analyses were carried out on pre-coated silica gel 60 F254 (Merck) using acetone-toluene mixtures as solvent systems and spots were visualized under short and long wavelength UV light and by spraying with Dragendorff reagent. The adsorbent used for column chromatography was silica gel 60/230–400 mesh (EM Science). X-ray diffraction data were recorded at 296 K on an Enraf-Nonius CAD-4 diffractometer (Cu-K_α radiation, graphite monochromator, $\lambda = 1.5418$ Å).

3.2. Plant material

Haplophyllum tuberculatum (Forssk.) A. Juss. was collected in April 1987, near the Riyadh-Gassim highway, 100 miles from Riyadh, in central Saudi Arabia.

The plant material was identified by Dr. Sultanul Abidin of the Department of Pharmacognosy, College of Pharmacy, King Saud University, Riyadh, Saudi Arabia, and voucher specimens are being kept at the local herbarium.

3.3. Extraction and isolation

The air-dried, aerial part (2.0 kg) was extracted with methylene chloride in a Soxhlet for 72 h. The extract (58 g) was partitioned between n-hexane and acetonitrile, 4×300 ml of each. The two solvents were presaturated with each other. The acetonitrile layer, after evaporation of the solvent, was subjected to flash chromatography on silica gel using toluene and increasing concentrations of acetone to give 6 fractions (A–F).

Fraction A was subjected to silica gel CC using ether/*n*-hexane (30:70) as eluent, to give first the known alkaloid buchapine, as previously reported (Al-Yahya et al., 1992) then the known alkaloid *N*-(2-phenylethyl)benzamide (**1**) (5 mg). Fraction B was flash chromatographed on silica gel using benzene/acetone (98:2) to yield first the known alkaloid 7-hydroxy-8-(3-methyl-2-butenyl)-4-methoxyfuro[2,3*b*]quinoline, as previously reported (Al-Yahya et al., 1992), followed by a yellow residue, which after crystallization from EtOAc–EtOH, furnished the known lignan diphyllin (**2**) (60 mg) as yellow needles. Further elution provided a fraction that yield upon crystallization the known alkaloid flindersine, as previously reported (Al-Yahya et al., 1992). Flash chromatography of the mother liquor on silica gel using *n*-hexane/acetone (60:40) afforded compound **3** as colorless crystals (100 mg) and compound **4** as an amorphous yellow powder (20 mg).

3.4. N-(2-Phenylethyl)benzamide (*1*)

White amorphous powder, mp 115.0–116.0°C (lit. Batsuren et al., 1992, 117.0–118.0°C); UV, IR, MS and NMR matched the literature data (Batsuren et al., 1992, Kita et al., 1986, Stamm et al., 1985).

3.5. Diphyllin (*2*)

Yellow needles, mp 282.0–285.0°C (lit. Sheriha et al., 1984, 282.0–285.0°C); UV, IR, MS and NMR were indistinguishable from those reported (Gozeler and Gozeler, 1984).

3.6. Haplotubinone (*3*)

Colorless crystals from ether, mp 177.0–178.0°C; $[\alpha]_D^{22}$ zero° (*c*; 0.500 in CH_2Cl_2); UV λ_{max} (MeOH) nm (log ε): 237 (4.40), 262 (*sh*) (3.50), 352 (3.70); IR ($CHCl_3$) ν_{max} cm^{-1}: 3450, 2976, 2930, 1702, 1673, 1611, 1486, 1371, 907 and 755; ^1H NMR ($CDCl_3$, 500 MHz) and ^{13}C NMR ($CDCl_3$, 125 MHz), see Table 1; EIMS *m*/*z* (rel. int. %) 330 $[M+H]^+$ (4.7), 256 (13.3), 242 (16.4), 214 (24.8), 200 (23.3), 177 (89.9), 161 (27.8) and 43 (100); HRMS: obsd 352.1586 (calc. for $C_{19}H_{23}NO_4$ + Na 352.1524).

3.7. Haplotubine (*4*)

Amorphous yellow powder; $[\alpha]_D^{22}$ −6° (*c*; 1.2 in CH_2Cl_2); UV λ_{max} (MeOH) nm (log ε): 250 (4.87), 320 (3.90), 332 (3.88); IR ($CHCl_3$) ν_{max} cm^{-1}: 3430, 2973, 2936, 2870, 1627, 1614, 1581, 1507, 1492, 1369, 1267, 1336, 1098, 1045 and 966; ^1H NMR ($CDCl_3$, 400 MHz) and ^{13}C NMR ($CDCl_3$, 100 MHz), see Table 2; EIMS *m*/*z* (rel. int. %) 415 $[M]^+$ (1.2), 400 (1.2), 356 (3), 245 (100) and 227 (96); HRMS: obsd 438.1888 (calc. for $C_{23}H_{29}NO_6$ + Na 438.1892).

3.8. X-ray crystal structure analysis of haplotubinone (*3*)

Crystal data: $C_{19}H_{23}NO_4$, $M_r = 329.40$, monoclinic, space group $P2_1/c(C_{2h}^5)$, $a = 15.939(2)$, $b = 6.123(1)$, $c = 19.041(3)$ Å, $\beta = 110.53(1)°$, $V = 1740.3(9)$ Å, $Z = 4$, $D_c = 1.257$ g cm^{-3}, μ(Cu-K_α radiation, $\lambda = 1.5418$ Å) = 6.8 cm^{-1}; crystal dimensions: 0.02×0.14×0.60 mm.

Check reflections remeasured every 2 h throughout data collection showed no significant decay (< 1.0%). Intensity data ($\theta_{max} = 65°$; 3064 + h, + k, ±1 total reflections, 2947 independent after merging equivalent reflections, $R_{merge} = 0.04$) were corrected for Lorentz, polarization, and absorption [$T_{max.}$:$T_{min.}$(rel.) = 1.00:0.92] effects. The crystal structure was solved by direct methods. Full-matrix least-squares refinement of atomic parameters (anisotropic C, N, O; calculated hydrogen positions), during which $\Sigma w\Delta^2\left[w = 1/\sigma^2(|F_o|), ?\Delta = (|F_o| - |F_c|)\right]$ was minimized, converged (max. shift: esd = 0.03) at $R = 0.055$ ($R_w = 0.063$, GOF = 1.21) over 1225 reflections with $I > 2.0\sigma(I)$. A final difference Fourier synthesis contained no unusual features $\left[\Delta\rho\left(e/\mathring{A}^3\right) = 0.18(\max), -0.22 (\min)\right]$. Atomic coordinates and thermal parameters, bond lengths, bond angles, and torsion angles have been deposited at the Cambridge Crystallographic Data Centre, Lensfield Road, Cambridge CB2 1EZ, UK.

Acknowledgements

This study was financially supported by the Research Center of the College of Pharmacy, King Saud University, for which the authors are grateful. We also wish to thank Professor Paul Schiff Jr., Department of Pharmaceutical Sciences, School of Pharmacy, University of Pittsburgh, Pittsburgh, Pennsylvania, USA, for his assistance.

References

Allen, F.H., Kennard, O., Watson, D.G., Brammer, L., Orpen, A.G., Taylor, R., 1987. Tables of bond lengths determined by X-ray and neutron diffraction. Part 1. Bond lengths in organic compounds. Journal of the Chemical Society Perkin Trans. 2, S1-S19.

Al-Rehaily, A.J., 1992. Novel alkaloids from *Haplophyllum tuberculatum*, MS thesis, King Saud University, Saudi Arabia.

Al-Yahya, M.A., El-Domiaty, M.M., Al-Meshal, I.A., Al-Said, M.S., El-Feraly, F.S., 1991. (+)-Dihydroperfamine: an alkaloid from *Hyplophyllum tubercullatum*. International Journal of Pharmacognosy 29, 268–272.

Al-Yahya, M.A., Al-Rehaily, A.J., Ahmad, M.S., Al-Said, M.S., El-Feraly, F.S., Hufford, C.D., 1992. New alkaloids from *Haplophyllum tuberculatum*. Journal of Natural Products 55, 899–903.

Ayafor, J.F., Okogun, J.I., 1982. Nkolbisine, a new furoquinoline alkaloid, and 7-acetylazadirone from *Teclea verdoorniana*. Journal of Natural Products 45, 182–185.

Batsuren, S.T., Batbayar, N., Dungerdorzh, D., Akhmedzhanova, V.I., Milgrom, Yu.M., Tashkes, Ya.V., Ibragimov, A.A., 1992. Alkaloids of oxytropis. Chemistry of Natural Compounds 28, 340–344.

Gozler, T., Gozler, B., 1984. Konyanin (a new lignan from *Haplophyllum vulcanicum*). Tetrahedron 40, 1145–1150.

Kita, Y., Akai, S., Ajimura, N., Yoshigi, M., Tsugoshi, T., Yasuda, H., Tamura, Y., 1986. Facile and efficient synthesis of carboxylic anhydrides and amides using trimethyl(silyl)ethoxyacetylene. Journal of Organic Chemistry 51, 4150–4159.

McPhail, A.T., McPhail, D.R., Al-Said, M.S., El-Domiaty, M.M., El-Feraly, F.S., 1990. Revision of the stereochemistry of (+)-tuberine, an alkaloid from *Haplophyllum tuberculatum*. Phytochemistry 29, 3055–3057.

Panichpol, K., Waterman, P.G., 1978. Novel flavonoids from the stem of *Popowia cauliflora*. Phytochemistry 17, 1363–1367.

Robertson, A.V., 1963. The proton magnetic resonance of furoquinoline alkaloids and related compounds. Australian Journal of Chemistry 16, 451–458.

Sangster, A.W., Stuart, K.L., 1965. Ultraviolet spectra of alkaloids. Chemical Reviews 65, 69–130.

Sheriha, G.M., Abouamer, K., Elshtaiwi, B.Z., Ashour, A.S., Abed, F.A., Alhallaq, H.H., 1987. Quinoline alkaloids and cytotoxic lignans from *Haplophyllum tuberculatum*. Phytochemistry 26, 3339–3341.

Sheriha, G.M., Abou Amer, K., 1984. Lignans of *Haplophyllum tuberculatum*. Phytochemistry 23, 151–153.

Stamm, H., Sommer, A., Woderer, A., Wiesert, W., Mall, T., Assithianakis, P., 1985. Highly regioselective ring cleavage of *N*-acylaziridines by "anthracene hydride" (anion of 9,10-dihydroanthracene). Intermediacy of a carbonyl adduct. Influence of nitrogen inversion on the ring opening. Journal of Organic Chemistry 50, 4946–4955.

Ulubelen, A., Gil, R.R., Cordell, G.A., Mericli, A.H., Mericli, F., 1995. Prenylated lignans from *Haplophyllum ptilostylum*. Phytochemistry 39, 417–422.

PERGAMON

Phytochemistry 57 (2001) 603–606

PHYTOCHEMISTRY

www.elsevier.com/locate/phytochem

Methyl chanofruticosinates from leaves of *Kopsia flavida* Blume

Khairana Husain[a,*], Ibrahim Jantan[a], Norasmawati Kamaruddin[a], Ikram M. Said[b], Norio Aimi[c], Hiromitsu Takayama[c]

[a]*Department of Pharmacy, Faculty of Allied Health Sciences, Universiti Kebangsaan Malaysia, Jalan Raja Muda Abdul Aziz, 50300 Kuala Lumpur, Malaysia*

[b]*School of Chemical Sciences and Food Technology, Faculty of Science and Technology, Universiti Kebangsaan Malaysia, 43600 Bangi, Malaysia*

[c]*Faculty of Pharmaceutical Sciences, Chiba University, 1-33, Yayoi-cho, Inage-ku, Chiba 263-8522, Japan*

Received 4 October 2000; received in revised form 8 February 2001

Abstract

Three new indole alkaloids with methyl chanofruticosinates skeletal system, viz., methyl 12-methoxy-N_1-decarbomethoxychanofruticosinate, methyl 12-methoxychanofruticosinate and methyl 11,12-dimethoxychanofruticosinate, in addition to methyl 11, 12-methylenedioxy-N_1-decarbomethoxychanofruticosinate, have been isolated from the leaves of *Kopsia flavida* Blume. The structures of these three new indole alkaloids were assigned by NMR spectral data using various 2D-techniques. © 2001 Elsevier Science Ltd. All rights reserved.

Keywords: *Kopsia flavida* Blume; Apocynaceae; Leaves; Indole alkaloids; Methyl chanofruticosinate skeletal system

1. Introduction

Many *Kopsia* species have been investigated chemically and are known to contain indole alkaloids of various structural types (Sevenet et al., 1994). In Penisular Malaysia, about 18 species are found distributed in the lowland forests including four species in Sarawak and north Borneo (Markgraf, 1970; Ashton, 1988; Sevenet et al., 1994). Some of these species have been subjected to phytochemical studies by several workers, which has resulted in the discovery of many novel compounds as well as some useful bioactivities (Awang et al., 1992; Kam et al., 1993b, 1994, 1996a,b,c, 1999; Kam and Yoganathan, 1996). In Malaysia, the roots of many *Kopsia* species are used in traditional medicine for the treatment of ulcerated noses in tertiary syphilis (Burkill, 1966). In the present paper, we report the isolation of three new indole alkaloids with methyl chanofruticosinate skeletal system together with a known alkaloid from the leaves of the yet uninvestigated *K. flavida* Blume (family: Apocynaceae).

2. Results and discussion

The alkaloidal extract of the leaves of *K. flavida* was obtained in the usual manner. Flash column chromatography of the crude mixture on silica gel, followed by

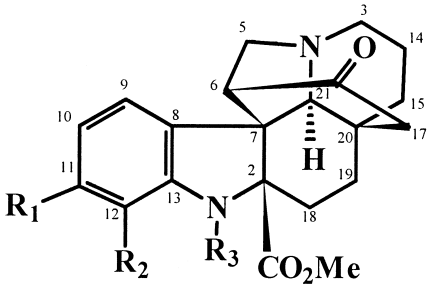

	R_1	R_2	R_3
1	H	OMe	H
2	H	OMe	CO_2Me
3	OMe	OMe	CO_2Me
4	-O-CH_2-O-		H

* Corresponding author. Tel.: +603-40405306; fax: +603-2983271.
E-mail address: khairana@medic.ukm.my (K. Husain).

0031-9422/01/$ - see front matter © 2001 Elsevier Science Ltd. All rights reserved.
PII: S0031-9422(01)00119-4

extensive column and preparative thin layer chromatography yielded four indole alkaloids with methyl chanofruticosinate skeletal system, viz., methyl 12-methoxy-N_1-decarbomethoxychanofruticosinate **1**, methyl 12-meth-x11dummy;oxychanofruticosinate **2**, methyl 11,12-dimethoxychano-fruticosinate **3** and methyl 11, 12-methylenedioxy-N_1-decarbomethoxychano-fruticosinate **4**. The first three are new alkaloids.

The structures of the new compounds were elucidated by a combination of EI mass spectrometry, ^{1}H and ^{13}C NMR spectra in combination with 2D NMR techniques (COSY-45, HMQC and HMBC). The known compound **4** was identified by comparison of their spectroscopic properties (UV, ^{1}H and ^{13}C NMR) (Chen et al., 1981; Kam et al., 1993a). The UV spectrum of all four alkaloids showed absorption maxima typical of a dihydroindole chromophore. The mass spectra of all the compounds exhibited fragmentation patterns typical of indole alkaloids with methyl chanofruticosinate skeletal system, with typical base peak corresponding to $[M-CO_2Me]^+$ fragment.

The HREIMS mass spectrum of compound **1** showed a $[M]^+$ molecular ion at m/z 382.1897 corresponding to $C_{22}H_{26}N_2O_4$. The ^{1}H and ^{13}C NMR spectra (Tables 1 and 2, respectively) of **1** showed that it is the methoxy derivative of methyl N_1-decarbomethoxychanofruticosinate which has been reported in *K. arborea* (Kam et al., 1993a), as indicated by appearance of a singlet (3H) at δ 3.84 belonging to an aromatic methoxy group signal in ^{1}H NMR. The position of the methoxy group was assigned to the 12-position in the benzene ring by the HMQC and HMBC experiments.

The mass spectrum of compounds **2** and **3** showed $[M]^+$ at m/z 440.1952 and 470.2061, corresponding to the formulae $C_{24}H_{28}N_2O_6$ and $C_{25}H_{30}N_2O_7$, respectively. Based on the ^{1}H NMR and ^{13}C NMR spectrums, compounds **2** and **3** were very similar to each other except for the presence of an additional methoxyl moiety in the latter. The connectivities between protons and carbons in the HMBC and HMQC spectrums indicated that proton singlets at δ 3.85 in both compounds were due to methoxyl attached to C-12. Another methoxyl signal at δ 3.79 in spectrum for compound **3** was connected to C-11. The coupling patterns of the aromatic protons in the ^{1}H NMR spectrums support the assignment of compound **2** and **3** as methyl 12-methoxychanofruticosinate and methyl 11,12-dimethoxychano-fruticosinate, respectively.

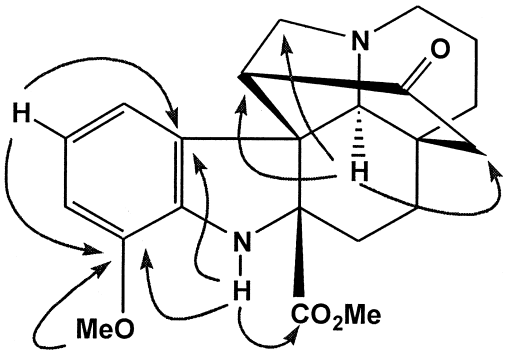

Compound **1**

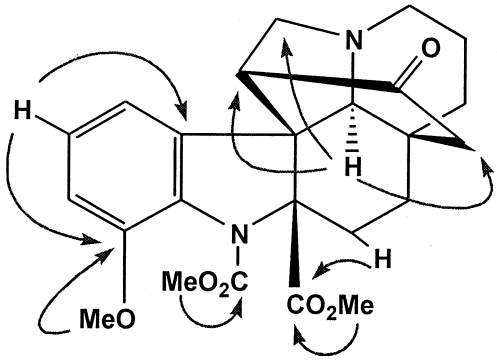

Compound **2**

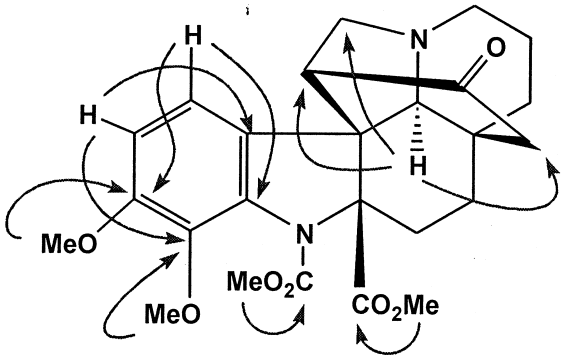

Compound **3**

Selected HMBC correlations of compounds **1**, **2** and **3**.

3. Experimental

3.1. Plant material

The plant material were collected from the Forest Research Institute of Malaysia (FRIM), Malaysia and identified as *Kopsia flavida* by taxonomist Norseha Ayop from FRIM and deposited as a voucher specimen in the herbarium of FRIM, Malaysia.

3.2. Extraction and isolation

The dry powdered sample of the leaves (624.5 g) was extracted with MeOH (2 l) for 3 days at room tempera-

Table 1
^{1}H NMR (500 MHz, $CDCl_3$) spectral data for compounds **1**, **2** and **3**[a]

Proton	Compound **1**		Compound **2**		Compound **3**	
	δ (ppm)	J (Hz)	δ (ppm)	J (Hz)	δ (ppm)	J (Hz)
H-3 α	2.99–3.03 (*m*)	–	3.00–3.04 (*m*)	–	2.98–3.03 (*m*)	–
H-3 β	2.99–3.03 (*m*)	–	3.00–3.04 (*m*)	–	2.98–3.03 (*m*)	–
H-5 α	2.94 (*d*)	3.0	2.96 (*d*)	11.0	2.94 (*d*)	11.3
H-5 β	3.75 (*dd*)	11.3, 6.1	3.80 (*dd*)	10.0, 7.8	3.74–3.79 (*m*)	–
H-6	3.32 (*d*)	6.1	3.21(*d*)	6.1	3.11 (*d*)	5.8
H-9	6.74 (*br d*)	7.4	6.90 (*d*)	7.0	6.90 (*d*)	8.6
H-10	6.78 (*t*)	7.3	7.02 (*t*)	16.9	6.60 (*d*)	8.5
H-11	6.70 (*dd*)	6.7, 2.8	6.84 (*d*)	8.2	–	–
H-14 α	1.34–1.37 (*m*)	–	1.37–1.40 (*m*)	–	1.34–1.36 (*m*)	–
H-14 β	1.34–1.37 (*m*)	–	1.93–2.00 (*m*)	–	1.95–2.00 (*m*)	–
H-15 α	1.34–1.37 (m)	–	1.37–1.40 (*m*)	–	1.35–1.38 (*m*)	–
H-15 β	1.51–1.53 (*m*)	–	1.54–1.60 (*m*)	–	1.55 (*s*)	–
H-17 α	2.02 (*d*)	18.9	2.07 (*d*)	18.9	2.09 (*d*)	18.6
H-17 β	2.82 (*d*)	18.6	2.90 (*d*)	18.6	2.88 (*d*)	18.9
H-18 α	1.80–1.90 (*m*)	–	1.92–2.00 (*m*)	–	1.95–2.00 (*m*)	–
H-18 β	1.97–1.99 (*m*)	–	3.30 (*dt*)	12.8, 3.7	3.28 (*dt*)	12.0, 4.0
H-19 α	1.26–1.29 (*m*)	–	1.32 (*brd*)	13.1	1.33 (*brd*)	13.1
H-19 β	1.80–1.90 (*m*)	–	1.37–1.40 (*m*)	–	–	–
H-21	2.53 (*s*)	–	2.51 (*s*)	–	2.47 (*s*)	–
N-H	4.63 (*s*)	–	–	–	–	–
Ar_{11}OMe	–	–	–	–	3.85 (*s*)	–
Ar_{12}OMe	3.84 (*s*)	–	3.85 (*s*)	–	3.79 (*s*)	–
NCOOMe	–	–	3.82 (*s*)	–	3.85 (*s*)	–
COOMe	3.64 (*s*)	–	3.57 (*s*)	–	3.58 (*s*)	–

[a] Assignments were by COSY, HMQC and HMBC 2D-NMR experiments.

Table 2
^{13}C NMR (100 MHz, $CDCl_3$) spectral data for compounds **1**, **2**, and **3**

Carbon	**1**	**2**	**3**
2	74.4	77.3	77.8
3	46.6	46.4	46.5
5	52.6	53.0	53.0
6	55.3	54.7	54.8
7	58.3	60.0	59.2
8	134.3	130.0	129.8
9	116.4	116.1	118.2
10	120.3	124.9	107.5
11	109.9	112.3	153.1
12	145.4	148.7	138.2
13	136.7	138.0	134.5
14	17.5	17.5	17.5
15	34.7	34.5	34.4
16	209.4	208.6	208.4
17	42.6	43.2	43.0
18	27.6	23.4	23.3
19	35.0	35.7	35.7
20	36.2	36.7	36.6
21	68.5	68.8	68.6
Ar_{11}OMe	–	–	56.0
Ar_{12}OMe	55.4	56.2	60.1
NCOOMe	–	52.9	53.1
NCOOMe	–	153.3	153.4
COOMe	175.0	171.3	171.5
COOMe	52.2	52.6	52.5

ture (30°C) and concentrated under reduced pressure to yield 48.5 g of the crude extract which was then triturated in 5% aqueous H_2SO_4 (150 ml) followed by basification with 10% Na_2CO_3 and then extracted into $CHCl_3$. The organic layer was washed with distilled water, dried (Na_2SO_4) and concentrated to yield 2.9 g of crude alkaloids. The alkaloid mixture (2.5 g) was purified by flash column chromatography (silica gel, MERCK 230–400 mesh) using *n*-hexane–EtOAc (1:1; 200 ml), $CHCl_3$ (100%; 150 ml), EtOAc (100%, 150 ml) and then MeOH (100%, 100 ml) as eluents. Several fractions (50 ml each) were collected, analysed by TLC and grouped accordingly. The *n*-hexane–EtOAc (1:1) eluates were subjected to repeated column chromatography followed by SiO_2 medium-pressure liquid chromatography (acetone–$CHCl_3$; 1:25) to afford methyl 12-methoxy-N_1-decarbomethoxychanofruticosinate **1** (1.5 mg). Further purification of the same fraction using ODS reverse phase column chromatography (H_2O–MeOH; 1:1) gave methyl 11, 12-methylenedioxy-N_1-decarbomethoxychanofruticosinate **4** (4.5 mg). Methyl 12-methoxychanofruticosinate **2** (54.8 mg) and methyl 11,12-dimethoxychanofruticosinate **3** (2.5 mg), were obtained from EtOAc fractions (100%) after further purification by preparative TLC (SiO_2, *n*-hexane–EtOAC; 1:1).

3.3. Methyl 12-methoxy-N_1-decarbomethoxychanofruticosinate **1**

UV (EtOH), λ_{max} nm (log ε): 210 (4.53), 293 (3.52). EIMS, (70 eV) *m/z* (rel. int.): 382 (M^+, $C_{22}H_{26}N_2O_4$, 21), 353 (2), 323 (100). HREIMS, [M+], found:

382.1897, calc. for $C_{22}H_{26}N_2O_4$: 382.1893.^{1}H NMR and ^{13}C NMR: Tables 1 and 2. CD (0.27 mM, MeOH, 24°C), λnm ($\Delta\ \varepsilon$) : 330 (0), 296 (+4.0), 275 (0), 268 (−0.6), 260 (0), 216 (+13.7), 205 (0).

3.4. Methyl 12-methoxychanofruticosinate **2**

UV (EtOH), λ_{max} nm (log ε): 215 (4.24), 246 (3.65), 289 (2.90). EIMS, (70 eV) *m/z* (rel. int.): 440 (M^+, $C_{24}H_{28}N_2O_6$, 29), 381 (100), 321 (16). HREIMS, [M+], found: 440.1952, calc. for $C_{24}H_{28}N_2O_6$: 440.1947. ^{1}H NMR and ^{13}C NMR: Tables 1 and 2. CD (0.3 mM, MeOH, 24°C), λnm ($\Delta\ \varepsilon$): 325 (0), 294 (+1.2), 280 (0), 252 (-7.5), 235 (0), 220 (+22.2), 208 (0).

3.5. Methyl 11,12-dimethoxychanofruticosinate **3**

UV (EtOH), λ_{max} nm (log ε): 221(4.04), 279 (2.95). EIMS, (70 eV) *m/z* (rel. int.): 470 (M^+, $C_{25}H_{30}N_2O_7$, 28), 411 (100), 351 (18). HREIMS, [M+], found: 470.2061, calc. for $C_{25}H_{30}N_2O_7$: 470.2053. ^{1}H NMR and ^{13}C NMR: Tables 1 and 2. CD (0.28 mM, MeOH, 24°C) λnm ($\Delta\ \varepsilon$): 325 (0), 298 (+0.7), 285 (0), 278 (-0.3), 224 (0), 266 (+0.2), 275 (0), 256 (-0.6), 253 (0), 226 (+14.6), 215 (0).

3.6. Methyl 11, 12-methylenedioxy-N_1-decarbomethoxychanofruticosinate **4**

UV (EtOH), λ_{max} nm (log ε): 242 (3.60), 292 (2.95). EIMS, (70 eV) *m/z* (rel. int.): 396 (M^+, $C_{22}H_{24}N_2O_5$, 7), 338 (20), 337 (100), 335 (15), 293 (8). ^{1}H NMR $CDCl_3$, 500 MHz): δ1.27–1.30 (*m*, H-19α), 1.35–1.38 (*m*, H-14α, H-15α), 1.54 (*brd*, *J* = 14.7 Hz, H-19β), 1.68–2.00 (m, H-14β, H-15β, H-18), 2.01 (*d*, *J* = 18.6 Hz, H-17α), 2.49 (s, H-21), 2.82 (*d*, *J* = 18.9 Hz, H-17β), 2.84–3.06 (*m*, H-3, H-5α), 3.25 (*d*, *J* = 6.4 Hz, H-6), 3.63 (*s*, COOMe), 3.72 (*dd*, *J* = 11.0, 6.4 Hz, H-5β), 4.46 (*s*, N-H), 5.88 (*d*, *J* = 1.5 Hz, OCH_2O), 5.93 (*d*, *J* = 1.5 Hz, OCH_2O), 6.33 (*d*, *J* = 7.6 Hz, H-10), 6.62 (*d*, *J* = 7.9 Hz, H-9). ^{13}C NMR ($CDCl_3$, 100 MHz): δ 17.5 (C-14), 27.6 (C-18), 34.7 (C-19), 34.9 (C-15), 36.3 (C-20), 42.6 (C-17), 46.6 (C-3), 52.3 (COOMe), 52.6 (C-5), 55.4 (C-6), 57.6 (C-7), 68.4 (C-21), 74.7 (C-2), 100.3 (C-10),101.0 (OCH_2O), 116.6 (C-9),129.4 (C-12), 130.0 (C-8), 131.6 (C-13), 148.1 (C-11), 174.6 (COOMe), 209.2 (C-16).

Acknowledgements

We wish to thank UKM for financial support (Grant No: UKM N4/99) and Encik Asri Ngah of FRIM for collecting the sample.

References

Ashton, P.S., 1988. Manual of the Non-Dipterocarp Trees of Sarawak, Vol. II. Dewan Bahasa & Pustaka, Sarawak Branch for Forest Department, Sarawak.

Awang, K., Sevenet, T., Hadi, A.H.A., David, B., Pais, M., 1992. Lapidilectine A and lapidilectine B, two new alkaloids from *Kopsia lapidilecta*. Tetrahedron Letters 33, 2493.

Burkill, I.H., 1966. A Dictionary of the Economic Products of the Malay Peninsula. The Ministry of Agriculture and Cooperatives, Kuala Lumpur.

Chen, W.S., Li, S.H., Kirfel, A., Will, G., Breitmaier, E., 1981. Drei Indoline aus *Kopsia officinalis* Tsiang. Liebigs Annalen der Chemie 1886.

Kam, T.S., Sim, K.M., Koyano, T., Komiyama, K., 1999. Leishmanicidal alkaloids from *Kopsia griffithii*. Phytochemistry 50, 75.

Kam, T.S., Tan, P.S., Hoong, P.Y., Chuah, C.H., 1993a. Methyl chanofruticosinates from leaves of *Kopsia arborea*. Phytochemistry 32, 489.

Kam, T.S., Yoganathan, K., 1996. Three aspidofractinine-type alkaloids from *Kopsia teoi*. Phytochemistry 42, 539.

Kam, T.S., Yoganathan, K., Chuah, C.H., 1993b. Kopsidine A and kopsidine B, two novel indole alkaloids from a Malaysian *Kopsia*. Tetrahedron Letters 34, 1819.

Kam, T.S., Yoganathan, K., Chuah, C.H., 1994. Kopsinitarines A, B and C, novel cage alkaloids from a Malaysian *Kopsia*. Tetrahedron Letters 35, 4457.

Kam, T.S., Yoganathan, K., Li, H.Y., 1996b. Tenuisines A, B and C, novel bisindoles with C_2 symmetry from *Kopsia tenuis*. Tetrahedron Letters 37, 8811.

Kam, T.S., Yoganathan, K., Koyano, T., Komiyama, K., 1996c. Pauciflorines A and B, novel melanin biosynthesis inhibitors from *Kopsia*. Tetrahedron Letters 37, 5765.

Kam, T.S., Yoganathan, K., Wei, C., 1996a. Novel cage indoles from a Malaysian *Kopsia*. Journal of Natural Products 59, 1109.

Markgraf, F., 1970. Apocynaceae II. Blumea 20, 416.

Sevenet, T., Allorge, L., David, B., Awang, K., Hadi, A.H.A., Kan-Fan, C., Quirion, J.C., Remy, F., Schaller, H., Teo, L.E., 1994. A preliminary chemotaxonomic review of *Kopsia* (Apocynaceae). Journal of Ethnopharmacology 41, 147.

PERGAMON

Phytochemistry 57 (2001) 607–611

PHYTOCHEMISTRY

www.elsevier.com/locate/phytochem

Polyhalogenated homosesquiterpenic fatty acids from *Plocamium cartilagineum*

Tomáš Řezanka[a,*], Valery M. Dembitsky[b]

[a]*Institute of Microbiology, Vídeňská 1083, Prague 14220, Czech Republic*

[b]*Department of Pharmaceutical Chemistry and Natural Products School of Pharmacy, PO Box 12065, Hebrew University of Jerusalem, Jerusalem 91120, Israel*

Received 13 November 2000; received in revised form 19 February 2001

Abstract

We describe the composition of novel polyhalogenated homosesquiterpenic acids from the red alga *Plocamium* collected during summer on Maltese Islands and Corsica. The compounds, predominantly derivatives with unique groups (bromine, chlorine, and diene), were identified by means of ^{1}H and ^{13}C NMR, MS, IR and UV spectra. © 2001 Elsevier Science Ltd. All rights reserved.

Keywords: Polyhalogenated homosesquiterpenic acids; Red alga; *Plocamium*; NMR, MS, IR and UV spectra

1. Introduction

Plocamium cartilagineum (L.) Dixon (Gigartinales) has a wide range of distribution (Cormaci et al., 1997; Frick et al., 1996). This species is cosmopolitan in all of the worlds' temperate oceans. *P. cartilagineum* grows in the mid to low intertidal zone and down to 20 m subtidally. It can live in sheltered to moderately exposed and exposed open coast habitats. This species is generally epilithic, growing on rocks, sand covered rocks or shell fragments. *P. cartilagineum* has also been found as an epiphyte on articulated coralline algae (Bischoff-Bäsmann and Wiencke, 1996).

Red algae of the genus *Plocamium* have been shown to be a rich source of halogenated monoterpenes and other compounds (Faulkner, 2000; Abreu et al., 1997). In the course of our investigation of the chemical composition of algae of fresh water (Rezanka et al., 1983; Rezanka and Podojil, 1984) and marine origin (Rezanka et al., 1988; Dembitsky et al., 1993), we describe in this paper the elucidation of the structure of four new polyhalogenated homosesquiterpenic acids from *P. cartilagineum* collected on Maltese Islands and Corsica.

2. Results and discussion

A fresh sample of *P. cartilagineum* was separately and successively extracted with a mixture of CH_2Cl_2 and MeOH. Fractionation of the extracts by chromatography on Sephadex LH-20 afforded three main fractions. The third fractions were purified by means of a preparative RP–HPLC to yield four acids (Table 1 and Fig. 1). Compound (**1**) was determined to have the molecular formula $C_{16}H_{19}O_3BrCl_2$ by HREIMS with major fragment peaks at m/z 372, 374 and 376 $[M–HCl]^+$, m/z 293 and 295 $[M–HCl–Br]^+$ and m/z 257 $[M–2xHCl–Br]^+$. The IR spectrum was consistent with the presence of an α, β-unsaturated ketone (1685 cm^{-1}) and a carboxylic group (1710 cm^{-1}). Compound **1** showed an UV maximum at 243 nm, typical for a conjugated en-one system. The ^{1}H NMR spectrum showed vinylidene protons at δ_H 6.16 and 5.86, which were found to be attached to C-14 (δ_C 126.8) from the HMQC experiment, and showed long-range correlations with C-4 (^{3}J) and C-3 (^{2}J) (δ_C 200.8 and 143.4, respectively) in the HMBC spectrum.

A weak carbon signal at δ_C 173.9 (C-1), which showed a ^{2}J interaction with δ_H 3.24 (H_2-2), was assigned to a carboxylic acid. The H_2-2 signal also exhibited HMBC interactions with C-3, C-4 and C-14. Finally, the positions of the two methyl groups were determined by the HMBC experiment (see Table 2). For example, Me-15

* Corresponding author. Tel.: +420-2-4752300; fax: +420-2-4752347.

E-mail address: rezanka@biomed.cas.cz (T. Řezanka).

0031-9422/01/$ - see front matter © 2001 Elsevier Science Ltd. All rights reserved.
PII: S0031-9422(01)00086-3

Table 1
Content of novel polyhalogenated homosesquiterpenic acids from the red alga *Plocamium cartilagineum* collected on Maltese Islands and Corsica (in mg on 100 g of dried alga)

Acid	Maltese Islands	Corsica
A (**1**)	5.4	–
B (**2**)	2.3	–
C (**3**)	–	3.8
D (**4**)	–	1.9

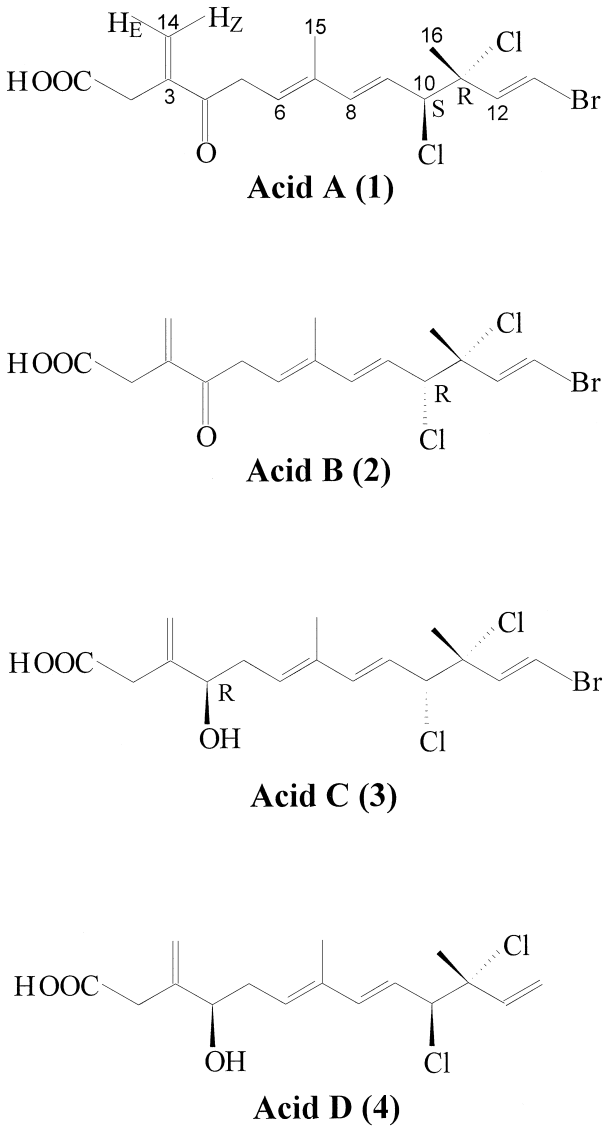

Fig. 1. The structure of acids A–D (**1**–**4**) from *Plocamium cartilagineum*.

had correlations with C-6, C-7 and C-8 and Me-16 with C-10, C-11 and C-12. The ^{1}H NMR spectrum of **1** (Table 2) displayed also two methyl signals at δ 1.78 and 1.56. DQF–COSY measurements allowed the following spin systems to be discerned: an AB quartet $-$CH=CHX at δ 6.45 (H-12) and δ 6.58 (H-13) and a three-proton AMX system $(R)_3C$–CH=CH–CHX– at δ 6.36 (H-8), δ 6.42 (H-9) and δ 4.55 (H-10).

The *E* stereochemistry of trisubstituted Δ^6 double bond is based on the relative upfield shift of the vinylic methyl group (C-15) (δ_C 15.7) and NOESY γ-correlations between this methyl group and the methylene group at C-5 (Blunt et al., 1985).

The stereochemistry of the double bonds Δ^8 and Δ^{12} was assigned as *E* on the basis of the interproton coupling constants J_{8H-9H} = 16.1 Hz and $J_{12H-13H}$ = 13.4 Hz. The coupling constants of olefinic protons in (3*E*,7*E*)-2,6-dimethyloctadiene polyhalogenated monoterpenes lie in the range of 13.5 to 15.9 Hz (Jongaramruong and Blackman, 2000). In the ^{13}C NMR spectrum of **1** (Table 3), the chemical shift of C-13 δ 110.8 indicated a vinyl bromide functionality. The remaining three sp^2 olefinic carbons absorb at δ 132.4 (C-12), δ 124.6 (C-8), and δ 136.5 (C-9). The halogen substitution at C-5 and C-6 was established by comparison of the ^{1}H NMR, ^{13}C NMR, and MS of 1 with those of known compounds (Grible, 1996). The proton and carbon chemical shifts of the C-16 methyl group δ 1.56 and δ 26.2 suggest a (10*S**,11*R**) stereochemistry, in accordance with the empirical rules of Mynderse and Faulkner (1975) and Crews and Kho-Wiseman (1974).

Thus, NMR spectroscopy indicated that the structure of compound **1** is that of (6*E*,8*E*,12*E*)-3-methylene-4-oxo-7,11-dimethyl-(10*S**,11*R**)-dichloro-13-bromo-trideca-6,8,12-trienoic acid.

Acid B (**2**) was isolated from the same fraction as **1** and a sesquiterpene skeleton with the formula $C_{16}H_{19}O_3BrCl_2$ was indicated by HREIMS; it had the same molecular weight as **1** but the some spectral characteristics were different. In support of this, the main MS fragment peaks were at *m*/*z* 293 and 295. The ^{13}C NMR spectrum (Table 3) indicated that Cl on C-10 had an opposite configuration, i.e. *R**. This assumption was proved by the ^{1}H NMR chemical shift of H-16 protons, in keeping with literature data (Mynderse and Faulkner, 1975; Crews and Kho-Wiseman, 1974). The stereochemistry at the C-10 and C-11 centers was assigned on the basis of NMR spectra (see above) and positive optical rotation ($[\alpha]_D^{21} = +37.6^\circ$). Acid B (**2**) is (6*E*,8*E*,12*E*)-3-methylene-4-oxo-7,11-dimethyl-(10*R**,11*R**)-dichloro-13-bromo-trideca-6,8,12-trienoic acid.

Acid C (**3**), the most polar of the four compounds, had the formula $C_{16}H_{21}O_3BrCl_2$, as determined by HREIMS. Comparison of its ^{1}H and ^{13}C NMR spectral data with those of compounds **1** and **2** suggested that the structure of **3** was similar, except for the presence of one substituent. The change of ketone group on C-4 to a hydroxyl group. Giving rise to another chiral carbon was indicated by the optical rotation. The fact that the end of the molecule has the same chemical shifts in ^{1}H and ^{13}C NMR as acid B (**2**), proved that the two were

Table 2
^{1}H NMR data of homosesquiterpenic acids (**1**–**4**) from *Plocamium cartilagineum*

Hydrogen no.	**1**	**2**	**3**	**4**
2	3.24 *d* (1H, *J* = 16.3)	3.21 *dd* (1H, *J* = 16.8)	3.26 *dd* (1H, *J* = 16.6)	3.28 brs (2H)
	3.29 *dd* (1H, *J* = 16.3)	3.29 *dd* (1H, *J* = 16.8)	3.31 *dd* (1H, *J* = 16.6)	
4	–	–	4.02 *dd*(1H, *J* = 8.1;6.1)	3.95 *dd*(1H, *J* = 7.9;5.2)
5	2.85 (1H, *J* = 16.1)	2.94 *dd* (1H, *J* = 15.6)	2.28 *m* (1H)	2.24 *m* (1H)
	2.64 (1H, *J* = 16.1)	2.81 *dd* (1H, *J* = 15.6)	2.31 *m* (1H)	2.33 *m* (1H)
6	5.75 *d* (1HJ = 0.7)	5.72 *dd* (1H, *J* = 0.9)	5.12 *sept* (1H, *J* = 6.5;1.1)	5.15 *sept* (1H, *J* = 6.9;1.4)
8	6.36 *dd* (1H, *J* = 16.1;0.7)	6.31 *dd* (1H, *J* = 15.9;0.9)	6.31 *dd* (1H, *J* = 15.9;0.9)	6.34 *dd* (1H, *J* = 15.3)
9	6.42 *dd* (1H, *J* = 8.6;16.1)	6.47 *dd* (1H, *J* = 8.4;15.9)	6.49 *dd* (1H, *J* = 8.4;15.9)	6.53 *dd* (1H, *J* = 15.3;8.5)
10	4.55 *dd* (1H, *J* = 0.7;8.6)	4.57 *dd* (1H, *J* = 0.9;8.4)	4.54 *dd* (1H, *J* = 0.9;8.4)	4.45 *dd* (1H, *J* = 8.5;1.0)
12	6.45 *dd* (1H, *J* = 13.4)	6.41 *dd* (1H, *J* = 13.8)	6.41 *dd* (1H, *J* = 13.8)	6.02 *dd* (1H, *J* = 10.6;16.5)
13	6.58 *dd* (1H, *J* = 13.4)	6.60 *dd* (1H, *J* = 13.8)	6.60 *dd* (1H, *J* = 13.8)	5.21 *dd* (1H, *J* = 10.6;1.0)
				5.38 *dd* (1H, *J* = 16.5;1.0)
14E	5.86 *brs* (1H)	5.91 *brs* (1H)	5.88 *brs* (1H)	5.91 *brs* (1H)
14Z	6.16 *brs* (1H)	6.18 *brs* (1H)	6.17 *brs* (1H)	6.15 *brs* (1H)
15	1.78 *s* (3H)	1.84 *s* (3H)	1.85 *s* (3H)	1.78 *s* (3H)
16	1.56 *s* (3H)	1.58 *s* (3H)	1.59 *s* (3H)	1.56 *s* (3H)

Table 3
^{13}C NMR data of homosesquiterpenic acids (1–**4**) from *Plocamium cartilagineum*

Carbon no.	**1**	**2**	**3**	**4**
1	173.9	174.1	175.8	174.4
2	37.4	37.1	37.2	37.1
3	143.4	141.9	143.2	142.9
4	200.8	199.5	74.6	77.0
5	44.8	44.1	36.2	34.7
6	123.9	122.4	124.7	120.8
7	136.1	134.9	135.7	134.0
8	124.6	125.5	124.9	125.8
9	136.5	135.8	136.2	137.1
10	68.2	69.7	69.3	70.6
11	72.1	73.0	72.9	71.8
12	132.4	133.1	132.7	139.1
13	110.8	111.2	110.1	115.8
14	126.8	126.9	127.0	126.5
15	15.7	15.8	15.8	15.9
16	26.2	29.6	29.7	24.6

identical. The strongly shielded nature of H-4 (δ 4.02) and C-4 (δ 74.6) indicated the presence of a hydroxyl group, and its *R** configuration was determined by means of Mosher's esters. Treatment of each hydroxy acid with (*R*)-(−)-MTPACl or (*S*)-(+)-MTPACl converted them into (*S*)- and (*R*)-2-methoxy-2-trifluoromethyl phenylacetic acid (MTPA) esters (**3s**, and **4s** and **3r** and **4r**, respectively). The values of $\Delta\delta = [\delta$(S-MTPA ester) − δ(R-MTPA ester)] in the ^{1}H NMR spectra suggested that the absolute configurations at C-4 of compounds **3** and **4** were (R) (Ohtani et al., 1991a,b). The data are shown in Table 4. Compound **3** could also be denoted (6*E*,8*E*,12*E*)-3-methylene-(4*R*)-hydroxy-7,11-dimethyl-(10*R**,11*R**)-dichloro-13-bromo-trideca-6,8,12-trienoic acid.

Table 4
^{1}H NMR (500 MHz) spectral data for Mosher's esters ($CDCl_3$)

Hydrogen no	Compound no. (Δin Hz)[a]	
	3	**4**
2	+27	+31
5a	−7	−8
5b	−21	−23
6	−34	−39
14*E*	+11	+10
14*Z*	+23	+19

[a] Resonances of H directly attached to esterified carbon are not analyzed and/or values < |3 Hz| have not been included.

Acid D (**4**), with the molecular formula $C_{16}H_{22}O_3Cl_2$, had a homosesquiterpene structure, as in **1**. However, the chain lacked one bromine atom. A 3-chloro-1-butenyl end of the chain was indicated by mass fragmentation (base peak at *m*/*z* 89) and ^{1}H NMR assignments of a tertiary methyl group and clean vinylic ABX system at δ 5.21 (H-13a), δ 5.38 (H-13b) and δ 6.02 (H-12). Therefore, the bromine at the end of chain (on C-13) is obviously missing. The further part of the molecule is the same as that of acid C (**3**). All the above data indicate that acid D (**4**) is (6*E*,8*E*,12*E*)-3-methylene-(4*R*)-hydroxy-7,11-dimethyl-(10*S**,11*R**)-dichloro-13-bromo-trideca-6,8,12-trienoic acid.

In terms of biosynthesis, halogenated homosesquiterpenic acids may be biosynthesized by elongation of the know a halogenated monoterpenes described in *Plocamium* many times (Jongaramruong and Blackman, 2000; Crews and Kho-Wiseman, 1974; König at al., 1990).

Although this alga has a worldwide distribution, which is restricted to temperate seas, it is of interest to

note that this Mediterranean Sea collection afforded new metabolites and provides yet another example of chemical variability of marine natural products.

3. Experimental

The algal material *Plocamium cartilagineum* (L.) Dixon (Gigartinales) was collected at two places at Maltese Islands and Corsica.

UV spectra were measured by a Cary 118 (Varian) apparatus in EtOH within the range of 200–350 nm. A Perkin-Elmer Model 1310 (Perkin-Elmer, Norwalk, CT, USA) infrared spectrophotometer was used for scanning infrared spectroscopy of methyl esters as neat film. NMR spectra were recorded on a Brüker AMX 500 spectrometer (Bruker Analytik, Karlsruhe, Germany) at 500.1 MHz (^{1}H), 125.7 MHz (^{13}C). High- and also low-resolution mass spectra were recorded using a VG 7070E-HF spectrometer (Micromass, Manchester, UK). The ionizing condition was 70 eV.

The air dried samples (250 and 300 g) from both collections were separately extracted with mixture of CH_2Cl_2–MeOH (1:1, v/v). The extracts were concentrated under N_2. The total lipid extract, viscous dark oil, was subjected to a Sephadex LH-20 column with CH_2Cl_2–MeOH (1:5) and further separated by semi-preparative RP–HPLC, a C_{18} reversed phase column (5 μm, 7.8×250 mm, Supelco, USA) was employed. A linear gradient from 20% H_2O and 80% acetonitrile to 1% water and 99% acetonitrile over 25 min, flow rate 2 ml/min was used to separate all of the compounds in crude extract. The acids **1**–**4** were detected by UV absorption at 208 nm.

(*S*)-MTPA esters. To a stirred solution of ~1.0 mg of hydroxy compound in 0.3 ml of dry pyridine was added 20 μl of (−)-MTPA chloride. After stirring the mixture under N_2 at room temperature for 1 h, the solvent was removed by blowing with N_2. The residue was redissolved in 2 ml of 30 ml EtOAc–hexane and filtered through a Sep-Pak silica column. After removing the solvent under vacuum, the residue was separated by reversed-phase HPLC (ODS column, 100% MeCN) to yield ~1.0 mg of *S* ester as a colorless gum; ^{1}H NMR spectra ($CDC1_3$), see Table 4.

(*R*)-MTPA esters. Prepared as described for ***S*** esters. From ~1.0 mg of compound and 20 μl of (+)-MTPA chloride 0.9 mg of *R* esters were obtained as a colorless gum; ^{1}H NMR spectra ($CDCl_3$), see Table 4.

Acid A (**1**) is (6*E*,8*E*,12*E*)-3-methylene-4-oxo-7,11-dimethyl-(10*S**,11*R**)-dichloro-13-bromo-trideca-6,8,12-trienoic acid (5.4 mg; 0.0054%), $[\alpha]_D$ −43.1° (*c* 0.17, MeOH); UV λ_{max}(EtOH) (log ε) 243 nm (2.37); IR (film) ν_{max} 2950, 2910, 1710 (COOH), 1685 cm^{-1} (α, β-unsaturated ketone); LREIMS *m*/*z* (% of base peak) 372 (15), 374 (16) and 376 (5) [M–HCl]$^+$, *m*/*z* 293 (11) and 295 (5) [M–HCl–Br]$^+$, *m*/*z* 257 (15) [M–2xHCl–Br]$^+$ HREIMS (*m*/*z*) 408.3247, (calc. for $C_{16}H_{19}O_3{}^{79}Br^{35}Cl_2$ 408.3251). NMR data, see Tables 2 and 3.

Acid B (**2**) is (6*E*,8*E*,12*E*)-3-methylene-4-oxo-7,11-dimethyl-(10*R**,11*R**)-dichloro-13-bromo-trideca-6,8,12-trienoic acid (2.3 mg; 0.0023%), $[\alpha]_D$ +37.6° (*c* 0.14, MeOH); UV λ_{max} (EtOH) (log ε) 243 nm (2.37); IR (film) ν_{max} 2950, 2910, 1710 (COOH), 1685 cm^{-1} (α, β-unsaturated ketone); LREIMS *m*/*z* (% of base peak) 372 (14), 374 (15) and 376 (4) [M-HCl]$^+$, *m*/*z* 293 (9) and 295 (4) [M–HCl–Br]$^+$, *m*/*z* 257 (13) [M–2xHCl–Br]$^+$ HREIMS (*m*/*z*) 408.3247, (calc. for $C_{16}H_{19}O_3{}^{79}Br^{35}Cl_2$ 408.3251). NMR data, see Tables 2 and 3.

Acid C (**3**) is (6*E*,8*E*,12*E*)-3-methylene-(4*R*)-hydroxy-7,11-dimethyl-(10*R**,11*R**)-dichloro-13-bromo-trideca-6,8,12-trienoic acid (3.8 mg; 0.0038%), $[\alpha]_D$ +30.1° (*c* 0.14, MeOH); UV λ_{max} (EtOH) (log ε) 243 nm (2.37); IR (film) ν_{max} 3450 (OH), 2950, 2910, 1715 (COOH); LREIMS *m*/*z* (% of base peak) 374 (17), 376 (19) and 378 (7) [M–HCl]$^+$, *m*/*z* 295 (10) and 297 (4) [M–HCl–Br]$^+$, *m*/*z* 259 (11) [M–2xHCl–Br]$^+$ HREIMS (*m*/*z*) 410.3406, (calc. for $C_{16}H_{21}O_3{}^{79}Br^{35}Cl_2$ 410.3409). NMR data, see Tables 2 and 3.

Acid D (**4**) is (6*E*,8*E*,12*E*)-3-methylene-(4*R*)-hydroxy-7,11-dimethyl-(10*S**,11*R**)-dichloro-13-bromo-trideca-6,8,12-trienoic acid oil (1.9 mg; 0.0019%), $[\alpha]_D$ 15.4° (*c* 0.18, MeOH); UV λ_{max}(EtOH) (log ε) 243 nm (2.37); IR (film) λ_{max} 3450 (OH), 2950, 2910, 1715 (COOH); LREIMS *m*/*z* (% of base peak) 296 (14) and 298 (6) [M–HCl]$^+$, *m*/*z* 259 (17) [M–2xHCl]$^+$ HREIMS (*m*/*z*) 332.3483, (calc. for $C_{16}H_{22}O_3{}^{35}Cl_2$ 332.3489). NMR data, see Tables 2 and 3.

References

Abreu, P.M., Galindro, J.M., Relva, A.M., Ramos, A.M., 1997. Non-terpenoid compounds from *Plocamium cartilagineum*. Phytochemistry 45, 1601–1603.

Bischoff-Bässmann, B., Wiencke, C., 1996. Temperature requirements for growth and survival of Antarctic Rhodophyta. J. Phycology 32, 525–535.

Blunt, J.W., Bowman, N.J., Munro, M.H.G., Parsons, M.J., Wright, G.J., Kon, Y.K., 1985. Polyhalogenated monoterpenes of the New Zealand marine red alga *Plocamium cartilagineum*. Austral. J. Chem. 38, 519–525.

Cormaci, M., Lanfranco, E., Borg, J.A., Buttigieg, S., Furnari, G., Micallef, S.A., Mifsud, C., Pizzuto, F., Scammacca, B., Serio, D., 1997. Contribution to the knowledge of benthic marine algae on rocky substrata of the Maltese Islands (Mediterranean Sea). Botanica Marina 40, 203–215.

Crews, P., Kho-Wiseman, E., 1974. Cartilagineal. An unusual monoterpene aldehyde from marine alga. J. Org. Chem. 39, 3303–3304.

Dembitsky, V.M., Rezanka, T., Rozentsvet, O.A., 1993. Lipid composition of three macrophytes from the Caspian sea. Phytochemistry 33, 1015–1019.

Faulkner, D.J., 2000. Marine natural products. Natural Product Reports 17, 7–55.

Frick, H.G., Boudouresque, C.F., Verlaque, M., 1996. A checklist of marine algae of the Lavezzi Archipelago, with special attention to

species rare or new to Corsica (Mediterranean). Nova Hedwigia 62, 119–135.

Grible, G., 1996. Naturally occurring organohalogen compounds: a comprehensive review. In: Hertz, W., Kirby, G.W., Moore, R.E., Steglich, W., Tamm, C. (Eds.), Progress in the Chemistry of Organic Natural Products, vol. 63. Springer Verlag, Vienna and New York, pp. 24–36.

Jongaramruong, J., Blackman, A.J., 2000. Polyhalogenated monoterpenes from a Tasmanian collection of the red seaweed *Plocamium cartilagineum*. J. Natural Products 63, 272–275.

König, G.M., Wright, A.D., Sticher, O., 1990. A new polyhalogenated monoterpene from the red alga *Plocamium cartilagineum*. J. Natural Products 53, 1615–1618.

Mynderse, J.S., Faulkner, D.J., 1975. Polyhalogenated monoterpenes from the red alga *Plocamium cartilagineum*. Tetrahedron 31, 1963–1967.

Ohtani, I., Kusumi, T., Kashman, Y., Kakisawa, H., 1991a. High-field FT NMR application of Mosher method — the absolute-configurations of marine terpenoids. J. Am. Chem. Soc. 113, 4092–4095.

Ohtani, I., Kusumi, T., Kashman, Y., Kakisawa, H., 1991. A new aspect of the high-field NMR application of Mosher method — the absolute-configuration of marine triterpene Sipholenol-A. J. Org. Chem. 56, 1296–1298.

Rezanka, T., Podojil, M., 1985. The very long chain fatty acids of the green alga *Chlorella kessleri*. Lipids 19, 472–473.

Rezanka, T., Vokoun, J., Slavicek, J., Podojil, M., 1983. Determination of fatty acids in algae by capillary gas chromatography mass spectrometry. J. Chromatogr. 268, 71–78.

Rezanka, T., Vyhnalek, O., Podojil, M., 1988. Separation and identification of lipids and fatty acids of the marine alga *Fucus vesiculosus* by TLC and GC–MS. Folia Microbiol. 33, 309–313.

PERGAMON

Phytochemistry 57 (2001) 613–619

PHYTOCHEMISTRY

www.elsevier.com/locate/phytochem

Nostocyclamide M: a cyanobacterial cyclic peptide with allelopathic activity from *Nostoc* 31

Friedrich Jüttner [a,*], Albena K. Todorova [a], Nadja Walch [b], Wolfgang von Philipsborn [b]

[a] *Institute of Plant Biology, Limnology, Limnological Station, University of Zürich, Seestrasse 187, CH-8802 Kilchberg, Switzerland*
[b] *Institute of Organic Chemistry, University of Zürich, Winterthurerstrasse 190, CH-8057 Zürich, Switzerland*

Received 27 July 2000; received in revised form 13 November 2000

Abstract

A cyclic peptide containing thiazole and oxazole moieties was isolated from *Nostoc* 31 and its structure determined by chemical degradation detailed NMR and mass spectroscopic analyses. The compound is stereochemically pure and closely related to nostocyclamide in which D-valine is replaced by D-methionine. Therefore, it differs from tenuecyclamide C reported to contain L-methionine. It shows allelopathic activity against *Anabaena* 7120, but is inactive against grazers. © 2001 Elsevier Science Ltd. All rights reserved.

Keywords: Cyanobacteria; *Nostoc*; Cyclic peptide; Thiazole; Allelopathic compounds; NMR

1. Introduction

Thiazole-containing cyclic and linear peptides have recently gained much pharmacological interest. Some of them turned out to be potent agents against multidrug resistance (Williams and Jacobs, 1993; Ogino et al., 1996) that develops in cancer cells resistant to chemotherapy. Marine seahares and ascidians were the first sources of several structural variants, among them dolastatins, patellamides and tawicyclamides (Michael and Pattenden, 1993; McDonald et al., 1992). The extreme variability of concentration of these compounds in the animals was taken as an indication that in ascidians these compounds were accumulated from symbiotic prochlorophytes and in seahares from cyanobacterial food rather than synthesized by the animals. In recent years similar cyclopeptides have been isolated from cultured freshwater and terrestrial cyanobacteria. The importance of the diet for the accumulation of cyclic peptides became clear when the same compound was isolated from the ascidian *Lissoclinum bistratum* and a pure cyanobacterial culture (*Westiellopsis prolifica*). The compounds were independently named cycloxazoline (Hambley et al., 1992) and westiellamide (Prinsep et al., 1992) In *Stigonema dendroideum*, three cyclic peptides were found which were called dendroamides (Ogino et al., 1996). They exhibited a basic structure in which two thiazole rings and a methyloxazole moiety were connected via amide bonds and which differed only in their substituents. *Nostoc spongiaeforme* was the source of several tenuecyclamides (Banker and Carmeli, 1998) and raocyclamides were isolated from *Oscillatoria raoi* (Admi et al., 1996, Freeman and Pattenden, 1998). Recently we described nostocyclamide (**2**) that was isolated from a freshwater *Nostoc* strain and exhibited grazer toxicity and allelopathy against related cyanobacteria (Todorova et al., 1995). In this investigation we report on another cyclic peptide from this cyanobacterium that reveals anticyanobacterial activity.

2. Results and discussion

During the investigation of nostocyclamide from the freshwater cyanobacterium *Nostoc* 31 (Todorova et al., 1995) a second component was observed that had the features of a cyclic peptide, but the small amounts available at that time did not allow the structural elucidation. In the present study this component was isolated

* Corresponding author. Tel.: +41-1-716-1210; fax: +41-1-716-1225.
E-mail address: juttner@limnol.unizh.ch (F. Jüttner).

0031-9422/01/$ - see front matter © 2001 Elsevier Science Ltd. All rights reserved.
PII: S0031-9422(00)00470-2

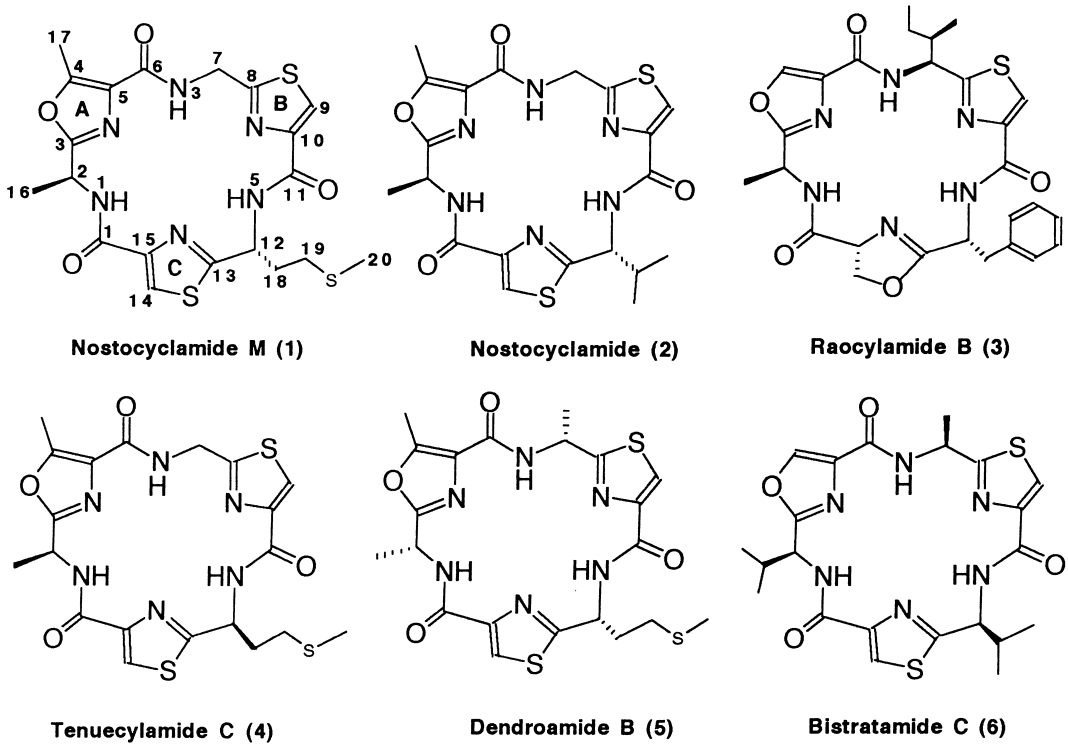

in amounts that were sufficient to determine its structure. Several features of this compound resembled those of nostocyclamide, such as the strong UV absorption and the intense sulfur signal shown by a sulfur specific detector during separation on a GC column, and some identical products that were obtained after acid hydrolysis. Mass spectrometric, chemical, and NMR studies showed that this compound has the same basic structure as the one for nostocyclamide, but the valine moiety is replaced by methionine. Using the one letter code of amino acids we named this compound nostocyclamide M (**1**).

Nostocyclamide M exhibits a quasi-molecular ion of *m/z* 507 $[M+H]^+$ when ESMS is applied in the positive mode. After GC separation of the underivatized molecule electron impact ionization affords a molecular ion (EIMS *m/z* 506 $[M^+]$) and important fragment ions that are indicative for thiazole (*m/z* 139) and oxazole (*m/z* 136) fragments. Intense sulfur-containing fragment ions at *m/z* 47 (CH_3–S), *m/z* 61 (CH_3–S–CH_2) and *m/z* 75 (CH_3–S–CH_2–CH_2) are observed along with the corresponding cleavage products of the molecule, *m/z* 458 (M-48 [CH_3–SH]), *m/z* 445 (M-61 [CH_3–S–CH_2]) and the base peak *m/z* 432 (M-74 [CH_3–S–CH=CH_2]). The molecular ion and the base peak obtained with the ^{15}N labelled molecule exhibit a shift of 6 mass units from *m/z* 506 to 512 and *m/z* 432 to 438, and indicate the presence of six nitrogen atoms in the molecule. The products of acid hydrolysis, that were trifluoroacetylated and transferred into the methyl ester for GC–MS analysis, afford alanine and two thiazole-containing amino acids derived from ring B and C. The derivative of ring B is identical in the retention time and mass fragmentation pattern (*m/z* 268 $[M^+]$ and strong fragment ions at *m/z* 236, 208 and 139) with that obtained from nostocyclamide. The derivative of ring C (*m/z* 342 $[M^+]$ exhibits prominent sulfur-containing fragment ions at *m/z* 47 [CH_3–S], *m/z* 61 [CH_3–S–CH_2], *m/z* 75 [CH_3–S–CH_2–CH_2] and *m/z* 268 [M-74] as the base peak. The fragmentation pattern is consistent with the presence of a CH_3–S–CH_2–CH_2 substituent.

The pure compound is sparingly soluble in MeOH and MeCN but easily soluble in DMSO and CH_2Cl_2. It crystallizes from aqueous solutions in very thin needles. Suitable crystals for X-ray diffraction have not been obtained so far. The molecular formula $C_{20}H_{22}N_6O_4S_3$ for nostocyclamide M was deduced from mass spectral data and NMR spectroscopy.

Nostocyclamide M was subjected to a detailed ^1H and ^{13}C NMR investigation. The 1D proton and carbon-13 and the 2D ^1H,^1H and ^1H,^{13}C correlated spectra were obtained in $CDCl_3$ solution on a 600 MHz spectrometer. For further details see the experimental section. The proton spectrum exhibits signals for the following groups: 1 C*H*$_3$(CH), 1 C*H*$_3$(C), 1 C*H*$_3$(S), 3 C*H*$_A$*H*$_B$, 1 C*H*(CH$_3$), 1 C*H*(CH$_2$), 2 H-C(sp^2), and 3 NH signals in the 8.5-8.6 ppm region, corresponding to a total of 22 hydrogen atoms (Table 1). The carbon-13 spectrum obtained with proton decoupling shows eight signals in the aliphatic region and 12 signals in the sp^2-carbon range. Based upon ^1H,^{13}C 2D correlation experiments (HSQC and HMBC) there are 3 CH_3, 3 CH_2, 2 (sp^3)

CH, 2 (sp^2)CH, and 10 nonprotonated carbon atoms (Table 1). Thus, nostocyclamide M has a $C_{20}H_{22}$ skeleton just as nostocyclamide.

Closer inspection of the 1D spectra reveals that there are no signals for an isopropyl group (valine) while the typical AB system of the glycine methylene group and the CH_3CHNH group of alanine are still present. As a new feature, compared with nostocyclamide, the aliphatic region of the proton spectrum reveals the presence of a $–CH(CH_2CH_2SCH_3)$ side chain for which we also have strong evidence from the mass spectrum (M-74, M-75). On the other hand, the characteristic $CH_3C(O)$ signal from the oxazole methyl group and the two isolated thiazole CH signals of nostocyclamide are still present in the new compound which points to the same basic skeleton of both structures.

The tentative conclusions are corroborated by 2D COSY and TOCSY $^1H,^1H$-correlations and $^1H,^{13}C$ 2D HSQC and HMBC correlations. The most significant correlation cross peaks are also listed in Table 1 and support the common skeleton for the two nostocyclamides. Moreover, from the TOCSY pattern the new side chain can be identified as arising from methionine ($HN(5)–C(12)H–C(18)H_AH_B–C(19)H_AH_B–S–CH_3$) that is replacing valine in nostocyclamide.

Nostocyclamide M (**1**) thus proves to have the same constitution as tenuecyclamide C (**4**) (Banker and Carmeli, 1998), and the ^1H and ^{13}C chemical shifts can be fully assigned. In fact, the ^1H and ^{13}C spectral data of the two compounds are virtually identical within experimental error limits. However, tenuecyclamide C differs in the UV absorption and was reported to contain L-methionine whereas our chemical degradation of nostocyclamide M gave D-methionine as the dominating sulfur containing cleavage product (vide infra). The excellent agreement of the NMR data of both compounds, in particular of the methionine side chain and its immediate surrounding is not what one would expect for a diastereoisomeric relationship. The open question remains to be settled by X-ray diffraction of suitable crystals.

The absolute configuration of the two chiral centers of nostocyclamide M was determined with the amino acids obtained after acid hydrolysis. The trifluoroacetylated methyl ester of alanine resulting after methanolysis from the oxazole ring was separated on a chiral GC column to give the pure L-stereoisomer. To analyze the configuration at C(12), the thiazole ring was reacted with ozone that gave methionine sulfone upon acid hydrolysis. The D-enantiomer was found to represent 91% of the total

Table 1
^1H and ^{13}C NMR chemical shifts (δ/ppm), $^1H,^1H$ coupling constants (J/Hz), and long-range C,H correlations[a]

	δ (H)	δ (C)	J (H,H)	Correlation C–H
C(1)		160.03[c] (*s*)[b]		N(1)H
C(2)H	5.150 (*dq*)	45.03 (*d*)	5.6; 6.7	C(16)H
C(3)		161.60 (*s*)		N(1)H; C(2)H; C(16)H
C(4)		153.88 (*s*)		C(17)H
C(5)		128.34 (*s*)		C(17)H
C(6)		160.91 (*s*)		$C(7)H_A$; C(17)H
$C(7)H_2$	H_A:4.979 (*dd*)	41.05 (*t*)	17.7; 4.7	
	H_B:4.814 (*dd*)		17.7; 3.3	
C(8)		165.34 (*s*)		$C(7)H_AH_B$; C(9)H
C(9)H	8.203 (*s*)	124.63[d] (*d*)		
C(10)		148.74[e] (*s*)		C(9)H
C(11)		159.77[c] (*s*)		N(5)H
C(12)H	5.795 (*dt*)	51.03 (*d*)	7.4; 5.4	$C(18)H_AH_B$; $C(19)H_AH_B$
C(13)		169.34 (*s*)		C(12)H; C(14)H; $C(18)H_AH_B$
C(14)H	8.187 (*s*)	124.24[d] (*d*)		
C(15)		149.11[e] (*s*)		C(14)H
$C(16)H_3$	1.695 (*d*)	20.24 (*q*)	6.7	C(2)H
$C(17)H_3$	2.700 (*s*)	11.59 (*q*)		
$C(18)H_2$	H_A: 2.514 (*ddt*)	37.37 (*t*)	14.1; 9.8; 5.2	C(12)H
	H_B: 2.203 (*ddt*)		14.1; 10.0; 5.7	
$C(19)H_2$	H_A: 2.616 (*ddd*)	28.99 (*t*)	13.1; 10.0; 5.1	C(12)H; $C(18)H_AH_B$, C(20)H
	H_B: 2.347 (*ddd*)		13.1; 10.0; 5.7	
$C(20)H_3$	2.075 (*s*)	15.42 (*q*)		$C(19)H_AH_B$; $C(18)H_B$
N(1)H	8.62 (*s*)			
N(3)H	8.51 (*t*)			
N(5)H	8.61 (*d*)			

[a] From ^1H-detected HMBC experiments.
[b] Refers to one-bond C,H coupling multiplicity.
[c,d,e] Pairwise ambiguous.

methionine, indicating that racemization has taken place only at a low rate. The presence of L-alanine and D-methionine sulfone upon ozone treatment and acid hydrolysis was also confirmed by Marfey's analysis on a C18 HPLC column by superposition with authentic compounds.

Stereochemically pure amino acids were only obtained when nostocyclamide M was analyzed that had undergone a short isolation procedure. Extracts separated on silica gels exhibited upon HPLC separation several isomers of nostocyclamide M that eluted closely to each other. Stereochemical analysis of these isomers gave mixture of the stereoisomeric alanines and methionine sulfones. Because these isomers turned out to be artifacts, they were not further investigated, and only freshly isolated material served for the final analysis.

In the HPLC chromatograms of cartridge-purified extracts of *Nostoc* an additional peak was observed that eluted much earlier (8.2 min) than nostocyclamide M (12.4 min) and exhibited an ESMS that was consistent with the two diastereomeric nostocyclamide M sulfoxides. These compounds were present in much lower concentrations in fresh extracts that have not been concentrated in a rotary evaporator. When purified nostocyclamide M was brought to dryness and redissolved, around 12% of the nostocyclamide M was oxidized to these sulfoxides. The same compounds were obtained by treatment of nostocyclamide M with hydrogen peroxide. Fresh extracts from *Nostoc* that were isolated under strict exclusion of oxygen under a nitrogen gas atmosphere in a closed apparatus (Wendel and Jüttner, 1996) afforded only a small signal in the HPLC chromatograms of which it was not clear whether it was the sulfoxides or another contaminant. These experiments indicate that the sulfoxides are not, or in only very small amounts, present in the live *Nostoc* and are in the observed amounts actually isolation artifacts.

Small portions of 100 ml standing cultures of *Nostoc* (0.7 mg d.w.) were used to determine quantitatively nostocyclamide M and nostocyclamide by integration of the UV absorption peaks of HPLC chromatograms. For calculating the concentrations of the nostocyclamide M sulfoxides the same molar extinction coefficient was used as for nostocyclamide M. The concentration of nostocyclamide M and nostocyclamide M sulfoxides, which were taken together, and nostocyclamide were 10 and 26 μg per mg chlorophyll *a*, respectively, in a four week old standing culture.

The low solubility of nostocyclamide M in water did not allow us to perform bioassays in liquid media without addition of solubilizers. Even at low concentrations of around 4 nM white needles, the typical crystalline form of nostocyclamide M, were observed. The much lower water solubility in comparison to nostocyclamide caused by the $(CH_2)_2$–S–CH_3 group may be the reason that toxicity was not observed in the *Thamnocephalus platyurus* bioassay. However, allelopathic activity was easily detectable by the agar plate diffusion assay with cyanobacteria as the indicator organisms. *Anabaena* 7120 was more sensitive than *Anabaena* P-9, and cleared zones in the lawn of *Anabaena* 7120 were obtained when 217 nmol nostocyclamide M were spotted on the mineral ground agar.

Nostocyclamide M is a member of the cyclic peptides which have been found in several structural variations in cyanobacteria and marine ascidians. Most likely the ascidians (*Lissoclinum*) accumulate these compounds from symbiotic prochlorophytes, a subgroup of cyanobacteria, and are not the producers. Peptides of this type are most probably synthesized nonribosomally by a multienzyme thiotemplate mechanism (Marahiel et al., 1997) on peptide synthetases. Amino acids are first activated by ATP, then bound as a thioester, and finally a peptide bond formation takes place. In the state of the thioester, epimerases are known that convert L-amino acids into their D-configuration. The strict control of the amino acid configuration in the cyclic peptides is evident by the occurrence of compounds that are stereochemically pure and characteristic in their configuration for a particular organism. Racemates which have also been observed are most likely produced during the rather lengthy isolation procedures.

In the nostocyclamides **1** and **2**, tenuecyclamide C (**4**), and raocyclamide A (**3**) the alanine moiety has the L-configuration. Both valine and methionine, which replace each other in nostocyclamide and nostocyclamide M, exhibit D-configuration, as does phenylalanine in raocyclamide A. An exception is methionine that is placed in the same position in tenuecyclamide C and has been reported to be in the L-configuration. The dendroamides differ essentially as all amino acids are in the D-configuration, c.f. dendroamide B (**5**), while the structurally related bistratamide C (**6**) that was isolated from *Lissoclinum* (Foster et al., 1992) had the amino acids in the all L-configuration.

It is interesting to note that structurally closely related cyclic peptides are found in phylogenetically very distant cyanobacteria. The heterocyst-forming *Nostoc* 31 and *N. spongiaeforme* are closely related to each other but *Oscillatoria raoi* belongs to the very distant hormogonia-forming group of cyanobacteria.

3. Experimental

3.1. Physical measurements

UV spectra were measured in MeOH on a spectrophotometer Cary 3 (Varian). Low-resolution EIMS were obtained on a combined GC–MS (Fisons MD 800), and ESMS in the positive mode on a mass spectrometer with an electrospray ion source (Vestec VT 201).

The ^{1}H and ^{13}C NMR spectra were measured at 300 K on a Bruker DRX-600 spectrometer at 600 and 150 MHz, respectively. Solutions of 2–3 mg in 0.4 ml of $CDCl_3$ were used. All chemical shifts are referred to TMS as internal standard. 2D spectra were obtained with standard pulse sequences i.e. double-quantum-filtered phase-sensitive COSY, TOCSY, HSQC, and HMBC. For the latter experiments a delay time corresponding to $^{n}J(C,H) = 9$ Hz was used and, therefore, not all conceivable C–H correlation peaks were actually observed.

3.2. Growth

The origin of the axenic culture of *Nostoc* sp. 31 and the conditions of the small and large scale culture to obtain 100-g amounts of wet biomass were described recently (Todorova et al., 1995).

3.3. Analysis

The procedure to obtain EI mass spectra after GC separation, the analysis of products of acid hydrolysis and ^{15}N labeling of the molecule were published previously (Todorova et al., 1995).

3.4. Isolation

The cyanobacterial biomass (160 g fr. wt) that was stored at −20°C was first suspended in 90 ml H_2O. 250 ml of ethanol were added for extraction in an ultrasound water bath (15 min). After centrifugation, the pellets were twice extracted with 125 ml 50% aq. EtOH. The combined extracts were partitioned between aq. EtOH and *tert*-butyl methyl ether (TBME), and the ether phase was washed several times with water and dried with dry Na_2SO_4. The TBME was replaced by 3×20 ml 90% aq. EtOH and supplied to three equilibrated reversed phase C18 cartridges (2 g, Mega Bond Elut, Varian). The first 20 ml of the elutes were collected, brought to dryness in a rotary evaporator, and the residue was dissolved in a minimum of MeOH. 100–300 μl were injected onto a semipreparative reversed phase HPLC column (250×10 mm Spherisorb S 5 ODS, LC-18, 5 μm, Supelco). A gradient (MeOH/H_2O; 50:50 in 12 min up to 100% MeOH and 10 min isocratic, flow rate 3 ml/min) was used to separate (in about 50 runs) a mixture of nostocyclamide and nostocyclamide M (180 mg) at R_t 12.6 min. To remove the major part of nostocyclamide from nostocyclamide M, the crystalline residue was extracted four times with 0.5 ml portions of cold MeOH. The enriched residue of nostocyclamide M was dissolved in MeOH and a small amount of CH_2Cl_2 and separated on a semipreparative HPLC column (Grom-Sil ODS-4 HE, 5 μm, 8.0×250 mm) in a 15 min linear gradient (aq. acetonitrile: 0.01% trifluoroacetic acid (15:85) to 100% acetonitrile). The first eluting peak at R_t 12.4 min was nostocyclamide M and the second at R_t 12.8 min nostocyclamide. The yield of nostocyclamide M was ca. 25 mg and of nostocyclamide ca.100 mg. To obtain nostocyclamide M in high purity, the collected substance was rechromatographed (ca. 100 μg per run) under the same conditions.

3.5. Nostocyclamide M

Nostocyclamide M (**1**): white thin needles, UVλ_{max} (MeOH) 220 nm (ε 41000); EIMS m/z (% rel. int.) 506 (27) [M^+], 432 (100), 139 (84), 61 (79), 136 (61), 112 (56), 75 (54), 141 (49), 276 (49), 235 (45), 249 (37) and 445 (17). For ^{1}H and ^{13}C NMR data see Table 1.

3.6. Hydrolysis

Nostocyclamide M was hydrolysed in 3 M HCl/MeOH at 110°C for 48 h. The dried residue was treated with trifluoroacetic anhydride in CH_2Cl_2 for 60 min at 80°C. The reagent and solvent were blown off with He; the residue was dissolved in 50 μl MeOH. The trifluoroacetylated esters were separated on a DB-1301 (30 m, 0.32 mm i.d., 0.25 μm film thickness) with a temperature program of 1 min 70°C, 10°C/min, 250°C isothermal for 20 min. Three trifluoroacetylated esters were obtained that could easily be deduced from the structure of the molecule: the alanine derivative (R_t 3.87 min) was identical to a reference compound, the amino acid B (R_t 14.35 min) exhibited ions at m/z 268 (M^+, 58%), 236 (100%), 208 (96%), 139 (93%), 69 (82%), 57 (64%), 171 (54%), 45 (52%), 112 (51%), 237 (47%) and the amino acid C (R_t 17.80 min) at m/z 342 (M^+, 1.3%), 268 (100%), 61 (69%), 45 (65%), 69 (63%), 208 (56%), 139 (38%), 236 (37%) and 171 (31%). Further indicative ions of this compound were 281 (M-61, 6.2%), 47 (CH_3S, 18%) and 75 ($CH_3SCH_2CH_2$, 13%).

3.7. Analysis of stereochemistry by chiral GC–MS

The cleavage of the thiazole moieties by ozone and acid hydrolysis was conducted as stated by Ogino (Ogino et al., 1996). 0.7 mg of nostocyclamide M was dissolved in CH_2Cl_2 and bubbled for 10 min with a stream of ozone to give a bluish solution. The solvent was removed in a stream of nitrogen and the residue was treated with 200 μl 3 M HCl/MeOH for 24 h at 110°C. The sample was brought to dryness in a nitrogen gas stream and treated with 100 μl TFA in 100 μl CH_2Cl_2 for 1 h at 80°C. The sample was dried with nitrogen gas and the residue dissolved in 100 μl CH_2Cl_2. 1-μl samples were subjected to gas chromatography–mass spectrometry on a chiral column (25 m, 0.25 mm i.d., Permabond-L-Chirasil-Val, Macherey & Nagel, Düren, Germany) in a temperature program (1 min

80°C, 5°C/min up to 120°C, 20°C/min at 190°C). The retention times were: D-alanine (R_t 4.71 min), L-alanine (R_t 4.98 min), D-methionine sulfone (R_t 25.54 min), and L-methionine sulfone (R_t 26.02 min). The identity of the stereoisomers was established by comparison with authentic compounds and confirmed by superposition. Reference substances were obtained from Sigma.

3.8. Analysis of stereochemistry by Marfey's method

Nostocyclamide M was treated with ozone as stated above for 10 min; the solvent was evaporated in a stream of nitrogen gas and the residue was subjected to vigorous hydrolysis in 6 M HCl. Marfey's analysis was conducted essentially as described by Ogino (Ogino et al., 1996) on a HPLC column (Grom-Sil 120 ODS 4 HE, 5 μm, 4.6×250 mm) at 30°C using a linear gradient of 10–50% acetonitrile and 0.05% aq. triethylamine / phosphate buffer pH 3. 5-Fluoro-2,4-dinitrophenyl-L-alaninamide was used as the reagent. The typical absorption spectra of the amino acid derivatives with maxima at 341 nm and 417 nm were recorded on a Shimadzu LC 10 diode array detector SPDM 10 Avp. D-Alanine and L-alanine were separated efficiently to determine the L-configuration by superposition with an authentic compound, however, separation of the methionine sulfone stereoisomers was not achieved with this and another acidic solvent gradient (acetonitrile/ 0.05% aq. TFA according to Fujii et al. (1997). Separation of the latter isomers was achieved applying an acetonitrile/0.05 M ammonium acetate gradient (10–50% acetonitrile) as stated by Harrigan et al. (1998). L-Methionine sulfone eluted at R_t 24.8 min and D-methionine sulfone at R_t 28.6 min.

3.9. Quantitative analysis

Fresh wet biomass of 20 ml suspension of *Nostoc* was collected on a glass fibre filter (Schleicher & Schuell GF 6) by vacuum filtration. The filter was extracted with 4 ml 85% aq. acetonitrile containing 0.05% trifluoroacetic acid. The extract was separated on a HPLC column. The integrated peak areas at 220 nm were used for quantification of the compounds. The molar extinction coefficient of nostocyclamide M was used to quantify the nostocyclamide M sulfoxides and a redetermined molar extinction coefficient (UVλ_{max} (MeOH) 220 nm (ε 40000) for nostocyclamide.

3.10. Bioassays

The growth of axenic cyanobacteria (Todorova and Jüttner, 1996) and the cyanobacterial agar plate diffusion bioassays were essentially performed as described (Todorova et al., 1995). Samples of nostocyclamide M dissolved in CH_2Cl_2 were spotted on a ground agar (50% cyanobacterial medium solidified with 2% agar). After drying in a sterile bench, an overlay of *Anabaena* 7120 or *Anabaena* P-9 in 0.5% agar was poured over the ground agar and incubated at 25°C and 32 μmol quanta m^{-2} s^{-1} measured at the surface of the Petri dishes. Chlorophyll *a* was determined in methanolic solution using the molar extinction coefficient given by Ogawa and Vernon (1971).

Acknowledgements

We thank Dr. S. Carmeli, Tel Aviv, for NMR spectral information and Professor R.E. Moore for help in HPLC separation of the optical isomers of methionine sulfone and E. Loher, H. Lüthi, and A. Mechsner for valuable technical assistance. F.J. is grateful for financial support from the Swiss National Science Foundation, Bern, and W.v.P. acknowledges generous funding by the Dr. Helmut-Legerlotz Stiftung.

References

Admi, V., Afek, U., Carmeli, S., 1996. Raocyclamides A and B, novel cyclic hexapeptides isolated from the cyanobacterium *Oscillatoria raoi*. Journal of Natural Products 59, 396–399.

Banker, R., Carmeli, S., 1998. Tenuecyclamides A-D, cyclic hexapeptides from the cyanobacterium *Nostoc spongiaeforme* var. *tenue*. Journal of Natural Products 61, 1248–1251.

Foster, M.P., Concepción, G.P., Caraan, G.B., Ireland, C.M., 1992. Bistratamides C and D. Two new oxazole-containing cyclic hexapeptides isolated from a Philippine *Lissoclinum bistratum* ascidian. Journal of Organic Chemistry 57, 6671–6675.

Freeman, D.J., Pattenden, G., 1998. Total synthesis and assignment of stereochemistry of raocyclamide cyclopeptides from cyanobacterium *Oscillatoria raoi*. Tetrahedron Letters 39, 3251–3254.

Fujii, K., Ikai, Y., Oka, H., Suzuki, M., Harada, K., 1997. A nonempirical method using LC/MS for determination of the absolute configuration of constituent amino acids in a peptide: combination of Marfey's method with mass spectrometry and its practical application. Analytical Chemistry 69, 5146–5151.

Hambley, T.W., Hawkins, C.J., Lavin, M.F., Vandenbrenk, A., Watters, D.J., 1992. Cycloxazoline — a cytotoxic cyclic hexapeptide from the ascidian *Lissoclinum bistratum*. Tetrahedron 48, 341–348. .

Harrigan, G.G., Luesch, H., Yoshida, W.Y., Moore, R.E., Nagle, D.G., Paul, V.J., Mooberry, S.L., Corbett, T.H., Valeriote, F.A., 1998. Symplostatin 1: a dolastatin 10 analogue from the marine cyanobacterium *Symploca hydnoides*. Journal of Natural Products 61, 1075–1077.

Marahiel, M.A., Stachelhaus, T., Mootz, H.D., 1997. Modular peptide synthetases involved in nonribosomal peptide synthesis. Chemical Reviews 97, 2651–2673.

McDonald, L.A., Foster, M.P., Phillips, D.R., Ireland, C.M., Lee, A.Y., Clardy, J., 1992. Tawicyclamides A and B, new cyclic peptides from the ascidian *Lissoclinum patella*: studies on the solution- and solid-state conformations. Journal of Organic Chemistry 57, 4616–4624.

Michael, J.P., Pattenden, G., 1993. Marine metabolites and metal-ion chelation — the facts and the fantasies. Angewandte Chemie International Edition in English 32, 1–23.

Ogawa, T., Vernon, L.P., 1971. Increased content of cytochromes 554

and 562 in *Anabaena variabilis*. Biochimica Biophysica Acta 226, 88–97.

Ogino, J., Moore, R.E, Patterson, G.M.L., Smith, C.D., 1996. Dendroamides, new cyclic hexapeptides from the blue-green alga. Multidrug-resistance reversing activity of dendroamide A. Journal of Natural Products 59, 581–586.

Prinsep, M.R., Moore, R.E., Levine, I.A., Patterson, G.M.L., 1992. Westiellamide, a bistratamide-related cyclic peptide from the blue-green alga *Westiellopsis prolifica*. Journal of Natural Products 55, 140–142.

Todorova, A.K., Jüttner, F., Linden, A., Plüss, T., von Philipsborn, W., 1995. Nostocyclamide: a new macrocyclic, thiazole-containing allelochemical from *Nostoc* sp. 31 (cyanobacteria). Journal of Organic Chemistry 60, 7891–7895.

Todorova, A., Jüttner, F., 1996. Ecotoxicological analysis of nostocyclamide, a modified cyclic hexapeptide from *Nostoc*. Phycologia 35 (Suppl. 6), 183–188.

Wendel, T., Jüttner, F., 1996. Lipoxygenase-mediated formation of hydrocarbons and unsaturated aldehydes in freshwater diatoms. Phytochemistry 41, 1445–1449.

Williams, A.B., Jacobs, R.S., 1993. A marine natural product, patellamide D, reverses multidrug resistance in a human leukemic cell line. Cancer Letters 71, 97–102.

PERGAMON

Phytochemistry 57 (2001) 621–623

PHYTOCHEMISTRY

www.elsevier.com/locate/phytochem

Editorial comment

Global phytochemistry: the Brazilian approach[☆]

One of the hottest issues worldwide is the preservation and sustainable use of biodiversity in the tropics (Fig. 1), and its exploitation by pharmaceutical companies in the race to discover and develop new drug candidates. In Brazil, the Convention on Biological Diversity signed in Rio de Janeiro in 1992 called the attention of a broad audience of scientists, politicians and non-governmental organizations (NGOs). Following the Convention, the issue of biodiversity went through extensive discussions in the media, well beyond the frontiers of research institutes and universities. Last year, Brazil celebrated 500 years of discovery and coincidently the July issue of *Nature* (406, 13 July 2000) published in its cover report the news about an important scientific achievement that made the country of soccer and samba to gain the additional status of a "genomic country" (*The Economist,* 22 July 2000). This was possible as a result of the financial support provided by Fapesp (São Paulo State Foundation for Scientific Research) which enabled a group of 35 laboratories and 200 researchers to describe the first DNA sequence of a plant pathogen — the bacteria *Xylella fastidiosa* — responsible for the citrus variegated chlorosis, a disease causing almost 30% loss in citrus culture every year. Such investment had an immediate and continuing impact. The genome of *Xanthomonas citri* — another citrus disease agent — was next described, and several other important targets of agricultural interest are waiting for sequencing. Solutions to problems related to agriculture, cancer and tropical diseases, and to biological and evolutionary interactions, will emerge from the acquisition and development of sophisticated techniques and mainly by the established competence of the research groups participating in this project.

The ripening of the scientific community in Brazil can also be seen in its awareness of the importance of biodiversity studies, including the bioprospecting of natural products. As an outcome of academic discussions, in public and private sectors, and with the support of the Ministry of Environment and its Secretary of Coordination of Amazonia, the Brazilian Program of Molecular Ecology for the Sustainable Use of the Biodiversity of Amazonia — (PROBEM) was launched and is one of the priorities of the government plan "Avança Brasil", which includes a dozen fast-tracking projects to accelerate the economic development in Amazonia. PROBEM was designed to foster the development of new products from biodiversity, and to encourage the settlement of new enterprises in Amazonia. To steer PROBEM and overcome the bureaucratic hurdles, a social organization (QUANGO — *quasi* autonomous non-governmental organization) named Bioamazônia was created. Its goals include the construction of the Amazonia Biotechnology Center (ABC) in Manaus, the city capital of the Amazon state, and the establishment of a network of Brazilian laboratories to research and develop products from biodiversity. An additional initiative within Bioamazônia is the Amazonia Permanent Trust Fund, created in association with A2R, a financial institution. Inspired by the framework of the Alaska Permanent Fund, which obtains royalties from the oil industry, the APTF will channel its revenues to the environmental management and social development in Amazonia.

The opportunities for investments in Brazil are unique and greater than never before. A recent survey by A.T. Kearney shows that Brazil ranks third, after the USA and China, in terms of reliability for investors, and is at the top position for new investments. Companies as important as Novartis Pharma and Glaxo Wellcome have already established partnership with Bioamazonia, universities, and business interested in the use of biodiversity, even though, insufficiencies in the Brazilian laws have brought about embarrassing, serious bottlenecks for all parties. Since then, the Brazilian federal government issued the provisional act no. 2042 (dated 29/08/2000) ruling the conservation and utilization of components of biological diversity, and the sharing of benefits from its exploitation, including rewards to indigenous and other local communities. The scientific community welcomes the new law, but the bureaucratic hurdles are expected to be many, in different instances, especially regarding the official permits to collect biological materials. Appropriate solutions will be needed in the near future.

Another important initiative in São Paulo State — the Biota Program — is also supported by Fapesp. The

[☆] The views expressed in Editorial comment articles are the sole opinion of the authors, and publication shall not imply the concurrence of the Editors or publisher.

PII: S0031-9422(01)00125-X

Fig. 1. Examples of Brazilian biodiversity. (a) *Virola venosa* (Benth.) Warb. (“ucu-úba” fruit), Myristicaceae. (b) *Teloschistes flavicans* (Sw.) Norm. (lichen on a cactus), Teloschistaceae. (c) *Palicourea markgravii* St. Hil. (“erva-de-rato”), Rubiaceae. (d) *Peperomia nitida* Dahlst (“peperomia”), Piperaceae.

Biodiversity Virtual Institute (www.biotasp.org.br) program, differently from Bioamazônia, does not involve the physical construction of a research institute. Instead, it focus mostly on the strengthening of interdisciplinary groups aiming to systematically evaluate the biodiversity of São Paulo State, including flora, fauna, microorganisms and the development of potential bioactive compounds from plants. The total budget of approximately eighteen million dollars provided for the initial four years is not large considering the number of researchers involved and the benefits expected in terms of basic knowledge to be achieved. Judging from the progress reported at the Fapesp workshop last January by project leaders, researchers, graduate and undergraduate students, additional funds certainly can be expected to continuously support these and other thematic projects.

Both successful programs funded by Fapesp — Genoma and Biota — demonstrate that significant changes in the scientific policy are taking place, but whether or not we are going to have an economy based on genome sequencing or on biodiversity exploitation depends on the establishment of long-term programs such as these. The discovery of new drug candidates to cure diseases from malaria to cancer, using thousands of plants or micro-organisms, is expected to be achieved in the near future with the access to high-throughput screening technologies and interdisciplinary approaches. Further developments to marketable drugs, and the involvement of small local companies are also highly expected. The genome blueprint for biosynthetic pathways of bioactive compounds, or even for a basic process such as that of lignification and its role in the evolution of land plants, plus several other important questions, will certainly be pursued in the near future. Nevertheless, the scientific and technological cooperation among the countries are in need of stimulation simply because a number of basic problems such as the taxonomy of our biodiversity cannot be solved fast enough or independently.

The organization of the phytochemical research community in Brazil has advanced significantly, through the Division of Natural Product Chemistry of the Brazilian Society of Chemistry. This Division, with approximately

220 members, enthusiastically discusses crucial topics related to biodiversity in all their annual meetings. Several new groups have emerged all over Brazil, and equipment facilities for phytochemical investigations are now easily available. A few groups are focused on the search for bioactive compounds, ecological studies, marine compounds, and also on cell tissue cultures and biosynthesis of natural products. The intellectual property rights of the new findings are also under discussion in a number of symposia and courses, and entrepreneurs and scientists alike are finally getting together in meetings. In the South American context, the debate has been initiated by the Latin American Society of Phytochemistry, but the management and the study of biodiversity in the continent as a whole waits for regulation as well.

Following the pressures raised by contracts signed with pharmaceutical companies, the establishment of solid and clear legislation regarding bioprospecting is a top priority for Brazilians, otherwise the hesitation could impair the creativity and the initial successful achievements such as those promoted by the genomic projects. There is an urgent need to develop basic science by means of long-term investment, to ensure a broad range of expertise. Additionally, specific actions from the federal government are required to improve our capacity to solve our own problems and to seed research companies and other enterprises. In this sense, the Ministry of Science and Technology and CNPq (National Council of Scientific and Technological Development) have announced that new funds for the Brazilian Genome Project, and specifically for the biodiversity studies, are on the way.

A new model of exploitation and conservation of biodiversity as the basis of economic development must be the next paradigm for Brazil and this is the way to establish a successful economic and scientific partnership in the globalized world.

Massuo Jorge Kato
Departamento de Química Fundamental
Instituto de Química
Universidade de São Paulo, Brazil
E-mail address: majokato@iq.usp.br

PERGAMON

Phytochemistry 57 (2001) 625–631

PHYTOCHEMISTRY

www.elsevier.com/locate/phytochem

Primary sequence determination of a Kunitz inhibitor isolated from *Delonix regia* seeds

Silvana C. Pando[a], Maria L.V. Oliva[b,*], Claudio A.M. Sampaio[b], Luciana Di Ciero[a], José C. Novello[a], Sérgio Marangoni[a]

[a]*Department of Biochemistry, Institute of Biology, UNICAMP, 13083-970, Campinas-SP, Brazil*
[b]*Department of Biochemistry, Escola Paulista de Medicina, UNIFESP, 04044-900, São Paulo-SP, Brazil*

Received 18 September 2000; received in revised form 23 January 2001

Abstract

A serine proteinase inhibitor was purified from *Delonix regia* seeds a Leguminosae tree of the Caesalpinioideae subfamily. The inhibitor named DrTI, inactivated trypsin and human plasma kallikrein with K_i values 2.19×10^{-8} M and 5.25 nM, respectively. Its analysis by SDS-PAGE 10–20% showed that the inhibitor is a protein with a single polypeptide chain of M_r 22 h Da. The primary sequence of the inhibitor was determined by Edman degradation, thus indicating that it contained 185 amino acids and showed that it belongs to the Kunitz type family; however, its reactive site did not contain Arg or Lys at the putative reactive site (position 63, SbTI numbering) or it was displaced when compared to other Kunitz-type inhibitors. © 2001 Elsevier Science Ltd. All rights reserved.

Keywords: *Delonix regia*; Leguminosae; Kunitz inhibitor; Serine proteinase; Trypsin; Human plasma kallikrein

1. Introduction

Serine proteinase inhibitors are found in animal tissues, micro-organisms as well as plant tissues. The inhibitors occur in large quantities in legume seeds and in smaller amounts in cereals, cucurbits, potatoes and others tubers (Richardson, 1991). Two families of plant serine proteinase inhibitors are well characterized, Kunitz-type inhibitors with M_r of 18,000–22,000 Da, a low cystine content and one reactive site; Bowman-Birk-type are proteins with relative molecular mass of 8000–10,000 Da, high cystine content and two reactive sites (Birk, 1985).

The presence of proteinase inhibitors in living tissues seems to be essential for natural regulatory processes, for example, plants protecting themselves against insect predation (Garcia-Carrenõ, 1996). The stability of proteinase inhibitors towards enzymes as well as the large quantities present in seeds indicates the importance of protease inhibitors as storage proteins (Ryan, 1973). Besides their biological function, proteinases inhibitors are useful tools in biochemical and physiological studies of proteinases functions (Oliva et al., 1999b); for purification of proteolytic enzymes by affinity chromatography (Sampaio et al., 1974) and for understanding the role of proteolytic enzymes in blood clotting (Hayashi et al., 1994; Oliva et al., 2000a). As a consequence, many aspects of these inhibitors such as occurrence, tissue localization, inhibition specificity, molecular and structural properties, possible regulatory and/or protective function and nutritional significance have been investigated (Bode and Huber, 1992).

Delonix regia (Leguminosae-Caesalpinioideae) is distributed in the north and western parts of Madagascar and is widely cultivated in many tropical countries. The trees of the genus *Delonix* are used as ornamental trees and the seeds of many species are crushed and eaten raw (Puy et al., 1995). The description of a potent inhibitor isolated from *Delonix regia* may contribute to a through understanding of a plasma kallikrein action and eventually to the development of synthetic inhibitors based on its structural properties. In the present work we describe the purification, the primary structure and inhibitory

* Corresponding author. Tel.: +55-11-5576-44-44; fax: +55-11-5572-30-06.
E-mail address: maysa.bioq@epm.br (M.L.V. Oliva).

0031-9422/01/$ - see front matter © 2001 Elsevier Science Ltd. All rights reserved.
PII: S0031-9422(01)00080-2

characteristics of the serine proteinase inhibitor isolated from *Delonix regia* seeds.

2. Results

The inhibitory fraction eluted from a DEAE Sephadex A-50 column was gel filtered on a Sephadex G-75 column and it emerged in the main peak, indicated by "Pool 2" (Fig. 1a). This fraction was further purified on a C-18 μBondapak reversed phase column and then purified further using other reversed phase columns (Fig. 1b). Electrophoretic analysis showed that the inhibitor is constituted by a single polypeptide chain in both its native and reduced conditions and the single protein peak eluted from the column corresponds to the inhibitor. The M_r of inhibitor, estimated by SDS-PAGE10–20%, was ca 22 h Da (inset Fig. 1b). The homogenous form of the inhibitor from reversed phase chromatography in HPLC was used for primary structure determination.

The *N*-terminal region sequence protein, up to residue 50 was established by automated Edman degradation of the protein. Peptide fragments produced by Lys-C, Glu-C and Asp-N cleavage of 4-vinyl pyridine reduced protein, were sequenced following the isolation by reversed phase chromatography. Enough overlaps were obtained to define the primary sequence (Fig. 2). DrTI is related to the Kunitz inhibitor family, the four cysteines residues are conserved, however, in the putative reactive site a glutamic acid was found in the P_1 position instead of Arg or Lys as in most Kunitz inhibitors (Fig. 3).

DrTI inhibited trypsin (K_i 2.19×10^{-8} M) following the slow-tight binding mechanism (Morrison, 1982). Besides trypsin, the inhibitory effect was also assayed on human plasma kallikrein, chymotrypsin, plasmin, factor Xa, tissue kallikrein and thrombin. The inhibitor presented higher affinity toward of human plasma kallikrein (K_i 5.25 nM) with 1:1 stoichiometry. The inhibitory effect of DrTI on trypsin and human plasma kallikrein can be seen in Fig. 4A and B respectively. DrTI did not inhibited factor Xa, plasmin, chymotrypsin, tissue kallikrein and thrombin.

3. Discussion

The purification procedure used to obtain the protein, which show trypsin inhibitor properties, is satisfactory since the products exhibited a single band in SDS-PAGE under reductive conditions, indicating no dimerization of the native inhibitor. DrTI showed M_r of ca 22 h Da, similar to proteinase inhibitors of the Kunitz-type (Richardson, 1991) and the primary structure confirmed this inhibitor as a member of the Kunitz family. The two loops composed by the four half-cysteine show high similarity to other Kunitz inhibitors. This result confirmed the preliminary crystallographic study of DrTI (Polikarpov et al., 1999). An interesting peculiarity of DrTI is that a glutamic acid was found in the expected position for the reactive site (residue 63, SbTI numbering) instead of an Arg or Lys, usually present in other Kunitz inhibitors. The other possibility would be the interaction

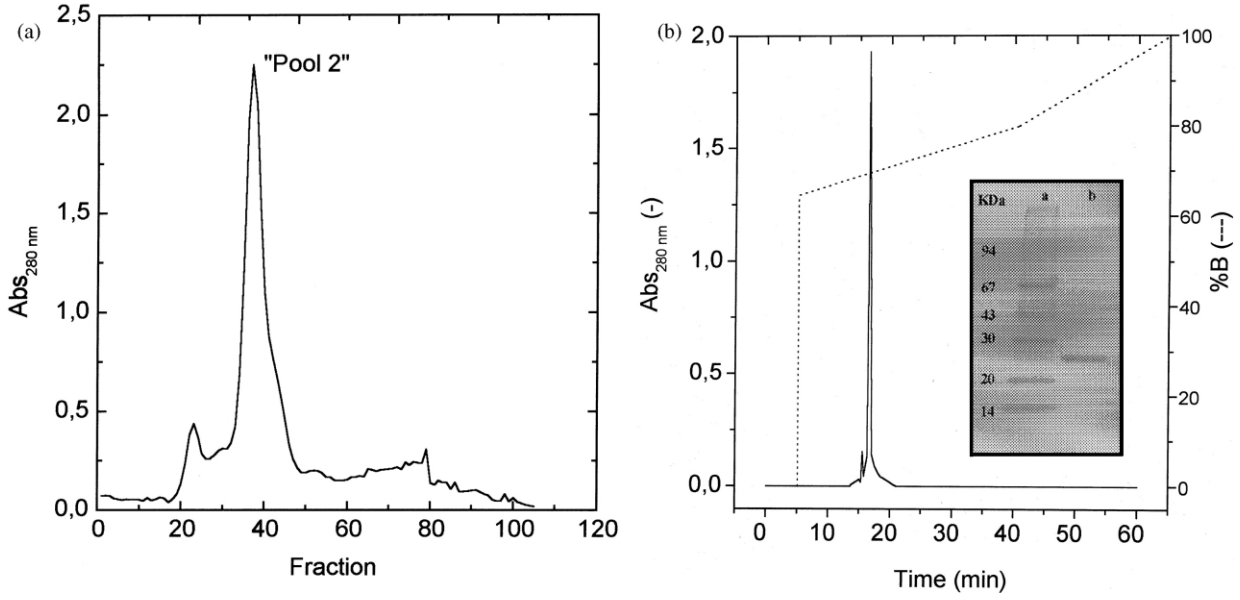

Fig. 1. (a) Gel filtration chromatography profile on Sephadex G-75 column of the DrTI eluted from DEAE Sephadex column. Eluting buffer: 0.05 M Tris–HCl, pH 8.0, 0.15 M NaCl. Flow rate: 12 ml h^{-1}. "Pool 2" indicates antitrypsin activity fraction. (b) Repurification by reversed phase HPLC [C-18 μBondapack column 3.9×300 mm]. Sample: 2.5 mg of the inhibitor eluted from C-18 μBondapack column (7.8×300 mm), using a 0–100% linear gradient of solvent B. Solvent A: 0.1% TFA (ml/ml); solvent B: 60% (ml/ml) acetonitrile in solvent A. Flow rate: 1 ml min^{-1}.

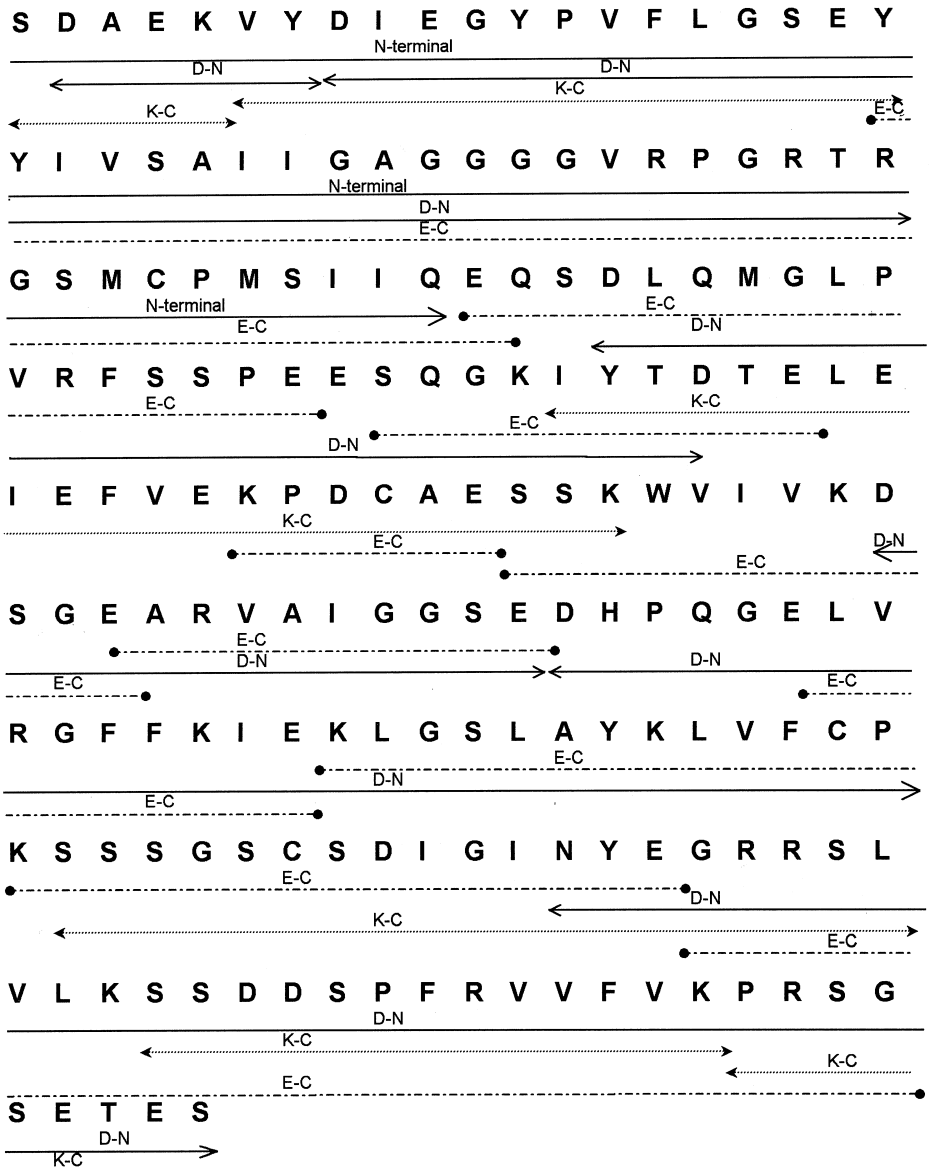

Fig. 2. Amino acid sequence of DrTI. The peptides obtained after fragmentation by enzyme digestion with trypsin, endoproteases Lys-C, Glu-C and Asp-N, are indicated.

of Ser^{64} with the pocket for Arg or Lys found in trypsin and other related proteases. The inhibitor isolated from *Swartzia pickellii* (SwTI) contain a glutamine in the P1 position for the reactive site (Cavalcanti et al., 2001).

Caesalpinia pulcherrima, which also belongs to the subfamily Caesalpinioideae, as well as the *Delonix regia* species, contained only inhibitors of the Kunitz-type, this species is considered to be the most primitive while the species of the subfamily Papilionoideae had only inhibitors of Bowman–Birk type. These facts suggest that there is some relationship between the families of the inhibitors found in leguminous seeds and the evolution of these plants (Norioka and Ikenaka, 1983).

The Bowman Birk-type inhibitors from legume seeds have been found to inhibit both trypsin and chymotrypsin at independent reactive sites. On the other hand, the inhibitory activity characteristics of the Kunitz-type proteinase inhibitor are varied. A few inhibitors are reported to be specific for chymotrypsin and do not inhibit trypsin (Joulbert et al., 1981). Some Kunitz-type inhibitors are potent inhibitors for trypsin but they also inhibit chymotrypsin to varying degrees (Odani et al., 1979). DrTI inhibited trypsin but not chymotrypsin.

There are many physiological inhibitors, such as α-2-macroglobulin and the C1 inhibitor, that efficiently act in control of the cascade of proteins during blood clotting (Travis and Salvesen, 1983). However there are vegetable inhibitors that are relatively easy to obtain and which are also efficient for the study of many properties of those proteins (Sampaio et al., 1990).

```
          1                                                  50
DrTI      SDAEKVYDIE GYPVFL.GSE YYIVSAIIGA GGGGVRPGRT RGSMCPMSII
SbTI   ..   .DFVLDNE GNPLEN.GGT YYILSDITAF GG..IRAAPT GNERCPLTVV
SwTI   ...   EFVLDTD GEPLRN.GGS YYIVSAIRGA GGGGVKLAKT GNETCPLTVV
LlTI   ...   .QLVDLD GDPLYN.GMS YYILPVARGK GGG.LELART GSESCPRTVV
EcTI   ...   KELLDSD GDILRN.GGT YYILPALRGK GGG.LELAKT GDETCPLNVV
BvTI-3c  ...DTLLDTD GEVVRNSGGR YYIIPAFRGN GGG.KTLS.T GWESCPRTVV

          51                                                 100
DrTI      QEQSDLQMGL PVRFSSPEES QGKIYTDTEL EIEFVEK...  PDCA.ESSKW
SbTI      QSRNELDKGI GTIISSPYRI R.FIAEGHPL SLKFDSFAVI MLCVGIPTEW
SwTI      QARSDLDYGK PVRISSPYQI A.YIYPDLIL NLAFES...V PTCANTPSEW
LlTI      QTRSETSRGL PARLASPYRI ..LIGSNIPL TIEFQPQK.P YSCHGHSSRS
EcTI      QARGETKRGR PAIIWTPPRI A.ILTPAFYL NIEFQTKD.L PACLREYSR.
BvTI-3c   QA.NETSDGL PRLIWTTSRI L.FIPTGFEL I..FFVEA.V PPCNGKPSLW

          101                                                150
DrTI      VIVKDSGEAR VAIGGSEDHP QGELVRGFFK IEKLGSLAYK LVFCPKSSS.
SbTI      SVVEDLPEGP AVKIGENKDA MDGWFRLERV SDDEFN.NYK LVFCPQQAED
SwTI      TVVDEQGL.K SLKITGYNDP LPGWFRIEKS SLE..S.AYK LMFSPHSGVT
LlTI      LQWKVEKT.Q MVKIASSDEE QRLFGPFQIQ PYR..N.HYK LVYCESESRN
EcTI      LPREEEQH.S EVKLAPK.EE AAAFGXEKLK PYR..D.DYK IVYCEGGSDD
BvTI-3c   TKVEGESE.G SVKIGASDSK EPFL..FRIK SPE..D.TYK LMYCPQNS..

          151                                                200
DrTI      ..GSCSDIGI NY...EGRRS LVLKSSDDSP FRVVFVKPRS GSETES....
SbTI   ..   DKCGDIGI SIDHDDGTRR LVVS..KNKP LVVQFQKLDK ESL
SwTI   ..   S..GNVAI EVD.DEGYRR LVVTDDKDRA FHVVFKKADS ..........
LlTI      HHDDCRDLGI SID.DQQNRL LVVKN..GDP LVVQFAKANR GGDDD.....
EcTI   .    .DSCKDLGI SID.DENNRR LVVKD..GDP LAVRFVKAHR RG........
BvTI-3c   ..DTCADLGI SID..EGNRR LVVTD..DNP LTVRFKKADR S.........
```

Fig. 3. Comparative sequences of related Kunitz inhibitors.1, DrTI (*Delonix regia* trypsin inhibitor); 2, SBTI (soybean trypsin inhibitor, Koide and Ikenaka, 1973); 3, SwTI (*Swartzia pickellii* trypsin Inhibitor, Cavalcanti et al., 2001); 4, LlTI (*Leucaena leucocephala* trypsin Inhibitor, Oliva et al., 2000b); 5, EcTI (*Enterolobium contortisiliquum* trypsin inhibitor, Batista et al., 1996); 6, BvTI-3c (*Bauhinia variegata*, var. *candida* trypsin inhibitor, Di Ciero et al., 1998). Reactive sites are in the box and the cysteine residues are indicated by the gray color. Multiple sequence alignment with hierarchical clustering (Corpet et al., 1998).

DrTI does not inhibit plasmin, tissue kallikrein, factor Xa and thrombin but it is an effective inhibitor of human plasma kallikrein (K_i 5.25 nM) and trypsin (K_i 2.19×10^{-8} M). It is of interest that proteases such as plasmin, tissue kallikrein, factor Xa and thrombin require special structural features of plant inhibitors to suit these enzymes. For example, either Kunitz-type or Bowman–Birk type inhibitors do not inhibit tissue kallikrein, factor Xa and thrombin. Plasma kallikrein, which is not inhibited by Bowman–Birk inhibitors such as lima bean trypsin inhibitor, is usually inhibited by Kunitz-type trypsin inhibitors (Oliva et al., 1999a,b) but not by a Kunitz-type chymotrypsin inhibitor (Souza et al., 1995).

The selectivity of the inhibitor for different proteases, in opposition to SwTI (Cavalcanti et al., 2001), was changed by the presence of Glu^{63} at the putative reactive site

The *Delonix regia* trypsin inhibitor (DrTI) may, therefore, be useful as a tool to investigate the catalytic mechanism of plasma kallikrein. Clinical application of the plant inhibitors might be feasible in the future (Hayashi et al., 1994). Furthermore, as the role of inhibitors in plant seeds is not fully understood, further knowledge concerning trypsin inhibitors in plant seeds such as *Delonix regia* may contribute to the understanding of the interactions between plant protease inhibitors and endogenous animal proteases (Xavier-Filho et al., 1989).

4. General experimental procedures

4.1. Enzymes

Human plasma kallikrein (EC 3.4.21.34) was purified by a previous procedure (Oliva et al., 1982). Tissue kallikrein (EC 3.4.21.35) was from Bayer; Bovine trypsin (EC 3.4.21.4), factor Xa (EC 3.4.21.6), human thrombin (EC 3.4.31.5) and chymotrypsin (EC 3.4.21.1) were Sigma products.

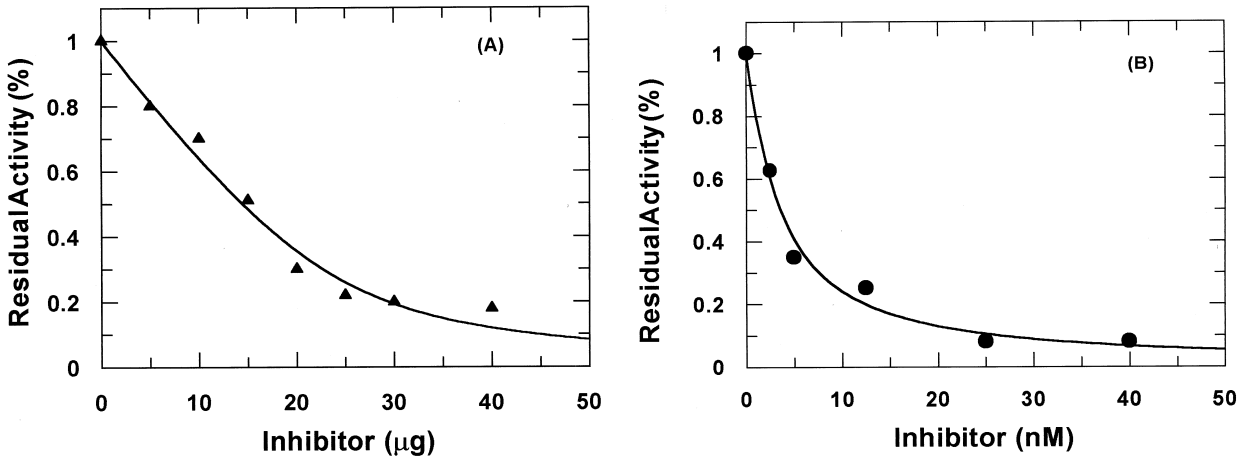

Fig. 4. Curves of trypsin and human plasma kallikrein inhibition by DrTI. (A) trypsin (5 μg) was preincubated (10 min, 37°C, 0.1 M Tris–HCl buffer, pH 8.0) with increasing concentration of the inhibitor. The residual trypsin activity was assayed on DL- Bz-Arg-pNan (0.1 M) as substrate, as described in Experimental. (B) HuPK (40 nM) was preincubated (10 min, 37°C, 0.05 M Tris–HCl buffer, pH 8.0) with increasing amounts of inhibitor. The residual HuPK activity was assayed on Ac-Phe-Arg-pNan (0.8 mM) as substrate, as described in the Experimental.

4.2. Substrates

H-D-Phe-L-Pip-L-Arg-pNan, DL-Bz-Arg-pNan, Bz-Tyr-pNan and Suc-Phe-pNan were from Sigma Chemical Company; *p*-nitrophenyl-*p*′-guanidinobenzoate (NPGB) was from Merck; H-Pro-Phe-Arg-pNan and MeO-Suc-Ala-Ala-Pro-Val-pNan were from Calbiochem; Ac-Phe-Arg-pNan was a gift of Dr Maria Juliano, UNIFESP, Brazil.

4.3. Inhibitor purification

Mature seeds of *Delonix regia* (70 g) were milled to a fine powder and submitted to agitation for 1 h at room temperature with 0.15 M NaCl (10%, wt/ml). The suspension was clarified by centrifugation (3000 *g*, 20 min), the ppt. was eliminated and the supernatant was used for inhibitor purification. Proteins were precipitated with 80% (ml/ml) aqueous acetone with stirring at 4°C. The acetone-dried powder was dissolved in 0.05 M Tris–HCl buffer, pH 8.0 and centrifuged 3000 *g*, 20 min. The clear supernatant solution was applied to a DEAE Sephadex A-50 column (27×1.8 cm), equilibrated with 0.05 M Tris–HCl buffer, pH 8.0, at a flow rate 30 ml h^{-1}. Fractions of 3 ml were collected. The active material from the previous step was submitted to gel filtration on a Sephadex G-75 column (102×1.9cm), equilibrated with 0.05 M Tris–HCl buffer, pH 8.0, 0.15 M NaCl at a flow rate 12 ml h^{-1}. The fractions with inhibitory activity were combined, dialyzed against distilled water, lyophilized then applied to a C-18 μBondapak reversed phase column (Waters System, 7.8×300 mm). A linear gradient of 0–100% of solvent B (60% acetonitrile in 0.1% trifluoroacetic acid, ml/ml) at a flow rate of 2 ml min^{-1} was used. The inhibitor was repurified on a C-18 μBondapak reversed phase HPLC column (3.9×300 mm) at a flow rate 1 ml min^{-1}. The absorbance at 280 nm was used to follow protein elution. Bovine trypsin inhibitory activity was verified as described in the Experimental.

4.4. SDS-PAGE

SDS-PAGE was carried out according to (Laemmli, 1970), using 10–20% polyacrylamide as separation gel and 5% as stacking gel. Samples containing 10 μg of the purified inhibitor, under reducing conditions, were dissolved in 0.08 M Tris–HCl buffer, 2% SDS, 10% glycerol (wt/ml) and 0.02% bromophenol blue, adjusted to pH 6.8 with HCl. Protein bands were stained by Coomassie Brilliant Blue. The M_r standards (Pharmacia) used were phosphorylase B (M_r 94 h Da), bovine serum albumin (67 h Da), ovalbumin (43 h Da), carbonic anhydrase (30 h Da), trypsin inhibitor (20100 Da) and α-lactalbumin (14.4 h Da).

4.5. Sequence determination

DrTI reduction with S-4-pyridylethylation was performed as described by (Friedman et al., 1970).

4.6. Endopeptidase Asp-N, Glu-C and Lys-C cleavage

Samples of S-pyridinethylated-DrTI (20 nmol) were incubated with endopeptidase Asp-N and with endopeptidase Glu-C in 0.05 M ammonium acetate buffer, pH 6.5 and pH 4.0 respectively, for 14 h at 37°C, using an enzyme: DrTI ratio of 1:20. The reaction was terminated by adjusting the pH to pH 2.0 and the produced peptides were separated as described by (Oliva et al., 2000a).

4.7. Sequence analysis and mass spectrometry

Edman degradation was performed with a gas-phase sequence equipment (Shimadzu and 473 Applied Biosystem) using the conditions recommended by the manufacturer.

4.8. Sequence comparison

The database from Max Planck Institute for Biochemistry at Martinsried, Germany, was searched using the Lipmann and Pearson fast protein-searching algorithm FASRP (Lipmann and Pearson, 1985). Alignments were optimized using a computer program (Corpet et al., 1998).

4.9. Trypsin inhibition

The concentration of the inhibitor was determined by its absorbance at 280 nm and the extinction coefficient was determined by experimental determination. The inhibitory activity of DrTI on trypsin was determined by measuring the hydrolysis of DL-Bz-Arg-pNan at pH 8.0, according to (Erlanger et al., 1961). The inhibitor was pre-incubated in different concentrations with enzymes (5 μg) prior to substrate addition in 0.1 M Tris–HCl buffer, pH 8.0, for 10 min at 37°C in 1ml final volume. The reaction was interrupted by addition of 500 μl of 30% acetic acid (ml/ml). The substrate hydrolysis was followed by absorbance of released *p*-nitroaniline at 405 nm.

4.10. Inhibitory activity on other serine proteinases

The inhibitory activities on human plasma Kallikrein, tissue kallikrein, chymotrypsin, plasmin and thrombin were determined by measuring remaining hydrolytic activity towards synthetic specific substrates after pre-incubation with DrTI. Enzymes or enzyme-inhibitor mixtures (20 μl) were added to a solution containing 1 mM substrate in 0.05 M Tris–HCl buffer, pH 8.0, 37°C, in 200 μl final volume. The reaction was followed for 15–30 min and stopped by addition of 50 μl of 30% acetic acid and the substrate hydrolysis was followed by absorbance at 405 nm in an ELISA reader.

4.11. K_i Determination

The dissociation constants of the enzyme-inhibitor complexes were measured following the procedure described by (Morrison, 1982) and the inhibition constants (K_i) were calculated using a graphite program (Knight, 1986).

4.12. Active site titration

Both trypsin and kallikrein site concentration was determined by *p*-nitrophenyl-*p*-guanidinobenzoate (NPGB) titration, as described previously (Sampaio et al., 1984).

Acknowledgements

This work was partially supported by FAPESP, CAPES, CNPq, SFB 4697 and VW Foundation. We thank the technical assistance of Lucimeire Santana, Reini Mentele and Sonia Andrade for performing the coagulation tests.

References

Batista, I.F.C., Oliva, M.L.V., Araujo, M.S., Sampaio, M.U., Richardson, M., Fritz, H., Sampaio, C.A.M., 1996. Primary structure of a Kunitz-type trypsin inhibitor from *Enterolobium contortisiliquum* seeds. Phytochemistry 41, 1017–1022.

Birk, Y., 1985. The Bowman–Birk inhibitor. International Journal of Peptide and Protein Research 25, 113–131.

Bode, W., Huber, R., 1992. Naturals protein proteinase inhibitors and their interaction with proteinases. European Journal of Biochemistry 204, 433–441.

Cavalcanti, M.S.M., Oliva, M.L.V., Torquato, R.J., Auerswald, E., Coelho, L.C.B.B., Sampaio, M.U., Sampaio, C.A.M., 2001. Determination of the primary structure of a Kunitz-type inhibitor from Swartzia pickellii with only one disulfide bridge and one N-glycosylation site. Biochemical and Biophysical Research Communications, submitted.

Corpet, F., Gouzy, J., Kahn, D., 1998. The ProDom database of protein domain families. Nucleic Acids Research 26 (1), 323–326.

Di Ciero, L., Oliva, M.L.V., Torquato, R., Köhler, P., Weder, J.K.P., Novello, J.C., Sampaio, C.A.M., Oliveira, B., Marangoni, S., 1998. The complete amino acid sequence of a trypsin inhibitor from *Bauhinia variegata* var. *candida* seeds. Journal of Protein Chemistry 17, 827–834.

Erlanger, B.F., Kolowsky, N., Cohen, N., 1961. Preparation and properties of two new chromogenic substrates of trypsin. Archives of Biochemistry and Biophysics 95, 271–278.

Friedman, M., Krull, L.H., Cavins, J.F., 1970. The chromatographic determination of cystine and cysteine residues in proteins as S-beta-(4-pyridylethyl) cysteine. Journal of Biological Chemistry 245, 3868–3871.

Garcia-Carreño, F.L., 1996. Proteinase inhibitors. Trends in Food Science Technology 7, 197–204.

Hayashi, K., Takehisa, T., Hamato, N., Takano, R., Hara, S., Miyata, T., Kato, H., 1994. Inhibition of serine proteinases of the blood coagulation system by squash family protease inhibitors. Journal of Biochemistry 116, 1013–1018.

Joulbert, F.J., Carlsson, F.H., Haylett, T., 1981. Purification and some properties of two proteinase inhibitors (DE-1 and DE-3) from *Erythrina latissima* (Broad leaved *Erythrina* seed). Hoppe-Seyler's Zeitschrift Fur Physiologische Chemie 362, 531–538.

Knight, C.G., 1986. The characterization of enzyme inhibition. In: Barret, A.J., Salvesen, G. (Eds.), Proteinase Inhibitors. Elsevier, Amsterdam, pp. 23–51.

Koide, T., Ikenaka, T., 1973. Studies on soybean trypsin inhibitor: amino acid sequence of the carboxyl terminal region and the complete amino acid sequence of soybean trypsin inhibitor (Kunitz). European Journal of Biochemistry 32, 417–431.

Laemmli, U.K., 1970. Cleavage of structural proteins during the assembly of the head of bacteriophage T4. Nature 227, 680–685.

Lipmann, D.J., Pearson, W.R., 1985. Improved tools for biological sequence comparison. Proceedings of the National Academy of Science, USA 85, 2444–2448.

Morrison, J.F., 1982. The slow-binding and slow tight-binding inhibition of enzyme catalyzed reactions. Trends in Biochemical Science 7, 102–105.

Norioka, S., Ikenaka, T., 1983. Amino acid sequences of trypsin-chymotrypsin inhibitors (A-I, A-II, B-I and B-II) from peanut (*Arachis hipogaea*): a discussion on the molecular evolution of legume Bowman-Birk type inhibitors. Journal of Biochemistry 94, 589–599.

Odani, S., Ono, T., Ikenaka, T., 1979. Proteinase inhibitors from Mimosoideae Legume, *Albizzia julibrissin*. Journal of Biochemistry 86, 1795–1805.

Oliva, M.L.V., Andrade, S., Batista, I.F.C., Sampaio, M.U., Juliano, M., Fritz, H., Auerswald, E.A., Sampaio, C.A.M., 1999a. Human plasma kallikrein and tissue kallikrein binding to a substrate based on the reactive site of a factor Xa inhibitor isolated from *Bauhinia ungulata* seeds. Immunopharmacology 45, 141–149.

Oliva, M.L.V., Grisolia, D., Sampaio, M.U., Sampaio, C.A.M., 1982. Properties of highly purified human plasma kallikrein. Agents and Actions 9, 52–57.

Oliva, M.L.V., Mendes, C.R., Juliano, M.A., Chagas, J.R., Rosa, J.C., Greene, L.J., Sampaio, M.U., Sampaio, C.A.M., 1999b. Characterization of a tissue kallikrein inhibitor isolated from *Bauhinia bauhinioides* seeds: inhibition of the hydrolysis of kininogen related substrates. Immunopharmacology 45, 163–169.

Oliva, M.LV., Souza-Pinto, J.C., Batista, I.F.C., Araujo, M.S., Silveira, V.F., Auerswald, E.A., Mentele, R., Eckerskorn, C., Sampaio, M.U., Sampaio, C.A.M., 2000a. Effect of a serine proteinase inhibitor from *Leucaena leucocephala* on plasma kallikrein and plasmin. Biochimica et Biophysica Acta 1477, 1–2.

Oliva, M.L.V., Souza-Pinto, J.C., Batista, I.F.C., Araujo, M.S., Silveira, V.F., Auerswald, E.A., Mentele, R., Eckerskorn, C., Sampaio, M.U., Sampaio, C.A.M., 2000b. *Leucaena leucocephala* serine proteinase inhibitor: primary structure and action on blood coagulation, kinin release and rat paw edema. Biochimica et Biophysica Acta 1477, 64–74.

Polikarpov, I., Golubev, A.M., Perles, L., Pando, S.C., Novello, J.C., Marangoni, S., 1999. Purification, crystallization and preliminary crystallographic study of a Kunitz-type trypsin inhibitor from *Delonix regia* seeds. Acta Crystallographica Section D 55, 1611–1613.

Puy, D.J.Du., Phillipson, P.B., Rabevohitra, R., 1995. The genus *Delonix* (Leguminosae-Caesalpinioideae) in Madagascar. Kew Bulletin 50, 445–475.

Richardson, M., 1991. Seed storage proteins: the enzyme inhibitors. In: Dey, P.M., Harborne, J.B. (Eds.), Methods in Plant Biochemistry. Academic Press, New York, pp. 259–305.

Ryan, C.A., 1973. Proteolytic enzymes and their inhibitors in plants. Annual Review of Plant Physiology 24, 173–196.

Sampaio, C.A.M., Sampaio, M.U., Prado, E.S., 1984. Active titration of horse urinary kallikrein. Hoppe-Seyler Physiologische Chemie 365, 297–302.

Sampaio, M.U., Tanaka, A.S., Oliva, M.L.V., Batista, I.F.C., Motta, G., Stella, R.C.R., Sampaio, C.A.M., 1990. Plant proteinase inhibitors. Action on blood clotting contact phase enzymes. In: Filho, B.O., Sgarbieri, V. (Eds.), Proceedings of the First Brazilian Congress on Proteins. Unicamp, Campinas, pp. 57–65.

Sampaio, C., Wong, S.C., Shaw, E.N., 1974. Human plasma kallikrein. Purification and preliminary characterization. Archives of Biochemistry and Biophysics 165, 133–139.

Souza, E.M.T., Mizuta, K., Sampaio, M.U., Sampaio, C.A.M., 1995. Purification and partial characterization of a *Schizolobium parahyba* chymotrypsin inhibitor. Phytochemistry 39, 521–525.

Travis, J., Salvesen, G.S., 1983. Human plasma proteinase inhibitors. Annual Review of Biochemistry 52, 655–709.

Xavier-Filho, J., Campos, F.A.P., Ary, M.B., Silva, C.P., Carvalho, M.M.M., Macedo, M.L.R., Lemos, F.J.A., Grant, G., 1989. Poor correlation between the levels of proteinase inhibitors found in seeds of different cultivars of cowpea (*Vigna unguiculata*) and the resistance/susceptibility to predation by *Callosobruchus maculatus*. Journal of Agricultural Food Chemistry 37, 1139–1143.

PERGAMON

Phytochemistry 57 (2001) 633–642

PHYTOCHEMISTRY

www.elsevier.com/locate/phytochem

Vanadium haloperoxidases from brown algae of the Laminariaceae family

M. Almeida[a], S. Filipe[a], M. Humanes[a], M.F. Maia[a], R. Melo[b], N. Severino[a], J.A.L. da Silva[c], J.J.R. Fraústo da Silva[c,*], R. Wever[d]

[a]*Centro de Electroquímica e Cinética, Departamento de Química e Bioquímica, Faculdade de Ciências da Universidade de Lisboa, Edifício C1-5° piso, Campo Grande, 1749-016 Lisbon, Portugal*

[b]*Instituto de Oceanografia, Faculdade de Ciências da Universidade de Lisboa, Campo Grande, 1749-016 Lisbon, Portugal*

[c]*Centro de Química Estrutural, Complexo 1, Instituto Superior Técnico, Av. Rovisco Pais,1, 1049-001 Lisbon, Portugal*

[d]*Institute for Molecular Chemistry, University of Amsterdam, Nieuwe Achtergracht 129, 1018 WS, Amsterdam, The Netherlands*

Received 25 July 2000; received in revised form 21 February 2001

Abstract

Vanadium haloperoxidases were extracted, purified and characterized from three different species of Laminariaceae — *Laminaria saccharina* (Linné) Lamouroux, *Laminaria hyperborea* (Gunner) Foslie and *Laminaria ochroleuca* de la Pylaie. Two different forms of the vanadium haloperoxidases were purified from *L. saccharina* and *L. hyperborea* and one form from *L. ochroleuca* species. Reconstitution experiments in the presence of several metal ions showed that only vanadium(V) completely restored the enzymes activity. The stability of some enzymes in mixtures of buffer solution and several organic solvents such as acetone, ethanol, methanol and 1-propanol was noteworthy; for instance, after 30 days at least 40% of the initial activity for some isoforms remained in mixtures of 3:1 buffer solution/organic solvent. The enzymes were also moderately thermostable, keeping full activity up to 40°C. Some preliminary steady-state kinetic studies were performed and apparent Michaelis–Menten kinetic parameters were determined for the substrates iodide and hydrogen peroxide. Histochemical studies were also performed in fresh tissue sections from stipe and blade of *L. hyperborea* and *L. saccharina*, showing that haloperoxidase activity was concentrated in the external cortex near the cuticle, although some activity was also observed in the inner cortical region. © 2001 Elsevier Science Ltd. All rights reserved.

Keywords: *Laminaria saccharina*; *Laminaria hyperborea*; *Laminaria ochroleuca*; Laminariaceae; Vanadium in biology; Vanadium-dependent haloperoxidases

1. Introduction

The bioinorganic chemistry of vanadium has aroused much interest in recent years due to the curious roles and states of this metal in various lower organisms (see reviews by Chasteen, 1990; Wever and Kustin, 1990; Butler and Carrano, 1991; Redher, 1991; Sigel and Sigel, 1995; Tracey and Crans, 1998). One case which received more attention in the last few years is that of the vanadium haloperoxidases, a new class of enzymes that contain vanadium(V), as vanadate, in the active site and catalyse halogenation reactions of several substrates. These enzymes are found in many brown, in some red and in one green marine alga (Butler and Walker, 1993) and in the lichen *Xantoria parietina* (Plat et al., 1987). Recently, vanadium dependent haloperoxidases were also found in some fungi (van Schijndel et al., 1993; Barnett et al., 1998).

All the vanadium haloperoxidases isolated to date share some common features: they are composed of one or more subunits of relative molecular mass around 67 kDa; they can be inactivated by dialysis against EDTA at low pH; their activity is only restored by addition of vanadium (as vanadate) and they seem to have similar coordination of vanadium in the active site (Messerschmidt and Wever, 1996; Messerschmidt et al., 1997; Weyand et al., 1999).

* Corresponding author. Tel.: +351-1841-9000; fax: +351-2136-12510.

E-mail address: pcd1950@alfa.ist.utl.pt (J.J.R. Fraústo da Silva).

0031-9422/01/$ - see front matter © 2001 Elsevier Science Ltd. All rights reserved.
PII: S0031-9422(01)00094-2

Vanadium haloperoxidases have been traditionally classified as chloro, bromo and iodoperoxidases. Vanadium chloroperoxidases have only been detected in terrestrial organisms, whereas bromo and iodoperoxidases are dominant in the marine environment.

Marine organisms, particularly seaweeds, produce large quantities of halometabolites, which are held within algal membrane bound vesicles and are thought to result from the catalytic activity of haloperoxidases. These halometabolites probably act as hormones or as repellents in biological defence mechanisms (Jordan and Vilter, 1991). Interestingly in this respect, thirty years ago, Siegel and Siegel (1970) proposed that an anomalous substrate specificity of haloperoxidases might be the reason why seaweeds are not lignificated. More recently, Küpper et al. (1998) reported that haloperoxidases might be involved in the uptake of iodide from seawater, a process that, according to these authors, may be related to conditions of oxidative stress. In the same year, ten Brink et al. (1998) reported that marine vanadium haloperoxidases were able to catalyse enantioselective sulfoxidation reactions. Despite these many studies, the reason for the selection of vanadium for these enzymes remains elusive since other more common biological metals, e.g. iron (heme) or manganese could also have been used (Fraústo da Silva and Williams, 1991).

The isolation of more than one form of vanadium haloperoxidase has been reported for *Ascophyllum nodosum* (Krenn et al., 1989). Recently, two papers from our laboratory were published showing that it is also possible to purify more than one form of the enzyme (Almeida et al., 1998; Almeida et al., 2000) from the brown seaweeds *Sacchoriza polyschides* and *Pelvetia canaliculata*. Histochemical tests are a very important control tool in this kind of studies, since contamination of the collected seaweeds with symbiont organisms living in and on the seaweeds is very common (Pedérsen and Fries, 1977). These controls were performed on *A. nodosum* and indicated that the enzyme activity was located on the surface of the cell wall of the thallus and inside the alga between the cortex and the medulla and especially around the conceptacles (Krenn et al., 1989). Similar experiments in *P. canaliculata* revealed that enzyme activity was located, on the surface cuticle of the thallus (Almeida et al., 2000).

Strangely, the seaweeds collected along the Portuguese coast, which were previously studied, exhibited lower haloperoxidase activities than most of the algae from northern regions of the Atlantic Ocean (Almeida et al., 1998; Almeida et al., 2000). To confirm if this is a general trend, which would suggest an environment dependence of the activity, we decided to carry out a comparative study of the properties of the haloperoxidases extracted from *L. saccharina, L. hyperborea* and *L. ochroleuca* since the Portuguese coast is the southern European habitat limit for these species.

2. Results and discussion

2.1. Extraction of the enzymes

The algae from the Laminariaceae family are extremely rich in alginates and polyphenolic compounds that complicate the extraction and purification of these proteins. An aqueous salt/polymer two-phase system was employed for the extraction. We have used polyethyleneglycol (PEG) and potassium carbonate in this system, since previous experience has shown that this salt is the most adequate for the extraction of this particular type of seaweed (Jordan and Vilter, 1991). From several compositions tested, the medium with 22.5% (w/v) K_2CO_3 and 15% (w/v) PEG 1500 in water was found to be the most efficient for the extraction of the haloperoxidases from these algae. The vanadium haloperoxidases (V-HPOs) were mainly found in the top-phase, bounded to the polymer (PEG); the bottom aqueous phase, rich in salts, accumulated most of the alginates and hydrophilic compounds. The separation of the enzyme from the polymer was easily achieved by the addition of acetone. After centrifugation the pellet thus obtained was dissolved in the minimum amount of 50 mM Tris–HCl (pH 9.0). Since the pH is quite high, a partial loss of the prosthetic group occurred; activity was fully restored by addition of vanadate (20 mM).

2.2. Purification of the enzyme — isoforms

The extracts from the three seaweeds were subjected to several chromatographic steps to purify the enzymes. The first stage was a hydrophobic interaction step with phenyl-sepharose. For *L. saccharina* and *L. ochroleuca* two sets of fractions with activity (named Ls1 and Ls2; Lo1 and Lo2, respectively) were obtained, whereas for the *L. hyperborea* extract only one set of active fractions was obtained. When subjected to electrophoresis under non-denaturing conditions all these fractions revealed several bands (results not shown); hence, a second chromatographic step was necessary.

Two different approaches were used for the second purification step; a further hydrophobic interaction chromatography with butyl-sepharose, for *L. saccharina* and *L. hyperborea,* and an ion exchange chromatography with DEAE-Sephacel for *L. ochroleuca*.

The active fraction from *L. hyperborea* yielded, after this second chromatographic step two active bands (named Lh1 and Lh2), while for *L. saccharina* this second step provided separation from most of the contaminants. A chromofocusing chromatography was used as the final purification step and yielded the two forms of the vanadium-haloperoxidases (V-HPO) from *L. saccharina* and *L. hyperborea* species. For *L. ochroleuca* the ion exchange chromatographic step with DEAE-Sephacel resolved the Lo2 fraction into a major fraction

(named α) and a minor fraction (named β). The Lo1 fraction lost its activity very rapidly and could not be reactivated.

Table 1 shows the specific activities of the purified forms from the three Laminariaceae studied. It is clear that the *L. saccharina* isoforms exhibit considerably higher iodoperoxidase (IPO) and bromoperoxidase (BrPO) activities than the isoforms from *L. hyperborea*. It is also interesting to notice that the two forms of the enzyme purified from this seaweed show different types of activity (Lh1 is a IPO while Lh2 is a BrPO). The *L. ochroleuca* fractions exhibited very low IPO activity only, so that we limited the study of the corresponding enzyme to the activity tests, molecular mass determination and reactivation with vanadium(V).

The IPO activity values found for the *L. saccharina* two isoforms of V-HPO (1067 and 320 U/mg) are comparable to the values obtained by Jordan and Vilter (1991) for the two V-HPO isoforms from *L. digitata*, a species commonly related to *L. saccharina* and *L. hyperborea* at higher latitudes (1140 and 797 U/mg, respectively). In a previous work, de Boer et al. (1986), purified only one enzyme form from *L. saccharina* using a classical extraction method. This enzyme had a specific activity in the bromination reaction of 608 U/mg after reactivation with vanadate, which is also much higher than the values obtained in the present study for the same kind of activity. This had already been observed for the haloperoxidase extracted from *P. canaliculata* and *S. polyschides* (Almeida et al., 1998; Almeida et al., 2000) and suggests a decreasing trend in enzymatic power of the vanadium haloperoxidases as one goes south in the habitat of the algae. If real, this trend may derive from specific conditions along the Portuguese coast, perhaps the higher temperature of the seawater, but this requires confirmation since the effect of this variable is not obvious. Another important observation is that the extraction procedure may determine the number of forms of the enzyme purified from these seaweeds. Using aqueous two-phase systems, which involve a delicate balance between hydrophobic and hydrophilic interactions, several isoforms can be separated. The classical extraction procedure used by de Boer et al. (1986) is not so selective; thus the fact that we have used the two-phase aqueous system may explain why we found two isoforms in *L. saccharina*. The reason for the existence of different forms of the enzyme in the same seaweed is not yet understood. It is possible that they have different functions and distribute differently, see below the histochemical tests. A more extensive study is required to clarify both of these aspects. It can not be excluded, however, that the life cycle of the seaweeds determines the production of isoforms since we have observed that for other specimens of *L. saccharina* collected at the same sites but in a different period of the year only one isoform was isolated although we have used the same extraction and purification procedures described in this work.

Table 1
IPO and BrPO specific activity values for the isoforms of V-HPO separated from *Laminara saccharina*, *Laminaria hyperborea* and *Laminaria ochroleuca*

Isoforms	IPO (U/mg)	BrPO (U/mg)
Ls_1	320	12
Ls_2	1067	32
Lh_1	131	–[a]
Lh_2	300	16
Lo1	(0.3)	–[a]
Lo2 (α)	16	–[a]
Lo2 (β)	9	–[a]

[a] The fractions did not show BrPO activity under the test conditions.

2.3. Determination of molecular mass

Each form of V-HPO purified from *L. saccharina* and *L. hyperborea* yielded only one major band on polyacrylamide gels under non-denaturating conditions; these bands stained both for protein and for HPO activity. Compared to standard proteins, these enzymes hardly migrate, indicating a high relative molecular mass, probably due to aggregation of the enzyme. Determination of the relative molecular mass for the enzymes from *L. saccharina* and *L. hyperborea* was difficult at first since in the presence of 0.1% SDS, chosen for this purpose, they were still very strongly aggregated. Subsequently, gel filtration on Sephacryl S-300R was successful, giving two bands, corresponding to relative molecular masses of 169 and 58 kDa (results not shown). The first band probably corresponds to an aggregated form of the enzyme (all peroxidases extracted from seaweeds aggregate easily) while the second band corresponds to the molecular mass of the subunit. On sodium dodecyl sulfate–polyacrylamide gel electrophoresis (SDS–PAGE), the purified enzymes showed only one major band, with M_r around 67 kDa (Fig. 1). This is in agreement with the reported values for *L. saccharina* (64 and 66 kDa) subunits (de Boer et al., 1986). Recently, the molecular mass of the *A. nodosum* bromoperoxidase monomer was determined as 60 kDa (Weyand et al., 1999). For *L. ochroleuca* the relative molecular mass of fraction α was determined as 133 kDa on a non-denaturating polyacrylamide gel electrophoresis (Fig. 1) and 65 kDa on a SDS-denaturating polyacrylamide gel electrophoresis, which seem to indicate the presence of two subunits of identical molecular masses.

2.4. Inactivation and reactivation

By extensive dialysis with citrate–phosphate buffer in the presence of EDTA the enzymes were inactivated due to removal of the prosthetic group (Table 2). Some enzymes were easily deactivated, while for others deactivation was incomplete. It is also interesting to

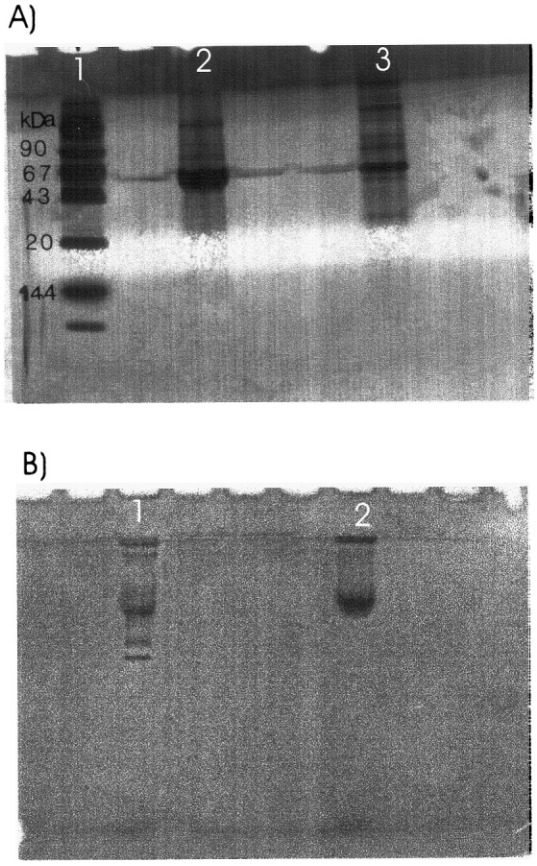

Fig. 1. SDS–PAGE 12.5% as laemmli of V-HPO: (A) V-HPO from *Laminaria saccharina* and *Laminaria hyperborea*: lane 1, standard proteins; lane 2, Ls1 enzyme; lane 3, Lh2 enzyme; (B) V-HPO from *Laminaria ochroleuca*: lane 1, standard proteins; lane 2, Lo2 (α) enzyme.

Table 2
Percentage of IPO specific activity of the isoforms of V-HPO, remaining after deactivation (specific IPO activity before the deactivation process was taken as 100%)[a]

Enzyme	% remaining IPO specific activity
Ls_1	1
Ls_2	9
Lh_1	5
Lh_2	3.5
Lo2 (α)	10
Phyllariopsis brevipes[b]	19

[a] For details see Experimental section.
[b] Almeida et al. (1996).

note the differences in deactivation between the two forms of the enzyme. For instance, Ls2 showed a higher resistance to deactivation than Ls1, whereas Lh1 is more resistant than Lh2. A similar behaviour has also been observed for the enzyme extracted from *P. canaliculata*, for which one of the forms showed a higher resistance to deactivation (Almeida et al., 2000). As Fig. 2 illustrates, the time required for complete reactivation of the enzymes was again different for each form of the enzyme. Since vanadium uptake (as vanadate) depends on the polypeptide chain and on the bonding of this species to the active site, the difference may be due to different conformations of the protein near the active site, which may alter the binding of vanadate. We note also, that the values of specific haloperoxidase activity were usually higher after reactivation with vanadate, which means that the vanadate group is not tightly bound at the active site and partial losses during the processes of purification may have occurred.

The effect of other metal ions, such as Mo(VI) (as molybdate), Mn(II) and Fe(III) on the reactivation of the apo-haloperoxidases was also tested; reactivation was always found to be less then 15% of that observed with vanadate.

2.5. Effect of organic solvents

The long term effect of organic solvents on haloperoxidase activity is shown in Fig. 3. After 1 month incubation, the Ls1 form showed the highest activity in the mixtures with 25% of organic solvent (Fig. 3A), especially in the case of acetone when the activity was actually higher than in aqueous media; a possible explanation may be that the enzyme is aggregated in the buffer media and the presence of acetone could contribute to its desaggregation. For the other two forms (Ls2 and Lh2) appreciable activity was still observed after 1 month. For mixtures with 50% of organic solvent (Fig. 3B) the behaviour was quite different. The stability of Ls1 decreased significantly, whereas for Ls2 and Lh2 the decrease was not so pronounced.

It is also curious to notice that for mixtures with 50% organic solvent the forms Ls2 and Lh2 were more stable than Ls1, in clear contrast to what was observed in the mixtures with 25% organic solvent. Clearly, further work is needed to clarify these features of the vanadium haloperoxidases.

2.6. Thermal stability

The thermal stability of *L. saccharina* enzymes was also investigated. For temperatures in the range 25–50°C the enzymes studied were quite stable, catalysing with considerable efficiency the formation of triiodide (Fig. 4). An enhanced activity was shown by the Ls1 enzyme in the range 30–50°C, with a maximum at 40°C, contrasting the behaviour of Ls2 (Fig. 4). Above 50°C, the catalytic activity of both the Ls1 and Ls2 isoforms is drastically reduced. The thermal stability has also been studied for the haloperoxidases from the red algae *Corallina officinalis* (Sheffield et al., 1993), *Ceramium rubrum* (Krenn et al., 1987), the brown algae *Phyllariopsis brevipes* (Almeida et al., 1996) and *A. nodosum* (Tromp et al., 1989), and the lichen *Xantoria parietina* (Plat et al., 1987). These studies indicate that the thermal stability

A) *L. saccharina*

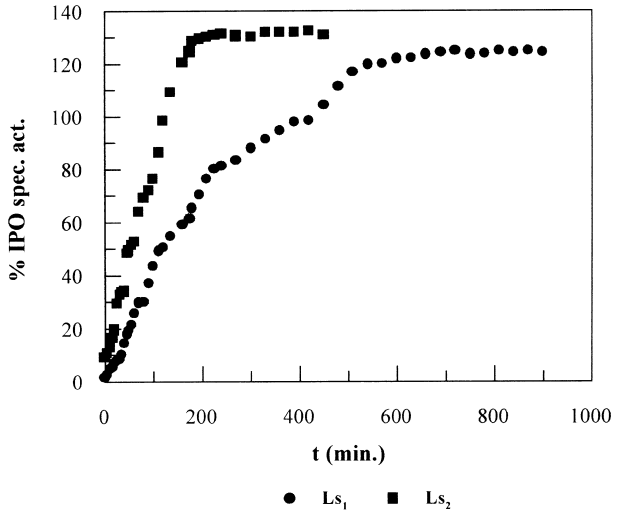

B) *L. hyperborea*

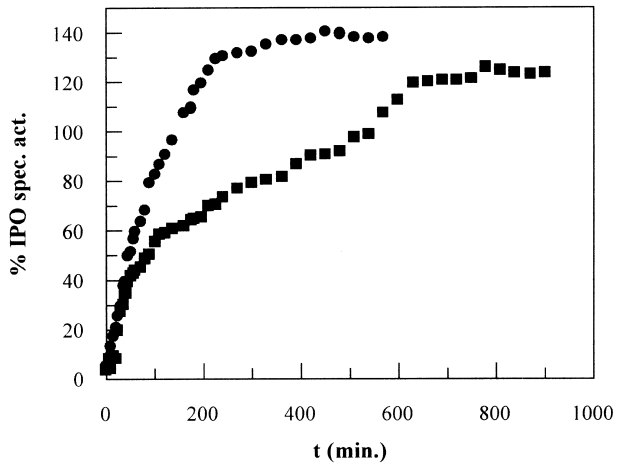

C) *L. ochroleuca* (Lo2(α))

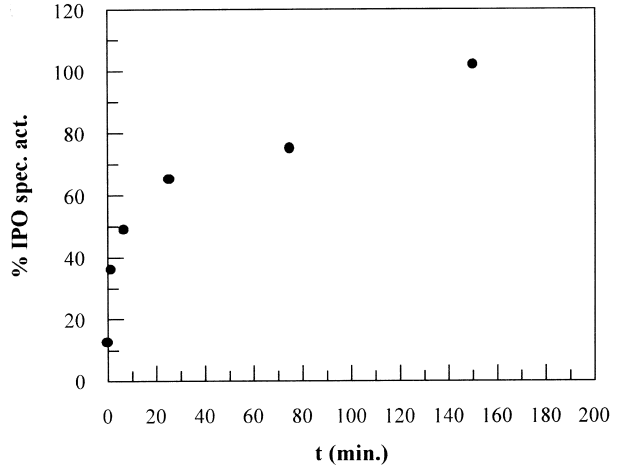

Fig. 2. Reactivaction with V(V) of the enzyme forms purified from *Laminaria saccharina, Laminaria hyperborea* and *Laminaria ochroleuca*. The values of IPO specific activity values the deactivaction/reactivaction process were taken as 100%. The values presented (% IPO specific activity) correspond to a percentage of those initial values.

of V-HPO is generally higher for the lichen comparatively to the seaweeds. This fact is probably related to the nature of the habitat, since *Xanthoria parietina* lives in the terrestrial environment, subject to larger temperature variation while seaweeds live in a more stable marine environment.

2.7. Steady-state kinetics

Some preliminary steady-state kinetic studies were performed by measuring the initial rate of I_3^- formation, catalysed by these enzymes, following the experimental conditions described in the Experimental section for the two substrates used (iodide and hydrogen peroxide) and for three pH values. Values of the apparent Michaelis–Menten constants for the two substrates and the values of maximum rate (V_{max}) were obtained and are presented in Table 3.

This table shows that there are no significant differences between kinetic parameters for the enzymes studied in this work. All the enzyme forms show a V_{max} at pH 6.1.

The apparent Michaelis–Menten constant for the substrate iodide ($K_m^{app\ I-}$) decreased slightly with the decrease of pH, showing that the affinity for iodide decreases when the pH increases. Previous studies on the bromoperoxidases from other seaweeds (de Boer and Wever, 1988; Everett and Butler, 1989; Soedjack and Butler, 1991) gave analogous results. It was not possible to increase the pH further since the non-catalysed reaction between H_2O_2 and I^- interferes strongly with the assay (Vilter, 1995).

The binding of hydrogen peroxide is affected in a different way; since the values of the apparent Michaelis–Menten constant for the substrate hydrogen peroxide ($K_m^{app\ H_2O_2}$) decreased with the increase in pH, this implies that the affinity of hydrogen peroxide for the enzyme increases with the increase of pH. Probably, protonation of a group at lower pH values, possibly a histidine side chain, prevents the reaction with peroxide. Studies carried out with the bromoperoxidase extracted from *A. nodosum* (de Boer and Wever, 1988) did indeed indicate the presence of a group, probably a histidine residue, with a pK_a of 5.7, which may be responsible for the pH dependence of the catalytical process. In fact, it was found for other peroxidases that a histidine with a pK_a between 4 and 6 could control the binding of peroxide to the active center, reflecting the importance of the polypeptide chain on activity (de Boer and Wever, 1988). Recently, the detailed role of a particular histidine residue (His 496) in the catalytic behaviour of haloperoxidases was discussed (Renirie et al., 2000).

2.8. Histochemical tests

From the observation of *L. saccharina* and *L. hyperborea* stained sections, it is possible to confirm that the

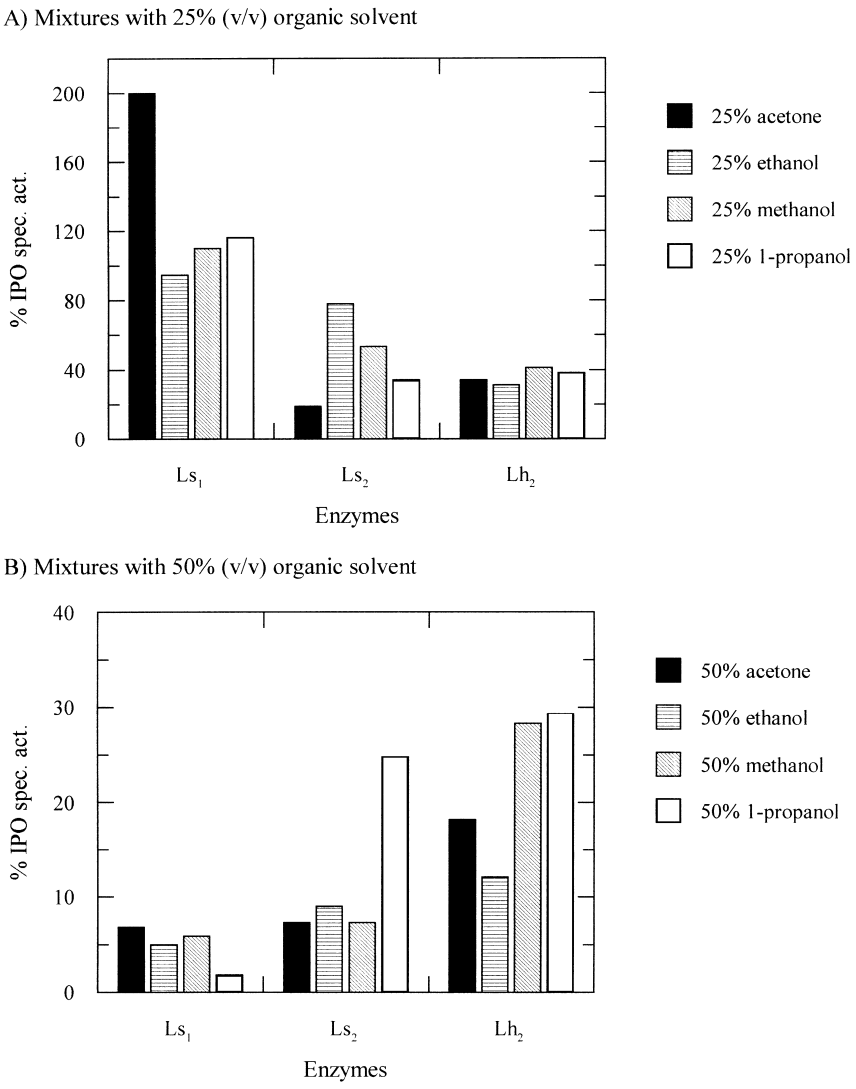

Fig. 3. Effect of buffer solution/organic solvent mixtures on IPO activity of the enzymes after 30 days incubation. IPO specific activity before mixture with organic solvent was taken as 100% (see Experimental section for details).

Table 3
Apparent kinetic parameters ($K_m^{app\ I-}$ and $K_m^{app\ H_2O_2}$) of the vanadium haloperoxidases from *Laminaria saccharina* and *Laminaria hyperborea*

pH	Enzyme	$K_m^{app\ I-}$ (mM)	$K_m^{app\ H_2O_2}$ (μM)	$V_{max}\times10^{-7}$ (M s^{-1})
5.5	Ls_1	1.3	376	7.6
	Ls_2	1.9	333	11.2
	Lh_1	1.9	334	9.8
	Lh_2	2.3	285	12.1
6.1	Ls_1	3.4	243	9.1
	Ls_2	2.7	273	12.1
	Lh_1	3.4	275	16.0
	Lh_2	3.8	217	17.5
6.7	Ls_1	3.7	120	8.3
	Ls_2	4.3	137	7.1
	Lh_1	3.5	166	9.4
	Lh_2	3.8	173	10.8

haloperoxidases are located, near the cuticle as well as in the external cortex region of the thallus (Fig. 5). However, the *L. hyperborea* sections exhibited also strong haloperoxidase activity around mucilaginous channels. The inner cortex region shows the presence of haloperoxidase activity for *L. saccharina*, absent in *L. hyperborea*. Some residual haloperoxidase activity was also observed in the medullar region of *L. hyperborea*. These results are in agreement with those of Krenn et al. (1989) and Almeida et al. (2000).

3. Experimental

3.1. Collection of algae

All the seaweeds were collected at low tide from the Portuguese west coast, in the northern part of the

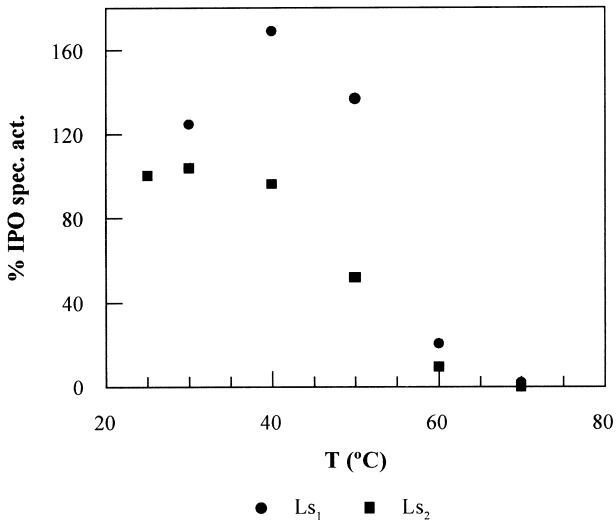

Fig. 4. The effect of temperature on the IPO activity for the two isoforms of V-HPO isolated from *Laminaria saccharina*. IPO specific activity before thermal treatment was taken as 100%.

country, near Viana do Castelo, at the end of summer (*L. hyperborea* and *L. saccharina*) and in spring (*L. saccharina* and *L. ochroleuca*). After collection, the algae were transported to the laboratory, thoroughly washed with distilled water, chopped and stored frozen until required.

3.2. Extraction and purification

For the extraction of HPO, two-phase aqueous systems, formed with an aqueous solution of PEG 1500 and an aqueous solution of potassium carbonate, were used. For each species, the process was optimised in order to select the most effective extraction media. In all cases, the media with 22.5% (w/v) K_2CO_3 and 15% (w/v) PEG 1500 proved to be the best.

After centrifugation for 30 min at 5000 *g* the upper phase was collected and the proteins precipitated by adding an equal volume of acetone. After a second centrifugation (30 min at 10,000 *g*) the resulting pellet was collected and resuspended in 50 mM Tris–HCl (pH

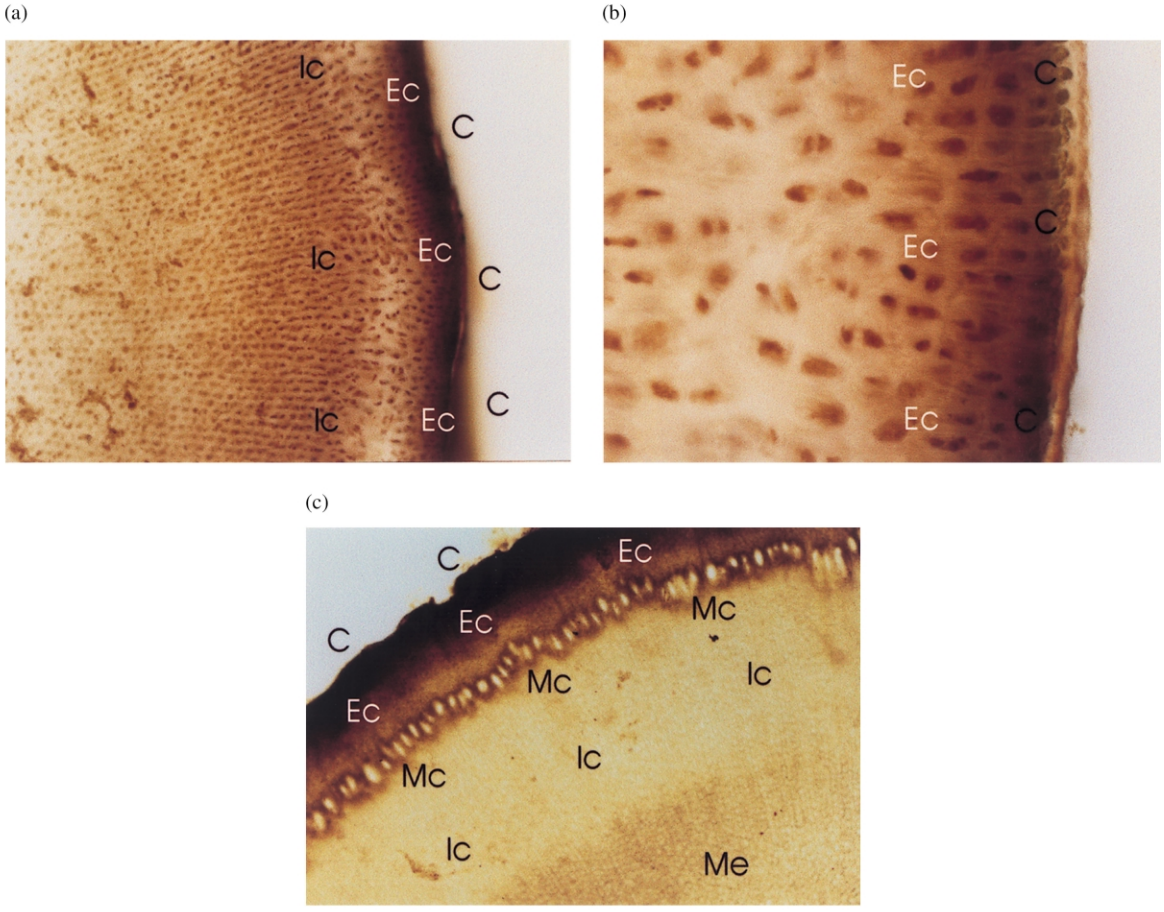

Fig. 5. Histochemical staining of fresh tissue samples of *Laminaria saccharina* and *Laminaria hyperborea*: (a) *Laminaria saccharina* (amplification: 10×); (b) *Laminaria saccharina* (amplification: 50×); (c) *L. hyperborea* (amplification: 10×); (C, cuticle; Ec, external cortex; Mc, mucilaginous channels; Ic, internal cortex; Me, medulla).

9.0) buffer. In order to reactivate the HPO, the extract was dialysed overnight against 20 mM $NaVO_3$ in 50 mM Tris–HCl (pH 9.0).

The sample was then loaded onto a hydrophobic interaction column (phenyl-sepharose from Pharmacia) and eluted with a decreasing linear gradient (1.3–0 M) of $(NH_4)_2SO_4$ in 50 mM Tris–HCl (pH 9.0). Resultant samples were then applied to another hydrophobic interaction column (butyl-sepharose from Pharmacia) and eluted also with a decreasing linear gradient (1.3–0 M) of $(NH_4)_2SO_4$ in 50 mM Tris–HCl (pH 9.0) or alternatively (*L. ochroleuca*) applied to an anionic exchange column (DEAE-Sephacel, from Pharmacia) and eluted with an increasing linear gradient of 0–1.3 M of $(NH_4)_2SO_4$ in 0.2 M Tris–Cl (pH 9.0). For the chromofocusing chromatography step (polybuffer exchanger-PBE 94, from Pharmacia) the samples were eluted with Polybuffer 74-imidazole (pH 4.0) also from Pharmacia.

3.3. Determination of protein content

Protein was determined by Bradford's method (Bradford, 1976), using bovine serum albumin as standard (Sigma).

3.4. Molecular mass determination and electrophoresis

The relative molecular mass was determined by FPLC/gel filtration chromatography on Sephacryl S-300R (Pharmacia) with a mobile phase of 0.5 M NaCl in 50 mM Tris–HCl (pH 9.0). Standard proteins from Pharmacia (ribonuclease A, M_r 13.7 kDa; chymotrypsinogen, M_r 25 kDa; ovalbumin, M_r 43 kDa; aldolase, M_r 158 kDa; and catalase, M_r 232 kDa) were used for the calibration of the column. SDS polyacrylamide gel electrophoresis was carried out on 12.5% gels according to Laemmli (1970). Standard proteins used for molecular mass determination were: phosphorylase b (94 kDa), bovine serum albumin (67 kDa), ovalbumin (43 kDa), carbonic anhydrase (30 kDa), trypsin inhibitor (20.1 kDa) and α-lactoalbumin (14.4 kDa), all from Pharmacia.

3.5. Reactivation studies

The HPO were inactivated at low pH by extensive dialysis for 24–72 h against a citrate–phosphate buffer at pH 3.8, in the presence of 1 mM EDTA, followed by dialysis against 50 mM Tris–HCl (pH 9.0). Reactivation studies with Na_3VO_4 were carried out in 50 mM Tris–HCl (pH 9.0). The final vanadium concentration for reactivation was 240 μM. The same conditions were used in the reactivation studies with other inorganic salts (ferric chloride, ammonium molybdate and manganese chloride).

3.6. Operational stability in organic solvents

The effect of organic solvents upon the haloperoxidase activity was determined by incubation of the enzyme with 25 and 50% (v/v) acetone, ethanol, methanol and 1-propanol mixed with 50 mM Tris–Cl pH 9.0, for 30 days at room temperature. The vials were tightly capped and kept in the dark. Each incubation was carried out in duplicate.

3.7. Thermal stability studies

The purified enzymes were incubated in a thermostated vessel for one hour at temperatures ranging from 25 to 70°C. Activity was determined after subsequent equilibration at room temperature.

3.8. Activity determinations

Activity as iodoperoxidase (IPO) was measured by following the conversion of I^- to I_3^- at 350 nm ($\varepsilon_M = 26400\ M^{-1}\ cm^{-1}$) using H_2O_2 as the electron acceptor (Björkstén, 1968). The H_2O_2 solutions were prepared by dilution of a 30% stock solution of Perhydrol (Merck) and their concentration was determined spectrophotometrically at 240 nm ($\varepsilon_M = 43.6\ M^{-1}\ cm^{-1}$). Bromination activity was measured spectrophotometrically at 290 nm in an assay system containing 50 μM monochlorodimedone ($\varepsilon_M = 20.2\ mM^{-1}\ cm^{-1}$), 2 mM H_2O_2, 100 mM KBr, in 100 mM phosphate buffer (pH 6.5) (Wever et al., 1985). Activity in native electrophoresis gels was detected by incubation of the gel in *o*-dianisidine, iodide and hydrogen peroxide (Vilter, 1981).

3.9. Steady-state kinetic experiments

These experiments were carried out in 0.1 M 2-(morpholino)ethanesulphonic acid (MES) (pH 5.5, 6.1 and 6.7) by measuring the oxidation of I^- by H_2O_2 to I_3^-. For each pH value the initial rate of formation of I_3^- was determined at a constant concentration of hydrogen peroxide (0.8 mM) and the potassium iodide concentration was varied between 0.2 and 10 mM. Alternatively, a constant concentration of potassium iodide (6 mM) was used and the hydrogen peroxide concentration was varied between 0.2 and 1.2 mM. Sodium sulphate was added to keep a constant ionic strength of 0.2 M when the potassium iodide concentration was varied. All measurements were performed at 25.0±0.5°C.

3.10. Steady-state kinetic analysis

The initial rates, v_0 plotted as a function of hydrogen peroxide or iodide concentration were fit to a Michaelis–Menten equation. The apparent kinetic parameters $K_m^{app\ I-}$ and $K_m^{app\ H_2O_2}$ as well as V_{max} were obtained from primary double reciprocal plots.

3.11. Histochemical studies

Tissue samples of fresh seaweeds cut with a blade razor, were immersed in filtered natural seawater followed by incubation with the haloperoxidase activity test solution, containing of 0.19 mM *o*-dianisidine, 6.06 mM KI and 0.8 mM H_2O_2 in distilled water.

After incubation, the tissue samples were washed with distilled water and observed in the light microscope.

The presence of haloperoxidase activity was ascertained from the development of a dark reddish brown colour due to *o*-dianisidine oxidation assisted by iodide. Control tests were performed for each tested tissue sample.

Acknowledgements

The authors thank the Portuguese Science Foundation for financial support (project: PRAXIS XXI/2/2.1/QUI/14/94 and PhD research grants: JNICT BD/2358/92-I, PRAXIS XXI-BD/5542/95 and GGPXXI/BD/2254/94).

References

Almeida, M., Humanes, M., Silva, J. A., Melo, R., Fraústo da Silva, J.J.R., 1996. *Phyllariopsis brevipes* — a brown algae with vanadium dependent iodoperoxidase. In: Obinger, C., Burner, U., Eberman, R., Penel, C., Greppin H. (Eds.), Plant Peroxidases: Biochemistry and Physiology, University of Geneve, pp. 146–152.

Almeida, M., Humanes, M., Silva, J.A., Melo, R., Fraústo da Silva, J.J.R., Vilter, H., Wever, R., 1998. *Saccorhiza polyschides* (Phaeophyceae; Phyllariaceae): a new source for vanadium-dependent haloperoxidases. Phytochemistry 48, 229–239.

Almeida, G., Humanes, M., Melo, R., Silva, J.A.L., Fraústo da Silva, J.J.R., Wever, R., 2000. Purification and characterisation of vanadium haloperoxidases from the brown algae *Pelvetia canaliculata*. Phytochemistry 54, 5–11.

Barnett, P., Hemrika, W., Dekker, H.L., Muijsers, A.O., Renirie, R., Wever, R., 1998. Isolation, characterization and primary structure of the vanadium chloroperoxidase from the fungus *Embellisia didymospora*. J. Biol. Chem. 273, 23381–23387.

Björkstén, F., 1968. A kinetic study of the horseradish peroxidase-catalysed oxidation of iodide. Eur. J. Biochem. 5, 133–184.

Bradford, M.M., 1976. A rapid and sensitive method for the quantitation of microgram quantities of protein utilizing the principle of protein-dye binding. Anal. Biochem. 72, 248.

Butler, A., Carrano, C.J., 1991. Coordination chemistry of vanadium in biological systems. Coord. Chem. Rev. 109, 61–105.

Butler, A., Walker, J.V., 1993. Marine haloperoxidases. Chem. Rev. 93, 1937–1944.

Chasteen, N.D., 1990. Vanadium in Biological Systems — Physiology and Biochemistry. Kluwer Academic Publishers, Dordrecht.

de Boer, E., Tromp, M.G.M., Plat, H., Kreen, B.E., Wever, R., 1986. Vanadium(V) as an essential element for haloperoxidase activity in marine brown algae: purification and characterisation of a vanadium(V)-containing bromoperoxidase from *Laminaria saccharina*. Biochim. Biophys. Acta 872, 104–115.

de Boer, E., Wever, R., 1988. The reaction mechanism of the novel vanadium-bromoperoxidase. A steady- state kinetic analysis. J. Biol. Chem. 263, 12326–12332.

Everett, R., Butler, A., 1989. Bromide-assisted hydrogen peroxide disproportionation catalyzed by vanadium bromoperoxidase: absence of direct catalase activity and implications for the catalytic mechanism. Inorg. Chem. 28, 393–395.

Fraústo da Silva, J.J.R., Williams, R.J.P., 1991. The Biological Chemistry of the Elements. Oxford University Press, Oxford.

Jordan, P., Vilter, H., 1991. Extraction of proteins from material rich in anionic mucilages: partition and fractionation of vanadate-dependent bromoperoxidases from the brown algae *Laminaria digitata* and *Laminaria saccharina* in aqueous polymer two-phase systems. Biochim. Biophys. Acta 1073, 98–106.

Krenn, B.E., Plat, H., Wever, R., 1987. The bromoperoxidase from the red alga *Ceramium rubrum* also contains vanadium as a prosthetic group. Biochim. Biophys. Acta 912, 287–291.

Krenn, B.E., Tromp, M.G.M., Wever, R., 1989. The brown alga *Ascophyllum nodosum* contains two different vanadium bromoperoxidases. J. Biol. Chem. 264, 19287–19292.

Küpper, F.C, Schweigert, N., Ar Gall, E., Legendre, J.-M., Vilter, H., Kloareg, B., 1998. Iodine uptake in *Laminariales* involves extracellular, haloperoxidase-mediated oxidation of iodide. Planta 207, 163–171.

Laemmli, U.K., 1970. Cleavage of structural proteins during the assembly of the head of bacteriophage. Nature 227, 680–685.

Messerschmidt, A., Wever, R., 1996. X-ray structure of a vanadium-containing enzyme: chloroperoxidase from the fungus *Curvularia inaequalis*. Proc. Natl. Acad. Sci. USA 93, 392–396.

Messerschmidt, A., Prade, L., Wever, R., 1997. Implications for the catalytic mechanism of the vanadium-containing enzyme chloroperoxidase from the fungus *Curvularia inaequalis* by X-ray structures of the native and peroxide form. J. Biol. Chem. 378, 309–315.

Pedérsen, M., Fries, N., 1977. Bromophenols identified in a marine ascomycete and its culture medium. Z. Pflanzenphysiol. 82, 363–366.

Plat, H., Krenn, B.E., Wever, R., 1987. The bromoperoxidase from the lichen *Xanthoria parietina* is a novel vanadium enzyme. Biochem. J. 248, 277–279.

Redher, D., 1991. The bioinorganic chemistry of vanadium. Ang. Chem. 30, 148–167.

Renirie, R., Hemrika, W., Piersma, S.R., Wever, R., 2000. Peroxidase and phosphatase activity of active-site mutants of vanadium CPO from the fungus *Curvularia inaequalis*. J. Biol. Chem. 275, 11650–11657.

Sheffield, D.J., Harry, T., Smith, A.J., Rogers, L.J., 1993. Purification and characterisation of the vanadium bromoperoxidase from the macroalga *Corallina officinalis*. Phytochemistry 32, 21–26.

Siegel, B.Z., Siegel, S.M., 1970. Anomalous substrate specificities among the algal peroxidases. Am. J. Bot. 57, 285–287.

Sigel, H., Sigel, A., 1995. Metal Ions in Biological Systems, Vol. 31. Marcel Dekker, New York.

Soedjak, H., Butler, A., 1991. Mechanism of dioxygen formation catalysed by vanadium bromoperoxidase from *Macrocystis pyrifera* and *Fucus distichus*: steady state kinetic analysis and comparison to the mechanism of V-BrPO from *Ascophyllum nodosum*. Biochim. Biophys. Acta 1079, 1–7.

ten Brink H., B., Tuynman, A., Dekker, H., L., Hemrika, W., Izumi, Y., Oshiro, T., Schoemaker, H.E., Wever, R., 1998. Enantioselective sulfoxidation catalyzed by vanadium haloperoxidases. Inorg. Chem. 37, 6780.

Tracey, S., Crans, D.C., 1998. Vanadium Compounds — Chemistry, Biochemistry and Therapeutic Applications. American Chemical Society Symposium, Series no 711. American Chemical Society, Washington.

Tromp, M.G.M., Olafsson, G., Krenn, B.E., Wever, R., 1989. Some structural aspects of vanadium bromoperoxidase from *Ascophyllum nodosum*. Biochim. Biophys. Acta 1040, 192–198.

van Schijndel, J.W.P.M., Vollenbroek, E.G.M., Wever, R., 1993. The chloroperoxidase from the fungus *Curvularia inaequalis*; a novel vanadium enzyme. Biochim. Biophys. Acta 1161, 249–256.

Vilter, H., 1981. PhD thesis, Rheinische Friedrich-Wilhelms Universität, Bonn.

Vilter, H., 1995. Vanadium-dependent haloperoxidases. In: Sigel, H., Sigel, A. (Eds.), Metal Ions in Biological Systems, vol. 31. Marcel Dekker, New York, pp. 325–362. (and references therein).

Wever, R., Kustin, K., 1990. Vanadium: a biological relevant element. Adv. Inorg. Chem. 35, 81–115.

Wever, R., Plat, H., de Boer, E., 1985. Isolation procedure and some properties of the bromoperoxidase from the seaweed *Ascophyllum nodosum*. Biochim. Biophys. Acta 830, 181–186.

Weyand, M., Hecht, H.-J., Kieß, M., Liaud, M.-F., Vilter, H., Schomburg, D., 1999. X-ray structure determination of a vanadium-dependent haloperoxidase from *Ascophyllum nodosum* at 2.0 Å resolution. J. Mol. Biol. 293, 595–611.

PERGAMON

Phytochemistry 57 (2001) 643–652

PHYTOCHEMISTRY

www.elsevier.com/locate/phytochem

Endoplasmic oleoyl-PC desaturase references the second double bond

Jennifer L. Schwartzbeck, Sook Jung, Albert G. Abbott, Erin Mosley, Shahed Lewis, Gina L. Pries, Gary L. Powell*

Department of Biological Sciences, Clemson University, Clemson, SC 29634-0326, USA

Received in revised form 16 January 2001

Abstract

The regiospecificity for the gene product of *fad2*,[1] the microsomal oleoyl-PC desaturase from higher plants, differs from some previous suggestions. Rather than only referencing the carboxyl group (a Δ^{12} desaturase) or the methyl terminus (an ω-6 desaturase), this desaturase locates the second double bond in its substrates by first referencing the existing double bond. This specificity was demonstrated for the oleoyl-PC desaturase cDNA from the developing seeds of peanut (*Arachis hypogaea* L) expressed in yeast (*Saccharomyces cerevisae*). The expressed enzyme was capable of desaturating monounsaturated fatty acyl groups in membrane lipids. Endogenous palmitoleate was desaturated to *cis*, *cis* 9,12 hexadecadienoate (9(*Z*)12(*Z*)C16:2), endogenous oleate to linoleate (9(*Z*)12(*Z*) octadecadienoate), and *cis* 10-nonadecenoate (provided as a supplement in the growth medium) to 10(*Z*)13(*Z*)C19:2. The rule, Δ^{x+3} where $x=9$ is the double bond location in the substrate, best describes the consistent placement of the second double bond in the above monounsaturated substrates for the oleoyl-PC desaturase of higher plants. © 2001 Elsevier Science Ltd. All rights reserved.

Keywords: *Arachis hypogaea* L.; Fabaceae; Peanut; Groundnut; Regiospecificity; Oleoyl-PC desaturase; Omega-6 desaturase; Delta-12 desaturase; Fatty acids; Polyunsaturated

1. Introduction

The desaturases introduce double bonds into fatty acid chains producing the mono- and polyunsaturated fatty acids that are important determinants for the quality of commercial plant oils. Mutants for reduced polyunsaturated fatty acid content in seed oils have been selected using conventional breeding practices (see Gorbert and Knauft, 1997 as an example). The oil becomes rancid less quickly, sharing the chemical composition and many of the qualities of olive oil. The oleoyl-PC desaturase is the enzyme that places the second double bond in the fatty acid and catalyzes the first step in polyunsaturated fatty acid biosynthesis. An agronomically important mutant for peanut (*Arachis hypogaea* L) with high oleate oil content has reduced oleoyl-PC desaturase activity (Ray et al., 1993). Mutants for reduced polyunsaturated fatty acid content for several agronomically important crop species have also been obtained using gene suppression technology directed to the oleoyl PC-desaturase (Mazur et al., 1999).

The question of the specificity of the desaturases (reviewed by Shanklin and Cahoon, 1998) is an interesting one because the substrates are featureless, unbranched, hydrocarbon chains with the ester group at one end and the methyl group at the other. The double bonds are found in the middle of this hydrocarbon. If one double bond is present, the usual double bond configuration is *cis* or *Z* (rather than *trans* or *E*). The most common plant monounsaturated fatty acid is oleate with the double bond exactly in the middle of an eighteen-carbon chain. This configuration can be abbreviated as 9(*Z*)C18:1, where 9 is the location of the double bond counted from the carboxyl or ester group, C18 gives the total number of carbons in the chain, and 2

* Corresponding author. Tel.: +1-864-656-2328; fax: +1-864-656-0435.

E-mail address: glpwl@clemson.edu (G.L. Powell).

[1] We will employ the convention of using *fad2* for the gene and oleoyl-PC desaturase or FAD2 for the gene product. This permits us to avoid describing the enzyme as a Δ^{12} desaturase, or an ω-6 desaturase. The latter designations involve an assertion about the substrate specificity no longer tenable based on this work. PC is the abbreviation for phosphatidylcholine, the most important phospholipid substrate for this activity. GLC is gas-liquid chromatography. GC/MS spectroscopy is separation by capillary gas chromatography with mass spectral, electron-impact detection.

0031-9422/01/$ - see front matter © 2001 Elsevier Science Ltd. All rights reserved.
PII: S0031-9422(01)00081-4

is the total number of double bonds. Second and subsequent double bonds are usually methylene interrupted and unconjugated. The most common polyunsaturated fatty acids in plant tissues are linoleate, 9(*Z*)12(*Z*)C18:2, and linolenate, 9(*Z*)12(*Z*)15(*Z*)C18:3.

Chemical nomenclature references the carboxyl group of the fatty acid as carbon one. This reference for the double bond location is given by the symbol Δ^9. But a desaturase could locate the double bond by starting from the methyl end and counting nine carbons before placing the double bond, i.e. ω-9 for oleate. Note that the result of the activity of a desaturase with Δ^{12} regiospecificity is identical to the product of a desaturase with ω-6 regiospecificity when the double bond is located precisely in the middle of the chain. Thus linoleate can be synthesized from oleate with a desaturase that may have ω-6 or Δ^{12} regiospecificity. Or, ignoring the ends, the desaturase could reference an existing double bond, Δ^{x+3}, placing the new double bond, methylene interrupted or $x+3$ towards the methyl group, from the first carbon of the pre-existing double bond, x. Gurr (1971), in an early consideration of this problem, stated the question of the regiospecificity of this desaturase nicely: "does the enzyme which introduces the second double bond measure from the carboxyl end of the chain, from the methyl end, or solely with reference to the first double bond?"

The regiospecificity of the second desaturation has been experimentally examined in plant materials using unsaturated fatty acids systematically varying in chain length and unsaturation (Gurr, 1971; Howling et al., 1972). *Chlorella,* or slices of castor bean seed, were supplemented with these fatty acids and the new products were identified. These groundbreaking experiments provided several important conclusions. They deduced that two desaturases with differing specificity were present. One desaturase was thought to derivatize monounsaturated fatty acids of variable chain length (C15–C19) but with the double bond at the Δ^9 position always forming the new double bond at Δ^{12} position. This desaturase was said to be a Δ^{12} desaturase. A second desaturase was thought to form the second double bond methylene-interrupted from the first double bond but with the initial double bond and the second double bond counted from the methyl or ω end; this desaturase was called an ω-6 desaturase. Thus, 8(*Z*)C17:1 (ω-9) was desaturated by the latter enzyme to form 8(*Z*)11(*Z*)C17:2 (ω-6 specificity) and 10(*Z*)C19:1 (ω-9) formed 10(*Z*)13(*Z*)C19:2 (also ω-6 specificity). Unfortunately these experimenters were unable to more directly evaluate the number and type of desaturases present in the algae or plant tissue acting on the fatty acids supplied. And β-oxidation of the desaturated products sometimes confused interpretation (Howling et al., 1972).

The question of regiospecificity of the desaturases has been reviewed (Heinz, 1993; Harwood, 1996; Shanklin and Cahoon, 1998; Napier et al., 1999). The *fad2* plant desaturase gene was first cloned using T-DNA tagged *Arabidopsis* mutants (Okuley et al., 1994) and the *fad3* was cloned using T-DNA tagged *Arabidopsis* together with map-based chromosome walking (Arondel et al., 1992). Four additional and different desaturase genes were then obtained by taking advantage of homologies to the above desaturases (reviewed by Ohlrogge and Browse, 1995). The two most common cloned desaturases that place the second double bond in the fatty acids of higher plants are *fad6* for the chloroplast, and *fad2* for the cytoplasm. This finding fulfilled the earlier prediction of the existence of two desaturases based on the substrate specificities (Howling et al., 1972). Cloning of these genes from *Arabidopsis* and other organisms has permitted the expression of the enzymes for desaturases in micro-organisms. Thus one can individually and directly test the specificity of each of the individual desaturases.

Yeast is a good expression system for the *fad2* gene encoding the oleoyl-PC desaturase from higher plants (Covello and Reed, 1996; Broun et al., 1998). *S. cerevisae* contains only a Δ^9 desaturase for the monoenoic fatty acids, palmitoleate and oleate; no desaturase specific for forming a second double bond is present. Significantly, *S. cerevisae* does not appreciably β-oxidize fatty acid supplements. Thus a variety of fatty acids can be provided as supplements to the growth medium. Diunsaturated fatty acids result from the desaturase being expressed. In the present studies, cloned *fad2* from developing peanut seeds was the only source of this desaturase activity in the engineered yeast. Using this system, questions about the specificity of the desaturation of monoenoic fatty acids by the oleoyl-PC desaturase from higher plants are unambiguously resolved.

Of the substrates employed in the study described here, many were either not taken up by the yeast or were not substrates for oleoyl-PC desaturase. However, the products of the desaturation of endogenous palmitoleate and oleate were 9(*Z*)12(*Z*)C16:2 and 9(*Z*)12(*Z*)C18:2 respectively. Supplemented 10(*Z*)C19:1 provided 10(*Z*)13(*Z*)C19:2. Because these products cannot all arise from either the action of a Δ^{12} or an ω-6 desaturase, the specificity for this oleoyl-PC desaturase must be Δ^{x+3}. The evidence suggests that the enzyme first references the location of the existing double bond and then places the new double bond methylene interrupted towards the methyl end of the fatty acid chain.

2. Results and discussion

The *fad2* cDNA from developing peanut seeds was directionally cloned into the multiple cloning site of the shuttle vector pYES2 (Bruner et al., 2001). This vector, containing *fad2,* was expressed in *Saccharomyces*

cerevisae under the control of the GAL1 promoter. When an empty vector was employed, gas chromatographic (GLC) analysis of the methyl esters revealed the monounsaturated fatty acids expected for this yeast, primarily palmitoleate and oleate (Fig. 1); as expected, no polyunsaturated fatty acids were present (Fig. 2). When FAD2 was induced, linoleate appeared, comprising 10–15% of the total fatty acids C16:0, C16:1, C18:0, C18:1, C18:2, and C19:1 (and C19:2, when present).

In a series of preliminary experiments not shown here, the regiospecificity of the oleoyl-PC desaturase was examined by supplying a variety of fatty acids to the medium for uptake and desaturation by the yeast. We were particularly interested in supplying fatty acids with chain lengths or with double bond locations that would demonstrate the specificity of the oleoyl-PC desaturase. While 10(*Z*)C17:1 or 11(*Z*)C20:1 were incorporated into lipids, no new desaturation products were observed. The 10(*Z*)C19:1 was incorporated to an extent of 15–20% and gave a new product readily observable in GLC chromatograms because of the longer retention time, comprising 3–4% of the total fatty acids. This new peak disappeared upon hydrogenation and was absent when cultures had been supplemented with 10(*Z*)C19:1 but were not induced.

These preliminary observations showed the presence of a new product produced by the desaturation of

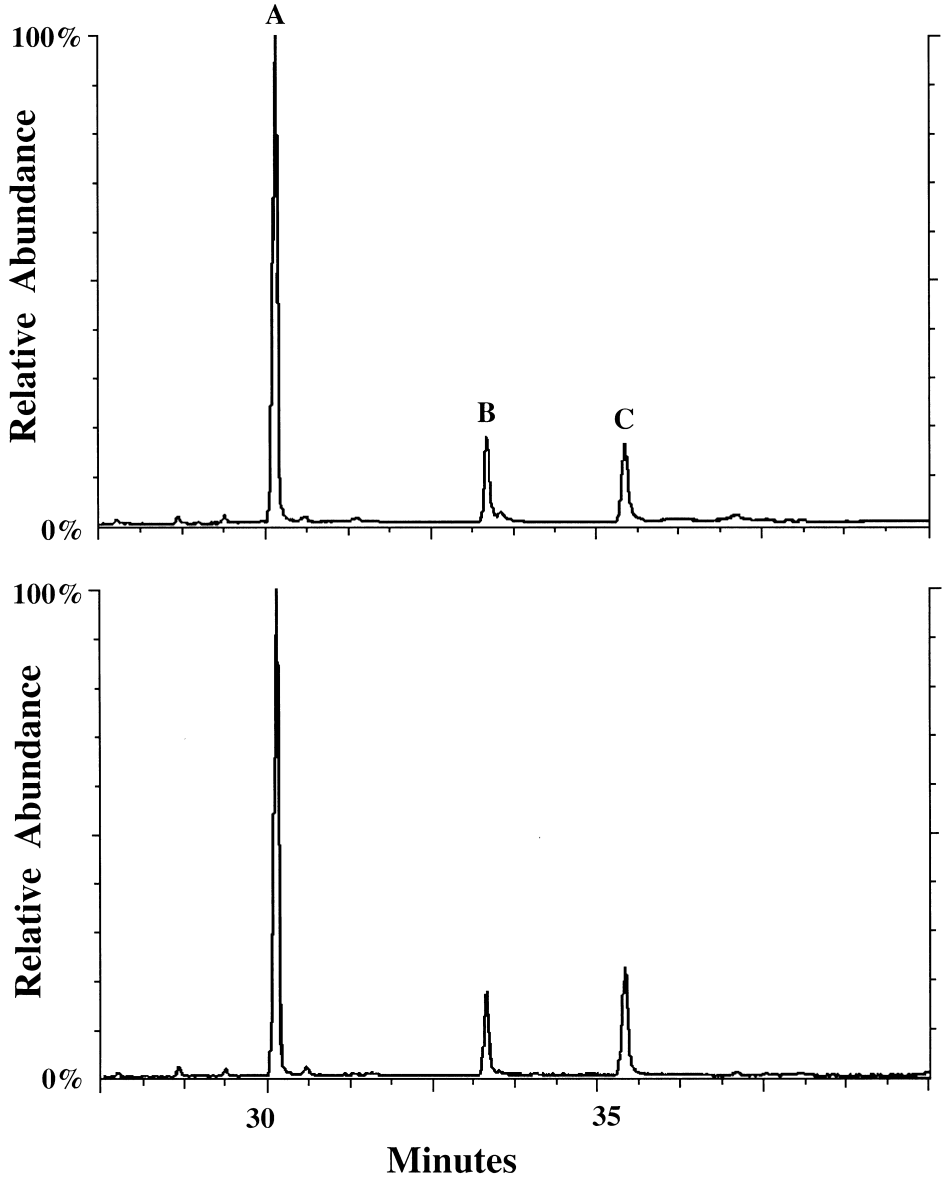

Fig. 1. Monounsaturated dimethyl disulfide methyl esters separated by gas chromatography with total ion mass spectral detection. Yeast fatty acid methyl esters were separated on silver ion columns and the monounsaturated fraction converted to dimethyl disulfide derivatives. (Top) composition after induction of the oleoyl-PC desaturase. (Bottom) composition without induction. The relative abundance scale for the bottom part of the figure is the same as for the top part. The fragmentation mass spectra (not shown) displayed prominent molecular ions and fragments identifying palmitoleate (A), oleate (B), and 9(*Z*) nonadecenoate (C).

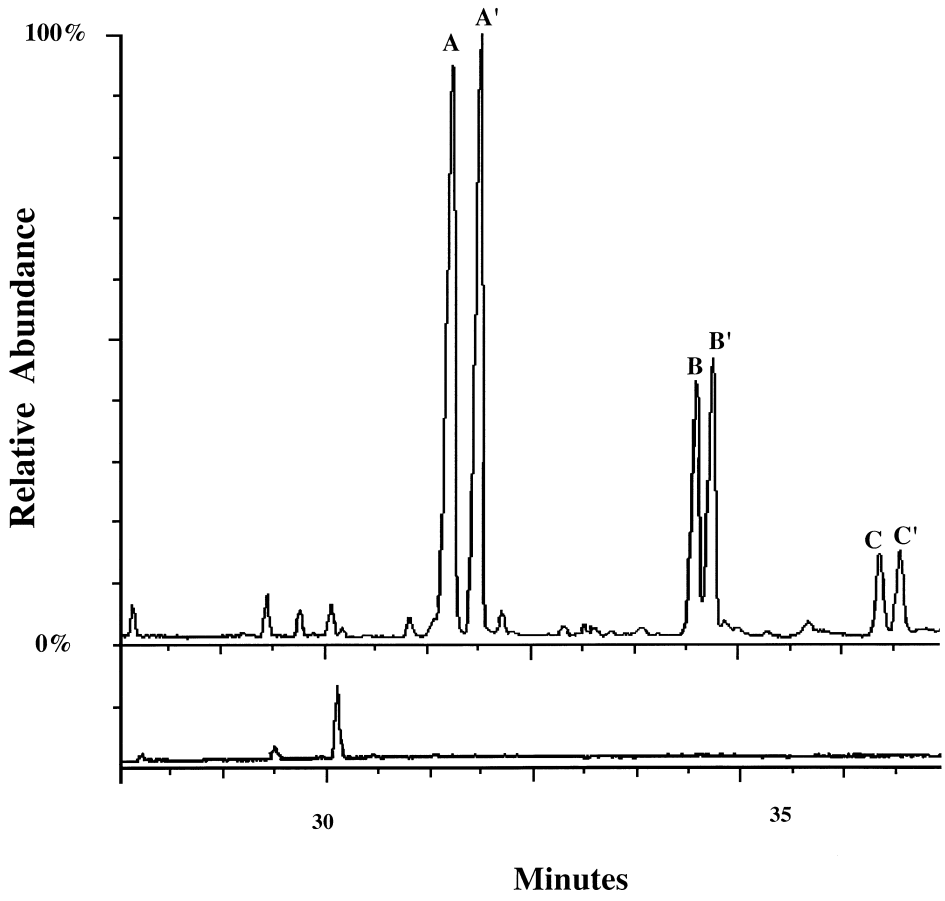

Fig. 2. Diunsaturated dimethyl disulfide methyl esters separated by gas chromatography with total ion mass spectral detection. Yeast fatty acid methyl esters were separated on silver ion columns and the diunsaturated fatty acid fraction converted to dimethyl disulfide derivatives. (Top) composition after induction of the oleoyl-PC desaturase. (Bottom) composition without induction. Peaks in the top spectra with longer retention times (not shown) correspond with rearranged dimethyl disulfide derivatives of diunsaturated fatty acids (Carballeira et al., 1994). The spectra for the pairs of peaks (AA′, BB′, CC′) are shown in Fig. 3.

10(*Z*)C19:1. If the oleoyl-PC desaturase were a Δ^{12} desaturase and referenced the ester group, the resulting doubly unsaturated product would be 10(*Z*)12(*Z*)C19:2, with conjugated double bonds. The product furnished by referencing the existing double bond and inserting the new one in a methylene-interrupted location (a Δ^{x+3} mechanism) would be 10(*Z*)13(*Z*)C19:2. These possibilities were distinguished by locating the double bonds as described below.

Mass spectroscopy was used for the identification of the location of double bonds, but direct electron impact fragmentation of the methyl esters of di-unsaturated fatty acids isomerizes and conjugates the double bond, obscuring their original location. Of the methods available (Christie, 1998), we employed the I_2 catalyzed addition of dimethyl disulfide to the double bonds of the fatty acids. Characteristic fragments result from cleavage between the vicinal methyl thioethers providing, for monoenoic fatty acids, two fragments readily identified with the two ends of the fatty acid. Dimethyl disulfide will randomly, but singly, add to one or another of the methylene-interrrupted double bonds of dienoic fatty acids after an hour of reaction at 37°C (Yamamoto et al., 1991). These dimethyl disulfide derivatives all have higher gas chromatographic retention times than the underivatized saturated fatty acid methyl esters. At higher temperatures and/or longer reaction times, thietane, tetrahydrothiophene and tetrahydrothiopyran structures are obtained from doubly unsaturated compounds (Vincenti et al., 1987; Carballeira et al., 1994). These compounds exhibit longer gas chromatographic retention times and bear a less obvious relationship to the original double bond positions.

Actively growing cultures of the engineered *S. cerevisae* and supplemented with the free fatty acid 10(*Z*)C19:1, were induced producing the oleoyl-PC desaturase. After 6 h of incubation, the fatty acyl moieties present in the yeast lipids were converted to methyl esters in situ. Note that unesterified fatty acids that have not been incorporated into lipid are not methylated by sodium methoxide. Silver ion column chromatography (Christie, 1989) was then used to resolve saturated, monoenoic and dienoic

fatty acid methyl esters. The first fraction, containing the saturated fatty acid methyl esters, was discarded and the separate fractions for monoenoic and dienoic fatty acid methyl esters retained and treated with dimethyl disulfide. The GC/MS total ion chromatograms for the monoenoic dimethyl disulfide derivatives are shown in Fig. 1 and the dienoic derivatives in Fig. 2. The mass spectra (not shown) for the three peaks in the chromatogram shown in Fig. 1 (top) and (bottom) verified their identities as dimethyl disulfide derivatives of palmitoleate, oleate, both endogenous, and *cis* Δ^9 nonadecenoate from the supplement. The amounts of monoenoic fatty acids were comparable for non-induced and induced cultures, as expected. In Fig. 2 (top), the characteristic double peaks from the fatty acids desaturated by oleoyl-PC desaturase were found. Fig. 2 (bottom) shows the absence of fatty acids in this dienoic fraction when the oleoyl-PC desaturase was not induced. The peak intensities of monoenoic fatty acid in the non-induced culture (Fig. 1, bottom) were similar to the induced culture (Fig. 1, top) implying that dienoic fatty acid derivatives would have been readily apparent if they had been present in uninduced cultures.

The mass spectra of each of the pairs of dimethyl disulfide derivative peaks from the gas chromatographic separation (Fig. 2, top) are shown in Fig. 3. The first pair of peaks (Fig, 3, A and A′) identify the product of the desaturation of endogenous palmitoleate as 9(*Z*)12(*Z*) C16:2 as has been previously observed (Covello and Reed, 1996). The second pair of peaks (Fig 3, B and B′) identify the product of desaturation of endogenous oleate as 9(*Z*)12(*Z*)C18:2 or linolenate. The third pair of peaks (Fig 3, C and C′) identify the product of the desaturation of *cis* Δ^9 nonadecenoate as 10(*Z*)13(*Z*)C19:2.

The possibilities for the specificity of the oleoyl-PC desaturase are depicted in Fig. 4. The oleoyl-PC desaturase present in developing peanut seeds and expressed in yeast was not that of a Δ^{12} desaturase because the enzyme can desaturate 10(*Z*)C19:1 to form 10(*Z*)13(*Z*)C19:2; the action of a Δ^{12} desaturase would have furnished 10(*Z*) 12(*Z*)C19:1, a conjugated fatty acid. The enzyme is not an ω-6 desaturase because it desaturated 9(*Z*)C16:1 to form 9(*Z*)12(*Z*)C16:2; ω-6 activity would have provided an allene, 9(*Z*)10(*Z*)C16:2, that was not observed. The specificity seems best to be described as Δ^{x+3} desaturase, where the key reference is the location of the existing double bond ($x=9$).

Others have previously observed that the remaining portions of the fatty acid chain, esterified to a polar lipid, are important in locating second double bonds. In intact plant systems supplemented with different fatty acids, those with a 10(*Z*) double bond and less than 19 carbon atoms were not desaturated; fatty acids with double bonds nearer than 9(*Z*) to the carboxyl group were not desaturated (Gurr, 1971; Howling et al., 1972; Heinz, 1993). Similar specificities were observed in our experiments with the oleoyl-PC desaturase expressed in yeast. Thus to locate the second double bond from the double bond system, the enzyme must be responsive both to the length of the hydrocarbon chain towards the polar portion of a complex lipid and the length of the chain towards the methyl group and the hydrophobic core of the membrane. Given the constraints, the ability of this enzyme to place a methylene-interrupted double bond so precisely in a hydrocarbon chain on the intact lipid within a membrane is extraordinary.

The regiospecificity demonstrated by using the *S. cerevisae* expression system is clearly the result of the expressed activity (compare Fig. 2, top and bottom). Results previously obtained by slices of tissue from higher plants or from other microorganisms could have been the result of one or more of the multiple desaturases present in these tissues (Gurr, 1971; Howling et al., 1972; Heinz, 1993). *S. cerevisae* contain monoenoic fatty acids in the absence of a plasmid containing *fad2*. Thus polyunsaturated fatty acids can only result from the desaturation of fatty acids by the *fad2* gene product and not from some cooperative interaction of more than one desaturase acting on a given fatty acid.

The specificity of membrane-associated desaturases from other organisms has also been explored by examining the products from feeding exogenous supplements. The enzyme from *Synechocystis* that inserts the second double bond at the Δ^{12} position has been cloned (Wada et al., 1993), and the deduced amino acid sequence differed considerably from that for oleoyl-PC desaturases of higher plants. Indeed, Southern blots using probes based on the *Synechocystis* sequence did not locate this protein in higher plants (our unpublished observations). The lipids of *Synechcystis* are primarily glycolipids, similar to plant chloroplasts lipids rather than the phospholipids of the endoplasmic reticulum where the oleoyl-PC desaturase is thought to reside. Thus the regiospecificity of this *Synechocystis* desaturase may or may not be similar to the oleoyl-PC desaturase of higher plants. When odd chain fatty acids were fed to the intact organism, the second double bond still appeared at the Δ^{12} position when the first double bond was Δ^9, suggesting that that desaturase did not count from the methyl end, i.e. it was not an ω-6 desaturase (Higashi and Murata, 1993).

The FAD6 enzyme also places double bonds at the Δ^{12} position in chloroplast lipids. This gene was cloned because of similarities in sequence to the *Synechocystis* enzyme and was successfully expressed in that organism (Hitz et al., 1994). The sequences of the FAD6 and the FAD2 (oleoyl-PC desaturase) differ markedly. Hitz et al., 1994 proposed the existence of three different desaturase families, with FAD6 and FAD2 representing two of the different families. Again one would not necessarily expect sequence-unrelated enzymes (especially those found in different compartments and acting on different

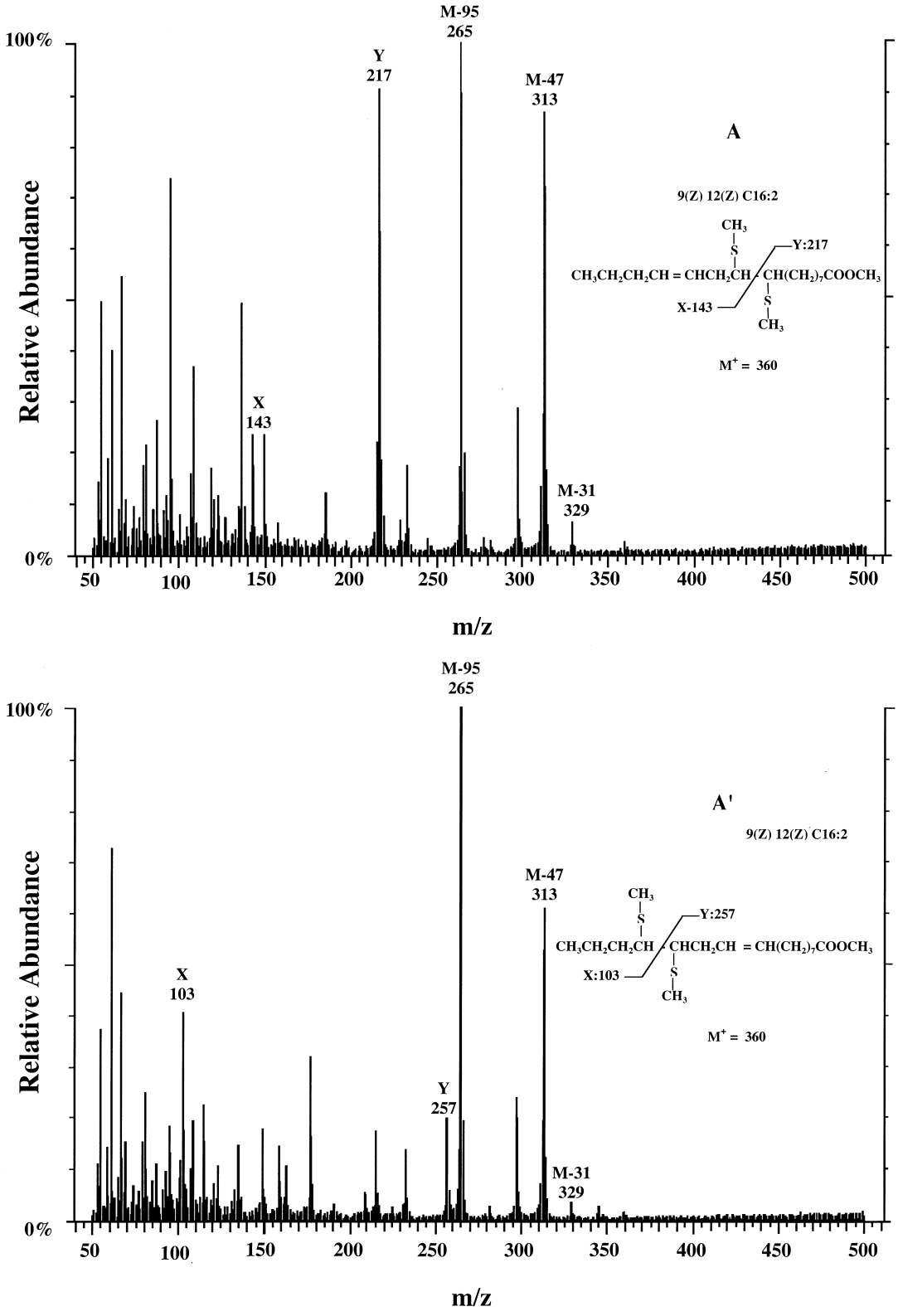

Fig. 3. Mass Spectra of the dimethyl disulfide derivatives of dienoic fatty acid methyl esters. The spectra are keyed to the labels given in Fig. 2. A and A′ identify 9(*Z*)12(*Z*)C16:2. B and B′ identify linoleic acid (9(*Z*)12(*Z*)C18:2). C and C′ identify 10(*Z*)13(*Z*)C19:2. The structures corresponding to fragments resulting from cleavage at the double bond in the location shown are provided. Sizeable molecular ions were not observed but characteristic losses of M-31 (CH_3O), M-47(CH_3S) and M-95(CH_3SSCH_3) were consistent with the calculated molecular masses (M^+) shown (*continued on next page*).

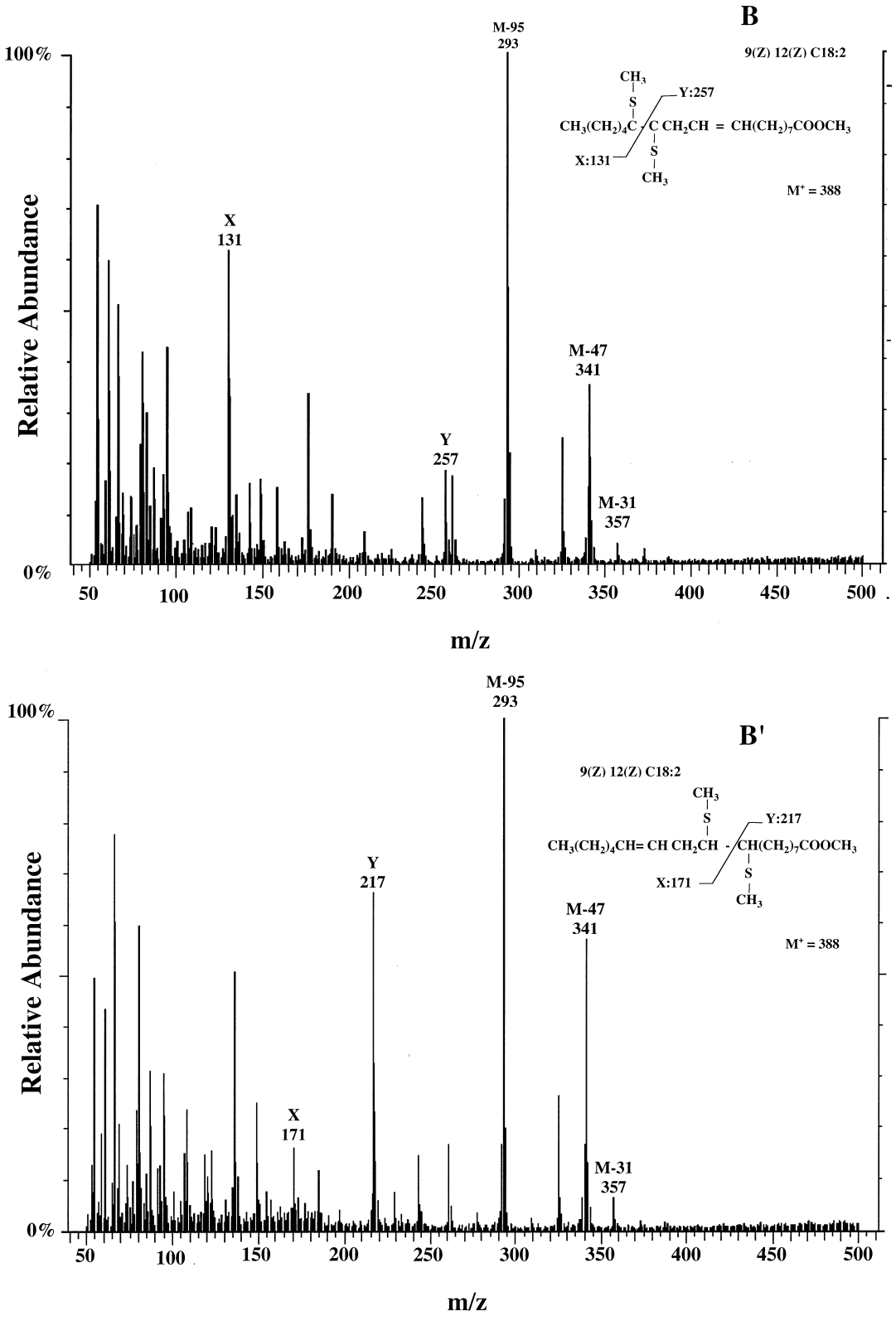

Fig. 3. (*continued*).

lipid substrates) to share similar substrate specificities. In this case, FAD6 desaturated endogenous palmitoleate to 9(*Z*)12(*Z*)C16:2 (ω-4 desaturation). Based on this desaturation, along with the desaturation of oleate to linoleate in the same construction (an ω-6 desaturation), Hitz et al., 1994 suggested that the enzyme measured from the existing double bond rather than from the methyl end.

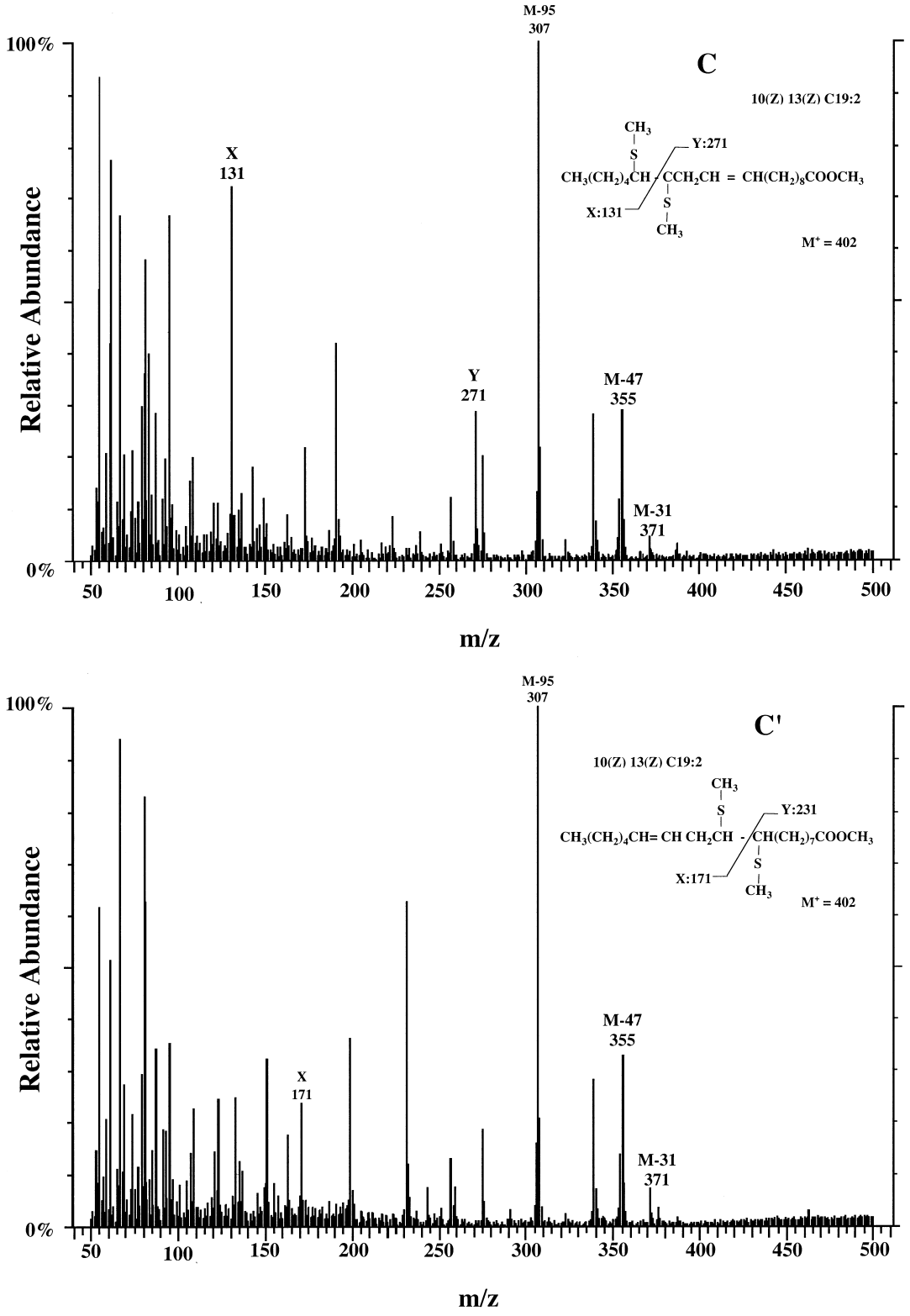

Fig. 3. (*continued*).

Although the cDNA for *fad2,* like that for the Δ^9 desaturase, encoded three conserved histidine motifs characteristic of diiron active sites (Shanklin et al., 1994), amino acid sequences of the enzymes that place the first and the second double bonds are clearly divergent. The oleoyl-PC desaturase is an intrinsic membrane enzyme and the Δ^9 desaturase is soluble; membrane-associated desaturases act on acyl groups of intact phospholipids

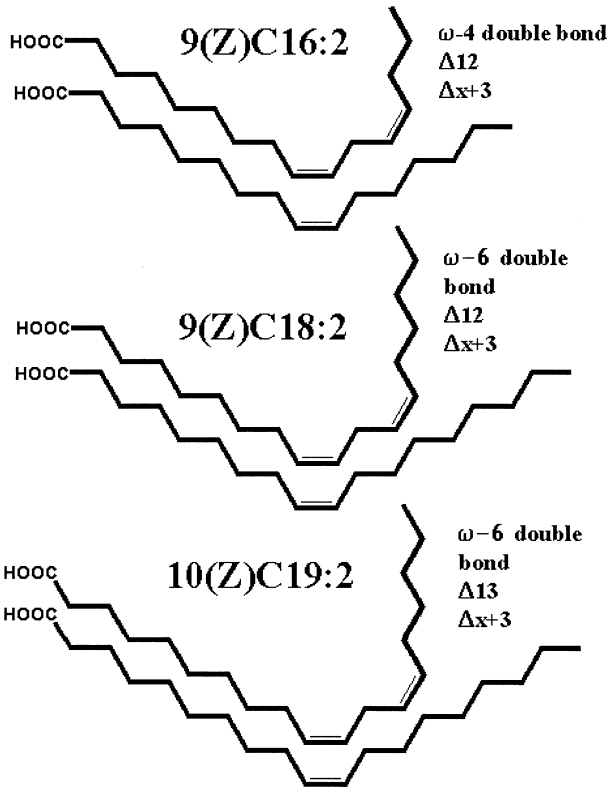

Fig. 4. Oleoyl-PC desaturase products. Three sets of fatty acids are shown. The starting monoenoic fatty acids, 9(*Z*)C16:1, 9(*Z*)C18:1 and 10(*Z*)C19:1, are the lower member of each pair. The action of oleoyl-PC desaturase provided the upper diunsaturated fatty acids. The designations on the left describe the location of the newly synthesized double bond relative to the methyl end (ω-4, ω-6 and ω-6), the ester end (Δ12, Δ12, and Δ13), and relative to the existing double bond (Δ^{x+3}).

oriented within the bilayer of the biological membrane while the soluble desaturases bind the lipoprotein acyl-ACP. The structures of the substrate binding sites for the electron carriers, cytochrome b_5 and ferredoxin, for the membrane-associated and soluble enzymes respectively, must differ as well, also accounting for some of the sequence differences between these proteins.

The most interesting information available for how double bonds are formed by desaturases comes from studies of the soluble desaturase for which a crystal structure is available (Lindqvist et al., 1996). A cavity was present that was postulated as being capable of accepting the methyl end of the acyl of the substrate. This saturated chain is bent in the vicinity of the nascent double bond. When the depth of the cavity was altered by amino acid substitution, the regiospecificity for the double bond was altered, implying that the depth of the cavity was the determinant for double bond location (Cahoon et al., 1997). In the absence of structural data for the membrane-localized oleoyl-PC desaturase, we may only speculate that a similar cavity exists. In such a model, the length of the hydrocarbon chain on either side of the existing double bond is important, regulating whether or not the unsaturated acyl chain present in the intact phospholipid can be productively accommodated within the cavity. Based on the present work, the oleoyl-PC desaturase would not place the new double bond in lipid acyl moieties relative to the methyl end (ω-6) or the ester of the intact lipid (Δ^{12}). The postulated cavity will accommodate monounsaturated acyl groups with the *cis* double bond (x) located $x+3$ from the diiron of the active site and the new double bond would be synthesized Δ^{x+3} to the existing double bond.

3. Experimental

3.1. Oleoyl-PC desaturase expression in yeast

The reading frame from the most active *fad2* from *Arachis hypogaea L.* (Jung et al., 2000; GenBank Accession Number AF03019) was directionally cloned into the pYES2 expression vector (Bruner et al., 2001). This plasmid is a centromeric expression vector containing the GAL1 promoter (Stratagene).

For expression, the cells were grown at 30°C on SC-ura liquid media containing 2% raffinose. When the A_{600} approached 0.5, 2% galactose (Acros, 99.9% purity) was added to induce the production of the *fad2* gene product. When cultures were supplemented with 1 mM 10(*Z*)C19:1 (Sigma Chemical Co.) (or other fatty acid supplements), the medium contained 0.1% Tergitol (NP-40, Sigma Chemical Co.). The cells were grown an additional six hours and were harvested by centrifugation.

3.2. Analysis of unsaturated fatty acids

The fatty acids were esterified by treatment of the cell pellets with 0.5 M sodium methoxide (Sigma Chemical Co.) in methanol for 30 min, neutralized with 125 mM H_2SO_4 and the methyl esters extracted into hexane. The methyl esters were fractionated by silver ion chromatography (Christie, 1989). The saturated fatty acid fraction was discarded. The monounsaturated and the diunsaturated fatty acid fractions were collected separately and the dimethyl disulfide derivatives (Yamamoto et al., 1991) were prepared. The fatty acid methyl esters were analyzed by gas chromatography with mass spectral detection (Varian Saturn System) using a 30 m×0.2 μ×25 mm Supelco 2380 column (Sigma/Aldrich/ Fluka/ Supelco). The temperature was programmed from 140°C (after 3 min) to 220°C at 3°C/min and the temperature held for a total run time of 50 min. The carrier gas was He with a flow rate of 20 cm/s and an injector split 100:1. GLC analysis of the fatty acid methyl esters using flame ionization detection was carried out with that column using similar conditions before and after hydrogenation of methyl esters (brief treatment in ethanol using Pd/C and H_2 gas).

Acknowledgements

We are pleased to thank Ed Cahoon and John Shanklin for introducing G.L. Powell to some of the techniques and concepts employed here. We are grateful for the technical assistance of Melissa Riley with GC/MS, Evanne Thies with GLC, and to Sally Brock for drawing the figures. Erin E. Mosley set up the silver ion column technique for separating monoenes and dienes and she with Gina L. Pries and Shahed Lewis used the silver ion column to obtain the fractions used for the mass spectra shown. The data reported was part of senior research problems for the Bachelor of Sciences Degree in Biochemistry for Schwartzbeck, Lewis, and Pries. Support was provided by the SC Experiment Station and by AgraTech, Atlanta, GA.

References

Arondel, V., Lemieux, B., Hwang, I., Gibson, S., Goodman, H.M., Somerville, C.R., 1992. Map-based cloning of a gene controlling omega-3 fatty acid desaturation in *Arabidopsis*. Science 258, 1353–1355.

Broun, P., Shanklin, J., Whittle, E., Somerville, C., 1998. Catalytic plasticity of fatty acid modification enzymes underlying chemical diversity of plant lipids. Science 282, 1315–1317.

Bruner, A.C., Jung, S., Abbott, A.G., Powell, G.L., 2001. The high oleate oil character in some naturally occurring peanut varieties was because of reduced oleoyl-PC desaturase activity from mutation of aspartate 150 to asparagine. Crop Science, in press.

Cahoon, E.B., Lindqvist, Y., Schneider, G., Shanklin, J., 1997. Redesign of soluble fatty acid desaturases from plants for altered substrate specificity and double bond position. Proc. Natl. Acad. Sci. USA 94, 4872–4877.

Carballeira, N.M., Shalabi, F., Cruz, C., 1994. Thietane, tetrahydrothiophene and tetrahydrothiopyran formation in reaction of methylene-interrupted dienoates with dimethyl disulfide. Tetrahedron Letters 35, 5575–5578.

Christie, W.W., 1989. Silver ion chromatography using solid-phase extraction columns packed with a bonded-sulfonic acid phase. Journal of Lipid Res. 30, 1471–1473.

Christie, W.W., 1998. Gas chromatography-mass spectrometry methods for structural analysis of fatty acids. Lipids 33, 343–353.

Covello, P.S., Reed, D.W., 1996. Functional expression of the extraplastidial *Arabidopsis thaliana* oleate desaturase gene (FAD2) in Saccharomyces cerevisiae. Plant Physiol. 111, 223–226.

Gorbet, D.W., Knauft, D.A., 1997. Registration of 'SunOleic 95R Peanut. Crop Science 37, 1392.

Gurr, M.I., 1971. The biosynthesis of polyunsaturated fatty acids in plants. Lipids 6, 266–273.

Harwood, J.L., 1996. Recent advances in the biosynthesis of plant fatty acids. Biochim. Biophys. Acta 1301, 7–56.

Heinz, E., 1993. Biosynthesis of polyunsaturated fatty acids. In: Moore, T.S. (Ed.), Lipid metabolism in plants. CRC Press, Boca Raton, FL, pp. 34–89.

Higashi, S., Murata, N., 1993. An in vivo study of substrate specificities of acyl lipid desaturases and acyltransferases in lipid synthesis in *Synechocystis* PCC6803. Plant Physiol. 102, 1275–1278.

Hitz, W.D., Carlson, T.J., Booth, J.R., Kinney, A.J., Stecca, K.L., Yadav, N.S., 1994. Cloning of a higher-plant plastid omega-6 fatty acid desaturase cDNA and its expression in a cyanobacterium. Plant Physiol. 105, 635–641.

Howling, D., Morris, L.J., Gurr, M.I., James, A.T., 1972. The specificity of fatty acid desaturases and hydroxylases. The dehydrogenation and hydroxylation of monoenoic acids. Biochim. Biophys. Acta 260, 10–19.

Jung, S., Swift, D., Sengoku, E., Patel, M., Teule, F., Powell, G., Moore, K., Abbott, A., 2000. High oleate trait in the cultivated peanut [*Arachis hypogaea L*]: I. Isolation and characterization of two microsomal oleoyl-PC desaturases. Mol. Gen. Genetics 263, 796–805.

Lindqvist, Y., Huang, W., Schneider, G., Shanklin, J., 1996. Crystal structure of a Δ^9 stearoyl-acyl carrier protein desaturase from castor seed and its relationship to other diiron proteins. EMBO 15, 4081–4092.

Mazur, B., Krebbers, E., Tingey, S., 1999. Gene discovery and product development for grain quality traits. Science 285, 372–375.

Napier, J.A., Michaelson, L.V., Stobart, A.K., 1999. Plant desaturases: harvesting the fat of the land. Curr. Opin. Plant Biol. 2, 123–127.

Ohlrogge, J., Browse, J., 1995. Lipid biosynthesis. Plant Cell 7, 957–970.

Okuley, J., Lightner, J., Feldmann, K., Yadav, N., Lark, E., Browse, J., 1994. *Arabidopsis* FAD2 gene encodes the enzyme that is essential for polyunsaturated lipid synthesis. Plant Cell 6, 147–158.

Ray, T.K., Holly, S.P., Knauft, D.A., Abbott, A.G., Powell, G.L., 1993. The primary defect in developing seed from the high oleate variety of peanut (*Arachis hypogaea L.*) is the absence of Δ^{12} desaturase activity. Plant Sci. 91, 15–21.

Shanklin, J., Cahoon, E.B., 1998. Desaturation and related modifications of fatty acids. Annu. Rev. Plant Physiol. Plant. Mol. Biol. 49, 611–641.

Shanklin, J., Whittle, E., Fox, B.G., 1994. Eight histidine residues are catalytically essential in a membrane-associated iron enzyme, stearoyl-CoA desaturase, and are conserved in alkane hydroxylase and xylene monooxygenase. Biochemistry 33, 12787–12794.

Vincenti, M., Guglielmetti, G., Cassani, G., Tonini, C., 1987. Determination of double bond position in diunsaturated compounds by mass spectroscopy of dimethyl disulfide derivatives. Anal. Chem. 59, 694–699.

Wada, H., Avelange-Macherel, M.H., Murata, N., 1993. The desA gene of the cyanobacterium *Synechocystis sp*. strain PCC6803 is the structural gene for Δ^{12} desaturase. J. Bacteriol. 175, 6056–6058.

Yamamoto, K., Shibahara, A., Nakayama, T., Kajimoto, G., 1991. Determination of double-bond position in methylene-interrupted dienoic fatty acids by GC–MS as their dimethyl disulfide adducts. Chem. Phys. Lipids 69, 39–50.

PERGAMON

Phytochemistry 57 (2001) 653–659

PHYTOCHEMISTRY

www.elsevier.com/locate/phytochem

Main glucosidase conversion products of the gluco-alkaloids dolichantoside and palicoside

Viviane Brandt*, Monique Tits, Jacques Penelle, Michel Frédérich, Luc Angenot

Service de Pharmacognosie, Institut de Pharmacie, Université de Liège, C.H.U., Tour 4, Avenue de l'Hôpital 1, 4000 Liege 1, Belgium

Received 9 October 2000; received in revised form 16 February 2001

Abstract

The enzymatic glucose cleavage of palicoside revealed the biosynthetic pathway to akagerine, whereas the conversion of dolichantoside led to a new quaternary heteroyohimbine alkaloid named N_b-methyl-21-β-hydroxy-mayumbine. The hypothetical models of reactions occurring after the conversion of both substrates are proposed. Dolichantoside and palicoside, as well as *Strychnos mellodora* stem bark crude ethanol extract, exhibit significant antimycotic activity against human pathogens in presence of specific glucosidase. © 2001 Elsevier Science Ltd. All rights reserved.

Keywords: *Strychnos mellodora*; *Loganiaceae*; Biosynthesis; Gluco-alkaloids; Dolichantoside; Palicoside; Akagerine; N_b-Methyl-21-β-hydroxy-mayumbine

1. Introduction

In our search for alkaloids in *Strychnos mellodora* S. Moore, an endemic species of East-Africa (Leeuwenberg, 1969) we isolated a wide range of gluco-alkaloids (Tits et al., 1996; Brandt et al., 1999) and particularly interesting amounts of the N_b-methylated alkaloids dolichantoside (**1**) and palicoside (**2**). Their structures are closely related to and present the same 3α configuration as strictosidine (**3**), the central intermediate in the biosynthesis of monoterpenoid indole and quinoline alkaloids (Rueffer et al., 1978; Bisset, 1980). The enzymatic cleavage of glucose in strictosidine (**3**) gives rise to a large variety of structure groups (Kisakürek et al., 1983). The intermediate isolated by Stevens (1994) after strictosidine conversion was 3α, 15α-$\Delta^{20(21)}$-didehydrocathenamine, a $\Delta^{20(21)}$-didehydro-heteroyohimbine. The amounts of dolichantoside (**1**) and palicoside (**2**) obtained from *Strychnos mellodora* gave us the opportunity to start phylogenetical studies in order to evaluate the potential biosynthetic pathway from those gluco-alkaloids. In our previous work, we mentioned the conversion of these two substrates by strictosidine glucosidase from *Catharanthus roseus* (SGD) and by a specific glucosidase isolated from *Strychnos mellodora* (SMGD) (Brandt et al., 2000). Here we present the isolation and identification of the main conversion products. An evaluation of the antimycotic activity before and after glucosidase conversion was carried out on the crude ethanol extract of *Strychnos mellodora* stem bark, as well as on dolichantoside (**1**) and palicoside (**2**).

2. Results and discussion

2.1. Identification and determination of conversion products

To check the invariability of the pattern of conversion products of dolichantoside (**1**) and palicoside (**2**), incubations were first compared in the presence of three different glucosidases: SGD, SMGD and a less specific one, the glucosidase from sweet almonds. Independent of the glucosidase used, the pattern of conversion products was the same. The kinetic parameters K_m and V_{max} were determined for the enzymes SGD and SMGD, in the presence of the substrates **1** and **2** (Brandt et al., 2000). This study clearly revealed that the conversion of substrates **1** and **2** was quicker and more complete with the enzyme SMGD (Table 1). The V_{max} or maximal

* Corresponding author at Laboratoires Ortis, Hinter der Heck, 46, 4750 Elsenborn, Belgium. Tel.: +32-80-440055; fax: +32-80-444280.
E-mail address: viviane.brandt@ortis.com (V. Brandt).

0031-9422/01/$ - see front matter © 2001 Elsevier Science Ltd. All rights reserved.
PII: S0031-9422(01)00085-1

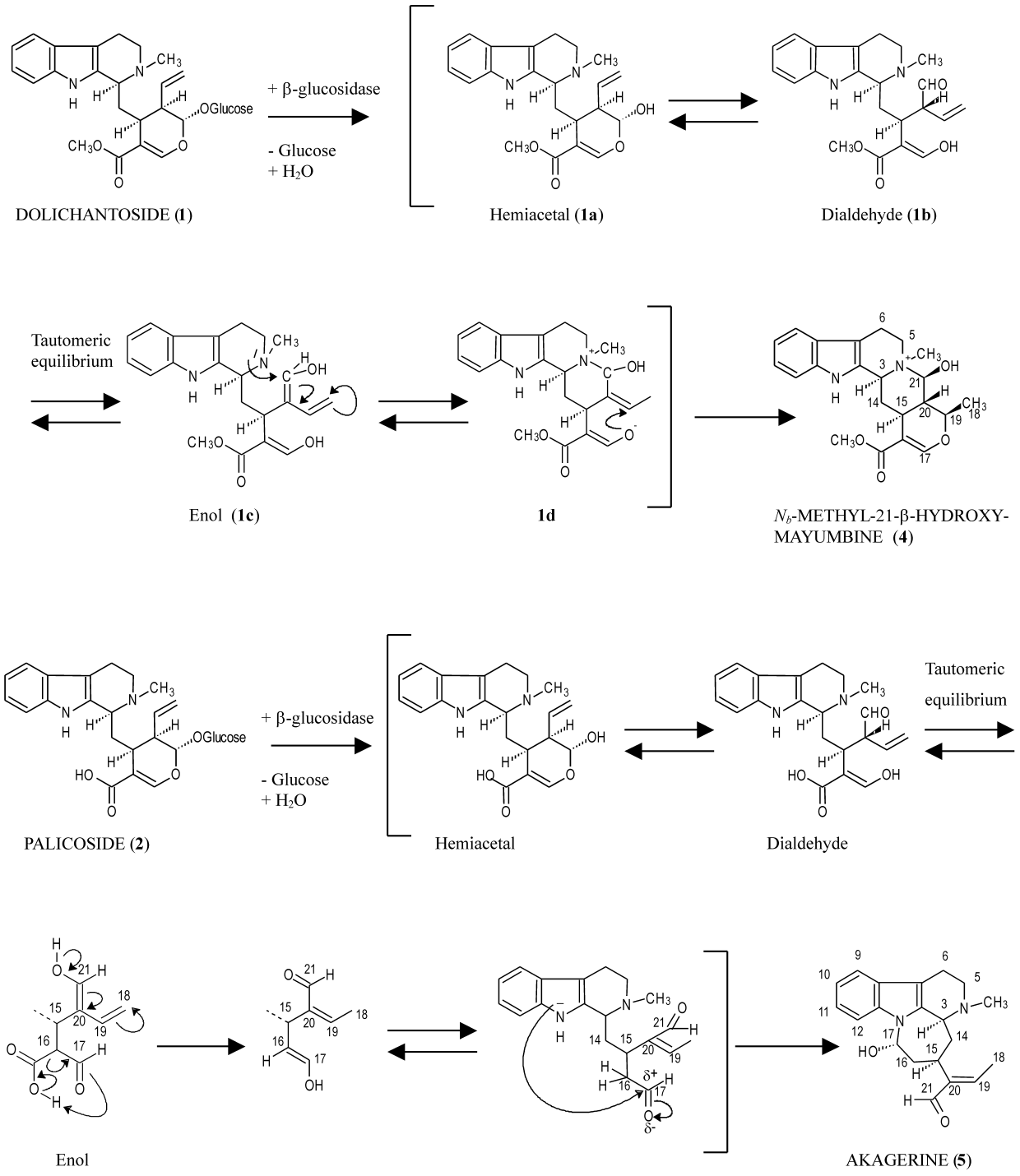

Scheme 2. Hypothetical model for the conversion of palicoside into akagerine.

conversion velocities were higher in the presence of SMGD and reached with lower substrate concentrations, as K_m represents half of the substrate concentration necessary to reach the maximal conversion velocity.

We thus incubated a larger amount of dolichantoside (**1**) in the presence of SMGD. After 72 h of incubation, dolichantoside was nearly completely converted into a main product (**4**) that was more polar. This product was compared in TLC and HPLC and stated to be identical to the one obtained after the 15 min incubation of a 1 mM dolichantoside solution. It was separated (see Experimental) from the incubation mixture and its structure determined by spectroscopic methods as N_b-methyl-21-β-hydroxy-mayumbine (**4**), a new heteroyohimbine quaternary alkaloid. Its UV spectrum revealed maxima of tetrahydro-β-carboline alkaloids. The high resolution mass spectrum exhibited a molecular peak corresponding to the molecular formula $C_{22}H_{27}N_2O_4^+$.

Table 1
Kinetic parameters of SGD and SMGD towards dolichantoside (**1**) and palicoside (**2**). Conditions used to determine these parameters are found in literature (Brandt et al., 2000)

Substrate	SGD		SMGD	
	K_m (μM)	V_{max} (nkat mg $^{-1}$ protein)	K_m (μM)	V_{max} (nkat mg $^{-1}$ protein)
(**1**)	1130	21.2	564	224
(**2**)	7015	11.1	335	39

The molecular peak also present in the ES–MS–MS spectrum at m/z 383 $(M)^+$ exactly corresponded to the loss of a glucose moiety from dolichantoside (**1**); an ion at m/z 365 suggested the easy loss of water and thus the presence of a hydroxyl function. In the ^{1}H-^{1}H NMR auto-correlation spectra, the most characteristic point for the formation of a heteroyohimbine structure was the presence of a methyl group at 1.55 ppm (d, $J_{18–19}$ = 6.7 Hz) (CH_3-18) correlated to H-19 at 3.75 ppm (q, $J_{19\text{-}20}$ = 8.6 Hz). Chemical shifts of those protons, in particular shielding of H-19, as well as high coupling constants, by comparison with the literature data concerning the eight possible diastereoisomers of heteroyohimbine type (Phillipson and Supavita, 1983), suggested α-configuration of H-19 and consequently β-configuration of the methyl group C-18 (19 *R* series). This configuration is related to 19-epiajmalicine or mayumbine (3α, 20β, *normal* diastereoisomeric type) (Uusvuori and Lounasmaa, 1981). The formation of a *normal* type alkaloid is predictable considering the initial H_3-α, H_{20}-α configuration of dolichantoside. On the other hand, the configuration α of H_{19}, characteristic of 19-epiajmalicine, is less evident but plausible if one considers the biomimetic scheme named "La Ronde" established by Lounasmaa and Hanhinen (1998). This scheme shows interconversions existing between the four $\Delta^{20(21)}$-didehydroheteroyohimbines (cathenamines), which, when combined with reduction steps, allow access to the eight basic heteroyohimbines. The option of H-19 α or β configuration takes place during the *Z–E* epimerisation of the ethylidene side chain (Lounasmaa et al., 1992; Uskoković et al., 1979). Closing of *E* ring is then achieved by a Michael addition of the enolate stereochemically exclusively possible on the β-face on the ethylidene chain (Brown, 1980). This ethylidene chain is moreover directly connected to H-20 (3.15 ppm), itself coupling with H-21 appearing in the form of a deshielded doublet at 4.45 ppm ($J_{20–21}$ = 7.5 Hz), compatible with the presence of an hydroxyl function on C-21 and the presence of an adjacent quaternary nitrogen. The coupling constant $J_{20–21}$ suggested the antiperiplanar position of H-20 and H-21, and thus the α position of H-21. H-20 is also correlated to H-15 at 2.85 ppm. The proton chemical shift of the *N*-methyl group is in accord with a C/D *cis* ring junction. Indeed, this stereochemistry is supported by the relatively low field position (^{1}H: 3.27; ^{13}C: 47.0 ppm) of the quaternary N_b-methyl, suggesting a *cis*-relationship between the N_b-methyl and the H-3 (Arata et al., 1975; Sugiura et al., 1977). The resonances of H-14a, H-14b and H-3 appear respectively at 2.45, 1.90 and 5.0 ppm. This latter deshielded value is likewise consistent with the presence of the adjacent quaternary nitrogen. All aromatic protons, including H-17 at 7.49 ppm, are detected. Carbons chemical shifts were determined on the base of HMQC spectra.

The second substrate, palicoside (**2**), was incubated with SMGD for 72 h. Its unfinished conversion gave rise to two main products. The first one, **5**, was apparently less polar than palicoside on TLC, in contrast to the second one, **6**, more polar. After a rapid chloroform extraction of **5** from the incubation mixture, its UV and MS spectra were measured. The UV spectrum exhibited maxima of an indole chromophore. The mass spectrum showed a molecular peak at m/z 325, corresponding to the molecular formula $C_{20}H_{24}N_2O_2$. We confronted this product **5** with available reference substances of identical molecular mass, and in particular to akagerine. They showed to possess the same behaviour when compared by HPLC and TLC in different systems. Moreover, the revelation of TLC plates by iodoplatinate reagent (Svendsen and Verpoorte, 1983) produced in each case a pink colour turning into red after a few minutes. We completed this identification by comparison of their 1D ^{1}H NMR spectra. The recorded resonances were identical, which confirmed that akagerine was the non-polar conversion product of palicoside (**2**). Akagerine (**5**) is a perhydroazepine alkaloid that accumulates in numerous species of *Strychnos* as *Strychnos usambarensis* (Angenot et al., 1975). It has showed convulsivant (Rolfsen et al., 1980) and antiprotozoal (Wright et al., 1991) properties on mice. Its enantioselective synthesis was proposed by Danieli et al. (1995). We completed the spectral data of this reference alkaloid by further ^{1}H and ^{13}C NMR contribution. The polar conversion product **6** could not be separated in sufficient amount to be identified and is, thus, still under studies.

2.2. Hypothetical models for the conversion reactions

For both conversions, we present hypothetical models of reactions occurring after enzymatic hydrolysis and removal of the glucose moiety. It should be noted that none of the intermediates depicted in Schemes 1 and 2 has ever been isolated as a product from any incubation mixture, or has ever been demonstrated in any other direct way. Their occurrence is described by mere theoretical organic chemistry. It has been reported that the deglucosylation of strictosidine leads also to reactive

and unstable intermediates, which may readily and quickly undergo different intra-molecular rearrangements (Hemscheidt and Zenk, 1980; Stöckigt, 1980; Stevens, 1994). The same situation is observed in our hands using systems with dolichantoside or palicoside as analogous substrates.

Reactions leading from dolichantoside (**1**) to N_b-methyl-21-β-hydroxy-mayumbine (**4**) are similar to those proposed in the conversion model of strictosidine (Stevens, 1994). They can be schematised as follows (scheme 1): removal of the glucose moiety of dolichantoside leads to an unstable hemiacetal (**1a**), which is rapidly converted into a high reactive aldehyde by opening of E ring. This aldehyde (**1b**) is in equilibrium with its enol tautomer (**1c**). This intermediate is then stabilised by a nucleophilic attack of the nitrogen N_b on C-21 to close D ring, with concomitant transformation of the vinyl chain into a *Z*-ethylidene chain (**1d**). Protonation of C-18 is ensured by the C-17 hydroxyl function, acting as proton donor. Closing of *E* ring is then achieved by a Michael addition of the enolate on the β face of the ethylidene side chain to form the quaternary alkaloid N_b-methyl-21-β-hydroxy-mayumbine (**4**).

Besides the cleavage of the glucose moiety, palicoside (**2**), during its conversion, further loses a group of 44 mass units equivalent to the carbonic gas CO_2. The conversion is thought to start by the two first steps occurring with dolichantoside (scheme 2). The loss of CO_2, happening in totally soft conditions (30°C, neutral pH), can take place at the stage of the tautomeric equilibrium between aldehyde and enol functions. This step is just characterised by the presence of a carboxylic function in β position from an aldehydic function where the start of CO_2 is favoured by a cyclic elimination process at six centres, identical to what occurs in the decarboxylation of malonic acid or β-cetonic acids (Carey and Sundberg, 1997). The double bond shift and the appearance of an ethylidene chain take place at the same time. Closing of perhydroazepine ring is then realised by the nucleophilic attack of the indole nitrogen N_a on C-17, to form a carbinolamine, akagerine (**5**). The loss of CO_2 would not be allowed in the case of dolichantoside, because of the presence of the methyl group on the carboxylic function, which prevents the six centres elimination process to take place.

2.3. Antimycotic activity of the substrates in presence of specific glucosidase

The antimycotic activity of dolichantoside (**1**) and palicoside (**2**), as well as of the crude ethanol extract of *Strychnos mellodora* stem bark (EtOH extract), was tested before and after enzymatic hydrolysis by SMGD against three standard strains of human pathogens, the yeasts *Candida albicans*, *Candida glabrata* and a filamentous fungus, *Aspergillus niger*. The substrates applied alone showed no activity at the higher tested concentrations (1.9 mg/ml of **1**; 1.8 mg/ml of **2**; 3.8 mg/ml of EtOH extract). This is in contrast with the significant antimycotic activity found against those same three pathogens when the substrates were tested in the presence of SMGD. The minimum inhibitory concentration (MIC) measured for each substrate in presence of SMGD against each strain is presented in Table 2. These products are, of course, far from competing with other antifungal agents such as miconazole that inhibits the growth of yeast strains *C. albicans* (1.6 μg/l), *C. glabrata* (0.2 μg/l) and *Aspergillus niger* (0.8 μg/l) at much lower concentrations in the same conditions (Piel et al., 1999).

Table 2
Minimal inhibitory concentration (MIC) of dolichantoside (**1**), palicoside (**2**) and the crude EtOH extract of *Strychnos mellodora* stem bark in presence of the glucosidase from *Strychnos mellodora* (SMGD) against three ATCC reference strains

	Minimum inhibitory concentration (mg/ml)		
	Candida albicans 10231	*Candida glabrata* 90030	*Aspergillus niger* 16404
Dolichantoside (**1**)/SMGD	0.38	0.76	0.38
Palicoside (**2**)/SMGD	0.14	1.48	0.74
EtOH extract /SMGD	2.28	0.38	0.76

3. Conclusion

The hypothesis formulated by Massiot and Delaude (1988) putting forward that N_b-methylated precursors lead to the formation of akagerine-type bases, monoterpenoid alkaloids with N_a–C_{17} bond, has been verified by the isolation and identification of a stable alkaloid, akagerine (**5**), after the conversion of palicoside (**2**). We have shown, moreover, that even in the presence of a methyl group, addition on N_b is possible and produces polar alkaloid, as in the case of the conversion of dolichantoside (**1**) into a new quaternary alkaloid, N_b-methyl-21-β-hydroxy-mayumbine (**4**).

We detected no presence of those conversion products in *Strychnos mellodora* organs, which may indicate that at the plant level substrates and glucosidase are contained in different cell compartments. Although the results of antimycotic activity do not concern vegetal pathogens, they may nevertheless suggest a constitutive "trigger mechanism" in the plant, in which an infection, by damage of the plant cell, results in substrate deglucosidation, thus allowing the active aglycone(s) to act against the intruder.

4. Experimental

4.1. Materials and methods

Dolichantoside (**1**) and palicoside (**2**) were isolated from *Strychnos mellodora* S. Moore stem bark according to Tits et al. (1996). Strictosidine β-glucosidase (SGD) was obtained by purification from suspension cultured cells of *Catharanthus roseus* L. G. Don according to Geerlings (1999). Strictosidine β-glucosidase from *Strychnos mellodora* (SMGD) was obtained by purification from dry leaves of *Strychnos mellodora* (Brandt et al., 2000). The β-glucosidase from sweet almonds was purchased from Merck (Germany). The reference akagerine has been isolated from *Strychnos usambarensis* and is kept in our laboratory.

The comparison of conversion products pattern was based on a HPLC method described by Pennings et al. (1989), but with a 4 × 250 mm Lichrospher 60 RP-Select B column (particle size 5 μm, cat. No. 00961; Merck). With this system the retention time of the substrates and conversion products were: **1** (18.5 min), **2** (5.4 min), **4** (24.2 min), **5** (4.3 min).

Protein concentrations were determined using the method described by Bradford (1976). UV spectra were recorded on a spectrophotometer Kontron Uvikon 922 with Hellma type 100-QS 10.00 mm thickness precision cuvettes.

^{1}H NMR and ^{13}C NMR 1D and 2D spectra of **4** were determined at 400 and 100 MHz respectively on a Bruker 400 MHz spectrometer. ^{1}H NMR and ^{1}H–^{1}H autocorrelation spectra of **5** and reference akagerine were determined at 600 MHz; ^{13}C NMR and HMQC spectra of reference akagerine were recorded at 150 MHz on a Bruker DMX 600 MHz spectrometer. Samples were run in deuterated solvents with TMS as internal standard.

HRMS was performed on a Micromass Ultima spectrometer (5.0 mDa resolution) in electrospray (MS–MS), positive ion; ES–MS–MS spectra was taken on a Micromass VG-Quattro II in electrospray, positive ion, ionisation energy 20 eV.

4.2. Conversion of dolichantoside (*1*) into N_b-methyl-21-β-hydroxy-mayumbine (*4*)

Half a milliliter of Na-Pi buffer pH 6.3 containing 50 mg dolichantoside (**1**) and 1 ml of enzymatic preparation (36.2 μg protein ml^{-1}) obtained from the leaves of *Strychnos mellodora* were mixed, homogenised and incubated in a bain-marie at 30°C until complete conversion of dolichantoside, after 72 h. The conversion was monitored by TLC analysis on silica gel with the mobile phase EtOAc–*iso*–prOH–NH_4OH 4.25% (60:25:15). In this system, dolichantoside (**1**) appears at R_f 0.43 and N_b-methyl-21-β-hydroxy-mayumbine (**4**) at R_f 0.13.

The dolichantoside (**1**) incubation mixture was then frozen and lyophilised. The dry residue was suspended in 2 ml MeOH, stirred and centrifuged 10 min at 3500 *g*. The supernatant was separated and evaporated to give a residue which was taken in 2 ml H_2O. This aq. soln was then extracted twice by *n*-BuOH and evaporated under reduced pressure. The residue dissolved in a few drops of MeOH gave by addition of Et_2O a voluminous white ppt. This latter was separated by centrifugation 10 min at 2500 *g*, dried and washed with Et_2O to obtain N_b-methyl-21-β-hydroxy-mayumbine (**4**) (27 mg) as an amorphous white powder; UV (MeOH) λ_{max} nm (log ε): 222 (4.19), 267 (3.54), 278 (3.55), 287 (3.43); ^{1}H NMR spectral data (400 MHz, CD_3OD): δ 1.55 (3H, *d*, $J=6.7$ Hz, H-18), δ 1.90 (1H, *m*, H-14b), δ 2.45 (1H, *m*, H-14a), δ 2.85 (1H, *m*, H-15), δ 3.15 (1H, *m*, $J=8.6$, 7.5 Hz, H-20), δ 3.20 (1H, H-6b), δ 3.27 (3H, *s*, N^+CH_3), δ 3.50 (1H, *d*, H-5a), δ 3.71 (3H, *s*, OCH_3), δ 3.75 (1H, *q*, $J=6.7$, 8.6 Hz, H-19), δ 4.30 (1H, H-5b), δ 4.45 (1H, *d*, $J=7.5$ Hz, H-21), δ 5.00 (1H, *d*, H-3), δ 7.07 (1H, *t*, $J=7.8$ Hz, H-0), δ 7.17 (1H, *t*, $J=8.2$ Hz, H-11), δ 7.37 (1H, *d*, $J=8.2$ Hz, H-12), δ 7.49 (1H, *s*, H-17), δ 7.50 (1H, *d*, $J=7.8$ Hz, H-9); ^{13}C NMR spectral data (100 MHz, CD_3OD): δ 10.8 (C-18), δ 17.5 (C-6), δ 25.6 (C-14), δ 32.7 (C-15), δ 47.0 (N^+CH_3), δ 51.3 (OCH_3), δ 59.5 (C-5), δ 61.7 (C-19), δ 69.0 (C-3), δ 75.0 (C-20), δ 97.0 (C-21), δ 114.4 (C-12), δ 118.2 (C-9), δ 119.6 (C-10), δ 122.4 (C-11), δ 144.0 (C-17); HRMS-MS–(EI) *m*/*z* (rel. int.): 383.1978 $[C_{22}H_{27}N_2O_4]^+$ (100), 365.2310 $[M-H_2O]^+$ (16), 352.2046 (20), 340.1962 (69), 322.1725 (41), 308.1646 (27), 144.0979 (53); Positive ES-MS-MS *m*/*z* (rel. int.): 383 $[M]^+$ (100), 365 $[M–H_2O]^+$ (13), 340 (28), 222 (30), 194 (64), 170 (50), 144 (97), 130 (42);

4.3. Conversion of palicoside (*2*) into akagerine (*5*)

Twenty milligrams of palicoside (**2**) dissolved in 200 μl of Na–Pi buffer pH 6.3 and 0.5 ml of enzymatic preparation (36.2 μg proteinml^{-1}) obtained from the leaves of *Strychnos mellodora* were mixed, homogenised and incubated in a bain-marie at 30°C. Lower specificity of the glucosidase in the presence of palicoside prevented to obtain a complete conversion of this substrate. Incubation was stopped after 72 h. In the TLC monitoring system described above palicoside (**2**) reaches a R_f of 0.09. Its conversion products, **5** and **6**, are characterised by R_f of 0.05 and 0.78 respectively. The palicoside (**2**) incubation mixture was then frozen and lyophilised. The residue was taken in 2 ml H_2O and then extracted by 2 ml CH_2Cl_2 until complete disappearance of **5** from the aq. layer. Each organic layer was separated by centrifugation 10 min at 2500 *g*. The joined organic layers were then conc. under reduced pressure and submitted to a prep. TLC in the system composed of silica gel and the mobile phase EtOAc–*iso*–prop-NH_4OH 4.25% (60:25:15). The elution was performed by CH_2Cl_2 and allowed

to obtain 7.38 mg of **5** as an amorphous white powder. UV (MeCN) λ_{max} nm (log ε): 229 (4.51), 276 (3.78), 283 (3.80), 293 (3.68); ^{1}H NMR spectral data (600 MHz, $CDCl_3$): δ 1.99 (1H, *d*, $J=12.8$ Hz, H-14b), δ 2.07 (3H, *d*, $J=7.2$ Hz, H-18), δ 2.09 (1H, *m*, H-16b), δ 2.19 (1H, *q*, $J=10.9$, 12.8 Hz, H-14a), δ 2.33 (1H, *t*, H-16a), δ 2.53 (3H, *s*, NCH_3), δ 2.72–2.78 (3H, *m*, H-5b, H-6a, H-6b), δ 3.07 (1H, *m*, H-5a), δ 3.66 (1H, *t*, $J=11.7$, 1.4 Hz, H-15), δ 3.82 (1H, *d*, $J=10.9$ Hz, H-3), δ6.24 (1H, *d*, $J=3.7$ Hz, H-17), δ 6.55 (1H, *q*, $J=7.2$ Hz, H-19), δ 7.11 (1H, *t*, $J=7.7$ Hz, H-10), δ7.18 (1H, *t*, $J=8.2$ Hz, H-11), δ 7.29 (1H, *d*, $J=8.2$ Hz, H-12), δ 7.48 (1H, *d*, $J=7.7$ Hz, H-9), δ 9.31 (1H, *d*, $J=1.4$ Hz, H-21); Positive ES–MS–MS *m*/*z* (rel. int.): 325 $[M+H]^+$ (93), 307 $[M+H\text{-}H_2O]^+$ (5), 282 (100), 264 (73), 144 (5), 130 (3); **5** has the same behaviour as reference akagerine in the TLC system described above ($R_f=0.78$), and with the mobile phases $CHCl_3$–CH_3OH (80:20) ($R_f=0.5$) and EtOAc–*iso*–prOH–NH_4OH 4.25% (45:35:5) ($R_f=0.73$); iodoplatinate reagent produces a pink color turning into red in a few minutes.

4.4. Reference akagerine

^{1}H NMR spectral data (600 MHz, $CDCl_3$) exactly match with **5** ones; ^{13}C NMR spectral data (150 MHz, $CDCl_3$): δ 15.2 (C-8), δ 19.8 (C-6), δ 29.1 (C-15), δ 36.3 (C-14), δ 37.4 (C-16), δ 42.5 (NCH_3), δ 50.4 (C-5), δ 60.8 (C-3), δ 75.7 (C-17), δ 108.3 (C-12), δ 108.8 (C-7), δ 118.3 (C-9), δ 119.4 (C-10), δ 121.3 (C-11), δ 126.7 (C-8), δ 136.0 (C-13), δ 137.0 (C-2), δ 147.9 (C-20), δ 150.5 (C-19), δ 194.9 (C-21).

4.5. Measure of antimycotic activity

The minimal inhibitory concentration (MIC) of **1**, **2** and the crude *Strychnos mellodora* EtOH extract against three ATCC® (American Type Culture Collection) reference strains were determined by using a broth microdilution method, based upon the National Committee for Clinical Laboratory Standards (NCCLS-USA) guidelines for broth microdilution technique (M-27A and M-38P) (NCCLS, 1997 and 1998). The three references strains, *Candida albicans* (ATCC 10231), *Candida glabrata* (ATCC 90030) and *Aspergillus niger* (ATCC 16404), were tested in duplicate and in parallel with the substrates alone and in presence of SMGD. Preparation of tested antifungal stock solns was not possible because of the low availability of the substrates. **1**, **2** and EtOH extract were dissolved in H_2O as acetates (by addition of the HOAc molar equivalent), filtered, frozen and then lyophilised. The residues were then weighed and dissolved in RPMI-1640 standard medium to give 7.6 mg/ml EtOH extract, 3.8 mg/ml **1** and 3.6 mg/ml **2**. These solns were incubated for 24 h in the presence of SMGD, then filtered to give solns of 6.08 mg/ml hydrolysed EtOH extract, 3.04 mg/ml hydrolysed **1** and 2.88 mg/ml hydrolysed **2**. Strains were pre-cultivated following the NCCLS guidelines. Cultures were realised in 96 wells microplates with lid. Wells 2–11 contained twofold decreasing dilutions of the different substrates. Well 1 served as sterility control with 0.1 ml RPMI 1640 medium and 0.1 ml sterile physiologic liquid while well 12 served as growing control with 0.1 ml strain suspension and 0.1 ml sterile physiologic liquid. Each well was inoculated with 0.1 ml of one of the three inoculum suspensions. The plates were then incubated at 35°C and examined on a spectrophotometer at 625 nm every 24 h until positive control reaches a optical density of 0.2. CMI is determined as the substrate concentration that allows a reduction of the strain growth to 20% of the positive control.

Acknowledgements

This research was supported by the "Fondation Léon Fredericq". We wish to thank the NMR laboratory of the Gorleaus Laboratories (University of Leiden-Netherlands) where the spectra of akagerine were measured; Mrs C. Prosperi (Physical Institute, University of Liège) for measuring the spectra of N_b-methyl-21-β-hydroxy-mayumbine; Dr. M.-P. Hayette (Department of Medical Microbiology, University of Liège) and Dr. G. Piel (Department of Pharmaceutical Technology, Institute of Pharmacy, University of Liège) who realised the antimycotic tests. The manuscript has benefited from the competence of Dr. P. DeTullio (Department of Pharmaceutical Organic Chemistry, Institute of Pharmacy, University of Liege).

References

Angenot, L., Dideberg, O., Dupont, L., 1975. Isolation and structure of akagerine: a new type of indole alkaloid. Tetrahedron Letters 16, 1357–1358.

Arata, Y., Aoki, T., Hanaoka, M., Kamei, M., 1975. Studies on 1-azabicyclo compounds. XXII. Stereochemistry of 9α-substituted quinolizidine methiodides. Chemical and Pharmaceutical Bulletin 23, 333–339.

Bisset, N.G., 1980. Alkaloids of the loganiaceae. In: Phillipson, J.D., Zenk, M.H. (Eds.), Indole and Biogenetically Related Alkaloids. Academic Press, London, pp. 34–35.

Bradford, M.M., 1976. A rapid and sensitive method for the quantitation of microgram quantities of protein utilizing the principle of protein dye binding. Analytical Biochemistry 72, 248–254.

Brandt, V., Geerlings, A., Tits, M., Delaude, C., van der Heijden, R., Verpoorte, R., Angenot, L., 2000. New strictosidine β-glucosidase from *Strychnos mellodora*. Plant Physiology and Biochemistry 38, 187–192.

Brandt, V., Tits, M., Geerlings, A., Frédérich, M., Penelle, J., Delaude, C., Verpoorte, R., Angenot, L., 1999. β-Carboline glucoalkaloids from *Strychnos mellodora*. Phytochemistry 51, 1171–1176.

Brown, R.T., 1980. Biomimetic conversion of secologanin into alkaloids.

In: Phillipson, J.D., Zenk, M.H. (Eds.), Indole and Biogenetically Related Alkaloids. Academic Press, London, pp. 171–184.
Carey, F.A., Sundberg, R.J., 1997. Chimie organique avancée. In: De Boeck (Ed.), Tome 2. Réactions et Synthèses. Université Paris, Bruxelles, pp. 14–15.
Danieli, B., Lesma, G., Mauro, M., Palmisano, G., Passarella, D., 1995. First enantioselective synthesis of (−)-akagerine by a chemoenzymatic approach. Journal of Organic Chemistry 60, 2506–2513.
Geerlings, A., 1999. Strictosidine β-D-glucosidase. PhD thesis, University of Leiden, The Netherlands.
Hemscheidt, T., Zenk, M.H., 1980. Glucosidases involved in indole alkaloid biosynthesis of *Catharanthus* cell cultures. FEBS Letters 110, 187–191.
Kisakürek, M.V., Leeuwenberg, A.J.M., Hesse, M., 1983. A chemotaxonomic investigation of the plant families of Apocynaceae, Loganiaceae, and Rubiaceae by their indole alkaloid content. In: Pelletier, S.W. (Ed.), Alkaloids — Chemical and Biological Perspectives, Vol. 1. John Wiley, New York, pp. 211–376.
Leeuwenberg, A.J.M., 1969. The Loganiaceae of Africa VIII–Strychnos III. University of Wageningen, pp. 180–181.
Lounasmaa, M., Hanhinen, P., 1998. Biomimetic formation and interconversion in the heteroyohimbine series. Heterocycles 48, 1483–1492.
Lounasmaa, M., Jokela, R., Miettinen, J., Halonen, M., 1992. New, short synthesis of (±)-geissoschizine. Heterocycles 34, 1497–1502.
Massiot, G., Delaude, C., 1988. African strychnos alkaloids. In: Brossi, A. (Ed.), The Alkaloids. Academic Press, San Diego, pp. 211–239.
National Committee for Clinical Laboratory Standard, 1997. Reference method for broth dilution antifungal susceptibility testing of yeasts; approved standard, M27-A.
National Committee for Clinical Laboratory Standard, 1998. Reference method for broth dilution antifungal susceptibility testing of Conidium-forming filamentous fungi; proposed standard, M38-P.
Pennings, E.J.M., van den Bosch, R.A., van der Heijden, R., Stevens, L.H., Duine, J.A., Verpoorte, R., 1989. Assay of strictosidine synthase from plant cell cultures by high performance liquid chromatography. Analytical Biochemistry 176, 412–415.
Phillipson, J.D., Supavita, N., 1983. Alkaloids of *Uncaria elliptica*. Phytochemistry 22, 1809–1813.
Piel, G., Hayette, M.-P., Evrard, B., Van Hees, T., De Mol, P., Delattre, L., 1999. A comparative study of the antimycotic activity of a miconazole HP-β-cyclodextrin solution and a surfactant solution. Journal de Pharmacie de Belgique 54, 87–88.
Rolfsen, W., Olaniyi, A., Hylands, P.J., 1980. New tertiary alkaloids of *Strychnos decussata*. Journal of Natural Products 43, 97–102.
Rueffer, M., Nagakura, N., Zenk, M.H., 1978. Strictosidine, the common precursor for monoterpenoid indole alkaloids with 3α and 3β configuration. Tetrahedron Letters 18, 1593–1596.
Stevens, L.H., 1994. Formation and conversion of strictosidine in the biosynthesis of monoterpenoid indole and quinoline alkaloids. PhD thesis, University of Leiden, The Netherlands.
Stöckigt, J., 1980. The biosynthesis of heteroyohimbine alkaloids. In: Phillipson, J.D., Zenk, M.H. (Eds.), Indole and Biogenetically Related Alkaloids. Academic Press, London, pp. 113–141.
Sugiura, M., Takao, N., Sasaki, Y., 1977. Stereochemistry of quinolizidines. II. Carbon-13 magnetic resonance spectra of *N*-methylquinolizidinium ions. Chemical and Pharmaceutical Bulletin 25, 960–963.
Svendsen, A.B., Verpoorte, R., 1983. Chromatography of alkaloids, part A: thin-layer chromatography. In: Journal of Chromatography Library, Vol. 23A. Elsevier Scientific Publishing Company, Amsterdam.
Tits, M., Brandt, V., Wauters, J.-N., Delaude, C., Llabres, G., Angenot, L., 1996. Glucoindole alkaloids from stem bark of *Strychnos mellodora*. Planta Medica 62, 73–74.
Uskoković, M.R., Lewis, R.L., Partridge, J.J., Despreaux, C.W., Pruess, D.L., 1979. Asymmetric synthesis of *allo*-heteroyohimbine alkaloids. Journal of American Chemical Society 101, 6742–6744.
Uusvuori, R., Lounasmaa, M., 1981. ^{13}C NMR data of 3-iso-ajmalicine and 19-epiajmalicine. Planta Medica 41, 406–407.
Wright, C.W., Bray, D.H., O'Neill, M.J., Warhurst, D.C., Phillipson, J.-D., Quetin-Leclercq, J., Angenot, L., 1991. Antiamoebic and antiplasmodial activities of alkaloids isolated from *Strychnos usambarensis*. Planta Medica 57, 337–340.

PERGAMON

Phytochemistry 57 (2001) 661–668

PHYTOCHEMISTRY

www.elsevier.com/locate/phytochem

Structure of fructans from excised leaves of New Zealand flax

Ian M. Sims[a,*], Andrew J. Cairns[b], Richard H. Furneaux[a]

[a]*Industrial Research Limited, PO Box 31-310, Lower Hutt, New Zealand*
[b]*Institute of Grassland and Environmental Research, Plas Gogerddan, Aberystwyth, Ceredigion, SY23 3EB, UK*

Received 28 September 2000; received in revised form 13 February 2001

Abstract

The accumulation of total water-soluble carbohydrate, and specifically sucrose and fructan, by excised leaves of *Phormium tenax* and *P. cookianum* (family Phormiaceae J. G. Agardh, order Asparagales) was investigated. Total water-soluble carbohydrate content of excised leaves of *P. tenax* and *P. cookianum* increased during 48 h of continuous illumination at an average rate of 1.3 and 0.9 mg g^{-1} fresh weight leaf per hour, respectively. The sucrose content of excised leaves increased throughout the experimental period. The fructan content of excised leaves of *P. tenax* increased slightly throughout the experimental period, whilst that of *P. cookianum* was variable and showed no overall change. Chemical and spectroscopic analysis of the fructans obtained from the two *Phormium* species showed that they were similar to each other and contained mostly 1-linked and terminal fructofuranosyl (Fru*f*) residues, together with smaller amounts of 6-linked Fru*f*, 1,6-branched Fru*f*, terminal and 6-linked glucopyranosyl residues. Separation of the fructans by thin-layer and high-performance anion-exchange chromatography revealed the presence of a complex mixture of fructo-oligosaccharides and higher molecular weight fructan. The branched structure of the fructans isolated from excised leaves of *Phormium* resembles that of fructans and fructo-oligosaccharides isolated from some related species within the order Asparagales (*Agave vera cruz*, *Cordyline australis* and *Urginea maritima*), but is distinct from the linear structure of fructans from others (*Allium cepa* and *Asparagus officinalis*). The structural heterogeniety of fructans within both the order Asparagales and superorder Liliiflorae may be a useful chemotaxonomic aid. © 2001 Elsevier Science Ltd. All rights reserved.

Keywords: *Phormium tenax*; *Phormium cookianum*; Phormiaceae; New Zealand flax; Water-soluble carbohydrate; Fructan; Accumulation; Structure

1. Introduction

Phormium is a genus of medium to tall monocotyledonous herbs within the family Phormiaceae J. G. Agardh, order Asparagales, superorder Liliiflorae (Watson and Dallwitz, 1992 onwards). In New Zealand there are two species, *Phormium tenax* (New Zealand flax), that was once extensively cultivated for its fibre, and *Phormium cookianum* (mountain flax). The presence of fructans (polyfructosylated sucrose) in other species within the order Asparagales, such as *Agave vera cruz* (Dorland et al., 1977), *Allium cepa* (onion; Henry and Darbyshire, 1980), *Asparagus officinalis* (asparagus; Shiomi, 1993), *Cordyline australis* (New Zealand cabbage tree; Brasch et al., 1988) and *Urginea maritima* (red squill; Spies et al., 1992), suggested that *Phormium* spp. may also contain fructans.

Preliminary experiments showed that fructans were present in leaves of *P. tenax* on one occasion, but was almost absent on another occasion. To enable the potential for fructan accumulation in *Phormium* species to be evaluated, an investigation was initiated to study the accumulation of water-soluble carbohydrate (WSC) in excised leaves of both *P. tenax* and *P. cookianum*. The excised leaf has been shown to be a convenient experimental system for inducing the accumulation of WSC in temperate grasses under controlled conditions. Continuous illumination of excised leaves of *Lolium temulentum* resulted in an initial accumulation of sucrose, followed by the onset of fructan biosynthesis and stabilisation of sucrose concentration (Cairns and Pollock, 1988).

Structural variation of fructans from species within the order Poales has been used to distinguish members of the supertribes Triticodae and Poodae. Branched fructans appear to be characteristic of the Triticodae, but are absent or present in only low proportions in the Poodae (Bonnett et al., 1997). The fructans from *C. australis* (Brasch et al., 1988) and *U. maritima* (Spies et

* Corresponding author. Tel.: +64-4-569-000; fax: +64-4-569-0055.

E-mail address: i.sims@irl.cri.nz (I.M. Sims).

0031-9422/01/$ - see front matter © 2001 Elsevier Science Ltd. All rights reserved.
PII: S0031-9422(01)00089-9

al., 1992), and the fructo-oligosaccharides from *A. vera cruz* (Dorland et al., 1977) are all branched to varying degrees, whereas those from *A. cepa* (Henry and Darbyshire, 1980) and *A. officinalis* (Shiomi, 1993) are linear. Thus, the structure of the fructans from members of the Asparagales may be a useful taxonomic aid.

We have now studied the accumulation of WSC in excised leaves of *P. tenax* and *P. cookianum* and in this publication we report on the characterisation of the accumulated fructan by glycosyl linkage analysis, nuclear magnetic resonance (NMR) spectroscopy, thin-layer chromatography (TLC) and high-performance anion-exchange chromatography (HPAEC). The structures of these *Phormium* fructans are compared to those from other species in the order Asparagales.

2. Results and discussion

2.1. Accumulation of water-soluble carbohydrate

Individual excised leaves of *P. tenax* and *P. cookianum* were harvested at various times during a 48 h period of continuous illumination, weighed and sequentially extracted with boiling aqueous ethanol and hot water. Total WSC and free reducing sugar contents of the extracts were estimated colorimetrically, and sucrose and fructan were determined using modifications of the Megazyme fructan assay procedure. The enzyme mixture used for the sucrose assay contained both sucrose and starch-degrading enzymes. However, starch, determined using the Megazyme total starch assay procedure, represented only 1–2% of the total WSC of the extracts at all harvest times and so was not considered separately in the determinations of sucrose content (see Experimental). The initial total WSC concentrations in leaves of *P. tenax* and *P. cookianum* were 26.1 and 32.7 mg g^{-1} fresh weight (FW) of leaf, respectively. Fig. 1 shows the changes in total WSC, sucrose and fructan extracted from excised leaves of *P. tenax* and *P. cookianum* over the 48 h illumination period.

The total WSC content of excised leaves of *P. tenax* and *P. cookianum* increased erratically. The total WSC content of leaves of *P. tenax* and *P. cookianum* generally increased throughout the 48 h experimental period at an average rate of 1.3 and 0.9 mg g^{-1} FW leaf per hour, respectively.

The initial concentrations of free reducing sugar, sucrose and fructan in excised leaves of *P. tenax* were 9.8, 7.0 and 4.6 mg g^{-1} FW leaf, respectively, and those in excised leaves of *P. cookianum* 7.1, 6.6 and 15.4 mg g^{-1} FW leaf, respectively. As the total WSC concentration in the excised and illuminated leaves increased the free reducing sugar concentrations remained almost constant. For clarity, these data are omitted from Fig. 1. The sucrose concentrations in excised leaves of *P. tenax* and *P. cookianum* increased at an overall rate of 0.7 and 0.8 mg g^{-1} FW leaf per hour, respectively. The fructan concentration of excised leaves of *P. tenax* increased at an overall rate of 0.3 mg g^{-1} FW leaf per hour. The fructan content of excised leaves of *P. cookianum* was variable and showed no overall change.

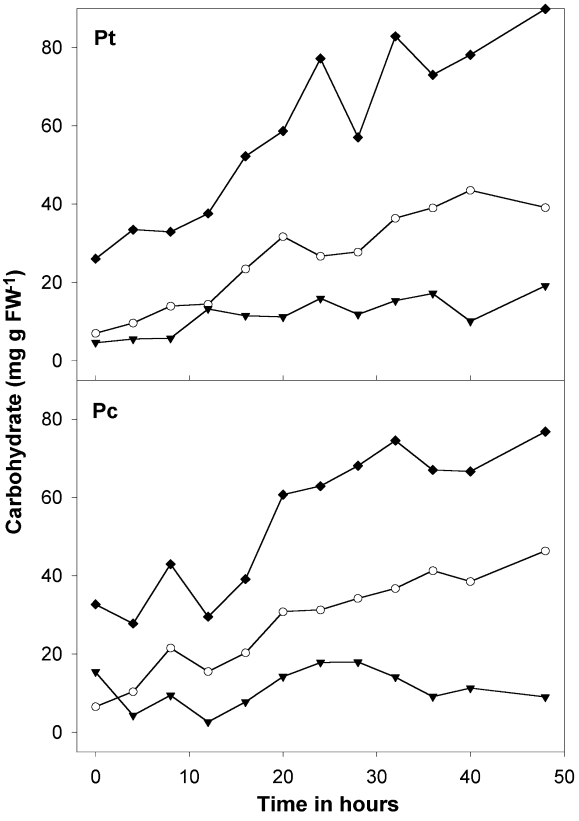

Fig. 1. Quantitative analysis of various water-soluble carbohydrate fractions from excised leaves of *Phormium tenax* (Pt) and *Phormium cookianum* (Pc) after various times of continuous illumination. Samples were assayed for total WSC (◆), sucrose (○) and fructan (▼).

2.2. Linkage composition of fructans

Fructans are a family of oligo- and polysaccharides in which one or more fructosyl-fructose linkages are present. All of the known fructans are based on three isomeric trisaccharides, 1-kestotriose (*O*-β-D-fructofuranosyl-(2 → 1)-β-D-fructofuranosyl-(2 → 1)-α-D-glucopyranoside), 6-kestotriose (*O*-β-D-fructo-furanosyl-(2→6)-β-D-fructofuranosyl-(2 → 1)-α-D-glucopyranoside) and 6_G-kestotriose (*O*-β-D-fructofuranosyl-(2 → 6)-α-D-glucopyranosyl-(1↔2)-*β*-D-fructofuranoside) (Waterhouse and Chatterton, 1993).

The linkage structures of the fructans from *Phormium* species were determined by GC–MS of partially methylated alditol acetates. Prior to derivatisation of total WSC extracts, sucrose was hydrolysed to fructose and glucose with a specific sucrase, and all monosaccharides

reduced with $NaBH_4$. Upon methylation, the resulting alditols gave highly volatile hexa-*O*-methyl derivatives which eluted much earlier than the partially methylated alditol acetate derivatives obtained from the fructans.

The linkage compositions of fructans from excised leaves of *P. tenax* and *P. cookianum* at various times after excision did not vary greatly. Table 1 shows the linkage compositions of the fructan from these two species immediately after excision and after 24 h of continuous illumination. Immediately after excision, fructan from *P. tenax* contained more terminal Fru*f* and less 1-linked Fru*f* than that from *P. cookianum*, but contained similar proportions of 6-linked Fru*f* and 1,6-branched Fru*f*. After 24 h continuous illumination the fructans from both *P. tenax* and *P. cookianum* contained similar proportions of the different fructofuranosyl linkages. Immediately after excision, the glucose residues of the fructan from leaves of *P. tenax* contained mostly terminal Glc*p* with only a small amount of 6-linked Glc*p*, while those from leaves of *P. cookianum* were mostly 6-linked Glc*p* with only a small amount of terminal Glc*p*. After 24 h continuous illumination both species contained similar amounts of both terminal and 6-linked Glc*p*.

Table 2 compares the average linkage composition of fructans extracted from excised leaves of *P. tenax* and *P. cookianum* after $t=0$, 8, 16 and 24 h of continuous illumination, with data reported for branched fructans from *C. australis* (Brasch et al., 1988), *U. maritima* (red squill; Spies et al., 1992) and the pentasaccharide fraction from *A. vera cruz* (Dorland et al., 1977). The linkage compositions of fructans from the two *Phormium* species were similar to that of fructan from the roots and stems of *C. australis* (Brasch et al., 1988), although the *Phormium* fructans contained more 6-linked Fru*f* and less 1,6-branched Fru*f*. Fructans from *Phormium* species also contained 6-linked Glc*p*, which was almost absent from *C. australis*. The fructan from *U. maritima* contained less terminal and 1-linked Fru*f*, and terminal Glc*p* than fructans from the *Phormium* species, but considerably more 6-linked and 1,6-branched Fru*f* (Spies et al., 1992). Oligosaccharide fractions from extracts of the stems of *A. vera cruz* also had similar linkage compostions to those of fructans from *Phormium* species (Dorland et al., 1977). The DP 5 oligosaccharide, for example, contained similar amounts of terminal, 1-linked and 1,6-branched Fru*f* to the *Phormium* fructans, although 6-linked Fru*f* was not present and the proportion of 6-linked Glc*p* was higher than that of fructans from *Phormium* species. *Phormium*, *Cordyline* and *Agave* have previously all been placed in the family Agavaceae (Pollard, 1978) and all contain varying proportions of different fructofuranosyl and glucopyranosyl linkages. *U. maritima* is a member of the family Hyacinthaceae and related species (e.g. *Scilla violacea*) were placed by Pollard (1978) in the Liliaceae. Therefore this species, containing branched fructans, is more closely related to *Allium* and *Asparagus* that contain linear fructans.

Table 1
Glycosyl linkage composition (mol%) of fructan in excised leaves of *Phormium tenax* and *Phormium cookianum* harvested immediately after excision and after 24 h continuous illumination

Species	Deduced glycosyl linkage	Time after excision (h)	
		0	24
P. tenax	Terminal Fru*f*	33	31
	1-Linked Fru*f*	39	46
	6-Linked Fru*f*	7	8
	1,6-Branched Fru*f*	8	5
	Terminal Glc*p*	11	6
	6-Linked Glc*p*	2	5
P. cookianum	Terminal Fru*f*	26	31
	1-Linked Fru*f*	48	44
	6-Linked Fru*f*	8	8
	1,6-Branched Fru*f*	8	7
	Terminal Glc*p*	3	6
	6-Linked Glc*p*	8	4

The detection in fructans extracted from excised leaves of *Phormium* species of both terminal and 6-linked Glc*p* suggested that oligosaccharides based on the trisaccharides 1-kestotriose and 6_G-kestotriose were present. The detection of 1-linked and 6-linked Fru*f* indicated that fructans were either a mixture of inulin (β-2,1-linked) and levan (β-2,6-linked) type fructan molecules, or mixed-linkage fructans such as those identified in the grass, *L. temulentum* (Sims et al., 1992). The existence of 1,6-branched Fru*f* indicated the presence of branched oligosaccharides such as those based on the tetrasaccharide (1 and 6)-kestotetraose (*O*-β-D-fructofuranosyl-(2 → 1)-*O*-[β-D-fructofuranosyl-(2 → 6)]-β-D-fructofuranosyl-(2 → 1)-α-D-glucopyranoside; Waterhouse and Chatterton, 1993).

2.3. ^{13}C NMR spectroscopy of fructans

Fructans from *Phormium* species, obtained after gel-permeation chromatographic fractionation of crude extracts to remove monosaccharides and sucrose, were analysed by ^{13}C NMR spectroscopy. The fructans in extracts from excised leaves of *P. tenax* and *P. cookianum* after 24 h of continuous illumination gave ^{13}C NMR spectra that were essentially the same (Fig. 2), and showed similarities to the spectra reported for fructans from *C. australis* (Brasch et al., 1988) and *U. maritima* (Spies et al., 1992).

The anomeric region contained a set of resonances at 104.7–105.6 ppm which were deduced to correspond to the C-2 of the various β-D-Fru*f* residues and a pair of resonances at 93.6 and 94.1 ppm which were deduced to correspond to the C-1 of the α-D-Glc*p* residues. The assignment of these anomeric chemical shifts shown in

Table 2
Average linkage composition (mol%) of fructans extracted from excised leaves of *Phormium tenax* and *Phormium cookianum* after $t = 0$, 8, 16 and 24 h of continuous illumination, and of fructans from *Cordyline australis* (Brasch et al., 1988), *Urginea maritima* (Spies et al., 1992) and the fructan pentasaccharide fraction from *Agave vera cruz* (Dorland et al., 1977)

Deduced	Species				
glycosyl linkage	*P. tenax*	*P. cookianum*	*C. australis*	*U. maritima*	*A. vera cruz* DP 5
Terminal Fru*f*	34	31	29	25	29
1-Linked Fru*f*	40	43	47	33	39
6-Linked Fru*f*	9	9	4	19	–
1,6-Branched Fru*f*	6	6	14	19	7
Terminal Glc*p*	8	5	5	1	5
6-Linked Glc*p*	3	6	tr	3	19

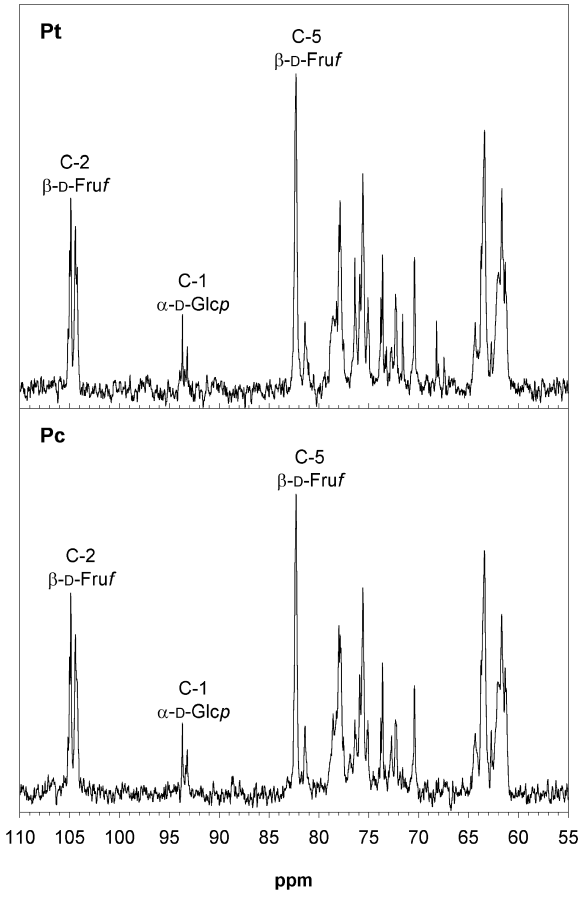

Fig. 2. ^{13}C NMR spectra of fructans from excised leaves of *Phormium tenax* (Pt) and *Phormium cookianum* (Pc), obtained after gel-permeation chromatography to remove monosaccharides and sucrose.

Table 3 was made by comparison with assignments made for the spectra for fructans from *Cichorium intybus* (chicory) and *Phleum pratense* (timothy grass), oligosaccharides from *Helianthus tuberosus* (Jerusalem artichoke) and *A. cepa* (onion), and sucrose, and by reference to published spectral data for fructans and fructo-oligosaccharides from various sources (Brasch et al., 1988; Carpita et al., 1991; Spies et al., 1992; Liu et al., 1993; Shiomi, 1993). Resonances at 104.7 and 104.9 ppm were assigned to → 1)-D-Fru*f*-β-(2→ residues and that at 105.3 ppm to D-Fru*f*-β-(2→ (Table 3). Based on the assignments of Liu et al. (1993) for chemical shifts for 1,1-kestotetraose and 1,1,1-kestopentaose, the chemical shift for →1)-D-Fru*f*-β-(2→ attached to a α-D-Glc*p* residue at O-1 was assigned at 104.9 ppm, 0.2 ppm downfield of that for →1)-D-Fru*f*-β-(2→ attached to a β-D-Fru*f* residue at O-1 (104.7 ppm).

Two resonances at 105.4 and 105.6 ppm in the spectra of fructans from *Phormium* species, downfield of that assigned to D-Fru*f*-β-(2→, did not correspond to any signals present in the spectra for fructans from *C. intybus*, *H. tuberosus* and *A. cepa*, but an intense resonance at 105.6 ppm was present in *P. pratense* fructan, which has a structure containing solely 6-linked Fru*f* with terminal Glc*p* (Cairns et al., 1999). Thus, the resonance at 105.6 ppm in spectra of fructans from *Phormium* species was assigned to →6)-D-Fru*f*-β-(2→ (Table 3). This assignment was supported by similar assignments for this residue in fructans from *C. australis* (Brasch et al., 1988), *F. arundinaceae* and *T. aestivum* (Carptia et al., 1991), and *Agropyron repens*, *Pucinella peisonis* and *U. maritima* (Spies et al., 1992) as being 0.4 ppm downfield of that for terminal β-D-Fru*f*. A resonance 0.1 ppm downfield of that for terminal β-D-Fru*f* has been assigned to the branched → 1,6)-D-Fru*f*-β-(2→ residue in fructans from *C. australis* (Brasch et al., 1988) and *U. maritima* (Spies et al., 1992), and thus, the chemical shift at 105.4 ppm in spectra of fructans from *Phormium* species was assigned to this residue. Interestingly, the chemical shift of →1,6)-D-Fru*f*-β-(2 → in fructans from *T. aestivum* (Carpita et al., 1991) and *A. repens* (Spies et al., 1992) has been assigned at 0.2 ppm upfield of that for D-Fru*f*-β-(2→, although no similar chemical shift could be detected in spectra of fructans from *Phormium* species.

The ^{13}C NMR spectra of fructans from *Phormium* species showed chemical shifts at 81.8 and 82.7 ppm which were deduced to be due to C-5 of β-D-Fru*f* residues carrying a substituent at O-6 or lacking a substituent at O-6, respectively, based on spectra for the predominantly 2,6-linked fructan from *P. pratense* and the predominantly 2,1-linked fructan from *C. intybus*. An

Table 3
Anomeric ^{13}C NMR chemical shifts (δ, ppm) of fructans extracted from excised leaves of *Phormium tenax* and *Phormium cookianum* after 24 h of continuous illumination, and of fructans from *Cichorium intybus, Phleum pratense* and *Allium cepa*, fructo-oligosaccharides from *Helianthus tuberosus* and sucrose

Residue	Chemical shifts (ppm)						
	P. tenax	*P. cookianum*	*C. intybus*	*Phleum pratense*	*A. cepa*	*H. tuberosus*	Sucrose
C-2							
D-Fru*f*-β-(2→	105.3	105.3	105.3	105.3	105.3	105.3	105.3
→1)-D-Fru*f*-β-(2→	104.7–104.9	104.6–104.8	104.9	–	104.7–104.9	104.7–104.9	–
→6)-D-Fru*f*-β-(2→	105.6	105.6	–	105.6		–	–
→1,6)-D-Fru*f*-β-(2→	105.4	105.4	–	–		–	–
C-1							
D-Glc*p*-α-(1→ (sucrose)	–	–	–	–	93.8	93.8	93.8
D-Glc*p*-α-(1→ (fructan)	94.1	94.1	94.1	94.1	94.1	94.1	–
→6)-D-Glc*p*-α-(1→	93.6	93.6	–	–	93.6	–	–

upfield shift of 0.9 ppm for the C-5 resonance of β-D-Fru*f* residues upon substitution at O-6 has been shown for purified 6-kestotriose in comparison to the resonance for C-5 of β-D-Fru*f* residues not substituted at O-6 (Liu et al. 1991). Although ^{13}C NMR spectroscopy is not entirely quantitative, the area ratio of the resonances at 82.7 and 81.8 ppm in spectra of fructans from both *P. tenax* and *P. cookianum* was ~4.5:1, close to the ~6:1 ratio of [terminal + 1-linked Fru*f*] to [6-linked + 1,6-branched Fru*f*] determined by linkage analysis.

The part of the anomeric region of the ^{13}C-NMR spectra of the *Phormium* fructans corresponding to the C-1 of the α-D-Glc*p* residues showed resonances at 93.6 and 94.1 ppm. The D-Glc*p*-α-(1 → residue from sucrose gave a resonance at 93.8 ppm, while a similar residue from *C. intybus* fructan gave a resonance at 94.1 ppm (Table 3). Fructo-oligosaccharides from *H. tuberosus* also contained resonances at both 93.8 and 94.1 ppm that were assigned to D-Glc*p*-α-(1 → from sucrose and fructan, respectively. In addition to these two signals, the spectrum of fructo-oligosaccharides from *A. cepa* gave a third signal at 93.6 ppm which was deduced to correspond to → 6)-D-Glc*p*-α-(1 →, based on the presence of oligosaccharides in the 6_G-kestotriose series in this species (Henry and Darbyshire, 1980). The signals at 93.6 and 94.1 ppm in ^{13}C NMR spectra of fructans from *Phormium* species were thus deduced to correspond to →6)-D-Glc*p*-α-(1 → and D-Glc*p*-α-(1 →, respectively (Table 3).

2.4. TLC and HPAEC of fructans

The linkage compositions and ^{13}C NMR spectra of the fructans extracted from excised leaves of *P. tenax* and *P. cookianum* suggested a complex mixture of isomeric oligosaccharides. To investigate this structural complexity, fructans obtained by gel-permeation chromatography were fractionated further by TLC and HPAEC.

Separation of *Phormium* fructans by TLC on silica gel plates revealed a complex pattern of oligosaccharides up to DP 7 and a smear of unresolved higher oligomers. Fig. 3 compares the oligosaccharides in extracts from excised leaves of *P. tenax* and *P. cookianum* after 24 h of continuous illumination with those from tubers of *H. tuberosus* and bulbs of *A. cepa*. *H. tuberosus* contains a series of linear β-2,1 linked fructo-oligosaccharides with terminal glucose, based on the trisaccharide 1-kestotriose (Bonnett et al., 1997). *A. cepa* accumulates two trisaccharides, 1-kestotriose and 6_G-kestotriose and their higher homologues (Henry and Darbyshire, 1980). The leaves of both *P. tenax* and *P. cookianum* contained two trisaccharides, with similar staining intensities,

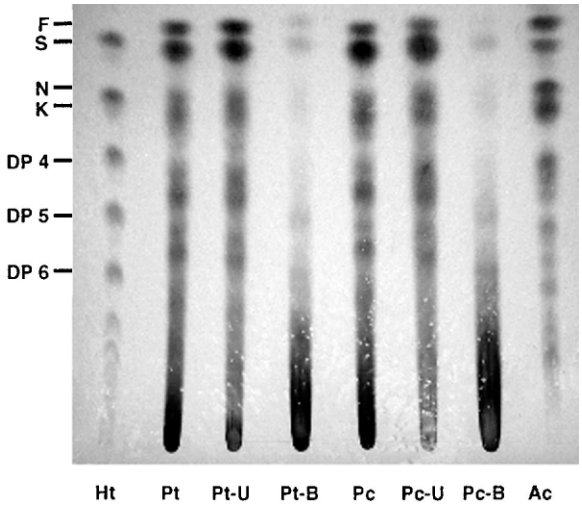

Fig. 3. Thin-layer chromatography of fructans extracted from excised leaves of *Phormium tenax* (Pt) and *Phormium cookianum* (Pc), compared with fructans extracted from tubers *Helianthus tuberosus* (Ht) and bulbs *Allium cepa* (Ac). Pt-U and Pc-U represent fructans not bound to C-18 cartridges and Pt-B and Pc-B represent fructans eluted from C-18 cartridges with methanol. Markers represent the mobilities of fructose (F), sucrose (S), 6_G-kestotriose (N), 1-kestotriose (K), and inulin tetrasaccharide (DP 4), pentasaccharide (DP 5) and hexasaccharide (DP 6).

which co-chromatographed with the deduced 1-kestotriose and 6_G-kestotriose. The trisaccharide fraction from *A. vera cruz* also contained these two trisaccharides (Dorland et al., 1977). The pattern of oligosaccharides > DP 3 from the *Phormium* species resembled the complex pattern of oligosaccharides from *A. cepa* rather than the simple series from *H. tuberosus* and added to the evidence from glycosyl linkage analysis (Table 1) which indicated that *Phormium* fructans contained oligosaccharides based on both 1-kestotriose and 6_G-kestotriose.

Separation of fructans in extracts from excised leaves of *P. tenax* and *P. cookianum* after 24 h of continuous illumination by HPAEC showed a complex pattern of oligosaccharides compared with the linear β-2,1 linked series of *H. tuberosus* and the linear β-2,6 linked series of *P. pratense* (Fig. 4). A large peak in both *P. tenax* (Fig. 4A) and *P. cookianum* (Fig. 4B) that eluted at about 13.7 min co-chromatographed with the trisaccharide from *H. tuberosus* and was thus identified as 1-kestotriose (K). The second trisaccharide, 6_G-kestoriose observed by TLC, could not be positively identified by HPAEC. This trisaccharide elutes from HPAEC between 1-kestotriose (K) and 1,1-kestotetraose (DP4, 17.6 min; Fig. 4C; Bancal et al., 1993). However, there was no peak in this region with a similar size to that of 1-kestotriose that would reflect their similar staining intensities on TLC, and unequivocal identification of this peak would require further chromatographic separation and characterisation. The complex mixture of oligosaccharides that eluted between 15 and 22 min ranged in size from DP 3 to DP7/8 as judged from the elution times of oligosaccharides of this size present in *H. tuberosus* (Fig. 4C) and *Phleum pratense* (Fig. 4D) extracts but could not be identified by their retention times. Material that was eluted from 22 to 33 min was not resolved into individual peaks and was assumed to contain a mixture of multiple isomeric fructans from DP 8 to > DP 30.

Fructans from both *P. tenax* and *P. cookianum* were passed through reverse-phase cartridges to remove hydrophobic material, giving unbound fractions (Pt-U and Pc-U) and bound fractions that was eluted with methanol (Pt-B and Pc-B). TLC showed that the distribution of oligosaccharides present in the unbound fractions, Pt-U and Pc-U, resembled that of the unfractionated material, but with less intense staining on the lower third of the plate and on the origin (Fig. 3). The bound fractions, Pt-B and Pc-B, contained material that was mostly > DP 6, with intense staining on the lower third of the plate and on the origin. Analysis of the reverse-phase unbound and bound fractions by HPAEC (not shown) gave a similar distribution of material to that observed on TLC. Reverse phase cartridges have been used previously in the preparation of fructan extracts to remove hydrophobic materials (Smouter and Simpson, 1989; Bonnett et al., 1997; St. John et al., 1997a,b), but this present study clearly shows that this results in the loss of higher molecular weight fructans, which can only be eluted with organic solvents.

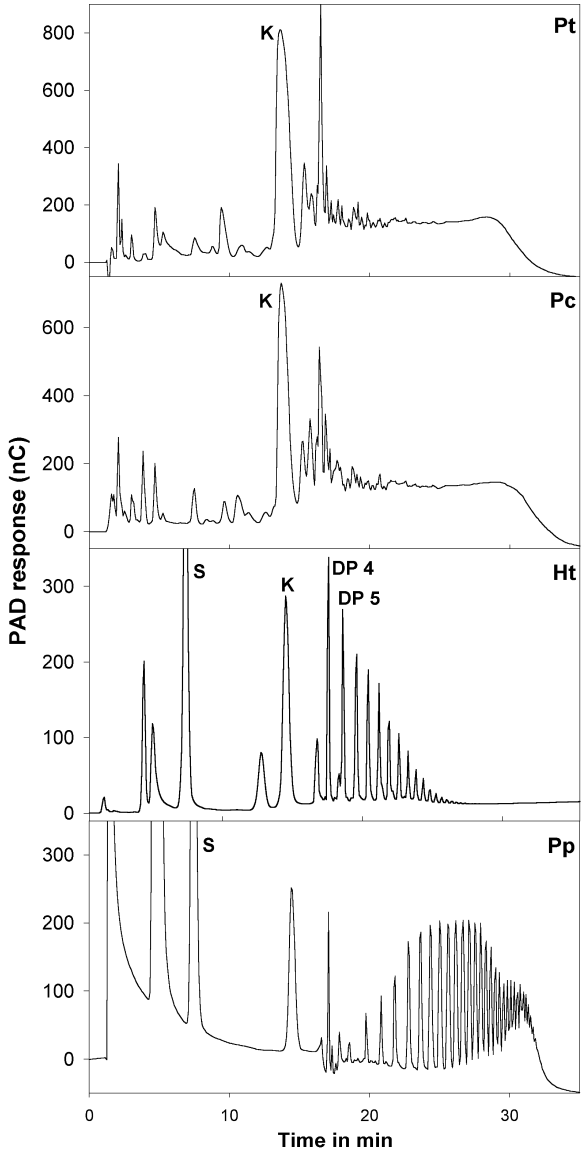

Fig. 4. HPAEC analysis of fructans extracted from excised leaves of *Phormium tenax* (Pt) and *Phormium cookianum* (Pc), compared with fructans extracted from tubers of *Helianthus tuberosus* (Ht) and leaves of *Phleum pratense* (Pp). Markers represent the mobilities of sucrose (S), 1-kestotriose (K), and inulin tetrasaccharide (DP 4) and pentasaccharide (DP 5).

2.5. Conclusions

The WSC accumulated by excised leaved of *Phormium* comprises mostly of sucrose with lesser amounts of fructan. The data indicate that there may be slight differences in the accumulation of fructan by leaves of *P. tenax* and *P. cookianum*, although more work is needed to confirm this. The fructans are based on the two trisacharides, 1-kestotriose and 6_G-kestotriose, and the

branched tetrasaccharide, (1 and 6)-kestotetraose, and have a complex distribution of oligosaccharides. The branched structure of the fructans isolated from excised leaves of *Phormium* resembles that of fructans and fructo-oligosaccharides isolated from the closely related species, *A. vera cruz* and *C. australis* and the less closely related *U. maritima*, but is distinct from the linear structure of fructans from *A. cepa* and *A. officinalis*. The detailed linkage analysis data for the branched fructans was able to separate the four species, but was not able to distinguish between the two *Phormium* species. The significance of this structural complexity is obscure, but it would be of considerable interest to use such structural heterogeniety as a chemotaxonomic aid within both the order Asparagales and superorder Liliiflorae.

3. Experimental

3.1. Fructans standards

Fructans were extracted from bulbs of *A. cepa* (obtained from a local market, UK) and tubers of *H. tuberosus* (obtained from a local market, UK) stored at 2–4°C for 6 weeks as described by Sims et al. (1991). Fructan was extracted from excised leaves of *P. pratense* as described by Cairns et al. (1999). Fructan from *C. intybus* was from Aldrich.

3.2. Plant material and induction of carbohydrate accumulation

Plants of *P. tenax* were to read and *P. cookianum* were obtained from a local nursery, NZ. Leaves approximately 50 cm long were excised and carbohydrate accumulation induced by immersing the cut ends in H_2O and illuminating at about 350 μmol m^{-2} s^{-1} photosynthetic photon flux density for up to 48 h.

3.3. Extraction of water-soluble carbohydrate

At various times after excision, individual leaves of *P. tenax* and *P. cookianum* were harvested and weighed. The leaves were cut into small pieces, killed in boiling 80% v/v EtOH (approx. 50 ml g^{-1} FW leaf), and the water-soluble carbohydrate extracted twice with H_2O (approx. 50 ml g^{-1} FW leaf, 70°C, 60 min). The pooled extracts were concentrated, filtered under vacuum (Whatman 541 filter paper), deionised by sequential passage through anion (Amberlite IR 120, Na^+ form) and cation (Amberlite IR 401, Cl^- form) exchange resins and freeze-dried.

3.4. Analyses of water-soluble carbohydrate

Total WSC was determined by the phenol-sulphuric acid method using fructose as a standard (Dubois et al., 1956). Total starch was determined using the Meagzyme Total Starch Assay Kit, Procedure B (Megazyme International Ireland Ltd.). Free reducing sugars (mostly fructose and glucose) were determined using the *p*-hydroxybenzoic acid hydrazide (PAHBAH) reducing-sugar assay (Lever, 1972). Sucrose and fructan were determined using the Megazyme Fructan Assay kit. For the determination of sucrose, the sucrase/β-amylase/pullulanase/maltase mixture was used to hydrolyse sucrose (assuming that the starch contents of the leaf extracts were negligible; see results) to glucose and fructose, and the increase in reducing-sugar content compared to unhydrolysed samples was used to calculate the sucrose content. Fructan was determined using the full Megazyme fructan assay procedure.

3.5. Fractionation of water-soluble carbohydrates

WSCs from excised leaves of *P. tenax* and *P. cookianum* illuminated continuously for 24 h were fractionated by gel-permeation chromatography on a column (90× 1.6 cm) of Fractogel TSK HW-40 (fine, Merck) in order to separate monosaccharides and sucrose from fructans. Samples (approx. 200 mg) dissolved distilled H_2O (2 ml) were loaded onto the column and eluted with distilled H_2O at 7 ml h^{-1} at room temperature. Fractions (4 ml) were collected and assayed for total carbohydrate using the phenol-sulphuric acid method (Dubois et al., 1956). Those corresponding to (A) fructans and (B) sucrose and monosaccharide were pooled and freeze-dried.

Fructans obtained following gel-permeation chromatography (20 mg) were dissolved in distilled water (1 ml). The samples were applied to reverse-phase cartridges (C-18 Sep-Pak, Waters Corporation, USA) and unbound material eluted with 5 ml distilled water. Bound material was then eluted with 5 ml MeOH, and both the bound and unbound fractions were freeze-dried.

3.6. Chromatographic analyses of fructans

Samples containing about 50 μg of fructan were applied to the origin of a 20 × 20 cm silica gel TLC plate (Schleicher & Schuell, Germany). Plates were developed three times in butan-1-ol/propan-2-ol/water (3:12:4, v/v/v) at room temperature (Kanaya et al., 1978). Compounds were visualised by spraying with the ketose-specific, urea-phosphoric acid stain (Wise et al., 1955).

Samples containing 100 μg of fructan dissolved in distilled H_2O (5 μg μl^{-1}) were separated by HPAEC at a flow rate of 1 ml min^{-1} on a Dionex BioLC using a CarboPac PA-100 column (4×250 mm; Dionex Corp., Sunnyvale, CA, USA) equilibrated in 100 mM NaOH. WSC was eluted with a gradient of NaOAc (0–0.4 M) starting 10 min after injection and ending 50 min after injection. Eluted material was monitored using pulsed amperometric detection (Dionex).

3.7. Glycosyl linkage analysis

Prior to derivatisation, sucrose was hydrolysed to fructose and glucose with a specific sucrase, and all monosaccharides were reduced to their respective alditols with $NaBH_4$. Samples of total WSC containing ~100 μg fructan were dissolved in 100 μl distilled water, 100 μl of sucrase (0.23 units) in Na-maleate (0.1 M, pH 6.5, Megazyme fructan assay kit) was added and incubated at 40°C for 1 h. $NaBH_4$ (100 μl, 10 mg ml^{-1}) was then added and the samples were incubated at 40°C for 1 h to reduce free reducing sugars to their respective alditols. Reduction was stopped by the addition of acetic acid (20 μl) and borate removed by repeated evaporation with 5% AcOH in MeOH (3×) and MeOH (3×). The samples were then dried and derivatised to partially methylated alditol acetates as described by Bonnett et al. (1994). The derivatives were separated by GC on a Hewlett Packard Ultra 2 capillary column (50 m×0.20 mm i.d., 0.33 μm film thickness) with the GC oven programmed from 130°C (held for 1 min) to 230°C at a rate of 3°C min^{-1} and analysed by MS using a HP 5970 MSD.

3.8. ^{13}C NMR spectroscopy

Fructans (~50 mg) were dissovled in 0.8 ml D_2O (99.96 atom%) in 5-mm tubes and spectra recorded at 30°C on a Brüker WM-300 spectometer (75 MHz). Chemical shifts were measured relative to internal DMSO at δ 40.4 ppm.

Acknowledgements

We are grateful to Dr. H. Wong for recording the ^{13}C NMR spectra and to Dr. R. Falshaw for critical assessment of the manuscript. This research was supported by the New Zealand Foundation for Research, Science and Technology and by the Biotechnology and Biological Sciences Research Council (UK). We are grateful to the ISAT Linkages Fund of the Royal Society of New Zealand for the provision of travel funds to I.M.S.

References

Bancal, P., Gibeaut, D.M., Carpita, N.C., 1993. Analytical methods for the determination of fructan structure and biosynthesis. In: Suzuki, M., Chatterton, N.J. (Eds.), Science and Technology of Fructans. CRC Press, Boca Raton, pp. 83–118.

Bonnett, G.D., Sims, I.M., Simpson, R.J., Cairns, A.J., 1997. Structural diversity of fructan in relation to the taxonomy of the Poaceae. New Phytol. 136, 11–17.

Bonnett, G.D., Sims, I.M., St. John, J.A., Simpson, R.J., 1994. Purification and characterization of fructans with β-2,1- and β-2,6-glycosidic linkages suitable for enzyme studies. New Phytol. 127, 261–269.

Brasch, D.J., Fankhauser, B.L., McDonald, A.G., 1988. A study of the glucofructofuranan from the New Zealand cabbage tree *Cordyline australis*. Carbohydr. Res. 180, 315–324.

Cairns, A.J., Pollock, C.J., 1988. Fructan biosynthesis in exised leaves of *Lolium temulentum* L. I. Chromatographic characterization of oligofructans and thier labelling patterns following $^{14}CO_2$ feeding. New Phytol. 109, 399–405.

Cairns, A.J., Nash, R., Machado de Carvalho, M.-A., Sims, I.M., 1999. Characterisation of the enzymatic polymerisation of 2,6-linked fructan by leaf extracts from timothy grass (*Phleum pratense*). New Phytol. 142, 79–91.

Carpita, N.C., Housley, T.L., Hendrix, J.E., 1991. New features of plant-fructan structure revealed by methylation analysis and carbon-13 n.m.r. spectroscopy. Carbohydr. Res. 217, 127–136.

Dorland, L., Kammerling, J.P., Vliegenthart, J.F.G., Satyanarayana, M.N., 1977. Oligosaccharides isolated from *Agave vera cruz*. Carbohydr. Res. 54, 275–284.

Dubois, M., Gilles, K.A., Hamilton, J.K., Rebers, P.A., Smith, F., 1956. Colorimetric method for determination of sugars and related substances. Anal. Chem. 28, 350–356.

Henry, R.J., Darbyshire, B., 1980. Sucrose:sucrose fructosyltransferase and fructan:fructan fructosyltransferase from *Allium cepa*. Phytochemistry 19, 1017–1020.

Kanaya, K.I., Chiba, S., Shimomura, T., 1978. Thin-layer chromatography of linear oligosaccharides. Agric. Biol. Chem. 42, 1947–1948.

Lever, M., 1972. A new reaction for colorimetric determination of carbohydrates. Anal. Biochem. 47, 273–279.

Liu, J., Waterhouse, A.L., Chatterton, N.J., 1991. Proton and carbon NMR chemical-shift assignments for 6-kestose and neokestose from two-dimensional N.M.R. measurments. Carbohydr. Res. 217, 43–49.

Liu, J., Waterhouse, A.L., Chatterton, N.J., 1993. Proton and carbon NMR chemical-shift assignments for [β-D-Fru*f*-(2→1)]$_3$-(2↔1)-α-D-Glc*p* (nystose) and [β-D-Fru*f*-(2→1)]$_4$-(2↔1)-α-DGlc*p* (1,1,1-kestopentaose) from two-dimensional NMR spectral measurements. Carbohydr. Res. 245, 11–19.

Pollard, C.J., 1978. Fructose oligosaccharides in monocotyledons: a possible delimitation of the order Liliales. Biochem. Systematics and Ecology 10, 245–249.

Shiomi, N., 1993. Structure of fructopolysaccharide (asparagosin) from roots of asparagus (*Asparagus officinalis* L.). New Phytol. 123, 263–270.

Sims, I.M., Pollock, C.J., Horgan, R., 1992. Structural analysis of oligomeric fructans from excised leaves of *Lolium temulentum*. Phytochemistry 31, 2989–2992.

Sims, I.M., Smouter, H., Pollock, C.J., Simpson, R.J., 1991. The separation of complex mixtures of fructo-oligosaccharides from plants. Plant Physiol. Biochem. 29, 257–267.

Smouter, H., Simpson, R.J., 1989. Occurrence of fructans in the Gramineae (Poaceae). New Phytol. 111, 359–368.

Spies, T., Praznik, W., Hofinger, A., Altmann, F., Nitsch, E., Wutka, R., 1992. The structure of the fructan sinistrin from *Urginea maritima*. Carbohydr. Res. 235, 221–230.

St. John, J.A., Sims, I.M., Bonnett, G.D., Simpson, R.J., 1997a. Identification of products formed by a fructan:fructan fructosyltransferase activity from *Lolium rigidum*. New Phytol. 135, 249–257.

St. John, J.A., Sims, I.M., Bonnett, G.D., Simpson, R.J., 1997b. Synthesis of fructans by partially purified fructosyltransferase activites from *Lolium rigidum*. New Phytol. 136, 39–51.

Waterhose, A.L., Chatterton, N.J., 1993. Glossary of fructan terms. In: Suzuki, M., Chatterton, N.J. (Eds.), Science and Technology of Fructans. CRC Press, Boca Raton, pp. 1–7.

Watson, L,. Dallwitz, M.J., 1992 onwards. The families of flowering plants: descriptions, illustrations, identification, and information retrieval. Version: 19 August 1999. http://biodiversity.uno.edu/delta.

Wise, C.S., Dimler, R.J., Davis, H.A., Rist, C.E., 1955. Determination of easily hydrolysable fructose units in dextran preparations. Anal. Chem. 27, 33–36.

PERGAMON

Phytochemistry 57 (2001) 669–673

PHYTOCHEMISTRY

www.elsevier.com/locate/phytochem

Biotransformation of (+)- and (−)-camphorquinones by plant cultured cells

Wen Chai[a], Hiroki Hamada[b], Jumpei Suhara[a], C. Akira Horiuchi[a,*]

[a]*Department of Chemistry, Rikkyo (St. Paul's) University, Nishi-Ikebukuro, Toshima-ku, Tokyo 171-8501, Japan*
[b]*Department of Applied Science, Faculty of Science, Okayama University of Science, Ridai-cho, Okayama 700-0005, Japan*

Received 15 August 2000; received in revised form 23 January 2001

Abstract

Biotransformation of (+)- and (−)-camphorquinones with suspension plant cultured cells of *Nicotiana tabacum* and *Catharanthus roseus* was investigated. It was found that the plant cultured cells of *N. tabacum* and *C. roseus* reduce stereoselectively the carbonyl group of (+)- and (−)-camphorquinones to the corresponding α-keto alcohols. © 2001 Elsevier Science Ltd. All rights reserved.

Keywords: *Nicotiana tabacum*; Solanaceae; *Catharanthus roseus*; Apocynaceae reduction; Biotransformation; (+)-Camphorquinone; (−)-Camphorquinone; 2-*exo*-Hydroxyepicamphor; 2-*endo*-Hydroxyepicamphor; 3-*exo*-Hydroxycamphor; 3-*endo*-Hydroxycamphor

1. Introduction

Asymmetric reductions of ketones by biocatalysts are useful preparative methods to obtain chiral alcohols (Sih and Chen, 1984). Chiral α-keto alcohols are useful and important intermediates for the synthesis of optically active natural products having stereodirecting groups. In previous work, microbes such as baker's yeast have been used widely to reduce camphorquinone. (Pfrunder and Tamm, 1969; Chenevert and Thiboutot, 1988; Rebolledo et al., 1991; Miyazawa et al., 1995). In the report of Miyazawa, (+)-camphorquinone (**1a**) was stereoselectivity reduced by *Glemerella cingulata* to give (−)-3*S*-*exo*-hydroxycamphor (**4a**).

On the other hand, plant cultured cells have been studied for the ability to transform foreign substrates into useful substances (Suga and Hirata, 1990). However, hitherto known biochemical reduction of the carbonyl group by plant culture cells is only NADH-dependent reduction of the C–C double bond of α,β-unsaturated ketones (Hirata et al., 1982; Shimoda et al., 1998). There is very little information on the biotransformation of diketones by plant cultured cells. Here, we report that the biotransformation of (+)- and (−)-camphorquinones (**1a** and **1b**) by *N. tabacum* and *C. roseus* yields the corresponding α-keto alcohols.

2. Results and discussion

2.1. Biotransformation of (+)-camphorquinone (*1a*) and (−)-camphorquinone (*1b*) by N. tabacum

It was found that cultured cells of *N. tabacum* reduce substrates **1a** and **1b** into α-keto alcohols. (−)-Camphorquinone (**1b**) afforded a mixture of diastereomeric isomers of four α-keto alcohols: (−)-2*S*-*exo*-hydroxy epicamphor (**3b**); (+)-3*R*-*exo*-hydroxycamphor (**2b**); (−)-3*S*-*endo*-hydroxycamphor (**4b**) and (+)-2*R*-*endo*-hydroxyepicamphor (**5b**). (+)-Camphorquinone (**1a**) was bioselectively transformed to give three corresponding enantiomers: (+)-2*R*-*exo*-hydroxyepicamphor (**3a**); (−)-3*S*-*exo*-hydroxycamphor (**4a**) and (+)-3*R*-*endo*-hydroxycamphor (**5a**). However, (−)-2*S*-*endo*-hydroxyepicamphor (**2a**) could not be formed from **1a** in this work (Schemes 1 and 2). Table 1 shows results of time-course experiments. (+)-Camphorquinone (**1a**) was easily reduced to obtain (−)-3*S*-*exo*-hydroxycamphor (**4a**, 57%) and (+)-2*R*-*exo*-hydroxyepicamphor (**3a**, 37%) as the major products after 10 h incubation. Substrate **1b** was transformed to (−)-2*S*-*exo*-hydroxy

* Corresponding author. Fax: +81-3-5992-3434.
E-mail address: horiuchi@rikkyo.ac.jp (C.A. Horiuchi).

0031-9422/01/$ - see front matter © 2001 Elsevier Science Ltd. All rights reserved.
PII: S0031-9422(01)00133-9

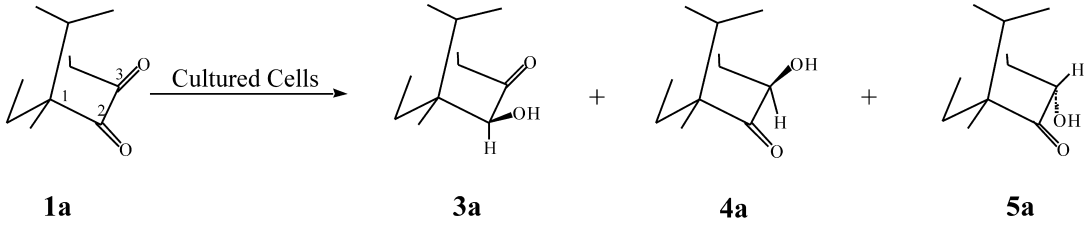

Scheme 1. Biotransformation of (+)-camphorquinone (**1a**) by plant cultured cells.

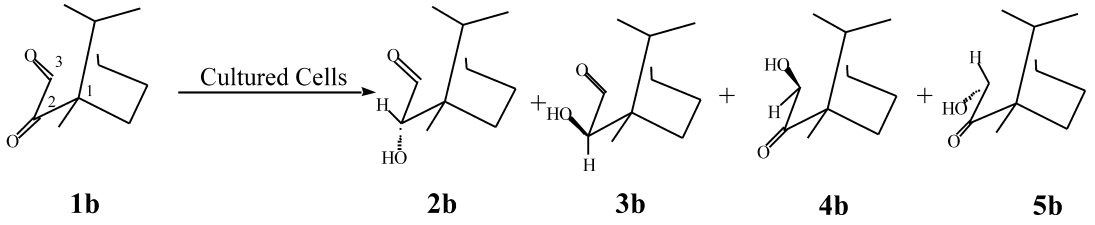

Scheme 2. Biotransformation of (−)-camphorquinone (**1b**) by plant cultured cells.

Table 1
Biotransformation of camphorquinone by plant cultured cells

Substrate	Plant cultured cells	T/h[a]	Total yield/%[b]	Product ratio/%			
(+)-Camphorquinone (**1a**)				**2a**	**3a**	**4a**	**5a**
	C. roseus	3	96	/	11	66	23
	N. tabacum	10	82	/	37	57	6
(−)-Camphorquinone (**1b**)				**2b**	**3b**	**4b**	**5b**
	C. roseus	10	93	25	5	29	41
	N. tabacum	18	98	8	49	37	6

[a] T is reaction time.
[b] Total yield is the yield of product isolated.

epicamphor (**3b**, 49%) and (−)-3*S*-*endo*-hydroxycamphor (**4b**, 37%) after 18 h. (Figs. 1 and 2).

2.2. Biotransformation of (+)-camphorquinone (*1a*) and (−)-camphorquinone (*1b*) by C. roseus

Incubation of substrates **1a** and **1b** with cultured cells of *C. roseus*, also gave the corresponding α-keto alcohols. Compound **1a** rapidly disappeared and was undetectable after 3 h incubation. Compound **1a** was converted to (−)-3*S*-*exo*-hydroxy-camphor (**4a**, 66%) as the major product. Compound **1b** was transformated to (+)-2*R*-*endo*-hydroxyepicamphor (**5b**, 41%) as the major product at the end of 10 h.

2.3. Discussion

After incubation, the column mixtures of α-keto alcohols were applied to a silica gel. Elution with *n*-hexane–Et_2O (3:1) gave two products: 2β-hydroxycamphor (**3**) and 3β-hydroxycamphor (**4**) were identified by their IR, GC–MS and NMR spectral data. In addition, the ^1H NMR spectral data of the proton at C_2 or C_3 position of products **3** and **4** agreed with those of the authentic samples (Thoren, 1970). From the ^1H NMR spectral data of the reaction mixtures, the presence of 2α-hydroxycamphor (**2**) and 3α-hydroxycamphor (**5**) has been shown (Table 2). Then, the structures and relative yields of the products were determined on the basis of the ^1H NMR spectral peak areas of the proton at C_2 or C_3 position. The transformation products and their yields are shown in Table 1.

In this paper, we have used plant suspension cells to transform camphorquinone. (+)-Camphorquinone (**1a**) was stereoselectively reduced by *C. roseus* and *N. tabacum* to give (−)-3*S*-*exo*-hydroxycamphor (**4a**) over a short time period (3–10 h). It was found that it is more rapid than the reduction of **1a** by *Glemerella cingulata* and *Mucor mucedo* (Miyazawa et al., 1995) with the same stereoselectivity (9–24 h).

3. Experimental

3.1. Analytical and substrates

IR: Jasco FT–IR 230; GC–MS: Shimadzu GCMS-QP5050 (EI–MS 70 eV) using DB1 (0.25 mm × 30 m,

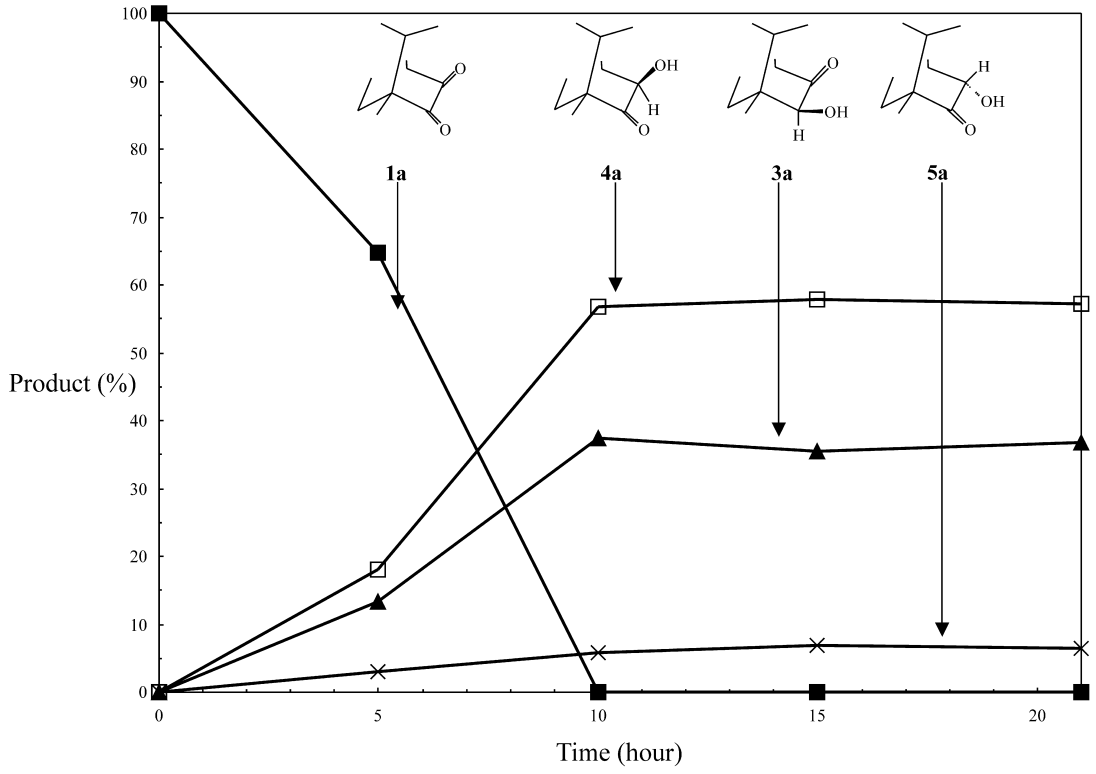

Fig. 1. Biotransformation of (1*S*)-(+)-camphorquinone (**1a**) using *Nicotiana tabacum*.

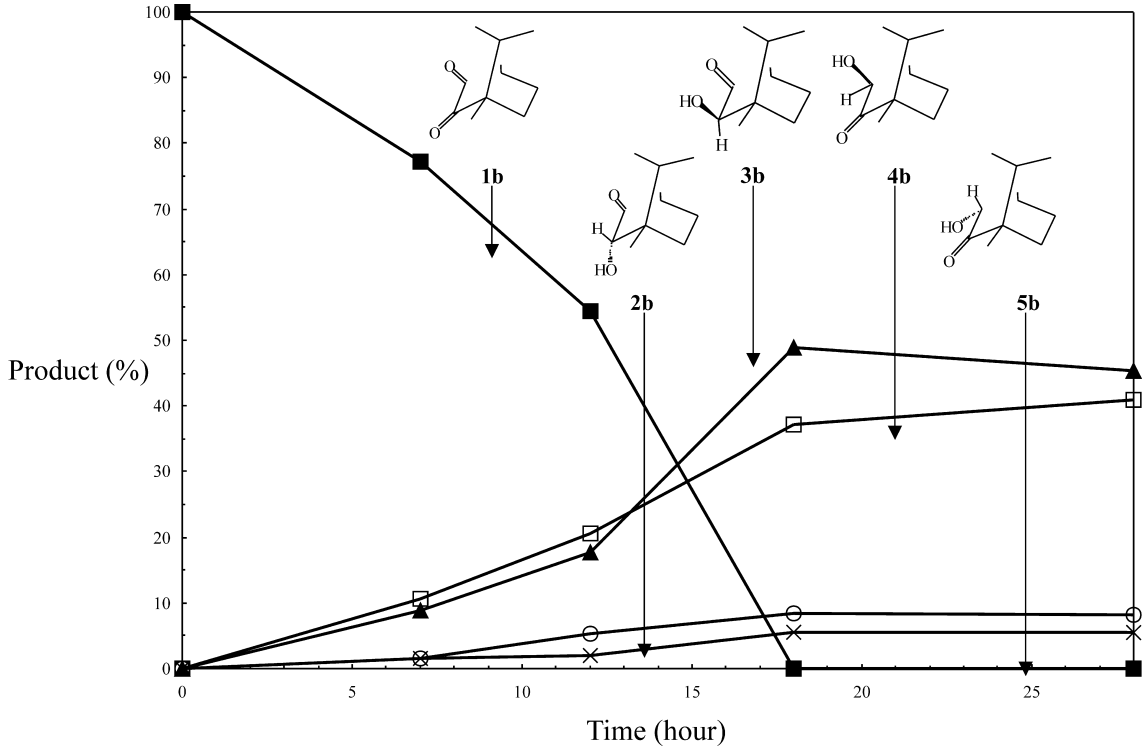

Fig. 2. Biotransformation of (1*R*)-(−)-camphorquinone (**1b**) using *Nicotiana tabacum*.

Table 2
^{1}H NMR spectra[a] of the α-ketols

Compound	$CDCl_3$: δ C_2 or C_3[b]	Compound	$CDCl_3$: δ C_2 or C_3
2α-Hydroxycamphor	3.87 (*s*, *b*, 1H)	**2**	3.86 (*s*, *b*, 1H)
2β-Hydroxycamphor	3.58 (*s*, 1H)	**3** (isolated)	3.54 (*s*, 1H)
3β-Hydroxycamphor	3.72 (*s*, 1H)	**4** (isolated)	3.75 (*s*, 1H)
3α-Hydroxycamphor	4.28 (*d*, *J* = 5 Hz, 1H)	**5**	4.21 (*d*, *J* = 5 Hz, 1H)

[a] Shifts are given in ppm downfield from the TMS signal; *s* = singlet; *d* = doublet; *b* = broadened.
[b] Thoren (1970).

0.25 μm) capillary column GC; GC: GC-17A at a column temp. of 80–200°C at 10°C/min; ^{1}H and ^{13}C NMR: Jeol GSX 400 spectrometer.

(1*S*)-(+)-Camphorquinone was purchased from Aldrich Chem. Co. (mp 200–202°C, $[\alpha]_D^{25}$ +100° (C_6H_5 CH_3; c 1.9)). (1*R*)-(−)-Camphorquinone was purchased from Tokyo Kasei Kogyo Co., Ltd (mp 200°C).

3.2. Cultivation of suspension cells of *N. tabacum* and *C. roseus*

The callus tissues of *N. tabacum* were transferred to freshly prepared MS medium (Murashige and Skoog, 1962) containing 1 ppm of 2,4-dichlorophenoxyacetic acid as auxin and 3% sucrose, and then were grown with continuous shaking (110 rpm) for 8 days at 25°C under the light. The callus tissues of *C. roseus* were transferred to freshly prepared SH medium (Schenk and Hildebrandt, 1976) containing 2 ppm of 2,4-dichlorophenoxyacetic acid as auxin and 3% sucrose, and then were grown with continuous shaking (110 rpm) for 8 days at 25°C under the light.

3.3. Time-course experiment

The details are described below using **1a** as an example. A part of the callus tissues (15 g) was transferred to 50 ml culture medium in a 200 ml Erlenmeyer flask and grown with continuous shaking for 8 days at 25°C under light (about 2000 Lux). The substrate **1a** (20 mg) was administered to the suspension cells and the cultures were incubated at 25°C in a rotary shaker (110 rpm) under light. At regular intervals, one of the flasks was taken out and the incubation mixture was filtered and extracted with EtOAc–Et_2O (1:1). The extract so obtained was then subjected to ^{1}H NMR spectral analysis. The yields of the products were determined on the basis of the peak area from ^{1}H NMR spectra and expressed as a relative percentage to the total amount of the total reaction mixture extracted.

3.4. Isolation of the metabolic products

After incubation, the culture medium was filtered. The supernatent was then saturated with NaCl and extracted with EtOAc–Et_2O (1:1). The resulting residue was applied to a silica gel column, that was eluted with *n*-hexane–Et_2O (3:1) to give: 2β-hydroxycamphor (**3**), (IR (KBr): ν 3448, 1751 and 1098 cm^{-1}; CI–MS *m*/*z*: $[M+H]^+$ 169; ^{1}H NMR ($CDCl_3$): δ (ppm) 0.94 (*s*, 3H), 1.03 (*s*, 3H), 1.04 (*s*, 3H), 1.18–1.94 (*m*, 4H), 2.18 (*d*, *J* = 7 Hz, 1H), 2.65 (*s*, *b*, 1H) and 3.54 (*s*, 1H); ^{13}C NMR ($CDCl_3$): δ (ppm) 10.3, 18.9, 20.3, 21.2, 33.9, 46.6, 49.2, 58.6, 79.5 and 218.7) and 3β-hydroxycamphor (**4**), (IR (KBr): ν 3448, 1751 and 1123 cm^{-1}; CI–MS *m*/*z*: $[M+H]^+$ 169; ^{1}H NMR($CDCl_3$): δ (ppm) 0.94 (*s*, 3H), 0.95 (*s*, 3H), 1.00 (*s*, 3H), 1.20–2.00 (*m*, 4H), 2.10 (*d*, *J* = 5 Hz, 1H), 2.59 (*s*, *b*, 1H) and 3.75 (*s*, 1H); ^{13}C NMR($CDCl_3$): δ (ppm) 9.03, 20.1, 21.0, 25.2, 28.6, 48.2, 49.2, 57.0, 77.4 and 220.0) (Thoren, 1970)

The ratios of the isomers were calculated from the peak areas of ^{1}H NMR spectral data: δ 3.86 (*s*, *b*, 1H for **2**), 3.54 (*s*, 1H for **3**), 3.75 (*s*, 1H for **4**) and 4.21 (*d*, *J* = 5 Hz, 1H for **5**).

References

Chenevert, R., Thiboutot, S., 1988. Baker's yeast reduction of 1,2-diketones. Preparation of pure (*S*)-(−)-2-hydroxy-1-phentl-1-propanone. Chem. Lett., 1191.

Hirata, T., Hamada, H., Aoki, T., Suga, T., 1982. Stereoselectivity of the reduction of carvone and dihydrocarvone by suspension cells of *Nicotiana tabacum*. Phytochemistry 21, 2209.

Miyazawa, M., Nobata, M., Hyakumachi, M., Kameoka, H., 1995. Biotransformation of (+)- and (−)-camphorquinones by fungi. Phytochemistry 39, 569.

Murashige, T., Skoog, F., 1962. A resised medium for rapid growth and bio assays with tobacco tissue cultures. Physiologia Plantarum 15, 473.

Pfrunder, B., Tamm, Ch., 1969. Mikrobiologische umwandlung von bicyclischen monoterpenen durch *Absidia orchidis* (VUILL) HAGEM. 1. Teil: reduktion von campherchinon und isofenchonchinon. Helvetica Chimica Acta 52, 1630.

Rebolledo, F., Roberts, S.M., Willetts, A.J., 1991. Biotransformation of cycloalkanediones by microorganisms; stereoselective reduction of (±)-camphorquinone. Biotechnology Letters 13, 245.

Schenk, R.U., Hildebrandt, A.C., 1972. Medium and techniques for induction and growth of monocotyledonous and dicotyledonous plant cell cultures. Canadian Journal of Botany 50, 199.

Shimoda, K., Hirata, T., Noma, Y., 1998. Stereochemistry in the reduction of enones by the reductase from *Euglena gracilisz*. Phytochemistry 49, 49.

Sih, C.J., Chen, C.S., 1984. Microbial asymmetric catalysis-enantioselective reduction of ketones. Angewandte Chemie International Edition in English. 23, 570.

Suga, T., Hirata, T., 1990. Review article number 55 biotransformation of exogenous substrates by plant cell cultures. Phytochemistry 29, 2393.

Thoren, S., 1970. Four isomeric α-hydroxybornanones. Acta Chemica Scandinavica 24, 93.

PERGAMON

Phytochemistry 57 (2001) 675–680

PHYTOCHEMISTRY

www.elsevier.com/locate/phytochem

Biotransformation of geranyl acetate to geraniol during palmarosa (*Cymbopogon martinii*, Roxb. wats. var. *motia*) inflorescence development

Vinod Shanker Dubey, Rajesh Luthra*

Biochemistry Division, Central Institute of Medicinal and Aromatic Plants, Lucknow- 226015 (U.P.), India

Received 24 May 2000; received in revised form 29 November 2000

Abstract

Only immature palmarosa (*Cymbopogon martinii*, Roxb. wats. var. *motia*) inflorescence with unopened spikelets accumulated essential oil substantially. Geraniol and geranyl acetate together constituted about 90% of the palmarosa oil. The proportion of geranyl acetate in the oil decreased significantly with a corresponding increase of geraniol, during inflorescence development. An esterase enzyme activity, involved in the transformation of geranyl acetate to geraniol, was detected from the immature inflorescence using a gas chromatographic procedure. The enzyme, termed as geranyl acetate cleaving esterase (GAE), was found to be active in the alkaline pH range with the optimum at pH 8.5. The catalysis of geranyl acetate was linear up to 6 h, and after 24 h of incubation, 75% of the geranyl acetate incubated was hydrolyzed. The GAE enzymic preparation, when stored at 4°C for a week, was quite stable with only 40% loss of activity. The physiological role of GAE in the production of geraniol during palmarosa inflorescence development has been discussed. © 2001 Elsevier Science Ltd. All rights reserved.

Keywords: Palmarosa; Cymbopogon; Essential oil; Geraniol; Geranyl acetate; Esterase; Biotransformation

1. Introduction

Cymbopogon martinii, Roxb. wats. var. *motia*, commonly known as palmarosa, is a wild perennial undershrub, whose flowering tops and leaves yield an essential oil rich in the acyclic monoterpenoid geraniol. Palmarosa oil is used for imparting rose like aroma to a wide range of perfumes, soaps, cosmetics, toiletry and tobacco products. The antiseptic, mosquito repellent and pain relieving properties of the oil makes it of considerable pharmaceutical significance as well. The characteristic odour of palmarosa oil lies in its high content of total alcohol mainly geraniol and a small but varying amount of esters, particularly geranyl acetate (Husain, 1994). Monoterpenoids, the major constituents of the essential oils, are derived from geranyl pyrophosphate (GPP), synthesized through head to tail fusion of isopentenyl pyrophosphate (IPP) with dimethylallyl pyrophosphate (DMAPP) (Singh et al., 1989b). IPP is in turn derived from the conventional mevalonate-isoprenoid pathway or the newly discovered non-mevalonate (pyruvate/triose-phosphate) pathway (McCaskill and Croteau, 1998; Lichtenthaler, 1999; Luthra et al., 1999; Rohmer, 1999). GPP may undergo cyclization, coupling, hydroxylation and/or rearrangement to produce the parent monoterpene carbon skeleton, followed by a variety of secondary chemical transformations viz. oxidation, reduction, acetylation, isomerization and hydration etc. to produce the myriad of monoterpenoids encountered in plants (Singh et al., 1989b). The biotransformation of monoterpenyl acetate to monoterpenol is of great interest as the monoterpenol–monoterpenyl acetate pair occur widely in aromatic plants. Furthermore they influence the quality of the essential oil distilled from such plants.

Geraniol which constitutes about 80% of the palmarosa oil is derived from pyrophosphorylysis of GPP. Our studies with developing palmarosa inflorescence have shown that in immature inflorescence, a substantial amount of geraniol undergoes acetylation to form geranyl acetate,

Abbreviations: DTE, dithioerythreitol; EDTA, ethylenediaminetetraacetic acid; GAE, geranyl acetate esterase; GC, gas chromatography

* Corresponding author. Tel.: +91-522-342676; fax: +91-522-342666.

E-mail address: cimap@satyam.net.in (R. Luthra).

0031-9422/01/$ - see front matter © 2001 Elsevier Science Ltd. All rights reserved.
PII: S0031-9422(01)00122-4

which gets hydrolyzed to produce geraniol, as the inflorescence matures. Thus, developing palmarosa inflorescence seems to be an ideal system to study the metabolism of acyclic monoterpenols. The interconversion of geraniol and geranyl acetate is presumably dependent on a complex interplay of different regulatory controls operating at the organ, cellular, subcellular and enzyme levels. There is, however, limited experimental support for these mechanisms. There are several reports with respect to chemical composition of the palmarosa oil (Saxena and Maheshwari, 1980; Akhila et al., 1984; Boelens, 1994), reproductive and breeding behaviour (Srivastava, 1987), mutational studies for crop improvement (Srivastava et al., 1998; Srivastava and Satpute, 1998), and plant tissue culture work in relation to salt tolerance (Patnaik and Debata, 1997). The present study was undertaken to understand the metabolism of geraniol and geranyl acetate during palmarosa inflorescence development. Emphasis has been presented to demonstrate the enzyme activity involved in the transformation of geranyl acetate into geraniol, the major secondary reaction occuring during palmarosa inflorescence development. The identification of an esterase enzyme activity involved in catalysis of acyclic monoterpenyl acetate is reported for the first time.

2. Results and discussion

2.1. Ontogenic changes in essential oil content and composition

Palmarosa (*Cymbopogon martinii*) inflorescence (flowering top), consisting of partially opened spikelets, contained a higher percentage of essential oil than the leaf (Table 1). Though geraniol was the major constituent of the inflorescence and leaf oil, the inflorescence oil contained a relatively higher percentage of geranyl acetate than the leaf oil (Luthra et al., 1995). The fresh weight (g/100 spikelets) of the inflorescence decreased appreciably as the spikelets opened (Fig. 1).

Table 1
Relative percentage of geraniol and geranyl acetate in leaf and inflorescence oil of palmarosa

Plant part[a]	Essential oil (% V/FW)	Relative % in essential oil[b]		
		Geraniol	Geranyl acetate	Unknown
Leaf	1.10	80.9	7.9	11.2
Inflorescence	1.30	53.5	34.0	12.5

[a] The leaf and the inflorescence sample was collected at partially opened spikelet stage.

[b] The leaf and inflorescence essential oil values significantly differ from each other by Student's *t*-test at $P < 0.05$.

The dry weight (g/100 spikelets) of the inflorescence, however, increased until the fully-opened spikelets (III) stage and then decreased (Fig. 1). An appreciable decrease in dry weight after the fully opened spikelets (III) stage suggests that the palmarosa inflorescence undergoes maturation after the spikelets were fully opened. Since fr. wt and dry wt of the spikelets vary with inflorescence development, the representation of the oil content on a unit weight basis (data not given) creates ambiguity with respect to the pattern of essential oil accumulation. The expression of results on spikelet development warrants more interest. Therefore, to avoid ambiguity, essential oil content, composition and other related parameters have been discussed only on spikelet basis during the inflorescence maturation.

The essential oil content exhibited phasic changes during palmarosa inflorescence development (Fig. 2). The essential oil content was maximum at the unopened spikelets (I) stage, and decreased significantly with their development. Since the observed levels of essential oil, accumulated during inflorescence development, are the net result of the anabolic and catabolic processes, the results suggest that only the immature inflorescence with unopened spikelets is biogenetically active to substantially accumulate essential oil (Fig. 2). One of the most important characteristics of essential oil accumulation is its dependence on the developmental stage of the concerned organ/plant part (Singh et al., 1989a,b). The concentration of volatile extracts has been, for example, reported to be highest in large buds prior to anthesis in *Boronia* flower (Mactavish and Menary, 1997), whereas in the rose flower, the essential oil content increased till open flower stage and then declined as

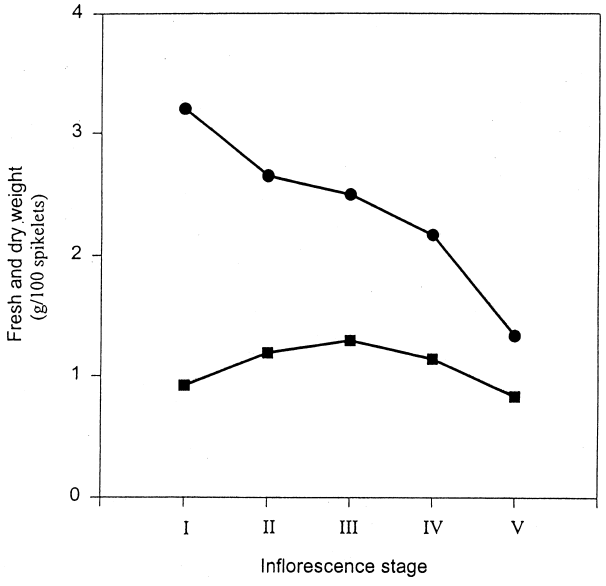

Fig. 1. Changes in fr. (●) and dry (■) wt of the spikelets during inflorescence development.

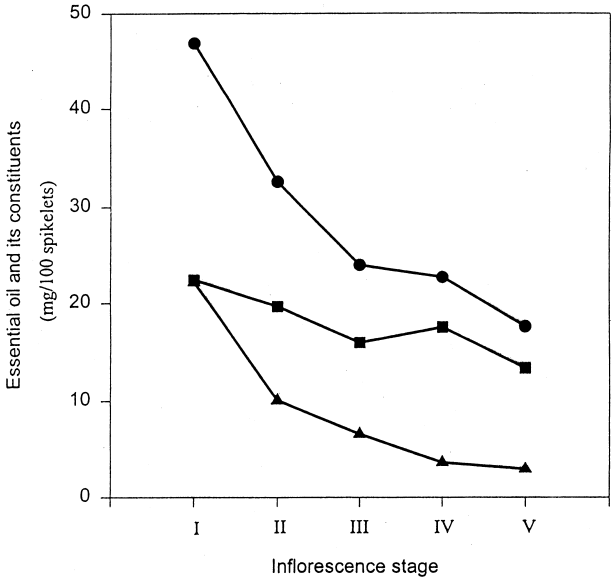

Fig. 2. Changes in essential oil content (●) and its major constituents, geraniol (■) and geranyl acetate (▲), during inflorescence development.

the flower became visibly senescent (Pogorel'skaya et al., 1980).

Gas chromatographic (GC) analysis of the essential oil from various developmental stages indicated that the geranyl acetate percentage in the oil decreased significantly from the unopened spikelets (I) stage (48%) to the partially mature spikelets (IV) stage (16%) with a corresponding increase in geraniol percentage (Fig. 3). These results suggest the role of an esterase enzyme in producing geraniol during this period. Geraniol% in the leaf oil increased from 81 to 86% with maturity, and is accompanied by a corresponding decrease in geranyl acetate (Luthra et al., 1995). The menthyl acetate content of the volatile oil in flowering peppermint, however, increased with maturity and resulted in an altered flavour characteristic of the essence distilled from flowering plants (Croteau and Hooper, 1978). Similar studies in lemongrass (*Cymbopogon flexuosus*) and citronella Java (*C. winterianus*) leaves indicated that the developmental phase influences the expression of monoterpene metabolism (Singh and Luthra, 1988; Singh et al., 1989a, 1990, 1991; Luthra et al., 1991). The relative percentage of geraniol and citronellol in the oil from immature citronella leaf increased with the tissue age along the leaf blade, and was accompanied by a corresponding decrease in geranyl acetate and citronellyl acetate (Luthra et al., 1991). The geraniol content in the palmarosa oil increases from the vegetative stage to the full flowering stage and is accompanied by a decrease in geranyl acetate content (Saxena and Maheshwari, 1980; Akhila et al., 1984). Though the geraniol percentage in the palmarosa inflorescence essential oil increased with inflorescence development, the absolute amount of geraniol decreased (Figs. 2 and 3). Since geraniol is the major constituent of the palmarosa oil at all the stages of inflorescence development, it is expected that the decrease in the essential oil content, as the inflorescence matured, shall be governed largely by the geraniol pool. Monoterpenyl glycosides have been implicated in terpene catabolism which involves their transport to the roots, where they are converted to primary metabolites (Croteau, 1987). Therefore, the decrease in geraniol content with maturity might be due to its glycosylation to form geranyl-D-glycosides for use in catabolic processes. Work in this direction needs to be carried out to determine the exact mechanism of catabolism.

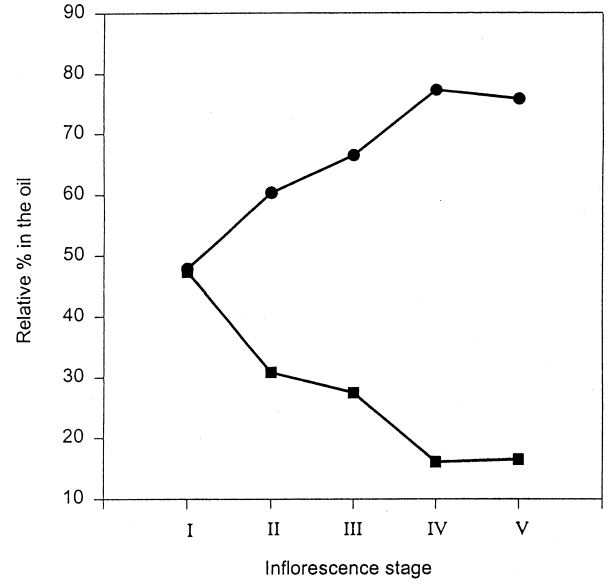

Fig. 3. Relative percentage of geraniol (●) and geranyl acetate (■) in the oil during inflorescence development.

2.2. Detection of geranyl acetate cleaving esterase activity

The enzyme which converts geranyl acetate to geraniol is named, after the reaction it catalyzes, as geranyl acetate cleaving esterase (GAE) (Dubey and Luthra, 1999). GAE activity was detected in palmarosa inflorescence using a gas chromatographic (GC) procedure. Geranyl acetate was incubated under defined conditions with respect to pH, temperature, substrate and enzyme concentration for a particular time and the amount of geraniol produced was used as an indicator of GAE activity (Fig. 4). Saturating levels (2 μmol/ml) of the substrate geranyl acetate and 0.5–1.0 mg of the enzyme protein were used in each assay. The enzyme GAE was most active in the pH range 8.0–9.0 and showed maximal activity at pH 8.5 (0.05 M Tris–HCl) and temperature 30°C. Preiss et al. (1988) have reported maximum esterase activity at pH 8.0 from tomato cell cultures hydrolyzing pyrethroid insecticide cyfluthrin, whereas, cell wall bound lanatoside 15′-*o*-acetyl esterase (LAE) from

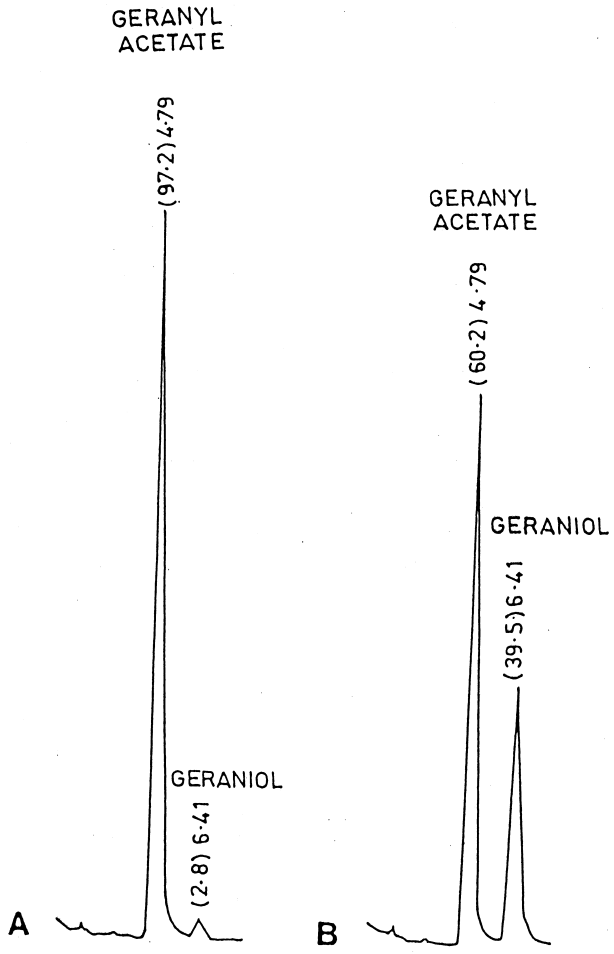

Fig. 4. Gas chromatograms (GC) of the geranyl acetate esterase (GAE) catalyzed reaction (A = control, B = assay) depicting hydrolysis of geranyl acetate (GA) to produce geraniol (G). The substrate GA was incubated with the enzymic preparation from palmarosa inflorescence for 4 h under defined conditions. The values in parentheses represent the relative% of G and GA, whereas the values outside parentheses represent the retention time.

Digitalis lanata cell suspension cultures (involved in cardenolides transformation) was found to be most active in the acidic range at pH 5.5 (Sutor and Kreis, 1996; Kandzia et al., 1998). A cyclic monoterpenyl acetate esterase from *Mentha piperita* leaves, which catalyzes transformation of menthyl acetate to menthol, also showed maximum activity at pH 8.0 (Croteau and Hooper, 1978). Thus esterases in plant system exhibited a wide pH range. The GAE activity increased linearly with protein concentration up to 1.0 mg per assay (data not given). The technical difficulty usually encountered in solubilization of geranyl acetate (substrate) was overcome by its dispersion in assay buffer containing Tween-20 (10 μg/μmol of substrate). Tween-20 had no adverse effect on the GAE activity even at concentrations much higher than that present in the assay system.

A time course experiment was performed to study the linearity of the hydrolysis of geranyl acetate during the incubation period. A linear catalytic rate was found up to 6 h of incubation at 30°C using 1 mg of enzyme protein. Almost 75% of the geranyl acetate was hydrolyzed after 24 h of incubation (Fig. 5). No geraniol was produced in the control using boiled enzyme. The enzyme in the crude preparation, when stored at 4°C, was quite stable for one week with 40% loss of activity. This is unlike other secondary metabolic enzymes, which are normally unstable in the crude preparations (Croteau, 1987; Singh et al., 1989b). The enzyme is being purified to study its kinetic attributes.

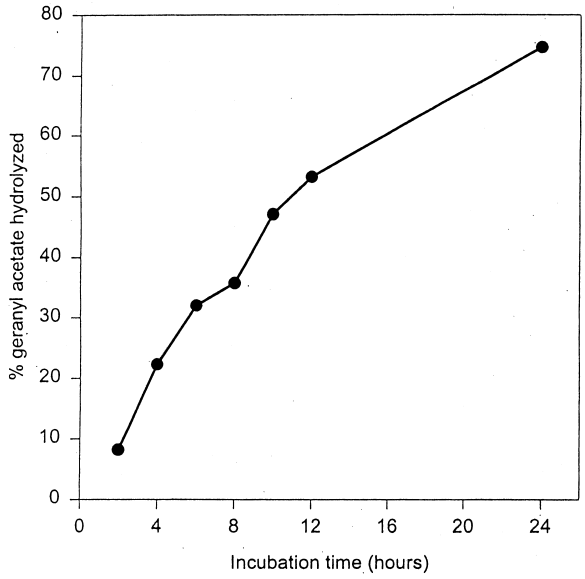

Fig. 5. Time course of hydrolysis of geranyl acetate by enzymic preparation from palmarosa inflorescence.

3. Conclusion

The geranyl acetate proportion in the oil decreased substantially with concomitant increase in geraniol during palmarosa inflorescence development, suggesting the role of an esterase in producing geraniol. A geranyl acetate hydrolyzing activity, referred to as geranyl acetate esterase (GAE), could be detected using a gas chromatographic procedure.

4. Experimental

4.1. Plant material and chemicals

Palmarosa (*Cymbopogon martinii*, Roxb. Wats. var. *motia*) plants were raised from seedlings at the experimental farm of the Central Institute of Medicinal and Aromatic Plants (CIMAP), Lucknow, by following the standard agronomic practices. The inflorescence (flowering top consisting of spikelets), was tagged at the time

of emergence. The samples were taken at 8 days interval, representing five developmental stages viz. stage I — unopened spikelets, stage II — partially opened spikelets (anthers partially visible), stage III — fully opened spikelets (yellow anthers fully visible), stage IV — partially mature spikelets (anthers brown and yellow), stage V — fully mature spikelets (brown inflorescence). The spikelets were removed from the inflorescence at each developmental stage and used for various studies. The leaf sample was collected at partially opened spikelet stage.

Geraniol and geranyl acetate were purchased from Sarsynthase (France) and the biochemicals from Sigma Chemical Co. (USA). Solvents and other chemicals used were of high purity (analytical reagent grade) and were obtained from E. Merck and Spectrochem (India).

4.2. Isolation and gas chromatographic analysis of essential oil

The essential oil was extracted from the freshly harvested spikelets (100 g) by steam distillation technique using a mini-Clevenger apparatus as described earlier (Luthra et al., 1991). The essential oil was collected in small stoppered tubes containing anhydrous sodium sulphate to remove moisture. The oil density was determined to convert the volume yields into their respective weights. The essential oil samples were analyzed for their major constituents viz. geraniol and geranyl acetate, using gas chromatography (GC). The GC analysis was performed using a Perkin Elmer (model 3920 B) apparatus equipped with FID (flame ionization detector) and a stainless steel column (2 m×3 mm i.d.) packed with 10% FFAP (free fatty acid phase) on chromosorb WAW (80–100 mesh). The operating conditions were: column temperature isothermal at 165°C, injector and detector temperatures 200 and 250°C, respectively. Nitrogen and hydrogen flow rates were adjusted to 30 and 28 ml/min., respectively. The geraniol and geranyl acetate peaks were identified by coinjecting authentic standards and quantified using a Varian integrator (model 4400). The quantitative values of the various oil constituents were computed from the relative percentage data and the amount of oil per 100 spikelets.

4.3. Enzyme extraction and assay

All the operations of enzyme isolation were carried out at 0–4°C unless specified. The extraction of the enzyme was optimized with respect to buffer, pH, protecting and stabilizing agents to obtain maximum extractable activity. Preliminary enzyme assays were done to standardize the assay conditions, and linearity of the reaction rate with time as well as protein concentration. The extraction medium consisted of 0.1 M NaPi buffer (pH 6.5) containing 50 mM sodium metabisulphite, 10 mM-mercaptoethanol, 10 mM ascorbic acid, 0.25 M sucrose and 1 mM EDTA-Na_2. The spikelets (partially opened stage) were homogenized in cold extraction medium (1 g tissue/ 3 ml) in the presence of 50% (w/w) insoluble PVPP (polyvinyl polypyrrolidone). The slurry was squeezed through four layers of muslin cloth and centrifuged at 15,000×g for 60 min. Purified amberlite XAD-4 resin (50% of the tissue weight) was added to the supernatant and kept for 5 min at 4°C to remove the endogenous terpenes of the tissue. The slurry thus formed was filtered through muslin cloth and the clear supernatant obtained was used to determine geranyl acetate cleaving esterase activity using geranyl acetate as substrate.

The terpenoid substrate geranyl acetate was solubilized by dispersion in the solution of Tween-20 (10 μg/μmol of the substrate) in assay buffer. The geranyl acetate cleaving esterase activity was determined by gas chromatographic (GC) monitoring of geraniol produced by the hydrolysis of geranyl acetate. The assay system consisted of 0.05 M Tris–HCl buffer (pH 8.5), 5 mM $MgCl_2$, 1 mM DTE, 2 mM geranyl acetate and the enzyme extract (0.5–1.0 mg protein), in a total volume of 0.5 ml. The reaction mixture was incubated at 30°C in a sealed capped tube for varying intervals (2–24 h). The geraniol produced and leftover geranyl acetate was then extracted with ether and subjected to GC analysis. The appearance of geraniol peak indicated the presence of geranyl acetate esterase activity. A blank with the boiled enzyme was also run simultaneously. The time course experiment was repeated three times to confirm the results.

4.4. Other determinations

For the determination of fr. wt and dry wt, a known number of spikelets (200) were weighed immediately after harvesting, and then oven dried at 65°C till a constant weight. Total soluble proteins were estimated by the Bradford (1976) method.

Acknowledgements

The authors are grateful to Dr. Sushil Kumar, Director, CIMAP, Lucknow, India, for providing facilities. The financial assistance from CSIR to V.S.D. as Senior Research Fellowship is gratefully acknowledged.

References

Akhila, A., Tyagi, B.R., Naqvi, A.A., 1984. Variation of essential oil constituents in *Cymbopogon martinii* (wats) var. *motia* at different stages of plant growth. Indian Perfumer 28, 126–128.

Boelens, M.H., 1994. Sensory and chemical evaluation of tropical grass oils. Perfumer and Flavorist 19, 29–45.

Bradford, M.M., 1976. A rapid and sensitive method for the quantitative determination of microgram quantities of protein utilizing the principle of protein-dye binding. Analytical Biochemistry 72, 248–254.

Croteau, R., 1987. Biosynthesis and catabolism of monoterpenoids. Chemical Review 87, 929–954.

Croteau, R., Hooper, C.L., 1978. Metabolism of monoterpenes: Acetylation of (−)-menthol by a soluble enzyme preparation from peppermint (*Mentha piperita*) leaves. Plant Physiology 61, 737–742.

Dubey, V.S., Luthra, R., 1999. Identification of an esterase as the key enzyme involved in geraniol formation in palmarosa inflorescence. Abstract in National Conference on Plant Biotechnology: Towards Strategic Agriculture and Drug Development held at CIMAP, Lucknow on 15–17 March, pp. 112.

Husain, A., 1994. Palmarosa. In: Essential Oil Plants and their Cultivation. Central Institute of Medicinal and Aromatic Plants (CIMAP), Lucknow, India, pp. 58-66.

Kandzia, R., Grimm, R., Eckerskorn, C., Lindermann, P., Luckner, M., 1998. Purification and characterization of lanatoside 15′-*O*-acetyl esterase (LAE) from *Digitalis lanata* Ehrh. Planta 204, 383–389.

Lichtenthaler, H.K., 1999. The 1-deoxy-D-xylulose-5-phosphate pathway of isoprenoid biosynthesis in plants. Annual Review of Plant Physiology and Plant Molecular Biology 50, 47–65.

Luthra, R., Dubey, V.S., Sangwan, R.S., 1995. Metabolism of monoterpenoids in *Cymbopogon martinii*. Abstract in 64th Annual Meeting of SBC (I) held at Lucknow, India on 6–8 October, pp. 127.

Luthra, R., Luthra, P.M., Kumar, S., 1999. Redefined role of mevalonate-isoprenoid pathway in terpenoid biosynthesis in higher plants. Current Science 76, 133–135.

Luthra, R., Singh, N., Sharma, S., 1991. Changes in monoterpene content accompanying development of *Cymbopogon winterianus* Jowitt leaves. Journal of Essential Oil Research 3, 349–354.

Mactavish, H.S., Menary, R.C., 1997. The effect of flower maturity and harvest timing on floral extract from *Boronia megastigma* (Nees). Annals of Botany 80, 299–303.

McCaskill, D., Croteau, R., 1998. Some caveats for bioengineering terpenoid metabolism in plants. Trends in Biotechnology 16, 349–355.

Patnaik, J., Debeta, B.K., 1997. Regeneration of plantlets from NaCl tolerant callus lines of *Cymbopogon martinii* (Roxb.) wats. Plant Science 128, 67–74.

Pogorel'skaya, A.N., Kholodova, V.P., Reznikova, S.A., 1980. Physiological aspect of essential oil accumulation in petals of the flowers of essential oil-rose. Soviet Plant Physiology 27, 279–284.

Preiss, U., Wallnofer, P.R., Engelhardt, G., 1988. Partial purification and properties of an esterase from tomato cell suspension cultures hydrolyzing the pyrethroid insecticide cyfluthrin. Pesticide Science 23, 13–24.

Rohmer, M., 1999. The discovery of a mevalonate-independent pathway for isoprenoid biosynthesis in bacteria, algae and higher plants. Natural Products Report 16, 565–574.

Saxena, D.B., Maheshwari, M.L., 1980. Terpenoids from palmarosa grass (*Cymbopogon martinii* var. *motia*). Indian Perfumer 24, 115–120.

Singh, N., Luthra, R., 1988. Sucrose metabolism and essential oil accumulation during lemongrass (*Cymbopogon flexuosus* Stapf.) leaf development. Plant Science 57, 127–133.

Singh, N., Luthra, R., Sangwan, R.S., 1989a. Effect of leaf position and age on the essential oil quantity and quality in lemongrass (*Cymbopogon flexuosus* Stapf.). Planta Medica 55, 254–256.

Singh, N., Luthra, R., Sangwan, R.S., Thakur, R.S., 1989b. Metabolism of monoterpenoids in aromatic plants. Current Research in Medicinal and Aromatic Plants 11, 174–197.

Singh, N., Luthra, R., Sangwan, R.S., 1990. Oxidative pathways and essential oil biosynthesis in the developing lemongrass (*Cymbopogon flexuosus*) leaf. Plant Physiology and Biochemistry 28, 703–710.

Singh, N., Luthra, R., Sangwan, R.S., 1991. Mobilization of starch and essential oil biogenesis during leaf ontogeny of lemongrass (*Cymbopogon flexuosus* Stapf.). Plant Cell Physiology 32, 803–811.

Srivastava, H.K., 1987. Phenotypic patterns in relation to herbage and oil yield in *Cymbopogon martinii* Wats. var. *motia* Burk. International Journal of Crude Drug Research 26, 22–28.

Srivastava, H.K., Misra, A., Satpute, G.K., 1998. Influence of ethophon as chemical hybridizing agent on growth, photosynthesis, chloroplastic pigments and essential monoterpene oils in palmarosa (*Cymbopogon martinii*). Journal of Herbs, Spices and Medicinal Plants 6, 24–30.

Srivastava, H.K., Satpute, G.K., 1998. Induction of mutations for enhanced essential oil in palmarosa (*Cymbopogon martinii*). Journal of Essential Oil Research 10, 287–291.

Sutor, R., Kreis, W., 1996. Partial purification and characterization of cell wall associated lanatoside 15′-*O*-acetyl esterase from *Digitalis lanata* suspension cultures. Plant Physiology and Biochemistry 34, 763–770.

PERGAMON

Phytochemistry 57 (2001) 681–687

PHYTOCHEMISTRY

www.elsevier.com/locate/phytochem

Seasonal variation of monoterpene emission from *Malus domestica* and *Prunus avium*

Francesca Rapparini*, Rita Baraldi, Osvaldo Facini

Istituto di Ecofisiologia delle Piante Arboree da Frutto, CNR, Via Gobetti 101, 40129 Bologna, Italy

Received 13 November 2000; received in revised form 6 March 2001

Abstract

Emission rates of monoterpenes released by apple (*Malus domestica* Borkh) and cherry (*Prunus avium* L.) were estimated at different phenological stages. These measurements employed a dynamic flow-through Teflon chamber, sample collection onto cartridges filled with graphitized carbon and thermal desorption gas chromatography–mass spectrometry (GC–MS) for identification and quantification of the emitted volatiles. At full bloom the release of monoterpene hydrocarbons from cherry flowers was 1213 ng g^{-1} dry weight (DW) h^{-1}, exceeding by approximately three-fold the emission rate of apple flowers (366 ng g^{-1} DW h^{-1}). Observed seasonal variations in biogenic volatile organic compound (VOC) emissions ranged over several order of magnitudes. At fruit-set and ripening stages, in fact, the hydrocarbon emission dramatically decreased reaching the lowest values at harvest time when leaves were fully mature (3–9 ng g^{-1} DW h^{-1}). Wide diversity in the composition of compounds from the species studied was also recorded. At blooming, linalool contributed significantly to the monoterpene emission from apple (94% of the emitted carbon) while α-pinene and camphene represented on average more than 60% of the total emitted volatiles from cherry flowers. Among the monoterpenes identified in flowers, α-pinene, camphene and limonene were also found in the foliage emission of both species. Fruit trees are relevant monoterpene emitters only at blooming and thus for a short period of the vegetative cycle. When leaves are fully developed, the carbon loss due to monoterpene emissions related to the photosynthetically carbon gain is negligible. © 2001 Published by Elsevier Science Ltd. All rights reserved.

Keywords: *Malus domestica*; *Prunus avium*; Rosaceae; Apple; Cherry; Emission; Monoterpenes; Flowers; Leaves; Seasonality

1. Introduction

It is well recognized that vegetation emits a wide range of photochemically reactive hydrocarbons in the atmosphere (Fehsenfeld et al., 1992; Hewitt et al., 1995), exceeding the anthropogenic emission of non-methane hydrocarbons by approximately one order of magnitude (Singh and Zimmerman, 1992). Isoprene and monoterpenes are the dominant classes of biogenic compounds released by terrestrial vegetation into the atmosphere (Guenther et al., 1995). In the last decade, a lot of attention has been given to characterizing volatile organic compounds (VOC) emission from plants (Benjamin et al., 1996; Kesselmeier and Staudt,1999) and to estimate the emission rates of these compounds from vegetable cover for a better understanding of the role of natural VOC in relation to the tropospheric air chemistry and to global change. Several inventories of biogenic hydrocarbons on regional and global scale have been published which focus on isoprene and monoterpene emissions (Guenther et al., 1995; Simpson et al., 1995). Terpenoids emitted from vegetation are in fact involved in processes regulating the oxidative capacity of the atmosphere and the formation of tropospheric ozone. Moreover, the emission of hydrocarbons represents a loss of carbon that was photosynthetically assimilated. According to the literature, this carbon loss ranges between a few thousands and some percent (Harley, 1994; Hansen et al., 1997; Kesselmeier et al., 1997, 1998).

A large surface of several European countries is covered by orchards, which represent an economically important resource in the Mediterranean area. To investigate the possible contribution of fruit trees to biogenic emissions from this area, the terpenoid emission pattern of several fruit species was determined during a preliminary study which was conducted in controlled condition on entire fruit plantlets at full bloom (Baraldi et al., 1999). This

* Corresponding author. Tel.: +39-051-6399014; fax: +39-051-6399024.

E-mail address: rapparini@istea.bo.cnr.it (F. Rapparini).

0031-9422/01/$ - see front matter © 2001 Published by Elsevier Science Ltd. All rights reserved.
PII: S0031-9422(01)00124-8

screening indicated that fruit trees are monoterpene emitters and that the amount and composition of flower emission varies mainly between pome and stone fruits.

Since seasonal variation has been observed in many cases (Lerdau et al., 1995; Street et al., 1996; Guenther, 1997; Staudt et al., 1997), it should always be considered for an accurate estimation of the annual VOC release from vegetation. The changes of seasonal emissions are in some cases linked to plant growth and phenological events such as budding, flowering, leaf development, fruiting etc (Robertson et al., 1995; Hakola et al., 1998).

The objective of this study was to follow the whole canopy emissions during the vegetation cycles of young cherry and apple trees, as representative of stone and pome fruit plants respectively, in order to better understand the potential contribution of fruit trees to the tropospheric air chemistry and to the global carbon cycle. The experiments were conducted in controlled chamber during different phenological stages: at blooming, when leaves are not yet developed, at fruit-set, when leaves are young, and at fruit ripening, when leaves are mature.

2. Results and discussion

Typical reconstructed chromatograms of air samples from flowers and leaves of fruit trees are illustrated in Fig. 1. At blooming stage (Fig. 2) the total monoterpene emission rate calculated on a flower dry weight (DW) basis was 1213 ng g^{-1} DW h^{-1} in cherry, about three times greater than that recorded in apple (366 ng g^{-1} DW h^{-1}). Thus, according to Guenther et al. (1996) who considered plant species to be high emitters if the total emissions exceed about 0.5 μg g^{-1} h^{-1}, cherry can be considered a high monoterpene emitter while, on the contrary, apple emitted negligible amounts of hydrocarbons. The different emissions were accompanied by characteristic differences in the emission composition. A higher number of monoterpene compounds were identified in cherry compared to apple (Table 1) but, as generally reported in the literature, only few predominating components characterized flower fragrance, accompanied by a larger number of minor compounds (Pellmyr et al., 1987; Matile and Altenburger, 1988). Indeed, the main portion of emitted monoterpenes was α-pinene and camphene, which on average counted for over 60% of the emitted carbon from cherry flowers. β-Myrcene alone represented 15% of the emitted volatiles while limonene, β-pinene, linalool and camphor, together constituted about 17% of the total hydrocarbon rates.

Linalool is by far the most abundant volatile of apple flowers accounting for 94% of the total emission. This result confirms the findings obtained in the previous screening which evidenced differences in monoterpene emission mainly between stone and pome fruit plants, being these last the highest emitters of linalool (Baraldi et al., 1999). On the other hand, an important ecophysiological functions of this alcohol is generally recognized since is a typical components of flowering fragrance attracting pollinators (Loughrin et al., 1990; Bergström, 1991; Knudsen and Tollsten, 1993). Among the other monoterpenes, Δ^3-carene, limonene and α-terpinolene were also reported as headspace constituents emitted in traces from living apple flowers by Buckbauer et al. (1993).

Similar rates of volatile emission were also observed when the blooming trees were kept in the dark (data not shown) as also reported in apple by Loughrin et al., (1990). Although different experimental approaches are needed to confirm these results, it is not surprising that these species are not vesperescent taking into account the biological significance of the flower fragrance emission in attracting insect pollinators and since fruit trees are primarily bee pollinated (Faust, 1989).

Despite of the larger biomass of the emitting organs, at fruit-set and ripening the release of monoterpenes from the leaves dramatically decreased in the tested species. In fact, average VOC emission rates calculated per gram dry weight of leaves, varied from 12 to 18 ng g^{-1} DW h^{-1} at fruit-set to 3–8 ng g^{-1}DW h^{-1} at ripening (Fig. 3).

Among the monoterpene hydrocarbons identified in flowers, α-pinene, camphene and limonene were also found in the foliar emission of both species. Limonene was always the major compound released by apple leaves. Δ^3-carene and α-phellandrene were characteristic compounds of apple and cherry emission, respectively, since they were released at all the phenological stages.

In our experimental condition (PPFD = 800 μmol m^{-2} s^{-1}; $T = 28°C$), CO_2 assimilation ranged on average from 15 to 20 μmol m^{-2} s^{-1}, values comparable to the data reported in the literature (Flore and Lakso, 1989; DeJong, 1983), and that corresponded to 540–720 μmol g^{-1} DW h^{-1} in apple and cherry, respectively. By consequence, the carbon loss as foliar emission by both species was irrelevant compared to the C-fixed during the photosynthetic activity.

In conclusion, this investigation confirmed a genotypic effect on the composition and total emission of biogenic volatiles released by fruit trees, and evidenced the existence of significant seasonal fluctuations in monoterpene emissions. Indeed, as observed for other species, the temporal variations of VOC emitted by fruit trees ranged from several order of magnitudes, suggesting that the developmental stages and the phenological status of the plant play a significant role on volatile production (Robertson et al., 1995; Guenther, 1997; Hakola et al., 1998).

The biological significance of fragrance emission by flowers for these entomophilic plants, which need to interact with their impollinators, is well known. Due to this ecological function, orchards represent a substantial source of reactive hydrocarbons only for a short period

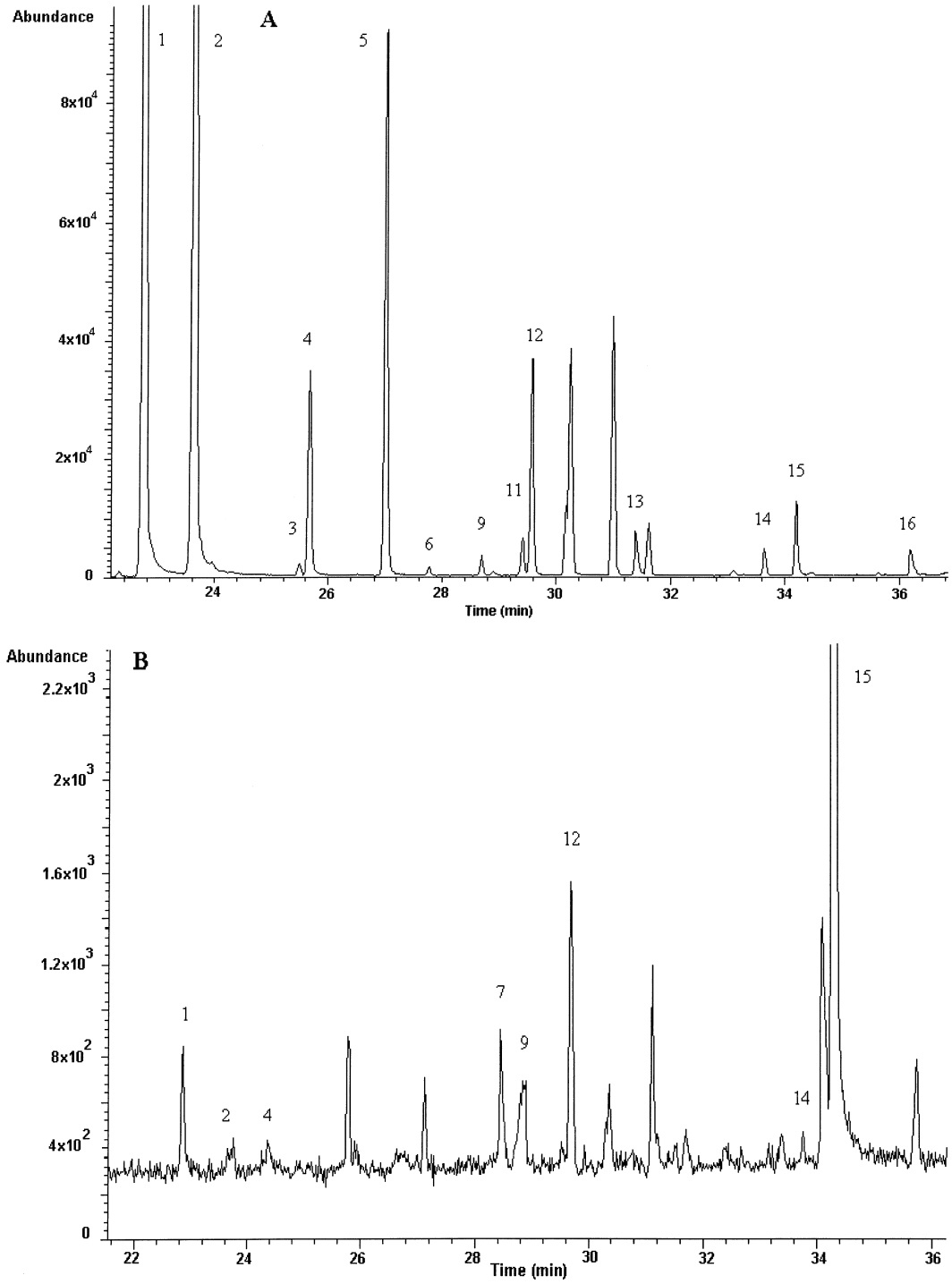

Fig. 1. Reconstructed mass chromatogram (m/z) obtained from GC–MS analysis of cherry (A) and apple (B) flower emission showing the profile of monoterpene hydrocarbons.

of the vegetation cycle, in spring, when the flowers are open and ready to be impollinated and the carbon sequestration by the not yet developed foliage is irrelevant. Later on in the season, when leaves develop or when they become mature, the total monoterpene emission rates become very low and the resulting carbon loss due to hydrocarbon emission is negligible compared to the carbon gain through the photosynthetic activity.

3. Experimental

3.1. Plant material

Three year-old plants of apple (*Malus domestica* Borkh. cv Earligold) and sweet cherry (*Prunus avium* L. cv Sunburst) were grown outdoors in 6 l pots in commercial soil under natural light conditions. Plants were

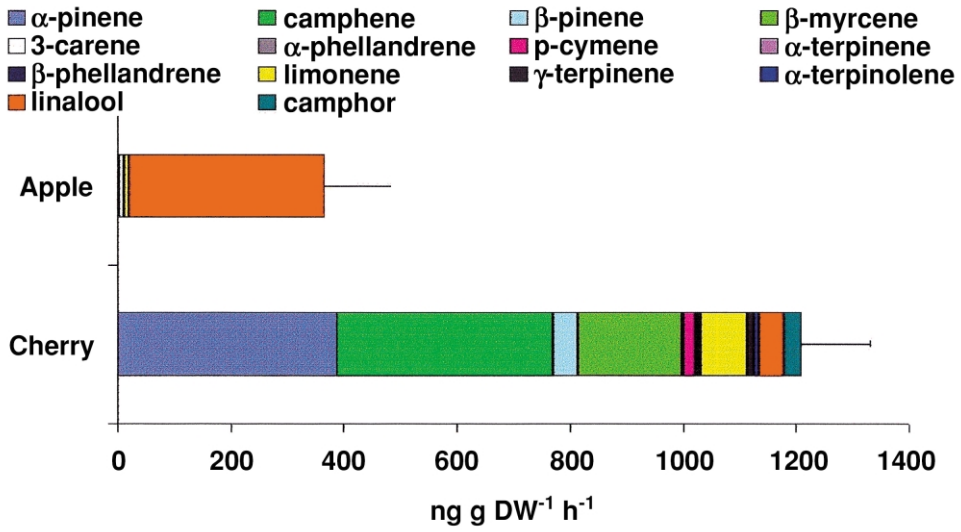

Fig. 2. Monoterpene emission rates given on a flower dry weight basis of apple and cherry at blooming. The error bars note the standard deviation of the mean sum of the monoterpene emissions at PPFD = 800 μmol m^{-2} s^{-1}.

Table 1
Percentage contribution of each identified compound to the total monoterpene emission of apple and cherry at different phenological stages[a]

Peak n.	Compound	SI[d]	Rt[e] (min)	Blooming (%)		Fruit-set (%)		Ripening (%)	
				Cherry	Apple	Cherry	Apple	Cherry	Apple
1	α-Pinene	93	22.7	31.9±0.9	0.2±0.1	12.1±2.8	14.6±3.6	12.9±3.1	5.3±1.5
2	Camphene	93	23.6	31.6±0.7	0.1±0.1	3.8±0.2	14.6±3.6	4.3±0.4	2.2±0.4
3	β-Pinene	93	25.7	3.6±1.1	0.5±0.3	3.0±0.5	nd	12.9±3.4	nd
4	β-Myrcene	41	27.0	15.3±4.3	nd	9.9±2.7	1.1± 0.9	4.3±1.5	0.5±0.1
5	α-Phellandrene	93	27.8	0.1±0.1	nd	15.8±3.5	nd	31.5±5.6	nd
6	Δ^3-Carene	93	28.3	nd[c]	2.2±0.2	nd	7.3±2.3	nd	6.5±1.5
7	D_{14}-Cymene (ISTD[b])	130	28.4	–	–	–	–	–	–
8	α-Terpinene	93	28.7	0.3±0.2	0.1±0.1	1.9±0.4	2.3±0.3	nd	4.1±1.3
9	ρ-Cymene	119	28.9	1.8±0.2	nd	31.3±7.1	0.6±0.2	nd	21.6±4.5
10	β-Phellandrene	93	29.4	0.4±0.1	nd	nd	nd	nd	nd
11	Limonene	68	29.7	6.7±1.9	2.4±0.6	15.4±4.8	35.4±9.0	21.4±5.9	25.8±4.5
12	γ-Terpinene	93	31.6	1.1±0.2	nd	0.5±0.2	2.8±1.2	4.3±0.3	4.4±1.4
13	α-Terpinolene	93	33.6	0.7±0.1	0.2±0.1	nd	1.7±0.5	nd	1.3±0.2
14	Linalool	71	34.2	3.5±0.4	94.3±1.6	5.7±2.2	11.8±5.3	nd	11.4±2.7
15	Camphor	95	36.2	2.8±0.5	nd	0.6±0.3	7.9±2.3	8.6±1.9	16.9±2.6

[a] Values represent the means±standard error of three experiments.
[b] ISTD = internal standard.
[c] nd = not detected.
[d] SI = selected ion.
[e] Rt = retention time.

regularly watered until the beginning of the laboratory experiments, which were carried out at times corresponding to full bloom, fruit-set and fruit ripening.

3.2. Volatile collection

Three plants of each species were individually transferred 24 h before the experiments to a 300 l flow-through Teflon growth chamber at 26–28°C under natural daylight conditions. A constant flow of filtered air (9 l min^{-1}) was maintained inside the chamber which was equipped with a ventilator to ensure a rapid mixing of the air. Attention was focused on minimizing physical damage to the plants. Plants were then adapted to the following experimental conditions: constant temperature (28°C), constant relative humidity (60%) and constant photosynthetic photon flux density (PPFD = 800 μmol m^{-2} s^{-1}). After 4 h, gas samples of 3 l were taken from the outlet of the chamber and collected at a flow rate of 50 ml min^{-1} onto carbonaceous traps

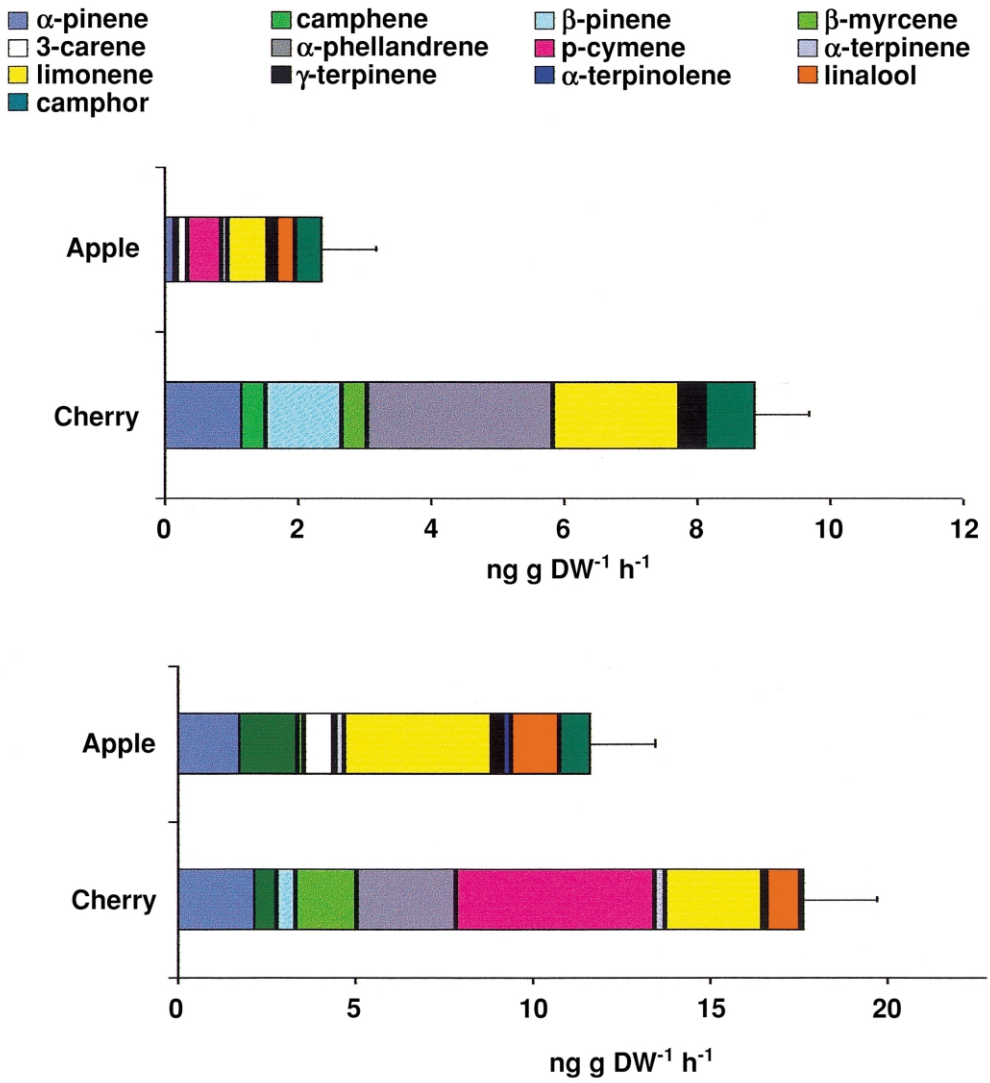

Fig. 3. Monoterpene emission rates given on a leaf dry weight basis of apple and cherry at fruit set (above) and ripening (below). The error bars note the standard deviation of the mean sum of the monoterpene emissions at PPFD = 800 μmol m^{-2} s^{-1}.

(Carbograph 1 and Carbograph 2, LARA, Rome, Italy) packed in glass tubes (Ciccioli et al., 1993). Two VOC samplings for each plant were taken simultaneously. The airflow rates were controlled with a mass-flow controller. The photon flux density in the photosynthetically active wavelength range was measured using a Li-Cor (NE, USA) 1800 spectroradiometer and the air temperature with copper constantan thermocouples (RS components, Vimodrone, Milan, Italy)

3.3. Biomass

In order to assess the biomass of the enclosed plants the dry weight of individual flowers and leaves was determined after drying the plant materials for 48 h at 70° C. The projected leaf area was determined using an image analysis method.

3.4. Analysis of volatiles and CO_2

The trapped compounds were thermodesorbed at 250°C and cryofocused at −150°C on a fused silica liner using a Thermal Desorption Cold Trap Injector (Chrompack, Middleburg, The Netherlands) connected to a Hewlett Packard 5890 gas chromatograph (GC) using a 5970 quadrupole mass spectrometer (MS) as detection system (Hewlett Packard, Palo Alto, CA, USA). The desorbed sample, enriched on the cryofocusing unit, was transferred to the capillary column (60 m × 0.25 mm I.D.; 0.25 μm film of polymethylsiloxane; HP-1, Hewlett Packard) by heating the fused silica liner to 230°C. The separation of terpenes was achieved maintaining the oven temperature at 40°C for 10 min and programming to 220°C at 5°C min^{-1}. Mass spectra and the reconstructed chromatogram were obtained by

automatically scanning in the mass range m/z from 20 to 200 a.m.u. Comparison of retention time and mass spectra of authentic standards achieved identification. Quantification of monoterpenes was performed after calculation of standard curves and response factors for each compound, and using d_{14}-cymene as internal standards (ISTD). The comparison of the response for the m/z 93 ion was generally used for quantification. Exceptions are reported in Table 1. The biogenic VOC emission rates were calculated by multiplying the concentration difference between chamber inlet and outlet air with the air flow through the chamber divided by the total biomass dry weight of the plant material (flowers or leaves).

Concurrently with the monoterpene emission measurements, CO_2 analyses were conducted using an infra-red gas analyzer (ADC 2250, Scientific Ltd Hoddesdon, Herts, UK) operating in a closed mode. The relationship between carbon loss due to monoterpene emissions and photosynthetically carbon uptake was then estimated.

Acknowledgements

We wish to thank Dr. Federica Rossi for suggestions in the design of this project, and Antonio Mazza and Matteo Mari for their careful technical assistance. We are also grateful to Dr. Ester Sztein for the revision of the manuscript. This paper is part of the EUROTRAC-BIATEX2 program.

References

Baraldi, R., Rapparini, F., Rossi, F., Latella, A., Ciccioli, P., 1999. Volatile organic compound emissions from flowers of the most occurring and economically important species of fruit trees. Phys. Chem. Earth (B) 24, 729–732.

Benjamin, M.T., Sudo, I.M., Bloch, L., Winer, A.M., 1996. Low-emitting urban forests: a taxonomic methodology for assigning isoprene and monoterpene emission rates. Atmos. Envir. 30, 1437–1452.

Bergström, G., 1991. Chemical ecology of terpenoids and other fragrances of angiosperm flowers. In: Harborne, J.B., Thomas-Barberan, F.A. (Eds.), Ecological Chemistry and Biochemistry of Plant Terpenoids. Clarendon Press, Oxford., pp. 287–296.

Buckbauer, G., Jirovetz, L., Wasicky, M., Nikiforov, A., 1993. Headspace and essential oil analysis of apple flowers. J. Agric. Food Chem. 41, 116–118.

Ciccioli, P., Brancaleoni, E., Cecinato, A., Sparapani, R., 1993. Identification and determination of biogenic and anthropogenic volatile organic compounds in forest areas of Northern and Southern Europe and a remote site of the Himalayan region by high resolution gas chromatography-mass spectrometry. J. Chrom. 643, 55–69.

DeJong, T.M., 1983. CO_2 assimilation characteristics of five *Prunus* tree fruit species. J. Am. Soc. Hort. Sci. 108, 303–307.

Faust, M., 1989. Physiology of Temperate Zone Fruit Trees. John Wiley and Sons, New York.

Fehsenfeld, F., Calvert, J., Fall, R., Goldan, P., Guenther, A.B., Hewitt, C.N., Lamb, B., Liu, S., Trainer, M., Westberg, H., Zimmerman, P., 1992. Emissions of volatile organic compounds from vegetation and the implications for atmospheric chemistry. Global Biogeochem. Cycles 6, 389–430.

Flore, J.A., Lakso, A.N., 1989. Environmental and physiological regulation of photosynthesis in fruit crops. Hort. Rev. 11, 111–157.

Guenther, A., 1997. Seasonal and spatial variations in natural volatile organic compound emissions. Ecol. Appl. 7, 34–45.

Guenther, A., Hewitt, C.N., Erickson, D., Fall, R., Geron, C., Graedel, T., Harley, P., Klinger-Leardau, M., McHay.W.A., Pierce, T., Scholes, B., Steinbrecher, R., Tallamraju, R., Taylor, J., Zimmerman, P., 1995. A global model of natural volatile organic compound emissions. J. Geophys. Res. 100, 8873–8892.

Guenther, A., Otter, L., Zimmerman, P., Greenberg, J., Scholes, R., Scholes, M., 1996. Biogenic hydrocarbon emissions from southern African savannas. J. Geophys. Res. 101, 25, 859–25, 865.

Hansen, U., Van Eijk, J., Bertin, N., Staudt, M., Kotzias, D., Seufert, G., Fugit, J.L., Torres, L., Cecinato, A., Brancaleoni, E., Ciccioli, P., Bomboi, T., 1997. Biogenic emission and CO_2 gas exchange investigated on four Mediterranean shrubs. Annals Bot. 60, 39–57.

Hakola, H., Rinne, J., Laurila, T., 1998. The hydrocarbon emission rates of Tea-Leafed Willow (*Salix phylicifolia*), Silver Birch (*Betula pendula*) and European Aspen (*Populus tremula*). Atmos. Environ. 32 (10), 1825–1833.

Harley, P.C., Litvak, M.E., Sharkey, T.D., Monson, R.K., 1994. Isoprene emission from Velvet bean leaves. Interaction among nitrogen availability, growth, photon flux density, and leaf development. Plant Physiol. 105, 279–285.

Hewitt, N.C., Cao, X.L., Boissard, C.H., Duckham, S.C., 1995. Atmospheric VOCs from natural sources. In: Hester, R.E., Harrison, R.M. (Eds.), Volatile organic compounds in the atmosphere, Issues in Environmental Science and Technology, Vol. 4. and The Royal Society of Chemistry, Cambridge, pp. 17–36.

Kesselmeier, J., Staudt, M., 1999. Biogenic volatile organic compounds (VOC): an overview on emission, physiology and ecology. J. Atmos. Chem. 33, 23–88.

Kesselmeier, J., Bode, K., Hofmann, U., Müller, H., Schäfer, L., Wolf, A., Ciccioli, P., Brancaleone, E., Cecinato, A., Frattoni, M., Foster, P., Ferrari, C., Jacob, V., Fugit, J.L., Dutaur, L., Simon, V., Torres, L., 1997. The BEMA-project: emission of short chain organic acids, aldehydes and monoterpenes from *Quercus ilex* L. and *Pinus pinea* L. in relation to physiological activities, carbon budget and emission algorithms. Atmos. Environ. 31, 119–134.

Kesselmeier, J., Bode, K., Schäfer, L., Schabeske, G., Wolf, A., Brancaleone, E., Cecinato, A., Ciccioli, P., Frattoni, M., Dutaur, L., Fugit, J.L., Simon, V., Torres, L., 1998. Simultaneous field measurements of terpene and isoprene emissions from two dominant Mediterranean oak species in relation to a North American species. Atmos. Environ. 32, 1947–1953.

Knudsen, J.T., Tollsten, L., 1993. Trends in floral scent chemistry in pollination syndromes: floral scent composition in moth-pollinated taxa. Bot. J. Linnean Soc. 113, 263–284.

Lerdau, M., Matson, P., Fall, R., Monson, R., 1995. Ecological controls over monoterpene emission from Douglas fir (*Pseudotsuga menziesii*). Ecology 76, 2640–2647.

Loughrin, J.H., Hamilton-Kemp, T.R., Andersen, R.A., Hildebrand, D.F., 1990. Volatiles from flowers of *Nicotiana sylvestris*, *N. otophora* and *Malus x domestica*: headspace components and day/night changes in their relative concentrations. Phytochem 29, 2473–2477.

Matile, P.H., Altenburger, R., 1988. Rhythms of fragrance emission in flowers. Planta 174, 242–247.

Pellmyr, O., Bergström, G., Groth, I., 1987. Floral fragrances in Actaea, using differential chromatograms to discern between floral and vegetative volatiles. Phytochem 26, 1603–1606.

Robertson, G.W., Griffiths, D.W., Woodford, J.A.T., Birch, A.N.E., 1995. Changes in the chemical composition of volatile released by the flowers and fruits of the red raspberry (*Rubus idaeus*) cultivar Glen Prosen. Phytochem 38, 1175–1179.

Simpson, D., Guenther, A., Hewitt, C.N., Steinbrecher, R., 1995. Biogenic emissions in Europe. Part I: estimates and uncertainties. J. Geophys. Res. 100, 22, 875–22, 890.

Singh, H.B., Zimmerman, P., 1992. Atmospheric distribution and sources of nonmethane hydrocarbons. In: Nriagu, J.D. (Ed.), Gaseous Pollutants Characterization and Cycles. Wiley, New York, pp. 117–235.

Staudt, M., Bertin, N., Hansen, U., Seufert, G., Ciccioli, P., Foster, P., Frenzel, B., Fugit, J.L., 1997. The BEMA-project: Seasonal and diurnal patterns of monoterpene emissions from *Pinus pinea* L. under field conditions. Atmos. Environ. 31, 145–156.

Street, R.A., Duckham, S.C., Hewitt, C.N., 1996. Laboratory and field studies of biogenic volatile organic compound emissions from Sitka spruce (*Picea sitckensis* Bong.) in the United Kingdom. J. Geophys. Res. 101, 22799–22806.

PERGAMON

Phytochemistry 57 (2001) 689–692

PHYTOCHEMISTRY

www.elsevier.com/locate/phytochem

Botrydial is produced in plant tissues infected by *Botrytis cinerea*

Nigel Deighton[a,*], Ingo Muckenschnabel[a], Ana J. Colmenares[b], Isidro G. Collado[b], Brian Williamson[a]

[a]*Scottish Crop Research Institute, Invergowrie, Dundee DD2 5DA, UK*
[b]*Departamento de Química Orgánica, Facultad de Ciencias, Universidad de Cádiz, Apdo. 40, 11510 Puerto Real, Cádiz, Spain*

Received 28 September 2000; received in revised form 14 February 2001

Abstract

The fungal metabolite botrydial was detected for the first time in ripe fruits of sweet pepper (*Capsicum annuum*) wound-inoculated with conidial suspensions of *Botrytis cinerea* and also in leaves of *Phaseolus vulgaris* and *Arabidopsis thaliana* inoculated without wounding. This phytotoxin was produced in soft rot regions of the infection. In *C. annuum*, the most aggressive isolate produced the highest botrydial concentrations *in planta*. The levels of botrydial produced by this isolate did not correlate with the reported relative susceptibilities of four *P. vulgaris* genotypes. The results suggest that botrydial is a pathogenicity factor for this fungus, but not a primary determinant of pathogenicity. © 2001 Elsevier Science Ltd. All rights reserved.

Keywords: *Botrytis cinerea*; Fungal metabolites; Phytotoxicity; *Capsicum annuum*; *Phaseolus vulgaris*; *Arabidopsis thaliana*

1. Introduction

A number of factors have been suggested as the primary causes of lesion development in grey mould disease caused by *Botrytis cinerea*, a ubiquitous necrotrophic pathogen affecting more than 200 crops, especially the leaves, flowers and fruits of plants of horticultural importance (Coley-Smith et al., 1980). The pathogen secretes numerous enzymes and other low molecular weight compounds that have been implicated in pathogenicity. These include cutinases (van Kan et al., 1997), cell wall degrading enzymes (Leone and van den Heuvel, 1987; Johnston and Williamson, 1992; Elad and Evensen, 1995; ten Have et al., 1998), aspartic proteases (Movahedi and Heale, 1990), oxidative enzymes and oxalic acid involved in production of active oxygen species (Edlich et al., 1989; von Tiedemann, 1997; Deighton et al., 1999; Muckenschnabel et al., 2001).

The pathogen also produces a number of toxic bicyclic sesquiterpenes with the botrydial skeleton in static liquid culture (Collado et al., 1995, 1996; Rebordinos et al., 1996; Durán-Patrón et al., 1999, 2000). In bioassays with floating tobacco leaf disks and attached leaves, purified botrydial (**1**) applied to the adaxial leaf surface was phytotoxic (Rebordinos et al., 1996). However,

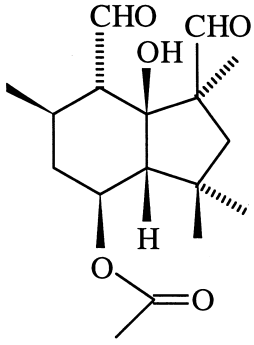

(1)

botrydial and these other metabolites have never been identified in plant tissues infected with isolates of *B. cinerea*. A greater understanding of the processes leading to disease onset and lesion expansion would be gained if this metabolite could be detected in infected whole plant tissues, at concentrations known to be phytotoxic in leaf disk assays (Rebordinos et al., 1996).

This paper describes experiments designed to determine whether botrydial has a role in pathogenicity of the grey mould pathogen. Sweet pepper (*Capsicum annuum*) fruits can be severely affected by the disease in glasshouse production and *B. cinerea* consistently produces

* Corresponding author. Fax: +44-1382-562426.
E-mail address: n.deighton@scri.sari.ac.uk (N. Deighton).

0031-9422/01/$ - see front matter © 2001 Elsevier Science Ltd. All rights reserved.
PII: S0031-9422(01)00088-7

large spreading soft rot lesions in the pericarp of these fruits that are amenable to chemical analysis when inoculated with the pathogen (Deighton et al., 1999). Therefore peppers were inoculated with three different fungal isolates and analysed for botrydial. Analyses were also made from leaves of French bean (*Phaseolus vulgaris*) and *Arabidopsis thaliana* inoculated with a single aggressive isolate.

2. Results and discussion

All three isolates produced substantial soft rot lesions in *C. annuum* after wound inoculation, the largest lesions forming within 6 days in attached fruits inoculated with isolate B05.10. Botrydial (**1**) was detected in peppers, but its appearance and concentration was isolate-dependent and varied considerably between individual fruits (Table 1). A typical chromatogram from a soft rot lesion of a pepper inoculated with isolate B05.10 is shown in Fig. 1A, and that from a non-inoculated pepper in Fig. 1B. The internal standard (DNP-FBz) elutes at ca. 22 min (m/z 303), the 2,4- dinitrophenylhydrazone of botrydial (DNP_2-bot) elutes at ca. 26 min (m/z 669).

In attached leaves of *P. vulgaris* inoculated with the most aggressive *B. cinerea* isolate, B05.10, all leaves in the experiment became infected and botrydial was detected in all lesions (Table 1). In *A. thaliana*, the compound was detected in only three of the eight infected leaves examined and at lower levels than in the other two host tissues.

This is the first evidence that botrydial can be produced *in planta*. The fact that the same aggressive isolate released the compound in attached tissues of members of the Solanaceae, Leguminoseae and Brassicaeae grown under controlled conditions suggests that botrydial has some role in pathogenicity. However, although large soft rot lesions were always produced, the compound was detectable only in 50% of peppers inoculated with one isolate (B1.19), and was never detected in these experiments with another (B1.4). It is possible that botrydial was present in these samples, but at concentrations lower than the current detection limit (0.04 nmol g^{-1}).

Table 1
Occurrence of botrydial in tissues of *Capsicum annuum*, *Phaseolus vulgaris* and *Arabidopsis thaliana* infected by *Botrytis cinerea*

Host[a]	Genotype	Isolate	No. positive samples	Botrydial conc. (range nmol g^{-1})
Capsicum annuum	Bendigo	B05.10	7/7	0.44–12.0 **2.8**[b]
	Bendigo	B1.19	4/8[c]	0.080–0.34 **0.17**[b]
	Bendigo	B1.4	0/8[c]	nd
Phaseolus vulgaris	Huron	B05.10	18/18	7.6–260 **140**[b]
	164214	B05.10	9/9	0.23–18 **7.7**[b]
	N90598	B05.10	18/18	5.8–120 **38**[b]
	416664	B05.10	14/14	4.0–35 **11**[b]
Arabidopsis thaliana	CS2360	B05.10	3/8[c]	0.097–0.48 **0.28**[b]

[a] Four days post inoculation (*C. annuum, P. vulgaris*), 6 days (*A. thaliana*).

[b] Mean value in tissues where detected; nd, not detected.

[c] Limit of detection = 0.04 nmol g^{-1} (fresh weight), therefore botrydial may be present at < 0.04 nmol g^{-1}.

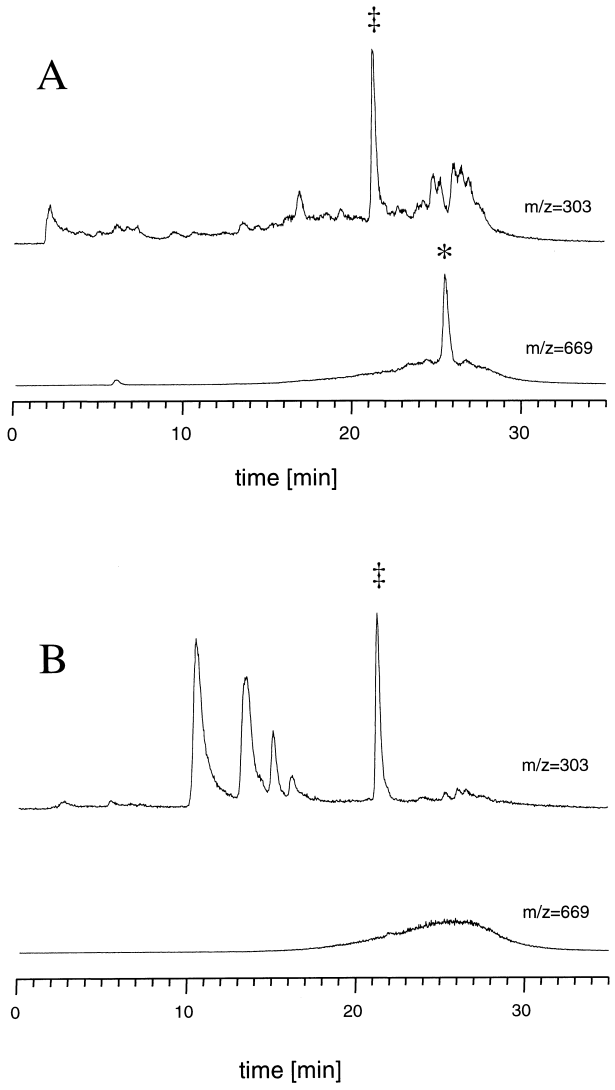

Fig. 1. Typical chromatograms from A: a soft rot lesion in the pericarp of a *Capsicum annuum* fruit inoculated with *Botrytis cinerea* isolate B05.10, and B: a non-inoculated control. Upper panels: m/z 303 ion trace. Lower panels: m/z 669 ion trace. Internal standard (DNP-FBz, ‡) elutes at ~22 min (m/z 303), botrydial derivative (DNP_2-bot, *) elutes at ~26 min (m/z 669).

These results suggest that isolates differ in their ability to produce substantial quantities of botrydial *in planta*.

Inoculation of four genotypes of *P. vulgaris* with the most aggressive *B. cinerea* isolate (B05.10) resulted in the accumulation of appreciably higher mean concentrations of botrydial than in *C. annuum*, the highest levels occurring in cv. Huron (140 nmol g^{-1}) and with very large differences between samples. There was no apparent relationship between botrydial concentration and lesion size, or the reported relative resistance of the genotypes to ozone toxicity — which in turn correlates with resistance to *B. cinerea* (von Tiedemann, 1997). In the case of the genotype Huron, botrydial was detected at concentrations 50-fold higher than those reported (Rebordinos et al., 1996) to be phytotoxic when tested in vitro on tobacco leaf disks (i.e. 1 ppm). Attempts to detect the compound at earlier stages in the infection may be difficult because of the sample size required for LC–MS. Another approach would be to take a series of samples across a leaf with a spreading soft rot lesions to indicate when production of the toxin begins in relation to appearance of lesions. Other compounds with the botryane skeleton may also be present in tissues, but the methodology applied in the present study is only applicable to aldehydic derivatives. Results therefore suggest that botrydial is associated with pathogenesis, but is not a primary determinant of the disease process.

3. Experimental

3.1. Plant material and methods of culture

Plants were grown from seeds in a standardised and quality controlled compost/sand mixture and given a minimum photoperiod of 14 h light at 20°C, with supplementary lighting provided by Hg-discharge lamps as described elsewhere (Muckenschnabel et al., 2001). Plants of *Capsicum annuum* cv. Bendigo were grown in the glasshouse to produce green fruits in excess of 10 cm in length and received no fungicide or insecticides. Seeds of *Phaseolus vulgaris* genotypes Huron (Kelly et al., 1994) and N90598 (from J.D. Kelly, Michigan State University, East Lansing, MI, USA) and 164214 and 416664 (from P.S. Benapal, Virginia State University, Petersburg, VA, USA) were grown under similar conditions to produce fully expanded primary leaves for inoculation. Seeds of *Arabidopsis thaliana* (CS2360 Wassilewskija, Ohio State University, Columbus, USA) were also grown under these conditions.

3.2. Fungal inoculum and inoculations.

Three isolates of the fungus *Botrytis cinerea* Pers.: Fr. [teleomorph *Botryotinia fuckeliana* (de Bary) Whetz.] were used in inoculations. Isolate B05.10 (Quidde et al., 1999), a haploid aggressive strain, was used on all plant hosts. Isolates B1.19 and B1.4 from *Vitis vinifera* were used only to inoculate pepper fruits. Conidial stock suspensions of all isolates remained viable in 75% glycerol at −80°C. Inoculum was obtained from 14-day-old cultures on potato dextrose agar containing an homogenate of leaves from *Phaseolus vulgaris* (50 g l^{-1} of media) and conidial suspensions at 1×10^5 conidia ml^{-1} were prepared as previously reported (Muckenschnabel et al., 2001).

In the glasshouse, attached pepper fruits were inoculated with 5 μl of the conidial suspension placed inside a tangential wound made by sterile scalpel in the proximal region. The adaxial surface of fully expanded leaves of *P. vulgaris* and *A. thaliana* (14 days old) were inoculated with two or one interveinal droplets (5 μl) of conidial suspension, respectively, and incubated in closed propagation boxes at high humidity for 4 days (*C. annuum*, and *P. vulgaris*) or 6 days (*A. thaliana*) as described by Muckenschnabel et al. (2001).

3.3. Sampling, extraction and analysis

The soft rotted areas of the fruit and leaves were excised, weighed and extracts prepared for LC–MS analyses. Briefly, leaf tissue (approx. 100 mg) was homogenised with methanol containing BHT (0.2 mM) as antioxidant (1 ml) in a MiniBead Beater (Biospec Products, Bartlesville, OK, USA) using a mixture of 0.5 g of 0.1 mm diameter and 0.5 g of 0.5 mm diameter glass beads. The methanolic extracts were then derivatised with 2,4-dinitrophenylhydrazine (35 mg 100 ml^{-1} in 1 M HCl) over a period of ca. 30 min at ca. 20°C. The dinitrophenylhydrazones (DNPHs) were extracted from the reaction mixture into dichloromethane (2×2 ml) and dried under nitrogen (40°C) in a Reacti-Therm heating module (Pierce, Rockford, IL, USA). These extracts were then made up in acetonitrile (200 μl) containing 1 μM of the DNPH-derivative of 4-fluorobenzaldehyde (DNP-FBz) as internal standard.

LC–MS analyses were carried out on a Finnigan MAT SSQ710C single quadrupole mass spectrometer with an APCI interface (ThermoQuest, Hemel Hempstead, UK) in negative ion mode with nitrogen as the reagent gas. The samples (5 μl) were eluted from a Hypersil C18 column (250×2 mm, Phenomenex, Macclesfield, UK) with a gradient from 60–90% acetonitrile in 40 mM ammonium acetate. Detection was by selected ion monitoring of the 2,4-dinitrophenylhydrazone derivatives of botrydial (DNP_2-bot, $[M\text{-}H]^-$ m/z 669) and 4-fluorobenzaldehyde (DNP-FBz, $[M\text{-}H]^-$ m/z 303). Alternate blank injections were made to ensure no carry-over from sample-to-sample. Quantification was made from a calibration curve (0.04–1250 nmol g^{-1} leaf tissue, fresh weight) prepared by injection of authentic standards (Collado et al., 1995, 1996) derivatised as above.

A second chromatographic system of different selectivity was used to ensure that the analyte from *B. cinerea*-inoculated hosts co-eluted with the authentic standard. A LUNA hexyl-phenyl (Phenomenex) column (150×2mm) was eluted with a linear gradient of 50–80% acetonitrile containing 40 mM ammonium acetate (25 min gradient, then 80% acetonitrile isocratic). With this chromatographic system, extracts from inoculated host plants gave rise to a peak (m/z 669) at approx. 28 min that co-eluted with that of DNPH-derivatised botrydial (results not shown).

Acknowledgements

This project was jointly funded by the European Union (FAIR project No. PL97-3351) and the Scottish Executive Rural Affairs Department (SERAD). We thank Professor P. Tudzynski (Münster University, Germany) for providing *B. cinerea* isolate B05.10 and Professor A. von Tiedemann (University of Rostock, Germany) for supplying isolates B1.19 and B1.4.

References

Coley-Smith, J.R., Verhoeff, K., Jarvis, W.R. (Eds.), 1980. The Biology of *Botrytis*. Academic Press, London.

Collado, I.G., Cantoral, J.M., Hernández-Galán, R., Durán-Patrón, R., 1995. Metabolites from a shake culture of *Botrytis cinerea*. Phytochemistry 38, 647–650.

Collado, I.G., Hernández-Galán, R., Prieto, V., Hanson, J.R., Rebordinos, L.G., 1996. Biologically active sesquiterpenoid metabolites from the fungus *Botrytis cinerea*. Phytochemistry 41, 513–517.

Deighton, N., Muckenschnabel, I., Goodman, B.A., Williamson, B., 1999. Lipid peroxidation and the oxidative burst associated with infection of *Capsicum annuum* by *Botrytis cinerea*. The Plant Journal 20, 485–492.

Durán-Patrón, R., Hernández-Galán, R., Collado, I.G., 2000. Secobotrytriendiol and related sesquiterpenoids, new phytotoxic metabolites from *Botrytis cinerea*. Journal of Natural Products 63, 182–184.

Durán-Patrón, R., Hernández-Galán, R., Rebordinos, L.G., Cantoral, J.M., Collado, I.G., 1999. Structure–activity relationships of new phytotoxic metabolites with the botryane skeleton from *Botrytis cinerea*. Tetrahedron 55, 2389–2400.

Edlich, W., Lorenz, G., Lyr, H., Nega, E., Pomme, E.-H., 1989. New aspects of the infection mechanisms of *Botrytis cinerea* Pers. Netherlands Journal of Plant Pathology 95 (Suppl 1), 53–62.

Elad, Y., Evensen, K., 1995. Physiological aspects of resistance to *Botrytis cinerea*. Phytopathology 85, 637–643.

Johnston, D.J., Williamson, B., 1992. Purification and characterization of four polygalacturonases from *Botrytis cinerea*. Mycological Research 96, 343–349.

Kelly, J.D., Hosfield, G.L., Varner, G.V., Uebersax, M.A., Brothers, M.E., Taylor, J., 1994. Registration of Huron navy bean. Crop Science 34, 1408.

Leone, G., van den Heuvel, J., 1987. Regulation by carbohydrates of the sequential in vitro production of pectic enzymes by *Botrytis cinerea*. Canadian Journal of Botany 65, 2133–2141.

Movahedi, S., Heale, J.B., 1990. The roles of aspartic proteinase and endo-pectin lyase enzymes in the primary stages of infection and pathogensis of various host tissues by different isolates of *Botrytis cinerea* Pers. Ex. Pers. Physiological and Molecular Plant Pathology 36, 303–324.

Muckenschnabel, I., Williamson, B., Goodman, B.A., Lyon, G.D., Stewart, D., Deighton, N., 2001. Markers for oxidative stress associated with soft rots in French bean (*Phaseolus vulgaris*) infected by *Botrytis cinerea*. Planta 212, 376–381.

Quidde, T., Büttner, P., Tudzynski, P., 1999. Evidence for three different specific saponin-detoxifying activities in *Botrytis cinerea* and cloning and functional analysis of a gene coding for a putative avenacinase. European Journal of Plant Pathology 105, 273–283.

Rebordinos, L.G., Cantoral, J.M., Prieto, V., Hanson, I.R., Collado, I.G., 1996. The phytotoxic activity of some metabolites of *Botrytis cinerea*. Phytochemistry 42, 383–387.

ten Have, A., Mulder, W., Visser, J., van Kan, J.A.L., 1998. The endopolygalacturonase gene *Bcpg*1 is required for full virulence of *Botrytis cinerea*. Molecular Plant-Microbe Interactions 11, 1009–1016.

van Kan, J.A.L., van't Klooster, J.W., Wagenmakers, C.A.M., Dees, D.C.T., vander Vlugt Bergmans, C.J.B., 1997. Cutinase A of *Botrytis cinerea* is expressed, but not essential, during penetration of gerbera and tomato. Molecular Plant-Microbe Interactions 10, 30–38.

von Tiedemann, A., 1997. Evidence for a primary role of active oxygen species in induction of host cell death during infection of bean leaves with *Botrytis cinerea*. Physiological and Molecular Plant Pathology 50, 151–166.

PERGAMON

Phytochemistry 57 (2001) 693–700

PHYTOCHEMISTRY

www.elsevier.com/locate/phytochem

Identification of glucosinolates on the leaf surface of plants from the Cruciferae and other closely related species

D. Wynne Griffiths[a,*], Nigel Deighton[a], A. Nicholas E. Birch[a], Bruno Patrian[b], Robert Baur[b], Erich Städler[b]

[a]*Scottish Crop Research Institute, Invergowrie, Dundee, Scotland, DD2 5DA, UK*
[b]*Swiss Federal Research Institute, CH 8820, Wädenswil, Switzerland*

Received 28 June 2000; received in revised form 1 March 2001; accepted 14 March 2001

Abstract

Leaf-surface extracts prepared from 18 non-cultivated (wild) plant species, derived from the *Capparidaceae*, *Cruciferae*, *Resedaceae* and *Tropaeolaceae* were ranked for their ability to stimulate oviposition by the cabbage root fly, and analysed for glucosinolates. A total of 28 different glucosinolates were identified. A clear relationship was detected between the indolyl-, benzyl- and the total glucosinolate composition on the leaf surface and oviposition preference by cabbage root fly females. However, as the results are not fully explained by differences in leaf surface glucosinolates, other important oviposition deterrents and stimuli on the leaf surface of these wild crucifers must also be present. © 2001 Elsevier Science Ltd. All rights reserved.

Keywords: Leaf surface glucosinolates; *Capparidaceae*; *Cruciferae*; *Resedaceae*; *Tropaeolaceae*; Cabbage root fly; *Delia radicum*

1. Introduction

The glucosinolates are a diverse group of secondary plant products whose generalised structure is outlined in Fig. 1. These sulfur-containing compounds, over a hundred of which have been identified (Fenwick et al., 1989), have been isolated from members of at least eleven plant families, but are most commonly associated with the Cruciferae (Kjaer, 1974). These compounds, when consumed at high concentration, have been shown to have a deleterious effect on vertebrate animal performance and their effects on domesticated livestock have been frequently reviewed (Fenwick et al., 1989; Duncan, 1991; Griffiths et al., 1998). However, the consumption of brassicas has also been linked with reduced risk of cancers and this protective role has been associated with the ability of the enzyme mediated breakdown products of glucosinolates to activate protective mechanisms within the body (Heaney and Fenwick, 1995).

The ecological role(s) of glucosinolates within the plant has not been fully elucidated although their presence has been linked to plant defence mechanisms against bacteria and fungi as well as acting as deterrents to non-adapted herbivores (Chew, 1988; Louda and Mole, 1991).

In crucifer-adapted insect species, such as the cabbage (*Delia radicum)* and turnip (*D. floralis*) root flies, glucosinolates on the leaf surface (phylloplane) of host plants are important as egg laying (oviposition) stimulants. Female flies orientate towards patches of cruciferous plants following upwind odours but the key step in host acceptance or rejection for oviposition takes place after landing on the plant. Recent research has shown that plant odour apparently may play some additional role in host selection after landing (De Jong and Städler, 1999). But more importantly, on the leaf surface the female fly perceives very low concentrations of specific glucosinolates and other polar plant compounds, which trigger the post-landing behavioural sequence resulting in oviposition (Roessingh et al., 1992; Simmonds et al., 1994; Baur et al., 1996; Hopkins et al., 1997, 1999). This normally occurs in the soil at the base of the chosen plant. These insects detect chemical oviposition stimuli by the activation of chemoreceptor neurons in sensilla on the ventral side of their tarsi (Roessingh et al., 1992) and on the proboscis (Simmonds et al., 1994).

* Corresponding author. Tel.: +44-1382-562731; fax: +44-1382-562426.
E-mail address: wgriff@scri.sari.ac.uk (D.W. Griffiths).

0031-9422/01/$ - see front matter © 2001 Elsevier Science Ltd. All rights reserved.
PII: S0031-9422(01)00138-8

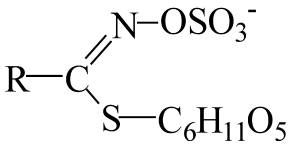

Fig. 1. Generalised glucosinolate structure.

Both field and glasshouse studies aimed at investigating the susceptibility of wild crucifers to the cabbage root fly (*D. radicum*) have indicated that several such species appear not to stimulate egg laying and do not support larval development (Finch and Ackley, 1977; Finch, 1978). Such crucifer species may therefore represent potential sources of host plant resistance to root flies, which is absent from most cultivated brassicas (Birch, 1988, 1989).

Although limited data is available on the glucosinolate composition of seeds (Kjaer, 1960; Horn and Vaughan, 1983; Daxenbichler et al., 1991) and foliage (Kjaer, 1960; Cole, 1976; Finch, 1978; Mithen et al., 1987) of wild crucifers and other closely related species, there appears to be no data regarding either the identification or quantification of glucosinolates on their leaf surfaces. Indeed, many of the earlier surveys of plant glucosinolate composition have been based on analysis of their enzymatically-derived breakdown products. Consequently these earlier studies were unable to distinguish between the various possible indolyl-based glucosinolates that are commonly present in both crucifer seeds and foliage and have been demonstrated to have an active role in some plant-insect interactions (Roessingh et al., 1992; Städler et al., 1995).

It has also been reported that the glucosinolates present in the seed and vegetative tissues may vary independently of each other (Rosa et al., 1997), with for example, the glucosinolates present in the foliage of double-low and single-low oilseed rape cultivars being similar despite the fact that those in the seed differ significantly between the two types. Similarly, foliar glucosinolate levels can vary with the developmental stage of the plant and may also be altered in response to environmental conditions (reviewed by Rosa et al., 1997). Glucosinolates on the surface of crucifer leaves have been reported to be qualitatively similar to those extracted from within the leaf, but the relative proportions of individual glucosinolates found on the phylloplane may differ from that of the leaf interior (Roessingh et al., 1992). Consequently, when evaluating the biological activity it would appear essential to both analyse and bioassay extracts simultaneously prepared from the same plants, thus ensuring that any differences seen in either insect behaviour or leaf surface chemistry can be meaningfully correlated.

The host plant preference of the cabbage root fly and other insects ovipositing on undamaged leaves of crucifers can only be understood if the leaf surface chemistry is analysed. Thus, the objective of this study was to identify and quantify the glucosinolates present in the leaf surface extracts of a range of Crucifers and other closely related plant species, which have also been ranked in order of their oviposition preference for cabbage root fly. This was performed using recently developed liquid chromatography–atmospheric pressure chemical ionisation–mass spectrometric (LC–APCI–MS) techniques for desulfo-glucosinolates (Ishida et al., 1997; Griffiths et al., 2000).

2. Results and discussion

2.1. Selection of plant material

Eighteen plant species from the Cruciferae (see Table 2) were selected on the basis of earlier published work (Finch and Ackley, 1977; Hardman and Ellis; 1978), which used development of *D. radicum* pupae after field and glasshouse exposure to egg laying females as a measure of host suitability providing a range of susceptibility to this pest. Leaf surface extracts were prepared from these 18 cruciferous plant species and sprayed onto surrogate waxed paper leaves in an oviposition choice bioasssay, as previously described (Roessingh et al., 1992; Baur et al., 1996). The percentage of the total (all plants in bioassay) eggs laid on each individual crucifer species was determined and used to rank the plants in order of increasing oviposition preference (Fig. 2).

2.2. Total glucosinolates

A total of 28 different glucosinolates (Table 1) were identified in the leaf surface extracts of the 18 plant species studied (Table 2, Fig. 2). Glucosinolates were detected on the leaf surfaces of all the species studied with the sole exception of *Capsella bursa-pastoris*. The concentration of total glucosinolates present on the leaf surfaces, expressed as μmoles/gram leaf equivalent (μmol/gle) ranged from 0.12 to 3.08 μmol/gle in *Isatis tinctoria* and *Lepidium sativum* respectively. These values were generally of the same order of magnitude as those previously reported for similarly prepared extracts from commercially available kale (0.07 μmol/gle) and swede (0.14 μmol/gle) cultivars (Hopkins et al., 1997). The absence of any detectable glucosinolates on the leaf surface of *Capsella bursa-pastoris* plants would appear to be somewhat anomalous, since earlier studies on the autolysis products released by whole plant extracts prepared from this species suggested the presence of sinigrin (prop-2-enyl glucosinolate) in the plant material (Cole, 1976). Similar studies also demonstrated the presence of sinigrin in the seeds of this species (Kjaer, 1960) whilst a more recent report concluded that *Capsella bursa-pastoris* seed contained high concentrations of methylsulfinylnonyl

Table 1
Abbreviations, trivial names and side-chain structures of the glucosinolates detected in this study

Abbreviation	Trivial name	Chemical structure	Basis of identity[a]
Methyl	Glucocapparin	CH_3-	a,b
Isopropyl	Glucoputranjivin	CH_3-(CH_3)CH-	a
1-Methylpropyl	Glucocochlearin	CH_3-CH_2-(CH_3)CH-	a,b
2-Propen	Sinigrin	CH_2=CH-CH_2-	a,b
3-Buten	Gluconapin	CH_2=CH-CH_2-CH_2-	a,b
4-Penten	Glucobrassicanapin	CH_2=CH-CH_2-CH_2-CH_2-	a,b
2-OH-3-Buten	Progoitrin	CH_2=CH-CH(OH)-CH_2-	a,b
2-OH-4-Penten	Napoleiferin	CH_2=CH-CH_2-CH(OH)-CH_2-	a
OH-Butyl[b]	Glucoconringiin	$(CH_3)_2$C(OH)-CH_2-	a
OH-Butyl[b]	Glucosisautricin	CH_2(OH)-(CH_3-CH_2)CH-	
4-MT-3-Buten	Glucodehydroerucin	CH_3S-CH=CH-CH_2-CH_2-	a
5-MTP	Glucoberteroin	CH_3S-CH_2-CH_2-CH_2-CH_2-CH_2-	a
4-MS-3-Buten	Glucoraphenin	CH_3SO-CH=CH-CH_2-CH_2-	a
4-MSB	Glucoraphanin	CH_3SO-CH_2-CH_2-CH_2-CH_2-	a,b
5-MSP	Glucoalyssin	CH_3SO-CH_2-CH_2-CH_2-CH_2-CH_2-	a,b
6-MSH	Glucohesperin	CH_3SO-CH_2-$(CH_2)_4$-CH_2-	a,b
7-MSHept	Glucosibarin	CH_3SO-CH_2-$(CH_2)_5$-CH_2-	a
8-MSO	Glucohirsutin	CH_3SO-CH_2-$(CH_2)_6$-CH_2-	a
9-MSN	Glucoaratin	CH_3SO-CH_2-$(CH_2)_7$-CH_2-	a
8-MSO_2O	8-Methylsulfonyloctyl	CH_3SO_2-CH_2-$(CH_2)_6$-CH_2-	a
9-MSO_2N	9-Methylsulfonylnonyl	CH_3SO_2-CH_2-$(CH_2)_7$-CH_2-	a
Bnz	Glucotropaeolin	C_6H_5-CH_2-	a,b
p-OH-Bnz	Sinalbin	*p*HO-C_6H_4-CH_2-	a,b
2-PhE	Gluconasturtiin	C_6H_5-CH_2-CH_2-	a,b
2-OH-2-PhE	Glucobarbarin	C_6H_5-CH(OH)-CH_2-	a
3-IM	Glucobrassicin	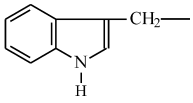	a,b
1-CH_3O-3-IM	Neoglucobrassicin	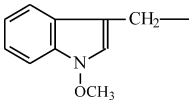	a,b
4-OH-3-IM	4-Hydroxyglucobrassicin	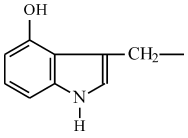	a,b
4-CH_3O-3-IM	4-Methoxyglucobrassicin	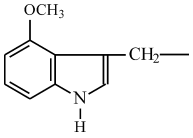	a,b

[a] a = Identity based on interpretation of mass spectrum; b = identity confirmed by both retention time and comparison of mass spectrum with either synthesised or isolated desulfoglucosinolates from other plant sources (see Griffiths et al., 2000).
[b] Mass spectral data insufficient to distinguish between these two possibilities.

and methylsulfinyldecyl glucosinolates (Daxenbichler et al., 1991). However, the fact that, under field conditions, this species does not attract the cabbage root fly to lay eggs (Finch and Ackley, 1977) would appear to be consistent with the absence of leaf surface glucosinolates. Clearly more detailed studies are required to confirm the veracity of these findings and to evaluate the effects of environment, stage of plant development and within-species variation on leaf surface glucosinolate concentration.

2.3. Aliphatic glucosinolates

Aliphatic glucosinolates were detected on the leaf surfaces of all but four of the plant species studied (Table 2, Fig. 2). In many species these glucosinolates predominated with for example methyl, isopropyl and 1-methylpropyl glucosinolates accounting for 97, 65 and 82% of the total leaf surface glucosinolates in *Cleome spinosa, Sisymbrium officinale* and *Cochlearia officinalis*

Table 2
Individual glucosinolates detected on the leaf surface of plants from the Cruciferae and other closely related species

Species[a]	Glucosinolates[b] (% total)				
	Aliphatic		Aromatic	Indolyl	Total (μmol/gle)
Aurinia saxatilis L.	3-Buten (51) 4-Penten (30)	5-MTP (1) 4-MSB (1) 5-MSP (15)		4-OH-3-IM (tr) 4-CH_3O-3-IM (1)	1.05
Barbarea vulgaris R.Br.			2-PhE (tr) 2-OH-2-PhE (97)	3-IM (3) 4-CH_3O-3-IM (1) (tr)	1.49
Brassica napus L. var. *napus*	3-Buten (7) 4-Penten (10)	2-OH-3-Buten(19) 5-MSP (11)	2-PhE (1)	3-IM (32) 4-CH_3O-3-IM (1) 1-CH_3O-3-IM (19)	0.35
Brassica rapa L. var. *silvestris* (Lam.) Briggs	3-Buten (8)	2-OH-3-Buten (8)	2-PhE (2)	3-IM (3)	
	4-Penten (45)	2-OH-4-Penten (14) 5-MSP (5)		4-OH-3-IM (8) 4-CH_3O-3-IM (5) 1-CH_3O-3-IM (2)	0.17
Cleome spinosa Jacq.	Methyl (97)			3-IM (3)	1.95
Cochlearia officinalis L.	Isopropyl (13) 1-Methylpropyl (82)	OH-butyl (3)		1-CH_3O-3-IM (2)	0.37
Isatis tinctoria L.	Methyl (2)			3-IM (98)	0.12
Lepidium campestre (L.) R.Br.		4-MSB (2) 5-MSP (24) 6-MSH (1)	p-OH-Bnz(73)	3-IM (tr)	3.05
Lepidium sativum L.			Bnz (100)		3.08
Raphanus raphanistrum L.		4-MT-3-Buten (9) 4-MS-3-Buten (60) 4-MSB (2)		3-IM (29) 4-CH_3O-3-IM (tr)	0.82
Reseda luteola L.		OH-Butyl (6)	2-OH-2-PhE (90)	3-IM (4)	0.49
Rorippa islandica (Oeder) Bess.		7-MSHept (tr) 8-MSO (10) 9-MSN (13)		3-IM (77)	0.66
Rorippa silvestris L.		8-MSO (96) 9-MSN (4)		4-CH_3O-3-IM (tr)	0.85
Sinapis arvensis L.		8-MSO_2O (15) 9-MSO_2N (40)	*p*-OH-Bnz (45)		1.08
Sisymbrium officinale L. (Scop.)	Isopropyl (65)			3-IM (35)	1.79
Thlaspi arvense L.	2-Propen (100)				0.63
Tropaeolum majus L.			Bnz (99) *p*-OH-Bnz (1)	3-IM (tr)	0.63

[a] All members of the Cruciferae except *Cleome spinosa* Jacq. (Capparidaceae), *Reseda luteola* L. (Resedeceae) and *Tropaeolum majus* L. (Tropaeolaceae).
[b] Abbreviated names as in Table 1.

respectively. Similarly, the only glucosinolate detected on the leaf surface of *Thlaspi arvense* was sinigrin.

Glucosinolates containing hydroxyalkene sidechains, namely progoitrin and napoliferin, were restricted to *Brassica napus napus* and *B. rapa silvestris* whilst leaf surface extracts from both *Cochlearia officinalis* and *Reseda luteola* appeared to contain a hydroxyalkane glucosinolate. Based on the presence of the diagnostic ions corresponding to $[M+H]^+$ and $[M+H\text{-}162]^+$ (Ishida et al., 1997; Griffiths et al., 2000) in the mass spectra of its desulfo analogue, this was identified as having an empirical formula equivalent to a hydroxybutyl glucosinolate. Previous studies on the seed of *Cochlearia officinalis* (Kjaer, 1960) have reported the presence of glucoconringiin (2-hydroxy-2-methylpropyl glucosinolate) which would be consistent with the empirical formulae found in the mass spectra of the leaf surface extracts. APCI mass spectra of desulfo-glucosinolates give little information regarding the exact structural nature of the glucosinolate side chain. Consequently, the possibility that this compound may be an alternative structural isomer such as glucosisautricin (2-hydroxy-1-ethylethylglucosinolate) which has also been found in the seeds of other wild crucifers (Daxenbichler et al., 1991) cannot be totally eliminated.

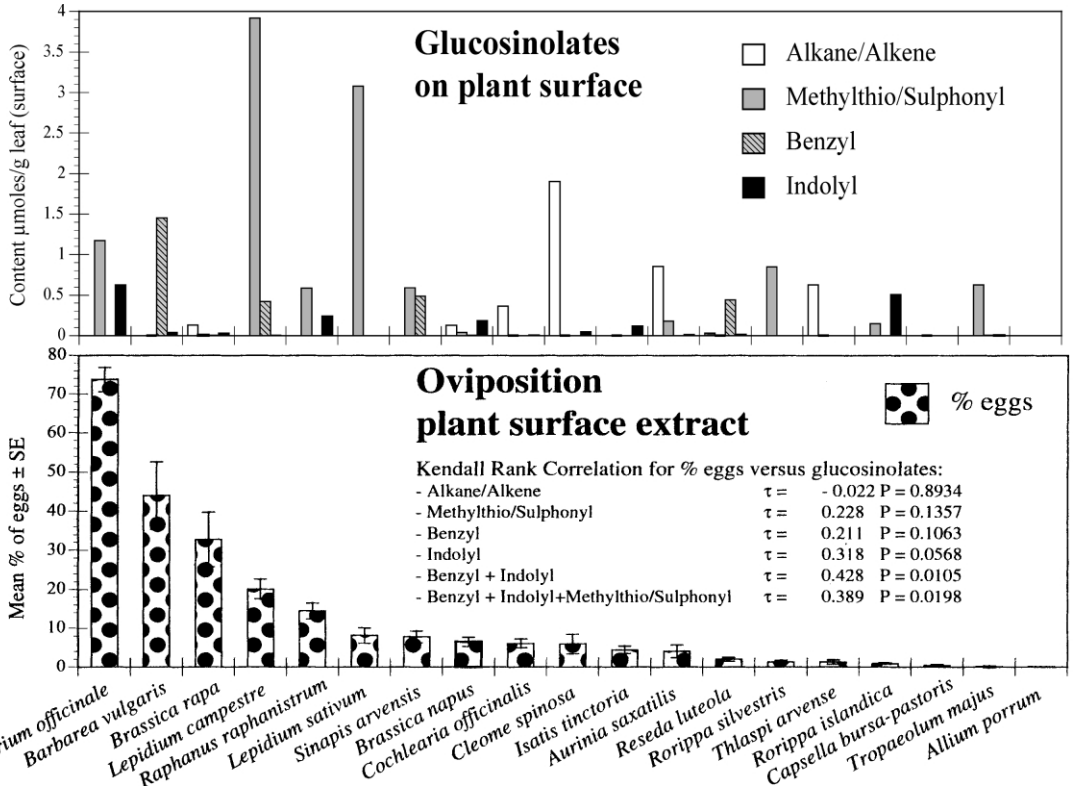

Fig. 2. The oviposition preference and glucosinolate content of leaf surface extracts prepared from a range of Cruciferae and other closely related species.

Sulfur-containing aliphatic glucosinolates were particularly common constituents of the leaf surface extracts with examples of methylthio, methylsulfinyl and methyl sulfonyl glucosinolates all being detected (Table 2). The identity of the 7-methylsulfinylheptyl, 8-methylsulfinyloctyl and 9-methylsulfinylnonyl glucosinolates in *Rorippa islandica* and *Rorippa silvestris* were based on the comparison of the mass spectra of their desulfo analogues with previously published spectra of their lower homologues (Griffiths et al., 2000). In each case, as for the lower homologues, the spectra contained, in addition to the expected ions corresponding to $[M+H]^+$ and $[M+H\text{-}162]^+$ a high intensity ion fragment with an empirical formulae equivalent to $[RCNOH]^+$. These high molecular weight methylsulfinyl glucosinolates have also been demonstrated as being the major constituents of the seed of both plant species (Daxenbichler et al., 1991).

Two methylsulfonyl containing glucosinolates, namely 8-methylsulfonyloctyl and 9-methylsulfonylnonyl glucosinolate, were detected in surface extracts from *Sinapis arvensis* and have been previously reported as major constituents of the seed of this species (Daxenbichler et al., 1991). Their identification was based on interpretation of the mass spectra of their respective desulfoglucosinolates. The mass spectra derived from both compounds contained ions with m/z values with empirical formulae weights corresponding with, and tentatively identified as: $[M+H]^+$; $[M+H\text{-}162]^+$; $[RNOH+H]^+$ (base peak) and $[ROH]^+$, all of which have been previously seen in spectra of other sulfur containing desulfo-glucosinolates (Griffiths et al., 2000). Additionally both spectra contained a fragment corresponding to $[M+H\text{-}155]^+$. This loss of neutral fragments totalling 155 mass units is difficult to reconcile, although on a purely mathematical basis, could arise by the loss of the following neutral molecules: SO_2, CH_4, HNCO and S. However, for such eliminations to occur considerable intra-molecular rearrangements would be required to produce the resultant stable fragment observed in the mass spectra of both methylsulfonyl glucosinolates.

2.4. Aromatic glucosinolates

Four aromatic glucosinolates, glucotropaeolin (benzyl glucosinolate), sinalbin (*p*-hydroxybenzyl glucosinolate) gluconasturtiin (2-phenylethyl glucosinolate) and glucobarbarin (2-hydroxy-2-phenylethyl glucosinolate), were detected. Glucobarbarin was identified as the major component on the leaf surfaces of *Barbarea vulgaris* and *Reseda luteola* and in both cases accounted for over 90% of the total leaf surface glucosinolates. This compound has been previously reported as the predominant seed glucosinolate in both these plant species (Daxenbichler et

al., 1991; Andersson et al., 1999). The mass spectrum of desulfo-glucobarbarin contained ions corresponding to $[M+H]^+$, $[M+H\text{-}18]^+$, and $[M+H\text{-}162]^+$, the last two corresponding to the loss of water and glucose respectively from the parent ion. Surprisingly, as with the methylsulfonyl-desulfoglucosinolates, the spectra from both plant sources also contained a major fragment ion equivalent to $[M+H\text{-}155]^+$. This could have arisen by the loss of C_6H_6, HNCO and H_2S but again highly complex intra-molecular rearrangements would be required.

Glucotropaeolin was the only glucosinolate detected on the leaf surface of *Lepidium sativum* plants and accounted for 99% of the leaf surface glucosinolates of *Tropaeolum majus*. Sinalbin accounted for 73% and 45% of the leaf surface glucosinolates of *Lepidium campestre* and *Sinapis arvensis* plants respectively and was also detected in quantifiable amounts on the leaves of *Tropaeolum majus*. Although gluconasturtiin was detected in three plant species (Table 2), the levels found were low and accounted in each case for less than 2% of the total leaf glucosinolates.

2.5. Indolyl glucosinolates

Indolyl containing glucosinolates were detected on the leaf surfaces of all but three of the plant species studied (Table 2, Fig. 2). The most common such glucosinolate was glucobrassicin (3-indolylmethyl glucosinolate) which was identified in extracts from eleven species and accounted for over 77% of the glucosinolates detected on the leaf surface of *Isatis tinctoria* and *Rorippa islandica* plants (Table 2). In comparison the relative concentrations of the other indolyl containing glucosinolates (4-hydroxy-, 4-methoxy- and 1-methoxy-3-indolylmethyl glucosinolates) were low, although 1-methoxy-3-indolylmethyl glucosinolate accounted for almost 20% of the total glucosinolates detected on the leaf surface of *Brassica napus* var. *napus* plants. All the indolyl glucosinolates detected have previously been reported as common constituents of cultivated brassicas (Griffiths et al., 1998).

2.6. Glucosinolate content and oviposition preference

The 18 species studied are shown in Fig. 2 in order of oviposition preference to cabbage root fly. These relative rankings were correlated with the presence or relative concentration of some, but not all, groups of glucosinolates (see Fig. 2 for significant correlations).

Significant rank correlations to the oviposition preference were found for the combined indolyl and benzyl groups and indolyl, benzyl and the sulphur-containing glucosinolate groups. This is in accordance with the findings by Roessingh et al., (1992), who found that the indolyl glucosinolate glucobrassicin and the benzyl glucosinolates glucotropaeolin and gluconasturtiin belong to compounds with the lowest threshold of activity (most stimulatory) both in the oviposition behaviour and the glucosinolate receptor neurons in the tarsal D sensilla.

But since none of the correlations were very high, this suggests that other leaf surface factors may also be responsible for the lower or higher than expected acceptability of some wild crucifers to cabbage root fly. Recently, three compounds, possibly structurally related to the brassica phytoalexins, have been isolated from cabbage leaf surface extracts and identified as potent stimulators of oviposition in cabbage root fly (Hurter et al., 1999; De Jong et al., 2000). It has been suggested that these may also be of importance in oviposition stimulation (Baur et al., 1996; Roessingh et al., 1997).

Additionally, there could be other groups of compounds present in wild crucifers that have additional positive or negative effects on the cabbage root fly's acceptance of a plant for oviposition. Indeed, some extracts have proven to inhibit the stimulation by glucosinolates (Städler et al., unpubl. results). Compounds such as the waxes, also present on the leaf surface, may affect the insect's ability to detect polar compounds already identified as oviposition stimulants (Roessingh and Städler, 1990; Spencer et al., 1999).

3. Experimental

3.1. Plant material

The seed of the plant species studied (see Table 2) were obtained from J.A.A. Renwick, Boyce Thompson Institute, Ithaca (*Aurinia saxatilis* and *Cleome spinosa*); Botanical Garden, University of Hohenheim (*Sisymbrium officinale*); Swiss Federal Research Station, Reckenholz (*Brassica napus* var. *napus* cv. Eurol, *B. rapa* var. *silvestris* cv. Hanko) and from the Botanical Garden of Zürich (all other species). The seeds were sown in mid April into compost and grown for three weeks in a glasshouse, transferred to a cold frame for acclimatisation, and then transplanted into soil. The plants were then grown under field conditions and leaf material harvested in July, prior to the onset of flowering.

3.2. Leaf surface extracts

The fresh leaf material was extracted using the method described by Städler and Roessingh (1991). After weighing, the leaves were dipped for 7–10 s into dichloromethane to remove the non-polar waxes and subsequently dipped twice for 5 s periods into methanol. The methanol fraction was filtered and evaporated under vacuum to produce a final solution containing the equivalent of between 1 and 5 g of plant material per ml of methanol (1–5gle/ml). All results are expressed in terms of gle (i.e. the

amount of a given substance extracted from the surface of 1 g of leaf material).

3.3. Oviposition bioassay

Oviposition preference tests were performed using *D. radicum* and surrogate leaves treated with leaf surface extracts of the selected wild crucifers, as previously described by Roessingh et al., (1992). In each assay about 100 female flies were given a choice of the leaf surface extracts and a methanol-treated control. The choice preference assays were performed in three partially overlapping sets of extracts and each set replicated at least 7 times, with the position of each treatment being re-randomised within the cages for each replicate. *Brassica oleracea* var "CC-Cross" was tested at two concentrations, 1 and 0.1 gle and included as a standard in all 3 sets. All the other extracts were applied at only one concentration of 1 gle. In all the three sets of extracts bioassayed, preferred, poor host plants and a non-host plant (*Allium porrum*) were included. This procedure resulted in 7–25 individual egg counts per plant species. The results (% on each treatment, of the total number of eggs laid in each assay) were averaged and the mean percent oviposition was correlated to the glucosinolate contents (μmoles / gle) using Kendall Rank Correlation statistical test (corrected for ties).

3.4. High performance liquid chromatography

The desulfo-glucosinolates were prepared using the on-column enzymatic desulfonation method of Heaney and Fenwick (1980). The resulting desulfo-glucosinolates were then separated and quantified by a reverse phase high performance liquid chromatographic method based on that of Spinks et al. (1984).

3.5. Liquid chromatography–mass spectrometry

Liquid chromatography–mass spectrometry was performed using a Finnigan MAT SSQ 710C single quadrupole instrument with an atmospheric pressure-chemical ionisation (APCI) interface (Thermo Quest, Hemel Hempstead, UK). The instrument was configured for positive chemical ionisation. Full details of instrument conditions and the gradients used have previously been published (Griffiths et al., 2000).

Acknowledgements

The Scottish Crop Research Institute receives Grant-in-Aid from the Scottish Executive Rural Affairs Department and E.S. a grant from the Swiss National Science Foundation No. 31.52409.97.

References

Andersson, A.A.M., Merker, A., Nilsson, P., Sørensen, H., Åman, P., 1999. Chemical composition of the potential new oilseed crops *Barbarea vulgaris, Barbarea verna* and *Lepidum campestre*. Journal of the Science of Food and Agriculture 79, 179–186.

Baur, R., Birch, A.N.E., Hopkins, R.J., Griffiths, D.W., Simmonds, M.S.J., Städler, E., 1996. Oviposition and chemosensory stimulation of the root flies *Delia radicum* and *D. floralis* in response to plants and leaf surface extracts from resistant and susceptible *Brassica* genotypes. Entomologia et Experimentalis Applicata 78, 61–75.

Birch, A.N.E., 1988. Field and glasshouse studies on components of resistance to root fly attack in swedes. Annals of Applied Biology 113, 89–100.

Birch, A.N.E., 1989. A field cage method for assessing resistance to turnip root fly in brassica. Annals of Applied Biology 115, 321–325.

Chew, F.S., 1988. Searching for defensive chemistry in the Cruciferae or do glucosinolates always control interactions of Cruciferae with their potential herbivores and symbionts? No! In: Spencer, K.C. (Ed.), Chemical Mediation of Coevolution. Academic, San Diego, pp. 81–112.

Cole, R.A., 1976. Isothiocyanates, nitriles and thiocyanates as products of autolysis of glucosinolates in *Cruciferae*. Phytochemistry 15, 759–762.

Daxenbichler, M.E., Spencer, G.F., Carlson, D.G., Rose, G.B., Brinker, A.M., Powell, R.G., 1991. Glucosinolate composition of seeds from 297 species of wild plants. Phytochemistry 30, 2623–2638.

De Jong, R., Maher, N., Patrian, B., Städler, E., Winkler, T., 2000. Rutabaga roots, a rich source of oviposition stimulants for the cabbage root fly. Chemoecology 10, 205–209.

De Jong, R., Städler, E., 1999. The influence of odour on the oviposition behaviour of the cabbage root fly. Chemoecology 9, 151–154.

Duncan, A.J., 1991. Glucosinolates. In: D'Mello, J.P.F., Duffus, C.M., Duffus, J.H. (Eds.), Toxic Substances in Crop Plants. The Royal Society of Chemistry, Cambridge, pp. 126–147.

Fenwick, G.R., Heaney, R.K., Mawson, R., 1989. Glucosinolates. In: Cheeke, R.R. (Ed.), Toxicants of Plant Origin, Vol II, Glycosides. CRC Press, Boca Raton, FL, pp. 1–41.

Finch, S., 1978. Volatile plant chemicals and their effect on host plant finding by the cabbage root fly (*Delia brassicae*). Entomologia et Experimentalis Applicata 24, 350–359.

Finch, S., Ackley, C.M., 1977. Cultivated and wild host plants supporting populations of cabbage root fly. Annals of Applied Biology 85, 13–22.

Griffiths, D.W., Bain, H., Deighton, N., Botting, N.P., Robertson, A.A.B., 2000. Evaluation of liquid chromatography-atmospheric pressure ionisation-mass spectrometry for the identification and quantification of desulfoglucosinolates. Phytochemical Analysis 11, 216–225.

Griffiths, D.W., Birch, A.N.E., Hillman, J.R., 1998. Antinutritional compounds in the Brassicaceae: analysis, biochemistry and dietary effects. Journal of Horticultural Science and Biotechnology 73, 1–18.

Hardman, J.A., Ellis, P.R., 1978. Host plant factors influencing the susceptibility of cruciferous crops to cabbage root fly attack. Entomologia et Experimentalis Applicata 24, 193–197.

Heaney, R.K., Fenwick, G.R., 1980. The analysis of glucosinolates in Brassica species using gas chromatography. Direct determination of the thiocyanate ion precursors, glucobrassicin and neoglucobrassicin. Journal of the Science of Food and Agriculture 31, 593–599.

Heaney, R.K., Fenwick, G.R., 1995. Natural toxins and protective factors in brassica species, including rapeseed. Natural Toxins 3, 233–237.

Hopkins, R.J., Birch, A.N.E., Griffiths, D.W., Baur, R., Städler, E., McKinlay, R.G., 1997. Leaf surface compounds and oviposition

preference of turnip root fly *Delia floralis*: the role of glucosinolate and non-glucosinolate compounds. Journal of Chemical Ecology 23, 629–643.

Hopkins, R.J., Wright, F., Birch, A.N.E., McKinlay, R.G., 1999. The decision to reject an oviparition site: sequential analysis of the post-alighting behaviour of *Delia floralis*. Physiological Entomology 24, 41–50.

Horn, P.J., Vaughan, J.G.. Seed glucosinolates of fourteen wild *Brassica* species (special issue). Phytochemistry 22465470.

Hurter, J., Ramp, T., Patrian, B., Städler, E., Roessingh, P., Baur, R., Jong, R., de, Nielsen, J. K., Winkler, T., Richter, W. J., Müller, D., Ernst, B., 1999. Oviposition stimulants for cabbage root fly: isolation from cabbage leaves. Phytochemistry 51, 377–382.

Ishida, M., Chiba, I., Okuyama, Y., Takahata, Y., Kaizuma, N., 1997. Separation and identification of desulfoglucosinolates in Japanese rapeseed by LC/APCI-MS. Japan Agricultural Research Quarterly 131, 73–80.

Kjaer, A., 1960. Naturally derived isothiocyanates (Mustard oils) and their parent glucosides. Progress in the Chemistry of Organic Natural Products 18, 122–176.

Kjaer, A., 1974. The natural distribution of glucosinolates: a uniform group of sulfur containing glucosides. In: Bendz, G., Santesson, J. (Eds.), Chemistry in Botanical Classification. Academic Press, New York, pp. 229–234.

Louda, S., Mole, S., 1991. Glucosinolates: chemistry and ecology. In: Rosenthal, G.A., Berenbaum, M.R. (Eds.), Herbivores: Their Interactions with Secondary Plant Metabolites, Vol. I, The Chemical Participants. Academic Press, New York, pp. 123–164.

Mithen, R.F., Lewis, B.G., Heaney, R.K., Fenwick, G.R., 1987. Glucosinolates of wild and cultivated *Brassica* species. Phytochemistry 26, 1969–1973.

Roessingh, P., Städler, E., 1990. Foliar form, color and surface characteristics influence oviposition behaviour in cabbage root fly *Delia radicum*. Entomologia et Experimentalis Applicata 57, 93–100.

Roessingh, P., Städler, E., Fenwick, G.R., Lewis, J.A., Nielsen, J.K., Hurter, J., Ramp, T., 1992. Oviposition and tarsal chemoreceptors of the cabbage root fly are stimulated by glucosinolates and host plant extracts. Entomologia et Experimentalis Applicata 65, 267–282.

Roessingh, P., Städler, E., Baur, R., Hurter, J., Ramp, T., 1997. Tarsal chemoreceptors and oviposition behaviour of the cabbage root fly (*Delia radicum*) sensitive to fractions and new compounds of host-leaf surface extracts. Physiological Entomology 22, 140–148.

Rosa, E.A., Heaney, R.K., Fenwick, G.R., Portas, C.A.M., 1997. Glucosinolates in crop plants. Horticultural Reviews 19, 99–215.

Simmonds, M.S.J., Blaney, W.M., Mithen, R., Birch, A.N.E., Lewis, J., 1994. Behavioural and chemosensory responses of the turnip root fly (*Delia floralis*) to glucosinolates. Entomologia et Experimentalis Applicata 71, 41–57.

Spencer, J.L., Pillai, S., Bernays, E.A., 1999. Synergism in the oviposition behaviour of *Plutella xylostella*: sinigrin and wax compounds. Journal of Insect Behaviour 12, 483–500.

Spinks, E.A., Sones, K., Fenwick, G.R., 1984. The quantitative analysis of glucosinolates in cruciferous vegetables, oilseeds and forage crops using high performance liquid chromatography. Fette Seifen Anstrichmittel 6, 228–231.

Städler, E., Roessingh, P., 1991. Perception of surface chemicals by feeding and ovipositing insects In: Jermy, T., Szentesi, A. (Eds.), Proceedings of 7th International Symposium on Insect-Plant Relationships. Symp. Biol. Hung. Vol. 39, pp. 71-86.

Städler, E., Renwick, J.A.A., Radke, C.D., Sachdev-Gupta, K., 1995. Tarsal contact chemoreceptor response to glucosinolates and cardenolides mediating oviposition in *Pieris rapae*. Physiological Entomology 20, 175–187.

PERGAMON

Phytochemistry 57 (2001) 701–710

PHYTOCHEMISTRY

www.elsevier.com/locate/phytochem

Antioxidant enzymes responses to cadmium in radish tissues

Angela P. Vitória[a], Peter J. Lea[b], Ricardo A. Azevedo[c,*]

[a]*Departamento de Ciências Biológicas, Universidade Estadual de Feira de Santana, Feira de Santana CEP 44031-460, BA, Brazil*
[b]*Department of Biological Sciences, University of Lancaster, Lancaster LA1 4YQ, UK*
[c]*Departamento de Genética, Escola Superior de Agricultura Luiz de Queiroz, Universidade de São Paulo, Piracicaba 13400-970, SP, Brazil*

Received 11 February 2000; received in revised form 28 December 2000

Abstract

To investigate the antioxidant responses of radish (*Raphanus sativus* L.) to cadmium (Cd) treatment, seedlings of a tolerant variety were grown in increasing concentrations of $CdCl_2$, ranging from 0.25–1 mM, for up to 72 h in a hydroponic system. Analysis of Cd uptake indicated that most of the Cd accumulated in the roots, but some was also translocated and accumulated in the leaves, especially at the higher concentrations of Cd used in the experiments. Roots and leaves were analysed for catalase, glutathione reductase and superoxide dismutase activities. Catalase and glutathione reductase activities increased considerably in the roots and leaves after 24 h exposure to the metal, indicating a direct correlation with Cd accumulation. The analysis of native PAGE enzyme activity staining, revealed several superoxide dismutase isoenzymes in leaves, with the two predominant isoenzymes exhibiting increases in activity in response to Cd treatment. The results suggest that in radish, the activity of antioxidant enzymes responds to Cd treatment. The main response may be via the activation of the ascorbate–glutathione cycle for the removal of hydrogen peroxide, or to ensure the availability of glutathione for the synthesis of Cd-binding proteins. © 2001 Elsevier Science Ltd. All rights reserved.

Keywords: *Raphanus sativus*; Radish; Antioxidant enzymes; Cadmium; Catalase; Glutathione reductase; Phytochelatins; Superoxide dismutase

1. Introduction

Cadmium (Cd) is a toxic element that normally occurs in low concentrations in soils (Wagner, 1993). However, in areas that have been subjected to mining the concentration can be high, varying from 100–600 mg kg^{-1} dry weight (Ernst and Neilssen, 2000; Lombi et al., 2000). In addition, following the application of sewage sludge to agricultural land, Cd can accumulate in the topsoil (Lombi et al., 2000). Although Cd is not an essential nutrient for plants, the metal ion is taken up rapidly by the roots (Leita et al., 1991; Hart et al., 1998) and on most occasions causes inhibition of growth (Di Toppi et al., 1999; Sneller et al., 1999). However, a number of plants (termed hyperaccumulators) that grow on metalliferous soils, are able to translocate Cd from the roots and accumulate it in high concentrations in the shoots (Chardonnens et al., 1998). It has been suggested that such plants would be of considerable value in the remediation of soils that are heavily contaminated with heavy metals (Zhu et al., 1999).

Cd may be detoxified in plants by combination with a family of sulphur rich peptides termed phytochelatins (Leopold et al., 1999; Cobbett, 2000). The peptides are structurally related to glutathione and contain a varying number (normally 2–5) of glutamate and cysteine, linked through the γ-carboxyl group of glutamate. Synthesis of these phytochelatins can be induced very rapidly in tissue culture cells and roots, and is accompanied by a fall in the concentration of glutathione, following the addition of Cd or other heavy metals (Grill et al., 1987). Glutathione synthesis may then be stimulated by induction of enzymes involved in sulphate uptake and reduction and γ-glutamylcysteine synthetase (Haag-Kerwer et al., 1999; Heiss et al., 1999). Phytochelatin synthase which carried out the conversion of glutathione to phytochelatins is activated by Cd, but is inactive in the absence of heavy metal ions (Cobbett, 2000).

Proof that phytochelatins are synthesised from glutathione has come from an investigation into enzyme deficient mutants and overexpressing plant lines. *cad2* mutants of Arabidopsis lacking γ-glutamylcysteine

* Corresponding author. Fax: +55-19-433-6706.
E-mail address: raazeved@carpa.ciagri.usp.br (R.A. Azevedo).

0031-9422/01/$ - see front matter © 2001 Elsevier Science Ltd. All rights reserved.
PII: S0031-9422(01)00130-3

synthetase are sensitive to Cd and are unable to synthesise glutathione, whilst the *cad1* mutants lacking phytochelatin synthase are sensitive to Cd and accumulate glutathione (Howden et al., 1995; Cobbett et al., 1998). Overexpression of both γ-glutamylcysteine synthetase and glutathione synthetase in Indian mustard has been shown to increase phytochelatin synthesis and confer resistance to Cd (Yong et al., 1999; Zhu et al., 1999).

Van Assche and Clijsters (1990) have reviewed in detail the early work showing that Cd has the capacity to inhibit a range of enzyme activities in plants, in particular those of the Calvin cycle and chlorophyll biosynthesis. Research into the effects of Cd on photosynthetic CO_2 assimilation has continued (Krupa, 1999), with evidence presented that the enzymes of the Calvin cycle and RUBP carboxylase/oxygenase are particularly sensitive to Cd (Chugh and Sawhney, 1999; Di Cagno et al., 1999).

Evidence that Cd causes the production of reactive oxygen species (ROS) (Foyer et al., 1997) in plants, came from observation that new isoenzymes of peroxidase were detectable in both the root and leaves of *Phaseolus vulgaris* (Van Assche and Clijsters, 1990). Further evidence of Cd induced oxidative stress came from the detection of lipid peroxidation and chlorophyll breakdown (Somashekaraiah et al., 1992; Gallego et al., 1996a; Chaoui et al., 1997; Dalurzo et al., 1997). Due to the multiplicity of processes that produce ROS during metabolism, including photosynthesis and photorespiration, fatty acid oxidation, response to pathogen attack and senescence, plants have developed a series of detoxification reactions. Peroxide can be metabolised directly by peroxidases, particularly in the cell wall, and by catalase (CAT) in the peroxisome (Azevedo et al., 1998; Polidoros and Scandalios, 1999). In the chloroplast, superoxide is converted by superoxide dismutase (SOD) to peroxide which is then detoxified to water and oxygen via the glutathione/ascorbate cycle, which involves the operation of ascorbate peroxidase, monohydroascorbate reductase/dehydroascorbate reductase and glutathione reductase (GR) (Foyer et al., 1997; Noctor and Foyer, 1998). Three distinct types of SOD activity have been detected in plants, which can be classified according to their metal cofactor, Mn, Fe and Cu/Zn. Mn–SOD is located in the mitochondria and peroxisomes, Fe–SOD (which is not found in all plants) is associated with the chloroplasts and the abundant Cu/Zn SODs are located in the cytosol, chloroplasts and peroxisomes (Bowler et al., 1992; Del Rio et al., 1998). The occurrence of SOD activity in such a wide range of metabolic compartments suggests that enzymes of the glutathione/ascorbate cycle, as well as peroxidases, may also play an important role outside the chloroplast. The synthesis of oxalate oxidase, that is present in the cytoplasm and apoplast of germinating wheat embryos and liberates peroxide, is stimulated by the presence of Cd (Berna and Bernier, 1999).

Given the above cited mechanisms utilised by plants to detoxify ROS, it is clearly important to establish whether exposing plants to Cd causes a detrimental or stimulatory effect on the enzymes involved in this detoxification process. Somewhat surprisingly, the limited number of experiments that have been carried out on the subject have frequently produced contradictory results. CAT activity has been shown to decline in *Phaseolus vulgaris* (Somashekariah et al., 1992), *Phaseolus aureus* (Shaw, 1995), *Pisum sativum* (Dalurzo et al., 1997), *Lemna minor* (Mohan and Hossetti, 1997) and *Amaranthus lividus* (Bhattacharjee, 1998), following the application of Cd to the growth medium. However in *Phaseolus vulgaris*, although decreases in CAT activity were detected in roots and leaves, there was no effect on the stem enzyme (Chaoui et al., 1997), and in *Agropyron repens* increases in CAT activity were detected in both leaves and stems (Brej, 1998). In *Helianthus annuus* (Gallego et al., 1996b, 1999) considerable variation in CAT activity was detected over a time period up to 22 days with similar variations being also detected in tolerant varieties of *Solanum tuberosum* (Stroinski and Kozlowska, 1997).

GR activity in *S. tuberosum* increased following the application of Cd, but this was followed by a rapid and total inactivation and then a slow recovery (Stroinski et al., 1999). In two species of *Alyssum,* GR activity increased at 0.02 mM Cd but decreased at 0.05 mM Cd (Schickler and Caspi, 1999). Increases in GR activity were observed in the leaves of *Phaseolus vulgaris* (Chaoui et al., 1997), but decreases had been noted previously in germinating seedlings of the same species (Somashekariah et al., 1992). Decreases in GR activity following the application of Cd, were detected in a series of experiments employing *H. annuus* (Gallego et al., 1996a,b, 1999). Increases in total SOD activity were detected following the application of Cd in *P. sativum* (Dalurzo et al., 1997) and two *Alyssum* species (Schickler and Caspi, 1999), along with a decrease and then an increase in SOD activity in *S. tuberosum* (Stroinski and Kozlowska, 1997). SOD activity remained constant or decreased in *H. annuus* (Gallego et al., 1996a, 1999) and declined in *A. lividus* (Bhattacharjee, 1998), following the application of Cd. As far as we are aware no attempt has been made to examine the effect of Cd on the different isoenzymes of SOD in higher plants.

In this work, we report new findings showing that the activities of all three enzymes (CAT, GR and specific isoenzymes of SOD) increased in the leaves and roots of a resistant variety of radish, following exposure to increasing concentrations of Cd. Although the concentrations of Cd used (0.25 and 1 mM) are high when compared to that found in contaminated soils, they have been used recently in testes on species of *Thlaspi* that are able to accumulate high concentrations of Cd (Lombi et al., 2000).

2. Results

2.1. $CdCl_2$ effect on plant growth

Four commercial varieties of radish were grown in the presence of increasing concentrations of $CdCl_2$ concentrations for a 7 day period in Hoagland's nutrient solution. All radish varieties exhibited reduced length in the $CdCl_2$ treatments based on root growth (Fig. 1). The variety Comprido Vermelho was more sensitive to $CdCl_2$, showing some reduction in growth at 0.012 mM. At low concentration of $CdCl_2$, the inhibition of root growth was very similar for Redondo Vermelho, Scarlett Globe and Grinson Gigante (Fig. 1). However, at concentrations higher than 0.5 mM, the variety Redondo Vermelho exhibited a greater degree of tolerance to $CdCl_2$ (Fig. 2). For the other varieties, 0.5, 1 and 5 mM $CdCl_2$ proved to be lethal after 4 days of Cd treatment. The variety Redondo Vermelho was chosen for further analysis.

2.2. Cd accumulation in roots and leaves

The accumulation of Cd in Redondo Vermelho was determined in the roots and leaves after growth in 0.5 and 1 mM $CdCl_2$ for 72 h (Fig. 3). Most of the Cd that entered the plant system accumulated in the roots and only a small amount was translocated to the leaves. Furthermore, it can be seen that Cd entered the roots very rapidly, with approximately 50% of the Cd being taken up within the first 12 h of growth in the presence of the metal.

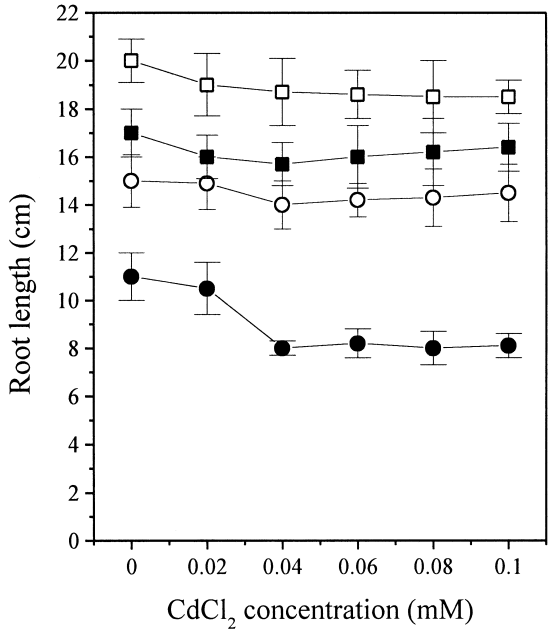

Fig. 1. Root length of four radish varieties (● Comprido Vermelho, ○ Redondo Vermelho, ■ Scarlett Globe, □ Grinson Gigante) grown in 0.02, 0.04, 0.06, 0.08 and 0.1 mM $CdCl_2$, for 7 days.

2.3. CAT activity

The specific activity of CAT expressed on a protein basis, was 2-fold higher in the leaves of the control plants, than in the roots. The CAT activity in the control plants was also shown to be very constant during the time-length of the experiment (Fig. 4). $CdCl_2$ induced an increase in CAT activity in both the roots and leaves of radish plants. A direct correlation was observed between Cd concentration and increased CAT activity in both tissues, so that higher concentrations of $CdCl_2$ produced a greater increase in CAT activity (Fig. 4). The percentage increase in CAT activity was higher in the roots than in leaves, especially at 1 mM $CdCl_2$ (Fig. 4). When $CdCl_2$ was tested on CAT activity determined by the spectrophotometric assay, no alteration in enzyme activity was observed, suggesting that $CdCl_2$ has no effect on CAT activity in vitro.

Extracts of leaves and roots treated with 0.5 mM $CdCl_2$ were applied to native PAGE gels and stained for CAT activity (Fig. 5). CAT activity staining revealed two major CAT isoenzymes in leaves (Fig. 5A), however some other minor bands were also observed in a few experiments, when much higher concentrations of protein were loaded onto the gels (data not shown). On the other hand, following electrophoresis of root extracts, one single diffuse band of CAT activity was observed (Fig. 5B), the position of which corresponded to the more electronegative band detected with leaf extracts (Fig. 5A). It can be seen in leaves exposed to 0.5 mM $CdCl_2$, that both CAT bands exhibited a major increase in activity over the 72 h time course, especially the most electropositive band (Fig. 5A). In roots, only a small increase in CAT activity was detected, after 48 h treatment with $CdCl_2$ (Fig. 5B).

Fig. 2. Radish (cv. Redondo Vermelho) seedlings grown for 7 days in 0 (A), 0.006 (B), 0.012 (C), 0.025 (D), 0.05 (E), 0.1 (F), 0.5 (G), 1.0 (H) and 5.0 (I) mM $CdCl_2$.

(colour)

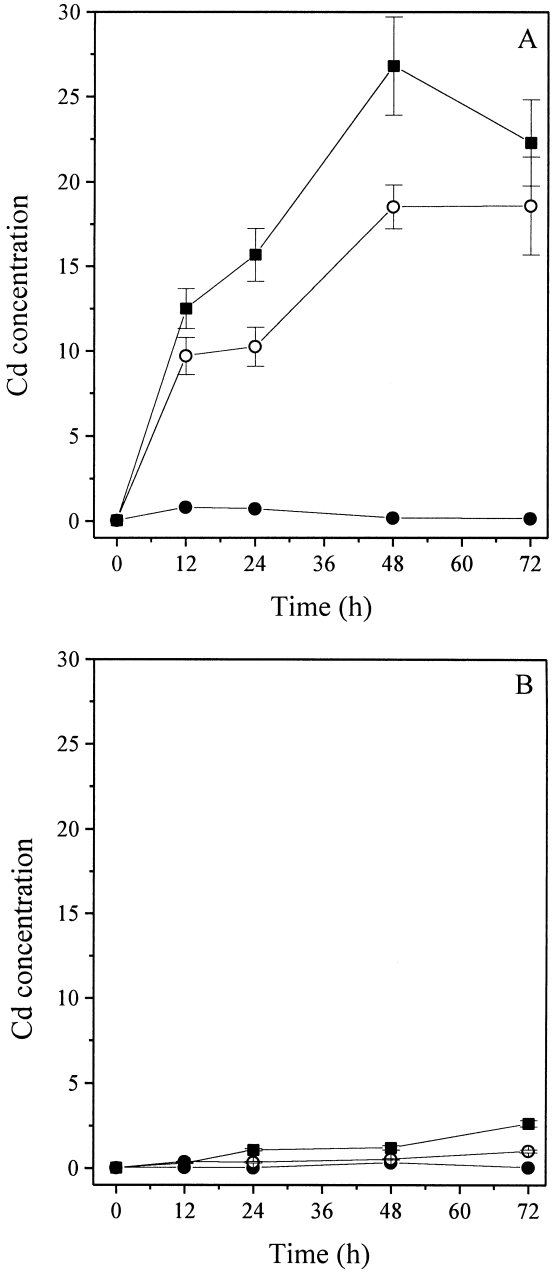

Fig. 3. Cd accumulation (μg g^{-1} dry weight) in radish (cv. Redondo Vermelho) seedlings. Cd concentrations were determined in the roots (A) and leaves (B) of plants grown over a 72 h period. Control zero $CdCl_2$ (●), 0.5 mM $CdCl_2$ (○) and 1 mM $CdCl_2$ (■).

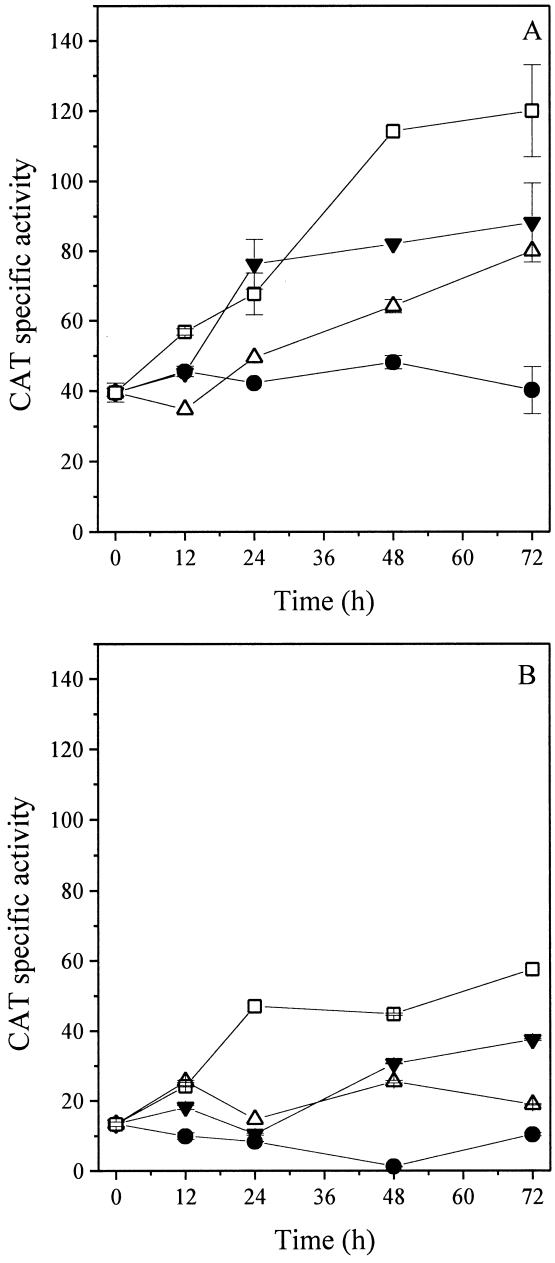

Fig. 4. The specific activity of CAT (μmol min^{-1} mg^{-1} prot) in the leaves (A) and roots (B) of radish (cv. Redondo Vermelho) seedlings grown for a 72 h period in four concentrations of $CdCl_2$. Control zero (●), 0.25 mM (△), 0.5 mM (▼) and 1.0 mM (□).

2.4. SOD activity

The same plant extracts used for CAT were also stained for SOD activity following native PAGE (Fig. 6). Several bands of SOD activity were observed in some experiments, depending on the protein concentration used in the gel. However, two major SOD bands, corresponding to ~95% of total SOD activity were observed in leaves (Fig. 6A), but only one band was present following the electrophoresis of root extracts (Fig. 6B). Both of the leaf SOD bands exhibited a continuous increase in activity after 24 h exposure to $CdCl_2$ (Fig. 6A), whereas in roots there was no significant variation in SOD activity (Fig. 6B). The incubation of gels in hydrogen peroxide and potassium cyanide was carried out to classify all the SOD isoenzymes observed in radish leaves. Two Fe–SOD (resistant to cyanide and inhibited by hydrogen peroxide) and four Cu/Zn–SOD (inactivated by both inhibitors) isoenzymes were identified, while Mn–SOD isoenzymes were not observed (data not

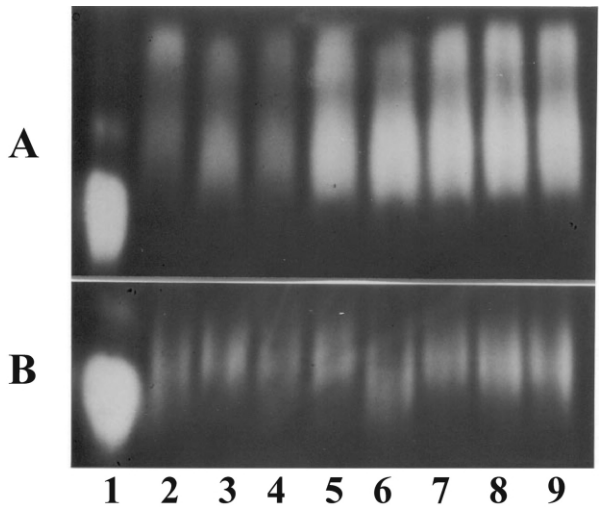

Fig. 5. Activity staining for CAT in radish (cv. Redondo Vermelho) leaves (A) and roots (B). Lane 1, CAT activity standard from bovine liver; lane 2, control (zero $CdCl_2$) after 72 h; lane 3, 3 h; lane 4, 6 h; lane 5, 9 h; lane 6, 12 h; lane 7, 24 h, lane 8, 48 h and lane 9, 72 h of growth in 0.5 mM $CdCl_2$; 60 and 15 μg of protein from leaves and roots, respectively, were loaded onto each gel lane.

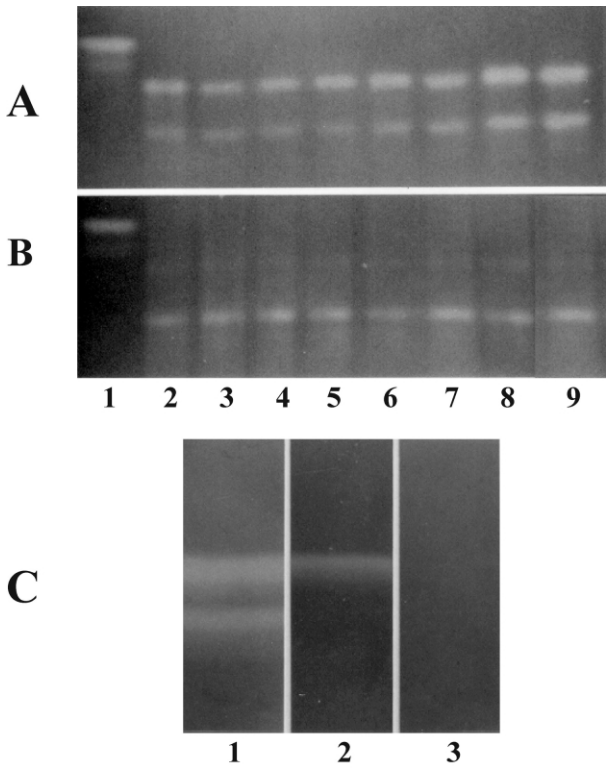

Fig. 6. Activity staining for SOD in radish (cv. Redondo Vermelho) leaves (A) and roots (B). Lane 1, Bovine SOD standard; lane 2, control (zero $CdCl_2$) after 72 h; lane 3, 3 h; lane 4, 6 h; lane 5, 9 h; lane 6, 12 h; lane 7, 24 h; lane 8, 48 h and lane 9, 72 h of growth in 0.5 mM $CdCl_2$; 30 μg of protein from leaves and roots were loaded onto each gel lane. In (C), a radish leaf protein sample (50 μg) was loaded onto the gel and stained for individual SOD isoenzymes. Lane 1, control SOD activity; lane 2, plus 2 mM potassium cyanide and lane 3, 5 mM hydrogen peroxide.

shown). Tobacco leaf SOD extracts were tested simultaneously and used as a control. The two major SOD bands of radish leaves, always present independent of the protein concentration, were classified as Fe–SOD and Cu/Zn–SOD (Fig. 6C). No other changes, such as the appearance or disappearance of bands, were detectable in the CAT and SOD isoenzyme patterns, that would suggest a specific response to $CdCl_2$ treatment.

2.5. GR activity

The activity of GR exhibited very little variation in the roots and leaves of control plants (Fig. 7A and B). However, GR activity in both tissues increased considerably with $CdCl_2$ treatment and time of exposure to the metal (Fig. 7A and B). The increase of GR activity was very rapid in roots reaching a 15-fold increase in the 1 mM $CdCl_2$ treatment, compared to the control (Fig. 7B), whereas in leaves the increase in GR activity in 1 mM $CdCl_2$ was only 7.5-fold after 72 h (Fig. 7A). In a similar manner to CAT, when $CdCl_2$ was tested in the spectrophotometric assay for GR activity, no significant alteration was observed, suggesting that $CdCl_2$ has no effect on GR activity in vitro.

3. Discussion

The impact of Cd uptake by living cells has been shown to be drastic, normally leading to cell death depending on the metal dose and time-length of exposure. Among some of the effects that heavy metals can cause is the generation of ROS. Relationship between Cd toxicity and oxidative reactions have been studied in more detail in animals and microrganisms. In mice, Cd daily administration led to inhibition of SOD activity (Patra et al., 1999). The responses of antioxidant enzymes in fish exposed to Cd have shown in general a reduction of CAT, GR and SOD activities (Zikic et al., 1997; Vaglio and Landriscina, 1999), whereas increased CAT and SOD activities were shown to be able to inhibit lipid peroxidation and Cd-induced cell injury to human fetal lung fibroblasts (Yang et al., 1997).

Increasing concentrations of $CdCl_2$ caused a decrease in the growth of the four varieties of radish under test (Fig. 1) and only one variety (Redondo Vermelho) was able to withstand 0.5 and 1 mM $CdCl_2$, albeit with a considerably reduced root growth (Fig. 2). Cd accumulated in the roots at a faster rate and to a much higher concentration than in the leaves, following the application of $CdCl_2$ (Fig. 3). In plants that are not hyperaccumulators of Cd, roots have been shown previously to be the major site of phytochelatin synthesis and hence Cd accumulation (Di Cagno et al., 1999; Zhu et al., 1999).

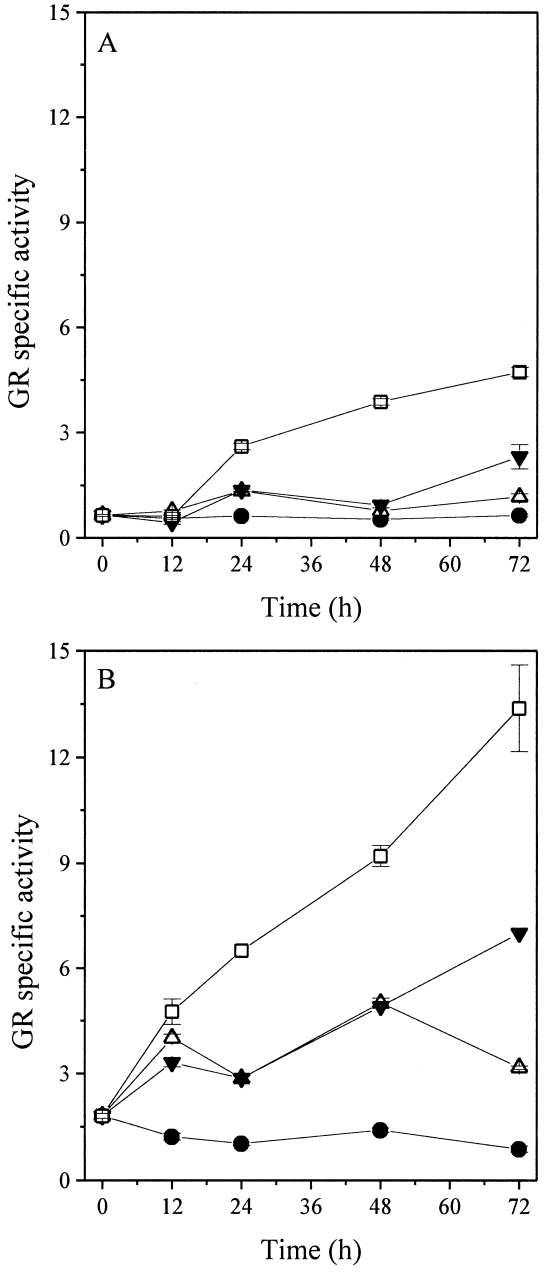

Fig. 7. The specific activity of GR (μmol min^{-1} mg^{-1} prot) in the leaves (A) and roots (B) of radish (cv. Redondo Vermelho) seedlings grown for a 72 h period in four concentrations of $CdCl_2$. Control zero (●), 0.25 mM (△), 0.5 mM (▼) and 1.0 mM (□).

As indicated in the Introduction, there have been a number of studies that have examined the effect of Cd on CAT activity in higher plants and the majority reported a decrease in activity, although there was some variation over longer time courses. Only Brej (1998), positively demonstrated a significant increase in CAT activity in the roots and leaves of some populations of *Agropyron repens* growing in highly contaminated soils. It can be clearly seen in Fig. 4, that there was a significant Cd induced increase in CAT activity in both the leaves and roots, and that the magnitude of this increase was proportional to the concentration of $CdCl_2$ in the external medium. Following the staining for CAT activity after native PAGE, two major bands were visible when leaf extracts were tested, both of which increased during the time course of exposure to 0.5 mM $CdCl_2$, although the more electropositive band seemed to respond earlier (Fig. 5A). Staining for CAT activity in root extracts was less clear and it was difficult to establish whether one or two isoenzymic bands were present. A definite increase in CAT activity was observed over the time course, although the magnitude was less than observed with leaf extracts (Fig. 5). The isoenzymic patterns for both leaves and roots in Fig. 5, are similar to those obtained by Anderson et al. (1995) in a study of chilling acclimation in maize.

A major function of CAT activity is to metabolise the peroxide liberated in the peroxisome following the conversion of glycollate to glyoxylate during photorespiration (Kendall et al., 1983). The activity of the enzyme is greatly reduced when plants are grown in elevated atmospheres of CO_2 (Azevedo et al., 1998). CAT is also important in the metabolism of peroxide liberated during the metabolism of fatty acids particularly in the germinating seed (Holtman et al., 1994). Isoenzymic forms of CAT have been studied extensively in higher plants, where there are frequently three genes encoding CAT. In *Nicotiana plumbaginofolia,* the transcription of two of the three genes was stimulated by ozone (Willekens et al., 1994), whilst the transcription of all three genes in maize has been shown to be increased by the addition of hydrogen peroxide, although the time course of the response varied between genes (Polidoros and Scandalios, 1999). The increase in CAT activity demonstrated in Figs. 4 and 5, is therefore circumstantial evidence to support the hypothesis that Cd causes the formation of ROS. The increase in CAT activity in the leaves was stimulated by much lower concentrations of Cd than in the roots, which may be due to light causing a greater formation of ROS in leaves (Noctor and Foyer, 1998; Foyer and Noctor, 1999). However there is also the possibility that there is a signal of oxidative stress transported from the roots to the leaves. Evidence that such a signalling mechanism can increase the transcription of ascorbate peroxidase has recently been reported (Karpinski et al., 1999).

Only two major bands of SOD activity were detectable following the staining of native PAGE gels for enzyme activity in the leaves (Fig. 6A). Inhibitor studies (Fig. 6C) indicated that the upper more electropositive band was a Fe–SOD, whilst the lower more electropositive band was a Cu/Zn–SOD. Although more SOD bands were visible when larger amounts of protein were loaded onto the gel, it was clear that these two isoenzymes comprised the major SOD activity in the leaves. Both activities increased in the leaves during the time course of exposure to $CdCl_2$. However, in the roots a Cu/Zn form of SOD predominated and the activity

did not vary over the time course. As indicated in the Introduction, previous work examining the effects of Cd on SOD activity in plants has produced varied results, although most have shown a decrease or no change in activity. Only in *P. sativum* (Dalurzo et al., 1997) and *Alyssum* species (Schickler and Caspi, 1999) has definite increases in SOD activity been detected, although no attempt was made to separate the different metal containing isoenzymes. However a range of different oxidative stresses have been shown to increase both the activity and expression of genes encoding SOD (Bowler et al., 1992; Willekens et al., 1994).

GR activity increased in both the leaves and roots (Fig. 7) during the time course of exposure to three different concentrations of $CdCl_2$ and as with CAT the magnitude of the response was dependent upon the concentration applied. However in contrast to the results obtained with CAT and SOD, the increase in GR activity was far greater in the roots. These data could be explained by two completely different scenarios (i) the glutathione/ascorbate cycle is operating at high rate in order to detoxify the ROS formed in the root, or (ii) it is essential to keep the glutathione in a reduced form, prior to its incorporation into phytochelatins (Cobbett, 2000). A number of previous workers have detected increases in GR activity in plants following exposure to Cd (Chaoui et al., 1997; Stroinski et al., 1999; Schickler and Caspi, 1999), although the response has often been dose dependent and variable over time. In a similar manner to CAT and SOD, oxidative stress has been shown to cause an increase in GR activity (Stevens et al., 1997). Taking into consideration data showing that ascorbate peroxidase also increases following exposure to cadmium (Shaw, 1995; Chaoui et al., 1997), the present data would indirectly suggest that the glutathione/ascorbate cycle does play a role in the detoxification of Cd-induced ROS.

In conclusion, the data presented in this paper have demonstrated that activities of the three major enzymes (CAT, SOD and GR) involved in the detoxification of ROS increase significantly following the supply of high concentrations of $CdCl_2$ to a tolerant variety of radish. However, the magnitude of these activity increases, varies with both the enzyme and the location, i.e. in the roots or leaves. It remains to be seen whether these increases in activity are due to induced gene transcriptional and de novo synthesis of protein, or are due to posttranslational modification of existing enzyme protein.

4. Experimental

4.1. Plant material

Seeds of four radish varieties (*Raphanus sativus* — cv. Redondo Vermelho, Comprido Vermelho, Grinson Gigante and Scarlett Globe) were germinated on moistened filter paper and then transferred to a glass house maintained at 25–30°C and a 16 h photoperiod at 300 μmol m^{-2} s^{-1} in a hydroponic system in pots containing 1.4 l of Hoagland's nutrient solution. Fourteen-day old plants grown in Hoagland's nutrient solution were further grown in the same solution, but containing 0.006, 0.012, 0.025, 0.05, 0.1, 0.5, 1.0 and 5.0 mM $CdCl_2$ for 12, 24, 48 and 72 h or 7 day periods. After these periods, growth was determined by measurement of root length.

Based on the growth of these varieties, Redondo Vermelho was selected and another experiment was carried out using 0.25, 0.5 and 1.0 mM $CdCl_2$ under the same conditions described above. Roots and leaves from each treatment were collected in liquid nitrogen and stored at −80°C for further analysis.

4.2. Enzyme extraction

The following steps were carried out at 4°C unless stated otherwise. The root or leaf tissue (3:1 buffer volume:-fresh weight) was homogenized in a pestle and mortar with 100 mM potassium phosphate buffer (pH 7.5) containing 1 mM EDTA, 3 mM DL-dithiothreitol and 5% (w/v) insoluble polyvynilpyrrolidone. The homogenate was centrifuged at 10,000 *g* for 30 min and the supernatant kept stored in separate aliquots at −80°C, prior to CAT, GR and SOD analysis.

4.3. CAT assay

CAT activity was determined as described by Azevedo et al. (1998), with some minor modifications. CAT activity was assayed spectrophotometrically at 25°C in a reaction mixture containing 1 ml 100 mM potassium phosphate buffer (pH 7.5), containing 2.5 μl H_2O_2 (30% solution) prepared immediately before use. The reaction was initiated by the addition of 15 μl of plant extract and activity determined by monitoring the degradation of H_2O_2 at 240 nm over 1 min against a plant extract-free blank.

4.4. GR assay

GR activity was determined as described by Barata et al. (2000). GR activity was assayed spectrophoto metrically at 30°C in a mixture consisting of 3 ml 100 mM potassium phosphate buffer (pH 7.5) containing 1 mM 5,5″-dithiobis(2-nitrobenzoic acid), 1 mM oxidized glutathione and 0.1 mM NADPH. The reaction was started by the addition of 50 μl of plant extract. The rate of reduction of oxidized glutathione was followed by monitoring the increase in absorbance at 412 nm over 2 min.

4.5. Polyacrylamide gel electrophoresis (PAGE)

Electrophoresis was carried out under native condition in 5–6% polyacrylamide gradient and 8%

polyacrylamide gels for CAT and SOD activity staining, respectively. A constant current of 20 mA/gel was applied for 8 h (gels to be stained for CAT activity) or 4 h (gels to be stained for SOD activity) and the temperature maintained at 4°C. Electrophoresis buffers and gels were prepared as described by Laemmli (1970) except that SDS was excluded. Equal amounts of protein were loaded on to each lane.

4.6. CAT activity staining

CAT activity in native PAGE gels was determined as described by Woodbury et al. (1971). Gels were incubated in 0.003% H_2O_2 for 10 min and developed in a 1% (w/v) $FeCl_3$ and 1% $K_3Fe(CN_6)$ (w/v) solution for 10 min.

4.7. SOD activity staining

After electrophoretic separation, SOD activity was determined as described by Beauchamp and Fridovich (1971) and modified by Azevedo et al. (1998). The gels were rinsed in distilled–deionized water and incubated in the dark for 30 min at room temperature in a reaction mixture containing 50 mM potassium phosphate buffer (pH 7.8), 1 mM EDTA, 0.05 mM riboflavin, 0.1 mM nitroblue tetrazolium and 0.3% (v/v) *N*,*N*,*N*′,*N*′-tetramethylethylenediamine (TEMED). At the end of this period, the reaction mixture was poured off, the gels were rinsed with distilled–deionized water and then illuminated in water until the development of colorless bands of SOD activity in a purple-stained gel was visible. To stop the reaction, the gels were transferred to 6% (v/v) acetic acid. Bovine SOD (Sigma Chemical Co.) was applied to all gels to serve as a positive control of SOD activity. SOD isoenzymes were classified by testing a leaf sample, as described previously by Azevedo et al. (1998). Prior to SOD staining, the gel was cut into three slices; the first was stained for SOD as above; the second and third slices were incubated for 20 min in 100 mM potassium phosphate buffer (pH 7.8) containing 2 mM KCN and 100 mM potassium phosphate buffer (pH 7.8) containing 5 mM H_2O_2, respectively. At the end of this period, both slices were washed in distilled–deionized water and then stained for SOD activity. The pre-treatment of the gels in H_2O_2 and KCN before SOD staining allowed the classification of the SOD into Cu/Zn–SOD, Fe–SOD or Mn–SOD isoenzymes. Mn–SOD is resistant to both inhibitors, Fe–SOD isoenzymes is resistant to KCN and inhibited by H_2O_2, and Cu/Zn–SOD is inhibited by both inhibitors.

4.8. Determination of protein concentration

The concentration of protein was determined by the method of Bradford (1976) using BSA as a standard.

4.9. Statistical analysis

The experiments were repeated three times. Data were statistically analysed within each experiment and the results expressed as mean (±S.E.) of four independent replicates for CAT and GR activities measurements.

4.10. Cd accumulation

The accumulation of Cd in roots and leaves was analysed in a ICP–MS (inductivily coupled plasma mass spectrometer). Samples of roots and leaves of control and Cd treated plants exposed to 0.5 and 1.0 mM of $CdCl_2$, were dried at 60°C for 4 days. The samples were then digested with 2 ml concentrated HNO_3 and applied to the ICP–MS spectrophotometer and analysed exactly as described by Wu et al. (1997).

Acknowledgements

The authors gratefully acknowledge the support of this work by the Fundação de Amparo à Pesquisa do Estado de São Paulo (FAPESP, Grant No. 99/06429-0) and the British Council (UK) — Conselho Nacional de Desenvolvimento Científico e Tecnológico (CNPq-Brazil). A.P.V. and R.A.A. received research fellowships from FAPESP and CNPq, respectively.

References

Anderson, M.D., Prasad, T.K., Stewart, C.R., 1995. Changes in isozyme profiles of catalase, peroxidase, and glutathione reductse during acclimation to chilling in mesocotyls of maize seedlings. Plant Physiology 109, 1247–1257.

Azevedo, R.A., Alas, R.M., Smith, R.J., Lea, P.J., 1998. Response of antioxidant enzymes to transfer from elevated carbon dioxide to air and ozone fumigation, in the leaves and roots of wild-type and a catalase-deficient mutant of barley. Physiologia Plantarum 104, 280–292.

Barata, R.M., Chapparro, A., Chabregas, S.M., Gonzalez, R., Labate, C.A., Azevedo, R.A., Sarath, G., Lea, P.J., Silva-Filho, M.C., 2000. Targeting of the soybean leghemoglobin to tobacco chloroplasts: effects on aerobic metabolism in transgenic plants. Plant Science 155, 193–202.

Beauchamp, C.H., Fridovich, I., 1971. Superoxide dismutase: improved assays and an assay applicable to acrylamide gels. Analytical Biochemistry 44, 276–287.

Berna, A., Bernier, F., 1999. Regulation by biotic and abiotic stress of a wheat germin gene encoding oxalate oxidase, a H_2O_2 — producing enzyme. Plant Molecular Biology 39, 539–549.

Bhattacharjee, S., 1998. Membrane lipid peroxidation, free radical scavengers and ethylene evolution in *Amaranthus* as affected by lead and cadmium. Biologia Plantarum 40, 131–135.

Bowler, C., Van Montagu, M., Inzé, D., 1992. Superoxide-dismutase and stress tolerance. Annual Review of Plant Physiology and Plant Molecular Biology 43, 83–116.

Bradford, M.M., 1976. A rapid and sensitive method for the quantitation of microgram quantities of protein utilizing the principle of protein-dye binding. Analytical Biochemistry 72, 248–254.

Brej, T., 1998. Heavy metal tolerance in *Agropyron repens* (L.) P. Bauv. Populations from Legnica copper smelter area, Lower Silesia. Acta Societatis Botanicorum Poloniae 67, 325–333.

Chaoui, A., Mazhoudi, S., Ghorbal, M.H., El Ferjani, E., 1997. Cadmium and zinc induction of lipid peroxydation and effects on antioxidant enzyme activities in bean (*Phaseolus vulgaris* L.). Plant Science 127, 139–147.

Chardonnens, A.N., TenBookum, W.M., Kuijper, L.D.J., Verkleij, J.A.C., Ernst, W.H.O., 1998. Distribution of cadmium in the leaves of cadmium tolerant and sensitive ecotypes of *Silene vulgaris*. Physiologia Plantarum 104, 75–80.

Chugh, L.K., Sawhney, S.K., 1999. Photosynthetic activities of *Pisum sativum* seedlings grown in the presence of cadmium. Plant Physiology and Biochemistry 37, 297–303.

Cobbett, C.S., 2000. Phytochelatins and their roles in heavy metal detoxification. Plant Physiology 123, 825–832.

Cobbett, C.S., May, M.J., Howden, R., Rolls, B., 1998. The glutathione deficient cadmium-sensitive mutant *cad2-1* of *Arabidopsis thaliana* is deficient in γ-glutamylcysteine synthetase. Plant Journal 16, 73–78.

Dalurzo, H.C., Sandalio, L.M., Gomez, M., Del Rio, L.A., 1997. Cadmium infiltration of detached pea leaves: effect on its activated oxygen metabolism. Phyton-Annales Rei Botanicae 37, 59–64.

Del Rio, L.A., Pastori, G.M., Palma, J.M., Sandalio, L.M., Sevilla, F., Corpas, F.J., Jimenez, A., Lopez-Huertas, E., Hernandez, J.A., 1998. The activated oxygen role of peroxisomes in senescence. Plant Physiology 116, 1195–1200.

Di Cagno, R., Guidi, L., Stefani, A., Soldatini, G.F., 1999. Effects of cadmium on growth of *Helianthus annus* seedlings: physiological aspects. New Phytologist 144, 65–71.

Di Toppi, L.S., Lambardi, M., Pechioni, N., Pazzagli, L., Durante, M., Gabbrielli, R., 1999. Effects of cadmium stress on hairy roots of *Daucus carota*. Journal of Plant Physiology 154, 385–393.

Ernst, W.H.O., Nielssen, H.J.M., 2000. Life-cycle phases of zinc and cadmium resistant ecotype of *Silene vulgaris* in risk assessment of polymetallic mine soils. Environmental pollution 107, 329–338.

Foyer, C.H., LopezDelgado, H., Dat, J.F., Scott, I.M., 1997. Hydrogen peroxide- and glutathione-associated mechanism of acclimatory stress tolerance and signalling. Physiologia Plantarum 100, 241–254.

Foyer, C.H., Noctor, G., 1999. Plant biology — leaves in the dark see light. Science 284, 599–601.

Gallego, S.M., Benavides, M.P., Tomaro, M.L., 1996a. Effects of heavy metal ions on sunflower leaves: evidence for involvement of oxidative stress. Plant Science 121, 151–159.

Gallego, S.M., Benavides, M.P., Tomaro, M.L., 1996b. Oxidative damage caused by cadmium chloride in sunflower. Phyton 58, 41–52.

Gallego, S.M., Benavides, M.P., Tomaro, M.L., 1999. Effect of cadmium ions on antioxidant defense system in sunflower cotyledons. Biologia Plantarum 42, 49–55.

Grill, E., Winnacker, E.-L., Zenk, M.H., 1987. Phytochelatins a class of heavy metal binding proteins from plants are functionally analogous to metallothioneins. Proceedings of the National Academy of Sciences of the United States of America 84, 439–443.

Haag-Kerwer, A., Schafer, H.J., Heiss, S., Walter, C., Rausch, T., 1999. Cadmium exposure in *Brassica juncea* causes a decline in transpiration rate and leaf expansion without effect on photosynthesis. Journal of Experimental Botany 50, 1827–1835.

Hart, J.J., Welch, R.M., Norvell, W.A., Sullivan, L.A., Kochian, L.V., 1998. Characterization of cadmium binding, uptake and translocation in intact seedlings of bread and durum wheat cultivars. Plant Physiology 116, 1413–1420.

Heiss, S., Schafer, H.J., Haag-Kerwer, A., Rausch, T., 1999. Cloning sulphur assimilation genes of *Brassica juncea* L.: cadmium differentially affects the expression of a putative low-affinity shuphate transporter and isoforms of ATP sulphurylase and APS reductase. Plant Molecular Biology 39, 847–857.

Holtman, W.L., Heistek, J.C., Mattern, K.A., Bakhuizen, R., Dumas, A.C., 1994. β-Oxidation of fatty acids is linked to the glyoxylate cycle in the aleurone but not in the embryo of germinating barley. Plant Science 99, 43–53.

Howden, R., Goldsbrough, P.B., Andersen, C.R., Cobbett, C.S., 1995. Cadmium sensitive cad1 mutants of *Arabidopsis thaliana* are phytochelatin deficient. Plant Physiology 107, 1059–1066.

Karpinski, S., Reynolds, H., Karpinska, B., Wingsle, G., Creissen, G., Mullineaux, P., 1999. Systematic signalling and acclimation in response to excess excitation energy in Arabidopsis. Science 284, 654–657.

Kendall, A.C., Keys, A.J., Turner, J.C., Lea, P.J., Miflin, B.J., 1983. The isolation and characterization of a catalase-deficient mutant of barley (*Hordeum vulgare* L.). Planta 159, 505–511.

Krupa, Z., 1999. Cadmium against higher plant photosynthesis — a variety of effects and where do they possibly come from? Zeitschrift fuer Naturforschung C 54, 723–729.

Laemmli, U.K., 1970. Cleavage of structural proteins during the assembly of the head of bacteriophage T4. Nature 227, 680–685.

Leita, L., Contin, M., Maggioni, A., 1991. Distribution of cadmium and induced Cd binding proteins in roots, stems and leaves of *Phaseolus vulgaris*. Plant Science 77, 139–147.

Leopold, I., Gunther, D., Schmidt, J., Neumann, D., 1999. Phytochelatins and heavy metal tolerance. Phytochemistry 50, 1323–1328.

Lombi, E., Zhao, F.J., Dunham, S.J., McGrath, S.P., 2000. Cadmium accumulation in populations of *Thlaspi caerulescens* and *Thlaspi goesingense*. New Phytologist 145, 11–20.

Mohan, B.S., Hosetti, B.B., 1997. Potential phytotoxicity of leaf and cadmium to Lemna minor grown in sewage stabilization ponds. Environmental Pollution 98, 233–238.

Noctor, G., Foyer, C.H., 1998. Ascorbate and glutathione: keeping active oxygen under control. Annual Review of Plant Physiology and Plant Molecular Biology 49, 249–279.

Patra, R.C., Swarup, D., Senapati, S.K., 1999. Effects of cadmium on lipid peroxides and superoxide dismutase in hepatic, renal, and testicular tissue of rats. Veterinary and Human Toxicology 41, 65–67.

Polidoros, A.N., Scandalios, J.G., 1999. Role of hydrogen peroxide and different classes of antioxidants in the regulation of catalase and glutathione S-transferase gene expression in maize (*Zea mays* L.). Physiologia Plantarum 106, 112–120.

Schickler, H., Caspi, H., 1999. Response of antioxidant enzymes to nickel and cadmium stress in hyperaccumulator plants of the genus *Alyssum*. Physiologia Plantarum 105, 39–44.

Shaw, B.P., 1995. Effects of mercury and cadmium on the activities of antioxidative enzymes in the seedlings of *Phaseolus aureus*. Biologia Plantarum 37, 587–596.

Sneller, F.E.C., Noordover, E.C.M., TenBookum, W.M., Schat, H., Bedaux, J.J.M., Verkleij, J.A.C., 1999. Quantitative relationship between phytochelatin accumulation and growth during prolonged exposure to cadmium in *Silene vulgaris*. Ecotoxicology 8, 167–175.

Somashekaraiah, B.V., Padmaja, K., Prasad, A.R.K., 1992. Phytotoxicity of cadmium ions on germinating seedlings of mung bean (*Phaseolus vulgaris*) — involvement of lipid peroxides in chlorophyll degradation. Physiologia Plantarum 85, 85–89.

Stevens, R.G., Creissen, G.P., Mullineaux, P.M., 1997. Cloning and characterisation of a cytosolic glutathione reductase cDNA from pea (*Pisum sativum* L.) and its expression in response to stress. Plant Molecular Biology 35, 641–654.

Stroinski, A., Kubis, J., Zielezinska, M., 1999. Effect of cadmium on glutathione reductase in potato tubers. Acta Physiologiae Plantarum 21, 201–207.

Stroinski, A., Kozlowska, M., 1997. Cadmium-induced oxidative stress in potato tuber. Acta Societatis Botanicorum Poloniae 66, 189–195.

Vaglio, A., Landriscina, C., 1999. Changes in liver enzyme activity in the teleost *Sparus aurata* in response to cadmium intoxication. Ecotoxicology and Environmental Safety 43, 111–116.

Van Assche, F., Clijsters, H., 1990. Effects of metals on enzyme activity in plants. Plant Cell and Environment 13, 195–206.

Yang, C.F., Shen, H.M., Shen, Y., Zhuang, Z.X., Ong, C.N., 1997. Cadmium-induced oxidative cellular damage in human fetal lung fibroblasts (MRC-5 cells). Environmental Health Perspectives 105, 712–716.

Yong, L.Z., Pilon-Smits, E.A.H., Tarun, A.S., Weber, S.U., Jouanin, L., Terry, N., 1999. Cadmium tolerance and accumulation in Indian mustard is enhanced by overexpression of γ-glutamylcysteine synthetase. Plant Physiology 121, 1169–1177.

Wagner, G.J., 1993. Accumulation of cadmium in crop plants and its consequences to human health. Advances in Agronomy 51, 173–212.

Willekens, H., Langebartels, C., Tire, D., Van Montagu, M., Inzé, D., Van Camp, W., 1994. Differential expression of catalase genes in *Nicotiana plumbaginifolia* (L.). Proceedings of the National Academy of Sciences of the United States of America 91, 10450–10454.

Woodbury, W., Spencer, A.K., Stahmann, M.A., 1971. Improved procedure using ferricyanide for detecting catalase isozymes. Analytical Biochemistry 44, 301.

Wu, S.L., Feng, X.G., Wittmeier, A., 1997. Microwave digestion of plant and grain reference materials in nitric acid or a mixture of nitric acid and hydrogen peroxide for the determination of multi-elements by inductively coupled plasma mass spectrometry. Journal of Analytical Atomic Spectrometry 12, 797–806.

Zikic, V., Stajn, A.S., Ognjanovic, B.I., Pavlovic, S.Z., Saicic, Z.S., 1997. Activities of superoxide dismutase and catalase in erythrocytes and transaminases in the plasma of carps (*Cyprinus carpio* L.) exposed to cadmium. Physiological Research 46, 391–396.

Zhu, Y.L., Pilon-Smits, A.H., Jouanin, L., Terry, N., 1999. Overexpression of glutathione synthetase in Indian Mustard enhances cadmium accumulation and tolerance. Plant Physiology 119, 73–79.

PERGAMON

Phytochemistry 57 (2001) 711–719

PHYTOCHEMISTRY

www.elsevier.com/locate/phytochem

3-*O*-Methyl-D-galactose residues in lycophyte primary cell walls

Zoë A. Popper[a], Ian H. Sadler[b], Stephen C. Fry[a,*]

[a]*The Edinburgh Cell Wall Group, Institute of Cell and Molecular Biology, The University of Edinburgh, Daniel Rutherford Building, The King's Buildings, Mayfield Road, Edinburgh EH9 3JH, UK*

[b]*Edinburgh High Field NMR Centre, Department of Chemistry, Joseph Black Chemistry Building, The King's Buildings, West Mains Road, Edinburgh EH9 3JJ, UK*

Received 22 December 2000; received in revised form 15 March 2001

Abstract

Acid hydrolysis of cell wall-rich material from young leaves of the lycophyte *Selaginella apoda* (L.) Spring yielded substantial amounts of 3-*O*-methyl-D-galactose (**1**) in addition to the usual major monosaccharides (glucose, galactose, arabinose, xylose and galacturonic acid). The yield of **1** approximately equalled that of galacturonic acid. Compound **1** was identified as 3-*O*-methylgalactose by its ^{1}H and ^{13}C NMR spectra, and shown to be the D-enantiomer by its susceptibility to D-galactose oxidase. Compound **1** was detected in acid hydrolysates of the alcohol-insoluble residues from young leaves of all lycophytes tested, both homosporous (*Lycopodium*, *Huperzia* and *Diphasiastrum*) and heterosporous (*Selaginella*). It was not detectable in the charophyte green algae *Coleochaete scutata*, *Chara coralina* or *Klebsormidium flaccidum*, any bryophytes [a hornwort (*Anthoceros*), four liverworts and three mosses], or any euphyllophytes [a psilopsid (*Psilotum*), a horsetail (*Equisetum*), eusporangiate and leptosporangiate ferns, the gymnosperm *Gnetum*, and diverse angiosperms]. A high content of **1** is thus an autapomorphy of the lycophytes. © 2001 Elsevier Science Ltd. All rights reserved.

Keywords: *Selaginella apoda*; *S. erythropus*; *Lycopodium pinifolium*; *Huperzia selago*; *Diphasiastrum alpinum*; Lycophytes; Euphyllophytes; Pteridophytes; Primary cell walls; Polysaccharides; 3-*O*-Methyl-D-galactose; NMR spectroscopy; HMBC; HMQC

1. Introduction

Within dicots and non-graminaceous monocots, the primary cell wall has a relatively constant sugar composition, major monosaccharide residues being Glc, Gal, Ara, Xyl, GalA, Rha, Fuc, GlcA and Man (McNeil et al., 1984; Fry, 1988; Brett and Waldron 1996). Graminaceous primary walls contain the same monosaccharide residues but usually have more Xyl and less Gal, Ara and Fuc (Burke et al., 1974; Carpita, 1996). Gymnosperms are also similar to dicots, but tend to be richer in Man residues (Edashige and Ishii, 1996). Despite these quantitative differences, no qualitative differences in the monosaccharide composition of primary cell walls have been noted between different groups of seed plants.

Few studies have been undertaken of cell wall composition in lower land plants (Chodat and Cortesi, 1939; Edelmann et al., 1998), probably because they are not major world crops. Among bryophytes (non-vascular land plants), liverworts broadly resemble gymnosperms in their cell wall sugar residue composition, the major neutral monosaccharide residues being Glc > Gal > Man > Xyl ≈ Ara > Fuc ≈ Rha (Thomas, 1977; Thomas et al., 1984). Uronic acid residues, stated to be mannuronic acid, are also present (Das and Rao, 1967).

We have not found any reports specifically dealing with the composition of the primary cell wall of pteridophytes (non-seed vascular plants), although a few reports on their secondary walls have appeared (Timell, 1962; Bremner and Wilkie, 1971). Modern pteridophytes are the few surviving progeny of a much greater diversity of extinct taxa, representing the explosive evolutionary experimentation which occurred among land plants in the Silurian (Raven, 1993; Kenrick and Crane, 1997). Since the primary cell wall plays several essential biological roles, including the regulation of cell expansion, tissue cohesion, defence (e.g. against microbes), ion-exchange, and the production of oligosaccharins (Fry, 1988; Kaplan and Hageman, 1991; Brett and Waldron, 1996; Stübler and Buchenauer, 1996; Goldberg, 1995; Cassab, 1998), we suggest that the demands placed on it, and thus its optimal

Abbreviations: AIR, alcohol-insoluble residue; HMBC, heteronuclear multiple bond correlation; HMQC, heteronuclear multiple quantum coherence; PC, paper chromatography

* Corresponding author. Tel.: +44-131-650-5320; fax: +44-131-650-5392.

E-mail address: s.fry@ed.ac.uk (S.C. Fry).

0031-9422/01/$ - see front matter © 2001 Elsevier Science Ltd. All rights reserved.
PII: S0031-9422(01)00140-6

composition, may have changed rapidly during periods of rapid plant evolution. It is certainly the case that some green algae have cell wall compositions very different from those of seed plants (Mackie and Preston, 1974; Roberts, 1974; Domozych et al., 1980).

We are, therefore, documenting the evolution of the primary cell wall in land plants. DNA sequence data (Raubeson and Jansen, 1992; Manhart, 1994, 1995; Kranz et al., 1995; Pryer et al., 1995; Malek et al., 1996; Wolf, 1997; Duff and Nickrent, 1999, Vangerow et al., 1999) have recently confirmed the morphology-based view that the lycophytes (club-mosses) diverged very early from the ancestors of the euphyllophytes (= plants with 'true' leaves, extant euphyllophytes being all seed-plants as well as non-lycophyte pteridophytes). Indeed, the lycophytes show a relatively close relationship to the bryophytes. In the present paper we report on an unusual chemical feature in the primary cell walls of the lycophytes, which is apparently related to their isolated evolutionary position.

2. Results

2.1. An unusual sugar residue in Selaginella cell walls

Acid hydrolysis of the alcohol-insoluble residue (AIR; i.e. cell wall-rich material) from young leaves of *Selaginella apoda* followed by paper chromatography (PC) yielded an unfamiliar monosaccharide (**1**) in addition to the major monosaccharides characteristic of the cell wall polysaccharides of seed plants. In chromatography system 2, **1** migrated between Ara and Xyl. However, unlike these pentoses, **1** stained yellow-brown with aniline hydrogen-phthalate, suggesting a hexose derivative.

Larger amounts of **1** were partially purified by preparative PC (in system 2) of the acid hydrolysate obtained from 1 g of *S. apoda* AIR. Of several PC and TLC systems tested for their ability to separate **1** from the last traces of Ara and Xyl (Table 1), preparative PC in system 3 was selected, followed by gel-permeation chromatography on Bio-Gel P-2. On TLC (cellulose) in system 3, cmpd **1** exhibited an unusually high R_F, similar to that of authentic 3-*O*-methylglucose and 2-deoxygalactose; it was well resolved from the common hexoses and pentoses. R_F values (cellulose TLC, system 3) were Glc, 0.30; Gal, 0.36; Man, 0.39; Xyl, 0.37; Ara, 0.46; Rib 0.63; 6-deoxymannose (= rhamnose), 0.61; 2-deoxygalactose, 0.73; 3-*O*-methylglucose, 0.72; cmpd **1**, 0.70.

2.2. Identification of 3-O-methylgalactose by NMR spectroscopy

The standard 1D single-pulse 600-MHz proton NMR spectrum of 100 μg of purified unknown **1** in D_2O as solvent is reasonably well resolved (Fig. 1a) The doublets at 4.60δ and 5.26δ suggest the presence of the α and β anomers of a glucose or galactose derivative and the sharp signal at 3.45 suggest the presence of one methoxy group. Careful examination of this spectrum confirms the presence of the requisite number of signals and their assignment follows immediately from the 2D-COSY spectrum (Fig. 1b). Significant signal overlap occurs only for the C-6 protons. In the β-anomer the C-6 protons have different chemical shifts, and each appears as a doublet of doublets. In the α-anomer the C-6 proton signals coincide so the coupling between them is not seen resulting in a single doublet. One peak of the doublet for the C-6 of the α-anomer virtually coincides with one peak from one of the C-6 protons of the β-anomer. The coupling constants of each multiplet, measured from the 1-D spectrum (Table 2) are consistent only with a galactose derivative.

The ^{13}C chemical shifts, obtained from a 2D 1-bond carbon–proton shift (HMQC) correlation spectrum, are similar to those for the anomers of galactose with the exception of that for C-3, which is about 10 ppm higher. This is consistent with methylation of the hydroxyl at C-3. The site of methylation is confirmed by correlation between the methyl protons and C-3 of each anomer in the 2D long range carbon–proton (HMBC) shift correlation spectrum. The ^1H and ^{13}C spectral data of the individual components of **1** are given in Table 2.

In conclusion, the spectroscopic data show unambiguously that, apart from a few unidentified minor impurities, **1** was a mixture of the α and β anomers of 3-*O*-methylgalactose.

2.3. Determination of enantiomeric form

Plant cell wall polysaccharides contain both D- and L-Gal residues, which are biosynthetically derived from UDP-D-Glc (via UDP-D-Gal) and from GDP-D-Man (via GDP-L-Gal), respectively (Feingold and Avigad, 1980). The D-Gal:L-Gal ratio has been reported at ~7.3:1 in cultured sycamore cells (Roberts and Harper, 1973) and ~70:1 in cultured spinach cells (Baydoun and Fry, 1988). D-Gal, the more abundant enantiomer, is found in pectins, xyloglucans and arabinogalactan-proteins. L-Gal has been reported in the side-chains of xylans (Whistler and Corbett, 1955) and some xyloglucans (Zablakis et al., 1996; Hantus et al., 1997). It was, therefore, of interest to determine whether **1** was a derivative of D- or L-Gal.

D-Galactose oxidase uses O_2 to oxidise the $-CH_2OH$ group of D-Gal and some of its derivatives, but not of L-Gal. Derivatives of D-Gal that can be oxidised by this enzyme include the 2- and 3- but not 4-*O*-methyl monoethers (Avigad et al., 1962; Schlegel et al., 1968; Cleveland et al., 1975). D-Galactose oxidase can therefore be used to distinguish 3-*O*-methyl-D-galactose from 3-*O*-methyl-L-galactose.

Table 1
R_f values of Xyl, Ara and **1** in various solvent systems

Compound	R_F value in system[a]							
	a	*b*	*c*	*d*	*e*	*f*	*g*	*h*
Ara	0.28	0.21	0.12	0.41	0.15	0.75	0.58	0.46
Xyl	0.38	0.29	0.13	0.52	0.21	0.79	0.49	0.37
1	0.24	0.18	(s)[c]	(s)	0.12 (s)	(u)[b]	0.80	0.70

[a] Chromatographic systems used were: *a*, TLC (silica-gel) in BuOH–HOAc–H_2O (3:1:1 by vol.); *b*, TLC (silica-gel) in BuOH–HOAc–H_2O (4:1:1 by vol.); *c*, TLC (silica-gel) in MeEtCO–H_2O (85:7 by vol.); *d*, TLC (silica-gel) in EtOAc–Py–HOAc-H_2O (5:3:1:1 by vol.); *e*, TLC (silica-gel) in *i*-PrOH–NH_4OH–H_2O (8:1:1 by vol.); *f*, TLC (silica-gel) in *i*-PrOH–nitromethane–H_2O (5:2:3 by vol.); *g*, PC (Whatman No. 1) in PhOH–H_2O (4:1, w/w); *h*, TLC (cellulose) in PhOH–H_2O (4:1, w/w).
[b] (u) = Unrecordable (did not separate from Ara and Xyl).
[c] (s) = Streaked.

We confirmed that the commercial sample of galactose oxidase was able to oxidise D- but not L-Gal; it also oxidised cmpd **1**. The substrates (D-Gal and **1**) were partially destroyed within 1 h; oxidation was complete within 4 days, yielding multiple reaction products (Fig. 2). In contrast, the enzyme had no effect on L-Gal, despite the incubation continuing up to 4 days (Fig. 2). During the 4-day incubation, reaction mixtures containing D-Gal or **1** turned yellow (presumably owing to the formation of unstable aldehyde products) whereas the L-Gal reaction mixture did not change colour.

Together the results show that **1**, isolated from *S. apoda*, was 3-*O*-methyl-D-galactose.

2.4. Occurrence of 3-*O*-methylgalactose in various green plants

To ascertain the distribution of 3-*O*-methylgalactose among land plants we analysed acid hydrolysates of AIR from young shoot tissue (leaves and/or immature stems) of various pteridophytes and the thalli of various bryophytes and algae by 2D PC (exemplified by Fig. 3). 3-*O*-Methylgalactose was present in all lycophytes tested, both homosporous and heterosporous (Table 3). Typical yields (estimated from staining intensity relative to authentic 3-*O*-methylglucose) were in the order of 5–10 mg of 3-*O*-methylgalactose per g of AIR. 3-*O*-Methylgalactose was, however, undetectable in all euphyllophytes tested: a psilopsid, a horsetail, eusporangiate and leptosporangiate ferns and a gymnosperm (Table 3) and numerous angiosperms (data not shown). 3-*O*-Methylgalactose was also undetectable in all bryophytes tested: three mosses, four liverworts and a hornwort (Table 3). In addition, it was undetectable in walls of the charophytes *Coleochaete*, *Chara* and *Klebsormidium*—green algae which are thought (Kenrick and Crane, 1997) to be relatively closely related to the hypothetical, extinct, green alga from which all land plants evolved.

3. Discussion

The presence of 3-*O*-methylgalactose in both homosporous and heterosporous lycophytes supports the proposed (Bateman, 1996; Kranz and Huss, 1996) monophyly of the lycophytes. Extant lycophytes are the relicts of a much more diverse group of extinct lycophytes. Morphological features suggest that lycophytes evolved from ancestral plants between the bryophytes and the euphyllophytes. Our findings suggest that this phase of very rapid evolutionary experimentation was accompanied by the adoption of 3-*O*-methyl-D-galactose as a major component of the primary cell wall.

3-*O*-Methyl-D-galactose was not detectable in either *Equisetum* or *Psilotum*, supporting the view that these plants are more closely related to the ferns than to the lycophytes. Gene sequence data have shown *Equisetum* and *Psilotum*, but not the lycophytes, to be within the euphyllophyte clade (Robeson and Jansen, 1992; Manhart, 1994, 1995; Kranz et al., 1995; Pryer et al., 1995; Malek et al., 1996; Wolf, 1997; Duff and Nickrent, 1999; Vangerow et al., 1999).

A 3-*O*-methylgalactose (enantiomer not determined) has been detected, in trace amounts, in an extracellular polysaccharide exuded by a soil-dwelling *Cryptomonas* sp. (Paulsen et al., 1992). *Cryptomonas* is a member of the Cryptophyta, a small group of biflagellate, eukaryotic algae which frequently have red photosynthetic pigments. Most are free-swimming but one member of the Cryptophyceae has been found as an endosymbiont in a marine cilliate as a complex known as *Mesodinium rubrum*. Since the lycophytes analysed by us are not aquatic, they are unlikely to have any cryptophycean endosymbionts in their shoot tissues (Dr. D.G. Mann, RBGE, personal communication).

3-*O*-Methyl-D-galactose has also been isolated from polymers present in certain strains of the aquatic green alga *Chlorella vulgaris* (Ogawa et al., 1994). *Chlorella* spp. are primarily free-swimming and unlikely to form a symbiotic relationship with terrestrial lycophytes.

3-*O*-Methyl-D-galactose has been reported to constitute about 5% of the total neutral sugar residues in the soluble extracellular polysaccharides produced by the freshwater red alga *Porphyridium aerugineum* (Percival and Foyle, 1979). Methylgalactoses are also present in the rhodophyte genera *Geldiliella* and *Gracilaria*, from which agar is extracted. However, in agar the *O*-methyl groups are attached to galactose at position 4 and/or 6 (Matsuhiro and Urzua, 1991; Mollion, 1992; Chiovitti et al., 1995, Mollet et al., 1998; Givernaud et al., 1999). Therefore, it is highly unlikely that 3-*O*-methyl-D-galactose occurred in our lycophyte samples as a contaminant from laboratory agar. The lycophytes were collected from diverse sites (Table 3); it is, therefore, unlikely that they had a common contaminant.

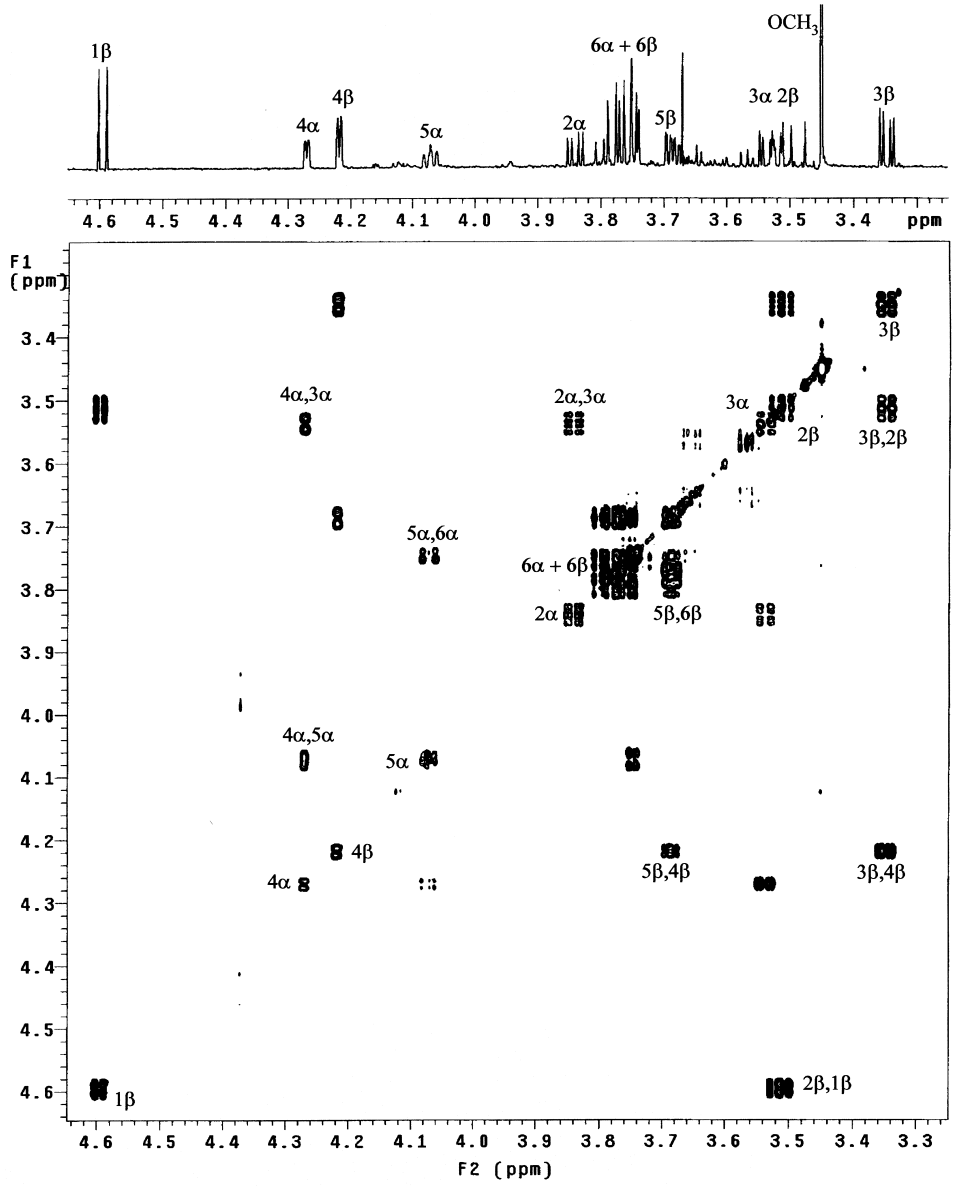

Fig. 1. NMR spectra of 3-*O*-methylgalactose (**1**): (a) 1D single-pulse 600 MHz proton NMR spectrum over the region 3.25δ–4.65δ [i.e. excluding the H-1α resonance at 5.26δ]; (b) 2D gradient selected proton COSY NMR spectrum over the same region as in (a) [i.e. excluding the H-1α diagonal resonance and the H-1α, H-2α off-diagonal resonances].

Among the fungi, 3-*O*-methyl-D-galactose has been detected as a polysaccharide component in *Armillaria mellea* (Bouveng et al., 1967) and a 3-*O*-methylgalactose (enantiomer not determined) in *Lamperomyces japonicus* (Fukuda and Hamada, 1978). 3-*O*-Methyl-D-galactose has also been reported as a component of haemocyanin, a glycoprotein from snails (Hall et al., 1977).

3-*O*-Methyl-D-galactose has been reported previously in land plants. For example, pectic polysaccharides from elm bark contain 3-*O*-methyl-D-galactose (Hirst et al., 1951; Barsett and Paulsen, 1985, 1991). These polymers have a backbone of 4-linked α-D-galacturonic acid interspersed with 2-linked α-L-rhamnose residues; some of the latter are substituted on O-4 with short side-chains containing 3-*O*-methylgalactose, galactose and/or glucuronic acid. It is possible that a similar polymer may occur in lycophytes since both rhamnose and galacturonic acid were detected in the hydrolysates of lycophyte AIRs. However, elm trees and lycophytes are not closely related and at present it is not known in which polysaccharide(s) 3-*O*-methyl-D-galactose occurs in the lycophyte cell wall.

3-*O*-Methyl-D-galactose was also detected as a component of a polysaccharide extracted from sassafras (*Sassafras albidum*) twigs (Springer et al., 1965), and a 3-*O*-methylgalactose (enantiomer not determined) was found in hydrolysates of the leaves of various dicot trees (Bacon and Cheshire, 1971). The yield from sweet-chestnut

Table 2
^{1}H and ^{13}C NMR spectral data of 3-*O*-methylgalactose (**1**)

Site	δ_C	δ_H	Multiplicity[a]	J_{HH} (Hz)
β-Galactose				
1	99.2	4.60	(*d*)	7.9
2	73.6	3.52	(*dd*)	9.9, 7.9
3	84.7	3.35	(*dd*)	9.9, 3.3
4	67.0	4.22	(*dd*)	3.3, 0.9
5	77.8	3.69	(*ddd*)	7.7, 4.4, 0.9
6	63.8	3.76	(*dd*)	11.6, 4.4
		3.80	(*dd*)	11.6, 7.7
O-Methyl	58.8	3.45	(*s*)	
α-Galactose				
1	94.9	5.26	(*d*)	4.0
2	70.1	3.84	(*dd*)	10.2. 4.0
3	81.2	3.54	(*dd*)	10.2, 3.2
4	67.6	4.27	(*dd*)	3.2, 1.3
5	73.0	4.08	(*ddd*)	6.7, 5.8, 0.9
6	64.0	3.74	(*d*)	nm[b]
O-Methyl	58.8	3.45	(*s*)	

[a] Key: *d* = doublet, *dd* = doublet of doublets, *ddd* = doublet of doublet of doublets, *s* = singlet.
[b] nm = Not measurable.

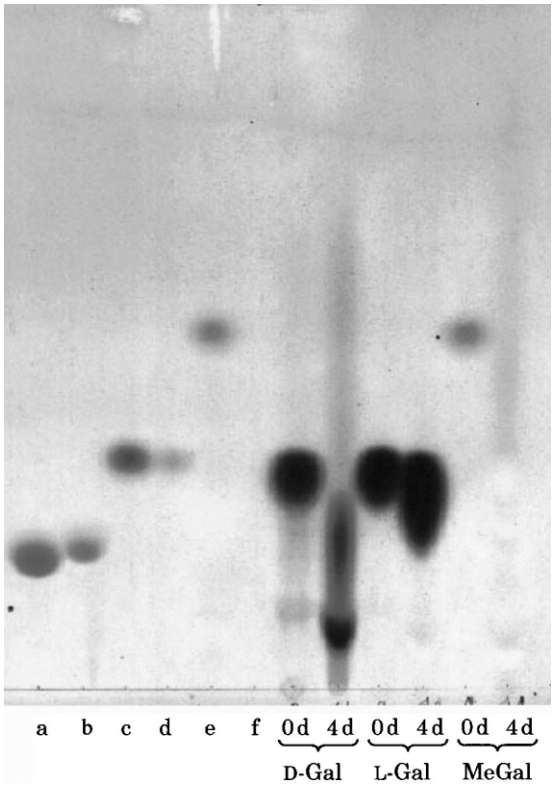

Fig. 2. Effect of D-galactose oxidase on D-Gal, L-Gal and 3-*O*-methylgalactose (**1**; MeGal) from *Selaginella apoda*. The three potential substrates were incubated with the enzyme for 0 or 4 days, as indicated, then analysed by TLC on cellulose in system 4 and stained with aniline hydrogen-phthalate. Markers used were: (a) D-GalA; (b) D-GlcA; (c) D-Gal; (d) L-Gal; (e) compound (**1**); (f) blank.

leaves was 11 mg of 3-*O*-methyl-D-galactose per 100 g AIR (Bacon and Cheshire, 1971), a very low concentration in comparison with the high levels detected in lycopod AIRs in our survey.

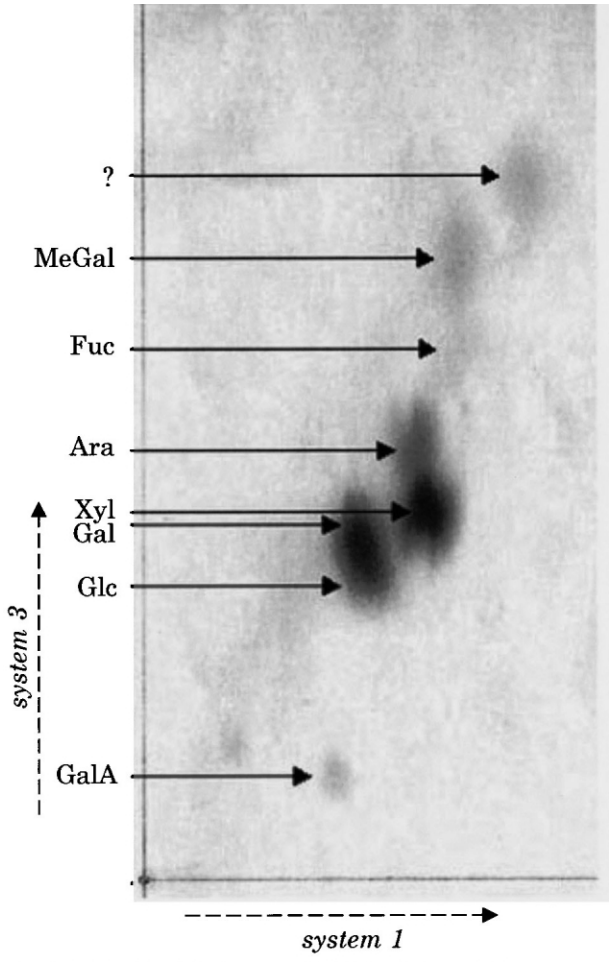

Fig. 3. Two-dimensional paper chromatogram showing 3-*O*-methylgalactose in an acid hydrolysate of AIR from *Lycopodium pinifolium* Blume. The PC was developed in system 1 (bottom to top, as photographed) followed by system 3 (left to right). Staining was with aniline hydrogen-phthalate. The spot marked '?' is unidentified: it was clearly distinguishable from rhamnose (not detectable in Fig. 3), which had an R_F higher than that of fucose in system 1 but approximately equal to that of fucose in system 3. Sugar '?' stained red with aniline hydrogen-phthalate and so is likely to have been a pentose derivative.

In conclusion, the adoption of 3-*O*-methyl-D-galactose as a quantitatively appreciable component of the primary cell wall appears to be an autapomorphy (a character which uniquely defines a taxon; Hennig, 1966) of the lycophytes that was acquired early during their evolution from hypothetical extinct ancestral land plants intermediate between the bryophytes and the euphyllophytes, and that has been retained by all extant lycophytes.

4. Experimental

4.1. Source of plant material

Sources of botanical material are listed in Table 3.

Table 3
Occurrence of 3-*O*-methylgalactose (MeGal) as a major component in acid hydrolysates of AIR from a range of lower plants

Classification		Species	MeGal[a]	Source[b]
Algae	Charophytes	*Chara coralina* (Klein ex Willd. Em. R.D.W.)	–	Culture, D. Sanders
		Coleochaete scutata Brébisson	–	CCAP 414/1
		Klebsormidium flaccidum (Kützing) Silva, Mattox et Blackwell	–	Culture, H. Sluiman
Bryophytes	Hornwort	*Anthoceros caucasicus* Spring.	–	Faial Island (R. Schumacker)
	Thalloid liverwort	*Pellia epiphylla* (L.) Corda	–	Roslin Glen
		Marsupella emarginata var *aquatica* (Lindb.) Dum.	–	Cairngorms
	Leafy liverworts	*Porella* sp.	–	Cairngorms
		Trichocolea tormentella (Ehrh.) Dum.	–	Glen Creran (D.S. Rycroft)
		Andrea rupestris Hedw. (*A. petrophila* Ehrh.)	–	Cairngorms (W.M.M. Eddie)
	Mosses	*Hypnum cupressiforme* Hedw.	–	Roslin Glen
		Sphagnum molle Sull.	–	Cairngorms
Lycophytes	Homosporous	*Lycopodium pinifolium* Blume	+	19835037(E)
		Huperzia selago (L.) Bernh. Ex. Schrank and Mart.	+	Cairngorms
		Diphasiastrum alpinum (L.) Holub.	+	Cairngorms
	Heterosporous	*Selaginella apoda* (L.) Spring.	+	19677705(E)
		Selaginella erythropus Spring.	+	19715473(E)
		Selaginella pallescens (C. Presl.) Spring.	+	19697710(E)
Euphyllophytes	Horsetail	*Equisetum debile* Roxb. Ex. Vaucher	–	19731694(E)
	Psilopsid	*Psilotum nudum* (L.) P. Beauv.	–	DRB
	Eusporangiate fern	*Marattia fraxinea* Sm.	–	19697183(E)
	Leptosporangiate ferns	*Osmunda regalis* L.	–	19578631(E)
		Onoclea sensiblis L.	–	19662802(E)
		Salvinia auriculata Aubl.	–	19830813(E)
		Platycerium bifurcatum (Car.) C. Chr.	–	19734554(E)
		Todea barbara (L.) T. Moore	–	19652792(E)
		Phyllitis scolopendrum L.	–	19731529(E)
		Asplenium australassium (J. Sm.) Hook.	–	19933661(E)
		Blechnum spicant (L.) Roth.	–	Cairngorms
		Dryopteris crispifolia Rasbach et al.	–	19920813(E)
	Gymnosperm	*Gnetum gnemon* L.	–	19902511(E)

[a] + Indicates 3-*O*-methylgalactose detectable after 2-dimensional PC as shown in Fig. 3.

[b] Accession numbers followed by (E) refer to material from the Royal Botanic Garden, Edinburgh (RGBE); CCAP = Culture Collection of Algae and Protozoa, Ambleside, Cumbria; DRB = glasshouses of the Daniel Rutherford Building, The University of Edinburgh. Additional material was kindly provided by Dr. D. Long and Dr. H. Sluiman (RBGE), Dr. D.S. Rycroft (Glasgow University), Dr. R. Schumacker (University of Liege), Dr. W.M.M. Eddie (University of Texas, Austin) and Prof. D. Sanders (University of York). Other material was collected by Z.A.P. Collection sites were: Cairngorm Hills (57°05–10′ N, 3°35–45′W.), Roslin Glen (55°51′ N, 3°10′ W), Glen Creran (56°36′ N, 5°12′ W) and Faial Island (38°40′ N, 28°40′ W).

4.2. Preparation and hydrolysis of AIR

About 30 g fr. wt of (fresh or frozen) young plant material was blended (two 1-min bursts) in an MSE 'Ato-Mix' with 150 ml 70% ethanol. The suspension was filtered through Miracloth (Calbiochem) and the residue ground to a fine powder in liquid N_2 with a ceramic pestle and mortar (both pre-cooled to −80°C). The powder was transferred to a flask with 150 ml 70% ethanol and incubated at 55°C for 5 days to solubilise free sugars. The suspension was then filtered again and repeatedly washed with 70% ethanol until colourless. The residue was finally washed in acetone and dried.

A portion (20 mg) of each AIR sample was subjected to hydrolysis in 1 ml 2 M TFA at 120°C for 1 h. The hydrolysate was dried in vacuo and re-dissolved in 50 μl water, of which 2 μl was subjected to 2-dimensional PC.

4.3. Paper chromatography and TLC

Analytical PC was on Whatman No. 1 paper; preparative PC was on Whatman 3MM. One-dimensional PC was by the descending method; 2-dimensional PC was by the ascending method. Solvent systems used were (1), BuOH–HOAc–H_2O (12:3:5 by vol.); (2), as system 1 for 16 h followed, in the same dimension, by EtOAc–pyridine–H_2O (8:2:1 by vol.) for 18 h; (3), PhOH–H_2O (4:1, w/w); (4), BuOH–HOAc–H_2O (2:1:1 by vol.) followed, in the same dimension, by EtOAc–pyridine–H_2O (10:4:3 by vol.); others are indicated in Table 1. TLC was on Merck silica-gel or microcrystalline cellulose. Chromatograms were stained with aniline hydrogen-phthalate; faint spots were more readily visible by their fluorescence when viewed under a 366-nm UV lamp (Fry, 1988).

4.4. NMR methods

The NMR spectra were measured on D_2O solutions using a Varian INOVA 600-MHz spectrometer operating at 599.9 MHz for protons and 150.9 MHz for ^{13}C nuclei.

The 2D gradient selected COSY proton spectrum was obtained using the sequence (von Kienlin, 1991): D1–90°–t1–zgrd–90°–zgrd–AQ with D1 = 1.5 s, AQ = 0.646 s, zgrad = 1 gauss/cm, 0.002 s. Other parameters were SW = 1586 Hz, 2K data points, 512 increments each with 16 transients per FID. The data were processed using sine-bell squared functions in both dimensions with zero filling of the F1-data to 2K data transformation resulting in digital resolution of 1.5 Hz/pt.

The 2-D proton detected one-bond ^{1}H–^{13}C correlation (HMQC) spectrum was obtained using the sequence (Summers et al., 1986): D1–90°(^{1}H)–D2–180°^{1}H); 180°(^{13}C)–D2–90°(^{1}H)–D3–90°(^{1}H)–D2–90°(^{13}C)–$t_1/2$–180°(^{1}H)–$t_1/2$–90°(^{13}C)–D2–AQ. The delays used were D1 = 1.6 s (pre-saturation), D2 = 3.7 ms ($1/2^{1}J_{CH}$) and D3 = 600 ms (to minimise signals from protons bonded to ^{12}C nuclei). The experiment was preceded by 64 scans to establish thermal equilibrium. A 4-step phase cycle (hypercomplex acquisition) was used with ^{13}C broad band decoupling during acquisition of the proton signals. Other parameters were SW(^{1}H) = 4632 Hz, 2K data points, SW(^{13}C) = 18000 Hz, AQ = 0.408 s, 200 increments each with 4 transients per FID. The data were processed using shifted sine-bell squared functions in both dimensions with zero filling of the F_1 data from 200 to 1024 W before transformation.

The 2D proton detected gradient selected long-range ^{1}H–^{13}C correlation (HMBC-g) spectrum was obtained using the sequence (Ruiz-Cabello et al., 1992): D1–90°(^{1}H)–D2–90°(^{13}C)–D3–90°(^{13}C)–zgrd1–$t_1/2$–180°(^{1}H)–$t_1/2$–zgrad1–90°(^{13}C)–zgrd2–AQ. The delays used were D1 = 1.4 s, D2 = 3.7 ms ($1/2^{1}J_{CH}$) and D3 = 55 ms (optimised for signals from protons with couplings to carbon of ca. 9 Hz), zgrad1 = 4 gauss/cm, 0.002 s, zgrad 2 = 2 gauss/cm, 0.002 s. A 16-step phase cycle (hypercomplex acquisition) was used with no ^{13}C broad band decoupling during the acquisition of the proton signals. Other parameters were SW(^{1}H) = 2500 Hz; 2K data points; SW(^{13}C) = 15,000 Hz, AQ = 0.410 s; 128 increments each with 192 transients per FID. The data were processed using shifted sine-bell squared functions in both dimensions with zero filling of the F_1 data from 200 to 1024 W before transformation.

4.5. Oxidation with D-galactose oxidase

D-Galactose (0.5 mg), L-galactose (0.5 mg) or cmpd **1** (trace) was incubated in an open vial containing 100 μl of 100 mM P_i (K^+) buffer, pH 6.0, containing 0.5% chlorobutanol, 15 'Sigma Units' of D-galactose oxidase (EC 1.1.3.9; from *Dactylium dendroides*) and 10 Units of bovine liver catalase (both enzymes from Sigma Chemical Co., Poole, UK). The K_m of galactose oxidase for D-galactose is reported to be 0.24 M (Avigad et al., 1962). One 'Sigma Unit' of D-galactose oxidase is the activity which will produce a ΔA_{425} of 1.0 per min in a reaction volume of 3.4 ml with D-Gal as substrate in the presence of a peroxidase–*o*-tolidine system to detect the H_2O_2 generated. After incubation for 1 h to 4 days at 20°C, 20-μl samples were analysed by TLC on cellulose in system 4.

Acknowledgements

We thank Dr. D. Long (RBGE) and Dr. D.S. Rycroft (Glasgow University), who kindly assisted in the provision and identification of several bryophytes. We are very grateful to horticultural staff at the RBGE, especially Mr. Philip O. Ashby, for supply of specimens. Z.A.P. thanks the BBSRC for a Research Studentship. We thank BBSRC/EPSRC for the provision of the NMR spectrometer at the Edinburgh High Field NMR Centre.

References

Avigad, G., Amaral, D., Asensio, C., Horecker, B.L., 1962. The D-galactose oxidase of *Polyporus circinatus*. Journal of Biological Chemistry 237, 2736–2743.

Bacon, J.S.D., Cheshire, M.V., 1971. Apiose and mono-*O*-methyl sugars as minor constituents of the leaves of deciduous trees and various other species. Biochemical Journal 124, 555–562.

Barsett, H., Paulsen, B.S., 1985. Separation of acidic polysaccharides from *Ulmus glabra* Huds. on Mono-P. Journal of Chromatography 329, 315–320.

Barsett, H., Paulsen, B.S., 1991. Separation, isolation and characterization of acidic polysaccharides from the inner bark of *Ulmus glabra* Huds. Carbohydrate Polymers 17, 137–144.

Bateman, R.M., 1996. An overview of lycophyte phylogeny. In: Camus, J.M., Gibby, M., Johns, R.J. (Eds.), Pteridology in Perspective. Royal Botanic Gardens, Kew, pp. 405–415.

Baydoun, E.A.-H., Fry, S.C., 1988. [2-^{3}H]Mannose incorporation in cultured plant cells: investigation of L-galactose residues of the primary cell wall. Journal of Plant Physiology 132, 484–490.

Bouveng, H.O., Fraser, R.N., Lindberg, B., 1967. polysaccharides elaborated by *Armillaria mellea* (Tricholomataceae). Part II. Water-soluble mycelium polysaccharides. Carbohydrate Research 4, 20–31.

Bremner, I., Wilkie, K.C.B., 1971. The hemicelluloses of bracken. II. A galactoglucomannan. Carbohydrate Research 20, 193–203.

Brett, C.T., Waldron, K.W., 1996. Physiology and Biochemistry of Plant Cell Walls, 2nd edn. Chapman and Hall, London.

Burke, D., Kaufman, P., McNeil, M., Albersheim, P., 1974. The structure of plant cell walls. VI. A survey of the walls of suspension-cultured monocots. Plant Physiology 54, 109–115.

Carpita, N.C., 1996. Structure and biogenesis of the cell walls of grasses. Annual Review of Plant Physiology and Plant Molecular Biology 47, 445–476.

Cassab, G.I., 1998. Plant cell wall proteins. Annual Review of Plant Physiology and Plant Molecular Biology 49, 281–309.

Chiovitti, A., Kraft, G.T., Saunders, G.W., Liao, M.L., Bacic, A., 1995. A revision of the systematics of the Nizymeniaceae (Gigartinales, Rhodophyta) based on polysaccharides, anatomy and nucleotide-sequences. Journal of Phycology 31, 153–166.

Chodat, F., Cortesi, R., 1939. Sur la coloration des membranes de mousses. Comptes rendus de la Société des Sciences physiques et naturelles de Genève 56, 58–61.

Cleveland, L., Coffman, R.E., Coon, P., Davis, L., 1975. An investigation of the role of copper in galactose oxidase. Biochemistry 14, 1108–1115.

Das, V.S.R., Rao, M.P., 1967. Cell wall sugars of the liverwort, *Riccardia*. Indian Journal of Experimental Biology 5, 193–194.

Domozych, D.S., Stewart, K.W., Mattox, K.R., 1980. The comparative aspects of cell wall chemistry in the green algae (Chlorophyta). Journal of Molecular Evolution 15, 1–12.

Duff, J.R., Nickrent, D.L., 1999. Phylogenetic relationships among land plants using mitochondrial small-subunit rDNA sequences. American Journal of Botany 86, 372–386.

Edashige, Y., Ishii, T., 1996. Structures of cell-wall polysaccharides from suspension-cultured cells of *Cryptomeria japonica*. Mokuzai Gakkaishi 42, 895–900.

Edlemann, H.G., Neinhuis, C., Jarvis, M.C., Evans, B., Fischer, E., Barthlott, W., 1998. Ultrastructure and chemistry of the cell wall of the moss *Rhacocarpus purpurascens* (Rhacocarpaceae): a puzzling architecture among plants. Planta 206, 315–321.

Feingold, D.S., Avigad, G., 1980. Sugar nucleotide transformations in plants. In: Preiss, J. (Ed.), The Biochemistry of Plants, Vol. 2. Academic Press, New York.

Fry, S.C., 1988. The Growing Plant Cell Wall: Chemical and Metabolic Analysis. Longman, Essex.

Fukuda, K., Hamada, A., 1978. 3-*O*-Methylgalactose found in polysaccharides of *Lampteromyces japonicus*. Biochimica et Biophysica Acta 544, 445–447.

Givernaud, T., El Gourjii, A., Mouradi-Givernud, A., Lemoine, Y., Chiadmi, N., 1999. Seasonal variations of growth and agar composition of *Gracilaria multipartita* harvested along the Atlantic coast of Morocco. Hydrobiologia 399, 167–172.

Goldberg, R., 1995. Cell wall isolation, general growth aspects. In: Linskens, H.F., Jackson, J.F. (Eds.), Modern Methods of Plant Analysis, New Series, Vol. 1: Cell Components. Springer-Verlag, Berlin, pp. 1–30.

Hall, R.L., Wood, E.J., Kamberling, J.P., Gerwig, G.J., Vliegenthart, F.G., 1977. 3-*O*-Methyl sugars as constituents of glycoproteins. Identification of 3-*O*-methylgalactose and 3-*O*-methylmannose in pulmonate gastropod haemocyanins. Biochemical Journal 165, 173–176.

Hantus, S., Pauly, M., Darvill, A.G., Albersheim, P., York, W.S., 1997. Structural characterization of novel L-galactose-containing oligosaccharide subunits of jojoba seed xyloglucan. Carbohydrate Research 304, 11–20.

Hennig, W., 1966. Phylogenetic Systematics. University of Illinois Press, Urbana.

Hirst, E.L., Hough, L., Jones, J.K.N., 1951. Constitution of the mucilage from the bark of *Ulmus fulva* (slippery elm mucilage). Part III. The isolation of 3-monomethyl-D-galactose from the products of hydrolysis. Journal of the Chemical Society1951, 323–325.

Kaplan, D.R., Hageman, W., 1991. The relationship of cell and organism in vascular plants. Bioscience 41, 693–703.

Kenrick, P., Crane, P.R., 1997. The origin and early evolution of land plants. Nature 389, 33–39.

Kranz, H.D., Huss, V.A.R., 1996. Molecular evolution of pteridophytes and their relationship to seed plants: evidence from complete 18S rRNA gene sequences. Plant Systematics and Evolution 202, 1–11.

Kranz, H.D., Mikš, D., Siegler, M.-L., Capesius, I., Sensen, C.W., Huss, V.A.R., 1995. The origin of land plants: phylogenetic relationships among charophytes, bryophytes and vascular plants inferred from complete small-subunit ribosomal RNA sequences. Journal of Molecular Evolution 41, 74–84.

Mackie, W., Preston, R.D., 1974. Cell wall and intercellular region polysaccharides. In: Stewart, W.D.P. (Ed.), Algal Physiology and Biochemistry. Blackwell, Oxford, pp. 40–85.

Malek, O., Lätting, K., Hiesel, R., 1996. RNA editing in bryophytes and a molecular phylogeny of land plants. EMBO Journal 15, 1403–1411.

Manhart, J.R., 1994. Phylogenetic analysis of green plant *rbc*L sequences. Molecular Phylogenetics and Evolution 3, 114–127.

Manhart, J.R., 1995. Chloroplast 165 rRNA sequences and phylogenetic relationships of fern allies and ferns. American Fern Journal 85, 182–192.

Matsuhiro, B., Urzua, C.C., 1991. Agars from Chilean Gelidiaceae. Hydrobiologia 221, 149–156.

McNeil, M., Darvill, A.G., Fry, S.C., Albersheim, P., 1984. Structure and function of the primary cell walls of plants. Annual Review of Biochemistry 53, 625–663.

Mollet, J.C., Rahaoui, A., Lemoine, Y., 1998. Yield, chemical composition and gel strength of agarcolloids of *Gracilaria gracilis*, *Gracilariopsis longissima* and the newly reported *Gracilaria* cf. *vermiculophylla* from Roscoff (Brittany, France). Journal of Applied Phycology 19, 59–66.

Mollion, J., 1992. On the agar from *Gelidium madagascariense* (Rhodophyceae). Hydrobiologia 232, 43–46.

Ogawa, K., Yamaura, M., Maruyama, I., 1994. Isolation and identification of 3-*O*-methyl-D-galactose as a constituent of neutral polysaccharide of *Chlorella vulgaris*. Bioscience, Biotechnology and Biochemistry 58, 942–944.

Paulsen, B.S., Vieira, A.A.H., Klaveness, D., 1992. Structure of extracellular polysaccharides produced by a soil *Cryptomonas* sp. (*Cryptophyceae*). Journal of Phycology 28, 61–63.

Percival, E., Foyle, R.A.J., 1979. The extracellular polysaccharides of *Porphyridium cruentum* and *Porphyridium aerugineum*. Carbohydrate Research 72, 165–176.

Pryer, K.M., Smith, A.R., Skog, J.E., 1995. Phylogenetic relationships of extant ferns based on evidence from morphological and *rbc*L sequences. American Fern Journal 85, 205–282.

Raven, J.A., 1993. The early evolution of vascular plants in relation to quantitative functioning of dead water-conducting cells and stomata. Biological Reviews 68, 337–363.

Roberts, K., 1974. Crystalline glycoprotein cell walls of algae: their structure, composition and assembly. Philosophical Transactions of the Royal Society of London B 268, 129–146.

Roberts, R.M., Harper, E., 1973. Determination of L-galactose in polysaccharide material. Phytochemistry 12, 2679–2682.

Robeson, L.A., Jansen, R.K., 1992. Chloroplast DNA evidence on the ancient evolutionary split in vascular land plants. Science 255, 1697–1699.

Ruiz-Cabello, J., Vuister, G.W., Moonen, C.T.W., van Gelderen, P., Cohen, J.S., van Zijl, P.C.M., 1992. Gradient-enhanced heteronuclear correlation spectroscopy-theory and experimental aspects. Journal of Magnetic Resonance 100, 282–302.

Schlegel, R.A., Gerbeck, C.M., Montgomery, R., 1968. Substrate specificity of D-galactose oxidase. Carbohydrate Research 7, 193–199.

Springer, G.F., Takahashi, T., Desai, P.R., Kolecki, B.J., 1965. Cross reactive human blood-group H(O) specific polysaccharide from *Sassafras albidum* and characterization of its hapten. Biochemistry 4, 2099–2012.

Stübler, D., Buchenauer, H., 1996. Antiviral activity of the glucan lichenan (poly-β-{1→3,1→4}-D-anhydroglucose). I. Biological activity in tobacco plants. Journal of Phytopathology 144, 37–43.

Summers, M.F., Marzilli, L.G., Bax, A., 1986. Complete ^{1}H and ^{13}C assignments of coenzyme B_{12} through the use of two-dimensional NMR experiments. Journal of the American Chemical Society 108, 4285–4294.

Thomas, R.J., 1977. Wall analyses of *Lophocolea* seta cells (Bryophyta) before and after elongation. Plant Physiology 59, 337–340.

Thomas, R.J., Behringer, F.J., Lombard, C.S., Sparkowski, J.J., 1984. Effects of auxin on wall polysaccharide composition and enzyme activity during extension-growth of *Pellia* (Bryophyta). Physiologia Plantarum 60, 502–506.

Timell, T.E., 1962. Studies on ferns (Filicineae). Part 1. The constitution of a xylan from cinnamon fern (*Osmunda cinnamomea*). Svensk Papperstidning 65, 122–125.

Vangerow, S., Teerkorn, T., Knoop, V., 1999. Phylogenetic information in the mitochondrial *nad5* gene of the pteridophytes: RNA editing and intron sequences. Plant Biology 1, 235–243.

von Kienlin, M., Moonen, C.T.W., van der Toorn, A., van Zijl, P.C.M., 1991. Rapid recording of solvent-suppressed 2D COSY spectra with inherent quadrature detection using pulsed field gradients. Journal of Magnetic Resonance 93, 423–429.

Whistler, R.L., Corbett, W.M., 1955. Oligosaccharides from partial acid hydrolysis of corn fiber hemicellulose. Journal of the American Chemical Society 77, 6328–6330.

Wolf, P.G., 1997. Evaluation of *atpB* nucleotide sequences for phylogenetic studies of ferns and other pteridophytes. American Journal of Botany 84, 1429–1440.

Zablackis, E., York, W.S., Pauly, M., Hantus, S., Reiter, W.D., Chapple, C.C.S., Albersheim, P., Darvill, A.G., 1996. Substitution of L-fucose by L-galactose in the cell walls of *Arabidopsis mur1*. Science 272, 1808–1810.

PERGAMON

Phytochemistry 57 (2001) 721–726

PHYTOCHEMISTRY

www.elsevier.com/locate/phytochem

Dihydroxynortropane alkaloids from calystegine-producing plants

Naoki Asano[a,*], Kae Yokoyama[a], Mio Sakurai[a], Kyoko Ikeda[a], Haruhisa Kizu[a], Atsushi Kato[b], Munehisa Arisawa[c], Dirk Höke[d], Birgit Dräger[d], Alison A. Watson[e], Robert J. Nash[e]

[a]*Faculty of Pharmaceutical Sciences, Hokuriku University, Ho-3 Kanagawa-machi, Kanazawa 920-1181, Japan*
[b]*Department of Hospital Pharmacy, Toyama Medical and Pharmaceutical University, Toyama 930-0194, Japan*
[c]*Faculty of Pharmaceutical Sciences, Toyama Medical and Pharmaceutical University, Toyama 930-0194, Japan*
[d]*Institut für Pharmazeutische Biologie, Martin-Luther-Universität Halle-Wittenberg, D-06120 Halle/Saale, Germany*
[e]*Institute of Grassland and Environmental Research, Plas Gogerddan, Aberystwyth, Cardiganshire SY23 3EB, UK*

Received 16 October 2000; received in revised form 16 January 2001

Abstract

Three dihydroxynortropanes, 2α,7β-dihydroxynortropane, 2α,3β-dihydroxynortropane, and 3α,7β-dihydroxynortropane, were isolated from calystegine-producing plants in the families Convolvulaceae and Solanaceae. 2α,7β-Dihydroxynortropane was isolated from six species in the Convolvulaceae whereas only *Calystegia soldanella* contained it and 2α,3β-dihydroxynortropane. Although neither of these were detectable in three species tested in the Solanaceae, 3α,7β-dihydroxynortropane was, however, isolated from *Duboisia leichhardtii*. © 2001 Elsevier Science Ltd. All rights reserved.

Keywords: Convolvulaceae; Solanaceae; Dihydroxynortropane; Calystegine; Swainsonine

1. Introduction

The tropane alkaloids mainly occur in the Solanaceae, but are found as well in the families Convolvulaceae, Erythroxylaceae, Proteaceae, and Rhizophoraceae, and occasionally in the Euphorbiaceae, Cruciferae, and Olacaceae (Lounasmaa, 1988; Lounasmaa and Tamminen, 1993). Nortropane alkaloids (i.e. those lacking the *N*-methyl group of tropane alkaloids) have rarely been isolated although they occasionally occur as minor constituents in plants producing tropane alkaloids. In 1988, Tepfer et al. (1988) reported the presence of a group of alkaloids in the underground organs and root exudates of *Calystegia sepium*, *Convolvulus arvensis* (both Convolvulaceae), and *Atropa belladonna* (Solanaceae). These compounds were named calystegines. Calystegines possess three structural features in common: a nortropane ring system; two to four secondary hydroxyl groups varying in position and stereochemistry; and a novel aminoketal functionality, which generates a tertiary hydroxyl group at the bicyclic ring bridgehead. The known members of the class have been subdivided into three groups on the basis of the number of hydroxyl groups present, namely calystegines A (with three hydroxyl groups), B (with four hydroxyl groups), and C (with five hydroxyl groups). Calystegines seem to be largely limited to the closely related families Solanaceae and Convolvulaceae, where they co-occur with tropane alkaloids (Asano et al., 2000). However, certain calystegines have also been found in species of *Morus* (Moraceae) (Asano, 1994a, b), which is a family not noted for the production of tropane alkaloids. In the course of isolating calystegines from species of the Solanaceae and Convolvulaceae, three dihydroxynortropane alkaloids were discovered. In the vast majority of tropane alkaloids, one or more of the hydroxyl groups on the tropane ring are esterified. However, Chinese researchers have isolated non-esterified dihydroxynortropane alkaloids, baogongten C (2β,6β-dihydroxynortropane) and erycibelline (2β,7β-dihydroxynortropane), from *Erycibe* species (Convolvulaceae) (Lu et al., 1986; Chen et al., 1986). In this report, we describe the isolation, structural determination, and the distribution of the new dihydroxynortropanes.

* Corresponding author. Tel.: +81-76-229-6196; fax: +81-76-229-2781.
E-mail address: naoki22@po.incl.ne.jp (N. Asano).

0031-9422/01/$ - see front matter © 2001 Elsevier Science Ltd. All rights reserved.
PII: S0031-9422(01)00131-5

2. Results and discussion

A hot water extract of the dried whole plants (550 g) of *Calystegia soldanella* (Convolvulaceae) was subjected to various ion-exchange resin chromatographic procedures to give alkaloids **1** (23 mg) and **2** (7 mg), and calystegines A_3 (7 mg), B_1 (100 mg), B_2 (530 mg), and B_3 (6 mg), respectively. From the aerial parts of *Duboisia leichhardtii* (Solanaceae), calystegines B_1, B_2, B_4, C_1, and C_2 were isolated previously (Kato et al., 1997). In the present studies, we isolated alkaloid **3** (3.6 mg), together with calystegines A_5 (6 mg), B_1 (5 mg), B_2 (25 mg), B_4 (25 mg), C_1 (810 mg), and C_2 (4 mg) from the dried aerial parts (1 kg) of *D. leichardtii* (Fig. 1).

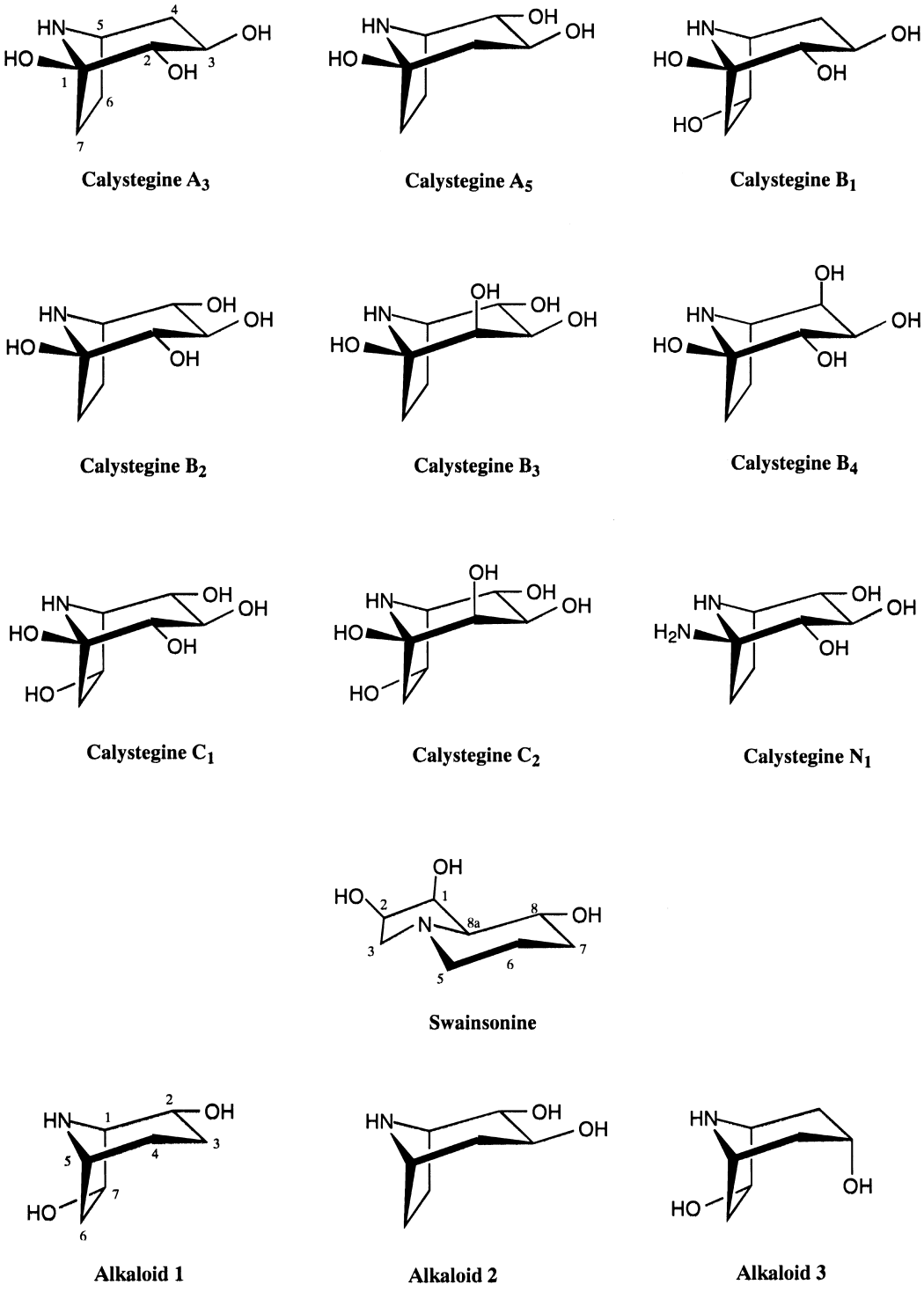

Fig. 1. Structures of the polyhydroxylated alkaloids included in this study.

The ^{13}C NMR spectrum of alkaloid **1** revealed the presence of three methylene and four methine carbon atoms. The HR–FABMS of **1** gave an $[M+H]^+$ ion at *m/z* 144.1026 ($C_7H_{14}O_2N$ requires 144.1025). The ^1H NMR spectral data, combined with extensive decoupling experiments and two-dimensional ^1H–^{13}C COSY spectral data, defined the complete connectivity of the carbon and hydrogen atoms for **1**. The methine doublets at δ 70.7 and 73.5 were assigned to C-2 and C-7, each bearing an OH group, due to the appearance in the low-field region of H-2 (δ 3.72) and H-7 (δ 4.45). The methine carbon at δ 70.1, with a doublet at δ 3.21 in the ^1H NMR spectrum, was identified as the bridgehead C-1, and the last methine at δ 57.0 was assigned to the other bridgehead C-5. There was no resolvable coupling between H-1 and H-7 in the ^1H NMR spectrum, indicating a dihedral angle close to 90° between them, and also an *endo* orientation of H-7. The strong NOE effect between H-7 and H-3ax also supports the *endo* orientation of H-7 (Fig. 2a). The coupling pattern of H-2 (*ddd*, $J_{1,2}=4.0$, $J_{2,3ax}=11.3$, $J_{2,3eq}=5.9$ Hz) and the NOE effect between H-2 and H-4ax indicate that H-2 is axial (Fig. 2a). Thus, alkaloid **1** was determined to be either 2α,7β-dihydroxynortropane or its enantiomer.

Alkaloid **2** was an isomer of **1** from HR–FABMS (*m/z* 144.1026 $[M+H]^+$) and ^{13}C NMR spectral data. The methines at δ 56.4 (C-5) and 61.0 (C-1) indicated that they must be bonded to the nitrogen of the heterocyclic ring. The coupling pattern of H-2 (δ 3.52, *dd*, $J_{1,2}=3.7$, $J_{2,3}=8.8$ Hz) indicates the *trans*-diaxial configuration of H-2 and H-3. The NOE effects between H-2 and H-4ax and between H-3 and H-6endo or H-7endo support this stereochemistry (Fig. 2b). Thus, alkaloid **2** was determined to be 2α,3β-dihydroxynortropane or its enantiomer.

Alkaloid **3** was also an isomer of **1** from HR–FABMS (*m/z* 144.1024 $[M+H]^+$) and ^{13}C NMR spectral data. The coupling pattern of H-7 (δ 4.83, *dd*, $J_{7,6endo}=7.3$, $J_{7,6exo}=2.2$ Hz), with no resolvable coupling with H-1 (δ 3.72, *t*, $J_{1,2ax}=J_{1,2eq}=4.0$ Hz), indicates an *endo* orientation for H-7. The small *J* value (4.0 Hz) between H-2ax and H-3, and the absence of an NOE effect between H-3 and H-7 or H-6endo indicate an equatorial orientation for H-3 (Fig. 2c). In addition, since alkaloid **3** was optically inactive, it was determined to be (±)-3α,7β-dihydroxynortropane.

In order to investigate the occurrence and distribution of these dihydroxynortropanes, nine species from the Convolvulaceae and three species from the Solanaceae were studied. All of the alkaloids were isolated by column chromatography using various ion-exchange resins. The known alkaloids were identified from their ^{13}C NMR chemical shifts. As shown in Table 1, 2α,7β-dihydroxynortropane (**1**) was isolated from six species in the Convolvulaceae and only *C. soldanella* produced both **1** and **2** (2α,3β-dihydroxynortropane). Although alkaloids **1** and **2** were not isolated from three species in the Solanaceae, the other alkaloid **3** (3α,7β- dihydroxynortropane) and calystegine A_5 were isolated from *D. leichhardtii*, in addition to known calystegines B_1, B_2, B_4, C_1, and C_2 (Kato et al., 1997). De Balogh et al. (1999) recently detected calystegine B_2 and swainsonine in *Ipomoea carnea* (Convolvulaceae) by GC–MS. In the present work, alkaloid **1** and calystegine B_1, in addition to calystegine B_2 and swainsonine, were isolated from the same plant. It is not known if the calystegines occur in *Erycibe* species (Convolvulaceae) (Lu et al., 1986; Chen et al., 1986), which are known to produce 2β,6β- and 2β,7β-dihydroxynortropanes. Major tropane alkaloids bear a hydroxyl group or an esterified one at C-3. Tropinone has been shown to be an intermediate on the biosynthesis of hyoscyamine and scopolamine in *Datura innoxia* (Landgrebe and Leete, 1990). Tropinone is

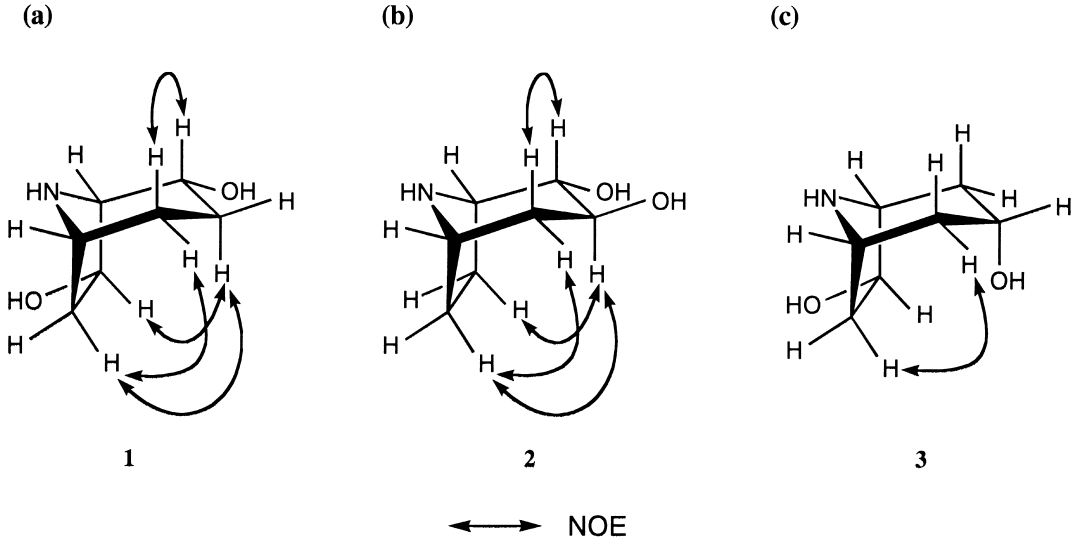

Fig. 2. NOE effects of 2α,7β-dihydroxynortropane (**1**) (a), 2α,3β-dihydroxynortropane (**2**) (b), and 3α,7β-dihydroxynortropane (**3**) (c).

Table 1
Distribution of polyhydroxylated alkaloids in the Convolvulaceae and Solanaceae

Plant	Organ[a]	**1**	**2**	**3**	A_3	A_5	B_1	B_2	B_3	B_4	C_1	C_2	N_1	Sw[b]
Convolvulaceae														
Calystegia japonica Choisy	C	●	–[c]	–	●	–	●	●	–	–	–	–	–	–
Calystegia sepium (L.) R. Br.	D	●	–	–	●	–	●	●	–	–	–	–	–	–
Calystegia soldanella (L.) Roem. et Schult.	A	●	●	–	●	–	●	●	●	–	–	–	–	–
Ipomoea batatas Lam. var. *edulis* Makino	B	●	–	–	–	–	●	●	–	–	–	–	–	–
Ipomoea carnea Jacq.	B	●	–	–	–	–	●	●	–	–	–	–	–	●
Ipomoea nil (L.) Roth	A	–	–	–	–	–	–	–	–	–	–	–	–	–
Ipomoea obscura Ker.	A	–	–	–	–	–	●	●	●	●	●	–	–	–
Ipomoea pes-caprae (L.) Sweet	B	–	–	–	–	–	–	●	–	–	–	–	–	–
Quamoclit angulata Bojer.	B	●	–	–	–	–	●	●	–	–	–	–	–	–
Solanaceae														
Cestrum nocturnum L.	B	–	–	–	–	–	–	–	–	–	–	–	–	–
Duboisia leichhardtii F. Muell	B	–	–	●	–	●	●	●	–	●	●	●	–	–
Solanum dulcamara L.	A	–	–	–	●	●	●	●	–	–	–	–	●	–

[a] A, whole parts; B, aerial parts; C, roots; D, root cultures.
[b] Swainsonine.
[c] Not detected.

reduced to specifically tropine in a cell-free system obtained from a root culture of *D. stramonium* (Koelen and Gross, 1983) or to pseudotropine as a major product in the same system of *Hyoscyamus niger* (Dräger et al., 1988). The structure of calystegines suggests that calystegines are formed by the biosynthetic pathway of tropane alkaloids. Although all of calystegines isolated from the root culture of *C. sepium* have a hydroxyl group at C-3, alkaloid **1** obtained from tha same plant does not have it. *Lycium chinense* (Solanaceae) produces calystegines A_6, A_7, and B_5 with no hydroxyl group at C-3 in addition to a lot of calystegines and *N*-methylcalystegines with a hydroxyl group at C-3 (Asano et al., 1997). The occurrence of nortropane alkaloids with no hydroxyl group at C-3 in the Convolvulaceae and Solanaceae is very interesting from the biosynthetic basis of tropane alkaloids.

3. Experimental

3.1. General

The purity of samples was checked by HPTLC on Silica Gel $60F_{254}$ (Merck) using the solvent system PrOH–AcOH–H_2O (4:1:1), and a chlorine/*o*-tolidine reagent was used for detection. Optical rotations were measured with a Jasco DIP-370 digital polarimeter. ^1H NMR (400 MHz) and ^{13}C NMR (100 MHz) spectra were recorded on a Jeol JNM-GX 400 spectrometer. Chemical shifts are expressed in ppm downfield from sodium **3**-(trimethylsilyl)propionate (TSP) in D_2O and TMS in CD_3OD as internal standards. MS were measured on a Jeol JMS-SX 102A spectrometer.

3.2. Plant material

Calystegia japonica and*C. soldanella* were collected in the wild in 1995 in Kanazawa City, Japan, and *Ipomoea obscura* and *I. pes-caprae* were collected in the wild in 1994 in Okinawa, Japan. *Quamoclit angulata* was collected in the wild in 1999 in Suwon, Korea. *I. batatas* var. *edulis*, *I. nil*, and *Solanum dulcamara* were cultivated in the field of the Medicinal Plants Garden, Hokuriku University, Japan, and *I. carnea* was grown in the greenhouse of the same facility. *Cestrum nocturnum* and *Duboisia leichhardtii* were cultivated in the greenhouse of Toyama Medical and Pharmaceutical University, Japan. Voucher specimens of all plants are deposited in the Medicinal Plants Gardens of Hokuriku University and Toyama Medical and Pharmaceutical University.

Transformed root cultures of *C. sepium* were established by transformation of leaf discs with *Agrobacterium rhizogenes* strain 8196, as described in the literature (Jung and Tepfer, 1987). Emerging roots were transferred to 25 ml of B5 liquid medium in 100 ml flasks containing 500 mg/l cefotaxim, but no phytohormones. After several subcultures, cefotaxim was omitted from the medium. For root mass production, roots were subcultured in 300 ml flasks with 70 ml of medium. Growth was typically 20–25-fold within 21 days.

3.3. Extraction and isolation

The dried whole plant (550 g) of *C. soldanella* was extracted with hot water (5 l) for 2 h. The extract (about 3 l) was applied to a column of Amberlite IR-120B (300 ml, H^+ form). The 0.5 M NH_4OH eluate was concentrated to give a brown oil (11.8 g), which was applied

to an Amberlite CG-50 column (2.5×95 cm, NH_4^+ form) with H_2O as eluant (fraction size 18 ml). The H_2O eluate was divided into five pools A (fractions 32–45, 580 mg), B (fractions 46–70, 176 mg), and C (fractions 75–100, 32 mg). The 0.5 M NH_4OH eluate from the same column was designated pool D. Pools A, B, and C were further subjected to Dowex 1-X2 (1.8×95 cm, OH^- form) column chromatorgraphy with H_2O as eluant to give calystegines B_2 (530 mg), B_1 (100 mg), and B_3 (6 mg), respectively. Pool D was applied to Dowex 1-X2 (1.8×65 cm, OH^- form) column with H_2O as eluant to give calystegine A_3 (7 mg) and a mixture of alkaloids (72 mg). The mixture was further subjected to CM-Sephadex C-25 (1.5×46 cm, NH_4^+ form) column chromatography with 0.01 M NH_4OH as eluant to give alkaloids **1** (23 mg) and **2** (7 mg).

The other plant materials were also extracted and purified in a similar manner. The yields of alkaloids from each plant are as follows.

C. japonica (300 g of dried roots): calystegines A_3 (33 mg), B_1 (42 mg), B_2 (186 mg), and alkaloid **1** (10 mg).

I. batatas var. *edulis* (2 kg of dried aerial parts): calystegines B_1 (65 mg), B_2 (95 mg), and alkaloid **1** (12 mg).

I. carnea (2 kg of dried aerial parts): swainsonine (86 mg), calystegines B_1 (39 mg) and B_2 (146 mg), and alkaloid **1** (20 mg).

I. obscura (416 g of dried whole parts): calystegines B_1 (14 mg), B_2 (88 mg), B_3 (6 mg), B_4 (10 mg), and C_1 (66 mg).

I. pes-caprae (480 g of dried aerial parts): calystegine B_2 (9 mg).

Q. angulata (330 g of dried aerial parts): calystegines B_1 (45 mg), B_2 (78 mg), and alkaloid **1** (18 mg).

Duboisia leichhardtii (1 kg of dried aerial parts): calystegines A_5 (8mg), B_1 (5 mg), B_2 (24 mg), B_4 (20 mg), C_1 (810 mg), C_2 (5 mg), and alkaloid **3** (3.6 mg).

Solanum dulcamara (250 g of dried whole parts): calystegines A_3 (34 mg), A_5 (19 mg), B_1 (6 mg), B_2 (48 mg), and N_1 (13 mg).

Fresh root cultures (1.2 kg) of *C. sepium* were extracted with 50% MeOH. The extract was concentrated and lyophilized to give a brown powder (46 g). The powder was subjected to chromatographic purification in a similar manner to give calystegines A_3 (25 mg), B_1 (32 mg), B_2 (49 mg), and alkaloid **1** (17 mg).

3.4. 2α,7β-Dihydroxynortropane (*1*)

$[\alpha]_D$ +13.1° (*c* 2.33, H_2O); HRFABMS: *m/z* 144.1026 $[M+H]^+$ ($C_7H_{14}O_2N$ requires 144.1025); ^1H NMR (400 MHz, CD_3OD) δ 1.18 (*ddt*, 1H, *J* = 6.2, 11.3, 14.8 Hz, H-3ax), 1.46 (*m*, 1H, H-4eq), 1.56 (*m*, 1H, H-4ax), 1.70 (*ddd*, 1H, *J* = 2.6, 7.0, 14.3 Hz, H-6exo), 1.84 (*m*, 1H, H-3eq), 2.15 (*dd*, 1H, *J* = 7.3, 14.3 Hz, H-6endo), 3.21 (*d*, 1H, *J* = 4.0 Hz, H-1), 3.61 (*m*, 1H, H-5), 3.72 (*ddd*, 1H, *J* = 4.0, 5.9, 11.3 Hz, H-2), 4.45 (*dd*, 1H, *J* = 2.6, 7.3 Hz, H-7); ^{13}C NMR (100 MHz, D_2O) δ 28.5 (*t*, C-3), 30.9 (*t*, C-4), 42.6 (*t*, C-6), 57.0 (*d*, C-5), 70.1 (*d*, C-1), 70.7 (*d*, C-2), 73.5 (*d*, C-7).

3.5. 2α,3β-Dihydroxynortropane (*2*)

$[\alpha]_D$ +48.4° (*c* 0.82, H_2O); HRFABMS: *m/z* 144.1026 $[M+H]^+$ ($C_7H_{14}O_2N$ requires 144.1025); ^1H NMR (400 MHz, D_2O) δ 1.48 (*ddd*, 1H, *J* = 3.7, 11.0, 13.2 Hz, H-4ax), 1.62 (m, 1H, H-6endo), 1.71 (*m*, 1H, H-7exo), 1.84 (*m*, 2H, H-6exo, H-7endo), 1.97 (*ddd*, 1H, *J* = 2.9, 6.6, 13.2 Hz, H-4eq), 3.46 (*dd*, 1H, *J* = 3.7, 6.6 Hz, H-1), 3.52 (*dd*, 1H, *J* = 3.7, 8.8 Hz, H-2), 3.57 (*ddd*, 1H, *J* = 2.9, 3.7, 6.6 Hz, H-5), 3.66 (*ddd*, 1H, *J* = 6.6, 8.8, 11.0 Hz, H-3); ^{13}C NMR (100 MHz, D_2O) δ 26.0 (*t*, C-7), 30.4 (*t*, C-6), 41.5 (*t*, C-4), 56.4 (*d*, C-5), 61.0 (*d*, C-1), 71.8 (*d*, C-3), 78.3 (*d*, C-2).

3.6. 3α,7β-Dihydroxynortropane (*3*)

HRFABMS: *m/z* 144.1024 $[M+H]^+$ ($C_7H_{14}O_2N$ requires 144.1025); ^1H NMR (400 MHz, D_2O) δ 1.85 (*m*, 1H, H-6endo), 1.96 (*m*, 1H, H-4eq), 2.03 (*m*, 1H, H-2eq), 2.12 (*m*, 1H, H-4ax), 2.17 (*dt*, 1H, *J* = 4.0, 15.8 Hz, H-2ax), 2.89 (*dd*, 1H, *J* = 7.3, 14.3 Hz, H-6endo), 3.72 (*t*, 1H, *J* = 4.0 Hz, H-1), 4.06 (*m*, 1H, H-5), 4.10 (*m*, 1H, H-3), 4.83 (*dd*, 1H, *J* = 2.2, 7.3 Hz, H-7); ^{13}C NMR (100 MHz, D_2O) δ 36.6 (*t*, C-2), 37.8 (*t*, C-4), 41.0 (*t*, C-6), 57.2 (*d*, C-5), 65.0 (*d*, C-3), 65.3 (*d*, C-1), 75.2 (*d*, C-7).

Acknowledgements

B. D. thanks Dr. Peter Bachman, Braunschweig, for the establishment of the *Calystegia sepium* root culture.

References

Asano, N., Nash, R.J., Molyneux, R.J., Fleet, G.W.J., 2000. Tetrahedron Asymm. 11, 1645–1680.

Asano, N., Tomioka, E., Kizu, H., Matsui, K., 1994a. Carbohydr. Res. 253, 235–245.

Asano, N., Oseki, K., Tomioka, E., Kizu, H., Matsui, K., 1994b. Carbohydr. Res. 259, 243–255.

Asano, N., Kato, A., Miyauchi, M., Kizu, H., Tomimori, T., Matsui, K., Nash, R.J., Molyneux, R.J., 1997. Eur. J. Biochem. 248, 296–303.

Chen, Z., Xu, P., Yao, T., 1986. Zhongcaoyao 17, 386–387; Chem. Abstr. 106, 153016s (1987).

De Balogh, K.K.I.M., Dimande, A.P., van der Lugt, J.J., Molyneux, R.J., Naudé, T.W., Welman, W.G., 1999. J. Vet. Diagn. Invest. 11, 266–273.

Dräger, B., Hashimoto, T., Yamada, Y., 1988. Agric. Biol. Chem. 52, 2663–2667.

Jung, G., Tepfer, D., 1987. Plant Sci. 50, 145–151.

Kato, A., Asano, N., Kizu, H., Matsui, K., Suzuki, S., Arisawa, M., 1997. Phytochemistry 45, 425–429.

Koelen, K.J., Gross, G.G., 1983. Planta Med. 44, 227–230.

Landgrebe, M.E., Leete, E., 1990. Phytochemistry 29, 2521–2524.

Lounasmaa, M., 1988. In: Brossi, A. (Ed.), The Alkaloids: Chemistry and Pharmacology, Vol. 33. Academic Press, New York, p. 1.

Lounasmaa, M., Tamminen, T., 1993. In: Cordell, G.A. (Ed.), The Alkaloids: Chemistry and Pharmacology, Vol. 44. Academic Press, New York, p. 1.

Lu, Y., Yao, T., Chen, Z., 1986. Yaoxue Xuebao 21, 829; 1987; Chemical Abstracts 106, 153028x.

Tepfer, D.A., Goldmann, A., Pamboukdjian, N., Maille, M., Lepingle, A., Chevalier, D., Denarie, J., Rosenberg, C., 1988. J. Bacteriol. 170, 1153–1161.

PERGAMON

Phytochemistry 57 (2001) 727–731

PHYTOCHEMISTRY

www.elsevier.com/locate/phytochem

Fatty acid profiles and their chemotaxonomy in planktonic species of *Anabaena* (Cyanobacteria) with straight trichomes

Renhui Li*, Makoto M. Watanabe[1]

National Institute for Environmental Studies, 16-2 Onogawa, Tsukuba, Ibaraki 305-0035, Japan

Received 13 October 2000; received in revised form 23 January 2001

Abstract

Twenty-four axenic strains of planktonic *Anabaena* with straight trichomes, assigned to 7 species, were investigated by analyzing the pattern and content of their fatty acid composition and comparing their fatty acid composition with their morphological properties. In general, the fatty acids in planktonic *Anabaena* contained 14:0, 16:0, 16:1(*cis*-), 18:0, 18:1, 18:2, and 18:3(α) as their major components, and were classified as Type 2 according to the Kenyon–Murata system. These strains were further divided into 2 subtypes: 18 strains belonging to Type 2A, which contains 16:2 and 16:3, and 6 strains to Type 2B, which lacks 16:2 and 16:3. Fatty acid compositions of strains of *A. solitaria*, *A. smithii,* and *A. kisseleviana* closely corresponded to morphological properties; however, 10 strains of *A. planctonica* were divided into 4 clusters, and 3 strains of *A. affinis* into 2 clusters. These clusters should be taxonomically evaluated based on other aspects such as genetic characteristics. © 2001 Elsevier Science Ltd. All rights reserved.

Keywords: Cyanobacteria; Fatty acid; Morphological characters; Planktonic *Anabaena*; Taxonomy

1. Introduction

Freshwater planktonic cyanobacteria *Anabaena* spp. are organisms that sometimes form water blooms in eutrophic lakes, reservoirs, and ponds. Like *Microcystis* species, these filamentous heterocystous cyanobacteria are also recognized as a threat to public health due to the production of toxic substances such as microcystin, anatoxin-a, and saxitoxin. (Carmichael, 1981; Skulberg et al., 1993; Humpage et al., 1994; Chorus and Bartram, 1999) and excretion of geosmin-like odor-producing substances (Izaguirre et al., 1981; Jüttner, 1987; Hayes and Burch 1989). In spite of the ecological significance of planktonic *Anabaena*, identification is problematic and often provisional (Hickel, 1982; Komárek and Anagnostidis, 1989). The current taxonomy of *Anabaena* is based mainly on morphological characteristics such as trichome form, shape of akinetes, size of cells, and relative position of the akinetes to heterocysts. According to Geitler (1942) "the determination of *Anabaena* species is very difficult and frustrating" (cf. Hickel, 1982). Some morphological criteria vary among different researchers (Fritsch, 1949; Nygaard, 1949; Komárek, 1958; Pankow, 1965; Komárková-Legenrová and Eloranta, 1992; Watanabe, 1992; Niiyama, 1996). Furthermore, taxonomic characters such as filament form and akinete cells are problematic because akinetes are occasionally absent and trichome form may be irreversibly changed by culture conditions. Recently, Castenholz and Waterbury (1989) strongly urged that bacterial approaches should be introduced to the taxonomy of cyanobacteria due to their prokaryotic properties. Therefore, it is apparent that planktonic *Anabaena* species require more taxonomic studies incorporating not only morphological characters but also physiological, chemical, and genetic features.

Fatty acid composition is a useful analytical tool in bacterial taxonomy (Welch, 1991; Embley and Wait, 1994). In the cyanobacteria, Kenyon (1972), Kenyon et al. (1972), and Murata et al. (1992) proposed that four types of fatty acid composition exist in cyanobacteria and demonstrated some correlations with morphological properties. Caudales and Wells (1992) investigated the cellular fatty acids of benthic cyanobacteria belonging to

* Corresponding author at present address: Department of Biological Sciences, Wright State University, Dayton, OH 45435, USA. Tel.: +1-937-775-2655; fax: +1-937-775-3320.

E-mail address: renhui.li@wright.edu (R. Li).

[1] Author for reprint request.

0031-9422/01/$ - see front matter © 2001 Elsevier Science Ltd. All rights reserved.
PII: S0031-9422(01)00082-6

the genera *Anabaena* and *Nostoc* and found significant differences between those genera. Krüger et al. (1995) evaluated the taxonomic importance of fatty acid composition at the genus and subgenus level by analyzing the fatty acid composition of different *Microcystis* isolates and other members of the order Chroococcales. However, there is little information about fatty acid composition and chemotaxonomy in planktonic species of *Anabaena*. According to Watanabe (1992, 1998), planktonic species of *Anabaena* are divided into two groups: species with straight trichomes and those with coiled trichomes. In the present study, we extensively examined 24 strains with straight trichomes by analyzing the pattern and content of fatty acids in these strains and established their chemotaxonomy by comparing their fatty acid composition with morphological properties.

2. Results

The 24 strains used in the present study (see Table 1) were identified as 7 species based on morphological observations: *Anabaena affinis* Lemmermann, *A. planctonica* Brunnthaler, *A. solitaria* Klenahn, *A. smithii* (Komárek) Watanabe, *A. viriguri* Denis et Fremy, *A. kisseleviana* Elenkin, *A. danica* (Nygaard) Komárková et Eloranta. The composition and content of fatty acids in these strains are shown in Table 2. The major components of fatty acids in these strains were 16:0, 16:1(*cis*-), 18:2, and 18:3(α); therefore, they are classified as Type 2 according to the Kenyon–Murata system (Kenyon, 1972; Kenyon et al., 1972; Murata et al., 1992). Our previous study indicated that Type 2 could be further divided into 2 subtypes: Type 2A (with 16:2 and 16:3), and Type 2B (without 16:2 and 16:3) (Li et al., 1998). As shown in Table 2, 18 strains belonging to *A. smithii*, *A. solitaria*, *A. planctonica* (8 strains), and *A. affinis* (2 strains) were Type 2A, and 6 strains belonging to *A. kisseleviana*, *A. danica*, *A. planctonica* (2 strains), and *A. affinis* (1 strain) were Type 2B. The simplified dendrogram created by a simplified unweighted pair-group method with arithmetic averages (UPGMA) using the NTSYS-pc program package and fatty acid data are shown in Fig. 1. In the dendrogram, the 24 strains are shown in relation to fatty acid compositions of Type 2A and 2B. In the strains of *A. smithii*, *A. solitaria,* and *A. kisseleviana*, there was a close correspondence between fatty acid composition and morphological characters; however, 10 strains of *A. planctonica* were divided into 4 separate clusters, AP 1∼4 (Fig. 1), of which 2 strains of AP-4 belonged to Type 2B and other clusters to Type 2A. In addition, 3 strains of *A. affinis* were separated into 2 clusters, AA-1 and AA-2, which belonged to Type 2A and 2B, respectively.

Table 1
Strains of *Anabaena* used in this study

Taxa	Strain	Source
A. affinis	NIES-40	NIES[a]
A. affinis	Inba3	Isolation, Chiba, Japan
A. affinis	Inba10	Isolation, Chiba, Japan
A. planctonica	TAC421	NSM[b]
A. planctonica	TAC422	NSM
A. planctonica	TAC424	NSM
A. planctonica	TAC434	NSM
A. planctonica	TAC435	NSM
A. planctonica	1403/19	CCAP[c]
A. planctonica	1403/27	CCAP
A. planctonica	Inba2	Isolation, Chiba, Japan
A. planctonica	Inba6	Isolation, Chiba, Japan
A. planctonica	NIVA66	NIVA[d]
A. solitaria	NIES-78	NIES
A. solitaria	NIES-80	NIES
A. smithii	TAC428	NSM
A. smithii	TAC431	NSM
A. smithii	TAC432	NSM
A. smithii	TAC450	NSM
A. smithii	TAC451	NSM
A. kisseloviana	NIES-74	NIES
A. kisseloviana	TAC34	NSM
A. viguieri	TAC433	NSM
A. danica	TAC453	NSM

[a] NIES: Microbial Culture Collection, National Institute for Environmental Studies, Tsukuba, Japan.
[b] NSM: National Science Museum, Tsukuba, Japan.
[c] CCAP: Culture Collection of Algae and Protozoa, Windermere, UK.
[d] NIVA: Norwegian Institute for Water Research, Oslo, Norway.

3. Discussion

Fatty acids of cyanobacteria have been investigated for their content, composition types, metabolism, and biotechnological application by different researchers (Cohen et al., 1987; Ahlgren et al., 1992; Murata et al., 1992; Matsunaga et al., 1995). In terms of chemotaxonomy by fatty acid composition, Cohen and Vonshak (1991) indicated that there should be a separation between freshwater and salt-tolerant strains in the genus *Spirulina* based on the difference in their fatty acid composition. Krüger et al. (1995) and Caudales and Wells (1992) also demonstrate the importance of fatty acid composition in the taxonomy of Cyanobacteria at the genus and subgenus level. Our previous study shows that fatty acid composition can be used in chemotaxonomy of cyanobacteria even at the species level based on examination of 28 strains of planktonic cyanobacteria (Li et al., 1998). In the present study, fatty acids and their chemotaxonomic values were further investigated using more strains of *Anabaena*. The results showed that both Type 2A and Type 2B are found in planktonic strains of *Anabaena* (Table 2 and Fig. 1).

Planktonic *Anabaena* species with straight trichomes were morphologically classified into *A. affinis* with bundle-

Table 2
Fatty acid composition of planktonic species of *Anabaena* with straight trichomes

Strain	14:0	16:0	16:1*[a]	16:1(*cis*-)	16:2*	16:3*	18:0	18:1	18:2	18:3(α)
A. affinis (NIES-40)	4.4	30.3	2.0	4.2	5.3	8.5	1.0	2.5	6.2	35.6
A. affinis (Inba3)	5.6	29.1	2.0	9.0	3.8	3.1	1.5	4.8	11.2	29.8
A. affinis (Inba10)	2.8	26.0	–[b]	15.8	–	–	1.3	1.6	10.7	41.9
A. planctonica (TAC421)	5.0	39.5	2.2	4.1	4.9	3.8	0.8	2.5	11.0	26.2
A. planctonica (TAC422)	4.4	36.0	2.0	3.3	4.7	4.0	1.0	2.5	13.4	28.6
A. planctonica (TAC424)	3.8	37.4	2.0	2.3	3.5	4.8	1.8	3.2	10.9	30.2
A. planctonica (TAC434)	2.7	37.0	–	16.1	–	–	0.8	0.8	7.6	35.0
A. planctonica (TAC435)	2.0	37.0	–	14.0	–	–	0.8	0.8	9.1	36.1
A. planctonica (1403/27)	2.6	39.7	2.5	6.6	2.1	3.4	1.0	7.6	9.8	24.7
A. planctonica (1403/19)	3.7	42.1	4.5	3.1	2.5	4.4	1.7	10.8	5.8	21.3
A. planctonica (NIVA66)	5.3	36.5	0.9	6.0	3.4	6.3	1.1	3.3	6.8	30.3
A. planctonica (Inba2)	4.7	35.3	1.1	3.3	5.9	8.8	1.6	1.1	10.1	27.1
A. planctonica (Inba6)	4.2	33.6	2.0	2.3	3.5	4.8	1.8	3.2	10.9	25.4
A. solitaria (NIES-78)	5.5	38.4	2.5	4.8	5.4	4.7	0.6	2.1	9.4	26.5
A. solitaria (NIES-80)	5.7	41.6	2.4	5.1	4.6	4.4	1.0	2.1	8.2	24.9
A. smithii (TAC428)	3.3	46.1	1.6	2.7	2.3	4.2	1.9	1.3	5.7	31.0
A. smithii (TAC431)	3.2	37.0	2.8	3.4	6.3	4.2	0.7	2.6	14.1	25.8
A. smithii (TAC432)	3.2	40.8	2.6	3.0	6.4	3.4	1.2	2.5	13.9	22.8
A. smithii (TAC450)	2.8	35.1	3.2	3.4	6.3	4.2	0.8	3.5	15.5	25.3
A. smithii (TAC451)	3.2	37.0	4.0	3.7	6.0	3.3	1.0	4.5	16.2	21.1
A. kisseloviana (NIES-74)	2.7	40.1	–	17.2	–	–	1.1	0.9	7.4	31.5
A. kisseloviana (TAC34)	2.7	43.4	–	17.6	–	–	tr	2.2	3.5	30.6
A. viguieri (TAC433)	3.4	30.3	1.5	2.7	4.8	6.0	1.9	2.3	10.9	36.2
A. danica (TAC453)	1.9	34.2	-	11.8	-	-	2.5	5.0	6.1	35.2

[a] *: Double band position not determined.
[b] –: Not detected.

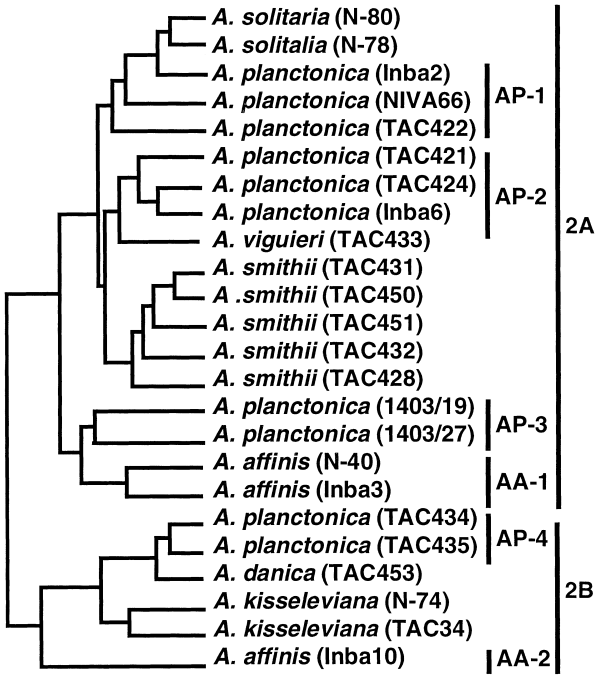

Fig. 1. Dendrogram of planktonic strains of *Anabaena* with straight trichomes based on fatty acid composition; 0.5 represents Euclidean distance. AA-1, 2 and AP-1∼4 represent clusters of *A. affinis* and *A. planctonica,* respectively.

forming trichomes and *Anabaena* spp. with solitary trichomes. The latter group was classified into *A. planctonica*, *A. solitaria*, *A. smithii*, *A. kisseleviana*, etc., based on the shape of the akinetes and their position relative to heterocysts. The results of this study indicate that the morphological classification agreed well with chemotaxonomy of fatty acids within *Anabaena* species having spherical akinetes (i.e. *A. smithii, A. kisseleviana*) and cylindrical akinetes (*A. solitaria*). However, the divergence of fatty acid composition in *A. planctonica* and *A. affinis* reflected current problems of morphological classification.

A. planctonica was established by Brunnthaler in 1903 and has many synonyms, including: *A. scheremetievi* Elenkin 1909; *A. scheremetievi* var. *recta* Elenkin f. *ovalispora* Elenkin 1938; *A. limnetica* G.M. Smith 1916; *A. solitaria* f. *solitaria* sensu Komárek 1958; *A. planctonica* f. *planctonica* (Brunnth.) Komárek 1958; *A. affinis* var. *intermedia* Griffith; *A. catenula* var. *intermedia* Geitler; and *A. affinis* var. *intermedia* f. *tenuis* Nygaard. Since it was first described, *A. planctonica* has been characterized mainly by its ellipsoidal akinetes. However, criteria for the size range of akinetes has varied among researchers (e.g. 14–18.8×21–37 μm by Watanabe, 1992, and 10–20×15–30 μm by Komárková-Legnerová and Eloranta, 1992), causing problems in classifying transient

forms and also resulting in overlap with other species, such as *A. macrospora* and *A. viguieri*. Baker (1991) suggested that there exists some variation in *A. planctonica* and described two morphotypes. To distinguish clusters of strains of *A. planctonica* by fatty acid composition, we tentatively designated them as AP-1, 2, 3, and 4. It is noteworthy that AP-4, with Type 2B fatty acids, included TAC434 and 435, which have higher salinity tolerance (up to 1.5%) than the other *A. planctonica* strains (with up to 0.78%) (Li, 1998), and they also have smaller vegetative cells and heterocysts than other clusters do (Li et al., 2001).

It is generally recognized that bundle formation in planktonic species of *Anabaena* occurs only in *A. affinis*. Akinetes of these bundle-forming *Anabaena* were occasionally absent in both field-collected and cultured specimens; consequently, the akinete shape and size were disregarded. In the genus *Aphanizomenon*, several species have been identified based on other morphological features besides bundle formation (Komárek and Kovácik, 1989). Therefore, it is possible that there are more than one species of bundle-forming *Anabaena*. Results of the fatty acid analysis in the present study suggest this possibility, which was further supported by results on growth temperature range (data not shown). Two clusters of *A. affinis* strains have been designated as AA-1 and AA-2. Clusters of *A. planctonica* and *A. affinis* should be taxonomically reevaluated based on other aspects such as genetic characteristics.

4. Experimental

4.1. Organisms and culture conditions

Axenic strains of 24 planktonic *Anabaena* with straight trichomes were used in the present study. Among these strains, 20 were obtained from different culture collections (NIES, TAC, CCAP, and NIVA; for abbreviations see Table 1), and 4 were isolated by the authors from Japan (Table 1). The unialgal strains were purified into the axenic state using the pipette washing method. Taxonomy of all the strains, based on morphological characteristics, are presented in Li et al. (2001). All the strains were cultivated in CT medium (Watanabe and Hiroki, 1997). The cultures were grown in 1 l of medium in 2-l flasks equipped with aeration by a filter with 0.22-μm pore size. All cultures were grown at 20°C under a 12:12 L/D cycle with a photon irradiance of 40 μmol m^{-2} s^{-1} provided by daylight fluorescent lamps.

4.2. Fatty acid analyses

About 5–10 mg of lyophilized cells were transmethylated with 5% HCl-methanol (TCI-SU, Japan) at 100°C for 3 h. The methylated acids were extracted with 1.5 ml hexane, washed with 0.5 ml distilled water, and filtered with quartz, then concentrated to 50 μl by nitrogen gas or by vacuum evaporation. A 1-μl portion of concentrated sample was injected into a Shimadzu GC-17A gas chromatograph equipped with a hydrogen flame ionization detector and a capillary column (25 m×0.25 mm×0.25 μm) coated with methyl silicone as a polar stationary phase (007-FFAP, Tokyo Kasei). The flow of helium gas was 40 ml min^{-1}, and column temperature was programmed to increase from 130–220°C at 5°C/min. The methyl esters were identified by co-chromatography of authentic standards (Sigma, USA) and by mass spectroscopy. The relative concentrations of fatty acids were calculated by comparing the areas under the chromatographic peaks with a data processor (C-R 6A, Shimadzu). All analyses were performed in triplicate. The quantitative fatty acid data were numerically analyzed using the NTSYS-pc program package (Applied Biostatistics, Inc., Setanket, NY), and the results are presented as dendrograms drawn using the unweighted pair-group arithmetic average (UPGMA) clustering method.

Acknowledgements

We thank Professors T. Hori and I. Inouye, University of Tsukuba, for their critical advice on this study and helpful encouragement. This work was supported by Special Coordination Funds from the Science and Technology Agency (STA) of Japan.

References

Ahlgren, G., Gustafsson, I., Boberg, M., 1992. Fatty acid content and chemical composition of freshwater microalgae. J. Phycol. 28, 37–50.

Baker, P.D., 1991. Identification of common noxious Cyanobacteria. Part I — Nostocales. Urban Water Res. Assoc. Aust. Res. Rep. 29, 20–102.

Carmichael, W.W., 1981. Freshwater blue-green algae (Cyanobacteria) toxins — a review. In: Carmichael, W.W. (Ed.), The Water Environment: Algal Toxins and Health. Plenum Press, New York, pp. 1–14.

Castenholz, R.W., Waterbury, J.B., 1989. Cyanobacteria. In: Staley, J.T., Bryant, M.P., Pfennig, N., Holt, J.G. (Eds.), Bergey's Manual of Systematic Bacteriology, Vol. 3. Williams & Wilkins, Baltimore, pp. 1710–1727.

Caudales, R., Wells, J.M., 1992. Differentiation of the free-living *Anabaena* and *Nostoc* cyanobacteria on the basis of fatty acid composition. Int. J. Syst. Bacteriol. 42, 246–251.

Chorus, I., Bartram, J., 1999. Toxic cyanobacteria in water. E. & F.N. Spon, London and New York.

Cohen, Z., Vonshak, A., 1991. Fatty acid composition of *Spirulina* and *Spirulina*-like cyanobacteria in relation to their chemotaxonomy. Phytochemistry 30, 205–206.

Cohen, Z., Vonshak, A., Richmond, A., 1987. Fatty acid composition of *Spirulina* strains grown under various environmental conditions. Phytochemistry 26, 2255–2258.

Embley, T.M., Wait, R., 1994. Structural lipids of eubacteria. In: Goodfellow, M., O'Donnell (Eds.), Chemical Methods in Prokaryotic

Systematics. John Wiley & Sons, Chichester, New York, Brisbane, Toronto, Singapore, pp. 121–161.
Fritsch, F.E., 1949. The genus *Anabaena*, with special reference to species recorded from India and from adjacent Asiatic Mainland. J. Indian Bot. Soc. 28, 135–161.
Geitler, H., 1942. Schizophyta: Klasse Schizophyceae. In: Engler, A., Prantl, K. (Eds.), Die natürlichen Pflanzenfamilien Bd. 1b. Leipzig, 232 pp.
Hayes, K.P., Burch, M.D., 1989. Odorous compounds associated with algal blooms in south Australia waters. Wat. Res. 23, 115–121.
Hickel, B., 1982. A helical, bloom-forming *Anabaena*-like blue-green alga (Cyanophyta) from hypertrophic lakes. Arch. Hydrobiol. 95, 115–124.
Humpage, A.R., Rositano, J., Bretag, A., Brown, R., Baker, P., Nicholson, B.C., Steffensen, D.A., 1994. Paralytic shellfish poisons from Australian blue-green algal (cyanobacterial) blooms. Aust. J. Mar. Freshwater Res. 45, 761–771.
Izaguirre, G., Hwang, C.J., Krasner, S.W., Mcguire, M.J., 1981. Geosmin and 2-methylisoborneol from cyanobacteria in three water supply systems. Appl. Environ. Microbiol. 43, 708–714.
Jüttner, F., 1987. Volatile organic substances. In: Fay, P., Baalen, C.V. (Eds.), The Cyanobacteria. Elsevier, Amsterdam, New York, Oxford, pp. 453–470.
Kenyon, C.N., 1972. Fatty acid composition of unicellular strains of blue-green algae. J. Bacteriol. 109, 827–834.
Kenyon, C.N., Rippka, R., Stanier, R., Y., 1972. Fatty acid composition and physiological properties of some filamentous blue-green algae. Arch. Microbiol. 83, 216–236.
Komárek, J., 1958. Die taxonomische Revision der planktischen Blaualgen der Tschechoslowakei. In: Komárek, J., Ettl, H. (Eds.), Algologische Studien. Tschechosl. Akad., Praha, pp. 10–206.
Komárek, J., Anagnostidis, K., 1989. Modern approach to the classification system of cyanophytes. 4. Nostocales. Arch. Hydrobiol. Suppl. Algological Studies 56, 247–345.
Komárek, J., Kovácik, L., 1989. Trichome structure of four *Aphanizomenon* taxa (Cyanophyceae) from Czechoslovakia, with notes on the taxonomy and delimitation of the genus. Pl. Syst. Evol. 164, 47–64.
Komárková-Legenrová, J., Eloranta, P., 1992. Planktonic blue-green algae (Cyanophyta) from central Finland (Jyvaskyla region) with special reference to the genus *Anabaena*. Arch. Hydrobiol. Suppl. 95, Algological Studies 67, 103–133.
Krüger, G.H.J., Wet, H.D., Kock, J.L.F., Pieterse, A.J.H., 1995. Fatty acid composition as taxonomic characteristic for *Microcystis* and other coccoid cyanobacteria (blue-green alga) isolates. Hydrobiologia 308, 145–151.
Li, R., 1998. Taxonomic Studies on Planktonic Species of *Anabaena* (Cyanobacteria). PhD thesis, University of Tsukuba.
Li, R., Watanabe, M., Watanabe, M. M., 2001. Taxonomic studies of planktic species of Anabaena based on morphological characteristics in cultured strains. Hydrobiologia, in press.
Li, R., Yokota, A., Sugiyama, J., Watanabe, M., Watanabe, M.M., 1998. Chemotaxonomy of planktonic cyanobacteria based on nonpolar and 3-hydroxy fatty acid composition. Phycol. Res. 46, 21–28.
Matsunaga, T., Takeyama, H., Miura, Y., Yamazaki, T., Furuya, H., Sode, K., 1995. Screening of marine cyanobacteria for high palmitoleic acid production. FEMS Microbiol. Lett. 133, 137–141.
Murata, N., Wada, H., Gombos, Z., 1992. Modes of fatty-acid desaturation in cyanobacteria. Plant Cell Physiol. 33, 933–941.
Niiyama, Y., 1996. Morphology and systematics of *Anabaena* strains in National Science Museum. Jpn. J. Phycol. 44: 1–8 (in Japanese with English abstract).
Nygaard, G., 1949. Hydrological studies on some Danish ponds and lakes. II. The quotient hypothesis and some new or little known phytoplankton organisms. Kongl. Danske Vidensk. Selskab., Biol. Skr. 7, 1–293.
Pankow, H., 1965. Bemerkungen zur systematik der *Anabaena*-formen mit spiralig schraubig oder kreisformig gewundenen trichomen. Limnologica (Berlin) 3, 163–172.
Skulberg, O.M., Carmichael, W.W., Codd, G.A., Skulberg, R., 1993. Taxonomy of toxic cyanophyceae (Cyanobacteria). In: Falconer, I.R. (Ed.), Algal Toxins in Seafood and Drinking Water. Academic Press, London, San Diego, New York, Boston, Sydney, Tokyo, pp. 145–164.
Watanabe, M., 1992. Studies on planktonic blue-green algae 4. Some *Anabaena* species with straight trichomes in Japan. Bull. Natn. Sci. Mus., Tokyo, ser. Bz 18, 123–137.
Watanabe, M., 1998. Studies on planktonic blue-green algae 8. *Anabaena* species with twisted trichomes in Japan. Bull. Natn. Sci. Mus., Tokyo, ser. B 18, 123–137.
Watanabe, M.M., Hiroki, M. (Eds.), 1997. NIES-Collection. List of Strains, Algae and Protozoa, 5th Edition. National Institute for Environmental Studies, Environment Agency, Japan, 140 pp.
Welch, D.F., 1991. Application of cellular fatty acid analysis. Clin. Microbiol. Rev. 4, 422–438.

PERGAMON

Phytochemistry 57 (2001) 733–736

PHYTOCHEMISTRY

www.elsevier.com/locate/phytochem

Chemical variability in the essential oil of *Hyptis suaveolens*

Neucírio R. Azevedo[a], Irani F.P. Campos[b], Heleno D. Ferreira[b], Tomás A. Portes[b], Suzana C. Santos[a], José C. Seraphin[c], José R. Paula[d], Pedro H. Ferri[a,*]

[a]*Laboratório de Bioatividade Molecular, Instituto de Química, Universidade Federal de Goiás, C.P. 131, 74001-970 Goiânia, GO, Brazil*
[b]*Departamento de Biologia Geral-ICB, Universidade Federal de Goiás, C.P. 131, 74001-970 Goiânia, GO, Brazil*
[c]*Núcleo de Estatística Aplicada, Instituto de Matemática e Estatística, Universidade Federal de Goiás, C.P. 131, 74001-970 Goiânia, GO, Brazil*
[d]*Laboratório de Farmacognosia, Faculdade de Farmácia, Universidade Federal de Goiás, C.P. 131, 74605-050 Goiânia, GO, Brazil*

Received 2 October 2000; received in revised form 29 December 2000

Abstract

The essential oils of *Hyptis suaveolens* plants collected from 11 localities of the Brazilian Cerrado region were investigated by GC–MS. Sabinene, limonene, biclyclogermacrene, β-phellandrene and 1,8-cineole were the principal constituents. The results were submitted to principal component and chemometric cluster analysis which allowed three groups of essential oils to be distinguished with respect to the content of *p*-mentha-2,4(8)-diene, limonene/β-phellandrene/γ-terpinene and germacrene D/bicyclogermacrene. In patterns of geographic variation in essential oil composition indicated that the sesquiterpenes are mainly produced in the samples grown at lower latitudes. © 2001 Elsevier Science Ltd. All rights reserved.

Keywords: *Hyptis suaveolens*; Lamiaceae; Essential oils; Chemical variability; Multivariate analysis

1. Introduction

Hyptis Jacq., with well over 300 species, exhibits a major morphological diversity in the Brazilian Cerrado region (Harley, 1988). Its species are quite aromatic and are frequently used for the treatment of gastrointestinal infections, cramps, and pain, as well as in the treatment of skin infections (Corrêa, 1931). The aggressive annual weedy species, *Hyptis suaveolens* (L.) Poit. is distributed in the tropics and subtropics, and it is not commonly found over 500 m. The plant is normally restricted to places where soils have been profoundly disturbed, and may be considered as a ruderal species (Wulff, 1973). Some work dealing with the composition and antifungal (Pandey et al., 1982; Singh et al., 1992; Zollo-Amvam et al., 1998), antibacterial (Iwu et al., 1990; Asekun et al., 1999), and anticonvulsant (Akah and Nwambie, 1993) activities of *H. suaveolens* leaf oil have been previously reported: these plants were obtained from various origins (Brazil, India, Malaysia, Nigeria, USA, Aruba). Although relatively few samples have been analysed, it appears from reported data that leaf or aerial parts oils of *H. suaveolens* exhibited several compositions characterised by the occurrence, as major components, of β-caryophyllene (Malaysia and Nigeria), 1,8-cineole and sabinene (USA, India and Aruba), 1,8-cineole and β-pinene (Brazilian Amazonian and Brazilian Northeast) (Craveiro et al., 1981; Gottlieb et al., 1981; Luz et al., 1984; Din et al., 1988; Iwu et al., 1990; Mallavarapu et al., 1993; Ahmed et al., 1994; Singh and Upadhyay, 1994; Asekun and Ekundayo, 2000). As part of our ongoing work on the characterisation of essential oils of aromatic plants growing wild in the Brazilian Cerrado region (Costa et al., 2000), we now report on the results obtained for the essential oil composition and variability of *H. suaveolens*. For that purpose, 11 different sampling sites (Fig. 1) were chosen, and the qualitative and quantitative analysis of the volatile oil of a representative population sample of each was performed by GC–MS. To study the chemical variability, the chemical constituents from the essential oil of samples from each locality were submitted to principal component and chemometric cluster analysis, in order to detect dome pattern distribution of samples and to identify which

* Corresponding author. Tel.: 55-62-521-1008; fax: 55-62-521-1008.
E-mail address: pedro@quimica.ufg.br (P.H. Ferri).

0031-9422/01/$ - see front matter © 2001 Elsevier Science Ltd. All rights reserved.
PII: S0031-9422(01)00128-5

constituents can differentiate between the groups of individuals.

2. Results and discussion

The essential oil of *H. suaveolens* plants collected from the eleven different sampling sites of Brazilian Cerrado (Fig. 1) gave an average yield of 0.7% (wt/wt). In total, 40 compounds were identified, accounting for 91–97% of the volatile constituents. Monoterpene hydrocarbons were the main group of constituents in most of the populations (36.89–73.40%). Nevertheless, important differences in the amounts of the major constituents were found, mainly of sabinene (2.93–31.13%) which had the highest percentage in population D, *p*-mentha-2,4(8)-diene (0.19–20.87%) as the principal constituent of populations E and G, β-phellandrene (0.92–18.17%), limonene (3.60–17.56%), γ-terpinene (0.52–17.33%) as the major components of population C. Populations A and B had the highest percentage of 1,8-cineole (0–15.08%), and populations H, J and K had bicyclogermacrene (2.38–12.68%) as the main constituent. The results showed some important differences between the populations, indicating the existence of chemical polymorphism. Results obtained from nearest neighbour complete linkage cluster analysis using Ward's technique (Ward, 1963) and principal component analysis (PCA) showed the existence of a highly chemical variability within the essential oil *H. suaveolens* (Fig. 2). First principal component separates monoterpene hydrocarbons (mean content 71.01%, S.D. = 2.39; populations C and D) from sesquiterpene samples (20.70%, S.D. = 11.40; populations B, H and I–K), and the second principal component distinguishes the populations A, E, F and G for the content of *p*-mentha-2,4(8)-diene. In Fig. 2, the strong negative correlation between sesquiterpenes and monoterpene hydrocarbons is clear. Additionally, there is a correlation between essential oil composition and geographic variation (Table 1). Sesquiterpenes were mainly produced at lower latitudes, whereas monoterpenes at higher ones. Therefore, three main types of essential oils were found: Cluster I was characterised by a high percentage of *p*-mentha-2,4(8)-diene (11.73%, S.D. 8.4); Cluster II had limonene (15.19%, S.D. = 3.35), β-phellandrene (16.48%, S.D. = 2.39) and γ-terpinene (10.65%, S.D. = 9.45) as the major compounds; and Cluster III showed substantial percentages of germacrene D (6.54%, S.D. = 2.43) and bicyclogermacrene (11.49%, S.D. = 1.22). The chemical composition of the oils from USA (Ahmed et al., 1994), India (Mallavarapu et al., 1993), Aruba (Fun and Svendsen, 1990) and Brazilian Amazonian (Gottlieb et al., 1981) are closed to the composition determined for

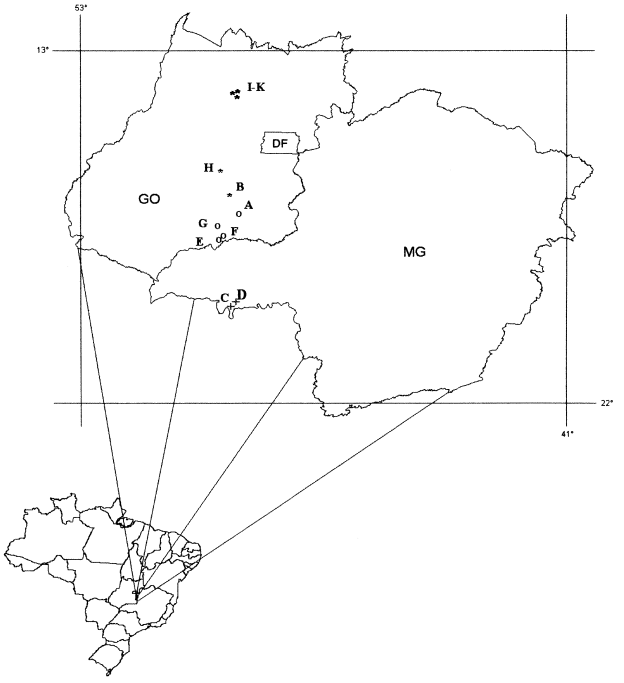

Fig. 1. Map of Brazilian Cerrado region showing the locations where *Hyptis suaveolens* plants were collected and to which cluster it belongs: I (○), II (+), and III (*). Goiás State (GO): (A) Caldas Novas (17° 41′ 26″ S/48° 42′ 23″ W), at an altitude of 763 m, 13 January 2000; (B) Piracanjuba (17° 13′ 56″ S/49° 4′ 40″ W), 734 m, 13 January 2000; (E) Itumbiara (18° 22′ 48″ S/49° 13′ 8″ W), 448 m, 29 January 2000; (F) Itumbiara (18° 22′ 30″ S/49° 13′ 12″ W), 448 m, 29 January 2000; (G) Goiatuba (18° 1′ 21″ S/49° 21′ 39″ W), 774 m, 14 January 2000; (H) Goiânia (16° 34′ 24″ S/49° 17′ 32″ W), 760 m, 15 January 2000; (I) Uruaçu (14° 30′ 32″ S/49° 7′ 22″ W), 524 m, 12 March 2000; (J) Uruaçu (14° 30′ 28″ S/49° 7′ 19″ W), 524 m, 12 March 2000; (K) Uruaçu (14° 30′ 35″ S/49° 7′ 27″ W), 523 m, 12 March 2000. Minas Gerais State (MG): (C) Frutal (20° 1′ 33″ S/48° 56′ 17″ W), 549 m, 29 January 2000; (D) Frutal (20° 1′ 27″ S/48° 56′ 14″ W), 549 m, 29 January 2000.

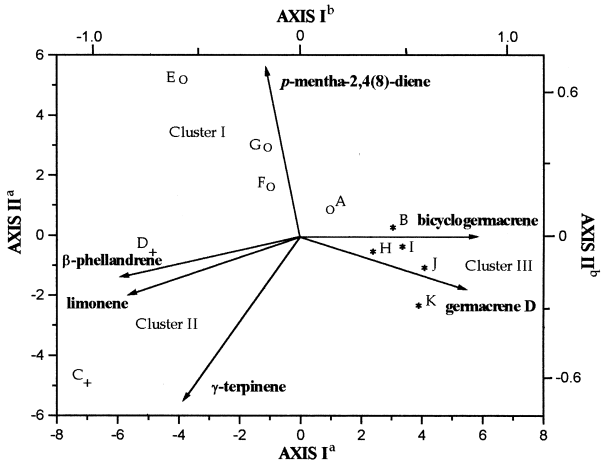

Fig. 2. Principal component analysis (PCA) ordination of *Hyptis suaveolens* plants collected from eleven populations (A-K) of Brazilian Cerrado. [a]Axes refer to the ordination scores obtained from the samples. [b]Axes refer to the ordination scores obtained for the discriminant oil components, which are represented as vectors from origin. Axis I[a] accounts for 38.5% of the total variance and Axes II[a] accounts for a further 17.6% of the total variance.

Table 1
Correlation coefficients between essential oil components and latitude (south) of sampling sites of *Hyptis suaveolens*[a]

Oil component	Latitude
Tricyclene	−0.84[b]
Myrcene	0.73
δ-2-Carene	0.86[b]
cis-*p*-Menth-2-en-1-ol	−0.61
Limonene	0.75[b]
β-Phellandrene	0.90[b]
β-Boubonene	−0.83[b]
β-Elemene	−0.93[b]
(E)-Caryophyllene	−0.69
cis-Thujopsene	0.64
Germacrene D	−0.89[b]
Bicyclogermacrene	−0.84[b]
Globulol	−0.77[b]
epi-α-Muurolol	−0.62
δ-Elemene	−0.82[b]

[a] All correlations have a significant level, $P < 0.05$ (Student's *t*-test).
[b] $P < 0.01$ (Student's *t*-test).

sample of cluster I. Otherwise, the content of the β-pinene in oil from Brazilian Amazonian is much higher than that of our samples. The chemical composition of Clusters II and III are original. The chemical variability presented in this paper corresponds well with the results from both polymorphism in seed germination and differential rate of growth in plantlets of *Hyptis suaveolens* (Wulff, 1973), which may be important factors in the colonising ability of this species.

3. Experimental

3.1. Plant material

H. suaveolens plants were collected at the vegetative stage in January and March 2000 and identified by two of the authors (I.F.P.C. and H.D.F.); 3–5 individuals, representing the local population, were collected from the each locality (Fig. 1). Voucher specimens of each sample are deposited in the Herbarium of the Universidade Federal de Goiás, Goiás State, Brazil. The aerial parts were air-dried at room temp. for 7 days. Then, the total plant material from each population was pulverized and submitted to hydrodistillation (6 h) using a Clevenger apparatus.

3.2. Analysis of essential oils

Oil samples analysis were performed on a GC–MS Shimadzu QP5050A instrument employing the following conditions: Column: CBP-5 (Shimadzu) fused silica capillary column (50 m long × 0.25 mm i.d. × 0.25 μm film thickness composed of 5% phenylmethylpolysiloxane) connected to an ion trap detector operating in EI mode at 70 eV; carrier gas: He (1 ml min^{-1}); injector and ion-source temperatures were 250°C and a split ratio of 1:5. Injection volume was 1 μl (20% in CH_2Cl_2) and the oven temperature was programmed from 60°C (isothermal for 2 min), with an increase of 3°C min^{-1}, to 240°C, then 10°C min^{-1} to 280°C, ending with a 10 min isothermal at 280°C. Individual components were identified by comparing their RR_t and mass spectra with those of the authentic samples, literature (Adams, 1995) and a computerized MS-data base using NIST libraries.

3.3. Chemical variability

Principal component analysis (PCA), using SPAD.N software package (Lebart et al., 1994), was applied to examine the interrelationships between different populations and its chemical constituents. Cluster analysis was also applied to the study of similarity of samples on the basis of constituent distribution. Nearest neighbour complete linkage technique by Benzécri algorithm (Benzécri, 1980) was used as an index of similarity and hierarchical clustering was performed according to the Wards variance minimising method (Ward, 1963).

Acknowledgements

We thank Dr. A.J. Marsaioli (IQ-Unicamp) for supplying the authentic samples. Thanks are also due to CNPq, PADCT III/QEQ (Grant No. 620166/97-5) and Fundação de Apoio à Pesquisa-FUNAPE/UFG for their financial support.

References

Adams, R.P., 1995. Identification of Essential Oil Components by Gas Chromatography/Mass Spectroscopy. Allured, Illinois.
Ahmed, M., Scora, R.W., Ting, I.P., 1994. Composition of leof oil of *Hyptis suaveolens* (L.) Poit. J. Essent. Oil Res. 6, 571–575.
Akah, P.A., Nwambie, A.I., 1993. Nigerian plants with anti-convulsant property. Fitoterapia 64, 42–44.
Asekun, O.T., Ekundayo, O., 2000. Essential oil constituents of *Hyptis suaveolens* (L.) Poit. (bush tea) leaves from Nigeria. J. Essent. Oil Res. 12, 227–230.
Asekun, O.T., Ekundayo, O., Adenivi, B.A., 1999. Antimicrobial activity of the essential oil of *Hyptis suaveolens* leaves. Fitoterapia 70, 440–442.
Benzécri, J.P., 1980. L'Analyse des Données: la Taxinomie, vol. 1. Dunod, Paris.
Corrêa, M.P., 1931. Dicionário das Plantas Úteis e das Exóticas Cultivadas. Imprensa Nacional, Rio de Janeiro.
Costa, R.T., Fernandes, O.F.L., Santos, S.C., Oliveira, C.M.A., Lião, L.M., Ferri, P.H., Paula, J.R., Ferreira, H.D., Sales, B.H.N., Silva, M. R. R., 2000. Antifungal activity of volative constituents of *Eugenia dysenterica* leaf oil. J. Ethnopharmacol. 72, 113–119.
Craveiro, A.A., Fernandes, A.G., Andrade, C.H.S., Matos, F.J.A., Alencar, J.W., Machado, M.I.L., 1981. Óleos Essenciais do Nordeste. Edições UFC, Fortaleza (68).

Din, L.B., Zakaria, Z., Sandudin, M.W., Brophy, J., Toia, R.F., 1988. Composition of the steam volatile oil from *Hyptis suaveolens*. Pertanika 11, 239–247.

Fun, C.E., Svendsen, A.B., 1990. The essential oil of *Hypis suaveolens* Poit. grown in Aruba. Flav. Frag. J. 5, 161–163.

Gottlieb, O.R., Koketsu, M., Magalhães, M.T., Maia, J.G.S., Mendes, P.H., Rocha, A.I., Silva, M.L., Wilberg, V.C., 1981. Essential oils of Amazonia. VII. Acta Amazonica 11, 143–148.

Harley, R.M., 1988. Revision of generic limits in *Hyptis* Jacq. and its allies. Bot. J. Linn. Soc. 98, 87–95.

Iwu, M.M., Ezeugwu, C.O., Okunji, C.O., Sanson, D.R., Tempesta, M.S., 1990. Antimicrobial activity and terpenoids of the essential oil of *Hyptis suaveolens*. Int. J. Crude Drug Res. 28, 73–76.

Lebart, L., Morineau, A., Lambert, T., Pleuvret, P., 1994. SAPD.N Versión 2.5. Sistema Compatible para el Análisis de Datos. Centre International de Statistique et d'Informatique Appliqueés, Saint Mandé, France.

Luz, A.I.R., Zoghbi, M.G.B., Ramos, L.S., Maia, J.G.S., Da Silva, M.L., 1984. Essential oils of some Amazonian Labiatae, 1. Genus *Hyptis*. J. Nat. Prod. 47, 745–747.

Mallavarapu, G.R., Ramesh, S., Kaul, P.N., Bhattacharya, A.K., Rao, B.R.R., 1993. The essential oil of *Hyptis suaveolens* (L.) Poit. J. Essent. Oil Res. 5, 321–323.

Pandey, D.K., Tripathi, N.N., Tripathi, R.D., Dixit, S.N., 1982. Fungitoxic and phytotoxic properties of the essential oil of *Hyptis suaveolens*. J. Plant Dis. Prot. 89, 344–349.

Singh, G., Upadhyay, R.K., 1994. Sesquiterpene alcohols from the essential oil of *Hyptis suaveolens*. Fitoterapia 65, 186–187.

Singh, G., Upadhyay, R.K., Rao, G.P., 1992. Fungitoxic activity of the volatile oil of *Hyptis suaveolens*. Fitoterapia 63, 462–465.

Ward, J.H., 1963. Hierarchical grouping to optimize an objective function. J. Am. Stat. Assoc. 58, 238–244.

Wulff, R., 1973. Intrapopulational variation in the germination of seeds in *Hyptis suaveolens*. Ecology 54, 646–649.

Zollo-Amvam, P.H., Biviti, L., Tchoumbougnang, F., Menut, C., Lamaty, G., Bouchet, P., 1998. Aromatic plants of tropical Central Africa. Part XXXII. Chemical composition and antifungal activity of thirteen essential oils from aromatic plants of Cameroon. Flav. Flag. J. 13, 107–114.

PERGAMON

Phytochemistry 57 (2001) 737–742

PHYTOCHEMISTRY

www.elsevier.com/locate/phytochem

3′,5′-Di-*C*-β-glucopyranosylphloretin, a flavonoid characteristic of the genus *Fortunella*

Kazunori Ogawa[a,*], Akemi Kawasaki[b], Mitsuo Omura[b], Toshio Yoshida[b], Yoshinori Ikoma[b], Masamichi Yano[b]

[a]*Okinawa Subtropical Station, Japan International Research Center for Agricultural Science, Ministry of Agriculture, Forestry, and Fishery, 1091-1, Maezato, Ishigaki, Okinawa 907-0002, Japan*

[b]*Department of Citriculture, National Institute of Fruit Tree Science, Ministry of Agriculture, Forestry, and Fishery, Okitsu, Shimizu, Shizuoka 424-0292, Japan*

Received 11 July 2000; received in revised form 20 December 2000

Abstract

Dihydrochalcone derivative, 3′,5′-di-*C*-β-glucopyranosylphloretin (**1**), is present in the genus *Fortunella*, (*F. crassifolia*, *F. japonica*, *F. margarita*, *F. polyandra* and *F. hindsii*). These species accumulate a large quantity of **1** in their fruits (peel, 6.5–15.2 mg/g in dry wt; juice sac, 1.5–10.5 mg/g) and in their leaves (21.3–60.2 mg/g). Twenty-seven Tanaka's *Citrus* species examined lack **1**, but *C. madurensis* and *C. halimii* contain **1** in large quantities in their peels (25.1 and 33.6 mg/g) and juice sacs (4.1 and 4.2 mg/g). *Poncirus* species do not contain **1**. *Fortunella*-citrus hybrids, the Orangequat [*C. unshiu*×*F. crassifolia*], the Thomasville citrangequat [*Fortunella* sp.×(*C. sinensis*×*Poncirus trifoliata*)], and seven hybrid progenies [*F. margarita*×*C. junos*], contain large amounts of **1** in their peels (17.0–7.9 mg/g) and juice sacs (2.0–9.9 mg/g). These facts suggest that accumulation of **1** is a generic trait of the genus *Fortunella* and that the inheritance of the trait among the intergeneric hybrids is controlled by a dominant allele. Thus *C. madurensis* and *C. halimii* are thought to originate from natural hybrids between the genera *Citrus* and *Fortunella*. Phloridzin, which has the same aglycon as **1**, was not detected in the citrus plants examined. © 2001 Elsevier Science Ltd. All rights reserved.

Keywords: *Fortunella*; *Citrus*; *Poncirus*; Rutaceae; Hybrid; Taxonomy; Dihydrochalcone; Flavonoid; 3′; 5′-Di-*C*-β-glucopyranosylphloretin

1. Introduction

The principal flavonoids of the genus *Citrus* are flavanone glycosides such as narirutin, naringin, hesperidin, and neohesperidin, and flavone aglycons such as nobiletin and tangeretin (Mizuno et al., 1991; Kanes et al., 1993; Tsuchida et al., 1997; Kawaii et al., 1999). The genus *Fortunella* is taxonomically close to the genus *Citrus*. Flavonoid compositions of *Fortunella* species, however, differ from those of *Citrus* species. While a flavanone glycoside, poncirin, has been reported, flavanones are thought to be minor constituents in plants of the *Fortunella* genus. A number of *C*-glycosylated flavones have also been identified in *F. japonica* and *F. crassifolia* (Kumamoto et al., 1985; Tsuchida et al., 1997), but quantities of flavonoids in *Fortunella* plants have been found to be rather low compared with plants of the *Citrus* genus (Kanes et al., 1993; Tsuchida et al., 1997). Our previous report demonstrated the presence and quantities of 24 flavonoid constituents in the edible portions of 66 citrus fruits (Kawaii et al., 1999). Narirutin was identified as a major constituent of plants of the *Fortunella* genus. As the result of reinvestigation, this "narirutin" is shown to be a new dihydrochalcone glucoside, 3′,5′-di-*C*-β-glucopyranosylphloretin (**1**), which was isolated from *F. margarita* as a major flavonoid. Also isolated were three flavone glycosides, 2′-*O*-α-L-rhamnopyranosylcytisoside (**2**), 2′-*O*-α-L-rhamnopyranosylisocytisoside (**3**), and acacetin 7-*O*-neohesperidoside (fortunellin, **4**), which had been isolated previously from plants of the *Fortunella* genus (Matsuno, 1958; Kumamoto et al., 1985). In this paper, we describe the structure determination of **1**. The distribution of major flavonoid species such as narirutin, naringin, hesperidin,

* Corresponding author. Tel.: +81-9808-2-2306; fax: +81-9808-2-0614.

E-mail address: kazunori@affrc.go.jp (K. Ogawa).

0031-9422/01/$ - see front matter © 2001 Elsevier Science Ltd. All rights reserved.
PII: S0031-9422(01)00132-7

and neohesperidin is applicable to the chemotaxonomy of the genus *Citrus*. Chemotaxonomy based on dihydrochalcones in citrus plants is a subject that has remained unexplored. We report the distribution and content of **1** and its related dihydrochalcone, phloridzin, in plants of the genus *Fortunella*, *Citrus*, and *Poncirus*, and moreover of the *Fortunella*-citrus hybrids. The generic relationship between the accumulation of **1** and citrus plants is discussed.

2. Results and discussion

The ^{1}H and ^{13}C NMR spectra of **1** indicated the presence of a *p*-substituted and a fully-substituted phenyl group. While the UV spectrum of **1** is similar to that of flavanones, ABX signals of H-2 and H_2-3 characteristic of flavanone were absent in the ^{1}H NMR spectrum of **1**. The presence of two methylene groups in **1** were indicated by ^{1}H (δ 3.34 and 2.85) and ^{13}C NMR signals (δ 47.8 and 31.0). These suggested that **1** had a dihydrochalcone skeleton. A partial structure of 3-(4-hydroxyphenyl)-1-propanone was deduced from the correlation of COSY, HMBC, and HMQC. The ^{13}C NMR special data indicated that the fully-substituted phenyl group consisted of three oxygenated carbons [δ 163.1 and 162.2 (2C)] and three carbons [δ 106.2 and 104.4 (2C)] having two adjacent oxygenated carbons. The presence of two pairs of equivalent carbons suggested that ring A had a symmetrical 2,4,6-trihydroxylphenyl structure. All of the NMR signals corresponding to hexapyranose moieties possessed double intensities; therefore, two equivalent hexapyranose moieties existed. The hexapyranose moieties were attached to the benzene ring in the manner of the *C*-glycosyl linkage because the anomeric carbon signals appeared at higher field (δ 76.7) compared with those of the *O*-glycosyl linkage. The fact that **1** resisted acid hydrolysis with 2 N HCl at 90°C for 3 h also indicated a *C*-glycosyl linkage. The HMBC correlation between anomeric protons and the carbons of ring A showed that the hexapyranose moieties were connected with C-3′ and C-5′. The ^{1}H NMR signals of the hexapyranose moieties at H-1, 2, 3 and 4 involve only axial-axial couplings ($J=8$ Hz). The manner of these couplings indicate that the hexapyranose moieties have a β-glucopyranose structure. The combined data suggested that the ring A had a symmetrical 2,4,6-trihydroxyl-3,5-di-*C*-β-glycopyranosylphenyl structure. Thus compound **1** was determined to be 3′,5′-di-*C*-β-glucopyranosylphloretin. Markham et al. (1976) reported phloretin-3′,5′-di-*C*-glycoside as a component of *Hymenophyton leptopodum* (Hepaticae). Its sugar structure was not determined. The spectral data described in their report are insufficient for discriminating between the two. We consider that the present paper is the first to describe and define **1**. Compounds **2**, **3**, and **4** were identified as 2′-*O*-α-L-rhamnopyranosylcytisoside (Kumamoto et al., 1985), 2′-*O*-α-L-rhamnopyranosyliso cytisoside (Kumamoto et al., 1985), and acacetin 7-*O*-neohesperioside (fortunellin) (Matsuno, 1958), respectively, as based on comparison of spectral data described in the literature and the results of hydrolysis.

Among the constituents isolated from *F. margarita* (Nagami kumquat), **1** is remarkable for the presence of the dihydrochalcone structure and for its high content. We have examined the distribution of **1** in other *Fortunella* plants. The genus *Fortunella* includes six species according to Tanaka's (1969) systematics. Five species except *F. obovata* (Changshou kumquat) were collected and analyzed as shown in Table 1. All of the *Fortunella* plants analyzed contained **1**. An HPLC profile of the peel of *F. margarita* is illustrated in Fig. 1. Compound **1** is actually a unique flavonoid glycoside, unlike more typical citrus flavanone glycosides such as narirutin, naringin, hesperidin, and neohesperidin. Tsuchida et al. (1997) reported the presence of an unidentified peak in the HPLC profile of the peel of *F. crassifolia* (Meiwa kumquat). The peak probably corresponds to **1**. The content of **1** in this fruit is as high as 6.5–15.2 mg/g (peels) in dry weight and 1.5–10.5 mg/g (juice sacs). It is notable that the leaves of the *Fortunella* species contained **1** in very large quantities (21.3–60.2 mg/g). In our previous report (Kawaii et al., 1999), we have consequently indicated the existence of narirutin instead of **1** in the edible portion of several *Fortunella species* and *C. madurensis* (Calamondin, see below) due to erroneous assignment.

Citrus species are rich sources of flavanone glycosides, but the presence of chalcones and dihydrochalcones, which are biosynthetic congeners of flavanones, is scarce in plants of the genus *Citrus*. We know of few species that contain chalcone or dihydrochalcone among the subfamily Aurantioideae: the root bark of *C. sinensis* (sweet orange) and *C. nobilis* (King mandarin) (Wu, 1989), the fruit of *Merrillia caloxylon* (Fraser and Lewis, 1974), and the apical stems and leaves of *Poncirus trifoliata* (trifoliate orange) and *C. jambhiri* (Rough lemon) (Bester and Rabe, 1996). Thus we assumed that the accumulation of **1** is a generic trait of the genus *Fortunella*, while the genera *Citrus* and *Poncirus* probably lack **1**. This was checked as mentioned below. Tanaka's systematics arranges 159 *Citrus* plants, which are divided into eight groups based upon a descriptive morphology (Tanaka, 1946, 1948, 1969 and 1980). Several species were selected from each group. Twenty-eight Tanaka's *Citrus* species and *C. halimii* were analyzed, as shown in Table 1. *C. halimii* is a recently described wild *Citrus* plant indigenous to peninsular Thailand and Malaya (Stone et al., 1973). Compound **1** was not detected in most *Citrus* species analyzed, with the exception of *C. madurensis* and *C. halimii*. These species accumulate a large quantity of **1** in their fruits. The contents of **1** in

Table 1
Distribution of 3′,5′-di-*C*-β-glucopyranosylphloretin in the peels, juice sacs, and leaves of various citrus plants[a]

Scientific name[b]	Common name	mg/g (dry wt) Peel	Juice sac	Leaf
Fortunella				
Protocitrus				
F. hindsii	Hong Kong wild kumquat	8.7	na[c]	27.8
Eufortunella				
F. crassifolia	Meiwa kumquat	6.5	2.6	60.2
F. japonica	Marumi kumquat	6.8	1.5	47.6
F. margarita	Nagami kumquat	15.2	4.6	46.1
F. polyandra	Malayan kumquat	10.1	10.5	21.3
Citrus				
Papeda				
C. hystrix	Purrut	nd[d]	nd	na
Limonellus				
C. latifolia	Tahiti lime	nd	nd	na
C. bergamia	Bergamot	nd	nd	na
Citrophorum				
C. medica	Citron	nd	nd	na
C. limon	Eureka lemon	nd	nd	na
C. limetta	Sweet lemon	nd	nd	na
Cephalocitrus				
C. grandis	Mato buntan	nd	nd	na
	Kao Pan	nd	nd	na
C. paradisi	Marsh grapefruit	nd	nd	na
C. hassaku	Hassaku	nd	nd	na
Aurantium				
C. natsudaidai	Natsudaidai	nd	nd	na
C. aurantium	Kabusu	nd	nd	na
C. sinensis	Valencia orange	nd	nd	na
C. iyo	Iyo	nd	nd	na
Osmocitrus				
C. ichangensis	Ichang papeda	nd	nd	na
C. junos	Yuzu	nd	nd	na
C. pseudo-aurantium	Henka mikan	nd	nd	na
C. wilsonii	Ichang lemon	nd	nd	na
C. sphaerocarpa	Kabosu	nd	nd	na
Acrumen				
C. nobilis	King mandarin	nd	nd	na
C. unshiu	Satsuma mandarin	nd	nd	na
C. reticulata	Ponkan	nd	nd	na
C. deliciosa	Mediterranean mandarin	nd	nd	na
C. succosa	Jimikan	nd	nd	na
C. suhuiensis	Shikaikan	nd	nd	na
C. tachibana	Tachibana	nd	nd	na
C. depressa	Shiikuwasha	nd	nd	na
Pseudofortunella				
C. madurensis	Calamondin	25.1	4.1	14.9
Other				
C. halimii		33.6	4.2	na
Poncirus				
P. trifoliata	Trifoliate orange	nd	nd	na

[a] Fruits specimens were collected in October 1998–February 1999 and in September–October 1999 (*C. ichangensis* and *C. halimii*); leaves in February–March 2000.
[b] The nomenclature of the plants is based mainly on Tanaka's systematics.
[c] na, Not analyzed.
[d] nd, Not detected.

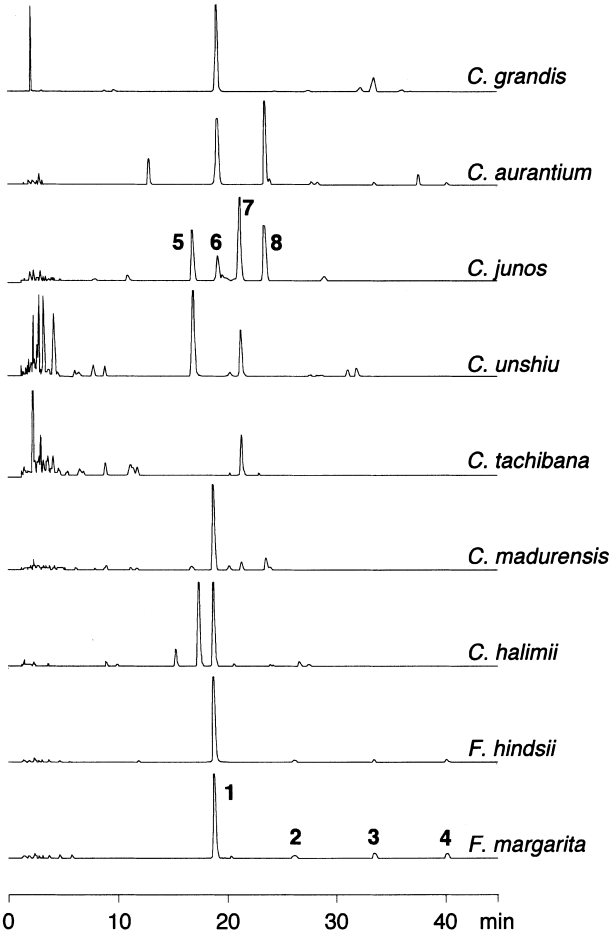

Fig. 1. HPLC profiles of the peels of some citrus plants. 1: 3′,5′-di-*C*-β-glucopyranosylphloretin; 2: 2′-*O*-α-L-rhamnopyranosylcytisoside; 3: 2′-*O*-α-L-rhamnopyranosylisocytisoside; 4: acacetin 7-*O*-neohesperioside; 5: nariruin; 6: naringin; 7: hesperidin; 8: neohesperidin.

the peels were 25.1 and 33.6 mg/g, respectively. *C. madurensis* contained the typical citrus flavanones in small quantities (Fig. 1), while *C. halimii* contained two unidentified constituents whose online-uv spectra suggested a flavone structure, instead of the typical citrus flavanones. The genus *Poncirus*, which consists of *P. trifoliata* alone, lacks **1**. Seasonal variation in the contents of **1** was not examined in the present study. The growth of the fruits generally decreases the flavonoid contents per fruit weight in *Citrus* fruits. Polymethoxylated flavones, tangeretin and heptametoxyflavone in the fruit of *C. aurantium* were seen to fall below undetectable quantities at the mature stage (Del Río et al., 1998). On the other hand, considerable amounts of flavanone diglycosides such as naringin and neohesperidin were maintained in the mature peels of several *Citrus* species (Tsuchida et al., 1996). The contents per fruit (*C. aurantium*) of naringin and neohesperidin were invariable after reaching their maximum levels (Castillo et al., 1993). These facts suggest that the diglycosides are end products of the flavonoid biosynthesis and their translo-

cation does not occur. We assume that seasonal variation in the contents of **1** is similar to that of the diglycosides. The fruits and leaves obtained from single trees growing in one area were used for the evaluation of the content of **1**. Tsuchida et al. (1996) reported that variations in the polymethoxylated flavone and coumarin contents in the fruit of *C. unshiu* (Satsuma mandarin) peels among trees growing in several individual areas were not larger than the variations among trees growing in one area. Thus we consider that constituents including **1** of citrus fruits are negligibly affected by the growing condition.

The *Citrus* species have undergone natural crossing for a long period (Hodgson, 1967). The genus *Citrus* comprises not only the true species but also many natural hybrids (Barret and Rhodes, 1976). Only *C. madurensis* belongs to the group Pseudofortunella according to Tanaka's systematics. Morphological and numerical taxonomic studies have suggested that *C. madurensis* probably originated from a natural hybrid between a *Fortunella* and a *Citrus species* (Swingle and Reece, 1967; Barret and Rhodes, 1976; Handa and Oogaki, 1985). The taxonomic position of *C. halimii* is uncertain, but this species has a leaf and fruit morphology intermediate between the genus *Fortunella* and the genus *Citrus* (Stone et al., 1973). A generic relationship deduced by analyses of isoenzymatic systems has indicated that *C. halimii* is located apart from the *Citrus* species and closer to the *Fortunella* species (Herrero et al., 1996). The accumulation of **1** in *C. madurensis* and *C. halimii* is reliable evidence that natural crosses between plants of the *Fortunella* genus and *Citrus* genus gave rise to these species.

A number of intergeneric crossbreedings between the genus *Fortunella* and related genera have been performed for the development of cold-hardy hybrids. The Orangequat and the Citrangequat are well-known hybrids that include *Fortunella* parentage. The Orangequat is a hybrid between *C. unshiu* (Satsuma mandarin) and *F. crassifolia*. Crossing between *F. margarita* and Willtis citrange, which is a hybrid of *C. sinensis* with *P. trifoliata,* yielded the Thomasville citrangequat. The fruit of the Orangequat contains a large amount of **1** (31.2 mg/g in peel and 2.0 mg/g in the juice sac), while the fruit of the Thomasville citrangequat also contains **1** in large quantities (47.9 mg/g in peel and 8.0 mg/g in juice sac). We have seven hybrid progenies produced by crossing *F. margarita* and *C. junos* (Yuzu). The fruits of these hybrid progenies showed morphologies between those of the *Fortunella* species and *C. junos*. The fruits of seven hybrids contain **1** in large quantities (peel, 17.0–28.7 mg/g; juice sac, 4.8–9.9 mg/g).

The above data indicated that the *Fortunella*-citrus hybrids certainly inherited accumulation of **1** from the *Fortunella* parent. Crossing *F. margarita* and *C. junos* has caused a unilateral accumulation of **1** in the resulting hybrids. The backcrossed hybrids do not exist, but there is a strong presumption that the accumulation of **1** in the intergeneric hybrids is controlled by a dominant allele, and that *Fortunella* species are probably homozygous for the allele. The biosynthesis of naringin has been established (Lewinsohn et al., 1989; McIntosh et al., 1990; Bar-Peled et al., 1991), while that of dihydrochalcone has not yet been clarified. Lewinsohn et al. (1989) showed that cell-free extract derived from the young fruit of*C. madurensis* possessed the capability to biosynthesize naringenin and 7-*O*-glucosylnarngenin, prunin, in the presence of the precursors, namely, *p*-coumaroyl-CoA, malonyl-CoA, and UDP-glucose. The fruit of *C. madurensis* accumulates small quantities of flavanone diglycosides such as hesperidin and neohesperidin (Kawaii et al., 1999) as shown in Fig. 1, while it did not contain naringenin. Flavanone biosynthesis occurs in the citrus plants involving the *Fortunella* parent. An immediate precursor of the aglycone of **1**, phloretin, is thought to be naringenin because phloretin is not synthesized during incubation. Phloretin 2′-*O*-glucoside, phloridzin, and **1** have a common aglycone. Bester and Rabe (1996) identified phloridzin in the leaves and stems of *P. trifoliata* and *C. jambhiri*. Our analysis did not detect its presence in the fruits and the leaves of citrus plants, regardless of whether or not they contained **1**. We assume that the *Fortunella* species possess a predominant flavonoid-biosynthetic pathway consisting of *C*-glucosylation of naringenin and the formation of phloretin and flavone structures occurring after the *C*-glucosylation, and that the true *Citrus* species lack the pathway.

Fortunella species and *Fortunella*-*Citrus* hybrids may be important plants for the elucidation of dihydrochalcone biosynthesis.

The fruits and leaves of *Fortunella* species have been used as the folk medicine in China (Jiangsu New Medical College, 1977). Phloridzin and its aglycone phloretin indicate biological and pharmacological activities; for example, they inhibit glucose transmembrane transport and tumor cell growth (Nelson and Falk, 1993). The activities of **1** have drawn a certain amount of interest. The dihydrochalcone glycosides, naringin dihydrochalcone and neohesperidin dihydrochalcone, have potential as sweetening agents (Borrego et al., 1995). The solution of **1** at a concentration of 10,000 ppm is tasteless.

3. Experimental

3.1. General

Narirutin, naringin, hesperidin, and neohesperidin were obtained from EXTRASYNTHESE (Funakoshi, Japan), and phloridzin from Sigma (St Louis, MO, USA). NMR spectra were recorded on a DPX400 spectrometer (Brüker, Japan). Mass spectra were measured

using an LC–MS apparatus (JMS 700, Jeol, Japan) equipped with FAB or APCI interfaces.

3.2. Isolation

Fresh fruits of *F. margarita* (225 g, harvested in December 1996) were extracted using EtOH at room temperature for a month. Concentrated ethanolic extract was partitioned between BuOH and water. The BuOH phase was concentrated, suspended in water, and subjected to HP-20 resin (Mitsubishi Kasei, Japan). The EtOH eluate (600 mg in dry weight) was applied to an ODS column (Tosoh ODS-Prep, 10 μm, 250 mm×22 mm i.d., Tosoh, Japan) using a MeOH–0.2%HOAc eluent (flow rate, 5.0 ml/min; gradient, 30–60% MeOH in 90 min) to afford **1** (220mg), **2** (21 mg), **3** (24 mg), and **4** (34 mg).

3.3. Identification

Compound **1**, 3′,5′-di-*C*-β-glucopyranosylphloretin. Yellow powder. $[\alpha]_D^{20}$ +83.6° (MeOH; *c* 1.0). UV λ_{max}^{MeOH} nm (log ε): 233 (4.3), 286 (4.1), 335 *sh*. Positive FABMS *m*/*z*: 599 $[M+H]^+$, 277, 249, 185. Negative FABMS *m*/*z*: 597 $[M-H]^-$, 183. Positive APCIMS (needle, 4.0 kV; orifice, 0 V; ring lens, 20 V) *m*/*z*: 599, 581, 569, 479, 461, 389, 359. IR ν_{max}^{KBr} cm^{-1}: 3350 (OH), 1620 (C=O). ^{13}C NMR (CD_3OD): phloretin moiety [δ 207.2 (C=O), 163.1 (C-4′), 162.2 (C-2′ and C-6′), 156.4 (C-4), 133.9 (C-1), 130.4 (C-2 and C-6), 116.1 (C-3 and C-5), 106.2 (C-1′), 104.4 (C-3′ and C-5′), 47.8 (C-α), 31.0 (C-β)]; glucose moiety [δ 82.7 (C-5), 79.1 (C-3), 76.7 (C-1), 74.2 (C-2), 71.1 (C-4), 61.9 (C-6)]×2. ^{13}C NMR (DMSO-d_6): phloretin moiety [δ 205.2, 161.2, 161.1, 155.4, 131.7, 129.3, 115.2×2, 104.7×2, 104.0, 46.2, 29.3]; glucose moiety [δ 81.1, 77.8, 74.7, 72.1, 69.2, 60.0]×2. ^1H NMR (CD_3OD): phloretin moiety [δ 7.03 (2H, *d*, *J*=8.4 Hz, H-2 and H-6), 6.75 (2H, *d*, *J*=8.4 Hz, H-3 and H-5), 3.34 (2H, *m*, H_2-α), 2.85 (2H, *m*, H_2-β)], glucose moiety [δ 4.94 (1H, *d*,*J*=9.8 Hz, H-1), 3.82 (2H, *ABX*, *J*=13, 4 and 2 Hz, H_2-6), 3.61 (1H, *dd*, *J*=8 and 8Hz, H-2), 3.54 (1H, *dd*, *J*=8 and 8Hz, H-4), 3.50 (1H, *dd*, *J*=8 and 8 Hz, H-3), 3.42 (1H, collapsed, H-5)]×2.

3.4. Plant material

Citrus plants, listed in Tables 1 and 2, were selected from germplasm reserved in the Department of Citriculture at the National Institute of Fruit Tree Science of Japan. Fruits in a mature or near mature stage were collected from each citrus tree in October 1998–Feburary 1999 (most of the species), in September–October 1999 (*C. ichangensis* and *C. halimii*), and in October 1999–January 2000 (Orangequat, Thomasville citrangequat, and *F. margarita–C. junos* hybrids). One-year leaves were collected from each citrus tree in February–March 2000. For all the fruit studied, the whole fruit was roughly cut. The samples were frozen at −80°C and freeze-dried. The fruits were divided into peel (epicarp and mesocarp), juice sacs, endocarp, and seeds. In this report, peel and juice sacs were analyzed. The samples were pulverized using a cutter and stored at −30°C for analysis.

3.5. Analytical procedure

Each Sample (1.000 g), which was a mixture of several fruits or leaves from single trees, was ground in MeOH–water (1:1, 15.0 ml) by using a mixer (Kinematica, Switzerland) for 3 min. The mixing generator was rinsed with MeOH–water (1:1) (5 ml×2). These solutions were combined and filtered through paper. The residue on the filter paper was washed with MeOH–water (1:1) (50 ml). The filtrate was concentrated, and then dissolved into MeOH-water (1:1), and adjusted to 5 ml in a volumetric flask. The HPLC analyses of **1** and phloridzin were carried out under the following conditions: column, YMC ODS M80 (4 μm, 150 mm×4.6 mm i.d.,

Table 2
Distribution of 3′,5′-di-*C*-β-glucopyranosylphloretin in the peels, juice sacs, and leaves of hybrids between *Fortunella* species and *Citrus* species[a]

Parents	Common name or tentative code	mg/g (dry wt)		
		Peel	Juice sac	Leaf
C. unshiu×*F. crassifolia*	Orangequat	31.2	2.0	46.5
Fortunella sp.×(*C. sinensis*×*Poncirus trifoliata*)	Thomasville citrangequat	47.9[b]	8.0	9.5
F. margarita×*C. junos*	NkY-A	20.2	9.1	na[c]
	NkY-B	20.6	8.5	na
	NkY-C	28.7	6.8	na
	NkY-D	24.9	9.9	na
	NkY-G	17.9	7.3	na
	NkY-6	17.0	5.6	na
	NkY-14	26.0	4.8	na

[a] Fruits were collected in October 1999–January 2000 and leaves in February–March 2000.
[b] S.D. = 16.4 (*n* = 3).
[c] na, Not analyzed.

YMC, Japan); injection volume, 5.0 μl; column temperature, 40°C; flow rate, 1.2 ml/min; elution schedule, an initial 5 min of 20% MeOH in 20 mM H_3PO_4 followed by a linear gradient with increasing concentration of MeOH from 20 to 45% in 45 min; detection, UV absorption at 286 nm. The purity of the authentic **1** was 97% as based on analysis by HPLC. The quantities of **1** were estimated using the absolute calibration method. The detection limit for determination of 1 using this procedure was 0.0002 mg/ml in sample solution. The peak for **1** was identified by its UV spectrum obtained by a diode-array detector. Since the chromatographic behavior, retention times, and UV spectrum of **1** are similar to those of the flavanone glycosides, the presence of **1** in *C. madurensis* and *C. halimii* was confirmed using an LC–MS equipped with an atmospheric pressure chemical ionization (APCI) interface. Statistical analyses of the quantitative values were not examined except in the Thomasville citrangequat (Table 2). Since each specimen was a mixture of several fruits or leaves, the quantities were practically considered to be the mean value.

References

Bar-Peled, M., Lewinsohn, E., Fluhr, R., Gressel, J., 1991. UDP-rhamnose: flavanone-7-*O*-glucoside-2″-*O*-rhamnosyltransferase: purification and characterization of an enzyme catalyzing the production of bitter compounds in citrus. J. Biol. Chem. 266, 20953–20959.

Barrett, H.C., Rhodes, A.M., 1976. A numerical taxonomic study of affinity relationships in cultivated Citrus and its close relations. Syst. Bot. 1, 105–136.

Bester, J.J., Rabe, E., 1996. Types and levels of phenolics in three citrus rootstocks of different vegetative vigour. J. S. Afr. Soc. Hort. Sci. 6, 75–77.

Borrego, F., Canales, I., Lindley, M.G., 1995. Neohesperidin dihydrochalcone: state of knowledge review. Z. Lebensm. Unters. Forsch. 200, 32–37.

Castillo, J., Benavente, O., Del Rio, J.A., 1993. Hesperetin 7-*O*-glucoside and prunin in *Citrus* species (*C. aurantium* and *C. paradisi*). A study of their quantitative distribution in immature fruits and as immediate precursors of neohesperidin and naringin in *C. aurantium*. J. Agric. Food Chem. 41, 1920–1924.

Del Río, J.A., Arcas, M.C., Benavente, O., Sabater, F., Ortuño, A., 1998. Changes of polymethoxylated flavones levels during development of *Citrus aurantium* (cv. Sevillano) fruits. Planta Med. 64, 575–576.

Fraser, A.W., Lewis, J.R., 1974. Flavonoids from *Merrillia caloxylon*. Phytochemistry 13, 1561–4564.

Handa, T., Oogaki, C., 1985. Numerical taxonomic study of *Citrus* L. and *Fortunella* Swingle using morphological characters. Application of multivariate analysis. J. Jap. Soc. Hort. Sci. 54, 145–154.

Herrero, R., Asins, M.J., Pina, J.A., Carbonell, E.A., 1996. Genetic diversity in the orange subfamily Aurantioideae. II. Genetic relationships among genera and species. Theor. Appl. Genet. 93, 1327–1334.

Hodgson, R.W., 1967. Horticultural varieties of citrus. In: Reuther, W., Webber, H.J., Batchelor, L.D. (Eds.), The Citrus Industry, Vol. I. Division of Agricultural Sciences. University of California Berkeley, California, pp. 431–592.

Jiangsu New Medical College, 1977. In: The Dictionary of Chinese Medicines. Shanghai Technologies Publisher, Shanghai.

Kanes, K., Tisserat, B., Berhow, M., Vandercook, C., 1993. Phenolic composition of various tissues of Rutaceae species. Phytochemistry 32, 967–974.

Kawaii, S., Tomono, Y., Katase, E., Ogawa, K., Yano, M., 1999. Quantitation of flavonoid constituents in *Citrus* fruits. J. Agric. Food Chem. 47, 3565–3571.

Kumamoto, H., Matsubara, Y., Iizuka, Y., Okamoto, K., Yokoi, K., 1985. Structure and hypotensive effect of flavonoid glycosides in kinkan (*Fortunella japonica*) peelings. Agric. Biol. Chem. 49, 2613–2618.

Lewinsohn, E., Britsch, L., Mazur, Y., Grssel, J., 1989. Flavone glycoside biosynthesis in *Citrus*. Chalcone synthase, UDP-glucose: flavone-7-*O*-glucosyl-transferase and -rhamnosyl-transferase activities in cell-free extracts. Plant Physiol. 91, 1323–328.

Markham, K.R., Porter, L.J., Campbell, E.O., Chopin, J., Bouillant, M.-L., 1976. Phytochemical support for the existence of two species in the genus *Hymenophyton*. Phytochemisry 15, 1517–1521.

Matsuno, T., 1958. Constituent of Cumquats: isolation of new flavone glycoside, fortunellin. Yakugaku Zasshi 78, 1311.

McIntosh, C.A., Latchinian, L., Mansell, R.L., 1990. Flavanone-specific 7-*O*-glucosyltransferase activity in *Citrus paradisi* seedlings: purification and characterization. Arch. Biochem. Biophys. 282, 50–57.

Mizuno, M., Iinuma, M., Ohara, M., Tanaka, T., Iwamasa, M., 1991. Chemotaxonomy of the genus *Citrus* based on polymethoxyflavones. Chem. Pharm. Bull. 39, 945–949.

Nelson, J.A.S., Falk, R.E., 1993. The efficacy of phloridzin and phloretin on tumor cell growth. Anticancer Res. 13, 2287–2292.

Stone, B.C., Lowry, J.B., Scora, R.W., Jong, K., 1973. Citrus halimii: A new species from Malaya and Peninsular Thailand. Biotropica 5, 102–110.

Swingle, W.T., Reece, P.C., 1967. The botany of citrus and its wild relatives. In: Reuther, W., Webber, H.J., Batchelor, L.D. (Eds.), The Citrus Industry, Vol. I. Division of Agricultural Sciences, University of California Berkeley, California, pp. 190–422.

Tanaka, T., 1946. Misunderstanding with regards citrus classification and nomenclature. Bulletin of the University of Osaka Prefecture Series B Agriculture and Biology 21, 139–145.

Tanaka, Y., 1946, 1948 and 1980. In: An Iconograph of Japanese Citrus Fruits, I, II and III. Yokendo, Tokyo.

Tsuchida, T., Yamamoto, T., Yamamoto, K., Hitomi, N., Kosaka, N., Shikano, E., Okada, M., Komatsu, K., Namba, T., 1996. Study on the botanical origins and the quality evaluation of crude drugs derived from *Citrus* and related genera (I). Chemical and anatomical changes of 5 *Citrus* peels along fruit ripening. Nat. Med. 50, 114–127.

Tsuchida, T., Yamamoto, T., Yamamoto, K., Hitomi, N., Kosaka, N., Okada, M., Komatsu, K., Namba, T., 1997. Study on the botanical origins and the quality evaluation of crude drugs derived from *Citrus* and related genera (III). Chemical constituents of peels of *Citrus*, *Fortunella* and *Poncirus*. Nat. Med. 51, 205–223.

Wu, T.-W., 1989. Flavonoids from root bark of *Citrus sinensis* and *C. nobilis*. Phytochemistry 28, 3558–3560.

PERGAMON

Phytochemistry 57 (2001) 743–747

PHYTOCHEMISTRY

www.elsevier.com/locate/phytochem

Antifungal polysulphides from *Petiveria alliacea* L.

Paulo José Coelho Benevides[a], Maria Claudia M. Young[b], Astréa M. Giesbrecht[a], Nídia F. Roque[a], Vanderlan da S. Bolzani[c,*]

[a]*Instituto de Química, Universidade de São Paulo, C.P. 26077, CEP 05599-970, SP, Brazil*
[b]*Departamento de Fisiologia e Bioquímica de Plantas, Instituto de Botânica, CP 4005, CEP 01161-970, São Paulo, SP, Brazil*
[c]*Instituto de Química, Universidade Estadual Paulista, C.P. 355, CEP 14800-900, Araraquara, SP, Brazil*

Received 27 October 2000; received in revised form 30 January 2001

Abstract

Bioactivity-directed fractionation of the CH_2Cl_2/MeOH (2:1, v/v) extract of the roots of *Petiveria alliacea,* using mutant yeast strains of *Saccharomyces cerevisiae* and fungi *Cladosporium cladosporioides* and *C. sphaerospermum* led to the isolation of dipropyl disulphide (**1**), dibenzyl sulphide (**2**), dibenzyl disulphide (**3**), dibenzyl trisulphide (**4**), dibenzyl tetrasulphide (**5**), benzylhydroxymethyl sulphide (**6**) and di(benzyltrithio) methane (**7**). Of these, **5**–**7** are new compounds and this is the first report of the natural occurrence of **2** and **3**. © 2001 Elsevier Science Ltd. All rights reserved.

Keywords: *Petiveria alliacea*; Phytolacaceae; Antifungal polysulphides

1. Introduction

Petiveria alliacea L. (Phytolacaceae) is a shrub widely distributed in South and Central America. It grows in all regions of Brazil where it is known by many popular names. Among these, ''erva-guiné'', ''guiné'', ''pipi'' and ''tipi''; and the Tupi-Guarani ''macuracaá'' are noteworthy (Hoehne, 1939; Pio Correa, 1969). In the State of Minas Gerais the roots of this plant are used to treat rheumatism (De Sousa et al., 1987) and in other Brazilian regions, both the roots and the leaves are popularly used as stimulants and abortefacients (Da Silva, 1935). Previous work on *P. alliacea* revealed the occurrence of coumarins, triterpenes and flavonoids (Rocha and Da Silva, 1969; Delle Monache and Suarez, 1992), amino acids and trisulphide (Adegosan, 1974). In continuing our search for biologically active compounds from the Brazilian flora (Carbonezi et al., 1999), a CH_2Cl_2/MeOH (2:1 v/v) extract of the roots of this plant was selected for phytochemical investigation due to its significant activity against some mutant yeast strains of *Saccharomyces cerevisiae* (Gunatilaka et al., 1994) and inhibition of the growth of *Cladosporium cladosporioides* and *C. sphaerospermum* (Homans and Fuchs, 1970). This study led to the isolation of five new polysulphides (**2**, **3**, **5**, **6** and **7**), together with two known compounds (**1**, **4**). Among the known compounds described in this study, only compound **4** had been previously isolated from this plant species (De Sousa et al., 1990).

2. Results and discussion

The CH_2Cl_2/MeOH (2:1) extract of roots of *P. alliacea* L. inhibited strains of *Saccharomyces cerevisiae* (RS 188N, RS 52YK and RS 321) indicating strong activity of this extract towards the mutant strains of yeast. This extract was also shown to possess potent inhibitory activity against *Cladosporium cladosporioides* and *Cladosporium sphaerospermum* fungi. Solvent–solvent partitioning of the bioactive crude extract afforded hexane, $CHCl_3$ and EtOAc fractions, in which the activities were concentrated. These fractions were individually subjected to silica gel column chromatography, using CH_2Cl_2 or CH_2Cl_2/MeOH as eluents, to obtain six major bioactive fractions. The purification of these fractions was performed on silica gel preparative TLC, reversed-phase Sep Pak cartridge and HPLC affording seven bioactive polysulphide compounds.

* Corresponding author. Tel.: +55-016-2016660; fax: +55-016-2227932.
E-mail address: bolzaniv@iq.unesp.br (V. da S. Bolzani).

0031-9422/01/$ - see front matter © 2001 Elsevier Science Ltd. All rights reserved.
PII: S0031-9422(01)00079-6

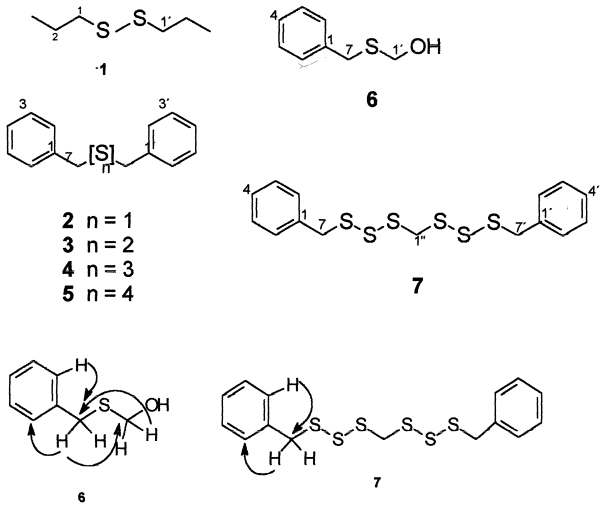

Fig. 1. Selected HMBC correlations for compounds **6** and **7**.

The molecular formula of compound **1** was determined as $C_6H_{14}S_2$, by ^1H, ^{13}C NMR, MS and elemental analysis. Three resonances at δ 2.66 *t* ($J=7.25$ Hz), δ 1.72 *dq* ($J=7.5$, 6.5) and 0.99 *t* ($J=7.26$ Hz) in the ^1H NMR spectrum were characteristic of a propyl moiety (Table 1). The ^{13}C NMR data also supported the propyl skeleton (Table 2). The proton resonance at δ 2.66, corresponding to a methylene group, was attributed to a sulfur-bearing carbon atom, which was confirmed by elemental analysis and interpretation of its mass spectrum. According to these data the structure of **1** was assigned as dipropyl disulphide, which is reported as a natural derivative in Phytolacaceae for the first time.

Compounds **2**–**5** exhibited common features in their MS, ^1H and ^{13}C NMR spectra. The presence of a significant ion peak at *m/z* 91, which is characteristic of a benzyl fragment was observed in all mass spectra of these compounds. The benzyl portion appeared to bear one, two, three and four sulfur atoms, respectively, based on the elemental analyses. The ^1H NMR spectra (Table 1) of **2**, **3**, **4** and **5** presented the same signal, around δ 7.30, compatible with a monosubstituted aromatic ring. The major differences observed in the ^1H NMR spectra of each compound was due to the chemical shift of the methylene benzylic hydrogens linked to the sulfur, which in compound **2** appeared at δ 3.66; **3** at δ 4.05; **4** at δ 4.15 (De Souza et al., 1990) and **5** at δ 4.19, respectively. The ^{13}C NMR spectral data (Table 2) of these compounds, interpreted with the aid of DEPT spectra, indicated the presence of one quaternary C and five CH's sp^2 carbons attributable to an aromatic monosubstituted ring and one sp^3 CH_2 assigned to a benzylic carbon. The elemental analysis and HRMS data of compounds **2**–**5** firmly established the number (and amount) of sulfur atoms in these polysulphides and confirmed their identities as dibenzyl sulphide (**2**), dibenzyl disulphide (**3**), dibenzyl trisulphide (**4**) and dibenzyl tetrasulphide (**5**),

Table 1
^1H NMR (300 MHz) spectral data for polysulphides **1**–**7**[a] ($CDCl_3$)

Position	1	2	3	5	6	7
1	2.66 *t* (7.5)	–	–	–	–	–
2	1.72 *dq* (7.5, 6.5)	7.30 *m*	7.32 *m*	7.30 *m*	7.30 *m*	7.33 *m*
3	0.99 *t* (6.5)	7.30 *m*	7.32 *m*	7.30 *m*	7.30 *m*	7.33 *m*
4	–	7.30 *m*	7.32 *m*	7.30 *m*	7.30 *m*	7.33 *m*
5	–	7.30 *m*	7.32 *m*	7.30 *m*	7.30 *m*	7.33 *m*
6	–	7.30 *m*	7.32 *m*	7.30 *m*	7.30 *m*	7.33 *m*
7	–	3.66 *s*	4.05 *s*	4.19 *s*	3.60 *s*	4.02 *s*
1′	2.66 *t* (7.5)	–	–	–	5.03 *s*	–
2′	1.72 *dq* (7.5, 6.5)	7.30 *m*	7.32 *m*	7.30 *m*	–	7.33 *m*
3′	0.99 *t* (6.5)	7.30 *m*	7.32 *m*	7.30 *m*	–	7.33 *m*
4′	–	7.30 *m*	7.32 *m*	7.30 *m*	–	7.33 *m*
5′	–	7.30 *m*	7.32 *m*	7.30 *m*	–	7.33 *m*
6′	–	7.30 *m*	7.32.	–	–	–
7′	–	3.66 *s*	4.05 *s*	4.19 *s*	–	4.02 *s*
1″	–	–	–	–	–	5.30 *s*

[a] ^1H chemical shifts based on COSY and HMQC experiments. The values are in ppm (δ) downfield from TMS. *J* values in Hertz in parentheses.

Table 2
^{13}C NMR spectral data for polysulphides **1**–**3**, **5**–**7**[a]

Carbon	1	2	3	5	6	7
1	41.08 *t*	137.38 *s*	136.52 *s*	136.71 *s*	136.00 *s*	136.55 *s*
2	22.42 *t*	127.82 *d*	127.80 *d*	127.22 *d*	127.82 *d*	127.57 *d*
3	13.01 *q*	128.73 *d*	128.73 *d*	128.76 *d*	128.73 *d*	128.62 *d*
4	–	129.56 *d*	129.56 *d*	129.56 *d*	129.51 *d*	129.44 *d*
5	–	128.73 *d*	128.73 *d*	128.73 *d*	128.73 *d*	128.62 *d*
6	–	127.82 *d*	127.80 *d*	127.80 *d*	127.82 *d*	127.57 *d*
7	–	43.38 *t*	43.15 *t*	44.27 *t*	44.32 *t*	43.19 *t*
1′	41.08 *t*	137.38 *s*	136.52 *s*	136.71 *s*	78.50 *t*	136.55 *s*
2′	22.42 *t*	127.82 *d*	127.80 *d*	127.22 *d*	–	127.57 *d*
3′	13.01 *q*	128.73 *d*	128.73 *d*	128.76 *d*	–	128.62 *d*
4′	–	129.56 *d*	129.56 *d*	129.56 *d*	–	129.44 *d*
5′	–	128.73 *d*	128.73 *d*	128.73 *d*	–	128.62 *d*
6′	–	127.82 *d*	127.80 *d*	127.80 *d*	–	127.57 *d*
7′	–	43.38 *t*	43.38 *t*	44.27 *t*	–	43.19 *t*
1″	–	–	–	–	–	106.32 *t*

[a] Spectra determined in $CDCl_3$; data reported in ppm (δ). Carbon type determined by DEPT.

respectively. Polysulphide **4** has previously been reported from this species (De Souza et al., 1990).

Compound **6**, isolated as an oil, gave IR absorption bands at 3335 (OH), 1580, and 1495 cm^{-1} (Ar). The EI MS showed a molecular ion peak $[M]^+$ at *m/z* 154 that together with ^{13}C NMR and elemental analysis established a molecular formula of $C_8H_{10}SO$. The ^1H and ^{13}C NMR spectra (Tables 1 and 2) of this compound resembled closely those of dibenzyl sulphide (**2**). Prominent differences in the ^1H and ^{13}C spectroscopic values between **2** and **6** were observed only in the aliphatic region; one extra methylene signal was observed at δ 5.03 *s* (δ 78.50, CH_2). These results allowed us to deduce that compound

6 had an hydroxymethyl group linked to the sulfur in place of the second benzylic group as in compound **2**. Interpretation of some HMBC data (Fig. 1) aided elucidation of this structure. Correlations observed between the methylene protons signal at δ 5.03 with the benzylic carbon at δ 44.27 and the methylene protons signal at δ 3.60 with the carbons at δ 78.50 and 127.42 established compound **6** as benzylhydroxymethyl monosulphide.

Polysulphide **7** is closely comparable with dibenzyl trisulphide (**4**); comparison of the ^{1}H and ^{13}C NMR spectra (Tables 1 and 2) data with those of **4** showed that the only differences observed were due to chemical shift of the benzylic hydrogens, which in **7** appeared at δ 4.20 ($\delta_C = 43.19$) and the presence of an additional singlet signal at δ 5.30, which was attributed to methylene protons by the analysis inferred by COSY, HMQC and DEPT spectral data. Analysis of ^{13}C NMR spectroscopic data recorded a methylene benzylic carbon at δ 43.19 and a second one, extremely unshielded at δ 106.32, whose chemical shift could be explained by the stereoeletronic effects of several sulfur atoms linked to methylene carbon. In fact, no correlations were observed in the spectra of the ^{1}H–^{1}H COSY and HMBC (Fig. 1) of the corresponding methylene protons with other protons or carbons, respectively in **7**. The elemental analysis, together with HRMS analysis established its molecular formula as $C_{15}H_{16}S_6$ and thus confirmed **7** to be di(benzyltrithio) methane.

Bioautography with the plant pathogenic fungi *C. cladosporioides* and *C. sphaerospermum* was employed to guide fractionation and isolation of the polysulphides **1**–**7**, these being responsible for the fungicidal activity detected in the crude extract (Table 3). Similar or higher to the reference compound Nystatin, the polysulphides **1**–**4** showed potent inhibition, while compounds **5**–**7** showed marginal activity against fungal growth (10.0 >25 and 5.0 μg, respectively), in both phytopathogenic strains tested. Furthermore, their potential anticancer activities were also tested, using a mechanism-based yeast bioassay for DNA-modifying agents (Gunatilaka et al., 1994). Compounds **1**, **3** and **5** had moderate effect on DNA, as deduced by the selective inhibition of the mutant strains RS 321 and RS 52YK, relative to the wild strain RS 188N (Table 3).

3. Experimental

3.1. Instrumentation

^{1}H NMR (300 MHz) spectra were recorded on a Bruker DPX-300 spectrometer, using TMS as an int. standard. The ^{13}C NMR (50 or 75 MHz) spectra were recorded on Bruker AC-200 and DPX-300 spectrometer. EI-MS were measured at 70 eV on a HP 5990/5988 A spectrometer and on a VG platform II spectrometer. Elemental analysis was performed on a Perkin-Elmer CHN Elemental Analyzer 2400. IR spectra were recorded on a FT-IR 1750 Perkin Elmer and FT-IR 510 Nicolet. UV spectra were recorded on a Perkin-Elmer UV/vis Hitachi U-3000.

3.2. Plant material

The species *Petiveria alliacea* L. was collected in September and October (1997) in the Instituto Butantã Reserve, in the city of São Paulo. Whole shrubs were collected and separated in their distinct parts: leaves, stems and roots. A voucher specimen was deposited in the Herbarium of the Instituto de Botânica-SMA, under the number SP112.6.84.

3.3. Biological testing

DNA-damaging assay with mutant yeast *S. cerevisiae*: Experimental screening methods utilizing mutant strains of *S. cerevisiae* have been described elsewhere (Gunatilaka et al., 1992). The IC_{12} values refer to the concentration in

Table 3
Bioactivity data of polysulphides **1**–**7** and three standards[a]

	Micro-organisms				
Compounds	RS 188N (rad +)	RS 321	RS 52YK (rad 52Y)	*Cladosporium sphaerospermum*	*Cladosporium cladosporioides*
1	389	68	11	0.1	1.0
2	402	381	412	1.0	1.0
3	332	66	16	0.1	1.0
4	73	64	62	1.0	1.0
5	328	53	104	10.0	10.0
6	67	58	76	>25	>25
7	76	58	67	5.0	5.0
Camptothecin	–	–	0.6	–	–
Streptonigrin	–	–	0.4	–	–
Nystatin	–	–	1.0	1.0	1.0

[a] Results are expressed as IC_{12} (RS 188N, RS 321, RS 322YK) (μg/ml) or MIC (*C. cladosporioides* and *C. sphaerospermum*) (μg) values.

μg/ml required to produce a inhibition zone of 12 mm in diameter around a 100 μl well during a 48 h incubation period at 30°C.

TLC bioautography assay: *Cladosporium cladosporioides* Fresen de Vries SPC 140 and *Cladosporium sphaerospermum* Penzig SPC 491 were maintained at the Instituto de Botânica-SMA. Ten microliters of the solutions of crude extracts, fractions and pure compounds were prepared, in different concentrations: corresponding to 20, 10, 1, 0.1 μg for pure compounds and 100, 50, 30 and 20 μg for the crude extracts or fractions, respectively. The samples were applied to TLC plates, these being eluted with the appropriate solvent system followed by complete removal of the solvent. The chromatographic plates were sprayed with spores suspension of *C. sphaerospermum* and *C. cladosporioides* in a nutritive medium and incubated for 48 h at 37°C. After incubation, clear inhibition zones appeared against a dark background chromatogram.

3.4. Extraction and isolation of constituents

Roots, stems, and leaves of *P. alliacea* L. were dried at room temperature, powdered and extracted three times with CH_2Cl_2:MeOH (2:1, v/v), for two days, at room temperature. The resulting extracts were filtered and concentrated in vacuo to yield 7.0, 8.0 and 15 g of root, stem and leaf extracts, respectively. Due to the higher bioactivity noted, half of the root extract was suspended in MeOH:H_2O (8:2) and successively extracted with hexane, chloroform, ethyl acetate and *n*-butanol. After liquid/liquid partition, the resulting residue was concentrated in vacuo and extracted with H_2O. Bioactivity-guided fractionation of the hexane, $CHCl_3$, and EtOAc solubles, using silica gel column chromatography and hexane, CH_2Cl_2, CH_2Cl_2:EtOAc and CH_2Cl_2:MeOH (with increasing polarity) as eluants, afforded several fractions, whose bioactivities were detected only in six of them. The first hexane fraction was applied to a Si gel column eluting with a hexane:CH_2Cl_2 gradient to afford compound **1** (22 mg). The fractions eluted with CH_2Cl_2:EtOAc were further subjected to silica gel column chromatography using a MeOH:H_2O gradient. The intermediary fractions of this column, purified by HPLC using a C-18 Econosil column, 5 mm, 250×4 mm i.d., with an elution gradient of MeOH:H_2O (70:30) 7 min; MeOH:H_2O (90:10) 15 min. and MeOH (100%) 20 min with flow rate of 1 ml/min yielded the compounds **2** (7.8 mg), **3** (4.5 mg), **4** (15.0 mg) and **5** (3.6 mg). The EtOAc soluble fraction, was subjected to Si gel column chromatography using CH_2Cl_2:EtOAc with increasing polarity. The fractions obtained with CH_2Cl_2: EtOAc (7:3) afforded **6** (3.8 mg). Compound **7** (2.0 mg) was isolated from the hexane fraction, by further purification over column chromatography on Si gel eluted with CH_2Cl_2:EtOAc (8:2).

3.4.1. Dipropyl disulphide (*1*)

Colorless volatile oil with a strong odour of garlic. $C_6H_{14}S_2$ requires 47.95% C, 9.39% H, 42.66% S; found 47.80% C, 9.40% H, 42.15% S. ^{1}H NMR (300 MHz, $CDCl_3$) and ^{13}C NMR (50 MHz, $CDCl_3$) (Tables 1 and 2). IR ν_{max}^{film} cm^{-1}: 2872, 1450, 1375, 720. MS *m*/*z* (rel. int.): $[M]^+$; 150(38),$[M+2]^+$ 152(2), 149(100), 108(36), 73 (37), 74(12).

3.4.2. Dibenzyl sulphide (*2*)

Yellow oil. $C_{14}H_{14}S$ requires 78.46% C, 6.58% H, 14.96% S; found 78.28% C, 6.56% H, 15.01% S. ^{1}H NMR (300 MHz, $CDCl_3$) and ^{13}C NMR (50 MHz, $CDCl_3$) (Tables 1 and 2). UV λ_{max}^{MeOH} nm (ε): 220 (8400), 265 (450). IR ν_{max}^{film} cm^{-1}: 3085, 3060, 3030, 2930, 1600, 1495, 1455, 712. MS *m*/*z* (rel. int.): $[M]^+$ 214(78), $[M+2]^+$ 216(1), 137(57), 124(100), 91(56), 78(33), 77 (28), 65(41).

3.4.3. Dibenzyl disulphide (*3*)

Yellow amorphous solid. $C_{14}H_{14}S_2$ requires 68.25% C, 5.73% H, 26.02% S; found 68.30% C, 5.61% H, 25.89% S. ^{1}H NMR (300 MHz, $CDCl_3$) and ^{13}C NMR (50 MHz, $CDCl_3$) (Tables 1 and 2). UV λ_{max}^{MeOH} nm (ε): 239 (9200), 279 (340). IR ν_{max}^{film} cm^{-1}: 3080, 3060, 3019, 3008, 1604, 1503, 1460, 700. MS *m*/*z* (rel. int.): $[M]^+$ 246(63), $[M+2]^+$ 248(3), 170(47), 156(100), 124(48), 91 (57), 78(45), 77(31), 65(29).

3.4.4. Dibenzyl trisulphide (*4*)

Yellow amorphous solid. $C_{14}H_{14}S_3$ requires 60.39% C, 5.07% H, 34.54% S; found 60.29% C, 4.94% H, 34.40% S. ^{1}H NMR (300 MHz, $CDCl_3$) and ^{13}C NMR (50 MHz, $CDCl_3$) (Tables 1 and 2). UV λ_{max}^{MeOH} nm (ε): 215 (9800), 260(320). IR ν_{max}^{film} cm^{-1}: 3076, 3025, 2988, 1598, 1489, 1456, 722. MS *m*/*z* (rel. int.): $[M]^+$ 278(71), $[M+2]^+$ 280(2), 202(56), 188(100), 124(32), 91(63), 78 (40), 77(27), 65(32).

3.4.5. Dibenzyl tetrasulphide (*5*)

Orange amorphous solid. $C_{14}H_{14}S_4$ requires 54.16% C, 4.54% H, 41.30% S; found 53.98% C, 4.53% H, 41.2% S. ^{1}H NMR (300 MHz, $CDCl_3$) and ^{13}C NMR (50 MHz, $CDCl_3$) (Tables 1 and 2). UV λ_{max}^{MeOH} nm (ε): 235 (11100), 256 (530). IR ν_{max}^{film} cm^{-1}: 3076, 3029, 2930, 1610, 1504, 1458, 719. MS *m*/*z* (rel. int.): $[M]^+$ 310(69), $[M+2]^+$ 312(1), 234(12), 220(100), 188(45), 156(29), 124 (19), 91(54), 78(33), 77(19), 65(28).

3.4.6. Benzyl hydroxymethyl sulphide (*6*)

Colorless oil. $C_8H_{10}OS$ requires 62.33% C, 6.49% H, 10.39% O, 20.77% S; found 63.12% C, 6.30% H, 10.12% O, 19.89% S. ^{1}H NMR (300 MHz, $CDCl_3$) and ^{13}C NMR (50 MHz, $CDCl_3$) (Tables 1 and 2). UV λ_{max}^{MeOH} nm (ε): 198 (13100), 264 (489). IR ν_{max}^{film} cm^{-1}: 3335, 3050, 1580, 1495, 1468, 1227, 757, 721. MS *m*/*z*

(rel. int.): 177(49)$[M+Na]^+$, $[M+2]^+$ 156(3), 137(71), 124 (100), 91(57), 78(12), 77(21), 65(33), 31(48).

3.4.7. Di(benzyltrithio) methane (7)

Orange amorphous solid. $C_{15}H_{16}S_6$ requires 46.36% C 4.15% H, 49.49% S; found 46.10% C, 4.09% H, 49.50% S. ^{1}H NMR (300MHz, $CDCl_3$) and ^{13}C NMR (50 MHz, $CDCl_3$) (Tables 1 and 2). UV λ_{max}^{MeOH} nm (ε): 238 (7200), 276 (240). IR ν_{max}^{film} cm^{-1}: 3079, 3057, 3007, 1585, 1498, 1456, 731, 708. MS *m/z* (rel. int.): $[M]^+$ 388(29), $[M+2]^+$ 390(2), 202(71), 188(100), 124(45), 91 (61), 78(35), 77(26), 65(29).

Acknowledgements

This work was funded by grants from BIOTA-FAPESP (Proc. # 98/05074-0). The authors are grateful to FAPESP for a PhD fellowship to Mr. Benevides and to CNPq for research fellowships (Drs. Bolzani and Young).

References

Adesogan, E.K., 1974. A trithiolaniacin, novel trithiolan from *Petiveria alliacea*. J.C.S. Chemical Communication, 906–907.

Carbonezi, C.A., Young, M.C.M., Lopes, M.N., Martins, D., Bolzani, V. da S., 1999. Iridoids from *Chioccoca alba* (Rubiaceae). Phytochemistry 51, 781–785.

Da Silva, R.A., 1935. Pipi (Plantas Medicinais do Brasil). Revista Flora Medicinal 9, 477–486.

De Sousa, J.R., Demuner, A.J., Pedersoli, J.L., Afonso, A.M.M., 1987. Guiné: Erva Medicinal ou Tóxica. Ciência and Cultura 39 (7), 645–646.

De Sousa, J.R., Demuner, A.J., Pinheiro, J.A., Breitmaier, E., Cassels, B.K., 1990. Dibenzyl trisulphide and *trans*-*N*-methyl-4-methoxyproline from *Petiveria alliacea*. Phytochemistry 29 (11), 3653–3655.

Delle Monache, F., Suarez, L.E.C., 1992. 6-C-Formyl and 6-C-hydroxymethyl flavanones from *Petiveria alliacea*. Phytochemistry 31 (7), 2481–2482.

Gunatilaka, A.A.L., Samaranayake, G., Kingston, D.G.I., Hoffmann, G., Johnson, R.K., 1992. Three bioactive 3β,5α-dihydroxyergost-5-enes from *Pseudobersama mossambicensis*. Journal of Natural Products 5, 1548–1554.

Gunatilaka, A.A.L., Kingston, D.G.I., Johnson, R.K., 1994. Mechanism-based isolation and structures of some anticancer active natural products. Pure and Applied Chemistry 66 (10/11), 2219–2222.

Hoehne, F. C., 1939. Plantas e Substâncias Vegetais Tóxicas e Medicinais. Departamento de Botânica do Estado de São Paulo, Graphicars Ed., São Paulo.

Homans, A.L., Fuchs, A., 1970. A direct bioautography on thin layer chromatograms as a method for detecting fungitoxic substances. Journal of Chromatography 51, 325–328.

Pio Correa, M., 1969. Dicionário das Plantas Úteis do Brasil e das Exóticas Cultivadas, Ministério da Agricultura, Rio de Janeiro.

Rocha, A.B., Da Silva, J.B., 1969. Análise cromatografica em camada delgada de alguns princípios ativos de *Petiveria alliaceae*. Revista de Farmacia e Odontologia Araraquara 3, 65–68.

PERGAMON

Phytochemistry 57 (2001) 749–758

PHYTOCHEMISTRY

www.elsevier.com/locate/phytochem

Endogenous gibberellins in immature seeds of *Prunus persica* L.: identification of GA_{118}, GA_{119}, GA_{120}, GA_{121}, GA_{122} and GA_{126}

Masayoshi Nakayama[a], Masaji Koshioka[a,*], Hiroyuki Matsui[b], Hitoshi Ohara[b], Lewis N. Mander[c], Sarah K. Leitch[c], Bruce Twitchin[c], Petra Kraft-Klaunzer[c], Richard P. Pharis[d], Takao Yokota[e]

[a]*Department of Genetics and Physiology, National Institute of Floricultural Science, 2-1 Fujimoto, Tsukuba, Ibaraki 305-8519, Japan*
[b]*Faculty of Horticulture, Chiba University, Chiba 271-8510, Japan*
[c]*Research School of Chemistry, Australian National University, Canberra, A.C.T. 0200, Australia*
[d]*Department of Biological Sciences, University of Calgary, Calgary, Alberta, T2N 1N4 Canada*
[e]*Department of Biosciences, Teikyo University, Utsunomiya 320-8551, Japan*

Received in revised form 12 January 2001

Abstract

The endogenous gibberellins in immature seeds of *Prunus persica* were analyzed by gas chromatography–mass spectrometry. Eleven known gibberellins, GA_3, GA_9, GA_{17}, GA_{19}, GA_{30}, GA_{44}, GA_{61}, GA_{63}, GA_{87}, GA_{95} and GA_{97} were identified. Additionally, several hitherto unknown gibberellins were detected and their putative structures were verified by synthesis of the authentic gibberellins. These gibberellins were then assigned trivial numbers, e.g. 1α-hydroxy GA_{20} (GA_{118}), 1α-hydroxy GA_9 (GA_{119}), 1,2-didehydro GA_9 (GA_{120}), 1,2-didehydro GA_{70} (GA_{121}), 1,2-didehydro GA_{69} (GA_{122}) and 1,2-didehydro GA_{77} (GA_{126}). GA_{118} and GA_{119} were the first 1α-hydroxy gibberellins identified from higher plants. The above profile of 1,2-didehydro gibberellins suggests that 1,2-dehydrogenation might occur prior to 3β-hydroxylation in biosynthesis of GA_3, GA_{30} and GA_{87} in immature seeds of *P. persica*. © 2001 Elsevier Science Ltd. All rights reserved.

Keywords: *Prunus persica*; Rosaceae; Peach; Immature seeds; Identification of gibberellins; GA_{118}; GA_{119}; GA_{120}; GA_{121}; GA_{122}; GA_{126}

1. Introduction

Gibberellins possessing a 1,2- double bond as well as a 3β-hydroxyl group, such as GA_3 (**1**) and GA_7 (**2**), exhibit high biological activity in many bioassay systems (Reeve and Crozier, 1974). The metabolic conversion of GA_5 (**14**) into GA_3 (**1**) has been shown in many plant systems, e.g. seedlings of *Zea mays* (Fujioka et al., 1990), cell suspensions cultures of *Prunus persica* (Koshioka et al., 1988), cell-free systems from seeds of *Marah macrocarpus* (Albone et al., 1990; MacMillan et al., 1997) and anthers of *Oryza sativa* (Kobayashi et al., 1991). Thus, GA_3 (**1**) in higher plants is currently thought to be biosynthesized from GA_5 (**14**) by 3β-hydroxylation which is accompanied by a rearrangement of the 2,3-double bond to the 1,2-location (Fujioka et al., 1990). Furthermore it has been shown that GA_7 (**2**) is formed in a similar manner from 2,3-didehydro GA_9 (**15**) in *M. macrocarpus* (Albone et al., 1990; MacMillan et al., 1997).

While investigating the presence of endogenous gibberellins in immature seeds of *Prunus cerasus*, we noted the co-occurrence of GA_3 (**1**) and GA_{95} (1,2-didehydro GA_{20}) (**5**); however, GA_5 (**14**) could not be detected (Nakayama et al., 1996). This led us to speculate that GA_{95} (**5**) could be the direct precursor of GA_3 (**1**) by 3β-hydroxylation without an A-ring double bond rearrangement. Additionally, GA_{30} (**3**) and GA_{87} (**4**), A-ring analogues of GA_3 (**1**) that possess both a 1,2-double bond and a 3β-hydroxyl group, were identified in immature seeds of *P. cerasus* (Nakayama et al., 1996). Hence GA_{30} (**3**) and GA_{87} (**4**) could also be biosynthesized from A-ring analogues of GA_{95} (**5**) by 3β-

* Corresponding author Tel.: +81-298-38-6811; fax: +81-298-38-6841.
E-mail address: masaji@nivot.affrc.go.jp (M. Koshioka).

0031-9422/01/$ - see front matter © 2001 Elsevier Science Ltd. All rights reserved.
PII: S0031-9422(01)00154-6

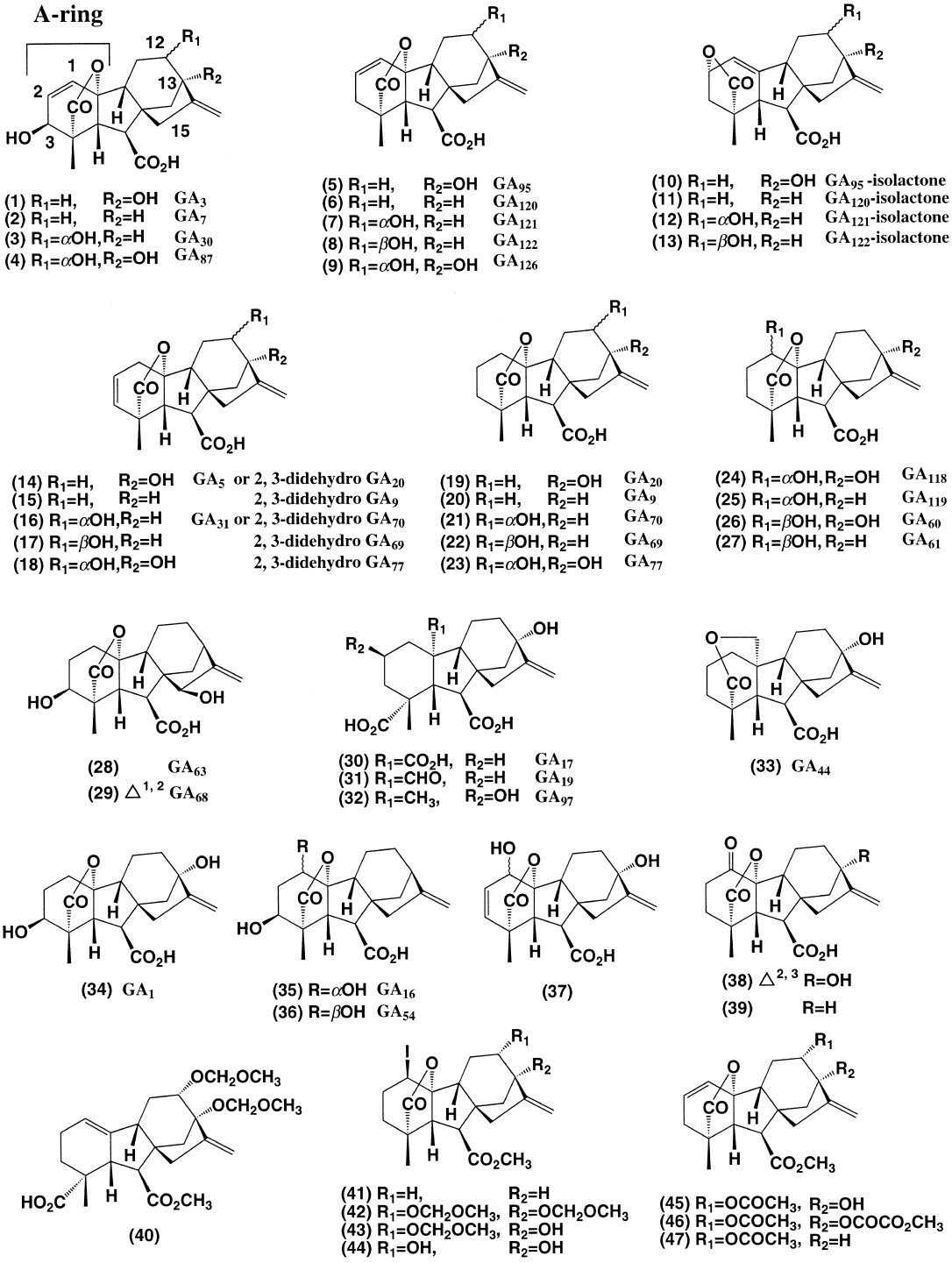

Fig. 1. Gibberellin structures.

hydroxylation without the double bond rearrangement in this plant tissue.

We analyzed the endogenous gibberellins in immature seeds of *P. persica*, with special emphasis on identifying potential precursors of GA_3 (**1**). Herein we report the co-occurrence of GA_3 (**1**) and GA_{95} (**5**) and their A-ring analogues in immature seeds of *P. persica*.

2. Results and discussion

The acidic EtOAc fraction of an extract from immature seeds of *P. persica* was analyzed by GC–MS. Based on comparisons of mass spectra and Kovats retention indices (KRIs) with methyl ester trimethylsilyl ether derivatives of authentic compounds, GA_3 (**1**), GA_9 (**20**),

GA_{17} (**30**), GA_{19} (**31**), GA_{30} (**3**), GA_{44} (**33**), GA_{63} (**28**), GA_{68} (**29**), GA_{87} (**4**), GA_{95} (**5**) and GA_{97} (**32**) were identified as endogenous gibberellins (Table 1). GA_{95} (**5**) had been found in immature seeds of *P. cerasus* (Nakayama et al, 1996). Its presence also in *P. persica* suggests that GA_{95} (**5**) may occur in a wide range of *Prunus* spp.

Several unknown gibberellin-like compounds were also detected. Mass spectra and KRIs of methyl ester trimethylsilyl ether derivatives of compounds **24** and **25** were respectively coincided with those of trimethylsilyl ether derivatives of 1α-hydroxy GA_{20} methyl ester and 1α-hydroxy GA_9 methyl ester, which had been already prepared (Tables 1 and 2). The authentic sample of compound **24** was synthesized by oxidation of the epimeric mixture of 1-hydroxy GA_5 methyl esters (**37**) obtained from the solvolysis of methyl gibberellate 3-methanesulfonate (Duri and Hanson, 1984), followed by reduction of the resulting enone of compound **38** with potassium tri-*sec*-butyl borohydride (Fortunato and Ganem, 1976) to remove the A-ring double bond and reduce the carbonyl function at C-1. An authentic sample of compound **25** was more readily obtained by oxidation of the carbinol group in GA_{61} (**27**) methyl ester (Kirkwood and MacMillan, 1982) followed by borohydride reduction. In both cases, reduction of the 1-oxo function gave the 1α-epimer as the major product.

Mass spectra of the methyl ester trimethylsilyl ether derivatives of the four remaining gibberellin-like compounds indicated that they might be either 1,2-didehydro derivatives (**6**–**9**) or 2,3-didehydro derivatives (**15**–**18**) of GA_9 (**20**), GA_{69} (**22**), GA_{70} (**21**) and GA_{77} (**23**).

Table 1
GC–MS data for endogenous gibberellins found in immature seeds of *Prunus persica*[a]

HPLC R_t (min)	Gibberellins	KRI	Characteristic ions m/z (rel. int.)
9–12	GA_{118}	2689	506 ($[M]^+$, 41), 491 (5), 459 (3), 451 (2), 447 (3), 375 (100), 235 (5), 207 (15), 194 (9), 167 (6)
11–12	GA_{87}	2853	592 ($[M]^+$, 84), 577 (6), 560 (15), 548 (14), 533 (15), 502 (81), 489 (100), 476 (26), 458 (17), 443 (17), 429 (40), 368 (27), 355 (31), 309 (47)
14–15	GA_{30}	2763	504 ($[M]^+$, 9), 472 (4), 444 (6), 414 (23), 382 (28), 369 (46), 355 (15), 310 (23), 279 (44), 221 (100), 193 (73), 179 (40)
	GA_{97}	2699	536 ($[M]^+$, 12), 504 (6), 477 (8), 446 (2), 417 (2), 387 (7), 371 (7), 327 (11), 297 (5), 251 (8), 239 (41), 207 (100)
17–18	GA_{126}	2659	504 ($[M]^+$, 72), 489 (8), 472 (14), 460 (6), 445 (10), 414 (57), 401 (100), 388 (26), 369 (22), 355 (30), 341 (26), 297 (20), 283 (18), 238 (46)
17–19	GA_3	2695	504 ($[M]^+$, 100), 489 (8), 475 (17), 460 (8), 445 (19), 431 (12), 387 (14), 370 (19), 355 (14), 341 (12), 311 (17), 297 (19), 221 (20), 208 (35)
21–24	GA_{95}-isolactone	2515	416 ($[M]^+$, 100), 401 (14), 387 (38), 371 (11), 357 (38), 343 (36), 313 (12), 311 (13), 298 (19), 238 (50), 207 (23), 193 (21)
21–22	GA_{121}	2563	416 ($[M]^+$, 15), 384 (17), 396 (11), 356 (19), 326 (28), 294 (63), 281 (32), 266 (41), 249 (40), 240 (66), 221 (100), 195 (46), 181 (44)
24–26	GA_{95}	2501[b]	416 ($[M]^+$, 100), 401 (12), 387 (24), 372 (15), 357 (34), 343 (25), 313 (11), 299 (60), 238 (26), 208 (31), 193 (31)
24–28	GA_{119}	2537	418 ($[M]^+$, 47), 403 (9), 386 (12), 371 (49), 359 (100), 347 (21), 327 (11), 300 (20), 296 (27), 274 (12), 241 (16), 223 (24), 185 (31)
27–28	GA_{122}	2524	416 ($[M]^+$, 29), 401 (10), 356 (14), 326 (14), 311 (12), 294 (62), 281 (32), 266 (38), 240 (42), 221 (100), 195 (61), 181 (52)
	GA_{122}-isolactone	2582	416 ($[M]^+$, 37), 384 (15), 356 (11), 326 (32), 311 (17), 294 (83), 282 (21), 266 (29), 240 (34), 221 (100), 195 (53), 181 (41)
27–29	GA_{44}	2791	432 ($[M]^+$, 27), 417 (2), 373 (16), 345 (4), 238 (28), 207 (100), 193 (11), 180 (18)
28–29	GA_{19}	2605	462 ($[M]^+$, 9), 434 (95), 402 (61), 374 (100), 359 (19), 345 (42), 315 (33), 285 (47), 258 (63), 239 (53), 208 (60), 207 (62), 193 (56)
	GA_{68}	2694	504 ($[M]^+$, 38), 489 (42), 444 (22), 414 (22), 382 (60), 370 (57), 355 (51), 310 (37), 280 (100), 221 (96), 193 (47), 156 (92)
29–30	GA_{63}	2713	506 ($[M]^+$, 100), 491 (41), 446 (57), 416 (18), 384 (29), 372 (20), 357 (13), 356 (29), 313 (15), 287 (44), 282 (57), 223 (59)
29–31	GA_{17}	2585	492 ($[M]^+$, 21), 460 (10), 432 (25), 401 (14), 373 (23), 313 (10), 293 (7), 280 (6), 251 (18), 208 (100), 207 (73), 193 (26)
33–36	GA_{120}	2331 2371[c]	328 ($[M]^+$, 11), 296 (62), 284 (100), 268 (49), 255 (16), 241 (29), 225 (85), 223 (86), 209 (60), 195 (34), 181 (75), 167 (39), 155 (63)
	GA_{120}-isolactone	2378 2428[c]	328 ($[M]^+$, 16), 296 (32), 284 (13), 282 (12), 268 (37), 255 (8), 253 (10), 223 (100), 209 (13), 195 (20), 181 (30), 167 (15), 155 (25)
36–37	GA_9	2332	330 ($[M]^+$, 12), 298 (90), 286 (0), 270 (100), 243 (67), 226 (42), 217 (29), 211 (26), 159 (37)

[a] In text, GA_9, GA_{120} and GA_{120}-isolactone were analyzed as methyl ester derivatives. All other gibberellins were analyzed as methyl ester and trimethylsilyl ether derivatives. HPLC R_ts were measured for non-derivatized gibberellins.
[b] The Kovat retention indices (KRI) was obtained with Program 2, otherwise Program 1 was used.
[c] The KRI was obtained by using an HP-5 column, otherwise a DB-1 column was used.

Table 2
GC–MS data for authentic gibberellins[a]

Gibberellins	KRI	Characteristic ions m/z (rel. int.)
GA_{118} (1α-hydroxy GA_{20})	2690	506 ([M]$^+$, 38), 491 (4), 459 (3), 451 (3), 447 (4), 375 (100), 235 (4), 207 (13), 194 (9), 167 (5)
GA_{119} (1α-hydroxy GA_9)	2538	418 ([M]$^+$, 35), 403 (8), 386 (7), 371 (41), 359 (100), 347 (20), 327 (13), 300 (18), 296 (24), 274 (17), 241 (25), 223 (29), 185 (47)
GA_{120}	2331	328 ([M]$^+$, 10), 296 (63), 284 (83), 268 (51), 255 (17), 241 (27), 225 (100),
(1,2-didehydro GA_9)	2371[b]	223 (94), 209 (66), 195 (43), 181 (90), 167 (44), 155 (67)
GA_{120}-isolactone	2378	328 ([M]$^+$, 13), 296 (32), 284 (15), 282 (12), 268 (37), 255 (10), 253 (10),
	2427[b]	223 (100), 209 (15), 195 (22), 181 (36), 167 (16), 155 (27)
2,3-Didehydro GA_9	2330	328 ([M]$^+$, 0), 297 (7), 284 (32), 269 (5), 252 (10), 224 (100), 209 (35),
	2368[b]	195 (19), 181 (39), 166 (31), 156 (35)
GA_{121}	2561	416 ([M]$^+$, 12), 384 (13), 369 (9), 356 (8), 326 (24), 294 (51), 281 (25),
(1,2-didehydro GA_{70})		266 (28), 249 (28), 240 (42), 221 (100), 195 (38), 181 (48)
GA_{121}-isolactone	2541	416 ([M]$^+$, 41), 384 (15), 369 (11), 356 (17), 326 (43), 294 (83), 281 (35), 266 (37), 249 (40), 240 (39), 221 (100), 195 (56), 181 (50)
GA_{31}	2557	416 ([M]$^+$, 3), 385 (5), 369 (8), 326 (5), 294 (15), 282 (30), 266 (27), 249 (16),
(2,3-didehydro GA_{70})		222 (100), 207 (35), 193 (42)
GA_{122}	2524	416 ([M]$^+$, 37), 401 (9), 356 (11), 326 (33), 311 (14), 294 (76), 281 (25),
(1,2-didehydro GA_{69})		266 (31), 240 (41), 221 (100), 195 (44), 181 (41)
GA_{122}-isolactone	2582	416 ([M]$^+$, 49), 384 (17), 356 (14), 326 (36), 311 (16), 294 (78), 282 (16), 266 (37), 240 (36), 221 (100), 195 (48), 181 (39)
2,3-Didehydro GA_{69}	2508	416 ([M]$^+$, 7), 401 (17), 384 (10), 369 (11), 326 (11), 294 (24), 282 (42), 266 (38), 249 (18), 222 (100), 207 (29), 193 (37), 181 (30)
GA_{126}	2659	504 ([M]$^+$, 69), 489 (7), 472 (9), 460 (8), 445 (10), 414 (45), 401 (100),
(1,2-didehydro GA_{77})		388 (28), 369 (18), 355 (60), 341 (22), 297 (16), 283 (17), 238 (40)
2,3-Didehydro GA_{77}	2641	504 ([M]$^+$, 44), 460 (14), 445 (7), 414 (45), 401 (100), 388 (25), 355 (17), 341 (8), 297 (18)

[a] In text, GA_{120}, GA_{120}-isolactone and 2,3-didehydro GA_9 were analyzed as methyl ester derivatives. All other gibberellins were analyzed as methyl ester and trimethylsilyl ether derivatives.
[b] The KRI was obtained by using an HP-5 column, otherwise a DB-1 was used.

The 2,3-didehydro derivatives (**15**–**18**) had been already synthesized and were available to use as authentic samples (Willis, 1987; Chu and Mander, 1988). 1,2-Didehydro GA_9 (**6**) methyl ester was prepared by elimination of the 1β-iodo group of compound **41** by 1,8-diazabicyclo[5.4.0]undec-7-ene (Furber et al., 1995). The remaining putative structures were assembled from compound **40**, a key intermediate in the preparation of several 12-hydroxy C_{20} gibberellins (Mander and Owen, 1997). Compound **40** was converted into iodolactone (**42**) and the methoxymethyl protecting groups at C-12 and C-13 were removed to afford compound **44**. The iodide of compound **44** was eliminated with 1,8-diazabicyclo[5.4.0]undec-7-ene to afford compound **9** methyl ester. The more reactive 12-hydroxyl group of compound **9** methyl ester was masked by acetylation and 13-methyloxalate (**46**) was prepared. After treatment with tributyltin hydride (Dolan and MacMillan, 1985), careful hydrolysis afforded compound **7** methyl ester. The 12-epimer of compound **7** methyl ester, namely compound **8** methyl ester, was prepared in an analogous manner, details of which have been published elsewhere (Leitch, 2000). Using GC–MS analysis we identified these unknown gibberellin-like compounds as 1,2-didehydro GA_9 (**6**), 1,2-didehydro GA_{70} (**7**) 1,2-didehydro GA_{69} (**8**) and 1,2-didehydro GA_{77} (**9**), respectively (Tables 1 and 2). Novel gibberellins detected in this study were assigned as the trivial numbers GA_{118} (**24**), GA_{119} (**25**), GA_{120} (**6**), GA_{121} (**7**), GA_{122} (**8**) and GA_{126} (**9**) according to convention (MacMillan and Takahashi, 1968; for allocation of GA_{117}, see Wynne et al., 1998; and allocation of GA_{123}, GA_{124} and GA_{125}, see Blake et al., 2000).

Methyl esters of GA_{120}-isolactone (**11**), GA_{121}-isolactone (**12**) and GA_{122}-isolactone (**13**) were synthesized by treatment with tetrakis-(triphenylphosphine)-palladium(0) (Serebryakov, 1980) and used as authentic samples in GC–MS analysis. Thus, GA_{95}-isolactone (**10**), GA_{120}-isolactone (**11**), and GA_{122}-isolactone (**13**) were also identified from immature seeds of *P. persica* (Tables 1 and 2). Because GA_{120} (**6**) could not be isomerized under our purification conditions (data not shown), we conclude that GA_{120}-isolactone (**11**) is a naturally occurring gibberellin in these tissues. GA_{95} (**5**) and GA_{122} (**8**) were easily converted to the isolactone form under our purification conditions (data not shown). So far it could not be determined whether GA_{95}-isolactones (**10**) and GA_{122}-isolactone (**13**) are naturally occurring gibberellins in *P. persica*.

Approximate quantitative levels of the identified gibberellins were estimated based on the total ion current areas over m/z 100 (as methyl ester or methyl ester trimethylsilyl ether derivatives) relative to a known amount of GA_1 (**34**) methyl ester trimethylsilyl ether derivative (Table 3). The most abundant gibberellin was

Table 3
Approximate amounts (ng/kg fw) of gibberellins present in immature seeds of *Prunus persica*. Estimates are based on total ion current peak areas obtained by GC–MS analysis, with a known amount of GA_1 as a quantitative standard

	1,2-Didehydro gibberellins				1α-Hydroxy gibberellins		Other gibberellins	
	Possessing 3β-hydroxyl group		Lacking 3β-hydroxyl group					
C_{19}-Gibberellins	GA_3	1550	GA_{95}	350	GA_{118}	400	GA_9	50
	GA_{30}	500	GA_{95}-isolactone	1700	GA_{119}	7950	GA_{63}	200
	GA_{68}	150	GA_{120}	350				
	GA_{87}	50	GA_{120}-isolactone	450				
			GA_{121}	150				
			GA_{122}	100				
			GA_{122}-isolactone	450				
			GA_{126}	200				
C_{20}-Gibberellins							GA_{17}	2250
							GA_{19}	350
							GA_{44}	1000
							GA_{97}	500

GA_{119} (**25**) followed by GA_{17} (**30**), GA_{95}-isolactone (**10**) and GA_3 (**1**).

While 1,2-didehydro derivatives of GA_9, GA_{20}, GA_{69}, GA_{70} and GA_{77} (**5**–**9**) were identified as endogenous gibberellins, their 2,3-didehydro derivatives (**14**–**18**) could not be detected. Because 2,3-didehydro GA_9 (**15**) methyl ester and GA_{120} (**6**) methyl ester could not be sufficiently separated to allow definitive identification using the DB-1 (100% dimethyl polysiloxane) column, we subjected these two gibberellins to HP-5 (5% diphenyl-95% dimethyl polysiloxane) column chromatography. This procedure allowed us to confirm the absence of 2,3-didehydro GA_9 (**15**) (Tables 1 and 2). Yamaguchi et al. (1975) first identified GA_5 (**14**) in immature seeds of *P. persica* by GC and MS. However we could not detect GA_5 (**14**) in the current collections of immature seeds of *P. persica*. Nor could we find endogenous GA_5 (**14**) in immature seeds of *P. cerasus* (Nakayama et al., 1996).

In immature seeds of *P. persica*, GA_3 (**1**), GA_{30} (**3**) and GA_{87} (**4**) were identified with their 3-deoxy derivatives, GA_{95} (**5**), GA_{121} (**7**) and GA_{126} (**9**). These co-occurrences suggest that 1,2-dehydrogenation might occur prior to 3β-hydroxylation in biosynthesis of GA_3 (**1**), GA_{30} (**3**) and GA_{87} (**4**) in this tissue. We are proceeding administering deuterated derivatives of the relevant gibberellins to the immature seed systems with a view to elucidating the speculative gibberellin biosynthetic pathways.

While several 1β-hydroxy gibberellins have been identified in higher plants, identification of 1α-hydroxy gibberellins in higher plants has not been reported. Once the detection of 1α-hydroxy gibberellin, GA_{16} (**35**), in *Secale cereale* had been reported by Dathe et al. (1978), but their reinvestigation elucidated the structure to be 1β-epimer, GA_{54} (**36**) (Dathe et al., 1989). Therefore GA_{118} (**24**) and GA_{119} (**25**) are the first 1α-hydroxy gibberellins identified from higher plants. The occurrence of GA_{118} (**24**) and GA_{119} (**25**) implies the presence of a 1α-hydroxylase in immature seeds of *P. persica*. Interestingly, GA_{61} (1β-hydroxy GA_9) (**27**) was found in *Ornithogalum thyrsoides* along with GA_7 (**2**), GA_9 (**20**) and GA_{120} (**6**) (Koshioka et al., 1999). It was shown in *Zea mays* that one enzyme can catalyze both 2,3-dehydrogenation and 3β-hydroxylation of gibberellins (Spray et al., 1996). The enzyme that catalyzes 1,2-dehydrogenation of gibberellins may also be multifunctional and catalyze 1-hydroxylation of gibberellins. Further research on these gibberellin biosynthetic enzymes would warrant this speculation.

3. Experimental

3.1. Extraction and isolation

Fruit of *Prunus persica* cv. Kansuke-hakutou growing at Chiba University, Japan, were collected 40 days after anthesis. After freezing on dry ice, the immature seeds (290 g fr. wt) were harvested and kept frozen at −80°C until extraction and analysis. The immature seeds were extracted once with MeOH, then twice with 80% aq. MeOH. The MeOH extracts were combined and reduced to the aq. phase in vacuo. The aq. residue was adjusted to pH 7.0 with 0.5 M K–Pi buffer (pH 7.3) and partitioned with EtOAc. The aq. fraction was then adjusted to pH 3.5 with 0.5 M K–Pi buffer (pH 2.3) and extracted with EtOAc, which was taken to dryness in vacuo. The acidic EtOAc soluble fraction was dissolved in 0.5 M K–Pi buffer (pH 3.5) and passed through a PVP column (25 g). The eluate was passed through an ODS column (6 g). The ODS column was washed with 0.1% HOAc and eluted with 80% aq. MeOH containing 0.1% HOAc. This later eluate was taken to dryness, then dissolved in

MeOH and loaded onto a Bondesil DEA column (8 g). This column was eluted with MeOH, followed by 0.5% HOAc in MeOH.

The later eluate was taken to dryness, then dissolved in 30% aq. MeOH containing 0.1% acetic acid and injected onto an Inertsil-2 ODS column (25×0.46 cm i.d.) in a Hewlett Packard 1100 HPLC system. Elution conditions were as follows: solvent, 0–2 min, 0% solvent A (MeOH containing 0.1% HOAc) in solvent B (30% aq. MeOH containing 0.1% HOAc); 2–42 min, 0–100% solvent A; 42–52 min, 100% solvent A; flow rate, 0.6 ml min^{-1}; column temp., 40°C; fractionation, every 1 min. The eluates were taken to dryness, methylated with ethereal diazomethane and then passed through a Bondesil NH_2 column for further purification.

3.2. GC–MS analysis

The methylated fraction from R_t 24 to 26 min was trimethylsilylated with *N*-methyl-*N*-(trimethylsilyl)-trifluoroacetamide at 60°C for 10 min. The other methylated fractions were trimethylsilylated at 80°C for 30 min. The derivatized samples were analyzed using a HP 5989B MS-system equipped with a HP 5890 GC-system fitted with a capillary column DB-1 (30 m×0.25 mm i.d., 0.25 μm film thickness), to which a retention gap column (5 m×0.25 mm i.d.) was attached. Ionization voltage was 70 eV. Helium carrier gas flow rate was 1 ml min^{-1} in the constant flow mode. Two column temp. programs were used. Program 1 was started at 60°C for 2 min, then raised to 210°C at 30°C min^{-1}, then raised to 280°C at 2°C min^{-1} and finally held at 280°C for 5 min. Temp. of the injection port, the separator, the ion source and the analyzer were 220, 280, 250 and 100°C, respectively. Program 2 was started at 60°C for 2 min, then raised to 225°C at 30°C min^{-1}, then raised to 280°C at 0.5°C min^{-1}, and finally held at 280°C for 5 min. Temp. of the injection port, the separator, the ion source and the analyzer were 180, 280, 250 and 100°C, respectively. HPLC fractions from R_t 33 to 36 min were analyzed also by a capillary column HP-5 (30 m×0.25 mm i.d., 0.25 μm film thickness) using the column temp. program 1, to which a retention gap column (5 m×0.25 mm i.d.) was attached.

3.3. Synthesis of methyl esters of novel gibberellins

3.3.1. GA_{118} (**24**) methyl ester

An epimeric mixture of 1-hydroxy GA_5 (**37**) methyl esters (300 mg), prepared by the procedure of Duri and Hanson (1984), was dissolved in CH_2Cl_2 (15 ml) and treated with pyridinium dichromate (1.0 g). After stirring overnight, Et_2O (15 ml) was added, the mixture was filtered through celite, solvent was removed and the residue was purified by flash chromatography on silica gel (EtOAc–pentane, 1:1). 1-Oxo-GA_5 (**38**) methyl ester (210 mg) was obtained as a white solid; ^1H NMR (300 MHz, $CDCl_3$): δ 1.36 (3H, *s*, H-18), 2.86 (1H, *d*, $J=10.4$ Hz, H-6), 3.42 (1H, *d*, $J=10.4$ Hz, H-5), 3.76 (3H, *s*, OCH_3), 4.98 (1H, *br s*, H-17) and 5.29 (1H, *t*, $J=2.5$ Hz, H-17′), 6.12 (1H, *d*, $J=9.5$ Hz, H-2), 6.99 (1H, *d*, $J=9.5$ Hz, H-3). A portion of this material (108 mg) dissolved in dry THF (2 ml) at −70°C was treated with potassium tri-*sec*-butylborohydride (1 M, 0.66 ml, 2.2 equivalent) and the mixture was stirred at −70°C for 30 min. EtOH (40 ml) was added and the mixture was stirred for 15 min, then potassium tri-*sec*-butylborohydride (0.9 ml) was added and stirring continued for 30 min at −70°C. The reaction vessel was transferred to an ice bath and 10% NaH_2PO_4 (0.5 ml) was added dropwise followed by the slow addition of H_2O_2 (100 vol) until gas evolution stopped. EtOAc (20 ml) was added and the mixture was washed with H_2O twice, brine, and dried Na_2SO_4. Removal of solvent in vacuo afforded a colorless gum (124 mg) and then flash chromatography on silica gel (EtOAc–pentane, 1:1 and 2:1) furnished GA_{60} (**26**) methyl ester (55 mg) followed by 1-*epi*-GA_{60} (GA_{118}) (**24**) methyl ester (40 mg) as an oil; ^1H NMR (300 MHz, $CDCl_3$): δ 1.05 (3H, *s*, H-18), 1.30–2.20 (11H, *m*), 2.4 (2H, *m*, 2×OH), 2.54 (1H, *d*, $J=10.5$ Hz, H-5), 2.71 (1H, *d*, $J=10.5$ Hz, H-6), 3.70 (3H, *s*, OCH_3), 3.72 (1H, *m*, H-1), 4.93 (1H, *s*, H-17), 5.24 (1H, *s*, H-17′); ^{13}C NMR (75 MHz, $CDCl_3$): δ 16.3 (C-18), 19.2 (C-11), 29.9 (C-3), 33.0 (C-2), 38.6 (C-12), 43.0 (C-14), 44.5 (C-15), 48.0 (C-4), 49.7 (C-8), 51.6 (C-6), 52.2 (OCH_3), 53.0 (C-9), 56.5 (C-5), 73.8 (C-1), 78.0 (C-13), 94.0 (C-10), 107.6 (C-17), 157.0 (C-16), 172.6 (C-7), 179.1 (C-19); EIMS *m*/*z* (rel. int.): 362 $[M]^+$ (76), 344 (5), 330 (25), 313 (29), 312 (85), 303 (100), 284 (16); HRMS *m*/*z*: Calc. for $[M]^+$ $C_{20}H_{26}O_6$: 362.1729; Found: 362.1731.

3.3.2. GA_{119} (**25**) methyl ester

To a soln. of GA_{61} (1β-hydroxy GA_9) (**27**) methyl ester (680.1 mg, 1.96 mmol) (Kirkwood and MacMillan, 1982) in CH_2Cl_2 (15 ml) was added Dess-Martin reagent (916 mg, 2.16 mmol) (Dess and Martin, 1983). The mixture was stirred overnight, followed by dilution with Et_2O (15 ml) and addition of 1 M NaOH soln. (20 ml), then stirred for a further 10 min. The organic layer was washed with 1 M NaOH soln. (20 ml), H_2O (20 ml), dried over $MgSO_4$, filtered, and the solvent was removed in vacuo. The crude material was applied to a silica gel column (EtOAc–petroleum ether, 1:4) to yield 1-oxo-GA_9 (**39**) methyl ester as a white foam (61%): R_f 0.40 (silica gel, EtOAc–petrol, 1:4); IR ν_{max} cm^{-1}: 2938, 1790, 1733, 1198; ^1H NMR (300 MHz, $CDCl_3$): δ 1.19 (3H, *s*, H-18), 1.42–1.90 (7H, *m*), 1.93–2.10 (3H, *m*), 2.44–2.74 (4H, *m*), 2.86 (1H, *d*, $J=10$ Hz, H-6), 2.91 (1H, *d*, $J=10$ Hz, H-5), 3.72 (3H, *s*, OCH_3), 4.86 (1H, *s*, H-17), 4.99 (1H, *s*, H-17′); ^{13}C NMR (75 MHz, $CDCl_3$): δ 16.2 (C-18), 16.3 (C-11), 31.2 (C-12), 33.8 (C-3), 35.1

(C-2), 36.9 (C-14), 38.5 (C-13), 44.1 (C-15), 46.6 (C-6), 48.1 (C-8), 51.1 (C-4), 52.2 (C-9 and OCH_3), 57.8 (C-5), 95.0 (C-10), 108.0 (C-17), 156.0 (C-16), 177.2 (C-7), 178.1 (C-19), 202.8 (C-1); EIMS *m/z* (rel. int.): 344 $[M]^+$ (75), 312 (34), 284 (100), 229 (34), 201 (36), 91 (51); HRMS *m/z*: Calc. for $[M]^+$ $C_{20}H_{24}O_5$: 344.1624; Found: 344.1630.

The above ketone (385.7 mg, 1.12 mmol) in EtOH (15 ml) was stirred at 0°C. Following the addition of $NaBH_4$ (850 mg, 22.5 mmol) the mixture was allowed to warm to room temp. and stirred for 15 min. H_2O was added dropwise to the solution followed by dilution with CH_2Cl_2 (20 ml). The aq. layer was extracted with CH_2Cl_2 (2×10 ml) and the combined organic extracts were dried over $MgSO_4$ and filtered, and solvent was removed in vacuo. The crude material was applied to a silica gel column (EtOAc–petroleum ether, 1:3) and appropriate fractions were combined to yield 1β-hydroxy GA_9 (GA_{61}) (**27**) methyl ester (19%) and 1α-hydroxy GA_9 (GA_{119}) (**25**) methyl ester (24%): mp 176-178°C; R_f 0.15 (silica gel, EtOAc–petroleum ether, 1:3); IR ν_{max} cm^{-1}: 3382, 1774, 1735, 1657, 1457, 1437, 1383, 1344, 1291, 1107; ^1H NMR (500 MHz, $CDCl_3$): δ1.05 (3H, *s*, H-18), 1.23–1.44 (2H, *m*), 1.52–1.58 (1H, *dt*, *J*=6,12 Hz, H-12), 1.62–1.73 (4H, *m*), 1.74–1.82 (2H, *m*), 1.93 (1H, *br s*, OH), 2.01–2.06 (3H, *m*), 2.15–2.20 (1H, *dt*, *J*=14.0, 6.2 Hz, H-11β), 2.53 (1H, *d*, *J*=11 Hz, H-5), 2.59 (1H, *br t*, *J*=8 Hz, H-13), 2.72 (1H, *d*, *J*=11, H-6), 3.69 (3H, *s*, OCH_3), 3.71–3.75 (1H, *m*, H-1β), 4.83 (1H, *s*, H-17), 4.96 (1H, *s*, H-17′); ^{13}C NMR (75 MHz, $CDCl_3$): δ 16.4 (C-18), 18.1 (C-11), 30.0 (C-2), 31.6 (C-12), 32.9 (C-3), 36.3 (C-14), 38.4 (C-13), 44.5 (C-15), 47.8 (C-8), 51.6 (C-6), 51.8 (C-4), 52.0 (OCH_3), 53.5 (C-9), 56.1 (C-5), 74.1 (C-1), 94.4 (C-10), 107.7 (C-17), 156.8 (C-16), 172.8 (C-7), 179.1 (C-19); EIMS, *m/z* (rel. int.): 346 $[M]^+$ (36), 314 (60), 286 (100), 91 (32); HRMS *m/z*: Calc. for $[M]^+$ $C_{20}H_{24}O_5$: 346.1780; Found: 346.1779.

3.3.3. GA_{120} (*6*) methyl ester

A soln. of 1β-iodo GA_9 methyl ester (**41**) (Furber et al, 1995) (100 mg, 0.219 mmol) in CH_2Cl_2 (1.0 ml) was treated with 1,8-diazabicyclo[5.4.0]undec-7-ene (0.45 ml) and the mixture heated under reflux for 6 h. CH_2Cl_2 was added, the soln. washed with 2 N HCl, then brine, and dried. Chromatography on silica gel (Et_2O–hexane, 1:4) afforded GA_{120} (**6**) methyl ester (71 mg, 99%), mp 160–162°C; IR ν_{max} cm^{-1}: 1770, 1740; ^1H NMR (300 MHz, $CDCl_3$): δ1.19 (3H, *s*, H-18), 1.22–1.40 (1H, *m*), 1.45–1.72 (4H, *m*), 1.47–1.86 (2H, *m*), 1.97–2.10 (2H, *m*), 2.25–2.30 (2H, *m*), 2.62-2.66 (1H, *m*, H-13), 2.66 (1H, *d*, *J*=10.9 Hz, H-6), 2.85 (1H, *d*, *J*=10.9 Hz, H-5), 3.64 (3H, *s*, OCH_3), 4.78 (1H, *br s*, H-17), 4.91 (1H, *br s*, H-17′), 5.78 (1H, *ddd*, $J_{1,2}$=9.3 Hz, $J_{2,3}$=3.3 Hz, $J_{2,3'}$=3.3 Hz, H-2), 6.10 (1H, *ddd*, $J_{1,2}$=9.3 Hz, $J_{1,3}$=2.2 Hz, $J_{1,3'}$=2.2 Hz, H-1); ^{13}C NMR (75 MHz, $CDCl_3$): δ 15.5 (C-11), 17.2 (C-18), 31.0 (C-12), 36.0 (C-14), 37.5 (C-3), 38.3 (C-13), 44.1 (15), 47.4 (C-4), 50.9 (C-6), 51.4 (C-9), 51.6 (OCH_3), 52.0 (C-8), 55.6 (C-5), 90.4 (C-10), 107.4 (C-17), 130.0, 130.6 (C-1, C-2), 156.8 (C-16), 173.1 (C-7), 179.8 (C-19); EIMS *m/z* (rel. int.): 328 $[M]^+$ (7), 297 (18), 296 (42), 285 (59), 268 (29), 225 (70), 224 (55), 209 (41), 183 (28), 181 (44), 156 (34), 155 (44), 143 (34), 141 (31), 129 (35), 128 (31), 115 (34), 105 (71), 93 (36), 91 (93), 81 (30), 79 (48), 77 (60), 65 (34), 55 (38), 53 (41), 51 (31), 41 (100); HRMS *m/z*: Calc. for $[M]^+$ $C_{20}H_{24}O_4$: 328.1675; Found: 328.1672.

3.3.4. GA_{126} (*9*) methyl ester

A soln. of compound **40** (Mander and Owen, 1997) (235.1 mg, 0.505 mmol) in THF (6 ml) and CH_2Cl_2 (6 ml) was treated with $NaHCO_3$ (5% aq. solution, 1 ml) followed by addition of iodine (102 mg, 0.81 mmol). The mixture was stirred overnight at room temp. Upon completion by TLC the reaction mixture was diluted with EtOAc (10 ml) and the entire soln. washed with satd. $Na_2S_2O_3$ soln. (10 ml). The organic layer was washed with brine, dried over dry $MgSO_4$, filtered and the solvent removed under reduced pressure. The crude material was applied to a silica gel column (EtOAc–petrol, 1:1 and 2:1) to afford the desired iodo lactone (**42**) (*ent*-12β, 13-bismethoxymethoxy-1α-iodogibberell-16-ene-7-oic acid 19, 10-lactone 7-methyl ester) (146.6 mg): R_f 0.8 (EtOAc–petrol, 1:1); ^1H NMR (300 MHz, $CDCl_3$): δ 1.08 (3H, *s*, H-18), 1.50–1.59 (1H, *dd*, *J*=13, 5 Hz, H-14), 1.82–2.28 (10H, *m*), 2.64 (1H, *d*, *J*=10 Hz, H-6), 3.30 (3H, *s*, $CH_2O\underline{CH_3}$), 3.34 (1H, *d*, *J*=8 Hz, H-5), 3.34 (3H, *s*, $CH_2O\underline{CH_3}$), 3.62 (1H, *t*, *J*=7 Hz, H-12), 3.71 (3H, *s*, $CO_2\underline{CH_3}$), 4.49 (1H, *d*, *J*=5 Hz, H-1), 4.56 (1H, *d*, *J*=7 Hz, $\underline{CH_2}OCH_3$), 4.63 (1H, *d*, *J*=7 Hz, $\underline{CH_2}OCH_3$), 4.68 (1H, *d*, *J*=7 Hz, $\underline{CH_2}OCH_3$), 4.86 (1H, *d*, *J*=7 Hz, $\underline{CH_2}OCH_3$), 5.17 (1H, *s*, H-17′), 5.19 (1H, *d*, *J*=2 Hz, H-17); ^{13}C NMR (75 MHz, $CDCl_3$): δ 16.8 (C-18), 25.8 (C-11), 27.2 (C-1), 30.8 (C-3), 31.6 (C-2), 37.0 (C-14), 43.2 (C-15), 47.3 (C-6), 49.3 (C-4), 50.9 (C-8), 52.0 (C-9), 54.9 ($CO_2\underline{CH_3}$), 55.1 (C-5), 55.2 [$(CH_2O\underline{CH_3})_2$], 79.5 (C-12), 84.9 (C-13), 91.9 ($\underline{CH_2}OCH_3$), 93.5 (C-10), 97.0 ($\underline{CH_2}OCH_3$), 111.5 (C-17), 150.7 (C-16), 172.3 ($\underline{CO_2}CH_3$), 177.9 (C-7); EIMS *m/z* (rel. int.): 576 $[M]^+$ (1), 531 (75), 327 (52), 283 (59), 195 (33), 149 (83), 129 (34), 91 (100); HRMS *m/z*: Calc. for $[M]^+$ $C_{24}H_{33}O_8I$: 576.1220; Found: 576.1224.

A soln. of iodo lactone (**42**) (146.6 mg, 0.254 mmol) in MeOH (10 ml) and H_2O (2 ml) containing Dowex resin (50W/H^+) was heated at reflux. After 16 h, TLC showed that all starting material had been consumed and two products were present. The reaction mixture was filtered through a plug of celite and diluted with EtOAc. The entire soln. was washed with KH_2PO_4 soln. (10%), brine, dried $MgSO_4$, filtered and the solvent removed in vacuo. The residue was applied to a silica

gel column (EtOAc–petrol, 1:1) to yield compound **43** (*ent*-13-hydroxy-1α-iodo-12β-methoxymethoxy-20-norgibberell-16-ene-7, 19-dioic acid 7-methyl ester 19, 10-lactone) (68.1 mg, 63%): R_f 0.75 (EtOAc–petrol, 2:1); IR $\nu_{max}cm^{-1}$: 3513, 2950, 1784, 1736; ^{1}H NMR (300 MHz, $CDCl_3$): δ 1.18 (3H, *s*, H-18), 1.57-1.59 (1H, *dd*, $J=14$, 5 Hz), 1.71–2.31 (12H, *m*), 2.63 (1H, *d*, $J=10$ Hz, H-6), 3.40 (3H, *s*, $CH_2O\underline{CH_3}$), 3.40 (1H, *d*, $J=8$ Hz, H-5), 3.50 (1H, *t*, $J=8$ Hz, H-12), 3.70 (3H, *s*, $CO_2\underline{CH_3}$), 4.50 (1H, *d*, $J=5$ Hz, H-1), 4.73 (2H, *s*, $\underline{CH_2}OCH_3$), 5.14 (1H, *s*, H-17′), 5.31 (1H, *d*, $J=2$ Hz, H-17); ^{13}C NMR (75 MHz, $CDCl_3$): δ 16.9 (C-18), 26.0 (C-11), 27.6 (C-1), 30.6 (C-3), 31.7 (C-2), 41.2 (C-14), 42.5 (C-15), 48.0 (C-8), 49.2 (C-6), 49.7 (C-4), 51.0 (C-9), 52.1 ($CO_2\underline{CH_3}$), 54.6 (C-5), 56.0 ($CH_2O\underline{CH_3}$), 77.8 (C-13), 81.1 (C-12), 93.7 (C-10), 96.8 ($\underline{CH_2}OCH_3$), 111.5 (C-17), 152.4 (C-16), 172.0 ($\underline{CO_2}CH_3$), 178.1 (C-7); EIMS *m*/*z* (rel. int.): 531 $[M]^+$ (6), 504 (48), 327 (52), 469 (34), 441 (33), 409 (44), 375 (40), 343 (82), 315 (56), 297 (36), 283 (100), 269 (48), 255 (59), 237 (60), 225 (38), 211 (62), 197 (49), 185 (36), 171 (40), 155 (40), 143 (50), 135 (44), 127 (60), 115 (45), 91 (69), 77 (53), 69 (42); HRMS *m*/*z*: Calc. for $[M]^+$ $C_{22}H_{29}O_7I$: 532.0958; Found: 532.0951, followed by compound **44** (*ent*-12β, 13-dihydroxy-1α-iodo-20-norgibberell-16-ene-7, 19-dioic acid 7-methyl ester 19, 10-lactone) (39.5 mg, 37%): R_f 0.6 (EtOAc–petrol, 2:1); IR $\nu_{max}cm^{-1}$: 3407, 2938, 1782, 1735; ^{1}H NMR (300 MHz, $CDCl_3$); δ 1.11 (3H, *s*, H-18), 1.57–2.37 (13H, *m*), 2.66 (1H, *d*, $J=10$ Hz, H-6),3.42 (1H, *d*, $J=10$ Hz, H-5), 3.63 (1H, *t*, $J=7$ Hz, H-12), 3.73 (3H, *s*, $CO_2\underline{CH_3}$), 4.52 (1H, *d*, $J=5$ Hz, H-1), 5.13 (1H, *s*, H-17′), 5.30 (1H, *d*, $J=2$ Hz, H-17); ^{13}C NMR (75 MHz, $CDCl_3$): δ 16.9 (C-18), 27.1 (C-11), 27.2 (C-1), 30.8 (C-3), 31.6 (C-2), 40.6 (C-14), 42.5 (C-15), 47.8 (C-6), 49.6 (C-8), 49.7 (C-4), 50.9 (C-9), 52.2 ($CO_2\underline{CH_3}$), 54.8 (C-5), 74.5 (C-12), 78.6 (C-13), 93.7 (C-10), 110.8 (C-17), 152.6 (C-16), 172.2 ($\underline{CO_2}CH_3$), 178.1 (C-7); EIMS *m*/*z* (rel. int.): 488 $[M]^+$ (38), 470 (50), 417 (70), 361 (48), 343 (51), 329 (70), 311 (50), 301 (82), 265 (32), 257 (88), 237 (70), 229 (48), 211 (64), 197 (46), 181 (30), 171 (34), 155 (36), 143 (44) 129 (52), 115 (46), 91 (70). HRMS *m*/*z*: Calc. for $[M]^+$ $C_{20}H_{25}O_6I$: 488.0696; Found: 488.0695.

Compound **44** (39.4 mg, 0.081 mmol) was dissolved in CH_2Cl_2 (4 ml) and 1,8-diazabicyclo[5.4.0]undec-7-ene (400 ml, mmol) was added. The mixture was heated until reflux began, this being maintained overnight and until the reaction was judged complete by TLC. After cooling, the mixture was diluted with EtOAc (10 ml) and washed with HCl (2 M, 2×20 ml), H_2O (10 ml) and brine (10 ml). The organic layer was dried $MgSO_4$, filtered and the solvent was removed under reduced pressure. The residue was subjected to silica gel column chromatography (EtOAc–petrol, 1:1) to afford GA_{126} (**9**) methyl ester (22.0 mg, 75%): R_f 0.4 (EtOAc–petrol, 2:1); IR ν_{max} cm^{-1}: 3348, 2925, 1773, 1734; ^{1}H NMR (300 MHz, $CDCl_3$): δ 1.19 (3H, *s*, H-18), 1.72 (1H, *d*, $J=11$ Hz), 1.82 (3H, *m*), 2.07 (1H, *br s*, OH), 2.12 (1H, *m*), 2.24 (2H, *m*), 2.34 (2H, *m*), 2.60–2.85 (1H, *br s*, OH), 2.76 (1H, *d*, $J=11$ Hz, H-6), 2.93 (1H, *d*, $J=11$ Hz, H-5), 3.66 (1H, *t*, $J=10$ Hz, H-12), 3.73 (3H, *s*, $CO_2\underline{CH_3}$), 5.11 (1H, *s*, H-17′), 5.31 (1H, *d*, $J=5$ Hz, H-17), 5.87 (1H, *dt*, $J=9$, 3 Hz, H-2), 6.14 (1H, *dt*, $J=9$, 2 Hz, H-1); ^{13}C NMR (75 MHz, $CDCl_3$): δ 17.6 (C-18), 27.5 (C-1), 37.8 (C-3), 40.7 (C-14), 43.3 (C-15), 48.0 (C-8), 48.3 (C-6), 50.6 (C-9), 51.0 (C-4), 52.2 ($CO_2\underline{CH_3}$), 56.2 (C-5), 74.8 (C-2), 78.6 (C-13), 89.7 (C-10), 110.8 (C-17), 129.4 (C-2), 131.2 (C-1), 152.9 (C-16), 172.6 (C-7), 179.2 (C-19); EIMS *m*/*z* (rel. int.): 360 $[M]^+$ (13), 342 (16), 329 (27), 316 (100), 284 (99), 271 (35), 256 (51), 238 (48), 211 (92), 195 (65), 183 (38), 167 (76), 155 (42), 143 (58), 121 (64), 105 (74), 91 (77), 77 (60); HRMS *m*/*z*: Calc. for $[M]^+$ $C_{20}H_{24}O_6$: 360.1573; Found: 360.1569.

3.3.5. GA_{121} (7) methyl ester

A soln. of GA_{126} (**9**) methyl ester (6.6 mg, 0.018 mmol) in CH_2Cl_2 (2 ml) was cooled to 0°C and triethylamine (6.4 ml, 0.046 mmol) was added, followed by addition of Ac_2O (4.31 ml, 0.046 mmol). The mixture was stirred overnight at room temp. Starting material was still present by TLC thus a further two equivalents of triethylamine and Ac_2O were added by the above method. Two h later all starting material was consumed. Ice was added and the reaction mixture stirred for 15 min, followed by dilution with EtOAc. The entire mixture was washed with HCl (1 M, 5 ml) and the aq. layer back extracted with EtOAc (2×10 ml). The combined organic layers were washed with brine (5 ml), dried $MgSO_4$, filtered and the solvent was removed under reduced pressure to give compound **45** (*ent*-12β-acetoxy-13-hydroxy-20-norgibberell-1, 16-ene-7, 19-dioic acid 7-methyl ester 19, 10-lactone) in quantitative yield (7.2 mg): R_f 0.6 (EtOAc–petrol, 2:1); ^{1}H NMR (300 MHz, $CDCl_3$): δ 1.19 (3H, *s*, H-18), 1.85 (3H, *m*), 2.12 (3H, *m*), 2.13 (3H, *s*, $OCO\underline{CH_3}$), 2.33 (3H, *m*), 2.67 (1H, *s*, O<u>H</u>), 2.77 (1H, *d*, $J=10$ Hz, H-6), 2.95 (1H, *d*, $J=6$ Hz, H-5), 3.74 (3H, *s*, $CO_2\underline{CH_3}$), 4.74 (1H, *t*, $J=7$ Hz, H-12), 5.22 (1H, *s*, H-17′), 5.40 (1H, *s*, H-17), 5.87 (1H, *dd*, $J=9$, 3 Hz, H-2), 6.12 (1H, *d*, $J=9$ Hz, H-1); ^{13}C NMR (75 MHz, $CDCl_3$): δ 17.6 (C-18), 21.3 ($OCO\underline{CH_3}$), 25.0 (C-11), 37.8 (C-14), 41.4 (C-15), 43.3 (C-3), 48.0, 48.1 (C-8, C-6), 50.6 (C-4), 51.0 (C-9), 52.2 ($CO_2\underline{CH_3}$), 56.2 (C-5), 76.4 (C-12), 77.8 (C-13), 89.6 (C-10), 112.4 (C-17), 129.3 (C-2), 131.3 (C-1), 152.0 (C-16), 171.0 ($O\underline{CO}CH_3$), 172.4 (C-7), 179.1 (C-19); EIMS *m*/*z* (rel. int.): 402 $[M]^+$ (36), 371 (27), 342 (78), 298 (72), 282 (100), 254 (35), 237 (60), 211 (72), 195 (43), 167 (47), 143 (40), 129 (30), 105 (44), 91 (83), 77 (34); HRMS *m*/*z*: Calc. for $[M]^+$ $C_{22}H_{26}O_7$: 402.1679; Found: 402.1668.

A soln. of compound **45** (7.3 mg, 0.018 mmol) in CH_2Cl_2 (2 ml) was treated with *N*,*N*-dimethyl-4-aminopyridine (small spatula amount) and pyridine (6.6 ml, 0.081 mmol) followed by addition of methyl oxalyl

chloride (7.47 ml, 0.081 mmol). After 2 h the reaction was complete by TLC. The reaction mixture was diluted with EtOAc (5 ml), washed with HCl (2M, 5 ml), sat. $NaHCO_3$ (5 ml), H_2O (5 ml) and brine (5 ml) and dried over $MgSO_4$, filtered and the solvent removed under reduced pressure. The residue was applied to a silica gel (EtOAc–petrol, 1:2) to afford compound **46** (*ent*-12β-acetoxy-13-methyloxalyloxy-20-norgibberell-1, 16-ene-7, 19-dioic acid 7-methyl ester 19, 10-lactone) (3.1 mg, 35%): R_f 0.6 (EtOAc–petrol, 1:1); ^{1}H NMR (300 MHz, $CDCl_3$): δ 1.21 (3H, *s*, H-18), 1.85 (1H, *dd*, $J=12$, 6 Hz), 1.98 (1H, *m*), 2.04 (1H, *dd*, $J=12$, 5 Hz), 2.12 (3H, *s*, $OCO\underline{CH_3}$), 2.13 (1H, *m*), 2.26 (2H, *m*), 2.34 (2H, *m*), 2.62 (1H, *d*, $J=10$ Hz), 2.79 (1H, *d*, $J=11$ Hz, H-6), 2.96 (1H, *d*, $J=11$ Hz, H-5), 3.76 (3H, *s*, $CO_2\underline{CH_3}$), 3.87 (3H, *s*, $OCOCO_2\underline{CH_3}$), 5.17 (1H, *t*, $J=8$ Hz, H-12), 5.23 (1H, *bs*, H-17′), 5.37 (1H, *d*, $J=2$ Hz, H-17), 5.89 (1H, *dt*, $J=9$, 3 Hz, H-2), 6.11 (1H, *d*, $J=9$ Hz, H-1); EIMS *m*/*z* (rel. int.): 488 $[M]^+$ (3), 457 (25), 428 (100), 401 (55), 384 (92), 341 (40), 297 (58), 280 (30), 237 (66), 193 (31); HRMS *m*/*z*: Calc. for $[M]^+$ $C_{25}H_{28}O_{10}$: 488.1682; Found: 488.1684.

A soln. of compound **46** (3.1 mg, 6.3 mmol) and azo-bisisobutyronitrile (0.5 mg, 3.2 mmol) in toluene (2 ml) was degassed and re-filled with N_2. Subsequent addition of tributyltin hydride (5.1 ml, 0.019 mmol) followed by gentle reflux for 15 min yielded a mixture of product and starting material (Dolan and MacMillan, 1985). After cooling the reaction mixture EtOAc (5 ml) was added. The solvent was removed under reduced pressure and the residue taken up in CH_3CN (5 ml) and layered with petrol (5 ml). The CH_3CN layer was washed with KF solution (1 M, 5 ml), and solvent removed under reduced pressure. The residue was applied to a silica gel column (EtOAc–petrol, 1:3) to yield the title compound **47** (*ent*-12β-acetoxy-20-norgibberell-1, 16-ene-7, 19-dioic acid 7-methyl ester 19, 10-lactone) (1.8 mg) and recovered starting material (1.3 mg): ^{1}H NMR (300 MHz, $CDCl_3$): δ 1.19 (3H, *s*, H-18), 2.05 (3H, *s*, $OCO\underline{CH_3}$), 1.85–2.16 (5H, *m*), 2.36 (1H, *dt*, $J=5$, 3 Hz), 2.70 (1H, *m*, H-13), 2.78 (1H, *d*, $J=11$ Hz, H-6), 2.96 (1H, *d*, $J=11$ Hz, H-5), 3.73 (3H, *s*, $CO_2\underline{CH_3}$), 4.69 (1H, *t*, $J=8$ Hz, H-12), 5.06 (1H, *s*, H-17′), 5.24 (1H, *s*, H-17), 5.86 (1H, *dd*, $J=9$, 3 Hz, H-2), 6.14 (1H, *d*, $J=9$ Hz, H-1).

Compound **47** (1.8 mg, 0.0047 mmol) was dissolved in MeOH, and K_2CO_3 (1 mg, 0.0072 mmol) was added. The resulting suspension was stirred for 30 min then more K_2CO_3 (1 mg, 0.0072 mmol) was added and stirred for 3 h by which time the reaction was judged complete by TLC. The mixture was diluted with EtOAc (5 ml) and washed with HCl (1 M, 5 ml). The organic layer was washed with $NaHCO_3$ (satd. soln., 5 ml), H_2O (5 ml) and brine and subsequently dried over $MgSO_4$, filtered and the solvent was removed under reduced pressure. The residue was washed with CH_3CN–hexane and the CH_3CN layer was condensed under reduced pressure. The residue was then taken up in EtOAc (5 ml) and washed with KF soln. (1 M, 5 ml). The organic layer was condensed under reduced pressure and the residue was applied to a silica gel column (progressive elution: 1% EtOAc to 100% EtOAc) to yield GA_{121} (**7**) methyl ester (0.4 mg, 27%): R_f 0.2 (EtOAc–petrol, 1:2) or 0.1 (EtOAc–petrol, 1:3); ^{1}H NMR (600 MHz, $CDCl_3$): δ 1.19 (3H, *s*, H-18), 1.53–1.74 (3H, *m*), 1.89 (2H, *dt*, $J=13$, 2 Hz), 1.95 (1H, *dd*, $J=11$, 2 Hz, H-14), 2.01-2.05 (2H, *m*), 2.09–2.14 (2H, *qt*, $J=19$, 2 Hz), 2.63 (1H, *d*, $J=5$ Hz, H-13), 2.78 (1H, *d*, $J=11$ Hz, H-6), 2.96 (1H, *d*, $J=11$ Hz, H-5), 3.73 (3H, *s*, $CO_2\underline{CH_3}$), 3.77 (1H, *t*, $J=8$ Hz, H-12), 5.00 (1H, *s*, H-17′), 5.11 (1H, *s*, H-17), 5.86 (1H, *dt*, $J=10$, 3 Hz, H-2), 6.15 (1H, *d*, $J=10$ Hz, H-1); ^{13}C NMR (600 MHz, $CDCl_3$): δ 17.6 (C-18), 27.1 (C-11), 33.8 (C-3), 37.8 (C-14), 44.7 (C-15), 47.9 (C-8), 48.2 (C-6), 49.3 (C-9), 50.7 (C-5), 52.1 ($CO_2\underline{CH_3}$), 52.5 (C-4), 56.3 (C-13), 75.1 (C-12), 89.9 (C-10), 110.1 (C-17), 129.7 (C-2), 131.0 (C-1), 151.1 (C-16), 172.8 (C-7), 179.3 (C-19); EIMS *m*/*z* (rel. int.): 344 $[M]^+$ (32), 326 (47), 312 (52), 294 (50), 239 (50), 221 (86), 195 (100), 181 (55), 167 (30), 155 (38), 143 (42), 119 (42), 105 (57), 91 (71); HRMS *m*/*z*: Calc. for $[M]^+$ $C_{20}H_{24}O_5$: 344.1624; Found: 344.1627.

3.3.6. Other novel gibberellins

The synthesis of 2,3-didehydro GA_9 (**15**) has been described in Willis (1987). The syntheses of 2,3-didehydro GA_{69} (**17**), 2,3-didehydro GA_{70} (GA_{31}) (**16**) and 2,3-didehydro GA_{77} (**18**) have been described in Chu and Mander (1988). GA_{122} (**8**) methyl ester was prepared in an analogous fashion to GA_{121} (**7**) methyl ester; detail will be published elsewhere (Leitch, 2000). GA_{120}-isolactone (**11**) methyl ester, GA_{121}-isolactone (**12**) methyl ester, and GA_{122}-isolactone (**13**) methyl ester were prepared from GA_{120} (**6**) methyl ester, GA_{121} (**7**) methyl ester and GA_{122} (**8**) methyl ester, respectively, as 3:2 mixtures with the parent gibberellins by treatment with tetrakis-(triphenylphosphine)-palladium(0) (Serebryakov, 1980).

References

Albone, K.S., Gaskin, P., MacMillan, J., Phinney, B.O., Willis, C.L., 1990. Biosynthetic origin of gibberellins A_3 and A_7 in cell-free preparations from seeds of *Marah macrocarpus* and *Malus domestica*. Plant Physiology 94, 132–142.

Blake, P.S., Taylor, D.R., Crisp, C.M., Mander, L.N., Owen, D.J., 2000. Identification of endogenous gibberellins in strawberry including the novel gibberellins GA_{123}, GA_{124} and GA_{125}. Phytochemistry 55, 887–890.

Chu, A.W.L., Mander, L.N. 1988. Synthesis of the 12-hydroxy gibberellins, GA_{31}, GA_{69} and GA_{70}. Tetrahedron Letters 2727–2730.

Dathe, W., Schneider, G., Sembdner, G., 1978. Endogenous gibberellins and inhibitors in caryopses of rye. Phytochemistry 17, 963–966.

Dathe, W., Jensen, E., Junttila, O., Schneider, G., Sembdner, G., 1989. Reinvestigation of endogenous gibberellins in immature rye ears. Biochemie und Physiologie der Pflanzen 184, 249–258.

Dess, D.B., Martin, J.C., 1983. Readily accessible 12-I-5 oxidant for the conversion of primary and secondary alcohols to aldehydes and lactones. Journal of Organic Chemistry 48, 4155–4156.

Dolan, S.C., MacMillan, J., 1985. A new method for deoxygenating secondary and tertiary alcohols. Journal of the Chemical Society Chemical Communications. 1588–1589.

Duri, Z.J., Hanson, J.R., 1984. Substitution reactions of the 3-epimeric methanesulphonates of methyl gibberellate. Journal of the Chemical Society. Perkin Transactions 1, 603–607.

Fortunato, J.M., Ganem, B., 1976. Lithium and potassium trialkylborohydrides. Reagents for direct reduction of α,β-unsaturated carbonyl compounds to synthetically versatile enolate anions. Journal of Organic Chemistry 76, 2194–2200.

Fujioka, S., Yamane, H., Spray, C.R., Phinney, B.O., Gaskin, P., MacMillan, J., Takahashi, N., 1990. Gibberellin A_3 is biosynthesized from gibberellin A_{20} via gibberellin A_5 in shoots of *Zea mays* L. Plant Physiology 94, 127–131.

Furber, M., Kraft-Klaunzer, P., Mander, L.N., Pour, M., Yamauchi, T., Murofushi, N., Yamane, H., Schraudolf, H., 1995. Synthesis and structure determination of gibberellin derived antheridiogens from fern gametophytes of the *Lygodium* genus. Australian Journal of Chemistry 48, 427–444.

Kirkwood., P.S., MacMillan, J., 1982. Gibberellins A_{60}, A_{61}, and A_{62}: partial syntheses and natural occurrence. Journal of the Chemical Society. Perkin Transactions 1, 689–697.

Kobayashi, M., Kwak, S.S., Kamiya, Y., Yamane, H., Takahashi, N., Sakurai, A., 1991. Conversion of GA_5 to GA_6 and GA_3 in cell-free systems from *Phaseolus vulgaris* and *Oryza sativa*. Agricultural and Biological Chemistry 55, 249–251.

Koshioka, M., Pharis, R.P., Matsuta, N., Mander, L.N., 1988. Metabolism of [^{3}H]gibberellin A_5 and [^{2}H]gibberellin A_5 in cell suspension cultures of *Prunus persica*. Phytochemistry 27, 3799–3805.

Koshioka, M., Roh, M., Nakayama, M., Hisamatsu, T., Mander, L.N., 1999. Identification of endogenous gibberellins in inflorescence of *Ornithogalum thyrsoides*. Journal of the Japanese Society for Horticultural Science 68, 1158–1160.

Leitch, S.K., 2000. PhD dissertation, Australian National University, Canberra, ACT, Australia.

MacMillan, J., Takahashi, N., 1968. Proposed procedure for the allocation of trivial names to the gibberellins. Nature 217, 170–171.

MacMillan, J., Ward, D.A., Phillips, A.L., Sánchez-Beltrán, M.J., Gaskin, P., Lange, T., Hedden, P., 1997. Gibberellin biosynthesis from gibberellin A_{12}-aldehyde in endosperm and embryos of *Marah macrocarpus*. Plant Physiology 113, 1369–1377.

Mander, L.N., Owen, D.J., 1997. Synthesis of 12-hydroxy C_{20}-gibberellins. Tetrahedron 53, 2137–2162.

Nakayama, M., Yokota, T., Sohma, R., Mander, L.N., Twitchin, B., Komatsu, H., Matsui, H., Bukovac, M.J., 1996. Gibberellins in immature seed of *Prunus cerasus*: Structure determination and synthesis of gibberellin, GA_{95} (1, 2 didehydro-GA_{20}). Phytochemistry 47, 587–593.

Reeve, D.R., Crozier, A., 1974. An assessment of gibberellin structure-activity relationship. Journal of Experimental Botany 25, 431–445.

Serebryakov, E.P. 1980. Transformations of gibberellin A_3 derivatives in the presence of palladium compounds. Izvestiya Akademii Nauk SSSR Seriya. Khimicheskaya, 2596–2603.

Spray, C.R., Kobayashi, M., Suzuki, Y., Phinney, B.O., Gaskin, P., MacMillan, J., 1996. The *dwarf-1* (*d1*) mutant of *Zea mays* blocks three steps in the gibberellin-biosynthetic pathway. Proceedings of the National Academy of Sciences of the USA 93, 10515–10518.

Willis, C.L., 1987. A new approach to the synthesis of 2β- and 3β-hydroxy gibberellins. Tetrahedron Letters 28, 6705–6708.

Wynne, G.M., Mander, L.N., Oyama, N., Murofushi, N., Yamane, H., 1998. A new antheridiogen from gametophytes of *Lygodium circinnatum*: 12α-hydroxy-gibberellin A_{73} (GA_{117}). Phytochemistry 49, 1837–1840..

Yamaguchi, I., Yokota, T., Murofushi, N., Takahashi, N., Ogawa, Y., 1975. Isolation of gibberellins A_5, A_{32}, A_{32} acetonide and (+)-abscisic acid from *Prunus persica*. Agricultural and Biological Chemistry 39, 2399–2403.

PERGAMON

Phytochemistry 57 (2001) 759–763

PHYTOCHEMISTRY

www.elsevier.com/locate/phytochem

Occurrence of cadaverine in hairy roots of *Brugmansia candida*

Carla N. Carrizo[a], Sandra I. Pitta-Alvarez[a], Marcelo J. Kogan[b], Ana M. Giulietti[a,*], María L. Tomaro[b]

[a]*Cátedra de Microbiología Industrial y Biotecnología, Facultad de Farmacia y Bioquímica, Universidad de Buenos Aires, Junín 956, (1113) Buenos Aires, Argentina*

[b]*Cátedra de Química Biológica Vegetal, Facultad de Farmacia y Bioquímica, Universidad de Buenos Aires, Junín 956 6to piso, Buenos Aires, Argentina*

Received 28 November 2000; received in revised form 26 January 2001

Abstract

The polyamine, cadaverine, was detected in transformed root cultures of *Brugmansia candida* (syn. *Datura candida*), a Solanaceae which produces the tropane alkaloids scopolamine and hyoscyamine. To the best of our knowledge, this is the first time that the existence of this uncommon polyamine has been detected in a *Datura* species. Cadaverine, however, could not be found in the whole plant. The occurrence of cadaverine in hairy roots could be a consequence of either the transformation or a response to stress. Also, cadaverine could be participating in other secondary pathways rather than to the tropane alkaloids. The common polyamines, putrescine, spermidine and spermine were also observed. © 2001 Elsevier Science Ltd. All rights reserved.

Keywords: *Brugmansia candida* (syn. *Datura candida*); Solanaceae; Cadaverine; *Agrobacterium rhizogenes*; Hairy roots; Polyamines

1. Introduction

Brugmansia candida (syn. *Datura candida*), a member of the Solanaceae, is a South American plant that produces the tropane alkaloids scopolamine and hyoscyamine (Roses et al., 1988). These alkaloids are extensively employed in medicine as anticholinergic agents. In our laboratory, we have worked with transformed (hairy) roots of *B. candida* in order to obtain these alkaloids (Pitta-Alvarez and Giulietti, 1995, 1997). The biosynthesis of these secondary metabolites uses the polyamine putrescine (Put) as a precursor (Scheme 1), a compound which can also diverge into the metabolic route leading to two other polyamines, spermidine (Spd) and spermine (Spm), both linked mainly to primary metabolism in this plant.

The common aliphatic polyamines Put, Spd and Spm, are ubiquitous in all types of organisms, and are considered to participate in a variety of events related to plant growth and development (Bagni and Torrigiani, 1992; Galston and Kaur Sawhney, 1995). However, besides these common polyamines, there are also some uncommon ones, such as 1,3-diaminopropane, cadaverine (Cad), norspermidine and homospermidine, which have been associated with the capacity of some biological systems to grow or function under extreme environments (Slocum and Flores, 1991). Cad (1,5-diaminopentane), is the penta homologue of Put, and it is present in many biological tissues. However, the existence of this diamine in plants is sporadic and less common than its homologue Put. Cad has been found in several genera of the Leguminosae, such as *Pisum*, *Glycine*, *Lathyrus*, *Trifolium*, *Lupinus* and *Vicia*; in *Hordeum* and *Oryza* (Gramineae), in *Zantedeschia* (Araceae), and in *Sedum* (Crassulaceae). In the Solanaceae, however, it has only been detected in *Nicotiana* and *Lycopersicon* (Slocum and Flores, 1991; Wink 1997).

The objective of our work was to evaluate the polyamine (Put, Spd and Spm) levels in hairy roots of *B. candida*. Unexpectedly, Cad was also found.

Abbreviations: Cad, Cadaverine; Put, putrescine; Spd, spermidine; Spm, spermine

* Corresponding author. Tel.: +54-11-4964-8269; fax: +54-11-4552-5017.

E-mail address: agiule@ffyb.uba.ar (A.M. Giulietti).

0031-9422/01/$ - see front matter © 2001 Elsevier Science Ltd. All rights reserved.
PII: S0031-9422(01)00127-3

2. Results and discussion

2.1. Time-course of growth and polyamine biosynthesis

Table 1 and Fig. 1 show the time course of growth of hairy root cultures of *B. candida* and the corresponding Put, Spd and Spm contents, respectively. The values obtained were similar to those observed by Robins et al. (1991) in hairy roots of *Datura stramonium*. The levels of the three polyamines decrease when the cultures enter into an exponential phase. This depletion could suggest that they are being used actively for cell division and growth.

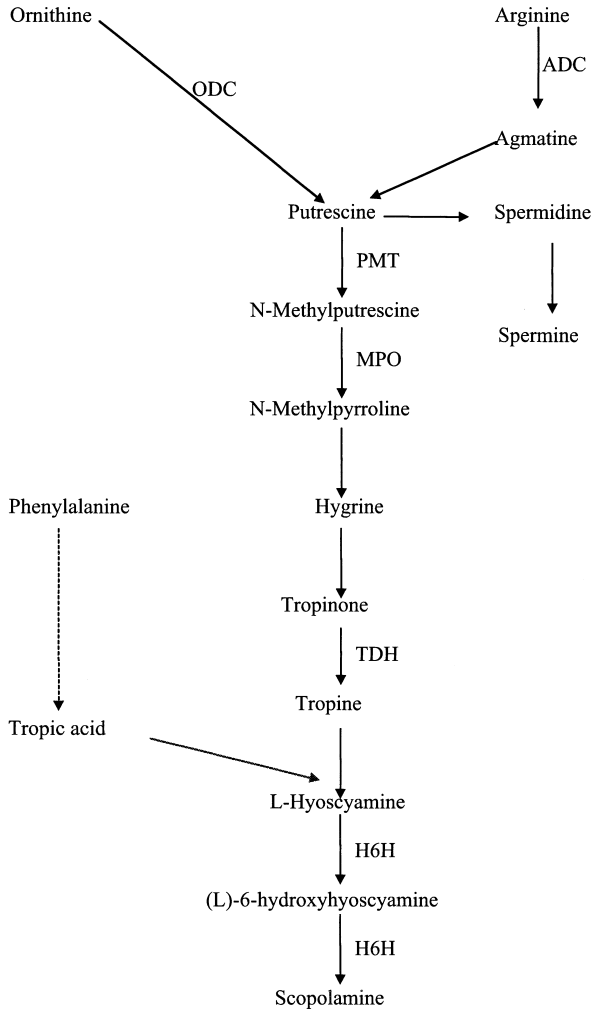

Scheme 1. Biosynthesis of hyoscyamine and scopolamine. ODC: ornithine-decarboxylase; ADC: arginine-decarboxylase; PMT: putrescine-methyltransferase; MPO: methylputrescine-oxidase; TDH: tropinone dehydrogenase; H6H: hyoscyamine 6-β-hydroxylase.

Table 1
Time course of growth of *Brugmarsia candida* hairy roots[a]

Time (days)	Fresh wt (g)
5	0.22±0.02
10	0.51±0.05
15	0.47±0.05
20	1.02±0.01
25	1.7±0.12
30	1.61±0.11

[a] Data are mean values of two independent experiments±S.E. Each point represents six replicates.

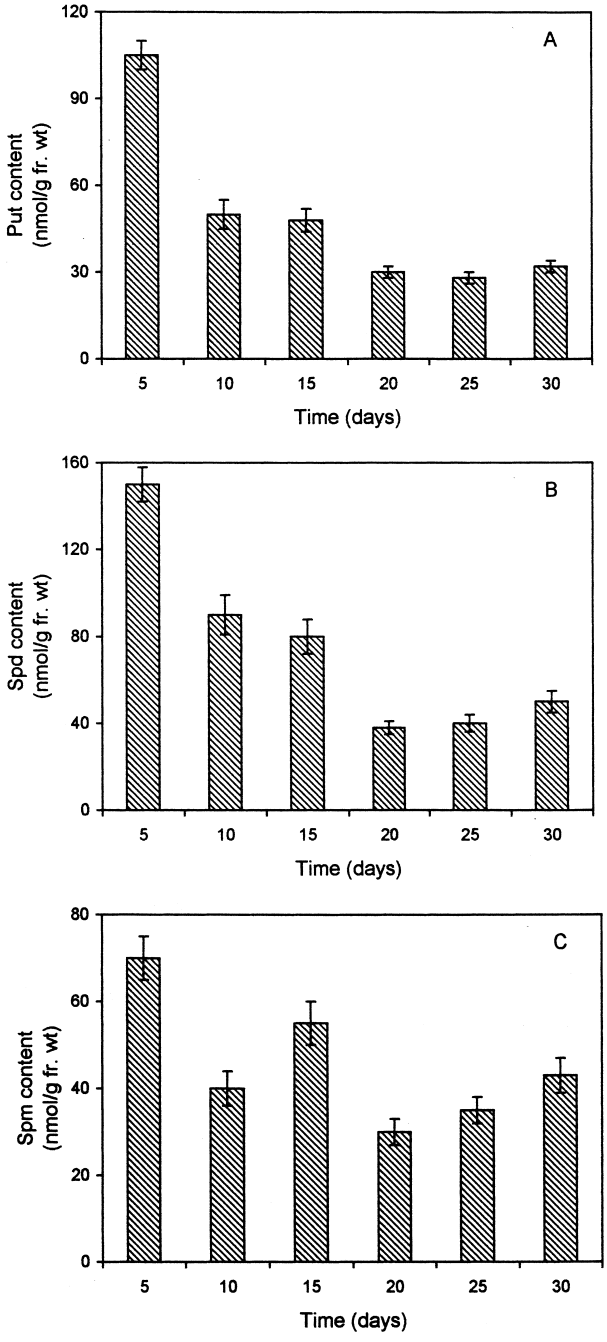

Fig. 1. Time course of accumulation of polyamines: (A) putrescine, (B) spermidine and (C) spermine in hairy roots of *Brugmarsia candida*. Values are the mean of two different experiments with three replicated measurements, and bars indicate S.E.

2.2. Cadaverine detection

When the TLCs of the perchloric extracts obtained from the cultures were examined, an additional band, which had the same R_f (in chloroform:triethylamine) as Cad, was detected. Moreover, this compound showed the same R_f as Cad in *n*-hexane:ethyl acetate. To confirm the identity of this compound, the FAB MS (positive ion mode) for the unknown compound and a Cad standard were performed. The presence of the characteristic ions, $[M+H]^+$ (m/z: 569) and $[(M+H)-C_{12}H_{10}N]^+$ (m/z: 399), were observed in both spectra coming from the two different solvent systems.

Data obtained from both TLC and mass spectrometric analyses clearly demonstrated that the unknown compound was Cad.

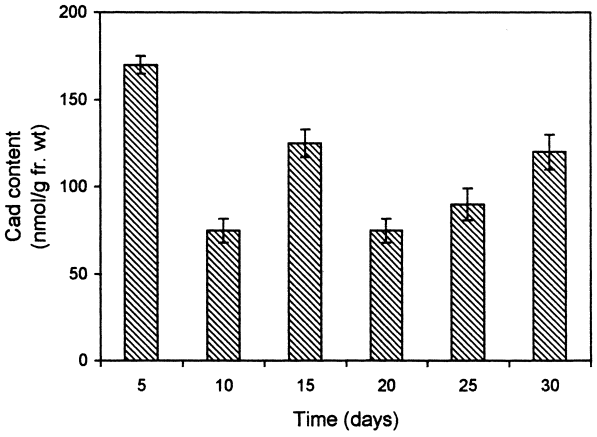

Fig. 2. Time course of accumulation of cadaverine in hairy roots of *Brugmansia candida*. Values are the mean of two different experiments with three replicated measurements, and bars indicate S.E.

2.3. Time-course of growth and cadaverine content

Table 1 and Fig. 2 show the time course of growth of hairy root cultures of *B. candida* and the corresponding Cad content, respectively. In comparison to the other three polyamines (Fig. 1), Cad was found in slightly higher quantities. However, the same phenomena of reduction of polyamine content concomitant with the exponential growth period, was observed. These results are in agreement with those found by Gamarnik and Frydman (1991) in soybean roots.

2.4. Occurrence of Cad in whole non-transformed plants

In view of the fact that the occurrence of Cad had not been described previously in *B. candida*, or to the best of our knowledge in any other *Datura* species, we decided to investigate whether it accumulated in different parts of the whole plant. No Cad was found either in leaves or roots of the plant. In contrast, there are reports of the presence of Cad in soybean radicles (Tajima et al., 1983) and in *Glycine max* cotyledons, embryonic axes and roots (Gamarnik and Frydman, 1991).

It is important to emphasize that the plant examined was the one whose explants had originated the transformed roots, and therefore shared with the latter the same genetic background.

The surprising finding of Cad in *B. candida* generates multiple hypotheses, whose robustness must be put to trial in the future. Several studies have indicated that *Agrobacterium rhizogenes* affects the levels of polyamines in transformed plants (Altabella et al., 1995; Martin-Tanguy et al., 1996). Also, the appearance of uncommon polyamines has been linked to stress (Tiburcio et al., 1997). In vitro cultures can be considered a stressful

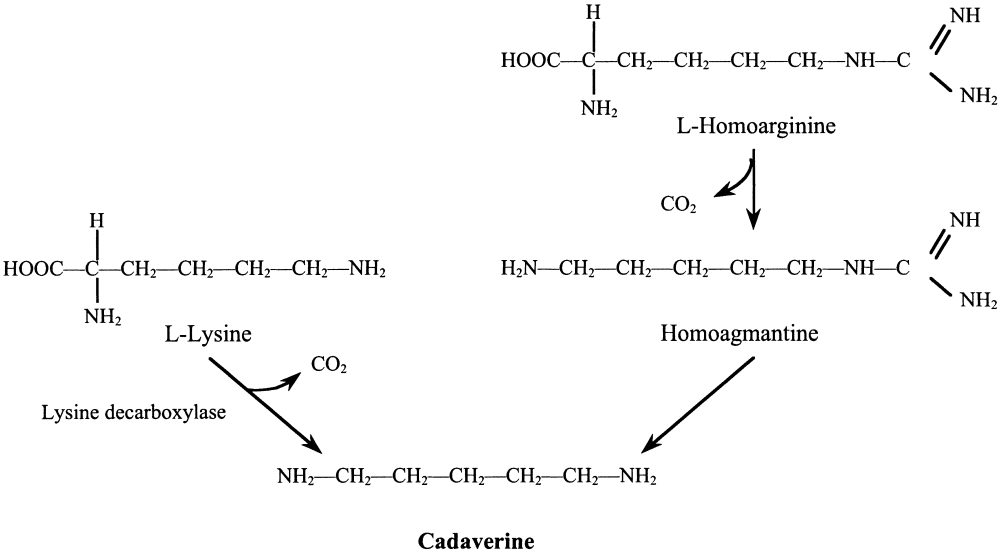

Scheme 2. Biosynthesis of cadaverine.

situation for plants, and the expression of the gene coding for the enzyme that synthesizes Cad could be triggered by it (Flores, 1991) either for transforming lysine into Cad in a reaction catalyzed by lysine decarboxylase or via an alternative route that involves L-homoarginine and homoagmatine (Wink, 1997) (Scheme 2).

Finally, the main question that remains unanswered is what is the role of Cad in hairy roots. As was mentioned previously, it could be part of the roots response to stress. Also, their participation in secondary routes, not necessarily to tropane alkaloids, might be possible.

3. Conclusions

Cadaverine (Cad), an uncommon polyamine, was detected for the first time in hairy roots of *Brugmansia candida*, and in comparison to the other three polyamines (Put, Spd and Spm), Cad was found in higher quantities. Cad levels decreased when the cultures entered into an exponential phase. This depletion could suggest that it is being used actively in cell division and growth.

Further studies will be necessary in order to assess more precisely the role of Cad in transformed roots of *Daturas* species.

4. Experimental

4.1. General experimental procedures

TLC was performed on high resolution silica gel plated (Merck, silica gel 60 F-254 plates). The silica gel used in column chromatography was Kieselgel DG (Riedel de Haen). All the chemical used were of analytical grade. Solvents were distilled before use. FAB MS spectra were obtained using a ZAB SEK (VG, Fisons) spectrometer.

4.2. Establishment and maintenance of axenic hairy root cultures

Transformed roots were obtained by infection of sterile leaves of *B. candida* with *A. rhizogenes* LBA 9402 according to the method described by Pitta-Alvarez and Giulietti (1995). The root tips were transferred to hormone-free Gamborg (Gamborg et al., 1969) medium, with half concentration of vitamin and minerals nutrients ($B5_{1/2}$) and with the addition of 15 g/l sucrose (Pitta-Alvarez and Giuletti, 1995). Cefotaxime 0.05% was added until axenic cultures were obtained. The transformation was confirmed according to the procedure described by Hamill et al. (1991). The roots that were used in the experiments were maintained in an hormone-free $B5_{1/2}$ medium, supplemented with 15 g/l sucrose and subcultured every 15–20 days. They were incubated at $24\pm2^{\circ}C$, in gyratory shakers at 100 rpm with a 16-h photoperiod using cool white fluorescent lamps, at a light intensity of approximately 1.8 W m^{-2}.

4.3. Time course of growth and polyamine content

Inocula of fresh weight (0.5 g) of 20-day-old hairy roots were inoculated in 50 ml of $B5_{1/2}$ (with 15 g/l sucrose) contained in 250 ml Erlenmeyers. The cultures were incubated as described above and samples were taken every 5 days during 30 days and fresh wt and free polyamines were determined in each one of them.

4.4. Analytical methods

Plant material (400 mg fresh wt of hairy roots, leaves and normal roots) was homogenized with 5% perchloric acid, kept 30 min on ice and centrifuged at 5000 rpm for 10 min. The supernatants (15 ml) were derivatized using the dansylation method described by Smith and Meeuse (1966) and 1,6 hexanediamine was used as internal standard. Standards of Put, Spd, Spm were dansylated simultaneously. The dansylated derivatives were extracted with 1 ml ethyl acetate. Polyamines (200 μl) were separated and identified by TLC with both chloroform–triethylamine (9:1) and *n*-hexane–ethyl acetate (2:1) solvent systems. Dansylated polyamines were identified by comparing the R_f values of dansylated standards. Silica plates were observed under UV light and the bands corresponding to polyamines in the samples and standards were scraped off the plates and eluted with EtOAc (1 ml). Their fluorescence was measured in a spectrofluorometer using an excitation wavelength of 365 nm and an emission wavelength of 510 nm.

For confirmation of the identity of Cad, the band with the same R_f as Cad was scraped from the plate and eluted off using chloroform–methanol (9:1). The solvent was evaporated and the residue was filtered through a small column of silica gel (2×1 cm) using the above-mentioned solvent. The fractions containing the product were evaporated in vacuum and afforded a white yellowish solid. FAB MS spectrometry was obtained using glycerol as a matrix: *m/z*: 569 $[M+H^+]$, 399$[(M+H)-C_{12}H_{10}N]^+$.

For fresh wt determinations, root tissues were separated from the medium by filtration and weighed.

Acknowledgements

This work was supported by grants from Universidad de Buenos Aires (Argentina) and the Consejo Nacional de Investigaciones Científicas y Técnicas (CONICET) (Argentina). A.M.G. and M.L.T. are career investigators from CONICET.

References

Altabella, T., Angel, E., Biondi, S., Palazon, J., Bagni, N., Pinol, M.T., 1995. Effect of the *rol* genes from *Agrobacterium rhizogenes* on polyamine metabolism in tobacco roots. Physiologia Plantarum 95, 479–485.

Bagni, N., Torrigiani, P., 1992. Polyamines: a new class of growth substances. In: Karssen, C.M., van Loon, L.C., Vreugdenhil, D. (Eds.), Progress in Plant Growth regulation. Kluwer Academic, Dordrecht, pp. 264–275.

Flores, H.E., 1991. Changes in polyamine metabolism in response to abiotic stress. In: Slocum, R.D., Flores, H.E. (Eds.), Biochemistry and Physiology of Polyamines in Plants. CRC Press, Boca Raton, FL., pp. 213–227.

Galston, A.W., Kaur Sawhney, R., 1995. Polyamines as endogenous plant growth regulators. In: Davies, P.J. (Ed.), Plant Hormones: Physiology, Biochemistry and Molecular Biology. Kluwer Academic, Dordrecht, pp. 158–178.

Gamarnik, A., Frydman, R.B., 1991. Cadaverine, an essential diamine for the normal root development of germinating soybean (Glycine *max*) seeds. Plant Physiology 97, 778–785.

Gamborg, O.L., Miller, R.A., Ojima, K., 1969. Nutrient requirements of suspension cultures of soybean root cells. Experimental Cellular Research 50, 151–158.

Hamill, J.D., Rounsley, S., Spencer, A., Todd, G., Rhodes, M.J.C., 1991. The use of the polymerase chain reaction in plant transformation studies. Plant Cell Reports 10, 221.

Martin-Tanguy, J., Sun, L.Y., Burtin, D., Vernoy, R., Rossin, N., Tepfer, D., 1996. Attenuation of the phenotype caused by the root-inducing, left-hand, transferred DNA and its *rol* gene-correlations with changes in polyamine metabolism and DNA methylation. Plant Physiology 111, 259–267.

Pitta-Alvarez, S.I., Giulietti, A.M., 1995. Advantages and limitations in the use of hairy root cultures for the production of tropane alkaloids: use of anti-auxins in the maintenance of normal root morphology. In Vitro Cellular and Developmental Biology — Plant 31 (4), 215–220.

Pitta-Alvarez, S.I., Giulietti, A.M., 1997. Effects of gibberellin GA_7 on kinetics of growth and tropane alkaloid accumulation in hairy roots of *Brugmansia candida*. In Vitro Cellular and Developmental Biology — Plant 33, 147–153.

Robins, J.R., Parr, A.J., Walton, N.J., 1991. Studies on the biosynthesis of tropane alkaloids in *Datura stramonium* L. transformed root cultures. Planta 183, 185–195.

Roses, O.C., Villamil, E.E., García Fernandez, J.C., 1988. Acción farmacodinámica de flores de *Brugmansia candida*. Fitoterapia 59, 120–127.

Slocum, R.D., Flores, H.E., 1991. Uncommon polyamines in plants and other organisms. In: Slocum, R.D., Flores, H.E. (Eds.), Biochemistry and Physiology of Polyamines in Plants. CRC Press, Boca Raton, FL, pp. 121–136.

Smith, M.A., Meeuse, B.J.D., 1966. Production of volatile amines in some *Arum lily* species. Plant Physiology 41, 343–347.

Tajima, S.H., Kato, N., Yamamoto, Y., 1983. Cadaverine involved in urate degrading activity (uricase activity) in soybean radicles. Plant Cell Physiology 24, 247–253.

Tiburcio, A.F., Altabella, T., Borrel, T., Masgrau, C., 1997. Polyamines metabolism and its regulation. Physiologia Plantarum 100, 664–674.

Wink, M., 1997. Special nitrogen metabolism. In: Dey, P.M., Harborne, J.B. (Eds.), Plant Biochemistry. Academic Press, San Diego, CA, pp. 439–485.

PERGAMON

Phytochemistry 57 (2001) 765–772

PHYTOCHEMISTRY

www.elsevier.com/locate/phytochem

The phenolic fraction of maize bran: evidence for lignin-heteroxylan association

Catherine Lapierre[a,*], Brigitte Pollet[a], Marie-Christine Ralet[b], Luc Saulnier[b]

[a]*Laboratoire de Chimie Biologique, INRA-INAPG, Institut National Agronomique, 78850, Thiverval-Grignon, France*
[b]*Unité de Recherche sur les Polysaccharides, leurs Organisations et Interactions, INRA, BP 71627-44316, Nantes Cedex 03, France*

Received 13 November 2000; received in revised form 22 February 2001

Abstract

Maize bran heteroxylan samples were extracted in various conditions of severity. Their ferulate and diferulate content was investigated by GC–MS of methyl ester-TMSi derivatives. When extracted by 0.5 M NaOH in mild conditions, the heteroxylan sample contained a low level of ferulic acid (0.032% by wt.) and the main diferulate surviving alkaline extraction was found to be the 8–8′ diferulate. On peroxidase treatment, this sample nevertheless produced a firm and brittle gel without any change in the diferulate profile. Typical lignin structures, mainly comprising syringyl units interconnected through β-*O*-4, β-1 and β-β interunit bonds, were evidenced in the maize bran sample. More importantly, these lignin structures were found to be tightly associated with the alkali-extracted heteroxylans. Thioacidolysis revealed the occurrence of 0.1–0.5% (by wt.) lignin structures in heteroxylan fractions extracted in mild or severe conditions, before and after purification of the polysaccharides. The gelling potential of the heteroxylan fractions was not only dependent on their ferulate level, but also influenced by associated lignin structures. These results argue for the occurrence of covalent linkages between heteroxylan chains and lignin structures which could participate in the peroxidase-driven gelation of feruloylated polysaccharides. They demonstrate the role of low lignin levels in the organization of native or reconstructed polysaccharide networks. © 2001 Elsevier Science Ltd. All rights reserved.

Keywords: *Zea mays*; *Gramineae*; Maize bran; Cell wall; Heteroxylans; Lignin; Polysaccharides; Ferulate; Dehydrodiferulate; Thioacidolysis

1. Introduction

Maize bran is an important by-product of the maize industry. This cell wall fraction, mainly composed of matrix polysaccharides and cellulose, originates from the pericarp tissues. The matrix polysaccharides, which represent more than 50% of the wall, are heteroxylans made primarily of xylose and arabinose units with minor amounts of galactose and glucuronic acid (Saulnier et al., 1995a). In addition, cinnamic acids represent up to 4–5% by weight of the destarched maize bran (Saulnier et al., 1999; Saulnier and Thibault, 1999). These acids, mainly ferulic acid (3-methoxy-4-hydroxycinnamic acid) together with a lower amount of *p*-coumaric acid (4-hydroxycinnamic acid), are esterified to the wall polymers (Kato and Nevins, 1985; Mueller-Harvey et al., 1986; Saulnier et al., 1995b). Many studies with grass cell walls or appropriate ferulate model compounds have demonstrated that ferulate esters can participate in peroxidase-mediated oxidative coupling (Ralph et al., 1994; Wallace and Fry, 1995; Grabber et al., 1995). Such coupling results in the cross-linking of polysaccharide chains, thereby decreasing the wall extensibility (Kamisaka et al., 1990; Sanchez et al., 1996; Wakabayashi et al., 1997) and enzymatic degradability (Grabber et al., 1998). In addition, during lignification, the oxidative coupling between lignin units and ferulate esters anchors lignins to polysaccharides and further strengthens grass cell walls (Jacquet et al., 1995). In contrast to ferulic acid, *p*-coumaric acid is not prone to peroxidase-mediated coupling (Russel et al., 1996; Wallace and Fry, 1999), but participates in photodimerization reactions (Ford and Hartley, 1988). In addition to the biological importance of the ferulate-based cross-linking, the oxidative gelation of feruloylated pectins isolated from sugar beet (Thibault, 1986; Oosteveld et al., 1997) or of feruloylated heteroxylans isolated from

* Corresponding author. Fax: +33-1-30-81-53-73.
E-mail address: lapierre@grignon.inra.fr (C. Lapierre).

0031-9422/01/$ - see front matter © 2001 Elsevier Science Ltd. All rights reserved.
PII: S0031-9422(01)00104-2

maize or wheat bran (Ng et al, 1997; Figueroa-Espinoza and Rouau, 1998; Schooneveld-Bergmans et al., 1998) has an interesting technological potential.

Because of the localization of maize heteroxylans in the secondary cell walls of pericarp tissues, their isolation requires alkaline conditions and their recovery yield varies with the severity of the treatment (Chanliaud et al., 1995). Accordingly, their gelling capacity depends on the ferulate content which can survive the extraction process (Ng et al., 1997). With the objective of further delineating the role of ferulate esters in the gelation of maize heteroxylans, we have examined herein the ferulate content of various heteroxylan fractions in relation to their gelling properties. Moreover and for the first time, we have examined the possibility that grass lignin structures remain associated to the alkali-extracted heteroxylans and thereby participate in the peroxidase gelation of these polysaccharides.

2. Results and discussion

2.1. Isolation and purification of maize bran heteroxylan fractions

Various heteroxylan samples were isolated from destarched maize bran, under mild (samples AX and AXP, Table 1) or more severe (samples HX and HXO, Table 1) conditions of alkaline extraction. The various heteroxylan fractions were purified by ion exchange chromatography. Crude polysaccharide fractions were yellowish in color and this colored material was retained on the column during the purification step. Glucose arising from residual starch was also eliminated from the purified fractions (see fractions AX and AXP in Table 1).

The sugar composition of purified fractions was similar, although HXO was slightly depleted in galactose compared to other samples. Size-exclusion chromatograms of the different fractions are presented in Fig. 1. Polysaccharides eluted as a main peak which presented a shoulder on the leading edge, indicating some heterogeneity in molar mass distribution. Weight average molar mass was about the same for AXP and HX, but was about two times lower for HXO (Table 1), which was extracted in the presence of hydrogen peroxide. Hydrogen peroxide did not improve the extraction yield, but might have catalyzed the cleavage of linkages labile in oxidative conditions. Heteroxylans with a similar low molar mass have been previously extracted from maize bran using acidic hypochlorite (Saulnier et al., 1995a).

2.2. Ferulate content of destarched maize bran and corresponding heteroxylan samples

The alkali-released ferulic and *p*-coumaric acids of destarched maize bran and of the corresponding heteroxylan fraction AX were analyzed by HPLC. Ferulic acid represented 2.82% (by weight) of the maize bran sample, versus 0.33% for *p*-coumaric acid (Table 2). A very small proportion of ester-linked ferulic acid (about 1% versus 18% for *p*-coumaric acid) survived the alkaline extraction used for the isolation of AX (Table 2). This alkali-releasable ferulic acid essentially resisted the purification step of the AX sample performed by ion exchange chromatography (data not shown). This result confirms that ferulic acid units surviving in the AX sample are covalently linked to the heteroxylan chains. Conversely, heteroxylans (HX and HXO) extracted in severe alkaline conditions did not contain ferulic acid.

The analysis of diferulates was performed by GC–MS in order to unambiguously identify the dimers from their mass fragmentation patterns. In addition, we observed that the 8–8′ diferulate could not be satisfactorily analyzed by HPLC, in agreement with recently reported results (Saulnier et al., 1999). The diferulates were analyzed by GC–MS of their methyl ester-TMSi derivatives after esterification with BF_3 methanol, then trimethylsilylation. This two-step derivatization mode was preferred to trimethylsilylation as TMSi derivatives of phenolic acids have been repeatedly reported to be somehow unstable during GC analyses (for review, see Wittkowski, 1985). Exhaustive methylation with diazomethane led to unsatisfactory results because of the formation of pyrazoline derivatives when the cinnamic compounds were subjected to a prolonged CH_2N_2 exposure. The diferulate derivatives obtained by the esterification/silylation procedure are outlined in Fig. 2. The corresponding GC trace and mass spectra are provided in Fig. 3 and Table 3. According to these results, we could observe that acyclic 8–5′ and 5–5′ diferulates (dimers **3** and **7**, in Fig. 2) were completely methylated at COOH,

Table 1
Characteristics of heteroxylan fractions isolated from destarched maize bran. Extractants were used in parallel, not in series

Fraction (isolation mode)	Recovery yield (wt.%)	Weight average molar mass (Da)	Carbohydrate content Ara/Xyl/Gal/GlcA/Glc (g/100 g)
AX (0.5 M NaOH, 30°C, 2 h)	19.1	270,000	24.1/41.8/6.1/5.7/1.3
AXP (as AX + purification on DEAE)	16.4	280,000	28.6/49.9/7.0/7.2/0
HX (1.5 M KOH, 100°C, 2 h + purification on DEAE)	48.4	264,000	30.7/51.2/6.8/6.3/0
HXO (as HX, but with 1% H_2O_2 during extraction)	51.5	124,000	29.9/51.4/4.9/5.8/0

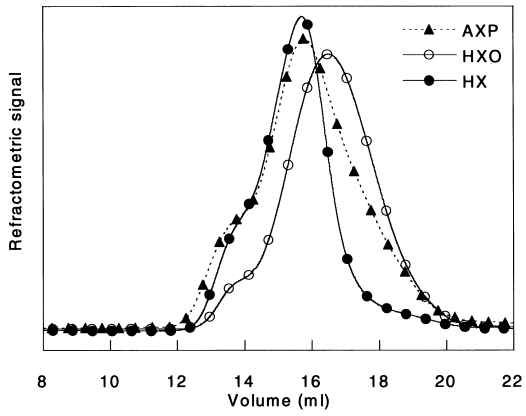

Fig. 1. Size exclusion chromatography of heteroxylan fractions. The void volume of the column is 10.5 ml. The included volume is 22.5 ml.

Table 2
Content of *p*-coumaric acid, ferulic acid and ferulic acid dehydrodimers for destarched maize bran and for the corresponding heteroxylan fraction AX isolated in mild conditions[a]

Hydroxycinnamic derivative (g/100 g)	Destarched maize bran	AX heteroxylan fraction
p-Coumaric acid	0.33	0.062
Ferulic acid	2.82	0.032
8–8′ diFA (**1** and **2**)	0.09	0.06
8–5′ diFA (**3** and **6**)	0.23	tr
8-*O*-4′ di FA (**4** and **5**)	0.13	tr
5–5′ diFA (**7**)	0.23	tr

[a] *p*-Coumaric and ferulic acid are analyzed by HPLC; dehydrodimers are analyzed by CPG–SM of their methyl ester-TMSi derivatives (structures outlined in Fig. 2) and by setting their response factor as 1.0; tr: trace amount.

similar to the case of ferulic and *p*-coumaric acid. In contrast, the cyclic 8–8′ and 8-*O*-4′ diferulates yielded two derivatives differing in their methylation degree (compounds **1** and **2**; compounds **4** and **5**, Fig. 2) and the cyclic 8-5′ diferulate provided only one derivative with one COOTMSi and one COOMe group (compound **6**, Fig. 2). More drastic methylation conditions were not attempted in order to avoid any diferulate degradation. Moreover, the recovery of partially methylated compounds did not hinder analysis of the reaction mixture (Fig. 3). The mass spectral fragmentation patterns of the methyl ester-TMSi derivatives of diferulates (Table 3) displayed some similarities with the ones of their fully trimethylsilylated analogues (data not shown). The common observed features were loss of formic acid (methylated or silylated) in 8–8′ and 8-*O*-4′ diferulates and of HOTMSi groups in diferulates **2** and **6** (giving rise to the fragment at *m*/*z* 467 from the ion at *m*/*z* 557 in **2** and to the *m*/*z* 454 base peak in **6**). However, an important attribute of the methyl ester-TMSi derivatives, relative to their fully trimethylsilylated analogues, was their abundant molecular ion (Table 3). The quantitative evaluation of the diferulates was carried out by setting their response factor as 1.0, due to the lack of appropriate standards in pure form. However, the data reported in Table 2 can be nevertheless comparatively discussed as follows. The only diferulate recovered from the AX sample in substantial amount was the cyclic 8–8′ diferulate (Table 2 and Fig. 3). In addition, the GC profile of AX displayed an additional compound (peak 8 in Fig. 3): its mass spectrum (M^+ at *m*/*z* 498 as the base peak) suggested that this compound originated from the decarboxylation of the 8–5′ diferulate **3**. The other diferulates could be detected only as trace components. The diferulate ester type which was, therefore, the less easily released from maize bran cell walls was the 8–8′ diferulate one. A similar conclusion has been recently reported in the case of maize coleoptile (Pena et al., 1998).

In contrast to similar studies carried out with maize bran heteroxylan (Ng et al., 1997), the diferulate profile of the maize heteroxylan AX fraction was not altered by the peroxidase gelation of the sample (GAX in Fig. 3). The amount of alkali-released 8–8′ diferulate was found similarly low (0.06% by weight) in AX and in GAX. Moreover, the GAX chromatographic profile did not reveal any increased amount of other diferulates (Fig. 3). In contrast, the amount of alkali-released ferulic acid was about two times lower in GAX than in the initial sample AX (data not shown). This result argues for the effective participation of ferulic units in cross-linking structures that cannot be released by mild alkaline hydrolysis, a phenomenon reminiscent of the situation met for lignified cell walls. Recent studies have established the propensity of ferulate esters to copolymerize with lignin units and demonstrated that most of the resulting cross-links are not measurable by solvolytic techniques (Grabber et al., 1995, 1998). Accordingly, the occurrence of lignin structures in the heteroxylan fractions isolated from maize bran was explored in order to tentatively account for the peroxidase-promoted disappearance of ferulic units without the concomitant formation of alkali-releasable diferulates.

2.3. Evidence for lignin structures in maize bran and in the corresponding heteroxylan samples

In order to unambiguously detect the occurrence of lignin structures that could putatively participate in the peroxidase cross-linking of maize heteroxylans, we subjected the heteroxylan fractions isolated in various conditions and the destarched maize bran to thioacidolysis. Thioacidolysis, that is solvolysis in dioxane-ethanethiol with boron trifluoride etherate, is an analytical degradation procedure which results in the depolymerization of lignins (Lapierre, 1993). The key reaction of thioacidolysis is the cleavage of the labile β-*O*-4 bonds which are the major interunit bonds in native lignins. The

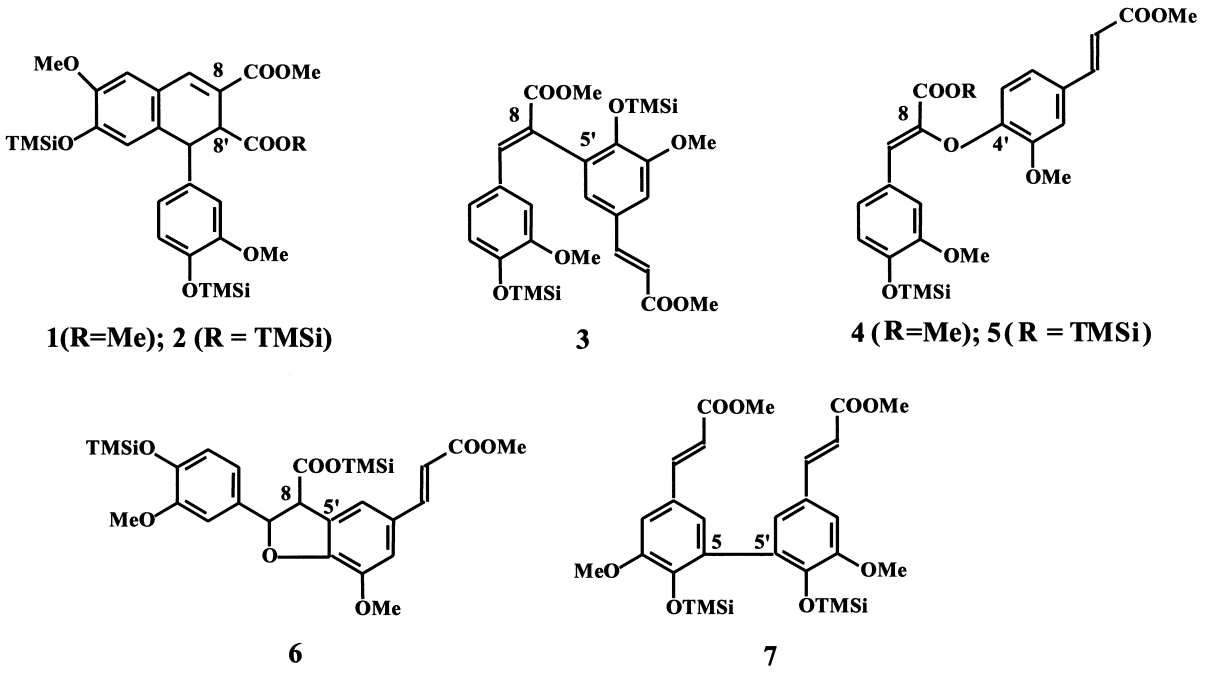

Fig. 2. Main diferulates recovered from maize bran and analyzed as methyl ester-TMSi derivatives. The compound numbers correspond to the peak quotation of the GC–MS profile shown in Fig. 3.

guaiacyl (G) and syringyl (S) lignin units only involved in β-*O*-4 bonds specifically and respectively give rise to thioethylated G and S monomers (Fig. 4), with a high reaction yield. In contrast, ferulic ester bonds are only partially cleaved, which give rise to free ferulic acid and to the corresponding product formed by addition of EtSH on the double bond (Lapierre, 1993). On this basis, thioacidolysis may be viewed as a diagnostic test for the presence of lignins in ferulic-containing samples.

Noticeable amounts of G and S thioethylated monomers were released from destarched maize bran (Table 4). The recovery yield was approximately one tenth of the yield obtained from mature maize internodes with 16–17% lignin content (Méchin et al., 2000), which suggests that the lignin content of destarched maize bran is in the 1–2% range (wt.%). Thioacidolysis revealed that the heteroxylan fractions extracted from maize bran by alkali in mild or in severe conditions were associated with β-*O*-4 structures, the most diagnostic lignin structures. The amount of β-*O*-4 lignin structures occurring in these maize heteroxylan fractions was only four times lower than that of the maize bran samples. According to the S/G proportion reported in Table 4, the β-*O*-4 linked lignin structures evidenced in maize bran and in corresponding heteroxylan fractions were particularly enriched in S units relative to the level observed for internode lignins (Table 4 and more comprehensive data in Méchin et al., 2000). In addition and as revealed by thioacidolysis of permethylated samples (Lapierre, 1993), maize bran lignins differed from maize stem lignins by the observation that ca. 12% of the β-*O*-4 linked S units were terminal units with a free phenolic group (versus 2% in maize stem lignins). This difference may support the hypothesis that lignin structures associated with maize bran are lower molecular weight phenolics relative to their maize stem analogues. About 75% of the lignin structures evidenced in the crude AX sample were lost

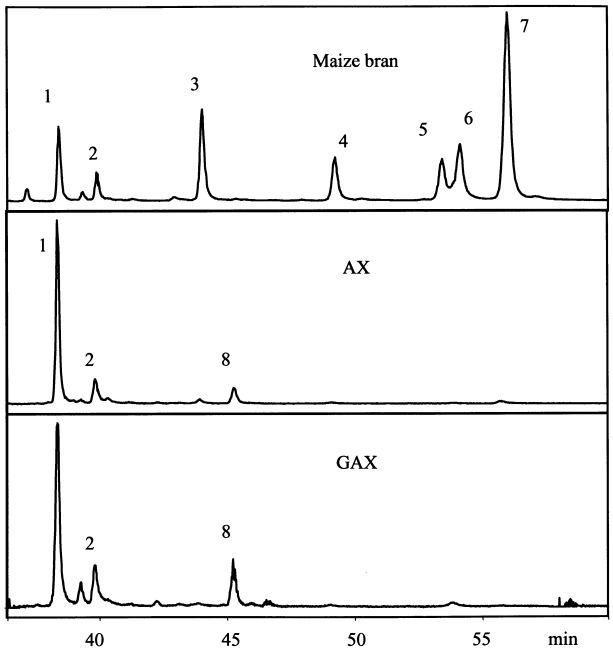

Fig. 3. Partial GC–MS trace of the various diferulates recovered from maize bran (upper trace) and from corresponding heteroxylan sample before (AX) and after (GAX) peroxidase gelation. On each trace, the y-scale (total ion current, arbitrary unit) is normalized on the highest peak. Numbers 1–8 on trace refer to specific diferulates (see Table 3).

Table 3
Abbreviated mass spectra of the methyl ester-TMSi derivatives of the main diferulates released by alkaline hydrolysis of destarched maize bran (electronic impact, 70 eV)

Diferulate[a]	M^+ (%)	Major diagnostic ions (%)
8–8′ Cyclic (**1**)	558 (5)	543 (10), 498 (100), 467 (40), 437 (10), 410 (8), 380 (5), 273 (5), 73 (60), 59 (17).
8–8′ Cyclic (**2**)	616 (5)	601 (20), 557 (45), 542 (6), 527 (5), 513 (10), 498 (25), 467 (25), 437 (10), 410 (10), 380 (5), 273 (5), 89 (10), 73 (100), 59 (10).
8–5′ (**3**)	558 (100)	543 (15), 527 (6), 511 (16), 453 (8), 423 (5), 393 (5), 89 (15), 73 (76), 59 (18).
8-*O*-4′ (**4**)	486 (100)	471 (5), 426 (63), 398 (15), 396 (41), 367 (10), 364 (14), 336 (8), 294 (11), 233 (7), 206 (10), 89 (15), 73 (100), 59 (20).
8-*O*-4′ (**5**)	544 (80)	529 (9), 426 (59), 396 (13), 367 (5), 364 (6), 294 (6), 206 (5), 89 (7), 73 (100), 59 (10).
8–5′ Cyclic (**6**)	544 (8)	486 (48), 454 (100), 439 (9), 424 (25), 394 (5), 364 (7), 350 (8), 234 (6), 196 (6), 73 (75), 59 (25).
5–5′ (**7**)	558 (100)	511 (22), 439 (9), 408 (9), 378 (7), 73 (50), 59 (5).

[a] Structure and peak number as shown in Figs. 2 and 3.

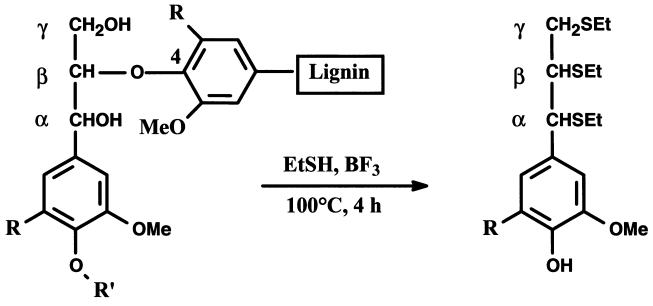

Fig. 4. Principle of the thioacidolysis analytical degradation. Thioethylated guaiacyl (R = H) and syringyl (R = OMe) monomers are specifically released from the typical β-*O*-4 lignin structures (R′ = H or side chain of lignin unit).

during the purification step (AXP, Table 4) which is in agreement with the decolorizing effect of ion-exchange chromatography. Taken together, the data of Table 4 argue for the tight association between alkali-extracted maize heteroxylans and a small percentage of lignin structures. Such associations which resist purification steps might involve alkali-resistant covalent linkages. With the assumption that these lignin structures give rise to thioacidolysis G and S monomers with reaction yields that approximate those of maize internode lignins and from the data of Table 4, we can evaluate the content of lignin structures in maize heteroxylan samples ranging between 0.1 and 0.5% by weight.

Further structural investigation of the lignin moiety associated with maize bran heteroxylans confirmed the occurrence of genuine lignin structures in these samples. The analysis of lignin-derived dimers recovered after thioacidolysis and Raney nickel desulfurization was carried out according to Lapierre (1993). The main lignin-derived dimers recovered from AX and HX samples were syringyl dimers representatives of the β-1 diarylpropane and of the syringaresinol bonding patterns (data not shown), which confirms the occurrence of typical lignin structures in maize heteroxylan samples before and after extensive purification.

Table 4
Yield of lignin-derived thioacidolysis G and S monomers recovered from destarched maize bran and the corresponding heteroxylan fractions obtained in various conditions (Table 1). The yield observed for an extractive-free maize internode sample (F292 line harvested at maturity) with 16.4% lignin (wt.%) content is given for comparison purpose

Sample	S + G (μmol per gram dry sample)	Molar proportion S/G
Maize internode (extractive-free) F292	129	59/41
Destarched maize bran	13.2	80/20
AX fraction	3.9	93/7
AXP fraction (= purified AX)	0.8	94/6
HX fraction (purified)	2.9	92/8
HXO fraction (purified)	4.4	90/10

When the various maize heteroxylan samples studied herein were subjected to peroxidase treatment, the very rapid formation of a firm and britlle gel was observed

only for the AX sample. In contrast, heteroxylan samples isolated in severe conditions did not yield any gel. When the peroxidase treatment was applied to the purified AXP sample, gelling was obtained, but very slowly and the resulting gel was soft and unstable. While the content in ferulate and diferulate units was not affected by the purification procedure, the content in lignin structures was four-fold reduced in AXP and relative to the unpurified AX sample. Taken together, these observations strongly support the hypothesis that lignin structures associated with maize heteroxylan samples may synergistically participate in the gelation phenomenon, at least when the amount of ferulic units available for cross-linking is very low. The fact that gelation induces a decrease in ester-linked ferulic acid without any correlated increase in alkali-releasable diferulates is compatible with the hypothesis that the cross-linking of maize heteroxylan chains may not exclusively involve ferulic units, but also lignin units.

3. Conclusions

The present work has provided the first evidence that typical lignin structures are tightly associated with maize bran heteroxylan extracted by alkali and extensively purified. The amount of lignin structures, as evaluated by thioacidolysis, ranged between 0.1 and 0.5% (wt.%) of the sample. These results argue for the occurrence of covalent linkages between heteroxylan chains and lignin structures. At this point, we cannot determine whether these linkages exist ab initio and/or are formed during the alkaline extraction of heteroxylan. The lignin structures evidenced in maize bran and in the heteroxylan fractions display the typical β-*O*-4, β-1 and β-β bonding patterns met in stem lignins. They differ from stem lignin by their high content in S units, including an unusually high level of S units with free phenolic groups.

In spite of a very low ferulate level, maize bran heteroxylan fractions could efficiently gel upon peroxidase treatment except when the lignin content was reduced to 0.1%. This point further supports a role for lignins, even when present in low amount, in the organization of native or reconstructed polysaccharide networks.

4. Experimental

4.1. Extraction of maize bran heteroxylan samples

Maize bran provided by ULICE (France) was destarched and deproteinized as previously reported (Saulnier et al., 1995b). Heteroxylan fractions were isolated from maize bran under mild or severe alkaline conditions as follows. Purified bran (25 g) was suspended in 500 ml of an alkaline solution (see precise conditions in the following). Solids were separated from solution by centrifugation (5000 *g*, 15 min) and the residue was rinsed with 500 ml of distilled water, centrifuged and rinsed again with 2×250 ml of distilled water. The extract and washings were pooled, acidified to pH 3–4, concentrated in a rotary evaporator at 40°C, dialyzed against distilled water. The pH was adjusted to 3.5 with conc. HOAc and polysaccharides were isolated by EtOH precipitation (4 vol, overnight at 4°C) as previously reported (Saulnier et al., 1995a). The heteroxylan fractions AX, HX and HXO were prepared using the following extraction conditions 0.5 M NaOH, 30°C, 2 h; 1.5 M KOH, 100°C, 2 h and 1.5 M KOH, 1% H_2O_2, 100°C, 2 h, respectively. Recovery yields of 19.1, 55.6 and 56.3% (wt.%) were observed for AX, HX and HXO, respectively.

4.2. Sugar analyses

Individual neutral sugars were determined after hydrolysis (1.5 h in 1 M H_2SO_4 at 100°C for extracted polysaccharides; 1 h in 72% H_2SO_4 at 25°C, then 2 h in 1 M H_2SO_4 at 100°C for the bran) by GC as their alditol acetates derivatives (Englyst and Cummings, 1988). Uronic acids were assayed by the automated *m*-hydroxydiphenyl method (Thibault, 1979) (after pre-hydrolysis for 1 h in 72% H_2SO_4 at 25°C for the bran), using glucuronic acid as standard

4.3. HPLC and GC–MS analyses of alkali-released hydroxycinnamic acid derivatives

Ferulic and diferulic acids were determined after alkaline treatment run according to Saulnier et al. (1999) and to Jacquet et al. (1995). The monomers were determined by HPLC analyses (Saulnier et al., 1999). The dimer fraction was analyzed after derivatization with BF_3 methanol (14% by wt., Supelco) at 80°C and for 30 min. The methylated reaction mixture was diluted with water, the pH adjusted to 3–4 (0.4 M aq. $NaHCO_3$) and the methyl ester derivatives were extracted with EtOAc–CH_2Cl_2 (1:1). Trimethylsilylation of the methylated compounds and subsequent GC–MS analysis of the methyl ester-TMSi derivatives were run according to Jacquet et al. (1995).

The quantitative determinations of diferulates by GC–MS were done relative to 5–5′ dieugenol added as internal standard and according to Jacquet (1997). A diferulate 8–5′ model compound, prepared by $FeCl_3$ oxidation of ferulate methyl ester in THF (data not shown), allowed us to check that the response factor of the 8–5′ dimer relative to dieugenol was 1 (relative concentration/relative surface). The other dimers were quantitatively determined using the same response factor, but without carrying out any precise calibration. Standard errors between duplicate experiments were in the 10–15% range.

4.4. Thioacidolysis experiments

Thioacidolyses were carried out from 10 to 50 mg of maize bran and corresponding heteroxylan fractions. The GC–MS analyses of the lignin-derived monomers and dimers were performed according to Lapierre et al. (1995). Standard errors between duplicate experiments were in the 5–10% range.

4.5. Ion-exchange chromatography

Ion-exchange chromatography was performed on a DEAE-Sepharose CL-6B column (2.6×28 cm) equilibrated with 0.05 M NaOAc buffer, pH 4.5. Heteroxylans (50 ml of a solution at 20 g/l) were loaded onto the column and the gel was washed with 400 ml of 0.05 M NaOAc buffer, pH 4.5. The bound material was eluted with 400 ml of 0.5 M NaOAc buffer, pH 4.5. Fractions (5 ml) were collected and analyzed for their contents of neutral sugars and uronic acids by the automated orcinol (Tollier and Robin, 1979) and *m*-hydroxydiphenyl (Thibault, 1979) assays, respectively. The bound fractions eluted with 0.5 M buffer were pooled, concentrated, extensively dialyzed against distilled water and freeze-dried to give purified heteroxylan fractions (AXP, HX or HXO, Table 1).

4.6. Gelation experiments

Heteroxylan fractions were dissolved in distilled water (ca. 30 mg/ml). One milliliter of the solution was put in a test tube together with 0.1 ml of 0.01 M aq. H_2O_2 and 0.1 ml of horseradish peroxidase aq. solution (110 U/ml, Type I, Sigma). The tube was left at room temperature for 2 h and then returned upside down to check gelation.

4.7. Molar mass determination

Heteroxylan samples were gently dispersed into 0.05 M aq. $NaNO_3$ containing 0.02% NaN_3 (by wt.) and left for dissolution overnight under magnetic stirring. The solutions (ca. 3 mg/ml) were centrifuged in a bench top centrifuge and filtered on 0.10 μm Minisart RC15 Sartorius membranes. Samples were then injected on a high-performance size exclusion chromatography (HPSEC) system constituted of a Shodex OH SB-G pre-column followed by two Shodex OH-pack 804 and 805 columns used in series. The elution was performed at room temperature with 0.05 M aq. $NaNO_3$, containing 0.02% NaN_3 as preservative, at a constant 0.7 ml/min flow rate. On-line molar mass determinations were performed using a multiangle laser light scattering (MALLS) detector (mini-Dawn, Wyatt, Santa Barbara, CA) operating at three angles (41°, 90° and 138) and a differential refractometer (ERC 7517 A) ($dn/dc = 0.146$ ml/g).

References

Chanliaud, E., Saulnier, L., Thibault, J.-F., 1995. Alkaline extraction and characterisation of heteroxylans from maize bran. J. Cereal Sci. 21, 195–203.

Englyst, H.N., Cummings, J.H., 1988. Improved method for measurement of dietary fiber and non-starch polysaccharides in plant foods. J. Assoc. Off. Anal. Chem. 71, 808–814.

Figueroa-Espinoza, M.C., Rouau, X., 1998. Oxidative cross-linking of pentosans by a fungal laccase and horseradish peroxidase: mechanisms of linkage between feruloylated arabinoxylans. Cereal Chem. 75, 259–265.

Ford, C.W., Hartley, R.D., 1988. Identification of phenols, phenolic acid dimers and monosaccharides by gas-liquid chromatography on a capillary column. J. Chromatogr. 436, 484–489.

Grabber, J.H., Hatfield, R.D., Ralph, J., Zon, J., Amrhein, N., 1995. Ferulate cross-linking in cell walls isolated from maize cell suspension. Phytochemistry 40, 1077–1082.

Grabber, J.H., Ralph, J., Hatfield, R.D., 1998. Ferulate cross-links limit the enzymatic degradation of synthetically lignified primary walls of maize. J. Agr. Food Chem. 46, 2609–2614.

Jacquet, G., 1997. Structure et Réactivité des Lignines de Graminées et Acides Phénoliques Associés. (Structure and Reactivity of Grass Lignins and Associated Phenolic Acids). PhD thesis, Université Aix-Marseille III, p. 181.

Jacquet, G., Pollet, B., Lapierre, C., Mhamdi, F., Rolando, C., 1995. New ether-linked ferulic acid-coniferyl alcohol dimers identified in grass straws. J. Agr. Food Chem. 43, 2746–2751.

Kato, Y., Nevins, D.J., 1985. Isolation and identification of *O*-(5-*O*-feruloyl-α-L-arabinofuranosyl)-(1→3)-*O*-β-D-xylopyranosyl-(1→4)-D-xylose as a component of *Zea* shoot cell walls. Carbohydr. Res. 137, 139–150.

Lapierre, C., 1993. Application of new methods for the investigation of lignin structure. In: Jung, H.J., Buxton, D.R., Hatfield, R.D., Ralph, J. (Eds.), Forage Cell Wall Structure and Digestibility. Am. Soc. Agronomy Inc., pp. 133–166.

Lapierre, C., Pollet, B., Rolando, C., 1995. New insights into the architecture of hardwood lignins by chemical degradative methods. Res. Chem. Intermed. 21, 397–412.

Kamisaka, S., Takeda, S., Takahashi, K., Shibata, K., 1990. Diferulic and ferulic acid in the cell wall of *Avena coleoptiles*:their relationships to mechanical properties of the cell wall. Physiol. Plant. 78, 1–7.

Méchin, V., Argillier, O., Menanteau, V., Barrière, Y., Mila, I., Pollet, B., Lapierre, C., 2000. Relationship of cell wall composition to in vitro cell wall digestibility of maize inbred line stems. J. Sci. Food Agric. 80, 574–580.

Mueller-Harvey, I., Hartley, R.D., Harris, P.J., Curzon, E.H., 1986. Linkage of *p*-coumaroyl and feruloyl groups to cell wall polysaccharides of barley straw. Carbohydr. Res. 148, 71–85.

Ng, A., Greenshields, R.R., Waldron, K.W., 1997. Oxidative cross-linking of corn bran hemicellulose formation of ferulic acid dehydrodimers. Carbohydr. Res. 303, 459–462.

Oosteveld, A., Grabber, J.H., Beldman, G., Ralph, J., Voragen, A.G.J., 1997. Formation of ferulic acid dehydrodimers through oxidative cross-linking of sugar-beet pectin. Carbohydr. Res. 300, 179–181.

Pena, M.-J., Sanchez, M., Zarra, I., Revilla, G., 1998. Sequential extraction of dehydroferulates show heterogeneity in their degree of association with *Zea mays* coleoptile cell walls. Phytochem. Anal. 9, 141–144.

Ralph, J., Quideau, S., Grabber, J.H., Hatfield, R.D., 1994. Identification and synthesis of new ferulic acid dehydrodimers present in grass cell walls. J. Chem. Soc. Perkin Trans. 1, 3485–3498.

Russel, W.R., Forrester, A.R., Chesson, A., Burkitt, M.J., 1996. Oxidative coupling during lignin polymerization is determined by unpaired electron delocalization with parent phenylpropanoid radicals. Arch. Biochem. Biophys. 332, 357–366.

Sanchez, M., Pena, M.J., Revilla, G., Zarra, I., 1996. Changes in

dehydrodiferulic acids and peroxidase activity against ferulic acid associated with cell walls during growth of *Pinus pinaster* hypocotyls. Plant Physiol. 111, 941–946.

Saulnier, L., Crépeau M.-J., Lahaye, M., Thibault, J.-F., Garcia-Conesa, M., Kroon, P.A., Williamson, G., 1999. Isolation and structural determination of two 5,5′-diferuloyl oligosaccharides indicate that maize heteroxylans are covalently cross-linked by oxidatively coupled ferulates. Carbohydr. Res. 320, 82–92.

Saulnier, L., Marot, C., Chanliaud, E., Thibault, J.-F., 1995a. Cell wall polysaccharide interactions in maize bran. Carbohydr. Polymers 26, 279–287.

Saulnier, L., Thibault, J.-F., 1999. Ferulic acid and diferulic acids as components of sugar-beet pectins and maize bran heteroxylans. J. Sci. Food Agric. 79, 396–402.

Saulnier, L., Vigouroux, J., Thibault, J.-F., 1995b. Isolation and partial characterization of feruloylated oligosaccharides from maize bran. Carbohydr. Res. 272, 241–253.

Schooneveld-Bergmans, M.E.F., Hopman, A.M.C.P., Beldman, G., Voragen, A.G.J., 1998. Extraction and partial characterization of feruloylated glucuronoarabinoxylans from wheat bran. Carbohydr. Polymers 35, 39–47.

Thibault, J.-F., 1979. Automatisation du dosage des substances pectiques par la méthode au méta-hydroxydiphényl. Lebensm. Wiss. u. Technol. 12, 247–251.

Thibault, J.-F., 1986. Some physicochemical properties of sugar-beet pectins modified by oxidative cross-linking. Carbohydr. Res. 155, 83–192.

Tollier, M.-T., Robin, J.-P., 1979. Adaptation de la méthode à l'orcinol sulfurique au dosage automatique des oses neutres et totaux. Ann. Technol. Agric. (Paris). 28, 1–15.

Wakabayashi, K., Hoson, T., Kamisaka, S., 1997. Osmotic stress suppresses cell wall stiffening and the increase in cell wall-bound ferulic and diferulic acids in wheat coleoptiles. Plant Physiol. 113, 967–973.

Wallace, G., Fry, S.C., 1995. In vitro peroxidase-catalysed oxidation of ferulic acid esters. Phytochemistry 39, 1293–1299.

Wallace, G., Fry, S.C., 1999. Action of diverse peroxidases and laccases on six cell wall-related phenolic compounds. Phytochemistry 52, 769–773.

Wittkowski, R., 1985. Phenole im Räucherrauch. Nachweis und Identifizierung. Verlag VCH, Weinheim.

PERGAMON

Phytochemistry 57 (2001) 773–779

PHYTOCHEMISTRY

www.elsevier.com/locate/phytochem

Triterpene glycosides from the roots of *Sanguisorba officinalis*

Yoshihiro Mimaki[a,*], Masato Fukushima[a], Akihito Yokosuka[a], Yutaka Sashida[a], Shigenori Furuya[b], Hiroshi Sakagami[b]

[a]*Laboratory of Medicinal Plant Science, School of Pharmacy, Tokyo University of Pharmacy and Life Science, 1432-1, Horinouchi, Hachioji, Tokyo 192-0392, Japan*

[b]*Department of Dental Pharmacology, Meikai University School of Dentistry, 1-1, Keyaki-dai, Sakado, Saitama 350-0283, Japan*

Received 2 November 2000; received in revised form 15 February 2001

Abstract

Five triterpene glycosides were isolated from the MeOH extract of *Sanguisorba officinalis* (Rosaceae) roots, as confirmed by detailed analysis of their ^{1}H, ^{13}C, and two-dimensional NMR data, and by the results of hydrolytic cleavage. Three known triterpenes and six known triterpene glycosides were also isolated and identified. The isolated compounds were evaluated for their cytotoxic activities against HSC-2 cells and HGF. © 2001 Elsevier Science Ltd. All rights reserved.

Keywords: *Sanguisorba officinalis*; Rosaceae; Triterpene glycosides; Cytotoxic activity; HSC-2 cells

1. Introduction

Sanguisorba officinalis L. (Rosaceae) is a perennial plant that occurs in the northern districts in China. Its roots have hemostatic, analgesic, and astringent properties, and have been used in traditional Chinese medicine for the treatment of burns, scalds, and internal hemorrhage (Cheng and Cao, 1992). A series of hydrolysable tannins were reported as characteristic constituents of *S. officinalis* roots and are considered to be partially responsible for the therapeutic effects of this crude drug (Tanaka et al., 1985). Apart from medicinal folklore background of *S. officinalis* as mentioned above, the discovery of a cytotoxic activity associated with inhibition of DNA topoisomerases of sanguiin H-6, a dimeric ellagitannin from *S. officinalis*, is noteworthy (Bastow et al., 1993). A communication dealing with the nitric oxide production-suppressing activity of sanguiin H-6 and H-11 has recently been published (Yokozawa et al., 2000). Furthermore, *S. officinalis* is known to contain a triterpene glycoside, ziyu-glycoside I, and its derivatives, including their corresponding aglycones (Cheng and Cao, 1992; Yosioka et al., 1971). However, triterpene constituents of *S. officinalis* seemed not to be completely known and thus deserved further study. We systematically examined the triterpene glycosides components of *S. officinalis* and isolated five new triterpene glycosides, along with three known triterpenes and six known triterpene glycosides. This paper deals with the structural elucidation of the new triterpene glycosides on the basis of spectroscopic analysis, including two-dimensional (2D) NMR spectroscopic techniques, and of the results of hydrolytic cleavage. The cytotoxic activities of the isolated triterpenes against human oral squamous cell carcinoma (HSC-2) cells and normal human gingival fibroblasts (HGF) are also reported.

2. Results and discussion

A concentrated MeOH extract of *S. officinalis* roots was passed through a polystyrene resin (Diaion HP-20) column, and the MeOH eluate fraction, in which triterpenes and triterpene glycosides were enriched, was subjected to column chromatography using silica gel and octadecylsilanized (ODS) silica gel, as well as preparative HPLC, to yield a total of 14 triterpenes and triterpene glycosides (compounds **1**–**14**). Compounds **6**–**14** are known constituents and identified as 3β,19α-dihydroxyurs-12-en-28-oic acid (**6**) (Cheng and Cao, 1992), 2α,3α,19α-trihydroxyurs-12-en-28-oic acid (**7**) (Cheng and Cao, 1992), 1β,2α,3α,19α-tetrahydroxyurs-12-en-28-oic acid

* Corresponding author. Tel.: +81-426-76-4577; fax: +81-426-76-4579.

E-mail address: mimakiy@ps.tokaku.ac.jp (Y. Mimaki).

0031-9422/01/$ - see front matter © 2001 Elsevier Science Ltd. All rights reserved.
PII: S0031-9422(01)00083-8

(**8**) (Guang-Yi et al., 1989), 3β,19α-dihydroxyurs-12-en-28-oic acid 28-β-D-glucopyranosyl ester (**9**) (Cheng and Cao, 1992), 2α,3β,19α-trihydroxyurs-12-en-28-oic acid 28-β-D-glucopyranosyl ester (**10**) (Jia et al., 1993), 2α,3α,19α-trihydroxyurs-12-en-28-oic acid 28-β-D-glucopyranosyl ester (**11**) (Jia et al., 1993), 3β-[(α-L-arabinopyranosyl)oxy]-19α-hydroxyurs-12-en-28-oic acid (**12**) (Cheng and Cao, 1992), 3β-[(α-L-arabinopyranosyl)oxy]-19α-hydroxyurs-12-en-28-oic acid 28-β-D-glucopyranosyl ester (**13**) (Cheng and Cao, 1992), 3β-[(α-L-arabinopyranosyl)oxy]-23-hydroxyolean-12-en-28-oic acid 28-β-D-glucopyranosyl ester (**14**) (Kizu et al., 1985), respectively. The physical and spectral data were consistent with the literature values.

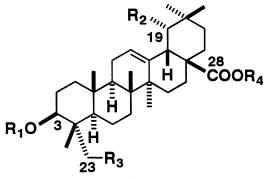

	R_1	R_2	R_3	R_4
1	Ara	OH	H	Glc
1a	H	OH	H	H
14	Ara	H	OH	Glc

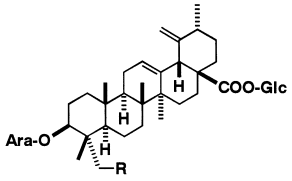

	R
2	H
3	OH

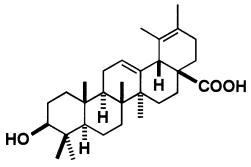

2a

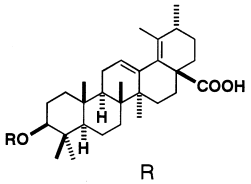

	R
2b	H
4	Ara

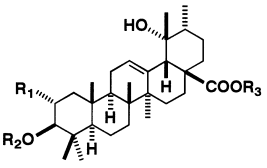

	R_1	R_2	R_3
5	H	Ara	6-*O*-Galloyl-Glc
6	H	H	H
9	H	H	Glc
10	OH	H	Glc
12	H	Ara	H
13	H	Ara	Glc

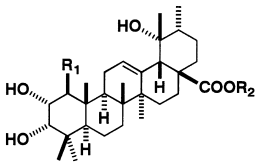

	R_1	R_2
7	H	H
8	OH	H
11	H	Glc

Ara: α-L-arabinopyranosyl
Glc: β-D-glucopyranosyl

Compound **1** was isolated as an amorphous solid with a molecular formula, $C_{41}H_{66}O_{13}$, as determined by elemental analysis combined with data of the positive-ion FABMS exhibiting an $[M+Na]^+$ ion at *m/z* 789. The IR spectrum showed a characteristic absorption attributable to an ester carbonyl group at 1731 cm^{-1}, as well as a broad absorption due to hydroxyl groups near 3418 cm^{-1}. The ^1H NMR spectrum of **1** (C_5D_5N) exhibited signals for seven tertiary methyl groups at δ 1.65, 1.27, 1.16×2, 1.00, 0.97, and 0.91 (each *s*), and an olefinic proton at δ 5.52 (*t*-like, $J=3.2$ Hz), which were characteristic of the oleanolic acid skeleton. Furthermore, two anomeric proton signals were identified at δ 6.39 (*d*, $J=8.1$ Hz) and 4.78 (*d*, $J=7.0$ Hz). Acid hydrolysis of **1** with 1 M HCl in dioxane–H_2O (1:1) gave a triterpene ($C_{30}H_{48}O_4$) (**1a**), and D-glucose and L-arabinose as the carbohydrate components. The monosaccharides, including their absolute configurations, were identified by direct HPLC analysis of the hydrolysate, with detection being carried out by using an optical rotation (OR) detector. Comparison of the ^1H and ^{13}C NMR spectroscopic assignments of **1a** with those of oleanolic acid (Kizu et al., 1995), taking into account the molecular formula of **1a**, suggested that **1a** was an oleanolic acid derivative with a hydroxyl group at the ring E portion. The proton signal at δ 3.66 showed long-range correlations with C-13 (δ 144.9), C-17 (δ 46.1), and C-28 (δ 180.9) in the HMBC spectrum, and was assigned to H-18. This proton had a proton spin-coupling correlation with the signal at δ 3.64, which was associated with the carbon signal at δ 81.3 (CH) in the HMQC spectrum. Thus, the presence of a hydroxyl group at C-19 was evident. The $^3J_{H,H}$ value of 2.8 Hz between H-18 and H-19, and NOE correlations from H-19 to Me-29 (δ 1.21) and Me-30 (δ 1.13) gave evidence for the C-19α hydroxy configuration. The ^1H and ^{13}C NMR signals of the glycoside moieties were readily assigned by interpretation of the ^1H–^1H COSY and HMQC spectra. Proton multiplet patterns and coupling constants, as well as the proton and carbon chemical shifts revealed that **1** contained that an α-L-arabinopyranosyl unit and a β-D-glucopyranosyl unit, which were directly linked to the aglycone. In the HMBC spectrum of **1**, correlation peaks were observed from δ 4.78 (anomer of arabinosyl) to δ 88.7 (C-3 of aglycone), and δ 6.39 (anomer of glucosyl) to δ 177.2 (C-28 of aglycone). Accordingly, the structure of **1** was characterized as 3β-[(α-L-arabinopyranosyl)oxy]-19α-hydroxyolean-12-en-28-oic acid 28-β-D-glucopyranosyl ester.

Compound **2** was obtained as an amorphous solid, and its molecular formula, $C_{41}H_{64}O_{12}$, was deduced from the positive-ion FABMS (*m/z* 771 $[M+Na]^+$) and the result of elemental analysis. The ^1H NMR spectrum of **2** (C_5D_5N) contained signals for five tertiary methyl groups at δ 1.29×2, 1.14, 0.97, and 0.89 (each *s*), a secondary methyl group at δ 1.07 (*d*, $J=6.4$ Hz), an exomethylene group at δ 5.21 and 5.06 (each *br s*), an olefinic proton at δ 5.55 (*t*-like, $J=3.3$ Hz), and two anomeric protons at δ 6.34 (*d*, $J=8.1$ Hz) and 4.79 (*d*, $J=7.1$ Hz). These data and the ^{13}C NMR spectral feature suggested that **2** was a triterpene bisdesmoside based upon ursolic acid. In the HMBC spectrum, the exomethylene protons showed long-range correlations with the carbons due to C-18 (δ 52.2) and C-20 (δ 37.5), indicating the location of the exomethylene group at C-19(29). Based on an NOE correlation between the protons of Me-30 and H-21α, Me-30 was assigned as α-configuration. Acid

hydrolysis of **2** with 1 M HCl resulted in the production of two artifactual triterpenes (**2a**, **2b**), together with D-glucose and L-arabinose. The ^{1}H NMR spectrum of **2a** showed seven three-proton singlet signals, and two of them were assigned as being located on a double bond. The UV spectrum of **2b** showed a λ_{max} at 226 nm (log ε 3.65), which implied the presence of a conjugated diene group, and the ^{1}H NMR spectrum included signals for five tertiary methyl groups, a secondary methyl group, and a methyl group on a double bond. These spectral properties combined with information from the MS, ^{13}C NMR, and various 2D NMR spectra allowed the identification of **2a** and **2b** as 3β-hydroxyurs-12,19(20)-dien-28-oic acid and 3β-hydroxyurs-12,18-dien-28-oic acid, respectively (Ahmad and Basha, 2000). These compounds were considered to be produced through migration of the C-19(29) double bond under acidic conditions. The ^{1}H, ^{13}C, and 2D NMR spectral data of **2** indicated that it had an α-L-arabinopyranosyl unit at C-3 and a β-D-glucopyranosyl unit at C-28 in the molecule, as in **1**. The structure of **2** was characterized as 3β-[(α-L-arabinopyranosyl)oxy]urs-12,19(29)-dien-28-oic acid 28-β-D-glucopyranosyl ester.

Compound **3** was shown to have the molecular formula, $C_{41}H_{64}O_{13}$, by the positive-ion FABMS (*m*/*z* 787 $[M+Na]^+$) and elemental analysis. The spectral properties of **3** were very similar to those of **2**. However, the molecular formula of **3** differed from **2** by containing an additional oxygen atom. When the ^{1}H NMR spectrum of **3** was compared with that of **2**, the signal for Me-23, which was observed at δ 1.29 in **2**, disappeared in **3**, and instead signals for an hydroxymethyl group were detected at δ 4.30 and 3.70 (AB*q*, $J=10.6$ Hz). The ^{13}C NMR spectrum of **3**, in which a signal at δ 64.5 was observed for an hydroxymethyl group rather than a tertiary methyl group, and an NOE correlation between the hydroxymethyl protons and H-6α equatorial proton (δ 1.67), also supported this structural modification. The structure of **3** was shown to be 3β-[(α-L-arabinopyranosyl)oxy]-23-hydroxyurs-12,19(29)-dien-28-oic acid 28-β-D-glucopyranosyl ester.

Compound **4** had the molecular formula $C_{35}H_{54}O_7$ on the basis of the positive-ion FABMS (*m*/*z* 609 $[M+Na]^+$) and elemental analysis. The ^{1}H NMR spectrum showed signals for six tertiary methyl groups at δ 1.89, 1.31, 1.18, 1.04, 0.97, and 0.89 (each *s*), a secondary methyl group at δ 1.13 (*d*, $J=6.9$ Hz), an olefinic proton at δ 5.73 (*t*-like, $J=2.8$ Hz), and an anomeric proton at δ 4.80 (*d*, $J=7.1$ Hz). The UV absorption at λ_{max} 226 (log ε 3.79) were attributable to a conjugated diene system. Acid hydrolysis of **4** gave **2b** and L-arabinose. The ^{13}C NMR spectrum of **4** showed data consistent with an arabinose moiety, and it was found to be attached at C-3 of the aglycone by an HMBC correlation from δ 4.80 to δ 88.7 (C-3 of aglycone). The structure of **4** was determined to be 3β-[(α-L-arabinopyranosyl)oxy]urs-12,18-dien-28-oic acid.

Compound **5** was obtained as a pale-yellow solid. Its molecular formula was determined as $C_{48}H_{70}O_{17}$ on the basis of the positive-ion FABMS (*m*/*z* 941 $[M+Na]^+$) and elemental analysis. The ^{1}H NMR spectrum included signals for seven triterpene methyls at δ 1.68 (*s*), 1.33 (*s*), 1.25 (*s*), 1.19 (*s*), 1.02 (*d*, $J=6.7$ Hz), 0.99 (*s*), and 0.93 (*s*), an olefinic proton at δ 5.53 (*t*-like, $J=3.3$ Hz), and two anomeric protons at δ 6.30 (*d*, $J=8.0$ Hz) and 4.76 (*d*, $J=7.0$ Hz). In addition, the presence of a galloyl ester group was suggested by the UV [λ_{max} 278 nm (log ε 3.75)], ^{1}H NMR [δ 7.87 (2H, s)], and ^{13}C NMR [δ 167.4 (C=O), 147.4 (C×2), 140.8 (C), 121.1 (C), 110.3 (CH×2)]. Alkaline treatment of **5** with 10% NH_3aq yielded **13** and gallic acid. When the ^{1}H and ^{13}C NMR spectra of **5** were compared with those of **13**, downfield shifts by *O*-acylation were detected at the H_2-6 signal at δ 5.01 (2H, *d*, $J=9.2$ Hz) and the C-6 signal at δ 64.6 of the glucosyl residue. Furthermore, an HMBC correlation was observed from δ 5.01 to the carbonyl carbon resonance of the galloyl group at δ 167.4. All of these data for **5** were consistent with the structure 3β-[(α-L-arabinopyranosyl)oxy]-19α-hydroxyurs-12-en-28-oic acid 28-(6-*O*-galloyl-β-D-glucopyranosyl) ester.

Compounds **1**–**5** are new triterpene glycosides, and this is the first report on the isolation of **8**, **10**, **11**, and **14** from *S. officinalis*.

The isolated compounds were evaluated for their cytotoxic activities against HSC-2 cells and HGF (Table 2). Compounds **3** and **14**, which are bisdesmosidic triterpenes with the oleanane or ursane skeleton bearing a hydroxyl group at C-23, showed cytotoxic activity against HSC-2 cells with the respective IC_{50} values of 15 and 18 μg/ml, although they were not cytotoxic against HGF at all ($IC_{50} > 200$ μg/ml).

3. Experimental

3.1. General

FABMS: Finnigan MAT TSQ-700 (San Jose, CA, USA) (matrix: Magic Bullet, a mixture of dithiothreitol and dithioerythritol, 3:1; Tokyo-Kasei, Tokyo, Japan). NMR (ppm, *J* Hz): Bruker DPX-400 (400 MHz for ^{1}H NMR, Karlsruhe, Germany) or Bruker AM-500 (500 MHz for ^{1}H NMR). CC: Diaion HP-20 (Mitsubishi-Kasei, Tokyo, Japan); silica gel (Fuji-Silysia Chemical, Aichi, Japan); ODS silica gel (Nacalai Tesque, Kyoto, Japan); Sephadex LH-20 (Pharmacia, Freiburg, Germany). TLC: precoated Kieselgel 60 F_{254} (0.25 mm thick, Merck, Darmstadt, Germany) and RP-18 $F_{254}S$ (0.25 mm thick, Merck). Preparative HPLC: a Tosoh HPLC system (pump, CCPM; controller, CCP controller PX-8010) equipped with an RI detector (Tosoh RI-8010, Tokyo, Japan) and a Capcell Pak C_{18} UG80 column (10 mm i.d.×250 mm, ODS, 5 μm, Shiseido,

Tokyo, Japan). Cell culture and assay for cytotoxic activity: Dulbecco's modified Eagle medium (DMEM) (Gibco, Grand Island, NY, USA); fetal bovine serum (FBS) (JRH Biosciences, Lenexa, KS, USA); penicillin, streptomycin, 3-(4,5-dimethylthiazol-2-yl)-2,5-diphenyl-2*H*-tetrazolium bromide (MTT), and α-minimum essential medium (α-MEM) (Sigma, St. Louis, MO, USA). All other chemicals used were of biochemical reagent grade.

3.2. Plant material

Sanguisorba officinalis was purchased from a wholesale firm in Uchida-Wakanyaku, Tokyo Japan in 1997. One of the authors, Y. Sashida., identified it by its morphological characters. A voucher specimen has been deposited in the laboratory of Y. Sashida (voucher No. SO-97-7, Laboratory of Medicinal Plant Science).

3.3. Extraction and isolation

The dessicated roots of the plant material (3 kg) were extracted with hot MeOH. The MeOH extract was concentrated under reduced pressure, and the viscous concentrate (320 g) was passed through a Diaion HP-20 column eluting with increased amounts of MeOH in H_2O (30% MeOH, 50% MeOH, and 80% MeOH), MeOH, EtOH, and EtOAc. Preliminary TLC analysis of these fractions suggested that the MeOH eluate portion contained a variety of triterpene and triterpene glycosides, on which further fractionation was carried out. CC of the MeOH eluate portion on silica gel and elution with a stepwise gradient mixture of $CHCl_3$–MeOH (9:1; 4:1; 2:1), and finally with MeOH alone, gave five fractions (I–V). Fraction I was applied to a silica gel column this being eluted with hexane–Me_2CO (1:1) and $CHCl_3$–MeOH (19:1) and ODS silica gel with MeOH–H_2O (4:1) to give **4** (9.0 mg), **6** (43.2 mg), **7** (7.5 mg), and **8** (5.5 mg). Fraction II was subjected to CC on silica gel eluting with $CHCl_3$–MeOH–H_2O (80:10:1; 50:10:1) and ODS silica gel with MeOH–H_2O (3:1) and MeCN–H_2O (2:3; 1:2) to yield **9** (7.0 mg), **11** (115 mg), and **12** (104 mg). Fraction III was subjected to a silica gel column eluting with $CHCl_3$–MeOH–H_2O (80:10:1; 50:10:1) and an ODS silica gel column with MeOH–H_2O (2:1) and MeCN–H_2O (1:2) to give **10** (3.2 mg). Fraction IV was applied to a silica gel column which was eluted with $CHCl_3$–MeOH–H_2O (50:10:1) and ODS silica gel with MeOH–H_2O (2:1) to give a mixture of **1** and **13**, and **2** with a few impurities. The mixture was separated by preparative HPLC using MeOH–H_2O (3:2) into **1** (40.2 mg) and **13** (180 mg). Compound **2** was completely refined by preparative HPLC using MeOH–H_2O (4:1) to furnish **2** (140 mg) as a pure compound. Fraction V was applied to a silica gel column eluted with $CHCl_3$–MeOH–H_2O (40:10:1) and ODS silica gel with MeOH–H_2O (2:1) and MeCN–H_2O (1:2) to give **3** (21.4 mg) and **5** (23.8 mg), and **14** with a few impurities. Compound **14** was purified by preparative HPLC using using MeOH–H_2O (2:1) to afford **14** (9.4 mg) as a pure compound.

3.4. Compound *1*

An amorphous solid. $[\alpha]_D^{25}$ +14.0° (MeOH: *c* 0.10). FABMS (positive mode) *m/z* 789 $[M+Na]^+$. (Found: C, 60.68; H, 8.64. Calc. for $C_{41}H_{66}O_{13}\cdot 5/2H_2O$: C, 60.66; H, 8.81%). IR ν_{max} (film) cm^{-1}: 3418 (OH), 2927 (CH), 1731 (C=O), 1455, 1388, 1260, 1190, 1071, 1028, 866. ^1H NMR (pyridine-d_5): δ; 6.39 (1H, *d*, *J* = 8.1 Hz, H-1″), 5.52 (1H, *t*-like, *J* = 3.2 Hz, H-12), 4.78 (1H, *d*, *J* = 7.0 Hz, H-1′), 3.59 (1H, *d*, *J* = 2.8 Hz, H-19), 3.34 (1H, *dd*, *J* = 11.7, 4.3 Hz, H-3), 1.65 (3H, *s*, Me-27), 1.27 (3H, *s*, Me-23), 1.16 (3H×2, *s*, Me-26 and Me-29), 1.00 (3H, s, Me-30), 0.97 (3H, *s*, Me-24), 0.91 (3H, *s*, Me-25). ^{13}C NMR: Table 1.

3.5. Acid hydrolysis of *1*

A solution of **1** (25 mg) in 1 M HCl (dioxane–H_2O, 1:1, 4 ml) was heated at 95° for 2 h under an Ar atmosphere. After cooling, the reaction mixture was neutralized by passage through an Amberlite IRA-93ZU (Organo, Tokyo, Japan) column and subjected to silica gel chromatography using a gradient mixture of $CHCl_3$–MeOH (19:1; 9:1; 1:1) to give an aglycone fraction and a sugar fraction (5.9 mg). The aglycone fraction was purified by silica gel CC eluting with hexane–Me_2CO (4:1) to give an aglycone (**1a**) (3.2 mg). HPLC analysis of the sugar fraction under the following conditions showed the presence of D-glucose and L-arabinose. Column: Capcell Pak NH_2 UG80 (4.6 mm i.d.×250 mm, 5 μm, Shiseido); detector: Shodex OR-2 (Showa-Denko, Tokyo, Japan); solvent: MeCN–H_2O (17:3); flow rate: 1.0 ml/min. R_t (min): 8.27 (L-arabinose, positive optical rotation); 13.39 (D-glucose, positive optical rotation).

3.6. Compound *1a*

An amorphous solid. $[\alpha]_D^{25}$ +20.0° (MeOH: *c* 0.10). EIMS *m/z* 472 $[M]^+$. IR ν_{max} (film) cm^{-1}: 3449 (OH), 2927 (CH), 1688 (C=O), 1455, 1388, 1260, 1071, 1028, 866. ^1H NMR (pyridine-d_5): δ 5.60 (1H, *t*-like, *J* = 3.3 Hz, H-12), 3.66 (1H, *d*, *J* = 2.8 Hz, H-18), 3.64 (1H, *d*, *J* = 2.8 Hz, H-19), 3.46 (1H, *dd*, *J* = 11.7, 4.3 Hz, H-3), 1.67 (3H, *s*, Me-27), 1.26 (3H, *s*, Me-23), 1.21 (3H, *s*, Me-29), 1.13 (3H, *s*, Me-30), 1.10 (3H, s, Me-26), 1.05 (3H, s, Me-24), 0.95 (3H, s, Me-25). ^{13}C NMR: Table 2.

3.7. Compound *2*

An amorphous solid. $[\alpha]_D^{25}$ +12.0° (MeOH: *c* 0.10). FABMS (positive mode) *m/z* 771 $[M+Na]^+$. (Found:

Table 1
^{13}C NMR spectral data for compounds **1**, **1a**, **2**, **2a**, **2b** and **3**–**5** in pyridine-d_5

C	1	1a	2	2a	2b	3	4	5
1	38.7	38.8	38.9	39.3	39.4	38.9	39.3	38.9
2	26.6	28.4	26.7	28.1	28.2	26.1	27.1	26.6
3	88.7	78.2	88.7	78.1	78.1	81.9	88.7	88.8
4	39.6	39.4	39.6	39.6	39.5	43.5	39.6	39.6
5	56.0	56.0	56.0	55.9	56.0	47.7	56.1	55.9
6	18.7	19.0	18.5	18.7	18.7	18.2	18.5	18.6
7	33.2	33.7	33.4	34.3	35.6	33.1	35.6	33.5
8	40.2	40.0	39.8	39.3	39.3	39.9	39.4	40.5
9	48.3	48.4	48.0	48.2	48.3	48.1	48.2	47.7
10	37.2	37.6	37.1	37.2	37.2	37.0	36.9	37.0
11	24.1	24.2	23.8	23.6	23.4	23.9	23.4	24.0
12	123.5	123.5	128.5	127.3	125.9	128.6	125.9	128.5
13	144.3	144.9	137.5	138.5	139.4	137.5	139.5	139.2
14	42.1	42.2	42.8	43.8	45.0	42.8	45.0	42.0
15	29.0	30.0	29.1	28.6	29.1	29.1	29.2	29.1
16	28.0	28.1	25.8	23.9	27.0	25.8	26.8	26.0
17	46.5	46.1	49.8	46.9	49.7	49.8	49.8	48.7
18	44.6	44.9	52.2	50.7	123.7	52.2	123.9	54.3
19	81.0	81.3	153.4	129.0	134.6	153.4	134.7	72.6
20	35.5	35.7	37.5	123.9	34.8	37.5	34.8	42.0
21	28.9	29.2	30.6	28.7	31.8	30.6	31.9	26.6
22	33.0	33.4	37.1	33.5	35.1	37.1	35.1	37.8
23	28.2	29.2	28.2	28.8	28.8	64.5	28.3	28.2
24	16.8	16.5	17.0	16.6	16.6	13.6	17.0	17.4
25	15.5	15.5	15.7	16.1	16.3	16.3	16.3	15.6
26	17.6	17.5	17.3	18.0	18.3	17.4	18.3	16.9
27	24.9	24.9	26.2	22.1	22.1	26.2	22.1	24.6
28	177.2	180.9	176.0	180.0	178.5	176.1	178.7	177.0
29	28.7	28.8	110.5	17.3	19.6	110.4	19.6	26.9
30	24.7	24.9	19.4	20.5	18.9	19.4	18.9	16.6
1′	107.6		107.6			106.6	107.5	107.4
2′	72.9		72.9			73.1	72.9	72.9
3′	74.6		74.7			74.7	74.6	74.6
4′	69.5		69.6			69.6	69.5	69.5
5′	66.8		66.8			67.0	66.7	66.6
1″	95.9		95.6			95.9		95.7
2″	74.1		74.1			74.1		74.0
3″	78.9		78.9			78.9		78.8
4″	71.1		71.1			71.1		71.3
5″	79.3		79.4			79.3		76.1
6″	62.2		62.2			62.3		64.6
1‴								121.1
2‴								110.3
3‴								147.4
4‴								140.8
5‴								147.4
6‴								110.3
7‴								167.4

C, 59.97; H, 8.66. Calc. for $C_{41}H_{64}O_{12}\cdot 4H_2O$: C, 59.98; H, 8.84%). IR ν_{max} (film) cm^{-1}: 3375 (OH), 2927 (CH), 1731 (C=O), 1455, 1388, 1260, 1200, 1136, 1071, 986. ^{1}H NMR (pyridine-d_5): δ 6.34 (1H, *d*, $J=8.1$ Hz, H-1″), 5.55 (1H, *t*-like, $J=3.3$ Hz, H-12), 5.21 and 5.06 (each 1H, *br s*, CH_2-29), 4.79 (1H, *d*, $J=7.1$ Hz, H-1′), 3.39 (1H, *dd*, $J=11.8$, 4.2 Hz, H-3), 1.29 (3H×2, *s*, Me-23 and Me-27), 1.14 (3H, *s*, Me-26), 1.07 (3H, *d*, $J=6.4$ Hz, Me-30), 0.97 (3H, *s*, Me-24), 0.89 (3H, *s*, Me-25). ^{13}C NMR: Table 2.

Table 2
Cytotoxic activites of compounds **1**–**14** against HSC-2 cells and HGF

Compounds	IC_{50} (μg/ml)	
	HSC-2	HGF
1	> 200	> 200
2	50	> 200
3	15	> 200
4	> 200	> 200
5	79	> 200
6	> 200	> 200
7	> 200	> 200
8	100	> 200
9	50	> 200
10	> 200	> 200
11	> 200	> 200
12	> 200	> 200
13	153	> 200
14	18	> 200

3.8. Acid hydrolysis of **2**

Compound **2** (20 mg) was subjected to acid hydrolysis as described for **1** to give **2a** (4.8 mg) and **2b** (3.5 mg), and a sugar fraction (4.1 mg). HPLC analysis of the sugar fraction under the same conditions as in the case of that of **1** showed the presence of D-glucose and L-arabinose.

3.9. Compound **2a**

An amorphous solid. $[\alpha]_D^{25}$ +4.0° (MeOH: *c* 0.10). EIMS *m*/*z* 454 $[M]^+$. IR ν_{max} (film) cm^{-1}: 3383 (OH), 2927 (CH), 1689 (C=O), 1449, 1378, 1256, 1091, 1025, 866. ^{1}H NMR (pyridine-d_5): δ 5.71 (1H, *t*-like, $J=3.5$ Hz, H-12), 3.64 (1H, *br s*, H-18), 3.46 (1H, *dd*, $J=11.3$, 4.3 Hz, H-3), 1.71 (3H, *s*, Me-29), 1.64 (3H, *s*, Me-30), 1.23 (3H, *s*, Me-23), 1.15 (3H, *s*, Me-27), 1.04 (3H, *s*, Me-26), 1.03 (3H, *s*, Me-25), 0.92 (3H, *s*, Me-24). ^{13}C NMR: Table 2.

3.10. Compound **2b**

An amorphous solid. $[\alpha]_D^{25}$ +166° (MeOH: *c* 0.10). EIMS *m*/*z* 454 $[M]^+$. UV λ_{max} (MeOH) nm: 226 (log ε 3.65). IR ν_{max} (film) cm^{-1}: 3412 (OH), 2927 (CH), 1689 (C=O), 1460, 1376, 1258, 1096, 1034. ^{1}H NMR (pyridine-d_5): δ 5.74 (1H, *t*-like, $J=2.8$ Hz, H-12), 3.48 (1H, *dd*, $J=11.3$, 4.3 Hz, H-3), 1.88 (3H, *s*, Me-29), 1.25 (3H, *s*, Me-23), 1.15 (3H, *s*, Me-27), 1.12 (3H, *d*, $J=6.9$ Hz, Me-30), 1.06 (3H, *s*, Me-26), 1.04 (3H, *s*, Me-24), 0.93 (3H, *s*, Me-25). ^{13}C NMR: Table 2.

3.11. Compound **3**

An amorphous solid. $[\alpha]_D^{25}$ +24.0° (MeOH: *c* 0.10). FABMS (positive mode) *m*/*z* 787 $[M+Na]^+$. (Found:

C, 63.28; H, 8.75. Calc. for $C_{41}H_{64}O_{13}\cdot 1/2H_2O$: C, 63.63; H, 8.47%). IR ν_{max} (film) cm^{-1}: 3376 (OH), 2935 (CH), 1733 (C=O), 1455, 1388, 1260, 1198, 1136, 1073. ^1H NMR (pyridine-d_5): δ 6.32 (1H, *d*, $J=8.2$ Hz, H-1″), 5.54 (1H, *t*-like, $J=3.1$ Hz, H-12), 5.18 and 5.03 (each 1H, AB*q*, $J=1.4$ Hz, CH_2-29), 4.79 (1H, *d*, $J=7.2$ Hz, H-1′), 4.31 (1H, overlapping, H-3), 4.30 and 3.70 (each 1H, AB*q*, $J=10.6$ Hz, CH_2-23), 1.19 (3H, *s*, Me-27), 1.16 (3H, *s*, Me-25), 1.06 (3H, *d*, $J=6.4$ Hz, Me-30), 0.99 (3H, *s*, Me-26), 0.93 (3H, *s*, Me-24). ^{13}C NMR: Table 2.

3.12. Compound **4**

An amorphous solid. $[\alpha]_D^{25}$ +112° (MeOH: *c* 0.10). FABMS (positive mode) *m/z* 609 $[M+Na]^+$. (Found: C, 63.86; H, 9.20. Calc. for $C_{35}H_{54}O_7\cdot 4H_2O$: C, 63.80; H, 9.48%). UV λ_{max} (MeOH) nm: 226 (log ε 3.79). IR ν_{max} (film) cm^{-1}: 3367 (OH), 2929 (CH), 1688 (C=O), 1449, 1388, 1367, 1256, 1136, 1083, 998. ^1H NMR (pyridine-d_5): δ 5.73 (1H, *t*-like, $J=2.8$ Hz, H-12), 4.80 (1H, *d*, $J=7.1$ Hz, H-1′), 3.40 (1H, *dd*, $J=12.0$, 4.1 Hz, H-3), 1.89 (3H, *s*, Me-29), 1.31 (3H, *s*, Me-23), 1.18 (3H, *s*, Me-27), 1.13 (3H, *d*, $J=6.9$ Hz, Me-30), 1.04 (3H, *s*, Me-26), 0.97 (3H, *s*, Me-24), 0.89 (3H, *s*, Me-25). ^{13}C NMR: Table 2.

3.13. Acid hydrolysis of **4**

Compound **4** (5 mg) was subjected to acid hydrolysis as described for **1** to give **2b** (2.7 mg) and a sugar fraction (0.7 mg). HPLC analysis of the sugar fraction under the same conditions as in the case of that of **1** showed the presence of L-arabinose.

3.14. Compound **5**

A pale-yellow amorphous solid. $[\alpha]_D^{25}$ +10.0° (MeOH: *c* 0.10). FABMS (positive mode) *m/z* 941 $[M+Na]^+$. (Found: C, 55.65; H, 7.74. Calc. for $C_{48}H_{70}O_{17}\cdot 13/2H_2O$: C, 55.63; H, 8.07%). UV λ_{max} (MeOH) nm: 278 (log ε 3.75). IR ν_{max} (film) cm^{-1}: 3418 (OH), 2931 and 2878 (CH), 1723 and 1714 (C=O), 1614 and 1538 (aromatic ring), 1455, 1350, 1228, 1137, 1078, 938, 870. ^1H NMR (pyridine-d_5): δ 7.87 (2H, *s*, H-2‴ and H-6‴), 6.30 (1H, *d*, $J=8.0$ Hz, H-1″), 5.53 (1H, *t*-like, $J=3.3$ Hz, H-12), 5.01 (2H, *d*, $J=9.2$ Hz, H_2-6″), 4.76 (1H, *d*, $J=7.0$ Hz, H-1′), 3.32 (1H, *dd*, $J=11.7$, 4.2 Hz, H-3), 1.68 (3H, *s*, Me-27), 1.33 (3H, *s*, Me-29), 1.25 (3H, *s*, Me-23), 1.19 (3H, *s*, Me-26), 1.02 (3H, *d*, $J=6.7$ Hz, Me-30), 0.99 (3H, *s*, Me-25), 0.93 (3H, *s*, Me-24). ^{13}C NMR: Table 2.

3.15. Alkaline hydrolysis of **5**

Compound **5** (8 mg) was treated with 10% NH_3aq (1 ml) at room temperature for 30 min. After evaporation of solvent, the reaction mixture was chromatographed on Sephadex LH-20 eluting with MeOH to furnish **13** (6.3 mg) and gallic acid (1.2 mg).

3.16. Cell culture

HSC-2 cells were maintained as monolayer cultures at 37° in DMEM medium supplemented with 10% heat-inactivated FBS in a humidified 5% CO_2 atmosphere. HGF were isolated, as described previously (Ito et al., 2000). Briefly, gingival tissues were obtained from healthy gingival biopsies from a 10-year-old girl, undergoing periodontal surgery. The tissue were cut into 1 to 2 mm^3 pieces, washed twice with phosphate-buffered saline (PBS, 0.01 M phosphate buffer, 0.15 M NaCl, pH 7.4) supplemented with 100 U/ml penicillin and 100 μg/ml streptomycin, and placed into 25 cm^2 tissue culture flasks. The explants were incubated in α-MEM supplemented with 30% FBS and antibiotics. When outgrowth of the cells was observed, the medium was replaced twice until the cells reached confluence. The cells were detached from the monolayer by trypsinization and recultured in 100 cm^2 tissue culture flasks until confluent monolayers were again obtained. Cells between the fifth and seventh passages were used.

3.17. Assay for cytotoxic activity

Cells were trypsinized and inoculated at 6×10^3 per each 96-microwell plate (Falcon, flat bottom, treated polystyrene, Becton Dickinson, San Jose, CA, USA), and incubated for 24 h. After washing once with PBS, they were treated with 24 h without or with test compounds. They were washed once with PBS and incubated for 4 h with 0.2 mg/ml MTT in DMEM medium supplemented with 10% FBS. After the medium was removed, the cells were lysed with 0.1 ml DMSO and the relative viable cell number was determined by measuring the absorbance at 540 nm of the cell lysate, using Labsystems Multiskan^R (Biochromatic, Helsinki, Finland) connected to a Star/DOT Matrix printer JL-10. The LD_{50} value, which reduces the viable cell number by 50%, was determined from the dose-response curve.

References

Ahmad., V.U., Basha, A., 2000. Spectroscopic Data of Saponins, Vol. III. CRC press, Boca Raton, p. 2831.

Bastow, K.F., Bori, I.D., Fukushima, Y., Kashiwada, Y., Tanaka, T., Nonaka, G., Nishioka, I., Lee, K.-H., 1993. Inhibition of DNA topoisomerases by sanguiin H-6, a cytotoxic dimeric ellagitannin from Sanguisorba officinalis. Planta Medica 59, 240–245.

Cheng, D.-L., Cao, X.-P., 1992. Pomolic acid derivatives from the root of *Sanguisorba officinalis*. Phytochemistry 31, 1317–1320.

Guang-Yi, L., Gray, A.I., Waterman, P.G., 1989. Pentacyclic triterpenes from the fruits of *Rosa sterilis*. Journal of Natural Products 52, 162–166.

Ito, H., Kobayashi, E., Takamatsu, Y., Li, S.-H., Hatano, T., Sakagami, H., Kusama, K., Satoh, K., Sugita, D., Shimura, S., Itoh, Y., Yoshida, T., 2000. Polyphenols from *Eriobotrya japonica* and their cytotoxicity against human oral tumor cell lines. Chemical and Pharmaceutical Bulletin 48, 687–693.

Jia, Z.-J., Liu, X.-Q., Liu, Z.-M., 1993. Triterpenoids from *Sanguisorba alpina*. Phytochemistry 32, 155–159.

Kizu, H., Hirabayashi, S., Suzuki, M., Tomimori, T., 1985. Studies on the constituents of *Hedera rhombea* BEAN. IV. On the Hederagenin Glycosides. (2). Chemical and Pharmaceutical Bulletin 33, 3473–3478.

Kizu, H., Shimana, H., Tomimori, T., 1995. Studies on the constituents of *Clematis* species. VI. The constituents of *Clematis stans* SIEB. *et* ZUCC. Chemical and Pharmaceutical Bulletin 43, 2187–2194.

Tanaka, T., Nonaka, G., Nishioka, I., 1985. Tannins and related compounds. Part 28. Revision of the structures of sanguiins H-6, H-2, and H-3, and isolation and characterization of sanguiin H-11, a novel tetrameric hydrolysable tannin, and several related tannins, from *Sanguisorba officinalis*. Journal of Chemical Research (M), pp. 2001–2029.

Yokozawa, T., Chen, C.P., Tanaka, T., Kitani, K., 2000. A study on the nitric oxide production-suppressing activity of Sanguisorbae Radix components. Biological and Pharmaceutical Bulletin 23, 717–722.

Yosioka, I., Sugawara, T., Ohsuka, A., Kitagawa, I., 1971. Soil bacterial hydrolysis leading to genuine aglycone. III. The structures of glycosides and genuine aglycone of Sanguisorba Radix. Chemical and Pharmaceutical Bulletin 19, 1700–1707.

PERGAMON

Phytochemistry 57 (2001) 781–785

PHYTOCHEMISTRY

www.elsevier.com/locate/phytochem

Investigation of Uña De Gato I. 7-Deoxyloganic acid and ^{15}N NMR spectroscopic studies on pentacyclic oxindole alkaloids from *Uncaria tomentosa*☆

Ilias Muhammad [a,*], D. Chuck Dunbar [a], Riaz A. Khan [a], Markus Ganzera [a], Ikhlas A. Khan [a,b]

[a] *National Center for Natural Products Research, Research Institute of Pharmaceutical Sciences, School of Pharmacy, University of Mississippi, University, MS 38677, USA*

[b] *Department of Pharmacognosy, Research Institute of Pharmaceutical Sciences, School of Pharmacy,University of Mississippi, University, MS 38677, USA*

Received 17 October 2000; received in revised form 23 January 2001

Abstract

The C-8-(*S*) isomer of deoxyloganic acid (7-deoxyloganic acid), together with β-sitosteryl glucoside, five known stereoisomeric pentacyclic oxindole alkaloids and the tetracyclic oxindole isorhyncophylline, were isolated from the inner bark of *Uncaria tomentosa*. Structures of the isolated compounds were based on ^{1}H and ^{13}C NMR data, mainly 2D NMR experiments, including ^{1}H–^{13}C HMBC and ^{1}H–^{1}H NOESY correlation. Furthermore, the hitherto unreported ^{15}N chemical shifts of the isomeric oxindole alkaloids, using ^{1}H–^{15}N HMBC experiments, were utilized to facilitate their characterization. Uncarine D showed weak cytotoxic activity against SK-MEL, KB, BT-549 and SK-OV-3 cell lines with IC_{50} values between 30 and 40 μg/ml, while uncarine C exhibited weak cytotoxicity only against ovarian carcinoma (IC_{50} at 37 μg/ml). © 2001 Elsevier Science Ltd. All rights reserved.

Keywords: *Uncaria tomentosa*; Rubiaceae; Cat's claw; Alkaloids; Oxindoles; ^{15}N NMR; Iridoid glucoside; 7-Deoxyloganic acid; β-Sitosteryl glucoside; Cytotoxic activity

1. Introduction

Uncaria tomentosa (Wild.) DC. (Uña de Gato; Cat's Claw) is considered one of the most valuable botanicals in the rainforest and is widely used in traditional medicine by native people of Peru for numerous ailments (Jones, 1995). This plant displays a diverse range of bioactive secondary metabolites, including tetracyclic and pentacyclic oxindole alkaloids, triterpenes, glycosides, flavonoids and procyanidins (Aquino et al., 1990, 1991, 1997; Jones, 1995; Van Ginkel, 1996; Wirth and Wagner, 1997). The pentacyclic oxindole alkaloids are considered to be biochemical markers of cat's claw and are responsible, in part, for immunomodulatory, cytotoxic, anti-AIDS and anti-amyloidosis (Alzheimer's disease) activities (Wagner et al., 1985; Keplinger et al., 1986; Keplinger and Keplinger, 1994; Jones, 1995; Lemaire et al., 1999; Castillo and Snow, 2000). To date, nine natural heteroyohimbine-type pentacyclic oxindole isomers have been isolated from *Uncaria* species and six of them are restricted to *U. tomentosa* inner bark (Shamma et al., 1967; Seki et al., 1993).

As part of our continuing program to isolate marker compounds from traditional medicines and evaluate their biological activity, the present study deals with the isolation and characterization of a new constituent, 7-deoxyloganic acid (**1**) from the inner bark of *U. tomentosa*. In addition, the ^{15}N NMR spectral assignments of the stereoisomeric oxindoles (uncarines C, D and E, mitraphylline and isomitraphylline) is described and cytotoxicity of the isolated compounds evaluated.

2. Results and discussion

Column chromatography of the ethanolic extract, using 1–5% MeOH in $CHCl_3$ mixture as eluent (see

☆ For part II, see Ganzera et al. (2001).

* Corresponding author. Tel.: +1-662-915-1051; fax: +1-662-915-7989.

E-mail address: milias@sunset.backbone.olemiss.edu (I. Muhammad).

0031-9422/01/$ - see front matter © 2001 Elsevier Science Ltd. All rights reserved.
PII: S0031-9422(01)00043-7

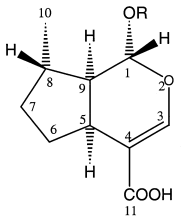

1 R=Glc

2 R=Glc(Ac)$_4$

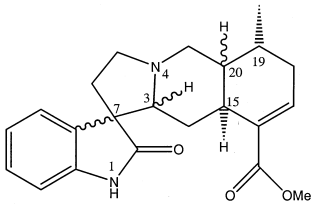

Uncarine C (**3**) 3*S*, 7*R*, 15*S*, 19*S*, 20*S*
Uncarine D (**4**) 3*R*, 7*S*, 15*S*, 19*S*, 20*S*
Uncarine E (**5**) 3*S*, 7*S*, 15*S*, 19*S*, 20*S*
Mitraphylline (**6**) 3*S*, 7*R*, 15*S*, 19*S*, 20*R*
Isomitraphylline (**7**) 3*S*, 7*S*, 15*S*, 19*S*, 20*R*

Experimental), resulted in the isolation of five known stereoisomeric oxindoles [namely, uncarines C, D and E, mitraphylline and isomitraphylline (**3**–**7**) (Shamma et al., 1967; Seki et al., 1993)], the tetracyclic oxindole isorhyncophylline (**8**) (Phillipson and Hemingway, 1973; Yu et al., 1989), as well as 7-deoxyloganic acid (**1**).

Compound **1**, $C_{16}H_{24}O_9$, was obtained as colorless amorphous granules: mp. 94–96°; $[\alpha]_D^{27}$ −81.9°; which exhibited the presence of carboxylic acid (ν_{max} 1680 cm^{-1}; δ_C 170.1) and β-D-glucose [$\delta_{C\text{-}1'}$ 99.1, $\delta_{C\text{-}2'}$ 73.8, $\delta_{C\text{-}3'}$ 77.0, $\delta_{C\text{-}4'}$ 70.6, $\delta_{C\text{-}5'}$ 77.3, $\delta_{C\text{-}6'}$ 61.9; δ 4.65, 1H, *d* (J=7.9 Hz, H-1′) (Murai et al., 1984)] substituents. The ^{13}C NMR spectrum of **1** (Table 1) was found to be similar to those reported for 8-(*S*) isomer of 7-deoxyloganic acid tetraacetate (**2**) (Tagawa and Murai, 1983), save for the differences associated with the presence of the β-D-glucose moiety at C-1. Furthermore, a close comparison of the ^{13}C NMR spectrum of **1** with those of other deoxyloganic acid isomers, such as 8-*epi*deoxyloganic acid [8-(*R*) isomer of 7-deoxyloganic acid], 1,5,9-*epi*deoxyloganic acid and 5-*epi*deoxyloganic acid, isolated from *Nepeta cataria* (Tagawa and Murai, 1983; Murai et al., 1984), led to the conclusion that indeed **1** was the C-8-(*S*)-isomer of deoxyloganic acid, which has not been reported previously as a natural product. Thus, the structure and stereochemistry of **1** was unambiguously established by detailed 2D NMR spectroscopic studies, including ^{1}H–^{13}C HMQC, ^{1}H–^{13}C HMBC and ^{1}H–^{1}H NOESY experiments. The ^{1}H–^{13}C HMBC experiment on **1** showed the key three-bond correlation between $\delta_{C\text{-}1'}$ 99.2 and δ 5.17 (H-1); $\delta_{C\text{-}11}$ 170.1 and δ 7.40 (H-3); $\delta_{C\text{-}9}$ 48.2 and δ 1.05 (H-10), confirming the placement of COOH, β-D-glucose and methyl substituents at C-1, C-4 and C-8, respectively.

The stereochemical assignment at the carbon centers C-1, C-5, C-8 and C-9 was inferred from 2D NMR ^{1}H–^{1}H NOESY experiments, which showed correlations between H-5 (δ 2.85), H-9 (δ 1.70) and H-10 (δ 1.05), indicating that they are *cis* (α-face) to each other. As a result, fusion between the five and six-member rings was also *cis* in **1**. Furthermore, the NOESY showed a *cis* (β-face) relationship between the protons H-1 (δ 5.17) and H-8 (δ 1.95), thereby confirming the assignment of β-D-glucose moiety at the α-face of the molecule. Compound **2** was previously reported as a catalytic hydrogenation product of asperuloside tetraacetate and its absolute configuration at C-8 was established as (*S*) (Inouye and Arai, 1964; Murai and Tagawa, 1980). Based on foregoing data compound **1** was established as the C-8 (*S*)-isomer of deoxyloganic acid.

The initial identity and purity of the isolated five stereoisomeric pentacyclic oxindoles (**3**–**7**) and the tetracyclic isorhyncophylline (**8**) were evaluated by HPLC (Ganzera et al., 2001), as well as by their optical purity ($[\alpha]_D$ values). All the oxindoles were found to be 99-99.5% pure by HPLC, except for isomitraphylline, which could only be purified up to 84.5%. The structures and relative stereochemistries of **3**–**7** were determined rigorously using high field 2D NMR spectroscopic studies, including ^{1}H–^{1}H NOESY and ^{1}H–^{13}C HMBC experiments and were found to be in agreement with those reported by Seki et al. (1993). In addition, the absolute stereochemistry of uncarine C (**3**) and uncarine E (**5**) were determined by single crystal X-ray crystallography,[1] which will be reported elsewhere. The pentacyclic oxindole isomers (**3**–**7**) are difficult and tedious to distinguish by simply comparing the ^{1}H or ^{13}C NMR spectral data. Therefore, the 2D ^{1}H–^{15}N NMR HMBC spectra were acquired to obtain ^{15}N chemical shifts that help to distinguish between most of the isomers (Table 2). The chemical shift of N-1 ranges from δ 136.9 to δ 135.1 and N-4 ranges from δ 54.6 to δ 64.8. The *allo*-type isomers (3*S*, 20*S*) uncarine C (**3**) and E (**5**) exhibited a drastic chemical shift differences at N-4 nitrogen (8-10 ppm) compared to those observed for *epiallo*-type (3*R*, 20*S*) uncarine D (**4**) and *normal*-type (3*S*, 20*R*) mitraphylline (**6**) and isomitraphylline (**7**). Although, the ^{15}N chemical shift differences between **4** and **6** are negligible, they can be very conveniently distinguished by their $[\alpha]_D^{27}$ values (+91° for **4** vs −8.6° for **6**). The ^{1}H–^{15}N HMBC experiment on uncarine C (**3**) demonstrated the correlation between the signals at δ_N 136.85 (N-1), $\delta_{N\text{–}H}$ 9.07 and $\delta_{H\text{-}12}$ 6.85; and δ_N 56.9 (N-4) and $\delta_{H\text{-}5}$ 1.95, $\delta_{H\text{-}6,14}$ 1.69, $\delta_{H\text{-}20}$ 1.53 and $\delta_{H\text{-}21}$ 3.29. All the correlated protons from ^{1}H–^{15}N HMBC data of five isomers studied (Table 2) were in good agreement with their original ^{1}H NMR spectroscopic assignments. Therefore, the ^{15}N chemical shifts and specific rotation values can be used as a valuable tool to distinguish quickly and conveniently all the five stereoisomers **3**–**7**. To our knowledge, this is the first report of ^{15}N NMR chemical shifts for *Uncaria* oxindole alkaloids.

All six oxindole alkaloids, as well as compound **1** and β-sitosteryl glucoside, were evaluated for cytotoxic activ-

[1] Fronczek, F.R., Department of Chemistry, Louisiana State University, Baton Rouge, LA 70803-1804, USA, pers. commun.

ity, using a microplate assay (Dou et al., 1996) against human cancer cell lines of malignant melanoma (SK-MEL), epidermoid carcinoma (KB), ductal carcinoma (BT-549) and ovarian carcinoma (SK-OV-3). The *epiallo*-type C-3(*R*)-isomer uncarine D (**3**) showed weak cytotoxic activity against all the cell lines with IC_{50} values at 30, 35, 34 and 30 μg/ml, respectively, while *allo*-type C-3(*S*-)-epimer uncarine C demonstrated weak cytotoxicitiy only towards SK-OV-3 at 37 μg/ml (Table 3). The other three isomers, *allo*-type uncarine E, *normal*-type mitraphylline and isomitraphylline as well as isorhyncophylline, compound **1** and β-sitosteryl glucoside were found to be inactive. Interestingly, uncarine C and uncarine E had previously been reported from *U. guianensis* to possess weak but selective DNA damaging activities (Lee et al., 1999).

Table 1
^1H and ^{13}C NMR chemical shift values for compound **1**[a]

Proton/carbon	^1H	NOESY	^{13}C
1	5.17 *d* (5.7)[b]	H-8 β	96.9 *d*[c]
2	–	–	–
3	7.40 *d* (1.0)	–	151.8 *d*
4	–	–	112.0 *s*
5	2.85 *dd br* (7.6, 7.3)	H-9 α H-10 α	34.3 *d*
6	2.16 *m* ; 1.38 *m*	–	32.4 *t*
7	1.84 *m*; 1.16 *m*	–	33.2 *t*
8	1.95 *m*	H-1 β	35.6 *d*
9	1.70 *dd br* (6.2, 12.5)	H-5 α H-10 α	48.2 *d*
10	1.05 *d* (6.7)	H-5 α H-9 α	19.9 *q*
11	–	–	170.1 *s*
1′	4.65 *d* (7.9)	–	99.2 *d*
2′	3.29 *m*	–	73.8 *d*
3′	3.37 *t* (8.8), 3.28 *m*	–	77.0 *d*
4′	3.28 *m*	–	70.6 *d*
5′	3.29 *m*	–	77.3 *d*
6′	3.64 *m* 3.86 *dd* (1.6, 13.2)	–	61.9 *t*

[a] Spectra recorded in CD_3OD at 500 MHz (^1H) and 125 MHz (^{13}C). Assignments were aided by 2D NMR COSY, HMQC and HMBC experiments.
[b] Values in parentheses are coupling constants, *J* values in Hz.
[c] Multiplicities of carbon signals were determined by DEPT experiments.

3. Experimental

3.1. General

Mp uncorr.; NMR: were acquired on a Brüker Avance DRX-500 instrument at 500 MHz (^1H), 125 MHz (^{13}C) and 50 MHz (^{15}N) in $CDCl_3$, unless otherwise stated, using the residual solvent as int. standard; Multiplicity determinations (DEPT) and 2D NMR spectra (COSY, HMQC, HMBC and NOESY) were obtained using standard Bruker pulse programs; ^1H–^{15}N HMBC spectra were calibrated using nitromethane as an external standard and setting the chemical shift to 380.2 resulting in ^{15}N chemical shifts are reported relative to liquid ammonia; HRMS: were obtained by direct injection using a Bruker Bioapex-FTMS with Electro-

Table 2
^1H–^{15}N NMR HMBC correlations and optical rotations of oxindoles **3**–**7**

Oxindoles	^{15}N (δ_N)		HMBC correlations with ^1H NMR (δ_H)								$[\alpha]_D^{27}$[a]
			N_1H[b]	H-3	H-5	H-6	H-12	H-14	H-20	H-21	
Uncarine C (**3**)	N-1	136.9	9.07	–	–	–	6.85	–	–	–	−106° (*c*, 0.2)
	N-4	56.9	–	–	1.95[d]	1.69[c]	–	1.69[c]	1.53[c]	3.29[d]	
Uncarine D (**4**)	N-1	135.1	9.31	–	–	–	6.85	–	–	–	+91° (*c*, 0.024)
	N-4	64.8	–	2.15[d]	–	1.99[d]	–	1.58[c]	–	–	
Uncarine E (**5**)	N-1	136.7	9.04	–	–	–	–	–	–	–	−80.5° (*c*, 0.554)
	N-4	54.6	–	–	3.18[d]	2.35[d]	–	–	1.60[c]	3.25[d]	
Mitraphylline (**6**)	N-1	135.1	8.41	–	–	–	6.85	–	–	–	−8.6° (*c*, 0.554)
	N-4	64.7	–	2.36[c]	3.36[d]	2.04[c]	–	2.36[c]	–	–	
Isomitraphylline (**7**)	N-1	135.8	9.02	–	–	–	6.85	–	–	–	+20° (*c*, 0.012)
	N-4	62.8	–	–	3.28[d]	1.97[c]	–	–	–	1.90[c]	

[a] All optical rotation values were measured in $CHCl_3$ at 27°C.
[b] One-bond N–H correlation.
[c] Two or three bond; α-protons.
[d] Two or three bond; β-protons.

Table 3
Cytotoxic activity of oxindole alkaloids[a]

Compounds	IC_{50} (μg/ml)				
	SK-MEL	KB	BT-549	SK-OV-3	VERO
Uncarine C (**3**)	> 50	> 50	> 50	37	> 50
Uncarine D (**4**)	30	35	34	30	39
Uncarine E (**5**)	> 50	–	–	> 50	–
DOX	< 1.1	1.7	2.0	1.9	> 10
5-FU	6.3	> 10	–	> 10	> 10

[a] SK-MEL, human malignant melanoma; KB, human epidermoid carcinoma; BT-549, human ductal carcinoma; SK-OV-3, human ovary carcinoma; VERO, (kidney, African green monkey) used as normal cell line; – inactive; DOX, doxorubicin; 5-FU, 5-fluorouracil.

Spray Ionization (ESI); Optical rotation measurements were taken on a JASCO DIP-370 digital polarimeter at 27°C; HPLC: was performed using a Waters 2690 alliance separation module with 996 PDA photodiode detector and a 3 μm Luna C-18 (Phenomenex) column; TLC: silica gel 60 F254 plates; solvent: hexane–EtOAc (4:6) and MeOH–$CHCl_3$(5:95); CC: flash-silica gel G (J.T. Baker, 40 μm); centrifugal preparative TLC (CPTLC, using Chromatotron®, Harrison Research Inc. Model 8924): 2 mm silica gel GF Chromatotron™ rotors (Analtech, Inc.), at a N_2 flow rate of 4 ml/min. The isolated compounds were visualized by observing under UV at 254 nm, followed by development in an iodine chamber or spraying with Dragendorff's reagent (Sigma Chemical Co.) and spraying with anisaldehyde–H_2SO_4 spray reagent.

3.2. Plant material

The inner stem bark of *Uncaria tomentosa* (Fam. Rubiaceae) was collected in April 2000 near Lima, Peru. A voucher specimen was deposited at the herbarium of University of Mississippi.

3.3. Extraction and isolation

The powdered inner stem bark of *U. tomentosa* (2.5 kg) was extracted by percolation with EtOH (3 × 2L). The combined extract was evaporated under reduced pressure and then freeze dried (yield 223 g). A portion of the crude extract (150g) was subjected to flash-CC over silica gel G (40 μm, 4.5 kg). Using 1% MeOH–$CHCl_3$ as solvent yielded uncarine E (**5**; needles, 500 mg), followed by mixture A, that was separated by a short flash-CC, using 25% EtOAc in *n*-hexane to afford uncarine C (**3**, plates, 225 mg) and isomitraphylline (**7**, amorphous powder, 180 mg). Further elution of the CC with 3–5% MeOH–$CHCl_3$ yielded mitraphylline (**6**, granules, 500 mg), followed by mixture B, which was purified by CPTLC (2 mm disc; solvent: 3% MeOH–$CHCl_3$) to give uncarine D (**4**, needles, 80 mg), followed by isorhyncophylline (**8**, needles, 100 mg; mp 138°, $[\alpha]_D^{27}$ +15°, lit.[2] mp 144°, $[\alpha]_D^{27}$ +8.3 ↔ +13°). Finally, elution with 6% MeOH in $CHCl_3$ yielded mixture C, which was separated and purified by CPTLC using 5% MeOH–$CHCl_3$ as eluent in a 2 mm disc to give **1** (80mg, R_f 0.30, solvent: 5% MeOH–$CHCl_3$) and β-sitosteryl glucoside (150 mg, R_f 0.25). The identity of β-sitosteryl glucoside was confirmed by the direct comparison with an authentic sample. The purity of the oxindoles was evaluated by an in-house HPLC method. The physical[2] and spectral data (Phillipson and Hemingway, 1975; Seki et al., 1993) of the oxindoles **3**–**7** were in agreement with those reported in literature.

3.4. 7-Deoxyloganic acid (*1*)

Obtained as colorless amorphous granules from $CHCl_3$, mp 94–96°; $[\alpha]_D^{27}$ −81.9° (MeOH, *c* 1.0); UV λ_{max}^{EtoH} nm (log ε): 220 sh (3.60), 238 (3.85) and 262 (3.88); IR ν_{max}^{KBr} cm^{-1}: 3357 (OH), 2952, 2870, 1680(COOH), 1630, 1548, 1071; ^1H and ^{13}C NMR: Table 1; HRMS (*m*/*z*): 361.1485 ($[MH]^+$, $C_{16}H_{24}O_9$.H); calculated for 361.1493.

3.5. Cytotoxicity assay

The in vitro cytotoxic activity was determined against four human cancer cell lines, SK-MEL, KB, BT-549, and SK-OV-3 (Table 3), obtained from American Type Culture Collection (ATCC, Rockville, MD). A primary assay for the oxindoles was conducted at a single concentration (100 μg/ml), followed by a secondary assay at three to six concentrations (between 50 and 1.56 μg/ml), using a culture-treated 96-well microplate (Dou et al., 1996). The level of toxicity of each sample was also determined by measuring their effect on fibroblast cell line from African green monkey kidney (VERO; non-transformed). The assay is based on the accumulation of neutral red dye in the lysosomes of viable cells. A subsequent addition of 2-propanol will lyse the cells releasing the dye into solution and the absorbance is measured at 490 and 630 nm. Corresponding growth inhibition was calculated and graphed. For secondary assays, IC_{50}s were determined from logarithmic graphs of growth inhibition values. The cytotoxic agents doxorubicin and 5-fluorouracil were used as positive controls, while the DMSO vehicle was used as negative control.

[2] The literature physical data (melting point and optical rotation values) were obtained from the Dictionary of Natural Products on CD ROM. 1999. Chapman and Hall, CR Cnet Base, Version 8:1, Chapman and Hall Numbers: CCG99-V, CCH03-T, CCH06-W, CGL89-T, CGL93-Q and CHF57-L.

Acknowledgements

The authors acknowledge Ms. Sharon Sanders, Mr. Charlie Dawson and Mr. John Trott for technical assistance and the financial support provided in part by United States Department of Agriculture ARS Specific Cooperative Research Agreement No. 58-6408-012 and ChromaDex™, Irvine, CA.

References

Aquino, R., De Simone, F., Vinceri, F.F., Pizza, C., Gacs-Baitz, E., 1990. New polyhydroxylated triterpenes from *Uncaria tomentosa*. J. Nat. Prod. 53, 559–564.

Aquino, R., De Feo, V., De Simone, F., Pizza, C., Cirino, G., 1991. Plant metabolites. New compounds and antiinflamatory activity of *Uncaria tomentosa*. J. Nat. Prod. 54, 453–459.

Aquino, R., De Tommasi, N., De Simone, F., Pizza, C., 1997. Triterpenes and quinovic acid glycosides from *Uncaria tomentosa*. Phytochemistry 45, 1035–1040.

Castillo, G. and Snow, A.D. (2000). Blended Composition for Treatment of Alzheimer's Disease and Other Amyloidoses. PCT Int. Appl. Application: WO 99-US19721. Priority: US 98-98473 19980831. AN 2000:161143.

Dou, J., McChesney, J.D., Sindelar, R.D., Goins, D.K., Walker, L.A., 1996. A new quassinoid from *Castela texana*. J. Nat. Prod. 59, 73–76.

Ganzera, M., Muhammad, I., Khan, R.A. and Khan, I.A., 2001. Improved method for the determination of oxindole alkaloids in *Uncaria tomentosa* by high performance liquid chromatography. Planta Medica, in press.

Inouye, H., Arai, T., 1964. Über die Monoterpengluckoside. II. Zur Stereochemie des Bisdesoxydihydromonoterpeins, eines Hydrierungsproduktes des Monoterpeins and des Asperulosides. Chem. Pharm. Bull. 12, 968–975.

Jones, K., 1995. Cat's Claw: Healing Vine of Peru. Sylvun Press, 1202 East Pike Street, Suite 746, Seattle, WA 98122, USA.

Keplinger, K., Keplinger, D. Pharmaceutical compositions containing oxindole alkaloids for stimulating the immunological system. 1994. PCT US. CODEN: USXXAM US 5302661 A19940412. Application: US 92-954040 19920930. Priority: AT 80-4971 19801007. AN 1994:418017.

Keplinger, K., Wagner, H. and Kreutzkamp, B. 1986. Oxindole alkaloids with properties for stimulating the immunity system. PCT Int. Appl. CODEN: PIXXD2 WO 8600524 A1 19860130. Application: WO 84-AT25 19840706. AN 1986:546231.

Lee, K.K., Zhou, B.-N., Kingston, D.G.I., Vaisberg, A.J., Hammond, G.B., 1999. Bioactive indole alkaloids from the bark of *Uncaria guianensis*. Planta Medica 65, 759.

Lemaire, I., Assinewe, V., Cano, P., Awang, D.V.C., Arnason, J.T., 1999. Stimulation of interleukin-1 and –6 production in alveolar macrophages by the neotropical liana, *Uncaria tomentosa* (uña de gato). J. Ethnopharmacology 64, 109–115.

Murai, F., Tagawa, M., 1980. The absolute configuration of boschnaloside and the chemical conversion of genipin into boschnaloside. Chem. Pharm. Bull. 28, 1730–1735.

Murai, F., Tagawa, M., Damtoft, S., Jensen, S.R., Nielsen, B.J., 1984. (1*R*, 5*R*, 8*S*, 9*S*)-Deoxyloganic acid from *Nepeta cataria*. Chem. Pharm. Bull. 32, 2809–2814.

Phillipson, J.D., Hemingway, S.R., 1973. Alkaloids from *Uncaria* species. III. Oxindole alkaloids from *Uncaria macrophylla*. Phytochemistry 12, 2795–2798.

Phillipson, J.D., Hemingway, S.R., 1975. Chromatographic and spectroscopic methods for the identification of alkaloids from herbarium samples of the genus *Uncaria*. J. Chromatography 105, 163–178.

Seki, A., Takayama, H., Aimi, N., Sakai, S.-I., Ponglux, D., 1993. Nuclear magnetic resonance study of the eleven stereoisomers of heteroyohimbine-type oxindole alkaloids. Chem. Pharm. Bull. 41, 2077–2086.

Shamma, M., Shine, R.J., Kompis, I., Sticzy, T., Morsingh, F., Poisson, J., Pousset, J.L., 1967. Stereochemistry of the pentacyclic oxindole alkaloids. J. Am. Chem. Soc. 89, 1739–1740.

Tagawa, M., Murai, F., 1983. 5-Epoxyloganic acid from *Nepeta cataria*. Planta Medica 47, 109–111.

Van Ginkel, A., 1996. Identification of the alkaloids and flavonoids from *Uncaria tomentosa* bark by tlc in quality control. Phytotherapy Research 10, S18–S19.

Yu, D.Q., Yang, J.S., Xie, J.X., 1989. Handbook of Analytical Chemistry. Part V, p. 635.

Wagner, H., Kreutzkamp, B., Jurcic, K., 1985. Alkaloids from *Uncaria tomentosa* and their phagocytosis enhancement effect. Planta Medica 5, 419–423.

Wirth, C., Wagner, H., 1997. Pharmacologically active procyanidins from the bark of *Uncaria tomentosa*. Phytomedicine 4, 265–266.

PERGAMON

Phytochemistry 57 (2001) 787–789

PHYTOCHEMISTRY

www.elsevier.com/locate/phytochem

Sterol composition of *Aureoumbra lagunensis*, the Texas brown tide alga

José-Luis Giner*, Xiaoyong Li, Gregory L. Boyer

Department of Chemistry, SUNY-ESF, Syracuse NY 13210, USA

Received 15 August 2000; received in revised form 31 October 2000

Abstract

Aureoumbra lagunensis, the alga responsible for the ''Texas brown tide'', contains (*E*)-24-propylidenecholesterol (35.7% of total sterols) as its dominant sterol, in common with other members of the Pelagophyceae. Other major sterols are stigmasterol (22.2%), sitosterol (19.2%), cholesterol (14.1%), and (24*R*)-24-propylcholesterol (5.2%). Trace amounts of 24-methylenecholesterol, crinosterol, clerosterol, campesterol, dihydrobrassicasterol, and 24-isopropylcholesterol were also detected. © 2001 Elsevier Science Ltd. All rights reserved.

Keywords: Texas brown tide; *Aureoumbra lagunensis*; Pelagophyceae; Chemotaxonomy; Algal sterols

1. Introduction

Aureoumbra lagunensis is a golden-brown picoplanktonic alga responsible for ''brown tides'' in lagoons along the Texas coast of the Gulf of Mexico (Stockwell et al., 1993; De Yoe et al., 1997). This organism is similar to *Aureococcus anophagefferens*, the alga responsible for the ''brown tide'' of the New York and Southern New England coasts (Cosper et al., 1987, 1989; Sieburth et al., 1988). Based on 18S rRNA analysis, ultrastructure, and pigmentation, these algae have recently been classified together with several other chrysophytic algae as members of a new taxon, the Pelagophyceae (DeYoe et al., 1997; Andersen et al., 1993; Saunders et al., 1997, 1995). The sterol composition of all members of this group examined to date is dominated by the unusual marine sterol (24*E*)-24-propylidenecholesterol (**1**) (Rohmer et al., 1980; Raederstorff and Rohmer, 1984; Giner and Djerassi, 1991). We have recently reported the sterol composition of *Aureococcus anophagefferens*, and have proposed that (24*Z*)-24-propylidenecholesterol may serve as a unique biomarker for this organism (Giner and Boyer, 1998). We hereby report the sterol composition of *Aureoumbra lagunensis*, the Texas brown tide alga.

2. Results and discussion

The sterols (Table 1) of cultured *Aureoumbra lagunensis* were separated by HPLC, and identified from their ^{1}H NMR spectra. The major sterol was (24*E*)-24-propylidenecholesterol (**1**) (35.7%), followed by stigmasterol (22.2%), sitosterol (**2**) (19.2%), cholesterol (14.1%), and (24*R*)-24-propylcholesterol (**3**) (5.2%). The configuration of the latter compound was determined by stereospecific synthesis (Giner and Li, 2000). Also isolated as minor sterols were 24-methylenecholesterol, crinosterol, clerosterol, campesterol, dihydrobrassicasterol, and 24-isopropylcholesterol. The 24-methylcholesterols (campesterol and dihydrobrassicasterol) were present in nearly equal amounts, with dihydrobrassicasterol predominating slightly.

We previously identified (24*Z*)-24-propylidenecholesterol as a sterol (12.4%) of the brown tide alga *Aureococcus anophagefferens*, and we proposed that it may be useful as a specific biomarker for this organism (Giner and Boyer, 1998). This sterol was not detected in the Texas brown tide alga *Aureoumbra lagunensis*. On the other hand, the (24*E*)-isomer (**1**), which represents a biomarker specific to pelagophyte algae, was found as

* Corresponding author. Tel.: +1-315-470-6895; fax: +z1-315-470-6856.

E-mail address: jlginer@syr.edu (J.-L. Giner).

0031-9422/01/$ - see front matter © 2001 Elsevier Science Ltd. All rights reserved.
PII: S0031-9422(01)00135-2

Table 1
Sterols of *Aureoumbra lagunensis*

Sterol	HPLC retention time	Total sterols (%)
24-Methylenecholesterol	42.6 min	0.4
Epibrassicasterol	44.8 min	0.9
Clerosterol	46.6 min	1.1
Cholesterol	49.8 min	14.1
(*E*)-24-Propylidenecholesterol (**1**)	51.9 min	35.7
Stigmasterol	53.3 min	22.2
24-Methylcholesterols	55.0 min	0.7
Sitosterol (**2**)	60.1 min	19.2
(24*R*)-24-Propylcholesterol (**3**)	65.7 min	5.2
24-Isopropylcholesterol	68.4 min	0.4
Sterol content: 0.16% wet wt		

35.7% of the total sterols. When compared with the sterol compositions of other pelagophyte algae (Rohmer et al., 1980; Raederstorff and Rohmer, 1984; Giner and Boyer, 1998), the sterol composition of *Aureoumbra* most closely resembles that reported for *Nematochrysopsis roscoffensis*, which also has a relatively high percentage of the stigmasterol (25%) and sitosterol (**2**) (6%), as well as cholesterol (12%) (Raederstorff and Rohmer, 1984). The use of stigmasterol and sitosterol (**2**) as biomarkers for terrestrial plant input in the marine environment should therefore be interpreted with caution (Volkman, 1986). It is interesting to note that 24-propylcholesterol (**3**, which also occurs in *Nematochrysopsis roscoffensis*, 9%) is found with the same configuration at C24 as the 24-ethyl sterols, stigmasterol and sitosterol (**2**). This suggests that the same sterol $\Delta^{24(28)}$-reductase may be involved in their biosynthesis (Fig. 1).

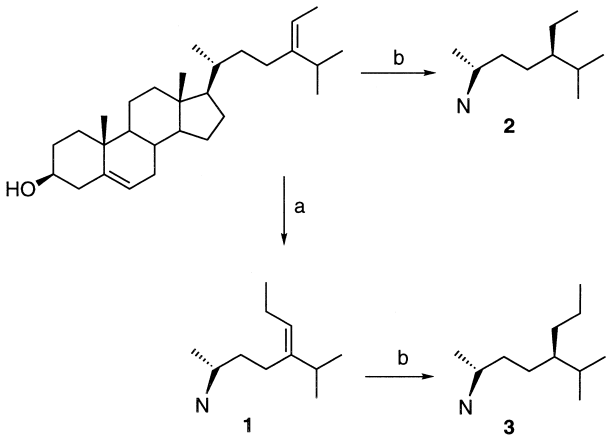

Fig. 1. Biosynthesis of *Aureoumbra lagunensis* sterols. (a) sterol methyltransferase; (b) sterol $\Delta^{24(28)}$-reductase.

3. Experimental

3.1. General procedures

NMR spectra were acquired using Brüker Avance-300 and Brüker Avance-600 instruments using $CDCl_3$ as the solvent and referenced to residual $CHCl_3$ signals (^1H: 7.26 ppm, ^{13}C: 77.0 ppm). GC–MS data was obtained using a Hewlett-Packard 5890 series II gas chromatograph with a Hewlett-Packard 5989B mass spectrometer. TLC was performed on glass backed plates coated with a 0.25 mm layer of Si gel 60 F254. HPLC was carried out using a Waters 6000A pump, Waters 410 differential refractometer, and two Altex Ultrasphere ODS 5-μm 10x250 mm columns in series, at a flow rate of 3 ml/min MeOH.

3.2. Culture conditions

Cultures of *Aureoumbra lagunensis* CCMP-1681 were grown at 18°C with aeration in 12 l glass carboys containing artificial seawater (Golmand and McCarthy, 1978) supplemented with F/2 trace metals (Guillard and Ryther, 1962) using a 14:10 h light/dark cycle (160 μE m^{-2} s^{-1}). Cell growth was measured using in vivo fluorescence and by visual cell counts under phase contrast. Cells were harvested in stationary phase by centrifugation (14,000 × *g*) and lyophilized. 2.7 g (wet wt) of cells were obtained from 8 l containing 3.7×10^6 cells ml^{-1}.

3.3. Sterol analysis

The cells were extracted at room temp. with 12 ml EtOAc overnight, then a second time for 3 h. The extracts were concentrated under reduced pressure and fractionated by TLC on silica gel (hexanes–EtOAc 2:1). The sterol band was further purified from contaminating pigments by chromatography on a small column of Florisil (hexanes–EtOAc 9:1 followed by 4:1). The sterols (4.4 mg) were separated by reversed phase HPLC. The relative proportions of sterols were determined from integration of the HPLC trace. The sterol fractions were evaporated with a stream of N_2 and characterized by ^1H NMR (300 MHz, $CDCl_3$). The NMR spectra matched those of known samples: (E)-24-propylidenecholesterol (**1**) (Rohmer et al., 1980); 24-methylenecholesterol (Hetzel et al., 1994); 24-methylcholesterols (dihydrobrassicasterol and campesterol) (Rubinstein et al., 1976); crinosterol (Rubinstein et al., 1976); clerosterol (Akihisa et al., 1991); 24-isopropylcholesterol (Hofheinz and Oesterhelt, 1979; Kokke et al., 1979).

3.4. (24*R*)-24-Propylcholesterol (*3*)

^1H NMR (300 MHz) 5.352 (*m*, 1H), 3.513 (*m*, 1H), 1.011 (*s*, 3H), 0.926 (*d*, $J=6.6$, 3H), 0.881 (*t*, $J=7.0$, 3H), 0.829 (*d*, $J=6.8$, 3H), 0.814 (*d*, $J=6.8$, 3H), 0.681 (*s*, 3H); ^{13}C NMR (150 MHz) 141.2, 122.1, 72.2, 57.2, 56.5, 50.6, 44.3, 42.7, 42.7, 40.2, 37.7, 36.9, 36.6, 34.4, 33.5, 32.3 (2), 32.1, 29.9, 28.6, 27.0, 24.7, 21.5, 21.2,

20.0, 19.8, 19.4, 19.2, 15.0, 12.2; low resolution mass spectrum, m/z (relative intensity) 428 (M^+, $C_{30}H_{52}O$, 100), 413 (22), 410 (38), 395 (18), 343 (28), 317 (17), 273 (11), 255 (10), 231 (7), 213 (10), 159 (13), 145 (18), 107 (23), 105 (23), 95 (21), 93 (18), 91 (19), 81 (23), 79 (18), 57 (42), 55 (27); HRMS m/z 428.4021 (calcd for $C_{30}H_{52}O$, 428.4018).

Acknowledgements

Financial support was provided by New York Sea Grant, and the National Oceanographic and Atmospheric Administration's Coastal Ocean Program.

References

Akihisa, T., Kokke, W.C.M.C., Tamura, T., Matsumoto, T., 1991. Sterols of *Kalanchoe petitiana*: first report of the isolation of both C-24 epimers of 24-Alkyl-Δ^{25}-sterols from a higher plant. Lipids 26, 660–665.

Andersen, R.A., Saunders, G.W., Paskind, M.P., Sexton, J.P., 1993. Ultrastructure and 18S rRNA gene sequence for *Pelagomonas calceolata gen. et sp. nov.* and the description of a new algal class, the Pelagophyceae *classis nov*. Journal of Phycology 29, 701–715.

Cosper, E.M., Bricelj, V.M., Carpenter, E.J. (Eds.), 1989. Novel Phytoplankton Blooms: Causes and Impact of Recurrent Brown Tides and Other Unusual Blooms. Springer-Verlag, New York.

Cosper, E.M., Dennison, W.C., Carpenter, E.J., Bricelj, V.M., Mitchell, J.G., Kuenstner, S.H., Colflesh, D.C., Dewey, M., 1987. Recurrent and persistent "brown tide" blooms perturb coastal marine ecosystem. Estuaries 10, 284–290.

DeYoe, H., Stockwell, D., Bidigare, R., Latasa, M., Johnson, P., Hargraves, P., Suttle, C., 1997. Description and characterization of the algal species *Aureoumbra lagunensis gen. et sp. nov.* and referral of *Aureoumbra* and *Aureococcus* to the Pelagophyceae. Journal of Phycology 33, 1042–1048.

Giner, J.-L., Boyer, G.L., 1998. Sterols of the brown tide alga *Aureococcus anophagefferens*. Phytochemistry 48, 475–477.

Giner, J.L., Djerassi, C., 1991. Evidence for a protonated cyclopropyl intermediate in the biosynthesis of 24-propylidenecholesterol. Journal of the American Chemistry Society 113, 1386–1393.

Giner, J.-L., Li, X., 2000. Stereospecific synthesis of 24-propylcholesterol isolated from the Texas brown tide. Tetrahedron 56, 9575–9580.

Goldman, J.C., McCarthy, J.J., 1978. Steady state growth and ammonium uptake of a fast growing marine diatom. Limnology and Oceanography 23, 695–703.

Guillard, R.R., Ryther, J.H., 1962. Studies of marine planktonic diatoms. Canadian Journal of Microbiology 8, 229–239.

Heltzel, C.E., Gunatilaka, A.A.L., Kingston, D.G.I., Hofmann, G.A., Johnson, R.K., 1994. Synthesis and structure-activity relationships of cytotoxic 7-hydroxy sterols. Journal of Natural Products 57, 620–628.

Hofheinz, W., Oesterhelt, G., 1979. 24-Isopropylcholesterol and 22-dehydro-24-isopropylchoelsterol, novel sterols from a sponge. Helvetica Chimica Acta 62, 1307–1309.

Kokke, W.C.M.C., Pak, C.S., Fenical, W., Djerassi, C., 1979. Occurrence of 24($R+S$)-isopropenylcholesterol, 24($R+S$)-methylcholesta-5,25-dien-3β-ol, and 24($R+S$)-methylcholesta-7,25-dien-3β-ol in the Caribbean sponge, *Verongia cauliformis*. Helvetica Chimica Acta 62, 1310–1318.

Raederstorff, D., Rohmer, M., 1984. Sterols of the unicellular algae Nematochrysopsis roscoffensis and Chrysotila lamellose: isolation of (24E)-24-*n*-propylidenecholesterol and 24-*n*-propylcholesterol. Phytochemistry 23, 2835–2838.

Rohmer, M., Kokke, W.C.M.C., Fenical, W., Djerassi, C., 1980. Isolation of two new C30 sterols, (24E)-24-*N*-propylidenecholesterol and 24ξ-*N*-propylcholesterol, from a cultured marine chrysophyte. Steroids 35, 219–231.

Rubinstein, I., Goad, L.J., Clague, A.D.H., Mulheirn, L.J., 1976. The 220 MHz NMR spectrum of phytosterols. Phytochemistry 15, 195–200.

Saunders, G.W., Potter, D., Paskind, M.P., Andersen, R.A., 1995. Cladistic analyses of combined traditional and molecular data sets reveal an algal lineage. Proceedings of the National Academy of Sciences United States of America 92, 244–248.

Saunders, G.W., Potter, D., Andersen, R.A., 1997. Phylogenetic affinities of the Sarcinochrysidales and Chrysomeridales (Heterokonta) based on analysis of molecular and combined data. Journal of Phycology 33, 310–318.

Sieburth, J.M., Johnson, P.W., Hargraves, P.E., 1988. Ultrastructure and ecology of *Aureococcus anophagefferens gen. et sp. nov.* (Chrysophyceae): the dominant picoplankter during a bloom in Narragansett Bay, Rhode Island, summer 1985. Journal of Phycology 24, 416–425.

Stockwell, D.A., Buskey, D.A., Whitledge, T.E., 1993. Studies on conditions conducive to the development and maintenance of a persistant brown tide in Laguna Madre, Texas. In: Smayda, T.J., Shimizu, Y. (Eds.), Toxic Phytoplankton Blooms in the Sea: Proc. 5th Int. Conf. on Toxic Marine Phytoplankton. Elsevier, New York, pp. 693–698.

Volkman, J.K., 1986. A review of sterol markers for marine and terrigenous organic matter. Organic Geochemistry 9, 83–99.

PERGAMON

Phytochemistry 57 (2001) 791–795

PHYTOCHEMISTRY

www.elsevier.com/locate/phytochem

Influence of *trans-cis* isomerisation of coumaric acid substituents on colour variance and stabilisation in anthocyanins

Florian George[a], Paulo Figueiredo[b], Kenjiro Toki[c], Fumi Tatsuzawa[d], Norio Saito[e], Raymond Brouillard[a,*]

[a]*Laboratoire de Chimie des Polyphénols, UMR 7509 du CNRS, Université Louis Pasteur, Faculté de Chimie, 1, rue Blaise Pascal, 67008 Strasbourg, France*

[b]*Department of Engenharia e Tecnologias, Universidade Lusófona de Humanidades e Tecnologias, Av. do Campo Grande, 376, 1749-024 Lisboa, Portugal*

[c]*Laboratory of Floriculture, Minami-Kyushu University, Takanabe, Japan*

[d]*Faculty of Horticulture, Chiba University, Matsudo, Chiba, Japan*

[e]*Chemical Laboratory, Meiji-Gakuin University, Totsuka-ku, Yokohama, Japan*

Received 25 July 2000; received in revised form 27 February 2001

Abstract

The recently isolated pigments from *Petunia integrifolia* and *Triteleia bridgesii* present a distinct feature that sheds new light on the understanding of intramolecular copigmentation of anthocyanins. These are among the infrequent anthocyanins that naturally present a coumaric acid substituent in both *cis* and *trans* forms. As a consequence, the two isomers demonstrate substantial variations of their thermodynamic and kinetic constants and also colour properties. A possible explanation for these characteristics is presented, making use of molecular modelling and taking into account the three-dimensional structures of the pigments. © 2001 Elsevier Science Ltd. All rights reserved.

Keywords: *Petunia integrifolia*; Solanaceae; *Triteleia bridgesii*; Liliaceae; Acylated anthocyanins; Coumaric acid; *trans-cis* Isomerisation; Intramolecular copigmentation; Molecular modelling

1. Introduction

Progress on extraction and purification techniques has afforded details of several forms of acylated anthocyanins (Toki et al., 1994a,b; Saito et al., 1995; Tatsuzawa et al., 1997). These recently discovered pigments possess, as a common trait, one or more aromatic acyl residues. Depending on the length of the "chains" that link them to the central chromophore, they may fold over the 2-benzopyrylium system and strongly influence its properties as a colourant (Brouillard and Dangles, 1994). A pattern is common to most of these recently discovered pigments: the hydroxycinnamic acid units occur in a *trans* configuration (Saito and Harborne, 1992; Strack and Wray, 1994). To our knowledge, only eight papers report the isolation and characterization of hydroxycinnamic acid residues present in a *cis* configuration, one on the Labiatae (Yoshida et al., 1990), one on the Commelinaceae (Kondo et al., 1991), three on Liliaceae (Hosokawa et al., 1995a,b; Toki et al., 1998) and three on the Solanaceae (Ando et al., 1999a,b; Slimestad et al., 1999) flowers. In all of the above-cited works, the *trans* isomer always predominates in vivo.

The present paper reports, for the first time, on the colour stabilisation and intensity changes brought about by the isomerisation of the coumaroyl residue. The results concern two pairs of acylated anthocyanins (Scheme 1): malvidin 3-*O*-[6-*O*-(4-*O*-(*trans-p*-coumaroyl) -α-L-rhamnopyranosyl)-β-D-glucopyranoside]-5-*O*-(β-D-glucopyranoside) (**1**) and malvidin 3-*O*-[6-*O*-(4-*O*-(*cis-p*-coumaroyl)-α-L-rhamnopyranosyl)-β-D-glucopyranoside]- 5-*O*-(β-D-glucopyranoside) (**2**) isolated from the red-purple flowers of *Petunia integrifolia* (Ando et al., 1999a,b) and delphinidin 3-*O*-[6-*O*-(*trans-p*-coumaroyl)-β-D-glucopyranoside]-5-*O*-[6-*O*-(malonyl)-β-D-glucopyranoside] (**3**) and

* Corresponding author. Tel.: +33-3-9024-1342; fax: +33-3-9024-1341.

E-mail address: brouil@chimie.u-strasbg.fr (R. Brouillard).

0031-9422/01/$ - see front matter © 2001 Elsevier Science Ltd. All rights reserved.
PII: S0031-9422(01)00105-4

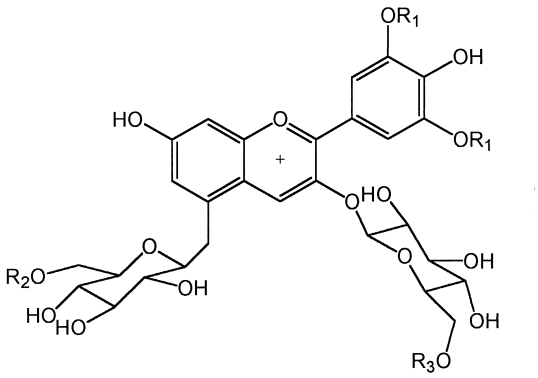

1. $R_1 = CH_3$, $R_2 = H$, R_3 = *trans*-4-*O*-(rhamnosyl)-*p*-coumaric acid
2. $R_1 = CH_3$, $R_2 = H$, R_3 = *cis*-4-*O*-(rhamnosyl)-*p*-coumaric acid
3. $R_1 = H$, R_2 = malonic acid, R_3 = *trans*-*p*-coumaric acid
4. $R_1 = H$, R_2 = malonic acid, R_3 = *cis*-*p*-coumaric acid

Scheme 1.

delphinidin 3-*O*-[6-*O*-(*cis*-*p*-coumaroyl)-β-D-glucopyranoside]-5-*O*-[6-*O*-(malonyl)-β-D-glucopyranoside] (**4**) extracted from the blue-purple flowers of *Triteleia bridgeseii* (Toki et al., 1998).

The thermodynamic and kinetic results gathered from the two pairs of natural pigments allowed the interpretation of intramolecular copigmentation from a new perspective, even supporting the hypothesis that such *cis*-hydroxycinnamic isomers may be more prolific in nature than has previously been thought, due to their aptitude to positively influence flower colour.

2. Results and discussion

Flower colour is, to a large extent, the consequence of the expression of the colouring properties of anthocyanins, the pigments residing in the vacuoles of plant cells. These pigments are, according to their chemical structure, capable of displaying an immense variety of tints and hues. In particular, acylated anthocyanins were shown to exhibit some of the more astonishing and stable colour capabilities ever found in plant pigments (Brouillard, 1981; Dangles et al., 1993a,b; Figueiredo et al., 1996a,b,1999). In this paper, we look at the changes brought about by the isomerisation around a coumaroyl residue on two sets of acylated anthocyanins (Scheme 1). In the vast majority of acylated anthocyanins extracted from plant material, the hydroxycinnamic acid units commonly appear as *trans* isomers, *cis* isomers being very rare. The two pairs of isomers presented in this work do not undergo isomerisation in aqueous solution, due to the high activation energy needed to convert between *trans* and *cis* forms. However, conversion between the two isomers was shown to take place in vitro, both with artificial (366 nm) and natural (sun) irradiation, for another set of structurally comparable anthocyanins (Yoshida et al., 1990).

The simple change from a *trans* to a *cis* configuration of the terminal coumaric acid on the molecules here studied produced some appreciable modifications both at the level of colour expression and colour stability. Table 1 reports those properties. Although the maximum absorbance wavelength in the visible, for the flavylium cation forms, does not greatly change among the four pigments concerned, their molar extinction coefficients do so (Fig. 1). In fact, *cis* isomers exhibit ε values about 1.5 times greater than *trans* ones, in both pairs of molecules. This increase in colour intensity may be due to differences in co-planarity between the central chromophore and the acyl residue. Computed structures for the two isomers **3** and **4** (Fig. 2), performed both in vacuo, in the AM1 (Dewar et al., 1985) parametrization, and in a simulated water container, with the MM+ (Allinger, 1977) force field, suggest that **4** has the coumaroyl residue almost parallel to the central anthocyanidin moiety, while **3** presents a quasi-perpendicular conformation.

The computed structures for anthocyanins **1**–**4** showed their ability to form folded structures (intramolecular copigmentation) that protect the pigments against the colour damaging hydration reaction. This is particularly true with the *cis* isomers (Fig. 2). The distance of the acyl residue in the *cis* isomer **4** to anthocyanidin moiety is smaller than in the *trans* isomer **3** (Fig. 2).

The hydration reaction is the primary cause of a marked colour loss in non-acylated anthocyanins, due to the formation of colourless equilibrium forms, in aqueous solution. This property is also affected by the change in configuration of the coumaroyl moiety from *trans* to *cis*. Calculated pK'_h values (Table 1) reveal that the *cis* isomers are less prone to undergo hydration than their *trans* counterparts. A closer look at the values obtained for the kinetic constants k_1 (hydration) and k_2 (reverse reaction) helps to understand this behaviour. While k_1 is of the same order of magnitude for both isomers, k_2 is always greater for the *cis* forms. This means that although

Table 1
Spectral characteristics (UV–vis.; pH = 1.0), hydration and deprotonation constant values for pigments **1**–**4**

	Pigment			
	1	**2**	**3**	**4**
λ_{max} (nm)	532	534	528	532
ε_{AH2+} (mol^{-1} dm^3 cm^{-1})	8500	12550	20900	35000
pK'_h	1.75±0.03	2.03±0.02	2.01±0.03	2.76±0.04
k_1 (min^{-1})	16.1±0.1	12.5±0.1	7.5±0.1	4.0±0.1
k_2 (mol^{-1} dm^3 cm^{-1})	914±7	1325±5	778±3	2300±10
pK_a	3.39±0.02	3.55±0.01	4.43±0.02	4.48±0.03

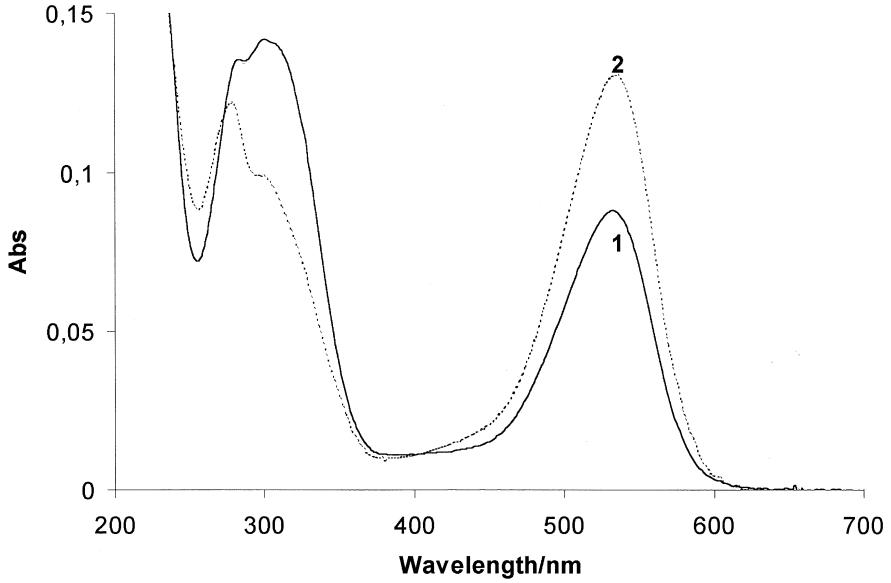

Fig. 1. Visible absorption spectra of pigments **1** (—) and **2** (- - -). pH = 1.0; conc. = 1.04×10^{-5} M.

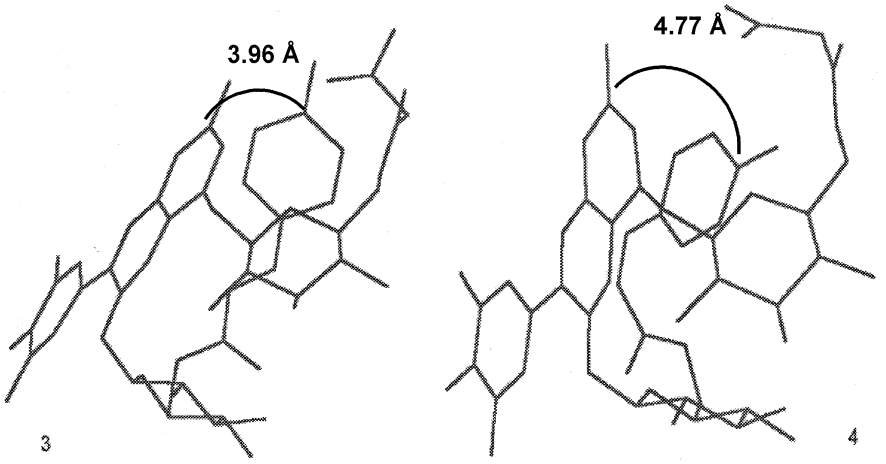

Fig. 2. Conformations of **3** and **4**, optimised by MM+. The arrows point to the coumaroyl moieties.

both forms have the same susceptibility to water addition to the charge deficient positions (C_2 and C_4), the *cis* isomer has a faster back reaction to reform the coloured flavylium cation. This may be due to a more favourable spatial arrangement of the molecules, conferred by *cis* isomerisation around the coumaroyl moiety. The computed (MM+) differences in formation energies between BH_2 (colourless hemiacetal) and AH_2^+ (coloured flavylium) indicate a more pronounced gap for anthocyanin **3** than for pigment **4**, which may account for the faster back reaction of **4**.

The present set of acylated anthocyanins presents pK_a values, for the proton transfer reaction transforming the coloured flavylium form in the also coloured quinonoidal base, within the characteristic range previously estimated for similar molecules (Dangles et al., 1993a,b; Figueiredo et al., 1996a, 1999). The influence of the *trans-cis* isomerisation seems not to be relevant in this particular case (Table 1). There is, however, a small variation in both pairs of anthocyanins, with *trans* isomers exhibiting slightly lower values in pK_a. The AM1 computed electronic charge densities for the atoms on C-7 and C-4' may account for such a difference. In all four molecules, the charge is more positive for C-7 than for C-4', in accordance with previously reported results (Figueiredo et al., 1999), indicating that the hydroxyl in position 7 of the aglycone is always the first to undergo proton transfer. Furthermore, in the present work, *trans* isomers yielded more positive values for the computed C-7 charges than their *cis* counterparts. However, no data clearly indicate that this feature is a consequence of structural variations caused by isomerisation about the coumaroyl moieties of the anthocyanins.

The results here reported once more stress the importance of the nature of substituents on colour stability of the anthocyanins. It is demonstrated, for the first time,

that one of the rarest features found in these pigments play an important role in preventing colour loss by nucleophilic water attack. In effect, the change from the common *trans* coumaroyl substituents to the unusual *cis* isomers confers an additional protection against hydration, reflected on an increase in pK'_h values. The more co-planar arrangement allowed by *cis* isomers is postulated as the rationale supporting the enhanced colour stability.

Knowing that *trans-cis* photoisomerisation may take place in vivo (Yoshida et al., 1990), we propose this mechanism as an additional means for preservation of flower colour, but one should bear in mind that the conversion between the two isomers in vivo is certainly rare due to low amounts of the *cis* configuration.

3. Experimental

3.1. Materials

Pigments were extracted according to published procedures and had their purity (always $\geqslant 98\%$) checked by ^{1}H NMR spectroscopy (Toki et al., 1998; Ando et al., 1999a). 3-*O*-[6-*O*-(4-*O*-(*trans*-*p*-coumaryl)-α-L-rhamnopyranosyl)-β-D-glucopyranosyl]-5-*O*-(β-D-glucopyranosyl) malvidin chloride (**1**) and 3-*O*-[6-*O*-(4-*O*-(*cis*-*p*-coumaryl)-α-L-rhamnopyranosyl)-β-D-glucopyranosyl]-5-*O*-(β-D-glucopyranosyl) malvidin chloride (**2**) were isolated from the red-purple flowers of *Petunia integrifolia* and 3-*O*-[6-*O*-(*trans*-*p*-coumaroyl)-β-D-glucopyranosyl]-5-*O*-[6-*O*-(malonyl)-β-D-glucopyranosyl] delphinidin chloride (**3**) and 3-*O*-[6-*O*-(*cis*-*p*-coumaryl)-β-D-glucopyranosyl]-5-*O*-[6-*O*-(malonyl)-β-D-glucopyranosyl] delphinidin chloride (**4**) were obtained from the blue-purple flowers of *Triteleia bridgeseii* and used without further purification. All other chemicals used were of analytical grade.

3.2. Absorption spectra

Absorption spectra were recorded with a Hewlett Packard diode-array spectrophotometer fitted with a quartz cell ($d = 1$ cm) equipped with a stirring magnet. A constant temperature of 25 ± 0.1°C, measured with a Comark thermocouple, was maintained in the spectrometer sample cell by use of a Bioblock water-thermostated external bath. Water used in sample preparations was bidistilled.

3.3. Data analysis

UV–visible absorption data were recorded on a Pentium P200 PC using the Hewlett Packard UV–visible Chemstation Programme. Mathematical treatments applied to the data were carried out with the Microsoft Excel 98 programme running on a PowerMacintosh G3/300 machine.

3.4. Thermodynamic measurements

Stock solns ranging from 6.6×10^{-5} M to 1.1×10^{-4} M of the 4 pigments were prepared in 0.1 M HCl and left to equilibrate in the dark for about 3 h. Then, for each pigment, 16 solns were prepared by 1:10 dilutions of the stock solns with different volumes of NaOH 0.1 M soln and H_2O so that the final pH covered a range of 1–3.5. After equilibration in the dark, the UV–vis spectra of these solns were recorded. The values of the global equilibrium constants ($K' = K'_h + K_a$) are gained from measuring the relative hyperchromic shift at the visible absorption maxima of the flavylium cation, for all the pigments studied, as a function of pH.

3.5. Kinetic measurements

One milliliter of each equilibrated aq. soln of anthocyanin, at different pH values (from 1.0 to 3.0, depending on the pigment) was magnetically stirred in the spectrophotometer cell. The concentrations of pigments **1**–**4** were respectively 8.54×10^{-6} M, 6.61×10^{-6} M, 1.07×10^{-5} M and 7.82×10^{-6} M. To these solns, 1 ml of acetate buffer solns, ranging in pH from 3.0 to 5.0, was quickly added and the visible absorbance at ca. 530 nm (near the visible absorption maxima for all the pigments) was immediately recorded every second over 120 s to guarantee that the hydration equilibrium is attained. The final pH was then measured and ranged from 2.4 to 4.6. The spectrophotometer software automatically computes the first order apparent rate constant of the hydration reaction (k).

3.6. Molecular modelling

Molecular mechanics [MM+ (Allinger, 1977)], inside a simulated periodic box of ca. 350 water molecules and semi-empirical quantum mechanical calculations [AM1 (Dewar et al., 1985)] were performed on a Pentium P350 PC using the Hyperchem programme (version 4, Hypercube, Inc., Ont., Canada).

References

Allinger, N.L., 1977. Conformational analysis 130. MM2. A hydrocarbon force field utilizing V_1 and V_2 torsional terms. J. Am. Chem. Soc. 99, 8127–8134.

Ando, T., Saito, N., Tatsuzawa, F., Kakefuda, T., Yamakage, K., Ohtani, E., Koshi-ishi, M., Matsusake, Y., Kokubun, H., Watanabe, H., Tsukamoto, T., Ueda, Y., Hashimoto, G., Marchesi, E., Asakura, K., Hara, R., Seki, H., 1999a. Floral anthocyanins in wild taxa of *Petunia* (Solanaceae). Biochem. Systematics Ecol. 27, 623–650.

Ando, T., Saito, N., Tatsuzawa, F., Kakefuda, T., Yamakage, K., Ohtani, E., Koshi-ishi, M., Matsusake, Y., Kokubun, H., Watanabe,

H., Tsukamoto, T., Hashimoto, G., Marchesi, E., 1999b. HPLC profiles of floral anthocyanins in the native taxa of *Petunia* (Solanaceae). Tech. Bull. Fac. Hort. Chiba Univ. 53, 135–144.

Brouillard, R., 1981. Origin of the exceptional colour stability of the *Zebrina* anthocyanin. Phytochemistry 20, 143–145.

Brouillard, R., Dangles, O., 1994. Flavonoids and flower colour. In: Harborne, J.B. (Ed.), The Flavonoids. Advances in Research since 1986. Chapman & Hall, London, pp. 565–588.

Dangles, O., Saito, N., Brouillard, R., 1993a. Anthocyanin intramolecular copigment effect. Phytochemistry 34, 119–124.

Dangles, O., Saito, N., Brouillard, R., 1993b. Kinetic and thermodynamic control of flavylium hydration in the pelargonidin-cinnamic acid complexation. Origin of the extraordinary flower color diversity of *Pharbitis nil*. J. Am. Chem. Soc. 115, 3125–3132.

Dewar, M.J.S., Zoebisch, E.G., Healy, E.F., Stewart, J.J.P., 1985. A new general purpose quantum mechanical model. J. Am. Chem. Soc. 107, 3902–3909.

Figueiredo, P., Elhabiri, M., Saito, N., Brouillard, R., 1996a. Anthocyanin intramolecular interactions. A new mathematical approach to account for the remarkable colorant properties of the pigments extracted from *Matthiola incana*. J. Am. Chem. Soc. 118, 4788–4793.

Figueiredo, P., Elhabiri, M., Toki, K., Saito, N., Dangles, O., Brouillard, R., 1996b. New aspects of anthocyanin complexation. Intramolecular copigmentation as a means for colour loss? Phytochemistry 41, 301–308.

Figueiredo, P., George, F., Tatsuzawa, F., Toki, K., Saito, N., Brouillard, R., 1999. New features of intramolecular copigmentation by acylated anthocyanins. Phytochemistry 51, 125–132.

Hosokawa, K., Fukunaga, Y., Fukushi, E., Kawabata, J., 1995a. Seven acylated anthocyanins in the blue flowers of *Hyacinthus orientalis*. Phytochemistry 38, 1293–1298.

Hosokawa, K., Fukunaga, Y., Fukushi, E., Kawabata, J., 1995b. Acylated anthocyanins from red *Hyacinthus orientalis*. Phytochemistry 39, 1437–1441.

Kondo, T., Yoshida, K., Yoshikane, M., Goto, T., 1991. Mechanism for color development in purple flower of *Commelina communis*. Agric. Biol. Chem. 55, 2919–2921.

Saito, N., Harborne, J.B., 1992. Correlations between anthocyanin type, pollinator and flower colour in the Labiatae. Phytochemistry 31, 3009–3015.

Saito, N., Ku, M., Tatsuzawa, F., Lu, T.S., Yokoi, M., Shigihara, A., Honda, T., 1995. Acylated cyanidin glycosides in the purple-red flowers of *Bletilla striata*. Phytochemistry 40, 1523–1529.

Slimestad, R., Aaberg, A., Andersen, Ø.M., 1999. Acylated anthocyanins from petunia flowers. Phytochemistry 50, 1081–1086.

Strack, D., Wray, V., 1994. The anthocyanins. In: Harborne, J.B. (Ed.), The Flavonoids. Advances in Research Since 1986. Chapman & Hall, London, pp. 1–22.

Tatsuzawa, F., Saito, N., Seki, H., Hara, R., Yokoi, M., Honda, T., 1997. Acylated cyanidin glycoside in the red-purple flowers of *Phalaenopsis*. Phytochemistry 45, 173–177.

Toki, K., Saito, N., Imura, K., Suzuki, T., Honda, T., 1994a. (Delphinidin 3-gentiobiosyl) (apigenin 7-glucosyl) malonate from the flowers of *Eichhornia crassipes*. Phytochemistry 36, 1181–1183.

Toki, K., Saito, N., Kawano, K., Lu, T.S., Shigihara, A., Honda, T., 1994b. An acylated delphinidin glycoside in the blue flowers of *Evolvulus pilosus*. Phytochemistry 36, 609–612.

Toki, K., Saito, N., Honda, T., 1998. Acylated anthocyanins from the blue-purple flowers of *Triteleia bridgesii*. Phytochemistry 48, 729–732.

Yoshida, K., Kondo, T., Kameda, K., Goto, T., 1990. Structure of anthocyanins isolated from purple leaves of *Perilla ocimoides* L. var. *crispa* Benththeir isomerisation by irradiation of light. Agric. Biol. Chem. 54, 1745–1751.

PERGAMON

Phytochemistry 57 (2001) 797–798

PHYTOCHEMISTRY

www.elsevier.com/locate/phytochem

Book reviews

Bioactive Compounds from Natural Sources: Isolation, Characterisation and Biological Properties
Edited by C. Tringali; Taylor & Francis, London and New York, 2001, 693 pp., ISBN 0-7484-0890-8, £65

There is a renewed interest in obtaining natural products for evaluation in high throughput screens and also a need to better understand the chemistry of herbal medicinal products and foods. This multi-author book is aimed at advanced students and research scientists from various disciplines working in areas related to natural products. This volume aims to focus on the modern approach to the isolation of biologically active natural products in general but there are also some very detailed research reviews by experts in the fields such as on limonoids, flavonoids, other potential anti-tumour compounds and marine natural products.

The book includes chapters on general modern methods of identifying and purifying natural products such as on-line identification of plant metabolites by LC–UV, LC–MS and LC–NMR and also NMR methods in structural elucidation (by the editor). An ethnobotanical approach is described using Mexican plants used to treat gastrointestinal disorders as an example and how cytotoxins and chemicals with activities as herbicides and insecticides were found. The other chapters deal with particular classes of compounds such as flavonoids in cancer prevention, anti-cancer drugs from higher plants, anti-HIV aromatic compounds, antioxidants from plants, antimalarial and anti-inflammatory compounds (affecting cyclo-oxygenase-2) and three chapters on marine metabolites including glycolipids as immunomodulators.

There is also an unusual chapter on phytotoxins from fungi which are pathogenic to agrarian, forestal and weedy plants. The taxoid chapter gives an interesting review of natural sources and the limonoid chapter has considerable detail of their biosynthesis, chemistry and anti-feedant properties to insects.

The title of the book gives a good description of the chapters, which are very detailed and interesting in their multi-disciplinary content of biology, biochemistry and chemistry. Since Professor Tringali is the editor, it is not surprising that the chapters tend to include useful details of NMR data. All of the chapters have a good literature reference list. This book is recommended to all natural products researchers.

Robert J. Nash
Institute of Grassland and Environmental Research
Plas Gogerddan, Aberystwyth, UK
E-mail address: robert.nash@bbsrc.ac.uk

PII: S0031-9422(01)00100-5

Molecular and Supramolecular Chemistry of Natural Products and Their Model Compounds
J.-H. Fuhrhop and C. Endisch, Marcel Dekker, New York, Basel, 1999, 602 pp., ISBN: 0-8247-8201-1, $195

Molecular and Supramolecular Chemistry of Natural Products and Their Model Compounds is primarily targeted at Masters and Doctoral students in chemistry and biochemistry who are interested in the basic structural properties and reactivity of common natural products. This book should provide an invaluable reference to researchers in this developing and exciting field and, perhaps, is the only book of its kind offering remarkable depth to each chapter. The book is logically presented covering all major natural compounds as well as extensively covering the properties of natural compounds in synkinetics (i.e. the reversible synthesis of complex molecular structures). The book is divided into nine chapters of which the first is essentially a review of the basic concepts covering the isolation and structure of natural compounds, the synthesis of natural compounds, their reactivity and finally synkinesis. The remaining eight chapters are organised systematically beginning with lipids and membranes, steroids, carbohydrates,

carotenes, porphyrins, vitamins, DNA and finally proteins. Of particular interest was the lipids and membranes chapter where applications relevant to monolayer technology were generously covered including atomic force microscopy of monolayers, two physical methods for measuring ion flow in black lipid membranes, large vesicular, and cell membranes as well as a method that works with a large population of vesicles using entrapped fluorescence dyes. The section on carbohydrates is focused on organic chemists who are working with cellulose and the structures of all known forms of cellulose are covered. The DNA and protein chapters will be of interest to molecular biologists who are familiar with manipulating DNA but not aware of the chemistry! The protein chapter covers a number of interesting examples of synkinesis with proteins. For example the assembly of peptide pores in membranes using bee venom melittin and gramicidine A as classical examples. Also discussed are examples of protein interactions with steroids (progesterone), carbohydrates, carotenes and porphyrins (using the heme pocket in myoglobin as an example). Finally, the most interesting section of the protein chapter is the section on the assemblies of proteins covering, zinc-finger proteins, leucine zippers and the formation of immunoglobulins.

One useful aspect of this book is that it covers new and emerging technologies such as cryo-electron, atomic force microscopy and scanning force microscopy as well as including established techniques such as black film methodology. One surprise for a book of this nature was the extensive illustrations with over 500 figures, almost equalling one per page. Perhaps, due to the large number of figures used some of the figures are very small and in places difficult to discern (this is particulary true of the DNA chapter). In addition, *Molecular and Supramolecular Chemistry of Natural Products and Their Model Compounds* is extensively referenced with over 900 references making this an ideal sourcebook for further study. The price of the book ($195) seems appropriate for an advanced reference book of this nature.

Simon Cutting
School of Biological Sciences
Royal Holloway University of London
Egham, Surrey TW20 0EX, UK
E-mail address: s.cutting@rhul.ac.uk

PII: S0031-9422(01)00074-7

PERGAMON

Phytochemistry 57 (2001) 799

PHYTOCHEMISTRY

www.elsevier.com/locate/phytochem

Corrigendum

Corrigendum to "Sesquiterpene coumarins and sesquiterpenes from *Ferula sinaica*" [Phytochemistry 50 (1999) 109–112]☆

Ahmed A. Ahmed*

Department of Chemistry, Faculty of Science, El-Minia University, El-Minia 61519, Egypt

The author regrets that there are two errors in this paper.

The structure of compound **6** on page 110 should read **5**.

Table 2 on page 111, the chemical shift of C-1′ of compounds **2** and **3** should read 65.8 and 65.9, respectively. The chemical shift of C-9 should read for C-10 and vice versa. The author apologises for any inconvenience or embarrassment caused.

☆ PII of original article: S0031-9422(98)00489-0

* Corresponding author. Tel.: +20-86-345-267; fax: +20-86-342-601.
E-mail address: abdellaahmed@hotmail.com

0031-9422/01/$ - see front matter © 2001 Elsevier Science Ltd. All rights reserved.
PII: S0031-9422(01)00152-2

PERGAMON

Phytochemistry 57 (2001) 801

PHYTOCHEMISTRY

www.elsevier.com/locate/phytochem

Erratum

Erratum to "7β-Oxygenated limonoids from *Trichilia elegans* ssp. *elegans*" [Phytochemistry 55 (2000) 733–740]☆

Fernanda R. Garcez [a,*], Walmir S. Garcez [a], Nídia F. Roque [b,c], Eduardo E. Castellano [b,d], Julio Zukerman-Schpector [b,d]

[a] *Departamento de Química, Universidade Federal de Mato Grosso do Sul, Campo Grande, MS, 79070-900, Brazil*
[b] *Instituto de Química, Universidade de São Paulo, 05599-970, SP, Brazil*
[c] *Instituto de Química, Universidade Federal da Bahia, 40170-290, Salvador, BA, Brazil*
[d] *Laboratório de Cristalografia, Estereodinâmica e Modelagem Molecular, DQ, Universidade Federal de São Carlos, São Carlos, SP, Brazil*

The Publisher regrets that one of the authors' names was spelt incorrectly. The author's name should be spelt "Eduardo E. Castellano".

We apologise for any inconvenience or embarrassment caused.

☆ PII of original article: S0031-9422(00)00287-9

* Corresponding author. Tel.: +55-67-7461034; fax: +55-67-7875314.
E-mail address: frgarcez@nin.ufms.br (F.R. Garcez).

0031-9422/01/$ - see front matter © 2001 Elsevier Science Ltd. All rights reserved.
PII: S0031-9422(01)00057-7

PERGAMON

Phytochemistry 57 (2001) 803–804

PHYTOCHEMISTRY

www.elsevier.com/locate/phytochem

Editorial

Special Issues Devoted to the Biosynthesis of Woody Plant Biopolymers and Related Substances

These Special Issues (Vol. 57/6 and 57/7) are largely derived from the presentation of papers given at the Millennium Symposium of the American Chemical Society (ACS) entitled, "Biosynthesis of Woody Plant Biopolymers and Related Substances", held in San Francisco from the 26–29 March 2000. It was organized by G.P. Bolwell and N.G. Lewis, under the auspices of the ACS Cellulose, Paper and Textile Division. The meeting was devoted to fundamental research on the biosynthesis, assembly and properties of plant cell walls which underpin their use as industrial feedstocks and other aspects that impinge on daily life such as dietary fiber. Of special interest was the way in which chemistry is being augmented with genomic, proteomic and metabolic studies to unravel the complex processes involved in plant cell wall assembly, and in combination with molecular breeding to improve fiber properties.

The rationale of the gathering was directed at integrating the present knowledge of the synthesis and assembly of carbohydrate and phenolic biopolymers in woody tissues. That notwithstanding, additional communications were given on those components that have been rather neglected in the past but which are important in preserving and enhancing both the integrity and function of specialized cell walls. These contributions focus upon specialized phenolics and lipids of secretory, cuticular, suberized and heartwood tissues.

We have organized these issues in several thematic sections, which mainly reflect the range of topics covered at the meeting. Authors were encouraged to update their contributions in the time since the meeting. The first section primarily deals with structural and anatomical aspects but contain protein and gene expression data that help understand the complexity of individual cell types within woody tissues. Four papers (McCann, Haigler and Lewis) largely relate to polysaccharide biosynthesis and cell wall assembly at the cellular level, while within the second group, two (Donaldson and Ruel) summarize spatial aspects of lignin biosynthesis and others (Lewis and Gross) describe the processes involving specialized depositions of lignins/lignans and tannins, in woody tissues, respectively.

The next section has an emphasis on chemical aspects and plant component analysis. The first begins with a comprehensive review on pectins (Mohnen) and is presented together with a research paper describing novel linkages between heterogeneous pectins (Ishii). Another contribution (Murray) describes an intriguing occurrence of oligosaccharides which might be related to glucan biosynthesis. A second chemistry section has two papers (Iiyama and Ralph) which describe some observations that they believe affect lignin assembly and a third by Stange indicates that the lignin formed by the wounding of cucumber is actually largely *p*-coumaraldehyde. Marton and Ferreira describe additional complex flavonoid derived structures found within specialized cell walls containing phenolic polymers, including that of heartwood. The final paper in this section (Stark) summarizes our knowledge of the lipid components associated with phenolics in cuticular structures.

The next sections address progress made on the biochemistry and molecular biology of carbohydrate and phenolic polymers. We begin with protein biochemistry and metabolism of wall carbohydrate synthesis. Further characterization of the synthesis of polysaccharides in vitro is described in two contributions (Carpita and Bolwell). This is followed by a study on metabolism of monosaccharides (Magel) which is also related to the provision of phenolic precursors for heartwood deposition. The biosynthesis of monolignols is reviewed with respect to metabolic channeling of individual monolignol pathways (Dixon) with three other papers following on coniferyl alcohol metabolism (Savidge and Ros Barcelo). Bernards and Cornish summarize the important advances being made in suberin and rubber biosynthesis, respectively. In the year in which the Arabidopsis genome was completed, molecular genetics have not been left out. It is apt that as we strive to identify the genes responsible for cell wall polysaccharide biosynthesis that we present a review that is germane to such studies (Brown). Five articles describe results on the regulation and manipulation of lignin biosynthesis, and these complete the two special issues (Kawaoka, Legrand, Ye, Grima-Pettenati and Bolwell). Such study represents the immediate take-off point for present commercially oriented work.

As Editors of this Special Issue, we are extremely grateful for the timely preparation and updating of

0031-9422/01/$ - see front matter © 2001 Published by Elsevier Science Ltd. All rights reserved.
PII: S0031-9422(01)00162-5

these articles by the authors. We hope that they and the readers will find these an important and stimulating series of articles on the present status of our yet very incomplete understanding of the biosynthesis of woody plant biopolymers and related substances. In this respect, we have strived in these two volumes to compile a range of views, which sometimes differ on the same topic.

Following this editorial, we provide a summary on our understanding of the remarkable processes involved in wood evolution. It would be remiss if we did not wholeheartedly thank financial support provided by a number of organizations without whose help neither symposium nor special issues would have been possible. These include, Applied Phytologics, Inc., American Chemical Society, Elsevier Science Ltd., the S.R. Noble foundation, Waters Corporation and the Weyerhaeuser Company.

Norman G. Lewis
G. Paul Bolwell

PERGAMON

Phytochemistry 57 (2001) 805–810

PHYTOCHEMISTRY

www.elsevier.com/locate/phytochem

Editorial comment

The Holy Grail of wood evolution — from wood anatomy to tissue-specific gene expression: to what extent do molecular studies of biosynthesis of cell wall biopolymers help the understanding of the evolution of woody species?

1. Introduction

During the assembly of these two Special Issues, we have been prompted in the review of the contributions to reflect on two main threads of study pursued for woody species. The first is the assessment of the current knowledge of how wood evolution occurred, drawing as far as we can at present upon the fields of genomics, proteomics, wood anatomy, plant chemistry and plant biology. The second is in the identification of the outstanding questions and opportunities that challenge us both now and in the future as regards strategic manipulations and optimization of wood and fiber quality. Thus, we attempt to highlight the progress made over nearly three centuries and apologize in advance for any omissions that may have occurred.

Woody vascular and herbaceous plant evolution was arguably the single most important development for sustenance of life in a terrestrial habitat. Moreover vascular plant life in general markedly defines and characterizes our terrestrial ecosystems, and their conquest of land has led to all of our modern soils and the varied life forms therein, as well as in providing the means to support the explosion of all terrestrial (metazoan) groups as they emerged (Graham et al., 2000). Vascular plant life has also markedly impacted the atmospheric chemistry and climate including the levels of gaseous CO_2. Humanity, of course, has long used woody plants for sundry purposes as a source of fiber, solid wood products, foods, medicines, intermediate chemicals, flavors and fragrances.

From its very early beginnings, phytochemistry has made many great advances into the chemical compositions and constituents of plant life, which in turn have set the foundation for the modern fields of plant chemotaxonomy, plant biochemistry and even genomics. However, phytochemistry now assumes perhaps its most compelling challenge, namely its integration with morphological and molecular studies, in order to comprehensively define how a plant both forms and compartmentalizes its various metabolic products. In this regard, what greater opportunity is there in defining how development of this heterogeneous tissue that we describe collectively as wood occurs? Arguably it represents one of nature's greatest engineering feats.

In this post-genomic age and with the ability to carry out molecular breeding at our disposal, we are now in a position to consider a technologically driven evolution of woody species with benefits for industrial processes including their impact on the environment. At this juncture, though, it is worth reflecting upon the course of evolution that has led to present day species. This is because the work presented at the meeting that has given rise to these Special Issues, and communications also published elsewhere recently, are adding to the insights into the evolution of woody species already developed in paleobotanical studies. Molecular analysis of the biochemistry and differential gene expression shown by present day plants is a culmination of 200 million years of evolution and carries the imprint of the early colonizers of terrestrial habitats. If woody species represent an evolutionary pinnacle from the point of view of mechanical success and as a bulk resource, then they are a product of many attempts to develop the vascular habit.

In terms of dicots, the advent of the vessel is thought to be significant in the evolution of woody species (Bailey, 1953; Cheadle, 1953). However, this and other genetic remnants of evolution ultimately led to the inherent variability found in the 250,000–350,000 plant species in existence today. This natural variability is observed not only in terms of both chemical compositions but also morphological patterns both between and within species.

Put in another way, while common biochemical themes clearly exist for cell wall assembly, individual species, nevertheless, generate specific patterns of formation of their extracellular matrices, e.g. through modulation of their biochemical pathways to the cell wall biopolymers. We simply do not know the limits to this variability at present, and one goal is to determine this and use it to humanity's benefit in a manner that is environmentally, societally and ethically responsible. Some of the questions to be asked include what are the desirable targets for change and is it really as simple as less lignin and more cellulose? Indeed the fundamental question may simply reside in defining the actual limits to cell wall variability. First impressions are that this variability is considerable and we review this in the context of these Special Issues.

Work of this type has, however, a number of ethical, societal and environmental ramifications, as noted from the ongoing GMO debates and related concerns. It is important that these aspects are not ignored by the scientific community during the period of research that will follow. This will require that we reach out to our communities and help explain both natural variability and the benefits that can accrue from such investigations, whether for new fiber sources, human health protection, and so forth.

2. What are the limits to structural variation?

Even without engineering mutations, wood development shows considerable variability in response to mechanical and environmental factors. One of the most common and widespread forms of this variability is in the generation of reaction wood, as is seen by compression wood in gymnosperms and tension wood in angiosperms. These serve to realign the stem when it is dislodged from its vertical alignment and restore the photosynthetic canopy, as well as being involved in determining the branching patterns and orientations. These effects arise by strategic synthesis of new wall material in the requisite areas of the developing stem or branch. In compression wood this takes the form of having a rounded phenotype and having a higher lignin content. Tension wood in contrast arises in the uppermost part of the leaning stem in the form of a gelatinous layer reflecting a higher cellulosic and lower lignin content than compression wood. Two papers Kwon et al. (2001a) and Levine et al. (2001) tackle the influence of mechanical factors from another angle by observing whether the effects of microgravity can override these programmable changes, and discovered that — in contrast to many reports in the literature-they do not.

Water status is also a factor. Besides the familiar effects of adverse conditions on ring growth the reciprocal effect of high water levels gives rise to the vesselless phenotype in willow and pea, as was recognized in the nineteenth century (Böhm, 1879; Vesque and Viet, 1881). It is, therefore, apparent that the study of xylem development needs to occur with the recognition that within the plant genome exists a flexibility that leads to different cell wall types and their constituents in order to maintain the particular biomechanical properties necessary for the tissue being formed. How plants perceive these needs and how the corrective actions are taken will be the focus of much research in the future.

3. Can wall polysaccharides be favorably altered?

Although cellulose is found universally there is considerable variation in its molecular weight ranges and extent of crystallinity both within and between species; this again presumably reflects the changes that this biopolymer has for individual cell types and subcellular layers.

There is also considerable variation in the associated polysaccharides which is found in its extreme in the dicots and monocots. The dicot primary wall contains three major pectin types and xyloglucan as the main hemicellulose. It is often overlooked that the middle lamella and primary wall, albeit subsequently lignified, is preserved in tracheids but the adjacent secondary wall that is laid down has a very different composition. There is little pectin and the major hemicellulose is xylan. In terms of composition this resembles the monocot primary wall, where the hemicellulose is mainly arabinoxylan together with *beta* $1\rightarrow3$; $1\rightarrow4$ mixed-linkage glucan. Indeed callose has been reported in secondary walls on occasion using histological staining (Currier, 1957) and can be detected using immunolocalization (M.E. Kerry and G.P. Bolwell, unpublished). Already there are reports that alteration in lignin in woody species brings about favorable increases in cellulose content (Hu et al., 1999). This has not yet been approached through direct manipulation of polysaccharide synthases due to the lack of genes available with the exception of cellulose synthase.

The paper by Saxena et al. (2001) illustrates how understanding the cellulose synthase may allow identification of further polysaccharide synthases in the genomic databases. Alternatively two papers [Buckeridge et al. (2001); Kerry et al. (2001)] describe the types of biochemical studies that are striving to identify the enzymes in order to lead to identification of new target genes. Already there are enough indications that these will be good targets to further explore the limits to wall variability. However, the differences between primary and secondary walls indicate that more sophisticated microscopic analysis, rather than chemical analyses of whole material, will be needed to understand the consequences of such manipulation such as those described by Ruel et al. (2001).

4. The pathway to lignin biosynthesis and polymerization; is there one pathway to lignification?

Understanding of the lignin pathway is truly in a state of flux at present! It is constantly being redrawn with revision of the functionality of some of the enzymes. Multiplicity of the number of genes coding for individual steps is adding a new complexity. This is described in a review (Dixon et al., 2001) which also introduces the concept of metabolic channeling.

5. Differential gene expression: do different cell types in wood express the same genes?

Differential gene expression in this context relates to the temporal and spatial activity of genes in the various vascular cell types. Several papers (Kwon et al., 2001b; Ye et al., 2001) together with work elsewhere suggest that different cell types express different genes and that this can give rise to micro-heterogeneity for both lignin biosynthesis and related substances in vessels and tracheids at least. In the paper by Ye et al. (2001) expression of CCOMT seemed to be confined to tracheids and fibers; there was a lack of a signal in the vessels. Does this reflect problems with detection limits, or is the lignin pathway in vessels lacking CCOMT? How also are the other pathways in woody plant cells using monolignols (not for lignification) kept separate. Clearly, as shown by Kwon et al. (2001b) and Burlat et al. (2001), we are just beginning to scratch the surface in unraveling the organizational frameworks of these complex biochemical machineries.

Structural genes in the lignin pathway are mainly regulated through transcriptional control (Kawaoka and Ebinuma, 2001). Cell-specific expression then resides in the regulatory sequences. If there is compelling evidence for considerable differential gene expression in tracheids and vessels then it does indeed support separate origins for the two cell types in primitive dicots. In addition to suppression of vessels by high humidity (Section 2) some species of dicot never form vessels particularly amongst the aquatic plants, saprophytes, parasites and succulents which have been considered to arise through a loss of the vessel habit (Bailey, 1953; Cheadle, 1953). There are also ten genera of dicots which are vessel-less and considered primitive. There does not seem to be any examples of tracheid-less dicots, although monocots and herbaceous dicots resemble vessel-type primitive land plants in the persistence of distinct vessel-rich vascular bundles rather than a continuous vasculature seen in woody plants. Since the presence of vessels would seem to be an advantage it is entirely feasible that it was selected for. In addition any crossing that introduced both cell types into a new hybrid would have conferred an enormous evolutionary advantage and would have been selected for.

6. Implications for understanding the evolution of woody species

This distinction between vessels and tracheids is important since the occurrence of vessels has been a focus of much of the work aimed at understanding the evolution of woody species (Bailey, 1953; Cheadle, 1953; Wheeler and Baas, 1991). As incomplete as the fossil records are, they provide evidence for migration of complex photosynthetic life forms, presumably derived from algal forerunners, to a land base some 470 million years ago (Edwards, 2000) (Fig. 1). This ultimately led to the development of tracheary elements as defined as imperforated cells with bordered pits, which following autolysis form reinforced water conducting cells. This pivotal progression ultimately led to complex multicellular plant forms and hence to the enormous proliferation of plant species in existence today.

Initially it has been proposed, based on the fossil record that three major classes of primitive plants then evolved, each possessing a characteristic tracheid type. All three differ markedly from the typical seed plant tracheids in existence today, and these differences shed important evolutionary insight into the success of land colonizing seed plants. Fig. 2 shows the three types of tracheary elements present in the S, G and P-type tracheids of early but now extinct land plants (Friedman and Cook, 2000). All three types contain a degradation-resistant layer adjacent to the cell lumen and a degradation-prone layer in the outer confines of the secondary wall thickening. In modern seed plant secondary thickenings there is no comparable degradable layer. In the S-type tracheids, present in the extinct Rhynia (Rhyniopsida), there are annular or helical wall thickenings as well as a lateral (degradation-prone layer) possessing spongy or reticulate material. In the G-type tracheids, present in the extinct Zosterophyllum (Lycophytina), there are again two layers — a resistant layer adjacent to the cell lumen and a degradation-prone layer in the external regions. Fossil evidence also suggests the presence of perforations in the primary wall and small pits in the decay-resistant secondary wall. The P-type tracheids present in *Psilophyton* (Euphyllophytina), resemble those of the G-type variants except for having bordered pits. It has been speculated that these early primitive land plants contained phenolics (lignin?) in their degradation resistant zones but lacked them in their degradation prone regions. This would reveal a situation at variance with present day gymno- and angio-sperms where essentially the whole wall is lignified in vascular cells. However, can the primitive condition be mimicked by altering patterns of micro-heterogeneity of lignification and loosening of wall structures (degradation-prone?). Interestingly, in a CCR down-regulated line this occurred, albeit in the reverse orientation (Ruel et al., 2001).

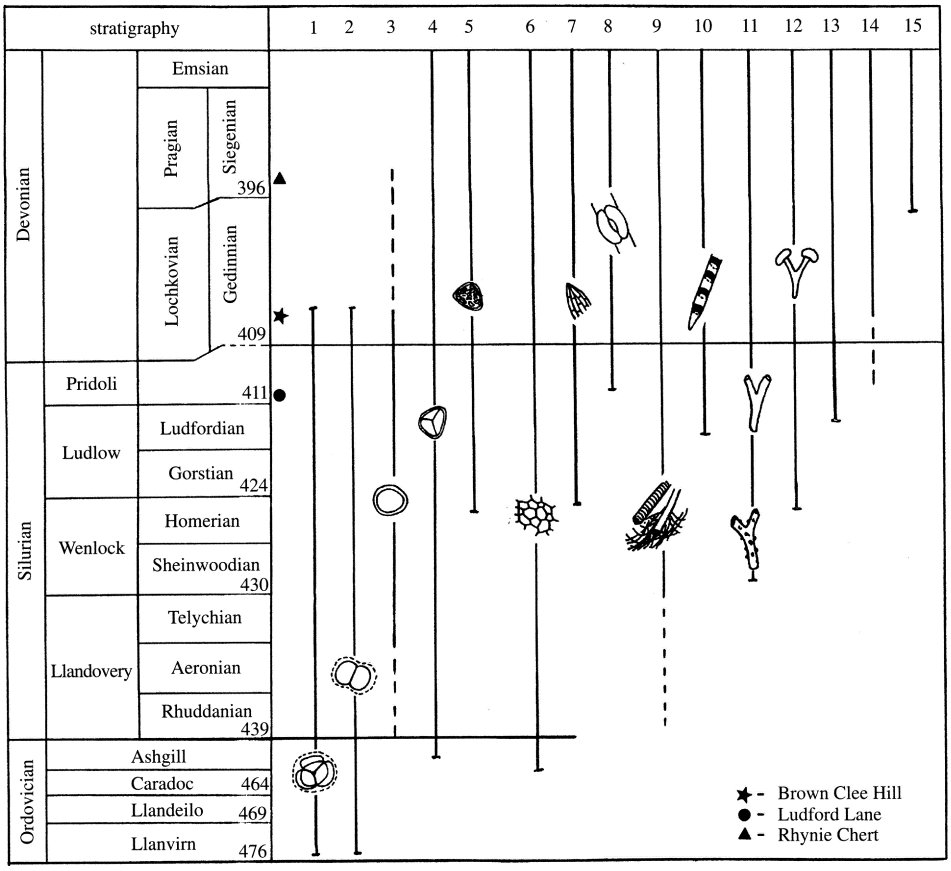

Fig. 1. Stratigraphic ranges of fossils. (1) Permanent (obligate) tetrads±envelope; (2) permanent dyads±envelopes; (3) hilate monads; (4) trilete laevigate monads; (5) ornamented trilete monads; (6) cuticular sheets (cf. *Nematothallus*); (7) sporangial cuticles; (8) stomata; (9) associations of tubes, solid line only indicates presence of banded tubes; (10) tracheids; (11) bifurcating axes of tracheophyte type; (12) *Cooksonia*/ Rhyniopsida; (13) Lycophytina sensu lato; (14) zosterophylls; (15) Trimerophytina. Redrawn from Edwards (2000) with permission.

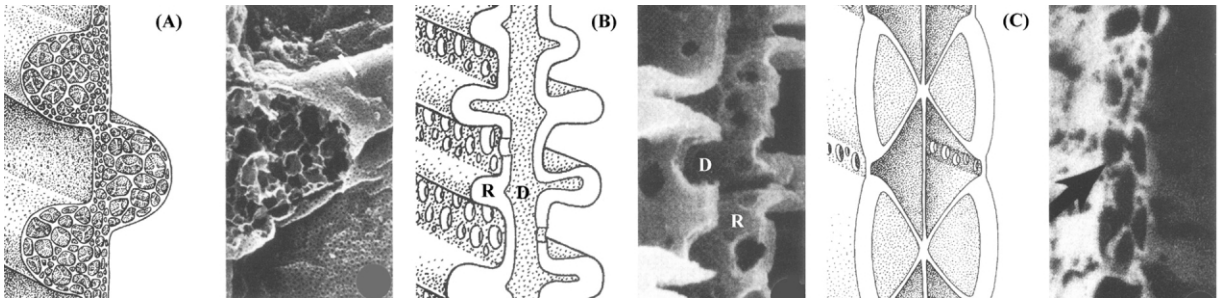

Fig. 2. The three major types of early tracheids. (A) Left: drawing of the wall of an S-type water-conducting cell showing the wall thickenings with a spongy (alveolate) structure and a thin microporate surface on the lumen face of the tracheid; right: SEM of a single gyre from a S-type cell of *Sennicaulis*, a member of the Rhyniopsida. (B) Left: drawing of the wall of a G-type water-conducting cell showing the wall thickenings that lack material in the core and holes in the surface of the lumen face of the tracheid; right: SEM of a portion of a G-type cell of *Gosslingia*, a member of the Lycophytina. (C) Left: drawing of the wall of a P-type water-conducting cell showing the wall thickenings that lack material in the core and continuity of the wall material that overlies the pits and has holes; right: SEM of a portion of a P-type cell of *Psilophyton*, a member of the Euphyllophytina. R = resistant, D = degradation prone. Reproduced from Friedman and Cook (2000) with permission.

Present day vascular cryptograms, of course, resemble the G, P and S type tracheids in that they possess only a very faintly lignified core at the base of their secondary wall thickenings (Bierhorst, 1958, 1960). Indeed, Friedman and Cook (Cook and Friedman, 1998; Friedman and Cook, 2000) have compared the cell walls of the extant lycopod Huperzia with those of the early fossil tracheids. Following deposition of the primary wall in Huperzia, a secondary wall is laid down as a "template" followed by a (lignified?) degradation-resistant layer. Although much remains to be established regarding secondary cell wall formation in primitive vascular plants it

is clear that the basic cell type, the tracheary elements, have been substantially modified through vascular plant evolution and coincided with the emergence of other vascular cell types.

Realization of the heterogeneity of cell types in vascular tissues dates from Antoni van Leeuwenhoek's (1673-1696) initial observations and led to the recognition of vessels in addition to tracheids and fiber cells. A large body of work resulted in the identification of "Baileyan trends". In this analysis, cryptograms are regarded as the most primitive with long tracheary elements with gymnosperms of an intermediate length. By contrast, angiosperms with their shorter tracheids and vessels are regarded as the most advanced. Germane to this advance must be the presence of vessels, currently defined as cells with pit perforations at the end walls.

In summary the evolution of woody plants occurred through stages of vesselless long tracheids, through intermediate stages of scalariform perforated and pitted vessels to arrive at woody plants with short, simply perforated, alternatively pitted vessels and libriform fibers. Vessels conferred the advantage in being more efficient conductors of water. These changes are summarized in Table 1 which shows the changes in wood anatomical features from the Cretaceous to the present. The vessel is thought to have appeared about 140 million years ago (Aloni et al., 2000). According to Bailey (1953) and Cheadle (1953), two lines of evolution occurred towards fibers or vessels. Vessels were thought to have arisen independently in lycopods, ferns, gymnosperms, monocotyledons and dicotyledons and arose several times independently in some of these groups, particularly the dicots. This is supported by more recent analysis of the fossil record (Wheeler and Baas, 1991) which concludes vessel evolution occurred in marked changes especially between the Cretaceous and Tertiary, whereas evolution in ray composition, storied structure and parenchymal patterns occurred very gradually.

7. Conclusions

It is obvious that considerations of evolution can tell us much about modern wood as it is a product of the

Table 1
Incidence (in percentages) of various wood anatomical features in extant families of different geological age according to their fossil pollen record, compared with character frequency in the extant woody flora of the world by families and genera (Baas, 1982)

	Families of Cretaceous origin (24)	Families of Paleocene origin (15)	Families of Tertiary origin as a whole (ca. 83)	Families of Cretaceous and Tertiary origin together (ca. 107)	Extant families (195)	Extant genera/species (sample of 1800)
Vessels						
Vesselless	4	0	0	1	2	0.5
Perforations exclusively scalariform	33	12	7	12	16	11
Perforations scalariform and simple	21	19	21	22	18	5
Perforations very rarely scalariform	17	31	24	22	18 } 83.5	–
Perforations exclusively simple	25	38	48	43	46 }	–
Fibres						
Typically fibre-tracheids	54	38	26	32	31	33
Intermediate or both fibre-tracheids and libriform	18	19	17	17	14 } 67	–
Typically libriform	28	43	57	51	55 }	–
Parenchyma						
Mostly apotracheal	54	27	20	27	34	36
Paratracheal and apotracheal	17	40	40	35	29	20
Mostly paratracheal	29	33	40	38	37	44
Rays						
Heterogeneous	62	47	55	56	67 } 79	–
Heterogeneous and/to homogeneous	17	33	35	31	21 }	–
Homogeneous	21	14	10	13	12	21
Storied structure						
Present	28	20	28	28	28	14
Spiral thickenings						
Present in vessels	60	69	57	58	52	9
Vestured pits						
Present	13	19	15	15	12	?

process. However, it also teaches us that there is a variability to be explored in woody species but warns us that our analysis of the effects of manipulation cannot be simple chemical analysis to show what has been changed. It must take into account cell types and the structure of the cell wall layers as exemplified by the study of Ruel et al. (2001).

References

Aloni, R., Feigenbaum, P., Kalev, N., Rozovsky, S., 2000. Hormonal control of vascular differentiation in plants: the physiological basis of cambium ontogeny and xylem evolution. In: Savidge, R.A., Barnett, J.R., Napier, R. (Eds.), Cell and Molecular Biology of Wood Formation. BIOS, Oxford, pp. 223–236.

Bailey, I.W., 1953. Evolution of the tracheary tissue of land plants. American Journal of Botany 40, 4–8.

Baas, P., 1982. Systematic, phylogenetic, and ecological wood anatomy. History and perspectives. In: Baas, P. (Ed.), New Perspectives in Wood Anatomy. Martinus Nijhoff, The Hague, pp. 23–58.

Bierhorst, D.W., 1958. The tracheary elements of *Equisetum* with observations on the ontogeny of the internodal xylem. Bulletin of the Torrey Botanical Club 85, 416–433.

Bierhorst, D.W., 1960. Observations on tracheary elements. Phytomorphology 10, 249–305.

Böhm, J., 1879. Über die Function der vegetabilischen Gefässe. Botanische Zeitung 37, 214–255.

Buckeridge, M.S., Vergara, C.E., Carpita, N.C., 2001. Insight into multi-site mechanisms of glycosyl transfer in (1→4) β-D-glycans provided by the cereal mixed-linkage (1→3),(1→4) β-D-glucan synthase. Phytochemistry 57, in press.

Burlat, V., Kwon, M., Davin, L.B., Lewis, N.G., 2001. Dirigent proteins and dirigent sites in lignifying tissues. Phytochemistry 57, 883–897.

Cheadle, V.I., 1953. Independent origin of vessels in the monocotyledons and dicotyledons. Phytomorphology 3, 23–44.

Cook, M.E., Friedman, W.E., 1998. Tracheid structure in a primitive extant plant provides an evolutionary link to earliest fossil tracheids. International Journal of Plant Sciences 159, 881–890.

Currier, H.B., 1957. Callose substances in plant cells. American Journal of Botany 44, 478–488.

Dixon, R.A., Chen, F., Guo, D., Parvathi, K., 2001. The biosynthesis of monolignols: a "metabolic grid", or independent pathways to guaiacyl and syringyl units? Phytochemistry 57, in press.

Edwards, D., 2000. The role of Mid-Palaeozoic mesofossils in the detection of early bryophytes. Philosophical Transactions of the Royal Society of London. Series B, Biological Sciences 355, 733–755.

Friedman, W.E., Cook, M.E., 2000. The origin and early evolution of tracheids in vascular plants: integration of palaeobotanical and neobotanical data. Philosophical Transactions of the Royal Society of London. Series B, Biological Sciences 355, 857–868.

Graham, L.E., Cook, M.E., Busse, J.S., 2000. The origin of plants: body plan changes contributing to a major evolutionary radiation. Proceedings of the National Academy of Sciences of the United States of America 97, 4535–4540.

Hu, W.-J., Harding, S.A., Lung, J., Popko, J.L., Ralph, J., Stokke, D.D., Tsai, C.-J., Chiang, V.L., 1999. Repression of lignin biosynthesis promotes cellulose accumulation and growth in transgenic trees. Nature Biotechnology 17, 808–812.

Kawaoka, A., Ebinuma, H., 2001. Transcriptional control of lignin biosynthesis by tobacco LIM protein. Phytochemistry 57, in press.

Kerry, M.E., Gregory, A.C.E., Bolwell, G.P., 2001. Differential behaviour of four plant polysaccharide synthases in the presence of organic solvents. Phytochemistry 57, in press.

Kwon, M., Bedgar, D.L., Piastuch, W., Davin, L.B., Lewis, N.G., 2001a. Induced compression wood formation in Douglas fir (*Pseudotsuga menziesii*) in microgravity. Phytochemistry 57, 847–857.

Kwon, M., Davin, L.B., Lewis, N.G., 2001b. In situ hybridization and immunolocalization of lignan reductases in woody tissues: implications for heartwood formation and other forms of vascular preservation. Phytochemistry 57, 899–914.

Levine, L.H., Heyenga, A.G., Levine, H.G., Choi, J.-W., Davin, L.B., Krikorian, A.D., Lewis, N.G., 2001. Cell-wall architecture and lignin composition of wheat developed in a microgravity environment. Phytochemistry 57, 835–846.

Ruel, K., Chabannes, M., Boudet, A.-M., Legrand, M., Joseleau, J.-P., 2001. Reassessment of qualitative changes in lignification of transgenic tobacco plants and their impact on cell wall assembly. Phytochemistry 57, 875–882.

Saxena, I. M., Brown, R.M. Jr., Dandekar, T., 2001. Structure-function characterization of cellulose synthase: relationship to other glycosyltransferases. Phytochemistry 57, in press.

van Leeuwenhoek, A., 1673–1696. The Collected Letters I–XI (to be continued). Swets & Zeitlinger, Amsterdam.

Vesque, J., Viet, C., 1881. Influence du milieu sur les végétaux. Annales des Sciences Naturelles, 6e série, Botanie 12, 165–176.

Wheeler, E.A., Baas, P., 1991. A survey of the fossil record for dicotyledonous wood and its significance for evolutionary and ecological wood anatomy. International Association of Wood Anatomists Bulletin 12, 275–332.

Ye, Z.-H., Zhong, R., Morrison, W.H., Himmelsbach, D.S., 2001. Caffeoyl coenzyme A *O*-methyltransferase and lignin biosynthesis. Phytochemistry 57, in press.

G. Paul Bolwell

Division of Biochemistry, School of Biological Sciences, Royal Holloway, University of London, Egham, Surrey, TW20 OEX, UK

Ann M. Patten, Norman G. Lewis

Institute of Biological Chemistry, Washington State University, Pullman, WA 99164-6340, USA

E-mail address: lewisn@wsu.edu

PII: S0031-9422(01)00149-2

PERGAMON

Phytochemistry 57 (2001) 811–821

PHYTOCHEMISTRY

www.elsevier.com/locate/phytochem

Approaches to understanding the functional architecture of the plant cell wall

Maureen C. McCann[a,*], Max Bush[a], Dimitra Milioni[a], Pierre Sado[a], Nicola J. Stacey[a], Gareth Catchpole[a], Marianne Defernez[b], Nicholas C. Carpita[c], Herman Hofte[d], Peter Ulvskov[e], Reginald H. Wilson[b], Keith Roberts[a]

[a]*Department of Cell Biology, John Innes Centre, Norwich Research Park, Colney, Norwich NR4 7UH, UK*
[b]*Department of Food Metrology, Institute of Food Research, Norwich Research Park, Colney, Norwich NR4 7UA, UK*
[c]*Department of Botany and Plant Pathology, Purdue University, West Lafayette, Indiana 47907-1155, USA*
[d]*Laboratoire de Biologie Cellulaire, INRA, Route de Saint-Cyr, 78026 Versailles cedex, France*
[e]*Biotechnology Group, DIAS, 40 Thornvaldsensvej, DK-1871 Frederiksberg C, Denmark*

Received 16 November 2000; received in revised form 9 March 2001

Abstract

Cell wall polysaccharides are some of the most complex biopolymers known, and yet their functions remain largely mysterious. Advances in imaging methods permit direct visualisation of the molecular architecture of cell walls and the modifications that occur to polymers during growth and development. To address the structural and functional relationships of individual cell wall components, we need to better characterise a broad range of structural and architectural alterations in cell walls, appearing as a consequence of developmental regulation, environmental adaptation or genetic modification. We have developed a rapid method to screen large numbers of plants for a broad range of cell wall phenotypes using Fourier transform infrared microspectroscopy and Principal Component Analysis. We are using model systems to uncover the genes that encode some of the cell-wall-related biosynthetic and hydrolytic enzymes, and structural proteins. © 2001 Elsevier Science Ltd. All rights reserved.

Keywords: *Arabidopsis*; Cruciferae; *Zinnia elegans*; Compositae; Solanum tuberosum; Solanaceae; Fourier transform infrared micro-spectroscopy; cDNA-AFLP; Reflectance confocal scanning laser microscopy; Pectin; Cellulose

1. Introduction

The plant cell wall is a highly organized composite of many different polysaccharides, proteins, and aromatic substances that undergo dynamic changes during cell division, expansion and differentiation (McCann and Roberts, 1991, Carpita and Gibeaut, 1993). However, it has been difficult to ascribe specific functions to these molecules. Molecules of the cell wall must provide mechanical strength, regulate porosity, and control cell-cell adhesion. The functions of the wall are not only mechanical, but also biological. Like the animal extracellular matrix, plant cell walls are a source of signalling molecules that elicit a range of cell behaviours, such as in response to pathogen invasion. Built largely from polysaccharides, the components of the wall are subject to many modifications between the processes of gene expression and assembly in the apoplast. Glycoproteins and polysaccharides are assembled in the Golgi apparatus, enter the secretory pathway in vesicles that release their contents into the apoplast, where cell–wall enzymes act upon their substrates and incorporate them into precise architectures. The current field of cell wall research must encompass the signal transduction mechanisms that result in up- or down-regulation of the

Abbreviations: cDNA-AFLP, complementary DNA-amplified fragment length polymorphism; FTIR, Fourier transform infrared; HGA, homogalacturonic acid; PCA, principal component analysis; PBS, phosphate-buffered saline; RCLSM, reflectance confocal laser scanning microsopy; RG I, rhamnogalacturonan I; TE, tracheary element.

* Corresponding author. Tel.: +44-1603-450687; fax: +44-1603-450022.

E-mail address: maureen.mccann@bbsrc.ac.uk (M.C. McCann).

0031-9422/01/$ - see front matter © 2001 Elsevier Science Ltd. All rights reserved.
PII: S0031-9422(01)00144-3

genes that encode biosynthetic and wall-modifying enzymes, the transcription and translation of those genes, the synthesis of wall polysaccharides by those gene products, and the assembly of the components of the wall into a functional architecture that responds during growth and differentiation to the changing needs of the cell and transmits information back to the protoplast. Such a goal requires both broad and directed views to address the specifics of function. In this paper, we discuss three approaches to characterising cell wall architecture: imaging techniques that probe the location of specific molecules; screening for variation in architecture using IR spectroscopy, and identifying differentially-expressed genes in a model system in which wall synthesis and deposition are the key events.

2. Results and discussion

2.1. Imaging the compositional diversity of walls at the single cell level

The fast-freeze rotary-shadow replica technique has previously been used to directly visualise cell-wall architecture of dicotyledonous species (McCann et al., 1990; Fujino et al., 2000). The images obtained are thought to preserve the native architecture of cell walls, and many thin cross-linking fibres are visible as well as cellulosic microfibrils. In dicots, these cross-linking glycans are xyloglucans — they have a glucan backbone that can hydrogen bond to the surface of cellulose microfibrils and are decorated with xylose-containing side-chains. Xyloglucans are long enough to link two or more microfibrils together to form a network. This network is embedded in a second independent but coextensive network of pectins, the most variable and complex component of the wall. Pectins are loosely defined as polymers rich in galacturonic acid and their associated side-chains, and comprise 20–50% of the wall. Homogalacturonans (HGAs) are long polymers of galacturonic acids that can be methyl-esterified. If methyl groups are removed, then calcium can bind to the carboxylate ions of the galacturonic acid to cross-link them (Goldberg et al., 1996). Some pectins called rhamnogalacturonan I (RGI) are built from a backbone of alternating rhamnose and galacturonic acid residues and carry side-chains of arabinans and galactans.

Dissection of a particular cell type at a specific developmental stage is seldom practical for chemical analysis, which requires microgram to milligram quantities of material. Thus, traditional methods of biochemistry average out the intrinsic heterogeneity of plant tissues (McCann et al., 1997). Two approaches offer the opportunity to analyse wall composition at the single cell level — the use of probes such as antibodies (Knox, 1997), and Fourier transform infrared (FTIR) microspectroscopy (McCann et al., 1997).

Longitudinal and transverse sections of plant stems, roots, or leaves, provide a developmental snapshot of cell growth and differentiation. In the light microscope, the use of probes, such as monoclonal antibodies coupled to fluorescent markers, has revealed the tissue-specific distributions of particular cell components in transverse sections of plant materials (Knox, 1997), whilst longitudinal sections reveal developmental regulation of those components. This is illustrated in Fig. 1 using monoclonal antibodies as designer stains for molecules of the pectin network in potato tubers. Reflectance confocal laser scanning microscopy (RCLSM) allows pectins to be localised to different domains within a wall, even at the light microscope level, by silver enhancement of immuno-gold-labelled tissue and imaging in the confocal microscope (Bush and McCann, 1999). Methyl-esterified pectin is present throughout the walls of parenchymal cells, the galactan side-chains of RGI are next to the plasma membrane but excluded from the middle lamella region that sticks two cells together, and the calcium cross-linked junction zones are localised to the cell corners (Fig. 1a–c). Different tissues contain combinations of different pectic epitopes. Fig. 1d and e shows that parenchymal cells contain both arabinans and galactans, whilst the vascular cells contain arabinans but very little galactan. In the potato stolon, developmental patterns rather than tissue specificity is marked by the presence of arabinan in all of the tissues from the tip to the hook of the stolon, and then calcium pectate and also galactans in all of the tissues beyond the hook (Bush et al., 2001).

Although antibodies are powerful tools, their availability is confined to a small number of wall epitopes and is not comprehensive of the structural complexity of the wall. An alternative technology, called chemical imaging, is becoming available, which combines spatial information with chemical information deduced from relative IR absorbances. In the IR spectrometer, a source emits radiation with a range of frequencies which is then passed through the sample. Particular chemical bonds in the sample absorb radiation of specific frequencies from the beam, and this is plotted as an absorbance spectrum against frequency. IR spectroscopy simultaneously reveals the type, distribution and relative abundances of chemical components within a particular system. However, a single IR spectrum also contains information about the molecular structure and intermolecular interactions among the individual sample components (McCann et al., 1992, 1997). A microscope accessory can be attached such that the infrared beam from the spectrometer is diverted to pass through a sample placed on the microscope stage. The sample can be imaged with visible light and apertures used to restrict the area of sample from which IR spectroscopic data are to be obtained. Therefore, determining the presence and distribution of the chemical constituents within a sample

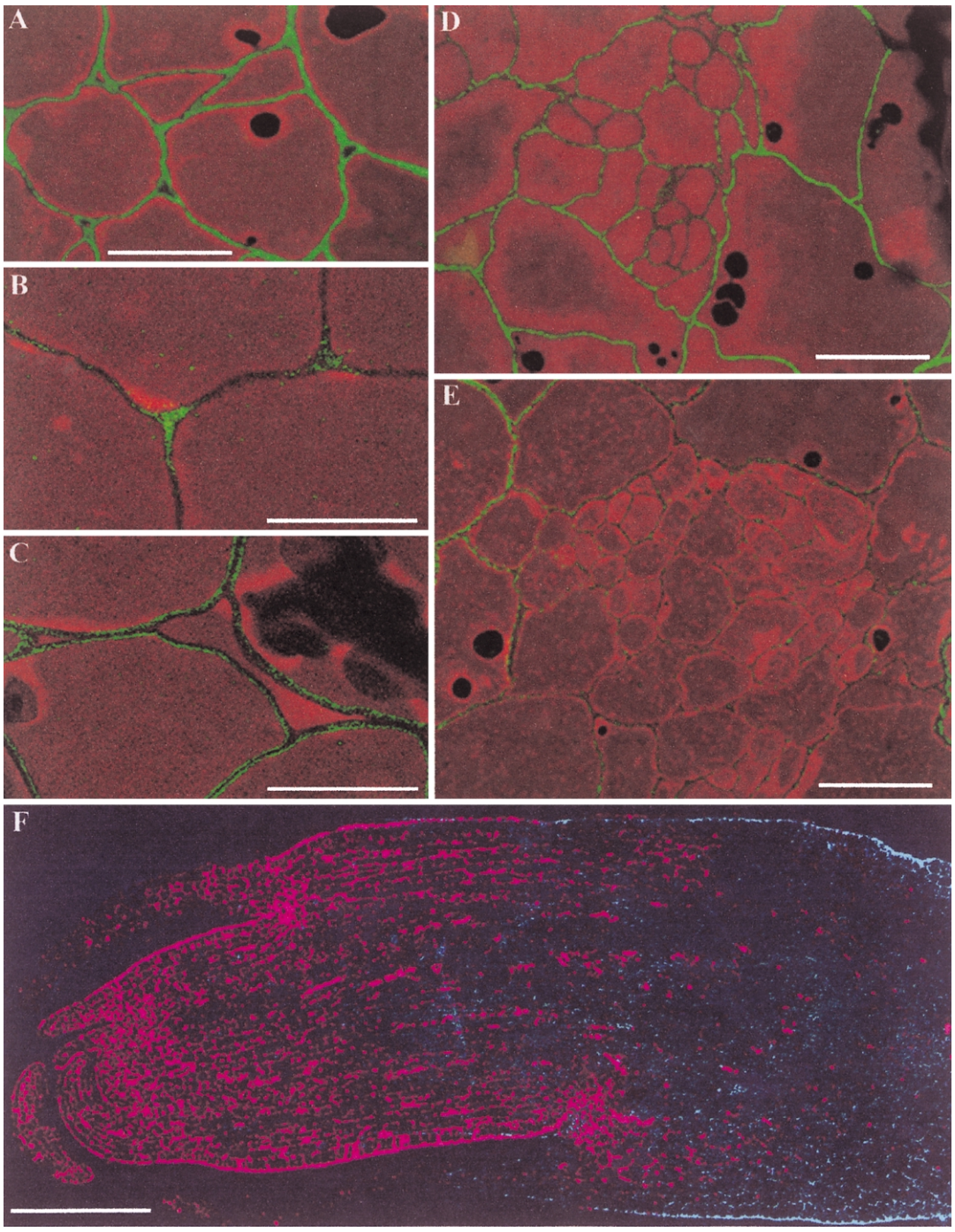

Fig. 1. Potato tuber sections of perimedullary tissue gold-labelled with mAbs (A) JIM 7, (B) 2F4 and (C) LM5 then silver-enhanced and viewed by reflectance confocal microscopy. (A) Methyl-esterified pectic epitopes are throughout the wall, (B) calcium pectate is localised to cell corners, and (C) galactans are present in a region close to the plasma membrane but excluded from the cell corners and middle lamellae. Vascular tissues are labelled with mAb LM6 (D) but label lightly with mAb LM5 (E), indicating the presence of arabinan but very few galactan side-chains of RG1 in these tissues. (F) Longitudinal section of a stolon tip labelled with mAbs 2F4 (blue) and LM6 (pink). The 2F4 epitope is only detected in walls from more proximal regions of the stolon, where it is concentrated in the epidermal and cortical walls. In contrast the LM6 arabinan epitope is localised to walls of young cells at the stolon tip. Scale bars for A, B, C, D, and E represent 20 μm, bar F is 0.5 mm.

depends only on the intrinsic spectral characteristics of the sample, and not on the addition of fluorescent tags or stains. The synergy of what have traditionally been two distinct methods for studying the chemistry and morphology of a sample, IR spectroscopy and optical microscopy, is called chemical imaging.

Current IR microscopes work in two modes. The first mode is single spectrum collection in which data are

collected from a region of the sample as small as 10×10 μm. This is accomplished by limiting the area of a sample illuminated by adjusting an aperture located at a remote image plane. During this process the size of the IR beam focus remains fixed as does the detector area. The maximum size from which a spectrum can be collected is 100×100 μm, which is the size of the detector area. When the smallest usable aperture of 10×10 μm is employed only a fraction of the detector area is illuminated. This small fraction of the detector generates the signal whilst the entire detector area generates noise. Consequently the spectroscopic performance falls dramatically with the size of aperture used.

The second mode of operation is mapping (McCann et al., 1997). In this mode the sample is moved under computer control such that different areas of the sample are measured in turn. Eventually an array of spectra is generated. These spectra can be correlated with visual images of the sample so that optically observed features can be associated with functional groups. While contrast in MRI images is determined by differences in the NMR spectrum of the sample components, contrast in IR spectroscopic imaging is determined by differences in the vibrational spectral response. It is possible to generate a contour plot (map) of the distribution of functional groups within a sample, using colour to represent absorbance intensities.

A 3-day-old maize coleoptile was sectioned transversely by hand, cleared of its soluble material and mounted on a barium fluoride window for chemical imaging. Mapping software allowed the collection of 273 individual FTIR spectra with an aperture size of 25×25 μm in an array encompassing epidermal, vascular and mesophyll cells from a transverse section of one-quarter of the coleoptile (Fig. 2a). The spectra in the data set were first area-normalised to compensate for any changes in thickness across the section. Peaks corresponding to phenolic esters (1720 cm^{-1}) or to methyl esters (1740 cm^{-1}) were enriched in the vascular bundle, and slightly enhanced in the outer epidermis (Fig. 2b, c). A peak corresponding to phenolic ring absorbance (1515 cm^{-1}) is enriched in the vascular tissue, and is decreased in the inner epidermis (Fig. 2d). The chemical images thus indicate some differences between the inner and outer epidermis. Absorbances at 1000 and 1020 cm^{-1} are enriched in the mesophyll layer (Fig. 2e, f), whilst absorbances at 1090 and 1034 cm^{-1} are enriched in the epidermal tissues (Fig. 2g, h). These latter two absorbances are potentially diagnostic for the presence of glucomannans (Kacuràková et al., 2000). These data demonstrate the ability of chemical imaging to localise different chemical species to specific cell types and the large heterogeneities in wall composition within the maize coleoptile. A new generation of instruments are becoming available that combine an IR microscope with focal plane array detector. These devices collect spectra simultaneously from all points in a field of view, reducing collection times for equivalent samples from a few hours to a few minutes.

2.2. Detecting cell walls of altered composition

Why cell walls are structurally complex seems obvious — cell walls must function in cell–cell adhesion, signal transduction both cell-to-cell and environment-to-cell, cell division, growth and differentiation, but how the molecular machinery of the wall is assembled and later modified to carry out those functions is still unknown. By studying cell walls with altered compositions, either as a consequence of developmental regulation, environmental adaptation, or genetic modification, we can assess the effect of such modifications on cell wall properties and on plant development. The selection of mutant plants with altered cell wall compositions and architectures is particularly useful because of the wide range of potential modifications and the possibility of uncovering novel genes that encode enzymes that participate in biosynthetic pathways, wall assembly, or in modifications to polymers in muro (Reiter, 1998). Mutants with altered cellulose deposition have been identified directly by birefringence (Potikha and Delmer, 1995). Other cell-wall mutations have appeared serendipitously in the course of screens for developmental phenotypes, such as a temperature-sensitive radial cell swelling mutant that was cellulose-deficient (Baskin et al., 1992, Arioli et al., 1998) or a collapsed xylem phenotype (Turner and Somerville, 1997).

Mutations in non-cellulosic polysaccharides may not always have visually abnormal or otherwise predictable phenotypes, and, hence, a general method is necessary to select for a broad range of potential modifications. One method that has been successfully applied is to screen directly for neutral sugars of cell-wall polymers that are over- or under-represented when compared with their distribution in the walls of a wild-type population (Reiter et al., 1997). This screen employs derivatisation of the cell-wall non-cellulosic sugars from leaves to alditol acetates, with subsequent quantitation by gas–liquid chromatography. Sugar composition can be assayed with great precision by this method, but the large numbers of plants involved in a mutant screen make it labour-intensive. FTIR microspectroscopy is an extremely rapid, non-invasive vibrational spectroscopic method that can quantitatively detect a range of functional groups including carboxylic esters, phenolic esters, protein amides and carboxylic acids, and can provide a complex "fingerprint" of carbohydrate constituents and their organization (McCann et al., 1992, 1997; Séné et al., 1994). The time taken to acquire a spectrum of a sample is roughly 30 s. It is non-destructive and does not require derivatization of the sample, so further assays can be applied to the same sample once potential mutants are identified.

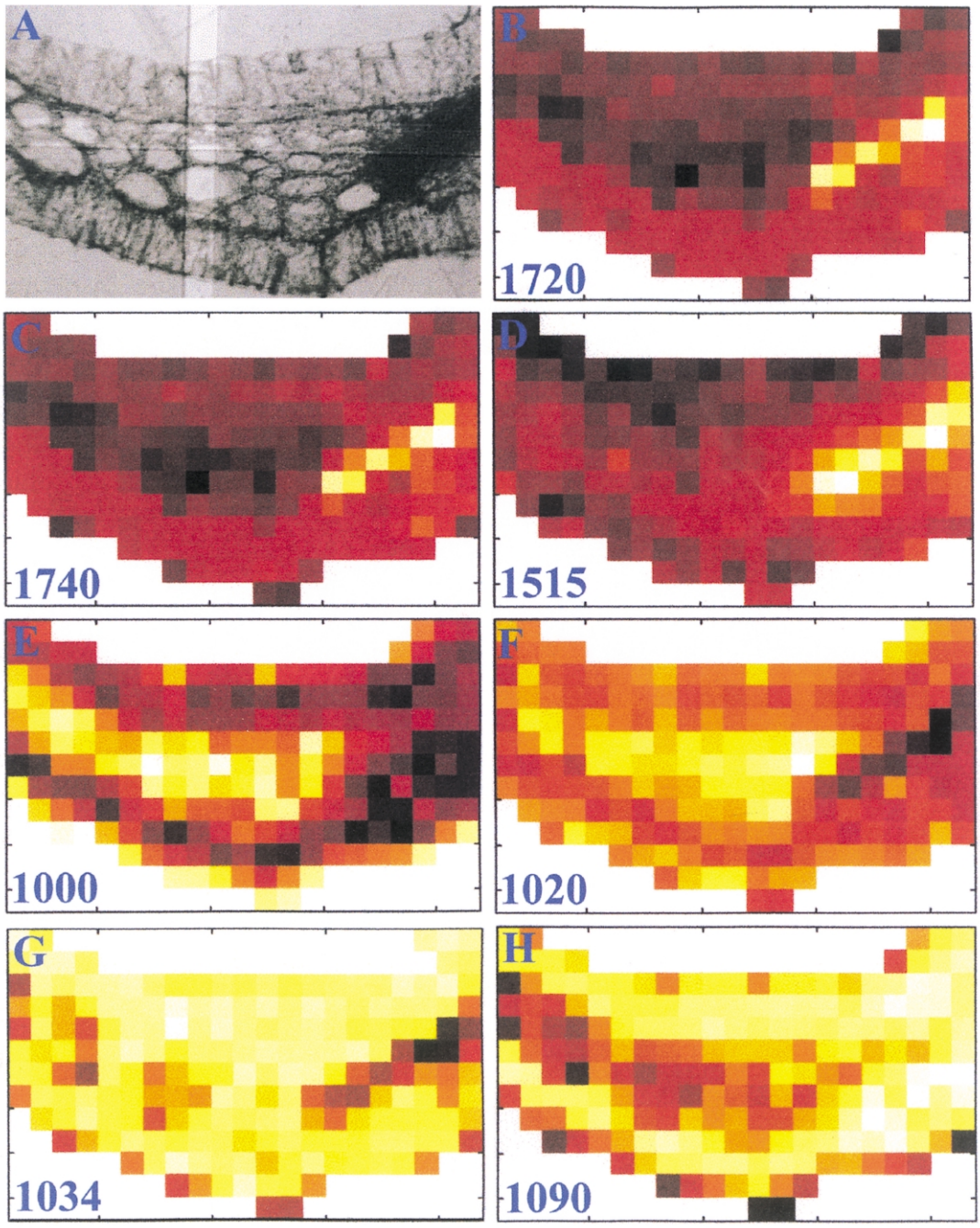

Fig. 2. Chemical images of a transverse section of 3-day-old maize coleoptile derived from FTIR spectra sampled with a 25×25 μm window. (A) Brightfield micrograph of the coleoptile section using mirror optics in the IR microscope. An example of the area from which IR data is sampled is delimited by a pair of transparent double-bladed apertures. (B) Phenolic esters of uronic acids sampled at 1720 cm^{-1}. (C) Carboxyl esters sampled at 1740 cm^{-1}. (D) Aromatic substances sampled at 1515 cm^{-1}. (E) Absorbance intensity at 1000 cm^{-1}. (F) Absorbance intensity at 1020 cm^{-1}. (G, H) Absorbances at 1034 and 1090 cm^{-1}, respectively, characteristic of glucomannan.

The effective analysis of large data sets of spectra is complex and the use of multivariate data reduction techniques (Massart et al., 1988) is now standard practice for many applications. Spectra are not analog, but are constructed from data points collected at intervals of 8 cm^{-1}. Principal component analysis (PCA) is a widely-used mathematical technique that is used to reduce the dimensionality of the data from the several hundred data points in the original spectra to a fewer number of dimensions (Kemsley, 1998). The variability in each individual spectrum relative to the mean of the population can then be represented as a smaller set of values (axes) termed principal components (see Fig. 3). The effect of this process is to concentrate the sources of

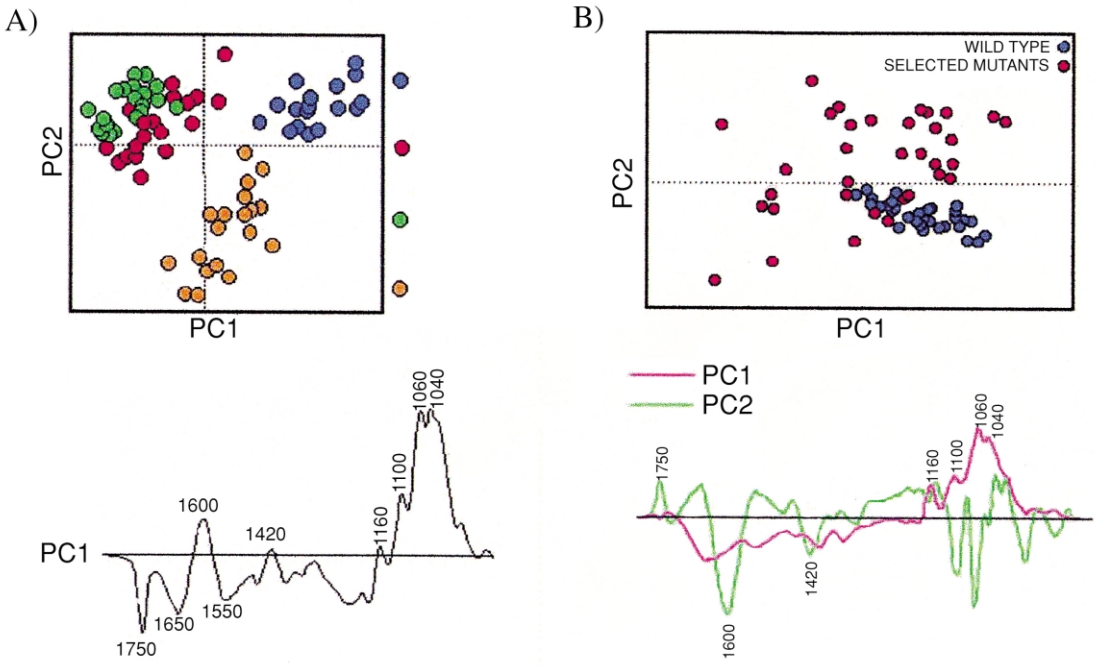

Fig. 3. Exploratory PCA of IR spectra sampled from populations of *Arabidopsis* hypocotyls. (A) Relative cellulose content of populations can be estimated from their scores on PC1, a loading with characteristic features of cellulose (Liang and Marchessault, 1959). Peaks associated with pectin are negatively correlated in the loading. The *rsw1* mutants discriminate on PC2 probably because they are in a different ecotype background. (B) Some dwarf hypocotyl mutants can be discriminated from wild-type on the basis of two principal components, PC1 has features of cellulose (Liang and Marchessault, 1959) whilst PC2 shows features of pectin (Sene et al., 1994).

variability in the data into the first few PCs. Plots of the so-called PC scores (projection on to PC axes) against one another can reveal clustering or structure in the data set.

We established and validated a model that can discriminate between the leaves of wild-type and a previously defined set of cell-wall mutants of *Arabidopsis*. Exploratory PCA indicated that mutants deficient in different cell-wall sugars are distinguished from each other (Chen et al., 1998). We have also used IR microspectroscopy to screen a population of hypocotyl mutants for alterations in their cell walls. The *Arabidopsis* hypocotyl mutants were selected from seedlings that are dwarf when dark-grown, and thus affected in cell elongation (Gendreau et al., 1997). The hypocotyl is laid down by a set of programmed cell divisions during early embryogenesis. Post-embryogenic growth of this organ involves no further cell divisions and so separates the events of cell division from those of cell expansion.

From a pre-selected sample of 40 dwarf mutants, PCA shows that both pectic (Sene et al., 1994) and cellulosic (Liang and Marchessault, 1959) features in the FTIR spectra can be used to discriminate mutants from a population of wild-type (Fig. 3). The wild-type population shows that a tight ratio exists under normal growth conditions, but this proportionality is disrupted in the mutants. PCA also revealed a dose-dependent reduction in cellulose content within hypocotyls treated with increasing concentrations of dichlorobenzonitrile (DCB), an inhibitor of cellulose synthesis. Cellulose deficiency was also detected in hypocotyl cell walls of *rsw1*, a temperature-sensitive mutant when grown at the restrictive temperature for a gene encoding the catalytic subunit of cellulose synthase (Arioli et al., 1998). The *kor* mutation (*korrigan*) is a mutation in a gene encoding an endo-glucanase (Nicol et al., 1998). Analysis of FTIR spectra of *rsw1*, *kor*, and DCB-treated seedlings showed that cellulose deficiency was invariably associated with an increased pectin content (Fig. 3). These observations are consistent with earlier results using suspension-cultured cells of tomato adapted to growth on DCB which make a pectin-rich wall that virtually lacks a cellulose-xyloglucan network (Shedletzky et al., 1990). The formation of one network has been prevented, while the other is still able to provide a cell wall with at least some of its usual functions.

Transgenic materials in which cell-wall-related genes have been up- or down-regulated provide a useful complement to mutants. We are also studying transgenic potato tubers in which fungal cell-wall enzymes have been over-expressed in a tuber-specific manner as a means to valorise the waste from starch production (Vincken et al., 2000). Removal of galactans by apoplastic expression of a fungal galactanase resulted in normal tuber development (Oxenbøll-Sørensen et al., 2000). We used PCA of IR spectra to screen a number

of transgenic lines, and selected one line that can be distinguished from the relevant control because of changes in pectic characteristics (Fig. 4a). Immuno-gold labelling confirmed that this line indeed had a greatly reduced galactan content (Fig. 4b–e).

2.3. Expression profiling — a molecular approach to identify genes that encode cell-wall related proteins

The wall contains structural proteins as well as hundreds of different cell-wall enzymes, and polysaccharides are the

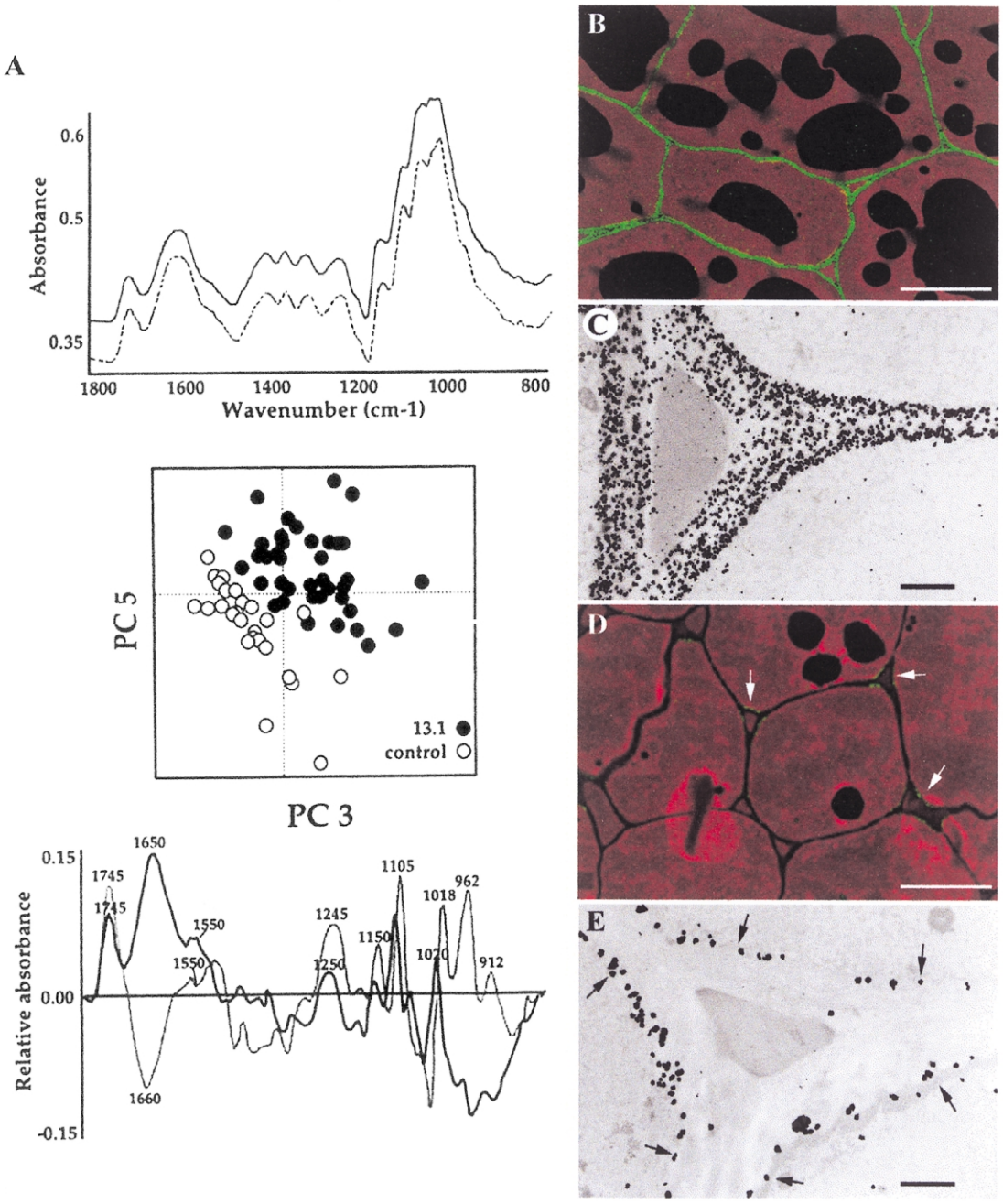

Fig. 4. (A) Top: averaged FTIR spectra of potato tuber cortex from 20 wild-type tubers (solid line) and 20 transgenic tubers (dashed line) over-expressing a fungal galactanase targetted to the apoplast. Middle. Exploratory PCA discriminates the transgenic population from the wild type, using the third and fifth PC scores. The loadings for PC3 (black line) and PC5 (gray line) show features characteristic of pectins at 1745, 1250, 1150, 1105 and 1018 cm^{-1}. Sections of wild-type tuber gold-labeled with mAb LM5, that recognises a galactan epitope, and imaged by RCLSM (B) and in the TEM (C), and equivalent of the galactanase transformant (D, E). The walls of wild-type parenchymal cells are strongly labelled (green in A, black particles in B) whereas in the transformant, the labelling density is greatly reduced and localised only to some cell corners (arrows) close to the plasma membrane. Scale bars represent 100 μm for RCLSM images and 2 μm for electron micrographs.

products of biosynthetic enzymes. The genes that encode these classes of cell-wall-related proteins belong to large multi-gene families. Much work remains to be done to elucidate the functions of the different family members, and to identify cell-wall-related genes without sequence identities. We are using a model system in which synthesis and deposition of cell wall is the main event, to identify cell-wall-related genes involved specifically in xylogenesis.

The construction of a tracheid or xylem element involves deposition of thick reinforcing hoops of secondary cell wall, waterproofing it with lignin followed by autolysis of the cell contents. In a plant, only a few cells are in the process of forming xylem, but we can study this entire developmental pathway in vitro using the *Zinnia* mesophyll cell system originally developed by Fukuda and Komamine (1980). In our laboratory, the *Zinnia* system consists of mesophyll and palisade cells isolated from the leaves of *Zinnia elegans* cv. Envy that are put into liquid culture and supplied with two plant growth factors, auxin and cytokinin, after 48 h (McCann et al., 2000). In a further 48 h, over half of the living cells have synchronously undergone trans-differentiation, making it possible to precisely stage the events involved in building a TE. Thus, one cell type can be reproducibly and synchronously switched, with known external signals, into a different cell type.

We have recently applied a novel RNA finger-printing technology, cDNA-AFLP (Bachem et al., 1996, Durrant et al., 2000), that allowed the detection of differentially-regulated genes across the time-course of xylo genesis. cDNAs are synthesized from mRNA populations isolated from the *Zinnia* cultures at five time-points, digested with a pair of restriction enzymes, adaptor-ligated and amplified by PCR to produce the primary template. A subset of this population of fragments is selectively amplified using primers with two selective nucleotides, and then analysed on polyacrylamide gels. Over 600 genes, whose transcription show overt changes in abundance over time, have been selected and partial sequences obtained. These sequences were then compared with databases from the plant and animal genome sequencing projects, allowing an identity to be assigned to about half of the predicted gene products, including about 10% that encode cell wall biosynthetic enzymes, hydrolytic enzymes or structural proteins (manuscript in preparation).

The deposition of hoops of secondary wall material occurs at 90–96 h of culture (between 42 and 48 h after

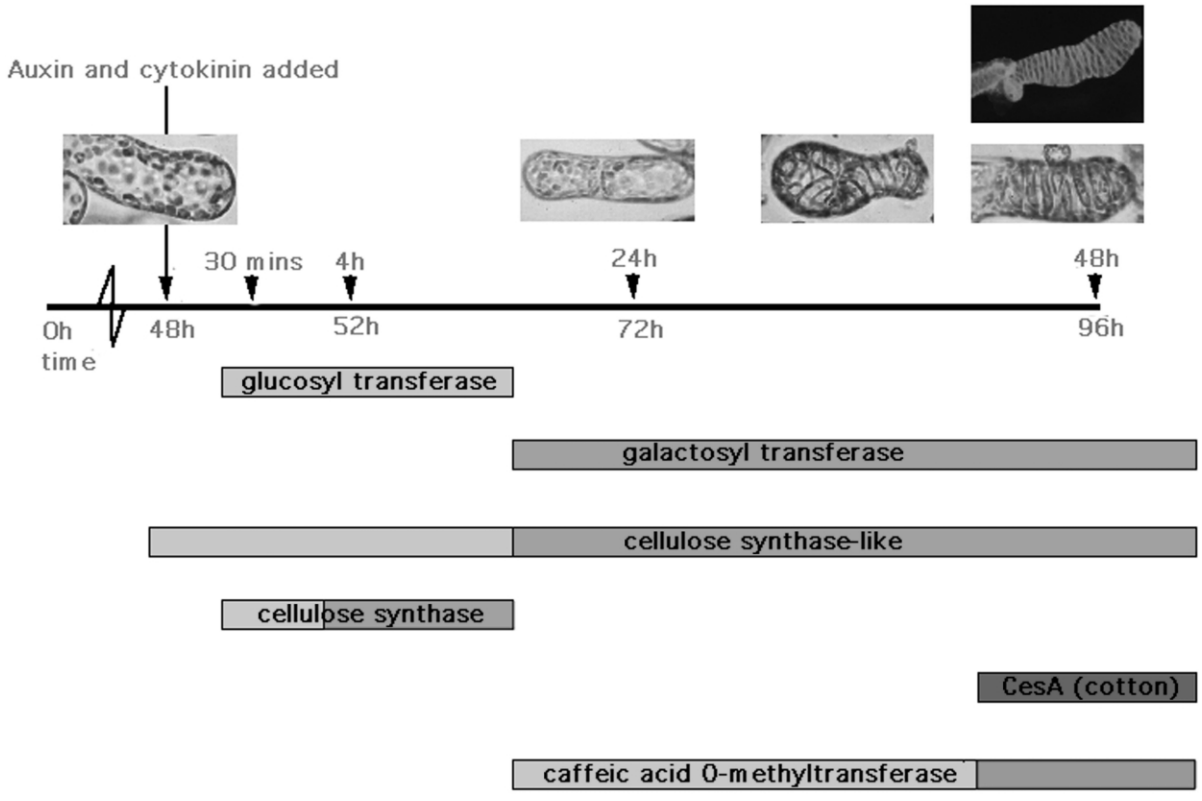

Fig. 5. Time course of the trans-differentiation of isolated *Zinnia* mesophyll cells to tracheary elements and the expression patterns of six cell wall biosynthetic genes identified so far by the cDNA-AFLP screen. Micrographs, left to right. (1) A palisade parenchyma cell appears unchanged after 48 h in liquid culture without TE-inducing growth factors. Auxin and cytokinin are added at 48 h, and RNA is extracted at this time and then 30 min, 4 h, 24 h and 48 h later. (2) At the 16 h point after induction, the chloroplasts move to the cell edges, and most of the cells have divided. (3) By 42 h after induction, the secondary wall thickenings have been deposited. (4) By 48 h after induction, the thickenings become lignified, and can be stained with phloroglucinol (above). Shading intensities of the bars indicate relative abundance of the cDNA-AFLP fragment in the gel.

addition of auxin and cytokinin). We have over 50 partial sequences of cell-wall related genes, many of which are hydrolytic enzymes (Milioni et al., 2001). Fig. 5 shows the expression patterns of six of the sequences that encode biosynthetic enzymes. A cellulose synthase is up-regulated early, perhaps simply induced by auxin, and a late-expressed cellulose synthase has high sequence identities with an Arabidopsis sequence (AB006703), the cotton cellulose synthase that is expressed in differentiating cotton fibers (Holland et al., 2000), and with a xylem-specific cellulose synthase gene from aspen (Wu et al., 2000). There are two sugar transferases for adding sugars to non-cellulosic polymers and a cellulose-synthase-like gene, which may encode a biosynthetic enzyme making a different polymer backbone. The enzyme caffeic acid *O*-methyltransferase from the lignin biosynthetic pathway is also expressed. About 40% of our sequences are unknowns — either hypothetical proteins in the *Arabidopsis* database or not represented in any of the plant or animal databases. As known genes encoding cell wall-related proteins comprise about 10% of our 600 sequences, then there may be further 30 sequences that represent cell-wall-related proteins of totally unknown function.

3. Conclusion

Genetically-defined variation through mutant approaches or transgenic technologies offers the best opportunity to identify a broad range of structural and architectural alterations in cell walls, leading to improved understanding of plant cell growth and differentiation. Gene discovery in the *Zinnia* system will have relevance for many commercially important tree species. By defining the key structural components in *Arabidopsis*, there is the opportunity to define wall properties in which variation is economically desirable include the length, substitution, and cross-linking of pectic polysaccharides, the relative levels of cellulose, the length and mechanical properties of fibres, the relative allocation of carbon to wall biomass, the regulation of cell–cell adhesion, wall-based growth control, and lignin composition, architecture, distribution and amount.

4. Experimental

4.1. Tissue preparation for immunocytochemistry

Elongating stolons and mature tubers were cut from mature *Solanum tuberosum* (L.) plants (cv. Karnico) and immersed in 2.5% (v/v) glutaraldehyde (EM grade) in 0.05 M sodium cacodylate containing 0.05% (v/v) NP-40 (Sigma, Poole, UK). All of the samples were processed for low temperature L.R. White resin embedding as described previously (Bush and McCann, 1999).

4.2. Immunogold labelling

Blocks of tissue were sectioned: 0.5-μm thick resin sections were collected on multi-well glass slides for light microscopy and ultrathin sections for electron microscopy were collected on Formvar-carbon coated gold grids. The sections were labelled as described previously (Bush and McCann, 1999), with mAbs that recognise the following pectic epitopes; JIM 7, $\geqslant$35% methyl-esterified homogalacturonan (Knox et al., 1990); 2F4, a calcium-dependent conformational epitope of at least nine contiguous galacturonic acid residues (Liners et al., 1989); LM5, (1→4)-β-D-galactan (Jones et al., 1997); LM6, (1→5)-α-L-arabinan (Willats et al., 1998). After three 10 min washes in phosphate-buffered saline (PBS) the sections were incubated with 5 nm gold conjugates (British BioCell International) overnight at 4°C. Sections were washed in PBS again, fixed in 1% (v/v) glutaraldehyde, and finally rinsed thoroughly with distilled water prior to silver enhancement. Control sections were treated in parallel but with the omission of the primary mAb. Silver enhancement of 5 nm gold probes was performed for 2 min at 20°C for electron microscopy, but this was extended to 10–15 min for light microscopy; the BioCell silver enhancement kit (British BioCell International) was used according to the manufacturer's instructions.

4.3. Reflectance confocal laser scanning microsopy (RCLSM)

Gold-labelled and silver-enhanced 0.5 μm-thick resin sections were counter-stained with basic fuchsin and examined with a Leica TCS NT laser scanning confocal microscope, using an RT 30/70 mirror and excitation and emission wavelengths of 488 and $>$515 nm, respectively. Images of autofluorescence and epi-reflectance were recorded separately, and merged and processed with Adobe Photoshop 4.0. Ultrathin sections counter-stained with uranyl acetate and lead citrate were examined in a Jeol 1200EX transmission electron microscope.

4.4. FTIR microspectroscopy and chemical imaging

The Arabidopsis hypocotyls were placed on 2-mm thick×13-mm diameter barium fluoride windows, and the materials were air-dried at 37°C for about 1 h. The windows were supported on the stage of a UMA500 microscope accessory of a Bio-Rad FTS175c FTIR spectrometer equipped with a liquid nitrogen-cooled mercury cadmium telluride detector. An area of wall (100×100 μm) was selected for spectral collection in

transmission mode. One hundred and twenty-eight interferograms were collected with 8 cm^{-1} resolution and co-added to improve the signal-to-noise ratio for each sample. Three spectra were collected from different areas of each hypocotyl, avoiding the stele and then averaged and baseline-corrected.

For chemical imaging, transverse sections were hand-cut from 3-day-old maize coleoptiles that were frozen in a cryosectioning medium (Tissue-Tek, Agar UK). Sections about 50 μm thick were picked up onto barium fluoride windows. The sections adhering to the surface were then washed extensively with water to remove all traces of the sectioning medium. A small amount of the sectioning medium was also streaked across a barium fluoride window as a control. FTIR spectra were acquired with an aperture size of 25×25 μm from an array encompassing epidermal, vascular and mesophyll cells from transverse sections comprising about 25% of the coleoptile area.

4.5. Preparation of cell cultures

Seeds of *Zinnia elegans* c. Envy (Chiltern Seeds Ltd, UK) were germinated in a peat/sand potting compost in a controlled environment room at 20°C with a 16 h day. The first true leaves of 14-day-old plants were removed, surface-sterilised in 5% commercial NaOCl, and rinsed three times in sterile distilled water. Single cells were isolated by gently grinding the leaves in 0.2 M mannitol in a mortar and pestle. The suspension was filtered through two layers of muslin and washed three times in 0.2 M mannitol by spinning at 800 rpm for 2 min. Cells were resuspended in culture medium (Fukuda and Komamine, 1980) with no hormones (maintenance medium), or 1 mg l^{-1} BAP and 1 mg l^{-1} NAA (inductive medium). Cultures were maintained at 27°C in the dark, shaking at 80 rpm, with 3 ml of cell suspension per well in six-well plates (Sterilin, UK) at a density of 10^6 cells ml^{-1}. At 48 h, cells were transferred by pipetting media and cells from the wells in the six-well plates into 30-ml screw-cap tubes (Sterilin, UK), spinning the tubes at 800 rpm for 2 min, pouring off the supernatant and re-suspending the cells in new medium at the same cell density of 10^6 cells ml^{-1}.

4.6. cDNA-AFLP

Total RNA was extracted from *Zinnia* cells at different stages of in vitro TE formation, according to Shirzadegan et al. (1991). Poly(A^+) RNA was obtained by using magnetic oligo(dT)25 Dynabeads, according to the manufacturer's (DYNAL, UK) instructions. Synthesis of the first strand of cDNA was carried out with Expand Reverse Transcriptase (Boehringer Mannheim), as described by the manufacturer. The second strand cDNA synthesis was performed according to Gubler et al. (1983). cDNA-AFLP was performed according to Bachem et al. (1996) and Durrant et al. (2000). The AFLP products were analyzed on a 6% polyacrylamide denaturing gel, at constant power (90 W) until the bromophenol blue dye reached the bottom. Gels were dried under vacuum at 80°C and exposed to X-ray films (KODAK X-OMAT AR) for autoradiography.

4.7. Isolation of cDNA clones and sequence data analysis

The cDNA bands of interest were marked and the X-ray films were repositioned on the radioactive gels. The segments of interest were cut out with a surgical blade, eluted and re-amplified with the same primer set as used for the initial amplification. The re-amplified cDNAs were subcloned using the pGEM-T easy vector system (PROMEGA). For each re-amplified fragment, several independent *E. coli* colonies were selected and the inserted fragments were sequenced on an automated sequencer using the BigDye Terminator kit (Applied Biosystems). Each sequence was analyzed against the sequences in Genbank non-redundant and expressed sequence tag (EST) databases using the BlastN programme for nucleic acids and the BlastX programme for proteins at the NCBI web server (Altschul et al., 1997). Default parameters of the programmes were used in both cases.

Acknowledgements

We are grateful to Drs. J.P. Knox and P. Van Cutsem for their kind gifts of mAbs. We would like to thank Kate Kemsley for advice on using PCA and LDA, Grant Calder for assistance with the Leica confocal microscope, Sue Bunnewell for photographic assistance, and Dr. Jonathon Jones and Dr. Wendy Durrant for assistance and advice with the cDNA-AFLP screen. NJS, MD, GC, RHW and KR gratefully acknowledge the financial support of the BBSRC. DM is funded by an EU Marie Curie Fellowship, MB is funded by an EU network grant, PS is funded by a BBSRC special studentship, NCC is funded by a grant from the US National Science Foundation Genome Research Program, and MCM is funded by a Royal Society University Research Fellowship.

References

Altschul, S.F., Madden, T.L., Schaffer, A.A., Zhang, J.H., Zhang, Z., Miller, W., Lipman, D.J., 1997. Gapped BLAST and PSI-BLAST: a new generation of protein database search programs. Nucl. Acid Res. 25, 3389–3402.

Arioli, T., Peng, L.C., Betzner, A.S., Burn, J., Wittke, W., Herth, W., Camilleri, C., Hofte, H., Plazinski, J., Birch, R., Cork, A., Glover,

J., Redmond, J., Williamson, R.E., 1998. Molecular analysis of cellulose biosynthesis in *Arabidopsis*. Science 279, 717–720.

Bachem, C.W.B., vanderHoeven, R.S., deBruijn, S.M., Vreugdenhil, D., Zabeau, M., Visser, R.G.F., 1996. Visualization of differential gene expression using a novel method of RNA fingerprinting based on AFLP: Analysis of gene expression during potato tuber development. Plant J. 9, 745–753.

Baskin, T.I., Betzner, A.S., Hoggart, R., Cork, A., Williamson, R.E., 1992. Root morphology mutants in *Arabidopsis thaliana*. Aust. J. Plant Physiol. 19, 427–437.

Bush, M.S., McCann, M.C., 1999. Pectic epitopes are differentially expressed in the cell walls of potato (*Solanum tuberosum*) tubers. Physiol. Plant. 107, 201–213.

Bush, M., Marry, M., Huxham, I.M., Jarvis, M.C., McCann, M.C., 2001. Developmental regulation of pectic epitopes during potato tuberisation Planta, in press.

Carpita, N.C., Gibeaut, D.M., 1993. Structural models of primary cell walls in flowering plants: consistency of molecular structure with the physical properties of the walls during growth. Plant J. 3, 1–30.

Chen, L., Carpita, N.C., Reiter, W-D., Wilson, R.H., Jeffries, C., McCann, M.C., 1998. A rapid method to screen for cell-wall mutants using discriminant analysis of Fourier transform infrared spectra. Plant J. 16, 385–392.

Durrant, W.E., Rowland, O., Piedras, P., Hammond-Kosack, K.E., Jones, J.D.G., 2000. cDNA-AFLP reveals a striking overlap in race-specific resistance and wound response gene expression profiles. Plant Cell 12, 163.

Fujino, T., Sone, Y., Mitsuishi, Y., Itoh, T., 2000. Characterization of cross-links between cellulose microfibrils, and their occurrence during elongation growth in pea epicotyl. Plant Cell Physiol 41, 486–494.

Fukuda, H., Komamine, A., 1980. Establishment of an experimental system for the tracheary element differentiation from single cells isolated from the mesophyll of *Zinnia elegans*. Plant Physiol. 52, 57–60.

Gendreau, E., Traas, J., Desnos, T., Grandjean, O., Caboche, M., Hofte, H., 1997. Cellular basis of hypocotyl growth in *Arabidopsis thaliana*. Plant Physiol. 114, 295–305.

Goldberg, R., Morvan, C., Jauneau, A., Jarvis, M.C., 1996. Methyl-esterification, de-esterification and gelation of pectins in the primary cell wall. In: Visser, J., Voragen, A.G.J. (Eds.), Pectins and Pectinases. Elsevier Science, Amsterdam, pp. 166–189.

Gubler, U., Monahan, J.J., Lomedico, P.T., Bhatt, R.S., Collier, K.J., Hoffman, B.J., Bohlen, P., Esch, F., Ling, N., 1983. Cloning and sequence analysis of cDNA for the precursor of human growth hormone-releasing factor, somatocirinin. Proct. Nat. Acad. Sci. 80, 4311–4314.

Holland, N., Holland, D., Helentjaris, T., Dhugga, K., Xoconostle-Cazares, B., Delmer, D.P., 2000. A comparative analysis of the plant cellulose synthase (CesA) gene family. Plant Physiol. 123, 1313.

Jones, L., Seymour, G.B., Knox, J.P., 1997. Localization of pectic galactan in tomato cell walls using a monoclonal antibody specific to (1→4)-β-D-galactan. Plant Physiol. 113, 1405–1412.

Kacuráková, M., Capek, P., Sasinková, V., Wellner, N., Ebringerová, A., 2000. FT-IR study of plant cell wall model compounds: pectic polysaccharides and hemicelluloses. Carbohydr. Polymers 43, 195–203.

Kemsley, E.K., 1998. Discriminant Analysis of Spectroscopic Data. John Wiley and Sons, Chichester, UK.

Knox, J.P., Linstead, P.J., King, J., Cooper, C., Roberts, K., 1990. Pectin esterification is spatially regulated both within cell walls and between developing tissues of root apices. Planta 181, 512–521.

Knox, J.P., 1997. The use of antibodies to study the architecture and developmental regulation of plant cell walls. Int. Rev. Cytol. 171, 79–120.

Liang, C.Y., Marchessault, R.H., 1959. Infrared Spectra of Crystalline Polysaccharides. II. Native Celluloses in the region from 640 to 1700 cm^{-1}. J. Polymer Science XXXIX, 269–278.

Liners, F., Letesson, J-J., Didembourg, C., Van Cutsem, P., 1989. Monoclonal antibodies against pectin, Recognition of a conformation induced by calcium. Plant Physiol. 91, 1419–1424.

Massart, D.L., Vandeginste, B.G.M., Deming, S.N., Michotte Y., Kaufman, L. 1988. In Vandeginste B.G.M., Kaufman, L. Data handling in Science and Technology. Vol. 2: Chemometrics, a Textbook. Elsevier Science, Amsterdam.

McCann, M.C., Wells, B., Roberts, K., 1990. Direct visualisation of cross-links in the primary plant cell wall. J. Cell Sci. 96, 323–334.

McCann, M.C., Roberts, K., 1991. Architecture of the primary cell wall. In: Lloyd, C.W. (Ed.), The Cytoskeletal Basis of Plant Growth and Form. Academic Press, London, pp. 109–129.

McCann, M.C., Hammouri, M.K., Wilson, R.H., Belton, P.S., Roberts, K., 1992. Fourier transform infrared microspectroscopy is a new way to look at plant cell walls. Plant Physiol. 100, 1940–1947.

McCann, M.C., Chen, L., Roberts, K., Kemsley, E.K., Séné, C., Carpita, N.C., Stacey, N.J., Wilson, R.H., 1997. Infrared microspectroscopy: sampling heterogeneity in plant cell wall composition and architecture. Physiol. Plant 100, 729–738.

McCann, M.C., Domingo, C., Stacey, N.J., Milioni, D., Roberts, K., 2000. Chapter 37: Tracheary element formation in an in vitro system. In: Savidge, R., Barnett, J., Napier, R. (Eds.), Cambium: the Biology of Wood Formation. BIOS Scientific Publishers LTD, Oxford, pp. 457–470.

Milioni, D., Sado, P-E., Stacey N.J., Roberts, K., McCann M.C. 2001. Differential expression of cell-wall-related genes during formation of tracheary elements in the *Zinnia* mesophyll cell system. Plant Molecular Biology.

Nicol, F., His, I., Jauneau, A., Vernhettes, S., Canut, H., Höfte, H., 1988. A plasma membrane-bound putative endo-1,4-β-D-glucanase is required for normal wall assembly and cell elongation in *Arabidopsis*. EMBO J. 17, 5563–5576.

Oxenbøll-Sørensen, S., Pauly, M., Bush, M., Skjøt, M., McCann, M.C., Borkhardt, B., Ulvskov, P., 2000. Pectin engineering: Modification of potato pectin by in vivo expression of an endo-1,4-β-D-galactanase. Proc. Natl. Acad. Sci. USA 97, 7639–7644.

Potikha, T., Delmer, D.P., 1995. A mutant *Arabidopsis thaliana* displaying altered patterns of cellulose deposition. Plant J. 7, 453–460.

Reiter, W-D., Chapple, C.C.S., Somerville, C.R., 1999. Mutants of *Arabisopsis thaliana* with altered cell wall polysaccharide composition. Plant J. 12, 335–345.

Reiter, W-D., 1998. *Arabidopsis thaliana* as a model system to study synthesis, structure, and function of the plant cell wall. Plant Physiol. Biochem. 36, 167.

Séné, C.F.B., McCann, M.C., Wilson, R.H., Grinter, R., 1994. FT-Raman and FT-infrared spectroscopy: an investigation of five higher plant cell walls and their components. Plant Physiol. 106, 1623–1633.

Shedletzky, E., Shmuel, M., Trainin, T., Kalman, S., Delmer, D.P., 1990. Adaptation and growth of tomato cells on the herbicide 2,6-dichlorobenzonitrile (DCB) leads to production of unique cell walls virtually lacking a cellulose-xyloglucan network. Plant Phys 94, 980–987.

Shirzadegan, M., Christie, P., Seemann, J.R., 1991. An efficient method for isolation of RNA from tissue cultured plant cells. Nucl. Acid Res. 19, 6055.

Turner, S.R., Somerville, C.R., 1997. Collapsed xylem phenotype of *Arabidopsis* identifies mutants deficient in cellulose deposition in the secondary cell wall. Plant Cell 9, 689–701.

Vincken, J.P., Borkhardt, B., Bush, M., Doeswijk-Voragen, C., Dopico, B., Labrador, E., Lange, L., McCann, M., Morvan, C., Muñoz, F., Oomen, R., Peugnet, I., Rudolph, B., Schols, H., Sørensen, S., Ulvskov, P., Voragen, A., Visser, R., 2000. Remodelling pectin structure in potato. In: de Vries, G.E., Metzlaff, K. (Eds.), Conference Proceedings of Phytosfere '99 European Plant Biotechnology Network. Elsevier Science, pp. 23–34.

Willats, W.G.T., Marcus, S.E., Knox, J.P., 1998. Generation of a monoclonal antibody specific to (1→5)-α-L-arabinan. Carbohydr. Res. 308, 149–152.

Wu, L.G., Joshi, S.P., Chiang, V.L., 2000. A xylem-specific cellulose synthase gene from aspen (*Populus tremuloides*) is responsive to mechanical stress. Plant J. 22, 495–502.

PERGAMON

Phytochemistry 57 (2001) 823–833

PHYTOCHEMISTRY

www.elsevier.com/locate/phytochem

Sucrose synthase localizes to cellulose synthesis sites in tracheary elements

Vadim V. Salnikov [a], Mark J. Grimson [a], Deborah P. Delmer [b], Candace H. Haigler [a,*]

[a] *Department of Biological Sciences, Texas Tech University, Box 43131, Lubbock, TX 79409, USA*
[b] *Section of Plant Biology, University of California-Davis, 1 Shields Avenue, Davis, CA 95616, USA*

Received 10 July 2000; received in revised form 17 October 2000

Abstract

The synthesis of crystalline cellulose microfibrils in plants is a highly coordinated process that occurs at the interface of the cortex, plasma membrane, and cell wall. There is evidence that cellulose biogenesis is facilitated by the interaction of several proteins, but the details are just beginning to be understood. In particular, sucrose synthase, microtubules, and actin have been proposed to possibly associate with cellulose synthases (microfibril terminal complexes) in the plasma membrane. Differentiating tracheary elements of *Zinnia elegans* L. were used as a model system to determine the localization of sucrose synthase and actin in relation to the plasma membrane and its underlying microtubules during the deposition of patterned, cellulose-rich secondary walls. Cortical actin occurs with similar density both between and under secondary wall thickenings. In contrast, sucrose synthase is highly enriched near the plasma membrane and the microtubules under the secondary wall thickenings. Both actin and sucrose synthase lie closer to the plasma membrane than the microtubules. These results show that the preferential localization of sucrose synthase at sites of high-rate cellulose synthesis can be generalized beyond cotton fibers, and they establish a spatial context for further work on a multi-protein complex that may facilitate secondary wall cellulose synthesis. © 2001 Elsevier Science Ltd. All rights reserved.

Keywords: *Zinnia elegans*; Compositae; Electron microscopic immunolocalization; Freeze substitution; Cellulose synthesis; Sucrose synthase; Actin; Microtubule; Tracheary element; Secondary cell wall

1. Introduction

The change of the millennium is paralleled by a change to the post-genomics era. For example, the genomes of *Arabidopsis* and rice have been completely sequenced, and the technology exists to obtain many cDNA sequences from any plant relatively quickly. Similarly, microarray technology will allow suites of genes that are expressed in particular developmental or physiological states to be analyzed and compared. Even for genes with known homology, the challenge will then be to elucidate how the cognate proteins cooperate in biochemical pathways and which enzymes exert most control within pathways. Genes with no or weak homology will be even harder to correlate with cellular functions. Analysis of mutant plants (in species where this is practical) and biochemistry will be important tools in functional genomics, and fluorescence and electron microscopy are also re-emerging as essential tools. This paper provides an example of the use of cryogenic immunoelectron microscopy to establish spatial relationships between structural proteins and enzymes that may facilitate cellulose synthesis.

Based on biochemical, molecular, and immunofluorescence evidence in secondary-wall-stage cotton fibers, a novel membrane-associated form of sucrose synthase (SuSy; EC 2.4.1.13) was proposed to channel UDP-glucose to cellulose synthase in a closely coupled reaction (Amor et al., 1995). When acting degradatively, SuSy degrades sucrose (with input of UDP) to release fructose and UDP-glucose. UDP-glucose is thought to be the immediate substrate for cellulose polymerization in higher plants, and direct channeling of UDP-glucose to cellulose synthase from SuSy may promote high-rate cellulose synthesis (Delmer and Amor, 1995). However, the previous immunofluorescence localization of SuSy

* Corresponding author. Tel.: +1-806-742-2707; fax: +1-806-742-2963.
E-mail address: candace.haigler@ttu.edu (C.H. Haigler).

0031-9422/01/$ - see front matter © 2001 Elsevier Science Ltd. All rights reserved.
PII: S0031-9422(01)00045-0

in cotton fibers (Amor et al., 1995) had insufficient resolution to establish clearly the spatial relationship of SuSy to the plasma membrane where cellulose synthases are located (Kimura et al., 1999). Also, there were no data to establish the generality of this model in other secondary-wall-stage, cellulose-synthesizing cells.

Biochemical evidence also indicated that SuSy is an actin-binding protein, but it did not establish a role for SuSy/actin in any particular process. Furthermore, it was suggested that soluble SuSy, not membrane-associated SuSy, was associated with F-actin (Winter et al., 1998). Cortical F-actin has frequently been discussed as a possible participant in cellulose synthesis (Heath and Seagull, 1982). When actin antagonists are applied to differentiating cotton fibers and differentiating TEs, both microtubules and newly deposited secondary wall thickenings occur in abnormal orientations relative to the cell axis (Kobayashi et al., 1988; Seagull, 1990). In addition, cortical actin networks have been visualized by immunofluorescence in both of these cell types during secondary wall deposition with a questionable degree of accuracy [(Kobayashi et al., 1987; Seagull, 1990); see also below and the discussion of Frost and Roberts, 1996)].

We set out to clarify the relationship of SuSy and actin to patterned secondary wall deposition using a cryogenic electron microscopic immunolocalization methods that greatly reduces artefacts (Nicolas and Bassot, 1993) and differentiating TEs as a model system (Fukuda and Komamine, 1980). Tracheary element differentiation is characterized by the deposition of cellulose-rich secondary walls in precise patterns. Proteins associated with cellulose synthesis accumulate within the plasma membrane in this pattern, as evidenced by the localization of protein aggregates called rosettes than contain the cellulose synthase (Herth, 1985; Kimura et al., 1999). Bands of cortical microtubules also underlie and help determine the secondary wall pattern of tracheary elements (Hepler, 1981). The specific, patterned, association of rosettes (cellulose synthases) and microtubules with the secondary wall thickenings of tracheary elements of *Zinnia elegans* differentiating in culture (the cell system used here) has been shown previously (Falconer and Seagull, 1985; Haigler and Brown, 1986). Therefore, we set out to test whether other proteins that might facilitate high-rate secondary wall cellulose synthesis, specifically sucrose synthase and actin, would also accumulate in the same pattern.

Cellulose synthesis is well-known to be easily disturbed. For example, from exogenous UDP-glucose, isolated membrane preparations of higher plants tend to synthesize callose (β-1,3 glucan) much more readily than cellulose (β-1,4 glucan) (Delmer and Amor, 1995), and rosettes of cellulose synthases are not detected after even low-speed centrifugation (Herth and Weber, 1984). Therefore, this research required immunolocalization methods that would not allow perturbation of molecules associated with cellulose synthesis in vivo. This was emphasized by our preliminary immunofluorescence studies that failed to show repeatable enrichment of SuSy over the thickenings (see below). Localization at the electron microscope level after freeze substitution was a preferred method, but the initial step of ultra-rapid freezing limited the depth of freezing that could be obtained without destructive ice crystal formation. This technical difficulty was overcome by use of TEs differentiating semi-synchronously in culture from isolated mesophyll cells of *Zinnia elegans L.* (Fukuda and Komamine, 1980). These single cells could be frozen without substantial ice crystal formation and processed for electron microscopy using techniques that should greatly hinder molecular movement (Echlin, 1992).

2. Results

2.1. Western blotting established antibody specificity in Zinnia elegans

Both antibodies used have been well-characterized in other systems. The rabbit polyclonal antibody to SuSy was raised against gel-purified cotton fiber SuSy (Amor et al., 1995). The mouse monoclonal antibody to actin (ICN, Costa Mesa, CA; clone C4) was raised against chicken gizzard actin, and it recognizes a conserved epitope in the N-terminal region of all actin monomers (Lessard, 1988). Western blots showed that both anti-SuSy and anti-actin each recognized one main band near the predicted size in whole cell protein extracts of differentiating *Zinnia* cultures (Fig. 1a and b). Thus, in *Zinnia* the band recognized by anti-SuSy ran below the 97 kDa marker, which is close to the 91 kDa molecular weight of cotton SuSy. The band recognized in *Zinnia* by anti-actin ran below the 50 kDa marker, which is consistent with the 41.8 kDa molecular weight of monomeric actin.

2.2. Immunofluorescence studies to detect SuSy yielded variable results

Immunofluorescence studies using anti-SuSy antibody revealed variable patterns in differentiating TEs, and SuSy was only rarely observed over thickenings. The cell in Fig. 2 was a differentiating TE as shown by birefringence of the thickenings in polarized light microscopy (Fig. 2a). Note that the secondary wall at the top of the cell is pitted, as shown by the horizontal white thickenings and the vertical black thickenings. The pitted wall, combined with the location of chloroplasts between thickenings, makes it appear that SuSy surrounds chloroplasts (Fig. 2b and c), but this is coincidental. Fig. 2b and c shows the fluorescence of

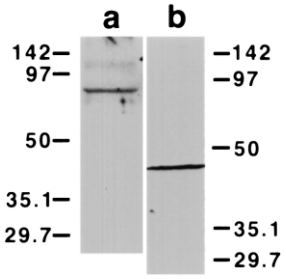

Fig. 1. Western blots against *Zinnia* protein: (a) anti-SuSy; (b) anti-actin. The location of the molecular weight standards run with each gel are indicated to the side.

FITC-labeled SuSy with (Fig. 2b; SuSy appears green) and without (Fig. 2c; SuSy appears yellow) a filter blocking chlorophyll autofluorescence. Without the chlorophyll-blocking filter, the chloroplasts were seen as orange spheres. Comparing the images in Fig. 2, FITC/SuSy was enriched over the thickenings at the top of the cell where chloroplasts remained normally placed for mesophyll cells (arrayed in a single layer of the cell cortex). However, SuSy was enriched between thickenings (leaving a "negative" image of thickenings) at the bottom of the cell where chloroplasts apparently moved from their normal location. This suggests that preparative methods for immunofluorescence caused variable and artefactual results. For example, since chloroplasts (and/or SuSy) might be tethered by actin, one possibility is that variable results arise due to inability to preserve actin structure and location during immunofluorescence protocols (see Section 3). We also observed that SuSy/FITC mainly retracted with the plasma membrane in an area of slight plasmolysis on the lower right side of the cell. Cells treated with the pre-immune serum at the same concentration showed only very dim, dull green fluorescence (data not shown).

2.3. Electron microscopic immunolocalization of SuSy and actin after freeze substitution established their pattern relative to secondary wall thickening

In contrast to the immunofluorescence results, using the superior technique of freeze substitution, SuSy was consistently highly-enriched close to the plasma membrane underlying secondary wall thickenings (Fig. 3a and b) and much less abundant between thickenings (Fig. 3a). Grazing sections that revealed longitudinal cross-sections of microtubules underneath a secondary cell thickening clarified that SuSy lies above the cortical microtubules and near the plasma membrane (Fig. 3c). No labeling was observed when similar sections were incubated with the same concentration of the pre-immune serum from the rabbit used to produce the antibody to SuSy (Fig. 3d). Equivalent results were obtained with a second polyclonal antibody raised against SuSy from Vicia faba (data not shown).

In differentiating TEs during active cellulose synthesis, labeling of SuSy over the cytoplasm or any organelle was rare (Fig. 3a–c). This low-frequency cytoplasmic labeling could well be background, non-specific, labeling. Therefore, these data showed that active secondary cell wall cellulose synthesis was characterized by the

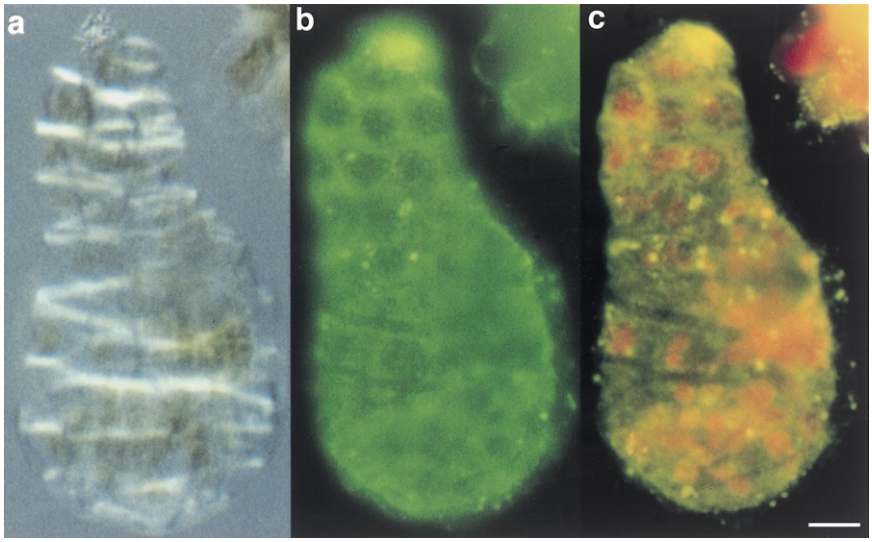

(Colour)

Fig. 2. Immunofluorescence of SuSy in a differentiating TE. (a) Polarization microscopy of the differentiating TE showed the birefringence of patterned cellulose. (The background was unusually bright for polarization microscopy because of the planapochromatic lens used to optimize fluorescence); (b) FITC labeling of SuSy was visualized as green with the chlorophyll blocking filter in place. SuSy was observed to be enriched over thickenings or between thickenings in the upper and lower parts of the cell, respectively; (c) FITC labeling of SuSy was visualized as yellow and chloroplasts were visualized as orange spheres with the chlorophyll blocking filter removed. Here, the "negative" images of thickenings in the lower left of the cell were enhanced. Note that different SuSy patterns correlate with different placement of the chloroplasts at the top and bottom of the cell. Bar is 5 μm.

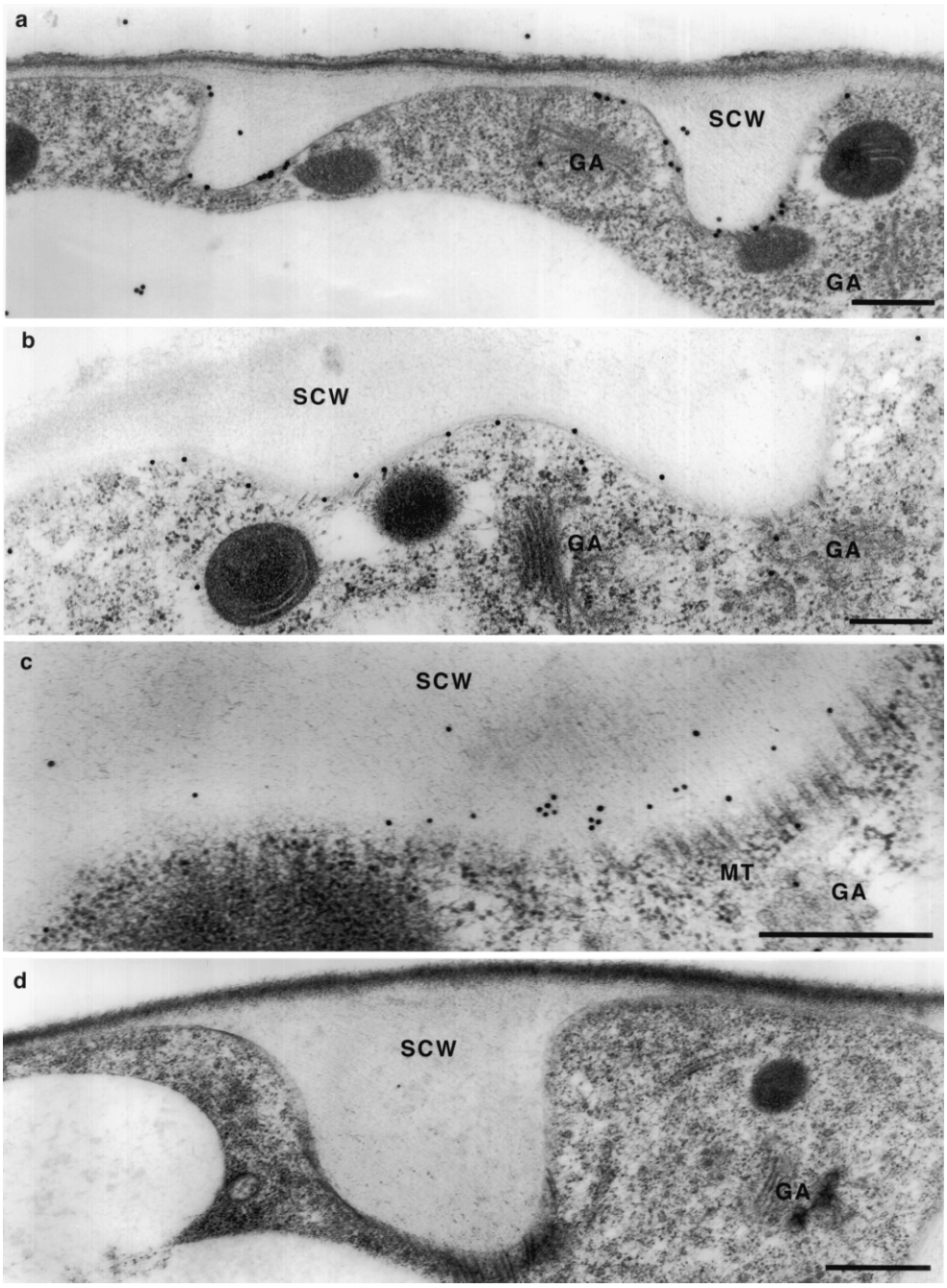

Fig. 3. Electron microscopic immunolocalization of SuSy in differentiating TEs. (a, b, c) Labeling occurred near the plasma membrane underneath secondary cell wall thickenings (SCW) and above the microtubules (MT), which are clearly shown in c. The Golgi apparatus (GA) was generally not labeled; (d) no labeling was observed after treatment of similar sections with the pre-immune serum. Bars are 0.2, 0.2, 0.5, and 1 μm in a, b, c and d, respectively.

preferential localization of SuSy at the plasma membrane.

Actin occurred in the vicinity of the plasma membrane all along the cortex of differentiating TEs, both between and over secondary wall thickenings (Fig. 4a). Labeling deep in the cytoplasm was also sometimes observed, and the labeling of a microfilament there confirmed the specificity of this monoclonal antibody (Fig. 4b).

Quantitative analysis of labeling of differentiating TEs (Fig. 5) was performed on cross-sections so that the difference between secondary wall thickenings and regions between thickenings was clearly apparent. Prior to patterned secondary wall deposition, the mesophyll cells thicken their primary wall uniformly (Burgess and Linstead, 1984), but cell walls between thickenings typically did not exceed 0.25 μm and patterned thickenings exceeded 0.5 μm. The label for SuSy was denser

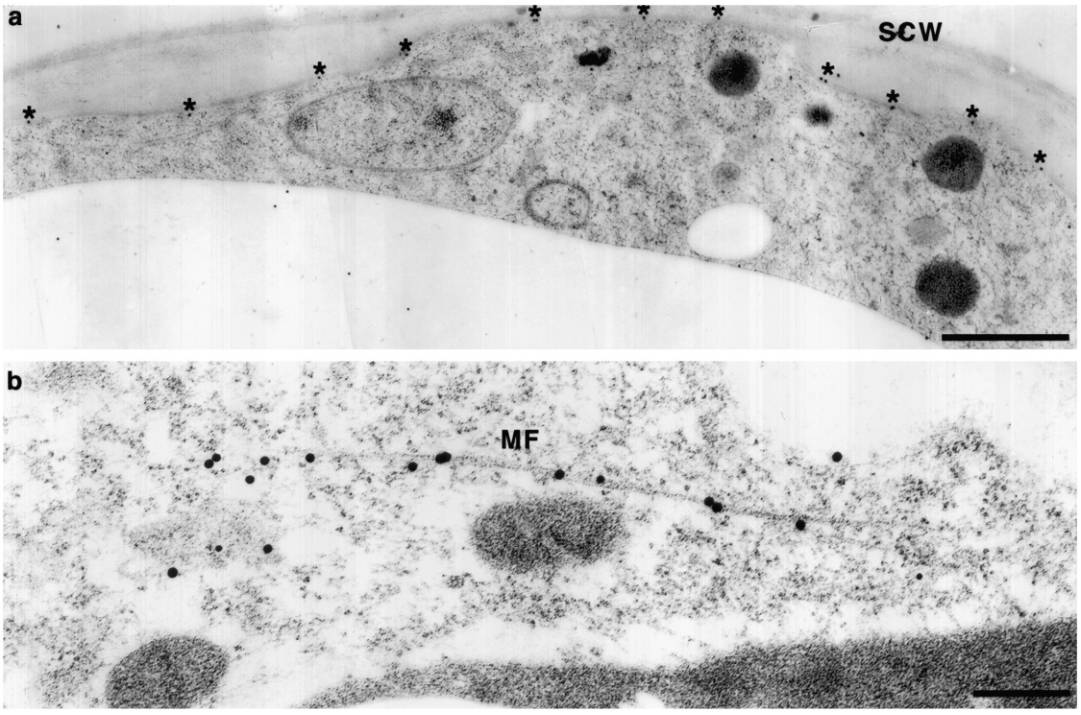

Fig. 4. Electron microscopic immunolocalization of actin in differentiating TEs. (a) Labeling of actin (as highlighted by asterisks) occurred near the plasma membrane both between and under secondary wall thickenings (SCW); (b) Labeling of a single microfilament (MF) deep in the cytoplasm. Bars are 1 and 0.2 μm in a and b, respectively.

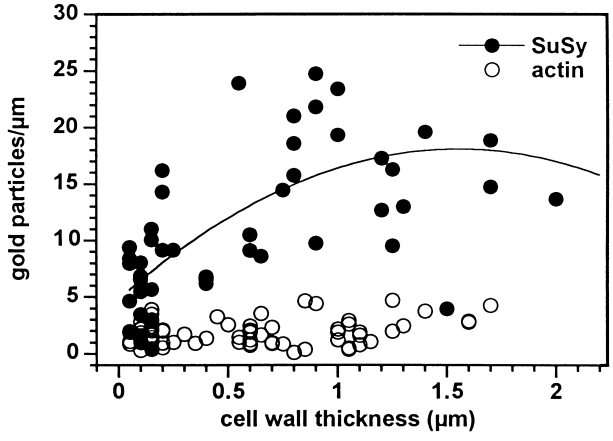

Fig. 5. Quantity of SuSy (●) and actin (○) labeling near the plasma membrane in relation to the thickness of the adjacent cell wall. Correlating observations and measurements, primary walls between thickenings typically did not exceed 0.25 μm and secondary wall thickenings exceeded 0.5 μm. The SuSy data were fitted with a second order polynomial equation ($R^2 = 0.44$).

over thickenings, whereas the label for actin had the same density regardless of cell wall thickness (Fig. 5). The best fit for the SuSy distribution data was obtained with a second order polynomial equation (coefficient of determination, $R^2 = 0.44$), whereas no type of line fitted the actin distribution data. Only cell walls that labeled are represented in the graph, which therefore over-represents the tendency of SuSy to label between thickenings. For both SuSy and actin, all the thickenings used for quantitation (25–26 in each case) had some associated label. In contrast, the areas between thickenings had more tendency not to label for SuSy (27% clean or 58% clean/sparsely labeled) than for actin (12% clean).

2.4. Double labeling of tangential sections established the spatial relationship of microtubules, SuSy, and actin relative to each other and the plasma membrane

Tangential sections that grazed between secondary cell wall and cytoplasm (Fig. 6a) clearly established the spatial relationships of molecules at the cell cortex. Little SuSy or actin label was observed when long lengths of longitudinally sectioned microtubules were revealed, a zone lying within the microtubule array below each secondary wall thickening (Fig. 6b, upper left). Instead, SuSy and actin labeled when the section traversed the region near the plasma membrane between the microtubules and the cell wall, indicating that SuSy and actin lie just above the microtubules. The area of the unlabeled microtubule array between the arrowheads in Fig. 6b does label in the next serial section outward toward the cell surface; the label is just above the microtubules (Fig. 6c). Actin labeled slightly closer to the microtubules than SuSy, as shown by these (Fig. 6b, lower right, and Fig. 6c; note the different placement of asterisks and arrows relative to the microtubules) and other micrographs (data not shown). In contrast to cross-sections (Figs. 4 and 5), actin

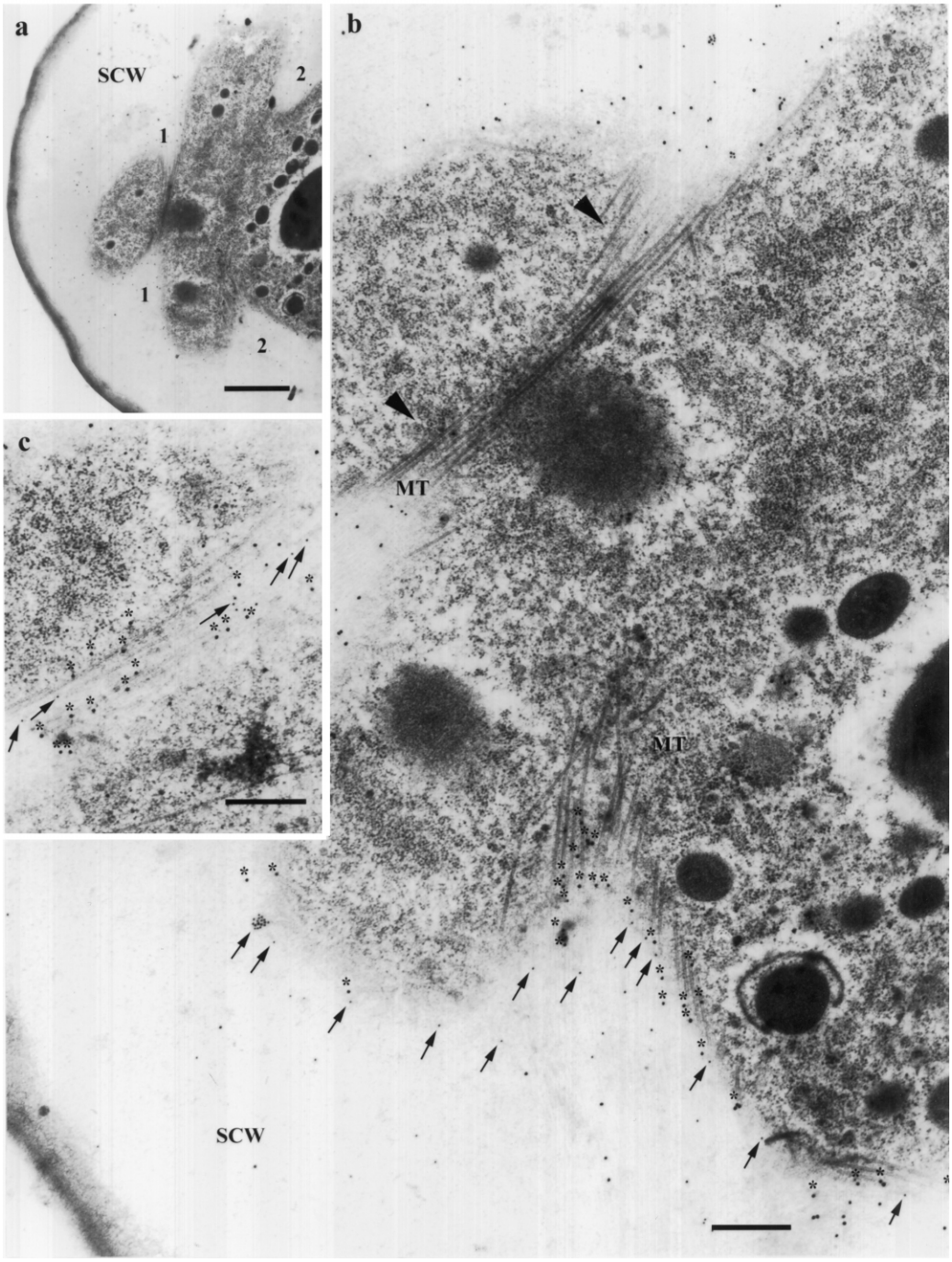

Fig. 6. Double labeling of SuSy (10 nm gold) and actin (20 nm gold) in a differentiating TE. To aid clarity in (b) and (c), sometimes the 10 nm gold labeling of SuSy is indicated by arrows and the 20 nm gold labeling of actin is indicated by asterisks. (a) A tangential section that includes secondary cell wall (SCW), deep cytoplasm, and all the intervening layers. The plane of section has just entered the zone of cytoplasm below the two secondary wall thickenings. (Opposite sides of each of the two thickenings — labeled 1 and 2 — point to each other at the top and bottom of the TE.); (b) high magnification view of one part of the section in (a) that grades between secondary cell wall (SCW) and cortical microtubules (MT). Note in the region between the arrowheads that neither SuSy nor actin occurs in the plane where the microtubule bundle under a thickening is visible along much of its length. However, the lower part of the micrograph shows that both SuSy and actin label in a plane between the microtubules and the cell wall. There is a tendency for actin to label more abundantly closer to the microtubules than SuSy (compare location of asterisks and arrows); (c) high magnification view of the next section outward toward the cell surface of the microtubule area between the arrowheads in (b). Note that the density of SuSy and actin labeling greatly increases in this plane above the microtubule bundle and below the thickening wall (beginning to appear as an unstained area devoid of organelles), which is consistent with close proximity to the plasma membrane. Bars are 2, 0.5, and 0.5 μm in a, b, and c, respectively.

labeled with a density ca. equal to SuSy in tangential sections (Fig. 6b), probably because longer regions of microfilaments are exposed in the section plane.

3. Discussion

The enrichment of SuSy underneath the patterned secondary wall thickenings of differentiating TEs is consistent with plasma membrane-associated SuSy being specifically related to high-rate cellulose synthesis. Organized cellulose synthases, rosettes, are specifically enriched over the thickenings (Haigler and Brown, 1986; Kimura et al., 1999). The rare labeling of SuSy in the cytoplasm could be partially explained by dilution in a large volume, but the data suggest that SuSy is strongly recruited to the plasma membrane during secondary wall deposition. Future biochemical experiments designed to discriminate between soluble and membrane-associated SuSy are planned to test this differential distribution, although it is possible that these cryogenic microscopic results are more definitive than extraction procedures that necessarily disrupt normal cellular organization.

SuSy is positioned so that it could interact with the inner bilayer of the plasma membrane and/or the cytoplasmic portion of the secondary wall cellulose synthase and/or actin (Fig. 7). Therefore, SuSy may channel UDP-glucose to cellulose synthase in diverse species and cell types, not only in cotton fibers that have unusual secondary walls composed of almost pure cellulose. In contrast to previous biochemical results that supported an interaction between soluble SuSy and F-actin (Winter et al., 1998), at least during active cellulose synthesis there is a possibility that membrane-associated SuSy is also interacting with F-actin. Membrane-associated SuSy extracted by EGTA from cotton fibers during secondary wall cellulose synthesis re-precipitated upon Ca^{2+} addition, along with other proteins including Ca^{2+}-independent kinase, tubulin, actin, and annexins (D. Delmer and M. Datcheva, unpublished). However, other methods such as fluorescence resonance energy transfer between GFP/BFP-tagged proteins (Mahajan et al., 1998) will be required to prove that direct binding between SuSy and other proteins exists in vivo.

In addition to cotton fibers, biochemical evidence of membrane-associated SuSy has been shown in maize endosperm and growing organs of maize and soybean (Carlson et al. 1996; Winter et al., 1998; Buckeridge et al., 1999). However, further work will be required to show that SuSy participates directly in primary wall cellulose synthesis or other endo- or plasma membrane-associated processes in these tissues. The Golgi apparatus of differentiating TEs did not commonly label for SuSy even though they are probably synthesizing abundant xylan, the predominant hemicellulose in *Zinnia*

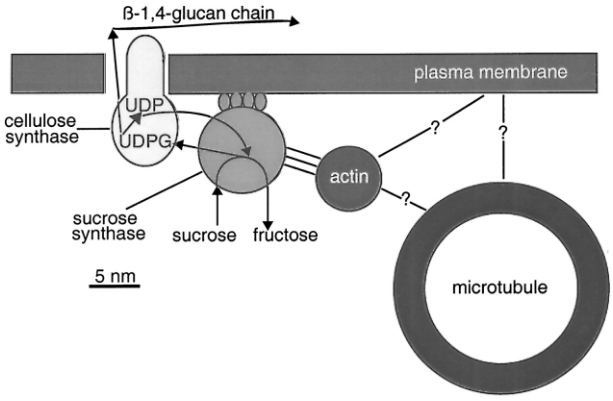

Fig. 7. Model depicting how cellulose synthase, SuSy, actin, and microtubules are positioned relative to each other in the cortex below secondary wall thickenings of differentiating tracheary elements and how they might interact to facilitate cellulose synthesis. The model takes into account the new data presented here and previously published findings. Sucrose synthase and actin are shown closer to the plasma membrane than microtubules, with SuSy being closest, as suggested by our data. Cellulose synthase is shown as a transmembrane protein that is enriched beneath secondary wall thickenings (Delmer, 1999; Haigler and Brown, 1986). The loops between SuSy and the plasma membrane indicate a hydrophobic region of the protein that may facilitate its membrane interaction (Carlson and Chourey, 1996), and the hatch marks between SuSy and actin indicate a peptide in SuSy that is homologous to known F-actin-binding amino acid sequences (Winter and Huber, 2000). The suggested channeling of UDP-glucose between SuSy and cellulose synthase is adapted from a previously published diagram (Delmer and Amor, 1995). The question marks indicate other possible binding interactions not addressed by our data. A gap remains in the plasma membrane to the left of the cellulose synthase to indicate that there is a still-undefined mechanism by which glucan chains reach the cell wall space. The scale of the drawing is approximately as indicated by the scale bar in the lower left (see Section 3).

secondary cell wall thickenings (Ingold et al., 1988). Therefore, membrane-associated SuSy might not be an obligatory part of xylan synthesis, which would require UDP-xylose rather than UDP-glucose as immediate substrate, whereas it has been proposed to participate in Golgi-associated β 1->3, 1->4 glucan synthesis in maize but not xyloglucan synthesis in soybean (Buckeridge et al., 1999). One possible explanation for this difference is that, among the UDP-glucose-requiring hemicellulose synthases, only the β 1->3, 1->4 glucan synthase may have a cellulose synthase ancestor (Buckeridge et al., 1999).

Multi-protein interactions highly related to cell structure and under complex cellular control may explain why cellulose has been difficult to synthesize reproducibly in vitro at high rates and in its native crystalline form (Blanton and Haigler, 1996). For example, related to the data presented here, the binding of SuSy to the plasma membrane, cellulose synthase, and/or actin in secondary wall synthesizing cells might be modulated very precisely by calcium. Elevated calcium hinders cellulose synthesis in vitro and in semi-permeablized cotton fibers (Amor et al., 1995; Delmer and Amor,

1995). F-actin can be degraded under elevated calcium (Frost and Roberts, 1996), which could destabilize an integrated cellulose synthase complex. However, uptake of extracellular calcium is required for tracheary element differentiation (Roberts and Haigler, 1990), microsomal SuSy remained in cotton fibers extracted with 200 nM free Ca^{2+}, and microsomal SuSy was released from cotton fibers by EGTA washing (D. Delmer and M. Ivanova-Datcheva, submitted). Elevated sucrose could also enhance the formation of a multi-protein cellulose synthesizing complex, as preliminarily suggested for actin/SuSy binding (Winter and Huber, 2000). In this case, secondary wall, cellulose synthesis would occur only when carbon was plentiful. The preference of cellulose synthesis for exogenous sucrose in semi-permeabilized cotton fibers (Amor et al., 1995) could be at least partially explained by promotion of the formation of such a multi-protein complex.

Only freeze substitution gave reproducible information about SuSy localization. Immunofluorescence techniques may have led to inconsistent and artefactual results for at least two reasons. First, aldehyde fixatives, which are usually used alone (without OsO_4) in order to preserve protein antigenicity, cross-link proteins but not lipids (Bozzola and Russell, 1999). Therefore, membrane flow might continue, carrying peripheral membrane proteins like SuSy to artefactual locations. Also, aldehyde fixatives and their buffers can degrade actin filaments (Frost and Roberts, 1996), possibly causing SuSy delocalization. Second, cellulases and/or pectinases that permeabilize the cell wall to antibodies in immunofluorescence protocols could disrupt cell wall/cytoskeleton linkages that stabilize localized plasma membrane domains and cortical organelles (Fowler and Quatrano, 1997). Similar reasons may explain why our electron microscope immunolocalization supports uniform distribution of cortical actin in differentiating TEs, whereas previous immunofluorescence supported its localization between thickenings (Kobayashi et al., 1988). In that paper, Fig. 1k shows actin only between thickenings in an image that is strikingly similar to the "negative" image of SuSy at thickenings in the bottom half of the cell in Fig. 2b and c. Therefore, immunofluorescence preparative procedures may disturb and allow secondary reorganization (Frost and Roberts, 1996) of specialized actin filaments (and bound SuSy) that normally underlie the thickenings. Protoplast undulations that occur due to continued, localized, plasma membrane/cell wall attachment after plasmolysis in TEs of several species (Seagull, 1991), including *Zinnia* (Roberts and Haigler, 1989), suggest that patterned cell wall/cortical interactions do exist in TEs.

This research provides a spatial context to guide further research on multi-protein interactions that may facilitate cellulose synthesis. A working model based on current knowledge is shown in Fig. 7, which is drawn with an approximately realistic scale and shows metabolic channeling between SuSy and cellulose synthase. The cellulose synthase is shown as an integral plasma membrane protein because of its eight predicted transmembrane helices and its identification there by freeze fracture labeling (Kimura et al., 1999). Its size and shape are predicted from the known molecular structure of membrane ATPases (Auer et al., 1998; Zhang et al., 1998), which have a molecular weight and topology similar to that known or predicted for cellulose synthase (Delmer, 1999). An approximate size for globular SuSy was derived from the relationship of its molecular weight (91 kDa for cotton) to cellulose synthase (110 kDa for cotton) (Kawagoe and Delmer, 1997). The gap beside cellulose synthase indicates that glucan chains must reach the cell wall space, which could occur through a pore formed by the trans-membrane helices (Delmer, 1999) or by the aggregation of multiple cellulose synthase proteins into rosettes (Emons, 1991). In Fig. 7, SuSy is shown to interact with the plasma membrane as a peripheral membrane protein through an identified hydrophobic region and with actin through a peptide identified in SuSy that has homology to known actin-binding peptides (Winter and Huber, 2000). Since we have no specific information about whether SuSy and cellulose synthase might be directly bound to each other, the diagram only shows them adjacent. However, cotton cellulose synthase has a LIM-like domain that could facilitate protein/protein interactions (Kawagoe and Delmer, 1997). Microtubules are shown furthest below the plasma membrane, but closest to cortical actin, as indicated by our data. The relationship of microtubules to a possible interaction between SuSy, actin, and cellulose synthase cannot be minimized. Unlike the actin that is distributed over the whole cortex, microtubules, SuSy, and cellulose synthases are specifically restricted to the sites of secondary wall deposition in differentiating tracheary elements. Therefore, the location of a possible complex between SuSy, cellulose synthase, actin, and other unidentified proteins may ultimately depend on the microtubules or microtubule-associate proteins underlying the thickenings. This possibility is consistent with the well-known effects of microtubule antagonists in disrupting secondary wall patterns, including in *Zinnia* tracheary elements (Falconer and Seagull, 1986). The question marks in the diagram indicate other possible linkages and/or sites for other interacting proteins not yet identified.

4. Concluding remarks

The diagram in Fig. 7 shows only one cellulose synthase and associated proteins, whereas many (about 24–36) of them are proposed to aggregate into one rosette to facilitate the crystallization of cellulose I microfibrils.

The rosettes are also proposed to move through the plasma membrane in prescribed patterns, spinning cellulose microfibrils behind them (Blanton and Haigler, 1996). This seems challenging enough for one rosette about 30 nm across (Kimura et al., 1999). If SuSy were directly linked to the rosette would this movement be hindered, or might SuSy linked to actin and microtubules serve only to saturate the cortex with UDP-glucose to be used by the moving cellulose synthases? Arguing against the latter possibility and for direct coupling, semi-permeabilized cotton fibers use sucrose for cellulose synthase much more readily than exogenous UDP-glucose (Amor et al., 1995). Another interesting question is what network of protein binding is required to cause SuSy to prefer the sites of secondary wall thickening? Might a different macromolecular organization of actin mediate this specific localization, or do the microtubules alone cause this? Is SuSy phosphorylation related or not to its recruitment to the cortex for cellulose synthesis? Questions like these will be answered as perturbed systems are analyzed and as more candidate proteins are discovered that may participate in a multi-protein complex regulating cellulose synthesis. Accurate placement of such proteins in their cellular context, as we have shown here, will be an essential part of future research.

5. Experimental

5.1. Cell cultures

Tracheary elements were induced to differentiate from isolated mesophyll cells of *Zinnia elegans* L. var. Envy as previously described (Fukuda and Komamine, 1980). Simplified medium (Roberts et al., 1992) was used to minimize salt crystals that hindered cell selection and sectioning. Cultures were frozen early in differentiation when about 20% of all cells were depositing cellulose in patterned secondary walls, but before extensive autolysis or lignification of TEs occurred.

5.2. Western blotting

Cells at the same stage of differentiation as described above were: pelleted by gentle centrifugation; suspended in 1× SDS sample buffer by addition of 5×buffer to the pellet; broken by sonication (Tekmar Sonic Disruptor Model TM300, Cincinnati OH, microtip, 2×10 s, duty 50, microlimit 5, pulse on, on ice, without foaming); boiled 3 min; and spun at 13,000 rpm to pellet debris. Samples were run in 10% SDS gels (10 μg protein/lane), and they were processed for Western blotting by standard methods with anti-SuSy (1:3000 in TBS/5% milk) or anti-actin (1:1000 in TBS/5% milk) and secondary antibodies for chemiluminescent detection on film (ECL kit; Amersham Pharmacia Biotech, Piscataway, NJ).

5.3. Sample preparation

For immunofluorescence, differentiating TEs were concentrated in medium without centrifugation by briefly slowing the rate of flask rotation to about 72 rpm so that cells clumped toward the middle. Using a wide-tip pipet, 0.5 ml cells in medium were removed and added to 1 ml fixative. After 10 min, cells were pelleted by low speed centrifugation and resuspended in fresh fixative for 1 h (RT). Fixatives used with equivalent results were: (a) Histochoice®, an acidic, buffered soln. containing glyoxal, a derivative of formaldehyde, and no chelators (Amresco, Solon, OH); or (b) 3.7% formaldehyde, 1 mM $MgSO_4$, and 5 mM EGTA in 50 mM PIPES, pH 6.9 (closely related to a previously-described buffer optimized for microtubules; Doonan and Clayton, 1986).

For immunoelectron microscopy, differentiating TEs concentrated as described above were placed in a microcentrifuge tube, and sprayed with an artist's air brush (Echlin, 1992) into resolidifying propane (near −168°C) cooled by liquid nitrogen within 3 min of removal from the incubator. [We also observed the same results in cells frozen on agar-coated loops (Lancelle et al., 1986), but the spray method resulted in a higher percentage of well-frozen cells.]

Cells were collected in the propane by a 10 μm nylon mesh funnel attached to a microcentrifuge tube "basket" then transferred to acetone at −80°C in 10 ml polypropylene vials contained within a pre-chilled, home-made, drilled brass block with cover (3.3 kg total mass to cause gradual temperature changes; design of Mark Grimson). Substitution at −80°C continued for 4 days and fixation (with acetone acting as a mild aldehyde; Newman and Hobot, 1993) occurred overnight at −40°C. Cells were washed in −40°C acetone, then infiltrated with gradually increasing percentages of resin (a 1:1 mix of Lowicryl K4M and HM20 acrylic resins, Electron Microscopy Sciences, Ft. Washington, PA; the resin was added in successive drops) for 2–3 days at −40°C followed by 3 changes of 100% resin (during a total period of 2 days) before embedding. The prolonged infiltration was necessary to optimize embedding of these thick-walled cells.

Cells were flat embedded between two slides treated with Paramount® release agent (#70880, Electron Microscopy Sciences, Ft. Washington, PA) using #1 thickness cover slips as spacers (Reymond and Pickett-Heaps, 1983). Polymerization proceeded with indirect 360 nm UV irradiation for 2 days at −20°C (light on within a −40°C freezer) and 1 day at 4°C. The upper slide was removed and differentiating TEs were selected by polarization microscopy (to detect patterned cellulose in secondary walls) and marked with a diamond "objective" (Leitz Optometric Inc., Richardson TX). Resin squares containing selected TEs were excised with

a razor blade and mounted with cyanoacrylate glue onto blank resin blocks. Ultrathin sections were taken (LKB Ultramicrotome III, Stockholm, Sweden) with a diamond knife (Diatome, Ft. Washington, PA) and mounted on Formvar-coated grids.

5.4. Immunolabeling

TBS and TBST refer to Tris-buffered saline (20 mM Tris–HCl, 150 mM NaCl, 0.02% azide, pH 7.5) minus or plus 0.05% (w/w) Tween 20, respectively. TB refers to 20 mM Tris, pH 8.2, 0.02% azide, used without salt for washing to minimize gold aggregation and background.

For immunofluorescence, after fixation cells were washed 2×10 min in TBS, 10 min in 0.05 M $C_2H_3NaO_2$ buffer, pH 5.0 and cells were permeabilized by 30 min digestion (RT) in 2.5 mg/ml pectinase (Sigma P2401), 2.5 mg/ml pectolyase (Sigma P3026), 2.5 mg/ml saponin (Sigma S2149), 0.25% (w/v) gelatin (Sigma G8150) in 0.05 M $C_2H_3NaO_2$ buffer, pH 5.0 plus protease inhibitors (0.57 mM PMSF, 2 mM N-CBZ-L-phenylalanine, and 5 mM 1,10-phenanthroline). After brief water washes (×3), cells were air-dried to poly-L-lysine-coated, multi-well slides, and autofluorescence was minimized by 10 min immersion in 0.1% $NaBH_4$ followed by 10 min washes (×2) in TBS. Cells were pre-blocked in 1% BSA in TBS (15 min, RT), and anti-SuSy was applied at 1:200 in TBS/BSA (overnight, 4°C). After 10 min washes in TBS (×3), goat anti-rabbit FITC (Organon Teknika, Durham, NC) was applied at 1:200 in TBS/BSA (1 h, RT). After 10 min washes in TBS (×3), an anti-fade mountant was applied [0.1% phenylenediamine in 90% glycerol/10% TBS (v/v), pH 8.6 adjusted with 0.5 M $CNa_2O_3/CHNaO_3$ buffer], and the edge of the coverslip was sealed with fingernail polish. As a control, the pre-immune serum was applied at the same concentration as anti-SuSy in the same protocol.

For immunoelectron microscopy, thin sections on nickel grids were: (a) blocked (15 min, RT, high humidity chamber) in TBST plus 5% normal goat serum (Sigma S-2007); (b) incubated in primary antibody (1–1.5 h, RT; anti-SuSy, 1:100 and/or anti-actin, 1:20 in TBST/5% normal goat serum); (c) washed in TB (×3); (d) incubated in secondary antibody [1–1.5 h, RT; 1:50 goat anti-rabbit and/or goat anti-mouse coupled to 10, 15, or 20 nm colloidal gold (Amersham Pharmacia Biotech, Piscataway, NJ) in TB plus 0.06% BSA]; and (e) washed in TB and dH_20. Grids were then stained for 15 min with 2% (w/v, aq.) uranyl acetate and 1.5 min with Reynold's lead citrate (Bozzola and Russell, 1999) before examination in the electron microscope. The pre-immune serum for polyclonal anti-SuSy was applied at the same dilution as the antibody as a control. For double labeling, the primary and secondary antibodies were applied together with each secondary antibody tagged with a different size of colloidal gold.

5.5. Microscopic observations

For immunofluorescence, samples were observed in an Olympus BH2 epi-fluorescence microscope equipped with polarization optics, a blue filter package for FITC (BP 490 with additional EY-455 excitation filter), an optional KP560 barrier filter (Carl Zeiss, Inc. Thornwood NY) to block chlorophyll autofluorescence, and a planapochromatic 40× lens with iris. Micrographs were recorded using an Olympus PM-10ADS automatic exposure device on Ektachrome 400 slide film. Images of cells for which pre-immune serum was substituted for the primary antibody in the same labeling protocol (not shown) were recorded at a manually set exposure time representing the average of several cells treated with anti-SuSy.

For immunoelectron microscopy, sections were observed and photographed in a transmission electron microscope (Hitachi HS-9 or Jeol 1200 EX).

5.6. Quantitation of immunoelectron microscopic labeling

We analyzed cross-sections near the middle of TEs so that thickenings and areas between thickenings were clearly revealed. For SuSy, 5 cells were analyzed and for actin, 8 cells were analyzed over about 1/2 or their circumference. The maximum width of the cell wall in a thickening or between thickenings was measured and the length of that segment of the plasma membrane was determined with a hand-operated measuring device (Map Mate; National Geographic Society). The number of gold particles lying not more than 0.1 μm from the membrane was counted and divided by the membrane length to determine density of labeling in each plasma membrane region. This value was plotted against cell wall thickness.

Acknowledgements

We thank: (a) James Lessard and Heather Ross, respectively, for gifts of monoclonal anti-actin (initial supply) and anti-SuSy (*Vicia faba*); (b) Marina Salnikova for assistance with ultramicrotomy and immunocytochemistry; (c) Trina Muehring for testing freeze substitution protocols for *Zinnia*; (d) Alison Roberts for development of the immunofluorescence digestion mixture; (e) Brett Kiedaisch for preparation of *Zinnia* cultures; (f) Larry Blanton for assistance in drawing Fig. 7; (g) the Electron Microscope Laboratory of Texas Tech University for access to instruments; and (h) NSF Plant Genomics grant R98RA1829 to D.P.D., C.H.H., and A.S.

References

Amor, Y., Haigler, C. H., Johnson, S., Wainscott, M., Delmer, D. P., 1995. A membrane-associated form of sucrose synthase and its potential role in synthesis of cellulose and callose. Proceedings of the National Academy of Sciences USA 92, 9353–9357.

Auer, M., Scarborough, G., Kühlbrandt, W., 1998. Three-dimensional map of the plasma membrane H+-ATPase in the open conformation. Nature 392, 840–843.

Blanton, R.L., Haigler, C.H., 1996. Cellulose biogenesis. In: Smallwood, M., Knox, J.P., Bowles, D.J. (Eds.), Membranes: specialized functions in plants. BIOS Scientific Pub, Oxford, UK, pp. 57–76.

Bozzola, J.J., Russell, L.D., 1999. Electron Microscopy. Jones & Bartlett, Sudbuy, MA.

Buckeridge, M.S., Vergara, C.E., Carpita, N.C., 1999. The mechanism of synthesis of mixed-linkage (1->3), (1->4) β-D-glucan in maize. Evidence for multiple sites of glucosyl transfer in the synthase complex. Plant Physiology 120, 1105–1116.

Burgess, J., Linstead, P., 1984. In-vitro tracheary element formation: structural studies and the effect of tri-iodobenzoic acid. Planta 160, 481–489.

Carlson, S.J., Chourey, P.S., 1996. Evidence for plasma membrane-associated form of sucrose synthase in maize. Molecular and General Genetics 252, 303–310.

Delmer, D.P., 1999. Celullose biosynthesis: exciting times for a difficult field of study. Annual Review of Plant Physiology 50, 245–276.

Delmer, D.P., Amor, Y., 1995. Cellulose biosynthesis. Plant Cell 7, 987–1000.

Doonan, J., Clayton, L., 1986. Immunofluorescent studies on the plant cytoskeleton. In: Wang, T.L. (Ed.), Immunology in Plant Science. Cambridge University Press, Cambridge, pp. 111–135.

Echlin, P., 1992. Low temperature microscopy and analysis. Plenum Press, New York.

Emons, A.M.C., 1991. Role of particle rosettes and terminal globules in cellulose synthesis. In: Haigler, C.H., Weimer, P.J. (Eds.), Biosynthesis and Biodegradation of Cellulose. Marcel Dekker, New York, pp. 71–98.

Falconer, M.M., Seagull, R.W., 1985. Immunofluorescent and Calcofluor white staining of developing tracheary elements in *Zinnia elegans* L. suspension cultures. Protoplasma 125, 190–198.

Falconer, M.M., Seagull, R.W., 1986. Xylogenesis in tissue culture II: microtubules, cell shape, and secondary wall patterns. Protoplasma 133, 140–148.

Fowler, J.E., Quatrano, R.S., 1997. Plant cell morphogenesis: Plasma membrane interactions with the cytoskeleton and cell wall. Annual Review of Cell and Developmental Biology 13, 697–743.

Frost, A.O., Roberts, A.W., 1996. Cortical actin filaments fragment and aggregate to form chloroplast-associated and free F-actin rings in mechanically isolated *Zinnia* mesophyll cells. Protoplasma 194, 195–207.

Fukuda, H., Komamine, A., 1980. Establishment of an experimental system for the study of tracheary element differentiation from single cells isolated from the mesophyll of *Zinnia elegans*. Plant Physiology 65, 57–60.

Haigler, C.H., Brown Jr., R.M., 1986. Transport of rosettes from the Golgi apparatus to the plasma membrane isolated mesophyll cells of *Zinnia elegans* during differentiation to tracheary elements in suspension culture. Protoplasma 134, 111–120.

Heath, I.B., Seagull, R., 1982. Oriented cellulose fibrils and the cytoskeleton: a critical comparison of models. In: Lloyd, C.W. (Ed.), The Cytoskeleton in Plant Growth and Development. Academic Press, New York, pp. 163–182.

Hepler, P.K., 1981. Morphogenesis of tracheary elements and guard cells. In: Kiermayer, O. (Ed.), Cytomorphogenesis in Plants. Springer Verlag, Berlin, pp. 327–347.

Herth, W., 1985. Plasma-membrane rosettes involved in localized wall thickening during xylem vessel formation of *Lepidium sativum* L. Planta 164, 12–21.

Herth, W., Weber, G., 1984. Occurrence of the putative cellulose-synthesizing "rosettes" in the plasma membrane of *Glycine max* suspension culture cells. Naturwissenschaften 71, 153–154.

Ingold, E., Sugiyama, M., Komamine, A., 1988. Secondary wall formation: changes in cell wall constituents during the differentiation of isolated mesophyll cells of *Zinnia elegans* to tracheary elements. Plant Cell Physiology 29, 295–303.

Kawagoe, Y., Delmer, D.P., 1997. Pathways and genes involved in cellulose biosynthesis. Genetic engineering 19, 63–87.

Kimura, S., Laosinchai, W., Itoh, T., Cui, X., Linder, R., Brown Jr., R.M., 1999. Immunogold labeling of rosette terminal cellulose-synthesizing complexes in the vascular plant *Vigna angularis*. The Plant Cell 11, 2075–2085.

Kobayashi, H., Fukuda, H., Shibaoka, H., 1987. Reorganization of actin filaments associated with the differentiation of tracheary elements in *Zinnia* mesophyll cells. Protoplasma 138, 69–71.

Kobayashi, H., Fukuda, H., Shiboka, H., 1988. Interrelation between the spatial disposition of actin filaments and microtubules during the differentiation of tracheary elements in cultured *Zinnia* cells. Protoplasma 143, 29–37.

Lancelle, S.A., Callaham, D.A., Hepler, P.K., 1986. A method for rapid freeze-fixation of plant cells. Protoplasma 131, 153–165.

Lessard, J.L., 1988. Two monoclonal antibodies to actin one muscle-selective and one generally reactive. Cell Motility and the Cytoskeleton 10, 349–362.

Mahajan, N.P., Linder, K., Berry, G., Gordon, G.W., Heim, R., Herman, G., 1998. Bcl-2 and Bax interactions in mitochondria probed with green fluorescent protein and fluorescence resonance energy transfer. Nature Biotechnology 16, 547–552.

Newman, G., Hobot, J., 1993. Resin microscopy and on-section immunocytochemistry. Springer Verlag, Berlin.

Nicolas, T.N., Bassot, J.M., 1993. Freeze substitution after fast-freeze fixation in preparation for immunocytochemistry. Microscopy Research and Technique 24, 474–487.

Reymond, O.L., Pickett-Heaps, J.D., 1983. A routine flat embedding method for electron microscopy of microorganisms allowing selection and precisely orientated sectioning of single cells by light microscopy. Journal of Microscopy 130, 79–84.

Roberts, A.W., Haigler, C.H., 1989. Rise in chlorotetracycline fluorescence accompanies tracheary element differentiation in suspension cultures of *Zinnia*. Protoplasma 152, 37–45.

Roberts, A.W., Haigler, C.H., 1990. Tracheary element differentiation in suspension cultures of *Zinnia* requires uptake of extracellular Ca^{2+}. Experiments with calcium-channel blockers and calmodulin inhibitors. Planta 180, 502–509.

Roberts, A.W., Koonce, L.T., Haigler, C.H., 1992. A simplified medium for in vitro tracheary element differentiation in mesophyll suspension cultures of *Zinnia elegans* L. Plant Cell, Tissue and Organ Culture 28, 27–35.

Seagull, R.W., 1990. The effects of microtubule and microfilament disrupting agents on cytoskeletal arrays and wall deposition in developing cotton fibers. Protoplasma 159, 44–59.

Seagull, R.W., 1991. Role of the cytoskeletal elements in organized wall microfibril deposition. In: Haigler, C.H., Weimer, P.J. (Eds.), Biosynthesis and Biodegradation of Cellulose. Marcel Dekker, New York, pp. 143–164.

Winter, H., Huber, J.L., Huber, S.C., 1998. Identification of sucrose synthase as an actin-binding protein. FEBS Letters 430, 205–208.

Winter, H., Huber, S.C., 2000. Regulation of sucrose metabolism in higher plants: localization and regulation of activity of key enzymes. Critical Reviews in Plant Science 19, 31–67.

Zhang, P., Toyoshima, C., Yonekura, K., Green, N.M., Stokes, D.L., 1998. Structure of the calcium pump from sarcoplasmic reticulum at 8 Å resolution. Nature 392, 835–839.

PERGAMON

Phytochemistry 57 (2001) 835–846

PHYTOCHEMISTRY

www.elsevier.com/locate/phytochem

Cell-wall architecture and lignin composition of wheat developed in a microgravity environment

Lanfang H. Levine[a,*], A. Gerard Heyenga[b], Howard G. Levine[a], Joon-Weon Choi[c], Laurence B. Davin[c], Abraham D. Krikorian[d], Norman G. Lewis[c,**]

[a]*Dynamac Corporation, DYN-3, Kennedy Space Center, FL 32899, USA*
[b]*Space Technology Division, NASA Ames Research Center, Moffett Field, CA 94035-1000, USA*
[c]*Institute of Biological Chemistry, Washington State University, Pullman, WA 99164-6340, USA*
[d]*Department of Biochemistry and Cell Biology, State University of New York, Stony Brook, NY 11794-5215, USA*

Received 17 July 2000; received in revised form 20 September 2000

Abstract

The microgravity environment encountered during space-flight has long been considered to affect plant growth and developmental processes, including cell wall biopolymer composition and content. As a prelude to studying how microgravity is perceived — and acted upon — by plants, it was first instructive to investigate what gross effects on plant growth and development occurred in microgravity. Thus, wheat seedlings were exposed to microgravity on board the space shuttle *Discovery* (STS-51) for a 10 day duration, and these specimens were compared with their counterparts grown on Earth under the same conditions (e.g. controls). First, the primary roots of the wheat that developed under both microgravity and 1 *g* on Earth were examined to assess the role of gravity on cellulose microfibril (CMF) organization and secondary wall thickening patterns. Using a quick freeze/deep etch technique, this revealed that the cell wall CMFs of the space-grown wheat maintained the same organization as their 1 *g*-grown counterparts. That is, in all instances, CMFs were randomly interwoven with each other in the outermost layers (farthest removed from the plasma membrane), and parallel to each other within the individual strata immediately adjacent to the plasma membranes. The CMF angle in the innermost stratum relative to the immediately adjacent stratum was ca 80° in both the space and Earth-grown plants. Second, all plants grown in microgravity had roots that grew downwards into the agar; they did not display "wandering" and upward growth as previously reported by others. Third, the space-grown wheat also developed normal protoxylem and metaxylem vessel elements with secondary thickening patterns ranging from spiral to regular pit to reticulate thickenings. Fourthly, both the space- and Earth-grown plants were essentially of the same size and height, and their lignin analyses revealed no substantial differences in their amounts and composition regardless of the gravitational field experienced, i.e. for the purposes of this study, all plants were essentially identical. These results suggest that the microgravity environment itself at best only slightly affected either cell wall biopolymer synthesis or the deposition of CMFs, in contrast to previous assertions. © 2001 Published by Elsevier Science Ltd. All rights reserved.

Keywords: *Triticum aestivum* L., Wheat; Gramineae; Space flight; Microfibrils; Secondary wall; Lignin; Microgravity

1. Introduction

Plant cell walls perform critical functions in plant development and survival (Taylor et al., 1992). Although the underlying reasons are poorly understood, the phenomena of differential syntheses of the various polymeric cell wall components and their concomitant organization into cell walls of distinct types are fundamental to plant morphogenesis and differentiation (Cosgrove, 1997; Hable et al., 1998; Lewis et al., 1999; Croteau et al., 2000). The cell wall helps control the direction of cell expansion through orientation of cellulose microfibrils (CMF), and also provides mechanical reinforcement through deposition of an additional layer of cellulose onto the primary wall. Then, depending upon the cell type being sculptured, subsequent impregnation and reinforcement by hemicelluloses and lignins can occur. For example, in tracheary and vessel elements, the

* Corresponding author. Tel.: +1-321-476-4269; fax: +1-321-853-4165.
E-mail address: lanfang.levine-1@ksc.nasa.gov (L.H. Levine).
** Corresponding author. Tel.: +1-509-335-8382; fax: +1-509-335-8206.
E-mail address: lewisn@wsu.edu (N.G. Lewis).

0031-9422/01/$ - see front matter © 2001 Published by Elsevier Science Ltd. All rights reserved.
PII: S0031-9422(01)00148-0

secondary thickenings arise in cell-specific patterns and ultimately allow effective water transportation upward against the gravitational force vector. Therefore, the investigation of cell wall formation and structure in an environment where the gravitational force is essentially absent or greatly diminished could be anticipated to yield important insight into how gravity impacts upon these processes. In early space-flight experiments, it was reported that cell wall assembly processes, including cellulose microfibril orientation and lignin composition and amount, were adversely affected in the microgravity environment (reviewed in Halstead and Dutcher, 1987) Additionally, the reports therein also indicated that various root tissues became disoriented, with all of these observations being related to the direct effect of microgravity.

Many environmental factors and chemical perturbations have been shown to alter the ultrastructure of the cell wall (Hogetsu and Shibaoka, 1978a; Lang et al., 1982; Roberts et al., 1985; Pritchard et al., 1993; Sauter et al., 1993). However, the effect of gravity on cell wall morphology is poorly understood due to the fact that gravitational forces cannot typically be eliminated (for extended durations) on Earth. A few qualitative observations concerning cell wall formation indicate that the cell wall was thinner and the cellulose microfibril organization was disturbed in the absence of gravity (Halstead and Dutcher, 1987; Claassen and Spooner, 1994). A recent study also demonstrated that a clinostat-based simulation of weightlessness decreased the percentage of *Brassica* protoplasts with cortical microtubules organized in parallel (Skagen and Iversen, 1999). However, the evidence of these growth patterns after exposure to microgravity is far from conclusive, and it was thus deemed important to ascertain the effects of the microgravity environment on the growth of wheat (*Triticum aestivum*) seedlings.

This paper thus presents the results of a space-flight experiment relevant to these cell wall-related questions: (i) Does greatly diminishing the gravitation vector (e.g. in microgravity in space) alter CMF organization and cell wall (including lignin) composition? (ii) Is the secondary wall thickening pattern modified in microgravity? Clarification to both questions is fundamental not just in delineating how gravity affects plant growth and development (e.g. cell wall formation and structure), but also in determining the suitability of plant growth in the microgravity environment during space exploration and utilization.

2. Results and discussion

2.1. *T. aestivum* plant growth and development

The growth in space (microgravity) of vascular plants and their subsequent study on Earth resulted in numerous reports claiming an enormous number of aberrations in various plant species, e.g. in terms of effects on the overall growth, the root orientation(s), the cell wall assembly processes and the biopolymer compositions — including lignin content reduction — as well as alterations in metabolic profiles (Cowles et al., 1984; reviewed in Halstead and Dutcher, 1987). However, these experiments were carried out during the initial stages of space exploration, and questions regarding the effects of nutrient and water transport were then unknown.

For this study, we considered it essential to devise a growth system whereby continual provision of water and nutrients could be assured for experimentation in a microgravity environment and for the corresponding 1 *g* controls. This was because of a growing concern that we had regarding some of the changes being claimed for the microgravity environment, which we rationalized might be due to stresses introduced as a consequence of an inadequate water/nutrient supply delivery while in microgravity (space-flight).

NASA utilizes a so-called plant growth unit (PGU) for growing plants in space, but which has no effective mechanism for adding water/nutrients as needed. We, therefore, designed a so-called nutrient pack (Fig. 1A) for continual growth of wheat (*T. aestivum*) from seed to seed. In this way, during a so-called pre-flight payload verification test (PVT), it was established that for the duration of the proposed space-flight (10 days), the plants grew "normally" following seed germination. That is, the sterilized germinated seeds were placed in the nutrient packs within the PGU and grew without provision of additional water and/or nutrients.

In the corresponding space-flight conditions, the plants (at the germinating stage) were placed in the PGU which was then loaded onto the space shuttle *Discovery*, and following lift-off were permitted to grow for 10 days, when the plants returned to Earth for analysis. A corresponding control experiment, carried out on Earth under identical growth conditions experienced during space-flight except for the gravitational vector, was started 1-h later.

As can be seen in Fig. 1B and C, both sets of plants grew "normally," and there were no obvious or significant differences in either the volume or mass of biomass produced (see Table 1). Additionally, the roots grew downwards (relative to the photosynthetic canopy) within either the agar medium (see Fig. 1D for an example) or alternately on nitex-foam. Consequently, these results contrasted markedly with other plant growth experiments, one of whose main differences was that previous studies had been conducted under conditions where no reliable provision of water/nutrients in microgravity had occurred. Thus, having observed no significant differences in vegetative growth profiles, it was next of interest to establish whether cell wall architecture or lignin contents were adversely affected or not.

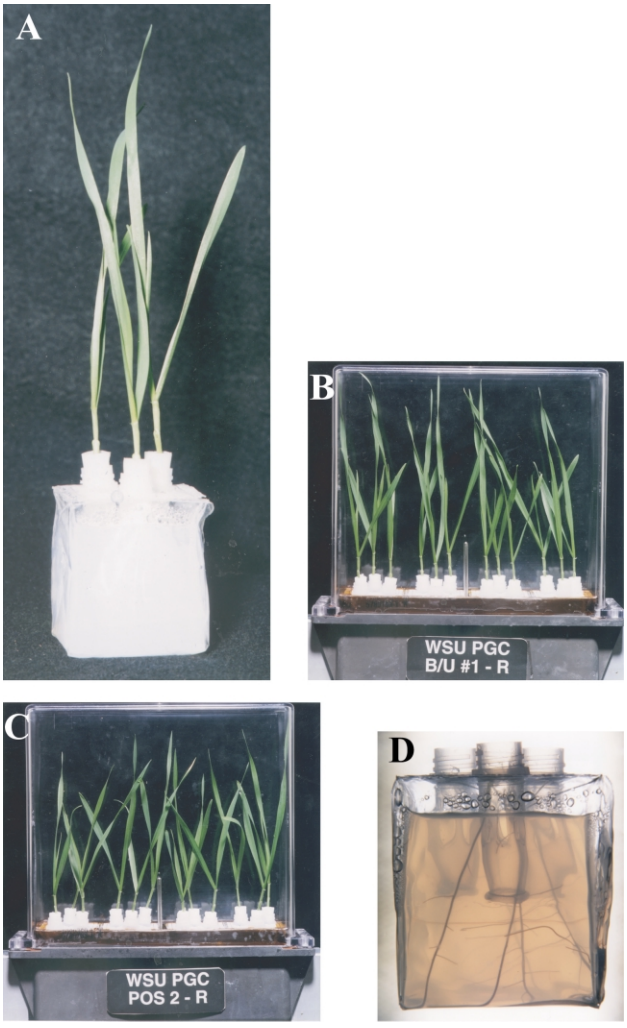

Fig. 1. Nutrient pack (A). Wheat grown (B) on Earth (1 *g* control) and (C) in microgravity aboard the space shuttle *Discovery* during the STS51 mission, as well as (D) the root sections that were also grown in space.

2.2. Cellulose microfibril (CMF) organization in cortical parenchyma cell walls of T. aestivum

The freeze-fracture/deep-etch technique (Hawes and Martin, 1986) was employed in order to visualize orientation patterns of CMFs in different strata of wheat plant cell walls. As described in the Experimental section, the tissues were pretreated with methylamine before freeze-fracture to remove non-cellulosic carbohydrates: Figs. 2 and 3 show representative electron micrographs of platinum/carbon replicates of the outer and inner surfaces of cortical parenchyma cell walls. The samples of the outer strata of the cortical parenchyma cell walls taken from the microgravity-exposed wheat primary roots were selected in such a way as to ensure that they came from tissue completely developed in space. Nevertheless, these tissues were essentially identical to those from the 1 *g*-developed cell wall controls (Fig. 2A and B), i.e. the microfibrils had no predominant orientation, and were interwoven with each other. It is well known that there are disordered microfibrils in the outer strata of the cell wall, as well as cell walls of isodiametric cells such as in suspension cultures of Earth-grown plants (Hogetsu and Shibaoka, 1978b; Satiat-Jeunemaitre et al., 1992; Carpita and Gibeaut, 1993). The same applies to wheat cell walls grown in space (microgravity).

In contrast to the outer layers, a higher order of cellulose microfibril organization was observed within the cell wall layers adjacent to the plasma membrane in both the Earth-grown and microgravity (space-flight) wheat (Fig. 3A and B). Microfibrils within any one layer were parallel to each other and regularly spaced, although their orientation underwent an abrupt change relative to the adjacent layers. Although the mechanism by which CMF orientation shifts from one layer to another is still worthy of debate, this arrangement is a typical feature of the helicoidal wall (Lang et al., 1982; Roland et al., 1987), and was not disrupted by the microgravity environment. Examination of the plants grown in both agar-based and nitex-foam media under microgravity gave essentially the same result. This contrasts markedly to previous reports (Sytnik et al., cited in Halstead and Dutcher, 1987).

Furthermore, the tissue before methylamine treatment was also examined to ensure the treatment does not induce any artifacts. Successful fracture and replication of the inner surfaces of cortical parenchyma cells gave rise to the same ordered arrangement of the CMFs (Fig. 4) as that of the treated tissue. However, under these conditions, the individual microfibril bundles were less distinct: i.e. they were flatter due to the presence of non-cellulosic embedding materials. Notably, as expected, the untreated tissue did not give large fracture surfaces, especially between cells.

In an effort to quantify the offset of CMF orientation between adjacent strata, electron microscopic images were next digitized and analyzed. Cell walls of primary roots grown in the agar-nutrient pack exhibited statistically indistinguishable relative microfibril angles of 82 ± 4.87 and 76 ± 11.06 for microgravity and 1 *g* grown plants respectively (data not shown). The result for the

Table 1
Growth characteristics of wheat (*Triticum aestivum*) plants grown on space aboard shuttle *Discovery* and on Earth

	Shoot length (cm)	Shoot weight (g)	Root length (cm)	Root weight (g)
Flight	14.23 ± 1.25	0.20 ± 0.03	13.18 ± 4.26	0.26 ± 0.08
Control	15.13 ± 1.61	0.20 ± 0.03	11.99 ± 3.71	0.23 ± 0.08

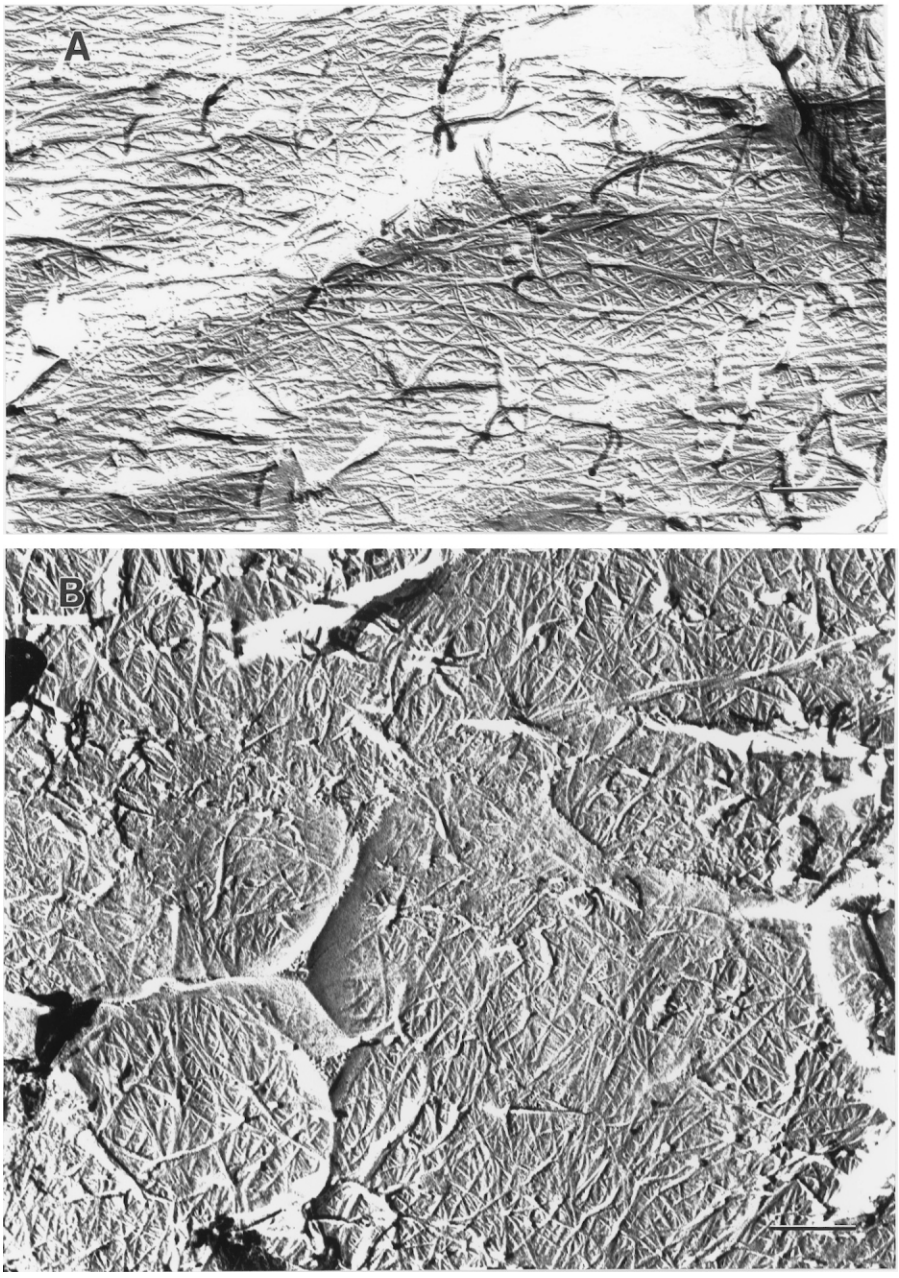

Fig. 2. Cellulose microfibril organization in the outer strata of cortical parenchyma cells of wheat primary roots developed under 1 *g* on Earth (A) and in microgravity (B), scale bar: 0.25 μm.

foam-nitex grown wheat was similar. Although no attempt was made to determine the absolute orientation of CMFs relative to the cell axis, one can assume that the microfibrils on those load-bearing (innermost) layers had a helical pattern, i.e. this offset suggests an oblique (within a ca 40 degree angle) orientation of the CMFs. These results imply that microgravity and its associated conditions do not perturb the deposition of ordered CMFs in the primary walls of wheat. This is contrary to the observation of Sytnik et al. (cited in Halstead and Dutcher, 1987) in which cellulose microfibrils were claimed to be randomized in relation to the longitudinal axis of cells developed under microgravity conditions.

Further interpretation of these observations requires consideration of the hypothetical mechanism by which CMF orientation is governed, and of the roles of CMFs in controlling cell growth and cell anisotropy. CMFs are precisely deposited onto cell walls through the guidance of underlying cortical microtubules (MTs) (Cyr, 1994; Wymer and Lloyd, 1996; Hable et al., 1998), and hence provide the mechanical strength to withstand isotropic turgor pressure and to permit preferential cell expansion in one direction (growth anisotropy). Thus, the ability of CMFs to control anisotropic growth lies in their mechanically anisotropic behavior, i.e. the cellulose macromolecules have higher tensile moduli and greater

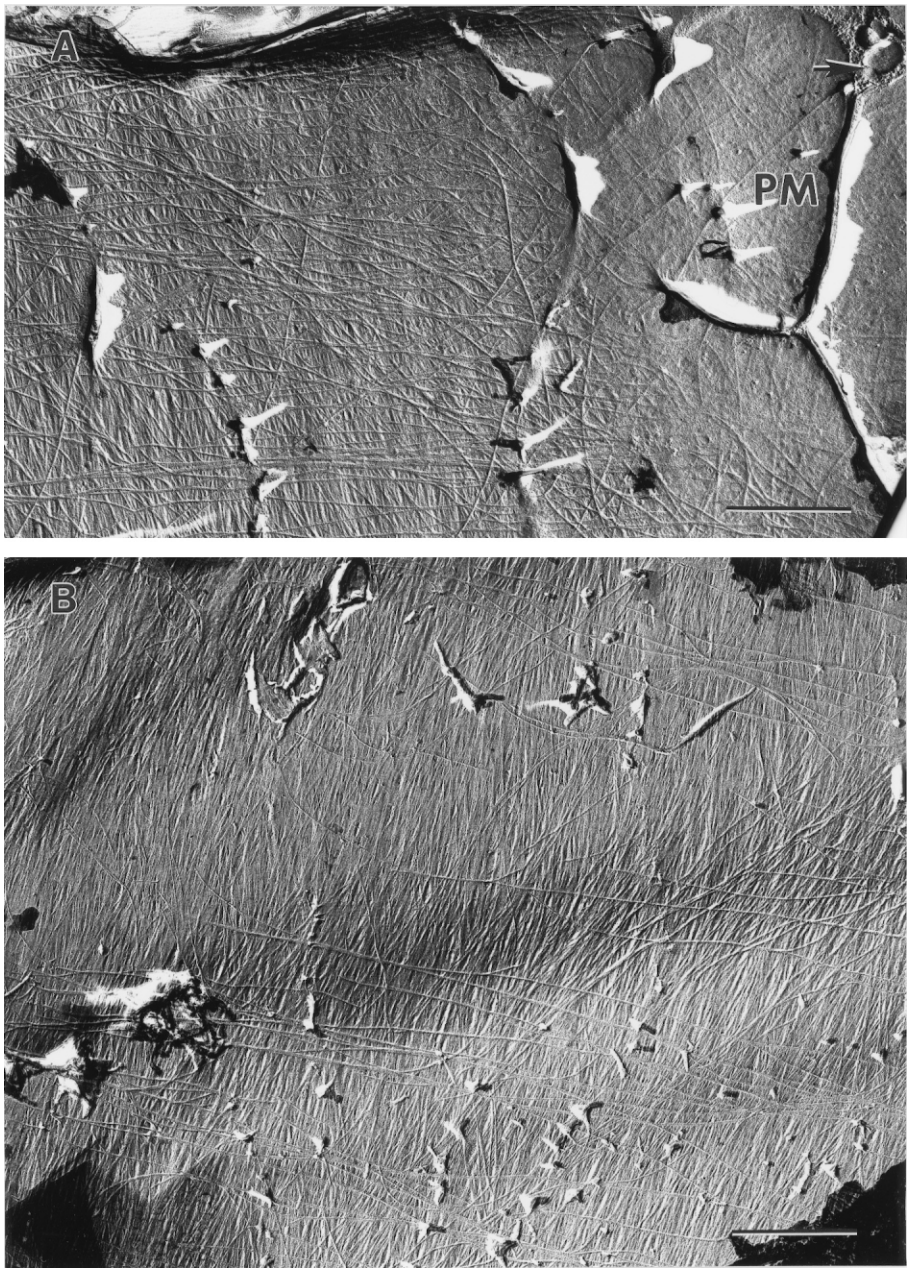

Fig. 3. Cellulose microfibril organization in the inner strata (facing the plasma membrane, PM) of cortical parenchyma cells of wheat primary roots developed under 1 *g* on Earth (A) and microgravity (B), scale bar: 0.5 μm.

tensile strength when stressed along their longitudinal axes than when stressed along the transverse axis (Niklas, 1992). Anisotropic expansion is also characterized by the direction in which maximal expansion rate occurs and in the degree to which this exceeds the minimal rate. The preponderance of evidence, therefore, suggests that the direction of maximal expansion is dictated by the mean orientation of the CMFs (Baskin et al., 1999 and references cited within), whereas the randomly oriented CMFs physically restrict directional expansion. Ordered cellulose microfibrils are also essential for directional expansion and proper differentiation. The fact that mature cells in space-grown wheat were properly elongated (Fig. 6) also supports the observation of well-organized CMFs with a preferred orientation.

Yet, previous studies under microgravity had suggested that mitotic activity in the root meristem following space flight was reduced (Krikorian et al., 1992; Claassen and Spooner, 1994). However, given that plant growth principally relies upon cell division and cell expansion, then if cellulose synthesis and CMF organization were dramatically disrupted by microgravity, it would be anticipated that cell elongation would have correspondingly been inhibited and the primary roots would have been shorter than their Earth-grown counterparts. On the contrary, the roots of the space-grown

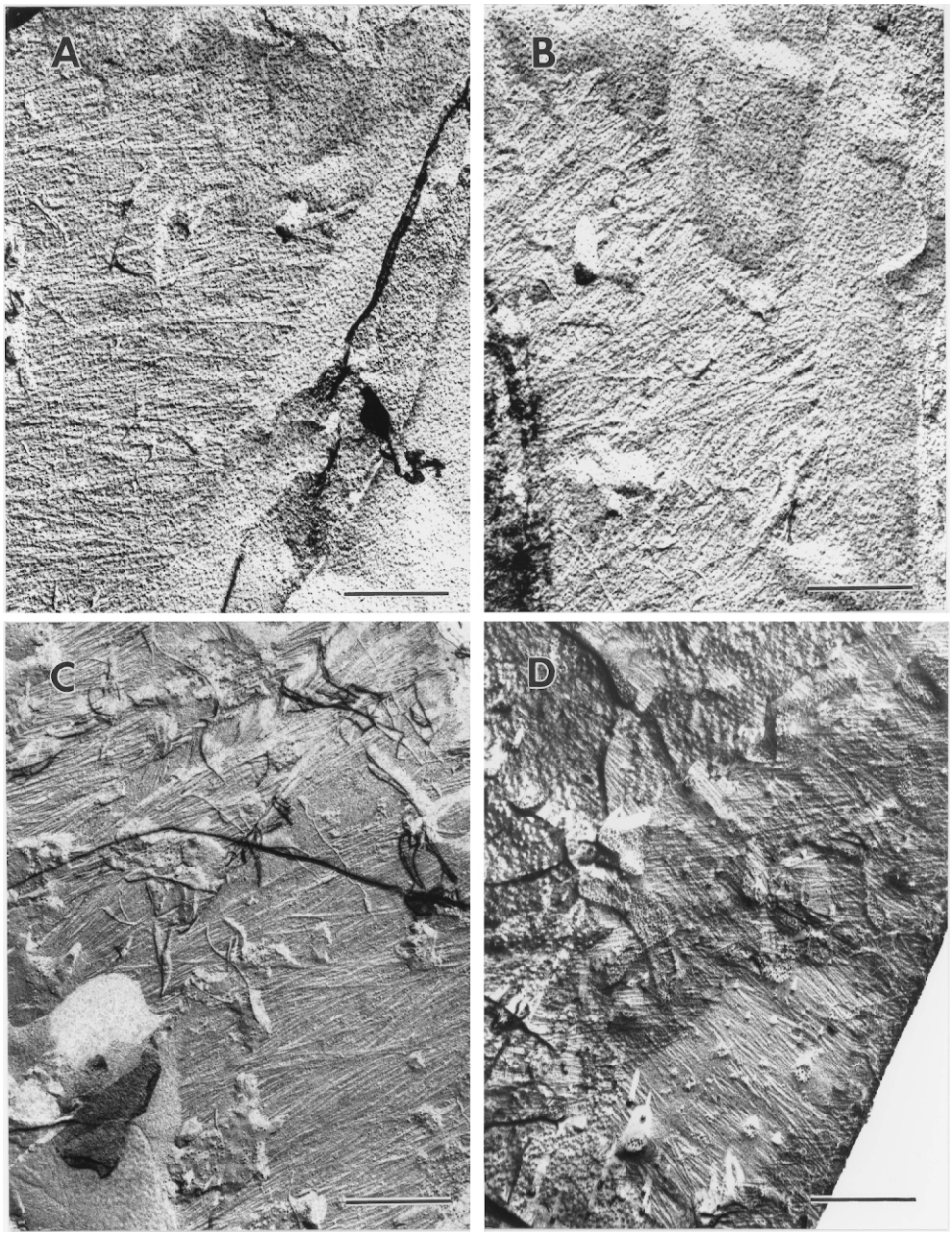

Fig. 4. Replicas of CMF arrangement on the innermost layer of untreated primary walls of cortical parenchyma cells in wheat primary roots developed under 1 *g* on Earth (A and B) and in microgravity (C and D), scale bar: 0.5 μm.

wheat were not significantly different from their Earth-grown controls (13.18 cm±4.26 vs. 11.99 cm±3.71, respectively). Furthermore, instances of even longer root lengths being formed under space-flight conditions, relative to the 1 *g* controls, have been reported (Levine et al., 1991, 2000; Levine and Krikorian, 1992).

2.3. *T. aestivum* secondary wall thickening patterns in water-conducting elements

Fig. 5A and B present transmission electron microscopy views of the cross-section of a vessel element and an adjacent parenchyma cell wall from ground and space-grown wheat roots, respectively. There is extensive thickening of the secondary wall (SW) in both vessel elements. The SW is slightly thinner in the space-developed vessel element in the micrographs shown, but the inherent variability in thickening over the entire surface of the primary walls negates any ability to claim significance in this respect. Serial longitudinal sections (Fig. 6) also revealed uneven secondary thickenings (as indicated by arrows) for both Earth- (1 *g*) and microgravity-grown plants. Three distinct types of thickenings were observed in both the space- and Earth-grown plants (Fig. 6), i.e. ring or spiral, regularly pitted and reticulate patterns. It seems that a single protoxylem

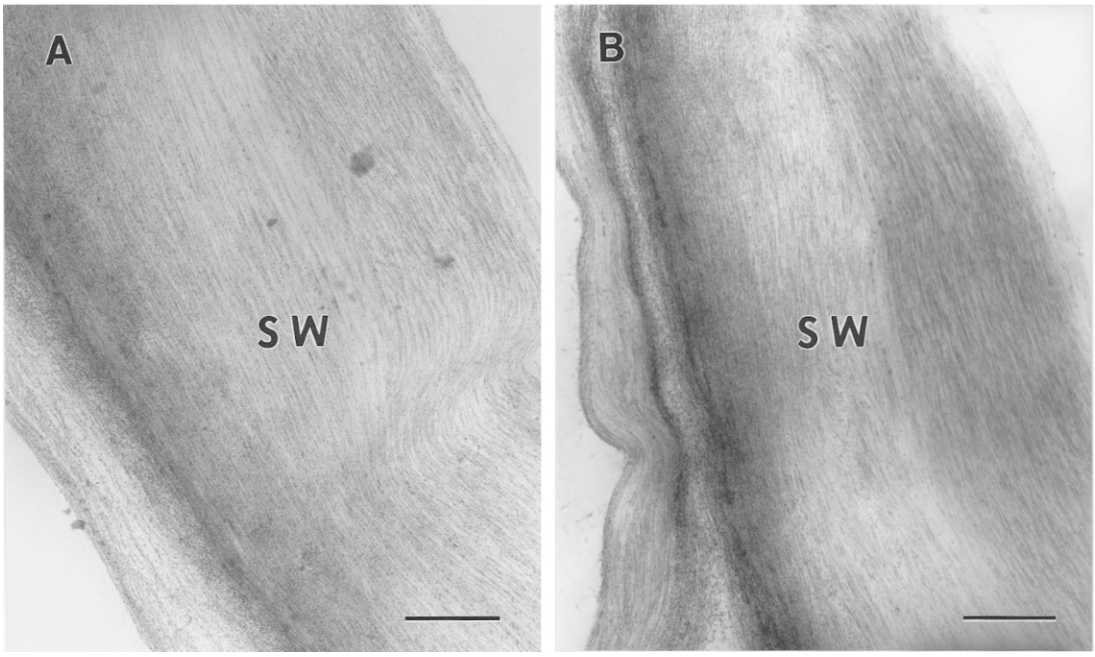

Fig. 5. Cross-sections of a vessel element and an adjacent parenchyma cell wall of wheat primary roots developed under 1 *g* on Earth (A) and in microgravity (B), scale bar: 0.5 μm.

vessel element has different patterns from one end to another (Fig. 6C), a feature commonly noted in plants (Hogetsu, 1991).

Next, a three-dimensional visualization of the secondary wall thickenings of both Earth- (1 *g*) and microgravity-grown wheat plants, was obtained by tissue maceration of the primary roots followed by staining with a fluorescent dye (see Experimental Section and Fig. 7). This method verified not only the thickenings in the protoxylem, but also allowed the examination of a broad range of distinctive vessel elements. Metaxylem vessels of larger diameter exhibited reticulate thickenings in the lateral walls (Fig. 7A and D), whereas medium sized vessel elements had both regularly arranged pits and randomly distributed pits (Fig. 7B and E). The protoxylem vessels, by contrast, had lattice thickenings (Fig. 7C and F) in addition to spiral thickenings (data not shown). Importantly, no twisted, deformed or mutated patterns of cell wall assembly were found in space-developed cell walls relative to those from ground control plants. However, the intensity of the fluorescent stain on the space-developed cell walls was less intense, as indicated by lower levels of contrast in the micrographs (Fig. 7D, E and F). This may be an indication of reduced cellulose deposition and thinner secondary walls in the space-grown wheat.

The secondary wall is an additional layer of cellulose deposited onto the primary wall with impregnation by hemicellulose and lignin to reinforce a specific group of cells (such as vessel elements). Carbohydrate synthesis is a key component in secondary wall formation. Previous studies demonstrated that the treatment of differentiating *Zinnia* cells with a cellulose synthesis inhibitor (2,6-dichlorobenzonitrile, DCB) results in less significant and less regular secondary thickenings (Suzuki et al., 1992; Taylor et al., 1992). Furthermore, the presence of the microtubule-disrupting agent, amiprophosmethyl, disrupted the deposition of cellulose and hemicellulose, resulting in deformed secondary thickening patterns in tracheary elements of *Pisum* roots and epicotyl and *Commelina* roots (Hogetsu, 1991). Therefore, the finding of normal thickenings in the water conducting elements of space-grown primary roots could be an indication that neither cell wall biopolymer synthesis nor microtubule assembly and functions involved in secondary thickenings were adversely affected by the microgravity environment to any appreciable extent. These results also imply that cells grown under microgravity conditions undergo successful differentiation according to their predetermined functions.

2.4. Lignin analyses of *T. aestivum* leaves and roots

It was next deemed instructive to ascertain the lignin content, determined as % acetyl bromide lignin (Iiyama and Wallis, 1990), and the lignin monomeric composition, using the thioacidolysis procedure (Lapierre et al., 1985), to determine relative amounts of guaiacyl and syringyl moieties (Table 2). The results obtained for removal of extractives, gave higher yields for flight-grown shoots and roots relative to Earth-grown plants. By contrast, acetyl bromide lignin determinations of the flight grown tissues were very slightly lower (~7%) than that of the Earth-grown counterparts, and not statistically

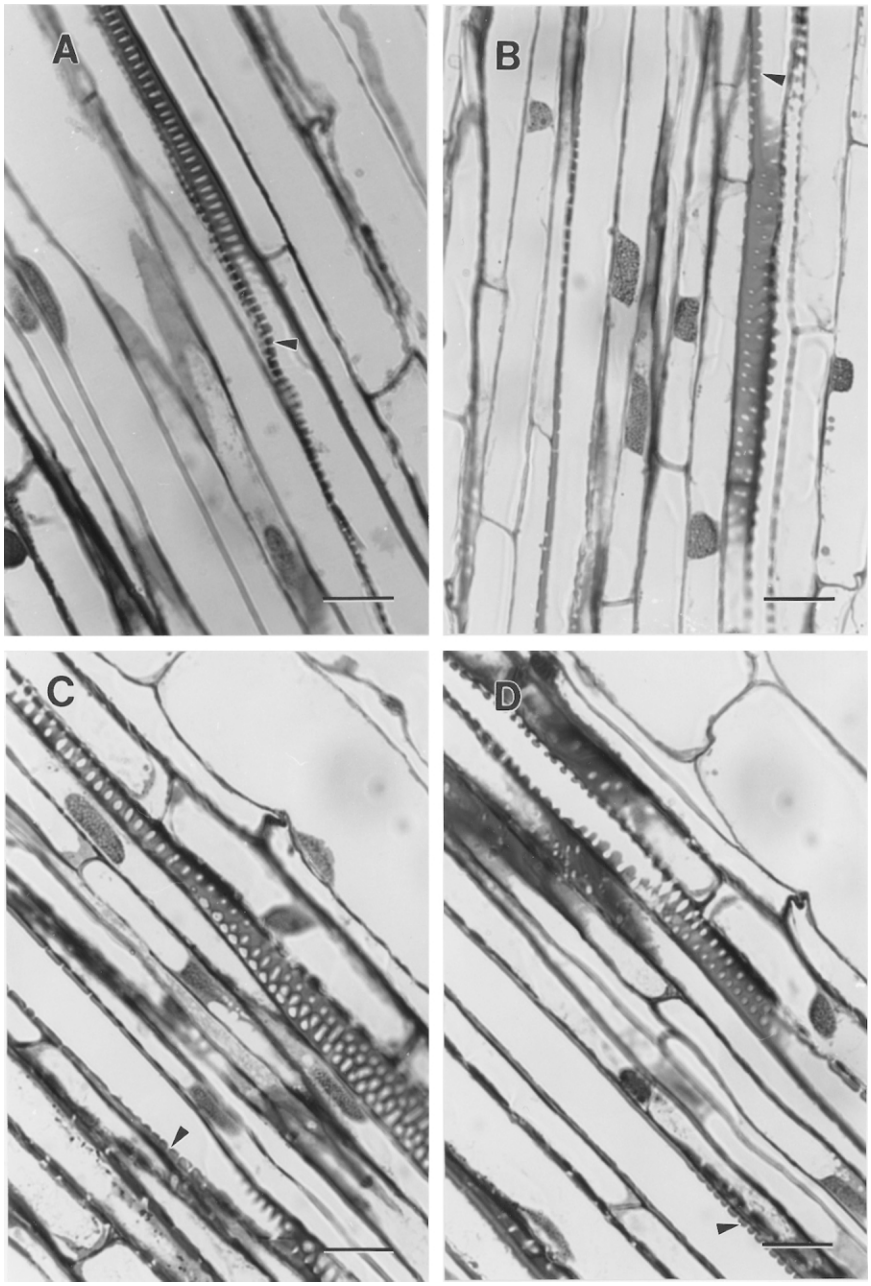

Fig. 6. Longitudinal sections of wheat primary roots revealing secondary thickening patterns developed under 1 *g* on Earth (A and B) and in microgravity (C and D), scale bar: 20 μm.

very different. Thioacidolysis also revealed that the *S*/*G* ratio for both shoots and roots were essentially the same. In conclusion, there were no substantial differences in either lignin contents or composition.

2.5. Concluding remarks

We report herein on several aspects of cell wall formation under microgravity conditions. Primary roots of wheat developed under space-flight conditions possessed normal primary and secondary wall frameworks, i.e. equivalent to those noted at 1 *g*, with lignin contents and compositions only slightly changed relative to the 1 *g* counterparts. It is possible, that while seedlings initiated on Earth did not exhibit any microgravity effects during the course of these relatively short space shuttle missions, a different result might be obtained for either seedlings actually initiated in space and/or grown for much longer duration. In addition, there may be multiple gravisensing thresholds which come into effect for different graviresponses. Note also that while the convention is to refer to the gravitational environment on a space shuttle as a microgravity (10^{-6} *g*) environment, in reality the term milligravity (10^{-3}–10^{-4} *g*) may be more appropriate (Krikorian and Levine, 1991). Thus, we cannot eliminate the possibility that more striking

Fig. 7. Fluorescence-stained whole cell mounts demonstrating reticulate, regular pits and latticed secondary thickenings of metaxylem, medium-sized and protoxylem vessel elements from wheat primary roots grown under 1g (A–C) and microgravity conditions (D–F), scale bar: 40 μm.

Table 2
Lignin content and compositional analyses of wheat (*Triticum aestivum*) plants grown in space aboard space shuttle *Discovery* and on Earth

	Extractives (%)	Lignin content (%)	*S*/*G* ratio
Flight			
Shoots	63.6	9.15±0.18	0.145
Roots	75.8	11.72±0.28	0.380
Control (1 g)			
Shoots	41.0	10.32±0.33	0.150
Roots	70.2	12.04±0.26	0.430

responses would have been evident under conditions closer to a zero *g* environment. Finally, metabolic and morphological responses may differ based upon the physiological state of the plant when the critical stimulus is exerted. Given these variable factors, this may in part explain some of the conflicting results obtained from previous space flight experiments which were conducted using different species at different life stages and using different protocols and hardware. Clearly, more studies are required in order to dissect and explain the role that gravity has in plant growth and development. However, a growth and development system has now been developed to study these processes, and to help identify what effects the microgravity environment has.

3. Experimental

3.1. Plant material

Dwarf wheat (*Triticum aestivum*, var. Super Dwarf) seeds obtained as a gift from Dr. Bruce Bugbee (Crop

Physiology laboratory, Utah State University, Logan) were planted in Washington State University greenhouse facilities, grown to maturation and the seeds harvested. The corresponding seeds were then used in all further experiments.

3.2. Plant growth unit (PGU)

The plant growth unit (PGU) used in this experiment is as described in Kwon et al. (2001).

3.3. "Nutrient pack" for support of T. aestivum growth and development

A nutrient support system was designed in order to immobilize the nutrients and water in a gel matrix, and this configuration was named "nutrient pack" (see Fig. 1A).

The non-media components of the "nutrient pack" consist of the medium enclosure membranes, prepared from 55 μm gauge autoclavable polypropylene film, fused with a 24 mm 0.02 μm-disc gas diffusion membrane (Sun bags, Sigma). This material was sectioned and heat sealed to form square packs (4.2×4.5×6.5 cm; L×W×H), with the diffusion membrane positioned in the upper face of the pack. The upper face was also used to incorporate three open ended columns (3.0 cm in length; prepared from 1.5 ml polypropylene Eppendorf tubes). Each column was sectioned with 8 longitudinal slits (15×1.0 mm) to provide mechanical support for the germination media plug on which the seeds are originally planted.

Four empty packs were autoclaved in each PGC. Under aseptic conditions, 50 ml of enriched medium (see composition below) were added to each pack and allowed to set before a further addition of normal strength medium (50–60 ml, see composition below) leaving an air phase of ca 1.0 cm in depth. Columns prepared with solidified germination medium (see composition below) were finally secured to the upper face of the nutrient pack and partially submerged to a depth of 1.0–1.5 cm into the normal strength medium.

3.4. Nutrient media

3.4.1. Normal strength medium

Macroelements: $CaNO_3$ (4 mM), KNO_3 (6 mM), $MgSO_4$ (2.0 mM), KCl (0.32 mM), NaH_2PO_4 (0.81 mM), and KH_2PO_4 (0.93 mM).

Microelements: H_3BO_3 (24.25 μM), $MnSO_4$ (13.24 μM), $ZnSO_4$ (13.92 μM), Na_2MoO_4 (1.03 μM), $CuSO_4$ (0.4 μM), $CoCl_2$ (0.105 μM), KI (4.52 μM), NaFe-EDTA (2.7 μM), and $FeSO_4$ (5.0 μM).

The pH of the medium was adjusted to 5.6 (NaOH, 100 mM) and 1.0% (w/v) agar was added prior to autoclaving for 20 min.

3.4.2. Enriched medium

This medium was prepared as above but with KNO_3 (9.0 mM), NaFe-EDTA (5.4 μM) and $FeSO_4$ (10.0 μM).

3.4.3. Germination medium

This medium consisted of 0.7% agar only.

3.5. T. aestivum seed germination and transfer of germinated seeds to the plant growth chamber (PGC)

Seeds were sterilized in a 25% (v/v) aqueous solution of bleach (6.25% sodium hypochlorite) containing 2% (v/v) Triton X100 for 10 min then washed with sterile distilled water (5 times). The seeds were next transferred to Petri dishes (24 seeds/dish) containing the normal strength medium diluted 1:1 with H_2O and these were placed in an incubator at 25° in the dark. After 2 days, the germinated seeds were individually transferred to "nutrient agar plugs", with the emerging shoot placed in a vertical position. Two days later the nutrient agar plugs were inserted into the support column of the nutrient bag. The PGC was then closed and transferred to the PGU.

3.6. Payload verification test

The PGU was placed in the orbiter environmental simulator (OES) which uses space shuttle calibrated ancillary data (CAS) to mimic the middeck environment. Following a 9-day mission the PGU was removed from the OES, photographs were taken, and the plants were harvested and fixed as described in Section 3.8.

3.7. Flight experiment

On day 1 (11:00 am), the nutrient agar plugs were inserted into the support columns of the nutrient packs. Two PGCs were prepared under these conditions. Wheat plants were also grown in a foam-nitex matrix (2 other PGC's) as described in Tripathy et al. (1996). The PGCs were closed, photographs were taken, and then transferred to the PGU. The PGU was stored in the orbiter environmental simulator until 4:30 PM where it was taken and stowed in the space shuttle *Discovery*. *Discovery* took off on day 2 at 7:45 am EDT at Cape Canaveral, FL, and returned to Earth after 9 days, 20 h, 11 min, 11 s. Seedlings were allowed to grow under continuous light, with an intensity of 30–60 μmol sec^{-1} m^{-2}, and at a temperature range of 22–26°C.

3.8. Space-grown T. aestivum tissue fixation

Plants were harvested within 3–4 h following landing at Kennedy Space Center. Four representative wheat plants grown in the "nutrient pack" and 6 in the foam-nitex matrix were chosen. Segments (2–3 mm long) of

primary roots were dissected from a point one centimeter basal to the root tips, thereby assuring that growth had occurred during the space flight. The segments were immediately immersed in fixative containing 3% glutaraldehyde and 2% paraformaldehyde in PIPES buffer (1,4-piperazinediethanesulfonic acid, 100 mM, pH 7.4) and placed at 4°C until further processing.

3.9. Postfixation and embedding

Chemically fixed plant tissues were rinsed with 0.1 M PIPES buffer and postfixed in 1% osmium tetraoxide overnight at 4°C. Specimens were thoroughly rinsed and dehydrated with an alcohol series (30, 50, 70, 80, 95 and 100% × 2). The dehydrated specimens were infiltrated with Spurr's resin and embedded by heating the resin at 70°C overnight. Longitudinal sections (1 μm thick) of the wheat roots were prepared and stained with methylene-blue. Sections were observed using an Olympus BH2 microscope, and micrographs were recorded on Technical pan 100 black-white film.

3.10. Freeze-fracture/transmission electron microscopy

Prefixed root tissues were further cut into short segments (1–2 mm) and treated with methylamine for 18 h. The root segments were next placed onto a Balzers specimen holder using starch paste (1 g/1.5 ml), then quickly immersed into liquid nitrogen cooled Cryokwik (dichlorodifluoromethane, CCl_2F_2) slurry for 30 sec. Frozen specimens were carefully but rapidly transferred to a precooled (−140°C) Balzers specimen stage in a freeze-etch unit (BA-360 M), fractured at −120°C, and etched for 15 min at −110°C under 10^{-6} Torr. Exposed etched surfaces were replicated by shadowing with platinum/carbon at an angle of 30–40° and backed with deposition of carbon at an angle of 90°. The replicas were floated onto distilled water and subsequently transferred to 30% chromic acid (v/v) to digest away tissue remnants. These were then thoroughly washed with distilled water and loaded onto formvar-coated 200-mesh grids (Ted Pella, Inc.). The platinum/carbon cell wall replicas were observed with a Hitachi H-600 at 100 kV and photographed with Kodak film 4489.

3.11. Measurement of microfibril angle

Digitized versions of micrographs were analyzed for the relative angle of the cellulose microfibrils in adjacent cell wall layers using the NIH Image 1.54 image processing program in a manner similar to that described by Seagull (1992). Micrographs of 3–5 replicates were measured. The mean microfibrillar angles for both layers within each micrograph were then used to calculate the angular offset between the two layers. Thus each micrograph yielded one final value reflecting the degree to which the two microfibril layers were offset from one another.

3.12. Whole cell mounts and fluorescence microscopy

Excised wheat root segments were macerated in a solution of HCl-95% ethanol (1:3) at room temperature for 24 h followed by an additional 2 h treatment at 70°C. The tissue was then rinsed with distilled water thoroughly and stained with 0.01% (wt/v) Fluorescent brightener 28 (Sigma) for 30 s. Samples were placed onto a microscope slide in a drop of 50% glycerol and squashed gently with a coverslip. Observations were made with an Olympus BH 2 microscope equipped with epifluorescence optics and using a blue-filter package. Micrographs were recorded using an Olympus PM 20 automatic exposure unit on TMAX 400 film.

3.13. Lignin analyses

Aerial portions and roots of plants grown both in space and on Earth (control) were freeze dried and reduced to a powder by means of a ball-mill. Aerial portions (~200 mg) and roots (~50–60 mg) were sequentially extracted with water, ethanol, and toluene/ethanol (1:1) as described in Yahiaoui et al. (1998). The resulting extracted residue was dried and subjected to both acetyl bromide (Iiyama and Wallis, 1990) and thioacidolysis (Lapierre et al., 1985; Blee et al., 2001) analyses, respectively.

Acknowledgements

The authors wish to thank NASA (NAG10-0086, NAG10-0164, NAS10-12180) for financial support for this study.

References

Baskin, T.I., Meekes, H.T.H.M., Liang, B.M., Sharp, R.E., 1999. Regulation of growth anisotropy in well-watered and water-stressed maize roots. II. Role of cortical microtubules and cellulose microfibrils. Plant Physiology 119, 681–692.

Blee, K., Choi, J.W., O'Connell, A.P., Jupe, S.C., Schuch, W., Lewis, N.G., Bolwell, G.P., 2001. Antisense and sense expression of cDNA coding for CYP3A15, a class II cinnamate 4-hydroxylase, leads to a delayed and reduced production of lignin in tobacco. Phytochemistry 57, in press.

Carpita, N.C., Gibeaut, D.M., 1993. Structural models of primary cell walls in flowering plants: consistency of molecular structure with the physical properties of the walls during growth. The Plant Journal 3, 1–30.

Claassen, D.E., Spooner, B.S., 1994. Impact of altered gravity on aspects of cell biology. International Review of Cytology 156, 301–373.

Cosgrove, D.J., 1997. Relaxation in a high-stress environment: the molecular bases of extensible cell walls and cell enlargement. The Plant Cell 9, 1031–1041.

Cowles, J.R., Scheld, H.W., Lemay, R., Peterson, C., 1984. Growth and lignification in seedlings exposed to eight days of microgravity. Annals of Botany 54, 33–48.

Croteau, R., Kutchan, T.M., Lewis, N.G., 2000. Secondary metabolites. In: Buchanan, B.B., Gruissem, W., Jones, R.L. (Eds.), Biochemistry and Molecular Biology of Plants. American Society of Plant Physiologists, Rockville, MD, pp. 1250–1318.

Cyr, R.J., 1994. Microtubules in plant morphogenesis: role of the cortical array. Annual Review of Cell Biology 19, 153–180.

Hable, W.E., Bisgrove, S.R., Kropf, D.L., 1998. To shape a plant — the cytoskeleton in plant morphogenesis. The Plant Cell 10, 1772–1774.

Halstead, T.W., Dutcher, F.R., 1987. Plants in space. Annual Review of Plant Physiology 38, 317–345.

Hawes, C., Martin, B., 1986. Deep etching of plant cells: cytoskeleton and coated pits. Cell Biology International Reports 10, 985–992.

Hogetsu, T., 1991. Mechanism for formation of the secondary wall thickening in tracheary elements: microtubules and microfibrils of tracheary elements of *Pisum sativum* L., *Commelina communis* L., the effects of amiprophosmethyl. Planta 185, 190–200.

Hogetsu, T., Shibaoka, H., 1978a. Effects of colchicine on cell shape and on microfibril arrangement in the cell wall of *Closterium acerosum*. Planta 140, 15–18.

Hogetsu, T., Shibaoka, H., 1978b. The change of pattern in microfibril arrangement on the inner surface of the cell wall of *Closterium acerosum* during cell growth. Planta 140, 7–14.

Iiyama, K., Wallis, A.F.A., 1990. Determination of lignin in herbaceous plants by an improved acetyl bromide procedure. Journal of Food Science and Agriculture 51, 145–161.

Krikorian, A.D., Levine, H.G., 1991. Development and growth in space. In: Bidwell, R.G.S., Steward, F.C. (Eds.), Plant Physiology: A Treatise, Vol. 10. Academic Press, London, pp. 491–555.

Krikorian, A.D., Levine, H.G., Kann, R.P., O'Connor, S.A., 1992. Effects of Spaceflight on Growth and Cell Division in Higher Plants. JAI Press, Inc, Greenwich, CT.

Kwon, M., Bedgar, D.L., Piastuch, W., Davin, L.B., Lewis, N.G., 2001. Induced compression wood formation in Douglas fir (*Pseudotsuga menziesii*) in microgravity. Phytochemistry 57, 847–857.

Lang, J.M., Eisinger, W.R., Green, P.B., 1982. Effects of ethylene on the orientation of microtubules and cellulose microfibrils of pea epicotyl cells with polylamellate cell walls. Protoplasma 110, 5–14.

Lapierre, C., Monties, B., Rolando, C., 1985. Thioacidolysis of lignin: comparison with acidolysis. Journal of Wood Chemistry and Technology 5, 277–292.

Levine, H.G., Kann, R.P., Krikorian, A.D., 1991. Plant development in space: observations on root formation and growth. The Fourth European Symposium on Life Sciences Research in Space, ESTEC, Noordwijk, Netherlands, ESA SP-307, pp. 503–508.

Levine, H.G., Krikorian, A.D., 1992. Shoot growth in aseptically cultured daylily and *Haplopappus* plantlets after a 5-day space-flight. Physiologia Plantarum 86, 349–359.

Levine, H.G., Sharek, J.A., Johnson, K.M., Stryjewski, E.C., Prima, V., Martynenko, O., Piastuch, W.C., 2000. Growth protocols for etiolated soybeans germinated within BRIC-60 canisters under spaceflight conditions. Advances in Space Research 26, 311–314.

Lewis, N.G., Davin, L.B., Sarkanen, S., 1999. The nature and function of lignins. In: Barton, Sir. D.H.R., Nakanishi, K., Meth-Cohn, O. (Eds.), Comprehensive Natural Products Chemistry, Vol. 3. Elsevier, London, pp. 617–745.

Niklas, K.J., 1992. Plant Biomechanics-an Engineering Approach to Plant Form and Function. The University of Chicago Press.

Pritchard, J., Hetherington, P.R., Fry, S.C., Tomos, A.D., 1993. Xyloglucan endotransglycosylase activity, microfibril orientation and profiles of cell wall properties along growth regions of maize roots. Journal of Experimental Botany 44, 1281–1289.

Roberts, I.N., Lloyd, C.W., Roberts, K., 1985. Ethylene-induced microtubule reorientations: mediation by helical arrays. Planta 164, 439–447.

Roland, J.C., Reis, D., Vian, B., Satiat-Jeunemaitre, B., Mosiniak, M., 1987. Morphogenesis of plant cell walls at the supramolecular level: internal geometry and versatility of helicoidal expression. Protoplasma 140, 75–91.

Satiat-Jeunemaitre, B., Martin, B., Hawes, C., 1992. Plant cell wall architecture is revealed by rapid-freezing and deep-etching. Protoplasma 167, 33–42.

Sauter, M., Seagull, R.W., Kende, H., 1993. Internodal elongation and orientation of cellulose microfibrils and microtubules in deepwater rice. Planta 90, 354–362.

Seagull, R.W., 1992. A quantitative electron microscopic study of changes in microtubule arrays and wall microfibril orientation during in vitro cotton fiber development. Journal of Cell Science 101, 561–577.

Skagen, E.B., Iversen, T.H., 1999. Simulated weightlessness and hyper-*g* results in opposite effects on the regeneration of the cortical microtubule array in protoplasts from *Brassica napus* hypocotyls. Physiologia Plantarum 106, 318–325.

Suzuki, K., Ingold, E., Sugiyama, M., Fukuda, H., Komamine, A., 1992. Effect of 2,6-dichlorobenzonitrile on differentiation to tracheary elements of isolated mesophyll cells of *Zinnia elegans* and formation of secondary cell walls. Physiologia Plantarum 86, 43–48.

Taylor, J.G., Owen Jr, T.P., Koonce, L.T., Haigler, C.H., 1992. Dispersed lignin in tracheary elements treated with cellulose synthesis inhibitors provides evidence that molecules of secondary cell wall mediate wall patterning. The Plant Journal 2, 959–970.

Tripathy, B.C., Brown, C.S., Levine, H.G., Krikorian, A.D., 1996. Growth and photosynthetic responses of wheat plants grown in space. Plant Physiology 110, 801–806.

Wymer, C., Lloyd, C.W., 1996. Dynamic microtubules: implications for cell wall patterns. Trends in Plant Sciences 1, 222–228.

Yahiaoui, N., Marque, C., Myton, K.E., Negrel, J., Boudet, A.M., 1998. Impact of different levels of cinnamyl alcohol dehydrogenase downregulation on lignins of transgenic tobacco plants. Planta 204, 8–15.

PERGAMON

Phytochemistry 57 (2001) 847–857

PHYTOCHEMISTRY

www.elsevier.com/locate/phytochem

Induced compression wood formation in Douglas fir (*Pseudotsuga menziesii*) in microgravity

Mi Kwon[a], Diana L. Bedgar[a], William Piastuch[b], Laurence B. Davin[a], Norman G. Lewis[a,*]

[a]*Institute of Biological Chemistry, Washington State University, Pullman, WA, 99164-6340, USA*
[b]*Dynamac Corporation, Mail Code: DYN-3, Kennedy Space Center, FL 32899, USA*

Received 12 September 2000; received in revised form 30 November 2000

Abstract

In the microgravity environment of the Space Shuttle Columbia (Life and Microgravity Mission STS-78), were grown 1-year-old Douglas fir and loblolly pine plants in a NASA plant growth facility. Several plants were harnessed (at 45°) to establish if compression wood biosynthesis, involving altered cellulose and lignin deposition and cell wall structure would occur under those conditions of induced mechanical stress. Selected plants were harnessed at day 2 in orbit, with stem sections of specific plants harvested and fixed for subsequent microscopic analyses on days 8, 10 and 15. At the end of the total space mission period (17 days), the remaining healthy harnessed plants and their vertical (upright) controls were harvested and fixed on earth. All harnessed (at 45°) plant specimens, whether grown at 1 *g* or in microgravity, formed compression wood. Moreover, not only the cambial cells but also the developing tracheid cells underwent significant morphological changes. This indicated that the developing tracheids from the primary cell wall expansion stage to the fully lignified maturation stage are involved in the perception and transduction of the stimuli stipulating the need for alteration of cell wall architecture. It is thus apparent that, even in a microgravity environment, woody plants can make appropriate corrections to compensate for stress gradients introduced by mechanical bending, thereby enabling compression wood to be formed. The evolutionary implications of these findings are discussed in terms of "variability" in cell wall biosynthesis. © 2001 Published by Elsevier Science Ltd. All rights reserved.

Keywords: *Pseudotsuga menziesii*; Douglas fir; *Pinus taeda*; Loblolly pine; Pinaceae; Lignin; Cellulose; Compression wood; Microgravity

1. Introduction

Douglas fir (*Pseudotsuga menziesii*) and loblolly pine (*Pinus taeda*) represent two important gymnospermous tree species used today for pulp and paper manufacture, and for other solid wood products. Understanding how to optimize both the quality and the texture of such woody (secondary xylem) tissue is an important biotechnological goal, particularly with current trends towards "fast-growing" plantations as sources of both fiber and wood (Lewis and Davin, 1994). A highly deleterious feature in terms of wood properties for such applications arises when their stems form reaction wood. This specialized tissue is manifested as "compression" wood in the Coniferales, Ginkgoales and Taxales, and as "tension" wood in the woody angiosperms.

The physiological function of such specialized reaction wood tissues (and corresponding cell types) provides woody stems with a mechanism by which they can realign their orientations when displaced away from the vertical axis. Branches also form such tissues in a way whereby this provides the means for continually orientating (or reorientating) branching angles. Compression wood is formed on the underside of leaning stems and branches, and manifests its effect by slowly buttressing (pushing) the stem or branches until the requisite (re)orientation is achieved. Tension wood, on the other hand, is formed on the upper side of woody angiosperm branches and leaning stems, and functions by "pulling" the branches and stems to the needed orientation (Westing, 1965; Scurfield, 1973; Timell, 1986; Lewis et al., 1999; Croteau et al., 2000).

* Corresponding author. Tel.: +1-509-335-2682; fax: +1-509-335-8206.
E-mail address: lewisn@wsu.edu (N.G. Lewis).

0031-9422/01/$ - see front matter © 2001 Published by Elsevier Science Ltd. All rights reserved.
PII: S0031-9422(01)00145-5

The formation of compression/tension wood is an inducible process (Cronshaw and Morey, 1965; Wilson and Archer, 1977; Fisher, 1985; Baba et al., 1995), although how this is achieved is not understood in terms of: the nature of the stimulus (gravity, "stress", and/or other factors); how the signal(s) is (are) perceived by the plant(s); how signal transduction occurs resulting in activation of cascades of various biochemical pathways, and, thus, which ultimately affords these specialized cell wall structures. Fig. 1a shows the effect of prolonged compression wood deposition in a sequoia (*Sequoia sempervirens*), a gymnosperm, which unsuccessfully attempted to restore its vertical alignment over several centuries. There are two distinct regions observable in the transverse section, namely that of compression wood on the underside and so-called opposite wood on the upperside. For comparative purposes, Fig. 1b displays a transverse section of "normal" wood tissues in a gymnosperm. Clearly, these corrective processes when induced can be sustained over extremely long periods if the required effect is not achieved.

In gymnosperms, the wood opposite to compression wood has "normal" tracheids of a squared or rectangular shape, with apparently no significant differences to those of "normal" xylem (Timell, 1986). In "opposite" wood, the relative proportions of the plant cell wall biopolymers (lignin, cellulose and hemicelluloses) appear to be essentially identical to that of "normal" wood (Timell, 1986). However, compression wood tracheids are markedly different from "normal" tracheids. For example, in loblolly pine (*P. taeda*), the compression wood tracheids are 10–40% shorter than normal (Yoshizawa and Idei, 1987) with frequently distorted tips (Wardrop and Dadswell, 1952). Fig. 2 shows a Douglas fir cross-section of normal wood (Fig. 2a) and compression wood (Fig. 2b), where the tracheids of the latter (Fig. 2b) have a rounded outline with large intercellular spaces in the cell corner regions, with three or four tracheids in contact with each other; the "normal" tracheids by contrast have a rectangular shaped outline with no intercellular spaces (Fig. 2a). Anatomically, compression wood tracheids differ from those of normal wood as follows: the S1 and S2 layers of compression wood secondary cell walls are thicker (Fig. 2d) than those of "normal" wood (Fig. 2c), with the S2 layer deeply fissured along the direction of the cellulose microfibrils (Wardrop and Dadswell, 1950; Wardrop and Davies, 1964); there is no S3 layer (Westing, 1965, 1968; Yoshizawa and Idei, 1987).

In general, compression wood cellulose has a lower degree of polymerization, is less crystalline (Lee, 1961) and has an altered cellulose microfibril orientation in the secondary cell wall (Timell, 1986). In "normal" tracheids (Fig. 2c), the cellulose microfibrils are relatively flat (70° to 50° to the cell length) in the Sl and S3 sublayers, while in the S2 sublayers they are relatively steep (45° to 10° to the cell length; Scurfield, 1973). By contrast, compression wood tracheids are aligned more or less transversely in the S1 sublayer, whereas in the S2 sublayer they are, for the most part, at an angle of 30–45° to the longitudinal axis of the cell (Fig. 2d; Scurfield, 1973). This suggests that microtubular assembly/orientation is greatly affected during compression wood cell wall assembly.

Woody angiosperms biosynthesize a different kind of reaction wood tissue known as tension wood. In this

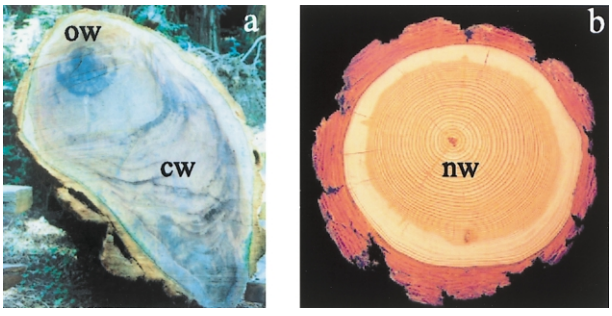

Fig. 1. Transverse sections showing compression wood of (a) *Sequoia sempervirens* and (b) normal wood of western larch *(Larix occidentalis)*. Abbreviations: cw: compression wood; nw: normal wood; ow: opposite wood.

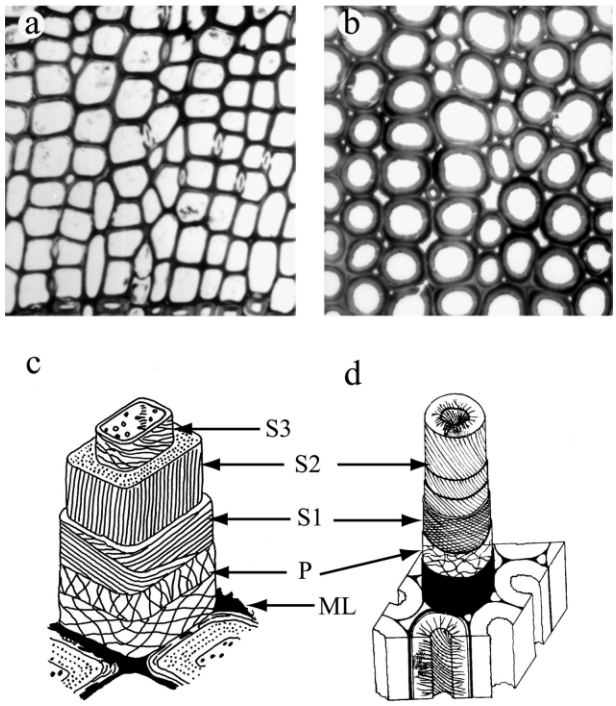

Fig. 2. Cross-section of Douglas fir seedling stems displaying (a) "normal" wood and (b) compression wood, as well as idealized schematic models for the cell wall structures of xylary cells (tracheid and libriform fibers) in (c) "normal" wood and (d) compression wood secondary xylem. Solid lines approximate the cellulose microfibril orientations. Abbreviations: ML: middle lamella; P: primary cell wall; S1: outermost layer of secondary wall; S2: middle layer of secondary cell wall; S3: innermost layer of secondary cell wall [c and d: redrawn from Fengel and Wegener (1984) and Timell (1986), respectively].

case, the accentuated growth is generated on the upper side of the branches and leaning stems as they attempt to (re)gain a particular alignment or orientation (Scurfield, 1973). Relative to "normal" wood (Fig. 3a), the most characteristic feature of tension wood is in the deposition of a new cell wall layer, the so-called gelatinous (G) layer (see Fig. 3b–d). "Tension" wood contains conspicuously thickened inner cell wall layers (i.e. non-lignified G-layers; Scurfield, 1964), which are composed almost entirely of cellulose (Norberg and Meier, 1966). Moreover, three distinct types of secondary walls in tension wood fibers have been reported; these include cells which either have not formed the S2 and S3 sublayers (Fig. 3b), and the S3 sublayer (Fig. 3c), or those which also contain an additional G layer (Fig. 3d), respectively. Interestingly, the microfibrils in the G layer are oriented (nearly) parallel to the longitudinal axis and have a high degree of crystallinity (Mia, 1968; Côté et al., 1969; Scurfield, 1973).

Another important distinction between both forms of reaction wood is in the differences in their cell wall polymeric constituents. In compression wood, for example, the lignin content is significantly higher, with a large increase in the amount of *p*-coumaryl alcohol present relative to that of coniferyl alcohol (Bland, 1961; Nimz et al., 1981; Timell, 1986; Lapierre and Rolando, 1988; Lapierre et al., 1988). Indeed, the darker color of compression wood might be attributed in part to this increase in the amount of lignin (e.g. from ca 25% in "normal" wood to ca 34% in compression wood of *Abies balsamea*; Westing, 1965). Tension wood, by contrast, may have lower lignin contents although this is still somewhat controversial (Timell, 1986).

Although both the content and monomeric composition of compression wood lignins are quite different from that of "opposite" wood, essentially nothing is known yet about how each is formed. In compression wood of *Thuja orientalis* and *Metasequoia glyptostroboides,* the activities of certain enzymes involved in lignin precursor biosynthesis were marginally higher than that of "normal" wood, i.e. phenylalanine ammonia lyase (PAL), 3-*O*-methyltransferase (OMT), *p*-hydroxycinnamate:CoA ligase (4CL) and cinnamyl alcohol dehydrogenase (CAD) (Kutsuki and Higuchi, 1981).

More recently, an important clue as to how monolignol composition and content is controlled was obtained through the study of monolignol biosynthesis in *P. taeda* cell suspension cultures (Anterola et al., 1999). By provision of increasing amounts of phenylalanine, a differential induction of formation of its monolignols was observed, i.e. the formation of coniferyl and *p*-coumaryl alcohols was differentially induced, with their ratios changing from ca 8:1 to 1:1, respectively (Anterola et al., 1999). This observation may provide an

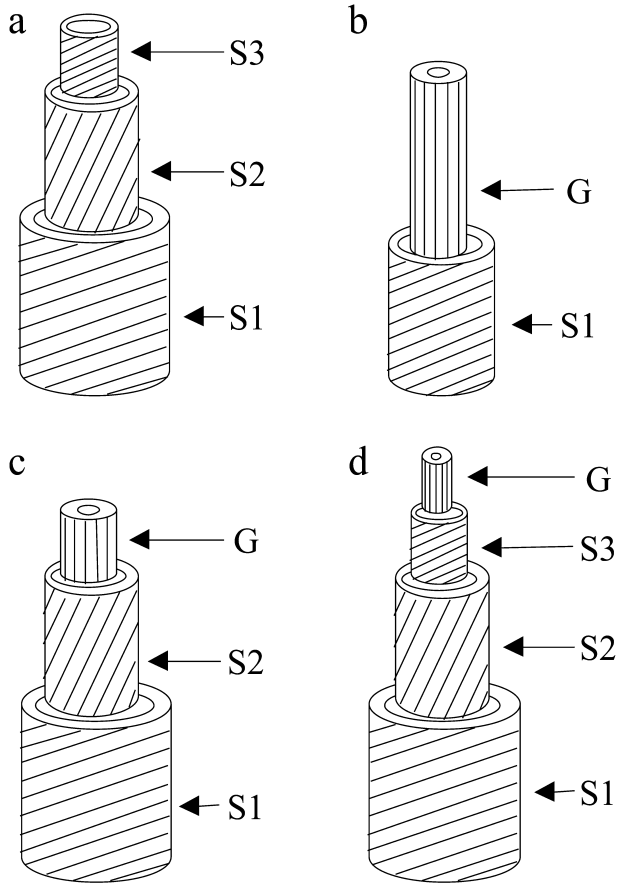

Fig. 3. Idealized diagrammatic representation of the organization of normal angiosperm wood (a), and three types of secondary walls observed in tension wood formation (b, c, and d). S1: outermost layer; S2: middle layer; S3: innermost layer; G; gelatinous layer of tension wood fibers. Solid lines indicate the cellulose microfibril orientation [redrawn from Wardrop and Dadswell (1955)].

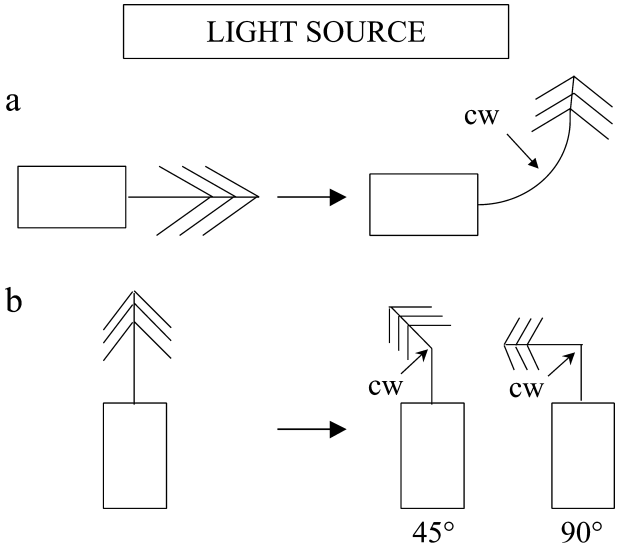

Fig. 4. Preferred plant configuration for studying compression wood formation in microgravity (a) and the configuration adopted for this study to induce compression wood formation of Douglas fir (*Pseudotsuga menziesii*) and loblolly pine (*Pinus taeda*) seedlings by mechanical bending at 45 and 90° (b).

explanation for the noted increases in the *p*-coumaryl alcohol content of compression wood lignins.

In this study, 1-year-old Douglas fir (*P. menziesii*) and loblolly pine (*P. taeda*) plants were placed under mechanical strain (harnessed at 45°) in a microgravity environment, aboard the Space Shuttle, Columbia (STS-78 mission), in order to determine whether compression wood formation would still occur. Because of the time constraints of the flight experiment (~17 days), the plant stems were oriented (bent) to a 45° angle from the vertical axis by mechanical stimulation. This procedure was initiated after 48 h in flight. This study describes the results from this research, i.e. as a first step to establishing how regulation of reaction wood formation occurs, and how the processes of both compression and tension wood have differentially evolved.

2. Results and discussion

The STS-78 mission objective was to establish whether compression wood formation could be engendered in a true microgravity environment when the plant species of interest were placed under mechanical strain. In order to investigate this question, various experimental protocols needed to be developed prior to embarking upon space-flight. These included: (1) verifying that compression wood was formed within the duration of the proposed space-flight and then (2) adapting an experimental protocol for space-flight that would result in compression wood being biosynthesized under normal gravitational loads (at 1 *g*).

Eventually, in order to test whether compression wood formation is manifested in microgravity, the preferred experimental design would be growth of the woody plants in space in an horizontal orientation relative to the light source (Fig. 4a). Following unassisted phototropic mediated reorientation of the stem and the photosynthetic canopy over an extended duration of time (weeks, months), the resulting xylem formed could then be analyzed to establish if compression wood resulted. Under such conditions, there would presumably be no external stresses imposed (e.g. by mechanical bending) on the plants, and hence this would represent the most ideal growth conditions to investigate the effects of a greatly diminished gravitational load (microgravity). Such an experiment is not yet possible since the duration of space-flight experiments on the space shuttle cannot be extended to the lengthy timeframes required. This study, therefore, must await scientific utilization of the International Space Station research platform in the future.

As a preliminary experiment, it was instructive to first ascertain whether compression wood formation might result by mechanical stimulation in microgravity. This involved the harnessing (bending) of woody plants aboard the 17 day STS-78 space shuttle mission.

Conditions for compression wood formation and its detection at normal gravitational loads (1 *g*) were first verified as follows: soil-grown Douglas fir and loblolly pine seedlings (four each) were mechanically bent at 45° and 90° (Fig. 4b), for different time intervals (9 and 15 days). The plants were then restored to a vertical alignment, and at the end of 17 days, were harvested and analyzed. All plants when bent at 45° and 90° to the vertical axis had formed compression wood, i.e. as evidenced by the presence of the characteristic compression wood round-shaped tracheids and intercellular spaces (see Fig. 5a and b which show only the results for Douglas fir). Since progression of compression wood development could be observed when plants were mechanically bent at a 45° angle, this particular orientation was adopted for all subsequent experiments.

With a timeframe suitable for the study of possible compression wood development on the space shuttle flight, the next technical development was to identify

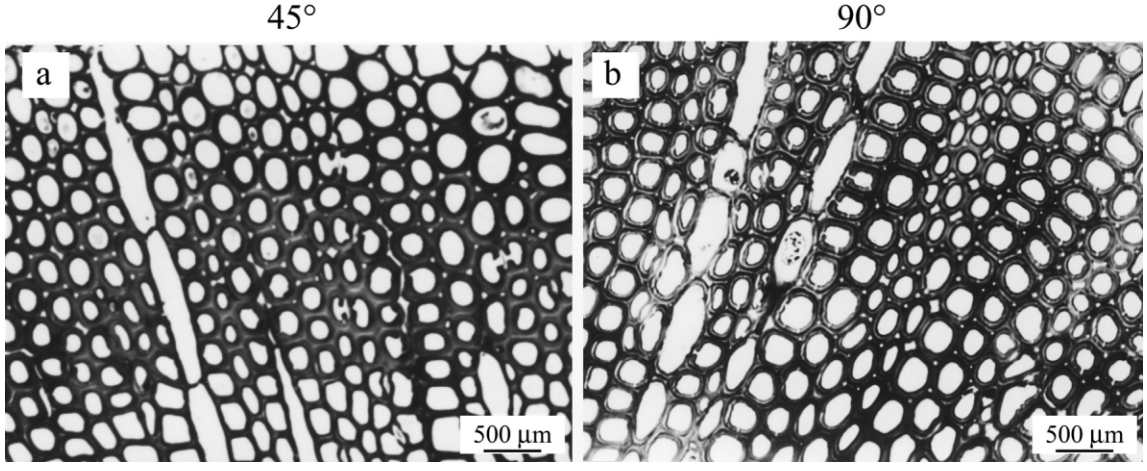

Fig. 5. Partial cross-sections of Douglas fir seedlings grown for 9 days at (a) 45° and (b) 90° configuration, respectively, then allowed to further grow for an additional 8 days in an upright (vertical) orientation.

suitable plant growth conditions using the NASA supplied plant growth chambers (PGCs). Plant growth in space in general has long been problematic, mainly because applied liquids (water) in space tend to ball up and not diffuse (spread) throughout the solid root supporting system(s). Additionally, the NASA plant growth unit (PGU), which can house up to six PGCs, has no ability to readily add water and nutrients to plants on an ongoing basis during space-flight. Moreover, although lighting is provided, the temperature regimen experienced cannot be controlled, i.e. the plant growth temperature is dictated by, as a minimum value, the ambient temperature of the space shuttle cabin.

Nutrient packs (agar gels containing the requisite amount of water and nutrients required for the duration of the Space-Shuttle flight, see Section 4) were next developed, and these were adapted for growth of both Douglas fir and loblolly pine seedlings (Fig. 6a, showing only loblolly pine). The overall dimensions of the PGCs necessitated trimming of the plants at the crown (via decapitation) in order for them to fit snugly into the growth chamber (Fig. 6b, showing only loblolly pine). In earlier studies (Wardrop, 1957; Westing, 1961), both girdling of trees and decapitation had no noticeable effect on the ability to form reaction wood. Decapitation of the Douglas fir and loblolly pine plants in our studies also had no deleterious effect on compression wood formation (data not shown). Thus, with the various experimental parameters [light levels, temperatures, orientation and use of trimmed (decapitated) plants] so defined, attention was next directed to establishing the precise protocol to be employed for space-flight.

Space shuttle flight experiments must undergo rigorous pre-flight controls at Kennedy Space Center at Cape Canaveral [so-called payload verification tests (PVTs)] in order to verify conditions necessary for successful space-flight experimentation, and thus to ensure that reliable scientific data is collected on the effects of the microgravity environment proper. The PVT thus established that (1) decapitated Douglas fir and loblolly pine seedlings grew ''normally'' in the nutrient pack within the plant growth chambers (of the PGU) for the duration of the proposed flight(s); (2) that compression wood was formed in the plants used, when their stems were bent at a 45° angle to the vertical axis, while housed in the nutrient packs in the PGC for periods of 8, 10 and 15 days, respectively; and (3) that plant tissues were well preserved when fixed at room temperature in 2% paraformaldehyde/2.5% glutaraldehyde, using a specially designed fixation kit suitable for handling and containing liquid samples in space (microgravity; see Fig. 6c and d, respectively).

To summarize, the decapitated Douglas fir and loblolly pine seedlings, when placed in the nutrient packs housed in the PGC, grew either normally (upright) or developed compression wood (45° harnessing) during the time-frame examined (see Fig. 7a–e and 7b–d, respectively).

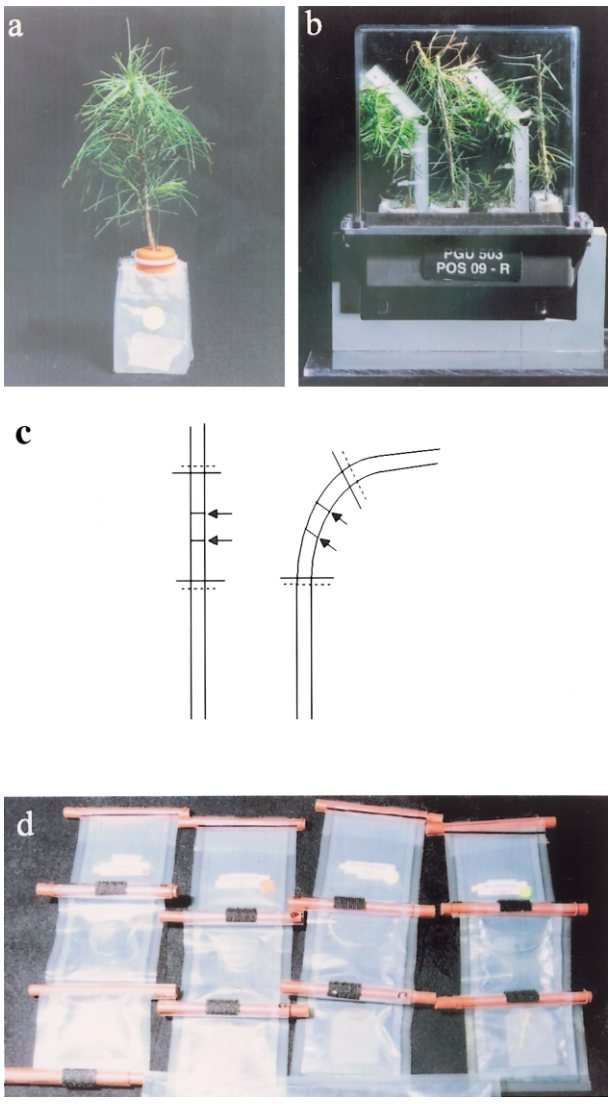

Fig. 6. Loblolly pine seedling inserted in a nutrient pack (a) and a plant growth chamber (PGC) containing decapitated loblolly pine seedlings which were grown in an upright (vertical) position and at a 45° configuration, respectively (b); a comparable system was used for Douglas fir seedlings. Diagram showing the regions of plant stem samples that were selected and harvested for fixation and microscopic analysis (c) and the fixative bags designed for plant tissue fixation in space (d). The dotted lines approximate the sites of initial sectioning with wire cutters, and the second solid line shows the region subsequently sectioned using mechanical clippers. The plant tissue segment between the two arrows was subsequently fixed and utilized for microscopic analyses.

By contrast, the corresponding opposite wood (Fig. 7f–h) only developed ''normal'' secondary xylem with rectangular shaped tracheids and no intercellular spaces.

It was possible to identify cells designated to become compression wood tracheids as early as at the beginning of primary wall differentiation, i.e. when the cells undergo expansion just after cell division has occurred

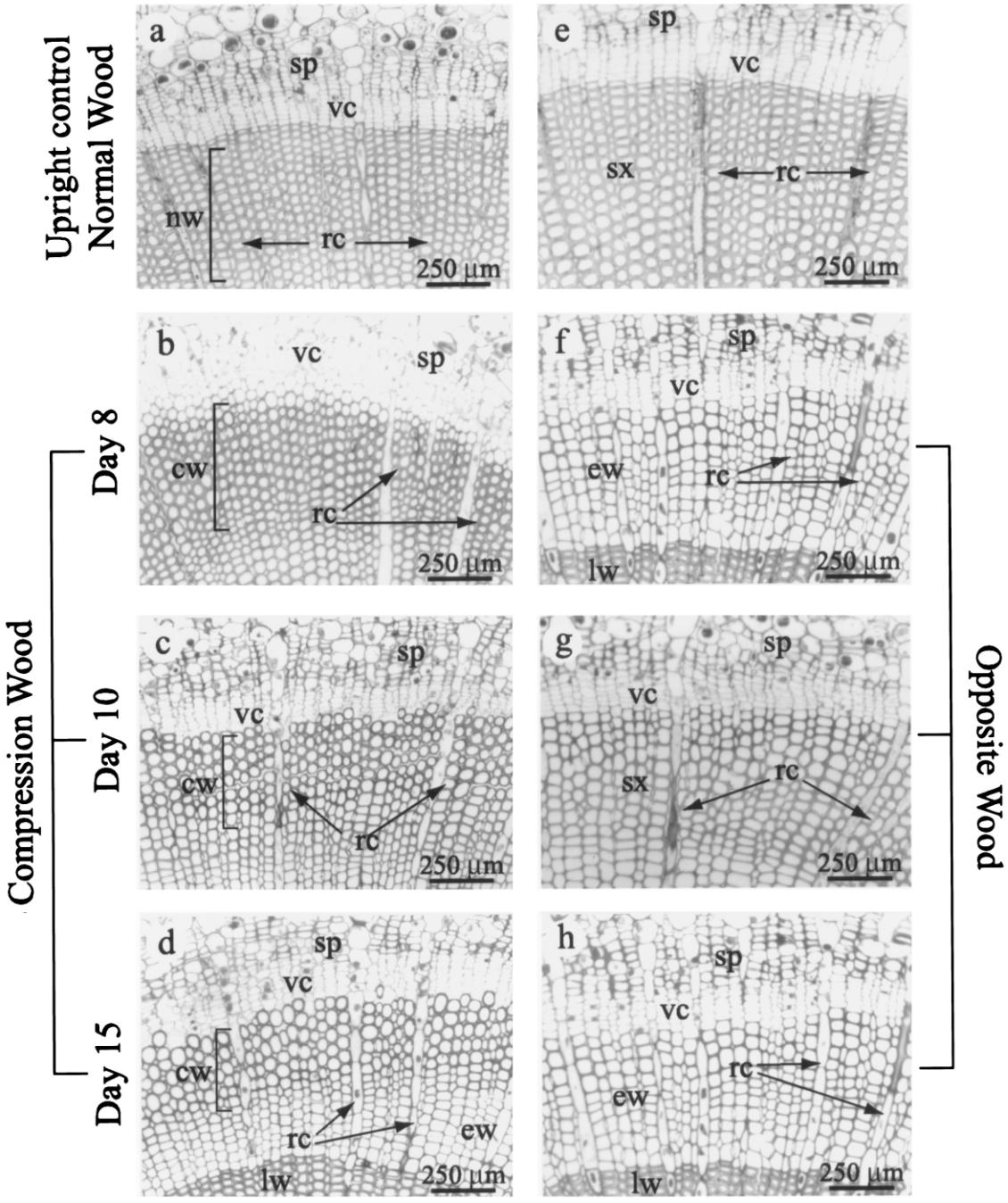

Fig. 7. Cross-sections of Douglas fir seedlings grown in an upright vertical position for 17 days (a, e) and at a 45° orientation for 8 (b and f), 10 (c and g) and 15 (d and h) days in nutrient packs within the PGC during the Payload Verification Test (PVT). Abbreviations: cw: compression wood; ew: early wood; lw: late wood; nw: normal wood; rc: ray cells; sp: secondary phloem; sx: secondary xylem; vc: vascular cambium.

in the vascular cambium region. This suggests that the perception and transduction of the external signal(s) stipulating compression-wood formation is perceived by cambial-derived tracheid initials in the cambial zone, as proposed earlier by Sinnott and Westing (Sinnott, 1952; Westing, 1965). However, maturing tracheids were also able to undergo dramatic morphological changes during secondary cell wall formation and lignification. This additionally suggests that developing xylem (i.e. from initial primary cell expansion to secondary maturation) is influenced by the stimulus of the stresses/strains perceived as a consequence of the mechanical load and/or gravitational force experienced. Indeed, the compound middle lamella region of the cell corners of the compression wood so formed undergoes major morphological modifications relative to that of "normal" tracheids, i.e. as evidenced by development of large intercellular spaces. Furthermore, these regions generally undergo

the initial stages of lignin deposition (Bland, 1961; Donaldson, 1994). Accordingly, it will be of considerable interest to ascertain at the molecular level how the changes in a stress/strain gradient ultimately result in a different form of cell wall being sculptured for the particular cells "sacrificed" for buttressing.

Space Shuttle Columbia (STS-78) carried 16 Douglas fir and 4 loblolly pine plants. Following 48 h in orbit in space, the PGU was opened with the sterilized PGCs having their casings removed. The mechanical harnessing devices in the PGCs were then adjusted to place two plants per PGC at 45° to the vertical axis (i.e. to the light source of the PGC; Fig. 6b). The PGCs were then reassembled, placed back into the PGU, which was powered as before. After ten days in orbit, a plant retrieval protocol was employed whereby the PGU was again opened. All plants (both upright vertical controls and those harnessed at 45° for 8 days, two each) were removed from one PGC, and harvested in space by clipping stem regions adjacent to the area undergoing bending (see Fig. 6c). The plant sections obtained were immediately fixed in 2% paraformaldehyde/2.5% glutaraldehyde, using a device designed to give three levels of containment (against liquid/vapor leakage; Fig. 6d). Comparable sections were collected for the same anatomical regions for the stems of "vertical" controls (see Fig. 6c). Additional sampling was made at day 12 (2 days upright and 10 days harnessed at 45°, as well as the corresponding vertical controls). Remaining plant specimens in the PGU/PGCs were returned at the end of the space flight (2 days upright and 15 days harnessed at 45° and their corresponding controls) on earth, harvested

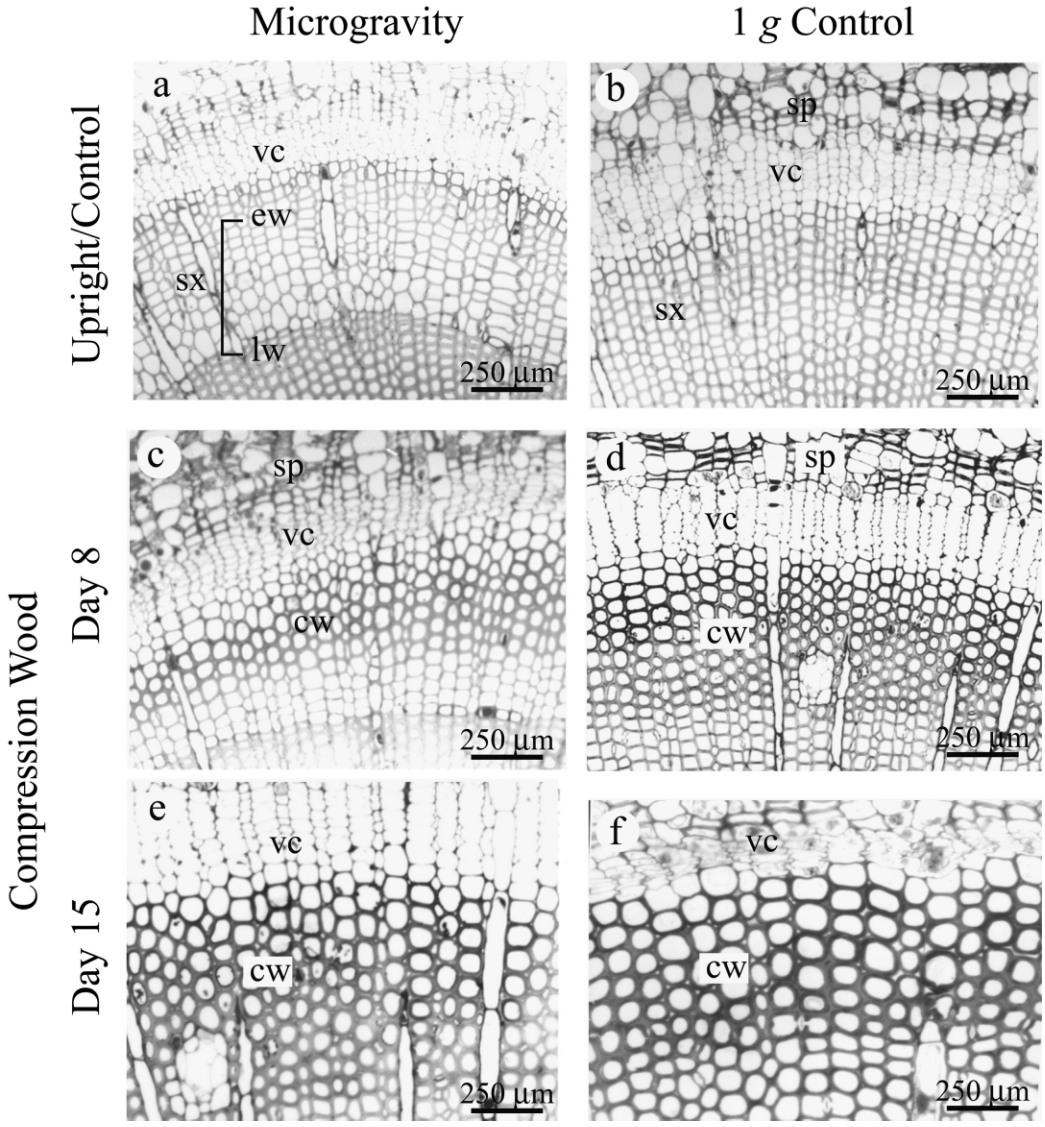

Fig. 8. Cross-sections of Douglas fir seedlings grown in microgravity (a, c, and e) and at 1 *g* (b, d, and f). Specimens were either placed in an upright vertical orientation for 17 days (a and b) or at a 45° orientation for 8 (c and d) and 15 (e and f) days. Abbreviations: cw, compression wood; ew, early wood; 1w, late wood; sp, secondary phloem; sx, secondary xylem; vc, vascular cambium.

and fixed as above. Additionally, a flight simulation experiment, except for being conducted at 1 *g*, was initiated 48 h after launch, with plant processing protocols following those used for space-flight.

The space-flight experiment established that compression wood development was able to occur in the near absence of gravity, provided that the stems were harnessed (at 45°). However, the study was not without technical difficulty, this resulting from high temperatures (>29°) due to an extremely warm space shuttle cabin environment, which was significantly higher than any other previous mission. This had a deleterious effect on the growth and survival of several plant specimens, particularly the loblolly pine, with only about 20% returning healthy (i.e. still containing new growth).

Nevertheless, the (healthy) plant specimens, whether grown under microgravity conditions or at 1 *g* gave essentially identical results, i.e. they all formed compression wood when oriented at a 45° angle (Fig. 8), and "normal" wood when grown in a vertical orientation, i.e. the Douglas fir seedlings grown in a vertical (upright) orientation for 17 days, under either microgravity or 1 *g* conditions, only developed normal secondary xylem as expected (Fig. 8a and b). On the other hand, those harnessed at a 45° configuration for 8 days developed compression wood in their developing secondary xylem region (Fig. 8c), and its formation was even more pronounced with samples harnessed for 15 days (Fig. 8e). As expected, Douglas fir seedlings harnessed at 45° under the 1 *g* controls displayed similar patterns of compression wood development (Fig. 8d and f), with no significant differences compared to those grown in microgravity (Fig. 8c and e).

3. Concluding remarks

To account for compression wood formation in space, two possibilities can be considered: First, the greatly reduced gravitational forces of the microgravity environment are still sufficient that the plants can still respond to this stimulus. Second, and more likely, the effect of induced stress through mechanical loading (harnessing at 45°) overrides the gravitactic responses (due to overlapping signal transduction, perception and response mechanisms). The plants then compensate to limit the effect of the mechanical stresses and strains imposed through certain cells undergoing compression wood formation. That is, even in microgravity, the woody plants can make appropriate corrections to alleviate stress gradients introduced by mechanical bending.

Given that compression wood induction can occur in a microgravity environment, studies will be conducted in the future to ascertain whether it is still formed when plants restore their "vertical" alignment unassisted relative to tracking of the lighting source in microgravity, i.e. when placed in a configuration (horizontal) parallel to the light source (see Fig. 4a).

The results obtained have important evolutionary implications. They raise questions as to which point during the evolution of land plant growth and development did the cambial cells initiate secondary thickening processes leading to woody tissue development? At what point did the earliest plant forms evolve these complex biological systems whereby reaction wood tissues were generated in order to both maintain stem orientation (relative to the vertical axis) and to regulate branching patterns? The gymnosperms have perhaps deployed buttressing of woody tissue by compression wood formation for up to the ~360 million years that they have been in existence. It is intriguing to contemplate what advantages were conferred, if any, by changing this buttressing mechanism in gymnosperms to the generation of tension wood tissues (both spatially and chemically) in the angiosperms. How did such different processes achieving comparable physiological functions differentially evolve? Much remains to be learned about these fascinating biochemical systems at the molecular, biochemical, chemical and anatomical levels and which ultimately lead to these remarkable morphologies. This will be the subject of additional study in the future.

4. Experimental

4.1. Plant material

One-year-old Douglas fir (*Pseudotsuga menziesii* (Mirb.) Franco), obtained from the University of Idaho Forest Experimental Station, and 1-year-old loblolly pine (*Pinus taeda*,) grown from seeds, were maintained in Washington State University greenhouse facilities. Plant specimens for the payload verification test (PVT), the space shuttle flight and simulation experiments were transported by air while being maintained throughout in a vertical position. Plants were transferred into walk-in growth chambers (23°C, 16 h light and 8 h dark) at NASA (Kennedy Space Center, Cape Canaveral, FL) until needed. Payload verification tests and flight simulations were conducted in walk-in growth chambers under temperature and lighting conditions used for the flight experiment.

4.2. Mechanical harnessing and tip decapitation of Douglas fir and loblolly pine seedlings

In order to establish the effects of bending and decapitation on compression wood formation, soil grown one year old Douglas fir and loblolly pine seedlings were decapitated by removing the tips of their stems. The decapitated stems were then harnessed at 45° or 90° for 9 and 15 days, respectively, then harvested as

described in Section 4.8 and processed as described in Section 4.9.

4.3. Plant growth unit

The NASA plant growth unit (PGU) has overall dimensions of 51×45×26 cm (L×W×H) and fits in a middeck locker on the space shuttle. It includes housing controls for electronic regulation of light, temperature and aeration. Lighting was provided by a bank of three fluorescent lamps containing Duratest Vitalite phosphor lenses, a reflector and an aluminium housing. Each PGU has a cavity region able to hold up to five plant growth chambers (PGC) as well as an Atmospheric Exchange System which circulates filtered cabin air through four of the PGCs, with the fifth serving as a control with no air flow. Temperature was controlled by heat from the lamps, one 20 W strip heater and the flow of middeck cabin air through the PGU: in order to be controlled, the temperature has to be above the middeck temperature. The PGU also contains a Data Acquisition System to record data such as day/night cycles and temperature. (A fuller description of the PGU/PGC can be found at http://lsda.ksc.nasa.gov/payload/payload_web/hdw_home.htm.) Inside each PGC was installed a mechanical device to either mechanically bend each of the Douglas fir/loblolly pine plants to an angle of 45° from the vertical axis or to maintain them in an upright position.

4.4. Plant "nutrient" packs

Plant nutrient packs were prepared as described in Levine et al. (2001) with the following modifications: the overall dimensions of the pack were 3.5×1.5×6.5 cm (L×W×H). To each pack was added a sterile (autoclaved) solution, which consisted of 5% (v/v) modified Brown and Lawrence medium (Eberhardt et al., 1993) containing 1% (v/v) antibiotic solution [antimycotic lyophilized powder: 10,000 U penicillin, 10 mg streptomycin and 25 μg amphotericin B per ml in 0.9% NaCl (Sigma)], 3.0% (w/v) thiabendazole (Sigma) in DMF (N, N-dimethylformamide, Sigma) and 1% (w/v) phytoagar (Gibco BRL Life Technology). Prior to the medium gelling, a conical tube (15 ml, Corning), filled with glass beads (2 mm in diameter), was inserted into the center of each nutrient pack, and following gelling through cooling, each conical tube was removed. Into the void created by the tube was inserted the upper part (2.5 cm) of a 15 ml-Corning tube through which four holes (6 mm in diameter) had previously been drilled equidistant from each other to facilitate subsequent root growth. One-year-old Douglas fir/loblolly pine plants, freshly depotted and with root systems individually washed successively with tap and distilled water, were soaked for 10 min in a 10% (v/v) bleach (Clorox) solution and then for 2 min in the 1% (v/v) antibiotic solution (see earlier) containing 0.9% (w/v) thiabendazole in DMF. The plants were individually inserted into nutrient packs, with roots placed through the 2.5 cm-long Corning tube, in the void originally housing the conical tube. Freshly prepared liquid growth medium at ca 50°C with 1% (w/v) low melting point agar (Gibco BRL Life Technology), instead of 1% phytoagar, was slowly added to the root tissue compartment of the nutrient pack until filled. The screw cap of the Corning tube which had a hole drilled through the middle (6 mm in diameter) as well as an opening (slit) at the side, was inserted around the Douglas fir/loblolly pine stem and loosely tightened. Following gelling through cooling, the screw cap was removed, the empty space around the Douglas fir/loblolly pine plant was packed with sterilized (autoclaved) cotton wool (see Fig. 6a) and the cap again tightened loosely. Four nutrient packs were placed inside each PGC and these were kept in an incubator (23°C; 16 h light and 8 h dark) until needed.

4.5. Payload verification test

A payload verification test (PVT) was conducted during which all phases of the pre/post and in-flight operations were performed using flight hardware. Two PGU's were prepared containing 20 plants each (four plants/PGC) as described in Section 4.4 with the trees secured along the mechanical devices of the PGC's with 4-inch cable tie. The regions of the stems stipulated to undergo either mechanical bending, or for the vertical controls corresponding to the same anatomical regions, were marked with red (top) and blue (bottom) lines by means of permanent markers to facilitate harvesting (see Fig. 6c). Both PGUs were placed in the Orbiter Environmental Simulator (OES) which uses space shuttle calibrated ancillary data to mimic the middeck environment. Ten of the plants (2/PGC) in both PGUs had their stems reorientated at 45° to the vertical axis by activating the mechanical device (see Fig. 6b) 48 h after transfer to the OES. At day 8 after bending, two vertical and two specimens at 45° were harvested from one PGC (from both PGUs) and fixed as described in Section 4.8; this procedure was repeated at day 10 after bending with another PGC. The stem segments were held in fixative bags at the temperature of the OES until the end of PVT; these were further processed as described in Section 4.9. The remaining plants from one PGU were harvested on day 17 and from the other on day 19 (17-day mission plus 2 contingency days). Trees were photographed at the time of harvest for record-keeping purposes.

4.6. Flight experiment

Sixteen Douglas fir and four loblolly pine seedlings were transferred to "nutrient packs", respectively, as before, these being placed inside five PGC's. After

securing the trees along the mechanical device with 4-inch cable tie, they were marked as described in Section 4.5. The PGC's were next stored in an incubator (23°C, 16 h light, 8 h dark). Two days prior to flight (13:00 to 15:00 EDT), the PGCs were transferred to the PGU. Photographs of each PGC were taken during the transfer, and the PGU was stored in the OES. The next day 17:00 EDT, the PGU was taken from the Life Science Support Facility and stowed in the middeck of the Columbia Space Shuttle. Columbia (STS-78 mission) lifted-off at 10:49:00 EDT on June 20, 1996 at Cape Canaveral, FL, and climbed to a 278 km-high orbit with a 39° inclination to the earth's equator. Following 48 h of growth in orbit, the astronauts placed two Douglas fir/loblolly pine plants from each PGC in a 45° orientation through activation of the mechanical device shown in Fig. 6b; the remaining two plants in each PGC were left in an upright (vertical) orientation. Plants (vertical controls and 45° oriented specimens from one PGC) were harvested, sectioned, and fixed in flight on day 10 and again at day 12 (2 days upright and 8 and 10 days harnessed at 45°, respectively, as well as the corresponding controls) as described in Section 4.8. The stem segments were held in the fixative bag at the Shuttle ambient temperature until the end of the mission. Photographs of the plants were also taken during bending and harvesting. Space Shuttle Columbia returned to Kennedy Space Center at 8:36:45 EDT on July 7, 1996, giving a total mission elapsed time of 16 days 21 h 47 mm 45 s. The PGU was returned to the Life Science Support Facility approximately at 12:00 EDT. Photographs were next taken with the remainder of the plants then being harvested, sectioned, and fixed as described in Section 4.8. All the specimens in fixative bags were processed as described in Section 4.9. PGC temperatures were recorded during the flight, and these ranged in average from 23.5°C to 30.5°C. Note that all loblolly pine plants died during the space flight experiment due to shuttle cabin overheating.

4.7. Flight simulation experiment (2 days after launch)

An additional control experiment was carried out under identical conditions to that of the space flight experiment except for being conducted at 1 *g*. This was initiated 2 days following lift-off, with a time-lapse being employed in order to download temperature data from the shuttle to Kennedy Space Center; these conditions were then used for flight simulation. Thus, plants were transferred to the PGC/PGU exactly as described for the flight experiment (Section 4.6), albeit 48 h later. Growth conditions (temperature and lighting) were maintained exactly as for that of the flight experiment, since the control PGU was located in the OES. Douglas fir (two per PGC) and loblolly pine plants were placed in a 45° orientation at the same flight times as for the microgravity-grown plants. At days 8 and 10 (same overall time period as the flight specimens), the plants from two PGCs were sectioned and fixed as described Section 4.8. The fixative bags were held at the same temperature as the samples harvested in space, until the end of the simulation (16 days 21 h 47 mm 45 s) at which time the remaining plants were sectioned and fixed as described in Section 4.8. All specimens were processed as described in Section 4.9. Photographs were taken at time of bending and harvesting.

4.8. Sample harvest and fixation in space and on Earth

Douglas fir and loblolly pine plants were harvested during the PVT, space flight, and flight simulation experiment, as follows: stem segments (3 cm in length) were collected from the marked-up areas flanking the region of the stem that had undergone either mechanical bending, or were from vertical controls corresponding to the same anatomical region (3 cm in length). Coarse stem sections were initially harvested above the red and below the blue marks with a wire cutter, and then more precisely trimmed by means of a mechanical clipper at both sides of the marked up zones (Fig. 6c). Any plant debris was collected by means of a small hand held vacuum cleaner for the operation in space aboard the space shuttle. Harvested stem segments were immediately placed into fixative bags (Fig. 6d) containing 2% paraformaldehyde/2.5% glutaraldehyde in 0.05 M phosphate buffer (pH 7.2). All fixation procedures were carried out inside a glove-box in order to achieve four levels of containment as required by NASA for occupational exposure.

4.9. Microscopy analyses offlight and control (1 g) plant tissue stein sections

Stem segments stored in the fixative bags were briefly washed three times in 0.05 M phosphate buffer (pH 7.2) and then further dissected into smaller pieces (0.5 cm in length) and dehydrated gradually in 30, 50, 70, 90, 95, and 100% ethanol (10 min each). After dehydrating two more times in 100% EtOH, the samples were transferred gradually to solutions of EtOH–acetone 1:3, 1:2, 1:1, and 0:1. After infiltration in Spurr's resin in acetone (10, 30 50, 70, 90 and 100%, four times each) at room temperature, the stem segments were finally embedded overnight in fresh Spurr's resin in a 70°C oven. Thick sections (800 nm) were obtained by means of a glass knife using an ultramicrotome (Reichert). Sections were next mounted on microscopic slides (VWR Scientific Inc.) and stained with Stevanels' blue for morphological observation. The anatomy of sections was recorded using an Olympus BH2 photomicroscope housing Tech pan film (Kodak). Photographs were developed and scanned using a ScanMaker III (Microtek).

Acknowledgements

The authors thank NASA (NAG 10-0164) for generous financial support of this study, and Deborah Vordermark-Wells, Rina Thompson and Chung Wang (for designing the mechanical device to bend the trees in a 45° configuration), the Bionetics Corporation, Kennedy Space Center, for excellent technical assistance. Special thanks are also expressed to astronauts, Jean-Jacques Favier and Susan Helms, for their participation in this study.

References

Anterola, A.M., van Rensburg, H., van Heerden, P.S., Davin, L.B., Lewis, N.G., 1999. Multi-site modulation of flux during monolignol formation in loblolly pine (*Pinus taeda*). Biochemical and Biophysical Research Communications 261, 652–657.

Baba, K.-i., Adachi, K., Take, T., Yokoyama, T., Itoh, T., Nakamura, T., 1995. Induction of tension wood in GA_3-treated branches of the weeping type of Japanese cherry, *Prunus spachiana*. Plant Cell Physiology 36, 983–988.

Bland, D.E., 1961. The chemistry of reaction wood. III. The milled wood lignins of *Eucalyptus goniocalyx* and *Pinus radiata*. Holzforschung 15, 102–106.

Côté Jr, W.A., Day, A.C., Timell, T.E., 1969. A contribution to the ultrastructure of tension wood fibers. Wood Science and Technology 3, 257–271.

Cronshaw, J., Morey, P.R., 1965. Induction of tension wood by 2,3,5-tri-iodobenzoic acid. Nature 205, 816–818.

Croteau, R., Kutchan, T.M., Lewis, N.G., 2000. Natural products (secondary metabolites). In: Buchanan, B.B., Gruissem, W., Jones, R.L. (Eds.), Biochemistry and Molecular Biology of Plants. American Society of Plant Physiologists, Rockville, MD, pp. 1250–1318.

Donaldson, L.A., 1994. Mechanical constraints on lignin deposition during lignification. Wood Science and Technology 28, 111–118.

Eberhardt, T.L., Bernards, M.A., He, L., Davin, L.B., Wooten, J.B., Lewis, N.G., 1993. Lignification in cell suspension cultures of *Pinus taeda: In situ* characterization of a gymnosperm lignin. The Journal of Biological Chemistry 268, 21088–21096.

Fengel, D., Wegener, G., 1984. Wood. Chemistry, Ultrastructure, Reactions. Walter de Gruyter, Berlin.

Fisher, J.B., 1985. Induction of reaction wood in *Terminalia* (Combretaceae): roles of gravity and stress. Annals of Botany 55, 237–248.

Kutsuki, H., Higuchi, T., 1981. Activities of some enzymes of lignin formation in reaction wood of *Thuja orientalis, Metasequoia glyptostroboides* and *Robinia pseudoacacia*. Planta 152, 365–368.

Lapierre, C., Rolando, C., 1988. Thioacidolyses of pre-methylated lignin samples from pine compression and poplar woods. Holzforschung 42, 1–4.

Lapierre, C., Monties, B., Rolando, C., 1988. Thioacidolyses of diazomethane-methylated pine compression wood and wheat straw *in situ* lignins. Holzforschung 42, 409–411.

Lee, C.L., 1961. Crystallinity of wood cellulose fibers studied by X-ray methods. Forest Product Journal 11, 108–112.

Levine, L.H., Heyenga, A.G., Levine, H.G., Choi, J.W., Davin, L.B., Krikorian, A.D., Lewis, N.G., 2001. Cell-wall architecture and lignin composition of wheat developed in a microgravity environment. Phytochemistry 57, 835–846.

Lewis, N.G., Davin, L.B., 1994. Evolution of lignan and neolignan biochemical pathways. In: Nes, W.D. (Ed.), Isopentenoids and Other Natural Products: Evolution and Function, Vol. 562. ACS Symposium Series, Washington, DC, pp. 202–246.

Lewis, N.G., Davin, L.B., Sarkanen, S., 1999. The nature and function of lignins. In: Barton Sir, D.H.R., Nakanishi, K., Meth-Cohn, O. (Eds.), Comprehensive Natural Products Chemistry, Vol. 3. Pergamon, London, pp. 617–745.

Mia, A.J., 1968. Organization of tension wood fibres with special reference to the gelatinous layer in *Populus tremuloides* Michx. Wood Science 1, 105–115.

Nimz, H.H., Robert, D., Faix, O., Nemr, M., 1981. Carbon-13 NMR spectra of lignins: structural differences between lignins of heartwoods, softwoods, grasses, and compression woods. Holzforschung 35, 16–26.

Norberg, H., Meier, H., 1966. Physical and chemical properties of the gelatinous layer in tension wood fibres of aspen (*Populus tremula* L.). Holzforschung 20, 174–178.

Scurfield, G., 1964. The nature of reaction wood. IX. Anomalous cases of reaction anatomy. Australian Journal of Botany 12, 173–184.

Scurfield, G., 1973. Reaction wood: its structure and function. Science 179, 647–655.

Sinnott, E.W., 1952. Reaction wood and the regulation of tree form. American Journal of Botany 39, 69–78.

Timell, T.E., 1986. Compression Wood in Gymnosperms. Springer-Verlag, Berlin (and references therein).

Wardrop, A.B., 1957. The phase of lignification in the differentiation of wood fibers. TAPPi 40, 225–243.

Wardrop, A.B., Dadswell, H.E., 1950. The nature of reaction wood. II. The cell wall organization of compression wood tracheids. Australian Journal of Scientific Research, Series B, Biological Sciences 3, 1–13.

Wardrop, A.B., Dadswell, H.E., 1952. The nature of reaction wood. III. Cell division and cell wall formation in conifer stems. Australian Journal of Scientific Research, Series B, Biological Sciences 5, 385–398.

Wardrop, A.B., Dadswell, H.E., 1955. The nature of reaction wood. IV. Variations in cell wall organization of tension wood fibres. Australian Journal of Botany 3, 177–189.

Wardrop, A.B., Davies, G.W., 1964. The nature of reaction wood. VIII. The structure and differentiation of compression wood. Australian Journal of Botany 12, 24–38.

Westing, A.H., 1961. Changes in radical symmetry in the leaders of eastern white pine following inclination. Journal of Forestry 59, 17–19.

Westing, A.H., 1965. Formation and function of compression wood in gymnosperms. The Botanical Review 31, 381–480.

Westing, A.H., 1968. Formation and function of compression wood in gymnosperms. II. The Botanical Review 34, 51–78.

Wilson, B.F., Archer, R.R., 1977. Reaction wood: induction and mechanical action. Annual Review of Plant Physiology 28, 23–43.

Yoshizawa, N., Idei, T., 1987. Some structural and evolutionary aspects of compression wood tracheids. Wood and Fiber Science 19, 343–352.

PERGAMON

Phytochemistry 57 (2001) 859–873

PHYTOCHEMISTRY

www.elsevier.com/locate/phytochem

Review

Lignification and lignin topochemistry — an ultrastructural view

Lloyd A. Donaldson *

Forest Research, Private Bag 3020, Rotorua, New Zealand

Received 27 June 2000; received in revised form 26 October 2000

Abstract

This review discuses the ultrastructural aspects of cell wall lignification and lignin topochemistry. Lignification results from the enzyme mediated polymerization of monolignols initiated by unknown factors (initiation sites) located at the corners of cells and in the middle lamella. Lignification results in the filling of pores within the carbohydrate matrix following a sequence from the outer regions of the wall towards the lumen. The amount and chemical characteristics of lignin vary across the cell wall, with the presence of reaction wood, and among cell types. © 2001 Elsevier Science Ltd. All rights reserved.

Keywords: Lignification; Lignin topochemistry; Lignin distribution; Monolignol; Guaiacyl; Syringyl; *p*-Hydroxyphenyl; Angiosperms; Gymnosperms; Reaction wood; Ultrastructure

Contents

1. Introduction 859

2. Ultrastructure of lignifying xylem 860
   2.1. Lignin formation 860
   2.2. Topochemistry of lignification 862
   2.3. Seasonal and environmental effects on lignification 864

3. Lignification of reaction wood 864

4. Lignin distribution in gymnosperms 865

5. Lignin distribution in angiosperms 866

6. Lignin distribution in reaction wood 867

7. Conclusions 869

References 869

1. Introduction

Lignin is a complex 3-dimensional polymer that occurs predominantly in the xylem of most land plants, forming about 1/3 of the terrestrial woody biomass. As a major component of the cell wall of tracheids, vessels and fibers, lignin contributes to the compression strength of woody stems, and to the water proofing of conductive elements within the xylem. Lignification has allowed the evolution of large arborescent land plants capable of survival in relatively arid environments. As a major component of wood lignin is of major technological significance, particularly in the pulp and paper industry

* Tel.: +64-7-373-5899; fax: +64-7-348-0952.
E-mail address: lloyd.donaldson@forestresearch.co.nz

0031-9422/01/$ - see front matter © 2001 Elsevier Science Ltd. All rights reserved.
PII: S0031-9422(01)00049-8

where lignin removal is often a major processing step. Because the distribution of lignin, or its topochemistry, influences commercial utilization of wood for both pulp and paper, and solid wood (although the latter is often not considered), this has been a topic of considerable interest since the early 1950s.

2. Ultrastructure of lignifying xylem

Lignification is one of the final stages of xylem cell differentiation, where lignin is deposited within the carbohydrate matrix of the cell wall by infilling of interlamellar voids, and at the same time, formation of chemical bonds with the non-cellulosic carbohydrates. The process of lignification has been studied by a variety of microscopy techniques including microautoradiography, histochemistry, UV absorbance, interference microscopy, fluorescence microscopy, and transmission electron microscopy. Lignification begins at the cell corners in the middle lamella and S1 regions, eventually spreading across the secondary wall towards the lumen. Lignification of the middle lamella and primary wall typically begins after the start of secondary wall formation, while lignification of the secondary wall usually begins when secondary wall formation is complete, as judged by the presence of an S3 layer (Wardrop, 1957, 1976; Hepler et al., 1970; Kutscha and Schwarzmann, 1975; Imagawa et al., 1976; Takabe et al., 1981, 1986; Saka and Thomas, 1982; Donaldson 1991, 1992).

2.1. Lignin formation

Lignin biosynthesis has recently been reviewed by Higuchi (1990) and Boudet (2000). Lignin monomers (coniferyl alcohol, sinapyl alcohol, *p*-coumaryl alcohol) are synthesized in the cytoplasm (golgi or endoplasmic reticulum), and are released into the cell wall from vesicles as monolignols or monolignol glucosides (Freudenberg et al., 1955; Wardrop, 1965; Pickett-Heaps, 1968; Hepler et al., 1970; Fujita et al., 1978b). Enzymes located within the cell wall during lignification, in either the free or bound state, including various types of peroxidase and oxidase (including laccase), have been shown to have a role in monolignol polymerization, both in vivo and in vitro (Goldberg et al., 1985; Nakashima et al., 1992; Terashima et al., 1995, 1996; Tsutsumi et al., 1998; Deighton et al., 1999). Oxidase activity may be associated with the earliest stages of lignification and peroxidase with the later stages so that the phytotoxic effects of H_2O_2 are avoided until apoptosis has commenced (Sterjiades et al., 1993). Both oxidase and peroxidase with specific activity against coniferyl or sinapyl alcohol have been identified (Tsutsumi et al., 1998; Deighton et al., 1999).

Because lignification starts in the region furthest from the protoplast, it has been suggested that there are initiation sites bound to specific regions of the cell wall, which begin the polymerization process as shown diagrammatically in Fig. 1 (Donaldson, 1994). Enzymes bound to specific locations in the cell wall could act as initiating sites. However, the observation that oxidase and peroxidase activities are restricted to lignifying cells during xylem formation (Hepler et al., 1972; Fukuda and Komamine, 1982; Goldberg et al., 1985; Yoshizawa et al., 1991; Czaninski et al., 1993; Nose et al., 1995; Deighton et al., 1999), suggests that these enzymes are not initiating sites. Ideally, initiating sites should be built into the wall during its formation (and thus be present in differentiating xylem prior to the onset of lignification), rather than relying on diffusion of enzymes to secondary binding sites in the primary wall or middle lamella. Although these enzymes are known to be present in cell walls undergoing lignification, little or no information is available on their exact location within the cell wall and how their distribution changes during the lignification process. For example it is not known if the complement of enzymes within the cell wall changes in relation to the type of lignin being formed, or if it is the substrate that changes, or both. Ultrastructural localization of both enzymes and substrates is needed to confirm their relative roles in controlling lignin topochemistry. This is no easy task given the nature of the substrates, which would readily diffuse

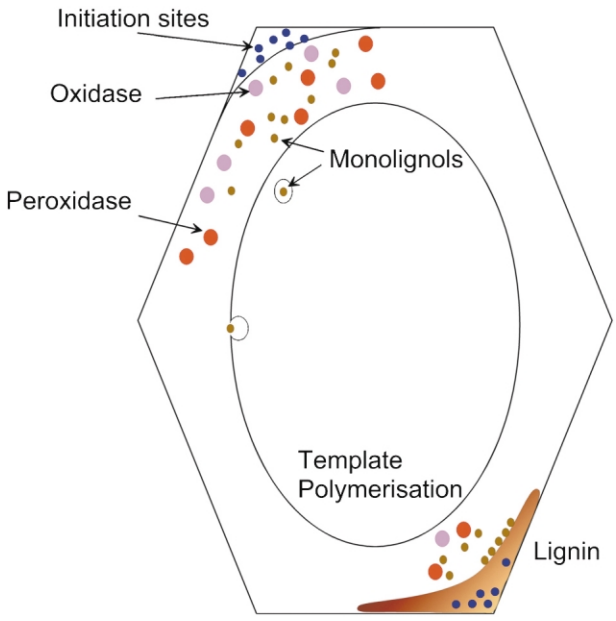

Fig. 1. A tentative scheme for the lignification process in xylem cell walls. Monolignols are released into the cell wall from the protoplast and diffuse towards initiation sites where the polymerisation process begins. Lignification is mediated by a range of free and bound enzymes and occurs by addition of monolignols to the expanding lignin polymer in a process known as template polymerisation. The nature of initiating sites and the way in which the amount and type of lignin formation is controlled across the cell wall are poorly understood.

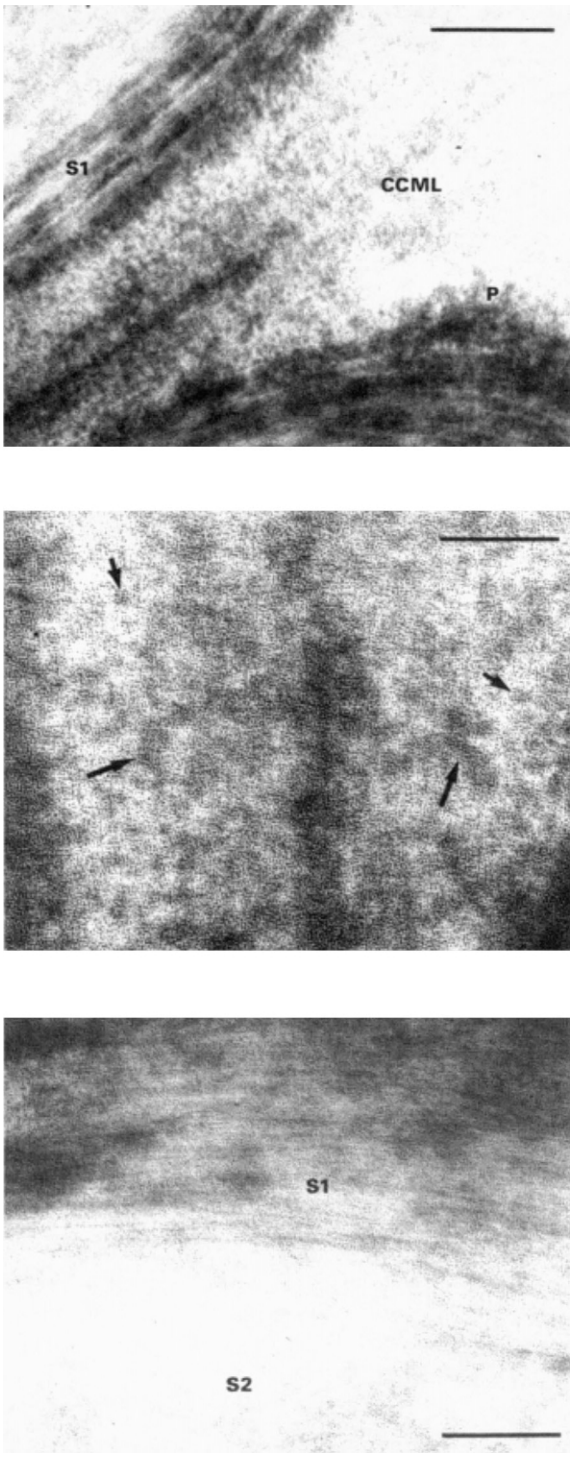

Fig. 2. Transmission electron microscopy of lignifying cell corner middle lamella (ccml), primary wall (P) and S1 regions in *Pinus radiata* after permanganate staining for lignin. Lignification is initiated in the central zone of the middle lamella and in the S1 region of the secondary wall. Arrows indicate small particles of lignin associated with initiation sites. The particles eventually coalesce (long arrows) to form a continuous matrix. Particles are rounded in the middle lamella region but form greatly elongated structures in the S1 region because of the orienting effect of the cellulose microfibrils. Scalebars top 440 nm, middle 170 nm, bottom 250 nm. (Reproduced with permission from Donaldson, 1994.)

out of the sample during most types of preparation for microscopy. The use of some form of cryo-microscopy may prove effective at fixing the substrates within the cell wall although localization remains a problem.

Initiating sites may be rich in calcium, thought to be needed for H_2O_2 formation via enzymatically produced superoxide radicals, a prerequisite for polymerization of coniferyl alcohol in the absence of laccase or oxidase activity (Wardrop, 1976; Westermark, 1982; Westermark et al., 1986). Other candidates for initiating sites include arrays of dirigent sites (proline-rich proteins, extensins) (Nose et al., 1995; Müsel et al., 1997; Davin et al., 1997; Devin and Lewis, 2000), and cell wall polysaccharides (Terashima et al. 1995, 1996). Little is known about the nature and distribution of cell wall proteins in differentiating xylem, especially in relation to lignification (Westermark et al., 1986; Bao et al., 1992; Ryser and Keller 1992). Bao et al. (1992) describe an extensin-like protein from differentiating xylem and mature wood of loblolly pine (*Pinus taeda* L.). Müsel et al. (1997) studied lignification in primary xylem and showed that proline-rich proteins were localized in secondary wall thickenings prior to lignification. Because primary and secondary xylem lignify differently (typically only the secondary wall lignifies in primary xylem), a comparison of these two tissues may provide useful insight in to the problem of initiation. Dirigent (non-enzymatic) proteins are known to have a role in lignan biosynthesis (Davin et al., 1997) but their involvement in lignification [proposed as arrays of dirigent (monomer binding) sites] remains a controversial issue (Davin and Lewis, 2000). It is thought that the lignin macromolecules themselves act as templates for further lignification once the process has been initiated (Sarkanen, 1998).

Lignification is influenced by the carbohydrate matrix in which it occurs. Donaldson (1994) studied the early stages of lignification in radiata pine by transmission electron microscopy. Growing lignin particles in the middle lamella and primary wall form roughly spherical structures within the randomly arranged matrix, while in the secondary wall, lignin lamellae form greatly elongated structures, following the orientation of microfibrils in this region of the cell wall (Fig. 2). It was concluded that the carbohydrate components of the cell wall exert a mechanical influence on the expanding lignin lamellae during lignification. Using a Raman microprobe, Atalla and Agarwal (1985) have shown that the aromatic rings of lignin are often oriented within the plane of the cell wall, possibly also as a result of the mechanical or chemical influence of the carbohydrate wall components. At the same time, lignin is forming chemical bonds with the hemicellulose component of the cell wall, which acts as a bridge or adhesive, ensuring coherence between the matrix phase and the cellulose microfibrils (Meshitsuka et al., 1982; Minor, 1986; Iversen et al., 1987; Tanabe and Kobayashi 1988; Hansen and Björkman 1998;

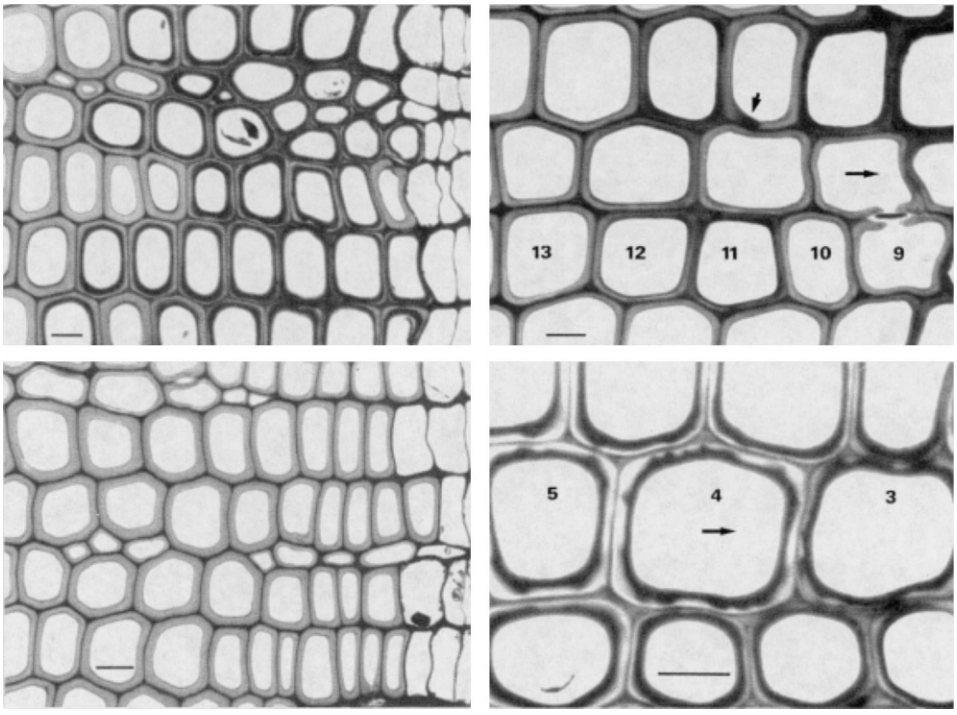

Fig. 3. Lignifying earlywood and latewood tracheids stained with toluidine blue in *Pinus radiata*. The numbers indicate the distance (cell number) from the cambium. The long arrows indicate the direction of the cambium while the short arrow indicates non-uniform lignification. The two images on the left show normal latewood, one sample showing partial lignification, the other showing full lignification. Both trees were sampled during the winter. The two images on the right show lignifying normal earlywood cells. Scalebars are all 10 μm. (Reproduced with permission from Donaldson, 1992.)

Salmén and Olsson 1998). The chemical nature of the carbohydrate environment in which lignin forms also has a recognized role in controlling the properties of the resulting polymer (Roussel and Lim, 1995; Terashima et al., 1995, 1996).

2.2. Topochemistry of lignification

In normal wood of Balsam fir (*Abies balsamea* (L.) Mill.) lignification starts in the middle lamella between pit borders, extending into the initial pit borders and cell corners, and then into the secondary wall (Kutscha and Schwarzmann, 1975). Similar patterns have been observed in *Pinus radiata* D. Don (Wardrop and Bland, 1959), *Larix leptolepis* Gord. (Imagawa et al., 1976), *Pinus thunbergii* Parl. (Takabe et al., 1981), and *Cryptomeria japonica* D. Don (Takabe et al., 1986). Cell corners adjacent to rays may lignify earlier than those more distant from the rays. All regions of the cell wall undergo continuing lignification until cell death and loss of the protoplast.

Lignification in loblolly pine was studied using bromination/EDXA by Saka and Thomas (1982). The middle lamella lignin concentration reached approximately 50% of its maximum before lignification of the secondary wall commenced. An S3 layer was detected prior to the start of secondary wall lignification, which was a more gradual process than the relatively rapid lignification of the middle lamella.

In lignifying xylem of *Picea glauca* (Moench) Voss, Yumoto et al. (1982) observed groups of tangentially arranged cells that differed from the surrounding lignifying cells when stained with hematoxylin-orange G, indicating these cells had not yet begun to lignify. Donaldson (1992) also observed differences in the state of lignification among adjacent cells (Fig. 3) suggesting that the lignification process is controlled to a significant extent by individual tracheids.

Lignification of secondary xylem has been studied by incorporation of radioactive precursors of lignin and subsequent microautoradiography. Saleh et al. (1967) treated cuttings of poplar, Douglas fir and wheat with tritiated ferulic acid[1] and demonstrated labeling of lignin, first in the primary wall at the cell corners, and subsequently in the middle lamella of radial and then tangential walls. Fujita and Harada (1979) later observed labeling of lignin in the secondary wall, also using tritiated ferulic acid as a precursor. Further studies by Terashima and coworkers demonstrated the formation and localization of *p*-hydroxyphenyl, guaiacyl, and syringyl lignins using a variety of labeled precursors including monolignol glucosides in pine, *Ginkgo*, sugarcane, *Magnolia*, *Syringa*, poplar, lilac, beech, rice, bamboo grass and orchid. In pine (Terashima and Fukushima, 1988; Terashima et al.,

[1] Ferulic acid is no longer considered a significant precursor for syringyl lignin (Li et al., 2000).

1988) and *Ginkgo* (Fukushima and Terashima, 1991a), *p*-hydroxyphenyl lignin is formed in the compound middle lamella and cell corner at an early stage of the lignification process. Guaiacyl lignins are first deposited in the middle lamella region and later in the secondary wall, while syringyl lignins are deposited in trace amounts during the late stages of secondary wall lignification. In pine, lignification was found to proceed in three stages (Terashima et al., 1988), lignification of the cell corner and middle lamella after S1 formation, slow lignification during secondary wall formation, and the main lignification after S3 formation. In magnolia (*Magnolia kobus* DC.) and poplar (*Populus maximowiczii* A. Henry *x berolinensis* C. Koch) (Terashima et al., 1986a,b), lignification was first observed in the vessel wall, cell corner and middle lamella, with formation of guaiacyl lignin, followed at a later stage by lignification of the fiber walls with a mixed guaiacyl-syringyl lignin. Deposition of *p*-hydroxyphenyl lignin occurred in the compound middle lamella of vessel and fiber cell walls during the early stages of secondary wall formation (Fukushima and Terashima, 1990).

Similar patterns of lignification are found in monocotyledons, with the additional formation of phenolic acids among all cell types. Ferulic acid is deposited in the middle lamella and cell corners during early lignification, while *p*-coumaric and sinapic acids are deposited in the secondary walls (He and Terashima, 1989a,b, 1990). The polylamelate walls of monocotyledonous fibers such as palms and bamboo show concentric variations in lignification corresponding to each wall layer (Itoh, 1990; Weiner et al., 1996). Such fibers remain living for extended periods and continue to develop new lamellae, which then undergo lignification.

During latewood formation in Japanese oak (*Quercus mongolica* Fisch.) (Yoshinaga et al., 1997a, b), guaiacyl lignin is deposited in vessel elements and vasicentric tracheids at all stages of lignification, while syringyl lignins are deposited in the later stages of lignification in fibers. Similar results were found in *Betula grossa* Sieb. et. Zucc., and *Aesculus turbinata* Blume (Yoshinaga et al., 2000). By comparing the rates of cell wall formation and lignification these authors conclude that cell walls rich in guaiacyl lignin are thickened rapidly and lignify slowly, while walls rich in syringyl lignin both thicken and lignify slowly.

Fujino and Itoh (1998) studied the lignification process in *Eucalyptus tereticornis* Sm. using rapid-freeze deep-etching electron microscopy to provide a 3D perspective on lignin deposition. This study clearly demonstrates the loss of wall porosity as lignin deposition proceeds, illustrating the likely reason for differences in lignin concentration among wall regions in mature wood. The highly porous carbohydrate matrix in the middle lamella and primary wall allows greater lignin deposition by space filling than the more densely packed secondary cell wall. Whether the uneven distribution of lignin in mature wood results entirely from differences in porosity of the carbohydrate matrix, or is a more actively controlled process, requires further investigation. For example there is evidence that the lignification of the middle lamella is reduced when the middle lamella and secondary wall lignify concurrently, presumably as a result of restricted access by monolignols due to blockage of diffusion pathways (Donaldson, 1991).

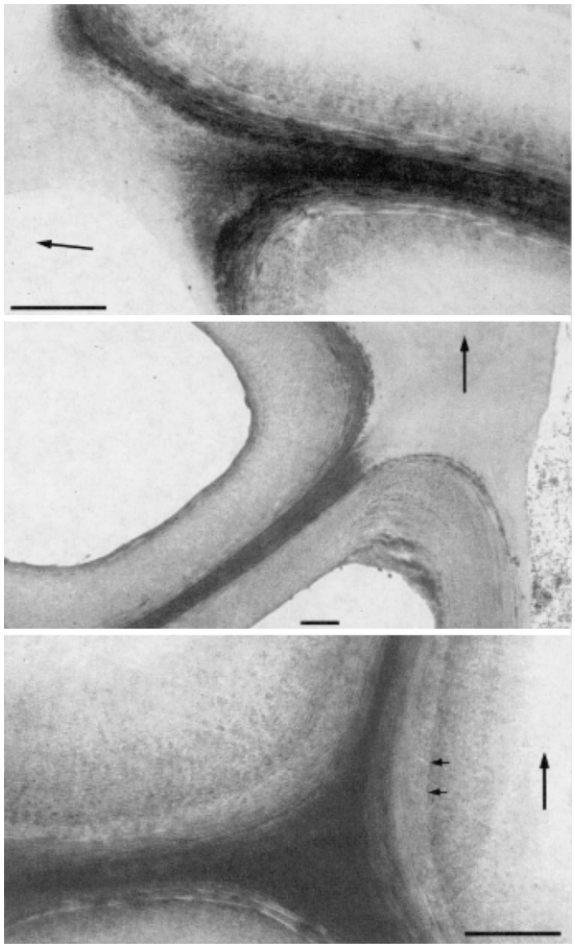

Fig. 4. Lignifying latewood tracheids stained with potassium permanganate and imaged by transmission electron microscopy in *Pinus radiata*. The three micrographs indicate different stages of secondary wall lignification. The top image shows an early stage of lignification, the middle image an almost complete state of lignification, and the bottom image an intermediate stage. The long arrows indicate the direction of the cambium. The short arrows indicate a lignification boundary within the S2 region. Scalebars are all 1 μm. (Reproduced with permission from Donaldson, 1992.)

The only known case of a lignification sequence markedly different to what is considered typical, is described by Engels and Jung (1998) in the primary phloem fibers of alfalfa stems. The primary phloem fibers show a 3-step pattern of cell wall development including a localized thickening of the primary wall, lignification of a thin region of primary wall at the lumen boundary,

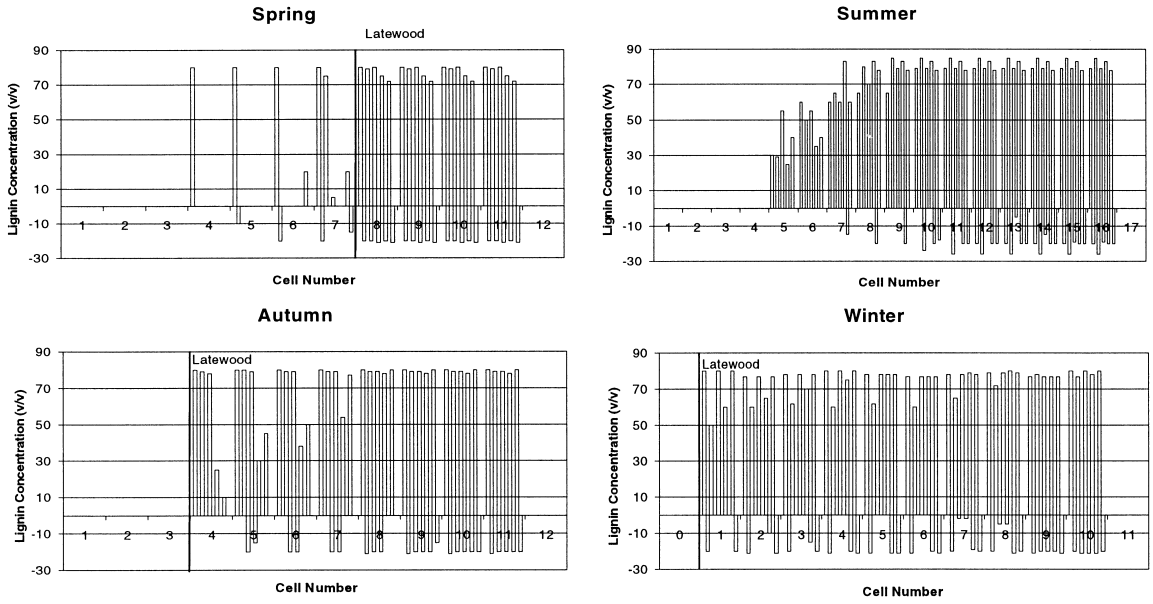

Fig. 5. Variations in lignification of the middle lamella and secondary wall during one growth season comparing 5 trees at each sample time. The upper values in each graph are for the cell corner middle lamella, while the lower values are for the S2 region. The cell numbers refer to the cells that were measured and not to the distance from the cambium as in previous figures. Varying numbers of cells were measured as required to cover the range from unlignified to fully lignified. In the case of spring and summer, the cambium is located beyond the left margin of each figure. In the case of autumn and winter, the cambium is located immediately to the left of the latewood boundary (Reproduced with permission from Donaldson 1991, 1992.)

and subsequent deposition of a thick unlignified secondary wall. These authors conclude that the lignified "ring" forms as a result of polymerization of monolignols at the lumen surface, thus preventing diffusion of monolignols into the middle lamella, which remains unlignified. This study is significant because it appears to describe a pattern of lignification that would be expected in the absence of initiating sites, i.e. where lignin forms adjacent to the protoplast rather than at some more remote location in the cell wall.

2.3. Seasonal and environmental effects on lignification

Donaldson (1991) studied the seasonal variations in lignification during one growth season in radiata pine. Although the pattern of lignification remained the same, the number of lignifying cells reached a maximum during the summer. Lignification of the secondary wall of latewood tracheids was often incomplete at the onset of winter (Figs. 3–5), with secondary walls remaining in a partially lignified state until early the following spring, suggesting that lignification is quite sensitive to environmental conditions such as temperature. Winter is thus the ideal time for microscopic study of lignification when the rapid early stages are well represented. Similarly Grand et al. (1979) found that light is necessary for incorporation of guaiacyl but not syringyl residues from radioactively labeled phenylalanine in poplar stems.

In one of the trees examined by Donaldson (1991) lignification occurred concurrently in both the middle lamella and secondary wall, and as a result, the middle lamella of mature wood showed below average lignin concentrations. Reduced lignification, especially in the middle lamella, has been reported for Cu deficient trees of *P. radiata* although the change in lignification was not directly attributed to the physiological effects of Cu deficiency (Downes et al. 1991).

3. Lignification of reaction wood

In view of the significant differences in lignin distribution between compression wood and normal wood, with the presence of a highly lignified S2L layer, it is surprising that many studies of the lignification process in compression wood describe a lignification sequence largely the same as in normal wood. The first investigation of lignification in any tree was a study of compression wood in *Pinus sylvestris* L. (Sanio, 1873). Sanio found that lignification started at the cell corners and progressed through the secondary wall towards the lumen. In radiata pine compression wood, the S1 region may show a reduction in lignification (Wardrop and Bland, 1961). Scurfield (1967) found that lignin was first deposited at the apex of intercellular spaces and subsequently spread into the secondary wall in radiata pine compression wood. The lignification process in compression wood of *Abies balsamea* has been studied by Kutscha (1968) using permanganate fixation and transmission electron microscopy, showing that the lignifica-

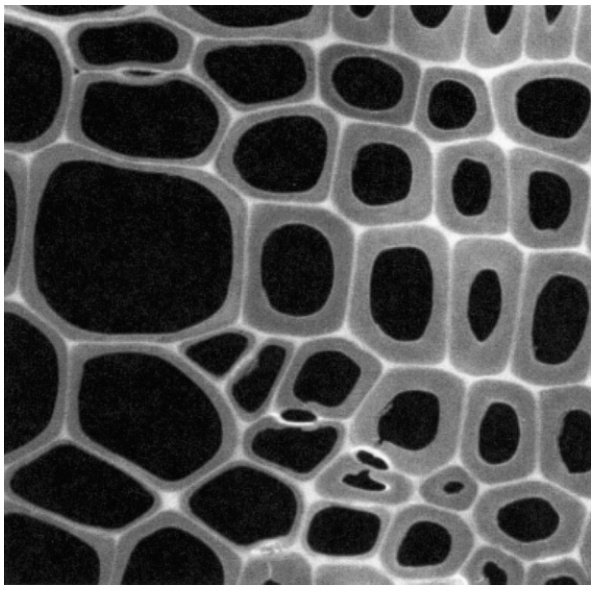

Fig. 6. Confocal fluorescence micrograph of *Pinus radiata* wood showing lignin autofluorescence at 530 nm. Increased brightness reflects higher lignin concentration. This image shows a growth ring boundary with thick walled latewood tracheids on the right. The image is 160 × 160 μm.

tion process was similar to that in normal wood. Fujita et al. (1978a,b) studied lignification in compression wood of *Cryptomeria japonica* and also observed a process similar to that of normal wood.

Fujita et al. (1978a,b) indicate that the lignification of the middle lamella is more distinctly separate from lignification of the secondary wall in compression wood compared to normal wood. These results were later confirmed by Fujita and Harada (1979) using autoradiography, indicating that lignification of the S2L region where most of the lignin is deposited, takes place after completion of secondary wall formation.

In a significant study, Fukushima and Terashima (1991b) used microautoradiography to study lignification of compression wood in *Pinus thunbergii*. Lignin was deposited in the order *p*-hydroxyphenyl, guaiacyl, and syringyl, which is the same sequence as normal wood. However *p*-hydroxyphenyl units were deposited in both the compound middle lamella and the S2 region in compression wood, in contrast to normal wood, where these units are deposited only in the compound middle lamella. Lignification of the secondary wall took place for an extended period in compression wood while S2 formation was still taking place, the most active lignification occurring in the outer S2 (S2L) region. In contrast, S2 lignification in normal wood became active only after S3 formation was complete. This study is one of the few to show distinct differences in the lignification process of normal and compression wood.

It is important to note that intercellular spaces present in severe compression wood do not lignify. If initiating sites are usually located in the cell corner region they must obviously be located elsewhere in this type of material, thus potentially accounting for the altered lignin distribution of compression wood. In mild compression wood the reduced lignification of the middle lamella may be due to an effect of the highly lignified S2L region on diffusion pathways into the middle lamella in the event of concurrent lignification in these two regions (Fukushima and Terashima, 1991b; Donaldson et al., 1999).

4. Lignin distribution in gymnosperms

Two distinct approaches have been used to study the distribution of lignin across the cell wall. Cell walls can be thin sectioned and examined by histochemistry or by other microscopy techniques such as UV absorbance. Alternatively, wood material can be finely ground to form minute cell wall fragments, which can subsequently be separated, purified according to their origin in the cell wall, and chemically analyzed.

A number of early investigations established that the compound middle lamella is more highly lignified than the secondary wall in typical softwood tracheids (Crocker, 1921; Ritter, 1925; Kerr and Bailey, 1934; Bailey, 1936; Bailey and Kerr, 1937; Staudinger, 1942; Lange, 1944, 1950; Lange and Kjaer, 1957; Jayme and Fengel, 1961; Hepler and Newcomb, 1963; Sachs et al., 1963; Meier, 1964; Côté et al., 1966, 1968; Bucher, 1968; Côté and Day, 1969; Norberg, 1969; Hepler et al., 1970; Parham and Côté, 1971; Kutscha and Gray, 1972; Parham, 1974). Some inference was also made from comparison of lignin content with the morphological variability of the tracheid walls (Ritter and Fleck, 1926; Hale and Clermont, 1963; Berlyn and Mark, 1965; Larson, 1966; Stamm and Sanders, 1966; Siddiqui, 1976). However, detailed quantitative information on the distribution of lignin in the tracheid wall was not available until the development of quantitative methods such as UV microscopy (Scott et al., 1969; Scott and Goring, 1970b; Wood and Goring, 1974).

The compound middle lamella region of the cell wall typically contains more than 50% lignin concentration (w/w) while the S2 region contains about 20% (Fig. 6). However, because the secondary wall represents a much greater volume than the relatively thin middle lamella, most of the lignin in wood is located in the secondary wall, a point which caused much confusion in the early literature. It is thus important to differentiate between lignin concentration (within a cell wall region) and lignin content (a measure of lignin in bulk samples which is thus dependent on variations in anatomy such as cell wall thickness and earlywood/latewood proportion). The cell corner middle lamella is often more highly lignified than the compound middle lamella with reported values above 70% lignin concentration (Fergus et al., 1969;

Wood and Goring, 1971; Boutelje, 1972; Fukazawa and Imagawa, 1981; Saka et al., 1981; Boutelje and Eriksson, 1982, 1984; Takano et al., 1983; Donaldson, 1985, 1986, 1993; Donaldson et al., 1997; Westermark et al., 1988). Comparisons of earlywood and latewood tracheids indicate little if any difference in lignin distribution as is the case for juvenile and mature wood (Fergus et al., 1969; Wood and Goring, 1971; Fukazawa and Imagawa, 1981; Takano et al., 1983; Donaldson, 1985; Gindl et al., 2000). Differences in the lignin content of earlywood and latewood probably arise almost entirely from variations in cell wall morphology within the growth ring. A thicker secondary wall in latewood tracheids reduces the contribution of the high middle lamella lignin concentration, resulting in a slightly lower lignin content for latewood (Siddiqui, 1976). However Gindl et al. (2000) using *Picea abies* (L.) Karst. and UV microscopy, have reported a reduction in the lignin concentration of the S2 region of the terminal latewood cells. The lignin concentration of these cells was found to be correlated with autumn temperature under alpine growing conditions.

Values determined by microscopy seem to agree quite well with those determined by analysis of cell wall fractions (Hardell et al., 1980a; Whiting et al., 1981; Whiting and Goring, 1982a; Sorvari et al., 1983, 1986).

Significant variation among trees in lignin concentration, especially in the cell corner middle lamella, has been reported for radiata pine using interference microscopy (Donaldson, 1985, 1986). Later studies with clones confirmed that this between tree variation is genetic in origin (Donaldson, 1993; Donaldson et al., 1997).

Although the S2 layer in normal wood is typically uniformly lignified it may occasionally show concentric variations in lignification (Daniel and Nilsson, 1984).

Lignification of the S1 region is variously described as similar to the middle lamella, intermediate between the middle lamella and S2 region, or similar to the S2 region, depending on species and technique used (Sachs et al., 1963; Bland et al., 1971; Parham and Côté, 1971; Timell, 1973; Saka et al., 1979, 1981). Maurer and Fengel (1991) describe lignin distribution in the S1 region as being in two distinct parts, high in the outer and low in the inner regions for *Picea abies*. Donaldson (1995) describes the lignification of the S1 region in *P. radiata* as patchy and generally lower than that of the S2 layer, especially at the S1/S2 boundary. This reduced lignification has been ascribed to the occurrence of cell wall fracturing at the S1/S2 boundary during processing in radiata pine.

The S3 layer has often been reported to be more highly lignified than the adjacent S2 layer (Jayme and Fengel, 1961; Sachs et al., 1963, 1965; Wergin, 1965; Côté et al., 1966; Scott and Goring, 1970a; Bland et al., 1971; Parham and Côté, 1971; Timell, 1973; Saka et al., 1981; Donaldson, 1987). Quantitative studies indicate values intermediate between the S2 and compound middle lamella but the general opinion is that the lignification state of the S3 layer is a variable feature (Scott and Goring, 1970a). Lignin concentration in the S3 layer is similar to that in the S2 region in both Douglas fir and Larch. Little information is available on species outside of the Pinaceae.

Initial pit borders (part of the primary cell wall) are more lignified than adjacent parts of the pit border (Singh, 1997). Pit membranes including the torus of bordered pits, are unlignified, although in heartwood, impregnation with extractives may be confused with lignification (Bamber, 1961; Bauch et al., 1968; Bauch and Berndt, 1973).

Analysis of cell wall fractions has indicated that secondary wall lignin of *Picea abies*, *Picea mariana* (Mill.) B.S.P., and *Pseudotsuga menziesii* (Mirb.) Franco, contains about twice as many phenolic-OH groups as lignin from the middle lamella (Sorvari et al., 1983, 1986; Whiting and Goring, 1982a,b; Hardell et al., 1980a; Yang and Goring, 1978, 1980). Middle lamella lignin has a higher molecular weight and a higher oxygen content compared to secondary wall lignin (Sorvari et al., 1983, 1986).

Using microautoradiography, Terashima and Fukushima (1988) found high levels of *p*-hydroxyphenyl lignin in the compound middle lamella in *Pinus thunbergii*. Condensed guaiacyl units were also higher in the middle lamella compared to the secondary wall. Traces of syringyl lignin were found in the inner secondary wall. In contrast, Westermark (1985) found that normal wood of *Picea abies* contains low levels of *p*-hydroxyphenyl units in the middle lamella.

Little information is available on the lignification of ray cells, which probably varies with cell type and species. Harada and Wardrop (1960) examined the lignification of ray parenchyma in *Cryptomeria japonica* using UV microscopy and interference microscopy, indicating a relatively high lignin concentration (44%) with lignin distributed evenly across the cell wall. A high lignin concentration in ray cells was also reported in spruce by Westermark et al. (1988). In pines, thick-walled ray parenchyma and ray tracheids are lignified, while thin walled parenchyma are unlignified (both types may be present within a species). Thick-walled ray parenchyma cells and axial tracheids are lignified to a similar extent in larch (Côté et al., 1968). Bamber and Davies (1969) suggest that thin walled ray parenchyma cells may become lignified during heartwood formation in radiata pine.

Resin canal epithelial cells are unlignified while associated strand tracheids are lignified to the same extent as axial tracheids (Bamber, 1972).

5. Lignin distribution in angiosperms

In contrast to gymnosperms where lignin is predominantly made up of guaiacyl units, angiosperm lig-

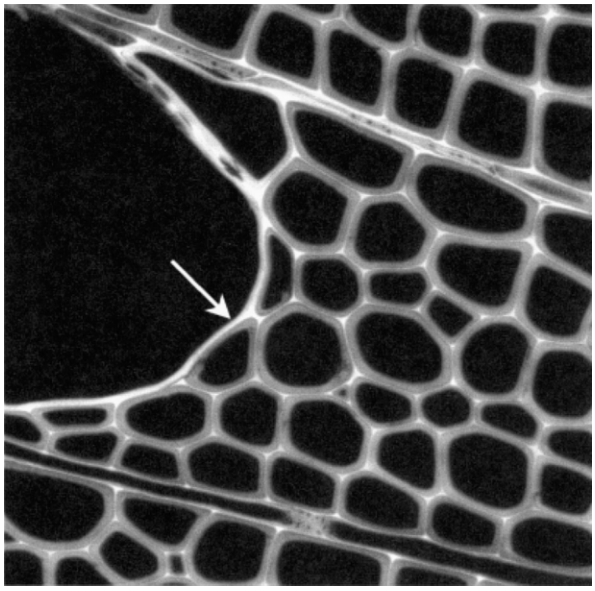

Fig. 7. Confocal fluorescence micrograph of *Populus nigra* Du Roi, stained with acriflavine to show lignin distribution. Increased brightness reflects higher lignin concentration. Note the more highly lignified vessel cell wall (arrow). The image is 160×160 μm.

nin contains a mixture of guaiacyl and syringyl units. The vessel secondary wall and middle lamella of typical hardwoods contains guaiacyl units while the secondary walls of fibers and the cell walls of parenchyma cells contains a mixture of guaiacyl and syringyl units with the latter predominating (Fergus and Goring, 1970a,b; Musha and Goring, 1975a,b; Hardell et al., 1980b; Kolar et al., 1982; Saka and Goring, 1988; Wu et al., 1990, 1992; Takabe et al., 1992; Yoshinaga et al., 1992; Peng and Westermark, 1997; Ruel et al., 1999). In white birch the G/S ratio of vessel secondary walls was found to be 88:12 while in fiber walls the ratio was 12:88, and in parenchyma walls 49:51 (Saka and Goring, 1988). However, these ratio's may vary significantly among species (Fujii et al., 1987). Wu et al. (1992) in a survey of 25 hardwood species from China, found that the monomeric composition of lignin was influenced by cell type, location within a growth ring, vessel arrangement and tree habitat. Three major patterns were found including:

1. All elements rich in guaiacyl lignin represented by vessel-less hardwoods and some tropical diffuse porous woods.
2. Vessels with guaiacyl lignin and fibers with guaiacyl/syringyl lignin, represented by diffuse porous woods.
3. Vessels with guaiacyl/syringyl lignin in variable ratios, represented by ring-porous and radial porous woods.

Vessel secondary walls may be more highly lignified in some species (Fig. 7). Vessel cell walls must withstand the large compressive forces resulting from the transpiration stream in plants and hence an increased lignification of the cell wall would be expected to increase the compression strength of the vessel and reduce its susceptibility to collapse (Yoshinaga et al., 1992). Takabe et al. (1992) examined lignin distribution in secondary xylem of *Fagus crenata* Blume, using UV microscopy. Their micrographs clearly show increased lignification of vessel secondary walls in earlywood, but not in latewood. Yoshizawa et al. (1993a, b) studied lignin distribution in normal and "compression wood" of *Buxus microphylla* Nakai, using UV microscopy and fluorescence microscopy, both techniques showing vessel secondary walls to be more highly lignified than adjacent fibers. Using mercurisation combined with EDXA, Eriksson et al. (1988) found the cell wall of vessels and ray cells had a lignin concentration 1.5–1.6× that of the fiber secondary wall.

The lignin distribution between secondary wall and middle lamella in hardwood fibers is similar to that in softwoods, however the secondary wall of hardwood fibers is often less lignified than the secondary wall of softwood tracheids. Fergus and Goring (1970b) examined lignin distribution in white birch using UV microscopy and found values for lignin concentration of 16–19% for the secondary wall of fibers, and 72–85% for the middle lamella. Saka and Goring (1988) determined the lignin concentration in the S2 and middle lamella regions of fibers and vessels of white birch using bromination combined with TEM/EDS. The average value for the S2 region of fiber walls was 16% (w/w) while for vessels the comparable value was 22%. The average value for the middle lamella region was 72%.

Cho et al. (1980) examined the chemical characteristics of middle lamella lignin isolated from birch (*Betula ermanii* (Nakai) T. Shimizu). The lignin content of this fraction was found to be 44% with a lower syringaldehyde/vanillin molar ratio among the nitrobenzene oxidation products and fewer methoxyl groups compared to the secondary wall fraction.

Variability in lignification within the middle lamella region has been reported in several studies. Singh and Schmitt (2000) studied lignin distribution in *Hevea brasiliensis* Engl. (rubber wood) with transmission electron microscopy and permanganate staining. They describe poorly lignified areas within the otherwise highly lignified cell corner regions between fibers, later confirmed by UV absorbance measurements on the same material. Similar observations have been made by Daniel et al. (1991) and by Tirumalai et al (1996), in birch.

6. Lignin distribution in reaction wood

Several studies of lignin distribution in compression wood have shown that the middle lamella region is less lignified than in normal wood (Côté et al., 1968; Wood

and Goring, 1971; Fukazawa, 1974; Donaldson, 1991; Donaldson et al., 1999). The presence of intercellular spaces at the cell corners, reduces the contribution of middle lamella lignin to the lignin content of compression wood. Lignin content is generally much higher than normal wood as a result of the more highly lignified secondary wall (Watson and Dadswell, 1957; Bland, 1958; Young et al., 1970). The highly lignified S2L layer (Fig. 8) (Lange, 1950; Wardrop and Davies, 1964; Wood and Goring, 1971; Fukazawa, 1974; Donaldson et al., 1999; Singh and Donaldson, 1999; Wi et al., 2000) is characteristic of both mild and severe forms of compression wood, not only in the Coniferales but also in the Ginkgoales and Taxales (Timell, 1978a,b; Yumoto et al., 1983; Yoshizawa et al., 1992; Wi et al., 2000). The increased lignification of the outer secondary wall in compression wood is thought to contribute to the formation of helical checking and the resulting longitudinal swelling is the mechanism by which compression wood achieves the correction of stem lean in standing trees (Boyd, 1973).

Lignin distribution may be highly variable within a single sample of compression wood. Donaldson et al. (1999) found concentrations of 26, 46, and 57% (v/v) for the S2, S2L, and cell corner middle lamella regions respectively in mild compression wood of *Pinus radiata*, with significant variation among adjacent cells. The inner S2 region of compression wood tracheids often shows radial lignin striations parallel to, and associated with, helical checking (Singh et al., 1998). The distribution of lignin subunits also varies in compression wood. *p*-Hydroxyphenyl units occur in both the compound middle lamella and in the secondary wall especially in the S2L region (Fukushima and Terashima, 1991b).

Lignin distribution in reaction wood of the more primitive angiosperms is similar to that in the compression wood of gymnosperms. Yoshizawa et al. (1993a,b, 1999) studied lignin distribution in the "compression wood" of *Buxus microphylla* using UV microscopy and fluorescence microscopy, both techniques showing vessel secondary walls to be more highly lignified than adjacent fibers. A highly lignified S2L region was observed in both vessel and fiber-tracheid cell walls. While normal wood of this species contains a mixture of guaiacyl and syringyl lignins, compression wood showed an increased content of guaiacyl lignin (Yoshizawa et al., 1993a,b, 1999).

Very few studies of lignin distribution in tension wood have been completed, especially using modern techniques (Fig. 8). Tension wood is characterized by the presence of a gelatinous layer forming part of the secondary wall in fibers. This gelatinous layer is considered to be unlignified and to consist of highly crystalline cellulose (Lange, 1950; Wardrop and Dadswell, 1955; Norberg and Meier, 1966; Robards, 1966, 1967; Robards and Purvis, 1967). The lignification of the S2 and S3 layers if present may be variable. Ruel et al. (1999) studied the distribution of lignin subunits in *Eucalyptus gunnii* Hook.f. tension wood, indicating a low proportion of condensed guaiacyl-syringyl subunits in the S2 region of the fiber walls. Distribution of lignin in tension wood of *Acer rubrum* L., *Fagus grandifolia* Ehrh., *Populus tremuloides* Michx., and *Ulmus americana* L., has been studied using the lignin skeleton method (Bentum et al., 1969). Normal and tension wood in these species showed a similar lignin distribution except for the unlignified G layer. The ultrastructure of tension wood in *Populus tremuloides* and *Acer rubrum* has been examined by Blanchette et al. (1994) who found a complete lack of

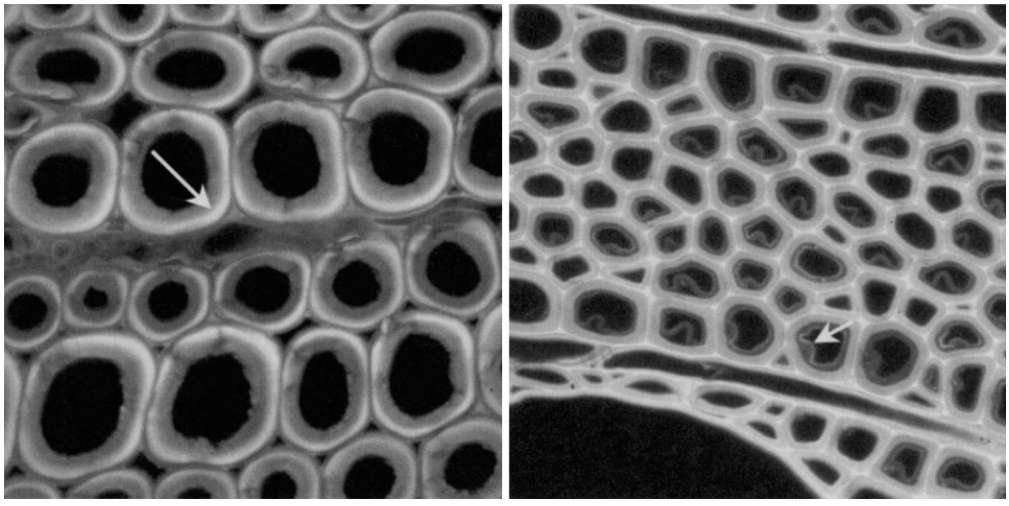

Fig. 8. Confocal fluorescence micrographs of compression wood (*Pinus radiata* left) and tension wood (*Populus nigra* right) stained with acriflavine showing lignin distribution. Increased brightness reflects higher lignin concentration. Note the presence of a highly lignified S2L region in the secondary wall (long arrow) The poplar micrograph has been overexposed to enable visualization of the unlignified G layer (short arrow) adjacent to the fiber lumen. In this case the G layer is unstained and is visualized by its extremely weak autofluorescence. Each image is 160×160 μm.

lignin in the G layer but normal lignin distribution in the rest of the secondary wall.

7. Conclusions

The process of lignin deposition within the cell wall during xylem formation appears to be highly controlled, requiring initiation sites and a complement of cell wall localized enzymes. The process of lignin deposition is thought to be an example of template polymerization and is still poorly understood. Further research is needed to understand the role of initiating sites including identifying the nature of such sites, and to understand the roles of enzymes and the cell wall matrix during lignin deposition. The involvement of peroxidase, laccase and oxidase enzymes, and arrays of dirigent (monomer binding) sites in the lignification process remain controversial. There is ample scope for immunolocalisation of these proteins in order to understand their spatial relationship to the lignification process. There is a need for novel histochemical techniques to localize specific monolignols or their glucosides within the cell walls of lignifying cells. Similarly there is a need to localize both enzymes and substrates involved in monolignol biosynthesis within the cytoplasm. It is anticipated that molecular biology will play an increasing role in the understanding of the lignification process.

Lignin shows a variety of qualitative and quantitative differences in its distribution. Typically there is a highly lignified middle lamella containing a predominance of guaiacyl units, and a less lignified secondary wall containing guaiacyl units in gymnosperms, or a mixture of guaiacyl and syringyl units in angiosperms. The type of lignin structural units in angiosperm xylem can often be distinguished on the basis of cell function (structural support versus water conduction — the former favoring a less highly lignified secondary wall containing syringyl units, the latter favoring a more highly lignified secondary wall containing guaiacyl units). Work continues to explore the natural diversity of lignified cell walls. More studies are needed on the influence of environment on lignification and its interaction with genotype.

References

Atalla, R.H., Agarwal, U.P., 1985. Raman microprobe evidence for lignin orientation in cell walls of native woody tissue. Science 227, 636–638.

Bailey, I.W., 1936. Lignin in Douglas fir. Composition of the middle lamella. Ind. Eng. Chem. 8, 52–55.

Bailey, I.W., Kerr, T., 1937. The structural variability of the secondary wall as revealed by lignin residues. J. Arnold Arbor. 18, 261–272.

Bamber, R.K., 1961. Staining reaction of the pit membrane of wood cells. Nature 191, 409–410.

Bamber, R.K., 1972. Properties of the cell walls of the resin canal tissue of the sapwood and heartwood of *Pinus lambertiana* Dougl. and *P. radiata* D. Don. J. Inst. Wood Sci. 6, 32–35.

Bamber, R.K., Davies, G.W., 1969. Lignification of ray parenchyma cell walls in the wood of *Pinus radiata* D. Don. Holzforschung 23, 83–84.

Bao, W., O'Malley, D.M., Sederoff, R.R., 1992. Wood contains a cell-wall structural protein. Proc. Natl. Acad. Sci. USA 89, 6604–6608.

Bauch, J., Berndt, H., 1973. Variability of the chemical composition of pit membranes in bordered pits of gymnosperms. Wood Sci. Technol. 7, 6–19.

Bauch, J., Liese, W., Scholz, F., 1968. On the development and chemical composition of the membranes in bordered pits of conifers. Holzforschung 22, 144–153.

Bentum, A.L.K., Côté, W.A., Day, A.C., Timell, T.E., 1969. Distribution of lignin in normal and tension wood. Wood Sci. Technol. 3, 218–231.

Berlyn, G.P., Mark, R.E., 1965. Lignin distribution in wood cell walls. For. Prod. J. 16, 140–141.

Blanchette, R.A., Obst, J.R., Timell, T.E., 1994. Biodegradation of compression wood and tension wood by white and brown rot fungi. Holzforschung 48 (Suppl.), 34–42.

Bland, D.E., 1958. The chemistry of reaction wood. I. The lignins of *Eucalyptus goniocalyx* and *Pinus radiata*. Holzforschung 12, 36–43.

Bland, D.E., Foster, R.C., Logan, A.F., 1971. The mechanism of permanganate and osmium tetroxide fixation and distribution of lignin in the cell wall of *Pinus radiata*. Holzforschung 25, 137–143.

Boudet, A.-M., 2000. Lignins and lignification: selected issues. Plant Physiol. Biochem. 38, 81–96.

Boutelje, J.B., 1972. Calculation of lignin concentration and porosity of the cell wall regions by interference microscopy. Sven. Papperstidn. 75, 683–686.

Boutelje, J.B., Eriksson, I., 1982. An UV-microscopic study of lignin in middle lamella fragments from fibers of mechanical pulp of spruce. Sven. Papperstidn. 85, R39–42.

Boutelje, J.B., Eriksson, I., 1984. Analysis of lignin in fragments from thermomechanical spruce pulp by ultraviolet microscopy. Holzforschung 38, 249–252.

Boyd, J.D., 1973. Helical fissures in compression wood cells: Causative factors and mechanics of development. Wood Sci. Technol. 7, 92–111.

Bucher, H., 1968. Der mikroskopische Nachweis von Lignin in verholzten Fasern durch Jod-Malachitgrün. Papier 22, 390–396.

Cho, N.S., Lee, J.Y., Meshitsuka, G., Nakano, J., 1980. On the characteristics of hardwood compound middle lamella lignin. Mokuzai Gakkaishi 26, 527–533.

Côté, W.A., Day, A.C., 1969. Wood ultrastructure of the southern pines. NY Coll. For. Syracuse Tech. Publ. 95, p. 70.

Côté, W.A., Day, A.C., Timell, T.E., 1968. Studies on compression wood VII. Distribution of lignin in normal and compression wood of tamarack *Larix laricina* (Du Roi, K. Koch). Wood Sci. Technol. 2, 13–37.

Côté, W.A., Timell, T.E., Zabel, R.A., 1966. Studies on compression wood I. Distribution of lignin in compression wood of red spruce (*Picea rubens* Sarg.). Holz Roh-Werkstoff 24, 432–438.

Crocker, E.C., 1921. An experimental study of the significance of lignin color reactions. Ind. Eng. Chem. 13, 625–627.

Czaninski, Y., Sachot, R.M., Catesson, A.M., 1993. Cytochemical localization of hydrogen peroxide in lignifying cell walls. Ann. Bot. 72, 547–550.

Daniel, G., Nilsson, T., 1984. Studies of the S2 Layer of *Pinus sylvestris* L. Swedish University of Agricultural Sciences, Uppsala, Sweden. Report no. 154, pp. 1–34.

Daniel, G., Nilsson, T., Pettersson, B., 1991. Poorly and non-lignified regions in the middle lamella cell corners of birch (*Betula verrucosa*) and other wood species. IAWA Bull. n.s. 12, 70–83.

Davin, L.B., Wang, H.-B., Crowell, A.L., Bedgar, D.L., Martin, D.M., Sarkanen, S., Lewis, N.G., 1997. Stereoselective bimolecular phenoxy radical coupling by an auxiliary (dirigent) protein without an active center. Science 275, 362–366.

Davin, L.B., Lewis, N.G., 2000. Dirigent proteins and dirigent sites explain the mystery of specificity of radical precursor coupling in lignan and lignin biosynthesis. Plant Physiology 123, 453–461.

Deighton, N., Richardson, A., Stewart, D., McDougall, G.J., 1999. Cell-wall associated oxidases from the lignifying xylem of angiosperms and gymnosperms: monolignol oxidation. Holzforschung 53, 503–510.

Donaldson, L.A., 1985. Within- and between-tree variation in lignin concentration in the tracheid cell wall of *Pinus radiata*. NZ Journal of Forestry Science 15, 361–369.

Donaldson, L.A., 1986. Between-tree variation in lignin concentration in *Pinus radiata* tracheids with growth rate, stem eccentricity, site and silvicultural treatment. NZ Journal of Forestry Science 16, 118–123.

Donaldson, L.A., 1987. S3 Lignin concentration in radiata pine tracheids. Wood Sci. Technol. 21, 227–234.

Donaldson, L.A., 1991. Seasonal changes in lignin distribution during tracheid development in *Pinus radiata* D. Don. Wood Sci. Technol. 25, 15–24.

Donaldson, L.A., 1992. Lignin distribution during latewood formation in *Pinus radiata* D. Don. IAWA Bull. n.s. 13, 381–387.

Donaldson, L.A., 1993. Lignin distribution in wood from a progeny trial of genetically selected *Pinus radiata* D. Don. Wood Sci. Technol. 27, 391–395.

Donaldson, L.A., 1994. Mechanical constraints on lignin deposition during lignification. Wood Sci. Technol. 28, 111–118.

Donaldson, L.A., 1995. Cell wall fracture properties in relation to lignin distribution and cell dimensions among three genetic groups of radiata pine. Wood Sci. Technol. 29, 51–63.

Donaldson, L.A., Croucher, M., Uprichard, J.M., 1997. Clonal variation of wood chemistry variables in radiata pine (*Pinus radiata* D. Don.) wood. Holzforschung 51, 537–542.

Donaldson, L.A., Singh, A.P., Yoshinaga, A., Takabe, K., 1999. Lignin distribution in mild compression wood of *Pinus radiata* D. Don. Can J. Bot. 77, 41–50.

Downes, G.M., Ward, J.V., Turvey, N.D., 1991. Lignin distribution across tracheid cell walls of poorly lignified wood from deformed copper deficient *Pinus radiata* (D. Don). Wood Sci. Technol. 25, 7–14.

Engels, F.M., Jung, H.G., 1998. Alfalfa stem tissues: Cell-wall development and lignification. Ann. Bot. 82, 561–568.

Eriksson, I., Lidbrandt, O., Westermark, U., 1988. Lignin distribution in Birch (*Betula verrucosa*) as determined by mercurisation with SEM-TEM-EDXA. Wood Sci. Technol. 22, 251–257.

Fergus, B.J., Goring, D.A.I., 1970a. The location of guaiacyl and syringyl lignins in birch xylem tissue. Holzforschung 24, 113–117.

Fergus, B.J., Goring, D.A.I., 1970b. The distribution of lignin in birch wood as determined by ultraviolet microscopy. Holzforschung 24, 118–124.

Fergus, B.J., Procter, A.R., Scott, J.A.N., Goring, D.A.I., 1969. The distribution of lignin in Spruce wood as determined by ultraviolet microscopy. Wood Sci. Technol. 3, 117–138.

Freudenberg, K., Reznik, H., Fuchs, W., Reichert, M., 1955. Untersuchungen über die Entstehung des Lignins und des Holzes. Die Naturwissenschaften 42, 29–35.

Fujii, T., Shimizu, K., Yamaguchi, A., 1987. Enzymatic saccharification on ultrathin sections and ultraviolet spectra of Japanese hardwood and softwoods. Mokuzai Gakkaishi 33, 400–407.

Fujino, T., Itoh, T., 1998. Changes in the three dimensional architecture of the cell wall during lignification of xylem cells in *Eucalyptus tereticornis*. Holzforschung 52, 111–116.

Fujita, M., Harada, H., 1979. Autoradiographic investigations of cell wall development. II. Tritiated phenylalanine and ferulic acid assimilation in relation to lignification. Mokuzai Gakkaishi 25, 89–94.

Fujita, M., Saiki, H., Harada, H., 1978a. The secondary wall formation of compression wood tracheids. II. Cell wall thickening and lignification. Mokuzai Gakkaishi 24, 158–163.

Fujita, M., Saiki, H., Harada, H., 1978b. The secondary wall formation of compression wood tracheids. III. Cell organelles in relation to cell wall thickening and lignification. Mokuzai Gakkaishi 24, 353–361.

Fukazawa, K., 1974. The distribution of lignin in compression- and lateral-wood of *Abies sachalinensis* using ultraviolet microscopy. Res. Bull. Coll. Exp. For. Hokkaido Univ. 31, 87–114.

Fukazawa, K., Imagawa, H., 1981. Quantitative analysis of lignin using an UV microscopic image analyzer. Variation within one growth increment. Wood Sci. Technol. 15, 45–55.

Fukuda, H., Komamine, A., 1982. Lignin synthesis and its related enzymes as markers of tracheary element differentiation in single cells isolated from the mesophyll of *Zinnia elegans*. Planta 155, 423–430.

Fukushima, K., Terashima, N., 1990. Heterogeneity in formation of lignin XIII. Formation of *p*-hydroxyphenyl lignin in various hardwoods visualized by microautoradiography. J. Wood Chem. Technol. 10, 413–433.

Fukushima, K., Terashima, N., 1991a. Heterogeneity in formation of lignin XIV. Formation and structure of lignin in differentiating xylem of *Ginkgo biloba*. Holzforschung 45, 87–94.

Fukushima, K., Terashima, N., 1991b. Heterogeneity in formation of lignin. Part XV: Formation and structure of lignin in compression wood of *Pinus thunbergii* studied by microautoradiography. Wood Sci. Technol. 25, 371–381.

Gindl, W., Grabner, M., Wimmer, R., 2000. The influence of temperature on latewood lignin content in treeline Norway spruce compared with maximum density and ring width. Trees 14, 409–414.

Goldberg, R., Lê, T., Catesson, A.M., 1985. Localization and properties of cell wall enzyme activities related to the final stages of lignin biosynthesis. J. Exp. Bot. 36, 503–510.

Grand, C., Ranjeva, R., Boudet, A.M., Alibert, G., 1979. Photoregulation of the incorporation of guaiacyl units into lignins. Planta 146, 281–286.

Hale, J.D., Clermont, L.P., 1963. Influence of prosenchyma cell-wall morphology on basic physical and chemical characteristics of wood. J. Polym. Sci. C-2, 253–261.

Hansen, C.M., Björkman, A., 1998. The ultrastructure of wood from a solubility parameter point of view. Holzforschung 52, 335–344.

Harada, H., Wardrop, A.B., 1960. Cell wall structure of ray parenchyma cells of a softwood (*Cryptomeria japonica*). Mokuzai Gakkaishi 6, 34–41.

Hardell, H.-L., Leary, G., Stoll, M., Westermark, U., 1980a. Variations in lignin structure in defined morphological parts of spruce. Svensk Papperstidn. 83, 44–49.

Hardell, H.-L., Leary, G., Stoll, M., Westermark, U., 1980b. Variations in lignin structure in defined morphological parts of birch. Svensk Papperstidn. 83, 71–74.

He, L., Terashima, N., 1989a. Formation and structure of lignin in monocotyledons I. Selective labeling of the structural units of lignin in rice plant (*Oryza sativa*) with ^{3}H and visualization of their distribution in the tissue by microautoradiography. Mokuzai Gakkaishi 35, 116–122.

He, L., Terashima, N., 1989b. Formation and structure of lignin in monocotyledons II. Deposition and distribution of phenolic acids and their association with cell wall polymers in rice plants (*Oryza sativa*). Mokuzai Gakkaishi 35, 123–129.

He, L., Terashima, N., 1990. Formation and structure of lignin in monocotyledons. III. Heterogeneity of sugarcane (*Saccharum officinarum* L.) lignin with respect to the composition of structural units in different morphological regions. J. Wood Chem. Technol. 10, 435–459.

Hepler, P.K., Fosket, D.E., Newcomb, E.H., 1970. Lignification during secondary wall formation in *Coleus*: An electron microscope study. Am. J. Bot. 57, 85–96.

Hepler, P.K., Newcomb, E.H., 1963. The fine structure of young tracheary xylem elements arising by redifferentiation of parenchyma in wounded *Coleus* stem. J. Exp. Bot. 14, 496–503.

Hepler, P.K., Rice, R.M., Terranova, W.A., 1972. Cytochemical localization of peroxidase activity in wound vessel members of Coleus. Can. J. Bot. 50, 977–983.

Higuchi, T., 1990. Lignin biochemistry: biosynthesis and biodegradation. Wood Sci. Technol. 24, 23–63.

Imagawa, H., Fukazawa, K., Ishida, S., 1976. Study of the lignification of Japanese larch, *Larix leptolepis* Gord. Res. Bull. Coll. Exp. For. Hokkaido Univ. 33, 127–138.

Itoh, T., 1990. Lignification of bamboo (*Phyllostachys heterocycla* Mitf.) during its growth. Holzforschung 44, 191–200.

Iversen, T., Westermark, U., Samuelsson, B., 1987. Some comments on the isolation of galactose-containing lignin-carbohydrate complexes. Holzforschung 41, 119–121.

Jayme, G., Fengel, D., 1961. Beitrag zur Kenntnis des Feinbaus der Fichtenholztracheiden. II. Beobachtungen an Ultradünnschnitten von delignifiziertem Holz und Ligningerüsten. Holzforschung 15, 98–102.

Kerr, T., Bailey, I.W., 1934. The cambium and its derivative tissues. IV. Structure, optical properties and chemical composition of the so-called middle lamella. J. Arnold Arb. 15, 327–349.

Kolar, J.J., Lindgren, B.O., Treiber, E., 1982. The distribution of lignin between fiber wall and middle lamella. Svensk. Papperstidn. 83, R21–A26.

Kutscha, N.P., 1968. Cell wall development in normal and compression wood of balsam fir *Abies balsamea* (L) Mill. PhD thesis State Univ. Coll. For., Syracuse NY, pp. 231.

Kutscha, N.P., Gray, J.R., 1972. The suitability of certain stains for studying lignification in balsam fir, *Abies balsamea* (L) Mill. Life Sci. Agric. Expt. Station, University of Maine, Orono, Technical bulletin 50, pp. 53.

Kutscha, N.P., Schwarzmann, J.M., 1875. The lignification sequence in normal wood of balsam fir. Holzforschung 29, 79–84.

Lange, P.W., 1944. Om ligninets natur och fördelning i granved (On the nature of the lignin and its distribution in spruce wood). Svensk. Papperstidn. 47, 262–265.

Lange, P.W., 1950. The distribution of lignin in the cell wall of normal and reaction wood from spruce and a few hardwoods. Svensk. Papperstdn. 57, 525–532.

Lange, P.W., Kjaer, A., 1957. Kvantitative kemisk analys av cellväggens delar i ved-och cellulosafiberr med användning av interferensmikroskopi. (Quantitative chemical analysis of the different parts of the cell wall in wood and cellulose fibers by interference microscopy). Nor. Skogind. 11, 425–432.

Larson, P.R., 1966. Changes in chemical composition of wood cell walls associated with age in *Pinus resinosa*. For. Prod. J. 16, 37–45.

Li, L., Popko, J.L., Umezawa, T., Chiang, V.L., 2000. 5-Hydroxyconiferyl aldehyde modulates enzymatic methylation for syringyl monolignol formation, a new view of monolignol biosynthesis in Angiosperms. J. Biol. Chem. 275, 6537–6545.

Maurer, A., Fengel, D., 1991. Electron microscopic representation of structural details in softwood cell walls by very thin ultramicrotome sections. Holz Roh-Werkstoff 49, 53–56.

Meier, H., 1964. General chemistry of cell walls and distribution of the chemical constituents across the walls. In: Zimmermann, M.H. (Ed.), The formation of wood in forest trees. Academic Press, New York, London, pp. 137–151.

Meshitsuka, G., Lee, Z.Z., Nakano, J., Eda, S., 1982. Studies on the nature of lignin-carbohydrate bonding. J. Wood Chem. Technol. 2, 251–267.

Minor, J.L., 1986. Chemical linkage of polysaccharides to residual lignin in loblolly pine kraft pulps. J. Wood Chem. Technol. 6, 185–201.

Müsel, G., Schindler, T., Bergfeld, R., Ruel, K., Jacquet, G., Lapierre, C., Speth, V., Schopfer, P., 1997. Structure and distribution of lignin in primary and secondary cell walls of maize coleoptiles analyzed by chemical and immunological probes. Planta 201, 146–159.

Musha, Y., Goring, D.A.I., 1975a. Cell dimensions and their relationship to the chemical nature of the lignin from the wood of broad-leaved trees. Can. J. For. Res. 5, 259–268.

Musha, Y., Goring, D.A.I., 1975b. Distribution of syringyl and guaiacyl moieties in hardwoods as indicated by ultraviolet microscopy. Wood Sci. Technol. 9, 45–58.

Nakshima, J., Takabe, K., Saiki, H., 1992. Artificial lignification within unlignified cell walls of *Populus koreana*. Mokuzai Gakkaishi 38, 1136–1142.

Norberg, P.H., 1969. Electron microscope studies of the morphology of fibers subjected to different pulping conditions. Svensk. Papperstidn 72, 575–582.

Norberg, P.H., Meier, H., 1966. Physical and chemical properties of the gelatinous layer in tension wood fibers of aspen (*Populus tremula* L.). Holzforschung 20, 174–178.

Nose, M., Bernards, M.A., Furlan, M., Zajicek, J., Eberhardt, L., Lewis, N.G., 1995. Towards the specification of consecutive steps in macromolecular lignin assembly. Phytochemistry 39, 71–79.

Parham, R.A., 1974. Distribution of lignin in kraft pulp as determined by electron microscopy. Wood Sci. Technol. 5, 49–62.

Parham, R.A., Côté, W.A., 1971. Distribution of lignin in normal and compression wood of *Pinus taeda* L.. Wood Sci. Technol. 5, 49–62.

Peng, F., Westermark, U., 1997. Distribution of coniferyl alcohol and coniferaldehyde groups in the cell wall of spruce fibers. Holzforschung 51, 531–536.

Pickett-Heaps, J.D., 1968. Xylem wall deposition — radioautographic investigations using lignin precursors. Protoplasma 65, 181–205.

Ritter, G.J., 1925. Distribution of lignin in wood. Microscopical study of changes in wood structure upon subjection to standard methods of isolating cellulose and lignin. Ind. Eng. Chem. 17, 1194–1197.

Ritter, G.J., Fleck, L.C., 1926. Chemistry of wood. IX. Springwood and summerwood. Ind. Eng. Chem. 18, 608–609.

Robards, A.W., 1966. The application of the modified sine rule to tension wood production in the stem of crack willow (*Salix fragilis* L.). Ann. Bot. 30, 513–523.

Robards, A.W., 1967. The xylem fibers of *Salix fragilis* L.. J. Roy. Micr. Soc. 87, 329–352.

Robards, A.W., Purvis, M., 1967. Chlorazol black E as a stain for tension wood. Stain Technol. 39, 309–315.

Roussel, M.R., Lim, C., 1995. Dynamic model of lignin growing in restricted spaces. Macromolecules 28, 370–376.

Ruel, K., Burlat, V., Joseleau, J.-P., 1999. Relationship between ultrastructural topochemistry of lignin and wood properties. IAWA J. 20, 203–211.

Ryser, U., Keller, B., 1992. Ultrastructural localization of a bean glycine-rich protein in unlignified primary cell walls of protoxylem cells. The Plant Cell 4, 773–783.

Sachs, I.B., 1965. Evidence of lignin in the tertiary wall of certain wood cells. In: Côté, W.A. (Ed.), Cellular Ultrastructure of Woody Plants. Syracuse Univ. Press, Syracuse, pp. 335–339.

Sachs, I.B., Clark, I.T., Pew, J.C., 1963. Investigation of lignin distribution in the cell wall of certain woods. J. Polym. Sci. C-2, 203–212.

Saka, S., Goring, D.A.I., 1988. The distribution of lignin in white birch wood as determined by bromination with TEM-EDXA. Holzforschung 42, 79–83.

Saka, S., Thomas, R.J., 1982. A study of lignification in loblolly pine tracheids by SEM-EDXA technique. Wood Sci. Technol. 16, 167–179.

Saka, S., Thomas, R.J., Gratzl, J.S., 1979. Lignin distribution in soda-oxygen and kraft fibers as determined by conventional electron microscopy. Wood Fiber 11, 99–108.

Saka, S., Thomas, R.J., Gratzl, J.S., 1981. Lignin distribution in Douglas fir and loblolly pine as determined by energy dispersive x-ray analysis. ISWPC, Stockholm 1, 35–42.

Saleh, T.M., Leney, I., Sarkanen, K.V., 1967. Radiographic studies of cottonwood, Douglas fir, and wheat plants. Holzforschung 21, 116–120.

Salmén, L., Olsson, A.-M., 1998. Interaction between hemicelluloses, lignin and cellulose: Structure-property relationships. J. Pulp Pap. Sci. 24, 99–103.

Sanio, K., 1973. Anatomie der gemeinen Kiefer (*Pinus sylvestris* L.). Jarb. Wiss. Bot. 9, 50–126.

Sarkanen, S., 1998. Template polymerization in lignin biosynthesis. In: Lewis, N.G., Sarkanen, S. (Eds.), Lignin and Lignan Biosynthesis. American Chemical Society Symposium Series 697, Washington, DC, pp. 194–208.

Scott, J.A.N., Goring, D.A.I., 1970a. Lignin concentration in the S3 layer of softwoods. Cellulose Chem. Technol. 4, 83–93.

Scott, J.A.N., Goring, D.A.I., 1970b. Photolysis of wood microsections in the ultraviolet microscopy. Wood Sci. Technol. 4, 237–239.

Scott, J.A.N., Procter, A.R., Fergus, B.J., Goring, D.A.I., 1969. The application of ultraviolet microscopy to the distribution of lignin in wood. Description and validity of the technique. Wood Sci. Technol. 3, 73–92.

Scurfield, G., 1967. Histochemistry of reaction wood differentiation in *Pinus radiata* D. Don. Aust. J. Bot. 18, 377–392.

Siddiqui, K.M., 1976. Relationship between cell wall morphology and chemical composition of earlywood and latewood in two coniferous species. Pakistan J. For. 26, 21–34.

Singh, A.P., 1997. Initial pit borders in *Pinus radiata* are resistant to degradation by soft rot fungi and erosion bacteria but not tunneling bacteria. Holzforschung 51, 15–18.

Singh, A.P., Donaldson, L.A., 1999. Ultrastructure of tracheid cell walls in radiata pine (*Pinus radiata* D. Don) mild compression wood. Can. J. Bot. 77, 32–40.

Singh, A.P., Schmitt, U., 2000. High variability in the distribution of lignin in the middle lamella of rubber-wood (*Hevea brasiliensis*) cells. In: Kim, Y.S. (Ed.), New Horizons in Wood Anatomy. Chonnam Nat'l Univ. Press, Kwanju, Korea, pp. 203–207.

Singh, A.P., Sell, J., Schmitt, U., Zimmermann, T., Dawson, B., 1998. Radial striation of the S2 layer in mild compression wood tracheids of *Pinus radiata*. Holzforschung 52, 563–566.

Sorvari, J., Pietarilla, V., Nygren-Konttinen, A., Klemola, A., Laine, J.E., Sjöström, E., 1983. Attempts at isolating and characterizing secondary wall and middle lamella from spruce wood (*Picea abies*). Pap. Puu 3, 117–121.

Sorvari, J., Sjöström, E., Klemola, A., Laine, J.E., 1986. Chemical characterization of wood constituents, especially lignin, in a fraction separated from middle lamella and secondary wall of Norway spruce (*Picea abies*). Wood Sci. Technol. 20, 35–52.

Stamm, A.J., Sanders, H.T., 1966. Specific gravity of the wood substance of loblolly pine as affected by chemical composition. Tappi 49, 397–400.

Staudinger, M., 1942. Chemische Anatomie des Holzes. Holz. Roh-Werkst. 5, 193–201.

Sterjiades, R., Dean, J.F.D., Gamble, G., Himmelsbach, D.S., Eriksson, K-E.L., 1993. Extracellular laccases and peroxidases from sycamore maple (*Acer pseudoplatanus*) cell suspension cultures. Reactions with monolignols and lignin model compounds. Planta 190, 75–87.

Takabe, K., Fujita, M., Harada, H., Saiki, H., 1981. Lignification process of Japanese black pine (*Pinus thunbergii* Parl.) tracheids. Mokuzai Gakkaishi 27, 813–820.

Takabe, K., Fujita, M., Harada, H., Saiki, H., 1986. Lignification process in *Cryptomeria* (*Cryptomeria japonica* D. Don) tracheid: Electron microscopic observation of lignin skeleton of differentiating xylem. Res. Bull. Coll. Exp. For. Hokkaido Univ. 43, 783–788.

Takabe, K., Miyauchi, S., Tsunoda, R., Fukazawa, K., 1992. Distribution of guaiacyl and syringyl lignins in Japanese beech (*Fagus crenata*): Variation within an annual ring. IAWA Bull. n.s. 13, 105–112.

Takano, T., Fukazawa, K., Ishida, S., 1983. Within-a-ring variation of lignin in *Picea glehnii* by UV microscopic image analysis. Res. Bull. Coll. Exp. For. Hokkaido Univ. 40, 709–722.

Tanabe, H., Kobayashi, Y., 1988. Aggregate of pectic substances and lignin-carbohydrate complex in Mitsumata (*Edgeworthia papyrifera* Sieb. Et Zucc.) bast and its degradation by pectinolytic enzymes from *Erwinia carotovora*. Holzforschung 42, 47–52.

Terashima, N., Atalla, R.H., Ralph, S.A., Landucci, L.L., Lapierre, C., Monties, B., 1995. New preparations of lignin polymer models under conditions that approximate cell wall lignification. I. Synthesis of novel polymer models and their structural characterization by ^{13}C NMR. Holzforschung 49, 521–527.

Terashima, N., Atalla, R.H., Ralph, S.A., Landucci, L.L., Lapierre, C., Monties, B., 1996. New preparations of lignin polymer models under conditions that approximate cell wall lignification. II. Structural characterization of the models by thioacidolysis. Holzforschung 50, 9–14.

Terashima, N., Fukushima, K., 1988. Heterogeneity in formation of lignin — XI: an autoradiographic study of the heterogeneous formation and structure of pine lignin. Wood Sci. Technol. 22, 259–270.

Terashima, N., Fukushima, K., Sano, Y., Takabe, K., 1988. Heterogeneity in formation of lignin. X. Visualization of lignification process in differentiating xylem of pine by microautoradiography. Holzforschung 42, 347–350.

Terashima, N., Fukushima, K., Takabe, K., 1986a. Heterogeneity in formation of lignin. VIII. An autoradiographic study on the formation of guaiacyl and syringyl lignin in *Magnolia kobus* DC. Holzforschung 40 (Suppl.), 101–105.

Terashima, N., Fukushima, K., Tsuchiya, S., 1986b. Heterogeneity in formation of lignin. VII. An autoradiographic study on the formation of guaiacyl and syringyl lignin in poplar. J. Wood Chem. Technol. 6, 495–504.

Timell, T.E., 1973. Studies on opposite wood in conifers Part III: distribution of lignin. Wood Sci. Technol. 7, 163–172.

Timell, T.E., 1978a. Helical thickenings and helical cavities in normal and compression wood of *Taxus baccata*. Wood Sci. Technol. 12, 1–15.

Timell, T.E., 1978b. Ultrastructure of compression wood in *Ginkgo biloba*. Wood Sci. Technol. 12, 89–103.

Tirumalai, V.C., Agarwal, U.P., Obst, J.R., 1996. Heterogeneity of lignin concentration in cell corner middle lamella of white birch and black spruce. Wood Sci. Technol. 30, 99–104.

Tsutsumi, Y., Matsui, K., Sakai, K., 1998. Substrate-specific peroxidases in woody angiosperms and gymnosperms participate in regulating the dehydrogenative polymerization of syringyl and guaiacyl type lignins. Holzforschung 52, 275–281.

Wardrop, A.B., 1957. The phase of lignification in the differentiation of wood fibers. Tappi 40, 225–243.

Wardrop, A.B., 1965. Cellular differentiation in xylem. In: Côté, W.A. (Ed.), Cellular ultrastructure of woody plants. Syracuse University Press, Syracuse, New York, pp. 61–97.

Wardrop, A.B., 1976. Lignification of the plant cell wall. Appl. Polym. Symp. 28, 1041–1063.

Wardrop, A.B., Bland, D.E., 1959. The process of lignification in woody plants. IV. Int. Congr. Biochem. Vol. 11, Biochemistry of wood, pp. 92–116.

Wardrop, A.B., Bland, D.E., 1961. Lignification in reaction wood. 140th Meeting Am. Chem. Soc., Chicago, IL, 5E.

Wardrop, A.B., Davies, G.W., 1964. The nature of reaction wood. VIII. The structure and differentiation of compression wood. Aust. J. Bot. 12, 24–38.

Wardrop, A.B., Dadswell, H.E., 1955. The nature of reaction wood. IV. Variations in cell wall organisation of tension wood fibers. Aust. J. Bot. 3, 177–189.

Watson, A.J., Dadswell, H.E., 1957. Papermaking properties of compression wood from *Pinus radiata*. Appita 11, 56–70.

Weiner, G., Liese, W., Schmitt, U., 1996. Cell wall thickening in fibers of the palms *Rhapis excelsa* (Thunb.) Henry and *Calamus axillaris* Becc. In: Donaldson, L.A., Singh, A.P., Butterfield, B.G., Whitehouse, L. (Eds.), Recent Advances in Wood Anatomy. NZFRI Ltd, Rotorua, New Zealand, pp. 191–197.

Wergin, W., 1965. Über Entstehung und Aufbau von Reaktionsholzzellen. 4. Mitt.: Nachweise der Ligninverteilung un den Zellwänden des Druckholzes durch Untersuchungen im UV-Licht. Flora 156, 322–331.

Westermark, U., 1982. Calcium promoted phenolic coupling by superoxide radical — a possible lignification reaction in wood. Wood Sci. Technol. 16, 71–78.

Westermark, U., 1985. The occurrence of *p*-hydroxyphenylpropane units in the middle lamella lignin of spruce (*Picea abies*). Wood Sci. Technol. 19, 223–232.

Westermark, U., Hardell, H.-L., Iverson, T., 1986. The content of protein and pectin in the lignified middle lamella/primary wall from spruce fibers. Holzforschung 40, 65–68.

Westermark, U., Lidbrandt, O., Eriksson, I., 1988. Lignin distribution in spruce (*Picea abies*) determined by mecurisation with SEM-EDXA technique. Wood Sci. Technol. 22, 243–250.

Whiting, P., Goring, D.A.I., 1982a. Chemical characterization of tissue fractions from the middle lamella and secondary wall of spruce tracheids. Wood Sci. Technol. 16, 261–267.

Whiting, P., Goring, D.A.I., 1982b. Relative reactivities of middle lamella and secondary wall lignin of black spruce wood. Holzforschung 36, 303–306.

Whiting, P., Favis, B.D., St Germain, F.G.T., Goring, D.A.I., 1981. Fractional separation of middle lamella and secondary wall tissue from spruce wood. J. Wood Chem. Technol. 1, 111–122.

Wi, S.G., Lim, K.P., Kim, Y.S., 2000. Inhomogenous distribution of lignin in compression wood of *Pinus densiflora* and *Ginkgo biloba*. In: Kim, Y.S. (Ed.), New Horizons in Wood Anatomy. Chonnam Nat'l Univ. Press, Kwangju, Korea, pp. 208–212.

Wood, J.R., Goring, D.A.I., 1971. The distribution of lignin in stem and branch wood of Douglas fir. Pulp Pap. Mag. Can. 72, T95–T102.

Wood, J.R., Goring, D.A.I., 1974. Ultraviolet microscopy at wavelengths below 240 nm. J. Microscopy 100, 105–111.

Wu, J., Fukazawa, K., Ohtani, J., 1990. Lignin analysis in some tropical hardwoods using ultraviolet microscopy. Res. Bull. Col. Exp. For. Hokkaido Univ. 47, 353–386.

Wu, J., Fukazawa, K., Ohtani, J., 1992. Distribution of syringyl and guaiacyl lignins in hardwoods in relation to habitat and porosity form in wood. Holzforschung 46, 181–185.

Yang, J.M., Goring, D.A.I., 1978. A comparison of the concentration of free phenolic hydroxyl groups in the secondary wall and middle lamella regions of softwoods. Trans. Tech. Sect. CPPA 4, 2–5.

Yang, J.M., Goring, D.A.I., 1980. The phenolic hydroxyl content of lignin in spruce wood. Can. J. Chem. 58, 2411–2414.

Yoshinaga, A., Akiyoshi, K., Fujita, M., 2000. Secondary wall thickening and lignification of xylem components in *Betula grossa* and *Aesculus turbinata*. In: Kim, Y.S. (Ed.), New Horizons in Wood Anatomy. Chonnam Nat'l Univ. Press, Kwangju, Korea, pp. 208–212.

Yoshinaga, A., Fujita, M., Saiki, H., 1992. Relationships between cell evolution and lignin structural varieties in oak xylem evaluated by microscopic spectrophotometry with separated cell walls. Mokuzai Gakkaishi 38, 629–637.

Yoshinaga, A., Fujita, M., Saiki, H., 1997a. Secondary wall thickening and lignification of oak xylem components during latewood formation. Mokuzai Gakkaishi 43, 377–383.

Yoshinaga, A., Fujita, M., Saiki, H., 1997b. Cellular distribution of guaiacyl and syringyl lignins within an annual ring in oak wood. Mokuzai Gakkaishi 43, 384–390.

Yoshizawa, N., Satoh, I., Yokota, S., Idei, T., 1992. Response of differentiating tracheids to stem inclination in young trees of *Taxus cuspidata*. IAWA Bull. n.s. 13, 187–194.

Yoshizawa, N., Ohba, H., Uchiyama, J., Yokota, S., 1999. Deposition of lignin in differentiating xylem cell walls of normal and compression wood of *Buxus microphylla* var. *insularis* Nakai. Holzforshung 53, 156–160.

Yoshizawa, N., Satoh, M., Yokota, S., Idei, T., 1991. Lignification and peroxidase activity in bamboo shoots (*Phyllostachys edulis* A. et C. Riv.). Holzforshung 45, 169–174.

Yoshizawa, N., Satoh, M., Yokota, S., Idei, T., 1993a. Formation and structure of reaction wood in *Buxus microphylla* var. *insularis* Nakai. Wood Sci. Technol. 27, 1–10.

Yoshizawa, N., Satoh, M., Yokota, S., Idei, T., 1993b. Distribution of guaiacyl and syringyl lignins in normal and compression wood of *Buxus microphylla* var. *insularis* Nakai. IAWA J. 14, 139–151.

Young, W.D., Laidlaw, R.A., Packman, D.F., 1970. Pulping of British-grown softwoods. VI. The pulping properties of Sitka spruce compression wood. Holzforschung 24, 86–98.

Yumoto, M., Ishida, S., Fukazawa, K., 1982. Studies on the formation and structure of the compression wood cells induced by artificial inclination in young trees of *Picea glauca* I. Time course of the compression wood formation following inclination. Res. Bull. Coll. Exp. For. Hokkaido Univ. 39, 137–162.

Yumoto, M., Ishida, S., Fukazawa, K., 1983. Studies on the formation and structure of the compression wood cells induced by artificial inclination in young trees of *Picea glauca* IV. Gradation of the severity of compression wood tracheids. Res. Bull. Coll. Exp. For. Hokkaido Univ. 39, 137–162.

PERGAMON

Phytochemistry 57 (2001) 875–882

PHYTOCHEMISTRY

www.elsevier.com/locate/phytochem

Reassessment of qualitative changes in lignification of transgenic tobacco plants and their impact on cell wall assembly

Katia Ruel[a], Matthieu Chabannes[b], Alain-Michel Boudet[b], Michel Legrand[c], Jean-Paul Joseleau[a,*]

[a]*Centre de Recherches sur les Macromolécules Végétales, CNRS (UPR 5301), BP 53, 38041 Grenoble Cedex 9, France*
[b]*UMR CNRS/UPS 5546, Signaux et Messages Cellulaires chez les Végétaux, Pôle de Biotechnologie végétale, chemin de Borde Rouge, BP 17 Auzeville, 31326 Castanet-Tolosan, France*
[c]*Institut de Biologie Moléculaire des Plantes, CNRS, Université Louis Pasteur, 67084 Strasbourg Cedex, France*

Received 1 November 2000; received in revised form 16 February 2001

Abstract

In tobacco plants the effect of antisense down-regulation of various genes encoding enzymes of the monolignol biosynthetic pathway resulted in quantitative and qualitative changes in lignin distribution and in diverse alterations of the secondary wall assembly of modified tobacco plants. Total lignin content, composition in syringyl and guaiacyl units, and absolute proportions of condensed and non-condensed substructures occurring in the cell walls, were differentially modified according to the repressed gene. Immunocytochemical characterisation and visualisation of the distribution of condensed and non-condensed lignin substructure epitopes in transmission electron microscopy (TEM) revealed that some transformations entailed profound and specific alterations in the secondary wall biogenesis. Correlation between micro-morphological cell wall alterations and semi-quantitative immunoanalysis of the topochemical distribution of lignin sub-units suggests that the mode of polymerisation of monolignols into non-condensed units, favoured by the microfibril matrix of the secondary wall, plays an important part in the lignified cell wall assembly.
© 2001 Elsevier Science Ltd. All rights reserved.

Keywords: *Nicotiana tabacum* L. cv Samsun NN; Solanaiece; Transgenic plants; Lignin biosynthesis; Plant cell wall architecture; Immunocytochemisty

1. Introduction

Lignin has long been recognised as essential in the cell wall architecture of land plant vascular tissues. However, the sequence of events that relate lignin monomer biosynthesis and their insertion and polymerisation within the pre-existing extracellular carbohydrate matrix is far from being known. Genetically modified plants, aside from their potential economical interest, constitute versatile tools for the study of plant physiology and biochemistry (Reiter, 1998). Tobacco plants have been modified by down-regulating various lignin biosynthetic genes leading to transformed lines differentially modified in their lignin content as well as their lignin monomer composition. These plants may be regarded as potential models towards the understanding of the role of lignin in plant cell wall assembly. Lignin monomer biosynthesis is derived from the shikimic acid pathway (Higuchi, 1990) and consists of a multistep process (Whetten and Sederoff, 1995) which offers various possibilities for selective targeting of genes that control the flux of monolignol production. There are still several unclear points regarding alternative enzymatic steps and the extent of inter-relationships between enzymes. Because of that it is still impossible to predict the exact impact of gene down regulation upon lignin content and composition in the derived transgenic plants, as well as the consequence of such modification on the plant cell wall assembly.

To assess the structural changes arising after lignin biosynthesis modification, chemical analysis has been the principal way to estimate the monomeric composition and the nature of the inter-unit linkages. Lignins from genetically modified plants have been analysed principally by thioacidolysis (Lapierre et al., 1999) and

* Corresponding author. Tel.: +33-476-03-76-61; fax: +33-476-54-72-03.
E-mail address: joseleau@cermav.cnrs.fr (J.-P. Joseleau).

0031-9422/01/$ - see front matter © 2001 Elsevier Science Ltd. All rights reserved.
PII: S0031-9422(01)00118-2

by nuclear magnetic resonance (NMR) (Ralph et al., 1998). The thioacidolysis method provides information on the relative proportions of syringyl and guaiacyl nuclei and on the proportion of non-condensed linkages in a lignin fraction. Similarly, NMR spectroscopy gives qualitative and quantitative indications about the monomer composition of lignins. Thus, ^{13}C–^{1}H NMR spectroscopy provided evidence for unusual and new aldehyde units, suggesting that other phenols than the usual monolignols may be utilised through redirected pathways (Ralph et al., 1998). Thioacidolysis analysis and NMR spectroscopy clearly identify differences between the lignins from control and transgenic plants. However, the compositional and structural information provided by these methods are limited to a certain fraction of lignin and it could be misleading to extend the results provided by these methods to the whole lignin present in cell walls.

In this paper, in order to partly overcome these limitations in view of the assessment of lignification following genetic transformation, we have used a non-invasive in situ immunocytochemical characterisation of lignin structural features by transmission electron microscopy (TEM). This approach allows the visualisation and characterisation of the diversity of lignin types in all the different parts of a cell wall, and in the various cell types. The antibodies used in this study were directed against condensed and non-condensed inter-unit linkages, respectively, as described in Ruel et al. (1994). Immuno-gold labelling in TEM allowed identification and ultrastructural localisation of specific lignin subunit epitopes in a comparative way between control and transgenic plants. Semi-quantitative results regarding the most typical lignin features synthesised in the different tissues of transformed tobacco could thus be obtained. Tobacco plants respectively down-regulated on the enzymes caffeic acid/5-OH-ferulic *O*-methyl transferase (COMT1), cinnamyl CoA reductase (CCR), and cinnamyl alcohol deshydrogenase (CAD) were used for the study together with a double transformed plant (CADxCCR) (Halpin et al., 1994; Atanassova et al.,1995; Piquemal et al., 1998; Chabannes et al., 2001).

The aim of this study was to investigate how changes in the content and/or the composition and molecular structure of lignin had influenced cell wall assembly and microstructure.

2. Results and discussion

The impact of modifications of lignin composition and structure on cell wall assembly was investigated at the ultrastructural level on a series of genetically engineered tobacco lines. Immunocytochemical identification and distribution of lignin sub-units was studied on ultra-thin sections from the stem of three simple transformants respectively down-regulated in expression of CAD, CCR and COMT1, and the double transformant resulting from the sexual crossing between CAD and CCR single transformants. These lines were selected according to previously obtained analytical data (Halpin et al., 1994; Atanassova et al., 1995; Piquemal et al., 1998; Chabannes et al., 2001; Pinçon et al., 2001) indicating that two of the transformed plants, CAD and COMT1, had almost no change in their lignin content, whereas the two other lines, CCR and CAD x CCR had considerable reduction of their lignin contents. Down-regulation of genes encoding key-step enzymes in the lignin biosynthetic pathway is also known to modify lignin composition and structure. Thus, examination of the respective amounts of lignin subunits in terms of non-condensed linkages versus condensed linkages (Lapierre et al., 1995) and recalculation of their respective amounts relative to total lignin content and to total cell wall material showed that the amount of condensed sub-units were always largely predominant in all tobacco lines (Table 1). Interestingly, the lignin of the double transformant, whose content had been lowered, had almost the same proportion of non-condensed linkages as the wild type plant. In spite of that, the monomer composition of the non-condensed subunits (S/G ratio) were very different between the control (S/G, 0.9) and the double transformant (S/G, 2.5). This observation can be extended to the CAD and CCR single transformants which had dramatically different total lignin contents, whose lignin showed very close proportions of non-condensed substructures (84.2 and 82.4%, respectively) in spite of their highly different composition in syringyl and guaiacyl monomers (S/G 0.4 and 3.2, respectively). This suggests that the strict guaiacyl and syringyl composition may not have a direct influence on the type of inter-unit linkages in the final lignin polymer and that other factors may be considered. Among those, the role of the environment in which the coupling reaction between monolignols occurs may be taken into account. In fact, the polymer matrix constituted by the pre-deposited cell wall polymers has been considered a determinant in the control of the course of the polymerisation of monolignols (Siegel, 1957). Of particular importance are the effects induced by different types of polysaccharides localised in different zones of the cell wall (Yoshida et al., 1994; Houtman and Atalla, 1995; Terashima et al., 1995). The calculation of absolute amounts of non-condensed and condensed lignins occurring in the cell walls (Table 1) show that the wild type plant harbours the highest amounts of both lignin types, whereas the CCR transformant had the lowest amounts of both. Interestingly, it appears that the cell walls of the parent CCR and of the double transformant CADxCCR had in common the same content of condensed subunits (ca 9% of the wall material) but markedly differed in the amount of non-condensed subunits (1.7 vs 2.8%, respectively).

Table 1
Respective amounts of non-condensed and condensed subunits in normal and transformed tobacco plants

Plant	Lignin %[b]	Non-condensed subunits[a]		Condensed subunits[a]		S/G in non-condensed subunits
		% of lignin	% in cell wall	% of lignin	% in cell wall	
Normal plant (wt)[c]	22.2	23.4	5.2	76.6	17	0.9
CCR (−)	10.7	15.8	1.7	84.2	9	3.2
CAD(−)	21.05	17.6	3.7	82.4	17.3	0.4
$COMT_1$ (−)	21.2	–	–	–	–	–
CAD^- x CCR^-	11.82	23.7	2.80	76.3	9	2.51

[a] The respective amounts of lignin subunits were recalculated from Halpin et al., 1994 Atanassova et al., 1995; Piquemal et al., 1998; Pinçon et al., 2000; Chabannes et al., 2001.
[b] As Klason lignin.
[c] Abbreviations: wt; wild type, CCR, cinnamoyl CoA reductase; CAD, cinnamyl alcohol dehydrogenase; COMT., caffeic acid *O*-methoyl transferase.

The effects of CCR anti-sense inhibition on the micromorphology of the secondary xylem elements, as observed in TEM, were characterised by a dramatic loosening between cellulose microfibrils, and a perturbation in their orientation, occurring in most of the S2 layer of vessels and fibres [Fig. 1(B)]. Interestingly, in both cell types, the S1 layer was not affected by the loosening. This suggests that there is a clear and distinct control in the assembly of lignin in the S1 and S2 layers. Further evidence of the spatio-temporal and cell specific regulation of lignification in secondary walls was shown by the fact that the ultrastructural alteration of S2 concerned only fibres and vessels of the metaxylem but not vessels of the protoxylem (data not shown). This shows that cell types and even sublayers of cell walls are differently and specifically affected when one of the genes of the pathway leading to lignin monomers is down-regulated.

The fact that the high reduction in the total lignin content resulting from the inhibition of CCR activity (Piquemal et al., 1998) is accompanied by an intense wall loosening shows the global importance of lignin in cell wall cohesion. However, in spite of a similar reduction of lignin content, the double transformant CADxCCR was not affected in the formation of secondary walls which did not show ultrastructural loosening and exhibited the same cohesion as the normal plant [Fig. 1 (E)]. This indicates that other factors besides the total amount of lignin must prevail for maintaining cohesion between cellulose micro-fibrils during cell wall assembly. It is indeed worth noting that the nature of the lignin varies between the normal plant and the different transformants. The variations which were found at the level of the relative proportions of syringyl and guaiacyl units and at the level of the nature of the inter-unit linkages (i.e. condensed and non-condensed) (Table 1) may have different effects on the process of cell wall assembly. To verify whether the type of lignin deposited in the cellulose–hemicellulose matrix of the secondary walls could have a specific impact on the wall cohesion, the ultrathin sections were assayed with our immunospecific probes respectively directed against condensed and non-condensed guaiacyl–syringyl subunits (Joseleau and Ruel, 1997). This allowed us to establish the topochemistry of lignin structural epitopes in each transformant. The results are illustrated in Fig. 1 with the labelling of non-condensed subunits. In view of comparing the respective intensities of the labelling, all the transformants and the normal plants were treated in parallel with the same antiserum at the optimal dilution. This insured that semi-quantitative evaluation of the labelling could be done for each antibody assayed. It is important to recall here that one cannot compare quantitatively the intensities of labelling given by two antibodies of different specificity. Therefore, semi-quantitative results are expressed separately for each antibody. The figures reported in Tables 2–5 were calculated from the number of gold particles per μm^2 in the three sub-layers of fibre and vessel walls, respectively, and are expressed relative to the highest concentration of gold particles found in any one of the sub-layers of the normal plant taken as control. Thus, comparative intensities of labelling between normal plant and transformants could be evaluated for each antibody.

As expected from the strongly altered ultrastructure of fibres and vessels of the CCR down-regulated transformant, striking variations in the labelling of fibres and vessels were observed. The strong loosening of S2 and S3 coincides with a very weak concentration of non-condensed GS epitopes in these regions of the walls, both in fibres and vessels (Tables 2 and 4). Conversely, the condensed GS epitopes appear relatively well represented in the less disorganised outer part of the S2 in the walls of the CCR plant (Tables 3 and 5) and do not show dramatic variations of concentration compared to the normal plant. This indicates that the overall 50% diminution of total lignin brought about by the anti-sense inhibition of CCR activity had repercussions

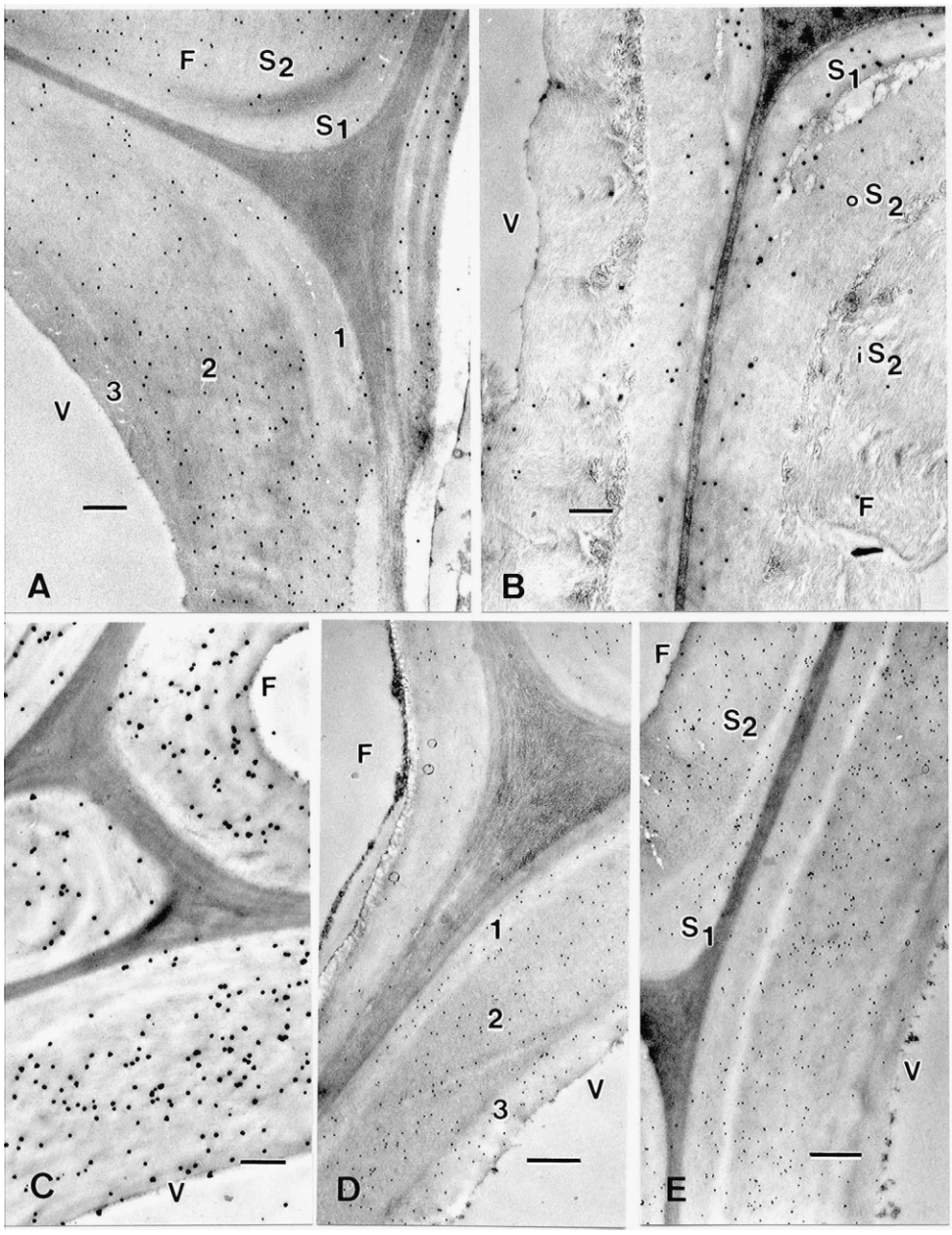

Fig. 1. Immunocytochemical localisation of non-condensed mixed guaiacyl–syringyl lignin sub-units in lignified tissues of wild type tabacco, CCR down-regulated, CAD down-regulated, COMT I down-regulated and CADxCCR double transformant lines. N.B.: The gold particles (5 nm in diameter) were silver enhanced. As a result, the size of silver grains may vary from one preparation to the other due to temperature and time. However, the actual number of grains remains unchanged. Bar = 0.5 μm; V = vessel; F = fibre; S1, S2, S3, and 1, 2, 3 = sub-layers in fibres and vessels, respectively; iS, oS = inner and outer parts of S2 layers. (A) In wild type plants, gold particles cover the three sub-layers of fibre walls with a lower labelling in the part of S1 adjacent to cell corners. In vessels, gold particles are essentially concentrated in S2. Middle lamellae and cell corners do not contain these subunits. (B) In CCR down-regulated line, gold particles have become mostly localised in S1, in fibres and vessels. An extensive loosening of the cellulose framework is visible in S2 of both fibres and vessels. Cellulose microfibrils appear irregularly oriented. (C) In CAD down-regulated line, the distribution of the gold particles is similar to that the wild type plant. (D) In the COMT I down-regulated line, the fibre presents an immature aspect. The distribution of gold particles seems to be weak. In vessel walls, gold grains are homogeneously distributed in the three sub-layers. (E) In the double transformant (CADxCCR), the distribution of gold particles in fibres and vessels is abundant in S1 and S2 where it predominates. However, in vessels, the newly formed S3 is only weakly labelled.

mostly on the formation of non-condensed sub-structures. These results are consistent with the general trends given by chemical analyses (Table 1), indicating that the lignin of CCR down-regulated lines was more severely depressed in non-condensed (ca. three times less than in a normal plant) rather than in condensed sub-units.

On the basis of analytical results (Table 1), one could expect the respective labelling in the double transformant CADxCCR to be stronger for the non-condensed

Table 2
Semi-quantitative distribution of non-condensed GS epitopes in fibres of transformants relative to wild type[a]

	wt[b]	CCR	CAD	$COMT_1$	CADxCCR
S_1	0.30 (± 0.09)	0.25 (±0.08)	0.22 (±0.08)	0.25 (±0.08)	0.45 (±0.10)
S_2	1.00 (±0.13)	0.05 (±0.01)	0.33 (±0.10)	0.30 (±0.09)	1.00 (±0.14)
S_3	0.45 (± 0.09)	0.00	0.35 (±0.09)	0.30 (±0.09)	0.5 (±0.09)

[a] Values correspond to mean number of gold particles per μm^2, and are expressed relative to the highest labelling found in anyone of wild type wall sublayers to which value 1.00 has been assigned.
[b] For explanations of abbreviations, see Table 1 footnotes.

Table 3
Semi-quantitative distribution of condensed GS epitopes in fibres from transformants relative to wild type[b]

	wt[c]	CCR	CAD	$COMT_1$	CAD x CCR
S_1	1.00	1.00	1.10	1.00	0.50
S_2	0.30	1.20[(a)]	0.15	0.10	1.33[a]
S_3	0.10	0.00	0.30	0.10	0.20

[a] Only concentrated in oS_2 (outer S_2 sub-layer).
[b] Standard deviations were of the same order of magnitude as in Table 2.
[c] For explanations of abbreviations, see Table 1 footnotes.

Table 4
Semi-quantitative distribution of non-condensed GS epitopes in vessels from transformants relative to wild type[a]

	wt[c]	CCR	CAD	$COMT_1$	CADxCCR
S_1	0.05	0.15	0.31	1.10	0.35
S_2	1.00	0.08	0.45	1.00	(PX) 1.40[b]
S_3	0.10	0.05	0.45	1.00	0.08

[a] Standard deviations as in Table 2.
[b] PX, proto xylem.
[c] For explanations of abbreviations, see Table 1 footnotes.

Table 5
Semi-quantitative distribution of condensed GS epitopes in vessels from transformants relative to wild type[a]

	wt[c]	CCR	CAD	$COMT_1$	CADxCCR
S_1	1.00	0.65	0.50	1.20	1.00
S_2	0.60	0.60	0.20	1.20	n.d.[b]
S_3	0.80	0.10	0.55	1.20	n.d.

[a] Standard deviations as in Table 2.
[b] n.d., not detectable.
[c] For explanations of abbreviations, see Table 1 footnotes.

subunits, whose relative abundance is higher than in the single CCR transformant, and the labelling of condensed units to be of comparable intensities since both the single (CCR) and double transformants harbour the same amount of these subunits in their cell walls. The results of semi-quantitative evaluation of the immunological labelling (Tables 2 and 4) confirm that the double transformant was richer in non-condensed sub-units than the CCR transformant, mostly in vessels. The TEM images showed also that the ultrastructural distribution of non-condensed GS epitopes had not been significantly modified in the double transformant, as compared to the normal plant [Fig. 1(A) and (E)]. Contrarily, the ultrastructural distribution of the condensed epitopes (Tables 3 and 5), particularly in the outer S2 of fibres, was significantly modified. Also, the pattern of condensed epitopes in vessels, concentrated almost exclusively in S1, was much different from that of the normal plant and of the CCR parent. However, according to analysis and calculations (Table 1), the global amount of condensed forms in the cell walls are expected to be similar between the CCR parent and the double transformant. Added to the fact that the double transformant did not display the strong loosening observed in the CCR simple transformant, these results support the conclusion that the non-condensed moiety of lignin could have a preferential structural participation in the cohesion of the micro-fibril matrix of the secondary walls. This seems particularly significant in the case of fibres. This view is further supported by the results obtained with the anti-sense CAD and anti-sense COMT down-regulated lines which showed the non-condensed GS epitopes to be distributed in significant amounts in the S2 of both fibres and vessels without signs of loosening of the micro-fibril matrix. A peculiar feature of CAD modified plants is the accumulation of 4-hydroxy-3methoxycinnamaldehyde whose coupling would be similar to the corresponding alcohol, with the possibility of increasing the number of 8-*O*-4′ linkages (Russel et al., 2000). This could explain the high value of non-condensed sub-units in CAD cell walls (Table 1), and the rather large distribution of non-condensed epitopes observed in all sub-layers of fibres and vessels. On the other hand, the condensed GS epitopes were present in highly variable amounts in these two lines (Tables 3 and 5) without noticeable consequence on the ultrastructural wall assembly in S2. It seems thus that condensed substructures might be less implicated in secondary wall cohesion than their non-condensed counter part.

3. Conclusions

The effect of anti-sense down-regulation of various genes encoding enzymes of the monolignols biosynthetic pathway resulted in diverse alterations of the secondary wall assembly. Immunological characterisation showed that the topochemical distribution of lignin substructure epitopes was also modified (already described, Ruel et al., 2000; Chabannes et al., 2001). Inhibition of CCR activity resulted in an important loosening of the microfibrillar cellulose-hemicellulose matrix, together with a perturbation in the microfibrils orientation. Taken together with the reduction of 50% in total lignin content, it might be deduced that a minimum amount of lignin is necessary to insure cohesion between microfibrils in the secondary wall. However, with the same reduction in total lignin content, the double transformant resulting from the cross between individual homozygous CCR and CAD down-regulated lines (Chabannes et al., 2001), did not show loosening of its xylem walls. This constitutes a clear evidence that the global amount is not sufficient to explain the participation of lignin in the maintaining of cohesion in secondary wall assembly.

The deposition of lignin during the formation of the composite secondary wall has been suggested to be a highly regulated phenomenon (Lewis et al., 1999). This view is further supported by in vitro model of lignin biosynthesis suggesting that in the natural microenvironment lignin polymerisation would involve an alternating sequence of radical and ionic steps leading to an ordered structure with repeating units (De Angelis et al., 1999). Our results show that the condensed and non-condensed GS substructure epitopes underwent modifications in their repartition that depended on the genetic transformation. The alteration of ultrastructure in CCR transformant coinciding with a dramatic depletion in non-condensed GS epitopes suggests that this type of lignin substructure must be implicated in the morphogenesis of the secondary wall. The fact that it is the non-condensed form rather than the condensed form of lignin that has a special role in secondary wall assembly agrees with the view that the restricted space (ca. 30 Å) between the cellulose-hemicellulose microfibrillar template favours the extended macromolecule conformation of the non-condensed lignin molecule over the bulky one of condensed lignin (Terashima and Fukushima, 1989; Higuchi, 1990; Roussel and Lim, 1995; Joseleau and Ruel, 1997). The occurrence of the extended non-condensed lignin between microfibrils is further supported by the results of calculation of lignin morphology by computer modelling, predicting in the secondary wall a high degree of orientation of the phenylpropane sub-units parallel with cellulose microfibrils (Agarwal and Atalla, 1986; Jurasek, 1996, 1998).

Our results of immuno-labelling show that variations in the ultrastructural distribution of lignin substructures were observed whenever lignin composition and structure had been modified. This must be related to the metabolic flux and availability of the precursor monolignols, on the one hand (Roussel and Lim, 1995), and to the influence of the polysaccharide matrix on lignin polymerisation, on the other hand. This is also in favour of a fast and irreversible coupling of monolignols within the microfibril template placed under kinetic control suggested by Houtman (1999). The question of the implication of stereo-specific proteins (Davin et al., 1997) in the control of orientation of the coupling reactions of monolignols still remains unresolved. The variability in lignin ultrastructural distribution would therefore depend on the respective rate of synthesis of the monolignols and the fact that the different saccharides of the secondary wall interact differently with the different lignin precursors (Houtman and Atalla, 1995). These views are consistent with the irregular and within-wall specific distribution of the different types of lignins in the secondary walls depicted in all cell walls with the immunological probes. They are also consistent with a spatially-controlled organisation of lignification.

The increasing availability of engineered plant cell walls should help in uncovering the complex biochemical and physicochemical machinery underlying secondary wall assembly.

4. Experimental

4.1. Plant materials

The transgenic tobacco lines used in this work have been described previously. They consisted of three single transformants, a CAD down-regulated line (Halpin et al., 1994), a CCR down-regulated line (Piquemal et al., 1998) a COMT I down-regulated line (Atanassova et al., 1995), and a double transformant originating from cross-pollination between CAD and CCR transformants (Chabannes et al., 2001).

The chemical and microscopy analyses were performed on the basis of the stems of mature plants grown in a culture room.

4.2. Immunocytochemistry

Two specific polyclonal antibodies prepared and characterised as described in Ruel et al. (1994); Joseleau and Ruel (1997) were used as anti-sera. They were directed respectively against: mixed guaiacyl/syringyl (GS) lignin polymer containing non-condensed inter-unit linkages (8-*O*-4), and, mixed guaiacyl/syringyl lignin polymer containing condensed inter-units.

Small slices (1 mm in thickness) obtained by free hand sectioning with a razor blade were fixed in a freshly prepared mixture of 0.1% glutaraldehyde (v/v), 2%

paraformaldehyde (w/v) in 0.05 M phosphate buffer (pH 7–7.2). After rinsing in phosphate buffer, they were dehydrated through a graded ethanol series up to 80% (v/v), then infiltrated and embedded in LR White resin (hard mixture, TAAB) and polymerised 24 h at 50°C as described earlier (Ruel et al., 1994).

In TEM, immunolabelling was done on ultra-thin transverse sections (500 Å) floating downward in plastic rings passed on 50 µl drops of reagents deposited on parafilm. The sections were first treated with 0.15 M glycine in Tris–HCL buffer 0.01 M, pH 7.6, containing 500 mM NaCl, for blocking remaining aldehyde functions. This was followed by 2 min rinse (×5) on TBS500. Protein-protein interactions were blocked for 30 min by incubating on 5% (w/v) non-fat dried milk in TBS500. The sections were then incubated on each antiserum diluted 1/50–1/100 in the blocking buffer. Incubation time was 3 h at room temperature followed by one night at 4°C. After 4 washes (2 min each) in TBS500 followed by 3 rinses in Tris–HCl buffer (0.01 M Tris–HCl, pH 7.4–7.6), the sections were floated on the secondary marker [protein A-gold (pA 5), (Amersham)] diluted 1/25 in Tris–HCl buffer containing 0.2% fish gelatin for 90 min at room temperature. They were washed 5 times (2 min each) in Tris–HCl buffer and 3 times in H_2O. The sections were then post-fixed in 2.5% glutaraldehyde in H_2O and washed 3 times in H_2O. At this stage, the diameter of the 5 nm gold particles was further enhanced using a silver enhancing kit from Amersham. Finally, thin sections were transferred on carbon-coated copper grids and post-stained in 2.5% aqueous uranyl acetate. Observations were performed at 80 kV with a Philips CM 200 Cryo-electron microscope.

All comparative immunolabelling experiments were carried out in parallel in order to keep the same experimental conditions (dilutions of antibodies, times of contact et) and pre-immune serum for each antibody was assayed on the different tobacco lines, in the same conditions as described for the immuno-gold labelling.

Quantitative estimation of the labelling was carried out by counting the gold particles per μm^2. In each case, a section of the wild type plant was used as control for immunolabelling. Value 1.00 was assigned to the highest labelled sub-layer in the control. The labelling in the transformed samples are expressed relative to the normal plant.

References

Agarwal, U.P., Atalla, R.H., 1986. In situ Raman microprobe studies of plant cell walls: macromolecular organisation and composition variability in the secondary wall of *Picea mariana*. Planta 169, 325–332.

Atanassova, R., Favet, N., Martz, F., Chabbert, B., Tollier, M-T., Monties, B., Fritig, B., Legrand, M., 1995. Altered lignin composition in transgenic tobacco expressing *O*-methyltranferase sequences in sense and anti-sense orientation. Plant J. 8, 465–477.

Chabannes, M., Ruel, K., Yoshinaga, A., Chabbert, B., Jauneau, A., Joseleau, J.-P., Boudet, A.-M., 2001. In situ investigation of specifically engineered tobacco lignins reveals a differential impact of individual transformations on the patterns of lignin deposition, at the cellular and sub-cellular levels. Plant J., in press.

Davin, L.B., Wang, B.H., Crowell, A.L., Bedgar, D.L., Martin, D.M., Sarkanen, S., Lewis, N.G., 1997. Stereo-selective bimolecular phenoxy radical coupling by an auxiliary (dirigent) protein without an active center. Science 275, 362–366.

De Angelis, F., Nicoletti, R., Spreti, N., Veri, F., 1999. A new model of lignin biosynthesis. Angew. Chem. Int. Ed. 9, 1283–1285.

Halpin, C., Knight, M., Foxon, G., Campbell, M., Boudet, A.M., Boon, J., Chabbert, B., Tollier, M.-T., Schuch, W., 1994. Manipulation of lignin quality by down-regulation of cinnamyl alcohol dehydrogenase. Planta 6, 339–350.

Higuchi, T., 1990. Lignin biochemistry: biosynthesis and biodegradation. Wood Sci. Technol. 24, 23–63.

Houtman, C.J., 1999. What factors control dimerization of coniferyl alcohol? Holzforschung 53, 585–589.

Houtman, C.J., Atalla, R.H., 1995. Cellulose-lignin interactions. A computational study. Plant Physiol. 107, 977–984.

Joseleau, J.-P., Ruel, K., 1997. Study of lignification by noninvasive techniques in growing maize internodes — an investigation by Fourier tranform infrared, cross-polarisation-magic angle spinning ^{13}C-nuclear magnetic resonance spectroscopy and immunocytochemical transmission electron microscopy. Plant Physiol. 114, 1123–1133.

Jurasek, L., 1996. Morphology of computer-modeled lignin structures: fractal dimensions, orientation and porosity. J. Pulp Paper Sci. 22, 376–380.

Jurasek, L., 1998. Experimenting virtual lignins. In: Lewis, N.G., Sarkanen, S. (Eds.), ACS Symposium series, Vol. 697, Lignin and Lignin Biosynthesis, pp. 276–293.

Lapierre, C., Pollet, B., Petit-Conil, M., Toval, G., Romero, J., Pilate, G., Leplé, J.-C., Boerjan, W., Ferret, V., de Nadai, V., Jouanin, L., 1999. Structural alterations of lignins in transgenic poplars with depressed cinnamyl alcohol dehydrogenase or caffeic acid-*O*-methyl transferase activity have an opposite impact on the efficiency of industrial Kraft pulping. Plant Physiol. 119, 153–163.

Lapierre, C., Pollet, B., Rolando, M., 1995. New insignts into the molecular architecture of hardwood lignins by chemical degradative methods. Res. Chem. Intermed. 21, 397–412.

Lee, D., Meyer, K., Chapple, C., Douglas, C.J., 1997. Antisense suppression of 4-coumarate:coenzyme A ligase activity in *Arabidopsis* leads to altered lignin sub-unit composition. Plant Cell 9, 1985–1998.

Lewis, N.G., Davin, L.B., Sarkanen, S., 1999. The nature and function of lignins. In: Pinto, B.M. (Ed.), Comprehensive Natural Products Chemistry. Vol. 3.

Pinçon, G., Chabannes, M., Lapierre, C., Pollet, B., Ruel, K., Joseleau, J.-P., Boudet, A., Legrand, M., 2001. Simultaneous down-regulation of caffeic/5-OH ferulic acid-*O*-methyltransferase I (COMT I) in the progeny from a cross between tobacco lines homozygous for each transgene: consequences for plant development and lignin synthesis. Plant Physiol. 126, 1–11.

Piquemal, J., Lapierre, C., Myton, K., O'Connell, A., Schuch, W., Grima-Pettenati, J., Boudet, A.-M., 1998. Down-regulation of cinnamoyl–CoA reductase induces significant changes of lignin profiles in tobacco plants. Plant J. 13, 71–83.

Ralph, J., Hatfield, R.D., Piquemal, J., Yahiaoui, N., Pean, M., Lapierre, C., Boudet, A.-M., 1998. NMR characterization of altered lignins extracted from tobacco plants down-regulated for lignification enzymes cinnamyl-alcohol dehydrogenase and cinnamoyl — alcohol reductase. Proc. Natl. Acad. Sci. USA 95, 12803–12808.

Reiter, W.-D., 1998. *Arabidopsis thaliana* as a model system to study synthesis, structure, and function of the plant cell wall. Plant Physiol. Biochem. 36, 167–176.

Roussel, M.R., Lim, C., 1995. Dynamic model of lignin growing in restricted spaces. Macromolecules 28, 370–376.

Ruel, K., Chabannes, M., Pinçon, G., Piquemal, J., Boudet, A.-M., Legrand, M., Joseleau, J.-P., 2000. Modifications in lignin biosynthesis pathways affect plant cell wall assembly. 219th ACS Symposium, San-Francisco, CA, Cellulose, Paper, and Textile Chemistry Division. Symposium: Biosynthesis of Plant Biopolymers and Related Substances, Part 1 of 2, Abstract No. 134.

Ruel, K., Faix, O., Joseleau, J.-P., 1994. New immunogold probes for studying the distribution of the different lignin types during plant cell wall biogenesis. J. Trace Microprobe Techniques 12, 247–265.

Russell, W.R., Provan, G.L., Burkitt, M.J., Chesson, A., 2000. Extent of incorporation of hydroxycinnamaldehydes into lignin in cinnamyl alcohol dehydrogenase-downregulated plants. J. Biotechnol. 79, 73–85.

Siegel, S., 1957. Non-enzymatic macromolecules as matrices in biological synthesis: the role of polysaccharides in peroxidase-catalysed lignin polymer from eugenol. J. Am. Chem. Soc. 79, 1628–1632.

Terashima, N., Fukushima, K., 1989. Biogenesis and structure of macromolecular lignin in the cell wall of tree xylem as studied by microautoradiography. In: Lewis, N.G., Paice, M.G. (Eds.), Plant Cell Wall Polymers, Biogenesis and Biodegradation. Am. Chem. Soc. Symposium Series 339, Washington DC, pp. 160–168.

Terashima, N., Atalla, R.H., Ralph, S.A., Landucci, L.L., Lapierre, C., Monties, B., 1995. preparations of lignin polymer models under conditions that approximate cell wall lignification. Holzforschung 49, 521–527.

Wetten, R., Sederoff, R., 1995. Lignin biosynthesis. Plant Cell 7, 1001–1013.

Yoshida, S., Tanahashi, M., Shigematsu, M., Shinoda, Y., 1994. Effect of reaction medium on dehydrogenative polymerization of sinapyl alcohol. Mokuzzai Gakkaishi 40, 974–979.

PERGAMON

Phytochemistry 57 (2001) 883–897

PHYTOCHEMISTRY

www.elsevier.com/locate/phytochem

Dirigent proteins and dirigent sites in lignifying tissues

Vincent Burlat, Mi Kwon, Laurence B. Davin, Norman G. Lewis*

Institute of Biological Chemistry, Washington State University, Pullman, WA 99164-6340, USA

Received in revised form 18 January 2001

Abstract

Tissue-specific dirigent protein gene expression and associated dirigent (site) localization were examined in various organs of *Forsythia intermedia* using tissue printing, in situ mRNA hybridization and immunolabeling techniques, respectively. Dirigent protein gene expression was primarily noted in the undifferentiated cambial regions of stem sections, whereas dirigent protein sites were detected mainly in the vascular cambium and ray parenchyma cell initials. Immunolocalization also revealed cross-reactivity with particular regions of the lignified cell walls, these being coincident with the known sites of initiation of lignin deposition. These latter regions are considered to harbor contiguous arrays of dirigent (monomer binding) sites for initiation of lignin biopolymer assembly. Dirigent protein mRNA expression was also localized in the vascular regions of roots and petioles, whereas in leaves the dirigent sites were primarily associated with the palisade layers and the vascular bundle. That is, dirigent protein mediated lignan biosynthesis was initiated primarily in the cambium and ray cell initial regions of stems as well as in the leaf palisade layers, this being in accordance with the occurrence of the lignans for defense purposes. Within lignified secondary xylem cell walls, however, dirigent sites were primarily localized in the S_1 sublayer and compound middle lamella, these being coincident with previously established sites for initiation of macromolecular lignin biosynthesis. Once initiation occurs, lignification is proposed to continue through template polymerization. © 2001 Elsevier Science Ltd. All rights reserved.

Keywords: *Forsythia intermedia*; Oleaceae; Immunolocalization; In situ hybridization; Dirigent proteins; Dirigent sites; Lignans; Lignins

1. Introduction

The biochemical processes involved in stipulating the outcome of monolignol coupling to afford vascular plant lignin biopolymers and (oligomeric) lignans, nature's second most abundant substances, are only now beginning to yield to inquiry (Davin et al., 1997; Lewis and Davin, 1998, 1999; Sarkanen, 1998; Gang et al., 1999; Lewis, 1999; Lewis et al., 1999). The lignins are heterogenous structural biopolymers mainly laid down within cell-walls of primary and secondary xylem, as well as phloem fibers (Lewis et al., 1999). Their compositions can vary both between and within plant species according to the type of monolignols present (i.e. *p*-coumaryl, coniferyl and sinapyl alcohols, Fig. 1A), as well as by the various intermonomeric linkages involved (Lewis and Yamamoto, 1990; Brunow et al., 1998). Lignin heterogeneity results from predetermined differences in the *organized* distribution of individual monolignols in lignins within different cell types and even within distinct cell wall layers of the same cell type (Fergus and Goring, 1970; Hardell et al., 1980; Saka et al., 1982; Tollier et al., 1986; Lewis and Yamamoto, 1990; Fukushima and Terashima, 1991; Burlat et al., 1997; Joseleau and Ruel, 1997).

It has long been known that lignin formation begins at so-called lignin initiation sites located at the furthermost outer reaches within the preformed wall (Wardrop and Bland, 1959; Donaldson, 1994). That is, lignification is initiated at the outermost regions and then works its way back towards the plasma membrane/lumen after which the cell dies. The evolution of this remarkable biochemical system thus provided the means for not only ensuring that lignification occurs throughout the entire plant cell wall, but also affords the means for the cytoplasm to control both lignin assembly and monomer composition throughout the wall. However, we still have a very incomplete understanding of how the monomers are transported to the lignin initiation sites and their precise interactions with the lignin forming proteins and

* Corresponding author. Tel.: +1-509-335-2682; fax: +1-509-335-8206.

E-mail address: lewisn@wsu.edu (N.G. Lewis).

0031-9422/01/$ - see front matter © 2001 Elsevier Science Ltd. All rights reserved.
PII: S0031-9422(01)00117-0

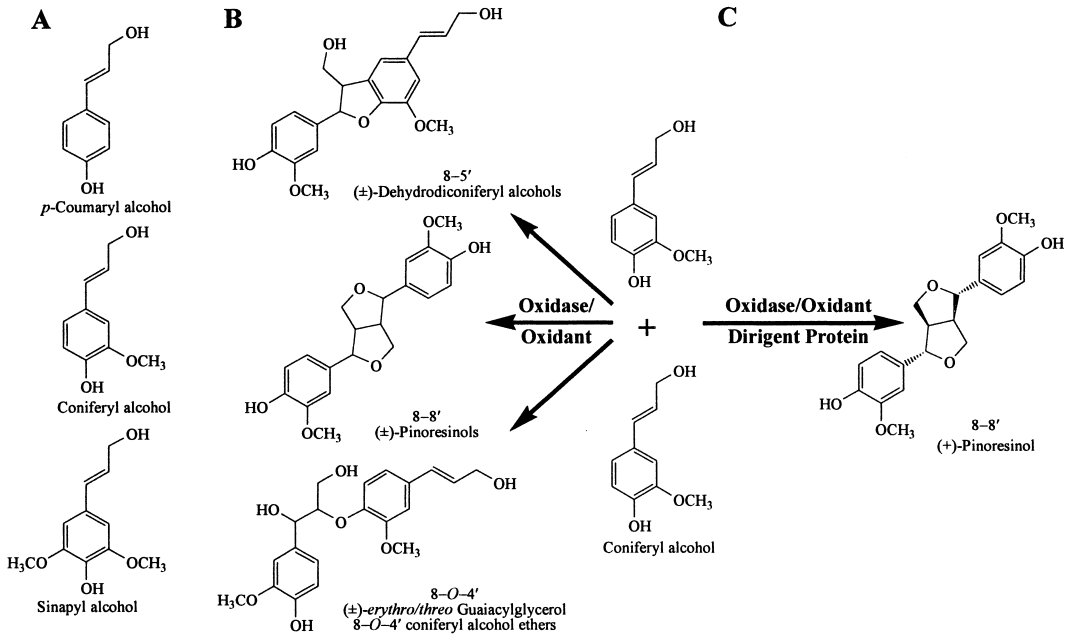

Fig. 1. Monolignols and oxidative coupling. (A) Chemical structures of monolignols, (B) non-specific, racemic phenoxy-radical coupling of *E*-coniferyl alcohol in presence of an oxidant/oxidase, and (C) an example of stereoselective phenoxy-radical coupling of *E*-coniferyl alcohol, in this case, in the presence of an oxidant/oxidase and the *Forsythia intermedia* dirigent protein (psd-Fi1).

enzymes in the wall. Nevertheless, the regiospecificity of coupling affords a polymer typically having 50–70% of 8-*O*-4′ linkages (Adler, 1977), with this perhaps even being as much as 80% in transgenic *Arabidopsis* (Meyer et al., 1998; Marita et al., 1999). Following lignin initiation, it has been proposed that subsequent lignification occurs back toward the plasma membrane through a template polymerization process (Guan et al., 1997; Sarkanen, 1998).

Lignification has been temporally and spatially correlated with secretion from the Golgi apparatus of specific glycine-rich proteins (GRPs) (Keller et al., 1988; Ye et al., 1991; Ye and Varner, 1991; Ryser et al., 1997) and proline-rich proteins (PRPs) (Marcus et al., 1991; Ye et al., 1991; Müsel et al., 1997). Although these ultimately become an integral part of the maturing cell wall architecture, no explicit biochemical function was demonstrated in vitro for either class of proteins.

The lignans are a widespread class of related, but biochemically distinct, metabolites, which are frequently found as 8-8′ linked dimers, although other interunit linkages abound (e.g. 8-5′, 8-*O*-4′) (for reviews, see Lewis and Davin, 1994, 1998, 1999). They are found in *all* plant tissues examined thus far. Many lignans are optically active; they can exist as higher molecular weight oligomeric entities, such as major heartwood constituents in western red cedar (*Thuja plicata*) (Beatson et al., 1998; Fujita et al., 1999). Their roles appear to be primarily in plant defense, with their formation being either under constitutive or inducible control (Lewis and Davin, 1994, 1999); their deposition can have important positive contributions to plant tissue durability, color and quality. Various lignans have been demonstrated to have antioxidant (Osawa et al., 1985; Harper et al., 1999), antiviral (Gnabre et al., 1995; Asano et al., 1996), bactericidal (Nitao et al., 1991), antifungal (Atta-ur-Rahman et al., 1995; Miyazawa et al., 1996), and cytotoxic (Kupchan et al., 1978; Day et al., 1999) properties.

A new perspective on control of monolignol coupling was obtained with the discovery of dirigent proteins (Latin: *dirigere*, to guide or to align) (Davin et al., 1997; Gang et al., 1999). Discovered first in *Forsythia intermedia*, the dirigent glycoprotein stipulates, at both the regio- and stereochemical levels, the outcome of coupling of two molecules of *E*-coniferyl alcohol to give the lignan, (+)-pinoresinol, as shown in Fig. 1C rather than racemic products (Fig. 1B) (Davin et al., 1997). A requirement of the protein is, however, provision of one-electron oxidation through an auxiliary source (e.g. laccase, peroxidase, cytochrome P-450, and ammonium peroxydisulfate). Significantly, only *E*-coniferyl alcohol derived substrates were utilized by this protein, and not *p*-coumaryl or sinapyl alcohols which differ only in the degree of methoxylation (see Fig. 1A).

The discovery of dirigent proteins established the long anticipated existence of *specific* monolignol (radical) binding proteins. The gene encoding the ~18 kDa dirigent protein subunit was cloned, with the fully functional glycosylated recombinant form (~26 kDa subunit) obtained using a *Spodoptera*/baculovirus expression system (Gang et al., 1999). It had no significant level of similarity or identity to any other protein of known function. Thus far, dirigent proteins and their homologues have only been reported in vascular plants (Davin and Lewis, 2000).

This discovery led to the central question of whether or not arrays of dirigent (monomer binding) sites might be the means for initiating the onset of lignification at the so-called lignin initiation sites. This does not, however, imply that the dirigent proteins and arrays of dirigent (monomer) binding sites are synonymous. Indeed they could not be, as the former are required for optically active lignan biosynthesis. A dual deployment of dirigent proteins for lignan biosynthesis and dirigent (monomer binding) sites in other proteins for lignin biosynthesis initiation would place this main branch of metabolism in alignment with all other major branches of plant metabolism. That is, in terpenoid, carbohydrate and lipid metabolism, there are recurring biochemical (enzymological) processes which account for dimer, oligomer and biopolymer biosyntheses in each metabolic class, e.g. glycosyl transferases and prenyl transferases. It is therefore tempting to consider that there are recurring themes in free-radical coupling also, and which would control lignan and lignin biosynthesis assembly processes. Furthermore, a mechanism employing template polymerization could explain how lignins proper have relatively few cross-links and types of inter-unit linkages, and lack any apparent optical activity.

This study undertook the objectives of establishing, at the ultrastructural level, the specificity of both dirigent protein gene expression (i.e. mRNA localization) and dirigent site localization, in different tissues and subcellular compartments of the angiosperm *F. intermedia*. Polyclonal antibodies were employed not only to localize the dirigent protein involved in (+)-pinoresinol biosynthesis, but also to ascertain whether related proteins harboring (arrays of) dirigent (monomer binding) sites were co-localized with the established initiation sites of lignin formation (Donaldson, 1994). The results described below provide further evidence for the involvement of dirigent proteins and dirigent sites in lignan and lignin biosynthesis, respectively.

2. Results and discussion

The morphology of cross-sections of different tissues of *F. intermedia* is conveniently revealed (Fig. 2) by toluidine blue staining. Fig. 2A and D [1st, young, and 10th, more mature, internodes, respectively] show stem morphology at two developmental stages, whereas Fig. 2G, J and M display the relative morphologies of petiole, root and leaf tissues. Three broad tissue categories are observed in the stem sections (Fig. 2A and D): the cortex, the differentiating cambial layers, and the lignified developing xylem. With increased maturity (Fig. 2D), the vascular cambium cells are readily distinguished from the secondary phloem located beneath the phloem fibers, and the pith progressively collapses to give the central hollow. In petioles (Fig. 2G), the crescent-shaped vascular bundle embodying the vascular cambium is flanked by secondary phloem and the lignified developing xylem/ground parenchyma. In the roots (Fig. 2J), the meristematic cambial region is constituted by the pericycle, with vascular lignified tissues forming the stele, whereas in leaves (Fig. 2M), the bundle sheath cells are embodied within the paraveinal mesophyll, these cells being flanked by the palisade parenchyma above and the spongy mesophyll below.

Using phloroglucinol-HCl histochemical staining (Johansen, 1940), patterns of lignin deposition are readily visualized within the stem xylem cell walls, phloem fibers and sclerified pith parenchyma (Fig. 2B and E). Patterns of lignin deposition are also observed inside the developing xylem of the petiole (Fig. 2H), the stele of the root (Fig. 2K), and the bundle sheath cells of the leaves (Fig. 2N). The application of autofluorescence (Franceschi et al., 1998) permits an assessment of the gross localization of phenolics in the various lignin and lignan containing tissues of *Forsythia*; this revealed that beside the lignified cell walls (and the cutinized and/or suberized epidermis), additional light blue signals were present in both the cortex and the vascular cambium-secondary phloem region of stems (Fig. 2C and F). Similar observations were made in the cambium-secondary phloem region and ground parenchyma of the petiole (Fig. 2I), as well as in the pericycle and cortex regions of the root (Fig. 2L). Finally, in leaf tissues (Fig. 2O), where lignins are scarcely present but where lignans accumulate (Rahman et al., 1990), an intense phenolic autofluorescence was observed in the palisade parenchyma and the paraveinal spongy mesophyll, as well as the vascular bundles. Thus, beside the lignin patterning in the cell walls of vascular tissues, other populations of phenolics, which typically include lignans, are present in various different cell types. Lignans are also present in all of the other *Forsythia* tissues (Chiba et al., 1979; Kitagawa et al., 1988; Rahman et al., 1990).

2.1. Tissue specific expression of dirigent transcripts

The expression patterns of the dirigent protein gene psd-Fi1 was examined in *F. intermedia* stem, root and petiole tissues, using tissue print mRNA hybridization (McClure and Guilfoyle, 1989; Ye et al., 1991; Ye and Varner, 1991) and in situ hybridization (Bochenek and Hirsch, 1990) techniques; this dirigent protein gene is from a multigene family with at least three members in the *Forsythia* species (Gang et al., 1999, Jeon and Lewis, unpublished data).

Physical prints onto sobo glue (polyvinyl acetate) first revealed the gross morphology of the different tissues (Fig. 3A, D, G, J and M). Tissue-print blotting was next used to define patterns of dirigent protein mRNA accumulation. Hybridization with the radiolabeled antisense probe (Fig. 3B, E, H, K and N) revealed specific

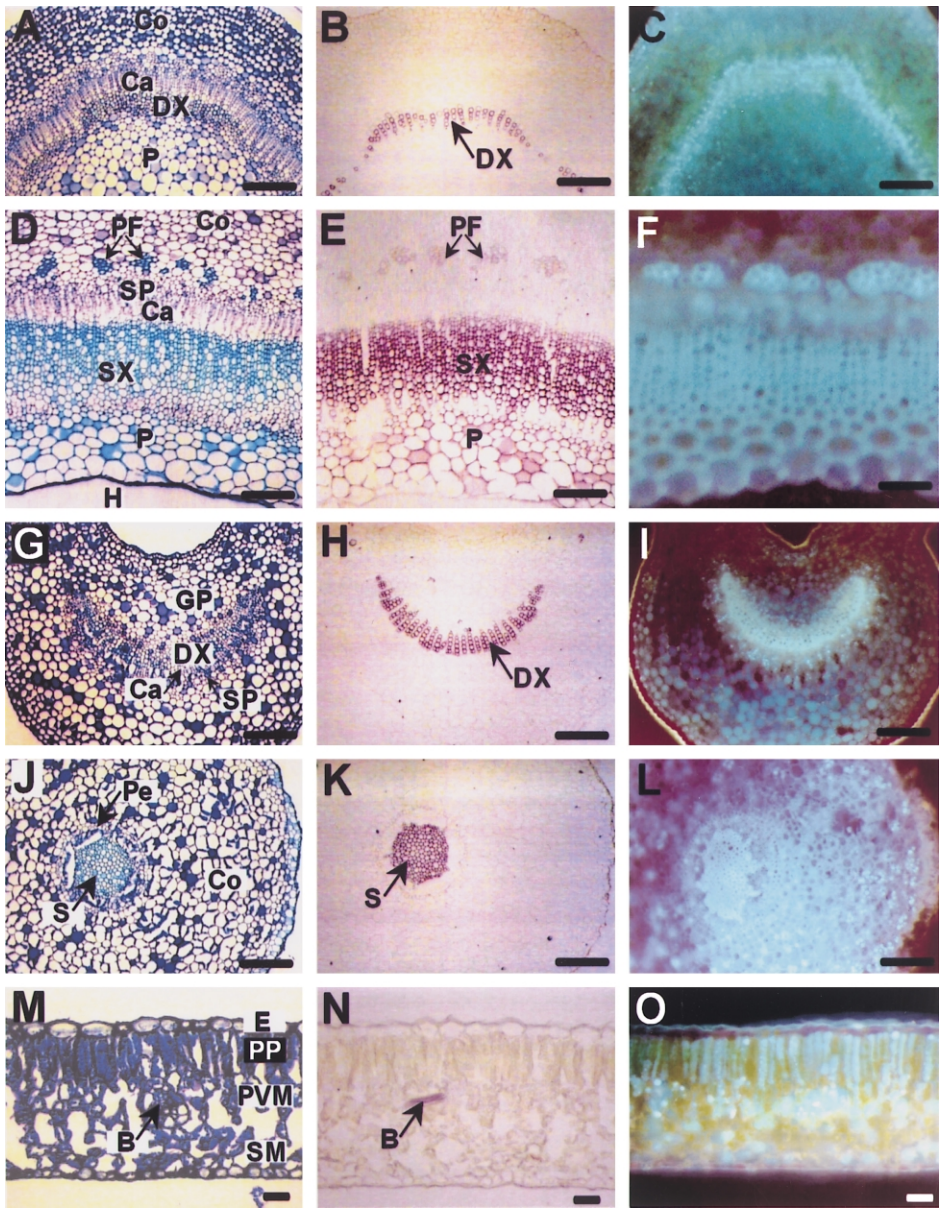

Fig. 2. Distribution of lignin and other phenolics (i.e. lignans) within cross-sections of *Forsythia intermedia* tissues. (A)–(C) Stem 1st developing internode, (D)–(F) stem 10th mature internode, (G)–(I) mature petiole, (J)–(L) root and (M)–(O) leaf, respectively. Morphological features are revealed with toluidine blue staining (A), (D), (G), (J), and (M), whereas histochemical aspects of lignin deposition are displayed by phloroglucinol-HCl staining (B), (E), (H), (K), and (N), and the phenolics are exposed via light blue autofluorescence (C), (F), (I), (L), and (O). Note in addition to the lignin deposition detected in vascular tissues with both phloroglucinol-HCl and phenolic autofluorescence, the additional phenolic populations detected as autofluorescence in different cell types/tissues. B, bundle sheath; Ca, cambium; Co, cortex; DX, developing xylem; E, epidermis; GP, ground parenchyma; H, hollow; P, pith; Pe, pericycle; PF, phloem fibers; PP, palisade parenchyma; PVM, paraveinal mesophyll; S, stele; SM, spongy mesophyll; SP, secondary phloem; SX, secondary xylem. Bars: 50 μm.

and intense signals in all cases examined, as compared to the corresponding sense controls (Fig. 3C, F, I, L and O). In stem cross-sections, the dirigent protein mRNA signals were predominantly present in the cambial region in all three developmental stages examined [young (1st, Fig. 3B), intermediate (10th, Fig. 3E) and oldest (20th, Fig. 3H) internode, respectively]. Additional signals were detected at the youngest (1st internode) developmental stage in the cortex, developing xylem and pith tissues (Fig. 3B). The intensity of this particular labeling pattern decreased with maturation, with the signal becoming essentially restricted to the cambial region (Fig. 3H). Petiole cross-sections (Fig. 3K) also displayed a specific, albeit weaker, signal, this being in the cambial tissue adjacent to the differentiating lignified vascular region. A similar observation was made with root cross-sections (Fig. 3N), where a relatively weak but specific signal was noted with the anti-sense probe in the pericycle surrounding the central vascular tissues (stele). Thus, the tissue printing hybridization technique established that

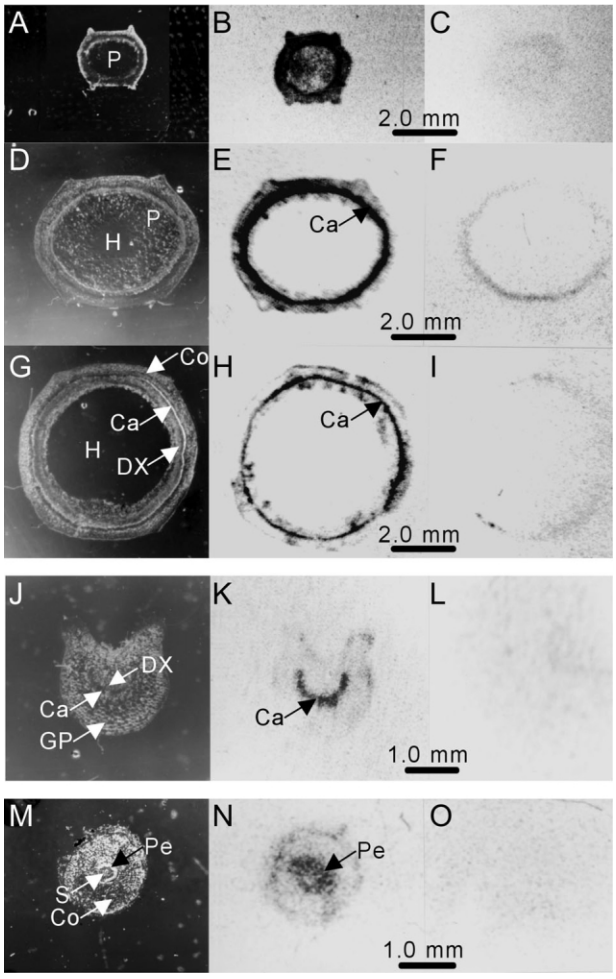

Fig. 3. Dirigent protein mRNA localization via tissue-print hybridization of fresh cross-sections of *Forsythia intermedia* tissues. (A)–(C) Stem 1st developing internode, (D)–(F) stem 10th mature internode, (G)–(I) stem 20th mature internode, (J)–(L) petiole, and (M)–(O) root, respectively. (A), (D), (G), (J) and (M) Physical prints of cross-sections displaying gross tissue morphology. Each of the blots from adjacent cross-sections within the same tissue were hybridized in parallel with the ^{35}S-thio UTP-labeled anti-sense (B), (E), (H), (K) and (N) and sense (C), (F), (I), (L) and (O) probes for dirigent protein mRNA labeling and for negative controls, respectively. Note: (i) the intense dark signals (anti-sense experiments) due to localization of dirigent protein mRNA in the differentiating cambial region of the stems and petiole, and in the pericycle of root; (ii) the fainter signal observed in the outer cortex of the young differentiating internodes that disappeared during maturation of the stem, with the mRNA localization subsequently becoming restricted to the cambial region. Ca, vascular cambial region; Co, cortex; DX, developing xylem; GP, ground parenchyma; H, hollow; P, pith; Pe, pericycle; S, stele.

gross localization of the dirigent mRNA was mainly associated with the cambial regions (Burlat et al., 1999; Kwon et al., 1999); it should be noted that historically the cambial region/differentiating xylem has hitherto been viewed by many researchers as exclusively restricted to lignin biosynthesis (Freudenberg, 1968; Bao et al., 1993).

In situ hybridization experiments were conducted using 1st and 10th internode stem cross-sections as a means to obtain resolution at the cellular level (Fig. 4). These particular samples were chosen for the relatively high dirigent gene expression level as noted from both tissue print hybridization (Fig. 3B and E) and northern analysis (Kwon et al., 1999). These experiments confirmed the observations with tissue printing hybridization, with the main signal again being present in the cambial regions of the 1st internode (Fig. 4A and C) and 10th internode (Fig. 4E and G), respectively. At the youngest stage of development, dirigent protein expression was also observed in the cortex and the pith (Fig. 4A); however, the strongest signals were restricted to the cambial region and ray parenchyma cell initials (Fig. 4C). Interestingly, the latter cells are *adjacent* to the lignified tracheary elements which, by comparison, only display a weak signal, especially in the oldest lignified tracheary elements adjacent to the pith. The more mature stem, in contrast, showed a relatively weaker signal, which was specifically localized along the vascular cambium, and, to a lesser extent, the secondary phloem (Fig. 4E and G). Negative controls with the sense probe gave essentially no background signals (Fig. 4B, D, F and H).

Both methods thus gave complementary results illustrating that among the tissues studied, dirigent gene expression was mainly associated with the vascular cambium region, in the cambium and secondary phloem of mature stem and petiole tissues, i.e. regions previously described as the exclusive domain of lignification (Freudenberg, 1968; Bao et al., 1993).

2.2. Tissue specific and sub-cellular localization of dirigent protein and proposed arrays of dirigent (monomer binding) sites

The next objective was to localize the dirigent protein (and/or related dirigent sites) at the tissue and subcellular levels. For this purpose, polyclonal antibodies were specifically employed with the rationale that they would not only immunolocalize dirigent proteins involved in lignan biosynthesis, but would perhaps display an antigenic response with related dirigent binding sites (for coniferyl alcohol derived substrate) involved in the initiation of lignin deposition. Thus, the glycosylated dirigent protein obtained in functional recombinant form through heterologous expression of psd-Fi1 in a *Spodoptera*/baculovirus expression system (Gang et al., 1999) was used to raise polyclonal antibodies in two rabbits.

The titers of both rabbit sera (raised against the dirigent protein and the pre-immune serum controls, respectively) were first evaluated using the indirect ELISA technique. It was found that neither of the two pre-immune sera bound the antigen, even at the lowest dilutions tested, i.e. 1:100 (data not shown). The best titer (highest dilution to obtain an $\frac{1}{2}$ OD 490 nm max reading) was observed after 7 weeks for the first rabbit ($\sim$1:2500), and 11 weeks for the second ($\sim$1:2500), in harmony

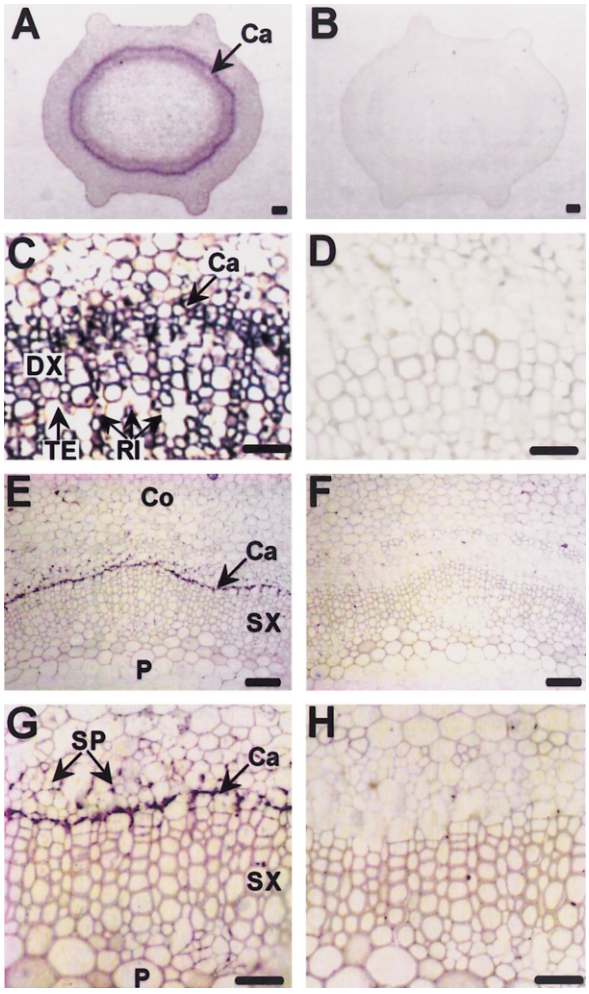

Fig. 4. In situ hybridization of *Forsythia intermedia* dirigent protein mRNA with digoxigenin-labeled riboprobes. (A), (C), (E), and (G) Labeling with anti-sense probe, and (B), (D), (F), and (H) controls using the sense probe. The data shown are for the *F. intermedia* stem differentiating 1st internode (A)–(D) and mature 10th internode (E)–(H), and are given at two different enlargements in each case. Note the evolution of the dark purple signal with maturation of the stem. This became restricted to the cambium and secondary phloem in the differentiated 10th internode, whereas it was also present, to a lesser extent, in the cortex of the young differentiating 1st internode. Ca, cambium; Co, cortex; DX, developing xylem; P, pith; RI, ray initials; SP, secondary phloem; SX, secondary xylem; TE, tracheary elements. Bars: 50 μm (A), (B), (E) and (F), 25 μm (C), (D), (G) and (H).

with previous observations using the whiffle-ball technique to raise antibodies (Hillam et al., 1974; Ried et al., 1992). The 7-week immune serum of the first rabbit and its corresponding pre-immune serum were chosen for subsequent experiments.

Note, however, that SDS–PAGE followed by western blot analysis had previously demonstrated that the dirigent protein immune serum specifically recognized the recombinant *Forsythia* dirigent protein (even after deglycosylation), as well as both the dirigent in a crude protein extract from *Forsythia* stems and the purified native *Forsythia* dirigent (Gang et al., 1999). The same specific band (~26 kDa for the glycosylated subunit) was also observed on western blots of crude protein extracts from petioles, roots and leaves (data not shown).

Antiserum specificity was further confirmed by indirect competitive ELISA experiments. These demonstrated that, among the pre-adsorbed competitors tested, only the dirigent protein inhibited antiserum binding of the pure recombinant dirigent (Fig. 5A). This clearly established the specificity of the antiserum for both recombinant and native dirigent forms, as compared to other *F. intermedia* proteins (e.g. pinoresinol/lariciresinol reductase and laccase). Furthermore, none of the plant cell-wall polymers tested (xylan, cellulose, and three types of pectins) or other related preparations (i.e. synthetic lignins) displayed any significant competitive inhibitory properties. Additionally, the total crude protein extract from *F. intermedia* stems functioned in an analogous manner (Fig. 5B). Therefore, the antiserum appeared to be very useful for the study of the localization of dirigent and/or dirigent sites in vascular (lignifying) tissues.

Using thick sections of paraffin embedded samples, immunolabeling of different *F. intermedia* anatomical tissues revealed intense specific signals with the dirigent immune protein serum (Fig. 6A, C, E, G, I, K and M), as compared to the pre-immune serum control of serial sections (Fig. 6B, D, F, H, J, L and N). Essentially, the 1st internode stem cross-sections displayed a strong dark signal in both the vascular cambium region and young developing xylem, together with labeling in the outer layers of the cortex (Fig. 6A). With stem maturation the signal became primarily restricted to the vascular cambium region (cambium and secondary phloem), and the lignified cells of the secondary xylem, sclerified pith parenchyma, and phloem fibers (Fig. 6C and E). Dirigent protein immune serum also gave a very intense signal in all tissues of young developing leaves and their central veins (Fig. 6G). Interestingly, fully mature leaves displayed the strongest immunolabeling response within the palisade parenchyma layers, and to a somewhat lesser extent in the paraveinal and spongy mesophyll (Fig. 6I). The labeling pattern observed in young differentiating petioles was also identical to those of the central vein extension (data not shown). In a similar manner, as observed during stem maturation, the signal observed in mature petioles was mainly restricted to the cambial layers and secondary phloem, as well as in the developing xylem (Fig. 6K). Roots displayed an uniform labeling pattern in the pericycle layers together with the vascular tissues of the stele at all maturation stages observed (see Fig. 6M for example).

These findings were generally consistent with observations made for dirigent protein gene expression in the cambial regions of stem, petiole and, to a lesser extent, root sections (Figs. 3 and 4). Moreover, during stem maturation, development of the patterns of both gene expression and protein accumulation also displayed

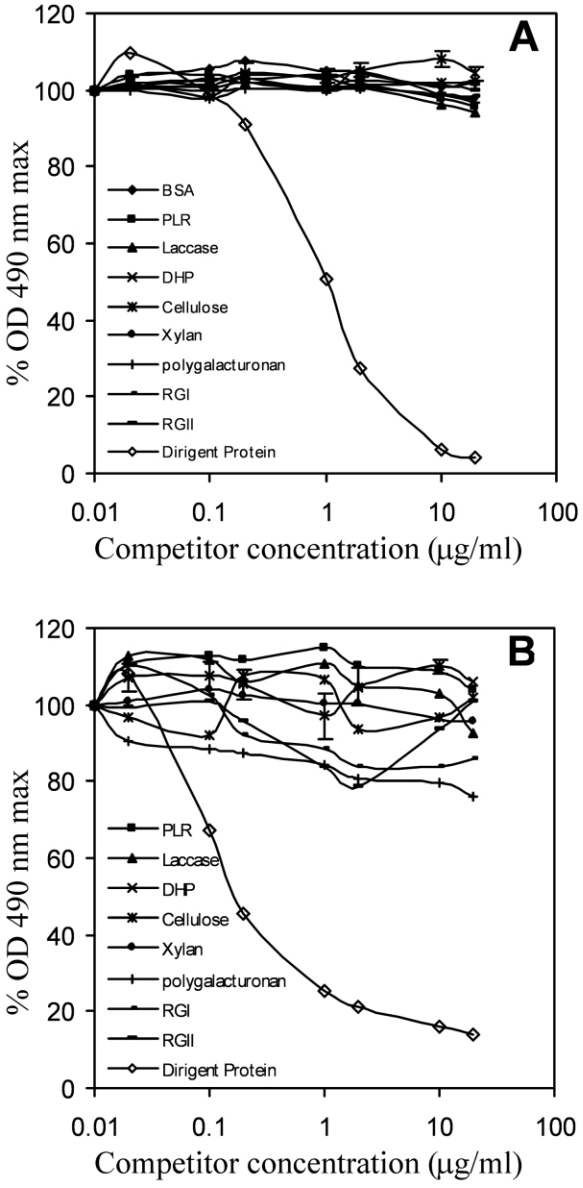

Fig. 5. Specificity of the *Forsythia intermedia* dirigent protein antiserum as revealed by indirect competitive ELISA. (A) Pure recombinant dirigent protein and (B) a crude extract of total protein from *F. intermedia* young stems were used as antigens to coat 96-well ELISA plates. Different competitors were pre-incubated with the antiserum at different concentrations as described in the Experimental. Abbreviations: BSA, bovine serum albumin; DHP, dehydrogenative polymer (synthetic lignin); PLR, pinoresinol/lariciresinol reductase; RGI, rhamnogalacturonan I; RGII, rhamnogalacturonan II. Note that, among the competitors tested, only the dirigent protein itself was able to significantly reduce the cross-reaction of the dirigent protein immune serum with the pure recombinant dirigent protein, as well as with a crude protein extract from *Forsythia* stems.

striking similarities, namely decrease of the signal in the outer cortex and restriction to the cambial region. It was interesting to note that immunolabeling experiments revealed the presence of a population of dirigent sites within the lignified tissues, which had not been detected at the gene expression level. Even though the secondary xylem has originated from cambial cells, the dirigent protein gene expression observed in these cells is unlikely to be the forerunners of dirigent sites detected in the developed secondary xylem. This is because it is highly unlikely that the dirigent proteins are incorporated into developing cell walls — particularly at the sites of lignin initiation; instead they are considered to be involved in lignan deposition within the cell itself. It is much more likely that the epitopes detected are from related proteins having [arrays of] lignin monomer binding sites (coniferyl alcohol derived), and which are involved in initiation of lignin biosynthesis proper. However, much remains to be done to characterize these sites, the mechanism of lignin monomer transport, the interactions between lignin monomers and the arrays of dirigent sites, as well as determination of the placement and catalytic functions of the various oxidases involved in lignin assembly(ies).

Immunolabeling experiments were next conducted on resin embedded sections in order to obtain better resolution. A strong signal was again detected in the lignified cell walls of secondary xylem cells, sclerified pith parenchyma, and phloem fibers but not in either the cambial region or young cortex tissues (data not shown) (Gang et al., 1999); this was true for all developmental stages and different tissues examined. A comparable observation had been made for glycine-rich proteins in both tobacco (*Nicotiana tabacum*) and petunia (*Petunia hybrida*) stems (Ye et al., 1991). That is, while the encoding gene was specifically expressed in the cambial region as determined by tissue printing hybridization, the corresponding protein was only observed in the cell walls of vascular tissues with resin embedded sections. The differences in detection and relative intensity between the two procedures (paraffin and resin sections, respectively), are thus attributed to one or more of the following *three* reasons: Firstly, the resin fixation method (i.e. using paraformaldehyde/glutaraldehyde) is employed *primarily* for ultrastructural preservation; however, this can be anticipated to result in a higher loss of antigenicity of dirigent protein epitopes in the cytoplasmic rich regions such as the cambial region and the young cortex tissues, i.e. as compared to those within fully lignified secondary cell walls where the cross-linking agent is not as readily accessible. This could result in either differences in relative solubility/extractability of the two populations of dirigent (epitope)s, and/or to differences in aldehyde resin accessibility in both regions. Secondly, since thick (8 μm) paraffin sections were deparaffinized prior to immunolabeling, this might result in an overestimation of the antigenicity of the more soluble dirigent protein epitopes in the cambial region relative to those dirigent sites less accessible in the immobilized lignified cell wall regions. Thirdly, with resin-embedded sections, a more representative surface reaction is anticipated, even with the

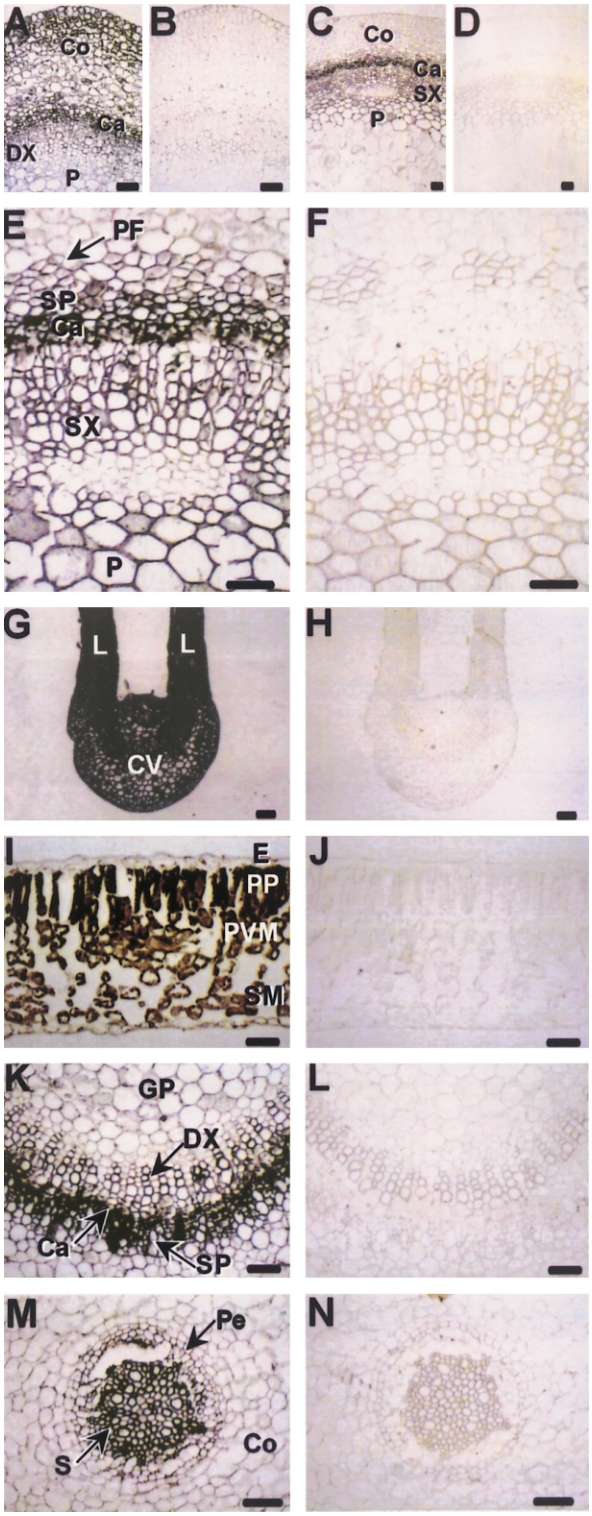

Fig. 6. Tissue-specific immunolocalization of dirigent protein and dirigent site epitopes on cross-sections of paraffin-embedded tissues of *Forsythia intermedia*. (A), (C), (E), (G), (I), (K), and (M) Dirigent protein immune serum and (B), (D), (F), (H), (J), (L), and (N) corresponding pre-immune serum negative control were applied to serial cross-sections of the following: differentiating 1st internode (A) and (B), more mature 10th internode (C)–(F), differentiating leaf with its central vein (G) and (H), mature leaf (I) and (J), mature petiole (K) and (L) and root (M) and (N). The localization of the major dirigent protein epitopes (dark black signal) was in the same tissues where the dirigent protein gene was expressed, i.e. vascular cambium and secondary phloem of the stem and petiole, as well as in the cortex of young differentiating stem and root pericycle. Additional strong specific signals were also observed in the lignified regions of stem, petiole and root tissues, whereas the strong dark signal in the differentiating leaves became mainly restricted to the palisade parenchyma layers at maturation. Ca, vascular cambium region; Co, cortex; CV, central vein; DX, developing xylem; E, epidermis; L, leaf; P, pith; Pe, pericycle; PP, palisade parenchyma; PF, phloem fibers; PVM, paraveinal mesophyll; S, stele; SM, spongy mesophyll; SP, secondary phloem; SX, secondary xylem; X, xylem. Bars: 50 μm.

different levels of epitope conservation and accessibility in various tissues. Furthermore, even when other fixation protocols, such as with cryofixation (Fisher and Housley, 1972) and microwave-curing (Turner et al., 1999), were evaluated for resin embedding using different mixtures of aldehydes, the same labeling pattern restricted to the lignified cell walls, albeit with poorer ultrastructural preservation, was obtained (data not shown).

Thus, there are two main regions of dirigent proteins (or dirigent sites), namely in the cambial region for lignan formation and in the lignified elements of mature stem, petiole and root tissues for lignification, respectively. Interestingly, downstream lignan metabolic processes involving expression of the genes encoding pinoresinol-lariciresinol reductases are also localized in the cambial regions as well (Kwon et al., 2001), as evidenced by in situ hybridization. This again demonstrates that this region can no longer be viewed as the exclusive domain of lignin biosynthesis. Mature leaves also gave a very tissue specific localization of dirigent protein (site)s, with a stronger signal in the palisade parenchyma layers (lignans), relative to that of the lignified bundle sheath and the spongy mesophyll cells.

High-resolution transmission electron microscopy was next employed to estimate the sub-cellular locations of dirigent sites within different *types* of lignified cell walls of stems. In this way, distinct, but specific, patterns of labeling (see Fig. 7) were clearly observed with the various cell types present in *F. intermedia* serial sections. In all cases, in order to provide a comparative analysis of a particular anatomical region, experiments were conducted with both immune and pre-immune (control) sera; these controls gave, as expected, no labeling (Gang et al., 1999).

An examination of the immunolabeling patterns in fully developed vessels (Fig. 7A) and in developing ray cells (Fig. 7B) was first undertaken. This revealed that immunolabeling was predominantly in the S_1 sub-layer and the compound middle lamella, as well as, to a lesser extent, in the S_3 sub-layer — with the latter only being detected when the S_3 layer was completed. No significant degree of labeling was noted in either the S_2 sub-layer or the cell corners. These immunolabeled regions are consistent with the placement of lignin initiation sites.

The patterns of dirigent sites were also examined in lignified phloem at two stages of fiber cell development, namely at an early stage of development (Fig. 7C) and when more fully mature (Fig. 7D). As can be seen, the labeling of the phloem fiber cells was again essentially only associated with the S_1 sub-layer, as previously noted for vessels (Fig. 7A), possessing layered cell walls. Thus, in summary, the patterns of labeling in the ray cells, vessels and fibers were essentially the same, despite the ray cells having much thinner cell walls.

It was next of interest to establish whether immunolabeling patterns were similar in both secondary xylem and primary xylem (in this case, metaxylem), with the latter lacking any distinctive secondary cell wall layering, i.e. the metaxylem has an uniform cell wall thickening (Fig. 8A), in contrast, for example, to the layered vessels of the secondary xylem (Fig. 8C).

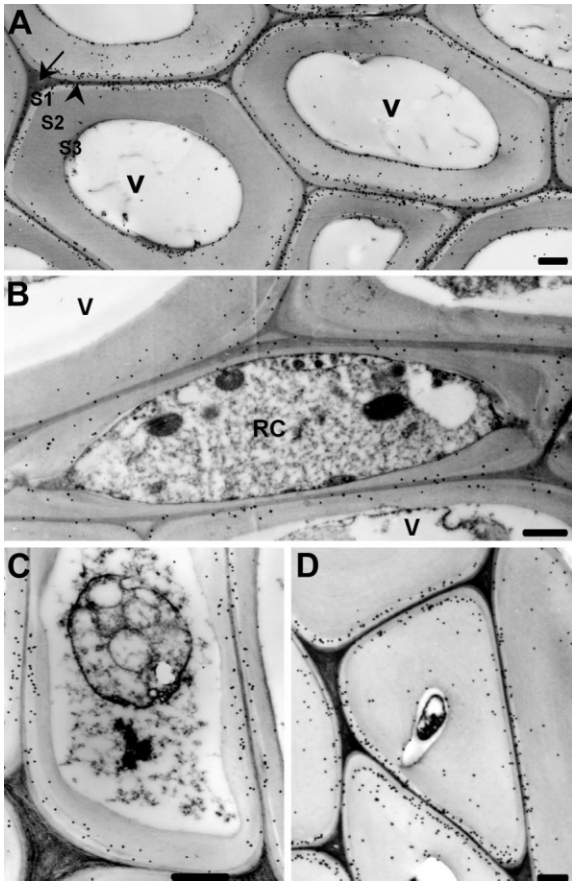

Fig. 7. Sub-cellular immunolocalization of dirigent protein epitopes (or dirigent sites) in various cell types present in *Forsythia intermedi*a young stem cross-sections using transmission electron microscopy. Representative immunolabeling of the S_1 sub-layer and compound middle lamella, and to a lesser extent of the S_3 sub-layer, observed in fully developed vessels (A), ray cells (B) as well as in young (C) and mature (D) phloem fibers. Arrow, cell corner; arrowhead, compound middle lamella (middle lamella with very thin primary walls on each side); RC, ray cell; S_1; S_2; S_3, successive sub-layers of secondary walls with numerical labeling of each moving inward from the outer to the inner part; SW, secondary wall; V, vessel. Bars: 1 μm.

In Fig. 8A and C, the patterns of both secondary cell wall layering and lignin distribution in the different cell types were revealed using the $KMnO_4$ lignin staining technique (Donaldson, 1994); as noted, the *secondary* cell walls of both metaxylem (Fig. 8A) and vessels (Fig. 8C) were stained uniformly, indicative of the presence of lignins throughout both wall types. Next, the patterning of dirigent sites was investigated and found to differ markedly: these were now uniformly distributed throughout the metaxylem secondary wall (Fig. 8B), in sharp contrast to that of lignified vessels (Fig. 7A) where they predominated in the S_1 sublayer. This is most

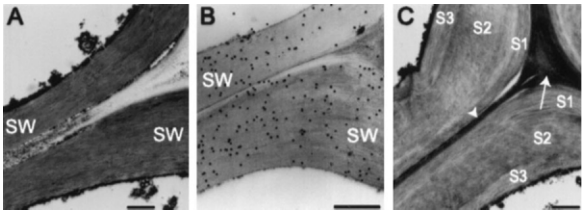

Fig. 8. $KMnO_4$ histochemical lignin staining of single-layered secondary wall metaxylem vessels (A) and dirigent site immunolocalization (B). For comparison, $KMnO_4$ lignin staining of triple-layered (S_1, S_2, S_3) secondary wall vessels is shown (C). For legend see Fig. 7.

interesting since it suggests a different pattern of arrays of dirigent site distribution during lignin macromolecular assembly in cell walls lacking distinct layers.

Overall, the main pattern of sub-cellular localization of dirigent sites was associated with the S_1 sub-layer and compound middle lamella of lignified secondary xylem cells, and to a lesser extent inside the corresponding S_3 sublayers, whereas in the primary (meta)xylem tissue it was uniformly distributed throughout the entire wall. It must again be emphasized, however, that none of the other cell wall polymers examined cross-reacted in any detectable manner with dirigent immune serum, e.g. xylan (4-*O*-methyl-D-glucurono-D-xylan). The latter polymer was of particular interest for two reasons: it contained sugar residues common to the glycosylated portion of the dirigent protein (data not shown), and these xylans are known to be present in the S_1 sub-layer of xylem cells of dicotyledonous woody plants, such as *Betula verrucosa* (Meier, 1964).

Taken together, these data provided compelling evidence that dirigent mediated lignan biosynthesis occurs within all of the cell and tissue types previously associated with lignification. However, given that control over one form of monolignol coupling was occurring to afford the lignans, this raised the central question of whether an analogous level of control was being exercised over lignification in the same tissues.

In this regard, it should be recognized that the first stage of plant wall development is that of expansion, which, in essence, establishes the nature of the cell (vessel, tracheid, ray cells, etc.) and its overall dimensions; during this phase, the primary wall has been laid down. The plasma membrane then gradually contracts inwards, sculpturing in its wake the various layers (S_1, S_2, S_3, etc.) of the secondary xylem cell wall. During this developmental phase, the carbohydrates (celluloses, hemicelluloses) are deposited in a defined temporal and spatial manner, as well as that of various proteins and oxidative enzymes (e.g. those containing the proteins proposed as harboring arrays of dirigent sites, glycine and proline-rich proteins, peroxidases and laccases). That is, such proteins and enzymes are *strategically* incorporated into specific regions of the growing cell wall in a manner whereby the cytoplasm can maintain control over subsequent cell wall developmental events.

In this way, the living part of the cell establishes not only the overall architecture of the developing wall, but it can also subsequently target the monolignol-derived radicals to (specific) dirigent binding sites where lignification is initiated. The evidence for such a viewpoint now seems to be quite compelling: secondary xylem cell wall lignification indeed begins at lignin initiation sites in regions farthest from the plasma membrane, such as in the S_1 sublayer and the compound middle lamella (Wardrop and Bland, 1959; Donaldson, 1994). That the presumed arrays of dirigent (coniferyl alcohol derived monomer binding) sites are immuno-detected in those very regions (Fig. 7A–D) provides a facile explanation as to why lignification is indeed initiated at these key sites. If such a control mechanism were *not* in place, the monomers would then presumably undergo oxidation and coupling following immediate passage through the plasma membrane, and lignification might inevitably be restricted to regions directly adjacent to the plasma membrane and not throughout the wall. Furthermore, following the initiation of lignin biosynthesis at these initiation sites far removed from the plasma membrane, the lignifying regions begin to expand gradually inward until the entire wall is reinforced, and the cell then dies (Donaldson, 1994). Sarkanen (Guan et al., 1997; Sarkanen, 1998) has proposed that this expansion phase of lignification occurs through an iterative process of lignin assembly (following primary chain formation) in a template guided manner. Overall, this process is presumed to favor the observed 8-*O*-4′-linked regiospecificity observed in native lignins.

These results, however, only serve to illustrate how much we still have to learn about lignification: for example, how are the monolignol-derived monomers differentially translocated from the plasma membrane to specific cell wall regions? How are the proposed arrays of dirigent sites oriented in such a way as to promote regiospecific linkage formation of the incoming monomers? Or are they just involved in initial binding and more than one protein is involved in dictating lignin assembly? What are the precise roles of each of the various oxidative enzymes in the cell wall, and what are their precise subcellular localizations and in which cell types? Why are the lignin chains [apparently] formed in mirror image form? Why is it that within primary xylem (e.g. metaxylem cells), which lack any distinctive cell wall layering (Fig. 8A), the proposed arrays of dirigent protein epitopes appear to be uniformly distributed throughout the wall (Fig. 8B)? Each of these aspects require full explanation, and these must be the subject of future investigation. It must be emphasized, however, that we are in the infancy of understanding how cell wall macromolecular assemblies are controlled, not just lignification. It is likely that cell wall ''organelles'' utilize tens — if not hundreds — of different proteins to ensure biopolymer orientation, ''self-assembly'' and control of lignification. Certainly, the

recent advances in genomics and proteomics and the vast number of presumed cell wall proteins of unknown function so identified underscore how little we yet understand about cell wall biosynthesis and its control.

3. Experimental

3.1. Plant materials

Forsythia intermedia plants, grown in Washington State University greenhouse facilities, were harvested in Spring 1998 and 1999.

3.2. Tissue preparation for light microscopy (LM) and histochemical detection of lignin

F. intermedia stems, petioles, leaves and roots were fixed in FAA solution (10% formalin, 5% glacial acetic acid, 50% ethanol, v/v) at 4°C overnight. Tissues were processed under vacuum using an histomatic tissue processor 166A (Fisher Scientific) as follows: sequential dehydration at room temperature in 70, 80, 95 and 100% (3 times) ethanol (20 min each). Tissues were infiltrated and embedded in paraffin at room temperature using hemo-De (Fisher Scientific) (Ruzin, 1999). Thick sections (~8 μm), obtained using a rotary microtome (Jung Biocut, Leica), were subsequently mounted on silane (3-aminopropylsilane) coated microscopic slides. Paraffin was solubilized by immersion of the slides in hemo-De for 10 min, and then 100% ethanol. Sections were re-hydrated (5 min each) in 90 and 70% (v/v) ethanol and finally H_2O (twice), and allowed to dry. For morphological observations and lignin histochemistry, the sections were stained with toluidine blue (0.05% aqueous solution) and phloroglucinol-HCl (Johansen, 1940), respectively.

3.3. Autofluorescence of phenolics

Hand-cut cross-sections of fresh *F. intermedia* tissues were mounted in water and directly observed using a Leitz Aristoplan photomicroscope operated in an epifluore scence mode (Franceschi et al., 1998). UV light (340–380 nm) was used as the excitation wavelength with a long bandpass filter (440 nm and above) being employed for visualization of the light blue induced fluorescence. Images were captured on Kodak Gold 100 film.

3.4. Tissue print hybridization

Tissue print mRNA hybridization was performed with fresh *F. intermedia* stems, roots and petioles, using the protocol of Ye et al. (1991) which was modified as follows. Freshly cut cross-sections of tissues of interest were pressed onto nylon membranes (Genescreen, NEN Research Products, Boston), air dried, and UV cross-linked. pBluescript plasmids, containing the psd-Fi1 cDNA insert (Gang et al., 1999), were linearized by either *Bam* HI or *Xho* I and ^{35}S-thio-UTP was incorporated using T7 or T3 RNA polymerase in order to obtain the antisense and sense probes, respectively. Membranes were prehybridized at 68°C for 4 h in 1.5×SSPE, 1% SDS, 1% BSA, 100 mM DTT and then hybridized at 68°C for 16 h in the same solution containing ^{15}S-thio-UTP labeled probe. Membranes were washed successively in 4×SSPE, 2×SSPE and 1×SSPE, for 30 min each, at room temperature and finally in 0.1×SSPE, for 1 h at 68°. For image evaluation, membranes were exposed for 5 days at room temperature to Kodak scientific imaging film. Additionally, the corresponding tissue prints showing anatomical features were obtained by pressing the surface of freshly cut cross-sections onto sobo glue (polyvinyl acetate) coated microscopic slides. Physical prints and membranes were photographed using Kodak Technical Pan film with a stereomicroscope (Wild Heerbrugg) and then scanned (ScanMaker III, Microtek).

3.5. In situ hybridization

Stem tissues were harvested at various stages of development and fixed in paraffin as above. Deparaffinized and rehydrated tissue sections were treated with proteinase K (2 μg/ml) (Boehringer Mannheim). Digoxigenin-labeled antisense and sense riboprobes were synthesized as above but with digoxigenin-11-dUTP (Boehringer Mannheim) instead of ^{35}S-thio-UTP. RNA transcripts were fragmented into 150 bp by alkaline hydrolysis prior to hybridization (Duck, 1994). Slides were prehybridized for 2 h at room temperature in 50% formamide, 30 mM NaCl, 10 mM Tris–HCl (pH 7.5), 1 mM EDTA, 1×Denhardt's solution, 10% dextran sulfate, 100 mM DTT, 500 μg/ml denatured salmon sperm DNA (Sigma) and 150 μg/ml yeast tRNA (Sigma). Tissue sections were hybridized in the same solution containing 0.05 μg/ml digoxigenin-labeled probe for 16 h at 38°C, then washed at room temperature in 2×SSC, 1×SSC, 0.5× SSC, for 30 min each, and finally at 38°C, in 0.1×SSC, for 1 h. Hybridization of riboprobes was detected with anti-digoxigenin antibodies conjugated to alkaline phosphatase (Boehringer Mannheim) and visualized by color development according to the manufacturer's instructions.

3.6. Antigen and immunization

Dirigent protein, heterologously expressed in a *Spodoptera frugiperda*/*Autographa californica* system (Gang et al., 1999) and purified to apparent homogeneity (Davin et al., 1997; Gang et al., 1999), was used for immunization of two male New Zealand rabbits in facilities of the Laboratory Animal Resource Center at Washington State University. Immunization used the

subcutaneous implanted-ball (whiffle ball) technique which permits introduction of microgram quantities of immunizing antigen without adjuvant, and subsequent removal of large amounts of antibody-containing fluid from the implanted-ball (Hillam et al., 1974; Ried et al., 1992). Initially, a 45 μg-injection of dirigent protein was followed by two 22 μg-booster injections after 5 and 7 weeks, respectively. Prior to each injection, serum (10–20 ml) was withdrawn from the whiffle ball, this being centrifuged for 30 min at 1000 *g* at 4°C, and stored in aliquots (0.5 ml) at −20°C until needed. The titer of the resulting polyclonal antibodies was monitored using the indirect ELISA technique as described below.

3.7. Indirect ELISA

Unless otherwise stated, all steps were performed at room temperature. Each well of Immulon 2 ELISA plates (Dynatech Laboratories, Inc., Chantilly, VA) was coated with recombinant dirigent (100 μl, 1 μg/ml in 0.05 M carbonate buffer, pH 9.6) for 16 h at 4°C. After washing 3 times with PBS-Tween 20 [150 μl, 0.1 M phosphate buffer (pH 7.4), 150 mM NaCl, containing 0.05% (wt/v) Tween 20] for 2 min each, the wells were blocked for 1 h with 0.5% (wt/v) gelatin (fish skin gelatin, Sigma) in PBS-Tween 20. Then, 100 μl of a two-fold serial dilution (from 1:100 to 1:102,400) of the sera (whether pre-immune or immune-sera, for each rabbit), in the same blocking buffer was added and further incubated for 2 h. After washing with PBS-Tween 20 (4×150 μl) for 2 min, the secondary antibody (goat anti-rabbit-horse radish peroxidase; Pierce, Rockford, IL), diluted 1:10,000 in PBS-Tween 20 containing 0.25% (wt/v) gelatin, was added and incubated for 2 h. The wells were then washed 3 times as before, and incubated with 100 μl of chromogenic substrate (*O*-phenylenediamine dihydrochloride, Sigma) as directed by the manufacturer. The reaction was terminated by addition of H_2SO_4 (50 μl, 10% aqueous solution), with the absorbance (A_{490}) measured using an ELISA plate reader (Spectra Max 250, Molecular Devices). Serum giving the best titer, expressed as the dilution giving A_{490} max/2, together with the corresponding rabbit pre-immune serum, were used as outlined below.

3.8. Crude protein extraction

Crude protein extracts from *F. intermedia* stems were obtained using the TRI Reagent™ Kit (Molecular Research Center, Cincinnati, OH) (Chomczynski, 1993), according to the manufacturer's instructions.

3.9. Indirect competitive ELISA

Purified recombinant dirigent protein and crude total protein extracts from *F. intermedia* stems were coated in the wells as described above. The same protocol, previously employed for indirect ELISA experiments, was also used, except that the dirigent immune-serum (50 μl, diluted 1:250 in the blocking buffer) was first mixed with solutions of potential competitors in blocking buffer (50 μl) at different concentrations. That is, each potential competitor was diluted to eight different concentrations (0.01 to 20 μg/ml) in blocking buffer (1:500 final dilution of the antiserum) for testing, with each sample individually incubated under mild agitation for 16 h at 4°C before being applied to the coated wells. Bovine serum albumin (Sigma), recombinant *F. intermedia* pinoresinol-lariciresinol reductase (PLR) (Dinkova-Kostova et al., 1996), purified native *F. intermedia* laccase, guaiacyl-dehydrogenative polymeric (DHP) synthetic lignin obtained using the Zutropf method (G-DHPzt) (Lewis et al., 1987), cellulose powder (Whatman, Fairfield, NJ), 4-*O*-methyl-D-glucurono-D-xylan (Sigma), polygalacturonic acid methyl ester (Sigma), rhamnogalacturonan I (gift from Dr. M. Vignon, CERMAV, CNRS, France), rhamnogalacturonan II (gift from Pr. J.P. Joseleau, CERMAV, CNRS, France), and purified recombinant dirigent protein from *F. intermedia*, were used as potential competitors. In the case of the DHP, five different samples were solubilized in DMSO (10 μg/μl stock solutions) before further use in the same buffer as the other competitors. This resulted in a 2% (v/v) maximum concentration of DMSO in the pre-adsorbed antibody solutions, with no effect on the antibody-antigen interaction being observed (data not shown). The average of these five DHP samples ± standard deviation is displayed in Fig. 5A and B. Optical density values were corrected by subtracting the very low pre-immune serum background, and results were expressed as percentages of the maximal reaction (immune-serum pre-incubated with buffer only).

3.10. Preparation of resin embedded samples for light microscopy (LM) and transmission electron microscopy (TEM)

Several protocols (i.e. cryofixation (Fisher and Housley, 1972), microwave fixation (Turner et al., 1999) and different fixative mixtures) were evaluated in order to optimize both antigenicity conservation and ultrastructural preservation; conditions adapted from Klauer et al. (1991) were finally utilized. Freshly cut samples were dissected into small pieces in fresh fixative solution (1.25% glutaraldehyde/2% paraformaldehyde in 50 mM Pipes buffer, pH 7.2), these being placed under gentle vacuum (1 atm, few seconds), then fixed for 2 h at room temperature in this solution under mild agitation. Samples were individually rinsed in 50 mM Pipes (3×20 min) at room temperature, and dehydrated (30, 50, 70, 95 and 100% ethanol; 20 min each). Subsequent infiltration used a mixture of L. R. White acrylic

resin (hard mixture, Ted Pella, Inc.) and 100% ethanol (3:1, v/v) for 20 min, with subsequent pure L. R. White resin changes (4–5) within one week at 4°C. Sample embedding in L. R. White resin was performed in 0.2 ml gelatin capsules with a 24 h polymerization at 50°C.

3.11. Immunolabeling for light microscopy (LM)

Semi-thin sections (800 nm) were obtained using an ultramicrotome (Reichert) with glass knives. Floating sections were collected using plastic rings as previously described (Burlat et al., 1997). Immunolabeling was attained by floating the plastic rings, containing the semi-thin sections, on 50 μl drops of either the different incubation or washing solutions. These solutions were distributed in plastic molds (Pelco) and placed in a moist chamber to prevent evaporation. For dirigent protein immune serum the labeling steps were as for Klauer et al. (1991), with the following modifications. Experiments were carried out at room temperature, except for the washing steps following primary antibody incubation, which were conducted at 37°C for background reduction. Quenching of residual aldehydic functionalities was carried out by incubation with 0.15 M glycine in TBS_{500} (0.01 M Tris–HCl, 500 mM NaCl, pH 7.6) for 30 min, with resulting sections washed with TBS_{500} (4×5 min) and blocked for 1 h with 1% (wt/v) BSA in TBS_{500} (TBS-BSA). Sections were incubated for 3 h with dirigent protein immune serum diluted 1:50 to 1:100 in TBS-BSA, then washed at 37°C with TBS-BSA (6×5 and 2×15 min) and incubated for 3 h with the secondary antibody (Goat anti-rabbit-1nm gold particle, Auro Probe One; Amersham-Pharmacia Biotech Inc.) diluted 1:50 in TBS-BSA containing 0.1% gelatin (Amersham-Pharmacia Biotech Inc.). Sections were sequentially washed with TBS-BSA (3×10 min), TBS_{500} (3×10 min) and H_2O (3×5 min), then post-fixed with 2.5% (v/v) glutaraldehyde for 5 min and rinsed with H_2O (3×2 min). Silver enhancement was carried out for 15 min at 20°C with intenSE M (Amersham-Pharmacia Biotech Inc.), in accordance with the manufacturer's instructions. Sections were finally deposited onto gelatin-coated slides and dried before counter-staining for 30 s with 0.5% (wt/v) *O*-Safranin with mounting under a cover slip in immersion oil.

The same protocol was used for immunolabeling of paraffin sections (prepared as described above for in situ hybridization) except that they were immobilized on gelatin coated slides covered with 1 ml of the different incubating and washing solutions containing 0.3% (wt/v) Tween 20 under gentle shaking (30–50 rpm). Sections were analyzed without counterstaining under a Olympus BH2 microscope equipped with a Pulnix TM-7 CN color CDD camera.

3.12. Immunolabeling for transmission electron microscopy (TEM)

The same protocol as for LM was used, with the following modifications. Ultrathin sections (100 nm), precisely obtained using an ultramicrotome (Reichert) and a diamond knife (Delaware Diamond Knifes, Wilmington, DE), were positioned on uncoated 300 mesh nickel grids so that both sides of the ultrathin section were accessible to the incubation and washing solutions. Labeling was attained by immersing grids in 50 μl drops of the different solutions contained in plastic molds as before and gently agitating them by means of a magnetic stirrer. The resulting steps employed were as for the LM protocol, except that 0.3% (wt/v) Tween 20 was added to the TBS and TBS-BSA buffers. Pre-immune or immune sera were diluted from 1:10 to 1:25; the grids were incubated for 1 h with secondary marker (protein A conjugated to 10 nm gold particles; Amersham-Pharmacia Biotech Inc.), with silver enhancement performed for a 3–5 min duration as above. Post-staining employed 2% (wt/v) uranyl acetate, and grids were observed at 80 kV using a Jeol 1200 EX transmission electron microscope.

3.13. Immunolabeling controls

Pre-immune sera were employed under the same conditions and dilutions as for immune sera. Negative controls, with omission of immune serum, and pre-adsorption of the antiserum by the antigen (competitive inhibition) were also performed. As an additional control, it is emphasized that the pattern of immunolocalization of dirigent protein epitopes was exactly the same when polyvinyl pyrolidone (PVP) was used during the labeling protocol, this being carried out to quench the different phenolic sites (Franceschi et al., 1998).

Acknowledgements

The authors thank Professor Vincent R. Franceschi (Director of the Electron Microscopy Center, Washington State University) for use of the facilities, helpful technical assistance and critical reading of the paper. Thanks are extended to Christine M. Davitt and Valerie J. Lynch-Holm (EM Center, Washington State University), as well as to Jean-Paul Joseleau and Michel Vignon (CERMAV, CNRS, Grenoble, France) for the gift of RGII and RGI samples, respectively. We gratefully acknowledge the United States Department of Energy (DE-FG03-97ER20259), the National Science Foundation (MCB-9976684), the National Aeronautics and Space Administration (NAG 21198), the United States Department of Agriculture (99-35103-8037), McIntire-Stennis, the Arthur M. and Kate Eisig Tode Foundation and

the Lewis B. and Dorothy Cullman and G. Thomas Hargrove Center for Land Plant Adaptation Studies for generous support of this and related studies.

References

Adler, E., 1977. Lignin chemistry. Past, present and future. Wood Science and Technology 11, 169–218.

Asano, J., Chiba, K., Tada, M., Yoshii, T., 1996. Antiviral activity of lignans and their glysosides from *Justicia procumbens*. Phytochemistry 42, 713–717.

Atta-ur-Rahman Ashraf, M., Iqbal Choudhary, M., Habib-ur-Rehman, Kazmi, M.H., 1995. Antifungal aryltetralin lignans from leaves of *Podophyllum hexandrum*. Phytochemistry 40, 427–431.

Bao, W., O'Malley, D.M., Whetten, R., Sederoff, R.R., 1993. A laccase associated with lignification in loblolly pine xylem. Science 260, 672–674.

Beatson, R. P., Wang, W., Johansson, C. I., Saddler, J. N., 1998. The use of enzymes to produce, characterize and degrade chromophores present in western red cedar mechanical pulp. In: 7th International Conference on Biotechnology in the Pulp and Paper Industry, Technical Section, Canadian Pulp and Paper Association, Vancouver, BC, Canada, pp. A211–A215.

Bochenek, B., Hirsch, A.M., 1990. In situ hybridization of nodulin mRNAs in root nodules using non-radioactive probes. Plant Molecular Biology Report 8, 237–248.

Brunow, G., Kilpeläinen, I., Sipilä, J., Syrjänen, K., Karhunen, P., Setälä, H., Rummakko, P., 1998. Oxidative coupling of phenols and the biosynthesis of lignin. In: Lewis, N.G., Sarkanen, S. (Eds.), Lignin and Lignan Biosynthesis, vol. 697. ACS Symposium Series, Washington, DC, pp. 131–147.

Burlat, V., Ambert, K., Ruel, K., Joseleau, J.-P., 1997. Relationship between the nature of lignin and the morphology of degradation performed by white-rot fungi. Plant Physiology and Biochemistry 35, 645–654.

Burlat, V., Kwon, M., Davin, L. B., Lewis, N. G., 1999. Dirigent proteins. Tissue specific expression of genes and subcellular localization of proteins. Correlation with lignan and lignin formation. In: 10th International Symposium on Wood and Pulping Chemistry, Yokohama, Japan. Vol. I, pp. 114–119.

Chiba, M., Tsukamoto, H., Hisada, S., Nishibe, S., 1979. Studies on the Chinese crude drug "Forsythiae fructus" (IV) On the constituents of fruits of *Forsythia koreana* and Forsythiae fructus from Korea on the market. Shoyakugaku Zasshi 33, 150–154.

Chomczynski, P., 1993. A reagent for the single-step simultaneous isolation of RNA, DNA and proteins from cell and tissue samples. BioTechniques 15, 532–537.

Davin, L.B., Lewis, N.G., 2000. Dirigent proteins and dirigent sites explain the mystery of specificity of radical precursor coupling in lignan and lignin biosynthesis. Plant Physiology 123, 453–461.

Davin, L.B., Wang, H.-B., Crowell, A.L., Bedgar, D.L., Martin, D.M., Sarkanen, S., Lewis, N.G., 1997. Stereoselective bimolecular phenoxy radical coupling by an auxiliary (dirigent) protein without an active center. Science 275, 362–366.

Day, S.H., Chiu, N.Y., Won, S.J., Lin, C.N., 1999. Cytotoxic lignans of *Justicia ciliata*. Journal of Natural Products 62, 1056–1058.

Dinkova-Kostova, A.T., Gang, D.R., Davin, L.B., Bedgar, D.L., Chu, A., Lewis, N.G., 1996. (+)-Pinoresinol/(+)-lariciresinol reductase from *Forsythia intermedia*: protein purification, cDNA cloning, heterologous expression and comparison to isoflavone reductase. The Journal of Biological Chemistry 271, 29473–29482.

Donaldson, L.A., 1994. Mechanical constraints on lignin deposition during lignification. Wood Science and Technology 28, 111–118.

Duck, N.B., 1994. RNA in situ hybridization in plants. Plant Molecular Biology Manual G1, 1–13.

Fergus, B.J., Goring, D.A.I., 1970. The distribution of lignin in birch wood as determined by ultraviolet microscopy. Holzforschung 24, 118–124.

Fisher, D.B., Housley, T.L., 1972. The retention of water-soluble compounds during freeze-substitution and microautoradiography. Plant Physiology 49, 166–171.

Franceschi, V.R., Krekling, T., Berryman, A.A., Christiansen, E., 1998. Specialized phloem parenchyma cells in Norway spruce (Pinaceae) bark are an important site of defense reactions. American Journal of Botany 85, 601–615.

Freudenberg, K., 1968. The constitution and biosynthesis of lignin. In: Freudenberg, K., Neish, A.C. (Eds.), Constitution and Biosynthesis of Lignin. Springer-Verlag, New York, pp. 47–122.

Fujita, M., Gang, D.R., Davin, L.B., Lewis, N.G., 1999. Recombinant pinoresinol/lariciresinol reductases from western red cedar (*Thuja plicata*) catalyze opposite enantiospecific conversions. The Journal of Biological Chemistry 274, 618–627.

Fukushima, K., Terashima, N., 1991. Heterogeneity in formation of lignin. XIV. Formation and structure of lignin in differentiating xylem of *Ginkgo biloba*. Holzforschung 45, 87–94.

Gang, D.R., Costa, M.A., Fujita, M., Dinkova-Kostova, A.T., Wang, H.-B., Burlat, V., Martin, W., Sarkanen, S., Davin, L.B., Lewis, N.G., 1999. Regiochemical control of monolignol radical coupling: a new paradigm for lignin and lignan biosynthesis. Chemistry and Biology 6, 143–151.

Gnabre, J.N., Brady, J.N., Clanton, D.J., Ito, Y., Dittmer, J., Bates, R.B., Huang, R.C.C., 1995. Inhibition of human immunodeficiency virus type 1 transcription and replication by DNA sequence-selective plant lignans. Proceedings of the National Academy of Sciences of the United States of America 92, 11239–11243.

Guan, S.-y., Mlynár, J., Sarkanen, S., 1997. Dehydrogenative polymerization of coniferyl alcohol on macromolecular lignin templates. Phytochemistry 45, 911–918.

Hardell, H.-L., Leary, G.J., Stoll, M., Westermark, U., 1980. Variations in lignin structure in defined morphological parts of birch. Svensk Papperstidning 83, 71–74.

Harper, A., Kerr, D.J., Gescher, A., Chipman, J.K., 1999. Antioxidant effects of isoflavonoids and lignans, and protection against DNA oxidation. Free Radical Research 31, 149–160.

Hillam, R.P., Tengerdy, R.P., Brown, G.L., 1974. Local antibody production against the murine toxin of *Yersinia pestis* in a golf ball-induced granuloma. Infection and Immunity 10, 458–463.

Johansen, D.A., 1940. Plant microtechnique. McGraw-Hill, New York, NY.

Joseleau, J.-P., Ruel, K., 1997. Study of lignification by noninvasive techniques in growing maize internodes. An investigation by Fourier transform infrared cross-polarization-magic angle spinning ^{13}C-nuclear magnetic resonance spectroscopy and immunocytochemical transmission electron microscopy. Plant Physiology 114, 1123–1133.

Keller, B., Sauer, N., Lamb, C.J., 1988. Glycine-rich cell wall proteins in bean: gene structure and association of the protein with the vascular system. The EMBO Journal 7, 3625–3633.

Kitagawa, S., Nishibe, S., Benecke, R., Thieme, H., 1988. Phenolic compounds from *Forsythia* leaves (II). Chemical and Pharmaceutical Bulletin 36, 3667–3670.

Klauer, S.F., Franceschi, V.R., Ku, M.S.B., 1991. Protein compositions of mesophyll and paraveinal mesophyll of soybean leaves at various developmental stages. Plant Physiology 97, 1306–1316.

Kupchan, S.M., Stevens, K.L., Rohlfing, E.A., Sickles, B.R., Sneden, A.T., Miller, R.W., Bryan, R.F., 1978. New cytotoxic neolignans from *Aniba megaphylla* Mez. Journal of Organic Chemistry 43, 586–590.

Kwon, M., Burlat, V., Davin, L.B., Lewis, N.G., 1999. Localization of dirigent protein involved in lignan biosynthesis: implications for lignification at the tissue and subcellular level. In: Gross, G.G., Hemingway, R.W., Yoshida, T. (Eds.), Plant Polyphenols: Chemistry, Biology, Pharmacology, Ecology, vol. 2. Kluwer Academic/Plenum Publishers, New York, pp. 393–411.

Kwon, M., Davin, L.B., Lewis, N.G., 2001. In situ hybridization and immunolocalization of lignan reductases in woody tissues: implications for heartwood formation and other forms of vascular tissue preservation. Phytochemistry 57, 899–914.

Lewis, N.G., 1999. A 20th century roller coaster ride: a short account of lignification. Current Opinion in Plant Biology 2, 153–162.

Lewis, N.G., Davin, L.B., 1994. Evolution of lignan and neolignan biochemical pathways. In: Nes, W.D. (Ed.), Isopentenoids and Other Natural Products: Evolution and Function, vol. 562. ACS Symposium Series, Washington, DC, pp. 202–246.

Lewis, N.G., Davin, L.B., 1998. The biochemical control of monolignol coupling and structure during lignan and lignin biosynthesis. In: Lewis, N.G., Sarkanen, S. (Eds.), Lignin and Lignan Biosynthesis, vol. 697. ACS Symposium Series, Washington, DC, pp. 334–361.

Lewis, N.G., Davin, L.B., 1999. Lignans: biosynthesis and function. In: Barton, Sir D.H.R., Nakanishi, K., Meth-Cohn, O. (Eds.), Comprehensive Natural Products Chemistry, vol. 1. Elsevier, London, pp. 639–712.

Lewis, N.G., Davin, L.B., Sarkanen, S., 1999. The nature and function of lignins. In: Barton, Sir D.H.R., Nakanishi, K., Meth-Cohn, O. (Eds.), Comprehensive Natural Products Chemistry, vol. 3. Elsevier, London, pp. 617–745.

Lewis, N.G., Newman, J., Just, G., Ripmeister, J., 1987. Determination of bonding patterns of ^{13}C specifically enriched dehydrogenatively polymerized lignin in solution and solid state. Macromolecules 20, 1752–1756.

Lewis, N.G., Yamamoto, E., 1990. Lignins: occurrence, biogenesis and biodegradation. Annual Review of Plant Physiology and Plant Molecular Biology 41, 455–496.

Marcus, A., Greenberg, J., Averyhart-Fullard, V., 1991. Repetitive proline-rich proteins in the extracellular matrix of the plant cell. Physiologia Plantarum 81, 273–279.

Marita, J.M., Ralph, J., Hatfield, R.D., Chapple, C., 1999. NMR characterization of lignins in *Arabidopsis* altered in the activity of ferulate 5-hydroxylase. Proceedings of the National Academy of Sciences of the United States of America 96, 12328–12332.

McClure, B.A., Guilfoyle, T.J., 1989. Tissue print hybridization. A simple technique for detecting organ- and tissue-specific gene expression. Plant Molecular Biology 12, 517–524.

Meier, H., 1964. General chemistry of cell walls and distribution of the chemical constituents across the walls. In: Zimmermann, M.H. (Ed.), The Formation of Wood in Forest Trees. Academic Press, New York, pp. 137–151.

Meyer, K., Shirley, A.M., Cusumano, J.C., Bell-Lelong, D.A., Chapple, C.C.S., 1998. Lignin monomer composition is determined by the expression of a cytochrome P450-dependent monooxygenase in *Arabidopsis*. Proceedings of the National Academy of Sciences of the United States of America 95, 6619–6623.

Miyazawa, M., Kasahara, H., Kameoka, H., 1996. Antifungal activities of 8-*O*-4′-neolignans from *Myristica fragrans*. Natural Product Letters 8, 271–273.

Müsel, G., Schindler, T., Bergfeld, R., Ruel, K., Jacquet, G., Lapierre, C., Speth, V., Schopfer, P., 1997. Structure and distribution of lignin in primary and secondary walls of maize coleoptiles analyzed by chemical and immunological probes. Planta 201, 146–159.

Nitao, J.K., Nair, M.G., Thorogood, D.L., Johnson, K.S., Scriber, J.M., 1991. Bioactive neolignans from the leaves of *Magnolia virginiana*. Phytochemistry 30, 2193–2195.

Osawa, T., Nagata, M., Namiki, M., Fukuda, Y., 1985. Sesamolinol, a novel antioxidant isolated from sesame seeds. Agricultural and Biological Chemistry 49, 3351–3352.

Rahman, M.M.A., Dewick, P.M., Jackson, D.E., Lucas, J.A., 1990. Lignans of *Forsythia intermedia*. Phytochemistry 29, 1971–1980.

Ried, J.L., Walker-Simmons, M.K., Everard, J.D., Diani, J., 1992. Production of polyclonal antibodies in rabbits is simplified using perforated plastic golf balls. BioTechniques 12, 660–666.

Ruzin, S.E., 1999. Plant microtechnique and microscopy. Oxford University Press, New York, Oxford.

Ryser, U., Schorderet, M., Zhao, G.-F., Studer, D., Ruel, K., Hauf, G., Keller, B., 1997. Structural cell-wall proteins in protoxylem development: evidence for a repair process mediated by a glycine-rich protein. The Plant Journal 12, 97–111.

Saka, S., Whiting, P., Fukazawa, K., Goring, D.A.I., 1982. Comparative studies on lignin distribution by UV microscopy and bromination combined with EDXA. Wood Science and Technology 16, 269–277.

Sarkanen, S., 1998. Template polymerization in lignin biosynthesis. In: Lewis, N.G., Sarkanen, S. (Eds.), Lignin and Lignan Biosynthesis, vol. 697. ACS Symposium Series, Washington, DC, pp. 194–208.

Tollier, M.-T., Monties, B., Lapierre, C., Hervé du Penhoat, C., Rolando, C., 1986. Inhomogeneity of angiosperm lignin. Comparison of the monomeric composition of lignin fractions isolated from different wood species. Holzforschung 40 (Suppl.), 75–79.

Turner, G., Gershenzon, J., Nielson, E.E., Froehlich, J.E., Croteau, R., 1999. Limonene synthase, the enzyme responsible for monoterpene biosynthesis in peppermint, is localized to leucoplasts of oil gland secretory cells. Plant Physiology 120, 879–886.

Wardrop, A.B., Bland, D.E., 1959. The process of lignification in woody plants. In: Kratzl, K., Billek, G. (Eds.), Biochemistry of Wood. Pergamon Press, London, pp. 92–116.

Ye, Z.-H., Song, Y.-R., Marcus, A., Varner, J.E., 1991. Comparative localization of three classes of cell wall proteins. The Plant Journal 1, 175–183.

Ye, Z.-H., Varner, J.E., 1991. Tissue-specific expression of cell wall proteins in developing soybean tissues. The Plant Cell 3, 23–37.

PERGAMON

Phytochemistry 57 (2001) 899–914

PHYTOCHEMISTRY

www.elsevier.com/locate/phytochem

In situ hybridization and immunolocalization of lignan reductases in woody tissues: implications for heartwood formation and other forms of vascular tissue preservation

Mi Kwon, Laurence B. Davin, Norman G. Lewis*

Institute of Biological Chemistry, Washington State University, Pullman, WA, 99164-6340, USA

Received 6 October 2000; received in revised form 29 November 2000

Abstract

Vascular plants have evolved with remarkable ways to form and protect the vasculature apparatus. In certain woody shrubs, the secondary xylem can have within its center a hollowed pith surrounded by secondary xylem, whereas in most trees there is a solid core of heartwood. Both types of woody systems have, however, the commonality of accumulating so-called 'secondary' metabolites, albeit to different extents, whose roles are to protect and preserve the vascular (lignified) tissues. This investigation had as its purpose establishing the nature of the cells involved in the biosynthesis of these specialized 'secondary' metabolites in plants forming heartwood and hollow piths, respectively. This was achieved by determining the tissue-specific expression of two lignan biosynthetic pathway enzymes: pinoresinol-lariciresinol reductase (PLR) and phenylcoumaran benzylic ether reductase (PCBER), soluble enzymes which catalyze analogous benzylic ether reductions of 8–8′ and 8–5′ linked lignans, respectively. Using *Forsythia intermedia*, reverse transcription-PCR (RT–PCR) and northern blots revealed that PLR mRNA accumulated mainly in young stems, as well as in young roots and petioles. Furthermore, PLR-specific DIG-labeled riboprobes established that in the stems its mRNA accumulated in the radial parenchyma cells [and to a lesser extent in the developing vessels], as well as in the cambial cells of developing secondary xylem. In addition, immunocytochemical localization of PCBER in *Pinus taeda* established that it was in the axial and radial parenchyma cells of secondary xylem of stems. That is, irrespective of whether the woody plants formed hollowed piths or heartwood, the 'secondary' metabolite pathways leading to the protective lignans predominantly involved axial and radial parenchyma cells. This is in contrast to monolignol coupling (i.e. the entry point to both the lignans and lignins), which appears to be more restricted to the vascular cambial regions. © 2001 Elsevier Science Ltd. All rights reserved.

Keywords: *Forsythia intermedia*; *Pinus taeda*; Oleaceae; Pinaceae; Heartwood; Vascularization; Immunolocalization; In situ hybridization; Lignans; Pinoresinol/lariciresinol reductase; Phenylcoumaran benzylic ether reductase

1. Introduction

Vascular woody plants represent some of the most successful life forms to have evolved, in terms of longevity and durability through self-protective (preservation) mechanisms, as well as in relative orders of magnitude (size). Certain conifers, for example, such as California redwood (*Sequoia sempervirens*), western red cedar (*Thuja plicata*) and bristlecone pine (*Pinus longaeva*) can have life spans of 2000–5000 years (Lewis and Davin, 1999). Indeed, in general, the longevity, durability and relatively large sizes of woody plants are very much a consequence of an extraordinary ability to form highly specialized (vascularized) secondary bodies, such as lignified stems and bark (cork layers). However, the precise form of vascularization conferred can differ substantially, and the pattern of metabolites deposited is quite species-specific. Differences in vascularization can include both the type and amounts of bark and heartwood formed, and in their relative chemical compositions. Some species do not, for example, form heartwood but instead have discontinuous (pigmented) secondary xylem tissues, and others have hollow piths within the vascular apparatus. While these variations are all presumably consequences of differences in evolutionary adaptation, the biochemical processes associated with such developments are only now beginning to yield to enquiry (Magel et al., 1997; Gang et al., 1998;

* Corresponding author. Tel.: +1-509-335-2682; fax: +1-509-335-8206.

E-mail address: lewisn@wsu.edu (N.G. Lewis).

0031-9422/01/$ - see front matter © 2001 Elsevier Science Ltd. All rights reserved.
PII: S0031-9422(01)00108-X

Hauch and Magel, 1998; Fujita et al., 1999; Burlat et al., 2001).

Another fascinating aspect of overall woody plant growth and development is that such plants apparently must continually replace their water and nutrient conducting elements. That is, the original elements designated for this purpose are gradually converted into non-conducting tissues, such as in the heartwood of secondary xylem. In this way, plants have evolved systems which permit growth to enormous heights, and for the management of massive weights including the accompanying associated stresses and strains so encountered. Accordingly, it can be considered that this continual replacement of water/nutrient conducting cells has evolved as a fail-safe mechanism, i.e. before the individual cells designated for this purpose became unable to fulfill their functions due to deterioration through aging.

Concomitant with the continual displacement/renewal of conducting cells is the often massive accumulation of distinctive 'secondary' metabolites, whose deposition helps impart desirable properties to specific woody tissues. Examples of this include the black colored phlobaphene metabolites in the highly valued ebony (*Diospyros ebenum* Koenig) (Hillis and Soenardi, 1994) and the orange-red lignan-derived substances in highly durable western red cedar (Swan et al., 1969) heartwoods. Furthermore, the longevity of such plant species may also be positively impacted by the deposition of these complex 'secondary metabolite' mixtures, since they frequently contain bioactive plant products and thus help protect against opportunistic pathogens and other encroachers. Interestingly, the precise composition of such secondary constituents is often species specific, and hence their individual metabolic profiles frequently provide characteristic chemical 'fingerprints' for a particular species. For example, western red cedar heartwood contains nearly 20% of its weight as highly colored, but distinctive lignans, derived from plicatic acid (Swan et al., 1969), whereas in Douglas fir (*Pseudotsuga menziesii*) characteristic flavonoids and other lignans, such as α-conidendrin, accumulate (Hemingway and Hillis, 1970). Another example is in the heartwood of *Eucalyptus sideroxylon*, which contains, amongst other metabolites, a variety of stilbenes (Hart and Hillis, 1974) important in resisting fungal decay (Scheffer and Cowling, 1966).

In spite of their enormous importance, the accompanying biochemical and molecular processes involved in vascularization leading to, for example, heartwood and secondary phloem formation, are essentially unknown (Gang et al., 1998). In the case of heartwood, Chattaway had proposed that its formation is largely a consequence of accumulation of heartwood-forming metabolites (or the corresponding precursors) in the ray parenchyma cells, these being exuded into adjacent tracheary elements during heartwood maturation (Chattaway, 1952). Recently, using western red cedar, the first specific genes and enzymes involved in the biochemical pathways leading to its heartwood metabolites were reported (Gang et al., 1998; Fujita et al., 1999), although no specific cell types were identified at that point. Other studies, using black locust (*Robinia pseudoacacia*), have suggested a complex range of biochemical processes as being operative during heartwood formation, these occurring between the cambial cells and the so-called heartwood-sapwood transition zone (Hauch and Magel, 1998). In that study, various conversions of carbohydrates into heartwood flavonoids were reported to occur between the cambium cells and the heartwood-sapwood transition zone, although no specific cell types were implicated.

Not all woody plant species, however, produce heartwood such as with western red cedar and black locust. For example, the sapwood of several species including alder (*Alnus glutinosa*), British sycamore (*Acer pseudoplatanus*), quaking aspen (*Populus tremuloides*) and Norway maple (*Acer platanoides*) has a different mechanism involved in the further maturation of its secondary xylem (Magel et al., 1997). That is, under 'normal' growing conditions, these species still contain living parenchyma cells at the pith of the stem even after considerable trunk cambial expansion/growth (Bosshard, 1966; Magel et al., 1997). It is believed that in such species changes characteristic of heartwood formation are considerably delayed or are absent (Bosshard, 1966). Yet when, for example, species such as European ash (*Fraxinus excelsior*), European beech (*Fagus sylvatica*), and quaking aspen are injured by pathogen attack, they can also form discolored wood (Sucoff et al., 1967) similar in appearance to normal heartwood, albeit discontinuous in its occurrence in secondary xylem (Farkas and Király, 1962; Shigo and Hillis, 1973). This irregular discolored wood is formed by deposition of phenols and other substances (Gagnon, 1967), these appearing as inclusions in parenchyma cells; however, interestingly, the cell walls of fibers and vessels apparently typically remain unpigmented in such cases (Bosshard, 1968).

Other species, such as *Forsythia*, have evolved additional means for preservation/protection of their vascular apparatus. Rather than forming heartwood tissue, the parenchyma cells within the pith collapse as the stem matures (ages) to give a hollow pith (Kwon et al., 1999). However, the lignified secondary xylem in *Forsythia* contains significant levels of lignan-derived metabolites which provide both color and protection to the mature secondary xylem tissues. Thus, these three different examples [i.e. (a) heartwood-forming conifers, (b) formation of discontinuous pigmented wood upon injury in poplar and related species, and (c) others, such as *Forsythia*, having a hollow pith] illustrate some of the different forms of successful vascularization that have evolved in woody plants. Significantly, however, each type of woody tissue is linked through a common process

of enhanced protection and preservation via deposition of complex 'secondary' metabolic products.

The purpose of this particular study was thus to begin to define the cellular processes involved during both the formation and deposition of these important protective 'secondary' metabolites. Lignan biosynthesis was selected for this study using *F. intermedia* and *P. taeda*. Both species are intimately involved in 'secondary' metabolite deposition processes and they form a hollow pith and heartwood, respectively. The approaches utilized in this investigation involved both in situ hybridization and immunolocalization, these being carried out in order to define the specific cells and tissues involved.

In this regard, the lignans, primarily derived from the monolignols, *E*-coniferyl, *E*-sinapyl and *E*-*p*-coumaryl alcohols, are typically dimeric substances — although higher oligomers exist as well (Lewis and Davin, 1999). While mainly present in heartwood and bark tissues, lignans can also accumulate in other organs and tissues including sapwood, leaves, fruits, seeds and roots; (MacRae and Tower, 1984; Ayres and Loike, 1990; San Feliciano et al., 1992). Lignans have broad roles in defense based on their profound biological activities which include antioxidant (Osawa et al., 1985; Fauré et al., 1990), antifungal (Belmares et al., 1979), antibacterial (Hattori et al., 1986), antiviral (Gnabre et al., 1996), insect antifeedant (Harmatha and Nawrot, 1984), phytotoxic (Elakovich and Stevens, 1985) and cytotoxic properties (Binns et al., 1987).

F. intermedia was chosen for study since its lignan biosynthetic pathway has been fully delineated from *E*-coniferyl alcohol (**1**) to the 8–8′ linked lignan, (−)-matairesinol (**2**) (Fig. 1) (Umezawa et al., 1991; Chu et al., 1993; Dinkova-Kostova et al., 1996; Davin et al., 1997) and the genes for each transformation are now available (Dinkova-Kostova et al., 1996; Gang et al., 1999a; Xia et al., 2001). Significantly, (−)-matairesinol (**2**) is a precursor of heartwood lignans, such as plicatic acid (**3**) and α-conidendrin (**4**), in *T. plicata* and *T. heterophylla*, respectively (Lewis and Davin, 1999), and some of the genes involved in the biochemical pathway to matairesinol (**2**) have been characterized in both species (Gang et al., 1998; Gang et al., 1999a). Moreover, even though *F. intermedia* itself does not form heartwood, it was, nevertheless, considered to be able to provide meaningful information regarding sites (cells and tissues) involved in 8–8′-linked lignan biosynthesis, and thus important insight into the processes likely involved during heartwood formation in *T. plicata* and *T. heterophylla*. The first objective therefore addresses defining the tissue specific expression of the (+)-pinoresinol/(+)-lariciresinol reductase gene in *F. intermedia*; this enzyme catalyzes the first step in 8–8′-lignan biosynthesis, en route to (−)-matairesinol (**2**).

(+)-Pinoresinol/(+)-lariciresinol reductase was purified from *F. intermedia* stem tissue (Dinkova-Kostova et al., 1996); this soluble, 35 kDa, NADPH dependent, bifunctional enzyme catalyzes the sequential enantiospecific conversions of (+)-pinoresinol (**5**) into (+)-lariciresinol (**6**), and (+)-lariciresinol (**6**) into (−)-secoiso lariciresinol (**7**), respectively (see Fig. 1): the corresponding antipodes do not serve as substrates. The gene encoding PLR (*plr-Fi1*) was also obtained and cloned, this having considerable homology (~50% identity, ~ 65% similarity) to both isoflavone reductases (IFRs) and PLR/IFR homologs (Gang et al., 1997). The IFRs catalyze analogous reductions of α, β unsaturated ketones during isoflavonoid phytoalexin formation, and appear to be evolutionarily related to the PLRs in plant defense (Gang et al., 1997). The PLR/IFR homologs, however, appear to be mainly involved in phenylcoumaran benzylic ether reductions (Gang et al., 1999b) in lignan (8–5′-linked) biosynthesis.

Pinus taeda was also chosen for study, since it largely accumulates the 8–5′-linked lignans, dehydrodiconiferyl alcohol (**8**) and its derivatives in its heartwood (Fig. 2) (Gang et al., 1999b). Interestingly, formation of such metabolites is apparently inducible in the Pinaceae, given the increase in their amounts during gall formation in *Picea glauca*, resulting from attack by the gall-forming aphid *Adelges abietis* (Kraus and Spiteller, 1997). In this regard, one of the first 8–5′-lignan post-coupling transformations in *P. taeda* and *Cryptomeria japonica* (Lewis and Davin, 1999) involves benzylic ether reductions (Fig. 2) (Gang et al., 1999b). The presumed enzyme catalyzing this conversion, phenylcoumaran benzylic ether reductase (PCBER), has been obtained from both species, with the encoding genes cloned and functional proteins over-expressed in recombinant form (Gang et al., 1999b). The second objective of this investigation was thus directed toward employing immunocytochemistry to ascertain the tissue localization of PCBER. The results described below were presented at the 219th American Chemical Society National Meeting in San Francisco, March 2000 (Lewis et al., 2000).

2. Results

Using primers designed from the *plr-Fi1* sequence (GeneBank accession number U81158), the cDNAs for two PLR/IFR homologs and two other PLRs were isolated from different species, i.e. from *F. intermedia* was obtained the PLR/IFR homolog, *plrh-Fi1* (Dinkova-Kostova et al., 1996), and from *T. plicata* were genes encoding the PLR isoforms, *plr-Tp1* (GeneBank accession number AF242503) and *plr-Tp2* (GeneBank accession number AF242504) (Fujita et al., 1999). A comparable screening of a *P. taeda* cDNA library afforded the PLR/IFR homolog, the phenylcoumaran benzylic ether reductase (PCBER, *plrh-Pt1*, GeneBank accession number AF242490) (Gang et al., 1999b): The latter has rather

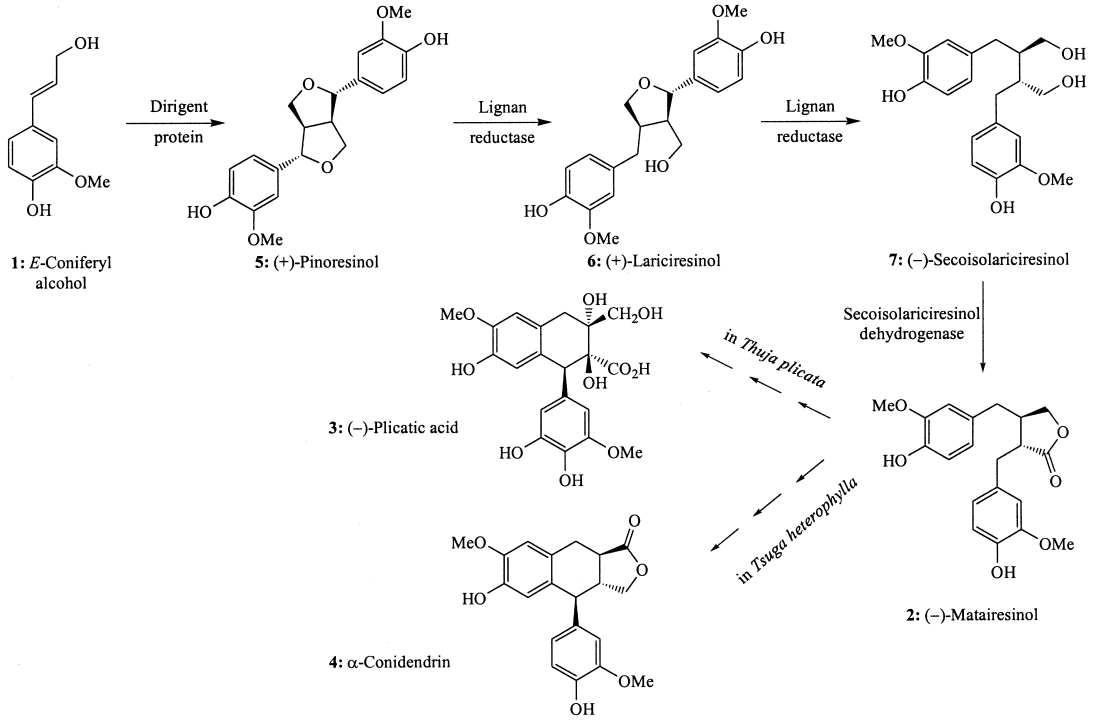

Fig. 1. The biosynthetic pathway to various 8–8′-linked lignans in *Forsythia intermedia*, *Thuja plicata* and *Tsuga heterophylla*. Two molecules of *E*-coniferyl alcohol (**1**) are stereoselectively coupled to afford (+)-pinoresinol (**5**) via dirigent protein mediation, which then undergoes sequential enantiospecific reduction to first give (+)-lariciresinol (**6**) and then (−)-secoisolariciresinol (**7**). (−)-Matairesinol (**2**) is subsequently formed via dehydrogenation of (−)-secoisolariciresinol (**7**), the further metabolism of which affords lignans, such as (−)-plicatic acid (**3**) and (−)-α-conidendrin (**4**), which accumulate in large amount in the heartwood of *T. plicata* and *T. heterophylla*, respectively.

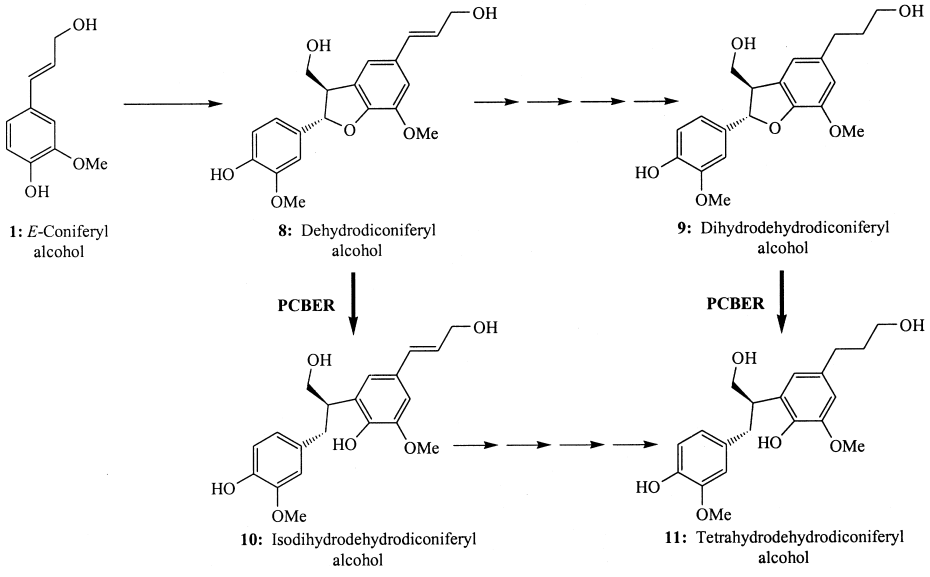

Fig. 2. The biosynthetic pathway to the 8–5′-linked lignans of *Pinus taeda* and *Cryptomeria japonica*. NADPH-dependent allylic double bond reduction of dehydrodiconiferyl alcohol (**8**) to its analog, dihydrodehydrodiconiferyl alcohol (**9**), occurs in several steps (Kasahara et al., manuscript in preparation), with a similar conversion also occurring for isodihydrodehydrodiconiferyl alcohol (**10**) and tetrahydrodehydrodiconiferyl alcohol (**11**). PCBER catalyzes the NADPH-dependent conversion of either dehydrodiconiferyl alcohol (**8**) or dihydrodehydrodiconiferyl alcohol (**9**) leading to the benzylic ether cleavage products isodihydrodehydrodiconiferyl alcohol (**10**) and tetrahydrodehydrodiconiferyl alcohol (**11**), respectively.

low enzymatic activity; nevertheless, it catalyzes the regiospecific, NADPH dependent, reduction of both dehydrodiconiferyl alcohol (**8**) and dihydrodehydrodiconiferyl alcohol (**9**) into isodihydrodehydrodiconiferyl alcohol (**10**) and tetrahydrodehydrodiconiferyl alcohol (**11**), respectively, in *P. taeda* (Fig. 2), with a

slightly higher affinity for dehydrodiconiferyl alcohol (**8**) based on the K_m and V_{max} determinations (Gang et al., 1999b). Interestingly, 8–5′-lignan dehydrodiconiferyl alcohol (**8**) derived substances are widespread throughout the Pinaceae, and mainly result from allylic double bond reductions, demethylations, and phenylcoumaran ring cleavage (Suga et al., 1993; Pan and Lundgren, 1995; Su et al., 1995; Lewis and Davin, 1999). Such substances and their higher oligomeric forms are present in both sapwood and heartwood of the Pinaceae, although they are typically 10-fold higher or so in the latter (Kraus and Spiteller, 1997).

2.1. PLR gene expression/mRNA accumulation are organ specific and developmentally regulated in F. intermedia

In order to initially establish the organ specificity of PLR (*plr-Fi1*) gene expression in *F. intermedia*, both RNA gel blot (Fig. 3a) and RT–PCR (Fig. 3b) analyses were conducted. For RNA gel blot analysis, a ^{32}P-labeled DNA probe was first obtained from the purified PCR product amplified from a near full-length *plr-Fi1* cDNA (28–936 bp) inserted in the pBluescript vector (SK$^-$) using T7 DNA polymerase (see Experimental). Subsequent RNA gel blot analyses (Fig. 3a) indicated that *plr-Fi1* mRNA accumulation was highest in the stems as compared to the roots and petioles (Fig. 3a, lower panel), this assumption being based on comparison of accumulation levels relative to that of ribosomal RNA from each tissue (Fig. 3a, upper panel).

RT–PCR analysis was next carried out in order to compare the levels of PLR mRNA accumulation at different stages of stem development. cDNA libraries, individually constructed from RNA samples from both young (first to second internodes) and mature stems (tenth to twentieth internodes), respectively, were amplified using primers designed from the 3′ region of the *plr-Fi1* cDNA (from 808 to 955 bp). The resulting amplified PCR products were then examined by gel electrophoresis as before whereby only the one expected band (circa 140 bp) (Fig. 3b, lower panel, lanes 1 and 2) was observed in each case. However, relative to similar amounts of 5.8S rRNA (Fig. 3b, upper panel), the PLR mRNA accumulation was highest in the young stems as compared to that of more mature stem tissue (Fig. 3b, lower panel, lanes 1 and 2). A similar trend was also noted for young roots relative to the more mature root tissues (data not shown). Finally, cDNA libraries were constructed from total RNA, isolated from both stem xylem and bark (first to twentieth internodes) regions, respectively, with the corresponding cDNA pools subsequently amplified using the same primers and PCR conditions as before. This revealed that PLR gene expression/mRNA accumulation were essentially only in the xylem tissues and not bark (Fig. 3b, lower panel, lanes 3 and 4).

2.2. PLR gene expression/mRNA accumulation in the cambium tissues of F. intermedia

With the gross tissue/organ specificity of the PLR gene having been demonstrated, it was next of interest to examine which cell types were associated with its specific mRNA accumulation. However, given the considerable level of homology (55.8% similarity, 55.8% identity), between PLR (*plr-Fi1*) and its homolog (*plrh-Fi1*), a *plr-Fi1* specific riboprobe was first designed in order to reduce and/or eliminate the potential for unwanted cross-reactivity and nonspecific binding (see Experimental). The specificity of both antisense and sense riboprobes was next evaluated by hybridizing each riboprobe (circa 210 nt, Fig. 4b and c) with the cDNAs encoding the *F. intermedia* PLR (*plr-Fi1*) and its homolog (*plrh-Fi1*) (see Fig. 4a). As an additional control, a PLR cDNA from *T. plicata* (*plr-Tp1*) was also examined for cross-reactivity. Thus, following employment of the anti-DIG antibodies conjugated to alkaline phosphatase with a chemiluminescent substrate both antisense (Fig. 4b) and sense (Fig. 4c) riboprobes were found to be only specifically hybridized to the *plr-Fi1* cDNA (1060 bp) but not to either the *plrh-Fi1* (954 bp) or the *plr-Tp1* (1190 bp).

However, prior to discussing the results obtained for in situ hybridization, it is first necessary to briefly

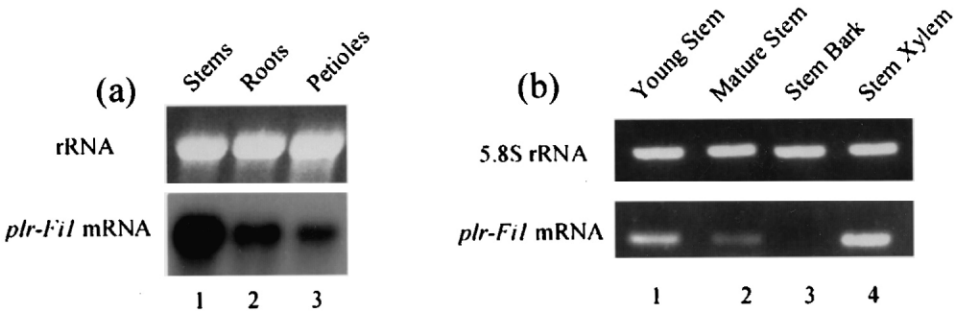

Fig. 3. Relative abundance of *plr-Fi1* mRNA in various *Forsythia intermedia* organs, and at different stem developmental stages. (a) RNA gel blot analysis using full-length *plr-Fi1* cDNA as template for synthesis of ^{32}P-labeled DNA probes using T7 DNA polymerase. (b) RT-PCR using gene specific primers for cDNA library amplification.

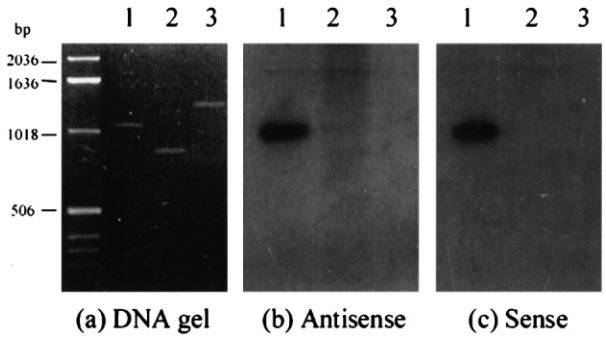

Fig. 4. Antisense and sense riboprobe specificity of *plr-Fi1* cDNA and reductase homologs, *plrh-Fi1* and *plr-Tp1*. (a). Gel fractionation of double digested fragments released following *Eco*RI and *Kpn*I restriction enzyme digestion. This released double-stranded full length cDNA coding for *plr-Fi1* (1060 nt, lane 1), *plrh-Fi1* (954 nt, lane 2) and *plr-Tp1* (1190 nt, lane 3), respectively, from their individual cDNAs cloned into the pBluescript vector (SK^-). (b) and (c). Probe specificity of *plr-Fi1* (lane 1) versus that of *plrh-Fi1* and *plr-Tp1* (lanes 2 and 3, respectively) using antisense (b) and sense (c) probes from *plr-Fi1*, respectively. Note: antisense (b) and sense (c) specifically bind to the *plr-Fi1* cDNA and not to the homologs *plrh-Fi1* and *plr-Tp1*.

describe the morphology of the tissues that were examined. Thus, in Fig. 5, the panels on the left column reveal the gross morphology as described following Saffranin-O staining of thick sections (8 μm) of the different organs selected for study. These were obtained from stems e.g. the first (Fig. 5a), second (Fig. 5d), tenth (Fig. 5g), and twentieth (Fig. 5j) internodes as well as from the young roots (Fig. 5m), the petioles (Fig. 5p) and the leaves (Fig. 5s). With the first internode (Fig. 5a), the vascular cambium (vc), the pith (p) and the cortex (co) are readily visible, as is the secondary xylem (sx) which has begun to develop from the vascular cambium (vc). As the stem grows and matures further (Fig. 5d,g and j), the stem diameter increases mainly as a consequence of secondary xylem development, as clearly visible from the second internode (Fig. 5d) onwards. By development of the tenth internode (Fig. 5g), the pith (p) has partially collapsed as evidenced by the hollow developing in the center, and it has completely collapsed by the twentieth internode (Fig. 5j), which contains highly lignified secondary xylem (sx) tissues. In the cross-sections of the young roots (Fig. 5m), both the cortex (co) and the stele (st) are clearly visible, as are the cortex (co), the midrib (mr) and the vascular bundles (vb) of the petioles (Fig. 5p) and leaf (Fig. 5s) tissues.

Accordingly, with the gene specific riboprobes in hand, in situ hybridization of PLR mRNA was next carried out using these *F. intermedia* stems, roots, petioles and leaves. Initially, serial sections were prepared from paraffin-embedded tissues and subjected to in situ hybridization using antisense and sense (negative controls) riboprobes described above.

In this way, in situ hybridization revealed that the strongest signal was detected in the stems (Fig. 5b,e,h and k) when compared to other organs such as the roots (Fig. 5n), the petioles (Fig. 5q) and the leaves (Fig. 5t). In the stem sections, the PLR gene expression/mRNA accumulation were mainly associated with the vascular cambium/differentiating xylem region (Fig. 5b,e,h and k), together with faint signal in the cortex in the early stages of maturation (Fig. 5b and e). However, as maturation proceeded, the levels of detectable PLR mRNA decreased (Fig. 5h and k), this being in agreement with the previous RT-PCR analysis (Fig. 3b). The negative controls, on the other hand, using the sense probe gave essentially only background signals in each case (Fig. 5c,f,i and l). Accumulation levels were also lower in the roots (Fig. 5n), the petioles (Fig. 5q) and the leaves (Fig. 5t), as predicted from the previous RNA gel blot analyses (Fig. 3a). It is noteworthy, however, that in each case, PLR gene expression was only associated with the meristematic tissues. For example, in the young root section (Fig. 5n), which contains both cortex and a centralized vascular network, the PLR mRNA accumulation was associated only with the pericycle (pe), the outermost layer of the stele (st); no signal was detected in the negative control (Fig. 5o). In the petioles, it was mainly in the cambium (ca), vascular bundles (vb) and the midrib (mr) (Fig. 5q), with again no signal being observed with the negative control (Fig. 5r). Lastly, in the leaf tissues, PLR mRNA accumulation was observed in the leaf blade as well as in the midrib cambium (ca) region (Fig. 5t), and the sense probe also gave essentially no signal as expected (Fig. 5u). Thus, taken together, PLR gene expression/mRNA accumulation in each case were broadly confined to the cambium regions typically associated with the onset of vascularization. Similar results were obtained with tissue printing (data not shown).

2.3. PLR mRNA accumulation in radial parenchyma cells, vessels, and the vascular cambium of F. intermedia stems

Fig. 6 displays the differences encountered in stem morphology, secondary xylem development and PLR mRNA accumulation during stem maturation at the 1st, 2nd and 20th internodes, respectively. Saffranin-O staining reveals the anatomical features at both lower (see Fig. 6a, d and g) and higher magnification (Fig. 6b, e and h), with the latter focusing on the vascular cambium and developing secondary xylem regions. In the cross-section of the shoot apex of the first internode (Fig. 6a and b), the vascular cambium (vc) has clearly developed from the interfascicular (ifc) and procambium-derived fascicular (fc) cambium. That is, the meristematic vascular cambium (vc), the cortex (co) and the pith (p) (Fig. 6a) consist of essentially only parenchyma cells, with the vascular cambium containing phloem- and xylem-parent cells and their undifferentiated daughter cells. At higher magnification

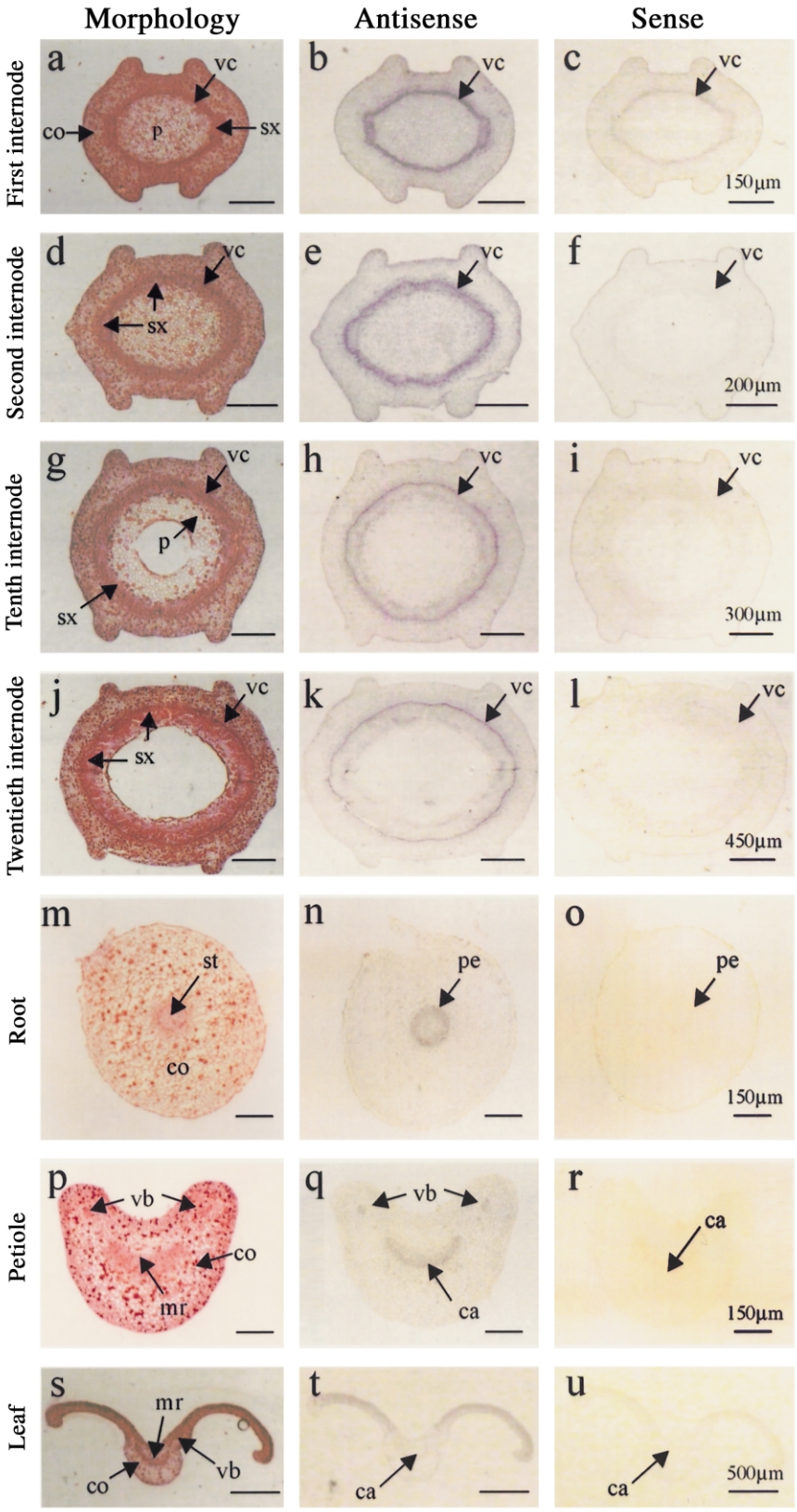

Fig. 5. Morphology of different *Forsythia intermedia* organs and the in situ hybridization of *plr-Fi1* mRNA expression. For morphology, tissue sections were stained with Saffranin-O (red-color). Serial sections of various tissues were used for direct comparisons between antisense and sense experiments. Antisense probes to *plr-Fi1* were specifically detected in the stem, root, petiole and leaf sections, whereas negative controls gave no signal. Abbreviations: ca, cambium; co, cortex; mr, midrib; p, pith; pe, pericycle; sx, secondary xylem; st, stele; vb, vascular bundle; vc, vascular cambium.

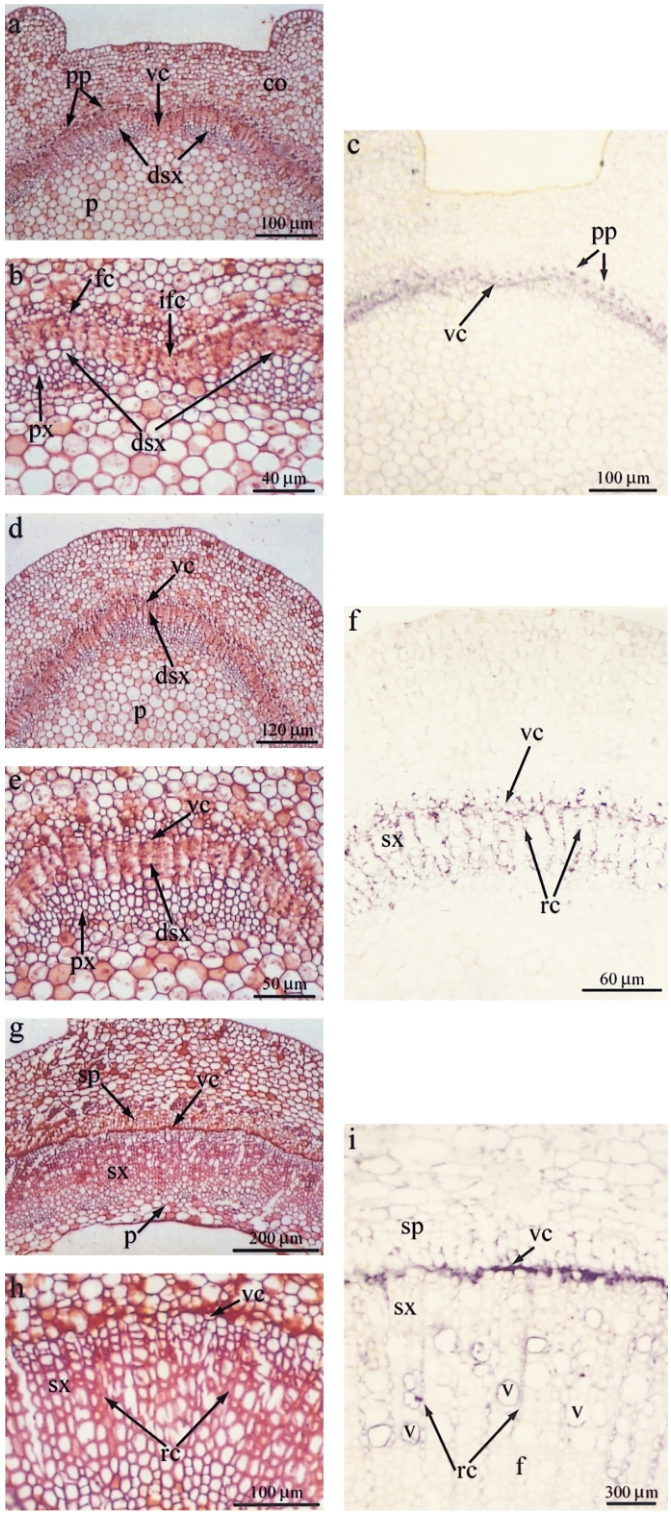

Fig. 6. Stem morphology, secondary xylem differentiation and PLR mRNA accumulation in the secondary xylem of *Forsythia intermedia* stems at different developmental stages. (a) through (c): first internode; (d) through (f): second internode; (g) through (i): twentieth internode. Partial cross sections revealed stages of secondary xylem development (a, d and g). Higher magnification of the vascular cambium region show development of the different cell and tissue types of interest (b, e and h). Sections were incubated with the antisense probe to *plr-Fi1* (c, f and i). PLR mRNA strongly accumulated in the vascular cambium regions (vc), and in the primary phloem (pp). As the stem matures and in the second and twentieth internodes, the *plr-Fi1* mRNA expression was in the vascular cambium, and in the ray parenchyma cells (rc). In the twentieth stem internode, the *plr-Fi1* mRNA was mainly expressed in the vascular cambium, as well as in the vessels (v) adjacent to the radial parenchyma cells, but not in the fibers (f) of secondary xylem. Abbreviations: co, cortex; dsx, developing secondary xylem; f, fiber; fc, fascicular cambium; ifc, interfascicular cambium; p, pith; pp, primary phloem; px, primary xylem; rc, radial parenchyma cells (or ray cells); sp, secondary phloem; sx, secondary xylem; v, vessel; vb, vascular bundle; vc, vascular cambium.

(Fig. 6b), the differentiating secondary xylem (dsx) is more clearly visible and the primary xylem (px), formed during primary growth, has separated away from the vascular cambium as secondary xylem development has proceeded. By development of the second internode (Fig. 6d and e), the differentiating secondary xylem (dsx) is more clearly detectable on the interior relative to that of the vascular cambium (vc). That is, the vascular cambium derived daughter cells have begun to differentiate into either lignifying cells (vessels and fibers) or into parenchyma cells. At this stage, cell wall lignin deposition in the secondary xylem is clearly detectable (Kwon et al., 1999). As the stems grow and mature further (Fig. 6g and h), both the secondary phloem (sp) and the secondary xylem (sx) were clearly distinguishable, with the latter being more highly lignified. At the twentieth internode stage (Fig. 6g and h), the conducting vessels, fibers, ray parenchyma cells and the collapsed pith tissues in the secondary xylem are now essentially fully developed. As noted earlier by the tenth internode (Fig. 5g), the *F. intermedia* stem had partially developed a hollow pith (Fig. 6g).

With these developmental observations, the differential patterns of PLR mRNA accumulation noted were instructive. At the first internode developmental stage, which lacks both developed secondary phloem and xylem formation, the PLR gene was strongly expressed in the vascular cambium (vc), together with a very faint level of mRNA accumulation in the primary phloem (pp) (Fig. 6c). However, at the second internodal developmental stage, where both the differentiating secondary xylem (sx) and vascular cambium (vc) are readily visible, the PLR mRNA clearly accumulated in both the vascular cambium and the differentiating radial parenchyma cells (rc) (Fig. 6f). As maturation continued (e.g. by development of the 20th internode), the strongest signal was detected in the vascular cambium and to a lesser extent, in the fully differentiated radial parenchyma cells (rc) of the secondary xylem (Fig. 6i). In addition, PLR mRNA accumulation was also faintly detectable in the vessels (v) adjacent to the ray parenchyma cells, but not in the xylem fibers (Fig. 6i). In summary, therefore, PLR gene expression/mRNA accumulation were not only mainly associated with the vascular cambium, but also to a lesser extent with radial parenchyma cells and vessels of the secondary xylem.

2.4. PCBER localization in P. taeda stems

The next objective was to localize the 8–5′-lignan reductase, the phenylcoumaran benzylic ether reductase (PCBER), at the cell and tissue levels. For this purpose, polyclonal antibodies were first raised in rabbits against the purified recombinant 35 kDa PCBER, with both the 35-week immune and the corresponding pre-immune serum chosen for subsequent experimentation. The

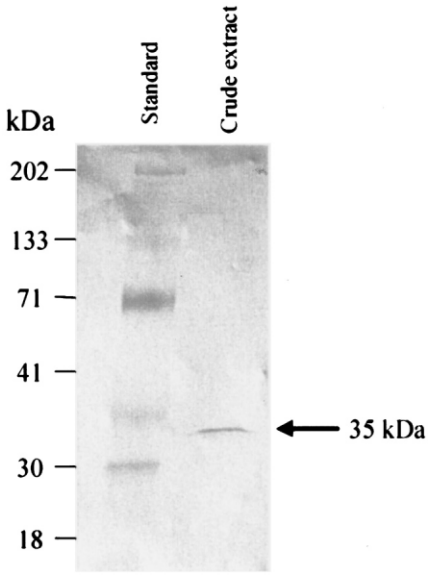

Fig. 7. Western blot analysis of a crude protein extract from *Pinus taeda* using PCBER polyclonal antibodies for detection. Polyclonal antibodies against purified functional recombinant PCBER specifically binds to PCBER (35 kDa) in *Pinus taeda* crude extract. Lane 1: standards; Lane 2: *P. taeda* stem crude extract.

polyclonal PCBER antibodies were found only to cross-react with the purified recombinant PCBER but not to its homologs, the PLR's from *F. intermedia* and *T. plicata* (data not shown). Next, western blot analysis of the total crude protein extract from *P. taeda* seedling stem tissues revealed that the polyclonal antibodies raised against PCBER specifically cross-reacted with PCBER, to give the expected band of circa 35 kDa molecular size (Fig. 7). With the specificity of the PCBER polyclonal antibodies thus established, *P. taeda* seedlings stem sections (1 year old) were next examined in order to define the cell and tissue specificities of PCBER. Two tissue sections were evaluated, namely that of both the green shoot (newly growing tissue) and the basal woody stem. For the green shoot section (Fig. 8a and b), although the secondary xylem has begun to develop, cells and tissues had not yet fully differentiated. By contrast, at the basal part of the more mature stem (Fig. 8c and d), the vascular cambium derived secondary xylem cells are now differentiated into specific cell types, such as tracheid (t), and radial (rc)/axial (ap) parenchyma cells. Characteristic brown spots in both the green shoot and woody stem are due to the presence of resinous material, some of which may also be phenolic.

At the green shoot developmental stage, PCBER was found to be localized in the differentiating secondary xylem regions, i.e. in the regions containing undifferentiated tracheids, undifferentiated fibers and the initials of both axial and radial parenchyma cells (Fig. 8a). As expected, the pre-immune control gave essentially no signals (Fig. 8b). In the more mature woody stem

(Fig. 8c), however, PCBER was now specifically localized in the fully differentiated axial (ap) and radial (rc) parenchyma cells, and, by contrast, to a much lesser extent in the vascular cambium (vc). Indeed, the latter observation in the vascular cambium might correspond to either axial or radial parenchyma cell initials. Again, the pre-immune controls gave background signals (Fig. 8d). Thus these findings clearly established that the PCBER was mainly localized in the radial and axial parenchyma cells of *P. taeda*. [Note added in proof: Somewhat analogous findings for PCBER have been reported also for poplar (Vander Mijnsbrugge et al., 2000).]

3. Discussion

These results are beginning to reveal how different species have evolved their distinctive mechanisms for long-term survival, i.e. where the monolignols are differentially deployed for both protective and structural roles as in *F. intermedia* secondary xylem and *P. taeda* heartwood formation. In the case of *F. intermedia*, the central parenchyma-rich pith tissues partially collapse and this part of the stem hollows out over time with the protective lignans being deposited in the remaining lignified secondary xylem. In *P. taeda*, on the other hand, the heartwood forming substances, including lignans, are synthesized and/or transported along axial and radial parenchyma cells; these are presumably converted subsequently into the corresponding heartwood-characteristic metabolites at the sapwood and heartwood boundary zone, where they are later infused into adjacent pre-lignified tracheary elements.

In earlier studies (Chattaway, 1952; Gang et al., 1998), the ray cells (radial parenchyma cells) had been proposed as possible sites for specialized secondary metabolite biosynthesis and thus for the formation of heartwood metabolites (e.g., such as lignans). According to this model, heartwood metabolites were biosynthesized and/or translocated along the ray cells, with these then being infused through the pits in the so-called transition zone, between the heartwood and sapwood, and into adjacent cell lumens. Indeed, this presumably explains why lignans often accumulate in lignified tissues as non-structural components, even when originating from axial and radial parenchyma cells (Hillis, 1971). It is also very significant that during heartwood formation, lignan biosynthetic and deposition processes are also clearly highly controlled: for example, in western hemlock (*T. heterophylla*) heartwood, the lumen of some tracheid cells can contain 7′-hydroxymatairesinol, whereas adjacent cells can accumulate α-conidendrin (**4**) (Krahmer et al., 1970). Moreover, the lignans can also have quite marked variations in molecular sizes: in western red cedar (*T. plicata*) heartwood, for example, the 8–8′-lignans derived from plicatic acid (**3**) can range in size from dimers up to oligomers of at least MW∼10,000 (Beatson et al., 1998). Furthermore, since a portion of these are also solubilized under conditions required for lignin removal, their presence had originally led to the erroneous consideration that they were formed through the 'aging' of lignin (Li and Sarkanen, 1971).

The discovery of lignan-specific biosynthetic enzymes thus provided not only a means to localize the cellular sites involved in lignan heartwood metabolite formation, but also that of related processes in non-heartwood

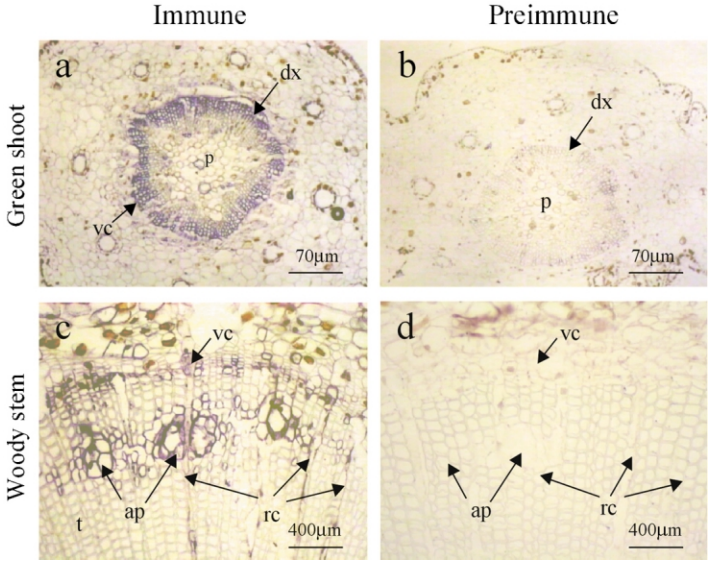

Fig. 8. PCBER localization in *P. taeda* (1 year old) seedlings. PCBER was in the developing xylem regions (dx) of young green shoots. In the basal stem section, PCBER was present in the axial (ap) and radial (rc) parenchyma cells, and to a lesser extent in the vascular cambium regions (vc). Abbreviations: ap, axial parenchyma cells; dx, developing xylem; p, pith; rc, radial parenchyma cells; t, tracheid; vc, vascular cambium.

forming species, e.g. during secondary xylem/hollow pith generation. Interestingly, the initial steps of the lignan and lignin pathways, namely that of monolignol coupling, were previously noted to occur mainly in the vascular cambial cells at all stages of stem development in *F. intermedia* as demonstrated by dirigent protein mRNA accumulation (Kwon et al., 1999; Davin and Lewis, 2000; Burlat et al., 2001). To a lesser extent, dirigent gene expression was also noted in the developing secondary xylem and in undifferentiated ray parenchyma cells as shown by in situ hybridization (Kwon et al., 1999; Burlat et al., 2001), but, importantly, not in the fully differentiated radial parenchyma cells of mature secondary xylem. This, in turn, suggests that monolignol partitioning into the lignan and lignin biosynthetic pathways occurs predominantly in the cambial regions.

On the other hand, while the *F. intermedia* PLR gene was expressed in the vascular cambium region of young stems, significant levels of mRNA accumulation were also noted along the ray parenchyma cells of mature secondary xylem (Fig. 6i). Furthermore, another downstream lignan-forming enzyme, secoisolariciresinol dehydrogenase, is also largely localized in the ray parenchyma cells of mature stem secondary xylem of *F. intermedia* (Pélissier, Franceschi, Davin and Lewis, unpublished results). Therefore, based on expression of several enzymes involved in the early stages of 8–8′-lignan biosynthesis (Kwon et al., 1999; Davin and Lewis, 2000; Burlat et al., 2001), it appears that monolignol coupling occurs mainly in the vascular cambium whereas post-coupling transformations are manifested along the radial parenchyma cells in addition to the vascular cambium.

A low level of PLR mRNA accumulation was also specifically noted in the developing vessels adjacent to radial parenchyma cells in the secondary xylem of mature *F. intermedia* stems, but not in the fibers. However, since vessels have relatively well developed pit systems which link adjacent axial/radial parenchyma cells, this finding also supports the possibility of lignan metabolite infusion into these tracheary elements. On the other hand, it is also possible that the PLR gene is expressed at lower levels in the vessels prior to programmed cell death. Whatever case holds, this may further explain the presence of heartwood (lignan) metabolites in heartwood tracheary elements.

The involvement of both radial and axial parenchyma cells was also supported further by the immunolocalization of PCBER, presumed to be involved in the post-coupling modification of 8–5′-lignans in *P. taeda*. Since PCBER was localized mainly in the axial/radial parenchyma cells of secondary xylem of maturing stem sections, this gave additional evidence at the molecular level for the involvement of these cells in the biosynthesis of the heartwood characteristic substances. Therefore, it can be considered that the involvement of axial/radial parenchyma cells is important in generating the properties of lignan-rich woody tissues (including that of heartwood). However, for heartwood formation, the precise metabolic function of the sapwood-heartwood transition zone still remains to be fully established; i.e. as to the precise nature of the specific metabolic events occurring in this region whereby the transition from sapwood to heartwood occurs. Nevertheless, it is clear that the axial and ray parenchyma cells are involved in this process, and it will be of considerable importance to ultimately define the precise metabolic processes operative, and how they differ between species.

Until this study, the co-occurrence of lignans and lignins in secondary xylem was not well understood. For example, for secondary xylem formation to occur, the vascular cambium derived cells need to undergo active expansion and elongation in order to differentiate into the specific cell types, such as xylary cells (tracheary elements and fibers) as well as in generating axial/radial parenchyma cells (Bosshard, 1965). These xylary cells (tracheary elements and fibers) then undergo a process involving massive monolignol deposition, these being mainly directed to the secondary cell wall regions prior to cell death; however, by the stage where monolignol infusion for lignification occurs, the cell walls already contain other constituents such as cellulose microfibrils, the hemicelluloses, cell wall structural proteins (e.g. glycine and proline-rich proteins), and various oxidative enzymes (apoplastic peroxidase and laccases). Hitherto, the enzymes localized in the radial parenchyma cells of secondary xylem were considered only in terms of lignin biosynthesis, even though these cells were not (immediately) lignified in contrast to the tracheary elements and fibers. Accordingly, the radial/axial parenchyma cell expression/localization of PLR and PCBER now establishes an involvement in lignan biosynthesis, with lignification being — at least initially — restricted to other cell types, such as the tracheary elements and fibers.

In conclusion, there are significant spatial and temporal differences emerging between lignan and lignin biosynthesis, even though both are formed via monolignol coupling; these observations are in harmony with their distinct physiological roles and functions.

4. Experimental procedures

4.1. Plant materials

F. intermedia (var. Lynwood Gold) and *P. taeda*, obtained from Bailey's Nursery (St. Paul, MN) and Gulf States Nursery (Tuscaloosa, AL), respectively, were maintained in greenhouse facilities at Washington State University. In this study, *Forsythia* plant tissues were harvested in the spring of 1998 and 1999, whereas *P. taeda* tissues from one year old specimens were collected during the summer of 1999.

4.2. RNA isolation from F. intermedia

Total RNA samples were extracted and utilized for gene expression analysis as follows. Tissues (3 g, fresh weight) from different organs were individually pulverized in liquid nitrogen in a mortar with a pestle. Each was homogenized in 5 volumes of extraction buffer [50 mM Tris–HCl, pH 8.0, 300 mM NaCl, 5 mM EDTA, 2% SDS, 0.5% (w/v) soluble polyvinylpyrrolidone (PVP), 0.5 mM aurintricarboxylic acid and 10 mM dithiothreitol (DTT)] for 10 min at 65°C. Each homogenate was next filtered through a single layer of miracloth (Calbiochem, La Jolla, CA) and centrifuged for 10 min at 4°C at 10,000× *g*. Potassium acetate solution (0.42 ml, 5 M, pH 4.8) was added to each supernatant with the resulting suspension centrifuged at 10,000 *g* (30 min, 4°C) and further incubated on ice for 30 min. Next, a lithium chloride solution (5 ml, 8 M) was added to each supernatant with the corresponding mixture incubated overnight at 4°C. The nucleic acids were recovered by centrifugation at 2000× *g* (20 min, 4°C), resuspended in 5 ml DEPC (diethylpyrocarbonate)-treated distilled H_2O, and extracted with 2 volumes of phenol-chloroform-isoamyl alcohol (24:23:1) mixture, and finally with 2 volumes of chloroform. Following addition of 0.1 volume of sodium acetate (500 μl, 3 M) to the recovered aqueous phase, the nucleic acids were precipitated overnight at −20°C in ethanol [final concentration 33% (v/v)] and recovered by centrifugation at 10,000× *g* (10 min, 4°C). Each RNA pellet was resuspended in DEPC-treated distilled H_2O and stored at −80°C until needed.

4.3. RNA gel blot analysis

A DNA probe was prepared from *plr-Fi1* cDNA (50 ng, GeneBank accession number U81158) which had previously been isolated and cloned into pBluescript (SK$^-$) vector (Dinkova-Kostova et al., 1996). The probe was labeled from the purified PCR product amplified from the near full-length *plr-Fi1* cDNA (from 28 to 936 bp) with 50 μCi of [α-^{32}P] dCTP (3000 Ci/mmol) at 37°C for 15 min using T7 DNA polymerase (6 units, T7 Quick Prime Kit), according to the manufacturer's instructions (Amersham Pharmacia Biotech, Inc., Piscataway, NJ). The ^{32}P-labeled DNA probe was next purified by centrifugation using Micro Bio-Spin Chromatography Columns (Bio-Rad, Hercules, CA) in order to remove unincorporated nucleic acids.

Total RNA samples (15 μg) were individually denatured at 70°C, and resolved in 1.2% formaldehyde-containing gels (Sambrook et al., 1989). Each RNA gel was blotted onto a Hybond^{TM}-N$^+$ nylon membrane (Amersham Pharmacia Biotech, Inc.) in 10×SSPE (1.8 M NaCl, 0.1 M sodium phosphate, 0.01 M EDTA) overnight, with each blot irradiated under UV light (1.2×10^5 μJ cm^{-2}) for 30 s (UV Stratalinker^{TM} 2400, Stratagene, La Jolla, CA). The blots were then prehybridized for 4 h at 68°C in 5×SSPE, 5×Denhardt's solution, 1% SDS, 10% dextran sulfate and subsequently hybridized in the same solution containing the ^{32}P-labeled DNA probe which had previously been denatured by boiling for 10 min. Hybridization was carried out for 16 h at 68°C, with the blots next washed at high stringency (final wash 0.1×SSPE and 0.1% SDS) at 68°C and finally subjected to autoradiography at −80°C using intensifying screens.

4.4. Reverse transcription polymerase chain reaction (RT–PCR) analysis

First-strand cDNAs were synthesized by incubating *F. intermedia* total RNA (4 μg), previously heat-denatured at 70°C for 10 min, with reaction buffer [50 mM Tris–HCl (pH 8.3), 75 mM KCl, 3 mM $MgCl_2$ and 10 mM DTT], 0.5 mM each deoxyribonucleoside triphosphate (dNTP), 1 mM random hexamer (Amersham Pharmacia Biotech, Inc.) and 200 units of Superscript II (Life Technologies, Rockville, MD) in a total volume of 20 μl for 50 min at 42°C. Following incubation, the resulting first-strand cDNAs (1 μl) were individually amplified by PCR. PCR conditions were as follows: 35 cycles, each consisting of 30 s denaturation at 95°C, 30 s annealing at 60°C, 1 min extension at 72°C with an additional 7 min extension after the final cycle. Amplification was carried out in reaction buffer [10 mM Tris–HCl (pH 7.5), 50 mM KCl, 0.5 mM DTT, 7.5 mM $MgCl_2$, 0.05 mM EDTA, 0.25% Tween 20 (v/v), 100 μM each dNTP] with 2.6 units of enzyme mixture consisting of *Taq* DNA and *Pwo* DNA polymerases (total volume of 50 μl) using the Expand^{TM} High Fidelity PCR system (Boehringer Mannheim, Indianapolis, IN) and gene specific primers (0.5 μM each). The sequences of the primers used in this amplification were 5′-CTCGAGTATGCTCAGCAAGTGGG-3′ (from 808 to 830 bp) and 5′-GCTTGAGGTACTCTTCCACAC-3′ (from 935 to 955 bp). For a positive control, *F. intermedia* rRNA was amplified under the same conditions as above, but with the following primers 5′-TCG GCAACGGATATCTCGGCTCT-3′ and 5′-GCGTGA CGCCCAGGCAGACGT-3′ designed from the tobacco (*Nicotiana tabacum*) 5.8S rRNA (GeneBank accession number AJ012367). RT-PCR products were analyzed on 1.2% agarose gel with UV visualization after ethidium bromide staining.

4.5. Run-off transcription and RNA probe preparation

Because of the considerable homology of *plr-Fi1* to a pinoresinol/lariciresinol reductase homolog in *F. intermedia* (*plrh-Fi1*, GeneBank accession number AF242491, 55.8% similarity, 55.8% identity), efforts were made to synthesize gene-specific probes for the detection of *plr-Fi1*

mRNA as follows. First, a 210 bp *Pst* I/*Hind* III fragment, located at 761/971 bp in the *plr-Fi1* cDNA, was subcloned into the corresponding sites of pBluescript vector (SK^-). Digoxigenin (DIG)-labeled antisense and sense RNA probes were next synthesized by an in vitro transcription reaction from the pBluescript SK^- template containing the partial sequence of *plr-Fi1* cDNA using the DIG-RNA Labeling Kit (Boehringer Mannheim): plasmids were linearized by cleavage using either *Pst* I or *Hind* III, and digoxigenin-11-dUTP (Boehringer Mannheim) was incorporated using either T7 or T3 polymerase for the antisense or sense probes, respectively. These were then individually fragmented to about 150 nt in size by alkaline hydrolysis prior to hybridization according to Duck (Duck, 1994). The specific activities of both sense and antisense riboprobes were determined using DIG-Quantitation Teststrips (Boehringer Mannheim) according to the manufacturer's instructions.

4.6. Riboprobe specificity

cDNA inserts from the *Forsythia* PLR homolog (*plrh-Fi1*), and as an additional control from an authentic PLR from *T. plicata* (*plr-Tp1*), were cross-hybridized with a riboprobe specifically designed for *plr-Fi1* mRNA detection in order to test for its specificity. That is, both the *F. intermedia* pinoresinol/lariciresinol reductase homolog (*plrh-Fi1*, GeneBank accession number AF242491) and the *T. plicata* pinoresinol/lariciresinol reductase (*plr-Tp1*, GeneBank accession number AF242503), were individually tested to verify the specificity of the *plr-Fi1* RNA probe as well as the specificity to *plr-Fi1* itself. Each cDNA (*plr-Fi1*, *plrh-Fi1*, *plr-Tp1*) sample was digested with *Eco*RI/*Kpn*I, with 15 ng of each fragment subjected to agarose gel electrophoresis (Fig. 3a). The gels were next blotted onto Hybond^{TM}-N^+ nylon membranes (Amersham Pharmacia Biotech Inc.) in alkaline solution (0.4 M NaOH) overnight, with each blot cross-linked under UV light (1.2×10^5 μJ cm^{-2}) for 30 s to immobilize the DNA. The blots were then prehybridized for 1 h at 65°C in prehybridization buffer containing 5×SSPE, 5×Denhardt's solution, 10% SDS, and denatured salmon sperm DNA (0.5 mg ml^{-1}). These were next individually hybridized for 16 h at 65°C in fresh prehybridization buffer containing either DIG-labeled antisense or sense RNA probes (0.05 μg ml^{-1}) which had been hydrolyzed and denatured prior to hybridization as described previously. The blots were rinsed in 2×SSPE, 0.1% (w/v) SDS at room temperature, and finally in 1×SSPE, 0.1% (w/v) SDS at 65°C. These were then incubated for 30 min at room temperature, with sheep anti-DIG-alkaline phosphatase antibodies diluted (1:25,000) in maleic acid buffer (0.1 M, pH 7.5) containing 0.15 M NaCl and 10×blocking reagent (Boehringer Mannheim). After washing in maleic acid buffer (0.1 M, pH 7.5) containing 0.15 M NaCl and 0.3% (v/v) Tween 20, the blots were next incubated with CSPD (disodium 3-(4-methoxyspiro{1,2-dioxetane-3,2′-(5′-chloro)tricyclo[3.3.1.$1^{3,7}$]decan}-4-yl) phenyl phosphate, 25 mM), a chemiluminescent substrate for alkaline phosphatase, diluted (1:100) in Tris buffer (0.1 M Tris–HCl, pH 9.5), containing 0.1 M NaCl according to the manufacturer's instructions (Boehringer Mannheim). After 15 min at 37°C, the blots were exposed to a Hyper film ECL^{TM} (Amersham Pharmacia Biotech Inc.) for 5 min and the films were then developed.

4.7. Tissue preparation and RNA in situ hybridization of PLR in F. intermedia

To protect samples from the effects of exogenous RNase during experimentation, each solution was treated with DEPC and autoclaved. In addition, all glassware, metal items, microscopic slides and cover slips were baked at 180°C.

Stems at various developmental stages, as well as roots, petioles and leaves were harvested from *F. intermedia* and immediately fixed in FAA solution (10% formaldehyde, 5% glacial acetic acid, 50% ethanol, v/v) overnight at 4°C. Tissues were next dehydrated gradually in 50, 70, 80, 95 and 100% ethanol solutions and transferred to a histomatic tissue processor (166A, Fisher Scientific) for infiltration and paraffin embedding. Thick sections (8 μm) were then obtained and directly mounted onto silane (3-aminopropylsilane) coated microscopic slides (Fisher Scientific), with the paraffin being removed by immersion of the slides in a hemo-D (Fisher Scientific) solution. The sections were subsequently rehydrated in 100, 95, 80, 50 and 30% ethanol and distilled water and finally air dried. Several treatments, prior to prehybridization, were applied to increase the accessibility of each probe to the target mRNA as well as to minimize nonspecific binding as follows: First, tissue sections were incubated with protease K solution (1 μg ml^{-1}) in TE buffer (50 mM Tris–HCl, 5 mM EDTA, pH 7.4) for 30 min at 37°C. After washing with TE buffer and then water, sections were sequentially incubated in a solution of aqueous soluble PVP (1%, w/v) at room temperature for 20 min in order to quench any background reaction caused by phenolics. Tissue sections were next prehybridized in a prehybridization solution containing 50% formamide (v/v), 30 mM NaCl, 10 mM Tris–HCl (pH 7.5), 1 mM EDTA, 1×Denhardt's solution, 10% dextran sulfate, 100 mM DTT and 150 μg ml^{-1} yeast tRNA (Sigma) for 2 h at room temperature. Tissue sections were hybridized overnight at 38°C in the same solution but which also contained the denatured digoxigenin-labeled probe (0.1 μg ml^{-1}), which had previously been hydrolyzed into 150 nt segments as described above. Following hybridization, sections were washed in 2×SSC, 1×SSC, and 0.5×SSC at room temperature for 30 min each, then in 0.1×SSC for 1 h at 38°C and finally

with Tris-buffered saline–Tween (TBST; 10 mM Tris–HCl, 500 mM NaCl, 0.3% Tween 20, pH 8.2). Sections were first incubated in TBST solution containing 1% (w/v) BSA, 0.1% (w/v) PVP and 0.5% whole sheep serum (Ted Pella, Inc., Redding, CA), for 1 h at room temperature and then in sheep anti-DIG-antibodies conjugated with alkaline phosphatase (Boehringer Mannheim) [(1:1000 in TBST containing 1% w/v BSA (TBST + BSA)] for 2 h at room temperature. After three washes (10 min each) in TBST, PLR mRNA was detected by incubating the slides with the chromogenic substrates, nitroblue tetrazolium chloride (NBT) and 5-bromo-4-chloro-3-indolyl-phosphate, 4-toluidine salt (BCIP) in 100 mM Tris–HCl (pH 9.2) containing 100 mM NaCl and 50 mM $MgCl_2$. Incubation was carried out in the dark, for up to 10 min, at room temperature according to the manufacturer's instructions (Boehringer Mannheim). In order to remove endogenous alkaline phosphatase activity in the tissue sections, levamisol (Sigma, 0.24 mg ml^{-1}) was additionally added to the color developing solution as described in Bochenek and Hirsch (1990). Progression of the color reaction was terminated by washing the slides for 5 min in H_2O, followed by air drying in the dark at room temperature. Slides were next covered with cover-slips for microscopy analyses using a Permount (Fisher Scientific) as a mounting media without counter-staining.

4.8. Western blot analysis using PCBER antibodies

P. taeda stems were ground in liquid N_2 to a powder by means of a mortar and pestle. The powder was next homogenized in potassium phosphate buffer (0.1 M, pH 7.9). The resulting slurry was passed through one layer of miracloth, then centrifuged (10,000 *g* for 5 min) and the total crude protein extract so obtained was used for western blot analysis. Total proteins [4 μg, based on absorbance at 595 nm with the Bradford reagent (Bradford, 1976)] were next loaded onto a polyacrylamide gel (4–15% acrylamide) (Bio-Rad) and subjected to electrophoresis (20 mA) according to Laemmli (1970), using Kaleidoscope prestained standards (Bio-Rad). The resulting gel was then blotted onto a PVDF membrane (Bio-Rad), presoaked in transfer buffer containing 20% MeOH, and 80% [25 mM Tris buffer, and 192 mM glycine]. This was then blotted at 150 mA for 1 h using the corresponding transfer apparatus, with the resulting membrane washed briefly in distilled water and blocked in TBS (20 mM Tris–HCl, pH 7.5, 500 mM NaCl) buffer containing 5% powdered milk for 30 min at room temperature. After briefly washing the membrane in 20 mM Tris–HCl buffer (pH 7.5) containing 500 mM NaCl and 0.05% Tween 20 (TBST), it was next incubated with PCBER antibodies, diluted (1:5000) in TBST buffer containing 5% powdered milk. After washing with TBST twice for 10 min each, the membrane was incubated with goat anti-rabbit antibody conjugated to horseradish peroxidase (Pierce, Rocklord, IL) diluted (1:10,000) in TBST containing 5% powdered milk, for 2 h at room temperature. After washing the membrane three times in TBST for 5 min each, and then twice in TBS for 5 min each, the antibody binding was visualized using 4-chloro-1-naphthol and hydrogen peroxide in TBS.

4.9. Immunocytochemistry of PCBER in Pinus taeda

Stems of 1 year old *Pinus taeda* seedlings were harvested and embedded in paraffin after FAA fixation as described above. Thick sections (10 μm) were obtained using a rotary microtome (Jung Biocut, Leica) and mounted on silane coated-microscopic slides (Fisher Scientific). The paraffin was removed by immersion of the slides in a hemo-D (Fisher Scientific) solution and subsequently rehydrated in 100, 95, 80, 50 and 30% EtOH, and finally in distilled water. After air drying, sections were blocked for 1 h in TBST containing 1% (w/v) BSA, 0.1% (w/v) PVP, 0.5% whole rabbit serum (Ted Pella, Inc). All incubations were carried out at room temperature with gentle shaking. Sections were next transferred to a solution containing either rabbit polyclonal antibodies raised against purified recombinant PCBER protein expressed in *E. coli* or the preimmune serum as a control, each of which had been diluted 1:10 in TBST containing 1% (w/v) BSA (TBST + BSA). After incubation for 4 h, sections were immersed and rinsed in TBST + BSA for four times 15 min, then finally transferred to and incubated in blocking solution (TBST + BSA containing 0.5% (v/v) whole sheep serum) for 30 min. Sections were next incubated for 2 h with sheep anti-rabbit antibody conjugated to alkaline phosphatase (Boehringer Mannheim) (1:50, in TBST + BSA). Tissue sections were washed with TBST + BSA, TBST and with distilled water (3 times each), successively, and then each was incubated with chromogenic substrates, NBT and BCIP as described above (Bochenek and Hirsch, 1990). Color development was carried out at room temperature for 10 min in the dark according to manufacturer's instructions (Boehringer Mannheim). Slides were treated as described above for microscopy analyses.

4.10. Image processing

Photographs of sections were archived using a Stereomicroscope (Wild Heerbrugg) and an Olympus BH2 microscope equipped with a Pulnix TM-7 CN color CDD camera.

Acknowledgements

We gratefully acknowledge the National Science Foundation (MCB-9976684), the United States Department of

Energy (DE-FG03-97ER20259), the United States Department of Agriculture (99-35103-8037), McIntire-Stennis, and the Arthur M. and Kate Eisig-Tode Foundation, and the Lewis B. and Dorothy Cullman and G. Thomas Hargrove Center for Land Plant Adaptation Studies for generous support of this and related studies.

References

Ayres, D.C., Loike, J.D., 1990. Lignans: Chemical, Biological and Clinical Properties. Cambridge University Press, Cambridge, UK.

Beatson, R.P., Wang, W., Johansson, C.I., Saddler, J.N., 1998. The use of enzymes to produce, characterize and degrade chromophores present in western red cedar mechanical pulp. In: 7th International Conference on Biotechnology in the Pulp and Paper Industry, Vol. A. Technical Section, Canadian Pulp and Paper Association, Vancouver, BC, Canada, pp. 211–215.

Belmares, H., Barrera, A., Castillo, E., Ramos, L.F., Hernandez, F., Hernandez, V., 1979. New rubber antioxidants and fungicides derived from *Larrea tridentata* (creosote bush). Industrial and Engineering Chemistry Product Research and Development 18, 220–226.

Binns, A.N., Chen, R.H., Wood, H.N., Lynn, D.G., 1987. Cell division promoting activity of naturally occurring dehydrodiconiferyl glucosides: do cell wall components control cell division? Proceedings of the National Academy of Sciences of the United States of America 84, 980–984.

Bochenek, B., Hirsch, A.M., 1990. In situ hybridization of nodulin mRNAs in root nodules using non-radioactive probes. Plant Molecular Biology Report 8, 237–248.

Bosshard, H.H., 1965. Aspects of the aging process in cambium and xylem. Holzforschung 19, 65–69.

Bosshard, H.H., 1966. Notes on the biology of heartwood formation. International Association of Wood Anatomists 1966, 11–14.

Bosshard, H.H., 1968. On the formation of facultatively colored heartwood in *Beilschmiedia tawa*. Wood Science and Technology 2, 1–12.

Bradford, M.M., 1976. A rapid and sensitive method for the quantitation of microgram quantities of protein utilizing the principle of protein-dye binding. Analytical Biochemistry 72, 248–254.

Burlat, V., Kwon, M., Davin, L.B., Lewis, N. G., 2001. Dirigent proteins and dirigent sites in lignifying tissues. Phytochemistry 57, 883–897.

Chattaway, M.M., 1952. The sapwood-heartwood transition. Australian Forestry 16, 25–34.

Chu, A., Dinkova, A., Davin, L.B., Bedgar, D.L., Lewis, N.G., 1993. Stereoselectivity of (+)-pinoresinol and (+)-lariciresinol reductases from *Forsythia intermedia*. Journal of Biological Chemistry 268, 27026–27033.

Davin, L.B., Lewis, N.G., 2000. Dirigent proteins and dirigent sites explain the mystery of specificity of radical precursor coupling in lignan and lignin biosynthesis. Plant Physiology 123, 453–461.

Davin, L.B., Wang, H.-B., Crowell, A.L., Bedgar, D.L., Martin, D.M., Sarkanen, S., Lewis, N.G., 1997. Stereoselective bimolecular phenoxy radical coupling by an auxiliary (dirigent) protein without an active center. Science 275, 362–366.

Dinkova-Kostova, A.T., Gang, D.R., Davin, L.B., Bedgar, D.L., Chu, A., Lewis, N.G., 1996. (+)-Pinoresinol/(+)-lariciresinol reductase from *Forsythia intermedia*. Protein purification, cDNA cloning, heterologous expression and comparison to isoflavone reductase. Journal of Biological Chemistry 271, 29473–29482.

Duck, N.B., 1994. RNA in situ hybridization in plants. Plant Molecular Biology Manual G1, 1–13.

Elakovich, S.D., Stevens, K.L., 1985. Phytotoxic properties of nordihydroguaiaretic acid, a lignan from *Larrea tridentata* (creosote bush). Journal of Chemical Ecology 11, 27–33.

Farkas, G.L., Király, Z., 1962. Role of phenolic compounds in the physiology of plant diseases and disease resistance. Phytopathologische Zeitschrift 44, 105–150.

Fauré, M., Lissi, E., Torres, R., Videla, L.A., 1990. Antioxidant activities of lignans and flavonoids. Phytochemistry 29, 3773–3775.

Fujita, M., Gang, D.R., Davin, L.B., Lewis, N.G., 1999. Recombinant pinoresinol-lariciresinol reductases from western red cedar (*Thuja plicata*) catalyze opposite enantiospecific conversions. The Journal of Biological Chemistry 274, 618–627.

Gagnon, C., 1967. Polyphenols and discoloration in the elm disease investigated by histochemical techniques. Canadian Journal of Botany 45, 2119–2124.

Gang, D.R., Costa, M.A., Fujita, M., Dinkova-Kostova, A.T., Wang, H.-B., Burlat, V., Martin, W., Sarkanen, S., Davin, L.B., Lewis, N.G., 1999a. Regiochemical control of monolignol radical coupling: a new paradigm for lignin and lignan biosynthesis. Chemistry and Biology 6, 143–151.

Gang, D.R., Dinkova-Kostova, A.T., Davin, L.B., Lewis, N.G., 1997. Phylogenetic links in plant defense systems: lignans, isoflavonoids, and their reductases. In: Hedin, P. (Ed.), Phytochemical Pest Control Agents, Vol. 658. ACS Symposium Series, Washington, DC, pp. 58–89.

Gang, D.R., Fujita, M., Davin, L.B., Lewis, N.G., 1998. The 'abnormal lignins': mapping heartwood formation through the lignan biosynthetic pathway. In: Lewis, N.G., Sarkanen, S. (Eds.), Lignin and Lignan Biosynthesis, Vol. 697. ACS Symposium Series, Washington, DC, pp. 389–421.

Gang, D.R., Kasahara, H., Xia, Z.-Q., Vander Mijnsbrugge, K., Bauw, G., Boerjan, W., Van Montagu, M., Davin, L.B., Lewis, N.G., 1999b. Evolution of plant defense mechanisms: relationships of phenylcoumaran benzylic ether reductases to pinoresinol lariciresinol and isoflavone reductases. The Journal of Biological Chemistry 274, 7516–7527.

Gnabre, J.N., Ito, Y., Ma, Y., Huang, R.C., 1996. Isolation of anti-HIV-1 lignans from *Larrea tridentata* by counter-current chromatography. Journal of Chromatography A 719, 353–364.

Harmatha, J., Nawrot, J., 1984. Comparison of the feeding deterrent activity of some sesquiterpene lactones and a lignan lactone towards selected insect storage pests. Biochemical Systematics and Ecology 12, 95–98.

Hart, J.H., Hillis, W.E., 1974. Inhibition of wood-rotting fungi by stilbenes and other polyphenols in *Eucalyptus sideroxylon*. Phytopathology 64, 939–948.

Hattori, M., Hada, S., Watahiki, A., Ihara, H., Shu, Y.-Z., Kakiuchi, N., Mizuno, T., Namba, T., 1986. Studies on dental caries prevention by traditional medicines. X. Antibacterial action of phenolic components from mace against *Streptococcus mutans*. Chemical and Pharmaceutical Bulletin 34, 3885–3893.

Hauch, S., Magel, E., 1998. Extractable activities and protein content of sucrose-phosphate synthase, sucrose synthase and neutral invertase in trunk tissues of *Robinia pseudoacacia* L. are related to cambial wood production and heartwood formation. Planta 207, 266–274.

Hemingway, R.W., Hillis, W.E., 1970. Heartwood formation in living stumps of Douglas-fir. Wood Science and Technology 4, 246–254.

Hillis, W.E., 1971. Distribution, properties and formation of some wood extractives. Wood Science and Technology 5, 272–289.

Hillis, W.E., Soenardi, P., 1994. Formation of ebony and streaked woods. International Association of Wood Anatomists Journal 15, 245–437.

Krahmer, R.L., Hemingway, R.W., Hillis, W.E., 1970. The cellular distribution of lignans in *Tsuga heterophylla* wood. Wood Science and Technology 4, 122–139.

Kraus, C., Spiteller, G., 1997. Comparison of phenolic compounds from galls and shoots of *Picea glauca*. Phytochemistry 44, 59–67.

Kwon, M., Burlat, V., Davin, L.B., Lewis, N.G., 1999. Localization of dirigent protein involved in lignan biosynthesis: implications for

lignification at the tissue and subcellular level. In: Gross, G.G., Hemingway, R.W., Yoshida, T. (Eds.), Plant Polyphenols: Chemistry, Biology, Pharmacology, Ecology, Vol. 2. Kluwer Academic/Plenum Publishers, New York, pp. 393–411.

Laemmli, U.K., 1970. Cleavage of structural proteins during the assembly of the head of bacteriophage T4. Nature 227, 680–685.

Lewis, N.G., Davin, L.B., 1999. Lignans: biosynthesis and function. In: Barton Sir, D.H.R., Nakanishi, K., Meth-Cohn, O. (Eds.), Comprehensive Natural Products Chemistry, Vol. 3. Pergamon, Oxford, pp. 639–712.

Lewis, N.G., Kwon, M., Kasahara, H., Bedgar, D.L., Burlat, V., Davin, L.B., 2000. Carbon partitioning into the lignan pathway in active cambial, differentiating xylem and heartwood-forming tissues. 219th American Chemical Society National Meeting, San Francisco, CA, March 2000.

Li, Z., Sarkanen, K.V., 1971. Isolation and structural studies. In: Sarkanen, K.V., Ludwig, C.H. (Eds.), Lignins. Occurrence, Formation, Structure and Reactions. Wiley Interscience, New York, NY, pp. 165–240.

MacRae, W.D., Tower, G.H.N., 1984. Biological activities of lignans. Phytochemistry 23, 1207–1220.

Magel, E., Hillinger, C., Höll, W., Ziegler, H., 1997. Biochemistry and physiology of heartwood formation: role of reserve substances. In: Rennenberg, H., Eschrich, W., Ziegler, H. (Eds.), Trees-Contributions to Modern Tree Physiology. Backhuys Publisher, Leiden, The Netherlands, pp. 477–506.

Osawa, T., Nagata, M., Namiki, M., Fukuda, Y., 1985. Sesamolinol, a novel antioxidant isolated from sesame seeds. Agricultural and Biological Chemistry 49, 3351–3352.

Pan, H., Lundgren, L.N., 1995. Phenolic extractives from root bark of *Picea abies*. Phytochemistry 39, 1423–1428.

Sambrook, J., Fritsch, E.F., Maniatis, T., 1989. Molecular Cloning: A Laboratory Manual. Cold Spring Harbor Laboratory Press, Cold Spring Harbor, NY.

San Feliciano, A., Miguel Del Corral, J.M., Lopez, J.L., De Pascual-Teresa, B., 1992. Lignans from polar extracts of *Juniperus thurifera*. Phytochemistry 31, 267–270.

Scheffer, T.C., Cowling, E.B., 1966. Natural resistance of wood to microbial deterioration. Annual Review of Phytopathology 4, 147–170.

Shigo, A.L., Hillis, W.E., 1973. Heartwood, discolored wood, and microorganisms in living trees. Annual Review of Phytopathology 11, 197–222.

Su, W.-C., Fang, J.-M., Cheng, Y.-S., 1995. Flavonoids and lignans from leaves of *Cryptomeria japonica*. Phytochemistry 40, 563–566.

Sucoff, E., Ratsch, H., Hook, D.D., 1967. Early development of wound-initiated discoloration in *Populus tremuloides* Michx. Canadian Journal of Botany 45, 649–656.

Suga, T., Ohta, S., Munesada, K., Ide, N., Kurokawa, M., Shimizu, M., Ohta, E., 1993. Endogenous pine wood nematicidal substances in pines, *Pinus massoniana*, *P. strobus* and *P. palustris*. Phytochemistry 33, 1395–1401.

Swan, E.P., Jiang, K.S., Gardner, J.A.F., 1969. The lignans of *Thuja plicata* and the sapwood-heartwood transformation. Phytochemistry 8, 345–351.

Umezawa, T., Davin, L.B., Lewis, N.G., 1991. Formation of lignans (−)-secoisolariciresinol and (−)-matairesinol with *Forsythia intermedia* cell-free extracts. The Journal of Biological Chemistry 266, 10210–10217.

Vander Mijnsbrugge, K., Beeckman, H., De Rycke, R., Van Montagu, M., Engler, G., Boerjan, W., 2000. Phenylcoumaran benzylic ether reductase, a prominent poplar xylem protein, is strongly associated with phenylpropanoid biosynthesis in lignifying cells. Planta 211, 502–509.

Xia, Z.-Q., Costa, M.A., Pélissier, H.C., Davin, L.B., Lewis, N.G., 2001. Secoisolariciresinol dehydrogenase purification, cloning and functional expression. Implications for human health protection. The Journal of Biological Chemistry 276, 12614–12623.

PERGAMON

Phytochemistry 57 (2001) 915–927

PHYTOCHEMISTRY

www.elsevier.com/locate/phytochem

Biosynthesis and subcellular distribution of hydrolyzable tannins

Petra Grundhöfer[a], Ruth Niemetz[a], Gerhard Schilling[b], Georg G. Gross[a,*]

[a]*Molekulare Botanik, Universität Ulm, D-89069 Ulm, Germany*
[b]*Universität Heidelberg, Organisch-Chemisches Institut, Im Neuenheimer Feld 270, D-69120 Heidelberg, Germany*

Received 29 June 2000; received in revised form 29 August 2000

Abstract

Pathways to complex gallotannins have been elucidated by enzyme studies, indicating that β-glucogallin is required as principal acyl donor. Evidence for the in vitro oxidation of pentagalloylglucose, the pivotal metabolite in this sequence, to ellagitannins, is presented. Immunohistochemical studies with antibodies raised against pentagalloylglucose and the galloyltransferase catalyzing the formation of this ester revealed that leaf mesophyll cell walls were a typical site of origin and deposition of hydrolyzable tannins. Seasonal changes of these compounds were studied with extracts from cell walls and intracellular space of oak leaves. © 2001 Published by Elsevier Science Ltd. All rights reserved.

Keywords: *Quercus robur* (*Q. pedunculata*); Fagaceae; Pedunculate oak; *Rhus typhina*; Anacardiaceae; Staghorn sumac; *Tellima grandiflora*; Saxifracaceae; Biosynthesis; Immunohistochemistry; Transmission electron microscopy; Gallotannins; Ellagitannins

1. Introduction

Vegetable tannins, nowadays often called 'plant polyphenols' as an attempt to describe their heterogenous chemical structures and manifold reactions more adequately (cf. Haslam, 1989, 1999), have exerted a strong impact on human life for millenia. As common components of food and beverages of plant origin, they influenced their taste by providing a more or less appreciated astringency (which must not necessarily be negative if one considers the recently intensively discussed 'French paradox' (cf. Carando and Teissedre, 1999), i.e. reduced incidence of coronary artery disease supposed to be caused by ingestion of red wine tannins). They were later recognized as valuable chemicals for technical processes (e.g. in tannery to convert raw hides to durable leather or for the production of dyes and inks) and as versatile medicinal agents that have been widely used in traditional folk medicine to cure a variety of physical disorders (cf. Haslam et al., 1989; Haslam, 1996) and that appear to experience now a renaissance as potent antioxidant, antimicrobial, antiviral and antitumor agents (for recent reviews related to these topics, see Gross et al., 1999). It is, thus, not surprising that chemists started studies on the structure of tannins already more than a century ago. These efforts were, however, awarded by significant progress only during the past decades when the problems that arose from the complexity of these substances and that prevented their facile isolation and unequivocal characterization had been solved by the introduction of modern chromatographic and analytical techniques, like high-performance liquid chromatography (HPLC), mass spectrometry (MS) and nuclear magnetic resonance (NMR) spectroscopy. The rich body of different tannin structures isolated from many plant species that became available by such investigations stimulated subsequent considerations on the then completely unknown biosynthesis of these compounds. Experiments on this latter challenging question, focussed on the biogenetic routes to the class of hydrolyzable tannins, were performed in the authors' laboratory by enzyme studies with cell-free extracts from leaves of staghorn sumac (*Rhus typhina*), pedunculate oak (*Quercus pedunculata*, syn. *Q. robur*) and the weed *Tellima grandiflora* (Saxifragaceae). [According to the already classical definition proposed by Freudenberg (1920), plant tannins are divided into hydrolyzable tannins and flavonoid derived condensed tannins, *syn.* proanthocyanidins, which are not the subject of this contribution]. In close connection with this research project it became

* Corresponding author. Tel.: +49-731-50-22624; fax: +49-731-50-22809.
E-mail address: georg.gross@biologie.uni-ulm.de (G.G. Gross).

0031-9422/01/$ - see front matter © 2001 Published by Elsevier Science Ltd. All rights reserved.
PII: S0031-9422(01)00099-1

increasingly interesting to investigate the subcellular localization of the enzymes involved in the biosynthesis of hydrolyzable tannins and also to determine the compartments for the deposition of their reaction products. Results of biochemical and histochemical studies related to these topics, including recent unpublished findings, are summarized in this article.

2. Biosynthesis of hydrolyzable tannins

The biogenetic pathways to hydrolyzable tannins can be logically divided into three smaller sections that reflect typical structural features of the intermediates involved in these conversions. A starting sequence comprises the reactions from free gallic acid (**1**) to 1,2,3,4,6-penta-*O*-galloyl-β-D-glucopyranose (**6**) (Fig. 1). The compounds of this route are often referred to as 'simple galloylglucose esters', primarily to differentiate them unequivocally from higher substituted polygalloylglucoses (gallotannins sensu strictu, for clarity referred to as 'complex gallotannins' here) and neglecting the fact that tetra- and pentagalloylglucoses are very potent tanning agents. Many details of this reaction sequence have recently been described in comprehensive review articles (Gross, 1999a,b; Niemetz et al., 1999); consequently, only the most prominent features of this pathway will be discussed here. As theorized already decades ago (e.g. Haslam, 1989), the end-product of this first sequence, pentagalloylglucose (**6**), has a pivotal role as immediate precursor of two subsequent routes, one leading to (complex) gallotannins which are characterized by additional galloyl residues bound to the pentagalloylglucose core. In an alternative pathway, ellagitannins are formed by oxidative processes that yield C–C linkages between adjacent galloyl groups of pentagalloylglucose and that often lead to the subsequent formation of dimeric and oligomeric derivatives.

2.1. The pathway from gallic acid to pentagalloylglucose

In recent experiments on the still not completely clarified origin of gallic acid (Fig. 1, **1**), the principal phenolic unit of hydrolyzable tannins, [^{13}C]glucose was administered to the fungus *Phycomyces blakesleeanus* and to the dicotyloneous plant *R. typhina,* followed by NMR spectroscopical determination of the isotope distribution of gallic acid and aromatic amino acids isolated from these species. Interpretation of the isotopomer patterns of these metabolites by a retrobiosynthetic approach showed that gallic acid was derived from an early intermediate of the shikimate pathway, most likely 5-dehydroshikimic acid, suggesting that dehydrogenation of this compound was the predominant pathway to gallic acid (Werner et al., 1999). However, alternative routes cannot be excluded.

For thermodynamic reasons, esterification of gallic acid and glucose to yield β-glucogallin (1-*O*-galloyl-β-D-glucose, **2**), the often proposed primary specific metabolite in the route to hydrolyzable tannins, depends on the participation of an 'activated' intermediate with a high group-transfer potential. Enzyme studies revealed that this requirement was met by a common metabolite, UDP-glucose, which was utilized by a glucosyltransferase from oak leaves for the (reversible) synthesis of β-glucogallin (cf. Fig. 1) and of related 1-*O*-acyl-β-D-glucoses

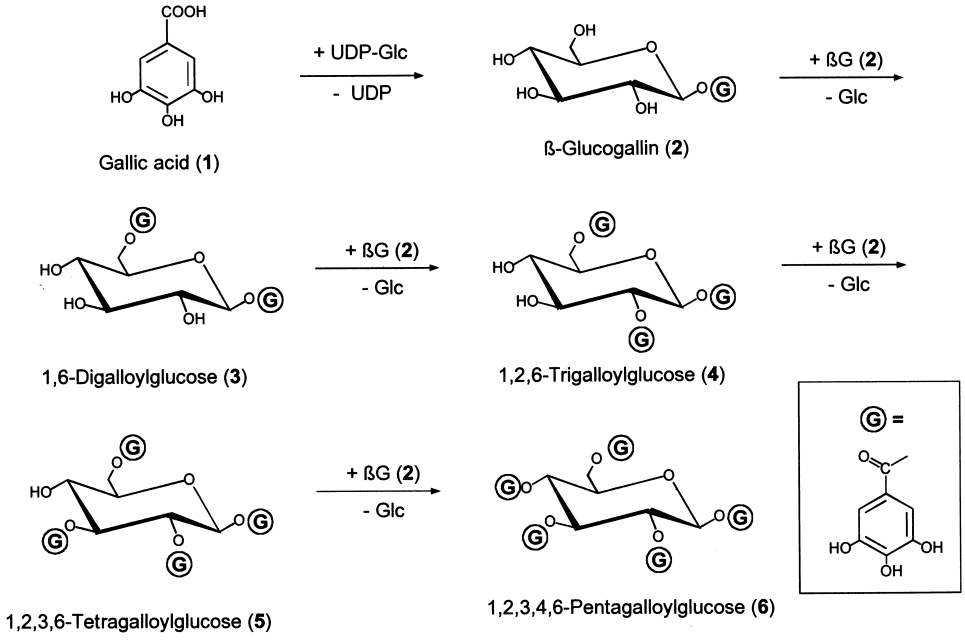

Fig. 1. Enzyme reactions catalyzing the biosynthesis of 1,2,3,4,6-pentagalloylglucose (**6**).

(Gross, 1983a). Cell-free extracts from this plant were also found to catalyze the subsequent transformation of β-glucogallin to di- and trigalloylglucoses, a reaction that surprisingly ocurred in the absence of any other cofactors and which could be explained only by the assumption that β-glucogallin exerted a dual role, functioning not only as acyl acceptor, but also as an efficient acyl donor (Gross, 1983b). Such a behavior would necessarily require that β-glucogallin had the then unexpected characteristic of an energy-rich 'activated' compound. This question was answered by the discovery of Mock and Strack (1993) that a related ester, 1-*O*-sinapoyl-β-D-glucose, had an unexpectedly high $\Delta G_o'$ of 35.7 kJ mol^{-1}, i.e. a value that is comparable to the well-known data for acyl-CoA thioesters. Numerous examples for the reactivity of such acetal esters have been reported meanwhile (for references, see Gross, 1999a,b; Niemetz et al., 1999). It is evident now that phenolic 1-*O*-acylglucose esters, often regarded in the past as metabolically inert compounds, have acquired a prominent position in the secondary metabolism of higher plants.

Further studies with enzymes isolated from oak or sumac revealed that this mechanism applied to the entire route from β-glucogallin (**2**) to pentagalloylglucose (**6**). As depicted in Fig. 1, substitution of glucose hydroxyls was not randomly distributed in these conversions but displayed extreme specificity, thus constituting the metabolic sequence β-glucogallin (**2**)→1,6-digalloylglucose (**3**, Schmidt et al., 1987)→1,2,6-trigalloylglucose (**4**, Gross and Denzel, 1991)→1,2,3,6-tetragalloylglucose (**5**, Hagenah and Gross, 1993)→1,2,3,4,6-pentagalloyl glucose (**6**, Cammann et al., 1989). Interestingly, an identical pattern has been reported for the chemical substitution of glucose hydroxyls in experiments with 1-benzyl or 1-methyl-β-D-glucopyranose which was explained as a combination of reactivity differences according to variations in chemical nature (primary vs secondary hydroxyls), neighboring group activation effects and steric hindrance (Williams and Richardson, 1967; Reinefeld and Ahrens, 1971).

These enzyme studies gave the impression of a straight, forward-directed pathway that depended on β-glucogallin as sole and general acyl donor. However, the existence of other enzymes was encountered that led to side-reactions and ramifications of the main pathway. An acyltransferase was isolated from oak leaves that catalyzed an unusual galloyl exchange between β-glucogallin and free glucose, a reaction that was detectable only by the use of labeled substrates and whose physiological significance is still obscure (Gross et al., 1986). Another enzyme that had been isolated from sumac leaves interfered with the acylation of 1,6-digalloylglucose (**3**) to 1,2,6-trigalloylglucose (**4**) by promoting this reaction without any requirement of the established acyl donor, β-glucogallin (**2**). It was recognized that this enzyme catalyzed a 'disproportionation' reaction in which two molecules 1,6-digalloylglucose were converted to 1,2,6-trigalloylglucose and anomeric 6-*O*-galloylglucose as partially deacylated byproduct (Denzel and Gross, 1991). This latter finding stimulated ideas that, besides β-glucogallin, also higher substituted galloylglucoses could act as acyl donors, provided that they possessed the energetically indispensable 1-*O*-galloyl group. This interpretation was corroborated by substrate specificity studies which, however, revealed that the reactivity of higher substituted analogs was drastically diminished, most likely because of steric hindrance due to excessive bulkiness of these molecules, thus leaving 1-mono- and, within certain limits, 1,6-di-esters as predominating galloyl donors (Denzel and Gross, 1991).

The pathway to pentagalloylglucose, as summarized in Fig. 1, has long been assumed to be unique. However, striking similarities have been reported for the biosynthesis of isobutyroyl-β-D-glucoses in wild tomato (*Lycopersicon penellii*) leaves. A UDP-glucose dependent glucosyltransferase catalyzed the formation of 1-*O*-isobutyroyl-β-D-glucose. This ester, in turn, was utilized as activated acyl donor in a series of substitution reactions that afforded 1,3-di-, 1,2,3-tri- and 1,2,3,4-tetra-*O*-isobutyroyl derivatives, and was also involved in an acyl exchange reaction with free glucose as an analogy to the above mentioned galloyl exchange reaction (Ghangas and Steffens, 1993, 1995; Kuai et al., 1997).

2.2. Biosynthesis of gallotannins

Formally, 'simple' galloylglucoses are converted to complex gallotannins by the addition of further galloyl residues to 1,2,3,4,6-pentagalloylglucose (**6**) to yield the *meta*-depside groups that characterize this class of

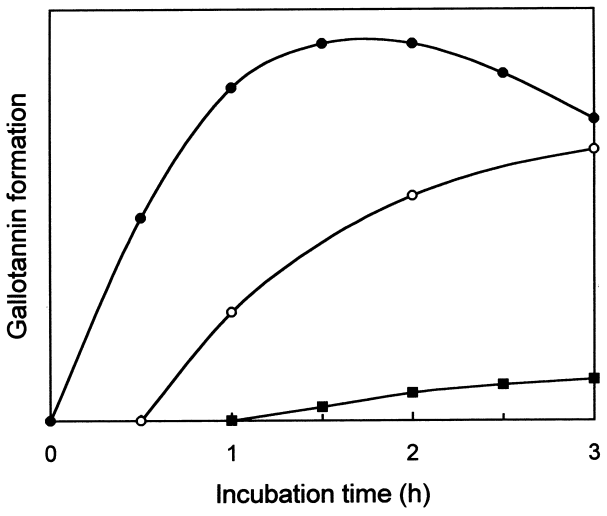

Fig. 2. Enzymatic synthesis of complex gallotannins by galloylation of 1,2,3,4,6-pentagalloylglucose (**6**) in the presence of β-glucogallin with crude enzyme extracts from leaves of *Rhus typhina*. (●), Hexa-, (○), hepta-, (■), octagalloylglucoses (from Gross, 1999a).

phenolic plant constituents (cf. Ⓖ▸Ⓖ in Fig. 3). It must be emphasized that this process is not a mere continuation of the esterification reactions of the preceding steps because the newly introduced galloyl moieties now combine with phenolic hydroxyls whose chemical properties differ significantly from those of the aliphatic OH-groups of glucose. It was thus surprising to discover that crude enzyme preparations from sumac (*R. typhina*) leaves catalyzed the sequential transformation of pentagalloylglucose to complex gallotannins according to the same reaction mechanism as above, i.e. by utilizing β-glucogallin (**2**) as specific galloyl donor (Fig. 2). Such assays afforded a mixture of hexa-, hepta-, octa- and nonagalloylglucoses, together with traces of decagalloyl glucoses, and eventually even of undecagalloylglucoses, as shown by HPLC with normal-phase (Si 60) and reversed-phase (RP-18) columns (Hofmann and Gross, 1990). Evidence for the presumed gallotannin nature of the most abundant enzyme reaction products, hexa- to octagalloylglucoses that had been purified from scaled-up in vitro assays, was obtained by hydrolysis with fungal tannase, leaving gallic acid (**1**) as sole phenolic component. Upon methanolysis, known to exclusively cleave *meta*-depside bonds, these compounds were degraded to 1,2,3,4,6-pentagalloylglucose (**6**) and methyl gallate in the expected molar ratios of 1:1, 1:2, and 1:3, respectively. Structural proof of hexa- and hepta-galloylglucoses was obtained by ^{1}H and ^{13}C NMR spectroscopic analyses and comparison with previously published data on the components of Chinese gallotannin from the related species *R. semialata* (Nishizawa et al., 1982; cf. Fig. 3).

Recent enzyme studies revealed the existence of numerous isoenzymes in sumac (*R. typhina*) leaves that participated in the in vitro acylation of pentagalloylglucose (**6**) to higher substituted derivatives. Among these, four galloyltransferases (transferases A–D) have been isolated and characterized to date. The general properties of these enzymes were found to vary significantly, particularly with respect to the enormous band-width of their molecular weights. It was also apparent that their substrate and product specificities were rather low, a feature that, however, is not uncommon to enzymes of secondary plant metabolism. Accordingly, in order to maintain a clear overall view of the major biogenetic interrelationships, only the most prominent reactions of the pathways from penta- to heptagalloylglucoses (higher substituted gallotannins of defined structure were not available) are reported below (cf. Fig. 3).

Galloyltransferase A has been purified to apparent homogeneity. It had a molecular weight (M_r) of 360,000 and was found to preferentially acylate pentagalloyl glucose (**6**) in the 4-position, followed by substitution of the 2-position, yielding the hexagalloylglucose, 4-*O*-digalloyl-1,2,3,6-tetra-*O*-galloylglucose (**7**), and the hepta galloylglucose, 2,4-bis-*O*-digalloyl-1,3,6-tri-*O*-galloyl-glucose (**10**). Compound (**7**) was the preferred substrate (Niemetz and Gross, 1999). Transferase B (M_r 260,000) also catalyzed the sequence (**6**)→(**7**)→(**10**) but was more effective in the formation of the hexagalloylglucose, 3-*O*-digalloyl-1,2,4,6-tetra-*O*-galloylglucose (**9**), and particularly of the heptagalloylglucose, 3-*O*-trigalloyl-1,2,4,6-tetra-*O*-galloylglucose (**12**) (Niemetz and Gross, unpublished results). Transferase C could also be purified to

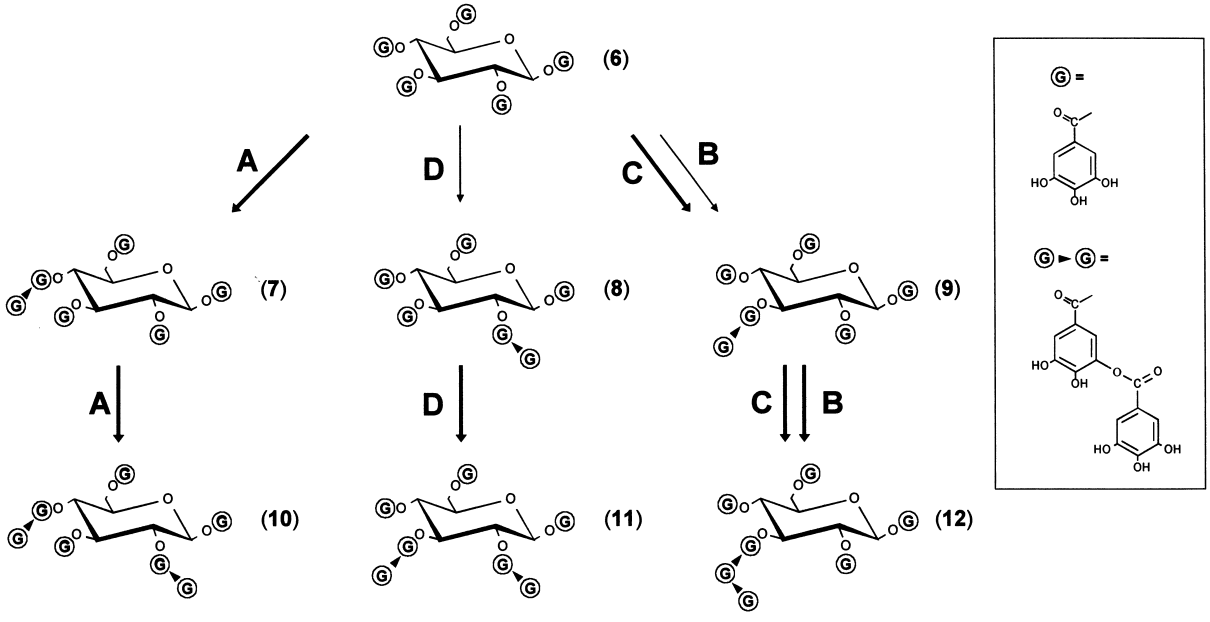

Fig. 3. Major routes in the transformation of pentagalloylglucose (**6**) to hexagalloylglucoses (**7**–**9**) and heptagalloylglucoses (**10**–**12**), catalyzed by galloyltransferases **A**–**D** from sumac (*Rhus typhina*) leaves. Main reactions are symbolized by bold arrows, minor reactions by thin arrows.

apparent homogeneity; it had an M_r of 170,000 and was found to be composed of four identical subunits of M_r 42,000. The preferred substrate for this enzyme was pentagalloylglucose (**6**) which was preferentially acylated to hexagalloylglucose (**9**) and heptagalloylglucose (**12**) (Niemetz and Gross, 1998). Transferase D (M_r 300,000) was detected in a different screening experiment in which hexagalloylglucose (**8**) replaced the standard acceptor substrate of the above investigations, pentagalloylglucose (**6**). This enzyme displayed rather low affinity toward pentagalloylglucose, which was preferentially acylated to the hexagalloylglucose, 2-*O*-digalloyl-1,3,4,6-tetra-*O*-galloylglucose (**8**), but was very effective in acylating this latter compound to the heptagalloylglucose, 2,3-bis-*O*-digalloyl-1,4,6-tri-*O*-galloylglucose (**11**) (Fröhlich and Gross, unpublished results). In summary, the specificities of these enzymes support earlier findings that the C-1 and C-6 positions of 'Chinese gallotannin' from *Rhus semialata* generally remain free of depsidic substituents (Nishizawa et al., 1982), in contrast to the gallotannins from *Quercus infectoria* ('Turkish gallotannin'; Nishizawa et al., 1983a) or *Paeonia lactiflora* (Nishizawa et al., 1980, 1983b) where depside bonds occur also at C-6 of the glucose core.

It should finally be mentioned that the reported reactions bear the risk of interference with nonenzymatic, chemical acyl migrations. We observed, for instance, a significant translocation of the distal, *meta*-depsidically bound galloyl group of hexagalloylglucose (**9**) from the 3-position to the adjacent 4-position to yield hexagalloylglucose (**7**) under slightly acidic conditions (Bayer and Gross, unpublished results).

2.3. Biosynthesis of ellagitannins

In contrast to the rather limited distribution of gallotannins in nature, ellagitannins are typical constituents of many plant families. These compounds display an enormous structural variability that results from the manifold possible sites for the linkage of HHDP (**14**) residues with the glucose moiety (which, in turn, can adopt several conformations that control the range of possible spatial arrangements of reactive ligands), and particularly by their strong tendency to form a multitude of dimeric and oligomeric derivatives being interconnected by C–C and C–O–C linkages (recently reviewed by Haslam, 1998). This structural diversity of ellagitannins, together with their recently recognized role as promising chemotherapeutic agents (e.g. Yoshida et al., 1999; Miyamoto et al., 1999), have attracted the interest of chemists for decades, culminating in recent successful efforts on the extreme challenge of synthesizing ellagitannins by chemical means (Feldman et al., 1999).

Progress in the study of the biosynthesis of ellagitannins was significantly slower (cf. Helm et al., 1999). It has been postulated very early that the HHDP residues of ellagitannins should originate from the dehydrogenation of neighboring galloyl groups of 1,2,3,4,6-pentagalloylglucose (**6**) (reviewed by Haslam, 1989). In the case of the preferred $^4C_1$ configuration of pentagalloylglucose, for instance, the two galloyl groups at C-4 and C-6 were thought to be interconnected to form one HHDP group, thus yielding tellimagrandin II (**13**) as a primary ellagitannin metabolite that can be subjected to further oxidation reactions. Hydrolysis of (**13**) would afford both free gallic acid (**1**) and hexahydroxydiphenic acid (**14**), the latter possessing a strong tendency to spontaneously undergo lactonization to give ellagic acid (**15**) (Fig. 4).

Many attempts to unravel the mechanism of ellagitannin biosynthesis have been carried out by experiments with chemical oxidants (e.g. O_2, Fe^{3+}) or by studies with the enzymes laccase and peroxidase, using gallic acid, methyl gallate, β-glucogallin, 3,6-digalloylglucose or pentagalloylglucose as substrates (references in Gross, 1999b). Only free ellagic acid (**15**), however, was detected as a typical product in these experiments, while the formation of true ellagitannins, characterized by glucose-bound HHDP residues, was never observed.

Considering these negative results, it was apparent that new strategies were required that combined both increased specificity and higher sensitivity to tackle the question of ellagitannin biosynthesis. A common way to eliminate such problems is the use of radioactively labeled compounds, which in this specific case also would provide an excellent tool to discriminate between true in vitro enzyme reaction products and any contaminating ellagitannins that had been formed in vivo and were transferred to the assays by unspecific binding to proteins due to their tannin nature. We therefore synthesized [U–^{14}C]pentagalloylglucose by photoassimilation of $^{14}CO_2$ in leaves of *R. typhina* (Rausch and Gross, 1996). Using this compound as standard substrate in an extended screening program, based on the considerations depicted in Fig. 4 and aiming at the detection of in vitro formed [^{14}C]ellagic acid-liberating products, we were finally able to isolate and partially purify a soluble enzyme fraction from leaves of *Tellima grandiflora* (saxifragaceae) that catalyzed the conversion of [U–^{14}C]pentagalloylglucose to several radioactively labeled products (Fig. 5A). Major components among these products were purified by semipreparative HPLC and subsequently hydrolyzed, releasing [^{14}C]glucose, [^{14}C]gallic acid (**1**) and [^{14}C]ellagic acid (**15**) as labeled degradation products (cf. Fig. 5B), thus indicating the preceding in vitro formation of true ellagitannins (Niemetz et al., 2001). ^{1}H NMR spectroscopy (500 MHz) of one of the most prominent enzyme reaction products obtained in these experiments showed signals that were analogous to those of an authentic sample of tellimagrandin II (**13**), i.e. the compound that traditionally

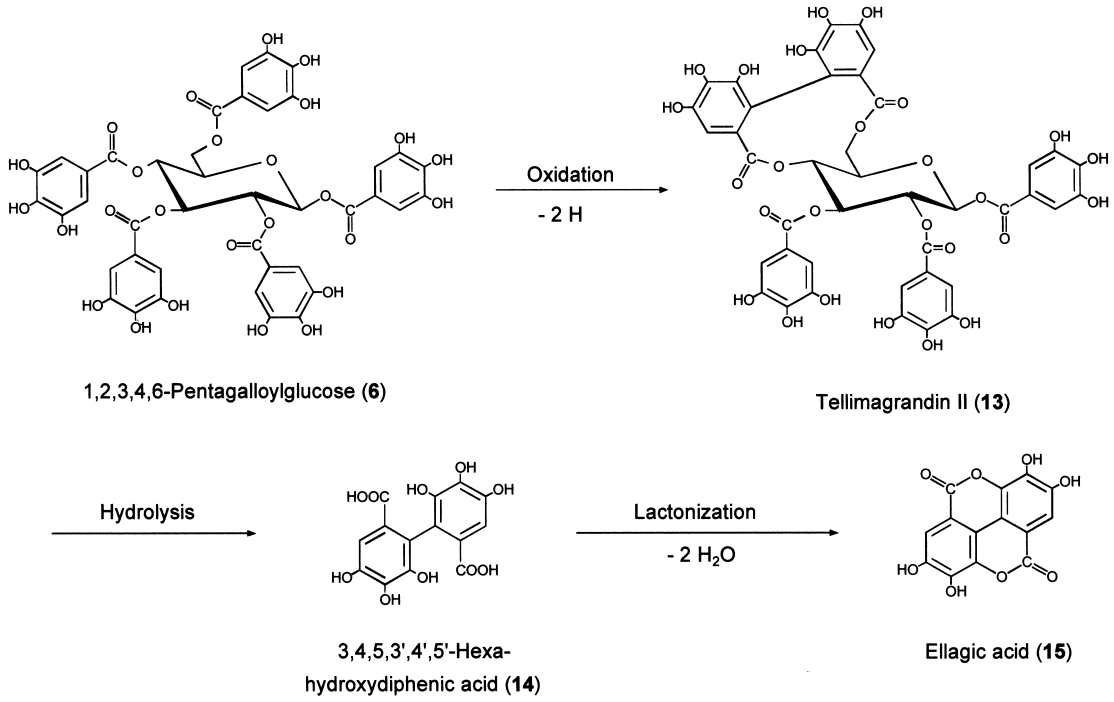

Fig. 4. Oxidation of pentagalloylglucose to the ellagitannin, tellimagrandin II (**13**), and formation of ellagic acid (**15**) via hydrolytically released hexahydroxydiphenic acid (**14**) as characteristic degradation product of ellagitannins.

has been proposed as primary metabolite in the oxidation of pentagalloylglucose to ellagitannins. In particular, three prominent singlets at δ ppm (TMS) 7.04 (2H), 6.94 (2H) and 6.92 (2H) were detected in methanol-d_4 that corresponded to the aryl-2,6 hydrogens at C-1, C-2 and C-3 of tellimagrandin II (**13**), respectively, while the singlets at δ 6.60 (1H) and 6.47 (1H) were due to the 2- and 2′-hydrogens of diphenic acid at C-4,6. Furthermore, also the chemical shifts for the glucose moiety were in full agreement with those of the authentic sample of (**13**). Additional signals were observed that were interpreted to result from a C-2,3 linked HHDP unit, suggesting the eventual in vitro formation also of compounds like casuarictin (**16**) or pedunculagin (**17**) (Fig. 6). Summarizing these data, it is evident that the evasive clue to clarify the mechanism of ellagitannin biosynthesis has been found in these investigations.

3. Subcellular sites of biosynthesis and deposition of hydrolyzable tannins

In the course of the above reported biochemical investigations it became increasingly evident that only limited reliable data was available on all aspects related to the histology of hydolyzable tannins, and tannins in general. This was not really surprising with respect to considerations on their biogenesis, an aspect that has been investigated only recently in the case of hydrolyzable tannins while the routes to condensed tannins are still a matter of speculation. However, also reports on

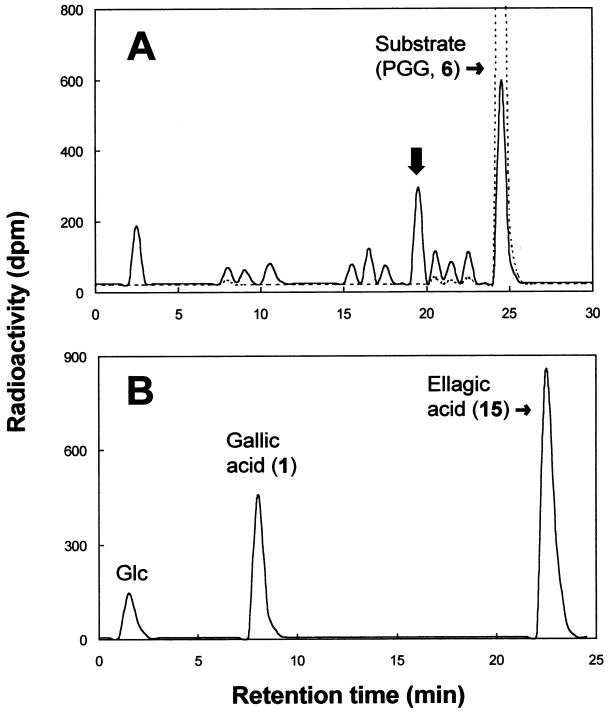

Fig. 5. In vitro oxidation of [^{14}C]pentagalloylglucose to ellagitannins with an enzyme from *Tellima grandiflora* leaves. A: RP-18 HPLC analysis of in vitro formed reaction products. (—), Enzyme assay; (.....), blank with acid-denatured enzyme; PGG, pentagalloylglucose. The major reaction product, marked with a bold arrow (↓), was collected and hydrolyzed. B: RP-18 HPLC of hydrolysis products of marked (↓) component in panel A. Glc, glucose. Radioactivity of eluates was determined by fractionation of eluates and liquid-scintillation counting.

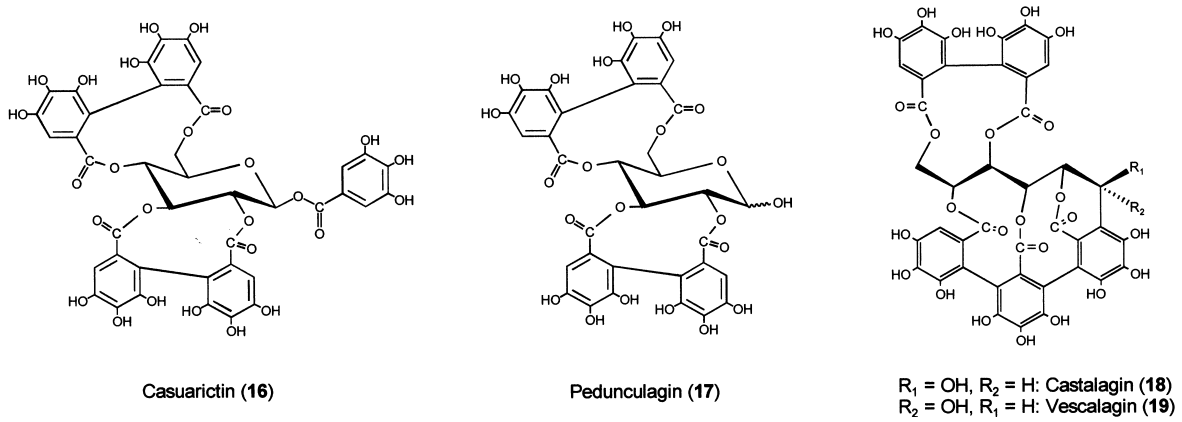

Fig. 6. Structures of prominent ellagitannins (**16**–**19**) from oak.

the localization of tannins are characterized by remarkable ambiguity, despite abundant knowledge of the structures and properties of these compounds that should have facilitated studies in this area. Consequently, such different epitopes like plastids, dictyosomes, smooth or rough endoplasmatic reticulum and vacuoles (including 'tannin vacuoles') have been proposed as subcellular compartments of polyphenolic compounds (references in Kaspar et al., 1998).

It must be emphasized that all these histological studies had been performed with common but rather unspecific staining reagents (e.g. Fe^{3+} or Fe^{2+} ions, $Cr_2O_7^{2-}$, vanillin/HCl, neutral red, methylene blue, toluidine/molybdate, etc.), thus preventing their unequivocal identification and discrimination from other phenolic plant constituents. When closer identification of tannins had been attempted in a few cases, they were classified as proanthocyanidins on the mere basis of the above unspecific criteria.

A well established method that avoids such problems is the use of immunocytochemical techniques that combine both specificity and sensitivity. Besides their traditional application to localize macromolecules they have also gained increasing importance in the detection of low-molecular weight compounds. Considering the essential role of 1,2,3,4,6-pentagalloylglucose (**6**) in the biosynthesis of gallotannins and ellagitannins, and hence also of the acyltransferase catalyzing the synthesis of this pivotal metabolite, we decided to use this representative metabolic step as a specific marker to detect the sites of synthesis and cellular localization of hydrolyzable tannins (Fig. 7). For this purpose, we produced two antibodies, one raised against pentagalloylglucose as antigen, and a second one which was directed against

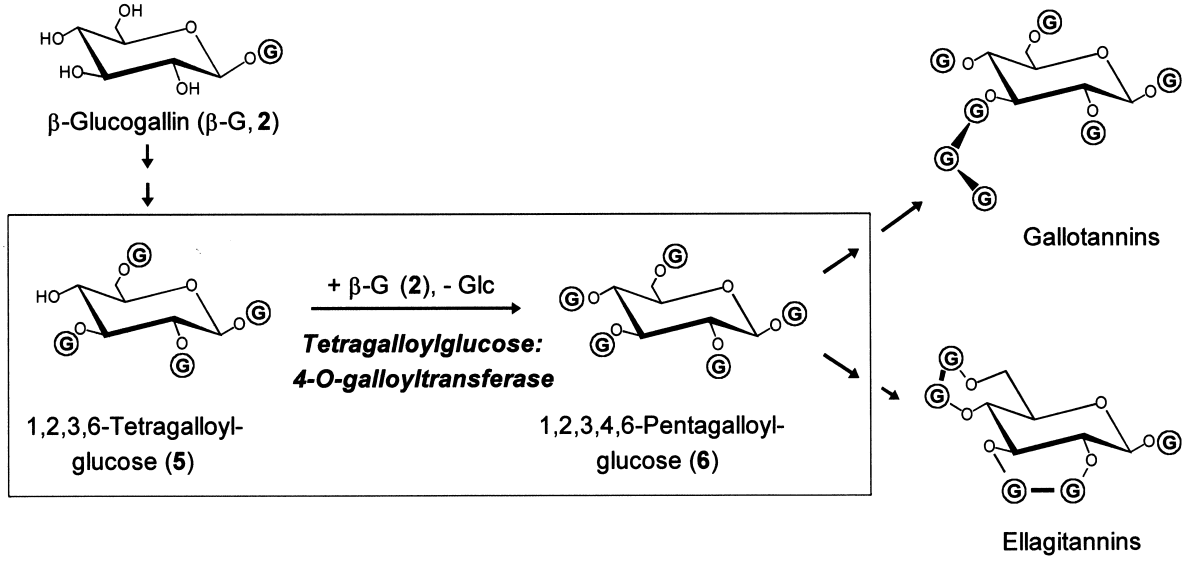

Fig. 7. Key function of the enzyme, β-glucogallin: 1,2,3,6-tetra-*O*-galloyl-β-D-glucose 4-*O*-galloyltransferase, in the pathway from β-glucogallin to gallotannins (example: heptagalloylglucose **12**) and ellagitannins (example: casuarictin 16) via 1,2,3,4,6-penta-*O*-galloyl-β-D-glucose as immediate common precursor. Ⓖ, Galloyl; Ⓖ▸Ⓖ, *meta*-digalloyl; Ⓖ–Ⓖ, hexahydroxydiphenoyl (HHDP) residue; Glc, glucose.

the enzyme, β-glucogallin: 1,2,3,6-tetragalloylglucose 4-*O*-galloyltransferase, for immunohistochemical studies.

3.1. Preparation and characterization of antibodies

As a preriquisite for the production of antibodies against 1,2,3,4,6-penta-*O*-galloyl-β-D-glucose (**6**) it was necessary to bind this low-molecular compound (M_r 940) on a macromolecule, preferentially a protein, to give it immunogenic properties. Bovine serum albumin or keyhole limpet hemocyanin were therefore substituted with *p*-aminohippuric acid, followed by diazotation of this linking unit and final coupling with the hapten, pentagalloylglucose. Crude antisera obtained by immunization of rabbits with these antigens were purified by affinity chromatography on Sepharose-coupled pentagalloylglucose (Kaspar et al., 1998). Cross reactivities of this pure antibody were analyzed in a heterogenous competitive ELISA (Weiler et al., 1981) with solid-phase adsorbed anti-pentagalloylglucose IgG and chemically synthesized antigen-peroxidase conjugate. Not unexpectedly owing to the polyphenolic nature of the antigen, high reactivities were observed with penta- to nonagalloylglucoses and with structurally related ellagitannins, pedunculagin (**18**) and vescalagin (**19**). In contrast, insignificant cross-reactivity, or none at all, was displayed with biogenetic precursors or degradation products of hydrolyzable tannins, i.e. glucose, gallic acid (**1**), β-glucogallin (**2**) and ellagic acid (**15**), as well as with numerous low-molecular phenolics, including coniferyl alcohol as the principal monomeric unit of the polyphenolic cell wall constituent lignin. In contrast to the highly cross-reactive hydrolyzable tannins, condensed tannins (procyanidin B-3 and B-4) and their monomeric precursors, e.g. catechin and structurally related flavanoids, were inactive. Monomeric, dimeric and polymeric carbohydrates, including high-molecular plant cell wall components (pectin, polygalacturonic acid, xylan), exhibited no affinity toward the antibody. In summary, this pentagalloylglucose-derived polyclonal antibody (referred to as 'anti-tannin' serum below) provided a reliable tool for the specific detection of hydrolyzable tannins (i.e. gallotannins and ellagitannins) without interference with proanthocyanidins, low-molecular polyphenolic substances or aliphatic polyhydroxylated compounds.

For the preparation of anti-galloyltransferase, rabbits were vaccinated with pure denatured 4-*O*-galloyltransferase from oak leaves. Crude antisera were purified by ammonium sulfate precipitation, chromatography on protein-A and gel filtration and a final affinity complexation step (Olmsted, 1981), affording pure polyclonal antibodies that showed no cross-reactivity with cell-free extracts from staghorn sumac (*Rhus typhina*), known to produce high concentrations of gallotannins via a metabolic pathway identical to that in oak, nor with extracts from leaves of *Tellima grandiflora*, a rich source of pentagalloylglucose-derived ellagitannins, nor with spinach (*Spinacia oleracea*) leaves being devoid of tannins (Grundhöfer and Gross, 2000).

3.2. Immunohistochemical studies

Tannin and galloyltransferase epitopes were analyzed by light-microscopical examination of semi-thin cross sections (0.5 μm) from pedunculate oak (*Q. robur*) leaves. After specifically blocking endogenous peroxidase with trypsin/H_2O_2, sections were successively treated with anti-tannin or anti-transferase serum (replaced by corresponding pre-immune sera in controls), respectively, followed by goat anti-rabbit IgG-peroxidase complex and diaminobenzidine (DAB) which resulted in significant staining of chloroplasts and cell walls (Fig. 8). Similar staining patterns were obtained with anti-rabbit IgG-alkaline phosphatase complex as secondary antibody. Analogous experiments with sumac (*R. typhina*) revealed an identical staining of chloroplasts and cell walls upon treatment with anti-tannin serum, while no reaction occurred with anti-galloyltransferase IgG, thus demonstrating the high specificity of this antibody that had been raised against enzyme from oak (Grundhöfer and Gross, 2000). Cross sections from (tannin-free) spinach, used as control in these experiments, were inactive with both antisera.

More conclusive information was obtained by transmission electron microscopy of ultra-thin sections (0.1 μm) from oak leaves that had been treated with anti-galloyltransferase and anti-rabbit immunogold IgG, revealing that the enzyme occurred in the undifferentiated cytosol and in the intercellular space, displayed more pronounced affinity to chloroplasts (particularly to starch grains), and was preferentially associated with cell walls, as depicted in Fig. 9A. Parallel experiments with anti-tannin IgG applied to ultra-thin sections from caffeine-pretreated tissues (to prevent leaching of phenolics into the cytoplasm; Mueller and Greenwood, 1978) revealed that immunogold labeling was primarily associated with cell walls (Fig. 9B), while the cytoplasmatic regions beetwen cell walls and chloroplasts showed only traces of gold particles. In both cases, no reaction was observed in controls with pre-immune serum (Fig. 9D and E). Of particular interest were results from double-labeling experiments with both antibodies which revealed a close association of 4-*O*-galloyltransferase and hydrolyzable tannins to form characteristic 'clusters' that were preferentially located in the cell walls, but also occurred in the intracellular space and the cytoplasm (Fig. 9C). Similar tannin deposition patterns were observed with ultra-thin sections from leaves of sumac (*R. typhina*) and *T. grandiflora* which, however, displayed no affinity toward the antibody directed against the 4-*O*-galloyltransferase from oak. As above, controls with spinach leaves where inactive throughout.

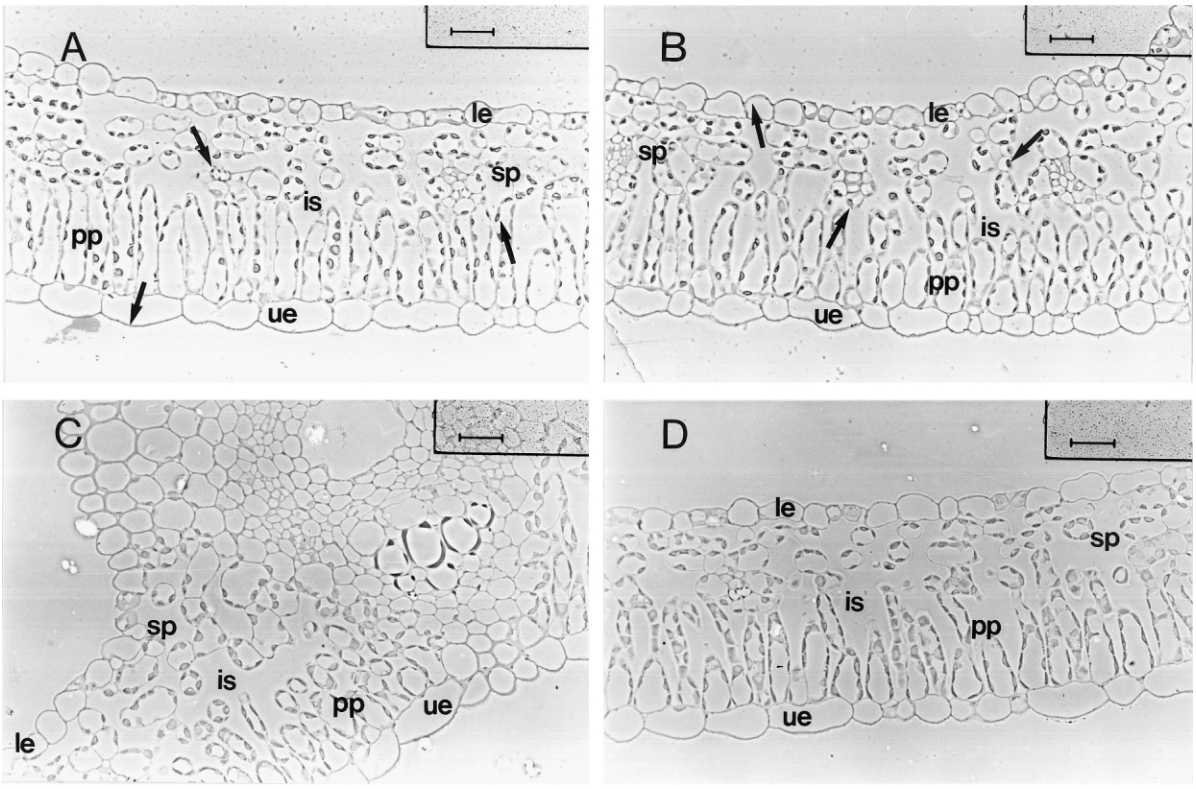

Fig. 8. Light microscopical determination of 4-*O*-galloyltransferase and hydrolyzable tannin epitopes in semi-thin cross-sections from leaves of *Quercus robur* by treatment with anti-galloyltransferase (A) and anti-tannin IgG (B), respectively, and subsequent peroxidase-diaminobenzidine staining; (C, D), controls with pre-immune sera. Arrows point to characteristic color reactions of cell walls and chloroplasts. is, Intercellular space; le, lower epidermis; pp, palisade parenchyma; sp, spongy parenchyma; ue, upper epidermis. Bars represent 15 μm (A, C; ×40) and 25 μm (B, D; ×60).

The logical assumption of a largely apoplasmatic origin and deposition site of hydrolyzable tannins, comprising both cell walls and intracellular space, was confirmed by analyzing these compartments for the occurrence of 4-*O*-galloyltransferase and galloylglucose esters. For this purpose, we used an unpublished washing method (G. Hrazdina, Cornell University) in which young oak leaves were infiltrated with water under slight vacuum (200 mbar). After slowly releasing the vacuum to avoid cell rupture, the leaves were centrifuged at 3000 *g* to yield cell wall extracts that contained gallic acid and mono- to hexagalloylglucoses esters, together with activity of the marker enzyme, 4-*O*-galloyltransferase, as shown by HPLC, enzyme assays and immuno dot blot tests (unpublished results). Similar results were obtained with extracts from *R. typhina* and *Q. robur* leaves.

Summarizing these data, it is evident that walls of leaf mesophyll cells represent a major site for the formation and deposition of hydrolyzable tannins. This conclusion is in clear contrast to numerous earlier reports on 'tannin vacuoles' (e.g. Chafe and Durzan, 1973; Diers et al., 1973; Zobel, 1986; Lees et al., 1993). Considering the rather unspecific staining procedures employed in these studies, however, it is uncertain what phenolic plant metabolites have actually been detected in these investigations. On the other hand, our data are consistent with observations on the immunocytochemically determined accumulation of flavonoids in cell walls of *Chrysosplenium americanum* (Charest et al., 1986; Marchand et al., 1987) and they are further supported by recent considerations on chemical interactions between lignins and hydrolyzable tannins in wood (Helm et al., 1997). An obvious explanation for the currently available data is that cytotoxic hydrolyzable tannins are rapidly excreted into the apoplast or, more efficiently, that they are directly produced and deposited in this compartment where they can exert their protecting potential without harming cytoplasmatic components.

4. Seasonal turnover of hydrolyzable tannins in cell walls

It was apparent that the above cell wall extraction method provided an excellent tool to study the concentrations of hydrolyzable tannins in this compartment without requiring abundant quantities of plant material. We thus determined the amounts of gallic acid and mono- to hexagalloylglucoses (the occurrence of higher substituted derivatives and ellagitannins was not analyzed in these experiments) in 3-month-old leaves of *Q. robur*, i.e. at a developmental stage in which the activity

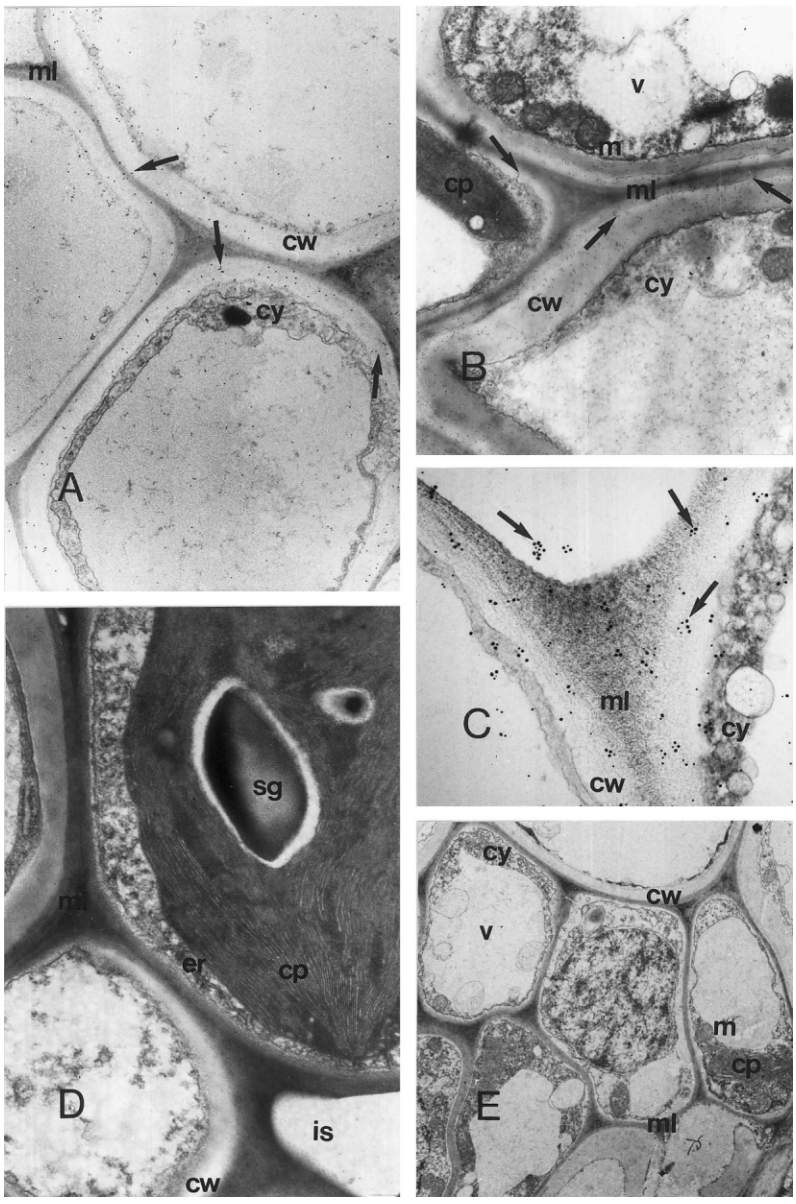

Fig. 9. Transmission electron microscopy of immunogold-labeled ultra-thin cross-sections from leaves of *Q. robur*. A: Anti-galloyltransferase treated mesophyll cells (10 nm gold particles; ×11,000); B: anti-tannin treated mesophyll (20 nm gold particles; ×30,000); C: double labeling with anti-galloyltransferase and anti-tannin IgG (particle sizes as above; ×34,000); D: control to A with pre-immune serum (×30 000): E: control to B (×5,000). Arows indicate typical epitopes of enzyme and hydrolyzable tannins. cp, Chloroplast; cw, cell wall; cy, cytoplasm; er, endoplasmatic reticulum; is, intercellular space; m, mitochondrium; ml, middle lamella; sg, starch grain; v, vacuole.

of the marker enzyme, 4-*O*-galloyltransferase, had reached its maximum as shown by immuno dot blot tests. Tetra- and particularly pentagalloylglucose were found to be the most prominent metabolites, while the concentration of hexagalloylglucoses was significantly lower. A similar pattern was determined with extracts from *T. grandiflora*, in contrast to *R. typhina* where hexagalloylglucoses represented the predominant galloylglucose fraction. It is feasible to assume that these data reflect the marked biogenetic differences between these plants, according to which complex gallotannins are exclusively formed from pentagalloylglucose in *R. typhina*, while *Q. robur* and *T. grandiflora* oxidize this intermediate to ellagitannins.

These observations stimulated experiments in which the seasonal changes of hydrolyzable tannins and their precursors in oak leaves were analyzed. As depicted in Fig. 10, the concentrations of gallic acid (**1**) and of monogalloylglucoses, in particular β-glucogallin (**2**), were constantly rather low but nevertheless displayed a maximum in the third month. The tetragalloylglucose fraction had a first maximum in the second month that corresponded to 1,2,3,6-tetragalloylglucose (**5**), and a second peak late in the year with high concentrations of

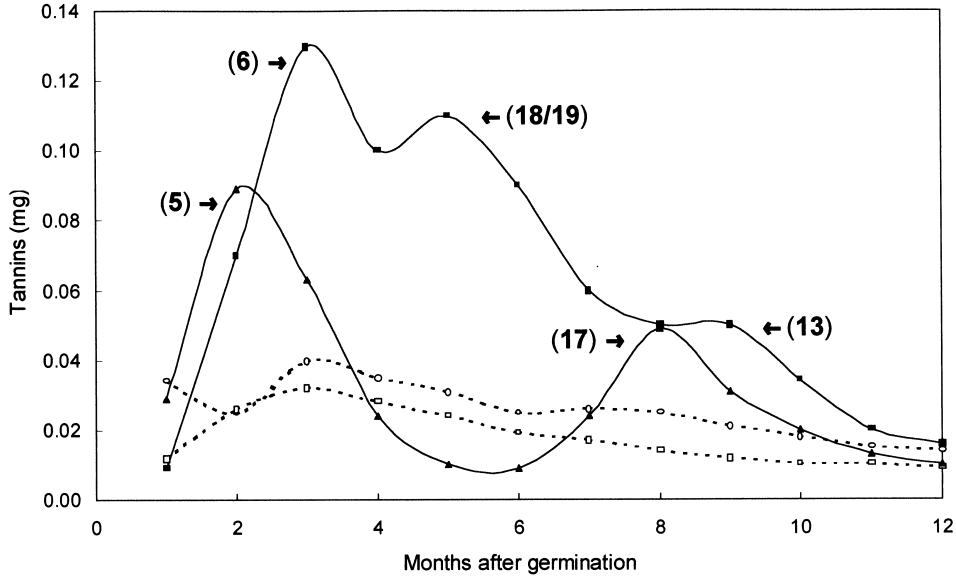

Fig. 10. Seasonal changes of hydrolyzable tannins and their precursors in extracts from cell walls and intercellular space of greenhouse-grown *Quercus robur* leaves. ○, Gallic acid (**1**); □, monogalloylglucoses, e.g. β-glucogallin (**2**); ▲, tetragalloylated derivatives; ■, pentagalloylated derivatives. The following tannin metabolites were identified: 1,2,3,6-tetragalloylglucose (**5**), 1,2,3,4,6-pentagalloylglucose (**6**), tellimagrandin II (**13**), pedunculagin (**17**), castalagin/vescalagin (**18**, **19**).

an ellagitannin, pedunculagin (**17**). Pentagalloylglucoses displayed a first maximum after three months, with 1,2,3,4,6-pentagalloylglucose (**6**) as characteristic metabolite which was transformed to ellagitannins like castalagin/vescalagin (**18**, **19**) accumulating in the fifth month, and tellimagrandin II (**13**) that appeared in late fall. It is evident from these results that 'simple' galloylglucoses were preferentially formed in spring, followed by oxidation to ellagitannins in summer and eventual degradation reactions in fall. Similar observations have been reported for the hydrolyzable tannins from leaves of *Liquidambar formosana* (Hamamelidaceae) by Hatano et al. (1986).

5. Conclusions

The above reported enzyme studies describe the intermediates and reaction principles involved in an extended biochemical pathway that ranges from a simple phenolic plant constituent, gallic acid, to highly substituted complex gallotannins. This laborious but highly evidential technique has also provided first insights into the transition of pentagalloylglucose, often regarded as the pivotal metabolite in the biosynthesis of hydrolyzable tannins, to ellagitannins, thus superseding critical statements that have still been formulated only one year ago (Gross, 1999a; Niemetz et al., 1999). It is hoped that the mechanism(s) of these oxidative processes will be understood in the near future to solve the old enigma of ellagitannin biosynthesis.

An unexpected result was obtained in the above described immunohistochemical studies on the origin and intracellular deposition of hydrolyzable tannins. In clear contrast to numerous reports describing the existence of tannin vacuoles, we were unable to find evidence supporting this view in experiments with specific antibodies. Instead, we observed pronounced affinities to leaf mesophyll cell walls, giving this apoplasmatic compartment a characteristic role as deposition site of hydrolyzable tannins (in addition to established cell wall polyphenols like lignins or suberin-associated aromatic derivatives), while the contents of tannin vacuoles must be considered now as (poly)phenolic compounds of uncertain nature that were detected by unspecific color reactions. We are confident that the *bon mot* of R. H. Davis (cited from Hrazdina, 1992) that *"the subcellular localization of small molecules is easy to believe, but difficult to prove"* does not apply to our studies related to hydrolyzable tannins.

Acknowledgements

We thank Angelika Müller (Ulm) for excellent technical assistence, and Professor Geza Hrazdina (Cornell University, Geneva) for valuable suggestions and making available unpublished methods. Generous financial support from the Deutsche Forschungsgemeinschaft (Bonn), the Fonds der Chemischen Industrie (Frankfurt/M.) and from research grants of the University of Ulm are gratefully acknowledged.

References

Cammann, J., Denzel, K., Schilling, G., Gross, G.G., 1989. Biosynthesis of gallotannins: β-glucogallin-dependent formation of 1,2,3,4,6-pentagalloylglucose by enzymatic galloylation of 1,2,3,6-tetragalloylglucose. Archives of Biochemistry and Biophysics 73, 58–63.

Carando, S., Teissedre, P.L., 1999. Catechin and procyanidin levels in French wines: contribution to dietary intake. In: Gross, G.G., Hemingway, R.W., Yoshida, T. (Eds.), Plant Polyphenols 2. Chemistry, Biology, Pharmacology, Ecology. Kluwer Academic/Plenum Publishers, New York, pp. 725–737.

Chafe, S.C., Durzan, D.J., 1973. Tannin inclusions in cell suspension cultures of white spruce. Planta 113, 251–262.

Charest, P.M., Brisson, L., Ibrahim, R.K., 1986. Ultrastructural features of flavonoid accumulation in leaf cells of *Chrysosplenium americanum*. Protoplasma 134, 95–101.

Denzel, K., Gross, G.G., 1991. Biosynthesis of gallotannins. Enzymatic 'disproportionation' of 1,6-digalloylglucose to 1,2,6-trigalloylglucose and 6-galloylglucose by an acyltransferase from leaves of *Rhus typhina* L. Planta 184, 285–289.

Diers, L., Schötz, F., Meyer, B., 1973. Über die Ausbildung von Gerbstoffvakuolen bei Oenotheren. Cytobiologie 7, 10–19.

Feldman, K., Sahasrabudhe, K., Quideau, S., Lawlor, M.D., 1999. Synthesis studies on complex ellagitannins. In: Gross, G.G., Hemingway, R.W., Yoshida, T. (Eds.), Plant Polyphenols 2. Chemistry, Biology, Pharmacology, Ecology. Kluwer Academic/Plenum Publishers, New York, pp. 101–125.

Freudenberg, K., 1920. Die Chemie der natürlichen Gerbstoffe. Springer Verlag, Berlin.

Ghangas, G.S., Steffens, J.C., 1993. UDP glucose: fatty acid transglucosylation and transacylation in triacylglucose biosynthesis. Proceedings of the National Academy of Sciences USA 90, 9911–9915.

Ghangas, G.S., Steffens, J.C., 1995. 1-*O*-Acyl-β-D-glucoses as fatty acid donors in transacylation reactions. Archives of Biochemistry and Biophysics 316, 370–377.

Gross, G.G., 1983a. Partial purification and properties of UDP-glucose: vanillate 1-*O*-glucosyl transferase from oak leaves. Phytochemistry 22, 2179–2182.

Gross, G.G., 1983b. Synthesis of mono-, di- and trigalloyl-β-D-glucose by β-glucogallin-dependent galloyltransferases from oak leaves. Zeitschrift für Naturforschung 38c, 519–523.

Gross, G.G., 1999a. Biosynthesis, biodegradation, and cellular localization of hydrolyzable tannins. In: Romeo, J.T. (Ed.), Phytochemistry in Human Health Protection, Nutrition and Plant Defense. Recent advances in Phytochemistry, Vol. 33. Kluwer Academic/Plenum Publishers, New York, pp. 185–213.

Gross, G.G., 1999b. Biosynthesis of hydrolyzable tannins. In: Pinto, B.M. (Ed.), Comprehensive Natural Products Chemistry. vol. 3. Carbohydrates and their Derivatives Including Tannins, Cellulose, and Related Lignins. Elsevier, Amsterdam, pp. 799–826.

Gross, G.G., Denzel, K., 1991. Biosynthesis of gallotannins. β-Glucogallin-dependent galloylation of 1,6-digalloylglucose to 1,2,6-trigalloylglucose. Zeitschrift für Naturforschung 46c, 389–394.

Gross, G.G., Hemingway, R.W., Yoshida, T., 1999. Plant Polyphenols 2. Chemistry, Biology, Pharmacology, Ecology. Kluwer Academic/Plenum Publishers, New York.

Gross, G.G., Schmidt, S.W., Denzel, K., 1986. β-Glucogallin-dependent acyltransferase from oak leaves. I. Partial purification and characterization. Journal of Plant Physiolology 126, 173–179.

Grundhöfer, P., Gross, G.G., 2000. Purification of tetragalloylglucose 4-*O*-galloyltransferase and preparation of antibodies against this key enzyme in the biosynthesis of hydrolyzable tannins. Zeitschrift für Naturforschung 55c, 582–587.

Hagenah, S., Gross, G.G., 1993. Biosynthesis of 1,2,3,6-tetra-*O*-galloyl-β-D-glucose. Phytochemistry 32, 637–641.

Haslam, E., 1989. Plant polyphenols. Vegetable tannins revisited. Cambridge University Press, Cambridge.

Haslam, E., 1996. Natural polyphenols (vegetable tannins) as drugs: possible modes of action. Journal of Natural Products 59, 205–215.

Haslam, E., 1998. Practical polyphenols. From structure to molecular recognition and physiological action. Cambridge University Press, Cambridge.

Haslam, E., 1999. Che farò senza polifenoli? In: Gross, G.G., Hemingway, R.W., Yoshida, T. (Eds.), Plant Polyphenols 2. Chemistry, Biology, Pharmacology, Ecology. Kluwer Academic/Plenum Publishers, New York, pp. 15–40.

Haslam, E., Lilley, T.H., Cai, Y., Martin, R., Magnolato, D., 1989. Traditional herbal medicines the role of polyphenols. Planta Medica 55, 1–8.

Hatano, T., Kira, R., Yoshizaki, M., Okuda, T., 1986. Seasonal changes in the tannins of *Liquidambar formosana* reflecting their biogenesis. Phytochemistry 25, 2787–2789.

Helm, R.F., Ranatunga, T.D., Chandra, M., 1997. Lignin-hydrolyzable tannin interactions in wood. Journal of Agricultural and Food Chemistry 45, 3100–3106.

Helm, R.F., Zhentian, L., Ranatunga, T., Jervis, J., Elder, T., 1999. Toward understanding monomeric ellagitannin biosynthesis. In: Gross, G.G., Hemingway, R.W., Yoshida, T. (Eds.), Plant Polyphenols 2. Chemistry, Biology, Pharmacology, Ecology. Kluwer Academic/Plenum Publishers, New York, pp. 83–99.

Hofmann, A.S., Gross, G.G., 1990. Biosynthesis of gallotannins: Formation of polygalloylglucoses by enzymatic acylation of 1,2,3,4,6-penta-*O*-galloylglucose. Archives of Biochemistry and Biophysics 283, 530–532.

Hrazdina, G., 1992. Compartimentation in aromatic metabolism. In: Stafford, H.A., Ibrahim, R.K. (Eds.), Phenolic Metabolism in Plants. Plenum Press, New York, pp. 1–23.

Kaspar, D., Grundhöfer, P., Gross, G.G., 1998. Preparation of antibodies against hydrolyzable plant tannins. Phytochemical Analysis 9, 107–111.

Kuai, J.P., Ghangas, G.S., Steffens, J.C., 1997. Regulation of triacylglucose fatty acid composition. Uridine diphosphate glucose: fatty acid glucosyltransferase with overlapping chain-length specificity. Plant Physiology 115, 1581–1587.

Lees, G.L., Suttill, N.H., Gruber, M.Y., 1993. Condensed tannins in sainfoin. 1. A histological and cytological survey of plant tissues. Canadian Journal of Botany 71, 1147–1152.

Marchand, L., Charest, P.M., Ibrahim, R.K., 1987. Localization of partially methylated flavonol glucosides in *Chrysosplenium americanum*: Immunogold labeling. Journal of Plant Physiology 131, 339–348.

Miyamoto, K., Murayama, T., Hatano, T., Yoshida, T., Okuda, T., 1999. Host-mediated anticancer activities of tannins. In: Gross, G.G., Hemingway, R.W., Yoshida, T. (Eds.), Plant Polyphenols 2. Chemistry, Biology, Pharmacology, Ecology. Kluwer Academic/Plenum Publishers, New York, pp. 643–663.

Mock, H.P., Strack, D., 1993. Energetics of the uridine 5′-diphosphoglucose: hydroxycinnamic acid acyl-glucosyltransferase reaction. Phytochemistry 32, 575–579.

Mueller, W.C., Greenwood, A.D., 1978. The ultrastructure of phenolic-storing cells fixed with caffeine. Journal of Experimental Botany 29, 757–764.

Niemetz, R., Gross, G.G., 1998. Gallotannin biosynthesis: Purification of β-glucogallin: 1,2,3,4,6-pentagalloyl-β-D-glucose galloyltransferase from sumac leaves. Phytochemistry 49, 327–332.

Niemetz, R., Gross, G.G., 1999. Gallotannin biosynthesis: a new β-glucogallin-dependent galloyltransferase from sumac leaves acylating gallotannins at positions 2 and 4. Journal of Plant Physiology 155, 41–446.

Niemetz, R., Niehaus, J.U., Gross, G.G., 1999. Biosynthesis and biodegradation of complex gallotannins. In: Gross, G.G., Hemingway, R.W., Yoshida, T. (Eds.), Plant Polyphenols 2. Chemistry, Biology, Pharmacology, Ecology. Kluwer Academic/Plenum Publishers, New York, pp. 63–82.

Niemetz, R., Schilling, G. Gross, G.G., 2001. Ellagitannin biosynthesis:

oxidation of pentagalloyl glucose to tellimagrandin II by an enzyme from *Tellima grandiflora* leaves. JCS Chemical Communications, 35–36.

Nishizawa, M., Yamagishi, T., Nonaka, G., Nishioka, I., 1980. Structure of gallotannins in *Paeoniae radix*. Chemical and Pharmaceutical Bulletin (Tokyo) 28, 2850–2852.

Nishizawa, M., Yamagishi, T., Nonaka, G., Nishioka, I., 1982. Tannins and related compounds. Part 5. Isolation and characterization of polygalloylglucoses from Chinese gallotannin. Journal of the Chemical Society, Perkin Transactions I 2963–2968.

Nishizawa, M., Yamagishi, T., Nonaka, G., Nishioka, I., 1983a. Tannins and related compounds. Part 9. Characterization of polygalloylglucoses from Turkish galls. Journal of the Chemical Society, Perkin Transactions 1, 961–965.

Nishizawa, M., Yamagishi, T., Nonaka, G., Nishioka, I., Nagasawa, T., Oura, H., 1983b. Tannins and related compounds. XII. Isolation and characterization of galloylglucoses from Paeoniae radix and their effect on urea–nitrogen concentration in rat serum. Chemical and Pharmaceutical Bulletin (Tokyo) 31, 2593–2600.

Olmsted, J.B., 1981. Affinity purification of antibodies from diazotised paper blots of heterogeneous protein samples. Journal of Biological Chemistry 256, 11955–11957.

Rausch, H., Gross, G.G., 1996. Preparation of [^{14}C]-labelled 1,2,3,4,6-penta-*O*-galloyl-β-D-glucose and related gallotannins. Zeitschrift für Naturforschung 51c, 473–476.

Reinefeld, E., Ahrens, D., 1971. Der Einfluss der Konfiguration auf die partielle Verestererung von D-Glucopyranosiden. Liebigs Annalen der Chemie 747, 39–44.

Schmidt, S.W., Denzel, K., Schilling, G., Gross, G.G., 1987. Enzymatic synthesis of 1,6-digalloylglucose from β-glucogallin by β-glucogallin: β-glucogallin 6-*O*-galloyltransferase from oak leaves. Zeitschrift für Naturforschung 42c, 87–92.

Weiler, E.W., Jourdan, P.S., Conrad, W., 1981. Levels of indole-3-acetic acid in intact and decapitated coleoptiles as determined by a specific and highly sensitive solid-phase enzyme immunoassay. Planta 153, 561–571.

Werner, I., Bacher, A., Eisenreich, W., 1999. Analysis of gallic acid biosynthesis via quantitative prediction of isotope labeling patterns. In: Gross, G.G., Hemingway, R.W., Yoshida, T. (Eds.), Plant Polyphenols 2. Chemistry, Biology, Pharmacology, Ecology. Kluwer Academic/Plenum Publishers, New York, pp. 43–61.

Williams, J.M., Richardson, A.C., 1967. Selective acylation of pyranosides. I. Benzoylation of methyl α-D-glycopyranosides of mannose, glucose and galactose. Tetrahedron 23, 1369–1378.

Yoshida, T., Hatano, T., Ito, H., Okuda, T., 1999. Highly oxidized ellagitannins and their biological activity. In: Gross, G.G., Hemingway, R.W., Yoshida, T. (Eds.), Plant Polyphenols 2. Chemistry, Biology, Pharmacology, Ecology. Kluwer Academic/Plenum Publishers, New York, pp. 127–144.

Zobel, A.M., 1986. Localization of phenolic compounds in tannin-secreting cells from *Sambucus racemosa* L. shoots. Annals of Botany 57, 801–810.

PERGAMON

Phytochemistry 57 (2001) 929–967

PHYTOCHEMISTRY

www.elsevier.com/locate/phytochem

Review

Pectins: structure, biosynthesis, and oligogalacturonide-related signaling

Brent L. Ridley, Malcolm A. O'Neill, Debra Mohnen*

Complex Carbohydrate Research Center and Department of Biochemistry and Molecular Biology, University of Georgia, 220 Riverbend Road, Athens, GA 30602-4712, USA

Received 2 October 2000; received in revised form 11 December 2000

Abstract

Pectin is a family of complex polysaccharides present in all plant primary cell walls. The complicated structure of the pectic polysaccharides, and the retention by plants of the large number of genes required to synthesize pectin, suggests that pectins have multiple functions in plant growth and development. In this review we summarize the current level of understanding of pectin primary and tertiary structure, and describe new methods that may be useful to study localized pectin structure in the plant cell wall. We also discuss progress in our understanding of how pectin is biosynthesized and review the biological activities and possible modes of action of pectic oligosaccharides referred to as oligogalacturonides. We present our view of critical questions regarding pectin structure, biosynthesis, and function that need to be addressed in the coming decade. As the plant community works towards understanding the functions of the tens of thousands of genes expressed by plants, a large number of those genes are likely to be involved in the synthesis, turnover, biological activity, and restructuring of pectin. A combination of genetic, molecular, biochemical and chemical approaches will be necessary to fully understand the function and biosynthesis of pectin. © 2001 Elsevier Science Ltd. All rights reserved.

Keywords: Cell wall; Homogalacturonan; Oligogalacturonides; Pectin; Polysaccharide; Rhamnogalacturonan

Contents

1. Structure 930
   1.1. Introduction 930
   1.2. The chemical structure of primary cell wall pectins 930
   1.3. Advances in the structural analysis of cell wall pectic polysaccharides 932
      1.3.1. Homogalacturonan and rhamnogalacturonan I 932
      1.3.2. Rhamnogalacturonan II 933
   1.4. The macromolecular organization of HG, RG-I, and RG-II in the primary wall 935
      1.4.1. Are homogalacturonan, rhamnogalacturonan I, and RG-II linked together covalently? 935
      1.4.2. Is pectin cross-linked to other wall components? 935
      1.4.3. Borate-ester cross-linked pectin 936
      1.4.4. Anionic cross-links 936
      1.4.5. Other cross-links 936
      1.4.6. Biophysical methods for determining the properties and functions of primary wall pectin 937
      1.4.7. Are there pectin-membrane-cytoskeleton connections? 938
   1.5. The distribution of pectic polysaccharides in the primary wall 939
   1.6. Probing the structure and function of pectin with cell wall mutants 940

* Corresponding author. Tel.: +1-706-542-4458; fax: +1-706-542-4412.

E-mail address: dmohnen@ccrc.uga.edu (D. Mohnen).

0031-9422/01/$ - see front matter © 2001 Elsevier Science Ltd. All rights reserved.
PII: S0031-9422(01)00113-3

2. Biosynthesis 941
2.1. Introduction 941
2.2. Setting the stage for pectin synthesis 942
2.3. Nucleotide sugars, transporters, and a general model for the topology of pectin biosynthesis 943
2.4. Synthesis of homogalacturonan 945
2.4.1. α1,4Galacturonosyltransferase (GalAT) 945
2.4.2. HG-methyltransferase (HG-MT) 946
2.4.3. HG-acetyltransferase (HG-AT) 948
2.5. Synthesis of rhamnogalacturonan-I (RG-I) 948
2.5.1. RG-I-galactosyltransferase (RG-I-GalT) 948
2.5.2. RG-I-arabinosyltransferase 948
2.5.3. RG-I-methyltransferase (RG-I-MT) 948
2.5.4. RG-I-acetyltransferase (RG-I-AT) 949
2.6. Synthesis of rhamnogalacturonan-II (RG-II) 949
2.6.1. RG-II-methyltransferase (RG-II-MT) 949
2.6.2. Pressing needs in pectin biosynthesis research 949

3. Biological activities of oligogalacturonides 949
3.1. Introduction 949
3.2. Oligogalacturonide-induced responses involved in plant defense 950
3.3. Biological responses involved in plant growth and development 951
3.4. The structural requirements for the biological activity of oligogalacturonides 952
3.5. Presence and fate of biologically active oligogalacturonides in plant tissues 952
3.6. Oligogalacturonide receptors 953
3.7. Oligogalacturonide induced signaling cascades 954
3.7.1. Suspension-cultured soybean cells: early signaling events 954
3.7.2. Suspension-cultured carrot cells: the role of calcium 955
3.7.3. Suspension-cultured tobacco cells: a role for cytosolic acidification 956
3.7.4. Tomato wound response: oligogalacturonide signaling in intact plant tissues 956
3.7.5. Conclusions and relevance to future work 958

Acknowledgements 958

References 958

1. Structure

1.1. Introduction

A generally accepted primary structure of pectin has emerged from cumulative studies spanning the last 70 years. The pectins used in these studies were typically isolated from plants of economic importance (e.g. citrus, tomato, sugar beet, apple) or from suspension-cultured cells (e.g. sycamore, carrot, spinach, and rose). However, these plants represent only a small fraction of the total number of known flowering plants (~235,000 species), and little is known about the pectin of green algae, liverworts, mosses, and ferns. The characterization of pectin from lower plants, from cell wall mutants, and from plants that grow in extreme environments may reveal hitherto unknown pectin structures and provide further insight into the origins and functions of these complex polysaccharides.

In this section we briefly describe what is currently known about the chemical structures of pectin. We also provide an overview of some new approaches to studying localized pectin structure that may increase our knowledge of the biological functions of pectin.

1.2. The chemical structure of primary cell wall pectins

Pectins are a family of complex polysaccharides that contain 1,4-linked α-D-galactosyluronic acid (Gal*p*A) residues. Three pectic polysaccharides (homogalacturonan, rhamnogalacturonan-I, and substituted galacturonans) have been isolated from primary cell walls and structurally characterized (O'Neill et al., 1990; Visser and Voragen, 1996).

Homogalacturonan (HG) is a linear chain of 1,4-linked α-D-galactopyranosyluronic acid (Gal*p*A) residues in which some of the carboxyl groups are methyl esterified (Fig. 1). HGs may, depending on the plant

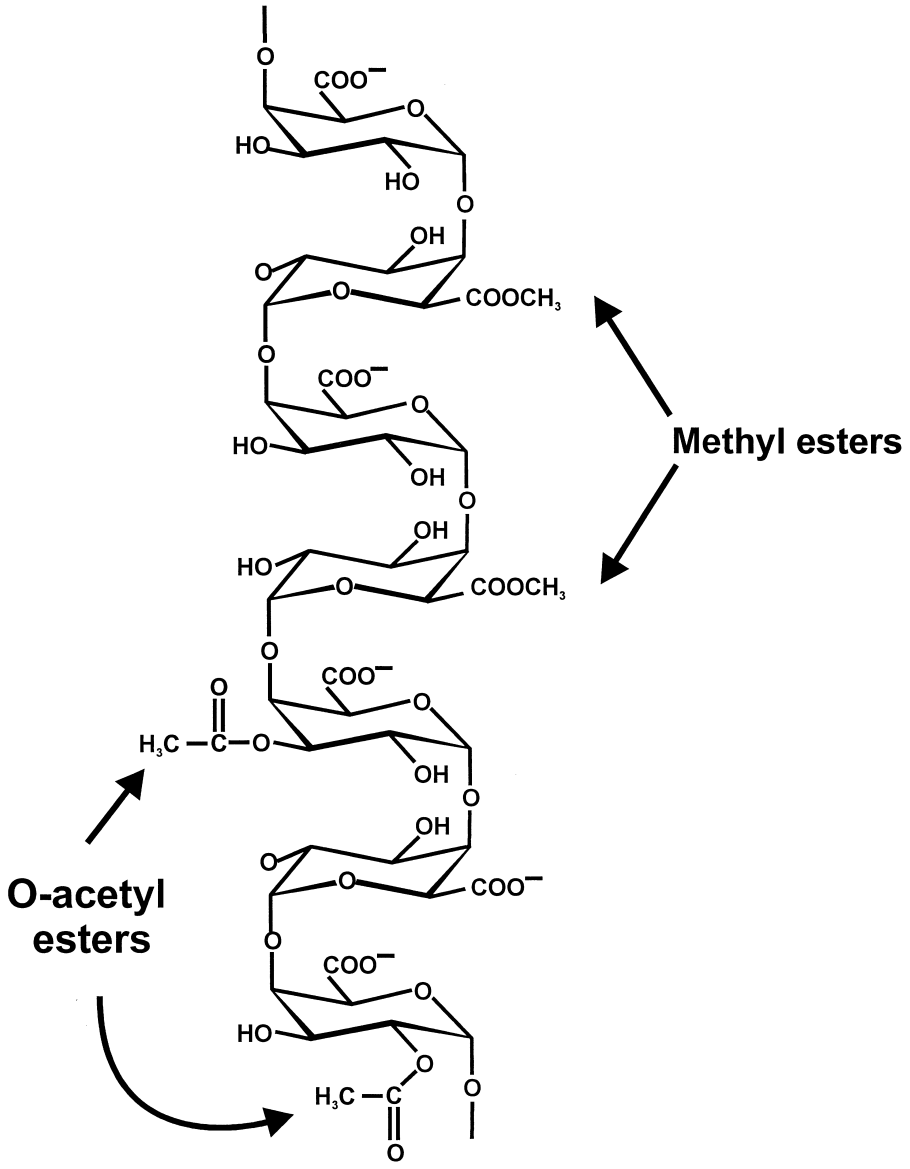

Fig. 1. The primary structure of homogalacturonan. Homogalacturonan is a linear polymer of 1→4 linked α-D-Gal*p*A residues. Some of the carboxylates of the Gal*p*A residues are esterified with methanol. The Gal*p*A residues may also be esterified with acetic acid at C2 and C3. At least three enzymes homgalacturonan galacturonosyltransferase, homogalacturonan methyltransferase, and homogalacturonan acetyltransferase are required for the synthesis of HG (see Table 1 for details).

source, also be partially O-acetylated at C-3 or C-2 (Ishii, 1995, 1997a).

Rhamnogalacturonan-I (RG-I) is a family of pectic polysaccharides that contain a backbone of the repeating disaccharide [→4)-α-D-Gal*p*A-(1→2)-α-L-Rhap-(1→] (Fig. 2). The backbone Gal*p*A residues may be *O*-acetylated on C-2 and/or C-3 (Komalavilas and Mort, 1989). There is no conclusive chemical evidence that the Gal*p*A residues are methyl esterified, however, an enriched RG-I-like wall fraction from flax has been reported to contain methyl esters (Rihouey et al., 1995). The Gal*p*A residues typically are not substituted with mono- or oligosaccharide side chains, although a recent study reported that a single β-D-Glc*p*A residue is linked to C-3 of ~2% of the Gal*p*A in the backbone of sugar beet RG-I (Renard et al., 1999). In contrast, 20–80% of the rhamnosyl (Rha*p*) residues are, depending on the plant source and method of isolation, substituted at C-4 with neutral and acidic oligosaccharide side chains (O'Neill et al., 1990). The predominant side chains contain linear and branched α-L-arabinofuranosyl (Ara*f*), and/or β-D-galactopyranosyl (Gal*p*) residues (Fig. 2), although their relative proportions and chain lengths may differ depending on the plant source (Lerouge et al., 1993). The glycosyl residues α-L-fucosyl (Fucp), β-D-glucuronosyl (Glc*p*A), and 4-*O*-methyl β-D-glucuronosyl (4-*O*-Me GlcpA) may also be present (O'Neill et al., 1990), as may ferulic and coumaric acid (Saulnier and Thibault, 1999).

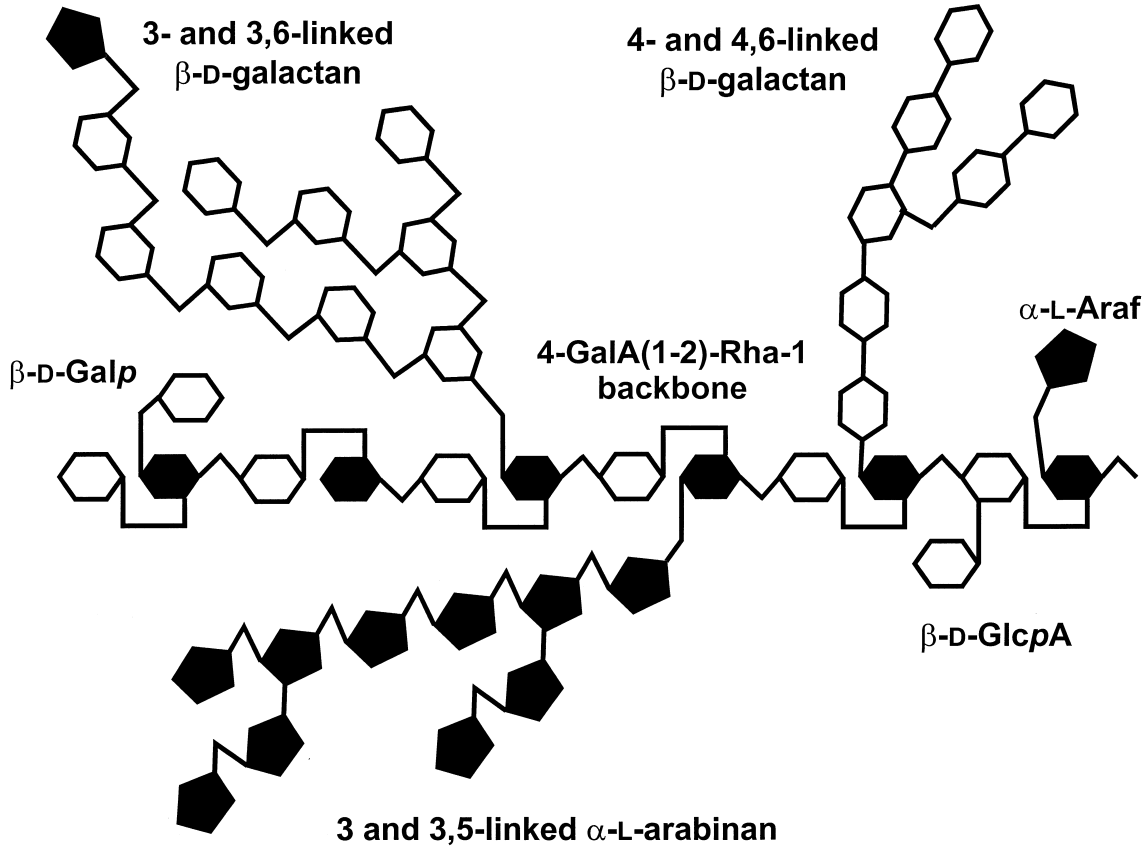

Fig. 2. A model showing the major structural features of rhamnogalacturonan I. The backbone is composed of the disaccharide repeating unit [→4-α-D-Gal*p*A-(→2)-α-L-Rhap-(1→]. Branched and linear oligosaccharides composed predominantly of α-L-Ara*f* and β-D-Gal*p* residues are linked to C4 of some of the Rha*p* residues. Some of the Rha*p* residue may also be *O*-acetylated at C2 and/or C3. More than ten glycosyltransferase activities are required for the biosynthesis of RG-I (see Table 2 for details).

Substituted galacturonans (SG) are a diverse group of polysaccharides that contain a backbone of linear 1,4-linked α-D-Gal*p*A residues (O'Neill et al., 1990). The substituted galacturonan referred to as rhamnogalacturonan II (RG-II) is present in all higher plant primary walls analyzed to date (O'Neill et al., 1990). The demonstration that wine and other fruit juices contain relatively high amounts (20–150 mg/l) of RG-II (Doco et al., 1997), that RG-II binds heavy-metals (Pellerin et al., 1997, Pellerin and O'Neill, 1998; Szpunar et al., 1999; Tahiri et al., 2000), and that RG-II has immunomodulating activities (Shin et al., 1998) has led to a greater interest in the structure of RG-II and to the role of this enigmatic pectic polysaccharide in human nutrition and health.

RG-II is *not* structurally related to RG-I since its backbone is composed of 1,4-linked α-D-Gal*p*A residues rather than the repeating disaccharide [→4)-α-D-Gal*p*A-(1→2)-α-L-Rhap-(1→] (O'Neill et al., 1990). A nonasaccharide (side chain B) and an octasaccharide (side chain A) are attached to C-2 of some of the backbone GalA residues and two structurally different disaccharides (side chains C and D) are attached to C-3 of the backbone (Fig. 3). The locations on the backbone of the side chains with respect to one another have not been established with certainty.

Other substituted galacturonans have been described that are present in the walls of a restricted number of plants. For example, xylogalacturonans (XGA), which contain β-D-xylosyl (Xylp) residues attached to C-3 of the backbone (Kikuchi et al., 1996; Yu and Mort, 1996; Schols et al., 1995; O'Neill et al., 1990; Aspinall, 1980), are present in the walls of reproductive plant tissues (e.g. apple, carrot, cotton, and pine). Apiogalacturonans, which are present in the walls of some aquatic monocotyledons (e.g. *Lemna* and *Zostera*), contain β-D-apiofuranosyl (Api*f*) residues attached to C-2 and C-3 of the backbone either as a single Api*f* residue or as the disaccharide β-D-Api*f*-(1→3′)- β-D-Apif-(1→(Hart and Kindel, 1970a,b; Cheng and Kindel, 1997).

1.3. Advances in the structural analysis of cell wall pectic polysaccharides

1.3.1. Homogalacturonan and rhamnogalacturonan I

The availability of exo- and endoglycanases, and endolyases that fragment HG and RG-I has led to a greater understanding of the structure of these pectic

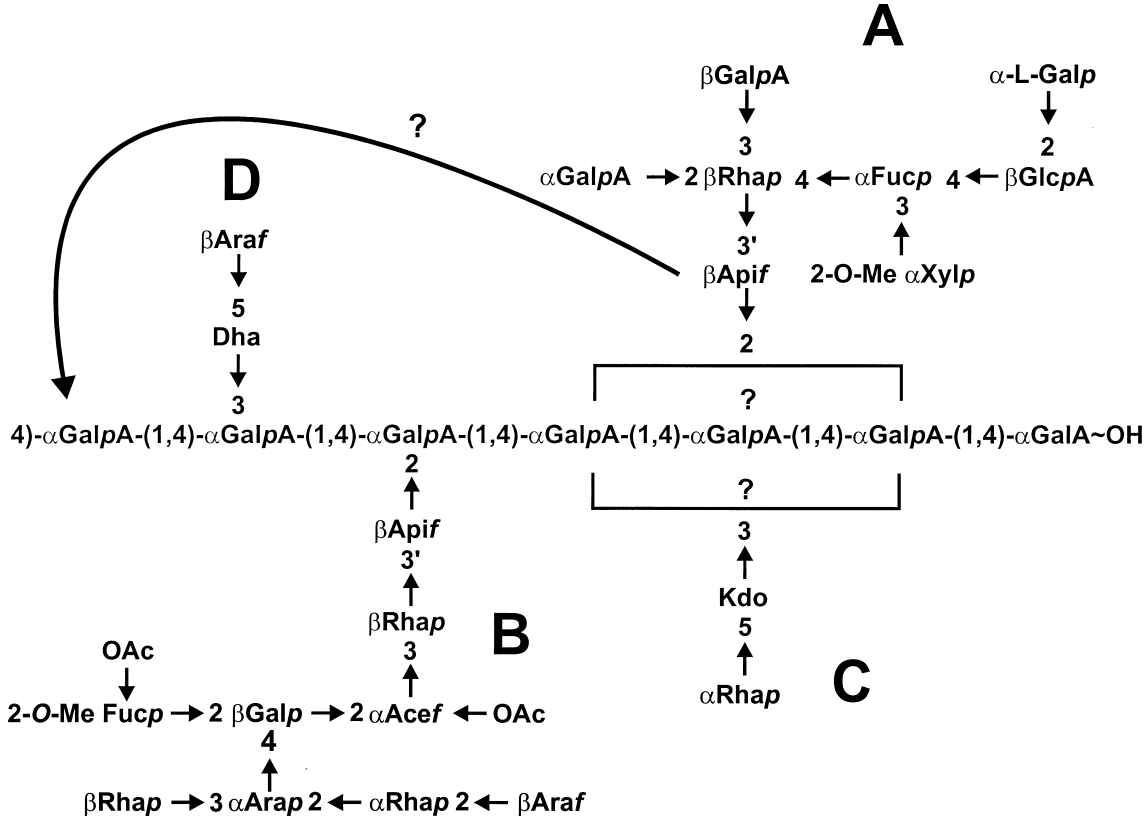

Fig. 3. The primary structure of rhamnogalacturonan II. The backbone of RG-II is composed of at least seven 1→4 linked α-D-Gal*p*A residues. Four structurally different oligosaccharide side chains (A–D) are linked to the RG-II backbone. The anomeric configurations of the glycosyl residues present in side chain B have been determined by high resolution NMR spectroscopy. The anomeric configurations of the glycosyl residues in side chain A are taken from Melton et al., 1986, but have not been confirmed by high resolution NMR spectroscopy. The order of the side-chains has not been unambiguously determined. At least 20 glycosyltransferase activities are required for the biosynthesis of RG-II (see Table 3 for details).

polysaccharides (Prade et al., 1999). For example, rhamnogalacturonase, rhamnogalacturonan lyase, rhamnogalacturonan-rhamnohydrolase, rhamnogalacturonan-galacturonohydrolase, and exo- and endogalacturonases, arabinanases and galactanases have been used to refine the structural features of RG-I (Prade et al., 1999). These enzymes, which have been isolated from fungi and bacteria, also provide insight into the wide range of enzymes that microorganisms secrete to fragment HG and RG-I (De Vries et al., 2000).

The distribution of methyl esters in HG has been investigated using chemical methods (Mort et al., 1993) and by treating walls, or isolated pectin, with pectin methylesterase (PME), endopolygalacturonase (EPGase), and endopectin lyase (PL) in combination with NMR spectroscopy (Grasdalen et al., 1988) and mass spectrometry (Daas et al., 1998; Limberg et al., 2000a). The results of such studies have demonstrated that commercially prepared pectin typically has a less regular pattern of methyl esterification than HGs isolated from cell walls, presumably due to the methods used to extract the pectin from the plant material. Mass spectrometry and anion-exchange chromatography, in combination with EPGase and PL fragmentation, have been used to show that plant PMEs cause blockwise de-esterification of pectin, whereas microbial PMEs typically cause random de-esterification (Limberg et al., 2000b).

1.3.2. Rhamnogalacturonan II

RG-II is present in primary walls predominantly as a dimer that is cross-linked by a 1:2 borate-diol ester (Kobayashi et al, 1996; Ishii et al., 1999). This cross-link is formed between OH-2 and OH-3 of the apiosyl residues in each monomeric RG-II subunit. Two diastereoisomers are formed (see Fig. 4) when methyl β-D-apiofuranoside is reacted with borate at pH 8 (Ishii and Ono, 1999). It is not known whether the naturally occurring dimer contains one or both of the diastereoisomers (O'Neill et al., 1996). Chemical analysis of naturally occurring and in vitro formed dimer suggests that the apiosyl residue of each side chain A, but not those of side chain B (see Fig. 3), are cross-linked by borate (Ishii et al., 1999). However, the possibility cannot be discounted that borate esters may cross-link the apiosyl residues of side chains A and B (Matoh et al., 2000).

RG-II dimer formation is a self-assembly process since it occurs in vitro in the absence of a catalytic protein. The anionic nature and chemical structure of RG-II

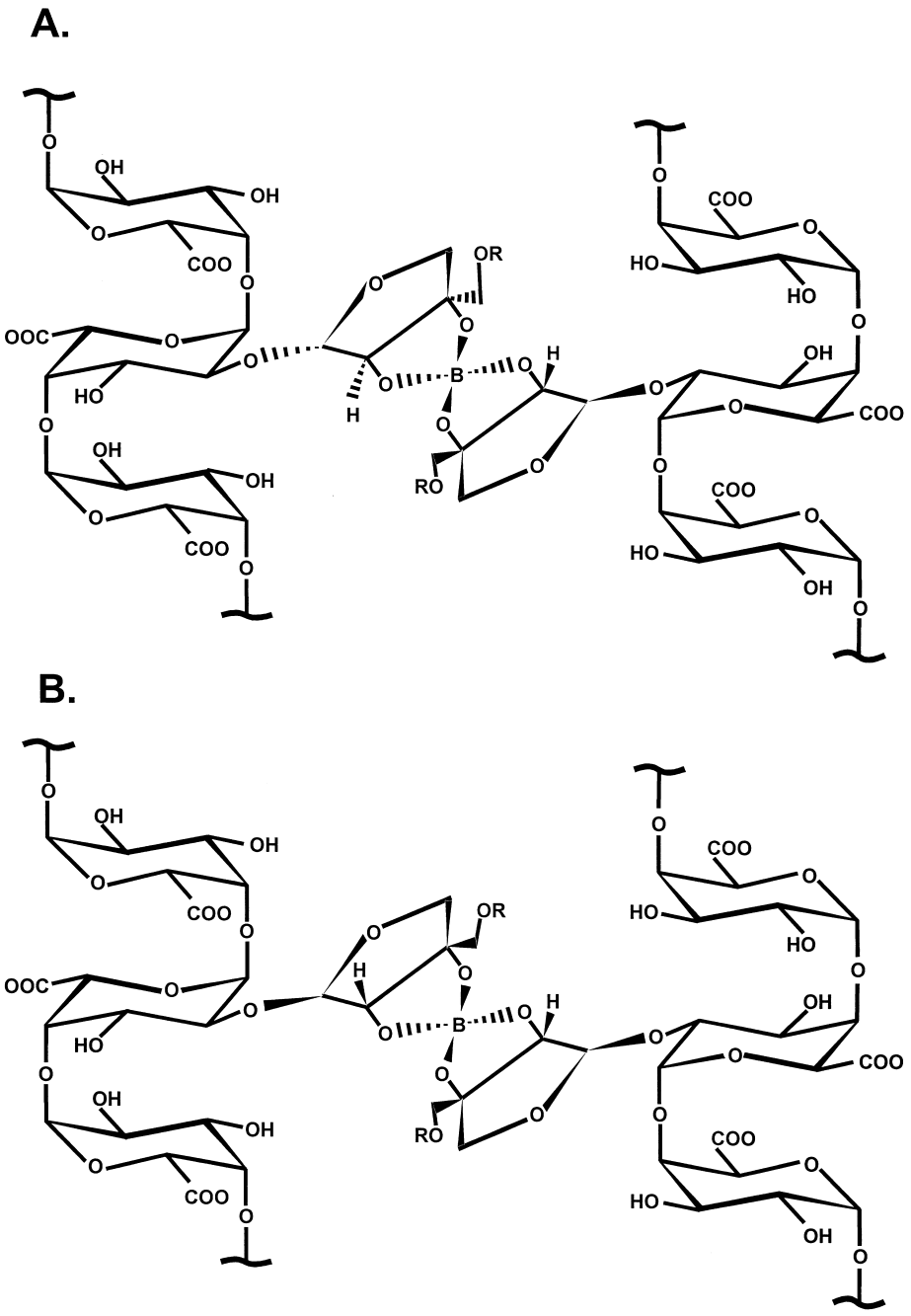

Fig. 4. The borate 1:2 diol ester that cross links two monomeric units of RG-II. The borate ester is formed between OH-2 and OH-3 of the 3′ linked apiosyl residues. "R" represents the oligoglycose that is linked to 3′ of the apiosyl residues. The ester can exist in either of two diastereomeric forms. In A one "R" group is pointing upward and the other is pointing downward. In B both "R" groups are pointing upward.

are likely to be major factors in determining the optimum pH (pH 3.0–4.0) for dimer formation in vitro (O'Neill et al., 1996) since 1:2 borate-diol esters of methyl β-D-apiofuranoside do not form below pH 5 (Ishii and Ono, 1999). The rate and extent of RG-II dimer formation in vitro are increased in the presence of di- and trivalent cations with ionic radii >1.0 Å (Ishii et al., 1999). Calcium at low concentrations (1 mM) is less effective than the larger cations (Ishii et al, 1999). However, higher concentrations (10 mM) of calcium and boric acid do increase the rate of dimer formation in vitro (Matoh and Kobayashi, 1998). The role of Ca^{2+} in dimer formation in vivo is not fully understood but there is evidence that it increases the stability of the RG-II dimer (Fleischer et al., 1999; Kobayashi et al., 1999).

The chemical structure of RG-II has been increasingly refined using high-field NMR spectroscopy in combination with electrospray and matrix-assisted laser desorption mass spectrometry. As a result, some of the previously published structures (Spellman et al., 1983) have been

revised (Vidal et al., 2000). The aceric acid-containing side chain (B in Fig. 3) is most likely a nonasaccharide (Whitcombe et al., 1995; Shin et al 1998; Terrell, M. and Prestegard, J., personal communication) and not a heptasaccharide as had previously been reported (Spellman et al., 1983). Side chain B is linked to *O*2 of the fifth Gal*p*A residue from the reducing end of the backbone, whereas side chain D [β-L-Araf-(1→5)-α-D-Dha-(1→] is most likely linked to *O*3 of the sixth Gal*p*A residue from the reducing end (Vidal et al., 2000). This study also provided evidence that the aceryl acid residue is α linked and that the galactosyl residue is β-linked, thus reversing the previously published anomeric configurations of these residues (Spellman et al., 1983). Somewhat unexpectedly, the terminal Gal*p* residue on side chain A (see Fig. 3) has been shown to have the L rather than the D configuration (Reuhs et al., submitted) thereby confirming that L-galactose is a minor component of primary walls (Baydoun and Fry, 1988).

A preliminary assignment of the ^{1}H and ^{13}C resonances in the NMR spectra of the $NaBH_4$-reduced RG-II monomer have been made and used to propose an NMR solution structure for RG-II (Du Penhoat et al., 1999). The ^{1}H and ^{13}C resonance assignments appear to be based in part on the published, and in some cases incorrectly assigned, anomeric configurations of the glycosyl residues present in RG-II. Inter-glycosidic NOEs and long-range NOEs were measured and interpreted on the basis of these assignments. The specific attachment site of each side-chain was not determined, although the authors suggest that only two arrangements of the side-chains (A, C, B, D or A, D, B, C) are consistent with the NMR spectroscopic data (Du Penhoat et al., 1999). Additional data are required before the validity of this conclusion can be assessed since the unambiguous assignment of all the resonances and the interpretation of NOE data for RG-II is a challenging endeavor. This is largely due to the considerable signal overlap and degeneracy that result from the relatively narrow spectral dispersion of complex carbohydrates (Van Halbeek, 1994). Complete assignment of the resonances in crowded regions of the NMR spectra of RG-II may be achieved by using selective excitation techniques (Freeman, 1992) or by 3D NMR spectroscopy. 3D NMR techniques were developed to facilitate the assignment of resonances in NMR spectra of isotopically-enriched proteins (Marion et al., 1989; Zuiderweg and Fesik, 1989) and have also been used to analyze ^{13}C-labeled complex carbohydrates (Van Halbeek, 1994; Bush et al., 1999). The availability of ^{13}C-enriched RG-II (York, W.S., O'Neill, M.A., Terrell, M., Prestegard, J., unpublished results) now makes 3D NMR spectroscopic analysis of this polysaccharide possible.

Molecular modeling procedures have been used to generate several possible three-dimensional structures for the side-chains of RG-II (Mazeau and Perez, 1998; Perez et al., 2000). The reader should consult Woods (1998) for a concise discussion of the computational methods that are used to model complex carbohydrates. The validity of the RG-II side chain models remain to be established, particularly in light of the evidence showing that in side-chain B the Ace*f*A residue is α- rather than β-linked, and that the 2,4-linked Gal*p* residue is β- and not α-linked. The computer-generated conformations of side-chain A need to be reexamined since they were obtained by assuming that the previously published anomeric configurations of the glycosyl residues (Melton et al., 1986) were correct and that the galactosyl residue was D rather than L.

1.4. The macromolecular organization of HG, RG-I, and RG-II in the primary wall

1.4.1. Are homogalacturonan, rhamnogalacturonan I, and RG-II linked together covalently?

Homogalacturonan, RG-I, and RG-II are solubilized from insoluble walls by treating the walls with aqueous buffers or calcium chelators. The polysaccharides, however, are not separated from each other by size-exclusion chromatography (e.g. Superose 6 and 12) since they elute in the column void volume (molecular masses >200 kDa). Fractions enriched in RG-I, RG-II, and oligogalacturonides are generated by treating the high molecular weight material with EPGase (O'Neill et al., 1990). Thus, it is often assumed that in primary walls HG, RG-I, and RG-II are covalently linked to one another and models have been proposed for the distribution of RG-I and HG in pectin (Matsuhashi et al., 1993).

Homogalacturonan and RG-II are likely to be covalently linked since they both have backbones composed of 1→4-linked α-D-Gal*p*A residues and they are both solubilized by treating walls with EPGase. The backbone of EPGase-solubilized RG-II contains up to 15 1,4-linked α-D-Gal*p*A residues, providing indirect evidence that RG-II is linked to HG (Whitcombe et al., 1995). RG-I is also solubilized by treating walls with EPGase even though there are no glycosyl residues in RG-I that are susceptible to EPGase. However, no oligosaccharides composed of the RG-I backbone disaccharide repeating unit covalently linked to fragments of HG have been isolated, nor is there evidence that HG is glycosidically linked to the side-chains of RG-I. The notion that HG chains are interrupted by the insertion of a single Rhap residue between regions containing 20–30 Gal*p*A residues is almost certainly incorrect (Zhan et al., 1998).

1.4.2. Is pectin cross-linked to other wall components?

Early models of the primary cell wall postulated that xyloglucans and pectic polysaccharides, as well as structural glycoproteins, are covalently linked together

to form a continuous macromolecular network (Keegstra et al., 1973). This view has gradually changed and current models emphasize the predominance of non-covalent linkages between wall polymers (Carpita and Gibeaut, 1993). Nevertheless, there is a substantial body of data showing that RG-II molecules are covalently cross-linked by borate esters.

1.4.3. Borate-ester cross-linked pectin

There is accumulating evidence that borate ester cross-linking of RG-II is required for the formation of a macromolecular pectic network within the plant cell wall (Matoh and Kobayashi, 1998). The function of this network is not understood, although it may have a role in controlling the mechanical properties of the primary wall (Loomis and Durst, 1992; Flesicher et al., 1998, 1999). For example, boron-mediated cross-linking of RG-II in the walls of living plant cells generates a pectin network with a decreased size-exclusion limit for polymers (Fleischer et al., 1999). Such results are consistent with previous studies showing that the size of molecules able to diffuse through the wall is increased by enzymic and chemical fragmentation of wall-bound pectin (Baron-Epel et al., 1988; Ehwald et al., 1992).

Chenopodium album cells divide and grow in the absence of added boron (Fleischer et al., 1998) and their walls contain monomeric RG-II, but no discernible amounts of dimeric RG-II. Thus, borate ester cross-linking of RG-II is unlikely to be required for cell division and growth in these cells. Boron-deficient *C. album* cells, in contrast to their boron-grown counterparts, are unable to reduce their wall pore size and thereby undergo excessive cell enlargement and experience wall rupture during their transition to the stationary phase (Fleischer et al., 1998). Thus, it appears that the size-exclusion or cross-linking effects of the pectic network may become essential for the stability of *C. album* cells only when growth has ceased. In contrast, tobacco cells do not grow in a boron-free medium but do grow in media containing a low amount (10 μg/l) of added boric acid (Matoh et al., 2000). Most (~60%) of the RG-II is present as the monomer in the boron-deficient cells and the walls are swollen suggesting that the cross-linking and organization of the pectin network has been altered (Matoh et al., 2000). The inability to form a borate ester cross-linked pectic network may influence physiologically important processes including the incorporation of polymers into the wall, the access of wall modifying enzymes or proteins to their substrates or ligands, and the transport of polymers from the protoplast into the wall.

Kobayashi et al. (1999) have provided evidence that cyclohexanediaminetetraacetic acid (CDTA) promotes the hydrolysis of the RG-II dimer and that the release of the most tightly bound wall calcium is correlated with the solubilization of wall-bound RG-II. Divalent cations promote soluble dimer formation in vitro (O'Neill et al., 1996; Matoh and Kobayashi, 1998) and together with boric acid prevent the low-pH mediated increase in wall pore size (Fleischer et al., 1999). These results, when taken together with the ability of calcium to stabilize borate complexes in root tips (Wimmer and Goldbach, 1999), suggest that in muro calcium has a role at specific, but as yet unidentified, sites close to the borate ester cross-link.

1.4.4. Anionic cross-links

Pectins are the predominant anionic polymer in the primary walls of dicots and non-graminaceous monocots and thus many of their properties are believed to be determined by ionic interactions. The properties of pectin gels and the mechanism of gelation have been the subject of numerous studies (Grant et al., 1973; Powell et al., 1982; Morris et al., 1982; Thibault and Rinaudo, 1986; Thakur et al., 1997). The pectins used for many of the gelation experiments, however, were often solubilized from plant tissue by degradative treatments (e.g. hot aqueous acid). Thus, the relevance of such studies for the macromolecular properties of cell wall-bound pectin has been questioned (MacDougall et al., 1996).

Pectin gels have also been studied using pectin isolated from cell walls by nondegradative conditions. For example, CDTA treatment of unripe tomato fruits has been shown to result in cell separation and the solubilization of a high methoxy pectin (DM 68%). This pectin is believed to originate from the middle lamella and may have an important role in maintaining cell adhesion (MacDougall et al., 1996). The CDTA-soluble pectin forms elastic gels in the presence of calcium. These gels have a higher affinity for calcium than aqueous solutions of the same polysaccharide (Tibbits et al., 1998). A fraction of the Gal*p*A residues in the gel does not participate in ionic cross-linking but may contribute to gel swelling particularly at low ionic strength (Tibbits et al., 1998). The maximum swelling of the gel and the minimum shear modulus (strength of the gel) occur at pH 3 which is close to the pK_a of the carboxyl group of galacturonic acid (Tibbits et al., 1998). This pH value is also similar to the optimum pH required for borate ester cross-linking of RG-II in vitro (O'Neill et al., 1996). The question of what role RG-II cross-linking has on the properties of CDTA-soluble pectin gels has not yet been addressed.

1.4.5. Other cross-links

A portion of primary wall pectin is not solubilized by treatment with aqueous buffers, calcium chelators, or EPGase, but is solubilized by aqueous base (Bauer et al., 1973; Selvendran, 1985). Thus, the existence of esters that form between the carboxyl group of a 4-linked Gal*p*A residue and a hydroxyl group of another glycosyl residue has been hypothesized (Fry, 1986). The presence of

non-methyl galacturonosyl esters has been implied from chemical analysis of maize cell walls (Kim and Carpita, 1992) and by chemical and infra-red spectroscopic analysis of tobacco cell walls (McCann et al., 1994). Non-methyl esters have also been reported to be present in the walls of spinach (Brown and Fry, 1993) and carrot (Needs et al., 1998), although no fragments of HG containing unusual esters have been isolated and structurally characterized. The trans-esterification of pectin has been reported to be catalyzed by pectin methyl esterase (Hou and Chang, 1996), but additional structural evidence is required to substantiate this claim.

In the walls of the *Chenopodiaceae* (e.g. sugar beet and spinach) some of the pectic arabinosyl and galactosyl residues are esterified with ferulic or coumaric acid and these phenolic residues are potential sites for cross-linking via oxidative coupling (Ishii, 1997b; Saulnier and Thibault, 1999). However, the existence in muro of intermolecular dehydrodiferuloyl cross-linked pectin has not been demonstrated. Hemicellulose-pectin complexes that may be cross-linked by as yet unidentified phenolic material have been reported to be present in the walls of cauliflower (Femenia et al., 1999), asparagus stems (Waldron and Selvendran, 1992), and olive seed hulls (Coimbra et al., 1995).

Pectin and xyloglucan are both solubilized by treating primary walls with alkali (Bauer et al., 1973; Selvendran, 1985; Thompson and Fry, 2000). A portion of the xyloglucan and pectin is assumed to be covalently cross-linked since these polymers co-elute from anion-exchange columns and xyloglucans themselves contain no acidic glycosyl residues (Thompson and Fry, 2000). However, the nature of the covalent linkage between xyloglucan and pectin, if it exists, has not been established. The wall material remaining after 4M KOH treatment is rich in cellulose but may also contain Rhap and Gal*p*A residues and Hyp-rich glycoprotein. Linkages between pectin and wall glycoprotein have been inferred from chemical analysis (Qi et al., 1995; Fu and Mort, 1996; Peronne et al., 1998) and from solid state NMR spectroscopic studies (Pan, 1992) but compelling evidence for these cross-links is lacking.

Although numerous studies have reported cross-linking between pectic and hemicellulosic polysaccharides and between pectin and wall glycoprotein, conclusive evidence for their existence is lacking. Future research should be directed towards the isolation and structural characterization of these putative cross-links.

1.4.6. Biophysical methods for determining the properties and functions of primary wall pectin

The current lack of understanding of the macromolecular organization of pectin in the primary wall is largely due to a paucity of evidence for all but a few of the postulated cross-links and ionic interactions. One interpretation of the available, albeit inadequate, data is that primary wall pectin exists as a continuous three-dimensional cross-linked network. The functional characteristics of this network depend on the chemical structures, the conformations, and the interactions of the individual macromolecules. Thus, techniques are required that can examine primary walls in their native state. Such techniques include solid state NMR spectroscopy, Fourier transform infra-red spectroscopy, and atomic force microscopy.

Solid state ^{13}C NMR spectroscopy is a useful tool for the characterization of synthetic polymers (Andrew and Szczesniak, 1995), biological solids (McDowell and Schaefer, 1996), and plant cell walls (Jarvis and McCann, 2000). Chemical shift data provide information on the local chemical environment and structure whereas local dynamics, including the thermal motion of polymers in the solid state, are derived from various relaxation measurements (Jarvis and McCann, 2000). Such relaxation experiments have led to the general conclusion that pectic galacturonans have a range of thermal mobilities and that highly methyl esterified pectins are more mobile than low esterified pectins (Ha et al., 1997; Jarvis and McCann, 2000; Tang et al., 2000). The most mobile portions of pectin are the galactan and arabinan side chains of RG-I which are suggested to behave as "tethered liquids" (Jarvis and McCann, 2000).

Conventional solid state ^{13}C NMR spectra are typically interpreted primarily in terms of a single polymer chain. Thus, the relationship between the microscopic structure of a polymer, the mobility of a polymer, and its macroscopic properties can only be inferred indirectly. However, an accurate and direct characterization of inter-chain packing is required to understand the mechanical properties of the cell wall. The inter-nuclear distances (10–15 Å) between packed chains can be determined from long-range, weak dipolar couplings using rotational echo double resonance (REDOR) and transferred echo double resonance (TEDOR) NMR (McDowell and Schaefer, 1996; Schaefer, 1998). These technically challenging experiments are complicated because observation of the appropriate dipolar couplings necessitates selective enrichment of the polymers with isotopes (e.g. ^{13}C–^{15}N, ^{13}C–^{2}H, ^{19}F–^{31}P), whose abundance is low in naturally occurring samples. REDOR NMR has been used to investigate the structure and dynamics of cross-links in *Staphylococcus aureus* cell walls (Tong et al., 1997), in mussel byssal plaques (McDowell et al., 1999), in insect cuticle (Merritt et al., 1996), and in the binding sites of several proteins (Schaefer, 1998). REDOR ^{15}N NMR analysis, in combination with double cross-polarization magic angle spinning ^{13}C NMR analysis, of ^{15}N- and ^{13}C-enriched tomato cell walls have provided evidence that some carbonyl carbons, presumably from pectin, are cross-linked to histidine (Pan, 1992). However, additional experimental evidence is required to support this conclusion.

Fourier transform infra-red (FTIR) spectroscopy is a valuable tool for determining the bulk structural features of polysaccharides and cell walls (Jarvis and McCann, 2000; Kacurakova et al., 2000). The IR beam is focused onto a small ($\geqslant$10 μm) sample area using a FTIR microscope and information is obtained for the distribution of wall polysaccharides within a tissue. Information on the mean orientation of pectin and cellulose in the wall can be obtained using polarized IR beams (Jarvis and McCann, 2000).

The IR spectra of polysaccharides are complex. The major classes of cell wall polysaccharide (HG, RG-I, arabinan, galactan, arabinogalactan, xyloglucan, arabinoglucuronoxylan, glucomannan, and galactoglucomannan) each have distinctive absorption bands (Kacurakova et al., 2000). Nevertheless, partial overlap of the absorption bands in the 1200–800 cm^{-1} region of the spectra complicates determining the polysaccharide composition of a wall by IR spectroscopy. The carboxylate and ester bands of pectin at 1607 and 1740 cm^{-1}, respectively, are reasonably well resolved from other absorption bands and their relative intensities provide information on the degree of esterification of HG (Bociek and Welti, 1975). However, the IR spectra of walls containing a large amount of protein are likely to contain a significant amide band (1650 cm^{-1}) and this may overlap with the carboxylate band (Bociek and Welti, 1975).

Scanning probe microscopy encompasses several distinct techniques that have been used to characterize cell surfaces and cell wall polysaccharides (Brant, 1999; Morris et al., 1999). Atomic force microscopy (AFM) is an imaging technique that has been used to visualize plant cell walls (Morris et al., 1997), cellulose (Baker et al., 1997) and pectin (Round et al., 1997). The polysaccharides are imaged directly under butanol and the images are likely to contain less artifacts than electron microscope images which are obtained from rotary-shadowed replicas of polysaccharides (Seymour and Harding, 1987).

AFM images of a sodium carbonate-soluble pectin from tomato show the presence of a mixed population of single chains and aggregates (Round et al., 1997). Somewhat unexpectedly, the AFM images revealed branched structures that have been interpreted as evidence that HG chains are covalently linked to one another or that the neutral-sugar side chains of pectin are considerably longer than previously believed (Round et al., 1997).

Single-molecule force spectroscopy is a technique that has been used to measure the mechanical properties of proteins (Leckband, 2000) and polysaccharides (Brant, 1999). A single polymer chain is tethered at one point to a fixed substrate and at another point to an AFM tip. The application of a stretching force elastically deforms the molecule and may also induce conformational transitions (Marszalek et al., 1998, 1999). The force-extension curves for citrus pectin show two reversible yield domains that correspond to abrupt increases in the length of the polysaccharide chain (Marszalek et al., 1999). The yield domains may result from the conversion of D-Gal*p*A residues in the $^4C_1$ chair to an intermediate boat/skew-boat conformer and then to the $^1C_4$ chair. Such conformational changes are suggested to result in a increase in chain length since the distance spanned by the $^1C_4$ ring conformer is larger than the $^4C_1$ ring conformer (Marszalek et al., 1999). The force-extension curves of cellulose contain no yield domains since the virtual bond length of the glucosyl residues is not increased by a change in ring conformation (Marszalek et al., 1999). Thus, differences in the extensibility of pectin and cellulose may allow plant cells to finely control the extensibility of their walls (Marszalek et al., 1998).

1.4.7. Are there pectin-membrane-cytoskeleton connections?

There is an increasing awareness that the mechanical and biochemical properties of the primary wall influence the growth and development of plant cells and tissues, although the mechanisms by which a cell perceives and responds to changes in wall properties are not understood (Roberts, 1990; Wyatt and Carpita, 1993). The limited available data suggest that the primary wall and the cytoskeleton are connected by membrane associated proteins, although the nature of the connecting proteins and the wall components they interact with are largely unidentified (Miller et al., 1997; He et al., 1996). In contrast, the role of the extracellular matrix in the growth and development of animal cells has been studied in detail (Chothia and Jones, 1997; Deller and Jones, 2000) and models have been proposed to explain how mechanical forces affect the behavior of animal cells (Ingber, 1998).

Homologs of animal cell adhesion molecules (integrins, proteoglycans, vitronectin, and fibronectin) have been detected in plant cell walls and membranes using antibodies and synthetic peptides (Miller et al., 1997). *A. thaliana* plasma membranes contain proteins with homology to animal β-integrins (Laval et al., 1999). Purified plasma membranes from *Arabidopsis* cells have also been reported to contain two types of high-affinity binding sites for the RGD (Arg–Gly–Asp) peptide, a sequence typically required for binding to integrin receptors (Canut et al., 1998). A heptapeptide containing the RGD motif has been reported to cause a loss of wall-membrane attachments (Hechtian threads) in plasmolyzed onion epidermal cells and suspension-cultured *arabidopsis* cells (Canut et al., 1998). However, it was not shown whether the effects of the RGD motif result from an interaction with the cell wall or plasma membrane. RGD peptides have been reported to enhance cell division in soybean (Schindler et al., 1989), to inhibit gravity perception in Chara (Wayne et al., 1992), and to disrupt protoplast adhesion in NaCl-adapted tobacco cells (Zhu et al., 1993), although the mechanisms of action remain unidentified.

Fibronectin-like molecules and wall-associated kinases have been identified in plants and these proteins may bind directly or indirectly to pectic polysaccharides (He et al., 1996; Miller et al., 1997). No direct evidence has been obtained to show that pectic polysaccharides are linked to the plasma membrane, although a narrow zone of the wall adjacent to the plasma membrane is often enriched with unesterified HG (Knox et al., 1990), RG-II (Williams et al., 1996; Matoh et al., 1998), β1→4 linked galactan and β1→6 linked galactans (Jauneau et al., 1998; Sorensen et al., 2000). Such labeling patterns must be interpreted with caution since the pectin located in the region of the wall adjacent to the plasma membrane is likely to be the most recently deposited wall material and may be more accessible to the antibodies than pectin in the rest of the wall.

1.5. The distribution of pectic polysaccharides in the primary wall

Antibodies that recognize specific structural features of primary cell wall pectin are powerful tools for determining the location and distribution of these polysaccharides within a single wall and for following changes in pectin structure during cell and tissue development (Knox, 1997; Vicre et al., 1998; Willats et al., 2000b). Antibodies have been described that are believed to recognize HG with different degrees of esterification including JIM 5 (VandenBosch et al., 1989; Knox et al., 1990); Jim 7 (Knox et al., 1990) and PAM1 (Willats et al., 1999a). Other anti-pectin antibodies are 2F4 that recognizes calcium cross-linked pectin (Liners et al. 1989), and LM5 and LM6 that recognize, respectively, 1→4-linked β-D-galactan (Jones et al., 1997) and 1→5-linked α-L-arabinan (Willats et al., 1998) in the side chains of RG-I. Another series of antibodies includes CCRC-M1 that recognizes polysaccharides containing a terminal non-reducing α-L-fucosyl residue (Puhlmann et al., 1994), CCRC-M2 that recognizes RG-I (Puhlmann et al., 1994), CCRC-M7 that recognizes arabinosylated 1→6-linked β-D-galactan (Steffan et al., 1995), and CCRC-R1 that recognizes RG-II (Williams et al., 1996).

The epitopes recognized by LM5 and LM6 are known with some certainty since these antibodies were generated against specific oligosaccharides coupled to proteins (Jones et al., 1997; Willats et al., 1998). The epitope recognized by CCRC-M1 has been shown, using a series of structurally related oligosaccharides, to contain a terminal 1→2 linked α-L-fucosyl residue (Puhlman et al., 1994). The binding characteristics of PAM1, JIM5, and JIM7 have been compared using pectin of varying degrees and patterns of methyl esterification (Willats et al., 1999a, 2000a). PAM1 binds most effectively to fully de-esterified pectin whereas JIM5 and JIM7 bind to pectin with a wide range of degrees of methyl esterification. Some published studies, however, have been interpreted based on the assumption that JIM5 recognizes deesterified HG and JIM7 recognizes methylesterified HG. Thus, the results of immunolocalization studies using JIM5 and JIM7 must be interpreted with caution (Willats et al., 2000a).

Immunolocalization studies have provided evidence that the localization and structure of pectin may have an impact on plant cell growth and development. For example, the presence of a pectin sheath on the primary walls of developing cotton fibers is correlated with the ability of epidermal cells to differentiate into elongating fiber cells (Vaughn and Turley, 1999), while epidermal cells that do not have a pectin sheath do not elongate. The role of the external pectin-rich layer in cell elongation, however, remains to be determined since epidermal cells in maize coleoptiles (Schindler et al., 1995), flax (Jauneau et al., 1997), and pea stems (Fujino and Itoh, 1998) have an asymmetric distribution of pectin but do not elongate.

Differences in the distribution of pectic epitopes in different cell and tissue types have also been reported in pea cotyledons (McCartney et al., 2000), tomato pericarp (Roy, 1994; Steele et al., 1997; Orfila and Knox, 2000); flax roots and hypocotyls (Jauneau et al., 1997, 1998), potato tubers (Bush and McCann, 1999), Arabidopsis roots (Freshour et al., 1996; Dolan et al., 1997), aspen cambium (Ermel et al., 2000), poplar cambium (Guglielmino, 1997), pollen (Geitmann et al., 1995; Juah and Lord, 1996), *Zinnia* cells (Stacey et al., 1995), suspension-cultured cells (McCann et al., 1994; Williams et al., 1996; Matoh et al., 1998), and cauliflower stems (Femenia et al., 1998). The results of these studies, when taken together, lead to the general conclusion that unesterified HG is localized to the middle lamella, to cell corners, and around air spaces whereas esterified HG is typically present throughout the wall. The immunocytochemistry results also suggest that the presence and location of the arabinan and galactan side chains of RG-I are often correlated with stages of cell and/or tissue development. The appearance of 1→4-linked β-D-galactan and a decrease of 1→5-linked α-L-arabinan in carrot cell walls has been correlated with the transition from cell division to cell elongation (Willats et al., 1999b). The α1,5-arabinan epitopes are also expressed specifically in the central meristem of carrot roots and in proliferating carrot suspension-cultured cells, while the 1,4-galactan epitopes are not expressed in these cells but rather in the root cap and differentiating stele and cortical cells of the carrot root and in non-proliferating induced carrot suspension cultures (Willats et al., 1999a,b). The expression of the arabinan and galactan side chains of RG-I also appears to be developmentally regulated in other plants and tissues. HG and α1,5-arabinan epitopes are present in the pea cotyledon throughout development while the β1,4-galactan-epitope is restricted to a specific stage of cotyledon development

(26–30 days after anthesis) and is present in a thin layer at the plasma membrane face of the cell wall (McCartney et al., 2000). The HG, α1,5-arabinan and β1,4-galactan epitopes in the wall surrounding pit fields in the tomato pericarp are also spatially regulated, with HG present in the pit fields, α1,5-arabinan surrounding the pit fields, and β1,4-galactan absent from the pit field (Orfila and Knox, 2000).

The results of immunocytochemical studies showing the differential labeling of a particular wall epitope may suggest that the synthesis of the epitope is regulated, however, additional experiments are required to determine if the lack of binding of an antibody to a tissue section is due to the absence of the epitope or to the masking of an epitope. For example, Masuda et al. (1984) reported that in elongating carrot walls the ratio of 3,5- to 5-linked arabinosyl residues increased. Thus, increased branching of the 1,5-linked arabinan may account for the reduced labeling of elongating cell walls by the 1→5-linked α-L-arabinan antibody (Willats et al., 1999b). Evidence that the antibody labeling pattern of the tissues is due to the differential expression of arabinan, rather than to the masking of the epitope(s) recognized by the antibody, is not easily obtained by independent methods since it is difficult to excise discrete cell populations and prepare their walls in amounts sufficient for conventional chemical or biochemical analyses.

Another example of a differentially labeled cell wall epitope is an RG-II epitope recognized by polyclonal anti-RG-II antibodies (Matoh et al., 1998). The RG-II epitope is present in dicot and monocot walls, but is not detected in the middle lamella (Matoh et al., 1998). This epitope, however, may be masked by a base-labile component since alkali treatment of the walls typically results in a dramatic increase in the density of labeling (Williams et al., 1996; Matoh et al., 1998). This example again illustrates that care must be taken in interpreting the results of immunolabeling studies. Furthermore, it is difficult to determine whether the changes in the ability of specific antibodies to bind to tissue sections results from a change in the glycosyl residue composition of the wall or to changes in the physical properties of the wall (e.g. permeability). Additional antibodies with well defined epitopes and methods to structurally analyze the walls surrounding single cells are required to address this issue.

The differential expression of a wall carbohydrate epitope may, or may not, indicate that the specific epitope plays a role in plant growth or development. For example, despite the differential expression of the β-D-galactan epitope, the role of 1→4-linked β-D-galactan in plant growth is unclear since the walls of potato tubers transformed with a fungal endo-1,4-β-D-galactanase contain ~30% of the normal amount of galactose and yet the plants have no apparent change in phenotype (Sorensen et al., 2000).

1.6. Probing the structure and function of pectin with cell wall mutants

Our knowledge of the primary structure of wall pectin, its distribution within the wall, and some of its interactions with itself and other wall components has increased dramatically over the last 10 years. In contrast, our understanding of the biological functions of pectic polysaccharides remains inadequate. The increasing availability of cell wall mutants provides new opportunities to study pectin structure and function (Fagard et al., 2000).

Many of the cell wall mutants currently available have been generated using Arabidopsis, although only a limited number of them have been shown to have altered pectin structure or metabolism (Fagard et al., 2000). Arabidopsis mutants (*Mur1–Mur11*) have been described that have reduced levels of Fuc, Ara, Gal, or Rha in their walls (Reiter et al., 1997). These glycosyl residues are typically present in RG-I and RG-II, although Fuc, Ara, and Gal are also components of xyloglucan and arabinogalactan proteins. Thus, some of these mutants are likely to have structural changes in more than one wall component.

Mur1 and *Mur4* have each been shown to be defective in a single gene that is required for the biosynthesis of a specific monosaccharide. For example, the aerial portions of *Mur1* plants are defective in an isoform of GDP-mannose-4,6-dehydratase and thus their walls contain ~5% of the wild type fucose (Bonin et al., 1997). The reduced fucose content is reflected in the almost total absence of fucosyl residues in *Mur1* xyloglucan (Zablackis et al., 1996) and RG-II (Reuhs et al., submitted). Somewhat unexpectedly, ~30% of the β-D-galactosyl residues that would normally be substituted with a L-fucosyl residue are substituted with an α-L-galactosyl residue (Zablackis et al., 1996). Similarly, the 2-*O*-Me α-L-fucosyl and α-L-fucosyl residues in *Mur1* RG-II are replaced with terminal 2-*O*-Me α-L-galactosyl and α-L-galactosyl residues (Reuhs et al., submitted). L-galactosyl residues are believed to be generated from GDP-mannose by GDP-mannose-3,5-epimerase, a enzyme required for the biosynthesis of vitamin C (Wheeler et al. 1998). *Mur4* plants are defective in a membrane-bound UDP-D-xylose 4-epimerase and thus have reduced levels of arabinose in their walls (Burget and Reiter, 1999). *Mur4* plants have no visible phenotype, although the double mutant *Mur4*/*Mur1* has been reported to have an extreme dwarf phenotype (Reiter et al., 1997). The walls of *Mur4*/*Mur1* plants are likely to contain structurally modified RG-II, xyloglucan, and possibly RG-I, although no structural analysis of the individual polysaccharides has been reported.

Mutant plant populations are generated by random mutagenesis of seeds with ethylmethanesulfonate or through T-DNA or transposon-mutagenesis. Typically,

this results in many thousands of M2 lines that must be screened. The identification of wall mutants is labor-intensive since no rapid screening procedures are currently available, although sample throughput may be increased using FTIR spectroscopy (Chen et al., 1998) and immunocytochemical methods (Willats et al., 2000b). Thus, more direct methods for generating transgenic plants with altered pectin structure and/or metabolism are now being exploited.

Antisense mRNA technology has been used to investigate the role of EPGase in the ripening and softening of tomato fruit. Transgenic tomato fruits containing $<1\%$ of the normal EPGase activity ripen normally showing that EPGases are not responsible for ripening-associated softening (Tieman and Handa, 1994). Nevertheless, these fruits have improved storage characteristics since tissue integrity is maintained during fruit senescence. Normal ripening also occurs in transgenic tomato plants with reduced PME activity but there is a significant decrease in tissue integrity during fruit senescence, and the fruits are more susceptible to microbial attack (Tieman and Handa, 1994). Antisense mRNA has also been used to show that in pea root tips the PME-catalyzed de-esterification of pectin has a role in border cell release and in root growth (Wen et al., 1999).

An alternative approach to antisense mRNA approaches to modify the wall is to transform plants with glycanases that are known to fragment cell wall polysaccharides. For example, the walls of transgenic potato tubers expressing a fungal endo-β1,4-galactanase contain reduced amounts of galactose, although plant growth is not affected (Sorensen et al., 2000).

Virus-induced gene silencing of a putative cellulose synthase gene has been used to generate transiently dwarf tobacco plants (Burton et al., 2000). The walls of the infected leaves have a reduced cellulose content, the HG content is increased, and the HG is reported to be less esterified than the HG in the walls of control plants. Pectin also accounts for a greater proportion of the walls of plant cells grown in the presence of the cellulose synthesis inhibitor dichlorobenzonitrile (Shedletzky et al., 1992). Thus, a plant may compensate for reduced cellulose production by increasing the amount of HG in its wall (Burton et al., 2000).

Several Arabidopsis mutants that may yield insights into pectin function have been generated in studies not directly related to primary cell walls. For example, transgenic arabidopsis plants expressing a fungal cutinase exhibit postgenital organ fusion in epidermal tissue that lacks an intact cuticle. These fusions are due in part to pectin-mediated cell-cell adhesion and have been observed in the leaves, stems, and flowers but not in the roots (Sieber et al., 2000). Fusions occur in epidermal cells only early in organ development when the organs are close together and often results in the formation of cell bridges (Sieber et al., 2000). The material in the junctions of the fusions and cell bridges is rich in pectin with low and high degrees of esterification. Thus, in the absence of an intact cuticle, the walls of closely appressed epidermal cells partially fuse by co-polymerization of pectin (Sieber et al., 2000). A second example of abnormal pectin-mediated cell-cell adhesion has been observed in the *Qrt* mutant of arabidopsis. In wild type plants, the pollen mother cell wall consists of an inner callose layer and an outer pectin-rich layer. These layers are both removed during pollen maturation and the four microspores separate before deposition of the exine. Callose is fragmented normally in *Qrt* mutants but the pectin layer persists and the microspores remain attached to one another. The exine is then deposited simultaneously on all four microspores. The nature of the QRT gene product is not known but it is likely to have a role in pectin metabolism (Rhee and Somerville, 1998).

A vitamin C deficient mutant (*Vtc1*) has recently been shown to be partially defective in GDP-mannose pyrophosphorylase (Conklin et al., 1999). This mutation may affect the fucosyl, mannosyl, and L-galactosyl contents of the wall since these glycosyl residues are derived from GDP-mannose (Conklin et al., 1999). The arabidopsis mutant *Cyt1-2* is believed to contain a completely defective GDP-mannose pyrophosphorylase (Conklin et al., 1999). *Cyt1-2* is an embryo-lethal mutant with severely deformed walls, although it has not been shown that the wall defects themselves are directly responsible for the observed phenotype.

The identification of cell wall-related genes in arabidopsis via sequence similarities to *Acetobacter xylinum* and *Agrobacterium tumefaciens* genes involved in cellulose synthesis has met with considerable success (Delmer, 1999; Pear et al., 1996). This approach also has the potential to identify genes involved in the biosynthesis of pectic polysaccharides (Bonin and Reiter, 2000). No bacteria are known that synthesize HG, RG-I, or RG-II. Nevertheless, the glycosyl residues present in pectin are, with the exception of apiose and aceric acid, also present in various bacterial polysaccharides. For example, a 4-linked α-D-Gal*p*A residue and a 2-linked α-L-Rha*p* are present in the hexasaccharide repeating unit of the extracellular polysaccharide synthesized by *Erwinia chrysanthemi* A350 (Gray et al., 2000). The ability to selectively mutate genes involved in cell wall formation and metabolism clearly presents new opportunities for determining the function of pectic polysaccharides in plant growth and development.

2. Biosynthesis

2.1. Introduction

The study of pectin biosynthesis is challenging and progress in this area has been slow. The complex structure

of pectin requires the action of at least 53 different enzymatic activities (Mohnen, 1999). Some of the nucleotide sugar substrates for the pectin biosynthetic enzymes are unknown, most are not commercially available, and the oligo/polysaccharide acceptors required to assay the enzymes must be generated by chemical or enzymatic cleavage of pectin and then purified. In order to understand how the activity of the 53 distinct enzymatic activities required for pectin synthesis (see Tables 1–3) are coordinated, and how that process is regulated, the pectin biosynthetic enzymes must be identified and the corresponding genes cloned. No pectin biosynthetic enzyme has yet been purified to homogeneity, and no pectin biosynthetic glycosyl-, methyl- or acetyltransferase has been cloned. Nevertheless, recent progress in the area of pectin biosynthesis, including the partial purification of some of the pectin biosynthetic enzymes, make it likely that the first genes for pectin biosynthetic enzymes will be identified in the near future. The published literature on pectin biosynthesis has recently been reviewed (Mohnen, 1999), thus only recent developments in our understanding of pectin biosynthesis will be presented here.

2.2. Setting the stage for pectin synthesis

The synthesis of pectin must be regulated in a temporally, spatially, and developmentally specific manner since the pectic polysaccharides are largely absent from many secondary walls while they show cell type and developmental expression in primary walls. A discussion of pectin synthesis must first address where synthesis occurs. Immunocytochemistry using antibodies directed against cell wall carbohydrate epitopes (Hoson, 1991; Moore et al., 1991; Knox, 1992; Staehelin and Moore, 1995) showed that HG and RG-I-like epitopes are present in both the *cis*- and medial-Golgi. Thus, it is likely that the synthesis of these epitopes begins in *cis* Golgi (Lynch and Staehelin, 1992; Zhang and Staehelin, 1992) and continues into the medial Golgi (Moore et al., 1991; Zhang and Staehelin, 1992; Staehelin and Moore, 1995). The esterification of HG appears to occur in the medial and trans Golgi (Vian and Roland, 1991; Liners and Van Cutsem, 1992; Zhang and Staehelin, 1992; Sherrier and VandenBosch, 1994; Staehelin and Moore, 1995), while more extensive branching of pectin occurs in the trans Golgi cisternae (Zhang and Staehelin, 1992; Staehelin and Moore, 1995). Final pectin assembly may occur as the Golgi vesicles are transported to the plasma membrane and the pectin is inserted into the wall, often as a highly methyl esterified polymer (Carpita and Gibeaut, 1993; Liners et al., 1994; Dolan et al., 1997). Some cell types, however, appear to secrete relatively unesterified pectin in the wall. For example, melon callus cells (Vian and Roland, 1991) and slime-secreting clover root epidermal cells (Lynch and Staehelin, 1992) contain unesterified HG in the trans Golgi. Also, unesterified HG epitopes have been found at the plasma membrane-cell wall interface by immunocytochemistry, suggesting that HG can also be inserted into the wall in a relatively unesterified form and that HG is not necessarily synthesized in a highly esterified form (Knox et al., 1990; Casero and Knox, 1995). The extent to which HG is esterified during synthesis thus remains an open question.

Table 1
List of glycosyltransferase activities required for homogalacturonan (HG) biosynthesis

Type of transferase	Working[a] number	Enzyme[b]		Ref.[c] for structure
		Acceptor substrate	Enzyme activity	
Glycosyl-				
D-GalAT	I	*GalAα1,4-GalA	*α1,4-GalAT*	(O'Neill et al., 1990)
D-GalAT	II[d]	GalAα1,2-L-Rha	*α1,4-GalAT*	–
D-XylT	I	GalAα1,4-GalA	*β1,3 XylT*	(Aspinall, 1980; Yu and Mort, 1996; Kikuchi et al., 1996; Schols et al., 1995)
Methyl-				
HG-methyltransferase (HG-MT)		$GalA\alpha1,4\text{-}GalA_{(n)}$		(Goubet et al., 1998; Vannier et al., 1992; Kauss and Hassid, 1967)
Acetyl-				
HG: GalA-3-*O*-acetyltransferase (HG-AT)		$GalA\alpha1,4\text{-}GalA_{(n)}$		(Ishii, 1997a,b; De Vries et al., 1986; Ishii, 1995; Rombouts and Thibault, 1986)

[a] Enzymes that transfer the same type of glycosyl residue to different acceptors are given numbers to facilitate identification of the specific glycosyltransferase activities. Note that the numbers are different from those in (Mohnen, 1999) since the glycosyltransferases have been grouped according to the type of pectic polysaccharide they synthesize.

[b] All sugars are D sugars and have pyranose rings unless otherwise indicated. Glycosyltranferases add to the glycosyl residue on the left* of the indicated acceptor.

[c] Refs. for the structure.

[d] Enzyme that may be required to make an RG-I/HG junction.

Table 2
List of glycosyltransferase activities required for RG-I biosynthesis

Type of glycosyl-transferase	Working[a] number	Parent polymer	Enzyme[b]		Ref.[c] for structure
			Acceptor substrate	Enzyme activity	
D-GalAT	I	RG-I	*L-Rhaα1,4-GalA	*α1,2-GalAT*	(O'Neill et al., 1990; Eda et al 1986; Lau et al., 1985)
D-GalAT	II[d]	RG-I/HG	GalAα1,2-L-Rha	*α1,4-GalAT*	–
L-RhaT	I	RG-I	GalAα1,2-L-Rha	α1,4-L-RhaT	(O'Neill et al.,1990; Eda et al., 1986; Lau et al, 1985)
L-RhaT	II[d]	HG/RG-I	GalAα1,4-GalA	*α1,4-L-RhaT*	–
D-GalT	I	RG-I	L-Rhaα1,4-GalA	*β1,4-GalT*	(O'Neill et al., 1990; Lau et al., 1987)
D-GalT	II	RG-I	Galβ1,4-Rha	*β1,4-GalT*	(O'Neill et al., 1990; Lau et al., 1987)
D-GalT	III	RG-I	Galβ1,4-Gal	*β1,4-GalT*	(Morita. 1965a,b; Aspinall et al., 1967; Stephen. 1983; Aspinall. 1980; O'Neill et al., 1990; Lau et al., 1987)
D-GalT	IV	RG-I	Galβ1,4-Gal	*β1,6-GalT*	(O'Neill et al., 1990; Lau et al., 1987)
D-GalT	V	RG-I/AGP[e]	Galβ1,3-Gal	*β1,3-GalT*	(Carpita and Gibeaut, 1993)
D-GalT	VI	RG-I/AGP	Galβ1,3-Gal	*β1,6-GalT*	(Carpita and Gibeaut, 1993)
D-GalT	VII	RG-I/AGP	Galβ1,6-Galβ1,3-Gal	*β1,6-GalT*	(Carpita and Gibeaut, 1993)
L-AraT	I	RG-I	Galβ1,4-Rha	*α1,3-l-ArafT*	(O'Neill et al., 1990; Lau et al., 1987)
L-AraT	II	RG-I	L-Ara*f*α1,3-Gal	*α1,2-L-ArafT*	(O'Neill et al., 1990; Lau et al., 1987)
L-AraT	III	RG-I	L-Ara*f*α1,2-Ara	*1,5-L-ArafT*	(O'Neill et al., 1990; Lau et al., 1987)
L-AraT	IV	RG-I	L-Rhaα1,4-GalA	*ArafT*	(Lau et al., 1987)
L-AraT	V	RG-I	L-Ara*f*α1,5-Araf	*α1,5-L-ArafT*	(Carpita and Gibeaut, 1993)
L-AraT	VI	RG-I	L-Araα1,5-Araf	*α1,2-L-ArafT*	(Carpita and Gibeaut, 1993)
L-AraT	VII	RG-I	L-Ara*f*α1,5-Araf	*α1,3-L-ArafT*	(Carpita and Gibeaut, 1993)
L-AraT	VIII	RG-I	L-Ara*f*α1,3-Araf	*α1,3-L-ArafT*	(Carpita and Gibeaut, 1993)
L-AraT	IX	RG-I	Galβ1,4-Gal	*α1,3-L-ArafT*	(Morita, 1965a,b; Aspinall, et al., 1967; Stephen, 1983; Aspinall, 1980; O'Neill et al., 1990; Carpita and Gibeaut, 1993)
L-AraT	X	RG-I	L-Ara*f*-1,3-Gal	*1,5-L-ArafT*	(Morita, 1965a,b; Aspinall et al., 1967b; Stephen, 1983b; Aspinall, 1980)
L-AraT	XI	RG-I/AGP	Galβ1,6-Gal	*α1,3-L-ArafT*	(Carpita and Gibeaut, 1993)
L-AraT	XII	RG-I/AGP	Galβ1,6-Gal	*α1,6-L-ArafT*	(Carpita and Gibeaut, 1993)
L-FucT	I	RG-I	Galβ1,4-Gal	*α1,2-L-FucT*	(O'Neill et al., 1990; Lau et al., 1987)
D-GlcAT	I	RG-I	Gal....	*β1,6GlcAT*	(An et al., 1994)
D-GlcAT	II	RG-I	Gal....	*β1,4GlcAT*	(An et al., 1994)
Methyl- RG-I: GlcA-4-*O*-methyltransferase	–	RG-I	GlcAβ1,6-Gal		(An et al., 1994)
Acetyl- RG-I: GalA-3-O/2-*O*-acetyltransferase	–	RG-I	GalAα1,2-L-Rhaα1,4$_{(n)}$		(Lerouge et al., 1993; Ishii, 1997a; O'Neill et al., 1990; Bacic et al., 1988; Komalavilas and Mort, 1989)

[a] Enzymes that transfer the same type of glycosyl residue to different acceptors are given numbers to facilitate identification of the specific glycosyltransferase activities. Note that the numbers are different from those in (Mohnen, 1999) since the glycosyltransferases have been grouped according to the type of pectic polysaccharide they synthesize.

[b] All sugars are D sugars and have pyranose rings unless otherwise indicated. Glycosyltranferases add to the glycosyl residue on the left* of the indicated acceptor.

[c] Refs. for the structure.

[d] Enzyme that may be required to make an HG/RG-I junction.

[e] This enzymatic activity would also be required to synthesize arabinogalactan proteins (AGPs).

Data from biochemical and structural studies of the pectic polysaccharides suggest that HG and RG-II are covalently linked in the wall. It is likely that HG serves as the backbone for RG-II synthesis. It is also possible that HG and RG-I are linked in the wall, however, definitive chemical evidence for that linkage has not been reported.

2.3. Nucleotide sugars, transporters, and a general model for the topology of pectin biosynthesis

The pectin biosynthetic glycosyltranferases studied to date all use nucleotide-sugars as substrates for in vitro enzymatic reactions and it is believed that nucleotide sugars are the immediate substrates for the reactions in

Table 3
List of glycosyltransferase activities required for RG-II biosynthesis

Type of glycosyltransferase	Working[a] number	Parent polymer	Enzyme[b]		Ref.[c] for structure
			Acceptor substrate	Enzyme activity	
D-GalAT	I	HG/RG-II[d]	*GalAα1,4-GalA	*α1,4-GalAT*	(O'Neill et al., 1990)
D-GalAT	II	RG-II	L-Rhaβ1,3′-Apif	*α1,2-GalAT*	(O'Neill et al., 1997; Carpita and Gibeaut, 1993)
D-GalAT	III	RG-II	L-Rhaβ1,3′-Apif	*β1,3GalAT*	(O'Neill et al., 1997; Carpita and Gibeaut, 1993)
L-RhaT	I	RG-II	Apifβ1,2-GalA	*β1,3′-L-RhaT*	(O'Neill et al., 1997; Carpita and Gibeaut, 1993)
L-RhaT	II	RG-II	Kdo2,3GalA	*α1,5-L-RhaT*	(O'Neill et al., 1997; Carpita and Gibeaut, 1993)
L-RhaT	III	RG-II	L-Arapα1,4-Gal	*α1,2- L-RhaT*	(O'Neill et al., 1997; Carpita and Gibeaut, 1993)
L-RhaT	IV	RG-II	L-Arapα1,4-Gal	*β1,3- L-RhaT*	
L-GalT	I	RG-II	GlcAβ1,2-Fuc	*α1,2-L-GalT*	(Reuhs et al., submitted; O'Neill et al., 1997; Carpita and Gibeaut, 1993)
D-GalT	II	RG-II	L-Ace*f*Aα1,3-Rha	*β1,2GalT*	(Vidal et al., 2000; O'Neill et al., 1997; Carpita and Gibeaut, 1993)
L-AraT	I	RG-II	Dha2,3-GalA	*β1,5-L-ArafT*	(O'Neill et al., 1997; Carpita and Gibeaut, 1993)
L-AraT	II	RG-II	Galβ1,2- L-Ace*f*A	*α1,4-L-ArapT*	(Vidal et al., 2000; O'Neill et al., 1997; Carpita and Gibeaut, 1993)
L-AraT	III	RG-II	L-Rhaα1,2-L-Ara	*β1,2- L-ArafT*	(O'Neill et al., 1997; Carpita and Gibeaut, 1993)
L-FucT	I	RG-II	L-Rhaβ1,3′-Api*f*	*α1,4-L-FucT*	(O'Neill et al., 1997; Carpita and Gibeaut, 1993)
L-FucT	II	RG-II	Galβ1,2-L-Ace*A*f	*α1,2-L-FucT*	(Vidal et al., 2000; O'Neill et al., 1997; Carpita and Gibeaut, 1993)
D-ApifT	I	RG-II	GalAα1,4-GalA	β1,2-Api*f*T	(O'Neill et al., 1997; Carpita and Gibeaut, 1993)
D-XylT	I	RG-II	L-Fucα1,4-L-Rha	*α1,3XylT*	(O'Neill et al., 1997; Carpita and Gibeaut, 1993)
D-GlcAT	III	RG-II	L-Fucα1,4-L-Rha	*β1,4GlcAT*	(O'Neill et al., 1997; Carpita and Gibeaut, 1993)
D-KdoT	I	RG-II	GalAα1,4-GalA	*2,3KdoT*	(O'Neill et al., 1997; Carpita and Gibeaut, 1993)
D-DhaT	I	RG-II	GalAα1,4-GalA	*2,3DhaT*	(O'Neill et al., 1997; Carpita and Gibeaut, 1993)
L-AcefA	I	RG-II	L-Rhaβ1,3′-Api*f*	*α1,3AceAfT*	(Vidal et al., 2000; O'Neill et al., 1997; Carpita and Gibeaut, 1993)
Methyl-					
RG-II: xylose-2-*O*-methyltransferase	–	RG-II	D-Xylα1,3-L-Fuc		(O'Neill et al., 1997; Carpita and Gibeaut, 1993)
RG-II: fucose-2-*O*-methyltransferase	–	RG-II	L-Fucα1,2-D-Gal		(O'Neill et al., 1997; Carpita and Gibeaut, 1993)
Acetyl-					
RG-II: fucose-acetyltransferase	–	RG-II	L-Fucα1,2-D-Gal		(O'Neill et al., 1997; Carpita and Gibeaut, 1993)
RG-II: aceric acid-3-*O*-acetyltransferase	–	RG-II	L-Ace*f*Aα1,3-L-Rha		(Vidal et al., 2000; O'Neill et al., 1997; Carpita and Gibeaut, 1993)

[a] Enzymes that transfer the same type of glycosyl residue to different acceptors are given numbers to facilitate identification of the specific glycosyltransferase activities. Note that the numbers are different from those in (Mohnen, 1999) since the glycosyltransferases have been grouped according to the type of pectic polysaccharide they synthesize.

[b] All sugars are D sugars and have pyranose rings unless otherwise indicated. Glycosyltranferases add to the glycosyl residue on the left* of the indicated acceptor.

[c] Refs. for the structure.

[d] GalAT-I may be the same as GalAT-I for HG synthesis if RG-II is synthesized onto an existing HG backbone.

vivo (Mohnen, 1999). The nucleotide sugars required for pectin biosynthesis and progress towards understanding the biochemical pathways by which they are synthesized has recently been reviewed (Mohnen, 1999). The nucleotide sugars are, for the most part (see Hayashi et al., 1988, for a possible exception) believed to be synthesized on the cytosolic side of the Golgi. However, the transferase reactions that catalyze the synthesis and modification of the polysaccharide backbone and side chains are believed to occur in the Golgi. Thus, mechanisms are required to transport the nucleotide sugars across the Golgi membrane. Data from animal systems (Capasso and Hirschberg, 1984) and plants (Munoz et al., 1996; Wang et al., 1997; Neckelmann and Orellana, 1998) suggest that this transport is achieved by nucleotide-sugar:nucleoside monophosphate antiporters. The availability of nucleotide-sugars differentially labeled on both the nucleotide and sugar moieties will facilitate the study of Golgi-localized transporters involved in pectin biosynthesis (Orellana and Mohnen, 1999).

A working model for the topology of pectin synthesis is shown in Fig. 5. It is proposed that the nucleotide-sugars are synthesized on the cytosolic side of the Golgi

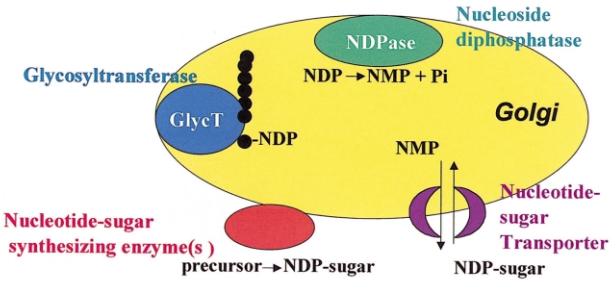

Fig. 5. A model for pectin biosynthesis. The model predicts that pectin biosynthesis is dependent upon the formation of the required nucleotide-sugars by nucleotide-sugar transformation reactions that occur on the cytosyolic side of the Golgi. The nucleotide-sugars are transported into the Golgi by specific nucleotide-sugar:nucleoside monophosphate antiporters. Once inside the Golgi, the nucleotide-sugar is used as a substrate by glycosyltransferases that are specific for the type of nucleotide sugar, the type of oligo/polysaccharide acceptor, and the nature of the anomeric configuration and linkage of the glycosyl linkage formed. The released nucleoside monophosphate is hydrolyzed by a Golgi-localized nucleoside diphosphatase and the nucleoside monophosphate and the inorganic phosphate are transported out of the Golgi by separate transporters (Munoz et al., 1996; Wang et al., 1997; Neckelmann and Orellana, 1998; Sterling et al., submitted).

and transported into the Golgi lumen by specific nucleotide-sugar:nucleoside monophosphate antiporters. The nucleotide-sugar is used as a substrate by the glycosyltransferase and the glycosyl residue is transferred onto a growing polysaccharide chain. The released nucleoside diphosphate (NDP) is hydrolyzed by a Golgi-localized nucleoside-5′-diphosphatase (Orellana et al., 1997) into NMP and inorganic phosphate, making available the nucleoside monophosphate for the nucleotide-sugar:nucleoside monophosphate antiporter. The regulation of pectin biosynthesis could occur during the formation of the nucleotide-sugar, the transport of the nucleotide-sugar into the Golgi, or at the level of the glycosyltransferase or other polymer modifying enzymes. One challenge for the next decade is to identify the molecular components required for each step of pectin biosynthesis. Many questions need to be addressed including: Does the proposed model hold for all of the glycosyl residues found in pectin? Are nucleotide-sugars the immediate glycosyl donors for all the pectin biosynthetic glycosyltransferases or are lipid-linked donors involved? Are all the required nucleotide-sugars made outside the Golgi, or are some made in the Golgi as has been suggested for UDP-Xyl (Hayashi et al., 1988)? Do the levels of nucleotide-sugars in the Golgi fluctuate and, if so, does this level regulate the relative activity of different types of glycosyltransferases? What is the organization of the different glycosyltransferases in the Golgi? How is this organization made and maintained? How is the inorganic phosphate generated by the nucleoside diphosphatase transported out of the Golgi? Does the transport of phosphate establish or maintain an ion gradient in the Golgi that is required for pectin synthesis?

2.4. Synthesis of homogalacturonan

Most effort towards understanding pectin biosynthesis has been directed towards two enzymes believed to be involved in the synthesis of homogalacturonan (HG) in planta: a homogalacturonan-α1,4galacturonosyltransferase (also referred to as polygalacturonate:α1,4-galacturonosyltranferase) and homogalacturonan-methyltransferase (also referred to as pectin methyltransferase) (see Table 1).

2.4.1. α1,4Galacturonosyltransferase (GalAT)

A membrane-bound α1,4galacturonosyltransferase (GalAT) has previously been identified and partially characterized in mung bean (Kauss and Swanson. 1969; Villemez et al., 1966), tomato (Lin et al., 1966), turnip (Lin et al., 1966), and sycamore (Bolwell et al., 1985), and more recently in suspension cultured tobacco cells (Doong et al., 1995), radish roots (H.F. Quigley, and D. Mohnen, unpublished results), enriched Golgi from elongating pea epicotyls (Sterling et al., submitted) and arabidopsis (J. Sterling and D. Mohnen, unpublished results). The GalAT from tobacco has been most extensively characterized. GalAT adds [^{14}C]GalA from UDP-[^{14}C]GalA (Liljebjelke et al., 1995) onto endogenous acceptors in membrane preparations to produce a radiolabeled product of large M_r (i.e. ~105 kDa in tobacco microsomal membranes (Doong et al., 1995) and ⩾500 kDa in pea Golgi (Sterling et al., submitted). The cleavage of up to 89% of the radiolabeled tobacco product into GalA, diGalA and triGalA upon exhaustive hydrolysis with a purified endopolygalacturonase confirmed that the product synthesized was largely HG. Since approximately 90% of the GalA in the primary wall is present in HG (Mohnen et al., 1996), these results suggest that the identified activity may be the GalAT responsible for the elongation of HG. The enzyme was thus named polygalacturonate α-4-galacturonosyltransferase (EC 2.4.1.43) (PGA-GalAT) in accordance with the nomenclature for a comparable enzyme activity in mung bean microsomes (Villemez et al., 1965, 1966; Lin et al., 1966; Kauss and Swanson, 1969). The product synthesized in vitro in tobacco microsomes is ~ 50% esterified and at least 40% of the ester is a C-6 methylester (Doong et al., 1995). These results are consistent with a model of pectin biosynthesis in which the newly synthesized HG is directly, or somewhat belatedly, esterified during synthesis.

Fractionated membranes from pea were recently used to localize GalAT to the Golgi and to demonstrate that the catalytic site of GalAT is on the lumenal side of the Golgi (Sterling et al., submitted). These results provide the first direct enzymatic evidence that a pectin biosynthetic glycosyltransferase (i.e. GalAT) resides in the Golgi.

GalAT was solubilized from membranes and shown to add GalA onto the non-reducing end (Scheller et al.,

1999) of exogenous HG acceptors (oligogalacturonides; OGAs) of a degree of polymerization $\geqslant 10$ (Doong and Mohnen, 1998). Surprisingly, the bulk of the HG is elongated by a single GalA residue in vitro using either solubilized GalAT from tobacco membranes (Doong and Mohnen, 1998) or detergent-permeabilized Golgi from pea (Sterling et al., submitted). Thus, the solubilized GalAT does not express the processivity expected for a polymer synthase. The lack of processivity of the solubilized GalAT may be due to the dissociation of an enzyme complex during solubilization, to the loss of a factor/activator required for processivity, or to the absence of a required substrate(s). Alternatively, the GalAT may not be a processive GalAT but rather a GalAT involved in a priming reaction for HG or in some other pectin biosynthetic reaction. One question that needs to be resolved is: How many contiguous GalA residues are added onto the endogenous acceptor in Golgi or microsomal preparations? In other words, how processive is the membrane-bound GalAT?

The possibility that an acceptor other than oligogalacturonides (OGAs) of DP 10-23 is required to convert the solubilized GalAT into a processive enzyme has been investigated. Specific oligosaccharide acceptor structures have been shown to be required for the processivity of other types of glycosyltransferases (Kojima et al., 1996). For example, a mammalian α2,8-polysialic acid synthase acts processively only when its protein acceptor has a specific α-1,6-linked fucose in its N-linked glycans (Kojima et al., 1996). In this case only one, or a few, sialic acid residues are added to structurally related acceptors without the α-1,6-linked fucose. Studies with GalAT suggest that neither polygalacturonic acid nor pectins of various degrees of esterification (31–90%) stimulate GalAT activity above the rate achieved with OGAs (R.L. Doong and D. Mohnen, unpublished results). GalAT activity is also not stimulated by GalA, diGalA or triGalA as individual acceptors. A question that must still be addressed is: Is endogenous HG in Golgi and in microsomal membranes a better substrate to promote processivity of GalAT in vitro than HG oligomers or commercially available PGA or pectin?

The possibility that high (>1 mM) concentrations of the substrate UDP-GalA might convert solubilized GalAT into a processive mode of action has also been tested. An effect of substrate concentration on the structure of a polymer synthesized by a glycosyltransferase has been reported for the in vitro synthesis of (1→3),(1→4) β-glucan in which the ratio of cellotriosyl to cellotetraosyl sequences increases from 1.5 to 11 as the concentration of UDP-Glc is increased from 5 μM to 30 mM (Buckeridge et al., 1999). The results of preliminary studies with GalAT, however, suggest that high concentrations (>1 mM) of UDP-GalA do not convert in vitro GalAT into a processive mode of action (H.F. Quigley and D. Mohnen, unpublished results).

HG isolated from the wall is partially methyl esterified and acetylated. Thus, it is possible that processivity of GalAT requires the simultaneous action of GalAT, HG-methyltransferase and/or HG-acetyltransferase. The in vitro synthesis of HG by GalAT in microsomal membranes, however, is not stimulated by the methyl donor S-adenosylmethionine (Kauss and Swanson, 1969; Doong et al., 1995) and/or the acetyl donor acetylCoA (D. Mohnen, unpublished results). Thus, no evidence has been obtained to support the idea that in vitro synthesis of HG by membrane bound GalAT requires concurrent methylation and/or acetylation of HG.

An obstacle to the study of GalAT is the time and expense required to synthesize UDP-[^{14}C]GalA. Radiolabeled UDP-GalA can be produced by the enzymatic epimerization of UDP-[^{14}C]GlcA to UDP-[^{14}C]GalA (Liljebjelke et al., 1995). Recently, a procedure for the one step production of UDP-[^{14}C]GalA has been reported (Basu et al., 2000). The procedure is based on the enzymatic oxidation of UDP-[^{14}C]Gal to UDP-[^{14}C]GalA (Rao and Mendicino, 1976; Kelleher and Bhavanandan, 1986). Basu et al. (2000) report a yield of $>90\%$ UDP-[^{14}C]GalA using a polyethyleneimine (PEI-cellulose) column chromatography purification step. We have found, using a slightly modified verison of this procedure, that it is necessary to purify the synthesized UDP-[^{14}C]GalA by HPLC in order to remove contaminants that inhibit GalAT activity. Under these conditions our final yield of UDP-[^{14}C]GalA was 32% (J. Sterling, and D. Mohnen, unpublished results). Further work is required to establish whether the epimerization procedure (approximately 20% yield) or the oxidation procedure (Basu et al., 2000) will prove more useful for the routine synthesis of the radiolabeled UDP-GalA required for studies of pectin biosynthesis.

The purification of GalAT has not yet been reported. Progress towards understanding the role of GalAT in HG synthesis requires that the enzyme be purified and its gene identified.

2.4.2. HG-methyltransferase (HG-MT)

HG-methyltransferase (HG-MT) [the term HG-MT is used in preference to pectin methyltransferase to specify the enzyme that methylates HG rather than RG-I or RG-II] has been identified in microsomal membranes from mung bean (Kauss et al., 1967, 1969; Crombie and Reid, 1998), flax (Vannier et al., 1992; Schaumann et al., 1993), tobacco (Goubet et al., 1998) and soybean hypocotyls (Ishikawa et al., 2000) (see Table 4). The membrane-bound HG-MTs from flax (Bruyant-Vannier et al., 1996; Bourlard et al., 1997a) and from tobacco (Goubet and Mohnen, 1999a) have been solubilized in an active form and the flax enzyme(s) has been partially purified (Bruyant-Vannier et al., 1996). The HG-MT from detergent-treated etiolated soybean hypocotyls is significantly more active (1360 pmol mg^{-1} min^{-1}) than the HG-MT

Table 4
Comparison of catalytic constants and pH optima for HG-methyltransferases involved in, or potentially involved in, pectin biosynthesis[a]

Enzyme[b]	Plant source	Apparent K_m for SAM[c]	pH optimum	V_{max}[d]	Ref
HG-MT[b]	Mung bean	59 μM	6.6–7.0	2.7[e]	(Kauss and Hassid, 1967; Kauss et al., 1969; Kauss et al., 1967)
PMT	Flax	10–30 μM	6.8	n.d.[g]	(Schaumann et al., 1993; Vannier et al., 1992)
PMT (sol)[f]	Flax	0.5 μM	7.1[h] or 5.5[i]	n.d.	(Bourlard et al., 1997a,b; Bruyant-Vannier et al., 1996)
HG-MT	Tobacco	38 μM	7.8	49	(Goubet et al., 1998)
HG-MT (sol)	Tobacco	18 μM	7.8	7.3	(Goubet and Mohnen, 1999a)
PMT-MT	Soybean	230 μM	6.8	1360	(Ishikawa et al., 2000)

[a] Unless indicated, all enzymes are measured in particulate preparations.
[b] All enzymes are thought to be HG-MT. However, since some authors use the previous name, pectin methyltransferase, it is included for clarity.
[c] Apparent K_m for *S*-adenosylmethionine.
[d] V_{max} in pmol min^{-1} mg^{-1} protein.
[e] The V_{max} is our calculation using data from Kauss et al. (1969).
[f] (sol): Detergent-solublized enzyme.
[g] n.d.: Not determined.
[h] From Bruyant-Vannier et al. (1996).
[i] From Bourlard et al. (1997a,b).

from mung bean, flax and tobacco (i.e. 3–49 pmol mg^{-1} min^{-1}, reviewed in Goubet et al., 1998). The apparent K_m of 0.23 mM for *S*-adenosylmethionine (SAM) reported for the soybean enzyme (Ishikawa et al., 2000) is much higher than the values reported for the other HG-MTs, 30–59 μM for membrane-bound HG-MTs (see Table 4 and Goubet et al., 1998) and 0.5–18 μM for solubilized HG-MT.

The low HG-MT activity recovered has hampered the purification of HG-MT or other pectin methyltransferases (Bourlard et al., 1997a). Thus, the increased activity recovered from soybean is noteworthy. The HG-MT from soybean (Ishikawa et al., 2000) was assayed by spotting the radiolabeled product onto paper, followed by paper chromatography to remove the unincorporated radiolabeled SAM. The product immobilized at the base of the paper chromatogram strip was analyzed by scintillation counting. Most other studies of HG-MT have employed a precipitation method to recover synthesized product. The precipitation method may not recover all of the methylated product (Pauly and Scheller, 2000). Alternatively, differences in the recovered HG-MT activity may depend on the plant species, on the amount and type of exogenous pectic acceptors used, or on whether intact membranes, detergent permeabilized membranes, or solubilized enzyme are used.

A question regarding the synthesis and methylation of HG is: How are the activities of GalAT and HG-MT coordinated during the synthesis of HG? The methylesterification of HG in membranes from mung bean (Kauss and Swanson, 1969) and tobacco (Goubet et al., 1998) is increased by the addition of UDP-GalA, a substrate for HG synthesis. The stimulation of HG-MT activity by UDP-GalA would be expected if either HG synthesis, or HG substrate, was required for endogenous methylation of HG. Evidence from studies with intact membranes in which UDP-GalA stimulates HG-MT activity (Kauss and Swanson, 1969; Goubet et al., 1998), and from studies using detergent-permeabilized membranes and solubilized HG-MT in which polygalacturonic acid or partially methylesterified pectin serve as acceptors of HG-MT, support the hypothesis that at least a small stretch of HG is synthesized prior to its methylation by HG-MT in the Golgi. However, the available results regarding the relationship between the action of GalAT and HG-MT need to be confirmed by reconstitution experiments using cloned and/or purified enzymes, and by using plants transgenically modified in the pectin biosynthetic genes.

Tobacco membrane-bound HG-MT has been localized to the Golgi and its catalytic site shown to face the Golgi lumen (Goubet and Mohnen, 1999b). These observations are consistent with earlier reports that mung bean HG-MT resides in a membrane compartment (Kauss and Swanson, 1969), and that a pectin methyltransferase from pea epicotyls is located in the Golgi (Baydoun et al., 1999). Similarly, about half of the pectin methyltransferase activity from flax co-fractionates with Golgi vesicles (Vannier et al., 1992; Bourlard et al., 1997b). The co-localization of the catalytic sites of GalAT and HG-MT in lumen of the Golgi support the notion that these enzymes act together, either sequentially or as a complex, during the synthesis of HG. Two questions that must be addressed are: How many different HG-MTs are required for HG synthesis?, and What is the substrate specificity of the HG-MT(s)? The fact that at least one HG-MT in detergent-permeabilized membranes from flax and soybean shows a preference for partially esterified pectin over polygalacturonic acid (Bourlard et al., 1997b; Ishikawa et al., 2000), suggests

that multiple HG-MTs may exist that either initiate the methylation of HG or enhance the further methylation of HG. Different HG-MTs may also exist that recognize other structural differences in HG (e.g. degree of acetylation or other modifications).

2.4.3. HG-acetyltransferase (HG-AT)

A pectin *O*-acetyltransferase activity has been identified in microsomes from suspension-cultured potato cells (Pauly and Scheller, 2000). Incubation of potato microsomes with [^{14}C]acetyl-CoA resulted in the recovery of a NaCl/ethanol precipitable product. Approximately 8% of the radiolabeled product was specifically solubilized by treatment EPGase and PME indicating that [^{14}C]acetate had been transferred either to HG, or to RG-II or RG-I that was covalently attached to HG. Further work is required to establish whether the described activity is an HG-AT or an acetyltransferase that acetylates one of the other pectic polysaccharides that is covalently linked to HG.

2.5. Synthesis of rhamnogalacturonan-I (RG-I)

2.5.1. RG-I-galactosyltransferase (RG-I-GalT)

Galactosyltransferase activity has been identified in particulate cell free homogenates from mung bean (McNab et al., 1968; Panayotatos and Villemez, 1973). It is possible that RG-I biosynthetic galactosyltransferases (see Table 2) were among those present in the homogenate since the synthesized product contained some β-1,4-galactan and a lesser amount of β-1,3-galactan (Panayotatos and Villemez, 1973). More recently, a β-1,4-galactosyltransferase activity with a pH of optimum of 6.5 has been identified in membrane preparations from mung bean hypocotyls based on sensitivity of the product to fragmentation by endo-β-1,4-galactanase (Brickell and Reid, 1996). Such results are consistent with an RG-I biosynthetic β-1,4-galactosyltransfserase in mung bean microsomal membranes. Galactosyltransferases have also been studied in particulate homogenates (Goubet and Morvan, 1993, 1994) and solubilized enzymes (Goubet, 1994) from flax. The chemical properties of some of the products synthesized in flax are consistent with those expected for GalTs involved in RG-I or arabinogalactan protein synthesis. However, glycosyl-linkage composition analysis of the synthesized product, or proof that the products are cleaved with RG-I-specific enzymes, is required to confirm this interpretation.

An RG-I:β-1,4-galactosyltransferase in suspension-cultured potato cells transfers [^{14}C]Gal from UDP-[^{14}C]Gal onto endogenous acceptor(s) in the membranes (Geshi et al., 2000). The synthesized product was fragmented by a purified endo-β-1,4-galactanase and rhamnogalacturonase A (an endohydrolase that cleaves the glycosidic linkage between the GalA and the Rha in the backbone of RG-I; Azadi et al., 1995), showing that the GalT catalyzed the transfer of galactose to RG-I. The β-1,4-galactosyltransferase had a pH optimum of 6.0–6.5 and required Mn^{2+} for maximum activity. The intact [^{14}C]Gal-labeled product synthesized in potato membranes had an estimated size of >500 kDa. Fragmentation of the intact product using endo-β-1,4-galactanase yielded [^{14}C]Gal and [^{14}C]galactobiose as the primary radiolabeled products. Cleavage of the intact and de-esterified (to remove methyl and acetyl groups from the RG-I backbone) product with rhamnogalacturonase A fragmented the product into material between 50 and 180 kDa in size. Subsequent treatment of the [^{14}C]Gal-labeled fragments with endo-β-1,4-galactanase yielded [^{14}C]Gal and slightly larger fragments that themselves could be cleaved to [^{14}C]Gal by a purified β-galactosidase. Taken together, these results support the conclusion that potato microsomal membranes contain enzymes that both initiate, and elongate, β-1,4-galactan side chains of RG-I.

2.5.2. RG-I-arabinosyltransferase

Arabinosyltransferases putatively involved in the synthesis of RG-I side chains have been recently reviewed (Mohnen, 1999). One advance in this area is the description of an improved procedure for the synthesis and purification of non-radiolabeled and radiolabeled UDP-β-L-arabinopyranose (Pauly et al., 2000). The UDP-Ara is produced by the enzymatic 4-epimerization of UDP-Xyl to UDP-Ara using a partially purified UDP-xylose-4-epimerase from wheat germ (Fan and Feingold, 1970; Feingold and Avigad, 1980). The UDP-Ara is purified by high performance anion exchange chromatography (HPAEC), a method that also allows quantitation of the product (Pauly et al., 2000).

2.5.3. RG-I-methyltransferase (RG-I-MT)

Detergent-solubilized pectin methyltransferase (PMT) from suspension-cultured flax cells uses an RG-I-enriched fraction from flax fibers as an exogenous acceptor (Bourlard et al., 1997a). In the presence of the RG-I fraction, methyltransferase activity was stimulated 1.5- to 1.7-fold above the endogenous acceptor activity and the radiolabeled product recovered had a size similar to the RG-I fraction. While these results suggest that an RG-I methyltransferase activity may have been identified, it has not yet been shown where in RG-I the methylation occurred. Methylation may have occurred on HG tails covalently linked to RG-I. Thus, the identified activity may result from methylesterification of HG rather than methylesterification of the galacturonic acid in the RG-I backbone. Alternatively, the methylation could have occurred on a non-galacturonic substituent. Some of the side chains of RG-I contain 4-*O*-methylGlcA (An et al., 1994). Further work is required to determine the site(s) of methylation and thus, the identity of the enzyme reported.

2.5.4. RG-I-acetyltransferase (RG-I-AT)

An RG-I acetyltransferase has been identified in microsomes from suspension-cultured potato cells (Pauly and Scheller, 2000). Incubation of potato microsomes with [^{14}C]acetyl-CoA resulted in the recovery of a NaCl/ethanol precipitable product that consisted of at least 19% acetylated RG-I based on the release of [^{14}C]acetate by treatment with a purified rhamnogalacturonan *O*-acetyl esterase (Pauly and Scheller, 2000). The product recovered from the microsomes had a mass >500 kDa and was partially fragmented by treatment with rhamnogalacturonan lyase (RGase B). An assay for RG-I-AT was developed based on specific solubilization of the product with RGase B. RG-I-AT has a pH optimum of 7.0 with 80% of activity retained from pH 6.5 to 8.0. The potato RG-I-AT has an apparent K_m for acetyl-CoA of 35 μM and an apparent V_{max} of 54 pmol min^{-1} mg^{-1} protein.

2.6. Synthesis of rhamnogalacturonan-II (RG-II)

2.6.1. RG-II-methyltransferase (RG-II-MT)

Detergent-solubilized pectin methyltransferase (PMT) from suspension-cultured flax cells is able to use RG-II isolated from wine as an exogenous acceptor (Bourlard et al., 1997a). In the presence of RG-II, the methyltransferase activity was stimulated 7-fold above the endogenous acceptor activity and the radiolabeled product had a size similar to RG-II monomers and RG-II dimers. While these results suggest that an RG-II-MT activity (see Table 3) may have been identified, it has not yet been shown where in RG-II the methylation occurred. Methylation of the HG "tails" covalently linked to RG-II, would represent methylesterification of HG rather than methylesterification of RG-II. Alternatively, the activity may represent methyletherification of side chain residues since RG-II side chains contain 2-*O*-methyl xylose and 2-*O*-methyl fucose (Darvill et al., 1978). Further research is required to determine the location of methylation and thus, the identity of the potentially novel enzyme activity.

2.6.2. Pressing needs in pectin biosynthesis research

Progress in understanding how pectin is synthesized requires that genes that encode the biosynthetic enzymes be identified. The genes are essential to generate the tools (e.g. antibodies against the biosynthetic enzymes and transgenic plants modified in pectin biosynthesis) needed to elucidate the structure and function of each enzyme and to determine how the enzymes work together to synthesize the structurally complex pectic polysaccharides. Furthermore, a study of the regulation of the pectin biosynthetic genes may indicate how the fine structure of pectin is altered during plant growth and development. The production of transgenic plants modified in the synthesis of pectin will allow the testing of hypotheses, the establishment of models of pectin biosynthesis, and the elucidation of the function(s) of pectin in the plant.

As noted above, the identification of pectin biosynthetic genes will undoubtedly come, in part, through the purification of the biosynthetic enzymes and the use of amino acid sequences to identify the genes in plant DNA databases. It is also likely that putative pectin mutants will be useful for identifying candidate genes, as will DNA sequence/motif similarity computer searches. Gene families for some of the hemicellulose biosynthetic enzymes such as xyloglucan:α1,2-fucosyltranferase (Perrin et al., 1999) and galactomannan: α1,6-galactosyltransferase (Edwards et al., 1999) have been identified. Some of the putative fucosyltransferase and galactosyltransferase genes may encode enzymes involved in RG-II and/or RG-I synthesis. Once the first genes for pectin biosynthetic enzymes are cloned, it is likely that web-based sequence analysis sites, such as the "carbohydrate active enzyme server (CAZY)" established by Bernard Henrissat (http://afmb.cnrs-mrs.fr/~pedro/CAZY/db.html), will be useful aids for the identification of genes for other pectin biosynthetic enzymes. For example, the section of the CAZY site devoted to glycosyltransferases currently contains 51 sequence-based families that are expected to have similar tertiary structure. Thus, once the first pectin galacturonosyltransferase gene (for example) is identified, such sequence/structure-based databases may allow the rapid identification of other putative pectin galacturonosyltransferases. The definitive identification of pectin biosynthetic genes, however, will require proof of enzymatic activity. Thus, one major area of need is the generation of the required nucleotide-sugar and oligo/polysaccharide substrates for the biosynthetic enzymes. This is a challenging problem since many of the chemical or enzymatic methods required to generate the specific fragments needed for use as acceptors for the enzymes are not available. Thus, progress in identifying pectin biosynthetic genes, and in studying the biosynthetic enzymes, will require the combined use of carbohydrate chemistry, biochemistry, molecular biology and genetics.

3. Biological activities of oligogalacturonides

3.1. Introduction

Biologically active carbohydrates that act as signal molecules are called oligosaccharins (reviewed by Côté and Hahn, 1994; Côté et al., 1998). Oligogalacturonides (OGAs), which are linear molecules of two to about twenty α-1,4-D-galactopyranoslyuronic acid (GalA) residues, were the first plant oligosaccharins to be discovered (Bishop et al., 1981; Hahn et al., 1981). OGAs are released upon fragmentation of homogalacturonan (HG) from the plant primary cell wall (reviewed by Côté

et al., 1998). Biological responses to OGAs occur in at least five of the six subclasses of dicotyledonous plants; Magnoliidae, Hamamelidae, Asteridae, Rosidae, Dilleniidae (Côté and Hahn, 1994; Reymond, et al., 1996); in a monocot (Moerschbacher et al., 1999); and a gymnosperm (Asiegbu et al., 1994). A number of different biological responses to OGAs have been reported, and the particular response observed depends on the plant species, the bioassay, and the chemical structure of the OGA used (Côté et al., 1998). A spectrum of modified and unmodified OGAs of various lengths are active in different systems (reviewed by Côté and Hahn, 1994; for recent examples see Reymond et al., 1996; Weber et al., 1996; Simpson et al., 1998; Spiro et al., 1998; Moerschbacher et al., 1999). The biological responses of plants to OGAs can be divided into two broad categories: plant defense, and plant growth and development (Côté and Hahn, 1994).

3.2. Oligogalacturonide-induced responses involved in plant defense

Pathogens enter plant tissues in at least three ways: digesting cell walls, entering through wounds, and invading through natural openings such as stomata. Pectins are one of the first targets of digestion by invading pathogens (Pagel and Heitifuss, 1990). OGAs are released when endopolygalacturonases (EPGases) and endopectate lyases (ePLases) secreted from the pathogen degrade the homogalacturonan in the cell wall (Côté et al., 1998). The OGAs released are a carbon source for the pathogens, but can also be detected by plants as signals to initiate defense responses. A plant may attempt to limit introgression by the pathogen in several ways. For example, the plant may strengthen its cell walls, close its stomata, synthesize phytoalexins and other antibiotic compounds, synthesize pathogenesis-related (PR) proteins and toxic peptides, contain the infection by means of localized cell death resulting from the hypersensitive response (HR), and produce cytotoxic active oxygen species (Low and Merida, 1996; Côté et al., 1998; Bolwell, 1999). Exogenously added OGAs inhibit the light-induced opening of stomata in tomato and *Commelina communis* L. leaves (Lee et al., 1999). Stomatal openings provide access to inner leaf tissues required by many plant pathogens (Agrios, 1997), suggesting that the constriction of stomatal apertures is beneficial for plant defense.

The first response observed after the addition of OGAs that is clearly involved in plant defense is the production of active oxygen species, including H_2O_2, and O_2^- (Low and Merida, 1996). This response, termed the oxidative burst, occurs within a few minutes after the addition of OGAs to suspension-cultured soybean (Legendre et al., 1993a), tobacco (Rout-Mayer et al., 1997; Binet et al., 1998), and tomato (Stennis et al., 1998) cells. Protein synthesis was not required for tomato suspension-cultures to initiate an oxidative burst, suggesting that changes in gene expression are not required (Stennis et al., 1998). Intact tomato leaves have been reported to produce active oxygen species in response to systemically (Orozco-Cardenas and Ryan, 1999) or locally (Lee et al., 1999) applied OGAs.

The oxidative burst is an immediate and localized reaction that is believed to have several roles in plant defense (Low and Merida, 1996; Bolwell, 1999). The quantities of reactive oxygen species produced can be cytotoxic and thus are expected to be antimicrobial. Reactive oxygen species are thought to have direct (through cytotoxicity) and indirect (through signaling) roles in the plant cell death required for the HR. Reactive oxygen species induce the expression of defense related genes (Lamb and Dixon, 1997), and are implicated as second messengers that elicit other defense responses, including systemic acquired resistance (SAR) and the HR (Bolwell, 1999). SAR is the induction of defense mechanisms at locations remote from the original wound or infection site that serve to prepare the plant to defend itself against new attacks by pathogens (Sticher et al., 1997). In addition, reactive oxygen species drive the rapid peroxidase-mediated oxidative cross-linking of cell wall lignins, proteins, and carbohydrates, thereby reinforcing the wall against enzymatic maceration by the pathogen (Côté and Hahn, 1994).

OGAs initiate signaling cascades that activate a plant's defense responses and many examples of OGA-elicited induction of defense related genes and proteins have been reported (Côté and Hahn, 1994). The exogenous application of OGAs elicit the expression of proteinase inhibitors (PIs) in tomato plants (Bishop et al., 1984; Moloshok et al., 1992). These PIs inhibit insect proteases and thereby decrease the digestability of plant proteins and reduce the nutrients available to feeding insects (Orozco-Cardenas et al., 1993). OGAs have been shown to induce phenylalanine ammonia-lyase (PAL), the activity of the first enzyme in the phenylpropanoid pathway, in suspension-cultured carrot (Messiaen and VanCutsem, 1994) and tobacco (Lapous, et al., 1998) cells, and in bean cotyledons (Dixon et al., 1989; Tepper and Anderson, 1990). This biochemical pathway leads to the production of phytoalexins and lignin. The activity of chalcone synthase (CHS), which is part of a branch in the phenylpropanoid pathway leading to the production of flavonoids including some phytoalexins, is induced by OGAs in bean cotyledons (Tepper and Anderson, 1990; Rose et al., 1999). The activity of casbene synthetase, an enzyme required for the synthesis of the phytoalexin casbene, is induced by OGAs in castor bean seedlings (Walker-Simmons et al., 1984). Accordingly, OGA-induced phytoalexin accumulation has been observed in soybean cotyledons (Davis et al., 1986a; Komae et al., 1990), bean cotyledons (Dixon et al., 1989; Tepper and Anderson, 1990), castor bean seedlings (Walker-Simmons

et al., 1984), pea pods (Walker-Simmons et al., 1984), and parsley suspension-cultured cells (Davis and Hahlbrock, 1987).

OGAs have a role in the induction of cell wall strengthening in response to pathogenic infection (Côté and Hahn, 1994). OGAs induce a series of cell wall peroxidase isoenzymes in suspension-cultured castor bean cells (Bruce and West, 1989). In the presence of active oxygen species, such peroxidases catalyze the free-radical mediated cross-linking of lignins, proteins, and carbohydrates, thereby strengthening the wall. OGA treatment of bean seedlings induced the accumulation of hydroxyproline-rich glycoproteins (HRGPs) which may also reinforce the cell wall after free-radical mediated cross-linking (Boudart et al., 1995). In addition, OGAs have been shown to induce lignin deposition in suspension-cultured castor bean cells (Bruce and West, 1989), cucumber hypocotyls (Robertson, 1986), and bean cotyledons (Tepper and Anderson, 1990).

Exogenously added OGAs regulate the expression of some enzymes and polypeptides that are involved in extracellular polysaccharide metabolism. For example, OGAs induce β-1,3 glucanase in suspension-cultured parsley cells (Davis and Hahlbrock, 1987), and chitinase in tobacco leaves (Broekaert and Peumans, 1988). Both of these enzymes fragment fungal cell wall polysaccharides. OGAs also elicit the expression of the mRNA and activity of an endogenous EPGase and of endopolygalacturonase-inhibiting protein (PGIP); two proteins involved in the metabolism of homogalacturonans in the cell wall. The elicited EPGase is present in tomato leaves and may have a role in the SAR response to insect feeding (Orozco-Cardenas and Ryan, 1999). PGIP, which was shown to be elicited by OGAs in suspension-cultured bean cells, binds to fungal EPGases in vitro and slows the rates of their enzymatic reactions (Bergmann et al., 1994). Thus PGIP is thought to expedite the plant's defense response by prolonging the life of the elicitor active OGAs in the apoplasm, and slowing the degradation of cell wall pectins (Cervone et al., 1993).

OGAs have been implicated in HR, but their role is unclear. OGAs may have a role in protecting potato tubers from maceration by the bacterial pathogen *Erwinia carotovora*, which causes potato soft rot (Weber et al., 1996). The protection may be mediated by OGA-induced cell death, but more work is needed to confirm this. Indeed, injection of OGAs into tobacco leaves prior to their inoculation with the pathogenic bacteria *Pseudomanas syringae* pv. syringae, completely inhibited the expected hypersensitive reaction (Baker et al., 1990). In contrast, the hypersensitive reaction is only partially inhibited when wheat leaves are injected with OGAs prior to their inoculation with the wheat rust fungus *Puccina graminis* Pers. f. sp. tritici (Moerschbacher et al., 1999).

3.3. Biological responses involved in plant growth and development

Exogenously added OGAs influence the growth and development of plant tissues (Côté and Hahn, 1994). OGAs inhibit auxin-induced pea stem elongation (Branca et al., 1988) and are also active in the tobacco thin-cell layer (TCL) (Tran Thanh Van et al., 1985; Mohnen et al., 1990), and the tobacco leaf explant (Bellincampi et al., 1993) bioassays. When biologically active OGAs are added to media containing specific phytohormone concentrations, TCLs that would normally form few or no organs form flowers, while TCLs that normally form roots form significantly fewer roots (Eberhard et al., 1989; Marfà et al., 1991). Biologically active OGAs inhibit root formation (Bellincampi et al., 1993) and increase stomata formation (Altamura et al., 1998) on tobacco leaf explants incubated in media with specific phytohormone concentrations. All of the affects OGAs have on tobacco explant morphogenesis could be mimicked if the explants were cultured on media containing a lower auxin concentration (Branca et al., 1988; Eberhard et al., 1989; Altamura et al., 1998).

OGAs are involved in fruit ripening. They have been shown to induce ethylene production in the fruits of tomato (Brecht and Huber, 1988; Campbell and Labavitch, 1991) and citrus (Baldwin and Biggs, 1988). Pectic fragments that elicit ethylene production have been extracted from tomato fruit at the breaker stage of ripeness. This suggests that OGAs, presumably released by EPGase, could be involved in initiating the ripening process (Melotto et al., 1994), since exogenous ethylene initiates the ripening process and the production of ethylene is required for ripening (Theologis et al., 1993; Giovannoni, 1997). The role of OGAs in fruit ripening, however, seems to be complex and is not understood. Tomato fruits expressing antisense EPGase mRNA exhibited a 99% reduction in EPGase activity and a substantial reduction in pectin depolymerization, but were unaffected in their ethylene production and overall ripening (Smith et al., 1990). Moreover, the increase in ethylene production during ripening is detected prior to the increase in EPGase production (Grierson and Tucker, 1983), and elevated ethylene levels can induce the accumulation of EPGase mRNA (Sitrit and Bennett, 1998). The addition of trigalacturonide to ripening tomato fruit tissue inhibits the increase in EPGase mRNA and enzyme activity, as well as fruit ripening (Mignani, et al., 1995). These data indicate that although OGAs are involved in tomato fruit ripening, their role in the process is not clear (discussed in Rose et al., 1998).

In every case reported to date where OGAs regulate the growth and development of plant tissues, with the exception of fruit ripening, their effect is the opposite of the effect of added auxin (Branca et al., 1988; Eberhard et al., 1989; Altamura et al., 1998). Accordingly, OGAs

inhibit the auxin-induced expression of the plant oncogene rolB (Bellincampi et al., 1996), and the auxin-induced division of phloem parenchyma cells (Altamura et al., 1998) in tobacco leaf disk explants. OGAs also induce the tobacco leaf explants to produce extracellular H_2O_2 (Bellincampi et al., 2000). However, the H_2O_2 does not appear to have a role in the OGA induced signal transduction pathway leading to the inhibition of rolB expression (Bellincampi et al., 2000). The mechanism by which OGAs act in opposition to the action of auxin is presently unknown.

3.4. The structural requirements for the biological activity of oligogalacturonides

Many studies attributing biological responses to OGAs have used impure mixtures of OGA oligomers that often contain sugars other than galacturonic acid (Côté and Hahn, 1994). The results of such studies must be considered carefully, since molecules other than OGAs may be responsible for the observed biological activities. Furthermore, studies using mixtures of different sizes of OGA oligomers reveal little about the OGA structure that is required for biological activity. Homogeneous, size-fractionated OGAs are relatively easy to prepare, and have been used in some studies (Spiro et al., 1993, 1998). Thus, only studies using size fractionated OGAs will be discussed in this section.

Most biological responses have been attributed to OGAs with a degree of polymerization (DP) from 10 to 16, with the most active sizes being around DP 12 (Côté and Hahn, 1994). These responses include: the induction of phytoalexins in soybean (Davis et al., 1986a; Komae, et al., 1990), the induction of casbene synthetase in castor bean (Jin and West, 1984), the induction of PAL in suspension-cultured carrot cells (Messiaen and Van Cutsem, 1994), the induction of rolB expression in tobacco leaf explants (Bellincampi et al., 1993), the induction of Ca^{2+} influx in suspension-cultured tobacco cells (Mathieu et al., 1991), and the regulation of organogenesis in tobacco TCL and leaf explants (Marfà et al., 1991; Bellincampi et al., 1993). The same size range of OGAs (i.e. DP ~10-16) having a GalA or a Δ-4,5 unsaturated GalA residue at the non-reducing terminus induce the production of phytoalexins in soybean cotyledons, indicating that 4,5-unsaturation of the non-reducing terminal GalA does not greatly influence the biological activity of the OGAs (Hahn et al., 1981; Davis et al., 1986b; Komae et al., 1990). In contrast, modifications of the reducing terminus including biotinylation, tyramination, C_1 reduction, and C_1 oxidation decrease the biological activity of OGAs 2–6 fold in the tobacco TCL bioassay and 2–32 fold in suspension-cultured tobacco cell extracellular alkalinization bioassays (Spiro et al., 1998). Chemical esterification of the C_6 carboxylates of OGAs greatly diminishes their ability to elicit casbene synthetase in castor bean, whereas subsequent deesterification restores their biological activity (Jin and West, 1984). This shows that, at least in the case of induction of casbene synthetase, free carboxylates are necessary for activity.

The minimum size of OGAs required for most of the biological activities reported, and the minimum size requirement for the formation of a Ca^{2+}-dependent conformation often called the "egg-box" conformation, coincide at a DP of approximately 10 (Kohn, 1975; Côté and Hahn, 1994; Messiaen and Van Cutsem, 1994; Thakur et al., 1997). Millimolar Ca^{2+} is required for biological activity of OGAs in carrot and tobacco cell suspensions (Mathieu et al., 1991; Messiaen and Van-Cutsem, 1994) which suggests that a Ca^{2+}-dependent conformation formed by OGAs with DPs $\geqslant 10$ is required for biological activity in certain bioassays (Côté and Hahn, 1994; Messiaen and VanCutsem, 1994). The polyamines spermidine and spermine are believed to selectively prevent OGAs from adopting the Ca^{2+}-dependent conformation (Messiaen and Van Cutsem, 1999). Physiological concentrations of these polyamines inhibit the biological activity of OGAs in carrot cell suspensions, suggesting that they modulate the biological activity of OGAs by preventing the Ca^{2+}-dependent formation of an active conformation (Messiaen and VanCutsem, 1999).

There are several reports showing that OGAs other than those with DPs from 10 to 17 are biologically active (Côté and Hahn, 1994). For example, OGAs from DP 2 to 30 elicit the expression of proteinase inhibitors (PIs) in tomato seedlings, with the disaccharide being the most active (Farmer et al., 1990; Moloshok et al., 1992). In this system, di- and tri-GalA with Δ-4,5 unsaturated GalA at the non-reducing terminus are active, whereas C_1 reduced oligomers are not. OGAs with a DP from two to six induce ethylene biosynthesis in tomato plants, with the pentasaccharide being the most active (Simpson et al., 1998). Trigalacturonide is active in inhibiting the production of EPGase in ripening tomato fruit tissue (Mignani et al., 1995). Di- and tri- GalA elicit the accumulation of HGRPs in the cell walls of bean seedlings (Boudart et al., 1995). Di- and tri- GalA also suppress the induction of PAL and the hypersensitive response to a fungal pathogen in wheat leaves (Moerschbacher et al., 1999). Nonreducing-end Δ-4,5 unsaturated di-GalA is active in inhibiting tissue maceration in potato tuber tissue infected with the bacterial soft rot pathogen Erwinia carotovora (Weber et al., 1996).

3.5. Presence and fate of biologically active oligogalacturonides in plant tissues

Plant cells and plant pathogens secrete endo- and exo-polygalacturonases into their extracellular matrix.

EPGases are often found at sites where the application of exogenous OGAs elicit a biological response and thus, the EPGases are present at those locations where the release of biologically active OGAs would be expected (Côté et al., 1998; Hadfield and Bennett, 1998). However, a conclusive demonstration that EPGases release biologically active OGAs from a plant's cell wall at physiologically relevant locations and times is lacking. The best evidence to date comes from studies of ripening tomato fruit. Polygalacturonase activity is known to increase during tomato ripening, and pectic oligomers that elicit ethylene have been extracted from tomato fruits at the breaker stage of ripening (Melotto et al., 1994). Purified OGAs with a DP greater than eight initiate ethylene biosynthesis in tomato fruits (Brecht and Huber, 1988; Campbell and Labavitch, 1991). The OGA-enriched material isolated from ripening tomato fruit, and EPGase-generated OGAs have similar chromatographic profiles, suggesting that the active components in the fruit extracts are OGAs. However, the individual OGA oligomers isolated from the fruit cell wall material are contaminated with the neutral sugars present in RG I and RG II.

There have been conflicting reports concerning the movement of OGAs in plants. When crude ^{3}H-labeled pectic fragments (Bishop et al., 1981) or ^{3}H-labeled OGAs (MacDougall et al., 1992) are introduced into the xylem of tomato plants through cut stems, the radiolabel moves through the plant with the transpiration stream. Ninety minutes after being introduced, the label was found throughout the plant (MacDougall et al., 1992). Labeled OGAs recovered from the plants had been fragmented into smaller oligomers, and some were esterified with an unidentified alcohol. In contrast, ^{14}C-labeled pectin and ^{3}H-labeled pectic fragments were immobile when applied to wounds on the leaves of tomato plants (Baydoun and Fry, 1985). The label would have needed to move out of the leaves via the phloem, since xylem flow is transpiration driven and normally flows into leaves. The immobility of the label indicates that OGAs do not move in the phloem, and that biologically active OGAs generated in infected leaves cannot move through the plant and induce SAR. In contrast, OGAs released during infection of the roots or stems could move throughout the plant's xylem and induce SAR (MacDougall et al., 1992).

To function as signal molecules, biologically active OGAs must be present when the physiological responses they induce are required and are likely to be absent when the responses are not required. Therefore, it is likely that OGA signal molecules are removed or inactivated following the activation of a physiological response. Endogenous EPGases are often found in plant tissues where the exogenous application of OGAs would elicit physiological responses. For example, polygalacturonase activity has been found in suspension-cultured tobacco (Mathieu et al., 1998), carrot (Konno et al., 1989) and rose (García-Romera and Fry, 1995) cells, as well as in cotton cotyledons (Zhang et al., 1996). In the tobacco and rose cells, the enzymes do not release biologically active concentrations of OGAs from the plant cell walls, suggesting that the enzymes are maintained in an inactive state or that their substrates are inaccessible (Mathieu et al., 1998; García-Romera and Fry, 1995). On the other hand, exogenously added OGAs are rapidly sequestered into the cell wall or degraded in tobacco (Mathieu et al., 1998) and rose (García-Romera and Fry, 1997) suspension-cultured cells. These findings indicate that endogenous endo- and exo- polygalacturonases capable of degrading biologically active OGAs after initiation of a physiological response are present in suspension-cultured cells (Mathieu et al., 1998; García-Romera and Fry, 1997).

3.6. Oligogalacturonide receptors

Considering the diversity of biologically active OGA structures, and the range of biological activities attributed to these structures, it would not be surprising to find that OGAs are perceived through multiple mechanisms (Côté and Hahn, 1994; Spiro et al., 1998). It is generally believed that biologically active macromolecules are recognized by receptor proteins and that this recognition event elicits a biological response via a signal transduction cascade (Hahn, 1996). The widely variable concentrations of OGAs required for bioactivity (from 10^{-4} to 10^{-7} M) supports the notion that OGAs are recognized by a number of receptors with different affinities (Côté and Hahn, 1994). However, OGAs can bind to each other and to other homogalacturonans in the cell wall. A significant portion of the OGAs added to suspension-cultured tobacco cells was found to be ionically bound to the cell wall (Mathieu et al., 1998). Thus, OGAs may saturate binding sites in the wall before they can be perceived at the plasma membrane. If this is the case, the concentration required for biological activity would not reflect the affinity of the receptor.

The possibility that the cell wall itself could be the 'receptor' for OGAs has been discussed (Mohnen and Hahn, 1993). OGAs may intercalate into the junction zones formed by the self-association of homogalacturonans, thereby releasing some of the tension in the wall (Carpita and Gibeaut, 1993; Rose et al., 1999). Changes in the tension of cell wall polymers may be transmitted to the cytoskeleton and initiate signaling cascades through transmembrane proteins similar to integrins (Schwartz et al., 1995; Miller et al., 1997; Faik et al., 1998).

Suspension-cultured soybean cells have been reported to respond to OGAs in a process of receptor mediated endocytosis in (Horn et al., 1989). An OGA of DP 14,

derivatized with fluorescein via a thiosemicarbazone linkage, bound to the surface of soybean suspension-cultured cells and was internalized. The fluorescence traveled from the plasma membrane to the vacuole over the course of two hours. OGAs labeled with I^{125} after derivatization with tyrosine via a hydrazone linkage were used to measure the binding kinetics. The binding was competitively inhibited by an excess of non-labeled OGA (Horn et al., 1989), and was saturated at a concentration about five times higher than that required for maximum biological activity (Low et al., 1993). To date, no connection has been made between this binding and a biological response elicited by OGAs. It should be noted that the thiosemicarbazone and hydrazone linkages used in these derivatives are chemically unstable (Ridley et al., 1997). Thus, it is not certain whether OGA was covalently linked to all the fluorescence or iodinated signals observed.

A 34 kilodalton (kd) plasma membrane protein that is phosphorylated in response to OGAs with a DP from 13 to 30 has been cloned from potato (Farmer et al., 1991; Reymond et al., 1996). This protein, called remorin, binds to, and is phosphorylated in vitro in response to, OGAs of the same size range (Reymond et al., 1995, 1996). Immunologically similar proteins that are phosphorylated in response to OGAs were found in several widely divergent species of dicots. The OGA size requirement for phosphorylation of remorin does not match the size requirement for any of the known OGA-induced biological responses and remorin has not been implicated in any of the known biological responses elicited by OGAs. Remorin does not have homology to any known receptor proteins, although it does share properties such as plasma membrane-association, binding to polyanions, and phosphorylation, with the 30-kd cell-to-cell movement protein of tobacco mosaic virus (Reymond et al., 1996). Interestingly, viral cell movement proteins bind pectin methylesterase in the wall (Dorokhov et al., 1999) and deletion of the PME-binding region of the movement protein inhibits cell-to-cell viral movement through plasmodesmata (Chen et al., 2000). The hypothesis that remorin plays a role in plant driven transport or signaling through plasmodesmata has been prosposed (Reymond et al., 1996).

3.7. Oligogalacturonide induced signaling cascades

Much information is available concerning the signaling events underlying a plant's responses to OGAs and a coherent picture of these events is now beginning to emerge. Selected elements of the signaling cascades have been studied in suspension-cultured soybean, tobacco, and carrot cells, and in tomato plants, but in no case have all elements been studied in one system. Several potential limitations of these studies should be considered when general conclusions are made. The OGAs used in many of these studies were not size-fractionated or completely pure. Since differently-sized OGAs can elicit unique sets of responses, the responses obtained using mixtures of differently-sized OGAs could result from multiple receptors and/or the induction of multiple signal transduction pathways. Furthermore, cultured plant cells are in vitro systems that are subject to genetic and epigenetic variation and extrapolating results obtained with such cells to the physiology of whole plants can be difficult. Finally, much of the information available is based on the use of pharmacologic inhibitors whose specificity and affects are not well characterized in plants.

3.7.1. Suspension-cultured soybean cells: early signaling events

Cultured soybean cells produce H_2O_2 within seconds to a few minutes after the addition of partially purified pectic fragments (Legendre et al., 1992, 1993a). OGA elicited H_2O_2 production appears to be tightly regulated since the quantity and duration of H_2O_2 production are limited, and are relatively consistent between experiments (Legendre et al., 1993a,b). Furthermore, the cells become desensitized to an additional dose of OGAs for a defined period (refractory period). It is noteworthy that OGA-elicited H_2O_2 production in suspension-cultured soybean cell is not accompanied by transient extracellular alkalinization (Horn et al., 1992), as it is in suspension-cultured carrot and tobacco cells (Messiaen and VanCutsem, 1994; Matheiu et al., 1996b).

Signaling events that require protein phosphorylation and GTP binding proteins (G-proteins) may be required for H_2O_2 production (Fig. 6). The protein kinase inhibitors, K252a and staurosporine block the OGA-induced oxidative burst in a concentration dependent manner, whereas the phosphatase inhibitors, okadaic acid and calyculin A elicit an oxidative burst in the absence of OGAs (Chandra and Low, 1995). This suggests that kinase activity is required for the oxidative burst, and that in the absence of phosphatase activity a basal level of kinase activity can activate the signaling cascades leading to H_2O_2 production in the absence OGAs. The G-protein activator, mastoparan, also elicits an oxidative burst in soybean cells, suggesting that G-protein activation is required for the oxidative burst (Legendre et al., 1992). However, direct G-protein involvement in OGA-elicited oxidative burst has not been demonstrated, and more than one signal transduction pathway leading to oxidative burst is likely to exist in plants (Low and Merida, 1996; Bolwell, 1999). Phospholipase C activation resulting in the release of inositol triphosphate (IP_3) may be part of OGA activated signaling in suspension-cultured soybean cells (Legendre et al., 1993b). OGAs promote a transient increase in the intracellular level of IP_3 prior to the biosynthesis of H_2O_2. Furthermore neomycin sulfate, an inhibitor of

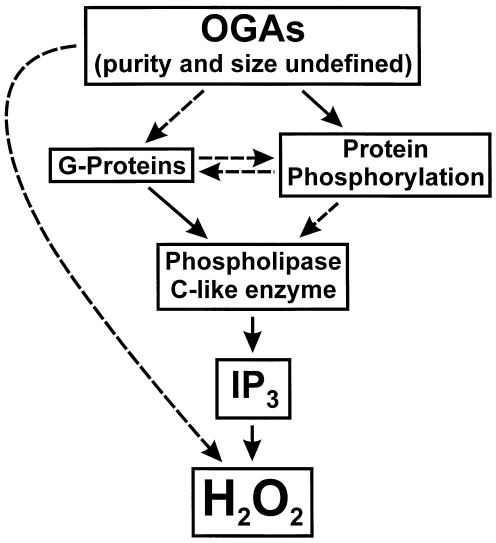

Fig. 6. A working model of OGA-induced signaling in suspension-cultured soybean cells. The solid arrows indicate potential pathways supported by experimental evidence. The dashed arrows indicate hypothetical interactions/pathways that are implied from experimental evidence. The arrows are not meant to suggest that a particular number of biochemical steps are involved in any of the interactions.

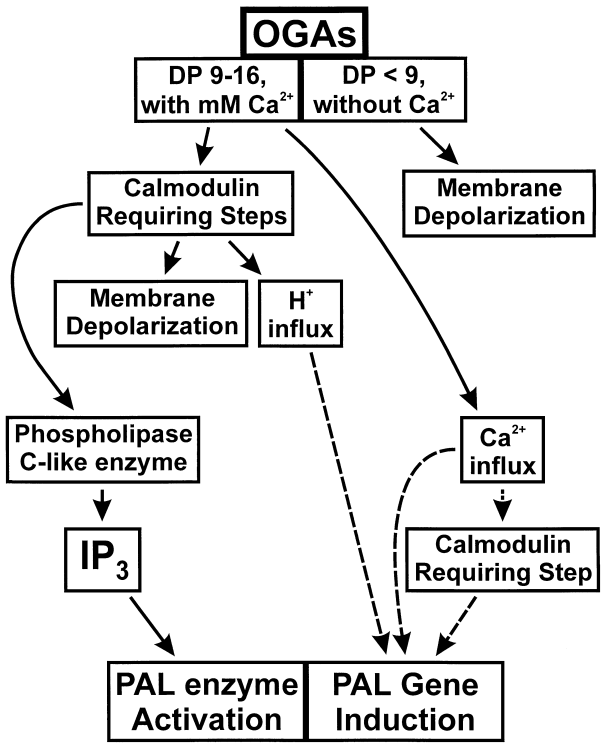

Fig. 7. A working model of OGA-induced signaling in suspension-cultured carrot cells. The solid arrows indicate potential pathways whose existence is supported by experimental evidence. The dashed arrows indicate hypothetical interactions/pathways that are implied from experimental evidence. The arrows are not meant to suggest that a particular number of biochemical steps are involved in any of the interactions.

polyphosphoinositide hydrolysis, partially inhibits the OGA induced biosynthesis of H_2O_2, suggesting that IP_3-independent signaling may also exist.

3.7.2. Suspension-cultured carrot cells: the role of calcium

OGAs with a DP from 9 to 16 induce a transient cytosolic Ca^{2+} mobilization, cytosolic acidification, and plasma membrane depolarization accompanied by an induction of PAL mRNA and enzyme activity in carrot cells (Fig. 7; Messiaen and VanCutsem, 1994). The most active size of OGA is DP 11. Externally supplied Ca^{2+} is required for all of these responses except for membrane depolarization. OGAs with a DP <9 elicit plasma membrane depolarization irregardless of the presence of Ca^{2+}, but do not elicit any of the other responses measured (Messiaen and VanCutsem, 1994). This is a particularly significant result since it suggests that the two different size classes of OGAs interact with the same cells to activate distinct signal transduction pathways.

The calcium channel blockers, verapamil and nifedipine, block OGA (DP 9–16) elicited cytosolic Ca^{2+} mobilization and PAL mRNA induction, but do not block cytosolic acidification or membrane depolarization (Fig. 7, Messiaen and VanCutsem, 1994). Furthermore, when the calcium ionophore A23187 is used to increase the cytosolic free Ca^{2+}, PAL mRNA is induced but cytosolic acidification and membrane depolarization are not. The inhibitor of the ATP-dependent plasma membrane proton-pump, vanadate, causes membrane depolarization and cytosolic acidification, but not PAL induction (Fig. 7; Messiaen and VanCutsem, 1994). Conversely, the activator of the ATP-dependent plasma membrane proton-pump, fusicoccin, causes a slight cytosolic alkalinization and inhibits OGA-elicited cytosolic acidification, membrane depolarization, and PAL mRNA induction. Together, these data suggest that transient cytosolic Ca^{2+} mobilization is required for induction of PAL mRNA induction, whereas transient cytosolic acidification and membrane depolarization do not require Ca^{2+} mobilization and may or may not be involved in PAL mRNA induction (Fig. 7; Messiaen and VanCutsem, 1994).

Neomycin sulfate, an inhibitor of polyphosphoinositide hydrolysis, inhibits the OGA-elicited induction of PAL enzyme activity by about 50%, suggesting that phospholipase C- mediated IP_3 turnover is involved in activation of the enzyme (Messiaen and VanCutsem, 1994). Neomycin sulfate has a small quantitative affect on OGA induced cytosolic Ca^{2+} mobilization, but does not affect cytosolic acidification, plasma membrane depolarization or PAL mRNA induction. The calmodulin inhibitor, calmidazolium, does not affect cytosolic Ca^{2+} mobilization, but blocks OGA elicited induction of cytosolic acidification, membrane depolarization, and PAL mRNA and enzyme activity (Messiaen and VanCutsem, 1994). This suggests that calmodulin is required for

steps affecting all of these responses except cytosolic Ca^{2+} mobilization (Fig. 7).

3.7.3. Suspension-cultured tobacco cells: a role for cytosolic acidification

OGAs with a DP from 10 to 15 (DP 12 is most active) induce a transient K^+ efflux, Cl^- efflux, cytosolic acidification, cytosolic Ca^{2+} mobilization, oxidative burst, plasma membrane depolarization, and induction of PAL mRNA accumulation in suspension-cultured tobacco cells (Fig. 8; Mathieu et al., 1991; Lapous et al., 1998; Spiro et al., 1998). Degradation of the OGA elicitor molecules is not responsible for the transient nature of the responses (Mathieu et al., 1998). The protein kinase inhibitors, staurosporine and 6-dimethylaminopurine, block OGA elicited oxidative burst, cytosolic acidification, and induction of PAL, whereas the protein phosphatase inhibitors, calyculin A and cantharidin induce these responses in the absence of OGAs (Mathieu et al., 1996a,b). Furthermore, OGA-induced changes in the phosphorylation of membrane-associated proteins from suspension-cultured tobacco cells have been detected (Droillard et al., 1997). As with soybean cells, protein kinase activity seems to be required, and in the absence of phosphatase activity a basal level of kinase activity may activate the signaling cascades in the absence of added OGAs.

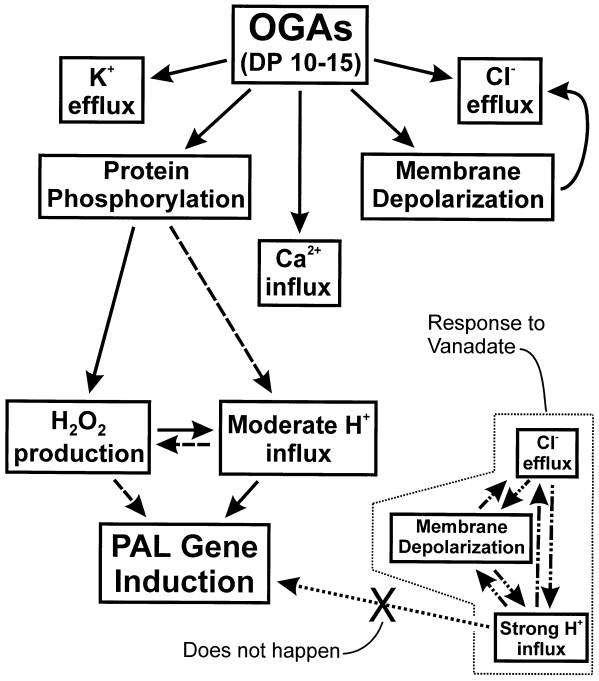

Fig. 8. A working model of OGA-induced signaling in suspension-cultured tobacco cells. The solid arrows indicate potential pathways whose existence is supported by experimental evidence. The dashed arrows indicate hypothetical interactions/pathways that are implied from the experimental evidence. The dot-dashed arrows indicate hypothetical interactions that potentially interconnect the responses induced by vanadate in the absence of OGA's. The arrows are not meant to suggest that a particular number of biochemical steps are involved in any of the interactions.

The inhibitors of the ATP dependent plasma membrane proton pump, vanadate and erythrosine B, cause plasma membrane depolarization, cytosolic acidification, and Cl^- efflux (Fig. 8; Zimmermann et al., 1998). Patch clamp experiments suggest that activation of a voltage-gated anion channel is responsible for the Cl^- efflux. Treatment of tobacco cells with the hydrophobic acid propionate, which moves protons across the plasma membrane with the proton gradient to cause cytosolic acidification, elicits PAL mRNA production. On the other hand, the cytosolic acidification caused by the proton pump inhibitor erythrosin B does not induce PAL mRNA (Lapous et al., 1998). It is suggested that the moderate cytosolic acidification induced by propionate stimulates production of PAL mRNA, while the strong cytosolic acidification induced by vanadate or erythrosine B is inhibitory (Fig. 8). In light of these results, the role of OGA-induced cytosolic acidification in the induction of PAL in carrot suspension-cultured cells merits reexamination.

The oxidative burst inhibitor, iodonium diphenyl, completely inhibited the OGA induced oxidative burst in suspension-cultured tobacco cells and inhibited cytosolic acidification (Rout-Mayer et al., 1997). This suggests that H_2O_2 may induce cytosolic acidification, although inverse experiments involving the addition of exogenous H_2O_2 were not reported.

3.7.4. Tomato wound response: oligogalacturonide signaling in intact plant tissues

When tomato seedlings with their roots excised are placed in a solution containing OGAs, these elicitors travel through the xylem and induce the expression of PIs, EPGase, and oxidative burst throughout the plant (MacDougall et al., 1992; Moloshok et al., 1992; Bergey et al., 1999; Orozco-Cardenas and Ryan, 1999). OGAs from DP 2 to 30 induce the expression of PIs, and other systemic wound response proteins (SWRPs) in these plants (Fig. 9; Moloshok et al., 1992; Bergey et al., 1996, 1999). PIs and SWRPs have been shown to help protect the plant from insect damage by reducing the nutrients available to feeding insects (Orozco-Cardenas et al., 1993). Xylem transport of OGAs is, however, thought to be physiologically insignificant in the normal tomato systemic wound response (SWR) to herbivore attack. Herbivores normally feed on leaves, and OGAs released in leaves are not transported in the phloem and do not move from the leaves to initiate a systemic reaction (Baydoun and Fry, 1985). For this reason, OGAs are thought to constitute a localized signal in the induction of SWR. The peptide hormone, systemin, is transported throughout the plant via the phloem and the xylem after its proteolytic release from its precursor in response to wounding or insect feeding (Doares et al., 1995; Narvaez-

Vasquez et al., 1995; Bergey et al., 1996; Ryan and Pearce, 1998). The signal from systemin propagates very rapidly, perhaps by means of rapid pressure changes in the xylem that are perceived throughout the plant (Malone, 1996; Stratmann and Ryan, 1997). Like OGAs, systemin and wounding induce the expression of PIs, SWRPs, EPGase, and H_2O_2 (Stratmann and Ryan, 1997; Bergey et al., 1999; Orozco-Cardenas and Ryan, 1999). Tomato plants expressing an antisense prosystemin gene respond to OGAs and systemin normally, but do not produce PIs, SWRPs, EPGase, or H_2O_2 in response to wounding, indicating that the activation of systemin is not required for the response to OGAs (Orozco-Cardenas and Ryan, 1999).

Jasmonic acid is required for the induction of H_2O_2, EPGase, PIs, and SWRPs by either OGAs or systemin (Fig. 9; Doares et al., 1995; Howe et al., 1996). Jasmonic acid is synthesized via the octadecanoid pathway from linolenic acid which, presumably, is released from phospholipids by phospholipase A activity (Howe et al., 1996). Tomato plants with a mutation in the octadecanoid pathway do not make jasmonic acid and do not produce PIs in response to OGAs, systemin, or wounding (Howe et al., 1996). Two inhibitors of the octadecanoid pathway, salicylic acid and diethylthiocarbamic acid, severely inhibit the induction of PIs by OGAs, systemin, and wounding (Doares et al., 1995). Wounding, OGAs, systemin, and jasmonic acid all induce tomato plants to produce ethylene and PIs (O'Donnell et al., 1996; Simpson et al., 1998). The induction of PIs is blocked by the ethylene biosynthesis inhibitors, silver thiosulphate and norbornadiene (O'Donnell et al., 1996), suggesting that ethylene is required as a second messenger when wounding, or treatment with OGAs, systemin, or jasmonic acid induce PIs. The ethylene requirement was not readily apparent because the addition of jasmonic acid induces the ethylene biosynthesis required for elicitation (Farmer and Ryan, 1992; O'Donnell et al., 1996; Orozco-Cardenas and Ryan, 1999). Taken together these results indicate that both ethylene and jasmonic acid are required for the induction of PIs by OGAs, systemin or wounding.

A 48 kd myelin basic protein kinase is activated in response to wounding, systemin, and OGAs (Stratmann and Ryan, 1997). The kinase is also activated by the same signals in plants that have a genetic defect in the octadecanoid pathway blocking the normal induction of PIs and SWRPs (Howe et al., 1996) (see Fig. 9). A synthetic analogue of the peptide hormone systemin strongly inhibits activation of the kinase and the induction of SWRPs by systemin (Stratmann and Ryan, 1997). This suggests that the 48 kd myelin basic protein kinase functions between these primary signals and the octadecanoid biosynthetic pathway as part of the signaling cascade leading to the SWR (Stratmann and Ryan, 1997).

Systemin elicits the systemic production of an endogenous EPGase in the leaves of tomato plants (Orozco-Cardenas and Ryan, 1999). This EPGase could generate biologically active OGAs, which act locally in concert with systemin to augment the SWR (Fig. 9; Bergey et al., 1999). Accordingly, the simultaneous addition of OGAs and systemin to suspension-cultured tomato cells produces an oxidative burst at least an order of magnitude larger than when OGAs are added alone (Stennis et al., 1998). This suggests that the two signals could act synergistically in the induction of the SWR in whole plants. Systemin is inactive in eliciting an oxidative burst in the suspension-cultured cells, suggesting that intact plant tissues are required (Stennis et al., 1998). Comparison of the timing and location of EPGase mRNA accumulation with H_2O_2 biosynthesis in whole plants treated with systemin suggests that OGAs

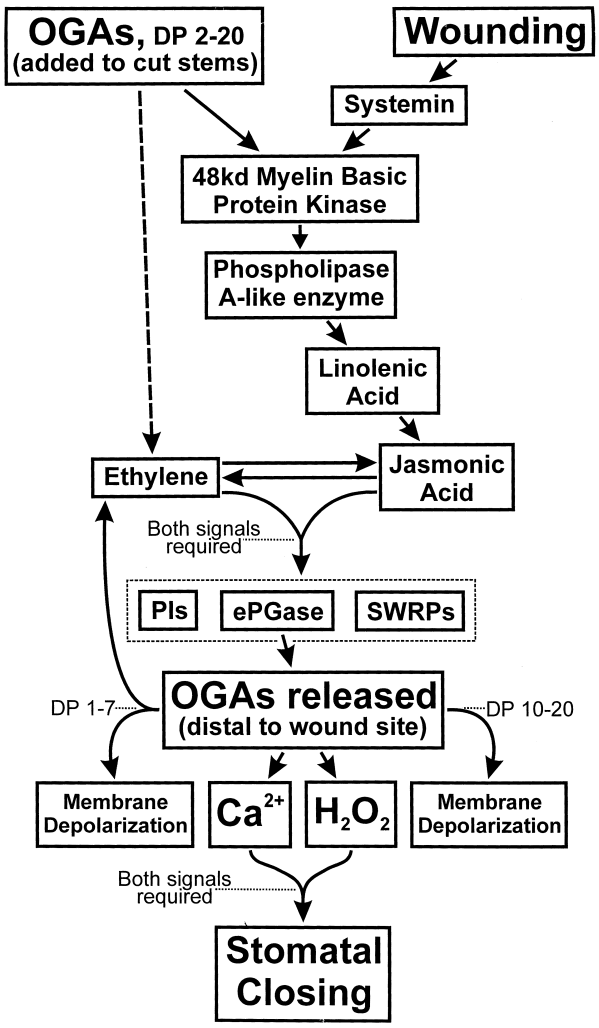

Fig. 9. A working model of OGA-induced signaling in tomato plants. As indicated in the text, the potential existence of some of the interactions shown is based on experiments using tomato tissues other than whole plants. The solid arrows indicate potential pathways whose existence is supported by experimental evidence. The dashed arrows indicate hypothetical interactions/pathways that are implied from experimental evidence. The arrows are not meant to suggest that a particular number of biochemical steps are involved in any of the interactions.

released by this enzyme could be responsible for the systemically induced oxidative burst associated with the SWR (Orozco-Cardenas and Ryan, 1999).

Another response that may be involved in the SWR is the OGA-induced closing of stomata (Fig. 9; Agrios, 1997; Lee et al., 1999). The Ca^{2+} chelater, EGTA, as well as the H_2O_2 scavengers, catalase and ascorbate, completely inhibit OGA induced stomatal closing in tomato leaf epidermal peels (Lee et al., 1999). This suggests that both Ca^{2+} and H_2O_2 signals are required for OGA-induced stomatal closing (Fig. 9).

A unique feature of the induction of SWR by OGAs in tomato plants is that a broad range of OGA sizes are biologically active (Farmer et al., 1990). OGAs with a DP from 1 to 7, as well as those with a DP from 10 to 20 are active in inducing membrane depolarization in tomato leaf mesophyll cells and in inducing PI activity in tomato plants (Thain et al., 1990). However, the membrane depolarization responses elicited by the two size ranges of OGAs are quantitatively and kinetically different. Furthermore, OGAs with a DP from 4 to 6 induce ethylene biosynthesis in tomato plants, whereas other sizes do not (Simpson et al., 1998). In light of these findings, it seems likely that tomato plants recognize OGAs by at least two different mechanisms.

3.7.5. Conclusions and relevance to future work

Oligogalacturonides participate in an information network of branched and interconnecting signal transduction pathways that lead to the more integrated tissue level responses. Plants are able to respond adaptively to changing environmental conditions by means of such information networks. It is of great importance to understand how plants accomplish this remarkable feat. Our understanding of OGA signal transduction is sketchy, and in some cases, conflicting. A variety of OGA signaling elements have been implicated in different plant species, but the role of each element has not been investigated in a single species. A major limitation has been the difficulty of isolating and directly characterizing the components of the OGA signaling cascades, including the receptors. In similar research with animals, the isolation of receptors and other signaling components has allowed interacting signaling elements to be identified.

Acknowledgements

We thank Jason Sterling for critical reading of the manuscript and our colleagues at the CCRC for their helpful discussions. This work was supported in part by NSF grant No. INT-9722509, NRI competitive USDA award 98-35304-6772, NIH grant 5R01GM39583, DOE grant DE-FG02-96ER20220 and DOE-funded center grant DE-FG05-93-ER20097.

References

Agrios, G.N., 1997. Plant pathology, 4th Edition. Academic Press, San Diego, pp. 46–52.

Altamura, M.M., Zaghi, D.Z., Salvi, G., DeLorenzo, G., Bellincampi, D., 1998. Oligogalacturonides stimulate pericycle cell wall thickening and cell divisions leading to stoma formation in tobacco leaf explants. Planta 204, 429–436.

An, J., O'Neill, M.A., Albersheim, P., Darvill, A.G., 1994. Isolation and structural characterization of β-D-glucosyluronic acid and 4-*O*-methyl β-D-glucosyluronic acid-containing oligosaccharides from the cell-wall pectic polysaccharide, rhamnogalalcturonan I. Carbohydr. Res. 252, 235–243.

Andrew, E.R., Szczesniak, E., 1995. A historical account of NMR in the solid state. Prog. Nuc. Mag. Spec. 28, 11–16.

Asiegbu, F.O., Daniel, G., Johansson, M., 1994. Defense related reactions of seedling roots of Norway spruce to infection by *Heterobasidion annosum* (Fr.) Bref. Physiol. Mol. Plant Pathol. 45, 1–19.

Aspinall, G.O., 1980. Chemistry of cell wall polysaccharides. In: Preiss, J. (Ed.), The Biochemistry of Plants, Vol. 3. Academic Press, New York, pp. 473–500.

Aspinall, G.O., Begbie, R., Hamilton, A., Whyte, J.N.C., 1967. Polysaccharides of soy beans. Part III. Extraction and fractionation of polysaccharides from cotyledon meal. J. Chem. Soc. 1065–1070.

Azadi, P., O'Neill, M.A., Bergmann, C., Darvill, A.G., Albersheim, P., 1995. The backbone of the pectic polysaccharide rhamnogalacturonan I is cleaved by an endohydrolase and an endolyase. Glycobiology 5, 783–789.

Bacic, A., Harris, P.J., Stone, B.A., 1988. Structure and function of plant cell walls. In: Preiss, J. (Ed.), The Biochemistry of Plants. Academic Press, New York, pp. 297–371.

Baker, A.A., Helbert, W., Sugiyama, J., Miles, M.J., 1997. High-resolution atomic force microscopy of native Valonia cellulose I microcrystals. J. Struct. Biol. 119, 129–138.

Baker, C.J., Mock, N., Atkinson, M.M., Hutcheson, S., 1990. Inhibition of the hypersensitive response in tobacco by pectate lyase digests of cell wall and of polygalacturonic acid. Physiol. Mol. Plant Pathol. 37, 155–167.

Baron-Epel, O., Gharyal, P.K., Schindler, M., 1988. Pectins as mediators of wall porosity in soybean cells. Planta 175, 389–395.

Baldwin, E.A., Biggs, R.H., 1988. Cell-wall lysing enzymes and product of cell-wall digestion elicit ethylene in citrus. Physiol. Plant. 73, 58–64.

Basu, S.S., Dotson, G.D., Raetz, C.R.H., 2000. A facile enzymatic synthesis of uridine diphospho-[^{14}C]galacturonic acid. Anal. Biochem. 280, 173–177.

Bauer, W.D., Talmadge, K.W., Keegstra, K., Albersheim, P., 1973. The structure of plant cell walls II. The hemicellulose of the walls of suspension-cultured sycamore cells. Plant Physiol. 51, 174–187.

Baydoun, E.A-H., Fry, S.C., 1985. The immobility of pectic substances in injured tomato leaves and its bearing on the identity of the wound hormone. Planta 165, 269–276.

Baydoun, E.A-H., Fry, S.C., 1988. [2-^{1}H] mannose incorporation in cultured plants cells — investigation of L-galactose residues of the primary cell wall. J. Plant Physiol. 132, 484–490.

Baydoun, E.A.H., Rizk, S.E., Brett, C.T., 1999. Localisation of methyltransferases involved in glucuronoxylan and pectin methylation in the Golgi apparatus in etiolated pea epicotyls. J. Plant Physiol. 155, 240–244.

Bellincampi, D., Salvi, G., DeLorenzo, G., Cervone, F., Marfà, V., Eberhard, S., Darvill, A., Albersheim, P., 1993. Oligogalacturonides inhibit the formation of roots on tobacco explants. Plant J. 4, 207–213.

Bellincampi, D., Cardarelli, M., Zaghi, D., Serino, G., Salvi, G., Gatz, C., Cervone, F., Altamura, M.M., Costantino, P., DeLorenzo, G., 1996. Oligogalacturonides prevent rhizogenesis in rolB-transformed tobacco explants by inhibiting auxin-induced expression of the rolB gene. Plant Cell 8, 477–487.

Bellincampi, D., Dipierro, N., Salvi, G., Cervone, F., DeLorenzo, G., 2000. Extracellular H_2O_2 induced by oligogalacturonides is not involved in the inhibition of the auxin-regulated rolB gene expression in tobacco leaf explants. Plant Physiol. 122, 1379–1385.

Bergey, D.R, Howe, G.A., Ryan, C.A., 1996. Polypeptide signaling for plant defense genes exhibits analogies to defense signaling in animals. Proc. Natl. Acad. Sci. USA 93, 12053–12058.

Bergey, D.R., Orozco-Cardenas, M., De Moura, D.S., Ryan, C.A., 1999. A wound- and systemin-inducible polygalacturonase in tomato leaves. Proc. Natl. Acad. Sci. USA 96, 1756–1760.

Bergmann, C.W., Ito, Y., Singer, D., Albersheim, P.A., Darvill, A.G., 1994. Polygalacturonase-inhibiting protein accumulates in *Phaseolus vulgaris* L. in response to wounding, elicitors and fungal infection. Plant J. 5, 625–634.

Bishop, P.D., Makus, D.J., Pearce, G., Ryan, C.A., 1981. Proteinase inhibitor-inducing factor activity in tomato leaves resides in oligosaccharides enzymatically released from cell walls. Proc. Natl. Acad. Sci. USA 78, 3536–3540.

Bishop, P.D., Pearce, G., Bryant, J.E., Ryan, C.A., 1984. Isolation and characterization of the proteinase inhibitor-inducing factor from tomato leaves. J. Biol. Chem. 259, 13172–13177.

Binet, M.-N., Bourque, S., Lebrun-Garcia, A., Chiltz, A., Pugin, A., 1998. Comparison of the effects of cryptogein and oligogalacturonides on tobacco cells and evidence of different forms of desensitization induced by these elicitors. Plant Sci. 137, 33–41.

Bociek, S.M., Welti, D., 1975. The quantitative analysis of uronic acid polymers by infrared spectroscopy. Carbohydr. Res. 42, 217–226.

Bolwell, P.G., 1999. Role of active oxygen species and NO in plant defense responses. Curr. Opin. Plant Biol. 2, 287–294.

Bolwell, G.P., Dalessandro, G., Northcote, D.H., 1985. Decrease of polygalacturonic acid synthase during xylem differentiation in sycamore. Phytochemistry 24, 699–702.

Bonin, C.P., Reiter, W.-D., 2000. A bifunctional epimerase-reductase acts downstream of the MUR1 gene product and completes the de novo synthesis of GDP-L-fucose in *Arabidopsis*. Plant J. 21, 445–454.

Bonin, C.P., Potter, I., Vanzin, G., Reiter, W-D., 1997. The *MUR1* gene of *Arabidopsis thaliana* encodes an isoform of GDP-mannose-4,6-dehydratase, catalyzing the first step in the de novo synthesis of GDP-L-fucose. Proc. Natl. Acad. Sci. USA 94, 2085–2090.

Boudart, G., Dechamp-Guillaume, G., LaFitte, C., Ricart, G., Barthe, J.-P., Mazau, D., Esqurré-Tugayé, M.-T., 1995. Elicitors and suppressors of hydroxyproline-rich glycoprotein accumulation are solubilized from plant cell walls by endopolygalacturonase. Eur. J. Biochem. 232, 449–457.

Bourlard, T., Pellerin, P., Morvan, C., 1997a. Rhamnogalacturonans I and II are pectic substrates for flax-cell methyltransferases. Plant Physiol. Biochem. 35, 623–629.

Bourlard, T., Schaumann-Gaudinet, A., Bruyant-Vannier, M.-P., Morvan, C., 1997b. Various pectin methyltransferase activities with affinity for low and highly methylated pectins. Plant Cell Physiol. 38, 259–267.

Branca, C., DeLorenzo, G., Cervone, F., 1988. Competitive inhibition of the auxin-induced elongation by α-D-oligogalacturonides in pea stem segments. Physiol. Plant. 72, 499–504.

Brant, D.A., 1999. Novel approaches to the analysis of polysaccharide structures. Curr. Opin. Struct. Biol. 9, 556–562.

Brecht, J.K, Huber, D.J., 1988. Products released from enzymically active cell wall stimulate ethylene production and ripening in preclimacteric tomato (*Lycopersicon esculentum* Mill.) fruit. Plant Physiol. 88, 499–504.

Brickell, L.S., Reid, J.S.G., 1996. Biosynthesis in vitro of pectic (1-4)-β-D-galactan. In: Visser, J., Voragen, A.G.J. (Eds.), Pectins and Pectinases. Elsevier Science, Amsterdam, pp. 127–134.

Broekaert, W.F., Peumans, W.J., 1988. Pectic polysaccharides elicit chitinase accumulation in tobacco. Physiol. Plant. 74, 740–744.

Brown, J.A., Fry, S.C., 1993. Novel *O*-D-galacturonosyl esters in the pectic polysaccharides of suspension-cultured plant cells. Plant Physiol. 103, 993–999.

Bruce, R.J., West, C.A., 1989. Elicitation of lignin biosynthesis and isoperoxidase activity by pectic fragments in suspension-cultures of castor bean. Plant Physiol. 91, 889–897.

Bruyant-Vannier, M.-P., Gaudinet-Schaumann, A., Bourlard, T., Morvan, C., 1996. Solubilization and partial characterization of pectin methyltransferase from flax cells. Plant Physiol. Biochem. 34, 489–499.

Buckeridge, M.S., Vergara, C.E., Carpita, N.C., 1999. The mechanism of synthesis of a mixed-linkage (1-3),(1-4)β-D-glucan in maize (*Zea mays* L.). Evidence for multiple sites of glucosyl transfer in the synthase complex. Plant Physiol. 120, 1–12.

Burget, E.G., Reiter, W.-D., 1999. The *mur4* mutant of arabidopsis is partially defective in the de novo synthesis of uridine diphospho L-arabinose. Plant Physiol. 121, 383–389.

Burton, R.A., Gibeaut, D.M., Bacic, A., Findlay, K., Roberts, K., Hamilton, A., Baulcombe, D.C., Fincher, G.B., 2000. Virus-induced silencing of a plant cellulose synthase gene. Plant Cell 12, 691–705.

Bush, M.S., McCann, M.C., 1999. Pectic epitopes are differentially distributed in the cell walls of potato (*Solanum tuberosum*) tubers. Physiol. Plant. 107, 201–213.

Bush, C.A., Martin-Pastor, M., Imberty, A., 1999. Structure and conformation of complex carbohydrates of glycoproteins, glycolipids, and bacterial polysaccharides. Ann. Rev. Biophys. Biomol. Struct. 28, 269–293.

Campbell, A.D., Labavitch, J.M., 1991. Induction and regulation of ethylene biosynthesis and ripening by pectic oligomers in tomato pericarp discs. Plant Physiol. 97, 706–713.

Canut, H., Carrasco, A., Galaud, J.-P., Cassan, C., Bouyssou, H., Ita, N., Ferrara, P., Pont-Lezica, R., 1998. High affinity RGD-binding sites at the plasma membrane of *Arabidopsis thaliana* links the cell wall. Plant J. 16, 63–72.

Capasso, J.M., Hirschberg, C.B., 1984. Mechanisms of glycosylation and sulfation in the Golgi apparatus: evidence for nucleotide sugar/nucleoside monophosphate and nucleotide sulfate/nucleoside monophosphate antiports in the Golgi apparatus membrane. Proc. Natl. Acad. Sci. USA 81, 7051–7055.

Carpita, N.C., Gibeaut, D.M., 1993. Structural models of primary cell walls in flowering plants-consistency of molecular structure with the physical properties of the walls during growth. Plant J. 3, 1–30.

Casero, P.J., Knox, J.P., 1995. The monoclonal antibody JIM5 indicates patterns of pectin deposition in relation to pit fields at the plasma-membrane-face of tomato pericarp cell walls. Protoplasma 188, 133–137.

Cervone, F., DeLorenzo, G., Caprari, C., Clark, A.J., Desiderio, A., DeVoto, A., Leckie, F., Nuss, L., Salvi, G., Toubart, P., 1993. The interaction between fungal endopolyglacturonase and plant cell wall PGIP (polygalacturonase inhibiting protein). In: Fritig, B., Legrand, M. (Eds.), Mechanisms of Plant Defense Responses. Kluwer, Dordrecht, pp. 64–67.

Chandra, S., Low, P.S., 1995. Role of phosphorylation in elicitation of the oxidative burst in cultured soybean cells. Proc. Natl. Acad. Sci., USA 92, 4120–4123.

Chen, L.M., Carpita, N.C., Reiter, W.D., Wilson, R.H., Jeffries, C., McCann, M.C., 1998. A rapid method to screen for cell-wall mutants using discriminant analysis of Fourier transform infrared spectra. Plant J. 16, 385–392.

Chen, M.-H., Sheng, J., Hind, G., Handa, A.K., Citrovsky, V., 2000. Interaction between the tobacco mosaic virus movement protein and host cell pectin methylesterase is required for virus cell-to-cell movement. EMBO J. 19, 913–920.

Cheng, L., Kindel, P.K., 1997. Detection and homogeneity of cell wall pectic polysaccharides of *Lemna minor*. Carbohydr. Res. 301, 205–212.

Chothia, C., Jones, E.Y., 1997. The molecular structure of cell adhesive molecules. Ann. Rev. Biochem. 66, 823–862.

Coimbra, M.A., Waldron, K.R., Selvendran, R.R., 1995. Isolation and characterisation of cell wall polymers from the heavily lignified tissues of olive (*Olea europaea*) seed hull. Carbohydr. Polym. 27, 285–295.

Conklin, P.L., Norris, S.R., Wheeler, G., Williams, E.H., Smirnoff, N., Last, R.L., 1999. Genetic evidence for the role of GDP-mannose in plant ascorbic acid (vitamin C) biosynthesis. Proc. Natl. Acad. Sci. USA 96, 4198–4203.

Côté, F., Hahn, M.G., 1994. Oligosaccharins: structure and signal transduction. Plant Molec. Biol. 12, 1379–1411.

Côté, F., Ham, K.-S., Hahn, M.G., Bergman, C.W., 1998. Oligosaccharide elicitors in host-pathogen interactions: Generation, perception, and signal transduction. In: Biswas, B.B., Das, H. (Eds.), Subcellular biochemistry, Vol. 29, Plant-microbe interactions. Plenum Press, New York, pp. 385–431.

Crombie, H.J., Reid, J.S.G., 1998. Pectin methyltransferase: activities in particulate and solubilised preparations from mung bean (*Vigna radiata*) hypocotyls and tomato (*Lycopersicon esculentum*) pericarp. In: Cell Walls '98: 8th International Cell Walls Meeting: John Innes Centre, Norwich, UK: 1–5 September 1998.

Daas, P.J.H., Arisz, P.W., Schols, H.A., DeRuiter, G., Voragen, A.G.J., 1998. Analysis of partially methyl-esterified galacturonic acid oligomers by high-performance anion-exchange chromatography and matrix-assisted laser desorption/ionization time-of-flight mass spectrometry. Anal. Biochem. 257, 195–202.

Darvill, A., McNeil, M., Albersheim, P., 1978. Structure of plant cell walls: VIII. A new pectic polysaccharide. Plant Physiol. 62, 418–422.

Davis, K.R., Darvill, A.G., Albersheim, P., Dell, A., 1986a. Host-pathogen interactions. XXX. Characterization of elicitors of phytoalexin accumulation in soybean released from soybean cell walls by endopolygalacturonic acid lyase. Z. Naturforsch. 41c, 39–48.

Davis, K.R., Darvill, A.G., Albersheim, P., Dell, A., 1986b. Host-pathogen interactions XXIX. Oligogalacturonide released from sodium polypectate by endopolygalacturonic lyase are elicitors of phytoalexins in soybean. Plant Physiol. 80, 568–577.

Davis, K.R., Hahlbrock, K., 1987. Induction of defense responses in cultured parsley cells by plant cell wall fragments. Plant Physiol. 85, 1286–1290.

Deller, M.C., Jones, E.Y., 2000. Cell surface receptors. Curr. Opin. Struct. Biol. 10, 213–219.

Delmer, D.P., 1999. Cellulose biosynthesis: exciting times for a difficult field of study. Annu. Rev. Plant Physiol. Plant Mol. Biol. 50, 245–276.

DeVries, R.P., Kester, H.M., Poulsen, C.H., Benen, J.A.E., Visser, J., 2000. Synergy between enzymes from *Aspergillus* involved in the degradation of plant cell wall polysaccharides. Carbohydr Res. 327, 401–410.

De Vries, J.A., Voragen, A.G.J., Rombouts, F.M., Pilnik, W., 1986. Structural studies of apple pectins with pectolytic enzymes. In: Fishman, M.L., Jen, J.J. (Eds.), Chemistry and function of pectins. American Chemical Society, Washington, DC, pp. 38–48.

Dixon, R.A., Jennings, A.C., Davis, L.A., Gerrish, C., Murphy, D.L., 1989. Elicitor-active components from French bean hypocotyls. Physiol. Mol. Plant Path. 34, 99–115.

Doares, S.H., Syrovets, T., Weiler, E.W., Ryan, C.W., 1995. Oligogalacturonides and chitosan activate plant defensive genes through the octadecanoid pathway. Proc. Natl. Acad. Sci. USA. 92, 4095–4098.

Doco, T., Williams, P., Vidal, S., Pellerin, P., 1997. Rhamnogalacturonan II, a dominant polysaccharide in juices produced by enzymic liquefaction of fruits and vegetables. Carbohydr. Res. 297, 181–186.

Dolan, L., Linstead, P., Roberts, K., 1997. Developmental regulation of pectic polysaccharides in the root meristem of *Arabidopsis*. J. Exp. Bot. 48, 713–720.

Doong, R.L., Liljebjelke, K., Fralish, G., Kumar, A., Mohnen, D., 1995. Cell free synthesis of pectin: identification and partial characterization of polygalacturonate 4-α-galacturonosyltransferase and its products from membrane preparations of tobacco (*Nicotiana tabacum* L. cv samsun) cell suspension cultures. Plant Physiol. 109, 141–152.

Doong, R.L., Mohnen, D., 1998. Solubilization and characterization of a galacturonosyltransferase that synthesizes the pectic polysaccharide homogalacturonan. Plant J. 13, 363–374.

Dorokhov, Y.L., Mäkinen, K., Frolova, O.Y., Merits, A., Saarinen, J., Kalkkinen, N., Atabekov, J.G., Saarma, M., 1999. A novel function for a ubiquitous plant enzyme pectin methylesterase: the host-cell receptor for the tobacco mosaic virus movement protein. FEBS Letters 461, 223–228.

Droillard, M.-J., Güclü, J., Le Care, J.-P., Mathieu, Y., Guern, J., Laurière, C., 1997. Identification of calreticulin-like protein as one of the phosphoproteins modulated in response to oligogalacturonides in tobacco cells. Planta 202, 341–249.

du Penhoat, C.H., Gey, C., Pellerin, P., Perez, S., 1999. An NMR solution study of the mega-oligosaccharide rhamnogalacturonan II. J. Biomol. NMR. 14, 253–271.

Eberhard, S., Doubrava, N., Marfà, V., Mohnen, D., Southwick, A., Albersheim, P., Darvill, A., 1989. Pectic cell wall fragments regulate tobacco thin-cell-layer explant morphogenesis. Plant cell 1, 747–755.

Eda, S., Miyabe, K., Akiyama, Y., Ohnishi, A., Kato, K., 1986. A pectic polysaccharide from cell walls of tobacco (*Nicotiana tabacum*) mesophyll. Carbohydr. Res. 158, 205–216.

Edwards, M.E., Dickson, C.A., Chengappa, S., Sidebottom, C., Gidley, M.J., Reid, J.S.G., 1999. Molecular characterisation of a membrane-bound galactosyltransferase of plant cell wall matrix polysaccharide biosynthesis. Plant J. 19, 691–697.

Ehwald, R., Woehlecke, H., Titel, C., 1992. Cell wall microcapsules with different porosity from suspension cultured *Chenopodium album*. Phytochemistry 31, 3033–3038.

Ermel, F.F., Follet-Gueye, M.-L., Cibert, C., Vian, B., Morvan, C., Catesson, A-M., Goldberg, R., 2000. Differential localization of arabinan and galactan side chains of rhamnogalacturoanan I in cambial derivatives. Planta 210, 732–740.

Fagard, M., Hofte, H., Vernhettes, S., 2000. Cell wall mutants. Plant Physiol. Biochem. 38, 15–25.

Faik, A., Laboure, A.M., Gulino, D., Mandaron, P., Falconet, D., 1998. A plant surface protein sharing structural properties with animal integrins. Eur. J. Biochem. 153, 552–559.

Fan, D.-F., Feingold, D.S., 1970. Nucleoside diphosphate-sugar 4-epimerases. II. Uridine diphosphate arabinose 4-epimerase of wheat germ. Plant Physiol. 46, 592–595.

Farmer, E.E., Moloshok, T.D., Ryan, C.A., 1990. In vitro phosphorylation in response to oligouronide elicitors: structural and biological relationships. Curr. Topics Plant Biochem. Physiol. 9, 249–258.

Farmer, E.E., Moloshok, T.D., Saxton, M.J., Ryan, C.A., 1991. Oligosaccharide signaling in plants. Specificity of oligouronide-enhanced plasma membrane protein phosphorylation. J. Biol. Chem. 266, 3140–3145.

Farmer, E.E., Ryan, C.A., 1992. Octadecanoid precursors of jasmonic acid activate the synthesis of wound-inducible proteinase inhibitors. Plant Cell 4, 129–134.

Feingold, D.S., Avigad, G., 1980. Sugar nucleotide transformations in plants. In: Preiss, J. (Ed.), The Biochemistry of Plants, Vol.3.. Academic Press, New York, pp. 101–170.

Femenia, A., Garosi, P., Roberts, K., Waldron, K.W., Selvendran, R.R., Robertson, J.A., 1998. Tissue-related changes in methylesterification of pectic polysaccharides in cauliflower (*Brassica oleracea* L. var. botrytis) stems. Planta 205, 438–444.

Femenia, A., Rigby, N.M., Selvendran, R.R., Waldron, K.W., 1999. Investigation of the occurrence of pectic–xylan–xyloglucan complexes in the cell walls of cauliflower stem tissues. Carbohydr. Polym. 39, 151–164.

Fleischer, A., Titel, C., Ehwald, R., 1998. The boron requirement and cell wall properties of growing- and stationary-phase suspension-cultured *Chenopodium album* L. cells. Plant Physiol. 117, 1401–1410.

Fleischer, A., O'Neill, M.A., Ehwald, R., 1999. The pore size of non-graminaceous plant cell walls is rapidly decreased by borate ester cross-linking of the pectic polysaccharide rhamnogalacturonan II. Plant Physiol. 121, 829–838.

Freeman, R., 1992. High-resolution NMR using selective excitation. J. Mol Struct. 266, 39–51.

Freshour, G., Clay, R.P., Fuller, M.S., Albersheim, P., Darvill, A.G., Hahn, M.G., 1996. Development and tissue specific structural alterations of the cell wall polysaccharides of *Arabidopsis thaliana* roots. Plant Physiol. 110, 1413–1429.

Fry, S.C., 1986. Cross-linking of matrix polymers in the growing cell walls of angiosperms. Annu. Rev. Plant Physiol. 37, 165–186.

Fu, J., Mort, A.J., 1996. Progress toward identifying a covalent linkage between xyloglucan and rhamnogalacturonan in cotton cell walls. Plant Physiol. 111 (suppl), 147.

Fujino, T., Itoh, T., 1998. Changes in pectin structure during epidermal cell elongation in pea (*Pisum sativum*) and its implications for cell wall architecture. Plant cell Physiol. 39, 1315 – 1323.

García-Romera, I., Fry, S.C., 1995. The longevity of biologically-active oligogalacturonides in rose cell cultures: degradation by exo-polygalacturonase. J. Exp. Bot. 150, 241–246.

García-Romera, I., Fry, S.C., 1997. Upper limits for endogenous oligogalacturonides and free galacturonic acid in rose cell-suspension cultures: implications for the action of exo- and endo- polygalacturonase in vivo. J. Plant Physiol. 150, 241–246.

Geitmann, A., Li, Y.Q., Cresti, M., 1995. Ultrastructural immunolocalization of periodic pectin depositions in the cell wall of *Nicotiana tabacum* pollen tubes. Protoplasma 187, 168–171.

Geshi, N., Jorgensen, B., Scheller, H.V., Ulvskov, P., 2000. In vitro biosynthesis of 1,4-β-galactan attached to rhamnogalacturonan I. Planta 210, 622–629.

Giovannoni, J.J., 1997. Molecular genetic analysis of ethylene-regulated and developmental components of tomato fruit ripening. In: Kanellis, A., Chang, C., Kende, H., Grierson, D. (Eds.), Biology and Biotechnology of the Plant Hormone Ethylene. Kluwer Academic, Dordrecht, pp. 133–140.

Goubet, F., 1994. Etude de la Biosynthese de Polysaccharides Parietaux des Fibres Cellulosiques au Cours du Developpement du Lin. PhD Dissertation, Université de Rouen, pp. 1–176.

Goubet, F., Council, L.N., Mohnen, D., 1998. Identification and partial characterization of the pectin methyltransferase "homogalacturonan-methyltransferase" from membranes of tobacco cell suspensions. Plant Physiol 116, 337–347.

Goubet, F., Mohnen, D., 1999a. Solubilization and partial characterization of homogalacturonan-methyltransferase from microsomal membranes of suspension-cultured tobacco cells. Plant Physiol. 121, 281–290.

Goubet, F., Mohnen, D., 1999b. Subcellular localization and topology of homogalacturonan methyltransferase in suspension-cultured Nicotiano tabacum cells. Planta 209, 112–117.

Goubet, F., Morvan, C., 1993. Evidence for several galactan synthases in flax (*Linum usitassimum* L.) suspension-cultured cells. Plant Cell Physiol. 34, 1297–1303.

Goubet, F., Morvan, C., 1994. Synthesis of cell wall galactans from flax (*Linum usitatissimum* L.) suspension-cultured cells. Plant Cell Physiol. 35, 719–727.

Grant, G.T., Morris, E.R., Rees, D.A., Smith, P.J.C., Thom, D., 1973. Biological interactions between polysaccharides and divalent cations: the "egg box" model. FEBS Lett. 32, 195–198.

Grasdalen, H., Bakoy, O.E., Larsen, B., 1988. Determination of the degree of esterification and the distribution of methylated and free carboxyl groups in pectin by ^{1}H-N.M.R. spectroscopy. Carbohydr. Res. 184, 183–191.

Gray, J.S.S., Yang, B.Y., Montgomery, R., 2000. Extracellular polysaccharides of Erwinia chrysanthemi A350 and ribotyping of *Erwinia chrysanthemi* spp. Carbohydr. Res. 324, 255–267.

Grierson, D., Tucker, G.A., 1983. Timing of ethylene and polygalacturonase synthesis in relation to the control of tomato fruit ripening. Planta 157, 263–271.

Guglielmino, N., Liberman, M., Jauneau, A., Vian, B., Catesson, A.M., GoldbergR., 1997. Pectin immunolocalization and calcium visualization in differentiating derivatives from poplar cambium. Protoplasma 199, 151–160.

Ha, M.A., Apperley, D.C., Jarvis, M.C., 1997. Molecular rigidity in dry and hydrated onion cell walls. Plant Physiol. 115, 593–598.

Hadfield, K.A., Bennett, A.B., 1988. Polygalacturonases: Many genes in search of a function. Plant Physiol. 117, 337–343.

Hahn, M.G., 1996. Signal perception at the plasma membrane: binding protine and receptors. In: Smallwood, M., Knox, J.P., Bowles, D.J. (Eds.), Membranes: Specialized Functions in Plants. Bios Scientific Publishers, Oxford, pp. 103–136.

Hahn, M.G., Darvill, A.G., Albersheim, P., 1981. Host-pathogen interactions. XIX. The endogenous elicitor, a fragment of a plant cell wall polysaccharide that elicits phytoalexin accumulation in soybeans. Plant Physiol. 68, 1161–1169.

Hart, D.A., Kindel, P.K., 1970a. A novel reaction involved in the degradation of apiogalacturonans from *Lemna minor* and the isolation of apiobiose as a product. Biochemistry 9, 2190–2196.

Hart, D.A., Kindel, P.K., 1970b. Isolation and partial characterization of apiogalacturonans from the cell wall of *Lemna minor*. Biochem. J. 116, 569–579.

Hayashi, T., Koyama, T., Matsuda, K., 1988. Formation of UDP-xylose and xyloglucan in soybean. Plant Physiol. 87, 341–345.

He, Z., Fujiki, M., Kohorn, B.D., 1996. A cell wall-associated, receptor-like protein kinase. J. Biol. Chem. 271, 19789–19793.

Horn, M.A., Heinstein, P.F., Low, P.S., 1989. Receptor-mediated endocytosis in plant cells. Plant Cell 1, 1003–1009.

Horn, M.A., Meadow, R.P., Apostol, I., Jones, C.R., Gorenstein, D.G., Heinstein, P.F., Low, P.S., 1992. Effect of elicitation and changes in extracellular pH on the cytoplasmic and vacuolar pH of suspension-cultured soybean cells. Plant Physiol. 98, 680–686.

Hoson, T., 1991. Structure and function of plant cell wall: immunological approaches. International Review of Cytology 130, 233–268.

Hou, W.-C., Chang, W.H., 1996. Pectin esterase-catalyzed firming effects during precooking of vegetables. J. Food Biochem. 20, 397–416.

Howe, G.A., Lightner, J., Browse, J., Ryan, C.A., 1996. An octadecanoid pathway mutant (JL5) of tomato is compromised in signaling for defense against insect attack. Plant Cell 8, 2067–2077.

Ingber, D., 1998. How cells might sense gravity. FASEB J. 13, S3–S15.

Ishii, T., 1995. Pectic polysaccharides from bamboo shoot cell walls. Mokuzai Gakkaishi 41, 669–676.

Ishii, T., 1997a. *O*-acetylated oligosaccharides from pectins of potato tuber cell walls. Plant Physiol. 113, 1265–1272.

Ishii, T., 1997b. Structure and function of feruloylated polysaccharides. Plant Sci. 12, 111–127.

Ishii, T., Ono, H., 1999. NMR spectroscopic analysis of the borate diol esters of methyl apiofuranoside. Carbohydr. Res. 321, 257–260.

Ishii, T., Matsunaga, T., Pellerin, P., O'Neill, M.A., Darvill, A., Albersheim, P., 1999. The plant cell wall polysaccharide rhamnogalacturonan II self-assembles into a covalent cross-linked dimer. J. Biol. Chem. 274, 13098–13109.

Ishikawa, M., Kuroyama, H., Takeuchi, Y., Tsumuraya, Y., 2000. Characterization of pectin methyltransferase from soybean hypocotyls. Planta 210, 782–791.

Jarvis, M.C., McCann, M.C., 2000. Macromolecular biophysics of the plant cell wall: concepts and methodology. Plant Physiol. Biochem. 38, 1–13.

Jauh, G.Y., Lord, E.M., 1996. Localization of pectins and arabinogalactan-proteins in lily (*Lilium longiflorum* L) pollen tube and style, and their possible roles in pollination. Planta 199, 251–261.

Jauneau, A., Quentin, M., Driouich, A., 1997. Micro-heterogeneity of pectins and calcium distribution in the epidermal and cortical parenchyma cell walls of flax hypocotyl. Protoplasma 198, 9–19.

Jauneau, A., Roy, S., Reis, D., Vian, B., 1998. Probes and microscopical methods for the localization of pectins in plant cells. Int. J. Plant Sci. 159, 1–13.

Jin, D.F., West, C.A., 1984. Characteristics of galacturonic acid oligomers as elicitors of casbene synthetase activity in castor bean seedlings. Plant Physiol. 74, 989–992.

Jones, L., Seymour, G.B., Knox, J.P., 1997. Localization of pectic galactan in tomato cell walls using a monoclonal antibody specific to (1-4)-β-D-galactan. Plant Physiol. 113, 1405–1412.

Kacurakova, M., Capek, P., Sasinkova, V., Wellner, N., Ebringerova, A., 2000. FT-IR study of plant cell wall model compounds: pectic polysaccharides and hemicelluloses. Carbohydr. Polymers 43, 195–203.

Kauss, H., Hassid, W.Z., 1967. Enzymatic introduction of the methyl ester groups of pectin. J. Biol. Chem. 242, 3449–3453.

Kauss, H., Swanson, A.L., 1969. Cooperation of enzymes responsible for polymerization and methylation in pectin biosynthesis. Z. Naturforsch. 24, 28–33.

Kauss, H., Swanson, A.L., Arnold, R., Odzuck, W., 1969. Biosynthesis of pectic substances. Localization of enzymes and products in a lipid-membrane complex. Biochim. Biophys. Acta 192, 55–61.

Kauss, H., Swanson, A.L., Hassid, W.Z., 1967. Biosynthesis of the methyl ester groups of pectin by transmethylation from *S*-adenosyl-L-methionine. Biochem. Biophys. Res. Commun. 26, 234–240.

Keegstra, K., Talmadge, K.W., Bauer, W.D., Albersheim, P., 1973. The structure of plant cell walls. III. A model of the walls of suspension-cultured sycamore cells based on the interconnections of the macromolecular components. Plant Physiol. 51, 188–196.

Kelleher, F.M., Bhavanandan, V.P., 1986. Re-examination of the products of the action of galactose oxidase. J. Biol. Chem. 261, 11045–11048.

Kikuchi, A., Edashige, Y., Ishii, T., Satoh, S., 1996. A xylogalacturonan whose level is dependent on the size of cell clusters is present in the pectin from cultured carrot cells. Planta 200, 369–372.

Kim, J.-B., Carpita, N.C., 1992. Changes in esterification of the uronic acid groups of cell wall polysaccharides during elongation of maize coleoptiles. Plant Physiol. 98, 646–653.

Knox, J.P., 1992. Molecular probes for the plant cell surface. Protoplasma 167, 1–9.

Knox, P.J., 1997. The use of antibodies to study the architecture and developmental regulation of plant cell walls. Int. Rev. Cytol. 171, 79–120.

Knox, P.J., Linstead, P.J., King, J., Cooper, C., Roberts, K., 1990. Pectin esterification is spatially regulated both within cell walls and between between developing tissues of root apices. Planta 181, 512–521.

Kobayashi, M., Matoh, T., Azuma, J., 1996. Two chains of rhamnogalacturonan II are cross linked by borate-diol ester bonds in higher plant cell walls. Plant Physiol. 110, 1017–1020.

Kobayashi, M., Nakagawa, H., Asaka, T., Matoh, T., 1999. Borate-rhamnogalacturonan II bonding reinforced by Ca^{2+} retains pectic polysaccharides in higher plants cell walls. Plant Physiol. 119, 199–203.

Kohn, R., 1975. Ion binding on polyuronates-alginate and pectin. Pure Appl. Chem. 42, 371–397.

Kojima, N., Tachida, Y., Yoshida, Y., Tsuji, S., 1996. Characterization of mouse ST8Sia II (STX) as a neural cell adhesion molecule-specific polysialic acid synthase. Requirement of core α1,6-linked fucose and a polypeptide chain for polysialylation. J. Biol. Chem. 271, 19457–19463.

Komae, K., Komae, A., Misaki, A., 1990. A 4,5-unsaturated low molecular weight oligogalacturonide as a potent phytoalexin-elicitor isolated from polygalacturonide of Ficus awkeotsang. Argic. Biol. Chem. 54, 1477–1484.

Komalavilas, P., Mort, A.J., 1989. The acetylation at *O*-3 of galacturonic acid in the rhamnose-rich region of pectins. Carbohydr. Res. 189, 261–272.

Konno, H., Yamasaki, Y., Katoh, K., 1989. Extracellular exo-polygalacturonase secreted form carrot cell cultures. Its purification and involvement in pectic polymer degradation. Physiol. Plant. 76, 514–520.

Lamb, C.J., Dixon, R.A., 1997. The oxidative burst in plant disease resistance. Annu. Rev. Plant Physiol. Plant Mol. Biol. 179, 45–51.

Lapous, D., Mathieu, Y., Guern, J., Lauriére, C., 1998. Increase of defense gene transcripts by cytoplasmic acidification. Planta 205, 452–458.

Lau, J.M., McNeil, M., Darvill, A.G., Albersheim, P., 1985. Structure of the backbone of rhamnogalacturonan I, a pectic polysaccharide in the primary cell walls of plants. Carbohydr. Res. 137, 111–125.

Lau, J.M., McNeil, M., Darvill, A.G., Albersheim, P., 1987. Treatment of rhamnogalacturonan I with lithium in ethylenediamine. Carbohydr. Res. 168, 245–274.

Laval, V., Chabannes, M., Carriere, M., Canut, H., Barre, A., Rouge, P., Pont-Lezica, R., Galaud, J.-P., 1999. A family of *Arabidopsis* plasma membrane receptors presenting animal β-integrin domains. Biochim. Biophys. Acta. 1435, 61–70.

Leckband, D., 2000. Measuring the forces that control protein interactions. Ann. Rev. Biophys. Biomol. Struct. 29, 1–26.

Lee, S., Choi, H., Suh, S.S., Doo, I.-S., Oh, K.-Y., Choi, E., Schroeder-Taylor, A.T., Low, P.S., Lee, Y., 1999. Oligogalacturonic acid and chitosan reduce stomatal aperture by inducing the evolution of reactive oxygen species from guard cells of tomato and *Commelina communis*. Plant Physiol. 121, 147–152.

Legendre, L., Heinstein, P.F., Low, P.S., 1992. Evidence for participation of GTP-binding proteins in elicitation of the rapid oxidative burst in cultured soybean cells. J. Biol. Chem. 267, 20140–20147.

Legendre, L., Rueter, S., Heinstein, P.F., Low, P.S., 1993a. Characterization of the oligogalacturonide-induced oxidative burst in cultured soybean (*Glycine max*) cells. Plant Physiol. 102, 233–240.

Legendre, L., Yir, Y.G., Crain, R., Haddock, N., Heinstein, P.F., Low, P.S., 1993b. Phospholipase C activation during elicitation of the oxidative burst in cultured plant cells. J. Biol. Chem. 268, 24559–24563.

Lerouge, P., O'Neill, M.A., Darvill, A.G., Albersheim, P., 1993. Structural characterization of endo-glycanase-generated oligoglycosyl side chains of rhamnogalacturonan I. Carbohydr. Res. 243, 359–371.

Liljebjelke, K., Adolphson, R., Baker, K., Doong, R.L., Mohnen, D., 1995. Enzymatic synthesis and purification of uridine diphosphate [^{14}C]galacturonic acid: a substrate for pectin biosynthesis. Anal. Biochem. 225, 296–304.

Limberg, G., Korner, R., Bucholt, H.C., Christensen, T.M.I.E., Roepstorff, P., Mikkelsen, J.D., 2000a. Quantification of the amount of galacturonic acid residues in block sequences in pectin homogalacturonan by enzymatic fingerprinting with *exo*- and *endo*-polygalacturonase II from *Aspergillus niger*. Carbohydr. Res. 327, 321–332.

Limberg, G., Korner, R., Bucholt, H.C., Christensen, T.M.I.E., Roepstorff, P., Mikkelsen, J.D., 2000. Analysis of different de-esterification mechanisms for pectin by enzymatic fingerprinting using endopectin lyase and endopolygalacturonase II from *A. niger*. Carbohydr. Res. 327, 293–307.

Lin, T.-Y., Elbein, A.D., Su, J.C., 1966. Substrate specificity in pectin synthesis. Biochem. Biophys. Res. Commun. 22, 650–657.

Liners, F., Gaspar, T., Van Cutsem, P., 1994. Acetyl- and methyl-esterification of pectins of friable and compact sugar-beet calli: consequences for intercellular adhesion. Planta 192, 545–556.

Liners, F., Letesson, J.-J., Didembourg, C., Van Cutsem, P., 1989. Monoclonal antibodies against pectin. Recognition of a conformation induced by calcium. Plant Physiol. 91, 1419–1424.

Liners, F., Van Cutsem, P., 1992. Distribution of pectic polysaccharides throughout wall of suspension-cultured carrot cells. Protoplasma 170, 10–21.

Loomis, W.D., Durst, R.W., 1992. Chemistry and biology of boron. BioFactors 3, 229–239.

Low, P.S., Legendre, L., Heinstein, P.F., Horn, M.F., 1993. Comparison of elicitor and vitamin receptor- mediated endocytosis in cultured soybean cells. J. Exp. Bot. 44 (Suppl.), 269–274.

Low, P.S., Merida, J.R., 1996. The oxidative burst in plant defense: function and signal transduction. Physiol. Plant. 96, 533–542.

Lynch, M.A., Staehelin, L.A., 1992. Domain-specific and cell type-specific localization of two types of cell wall matrix polysaccharides in the clover root tip. J. Cell Biol. 118, 467–479.

MacDougall, A.J., Needs, P.W., Rigby, N.M., Ring, S.G., 1996. Calcium gelation of pectic polysaccharides isolated from unripe tomato fruit. Carbohydr. Res. 293, 235–249.

MacDougall, A.J., Rigby, N.M., Needs, P.W., Selvendran, R.R., 1992. Movement and metabolism of oligogalacturonide elicitors in tomato shoots. Planta 188, 566–574.

Malone, M., 1996. Rapid, long-distance signal transmission in higher plants. Adv. Bot. Res. 22, 163–228.

Marfà, V., Gollin, D., Eberhard, S., Mohnen, D., Albersheim, P., Darvill, A., 1991. Oligogalacturonides are able to induce flowers to form on tobacco explants. Plant J. 1, 217–225.

Marion, D., Driscoll, P.C., Kay, L.E., Wingfield, P.T., Bax, A., Gronenborn, A., Clore, G.M., 1989. Overcoming the overlap problem in the assignment of H-1 NMR spectra of larger proteins by use of 3-dimensional heteronuclear H-1-N-15 Hartmann-Hahn multiple quantum coherence spectroscopy — application to interluekin-1-beta. Biochem. 28, 6150–6156.

Marszalek, P.E., Oberhauser, A.F., Pang, Y.-P., Fernandez, J.M., 1998. Polysaccharide elasticity governed by chair-boat transitions of the glucopyranose ring. Nature (London) 396, 661–664.

Marszalek, P.E., Pang, Y.-P., Li, H., El Yazal, J., Oberhauser, A.F., Fernandez, J.M., 1999. Atomic levers control pyranose ring conformations. Proc. Natl. Acad. Sci. USA 96, 7894–7898.

Masuda, H., Ozeki, Y., Amino, S.-I., Komamine, A., 1984. Changes in cell wall polysaccharides during elongation in a 2,4-D free medium in a carrot suspension culture. Physiol. Plant. 62, 65–72.

Mathieu, Y., Guern, J., Spiro, M.D., O'Neill, M.A., Kates, K.A., Darvill, A., Albersheim, P., 1998. The transient nature of the oligogalacturonide-induced ion fluxes of tobacco cells is not correlated with fragmentation of the oligogalacturonides. Plant J. 16, 305–311.

Mathieu, Y., Kurkdjian, A., Xia, H., Guern, J., Koller, A., Spiro, M.D., O'Niell, M., Albersheim, P., Darvill, A., 1991. Membrane responses induced by oligogalacturonides in suspension-cultured tobacco cells. Plant J. 1, 333–343.

Mathieu, Y., Lapous, D., Thomine, S., Laurière, C., Guern, J., 1996a. Cytoplasmic acidification as an early phosphorylation-dependent response of tobacco cells to elicitors. Planta 199, 416–424.

Mathieu, Y., Sanchez, F.J., Droillard, M.-J., Lapous, D., Laurière, C., Guern, J., 1996b. Involvement of protein phosphorylation in the early steps of transduction of the oligogalacturonide signal in tobacco cells. Plant Physiol. Biochem. 34, 399–408.

Matoh, T., Kobayashi, M., 1998. Boron and calcium, essential inorganic constituents of pectic polysaccharides in higher plant cell walls. J. Plant Res. 111, 179–190.

Matoh, T., Takahashi, M., Takabe, K., Kobayashi, M., 1998. Immunochemistry of rhamnogalacturonan II in cell walls of higher plants. Plant Cell Physiol. 39, 483–491.

Matoh, T., Takasaki, M., Kobayashi, M., Takabe, K., 2000. Boron nutrition of cultured tobacco BY-2 cells. III. Characterization of the boron-rhamnogalacturonan II complex in cells acclimated to low levels of boron. Plant Cell Physiol. 41, 363–366.

Matsuhasi, S., Nishikawa, N., Negishi, T., Hatanaka, C., 1993. Enzymic-HPLC determination of the amount and distribution of the galacturonan region in pectate molecules. J. Liquid Chromatogr. 16, 3203–3215.

Mazeau, K., Perez, S., 1998. The preferred conformations of four oligomeric fragments of rhamnogalacturonan II. Carbohydr. Res. 311, 203–217.

McCann, M.C., Shi, J., Roberts, K., Carpita, N.C., 1994. Changes in pectin structure and localization during the growth of unadapted and NaCl-adapted tobacco cells. Plant Journal 5, 773–785.

McCartney, L., Ormerod, A.P., Gidley, M.J., Knox, J.P., 2000. Temporal and spatial regulation of pectic (1→4)-β-D-galactan in cell walls of developing pea cotyledons: implications for mechanical properties. Plant J. 22, 105–113.

McNab, J.M., Villemez, C.L., Albersheim, P., 1968. Biosynthesis of galactan by a particulate preparation from *Phaseolus aureus* seedlings. Biochem. J. 106, 355–360.

McDowell, L.M., Schaefer, J., 1996. High-resolution NMR of biological solids. Curr. Opin. Struct. Biol. 6, 624–629.

McDowell, L.M., Burzios, L.A., Waite, J.H., Schaefer, J., 1999. Rotational echo double resonance detection of cross-links formed in mussel byssus under high-flow stress. J. Biol. Chem. 274, 20293–20295.

Melotto, E., Greve, L.C., Labavitch, J.M., 1994. Cell wall metabolism in ripening fruit VII. Biologically active pectin oligomers in ripening tomato (*Lycopersicon esculentum* Mill.) fruits. Plant Physiol. 106, 575–581.

Melton, L.D., McNeil, M., Darvill, A.G., Albersheim, P., 1986. Structure of plant cell walls. 17. Structural characterization of oligosaccharides isolated from the pectic polysaccharide rhamnogalacturonan II. Carbohydr. Res. 146, 279–305.

Merritt, M.E., Christensen, A.M., Kramer, K.J., Hopkins, T.L., Schaefer, J., 1996. Detection on intercatechol cross-links in insect cuticle by solid-state carbon-13 and nitrogen-15 NMR. J. Am. Chem. Soc. 118, 11278–11282.

Messiaen, J., Van Cutsem, P., 1994. Pectic signal transduction in carrot cells: membrane, cytosolic nuclear responses induced by oligogalacturonides. Plant Cell Physiol. 35, 677–689.

Messiaen, J., Van Cutsem, P., 1999. Polyamines and pectins. II. Modulation of pectic-signal transduction. Planta 208, 247–256.

Mignani, I., Greve, C., Ben-Arie, R., Stotz, H.U., Li, C., Shackel, K.A., Labavitch, J.M., 1995. The effects of GA_3 and divalent cations on aspects of pectin metabolism and tissue softening in ripening tomato pericarp. Physiol. Plant. 93, 108–115.

Miller, D., Hable, W., Gottwald, J., Ellard-Ivey, M., Demura, T., Klomax, T., Carpita, N.C., 1997. Connections: the hard wiring of the plant cell for perception, signaling, and response. Plant Cell 9, 2105–2117.

Moerschbacher, B.M., Mierau, M., Graebner, B., Noll, U., Mort, A.J., 1999. Small oligomers of galacturonic acid are endogenous suppressors of disease resistance reactions in wheat leaves. J. Exp. Bot. 50, 605–612.

Mohnen, D., 1999. Biosynthesis of pectins and galactomannans. In: Pinto, B.M. (Ed.), Comprehensive Natural Products Chemistry, Vol. 3, Carbohydrates and their Derivatives Including Tannins, Cellulose, and Related Lignins. Elsevier, Oxford, pp. 497–527.

Mohnen, D., Doong, R.L., Liljebjelke, K., Fralish, G., Chan, J., 1996. Cell free synthesis of the pectic polysaccharide homogalacturonan. In: Visser, J., Voragen, A.G.J. (Eds.), Pectins and Pectinases. Elsevier Science, Amsterdam, pp. 109–126.

Mohnen, D., Eberhard, S., Marfà, V., Doubrava, N., Toubart, P., Gollin, D., Gruber, T.A., Nuri, W., Albersheim, P., Darvill, A., 1990. The control of root, vegetative shoot and flower morphogenesis in tobacco thin cell-layer explants (TCLs). Development 108, 191–201.

Mohnen, D., Hahn, M.G., 1993. Cell wall carbohydrates as signals in plants. Sem. Cell Biol. 4, 93–102.

Moloshok, T., Pearce, G., Ryan, C.A., 1992. Oligouronide signaling of proteinase inhibitor genes in plants: structure–activity relationships of di- and trigalacturonic acids and their derivatives. Arch. Biochem. Biophys. 294, 731–734.

Moore, P.J., Swords, K.M.M., Lynch, M.A., Staehelin, L.A., 1991. Spatial organization of the assembly pathways of glycoproteins and complex polysaccharides in the Golgi apparatus of plants. J. Cell Biol. 112, 589–602.

Morita, M., 1965a. Polysaccharides of soybean seeds. Part I. Polysaccharide consituents of "hot-water-extract" fractions of soybean seeds and an arabinogalactan as its major component. Agric. Biol. Chem. 29, 564–573.

Morita, M., 1965b. Polysaccharides of soybean seeds. Part II. A methylated arabinogalactan isolated from methylated product of "hot-water extract" fraction of soybean seed polysaccharides. Agric. Biol. Chem. 29, 626–630.

Morris, E.R., Powell, D.A., Gidley, M.J., Rees, D.A., 1982. Conformations and interactions of pectins. 1. Polymorphism between gel and solid states of calcium polygalacturonate. J. Mol. Biol. 155, 507–516.

Morris, V.J., Kirby, A.R., Gunning, A.P., 1999. Atomic force microscopy for biologists. Imperial College Press, London.

Morris, V.J., Gunning, A.P., Kirby, A.R., Round, A.N., Waldron, K.W., Ng, A., 1997. Atomic force microscopy of plant cell walls, plant cell wall polysaccharides and gels. Int. J. Biol. Macromol. 21, 61–66.

Mort, A.J., Qiu, F., Maness, N.O., 1993. Determination of the pattern of methyl esterification in pectins. Distribution of contiguous non-esterified residues. Carbohydr Res. 247, 21–35.

Munoz, P., Norambuena, L., Orellana, A., 1996. Evidence for a UDP-glucose transporter in Golgi apparatus-derived vesicles from pea and its possible role in polysaccharide biosynthesis. Plant Physiol. 112, 1585–1594.

Narvaez-Vasques, J., Pearce, G., Orozco-Cardenas, M.L., Franceschi, V.R., Ryan, C.A., 1995. Autoradiographic and biochemical evidence for the systemic translocation of systemin in tomato plants. Planta 195, 593–600.

Neckelmann, G., Orellana, A., 1998. Metabolism of uridine 5′-diphosphate-glucose in Golgi vesicles from pea stems. Plant Physiol. 117, 1007–1014.

Needs, P.W., Rigby, N.M., Colquhoun, I.J., Ring, S.G., 1998. Conflicting evidence for non-methyl galacturonosyl esters in *Daucus carota*. Phytochemistry 48, 71–77.

O'Donnell, P.J., Calvert, C., Atzorn, R., Wasternach, C., Leyser, H.M.O., Bowles, D.J., 1996. Ethylene as a signal mediating the wound response of tomato plants. Science 274, 1914–1917.

O'Neill, M., Albersheim, P., Darvill, A., 1990. The pectic polysaccharides of primary cell walls. In: Dey, D.M. (Ed.), Methods in Plant Biochemistry, Vol. 2. Academic Press, London, pp. 415–441.

O'Neill, M.A., Warrenfeltz, D., Kates, K., Pellerin, P., Doco, T., Darvill, A.G., Albersheim, P., 1996. Rhamnogalacturonan-II, a pectic polysaccharide in the walls of growing plant cell, forms a dimer that is covalently cross-linked by a borate ester — in vitro conditions for the formation and hydrolysis of the dimer. J. Biol. Chem. 271, 22923–22930.

O'Neill, M.A., Warrenfeltz, D., Kates, K., Pellerin, P., Doco, T., Darvill, A.G., Albersheim, P., 1997. Rhamnogalacturonan-II, a pectic polysaccharide in the walls of growing plant cell, forms a dimer that is covalently cross-linked by a borate ester — in vitro conditions for the formation and hydrolysis of the dimer. J. Biol. Chem. 272, 3869.

Orellana, A., Mohnen, D., 1999. Enzymatic synthesis and purification of [^{3}H]uridine diphosphate galacturonic acid for use in studying Golgi-localized transporters. Anal. Biochem. 272, 224–231.

Orellana, A., Neckelmann, G., Norambuena, L., 1997. Topography and function of Golgi uridine-5′-diphosphatase from pea stems. Plant Physiol. 114, 99–107.

Orfila, C., Knox, J.P., 2000. Spatial regulation of pectic polysaccharides in relation to pit fields in cell walls of tomato fruit pericarp. Plant Physiol. 122, 775–781.

Orozco-Cardenas, M., McGurl, B., Ryan, C.A., 1993. Expression of an antisense prosystemin gene in tomato plants reduces resistance toward Manduca sexta larvae. Proc. Natl. Acad. Sci. USA 90, 8273–8276.

Orozco-Cardenas, M., Ryan, C.A., 1999. Hydrogen peroxide is generated systemically in plant leaves by wounding and systemin via the octadecanoid pathway. Proc. Natl. Acad. Sci. USA 96, 6553–6557.

Pagel, W., Heitifuss, R., 1990. Enzymatic activities in soft rot pathogenesis of potato tubers: effects of calcium, pH, and degree of pectin esterification on the activities of polygalacturonase and pectate lyase. Physiol. Mol. Plant Pathol. 37, 9–25.

Pan, Y., 1992. NMR Studies of the Structure of Hydroxyproline-rich Glycoproteins of Plant Cell Walls (Tomato). PhD thesis, Washington University, St Louis MO, USA.

Panayotatos, N., Villemez, C.L., 1973. The formation of a β-(1->4)-D-galactan chain catalysed by a *Phaseolus aureus* enzyme. Biochem. J. 133, 263–271.

Pauly, M., Porchia, A., Olsen, C.E., Nunan, K.J., Scheller, H.V., 2000. Enzymatic synthesis and purification of UDP-β-L-arabinopyranose, a substrate for the biosynthesis of plant polysaccharides. Anal. Biochem. 278, 69–73.

Pauly, M., Scheller, H.V., 2000. *O*-acetylation of plant cell wall polysaccharides: identification and partial characterization of rhamnogalacturonan *O*-acetyl-transferase from potato suspension cultured cells. Planta 210, 659–667.

Pear, J.R., Kawagoe, Y., Schreckengost, W.E., Delmer, D.P., Stalker, D.M., 1996. Higher plants contain homologs of the bacterial *celA* genes encoding the catalytic subunit of cellulose synthase. Proc. Natl. Acad. Sci. USA 93, 12367–12642.

Pellerin, P., O'Neill, M.A., 1998. The interaction of the pectic polysaccharide rhamnogalacturonan II with heavy metals and lanthanides in wines and fruit juices. Analusis 26, M32–M36.

Pellerin, P., O'Neill, M.A., Pierre, C., Cabanis, M-T., Darvill, A.G., Albersheim, P., Moutounet, M., 1997. Lead complexation in wines with the dimers of the grape pectic polysaccharide rhamnogalacturonan II. J. Int. Sci. Vigne et Vin. 31, 33–41.

Perez, S., Mazeau, K., Herve du Penhoat, C., 2000. The three-dimensional structures of the pectic polysaccharides. Plant Physiol. Biochem. 38, 37–55.

Perrin, R.M., DeRocher, A.E., Bar-Peled, M., Zeng, W., Norambuena, L., Orellana, A., Raikhel, N.V., Keegstra, K., 1976. Xyloglucan fucosyltransferase, an enzyme involved in plant cell wall biosynthesis. Science 284.

Perrone, P., Hewage, C.M., Sadler, I.H., Fry, S.C., 1998. N alpha- and N epsilon-D-galacturonoyl-L-lysine amides: Properties and possible occurrence in plant cell walls. Phytochemistry 49, 1879–1890.

Powell, D.A., Morris, E.R., Gidley, M.J., Rees, D.A., 1982. Conformations and interactions of pectins. II. Influence of residue sequence on chain association in calicium pectate gels. J. Mol. Biol. 155, 517–531.

Prade, R.A., Zhan, D., Ayoubi, P., Mort, A.J., 1999. Pectins, pectinases and plant-microbe interactions. Biotechnol. Genet. Eng. Rev. 16, 361–391.

Puhlmann, J., Bucheli, E., Swain, M.J., Dunning, N., Albersheim, P., Darvill, A.G., Hahn, M.G., 1994. Generation of monoclonal antibodies against plant cell wall polysaccharides. 1. Characterization of a monoclonal antibody to a terminal α-(1,2)-linked fucosyl-containing epitope. Plant Physiol. 104, 699–710.

Qi, X., Behrens, B.X., West, P., Mort, A.J., 1995. Solubilization and partial characterization of extensin fragments from cell walls of cotton suspension cultures. Evidence for a covalent crosslink between extensin and pectin. Plant Physiol. 108, 1691–1701.

Rao, A.K., Mendicino, J., 1976. Preparation of UDP-D-[U-^{14}C]Galacturonic acid and UDP-D-[6-^{3}H]Galactose with high specific activities. Anal. Biochem. 72, 400–406.

Reiter, W.-D., Chapple, C., Somerville, C.R., 1997. Mutants of *Arabidopsis thaliana* with altered cell wall polysaccharide composition. Plant J. 12, 335–345.

Renard, C.M.C.G., Crepeau, M.J., Thibault, J.-F., 1999. Glucuronic acid directly linked to galacturonic acid in the rhamnogalacturonan backbone of beet pectins. Eur. J. Biochem. 266, 566–574.

Reuhs, B.L., Glenn, J., Stephens, S.B., Kim, J.S., Christie, D.B., Eberhard, S., Zablackis, E., O'Neill, M.A., Albersheim, P., Darvill, A.G. The substitution of L-galactose for L-fucose in the cell wall

polysaccharide rhamnogalacturonan II results in changes in the properties of borate cross-linked pectin (submitted).

Reymond, P., Grünberger, S., Paul, K., Müller, M., Farmer, E.E., 1995. Oligogalacturonide defense signals in plants: large fragments interact with the plasma membrane in vitro. Proc. Natl. Acad. Sci. USA 92, 4145–4149.

Reymond, P., Kunz, B., Paul-Pletzer, K., Grimm, R., Eckerskorn, C., Farmer, E.E., 1996. Cloning of a cDNA encoding a plasma membrane-associated, uronide binding phosphoprotein with physical properties similar to viral movement proteins. Plant Cell 8, 2265–2276.

Ridley, B.L., Spiro, M.D., Glushka, J., Albersheim, P., Darvill, A., Mohnen, D., 1997. A method for biotin labeling of biologically active oligogalacturonides using a chemically stable hydrazide linkage. Anal. Biochem. 249, 10–19.

Rihouey, C., Morvan, C., Borissova, I., Jauneau, A., Demarty, M., Jarvis, M., 1995. Structural features of CDTA-soluble pectins from flax hypocotyls. Carbohydr. Polym. 28, 159–166.

Rhee, S., Somerville, C., 1988. Tetrad pollen formation in *quartet* mutants of *Arabidopsis thaliana* is associated with the persistence of pectic polysaccharides of the pollen mother cell wall. Plant J. 15, 79–88.

Roberts, K., 1990. Structures at the plant cell surface. Curr. Opin. Cell Biol. 2, 920–92.

Robertson, B., 1986. Elicitors of the production of lignin-like compounds in cucumber hypocotyls. Physiol. Mol. Plant Pathol. 28, 137–148.

Rombouts, F.M., Thibault, J.F., 1986. Sugar beet pectins: chemical structure and gelation through oxidative coupling. In: Fishman, M.L., Jen, J.J. (Eds.), Chemistry and Function of Pectins. American Chemical Society, Washington, DC, pp. 49–60.

Rose, J.K.C., Hakfield, K.A., Labavitch, J.M., Bennett, A.B., 1998. Temporal sequence of cell wall disassembly in rapidly ripening melon fruit. Plant Physiol. 17, 345–361.

Rose, J.K.C., O'Neill, M.A., Albersheim, P., Darvell, A., 1999. The primary cell walls of higher plants. In: Ernst, W., Hart, E.W. (Eds.), Oligosaccharides in Chemistry and Biology. Wiley, London, pp. 783–803.

Round, A.N., MacDougall., A.J., Ring, S.G., Morris, V.J., 1997. Unexpected branching in pectin observed by atomic force micrsocopy. Carbohydr. Res. 303, 251–253.

Rout-Mayer, M.-A., Mathieu, Y., Cazalé, A.-C., Guern, J., Laurière, C., 1997. Extracellular alkalinization and oxidative burst induced by fungal pectin lyase in tobacco cells are not due to the perception of oligogalacturonide fragments. Plant Physiol. Biochem. 35, 321–330.

Roy, S., 1994. Analytical detection of calcium and immunocytochemical visualization of homogalacturonic acid sequences in the ripe cherry tomato. Plant Physiol. Biochem. 32, 633–640.

Ryan, C.A., Pearce, G., 1998. Systemin: a polypeptide signal for plant defensive genes. Annu. Rev. Dev. Biol. 14, 1–17.

Saulnier, L., Thibault, J.-F., 1999. Ferulic acid and diferulic acids as components of sugar-beet pectins and maize bran heteroxylans. J. Sci. Food Agric. 79, 396–402.

Schaefer, J., 1998. REDOR NMR of biological solids: from protein binding sites to bacterial cell walls. In: Diederich, F., Künzer, H. (Eds.), Proceedings of the 26th Ernst Schering Research Foundation Workshop on Recent Trends in Molecular Recognition. Springer-Verlag, New York, pp 26–52.

Schaumann, A., Bruyant-Vannier, M.-P., Goubet, F., Morvan, C., 1993. Pectic metabolism in suspension-cultured cells of flax, *Linum usitatissimum*. Plant Cell Physiol. 34, 891–897.

Scheller, H.V., Doong, R.L., Ridley, B.L., Mohnen, D., 1999. Pectin biosynthesis: a solubilized galacturonosyltransferase from tobacco catalyzes the transfer of galacturonic acid from UDP-galacturonic acid onto the non-reducing end of homogalacturonan. Planta 207, 512–517.

Schindler, M., Meiners, S., Cheresh, D.A., 1989. RGD-dependent linkage between plant cell wall and plasma-membrane — consequences for growth. J. Cell Biol. 108, 1955–1965.

Schindler, T.M., Bergfeld, R., Van Cutsem, P., von Sengbusch, D., Schopfer, P., 1995. Distribution of pectins in cell walls of maize coleoptiles and evidence against their involvement in auxin-induced extension growth. Protoplasma 188, 213–224.

Schols, H.A., Bakx, E.J., Schipper, D., Voragen, A.G.J., 1995. A xylogalacturonan subunit present in the modified hairy regions of apple pectin. Carbohydr. Res. 279, 265–279.

Schwartz, M.A., Schaller, M.D., Ginsberg, M.H., 1995. Integrins: Emerging paradigms of signal transduction. Annu. Rev. Cell Biol. 11, 549–599.

Seymour, G.B., Harding, S.E., 1987. Analysis of the molecular size of tomato (*Lycopersicon esculentum*) fruit polyuronides by gel-filtration and low-speed sedimentation equilibrium. Biochem. J. 245, 463–466.

Selvendran, R.R., 1985. Developments in the chemistry and biochemistry of pectic and hemicellulosic polymers. J. Cell Sci. (Suppl.) 2, 51–88.

Shedletzky, E., Schmuel, M., Trainin, T., Kalman, S., Delmer, D., 1992. Cell wall structure in cells adapted to grow on the cellulose synthesis inhibitor 2,6-dichlorobenzonitrile. A comparison between 2 dicotyledonous plants and a gramineous monocot. Plant Physiol. 100, 120–130.

Sherrier, D.J., VandenBosch, K.A., 1004. Secretion of cell wall polysaccharides in *Vicia* root hairs. Plant J. 5, 185–195.

Shin, K.S., Kiyohara, H., Matsumoto, T., Yamada, H., 1998. Rhamnogalacturonan II dimers cross-linked by borate diesters from the leaves of *Panax ginseng* C.A. Meyer are responsible for expression of their IL-6 production enhancing activities. Carbohydr. Res. 307, 97–106.

Sieber, P., Schorderet.M., Ryser, U., Buchala, A., Kolattukudy, P., Metraux, J.-P., Nawrath, C., 2000. Transgenic *Arabidopsis* plants expressing a fungal cutinase show alterations in the structure and properties of the cuticle and postgenital organ fusions. Plant Cell 12, 721–737.

Simpson, S.D., Ashford, D.A., Harvey, D.J., Bowles, D.J., 1998. Short chain oligogalacturonides induce ethylene production and expression of the gene encoding aminocyclopropane 1-carboxylic acid oxidase in tomato plants. Glycobiology 8, 579–583.

Sitrit, Y., Bennett, A.B., 1998. Regulation of tomato fruit polygalacturonase mRNA accumulation by ethylene: a re-examination. Plant Physiol. 116, 1145–1150.

Smith, J.S., Watson, C.F., Morris, P.C., Birs, C.R., Seymour, G.B., Gray, J.E., Arnold, C., Tucker, G.A., Schuch, W., Harding, S., Grierson, D., 1990. Inheritance and effect on ripening of antisense polygalacturonase genes in transgenic tomatoes. Plant Mol. Biol. 14, 369–379.

Sorensen, S.O., Pauly, M., Bush, M., Skjot, M., McCann, M.C., Borkhardt, B., Ulvskov, P., 2000. Pectin engineering: Modification of potato pectin by in vivo expression of an endo-1,4-β-D-galactanase. Proc. Natl. Acad. Sci. USA. 97, 7639–7644.

Spellman, M.W., McNeil, M., Darvill, A.G., Albersheim, P., Dell, A., 1983. Structure of plant cell walls. 14. Characterization of a structurally complex heptasaccharide isolated from the pectic polysaccharide rhamnogalacturonan II. Carbohydr Res. 122, 131–153.

Spiro, M.D., Kates, K.A., Koller, A.L., O'Neill, M.A., Albersheim, P., Darvill, A., 1993. Purification and characterization of biologically active 1,4-linked α-D-oligogalacturonides after partial digestion of polygalacturonic acid with endopolyglacturonase. Carbohydr. Res. 247, 9–20.

Spiro, M.D., Ridley, B.L., Eberhard, S., Kates, K.A., Mathieu, Y., O'Neill, M.A., Mohnen, D., Guern, J., Darvill, A., Albersheim, P., 1998. Biological activity of reducing-end-derivatized oligogalacturonides in tobacco tissue cultures. Plant Physiol. 116, 1289–1298.

Stacey, N., Roberts, K., Carpita, N.C., Wells, B., McCann, M.C., 1995. Dynamic changes in cell surface molecules are very early events in the differentiation of mesophyll cells from *Zinnia elegans* into tracheary elements. Plant J. 8, 891–906.

Staehelin, L.A., Moore, I., 1995. The plant Golgi apparatus: structure, functional organization and trafficking mechanisms. Annu. Rev. Plant Physiol. Plant Mol. Biol. 46, 261–288.

Steele, N.M., McCann, M.C., Roberts, K., 1997. Pectin modification in cell walls of ripening tomatoes occurs in distinct domains. Plant Physiol. 114, 373–381.

Steffan, W., Kovac, P., Albersheim, P., Darvill, A.G., Hahn, M.G., 1995. Characterization of a monoclonal antibody that recognizes an arabinosylated (1-6)-β-D-galactan epitope in plant complex carbohdyrates. Carbohydr. Res. 275, 295–307.

Stennis, M.J., Chandra, S., Ryan, C.A., Low, P.S., 1998. Systemin potentiates the oxidative burst in cultured tomato cells. Plant Physiol. 117, 1031–1036.

Stephen, A.M., 1983. Other plant polysaccharides. In: Aspinall, G.O. (Ed.), The Polysaccharides, Vol. 2. Academic Press, New York, pp. 97–193.

Sterling, J., Quigley, H.F., Orellana, A., Mohnen, D. α1,4-galacturonosyltransferase is located in the lumen of the Golgi (submitted) .

Sticher, L., Mauch-Mani, B., Métraux, J.P., 1997. Systemic acquired resistance. Annu. Rev. Phytopathol. 37, 235–237.

Stratmann, J.W., Ryan, C.A., 1997. Mylen basic protein kinase activity in tomato leaves is induced systemically by wounding and increases in response to systemin and oligosaccharide elicitors. Proc. Natl. Acad. Sci. USA 94, 11085–11089.

Szpunar, J., Pellerin, P., Makarov, A., Doco, T., Williams, P., Lobinski, R., 1999. Speciation of metal-carbohydrate complexes in fruit and vegetable samples by size-exclusion HPLC-ICP-MS. J. Anal. Atomic Spectrom. 14, 639–644.

Tahiri, M., Pellerin, P., Tressol, J.C., Doco, T., Pepin, D., Rayssiguier, Y., Coudray, C., 2000. The rhamnogalacturonan-II dimer decreases intestinal absorption and tissue accumulation of lead in rats. J. Nutr. 130, 249–253.

Tang, H.-R., Wang, Y.-L., Belton, P.S., 2000. ^{13}C CPMAS studies of plant cell wall material and model systems using proton relaxation-induced spectral editing techniques. Solid State Nucl. Magn. Res. 15, 239–248.

Tepper, C.S., Anderson, A.J., 1990. Interactions between pectic fragments and extracellular components from the fungal pathogen *Colletotrichum lindemuthianm*. Physiol. Molec. Plant Path. 36, 147–158.

Thain, J.F., Doherty, H.M., Bowles, D.J., Wildon, D.C., 1990. Oligogalacturonides that induce proteinase inhibitor activity in tomato plants cause depolarization of tomato leaf cells. Plant Cell Environ. 13, 569–574.

Thakur, B.R., Singh, R.K., Handa, A.K., 1997. Chemistry and uses of pectin — a review. Crit. Rev. Food Sci. Nutrition 37, 47–73.

Theologis, A., Oeller, P.W., Wong, L., Rottmann, W.H., Gantz, D.M., 1993. Use of a tomato mutant constructed with reverse genetics to study fruit ripening, a complex developmental process. Dev. Genet. 14, 282–295.

Thibault, J.-F., Rinaudo, M., 1986. Chain association of pectic molecules during calcium-induced gelation. Biopolymers 25, 455–468.

Thompson, J.E., Fry, S.C., 2000. Evidence for covalent linkage between xyloglucan and acidic pectins in suspension-cultured rose cells. Planta 211, 275–286.

Tibbits, C.W., MacDougall, A.J., Ring, S.G., 1998. Calcium binding and swelling behaviour of a high methoxy pectin gel. Carbohydr. Res. 310, 101–107.

Tieman, D., Handa, A., 1994. Reduction in pectin methyl-esterase activity modifies tissue integrity and cation levels in ripening tomato (*Lycopersicon esculentum*). Plant Physiol. 106, 429–436.

Tong, G., Pan, Y., Dong, H., Pryor, R., Wilson, G.E., Schaefer, J., 1997. Structure and dynamics of pentaglycyl bridges in the cell walls of *Staphylococcus aureus* by ^{13}C-^{15}N REDOR NMR. Biochem. 36, 9859–9866.

Tran Thanh Van, K., Toubart, P., Cousson, A., Darvill, A.G., Collin, D.J., Chelf, P., Albersheim, P., 1985. Manipulation of the morphogenetic pathways of tobacco explants by oligosaccharins. Nature 314, 615–617.

Van Halbeek, H., 1994. NMR developments in structural studies of carbohydrates and their complexes. Curr. Opin. Struct. Biol. 4, 697–709.

VandenBosch, K.A., Bradley, D.J., Knox, J.P., Perotto, S., Butcher, G.W., Brewin, N.J., 1989. Common components of the infection thread matrix and the intercellular space identified by immunocytochemical analysis of pea nodules and uninfected roots. EMBO J. 8, 335–342.

Vannier, M.P., Thoiron, B., Morvan, C., Demarty, M., 1992. Localization of methyltransferase activities throughout the endomembrane complex system of flax (*Linum usitatissimum* L) hypocotyls. Biochem. J. 286, 863–868.

Vaughn, K.C., Turley, R.B., 1999. The primary walls of cotton fibers contain an ensheathing pectin layer. Protoplasma 209, 226–237.

Vian, B., Roland, J.-C., 1991. Affinodetection of the sites of formation and of the further distribution of polygalacturonans and native cellulose in growing plant cells. Biol. Cell 71, 43–55.

Vicre, M., Jauneau, A., Knox, J.P., Driouich, A., 1998. Immunolocalization of β-(1→4) and β-(1→6)-D-galactan epitopes in the cell wall and Golgi stacks of developing flax root tissue. Protoplasma 203, 26–34.

Vidal, S., Doco, T., Williams, P., Pellerin, P., York, W.S., O'Neill, M.A., Glushka, J., Darvill, A.G., Albersheim., P., 2000. Structural characterization of the pectic polysaccharide rhamnogalacturonan II: evidence for the backbone location of the aceric acid-containing oligoglycosyl side chain. Carbohydr. Res. 326, 277–294.

Villemez, C.L., Lin, T.-Y., Hassid, W.Z., 1965. Biosynthesis of the polygalacturonic acid chain of pectin by a particulate enzyme preparation from phaseolus aureus seedlings. Proc. Natl. Acad. Sci. USA 54, 1626–1632.

Villemez, C.L., Swanson, A.L., Hassid, W.Z., 1966. Properties of a polygalacturonic acid-synthesizing enzyme system from *Phaseolus aureus* seedlings. Arch. Biochem. Biophys. 116, 446–452.

Visser, J., Voragen, A.G.J. (Eds.), 1996. Pectins and pectinases, progress in biotechnology Vol. 14. Elsevier, Amsterdam.

Waldron, K.R., Selvendran, R.R., 1992. Cell-wall changes in immature asparagus stem tissue after excision. Phytochemistry 31, 1931–1940.

Walker-Simmons, M., Jin, D., West, C.A., Hakwiger, L., Ryan, C.A., 1984. Comparison of proteinase inhibitor-inducing activities and phytoalexin elicitor activities of a pure fungal endopolygalacturonase, pectic fragments, and chitosan. Plant Physiol. 76, 833–836.

Wang, J., Dudareva, N., Bhakta, S., Raguso, R.A., Pichersky, E., 1997. Floral scent production in *Clarkia breweri* (Onagraceae) II. Localization and developmental modulation of the enzyme *S*-adenosyl-L-methionine: (Iso)Eugenol *O*-methyltransferase and phenylpropanoid emission. Plant Physiol. 114, 213–221.

Wayne, R., Staves, M.P., Leopold, A.C., 1992. The contribution of the extracellular matrix to gravisensing in characean cells. J. Cell Sci. 101, 611–623.

Weber, J., Olsen, O., Wegener, C., von Wettstein, D., 1996. Digalacturonates from pectin degradation induce tissue responses against potato soft rot. Physiol. Molec. Plant Path. 48, 389–401.

Wen, F., Zhu, Y., Hawes, M., 1999. Effect of pectin methyl esterase gene expression on pea root development. Plant Cell 11, 1129–1140.

Wheeler, G.L., Jones, M.A., Smirnoff, N., 1998. The biosynthetic pathway of vitamin C in higher plants. Nature (London) 393, 365–369.

Whitcombe, A.J., O'Neill, M.A., Steffan, W., Darvill., A.G., Albersheim, P., 1995. Structural characterization of the pectic polysaccharide rhamnogalacturonan II. Carbohydr. Res. 271, 15–29.

Willats, W.G.T., Gilmartin, P.M., Mikkelsen, J.D., Knox, J.P., 1999a. Cell wall antibodies without immunization: generation and use of de-esterified homogalacturonan block-specific antibodies from a naive phage display library. Plant J. 18, 57–65.

Willats, W.G.T., Limberg, G., Bucholt, H.C., van Alebeck, G-J., Benen, J., Christensen, T.M.I.E., Visser, J., Voragen, A., Mikkelsen, J.D., Knox, J.P., 2000a. Analysis of pectic epitopes recognized by hydridoma and phage display monoclonal antibodies using defined oligosaccharides, polysaccharides, and enzymatic degradation. Carbohydr Res. 327, 309–320.

Willats, W.G.T., Marcus, S.E., Knox, J.P., 1998. Generation of a monoclonal antibody specific to (1→5)-α-L-arabinan. Carbohydr. Res. 308, 149–152.

Willats, W.G.T., Steele-King, C.G., Marcus, S.E., Knox, J.P., 1999bb. Side chains of pectic polysaccharides are regulated in relation to cell proliferation and cell differentiation. Plant J. 20, 619–628.

Willats, W.G.T., Steele-King, C.G., McCartney, L., Orfila, C., Marcus, S.E., Knox, J.P., 2000b. Making and using antibody probes to study plant cell walls. Plant Physiol. Biochem. 38, 27–36.

Williams, M.N.V., Freshour, G., Dravill, A.G., Albersheim, P., Hahn, M.G., 1996. An antibody Fab selected from a recombinant display library detects de-esterified pectic polysaccharide rhamnogalacturonan II in plant cells. Plant Cell 8, 673–685.

Wimmer, M.A., Goldbach, H.E., 1999. Influence of Ca^{2+} and pH on the stability of different boron fractions in intact roots of *Vicia faba* L. Plant Biol. 1, 632–637.

Woods, R.J., 1998. Computational carbohydrate chemistry: what theoretical methods can tell us. Glycoconjugate J. 15, 209–216.

Wyatt, S.E., Carpita, N.C., 1993. The plant cytoskeleton-cell-wall continuum. Trends Cell Biol. 3, 413–417.

Yu, L., Mort, A.J., 1996. Partial characterization of xylogalacturonans from cell walls of ripe watermelon fruit: inhibition of endopolygalacturonase activity by xylosylation. In: Visser, J., Voragen, A.G.J. (Eds.), Pectins and Pectinases. Elsevier, Amsterdam, pp. 79–88.

Zablackis, E., York, W.S., Pauly, M., Hantus, S., Reiter, W-D., Chapple, C.C.S., Albersheim, P., Darvill, A.G., 1996. Substitution of L-fucose by L-galactose in cell walls of *Arabidopsis mur1*. Science 272, 1808–181.

Zhan, D., Janssen, P., Mort, A.J., 1998. Scarcity or complete lack of single rhamnose residues interspersed within the homogalacturonan regions of citrus pectin. Carbohydr. Res. 308, 373–380.

Zhang, Z., Pierce, M.L., Mort, A.J., 1996. Detection and differentiation of pectic enzyme activity in vitro and in vivo by capillary electrophoresis of products for fluorescent-labeled substrate. Electrophoresis 17, 372–378.

Zhang, G.F., Staehelin, L.A., 1992. Functional compartmentation of the Golgi apparatus of plant cells; immunocytochemical analysis of high-pressure frozen- and freeze-substituted sycamore maple suspension culture cells. Plant Physiol. 99, 1070–1803.

Zhu, J.K., Shi, J., Singh, U., Wyatt, S.E., Bressan, R.A., Hasegawa, P.M., Carpita, N.C., 1993. Enrichment of vitronectin-like and fibronectin-like proteins in NaCl-adapted plant cells and evidence for their involvement in plasma-membrane cell-wall adhesion. Plant J. 3, 637–646.

Zimmermann, S., Frachisse, J.-M., Thomine, S., Barbier-Brygoo, H., Guern, J., 1998. Elicitor-induced chloride efflux and anion channels in tobacco cell suspensions. Plant Physiol. Biochem. 36, 665–674.

Zuiderweg, E.R.P., Fesik, S.W., 1989. Heteronuclear 3-dimensional NMR spectroscopy of the inflamatory protein C5A. Biochem. 28, 2387–2391.

PERGAMON

Phytochemistry 57 (2001) 969–974

PHYTOCHEMISTRY

www.elsevier.com/locate/phytochem

Pectic polysaccharide rhamnogalacturonan II is covalently linked to homogalacturonan

Tadashi Ishii [a,*], Toshiro Matsunaga [b]

[a] *Forestry and Forest Products Research Institute, PO Box 16, Tsukuba Norin Kenkyu, Danchi-nai, Ibaraki, 305-8687 Japan*
[b] *Kyushu National Agricultural Experiment Station, Nishigoshi, Kumamoto, 861-1192 Japan*

Received 2 June 2000; received in revised form 1 December 2000

Abstract

A borate-containing pectin was solubilized from sugar beet (*Beta vulgaris* L.) cell walls by treatment with 0.5 M imidazole, pH 7. The molecular weight of the pectin was reduced when the borate ester was hydrolyzed by treatment with 1 N HCl. Treatment of the acid-treated pectin with boric acid in the presence of Pb^{2+} gave a product whose molecular weight distribution was similar to the imidazole-soluble pectin. The imidazole-soluble pectin was saponified and then digested with *endo*- and *exo*-polygalacturonases. These treatments shifted the boron peak at the high molecular weight region to the low molecular weight (10 kDa), which corresponds to rhamnogalacturonan II-borate ester cross-linked dimer (dRG-II-B). The treatment also generated rhamnogalacturonan I (RG-I), dRG-II-B, monomeric rhamnogalacturonan II and galacturonic acid. These results show that imidazole solubilizes a high molecular weight borate-containing pectic complex composed of homogalacturonan-rhamnogalacturonan II and RG-I. Our data suggest that borate esters formed between rhamnogalacturonan II molecules cross-link the macromolecular pectin. © 2001 Elsevier Science Ltd. All rights reserved.

Keywords: *Beta vulgaris*; Chenopodiaceae; Borate esters; Cross-linking; *endo*-Polygalacturonase; Homogalacturonan; Rhamnogalacturonan I; Rhamnogalacturonan II; Pectin; Sugar beet

1. Introduction

Pectin consists of three structurally well characterized polysaccharides: homogalacturonan (HG), rhamnogalacturonan I (RG-I) and rhamnogalacturonan II (RG-II) (O'Neill et al., 1990). These polysaccharides are believed to be covalently linked to one another because they are all solubilized by *endo*-polygalacturonase (EPG) treatment of primary cell walls. As far as we are aware there is no compelling evidence showing that HG, RG-I and RG-II are covalently linked to each other to form a macromolecular pectin complex.

Recent studies have shown that RG-II is present in the primary cell wall predominantly as a dimer (dRG-II-B) that is cross-linked by a borate diol diester (Ishii and Matsunaga, 1996; Kobayashi et al., 1996; O'Neill et al., 1996). RG-II is the only known borate-binding polysaccharide in the primary cell wall (Ishii and Matsunaga, 1996; Kobayashi et al., 1996; O'Neill et al., 1996). These results provide support for the hypothesis that one of the physiological functions of boron (B) in the normal cell growth and development of higher plants is to cross-link cell wall pectins. Nevertheless, the effects on the macromolecular organization of pectin and on the structure of the cell wall that result from borate ester cross-linking of pectin are poorly understood (Fliescher et al., 1999). In this report we show that a high molecular weight boron-containing pectin is solubilized by treating sugar beet walls with 0.5 M imidazole, pH 7, and that this pectin is composed of HG, RG-I and borate ester cross-linked RG-II. The molecular weight distribution of the pectin is decreased after hydrolysis of the borate ester cross-link and is increased when the ester cross-link is reformed in vitro. Our data provide evidence that RG-II and HG are covalently linked together.

2. Results

2.1. Isolation of a borate-containing pectin from sugar beet cell walls

Imidazole, 0.5 M, pH 7.0 (Mort et al., 1991; Marry et al., 2000) was used to solubilize pectin from sugar beet

* Corresponding author. Tel.: +81-298-73-3211; fax: +81-298-73-3795.
E-mail address: tishii@ffpri.affrc.go.jp (T. Ishii).

0031-9422/01/$ - see front matter © 2001 Elsevier Science Ltd. All rights reserved.
PII: S0031-9422(01)00047-4

cell walls rather than the chelating reagent cyclohexanediamine tetraacetate (CDTA) (Selvendran and O'Neill, 1986) since CDTA converts dRG-II-B to mRG-II (Kobayashi et al., 1999). In our study we found that ~70% of dRG-II-B was converted to mRG-II by treatment for 16 h at room temperature with 50 mM CDTA, pH 6.5. In contrast, dRG-II-B was stable in 0.5 M imidazole-HCl, pH 7.

Approximately 12% of the weight of the sugar beet cell walls was solubilized by 0.5 M imidazole, pH 7. The soluble material was subjected to ion-exchange chromatography to give Fraction I (Fig. 1a), which was subsequently subjected to size-exclusion chromatography (SEC) to give Fraction II (Fig. 1b). Fraction II was further characterized and appeared to be a boron-containing macromolecule. The pectin was shown to be a boron-containing macromole (69 μgB/g dry wt) with an apparent molecular mass of 200–150 kDa by SEC with a refractive index detector (SEC/RI, Fig. 2a) and by SEC with inductively coupled mass spectrometry SEC/(ICP-MS) (Fig. 2d). The ^{11}B NMR spectrum of the pectin contained a single signal at δ-9.5, thereby establishing the presence of a borate diol diester (van Duin et al., 1985).

2.2. Hydrolysis of the borate ester reduces the molecular weight distribution of the borate-containing pectin

The borate ester in the imidazole-soluble pectin was completely hydrolyzed by treatment for 1 h with 1 N HCl, which was confirmed by SEC/ICP–MS that the acid-treated pectin contained no B (data not shown). Moreover, the molecular weight distribution of the native (Fig. 3, curve 1) and acid-treated pectin (Fig. 3, curve 2) were not the same. The acid treatment had broadened the molecular weight distribution and increased the amount of material eluting in the lower molecular weight region (compare curves 1 and 2 in Fig. 3). To obtain evidence that borate ester formation alters the molecular weight distribution of pectin, the acid-treated pectin was kept for 16 h in K hydrogen phthalate/HCl, pH 3.7, containing

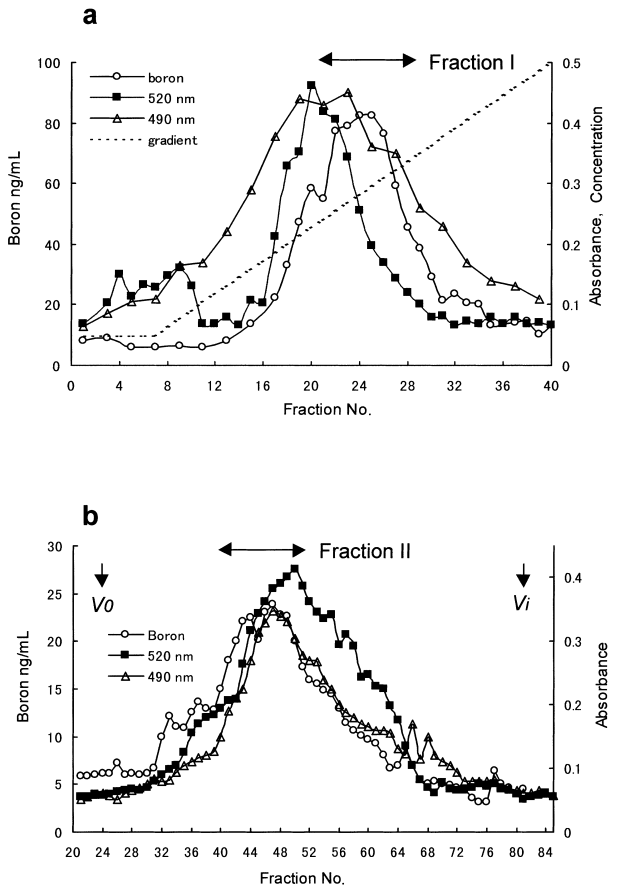

Fig. 1. Purification of the borate-containing pectin by (a) ion-exchange chromatography on DEAE-Sepharose Fast Flow and (b) size-exclusion chromatography on Sepharose CL-6B. Fractions were assayed for B (○), uronic acid (■), and total sugar (△) by ICP–MS, *m*-hydroxybiphenyl and phenol-sulfuric acid methods, respectively. The boron and polysaccharide-containing fractions were pooled as indicated. Gradient: a linear gradient from 50 mM to 1 M HCOONH4, pH 5.3.

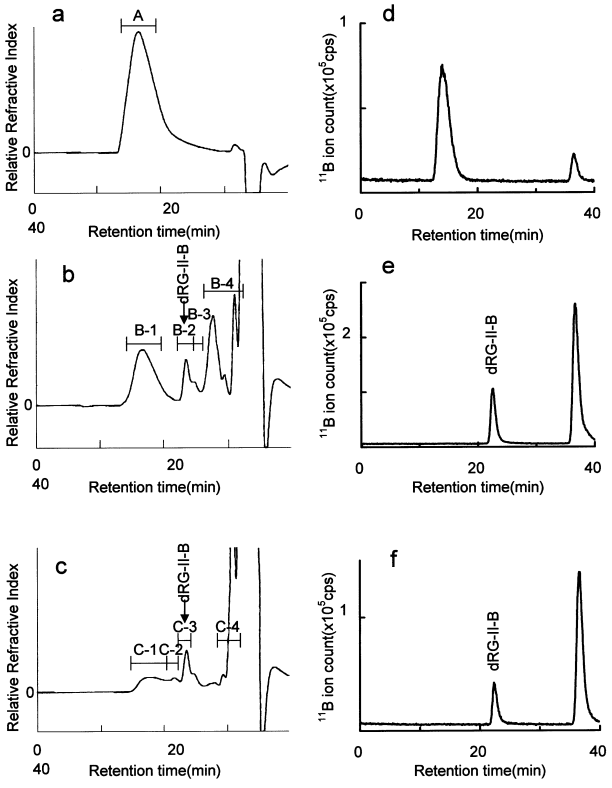

Fig. 2. Size-exclusion chromatograms of the enzyme-treated borate-containing pectin with refractive index (RI) detection (a–c) and with ICP–MS detection (d–f). (a) and (d), SEC profile of the imidazole-soluble pectin. (b) and (e), SEC profile of the saponified and EPG-treated pectin. (c) and (f), SEC profile of the saponified and EPG, arabinanase and α-L-arabinofuranosidase-treated pectin. The RG-II dimer (dRG-II-B) and monomer (mRG-II) eluted at 23.5 and 24.9 min, respectively (b) and (c).

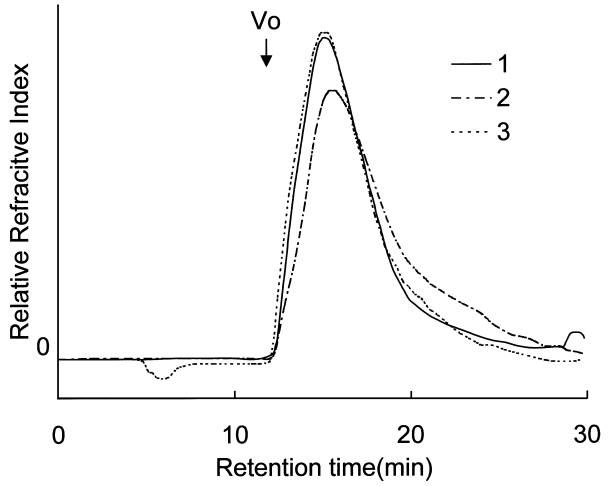

Fig. 3. Size-exclusion chromatograms with refractive index (RI) detection of the borate-containing pectin. 1. (–) The elution profile of the borate-containing pectin. 2. (---) The elution profile of the pectin after treatment for 1h at 30°C with 1 N HCl. 3. (- - - -) The elution profile after the acid-treated pectin was kept for 16 with boric acid and lead acetate at pH 3.7. Pullulan P-800 (854 kDa, V_0) and glucose (V_i) eluted at 13.3 and 32.3 min, respectively. The chromatograms were normalized.

boric acid (6 mM) and lead acetate (4 mM). These conditions have been known to completely convert mRG-II to dRG-II-B in vitro (O'Neill et al., 1996). The molecular weight distribution of the acid-treated pectin that had been treated with boric acid and Pb^{2+} and the original pectin are similar (Fig. 3, curves 1 and 3). The reconstructed pectin contained 79 μgB/g dry wt and its ^{11}B NMR spectrum contained a signal at δ −9.5 that corresponds to a borate diol diester. These results suggest that borate ester cross-links in part determine the molecular size of the pectin.

2.3. The imidazole-soluble pectin is composed of HG, RG-I and RG-II

The glycosyl composition and linkage analyses of the borate-containing pectin (Tables 1 and 3, Fr. A) indicate that it contained RG-I, RG-II and HG. Additional evidence for the presence of these polysaccharides was obtained by saponifying the pectin and treating the resulting material with a mixture of *endo*- and *exo*-polygalacturonase. Approximately 50% of the material was recovered after enzymatic treatment and dialysis. This material was shown by SEC to contain four major components (Fig. 2b). The boron eluted as a sharp peak in the region corresponding to dRG-II-B (~10 kDa) (Fig. 2e) rather than as a broad, high molecular weight boron-containing peak in the native pectin (Fig. 2d). The results show that dRG-II-B is linked to HG in the pectin. A free boric acid peak eluted at the lower molecular weight region was partly due to the degradation of the borate complex during the sample preparation

Table 1
Glycosyl-residue compositions of the borate-containing pectin and the fractions obtained after EPG treatment of the borate-containing pectin

Glycosyl residue	Untreated pectin	Fractions generated by EPG treatment			
	A[a]	B1[b]	B2[b] mol%	B3[b]	B4[b]
Ara	38	38	25	20	–
Rha	10	8	9	9	–
Fuc	2	1	1	2	–
Me-Fuc	T[b]	–[c]	1	3	–
Xyl	2	4	–	–	–
Me-Xyl	T	–	1	2	–
Api	2	–	7	9	–
Man	2	2	–	–	–
Gal	21	34	15	11	–
GalA	23	13	21	24	100
GlcA	T	–	5	4	–
AcericA	T	–	4	4	–
Dha	T	–	4	5	–
Kdo	T	–	4	6	–

[a] The origins of Fractions A and B1–B4 are shown in Fig. 2a and b, respectively.
[b] T: trace (less than 1%).
[c] 3−: Not detected.

Table 2
Glycosyl-residue compositions of the fractions obtained after treating the borate-containing pectin with EPG, arabinanase and arabinofuranosidase

Glycosyl residue	C1[a]	C2[a]	C3[a]	C4[a]
		mol%		
Ara	13	10	11	55
Rha	10	12	12	–[b]
Fuc	4	3	2	–
Me-Fuc	–	–	2	–
Xyl	8	5	–	–
Me-Xyl	–	–	2	–
Api	–	–	8	–
Man	6	5	–	–
Gal	30	22	8	–
GalA	29	43	39	45
GlcA	–	–	5	–
AcericA	–	–	3	–
Dha	–	–	4	–
Kdo	–	–	3	–

[a] The origins of Fractions C1–C4 are shown in Fig. 2c.
[b] –: Not detected.

(Fig. 2d–f). Glycosyl composition analysis of the four fractions (B1–B4, see Fig. 2b) generated by enzymatic treatment showed that Fraction B1 contained RG-I with a high content of arabinosyl and galactosyl residues but no RG-II (Table 1). In contrast, Fractions B2 and B3 both contained those glycoses [(2-*O*-Me-Xyl, 2-*O*-Me-Fuc, aceric acid, apiose, 3-deoxy-D-*manno*-2-octulosonic acid (Kdo) and 3-deoxy-D-*lyxo*-heptulosaric acid (Dha)] that are diagnostic for RG-II (O'Neill et al.,

Table 3
Glycosyl-linkage analysis of the borate-containing pectin and the fractions obtained after enzyme treatment of the pectin

Glycosyl residue	Linkage	Untreated pectin	Fractions generated by enzyme treatment			
		A[a]	B1[a]	C1[a] mol%	C2[a]	C3[a]
Ara	T_f^-	14	21	4	2	7
	T_p^-	1	–[c]	–	–	4
	5^-	12	12	4	2	–
	$3,5^-$	9	10	–	–	–
Rha	T^-	1	–	–	–	3
	2^-	3	1	2	3	2
	3^-	1	2	1	3	5
	$2, 4^-$	4	2	6	3	–
	$3, 4^-$	1	T	4	4	–
	$2, 3, 4^-$	5	8	6	7	6
Fuc	T^-	1	–	–	–	4
	$3, 4^-$	T[b]	–	–	–	4
Xyl	T^-	1	T	4	1	6
Api	$3'^-$	1	–	–	–	5
	$2, 3, 3'^-$	–	–	–	–	5
Gal	T^-	5	2	4	3	–
	3^-	3	2	13	4	–
	4^-	6	4	9	5	–
	6^-	4	15	8	20	–
	$2, 4^-$	T[b]	2	1	–	5
	$3, 6^-$	6	4	7	–	–
GlcA	2^-	T[b]	–	–	–	4
GalA	T^-	–	–	–	–	11
	4^-	22	15	25	43	8
	$2, 4^-$	T	T	1	T	4
	$3, 4^-$	T	T	1	T	5
	$2, 3, 4^-$	T	T	T	T	6

[a] The origins of Fractions A, B1 and C1–C3 are shown in Fig. 2a, b and c, respectively.
[b] T: trace (less than 1%).
[c] –: Not detected.

1990). Fraction B4 was shown by high pH anion-exchange chromatography with pulsed amperometic detection (HPAEC-PAD) to contain di- and trigalacturonides, in addition to galacturonic acid. These are the expected products resulting from *endo*- and *exo*-polygalacturonase treatment of HG. Taken together these results establish that the imidazole-soluble pectin contains HG, RG-I and borate ester cross-linked RG-II. These results provide evidence that dRG-II-B is covalently inserted with HG chains.

To characterize the high molecular weight fraction and to determine the content of RG-I in the pectin, the pectin was treated with EPG together with arabinanase and α-L-arabinofuranosidase since Fraction B1 (see Fig. 2b) contained a high level of arabinosyl residues (Table 1). Approximately 15% of the material was recovered after enzyme treatment and dialysis. This treatment resulted in a decrease in the amount of the high molecular weight peak (Fraction B1, see Fig. 2b) and the appearance of a broad, lower molecular weight fraction (Fig. 2c, Fractions C1 and C2). As expected the arabinosyl residue content of Fraction B1 was decreased by the enzyme treatment. Fractions C1 and C2 most likely contain RG-I since they are enriched with terminal non-reducing Ara_f and Gal, 2-Rha, 2, 4-Rha, 5-Ara_f, 4-Gal and 4-linked GalA residues (Table 3) (Ishii et al., 1989). These fractions may also contain xylogalacturonan since small amounts of terminal non reducing-Xyl and 3, 4-linked GalA residues were also detected (Schols and Voragen, 1996). The molecular weight distribution of the original pectin and Fractions C1 and C2 was similar, indicating that RG-I and xylogalacturonan in the pectin were likely to be a contaminant. Glycosyl-residue composition (Table 2) and glycosyl-linkage composition analyses (Table 3) confirmed that Fraction C-3 contained RG-II. Fraction C4 was shown by HPEAC-PAD to contain galacturonic acid and arabinose.

3. Discussion

A high molecular weight pectin containing HG, RG-I and RG-II was solubilized by treating sugar beet cell walls with imidazole-HCl. The pectin contained 69 μg B/g and had a molecular weight of 150–200 kDa. Previous results showed that dRG-II-B having a molecular weight 10 kDa contained one mole boron (Ishii and Matsunaga, 1996; Kobayashi et al., 1996; O'Neill et al., 1996). It can be estimated that approximately one mole of dRG-II-B/mol pectin was present. *Endo*-polygalacturonase treatment of the pectin fragmented the homogalacturonan region of the molecule and generated RG-II with an apparent molecular mass of 5–10 kDa. Thus, it is likely that the pectin contains RG-II covalently linked within homogalacturonan chains. *Endo*-polygalacturonase, arabinanase and α-L-arabinofuranosidase treatment fragmented some of the arabinosyl-containing side chains of RG-I, in addition to homogalacturonan. Nevertheless, a portion of this material still eluted in the high molecular weight region of the column (Fig. 2c, C1 and C2). This material contained RG-I with short side chains and xylogalacturonan. If the pectin contains RG-I and xylogalacturonan as a contaminant, their content is less than 10%. It is uncertain from the present results that RG-I is linked to HG and that RG-I, RG-II and HG are on the same molecule. Isolation and characterization of oligogalacturonides carrying oligosaccharides derived from RG-I is essential for providing evidence for the above notion.

The molecular weight distribution of the imidazole-soluble pectin decreased after hydrolysis of the borate ester. The in vitro reformation of the borate ester gave a pectin that had a molecular weight distribution pattern similar to native pectin (Fig. 3, curves 1 and 3). Such a result indicates that RG-II being covalently linked to

HG can itself assemble into a borate ester cross-linked dimer and that the formation of this cross-link increases the molecular size of the pectin. Sugar beet pectin contains ferulic and diferulic acids ester-linked to arabinan and galactan side chains of RG-I (Ishii, 1997a). Ferulate and diferulate esters are stable under acid treatment used to cleave borate esters (Ishii, unpublished results). These results exclude the possibility of the involvement in diferulate cross-linking of pectin. In previous studies, dRG-II-B has been isolated as a low molecular weight component (10 kDa) from *endo*-polygalacturonase digests of plant cell walls (Ishii and Matsunaga, 1996; Kobayashi et al., 1996; O'Neill et al., 1996). RG-II has also been solubilized as a high molecular weight pectin (>25 kDa) by 0.5 M phosphate-buffer treatment of *Chenopodium album* (Fleischer et al., 1999). The RG-II in these macromolecules is converted to a low molecular weight (5–10 kDa) component by *endo*-polygalacturonase treatment. The results of the present study have established that borate ester cross-linking of RG-II determines the macromolecular properties of pectin.

4. Experimental

4.1. Plant material

Sugar beet pulp was a gift from Hokkaido Prefecture Konsen Agricultural Experimental Station (Nakashibetsu, Hokkaido). The pulp was ground with a hammer mill, refluxed with MeOH for 16 h, and the alcohol-insoluble residue (AIR) (B content 37 μg/g dry AIR) was used as the cell wall material.

4.2. Isolation of a borate-containing pectin

Sugar beet cell walls (10 g) were stirred for 16 h at room temperature in 0.5 M imidazole-HCl, pH 7.0, (1 l). The suspension was centrifuged for 10 min at 5000 g. The insoluble residue was suspended in 500 ml of 0.5 M imidazole, pH 7 and extracted for 4 h at room temperature, and then centrifuged. The supernatants were combined and dialyzed against deionized H_2O with 12 kDa cutoff dialysis tube. The retentate was applied to a column (2.5×30 cm) of DEAE-Sepharose Fast Flow that had been equilibrated with 50 mM $HCOONH_4$, pH 5.3. The column was washed with equilibration buffer (500 ml) to remove unbound material and then eluted with a linear gradient from 50 mM to 1 M $HCOONH_4$, pH 5.3 (total volume 800 ml). Fractions (10 ml) were collected and assayed for their B, total sugars and uronic acid contents. Fraction I (Fraction Nos. 21–28 in Fig. 1a) was pooled, dialyzed (12 kDa cutoff), and freeze-dried. A solution of Fraction I in 50 mM $HCOONH_4$, pH 5.3 (5 ml) was loaded onto a column (2.5×90 cm) of Sepharose CL-6B, equilibrated with 50 mM $HCOONH_4$, pH 5.3, and eluted with the same buffer. Fractions (2 ml) were collected and assayed for their B, uronic acid and total sugar contents. Fraction II (Fraction Nos. 41–52 in Fig. 1b) was pooled, dialyzed (12 kDa cutoff), and freeze-dried.

4.3. Acid treatment of the borate-containing pectin and reformation of the borate ester in the acid-treated pectin

The pectin (2 mg) was treated for 1 h at 30°C with 1 N HCL solution (0.5 ml). The acid-treated pectin was dialyzed (1 kDa cutoff) and freeze-dried. The acid-treated pectin (1 mg) was kept for 16 h in K^+ hydrogen phthalate/HCl, pH 3.7, (200 μl) containing boric acid (6 mM) and lead acetate (4 mM) (O'Neill et al., 1996). This solution was then dialyzed (1 kDa cutoff) and freeze-dried.

4.4. Enzymic treatments of the borate-containing pectin

The borate-containing pectin (5 mg) was saponified to remove ester bonds by treatment for 4 h at 4°C with 0.1 N NaOH (0.2 ml). The solution was then adjusted to pH 5.0 with 10% AcOH . The saponified pectin was treated for 16 h at 30°C with homogeneous preparations of recombinant *endo*-polygalacturonase (3 units) and *exo*-polygalacturonase (2 units). The recombinant *endo*-polygalacturonase (EPG-II) from *Aspergillus niger* and *exo*-polygalacturonase (ExoPG) from *A. tubingensis* (Biely et al., 1996) were over-expressed in *A. niger* and then purified to apparent homogeneity; these were a gift of J. Visser (Wageningen, The Netherlands). One unit of EPG and one unit ExoPG, respectively, releases 1 μmol of reducing sugar/min from polygalacturonic acid at pH 5. The solution was dialyzed (1 kDa cutoff) and freeze-dried. In a second experiment, the saponified pectin was digested for 16 h at 30°C with a mixture of *endo*- and *exo*-polygalacturonase, arabinanase (2 units) and α-L-arabinofuranosidase (2 units) from *A. niger* (Megazyme, Ireland), dialyzed (1 kDa cutoff), and freeze-dried. The arabinanase preparation contained arabinanase, arabinofuranosidase, and α-D-galacturonase activities, but it did not degrade RG-I (Lerouge et al., 1993).

4.5. Analytical methods

The enzymatic digests were separated by HPLC using a Shimadzu LC6A liquid chromatograph with a Superose 12 HR 10/30 column (Pharmacia, Uppsala) and a refractive index detector (Shimadzu model RID-6A) eluted with 50 mM $HCOONH_4$, pH 5. 3 at 0.6 ml/min. SEC/ICP–MS was performed with the same column using a JASCO PU-1580i pump and a SII SPQ9000 ICP mass spectrometer. The column elution conditions were the same as above. The pectin solution (2 mg/ml) was prepared and 100 and 20 μl were injected for SEC-HPLC and SEC/ICP-MS, respectively. The monosaccharides

released by enzymatic treatment were determined by HPAEC-PAD with a Dionex BioLC as described (Ishii, 1997b).

The boron concentrations in each fraction (Fig. 1) were determined by ICP–MS (Ishii and Matsunaga, 1996). ^{11}B NMR spectra were recorded with a Jeol Alpha 500 NMR spectrometer (Ishii and Matsunaga, 1996).

Uronic acids and total sugars were determined by the *m*-hydroxybiphenyl method (Blumenkrantz and Asboe-Hansen, 1973), and phenol-sulfuric acid methods (Hodge and Hotreiter, 1962), respectively. The neutral and acidic glycosyl residue compositions of the pectin were determined by GC–MS analysis of the alditol acetate derivatives and trimethylsilyl methyl glycoside derivatives, respectively (York et al., 1985). The glycosyl linkage compositions were determined by a modified Hakomori procedure method (Ishii et al., 1999).

Acknowledgements

We thank C. Bergmann and M.A. O'Neill, Complex Carbohydrate Research Center, the University of Georgia, Athens, Georgia, for providing of the *endo*- and *exo*-polygalacturonases and for critical reading of the manuscript, respectively. M. Ishikawa is acknowledged for preparing the manuscript. This work was supported by a research grant (BDP-01-II-1-1) from the Ministry of Agriculture, Forestry and Fisheries.

References

Biely, P., Benen, J., Heinrichova, K., Kester, H.C., Visser, J., 1996. Inversion of configuration during hydrolysis of α-1, 4-galacturonidic linkage by three *Aspergillus* polygalacturonases. FEBS Lett. 382, 249–255.

Blumenkrantz, N.J., Asboe-Hansen, B., 1973. A new method for the quantitative determination of uronic acid. Anal. Biochem. 54, 484–489.

Fleischer, A., O'Neill, M.A., Ehwald, R., 1999. Pore size of non-graminaceous plant cell walls is rapidly decreased by borate ester cross-linking of the pectic polysaccharide rhamnogalacturonan II. Plant Physiol. 121, 829–838.

Hodge, J.E., Hofreiter, B.T., 1962. Determination of reducing sugars and carbohydrates. In: Whistler, R.L., Wolfrom, M.W. (Eds.), Methods in Carbohydrate Chemistry, Vol. I. Academic Press, New York, pp. 380–399.

Ishii, T., Thomas, J., Darvill, A.D., Albersheim, P., 1989. Structure of plant cell walls, XXVI. The walls of suspension-cultured sycamore cells contains a family of rhamnogalacturonan-I-like pectic polysaccharides. Plant Physiol. 89, 421–428.

Ishii, T., Matsunaga, T., 1996. Isolation and characterization of a boron-rhamnogalacturonan II complex from cell walls of sugar beet pulp. Carbohydr. Res. 284, 1–9.

Ishii, T., 1997a. Structure and functions of feruloylated polysaccharides. Plant Sci. 127, 111–127.

Ishii, T., 1997b. O-Acetylated oligosaccharides from pectins of potato tuber cell walls. Plant Physiol. 113, 1265–1272.

Ishii, T., Matsunaga, T., Pellerin, P., O'Neill, M.A., Darvill, A., Albersheim, P., 1999. The plant cell wall polysaccharide rhamnogalacturonan II self-assembles into a covalently cross-linked dimer. J. Biol. Chem. 274, 13098–13104.

Kobayashi, M., Matoh, T., Azuma, J., 1996. Two chains of rhamnogalacturonan II are cross-linked by borate-diol ester bonds in higher plant cell walls. Plant Physiol. 110, 1017–1020.

Kobayashi, M., Nakagawa, H., Asaka, T., Matoh, T., 1999. Borate-rhamnogalacturonan II bonding reinforced by Ca^{2+} retains pectic polysaccharides in higher-plant cell walls. Plant Physiol. 119, 199–204.

Lerouge, P., O'Neill, M.O., Darvill, A.G., Albersheim, P., 1993. The purification of commercially available *endo* α-L-arabinanase and α-L-arabinofuranosidase for use in the structural analysis of pectic polysaccharides. Carbohydr. Res. 243, 373–378.

Marry, M., McCann, M.C., Kolpak, F., White, A.R., Stacey, N.J., Roberts, K., 2000. Extraction of pectic polysaccharides from sugar-beet cell walls. J. Sci. Food Agric. 80, 17–28.

Mort, A.J., Moreschbacher, B.M., Pierce, M.L., Maness, N.O., 1991. Problems encountered during the extraction, purification and chromatography of pectic fragments and some solutions to them. Carbohydr. Res. 215, 219–227.

O'Neill, M.A., Albersheim, P., Darvill, A., 1990. The pectic polysaccharides of primary cell walls. In: Dey, P.M., Harborne, J.B. (Eds.), Methods in Plant Biochemistry, Vol. 2, Carbohydrates. Academic Press, London, pp. 415–441.

O'Neill, M.A., Warrenfeltz, D., Kates, K., Pellerin, P., Doco, T., Darvill, A.G., Albersheim, P., 1996. Rhamnogalacturonan II, a pectic polysaccharide in the walls of growing plant cells, forms a dimer that is covalently cross-linked by a borate ester. J. Biol. Chem. 271, 22923–22930.

Schols, H.A., Voragen, A.G.J., 1996. Complex pectins. In: Visser, J.A., Voragen, G.J. (Eds.), Pectin and Pectinase. Elsevier Science, The Netherlands, pp. 3–19.

Selvendran, R.R., O'Neill, M.A., 1986. Isolation and analysis of cell walls from plant material. Methods Biochem. Anal. 32, 25–153.

van Duin, M., Peters, J.A., Kieboom, A.P.G., van Bekkum, H., 1985. Studies on borate esters II. Tetrahedron 41, 3411–3421.

York, W.S., Darvill, A.G., McNeil, M., Stevenson, T.T., Albersheim, P., 1985. Isolation and characterization of cell walls and cell wall components. Methods Enzymol. 118, 3–40.

PERGAMON

Phytochemistry 57 (2001) 975–986

PHYTOCHEMISTRY

www.elsevier.com/locate/phytochem

Cell wall biosynthesis: glycan containing oligomers in developing cotton fibers, cotton fabric, wood and paper

Allen K. Murray[a,*], Robert L. Nichols[b], Gretchen F. Sassenrath-Cole[c]

[a]*Glycozyme, Inc., 17935 Sky Park Circle, Ste. E, Irvine, CA 92614, USA*
[b]*Cotton Incorporated, 6399 Weston Parkway, Cary, NC 27513, USA*
[c]*USDA, ARS, APTRU, POB 36, Stoneville, MS 38776, USA*

Received 21 August 2000; received in revised form 22 December 2000

Abstract

A series of oligomeric glycans can be extracted from the cell walls of developing cotton fibers with weak acid. Glycans that produce similar profiles on high pH anion chromatography with pulsed amperometric detection (HPAEC-PAD) are also found in a protein complex extracted from developing fibers and in amorphous aggregates found in association with immature fibers in developing, but not in mature cotton bolls. The quantity and composition of the glycans recovered from the carbohydrate–protein complex varies significantly with the time of day when the bolls are harvested. This diurnal variation is consistent with the hypothesis that secondary cell walls are deposited primarily at night. Incubation of re-hydrated cotton fibers in the presence of exogenous oligosaccharides, *myo*-inositol and glycerol substantially alters the apparent quantity of the oligomers extracted from the fibers. The same and similar glycans have also been extracted from cotton fabric, marine algae, various paper products and wood. While many of the oligomers isolated from the various cellulose sources display the same peaks by HPAEC-PAD, the specific number of oligomers and their relative quantities appear unique for each source of cellulosic material. Oligomeric glycans, as described in the preceding, are present in all cellulose sources that have been investigated. Their relative abundance changes in response to source, stage of development and other physiological variables. We hypothesize that the glycans are intermediates in the biological assembly of cellulose, and that their incorporation in cellulose is mediated by physicochemical and enzymatic mechanisms. © 2001 Elsevier Science Ltd. All rights reserved.

Keywords: *Gossypium hirsutum*; Cell wall; Biosynthesis; Cotton; Fiber; Glycans; Oligomers; Development; Cellulose; HPAEC-PAD

1. Introduction

Cell wall biosynthesis is a highly complex process which involves soluble substrates being converted to insoluble products at the surface of the cell membrane or external to it. This is complicated by the synthesis of a primary wall followed by the synthesis of the secondary wall often with overlap of the synthesis of both. The products include polysaccharides, glycoproteins, proteins and enzymes which may exist in complexes or be covalently linked to each other. Correlations between cell growth and substrate concentrations and the activities of several enzymes have been made (Murray and Bandurski, 1975; Murray and Brown, 1997). The fact that hydrolysis of sucrose to glucose and fructose is an integral part of fiber wall synthesis (Basra et al., 1990) is consistent with observations in this laboratory. A direct relationship between cell growth and acid invertase activity has been demonstrated in several plant tissues (Morris and Arthur, 1985; Sturm and Chrispeels, 1990; Basra et al., 1990; Sturm et al., 1995; Buchala, 1987). The increased invertase activity is the result of transcription of messenger RNA, rather than simply an enzyme kinetic effect, therefore, the invertase response is specific and induced (Sturm and Chrispeels, 1990; Sturm et al., 1995).

The secondary cell wall of cotton fibers consists almost entirely of cellulose which directs interest to cellulose biosynthesis. The potential role of sucrose synthase with the cellulose synthetic apparatus has been proposed (Amor et al., 1995; Delmer, 1999). The possible role of the invertase mentioned above, the possible role of

* Corresponding author. Tel.: +1-949-261-9664; fax: +1-949-261-9078.
E-mail address: amurray@glycozyme.com (A.K. Murray).

0031-9422/01/$ - see front matter © 2001 Elsevier Science Ltd. All rights reserved.
PII: S0031-9422(01)00143-1

lipid-bound intermediates (Matthysse et al., 1995; Brett, 2000) and the suggestion of self-assembly mechanisms (Brett, 2000) remain observations in search of explanations.

Our interest is in understanding the dynamics of carbohydrate metabolism during cotton fiber development. Since a plant cell must synthesize cell wall material in order to grow and develop, knowledge of the events in cell wall biosynthesis can be used to monitor plant growth and to detect aberrations in growth due to environmental influences (Murray, 1998, 2000). The cotton fiber is unique in its development since it is a plant cell that usually does not divide or store starch. During the period of fiber elongation, it is generally synthesizing primary cell wall (Graves and Stewart, 1988). Following the period of cell elongation, the fiber cell thickens as it synthesizes secondary cell wall, which consists almost entirely of cellulose. The period of cotton lint development, from pollination to dry, mature fiber extends only about 45 days. The rates of cellulose deposition, on a per mm fiber length basis, vary with one maximum at 16 days post anthesis (DPA) and a greater maximum at 28DPA (Meinert and Delmer, 1977). Prior to 21 DPA well-defined fibers are usually not present in developing bolls. However, only after the first 21 days have elapsed, can fibers be excised from developing bolls.

The present work shows that several carbohydrates and the carbohydrate–protein complex vary in a manner that is consistent with known characteristics of cell wall development in plants. We have identified a series of glucose containing oligomers, which are ubiquitous in all plant tissues investigated to date including monocots, dicots, and marine algae. The quantitative distribution and presence of specific oligomers appears to be unique to each plant and tissue as well as to the developmental stage. These glycans constitute another piece of the cell wall biosynthetic process. Since they can be extracted from developing cotton fibers, mature cotton fibers and aging cotton fibers in fabric, they may be subunits of the cotton fiber. Since they have been extracted from every sample of plant cell wall material examined suggests that they are fundamental elements, which occur with cellulose.

2. Results

2.1. Effects of physiological factors on oligomers in fibers

A practical way to investigate cotton fiber development is to freeze bolls in the field, and subsequently lyophilize them. Fractionation of the re-hydrated, developing fibers yields mono- and oligosaccharides, oligomers, an oligomer–protein complex, as well as insoluble fiber material as shown in Fig. 1. The oligomers can be extracted using weak acid from developing cotton fibers, mature cotton fibers, cotton dust and cotton fabric at various stages of processing as well as from old fabric, paper and wood.

Chromatograms of the carbohydrate oligomers show that many of the peaks appear in a pattern of slightly decreasing retention time increments. Such increments suggest a series of oligomers differing in length by a repeating unit. Fig. 2 shows this pattern for oligomers extracted from first position cotton bolls collected from sequential fruiting branches on the same plant at the same time from 15 to 39 days post anthesis (DPA). Extracts of the older bolls contain the same oligomers, but less material is extracted on a dry weight basis. The relative abundance of the oligomers in extracts from developing cotton fibers correlates with the deposition of secondary cell wall and changes in the content of soluble oligosaccharides (Murray and Brown, 1997). The oligomers extracted are most abundant at about 21 DPA, which is the time when secondary cell wall synthesis is rapidly occurring. The quantitative decrease in the oligomers extracted with age corresponds to decreased synthesis, and probable incorporation of these glycans into linkages that are not cleaved by the weak acid extraction. The pattern of oligomers extracted from a plant stunted due to periodic drought stress is shown in Fig. 3. The relative abundance of the oligomers changes particularly with those eluting at 15–20 minutes of retention time. Changes in the number and relative quantities of oligomers are a sensitive detector of stress. As seen in this case, the first oligomer in the sequence is present in a large quantity, but it appears that the sequential oligomers, observed in the boll of a plant developing under favorable growing conditions are not present. In addition to the correlation of oligomers with developmental age the oligomers extracted from 24DPA fibers change with the time of day as shown in Fig. 4. They are more abundant in the early morning and evening. This difference correlates with the diurnal variation in soluble oligosaccharide content as well (data not shown).

Each chromatogram shows PAD response and A_{280} which is likely protein but could include other phenolic compounds. It appears that certain of the oligomers are associated with A_{280} absorbing material. Further, the nature of the A_{280} absorbing material also changes with the time of day. The chromatograms of extracts from bolls collected early and late in the day show an A_{280} triplet peak between 20 and 25 min, while the midday chromatogram shows a prominent A_{280} peak at about 35 min.

2.2. Characterization of oligomers

The glycans reported in this paper have been extracted at 100°C in 0.1 N HCl which has then been neutralized with an equivalent amount of 1 N NaOH. If these oligomers are allowed to stand in the refrigerator

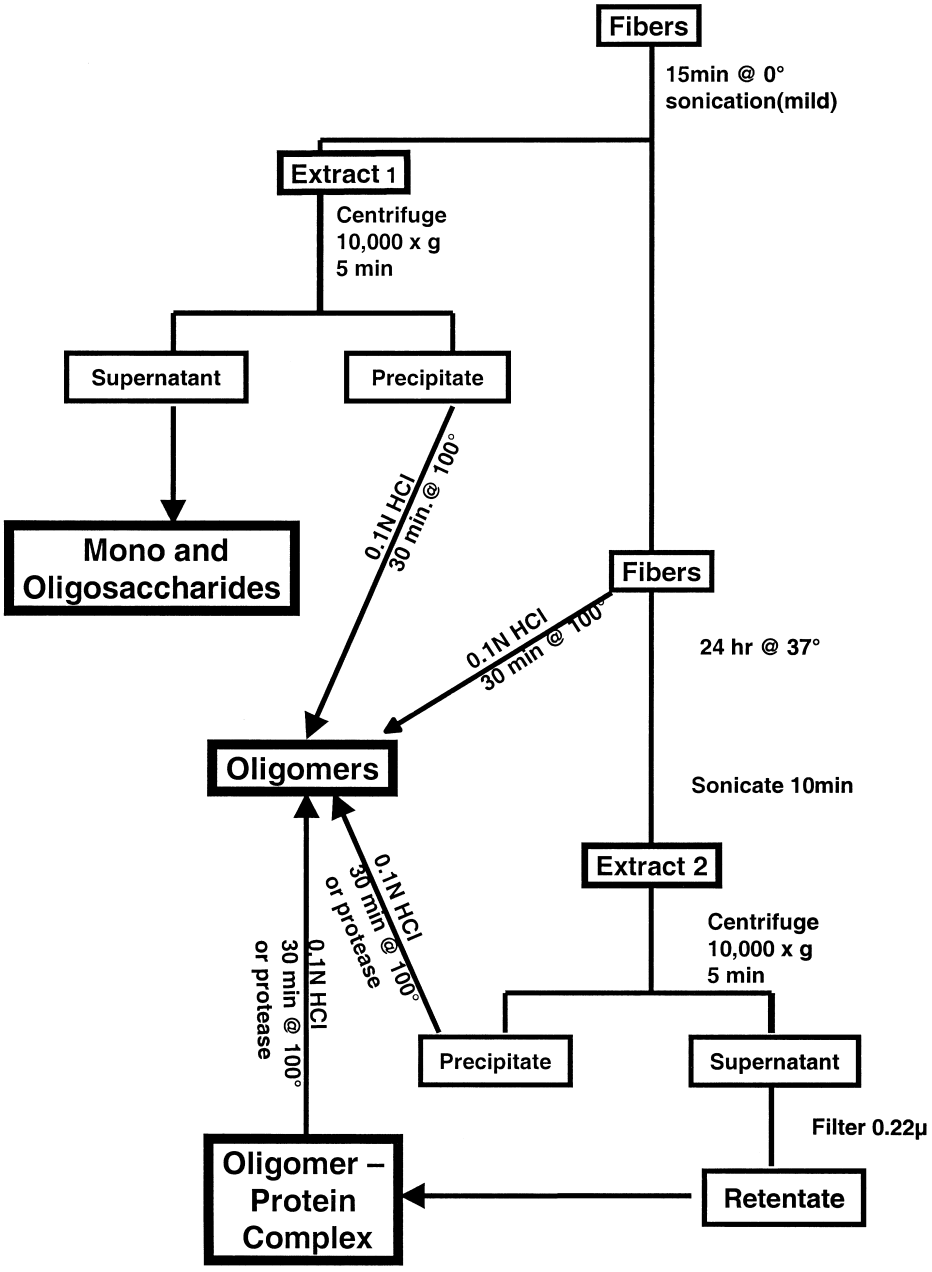

Fig. 1. Extraction procedures for cotton fibers.

at 4°C for a few days, they precipitate out of solution. If the solution of the oligomers is desalted by passage over ion exchange resins the oligomers precipitate out immediately and will plug up the filter (0.2 μm). Once precipitated out of solution, the material can be resolublized by boiling in 0.1 N HCl. The oligomers are reducing sugars as evidenced by the fact that they are susceptible to mild alkaline degradation, 0.1 N NaOH, boiling for 5–10 min (Whistler and BeMiller, 1958). Incubation with cellulase, in this case from *Trichoderma reesii* (Sigma), results in the degradation of the oligomers with retention times greater than 16 min, with a concomitant increase in the oligomers with retention times of approximately 14 and 16 min as shown in Fig. 5. In this system cellobiose elutes at about 10.5 min.

Treatment of the oligomers with ß-glucosidase, almond emulsin, results in a chromatogram with peaks quantitatively greater than the control. Presumably this is due to trimming of the longer oligomers which either are not resolved on the column or have a reduced detector response or both. A similar observation has been made in other work in which the oligomers with longer retention times, greater than 20 min, can be precipitated with alcohol. Subsequently, the precipitated oligomers can be dissolved and treated with a highly purified cellulase (endoß-1,4-glucanase, Megazyme, Ireland) which

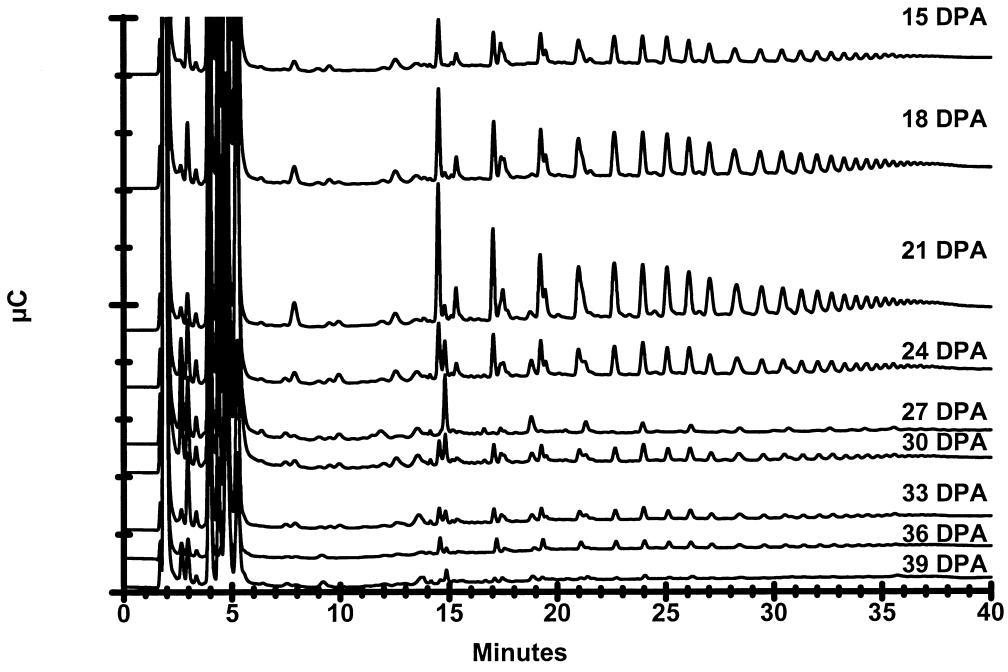

Fig. 2. Oligomers extracted from fibers from sequential first position bolls on a normal plant. In all cases essentially the same amount of fiber was extracted within 10%. Plots of detector response usually within 10%.

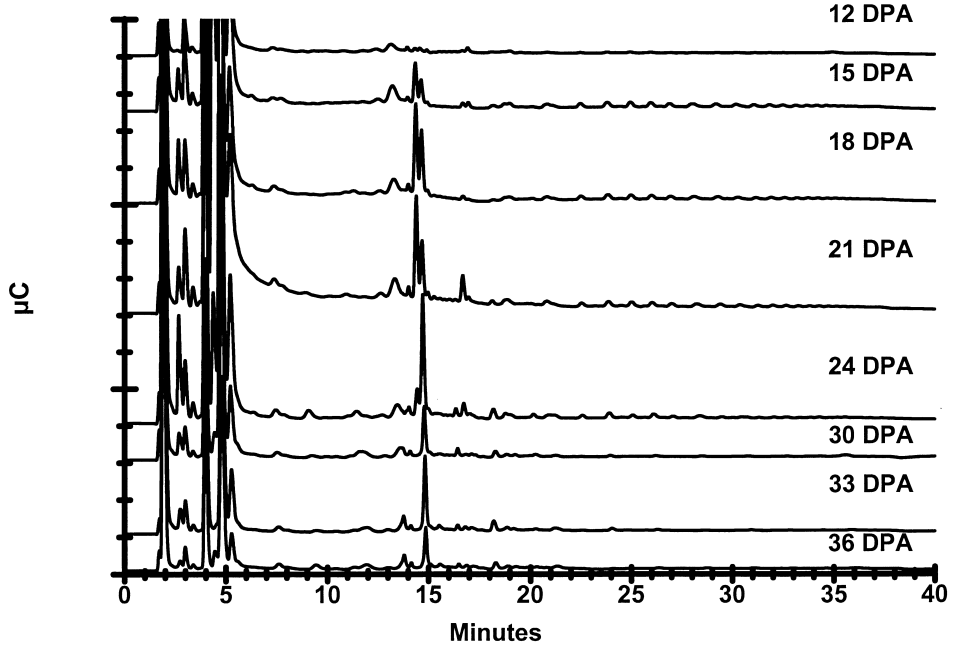

Fig. 3. Oligomers extracted from fibers from sequential first position bolls on a stunted plant. The amount of fiber extracted was the same as in Fig. 2.

then trims them back to the peaks with shorter retention times. The only monosaccharide released by this cellulase treatment is glucose. A preliminary investigation of the monosaccharide composition of the oligomers extracted from 21 DPA fibers has shown that the most prevalent monosaccharide is glucose, but that they also contain galactose, mannose, *m*-inositol and glycerol.

The major difference between successive oligomers from normal fibers is in the relative glucose content. That is, successive oligomers in a series have comparable amounts of galactose and mannose but different amounts of glucose. It is not yet known whether the apparently suppressed production of oligomers in the drought stressed plants follows this pattern. However, many of these

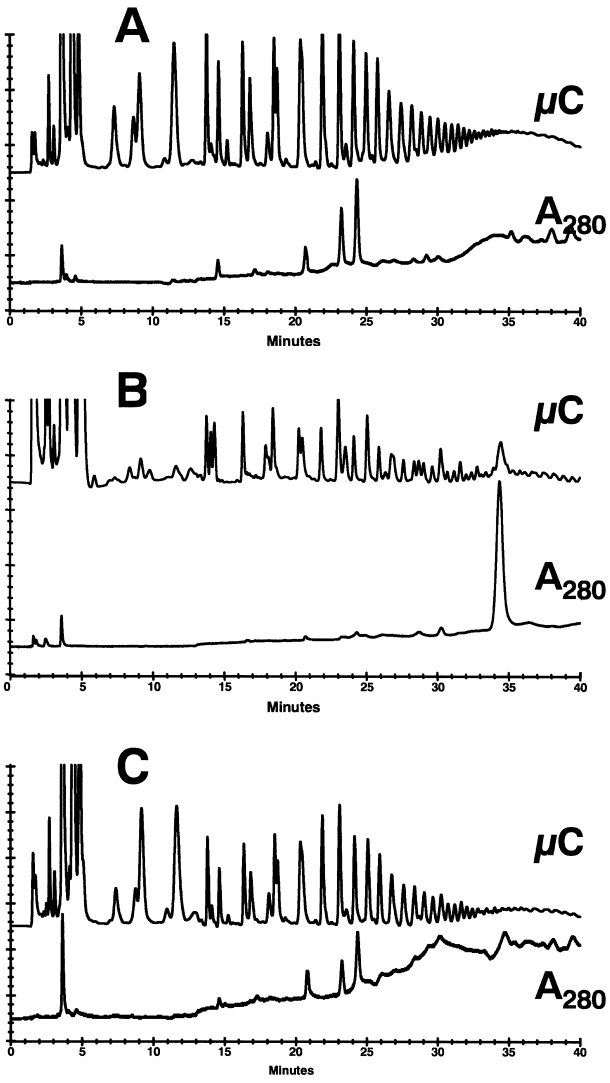

Fig. 4. Oligomers extracted from 24DPA fibers from bolls collected at 7 am (A), noon (B) and 7 pm (C).

same oligomers are found in a variety of cell walls although the data are not presented here.

2.3. Effect of incubation temperature, substrates, and tunicamycin on oligomers released

Fibers were rehydrated for 15–30 min prior to the beginning of the incubation with substrates. Oligomers were extracted from fibers, incubated for 24 h at 37°C under toluene with the substrates glycerol, *m*-inositol, sucrose, raffinose and cellobiose: control fibers had no exogenous substrates added. The control treatment resulted in oligomers as extracted from unamended fibers. The important point is that the addition of certain substrate combinations appear to reduce the quantities of oligomers which are extracted. Presumably such combinations of putative substrates affect the association of the oligomers with insoluble cell wall components. We hypothesize that these data suggest association of the oligomers with insoluble cellulosic structures, resulting in reduced extraction of oligomers by the weak acid procedure. The substrates were chosen due to their presence in aqueous extracts or hydrolyzates of fibers with the exception of cellobiose. However, the concentrations used are much higher than found in the aqueous extracts.

The effect of tunicamycin during incubation on the oligomers extracted from cotton fibers was investigated. Fibers were extracted with cold water to remove endogenous substrates and then incubated for 24 h with or without tunicamycin (10 μg/ml) both with and without added substrates 25 mM raffinose and 25 mM cellobiose. Tunicamycin specifically inhibits the formation of the bond between asparagine and *N*-acetylglucosamine in *N*-linked glycoproteins (Elbein, 1979) and it has been shown to inhibit other glycolipid mediated carbohydrate transfer reactions (Elbein, 1979; Barr et al., 1989; Müller et al., 1981). Without added substrates, tunicamycin had no appreciable effect, but with added substrates such as cellobiose and raffinose, the effect was substantial as the tunicamycin inhibited the relative quantities of oligomers extracted as shown in Fig. 6. In other experiments, not shown here, the tunicamycin effect was variable if the endogenous substrates were not removed by cold water extraction prior to addition of tunicamycin.

Incubation of developing fibers in water for up to 72 h at various temperatures results in the release of a white material to the medium, resulting in turbidity which can be precipitated by centrifugation. Cotton fibers (25 DPA) were extracted with water at three different temperatures, 37, 25 and 4°C for up to 30 days. The extraction tubes were sonicated for 15 min, and extracts were removed each day and centrifuged to yield a white particulate pellet. Microbial growth was retarded by a layer of toluene on the surface of the water in the tube. Following removal of the extracts fresh water was added back with the toluene layer on top. From 3 to 9 days of extraction, the fibers extracted at 4°C were characterized by one obvious difference. Before sonication all tubes were clear, but following sonication the extract in the tubes incubated at 4°C became turbid. The turbidily appeared as a very fine particulate suspension. Yet on centrifugation, the pellets obtained from all of the tubes were similar in the quantity of precipitate, and in the relative quantities of oligomers obtained. This result is indicative of a temperature dependent, and thus probably an enzymatic process which produces larger particles at the warmer temperatures. This precipitate material, when subjected to the 0.1 N HCl treatment, is completely dissolved, and is a rich source of the oligomers. The chromatograms of the oligomers obtained from this source appear to be more uniform with a smoother baseline between the peaks than from intact fibers.

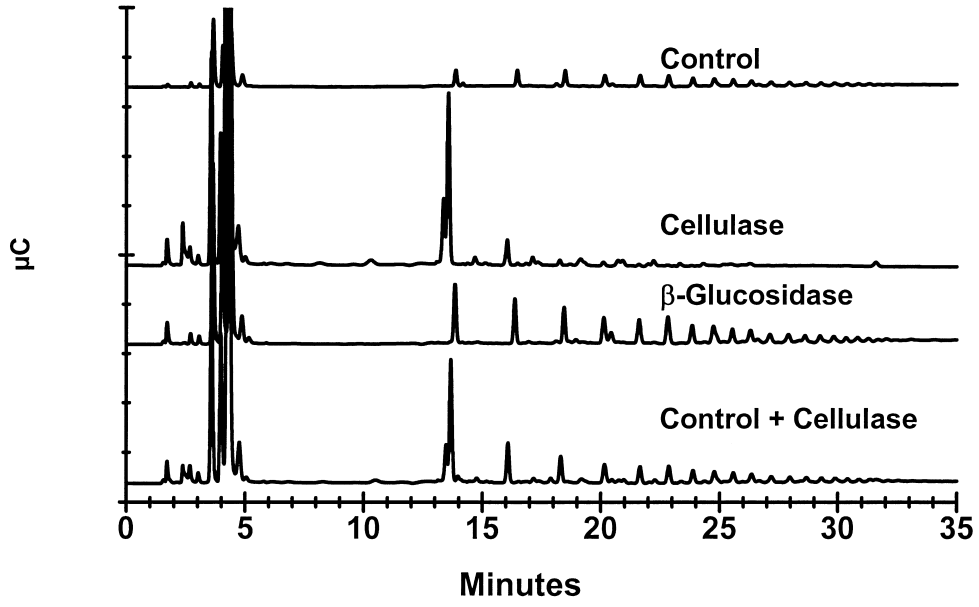

Fig. 5. Oligomers following treatment with cellulase or ß-glucosidase and the control without treatment. The bottom plot is a mixture of equal parts of the samples from the control oligomers and those treated with cellulase. This was done to determine if there were shifts in retention time of any of the peaks.

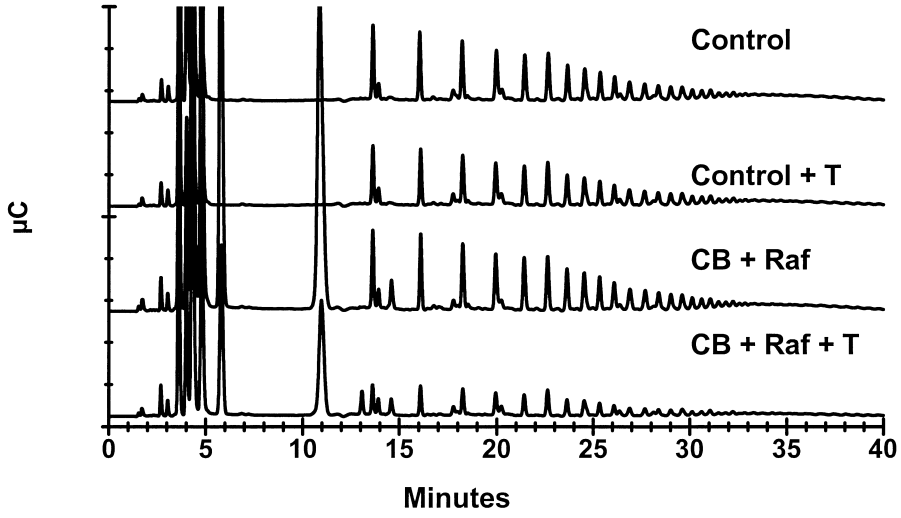

Fig. 6. Effect of tunicamycin on oligomers released following incubation. (CB: cellobiose; Raf: raffinose; T: tunicamycin).

2.4. An oligomer-protein colloid

In addition to the precipitate, another material remaining in solution, has been isolated by filtration on 0.22 μm filters. This material may be subjected to the weak acid treatment to yield the oligomers. Treatment with proteases also releases the oligomers from this carbohydrate-protein complex, after which it does pass through the 0.22 μm filter. Of four proteases investigated (proteinase K, trypsin, chymotrypsin and Pronase®), chymotrypsin is the most efficient in releasing the oligomers, being some 500-fold more active than trypsin on a molar basis. Proteases will also dissolve the white precipitate material and release the oligomers.

The carbohydrate-protein complex extracted from developing fibers varies with the time of day when the bolls were picked. If the fibers are boiled for 10 min prior to the extraction of the carbohydrate-protein complex , differences in the oligomers released are observed. The oligomer pattern of the carbohydrate-protein complex from boiled fibers and fibers that were not boiled is characterized by the absence of one peak in fibers from bolls harvested at 7 am, as shown in Fig. 7A , but the difference is very large in fibers from bolls harvested at noon, with most of the peaks being absent as shown in Fig. 7B.

While cotton fibers are still immature, external agglo merations appear as white flakes on the lyophilized fibers and in freshly opened bolls, until at least 39PDA.

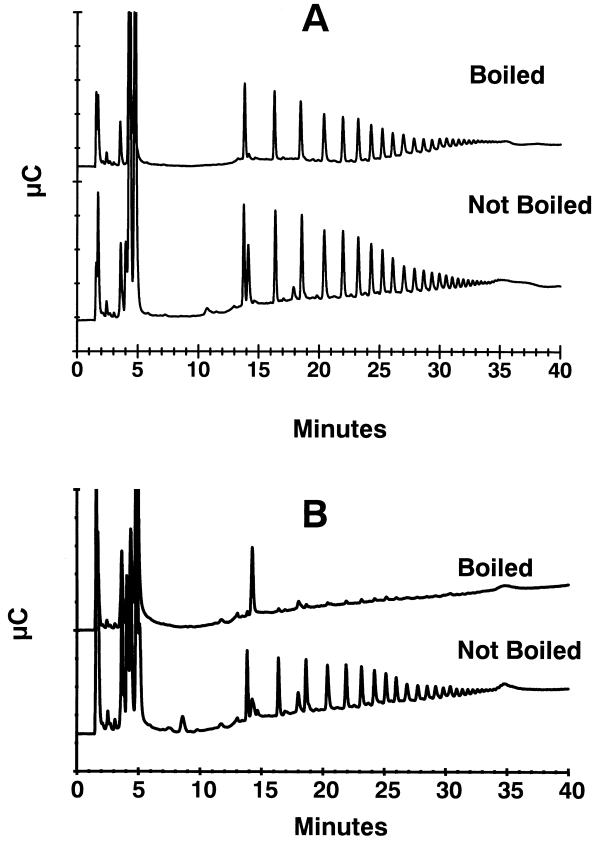

Fig. 7. Oligomers released from carbohydrate-protein complex from fibers from bolls collected at 7 am (A) and noon (B), which were boiled or not boiled before extraction.

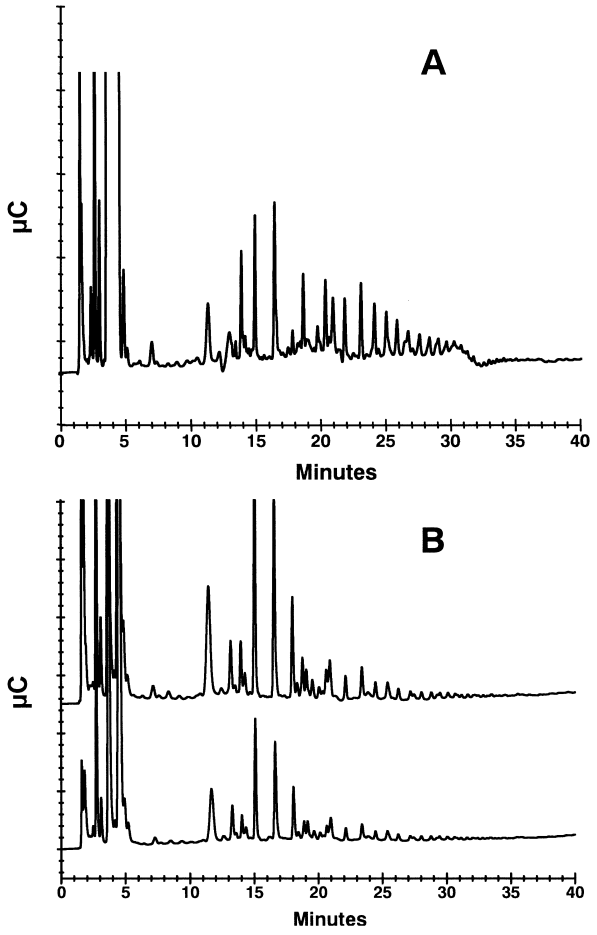

Fig. 8. Oligomers extracted from old denim fabric (A) and a towel dyed ivory in color (B). In (B) the upper plot is a newly manufactured towel and the lower plot is the same towel after one washing.

Such flakes have not been observed in later stages of development, nor in mature bolls. Although several investigators have mentioned observing the white flakes, we find no detailed characterization of them in the literature. Dissection of white flakes from the fibers, followed by both the cold water and weak acid extractions, demonstrated that they were rich sources of the same soluble oligosaccharides and oligomers as found in the fibers. On a dry weight basis, white flakes release at least 5-10 times the quantity of oligomers as do the fibers. Since these white flakes contain oligomers, that we hypothesize are incorporated into the fibers, we also infer that the white flakes contain materials that will be precursors of the fiber wall. If this is the case, then all of the developing fiber wall material does not reside within the cylindrical interior of the individual fiber during cellulose synthesis. However, the origin and role of such extra-fibril oligomers are not known at this time.

2.5. Oligosaccharides and oligomers in cotton textiles, wood, and paper products

Not only are oligosaccharides and oligomers found in extracts of fibers sampled directly from cotton bolls, but extracts of cotton textiles produce peaks having the same retention times, relative to know compounds, as do the extracts of fibers from plant material (Fig. 9, see also Fig. 2). Moreover, the same oligosaccharides and oligomers can be recovered from cotton textiles, e.g. denim, sheets and towels after prolonged wear and washings (data not shown). The effect of washing is to reduce the quantity of the oligosaccharides and oligomers extracted, relative to those found in newly-manufactured textile products or cotton fibers sampled from bolls (Fig. 8).

Similar oligosaccharides and oligomers may also be extracted from woods (Fig. 9). Twenty-two different woods have been extracted. While many of the same oligosaccharides and oligomers are found in the woods and in cotton, no two species of wood have been found to be display identical chromatograms. Thus each species of wood has a distinct signature. For example, birch and pine vary in peaks eluting between approximately 15 and 20 min; while balsa, a very low density wood has lower levels overall. (Note that in Fig. 9 the scale for balsa is expanded 5×). As with the new and old cotton products, there appears to be an effect of washing and aging

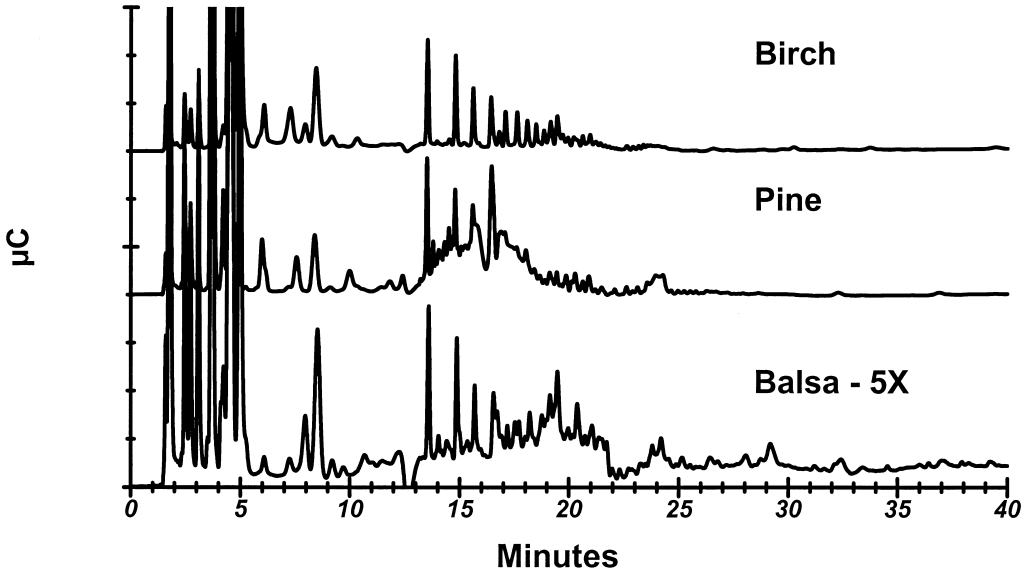

Fig. 9. Oligomers extracted from three different woods, birch, pine and balsa.

with woods as well. Note that the chromatograms of teak that has been part of the deck of a sea-going vessel for nineteen years is almost indistinguishable from that of recently-harvested teak, except that the scale of the weathered teak must be expanded 4× for the chromatographs to appear congruent (Fig. 10) for both the cotton and the wood, a probable hypothesis is that fractions of oligosaccharides and oligomers have leached out of the cellulose with successive exposure to water and salts. Loss of the oligosaccharides and oligomers may indicate, and may in fact constitute, wear and loss of integrity of the fabric and wood fibers.

Various paper products also display oligosaccharides and oligomers similar to those found in cotton and wood (Fig. 11) As with woods, every paper product tested to date has produced a unique chromatograph. Whereas the difference among the woods are probably due to differences in biochemistry and patterns of growth, the differences among the paper products illustrate differences in both cellulose source and in processing, such as type and degree of bleaching, coloring, and surface finishing.

3. Discussion

The relative amounts of oligomers extracted from the developing fibers vary with age of the tissues. The period of greatest abundance of the lower molecular weight oligomers coincides with the time considered to be the

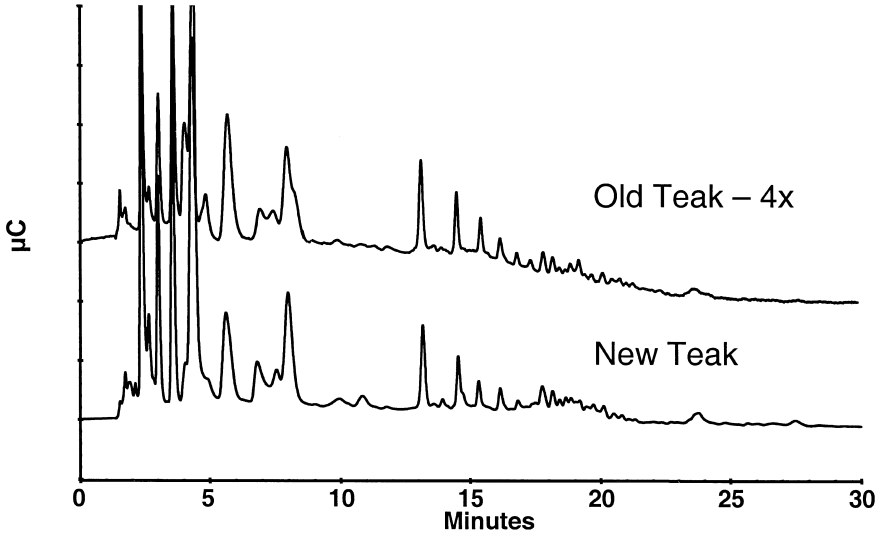

Fig. 10. Oligomers extracted from new teak and old teak which was weathered on a boat deck for 19 years.

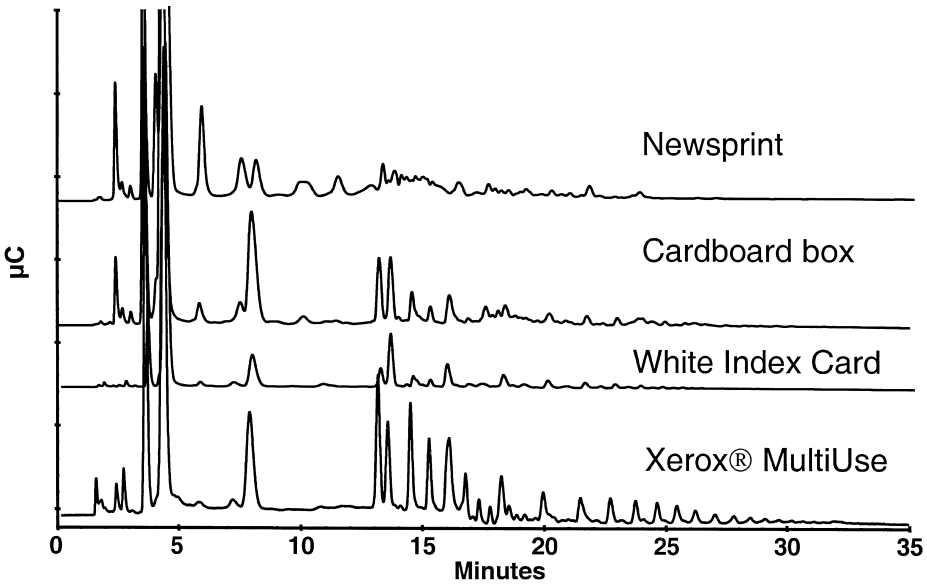

Fig. 11. Oligomers extracted from newsprint, cardboard, m indexcard and Xerox® MultiUse paper.

onset of secondary cell wall synthesis. This correspondence suggests a role of the oligomers in the biosynthetic process. Such a role is also supported by the skewed distribution of the oligomers in the sequential bolls from the a plant stunted due to periodic drought stress. The roles of UDPG, sucrose and sucrose synthase have been well described (Delmer, 1999). Correlation between the levels of sucrose and the sucrosyl oligosaccharides and the cyclical changes in the relative quantities of the oligomers with the time of day is suggestive of a role for these sugars in the synthesis of the oligomers. The influence of the concentrations of *myo*-inositol, sucrose, raffinose, cellobiose and glycerol on the oligomers extracted from fibers following incubation also supports the notion that a number of these sugars may function as substrates. The prospect of substrates originating external to the fiber being incorporated into the cellulose of the fiber wall was first raised by Delmer et al. (1974).

The extraction of the carbohydrate–protein complex containing the oligomers is also suggestive of a biosynthetic role for the oligomers. The fact that this material can be isolated by filtration, but that it appears to be incorporated into a larger material which precipitates with increased incubation time, is consistent with such a role. A likely scenario is that the rehydrated fibers are capable of carrying out some but not all of the enzymatic steps involved in the biosynthetic pathway.

The inhibition of the production of extractable oligomers by tunicamycin is very suggestive of a role of lipid linked intermediates (Elbein, 1979; Barr et al., 1989; Müller et al., 1981). In our case, incubation of fibers with tunicamycin results in a significant decrease in the oligomers which can be extracted if exogenous substrate is added (Fig. 6). Without exogenous substrate tunicamycin did not greatly decrease the oligomers which could be extracted. In contrast, experiments by Pillonel and Meier (1985) showed that fibers incubated with tunicamycin, at the same concentration, did not result in the reduction of ^{14}C incorporated into either ß-1,3 or ß-1,4 glucans using sucrose as the substrate. In fact, the incorporation was increased slightly. This apparent discrepancy may be explained by the different extraction methods used in the work of Pillonel and Meier, which utilized hot ethanol followed by precipitation of insoluble material. This procedure very likely included higher molecular weight glycans than have been extracted by the methods used herein (Fig. 1.) Also extraction with hot ethanol would very likely have destroyed the functionality of any associated proteins, such as that associated with the carbohyrdrate-protein complex isolated by the procedures used in this work. In ovule culture experiments the inclusion of tunicamycin in the culture medium resulted in the inhibition of secondary cell wall biosynthesis (Davidonis, 1993). An effect of tunicamycin similar to the ovule culture experiment and to what we report here has also been observed for the inhibition of cellulose biosynthesis in cell walls of *Arabidopsis* by tunicamycin (C. Somerville, personal communications).

The diurnal cycling of the carbohydrate-protein complex extracted from fibers harvested at different times of day coincides with the documented biosynthetic pattern of plant metabolism (Kehr et al., 1998). Although the the structure of the carbohydrate–protein complex has not been completely determined, the fact that the oligomers are released by weak acid suggests that they might have been released from a glycolipid. The possible role of intermediates other than glycolipids must also be kept open with the description of an *N*-glucosylated protein intermediate in the biosynthesis of a cell wall ß-1,6-glucan in *Saccharomyces cerevisiae* (Shahinian et al., 1998) and

an autoglycosylated protein implicated in plant cell wall biosynthesis (Delgado et al., 1998). The differences in the monosaccharide composition of oligomers subjected to differing conditions, as illustrated by those between oligomers extracted from fibers immediately following the cold water treatment versus those extracted from fibers following a 2 h incubation at 37°C also suggests biosynthetic activity. Such differences could be due to metabolic incorporation of the non-glucose components during the incubation, the addition of glucose to the oligomers, or differences in binding by other components of the system. A rigorous study employing thorough washing of the fibers prior to extraction with weak HCl following hydration or hydration and incubation is required to address these issues. The release by proteases suggests that the oligomers may be bound by a protein complex, also suggesting the possibility of a biosynthetic process. Invertase activity is present in the carbohydrate–protein complex, but the possibility of the presence of other enzyme activities remains open.

Clearly, biosynthesis of a polymer as large as cellulose may involve carbohydrates larger than sucrose. That such intermediates have not been described may be attributable to the complexity of carbohydrate biochemistry, and the relative fragility of glycoprotein associations, in the presence of rigorous extraction procedures. In this work, the use of mild extraction procedures, together with HPAEC-PAD, has revealed a number of, as yet not fully-characterized, oligomers. Such oligomers have been found in a number of cellulosic materials. The relative abundance of these oligomers varies with source and with developmental variables within a source. Moreover, the oligomers have been found in association with protein and, in certain experimental incubations, have behaved as if their solubility, acid-liability, and associated soluble products were affected by temperature and by amendment with biologically active saccharides. In short, they have behaved as if they were components of a biosynthetic apparatus. It is probable that the process of cellulose synthesis involves as yet un-described enzymatic activity, and that such activity is energetically favored by the conformation of glycan and glycoprotein conformations that are amenable to low-energy and possibly low-bioenergetic interconversion. We propose that the oligomers herein described are a fertile area for further research in elucidation of a model of cellulose biosynthesis.

4. Experimental

4.1. General experimental procedures

All water extractions were done using 18.3 megohm water from a Barnstead Nanopure water system. Enzymes used were obtained from Sigma Chemical Company. Chromatography was performed on a Dionex Bio-LC.

4.1.1. Plant material

Cotton, *Gossypium hirsutum* var. DP-50, was grown in the Mississippi Delta region for the time of day samples which were collected at 7 am, noon and 7 pm at 25 DPA. Plants for the sequential bolls were also *G. hirsutum* var. DP-50 grown in the Sacramento Valley of California. Sequential bolls were taken at the same time on the same plant. Bolls were placed on ice and frozen on dry ice as soon as possible following collection.

4.2. Extraction of fibers

The lyophilized fibers were first extracted with water at 0°C to remove soluble oligosaccharides and monosaccharides (Murray, 1998) (Fig. 1.). Typically, a 20 mg sample of fibers was placed in a 1.7 ml screw cap plastic tub to 0.5 ml water was added, the tube shaken, then placed in a Branson 85 W sonicator filled with ice water. Following removal of the cold water extract with a Pasteur pipette, 0.5 ml of 0.1 N HCl was added and the tube was placed in a boiling water bath for 30 min to extract the glucose containing oliogmers (Murray, 2000). The mono- and oligosaccharides extracted by the cold water procedure include *myo*-inositol, galactinol, arabinose, glucose, fructose, melibiose, sucrose, manninotriose, verbascotetraose, raffinose, stachyose, verbascose and, tentatively, ajugose which can be used as indicators of fiber development (Murray, 1998, 2000). The oligosaccharides extracted by the 0.1 N HCl procedure can also be used as indicators of cell wall biosynthesis and fiber development (Murray, 2000). The HCl extracts were neutralized with an equivalent amount of 1 N NaOH prior to HPAEC-PAD. In the case of fabric, wood or paper products typically 40–60 mg of material was extracted in a volume of 1.0 ml.

4.3. Isolation of oligomer–protein colloid

To obtain the oligomer–protein colloid, the cold water extract was removed and 0.5 ml of water was added, with 50 μl of toluene layered on top to prevent microbial growth, the cap was screwed on tightly and the tube was placed in a 37°C water bath for 24 h. Following the incubation, the oligomer–protein colloid was isolated by first centrifugation at 15,000 × *g* for 5 min after which the supernatant was filtered through a 0.22 μm Z-Spin filter (Gelman) with the oligomer–protein colloid being retained by the filter. The oligomers were released from the oligomer–protein colloid by either chymotrypsin or by the weak acid extraction.

4.4. Enzyme treatments

Extracted multimers were subjected to incubation with a cellulase (*Trichoderma reesei*) or a β-glucosidase (almond emulsin) both obtained from Sigma Chemical

Company. The enzymes were used at a concentration of 1 mg/ml in 50 mM sodium acetate buffer, pH 4.8. The effect of the β-glucosidase appeared to be to increase the heights of the multimer peaks significantly and to generate one additional small peak with a retention time slightly greater than 20 min. Presumably this is the result of removing terminal glucose unit(s) that results in a compound with an increased detector response. The cellulase gave a very different result since it resulted in the near elimination of many peaks and great reductions in many peak heights with a great increase in the peak height of the first peak in the series of multimers as shown in Fig. 5. Protease treatments of the carbohydrate-protein colloid were performed using a protein concentration of 1 mg/ml in water.

4.5. Chromatography

HPAEC-PAD was performed using a CarboPac PA-1 column. The eluent was 150 mM sodium hydroxide, isocratic from 0 to 5 min then a linear sodium acetate gradient from 5 to 40 min going from 0 to 500 mM in 150 mM NaOH at a flow rate of 1 ml/min. The detector wave form was the following: 0–0.50 s, 0.1 V; 0.51–0.59 s, 0.6 V; 0.60–0.65 s, −0.6 V; integration 0.30–0.50 sec. For monosaccharide composition, oliogomers were obtained by collecting fractions of the HPAEC-PAD eluent, which was passed through a Dionex ASRS-II anion suppressor to remove salt. Fractions were then lyophilized and taken up in 200 μl of water, made up to 2N trifluoroacetic acid (TFA)(Manzi and Varki, 1993). flushed with argon and sealed in screw cap plastic vials with O-rings. The samples were then placed in a heating block at 100°C for 2–4 h. Following hydrolysis, the samples were taken to dryness in a Speed-Vac overnight and then taken up in 200 μl of water for HPAEC-PAD on a Dionex CarboPac-PA10 column under isocratic conditions in 15 mM NaOH.

Acknowledgements

The authors would like to thank Judy Brown, Finch Ranch, Orland, CA, for collecting the sequential boll samples. Supported in part by Cotton Incorporated, 98-638. A portion of the work was performed under USDA CRADA No. 58-3K95-M415.

References

Amor, Y., Haigler, C.H., Johnson, S., Wainscott, M., Delmer, D.P., 1995. A membrane-associated form of sucrose synthase and its potential role in synthesis of cellulose and callose in plants. Proc. Natl. Acad. Sci. USA 92, 9353–9357.

Barr, K., Nunes-Edwards, P., Rick, P.D., 1989. In vitro synthesis of a lipid-linked trisaccharide involved in synthesis of enterobacterial common antigen. J. Bacteriol. 171, 1326–1332.

Basra, A.S., Sarlach, R.S., Nayyar, H., Malik, C.P., 1990. Sucrose hydrolysis in relation to development of cotton (*Gossypium* Spp.) fibres. Indian J. Exp. Biol. 28, 958–988.

Brett, C.T., 2000. Cellulose microfibrils in plants: biosynthesis, deposition, and integration into the cell wall. Int. Rev. Cytology 199, 161–199.

Buchala, A., 1987. Acid ß-fructofuranoside fructohydrolase (invertase) in developing cotton (*Gossypium arboreum* L.) fibres and its relationship to ß-glucan synthesis from sucrose fed to the fibre apopoplast. J. Plant Physiol. 127, 219–230.

Davidonis, G., 1993. Cotton fiber growth and development in vitro: effects of tunicamycin and monensin. Plant Sci. 88, 229–236.

Delgado, I.J., Wang, Z., de Rocher, A., Keegstra, K., Raikhel, N., 1998. Cloning and characterization of *AtRGP1*: a reversibly autoglucosylated arabidopsis protein implicated in cell wall formation. Plant Physiol. 116, 1339–1349.

Delmer, D.P., 1999. Cellulose biosynthesis: exciting times for a difficult field of study. Ann. Rev. Plant Physiol. Plant Mol. Biol. 50, 245–276.

Delmer, D.P, Beasley, C.A., Ordin, L., 1974. Utilization of nucleoside diphosphate gucoses in developing cotton fibers. Plant Physiol. 53, 149–153.

Elbein, A.D., 1979. The role of lipid-linked saccharides in the biosynthesis of complex carbohydrates. Ann. Rev. Plant Physiol. 30, 239–272.

Graves, D.A., Stewart, J.McD., 1988. Analysis of the protein constituency of developing cotton fibres. J. Exp. Bot. 39, 59–69.

Kehr, J., Hustiak, F., Walz, C., Willmitzer, L., Fisahn, J., 1998. Transgenic plants changed in carbon allocation pattern display a shift in diurnal growth pattern. The Plant Journal 16, 497–503.

Manzi, A.E., Varki, A., 1993. Compositional analysis of glycoproteins, in glycobiology. In: Fukuda, M., Kobata, A. (Eds.), A Practical Approach. Oxford University Press, Oxford, pp. 27–77.

Matthysse, A.G., Thomas, D.L., White, A.R., 1995. Methanism of cellulose synthesis in *Agrobacterium tumefaciens*. J. Bacteriol. 117, 1076–1081.

Meinert, M.C., Delmer, D.P., 1977. Changes in biochemical composition of the cell wall of the cotton fiber during development. Plant Physiol. 59, 1088–1097.

Morris, D.A., Arthur, E.D., 1985. Invertase activity, carbohydrate metabolism and cell expansion in the stem of *Phaseolus vulgaris* L. J. Exp. Bot. 36, 623–633.

Müller, T., Bause, E., Jaenicke, L., 1981. Glycolipid formation in *Volvox carterif*. FEBS Lett. 128, 208–212.

Murray, A.K., 1998., Method for monitoring growth and detection of environmental stress in plants. US Patent No. 5,710,047.

Murray, A.K., 2000., Method for detecting growth and stress in plants. US Patent No. 6,051,435.

Murray, A.K., Bandurski, R.S., 1975. Correlative studies on cell wall enzymes and growth. Plant Physiol. 56, 143–147.

Murray, A.K., Brown, J., 1997. Glycoconjugate profiles of developing fibers from different fruiting branches on the same plant. 1997 Proceedings Beltwide Cotton Conferences, pp. 1496–1499.

Pillonel, Ch., Meier, H., 1985. Influence of external factors on callose and cellulose synthesis during incubation in vitro of intact cotton fibres with [^{14}C]sucrose. Planta 165, 76–84.

Shahinian, S., Dijkgraaf, G.J.P., Sdicu, A.-M., Thomas, D.Y., Jakob, C.A., Aebi, M., Bussey, H., 1998. Involvement of protein *N* — glycosyl chain glucosylation and processing in the biosynthesis of cell wall ß-1,6-glucan of *Saccharomyces cerevisiae*. Genetics 149, 843–856.

Sturm, A., Chrispeels, M.J., 1990. cDNA cloning of carrot exocellular ß-fructofuranosidase and its expression in response to wounding and bacterial infection. The Plant Cell 2, 1107–1119.

Sturm, A., Šebková, V., Lorenz, K., Hardegger, M., Lienhard, S., Unger, C., 1995. Development- and organ-specific expression of the genes for sucrose synthase and three isoenzymes of acid ß-frucdto-furanosidase in carrot. Planta 195, 601–610.

Whistler, R.L., BeMiller, J.N., 1958. Alkaline degradation of polysaccharides. Adv. Carbohydr. Chem. 13, 289–329.

PERGAMON

Phytochemistry 57 (2001) 987–992

PHYTOCHEMISTRY

www.elsevier.com/locate/phytochem

Bonding of hydroxycinnamic acids to lignin: ferulic and *p*-coumaric acids are predominantly linked at the benzyl position of lignin, not the β-position, in grass cell walls

T.B.T. Lam[a], K. Kadoya[b], K. Iiyama[c,*]

[a]*School of Biochemistry, La Trobe University, Bundoora, Victoria, 3083 Australia*
[b]*Graduate School of Agricultural and Life Sciences, University of Tokyo, Yayoi, Bunkyo-ku, Tokyo, 113-8657 Japan*
[c]*Asian Natural Environmental Science Centre, University of Tokyo, Yayoi, Bunkyo-ku, Tokyo, 113-8657 Japan*

Received 10 September 1999; received in revised form 2 October 2000

Abstract

A suspension in dichloromethane–water (18:1, v/v) of various fractions containing hydroxycinnamic acid ester–ether bridges between lignin and polysaccharides prepared from cell walls of matured oat (*Avena sativa* L.) internodes, and a solution of their acetates in the same solvent, were treated with 2,3-dichloro-5,6-dicyano-1,4-benzoquinone (DDQ). This reagent selectively cleaves benzyl ether and ester linkages of negatively charged aromatic nuclei. The sample treated with DDQ was directly hydrolysed either under mild (1 M NaOH, overnight at 37°C) or severe (4 M NaOH, for 2 h at 170°C) conditions. The hydroxycinnamic acids released in the hydrolysate were methylated with diazomethane and analysed quantitatively using gas chromatography. Significant portions of ether linkages between hydroxycinnamic acids and lignin were cleaved with DDQ, which suggests that most of the hydroxycinnamic acids were ether-linked at the benzyl position, and not the β-position, of the lignin side chain as previously claimed. © 2001 Elsevier Science Ltd. All rights reserved.

Keywords: *Avena sativa*; Gramineae; 2,3-Dichloro-5,6-dicyano-1,4-benzoquinone; Lignin; Polysaccharides; Ferulic acid; *p*-Coumaric acid; Selective cleavage; Benzyl ether

1. Introduction

The presence of both ether- and ester-linked hydroxycinnamic acids in cell walls of wheat (*Triticum aestivum* L.) straw and rice (*Oryza sativa* L.) straw has been reported by Scalbert et al. (1985, 1986), and Sharma et al. (1986), respectively. It has been suggested that ether-linked hydroxycinnamic acids, especially ferulic acid, form bridges between lignin and polysaccharides in cell walls of wheat internodes (Iiyama et al., 1990). By using the specific techniques of hydrogenation followed by borohydride reduction, Lam et al. (1992, 1994b) found that in wheat and phalaris internodes, most of the ferulic acid ether-linked to lignin (excluding *p*-coumaric acid) was also ester-linked to polysaccharides. We have also proposed that during primary cell wall formation, ferulic acid is esterified to polysaccharides and the ferulate is then linked to the benzyl position of a lignin side chain through a nucleophilic addition reaction to quinonemethide intermediates of lignin during lignification (Iiyama et al., 1990; Lam et al., 1994b).

Ralph et al. (1992) and Ralph and Helm (1993), using ^{13}C NMR spectroscopy of a lignin preparation of maize (*Zea mays*) which had been administered ^{13}C enriched ferulic acid, have suggested that ferulate is ether-linked to the β-position of a lignin side chain through a radical coupling reaction between ferulate and monolignol radicals, which are presumably produced by the action of peroxidase. They also suggested that ferulate radicals are coupled with monolignol radicals to form various inter-unit linkage types such as β-5 (phenylcoumaran type), β-β (pinoresinol type), 5-5 (biphenyl type) etc, i.e. that ferulate acts as a monolignol. Jacquet et al. (1995) also isolated a ferulic acid-coniferyl alcohol dimer as the β-ether linked dimer, in a reaction mixture recovered from mild alkaline hydrolysis (2 M NaOH for 2 h at

* Corresponding author. Tel.: +81-3-5841-2783; fax: +81-3-5841-5230.
E-mail address: uakenji@mail.ecc.u-tokyo.ac.jp (K. Iiyama).

0031-9422/01/$ - see front matter © 2001 Elsevier Science Ltd. All rights reserved.
PII: S0031-9422(01)00052-8

37°C) of mature wheat and oat samples. Under these conditions, only ester linkages are cleaved. So the fragment of coniferyl alcohol should be a monomer, not a polymer. Lignin, on the other hand, is polymeric. Isolation of the ferulic acid-coniferyl alcohol dimer, therefore, has no relationship to the existence of β-ether linkages between lignin and ferulic acid. Terashima et al. (1993) and Morrison et al. (1998) have also suggested that ferulic acid is ester-linked to cell wall polysaccharides and thus is an anchor of lignification.

The cell walls of grasses release significant amounts of ferulic acid upon alkaline hydrolysis under various conditions, but there are few species of dicotyledonous plants which have detectable amounts of ferulic acid (Hartley and Harris, 1981; Kim et al., 1995). In order to understand the biosynthetic pathway of hydroxycinnamic acid bridges as well as the biosynthesis of lignin, it is important to identify the positions at which the hydroxycinnamic acids are ether-linked to lignin.

In this paper, internode walls of oat (*Avena saliva* L.) and various fractions containing lignin-polysaccharide associations through ferulic acid prepared from internode cell walls of oat were treated with 2,3-dichloro-5,6-dicyano-l,4-benzoquinone (DDQ). This reagent is well known as an oxidant, which selectively cleaves benzyl ester and ether linkages through charge transfer intermediates with negatively charged aromatic nuclei (Oikawa et al., 1982, 1983). DDQ has been applied to investigate the linkage position of polysaccharides to lignin (Koshijima et al., 1984; Watanabe et al., 1986, 1989). The results described here clearly suggest that most of the hydroxycinnamic acids, ferulic and *p*-coumaric acids, are etherlinked to the benzylic and not the β-position.

2. Results and discussion

The total recovery of fractions containing lignin-associated polysaccharides was ca. 90% of the extract-free cell walls of oat internodes (Table 1). About 10% of the walls were lost during ball milling and centrifugation. A significant amount of xylan was soluble in aqueous dioxane and DMSO; the DMSO-residue (DMR) was mostly composed of cellulose (Table 1). The total yield of products released by alkaline nitrobenzene oxidation was slightly higher in both 90 and 50% dioxane-soluble fractions than in other fractions (Table 2).

We tried to identify the position of the ether linkage of ferulate using DDQ. It has been reported that DDQ is a specific oxidant used to cleave benzyl ether and ester linkages by the formation of charge transfer complexes with reactants (Fig. 1) (Oikawa et al., 1982, 1983). Benzyl ether and ester linkages attached to aromatic nuclei of lignin (which is negatively charged), can be selectively cleaved by DDQ treatment. This reagent has been applied to the identification of the linkage position of polysaccharides to lignin in a fraction containing lignin–carbohydrate complexes isolated from wood meal (Koshijima et al., 1984; Watanabe et al., 1986, 1989). These results showed that sugar residues are linked to the lignin side chain at the benzyl position.

As the reaction of DDQ to cleave benzyl linkages is due to formation of charge transfer complexes with lignin aromatic nuclei, dichloromethane–H_2O (19:1, v/v) was used as solvent for the reaction. However, because the samples were not completely soluble in this solvent system, a homogeneous reaction using acetylated samples was also tested. The DDQ treatment for the heterogeneous system was carried out at 37°C for 24 h and 2 h for the homogeneous system. After DDQ treatment, dichloromethane was removed by evaporation and the samples were directly hydrolysed under mild (1 M NaOH, overnight at 37°C) and severe (4 M NaOH, for 2 h at 170°C) conditions. The hydroxycinnamic acids released by hydrolysis were derivatised with *N,O*-bis(-trimethylsily1)acetamide (BSA) and analysed by gas chromatography (GC) as previously described (Lam et al., 1994a). However, trimethylsilylated ferulic acid could not be separated from 2,3-dichloro-5,6-dicyano-l,4-hydroquinone, so the DDQ products were methylated with freshly prepared diazomethane and analysed by GC under the same conditions used for the trimethylsilyl derivatives (Lam et al., 1994a) (Fig. 2).

Hydroxycinnamic acids ether-linked to the benzyl position of the lignin side chain could be hydrolysed

Table 1
Yield of fractions containing lignin-polysaccharide associations of cell walls of oat internodes, and lignin and neutral sugar composition of the fractions

Sample	Yield, % of extractive-free plant walls	Neutral sugar, % of sample							Lignin, % of sample
		Rha	Ara	Xyl	Man	Gal	Glc	Total	
Extractive-free sample	100	1.4±0.1	1.2±0.0	24.6±0.2	0.2±0.1	0.4±0.0	50.9±0.4	78.7±0.4	18.4±0.1
90% Dioxane sol. (90S)	1.6	0.9±0.1	1.3±0.1	12.5±0.2	0.0±0.1	0.4±0.0	2.4±0.1	17.5±0.2	73.2±0.3
50% Dioxane sol. (50S)	5.2	1.2±0.1	1.9±0.1	38.6±0.3	0.0±0.0	0.8±0.1	5.8±0.1	48.3±0.3	44.6±0.2
DMSO sol. (DMS)	7.4	2.7±0.2	1.4±0.0	40.9±0.3	0.0±0.0	1.4±0.2	22.3±0.2	68.7±0.2	23.8±0.2
DMSO res. (DMR)	75.1	1.3±0.1	1.2±0.1	22.6±0.1	0.0±0.0	0.3±0.1	57.5±0.3	82.9±0.4	14.6±0.1

Table 2
Nitrobenzene oxidation products of lignin-polysaccharide complex fractions (% of lignin)

Sample	Alkaline nitrobenzene oxidation products	
	S/V (molar ratio)	Total yield
Extractive-free sample	1.76±0.02	27.1±0.1
90% Dioxane sol. (90S)	1.90±0.01	37.5±0.2
50% Dioxane sol. (505)	1.73±0.02	35.4±0.2
DMSO sol. (DMS)	1.49±0.01	29.4±0.1
DMSO res. (DMR)	1.77±0.02	28.0±0.2

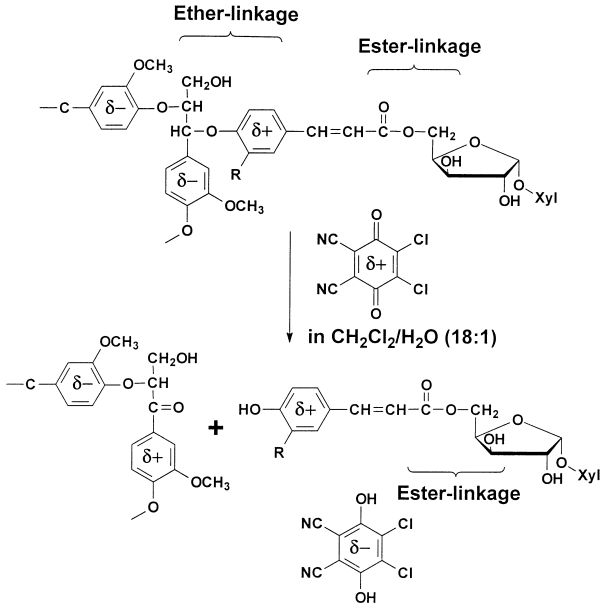

Fig. 1. Benzylic ether cleavage reaction with 2,3-dichloro-5,6-dicyano-l,4-benzoquinone.

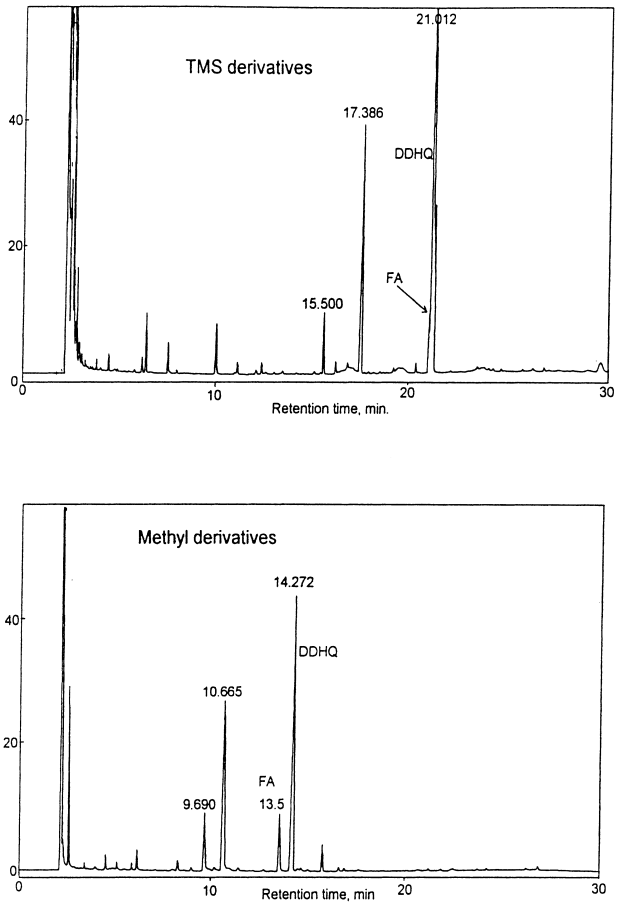

Fig. 2. Gas chromatograms of TMS derivatives and methyl derivatives of the products of alkaline hydrolysates.

using mild alkaline treatment. While the overall quantities of *p*-coumaric and ferulic acids liberated through mild and severe alkaline hydrolysis of each particular wall fraction (or its acetylated derivative) remained approximately constant, the amounts of both of the hydroxycinnamic acids released by mild alkaline hydrolysis alone increased substantially as a result of prior treatment with DDQ (Table 3). Thus, the results clearly showed that a significant portion of ether-linked hydroxycinnamic acids were cleaved by DDQ treatment. The data suggested that more than 80% of ether-linked hydroxycinnamic acids (both *p*-coumaric and ferulic acids) were linked to the benzyl position [Fig. 3(a)], and not to the β-position [Fig. 3(b)]. Therefore, the hypotheses of Ralph et al. (1992) and Ralph and Helm (1993), Terashima et al. (1993), Jacquet et al. (1995) and Morrison et al. (1998) that ferulate radicals produced by the action of peroxidase might be an anchor of lignification, should be reconsidered.

3. Experimental

3.1. Plant material and fractionation

Internodes of oat (*Avena saliva* L.) were harvested on 4 June, 1996 from the experimental field at the University of Tokyo, the Graduate School of Agricultural and Life Sciences, immediately frozen at −20°C, then freeze-dried. The dry internodes were ground in a Wiley mill and passed through a 420 μm sieve, then extracted successively with boiling Et_2O for 1 h (×3), boiling 80% (v/v) aqueous EtOH for 1 h (×3), and H_2O at 37°C overnight on a shaker. Solid material remaining following extraction was washed with $(CH_3)_2CO$ then dried in a vacuum oven at 40°C. The dried sample was finely ground for a further 96 h with water cooling (<25°C) using a stainless steel vibratory ball mill without solvent (Koshijima et al., 1972). The finely ground sample was extracted with 90% (v/v) aqueous dioxane at 37°C overnight on a shaker. The soluble sample was separated by filtration, and the residue was extracted again with 90% (v/v) aqueous dioxane. The extraction was performed in triplicate. The combined organic solution was

Table 3
Released hydroxycinnamic acids by alkaline hydrolysis before and after DDQ oxidation (% of sample)

Sample	Treatment	Alkaline hydrolysis			
		Ester linked		Ether linked	
		PCA[c]	FA[d]	PCA	FA
Oat cell wall	Untreated	0.40±0.01	0.35±0.00	0.17±0.01	0.90±0.03
	Untreated	1.26±0.02	0.73±0.01	0.63±0.01	0.91±0.02
90% Dioxane sol.	DDQ[a]	1.87±0.03	1.54±0.02	0.13±0.00	0.16±0.01
	Acetyl-DDQ[b]	1.75±0.02	1.06±0.03	0.20±0.01	0.51±0.02
	Untreated	0.92±0.01	0.82±0.01	0.52±0.02	0.89±0.03
50% Dioxane sol.	DDQ	1.44±0.02	1.62±0.02	0.08±0.01	0.12±0.00
	Acetyl-DDQ	1.26±0.01	1.18±0.01	0.23±0.00	0.52±0.02
	Untreated	0.63±0.02	0.81±0.03	0.32±0.01	1.21±0.03
DMSO[e] sol.	DDQ	1.07±0.01	2.00±0.03	0.06±0.00	0.10±0.01
	Acetyl-DDQ	0.86±0.02	1.44±0.01	0.86±0.02	1.44±0.01
	Untreated	0.45±0.02	0.31±0.02	0.31±0.02	1.31±0.02
DMSO residue	DDQ	0.68±0.01	0.95±0.02	0.11±0.01	0.30±0.00
	Acetyl-DDQ	0.38±0.01	0.78±0.01	0.16±0.00	0.76±0.02

[a] DQ: DDQ oxidation without acetylation.
[b] Acetyl-DDQ: DDQ oxidation of acetylated samples.
[c] PCA: *p*-coumaric acid.
[d] FA: ferulic acid.
[e] DMSO: dimethylsulfoxide.

concentrated in vacuo (45°C), then freeze-dried to give a 90% dioxane soluble fraction (90S).

The residue was further extracted with 50% (v/v) aqueous dioxane as described above, and the 50% aqueous dioxane soluble fraction (SOS) was recovered by freeze-drying. A dimethylsulfoxide (DMSO) soluble fraction was obtained by extraction of the residue of 50% aqueous dioxane extraction with DMSO at 37°C overnight with shaking. The extract was added dropwise into five volumes of MeOH with stirring, and the precipitate was collected by centrifugation (DMSO soluble fraction: DMS). The residue was washed several times with $(CH_3)_2CO$ and Et_2O, then dried in a vacuum oven at 40°C to give a DMSO insoluble fraction (DMR) (Fig. 4).

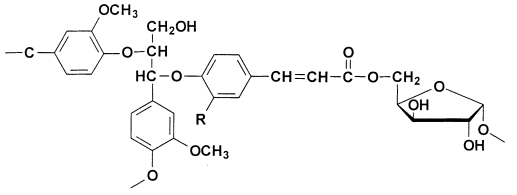

(a) α-ether linkage between lignin and hydroxycinnamates

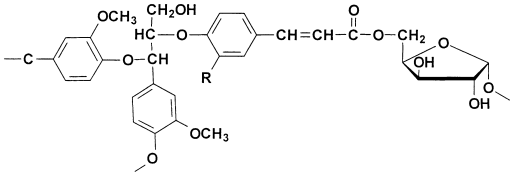

(b) β-ether linkage between lignin and hydroxycinnamates
R=H: *p*-coumarate, R=OCH_3: ferulate

Fig. 3. Possible linkages between lignin and hydroxycinnamic acids.

3.2. Chemical analysis

Hydroxycinnamic acids covalently bound to internode walls of oat and its fractions containing lignin-polysaccharide complex, were quantified as described by Lam et al. (1994a) using *m*-coumaric acid as an internal standard. Lignin content was determined using the acetyl bromide procedure (Iiyama and Wallis, 1990). Neutral sugar compositions of samples were determined by an alditol acetate procedure (Blakeney et al., 1983) which included some minor modifications. Digestion was carried out in 4% H_2SO_4 at 121°C for 60 min. Inositol was used as an internal standard, and a TC- 17 capillary column was used for gas chromatography (GC). The aromatic composition of lignin was analysed by alkaline nitrobenzene oxidation, and yields of products were corrected for products from *p*-coumaric and ferulic acids (Iiyama and Lam, 1990). All chemical analyses were carried out in duplicate.

3.3. Oxidation with 2,3-dichloro-5,6-dicyano-1, 4-benzoquinone (DDQ)

The samples (finely ground internode walls and fractions: 50 mg each) were suspended in CH_2Cl_2–H_2O (18:1, v/v, 25ml); DDQ (25 mg) was then added. The

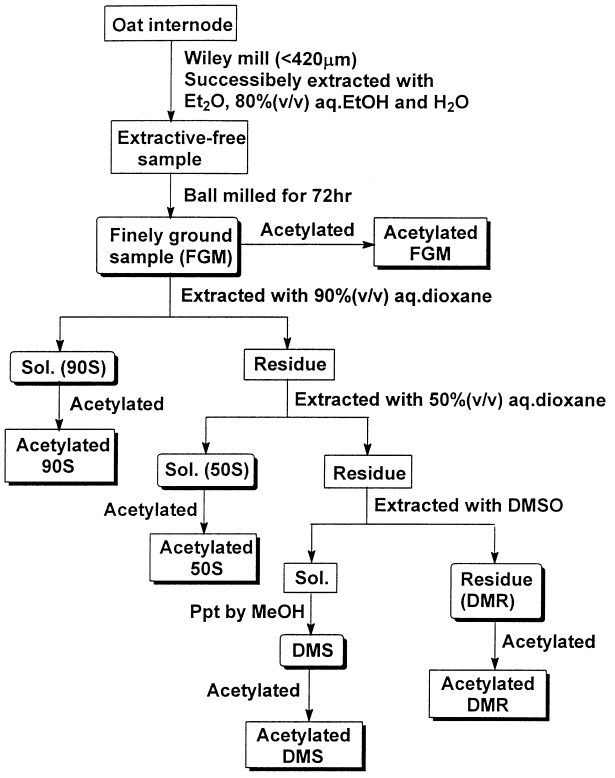

Fig. 4. Preparation of fractions containing lignins and polysaccharides.

suspension was stirred at room temperature for 24 h. Acetylated samples (50 mg) (except acetylated walls and DMSO-insoluble fraction) were dissolved in CH_2Cl_2–H_2O (18:1, v/v, 25 ml), then treated with DDQ for 2 h at room temperature with stirring. After DDQ oxidation, the solvent was removed by evaporation, and the reaction mixture was hydrolysed with 1 M NaOH (10 ml) at 37°C overnight on a shaker or with 4 M NaOH (5 ml) for 2 h at 170°C (Lam et al., 1994a). Products were extracted sequentially with CH_2Cl_2 (twice) and Et_2O, then dried (Na_2SO_4). The products were methylated with freshly prepared diazomethane, then analysed using GC under the same conditions with trimethylsilyl derivatives (Lam et al., 1994a).

Acknowledgements

This project was partially supported financially by a Grant-in-Aid from the Ministry of Education, Science, Sports and Culture (No. 10306011).

References

Blakeney, A.B., Harris, P.J., Henry, R.J., Stone, B.A., 1983. A simple and rapid preparation of alditol acetates for monosaccharide analysis. Carbohydrate Research 113, 291–299.

Hartley, R.D., Harris, P.J., 1981. Phenolic constituents of the cell walls of dicotyledons. Biochemical Systems and Ecology 9, 189–203.

Iiyama, K., Lam, T.B.T., 1990. Lignin in wheat internodes. Part 1. The reactivities of lignin units during alkaline nitrobenzene oxidation. Journal of the Science of Food and Agriculture 51, 481–491.

Iiyama, K., Wallis, A.F.A., 1990. Determination of lignin in herbaceous plants by an improved acetyl bromide procedure. Journal of the Science of Food and Agriculture 51, 145–161.

Iiyama, K., Lam, T.B.T., Stone, B.A., 1990. Phenolic acid bridges between polysaccharides and lignin in wheat internodes. Phytochemistry 29, 733–737.

Jacquet, G., Pollet, B., Lapierre, C., 1995. New ether-linked ferulic acid-coniferyl alcohol dimers identified in grass straw. Journal of Agriculture and Food Chemistry 43, 2746–2751.

Kim., Y.S., Iiyama, K., Kurahashi, A., Meshitsuka, G., 1995. Structural feature of lignin in cell walls of native and isogenic fast-grow aspen (*Populus maximowiczii* Henry): linkage types of wall-bound hydroxybenzoic and hydroxycinnamic acids in fast-grow aspen wood. Mokuzai Gakkaishi 41, 837–843.

Koshijima, T., Taniguchi, T., Tanaka, R., 1972. Lignin-carbohydrate complex. I. Influences of milling of wood upon the Björkman LCC. Holzforschung 26, 211–217.

Koshijima, T., Watanabe, T., Azuma, J., 1984. Existence of benzylated carbohydrate moiety in lignin-carbohydrate complex from pinewood. Chemistry Letters 1737–1740.

Lam, T.B.T., Iiyama, K., Stone, B.A., 1992. Cinnamic acid bridges between cell wall polymers in wheat and Phalaris internodes. Phytochemistry 32, 1179–1183.

Lam, T.B.T., Iiyama, K., Stone, B.A., 1994a. An approach to the estimation of ferulic acid bridges in unfractionated cell walls of wheat internodes. Phytochemistry 37, 327–333.

Lam, T.B.T., Iiyama, K., Stone, B.A., 1994b. Determination of etherified hydroxycinnamic acids in cell walls of grasses. Phytochemistry 36, 773–775.

Morrison., T.A., Jung, H.G., Buxton, D.R., Hatfield, R.D., 1998. Cell-wall composition of maize internodes of varying maturity. Crop Science 38, 455–460.

Oikawa, Y., Yoshioka, T., Yonemitsu, O., 1982. Specific removal of *p*-methoxybenzyl protection by DDQ oxidation. Tetrahedron Letters 23, 885–888.

Oikawa, Y., Nishi, T., Yonemitsu, O., 1983. Kinetic acetalization for 1,2- and 1,3-diol protection by the reaction of *p*-methoxyphenylmethyl methyl ether with DDQ. Tetrahedron Letters 24, 4037–4040.

Ralph, J., Helm, R.F., Quideau, S., Hatfield, R.D., 1992. Lignin-feruloyl ester cross-links in grasses. Part I. Incorporation of feruloyl esters into coniferyl alcohol dehydrogenation polymers. Journal of the Chemical Society Perkin Transaction 1, 2961–2969.

Ralph, J., Helm, R.F., 1992. Lignin/hydroxycinnamic acid-polysaccharide complexes: synthetic models for regiochemical characterization. In: Jung, H.G., Buxton, D.R., Hatfield, R.D., Ralph, J. (Eds.), Forage Cell Wall Structure and Digestibility. American Society of Agronomy, Crop Science Society of America, Soil Science Society of America, Madison, pp. 201–246.

Scalbert, A., Monties, B., Guittet, E., Lallemand, J.Y., 1986. Comparison of wheat straw lignin preparations. I. Chemical and spectroscopic characterizations. Holzforschung 40, 119–127.

Scalbert, A., Monties, B., Lallemand, J.Y., Guittet, E., Roland, C., 1985. Ether linkage between phenolic acids and lignin fractions from wheat straw. Phytochemistry 24, 1359–1362.

Sharma, V., Brillout, J.M., Scalbert, A., Monties, B, 1986. Studies on a brittle stem mutant of rice, *Oryza sativa* L.; characterization of lignin fractions, associated phenolic acids and polysaccharides from rice stem. Agronomie 6, 265–271.

Terashima, N., Fukushima, K., He, L.F., Takabe, K., 1993. Comprehensive model of the lignified plant cell wall. In: Jung, H.G.,

Buxton, D.R., Hatfield, R.D., Ralph, R.D. (Eds.), Forage Cell Wall Structure and Digestibility. American Society of Agronomy, Crop Science Society of America, Soil Science Society of America, Madison, pp. 247–270.

Watanabe, T., Kaizu, S.. Koshijima, T., 1986. Binding sites of carbohydrate moities toward lignin in "lignin-carbohydrate complex" from *Pinus densiflora* wood. Chemistry Letters, 1871–1874.

Watanabe, T., Ohnishi, J., Yamasaki, Y., Kaizu, S., Koshijima, T., 1989. Binding-site analysis of the ether linkages between lignin and hemicelluloses in lignin-carbohydrate complexes by DDQ-oxidation. Agricultural Biology and Chemistry 53, 2233–2252.

PERGAMON

Phytochemistry 57 (2001) 993–1003

PHYTOCHEMISTRY

www.elsevier.com/locate/phytochem

Elucidation of new structures in lignins of CAD- and COMT-deficient plants by NMR

John Ralph[a,b,*], Catherine Lapierre[c], Jane M. Marita[a,b], Hoon Kim[a,b], Fachuang Lu[a,b], Ronald D. Hatfield[a], Sally Ralph[d], Clint Chapple[e], Rochus Franke[e], Matt R. Hemm[e], Jan Van Doorsselaere[f], Ronald R. Sederoff[g], David M. O'Malley[g], Jay T. Scott[g], John J. MacKay[h], Nabila Yahiaoui[i], Alain-M. Boudet[i], Michel Pean[j], Gilles Pilate[k], Lise Jouanin[l], Wout Boerjan[f]

[a]*US Dairy Forage Research Center, USDA-Agricultural Research Service, 1925 Linden Drive West, Madison, WI 53706, USA*
[b]*Department of Forestry, University of Wisconsin, Madison, WI 53706, USA*
[c]*Laboratoire de Chimie Biologique, Institut National Agronomique, 78850 Thiverval-Grignon, France*
[d]*US Forest Products Laboratory, USDA-Forest Service, One Gifford Pinchot Drive, Madison, WI 53705, USA*
[e]*Department of Biochemistry, Purdue University, West Lafayette, IN 47907, USA*
[f]*Departement Plantengenetica, Vlaams Interuniversitair Instituut voor Biotechnologie, Ledeganckstraat 35, 9000 Gent, Belgium*
[g]*Department of Genetics, North Carolina State University, Raleigh, NC 27695, USA*
[h]*Institute of Paper Science and Technology, 500 10th Street N.W., Atlanta, GA, 30318, USA*
[i]*UMR 5546 Pôle de Biotechnologie Végétale, 24 Chemin de Borde Rouge, BP17 Auzeville, F31326 Castanet Tolosan, France*
[j]*Groupe de Recherches Appliquées en Phytotechnologie, Commissariat à l'Energie Atomique/Cadarache, DSV-DEVM, Saint-Paul-Lez-Durance Cedex, France*
[k]*Unité Amélioration, Génétique et Physiologie Forestières, Institut National Agronomique, Orleans, BP 20619 ARDON 45166 Olivet, France*
[l]*Biologie Cellulaire, Institut National Agronomique, 78026 Versailles Cedex, France*

Received 7 July 2000; received in revised form 16 November 2000

Abstract

Studying lignin-biosynthetic-pathway mutants and transgenics provides insights into plant responses to perturbations of the lignification system, and enhances our understanding of normal lignification. When enzymes late in the pathway are downregulated, significant changes in the composition and structure of lignin may result. NMR spectroscopy provides powerful diagnostic tools for elucidating structures in the difficult lignin polymer, hinting at the chemical and biochemical changes that have occurred. COMT (caffeic acid *O*-methyl transferase) downregulation in poplar results in the incorporation of 5-hydroxyconiferyl alcohol into lignins via typical radical coupling reactions, but post-coupling quinone methide internal trapping reactions produce novel benzodioxane units in the lignin. CAD (cinnamyl alcohol dehydrogenase) downregulation results in the incorporation of the hydroxycinnamyl aldehyde monolignol precursors intimately into the polymer. Sinapyl aldehyde cross-couples 8–O–4 with both guaiacyl and syringyl units in the growing polymer, whereas coniferyl aldehyde cross-couples 8–O–4 only with syringyl units, reflecting simple chemical cross-coupling propensities. The incorporation of hydroxycinnamyl aldehyde and 5-hydroxyconiferyl alcohol monomers indicates that these monolignol intermediates are secreted to the cell wall for lignification. The recognition that novel units can incorporate into lignins portends significantly expanded opportunities for engineering the composition and consequent properties of lignin for improved utilization of valuable plant resources. © 2001 Elsevier Science Ltd. All rights reserved.

Keywords: NMR; Transgenic; Mutant; *O*-Methyltransferase; Monolignol; Coniferyl aldehyde; Sinapyl aldehyde; 5-Hydroxyconiferyl alcohol

1. Introduction

NMR continues to become increasingly valuable as a tool for lignin structural elucidation. A number of powerful experiments stand out as being exceptionally useful. An extensively illustrated overview of solution-state NMR of lignins was recently published (Ralph et al., 1999c), so experimental details will not be given here. This paper will instead present recent NMR applications elucidating the structures of novel units in lignins from plants deficient in two monolignol biosynthetic pathway genes/enzymes.

* Corresponding author. Tel.: +1-608-264-5407; fax: +1-608-264-5275.
E-mail address: jralph@facstaff.wisc.edu (J. Ralph).

0031-9422/01/$ - see front matter © 2001 Elsevier Science Ltd. All rights reserved.
PII: S0031-9422(01)00109-1

Lignins are traditionally described as plant polymers resulting from dehydrogenative polymerization (via radical coupling reactions) of three primary phenylpropanoid monomers, *p*-coumaryl (4-hydroxy-cinnamyl), coniferyl (4-hydroxy-3-methoxy-cinnamyl), and sinapyl (3,5-dimethoxy-4-hydroxy-cinnamyl) alcohols, analogs varying in their degrees of methoxylation (Harkin, 1967; Freudenberg and Neish, 1968). They represent a class of complex polymeric natural products present in large quantities in the cell walls of terrestrial plants. The strict definition has, however, been long recognized as too narrow (Sarkanen and Ludwig, 1971). Other phenolic components, such as acylated hydroxycinnamyl alcohols and hydroxycinnamate esters may also intimately incorporate into lignins (Boudet, 1998; Sederoff et al., 1999; Ralph et al., 1999c). There has been considerable debate over what constitutes a "real" lignin (Lewis, 1999; Sederoff et al., 1999). We do not wish to revisit those issues here. We shall simply make the following observation. If a phenolic phenylpropanoid that is likely derived from the basic monolignol biosynthetic pathway couples (via radicals), as a monomer, with a growing oligomer/polymer of phenylpropanoids, and is further integrated into the polymer by endwise coupling with a new monolignol (or monomer), then we shall call this product lignin here. Ideally, histochemical studies should also be done to demonstrate that the polymer incorporating these units is in the cell wall.

Recent advances in genetic engineering have allowed researchers to perturb the monolignol biosynthetic pathway (Dixon and Ni, 1996; Baucher et al., 1998; Boudet, 1998; Whetten et al., 1998), allowing the abundance of normally minor components to be substantially enhanced and therefore structurally analyzed (Van Doorsselaere et al., 1995; Ralph et al., 1997, 1998, 1999b; Lapierre et al., 1999; Kim et al., 2000; Jouanin et al., 2000). This approach provides valuable insights into the control of lignification and into the remarkable biochemical flexibility of the lignification system.

The monolignol biosynthetic pathway in angiosperms has undergone considerable reevaluation recently. Fig. 1 derives from recent clarifications of the primary pathways, as deduced by Chiang's and Chapple's groups (Humphreys et al., 1999; Osakabe et al., 1999; Li et al., 2000). Studies to date indicate that downregulating any of the enzymes of the major pathways can affect the course and/or extent of lignification. General down-regulation of lignification (producing plants with reduced lignin levels) is possible. For example, NMR and other methods showed that the lignins from plants deficient in either a CoA ligase, Pt4CL1 (Hu et al., 1999) or an *O*-methyl transferase, CCoAOMT (Meyermans et al., 2000), were essentially normal in their composition and structure, despite having significantly lower than normal lignin levels. In both cases however, the levels of *p*-hydroxybenzoates on the lignins increased suggesting that the pathways to the monolignol esters might not be fully coupled to general monolignol synthesis (Li et al., 2000).

The most striking example of compositional flexibility in the normal monolignols came from the F5H (ferulate 5-hydroxylase) Arabidopsis mutants and transgenics produced by Chapple's group; F5H is sometimes now referred to as CAld5H to implicate coniferaldehyde as the preferred substrate for that enzyme (Humphreys et al., 1999; Osakabe et al., 1999). As shown by NMR (Marita et al., 1999) and other methods (Meyer et al., 1998), a chemical mutagenesis mutant of Arabidopsis had lignins devoid of syringyl units. More strikingly, when a suitably promoted *F5H* gene was introduced into the F5H-deficient mutant, up-regulation of sinapyl alcohol production was at such a high level that the lignin became extremely syringyl-rich. With an approximately 3% guaiacyl component, these plants' lignins have a far lower guaiacyl content than any plant reported to date (Marita et al., 1999). The up-regulation of F5H is therefore strikingly effective at diverting the monolignol pool toward sinapyl alcohol. In these examples massive compositional shifts in the traditional lignin components are apparent. As will be seen, compositional shifts can range considerably wider.

Here we present NMR data from recent studies on mutants and transgenics deficient in two of the later pathway enzymes, CAD (cinnamyl alcohol dehydrogenase) and COMT (caffeic acid *O*-methyl transferase, the favored substrate for which now appears to be 5-hydroxyconiferyl aldehyde (Li et al., 2000) although 5-hydroxyconiferyl alcohol must also be a viable substrate (Matsui et al., 1994; Chen et al., 1999; Humphreys et al., 1999; Maury et al., 1999). Downregulating these enzymes dramatically affects the composition of lignins and the structures contained in those lignins. We also reexamine the F5H-upregulated Arabidopsis transgenics where the methylation apparently can't keep pace with the increased hydroxylation rate.

2. CAD-deficient tobacco: aldehyde incorporation

CAD is the last enzyme on the pathway to the monolignols coniferyl and sinapyl alcohols **2**G and **2**S, from which lignins are normally derived, Figs. 1 and 2. When CAD is downregulated, the hydroxycinnamyl aldehyde precursors to the monolignols, coniferyl aldehyde **1**G and sinapyl aldehyde **1**S, build up and may be incorporated into the polymer by radical coupling (Halpin et al., 1994, 1998; Higuchi et al., 1994; Provan et al., 1997; Ralph et al., 1997, 1998; Stewart et al., 1997; Yahiaoui et al., 1998; Vailhe et al., 1998). Indeed, coniferyl aldehyde readily incorporated into synthetic lignins under biomimetic conditions (Higuchi et al., 1994). Recent studies have begun to elucidate the propensity for the mono-

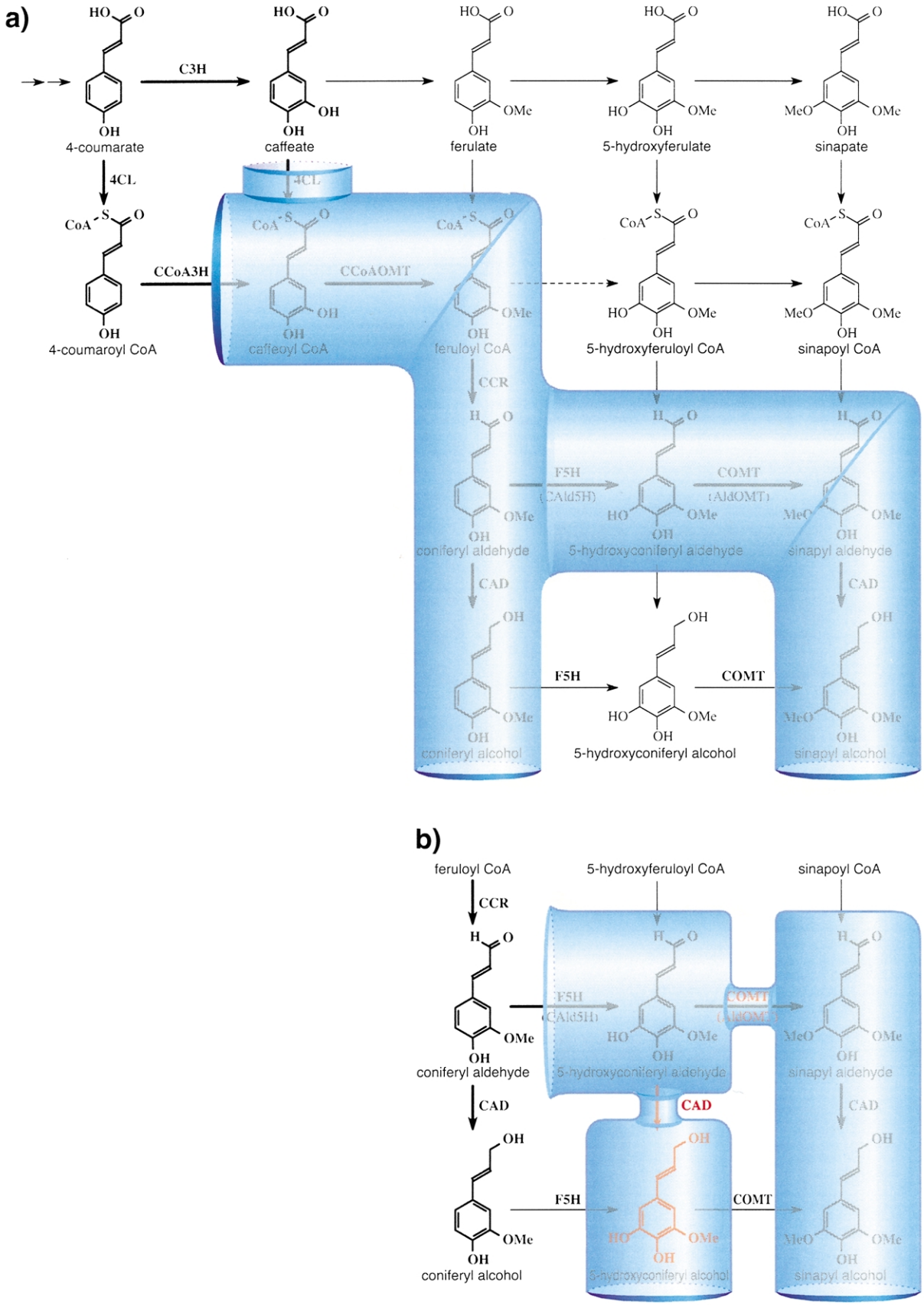

Fig. 1. (a) The monolignol biosynthetic pathway in angiosperms. Bolder structures and arrows (with large-diameter pipes) represent preferred pathways as recently clarified (Humphreys et al., 1999; Osakabe et al., 1999; Li et al., 2000). (b) When COMT activity is deficient, sinapyl alcohol production backs up the 5-hydroxyconiferyl aldehyde intermediate which can apparently be reduced by CAD; 5-hydroxyconiferyl alcohol then becomes a significant monomer in lignin biosynthesis.

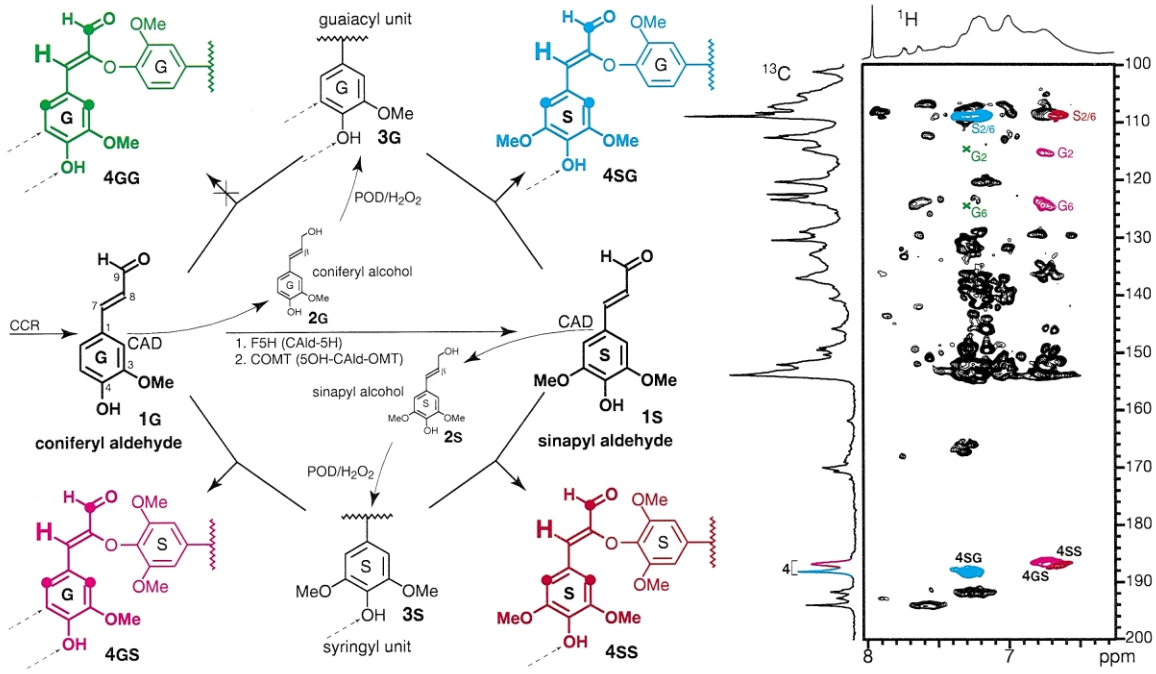

Fig. 2. Cross-coupling of hydroxycinnamyl aldehydes **1**G and **1**S with guaiacyl and syringyl lignin units **3**G and **3**S can potentially produce four 8–O–4-cross-coupled structures **4**. Only three of the four cross-products (**4**GS, **4**SG and **4**SS but not **4**GG) are significantly represented, as determined by analysis of the gradient-HMBC partial spectrum to the right. The HMBC section shows, in a lignin isolated from CAD-deficient tobacco stems, correlations from the aldehyde carbonyl carbons (185–195 ppm) to the H7 protons within three-bonds in structures **4** that have been further incorporated into lignin at positions indicated by the dashed arrows. These H7 protons diagnostically correlate with the 2- and 6-carbons of the cinnamyl aldehyde ring; the G2 and G6 carbons for guaiacyl units, and the higher-field equivalent S2/6 (syringyl) carbons are identified and colored correspondingly. Colored dots on the structures indicate the carbons correlated by $^{3}J_{C-H}$ to the H7-protons (which are shown in a larger font size) shown in the HMBC spectrum. The aldehydes at ~188.1 ppm, with their corresponding H7s at ~7.3 ppm result from hydroxycinnamyl aldehydes **1** 8–O–4-coupled to guaiacyl units **3**G in lignin; correlations from H7 indicate, however, that sinapyl aldehyde **1**S, but not coniferyl aldehyde **1**G, couples with guaiacyl units **3**G — the green X's show where correlations are present in a model for **4**GG. The aldehydes at ~186.7 ppm, with their corresponding H7s at ~6.7 ppm result from hydroxycinnamyl aldehydes **1** 8–O–4-coupled to syringyl units **3**S in lignin; correlations from H7 indicate that sinapyl aldehyde **1**S and coniferyl aldehyde **1**G each couple with syringyl units **3**S. S = syringyl, G = guaiacyl, CCR = cinnamoyl-CoA reductase, CAD = cinnamyl alcohol dehydrogenase, F5H = ferulate 5-hydroxylase which has recently also been termed CAld5H = coniferyl aldehyde 5-hydroxylase, to reflect the preferred in vivo substrate (Osakabe et al., 1999; Humphreys et al., 1999), COMT = caffeoyl *O*-methyl transferase (for which the preferred substrate appears to be 5-hydroxyconiferyl aldehyde, Li et al., 2000), POD = peroxidase. Convention for compound numbering: e.g. **4**GS = a guaiacyl aldehyde (coniferyl aldehyde **1**G) coupled 8–O–4 to a syringyl lignin unit (**3**S).

lignols to cross-couple with (free-phenolic) guaiacyl and syringyl units in lignins (Syrjanen and Brunow, 1998, 2000). With the availability of a ^{13}C-enriched lignin from a CAD-deficient tobacco transgenic (Ralph et al., 1998) and a series of model compounds (Kim et al., 2000), NMR methods can be used to ascertain hydroxycinnamyl aldehyde in vivo cross-coupling propensities. Data revealing such details of plant lignification are rarely obtained.

Radical cross-coupling of monolignols **2**, Fig. 2, with the growing lignin oligomer/polymer **3** is the major reaction occurring during lignification. Thus, the hydroxycinnamyl alcohol **2** (primarily at its β-position) couples with phenolic units **3** (at the 4–O- or 5-position for guaiacyl units **3**G, and almost exclusively at the 4–O-position for syringyl units **3**S) to form a chain-extended oligomer/polymer, also with the general formula **3**. Fig. 2 (right) shows a selected region of a long-range ^{13}C–^{1}H correlation (gradient-HMBC) spectrum from a CAD-deficient tobacco lignin, with peaks in the ^{13}C-projection and the resultant contours in the HMBC spectrum colored to match structures on the left for easy identification. In fact, the aldehyde structures in the lignins likely have been further incorporated into the polymer by primarily 4–O-coupling with the next monolignol, so they are not strictly the phenolic compounds **4** shown. Available coupling sites are indicated in Fig. 2 by the dashed arrows.

As the caption to Fig. 2 describes, correlation of the aldehyde carbonyl carbons in cross-products **4** to the H7-protons three-bonds away identifies the type of lignin units involved. Protons H7 resonate at ~7.3 ppm for hydroxycinnamyl aldehydes (either **1**G or **1**S) coupled 8–O–4 to guaiacyl units **3**G (compounds **4**GG and **4**SG, δ_C = 188.1 ppm), whereas they resonate considerably upfield, at ~6.7 ppm when coupled 8–O–4 to syringyl units **3**S (compounds **4**GS and **4**SS, δ_C = 186.8 ppm). Correlations from these H7 protons into the ring

identify the hydroxycinnamyl aldehyde involved in the coupling; three-bond correlations identify equivalent S2/6 carbons derived from sinapyl aldehyde **1**S units at higher field than the non-equivalent G2 and G6 carbons from units derived from coniferyl aldehyde **1**G. Therefore, for 8–O–4 cross-coupled units **4** in lignins, the G/S nature of both the hydroxycinnamyl aldehyde component (coupled 8-) and the lignin unit (coupled 4–O-) are diagnostically revealed. Other aromatic protons in the complex lignin polymer resonate in the H7 regions so correlations that are not of interest here will result; an absence of correlations is therefore more diagnostic, revealing the absence of a component.

Of the four possible aldehyde 8–O–4 incorporation products **4**, Fig. 2, only three can be detected in the antisense-CAD tobacco lignin by NMR methods. Product **4**GG is conspicuously absent. The data imply that sinapyl aldehyde **1**S cross-couples 8–O–4 with both guaiacyl and syringyl units (to form cross-coupled structures **4**SG and **4**SS), but that coniferyl aldehyde **1**G cross-couples 8–O–4 *only* with syringyl units **3**S and not with guaiacyl units **3**G. Thus, cross-coupling product **4**GS is readily detected, whereas **4**GG cannot be detected even when spectra are viewed at close to the baseplane noise level. This cross-coupling propensity is presumably the reason why 8–O–4-coupled structures are not found to be prominent in CAD-deficient softwood lignins (Ralph et al., 1997).

Attempting to prepare compounds modeling **4**GG by biomimetically cross-coupling coniferaldehyde **1**G (at the eight-position) with coniferyl alcohol **2**G or with a simple guaiacyl model 1-(4-hydroxy-3-methoxy)-ethanol (at the 4–O-position), also failed to produce 8–O–4-coupled cross-products. Apparently the same factors that promote cross-coupling in vitro apply in vivo, suggesting that these radical coupling reactions and those involved in "normal" lignification are likely to be under simple chemical control in the plant (Sederoff et al., 1999). In the cross-products, the chemical shifts match those in model compounds synthesized by traditional means (Kim et al., 2000). Also available from the HMBC spectrum in Fig. 2 is some information regarding the incorporation of the hydroxycinnamyl aldehydes **1** and their derived hydroxybenzyl aldehydes at ring 4–O-positions, as described elsewhere (Kim et al., 2000).

Examination of the spectra also provides significant information regarding the incorporation of hydroxycinnamyl aldehydes into "bulk" vs. "endwise" polymers (Sarkanen, 1971). "Bulk" lignins are characterized by frequent dimerization reactions, whereas endwise polymerization, the normal process occurring during lignification in the secondary cell wall, is from cross-coupling of monomers with the growing polymer. Dimerization of coniferaldehyde produces the 8–O–4-coupled dimer (analogous to **4**GG, Fig. 2), along with the other anticipated 8–8- and 8–5-coupled dimers (Connors et al., 1970). The absence of signals for coniferaldehyde coupled with G-units (of which the coniferaldehyde dimer **4**GG is an example), is evidence that coniferaldehyde does not dimerize at an appreciable level and therefore is not significantly involved in "bulk" lignification.

In summary, in 8–O–4-coupling reactions, coniferyl aldehyde cross-couples only with syringyl units, whereas sinapyl aldehyde cross-couples with both guaiacyl and syringyl units. These observations require no departure from the existing theory of radical coupling of phenols into polymeric lignins since they appear to reflect simple chemical coupling propensities.

3. CAD-deficient pine: incorporation of dihydroconiferyl alcohol and guaiacylpropane-1,3-diol

Preliminary observations (Ralph et al., 1997) on the novel lignins from a CAD-deficient pine (*Pinus taeda*) mutant are being strengthened as more diverse evidence accumulates (Dimmel et al., 1999; Ralph et al., 1999a; Lapierre et al., 2000). The plant, despite a reduction in CAD levels to $< 1\%$ of normal levels (MacKay et al., 1997), appeared to be producing normal levels of lignin (Klason lignin values were almost identical). A possible interpretation is that the CAD-deficiency is not sufficient to change the system and that there is still sufficient flux through the residual enzyme levels that normal lignification can proceed. The lignin in the CAD-deficient pine mutant however was highly colored and stained strongly with phloroglucinol, suggesting a higher aldehyde component. From NMR studies on isolated lignins, aldehydes and dihydroconiferyl alcohol were substantial components of that lignin (Ralph et al., 1997, 1999c).

New aldehyde components were misidentified originally (Ralph et al., 1997), but corrected in subsequent publications (Ralph et al., 1998, 1999b,c). A book chapter on NMR details how the incorrect assignment was made (Ralph et al., 1999c). The aldehyde components all stem from incorporation into the lignin of more significant quantities of coniferyl aldehyde (and its product vanillin) than in normal pine. The low aldehyde levels seen in normal lignins could possibly result from post-lignification oxidation, but the levels seen in this and other CAD-deficient plants suggest that incorporation of hydroxycinnamyl (and hydroxybenzyl) aldehydes into lignins is a normal process that becomes more significant when the pathway to the final monolignols is downregulated.

The CAD-deficient pine lignin had another feature that may or may not be attributable directly to the CAD-deficiency. Since this was a natural mutant other unknown enzymes may have also been impacted by the mutation(s); however, this is unlikely because the genetic determinant of the modified wood colocalized with the coding

sequence for the enzyme CAD (MacKay et al., 1997). Substantial levels of an unexpected unit derived from dihydroconiferyl alcohol (DHCA, **5**, Fig. 3) were identified in the mutant's lignin (Ralph et al., 1997, 1999c; Sederoff et al., 1999). DHCA is found at lower levels in normal plant lignins (Lundquist and Stern, 1989; Fukagawa et al., 1991; Brunow et al., 1998; Ralph et al., 1999c) but its derivation is not completely clear. Claims that the unit could only arise as a modified metabolic product *following* dimerization of traditional lignin monomers (Gang et al., 1998; Lewis et al., 1998) were incorrect; there is ample evidence that DHCA is formed as a monomer in the CAD-deficient pine and that the monomer is incorporated into the lignin via radical coupling processes (Ralph et al., 1997, 1999c; Sederoff et al., 1999; Lapierre et al., 2000). NMR showed that about half of the DHCA units in the soluble lignin fractions were involved in 5–5-coupled structures (Ralph et al., 1997, 1999c); coniferyl alcohol has never been shown to 5-5-dimerize. We were able to dissolve the (dioxane-water insoluble) residual lignin in acetyl or propionyl bromide. These reagents acylate and α-brominate the lignin, and cause some other structural changes, but in no way (other than acylation) affect the saturated aryl propanol sidechain. HMQC and COSY NMR experiments then unambiguously determined that DHCA was a component of that residual lignin although quantification was not possible (Ralph et al., 1999c).

More recently, guaiacylpropane-1,3-diols (GPDs) were also identified in lignins isolated from the CAD-deficient pine mutant, Fig. 3. This helped to unravel the nature of weak correlations often seen in pine lignin ^{13}C–^{1}H correlation NMR spectra; smaller amounts of GPDs are now recognized to be present in lignins from normal pines and presumably other softwoods. The structures in the complex lignin polymers are readily proven by NMR of isolated lignins.

Fig. 3a shows a subplot of the sidechain region from a 2D HMQC-TOCSY NMR experiment on an acetylated lignin isolated from the mutant pine, highlighting the new (acetylated) guaiacylpropane-1,3-diols **6** (red) along with the DHCA **5** units (green). Data from a model compound, 1,3-diacetoxy-1-(4–O-benzyl-3-methoxyphenyl)-propane (Ralph et al., 1999b), are at the center of the yellow circles and obviously match well.

As with other novel units found in lignins from transgenic or mutant plants, traces of the same components can be found in lignins from control plants. Fig. 3b shows the α-C/H region of an HSQC spectrum of the mutant's lignin, where the β-aryl ether units (blue) and the strong new GPD unit (red) appear most cleanly. Fig. 3c shows the same region in lignin from a

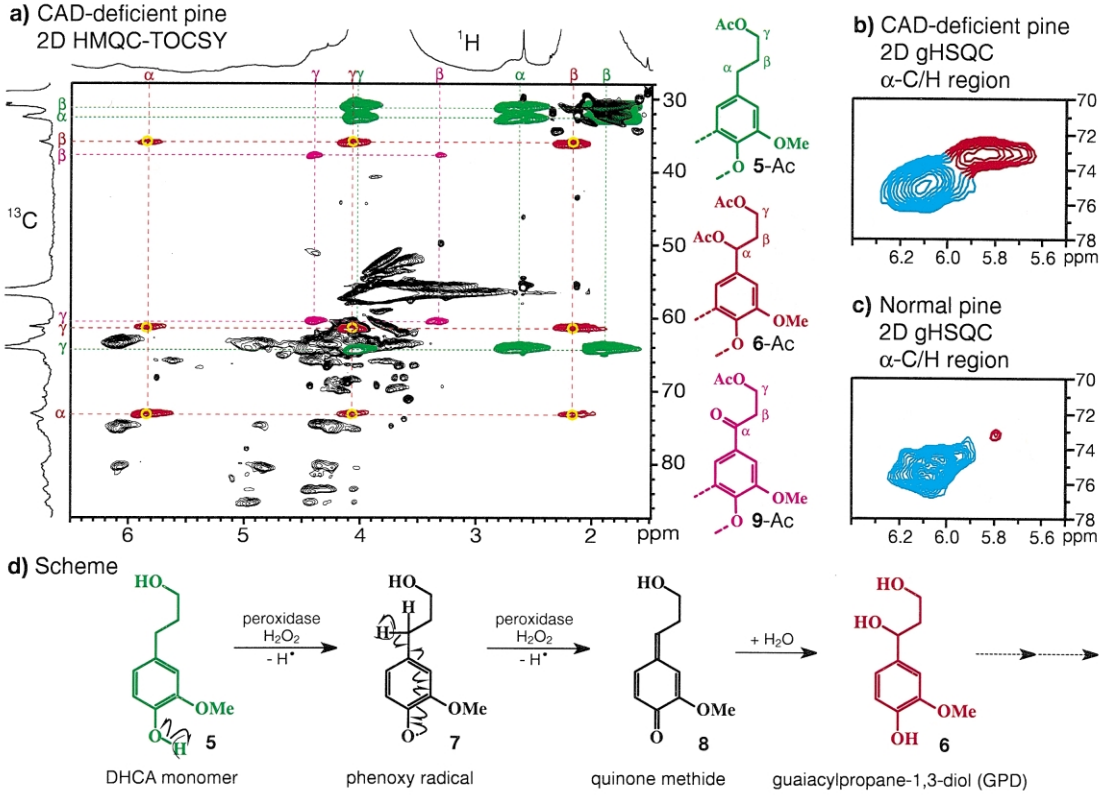

Fig. 3. NMR spectra showing new GPD **6** structures (red) and derived benzylic ketone analogs **9** (magenta), along with DHCA **5** units (green); data from acetylated model **6**–Ac are at the centers of the yellow circles; some β-aryl ether units are also shown (blue) in the HSQC spectra in b and c. The mechanism for producing GPD **6** from DHCA is shown in d.

normal pine control. Although the GPD peak is weak, it is diagnostic and, with other correlations evident (not shown), well authenticated.

GPD monomeric units derive from DHCA monomer **5** via the action of peroxidase and hydrogen peroxide, Fig. 3d. The mechanism, via a vinylogous quinone methide **8**, involves two H-radical abstractions. Abstraction from a benzylic CH_2 to produce quinone methides from phenoxy radicals has been noted previously (Zanarotti, 1982). When DHCA is subjected to peroxidase-H_2O_2, monomeric GPD **6** as well as the range of homo- and crossed-dimers involving DHCA and GPD are found (Peng and Ralph, unpublished).

Also evident in the HMQC-TOCSY spectrum, Fig. 3a, are (acetylated) ketones **9** (magenta contours). Products of benzylic alcohol oxidation are seen in various isolated lignins, notably from syringyl (3,5-dimethoxy-4-hydroxy-phenyl) units; they may arise during lignin isolation (particularly in the ball-milling step). Ketones **9** provide additional confirmatory evidence for the GPD structures **6** described earlier.

In summary, another previously unidentified unit present in small quantities in normal lignins is a major component of the hydroxyphenylpropanoid polymeric component of a pine mutant deficient in CAD. Those units, guaiacylpropane-1,3-diols, arise from conversion of dihydroconiferyl alcohol monomers by radical reactions and also incorporate into lignins as monomers. Like DHCA however, GPD **6**, which does not possess an unsaturated sidechain, is limited to coupling on the ring 4–O-, 5-, and possibly 1-positions, necessarily forming terminal units in lignin (except via 5–O–4-coupling). High MW polymers cannot be created without the incorporation of authentic hydroxycinnamyl alcohols (or other cinnamyl derivatives) as well. The CAD-deficient pine lignin is more soluble in alkali and has reduced molecular weight (Dimmel et al., 1999).

4. COMT-deficient poplar: benzodioxanes from incorporation of 5-hydroxyconiferyl alcohol

COMT is one of two enzymes required to 5-methoxylate guaiacyl monomeric units to produce sinapyl alcohol and eventually produce syringyl units in angiosperm lignins, Fig. 1. If COMT is downregulated, 5-hydroxyconiferyl aldehyde might build up and might be expected to be reduced to 5-hydroxyconiferyl alcohol if the next enzyme, CAD, is sufficiently non-specific. In fact, as illustrated in Fig. 1b, it appears that 5-hydroxyconiferyl alcohol is indeed formed, shipped out to the wall, and incorporated into lignin analogously to other lignin monomers (although it produces some novel structures in the final lignin).

NMR provides beautiful evidence that benzodioxane structures are produced in lignins which incorporate 5-hydroxyconiferyl alcohol. Fig. 4b shows the sidechain region of an HMQC spectrum from an (acetylated) isolated lignin from a COMT-deficient poplar (*Populus tremula* × *Populus alba*) described recently (Jouanin et al., 2000). The transgenic was actually the result of an attempt to up-regulate COMT by sense-methods that instead resulted in gene silencing. The degree of COMT suppression was higher than in other trials using antisense suppression (Van Doorsselaere et al., 1995; Lapierre et al., 1999). As with the dibenzodioxocins **D** (Karhunen et al., 1995a,b), the benzodioxanes **H** are readily apparent in short-range ^{13}C–^{1}H correlation spectra (HMQC or HSQC) of acetylated isolated lignins. Well separated contours at δ_C/δ_H of 76.8/4.98 (α), and 75.9/4.39 (β) are diagnostic for the benzodioxanes **H**; the γ-correlations overlap with those in other lignin units. Anticipated shifts occur following acetylation; in the unacetylated lignins (not shown), the correlations are centered at δ_C/δ_H of 76.5/4.87 (α), and 78.9/4.06 (β). As seen in Fig. 4b and d, the sidechain correlations are consistent with those in a model compound for the *trans*-benzodioxane **10**–Ac, synthesized by biomimetic cross-coupling reactions between coniferyl alcohol and a 5-hydroxyguaiacyl unit (Ralph et al., 2000). The α-proton shift deviated the most presumably since this is an acetylated (and therefore originally free-phenolic) model, rather than a phenol-etherified structure which would correspond to most of the units in the lignin polymer. Lignins from COMT antisense poplars also contain benzodioxane units (Ralph et al., 2000).

A reasonable quantification of this unit can be done by measuring volume integrals in the 2D spectra (Zhang et al., 2000), particularly if the similar Cα–Hα correlations are used. The ratios in the transgenic (and in the wild-type control in parentheses) are 53% (88%) aliphatic-sidechain β–O–4-units **A**, 13% (3%) phenylcoumarans **B**, 5% (7%) resinols **C**, 6% (0%) dibenzodioxocins **D**, 5% (2%) coniferyl alcohol endgroups **X**, and 18% (0%) of the new benzodioxane units **H**. The 5-hydroxyconiferyl alcohol-derived benzodioxane **H** units are therefore the second most abundant interunit type in this sample. Since the lignins analyzed by NMR represent 65% of the total lignin in this transgenic, it is logical that the benzodioxane structures would remain a significant component even if the lignins were drastically partitioned by the isolation process. The total β-ether frequency (normal β-ether **A** plus dibenzodioxocins **D** plus benzodioxanes **H**) in the transgenic is around 77%, lower than in the control because of the higher guaiacyl content. However, there are a few units not covered by these percentages since they have no resonances in the aliphatic sidechain region of the NMR spectra (cinnamaldehyde endgroups, β–1-structures). Although the data are limited at present, it appears that 5-hydroxyconiferyl alcohol may quantitatively make up for the sinapyl alcohol deficiency.

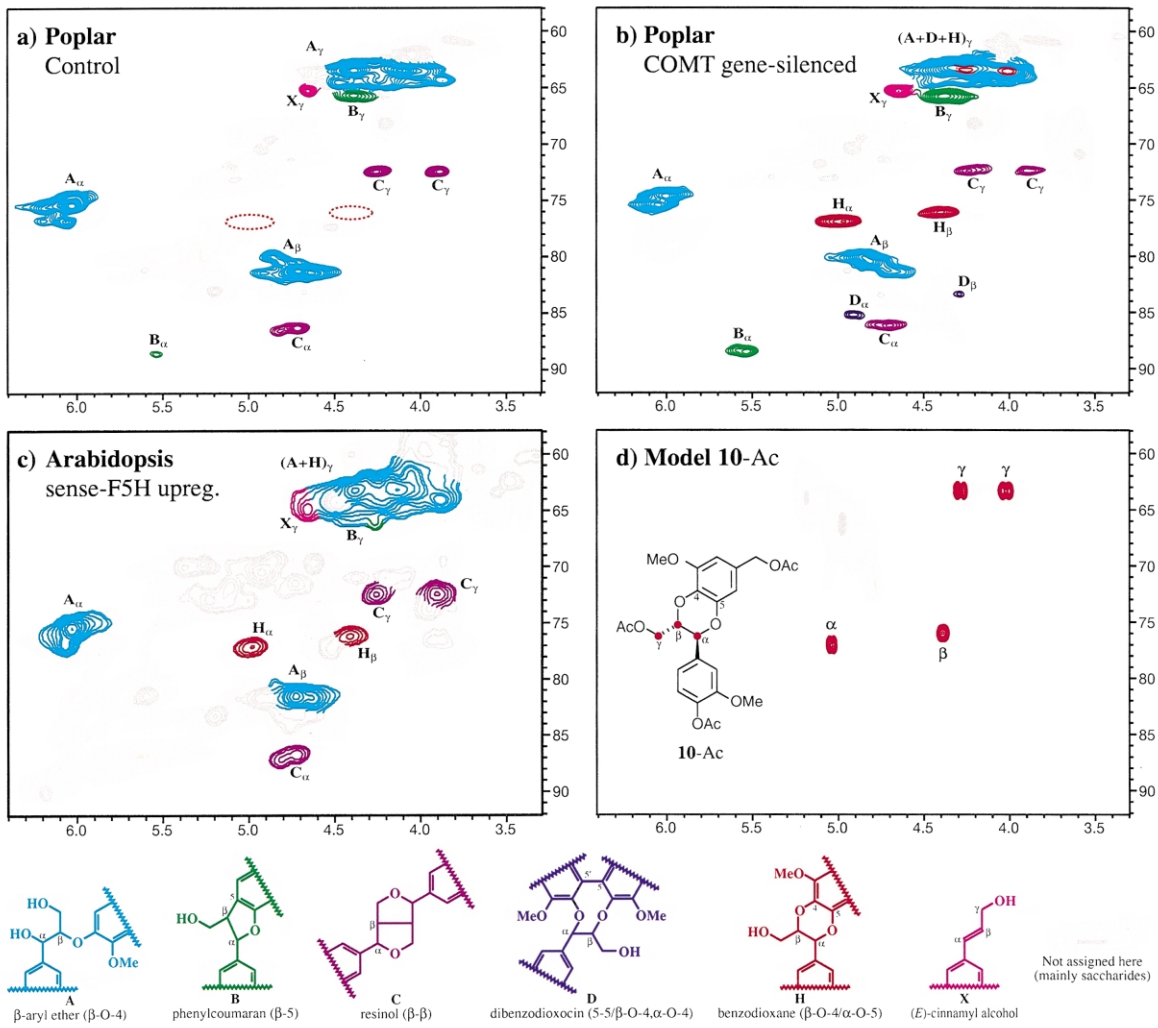

Fig. 4. Partial spectra from gradient HMQC NMR experiments highlighting new peaks for benzodioxane units **H**. Lignins were from (a) a control poplar, (b) a COMT-downregulated transgenic, (c) an F5H-upregulated Arabidopsis, and (d) similar correlations from a benzodioxane model **10**–Ac. The major unit coding is the same as that used in Ralph et al., 1999c and other references; it is suggested that **H** be reserved for 5-hydroxyguaiacyl benzodioxane units in lignin NMR spectra.

The incorporation of 5-hydroxyconiferyl alcohol into lignins has been documented several times (Hwang and Sakakibara, 1981; Lapierre et al., 1988; Jacquet, 1997; Suzuki et al., 1997). Benzodioxanes have been proposed to be in lignins previously (Hwang and Sakakibara, 1981; Jacquet, 1997; Jouanin et al., 2000), and analogous structures occur in lignans (Ishikawa et al., 1995; Su et al., 1997), but until now the occurrence of benzodioxanes in lignins has not been observed directly. The likely mechanism for formation of the novel benzodioxane units is shown in Fig. 5, as described in the caption.

There is another sample in which benzodioxanes are evident, an interesting variant in the COMT-deficiency class. Arabidopsis transgenics with upregulated F5H have previously been shown to have only a minor guaiacyl component (Meyer et al., 1998; Marita et al., 1999). Contours previously unidentified in the 2D NMR spectra of their lignins (Marita et al., 1999) now obviously result from benzodioxane structures, Fig. 4c. The observations here imply that, whereas syringyl production was enormously up-regulated in these transgenics, the methylation could apparently not keep pace with the accelerated production of 5-hydroxy units (e.g. 5-hydroxyconiferyl aldehyde and 5-hydroxyconiferyl alcohol). The result is a significant incorporation of 5-hydroxyconiferyl alcohol into the monolignol pool for the most heavily F5H-upregulated transgenics, ~10% as measured from contour volumes in the HMQC spectrum in Fig. 4c.

As further evidence accumulates from degradative and NMR methods that coniferyl and sinapyl alcohols couple with the new terminus created by incorporation of 5-hydroxyconiferyl alcohol monomers into the growing polymer (e.g. Jouanin et al., 2000), it becomes clear that 5-hydroxyconiferyl alcohol can be used as a

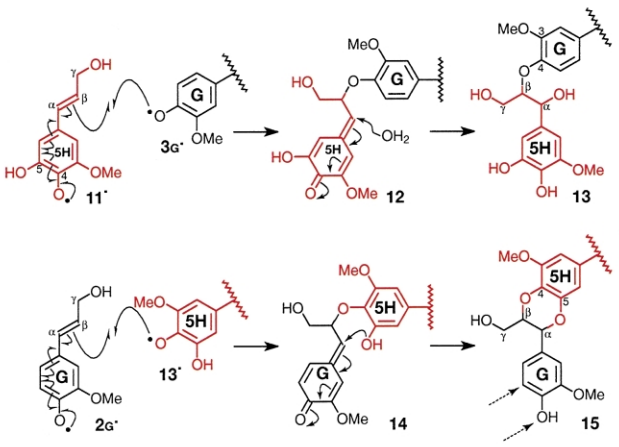

Fig. 5. Production of benzodioxanes **15** in lignins via incorporation of 5-hydroxyconiferyl alcohol **11** into a guaiacyl lignin. Only the pathways producing β-ether units are shown, but β–5-(phenylcoumaran) units are also possible. Cross-coupling with syringyl units is also possible but must be less pronounced in lignins which have a low syringyl content due to strong COMT downregulation. Cross-coupling of 5-hydroxyconiferyl alcohol **11**, via its radical **11·**, with a guaiacyl lignin unit **3**G, via its radical **3**G**·**, produces a quinone methide intermediate **12** which re-aromatizes by water addition to give the β-ether structure **13** (possessing a 5-hydroxyguaiacyl end-unit). This unit is capable of further incorporation into the lignin polymer via radical coupling reactions of radical **13·**. Reaction with the monolignol coniferyl alcohol **2**G, via its radical **2**G**·**, produces a quinone methide intermediate **14**. This time, however, quinone methide **14** can be internally trapped by the 5-OH phenol, forming a new 5–O–α-bond, and creating the benzodioxane ring system in **15**. The presence of structures **15** in COMT-deficient transgenic plants is diagnostically revealed by NMR, units **H** in Fig. 4.

lignin monomer by plants to offset the deficiency in sinapyl alcohol monomers. The recent statement that "There is, however, no known precedent for the free interchange of monomeric units in any biopolymer assembly, then or now, and no biochemical evidence..." (Lewis, 1999) needs to be revisited. In fact, plants and other organisms have long used loosely ordered chemistry to enhance their viability and resistance, as eloquently stated in a letter to Science (Denton, 1998).

5. Conclusions

Recent studies have shown that manipulating specific lignin-biosynthetic-pathway genes produces profound alterations in plant lignins. Although the lignins in mutant and transgenic plants may appear to be strikingly different from normal lignins, they often represent merely broad compositional shifts; most of the novel units that have been found to date appear to be (often previously unidentified) minor units in lignins from 'normal' plants. A salient observation is that the process of lignification appears to be flexible enough to readily incorporate phenolic phenylpropanoids other than the traditional monolignols. The incorporation of hydroxycinnamyl aldehyde monomers as well as 5-hydroxyconiferyl alcohol also implies that the plant is sending these products of incomplete monolignol biosynthesis out to the cell wall for incorporation. The resultant modified lignins apparently have properties sufficient to accommodate the water transport and mechanical strengthening roles of lignin and to allow the plant to be viable. Whether such plants will be able to confront the rigors of a natural environment replete with a variety of pathogens remains to be determined. However, the plants' flexible approach toward lignification, i.e. polymerizing monolignol precursors and derivatives along with the traditional monolignols, is a testament to their flexible strategy; in a single generation, these plants have circumvented genetic obstacles to remain viable. The recognition that novel units can incorporate into lignin provides significantly expanded opportunities for engineering the composition and consequent properties of lignin for improved utilization of valuable plant resources.

6. Experimental

6.1. Plant materials and lignin isolation

Isolation of the lignins for which NMR spectra are reported here were all previously described. All isolations follow the basic scheme: solvent extraction to remove major extractives and protein, ball milling, crude cellulases digestion to remove the bulk of the polysaccharides, dioxane–water (96:4) extraction to remove soluble lignin fractions, and some clean up of this lignin fraction by EDTA washing to remove some saccharide impurities and metal contaminants which can otherwise reduce the quality of the NMR data. All of the isolated lignins described here were acetylated and dissolved in acetone-d_6 (~60–100 mg in 0.4 ml) for NMR. In some cases, the proportion of the lignin that could be extracted and solubilized for NMR studies was as low as 17%; in poplar samples it is more typically 65%. Criticisms that these lignins are therefore not representative, or are contaminated by non-lignin extractives are slowly being dispelled as the results of more diverse studies, primarily using degradative methods, emerge. It is nevertheless important that this potential sample limitation be known, so the yields are reproduced here. Our comments on what constitutes a lignin for this study are delineated in the second paragraph of Section 1.

The sense-F5H-upregulated (C4H-promoted) Arabidopsis lignin (Fig. 4c) was obtained in 27.5% yield (Marita et al., 1999). The CAD-deficient (antisense downregulated) tobacco lignin (Fig. 2) was isolated in 24% yield (Ralph et al., 1998). Lignin from the CAD-deficient loblolly pine mutant (Fig. 3) was isolated in 17% yield (Ralph et al., 1997). Poplar lignins in Fig. 4a, b were isolated in 65% yields (Ralph et al., 2000).

6.2. NMR experiments

NMR spectra were acquired on a Bruker DRX-360 instrument fitted with a 5-mm ^{1}H/broadband gradient probe with inverse geometry (proton coils closest to the sample). The central acetone solvent peak was used as internal reference (δ_C 29.80, δ_H 2.04). We used the standard Bruker implementation (inv4gstp) of the gradient-selected inverse (^{1}H-detected) HMQC experiment for the spectra in Fig. 4, the standard (inv4gslplrnd) gradient-selected inverse-detected HMBC experiment with a 100 ms long-range coupling delay for the spectrum in Fig. 2, and a (non-gradient) HMQC-TOCSY (invbmltp) with a 100 ms mixing time for the spectrum in Fig. 3a. These experiments and their applications to lignins are detailed in a recent book chapter on "Solution-state NMR of Lignins" (Ralph et al., 1999c).

Acknowledgements

Partial funding for the Dairy Forage Research Center authors was from USDA-NRI (Plant Growth and Development No. 96-35304-3864; Improved Utilization of Wood and Wood Fiber No. 97-02208 and No. 99-02351) and the Division of Energy Biosciences, US Department of Energy 2000 awards (No. DE-AI02-00ER15067); for NCSU was by NIH (GM45344-07), DOE (DE-FG05-92ER20085), and the NCSU Forest Biotechnology Industrial Research Consortium; for French and Belgium collaborators, from the European Commission FAIR (OPLIGE, AGRE-0021-C), and "Tree improvement based on lignin engineering" (TIMBER-CT95-0424) projects; for the Purdue lab from the Division of Energy Biosciences, US Department of Energy (No. DE-FG02-94ER20138).

References

Baucher, M., Monties, B., Van Montagu, M., Boerjan, W., 1998. Biosynthesis and genetic engineering of lignin. Crit. Rev. Plant Sci. 17 (2), 125–197.

Boudet, A.-M., 1998. A new view of lignification. Trends in Plant Science 3 (2), 67–71.

Brunow, G., Ämmålahti, E., Niemi, T., Sipilä, J., Simola, L.K., Kilpeläinen, I., 1998. Labelling of a lignin from suspension cultures of *Picea abies*. Phytochemistry 47 (8), 1495–1500.

Chen, F., Yasuda, S., Fukushima, K., 1999. Evidence for a novel biosynthetic pathway that regulates the ratio of syringyl to guaiacyl residues in lignin in the differentiating xylem of *Magnolia kobus*. Planta 207 (4), 597–603.

Connors, W.J., Chen, C.-L., Pew, J.C., 1970. Enzymic dehydrogenation of the lignin model coniferaldehyde. J. Org. Chem. 35 (6), 1920–1924.

Denton, F.R., 1998. Beetle Juice. Science 281, 1285.

Dimmel, D.R., MacKay, J.J., Althen, E., Parks, C., Boon, J.J., 1999. Pulping, bleaching, and characterization of CAD-deficient wood. In: Tenth International Symposium on Wood and Pulping Chemistry, Yokohama, Japan, pp. 524–527.

Dixon, R.A., Ni, W., 1996. Genetic manipulation of the phenylpropanoid pathway in transgenic tobacco: new fundamental insights and prospects for crop improvement. Biotech. Biotechnol. Equipment 10 (4), 45–51.

Freudenberg, K., Neish, A.C., 1968. Constitution and Biosynthesis of Lignin. Springer-Verlag, Berlin.

Fukagawa, N., Meshitsuka, G., Ishizu, A., 1991. A two dimensional NMR study of birch milled wood lignin. J. Wood Chem. Technol. 11 (3), 373–396.

Gang, D.R., Fujita, M., Davin, L.D., Lewis, N.G.. In: Lewis, N.G., Sarkanen, S. (Eds.), Lignin and Lignan Biosynthesis. Am. Chem. Soc., Washington, DC, pp. 389–421.

Halpin, C., Knight, M.E., Foxon, G.A., Campbell, M.M., Boudet, A.-M., Boon, J.J., Chabbert, B., Tollier, M.-T., Schuch, W., 1994. Manipulation of lignin quality by downregulation of cinnamyl alcohol dehydrogenase. Plant J. 6 (3), 339–350.

Halpin, C., Holt, K., Chojecki, J., Oliver, D., Chabbert, B., Monties, B., Edwards, K., Barakate, A., Foxon, G.A., 1998. Brown-midrib maize (*bm1*) — a mutation affecting the cinnamyl alcohol dehydrogenase gene. Plant J. 14 (5), 545–553.

Harkin, J.M., 1967. In: Taylor, W.I., Battersby, A.R. (Eds.), Oxidative Coupling of Phenols. Marcel Dekker, New York, pp. 243–321.

Higuchi, T., Ito, T., Umezawa, T., Hibino, T., Shibata, D., 1994. Red-brown color of lignified tissues of transgenic plants with antisense CAD gene: wine-red lignin from coniferyl aldehyde. J. Biotechnol. 37 (2), 151–158.

Hu, W.-J., Lung, J., Harding, S.A., Popko, J.L., Ralph, J., Stokke, D.D., Tsai, C.-J., Chiang, V.L., 1999. Repression of lignin biosynthesis in transgenic trees promotes cellulose accumulation and growth. Nature Biotechnol. 17 (8), 808–812.

Humphreys, J.M., Hemm, M.R., Chapple, C., 1999. Ferulate 5-hydroxylase from Arabidopsis is a multifunctional cytochrome P450-dependent monooxygenase catalyzing parallel hydroxylations in phenylpropanoid metabolism. Proc. Natl. Acad. Sci. USA 96 (18), 10045–10050.

Hwang, B.H., Sakakibara, A., 1981. Hydrogenolysis of protolignin. XVIII. Isolation of a new dimeric compound with a heterocycle involving α-,β-diether. Holzforschung 35 (6), 297–300.

Ishikawa, T., Seki, M., Nishigaya, K., Miura, Y., Seki, H., Chen, I.-S., Ishii, H., 1995. Studies on the chemical constituents of *Xanthoxylum nitidum* (Roxb.) D. C. (*Fagara nitida* Roxb.). III. The chemical constituents of the wood. Chem. Pharm. Bull. 43 (11), 2014–2018.

Jacquet, G., 1997. Structure et réactivité des lignines de graminées et des acides phénoliques associés: développement des méthodologies d'investigation. PhD thesis, Laboratoire de Chemie Biologique, Institut National Agronomique, Paris-Grignon.

Jouanin, L., Goujon, T., de Nadaï, V., Martin, M.-T., Mila, I., Vallet, C., Pollet, B., Yoshinaga, A., Chabbert, B., Petit-Conil, M., Lapierre, C., 2000. Lignification in transgenic poplars with extremely reduced caffeic acid *O*-methyltransferase activity. Plant Physiol. 123 (4), 1363–1373.

Karhunen, P., Rummakko, P., Sipilä, J., Brunow, G., Kilpeläinen, I., 1995a. Dibenzodioxocins: a novel type of linkage in softwood lignins. Tetrahedron Lett. 36 (1), 169–170.

Karhunen, P., Rummakko, P., Sipilä, J., Brunow, G., Kilpeläinen, I., 1995b. The formation of dibenzodioxocin structures by oxidative coupling. A model reaction for lignin biosynthesis. Tetrahedron Lett. 36 (25), 4501–4504.

Kim, H., Ralph, J., Yahiaoui, N., Pean, M., Boudet, A.-M., 2000. Cross-coupling of hydroxycinnamyl aldehydes into lignins. Org. Lett. 2 (15), 2197–2200.

Lapierre, C., Tollier, M.T., Monties, B., 1988. A new type of constitutive unit in lignins from the corn *bm3* mutant. C. R. Acad. Sci., Ser. 3 307 (13), 723–728.

Lapierre, C., Pollet, B., Petit-Conil, M., Toval, G., Romero, J., Pilate, G., Leple, J.C., Boerjan, W., Ferret, V., De Nadai, V., Jouanin, L., 1999. Structural alterations of lignins in transgenic poplars with

depressed cinnamyl alcohol dehydrogenase or caffeic acid *O*-methyltransferase activity have an opposite impact on the efficiency of industrial kraft pulping. Plant Physiol. 119 (1), 153–163.

Lapierre, C., Pollet, B., MacKay, J.J., Sederoff, R.R., 2000. Lignin structure in a mutant pine deficient in cinnamyl alcohol dehydrogenase. Journal of Agricultural and Food Chemistry 48 (6), 2326–2331.

Lewis, N.G., 1999. A 20th century roller coaster ride: a short account of lignification. Curr. Opin. Plant Biol. 2 (2), 153–162.

Lewis, N.G., Davin, L.B., Sarkanen, S., 1998. In: Lewis, N.G., Sarkanen, S. (Eds.), Lignin and Lignan Biosynthesis. Am. Chem. Soc., Washington, DC, pp. 1–27.

Li, L., Popko, J.L., Umezawa, T., Chiang, V.L., 2000. 5-Hydroxyconiferyl aldehyde modulates enzymatic methylation for syringyl monolignol formation, a new view of monolignol biosynthesis in angiosperms. J. Biol. Chem. 275 (9), 6537–6545.

Lundquist, K., Stern, K., 1989. Analyisis of lignins by ^{1}H NMR spectroscopy. Nordic Pulp and Paper Res. J.1989, 210–213.

MacKay, J.J., O'Malley, D.M., Presnell, T., Booker, F.L., Campbell, M.M., Whetten, R.W., Sederoff, R.R., 1997. Inheritance, gene expression, and lignin characterization in a mutant pine deficient in cinnamyl alcohol dehydrogenase. Proc. Natl. Acad. Sci. USA 94 (15), 8255–8260.

Marita, J., Ralph, J., Hatfield, R.D., Chapple, C., 1999. NMR characterization of lignins in *Arabidopsis* altered in the activity of ferulate-5-hydroxylase. Proc. Natl. Acad. Sci. USA 96 (22), 12328–12332.

Matsui, N., Fukushima, K., Yasuda, S., Terashima, N., 1994. On the behaviour of monolignol glucosides in lignin biosynthesis. II. Synthesis of monolignol glucosides labeled with 3H at the hydroxymethyl group of side chain and incorporation of the label into magnolia and ginko lignin. Holzforschung 48, 375–380.

Maury, S., Geoffroy, P., Legrand, M., 1999. Tobacco *O*-methyltransferases involved in phenylpropanoid metabolism. The different caffeoyl-coenzyme A/5-hydroxyferuloyl-coenzyme A 3/5-*O*-methyltransferase and caffeic acid/5-hydroxyferulic acid 3/5-*O*-methyltransferase classes have distinct substrate specificities and expression patterns. Plant Physiol. 121 (1), 215–223.

Meyer, K., Shirley, A.M., Cusumano, J.C., Bell-Lelong, D.A., Chapple, C., 1998. Lignin monomer composition is determined by the expression of a cytochrome P450-dependent monooxygenase in *Arabidopsis*. Proc. Natl. Acad. Sci. USA 95 (12), 6619–6623.

Meyermans, H., Morreel, K., Lapierre, C., De Bruyn, A., De Vreese, B., Van Montagu, M., Messens, E., Marita, J.M., Ralph, J., Boerjan, W., 2000. Changes in lignin and *in vivo* accumulation of phenolic glucosides in poplar xylem upon downregulation of CCoAOMT, an enzyme involved in lignin biosynthesis. J. Biol. Chem., in press.

Osakabe, K., Tsao, C.C., Li, L., Popko, J.L., Umezawa, T., Carraway, D.T., Smeltzer, R.H., Joshi, C.P., Chiang, V.L., 1999. Coniferyl aldehyde 5-hydroxylation and methylation direct syringyl lignin biosynthesis in angiosperms. Proc. Natl. Acad. Sci. USA 96, 8955–8960.

Provan, G.J., Scobbie, L., Chesson, A., 1997. Characterisation of lignin from CAD and OMT deficient *bm* mutants of maize. J. Sci. Food Ag. 73 (2), 133–142.

Ralph, J., MacKay, J.J., Hatfield, R.D., O'Malley, D.M., Whetten, R.W., Sederoff, R.R., 1997. Abnormal lignin in a loblolly pine mutant. Science 277, 235–239.

Ralph, J., Hatfield, R.D., Piquemal, J., Yahiaoui, N., Pean, M., Lapierre, C., Boudet, A.-M., 1998. NMR characterization of altered lignins extracted from tobacco plants down-regulated for lignification enzymes cinnamyl-alcohol dehydrogenase and cinnamoyl-CoA reductase. Proc. Natl. Acad. Sci. 95 (22), 12803–12808.

Ralph, J., Hatfield, R.D., Marita, J.M., Lu, F., Peng, J., Kim, H., Grabber, J.H., MacKay, J.J., O'Malley, D.M., Sederoff, R.D., Chapple, C., Chiang, V., Boudet, A.M., 1999a. Lignin structure in lignin-biosynthetic-pathway mutants and transgenics: new opportunities for engineering lignin? In: Tenth International Symposium on Wood and Pulping Chemistry, Yokohama, Japan, pp. 138–145.

Ralph, J., Kim, H., Peng, J., Lu, F., 1999b. Arylpropane-1,3-diols in lignins from normal and CAD-deficient pines. Org. Lett. 1 (2), 323–326.

Ralph, J., Marita, J.M., Ralph, S.A., Hatfield, R.D., Lu, F., Ede, R.M., Peng, J., Quideau, S., Helm, R.F., Grabber, J.H., Kim, H., Jimenez-Monteon, G., Zhang, Y., Jung, H.-J.G., Landucci, L.L., MacKay, J.J., Sederoff, R.R., Chapple, C., Boudet, A.M., 1999c, In: Argyropoulos, D.S., Rials, T. (Eds.), Progress in Lignocellulosics Characterization. TAPPI Press, Atlanta, GA, pp. 55–108.

Ralph, J., Lapierre, C., Lu, F., Marita, J.M., Pilate, G., Van Doorsselaere, J., Boerjan, W., Jouanin, L., 2000. NMR evidence for benzodioxane structures resulting from incorporation of 5-hydroxyconiferyl alcohol into lignins of *O*-methyl-transferase-deficient poplars. J. Agric. Food Chem., in press.

Sarkanen, K.V., 1971. In: Sarkanen, K.V., Ludwig, C.H. (Eds.), Lignins, Occurence, Formation, Structure and Reactions. Wiley-Internaterscience, New York, pp. 95–163.

Sarkanen, K.V., Ludwig, C.H., 1971. In: Sarkanen, K.V., Ludwig, C.H. (Eds.), Lignins, Occurence, Formation, Structure and Reactions. Wiley-Interscience, New York, pp. 1–18.

Sederoff, R.R., MacKay, J.J., Ralph, J., Hatfield, R.D., 1999. Unexpected variation in lignin. Curr. Opin. Plant Biol. 2 (2), 145–152.

Stewart, D., Yahiaoui, N., McDougall, G.J., Myton, K., Marque, C., Boudet, A.M., Haigh, J., 1997. Fourier-transform infrared and Raman spectroscopic evidence for the incorporation of cinnamaldehydes into the lignin of transgenic tobacco (Nicotiana tabacum L.) plants with reduced expression of cinnamyl alcohol dehydrogenase. Planta 201 (3), 311–318.

Su, B.-N., Li, Y., Jia, Z.-J., 1997. Neolignan, phenylpropanoid and iridoid glycosides from *Pedicularis verticillata*. Phytochemistry 45 (6), 1271–1273.

Suzuki, S., Lam, T.B.T., Iiyama, K., 1997. 5-Hydroxyguaiacyl nuclei as aromatic constituents of native lignin. Phytochemistry 46 (4), 695–700.

Syrjanen, K., Brunow, G., 1998. Oxidative cross coupling of *p*-hydroxycinnamic alcohols with dimeric arylglycerol β-aryl ether lignin model compounds. The effect of oxidation potentials. J. Chem. Soc. Perkin Trans. 1 (20), 3425–3429.

Syrjanen, K., Brunow, G., 2000. Regioselectivity in lignin biosynthesis. The influence of dimerization and cross-coupling. J. Chem. Soc. Perkin Trans. 1 (2), 183–187.

Vailhe, M.A.B., Besle, J.M., Maillot, M.P., Cornu, A., Halpin, C., Knight, M., 1998. Effect of down-regulation of cinnamyl alcohol dehydrogenase on cell wall composition and on degradability of tobacco stems. J. Sci. Food Agric. 76 (4), 505–514.

Van Doorsselaere, J., Baucher, M., Chognot, E., Chabbert, B., Tollier, M.-T., Petit-Conil, M., Leplé, J.-C., Pilate, G., Cornu, D., Monties, B., Van Montagu, M., Inzé, D., Boerjan, W., Jouanin, L., 1995. A novel lignin in poplar trees with a reduced caffeic acid/5-hydroxyferulic acid *O*-methyltransferase activity. Plant J. 8 (6), 855–864.

Whetten, R.W., MacKay, J.J., Sederoff, R.R., 1998. Recent advances in understanding lignin biosynthesis. Annu. Rev. Plant Physiol. Plant Mol. Biol. 49, 585–609.

Yahiaoui, N., Marque, C., Myton, K.E., Negrel, J., Boudet, A.-M., 1998. Impact of different levels of cinnamyl alcohol dehydrogenase down-regulation on lignins of transgenic tobacco plants. Planta 204 (1), 8–15.

Zanarotti, A., 1982. Preparation and reactivity of 2,6-dimethoxy-4-allylidene-2,5-cyclohexadien-1-one (vinyl quinone methide). A novel synthesis of sinapyl alcohol. Tetrahedron Lett. 23 (37), 3815–3818.

Zhang, L., Gellerstedt, G., 2000. Achieving quantitative assignment of lignin structure by combining 13C and HSQC NMR techniques. In: Sixth European Workshop on Lignocellulosics and Pulp. Bordeaux, France, pp. 7–10.

PERGAMON

Phytochemistry 57 (2001) 1005–1011

PHYTOCHEMISTRY

www.elsevier.com/locate/phytochem

Acidolysis and hot water extraction provide new insights into the composition of the induced "lignin-like" material from squash fruit

Richard R. Stange Jr.[a,*], John Ralph[b], Junpeng Peng[b], James J. Sims[c], Sharon L. Midland[c], Roy E. McDonald[a]

[a] *USDA-ARS, Horticultural Research Laboratory, 2001 South Rock Road, Fort Pierce, FL 34945, USA*
[b] *USDA-ARS, US Dairy Forage Research Center, 1925 Linden Drive West, Madison, WI 53706-1108, USA*
[c] *Department of Plant Pathology, University of California, Riverside, CA 92521, USA*

Received 28 October 1999; received in revised form 6 June 2000

Abstract

Accumulation of "lignin-like" material (L-LM) by plant tissues in response to injury or disease has been observed in a wide variety of plant taxa. The most intensively studied L-LM is that produced by members of the Cucurbitaceae; this material is thought to be an unusual lignin rich in *p*-coumaryl alcohol derived subunits. Employing acidolysis we found the primary degradation product of L-LM from squash fruit was *p*-coumaryl aldehyde. These findings conflict with the current concept of L-LM, but would be consistent with L-LM being a polymer derived directly from *p*-coumaryl aldehyde or a gum containing this compound. Results of hot water extraction support the latter possibility. Further, we report on a simple TLC method useful for rapid qualitative characterization of acidolysis degradation products. © 2001 Elsevier Science Ltd. All rights reserved.

Keywords: *Cucurbita maxima*; Cucurbitaceae; Squash; Composition of induced lignin; *p*-Coumaryl alcohol; *p*-Coumaryl aldehyde

1. Introduction

The lignin-like material (L-LM) produced by many plants in response to injury or disease has been studied by numerous investigators and is frequently associated with resistance to fungal or bacterial pathogens (Ride, 1975; Vance et al., 1980; Nicholson and Hammerschmidt, 1992). Lignins are a complex class of compounds derived via the free radical polymerization of the three primary lignols (Fig. 1), *p*-coumaryl **1b**, coniferyl **2b** and sinapyl **3b** alcohols (Harkin, 1967; Freudenberg and Neish, 1968; Whetten et al., 1998). Lignins are classified based on the ratio of the different lignols present. Because of their high molecular weight and insolubility, precise knowledge of the composition of lignins cannot be obtained directly, but must be gained indirectly by NMR of soluble lignin fractions or by identification of lignin degradation products (Lewis and Yamamoto, 1990). Degradation methods used include pyrolysis-GC–MS, hydrolysis, and oxidation (Tanahashi and Higuchi, 1988; Ralph and Hatfield, 1991). In addition to providing subunit composition, a portion of the products from the first two methods retain their C-3 side chains, providing information about the interunit linkages in the parent lignin (Lundquist, 1992; Ralph and Hatfield, 1991). However, the sheer number of possible products complicates routine analysis of lignins by these methods. In contrast, oxidative methods degrade lignins to the benzaldehyde or benzoic acid analogues of their parent lignols. Because there are only three primary products, analyses of oxidative degradation products are relatively simple, (Tanahashi and Higuchi, 1988), but information on the nature of the sidechains is lost.

Deposition of L-LM has been reported in a wide variety of plant taxa (Vance et al., 1980; Rittinger et al., 1987). However, only in a relatively small number of plants has the composition of the L-LM been examined. The L-LM from members of the Cucurbitaceae is perhaps the best characterized, having been studied by four independent research groups using alkaline cupric oxide or nitrobenzene oxidization methods. L-LM induced by fungal infection in five species of cucurbits was

* Corresponding author. Tel.: +1-561-462-5838; fax: +1-561-462-5986.
E-mail address: rstange@ushrl.ars.usda.gov (R.R. Stange Jr.).

0031-9422/01/$ - see front matter © 2001 Elsevier Science Ltd. All rights reserved.
PII: S0031-9422(01)00096-6

characterized by Hammerschmidt et al. (1985) and in muskmelon by Grand and Rossignol (1982). L-LM in cucumber, induced by wounding of fruit (Walter et al., 1990) or by an elicitation of hypocotyls with a pectic elicitor (Robertsen and Svalheim, 1990) has also been characterized. In all these studies, degradation products of tissues containing L-LM contained an abundance of *p*-hydroxybenzaldehyde, with increases of up to 61-fold over control tissues (Grand and Rossignol, 1982; Hammerschmidt et al., 1985; Robertsen and Svalheim, 1990; Walter et al., 1990). Similar results have been reported in other plant taxa. Compared to controls, degradation products of L-LM-containing tissues of radish roots, wheat leaves, soybean cotyledons, and parsley suspension cells had 2.5, 6.7, 2.9, or 8.6 fold more *p*-hydroxybenzaldehyde (Asada and Matsumoto, 1972; Ride, 1975; Graham and Graham, 1991; Kauss et al., 1993). Thus, our current concept about L-LM is of a lignin that is unusually rich in *p*-coumaryl alcohol derived subunits. Consistent with their role in defense, lignins rich in this lignol may yield highly condensed lignins that are resistant to degradation (Hammerschmidt et al., 1985). Some lignins of unique function, such as compression wood lignin, also have unique compositions (Nimz et al., 1981; Timell, 1982, 1986).

Although there is a consensus that the function of L-LM is protective, investigators earlier in this century had a much different concept of its chemical nature. While these earlier investigators did not have a precise chemical model, the intense reaction with phloroglucinol-HCl (PG-HCl) was attributed to the presence of aromatic aldehydes held within a water insoluble gum, termed wound gum (Bloch, 1937; Rawlins and Takahashi, 1952). Both wound gum and lignin become strikingly colored in PG-HCl; however, on the basis of other histological, anatomical and developmental criteria, wound gum was thought to be biochemically distinct from lignin (Hewitt, 1938; Schneider, 1980).

We recently reported that squash tissue elicited with pectinase synthesizes and accumulates the antifungal compound *p*-coumaryl aldehyde **1a** (Stange et al., 1999). The appearance of this compound is coincidental with the deposition of L-LM (unpublished data). This compound is also the immediate biosynthetic precursor of *p*-coumaryl alcohol that is presumed to be the primary component of L-LM in cucurbits (Lewis and Yamamoto, 1990). Recent studies of novel lignins, formed by plants with reduced cinnamyl alcohol dehydrogenase activity, have dramatically expanded our concept of lignins (Whetten et al., 1998). In these plants, conversion of coniferyl aldehyde **2b** to coniferyl alcohol **2a** is partly or completely blocked and their lignins are synthesized, in part, from coniferyl aldehyde (Higuchi et al., 1994; Baucher et al., 1996; Ralph et al., 1997). Thus, aldehyde analogs of lignols can be directly polymerized into lignins or lignin-like materials. The oxidation methods used by earlier investigators to characterize the L-LM from cucurbits would not have differentiated between lignins derived from *p*-coumaryl aldehyde or alcohol (Grand and Rossignol, 1982; Hammerschmidt et al., 1985; Robertsen and Svalheim, 1990; Walter et al., 1990). Distinguishing the identity of L-LM's parent compounds requires use of methods which do not destroy the C3 side chain.

The close association between *p*-coumaryl aldehyde and L-LM accumulation in squash, together with the general doubts of earlier researchers that L-LM is even lignin at all, poses several fundamental questions. Is the L-LM an unusual lignin derived from *p*-coumaryl alcohol or aldehyde? Or, in fact, is the material a lignin at all? We attempt to begin to address these questions by using acidolysis to analyze tissues containing L-LM. In addition, we report on a TLC method for separation of the acidolysis degradation products which greatly simplifies the analyses of the hydrolysates of L-LM.

2. Results and discussion

Identification of components unique to L-LM depends on comparing degradation products of tissues having low lignin content with or without L-LM being present. Further, comparison of degradation products from L-LM containing tissue with highly lignified tissues would assist in the characterization of L-LM acidolysis products and provide confirmation of the methodology. Our experimental scheme utilized extractive-free cell wall preparations from squash fruit tissue elicited with pectinase and cured 24 h to promote accumulation of L-LM (Stange and McDonald, 1999), from unelicited freshly sliced fruit tissue, and from tissue of the highly lignified stem of the fruit.

Histochemical tests were performed to confirm the composition of these cell wall preparations. When the Mäule test was performed, the abundant, heavily sclerified cell walls in the stem tissue gave an intense reaction,

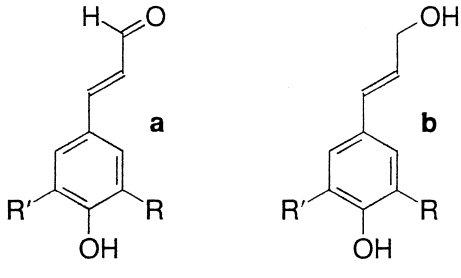

		R	R′
1a/b	*p*-coumaryl aldehyde/alcohol	H	H
2a/b	coniferyl aldehyde/alcohol	OMe	H
3a/b	sinapyl aldehyde/alcohol	OMe	OMe

Fig. 1. Primary lignols and their corresponding aldehydes.

turning a dark purple-red (Fig. 2, Mäule). However, microscopic examination revealed that remnants of xylem elements in the stem tissue gave no reaction with the Mäule test. Similarly, positively testing xylem components were observed in neither fresh nor elicited-cured fruit tissue preparations. The Mäule (-) reaction of the xylem is consistent with the observations of Walter et al. (1990) and with the results of Robertsen and Svalheim (1990), who reported finding no syringaldehyde in the CuO oxidation products of cucumber hypocotyls. Syringaldehyde is indicative of sinapyl alcohol **3b** derived constituents in lignin, which in turn, form colored products in the Mäule test (Iiyama and Plant, 1988). However, the xylem content of the stem tissue was low, relative to the abundant sclerified cells, which composed most of the sample.

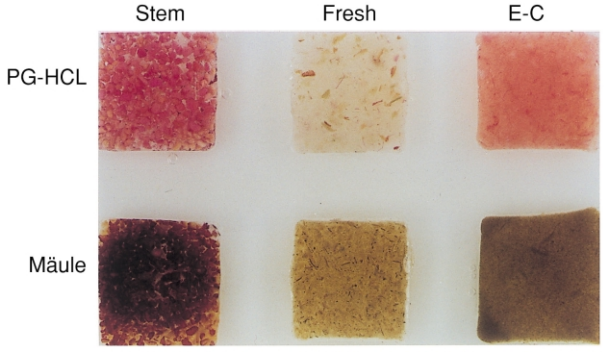

Fig. 2. Histochemical reactions of cell wall preparations. Each well contains similar volumes of extractive-free cell wall preparations from stem (Stem), fresh fruit (Fresh) and elicited-cured (E–C) fruit tissues. Cell wall preparations were subjected to the phloroglucinol-HCl test (PG-HCl) for aldehydes (upper) and the Mäule test for syringyl groups (lower). Wells are 1 cm^2.

Both sclerified cells and xylem remnants in the stem tissue sample reacted positively with PG-HCl, turning a purple-red color (Fig. 2, PG-HCl). The sclerifed tissue in the stem sample reacted positively with both reagents; this set of reactions is typical of angiosperm lignins (Towers and Gibbs, 1953; Lewis and Yamamoto, 1990). In fresh fruit cell wall preparations, only xylem elements reacted positively with PG-HCl. In contrast, a large portion of the elicited-cured fruit tissue reacted with the PG-HCl reagent, L-LM turned red while the xylem elements turned a purple-red color. The abundance of xylem in both fresh and elicited-cured fruit samples was quite low (Fig. 2, PG-HCl). The PG-HCl (+) and Mäule (-) histochemical reactions of L-LM are consistent with those reported by previous workers in cucurbits (Walter et al., 1990) and other crops (Schneider, 1980). Thus, the fruit tissue preparations provide samples with a low abundance of vascular lignin, with L-LM being either abundant in elicited cured tissue, or absent in fresh tissue. The stem sample has no L-LM, but contains an abundance of typical lignin.

Acid hydrolysis products of these three types of samples were obtained by the standard method, refluxing in dioxane-HCl (Tanahshi and Higuchi, 1988; Lundquist, 1992) and by mild acid hydrolysis [2 N HCl at 90°C]. Degradation products from both methods were separated by TLC and visualized with PG-HCl or Folin–Ciocalteu's phenol reagent. PG-HCl gives red to purple products with aromatic aldehydes and yellow to orange spots with furfurals (Feigl and Anger, 1966). Several compounds giving red to purple hued spots were observed in the stem tissue sample (Fig. 3). Two of these spots corresponded in mobility and color to the magenta spot of coniferyl aldehyde **2a** and the purple-brown spot of sinapyl aldehyde **3a**. Large quantities of staining material were

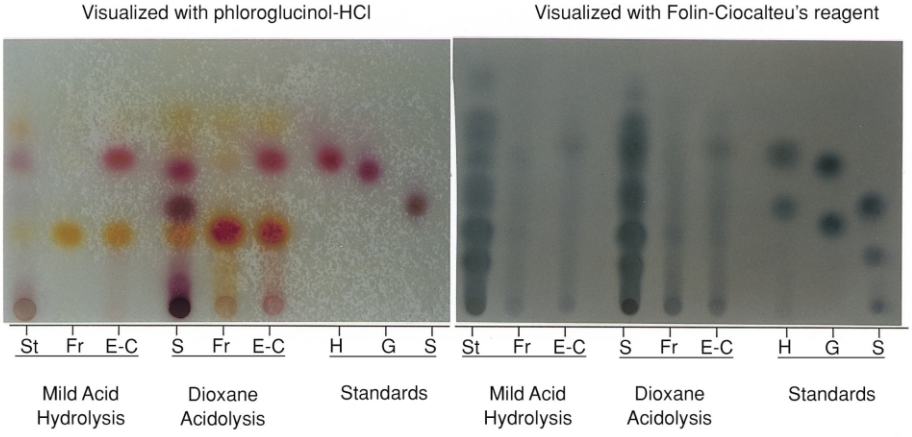

Fig. 3. Comparison of mild acid hydrolysis and dioxane acidolysis products from stem (St), fresh fruit (Fr) and elicited-cured fruit (E-C) extractive-free cell wall preparations. Standards are mixtures of *p*-coumaryl (H) **1**, coniferyl (G) **2** or sinapyl (S) **3** alcohol and aldehyde; 0.5 μg of each compound spotted. Plates were developed in hexane–EtOAc (1:1); solvent fronts travelled 90 mm, 60 mm of travel shown. TLC plate on left visualized with phloroglucinol-HCl to reveal aromatic aldehydes (red to purple colors) and furfurals (orange to yellow colors). Loading of hydrolysates equivalent to 1.5 mg cell wall preparation. TLC plate on right visualized with Folin–Ciocalteu's reagent to reveal phenolics. Loadings of hydrolysates equivalent to 0.5 mg cell wall preparation.

present at the origin, indicating that component(s) of the sample were of higher molecular weight or highly polar. No red hued spots were evident from the fresh fruit samples; this would be expected given the low abundance of lignin in the sample. The elicited-cured tissue yielded a single red spot, unique to this sample. This compound had similar color and mobility to *p*-coumaryl aldehyde **1a**. When plates were visualized for phenolics with Folin-Ciocalteu's reagent, similar patterns were observed. Products of the stem tissue sample were abundant and numerous (Fig. 3). By contrast, in fresh and elicited-cured fruit tissue samples products were far less abundant, indicating that very few phenolic components were present. The exception to this was *p*-coumaryl aldehyde **1a** in the elicited-cure sample, which produced a distinct spot with Folin–Ciocalteu's reagent. Both acid hydrolysis methods yielded similar products from fresh and elicited-cured fruit samples, but for the stem sample mild acid hydrolysis yielded fewer products and gave lower yields than dioxane acidolysis.

Hot water and mild acid hydrolysis of elicited tissue yielded 161 ± 25 ($n = 4$) and 303 ± 19 ($n = 4$) μg *p*-coumaryl aldehyde **1a** per gram cell wall material, respectively. When residues from hot water hydrolysis were subjected to mild acid hydrolysis, additional *p*-coumaryl aldehyde (130 ± 25 μg/g cell wall) was recovered. Because the hot water suspension was slightly acidic (initial pH, 5.7; final pH, 5.2), one possibility is that the *p*-coumaryl aldehyde recovered by this treatment was held by relatively easily hydrolyzed covalent bonds, such as ester linkages. However, the more probable interpretation is that the compound was contained within a gum which was dissolved by the hot water. We are attempting to address this technically difficult question presently.

A single furfural predominated in both fruit samples (orange spots, Fig. 3, PG-HCl), but furfurals were rare or lacking in the stem tissue sample. The abundance of furfurals in fruit samples was much greater with the dioxane acidolysis method than with mild acid hydrolysis.

GC–MS analysis of the stem tissue sample acidolysis products identified six guaiacyl and two syringyl derivatives. The presence of syringyl units is consistent with the positive Mäule reaction of the tissue (Iiyama and Plant, 1988). In the fresh fruit sample, no lignin related degradation products were found by GC–MS, again indicating the low abundance of lignified xylem in the fresh fruit samples. The identity of the compound giving a red colored spot in TLCs of the elicited-cured samples was confirmed by GC–MS and by NMR following separation by TLC. As suspected, the compound was *p*-coumaryl aldehyde **1a**. Further, this was the only lignin related product detectable by GC–MS.

The predominant furfurfal in both the fruit samples was 5-(hydroxymethyl)-2-furaldehyde. In addition, the elicited-cured sample contained 2-hydroxymethyl furan. Presence of this compound in the mixture interfered with the identification of *p*-coumaryl aldehyde **1a** by GC–MS. We are uncertain of the significance of this compound, but it may indicate differences in the carbohydrate composition between fresh and elicited-cured samples.

Our results confirm that the stem tissue contained a typical angiosperm lignin, composed primarily of guaiacyl and syringyl units. The fresh fruit tissue had a very low abundance of lignin. These results could be anticipated based on histochemical tests and microscopic observations. The colors developed by hydrolysates when TLC plates were visualized with PG-HCl corresponded very well to the colors of cell wall residues treated with this reagent. The elicited-cured tissue developed the same pure red color developed by *p*-coumaryl aldehyde **1a**. The stem tissue's more purple color suggests the magenta to purple colors developed by coniferyl **2a** and sinapyl **3a** aldehydes.

Finding *p*-coumaryl aldehyde as the sole acidolysis product of L-LM was unexpected. This result is strong evidence that L-LM is not derived from *p*-coumaryl alcohol **1b**. The exact nature of L-LM is, however, much less clear. If it were a lignin-like material derived from *p*-coumaryl aldehyde, we would have expected more related products, similar to the numerous products yielded from stem tissue. Because a *p*-coumaryl aldehyde based lignin might be highly condensed, these products could be quite rare, and more exhaustive are studies needed to determine if they exist. Attempts to dissolve the L-LM in acetyl bromide and subsequent application of the 'derivatization followed by reductive cleavage' method (Lu and Ralph, 1997a,b,1998) were unsuccessful, even with extended treatment periods. Only minor amounts of the fraction, mainly saccharide components, dissolved. We (Lu and Ralph, 1999, unpublished) have previously encountered difficulty in dissolving aldehyde-rich fractions in acetyl bromide. While our results do fit well with the concept of the material being a water-insoluble gum imbedded with *p*-coumaryl aldehyde, they do not rule out the possibility that a portion of this compound is covalently bound. Whatever it is, this material certainly differs from a lignin derived from *p*-coumaryl alcohol **1b**. More fundamental research, utilizing a wider variety of approaches based on the above models, is needed to determine the actual composition and structure of the so-called "lignin-like" material from elicited cured squash.

3. Experimental

3.1. Plant material, elicitation and isolation of lignin-like material

Green acorn squash, *Cucurbita maxima*, were purchased from retail outlets. Only recently harvested fruits

with green living stems were selected. Stems were air dried and ground through a #20 mesh screen using a Wylie® mill. Fresh fruit tissue was diced finely. Elicited-cured tissue was prepared as described earlier from squash sliced 5 mm thick (Stange et al., 1999). Extractive-free cell wall preparations were made by first homogenizing tissues 1 min in 10 mM phosphate buffer, pH 6 (25 ml per g dry wt). Cell wall material was pelleted by centrifugation (6000×*g*) and washed with two changes of buffer. The water-insoluble residue was further extracted with two changes over 24+ h of the following sequence of solvents: ethanol–water (4:1) (25 ml per g dry wt); chloroform–methanol–water (5:10:4); methanol; acetone (12 ml per g dry wt). Extractive-free cell wall preparations were stored at −20°C.

3.2. Chemicals

Coniferyl and sinapyl alcohols and aldehydes were purchased from commercial sources. *p*-Coumaryl alcohol **1b** was synthesized according to Quideau and Ralph (1992) and *p*-coumaryl aldehyde was prepared from **1b** by oxidation with 2,3-dichloro-5,6-dicyano-1,4-benzoquinone.

3.3. Histochemical tests

PG-HCl and Mäule tests were performed on cell wall preparations using standard methods (Rawlins and Takahashi, 1952). Microscopic examination of samples was done under bright and dark field illumination using a Nikon Optiphot microscope at 40 and 100× magnification.

3.4. Hydrolysis of extractive-free cell wall samples

A modification of the procedure of Tanahashi and Higuchi (1988) was used for acidolysis (Lundquist, 1992). Tissue, 400 mg, was refluxed under N_2 in 20 ml dioxane–2 M HCl (9:1) for 3 h. The suspension was filtered, and the residue washed with dioxane. The filtrate was adjusted to pH 3 with 0.4 M $NaHCO_3$ and stirred for 30 min. This solution was extracted with methylene chloride, and the organic phase was dried over Na_2SO_4, filtered, and evaporated under vacuum. Acidolysis products were dissolved in EtOAc–EtOH (3:1) and stored at −20°C.

For mild acid hydrolysis, 400 mg extractive-free cell wall residue was placed in a 100-ml volumetric flask with 40 ml 2 N HCl. The flask was purged with N_2, capped with a marble, and placed in a 90°C water bath for 3 h. The suspension was cooled, 40 ml 2-propanol added, and then filtered. The residue was washed with 20 ml 2-propanol. Combined filtrates were reduced to aqueous under vacuum, extracted 2× with methylene chloride, and the organic phase was dried over Na_2SO_4. This solution was filtered, dried, and the products dissolved and stored as the acidolysis samples above. Hot water hydrolysis products of elicited-cured tissue were also obtained using this procedure by substituting distilled water for 2 M HCl.

3.5. Analyses of hydrolysis products by TLC

Samples and standards were spotted onto polyester backed silica gel TLC plates (250 μm) and developed in hexane–EtOAc (1:1). Phenolics were visualized using Folin Ciocalteu's reagent as described by Fry (1988). Aromatic aldehydes and furfurals were visualized by first spraying with 1% phloroglucinol in ethanol–water (7:3), air drying, and spraying with conc HCl (Feigl and Anger, 1966). The quantity of *p*-coumaryl aldehyde present in mild acid and hot water hydrolysates was determined as follows. Samples and standards of *p*-coumaryl aldehyde were separated by TLC, spots corresponding to the compound were located under long-wave UV, scraped off, and dissolved in 1 ml 95% ethanol. Abundance of *p*-coumaryl aldehyde was quantified by A_{325}.

3.6. Analyses of hydrolysates by GC–MS

GC was run on a Hewlett-Packard (Atlanta, GA) 5980 gas chromatograph; column 0.2 μm film, 0.2 mm × 30 m SPB-5 (Supelco); He carrier gas, 1 ml/min; 30:1 split ratio; injector 220°C, initial column temperature 150°C, ramped at 10°C/min to 310°C, hold for 10 min, total running time 34 min. Mass spectra (EI, 70 eV) were collected on a Hewlett-Packard 5970 MS Detector connected directly to a similar column in the same GC.

Three samples were chosen for GC–MS analysis: mild acid hydrolysate of stem tissue, and dioxane acidolysis hydrolysates of fresh and elicited-cured fruit tissues. For trimethylsilylation hydrolysates (0.5 mg) were silylated using BSTFA {N,*O*-bis(trimethylsilyltrifluoroacetamide)} (80 μl) plus pyridine (20 μl) at 50°C for 15 min. For acetylation, hydrolysates (1 mg) were acetylated with 1:1 acetic anhydride:pyridine (0.5 ml) at RT for 4 h. Solvents were removed by co-evaporation with ethanol on a rotary evaporator. The acetylated products were dissolved in methylene chloride (0.2 ml) for GC.

3.6.1. GC–MS

Acetylated or trimethylsilylated samples (2 μl) were injected into the GC. Trimethylsilylated *p*-coumaraldehyde eluted at 6.01 min; acetylated *p*-coumaryl aldehyde at 5.76 min. Mass spectra were identical with those derived from authentic *p*-coumaryl aldehyde (Aldrich): trimethylsilyl *p*-coumaryl aldehyde 220 (M+, 66), 205 (47), 73 (100); 4-acetoxycinnamaldehyde 190 (M+, 14), 148 (100).

3.7. Confirmation of p-coumaryl aldehyde by NMR

The dioxane acidolysis hydrolysate of elicited fruit tissue (37 mg) was applied to a preparative TLC plate (2 mm thickness, Macherey-Nagel Products, Germany), and eluted with 10:2 CH_2Cl_2:EtOAc. The band at R_f 0.6 was isolated (2.5 mg) and shown by NMR (^{1}H, COSY) to be identical to authentic *p*-coumaryl aldehyde **1a** — NMR data were the same as for compound number 152 in the "NMR Database of Lignin and Cell Wall Model Compounds" (Ralph et al., 1998). The acetylated TLC fraction had spectra identical to acetylated *p*-coumaryl aldehyde, compound number 223 in the same database.

Acknowledgements

We thank anonymous reviewers, D. Akin, N.G. Lewis, W. Walter and C. West for their helpful suggestions on improving this manuscript and Hoon Kim for preparation of the *p*-coumaryl aldehyde. Henry Schneider's efforts in educating the first author on wound gum are greatly appreciated.

References

Asada, Y., Matsumoto, I., 1972. The nature of lignin obtained from downy mildew-infected Japansese radish root. Phytopathologische Zeitschrift 73, 208.

Baucher, M., Chabbert, B., Pilate, G., Van Doorsselaere, J., Tollier, M-T., Petit-Conil, M., Cornu, D., Monties, B., Van Montagu, M., Inzé, D., Jouanin, L., Boerjan, W., 1996. Red xylem and higher lignin extractability by down-regulating a cinnamyl alcohol dehydrogenase in poplar. Plant Physiology 112, 1479.

Bloch, R., 1937. Wound healing and necrosis in air roots of Phoenix reclinata and leaves of *Araucaria imbricata*. American Journal of Botany 24, 279.

Feigl, F., Anger, V., 1966. Spot Tests in Organic Chemistry, 7th Edition. Elsevier, Amsterdam.

Fry, S.C., 1988. The Growing Plant Cell Wall: Chemical and Metabolic Analysis. Longman Scientific & Technical, Essex.

Freudenberg, K., Neish, A. C., 1968. In: Freudenberg, K., Neish, A. C. (Eds.) Constitution and Biosynthesis of Lignin. Springer-Verlag, Berlin-Heidelberg-New York.

Graham, M.Y., Graham, T.L., 1991. Rapid accumulation of anionic peroxidases and phenolic polymers in soybean cotyledon tissues following treatment with *Phytophthora megasperma* f. sp. *Glycinea wall glucan*. Plant Physiology 97, 1445.

Grand, G., Rossignol, M., 1982. Changes in the lignification process induced by localized infection of muskmelons with *Colletotrichum lagenarium*. Plant Science Letters 28, 103.

Hammerschmidt, R., Bonnen, A.M., Bergstrom, G.C., Baker, K.K., 1985. Association of epidermal lignification with nonhost resistance of cucurbits to fungi. Canadian Journal of Botany 63, 2393.

Harkin, JM., 1967. In: Taylor, WI., Battersby, A.R. (Eds.), Oxidative Coupling of Phenols. Marcel Dekker, New York, p. 243.

Hewitt, W.B., 1938. Leaf-scar infection in relation to the olive-knot disease. Hilgardia 12, 39.

Higuchi, T., Ito, T., Umezawa, T., Hibino, T., Shibata, D., 1994. Red-brown color of lignified tissues of transgenic plants with antisense CAD gene: wine-red lignin from coniferyl aldehyde. Journal of Biotechnology 37, 151.

Iiyama, K., Plant, R., 1988. The mechanism of the Mäule colour reaction introduction of methylated syringyl nuclei into softwood lignin. Wood Science and Technology 22, 167.

Kauss, H., Franke, R., Krause, K., Conrath, U., Jeblick, W., Grimming, B., Matern, U., 1993. Conditioning of parsley (*Petroselinum crispum* L.) suspension cells increases elicitor-induced incorporation of cell wall phenolics. Plant Physiology 102, 459.

Lewis, N.G., Yamamoto, E., 1990. Lignin: occurrence, biogenesis and biodegradation. Annual Review of Plant Physiology and Plant Molecular Biology 41, 455.

Lu, F., Ralph, J., 1997a. Derivatization followed by reductive cleavage (DFRC method), a new method for lignin analysis: protocol of analysis of DFRC monomers. Journal of Agricultural and Food Chemistry 45, 2590.

Lu, F., Ralph, J., 1997b. DFRC method for lignin analysis. 1. New method for β-aryl ether cleavage: lignin model studies. Journal of Agricultural and Food Chemistry 45, 4655.

Lu, F., Ralph, J., 1998. Efficient ether cleavage in lignins: the derivatization followed by reductive cleavage procedure as a basis for new analytical methods. In: Lewis, N.G., Sarkanen, S. (Eds.), Lignin and Lignan Biosynthesis. American Chemical Society, Washington, DC, pp. 294.

Lundquist, K., 1992. Acidolysis. In: Lin, S.Y., Dence, C.W. (Eds.), Methods in Lignin Chemistry. Springer-Verlag, Berlin-Hiedelberg, pp. 289.

Nicholson, R.L., Hammerschmidt, R., 1992. Phenolic compounds and their role in disease resistance. Annual Review of Phytopathology 30, 369.

Nimz, H.H., Faix, R.D., Nemr, M., 1981. Carbon-13 NMR spectra of lignins, 8. Structural differences between lignins of hardwoods, softwoods, grasses and compresssion wood. Holzforschung 35, 16.

Quideau, S., Ralph, J., 1992. Facile large-scale synthesis of coniferyl, sinapyl, and *p*-coumaryl alcohol. Journal of Agricultural and Food Chemistry 40, 1108.

Ralph, J., Hatfield, R.D., 1991. Pyrolysis-GC–MS characterization of forage materials. Journal of Agriculture and Food Chemistry 39, 1426.

Ralph, J., MacKay, J.J., Hatfield, R.D., O'Malley, D.M., Whetten, R.W., Sederoff, R.R., 1997. Abnormal lignin in a loblolly pine mutant. Science 277, 235.

Ralph, SA., Ralph, J., Landucci, WL., and Landucci, LL., 1998. NMR database of lignin and cell wall model compounds. Available over Internet at http://www.dfrc.ars.usda.gov/software.html.

Rawlins, T.E., Takahashi, W.N., 1952. Techniques of Plant Histology and Virology. The National Press, Milbrae.

Ride, J.P., 1975. Lignification in wounded wheat leaves in response to fungi and its possible role in resistance. Physiological Plant Pathology 5, 125.

Rittinger, P.A., Biggs, A.R., Peirson, D.R., 1987. Histochemistry of lignin and suberin depositions in boundary layers formed after wounding in various plant species and organs. Canadian Journal of Botany 65, 1886.

Robersten, B., Svalheim, Ø., 1990. The nature of lignin-like compounds in cucumber hypocotyls induced by α-1,4-linkded oligogalacturonides. Physiologia Plantarum 79, 512.

Schneider, H., 1980. Deposition of wound gum, callose, and suberin as responses to disease and wounding of citrus. Bulletin de la Société Botanique de France, Actualités Botaniques 127, 143.

Stange Jr., R.R., McDonald, R.E., 1999. A simple and rapid method for determination of lignin in plant tissues — its usefulness in elicitor screening and comparison to the thioglycolic acid method. Postharvest Biology and Biotechnology 15, 185.

Stange Jr., R.R., Sims, J.J., Midland, S.L., McDonald, R.E., 1999. Isolation of a phytoalexin, *trans-p*-coumaryl aldehyde, from *Cucurbita maxima*, Cucurbitaceae. Phytochemistry 52, 41.

Timell, T.E., 1982. Recent progress in the chemistry and topochemistry of compression wood. Wood Science and Technology 16, 83.

Timell, T.E., 1986. Compression Wood in Gymnosperms. Springer-Verlag, Berlin-New York.

Tanahashi, M., Higuchi, T., 1988. Chemical degradation methods for characterization of lignins. Methods in Enzymology 161B, 101.

Towers, G.H.N., Gibbs, R.D., 1953. Lignin chemistry and the taxonomy of higher plants. Nature 172, 25.

Vance, C.P., Kirk, T.K., Sherwood, R.T., 1980. Lignification as a mechanism of disease resistance. Annual Review of Phytopathology 18, 259.

Walter Jr., W.M., Randall-Schadel, B., Schadel, W.E., 1990. Wound healing in cucumber fruit. Journal of the American Society for Horticultural Science 115, 444.

Whetten, R.W., MacKay, J.J., Sederoff, R.R., 1998. Recent advances in understanding lignin biosynthesis. Annual Review of Plant Physiology and Plant Molecular Biology 49, 585.

PERGAMON

Phytochemistry 57 (2001) 1013–1022

PHYTOCHEMISTRY

www.elsevier.com/locate/phytochem

A heartwood pigment in *Dalbergia* cell cultures

Mihály Czakó*, László Márton

Department of Biological Sciences, University of South Carolina, 700 Sumter Street, Columbia, SC 29208, USA

Received 18 October 1999; received in revised form 11 January 2000

Abstract

In an extensive survey of the genera *Baphia, Caesalpinia, Dalbergia, Haematoxylon,* and *Pterocarpus*, we have identified a number of species whose cell cultures accumulated pigments similar to those in heartwood. Thirteen rosewood (*Dalbergia*) species produced a purple quinonemethide pigment in the callus that was apparently identical between the species. The pigment was first purified from *D. retusa* cell culture and its structure was elucidated by mass, infrared, and detailed ^{1}H and ^{13}C NMR and NOE spectroscopic studies including 2D experiments (COSY, NOESY, HMQC, and HMBC). Retusapurpurin A (**1a**) is a C_{30} isoflavan of novel skeleton whose formation can be rationalized to occur via regioselective oxidative coupling of an isoflavan to 4,4′-dihydroxy-2′-methoxychalcone. Retusapurpurin A was also isolated from *D. parviflora* heartwood and cell culture indicating that stress metabolism pathways that are shared with heartwood-type secondary metabolism subpathways are initiated in *Dalbergia* cell cultures. Therefore, *Dalbergia* cell cultures afford a good model system for studying heartwood-type metabolic differentiation. © 2001 Published by Elsevier Science Ltd. All rights reserved.

Keywords: *Baphia*; *Caesalpinia*; *Dalbergia*; *Haematoxylon*; *Pterocarpus*; Leguminosae; Cell culture; Heartwood pigment; Isoflavan; Quinonemethide

1. Introduction

Despite the importance of wood as the depository of a large fraction of the fixed carbon stored in the global ecosystem and as a raw material for major global industries, we know little of the genes involved in the formation of wood. While there has been great progress in the understanding of the biology of xylem/sapwood formation (Fukuda, 1996; Whetten et al., 1998; Gang et al., 1999; Lewis, 1999), information on gene expression during heartwood formation is not available.

Wood (xylem), a tissue unique to higher plants, is a highly ordered arrangement of living, dying, and dead cells. Meristem cells of the vascular cambium differentiate into water-conducting and supportive fiber (and vessels for hardwoods) and intercalating parenchyma cells for food storage. Terminal differentiation of the fibers and vessels quickly ends with programmed cell death while there remain live parenchyma cells, sometimes deep in the no-longer-conducting sapwood (Allen and Hiatt, 1994); parenchyma cells can live for over a hundred years (Shigo, 1994) in certain trees.

Programmed cell death occurring during the terminal differentiation of ray and axial parenchyma is a developmental process probably under strict control since it occurs only within no-longer-conducting sapwood, spreading from the tree's center. Ray parenchyma's final function is the synthesis of secondary metabolites that impregnate the wood, and this wood is called heartwood (Higuchi, 1997). Ray parenchyma cells in the intermediate (or transition) wood, the sapwood adjacent to heartwood, undergo physiological differentiation and alter their metabolism. The similarity of the spectrum of substances found in heartwood to those in pathogen- or pest-challenged or stressed plants (Harborne, 1994) suggests that some heartwood- and active defense-related secondary metabolism (phytoalexin) pathways may be common.

Only a few of the enzymes of secondary metabolism have been characterized in wood. Phenylalanine ammonia-lyase (PAL) is active across the sapwood, while

* Corresponding author. Tel.: +1-803-777-8928; fax: +1-803-777-4002.

E-mail address: czako-mihaly@sc.edu (M. Czakó).

Abbreviations: APCI, atmospheric pressure chemical ionization; ESI, electrospray ionization; COSY, correlated spectroscopy; DQF-COSY, double-quantum COSY; DMSO, dimethylsulfoxide; HMBC (^{1}H,^{13}C-COSY-$^{n}J_{CH}$ = 18 Hz, n = 2 and 3), heteronuclear shift correlations via multiple bond connectivities (gradient enhanced); HMQC (^{1}H,^{13}C-COSY-$^{1}J_{CH}$) heteronuclear multiple quantum coherence; MS, mass spectroscopy; NMR, nuclear magnetic resonance; NOESY, nuclear Overhauser and exchange spectroscopy

0031-9422/01/$ - see front matter © 2001 Published by Elsevier Science Ltd. All rights reserved.
PII: S0031-9422(01)00111-X

chalcone synthase is active exclusively in the vicinity of the heartwood boundary (Magel et al., 1991, 1995; Magel and Huebner, 1997). PAL is involved both in the formation of lignin and flavonoid biosynthesis; an inhibitor of the enzyme fed to the sapwood prevented the formation of phenylpropanoid metabolites (Ohashi et al., 1991). The flavonoids in the heartwood thus are formed in situ; they are not transported to the heartwood via the phloem and the ray cells (Magel et al., 1991, 1995).

The characterization of novel genes involved in the biosynthesis of heartwood-specific secondary metabolites in intermediate wood should lead to a better understanding of mechanisms controlling this important differentiation pathway. Heartwood does not lend itself to biosynthetic studies or mRNA extraction because it does not contain living cells, and access to the transition zone or intermediate wood is limited. To overcome this difficulty, we sought a system of lower complexity where some aspect of heartwood-type metabolic differentiation is recreated in cell cultures. Cell cultures of gymnosperm trees (Campbell and Ellis, 1992; Eberhardt et al., 1993; Nose et al., 1995; Yamaguchi et al., 1997; Gang et al., 1999) and two angiosperm trees (Paré et al., 1994; Davin et al., 1997; Zhentian et al., 1999) have been utilized to study biochemical processes related to the formation of wood, but for heartwood formation the optimal indicator metabolite would be colored, easy to assay, not far off the charted biosynthetic pathways, yet specialized enough not to occur outside heartwood. These criteria narrowed the choices to relatively very few candidates including the quinonemethide pigments in angiosperm plants derived from precursors originating from the well studied isoflavonoid and flavonoid pathways in leguminous plants (Harborne, 1994; Dixon et al., 1998). In an extensive survey of leguminous woody plants, we have identified several species of *Dalbergia* that produce brilliantly colored pigments in cell cultures under controlled conditions. We describe herein the isolation and structural elucidation of a novel isoflavan-derived quinonemethide pigment, retusapurpurin A, from cell cultures and heartwood. The structure has been established by spectral analysis, mainly based on detailed ^{1}H and ^{13}C NMR and NOE studies including 2D experiments (COSY, NOESY, HMQC, and HMBC).

2. Results and discussion

As part of our ongoing research on heartwood development, cell cultures of a great number of leguminous plants were established in order to find species whose cell cultures undergo metabolic differentiation to produce heartwood secondary metabolites. This is the first report of in vitro culture of all the species listed under 'seeds and live plants' in the experimental procedures except for *C. pulcherrima* (Rahman et al., 1993), *P. indicus* (Lee and Rao, 1980), *D. latifolia,* and *D. sissoo* (Mandal et al., 1994).

Quinonemethide pigments were detected on the basis of their intensive color and electrophoretic mobility towards the cathode on paper after conversion into pyrylium ions by protonation in an acidic buffer. Species of *Caesalpinia* and *Haematoxylon* are well known for the intense colored brazilein and hematein heartwood pigments (Robinson, 1985) which, however, were not detectable in tissue cultures of 12 *Caesalpinia* and 2 *Haematoxylon* species despite the dark pigmentation in certain species. Similarly, tissue cultures of *Baphia nitida* and seven *Pterocarpus* species did not contain the santarubins and/or santalins characteristic for the heartwood (Arnone et al., 1975, 1977a,b, 1981). Heartwood extracts were used as references where available.

Since a quinonemethide pigment was also reported from a *Dalbergia* species (Hamburger et al., 1988), we tested callus cultures of numerous *Dalbergia* species for pigment production (Table 1). Several species of *Dalbergia* proved especially prone to pigment production in vitro. Pigmentation in most species was localized and most intense in the cells that were in contact with the medium and in adjacent cells, and the callus left a colored 'footprint' in the medium. The emergent portion of the callus usually was free of red, orange, brown, and purple pigments, with the exception of certain species where systemic coloration developed (Table 1).

Besides the apparently water insoluble immobile pigments in the 'footprint' and basal cell layers, diffusible pigments were also produced in certain species. Paper electrophoresis revealed a common major component in the pigment extracts of thirteen *Dalbergia* species (Table 1). It was a barely diffusible pigment located in the basal cell layers and the 'footprint'. It appeared orange-yellow in the acidic buffer, and turned purple with ammonia fumes. It showed strong fluorescence under UV. This component was easily extractable with ethanol. On silica thin layer chromatograms, it was the largest spot common to all the above thirteen species. It was conveniently detected by its yellow/orange fluorescence under UV, and by its pink fluorescence in ammonia fumes. The major component was accompanied by several similar fluorescent, as well as non-fluorescent, purple pigments. Since we first discovered pigment production in *D. retusa,* the major pigment was named retusapurpurin A. Pigmentation in cell cultures of other *Dalbergia* species was either not observed under the conditions tested, or the above purple pigment was not present and the color and solubility of the pigments were different (Table 1).

Rapid pigment accumulation can be induced by transferring the emergent portion of *D. retusa* callus on DM-2, and in *D. parviflora* callus upon transfer to DM-10 medium. Coloration started within 24 h and pigment accumulation continued thereafter. An orange to deep

Table 1
Culture conditions and pigment accumulation in *Dalbergia* cell cultures[a]

	Culture medium[b] for			
Dalbergia sp.	Callus initiation	Maintenance	Type of coloration[c]	Retusapurpurin A present
D. arbutifolia	DM-1	DM-1	*L*-Or, *S*-lBr	N
D. assamica	DM-1	DM-8	*L*-Or, *S*-dBr, *L*-RBr	N
D. balansae	DM-1	DM-7	*L*-RBr	Y
D. brownei	DM-3	DM-3	*L*-RBr	N
D. calycina	DM-1	DM-3	*L*-Re, *L*-Bl, *S*-Bl, *D*-Br	Y
D. candenatensis	DM-3	DM-3	*L*-Re, *L*-RBr	N
D. cochinchinensis	DM-1	DM-3	*L*-PRe	N
D. cultrata	DM-1	DM-3	*L*-Pu, *S*-Br	Y
D. densa	DM-1	DM-1	*L*-lBr	Y
D. ecastaphyllum	DM-1	DM-6	*L*-bRe	Y
D. glabra	DM-3	DM-3	*L*-ROr, *S*-dBr, *D*-Or	N
D. hainanensis	DM-1	DM-1	*L*-Br	N
D. hupeana	DM-1	DM-3	DM-1: *L*-dBr	Y
D. latifolia	DM-1	DM-3	*L*-Re, *D*-Or	N
D. martinii	DM-1	DM-1	*S*-Gy	N
D. melanocardium	DM-5	DM-6	*L*-dBr	N
D. melanoxylon	DM-1	DM-3	*L*-Pu, *S*-Pu	N
D. miscolobium	DM-1	DM-3	*L*-RBr, *S*-Bl	Y
D. nigra	DM-4	DM-8	*L*-dBr, *S*-dBr, *D*-dBr	Y
D. nigrescens	DM-1	DM-1	*L*-RBr	Y
D. obovata	DM-1	DM-6	*L*-dBr	N
D. oliveri	DM-1	DM-6	DM-3: *L*-Or	N
D. parviflora	DM-1	DM-9	DM-7: *L*-Bl, *L*-bRe	Y
D. retusa	DM-1	DM-1	DM-2: *L*-Bl, *L*-bRe, *S*-Bl, *D*-Or	Y
D. sericea	DM-1	DM-3	*L*-PBr, *S*-PBr	N
D. sissoo	DM-1	DM-3	*L*-Or	Y
D. trichocarpa	DM-1	DM-3	DM-1: *L*-PRe	Y
D. tucurensis	DM-1	DM-6	*L*-dBr, *S*-lOr	N

[a] Normal callus color is a light to dark, chlorophyllous green.
[b] Composition of media is given in the text.
[c] Coloration on maintenance medium unless indicated otherwise. Explanation of color codes: *L*: Localized to the tissue in contact with the medium and some of it is secreted into the medium but not very diffusible ('footprint'); *S*: systemic, expressed in nearly all cells; D: diffusible in the medium; b: bright; d: dark; l: light; Bl: black; Br: Brown; Gy: grey; Or: orange; P: purplish; Pu: purple; R: reddish; Re: red.

blood red stain, occasionally intensifying to black, was deposited at the foot and in the core of the compact callus.

Retusapurpurin A and the accompanying pigments were not soluble in water but were readily extractable by polar organic solvents. Retusapurpurin A (**1a**) was recovered from a methanol eluate of preparative TLC separated band as an amorphous deep reddish purple powder. It exhibited interesting physicochemical properties. The color was pH sensitive. The UV/vis spectrum of a fresh ethanol solution (red) retusapurpurin A dried in vacuo was close to what could be measured under pH controlled conditions in ethanol (pH 5.0). A bathochromic shift on addition of $NaHCO_3$ (purple red) suggested the presence of free phenolic hydroxyl groups. Identical UV spectra were obtained with addition of $AlCl_3$ and HCl or with HCl alone, indicating that the hypsochromic shift (orange solution) was solely caused by the acidity of $AlCl_3$. Retusapurpurin A also showed a pronounced solvatochromism: it dissolved in dimethylsulfoxide (DMSO) with a deep blue color. Color in DMSO was moisture dependent; unsealed solutions gradually turned the same color as can be obtained by addition of traces of water. Retusapurpurin A also displayed phase transition induced chromism in DMSO solution: it turned red upon freezing. The solution in acidified DMSO was dark orange that turned red on freezing.

The characteristic fluorescence, color, and electrophoretic mobility of retusapurpurin A facilitated identification of the cell culture-produced pigment in heartwood extracts. We searched for retusapurpurin A in heartwood containing samples of 50 *Dalbergia* species from both the Old and the New World tropics. *D. parviflora* was identified as the only species whose heartwood appeared to contain retusapurpurin A accompanied by similar UV fluorescent purple pigments in smaller amounts. Retusapurpurin A was also found in a sample of *Dalbergia* wood which was reported to be *D. candenatensis* (Hamburger et al., 1988; courtesy of the authors) and from which the quinonemethide pigment candenatone (**3**) was isolated. Comparison of the pigment profile of authentic *D. parviflora* wood (supported by a herbarium

voucher) and that of '*D. candenatensis*' (Hamburger et al., 1988), as well as a wood of identical appearance from a commercial source, suggested that these samples represent the same species, while a specimen of authentic *D. candenatensis* shoot containing traumatic wood near a split (also supported by a herbarium voucher) was very different in color and pigment composition. *D. parviflora* wood is dark reddish brown to blood red while the wood of *D. candenatensis* is blackish violet. *D. candenatensis* was not one of the species that produced retusapurpurin A in wood or in cell cultures under the conditions tested so far, while *D. parviflora* callus does produce it (Table 1).

Retusapurpurin A was most conveniently purified in a quantity sufficient for structure elucidation from *D. retusa* callus because of the high concentration and relative purity. The structure of retusapurpurin A (**1a**, Fig. 1) was determined on the basis of MS and IR spectroscopy as well as detailed ^{1}H and ^{13}C NMR and NOE studies including 2D experiments (COSY, NOESY, HMQC, and

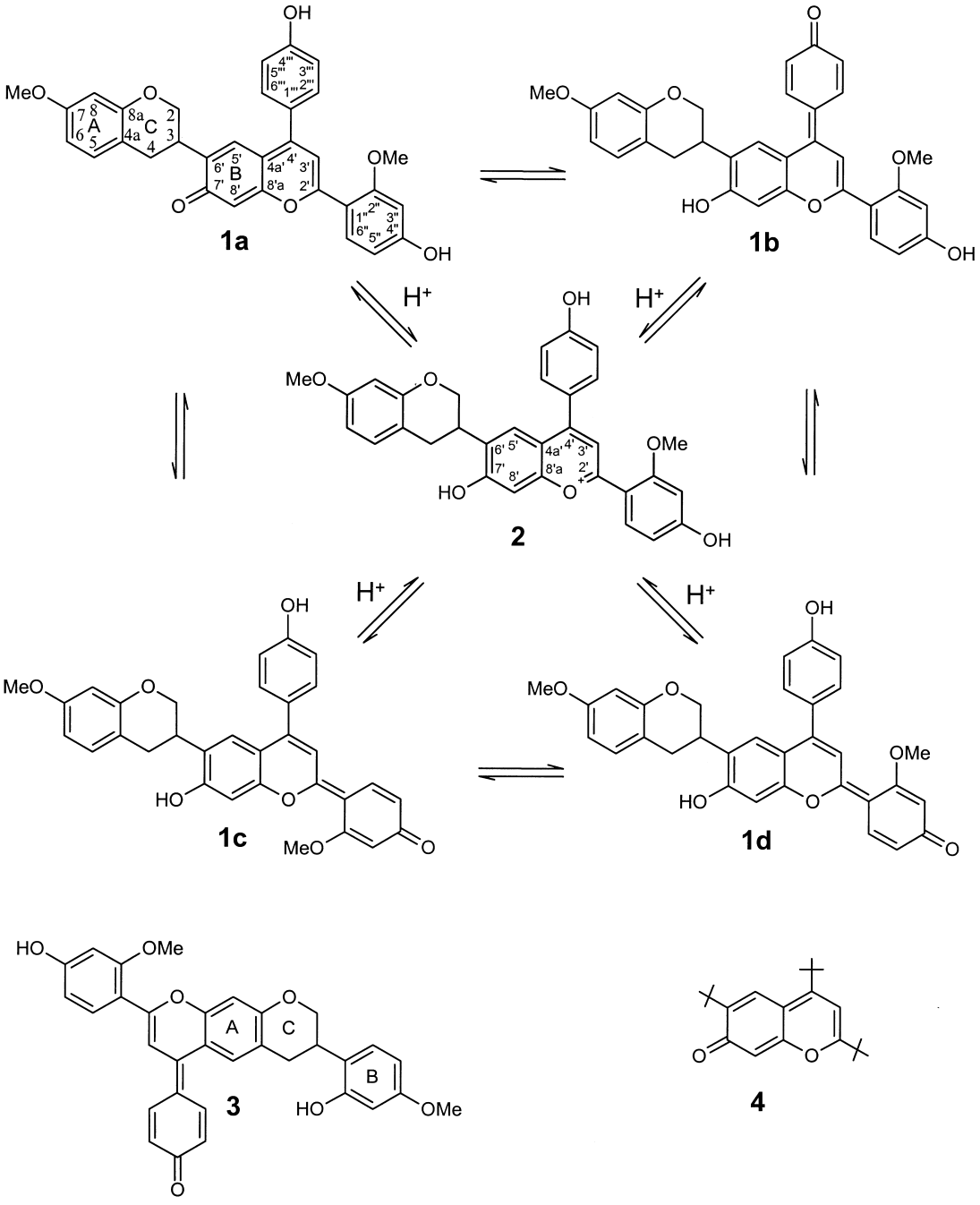

Fig. 1. Retusapurpurin A (**1a**), three of its possible tautomers (**1b–1d**), their protonated form (**2**), the partial structure (**4**), and the related pigment, candenatone (**3**).

HMBC) leading to complete assignment of the proton and carbon chemical shifts. Its molecular formula $C_{32}H_{26}O_7$ was deduced from the pseudo-molecular ion $[M+H]^+$ peak at m/z 523 in the ESI and APCI MS spectra. In the upfield region of the ^{1}H NMR spectrum of **1a** two pairs of methylene protons were observed (Table 2, at δ 2.71 and 2.89 and 4.02 and 4.19, respectively). The COSY spectrum revealed a methine proton hidden under the HDO peak at δ 3.43. The coupling patterns of the five aliphatic protons were typical for the C-ring of isoflavans (Kurosawa et al., 1978; Hamburger et al., 1988). This partial structure was further supported by the COSY cross-peaks (between H-2/H-3 and H-3/H-4), ^{13}C NMR (Table 2), and 2D NMR spectral data, which provided an overdetermined system of correlations.

Partially overlapping signals for 13 protons belonging to three aromatic rings were also observed in the ^{1}H NMR spectrum, in addition to two aromatic methoxy signals (Table 2). H-5 (*d*, δ 6.93) showed three-bond HMBC correlations with C-4 and C-8a (Fig. 2), in addition to COSY correlations with two protons (δ 6.31 (*d*) and 6.43 (*dd*)). The signal at δ 6.43 was assigned to H-6 since it was a double doublet and showed a three-bond interaction with C-4a and C-8, the latter also presenting an interaction with C-4a. These observations, also supported by the NOE between H-5 (*peri* position) and the methylene on C-4 NOE (Fig. 2 all NOEs were positive), confirmed (Hamburger et al., 1988) that **1a** had an isoflavan A/C-ring partial structure. C-7 showed correlation to a methoxy group (δ 3.70) (HMBC), and so did H-6 and H-8 (NOESY) (Fig. 2). From these observations it was concluded that **1a** has a 7-methoxy-substituted A-ring, similar to that of neovestitol (7-methoxy-2′,4-dihydroxyisoflavan; Ingham, 1979).

Three singlet signals were observed downfield in the ^{1}H spectrum of **1a** and they appeared to belong to a fifth ring or moiety because all other aromatic protons could be assigned to two additional aromatic rings. The proton signals at δ 6.38, 6.42, and 7.82 (Table 2) suggested a 1,2,4-tri-substituted ring. Their coupling was also confirmed by DQF-COSY. These chemical shifts were in good agreement with those obtained for

Table 2
^{1}H NMR and ^{13}C NMR assignments[a] of Retusapurpurin A

	Chemical shifts for 1a, δ TMS (ppm) in DMSO-d_6		Chemical shifts for 2, δ TMS (ppm) in DMSO-d_6 /DCl	
No.	δ ^{1}H (number, multiplicity, J_{HH} in Hz)	δ ^{13}C	δ ^{1}H (number, multiplicity, J_{HH} in Hz)	δ ^{13}C
2	4.02 (1H, *dd*, $^2J_{H2eq,H2ax}\approx$10.0, $^3J_{H2,H3}\approx$7.0)	69.03	4.25 (1H, *dd*, $^2J_{H2eq,H2ax}\approx$10.9, $^3J_{H2,H3}\approx$5.4)	68.46
	4.19 (1H, *dd*, $^2J_{H2eq,H2ax}$10.0, $^3J_{H2,H3}\approx$3.0)		4.30 (1H, *dd*, $^2J_{H2eq,H2ax}\approx$10.9, $^3J_{H2,H3}\approx$2.8)	
3	3.43 (1H, *m,* coupled to H2ax, H2eq, H4ax, H4eq)	31.64	3.61 (1H, *m,* coupled to H2ax, H2eq, H4ax, H4eq)	31.58
4	Hax 2.71 (1H *dd*, $^2J_{H4eq,H4ax}\approx$16.0, $^3J_{H3,H4ax}\approx$7.5)	28.98	Hax 3.11 (1H, *dd*, $^2J_{H4eq,H4ax}\approx$16.2, $^3J_{H3,H4}\approx$5.7)	28.91
	Heq 2.89 (1H, *dd*, $^2J_{H4ax,H4eq}\approx$16.0, $^3J_{H3,H4eq}\approx$5.5)		Heq 2.87 (1H, *dd*, $^2J_{H4ax,H4eq}\approx$16.2, $^3J_{H3,H4}\approx$5.5)	
4a		114.26		113.67
5	6.93 (1H, *d*, $^3J_{H6,H5}\approx$8.4)	130.71	6.98 (1H, *d*, $^3J_{H6,H5}\approx$8.5)	130.99
6	6.43 (1H, *dd*, $^3J_{H5,H6}\approx$8.4, $^4J_{H8,H6}\approx$2.6)	107.32	6.48 (1H, *dd*, $^3J_{H5,H6}\approx$8.5, $^4J_{H8,H6}\approx$2.4)	107.94
7		159.03		159.33
8	6.31 (1H, *d*, $^4J_{H6,H8}\approx$2.6])	101.56	6.32 (1H, *d*, $^4J_{H6,H8}\approx$2.0)	101.80
8a		155.21		155.20
2′		158.03		166.80
3′	7.27 (1H, *s*)	108.37	8.20 (1H, *s*)	115.65
4′		152.07		162.81
4′a		112.57		115.30
5′	7.28 (1H, *s*)	125.02	7.81 (1H, *s*)	127.98
6′		139.26		133.90[b]
7′		180.09		157.70
8′	6.33 (1H, *s*)	103.35	7.73 (1H, *s*)	103.10
8′a		159.31		165.52
1″		107.93		109.79
2″		161.31		163.70
3″	6.38 (1H, *d*, poorly res. $^4J_{H5'',H3''}\approx$2.1)	100.85	6.74 (1H, *d*, $^4J_{H5'',H3''}\approx$2.0)	100.68
4″		167.63		167.54
5″	6.42 (1H, *dd*, unres.$^3J_{H6'',H5''}\approx$8.9, $^4J_{H3'',H5''}\approx$2.6)	111.35	6.80 (1H, *dd*, $^3J_{H6'',H5''}\approx$9.0, $^4J_{H3'',H5''}\approx$2.0)	111.30
6″	7.82 (1H, *d*, $^3J_{H5'',H6''}\approx$8.9)	130.66	8.23 (1H, *d*, $^3J_{H5'',H6''}\approx$9.0)	133.81[b]
1‴		126.78		125.42
2‴/6″’	7.25 (2H, *d*, $^3J_{H3''',H2'''}\approx$8.6)	131.30	7.43 (2H, *d*, $^3J_{H3''',H2'''}\approx$8.5)	133.05
3‴/5‴	6.87 (2H, *d*, $^3J_{H2''',H3'''}\approx$8.6)	116.30	7.00 (2H, *d*, $^3J_{H2''',H3'''}\approx$8.5)	117.33
4‴		160.08		162.45
7OMe	3.70 (3H)	55.54	3.69 (3H)	55.78
2″OMe	3.83 (3H)	56.16	3.97 (3H)	57.21

[a] Assignments were confirmed by HMBC and HMQC.
[b] Interchangeable.

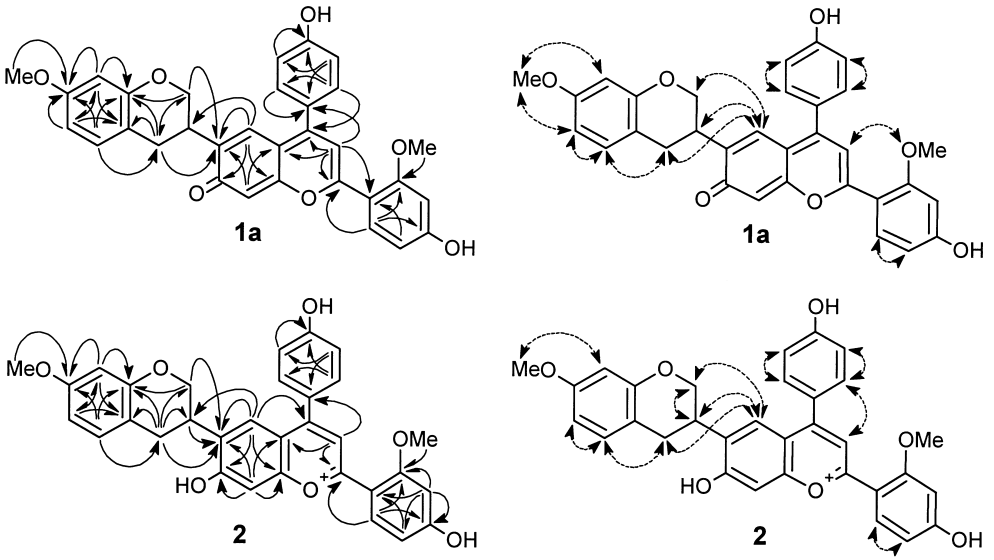

Fig. 2. Diagnostic HMBC (—) and NOE (- - - -) interactions in compounds **1a** and **2**.

the 2-methoxy-4-hydroxy substituted phenyl ring of candenatone (**3**), an isoflavan-chalcone dimer isolated from *Dalbergia* wood (Hamburger et al., 1988). The *ortho* position of the methoxy group (δ 3.83) was confirmed by HMBC. The doublets (showing the characteristic second order effects typical for an AA'XX' system) at δ 6.87 and 7.25 were assigned to a *para* substituted ring. Their coupling was confirmed in a DQF-COSY experiment. The signals for protons belonging to hydroxyl groups predicted by the molecular formula were apparently missing.

Considerations of possible biogenesis, the identical molecular formula and chemical and physicochemical similarity of retusapurpurin A to candenatone (**3**), the necessity to assign three singlets in the ^{1}H NMR spectra, and 2D NMR spectroscopic data obtained for retusapurpurin A led to the partial structure **4**.

The carbon at δ 139.26 was assigned to C-6′, which is linked to the isoflavan moiety, because it showed three-bond correlations in the HMBC spectrum with the aliphatic protons H-2 and H-4, and one of the two partially overlapping singlet signals at δ 7.27. The latter displayed NOEs with all aliphatic protons indicating that there is free rotation around the bond connecting the C-ring of the isoflavan A/C-ring system to the rest of the molecule. One of these two singlet signals was assigned to C-5′ because of its three-bond correlations to two oxygen-bearing carbons at δ 180.09 and 159.31. The singlet signal at δ 6.33 was assigned to C-8′ because of its two-bond correlation to the carbon at δ 159.31, assignable to C-8′a, and based on the three-bond HMBC correlations to C-6′ and a carbon at δ 112.57 assignable to C-4′a. The carbonyl carbon signal at δ 180.09 (supported by the carbonyl absorption at 1635 cm^{-1} in the IR spectrum) was left to be assigned to C-7′ thus suggesting a quinonemethide structure for the chromophore. The chromophore's complete structure was deduced from further HMBC correlations. C-4′a displayed a cross peak with δ 7.27 to which four other cross-peaks belonged, e.g. the carbon at δ 152.7 to C-4′, which also showed a three-bond correlation with the doublet at δ 7.25 belonging to a *para*-substituted ring, and to the carbon at δ 158.03, which showed a three-bond correlation to a doublet at δ 7.82 belonging to the *ortho* position of the 1,2,4-trisubstituted aromatic ring. The NOE between this latter proton and the singlet assigned to C-8′ allowed the deduction of the connectivity of the two aromatic rings to the chromophore. The NOE cross-peak between signals at δ 7.23 and 3.83 represents interaction between the proton at H-3′ and methyl protons confirming that the methoxy group is in the *ortho* position in the 1,2,4-trisubstituted aromatic ring whose connection to the central ring system is thus defined. NOEs were also expected between H-5′ and H-2‴/6‴, H-3′ and H-2‴/6‴, and between H-2 or H-4 and H-2‴/H-6‴ but were not detected due to spectral overlap (Table 2, Fig. 2). NOE was expected also between H-3′ and H-6'' but was not detected.

The assignment of a methoxy group to ring A of the isoflavan unit was corroborated by the positive ion ESI MS spectrum which exhibited a peak at m/z 387 which resulted from RDA cleavage of **1a** at the isoflavan C-ring.

The NMR and MS data established that retusapurpurin A is a quinonemethide represented by the structural formula **1a** (Fig. 1). The stability and simplicity of the ^{1}H NMR spectrum indicated that, of the at least four tautomeric structures of retusapurpurin A, **(1a)** is by far the most stable in DMSO solution at ambient temperatures. Addition of deuterium chloride (DCl) caused the color to change (hypsochromic shift) from blue to orange, consistent with the conversion of the quinonemethide into a pyrylium chromophore. Furthermore, the

addition of DCl shifted nearly all the signals downfield in the ^{1}H NMR spectrum. While most overlapping signals in the downfield region were resolved, some of the signals in the upfield region became congested. Comparison of the **1a** spectra and that of the protonated form (**2**), however, made assignment of the signals possible. The isoflavan partial structure was corroborated by 2D NMR spectral data obtained for the protonated form (**2**). All NOEs were positive except for the one between the protons at δ 4.30 and 3.61, which, we assume, was evidence of a three-spin effect between methine and methylene protons. NOE between the singlet at δ 8.20 and a 2H doublet (H-2‴ and 6‴) corroborated the connectivity of the *para*-substituted aromatic ring to the rest of the molecule. NOE between the singlet at δ 8.20 and the proton signal at δ 8.23 belonging to the 1,2,4-trisubstituted ring was expected but could not be detected because of spectral overlap. The signals for protons belonging to hydroxyl groups predicted by the molecular formula were apparently missing. ^{13}C NMR as well as 2D NMR spectroscopic data provided an overdetermined system of correlations from which the unambiguous structure **2** could be deduced. The 2,4-diarylbenzopyrylium structure of **2** is in complete agreement with **2** being the protonated form of the quinonemethide **1a**.

Retusapurpurin A (**1a**) is the first example of a new type of C_{30} isoflavan whose formation can be rationalized to occur via regioselective oxidative coupling of the isoflavan neovestitol (Ingham, 1979) to 4,4′-dihydroxy-2′-methoxychalcone (Carlson and Dolphin, 1982).

Retusapurpurin A belongs to a relatively small group of natural products: isoflavonoids condensed with a chalcone unit. The closest relative is candenatone (**3**), in which the A-ring of an isoflavan (Hamburger et al., 1988) is coupled to the chalcone unit (6→β linking). The orange pigments of sandalwood (*Pterocarpus santalinus, P. soyauxii,* and *P. osun*; Arnone et al., 1977a,b, 1981) and camwood (*Baphia nitida*; Arnone et al., 1975) have an entirely different fused ring system formally derived from two-point linking of an isoflavonoid to a chalcone.

The structures of the other fluorescent and non-fluorescent purple pigments of *D. parviflora* cell cultures have not been elucidated thus far. Based on chromatographic behavior, UV spectral data (not shown) and preliminary NMR spectroscopic data, at least some of these fluorescent pigments appear to have the same skeleton as retusapurpurin A (**1a**). The differences may be in ring substitution, and some of the minor pigments may be similar to candenatone (**3**) or represent other bimolecular coupling modes.

D. parviflora wood was reported to contain arylbenzofurans, neoflavonoids, and a benzophenone (Muangnoicharoen and Frahm, 1981, 1982). The wood from which candenatone (**3**) was isolated as the major heartwood pigment (Hamburger et al., 1988) was identified in our laboratory as *D. parviflora* by direct comparison to authentic samples of *D. parviflora* collected in Java and Borneo and *D. candenatensis* collected in Singapore, each supported with herbarium vouchers. Botanical literature also supports our determination of the red wood which is the source of both candenatone and retusapurpurin A. *D. parviflora* is a giant liana that develops a dark red heartwood; records of its use as a medicinal plant and for incense date back into the middle ages (Prain, 1904; Burkill, 1935). *D. candenatensis* is a climbing shrub of no economic importance (Chayamarit, 1986; Niyomdham et al., 1997). There exists a possible source of confusion about these two species which might have passed down in botanical literature since a monograph of Indian *Dalbergia* (Thothathri, 1987) apparently misquoted an earlier work (Kurz, 1877) attributing the red wood *D. parviflora* to *D. candenatensis*. Identification of the botanical sources of candenatone and retusapurpurin A as same means that candenatone and simple isoflavonoids hitherto attributed to *D. candenatensis* (Hamburger et al., 1987, 1988) should be referred to *D. parviflora*.

A rigorous comparison of the tissue culture- and heartwood-derived pigment has been carried out to support the premise that stress metabolism pathways that are shared with heartwood-type secondary metabolism subpathways are active in *Dalbergia* cell cultures. Retusapurpurin A purified from callus tissue of *D. retusa* and *D. parviflora*, respectively, and from *D. parviflora* wood had identical color reactions, fluorescence, UV/VIS spectrum, solvatochromic, and thermochromic behavior, molecular weight determined by ESI MS, and they comigrated in HPLC and several TLC solvent systems (see Experimental).

The subpathway to 4,4′-dihydroxy-2′-methoxychalcone (Carlson and Dolphin, 1982) is already known at the level of genes in alfalfa, and most of the genes for the isoflavan pathway are known (Akashi et al., 1998; Dixon et al., 1998). Retusapurpurin A represents an extension of the known isoflavonoid pathway in the direction of heartwood-type metabolism, and the biosynthetic gene(s) must be responsive to both stress and developmental cues. The next challenge is to identify the substrates undergoing coupling, and to determine whether the enzymatic coupling is as regioselective in vitro as in vivo. Identification of the enzyme(s) will afford access to genes involved in stress metabolism common to several species and possibly support research into the yet uncharted heartwood-type metabolic and cellular differentiation.

3. Experimental

3.1. General experimental procedures

For structural assignments, NMR spectra were recorded on solutions (0.8 ml) of **1a** and **2** in DMSO-d_6

(Cambridge Isotope Laboratories, Andover, MA) with a Varian INOVA 500 spectrometer (^{1}H NMR, 500.163 MHz, ^{13}C NMR, 125.781 MHz) at 25°C. The resonances were measured relative to internal DMSO-d_6 and the chemical shifts are expressed in parts per million (δ). Standard Varian supplied pulse sequences were used for gradient enhanced absolute value COSY, phase-sensitive double quantum filtered DQF-COSY, phase sensitive NOESY, and gradient enhanced HMQC and HMBC experiments. Mass spectra were recorded on a VG Trio 3 triple quadrupole instrument (Beverly, MA); the ESI and APCI sources were designed by Analytica (Branford, CT). IR spectrum of **1a** was recorded on a Perkin Elmer FTIR 1600 Series instrument (16 scans, resolution: 4 cm^{-1}).

3.2. Plant materials

The comparative phytochemical analysis included heartwood samples (h) and cell cultures (c) of the species listed below. Callus cultures were initiated from in vitro germinated seedlings or from explants of plants cultivated in the greenhouse.

Baphia nitida Lodd. (h,c), *Caesalpinia bonducella* (L.) Fleming (h,c), *C. cacalaco* Bonpl. (c), *C. coriaria* (Jacq.) Willd. (c), *C. decapetala* (Roth) Alston (c), *C. ferrea* Mart. (c), *C. gilliesii* (Wall. *ex* Hook.) Dietr. (c), *C. pulcherrima* (L.) Swartz (c), *C. sepiaria* Roxb. (c), *C. spinosa* (Mol.) O. Kuntze (c), *C. tinctoria* Dombey *ex* DC. (c), *C. vesicaria* L. (c), *C. violacea* (Mill.) Standl. (h,c), *Dalbergia arbutifolia* Baker (c), *D. assamica* Benth. (c), *D. balansae* Prain (a), *D. bariensis* Pierre (h), *D. baroni* Baker (h), *D. boehmii* Taubert (h), *D. brownei* (Jacq.) Urban (h,c), *D. calycina* Benth. (h,c), *D. cambodiana* Pierre (h), *D. candenatensis* (Dennst.) Prain (h,c), *D. cearensis* Ducke (h), *D. chermezonii* R. Viguier (h), *D. chlorocarpa* R. Viguier (h), *D. cochinchinensis* Pierre ex Laness. (h,c), *D. congestiflora* Pittier (h), *D. cubilquitzensis* (J. D. Smith) Pittier (h,c), *D. cultrata* Graham (h,c), *D. cuscatlanica* (Standley) Standley (h), *D. decipularis* Rizz. & A. Mattos (h), *D. densa* Benth. *var. australis* (c), *D. ecastaphyllum* (L.) Taubert (h,c), *D. floribunda* Craib (h), *D. foliolosa* Benth. (h), *D. frutescens* (Vell. Conc.) Britton (h), *D. funera* Standley (h), *D. fusca* Pierre (h), *D. glabra* (Miller) Standley (h,c), *D. granadillo* Pittier (h), *D. greveana* Baillon (h), *D. hainanensis* Merr. & Chun (c), *D. hupeana* Hance (h,c), *D. hypoleuca* Pittier (h), *D. latifolia* Roxb. (h,c), *D. lineata* Pittier (h), *D. louvelii* R. Viguier (h), *D. madagascariensis* Vatke (h), *D. maritima* R. Viguier (h), *D. mammosa* Pierre (h), *D. martinii* F. White (c), *D. melanocardium* Pittier (c), *D. melanoxylon* Guillemin & Perrottet (h,c), *D. miscolobium* Benth. (h,c), *D. nigra* (Vell.) Allemão ex Benth. (h,c), *D. nigrescens* Kurz (h,c), *D. nitidula* Welw. ex Baker (h), *D. obovata* E. Meyer (c), *D. obtusa* Lecomte (h), *D. oliveri* Gamble (h,c), *D. ovata* Graham (h), *D. palo-escrito* Rzedowski & L. I. Guridi-Gomez (h), *D. parviflora* Roxb. (h,c), *D. pterocarpifolia* Baker (h), *D. retusa* Hemsley (h,c), *D. sericea* G. Don (c), *D. sissoo* Roxb. (h,c), *D. spruceana* Benth. (h), *D. stevensonii* Standley (h), *D. trichocarpa* Baker (c), *D. tucurensis* J. D. Smith (h,c), *Haematoxylon braziletto* Karst. (h,c), *H. campechianum* L. (h,c), *Pterocarpus angolensis* DC. (h,c), *P. antunesii* (Taub.) Harms (c), *P. erinaceus* Poir. (c), *P. indicus* Willd. (h,c), *P. macrocarpus* Kurz (h,c), *P. rotundifolius* Druce (h,c), *P. santalinus* L.f. (h), *P. soyauxii* Taub. (h), *P. tinctorius* Welw. (h,c).

D. candenatensis stem and live plants were collected in Pulau Semakau (Singapore) and identified by Dr. Hugh T.W. Tan (School of Biological Sciences, The National University of Singapore, herbarium vouchers for our samples are SINU Nos. SM DC 27 Sep 1996, and SM DC 2). Sample labeled as '*D. candenatensis*' was a gift from Dr. N. Ruangrungsi (Faculty of Pharmaceutical Sciences, Chulalongkorn Univ., Bangkok). The sources of *D. parviflora* wood samples were as follows. Sample RTIw7917 (for abbreviations of institutional wood collections see Stern, 1988), collected in Indonesia (cut off from a larger sample supported by a voucher: Herbarium Bogoriense #8326) and sample without number, Borneo, were from Dr. Iep Wiselius (I.W.R.A. Consultancy, Woodsection, Westzaan, The Netherlands). Commercial samples identical to *D. parviflora* were from the Kamwo Trading Co., New York, NY (Herbal Catalog #HA108). Seeds were from Dr. Ir. Suhirman, Bogor Botanic Gardens, Indonesia. *D. retusa* seeds were from C. Elevich (AgroForester Tropical Seeds, Holualoa, Hawaii), and the wood samples were RBHw 4807, RBHw 16229, and MADw 42824. Additional information on the sources of plant materials can be obtained from the authors.

Seeds and leaves were surface sterilized with mercuric chloride (0.1% v/w, 15 min). The seeds were incubated in sterile moist cotton. Rescue of living tissue by excision from the testa was necessary with old seeds (*D. calycina*, *D. miscolobium, D. parviflora*) in which large portions of the cotyledon or the embryo were dead. The tissues rescued from seeds, cotyledons or leaves cut from germinated seeds, and the surface sterilized leaves were placed on callus induction medium (26–28 °C; continuous illumination, 30–50 μmol m^{-2} s^{-1}; mixture of incandescent and cool white fluorescent tubes: Sylvania and Power-Twist Vita-Lite 40 W).

All tissue culture media were supplemented with 30 g l^{-1} sucrose, solidified with Bacto agar 7 g l^{-1}, and sterilized in a pressure cooker (109 °C, 35 kPa, 25 min); the pH was adjusted to 5.8 before autoclaving. DM-1 medium contained MS (Murashige and Skoog, 1975) basal salts (Sigma Fine Chemicals) 4.3 g; KH_2PO_4 (6% [w/v]), 3 ml; *myo*-inositol, 100 mg; vitamin B_1, 1 mg; vitamin

B_6, 0.1 mg; glycine, 0.2 mg, nicotinic acid, 0.1 mg, folic acid, 0.05 mg, biotin, 0.1 mg, and supplemented with the plant growth regulators adenine hemisulfate, 10 mg; picloram, 0.12 mg; indole-3-butyric acid, 1 mg; 2,4-dichlorophenoxyacetic acid, 0.5 mg; isopentenyladenine, 0.5 mg; and *trans*-zeatin, 0.5 mg per liter. DM-2 medium was DM-1 supplemented with 0.1 M mannitol. DM-3 medium differs only in the plant growth regulators: adenine hemisulfate, 10 mg; 2,4-dichlorophenoxyacetic acid, 0.2 mg per liter; thidiazuron 0.022 mg. DM-4 contained Anderson's (Anderson, 1984) rhododendron basal salt mixture (Sigma Fine Chemicals) 1.89 g, vitamins of DM-1, and supplemented with the plant growth regulators; 2,4,5-trichlorophenoxy acetic acid, 0.04 mg per liter; thidiazuron 0.022 mg. DM-5 contained MS salts 4.3 g and 0.022 mg thidiazuron. DM-6 was MS salts, 4.3 g; vitamins of DM-1; adenine hemisulfate, 10 mg; 1-naphthaleneacetic acid, 0.2 mg l^{-1}; thidiazuron 0.022 mg. DM-7 was the same as DM-6 except that it contained 0.2 mg l^{-1} picloram instead of 1-naphthaleneacetic acid. DM-8 was the same as DM-1 except that it contained also 3 mg thidiazuron, and as much as 60 mg adenine hemisulfate per liter. DM-9 contained CLC/Ipomoea (CP) Basal salt mixture (Chée et al., 1992; Sigma Fine Chemicals) 6.7 g, vitamins of DM-1, and supplemented with the plant growth regulators; 2,4,5-trichlorophenoxyacetic acid, 0.04 mg per liter; thidiazuron 0.022 mg. DM-10 contained C2d vitis basal salt mixture (Chée and Pool, 1987, Sigma Fine Chemicals) 4.47 g, vitamins of DM-1, 2,4,5-trichlorophenoxyacetic acid, 0.04 mg, and thidiazuron, 0.022 mg.

All *Baphia*, *Caesalpinia*, *Haematoxylon*, and *Pterocarpus* as well as most *Dalbergia* species developed callus on DM-1 medium; the exceptions are listed in Table 1. In *D. melanocardium,* primary callus formed at the base of shoot tips excised from in vitro germinated seedlings and inserted into DM-5 medium, and this callus was maintained on DM-6 medium.

3.3. Pigment survey and isolation

Pigments extracted in ethanol were separated by paper electrophoresis (in 50% acetic acid, 25 V/cm on Whatman 3MM paper spanned between the buffer chambers connected to platinum electrodes) and TLC on silica gel (250 μm on polyester backed flexible plates, PE SIL G, Whatman) in solvent systems I (ethylacetate–methanol–water 100:16:13) and II (chloroform–methanol–water 80:20:2) (Hamburger et al., 1988).

For purification on a preparative scale, *Dalbergia retusa* callus pieces showing red coloration were repeatedly extracted with ethanol at 66 °C to give rise to a deep orange red solution. Crude pigment was precipitated from a preconcentrated ethanol extract by addition of H_2O. Fractionation was performed by suspending the precipitate in H_2O (1 g per 200 ml H_2O) with stirring. The resulting brownish red solid was collected by centrifugation and fractionation was repeated thrice with fresh H_2O (200 ml). The water insoluble pellet was further fractionated by suspending in benzene (1 g per 200 ml) with stirring and incubation at 50°C. Benzene extraction was repeated thrice. The insoluble pigment was collected by centrifugation, and redissolved in ethanol to give a dark brownish red solution. Preparative scale separation of the ethanol extract by TLC on Whatman PK5 preparative silica gel plates (1 mm on glass, pore size: 25–150 Å) was carried out first in solvent system II. There were at least three high mobility UV fluorescent (pink) and several UV absorbent purple/red components of lower mobility. The main component, retusapurpurin A (third band from top, R_f 0.63, color in HCl fumes is orange yellow, HCl + UV: orange yellow, in NH_3 red purple, NH_3 + UV: mauve pink, intermediate colors under neutral conditions), was subjected to rechromatography first in solvent system I (R_f 0.71) to separate it from traces of contaminants, then twice in solvent system II. Yield was approximately 0.01% of dry weight.

Retusapurpurin A was identified in the ethanol extract of *D. parviflora* heartwood as the main fluorescent pink band. It was isolated from the heartwood and callus by the procedure applied to *D. retusa* callus (yield was about 0.03 and 0.01% of dry weight, respectively).

3.4. Retusapurpurin A (*1a*)

Deep red amorphous powder. UV/VIS (EtOH–0.1 M Na-citrate (pH 5.0) 2:1 (v/v)): λ_{max} nm: 533 *sh*, 510, 392, 320 *sh*, 279. + $NaHCO_3$: 567, 533 sh, 419, 401, 323, 300, 288 sh, 271. + $AlCl_3$ + HCl or + HCl alone: 490, 420 *sh*, 284. λ_{max} (DMSO): 610, 571 sh, 526 *sh*, 433, 388, 338, 280. IR ν_{max} (KBr) cm^{-1}: 1635. MS (ESI, positive ion mode): 523 $[M+H]^+$ and *m/z* 413 (7), 399 (8), 387 (48), 371 (7), and 233 (10). MS (APCI, high capture voltage): $[M+H]^+$ 523. NMR: Table 2.

Retusapurpurin A isolated from *D. retusa* callus appeared homogeneous and comigrated on TLC with samples isolated from *D. parviflora* callus and wood in systems I (pink/red, UV: pink; R_f 0.71), II (R_f 0.63), III (toluene-methanol-water 140:77:3, R_f 0.60), IV (chloroform-tetrahydrofuran-water 40:70:2, R_f 0.33), V (ethylacetate–tetrahydrofuran–water 40:23:2, R_f 0.57), and in HPLC: 4.92 min (normal phase silica, 5 μm × 10 cm, 100 Å (Microsorb-MV) in MeOH-$CHCl_3$ (1:19), isocratic separation on a Beckman Model 332 gradient liquid chromatograph using a Model 165 variable wavelength detector).

Acknowledgements

We thank Perry Pellechia (Dept. Chemistry and Biochemistry) for NMR spectroscopy; Drs. Michael Walla

and William Cotham for MS; and Dr. Glenn Sauer for IR spectroscopy. This work was supported in part by US DA Grant No. 95-37302-1937 and SCUREF Cooperative Project No. USC 98-414.

References

Akashi, T., Aoki, T., Ayabe, S., 1998. Biochem. Biophys. Res. Commun. 251, 67–70.

Allen, R.M., Hiatt, E.N., 1994. Wood Fiber Sci. 26, 294–302.

Anderson, W.C., 1980. Proceedings of the Conference on Nursery Production of Fruit Plants Through Tissue Culture: Applications and Feasibility. 21–22 April 1980. Beltsville, MD, pp. 27–34.

Arnone, A., Camarda, L., Merlini, L., Nasini, G., 1977a. J. Chem. Soc. Perkin Trans. 1, 2118–2122.

Arnone, A., Camarda, L., Merlini, L., Nasini, G., Taylor, D.A.H., 1977b. J. Chem. Soc. Perkin Transa. 1, 2116–2118.

Arnone, A., Camarda, L., Merlini, L., Nasini, G., Taylor, D.A.H., 1981. Phytochemistry 20, 799–801.

Arnone, A., Camarda, L., Merlini, L., Nasini, G., 1975. J. Chem. Soc. Perkin Trans. 1, 186–194.

Burkill, I.H., 1935. A Dictionary of the Economic Products of the Malay Peninsula. Crown Agents for the Colonies, London, pp. 754–755.

Campbell, M.M., Ellis, B.E., 1992. Plant Physiol. 98, 62–70.

Carlson, R.E., Dolphin, D.H., 1982. Phytochemistry 21, 1733–1736.

Chayamarit, K., 1986. Thai For. Bull. 16, 119–153.

Chée, R.P., Leskovar, D.I., Cantliffe, D.J., 1992. J. Am. Soc. Hortic. Sci. 117, 663–667.

Chée, R., Pool, R.M., 1987. Sci. Hortic. (Amsterdam) 32, 85–95.

Davin, L.B., Bedgar, D.L., Katayama, T., Lewis, N.G., 1992. Phytochemistry 31, 3869–3874.

Davin, L.B., Wang, H.-B., Crowell, A.L., Bedgar, D.L., Martin, D.M., Sarkanen, S., Lewis, N.G., 1997. Science 275, 362–366.

Dixon, R.A., Howles, P.A., Lamb, C., He, X.-Z., Reddy, J.T., 1998. In: Manthey, J.A., Buslig, B.S., (Eds.), Flavonoids in the Living System. Plenum, New York, pp. 55–66.

Eberhardt, T.L., Bernards, M.A., He, L.F., Davin, L.B., Wooten, J.B., Lewis, N.G., 1993. J. Biol. Chem. 268, 21088–21096.

Fukuda, H., 1996. Annual Review of Plant Physiology. Plant Mol. Biol. 47, 299-325.

Gang, D.R., Costa, M.A., Fujita, M., Dinkova-Kostova, A.T., Wang, H-B., Burlat, V., Martin, W., et al., 1999. Chem. Biol. 6, 143–151.

Hamburger, M.O., Cordell, G.A., Tantivatana, P., Ruangrungsi, N., 1987. J. Nat. Prod. 50, 696–699.

Hamburger, M.O., Cordell, G.A., Ruangrungsi, N., Tantivatana, P., 1988. J. Org. Chem. 53, 4161–4165.

Harborne, J.B., 1994. The Flavonoids. Advances in Research Since 1986. Chapman & Hall, London.

Higuchi, T., 1997. Biochemistry and Molecular Biology of Wood. Springer, New York.

Ingham, J.L., 1979. Z. Naturforsch. 34c, 630–631.

Kurosawa, K., Ollis, W.D., Sutherland, I.O., Gottlieb, O.R., Oliveira, A.B.D.E., 1978. Phytochemistry 17, 1405–1411.

Kurz, S. (1877) Forest Flora of British Burma. Vol. 1., Calcutta.

Lee, S.K., Rao, A.N. (1980) In: Sala, F., Parisi, B., Cella, R., Cifferi, O. (Eds.), Plant Cell Cultures: Results and Perspectives. Elsevier/North-Holland Biomedical, Amsterdam, pp. 305–311.

Lewis, N.G., 1999. Curr. Opin. Plant Biol. 2, 153–162.

Magel, E.A., Drouet, A., Claudot, A.C., Ziegler, H., 1991. Trees (Berlin) 5, 203–207.

Magel, E., Huebner, B., 1997. Bot. Acta 110, 314–322.

Magel, E.A., Monties, B., Drouet, A., Jay-Allemand, C., Ziegler, H., 1995. In: Sandermann Jr. H. Bonnet-Masimbert, M. (Eds.), EUROSILVA: Contribution to Forest Tree Physiology. Institut National de la Recherche Agronomique, Paris, pp. 35–56.

Mandal, A.K., Subramanian, K.N., Nagarajan, B., 1994. Indian For. 120, 413–422.

Muangnoicharoen, N., Frahm, A.W., 1981. Phytochemistry 20, 291–293.

Muangnoicharoen, N., Frahm, A.W., 1982. Phytochemistry 21, 767–772.

Murashige, T., Skoog, F., 1962. Physiologia Plantarum 15, 473–497.

Niyomdham, C., Hô, P.H., Dy Phon, P., Vidal, J.E., 1997. Flore du Cambodge du Laos et du Viêtnam 29. Leguminosae-Papilionoideae-Dalbergieae. Muséum National d'Histoire Naturelle, Laboratoire de Phanérogamie, Paris.

Nose, M., Bernards, M.A., Furlan, M., Zajicek, J., Eberhardt, T.L., Lewis, N.G., 1995. Phytochemistry 39, 71–79.

Ohashi, H., Kato, N., Imai, T., Kawai, S., 1991. Holzforschung 45, 245–252.

Paré, P.W., Wang, H.-B., Davin, L.B., Lewis, N.G., 1994. Tetrahedron Lett. 35, 4731–4734.

Prain, D., 1904. Ann. Royal Bot. Gard. (Calcutta) 10, 1–114.

Rahman, S.M., Hossain, M., Biswas, B.K., 1993. Plant Cell Tiss. Org 32, 363–365.

Robinson, R.. , 1985. Bull. Soc. Chim. Fr. 1985, 125–134.

Shigo, A.L., 1994. Tree Anatomy. Shigo & Trees, Associates, Durham.

Stern, W.L., 1988. IAWA Bull. 9, 203–252.

Thothathri, K., 1987. Taxonomic Revision of the Tribe Dalbergieae in the Indian Subcontinent. Botanical Survey of India, Calcutta.

Whetten, R., MacKay, J.J., Sederoff, R.R., 1998. Annu. Rev. Plant Physiol. Plant Mol. Biol. 49, 585–609.

Yamaguchi, T., Itose, R., Sakai, K., 1997. J. Fac. Agr. Kyushu Univ. 42, 131–138.

Zhentian, L., Jervis, J., Helm, R.F., 1999. Phytochemistry 51, 751–756.

PERGAMON

Phytochemistry 57 (2001) 1023–1034

PHYTOCHEMISTRY

www.elsevier.com/locate/phytochem

Structure and stereochemistry of triflavanoids containing both ether and carbon–carbon interflavanyl bonds☆

Linette Bennie [a], Johan Coetzee [a], Elfranco Malan [a], Daneel Ferreira [b,*]

[a] *Department of Chemistry, University of the Orange Free State, PO Box 339, Bloemfontein, 9300 South Africa*
[b] *National Center for Natural Products Research, Research Institute of Pharmaceutical Sciences, School of Pharmacy, The University of Mississippi, University, MS 38677, USA*

Received 29 June 2000; received in revised form 29 August 2000

Abstract

The first triflavanoids with both C–C and C–O–C interflavanyl bonds, epioritin-(4β→6)-epioritin-(4α→4)-epioritin-4β-ol, epioritin-(4β→3)-epioritin-(4β→6)-epioritin-4β-ol and epioritin-(4β→3)-epioritin-(4β→6)-epimesquitol-4α-ol, were identified in the heartwood of *Acacia caffra*. The ethereal interflavanyl bond is readily susceptible to reductive cleavage with sodium cyanoborohydride in trifluoroacetic acid/dichloromethane which hence permits the unequivocal assignment of the absolute configuration of constituent flavanyl units. © 2001 Elsevier Science Ltd. All rights reserved.

Keywords: *Acacia caffra*; Leguminosae; Triflavanoids; Pro-/leucoanthocyanidins; Pro-/leucoteracacinidins; Pro-/leucomelacacinidins; Absolute configuration; Reductive cleavage

1. Introduction

The proanthocyanidin pool in heartwoods usually involves the presence of carbon–carbon bonds linking predominantly flavan-3-ol constituent moieties (Porter, 1994; Ferreira and Bekker, 1996; Ferreira and Li, 2000). Such an ensemble of flavan-3-ol units originates *via* electrophilic aromatic substitution of flavan-4-yl carbocations (or their equivalents) derived from flavan-3,4-diols and the nucleophilic centers of the *m*-oxygenated A-rings of flavan-3-ols (Hemingway, 1989; Ferreira et al., 1999). In the absence of these potent flavan-3-ol nucleophiles with their aptitude for the formation of carbon-carbon bonds, alternative centers emerge as participants in interflavanyl bond formation. This is especially prevalent in natural sources containing precursors with a 7,8-dihydroxy functionality of their A-rings where carbon-carbon coupled proanthocyanidins are often accompanied by ether-linked leucoanthocyanidins (Foo, 1989; Coetzee et al., 1998a, b; Bennie et al., 2000). We now report the structures of a new dimeric leucoteracacinidin, epioritin-(4β→4)-epioritin-4β-ol **1**, and the first triflavanoids with both a C–C and a C–O–C interflavanyl bond, epioritin-(4β→6)-epioritin-(4α→4)-epioritin-4β-ol **15**, epioritin-(4β→3)-epioritin-(4β→6)-epioritin-4β-ol **17**, and epioritin-(4β→3)-epioritin-(4β→6)-epimesquitol-4α-ol **19**, from *Acacia caffra*. Reductive cleavage of the ether bonds permits the unequivocal definition of the absolute configuration of constituent flavanyl units.

2. Results and discussion

Besides the known leucoteracacinidins *ent*-oritin-(4α→4)-epioritin-4α-ol, epioritin-(4β→4)-epioritin-4α-ol **3**, epioritin-(4β→3)-epioritin-4β-ol **9**, epioritin-(4β→3)-epioritin-4α-ol **11**, epioritin-(4β→3)-oritin-4α-ol **13**, and the 'mixed' leucomelacacinidin/leucoteracacinidin epimesquitol-(4β→4)-epioritin-4β-ol **5** (Bennie et al., 2000), the MeOH extract of the heartwood of *A. caffra* also affords epioritin-(4β→4)-epioritin-4β-ol **1**. The above dimers are accompanied by the first trimeric analogues, epioritin-(4β→6)-epioritin-(4α→4)-epioritin-4β-ol **15**, epioritin-(4β→3)-epioritin-(4β→6)-epioritin-4β-ol **17**, and epioritin - (4β→3) - epioritin - (4β→6) - epimesquitol - 4α - ol **19**. Owing to the complexity of the

☆ Part 33 in the series 'Oligomeric flavanoids'. Part 32 (Bennie et al., 2000).

* Corresponding author. Tel.: +1-91-662-915-1572; fax: +1-91-662-915-7062.

E-mail address: dferreir@olemiss.edu (D. Ferreira).

0031-9422/01/$ - see front matter © 2001 Elsevier Science Ltd. All rights reserved.
PII: S0031-9422(01)00044-9

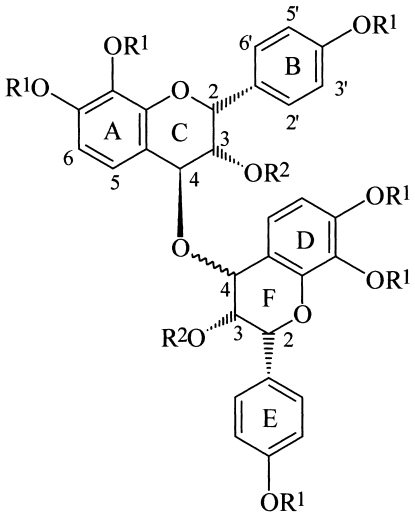

1 ⦚≡◭ , $R^1=R^2=H$
2 ⦚≡◭ , $R^1=Me, R^2=Ac$
3 ⦚≡≣ , $R^1=R^2=H$
4 ⦚≡≣ , $R^1=Me, R^2=Ac$

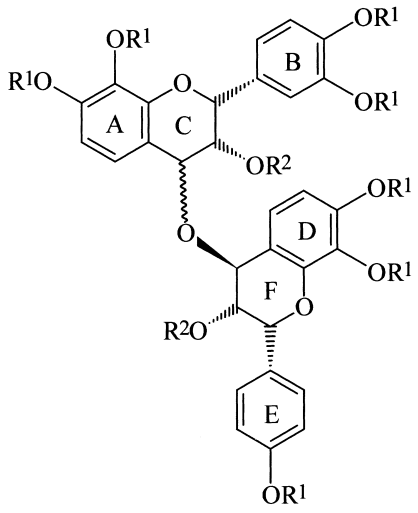

5 ⦚≡◭ , $R^1=R^2=H$
6 ⦚≡◭ , $R^1=Me, R^2=Ac$
7 ⦚≡≣ , $R^1=R^2=H$
8 ⦚≡≣ , $R^1=Me, R^2=Ac$

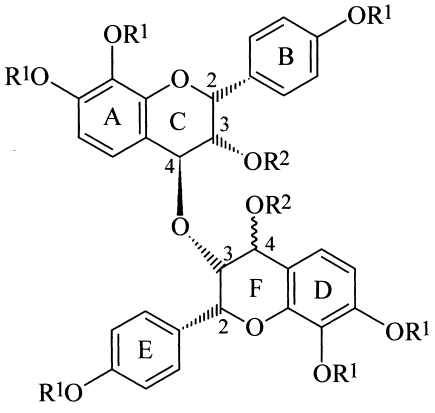

9 ⦚≡◭ , $R^1=R^2=H$
10 ⦚≡◭ , $R^1=Me, R^2=Ac$
11 ⦚≡≣ , $R^1=R^2=H$
12 ⦚≡≣ , $R^1=Me, R^2=Ac$

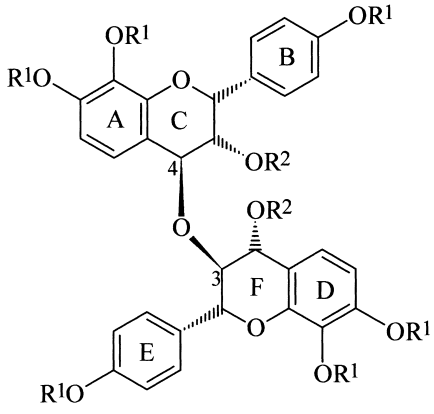

13 $R^1=R^2=H$
14 $R^1=Me, R^2=Ac$

phenolic mixture, these compounds were purified and identified as their permethylaryl ether acetate derivatives **2**, **16**, **18** and **20**.

In addition to the one *O*-acetyl and three *O*-methyl resonances the ^1H NMR spectral data (Table 1) of the epioritin-(4β→4)-epioritin-4β-ol derivative **2** only display an AB- and an AA′BB′-spin system in the aromatic region as well as only one AMX-system for protons of the heterocyclic ring. However, the chemical shifts of the latter protons are typical of similar derivatives of the (4-*O*-4)-bis-leucoanthocyanidins (Coetzee et al., 1998b; Bennie et al., 2000). The dimeric nature of compound 2 is accordingly confirmed by HREIMS analysis which indicates a molecular ion at $[M^+]$ 730.2703 ($C_{40}H_{42}O_{13}$).

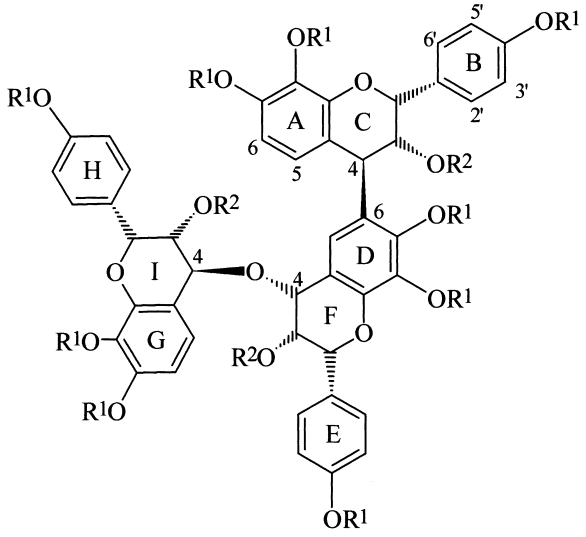

15 $R^1=R^2=H$
16 $R^1=Me$, $R^2=Ac$

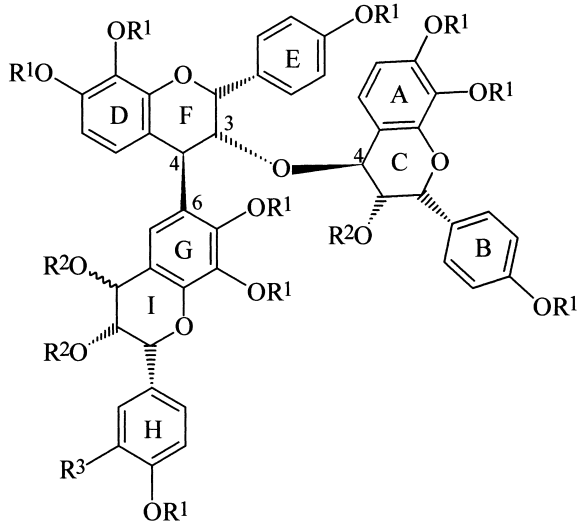

17 ≡ , $R^1=R^2=R^3=H$
18 ≡ , $R^1=Me$, $R^2=Ac$, $R^3=H$
19 ≡ , $R^1=R^2=H$, $R^3=OH$
20 ≡ , $R^1=Me$, $R^2=Ac$, $R^3=OMe$

Compound **2** is hence a symmetrical (4-*O*-4)-bis-leucoteracacinidin since only this mode of linkage could introduce a plane of symmetry into the molecule. The coupling constants ($^3J_{2,3}=1.5$; $^3J_{3,4}=3.0$ Hz) are reminiscent of 2,3-*cis*-3,4-*trans* relative stereochemistry (Malan and Sireeparsad, 1995; Coetzee et al., 1998a,b; Bennie et al., 2000). Although the CD spectrum of derivative 2 exhibits a high-amplitude negative Cotton effect at 246.7 nm ($[\theta]=-6.386\times10^4$), this cannot be related to chirality at C-4 due to the absence of a second phenyl chromophore in close proximity of this stereocenter (De Angelis and Wildman, 1969; Barrett et al., 1979; Botha et al., 1981; Van der Westhuizen et al., 1981). Reductive cleavage of the (4-*O*-4)-ether linkage with sodium cyanoborohydride [$Na(CN)BH_3$] in trifluoroacetic acid (TFA)/dichloromethane affords 3-*O*-acetyl-7,8,4-tri-*O*-methylepioritin **24** as the sole product (*vide infra*). Comparison of ^{1}H NMR and CD spectral data of **24** with those of an authentic sample supports the assignment of 2*R*,3*R* absolute configuration to both the C- and F-rings (Korver and Wilkins, 1971; Van Rensburg et al., 1999; Coetzee et al., 2000). The 4*S* configuration of both C- and F-rings of **2** is assigned using the $^3J_{3,4}$-value which indicates a 3,4-*trans* relative stereochemistry for each heterocyclic ring.

FAB-MS analyses of the permethylaryl ether acetate derivatives **16**, **18** and **20** of compounds **15**, **17** and **19** indicate molecular formulas of $C_{60}H_{62}O_{19}$ (*m*/*z* 1086) for **16** and **18**, and $C_{61}H_{64}O_{20}$ (*m*/*z* 1116) for **20**. When taken in conjunction with the number of *O*-methyl and *O*-acetyl resonances in their ^{1}H NMR spectra (Table 2) these formulas confirm the trimeric nature of all three analogues. The ^{1}H NMR spectra, conspicuously free of the effects of dynamic rotational isomerism about the interflavanyl bonds, indicate three *O*-acetyl resonances, one aromatic proton singlet, two aromatic AB- and three AA′BB′-spin systems as well as three AMX-spin systems for protons in the heterocyclic region for derivatives **16** and **18**. The data suggest trimeric structures comprising derivatized 7,8,4′-trihydroxyflavan-3-ol constituent units linked via one ether and one carbon–carbon interflavanyl bond. In the ^{1}H NMR spectrum of derivative **20**, one of the aromatic AA′BB′-spin systems is replaced by an ABX-system hence indicating a trimer comprising one derivatized 7,8,3′,4′-tetrahydroxy- and two derivatized 7,8,4′-trihydroxyflavan-3-ol constituent units.

The three heterocyclic AMX-spin systems of derivative **18** exhibit coupling constants reminiscent of 2,3-*cis*-3,4-*trans* ($^3J_{2,3}=1.5$; $^3J_{3,4}=3.0$ Hz for the I-ring, and $^3J_{2,3}=1.0$; $^3J_{3,4}=2.0$ Hz for the C- and F-rings) relative configuration (Steynberg et al., 1991; Malan and Sireeparsad, 1995). Two of the AMX-spin systems of derivatives **16** and **20** similarly indicate 2,3-*cis*-3,4-*trans* relative configuration ($^3J_{2,3}=1.5$, 1.0, and $^3J_{3,4}=3.0$, 2.0 for both **16** and **20**). The third AMX-system is reminiscent of 2,3-*cis*-3,4-*cis* ($^3J_{2,3}=1.0$; $^3J_{3,4}=4.5$ Hz for both **16** and **20**) relative stereochemistry (Coetzee et al., 1998b). Such all-*cis* configurations are confirmed by NOE associations between 2- and 4-H which indicate that these protons are coplanar hence occupying the same face of the heterocyclic ring. For the rings with 2,3-*cis*-3,4-*trans* relative configurations, these n.O.e. associations are conspicuously absent.

Longe range coupling ($^4J_{HH}$) observed from a COSY experiment, together with n.O.e. associations between the respective 2′,6′-protons (B-, E-, H-rings) and the

Table 1
^{1}H NMR (300 MHz, 296 K) spectral data of dimeric compounds **2**, **8**, **32**, **33** and **34** in $CDCl_3$. Splitting patterns and *J*-values are given in parentheses

Ring	H	**2**	**8**	**32**	**33**	**34**
A	5	7.13 (*d*, 8.5)	7.10 (*d*, 8.5)	6.73 (*d*, 9.0)	6.76 (*d*, 9.0)	6.75 (*d*, 9.0)
	6	6.72 (*d*, 8.5)	6.67 (*d*, 8.5)	6.59 (*d*, 9.0)	6.60 (*d*, 9.0)	6.60 (*d*, 9.0)
B	2, 6	7.44 (*d*, 9.0)	7.47 (*d*, 8.5)	7.29 (*d*, 9.0)	7.37 (*d*, 9.0)	7.38 (*d*, 9.0)
	3, 5	6.97 (*d*, 9.0)	6.92 (*d*, 8.5)	6.87 (*d*, 9.0)	6.93 (*d*, 9.0)	6.93 (*d*, 9.0)
C	2	5.37 (*br.s*, ca 1.5)	5.50 (*br.s*, ca 1.5)	5.12 (*br.s*, ca 1.5)	5.07 (*br.s*, ca 1.5)	5.07 (*br.s*, ca 1.5)
	3	5.40 (*dd*, 1.5, 3.0)	5.27 (*dd*, 1.5, 3.0)	5.39 (*dd*, 1.5, 3.0)	4.15 (*m*)	4.15 (*m*)
	4	4.82 (*d*, 3.0)	4.73 (*d*, 3.0)	4.48 (*d*, 3.0)	4.50 (*d*, 3.0)	4.51 (*d*, 3.0)
D	5	–	6.97 (*d*, 8.5)	6.19 (*br.s*)	6.17 (*br.s*)	6.18 (*br.s*)
	6	–	6.58 (*d*, 8.5)	–	–	–
E	2, 6	–	–	7.39 (*d*, 9.0)	7.39 (*d*, 9.0)	–
	3, 5	–	–	6.93 (*d*, 9.0)	6.93 (*d*, 9.0)	–
	2	–	7.09 (*d*, 2.0)	–	–	7.05 (*d*, 2.0)
	5	–	6.90 (*d*, 8.5)	–	–	6.89 (*d*, 8.5)
	6	–	7.06 (*dd*, 2.0, 8.5)	–	–	7.01 (*dd*, 2.0, 8.5)
F	2	–	5.36 (*br.s*, ca 1.0)	5.19 (*br.s*, ca 1.0)	5.10 (*br.s*, ca 1.0)	5.10 (*br.s*, ca 1.0)
	3	–	5.89 (*dd*, 1.0, 4.5)	5.37 (*m*)	5.37 (*m*)	5.40 (*m*)
	4	–	5.32 (*d*, 4.5)	3.17 (*dd*, 4.5, 17.0)	3.15 (*dd*, 4.5, 17.0)	3.16 (*dd*, 4.5, 17.0)
				2.78 (*dd*, 3.0, 17.0)	2.78 (*dd*, 2.5, 17.0)	2.79 (*dd*, 3.0, 17.0)
OMe		3.93, 3.89, 3.86 (each *s*)	3.95, 3.93, 3.92 (×3), 3.87, 3.83 (each *s*)	4.03, 4.01, 3.99, 3.92, 3.84, 3.81 (each *s*)	4.03, 4.00, 3.99, 3, 91, 3.84, 3.83 (each *s*)	4.01 (×2), 3.92 (×2), 3.91, 3.83 (×2) (each *s*)
OAc		1.94 (*s*)	1.98, 1.86 (each *s*)	1.91 (×2), *s*	1.91 (*s*)	1.91 (*s*)

Table 2
^{1}H NMR (300 MHz, 296 K) spectral data of trimeric derivatives **16**, **18** and **20** in $CDCl_3$. Splitting patterns and *J*-values are given in parentheses

Ring	H	**16**	**18**	**20**
A	5	6.56 (*d*, 9.0)	6.83 (*d*, 9.0)	6.82 (*d*, 9.0)
	6	6.64 (*d*, 9.0)	6.55 (*d*, 9.0)	6.54 (*d*, 9.0)
B	2, 6	7.30 (*d*, 9.0)	6.90 (*d*, 9.0)	6.91 (*d*, 9.0)
	3, 5	6.86 (*d*, 9.0)	6.80 (*d*, 9.0)	6.81 (*d*, 9.0)
C	2	5.18 (*br.s*, ca 1.0)	4.69 (*br.s*, ca 1.0)	4.74 (*br.s*, ca 1.0)
	3	5.42 (*dd*, 1.5, 3.0)	4.59 (*dd*, 1.0, 2.0)	4.65 (*dd*, 1.0, 2.0)
	4	4.50 (*d*, 3.0)	4.56 (*d*, 2.0)	4.58 (*d*, 2.0)
D	5	6.73 (*br.s*)	6.77 (*d*, 9.0)	6.80 (*d*, 9.0)
	6	–	6.58 (*d*, 9.0)	6.58 (*d*, 9.0)
E	2, 6	7.43 (*d*, 9.0)	7.43 (*d*, 9.0)	7.42 (*d*, 9.0)
	3, 5	6.94 (*d*, 9.0)	6.91 (*d*, 9.0)	6.92 (*d*, 9.0)
F	2	5.39 (*br.s*, ca 1.0)	5.12 (*d*, *br.s*, ca 1.0)	5.14 (*br.s*, ca 1.0)
	3	5.78 (*dd*, 1.0, 4.5)	4.18 (*dd*, 1.0, 2.0)	4.27 (*dd*, 1.0, 2.0)
	4	5.33 (*d*, 4.5)	4.76 (*d*, 2.0)	4.71 (*d*, 2.0)
G	5	6.77 (*d*, 9.0)	6.59 (s)	6.28 (*br.s*)
	6	6.51 (*d*, 9.0)	–	–
H	2, 6	7.50 (*d*, 9.0)	7.42 (*d*, 9.0)	–
	3, 5	6.92 (*d*, 9.0)	6.94 (*d*, 9.0)	–
	2	–	–	7.03 (d, 2.0)
	5	–	–	6.89 (d, 8.5)
	6	–	–	7.06 (dd, 2.0, 8.5)
I	2	5.21 (*br.s*, ca 1.5)	5.29 (*br.s*, ca 1.5)	5.33 (*br.s*, ca 1.0)
	3	5.15 (*dd*, 1.5, 3.0)	5.23 (*dd*, 1.5, 3.0)	5.63 (*dd*, 1.0, 4.5)
	4	4.50 (*d*, 3.0)	5.66 (*d*, 3.0)	6.17 (*d*, 4.5)
OMe		4.04, 3.98, 3.96, 3.93, 3.85, 3.84, 3.83, 3.80, 3.71 (each s)	3.99, 3.96, 3.94, 3.92, 3.87, 3.86, 3.84, 3.81, 3.77 (each s)	3.96, 3.95, 3.94, 3.92, 3.91, 3.88, 3.87, 3.86, 3.81, 3.78 (each s)
OAc		1.95, 1.90, 1.84 (each s)	2.09, 1.88, 1.82 (each s)	1.95, 1.87, 1.82 (each s)

heterocyclic 2-H resonances, differentiate between the three AA′BB′-systems in derivatives **16** and **18** hence establishing the C/B-, F/E- and I/H-ring junctions. Differentiation of the two AA′BB′-systems in derivative **20** is also possible *via* $^4J_{HH}$ coupling between the respective 2- and 2′,6′-protons of each constituent unit. The ABX-system of its H-ring is assigned in terms of the $^4J_{HH}$ coupling between 2′- and 6′-H (H-ring) and the corresponding 2-H (I-ring). Pronounced benzylic coupling between the respective 4- and 5-protons facilitates definition of the A- and C-, the D- and F-, as well as the G- and I-ring junctions.

The locations and mode of the interflavanyl linkage are accessible via NOE studies. Thus, the association between 5-H(D) and both 4-H(C) and 4-H(F) confirms the C-4(C)→C-6(D) interflavanyl bond in derivative **16**. N.O.e. correlations of 3-H(F) with both 3-H(I) and 4-H(I), and of 4-H(F) with both 3-H(I) and 4-H(I) confirm the C_4–*O*–C_4 linkage between the DEF- and GHI-epioritin moieties. Such a mode of linkage is supported by the chemical shifts of the heterocyclic protons of these units (Coetzee et al., 1998b; Bennie et al., 2000). One of the AMX-spin systems in the ^{1}H NMR spectra of derivatives **18** and **20** comprises a conspicuously deshielded 4-H resonance (δ5.66 and 6.17, respectively) that is indicative of a 4-*O*-acetyl substituent and hence a flavan-3,4-diol 'terminal' GHI-unit. Benzylic coupling and the observed n.O.e. associations of 5-H(G) with both 4-H(F) and 4-H(I) are reminiscent of the C-4(F)→C-4(G) interflavanyl linkages in derivatives **18** and **20**. The chemical shifts of the heterocyclic protons of the C- and F-rings are indicative of a C_4–*O*–C_3 bond between the ABC- and DEF-epioritin units (Coetzee et al., 1998a; Bennie et al., 2000). This is unequivocally confirmed via NOE associations of 3-H(F) with both 3- and 4-H(C) and of 4-H(F) with 5-H(A) for derivative **18**, and by associations of 4-H(F) with both 4-H(C) and 5-H(A) and of 3-H(C) with 3-H(F) for derivative **20**.

The 2*R*, 3*R*, 4*R*(C): 2*R*, 3*R*, 4*R*(F): 2*R*, 3*R*, 4*S*(I), 2*R*, 3*R*, 4*S*(C): 2*R*, 3*R*, 4*R*(F): 2*R*, 3*R*, 4*S*(I), and 2*R*, 3*R*, 4*S*(C): 2*R*, 3*R*, 4*R*(F): 2*R*, 3*R*, 4*R*(I) absolute configurations of **15**, **17** and **19**, respectively, are confirmed by reductive cleavage of the C–O–C interflavanyl bonds (vide infra) and subsequent comparison of CD and ^{1}H NMR spectral data of the resulting monomeric and dimeric units with those of authentic samples.

The absence of a second aromatic chromophore in close proximity of the C-4 stereocenter in ether linked leucoanthocyanidins at both the di- and trimeric levels, precludes assessment of its absolute configuration by chiroptical methods. The facile reductive cleavage of the C–O bond of the acetal functionality in A-type proanthocyanidins (Steynberg et al., 1997; Lou et al., 1999) thus prompts application of the same protocol to the ethereal bonds of leucoanthocyanidins in order to gain insight into the mode of the interflavanyl linkages and to assess the absolute configuration of the constituent flavanyl units.

Treatment of the epioritin-(4β→4)-epioritin-4α-ol hexamethylether diacetate **4** with $Na(CN)BH_3$ (7 molar excess) in TFA for 45 min at 0°C under N_2 (Scheme 1) affords epioritin-tri-*O*-methylether acetate **24** (35% yield) and the (2*R*)-1,3-diarylpropan-2-ol derivative **25** (32%). Thus, delivery of the equivalent of hydride ion at C-2(C) of the protonated intermediate **21** (Steynberg et al., 1995) effects the concurrent rupture of the O-C_2 bond of the pyran C-ring and the C–O–C interflavanyl bond to give the flavan-3,4-diol derivative **23** and the *o*-quinomethane **22**. The benzylic C_4–OH of the former is then further reduced to the epioritin derivative **24** and the latter to the (2*R*)-1,3-diarylpropan-2-ol derivative **25**. The retention of the absolute configuration at C-2 during the sequence leading to the formation of **25** has previously been demonstrated (Steynberg et al., 1995) and is confirmed by comparison of the CD data (see Experimental) of compound **25** with those of related analogs (Augustyn et al., 1990). Assignment of the 2*R*, 3*R* absolute configuration of **24** and hence its identification as an epioritin derivative is evident from comparison of its ^{1}H NMR and CD spectral data with those of an authentic sample (Van Rensburg et al., 1999; Coetzee et al., 2000). Preference for initial cleavage of the C_4 β–OH bond in the protonated intermediate **21** stems from the leaving group aptitude of such near-*axial* bonds and the remarkable stability of the equatorial C_4–OH bond of the F-ring towards similar fission (Clark-Lewis and Williams, 1967; Coetzee et al., 1999).

In an attempt to prevent cleavage of the heterocyclic ring of one of the constituent units and hence the formation of 1,3-diarylpropan-2-ols of type **25**, milder reaction conditions comprising CH_2Cl_2 containing 10 molar equivalents of TFA were employed. Treatment of the hexa-*O*-methylether diacetate **4** with $Na(CN)BH_3$ (7 molar excess) and TFA (10 molar excess) in CH_2Cl_2 for 45 min at 0°C under N_2 affords a mixture comprising the starting material 4 (7%) and epioritin-tri-*O*-methylether acetate **24** (65%) (Scheme 2). Under these conditions the protonated C_4 β-OH bond of the C-ring is presumably preferentially cleaved due to the anchimeric effect of the *axial* C_3-OH bond (Coetzee et al., 1998a,b). The flavan-3,4-diol derivative **23** that accompanies the epioritin derivative **24** is eventually reduced to afford the C_4-deoxy analogue **24**. Under similar conditions the hexamethylether diacetate derivative **2** also yields epioritin-tri-*O*-methylether acetate **24** (43%). The C_4–*O*–C_4 interflavanyl bond in the dimeric derivatives **6** and **8** (Bennie et al., 2000) with their epimesquitol and epioritin constituent units is similarly susceptible to reductive cleavage affording in each instance epioritin-tri-*O*-methylether acetate **24** (49 and 33%, resp.) and epimesquitol-tetra-*O*-methylether acetate **26** (28 and 62%, resp.).

Under similar conditions the C_4–*O*–C_3 interflavanyl bond in the dimeric leucoteracacinidin derivatives **10**, **12** and **14** is prone to facile cleavage to give the constituent

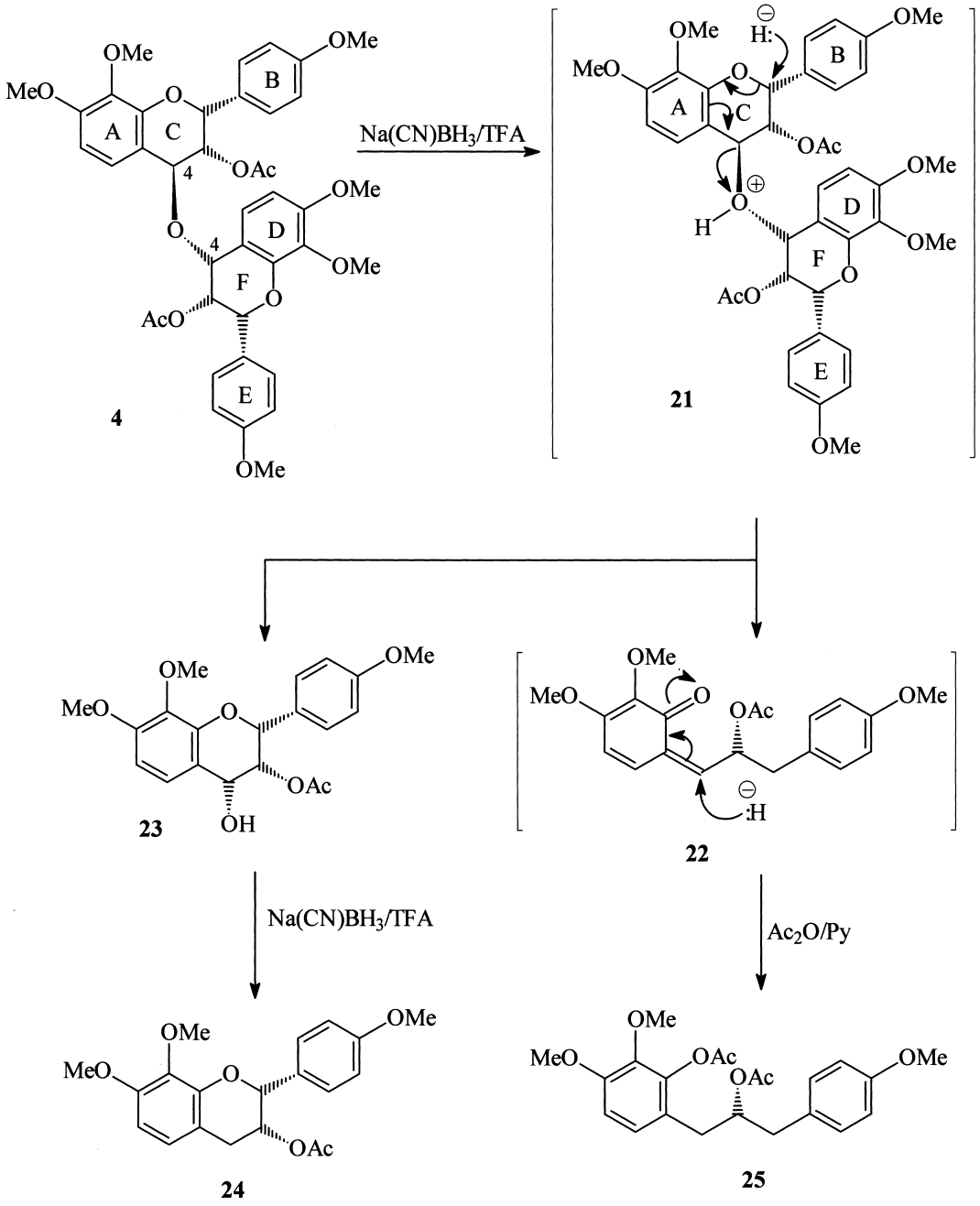

Scheme 1. Reductive cleavage of the C–O–C bond in dimeric leucoteracacinidin **4** using $Na(CN)BH_3$ in TFA.

flavan-3-ol units. Derivatives **10** and **12** are reduced to epioritin-tri-*O*-methylether acetate **24** (37 and 63%, resp.), representing the ABC constituent unit, and epioritin-tri-*O*-methylether **27** (49 and 21%, resp.), representing the DEF unit. Derivative **14** affords epioritin-tri-*O*-methylether acetate **24** (36%) and tri-*O*-methyloritin **28** (58%). The mechanism of the reactions leading to the formation of these products again involves reduction of the more labile protonated C_4 β–OH bond. Reduction of the C_4–OAc bond in the ensuing flavan-3,4-diol derivative of type **29** then leads to the formation of flavan-3-ol derivatives of types **27** and **28**, characterized by a 'labeled' C_3-hydroxyl group, *i.e.* an OH group at the point of the interflavanyl bond to one of the constituent units.

The CD spectra of derivatives **24**, **26** and **27** all exhibit the high-amplitude negative Cotton effects for both the ^1L_a ($[\theta]_{238,6} = -2.916\times10^3$ for **24**; $[\theta]_{240.5} = -2.063\times10^3$ for **26**; $[\theta]_{240.4} = -5.495\times10^3$ for **27**) and ^1L_b ($[\theta]_{274.2} = -3.270\times10^3$ for **24**; $[\theta]_{280.4} = -1.868\times10^3$ for **26**; $[\theta]_{277.4} = -2.105\times10^3$ for **27**) transitions that are reminiscent of (2*R*,3*R*)-flavan-3-ols (Van Rensburg et al., 1999). Derivative **28** similarly displays the Cotton effects for the ^1L_a and ^1L_b transitions ($[\theta]_{244.0} = +1.717\times10^4$; $[\theta]_{280.0} = -$

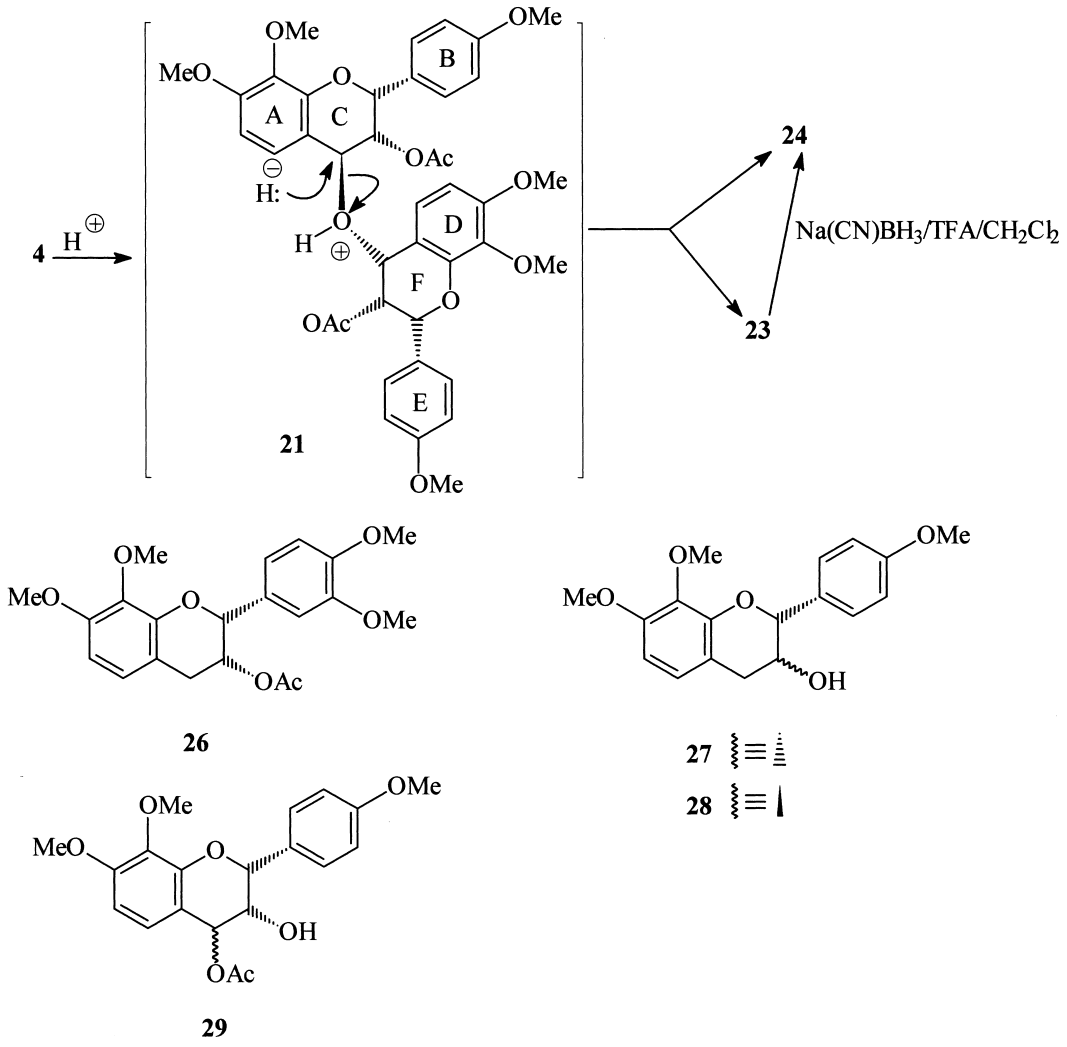

Scheme 2. Reductive cleavage of the C–O–C bond in leucoteracacinidin **4** using $Na(CN)BH_3$/TFA in CH_2Cl_2.

2.762×10^4) that characterize (2*R*,3*S*)-flavan-3-ols (Korver and Wilkins, 1971; Van Rensburg et al., 1999). Collectively the data then provide conclusive evidence for the absolute configurations of the C_4–*O*–C_4 and C_4–*O*–C_3 leucoanthocyanidins as indicated in formulations **1**, **3**, **5**, **7**, **9**, **11** and **13**.

The high-amplitude negative Cotton effects at ca 280 nm in the CD spectra of the trimeric derivatives **16**, **18** and **20** probably indicate the cumulative effects of the ^1L_b transitions of all the constituent flavanyl units exhibiting 2*R* absolute configuration (Korver and Wilkins, 1971; Van Rensburg et al., 1999). Positive Cotton effects in the 220–250 nm region are then reflecting ^1L_a transitions as well as contributions resulting from the biphenylmethylidine chromophore hence indicating a C-4β orientation of the flavanyl unit in the C-C coupled biflavanyl moieties (De Angelis and Wildman, 1969; Van der Westhuizen et al., 1981). In order to validate such chiroptical conclusions, these derivatives were also subjected to reduction of their C–O–C interflavanyl bonds.

Treatment of derivative **16** with $Na(CN)BH_3$ (7 molar excess) and TFA (10 molar excess) in CH_2Cl_2 for 2 h at 0°C under N_2 (Scheme 3), affords a mixture comprising starting material (26%), the epioritin-(4β→6)-epioritin hexa-*O*-methylether diacetate **32** (33%) and epioritin-tri-*O*-methylether acetate **24** (40%). Separate treatment of derivatives **18** and **20** under similar conditions gives the corresponding bis-epioritin and epioritin-(4β→6)-epimesquitol derivatives **33** (41%) and **34** (36%), respectively, as well as epioritin-tri-*O*-methylether acetate **24** (30 and 60%, resp.). These degradation products again form via preferential cleavage of the protonated C–4β ether bond of intermediate **30**, and subsequent reduction of the benzylic hydroxyl group of the flavan-3,4-diol unit in the dimeric intermediate **31**. Cleavage products **33** and **34** again carry a 'free' hydroxyl group at C-3 of the upper epioritin moiety, hence 'labeling' the location of the C–O–C ether linkage in the parent triflavanoid derivatives **18** and **20**.

The structures and relative configuration of the dimeric derivatives **32**, **33** and **34** are readily evident

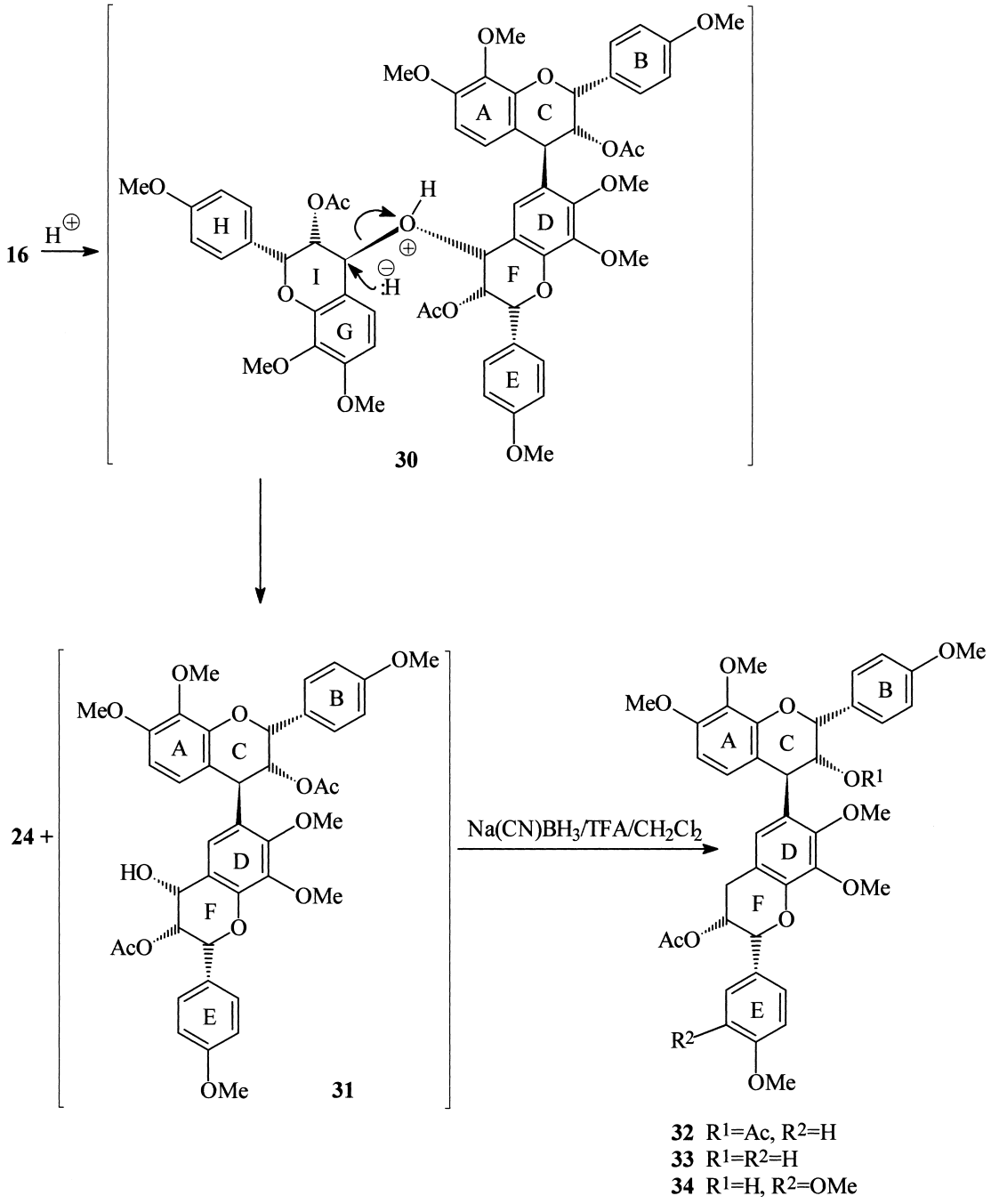

Scheme 3. Reductive cleavage of the C–O–C bond in trimeric derivative **16** using $Na(CN)BH_3$/TFA in CH_2Cl_2.

from the ^1H NMR spectral data that are collated in Table 1. The CD data of all three derivatives are virtually identical to those of the corresponding 4–OAc (F-ring) analogues that were previously synthesized (Malan and Sireeparsad, 1995). Thus, the high-amplitude negative Cotton effect at ca 280 nm is indicative of the ^1L_b transition of flavan-3-ol constituent units with 2*R* absolute configuration. The high-amplitude positive Cotton effect at ca 240 nm reflects the 4β-flavanyl substituent by application of the aromatic quadrant rule (De Angelis and Wildman, 1969). When taken in conjunction with CD data of the epioritin derivative **24** (vide supra), the absolute configuration of the natural products is thus unambiguously established as indicated in structures **15**, **17** and **19**.

We have thus developed a simple but concise protocol to unequivocally establish the structures and absolute configuration of the constituent flavanyl units in di- and trimeric ether-linked leucoanthocyanidins. Such rigorous structure elucidation is a prerequisite towards the understanding of the intricate physicochemical interaction of this class of compounds with other biomolecules.

The co-occurrence of the considerable number of ether-linked leucoteracacinidins and leucomelacacinidins in the heartwood of *A. caffra* in addition to some carbon–carbon bonded analogues, is yet a further manifestation of the much reduced nucleophilicity of the pyrogallol A-ring (Botha et al., 1981; Foo, 1989) which permits other centers to participate in the formation of interflavanyl bonds.

3. Experimental

^{1}H NMR spectra were recorded on a Bruker AVANCE DPX 300 spectrometer for solns. as indicated, with Me_4Si as internal standard. FAB mass spectra were recorded on a VG-70E instrument with a VG 11-250J data system and an iontech saddlefield FAB gun. TLC was performed on precoated Merck plastic sheets (silica gel 60 PF_{254}, 0.25 mm) and the plates were sprayed with H_2SO_4-HCHO (40:1, v/v) after development. Preparative plates (PLC) [20×22 cm, Kieselgel PF_{254} (1.0 mm)] were air dried and used without prior activation. Column chromatography was carried out on Sephadex LH-20 in various columns, solvent systems and flow rates (to be specified in each instance). Methylations were performed with an excess of CH_2N_2 in MeOH–Et_2O over a period of 48 h at −15°C while acetylations were conducted in Ac_2O–pyridine at ambient temperature. Evaporations were carried out under reduced pressure at ambient temp. in a rotary evaporator, and freeze drying of aqueous solutions on a Virtis 12 SL freezemobile.

3.1. General procedure for the sodium cyanoborohydride reductions with CH_2Cl_2 as solvent (mild conditions)

The appropriate dimer or trimer and $Na(CN)BH_3$ (7 eq.) were dissolved in CH_2Cl_2 (2 ml) under an N_2-atmosphere at 0°C. After 15 min trifluoroacetic acid (TFA, 10 eq.) was added and the mixture was stirred for a further 45 min at 0°C. The reaction was quenched by the careful addition of H_2O and the pH adjusted to ca 6.5 (saturated $NaHCO_3$-soln.). After extraction with EtOAc (10 ml×3) the combined organic layers were dried (Na_2SO_4) and evaporated under reduced pressure.

3.2. Synthesis of epioritin-(4β→4)-epimesquitol-4α-ol hepta-O-methylether diacetate **8**

Epioritin-4β-thiobenzylether (100 mg, 2.52×10^{-4} mole) and epimesquitol-4α-ol (155 mg, 5.04×10^{-4} mol, 2 eq.) were dissolved in dry THF (15 ml) and the mixture was stirred under an N_2-atmosphere for 15 min at 0°C before solid $AgBF_4$ (2.5 eq.) was added and the mixture stirred for a further 90 min. After the addition of H_2O (150 ml) and extraction with EtOAc (50 ml×6) the combined organic layers were dried (Na_2SO_4) and evaporated to dryness. Methylation of the residue and subsequent PLC separation in benzene–Me_2CO–EtOAc (7:2:1; v/v) gave three bands at R_f 0.60 (11.1 mg), 0.42 (15.5 mg) and 0.32 (91.7 mg).

3.3. Epioritin-(4β→4)-epimesquitol-4α-ol hepta-O-methylether diacetate **8**.

Acetylation of the R_f 0.42 band followed by PLC purification in benzene–Me_2CO (9:1; v/v) afforded compound **8** (R_f 0.33, 4.2 mg,) as a white amorphous solid. (Found: M^+, 760.2731. $C_{41}H_{44}O_{14}$ requires M, 760.2731); δ_H (Table 1); CD $[\theta]_{206.4}$ 20300, $[\theta]_{213.1}$ 6262, $[\theta]_{221.9}$ 13560, $[\theta]_{226.2}$ 184, $[\theta]_{228.6}$ −4458, $[\theta]_{232.7}$ −311, $[\theta]_{241.0}$ −14 70, $[\theta]_{256.9}$ −1104, $[\theta]_{274.2}$ −3976 and $[\theta]_{291.5}$ −204. The remaining bands afforded compounds that will be dealt with elsewhere.

3.4. Isolation of phenolic compounds

The extraction of the heartwood of *A. caffra* and column separation to give fractions A-UU were comprehensively described in Part 32 (Bennie et al., 2000) and need not be repeated.

3.5. Epioritin-(4β→4)-epioritin-4β-ol hexa-O-methylether diacetate **2**

Methylation of a portion (200 mg) of fraction W followed by PLC in benzene–Me_2CO–EtOAc (7:2:1; v/v) gave five bands at R_f 0.65 (12.6 mg), 0.57 (11.9 mg), 0.47 (12.8 mg), 0.39 (26.2 mg) and 0.19 (6.4 mg). Acetylation of the R_f 0.39 band followed by PLC in benzene–Me_2CO (9:1; v/v) afforded two main bands at R_f 0.53 (2.1 mg) and 0.41 (2.7 mg). The former band yielded compound **2** as a white amorphous solid. (Found: M^+, 730.2703. $C_{40}H_{42}O_{13}$ requires M, 730.2704); δ_H(Table 1); CD $[\theta]_{237.8}$ 6891, $[\theta]_{240.0}$ 197 $[\theta]_{246.7}$ −63860, $[\theta]_{267.4}$ −2628 and $[\theta]_{282.2}$ 3967. The remaining bands contain related leucoanthocyanidin-type compounds which were reported previously (Bennie et al., 2000).

3.6. Epioritin-(4β→6)-epioritin-(4α→4)-epioritin-4β-ol nona-O-methylether triacetate **16**

A portion (200 mg) of fraction HH was methylated and the mixture separated by PLC in benzene–Me_2CO–EtOAc (7:2:1; ×2; v/v) to give five bands at R_f 0.68 (14.4 mg), 0.63 (21.2 mg), 0.51 (19.7 mg), 0.47 (20.7 mg) and 0.39 (19.2 mg). Acetylation of the R_f 0.68 band followed by PLC in benzene–Me_2CO (9:1; v/v) afforded one main band at R_f 0.49 (3.3 mg). Further purification by PLC in hexane–Me_2CO–EtOAc (13:4:3; ×2; v/v) yielded compound **16** (R_f 0.17, 2.3 mg) as a white amorphous solid. (Found: M^+, 1086.3886. $C_{60}H_{62}O_{19}$ requires M, 1086.3885); δ_H(Table 2); CD $[\theta]_{221.7}$ 74, $[\theta]_{228.1}$ −6210,

$[\theta]_{232.2}$ 121, $[\theta]_{236.9}$ 3485, $[\theta]_{242.1}$ 6630, $[\theta]_{247.5}$ 67, $[\theta]_{252.8}$ −1732, $[\theta]_{283.3}$ −4788 and $[\theta]_{295.4}$ 5. The remaining bands yielded proanthocyanidin trimers that will be dealt with elsewhere.

3.7. Epioritin-(4β→3)-epioritin-(4β→6)-epioritin-4β-ol nona-O-methylether triacetate **18**

Methylation of a portion (179 mg) of fraction DD followed by PLC in benzene–Me_2CO–EtOAc (7:2:1; v/v) gave two bands at R_f 0.54 (19.3 mg) and 0.46 (32.4 mg). Acetylation of the R_f 0.54 band and PLC purification in benzene–Me_2CO (9:1; ×2; v/v) afforded two main bands at R_f 0.74 (2.9 mg) and 0.65 (4.5 mg). The latter band yielded compound **18** as a white amorphous solid. (Found: M^+, 1086.3884. $C_{60}H_{62}O_{19}$ requires M, 1086.3885); δ_H (Table 2); CD $[\theta]_{215.5}$ 47, $[\theta]_{221.3}$ 6666, $[\theta]_{233.1}$ 70, $[\theta]_{235.9}$ −1549, $[\theta]_{241.0}$ 470, $[\theta]_{246.8}$ −1459, $[\theta]_{255.4}$ −357, $[\theta]_{279.2}$ −4497 and $[\theta]_{297.2}$ 2. TLC showed that the remaining bands contained higher oligomeric material and were therefore not further investigated.

3.8. Epioritin-(4β→3)-epioritin-(4β→6)-epimesquitol-4α-ol deca-O-methyl-ether triacetate **20**

A portion (200 mg) of fraction LL was methylated and the mixture separated by PLC in benzene–Me_2CO–EtOAc (7:2:1; ×2; v/v) to give a main band at R_f 0.42 (29.8 mg). Acetylation and PLC purification in benzene–Me_2CO (9:1; ×2; v/v) yielded compound **20** (R_f 0.53, 3.1 mg) as a white amorphous solid. (Found: M^+, 1116.3990. $C_{61}H_{64}O_{20}$ requires M, 1116.3991); δ_H(Table 2); CD $[\theta]_{215.4}$ 49, $[\theta]_{226.0}$ 5688, $[\theta]_{233.6}$ 2368, $[\theta]_{244.7}$ 3416, $[\theta]_{258.3}$ 2, $[\theta]_{284.3}$ −7250 and $[\theta]_{297.2}$ 3.

3.9. Reductive cleavage of epioritin-(4β → 4)-epioritin-4α-ol hexamethylether diacetate **4** with TFA as solvent

The epioritin-(4β→4)-epioritin-4α-ol hexa-*O*-methylether diacetate derivative **4** (Bennie et al., 2000) (10 mg) was dissolved in TFA (2 ml) under an N_2-atmosphere at 0°C. After 15 min $Na(CN)BH_3$ (6 mg, 9.58×10^{-5} mol, 7 eq) was added in one portion and the mixture was stirred for another 45 min at 0°C. The reaction was quenched by the addition of H_2O and the pH adjusted to ca. 6.9 (saturated $NaHCO_3$–soln.) before extraction with EtOAc (15 ml×3). The combined organic layers were stirred for 15 min after the addition of 3 drops of a tetrabutylammonium fluoride (TBAF) soln. in THF. The solvent was dried (Na_2SO_4) and evaporated under reduced pressure.

3.10. Epioritin-tri-O-methylether acetate **24**

Acetylation of the residue and subsequent PLC separation in benzene–Me_2CO (95:5; ×2, v/v) afforded two main bands at R_f 0.58 (4.9 mg) and 0.49 (3.3 mg). The R_f 0.58 band yielded compound **24** (35.3%) as a white amorphous solid. δ_H (Table 3); CD and MS data identical to those in the literature (Coetzee et al., 2000).

3.11. 2R-Acetoxy-1-(2-acetoxy-3,4-dimethoxyphenyl)-3-(4-methoxyphenyl)-propane **25**

The R_f 0.49 band yielded compound **25** (31.7%) as a white amorphous solid. δ_H ($CDCl_3$) 7.12 (2H, *d*, 9.0, H-2,6), 6.91 (1H, *d*, 9.0, H-5), 6.83 (2H, *d*, 9.0, H-3,5), 6.76 (1H, *d*, 9.0, H-6), 5.14 (1H, *m*, H-2), 3.87 (OMe), 3.82 (OMe), 3.80 (OMe), 2.85–2.62 (4H, *m*, –CH_2–, H-2,3),

Table 3
^{1}H NMR (300 MHz, 296 K) spectral data of flavan-3-ol derivatives **24**, **26**, **27** and **28** in $CDCl_3$. Splitting patterns and *J*-values are given in parentheses

Ring	H	**24**	**26**	**27**	**28**
A	5	6.79 (*d*, 9.0)	6.79 (*d*, 9.0)	6.82 (*d*, 9.0)	6.81 (*d*, 9.0)
	6	6.57 (*d*, 9.0)	6.57 (*d*, 9.0)	6.57 (*d*, 9.0)	6.56 (*d*, 9.0)
B	2, 6	7.40 (*d*, 9.0)	–	7.47 (*d*, 9.0)	7.38 (*d*, 9.0)
	3, 5	6.92 (*d*, 9.0)	–	6.99 (*d*, 9.0)	6.96 (*d*, 9.0)
	2	–	7.07 (*d*, 2.0)	–	–
	5	–	6.89 (*d*, 8.5)	–	–
	6	–	7.01 (*dd*, 2.0, 8.5)	–	–
C	2	5.16 (*br.s*, ca 1.5)	5.16 (*br.s*, ca 1.5)	5.11 (*br.s*, ca 1.0)	4.85 (*d*, 7.5)
	3	5.41 (*m*)	5.44 (*m*)	4.29 (*m*)	4.10 (*m*)
	4	3.28 (*dd*, 4.5, 17.0)	3.28 (*dd*, 4.5, 17.0)	3.23 (*dd*, 4.0, 16.5)	3.06 (*dd*, 5.0, 16.0)
		2.95 (*dd*, 3.0, 17.0)	2.96 (*dd*, 3.0, 17.0)	2.95 (*dd*, 3.0, 16.5)	2.88 (*dd*, 8.5, 16.0)
OMe		3.93, 3.88, 3.84, (each *s*)	3.94, 3.91, 3.90, 3.89 (each *s*)	3.93, 3.88, 3.84, (each *s*)	3.88, 3.87, 3.84 (each *s*)
OAc		1.92 (*s*)	1.93 (*s*)	–	

2.24 (OAc), 1.96 (OAc); CD $[\theta]_{203.9}$ 94, $[\theta]_{207.9}$ 9640, $[\theta]_{211.7}$ 122, $[\theta]_{214.3}$ −4621, $[\theta]_{217.2}$ 27, $[\theta]_{223.4}$ 10340, $[\theta]_{229.9}$ 231, $[\theta]_{235.2}$ −8911, $[\theta]_{258.3}$ 190, $[\theta]_{272.8}$ −1511, $[\theta]_{284.0}$ 20 and $[\theta]_{294.7}$ 6.

3.12. Epimesquitol-tetra-O-methylether acetate 26

Reduction of epimesquitol-(4β→4)-epioritin-4β-ol hepta-*O*-methylether diacetate **6** (Bennie et al., 2000) (7 mg, 9.20×10^{-6} mol) according to the general procedure, followed by work-up and PLC separation in benzene–Me_2CO (9:1; v/v) afforded three main bands at R_f 0.57 (1.6 mg), 0.48 (1.0 mg) and 0.41 (1.0 mg). The R_f 0.57 band afforded compound **24** while the R_f 0.48 band yielded compound **26** as a white amorphous solid. (Found: M^+, 388.1526. $C_{21}H_{24}O_7$ requires M, 388.1522); δ_H (Table 3); CD $[\theta]_{219.0}$ 1326, $[\theta]_{224.8}$ 443, $[\theta]_{231.3}$ 838, $[\theta]_{235.2}$ −22, $[\theta]_{240.5}$ −2063, $[\theta]_{252.1}$ −269, $[\theta]_{280.4}$ −1868 and $[\theta]_{292.6}$−8.

3.13. Oritin-tri-O-methylether 28

Epioritin-(4β→3)-oritin-4α-ol hexa-*O*-methylether diacetate **14** (Coetzee et al., 1998a) (4 mg, 5.47×10^{-6} mol) was reduced according to the general procedure and afforded a mixture which was resolved by PLC in benzene–Me_2CO (9:1; v/v) to give two bands at R_f 0.57 (0.7 mg) and 0.30 (1.0 mg). The R_f 0.57 band comprised compound **24** (35.7%) while the R_f 0.30 band yielded compound **28** (57.7%) as a white amorphous solid. δ_H(Table 3); CD and MS data identical to those in the literature (Van Rensburg et al., 1999; Coetzee et al., 2000).

3.14. Epioritin-tri-O-methylether 27

Hexa-*O*-methylether diacetate derivatives **10** and **12** (10 mg, 1.37×10^{-5} mol) were separately reduced according to the general procedure. PLC separation in benzene–Me_2CO (9:1; v/v) afforded two bands at R_f 0.57 (3.1 and 1.8 mg for **10** and **12**, resp.) and 0.34 (1.0 and 2.1 mg for **10** and **12**, resp.). The R_f 0.57 bands comprised compound **24** while the R_f 0.34 band yielded compound **27** as a white amorphous solid. δ_H(Table 3); CD and MS data identical to those in the literature (Van Rensburg et al., 1999; Coetzee et al., 2000).

3.15. Epioritin-(4β→6)-epioritin hexa-O-methylether diacetate 32

Epioritin-(4β→6)-epioritin-(4α→4)-epioritin-4β-ol nona-*O*-methylether triacetate 16 (2.3 mg, 2.12×10^{-6} mol) was reduced according to the general procedure and PLC separation in benzene–Me_2CO (9:1; v/v) afforded three main bands at R_f 0.57 (0.3 mg), 0.53 (0.5 mg) and 0.47 (0.6 mg). The R_f 0.57 band comprised compound **24** while the R_f 0.53 band yielded compound **32** (33.2%) as a white amorphous solid. (Found: M^+, 714.2676. $C_{40}H_{42}O_{12}$ requires M, 714.2676); δ_H (Table 1); CD $[\theta]_{228.7}$ −49, $[\theta]_{231.5}$ −1920, $[\theta]_{233.5}$ −84, $[\theta]_{240.7}$ 25290, $[\theta]_{251.4}$ −26, $[\theta]_{282.7}$ −5474 and $[\theta]_{299.6}$ −233.

The R_f 0.47 band contained the unreacted starting material **16** (26.1%).

3.16. Epioritin-(4β→6)-epioritin hexa-O-methylether acetate 33

Epioritin-(4β→3)-epioritin-(4β→6)-epioritin-4β-ol nona-*O*-methylether triacetate **18** (8 mg, 7.36×10^{-6} mol) was reduced according to the general procedure. PLC separation in benzene–Me_2CO (9:1; v/v) afforded two main bands at R_f 0.57 (1.0 mg) and 0.26 (2.0 mg). The R_f 0.57 band comprised compound **24** while the R_f 0.26 band yielded compound **33** (40.5%) as a white amorphous solid. (Found: M^+, 672.2570. $C_{38}H_{40}O_{11}$ requires M^+, 672.2571); δ_H (Table 1); CD $[\theta]_{229.5}$ 364, $[\theta]_{235.4}$ 3010, $[\theta]_{239.1}$ 1491, $[\theta]_{246.3}$ 12870, $[\theta]_{259.7}$ −7, $[\theta]_{283.7}$ −5993 and $[\theta]_{298.2}$ −23.

3.17. Epioritin-(4β→6)-epimesquitol hepta-O-methylether acetate 34

Epioritin-(4β→3)-epioritin-(4β→6)-epimesquitol-4α-ol deca-*O*-methyl-ether triacetate **20** (3.1 mg, 2.78×10^{-6} mol) was reduced according to the general procedure. PLC separation in benzene–Me_2CO (9:1; v/v) afforded three main bands at R_f 0.57 (0.6 mg), 0.31 (0.7 mg) and 0.20 (0.1 mg). The R_f 0.57 band comprised compound **24** while the R_f 0.31 band yielded compound **34** (36.0%) as a white amorphous solid. (Found: M^+, 702.2679. $C_{39}H_{42}O_{12}$ requires M^+, 702.2676); δ_H (Table 1); CD $[\theta]_{220.3}$ 2218, $[\theta]_{224.4}$ 3250, $[\theta]_{231.3}$ 455, $[\theta]_{240.1}$ 16210, $[\theta]_{247.5}$ 19, $[\theta]_{249.5}$ −701, $[\theta]_{254.0}$ 18, $[\theta]_{257.3}$ 351, $[\theta]_{2261.9}$ 5, $[\theta]_{283.5}$ −3243 and $[\theta]_{292.6}$ 16.

The R_f 0.20 band contained unreacted starting material **20** (3.2%).

Acknowledgements

Financial support by the National Research Foundation, Pretoria and by the 'Sentrale Navorsingsfonds' of UOFS is acknowledged. This work was supported in part by the United States Department of Agriculture, Agricultural Research Service Specific Cooperative Agreement No. 58-6408-7-012.

References

Augustyn, J.A.N., Bezuidenhoudt, B.C.B., Swanepoel, A., Ferreira, D., 1990. Enantioselective synthesis of flavonoids. Part 2. Poly-oxygenated α-hydroxydihydrochalcones and circular dichroic assessment of their absolute configuration. Tetrahedron 46, 4429–4442.

Barrett, M.W., Klyne, W., Scopes, P.M., Fletcher, A.C., Porter, L.J., Haslam, E., 1979. Plant proanthocyanidins. Part 6. Chiroptical

studies. Part 94. Circular dichroism of procyanidins. Journal of the Chemical Society, Perkin Transactions 1, 2375–2377.

Bennie, L., Malan, E., Coetzee, J., Ferreira, D., 2000. Structure and synthesis of ether-linked proteracacinidin and promelacacinidin proanthocyanidins from *Acacia caffra*. Phytochemistry 53, 785–793.

Botha, J.J., Ferreira, D., Roux, D.G., 1981. Synthesis of condensed tannins. Part 4. A direct biomimetic approach to [4,6]- and [4,8]-biflavanoids. Journal of the Chemical Society, Perkin Transactions 1, 1235–1245.

Clark-Lewis, J.W., Williams, L.R., 1967. Flavan derivatives. Part XVII. Epimerization of the benzylic 4-hydroxyl group in flavan-3,4-diols and the formation of 4-alkyl ethers by solvolysis. Australian Journal of Chemistry 20, 2152–2167.

Coetzee, J., Malan, E., Ferreira, D., 1998a. Oligomeric flavanoids. Part 28, Structure and synthesis of ether-linked (4-O-3)-bis-teracacinidins, a novel class of naturally occurring proanthocyanidins. Journal of Chemical Research (S), 526–527; (*M*), 2287–2296.

Coetzee, J., Malan, E., Ferreira, D., 1998b. Oligomeric flavanoids. Part 29. Structure and synthesis of novel ether-linked [4-*O*-4] bis-teracacinidins. Tetrahedron 54, 9153–9160.

Coetzee, J., Malan, E., Ferreira, D., 1999. The formation and stability of flavans with 2,3-*cis*-3,4-*cis* configuration. Tetrahedron 55, 9999–10004.

Coetzee, J., Malan, E., Ferreira, D., 2000. Synthesis and reactions of flav-3-en-3-ols. Tetrahedron 56, 1819–1824.

De Angelis, G.G., Wildman, W.C., 1969. Circular dichroism studies-I. A quadrant rule for the optically active aromatic chromophore in rigid polycyclic systems. Tetrahedron 25, 5099–5112.

Ferreira, D., Bekker, R., 1996. Oligomeric proanthocyanidins. Naturally occurring *O*-heterocycles. Natural Product Reports 13, 411–433.

Ferreira, D., Li, X-C., 2000. Oligomeric proanthocyanidins-naturally occurring *O*-heterocycles. Natural Product Reports 17, 193–212.

Ferreira, D., Nel, R.J.J., Bekker, R. 1999. In: Barton, D.H.R. Nakanishi, K. Meth-Cohn O., Pinto B.M. (Eds.), Comprehensive Natural Products Chemistry, Vol. 3. Elsevier, New York, p. 723.

Foo, L.Y., 1989. Isolation of [4-0-4]-linked biflavanoids from *Acacia melanoxylon*: first examples of a new class of single ether-linked proanthocyanidin dimers. Journal of the Chemical Society, Chemical Communications 20, 1505–1506.

Hemingway, R.W., 1989. In: Rowe, J.W. (Ed.), Natural Products of Woody Plants, Vol. 1. Springer-Verlag, New York, p. 571.

Korver, O., Wilkins, C.K., 1971. Circular dichroism spectra of flavanols. Tetrahedron 27, 5459–5465.

Lou, H., Yamazaki, Y., Sasaki, T., Uchida, M., Tanaka, H., Oka, S., 1999. A-type proanthocyanidins from peanut skins. Phytochemistry 51, 297–308.

Malan, E., Sireeparsad, A., 1995. The structure and synthesis of the first dimeric proteracacinidins from *Acacia galpinii*. Phytochemistry 38, 237–239.

Porter, L.J., 1994. In Harborne, J.B. (Ed.), The Flavonoids. Advances in Research Since 1986. Chapman & Hall, London, p. 23.

Steynberg, J.P., Brandt, E.V., Ferreira, D., 1991. Conformational analysis of oligomeric flavanoids. Part 1. 4-Arylflavan-3-ols. Journal of the Chemical Society, Perkin Transactions 2 1569–1573.

Steynberg, P.J., Cronjé, A., Steynberg, J.P., Bezuidenhoudt, B.C.B., Brandt, E.V., Ferreira, D., 1997. Cleavage of the acetal functionality in A-type proanthocyanidins. Tetrahedron 53, 2591–2598.

Steynberg, P.J., Steynberg, J.P., Bezuidenhoudt, B.C.B., Ferreira, D., 1995. Oligomeric flavanoids. Part 19. Reductive cleavage of the interflavanyl bond in proanthocyanidins. Journal of the Chemical Society, Perkin Transactions 1 3005–3012.

Van der Westhuizen, J.H., Ferreira, D., Roux, D.G., 1981. Synthesis of condensed tannins. Part 2. Synthesis by photolytic rearrangement, stereochemistry, and circular dichroism of the first 2,3-*cis*-3,4-*cis*-4-arylflavan-3-ols. Journal of the Chemical Society, Perkin Transactions 1, 1220–1226.

Van Rensburg, H., Steynberg, P.J., Burger, J.F.W., Van Heerden, P.S., Ferreira, D., 1999. Circular dichroic properties of flaven-3-ols. Journal of Chemical Research 5, 450–451.

PERGAMON

Phytochemistry 57 (2001) 1035–1042

PHYTOCHEMISTRY

www.elsevier.com/locate/phytochem

NMR studies of molecular structure in fruit cuticle polyesters

Xiuhua Fang[a], Feng Qiu[b], Bin Yan[a], Hsin Wang[a], Andrew J. Mort[c], Ruth E. Stark[a,*]

[a]*Department of Chemistry, CUNY Graduate Center and College of Staten Island, 2800 Victory Blvd., Staten Island, NY 10314, USA*
[b]*Department of Chemistry, Oklahoma State University, Stillwater, OK 74078, USA*
[c]*Department of Biochemistry and Molecular Biology, Oklahoma State University, Stillwater, OK 74078, USA*

Received 22 September 2000; received in revised form 12 February 2001

Abstract

The cuticle of higher plants functions primarily as a protective barrier for the leaves and fruits, controlling microbial attack as well as the diffusion of water and chemicals from the outside environment. Its major chemical constituents are waxes (for waterproofing) and cutin (a structural support polymer). However, the insolubility of cutin has hampered investigations of its covalent structure and domain architecture, which are viewed as essential for the design of crop protection strategies and the development of improved synthetic waterproofing materials. Recently developed strategies designed to meet these investigative challenges include partial depolymerization using enzymatic or chemical reagents and spectroscopic examination of the intact polyesters in a solvent-swelled form. The soluble oligomers from degradative treatments of lime fruit cutin are composed primarily of the expected 10,16-dihydroxyhexadecanoic and 16-hydroxy-10-oxo-hexadecanoic acids; low-temperature HF treatments also reveal sugar units that are covalently attached to the hydroxyfatty acids. Parallel investigations of solvent-swollen cutin using 2D NMR spectroscopy assisted by magic-angle spinning yield well-resolved spectra that permit detailed comparisons to be made among chemical moieties present in the intact biopolymer, the soluble degradation products, and the unreacted solid residue. © 2001 Elsevier Science Ltd. All rights reserved.

Keywords: *Citrus aurantifolia*; Citrus; Rutaceae; Lime; Fruit; Cuticle; Cutin; Molecular structure; NMR; Magic-angle spinning; HMQC; MS; Hydrogen fluoride

1. Introduction

The leaves and fruit of terrestrial plants are protected by a cuticular membrane that mediates wettability, permeability, and microbial resistance. Plant cuticles consist of waxes and cutin, a polyester structural support (Fig. 1). Although it was established two decades ago that cutin's major monomeric constituents are C_{16} hydroxylated fatty acids (Kolattukudy, 1984), the molecular architecture responsible for its support functions has been more elusive because of the biopolymer's insolubility. Recently, partial degradation of tomato and lime fruit cutin by enzymatic or chemical means has been used to generate soluble oligomeric products that retain essential covalent connectivities from the native plant polyester (Osman et al., 1995; Ray et al., 1998; Ray and Stark, 1998).

The current report reviews the architectural information derived from these cutin oligomers and presents two new approaches to molecular structure determination in fruit cuticles. First, a low-temperature hydrogen fluoride treatment has been used to selectively cleave neutral sugar linkages (Mort and Bauer, 1982; Stark et al., 2000), producing both soluble oligomers and an insoluble residue for spectroscopic analysis. Secondly, the intact polymer has been swelled in organic solvents, generating a suspension from which high-resolution NMR spectra may be obtained using magic-angle spinning (Stark et al., 2000). The results of these studies provide evidence for both hydroxyfatty acid and glycoside building blocks of fruit cutins, and they validate novel spectroscopic strategies for molecular structure determination in cutins, suberins, and related plant materials.

* Corresponding author. Tel.: +1-718-982-3894; fax: +1-718-982-4077.
E-mail address: stark@postbox.csi.cuny.edu (R.E. Stark).

0031-9422/01/$ - see front matter © 2001 Elsevier Science Ltd. All rights reserved.
PII: S0031-9422(01)00106-6

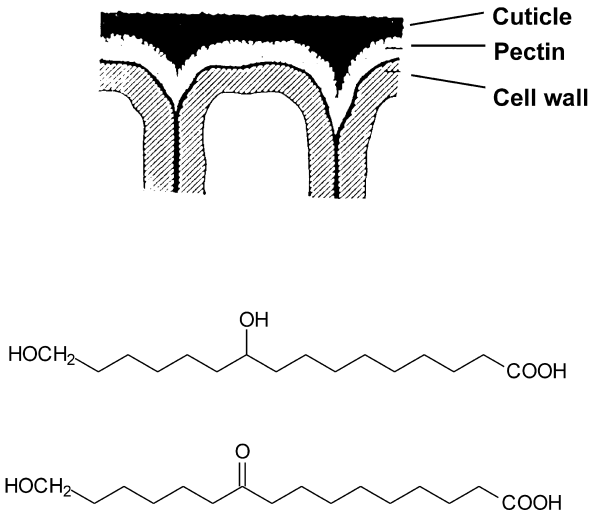

Fig. 1. Schematic organization of the plant cuticle (adapted from Kolattukudy (1984)) and the major monomeric constituents of lime fruit cutin.

2. Results

2.1. Oligomers from chemical and enzymatic treatments of fruit cutins

In order to augment the identification of molecular groupings in plant polyesters by solid-state ^{13}C NMR (Zlotnik-Mazori and Stark, 1988; Garbow et al., 1989), a variety of procedures have been developed for partial breakdown of covalent linkages in fruit cutins (Osman et al., 1995; Ray and Stark, 1998; Stark et al., 2000). With each of these approaches, the isolated oligomers retain valuable information regarding the covalent bonding patterns of the native biopolymers.

Using a strategy of partial alkaline hydrolysis, several monomers and a dimer were isolated from the tomato fruit cutin polyester (Osman et al., 1995). The proposed dimer structure contains a primary alcohol ester linkage between two units of 10,16-dihydroxyhexadecanoic acid, the most abundant tomato cutin monomer (Holloway, 1982). Any higher oligomers were deemed undetectable by chemical ionization mass spectrometry (MS). By contrast, enzymatic hydrolysis with *Fusarium solani* cutinase yielded only monomeric products. Nonetheless, this study clearly demonstrated the usefulness of partial degradation procedures in elucidating the essential covalent linkages of protective plant polymers.

Reaction of lime fruit cutin with the enzyme porcine pancreatic lipase, which requires the presence of substrate aggregates and specifically cleaves esters of primary alcohols (Hamosh, 1990), produced a mixture of soluble monomers and oligomers. The pentamer structure **1** was deduced from electron-impact MS experiments tailored for molecular weights up to 1500 amu and with supporting evidence from solution-state NMR spectroscopic analyses (Ray and Stark, 1998). Three of the four building blocks of the pentamer correspond to the principal monomeric fatty acid constituents of Citrus cutins: 10,16-dihydroxyhexadecanoic acid, hexadecanoic acid, and 10-hydroxyhexadecanoic acid (Holloway, 1982; Kolattukudy, 1984; Ray et al., 1995). Notably, this oligomer structure is assembled solely with linkages between the esters of secondary alcohols, and it lacks the ω-hydroxyoxo fatty acid monomers found abundantly in lime cutin. All four building blocks of the pentamer have molecular structures that render them capable of both polymer chain elongation and cross-link formation within the cutin support structure.

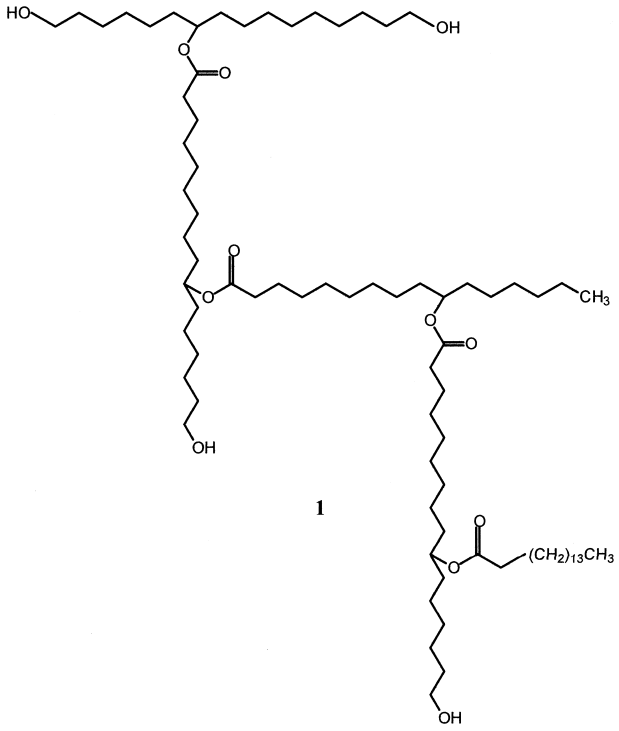

1

Using the mild chemical deprotecting reagent iodotrimethylsilane, which in organic solution is known to favor hydrolysis of sterically hindered esters of secondary alcohols (Purdy and Kolattukudy, 1975a,b), it was possible to improve the yield of soluble lime cutin fragments from ~5 to 22%. Both monomers and the soluble oligomers **2–4** were identified using two-dimensional multinuclear NMR and liquid secondary-ion mass spectrometry (Ray et al., 1998). The oligomeric materials are each comprised of the two most common Citrus cutin monomers, 16-hydroxy-10-oxo-hexadecanoic acid and 10,16-dihydroxyhexadecanoic acid. Although their covalent architectures are based exclusively on esterification of primary alcohols, the CHI moieties found in the oligomer structures also provide strong evidence for secondary ester linkages in the parent biopolymer.

Finally, we report herein a complementary chemical degradation strategy involving a low-temperature hydrogen fluoride treatment. This type of protocol is known to cleave sugars from glycoproteins (Mort and Lamport,

1977) and to break glycosidic linkages of neutral sugars in polysaccharides preferentially (Mort and Bauer, 1982). Thus, the resulting oligomeric fragments should retain any ester linkages to sugars from cell-wall polysaccharides of the cutin polyester. The low-temperature HF procedure was accompanied by a 23% loss in mass for lime fruit cutin, ensuring that the breakdown products reflect the molecular structure of the intact biopolymer to a significant degree.

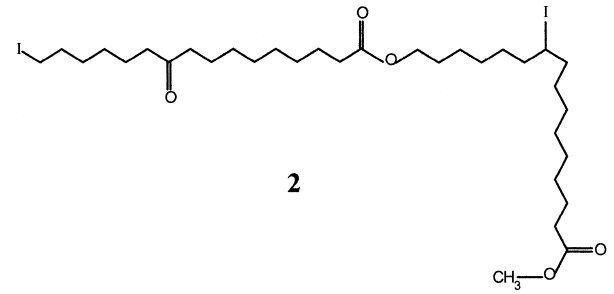

2

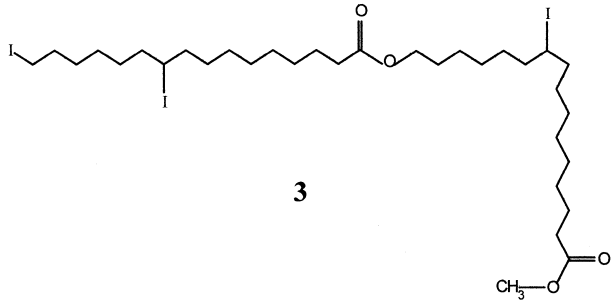

3

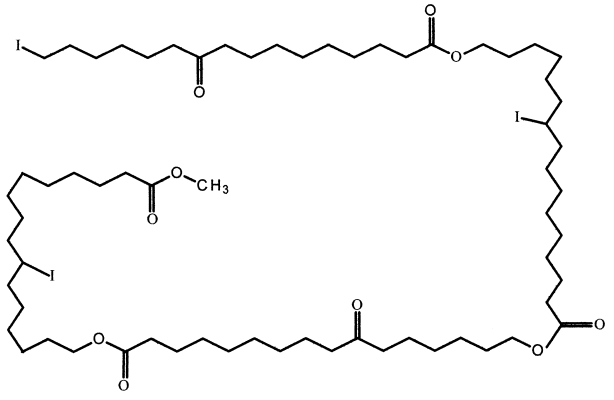

4

A complete structural determination of the soluble products and residues derived from HF treatment is in progress; however, the cutin oligomers examined to date by high-resolution NMR and MS reveal interesting compositional and architectural trends as well as impediments to structural elucidation. The conclusions outlined below are drawn from the following spectroscopic methods: ^{1}H and ^{13}C NMR chemical shifts and integrations; 2D total correlated spectroscopy (TOCSY; Griesinger et al., 1988); gradient-assisted heteronuclear-multiple quantum correlation (gHMQC; Hurd and John, 1991) and gradient-assisted heteronuclear-multiple-bond-correlation (gHMBC; Rinaldi and Keifer, 1994) experiments for through-bond connectivities *within* each monomeric constituent and *between* successive momomer units, respectively; and matrix-assisted laser desorption time-of-flight mass spectrometry (MALDI-TOF MS; Cotter, 1997) for molecular weights.

First, the most abundant Citrus cutin monomer (16-hydroxy-10-oxo-hexadecanoic acid) is present in all of the oligomers, but the other major lime fruit cutin monomer (10,16-dihydroxyhexadecanoic acid) is absent. The soluble products of low-temperature HF depolymerization also include units of hexadecanoic acid and 16-hydroxyhexadecanoic acid, which were reported previously among the lime cutin monomers and in the pentamer **1** derived from lipase treatment. At least one oligomer structure contains unanticipated sugar moieties, as detailed below. Thus, the significant diversity in monomer composition exhibited by the various oligomers underscores the importance of examining products from several complementary degradative treatments when assembling a molecular picture of the original biopolymer.

Second, the covalent linkages present in the products of low-temperature HF treatment (and the products of other chemical treatments) consist predominantly of primary alcohols esterified to carboxylic acids; only pentamer **1** exhibits secondary ester connectivities. Nevertheless, it would be inappropriate to conclude that lime fruit cutin is lacking in cross-links. Since the reported degradative treatments (Osman et al., 1995; Ray et al., 1995, 1998; Ray and Stark, 1998) are generally incomplete, it is reasonable to assume that heavily cross-linked regions of the insoluble biopolymer are less accessible to the reagents. Moreover, the presence of secondary ester cross links in the intact cutin polymer has been inferred from its extreme insolubility and confirmed by its solid-state ^{13}C NMR spectra and spin-relaxation times (Zlotnik-Mazori and Stark, 1988; Garbow and Stark, 1990). Supporting evidence for such sequestered regions of lime cutin also comes from the solvent swelling experiments described below.

Third, despite the definitive evidence for ester linkages obtained from long-range through-bond NMR connectivities (Ray et al., 1998; Stark et al., 2000), neither the position of the mid-chain oxo- groups nor the sequence of the monomeric units may be determined from these analyses. As illustrated by oligomer **4**, this limitation occurs because the carboxyl, carbonyl, and mid-chain hydroxyl functionalities occur repeatedly and are well separated by spectroscopically degenerate methylene groups. Nevertheless, 10-oxo and/or 10-hydroxy substitution patterns are likely based on the cutin monomer structures found in lime fruit (Ray et al., 1995) and other plant materials (Kolattukudy, 1984). It is also possible, for instance, to verify an alternating arrangement of 16-hydroxy-10-oxo-hexadecanoic acid and 16-

hydroxyhexadecanoic acid units, provided that MS fragmentation patterns or isolated dimers are available (Ray et al., 1998).

Fourth, at least one lime fruit cutin oligomer contains a sugar unit in addition to the hydroxyfatty acid moieties. GC analysis indicates arabinose, glucose, and other unidentified sugar moieties among the chloroform-soluble HF cleavage products, and both the NMR chemical shifts and scalar coupling networks of one purified oligomer are consistent with an unusual 2-deoxyfuranose structure. If the cutin polyester in native Citrus fruit is indeed bound covalently to polysaccharides, then this functionalization of the cell wall may reduce its vulnerability to microbial pathogens, as has been proposed for suberized wound periderm (Zucker and Hankin, 1970).

Finally, each of these cutin oligomers poses challenges for MS determination of molecular weights and fragmentation patterns. As noted for the tomato and lime cutin hydrolysates isolated previously (Osman et al., 1995; Ray et al., 1998), volatility will drop off precipitously for compounds larger than dimers. In our hands, liquid secondary-ion mass spectrometry (Aberth et al., 1982) and MALDI-TOF MS (Cotter, 1997) have sometimes failed to give molecular ions for cutin trimers and tetramers; in most cases these techniques will also fail to provide structurally informative fragments. Either derivatization or optimized MS protocols will be needed to confirm and augment the NMR-based structural elucidation of these intriguing plant materials.

2.2. High-resolution NMR of a solvent-swelled lime cutin polymer

Although intact plant cuticular materials may be examined directly by cross polarization magic-angle spinning (CPMAS) solid-state NMR spectroscopy, the resulting ^{13}C spectral lines are broader than those observed for monomeric and oligomeric fragments in solution (Stark et al., 1989). The corresponding ^{1}H NMR spectra display very broad features, even with rapid MAS. These spectral characteristics, which stem from the anisotropic chemical environment at each nucleus and the relative lack of molecular motion, limit the molecular-level structural information available in such amorphous solid materials. Nevertheless, it is possible to regain much of the desired information by swelling cutin in organic solvents (to enhance molecular mobility) and conducting the NMR experiments with MAS (to average chemical shift anisotropy, eliminate dipole-dipole interactions, and minimize magnetic susceptibility line-broadening) (Keifer et al., 1996; Millis et al., 1997; Stark et al., 2000).

Fig. 2 makes a quantitative comparison of MAS ^{1}H NMR spectroscopic data for dry and solvated lime cutin, verifying that all of the functional groups observable with vigorous magic-angle spinning are represented in their correct proportions upon swelling of the polyester. The potential of the swelling strategy for molecular structure determination is supported by the high-field MAS ^{1}H NMR spectrum of cutin in DMSO (Fig. 3), which exhibits all resonances typical of hydroxyalkanoic acids as well as the oxymethylenes that are diagnostic for esters of primary alcohols (Ray et al., 1998). The improved spectral resolution of this latter spectrum compares favorably with that of a typical lime cutin oligomer (data not shown), demonstrating that near solution-state linewidths may be achieved at slightly elevated temperatures (50°C) and using modest spinning rates (2.5 kHz).

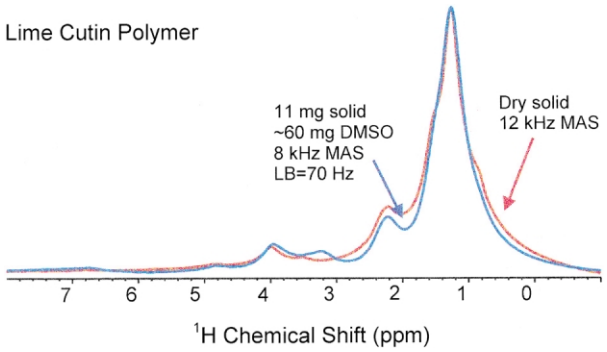

Fig. 2. 300-MHz MAS ^{1}H NMR spectrum of intact lime fruit cutin, prepared as a dry solid (red trace) and swelled at 1:6 (w/w) in DMSO (blue). Magic-angle spinning speeds were 12 and 8 kHz, respectively. NMR spectral data for the swelled sample were apodized to produce a line broadening of 70 Hz, in order to facilitate comparison with data for the dry solid.

When MAS NMR spectroscopy is combined with standard two-dimensional solution-state spectroscopy, it is possible to elucidate through-bond ^{1}H–^{13}C interactions and make detailed comparisons between the intact polymer, its soluble degradation products, and its HF-resistant residue. Comparable resolution is observed in the gHMQC contour plots of polymer, residue, and oligomer, again indicating the liquid-like state of the

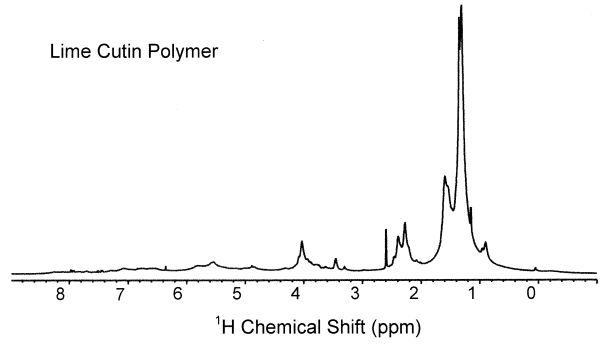

Fig. 3. 600-MHz MAS ^{1}H NMR spectrum of lime fruit cutin, swelled at 1:30 (w/w) in DMSO at 50°C and spun at 2.5 kHz. The sharp peak at 2.5 ppm comes from the solvent.

swelled moieties and showing the promise of the MAS NMR approach.

Fig. 4 displays the 2D MAS-assisted gHMQC data obtained for intact swelled lime cutin (center panel) and for a hydroxyfatty acid-based oligomer derived from low-temperature hydrogen fluoride treatment (top panel). The HMQC 'fingerprints' of directly-bonded carbon-hydrogen pairs are somewhat similar for the polymer and oligomer, supporting the presence of numerous distinguishable CH_2O and CH_2 groups in both materials. Surprisingly, no correlations to protonated carbons resonating above 70 ppm are observed in either 2D spectrum, though such resonances have been observed in prior CPMAS ^{13}C spectra of the dry solid (Zlotnik-Mazori and Stark, 1988) and attributed to CHOC=O, CHOH, aromatic, and doubly bonded functionalities. These signals could be missing from the spectrum of the soluble oligomer because of incomplete breakdown of the parent cutin (see above). Their absence from the gHMQC spectrum of the intact polymer suggests that despite solvent swelling, the combination of motional averaging and 2.5-kHz MAS is insufficient to produce high-resolution NMR spectra for its most heavily cross-linked regions.

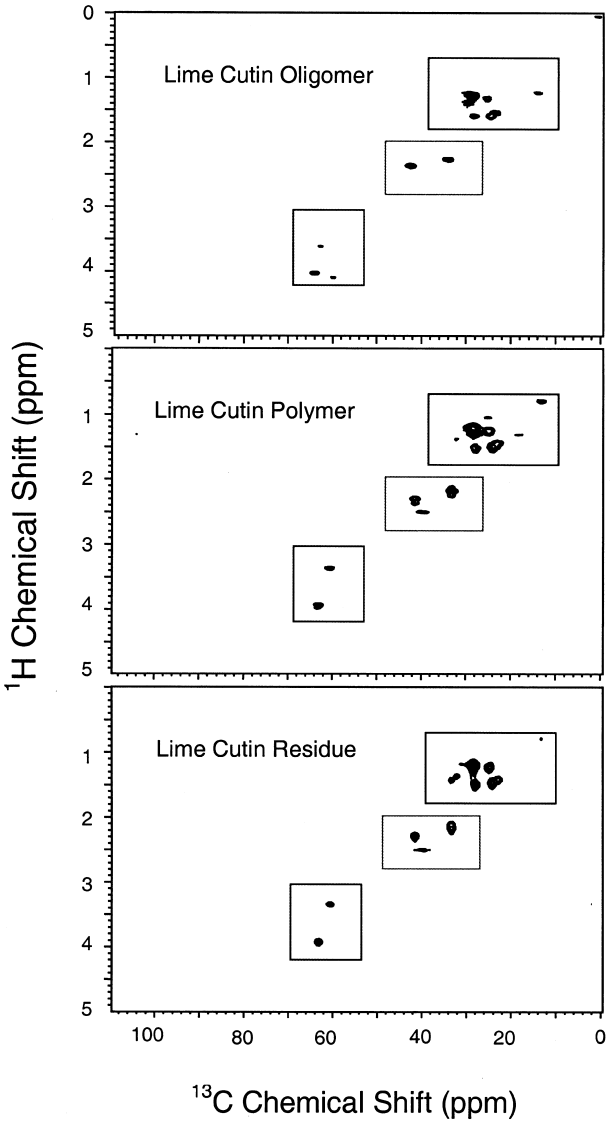

Fig. 4. Contour plots from 600-MHz gradient-assisted heterocorrelated multiple-quantum correlation (gHMQC) NMR of lime cutin, obtained with 2.5-kHz MAS and 11 G/cm z-axis pulsed field gradients. Top panel: a trimer dissolved in $CDCl_3$ at room temperature; center panel: intact plant polymer swelled in DMSO at 50°C; bottom panel: solid residue after HF treatment, swelled in DMSO at 50°C. The spectral regions highlighted by boxes are described in the text.

As compared with intact cutin, the upfield regions of the oligomer spectrum display cleaner correlation patterns for bulk methylene groups (highlighted by boxes in the upper right-hand corner of each plot) and segments alpha to ester and keto carbonyls (middle boxes). Specific changes in molecular structure are also evident among the oxymethylene groups (lower left boxes). The polymer $\underline{CH_2}OR$ resonance at (61, 3.4 ppm) disappears in the oligomer, while a new CH_2OH resonance (63, 3.6 ppm) suggests bond cleavage, and the appearance of $CH_3\underline{CH_2}OC{=}O$ (60, 4.1 ppm) and $\underline{CH_3}CH_2OC{=}O$ (14, 1.2 ppm) signals is indicative of a terminal ethyl ester. An analogous comparison between gHMQC spectra of the polymer and the unreacted residue after HF treatment is also shown in Fig. 4 (center and bottom panels). In this latter case the NMR fingerprints are almost identical, exhibiting differences only among the intensities of selected bulk methylene and terminal methyl cross peaks.

3. Discussion

A detailed understanding of the molecular architecture of plant cutins can point the way toward the design of improved crop protection protocols and robust synthetic waterproofing materials. Although the intractability of these and related plant biopolymers has slowed their structural characterization, it is possible to overcome many of these difficulties using two complementary strategies: partial depolymerization to produce soluble oligomers and high-resolution spectroscopy of the intact cuticular materials.

Soluble oligomers isolated from a variety of chemical and enzymatic degradation treatments on fruit cutins have revealed many of the essential primary and secondary ester linkages present in the native cuticular polymer. Although the through-bond correlations mapped out in 2D NMR spectra provide invaluable structural clues to the identity of these oligomeric materials, important information regarding their molecular weights and positional isomerism remains challenging to obtain routinely by MS methods. Taken together, the monomeric compositions of the oligomers are in reasonable accord with the expectations of exhaustive depolymerization studies, but no single protocol offers a reliable

molecular view of the biopolymer. Esters of secondary alcohols may be underrepresented among the soluble cutin oligomers, because the most heavily cross-linked regions of the biopolymer could be inaccessible to the depolymerization reagents. The possible presence of a novel glycoside oligomer also suggests a role for cutin in blocking access of pathogens or cell-wall degrading agents.

Insoluble cutin polymers and unreacted residues have been rendered amenable to high-resolution NMR structural analysis by swelling them in organic solvents and applying magic-angle spinning techniques. Although this hybrid (semi-solid) NMR strategy must be applied with caution to the cutin regions of heaviest cross-linking, it can provide well-resolved spectral data from both one- and two-dimensional NMR experiments. Thus, it has been possible to compare chemical moieties of the intact cutin polymer to both soluble oligomers and insoluble residues and to delineate some of the corresponding molecular transformations.

The results presented above for lime fruit cutin illustrate the feasibility of obtaining structural information on both oligomeric constituents and intact polymers. Such chemical and spectroscopic approaches also offer promise for detailed investigations of molecular architecture in a wide variety of complex plant materials, including suberins, lignins, and cell-wall polysaccharides.

4. Experimental

4.1. Isolation of lime fruit cutin

Fruit cutin was isolated from the skin of limes (*Citrus aurantifolia*) using a three-step protocol (Pacchiano et al., 1993): (1) peeling and separation of the cuticle by treatment with pectinase; (2) enzymatic digestion of cell-wall polysaccharides with successive cellulase, pectinase, and hemicellulase treatments; (3) exhaustive dewaxing using successive Soxhlet extraction with methanol, methylene chloride, and tetrahydrofuran. All reagents were obtained from Sigma or Aldrich Chemical Companies. In a typical preparation, 200 limes yielded 5.0 g of dry cutin.

4.2. Generation of lime cutin oligomers

In order to produce oligomeric fragments, 502 mg of powdered lime fruit cutin was reacted for 0.5 h with anhydrous HF at 0°C and quenched by diethyl ether in liquid nitrogen (Mort, 1983). After evaporating the ether-HF mixture (120 mg) to dryness, the reaction products were extracted to yield 22 mg of water solubles and 95 mg of chloroform solubles. The unreacted solid residue was reserved for analysis by magic-angle spinning NMR. The chloroform fraction was dried and then extracted with acetonitrile.

Purification of the acetonitrile extract was achieved using reversed-phase HPLC conducted on a Hewlett-Packard Model 1100 instrument equipped with a quaternary solvent delivery system, UV detector, and diode array detector. Separations were performed with 5 μm analytical and semi-preparative C_{18} columns, using UV detection at 210 nm, a 1-ml/min flow rate, and gradient elution (acetonitrile/H_2O/THF, varied from 75:20:5 to 95:0:5 during a period of 20 min). Isolated compounds (typical yield, 0.5 mg) were checked for purity by re-injection in two solvent systems.

4.3. Gas chromatography

Sugars were analyzed as their trimethylsilyl methyl glycosides using slight changes to the procedure of Chaplin, (1982) as previously modified by Komalavilas and Mort (Maness and Mort, 1989). After at least 3 h of methanolysis at 80°C using 1.5 M HCl in dry methanol containing 10% methyl acetate as a water scavenger, a few drops of *t*-butanol were added and the sample was evaporated to dryness. A 25–40 μl aliquot of a 1:3 v/v mixture of Tri-Sil concentrate (Pierce Chemical Co.): pyridine was added. After 15 min the sample was evaporated just to dryness and then dissolved in 100 μl isooctane. A 1-μl aliquot was injected via a cold on-column injector (J&W Scientific) fitted to a Varian 3300 chromatograph with a flame ionization detector. The column was a 30 m×0.25 mm I.D., 0.25-μm film DB-1 capillary from J&W Scientific with a constant head pressure of 12 psi helium for the carrier gas. During the injection the oven was held at 105°C. After a 1-min hold the temperature was raised to 160°C at a rate of 10°C/min. After a 4-min hold the temperature was then raised to 200°C at 2°C/min for the separation. The temperature was raised to 240°C after each separation to purge the column in preparation for subsequent injections.

4.4. Solution-state NMR spectroscopy

NMR spectra were acquired on a Varian ^{UNITY}INOVA spectrometer operating at ^{1}H and ^{13}C frequencies of 599.95 and 150.87 MHz, respectively. Cutin oligomer samples were dissolved in $CDC1_3$ to provide a field-frequency lock signal and contained 1% tetramethylsilane (TMS) to provide an internal chemical shift standard (Aldrich). One dimensional ^{1}H spectra were acquired using a Varian nanoprobe (see below). Typical experimental conditions included 16 repetitions, 2.0 s between successive acquisitions, 26,240 time-domain points, and a spectral width of 7200 Hz. Data processing and ^{1}H peak integration were done using VNMR software; ^{13}C chemical shift predictions were made using database software from Advanced Chemistry Development (Toronto, Canada).

Several two-dimensional NMR experiments were used to establish through-bond connectivities within and

between monomer units of the oligomer structures. ^{1}H–^{1}H total correlation spectroscopy ('clean' TOCSY) (Griesinger et al., 1988) was conducted with an effective spin-lock field of 6.25 kHz and a mixing period of 70 ms in order to allow magnetization transfer throughout each scalar-coupled spin system. Heteronuclear multiple quantum correlation (^{13}C HMQC) spectroscopy (Muller, 1979) was used to identify bonded proton-carbon pairs using a polarization transfer time corresponding to $^{1}J_{CH} = 140$ Hz. Heteronuclear multiple bond correlation (^{13}C HMBC) spectroscopy (Bax and Summers, 1986) was employed to delineate long-range proton-carbon bonded interactions, using a polarization transfer time corresponding to $^{3}J_{CH} = 10$ Hz. In proton-detected HMQC experiments, the GARP sequence (Shaka et al., 1985) was used for ^{13}C decoupling, and pulsed field gradients (Hurd and John, 1991; Rinaldi and Keifer, 1994) were used for coherence selection and to minimize spectral artifacts. The HMQC data were typically acquired with spectral widths of 7200 Hz for ^{1}H and 27,150 Hz for ^{13}C, a relaxation delay of 1.0 s between transients, and an array of 2 K× 256 points, zero-filled to 2K×1K points. The HMBC data were typically acquired with spectral widths of 7200 Hz for ^{1}H and 36,200 Hz for ^{13}C, a relaxation delay of 1.0 s between transients, and an array of 2K× 256 points, zero-filled to 2K×1K points.

Pentamer **1**: see Ray and Stark (1998). Dimer **2**, dimer **3**, tetramer **4**: see Ray et al. (1998).

4.5. Magic-angle spinning NMR spectroscopy

MAS ^{1}H spectra of swelled cutin samples were acquired either at 600 MHz (as described above) or on a Varian UNITY*plus* spectrometer operating at a ^{1}H frequency of 300.001 MHz. The former experiments were performed with a 4-mm Varian inverse-detection HX nanoprobe equipped with pulsed field gradients, using 1–2 mg of solid sample and magic-angle spinning typically regulated at 2.200±0.001 kHz. The latter experiments were performed on 30-mg samples in a Doty 5-mm XC5 probe spinning at 8.000±0.005 kHz. Spectra were obtained at either room temperature or 50°C, as noted. ^{1}H chemical shifts were referenced to DMSO at 2.50 ppm or $CDCl_3$ at 7.24 ppm, and ^{13}C chemical shifts were referenced to DMSO at 39.51 ppm.

4.6. Mass spectrometry

Electron-impact mass spectrometry was carried out at 70 eV using a Finnigan MAT-90 double focusing spectrometer and an accelerating potential of 5 keV, as described previously (Ray and Stark, 1998). Liquid secondary ion mass spectrometry was conducted with a VG ZAB-T high-resolution spectrometer equipped with a 30 kV cesium gun ionizing source, accelerating potential of 8 kV, and dithiothreitol/dithioerythritol matrix (Ray et al., 1998). Matrix-assisted laser desorption time-of-flight mass spectrometry (MALDI-TOF MS) was carried out using a Perseptive Biosystems Voyager instrument in the positive-ion mode. The matrices used in these experiments were trihydroxyacetophenol or indolacrylate (2 mg/ml) in acetone. Data were acquired by signal averaging of 40–70 scans, each obtained with an accelerating voltage of 25 kV and a low-mass gate of 300 amu.

Pentamer **1**: see Ray and Stark (1998). Dimer **2**, dimer **3**, tetramer **4**: see Ray et al. (1998). Oligomer from low-temperature HF treatment: m/z $(M+H)^{+}$ 853.

Acknowledgements

This work was supported by grants from the National Science Foundation (MCB/IBN-9728503) and the US Department of Agriculture (97-35106-4800). Funds to purchase the NMR spectrometers were provided by the National Science Foundation (BIR-9214560), the New York State Higher Education Applied Technology Program, the New York State Graduate Research Initiative, and the City University of New York (CUNY). The NMR facility is operated by the CUNY Center for Applied Biomedicine and Biotechnology (CABB) and by the College of Staten Island. The laser mass facility is operated by the Health Science Center of the University of Oklahoma. We gratefully acknowledge Mr. Shiying Tian and Dr. Xiaofang Cheng for assistance with the NMR experiments and analysis, and Mr. Bruce A. Baggenstoss for obtaining the MS data. Ms. Farah Jayman also assisted with the isolation of lime cutin and associated oligomers.

References

Aberth, W., Straus, S.K., Burlingame, A.L., 1982. Secondary-ion mass spectrometry with caesium-ion primary beam and liquid target matrix for analysis of bio-organic compounds. Analyical Chemistry 54, 2029–2034.

Bax, A., Summers, M.F., 1986. ^{1}H and ^{13}C assignments from sensitivity-enhanced detection of heteronuclear multiple-bond connectivity by 2D multiple quantum NMR. Journal of the American Chemical Society 108, 2093–2094.

Chaplin, M.F., 1982. A rapid and sensitive method for the analysis of carbohydrate components in glycoproteins using gas–liquid chromatography. Analytical Biochemistry 123, 334–341.

Cotter, R.J., 1997. Time-of-Flight Mass Spectrometry. American Chemical Society, Washington, DC.

Garbow, J.R., Ferrantello, L.M., Stark, R.E., 1989. ^{13}C nuclear magnetic resonance study of suberized potato cell wall. Plant Physiology 90, 783–787.

Garbow, J.R., Stark, R.E., 1990. Nuclear magnetic resonance relaxation studies of plant polyester dynamics. 1. Cutin from limes. Macromolecules 23, 2814–2819.

Griesinger, C., Otting, G., Wuthrich, K., Ernst, R.R., 1988. Clean TOCSY for ^{1}H spin system identification in macromolecules. Journal of the American Chemical Society 110, 7870–7872.

Hamosh, M., 1990. Lingual and Gastric Lipases: Their Role in Fat Digestion. CRC Press, Boca Raton, FL.

Holloway, P.J., 1982. The Plant Cuticle. Academic Press, New York, p. 45.

Hurd, R.E., John, B.K., 1991. Gradient enhanced proton-detected heteronuclear multiple-quantum coherence spectroscopy. Journal of Magnetic Resonance 91, 648–653.

Keifer, P.A., Baltusis, L., Rice, D.M., Tymiak, A.A., Shoolery, J.N., 1996. A comparison of NMR spectra obtained for solid-phase-synthesis resins using conventional high-resolution, magic-angle-spinning, and high-resolution magic-angle-spinning probes. Journal of Magnetic Resonance 119A, 65–75.

Kolattukudy, P.E., 1984. Biochemistry and function of cutin and suberin. Canadian Journal of Botany 62, 2918–2933.

Maness, N. O., Mort, A. J., 1989. Separation and quantitation of galacturonic acid oligomers from 3 to over 25 residues in length by anion-exchange high-performance liquid chromatography. Analytical Biochemistry 248–254.

Millis, K., Maas, W.E., Singer, S., Cory, D.G., 1997. Gradient, high-resolution, magic-angle spinning nuclear magnetic resonance spectroscopy of human adipocyte tissue. Magnetic Resonance in Medicine 38, 399–403.

Mort, A.J., 1983. An apparatus for safe and convienent handling of anhydrous, liquid hydrogen fluoride at controlled temperatures and reaction times. Application to the generation of oligosaccharides from polysaccharides. Carbohydrate Research 122, 315–321.

Mort, A.J., Bauer, W.D., 1982. Application of two new methods for cleavage of polysaccharides into specific oligosaccharide fragments. Structure of the capsular and extracellular polysaccharides of *Rhizobium japonicum* that bind soybean lectin. Journal of Biological Chemistry 257, 1870–1875.

Mort, A.J., Lamport, T.A., 1977. Anhydrous hydrogen fluoride deglycosylates glycoproteins. Analytical Biochemistry 82, 289–309.

Muller, L., 1979. Sensitivity enhanced detection of weak nuclei using heteronuclear multiple quantum coherence. Journal of the American Chemical Society 101, 4481–4484.

Osman, S.F., Gerard, H.C., Fett, W.F., Moreau, R.A., Dudley, R.L., 1995. Method for the production and characterization of tomato cutin oligomers. Journal of Agricultural and Food Chemistry 43, 2134–2137.

Pacchiano, R.A., Sohn, W., Chlanda, V.L., Garbow, J.R., Stark, R.E., 1993. Isolation and spectral characterization of plant cuticle polyesters. Journal of Agricultural and Food Chemistry 41, 78–83.

Purdy, R.E., Kolattukudy, P.E., 1975a. Hydrolysis of plant cuticle by plant pathogens. Purification, amino acid composition, and molecular weight of two isozymes of cutinase and a nonspecific esterase from *Fusarium solani f. pisi*. Biochemistry 14, 2824–2831.

Purdy, R.E., Kolattukudy, P.E., 1975b. Hydrolysis of plant cuticle by plant pathogens. Properties of cutinase I, cutinase II, and a nonspecific esterase isolated from *Fusarium solani f. pisi*. Biochemistry 14, 2832–2840.

Ray, A.K., Chen, Z., Stark, R.E., 1998. Chemical depolymerization studies of the molecular architecture of lime fruit cuticle. Phytochemistry 49, 65–70.

Ray, A.K., Lin, Y.Y., Gerard, H.C., Chen, Z., Osman, S.F., Fett, W.F., Moreau, R.A., Stark, R.E., 1995. Separation and identification of lime cutin monomers by high performance liquid chromatography and mass spectrometry. Phytochemistry 38, 1361–1369.

Ray, A.K., Stark, R.E., 1998. Isolation and molecular structure of an oligomer produced enzymatically from the cuticle of lime fruit. Phytochemistry 48, 1313–1320.

Rinaldi, P.L., Keifer, P.A., 1994. The utility of pulsed-field-gradient HMBC for organic structure determination. Journal of Magnetic Resonance A 108, 259–262.

Shaka, A.J., Barker, P.B., Freeman, R., 1985. Computer-optimized decoupling scheme for wideband applications and low-level operation. Journal of Magnetic Resonance 64, 547–552.

Stark, R.E., Yan, B., Ray, A.K., Chen, Z., Fang, X., Garbow, J.R., 2000. NMR studies of structure and dynamics in fruit cuticle polyesters. Solid State NMR 16, 37–45.

Stark, R.E., Zlotnik-Mazori, T., Ferrantello, L.M., Garbow, J.R., 1989. Molecular structure and dynamics of intact plant polyesters: solid-state NMR studies. ACS Symposium Series 399, 214–229.

Zlotnik-Mazori, T., Stark, R.E., 1988. Nuclear magnetic resonance studies of cutin, an insoluble plant polyester. Macromolecules 21, 2412–2417.

Zucker, M., Hankin, L., 1970. Physiological basis for a cycloheximide induced soft rot of potatoes-D by pseudomonas-fluorescens. Annals of Botany 34, 1047–1062.

PERGAMON

Phytochemistry 57 (2001) 1043–1044

PHYTOCHEMISTRY

www.elsevier.com/locate/phytochem

Editorial

Special Issues Devoted to the Biosynthesis of Woody Plant Biopolymers and Related Substances

These Special Issues (Vol. 57/6 and 57/7) are largely derived from the presentation of papers given at the Millennium Symposium of the American Chemical Society (ACS) entitled, "Biosynthesis of Woody Plant Biopolymers and Related Substances", held in San Francisco from the 26–29 March 2000. It was organized by G.P. Bolwell and N.G. Lewis, under the auspices of the ACS Cellulose, Paper and Textile Division. The meeting was devoted to fundamental research on the biosynthesis, assembly and properties of plant cell walls which underpin their use as industrial feedstocks and other aspects that impinge on daily life such as dietary fiber. Of special interest was the way in which chemistry is being augmented with genomic, proteomic and metabolic studies to unravel the complex processes involved in plant cell wall assembly, and in combination with molecular breeding to improve fiber properties.

The rationale of the gathering was directed at integrating the present knowledge of the synthesis and assembly of carbohydrate and phenolic biopolymers in woody tissues. That notwithstanding, additional communications were given on those components that have been rather neglected in the past but which are important in preserving and enhancing both the integrity and function of specialized cell walls. These contributions focus upon specialized phenolics and lipids of secretory, cuticular, suberized and heartwood tissues.

We have organized these issues in several thematic sections, which mainly reflect the range of topics covered at the meeting. Authors were encouraged to update their contributions in the time since the meeting. The first section primarily deals with structural and anatomical aspects but contain protein and gene expression data that help understand the complexity of individual cell types within woody tissues. Four papers (McCann, Haigler and Lewis) largely relate to polysaccharide biosynthesis and cell wall assembly at the cellular level, while within the second group, two (Donaldson and Ruel) summarize spatial aspects of lignin biosynthesis and others (Lewis and Gross) describe the processes involving specialized depositions of lignins/lignans and tannins, in woody tissues, respectively.

The next section has an emphasis on chemical aspects and plant component analysis. The first begins with a comprehensive review on pectins (Mohnen) and is presented together with a research paper describing novel linkages between heterogeneous pectins (Ishii). Another contribution (Murray) describes an intriguing occurrence of oligosaccharides which might be related to glucan biosynthesis. A second chemistry section has two papers (Iiyama and Ralph) which describe some observations that they believe affect lignin assembly and a third by Stange indicates that the lignin formed by the wounding of cucumber is actually largely *p*-coumaraldehyde. Marton and Ferreira describe additional complex flavonoid derived structures found within specialized cell walls containing phenolic polymers, including that of heartwood. The final paper in this section (Stark) summarizes our knowledge of the lipid components associated with phenolics in cuticular structures.

The next sections address progress made on the biochemistry and molecular biology of carbohydrate and phenolic polymers. We begin with protein biochemistry and metabolism of wall carbohydrate synthesis. Further characterization of the synthesis of polysaccharides in vitro is described in two contributions (Carpita and Bolwell). This is followed by a study on metabolism of monosaccharides (Magel) which is also related to the provision of phenolic precursors for heartwood deposition. The biosynthesis of monolignols is reviewed with respect to metabolic channeling of individual monolignol pathways (Dixon) with three other papers following on coniferyl alcohol metabolism (Savidge and Ros Barcelo). Bernards and Cornish summarize the important advances being made in suberin and rubber biosynthesis, respectively. In the year in which the Arabidopsis genome was completed, molecular genetics have not been left out. It is apt that as we strive to identify the genes responsible for cell wall polysaccharide biosynthesis that we present a review that is germane to such studies (Brown). Five articles describe results on the regulation and manipulation of lignin biosynthesis, and these complete the two special issues (Kawaoka, Legrand, Ye, Grima-Pettenati and Bolwell). Such study represents the immediate take-off point for present commercially oriented work.

As Editors of this Special Issue, we are extremely grateful for the timely preparation and updating of

0031-9422/01/$ - see front matter © 2001 Elsevier Science Ltd. All rights reserved.
PII: S0031-9422(01)00161-3

these articles by the authors. We hope that they and the readers will find these an important and stimulating series of articles on the present status of our yet very incomplete understanding of the biosynthesis of woody plant biopolymers and related substances. In this respect, we have strived in these two volumes to compile a range of views, which sometimes differ on the same topic.

It would be remiss if we did not wholeheartedly thank financial support provided by a number of organizations without whose help neither symposium nor special issues would have been possible. These include, Applied Phytologics, Inc., American Chemical Society, Elsevier Science Ltd., the S.R. Noble Foundation, Waters Corporation and the Weyerhaeuser Company.

Norman G. Lewis
G. Paul Bolwell

PERGAMON

Phytochemistry 57 (2001) 1045–1053

PHYTOCHEMISTRY

www.elsevier.com/locate/phytochem

Insight into multi-site mechanisms of glycosyl transfer in (1→4)β-D-glycans provided by the cereal mixed-linkage (1→3),(1→4)β-D-glucan synthase

Marcos S. Buckeridge[a], Claudia E. Vergara[b], Nicholas C. Carpita[b,*]

[a]*Instituto de Botânica, Secão de Fisiologia e Bioquímica Plantas, Caixa Postal 4005, CEP-01061970, São Paulo, SP, Brazil*
[b]*Department of Botany and Plant Pathology, Purdue University, West Lafayette, IN 47907-1155, USA*

Received 31 July 2000; received in revised form 23 October 2000

Abstract

Synthases of cellulose, chitin, hyaluronan, and all other polymers containing (1→4)β-linked glucosyl, mannosyl and xylosyl units have overcome a substrate orientation problem in catalysis because the (1→4)β-linkage requires that each of these sugar units be inverted nearly 180° with respect to its neighbors. We and others have proposed that this problem is solved by two modes of glycosyl transfer within a single catalytic subunit to generate disaccharide units, which, when linked processively, maintain the proper orientation without rotation or re-orientation of the synthetic machinery in 3-dimensional space. A variant of the strict (1→4)β-D-linkage structure is the mixed-linkage (1→3),(1→4)β-D-glucan, a growth-specific cell wall polysaccharide found in grasses and cereals. β-Glucan is composed primarily of cellotriosyl and cellotetraosyl units linked by single (1→3)β-D-linkages. In reactions in vitro at high substrate concentration, a polymer composed of almost entirely cellotriosyl and cellopentosyl units is made. These results support a model in which *three* modes of glycosyl transfer occur within the synthase complex instead of just two. The generation of odd numbered units demands that they are connected by (1→3)β-linkages and not (1→4)β-. In this short review of β-glucan synthesis in maize, we show how such a model not only provides simple mechanisms of synthesis for all (1→4)β-D-glycans but also explains how the synthesis of callose, or strictly (1→3)β-D-glucans, occurs upon loss of the multiple modes of glycosyl transfer to a single one. © 2001 Published by Elsevier Science Ltd.

Keywords: *Zea mays*; Poaceae; Maize coleoptile; Cellulose synthesis; Mixed-linkage β-glucans; Xyloglucan; Arabinoxylan; Glucomannan; Galactomannan; Sucrose synthase; Golgi apparatus; Plasma membrane

1. Introduction

The cell walls of higher plants are chemically characterized as amalgams of cellulose microfibrils tethered by several kinds of (1→4)β-linked cross-linking glycans and embedded in a pectin-rich matrix (McCann and Roberts, 1992; Carpita and Gibeaut, 1993). Research spanning over three decades has left us with yet a limited understanding of how plant polysaccharides are made. Cellulose synthesis in vitro has never been convincingly demonstrated with isolated membranes from plants (Delmer, 1999). The lack of progress in identifying polysaccharide synthase polypeptides to probe the mechanisms of catalysis has been attributed to the difficulties most investigators have encountered in maintaining synthase activities in vitro. In contrast, several non-cellulosic polysaccharide synthase activities have been stabilized in isolated Golgi membranes. These include the synthases of xyloglucan (Gordon and Maclachlan, 1989; Desveaux et al., 1998), glucuronoxylans (Hobbs et al., 1991), glucomannan (Piro et al., 1993), galactomannan (Reid et al., 1995), and the mixed-linkage (1→3),(1→4)-β-D-glucan (hereafter, called β-glucan) synthase (Gibeaut and Carpita, 1993).

Like cellulose, all major cross-linking glycans contain (1→4)β-linkages that invert one sugar residue almost

* Corresponding author. Tel.: +1-765-494-4653; fax: +1-765-494-0363.

E-mail address: carpita@btny.purdue.edu (N.C. Carpita).

Abbreviations: DTT, dithiothreitol; β-Glucan, mixed linkage (1→3), (1→4)β-D-glucan; Hepes, (*N*-[2-hydroxyethyl]piperazine-*N*′-[2-ethanesulfonic acid]); HPAEC-PAD, high performance anion exchange-high chromatography-pulsed amperometric detection; PMSF, phenylmethylsulfonate fluoride; SuSy, sucrose synthase

0031-9422/01/$ - see front matter © 2001 Published by Elsevier Science Ltd.
PII: S0031-9422(01)00110-8

180° with respect to each neighbor. This structural feature creates a fundamental problem in the mechanism of synthesis. With each single addition of glycosyl residue the position of the O-4 of the glycosyl acceptor at the non-reducing terminus is moved. This means that with each monosaccharide addition the catalytic site must also invert, the acceptor glycosyl unit at the terminus of the polysaccharide must invert, or the glycosidic bonds of both substrate and acceptor must be stretched or twisted alternatingly to rotate each sugar into its proper orientation to preserve linkage solely at the O-4 position (Fig. 1). Alternatively, we and others proposed that *two* sites of glucosyl transfer residing within a single catalytic subunit generate disaccharide units that are added iteratively (Carpita et al., 1996; Albersheim et al., 1997; Koyama et al., 1997; Carpita and Vergara, 1998; Buckeridge et al., 1999). In this model, glycobiosyl units, or even-numbered units, are added to the non-reducing end, assuring that (1→4)β-linkages are strictly preserved without inversion of substrate, active site, or terminus of the growing chain.

Our studies of the synthesis in vitro of the mixed-linkage β-glucan, a cell wall polysaccharide found in grasses and cereals (Carpita, 1996), lend support to a multiple-site model for catalysis of (1→4)β-linked polysaccharides. The glucan is not a random mixture of (1→3)β- and (1→4)β-linkages, but has a defined structure of cellotriosyl and higher cellodextrins each connected by single (1→3)β-linkages (Fig. 2). The cellotriosyl unit is the smallest and most abundant cellodextrin unit found in the polymer, i. e. no alternating (1→4)β- and (1→3)β-linkages are ever observed. The ratio of the odd-numbered cellodextrin oligomers is generally about two-fold greater in abundance than the next higher even-numbered oligomers in the series (Wood et al., 1994). This type of β-glucan is not found in angiosperm species outside the Poales (Smith and Harris, 1999). The only other organism known to synthesize β-glucan is the lichen *Cetraria islandica*, which has predominately a cellotriosyl unit structure comprising 86% of the polymer, with the remainder mostly cellopentosyl units (Wood et al., 1994).

Within this short review of (1→4)β-glycan synthases, we demonstrate how the linkage of primarily odd numbered cellodextrins by single (1→3)β-linkages at near saturating concentrations of UDP-Glc in vitro provides unique insight into comparative mechanisms inherent in the (1→4)β-glycan synthases. We proposed further that the trisaccharide unit of β-glucan can be formed if an ancestral cellulose synthase complex was modified to contain a third glucosyl transferase activity in addition to the cellobiose generating activity (Carpita et al., 1996). However, the acquisition of a mechanism to add primarily an odd number of glucosyl units means that the first and third residues are not inverted 180° with respect to each other, and this feature restricts the non-reducing terminal sugar of the growing chain so that it is always oriented to expose the O-3 hydroxyl for attachment instead of the O-4 (Fig. 1). Hence, the odd-numbered cellodextrin units of β-glucan will always be linked by single (1→3)β- rather than (1→4)β-linkages. An analysis of the deduced amino acid sequences of diverse members of the *Ces*A gene family give important

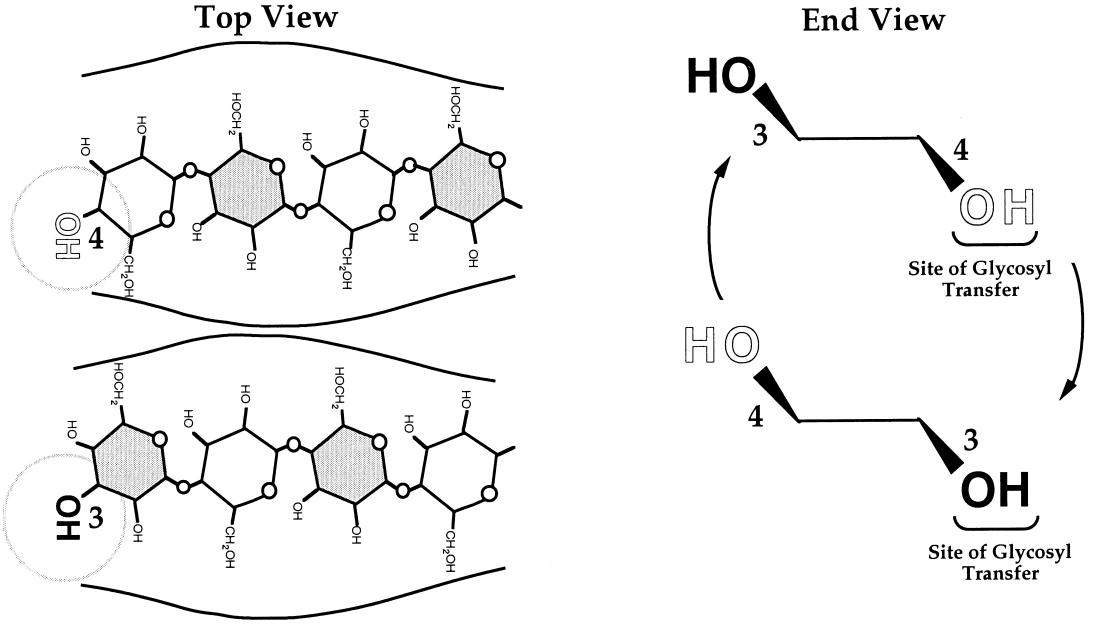

Fig. 1. *Top view*: Two possible positions of the non-reducing terminal acceptor glucosyl unit of a growing chain can be made either by rotating the chain over or processively adding a single glucosyl unit from a fixed site of glycosyl transfer. *End view*: Both (1→4)β- and (1→3)β- linkages are possible, so positioning of the non-reducing terminal sugar to expose either the O-3 or O-4 must be tightly controlled during synthesis of glucans with a defined linkage structure.

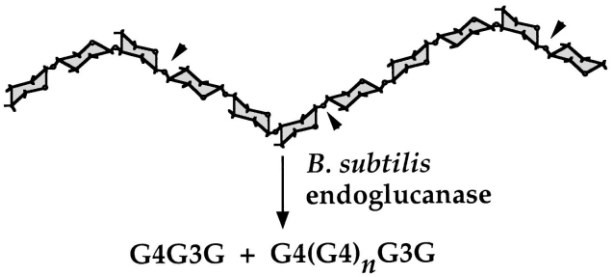

Fig. 2. General structure of the mixed-linkage (1→3),(1→4)β-D-glucan from cereal grasses. About 90–95% of the polymer is composed of cellotriosyl and cellotetraosyl units connected by single (1→3)β-linkages. The remainder of the polymer contains longer cellodextrins, with each connected by single (1→3)β-linkages. In the native polymer the cellotriose units outnumber the cellotetraosyl units about 2.5 to 1. The arrows marked the linkages that are hydrolyzed by the *Bacillus subtilis* endoglucanase, which cleaves (1→4)β-linkages when the previous linkage was (1→3)β.

clues as to the motifs that might be essential in modulating glycosyl transfer in (1→4)β-D-glycan synthases as well as differentiate them from β-glucan synthases.

2. Results

2.1. β-Glucan structure in the maize coleoptile

The structure of β-glucan is determined specifically with a sequence-dependent *Bacillus subtilis* endoglucanase (lichenase), which cleaves (1→4)β-D-glucosyl units only if preceded by (1→3)β-units. This hydrolysis yields primarily a diagnostic trisaccharide, cellobiosyl-(1→3)-D-glucose, and a tetrasaccharide, cellotriosyl-(1→3)-D-glucose (Anderson and Stone, 1975), which are separated and detected by HPAEC-PAD (Fig. 3A). Laminaribiose, or β-D-glucosyl-(1→3)-D-glucose, is not observed as a product, indicating that the polymer does not contain alternating (1→4)-D- and (1→3)-D-linked glucosyl units-the cellotriosyl unit is the smallest cellodextrin in the polymer. In β-glucans of the maize coleoptile, calculation of the mole fractions of each cellodextrin oligomer demonstrated that the cellotriose units are well over twice as abundant as the cellotetraose units, and the pentamer units are twice as abundant as the hexamers (Table 1).

2.2. β-Glucan synthesis in vitro

β-Glucan formed in vitro at suboptimal UDP-Glc concentrations of 5–250 μM was assayed by digestion with the *B. subtilis* endoglucanase, and the molar amounts synthesized were determined from the specific activity of the UDP-[^{14}C]-D-glucose provided to the membranes (Fig. 3B). At concentrations of UDP-Glc greater than 5 mM, radioactive substrate was no longer needed as the glucose incorporated could be determined by pulsed amperometry alone (Fig. 3C).

The incorporation of glucose into β-glucan is biphasic and appears to saturate between 5 and 20 mM UDP-Glc but then increases markedly above 20 mM UDP-Glc (Fig. 4A and B). The amounts of cellotriose formed relative to both cellotetraose and cellopentaose increased with increasing concentrations of UDP-Glc to about 250 μM (Fig. 4A). However, the marked increase in β-glucan synthase activity above 20 mM was primarily a result of the synthesis of cellotriosyl and cellopentaosyl units, but not cellotetraosyl units (Fig. 4B). The cellopentaose units are a small mole fraction of the total β-glucan at suboptimal UDP-Glc concentrations but become twice as abundant as cellotetraose units at high substrate concentrations (Table 1).

Table 1
Mol percentage contributions of each of the cellodextrin units of β-glucan from the maize coleoptile and that synthesized in vitro[a]

	β-Glucan source			
	Maize coleoptile	Reaction products		
Cellodextrin unit		5 μM	250 μM	30 mM
		Mol fraction[a]		
Cellotriose	0.68	0.56	0.75	0.76
Cellotetraose	0.26	0.37	0.20	0.07
Cellopentaose	0.04	0.05	0.03	0.14
Cellohexaose	0.02	0.02	0.01	0.03

[a] Values were determined from integration of HPAEC-PAD signals and response factors calculated from standards. The results are from at least two and typically three separate experiments. Variance was less

3. Discussion

3.1. Special features of β-glucan synthase in vitro

As a result of the early work on the synthesis of non-cellulosic polysaccharides at the Golgi apparatus, a common misconception developed that these synthases are saturated at μM concentrations of nucleotide-sugar substrate (for review, see Gibeaut and Carpita, 1994a). Originally thought to be true for xyloglucan synthase, Gordon and Maclachlan (1989) demonstrated that the

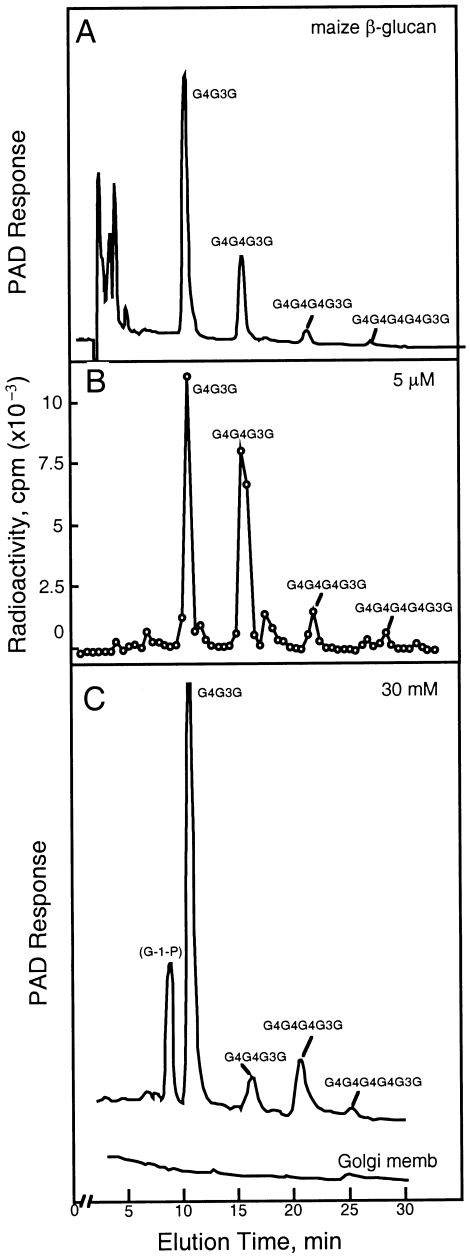

Fig. 3. HPAEC-PAD separation and detection of labeled cellodextrin-(1→3)-D-glucose oligosaccharides from β-glucan synthesized in vitro. A. Pulsed amperometric detection of cellodextrin-(1→3)-D-glucose oligosaccharides from β-glucan. B. Separation of the β-glucan cellodextrin products synthesized at low substrate concentrations. Radioactivity from 0.5-ml fractions was determined by liquid scintillation spectroscopy after acidification of the NaOH with acetic acid. C. Separation of the β-glucan cellodextrin products synthesized at high substrate concentrations. The cellodextrin-(1→3)-D-glucose oligosaccharides from β-glucan made in vitro were quantified by pulsed amperometric detection.

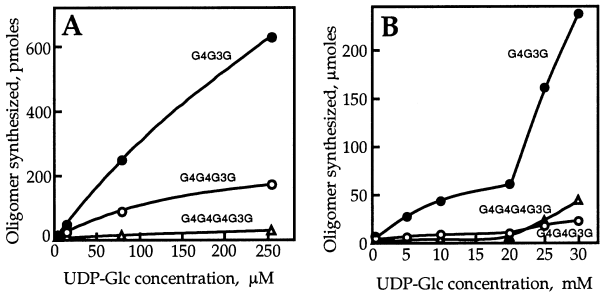

Fig. 4. A. Rates of β-glucan synthesis at low concentrations of UDP-Glc. Product made was determined from total radioactivity and specific activity of substrate or from calibration of the pulsed amperometric signal. B. Rates of β-glucan synthesis at high concentrations of UDP-Glc. The molar ratios based on incorporation of radioactivity were corrected based on the number glucosyl units per cellodextrin-(1→3)β-glucose oligosaccharide, whereas the mass detected by pulsed amperometry was calibrated by direct assay of eluted oligosaccharides.

synthesis demanded a precise ratio of UDP-Glc to UDP-Xyl but formation of hepta-saccharide units of true xyloglucan required mM, not μM concentrations of substrate. β-Glucan synthase has features that resemble cellulose synthase more than other Golgi-associated synthases (Buckeridge et al., 1999). The synthase requires Mg^{2+} (or Mn^{2+}) and has a high apparent K_m for UDP-Glc; maintenance of a high pH external to the Golgi lumen promotes prolonged synthesis of the glucan (Gibeaut and Carpita, 1993). The synthase activity preserved in vitro synthesizes a product containing a distribution of cellotriosyl and cellotetraosyl units similar to that of the native β-glucan when about 250 μM UDP-Glc is provided. Unlike non-gramineous plants, a callose synthase is associated with the Golgi apparatus as well as the plasma membrane, and increases in its activity coincide with loss of β-glucan synthase by action of protonophores or detergent solubilization of the Golgi membranes (Gibeaut and Carpita, 1993, 1994b).

Amor et al. (1995) proposed that the association of sucrose synthase (SuSy) with cellulose synthase provides a mechanism for metabolic channeling of UDP-Glc. In support of this idea, fibrils of callose were synthesized from sucrose and UDP on immobilized tobacco plasma membrane sheets (Hirai et al., 1998). In maize, SuSy is detected immunocytochemically in both a plasma membrane-enriched and Golgi membrane-enriched fractions, whereas in soybeans, the enzyme is detected only in plasma membranes (Buckeridge et al., 1999). Hence, if β-glucan synthase is derived from an ancestral cellulose synthase and possesses a similar mechanism of synthesis, then part of this mechanism may include the association of SuSy to control the supply of UDP-Glc to the active site(s) of the glucan synthase. For this mechanism to work, the catalytic domain of β-glucan synthase would reside on the cytosolic face of the Golgi membranes. The xyloglucan synthase complex is located completely within the lumen of the Golgi apparatus and dependent upon UDP-Glc transport (Muñoz et al., 1996), whereas the plasma membrane-associated callose synthase is predominately on the cytosolic face (Wu and Wasserman, 1993), consistent with the expected topology of substrate acceptor. The membrane topology of the β-

glucan synthase has never been established. We propose that the catalytic domain is on the cytosolic face of the Golgi membrane, and the β-glucan chains, like those of cellulose, are extruded through the membrane into the lumen of the Golgi apparatus.

The unit structure of β-glucan can be altered drastically depending on the UDP-Glc concentration (Fig. 4A and B). We found that sub-optimal UDP-Glc concentrations favor the synthesis of the longer cellodextrin units in β-glucan, particularly the cellotetraosyl unit, whereas at the highest UDP-Glc concentrations tested, the cellotriose and cellopentaose comprised over 90% of the total polymer synthesized (Table 1). The distribution of cellodextrin units in β-glucan synthesized in vitro at high concentrations of UDP-Glc is similar to that of the β-glucan from the lichen *Cetraria islandica* (Wood et al., 1994). Therefore, as saturation with substrate is approached, the polymers are composed of mostly cellotriose units, and cellopentaose units become the next most abundant unit (Fig. 4B).

The mechanism of glucosyl transfer indicated by our data suggest three different modes of glucosyl transfer from UDP-Glc to the non-reducing terminus of the glucan chain, instead of two as in the mechanism of cellulose synthase (Fig. 5A and B). The accumulation of cellopentaose units instead of cellotetraose units at high substrate concentration is fully consistent with the three-mode model of glycosyl transfer. If, as part of a structural regulatory mechanism, the additional mode is of lower affinity than the conserved modes of the ancestral cellulose synthase, then absence of substrate in the third site will introduce a cellobiosyl unit. This terminal unit will be inverted relative to its usual position when the unit moves into the non-reducing acceptor position. This inversion places the O-4 in the active position, and linkage of a subsequent cellotriose unit in the next round will generate a cellopentaosyl unit (Fig. 5C). Two consecutive cellobiosyl units form the cellotetraosyl unit, but such a linkage must create instability in the positioning of the growing chain in the synthase such that it inverts to once again place the O-3 of the non-reducing terminal unit in the acceptor position for the next round of processive transferase activity. Control of cellodextrin unit structure may occur by regulations of substrate concentration channeled to the sites of glycosyl transfer, e.g. via SuSy, or by conformational changes at the catalytic sites by changes from high affinity to low affinity states induced by other regulatory factors.

3.2. Possible relationship of cellulose and β-glucan synthase to callose synthase

Both cellulose and β-glucan synthases appear to "default" to callose synthases when disrupted (Delmer, 1977; Carpita and Gibeaut, 1993). Our model not only distinguishes the mechanisms of cellulose and β-glucan synthase but also predicts that callose synthase arises by loss of function of the multiple modes of glycosyl transfer and "default" to a single one (Fig. 5D). The best evidence for this default pathway comes from discovery of the cellulose synthase gene from *Dictyostelium* (Blanton et al., 2000). *Dictyostelium* makes no callose in vivo but exhibits cellulose and callose synthase activity in vitro (Blanton and Northcote, 1990). A mutation in the *Ces*A gene results in the inability to synthesize either (1→4)β- or (1→3)β-linked glucans, indicating that the product of the *Ces*A gene makes both products in vitro.

An *Agrobacterium* (1→3)β-glucan synthase gene contains the four U-motifs expected of a *Ces*A gene, even though the glucose units are not inverted during synthesis (Stasinopoulos et al., 1999). Such a gene may have derived from an ancestral cellulose synthase, but the encoded synthase may have lost the function of one of the two glycosyl transfer activities. Although it may be reasonable to suggest that callose synthesis may result from damage to cellulose and β-glucan synthases when the plasma membrane and Golgi membranes are disrupted, callose is made naturally at several stages of cell development and can be activated as a wound response. It is more likely that this callose is made by specific callose synthases encoded by genes unrelated to *Ces*A. Cui et al. (2001), Doblin et al. (2001) and Hong et al. (2001) have recently cloned distinct callose synthase homologs of fungal FKS1 synthases. These polypeptides are over 200 kD, are predicted to contain 16 membrane spanning domains, and are associated with other polypeptides thought to be part of the synthase mechanism or its regulation. However, while these findings indicate there may be several distinct synthases of 3-linked glucans, there are no precedents for distinct synthases of (1→4)β-glycans other than those with D,D,D,QxxRW domains.

3.3. Are β-glucan synthase and cellulose synthase both encoded by CesA genes?

The discovery of a higher plant cellulose synthase gene by Pear et al. (1996) has made it possible to compare the deduced amino acid structure of the active site with rational models of catalysis. The *Ces*A genes encode polypeptides of about 110 kDa with the presumed active site comprising a large cytosolic domain with four highly conserved "U" motifs. Each of the first three contains an essential aspartyl residue, and the fourth possesses a QxxRW motif. These four U-motifs of the *Ces*A gene are conserved in the genes encoding several processive glycosyl transferases in which repeating β-glycosyl unit structures are synthesized (Saxena et al., 1995). Some examples include hyaluronan synthases (DeAngelis et al., 1993; Spicer et al., 1997), chitin synthases (Bulawa et al., 1986), and the NodC synthase (Geremia et al., 1994), all of which make consecutive β-glycosidic linkages in which one sugar is oriented nearly

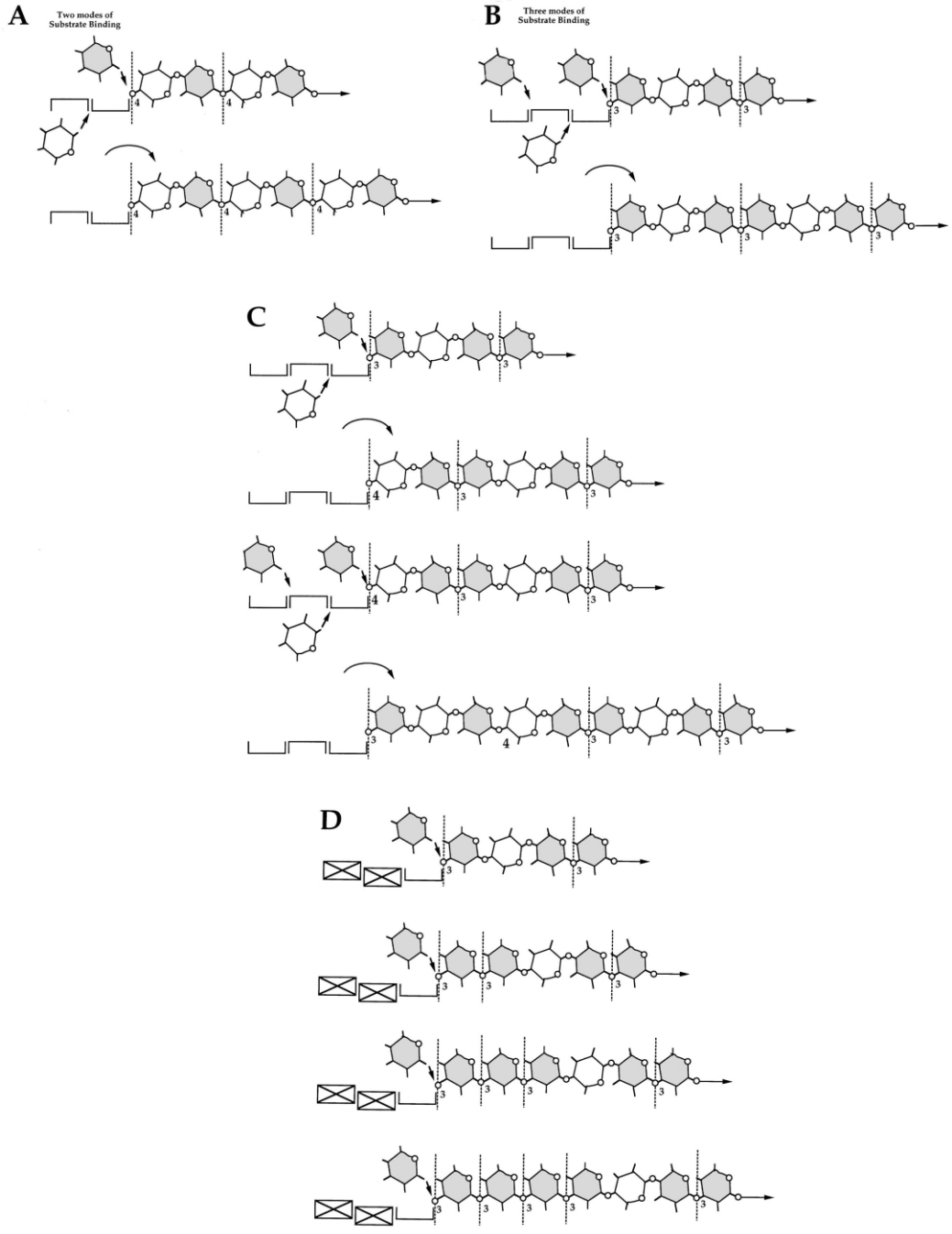

Fig. 5. A model to explain the mechanism of synthesis of (1→4)β-linked glycans, the special case of the (1→3),(1→4)β-D-glucans, and (1→3)β-D-glucans. A. If a single mode of linkage occurs without changing the position of the active site, then a polymer generates an alternating (1→4)β-, then (1→3)β-linkage pattern. However, if two complementary modes of glycosyl transfer occur juxtaposed to each other, then cellobiosyl units are generated and the non-reducing terminal unit will always expose its O-4 position for linkage. This two-mode mechanism assures that the entire polymer is composed of (1→4)β-linkages. A similar mechanism may have been adopted by synthases of the backbones of xyloglucans, xylans, and gluco- and galactomannans. B. Acquisition of a third mode of glucosyl transfer would generate cellotriosyl units instead of cellobiosyl units, and because the first and third units are not inverted, the non-reducing acceptor sugar exposes the O-3 for linkage instead of the O-4 position. Hence, when all three modes are used the polymer made is composed entirely of cellotriosyl-(1→3)β-D-glucosyl units. C. The third mode of transfer may be one of lower affinity than the cellobiosyl generating glucosyl transferases, and failure to fill it produces the longer cellodextrins. If only a cellobiose unit is formed, then its O-4 position is exposed in the active site when this unit occupies the non-reducing terminus position. If a cellotriose is generated in the next round, then a cellopentaosyl unit is made and the O-3 will once again be exposed in the next round of synthesis. Cellotetraosyl units are made if two consecutive cellobiosyl units are added, and cellohexaosyl units are made if three consecutive cellobiosyl units are added. Chain stability must be compromised in these instances because chain rotation to expose the O-3 must occur. Otherwise, celloheptaosyl and cellononaosyl units are made. D. If the multiple modes of glycosyl transfer collapse to a single mode, then no inversion of glucose residues occurs and the O-3 position will always be positioned at the non-reducing end of the growing chain. Callose becomes the only product possible.

180° with respect to each neighboring sugar. These and other "inverting" type processive synthases comprise the family 2 NDP-sugar glycosyl transferases (Campbell et al., 1997). A comparison of arabidopsis, maize, and other higher plant species reveals that the *Ces*A gene family clusters into several sub-classes (Holland et al., 2000). A unique feature of the *Ces*A genes is a plant-specific insertion of sequence that, upon examination of the few *Ces*A sequences, appeared to be highly mutable and was called the "hypervariable region" (Pear et al., 1996; Delmer, 1999). Analysis of the predicted amino acid sequences of a great many *Ces*A genes that had been examined since then revealed motifs of consecutive acidic and basic residues, cysteine residues, proline residues, and aromatic residues that are well conserved in a sub-class specific manner (Vergara and Carpita, 2001). Conservation of these motifs into specific sub-classes indicates that their roles in catalysis of glycosyl transfer or its regulation remain to be defined. However, determination of how these motifs alter the conformation of the active site to direct different modes of glycosyl transfer must await 3-dimensional structure determination and their possible interaction with other proteins. Several mutants of specific members of the *Ces*A gene family are now available and are beginning to shed light on the polymers made by them.

4. Experimental

4.1. Plant material and preparation of membranes

Maize (*Zea mays* L.) seeds (caryopses) were soaked overnight in deionized water bubbled with air at 30°C, sown in trays of moist medium-grade vermiculite, and incubated in darkness at 30°C for 2 days. All procedures were performed essentially as described by Buckeridge et al. (1999). Freshly isolated 2-day-old coleoptiles were collected in a chilled beaker and overlaid with an equal volume of ice-cold homogenization buffer (HB) of 84% sucrose in 20 mM Hepes [KOH], pH 7.2, containing 20 mM KCl, 5 mM EDTA, 5 mM EGTA, 10 mM DTT, and 0.2 mM PMSF. In addition, 2 g of activated charcoal was sprinkled on coleoptiles before addition of HB to absorb inhibitory phenolics released by the maize coleoptiles during mashing (Gibeaut and Carpita, 1993). The homogenate was squeezed through a nylon mesh (47-μm^2 pores), and about 15 ml of the homogenate was pipeted into a 38.5-ml Ultraclear centrifuge tube (Beckman) onto a cushion of 50% (w/v) sucrose in a gradient buffer 20 mM Hepes [BTP], pH 7.6, and overlaid with 8 ml each of 34 and 25% sucrose (w/v), 7 ml of 18% (w/v) sucrose in gradient buffer, and the remaining volume was made up with 9.5% (w/v) sucrose in the same buffer. After sucrose gradient centrifugation at 140,000 *g* in a Beckman SW28 rotor for 45 min, the interfaces containing the enriched Golgi membranes were collected with a Pasteur pipet. These membranes were used directly for β-glucan synthase reactions at low substrate concentration or were diluted with 1.08 M sucrose in gradient buffer and concentrated by centrifugation at 140,000 *g* for 30 min in an SW28 rotor for assays at high substrate concentration (Buckeridge et al., 1999). Samples of the other layers were also taken for protein determination and enzyme marker assays. Protein was determined by bicinchoninic acid assay (Pierce), and assays for IDPase (Golgi), NADH oxidase (mitochondria), vanadate-sensitive ATPase (plasma membrane), NADP reductase (endoplasmic reticulum), and NO_3-sensitive ATPase (vacuole) were performed as optimized for maize from published methods described in Gibeaut and Carpita (1994b).

4.2. Glucan synthase reactions

Reactions were performed with freshly isolated membranes at 30°C for up to 2 h. Reactions at low substrate concentrations were performed in 4-ml borosilicate glass vials and contained, at final substrate concentrations indicated, 0.5–2.0 μCi of UDP-D-[U-^{14}C]Glc (250 mCi/mmol; ICN Radiochemicals), 20 mM KCl, 1.08 M sucrose, 10 mM $MgCl_2$, 10 mM Hepes[BTP], pH 7.6. One-half of a milliliter each of a reaction buffer and membrane fraction (50 to 100 μg protein) were mixed in vials and placed at 30°C. Reactions without radioactivity at high substrate concentrations were performed with concentrated membranes (200 μg protein), and $MgCl_2$ concentrations were 1.5 times that of the UDP-Glc concentration. Reactions were stopped with 3 ml of ethanol, capped, and placed in an oven at 105°C for 5 min. The reaction mixtures were cooled to ambient temperature then centrifuged for 5 min at 10,000 *g*. The pellet was washed extensively with hot 80% ethanol after heating and recentrifuged.

4.3. Digestion with *B. subtilis* endoglucanase as a specific assay for (1→3),(1→4)β-D-glucan

The washed and dried products of the glucan synthase reactions were suspended in 200 μl of water. For reactions at low substrate concentration, 200 μg of barley β-glucan (Sigma) were added as carrier. Ten to fifty μl of a preparation of *B. subtilis* endo-β-D-glucanase (Gibeaut and Carpita, 1993) in 20 mM Na acetate, 20 mM NaCl, pH 5.5, were added, and the samples were incubated 3 h at 37°C. The products released from digestion of purified β-glucan are mostly cellobiosyl- and cellotriosyl-(1→3)-D-glucose, with decreasingly smaller amounts of cellotetraosyl- and cellopentaosyl-(1→3)-D-glucose. The reactions were terminated by heating for 2 min in a boiling water bath, cooled to ambient temperature, and centrifuged at 10,000 *g* for 5 min. Radioactivity in β-glucan was estimated as the difference in dpm in the supernatants

between digested and undigested samples. The remaining insoluble radioactivity from in vitro synthase reactions, which is greater than 90% (1→3)-linked glucosyl units was attributed to callose (Gibeaut and Carpita, 1993).

4.4. HPAEC-PAD

The oligomers from digestion of the in vitro reaction products were separated on a Carbo-Pac PA1 anion exchange column equilibrated in 0.5 N NaOH and eluted in a linear gradient of Na acetate in 0.5 N NaOH as described (Gibeaut and Carpita, 1993). With reactions products from low concentrations of UDP-Glc, the radioactivity in 0.5-ml fractions collected in 1.0 ml of 2 N acetic acid was determined by liquid scintillation spectroscopy, whereas the β-glucan products of high UDP-Glc concentrations and native β-glucans from alkali extracts were determined by pulsed amperometric detection (Buckeridge et al., 1999).

Acknowledgements

We thank Anna Olek for technical assistance. This work was supported by Contract DE-FG02-88ER13903 from the US Department of Energy, Energy Biosciences (to N.C.C.) and a grant from FAPESP (to M.S.B.). Journal paper #16,392 of the Purdue Agricultural Experiment Station.

References

Albersheim, P., Darvill, A., Roberts, K., Staehelin, L.A., Varner, J.E., 1997. Do the structures of cell wall polysaccharides define their mode of synthesis? Plant Physiology 113, 1–3.

Amor, Y., Haigler, C.H., Johnson, S., Wainscott, M., Delmer, D.P., 1995. A membrane-associated form of sucrose synthase and its potential role in synthesis of cellulose and callose in plants. Proceedings of the National Academy of Sciences USA 92, 9353–9357.

Anderson, M.A., Stone, B.A., 1975. A new substrate for investigating the specificity of β-glucan hydrolases. FEBS Letters 52, 202–207.

Blanton, R.L., Northcote, D.H., 1990. A 1,4-β-D-glucan synthase system from *Dictyostelium discoideum*. Planta 180 (3), 324–332.

Blanton, R.L., Fuller, D., Iranfar, N., Grimson, M.J., Loomis, W.F., 200. The cellulose synthase gene of *Dictyostelium*. Proceedings of the National Academy of Sciences of the United States of America 97, 2391–2396.

Buckeridge, M.S., Vergara, C.E., Carpita, N.C., 1999. The mechanism of synthesis of a cereal mixed-linkage (1→3),(1→4)-β-D-glucan: evidence for multiple sites of glucosyl transfer in the synthase complex. Plant Physiology 120, 1105–1116.

Bulawa, C.E., Slater, M., Cabib, E., Au-Young, J., Sburlati, A., Adair Jr, W.L., Robbins, P.W., 1986. The *S. cerevisiae* structural gene for chitin synthase is not required for chitin synthesis in vivo. Cell 46, 213–225.

Campbell, J.A., Davies, G.J., Bulone, V., Henrissat, B., 1997. A classification of nucleotide-diphospho-sugar glycosyltransferases based on amino acid sequence similarities. Biochemical Journal 326, 929–939.

Carpita, N.C., 1996. Structure and biogenesis of the cell walls of grasses. Annual Review of Plant Physiology and Plant Molecular Biology 47, 445–476.

Carpita, N.C., Gibeaut, D.M., 1993. Structural models of the primary cell walls in flowering plants: consistency of molecular structure with the physical properties of the walls during growth. The Plant Journal 3, 1–30.

Carpita, N.C., Vergara, C.E., 1998. A recipe for cellulose. Science 279, 672–673.

Carpita, N., McCann, M., Griffing, L.R., 1996. The plant extracellular matrix: news from the cell's frontier. The Plant Cell 8, 1451–1463.

Cui, X., Shin, H., Charlotte Song, C., Laosinchai, W., Amano, Y., Brown, R.M. Jr., 2001. A putative plant homology of the yeast β-1,3-glucan synthase subunit FKS1 from cotton (*Gossypium hirsutum* L.) fibers. Planta, in press.

DeAngelis, P.L., Papaconstantinou, J., Weigel, P.H., 1993. Molecular cloning, identification, and sequence of the hyaluronan synthase gene from Group A *Streptococcus pyrogenes*. Journal of Biological Chemistry 268, 19181–19184.

Delmer, D.P., 1977. Biosynthesis of cellulose and other plant cell wall polysaccharides. Recent Advances in Phytochemistry 11, 105–153.

Delmer, D.P., 1999. Cellulose biosynthesis: exciting times for a difficult field of study. Annual Review of Plant Physiology and Plant Molecular Biology 50, 245–276.

Desveaux, D., Faik, A., Maclachlan, G., 1998. Fucosyl transferase and the biosynthesis of storage and structural xyloglucan in developing nasturtium fruits. Plant Physiology 118, 885–894.

Doblin, M.S., de Melis, L., Newbigin, E., Bacic, A., Read, S., 2001. Pollen tubes of *Nicotiana alata* express two genes from different β-glucan synthase families. Plant Physiology, in press.

Geremia, R.A., Mergaert, P., Geelen, D., Van Montagu, M., Holsters, M., 1994. The *Nod*C protein of *Azorhizobium caulinodans* is an *N*-acetylglucosaminyltransferase. Proceedings of the National Academy of Sciences USA 91, 2669–2673.

Gibeaut, D.M., Carpita, N.C., 1990. Separation of membranes by flotation centrifugation for in vitro synthesis of plant cell wall polysaccharides. Protoplasma 156, 82–93.

Gibeaut, D.M., Carpita, N.C., 1993. Synthesis of (1→3),(1→4)-β-D-glucan in the Golgi apparatus of maize coleoptiles. Proceedings of the National Academy of Sciences USA 90, 3850–3854.

Gibeaut, D.M., Carpita, N.C., 1994a. Biosynthesis of plant cell-wall polysaccharides. FASEB Journal 8, 904–915.

Gibeaut, D.M., Carpita, N.C., 1994b. Improved recovery of (1→3),(1→4)-β-D-glucan synthase activity from Golgi apparatus of *Zea mays* (L.) using differential flotation centrifugation. Protoplasma 180, 92–97.

Gordon, R., Maclachlan, G., 1989. Incorporation of UDP-[^{14}C]glucose into xyloglucan by pea membranes. Plant Physiology 91, 373–378.

Hirai, N., Sonobe, S., Hayashi, T., 1998. In situ synthesis of β-glucan microfibrils on tobacco plasma membrane sheets. Proceedings of the National Academy of Sciences USA 95, 15102–15106.

Hobbs, M.C., Delange, M.H.P., Baydoun, E.A.-H., Brett, C.T., 1991. Differential distribution of a glucuronoyltransferase, involved in glucuronoxylan synthesis, with the Golgi apparatus of pea (*Pisum sativum* var. Alaska). Biochemical Journal 277, 653–658.

Holland, N., Holland, D., Helentjaris, T., Dhugga, K., Xoconostle-Cazares, B., Delmer, D.P., 2001. A comparative analysis of the plant cellulose synthase (*Ces*A) gene family. Plant Physiology 123, 1313–1323.

Hong, Z., Ashton, J., Delauney, A.J., Verma, D.P.S., 2001. A cell plate-specific callose synthase and its interaction with phragmoplastin. Plant Cell, in press.

Koyama, M., Helbert, W., Imai, T., Sugiyama, J., Henrissat, B., 1997. Parallel-up structure evidences the molecular directionality during biosynthesis of bacterial cellulose. Proceedings of the National Academy of Sciences of the United States of America 94, 9091–9095.

McCann, M.C., Roberts, K., 1991. Architecture of the primary cell wall. In: Lloyd, C.W. (Ed.), The Cytoskeletal Basis of Plant Growth and Form. Academic Press, London, UK, pp. 109–129.

Muñoz, P., Norambuena, L., Orellana, A., 1996. Evidence for a UDP-glucose transporter in Golgi apparatus-derived vesicles from pea and its possible role in polysaccharide biosynthesis. Plant Physiology 112, 1585–1594.

Pear, J.R., Kawagoe, Y., Schreckengost, W.E., Delmer, D.P., Stalker, D.M., 1996. Higher plants contain homologs of the bacterial *cel*A genes encoding the catalytic subunit of cellulose synthase. Proceedings of the National Academy of Sciences USA 93, 12637–12642.

Piro, G., Dalessandro, G., Northcote, D.H., 1993. Glucomannan synthesis in peas epicotyls: the mannose and glucose transferases. Planta 190, 206–220.

Reid, J.S.G., Edwards, M., Gidley, M.J., Clark, A.H., 1995. Enzyme specificity in galactomannan biosynthesis. Planta 195, 489–495.

Saxena, I.M., Brown, R.M., Dr., Fevre, M., Geremia, R.A., Henrissat, B. 1995. Multidomain architecture of β-glucosyl transferases: implications for mechanism of action. Journal of Bacteriology 177, 1419–1424.

Smith, B.G., Harris, P.J., 1999. The polysaccharide composition of Poales cell walls: poaceae cell walls are not unique. Biochemical Systematics and Ecology 27, 33–53.

Spicer, A.P., Olson, J.S., McDonald, J.A., 1997. Molecular cloning and characterization of a cDNA encoding the third putative mammalian hyaluronan synthase. Journal of Biological Chemistry 272, 8957–8961.

Stasinopoulos, S.J., Fisher, P.R., Stone, B.A., Stanisich, V.A., 1999. Detection of two loci involved in (1→3)-β-glucan (curdlan) biosynthesis by *Agrobacterium* sp. ATCC31749, and comparative sequence analysis of the putative curdlan synthase gene. Glycobiology 9, 31–41.

Vergara, C.E., Carpita, N.C., 2001. β-D-Glycan synthases and the *Ces*A gene family: lessons to be learned from the mixed-linkage (1→3),(1→4)-β-D-glucan synthase. Plant Molecular Biology, in press.

Wood, P.J., Weisz, J., Blackwell, B.A., 1994. Structural studies of (1→3),(1→4)-β-D-glucans by ^{13}C-nuclear magnetic resonance spectroscopy and by rapid analysis of cellulose-like regions using high-performance anion-exchange chromatography of oligosaccharides released by lichenase. Cereal Chemistry 71, 301–307.

Wu, A., Wasserman, B.P., 1993. Limited proteolysis of (1,3)-β-glucan (callose) synthase from *Beta vulgaris* L: topology of protease-sensitive sites and polypeptide identification using Pronase E. The Plant Journal 4, 683–695.

PERGAMON

Phytochemistry 57 (2001) 1055–1060

PHYTOCHEMISTRY

www.elsevier.com/locate/phytochem

Differential behaviour of four plant polysaccharide synthases in the presence of organic solvents

Maria E. Kerry, Abigail C.E. Gregory, G. Paul Bolwell*

Division of Biochemistry, School of Biological Sciences, Royal Holloway, University of London, Egham, Surrey TW20 0EX, UK

Received 1 September 2000; received in revised form 26 February 2001

Abstract

The behaviour of four membrane-bound glycosyl transferases involved in cell wall polysaccharide synthesis has been studied in relation to the effects of a graded series of organic solvents on their activity and type of product formed. Relative enzyme inhibition observed for some solvents was in direct relationship to the hydrophilicity of the product. This was in the order of arabinan synthase > callose synthase > xylan synthase > β-1,4-glucan synthase. The former two were always inhibited, the xylan synthase rather less so. However, the β-1,4-glucan synthase showed significant increases in substrate incorporation in the presence of solvents. A graded series of primary alcohols were much more effective in enhancing activity than acetone, ethyl acetate and dimethyl formamide. In the presence of the most effective solvent, methanol, there was considerable activation of β-1,4-glucan production. This reciprocal nature of the behaviour of the β-1,4- and β-1,3-glucan synthases in organic solvent is supportive of recent molecular data that the two types of glucans are catalysed by separate enzyme systems. However, the results reported here do not totally negate the proposition that either enzyme is capable of synthesising the other linkage in minor amounts in vitro. © 2001 Elsevier Science Ltd. All rights reserved.

Keywords: Glucan; Xylan; Arabinan; Glycosyl transferase; Organic solvent

1. Introduction

The plant cell wall represents a major component of the dry mass of plant tissue. It has long been the major source of dietary fibre and is recognised to play a critical role in determining the rheological properties of plants and food texture. Moreover, it is a dynamic structure and thus has a vital role during plant development and responses to pathogen attack and environmental stress (Bolwell, 1993; Carpita and Gibeaut, 1993). However, our understanding of the biosynthesis of plant cell wall components is limited particularly with respect to polysaccharides. Although considerable progress is at last being made with the molecular identification of the gene family coding for plant cellulose synthase (Pear et al., 1996; Arioli et al., 1999; Taylor et al., 1999), and cDNAs and genes coding for a fucosyl transferase (Perrin et al., 1999) and a galactosyl transferase (Edwards et al., 1999), there is still an enormous lack of knowledge of polysaccharide synthases at the protein level.

The site of synthesis of the matrix polysaccharides has been localised to the Golgi by biochemical studies of fractionated endomembranes (Bolwell, 1988), organelle subfractions (Baydoun and Brett, 1997), and by elegant immunogold localisation of the nascent polysaccharides within the Golgi stack (Moore et al., 1991). However, there are few reports of extensive direct characterisation and identification of the glycosyl transferases involved. A notable exception is the fucosyl transferase specific for a side chain of xyloglucan, a major hemicellulose of the dicot cell wall (Hanna et al., 1991; Perrin et al., 1999), which was purified as an M_r 51,000 protein before confirmation by molecular cloning. Other glycosyl transferases purified are arabinan and xylan synthases as M_r 70,000 and 50,000 proteins, respectively (Rodgers and Bolwell, 1992), and a number of callose synthases including that from French bean as a complex of M_r 65,000 and 55,000 polypeptides (McCormack et al., 1997) and from pea (M_r 70,000 and 55,000) (Dhugga and Ray, 1994). Most other polysaccharide synthases such as galacturonosyl transferases in pectin synthesis (Bolwell et al., 1985; Doong and Mohmen, 1998), glucosyl and xylosyl transferases of primary wall xyloglucan synthesis (White et al., 1993a,b) and glucuronosyl

* Corresponding author. Tel.: +44-1784-44-35-53; fax: +44-1784-43-43-26.

E-mail address: uhbc006@vms.rhbnc.ac.uk (G.P. Bolwell).

0031-9422/01/$ - see front matter © 2001 Elsevier Science Ltd. All rights reserved.
PII: S0031-9422(01)00126-1

transferases of secondary wall xylan synthesis (Baydoun and Brett, 1997) remain only partially characterised in membrane and solubilised preparations.

Although identification of the genes coding for such glycosyl transferases may well arise from large sequencing projects (Bolwell, 2000; Gibeaut, 2000), for instance there are many putative cellulose synthase genes in the Arabidopsis dbEST and genomic data bases, there will still be a need for the demonstration of activity in vitro for the expressed gene products. Part of the reason for the difficulties in purifying these enzymes is the loss of activity on solubilisation which is not entirely due to the release of hydrolytic activity.

In theory, the basis for some of these problems of loss of activity probably resides in their relationship to water (Bolwell, 1993). The glycosidic bond is of relatively low energy and can be readily made and broken. Thus, there are abundant reports of enzymatic transglycosylation reactions for plant glycosidases. The exclusion of water could, therefore, promote glycosidic bond formation and reflect a situation appertaining to proteins associated with membranes in vivo. There are now numerous examples in the literature that glycosidases can be driven in reverse under non-aqueous conditions. Examples include the synthesis of cellulose by *Trichoderma* cellulase using β-cellobioside fluoride as substrate (Kobayashi et al., 1991, 1996a) and polymers of xylan and chitin have also been produced in a similar manner (Kobayashi et al., 1996b,c). Even hetero-oligosaccharides have been produced using glycosidases (Bucke et al., 1999). We know of no reports of glycosyl transferases from plants being assayed under non-aqueous conditions as yet.

Overall there has been increasing interest recently in the behaviour of enzymes in organic media in general (Carrea and Riva, 2000; Kilbanov, 2001). Increased stability, catalysis of reactions impossible in water and changes in enzymatic selectivity even to the extent of inversion in the solvent have all been reported. We have tested such hypotheses by exposing plant glycosyl transferases, either in their membrane-bound or solubilised form, to aqueous environments and observing changes in their behaviour. A number of polysaccharide synthases were examined in relatively increased hydrophobic environments. Those enzymes that synthesise relatively hydrophilic products were inhibited whilst those with hydrogen-bonded products were stimulated. A dehydrating effect would be consistent with in vivo conditions for glycosyl transferase activity and may be useful for further characterisation of these enzymes.

2. Results and discussion

Membrane preparations were exposed to a graded series of organic solvents and assayed for arabinan synthase, xylan synthase and glucan synthase (Figs. 1 and 2). Arabinan synthase was inhibited by all solvents and at all concentrations used. Arabinan is a soluble plant polysaccharide therefore increasing the hydrophobicity of the assay medium might be expected to result in reduced production of product. Xylan synthase activity was much less affected by solvents although no marked stimulation of activity was observed. The glucan synthases showed significant differences in behaviour. Under conditions favouring the synthesis of callose, the effect of organic solvents was to almost universally inhibit callose synthase activity. This is consistent with callose being made under conditions of cell damage, reduced membrane integrity as at cell plates, or where the membranes are exposed to aqueous phases such as at plasmodesmata, sieve plates or during plasmolysis.

In contrast, organic solvents increased the activity of β-1,4-glucan synthase of which there are at least two cellular sites of activity in vivo. The synthesis of this linkage and the formation of aggregated polymers is likely to be favoured by the exclusion of water (Bolwell, 1993). Reduction of water activity by inclusion of organic solvents led to increased activity, particularly in the presence of methanol, ethanol (Fig. 1C) and ethyl acetate (Fig. 2B). It was not possible to synthesise enough product to attempt methylation analysis. However the products were characterised by solubility properties, susceptibility to specific enzyme digestion and chemical analysis (Table 1). This showed the β-1,4-synthase product to be polymeric in nature but showed no evidence of a crystalline structure. Enzyme digestion liberated both β-1,4- and β-1,3-linked glucose from the product synthesised under conditions favouring β-1,4-glucan synthesis. However, this ratio was markedly increased from 2:3 to 15:1 for release of β-1,4- and β-1,3-linked glucose in the product synthesised in the presence of organic solvent. In contrast, under the assay conditions favouring β-1,3-glucan synthase activity, the membrane preparation and a solublilised protein preparation synthesised products with the ratios 1:2 and 1:3, respectively, for release of β-1,4- and β-1,3-linked glucose (McCormack et al., 1997). Addition of 40% methanol under conditions favouring β-1,3 glucan synthesis virtually abolished this activity (Fig. 1D). Thus, the addition of organic solvent provided stimulatory assay conditions for β-1,4-glucan synthase, but inhibited β-1,3-glucan synthesis.

Glycosidases, including those from plants, have been the subject of a large number of investigations with regard to the reverse activity which is often promoted in the presence of organic solvents (Kobayashi et al., 1991; 1996a,b,c). This is important biotechnologically as it affords a method for the directed synthesis of biologically active oligosaccharides (Bucke et al., 1999). The present work describes the behaviour of plant glycosyl transferases involved in cell wall homopolymer biosynthesis as these may also be useful reagents in defined

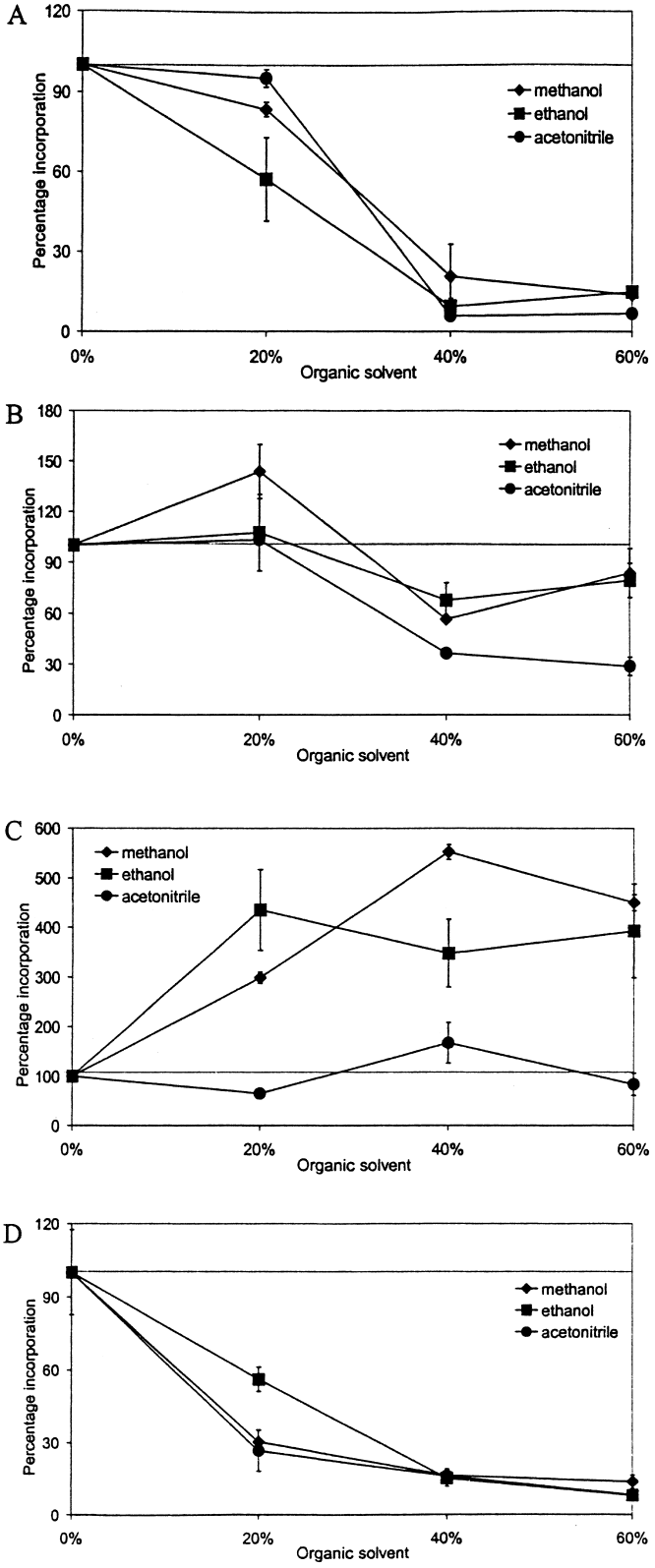

Fig. 1. Comparison of the effect of methanol (diamond), ethanol (square) and acetonitrile (circle) in H_2O on the activities of (A) arabinan synthase; (B) xylan synthase; (C) β-1,4-glucan synthase and (D) callose synthase in microsomal membranes from French bean. Two hundred grams of cells were used to derive the microsomal membranes from the different sources of French bean cells specific for each enzyme. The specific membrane fraction was used for the assay of each individual enzyme in the presence of various concentrations of organic solvent. Incorporation of radioactive substrate into characterised polysaccharide is shown as a percentage value in comparison to the same assay in the absence of organic solvent. Repeated experiments resulted in the same trends and the error bars are shown for three replicates of a representative experiment.

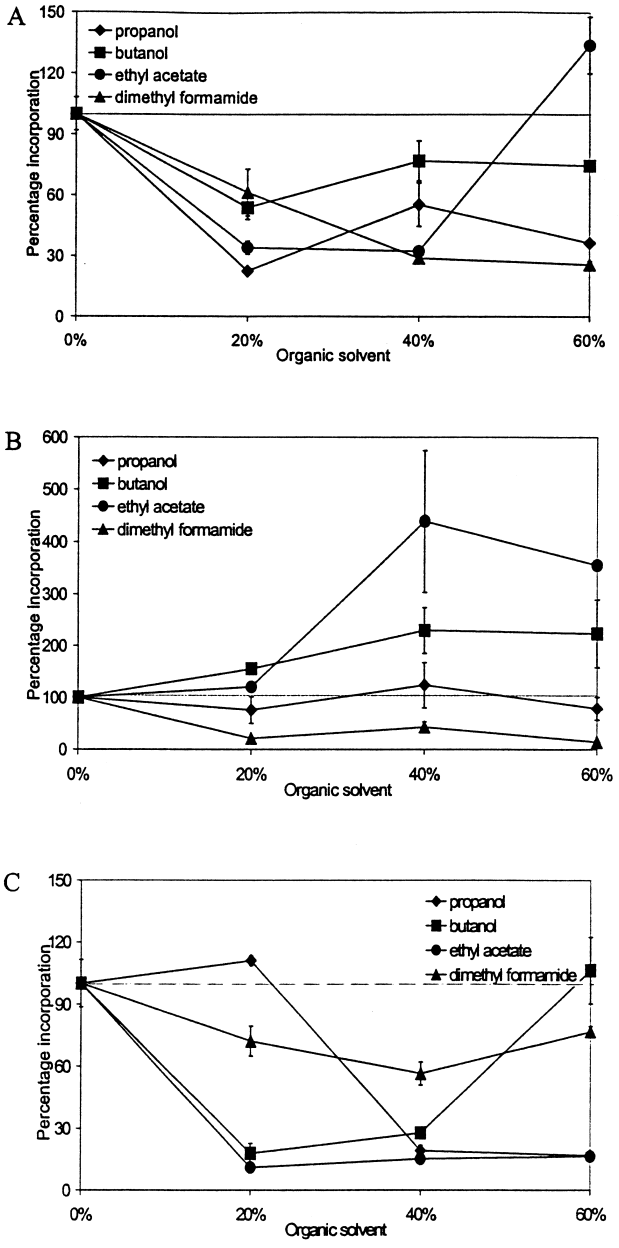

Fig. 2. Comparison of the effect of propan-2-ol (diamond), butan-2-ol (square), ethyl acetate (circle) and *N*,*N*-dimethylformamide (triangle) in H_2O on the activities of (A) xylan synthase; (B) β-1,4-glucan synthase and (C) callose synthase in microsomal membranes from French bean. Experiments were performed as for Fig. 1. Arabinan synthase was completely inhibited by these solvents at all concentrations.

synthesis of oligosaccharides. In addition if their activity were to be potentiated, this might be useful in improving recoveries during isolation and purification, so improving understanding and characterisation of these poorly described plant enzymes. Furthermore, suppression of competing reactions may also be desirable, as seen for the effect on the glucan synthases.

We have examined a number of polysaccharide synthases in relatively increased hydrophobic environments

Table 1
Characterisation of the β-1,4-glucan product synthesised with and without the addition of 40% methanol in H_2O[a]

Treatment	Product made by membranes	Product made in the presence of 40% methanol in H_2O
Radioactivity remaining in dialysis bag (%)	61.8	93
Radioactivity solubilised by laminarinase (%)	46	6.2
Radioactivity solubilised by cellulase (%)	75.1	92.4
Radioactivity soluble in DMSO (%)	98	83
Radioactivity soluble in NaOH (%)	97	67
β-1,4-:β-1,3-linked glucose liberated	2:3	15:1

[a] The polysaccharide product made under the conditions for β-1,4-glucan synthesis was analysed from membranes without the addition of organic solvent and in the presence of 40% methanol in H_2O, the condition observed to give highest stimulation of activity (five-fold).

and have found that those enzymes that synthesise relatively hydrophilic products were inhibited while those synthesising extensively hydrogen-bonded products were stimulated, particularly in the presence of primary and secondary alcohols. Thus, the synthesis of arabinan which is amongst the most soluble polysaccharide known was completely inhibited in the presence of organic solvent. Callose synthase which appears to be activated in situations where the plasmamembrane is exposed during stress, such as pathogen attack or developmentally at plasmodesmata or sieve plates (McCormack et al., 1997; Brown et al., 1998) was also inhibited by inclusion of organic solvents.

However, synthesis of the two products which favour hydrogen-bonding, xylan and β-1,4-glucan were relatively unaffected or increased. The dehydrating effect of organic solvent would be consistent with theoretical considerations of the optimum conditions for glycosyl transferase activity and may be useful in the further characterisation of these important but elusive plant enzymes. Clearly this favours β-1,4-glucan synthesis in preparations containing both β-1,4- and callose synthase activities. The fact that callose synthase activity can be virtually suppressed while β-1,4-glucan synthase is activated may support the growing molecular evidence that these are separate enzyme systems, which could not be resolved previously using biochemical data. However, there is no compelling reason to reject the notion that both enzymes have a limited capacity for synthesising small amounts of the other linkage in vitro. This would explain the apparent presence of mixed linkages in the products. However within the intact cell this specificity would be much less redundant due to the complex regulation of cellulose and callose synthesis.

3. Experimental

3.1. Materials

Suspension cultures were derived and maintained as previously described (Dixon and Lamb, 1979). Cell suspension cultures were subjected to biotic stress between 4 and 6 days after subculture. *Colletotrichum lindemuthianum*-derived elicitor was added to a concentration of 30 μg/ml glucose equivalents and cell samples taken at intervals. Over the period of elicitor treatment no gross effects on cell growth were observed (Bolwell et al., 1985). Uniformly labelled UDP-[^{14}C]-glucose (295 mCi mmol^{-1}) and UDP-[^{14}C]-xylose (266.7 mCi mmol^{-1}) was obtained from NEN, Stevenage, Herts., UK. UDP-[^{3}H]-arabinose was made as previously described (Bolwell and Northcote, 1981).

3.2. Preparation and treatment of plant extracts

For studies of glucan synthase activities, 4–6 day post sub-culture cells were homogenised in 50 mM Tris–HCl pH 7.2, 10 mM magnesium chloride, 1 mM dithiothreitol, 0.3 M sucrose, 1% (w/v) polyvinyl pyrrolidone at 4°C. The extract was filtered through three layers of muslin and centrifuged at 10,000 *g* for 10 min to remove cellular debris. The resultant supernatant was spun at 100,000 *g* for 90 min to pellet the microsomes, which were resuspended in 50 mM Tris pH 7.2 to give a final protein concentration of between 15 and 30 mg per ml, as determined using the Bradford protein assay (Read and Northcote, 1981).

Studies of arabinosyl transferase activity, were carried out using microsomes prepared from unelicited bean cell cultures 2–4 days after sub-culture (Rodgers and Bolwell, 1992). After harvesting the cells by vacuum filtration, microsomes were prepared as described above.

For studies of xylosyl transferase activity, 13 day old bean hypocotyls (Rodgers and Bolwell, 1992) were homogenised in 50 mM Tris–HCl pH 7.2, 10 mM magnesium chloride, 1 mM dithiothreitol, 0.3 M sucrose, 1% (w/v) polyvinyl pyrrolidone at 4°C. The extract was filtered through three layers of muslin and centrifuged at 10,000 *g* for 10 min to remove cellular debris. The resultant supernatant was spun at 100,000 *g* for 90 min to pellet the microsomes, which were resuspended in 50 mM Tris pH 7.2 to give a final protein concentration of between 15 and 30 mg per ml, as determined using the Bradford protein assay (Read and Northcote, 1981).

3.3. Enzyme assays

3.3.1. β-1,4-Glucan synthase

β-1,4-Glucan synthase activity was determined by a modification of the method of Ray (1980). Reaction mixtures contained membrane fractions in 40 mM Tris–HCl (pH 8.0), 3 mM $MgCl_2$ and 0.71 μM UDP-[^{14}C]-glucose final concentration in a total volume of 50 μl. Reactions were terminated after 10 min with the addition of 0.5 M EDTA to 10 mM and incorporation of radioactive glucose into polymeric products determined by high voltage paper electrophoresis which causes migration of the UDP-glucose away from the origin which contains the synthesized glucan (Bolwell and Northcote, 1981). Incorporation into lipid, glycoprotein and polysaccharide was determined after fractionation of the products (Bolwell and Northcote, 1983) and was a further check for incorporation into glucans.

3.3.2. Callose synthase

Callose synthase activity was determined by a modification of the method of Delmer (1987). Membranes were incubated in 100 mM HEPES buffer (pH 6.8) containing 3 mM $CaCl_2$, 1 mM UDP-glucose and 0.7 μM UDP-[^{14}C]-glucose final concentration in a total volume of 50 μl. Reactions were terminated after 10 min with the addition of 0.5 M EDTA to 10 mM. Total incorporations were determined by high voltage paper electrophoresis. The products were also fractionated as described.

3.3.3. Arabinan synthase and xylan synthase

Incubation conditions using radiolabelled substrate were as described previously (Bolwell and Northcote, 1981, 1983). Product analysis was carried out by high voltage paper electrophoresis in 8% acetic acid, 2% formic acid (w/w) also previously described (Bolwell and Northcote, 1981), or by precipitation and multiple washes of the polymer with cold 70% ethanol containing 1 mM EDTA before (Bolwell and Northcote, 1983). Determination of radioactivity was by liquid scintillation counting.

3.4. Characterisation of β-1,4-glucan product

The product was dialysed overnight to give an indication of the minimum M_r (30 kDa cut-off). and the radioactive material retained was determined by liquid scintillation. Enzyme digestion was performed with *Trichoderma* laminarinase (EC 3.2.1.6, Sigma) or *Aspergillus niger* cellulase (EC 3.2.1.4, Sigma) at 1 mg/ml in 50 mM sodium acetate buffer pH 5.0, at 37°C overnight. Following dialysis the remainder was counted by liquid scintillation. Solid ethanol-precipitated product was dissolved in dimethyl sulfoxide (DMSO) or 4 M sodium hydroxide. Dissolution and centrifugation of the pellet allowed observation of the ^{14}C remaining and incorporated into polymeric material.

Acknowledgements

G.P.B. thanks the BBSRC for funding. M.E.K. was the recipient of a BBSRC special research Studentship.

References

Arioli, T., Peng, L., Betzner, A.S., Burn, J., Wittke, W., Herth, W., Camilleri, C., Höfte, H., Plazinski, J., Birch, R., Cork, A., Glover, J., Redmond, J., Williamson, R.E., 1998. Molecular analysis of cellulose biosynthesis in *Arabidopsis*. Science 279, 717–720.

Baydoun, E., Brett, C.T., 1997. Distribution of xylosyltransferases and glucuronosyltransferase within the Golgi apparatus in etiolated pea (*Pisum sativum* L.) epicotyls. Journal of Experimental Botany 311, 1209–1214.

Bolwell, G.P., 1988. Synthesis of cell wall components: aspects of control. Phytochemistry 27, 1235–1253.

Bolwell, G.P., 1993. Dynamic nature of the plant extracellular matrix. International Review of Cytology 146, 261–323.

Bolwell, G.P., 2000. Biosynthesis of plant cell wall polysaccharides. Trends in Glycoscience and Glycotechnology 12, 143–160.

Bolwell, G.P., Northcote, D.H., 1981. Control of hemicellulose and pectin synthesis during differentiation of vascular tissue in bean (*Phaseolus vulgaris*) callus and in bean hypocotyl. Planta 152, 225–233.

Bolwell, G.P., Northcote, D.H., 1983. Arabinan synthase and xylan synthase activities of *Phaseolus vulgaris*: subcellular localization and possible mechanism of action. Biochemical Journal 210, 497–507.

Bolwell, G.P., Dalessandro, G., Northcote, D.H., 1985. Decrease of polygalacturonic acid synthase during xylem differentiation in sycamore. Phytochemistiy 24, 699–702.

Brown, I., Trethowan, J., Kerry, M., Mansfield, J., Bowell, G.P., 1998. Localization of components of the oxidative cross-linking of glycoproteins and of callose synthesis in papillae formed during the interaction between non-pathogenic strains of *Xanthomonas campestris* and French bean mesophyll cells. The Plant Journal 15, 333–343.

Bucke, C., Packwood, J., Suwasono, S., Rastall, R.A., 1999. Synthesis of homo- and hetero-oligosaccharides from underivatized sugars using glycosidases. In: Bucke, C. (Ed.), Methods in Biotechnology, Vol. 10. Humana Press, New Jersey, pp. 13–220.

Carpita, N.C., Gibeaut, D.M., 1993. Structural models of primaiy cell walls in flowering plants: consistency of molecular structure with the physical properties of the walls during growth. Plant Journal 3, 1–30.

Carrea, G., Riva, S., 2000. Properties and synthetic applications of enzymes in organic solvents. Angewandte Chemie International Edition 39, 2226–2254.

Delmer, D.P., 1987. Cellulose biosynthesis. Annual Review of Plant Physiology 38, 259–290.

Dhugga, K.S., Ray, P., 1994. Purification of 1,3-β-D-glucan synthase activity from pea tissue (two polypeptides of 55 kDa and 70 kDa copurify with enzyme activity). European Journal of Biochemistry 220, 943–953.

Dixon, R.A., Lamb, C.J., 1979. Stimulation of de novo synthesis of L-phenylalanine ammonia-lyase in relation to phytoalexin accumulation in *Colletotrichum lindemuthianum* elicitor-treated cell suspension cultures of French bean (*Phaseolus vulgaris*). Biochimica Biophysica Acta 586, 453–463.

Doong, R.L., Mohen, D., 1998. Solublization and characterization of a galacturonosyltransferase that synthesizes the pectic polysaccharide homogalacturonan. The Plant Journal 13, 363–374.

Edwards, M.E., Dickson, C.A., Chengappa, S., Sidebottom, C., Gidley, M.J., Reid, J.S.G., 1999. Molecular characterisation of a membrane-bound galactosyltransferase of plant cell wall matrix polysaccharide biosynthesis. The Plant Journal 19, 691–697.

Gibeaut, D.M., 2000. Nucleotide sugars and glycosyltransferases for synthesis of cell wall matrix polysaccharides. Plant Physiology and Biochemistry 38, 69–80.

Hanna, R., Brummell, D.A., Camirand, A., Hensel, A., Russell, E.F., Maclachlan, G.A., 1991. Solubilization and properties of GDP-fucose: xyloglucan 1,2-α-L-fucosyltransferase from pea epicotyl membranes. Archives of Biochemistry and Biophysics 290, 7–13.

Kilbanov, A.M., 2001. Improving enzymes by using them in organic solvents. Nature 409, 241–249.

Kobayashi, S., Kashiwa, K., Kawasaki, T., Shoda, S., 1991. Novel method for polysaccharide synthesis using an enzyme: the first in vitro synthesis of cellulose via a non-biosynthetic path using cellulase as catalyst. Journal of the American Chemical Society 113, 3079–3084.

Kobayashi, S., Okamoto, E., Wen, X., Shoda, S.I., 1996a. Chemical synthesis of native-type cellulose and its analogues via enzymatic polymerization. Journal of Macromolecular Sciences 33, 1375–1384.

Kobayashi, S., Wen, X., Shoda, S., 1996b. Specific preparation of artificial xylan: a new approach to polysaccharide synthesis by using cellulase as catalyst. Macromolecules 29, 2698–2700.

Kobayashi, S., Wen, X., Shoda, S., 1996c. Synthesis of artificial chitin: irreversible catalytic behaviour of a glycosyl hydrolase through a transition state analogue substrate. Journal of the American Chemical Society 118, 13113–13114.

McCormack, B.A., Gregory, A., Kerry, M., Smith, C., Bolwell, G.P., 1997. Purification of an elicitor-induced glucan synthase (callose synthase) from suspension cultures of French bean (*Phaseolus vulgaris* L.): purification and immunolocation of a probable M_r 65 000 subunit of the enzyme. Planta 203, 196–203.

Moore, P.J., Swords, K.M.M., Lynch, M.A., Staehelin, L.A., 1991. Spatial organization of the assembly pathways of glycoproteins and complex polysaccharides in the Golgi apparatus of plants. Journal of Cell Biology 112, 589–602.

Pear, J.R., Kawagoe, Y., Schreckengost, W.E., Delmer, D.P., Stalker, D.M., 1996. Higher plants contain homologs of the bacterial celA genes encoding the catalytic subunit of cellulose synthase. Proceedings of the National Academy of Sciences USA 93, 12637–12642.

Perrin, R.M., DeRocher, A.E., Bar-Peled, A.E., Zeng, W., Norambuena, L., Orellana, A., Raikhel, N.V., Keegstra, K., 1999. Xyloglucan fucosyltransferase, an enzyme involved in plant cell wall biosynthesis. Science 284, 1976–1979.

Ray, P., 1980. Cooperative action of β-glucan transferase and UDP-xylose xylosyl transferase of Golgi membranes in the synthesis of xyloglucan-like polysaccharide. Biochimica et Biophysica Acta 629, 431–444.

Read, S.M., Northcote, D.H., 1981. Minimization in the response to different proteins of the coomassie blue G dye-binding assay for protein. Analytical Biochemistry 116, 53–64.

Rodgers, M.W., Bolwell, G.P., 1992. Partial purification of arabinosyl transferase and two xylosyltransferases from French bean. Biochemical Journal 288, 817–822.

Taylor, N.G., Scheible, W.R., Cutler, S., Somerville, C.R., Turner, S.R., 1999. The irregular xylem 3 locus of Arabidopsis encodes a cellulose synthase required for secondary cell wall synthesis. Plant Cell 11, 769–779.

White, A.R., Xin, Y., Pezeshk, V., l993a. Xyloglucan glucosyltransferase in Golgi membranes from *Pisum sativum* (pea). Biochemical Journal 264, 231–238.

White, A.R., Xin, Y., Pezeshk, V., l993b. Separation of membranes from semiprotoplasts of suspension-cultured sycamore maple (*Acer pseudoplatanus*) cells. Physiologia Plantarum 87, 31–38.

PERGAMON

Phytochemistry 57 (2001) 1061–1068

PHYTOCHEMISTRY

www.elsevier.com/locate/phytochem

Oxidative pentose phosphate pathway and pyridine nucleotides in relation to heartwood formation in *Robinia pseudoacacia* L.

Elisabeth A. Magel[a,*], Claudia Hillinger[b], Thomas Wagner[c], Wolfgang Höll[c]

[a]*Department of Botany, University of Tuebingen, Auf der Morgenstelle 1, 72076 Tuebingen, Germany*
[b]*Max-Planck-Institut for Biogeochemistry, Carl-Zeiss-Promenade 10, 07745 Jena, Germany*
[c]*Department of Botany, Technical University of Munich, Am Hochanger 4, 85354 Freising - Weihenstephan, Germany*

Received 1 September 2000; received in revised form 17 November 2000

Abstract

Most tree species show in the inner parts of their woody axes often a dark colored zone, the heartwood. Its formation is a genetically determined, programmed cell death which is characterized by the activation of metabolic pathways which lead to the formation of phenolic heartwood extractives. In the present paper we report on the key position of the oxidative pentose phosphate pathway (OPP) for this process. The OPP plays a crucial role in anabolic processes and is involved in the interconversion and rearrangements of sugar-phosphates with the net production of NADPH. In tissues of *Robinia pseudoacacia* L. which are transferred to heartwood, enhanced activities of glucose-6-phosphate dehydrogenase (G6PDH) and 6-phosphogluconate dehydrogenase (6PGDH) are present. A consequence of these increased enzyme activities is a shift in the pyridine nucleotide pool towards NADP + NADPH at the expense of NAD + NADH. These alterations in the metabolism and the redox status probably provide precursors and reduction equivalents being required for the synthesis of heartwood phenolics. The non heartwood forming species *Acer pseudoplatanus* L. shows neither a radial gradient nor seasonal changes in the amounts of pyridine nucleotides across the trunkwood. The results are discussed in connection with programmed cell death, mitochondrial activity, and heartwood formation.
© 2001 Elsevier Science Ltd. All rights reserved.

Keywords: *Acer pseudoplatanus* L.; Glucose-6-phosphate dehydrogenase; Heartwood formation; Oxidative pentose phosphate pathway; Phenolic heartwood extractives; Pyridine nucleotides; 6-Phosphogluconate dehydrogenase; *Robinia pseudoacacia* L.

1. Introduction

In cross-sections of freshly felled trees at least two colored zones can usually be observed: a pale-colored outer zone — the sapwood — and a dark-colored inner core — the heartwood. The sapwood has been defined as "the portion of the wood that, in the living tree, contains living cells and reserve materials (e.g. starch)" (Anon., 1957). Heartwood, on the other hand, is defined as "the inner layers of the wood, which, in the growing tree, have ceased to contain living cells, and in which the reserve materials (e.g. starch) have been removed or converted into heartwood substances" (Anon., 1957).

This distinction into different colored zones of the trunk is not verified in all tree species. *Alnus glutinosa, Tilia cordata,* and species of *Acer* are examples for trees which do not form heartwood. These species are called sapwood trees. Heartwood must not necessarily be of darker color; e.g. trees of *Picea abies* contain a pale-colored heartwood, named ripewood. In roots, heartwood is formed in the region near the stem wood.

The formation of heartwood results from cell death due to internal factors and represents a phenomenon associated with the annual cycle of the life of a tree. It was demonstrated that cell death during heartwood formation starts with the depletion of starch components in the parenchyma cells which is based on enhanced amylolytic activity. Additionally, hydrolysis of sucrose plays an important role in the transformation of sapwood into heartwood. Recent findings make it plausible that enhanced enzyme activities are regulated by gene expression (Hauch and Magel, 1998). In the beginning of heartwood formation, products of sucrose breakdown are utilized as substrates for glycolytic and respiratory

* Corresponding author. Tel.: +49-7071-297-6941; fax: +49-7071-295635.
E-mail address: elisabeth.magel@uni-tuebingen.de (E.A. Magel).

0031-9422/01/$ - see front matter © 2001 Elsevier Science Ltd. All rights reserved.
PII: S0031-9422(01)00091-7

energy production (Magel, 2000). In a later stage of heartwood formation — when mitochondrial respiration is blocked — carbon compounds are increasingly used for the in situ synthesis of phenolic extractives. In *Robinia pseudoacacia* L. (black locust), flavonoids which accumulate within the heartwood are formed by an increased catalytic activity of the key enzymes of the phenyl propanoid pathway, phenylalanine ammonia-lyase, and of the flavonoid pathway, chalcone synthase. At least in *Robinia*, the accumulation and cellular distribution of these phenolic compounds within heartwood tissues seem to involve a mechanism of an enzymatically initiated but chemically driven copolymerization of the phenolic derivatives and the preexisting cell-wall macromolecular components including lignins and lignin-polysaccharide complexes (Magel et al., 1995). This mechanism explains the occurrence of a relative increase in lignin content of heartwood which, however, is not due to an increase in monolignol polymerization. Thus, at least in angiosperm trees, a de novo synthesis of lignin during heartwood formation can be excluded.

Histochemical investigations revealed that the oxidative pentose phosphate pathway (OPP) might be a prerequisite for the synthesis of heartwood phenolics (Baqui and Shah, 1985). Key enzymes of the pathway are two dehydrogenases, glucose-6-phosphate (G6PDH) and 6-phosphogluconate dehydrogenase (6PGDH). These two dehydrogenases are involved in the supply of sugar phosphates and reduction equivalents.

In the present paper, we give evidence for the important role of the OPP during heartwood formation. Applying enzymic cycling techniques we followed the generation of reduction equivalents starting in the transition zone between sapwood and heartwood. Simultaneously, we measured the catalytic activities of G6PDH and 6PGDH in the trunkwood of the heartwood forming *R. pseudoacacia* L. at different seasons of the year. As a reference, we used the non heartwood forming "sapwood" tree *Acer pseudoplatanus* L.

2. Results and discussion

The oxidative pentose phosphate pathway (OPP) plays a prominent role in plant metabolism. Metabolic challenges such as vigorous growth during cambial differentiation (Magel et al., 1996; Gahan et al., 1997), cold-hardening (Sagisaka, 1974), and dormancy release (De Meillon et al., 1990) are accompanied by enhanced activities of this pathway. Increased amounts of transcript and activities of the key enzymes of OPP characterize stress responses to heavy metals (Kampfenkel et al., 1995; Slaski et al., 1996) or infection (Norman et al., 1994; Fahrendorf et al., 1995; Batz et al., 1998; Sindelar et al., 1999). In these cases, the activity of the OPP is connected with the production of phenolics as part of an active defense mechanism. Recently, enzymes of OPP (G6PDH and 6PGDH) were ascribed to play an important role in the process of programmed cell death (Tian et al., 1999).

Many features of heartwood formation in trees resemble programmed cell death. Both events have loss of cell integrity and formation of phenolics in common. Thus, it seems reasonable to speculate that the oxidative pentose phosphate pathway might also be an important switch for carbon flow into the formation of heartwood phenolics. Our results show that both reduction equivalents and substrates for heartwood formation are provided by this pathway. This was proven by enhanced activities of the two key enzymes of the pathway, G6PDH and 6PGDH, and a dominance of the tri-phospho-pyridine nucleotides, NADP and NADPH, within the tissues transformed into heartwood.

2.1. Catalytic activities of glucose-6-phosphate dehydrogenase (G6PDH) and 6-phosphogluconate dehydrogenase (6PGDH)

Regarding enzyme properties such as Michaelis–Menten type saturation kinetics, apparent K_m values (40 μM G6P, 10 μM NADP for G6PDH and 54 μM 6PG and 7.5 μM NADP for 6PGDH), pH optima (7.8 and 7.4 for G6PDH and 6PGDH, respectively) and dependence on magnesium ions, G6PDH and 6PGDH from black locust sapwood tissues (data not shown) are very similar to respective enzymes from other green and non-green plant tissues (Guttenberger et al., 1994, and references therein).

Tree to tree variations of the enzyme activities were small as shown for four trees which were harvested in January (Fig. 1A and B). Thus we conclude that results from one tree are representative for the respective tissue and sampling date.

On a protein basis, the living bark contains low activities of both G6PDH and 6PGDH. In the wood, catalytic enzyme activities vary with trunk depth and season (Fig. 1A and B). In April, G6PDH and 6PGDH activities are high in the outer sapwood (Fig. 1A) and seem to be involved in xylem differentiation and cell wall synthesis, predominantly lignin (Magel et al., 1996). Involvement of the enzymes of OPP in xylem differentiation (including lignification) is reported for *Populus gelrica* (Sagisaka and Asada, 1981) and also for non-woody species (Pryke and apRees, 1976; Miller et al., 1985). Samples harvested in January or September showed enhanced enzyme activities both in the outermost, youngest tissue and at the sapwood heartwood transition zone. In November, however, the activity of G6PDH steadily increased from the bark to the inner sapwood. In any case, G6PDH activity dropped from the transition zone up to the heartwood boundary and was absent in the heartwood proper (Fig. 1A). For 6PGDH, the activity profile over

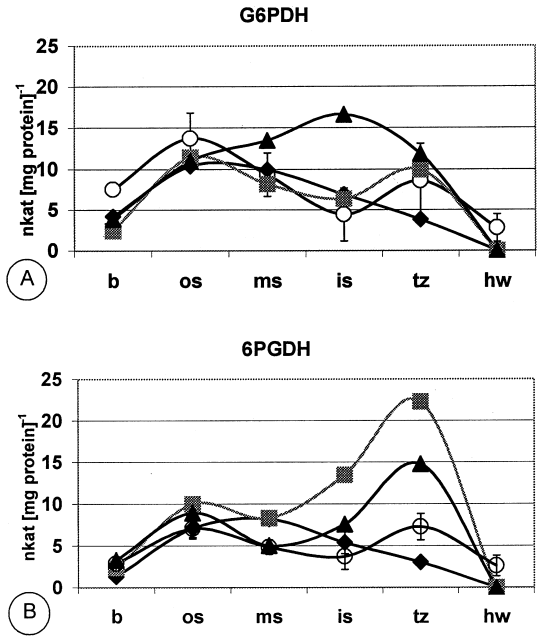

Fig. 1. Extractable catalytic activities of glucose-6-phosphate dehydrogenase (G6PDH; upper panel A) and 6-phosphogluconate dehydrogenase (6PGDH; lower panel B) in a radial stem transect of *Robinia pseudoacacia* L.. The samples were collected in January (○), April (◆), September (■), and November (▲). For the samples harvested in January standard deviation is given for four trees [bark (b), outer (os), middle (ms) and inner (is) sapwood, sapwood–heartwood transition zone (tz) and heartwood (hw)].

a radial transect peaked at the sapwood heartwood transition zone. This was most pronounced in samples collected in September and November. As no lignification takes place during heartwood formation (Magel et al., 1995), enzymes of the OPP should contribute to the supply of reduction equivalents and of precursors for the in situ synthesis of phenolic heartwood compounds. Activities of key enzymes of the OPP and those of flavonoid biosynthesis (phenylalanine ammonia-lyase and chalcone synthase) are closely correlated (Daniels et al., 1990; Magel et al., 1991; Magel and Hübner, 1997). Thus, these two pathways coincide in time and location with heartwood formation.

The activity of G6PDH depends on the water status of the tissue (Eichhorn and Corbus, 1988) and on the NADPH/NADP ratio (Ashihara and Komamine, 1974; Oka et al., 1981). The drop in the catalytic activities of G6PDH in contrast to that of 6PGDH (Fig. 1) within the transition zone in November might be due to a different sensitivity of this enzyme to the physiological changes and thus status of the tissues being transformed into heartwood. From the redox modulation of the G6PDH activities a presumable plastidic localization of the oxidative pentose phosphate pathway (Graeve et al., 1994, VonSchaeven et al., 1995) with only limited cooperation with the cytosolic OPP (Averill et al., 1998) can be concluded.

Commonly, the ratios of the activities of G6PDH/6PGDH are about 2 or higher (Guttenberger et al., 1994). In the trunkwood of black locust, however, the ratio is about 1 or even lower, indicating an optimized flux through the OPP (DeMeillon et al., 1990).

The ageing of the sapwood and heartwood formation in *Robinia* is accompanied by genetic alterations, as shown by changed similarity indices of the tissues based on RAPD-PCR investigations (DeFilippis and Magel, 1998). 6PGDH isoenzyme patterns are used for genetic studies in both woody (Solar et al., 1994; Bergmann and Gillet, 1997) and non-woody species (Bletsos et al., 1998). During heartwood formation, G6PDH (one activity band) and 6PGDH (two activity bands; data not shown) showed no differences in banding pattern. Thus, enzymes of the OPP do not contribute to the genetic differences connected with ageing of the sapwood.

2.2. Pool sizes of pyridine nucleotides

Pyridine nucleotides play a crucial role in such diverse processes like flower induction (Bonzon et al., 1983), wound reactions (Brinkman et al., 1982), leaf senescence (Meyer and Wagner, 1986), and cambial growth of trees (Magel et al., 1996). However, their role in one of the most important secondary differentiation processes of trees, the formation of heartwood, has still to be elucidated.

The total amounts of pyridine nucleotides in mature wood of *Robinia* and *Acer* are in the range of values reported for other green and non-green plant tissues and are considerably lower than within the actively growing, differentiating cambial tissue (Magel et al., 1996).

In the heartwood forming *R. pseudoacacia*, the pyridine nucleotides NAD, NADH, NADP, and NADPH were present in all stem tissues investigated. With increasing age of the sapwood and thus declining amount of living cells present within the tissue, the pool of total pyridine nucleotides decreased. In the dead, physiologically inactive heartwood, a low but constant pool is found (Fig. 2A–C).

Like in other plant tissues, NAD is the dominating pyridine nucleotide in bark and sapwood. Its contents are high in the bark and the outermost wood tissue, gradually decrease with increasing age of the sapwood and reach lowest values within the heartwood. The tissue specific contents of NADH, NADP and NADPH are lowest in the inner sapwood and increase towards both, the younger, physiologically active sapwood and the physiologically inactive heartwood (Figs. 2A–C). In specimens harvested in November, the amounts of the reduced forms (NADH and NADPH) peak in the youngest heartwood zone adjacent to the transition zone (Fig. 2C). In contrast, the wood of *A. pseudoplatanus* shows neither a pronounced radial gradient nor seasonal fluctuations in the amounts of pyridine nucleotides

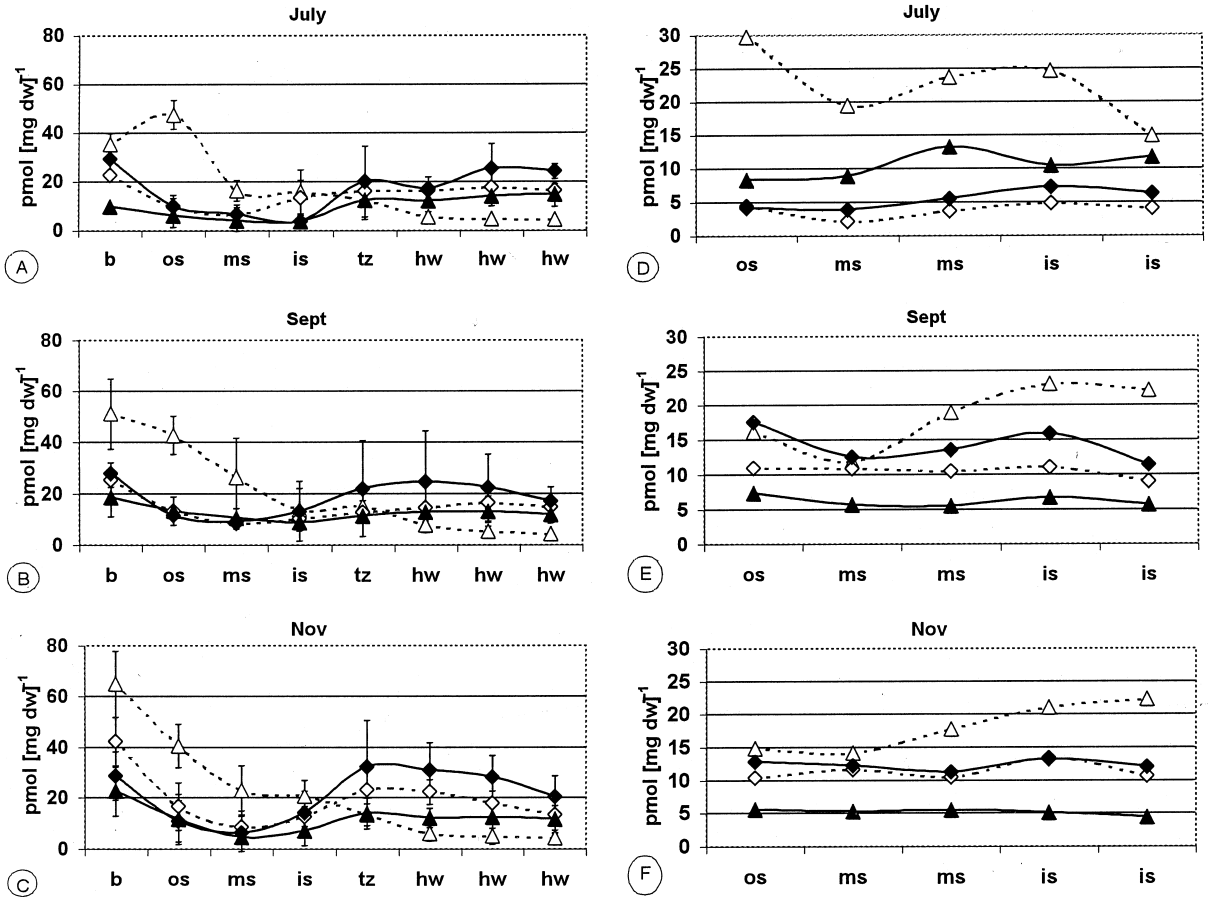

Fig. 2. Pools of the pyridine nucleotides NAD (△), NADH (◇), NADP (▲), and NADPH (◆) in radial stem transects of the heartwood forming *Robinia pseudoacacia* (A to C) and the sapwood tree *Acer pseudoplatanus* (D to F) are shown. The samples harvested in July (A, D), September (Sept; B, E) and November (Nov; C, F) are compared. Standard deviation is given for three trees [for legend, see Fig. 1, except that heartwood tissues of increasing age (hw) are shown].

(Figs. 2D–F and 3A). NAD constitutes the dominating pyridine nucleotide in all wood tissues.

Like in many other plant tissues showing predominantly maintenance metabolism, di-phospho-pyridine nucleotides dominate within the sapwood of maple and black locust. The ratio of tri-phospho-pyridine nucleotides to di-phospho-pyridine nucleotides is lower than 0.6 (Fig. 3A). In *Robinia*, the change in the pyridine nucleotide pool towards higher amounts of tri-phospho-pyridine nucleotides within the sapwood heartwood transition zone coincides with physiological alterations such as cell death, enhanced activities of the enzymes of the oxidative pentose phosphate pathway, and formation of phenolic substances. This shift is based on both a decrease in the pool of di-phospho-pyridine nucleotides and an increase in the pool of tri-phospho-pyridine nucleotides (Fig. 3B). It can be assumed that increased activities of a NAD-kinase (Magel et al., 1996) are involved in generating this shift. In dead heartwood tissue, the presence of pyridine nucleotides and the maintained preponderance of the NADP-system point towards a sudden cell death accompanied by an incomplete withdrawal of metabolites during heartwood formation.

Within the sapwood of black locust trunks, the redox state of the NAD-system (ratio of NADH to NAD; Fig. 4A) is below 1, and thus in a range reported for other plant tissues and species. The pronounced increase in this ratio up to 3.5 within the transition zone and the outermost heartwood is an indication for physiological and structural changes of these particular tissues. The increase in the NADH pool might be due to enhanced glycolysis, characteristic for heartwood formation (Hauch, 1997; Magel, 2000). The question whether the formation of NADH is due to reversible hydrogen transfer between NADPH and NAD by transhydrogenases (Bykova et al., 1999), or via the catalysis by phosphatases from NADPH (Schmidt and Schuck, 1996) cannot be answered at present. The redox state of the NADP-system (ratio of NADPH to NADP; Fig. 4A) ranged between 1 and 2.5 and is thus higher than in other plant tissues. In all tissues of the trunks harvested in July (except bark), the NADPH/NADP ratios were between 1.5 and 2, with no tissue specific pattern. In trunks collected in September

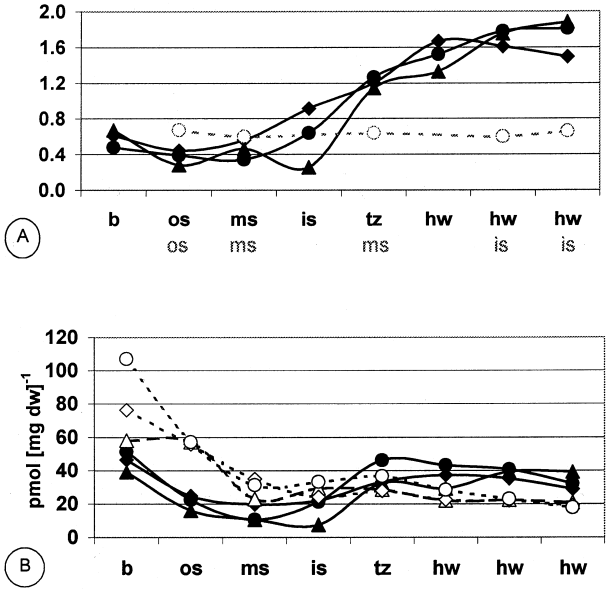

Fig. 3. (A) Calculated ratios of tri-phospho-pyridine nucleotides and di-phospho-pyridine nucleotides (NADP + NADPH/NAD + NADH) in radial stem transects of the heartwood forming *Robinia pseudoacacia* at different times of the season (▲, July; ◆, September; ●, November) and the sapwood tree *Acer pseudoplatanus* (○). (B) Content of tri-phospho-pyridine nucleotides (▲, ◆, ●) and di-phospho-pyridine nucleotides (△, ◇, ○) in radial stem transects of the heartwood forming *R. pseudoacacia* at different times of the season (▲, △, July; ◆, ◇, September; ●, ○, November). For legend, see Fig. 2.

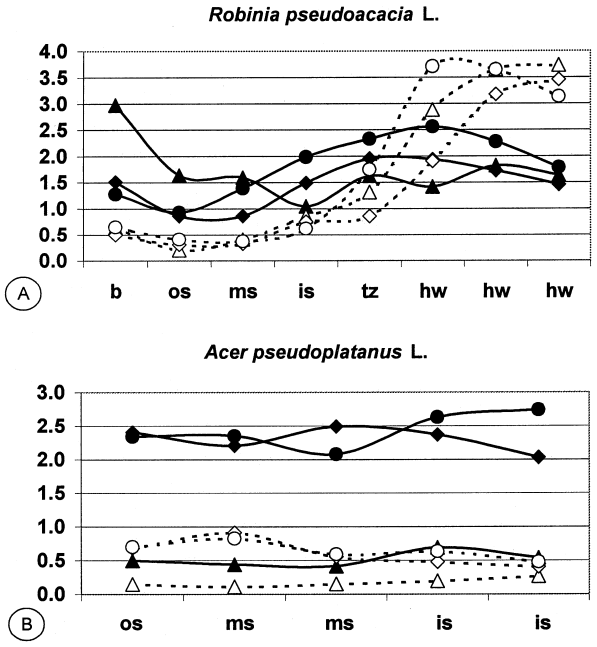

Fig. 4. Calculated redox state of the NADP-system (NADPH/NADP; ▲, ◆, ●), and the NAD-system (NADH/NAD; △, ◇, ○) in radial stem transects of the heartwood forming *Robinia pseudoacacia* (A) and the sapwood tree *Acer pseudoplatanus* (B) at three different times of the season (▲, △, July; ◆ ◇, September; ●, ○, November). For legend, see Fig. 2.

and November, the NADPH/NADP ratios were elevated in the transition zone and the outer heartwood. This coincided with the activation of the enzymes of the OPP. Increased pools of both NADH and NADPH within the innermost wood tissues might reflect reduced rates of NAD(P)H oxidation by NAD(P)H dehydrogenases (Moeller, 1997). The inactivation of these enzymes can be seen in context with the disturbance of the integrity of the mitochondria which was shown by electron microscopic investigations (Magel, unpublished data) or, as the activities of both enzymes are Ca^{2+} dependent, on free, cellular Ca^{2+}-concentrations (Hillinger, Magel and Wagner, unpublished data). NADH and NADPH inhibit in part the penetration of ADP through the outer mitochondrial membrane (Lee et al., 1996): the result is a rise in cytosolic NADH pools which in turn negatively affects glycolysis by inhibition of phosphofructokinase (Gottschalk and Kemp, 1981). This enhances metabolic flow through the OPP.

It is noteworthy that, in contrast to *Robinia*, the sapwood tree *Acer pseudoplatanus* L. showed no pronounced alterations in metabolism with ageing of the tissue. In this tree species no change in the redox state of the NAD-system or the NADP-system across the trunkwood occurs (Figs. 2 D–F, 3A and B and 4B). We thus conclude that during heartwood formation in *Robinia* the redox system of the pyridine nucleotide system is increased. As a consequence of these events catabolic pathways are inhibited and reducing equivalents are predominantly diverted to anabolic pathways, such as the synthesis of phenolic compounds which are accumulated in the heartwood.

3. Materials and methods

3.1. Plant material

Stem discs were collected from the heartwood forming tree species *Robinia pseudoacacia* L. and from *Acer pseudoplatanus* during one season in a forest near Munich, Germany. Freeze-stopping of metabolic processes within the specimen was achieved by deep-freezing the samples in liquid nitrogen immediately after withdrawal from the trunk. After freeze-drying, the specimens were divided into inner bark and individual growth ring tissues. In *Robinia*, the latter were separated into outer, middle, and inner sapwood, the sapwood–heartwood transition zone, and the heartwood proper by macroscopic (color) and microscopic (starch distribution), features. Depending on growth conditions of the individual trees, each tissue comprised, at least one growth ring. In the sapwood tree *Acer*, outer (2–5 years old growth rings), middle (10–11, and 14–15 year-old increments), and inner sapwood (oldest, 20–21, and 24–25 year-old tissue), were separated. Homogenization of the tissue to a fine powder was done by using a wood file.

3.2. Preparation of crude enzyme extracts

Lyophilized wood powder, PVPP and DOWEX 1×2-200 (pre-equilibrated with the extraction liquid; 1/1/1) were extracted with a 15-fold volume (w/v) of extraction buffer (0.1 M Tris–HCl pH 7.4, 0.01% BSA, 0.15% PEG (20000), 40 mM sucrose, 0.1 mM $CaCl_2$, 64 mM β-mercaptoethanol), for 20 min at 4°C. After filtration (Büchner filter), the filtrate was centrifuged for 18 min at 35,000 *g* (Beckman centrifuge J2-21). The supernatant was used as crude enzyme extract.

Protein was determined according to Bradford (1976), using the Bio-Rad Bradford microassay protein assay.

3.3. Assay of catalytic activities of glucose-6-phosphate dehydrogenase (G6PDH) and 6-phosphogluconate dehydrogenase (6PGDH)

In a total volume of 1 ml, 40-μl aliquots (three parallels each) of the crude enzyme extract were incubated at 37°C in a reaction mix containing 0.1 M Tris–HCl, 1.08 mM NADP, and 10 mM $MgCl_2$. For G6PDH, the reaction mix had a pH of 7.8 and was supplemented with 3 mM of G6P. For 6PGDH, the pH was 7.4 and 0.54 mM of 6PG was added. The reaction was followed in a thermostat-controlled chamber (37°C) over 20 min at 2.5-min intervals at 340 nm and in a microplate reader and rates were calculated from the linear parts of the kinetics. By different assays (containing only one or both substrates) it could be shown that 6-phosphogluconate dehydrogenase does not interfere with assaying glucose-6-phosphate dehydrogenase. Moreover, in order to trace possible losses of enzyme activity or interference of tissue-specific substances during sample preparation or measurement, commercially available enzyme preparations of known catalytic activity were added prior to extraction as internal standard. Recovery was around 92% for the enzymes analyzed. Thus, we conclude that neither interference of sample constituents with enzyme activities nor degradation of the reaction products occurred.

3.4. Determination of pyridine nucleotides

The oxidized (NAD and NADP) and reduced pyridine nucleotides (NADH, NADPH) were extracted from 10 mg of dry weight, with 50 mg of PVPP added, with 1 ml of 0.1 M HCl for 4 min at 95°C, or with 0.1 M 2-mercaptoethanol, pH 10.8, for 10 min at 80°C, respectively. Per sample, three replicates were done. Quantification of the individual metabolites was by enzymatic cycling (for details of this technique, see Lowry and Passonneau, 1972; Kato et al., 1973; Hampp et al., 1984, 1990). Twenty-five μl of the neutralized extracts (four parallels each) were incubated with 25 μl of cycling reagent for 60 min at ambient temperature for the NAD(H)-cycle, and 90 min at 37°C for the NADP(H)-cycle, respectively. After termination of the cycling step by heat (100°C, 20 min), one of the products formed during cycling [malate in the NAD(H)-cycle; 6-P-gluconate in the NADP(H)-cycle] was measured by addition of 1 ml of indicator reagent. In this last step, the product is coupled enzymatically to the reduction of pyridine nucleotides. The amount of NADH or NADPH formed in this indicator reaction was measured fluorometrically (340 nm excitation, 455 nm emission). In order to assay possible losses of pyridine nucleotides during handling, recovery experiments were carried out in which duplicate samples of different tissues were prepared. A measured amount of a mixture of oxidized (NAD, NADP) and reduced pyridine nucleotides (NADH, NADPH) was added as internal standard before extraction to one set of the samples. All samples were treated similarly, as outlined above, for extraction, cycling, and measurement. The recovery was 97 and 103% for NAD and NADH, and 87 and 96% for NADP and NADPH, respectively. Thus, the recovered redox status obviously reflects the in vivo situation.

3.4.1. Cycling reagents

The cycling reagent for the NAD(H)-cycle consisted of 0.25 M Tris, pH 8, 0.74 M ethanol, 5 mM 2-mercaptoethanol, 0.05% BSA, 5 mM oxalacetate, 24 U/ml malate dehydrogenase, and 72 U/ml alcohol dehydrogenase. The NADP(H)-cycle reagent was made from 0.25 M Tris-buffer, pH 8.1, containing 2.5 mM glucose-6-phosphate, 0.25 mM 5′-ADP, 20 mM 2-oxoglutarate, 25 mM NH_4Cl, 11.2 U/ml glucose-6-phosphate dehydrogenase, and 24 U/ml glutamate dehydrogenase.

3.4.2. Indicator reagents

The malate reagent (NAD, NADH cycle) contained 0.14 M 2-amino-2-methylpropanol, pH 9.9, 31 mM Na-glutamate, 1.2 mM NAD, malate dehydrogenase, 8 U/ml, and glutamate-oxalacetate-transaminase (GOT), 1.4 U/ml. The 6-P-gluconate reagent (NADP, NADPH cycle) consisted of 0.22 M Tris-buffer, pH 8.1, 0.28 mM EDTA, 170 mM NH_4Cl, 28 mM $MgCl_2$, 1.2 mM NADP, and 0.23 U/ml of 6-P-gluconate dehydrogenase.

References

Anon., 1957. International glossary of terms used in wood anatomy (prepared by the Int. Assoc. Wood Anatomists). Tropical Woods 107, 1–36.

Ashihara, H., Komamine, A., 1974. Regulation of the activities of some enzymes of the pentose phosphate pathway in *Phaseolus mungo*. Zeitschrift fuer Pflanzenphysiologie 36, 52–59.

Averill, R.H., Bailey-Serres, J., Kruger, N.J.R.P., Kruger, N.J., 1998. Co-operation between cytosolic and plastidic oxidative pentose phosphate pathways revealed by 6-phosphogluconate dehydrogenase-deficient genotypes of maize. Plant Journal 14, 449–457.

Baqui, S.A., Shah, J.J., 1985. Histoenzymatic studies in wood of *Acacia auriculiformis* Cunn. during heartwood formation. Holzforschung 39, 311–320.

Batz, O., Logemann, E., Reinold, S., Hahlbrock, K., 1998. Extensive reprogramming of primary and secondary metabolism by fungal elicitor or infection in parsley cells. Biological Chemistry 379, 1127–1135.

Bergmann, F., Gillet, E.M., 1997. Phylogenetic relationship among *Pinus* species (Pinaceae) inferred from different numbers of 6PGDH loci. Plant Systematics Evolution 208, 25–34.

Bletsos, F.A., Roupakias, D.G., Tsaktsira, M.L., Scaltsoyjannes, A.B., Thanassoulopoulos, C.C., 1998. Interspecific hybrids between three eggplant (*Solanum melongena* L.) cultivars and two wild species (*Solanum torvum* Sw. and *Solanum sisymbriifolium* Lam.). PlantBreeding 117, 159–164.

Bonzon, M., Simon, P., Greppin, H., Wagner, E., 1983. Pyridine nucleotides and redox-charge evolution during the induction of flowering in spinach leaves. Planta 159, 254–260.

Brinkman, F.G., Donkers, C.K., Smelt, J.J., van der Plas, L.H.W., 1982. Respiration rate and redox state of NAD during wound induced differentiation of potato tuber tissue (*Solanum tuberosum* L.). Plant Science Letters 27, 29–36.

Bradford, M.M., 1976. A rapid and sensitive method for the quantitation of microgram quantities of protein utilizing the principle of protein-dye binding. Analytical Biochemistry 72, 248–254.

Bykova, N.V., Rasmusson, A.G., Igamberdiev, A.U., Gardestrom, P., Moller, I.M., 1999. Two separate transhydrogenase activities are present in plant mitochondria. Biochemical Biophysical Research Communications 265, 106–111.

Daniels, S., Tiemann, K., Wittkampf, U., Bless, W., Hinderer, W., Barz, W., 1990. Elicitor-induced metabolic changes in cell cultures of chickpea (*Cicer arientinum* L.) cultivar resistant and susceptible to *Ascochyta rabiei* I. Investigations of enzyme activities involved in isoflavone and pterocarpan phytoalexin biosynthesis. Planta 182, 270–278.

DeFilippis, L., Magel, E., 1998. Differences in genomic DNA extracted from bark and from wood of different zones in *Robinia* trees using RAPD-PCR. Trees 12, 377–384.

DeMeillon, S.W., Small, J.G.C., VanDeVenter, H.A., 1990. The respiratory metabolism of *Strelitzia juncea* Ait. seeds. The effect of dormancy release through oxygen incubation of the seeds on the activity of glucose-6-phosphate dehydrogenase and 6-phosphogluconate dehydrogenase. Journal of Experimental Botany 41, 709–714.

Eichhorn, M., Corbus, B., 1988. Die Glucose-6-Phosphat Dehydrogenase im Stoffwechsel photoautotropher Organismen. Biochemie und Physiologie der Pflanzen 183, 449–475.

Fahrendorf, T., Ni, W., Shorrosh, B., Dixon, R., 1995. Stress response in alfalfa (*Medicago sativa* L.) XIX. Transcriptional activation of oxidative pentose phosphate pathway genes at the onset of isoflavonoid phytoalexin response. Plant Molecular Biology 28, 885–900.

Gahan, P.B., McGarry, A., Wang, L., Dore, T., Carmignac, D.F., 1997. Glucose-6-phosphate and UDP-glucose dehydrogenases: possible markers of vascular differentiation. Phytochemical Analysis 8, 110–114.

Gottschalk, M.E., Kemp, R.G., 1981. Interaction of dinucleotides with muscle phosphofructokinase. Biochemistry 20, 2245–2251.

Graeve, K., VonSchaeven, A., Scheibe, R., 1994. Purification, characterization, and cDNA sequence of glucose-6-phosphate dehydrogenase from potato (*Solanum tuberosum* L.). Plant Journal 5, 353–361.

Guttenberger, M., Schaeffer, C., Hampp, R., 1994. Kinetic and electrophoretic characterization of NADP dependent dehydrogenases from root tissues of Norway spruce [*Picea abies* (L.) Karst.] employing a rapid one-step extraction procedure. Trees 8, 191–197.

Hampp, R., Goller, M., Füllgraf, H., 1984. Determination of compartmented metabolite pools by a combination of rapid fractionation of oat mesophyll protoplasts and enzymatic cycling. Plant Physiology 75, 1017–1021.

Hampp, R., Rieger, A., Outlaw Jr., W.H., 1990. Microdissection and biochemical analysis of plant tissues. In: Linskens, H.F., Jackson, J.F. (Eds.), Physical Methods in Plant Sciences. Springer, Berlin/Heidelberg/New York, pp. 124–147.

Hauch, S., 1997. Saccharosestoffwechsel im Stamm der Scheinakazie (*Robinia pseudoacacia* L.) im Zusammenhang mit Wachstum, Stärkespeicherung und Kernholzbildung. PhD thesis, University of Tuebingen, Germany.

Hauch, S., Magel, E., 1998. Extractable activities and protein content of sucrose phosphate synthase, sucrose synthase and neutral invertase in trunk tissues of *Robinia pseudoacacia* L. are related to cambial wood production and heartwood formation. Planta 207, 266–274.

Kampfenkel, K., vanMontagu, M., Inze, D., 1995. Effects of iron excess on *Nicotiana plumbaginifolia* plants: implications to oxidative stress. Plant Physiology 107, 725–735.

Kato, T., Berger, S.J., Carter, J.A., Lowry, O.H., 1973. An enzymatic cycling method for nicotinamide-adenine dinucleotide with malic and alcohol dehydrogenases. Analytical Biochemistry 53, 86–97.

Lee, A.C., Xu, X., Colombini, M., 1996. The role of pyridine dinucleotides in regulating the permeability of the mitochondrial outer membrane. Journal of Biological Chemistry 271, 26724–26731.

Lowry, O.H., Passonneau, J.V., 1972. A Flexible System of Enzymatic Analysis. Academic Press, New York.

Magel, E.A., 2000. Biochemistry and physiology of heartwood formation. In: Savidge, R., Barnett, J., Napier, R. (Eds.), Cell and Molecular Biology of Wood Formation. BIOS, Oxford, UK, pp. 363–376.

Magel, E., Hübner, B., 1997. Distribution of phenylalanine ammonia-lyase (PAL) and chalcone synthase (CHS) within trunks of *Robinia pseudoacacia* L. Botanica Acta 110, 314–322.

Magel, E.A., Claudot, A.C., Drouet, A., Ziegler, H., 1991. Formation of heartwood substances in the stem of *Robinia pseudoacacia* L. I. Distribution of phenylalanine ammonium-lyase and chalcone synthase across the trunk. Trees 5, 203–207.

Magel, E.A., Monties, B., Drouet, A., Jay-Allemand, C., Ziegler, H., 1995. Heartwood formation: biosynthesis of heartwood extractives and "secondary" lignification. In: Sandermann, H., Bonnet-Masimbert, M. (Eds.), EUROSILVA — Contribution to Forest Tree Physiology. INRA, Paris, pp. 35–56.

Magel, E.A., Bleuel, H., Hampp, R., Ziegler, H., 1996. Pyridine nucleotide levels and activities of dehydrogenases in cambial derivatives of *Robinia pseudoacacia* L. Trees 10, 325–330.

Meyer, R., Wagner, K.G., 1986. Nucleotide pools in leaf root tissue of tobacco plants: influence of leave senescence. Physiologia Plantarum 67, 666–672.

Miller, A.R., Crawford, D.L., Roberts, L.W., 1985. Lignification and xylogenesis in *Lactuca* pith explants cultured *in vitro* in the presence of auxin and cytokinin: a role of endogenous ethylene. Journal of Experimental Botany 36, 110–118.

Moeller, I.M., 1997. The oxidation of cytosolic NAD(P)H by external NAD(P)H dehydrogenases in the respiratory chain of plant mitochondria. Physiologia Plantarum 100, 85–90.

Norman, E.G., Walton, A.B., Turpin, D.H., 1994. Immediate activity of respiration in *Petroselinum crispum* L. in response to the *Phytophthora megasporum* f.sp. glycinea elicitor. Plant Physiology 106, 1541–1546.

Oka, K.I., Takahashi, T., Hori, S.H., 1981. Differential effects of the NAPDH/NADP ratio on the activities of hexose-6-phosphate dehydrogenase and glucose-6-phosphate dehydrogenase. Biochimica et Biophysica Acta 662, 318–325.

Pryke, J.A., apRees, T., 1976. Activity of pentose phosphate pathway during lignification. Planta 132, 279–284.

Sagisaka, A., 1974. Transition of metabolism in living poplar bark from growing to wintering stages and vice versa: changes in glucose-6-phosphate and 6-phosphogluconate dehydrogenase activities and in the levels of sugar phosphates. Plant Physiology 54, 544–549.

Sagisaka, A., Asada, M., 1981. Coordinate and noncoordinate changes in enzyme activities in pentose phosphate cycle in poplar: a control of enzyme activities in differentiated xylem. Plant Cell Physiology 22, 1459–1568.

Schmidt, W., Schuck, C., 1996. Pyridine nucleotide pool size changes

in iron-deficient *Plantago lanceolata* roots during reduction of external oxidants. Physiologia Plantarum 98, 215–221.

Sindelar, L., Sindelarova, M., Burketova, L.R.P., Sindelar, L., 1999. Changes in activity of glucose-6-phosphate dehydrogenase and 6-phosphogluconate dehydrogenase isozymes upon potato virus Y infection in tobacco leaf tissues and protoplasts. Plant Physiology Biochemistry 37, 195–201.

Slaski, J.J., Zhang, G.C., Basu, U., Stephens, J.L., Taylor, G.J.R.P., 1996. Aluminum resistance in wheat (*Triticum aestivum*) is associated with rapid, Al-induced changes in activities of glucose-6-phosphate dehydrogenase and 6-phosphogluconate dehydrogenase in root apices. Physiologia Plantarum 98, 477–484.

Solar, A., Smole, J., Stampar, F., Virscek-Marn, M., 1994. Characterization of isozyme variation in walnut (*Juglans regia* L.). Euphytica 77, 105–112.

Tian, W.N., Braunstein, L.D., Apse, K., Pang, J.D., Rose, M., Tian, X.N., Staton, R.C., 1999. Importance of glucose-6-phosphate dehydrogenase activity in cell death. American Journal Physiology Cell Physiology 45, 1121–1131.

VonSchaeven, A., Langenkaemper, G., Graeve, K., Wenderoth, I., Scheibe, R., 1995. Molecular characterization of the plastidic glucose-6-phosphate dehydrogenase from potato in comparison to its cytosolic counterpart. Plant Physiology 109, 1327–1335.

PERGAMON

Phytochemistry 57 (2001) 1069–1084

PHYTOCHEMISTRY

www.elsevier.com/locate/phytochem

Review

The biosynthesis of monolignols: a ''metabolic grid'', or independent pathways to guaiacyl and syringyl units?

Richard A. Dixon*, Fang Chen, Dianjing Guo, Kota Parvathi

Plant Biology Division, Samuel Roberts Noble Foundation, 2510 Sam Noble Parkway, Ardmore, OK 73401, USA

Received 17 July 2000; received in revised form 16 October 2000

Abstract

Lignin is a complex polymer formed by the oxidative polymerization of hydroxycinnamyl alcohol derivatives termed monolignols. The major monolignols in dicotyledonous angiosperm lignin are monomethylated guaiacyl (G) units derived from coniferyl alcohol, and dimethylated syringyl (S) units derived from sinapyl alcohol. The biochemical pathways leading to the formation of monolignols feature successive hydroxylation and *O*-methylation of the aromatic ring and conversion of the side chain carboxyl to an alcohol function. The current view of the monolignol biosynthetic pathway envisages a metabolic grid leading to G and S units, through which the successive hydroxylation and *O*-methylation reactions may occur at different levels of side chain oxidation. The present article assesses biochemical and genetic evidence for and against such a model, including recent data on the methylation reactions of monolignol biosynthesis in alfalfa. We draw attention to portions of the currently accepted monolignol pathway that may require revision, and suggest an alternative model in which metabolic channeling allows for independent pathways to G and S lignin. © 2001 Elsevier Science Ltd. All rights reserved.

Keywords: Alfalfa (*Medicago sativa* L.); Leguminosae; Biosynthesis; Lignin; Monolignol; Genetic manipulation; Metabolic channeling; Metabolic grid

Contents

1. Introduction 1070

2. Developmental control of lignin composition 1071

3. A metabolic grid based on in vitro biochemistry 1071

4. In vivo labeling studies support novel routes to S lignin 1075

5. Cellular and subcellular localization of monolignol biosynthetic enzymes 1075

6. Are all the enzymes of monolignol biosynthesis accounted for? 1076

7. Genetic modification of monolignol pathways 1077

8. A metabolic channel model for monolignol biosynthesis? 1079

9. Conclusions 1080

References 1081

* Corresponding author. Tel.: +1+580-223-5810; fax: +1-580-221-7380.
E-mail address: radixon@noble.org (R.A. Dixon).

0031-9422/01/$ - see front matter © 2001 Elsevier Science Ltd. All rights reserved.
PII: S0031-9422(01)00092-9

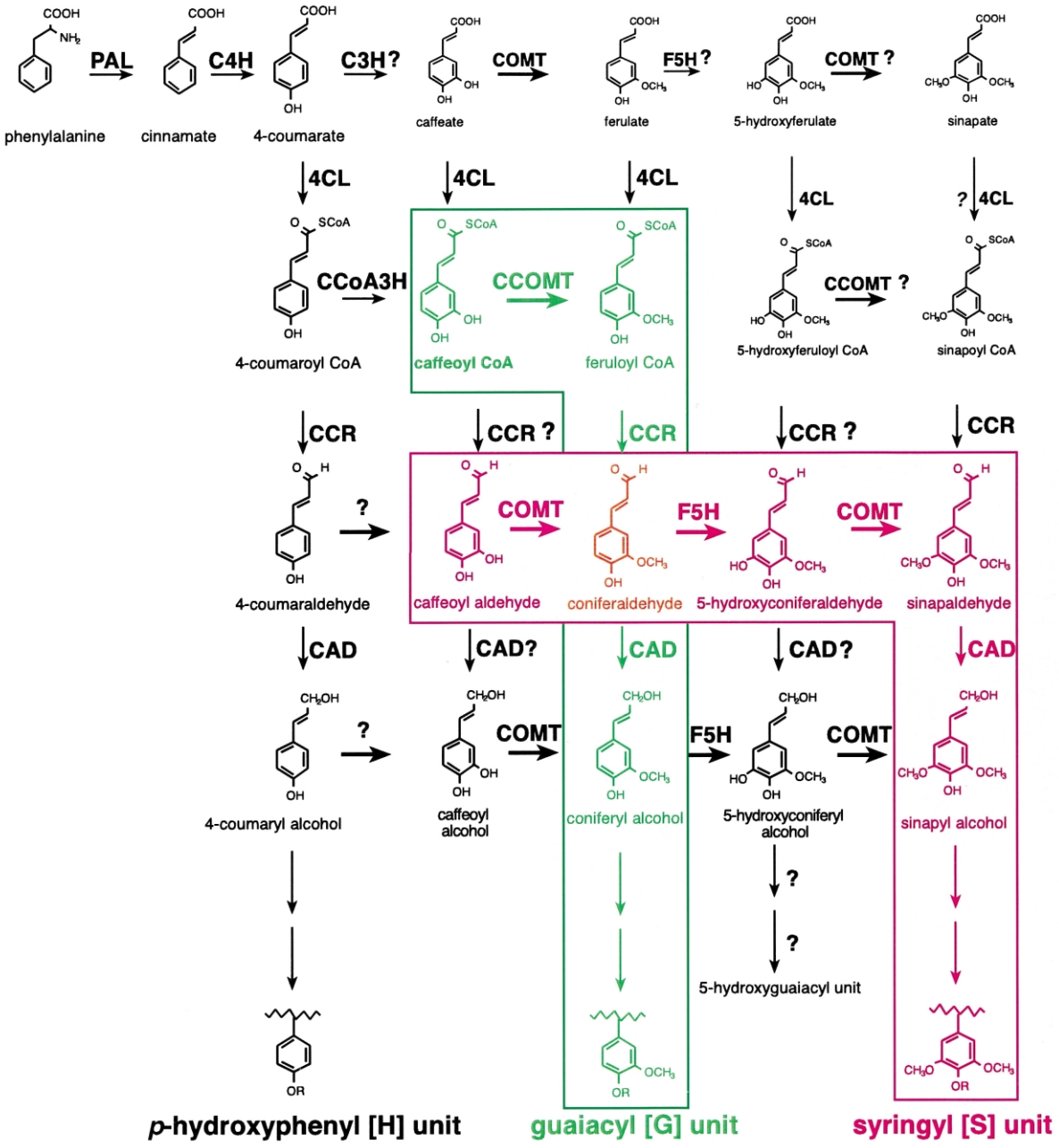

Fig. 1. Pathways to monolignols. The complete metabolic grid of reactions is shown. All enzyme reactions shown with a solid arrow have been demonstrated to occur in vitro. Reactions shown in smaller type may not occur in vivo. The reactions shown in green seem the most likely route to G lignin in vivo. The reactions in red represent those reactions consistent with both in vivo and in vitro evidence for being involved specifically in S lignin biosynthesis. The intermediate in orange is common to both G and S lignin pathways.

1. Introduction

Lignin is a major structural component of secondarily thickened plant cell walls. It is a complex polymer of hydroxylated and methoxylated phenylpropane units, linked via oxidative coupling that is probably catalyzed by both peroxidases and laccases (Boudet et al., 1995). Lignin imparts mechanical strength to plant stems and trunks, and hydrophobicity to water-conducting vascular elements. Dicotyledonous angiosperm lignins contain two major monomer species, termed guaiacyl (G) and syringyl (S) units (Fig. 1). G units are characterized by a single methoxyl substituent on the aromatic ring, whereas S units are di-methoxylated (Fig. 1). The S and G units in lignin are joined through at least five different types of linkages (Davin and Lewis, 1992). The mechanisms that determine the relative proportions of these linkage types in a particular lignin polymer are currently

unknown. It has, however, become increasingly apparent that lignin is not simply a random polymer of monolignol units, and lignin composition is developmentally programmed, both temporally and spatially (Terashima et al., 1993).

Softwood gymnosperm lignins essentially lack S residues and are, therefore, highly condensed. They are less amenable to chemical pulping than are hardwood lignins. Lignin levels increase with progressive maturity in stems of forage crops, including legumes such as alfalfa (Jung et al., 1997b) and in grasses such as tall fescue (Buxton and Redfearn, 1997). In addition, the lignin composition changes with advanced maturity towards a progressively higher S/G ratio (Buxton and Russell, 1988). Both lignin concentration (Albrecht et al., 1987; Casler, 1987; Jung et al., 1997a) and lignin methoxyl content (S/G ratio) (Sewalt et al., 1996) have been negatively correlated with forage digestibility for ruminant animals. Small reductions in lignin content may have correspondingly larger impacts on digestibility (Casler, 1987). Although a number of studies have linked decreased forage digestibility to increased S/G ratio as a function of increased plant maturity (Buxton and Russell, 1988; Grabber et al., 1992), other studies have questioned the effect of lignin composition on digestibility (Grabber et al., 1997).

Because of the impact of lignin on forage quality and paper pulping efficiency, there is considerable interest in genetic manipulation to alter the quantity and/or quality of the lignin polymer (Whetten and Sederoff, 1991; Dixon et al., 1996; Boudet and Grima-Pettenati, 1996; O'Connell et al., 1998). To predict the outcome of transgenic modification, it is necessary to understand the sequence of reactions in the pathway being manipulated. This understanding was believed to exist in the case of lignin biosynthesis until the mid 90s, when evidence emerged for previously unsuspected routes to the monolignols. Currently, the "text book" view of lignin biosynthesis presents the pathway as a metabolic grid, through which side chain reduction and ring hydroxylation/methylation can occur at several different levels (Fig. 1). Such a model appears, however, to be inconsistent with recent findings on enzyme specificity and the results of modification of lignin biosynthetic enzyme activities through transgenic approaches. Because of the complexity of lignin structure, the difficulty of accurately determining the composition of the entire lignin polymer, the complex temporal and spatial controls affecting lignin biosynthesis and deposition, and the possibility of significant species differences, any new hypothesis for lignin biosynthesis must be evaluated with caution. By critically evaluating the evidence for the metabolic grid model, and proposing an alternative model that is equally consistent with present evidence, at least for the forage legume alfalfa, we hope to stimulate experimental re-evaluation of the monolignol pathway.

2. Developmental control of lignin composition

In hardwoods, monolignols are first incorporated into the middle lamella of the primary cell wall during the S_1 and S_2 developmental stages of the secondary wall, whereas incorporation into the secondary wall takes place mainly after the S_3 stage (Terashima et al., 1993). Lignification of the vessel wall, cell corner and middle lamella starts in the early stages of xylem differentiation, whereas lignification of fiber secondary walls proceeds most actively in the middle and late stages.

High-resolution microautoradiography of developing hardwood xylem has revealed that the three monolignol units are incorporated at different stages of cell wall formation. H (*p*-hydroxyphenyl) units are incorporated in the earliest stages mainly in the cell corner and middle lamella during the period of formation of the S_1 layer. The deposition of G lignin continues through the early to late stages. S lignin is deposited mainly in the middle and late developmental stages, mostly in the secondary fiber wall, when formation of the inner layer of the secondary wall has already commenced (Terashima et al., 1986, 1993; Fukushima and Terashima, 1990). A somewhat similar situation appears to occur during development of vascular tissues of monocots (Lam et al., 1990; He and Terashima, 1991).

The fact that different monolignols are incorporated into the cell wall at different stages of vascular differentiation, and in different regions of the wall, strongly argues for tightly regulated pathways to G and S lignins that can function either independently or together. Independent pathways, rather than a metabolic grid, provide the greatest potential for such tight developmental control.

3. A metabolic grid based on in vitro biochemistry

Current ideas on the ring substitution reactions of lignin biosynthesis have evolved from the initial premise, based on substrate specificity studies with assumed substrates that were readily available, that successive ring hydroxylations and *O*-methylations take place at the level of hydroxycinnamic acid precursors (Neish, 1968). In angiosperms, the enzyme known as caffeic acid *O*-methyltransferase (COMT) was first identified as converting caffeic acid to ferulic acid, and was later shown to also convert 5-hydroxyferulic acid to sinapic acid (Davin and Lewis, 1992) (Fig. 1). Genes encoding this enzyme have been cloned from a variety of plant species (Ibrahim et al., 1998), initially based on enzyme purification using the hydroxycinnamic acids as substrates. COMT has a subunit M_r of approximately 43 kD, and characteristic sequence signatures of the plant *O*-methyltransferase superfamily (Ibrahim et al.,

1998; Joshi and Chiang, 1998). Its properties from a selection of species are summarized in Table 1.

The concept of a single pathway for ring methylation at the level of hydroxycinnamic acids received its first revision when it was demonstrated that caffeoyl CoA *O*-methyltransferase (CCOMT) was likely to be involved in lignin biosynthesis in differentiating tracheary elements of *Zinnia elegans* (Ye et al., 1994). CCOMT is also a bifunctional enzyme, converting caffeoyl CoA to feruloyl CoA and 5-hydroxyferuolyl CoA to sinapyl CoA (Inoue et al., 1998; Grimmig et al., 1999). CCOMT genes have now been cloned from many species, including *Z. elegans*, Arabidopsis, tobacco, parsley, and alfalfa. CCOMT has a subunit M_r of approximately 30 kD, and is more closely related at the amino acid sequence level to mammalian catechol OMT than to plant caffeic acid OMT (Joshi and Chiang, 1998). Its properties are summarized in Table 1.

The demonstration that both COMT and CCOMT are bi-specific, acting on both the 3, 4-dihydroxy- and 3-methoxy, 4, 5-dihydroxy-substituted aromatic nuclei, led to a picture of two pathways to monolignol biosynthesis, best designated, at least on paper, as the two upper parallel pathways in the metabolic grid shown in Fig. 1.

The three successive ring hydroxylation reactions of monolignol biosynthesis are catalyzed, respectively, by the well characterized cinnamate 4-hydroxylase (C4H) cytochrome P450 (Pierrel et al., 1994), a yet to be characterized enzyme believed to be a coumarate 3-hydroxylase, and the ferulate 5-hydroxylase (F5H) cytochrome P450 (Meyer et al., 1996). Although earlier studies had suggested that hydroxylation of coumarate might be carried out by a copper-containing phenolase enzyme (Bolwell and Butt, 1983), phenolase activity does not appear to be co-regulated, either temporally or spatially, with other enzymes of lignin biosynthesis. It has been suggested that a more specific membrane-associated hydroxylase might catalyze the aromatic 3-hydroxylation reaction (Kojima and Takeuchi, 1989). The mode of hydroxylation of the 4-hydroxycinnamoyl moiety represents the first "black box" in the monolignol pathway.

Recent enzyme specificity studies suggest that, if operational, the metabolic grid to monolignols could theoretically involve ring substitution at most, or all, levels of modification of the monolignol side chain, but that there may be kinetically favored paths through the resultant "grid". Thus, the enzyme designated as F5H has a higher affinity for coniferyl aldehyde than for ferulic acid, at least in sweet gum (Osakabe et al., 1999) and Arabidopsis (Humphreys et al., 1999) (Table 1) and may not hydroxylate ferulic acid itself in vivo. Likewise, COMT from aspen and alfalfa has a significantly higher affinity for 5-hydroxyconiferyl aldehyde than for caffeic or 5-hydroxyferulic acids (Table 1). It has been proposed that inhibition of COMT-mediated methylation of caffeic acid in vitro by 5-hydroxyconiferyl aldehyde could essentially prevent flux from caffeic acid to ferulic acid from occurring in vivo (Li et al., 2000).

The above substrate preferences are consistent with involvement of COMT primarily in the formation of S lignin via methylation of 5-hydroxyconiferyl aldehyde, a conclusion in agreement with the results of transgenic modification of COMT activity (see below). We have recently shown that recombinant alfalfa COMT exhibits significantly greater catalytic efficiency with caffeoyl aldehyde, caffeoyl alcohol, 5-hydroxyferuloyl aldehyde and 5-hydroxyferuolyl alcohol than it does with the corresponding hydroxycinnamic acids (Parvathi et al., 2001), suggesting that COMT could be involved in both the 3- and 5-methylation reactions of S lignin biosynthesis at either the aldehyde or alcohol levels.

If C3H turns out to be a P450 with similar substrate preference to F5H, it is possible that hydroxylation of the coumarate moiety also occurs at the aldehyde level, and that coumarate itself might not, therefore, be a natural intermediate in monolignol biosynthesis. This would then imply that caffeic acid is not a substrate for COMT in the monolignol pathway, consistent with the substrate preferences of this enzyme (Li et al., 2000; Parvathi et al., 2001) and the results of transgenic experiments outlined below.

Reduction of hydroxycinnamic acids to their corresponding alcohols is initiated by formation of coenzyme A thioesters, that are reduced successively to the corresponding aldehydes by cinnamoyl CoA reductase(s) (CCR) and cinnamyl alcohol dehydrogenase(s) (CAD). Hydroxycinnamate: CoA ligases have been characterized at the molecular level from many plant species. In general, these enzymes exhibit highest activity against coumaric, caffeic and ferulic acids, with little activity against cinnamic and sinapic acids (Ehlting et al., 1999), although there are reports of sinapate CoA ligase activity in extracts from some plants. For example, we have shown that, although crude extracts from alfalfa stems appear to lack sinapate CoA ligase activity, this activity can be recovered following ammonium sulfate fractionation (K. Inoue and R.A. Dixon, unpublished results). The apparent lack of activity of 4CL against sinapic acid in several plants does, however, call into question the role of sinapate as a lignin precursor, and therefore also questions whether the conversion of 5-hydroxyferulic acid to sinapic acid by COMT in vitro actually occurs in vivo. Thus, one must question whether any of the free hydroxycinnamic acids beyond coumaric acid is a natural substrate for monolignol biosynthesis, even though radiolabeling studies have indicated that ferulic acid and sinapic acid are incorporated into lignin in poplar (Terashima et al., 1986). In such labeling studies, it is possible that exogenously applied precursors do not enter the same pools used by endogenous precursors.

Table 1
Biochemical properties of the enzymes of monolignol biosynthesis[a]

Enzyme	Species	Substrate(s) tested	K_m (μM)	Preferred substrate	Reference
PAL	Alfalfa PAL1	L-phe	40	L-phe	Jorrin and Dixon, 1990
	PAL2		70		
	PAL3		110		
C4H	*Helianthus tuberosus*	cinnA			
		(tuber microsomes)	2.6	cinnA	Gabriac et al., 1991
		(yeast expressed)	3.9		Urban et al., 1994
C3H	*Vigna mungo*	coumA		coumA	Kojima and Takeuchi, 1989
CCoA3H	Parsley cell suspension culture	coumCoA	NR	coumCoA	Kneusel et al., 1989
		coumA	NR	coumCoA	
COMT	Aspen	caffA	75.1	5-OHconifALD	Li et al., 2000
		5-OHFA	15.0		
		5-OHconifALD	2.6		
		5-OHconifALC	NR		
	Tobacco COMT I		NR	5-OHconifALD	Maury et al., 1999
	COMT II		NR	catechol	
	Clarkia breweri			5-OHFA	Wang and Pichersky, 1999
	Wheat Early OMT		NR	caffA	Lam et al., 1996
	Late OMT		NR	5-OHFA	
	Alfalfa COMT I	caffA	26.0	5-OHFA	Inoue et al., 1998
		5-OHFA	3.5		
	COMT II	caffA	0.6	caffA	Inou et al., 2000
		5-OHFA	5.4		
	Aspen	caffA	40.0	5-OHFA	Meng and Campbell, 1996
		5-OHFA	19.0		
CCOMT	Alfalfa	caffCoA	NR	caffCoA	Inoue et al., 1998
		5-OHFCoA	NR		
	Tobacco	caffCoA	24.0		Martz et al., 1998
	Zinnia elegans		NR		Ye et al., 1994
	Parsley cell suspension	caffCoA	1.1		Pakusch and Matern, 1991
F5H	Sweetgum	FA	286	conifALD	Osakabe et al., 1999
		conifALD	2.77		
	Arabidopsis	FA	1000	conifALD	Humphreys et al., 1999
		conifALD	1.0	conifALC	
		conifALC	3.0		
	Magnolia kobus			conifALC	Chen et al., 1999
4CL	Arabidopsis	cinnA	6320	coumA (4CL1)	Ehlting et al., 1999
	4CL1	coumA	38		
		caffA	11		
		FA	199		
		SA	NC		
	4CL2	cinnA	6630	caffA (4CL2)	
		coumA	252		
		caffA	20		
		FA	NC		
		SA	NC		
	4CL3	cinnA	2070	coum A (4CL3)	
		coumA	23		
		caffA	374		
		FA	166		
		SA	NC		
	Tobacco	coumA	NR	coumA	Lee and Douglas, 1996
		caffA	NR		
		FA	NR		
		SA	NR		

(*continued on next page*)

Table 1 (*continued*)

Enzyme	Species		Substrate(s) tested	K_m (μM)	Preferred substrate	Reference
	Loblolly pine (normal wood)		coumA	6.8	coumA	Voo et al., 1995
			caffA	4.6		
			FA	9.1		
			cinnA	79.4		
	Poplar		5-OHFA	NR	5-OHFA	Grand et al., 1983
CCR	Spruce		coumCoA	NR	FCoA	Luderitz and Grisebach, 1981
	Soybean		caffCoA	NR		
	Poplar		FCoA	NR		Sarni et al., 1984
	Eucalyptus gunnii		SCoA	NR		Goffner et al., 1994
CAD	Loblolly pine		conifALD	1.8	conifALD	O'Malley et al., 1992
			SALD	147		
			cinnALD	5.3		
	Eucalyptus gunnii					
		Hetero CAD	conifALD	4.5	conifALD	Goffner et al., 1992
			SALD	6.8		
			coumALD	5.1		
			conifALC	2.3		
			SALC	6.6		
			coumALC	35		
		Homo CAD	conifALD	5.2	SALD	
			SALD	2.5		
			coumLAD	15.5		
			conifALC	23.1		
			SALC	4.5		
			coumLAC	63.8		
	Eucalyptus gunni					
		CAD1	conifALD	25	conifALD	Hawkins and Boudet, 1994
			SALD	NR		
			coumLAD	70		
			conifALC	560		
			SALC	NR		
			coumALC	760		
		CAD2	conifALD	1.7		
			SALD	1.5		
			coumALD	1.2		
			conifALC1	6.0		
			SALC	7.2		
			coumALC	4.9		
	Alfalfa	CAD1	SALD	12.3	conifALD	Brill et al., 1999
			conifALD	5.7		
			cinnALD	23.7		
		CAD2	SALD	6.9		
			conifALD	1.3		
			cinnALD	9.2		
	Spruce			NR	conifALC	Gallino et al., 1993
CBGase	*Pinus contorta*		coniferin	NR	with similar	Dharmawardhana et al., 1999
			syringin	NR	specificity	

[a] Abbreviations: caffA, caffeic acid; caffCoA, caffeoyl coenzyme A; CBGase, coniferin β-glucosidase; cinnA, cinnamic acid; cinnALD, cinnamaldehyde; conifALC, coniferyl alcohol; conifALD, coniferylaldehyde; coumA, 4-coumaric acid; coumALC, 4-coumaryl alcohol; coumALD, 4-coumaryl aldehyde; coumCoA, 4-coumaroyl coenzyme A; FA, ferulic acid; FCoA, feruolyl CoA; NC, no conversion; NR, not reported; 5-OHconifALC, 5-hydroxyconiferyl alcohol; 5-OH-conifALD, 5-hydroxyconiferaldehyde; 5-OHFA, 5-hydroxyferulic acid; 5-OHFCoA, 5-hydroxyferuolyl coenzyme A; SA, sinapic acid; SALC, sinapyl alcohol; SALD, sinapyl aldehyde; SCoA, sinapoly CoA.

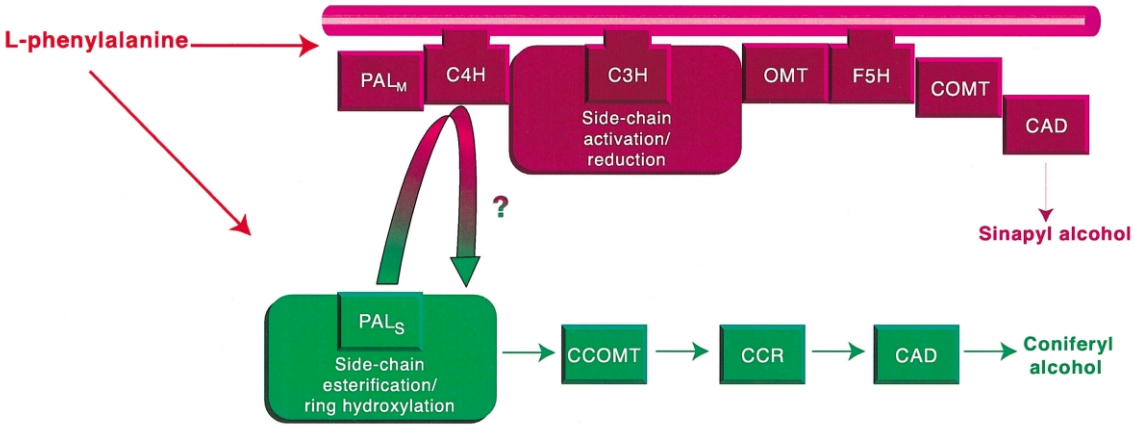

Fig. 2. A metabolic channel model for independent pathways to G and S monolignols. The hypothetical metabolic channel leading to S lignin (in red) is proposed to involve a microsomal-associated form of PAL (PAL_M) that directly channels its product, cinnamic acid, to the ER-associated cinnamate 4-hydroxylase (C4H) cytochrome P450. 3-Hydroxylation (possibly via a second P450 enzyme) and CoA esterification and reduction of the side chain then occur, although it is not clear whether hydroxylation occurs before or after side chain modification. These reactions are followed by the first *O*-methylation reaction (by COMT?) that produces coniferaldehyde, the substrate for the ER-associated F5H. The second methylation reaction is then catalyzed by COMT (perhaps associated with F5H) to yield sinapyl aldehyde, which is reduced by CAD to yield sinapyl alcohol. The hypothetical pathway to G units (in green) is proposed to involve a soluble form of PAL (PAL_S), that either provides cinnamate for C4H in an unchanneled reaction, or by-passes C4H by hydroxylation of the aromatic ring at the level of a side chain esterified intermediate. CCOMT then catalyzes the single *O*-methylation reaction, and coniferyl alcohol is formed via soluble forms of CCR and CAD. In an alternative model, the pathway to G units might also be membrane associated.

4. In vivo labeling studies support novel routes to S lignin

It has recently been shown by in vivo labeling studies in *Magnolia kobus* that S lignin can be derived from coniferyl alcohol. In these studies, side-chain labeled coniferyl alcohol was incorporated into S lignin with complete retention of label, indicating direct incorporation (Matsui et al., 1994; Chen et al., 1999). Consistent with a pathway for hydroxylation and methylation at the alcohol level, COMT from alfalfa has a significantly higher affinity for 5-hydroxyconiferyl alcohol than for caffeic acid (Parvathi et al., 2001). Furthermore, because alfalfa COMT is also active against caffeoyl aldehyde and alcohol (Parvathi et al., 2000), coniferyl alcohol could be formed from caffeoyl alcohol in addition to the accepted pathway from feruloyl CoA via coniferaldehyde. This idea finds support from a recent study indicating incorporation of labeled caffeoyl alcohol in both G and S lignin in several woody dicotyledonous angiosperms (Matsui et al., 2000). These new pathways to S lignin are indicated in red in Fig. 1.

5. Cellular and subcellular localization of monolignol biosynthetic enzymes

The cellular and subcellular localization of the enzymes is of critical importance in evaluating whether linear pathways, or a metabolic grid, underlie monolignol biosynthesis. Obviously, all the enzymes of the potential grid must be present in the same cell type for the metabolic grid hypothesis to hold.

There is ample evidence for the location of the enzymes of the core phenylpropanoid pathway at cellular sites of lignification. Early studies confirmed the localization of PAL to differentiating xylem (Rubery and Northcote, 1968). Subsequent studies with various *PAL* promoter reporter gene fusions in transgenic plants confirmed vascular specific expression of *PAL* genes in several species, including tobacco (Liang et al., 1989; Shufflebottom et al., 1993) and alfalfa (Guo et al., 2001). Likewise, the Arabidopsis C4H promoter confers vascular tissue specific expression of the GUS reporter gene in transgenic Arabidopsis (Bell-Lelong et al., 1997), and C4H has been immunolocalized to cells adjacent to differentiating xylem in bean (*Phaseolus vulgaris*) hypocotyls (Smith et al., 1994). The parsley *4CL1* promoter is active in vascular tissue of tobacco and Arabidopsis (Hauffe et al., 1991, 1993; Lee et al., 1995), and contains a series of positively acting *cis*-elements that confer xylem expression and a negative element that represses phloem expression (Hauffe et al., 1993).

PAL and 4CL are operationally soluble enzymes, although immunolocalization and biochemical fractionation studies have indicated that PAL may also be associated with the endomembrane system (Czichi and Kindl, 1977; Smith et al., 1994; Rasmussen and Dixon, 1999). C4H is a cytochrome P450 enzyme and is therefore localized to the outer surface of the endoplasmic reticulum by virtue of its N-terminal membrane anchor (Chapple, 1998).

As discussed above, the exact nature of the enzyme converting the coumarate moiety to the caffeate moiety during lignin biosynthesis is currently unknown. This 3-hydroxylation activity can be catalyzed by polyphenol oxidase type enzymes that, from different plant species, have been shown to act on 4-coumaric acid itself (Bolwell and Butt, 1983), 4-coumaroyl CoA (Wang et al., 1997) or 4-coumaroyl β-D-glucose (Tanaka and Kojima, 1991). The cellular and subcellular localization of these enzymes is not clear. In contrast, the enzyme known as ferulate 5-hydroxylase is presumably localized to cells producing lignin monomers in view of the blockage in S lignin biosynthesis in Arabidopsis lacking expression of this enzyme, and the increased effect of transgenic up-regulation of the enzyme if targeted to vascular tissues (Meyer et al., 1998; Franke et al., 2000).

Tissue print hybridization analysis indicated that both COMT and CCOMT transcripts are localized to developing xylem elements in alfalfa stems, whereas CCOMT transcripts are also found in phloem (Inoue et al., 1998). Immunolocalization studies at the light and electron microscope levels demonstrated expression of both COMT and CCOMT in the cytoplasm of primary and secondary xylem parenchyma cells in alfalfa stems (Kersey et al., 1999). Both enzymes were also localized to phloem in mature internodes, where COMT was found in cytoplasm and vacuoles, whereas CCOMT was only localized to cytoplasm (Kersey et al., 1999).

In in vitro differentiating tracheary elements of *Zinnia elegans*, COMT transcripts are much more apparent in phloem than in xylem in young internodes, whereas CCOMT transcripts are predominantly located in differentiating xylem (Ye et al., 1994; Ye and Varner, 1995). In mature internodes, both COMT and CCOMT transcripts appear in both xylem and phloem (Ye and Varner, 1995). In tobacco, three different classes of CCOMT transcripts are found in stem tissue, with different temporal patterns of developmental expression (Maury et al., 1999). The specific cell-type localizations of these different forms have yet to be reported.

CCOMT has been localized to secondary xylem in loblolly pine by direct biochemical assay, and the pine CCOMT promoter drives GUS expression in secondary xylem of transgenic tobacco (Li et al., 1999). The parsley CCOMT promoter also drives expression in xylem parenchyma in transgenic tobacco (Grimmig et al., 1999), consistent with the localization of CCOMT transcripts in parsley stems (Ye et al., 1994). Based on the above observations, there is at present no convincing evidence to suggest that the potential parallel pathways of lignin biosynthesis might take place in different cell types, thereby obviating the potential of a metabolic grid.

6. Are all the enzymes of monolignol biosynthesis accounted for?

Several of the enzymes of monolignol biosynthesis are multifunctional, such that more than one reaction in the hypothetical metabolic grid may be catalyzed by the same enzyme. However, it is also possible that other as yet unsuspected enzymes are involved in monolignol biosynthesis, and that new pathways may exist to S and G units. For example, interconversions of hydroxycinnamic acids are known to occur in plants at the levels of metabolically active glucose, shikimate or quinate esters (Strack and Bokern, 1984; Kuhnl et al., 1987; Kneusel et al., 1989; Tanaka and Kojima, 1991), and such alternate pathways have yet to be ruled out in lignin biosynthesis. A cinnamate: glucosyl transferase exists in alfalfa (Edwards et al., 1990), and an enzyme converting 4-coumaroyl glucose to caffeoyl glucose has been reported in sweet potato (Tanaka and Kojima, 1991), and may be present in other plants, where it could potentially by-pass the hydroxylation of coumarate.

Yet other enzymes may catalyze the methylation or hydroxylation reactions shown in Fig. 1. For example, young alfalfa internodes express a different form of COMT (COMT II), having preference for caffeic acid compared to 5-hydroxyferulic acid. This apparently new *O*-methyltransferase can be separated from the previously characterized COMT (COMT I) by anion exchange and hydrophobic interaction chromatography (Inoue et al., 2000). COMT I, but not COMT II, is found in mature internodes. COMT II is not recognized by anti-(COMT I) serum. In addition to substrate preference, COMT II differs from COMT I in its native Mr, pH optimum, and its very low Km for caffeic acid (Inoue et al., 2000). COMT II may therefore be the true caffeic acid OMT (although the enzyme is also active with coenzyme A esters and some flavonoids), and may be involved in formation of ferulic acid in the earliest stages of lignification in young tissues. A similar ''early'' form of COMT has been described in wheat seedlings (Lam, et al., 1996).

Loblolly pine xylem contains a further OMT, termed AEOMT, that methylates hydroxycinnamic acids and their coenzyme A esters with similar efficiency (Li et al., 1997). This enzyme has not been reported from angiosperms, and its subcellular localization has not been investigated.

Analysis of OMT substrate preferences in crude extracts from lignifying stems from wild-type and OMT down-regulated transgenic alfalfa plants has indicated that significant residual OMT activity against caffeoyl CoA and 5-hydroxyferuloyl CoA is observed in extracts that show no CCOMT protein by western blot analysis, and that extracts from lines with no COMT expression still have significant residual activity against caffeic and 5-hydroxyferulic acids, aldehydes and alcohols (Parvathi et al., 2001). These residual activities are greater

Table 2
Modification of lignin content and composition in transgenic plants and mutants with altered expression of lignin biosynthetic enzymes

Gene	Species	Method and activity	Lignin content	Lignin composition	Reference
PAL	Tobacco	Cosuppression to 20%	Decreased to 30%	Decreased G	Sewalt et al., 1997b
	Tobacco	Cosuppression to 17%	Decreased to 57%	Increased methoxyl content	Sewalt et al., 1997a
C4H	Tobacco	Cosuppression; antisense to 20%	Decreased to 20%	Decreased S	Sewalt et al., 1997a
F5H	Arabidopsis	Overexpression		Only S	Meyer et al., 1998
	Arabidopsis	Overexpression		Only S	Marita et al., 1999
	Tobacco; poplar	Overexpression	Decreased to 75%	Increased S	Franke et al., 2000
4CL	Arabidopsis	Antisense to 8%	Decreased to 70%	Decreased G	Lee et al., 1997
	Aspen	Antisense to 10%	Decreased to 55%	[Increased cellulose]	Hu et al., 1999
	Tobacco	Sense and antisense to 1%	Decreased to 66%	Decreased S	Kajita et al., 1996
	Tobacco	Antisense	Unchanged	Decreased S; Increased H	Kajita et al., 1997
COMT	Poplar	Antisense to 10%	Unchanged	Increased G	Lapierre et al., 1999
	Tobacco	Antisense to 40%	Decreased to 65%	More reduction of G than S	Sewalt et al., 1997a
	Aspen	Cosuppresion to 25%	Unchanged	Decreased S	Tsai et al., 1998
	Poplar	Antisense to 5%	Unchanged	Decreased S, new 5-OH G	Van Doorsselaere et al., 1995
	Tobacco	Antisense to 30%	Decreased to 42–85%	Unchanged	Ni et al., 1994
	Tobacco	Sense and antisense to 2–8%	Unchanged	Decreased S [and hemicellulose]	Bernard-Vailhe et al., 1996
	Tobacco	Antisense to 54%	Decreased to 88%	Decreased S	Dwivedi et al., 1994
	Tobacco	Sense and antisense to 2%	Unchanged	Decreased S, new 5-OH G	Atanassova et al., 1995
	Alfalfa	Antisense; cosuppression to 4%	Decreased to 71–87%	Reduction of G, near elimination of S, new 5-OH G	Guo et al., 2001
CCOMT	Tobacco	Antisense to 20-30%	Decreased to 53%	More reduction of G than S	Zhong et al., 1998
	Alfalfa	Antisense to 4%	Decreased to 83%	Reduction of G, no reduction of S	Guo et al., 2001
CCR	Tobacco	Antisense to 30%	Decreased to 53%	Decreased S and G increased S/G	Piquemal et al., 1998
CAD	Poplar	Antisense to 30%	Decreased (slight)	Increased S	Lapierre et al., 1999
	Alfalfa	Antisense to 30%	Unchanged	Decreased S	Baucher et al., 1999
	Tobacco	Antisense to 7–20%	Unchanged	Decreased S	Halpin et al., 1994
	Tobacco	Antisense to 7–20%	Unchanged	Decreased S	Bernard-Vailhé et al., 1998
	Tobacco	Antisense to 8–56%	Unchanged	Decreased S	Yahiaoui et al., 1998
	Loblolly pine	Mutant	Decreased to 91%	Increased coniferaldehyde units	MacKay et al., 1997
	Loblolly pine	Mutant		Increased units derived from DHCA	Ralph et al., 1997
	Sorghum	Mutant	Decreased to 75–85%		Pilonel et al., 1991

than can be accounted for by the activity of COMT for the CoA esters or of CCOMT for the non-esterified hydroxycinnamic acid derivatives, suggesting the involvement of other OMT enzymes. High transcript levels of candidate enzymes have been predicted from in silico analysis of *Medicago* stem ESTs (www.noble.org/medicago/), but the involvement of these enzymes in lignin biosynthesis must await analysis of enzymatic function and tissue-specific localization.

7. Genetic modification of monolignol pathways

Several studies have been published on the modification of lignin content and composition following transgenic up- or down-regulation of the enzymes discussed above, and several naturally occurring mutants in the monolignol pathway have been characterized. The results, which are summarized in Table 2, have often been difficult to interpret, although several consistent patterns have

emerged. The data confirm that COMT, CCOMT, F5H, CCR and CAD are indeed critical for normal wild-type lignin biosynthesis in the various species investigated. However, the data do not fully support the operation of a metabolic grid for monolignol biosynthesis through which intermediates find their way governed only by their cellular concentrations and the affinities of the various enzymes for their substrates.

Large reductions in lignin content have been obtained by down-regulation of PAL or C4H activities in transgenic tobacco, consistent with the positioning of these enzymes at the entry point into monolignol biosynthesis (Bate et al., 1994; Sewalt et al., 1997a,b). Down-regulation of PAL leading to an approximately 50% reduction in Klason lignin results in an increase in S/G ratio (from approximately 1.0 to 1.8). In contrast, down- regulation of C4H leading to a similar decrease in lignin content results in greatly reduced S/G ratio, tending towards complete elimination of S units (Sewalt et al., 1997a,b). This is quantitatively similar to the loss of S lignin observed following down-regulation of COMT (Atanassova et al., 1995; Van Doorsselaere et al., 1995) or F5H (Chapple et al., 1992), but none of the other enzymes of monolignol biosynthesis. There are three possible explanations for this finding: (1) the pathway to G lignin somehow bypasses C4H; (2) C4H catalyzes reactions in monolignol biosynthesis in addition to the 4-hydroxylation of cinnamic acid; (3) some kind of metabolic channeling places a form of C4H in a complex with other enzymes committed to S lignin biosynthesis.

Vascular tissue-directed over-expression of ferulate 5-hydroxylase in transgenic Arabidopsis leads to the formation of lignin composed almost totally of S residues linked predominantly in β-aryl ether units (Meyer et al., 1998; Marita et al., 1999; Franke et al., 2000), whereas down-regulation of F5H leads to lignin with very few S units (Marita et al., 1999). Thus, F5H is clearly a major control point in S lignin synthesis, consistent with the position of the enzyme in the "classical" pathway and its revised position acting primarily on 5-hydroxyconiferyl aldehyde.

There have been several reports on the effects of down-regulation of COMT activity on lignin content and composition in transgenic plants (Ni et al., 1994; Atanassova et al., 1995; Van Doorsselaere et al., 1995; Zhong et al., 1998; Guo et al., 2000), and the *brown midrib3* mutation in maize results from the insertion of a retrotransposon in the *COMT* gene (Vignols et al., 1995). In examples where COMT has been reduced to levels below approximately 20% of wild-type by expression of a homologous transgene, a strong reduction in S/G ratio is accompanied by no apparent change in lignin content (Atanassova et al., 1995; Van Doorsselaere et al., 1995). However, we have recently shown up to 30% decreases in Klason lignin levels in transgenic alfalfa in which COMT down-regulation was targeted using a vascular-tissue specific promoter that resulted in near total down-regulation of COMT transcripts and protein (Guo et al., 2001). However, acetyl bromide soluble lignin was not reduced. Determination of total G and S residues by thioacidolysis implied a greater down-regulation of lignin in COMT suppressed alfalfa plants than observed by determination of Klason lignin.

Studies with transgenic tobacco, poplar and alfalfa have indicated that down-regulation of COMT has a larger impact on S lignin than on G lignin, and that 5-hydroxyguaiacyl residues accumulate, albeit at a low level, in the lignin of COMT down-regulated plants (Atanassova et al., 1995; Van Doorsselaere., 1995). This is also the case in alfalfa, where a low level of 5-hydroxyguaiacyl residues accumulate in the lignin following near complete elimination of thioacidolysis-determined S units by reduction of COMT to 4.5% of wild-type level (Guo et al., 2001).

One problem with studies reporting transgenic modification of lignin biosynthesis is the use of analytical methods for lignin composition that report on only a fraction of the lignin polymer, namely the non-condensed portion. Using thioacidolysis followed by Raney nickel desulfurization, COMT down-regulation in alfalfa has been shown to lead to a loss of S residues in both the β-*O*-4-linked uncondensed fraction and in the condensed fraction resolved as a range of differently linked dimers (Guo et al., 2001). The effect of COMT down-regulation on S lignin therefore likely reflects a true metabolic reduction in S units, rather than a change in lignin composition resulting in appearance of more S units in the non-condensed fraction of the polymer.

In both tobacco and alfalfa, down-regulation of CCOMT leads to a corresponding decrease in Klason lignin levels (Zhong et al., 1998; Guo et al., 2001). However, although near elimination of CCOMT in alfalfa reduced G lignin with no effect on S lignin, the effect was at most an approximately 50% reduction in G units (Guo et al., 2000). This suggests that another methylation enzyme is also involved in the formation of G lignin in alfalfa. This might be COMT in view of the approximately 25% reduction in G lignin that accompanies the larger reduction in S lignin in strongly COMT down-regulated plants. However, it is also necessary to consider the possibility of other, yet to be determined *O*-methyltransferases, as discussed above. Whatever enzyme catalyzes the first step in S lignin biosynthesis in alfalfa, it may not be CCOMT.

The results of down-regulation of 4CL on lignin content and composition are somewhat contradictory. In tobacco, a reduction of 4CL activity resulted in a brownish coloration of the xylem cell walls, which correlated with reductions in overall lignin levels and in cinnamyl aldehyde and S residues in lignin. However, values for S/G ratio varied widely, from 0.45 to 2.0, in

plants with reduced 4CL activity due to large but variable reductions in G lignin (Kajita et al., 1996). In Arabidopsis, reduction of 4CL to less than 10% of wild-type activity resulted in strong reduction in G lignin with no reduction in S lignin, and it was therefore suggested that a route might exist to S lignin that is independent of 4CL activity (Lee et al., 1997). This idea is consistent with the lack of activity of Arabidopsis 4CL against sinapate (Lee et al., 1997), and the transgenic alfalfa data suggesting lack of involvement of CCOMT in S lignin biosynthesis. In quaking aspen (*Populus tremuloides*), it has been reported that down- regulation of 4CL can result in a striking decrease in lignin content with no apparent change in lignin composition (Hu et al., 1999).

Down-regulation of CCR leads to an orange/brown xylem coloration, reductions in lignin content, and increased S/G ratio due primarily to a decrease in extractable G units (Piquemal et al., 1998). However, there was some variation between lines, and one line also showed a significant reduction in S units. These data would, therefore, be consistent with the involvement of CCR in the synthesis of both G and S lignin. Down-regulation of CAD leads to lignin with an increased cinnamaldehyde content (Halpin et al., 1994; Hibino et al., 1995; Stewart et al., 1997). In alfalfa, CAD down-regulation has been reported to decrease the S/G ratio, primarily by causing a decrease in S units (Baucher et al., 1999). It should be noted that the effects of altered CCR or CAD on S/G ratio reported to date are far less striking than the effects of altered F5H or COMT. One explanation would be that F5H and COMT are specific for S lignin biosynthesis, whereas CAD and CCR are common to both S and G lignin biosynthesis.

The above inconsistencies between the results of in vitro and in vivo approaches to studying the monolignol pathway force us to re-evaluate how we have come to arrive at the current "metabolic grid" model for monolignol biosynthesis, namely by extrapolating perceived enzyme substrate preferences in vitro to pathways in vivo.

8. A metabolic channel model for monolignol biosynthesis?

Enzymes of secondary metabolism may be organized in complexes, variously described in the literature as "metabolic compartments", "metabolic channels" or "metabolons" (Hrazdina and Wagner, 1985; Srere, 1987; Hrazdina and Jensen, 1992; Winkel–Shirley, 1999). Metabolic complexes may contain arrays of consecutive, physically associated enzymes that are assembled on membranes or other physical structures, or that interact directly with one another (Cutler et al., 1981; Srere, 1987; Winkel-Shirley, 1999). This can result in the channeling of pathway intermediates from one enzyme to the next without their release into the total cellular metabolic pool.

Evidence for metabolic channeling in the phenylpropanoid pathway includes:

- Immunolocalization of operationally soluble enzymes on membranes or other cellular structures (Hrazdina et al., 1987).
- In vivo labeling and isotope dilution studies, in which potential pathway intermediates are only poorly incorporated into end products, or ineffectively compete with downstream intermediates for incorporation (Rasmussen and Dixon, 1999).
- In vitro channeling studies, in which isolated membrane preparations catalyze consecutive reactions, including at least one that is brought about by an operationally soluble enzyme, and in which the channeled intermediate is a poorer precursor for the end product than an upstream metabolite (Czichi and Kindl, 1975, 1977; Rasmussen and Dixon, 1999).
- Co-immunoprecipitation of consecutive pathway enzymes (Burbulis and Winkel-Shirley, 1999).
- Demonstration of direct physical interactions between consecutive pathway enzymes using the yeast two-hybrid system (Burbulis and Winkel-Shirley, 1999).
- Examination of the effects of genetic modification of pathway enzymes in transgenic plants. In some cases, the outcome is inconsistent with a simple linear pathway in which intermediates reach the next enzyme by a diffusion-limited process (e.g. Sewalt et al., 1997a,b), as discussed above.

The localization of monolignol biosynthesis to a small subset of cells in the developing stem makes it difficult to obtain suitable material for studying channeling of lignin biosynthesis in vivo or in isolated microsomes. Pine cell suspension cultures, which have provided excellent material for the analysis of flux into monolignols by in vivo labeling approaches (Anterola et al., 1999), or differentiating *Zinnia* tracheary elements (Ye et al., 1994), might provide suitable material for such studies in the future. In the pine cell culture system, the very low pool sizes of hydroxycinnamyl CoA, aldehyde and alcohol intermediates are consistent with metabolic channeling in which flux control is exerted upstream of the *O*-methyltransferase reactions (Anterola et al., 1999).

At the subcellular level, the involvement of at least two cytochrome P450 enzymes, C4H and F5H could, by way of the anchoring of such enzymes to the external surface of the ER, provide a basis for the assembly of metabolic complexes for G and S lignin formation. However, although immunolocalization studies indicate that other enzymes of the monolignol pathway are

localized to cytoplasm (Kersey et al., 1999), the resolution of these studies was insufficient to reveal whether these enzymes might exhibit loose ER association. Furthermore, COMT, CCOMT, 4CL, CCR and CAD are all operationally soluble enzymes, and do not appear to contain any sequence elements that might engender membrane localization. To the best of our knowledge, no attempts have been made to assess whether any of these enzymes might be structurally organized within the cell. However, studies on PAL, another operationally soluble enzyme, have suggested that it might be co-localized with C4H on membranes of the ER, and evidence has been presented for channeling of the product of PAL, *trans*-cinnamic acid, in the conversion of phenylalanine to 4-coumaric acid (Czichi and Kindl, 1977; Hrazdina and Jensen, 1992; Rasmussen and Dixon, 1999).

Tobacco contains two families of *PAL* genes (*PAL1* and *PAL2*), each family comprising two very closely related members. Protein gel blot analysis showed that PAL1 is localized in both soluble and microsomal fractions from tobacco stems and cell cultures, whereas PAL2 is only found in the soluble fraction (Rasmussen and Dixon, 1999). This suggests that PAL1 is the form of PAL involved in direct coupling to C4H. Extrapolating further, it is possible to envisage a metabolic complex to S lignin in which three cytochrome P450 enzymes, C4H, putative coumarate (or coumaraldehyde?) 3-hydroxylase and F5H (coniferaldehyde 5-hydroxylase) indirectly anchor other operationally soluble enzymes, including COMT and perhaps specific forms of PAL, 4CL and/or CCR, to the surface of the ER (Fig. 2). This complex might be molecularly and physically distinct from the metabolic system, utilizing CCOMT for 3-*O*-methylation, involved in G lignin biosynthesis. Based on the specificity of alfalfa COMT for caffeoyl and 5-hydroxyferuolyl aldehydes and alcohols, COMT alone could function as the only *O*-methyltransferase involved in the putative channel leading to S lignin.

The model in Fig. 2 does not present a clear picture of the necessary involvement of 4CL and CCR in the biosynthesis of S lignin. These enzymes are shown as interacting, perhaps as soluble enzymes recruited to the complex, with either the cinnamate 4-hydroxylase, coumarate hydroxylase, or the enzyme that catalyzes 3-*O*-methylation (most likely COMT, at least in alfalfa). The uncertainty arises because of our lack of understanding of the level at which the 3-hydroxyl group is introduced into the coumarate moiety, or, put another way, we do not know if CoA esterification and subsequent side chain reduction occur before or after 3-hydroxylation.

Alfalfa, as with most plants, contains a PAL multigene family (Gowri et al., 1991), and it is possible that different forms of PAL may be associated differentially with S and G lignin biosynthesis in the above model, consistent with over-expression of a specific (transgene) PAL form affecting S/G ratio in transgenic tobacco (Sewalt et al., 1997a,b). The advantage of such a channeled model for monolignol biosynthesis is that it allows for the fine control over production of G and S units that is required for the observed temporal and spatial regulation of lignin composition.

9. Conclusions

The currently accepted model for lignin monomer biosynthesis is inconsistent with the results of genetic manipulation experiments. In vitro biochemical studies favor preferred routes to G and S units, but do not provide evidence for the operation of these routes in vivo. Enzymes in addition to those currently identified may play a role in monolignol biosynthesis. Metabolic channeling has been demonstrated in several areas of plant natural product biosynthesis, and could explain how G and S units could be produced by completely separate pathways, even if some common enzymes were involved.

The G lignin pathway would first appear to involve hydroxylation of a coumarate moiety. This may occur at the level of conversion of coumaroyl CoA to caffeoyl CoA, inasmuch as this reaction has been demonstrated in vitro and the enzyme appears to be regulated in a manner consistent with involvement in cell wall phenolic biosynthesis (Kneusel et al., 1989); however, hydroxylation at the level of the free acid (or aldehyde) can not be discounted, in spite of the debate as to whether a specific coumarate hydroxylase exists. The remaining reactions are methylation of caffeoyl CoA by CCOMT, and reduction of feruloyl CoA to coniferyl alcohol via coniferaldehyde. The preferred reactions specific for S lignin biosynthesis in our model are the methylation of caffeoyl aldehyde by COMT, conversion of coniferaldehyde to 5-hydroxyconiferaldehyde by F5H, methylation of 5-hydroxyconiferaldehyde to sinapyl aldehyde (again by COMT), and final reduction of sinapyl aldehyde to sinapyl alcohol by CAD (Fig. 1). The hydroxylation and methylation steps might also take place at the alcohol level, utilizing the same enzyme complex. This pathway, that would still be distinct from the G lignin pathway, would require action of CAD at an earlier stage, such as caffeoyl aldehyde or coniferaldehyde. If hydroxylation of the 4-hydroxycinnamate moiety were to be catalyzed by a cytochrome P450 enzyme, the pathway from the 4-hydroxycinnamate moiety to S units would occur by the sequence P450- OMT-P450- OMT- CAD. This arrangement could exist as an enzyme complex anchored to the surface of the endoplasmic reticulum via the P450s (Fig. 2). In contrast, the G lignin pathway, involving hydrophilic coenzyme A esters as substrates for hydroxylation and methylation, could be localized in the soluble cytoplasm. The nature of the first methylation reaction in S lignin biosynthesis is, in our opinion, still questionable, although COMT is most

likely involved in alfalfa, and the above model does not address where the pathways to G and S lignin might initially diverge.

References

Albrecht, K.A., Wedin, W.F., Buxton, D.R., 1987. Cell-wall composition and digestibility of alfalfa stems and leaves. Crop Science 27, 735–741.

Anterola, A.M., van Rensburg, H., van Heerden, P.S., Davin, L.B., Lewis, N.G., 1999. Multi-site modulation of flux during monolignol formation in loblolly pine (*Pinus taeda*). Bichemical and Biophysical Research Communications 261, 652–657.

Atanassova, R., Favet, N., Martz, F., Chabbert, B., Tollier, M.T., Monties, B., Fritig, B., Legrand, M., 1995. Altered lignin composition in transgenic tobacco expressing *O*-methyltransferase sequences in sense and antisense orientation. The Plant Journal 8, 465–477.

Bate, N.J., Orr, J., Ni, W., Meroni, A., Nadler-Hassar, T., Doerner, P.W., Dixon, R.A., Lamb, C.J., Elkind, Y., 1994. Quantitative relationship between phenylalanine ammonia-lyase levels and phenylpropanoid accumulation in transgenic tobacco identifies a rate-determining step in natural product synthesis. Proceedings of the National Academy of Sciences USA 91, 7608–7612.

Baucher, M., Bernard-Vailhe, M.A., Chabbert, B., Besle, J.M., Opsomer, C., VanMontagu, M., Botterman, J., 1999. Down-regulation of cinnamyl alcohol dehydrogenase in transgenic alfalfa (*Medicago sativa* L.) and the effect on lignin composition and digestibility. Plant Molecular Biology 39, 437–447.

Bell-Lelong, D.A., Cusumano, J.C., Meyer, K., Chapple, C., 1997. Cinnamate-4-hydroxylase expression in Arabidopsis. Plant Physiology 113, 729–738.

Bernard-Vailhé, M.A., Besle, J.M., Maillot, M.P., Cornu, A., Halpin, C., Knight, M., 1998. Effect of down-regulation of cinnamyl alcohol dehydrogenase on cell wall composition and on degradability of tobacco stems. Journal of the Science of Food and Agriculture 76, 505–514.

Bernard-Vailhé, M.A., Migne, C., Cornu, A., Maillot, M.P., Grenet, E., Besle, J.M., 1996. Effects of modification of the *O*-methyltransferase activity on cell wall composition, ultrastructure and degradability of transgenic tobacco. Journal of the Science of Food and Agriculture 72, 385–391.

Bolwell, G.P., Butt, V.S., 1983. Photoinduced changes in *o*-diphenol oxidase and *p*-coumarate hydroxylase activities in spinach beet seedlings and leaves. Phytochemistry 22, 37–45.

Boudet, A.M., Grima-Pettenati, J., 1996. Lignin genetic engineering. Molecular Breeding 2, 25–39.

Boudet, A.M., Lapierre, C., Grima-Pettenati, J., 1995. Tansley review No. 80. Biochemistry and molecular biology of lignification. New Phytologist 129, 203–236.

Brill, E.M., Abrahams, S., Hayes, C.H., Jenkins, C.L.D., Watson, J.M., 1999. Molecular characterisation and expression of a wound-inducible cDNA encoding a novel cinnamyl-alcohol dehydrogenase enzyme in lucerne (*Medicago sativa* L.). Plant Molecular Biology 41, 279–291.

Burbulis, I.E., Winkel-Shirley, B., 1999. Interactions among enzymes of the Arabidopsis flavonoid biosynthetic pathway. Proceedings of the National Academy of Sciences USA 96, 12929–12934.

Buxton, D.R., Redfearn, D.D., 1997. Plant limitations to fiber digestion and utilization. Journal of Nutrition 127, S814–S818.

Buxton, D.R., Russell, J.R., 1988. Lignin constituents and cell-wall digestibility of grass and legume stems. Crop Science 28, 553–558.

Casler, M.D., 1987. In vitro digestibility of dry matter and cell wall constituents of smooth bromegrass forage. Crop Science 27, 931–934.

Chapple, C., 1998. Molecular-genetic analysis of plant cytochrome P450-dependent monooxygenases. Annual Review of Plant Physiology and Plant Molecular Biology 49, 311–343.

Chapple, C.C.S., Vogt, T., Ellis, B.E., Somerville, C.R., 1992. An Arabidopsis mutant defective in the general phenylpropanoid pathway. Plant Cell 4, 1413–1424.

Chen, F., Yasuda, S., Fukushima, K., 1999. Evidence for a novel biosynthetic pathway that regulates the ratio of syringyl to guaiacyl residues in lignin in the differentiating xylem of *Magnolia kobus* DC. Planta 207, 597–603.

Cutler, A.J., Hösel, W., Sternberg, M., Conn, E.E., 1981. The in vitro biosynthesis of taxiphyllin and the channeling of intermediates in *Triglochin maritima*. Journal of Biological Chemistry 256, 4253–4258.

Czichi, U., Kindl, H., 1975. Formation of *p*-coumaric acid and *o*-coumaric acid from L-phenylalanine by microsomal membrane fractions from potato: evidence of membrane-bound enzyme complexes. Planta 125, 115–125.

Czichi, U., Kindl, H., 1977. Phenylalanine ammonia-lyase and cinnamic acid hydroxylase as assembled consecutive enzymes on microsomal membranes of cucumber cotyledons: cooperation and subcellular distribution. Planta 134, 133–143.

Davin, L.B., Lewis, N.G., 1992. Phenylpropanoid metabolism: biosynthesis of monolignols, lignans and neolignans, lignins and suberins. Recent Advances in Phytochemistry 26, 325–375.

Dharmawardhana, D.P., Ellis, B.E., Carlson, J.E., 1999. cDNA cloning and heterologous expression of coniferin β-glucosidase. Plant Molecular Biology 40, 365–372.

Dixon, R.A., Lamb, C.J., Masoud, S., Sewalt, V.J.H., Paiva, N.L., 1996. Metabolic engineering: prospects for crop improvement through the genetic manipulation of phenylpropanoid biosynthesis and defense responses- a review. Gene 179, 61–71.

Dwivedi, U.N., Campbell, W.H., Yu, J., Datla, R.S.S., Bugos, R.C., Chiang, V.L., Podila, G.K., 1994. Modification of lignin biosynthesis in transgenic *Nicotiana* through expression of an antisense *O*-methyltransferase gene from *Populus*. Plant Molecular Biology 26, 61–71.

Edwards, R., Mavandad, M., Dixon, R.A., 1990. Metabolic fate of cinnamic acid in elicitor-treated cell suspension cultures of *Phaseolus vulgaris*. Phytochemistry 29, 1867–1873.

Ehlting, J., Buttner, D., Wang, Q., Douglas, C.J., Somssich, I.E., Kombrink, E., 1999. Three 4-coumarate: coenzyme A ligases in *Arabidopsis thaliana* represent two evolutionarily divergent classes in angiosperms. The Plant Journal 19, 9–20.

Franke, R., McMichael, C.M., Meyer, K., Shirley, A.M., Cusumano, J.C., Chapple, C., 2000. Modified lignin in tobacco and poplar plants over-expressing the Arabidopsis gene encoding ferulate 5-hydroxylase. The Plant Journal 22, 223–234.

Fukushima, K., Terashima, N., 1990. Heterogeneity in formation of lignin. XIII. Formation of *p*-hydroxyphenyl lignin in various hardwoods visualized by microautoradiography. Journal of Wood Chemistry and Technology 10, 413–433.

Gabriac, B., Werck-Reichhart, D., Teutsch, H., Durst, F., 1991. Purification and immunocharacterization of a plant cytochrome P450: the cinnamic acid 4-hydroxylase. Archives of Biochemistry and Biophysics 288, 302–309.

Galliano, H., Heller, W., Sandermann, J.H., 1993. Ozone induction and purification of spruce cinnamyl alcohol dehydrogenase. Phytochemistry 32, 557–563.

Goffner, D., Campbell, M.M., Campargue, C., Clastre, M., Borderies, G., Boudet, A., Boudet, A.M., 1994. Purification and characterization of cinnamoyl-coenzyme A: NADP oxidoreductase in *Eucalyptus gunnii*. Plant Physiology 106, 625–632.

Goffner, D., Joffroy, I., Grima-Pettenati, J., Halpin, C., Knight, M.E., Schuch, W., Boudet, A.M., 1992. Purification and characterization of isoforms of cinnamyl alcohol dehydrogenase from *Eucalyptus* xylem. Planta 188, 48–53.

Gowri, G., Paiva, N.L., Dixon, R.A., 1991. Stress responses in alfalfa (*Medicago sativa* L.) XII. Sequence analysis of phenylalanine ammonia-lyase (PAL) cDNA clones and appearance of PAL transcripts in elicitor-treated cell cultures and developing plants. Plant Molecular Biology 17, 415–429.

Grabber, J.H., Jung, G.A., Abrams, S.M., Howard, D.B., 1992. Digestion kinetics of parenchyma and sclerenchyma cell walls isolated from orchardgrass and switchgrass. Crop Science 32, 806–810.

Grabber, J.H., Ralph, J., Hatfield, R.D., Quideau, S., 1997. *p*-Hydroxyphenyl, guaiacyl, and syringyl lignins have similar inhibitory effects on wall degradability. Journal of Agricultural and Food Chemistry 45, 2530–2532.

Grand, C., Boudet, A., Boudet, A.M., 1983. Isoenzymes of hydroxycinnamate: CoA ligase from poplar stems. Properties and tissue distribution. Planta 158, 225–229.

Grimmig, B., Kneusel, R.E., Junghanns, K.T., Matern, U., 1999. Expression of bifunctional caffeoyl-CoA 3-*O*-methyltranferase in stress compensation and lignification. Plant Biology 1, 299–310.

Guo, D., Chen, F., Inoue, K., Dixon, R.A., 2001. Down-regulation of caffeic acid 3-O-methyltransferase and caffeoyl CoA 3-O-methyltransferase in transgenic alfalfa: impacts on lignin structure and implications for the biosynthesis of G and S lignin. Plant Cell 13, 73–88.

Hauffe, K.D., Lee, S.P., Subramaniam, R., Douglas, C.J., 1993. Combinatorial interactions between positive and negative *cis*-acting elements control spatial patterns of *4CL-1* expression in transgenic tobacco. The Plant Journal 4, 235–254.

Hauffe, K.D., Paszkowski, U., Schulze-Lefert, P., Hahlbrock, K., Dangl, J.L., Douglas, C.J., 1991. A parsley 4CL-1 promoter fragment specifies complex expression patterns in transgenic tobacco. Plant Cell 3, 435–443.

Halpin, C., Knight, M.E., Foxon, G.A., Campbell, M.M., Boudet, A.M., Boon, J.A., Chabbert, B., Tollier, M.-T., Schuch, W., 1994. Manipulation of lignin quality by down-regulation of cinnamyl alcohol dehydrogenase. The Plant Journal 6, 339–350.

Hawkins, S.W., Boudet, A.M., 1994. Purification and characterization of cinnamyl alcohol dehydrogenase isoforms from the periderm of *Eucalyptus gunnii* Hook. Plant Physiology 104, 75–84.

He, L., Terashima, N., 1991. Formation and structure of lignin in monocotyledons IV. Deposition process and structural diversity of the lignin in the cell walls of sugarcane and rice plant studied by ultraviolet microscopic spectroscopy. Holzforschung 45, 191–198.

Hibino, T., Yakabe, K., Kawazu, T., Shibata, D., Higuchi, T., 1995. Increase of cinnamaldehyde groups in lignin of transgenic tobacco plants carrying an antisense gene for cinnamyl alcohol dehydrogenase. Bioscience, Biotechnology and Biochemistry 59, 929–931.

Hrazdina, G., Jensen, R.A., 1992. Spatial organization of enzymes in plant metabolic pathways. Annual Review of Plant Physiology and Plant Molecular Biology 43, 241–267.

Hrazdina, G., Wagner, G.J., 1985. Metabolic pathways as enzyme complexes: evidence for the synthesis of phenylpropanoids and flavonoids on membrane associated enzyme complexes. Archives of Biochemistry and Biophysics 237, 88–100.

Hrazdina, G., Zobel, A.M., Hoch, H.C., 1987. Biochemical, immunological, and immunocytochemical evidence for the association of chalcone synthase with endoplasmic reticulum membranes. Proceedings of the National Academy of Sciences USA 84, 8966–8970.

Hu, W.-J., Harding, S.A., Lung, J., Popko, J.L., Ralph, J., Stokke, D.D., Tsai, C.-J., Chiang, V.L., 1999. Repression of lignin biosynthesis promotes cellulose accumulation and growth of transgenic trees. Nature Biotechnology 17, 808–812.

Humphreys, J.M., Hemm, M.R., Chapple, C., 1999. New routes for lignin biosynthesis defined by biochemical characterization of recombinant ferulate 5-hydroxylase, a multifunctional cytochrome P450-dependent monooxygenase. Proceedings of the National Academy of Sciences USA 96, 10045–10050.

Ibrahim, R.K., Bruneau, A., Bantignies, B., 1998. Plant *O*-methyltransferases: molecular analysis, common signature and classification. Plant Molecular Biology 36, 1–10.

Inoue, K., Parvathi, K., Dixon, R.A., 2000. Substrate preferences of caffeic acid/5-hydroxyferulic acid 3-*O*-methyltransferases in developing stems of alfalfa (*Medicago sativa* L.). Archives of Biochemistry and Biophysics 375, 175–182.

Inoue, K., Sewalt, V.J.H., Ballance, G.M., Ni, W., Stürzer, C., Dixon, R.A., 1998. Developmental expression and substrate specificities of alfalfa caffeic acid 3-*O*-methyltransferase and caffeoyl CoA 3-*O*-methyltransferase in relation to lignification. Plant Physiology 117, 761–770.

Jorrin, J., Dixon, R.A., 1990. Stress responses in alfalfa (*Medicago sativa* L.). II Purification, characterization and induction of phenylalanine ammonia-lyase isoforms from elicitor treated cell suspension cultures. Plant Physiology 92, 447–455.

Joshi, C.P., Chiang, V.L., 1998. Conserved sequence motifs in plant *S*-adenosyl-L-methionine-dependent methyltransferases. Plant Molecular Biology 37, 663–674.

Jung, H.G., Mertens, D.R., Payne, A.J., 1997. Correlation of acid detergent lignin and Klason lignin with digestibility of forage dry matter and neutral detergent fiber. Journal of Diary Science 80, 1622–1628.

Jung, H.G., Sheaffer, C.C., Barnes, D.K., Halgerson, J.L., 1997. Forage quality variation in the US alfalfa core collection. Crop Science 37, 1361–1366.

Kajita, S., Hishiyama, S., Tomimura, Y., Katayama, Y., Omori, S., 1997. Structural characterization of modified lignin in transgenic tobacco plants in which the activity of 4-coumarate: coenzyme A ligase is depressed. Plant Physiology 114, 871–879.

Kajita, S., Katayama, Y., Omori, S., 1996. Alterations in the biosynthesis of lignin in transgenic plants with chimeric genes for 4-coumarate: coenzyme A ligase. Plant and Cell Physiology 37, 957–965.

Kersey, R., Inoue, K., Schubert, K.R., Dixon, R.A., 1999. Immunolocalization of two lignin *O*-methyltransferases in stems of alfalfa (*Medicago sativa* L.). Protoplasma 209, 46–57.

Kneusel, R.E., Matern, U., Nicolay, K., 1989. Formation of *trans*-caffeoyl-CoA from *trans*-4-coumaroyl-CoA by Zn^{2+}-dependent enzymes in cultured plant cells and its activation by an elicitor-induced pH shift. Archives of Biochemistry and Biophysics 269, 455–462.

Kojima, M., Takeuchi, W., 1989. Detection and characterization of *p*-coumaric acid hydroxylase in mung bean, *Vigna mungo*, seedlings. Journal of Biochemistry 105, 265–270.

Kuhnl, T., Koch, U., Heller, W., Wellmann, E., 1987. Chlorogenic acid biosynthesis: characterization of a light-induced microsomal 5-*O*-(4-Coumaroyl)-D-quinate/shikimate 3′-hydroxylase from carrot (*Daucus carota* L.) cell suspension cultures. Archives of Biochemistry and Biophysics 258, 226–232.

Lam, T.B.T., Iiyama, K., Stone, B.A., 1990. Lignin in wheat internodes. Part 2: Alkaline nitrobenzene oxidation by wheat straw lignin and its fractions. Journal of the Science of Food and Agriculture 51, 493–506.

Lam, T.B.T., IIyama, K., Stone, B.A., 1996. Caffeic acid: *O*-methyltransferases and the biosynthesis of ferulic acid in primary cell walls of wheat seedlings. Phytochemistry 41, 1507–1510.

Lapierre, C., Pollet, B., PetitConil, M., Toval, G., Romero, J., Pilate, G., Leple, J.C., Boerjan, W., Ferret, V., DeNadai, V., Jouanin, L., 1999. Structural alterations of lignins in transgenic poplars with depressed cinnamyl alcohol dehydrogenase or caffeic acid *O*-methyltransferase activity have an opposite impact on the efficiency of industrial kraft pulping. Plant Physiology 119, 153–163.

Lee, D., Douglas, C.J., 1996. Two divergent members of a tobacco 4-coumarate: coenzyme A ligase (4CL) gene family. Plant Physiology 112, 193–2205.

Lee, D., Ellard, M., Wanner, L.A., Davis, K.R., Douglas, C.J., 1995. The *Arabidopsis thaliana* 4-coumarate: CoA ligase (*4CL*) gene: stress

and developmentally regulated expression and nucleotide sequence of its cDNA. Plant Molecular Biology 28, 871–884.

Lee, D., Meyer, K., Chapple, C., Douglas, C.J., 1997. Antisense suppression of 4-coumarate: coenzyme A ligase activity in Arabidopsis leads to altered lignin subunit composition. Plant Cell 9, 1985–1998.

Li, L., Osakabe, Y., Chandrashekhar, P.J., Chiang, V.L., 1999. Secondary xylem-specific expression of caffeoyl-coenzyme A 3-*O*-methyltransferase plays an important role in the methylation pathway associated with lignin biosynthesis in loblolly pine. Plant Molecular Biology 40, 555–565.

Li, L., Popko, J.L., Umezawa, T., Chiang, V.L, 2000. 5-Hydroxyconiferyl aldehyde modulates enzymatic methylation for syringyl monolignol formation, a new view of monolignol biosynthesis in angiosperms. Journal of Biological Chemistry 275, 6537–6545.

Li, L., Popko, J.L., Zhang, X.-H., Osakabe, K., Tsai, C.-J., Joshi, C.P., Chiang, V.L., 1997. A novel multifunctional *O*-methyltransferase implicated in a dual methylation pathway associated with lignin biosynthesis in loblolly pine. Proceedings of the National Academy of Science, USA 94, 5461–5466.

Liang, X., Dron, M., Schmid, J., Dixon, R.A., Lamb, C.J., 1989. Developmental and environmental regulation of a phenylalanine ammonia-lyase β-glucuronidase gene fusion in transgenic tobacco plants. Proceedings of the National Academy of Sciences, USA 86, 9284–9288.

Luderitz, T., Grisebach, H., 1981. Enzymic synthesis of lignin precursors. Comparison of cinnamoyl-CoA reductase and cinnamoyl alcohol: NADP+ dehydrogenase from spruce (*Picea abies* L.) and soybean (*Glycine max* L.). European Journal of Biochemistry 119, 115–124.

MacKay, J.J., O'Malley, D.M., Presnell, T., Booker, F.L., Campbell, M.M., Whetten, R.W., Sederoff, R.R., 1997. Inheritance, gene expression, and lignin characterization in a mutant deficient in cinnamyl alcohol dehydrogenase. Proceedings of the National Academy of Sciences USA 94, 8255–8260.

Marita, J.M., Ralph, J., Hatfield, R.D., Chapple, C., 1999. NMR characterization of lignins in Arabidopsis altered in the activity of ferulate 5-hydroxylase. Proceedings of the National Academy of Sciences USA 96, 12382–12332.

Martz, F., Maury, S., Picon, G., Legrand, M., 1998. cDNA cloning, substrate specificity and expression study of tobacco caffeoyl-CoA 3-*O*-methyltransferase, a lignin biosynthetic enzyme. Plant Molecular Biology 36, 427–437.

Matsui, N., Chen, F., Yasuda, S., Fukushima, K., 2000. Conversion of guaiacyl to syringyl moieties on the cinnamyl alcohol pathway during the biosynthesis of lignin in angiosperms. Planta 210, 831–835.

Matsui, N., Fukushima, K., Yasuda, S., Terashima, N., 1994. On the behavior of monolignol glucosides in lignin biosynthesis. Holzforschung 48, 375–380.

Maury, S., Geoffroy, P., Legrand, M., 1999. Tobacco *O*-methyltransferases involved in phenylpropanoid metabolism. The different caffeoyl-coenzyme A/5-hydroxyferuloyl-coenzyme A 3/5-*O*-methyltransferase and caffeic acid/5-hydroxyferulic acid 3/5-*O*-methyltransferase classes have distinct substrate specificities and expression patterns. Plant Physiology 121, 215–223.

Meng, H., Campbell, W.H., 1996. Characterization and site-directed mutagenesis of aspen lignin-specific *O*-methyltransferase expressed in *Escherichia coli*. Archives of Biochemistry and Biophysics 330, 329–341.

Meyer, K., Cusumano, J.C., Somerville, C., Chapple, C.C.S., 1996. Ferulate-5-hydroxylase from Arabidopsis thaliana defines a new family of cytochrome P450-dependent monooxygenases. Proceedings of the National Academy of Sciences USA 93, 6869–6874.

Meyer, K., Shirley, A.M., Cusumano, J.C., Bell-Lelong, D.A., Chapple, C., 1998. Lignin monomer composition is determined by the expression of a cytochrome P450-dependent monooxygenase in Arabidopsis. Proceedings of the National Academy of Sciences USA 95, 6619–6623.

Neish, A.C., 1968 In: Freudenberg, K. Neish, A. C. (Eds.), Constitution and Biosynthesis of Lignin. Springer-Verlag, Berlin, pp. 2–43.

Ni, W., Paiva, N.L., Dixon, R.A., 1994. Reduced lignin in transgenic plants containing an engineered caffeic acid *O*-methyltransferase antisense gene. Transgenic Research 3, 120–126.

O'Connell, A., Bolwell, P., Schuch, W., 1998 In: Lindsey, K., (Ed.), Transgenic Plant Research. Harwood Academic, Chur/Switzerland, pp. 175–186.

O'Malley, D.M., Porter, S., Sederoff, R.R., 1992. Purification, characterization, and cloning of cinnamyl alcohol dehydrogenase in loblolly pine (*Pinus taeda* L.). Plant Physiology 98, 1364–1371.

Osakabe, K., Tsao, C.C., Li, L., Popko, J.L., Umezawa, T., Carraway, D.T., Smeltzer, R.H., Joshi, C.P., Chiang, V.L., 1999. Coniferyl aldehyde 5-hydroxylation and methylation direct syringyl lignin biosynthesis in angiosperms. Proceedings of the National Academy of Sciences USA 96, 8955–8960.

Pakusch, A.E., Matern, U., 1991. Kinetic characterization of caffeoyl-coenzyme A-specific 3-*O*-methyltransferase from elicited parsley cell suspension. Plant Physiology 96, 327–330.

Parvathi, K., Chen, F., Guo, D., Blount, J.W., Dixon, R.A., 2001. Substrate preferences of O-methyltransferases in alfalfa suggest new pathways for 3-O-methylation of monolignols. Plant Journal 25, 193–202.

Pierrel, M.A., Batard, Y., Kazmaier, M., Mignotte-Vieux, C., Durst, F., Werck-Reichhart, D., 1994. Catalytic properties of the plant cytochrome P450 CYP73 expressed in yeast. European Journal of Biochemistry 224, 835–844.

Pillonel, C., Mulder, M.M., Boon, J.J., Forster, B., Binder, A., 1991. Involvement of cinnamyl-alcohol dehydrogenase in the control of lignin formation in *Sorghum bicolor* L. Moench. Planta 185, 538–544.

Piquemal, J., Lapierre, C., Myton, K., O'Connell, A., Schuch, W., Grima-Pettenati, J., Boudet, A.-M., 1998. Down-regulation of cinnamoyl-CoA reductase induces significant changes of lignin profiles in transgenic tobacco plants. The Plant Journal 13, 71–83.

Ralph, J., MacKay, J.J., Hatfield, R.D., O'Malley, D.M., Whetten, R.W., Sederoff, R.R., 1997. Abnormal lignin in a loblolly pine mutant. Science 277, 235–239.

Rasmussen, S., Dixon, R.A., 1999. Transgene-mediated and elicitor-induced perturbation of metabolic channeling at the entry point into the phenylpropanoid pathway. Plant Cell 11, 1537–1551.

Rubery, P.H., Northcote, D.H., 1968. Site of phenylalanine ammonia-lyase activity and synthesis of lignin during xylem differentiation. Nature 219, 1230–1234.

Sarni, R., Grand, C., Boudet, A.M., 1984. Purification and properties of cinnamoyl-CoA reductase and cinnamyl alcohol dehydrogenase from poplar stems (*Populus* X *euramericana*). European Journal of Biochemistry 139, 259–265.

Sewalt, V.J.H., Glasser, W.G., Fontenot, J.P., Allen, V.G., 1996. Lignin impact on fiber degradation. 1. Quinone methide intermediates formed from lignin during *in vitro* fermentation of corn stover. Journal of the Science of Food and Agriculture 71, 195–203.

Sewalt, V.J.H., Ni, W., Blount, J.W., Jung, H.G., Howles, P.A., Masoud, S.A., Lamb, C., Dixon, R.A., 1997. Reduced lignin content and altered lignin composition in transgenic tobacco down-regulated in expression of phenylalanine ammonia-lyase or cinnamate 4-hydroxylase. Plant Physiology 115, 41–50.

Sewalt, V.J.H., Ni, W., Jung, H., Dixon, R.A., 1997. Lignin impact on fiber degradation: Increased enzymatic digestibility of genetically engineered tobacco (*Nicotiana tabacum*) stems reduced in lignin content. Journal of Agricultural and Food Chemistry 45, 1977–1983.

Shufflebottom, D., Edwards, K., Schuch, W., Bevan, M., 1993. Transcription of two members of a gene family encoding phenylalanine ammonia-lyase leads to remarkably different cell specificities and induction patterns. The Plant Journal 3, 835–845.

Smith, C.G., Rodgers, M.W., Zimmerlin, A., Ferdinando, D., Bolwell,

G.P., 1994. Tissue and subcellular immunolocalisation of enzymes of lignin synthesis in differentiating and wounded hypocotyl tissue of French bean (*Phaseolus vulgaris* L.). Planta 192, 155–164.

Stewart, D., Yahiaoui, N., McDougall, G.J., Myton, K., Marque, C., Boudet, A.M., Haigh, J., 1997. Fourier-transform infrared and Raman spectroscopic evidence for the incorporation of cinnamaldehydes into the lignin of transgenic tobacco (*Nicotiana tabacum* L.) plants with reduced expression of cinnamyl alcohol dehydrogenase. Planta 201, 311–318.

Srere, P.A., 1987. Complexes of sequential metabolic enzymes. Annual Review of Biochemistry 56, 89–124.

Strack, D., Bokern, M., 1984. Metabolic activity of hydroxycinnamic acid glucose esters in cell suspension cultures of *Chenopodium rubrum*. Zeitschrift fur Naturforschung 39C, 902–907.

Tanaka, M., Kojima, M., 1991. Purification and characterization of *p*-coumaroyl-D-glucose hydroxylase of sweet potato (*Ipomoea batatas*) roots. Archives of Biochemistry and Biophysics 284, 151–157.

Terashima, N., Fukushima, K., He, L.-F., Takabe, K., 1993 In: Jung, H.G., Buxton, D.R., Hatfield, R.D., Ralph, J. (Eds.), Forage Cell Wall Structure and Digestibility, ASA-CSSA-SSSA, Madison, pp. 247–270.

Terashima, N., Fukushima, K., Tsuchiya, S., 1986. Heterogeneity in formation of lignin. VII. An autoradiographic study on the formation of guaiacyl and syringyl lignin in poplar. Journal of Wood Chemistry and Technology 6, 495–504.

Tsai, C.J., Popko, J.L., Mielke, M.R., Hu, W.J., Podila, G.K., Chiang, V.L., 1998. Suppression of *O*-methyltransferase gene by homologous sense transgene in quaking aspen causes red-brown wood phenotypes. Plant Physiology 117, 101–112.

Urban, P., Werck-Reichhart, D., Teutsch, H.G., Durst, F., Regnier, S., Kazmaier, M., Pompon, D., 1994. Characterization of recombinant plant cinnamate 4-hydroxylase produced in yeast. European Journal of Biochemistry 222, 843–850.

Van Doorsselaere, J., Baucher, M., Chognot, E., Chabbert, B., Tollier, M.-T., Petit-Conil, M., Leplé, J.-C., Pilate, G., Cornu, D., Monties, B., Van Montagu, M., Inzé, D., Boerjan, W., Jouanin, L., 1995. A novel lignin in poplar trees with a reduced caffeic acid/5-hydroxyferulic acid O-methyltransferase activity. The Plant Journal 8, 855–864.

Vignols, F., Rigau, J., Torres, M.A., Capellades, M., Puigdoménech, P., 1995. The *brown midrib3 (bm3)* mutation in maize occurs in the gene encoding caffeic acid *O*-methyltransferase. Plant Cell 7, 407–416.

Voo, K.S., Whetten, R.W., O'Malley, D.M., Sederoff, R.R., 1995. 4-coumarate: coenzyme A ligase from loblolly pine xylem- Isolation, characterization, and complementary DNA cloning. Plant Physiology 108, 85–97.

Wang, Z.X., Li, S.M., Löscher, R., Heide, L., 1997. 4-Coumaroyl coenzyme A 3-hydroxylase activity from cell cultures of *Lithospermum erythrorhizon* and its relationship to polyphenol oxidase. Archives of Biochemistry and Biophysics 347, 249–255.

Wang, J., Pichersky, E., 1999. Identification of specific residues involved in substrate discrimination in two plant *O*-methyltransferases. Archives of Biochemistry and Biophysics 368, 172–180.

Whetten, R., Sederoff, R., 1991. Genetic engineering of wood. Forest Ecology and Management 43, 301–316.

Winkel-Shirley, B., 1999. Evidence for enzyme complexes in the phenylpropanoid and flavonoid pathways. Physiologia Plantarum 107, 142–149.

Yahiaoui, N., Marque, C., Myton, K.E., Negrel, J., Boudet, A.M., 1998. Impact of different levels of cinnamyl alcohol dehydrogenase down-regulation on lignins of transgenic tobacco plants. Planta 204, 8–15.

Ye, Z.H., Kneusel, R.E., Matern, U., Varner, J.E., 1994. An alternative methylation pathway in lignin biosynthesis in *Zinnia*. Plant Cell 6, 1427–1439.

Ye, Z., Varner, J.E., 1995. Differential expression of two *O*-methyltransferases in lignin biosynthesis in *Zinnia elegans*. Plant Physiology 108, 459–467.

Zhong, R., Morrison, I.W.H., Negrel, J., Ye, Z.H., 1998. Dual methylation pathways in lignin biosynthesis. Plant Cell 10, 2033–2045.

PERGAMON

Phytochemistry 57 (2001) 1085–1093

PHYTOCHEMISTRY

www.elsevier.com/locate/phytochem

Coniferyl alcohol metabolism in conifers — I. Glucosidic turnover of cinnamyl aldehydes by UDPG: coniferyl alcohol glucosyltransferase from pine cambium

Valerie Steeves[a], Hartmut Förster[b,1], Ulrich Pommer[b], Rodney Savidge[a,*]

[a]*Faculty of Forestry and Environmental Management, University of New Brunswick, Fredericton, NB, E3B 6C2, Canada*
[b]*FSU Jena, Institut für Allgemeine Botanik, Bereich Pflanzenbiochemie, Kühnhäuser Str. 101, 99189 Erfurt-Kühnhäusen, Germany*

Received 25 July 2000; received in revised form 1 November 2000

Abstract

UDPG: coniferyl alcohol glucosyltransferase (CAGT; EC 2.4.1.111) isolated from cambial tissues of *Pinus strobus* was able to convert cinnamyl aldehydes as well as dihydroconiferyl alcohol into their corresponding 4-*O*-β-D-glucosides in vitro. Cinnamyl aldehydes were glucosylated with comparable efficiency to coniferyl alcohol, the physiological substrate for CAGT. Seasonal patterns of CAGT activity for aldehydes were similar to those of coniferyl alcohol. Formation of cinnamyl aldehyde and additional monolignol glucosides indicates that precursor flux and availability for lignification is likely greater than previously recognized.
© 2001 Elsevier Science Ltd. All rights reserved.

Keywords: *Pinus strobus*; Coniferophyta; Pinaceae; Eastern white pine; Cinnamyl aldehyde; Cinnamyl alcohol; Dihydroconiferyl alcohol; Glucoside; Glucosyltransferase; Seasonal cambial growth

1. Introduction

The 4-*O*-β-D-glucopyranosides of *trans*-cinnamyl alcohols, i.e. *E*-coniferin and *E*-syringin, frequently accumulate in the cambial region of woody plants, and they have long been considered as participants in lignification, conceivably as either storage reserves (see, for example, Terazawa and Miyake, 1984) or transported forms of monolignols (Freudenberg and Torres-Serres, 1967). While coniferin is known to accumulate in conifer cambial tissues (earlier examples include: Freudenberg and Harkin, 1963; Marcinowski and Grisebach, 1977; Schmid and Grisebach, 1982; Terazawa and Miyake, 1984; Terazawa et al., 1984a,b; Savidge, 1988, 1989, 1991), it has also been isolated from cambial tissues of various angiosperms (Terazawa et al., 1984a,b), needles of Douglas fir (Morris and Morris, 1990) and Norway spruce (Slimestad and Hostettmann, 1996), cell suspensions of *Linum flavum* (van Uden et al., 1990), *Paulownia tomentosa* bark (Sticher and Lahloub, 1982), flue-cured tobacco leaves (Ito et al., 2000), *Daphne oleides* stems (Ullah et al., 1999) and leaves and stems of *Viscum album* ssp. (Deliorman et al., 1999). However, its accumulation evidently is greatest in conifers, such as *Pinus banksiana* (Leinhos and Savidge, 1993; Leinhos et al., 1994; Förster and Savidge, 1995), *Larix laricina* (Savidge, 1991) and *Picea abies* (Schmid and Grisebach, 1982), where the contents of endogenous coniferin were reported to be as high as 10 mmol/g_{fw}. In isolated cambial protoplasts the concentration of coniferin reached 1.6 mM and accounted fully for the content found in tissue extracts (Leinhos and Savidge, 1993; Leinhos et al., 1994), indicating that very little if any was present in walls of the primary-walled radially expanded cambial derivatives from which the protoplasts were obtained.

In springtime, the cinnamyl alcohol glucosides accumulate in cambial derivatives of conifers in the complete absence of lignification (Savidge, 1988, 1989, 1991; Förster and Savidge, 1995; Fukushima et al., 1997; Rowland and Arora, 1997; Savidge et al., 1998); however, there is ample evidence that once lignification is

* Corresponding author. Tel.: +1-506-453-4919; fax: +1-506-453-3538.
E-mail address: savidge@unb.ca (R. Savidge).
[1] Joint first author

0031-9422/01/$ - see front matter © 2001 Elsevier Science Ltd. All rights reserved.
PII: S0031-9422(01)00107-8

underway they can contribute to that process (Förster et al., 1999, 2000), as earlier surmised by Freudenberg and Harkin (1963). In order for coniferin to accumulate to high levels, it must either be compartmentally shielded or produced many times more rapidly than it turns over (Marcinowski and Grisebach (1977) report a half-life of 60–120 h for coniferin) or is utilised in support of lignification. Freudenberg (1964) reported that when the coniferyl alcohol moiety of coniferin was radiolabelled, the radioactivity was readily incorporated into spruce lignin. The incorporation of isotopically labelled monolignol glucosides into lignin has been further investigated in autoradiographic studies by Terashima et al. (1986, 1993, 1995, 1997), Terashima and Fukushima (1988) and Eglinton et al. (2000). Monolignol glucosides enriched with carbon-13 at specific side chain carbons were administered to growing tree stems resulting in newly formed lignin shown to be carbon-13 enriched at the side chain carbons corresponding to those of the glucosides (Terashima et al., 1995; Xie and Terashima, 1991; Xie et al., 1994).

In agreement with the concept that the activity of coniferin-hydrolysing β-glucosidase may influence the rate of lignification (Grima-Pettenati and Goffner, 1999), a β-glucosidase specific to coniferin and of much lower abundance and/or activity than numerous other β-glucosidases of wood and cambial tissues was isolated, primarily on the basis of its unique ability to hydrolyse authentic coniferin to *E*-coniferyl alcohol, as confirmed by GC/MS (Leinhos et al., 1994). It remains unclear whether that coniferin-specific β-glucosidase is identical to the enzyme investigated by Dharmawardhana et al. (1995, 1999), the N-terminal sequences of the two being notably distinct although both evidently have similar p*I* values, or to the enzyme isolated from inner secondary cell walls in young spruce seedlings by Marcinowski et al. (1979), or that localized to xylem epi-, endo- and exodermis in stems and roots of chick pea seedlings by Burmeister and Hösel (1981). A problem may exist, however, in using antibodies for localisation; supposedly specific antibodies have been repeatedly observed to bind non-specifically with lignified secondary cell walls (R.A. Savidge, unpublished data).

Coniferin has been found present in the cambial zone and its derivatives throughout the period of cambial growth, but it becomes undetectable at the onset of cambial dormancy in autumn, before the last cambial derivatives have completed their maturation into latewood (Savidge, 1988, 1989, 1991; Förster and Savidge, 1995; Savidge et al., 1998). Coniferin has never been detected in stems during cambial dormancy (Freudenberg and Harkin, 1963; Terazawa and Miyake, 1984; Savidge, 1988, 1989, 1991; Förster and Savidge, 1995; Savidge et al., 1998). Quantitative investigations of endogenous indol-3-ylacetic acid, sucrose and coniferin in *Larix laricina* cambium revealed that, of the three, only coniferin content varied parallel to seasonal cambial activity (Savidge, 1991), and biochemical investigations revealed that the presence or absence of UDPG: coniferyl alcohol glucosyltransferase (CAGT; EC 2.4.1.111) activity is the explanation for the qualitative seasonal variation of coniferin, indicating that seasonal variation in coniferin has its explanation in seasonal change in gene expression (Förster and Savidge, 1995; Savidge and Förster, 1998; Förster et al., 2000).

Ibrahim and Grisebach (1976) were first to report purification and characterization of a CAGT, isolated from suspensions of Paul's scarlet rose. The enzyme catalysed the transfer of glucose from UDPG to coniferyl alcohol and had the highest substrate specificity reported to date for a CAGT ($K_m = 3.3\times10^{-9}$ M for coniferyl alcohol; $K_m = 2\times10^{-5}$ M for UDPG). In 1977, Ibrahim confirmed the substrate specificity using CAGT isolated from young lignifying stems of *Forsythia ovata*, demonstrating it to be distinct from other glucosyltransferases, which are capable of nonspecifically glucosylating hydroxy phenols, flavonols, anthocyanidins and phenolic acids.

Schmid and Grisebach (1982) purified and characterized CAGT from *Picea abies*, and found coniferin to inhibit CAGT in a noncompetitive manner, with product inhibition starting at approximately 10 mmol/g. Schmid et al. (1982) also immunolocalized CAGT to the epidermis, subepidermis and vascular bundles of young *P. abies* seedlings. Intracellularly, it was located in the parietal cytoplasmic layer, indicating that CAGT is a soluble enzyme of the cytoplasm, in agreement with Ibrahim (1977). Förster and Savidge (1995) reported that coniferin below 10 mmol/g_{tissue} showed no inhibitory effect on activity of CAGT of *Pinus banksiana*, but it did inhibit CAGT above 10 mmol/g. The catalytic activity of the coniferin-specific β-glucosidase isolated from lignifying tissues was not found to reside in CAGT obtained from the same tissues, at the same developmental stage (Savidge and Förster, 1998). Recently, Förster et al. (1999, 2000) confirmed the pronounced specificity of CAGT for UDPG; however, they unexpectedly found that CAGT from *P. strobus* also expressed high activity when UDP-galactose was supplied to the enzyme.

E-Coniferaldehyde has been detected in the cambial sap of conifers (Freudenberg and Neish, 1968), bamboo (Tanaka et al., 1998) and oak (Fernààndez de Simòn et al., 1996). Despite the generally low endogenous coniferylaldehyde levels in plants and the efficient reduction of cinnamyl aldehydes to cinnamyl alcohols, coniferyl aldehyde glucosides have nevertheless been isolated from bark of *Syringa velutina* (Park et al., 1999) and *Kolopanax pictus* (Sano et al., 1991).

Cinnamyl aldehydes have also been reported as suitable substrates for CAGT (Ibrahim and Grisebach, 1976; Schmid and Grisebach, 1982; Förster et al., 1999, 2000). Preliminary investigations indicated that CAGT

catalysed the conversion of cinnamyl aldehydes to their corresponding 4-*O*-β-D-glucosides in vitro (Förster et al., 1999, 2000). CAGT from *Pinus strobus* appeared to produce higher amounts of cinnamyl aldehyde glucosides than monolignol glucosides; however, the specific turnover rate (i.e. ratio between administered substrate and obtained product) was approximately 8 times lower (Förster et al., 2000). In seasonal investigations of CAGT activity, Förster et al. (2000) presented evidence for in vitro generation of coniferyl aldehyde glucoside to parallel similar seasonal patterns to that observed for coniferin. In the present study, we confirm, for the first time, by proton NMR spectroscopy, the enzymatic glucosidic turnover of cinnamyl aldehydes catalysed by CAGT isolated from pine cambial tissue. Seasonal patterns of CAGT activity for monolignols and cinnamyl aldehydes are provided and their K_m values reported for the first time. This is the first report of in vitro biosynthesis of dihydroconiferyl alcohol glucoside.

2. Results and discussion

Molecular structures of the predicted enzymatic products were confirmed by ^{1}H NMR spectroscopic analyses. Two-dimensional COSY and HMQC NMR spectra were obtained to aid in structure elucidation. For both semi-preparative and analytical HPLC, an assay was developed to effectively separate the cofactor uridine 5′-diphosophoglucose (UDPG), the monolignol substrates and the corresponding product glucosides, allowing exact quantitation of the catalysed reaction. Based on this assay, enzymatic products were separated using semi-preparative HPLC techniques, collected and lyophilized, resulting in mg quantities of the desired compounds.

The monolignol-specific UDPG was extracted and partially purified (Savidge and Förster, 1998) from approximately 400 g of differentiating xylem from *Pinus strobus* harvested in late May. IEF and native PAGE indicated purification to homogeneity, however, SDS–PAGE and N-terminal sequencing of the resulting major band revealed the presence of two proteins, one without any evident homology to known proteins and the other yielding perfect homology to the internal sequence of a glucosyltransferase precursor. Because of the almost identical physico-chemical features (p*I* 5.0 and molecular weight 43 kDa) of both proteins, complete purification could not yet be achieved (Förster et al., 2000).

All substrates tested in the assay were successfully converted to their 4-*O*-β-D-glucosides, as evidenced by the chemical shifts of the glucosyl moieties (not reported) in the ^{1}H NMR spectra. The glucosyl moiety did not bond to the alcoholic hydroxyl group of the phenylpropane side chain of the monolignol substrates (i.e. as in *iso*-coniferin), which is in agreement with Schmid and Grisebach's (1982) findings for *Picea abies*. Although Ibrahim (1977) obtained small amounts of *iso*-coniferin (i.e. *trans*-coniferyl alcohol-1-*O*-β-D-glucoside) from *Forsythia ovata*, this isomer of coniferin to our knowledge has not yet been reported in conifers.

^{1}H NMR data for the enzymatic products, along with that of coniferyl alcohol, are presented in Table 1, while corresponding molecular structures are found in Fig. 1. Carbon 9 (Table 1) refers to either the primary alcoholic carbon atom (i.e. as in coniferin (**1**), syringin (**2**), dihydroconiferyl alcohol glucoside (**5**) and coniferyl alcohol) or the aldehydic carbon atom (i.e. as in coniferyl aldehyde glucoside (**3**) and sinapyl aldehyde glucoside (**4**)). As evidenced by large coupling constants for the 7-H/8-H of the double bond (i.e. $J = 15.8$, 15.8, 16.6 and 14.8 Hz for **1–4**, respectively), products **1–4** maintained a *trans* orientation. Chemical shifts for glucosyl hydrogens are not reported, but were observed ranging from $\delta = 3.1$–3.8 ppm.

Chemical shifts of 9.61 and 9.63 ppm, corresponding to the aldehyde hydrogens for **3** and **4**, respectively, clearly demonstrate that the glucosyl moiety must have attached at the 4′-position of the aromatic ring, as opposed to the primary alcohol of the phenylpropane side chain.

When comparing the ^{1}H NMR spectra of coniferin and coniferyl alcohol, a larger up-field shift (i.e. up to 0.38 ppm) is observed for the aromatic hydrogens compared to the aliphatic ones. This suggests the glucose attached to the phenol oxygen, and not that of the primary alcohol. Since the structures and chemical shifts for **2** and **5** are similar to **1**, the same conclusions were obtained.

As previously mentioned, *E*-coniferin formation has been reported in various plants throughout the plant kingdom; however, by way of contrast, American beech exceptionally accumulates *cis*-monolignols. Yamamoto et al. (1990) reported a glucosyltransferase in bark of *Fagus grandifolia*, which showed an unusual preference for *Z*-coniferyl alcohol catalysing the formation of *Z*-coniferin. The glucosyltransferase isolated from cambial tissues of *Pinus strobus* did not accept *cis*-coniferyl alcohol and a mixture of *cis* and *trans* substrates always resulted in formation of *E*-coniferin, as evidenced by HPLC separation (results not shown). Plausibly, the maintenance of a *trans* orientation during catalysis is an essential requirement for converting suitable substrates to 4-*O*-β-D-glucosides in the cambium of *Pinus strobus*.

The catalytic activity of UDPG: CAGT in the formation of monolignol glucosides increased more than 3-fold in early June compared to CAGT isolated in mid-May (Fig. 2). The data agree with results obtained from cambial tissue of *Pinus banksiana* (Savidge and Förster, 1998); however, considerable differences in CAGT activity observed between cambium and developing xylem of *Pinus banksiana* did not appear in corresponding tissues of *Pinus strobus* (data not shown). Seasonal fluctuations in CAGT activity and levels of monolignol

Table 1
^{1}H NMR spectral data for the monolignol glucosides and coniferyl alcohol

	δ ^{1}H (ppm) [int, mult, *J* (Hz)]					
C	Coniferyl aldehyde glucoside	Sinapyl aldehyde glucoside	Dihydroconiferyl alcohol glucoside	Coniferin	Coniferyl alcohol	Syringin
2′	7.32 [1H, *d*, 1.6]	7.03 [1 of 2H, *s*]	6.86 [1H,*d*, 2.2]	7.06 [1H, *d*, 1.9]	7.00 [1H, *d*, 1.9]	6.74 [1 of 2H, *s*]
5′	7.21 [1H, *d*, 8.3]	–[a]	7.07 [1H, *d*, 8.2]	7.10 [1H, *d*, 8.3]	6.72 [1H, *d*, 8.0]	–[a]
6′	7.25 [1H, *d*, 8.3]	7.03 [1 of 2H, *s*]	6.74 [1H, *dd*, 8.2, 2.1]	6.94 [1H, *dd*, 8.3, 1.9]	6.84 [1H, *dd*, 8.1, 1.6]	6.74 [1 of 2H, *s*]
7	7.61 [1H, *d*, 16.0]	7.61 [1H, *d*, 16.0]	2.63 [2H, *t*, 7.6]	6.54 [1H, *br d*, 15.8]	6.50 [1H, *br d*, 15.9]	6.54 [1H, *br d*, 15.9]
8	6.71 [1H, *dd*, 16.6, 7.7]	6.78 [1H, *dd*, 14.8, 7.0]	1.82 [2H, *tt*, 7.7, 6.3]	6.27 [1H, *dt*, 15.8, 5.6]	6.19 [1H, *dt*, 15.6, 5.9]	6.32 [1H, *dt*, 15.8, 5.6]
9	9.61 [1H, *d*, 8.0]	9.63 [1H, *d*, 7.7]	3.55 [2H, *t*, 6.5]	4.20 [2H, *dd*, 5.8, 1.4]	4.19 [2H, *dd*, 6.0, 1.1]	4.21 [2H, *dd*, 5.6, 1.0]
OCH_3	3.91 [3H, *s*]	3.86 [6H, *s*]	3.85 [3H, *s*]	3.87 [3H, *s*]	3.85 [3H, *s*]	3.85 [6H, *s*]

[a] Both C3′ and C5′ methoxyls yield equivalent proton shifts.

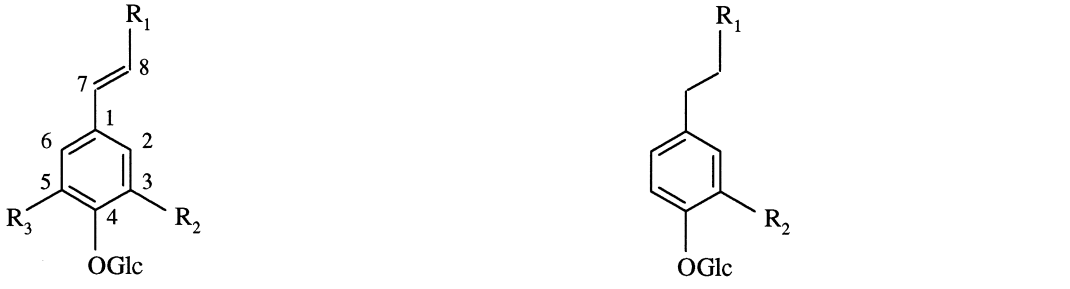

1. Coniferin: $R_1 = CH_2OH$, $R_2 = OCH_3$, $R_3 = H$

2. Syringin: $R_1 = CH_2OH$, $R_2 = OCH_3$, $R_3 = OCH_3$

3. Coniferaldehyde glucoside: $R_1 = CHO$, $R_2 = OCH_3$, $R_3 = H$

4. Sinapaldehyde glucoside: $R_1 = CHO$, $R_2 = OCH_3$, $R_3 = OCH_3$

5. Dihydroconiferyl alcohol glucoside: $R_1 = CH_2OH$, $R_2 = OCH_3$

Fig. 1. Structure of monolignol glucosides.

glucosides in cambial tissue parallel each other (Fig. 2, Savidge et al., 1998) with comparable efficiencies in the formation of aldehydic and alcoholic glucosides.

In addition, dihydroconiferyl alcohol (DHCA) was accepted as a suitable substrate for the pine CAGT and converted to its corresponding 4-*O*-β-D-glucoside (Fig. 1, Table 1). The 4-*O*-β-D-glucoside has been reported in needles of *Pinus contorta* (Higuchi et al., 1977). Ralph et al. (1997) recently reported dihydroconiferyl alcohol as a main constituent of lignin in a mutant loblolly pine. The involvement of dihydrophenylpropanoids in the biosynthesis of plant pigments (Schmitt and Schneider, 1999) suggests, in general, that dihydro-compounds play a role in secondary metabolism.

The effective turnover of both cinnamyl alcohols and cinnamyl aldehydes by CAGT during the growing season was confirmed by the determination of the apparent K_m values of the various substrates (Table 2). The apparent K_m values were obtained from Lineweaver–Burk plots at saturating concentrations of UDPG. For coniferyl alcohol, when assayed in phosphate buffer at pH 7.6, a K_m of 120 μM was obtained. Sinapyl alcohol, although not synthesized in pines, also served as a substrate with an apparent K_m of 154 μM. The data confirm former results for *Pinus banksiana*, where sinapyl alcohol reached 96% of the relative activity of coniferyl alcohol (Savidge and Förster, 1998). A comparable K_m value (250 μM) was reported for spruce (Schmid and Grisebach, 1982).

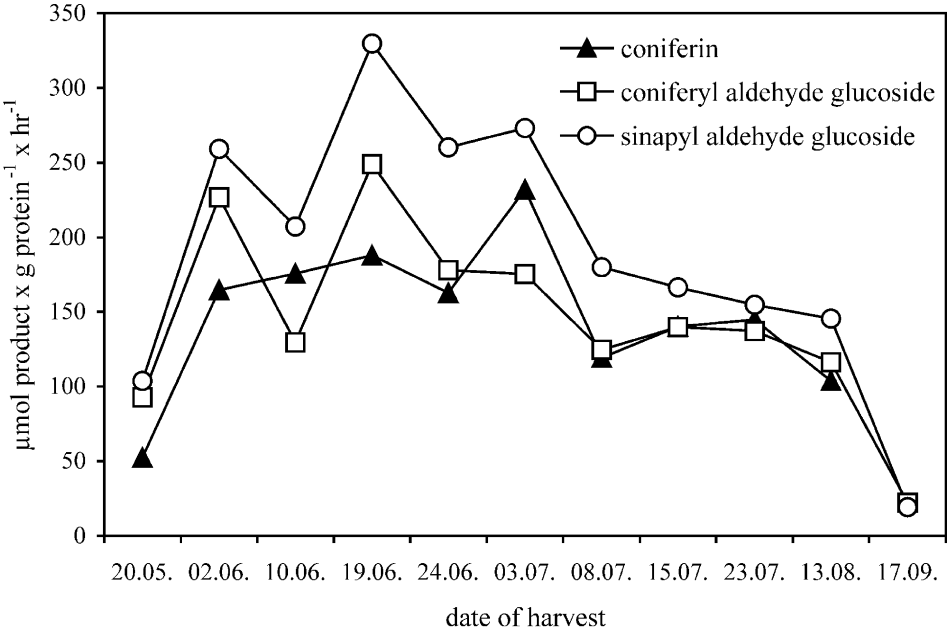

Fig. 2. Seasonal activity pattern of UDPG:CAGT in developing xylem of *Pinus strobus* as determined by in vitro experiments.

Table 2
Enzymatic parameters of the partially purified UDPG:CAGT from cambium of *Pinus strobus*

Substrate	Enzymatic product	K_m (µM)	V_{max} ($nM \times mg^{-1}_{protein} \times min^{-1}$)
Coniferyl alcohol	Coniferin	119.6	1.17
Sinapyl alcohol	Syringin	153.5	1.54
Coniferaldehyde	Coniferaldehyde-4-*O*-β-D-glucopyranoside	317.4	1.85
Sinapaldehyde	Sinapaldehyde-4-*O*-β-D-glucopyranoside	241.7	1.38

Coniferyl aldehyde and sinapyl aldehyde glucosylation resulted in K_m values of 317 and 242 µM, respectively, thus working in close proximity to the order of cinnamyl alcohols. Nevertheless, existing differences in the enzymatic turnover of cinnamyl alcohols and aldehydes, evident by the reported K_m values, underline that the hydroxyl group of the phenylpropane side-chain constitutes a more efficient substrate configuration. As reported before (Förster et al., 2000), cinnamyl alcohols and cinnamyl aldehydes compete with each other for CAGT when provided as dual substrates, with alcohols being more efficient in inhibiting the formation of cinnamyl aldehyde glucosides.

Cinnamyl aldehydes have been previously reported as appropriate substrates; however, structure and physiological relevance was not investigated. The amount of aldehydic glucosides obtained in investigations of the substrate specificity of CAGT in *Picea abies* (Schmid and Grisebach, 1982) and suspension cultures of Paul's Scarlet Rose (Ibrahim and Grisebach, 1976) was expressed as relative activity in comparison to coniferyl alcohol. Because of the lack of authentic compounds for co-chromatography, the structure of the presumed glucosidic products could not be unequivocally elucidated. Hence, the data in this report based on HPLC separation and NMR investigation (Table 2) confirm, to our knowledge for the first time the real structure of the enzymatic products (Fig. 1). In contrast to the glucosyltransferase purified from *Forsythia ovata* (Ibrahim, 1977) and in agreement with the glucosyltransferase purified from *Picea abies* (Schmid and Grisebach, 1982) the CAGT from *Pinus strobus* expressed almost no activity with cinnamic acids (Förster et al., 2000). The glucosylation of cinnamic acids (Nurmann and Strack, 1980; Lorenzen et al., 1996; Fons et al., 1998; Wang and Ellis, 1998) has been demonstrated previously, with the glucosyl moiety attached to the carboxyl group of the side-chain.

The observed seasonal fluctuations of both cinnamyl alcohol and aldehyde glucoside formation (Fig. 2) coincide with events of wood formation, i.e. formation of primary walled radially enlarged cells and the first appearence of differentiated tracheids undergoing secondary-wall formation and lignification (Savidge and Förster, 1998). Preliminary examination revealed both high activities of the glucosyltransferase and developmental processes during June and July (Fig. 2) in the cambial zone, thus concentrating the characterization and purification of the CAGT to this time of the season. Lignification is not developmentally correlated to the formation of monolignol glucosides as shown previously

(Leinhos and Savidge, 1994; Savidge and Förster, 1998). However, some observed metabolic connections to wood formation and lignification once the glucosides are produced in abundance needs further clarification.

CAGT, in catalyzing the formation of cinnamyl alcohol glucosides, evidently competes with coniferyl alcohol dehydrogenase (CAD) and monolignol oxidising enzymes for coniferyl alcohol. Our data (Fig. 2, Table 2) indicate that the glucosyltransferase must also compete with CAD for available cinnamyl aldehydes by forming the corresponding aldehydic glucosides (Fig. 1).

Results obtained in the past few years have prompted a reconsideration of the established lignin biosynthetic pathway. It is clear now that inter-conversions of lignin precursors may occur at varied points along the lignification pathway, and not necessarily solely at the phenylpropanoid acid stage. In addition, the ratio of guaiacyl to syringyl units can be modified at the level of CoA esters (Grimmig et al., 1999), cinnamyl aldehydes (Osakabe et al., 1999), cinnamyl alcohols (Chen et al., 1999a,b) and monolignol glucosides (Matsui et al., 1996).

Taken together, the questions of if and how CAGT (i.e. alone or in a regulatory manner with the coniferin-specific β-glucosidase) may participate in controlling availability of cinnamyl alcohols and/or cinnamyl aldehydes for lignin formation deserves further efforts.

3. Experimental

3.1. General experimental

Coniferyl alcohol, sinapyl alcohol, coniferyl aldehyde and sinapyl aldehyde were purchased from Aldrich. E-coniferin was isolated from *P. strobus* (Savidge, 1989) and dihydroconiferyl alcohol was obtained as previously described by Savidge (1987). Before processing and HPLC analysis, handcut sections of cambium and developing xylem were examined by microscopy as previously described by Savidge (1988).

3.2. Trees

Healthy *Pinus strobus* between 15 and 18 years old growing in the University of New Brunswick Woodlot, Fredericton, NB, Canada, were selected. Sufficient amounts of protein for this study were isolated for purification from a number of trees harvested in late May 1997. Individual trees were harvested during the growing season (April–September) for investigations into seasonal CAGT activity patterns. On each date, stem segments from the main axis were removed with a handsaw and brought directly to the laboratory for processing. The bark was peeled from the wood and the exposed inner bark surface (i.e. cambial zone) and wood surface (i.e. developing xylem) were scraped individually into cryogenic vials (Savidge et al., 1982). The tissue was then stored in liquid nitrogen until preparation for CAGT analysis.

3.3. Enzyme isolation

Buffer systems used include: extraction buffer (0.2 M phosphate (Na_2HPO_4, NaH_2PO_4), 10% polyvinylpyrroli done, 7.5% glycerol, 15 mM aminocaproic acid, 10 mM dithiothreitol, 14 mM β-mercaptoethanol, pH 7.6), equilibration buffer (0.1 M phosphate (Na_2HPO_4, NaH_2PO_4), 14 mM β-mercaptoethanol, pH 7.6), sodium phosphate buffer (Na_2HPO_4, NaH_2PO_4, 100 mM, pH 7.6). Cambial tissue was pulverized to a homogeneous powder and extracted for 1 h in extraction buffer. The suspension was filtered and the filtrate centrifuged for 20 min (4°C) at 15,500×*g*. The supernatant was centrifuged (1 h, 4°C) at 100,000×*g* to remove microsomes. Protein in the supernatant was precipitated with $(NH_4)_2SO_4$. Protein precipitated between 40 and 85% $(NH_4)_2SO_4$ was collected by centrifugation (23,300×*g*, 20 min, 4°C). The resulting pellet was resuspended in phosphate buffer (2.5 ml), then applied to Sephadex G-25 (20 mm i.d.×100 mm, previously equilibrated in equilibration buffer). One ml fractions of soluble protein were collected. Fractions showing transferase activity were pooled and concentrated by centrifugation at 2455×*g* using a Centricon YM-10 concentrator. All subsequent isolation and purification of UDPG: coniferyl alcohol glucosyltransferase (CAGT) was carried out according to Förster and Savidge (1995) and Savidge and Förster (1998).

3.4. Protein determination

Protein concentrations were determined using the method developed by Lowry et al. (1951), modifying final volumes to 40% of the original assay. The UDPG: CAGT was then applied in a 40-fold dilution, using bovine serum albumin as a standard, and measured at 578 nm.

3.5. Semi-preparative HPLC and product separation

Reversed-phase HPLC of the enzyme assay aliquots was performed according to Savidge (1989) on a Milton Roy system with a semi-preparative C18 ODS Ultrasphere column (Beckman, 5 μm spheres, 150×10 mm i.d.). Assays were carried out on a larger scale (i.e. total volume 2 ml) in order to obtain sufficient product for analytical investigations. The enzyme incubation mixture consisted of 100 mM phosphate buffer (pH 7.6), 2 mM UDPG, 1mM of the substrates in question and approximately 800 μg protein. Enzyme assay incubation time was 60 min at 36°C. Product separation was achieved with a linear gradient over 30 min (5–100% MeOH, adjusted to pH 3.0 with acetic acid) with a flow

rate of 5 ml/min and UV detection at 260 nm: R_t coniferin 8.0 min, 266 nm: R_t syringin 8.7 min, 330 nm: R_t coniferyl aldehyde glucoside 9.0 min, 320 nm: R_t sinapyl aldehyde glucoside 9.8 min, 262 nm: R_t *p*-coumaryl alcohol glucoside 8.7 min, 276 nm: R_t dihydroconiferyl alcohol glucoside 8.3 min., 266 nm. Enzymatic products were collected from semi-preparative HPLC eluant and freeze dried. The compounds were characterised by GC–MS and ^{1}H NMR and used as standards in analytical HPLC.

3.6. Ultraviolet-visible spectra

Ultraviolet-visible spectra of the purified enzymatic products were obtained using a computer-controlled UV/vis spectrophotometer (Shimazu, UV-2102-PC). Spectra were recorded from 195 to 450 nm and compared to spectra obtained in analytical HPLC work-up.

Coniferin (**1**) λ_{max} (MeOH) nm (log ε): 260 (1,3), 214, λ_{min} (MeOH) nm: 238, $\lambda_{shoulder}$ (MeOH) nm: 296; syringin (**2**) λ_{max} (MeOH) nm (log ε): 266, (1,23), 221, λ_{min} (MeOH) nm: 240; coniferyl aldehyde glucoside (**3**) λ_{max} (MeOH) nm (log ε): 330 (1,16), 236, λ_{min} (MeOH) nm: 266, $\lambda_{shoulder}$ (MeOH) nm: 306; sinapyl aldehyde glucoside (**4**) λ_{max} (MeOH) nm (log ε): 320 (0,55), 236, λ_{min} (MeOH) nm: 268; dihydroconiferyl alcohol glucoside (**5**) λ_{max} (MeOH) nm: 276, 224, λ_{min} (MeOH) nm: 248.

3.7. Nuclear magnetic resonance

Approximately 1–2 mg of coniferin, coniferyl aldehyde glucoside, syringin and sinapyl aldehyde glucoside were each dissolved in 600–700 μl deuterated methanol and placed in individual 5 mm NMR tubes. Only microgram quantities of dihydroconiferyl alcohol glucoside were available, which was subsequently dissolved in approximately 600 μl deuterated methanol, and placed in a 5 mm NMR tube. ^{1}H spectra were recorded on a 400 MHz, Unity 400 NMR spectrometer, at 25°C. The residual solvent peak, CHD_2OD, (3.30 ppm) was used as an internal standard. Two-dimensional COSY spectra and one-dimensional spectra were obtained.

3.8. Analytical HPLC and glucosyltransferase assay

Analytical HPLC was performed on a computer-controlled Jasco system consisting of an autosampler (AS950-10), multiwavelength detector (MD 910), ternary gradient unit (LG 980-02) and a 3-line-degasser (DG 980-50) on a Peltier-thermostated Sepsil C18 column (Jasco, 5 μm spheres, 125×3 mm i.d.). Cinnamyl alcohol glucosides were eluted in low pressure gradient mode in H_2O: MeOH (containing 1% HCO_2H) over 55 min (2–39% MeOH for 35 min, 39–100% MeOH for 15 min), and cinnamyl aldehyde glucosides over 70 min (2–60% MeOH for 50 min, 60–100% MeOH for 20 min) with a flow rate of 0.5 ml/min. Column temperature was adjusted to 26°C. Data analysis was accomplished using Borwin PDA (version 1.0) and chromatography (version 1.22.03 B) software.

The enzyme incubation mixture (i.e. total volume 200 μl) contained 200 nM UDPG in 10 μl H_2O, various amounts of substrate in 10 μl MeOH, 80 μl sodium phosphate buffer and approximately 100 μg protein dissolved in sodium phosphate buffer. The various substrates were incubated for 10 min at 36°C, then terminated using 20 μl HOAc (50%). K_m values were calculated at fixed concentration of UDPG (1 mM) by linear regression of 1/v vs. 1/s (Lineweaver-Burk plot) with Grafit (version 4.0.1). All experiments were performed in triplicate and compared to a control containing all constituents but terminated prior to catalytic activity by HOAc precipitation of the enzyme.

Acknowledgements

We would like to thank Dr. L. Calhoun for support on compilation of the NMR data for the cinnamyl glucosides. V.J.S. and R.A.S. thank NSERC for research funding. HF was supported by a Grant-in-Aid (FO 271/4-1) of the Deutsche Forschungsgemeinschaft (Bonn, Germany).

References

Burmeister, G., Hösel, W., 1981. Immunohistochemical localization of β-glucosidases in lignin and isoflavone metabolism in *Cicer arietinum* L. seedlings. Planta 152, 578–586.

Chen, F., Yasuda, S., Fukushima, K., 1999. Evidence for a novel biosynthetic pathway that regulates the ratio of syringyl to guaiacyl residues in lignin in the differentiating xylem of *Magnolia kobus* DC. Planta 207, 597–603.

Chen, F., Yasuda, S., Fukushima, K., 1999. Structural conversion of the lignin subunit at the cinnamyl alcohol stage in *Eucalyptus camaldulensis*. Journal of Wood Science 45, 487–491.

Dharmawardhana, D.P., Ellis, B.E., Carlson, J.E., 1995. A β-glucosidase from lodgepole pine xylem specific for the lignin precursor coniferin. Plant Physiology 107, 331–339.

Dharmawardhana, D.P., Ellis, B.E., Carlson, J.E., 1999. cDNA cloning and heterologous expression of coniferin β-glucosidase. Plant Molecular Biology 40, 365–372.

Deliorman, D., Calis, I., Ergun, F., Tamer, U., 1999. The comparative studies on phenylpropanoid glycosides of *Viscum album* subspecies by high performance liquid chromatography. Journal of Liquid Chromatography and Related Technologies 22, 3101–3114.

Eglinton, T.I., Goni, M.A., Boon, J.J., van der Hage, E.R.E., Terashima, N., Xie, Y., 2000. Incorporation of C-13-labeled coniferyl alcohol into developing *Ginkgo biloba* L. lignin revealed by analytical pyrolysis and CuO oxidation in combination with isotope ratio monitoring-gas chromatography-mass spectrometry. Holzforschung 54, 39–54.

Fernàndez de Simòn, B., Cadahia, E., Conde, E., Garcìa-Vallejo, M.C., 1996. Low molecular weight phenolic compounds in spanish oak woods. Journal of Agricultural and Food Chemistry 44, 1507–1511.

Fons, F., Rapior, S., Gueiffier, A., Roussel, J.-L., Gargadennec, A., Andary, C., 1998. (*E*)-*p*-coumaroyl-1-*O*-β-D-glucopyranoside accumulation in roots of *Plantago lanceolata* cultures. Acta Botanica Gallica 145, 249–255.

Förster, H., Savidge, R.A., 1995. Characterization and seasonal activity of UDPG: coniferyl alcohol glucosyltransferase linked to cambial growth in jackpine. In: Proceedings of the Plant Growth Regulation Society of America, 22nd Annual Meeting, pp. 402–407.

Förster, H., Pommer, U., Savidge, R.A., 1999. Metabolic activity of uridine 5′-diphosphoglucose: cinnamyl alcohol glucosyltransferase as an intrinsic indicator of cambial growth in conifers. In: Gross, G.G., Hemingway, R.W., Yoshida, T. (Eds.), Plant Polyphenols 2: Chemistry and Biology. Kluwer/Plenum, New York, pp. 371–392.

Förster, H., Steeves, V., Pommer, U., Savidge, R.A., 2000. UDPG: coniferyl alcohol glucosyltransferase and coniferin biosynthesis — a regulatory link to seasonal cambial growth in conifers. In: Savidge, R.A., Barnett, T.R., Napier, R. (Eds.), Cell and Molecular Biology of Wood Formation. BIOS, Oxford, pp. 189–202.

Freudenberg, K., 1964. The formation of lignin in the tissue and in vitro. In: Zimmermann, M.H. (Ed.), The Formation of Wood in Forest Trees. Academic Press, New York, pp. 203–218.

Freudenberg, K., Harkin, J.M., 1963. The glucosides of cambial sap of spruce. Phytochemistry 2, 189–193.

Freudenberg, K., Neish, A.C., 1968. Constitution and Biosynthesis of Lignin. Springer-Verlag, Berlin. (pp. 78–122).

Freudenberg, K., Torres-Serres, J., 1967. Umwandlung des Phenylalanins in Lignin-bildende Glucoside. Liebigs Annalen der Chemie 703, 225–230.

Fukushima, K., Taguchi, S., Matsui, N., Yasuda, S., 1997. Distribution and seasonal changes of monolignol glucosides in *Pinus thunbergii*. Mokuzai Gakkaishi 43, 254–259.

Grima-Pettenati, J., Goffner, D., 1999. Lignin genetic engineering revisited. Plant Science 145, 51–65.

Grimmig, B., Kneusel, R.E., Junghanns, K.T., Matern, U., 1999. Expression of bifunctional caffeoyl-CoA 3-*O*-methyltransferase in stress compensation and lignification. Plant Biology 1, 299–310.

Higuchi, R., Aritomi, M., Donnelly, D., 1977. Monolignol and dilignol glycosides from *Pinus contorta* leaves. Phytochemistry 16, 1007–1011.

Ibrahim, R.K., 1977. Glucosylation of lignin precursors by uridine diphosphate glucose: coniferyl alcohol glucosyltransferase in higher plants. Zeitschrift fuer Pflanzenphysiologie 85, 253–262.

Ibrahim, R.K., Grisebach, H., 1976. Purification and properties of UDP-glucose: coniferyl alcohol glucosyltransferase from suspension cultures of Paul's scarlet rose. Archives of Biochemistry and Biophysics 176, 700–708.

Ito, K., Tanabe, Y., Kato, S., Yamamoto, T., Saito, A., Mori, M., 2000. Glycosidic fraction of flue-cured tobacco leaves: its separation and component analysis. Bioscience Biotechnology and Biochemistry 64, 584–587.

Leinhos, V., Savidge, R.A., 1993. Isolation of protoplasts from developing xylem of *Pinus banksiana* and *Pinus strobus*. Canadian Journal of Forest Research 23, 343–348.

Leinhos, V., Savidge, R.A., 1994. Investigation of coniferin compartmentation in developing xylem of conifers during lignification. Acta Horticulturae 381, 97–103.

Leinhos, V., Udagama-Randeniya, P.V., Savidge, R.A., 1994. Purification of an acidic coniferin-hydrolysing β-glucosidase from developing xylem of *Pinus banksiana*. Phytochemistry 37, 311–315.

Lorenzen, M., Racicot, V., Strack, D., Chapple, C., 1996. Sinapic acid ester metabolism in wild type and a sinapoylglucose-accumulating mutant of Arabidopsis. Plant Physiology 112, 1625–1630.

Lowry, O.H., Rosebrough, N.J., Farr, A.L., Randall, R.J., 1951. Protein measurement with the Folin phenol reagent. Journal of Biological Chemistry 193, 265–275.

Marcinowski, S., Falk, H., Hammer, D.K., Hoyer, B., Grisebach, H., 1979. Appearance and localization of a β-glucosidase hydrolyzing coniferin in spruce (*Picea abies*) seedlings. Planta 144, 161–165.

Marcinowski, S., Grisebach, H., 1977. Turnover of coniferin in pine seedlings. Phytochemistry 16, 1665–1667.

Matsui, N., Fukushima, K., Yasuda, S., Terashima, N., 1996. On the behavior of monolignol glucosides in lignin biosynthesis. III. Synthesis of variously labelled coniferin and incorporation of the label into syringin in the shoot of *Magnolia kobus*. Holzforschung 50, 408–412.

Morris, J.W., Morris, R.O., 1990. Identification of an *Agrobacterium tumefaciens* virulence gene inducer from the pinaceous gymnosperm *Pseudotsuga menziesii*. Proceedings of the National Academy of Sciences USA 87, 3614–3618.

Nurmann, G., Strack, D., 1980. Formation of 1-sinapoylglucose by UDP-glucose: sinapic acid glucosyltransferase from cotyledons of *Raphanus sativus*. Zietschrift fuer Pflanzenphysiologie 102, 11–17.

Osakabe, K., Tsao, C.C., Li, L., Popko, J.L., Umezawa, T., Carraway, D.T., Smeltzer, R.H., Joshi, C., Chiang, V.L., 1999. Coniferyl aldehyde 5-hydroxylation and methylation direct syringyl lignin biosynthesis in angiosperms. Proceedings of the National Academy of Sciences USA 96, 8955–8960.

Park, H.-J., Lee, M.-S., Lee, K.-T., Sohn, I.-C., Han, Y.-N., Miyamoto, K., 1999. Studies on constituents with cytotoxic activity from the stem bark of *Syringa velutina*. Chemical and Pharmaceutical Bulletin 47, 1029–1031.

Ralph, J., MacKay, J.J., Hatfield, R.D., O'Malley, D.M., Whetten, R.W., Sederoff, R.R., 1997. Abnormal lignin in a loblolly pine mutant. Science 277, 235–239.

Rowland, J.J., Arora, R., 1997. Proteins related to endodormancy (rest) in woody perennials. Plant Science 126, 2119–144.

Sano, K., Sanada, S., Ida, Y., Shoji, J., 1991. Studies on the constituents of the bark of *Kalopanax pictus* Nakai. Chemical and Pharmaceutical Bulletin 39, 865–870.

Savidge, R.A., 1987. Dihydroconiferyl alcohol in developing xylem of *Pinus contorta*. Phytochemistry 26, 93–94.

Savidge, R.A., 1988. A biochemical indicator of commitment to tracheid differentiation in *Pinus contorta*. Canadian Journal of Botany 66, 2009–2012.

Savidge, R.A., 1989. Coniferin, a biochemical indicator of commitment to tracheid differentiation in conifers. Canadian Journal of Botany 67, 2663–2668.

Savidge, R.A., 1991. Seasonal cambial activity in *Larix laricina* saplings in relation to endogenous indol-3-ylacetic acid, sucrose and coniferin. Forest Science 37, 953–958.

Savidge, R.A., Heald, J.K., Wareing, P.F., 1982. Non-uniform distribution and seasonal variation of endogenous indol-3-yl-acetic acid in cambial region of *Pinus contorta* Dougl. Planta 155, 89–92.

Savidge, R.A., Förster, H., 1998. Seasonal activity of uridine 5′-diphosphoglucose: coniferyl alcohol glucosyltransferase in relation to cambial growth and dormancy in conifers. Canadian Journal of Botany 76, 486–493.

Savidge, R.A., Udagama-Randeniya, P.V., Xu, Y., Leinhos, V., Förster, H., 1998. Coniferyl alcohol oxidase, a new enzyme of lignification. In: Lewis, N.G., Sarkanen, S. (Eds.), Lignin and Lignan Biosynthesis. ACS Symposium Series Vol. 697, pp. 109–130.

Schmid, G., Grisebach, H., 1982. Enzymic synthesis of lignin precursors. Purification and properties of UDPglucose:coniferyl-alcohol glucosyltransferase from cambial sap of Spruce (*Picea abies* L.). European Journal of Chemistry 123, 363–370.

Schmid, G., Hammer, D.K., Ritterbusch, A., Grisebach, H., 1982. Appearance and immunohistochemical localization of UDP-glucose: coniferyl alcohol glucosyltransferase in spruce (*Picea abies* (L.) Karst.) seedlings. Planta 156, 207–212.

Schmitt, B., Schneider, B., 1999. Dihydrocinnamic acids are involved in the biosynthesis of phenylphenalenones in *Anigozanthos preissii*. Phytochemistry 52, 45–53.

Slimestad, R., Hostettmann, K., 1996. Characterization of phenolic constituents from juvenile and mature needles of Norway spruce by

means of high performance liquid chromatography-mass spectrometry. Phytochemical Analysis 7, 42–48.

Sticher, O., Lahloub, M.F., 1982. Phenolic glycosides of *Paulownia tomentosa* bark. Planta Medica 46, 145–148.

Tanaka, N., Wada, H., Fuchino, H., Inoue, T., Yasuda, D., Kanda, S., Kiyowaka, C., Ashida, N., Suzuki, T., Yamazaki, K., Hakamatsuka, T., 1998. Constituents of bamboos and bamboo grasses. Yakugaku Zasshi 118, 332–337.

Terashima, N., Fukushima, S., Takabe, K., 1986. Heterogeneity in formation of lignin. VIII. An autoradiographic study on the formations of guaiacyl and syringyl lignin in *Magnolia kobus* DC. Holzforschung 42, 347–350.

Terashima, N., Fukushima, S., 1988. Heterogeneity in formation of lignin. XI. An autoradiographic study of the heterogeneous formation and structure of pine lignin. Wood Science and Technology 22, 259–270.

Terashima, N., Fukushima, S., He, L., Takabe, K., 1993. Comprehensive model of the lignified plant cell wall. In: Jung, H.G., Buxton, D.R., Hatfield, R.D., Ralph, J. (Eds.), Forage Cell Wall Structure and Digestibility. American Society of Agriculture, Madison, WI, pp. 247–270.

Terashima, N., Atalla, R.H., Ralph, S.A., Landucci, L.L., Lapierre, C., Monties, B., 1995. New preparations of lignin polymer models under conditions that approximate cell wall lignification. I. Synthesis of novel lignin polymer models and their structural characterization by 13-C NMR. Holzforschung 49, 521–527.

Terashima, N., Atalla, R.H., Vanderhart, D.L., 1997. Solid-state NMR-spectroscopy of specifically C-13-enriched lignin in wheatstraw from coniferin. Phytochemistry 46, 863–870.

Terazawa, M., Miyake, M., 1984. Phenolic compounds in living tissues of woods. II. Seasonal variations of phenolic glycosides in the cambial sap of woods. Mokuzai Gakkaishi 30, 329–334.

Terazawa, M., Okuyama, H., Miyake, M., 1984a. Phenolic compounds in living tissues of woods. I. Phenolic β-glucosidases of 4-hydroxycinnamyl alcohol derivatives in the cambial sap of woods. Mokuzai Gakkaishi 30, 322–328.

Terazawa, M., Okuyama, H., Miyake, M., 1984b. Isolation of coniferin and syringin from the cambial tissue and inner-bark of some angiospermous woods. Mokuzai Gakkaishi 30, 409–412.

Ullah, N., Ahmad, S., Malik, A., 1999. Phenylpropanoid glycosides from *Daphne oleoides*. Chemical and Pharmaceutical Bulletin 47, 114–115.

van Uden, W., Pras, N., Batterman, S., Visser, J., Malingre, T.M., 1990. The accumulation and isolation of coniferin from a high-producing cell suspension of *Linum flavum* L. Planta 183, 25–30.

Wang, S.X., Ellis, B.E., 1998. Enzymology of UDP-glucose: sinapic acid glucosyltransferase from *Brassica nabus*. Phytochemistry 49, 307–318.

Xie, Y., Terashima, N., 1991. Selective carbon 13-enrichment of side chain carbons of Ginkgo lignin traced by carbon 13 nuclear magnetic resonance. Mokuzai Gakkaishi 37, 935–941.

Xie, Y., Robert, D., Terashima, N., 1994. Selective carbon 13 enrichment of side chain carbons of ginkgo lignin traced by carbon 13 nuclear magnetic resonance. Plant Physiology and Biochemistry 32, 243–249.

Yamamoto, E., Inciong, E.J., Davin, L.B., Lewis, N.G., 1990. Formation of *cis*-coniferin in cell-free extracts of *Fagus grandifolia* Ehrh bark. Phytochemistry 94, 209–213.

PERGAMON

Phytochemistry 57 (2001) 1095–1103

PHYTOCHEMISTRY

www.elsevier.com/locate/phytochem

Coniferyl alcohol metabolism in conifers — II. Coniferyl alcohol and dihydroconiferyl alcohol biosynthesis

Rodney A. Savidge[a,*], Hartmut Förster[b]

[a]*Faculty of Forestry and Environmental Management, University of New Brunswick, Fredericton, NB, E3B 6C2, Canada*
[b]*FSU Jena, Institut für Allgemeine Botanik, Bereich Pflanzenbiochemie, Kühnhäuser Str. 101, 99189 Erfurt-Kühnhausen, Germany*

Received 25 July 2000; received in revised form 26 January 2001

Abstract

Coniferaldehyde and NADPH when incubated with microsomes isolated from developing xylem of *Pinus strobus* yielded coniferyl alcohol and dihydroconiferyl alcohol in vitro. D-(+)-Pinitol was also found to be a microsomal constituent. Endogenous *E*-coniferyl alcohol content, quantified in dormant buds, cambium, bark and needles of *Pinus resinosa* and *P. strobus* by isotope-dilution combined gas chromatography mass spectrometry (GC/MS) using ring-$^{13}C_6$-coniferyl alcohol, was at a level similar to that of endogenous indol 3-ylacetic acid (IAA). Wounding (branch girdling) induced more than a 10-fold increase in content of endogenous *E*-coniferyl alcohol in dormant non-lignifying cambium, a clear indication that monolignol biosynthesis is not coupled to lignification. © 2001 Elsevier Science Ltd. All rights reserved.

Keywords: *Pinus resinosa*; *Pinus strobus*; Coniferophyta; Pinaceae; Red pine; Eastern white pine; Cambium; Phenylpropanoid; Lignification; Microsomes

1. Introduction

The potential to alter lignin content and chemistry of vascular tissues through recombinant DNA technologies, combined with perception of economic gains accruing from such genetic modification, has taken lignification research from a state of neglect less than two decades ago into an area of major activity today. Reports of new enzymes, precursors and products of phenylpropanoid metabolism have transformed the former three-pronged *p*-hydroxyphenyl (H), guaiacyl (G), syringyl (S) model of lignification biochemistry (Neish 1960; Freudenberg and Neish 1968) into a more complex metabolic network having competence to generate novel as well as H, G and S lignins (Li et al., 1997, 1998, 1999, 2000; Goffner et al., 1998; Chen et al., 1999; Humphreys et al., 1999; Osakabe et al., 1999; Halpin et al., 2000; Matsui et al., 2000). However, the overall mechanism of lignification still remains less than well elucidated, and immense strings of ''unknown-function'' DNA remain to find meaning within physiological genomics.

The overriding difficulty is one of definition: *What is lignin?* Lignin is commonly described as a complex ''polymer'' (singular) although there is abundant evidence that H, G and S lignins co-occur as distinct entities within the same cell-wall material. Microscopic observations based not only on varied histochemical reactions but also on quantitative differences in UV fluorescence, energy dispersive X-ray, autoradiographic and fine structural data have indicated lignin heterogeneity within cell-wall layers, across cell walls, and between woody cell types (Fergus and Goring, 1970; Parham and Côté, 1971; Wood and Goring, 1971; Kutscha and Gray, 1972; Wardrop, 1981; Saka et al., 1982; Terashima et al., 1986, 1988; Terashima and Fukushima, 1988; Maurer and Fengel, 1990; Daniel et al., 1991; Downes et al., 1991). Despite microscopically detectable differences, chemical analyses have with few exceptions (e.g. Kim et al., 1994) melded any molecular heterogeneity within woody tissues into one pot, and then attempted to deduce polymeric structure in terms of a singular substance (Obst and Kent Kirk, 1988). In addition to H, G and S lignins, wall-bound hydroxybenzoic acids of poplar wood, also found in cell walls of mosses, arguably qualify as a component of lignin (Wilson et al. 1989; Fukushima et al., 1994; Kim et al., 1995). Thus, the

* Corresponding author. Tel.: +1-506-453-4919; fax: +1-506-453-3538.
E-mail address: savidge@unb.ca (R.A. Savidge).

0031-9422/01/$ - see front matter © 2001 Elsevier Science Ltd. All rights reserved.
PII: S0031-9422(01)00142-X

statement by Neish (1960) that "no one knows how many different kinds of lignin exist" remains valid today.

Lignin-carbohydrate complexes are a well-known feature of in situ lignins in wood cell walls, and it could be that co-valent linkages between polysaccharide and H, G and/or S polyphenolic substances are what distinguish 'true' lignins from unbound or weakly bound cell-wall polyphenolics, in which case the catalytic mechanism for carbohydrate bonding is all important in defining and understanding lignification. Alternatively, whether or not H, G, S and other polyphenolics are linked to wall carbohydrates, they might be considered as lignins (as has been the case when synthetic model dehydrogenation polymers of *p*-coumaryl, coniferyl and sinapyl alcohols have been investigated), making precursor polymerisation mechanism(s) the focus (compare Gang et al., 1999; Kwon et al., 1999; Sederoff et al., 1999).

Progress in lignification biochemistry undoubtedly depends on development of improved separation methods as a preliminary to chemical analysis. In this respect, ethanol-soluble, 'organosolv' or native "lignin" macromolecules can be readily obtained (Desmet, 1961; Sakakibara et al., 1987), e.g. from *Populus* spp., and separated electrophoretically or by gel permeration chromatography (Desmet, 1961; Košíková et al., 1990; Niku-Paavola, 1991).

In addition to defining and solving the macromolecular structure(s) of lignin, there is a need to know what substances are able to serve as "precursor" (as opposed to "monomer") and to understand what cellular mechanisms facilitate precursor allocation as lignin is deposited. Coupling of monolignol radicals into "dilignols" (which pedantically could be considered as 'lignans') does not necessarily have anything to do with lignification, even in lignifying tissues where 'free' lignans and lignin co-exist (Lewis and Davin, 1998). Deciding whether low abundance moieties such as *p*-coumaryl, coniferyl and sinapyl aldehydes and the reduced dihydro forms of the corresponding monolignols are normal precursors, products of post-polymerative monolignol processing, or artefacts of chemical analysis ultimately requires answering several additional questions: (1) What putative precursors are actually present in the exoplasmic space during lignification? (2) What catalytic activities are actually present in relation to those precursors? (3) What is the exoplasmic environment (e.g. pH, $[O_2]$, $[H_2O_2]$, etc.) where catalysts and substrates generate lignin? Remarkably, after more than a century of research, definitive information remains crudely unfocussed and/or incomplete in relation to each of those three questions.

Here we address aspects of the first two of those three questions, focussing on coniferyl alcohol metabolism (Fig. 1). *E*-Coniferyl alcohol has often been portrayed as the immediate precursor for G lignin, but it is by no means

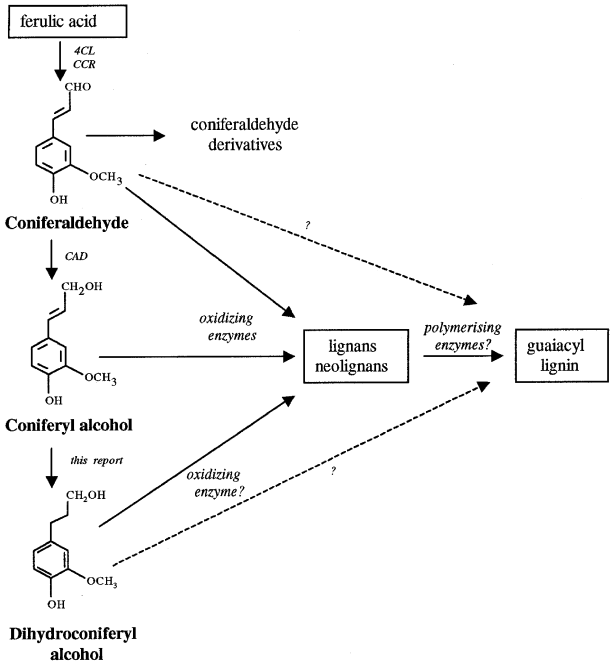

Fig. 1. Possible metabolic flow supporting guaiacyl lignin formation.

exclusively used in lignification, being convertible into coniferaldehyde, lignans, glucosides and, as indicated in the present study, also into dihydroconiferyl alcohol (Fig. 1). The coniferaldehyde moiety is found in G lignin at least in small quantities and was abundant in "lignin" of a mutant pine species (Peng and Westermark, 1997; Ralph et al., 1997, but compare Lewis, 1999). As indicated in Fig. 1, coniferaldehyde arises by 4-coumarate: CoA ligase (4CL) converting ferulic acid into the CoA thioester and the latter being de-esterified through the action of cinnamoyl-CoA reductase (CCR). Cinnamyl alcohol dehydrogenase (CAD) is well established to interconvert coniferaldehyde and coniferyl alcohol, but immense glucosyltransferase activity in the growing cambium (at least that of conifers) provides a mechanism to deplete the coniferyl alcohol pool in support of *E*-coniferin accumulation, thus ensuring that CAD favours the coniferaldehyde to coniferyl alcohol conversion (Savidge 1989; Förster et al., 1999, 2000). Coniferaldehyde can also be converted into various derivatives that, at best, affect lignification only indirectly by reducing substrate supply (Förster et al., 1999, 2000; Sy and Brown, 1999; Li et al., 2000). Thus, although coniferaldehyde conceivably is incorporated into the lignin matrix directly or, perhaps, as a component of a lignan, the mere presence of coniferaldehyde in a tissue is not an indication that lignification is either occurring or about to occur. For example, coniferaldehyde, vanillin and related compounds occur in non-lignified (but heavily suberized) bark of cork oak (Conde et al., 1997). Low concentrations of *E*-coniferaldehyde have been reported in cambial sap of conifers (Freudenberg and

Neish, 1968), as well as in extracts of bamboo (Tanaka et al., 1998) and oak (Fernàndez de Simòn et al., 1996).

Dihydroconiferyl alcohol has been obtained from kraft black liquors of conifer woods (Löwendahl et al., 1978; Niemelä, 1989), sap of maple (Lee et al., 1981), developing xylem of pine (Savidge, 1987), and pyrolysed *Cryptomeria japonica* wood (Kuroda et al., 1994). Dihydroconiferyl alcohol was also reported to be elevated in "lignin" of the same mutant pine tree containing abundant coniferaldehyde (Ralph et al., 1997). As explained above, it remains uncertain whether dihydroconiferyl alcohol per se serves as a precursor for lignification, or if it is even biosynthesised (Lewis, 1999).

2. Results and discussion

2.1. Coniferyl alcohol and dihydroconiferyl alcohol from coniferaldehyde

Pure coniferaldehyde and NADPH in phosphate buffer were provided to purified microsomes from lignifying xylem of *Pinus strobus*. Following 15 min, 1, 4 and 8 h, the incubations were stopped, centrifuged, the supernatants extracted into ethyl acetate (EtOAc), and each EtOAc fraction dried under a stream of nitrogen. The residue was taken up in a small volume of methanol (MeOH), adjusted to 95% water [pH 3.0 acetic acid (HOAc)] and the soluble constituents profiled by C18 reversed phase high performance liquid chromatography (HPLC) using a 95% water (pH 3.0 HOAc) to 100% MeOH gradient, monitoring UV absorbance at 262 nm, collecting all major peaks and, following trimethylsilylation, analyzing them by combined gas chromatography–mass spectrometry (GC/MS) in scanning mode. The HPLC data (Fig. 2) indicated that residual coniferaldehyde eluting at 13.2 min was present after all incubations, separating at baseline resolution from a major peak at 11.2 min.

To determine whether the unknown chromatographic peak was an endogenous microsomal constituent, as opposed to a product of coniferaldehyde/NADPH incubation, freshly prepared microsomes were extracted with phosphate buffer and analyzed by HPLC. Other freshly prepared microsomes were extracted with EtOAc, the EtOAc dried, and the residue trimethylsilylated and analyzed by GC/MS. Those investigations yielded no evidence for any of the aromatic substances shown in Fig. 1, but they did yield D-(+)-pinitol, distinguished by its GC retention time and highly diagnostic fragments, in particular *m*/*z* 260 (Fig. 3). Pinitol is a well known metabolite of general occurrence in conifers (Kretz, 1973) and is thought to modulate drought, salinity and low temperature stresses, also to scavenge hydroxyl radicals (Orthen et al., 1994). To our knowledge this is the first report of pinitol in microsomes.

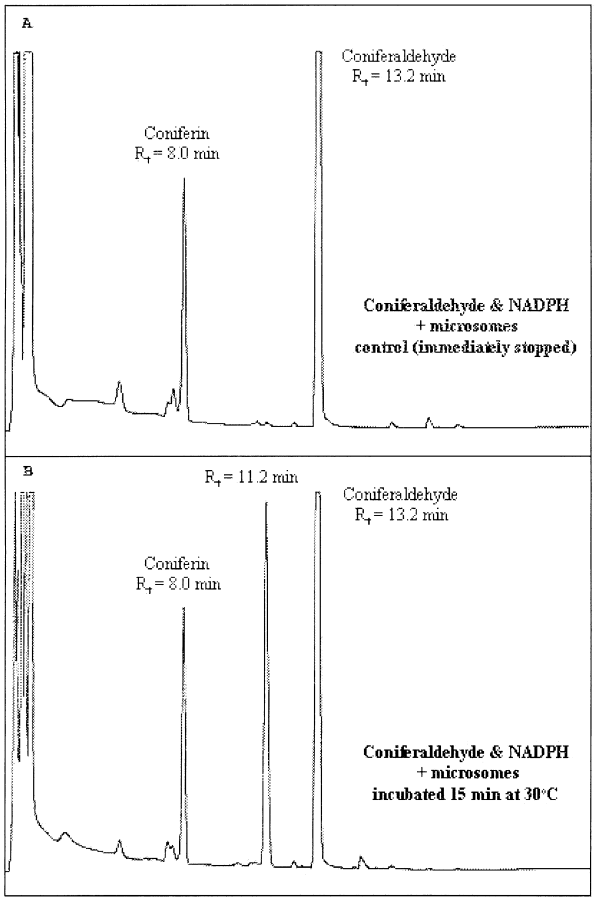

Fig. 2. HPLC traces showing λ 262 nm peaks generated after 0 min (A) and 15 min (B) incubation of coniferaldehyde and NADPH with microsomes. The fraction eluting at 11.2 min (B) yielded coniferyl alcohol and dihydroconiferyl alcohol by GC/MS. Note the residue of endogenous coniferin remaining despite extensive washing of the microsomes prior to incubation.

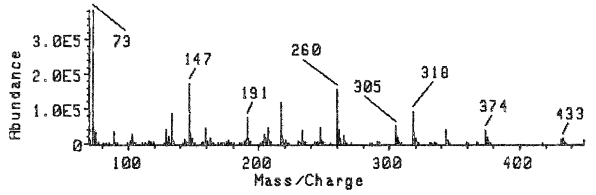

Fig. 3. EI mass spectrum of trimethylsilylated D-(+)-pinitol at 13.936 min obtained from microsome 'control' (no coniferaldehyde or NADPH provided).

The 11.2 min HPLC peak generated by incubating coniferaldehyde and NADPH with microsomes comprised two compounds by GC/MS: dihydroconiferyl alcohol and coniferyl alcohol (Figs. 4 and 5). Microsomes alone were devoid of both compounds. Dihydroconiferyl alcohol and coniferyl alcohol were both readily detected within the first 15 min of in vitro incubation (Fig. 2), and they exhibited increasing accumulation in the 1, 4 and 8 h incubations. *E*-Coniferyl alcohol abundance was approximately four times that of dihydroconiferyl alcohol. When coniferaldehyde and NADPH

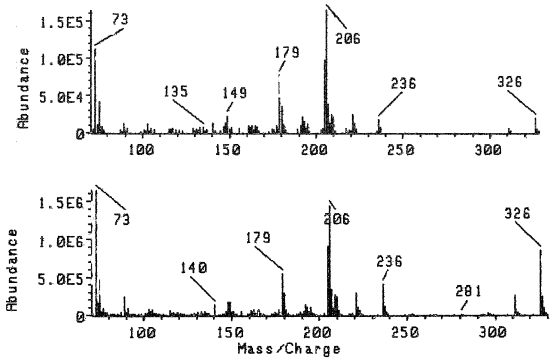

Fig. 4. EI mass spectra (70 eV) of dihydroconiferyl alcohol (as di-TMSi ether) produced in vitro in the presence of microsomes provided coniferaldehyde and NADPH (top), and as the synthetic standard (bottom), both with GC retention times of 13.5 min.

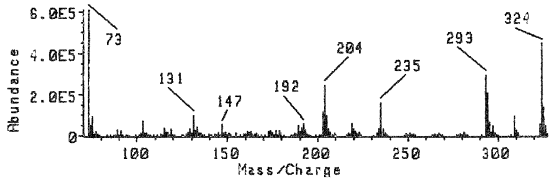

Fig. 5. 70 eV EI mass spectrum of the di-TMSi ether of coniferyl alcohol produced in vitro in the presence of microsomes incubated with coniferaldehyde and NADPH.

were incubated in buffer lacking microsomes, a trace amount of coniferyl alcohol was detected by selected-ion-monitoring (*m*/*z* 324), but no dihydroconiferyl alcohol was detected by either HPLC or GC/MS. Microsomes provided coniferaldehyde but not NADPH yielded neither coniferyl nor dihydroconiferyl alcohol. Coniferin was invariably associated with microsomes (Fig. 2); thus, some evidently is membrane associated. Based on data from our controls, microsomes contained little if any coniferin-specific β-glucosidase activity.

Dihydroconiferyl alcohol has previously been obtained from sap, bark, wood and other sources, as noted above; however, catalytic mechanisms for hydrogenation of C–C double bonds are still obscure, with a few exceptions (Hirata et al., 2000; Fillgrove and Anderson, 2000). Our data indicate that coniferaldehyde in the presence of NADPH is reduced to coniferyl alcohol which is further reduced to dihydroconiferyl alcohol by one or more microsomal enzymes. *Saccharomyces cerevisiae* evidently converts coniferaldehyde into coniferyl alcohol and dihydroconiferyl alcohol under fermentation conditions (Larsson et al., 2000). Acetaldehyde and ethanol are abundantly present in both hardwoods and conifers (MacDonald and Kimmerer, 1991; N. Forneris and R.A. Savidge, unpublished data), in agreement with O_2 not uncommonly being in short supply during cambial growth (Eklund and Klintborg, 2000). Thus, under anaerobic conditions dihydroconiferyl alcohol biosynthesis in cambium likely occurs by a mechanism similar to that occurring in yeast. Based on the extensive washing associated with preparation of the microsomal fraction (see Experimental), there can be little doubt that the hydrogenation catalyst(s) was somehow associated with the membrane fraction of developing xylem. Whether the reducing enzyme(s) is actually an integral part of microsomal membranes remains to be unequivocally determined, but there is evidence that the entire phenylpropanoid pathway is conducted on membrane associated enzyme complexes (Hrazdina and Wagner, 1985).

2.2. Endogenous coniferyl alcohol

Prior to this work, *E*-coniferyl alcohol had been repeatedly observed by GC/MS to be a common constituent in pine needles of different ages at all seasons (RAS, data not shown). We had also observed that *E*-coniferin accumulates in cambium above a girdle (Savidge, 1989; Steeves and Savidge, 2000) and that UDPG:coniferyl alcohol glucosyltransferase activity in both cambium and developing xylem is tightly coupled to seasonal cambial growth (Savidge and Förster, 1998). In view of an earlier report that ^{14}C-labelled quinic acid was transported from pine needles to the stem (Kretz, 1973), the possibility that coniferyl alcohol exported from needles to stem could explain coniferin accumulation above a girdle was investigated. To answer this question, ring-$^{13}C_6$-*E*-coniferyl alcohol was synthesized from $^{13}C_6$-vanillin and used as internal standard during extraction, purification and isotope dilution GC/MS (Figs. 6 and 7).

Applications (10 μg) of exogenous $^{13}C_6$-coniferyl alcohol were made to cut apical surfaces of *P. resinosa* needles intact on stem segments standing upright in water in the laboratory, followed by a time study over 1–24 h to determine whether the coniferyl alcohol was moving through the needle. At each time, needles were removed, cut into 2-cm segments, frozen and pulverized in liquid nitrogen, extracted with phosphate buffer, the latter extracted with EtOAc and the EtOAc dried down, trimethylsilylated and analyzed by GC/MS in selected-ion monitoring mode (*m*/*z* 309, 324, 315, 330). Analysis of the content of $^{13}C_6$-coniferyl alcohol present at increasingly more basal positions along the needle from the site of application of $^{13}C_6$-coniferyl alcohol, as well as in the cambium at the stem region associated with the needle, yielded no indication that coniferyl alcohol was exported from needles to stem (data not shown).

Endogenous *E*-coniferyl alcohol was present in dormant buds, needles and cambia of *Pinus resinosa* and *P. strobus* (Table 1). The content of coniferyl alcohol during dormancy was low, similar to endogenous IAA, and it is unclear what if any role such a low level of coniferyl alcohol fulfils in dormant tissues.

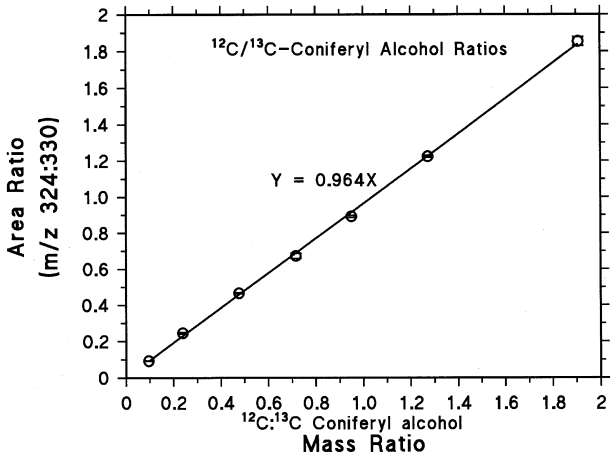

Fig. 6. Integrated peak area ratio as a function of mass ratio of *E*-coniferyl alcohol. Standard errors of the mean are indicated for triplicate analyses.

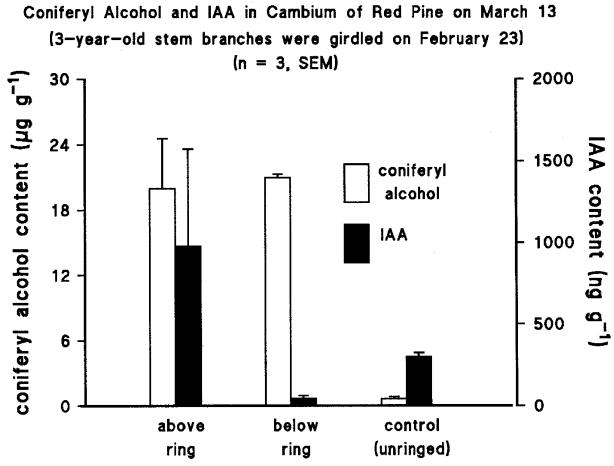

Fig. 7. Endogenous *E*-coniferyl alcohol and IAA per gram fresh weight of tissue found by isotope dilution GC/MS in dormant cambium of *Pinus resinosa* 18 days after branches were ring girdled at the three-year-old position. Standard errors of the mean are indicated for three distinct genotypes.

Coniferyl alcohol content began to increase in cambium immediately before initiation of cell-division activity in late winter (Table 1: 19 April). This perhaps explains the abrupt appearance of *E*-coniferin in early spring, it having been observed that UDPG:coniferyl alcohol glucosyltransferase activity resumes at that time (Savidge and Förster, 1998).

Our girdling experiments gave no indication that coniferyl alcohol specifically accumulated above the ring of removed bark (Fig. 7), and neither was coniferin detected by HPLC in either girdled or control tissues, in agreement with previous observations that coniferin is absent from conifer cambium during dormancy (Savidge et al., 1998). We were surprised to observe that stem girdling stimulated more than a 10-fold increase in cambial content of coniferyl alcohol below as well as above the girdle (Fig. 7). The elevated and similar levels of coniferyl alcohol above and below the girdle indicate that wounding induced coniferyl alcohol biosynthesis. Temperatures remained relatively cool from date of girdling until when tissues were harvested, ambient never exceeding 12°C and temperatures at nights commonly below zero. Water content in the tissue was that characteristic of the dormancy state (approximately 55%, in contrast to >90% during growth). Cambium both above and below the girdles remained dormant throughout the experiments, and no microscopy evidence was seen for lignification having occurred. Possibly our observations are related to induction of CAD activity by ozone and fungal elicitors (Walter et al., 1988; Galliano et al., 1993), but further research is needed to determine the nature and extent of ancillary metabolism needed to produce coniferyl alcohol in response to wounding under such limiting environmental conditions.

In contrast to coniferyl alcohol, the phytohormone IAA accumulated above the girdle and decreased below, relative to non-girdled control branches (Fig. 7). This confirms an earlier report of IAA being exported from needles and buds and moving basipetally in the dormant stem (Savidge and Wareing, 1982), and it is additional evidence that the heightened coniferyl alcohol content found below the girdles cannot be explained in terms of export from another source.

Biosynthesis of coniferyl alcohol by cambium when there is neither lignification occurring nor any obvious need for it in support of lignification agrees with the observation that coniferin is also generated quite precociously in relation to its perceived role in lignification (Savidge, 1989; Savidge et al., 1998; Savidge and Förster, 1998; Förster et al., 2000). As previously noted (Savidge, 1989), the evidence indicates that monolignol biosynthesis and lignification are distinct, developmentally uncoupled phenomena, and it follows that CAD activity is not specific to lignin synthesis. During xylogenesis, a mechanism must operate to allocate monolignols to lignification.

3. Experimental

3.1. General experimental procedures

Reversed-phase HPLC was performed at 5 ml/min according to Savidge (1989) on a Milton Roy system connected to a semi-preparative C18 ODS Ultrasphere column (Beckman, 5 µm spheres, 150×10 mm i.d.). Protein was determined by the method of Lowry et al. (1951) with bovine serum albumin for calibration, and measured at 578 nm.

Table 1
Endogenous coniferyl alcohol content per gram fresh weight in dormant tissues of *Pinus* spp. as estimated by isotope-dilution GC/MS

Tissue analyzed	Date harvested	Coniferyl alcohol (μg/g)	Comments
Terminal buds from a 15-year-old *P. resinosa*	6 February	0.44	Bud scales were included
One-year-old needles from a 15-year-old *P. resinosa*	6 February	0.91	
One-year-old phloem and cambium from a 15-year-old *P. resinosa*	6 February	0.32	Cambium dormant, bark did not peel
Two-year-old needles from a 15-year-old *P. resinosa*	6 February	0.87	
Three-year-old needles from a 15-year-old *P. resinosa*	6 February	0.93	
Three-year-old phloem and cambium from a 15-year-old *P. resinosa*	6 February	0.32	Cambium dormant, bark did not peel
Three-year-old outer bark from a 15-year-old *P. resinosa*	6 February	0.43	Cambium dormant, bark did not peel
Cambial region from a 3 year-old branch of a 15 year-old *P. resinosa*	13 March	0.42	Cambium dormant, bark did not peel
Cambial region from a 3 year-old branch of a 15 year-old *P. strobus*	31 March	1.85	Cambium dormant, bark did not peel
Cambial zone from the 3 year-old main stem of a 15 year-old *P. strobus*	9 April	1.81	Bark peeled, CZ on wood only, Cambium dormant
Cambial zone from the 4 year-old main stem of a 12 year-old *P. strobus*	19 April	6.52	Bark peeled, CZ on wood, protoplasm Cleaning but no cell division activity yet

3.2. Plant material

Eastern white pine (*Pinus strobus* L., 12- to 18-year-old) and red pine (*Pinus resinosa* Ait., 12-year-old) trees growing in the University of New Brunswick woodlot, Fredericton, NB, Canada, were used for these investigations. Girdling during winter of three red pine trees was done by cutting the bark with a sharp razor blade around the circumferences of branches. Two rings, one centimetre apart, were cut in the central region of three-year-old internodes of seven-year-old branches. The bark and cambial zone were removed from between the two cuts by scraping down to the wood with a knife. All lateral branches basal to the girdle were cut off and all basal-to-girdle needles were also removed from the main axis of each of the seven-year-old branches investigated. The investigation was repeated during two successive winters with the same result (Fig. 7).

3.3. Microsome preparation

Eastern white pine (12- to 18-year-old) was harvested in late May and thereafter. Stem segments from the main axis were removed by hand saw and immediately transferred to the laboratory for processing. Handcut sections were examined by microscopy to determine the stage of cambial growth, as previously described (Savidge et al., 1998; Savidge, 2000), and only developing xylem exhibiting secondary-wall formation was used. To isolate developing xylem, the bark was scored along the long axis with a razor sharp knife and peeled from the wood as previously described (Savidge et al., 1982, 1998). The tissue on the exposed wood surface was scraped into cryovials and immediately submerged in liquid nitrogen, where it was continually maintained until processed for microsomes.

All subsequent processing was done at 4°C, pre-cooling all equipment before use. Pre-weighed developing xylem (10–15 g) was ground in mortar with pestle in the presence of extraction buffer (1 mg ml^{-1} 0.2 M sodium phosphate, containing 150 ml glycerol, 0.744 g KCl, 2.032 g $MgCl_2 \cdot 6H_2O$, 180 μl mercaptoethanol, 0.932 g Na_2EDTA adjusted to pH and made up to 1.0 l with water), and left to stand at 4°C for 30 min. The suspension was filtered through 4 layers of cheesecloth and the filtrate centrifuged 10 min at 2500×*g*; then the supernatant was decanted and re-centrifuged 20 min at 23,500 ×*g*. The supernatant was decanted and again centrifuged 1 h at 100,000 ×*g*. The supernatant was discarded and the 100,000 ×*g* pellet re-suspended in extraction buffer, homogenized in a 15 ml Wheaton Tissue grinder, again centrifuged 1 h at 100,000×*g*, and the supernatant again discarded. The pellet was suspended in 3 ml of sodium phosphate buffer (0.1 M, pH 7.6), homogenized in a Wheaton Tissue grinder, measured for protein content, and adjusted to a protein content of 3 mg ml^{-1}. Microsomes prepared in this way were used immediately.

3.4. Microsomal incubation

Microsomes (3 mg protein equivalent) prepared as described and suspended in sodium phosphate buffer (0.1 M, pH 7.6) were provided 1 mM *E*-coniferaldehyde (Sigma-Aldrich) and 1 mM NADPH (Sigma-Aldrich), incubated at ambient temp. and stopped after 1, 4 and 8 h by addition of HOAc (100 μl). Controls containing microsomes and NADPH in buffer were stopped after 1 h. The stopped incubations were centrifuged (23,500×*g*, 4°C, 10 min). The supernatant was extracted three times

with an equal volume of EtOAc and the three EtOAc extracts combined and dried under nitrogen. The microsomal pellet was extracted overnight with EtOAc, centrifuged (23,500×*g*, 4°C, 10 min) and the EtOAc dried under nitrogen, derivatized with N,O-bis(trimethylsilyl)trifluoroacetimide (Pierce) and heated at 70°C for 1 h prior to GC/MS.

3.5. Gas chromatography — mass spectrometry

Fractions collected from the HPLC were freeze dried, transferred to tapered microvials in MeOH, dried under nitrogen, derivatised with *N,O*-bis(trimethylsilyl)trifluoroacetimide (BSTFA, Pierce), capped and heated at 70°C for 1 h prior to GC/MS. Combined gas chromatography–mass spectroscopy (HP 5890A GC, HP 5970B MS, HP 59970C ChemStation) was done in scanning mode (*m*/*z* 70–500) or selected-ion monitoring mode (coniferyl alcohol: *m*/*z* 309, 324, 315, 330; dihydroconiferyl alcohol: *m*/*z* 206, 311, 326; IAA: *m*/*z* 202, 208, 319, 325). Splitless injections into a deactivated glass liner at 200°C were separated using a 30-m HP-1 (0.25 mm i.d., 1 μm cross-linked methylsilicone) open tubular column, temperature programming from 40 to 300°C at 16°C/min, He flowing at 0.5 ml/min. The ion source (EI) was at 70 eV. Endogenous D-(+)-pinitol was confirmed to be associated with microsomes using a D-(+)-pinitol standard (Sigma-Aldrich) and analysing the pentatrimethylsilyl derivative.

3.6. $^{13}C_6$-coniferyl alcohol synthesis

$^{13}C_6$-Coniferyl alcohol was produced by a slightly modified method of Daubresse et al., 1994). Vanillin (100 mg, ring-$^{13}C_6$, 99%, Cambridge Isotope Laboratories CLM-1515) was acetylated using pyridine-acetic anhydride (1:1 v/v, 1.0 ml) in a sealed vial at 120°C for 1 h, cooled on ice and extracted thrice with equal volumes of CH_3Cl. The combined CH_3Cl extracts were dried under a stream of N_2. CH_2Cl_2 (1.76 ml), Tris-[2-(2-methoxyethoxy)-ethyl]amine (TDA-1, 0.167 g), and saturated aqueous K_2CO_3 (2.76 ml) were added to a 10 ml tapered reacti-vial and stirred vigorously to form an emulsion. Acetylated vanillin (~126 mg) dissolved in CH_2Cl_2 (1 ml) and (1,3-dioxolan-2-yl)methyltriphenylphosphonium bromide (0.333 g) were added to the emulsion, and it was left overnight at room temp., stirring slowly. The organic phase (upper layer) was removed to a clean 10 ml tapered reacti-vial, and the aqueous residue was extracted twice with CH_2Cl_2 (2×2.6 ml) and the CH_2Cl_2 extracts combined with the organic layer. HCl (10%, 2.6 ml) was added to CH_2Cl_2 and the solution was stirred for 12 h at room temp. The aqueous phase (upper layer) was decanted, diluted by addition of 4 ml H_2O, and extracted with CH_2Cl_2 (2×2.6 ml). After combining these CH_2Cl_2 extracts with the organic phase, it was washed with saturated $NaHCO_3$ (2 ml) followed by saturated NaCl (2 ml). Dry $MgSO_4$ (50 mg) was added to dry the organic layer, and the CH_2Cl_2 was then centrifuged (3000 × *g*) and the supernatant evaporated under a stream of N_2. The dry material was dissolved in CH_2Cl_2: EtOAc (90:10) and subjected to high performance liquid chromatography (normal phase silica gel, 5 μm, 10 mm i.d.×150 mm column, Jones Chromatography) using isocratic conditions (CH_2Cl_2–EtOAc 90:10, 5 ml min^{-1}) and monitoring at λ 260 nm. The major peak eluting from 2–4 min was collected, and that fraction combined from successive HPLC runs was dried under N_2 to yield a dark brown oil. The oil was dissolved in MeOH and stored at −18°C to yield, by GC–MS of the non-derivatized compound, crystals of *E*-3-(4-acetoxy-3-methoxyphenyl)-2-propenal. The crystals were recovered by filtration through GF/F glass microfibre (Whatman), dissolved in MeOH and transferred to a reacti-vial (7 ml MeOH). Under a stream of N_2, KH_2PO_4 (0.612 g) was added, then the solution was chilled in an ice bath and $NaBH_4$ (42.5 mg) slowly added, followed by stirring for 1 h at 0°C. Ice cold H_2O (7 ml) was added slowly and the solution adjusted to pH 4 (5% aqueous HCl) followed by removal of the MeOH in vacuo by rotary evaporation at 30°C. The aqueous residue was extracted with CH_2Cl_2 (3×5 ml), the combined CH_2Cl_2 extracts washed with H_2O (2×5 ml), dried with $MgSO_4$, centrifuged at 3000 rpm, and the CH_2Cl_2 dried to give a yellowish oil of *E*-3-(4-acetoxy-3-methoxyphenyl)-2-propen-1-ol (AMPP), which after trimethylsilylation yielded the expected M^+ 294 by GC–MS. AMPP was dissolved in 95% ethanol- 0.2 M KOH (8 ml) that had been pre-purged with N_2 and stirred for 12 h under N_2 at 0°C. H_2O (5 ml) was added and the pH of the suspension adjusted using 5% aqueous HCl with stirring until a clear solution was obtained (pH 4.0), followed by removal of the EtOH in vacuo by rotary evaporation at 30°C. The aqueous residue was extracted with peroxide-free diethyl ether (3×5 ml), the combined ether extracts washed with H_2O (2×2 ml), the ether dried with $MgSO_4$, centrifuged at 3000 rpm, and the supernatant evaporated under N_2. Following reversed phase C_{18} HPLC purification using conditions previously described (Savidge, 1989), pure ring-$^{13}C_6$ *E*-coniferyl alcohol, as confirmed by GC–MS, ^{13}C and ^1H NMR, was obtained. The yield was approximately 10 mg.

3.7. Coniferyl alcohol and IAA extraction, purification and quantification

Tissues were ground in liquid nitrogen in a mortar with a pestle. The powder was weighed and extracted with potassium phosphate buffer (0.1 M, pH 7.0) containing a known mass of $^{13}C_6$-coniferyl alcohol and a known mass of $^{13}C_6$-IAA (Cambridge Isotope

Laboratories). The samples were frozen and thawed, then centrifuged (20,000×*g*, 4°C, 10 min). The supernatant was partitioned thrice against ethyl acetate (EtOAc), the EtOAc extracts combined and dried under nitrogen. The dry residue was dissolved in a small volume of MeOH, adjusted to 5% MeOH with pH 3.0 acetic acid, and purified by reversed phase C_{18} HPLC, collecting the fractions corresponding to standard coniferyl alcohol and IAA. The collected fractions were dried in vacuo by rotary evaporation at 30°C, trimethylsilylated with BSTFA and analysed in selected ion monitoring mode by GC/MS (coniferyl alcohol *m*/*z* 330, 324, 315, 309; IAA *m*/*z* 325, 319, 208, 202).

Acknowledgements

The research was supported by an NSERC research grant to R.A.S. and a Grant-in-Aid (FO 271/4-1) of the Deutsche Forschungsgemeinschaft (Bonn, Germany) to H.F.

References

Chen, F., Yasuda, S., Fukushima, K., 1999. Evidence for a novel biosynthetic pathway that regulates the ratio of syringyl to guaiacyl residues in lignin in the differentiating xylem of *Magnolia kobus* DC. Planta 207, 597–603.

Conde, E., Cadahia, E., Garcia Vallejo, M.C., DeSimon, B.F., Adrados, J.R.G., 1997. Low molecular weight polyphenols in cork of *Quercus suber*. Journal of Agricultural and Food Chemistry 45, 2695–2700.

Daniel, G., Nilsson, T., Pettersson, B., 1991. Poorly and non-lignified regions in the middle lamella cell corners of birch (*Betula verrucosa*) and other wood species. IAWA Bulletin, new series 12, 70–83.

Daubresse, N., Francesch, C., Mhamdi, F., Rolando, C., 1994. A mild synthesis of coumaryl, coniferyl, sinapyl aldehydes and alcohols. Synthesis, April 1994, 369–371.

Desmet, J., 1961. Extraction et purification: deux problèmes fondamentaux dans l'étude des lignines. Association of Technical & Industrial Papermaking 1961, 67–70.

Downes, G.M., Ward, J.V., Turvey, N.D., 1991. Lignin distribution across tracheid cell walls of poorly lignified wood from deformed copper deficient *Pinus radiata* (D. Don). Wood Science & Technology 25, 7–14.

Eklund, L., Klintborg, A., 2000. Ethylene, oxygen and carbon dioxide in woody stems during growth and dormancy. In: Savidge, R.A., Barnett, J.R., Napier, R. (Eds.), Cell and Molecular Biology of Wood Formation. BIOS, Oxford, pp. 43–56.

Fergus, B.J., Goring, D.A.I., 1970. The location of guaiacyl and syringyl lignins in birch xylem tissue. Holzforschung 24, 113–117.

Fernàndez de Simòn, B., Cadahia, E., Conde, E., Garcìa-Vallejo, M.C., 1996. Low molecular weight phenolic compounds in spanish oak woods. Journal of Agricultural and Food Chemistry 44, 1507–1511.

Fillgrove, K.L., Anderson, V.E., 2000. Orientation of coenzyme A substrates, nicotinamide and active site functional groups in (di)enoyl-coenzyme A reductases. Biochemistry 39, 7001–7011.

Förster, H., Pommer, U., Savidge, R.A., 1999. Metabolic activity of uridine 5′-diphosphoglucose:cinnamyl alcohol glucosyltransferase as an intrinsic indicator of cambial growth in conifers. In: Gross, G.G., Hemingway, R.W., Yoshida, T. (Eds.), Plant Polyphenols 2: Chemistry, Biology, Pharmacology, Ecology. Kluwer/Plenum, New York, Boston, Dordrecht, London, Moscow, pp. 371–392.

Förster, H., Steeves, V., Pommer, U., Savidge, R.A., 2000. UDPG:-coniferyl alcohol glucosyltransferase and coniferin biosynthesis — a regulatory link to seasonal cambial growth in conifers. In: Savidge, R.A., Barnett, J.R., Napier, R. (Eds.), Cell and Molecular Biology of Wood Formation. BIOS, Oxford, pp. 189–201.

Freudenberg, K., Neish, A.C., 1968. Constitution and Biosynthesis of Lignin. Springer, New York.

Fukushima, K., Imai, T., Terashima, N., 1994. Heterogeneous lignification in one-year-old shoots of trees I. Characterization of cell wall components in the various tissues of a one-year-old poplar shoot. Mokuzai Gakkaishi 40, 958–965.

Galliano, H., Cabané, M., Eckerskorn, C., Lotspeich, F., Sandermann, H., Ernst, D., 1993. Molecular cloning, sequence analysis and elicitor — ozone-induced accumulation of cinnamyl alcohol dehydrogenase from Norway spruce (*Picea abies* L.). Plant Molecular Biology 23, 145–156.

Gang, D.R., Costga, M.A., Fujita, M., Dinkova-Kostova, A.T., Wang, H.B., Burlat, V., Martin, W., Sarkanen, S., Davin, L.B., Lewis, N.B., 1999. Regiochemical control of monolignol radical coupling: a new paradigm for lignin and lignan biosynthesis. Chemistry and Biology 6, 143–151.

Goffner, D., Vandoorsselaere, J., Yahiaoui, N., Samaj, J., Grimapettenati, J., Boudet, A.M., 1998. A novel aromatic alcohol dehydrogenase in higher plants. Molecular cloning and expression. Plant Molecular Biology 36, 755–765.

Halpin, C., Abbott, J., Barakate, A., 2000. Investigating lignin biosynthesis using transgenic mutant plants. In: Savidge, R.A., Barnett, J.R., Napier, R. (Eds.), Cell and Molecular Biology of Wood Formation. BIOS, Oxford, pp. 425–436.

Hirata, T., Shimoda, K., Gondai, T., 2000. Asymmetric hydrogenation of the C–C double bond of enones with the reductases from *Nicotiana tabacum*. Chemistry Letters 72, 850–851.

Humphreys, J.M., Hemm, M.R., Chapple, C., 1999. New routes for lignin biosynthesis defined by biochemical characterization of recombinant ferulate 5-hydroxylase, a multifunctional cytochrome P450-dependent monooxygenase. Proceedings of the National Academy of Sciences USA 96, 10045–10050.

Hrazdina, G., Wagner, G.J., 1985. Metabolic pathways as enzyme complexes: evidence for the synthesis of phenylpropanoids and flavonoids on membrane associated enzyme complexes. Archives of Biochemistry and Biophysics 237, 88–100.

Kim, Y.S., Meshnitsuka, G., Ishizu, A., 1994. Structural heterogeneity of lignin. Contribution of carbon–carbon bonds. Mokuzai Gakkaishi 40, 407–413.

Kim, Y., Iiyama, K., Kurahashi, A., Meshitsuka, G., 1995. Structural feature of lignin in cell walls of normal and fast-growing poplar (*Populus maximowiczii* Henry). Linkage types of wall-bound hydroxybenzoic and hydroxycinnamic acids. Mokuzai Gakkaishi 41, 837–843.

Košíková, B., Mlynár, J., Zákutná, L., Joniak, D., Micko, M., 1990. The relationship between ultrastructure and lignin extractability of steamed hardwoods. Holzforschung 44, 249–255.

Kretz, A., 1973. Zucker, Cyclite und organische Säuren des Cambialsaftes von *Pinus silvestris* L., *Picea abies* Karst. und *Abies alba* Mill. Planta (Berlin) 110, 1–14.

Kuroda, K., Yamaguchi, A., Sakai, K., 1994. Analysis of Sugi wood and its lignin preparation by pyrolysis–gas chromatography. Mokuzai Gakkaishi 40, 987–995.

Kutscha, N.P., Gray, J.R., 1972. The suitability of certain stains for studying lignification in balsam fir, *Abies balsamea* (L.) Mill. Tech. Bull. No. 53, Life Sciences Agricultural Experiment Station, University of Maine, Orono.

Kwon, M., Burlat, V., Davin, L.B., Lewis, N.G., 1999. Localization of dirigent protein involved in lignan biosynthesis: implications for lignification at the tissue and subcellular level. In: Gross, G.G., Hemingway, R.W., Yoshida, T. (Eds.), Plant Polyphenols 2: Chemistry, Biology, Pharmacology, Ecology. Kluwer/Plenum, New York, Boston, Dordrecht, London, Moscow, pp. 393–411.

Larsson, S., Quintana-Sainz, A., Reimann, A., Nilvebrant, N.O., Jonsson, L.J., 2000. Influence of lignocellulose-derived aromatic

compounds on oxygen-limited growth and ethanolic fermentation by *Saccharomyces cerevisiae*. Applied Biochemistry and Biotechnology 84- 86, 617–632.

Lee, T.S., Purse, J.G., Pryce, R.C., Horgan, R., Wareing, P.F., 1981. Dihydroconiferyl alcohol — a cell division factor from *Acer* species. Planta 152, 571–577.

Lewis, N.G., Davin, L.B., 1998. The biochemical control of monolignol coupling and structure during lignan and lignin biosynthesis. In: Lewis, N.G., Sarkanen, S. (Eds.), Lignin and Lignan Biosynthesis. ACS Symposium Series, Washington, DC, 697, pp. 334–361.

Lewis, N.G., 1999. A 20th century roller coaster ride: a short account of lignification. Current Opinion in Plant Biology 2, 153–162.

Li, L., Popko, J.L., Zhang, X.-H., Osakabe, K., Tsai, C.-J., Joshi, C.P., Chiang, V.L., 1997. A novel multifunctional *O*-methyltransferase implicated in a dual methylation pathway associated with lignin biosynthesis in loblolly pine. Proceedings of the National Academy of Sciences, USA 94, 5431–5466.

Li, L., Zhang, X.-H., Joshi, C.P., Chiang, V.L., 1998. Compression stress responsive expression of ferritin and peroxidase genes in developing xylem of loblolly pine (*Pinus taeda* L.). Plant Physiology 116, 1604–1605.

Li, L., Osakabe, Y., Joshi, C.P., Chiang, V.L., 1999. Secondary xylem-specific expression of caffeoyl-coenzyme A 3-*O*-methyltransferase plays an important role in the methylation pathway associated with lignin biosynthesis in loblolly pine. Plant Molecular Biology 40, 555–565.

Li, L., Popko, J.L., Umezawa, T., Chiang, V.L., 2000. 5-Hydroxyconiferyl aldehyde modulates enzymatic methylation for syringyl monolignol formation, a new view of monolignol biosynthesis in angiosperms. Journal of Biological Chemistry 275, 6537–6545.

Löwendahl, L., Petersson, G., Samuelson, O., 1978. Phenolic compounds in kraft black liquor. Svensk Papperstidn 81, 392–396.

Lowry, O.H., Rosebrough, N.J., Farr, A.L., Randall, R.J., 1951. Protein measurement with the Folin phenol reagent. Journal of Biological Chemistry 193, 265–275.

MacDonald, R.C., Kimmerer, T.W., 1991. Ethanol in the stems of trees. Physiologia Plantarum 82, 582–588.

Matsui, N., Chen, F., Yasuda, S., Fukushima, K.N., 2000. Conversion of guaiacyl to syringyl moieties on the cinnamyl alcohol pathway during the biosynthesis of lignin in angiosperms. Planta 210, 831–835.

Maurer, A., Fengel, D., 1990. A new process for improving the quality and lignin staining of ultrathin sections from wood tissue. Holzforschung 44, 453–460.

Neish, A.C., 1960. Biosynthetic pathways of aromatic compounds. Annual Review of Plant Physiology 11, 55–80.

Niemelä, K., 1989. GLC–MS studies on pine kraft black liquors. Holzforschung 43, 99–103.

Niku-Paavola, M.-L., 1991. Isoelectric focusing electrophoresis of lignin. Analytical Biochemistry 197, 101–103.

Obst, J.R., Kent Kirk, T., 1988. Isolation of lignin. In: Willis, A., Kellogg, S.T. (Eds.), Methods in Enzymology — Biomass, Part B, Lignin, Pectin, and Chitin, Vol. 167. Academic Press, San Diego, pp. 3–12.

Orthen, B., Popp, M., Smirnoff, N., 1994. Hydroxyl radical scavenging properties of cyclitols. Proceedings of the Royal Society of Edinburgh 102B, 269–272.

Osakabe, K., Tsao, C.C., Li, L., Popko, J.L., Umezawa, T., Carraway, D.T., Smeltzer, R.H., Joshi, C., Chiang, V.L., 1999. Coniferyl aldehyde 5-hydroxylation and methylation direct syringyl lignin biosynthesis in angiosperms. Proceedings of the National Academy of Sciences USA 96, 8955–8960.

Parham, R.A., Côté Jr., W.A., 1971. Distribution of lignin in normal and compression wood of *Pinus taeda* L.. Wood Science & Technology 5, 49–62.

Peng, F.H., Westermark, U., 1997. Distribution of coniferyl alcohol and coniferaldehdye groups in the cell wall of spruce fibers. Holzforschung 51, 531–536.

Ralph, J., MacKay, J.J., Hatfield, R.D., O'Malley, D.M., Whetten, R.W., Sederoff, R.R., 1997. Abnormal lignin in a loblolly pine mutant. Science 277, 235–239.

Saka, S., Whiting, P., Fukazawa, K., Goring, D.A.I., 1982. Comparative studies on lignin distribution by UV microscopy and bromination combined with EDXA. Wood Science & Technology 16, 269–277.

Sakakibara, A., Sasaya, T., Miki, K., Takahashi, H., 1987. Lignans and Brauns' lignins from softwoods. Holzforschung 41, 1–11.

Savidge, R.A., 1987. Dihydroconiferyl alcohol in developing xylem of *Pinus contorta*. Phytochemistry 26, 93–94.

Savidge, R.A., 1989. Coniferin, a biochemical indicator of commitment to tracheid differentiation in conifers. Canadian Journal of Botany 67, 2663–2668.

Savidge, R.A., 1996. Xylogenesis, genetic and environmental regulation — a review. IAWA Journal 17, 269–310.

Savidge, R.A., 2000. Biochemistry of seasonal cambial growth and wood formation — an overview of the challenges. In: Savidge, R.A., Barnett, J.R., Napier, R. (Eds.), Cell and Molecular Biology of Wood Formation. BIOS, Oxford, pp. 1–30.

Savidge, R.A., Förster, H., 1998. Seasonal activity of uridine 5′-diphosphoglucose: coniferyl alcohol glucosyltransferase in relation to cambial growth and dormancy in conifers. Canadian Journal of Botany 76, 486–493.

Savidge, R.A., Wareing, P.F., 1982. Apparent auxin production and transport in the non-growing pine tree. Canadian Journal of Botany 60, 681–691.

Savidge, R.A., Heald, J.K., Wareing, P.F., 1982. Non-uniform distribution and seasonal variation of endogenous indol-3-yl-acetic acid in cambial region of *Pinus contorda* Dougl.. Planta 155, 89–92.

Savidge, R.A., Udagama-Randeniya, P. V., Xu, Y., Leinhos, V., Förster, H., 1998. Coniferyl alcohol oxidase, a new enzyme of lignification. In: Lewis, N.G., Sarkanen, S. (Eds.), Lignin and Lignan Biosynthesis. ACS Symposium Series 697, pp. 109-130.

Sederoff, R.R., MacKay, J.J., Ralph, J., Hatfield, R.D., 1999. Unexpected variation in lignin. Current Opinion in Plant Biology 2, 145–152.

Steeves, V.J., Savidge, R.A., 2000. Cambial coniferin content as an indicator of the health status of conifers. In: Savidge, R.A., Barnett, J.R., Napier, R. (Eds.), Cell and Molecular Biology of Wood Formation. BIOS, Oxford, pp. 57–65.

Sy, L.K., Brown, G.D., 1999. Coniferaldehyde derivatives from tissue culture of *Artemisia annua* and *Tanacetum parthenium*. Phytochemistry 50, 781–785.

Tanaka, N., Wada, H., Fuchino, H., Inoue, T., Yasuda, D., Kanda, S., Kiyowaka, C., Ashida, N., Suzuki, T., Yamazaki, K., Hakamatsuka, T., 1998. Constituents of bamboos and bamboo grasses. Yakugaku Zasshi 118, 332–337.

Terashima, N., Fukushima, K., Takabe, K., 1986. Heterogeneity in formation of lignin VIII. An autoradiographic study on the formation of guaiacyl and syringyl lignin in *Magnolia kobus* DC. Holzforschung 40 (Suppl.), 101-105.

Terashima, N., Fukushima, K., 1988. Heterogeneity in formation of lignin — XI. An autoradiographic study of the heterogeneous formation and structure of pine lignin. Wood Science & Technology 22, 259–270.

Terashima, N., Fukushima, K., Sano, Y., 1988. Heterogeneity in formation of lignin X. Visualization of lignification process in differentiating xylem of pine by microautoradiography. Holzforschung 42, 347–350.

Walter, M.H., Grima-Pettenati, J., Grand, C., Boudet, A.M., Lamb, C.J., 1988. Cinnamyl-alcohol dehydrogenase, a molecular marker specific for lignin synthesis: cDNA clonging and mRNA induction by fungal elicitor. Proceedings of the National Academy of Sciences USA 85, 5546–5550.

Wardrop, A.B., 1981. Lignification and xylogenesis. In: Barnett, J.R. (Ed.), Xylem Cell Development. Castle House, Tunbridge Wells, UK, pp. 115–152.

Wilson, M.A., Sawyer, J., Hatcher, P.G., Lerch, H.E., 1989. 1,3,5-Hydroxybenzene structures in mosses. Phytochemistry 28, 1395–1400.

Wood, J.R., Goring, D.A.I., 1971. The distribution of lignin in stem wood and branch wood of Douglas fir. Pulp and Paper Magazine Canada 72, T95–T102.

PERGAMON

Phytochemistry 57 (2001) 1105–1113

PHYTOCHEMISTRY

www.elsevier.com/locate/phytochem

Oxidation of cinnamyl alcohols and aldehydes by a basic peroxidase from lignifying *Zinnia elegans* hypocotyls

A. Ros Barceló *, F. Pomar

Department of Plant Biology (Plant Physiology), University of Murcia, E-30100 Murcia, Spain

Received 7 June 2000; received in revised form 1 November 2000

Abstract

The xylem of 26-day old *Zinnia elegans* hypocotyls synthesizes lignins derived from coniferyl alcohol and sinapyl alcohol with a G/S ratio of 43/57 in the aryl-glycerol-β-aryl ether core, as revealed by thioacidolysis. Thioacidolysis of *Z. elegans* lignins also reveals the presence of coniferyl aldehyde end groups linked by β-*0*-4 bonds. Both coniferyl and sinapyl alcohols, as well as coniferyl and sinapyl aldehyde, are substrates of a xylem cell wall-located strongly basic peroxidase, which is capable of oxidizing them in the absence and in the presence of hydrogen peroxide. This peroxidase shows a particular affinity for cinnamyl aldehydes with k_M values in the μM range, and some specificity for syringyl-type phenols. The affinity of this strongly basic peroxidase for cinnamyl alcohols and aldehydes is similar to that shown by the preceding enzymes in the lignin biosynthetic pathway (microsomal 5-hydroxylases and cinnamyl alcohol dehydrogenase), which also use cinnamyl alcohols and aldehydes as substrates, indicating that the one-way highway of construction of the lignin macromolecule has no metabolic "potholes" in which the lignin building blocks might accumulate. This fact suggests a high degree of metabolic plasticity for this basic peroxidase, which has been widely conserved during the evolution of vascular plants, making it one of the driving forces in the evolution of plant lignin heterogeneity.
© 2001 Elsevier Science Ltd. All rights reserved.

Keywords: Cinnamyl alcohols; Cinnamyl aldehydes; Lignification; Peroxidase; Xylem; *Zinnia elegans*

1. Introduction

Lignins are complex cell wall phenolic heteropolymers covalently associated with both polysaccharides and proteins (Lewis et al., 1999). They are mainly localized in the impermeable water transport conduits of the xylem and other supporting tissues, and result from the oxidative polymerization of cinnamyl alcohols in a reaction that is mediated by both peroxidases (Ros Barceló, 1995; Wallace and Fry, 1999) and H_2O_2-independent oxidases (Bao et al., 1993; Sterjiades et al., 1993), leading to an optically inactive heteropolymer (Ros Barceló, 1997; Lewis, 1999). Although most of the building blocks found in natural lignins are mainly derived from cinnamyl alcohols, recent evidence has suggested that cinnamyl aldehydes are also incorporated in the growing lignin polymer (Higuchi et al., 1994; Lapierre et al., 1995), a situation which is especially evident in CAD (cinnamyl alcohol dehydrogenase)-depleted mutant or transgenic plants (Ralph et al., 1997; Lapierre et al., 1999). Even in wild-type plants, a certain amount of cinnamyl aldehydes escapes reduction by CAD, and accumulates in plant cells in their free forms (Osakabe et al., 1999) or as derivatives (Sy and Brown, 1999). These cinnamylaldehydes may then be deposited in the xylem cell walls, where they co-polymerize with cinnamyl alcohols to yield a highly heterogeneous alcohol/aldehyde lignin polymer (Higuchi et al., 1994). This escape of cinnamyl aldehydes from reduction to cinnamyl alcohols is co-substantial with the nature of the CAD-catalyzed reaction. In fact, CAD catalyzes the following reaction:

$$\text{cinnamyl aldehyde} + \text{NADPH} + \text{H}^+ \leftrightarrows \text{cinnamyl alcohol} + \text{NADP}^+$$

which is no more than an equilibrium. This means that if cinnamyl alcohols are not removed either by transport or conjugation, a certain amount of cinnamyl aldehydes,

* Corresponding author. Fax: +34-968-363-963.
E-mail address: rosbarce@um.es (A.R. Barceló).

0031-9422/01/$ - see front matter © 2001 Elsevier Science Ltd. All rights reserved.
PII: S0031-9422(01)00050-4

depending on the NADPH/$NADP^+$ cellular pool, will escape from CAD-mediated reduction. It might be expected that these aldehydes, together with their corresponding cinnamyl alcohols, would ultimately be incorporated into the cell wall lignins. The formation of these highly heterogeneous red lignins, which results from both cinnamyl aldehyde and cinnamyl alcohol copolymerization, apparently occurs in the xylem of *Z. elegans* hypocotyls, as is deduced from the dye reaction of the *Z. elegans* xylem with the phloroglucinol/HCl test (Ros Barceló and Aznar-Asensio, 1999), a specific reaction for cinnamaldehyde groups (Geiger and Fuggerer, 1979).

Zinnia elegans is a seasonal-cycle flowering plant belonging to the Asteraceae family, which is considered to be one of the most evolved families within the dicotyledon angiosperms. Cell walls of *Z. elegans* hypocotyls contain a basic peroxidase of high pI, which shows coniferyl alcohol oxidase activity (Ros Barceló and Aznar-Asensio, 1999) and which has a spectrum typical of a high spin heme class III peroxidase. This strongly basic peroxidase has been localized in the lignin-forming xylem from *Z. elegans* hypocotyls by means of competitive inhibitor-dissected histochemistry (Ros Barceló et al., 2000), and it is considered a marker of tracheary element differentiation in *Z. elegans* cell cultures (Sato et al., 1995a,b). In this work, the substrate specificity of this peroxidase, in the absence and the presence of hydrogen peroxide, for both cinnamyl alcohols and aldehydes is studied. The results illustrate that this cell wall peroxidase shows both a great affinity and a broad substrate specificity towards cinnamyl alcohols and aldehydes. This fact suggests a high degree of metabolic plasticity for this basic peroxidase, which has been widely conserved during the evolution of vascular plants (Ros Barceló et al., 1998), making it one of the driving forces in the evolution of plant lignin heterogeneity.

2. Results and discussion

2.1. Cinnamyl alcohols and cinnamyl aldehydes in the lignifying xylem of Z. elegans hypocotyls

The lignifying xylem from *Z. elegans* hypocotyls gives rise to an intense reaction with both the Maüle ($KMnO_4$) reagent and the Wiesner (phloroglucinol) test (Ros Barceló and Aznar-Asensio, 1999). Since the Maüle reaction is specific for syringyl moieties in lignins (Meshitsuka and Nakano, 1979), while the Wiesner test is specific for cinnamaldehyde groups (Geiger and Fuggerer, 1979), it was concluded that lignins from the *Z. elegans* xylem are rich in syringyl moieties and cinnamaldehyde groups.

To confirm these initial observations on the nature and heterogeneity of *Z. elegans* lignins, cell walls isolated from lignifying *Z. elegans* hypocotyls were subjected to thioacidolysis, and the recovered thioethylated monomers were analyzed by gas chromatography-mass spectrometry. The results showed that thioacidolysis of lignifying *Z. elegans* cell walls gave, as main products, the thioethylated monomers (both *erythro* and *threo* isomers) arising from aryl-glycerol-β-aryl ether structures derived from coniferyl [$m/z = 269$ (100), 75 (18) 73 (15) 235 (8)] and sinapyl [$m/z = 299$ (100), 73 (20) 265 (6)] alcohols. The guaiacyl (G)/syringyl (S) molar ratio for this β-*O*-4 lignin fraction was 43/57. In addition to these thioethylated monomers, thioacidolysis also revealed the presence of significant amounts of the thioethylated monomer arising from the coniferyl aldehyde end group [$m/z = 269$ (100), 73 (57) 135 (6), 209 (5), 295 (4), 239 (4), 192 (3), 418 (1)]. These results suggest that the linear β-*O*-4 lignin fraction from *Z. elegans* hypocotyls contains both coniferyl and sinapyl alcohols to approximately the same extent and, additionally, *O*-4 coniferyl aldehyde-end groups.

2.2. Oxidation of cinnamyl alcohols and cinnamyl aldehydes by cell walls isolated from lignifying Z. elegans hypocotyls

Since coniferyl alcohol, sinapyl alcohol and coniferyl aldehyde are incorporated in *Z. elegans* cell wall lignins, as revealed by thioacidolysis, the following step was to study the in situ ability of *Z. elegans* cell walls to oxidize cinnamyl alcohol and cinnamyl aldehydes. The results showed that cell walls isolated from lignifying *Z. elegans* hypocotyls were able to oxidize cinnamyl alcohols (coniferyl and sinapyl alcohol) and cinnamyl aldehydes (coniferyl and sinapyl aldehyde) in the absence and in the presence of H_2O_2 (Table 1). In fact, almost all the cinnamyl alcohols and cinnamyl aldehydes were oxidized in the presence of 500 μM H_2O_2 by lignifying cell walls within the first hour of incubation.

In the absence of H_2O_2, only minor percentages of oxidation, which never exceeded 10%, were observed (Table 1). This capacity of lignifying *Z. elegans* cell walls

Table 1
Oxidation of cinnamyl alcohols and cinnamyl aldehydes by cell walls isolated from lignifying *Zinnia elegans* hypocotyls

Substrate	μmol Substrate oxidized g^{-1} FW[a]	
	$-H_2O_2$	$+H_2O_2$
Coniferyl alcohol	0.04±0.03 (8.2)	0.48±0.00 (92)
Coniferyl aldehyde	0.02±0.01 (4.1)	0.52±0.02 (100)
Sinapyl alcohol	0.01±0.00 (1.1)	0.52±0.01 (100)
Sinapyl aldehyde	0.01±0.00 (1.9)	0.52±0.01 (100)

[a] The reaction medium contained 50 mM Tris–acetate pH 5.0, an amount of cell walls equivalent to 0.2 g FW, 50 μM of each substrate and, when used, 500 μM H_2O_2, in a total volume of 2.0 ml, which was incubated at 25°C for 2 h. Values are means±S.E. ($n = 3$). Values in parentheses correspond to the percentage of substrate oxidized.

to oxidize coniferyl alcohol, both in the absence and in the presence of H_2O_2, has previously been demonstrated to reside in a cell wall-located class III basic peroxidase (Ros Barceló and Aznar-Asensio, 1999), whose catalytic properties against cinnamyl alcohols and aldehydes were the next subject of study.

2.3. Oxidation of cinnamyl alcohols and cinnamyl aldehydes by the basic peroxidase isolated from lignifying Z. elegans hypocotyls

The oxidation of cinnamyl alcohols and aldehydes by the *Z. elegans* basic peroxidase was monitored by the decay in absorbance in the ultraviolet region. For this, the extinction coefficients for the substrates (coniferyl alcohol, coniferyl aldehyde, sinapyl alcohol and synapyl aldehyde), and the extinction coefficients for each one of the oxidative reactions, $\Delta\varepsilon = \varepsilon_s - \varepsilon_p$ (where ε_s is the extinction coefficient for the substrate and ε_p is the extinction coefficient for the oxidation products), were determined at maximal wavelength by measuring the oxidation of the respective substrates, in the presence of the *Z. elegans* basic peroxidase and an excess of H_2O_2, until no further changes in the spectra occurred. The extinction coefficients calculated are given in Table 2.

Similarly to lignifying *Z. elegans* cell walls (Table 1), the *Z. elegans* basic peroxidase was also capable of oxidizing the two cinnamyl alcohols and the two cinnamyl aldehydes, both in the absence and in the presence of H_2O_2 (Table 3). In the presence of H_2O_2, the catalytic activity of *Z. elegans* peroxidase was in the order: sinapyl alcohol > sinapyl aldehyde > coniferyl aldehyde > coniferyl alcohol (Table 3). This means that *Z. elegans* peroxidase oxidizes sinapyl moieties better than coniferyl moieties, this substrate preference being in accordance with that recently reported for other angiosperm plant peroxidases by Wallace and Fry (1999).

When the ability of the *Z. elegans* basic peroxidase to oxidize cinnamyl (coniferyl and sinapyl) alcohols was expressed on a protein basis, it was surprisingly found that, in the absence of H_2O_2, this protein oxidizes coniferyl and sinapyl alcohol with a similar specific activity to that shown by plant laccases (Table 4). Besides, it was much more able to oxidize coniferyl alcohol than the oxidase isolated from *Pinus strobus* (Table 4), despite the class III peroxidase nature of the *Z. elegans* enzyme (Ros Barceló and Aznar-Asensio, 1999). In the presence of H_2O_2, the specific activity of the *Z. elegans* basic peroxidase against cinnamyl alcohols was substantially greater than the specific activity shown by plant laccases (Table 4), confirming the observation made by Wallace and Fry (1999) on the better catalytic activities of peroxidases compared with laccases in the lignification process.

Table 2
Extinction coefficients calculated for cinnamyl alcohols and cinnamyl aldehydes, and for their corresponding oxidative reactions ($\Delta\varepsilon$) catalyzed by peroxidase

Substrate	ε (mM^{-1} cm^{-1}) (λ [nm])	$\Delta\varepsilon$ (mM^{-1} cm^{-1}) (λ [nm])[a]
Coniferyl alcohol	17.7±1.5 [262]	9.75±0.5 [262]
Coniferyl aldehyde	20.6±0.6 [341]	13.4±0.5 [341]
Sinapyl alcohol	8.12±0.5 [271]	4.14±0.0 [271]
Sinapyl aldehyde	18.6±0.1 [340]	11.9±0.2 [340]

[a] The extinction coefficients for the oxidative reactions ($\Delta\varepsilon$) were determined by oxidation of the respective substrates by *Zinnia elegans* peroxidase in the presence of an excess of H_2O_2 until no further change in the UV spectra occurred. Values are the mean±S.E. ($n=3$).

Table 3
Oxidation rates of cinnamyl alcohols and cinnamyl aldehydes by the *Zinnia elegans* basic peroxidase at 25°C

Substrate	nmol Substrate oxidized min^{-1} g^{-1} FW[a]	
	$-H_2O_2$	$+H_2O_2$
Coniferyl alcohol	3.83±3.10	143.4±6.32
Coniferyl aldehyde	1.20±0.65	352.2±11.0
Sinapyl alcohol	12.0±8.10	467.2±7.80
Sinapyl aldehyde	3.20±2.43	409.4±11.3

[a] The reaction medium contained 50 mM Tris–acetate pH 5.0, 100 μM of each substrate and, when used, 100 μM H_2O_2. Values are means±S.E. ($n=3$).

2.4. Kinetic of the oxidation of cinnamyl alcohols and aldehydes by the Z. elegans basic peroxidase

The oxidation of cinnamyl alcohols and aldehydes by the *Z. elegans* basic peroxidase yields hyperbolic curves, as was the case for sinapyl alcohol (Fig. 1). This fits wells with the irreversible ping-pong mechanism previously validated by us for peroxidase-catalyzed reactions involved in lignin biosynthesis (Ros Barceló et al., 1998), a mechanism which is characterized by a three-step cycle involving a two-electron enzyme oxidation:

$$\mathrm{FeIII} + \mathrm{H_2O_2} \xrightarrow{k_1} \mathrm{CoI} + \mathrm{H_2O} \quad (1)$$

followed by two one-electron reductions:

$$\mathrm{CoI} + \mathrm{RH} \xrightarrow{k_2} \mathrm{CoII} + \mathrm{R^\bullet} \quad (2)$$

$$\mathrm{CoII} + \mathrm{RH} \xrightarrow{k_3} \mathrm{FeIII} + \mathrm{R^\bullet} \quad (3)$$

where FeIII, CoI, CoII and RH are the native enzyme, compound I, compound II, and the phenolic compound, respectively. The most striking characteristic of this kinetic (see Ros Barceló et al., 1998, for details) is

Table 4
Specific activity, in the absence and in the presence of H_2O_2, of the *Zinnia elegans* basic peroxidase against coniferyl and sinapyl alcohols, in comparison with other oxidases involved in the polymerization of cinnamyl alcohols to lignins

Oxidase	Specific activity (nmol s^{-1} mg^{-1} protein)				
	Coniferyl alcohol		Sinapyl alcohol		Reference
	$-H_2O_2$	$+H_2O_2$	$-H_2O_2$	$+H_2O_2$	
Zinnia elegans basic peroxidase	3.16	341.5	28.3	1112.3	
Acer pseudoplatanus acidic peroxidase	–	680	–	55.5	Sterjiades et al. (1993)
Pinus taeda laccase	72[a]	–	46.7[a]	–	Bao et al. (1993)
Acer pseudoplatanus laccase	6.6	–	18.3		Sterjiades et al. (1993)
Pinus strobus oxidase	0.085	–	–	–	Udagama-Randeniya and Savidge (1995)

[a] Activity was monitored with an O_2 electrode (Bao et al., 1993).

the lineal continuous dependence of both the apparent V_{max}^{RH} values and the apparent k_M^{RH} values for the reducing substrate (i.e. cinnamyl alcohols and aldehydes) on the H_2O_2 concentration:

$$V_{max}^{RH} = 2Ek_1[H_2O_2] \quad (4)$$

and

$$k_M^{RH} = (k_1/k_3)[H_2O_2] \quad (5)$$

as well as the lineal dependence between V_{max}^{RH} and k_M^{RH} values:

$$V_{max}^{RH} = 2Ek_3k_M^{RH} \quad (6)$$

This is also true for the dependence of both the apparent $V_{max}^{H_2O_2}$ and the apparent $k_M^{H_2O_2}$ values for H_2O_2 on the RH (cinnamyl alcohols and aldehydes) concentration (Ros Barceló et al., 1998):

$$V_{max}^{H_2O_2} = 2Ek_3[RH] \quad (7)$$

and

$$k_M^{H_2O_2} = (k_3/k_1)[RH] \quad (8)$$

where there is also a lineal dependence between the $V_{max}^{H_2O_2}$ values and $k_M^{H_2O_2}$ values:

$$V_{max}^{H_2O_2} = 2Ek_1k_M^{H_2O_2} \quad (9)$$

As expected, these kinetic lineal relationships were completely fulfilled by the basic peroxidase isolated from *Z. elegans* hypocotyls for the four substrates (coniferyl and sinapyl alcohol, and coniferyl and sinapyl aldehyde). Figs. 2 and 3 illustrate these lineal plots in the case of sinapyl alcohol.

It should be pointed out that the lineal plots of $V_{max}^{H_2O_2}$ values and $k_M^{H_2O_2}$ values against sinapyl alcohol concentration cross the coordinate origin (Fig. 2B and D), while the lineal plots of V_{max}^{RH} values and k_M^{RH} values against H_2O_2 concentration intercept the ordinate axis at a positive (non zero) value (Fig. 2A and C). This means that there is a residual activity of the *Z. elegans* basic peroxidase at zero H_2O_2 concentration, i.e. the pseudo oxidase activity that is developed by this peroxidase in the absence of exogenous H_2O_2 (see Table 3).

2.5. k_M Values for the peroxidase reaction

The best way to know the affinity of an enzyme for its substrates is to compare the apparent k_M^{RH} values, which, in the case of peroxidase, show a special peculiarity frequently forgotten in the literature: they depend on H_2O_2 concentration [see Fig. 2C and Eq. (5)]. These apparent k_M^{RH} values may also suggest for which particular metabolic reaction of the complex process of lignin assembly a given enzyme has been designed in the course of the evolution of vascular plants. An example of the importance of these values is the recent observation that microsomal 5-hydroxylases, previously named ferulate-5-hydroxylases, hydroxylate coniferyl aldehyde ($k_M = 1$–2.7 μM) and coniferyl alcohol ($k_M = 3$ μM) with a greater affinity than ferulate ($k_M = 286$–1000 μM) (Humphreys et al., 1999; Osakabe et al., 1999), so that there is a tendency to call them coniferyl aldehyde-5-hydroxylases.

This observation is particularly important in the case of peroxidase, since this enzyme is capable of performing multiple metabolic functions (Morales and Ros Barceló, 1997), and is unable to discriminate between

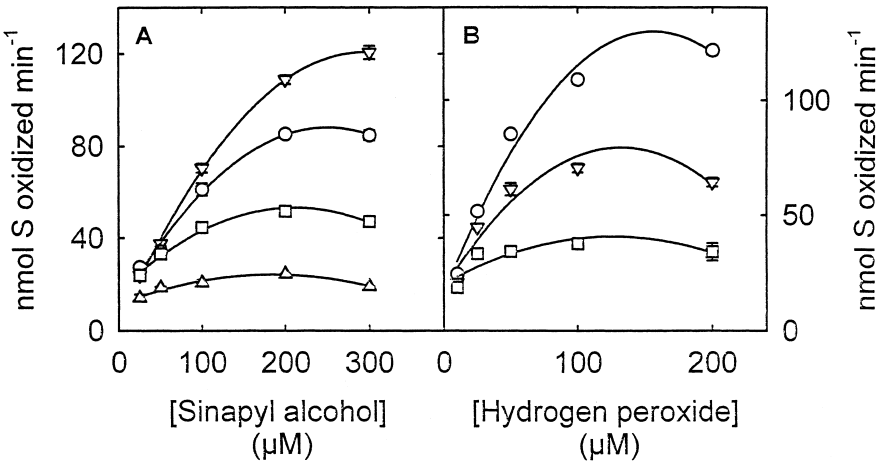

Fig. 1. Dependence of the sinapyl alcohol oxidation rate by the *Zinnia elegans* basic peroxidase on sinapyl alcohol (A) and H_2O_2 (B) concentration. In A, the reaction media contained 10 μM (Δ), 25 μM (□), 50 μM (○) and 100 μM (▽) H_2O_2. In B, the reaction media contained 50 μM (□), 100 μM (▽) and 200 μM (○) sinapyl alcohol. Other details are described in the Experimental section.

cinnamyl alcohols and cinnamyl aldehydes (Table 3). To cast light on this question, the k_M^{RH} values of the *Z. elegans* basic peroxidase for cinnamyl alcohol and aldehydes were examined in detail (Table 5). From these data, it can be concluded that the *Z. elegans* basic peroxidase shows k_M^{RH} values in the μM range, illustrating the great affinity of *Z. elegans* peroxidase for monomeric lignin precursors, especially for cinnamyl aldehydes, which were oxidized with greater affinity than the cinnamyl alcohols.

At this point, it should be recalled that the same weak preference is shown by other enzymes specific for the lignin biosynthetic pathway, such as the microsomal 5-hydroxylases (Humphreys et al., 1999). Nevertheless, the small differences in affinity shown by the *Z. elegans* basic peroxidase for cinnamyl aldehydes are apparently not sufficient to segregate its function towards cinnamyl aldehyde polymerization, since the local concentration of alcohols in the lignifying xylem is probably substantially greater than the local concentration of aldehydes, as may be deduced from their levels in cultured cells undergoing lignification (Anterola et al., 1999) and from the equilibrium constant of CAD (Lewis et al., 1999).

Table 5
k_M^{RH} Values for cinnamyl alcohols and cinnamyl aldehydes during their oxidation by the *Zinnia elegans* basic peroxidase at pH 5.0 for different H_2O_2 concentrations

Substrate	k_M^{RH} (μM)				
	H_2O_2 (μM)				
	5	10	25	50	100
Coniferyl alcohol	13.8	33.8	nd[a]	91.0	244.6
Coniferyl aldehyde	nd	8.7	20.7	30.0	106.3
Sinapyl alcohol	nd	21.2	40.1	73.7	174.0
Sinapyl aldehyde	nd	2.7	12.6	22.9	60.6

[a] nd, Not determined.

2.6. k_M Values for the pseudo oxidase reaction

A striking feature of the *Z. elegans* basic peroxidase is that it shows a hydrogen peroxide-independent oxidase activity against both cinnamyl aldehydes and cinnamyl alcohols (Table 3). The pseudo-oxidase activity of this peroxidase may be due, as occurs during the oxidation of other phenols (Singleton, 1987; Jiang and Miles, 1993), to a residual peroxidase activity that is switched on by the traces of hydrogen peroxide formed during the slow phase of both cinnamyl alcohol and cinnamyl aldehyde auto-oxidation:

$$2RH \rightarrow 2R^- + 2H^+ \quad (10)$$

$$2R^- + 2O_2 \rightarrow 2R^\bullet + 2O_2^- \quad (11)$$

$$2O_2^- + 2H^+ \rightarrow H_2O_2 + O_2 \quad (12)$$

where R^- is the phenoxy anion and $R^\bullet$ the phenoxy radical, and which yields, as balance, a net H_2O_2 production:

$$2RH + O_2 \rightarrow 2R^\bullet + H_2O_2 \quad (13)$$

This H_2O_2 formed at trace level could initiate the normal catalytic cycle of the enzyme described in Eqs. (1)–(3). Eqs. (10)–(13) could explain the partial sensitivity of such pseudo-oxidase reactions of peroxidase to both superoxide dismutase and catalase (Badiani et al.,

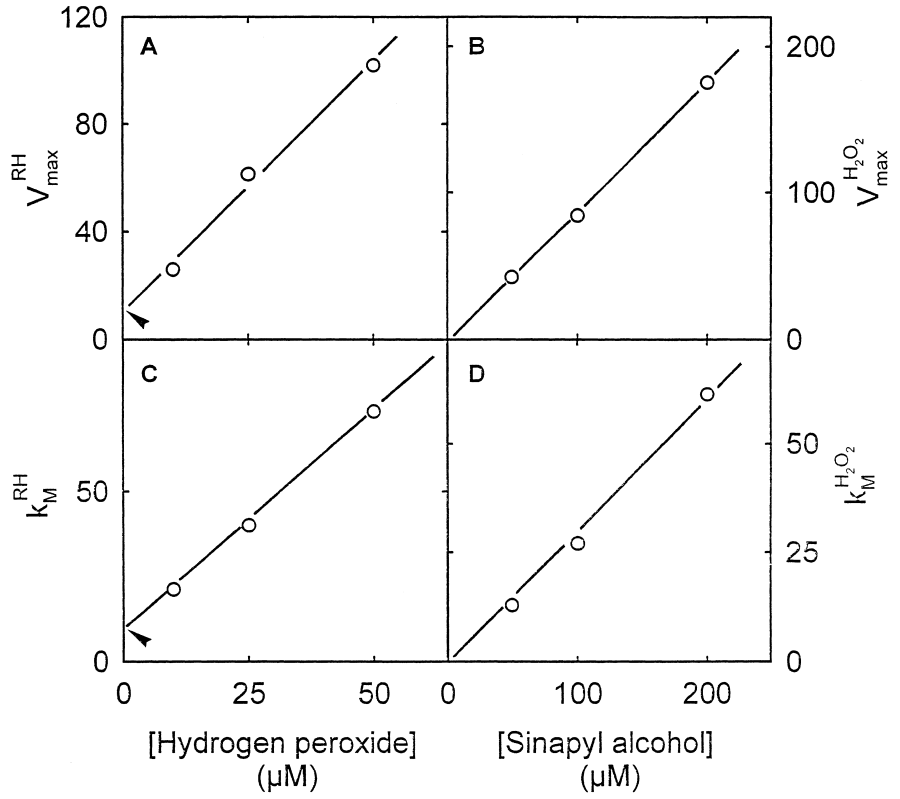

Fig. 2. Plot of V_{max}^{RH} values against H_2O_2 concentration (A), plot of $V_{max}^{H_2O_2}$ values against sinapyl alcohol concentration (B), plot of k_M^{RH} values against H_2O_2 concentration (C), and plot of $k_M^{H_2O_2}$ values against sinapyl alcohol concentration (D), for the oxidation of sinapyl alcohol by the *Zinnia elegans* basic peroxidase. Other details are described in Fig. 1 and in Experimental.

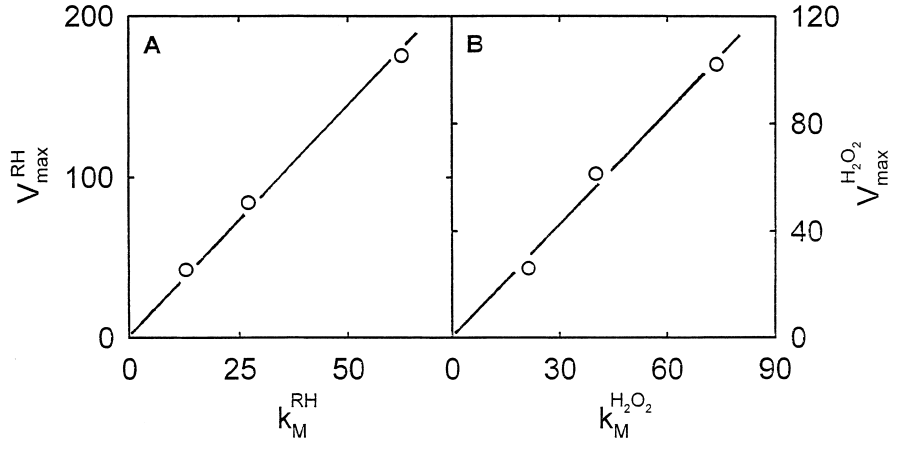

Fig. 3. Plot of V_{max}^{RH} values against k_M^{RH} values (A) and plot of $V_{max}^{H_2O_2}$ values against $k_M^{H_2O_2}$ values (B), for the oxidation of sinapyl alcohol by the *Z. elegans* basic peroxidase. Other details are described in Fig. 1 and in Experimental.

1990; Jiang and Miles, 1993), as well as the observation that basic peroxidases show a greater pseudo-oxidase activity than acidic peroxidases (Chabanet et al., 1993; Ros Barceló et al., 1998), due mainly to the special low k_M values of basic peroxidases for H_2O_2 (Ros Barceló et al., 1998).

The strong affinity of basic peroxidases for H_2O_2 is also true in the case of the *Z. elegans* basic peroxidase, which showed particularly low k_M values for H_2O_2 when coniferyl and sinapyl alcohols were used as reducing substrates (Table 6). These results suggest that this basic peroxidase is well adapted to the H_2O_2-containing lignifying xylem cells of *Z. elegans* hypocotyls (Ros Barceló, 1998a,b). In addition, that the pseudo-oxidase activity of the *Z. elegans* basic peroxidase is directly related to its capacity to use H_2O_2, especially at low concentrations, is clear when the oxidation rates of cinnamyl alcohols and aldehydes in the absence of H_2O_2

(Table 3) (which follow the order: sinapyl alcohol > coniferyl alcohol > coniferyl aldehyde) are compared with its efficacy ($V_{max}^{H_2O_2}/k_M^{H_2O_2}$ values) to use H_2O_2 (Table 7) (which follows the same order: sinapyl alcohol > coniferyl alcohol > coniferyl aldehyde).

Table 6
$k_M^{H_2O_2}$ Values for H_2O_2 during their reduction by the *Zinnia elegans* basic peroxidase at pH 5.0 for different cinnamyl alcohol and cinnamyl aldehyde concentrations

Substrate	$k_M^{H_2O_2}$ (μM)				
	Cinnamyl alcohol or aldehyde (μM)				
	6.25	12.5	25	50	75
Coniferyl alcohol	1.16	2.89	5.86	9.48	13.3
Coniferyl aldehyde	5.86	10.6	32.5	60.7	nd
Sinapyl alcohol	nd[a]	nd	nd	12.8	nd
Sinapyl aldehyde	5.4	22.1	68.1	121.5	nd

[a] nd, Not determined.

Table 7
Efficacy ($V_{max}^{H_2O_2}/k_M^{H_2O_2}$ values) in H_2O_2 utilization by the *Zinnia elegans* basic peroxidase at pH 5.0 for the different cinnamyl alcohol and cinnamyl aldehydes

Substrate	Efficacy ($V_{max}^{H_2O_2}/k_M^{H_2O_2}$) (nmols s^{-1} mg^{-1} protein μM^{-1})
Coniferyl alcohol	94.28 ± 12.38
Coniferyl aldehyde	18.09 ± 1.90
Sinapyl alcohol	282.83 ± 41.90
Sinapyl aldehyde	nd[a]

[a] nd, Not determined.

For this reason, the k_M values for cinnamyl alcohols and aldehydes during this particular pseudo-oxidase reaction were also calculated. This was done from an extrapolation of the dependence of the k_M values for cinnamyl alcohols and aldehydes on H_2O_2 at zero H_2O_2 concentration (Fig. 2C). The k_M^{RH} values for the pseudo-oxidase reactions are given in Table 8 and, like those obtained for the peroxidase reaction, they were in the μM range. In the absence of exogenous H_2O_2, the *Z. elegans* basic peroxidase also showed a great affinity for the monomeric lignin precursors, especially for coniferyl aldehyde, which is oxidized with greater affinity than coniferyl and sinapyl alcohols (Table 8). Furthermore, in the absence of exogenous H_2O_2, the *Z. elegans* basic peroxidase showed an affinity for the monomeric lignin precursors similar to that shown by an angiosperm (*Populus euroamericana*) laccase, and three orders of magnitude greater than that shown by a gymnosperm (*Pinus taeda*) laccase (Table 8).

Finally, all these k_M values for the lignin precursors shown by the *Z. elegans* basic peroxidase were in the same range as those shown by the peroxidase-preceding enzymes of the lignin biosynthetic pathway, cinnamyl alcohol dehydrogenase and microsomal 5-hydroxylases, which also use both cinnamyl alcohols and aldehydes as substrates (Table 8). The nature of these biochemical constants, which is in accordance with the predictions that may be made from the observed pools and metabolic fluxes of monolignols in lignifying cells (Anterola et al., 1999), implicitly indicates that the one-way highway of lignin macromolecule construction, which properly starts with the reduction of cinnamoyl-CoA's by cinnamoyl-CoA reductases, contains no metabolic "potholes", in which the lignin building blocks might be accumulated.

Table 8
k_M^{RH} Values for cinnamyl alcohols and cinnamyl aldehydes during their oxidation by the *Z. elegans* basic peroxidase at pH 5.0 in the absence of H_2O_2. For comparison, the k_M^{RH} values for cinnamyl alcohols and aldehydes for other enzymes involved in the lignin biosynthetic pathway which use cinnamyl alcohols and cinnamyl aldehydes as substrates are also shown

Enzyme	k_M^{RH} (μM)				
	Alcohol		Aldehyde		Reference
	Coniferyl	Sinapyl	Coniferyl	Sinapyl	
Zinnia elegans basic peroxidase	7.9	7.6	5.1	–	
Populus euroamericana laccase	1.5	17	25	2.7	Ranocha et al. (1999)
Pinus taeda laccase	12000	25400	–	–	Bao et al. (1993)
Eucalyptus gunnii cinnamyl alcohol dehydrogenases	2.3–23.1	4.5–6.6	4.5–5.2	2.5–6.8	Hawkins and Boudet (1994)
Arabidopsis thaliana ferulate 5-hydroxylase	3.0		1.0		Humphreys et al. (1999)
Liquidambar styraciflua coniferyl aldehyde 5-hydroxylase	–	–	2.77	–	Osakabe et al. (1999)

2.7. Conclusion

A strongly basic peroxidase, located in the aldehyde lignin-forming xylem from *Z. elegans* hypocotyls, is capable of oxidizing both cinnamyl alcohols and cinnamyl aldehydes in the absence and in the presence of H_2O_2. This basic peroxidase shows a particular affinity for cinnamyl aldehydes and some specificity for syringyl-type phenols. Its affinity for cinnamyl alcohols and aldehydes is similar to that shown by the preceding enzymes of the lignin biosynthetic pathway, which also use cinnamyl alcohols and cinnamyl aldehydes as substrates, indicating that the one-way highway of construction of the lignin macromolecule has no metabolic potholes where the lignin building blocks would accumulate. This fact suggests a high degree of metabolic plasticity (versatility) for this basic peroxidase, which has been widely conserved during the evolution of vascular plants, making it one of the driving forces in the evolution of plant lignin heterogeneity.

3. Experimental

3.1. Plant material

EC system standard seeds of *Zinnia elegans* were purchased from W.R. Vanderschoot (Hillegom, The Netherlands). Seedlings were grown for 26 days in a greenhouse under daylight conditions at 25°C (Ros Barceló and Aznar-Asensio, 1999). Fully grown (lignifying) hypocotyls were used for these studies. These hypocotyls showed a xylem cell wall lignification gradient which varied from the top (beginning) to the bottom (advanced), as tested by both the Wiesner test and the Mäule reaction.

3.2. Isolation of cell walls

Lignifying *Z. elegans* cell walls were prepared by a Triton X-100 washing procedure exactly as described (Ros Barceló and Aznar-Asensio, 1999).

3.3. Thioacidolysis of lignifying cell walls

Thioacidolysis of lignifying *Z. elegans* cell walls, which solubilizes the β-*O*-4 lignin core, and GC–MS (Hewlett Packard 5890-HP 5972) analyses were performed essentially as described by Lapierre et al. (1995). MS spectra were recorded at 70 eV.

3.4. Oxidation of cinnamyl alcohols and cinnamyl aldehydes by cell walls isolated from lignifying Z. elegans hypocotyls

To monitor both cinnamyl alcohol and cinnamyl aldehyde oxidation by isolated cell walls, an amount of purified cell walls, equivalent to 0.2 g FW, was incubated with stirring for 2 h at 25°C in an assay medium (2.0 ml) containing 50 μM of the substrate in 50 mM Tris–acetate buffer (pH 5.0), in the presence and in the absence of 0.5 mM H_2O_2. Controls were performed in the presence of a heat (100°C)-denatured cell wall fraction. After this time, the cell walls were centrifuged at 1100 *g* for 5 min at 5°C, the amount of cinnamyl alcohol and cinnamyl aldehyde oxidized being determined from the decay in absorbance at λ_{max} of the supernatants, using the $\Delta\varepsilon$ for each reaction given in Table 2.

3.5. Purification of the basic peroxidase from the intercellular washing fluid from lignifying Z. elegans hypocotyls

The *Z. elegans* basic peroxidase was obtained and purified from intercellular washing fluids of lignifying hypocotyls, as previously described (Ros Barceló and Aznar-Asensio, 1999).

3.6. Spectrophotometric determinations

The oxidation of cinnamyl alcohols and aldehydes by the *Z. elegans* basic peroxidase, in the presence and in the absence of H_2O_2, was assayed spectrophotometrically at 25°C in a reaction medium containing 50 mM Tris–acetate buffer (pH 5.0) using the $\Delta\varepsilon$ for each reaction given in Table 2. The reaction was initiated by the addition of 0.175 μg protein. Other assay conditions have been described previously (Ros Barceló and Aznar-Asensio, 1999), or are described in the figure legends and tables. Protein was determined according to Bradford (1976).

3.7. Chemicals

Coniferyl alcohol, coniferyl aldehyde, sinapyl alcohol and sinapyl aldehyde were purchased from Sigma (Madrid, Spain). The rest of the chemicals were obtained from various other suppliers and were of the highest purity available.

Acknowledgements

This work was supported by a grant from the MEC (project No. PB97-1042). F.P. holds a fellowship from the Xunta de Galicia.

References

Anterola, A.M., van Rensburg, H., van Heerden, P.S., Davin, L.B., Lewis, N.G., 1999. Multi-site modulation of flux during monolignol formation in loblolly pine (*Pinus taeda*). Biochemistry and Biophysics Research Communications 261, 652–657.

Badiani, M., de Biasi, M.G., Felici, M., 1990. Soluble peroxidase from winter wheat seedlings with phenoloxidase-like activity. Plant Physiology 92, 489–494.

Bao, W., O'Malley, D.M., Whetten, R., Sederoff, R.R., 1993. A laccase associated with lignification in loblolly pine xylem. Science 260, 672–674.

Bradford, M.G., 1976. A rapid and sensitive method for the quantitation of microgram quantities of protein utilizing the principle of protein dye binding. Analytical Biochemistry 72, 248–254.

Chabanet, A., Catesson, A.M., Goldberg, R., 1993. Peroxidase and phenoloxidase activities in mung bean hypocotyl cell walls. Phytochemistry 33, 759–763.

Geiger, H., Fuggerer, H., 1979. On the chemistry of the Wiesner reaction on lignins. Zeitscrift für Naturforschung 34b, 1471–1472.

Hawkins, S.W., Boudet, A.M., 1994. Purification and characterization of cinnamyl alcohol dehydrogenase isoforms from the periderm of *Eucalyptus gunnii* hook. Plant Physiology 104, 75–84.

Higuchi, T., Ito, T., Umezawa, T., Hibino, T., Shibata, D., 1994. Red-brown color of lignified tissues of transgenic plants with antisense CAD gene: wine-red lignin from coniferyl aldehyde. Journal of Biotechnology 37, 151–158.

Humphreys, J.M., Hemm, M.R., Chapple, C., 1999. New routes for lignin biosynthesis defined by biochemical characterization of recombinant ferulate 5-hydroxylase, a multifunctional cytochrome P450-dependent mono oxygenase. Proceedings of the National Academy of Science of USA 96, 10045–10050.

Jiang, Y., Miles, P.W., 1993. Generation of H_2O_2 during enzymatic oxidation of catechin. Phytochemistry 33, 29–34.

Lapierre, C., Pollet, B., Rolando, C., 1995. New insights into the molecular architecture of hardwood lignins by chemical degradative methods. Research Chemistry Intermediaries 21, 397–412.

Lapierre, C., Pollet, B., Conil, M.P., Toval, G., Romero, J., Pilate, G., Leplé, J.C., Boerjan, W., Ferret, V., de Nadai, V., Jouanin, L., 1999. Structural alterations of lignins in transgenic poplars with depressed cinnamyl alcohol dehydrogenase or caffeic acid o-methyltransferase activity have an opposite impact on the efficiency of industrial kraft pulping. Plant Physiology 119, 153–163.

Lewis, N.G., 1999. A 20th century roller coaster ride: a short account of lignification. Current Opinion in Plant Biology 2, 153–162.

Lewis, N.G., Davin, L.B., Sarkanen, S., 1999. The nature and function of lignins. In: Barton, D.H.R., Nakanishi, K. (Eds.), Comprehensive Natural Products Chemistry — Carbohydrates and their Derivatives Including Tannins, Cellulose and Related Lignins Vol. 3. Elsevier Science, New York, pp. 617–745.

Meshitsuka, G., Nakano, J., 1979. Studies on the mechanism of lignin color reaction. Mäule color reaction. Mokuzai Gakkaishi 25, 588–594.

Morales, M., Ros Barceló, A., 1997. A basic peroxidase from vacuoles and cell walls from *Vitis vinifera*. Phytochemistry 45, 229–232.

Osakabe, K., Tsao, Ch.Ch., Li, L., Popko, J.L., Umezawa, T., Carraway, D.T., Smeltzer, R.H., Joshi, C.P., Chiang, V.L., 1999. Coniferyl aldehyde 5-hidroxylation and methylation direct syringyl lignin biosynthesis in angiosperms. Proceedings of the National Academy of Sciences of USA 96, 8955–8960.

Ralph, J., MacKay, J.J., Hatfield, R.D., O'Malley, D.M., Whetten, R.W., Sederoff, R.R., 1997. Abnormal lignin in loblolly pine mutant. Science 277, 235–239.

Ranocha, P., McDougall, G., Hawkins, S., Sterjiades, R., Borderies, G., Stewart, D., Macheteau, M.C., Boudet, A.M., Goffner, D., 1999. Biochemical characterization, molecular cloning and expression of laccases — a divergent gene family- in poplar. European Journal of Biochemistry 259, 485–495.

Ros Barceló, A., 1995. Peroxidase and not laccase is the enzyme responsible for cell wall lignification in the secondary thickening of xylem vessels in *Lupinus*. Protoplasma 186, 41–44.

Ros Barceló, A., 1997. Lignification in plant cell walls. International Review of Cytology 176, 87–132.

Ros Barceló, A., 1998a. The generation of H_2O_2 in the xylem of *Zinnia elegans* is mediated by an NADPH-oxidase-like enzyme. Planta 207, 207–216.

Ros Barceló, A., 1998b. Hydrogen peroxide production is a general property of the lignifying xylem from vascular plants. Annals of Botany 82, 97–103.

Ros Barceló, A., Aznar-Asensio, G.J., 1999. Coniferyl alcohol oxidase activity of a cell wall-located class III peroxidase. Australian Journal of Plant Physiology 26, 411–419.

Ros Barceló, A., Morales, M., Pedreño, M.A., 1998. Specific compartmentalization of peroxidase isoenzymes in relation to lignin biosynthesis in the plant cell. In: Lewis, N.G., Sarkanen, S. (Eds.), American Chemical Society Symposium Series — Lignin and Lignan Biosynthesis, Vol. 697. American Chemical Society, Washington, DC, pp. 84–95.

Ros Barceló, A., Pomar, F., Pedreño, M.A., 2000. Competitive inhibitor-dissected histochemistry of the peroxidase responsible for syringyl lignin biosynthesis in *Z. elegans* xylem. Australian Journal of Plant Physiology 27, 1101–1107.

Sato, Y., Sugiyama, M., Komamine, A., Fukuda, H., 1995a. Separation and characterization of the isoenzymes of wall-bound peroxidase from cultured *Zinnia* cells during tracheary element differentiation. Planta 196, 141–147.

Sato, Y., Sugiyama, M., Takagi, T., Fukuda, H., 1995b. Purification of cationic peroxidases bound ionically to cell walls from the roots of *Zinnia elegans*. Journal of Plant Research 108, 463–468.

Singleton, V.L., 1987. Oxygen with phenols and related reactions in must, wines and model systems: observations and practical implications. American Journal of Enology and Viticulture 38, 69–77.

Sterjiades, R., Dean, J.F.D., Gamble, G., Himmelsbach, D.S., Eriksson, K.E.L., 1993. Extracellular laccases and peroxidases from sycamore maple (*Acer pseudoplatanus*) cell-suspension cultures. Planta 190, 75–87.

Sy, L.K., Brown, G.D., 1999. Coniferylaldehyde derivatives from tissue culture of *Artemisa annua* and *Tenacetum parthenium*. Phytochemistry 50, 781–785.

Udagama-Randeniya, P.V., Savidge, R.A., 1995. Coniferyl alcohol oxidase- a catechol oxidase? Trees 10, 102–107.

Wallace, G., Fry, S.C., 1999. Action of diverse peroxidases and laccases on six cell wall-related phenolic compounds. Phytochemistry 52, 769–773.

PERGAMON

Phytochemistry 57 (2001) 1115–1122

PHYTOCHEMISTRY

www.elsevier.com/locate/phytochem

The poly(phenolic) domain of potato suberin: a non-lignin cell wall bio-polymer

Mark A. Bernards *, Fawzi A. Razem

Department of Plant Sciences, University of Western Ontario, London, ON N6A 5B7, Canada

Received 6 July 2000; received in revised form 17 October 2000

Abstract

Suberized plant cell walls have three distinguishing features: (1) tissue specificity, (2) a poly(aliphatic) domain and (3) a unique, "lignin-like" poly(phenolic) domain. With respect to the latter, comparisons have often been made to lignin, but the unique phenolic composition of suberized cells yields a unique polymer better designated as a poly(phenolic) domain. Potato tubers that have been induced to suberize through wounding make an excellent model system with which the chemistry, biochemistry and macromolecular assembly of the suberin poly(phenolic) domain can be monitored. For example, wound healing potato tubers have been used to determine the unique hydroxycinnamic acid nature of its poly(phenolic) domain using specific carbon-13 labeling studies and specific chemical degradation techniques (e.g. thioacidolysis). Furthermore, a suberization-associated anionic peroxidase has been purified from suberizing potato tubers and subsequently shown to oxidize hydroxycinnamic acids (and their derivatives) in preference to monolignols, as well as yield an unique polymer in vitro. We have since extended these studies to begin analyzing the macromolecular assembly process leading to the deposition of this suberized tissue specific domain. To this end we have begun to describe an H_2O_2-generating system with NAD(P)H-dependent oxidase-like properties that is temporally associated with the formation of potato suberin poly(phenolics) during suberization. Herein we describe our progress to date. © 2001 Elsevier Science Ltd. All rights reserved.

Keywords: *Solanum tuberosum*; Solonaceae; Potato; Suberin poly(phenolic) domain; Wound healing; NAD(P)H-dependent oxidase; Peroxidase; Diphenyleneiodonium

1. Introduction

During normal growth and development the cell walls of many cell types, from both woody and herbaceous plant species, become modified to carry out specific functions. For example, xylem vessel and fiber cell walls become lignified to provide the necessary mechanical strength for axial water transport and an upright growth habit. Similarly, the epidermal tissues of underground plant parts (e.g. roots, stolons, tubers), the endodermis and the cells of bark tissue (i.e. cork, periderm) become suberized to provide a nearly perfect barrier to apoplastic water transport, as well as a pre-formed defense against many potential pathogens (e.g. Kolattukudy, 1980, 1984; Lulai and Corsini, 1998). In either case, lignification and suberization have the hallmark of being highly tissue/cell specific. Indeed, cells that ultimately become suberized or lignified either derive from specific progenitor cells in meristems or arise from a distinct cambium.

Both lignification and suberization involve the formation of a three dimensional poly(phenolic) matrix initially within the carbohydrate matrix of the primary cell wall followed by the deposition of additional carbohydrate, protein and poly(phenolic) containing layers, often referred to as secondary cell wall thickenings. In addition to this phenolic component, suberized cells develop a distinct poly(aliphatic) layer with associated phenolic acids (Kolattukudy, 1980), typically deposited between the primary cell wall and the plasma membrane prior to secondary wall formation (reviewed in Bernards and Lewis, 1998). This multi-layered aliphatic polymer, with its associated waxes, is thought to provide suberized tissues with their water impermeability (Soliday et al., 1979; Kolattukudy, 1980, 1984; Vogt et al., 1983; Lulai and Orr, 1994). The poly(aliphatic) domain of

* Corresponding author. Tel.: +1-519-661-2111-86477; fax: +1-519-661-3935.

E-mail address: bernards@uwo.ca (M.A. Bernards).

0031-9422/01/$ - see front matter © 2001 Elsevier Science Ltd. All rights reserved.
PII: S0031-9422(01)00046-2

suberized cells has been described as a polyester connected through primary ester bonds between the major aliphatic components (esp. α,ω-dioic acids and ω-hydroxyalkanoic acids), as well as phenolic acids. Recently, however, it has been shown that glycerol makes up a significant proportion of aliphatic suberins (up to 41% in *Pseudotsuga menziesii*) (Graca and Pereira, 1999), and may in fact act as a bridge between the poly(aliphatic) domain and the cell wall-bound poly(-phenolic) domain (PPD).

Given the duality of the cell wall modification that occurs during suberization (i.e. including both poly(-phenolic) and poly(aliphatic) domains), it is argued here that the term *suberin* is insufficient to describe it. Indeed, in the literature, the most common use of the term suberin is in reference to the poly(aliphatic) matrix. The (mis)use of the word suberin is exacerbated by other terms such as *suberinic acids* and *suberans* that have been used (Marques et al., 1996; Bolwell et al., 1997) to describe the aliphatic compounds released by alkaline hydrolysis and the fact that the tissue remaining after alkaline hydrolysis is considered to be "de-suberized"(e.g. Gil et al., 1997). The term *aromatic suberin* has been used to define the alkali-soluble hydroxycinnamic acids readily removed from suberized tissues, typically along with the aliphatics after alkaline hydrolysis or transesterification (e.g. Schreiber et al., 1999). This represents an important subset of phenolics found in suberized tissues and should be recognized as such. Historically, the PPD of suberized tissues has been likened to that of lignified tissues in both composition and structure (Kolattukudy, 1980, 1984), i.e. a polymer assembled from the common "monolignols" *p*-coumaryl alcohol **1**, coniferyl alcohol **2**, and/or sinapyl alcohol **3** (Scheme 1). But, as alluded to above, suberized and lignified tissues have evolved for different purposes in plants, and are found in distinct, specific tissues. These two characteristics argue against their being identical in structure and composition. Indeed, while most suberized tissues do contain small amounts of covalently-linked monolignols (i.e. lignin), relative to lignified tissues, they also contain a significant amount of associated hydroxycinnamic acids such as *p*-coumaric **4**, caffeic **5** and ferulic **6** acids, some of which are covalently cross-linked through bonds other than esters (see Bernards and Lewis, 1998). Interestingly, there is no direct evidence for sinapic acid **7** or its derivatives, other than the relatively large amounts of sinapaldehyde released by alkaline nitrobenzene oxidation (Borg-Olivier and Monties, 1989, 1993).

The common description of the PPD of suberized tissues as "lignin-like" is clearly misleading since it contains little monolignol, and a significant amount of hydroxycinammic acid. Therefore, a more appropriate term is simply "suberin poly(phenolic) domain" or SPPD, which distinguishes it from lignin and indicates its tissue/cell origins and unique phenolic composition.

It is essential to point out that not all suberized tissues are equivalent in the amount of PPD they contain or in their phenolic composition. For example there exists a wide variability in the degree of suberization in tissues ranging from highly suberized cork cells in the outer bark of woody plants to the radial-wall-restricted suberization of the Casparian band in the endodermis. Compared to lignified cells isolated from the same plant tissue, suberized cells studied thus far appear to have a lower monolignol content, higher hydroxycinnamate content and yield different relative amounts of both monomeric and dimeric products upon degradation (e.g. Schreiber, 1996; Zeier and Schreiber, 1997, 1999; Zeier et al., 1999). Indeed, the major difference between lignified and suberized cell wall phenolic polymers appears to be in the covalent incorporation of hydroxycinnamic acids into an otherwise monolignol-based macromolecule, during suberization (Bernards and Lewis, 1998). This may reflect the role of suberized tissues as antimicrobial barriers in plants since hydroxycinnamates are known to have antimicrobial properties (e.g. Friedman, 1997; Cowan, 1999).

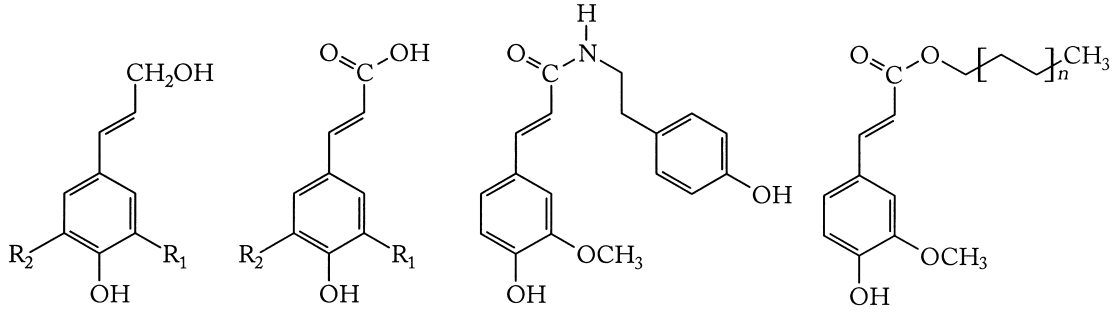

1, $R_1=R_2=H$
2, $R_1=OCH_3$, $R_2=H$
3, $R_1=R_2=OCH_3$

4, $R_1=R_2=H$
5, $R_1=OH$, $R_2=H$
6, $R_1=OCH_3$, $R_2=H$
7, $R_1=R_2=OCH_3$

8

9 n=7-13

Scheme 1. Phenylpropanoids found in the poly(phenolic) domain of suberized potatoes.

The predominantly hydroxycinnamate-based SPPD of potato tubers (Bernards et al., 1995; Negrel et al., 1996), which appears to contain a unique cell wall phenolic polymer, arguably represents an extreme example of how suberized cells can differ from typical lignified cells. Nevertheless, potato tubers have long been used as a model system to study the process of suberization since they suberize quickly and uniformly in response to wounding and are amenable to the exogenous application of metabolic precursors, inhibitors, etc. (e.g. Bernards and Lewis, 1992; Bernards et al., 1995).

The macromolecular assembly of potato SPPD is hypothesized to occur via a peroxidase-mediated free radical coupling process (Kolattukudy, 1980), analogous to the process suggested for lignin formation from monolignols. We have begun to characterize, at the biochemical level, an anionic peroxidase isolated from wound healing potatoes (Bernards et al., 1999) that was first purported to be associated with suberization by Kolattukudy's group (e.g. Espelie and Kolattukudy, 1985; Espelie et al., 1986). Interestingly, this enzyme shows a marked preference for hydroxycinnamates (esp. ferulic acid **6** and its derivatives, such as **8**) over the corresponding monolignols **1–3** and, when incubated with ferulic acid **6** in vitro, produces a polymer characterized by the retention of side chain unsaturation (Bernards et al., 1999). One question that remains is where does the H_2O_2 necessary for peroxidative oxidation of phenolics come from? While several H_2O_2 generating systems have been described in plants (e.g. Elstner and Heupel, 1976; Gross and Janse, 1977; Gross et al., 1977; Angelini and Federico, 1989; Vianello and Macri, 1989, 1991; Cross and Jones, 1991; Wojtaszek, 1997) an NADPH-dependent oxidase has been implicated in the generation of H_2O_2 during the lignification of *Zinnia elegans* (Ros Barceló, 1998a). Independent of this we have obtained data that supports a similar process during wound-induced suberization in potato tubers. In this report we describe our progress in characterizing a wound-induced oxidase that appears to be involved in suberization.

2. Results and discussion

2.1. Potato suberin poly(phenolic) domain: evidence for a unique polymer

Our current model for suberized potato tuber cells depicts a cell wall-associated poly(phenolic) domain with a covalently attached poly(aliphatic) domain residing between the cell wall and plasma membrane (Fig. 1; reviewed in Bernards and Lewis, 1998). The most significant revelation in our understanding of the potato SPPD came from specific carbon-13 labeling studies using [1-^{13}C]-, [2-^{13}C]- and [3-^{13}C]-phe coupled with in situ solid state carbon-13 CP-MAS NMR spectroscopy (Bernards et al., 1995), which demonstrated that the polymer contained a significant proportion of covalently cross-linked hydroxycinnamic acids. This was subsequently verified by the isolation of an *N*-feruloyltyramine **7** derivative from potato suberin after thioacidolysis (Negrel et al., 1996). Importantly, these conclusions were preceded by a series of studies (using spectroscopic and degradative techniques) that strongly suggested that the SPPD had a unique composition and therefore structure (reviewed in Bernards and Lewis, 1998). Equally important was the observation that the aromatic and aliphatic domains of suberized potato tubers are spatially distinct (Lulai and Morgan, 1992) but covalently linked (Stark and Garbow, 1992; Yan and Stark, 1998). These latter points have now also been demonstrated in the suberized cells of *Quercus suber* cork using sophisticated NMR relaxation studies (Gil et al., 1997). Moreover, glycerol has been described as a linker between domains, and as a site for phenolic acid esterification (e.g. Graca and Pereira, 1999) although its presence in suberized tissues has been described earlier (e.g. Schmutz et al., 1993, 1994). Finally, chemical analysis of isolated endodermal or hypodermal tissues from *Clivia miniata*, *Zea mays*, *Cicer arietum* and others (Schreiber, 1996; Zeier and Schreiber, 1997, 1999; Zeier et al., 1999) has revealed that these suberized tissues differ qualitatively and quantitatively from the lignified xylem tissues isolated from the same plants.

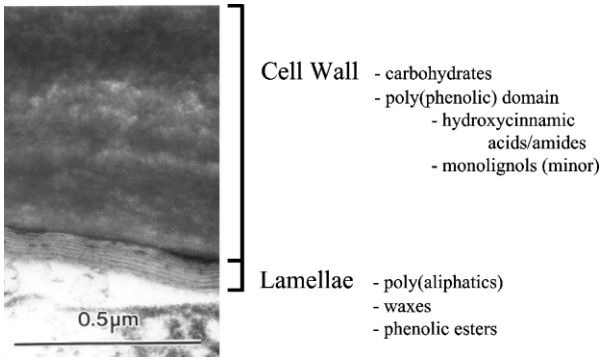

Fig. 1. Anatomy of a suberized potato tuber cell wall. Wound induced suberization of potato tubers results in the formation of a poly(-phenolic) domain, comprised of a hydroxycinnamic acid/amide-monolignol composite polymer embedded in the cellulosic matrix of the primary cell wall. A poly(aliphatic) matrix, evident as a series of alternating light and dark bands (lamellae) is also laid down, but between the cellulosic cell wall and the plasma membrane. This layer also contains waxes and esterified phenolic acids. The image is a TEM micrograph of a potato tuber cell wall, five days post wounding. (Courtesy of L.H. Levine.)

2.2. Biosynthesis of the suberin poly(phenolic) domain

The differences in phenolic biopolymer composition between lignifying and suberizing tissues is also apparent in the metabolic fate of hydroxycinnamoyl-CoA

thioesters during lignin/SPPD formation. For example, we have found that the enzyme hydroxycinnamoyl-coenzyme A oxido-reductase (CCR) is not induced in wounded (i.e. suberizing) potato tubers. By contrast, CCR is strongly induced in cell cultures of *Pinus taeda* when treated under culture conditions that induce lignification (Bernards et al., 2000). Instead, wounding of tubers induces hydroxycinnamoyl transferases (Negrel, et al., 1993, 1995; Lotfy et al., 1994) capable of biosynthesizing feruloyltyramine **8** and ferulate esters **9**. Together, these data suggest that during suberization of potato tubers, hydroxycinnamoyl-CoA derivatives are channeled into metabolic endpoints other than monolignols, (i.e. their apparent metabolic fate during lignification).

2.3. H_2O_2 generation during formation of the suberin poly(phenolic) domain

In order for phenolics to be assembled into the SPPD, they have to be polymerized. The current model used to describe this process involves the oxidative cross-linking of phenolics via an anionic peroxidase. We have begun to characterize this enzyme at the biochemical level (Bernards et al., 1999) and have shown it to prefer hydroxycinnamic acids (esp. **6**, and its derivatives, e.g. **8**) over their corresponding hydroxycinnamyl alcohols (e.g. **2**) in in vitro assays. Moreover, an in vitro polymer prepared from [8-^{13}C] ferulic acid using the purified anionic peroxidase and the slow addition of H_2O_2 had a number of unique features, principally the retention of side chain unsaturation (Bernards et al., 1999). Therefore, it seems as though, at least in suberizing potato tubers, the macromolecular assembly of a poly(phenolic) matrix during suberization favours the polymerization of hydroxycinnamates both in the biosynthesis of monomers as well as in their utilization. However, in order to be effective in the macromolecular assembly of the SPPD, the hydroxycinnamate-preferring anionic peroxidase must be localized to the cell wall, where it is needed. In part this has been done (Espelie et al., 1986), but the specificity of the antibody used was not confirmed, and the resolution of the detection method (fluorescence label) not sensitive enough to discriminate between cell walls and the plasma membrane–cell wall interface. To address this question, we are obtaining specific antibodies to the anionic peroxidase of potato (using deglycosylated native and denatured enzyme), with the intention of using them for immuno-gold-based immunocytochemical localization studies.

In order for peroxidases to function, they require H_2O_2 as oxidant. It follows that in order for the suberization-associated anionic peroxidase to function during SPPD formation, there must be a supply of H_2O_2 generated in situ. We have begun experiments to (1) demonstrate the requirement for H_2O_2 in the SPPD assembly process and (2) identify the source of H_2O_2 that is used.

Using the peroxidase-mediated oxidation of tetramethylbenzidine (TMB) as a histochemical marker (Ros Barceló, 1998b), it can be shown that H_2O_2 is actively synthesized de novo in the SPPD forming layers during wound healing (Fig. 2). Furthermore, the de novo synthesis of H_2O_2 can be inhibited by treatment with diphenyleneiodonium (DPI; Fig. 2), a known inhibitor of NAD(P)H-dependent oxidases (Deme et al., 1994; Dwyer et al., 1996). Still it is not clear whether the source of H_2O_2 is an NAD(P)H-dependent oxidase since it has also been shown that DPI can inhibit the H_2O_2 generating function of peroxidases (e.g. Baker et al., 1998; Bolwell et al., 1998). However, several observations combine to favour an NAD(P)H-dependent oxidase over a peroxidase in suberizing potato tubers during this process: (1) H_2O_2 generation is all but eliminated with $\leqslant$10 μM DPI (Fig. 2), a concentration that only partially inhibits this function of peroxidases (Bolwell et al., 1998), (2) NAD(P)H-dependent oxidases have been implicated in other Solanaceous species induced to generate H_2O_2 in response to stress (e.g. Doke and Miura, 1995; Allan and Fluhr, 1997; Bolwell et al. 1998; Amacucci et al., 1999) and (3) our experiments are

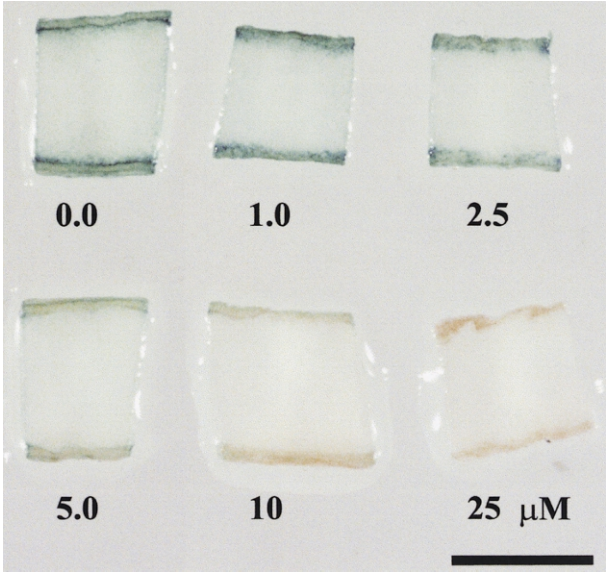

Fig. 2. Inhibition of hydrogen peroxide generation during suberin poly(phenolic) domain formation in wound healing potato tubers. Thin, hand-cut sections (250–500 μm) from wound healing potato tubers (5 days post wounding) were soaked in 1 mM ascorbic acid solution (1 min) and subsequently incubated with 0.0–25 μM diphenyleneiodonium (DPI) for 15 min. Tissues were transferred to 0.15 mg ml^{-1} TMB and the formation of blue-green stain taken as an indication of the presence of H_2O_2 (Ros Barceló, 1998b). Control tissue (0.0 μM DPI) was incubated with water only (after ascorbate treatment) followed by TMB staining. Note the restriction of staining to the layers of cells immediately below the sites of suberization. (Scale bar = 0.5 cm.)

performed without the addition of exogenous NAD(P)H. The last point is particularly important since the H_2O_2 generating capacity of peroxidases generally requires high levels (>1 mM) of NAD(P)H (Ros Barceló et al., 1998). Thus it seems likely that the H_2O_2 hypothesized to be required for SPPD formation is generated by an NAD(P)H-dependent oxidase, presumably present in the plasma membrane of suberizing cells. This observation, however, requires further experimental verification.

Notwithstanding the data presented above, it must also be verified that H_2O_2 is in fact *required* for SPPD formation. To address this question we have incubated potato disks on agar plates containing 25 μM DPI and compared both the soluble and cell wall bound phenolic compounds with those of controls (incubated on agar alone). As can be seen in Fig. 3, when incubated in the presence of DPI, wound healing tuber slices accumulate soluble compounds not present in control tissue (i.e. wound healed in the absence of DPI). For example, a large peak (retention time approx. 17 min) present in the chromatograms obtained from the extractives of DPI-treated tissues is all but absent from control extracts. The 17-min peak represents a pair of phenolic glycosides that remain unidentified to date. It is not clear at this point what role these compounds play in the suberization process, but it is proposed that if not for the presence of DPI in the treatment, both would have been covalently cross-linked into the SPPD.

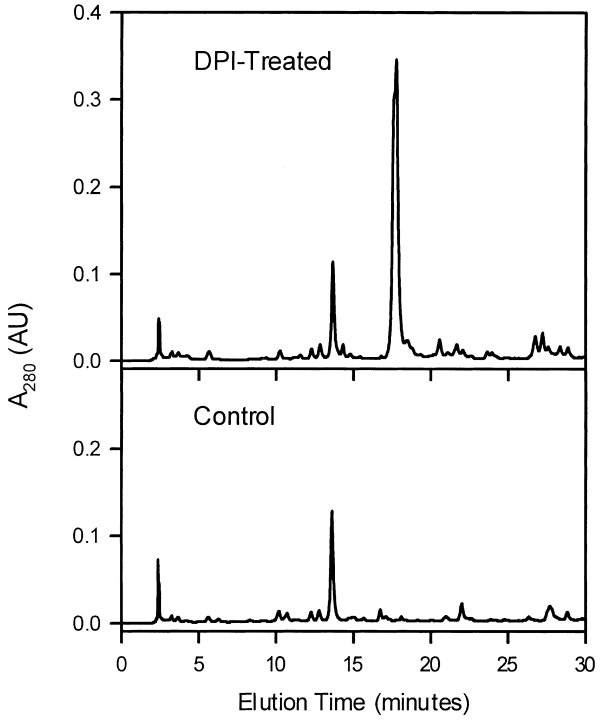

Fig. 3. High pressure liquid chromatographic analysis of soluble potato tuber extracts. Total soluble extracts (80% MeOH) prepared from wound healing potato tubers (7 days post wounding) incubated with (upper trace) and without (lower trace) 25 μM diphenyleneiodonium (DPI) were subject to Nucleosil C-18 reversed phase column chromatographic anaylses using a gradient of MeOH–CH_3CN–H_2O (1:1:1) in phosphoric acid (1.5% in H_2O) (see Experimental). The presence of new (phenolic) compound(s) is (are) evident in the large peak at approx. 17 min, present in the DPI-treated tissue. See text for details.

The presence of new soluble compounds in the extracts of DPI-treated tissues does not necessarily mean that the deposition of poly(phenolics) into the cell wall has also been inhibited by the treatment. Therefore, we also subjected extractive free cell walls of the suberized tissues isolated from control and DPI-treated tubers to both the thioacidolysis and DFRC methods of poly(phenolic) analysis. While the data remains preliminary (so far only single samples have been analyzed), yields were extremely low, as has been reported for suberized potato tubers before (Borg-Olivier and Monties, 1989, 1993; Lapierre et al., 1996). (These data do, however, point to a significant difference between suberized and lignified tissues, since the latter yield much larger amounts of product after either thioacidolysis or DFRC.) Notwithstanding the low yields, DPI-treated cells contained much lower amounts (in some cases only traces) of released phenolics, (data not shown) suggesting that formation of the SPPD was indeed interrupted by the treatment. Importantly, these data, support the need for H_2O_2 in the SPPD forming process, and a role for an NAH(P)H-dependent oxidase in its formation.

3. Concluding remarks

The question of how representative potato SPPDs are of suberized tissues in general remains to be answered, and it will be some time before the details revealed about it in the last decade can be readily transferred to other plant species (especially woody ones). Certainly, supportive evidence for the uniqueness of the PPD of suberized tissues has been obtained from endodermal and hypodermal tissues of several plant species including *Clivia miniata*, maize and *Cicer arietinun* (Schreiber, 1996, Zeier and Schreiber, 1997, 1999; Zeier et al., 1999). Arguably, the uniqueness of the SPPD has been evident in the literature for many years (Bernards and Lewis, 1998) but is now becoming more apparent, particularly through the careful chemical analysis of the suberized tissues from which they are found.

In the present paper, we have provided new preliminary evidence supporting the hypothesis that the SPPD of potatoes is assembled via an H_2O_2-dependent process, and that the H_2O_2 required for it is likely generated by an NAD(P)H-dependent oxidase system. Based on our data, and on models proposed for the oxidative burst that occurs during pathogenesis (Wojtaszek, 1997; Graham and Graham, 1999) and lignification in *Zinnia elegans* (Ros Barceló, 1998a), we have

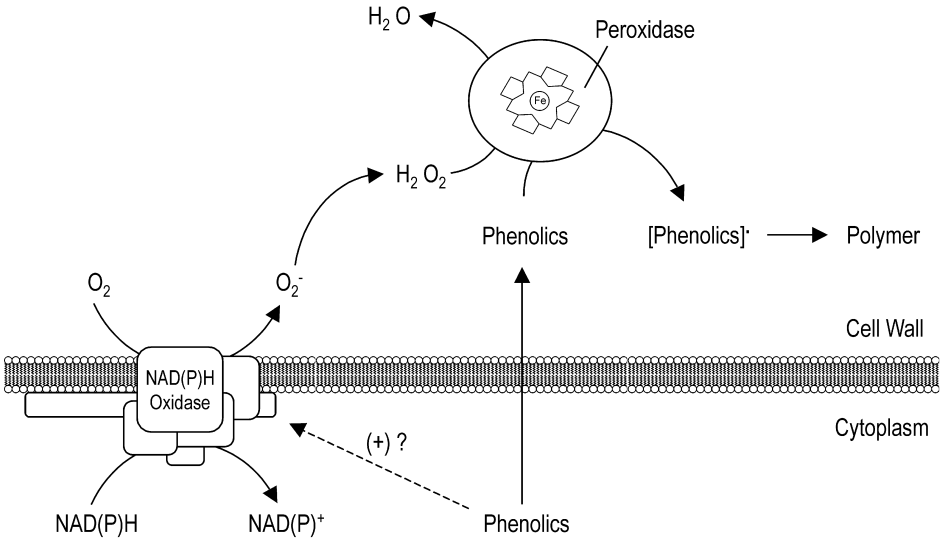

Fig. 4. Model for the macromolecular assembly of the potato suberin poly(phenolc) domain. Phenolics synthesized in the cytoplasm are transported to the carbohydrate matrix (by an as yet unknown mechanism) and may also act as stimulators of an NAD(P)H-dependent oxidase in the plasma membrane. The NAD(P)H-dependent oxidase generates superoxide on the exoplasmic face of the membrane, where it disproportionates to H_2O_2 in the presence of H^+ (or superoxide dismutase). The H_2O_2 formed can then be used by a cell wall associated peroxidase to catalyze the free radical-mediated coupling of phenolics into the poly(phenolic) domain. Adapted from Wojtaszek (1997) and Graham and Graham (1999).

constructed a model combining the H_2O_2-generating properties of a plasma membrane-bound NAD(P)H-dependent oxidase with the H_2O_2-utilizing properties of a cell wall bound peroxidase (Fig. 4) to account for the final stages of the macromolecular assembly of potato wound SPPD. Briefly, phenolics synthesized in the cytoplasm are transported to the cell wall (by an as yet unknown mechanism), where they are polymerized into the SPPD by a wall-associated peroxidase. The H_2O_2 required for this process likely comes from a plasma membrane-bound NAD(P)H-dependent oxidase. It is possible that soluble (cytoplasmic) phenolics serve to allosterically regulate the NAD(P)H-dependent oxidase in an analogous fashion to the "competency factor" role of genistein in soybeans (Graham and Graham, 1999). While speculative, our model is supported by the evidence collected to date, and continues to serve as a basis from which to design new experiments to explore the biosynthesis and macromolecular assembly of the potato SPPD.

4. Experimental

4.1. Plant material

Potato (*Solanum tuberosum* L. cv. Russet Burbank) tubers were grown locally from certified seed, and stored at 5°C until used. Suberization was initiated by cutting tubers (i.e. wounding) under sterile conditions as described (Bernards and Lewis, 1992).

4.2. DPI treatment, phenolic extraction and cell wall analysis

Tuber disks (1.5 cm diameter×0.5 cm thick) were incubated on water-agar plates (1.5% agar) with and without DPI (25 μM final concentration) for up to seven days. The suberized tissue collected from the lower surface of each disk was exhaustively extracted (i.e. 24 h) with 80% aqueous MeOH in a Soxhlet extractor. The MeOH solubles were concentrated and analyzed by HPLC on a Nucleosil C-18 reversed phase column (4.6× 150 mm, 5 μm, Machery-Nagel). Compounds were eluted using a gradient of organic solvent (MeOH–CH_3CN–H_2O, 1:1:1; solvent B) in 1.5% (v/v) aqueous phosphoric acid (solvent A). Initial column conditions: 10% solvent B in A. Gradient: 10–75% B in A over 30 min at 1 ml min^{-1}. The eluent was monitored over the range of 200–350 nm with a photodiode array detector.

The residues obtained from soxhlet extraction were dried with acetone and subjected to thioacidolysis according to Zeier and Schreiber (1997) and DFRC analysis according to Lu and Ralph (1997).

Acknowledgements

The authors would like to thank Dr. Lukas Schreiber (Universität Würzburg, Germany) for the use of facilities for thioacidolysis and the Natural Sciences and Engineering Research Council (NSERC) of Canada for financial support.

References

Allan, A.C., Fluhr, R., 1997. Two distinct sources of elicited reactive oxygen species in tobacco epidermal cells. Plant Cell 9, 1559–1572.

Amacucci, E., Gaschler, K., Ward, J.M., 1999. NADPH oxidase genes from tomato (*Lycopersicon esculentum*) and curly-leaf pondweed (*Potamogeton crispus*). Plant Biology 1, 524–528.

Angelini, R., Federico, R., 1989. Histochemical evidence of polyamine oxidation and generation of hydrogen peroxide in the cell wall. Journal of Plant Physiology 135, 212–217.

Baker, C.J., Deahl, K., Domek, J., Orlandi, E.W., 1998. Oxygen metabolism in plant/bacteria interactions: effect of DPI on the pseudo-NAD(P)H oxidase activity of peroxidase. Biochemical Biophysical Research Communications 252, 461–464.

Bernards, M.A., Fleming, W.D., Llewellyn, D.B., Priefer, R., Yang, X.L., Sabatino, A., Plourde, G.L., 1999. Biochemical characterization of the suberization-associated anionic peroxidase of potato. Plant Physiology 121 (1), 135–145.

Bernards, M.A., Lewis, N.G., 1992. Alkyl ferulates in wound healing potato tubers. Phytochemistry 31 (10), 3409–3412.

Bernards, M.A., Lewis, N.G., 1998. The macromolecular aromatic domain in suberized tissue: a changing paradigm. Phytochemistry 47 (6), 915–933.

Bernards, M.A., Lopez, M.L., Zajicek, J., Lewis, N.G., 1995. Hydroxycinnamic acid-derived polymers constitute the polyaromatic domain of suberin. Journal of Biological Chemistry 270 (13), 7382–7386.

Bernards, M.A., Susag, L.M., Bedgar, D.L., Anterola, A.M., Lewis, N.G., 2000. Induced phenylpropanoid metabolism during suberization and lignification: a comparative analysis. Journal of Plant Physiology 157, 401–407.

Bolwell, G.P., Gerrish, C., Salaun, J.-P., 1997. Changes in enzymes involved in suberisation in elicitor-treated french bean cells. Phytochemistry 45 (7), 1351–1357.

Bolwell, G.P., Davies, D.R., Gerrish, C., Auh, C.-K, Murphy, T.M., 1998. Comparative biochemistry of the oxidative burst produced by rose and french bean cells reveals two distinct mechanisms. Plant Physiology 116, 1379–1385.

Borg-Olivier, O., Monties, B., 1989. Characterization of lignins, phenolics acids and tyramine in the suberized tissues of natural and wound induced potatoe periderm. Comptes Rendus hebdomadaire des séances de l' Académiedes Sciences, Paris 308 (3), 141–147.

Borg-Olivier, O., Monties, B., 1993. Lignin, suberin, pheolic acids and tyramine in the suberized, wound-induced potato periderm. Phytochemistry 32 (3), 601–606.

Cowan, M.M., 1999. Plant products as antimicrobial agents. Clinical Microbiology Reviews 12 (4), 564–582.

Cross, A.R., Jones, O.T.G., 1991. Enzymic mechanisms of superoxide production. Biochimica et Biophysica Acta 1057, 281–298.

Deme, D., Doussiere, J., De Sandro, V., Dupuy, C., Pommier, J., Virion, A., 1994. The Ca^{2+}/NADPH-dependent H_2O_2 generation in thyroid plasma membrane: inhibition by diphenyleneiodonium. Biochemical Journal 301, 75–81.

Doke, N., Miura, Y., 1995. In vitro activation of NADPH-dependent O_2^- generating system in a plasma membrane-rich fraction of potato tuber tissues by treatment with an elicitor from *Phytophthora infestans* or with digitonin. Physiological and Molecular Plant Pathology 46, 17–28.

Dwyer, S.C., Legendre, L., Low, P.S., Leto, T.L., 1996. Plant and human neutrophil oxidative burst complexes contain immunologically related proteins. Biochimica et Biophysica Acta 1289, 231–237.

Elstner, E.F., Heupel, A., 1976. Formation of hydrogen peroxide by isolated cell walls from horseradish (*Armoracia lapathifolia* Gilib.). Planta (Berlin) 130, 175–180.

Espelie, K.E., Kolattukudy, P.E., 1985. Purification and characterization of an abscisic acid-inducible anionic peroxidase associated with suberization in potato (*Solanum tuberosum*). Archives of Biochemistry and Biophysics 240 (2), 539–545.

Espelie, K.E., Franceschi, V.R., Kolattukudy, P.E., 1986. Immunocytochemical localization and time course of appearance of an anionic peroxidase associated with suberization in wound-healing potato tuber tissue. Plant Physiology 81, 487–492.

Friedman, M., 1997. Chemistry, biochemistry and dietary role of potato polyphenols: a review. Journal of Agricultural and Food Chemistry 45, 1523–1540.

Gil, A.M., Lopes, M., Rocha, J., Pascoal Neto, C., 1997. A ^{13}C solid state nuclear magnetic resonance spectroscopic study of cork cell wall structure: the effect of suberin removal. International Journal of Biological Macromolecules 20, 293–305.

Graca, J., Pereira, H., 1999. Glyceryl-acyl and aryl-acyl dimers in *Pseudotsuga menziesii* bark suberin. Holzforschung 53 (4), 397–402.

Graham, T.L., Graham, M.Y., 1999. Role of hypersensitive cell death in conditioning elicitation competency and defense potentiation. Physiological and Molecular Plant Pathology 55, 13–20.

Gross, G.G., Janse, C., 1977. Formation of NADH and hydrogen peroxide by cell wall- associated enzymes from *Forsythia* xylem. Zeitschrift für Pflanzenphysiologie 84, 447–452.

Gross, G.G., Janse, C., Elstner, E.F., 1977. Involvement of malate, monophenols, and the superoxide radical in hydrogen peroxide formation by isolated cell walls from horseradish (*Armoracia lapathifolia* Gilib.). Planta 136, 271–276.

Kolattukudy, P.E., 1980. Biopolyester membranes of plants: cutin and suberin. Science 208, 990–1000.

Kolattukudy, P.E., 1984. Biochemistry and function of cutin and suberin. Canadian Journal of Botany 62, 2918–2933.

Lapierre, C., Pollet, B., Negrel, J., 1996. The phenolic domain of potato suberin: structural comparison with lignins. Phytochemistry 42 (4), 949–953.

Lotfy, S., Negrel, J., Javelle, F., 1994. Formation of ω-feruloyloxypalmitic acid by an enzyme from wound-healing potato tuber discs. Phytochemistry 35 (6), 1419–1424.

Lu, F., Ralph, J., 1997. Derivatization followed by reductive cleavage (DFRC method), a new method for lignin analysis: Protocol for analysis of DFRC monomers. Journal of Agricultural and Food Chemistry 45, 2590–2592.

Lulai, E.C., Corsini, D.L., 1998. Differential deposition of suberin phenolic and aliphatic domains and their roles in resistance to infection during potato tuber (*Solanum tuberosum* L.) wound-healing. Physiological and Molecular Plant Pathology 53 (4), 209–222.

Lulai, E.C., Morgan, W.C., 1992. Histochemical probing of potato periderm with neutral red: a sensitive cytofluorochrome for the hydrophobic domain of suberin. Biotechnic and Histochemistry 67 (4), 185–195.

Lulai, E.C., Orr, P.H., 1994. Techniques for detecting and measuring developmental and maturational changes in tuber native periderm. American Potato Journal 71, 489–505.

Marques, A.V., Pereira, H., Meier, D., Faix, O., 1996. Isolation and characterization of a guaiacyl lignin from saponified cork of *Quercus suber* L. Holzforschung 50, 393–400.

Negrel, J., Javelle, F., Paynot, M., 1993. Wound-induced tyramine hydroxycinnamoyl transferase in potato (*Solanum tuberosum*) tuber discs. Journal of Plant Physiology 142, 518–524.

Negrel, J., Lotfy, S., Javelle, F., 1995. Modulation of the activity of two hydroxycinnamoyl transferases in wound-healing potato tuber discs in response to pectinase or abscisic acid. Journal of Plant Physiology 146, 318–322.

Negrel, J., Pollet, B., Lapierre, C., 1996. Ether-linked ferulic acid amides in natural and wound periderms of potato tuber. Phytochemistry 43 (6), 1195–1199.

Ros Barceló, A., 1998a. The generation of H_2O_2 in the xylem of *Zinnia elegans* is mediated by an NADPH-oxidase-like enzyme. Planta 207 (2), 207–216.

Ros Barceló, A., 1998b. Hydrogen peroxide production is a general property of the lignifying xylem from vascular plants. Annals of Botany 82, 97–103.

Ros Barceló, A., Morales, M., Pedreño, M. A., 1998. Specific compartmentalization of peroxidase isoenzymes in relation with lignin biosynthesis in the plant cell. In: Lewis, N.G., Sarkenen, S. (Eds.), Lignin and Lignan Biosynthesis, ACS Symposium Series 697, pp. 1–11.

Schreiber, L., 1996. Chemical composition of Casparian strips isolated from *Clivia miniata* Reg. roots: evidence for lignin. Planta 199, 596–601.

Schreiber, L., Hartmann, K., Skrabs, M., Zeier, J., 1999. Apoplastic barriers in roots: chemical composition of endodermal and hypodermal cell walls. Journal of Experimental Botany 50, 1267–1280.

Schmutz, A., Jenny, T., Amrhein, N., Ryser, U., 1993. Caffeic acid and glycerol are constitutents of the suberin layers in green cotton fibres. Planta 189, 453–460.

Schmutz, A., Jenny, T., Ryser, U., 1994. A caffeoyl-fatty acid-glycerol ester from wax associated with green cotton fibre suberin. Phytochemistry 36 (6), 1343–1346.

Soliday, C.L., Kolattukudy, P.E., Davis, R.W., 1979. Chemical and ultrastructural evidence that waxes associated with the suberin polymer constitute the major diffusion barrier to water vapor in potato tuber (*Solanum tuberosum* L.). Planta 146, 607–614.

Stark, R.E., Garbow, J.R., 1992. Nuclear magnetic resonance relaxation studies of plant polyester dynamics. 2. Suberized potato cell wall. Macromolecules 25, 149–154.

Vianello, A., Macri, F., 1989. NAD(P)H oxidation elicits anion superoxide formation in radish plasmalemma vesicles. Biochimica et Biophysica Acta 980, 202–208.

Vianello, A., Macri, F., 1991. Generation of superoxide anion and hydrogen peroxide at the surface of plant cells. Journal of Bioenergetics and Biomembranes 23 (3), 409–423.

Vogt, E., Schonherr, J., Schmidt, H.W., 1983. Water permeability of periderm membranes isolated enzymatically from potato tubers (*Solanum tuberosum* L.). Planta 158, 294–301.

Wojtaszek, P., 1997. Oxidative burst: an early plant response to pathogen infection. Biochemical Journal 322, 681–692.

Yan, B., Stark, R.E., 1998. A WISE NMR approach to heterogeneous biopolymer mixtures: dynamics and domains in wounded potato tissues. Macromolecules 31 (8), 2600–2605.

Zeier, J., Schreiber, L., 1997. Chemical composition of hypodermal and endodermal cell walls and xylem vessels isolated from *Clivia miniata*: identification of the biopolymers lignin and suberin. Plant Physiology 113, 1223–1231.

Zeier, J., Schreiber, L., 1999. Fourier transform infrared-spectroscopic characterization of isolated endodermal cell walls from plant roots: chemical nature in relation to anatomical development. Planta 209, 537–542.

Zeier, J., Goll, A., Yokoyama, M., Karahara, I., Schreiber, L., 1999. Structure and chemical composition of endodermal and rhizodermal hypodermal walls of several species. Plant Cell and Environment 22 (3), 271–279.

PERGAMON

Phytochemistry 57 (2001) 1123–1134

PHYTOCHEMISTRY

www.elsevier.com/locate/phytochem

Review

Similarities and differences in rubber biochemistry among plant species

Katrina Cornish*

USDA-ARS, Western Regional Research Center, 800 Buchanan Street, Albany, CA 94710, USA

Received 19 September 2000; received in revised form 28 December 2000

Abstract

This report reviews aspects of the biochemical regulation of rubber yield and rubber quality in three contrasting rubber-producing species, *Hevea brasiliensis*, *Parthenium argentatum* and *Ficus elastica*. Although many similarities are revealed, considerable differences also exist in enzymatic mechanisms regulating biosynthetic rate and the molecular weight of the rubber biopolymers produced. In all three species, rubber molecule initiation, biosynthetic rate and molecular weight, in vitro, are dependent upon substrate concentration and the ratio of isopentenyl pyrophosphate (IPP, the elongation substrate, or monomer) and farnesyl pyrophosphate (FPP, an initiator), but these parameters are affected by intrinsic properties of the rubber transferases as well. All three rubber transferases are capable of producing a wide range of rubber molecular weight, depending upon substrate concentration, clearly demonstrating that the transferases are not the prime determinants of product size in vivo. However, despite these commonalities, considerable differences exist between the species with respect to cosubstrate effects, binding constants, effective concentration ranges, and the role of negative cooperativity in vitro. The *P. argentatum* rubber transferase appears to exert more control over the molecular weight it produces than the other two species and may, therefore, provide the best prospect for the source of genes for transformation of annual crop species.The kinetic data, from the three contrasting rubber-producing species, also were used to develop a model of the rubber transferase active site in which, in addition to separate IPP and allylic-PP binding sites, there exists a hydrophobic region that interacts with the linear portion of allylic-PP initiator proximal to the pyrophosphate. Substrate affinity increases until the active site is traversed and the rubber interior of the rubber particle is reached. The kinetic data suggest that the hydrophobic region in *H. brasiliensis* and *F. elastica* is about 1.8 nm long but only 1.3 nm in *P. argentatum*. The estimates are supported by measurements of the rubber particle monolayer membrane using electron paramagnetic resonance spectroscopy. Published by Elsevier Science Ltd.

Keywords: *Ficus elastica*; Moraceae; *Hevea brasiliensis*; Euphorbiaceae; *Parthenium argentatum*; Compositae; Natural rubber; Rubber transferase; Electron paramagnetic resonance spectroscopy

Contents

1. Introduction 1124

2. Rubber particles and their components 1125

3. Rubber biosynthesis 1127
   3.1. Regulation of initiation and biosynthetic rate 1127
   3.2. Regulation of molecular weight 1128
   3.3. The role of negative cooperativity 1130
   3.4. Competition and activation 1132

* Tel.: +1-510-559-5950; fax: +1-510-559-5663.
E-mail address: kcornish@pw.usda.gov

0031-9422/01/$ - see front matter Published by Elsevier Science Ltd.
PII: S0031-9422(01)00097-8

4. Conclusions....1132

Acknowledgements....1132

References....1132

1. Introduction

All natural rubber currently in commercial use comes from a single plant species, the Brazilian rubber tree (*Hevea brasiliensis*), and the United States is completely dependent on imports from developing countries (Davis, 1997), for the manufacture of more than 40,000 products, including more than 400 medical devices. Asia now produces about 90% of the world demand for *H. brasiliensis* natural rubber, which, in 1998, was 6.61 million tonnes [40% of the total rubber demand; the remaining 60% is synthetic rubber produced from petroleum (data from the International Rubber Study Group)]. The United States, with no natural rubber production, is the largest single consumer of this material. In 1998, the United States imported nearly 1.2 million tonnes of natural rubber for product manufacture, at a cost approaching $2,000,000,000. In addition, the United States imports a considerable quantity of finished goods: in 1998, valued at $8,060,000,000 containing 349,000 tonnes of natural rubber (data from US Department of Commerce, Office of Trade and Economic Analysis). Natural rubber consumption closely tracks production, preventing the accumulation of large stockpiles (Fig. 1) (Mooibroek and Cornish, 2000).

Primarily due to its molecular structure and high molecular weight (>1 million Da), natural rubber has high performance properties that cannot be matched by synthetic rubber produced from petroleum. These properties include resilience, elasticity, abrasion and impact resistance, efficient heat dispersion, and malleability at cold temperatures. Despite the best efforts of the chemical industry, these properties have not been achieved by synthetic materials, or non-rubber natural polymers or blends, in many high performance applications, including tires, and surgical gloves and latex balloon devices. As a result, the amount of synthetic rubber produced has reached a plateau, whilst annual natural rubber production is steadily increasing to meet demand (Fig. 2), and probably will soon exceed the synthetic rubber market share. The *H. brasiliensis* crop consists almost entirely of plantation-grown clonal trees, and is one of the most genetically-restricted crops under cultivation. This lack of genetic diversity leaves the crop highly susceptible to pathogenic attack and failure, as demonstrated by the devastation caused by leaf blight in South American plantations (Davis, 1997). A dependable supply is endangered by many other factors, including diminishing acreage as growers in developing countries move away from rubber farming toward higher value agriculture, increasing global demand, and changing political positions (Reisch, 1995; Davis, 1997). Higher-yielding germplasm cannot indefinitely meet increased natural rubber demand and many new plantations will be required. *H. brasiliensis* also has strict climatic requirements, which limit its cultivation to specific tropical regions.

In addition to strategic and economic incentives to develop a renewable US-based natural rubber supply, the recent widespread occurrence of life-threatening "latex allergy" to *H. brasiliensis* rubber products, which

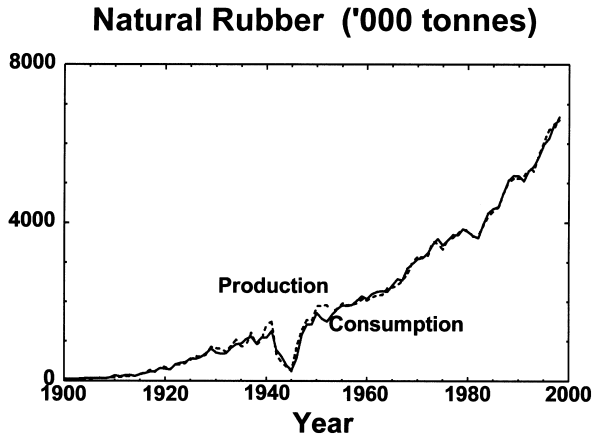

Fig. 1. Global production (dashed line) and consumption (solid line) of natural rubber during the twentieth century.

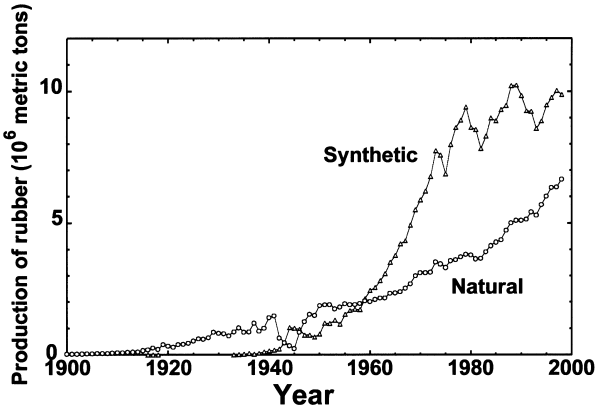

Fig. 2. Global production of natural (○) and synthetic (△) rubber during the twentieth century. Synthetic rubber production was established largely because of the drop in natural rubber production during World War II. Rubber consumption figures have closely tracked production.

affects an estimated 20,000,000 Americans, strengthens the need for development of alternative sources of natural rubber (Morales et al., 1989; Slater, 1989; Tomazic et al., 1992; Kekwick 1993; Pailhories, 1993; Ownby et al., 1994; Nakayama et al., 1996; Siler and Cornish, 1994a; Carey et al., 1995; Siler et al., 1996). Also, although synthetic rubber cannot replace natural rubber in many applications, the converse is not true. Large-scale, domestic natural rubber production will be needed in the future, even without a natural rubber supply crisis, to first supplement, then replace the 60% market share currently enjoyed by synthetic rubbers because these are derived from petroleum, a non-renewable resource. A decline in global oil production may begin within the next 10 (Campbell and Laherrere, 1998) or 20 (Monastersky, 1998) years. Thus, commercialization and natural rubber production from domestic crops is in the best short- and long-term interests of developed countries such as the United States.

Some 2500 plant species, many of which are tropical, produce natural rubber (Bowers, 1990; Ray, 1993). Most, however, do not produce the high molecular weight polymers required for high performance commercial products [molecular weight is strongly correlated with rubber quality (Swanson et al., 1979)]. Of the possible rubber-producing plant species for the US, *Parthenium argentatum* (guayule) has received the most sustained research and development effort over the years (Bowers, 1990; Whitworth and Whitehead, 1991) and is closest to domestication and commercial production. Currently, guayule is being introduced as a biennial crop in the southwestern United States to supply high performance, nonallergenic latex (Siler and Cornish, 1994a; Siler et al., 1996; Cornish and Lytle, 1999) to the medical products market (Cornish, 1996, 1998, patents exclusively licensed to Yulex Corporation). This crop may be able to fully supply the medical market but is unlikely to generate sufficient rubber for other large markets, such as tires, because it cannot tolerate the snowy winters and severe temperatures experienced by much of the United States and many other temperate countries. Also, although it may prove practical to generate new higher yielding lines, it cannot be grown as an annual crop because it produces its rubber in bark parenchyma cells and most of the rubber is synthesized during winter months. Thus, one season's growth gives a plant containing little bark parenchyma and little rubber. Additional alternative rubber-producing annual crops are, therefore, required to supply rubber to meet non-medical market requirements, and to engender a much-needed biodiversity.

Ideally, rubber-producing crop plants should be rapidly-growing, have large biomass, and be annual crops, which can be more readily included in on-farm crop rotations and farming systems, and could be readily planted and plowed-out in response to market needs and farmer production considerations. Cropping systems, such as trees, that must remain in place for many years are not well suited to changing market demand and fluctuations. Most of the 2500 known rubber-producing plant species produce small amounts of poor quality, low molecular weight rubber. Successful conversion of candidate crop species, whether or not they already produce rubber naturally, into domestic rubber-producing crops requires the generation of lines capable of producing commercially-viable yields of high quality rubber. This can only be accomplished by basing genetic engineering strategies upon a thorough understanding of biochemical factors affecting rubber yield (biosynthetic rate, substrate availability and rubber particle size, number and ontogeny) and rubber quality (primarily rubber molecular weight).

2. Rubber particles and their components

Many different dicotyledonous plants make natural rubber. Most of this review concentrates on the similarities and differences in rubber production among three plant species, each from a different superorder of the Dicotyledonae, i.e. *Hevea brasiliensi* Müll. Arg. (Rosidae), *Ficus elastica* Roxb. (Dilleniidae), and *Parthenium argentatum* Gray (Asteridae). In all three species, natural rubber is compartmentalized within subcellular rubber particles, located in the cytosol of cells, whether these be specialized laticifers (pipe-like anastomosized cell systems which produce latex), as in *H. brasiliensis* (d'Auzac et al., 1989) and *F. elastica* (Heinrich, 1970) or generalised cells, such as the bark parenchyma of *P. argentatum* (Whitworth and Whitehead, 1991). The average size of the particles varies among species [e.g. *F. elastica* 3.8 μm, *Euphorbia lactiflua* 0.42 μm (Siler et al., 1997; Wood and Cornish, 2000)], and differently-sized subsets of particles can even be found in the same plant. *H. brasiliensis*, for example, has two distinct subsets of particles with mean diameters of 1.0 and 0.2 μm (Cornish et al., 1993; Wood and Cornish, 2000).

Very little is known about rubber particle ontogeny, largely because small, electron-dense rubber particles cannot be readily distinguished from other small electron-dense particles in cytoplasm (Backhaus, 1985). However, studies of rubber particle structure and biochemical components suggest a likely origin in the rough endoplasmic reticulum. The overall structure of rubber particles is similar in all species examined so far, in that they contain a homogeneous rubber core surrounded by an intact monolayer membrane (Cornish et al., 2000; Wood and Cornish, 2000). The glycosylated moieties of some of the particle-bound proteins and the hydrophilic head groups of the phospholipids enable the particles to interface with the aqueous cytosol. However, within the shared architecture, the rubber particle components are quite different, the compartmentalized

rubber being of much lower molecular weight in *F. elastica* than in the other two species, and all three possessing a species-specific complement of lipids and proteins (Cornish et al., 1993; Siler et al., 1997). The lipid fraction of *P. argentatum* rubber particles is typical of many plant cell membranes, and appears to reflect the very ordinary cells (bark parenchyma) in which the rubber particles are formed. It seems likely that the rubber particle membrane in different species is made up of readily available lipid components, and that highly conserved structure and chemical composition are not required. Also, the amount of protein associated with rubber particles varies tremendously between species, ranging from 4.8% in *E. lactiflua* to less than 0.1% in *P. argentatum* (Siler et al., 1997), and the number of different proteins is remarkably different. The most complicated rubber particles currently known are those of *H. brasiliensis*. These contain upwards of 80 different proteins across a size range of 5 to over 200 kDa. However, other rubber particles contain far fewer proteins, perhaps less than 10 in *F. elastica* and *P. argentatum*, for example (Cornish et al., 1993). The architecturally-analogous cytoplasmic oil bodies (Huang, 1992) are much more highly conserved from one species to another in their protein and lipid components, but these organelles must export their contents, not merely retain them, and so require a sophisticated secretion system. Rubber is a secondary product that is not catabolized during the life of the plant, and rubber particles only need to effectively compartmentalize the rubber. The non-conserved nature of the particular rubber particle biomembrane components suggests that few, if any, specific genes may be required to generate a rubber particle once a rubber transferase enzyme begins rubber synthesis. Thus, normally non-rubber-producing species transformed with genes encoding rubber transferase may be able to effectively compartmentalize rubber using cytosolic membrane components. Information on factors regulating the number of rubber particles made in a tissue will probably not be obtained until transformed plants with enhanced rubber biosynthetic activity have been generated.

Very large proteins or protein complexes appear to be present in all species (Cornish et al., 1993; Siler and Cornish, 1993, 1994a,b), and they all contain an integral, membrane-bound, rubber-synthesizing *cis*-prenyl transferase enzyme or enzyme complex (rubber transferase, EC 2.5.1.20). This enzyme synthesizes rubber from hydrophilic substrates obtained from the cytoplasm and the hydrophobic polymer is compartmentalized into the rubber particle interior. Thus, the polymerization reaction must take place at the rubber particle surface, and it has been proven that rubber transferase is an integral membrane protein or protein complex (Madhavan et al., 1989; Cornish and Backhaus, 1990; Cornish, 1993; Cornish and Siler, 1996).

The identity of the rubber particle-bound rubber transferase remains equivocal. Two different proteins on *H. brasiliensis* rubber particles have been implicated in activity, namely the 14.6 kD "rubber elongation factor" (Dennis and Light, 1989) and the 24 kD "small rubber particle protein" (Oh et al., 1999). Although the case for both has yet to be substantiated, the data supporting the role of the 24 kD protein seems more convincing than for the 14.6 kD protein (Cornish, 1993), which relied solely on immunoinhibition of activity in latex, not in washed rubber particles. Oh et al. (1999), used a combination of immunoinhibition and direct addition of expressed protein to affect activity. However, it seems worthwhile to point out that meaningful immunoinhibition experiments must be performed using purified antibody. Crude sera can lead to reproducible and substantial inhibition of rubber transferase activity in washed rubber particles that is not antibody specific (Fig. 3). Also, immunoblots of sera against *H. brasiliensis* latex proteins have shown that experimental animals frequently contain antibodies to *H. brasiliensis* latex proteins before being challenged with purified protein(s) (Siler and Cornish, unpublished). The animals have presumably reacted to contact with the latex gloves worn by their handlers and/or the rubber stoppers commonly used to support the water supply tubes.

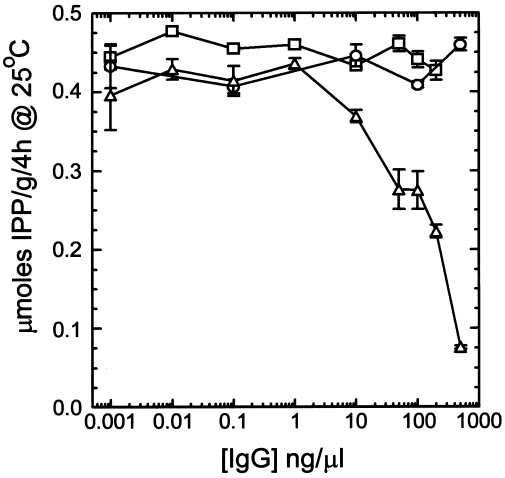

Fig. 3. Rubber transferase activity in rubber particles purified from *Hevea brasiliensis* latex. Ascites fluid (crude sera) from mice challenged with a low-density lipoprotein was the generous gift of Dr. Alex Karu, UC Berkeley Hybridoma Center. IgG was purified from the ascites fluid by chromatography on a 1 ml bed volume Protein G column (Hi-Trap, Pharmacia) according to the manufacturer's instructions. A non-specific purified mouse ascites IgG (Pierce) was used as a negative control. The serum and purified IgG samples were incubated with the rubber particles for 15 h on ice before the remaining rubber transferase activity was assayed as described (Cornish, 1993). 465 µg dw of rubber particles in 500 µl were assayed for 4 h at 25°C in imM IPP, 20 µM FPP and 1 mM Mg^{2+}. Each value is the mean of 3±S.E. In the absence of IgG or ascites, 0.412±0.034 µmol IPP were incorporated. The experiment was repeated with similar results (not shown).Key: (○) control IgG; (Δ) serum; (□) purified lipoprotein IgG.

Thus, pre-immune bleed evaluations are essential and, in this laboratory, we use animals born and reared in latex-free environments.

The situation has been complicated again recently by the identification and cloning of a bacterial gene encoding undecaprenyl diphosphate synthase (Shimizu et al., 1998), another member of the *cis*-prenyl transferase family, followed by the isolation of various related enzymes through sequence homology. Although it seemed possible that rubber transferase also might be identified as a homologue, it seems increasingly unlikely that the homology between the two enzymes is high enough for successful homogue-based cloning. This is perhaps not surprising, because the undecaprenyl diphosphate synthase is a soluble enzyme and makes relatively short polymer (55 carbons), whereas the rubber transferase is membrane-bound, possibly a complex, and can make product many thousands of carbons long (Cornish et al., 1993, 2000; Castillón and Cornish, 1999).

However, even though the degree of relationship between the UDP synthase and rubber transferase is unknown, immuno-inhibition experiments indicate that rubber transferase activity does appear to be associated with a 376 kDa rubber particle-bound protein in *F. elastica* (Cornish et al., 1994). Cross-specific immunoinhibition and immunoprecipitation studies, with purified IgG antibodies and purified rubber particles, also have indicated that some structural similarities probably exist between the rubber transferases of *F. elastica*, *H. brasiliensis* and *P. argentatum* (Siler and Cornish, 1993, 1994b; Cornish et al., 1994).

3. Rubber biosynthesis

3.1. Regulation of initiation and biosynthetic rate

Natural rubber is produced by a simple side-branch of the ubiquitous isoprenoid pathway (Chappell, 1995) from an allylic pyrophosphate (allylic-PP) and isopentenyl pyrophosphate (IPP) (Fig. 4). Several allylic-PP's, namely dimethylallyl-PP (DMAPP), geranyl-PP (GPP) and *trans,trans*-farnesyl-PP (FPP) are synthesized, by soluble enzymes, in the same cytosolic compartment as rubber transferase and so could be used by the rubber transferase. The IPP polymerized by the rubber transferase is probably derived from the mevalonate pathway, also located in the cytosol (Chappel, 1995). However, IPP derived from the deoxy-xylulose pathway (reviewed by Lichtenthaler, 1999) may diffuse from the plastids and join the cytosolic pool. The importance of the soluble *trans*-prenyl transferases in rubber biosynthesis lies in their synthesis of allylic-PP's, essential initiators of rubber biosynthesis.

The rubber particle-bound rubber transferases of *F. elastica*, *H. brasiliensis* and *P. argentatum* have considerable similarities in their substrate requirements,

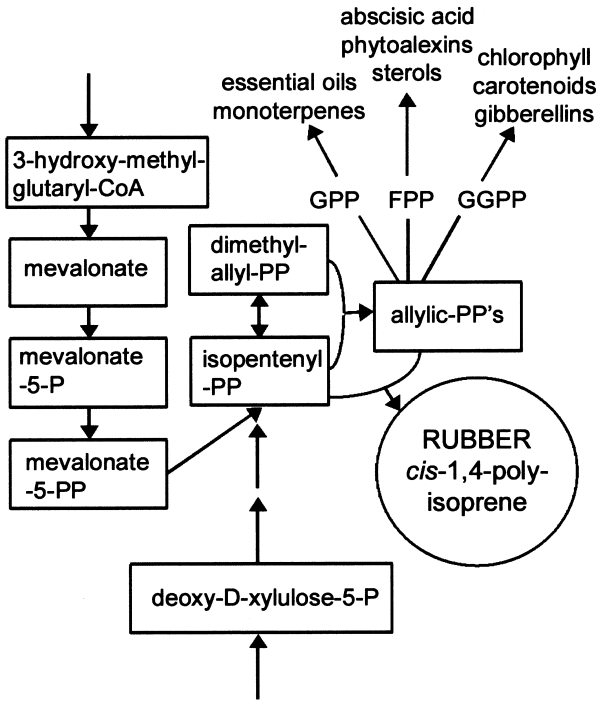

Fig. 4. The relationship of rubber biosynthesis to the isoprenoid pathway. The rubber particle membrane-bound rubber transferase (a *cis*-prenyl transferase) binds an allylic pyrophosphate (allylic-PP) to initiate a new rubber molecule and then elongates the polymer by *cis*-1,4-polymerization of isopentenyl monomers derived from isopentenyl pyrophosphate (IPP). Cytosolic IPP is produced by the mevalonate pathway, but the endogenous pool size may be supplemented by IPP produced by the deoxy-*D*-xylulose pathway in the plastids. Dimethyl allyl pyrophosphate (DMAPP) is produced by IPP-isomerase, and allylic-PP's larger than DMAPP are synthesized by soluble *trans*-prenyl transferases. All the allylic-PP's shown can be used as initiators by rubber transferase. All reactions shown require a divalent cation cofactor such as magnesium. Given the multidisciplinary nature of the intended audience of this paper, a brief summary of essential terms is given. IPP is the "elongation" or "polymerization" substrate, or the "monomer" in the rubber biosynthetic reaction. Polymer "elongation" is equivalent to "polymerization" and to "propagation". Allylic-PP is the initiation substrate, one being needed for each new polymer. Allylic-PP also can displace the elongating rubber molecule from the enzyme's active site and so acts as a "chain transfer agent" in addition to its role as an initiator. PP, pyrophosphate; GPP, geranyl pyrophosphate; FPP, farnesyl pyrophosphate; GGPP = geranylgeranyl pyrophosphate.

kinetic constants, and pH dependencies (Lynen, 1969; Archer and Audley, 1987; Madhavan et al., 1989; Cornish and Siler, 1996; Cornish et al., 1998). Rubber molecules are synthesized from one allylic-PP molecule, which initiates the reaction; the rubber polymer (*cis*-1,4-polyisoprene) is then made by sequential condensations of the non-allylic IPP (divalent cations, such as magnesium or manganese, are a required cofactor) with release of a diphosphate at each condensation (Archer et al., 1963). After initiation and elongation, a termination event occurs in which the rubber molecule is released from the enzyme. However, despite these similarities, remarkable differences exist between these species with

respect to enzymatic reaction mechanisms and product molecular weight.

Many different allylic-PP's are effective initiators of rubber biosynthesis, including DMAPP (C_5), GPP (*trans*, C_{10}), FPP (all-*trans*, C_{15}) and geranylgeranyl-PP (GGPP) (*trans*, C_{20}) (Lynen, 1969; Archer and Audley, 1987; Madhavan et al., 1989; Cornish et al., 1998). Only the first three of these are likely initiators of rubber biosynthesis in vivo because only the corresponding short-chain prenyl transferases share the cytosolic compartment with rubber transferase. Geranylgeranyl-PP synthase is located in the plastids (e.g. Dogbo and Camara, 1987). Also, GPP synthase is not a common cytosolic enzyme and is usually only found in abundance in specialized secretory cells such as in mint oil glands (Burke et al., 1999). However, the gene encoding a GPP synthase is present in *P. argentatum* (from EST homologues, Mau and Cornish, unpublished). Direct NMR-based structural evidence supports FPP as the principal initiator in vivo, at least in *H. brasiliensis* (Tanaka, 1989; Tanaka et al., 1996) and the mushroom *Lactarius volemus* (Ohya and Tanaka, 1998). Also, biochemical studies have shown that the apparent K_m value for FPP is lower than those for GPP or DMAPP in all three species (Table 1) (Cornish et al., 1998) and so the affinity of rubber transferase is greater for FPP than for the other two initiators.

In *H. brasiliensis*, *F. elastica* and *P. argentatum*, many other allylic-PP's can initiate rubber polymerization in vitro (Archer and Audley, 1987; Cornish et al., 1998). Thus, rubber transferases in general are very tolerant of both size and stereochemistry of the allylic-PP. This is in contrast to most known prenyl transferases which have strict substrate structural requirements for the elongation reactions they catalyze. Nonetheless, in vitro experiments have shown that the particular initiator supplied to the rubber transferase has a considerable impact on rubber biosynthetic rate. This appears to result from different initiation rates being caused by different $K_m^{\text{allylic-PP}}$'s as well as by direct effects on the IPP incorporation rate (Cornish and Siler, 1995; Castillón and Cornish, 1999; Cornish et al., 2000). In general, biosynthetic rate increases with the size of the *trans*-allylic-PP from DMAPP until either FPP (in *P. argentatum*) or GGPP (in *H. brasiliensis* and *F. elastica*) (Cornish and Siler, 1995; Cornish et al., 1998). In line with the increase in biosynthetic rate, the apparent K_m for the different allylic-PP's declines (Table 1).

Table 1
K_m's of three rubber transferases[a]

Initiator	*Hevea brasiliensis*	*Ficus elastica* (μM)	*Parthenium argentatum*
DMAPP	13.2	33.9	3.4
GPP	3.9	1.6	0.7
FPP	1.5	0.6	0.01
GGPP	1.4	0.3	0.01
IPP in FPP	363	115	385

[a] K_m's were determined from Hill plots of log $\upsilon/(V_{max}-\upsilon)$ against log substrate concentration. Assays in varying allylic-PP were performed at 25°C for *H. brasiliensis* and *F. elastica* and 16°C for *P. argentatum* in the presence of 1 mM [^{14}C]IPP. Assays in varying IPP were performed similarly except that 20 μM FPP was used.

Kinetic data were used to develop a model of the rubber transferase active site which contains a catalytic site and separate IPP and allylic-PP binding sites. The allylic-PP binding site is composed of a specific binding region which recognizes the allylic-PP moiety and a non-specific region which interacts with the hydrophobic portion of allylic-PP initiator. Increasing the length of the initiator increases the hydrophobic interaction and thus the affinity of the enzyme for the substrate. Substrate affinity increases until the active site is traversed and the interior of the rubber particle is reached. At this point, no additional change in affinity occurs with an increase in initiator length. The kinetic data indicate that FPP is of sufficient size to traverse the rubber transferase active site in *P. argentatum*, because V_{max} and K_m are similar for FPP and GGPP in this species, whereas GGPP is large enough to do the same in the rubber transferase active sites of *H. brasiliensis* and *F. elastica*. The model was successfully tested using a variety of stereoisomers of the allylic-PP's (unpublished data). The data suggest that the hydrophobic region in *H. brasiliensis* and *F. elastica* is about 1.8 nm long but is only 1.3 nm in *P. argentatum*. These estimates are supported by measurements of the *P. argentatum* rubber particle monolayer membrane using electron paramagnetic resonance spectroscopy (Cornish et al., 1999). When the hydrophilic pyrophosphate region of FPP is aligned with the hydrophilic phospholipid region of the monolayer membrane, the rubber interior of the particle is reached at almost exactly the same place (Fig. 5). This seems noteworthy because the tertiary structure of the enzyme or enzyme complex would not make such a coincidence actually necessary, even though a minimization of active site structure has obvious advantages.

3.2. Regulation of molecular weight

Many different plant species produce natural rubber, but only a few produce the high molecular weights required for high performance commercial products. As mentioned earlier, the biochemical regulation of molecular weight must be understood so that genetic-engineering strategies may be designed that increase yield while maintaining or conferring high molecular weight. In vitro investigations have now shown that, in the three different species discussed in this review, rubber

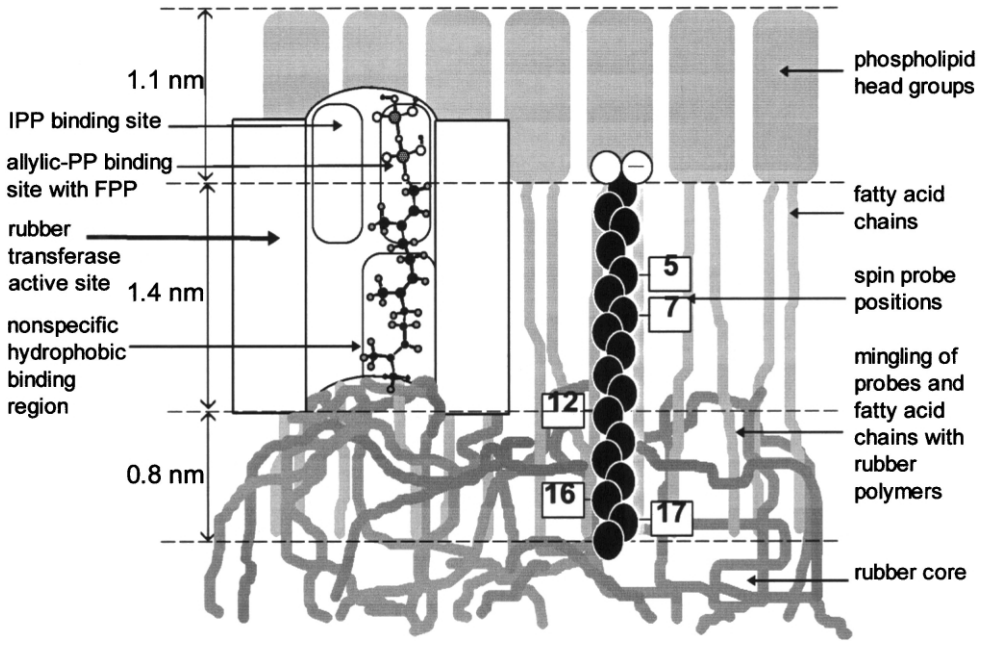

Fig. 5. A schema depicting, to scale, a section of the surface monolayer biomembrane surrounding a *Parthenium argentatum* rubber particle and the intermingling of the phospholipid fatty acid chains with the pure rubber core (from Cornish et al., 1999). The major phospholipids are phosphatidyl choline and the major fatty acids are 16:0, 18:0, 18:1, 18:2 and 18:3 comprising 95% of the phospholipids (Siler et al.,1997). The predominate protein, allene oxide synthese, a 52 kDa glycoprotein (Pan et al., 1995), is a partially embedded amphiphilic protein (not shown) that penetrates the monolayer only as far as the 5- and possibly the 7-doxyl spin probe positions. The orientation of the stearic acid spin probes in the monolayer is depicted with the stearic acid chain in the all *trans* configuration and the doxyl spin probe shown as a rectangular box attached to a specific methylene carbon (black ball) indicated by the number in the box. The positions of all the probes used are depicted on a single stearic acid instead of on individual ones for the sake of space, and indicate the region of the monolayer probed. The stearic acid chain is aligned parallel to the phospholipid fatty acid chains with its polar head group localized in the aqueous media between the phospholipid head groups. The intermingling of the fatty acid chains of the phospholipids with the pure rubber of the particle core begins at the C-12 doxyl position and ends somewhere in the vicinity of the terminal methyl of the stearic acid chain. The rubber transferase active site with FPP bound into the allylic-PP binding site is positioned so that the hydrophilic pyrophosphate of FPP is aligned to the polar head group region of the membrane. The kinetic studies suggest that FPP traverses the active site as shown. Both models show the same physical position for the membrane-rubber interface.

molecular weight is greatly affected by substrate concentration and type, and especially by the concentration of allylic-PP initiator. In general, the higher the allylic-PP concentration, the lower the rubber molecular weight that results, while the converse is true for IPP, i.e. the higher the concentration of IPP the greater the molecular weight (Castillón and Cornish, 1999; Cornish et al., 2000). It appears that competition for the allylic-PP binding (initiation) site occurs between free allylic-PP (although it should be noted that only FPP has been tested in all three species) and the allylic-PP moiety of the growing polymer. This site binds the original FPP initiator and all the allylic-PP intermediates formed as the rubber polymer grows (the terminal five-carbon unit always includes the pyrophosphate and allylic carbon). The higher the FPP concentration, the more likely that free FPP, acting as a reinitiation (or chain transfer) reagent, could displace the polymer and initiate a new rubber molecule, which in turn accounts for the shortening of the rubber polymer observed with increasing FPP concentration. The affinity of FPP would probably not be very much lower than the affinity of the growing rubber polymer because only a relatively small piece of the rubber molecule appears to be positioned within the active site at any time (see Fig. 5 and related discription). The same effect of increasing concentration causing shorter polymers is caused by GPP in *P. argentatum* and would probably occur in the other two species as well.

Presumably, the rubber transferase enzymes would be similarly affected in vivo. The polymer molecular weights produced by rubber transferase vary without exhaustion of free substrate, and in many cases without large changes in substrate concentration. Competition between FPP and the IPP donor site which could signal a non-productive terminal extensions and hence chain extension seems unlikely because such competition has only been observed in the *P. argentatum* rubber transferase (Castillón and Cornish, 1999) but not in the *H. brasiliensis* or *F. elastica* rubber transferases (Cornish et al., 2000). The rubber transferase system in vitro does appear to be able to terminate the polymers and initiate new molecules. For example, the incorporation rate of allylic-PP, under saturating concentrations of IPP and either FPP or GPP, was linear over 6 h in *P. argentatum* (Cornish and Siler, 1995) and so the rate of termination and reinitiation (the chain transfer reaction rate),

remained constant under these conditions. Very little is known about the termination event of rubber polymer biosynthesis. Different termination functional groups have been characterized by NMR spectroscopic analyses and indicate that rubber dephosphorylation and release may involve esterification, cyclization or hydrolysis in different species (Tanaka, 1989; Tanaka et al., 1996).

The studies of molecular weight regulation in vitro, summarized above, clearly indicate that additional mechanisms must be involved in regulating chain length in vivo. Also, although the three rubber transferases appear to be similar in many ways, a closer look at their regulation of rubber molecular weight reveals quite different mechanisms. For example, the *P. argentatum* and *H. brasiliensis* rubber transferase enzymes, despite their different allylic-PP kinetic constants and kinetic behavior in vitro (Table 1), produce similar molecular weights in any particular substrate mixture (Castillón and Cornish, 1999; Cornish et al, 2000). However, the *F. elastica* enzyme consistently produces rubber twice as large as in the other two species, even though this is primarily a low molecular weight producer in vivo (Cornish et al., 1993). This higher molecular weight may be caused by the lower K_m^{IPP} (Table 1), which is a third that of the other two species in the presence of FPP. The greater affinity of the *F. elastica* rubber transferase for IPP may lead to a more rapid polymerization (elongation or propagation) rate which, in turn, could produce the higher overall molecular weights observed over the four hour reaction period used. Also, K_m's reflect the substrate concentration around which the particular enzyme operates most effectively and are believed to reflect the endogenous, or physiological, substrate concentration in vivo (Segel, 1993). Thus, the rubber transferase K_m^{IPP} and the allylic-PP K_m's can be considered to predict the ideal conditions for the enzyme (high IPP levels, low allylic-PP levels). The high rubber transferase K_m^{IPP} ensures that rubber is made at times when IPP is non-limiting for other prenyl transferases, all of which have lower K_m^{IPP}'s much closer to the allylic-PP K_m's (reviewed by Ogura and Koyama, 1998). Under optimal conditions, and if no other factors are involved, the rubber molecular weight synthesized would presumably reflect the substrate equilibrium, and can be calculated from the K_m^{IPP} to $K_m^{allylic\text{-}PP}$ ratio. In *P. argentatum*, the ratio of K_m^{IPP} to K_m^{FPP} does translate to match the high molecular weight of over 1,000,000 Da produced in vivo (Table 2) in this species. Similarly, in *F. elastica* the same ratio is consistent with the low molecular weight it produces in vivo (Table 2). However, in *H. brasiliensis*, the K_m^{IPP} to $K_m^{allylic\text{-}PP}$ ratio predicts that *H. brasiliensis* would produce low molecular weight rubber in vivo (Table 2), which is, of course, untrue.

In vitro biochemical studies, showing that all three species can make high and low molecular weight rubber depending upon substrate concentrations, demonstrate that the rubber transferases, themselves, are not the cause of the low molecular weight rubber normally produced by *F. elastica*, nor of the high molecular weight produced by *P. argentatum* and *H. brasiliensis*. Other *cis*-prenyl transferases investigated make fixed product sizes as do most *trans*-prenyl transferases (Ogura and Koyama, 1998; Wang and Ohnuma, 1999). The rubber transferases clearly represent a distinct class of *cis*-prenyl transferases, despite similar substrate and cofactor requirements and similar pH dependencies.

Table 2
Some kinetic parameters and projected and in vivo rubber molecular weights produced by three different rubber transferases[a]

Parameter	*Hevea brasiliensis*	*Ficus elastica*	*Parthenium argentatum*
K_m^{IPP}/K_m^{FPP}	242	192	38,500
Projected M_r from K_m ratio (Da)	16,632	13,232	2,618,176
Actual rubber M_r in vivo (Da)	$>10^6$	10^3–10^4	$>10^6$

[a] The ratios of apparent K_m's were calculated from Table 1. The projected rubber molecular weight (M_r) from in vitro experiments (Refs. 41 and 42) was calculated, assuming that the ratio of K_m^{IPP}/K_m^{FPP} reflects the number of isoprene units incorporated, as (K_m^{IPP}/K_m^{FPP}) 68 + 176. (Molecular weight of isoprene subunit = 68, pyrophosphate with one negative charge = 176).

3.3. The role of negative cooperativity

It appears for rubber transferases, in general, that once an allylic-PP binds to the active site, the polymer that begins to form restricts access to the allylic-PP binding site by free allylic-PP. This probably occurs because the enzyme has a high affinity for the end of the rubber polymer. The enzyme product is not soluble and is certainly not fully released from the active site during the polymerization reaction. Thus, IPP polymerization can proceed even though the apparent K_m^{IPP} is much higher than K_m^{FPP} (Table 1). However, in addition to the affinity of the rubber transferases for the allylic-PP terminal C_{15} or C_{20} portion of the growing polymer, Hill plots of IPP incorporation rate as a function of FPP concentration demonstrate, by gradients $\ll 1$, that all three rubber transferases exhibit regions of strong negative cooperativity (Fig. 6) (Cornish et al., 2000). At these FPP concentrations, an additional hinderance to the binding of FPP to the allylic-PP binding site occurs, in that after one FPP has bound to the allylic-PP site it becomes much more difficult for a second molecule to bind. This change in binding affinity probably results from a conformational change in the enzyme caused by the first FPP binding event. Thus, free FPP cannot easily displace the elongating rubber polymer, i.e. the chain transfer reaction is inhibited over the FPP negative cooperativity concentration range. The *P. argentatum*

rubber transferase shows a remarkably wide concentration range of negative cooperativity, operating from its K_m^{FPP} to more than two orders of magnitude above it (Fig. 6). In contrast, *H. brasiliensis* and *F. elastica* have much shorter concentration ranges of strong negative cooperativity. In *H. brasiliensis*, the negative cooperativity region falls at the high end of the range for *P. argentatum*, whereas that of *F. elastica* falls just beyond the *P. argentatum* range (Fig. 6). Another measure of the negative cooperativity operating in these rubber transferases is reflected by the ratio of the FPP concentration at 0.75 V_{max} ($y=3$ in Fig. 6) to the FPP concentration at 0.5 V_{max} ($y=1$ in Fig. 6). Values of 3 reflect Michaelis-Menton kinetics, less than 3 indicate positive cooperativity, and greater than 3 indicate negative cooperativity (Segel, 1993). Using this measure, it is clear that negative cooperativity is much stronger in *P. argentatum* than in the other two species ($[S]_{0.75}/[S]_{0.5}$ for *H. brasiliensis* is 6.91, for *F. elastica* is 8.04, and for *P. argentatum* is 53.8).

The FPP negative cooperativity also appears directly to affect IPP incorporation rate, although IPP incorporation is dependent upon IPP concentration in *P. argentatum* (Castillón and Cornish, 1999). In *H. brasiliensis* and *F. elastica*, IPP only enhanced IPP incorporation at FPP concentrations where negative cooperative operated, when IPP and FPP concentrations were rate-limiting (Cornish et al., 2000).

When the regulation of molecular weight is considered, it is clear that the negative cooperativity properties of the different rubber transferases directly affect the molecular weight they produce under different substrate conditions, beyond the effects mediated by their different K_m's. For example, as described earlier, for *P. argentatum* rubber transferase, Hill plots of $\upsilon/(V_{max}-\upsilon)$ against [S] indicate negative cooperativity (gradient $\ll 1$, Fig. 6) over a much wider concentration range than in the other two species. Over this range, the *P. argentatum* rubber transferase active site is insensitive to the presence of unbound FPP, and the rubber polymers produced are considerably larger than would be the case if free FPP had the same ability to compete with the elongating polymers, and displace the rubber molecules from the active site, that it has at concentrations outside this negative cooperativity range (as discussed in the previous section). Also, in all three species, it appears that increasing IPP concentrations only can increase the molecular weight of the rubber polymers either when the initiator concentration is limiting (below the $K_m^{allylic\text{-}PP}$) or, under nonlimiting concentrations, when the particular enzyme exhibits negative cooperativity (Fig. 7; Cornish et al., 2000).

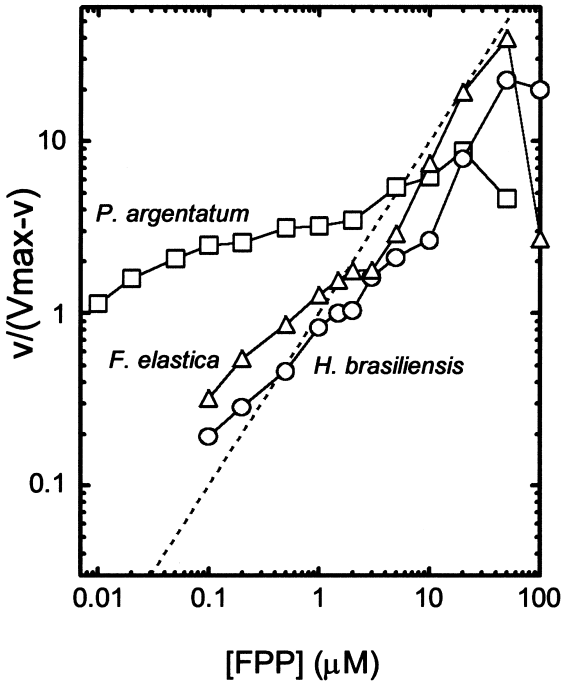

Fig. 6. Hill plot of IPP incorporation rate as a function of FPP concentration for *Hevea brasiliensis*, *Ficus elastica* and *Parthenium argentatum*. The intercept at $y=1$ is the K_m. Regions with a gradient $<<1$ indicate concentration ranges of negative cooperativity.

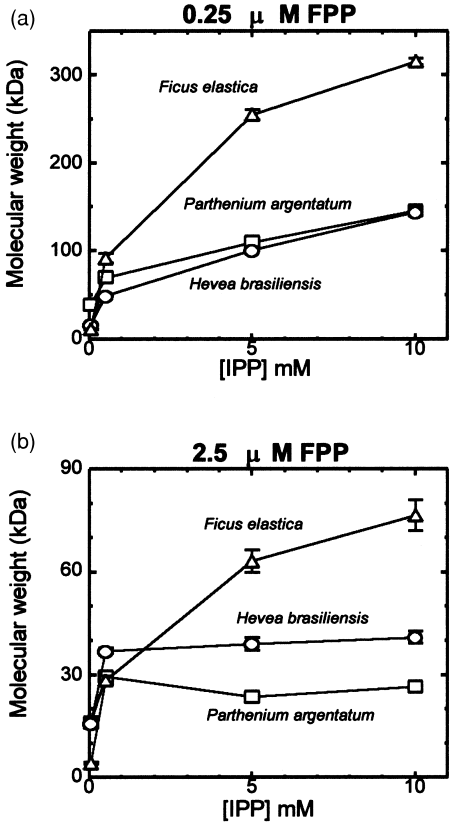

Fig. 7. Mean molecular weight (kDa) of rubber molecules synthesized by *Hevea brasiliensis*, *Ficus elastica* and *Parthenium argentatum* at various IPP concentrations at either (a) 0.25 μM or (b) 2.5 μM FPP. Each value is the mean of three replicates ± S.E.

3.4. Competition and activation

Additional similarities and differences between the three rubber transferases become apparent when co-substrate effects are considered (Castillón and Cornish, 1999; Cornish et al., 2000). For example, substrate activation appears to operate in the *P. argentatum* and *H. brasiliensis* rubber transferases. In these enzymes, IPP enhances the rate of FPP binding, but is significant in *H. brasiliensis* only at rate-limiting FPP concentrations instead of at all FPP concentrations as in *P. argentatum*. By contrast, the *F. elastica* rubber transferase was insensitive to increasing IPP concentrations and is the only species of the three in which IPP may slightly inhibit FPP incorporation at all FPP concentrations tested.

In all three species, the initiator FPP appears to activate IPP incorporation, but the *P. argentatum* rubber transferase differs from the other two in that IPP incorporation rate was enhanced by increasing FPP concentration at all IPP concentrations. By contrast, for the *H. brasiliensis* and *F. elastica* rubber transferases, IPP incorporation rates were only markedly FPP-dependent at rate-limiting IPP concentrations of near or below the K_m^{IPP}'s.

For the *H. brasiliensis* and *F. elastica* rubber transferases, under conditions where the FPP concentration is near or below the K_m^{FPP}, but when the IPP concentration is above K_m^{IPP}, IPP incorporation rate is a function of the IPP concentration and is insensitive to FPP concentration. This is apparent also for the *P. argentatum* rubber transferase when GPP is used is the initiator. It seems likely that the same result would be found with FPP, in this species, but lower FPP concentrations, than as yet explored, would be needed to achieve conditions below its K_m^{FPP}.

Although competition at the allylic-PP site has not been observed (Cornish et al., 2000), IPP and allylic-PP do appear to compete for the IPP binding site in the *P. argentatum* rubber transferase (Castillón and Cornish, 1999), although catalysis only occurs if IPP is bound. Interestingly, this also is a species-specific phenomenon, such competition not being apparent with either *H. brasiliensis* or *F. elastica* rubber transferase.

4. Conclusions

Prospects for the biotechnological development of alternative rubber producing crop plants suitable for temperate zone agriculture will improve as our knowledge of the factors regulating rubber biosynthesis progresses. In vitro investigations have indicated promising strategies for the enhancement of rubber yield, such as the transformation of rubber-producing plants with genes for substrate synthesis. However, the production of high molecular weight rubber seems more uncertain because in vitro biochemical studies have shown that a combination of factors must contribute to the molecular weight of rubber produced in vivo. The *P. argentatum* rubber transferase appears to exert more control over the molecular weight it produces than those from *H. brasiliensis* or *F. elastica* and the corresponding gene(s) may, therefore, provide the best prospect for genetic transformation of candidate annual crop species. However, in vitro experiments have not yet provided a unifying biochemical mechanism that could explain the different rubber molecular weights found in vivo in different plant species, such as the high molecular weight rubber in *H. brasiliensis* and *P. argentatum* and the low molecular weight rubber in *F. elastica*. It is possible that these evolutionarily-divergent species employ different mechanisms to regulate molecular weight but, given the general similarities in rubber biosynthesis enjoyed by the species, similar endogenous regulatory factors probably operate in vivo. Thus, molecular weight probably will be affected by endogenous substrate concentrations, the intrinsic properties of the rubber transferases involved and by other, as yet unknown, endogenous factors. These factors, and their interaction, must be understood before effective metabolic engineering strategies can be designed to maximize biosynthetic rate while simultaneously maintaining or conferring high rubber molecular weight. It may then be possible to achieve the goal of engineering temperate zone annual crops to produce commercially-viable yields of high quality rubber.

Acknowledgements

The author would especially like to thank past and present researchers, namely Javier Castillón, Mary H. Chapman, Christopher J.D. Mau, Deborah J. Scott and Deborah J. Siler, who, working in her laboratory, contributed considerably to our current knowledge of natural rubber biosynthesis.

References

Archer, B.L., Audley, B.G., 1987. New aspects of rubber biosynthesis. Botanical Journal of the Linear Society 94, 181–196.

Archer, B.L., Audley, B.G., Cockbain, E.G., McSweeney, G.P., 1963. The biosynthesis of rubber. Biochemical Journal 89, 565–574.

Backhaus, R.A., 1985. Rubber formation in plants — a mini-review. Israel Journal of Botany 34, 283–293.

Bowers, J.E., 1990. Natural rubber-producing plants for the United States. USDA, Cooperative State Research Service and National Agricultural Library. NAL, Beltsville, Maryland.

Burke, C.C., Wildung, M.R., Croteau, R., 1999. Geranyl diphosphate synthase: cloning expression, and characterization of this prenyl transferase as a heterodimer. Proceedings of National Academy of Sciences of the United States of America 96, 13062–13067.

Campbell, C.J., Laherrere, J.H., 1998. The end of cheap oil. Scientific American, March 1998, 78–83.

Carey, A.B., Cornish, K., Schrank, P.J., Ward, B., Simon, R.A., 1995. Cross reactivity of alternate plant sources of latex in subjects with systemic IgE mediated sensitivity to *Hevea brasiliensis* latex. Annals of Allergy, Asthma and Immunology 74, 317–320.

Castillón, J., Cornish, K., 1999. Regulation of polymer molecular weight by enzymatically-active rubber particles of *Parthenium argentatum*. Gray. Phytochemistry 51, 43–51.

Chappell, J., 1995. Biochemistry and molecular biology of the isoprenoid biosynthetic pathway in plants. Annual Review of Plant Physiology and Plant Molecular Biology 46, 521–547.

Cornish, K., 1993. The separate roles of plant *cis* and *trans* prenyl transferases in *cis*-1,4-polyisoprene biosynthesis. European Journal of Biochemistry 218, 267–271.

Cornish, K., 1996. Hypoallergenic Natural Rubber Products from *Parthenium argentatum* (Gray) and Other Non-*Hevea brasiliensis* Species. US Patent No. 5580942.

Cornish, K., 1998. Hypoallergenic Natural Rubber Products from *Parthenium argentatum* (Gray) and Other Non-*Hevea brasiliensis* species. US Patent No. 5717050.

Cornish, K., Backhaus, R.A., 1990. Rubber transferase activity in rubber particles of guayule. Phytochemistry 29, 3809–3813.

Cornish, K., Castillón, J., Chapman, M.H., 1998. Membrane-bound *cis*-prenyl transferase activity: regulation and substrate specificity. In: Steinbüchel, A. (Ed.), Biochemical Principles and Mechanisms of Biosynthesis and Biodegradation of Polymers. Wiley-VCH-Verlag, pp. 316–323.

Cornish, K., Castillón, J., Scott, D.J., 2000. Substrate-dependent rubber molecular weight regulation, in vitro, in plant species that produce high and low molecular weights in vivo. Biomacromolecules 1, 632–641.

Cornish, K., Lytle, C.D., 1999. Viral impermeability of hypoallergenic, low protein, guayule latex films. Journal of Biomedical Materials Research 47, 434–437.

Cornish, K., Siler, D.J., Grosjean, O.K., 1994. Immunoinhibition of rubber particle-bound *cis*-prenyl transferases in *Ficus elastica* and *Parthenium argentatum* (Gray). Phytochemistry 35, 1425–1428.

Cornish, K., Siler, D.J., Grosjean, O.K., Goodman, N., 1993. Fundamental similarities in rubber particle architecture and function in three evolutionarily divergent plant species. Journal of Natural Rubber Research 8, 275–285.

Cornish, K., Siler, D.J., 1996. Characterisation of *cis*-prenyl transferase activity localised in a buoyant fraction of rubber particles from *Ficus elastica* latex. Plant Physiol. Biochemical 34, 377–384.

Cornish, K., Siler, D.J., 1995. Effect of different allylic diphosphates on the initiation of new rubber molecules and on *cis*-1,4-polyisoprene biosynthesis in guayule (*Parthenium argentatum* Gray). Journal Plant Physiol. 147, 301–305.

Cornish, K., Wood, D.F., Windle, J.J., 1999. Rubber particles from four different species, examined by transmission electron microscopy and electron paramagnetic resonance spin labeling, are found to consist of a homogeneous rubber core enclosed by a contiguous, monolayer biomembrane. Planta 210, 85–96.

d'Auzac, J., Jacob, J.-L., Chrestin, H., 1989. Physiology of Rubber Tree Latex. CRC Press, Boca Raton, Florida, 470 pp.

Davis, W., 1997. The rubber industry's biological nightmare. Fortune, 4 August, 86–95.

Dennis, M.S., Light, D.R., 1989. Rubber elongation factor from *Hevea brasiliensis*. Identification, characterization and role in rubber biosynthesis. Journal of Biological Chemistry 264, 18608–18617.

Dogbo, O., Camara, B., 1987. Purification of isopentenyl pyrophosphate isomerase and geranylgeranyl pyrophosphate synthase from *Capsicum* chromoplasts by affinity chromatography. Biochimica Biophysica Acta 920, 140–148.

Heinrich, G., 1970. Elektronmikroskopische Untersuchung der Milchröhren von *Ficus elastica*. Protoplasma 70, 317–323.

Huang, H.C., 1992. Oil bodies and oleosins in seeds. Annual Review of Plant Physiology and Plant Molecular Biology 43, 177–200.

Kekwick, R.G.O., 1993. Origin and source of latex protein allergy. In: Latex protein allergy: the present position. Crain Commun Ltd, Rubber Consultants, Brickendonbury, Hertford, UK, 1993, p. 21–24.

Lichtenthaler, H.K., 1999. The 1-deoxy-D-xylulose-5-phosphate pathway of isoprenoid biosynthesis in plants. Annual Review of Plant Physiology and Plant Molecular Biology 50, 47–65.

Lynen, F., 1969. Biochemical problems of rubber synthesis. Journal Rubb. Res. Inst. Malaya 21, 389–406.

Madhavan, S., Greenblatt, G.A., Foster, M.A., Benedict, C.R., 1989. Stimulation of isopentenyl pyrophosphate incorporation into polyisoprene in extracts from guayule plants (*Parthenium argentatum* Gray) by low temperature and 2-(3,4-dichloro-phenoxy)triethyl amine. Plant Physiology 89, 506–511.

Monastersky, R., 1998. Geologists anticipate an oil crisis soon. Science News 154, 278–279.

Mooibroek, H., Cornish, K., 2000. Alternative sources of natural rubber. Appl. Microbiol. Biotechnol 53, 355–365.

Morales, C., Bascomba, A., Carrieira, J., Sastre, A., 1989. Anaphylaxis produced by rubber gloves contact: case reports and immunological identification of the antigens involved. Clinical and Experimental Allergy 19, 425–430.

Nakayama, F.S., Cornish, K., Schloman, W.W., 1996. Guayule natural rubber: a promising source of latex for medical products. Journal of Arid Land Studies 5, 203–206.

Ogura, K., Koyama, T., 1998. Enzymatic aspects of chain elongation. Chemical Reviews 98, 1263–1276.

Oh, S.K., Kang, H., Shin, D.H., Yang, J., Chow, K.-S., Yeang, H.Y., Wagner, B., Breiteneder, H., Han, K.-H., 1999. Isolation, characterization, and functional aspects of a novel cDNA clone encoding a small rubber particle protein from *Hevea brasiliensis*. Journal of Biological Chemistry 274, 17132–17138.

Ohya, N., Tanaka, Y., 1998. Structural characterization of rubber from *Lactarius* mushrooms: ^{1}H-NMR analysis of terminal groups in the rubber chain. Journal of Rubber Research 1, 84–94.

Ownby, D.R., Ownby, H.E., McCullough, J.A., Shafer, A.W., 1994. The prevalence of anti-latex IgE antibodies in 1000 volunteer blood donors. Journal of Allergy and Clinical Immunology 93, 282.

Pailhories, G., 1993. Reducing proteins in latex gloves. Clinical Reviews of Allergy 11, 391–402.

Pan, Z., Durst, F., Werck-Reichhart, D., Gardner, H.W., Camara, B., Cornish, K., Backhaus, R.A., 1995. The major protein of guayule rubber particles is a cytochrome P450; characterization based on cDNA cloning and spectroscopic analysis of the solubilized enzyme and its reaction products. Journal of Biological Chemistry 270, 8487–8494.

Ray, D.T., 1993. Guayule: a source of natural rubber. In: Janick, J., Simon, J.E. (Eds.), Advances in New Crops. John Wiley and Sons, pp. 338–342.

Reisch, M.S., 1995. Rubber consumption is rising, but producers' profits are squeezed. Chemical and Engineering News, August 14, 11–14.

Segel, I.H., 1993. Enzyme Kinetics. John Wiley and Sons, New York.

Shimizu, N., Koyama, T., Ogura, K., 1998. Molecular cloning, expression and purification of undecaprenyl diphosphate synthase. Journal of Biological Chemistry 273, 19476–19481.

Siler, D.J., Cornish, K., 1993. A protein from *Ficus elastica* rubber particles is related to proteins from *Hevea brasiliensis* and *Parthenium argentatum*. Phytochemistry 32, 1097–1102.

Siler, D.J., Cornish, K., 1994a. Hypoallergenicity of guayule rubber particle proteins compared to *Hevea* latex proteins. Industrial Crops and Products 2, 307–313.

Siler, D.J., Cornish, K., 1994b. Identification of *Parthenium argentatum* rubber particle proteins immunoprecipitated by an antibody that specifically inhibits rubber transferase activity. Phytochemistry 36, 623–627.

Siler, D.J., Cornish, K., Hamilton, R.G., 1996. Absence of cross-reactivity of IgE antibodies from *Hevea brasiliensis* latex allergic subjects with a new source of natural rubber latex from guayule (*Parthenium argentatum*). Journal of Allergy and Clinical Immunology 98, 895–902.

Siler, D.J., Goodrich-Tanrikulu, M., Cornish, K., Stafford, A.E., McKeon, T.A., 1997. Composition of rubber particles of *Hevea brasiliensis*, *Parthenium argentatum*, *Ficus elastica* and *Euphorbia lactiflua* indicates unconventional surface structure. Plant Physiology and Biochemistry 35, 281–290.

Slater, J.E., 1989. Rubber anaphylaxis. N. Engl. J. Med. 320, 1126–1130.

Swanson, C.L., Buchanan, R.A., Otey, F.H., 1979. Molecular weights of natural rubbers from selected temperate zone plants. Journal of Applied Polymer Science 23, 743–748.

Tanaka, Y., 1989. Structure and biosynthesis mechanism of natural polyisoprene. Progress in Polymer Science 14, 339–371.

Tanaka, Y., Aik-Hwee, E., Ohya, N., Nishiyama, N., Tangpakdee, J., Kawahara, S., Wititsuwannakul, R., 1996. Initiation of rubber biosynthesis in *Hevea brasiliensis*: Characterisation of initiating species by structural analysis. Phytochemistry 41, 1501–1505.

Tomazic, V.J., Withrow, T.J., Fisher, B.R., Dillard, S.F., 1992. Latex-associated allergies and anaphylactic reactions. Clinical Immunology and Immunopathology 64, 89–97.

Wang, K., Ohnuma, S., 1999. Chain length determination mechanism of isoprenyl diphosphate synthases and implications for molecular evolution. Trends in Biochemical Sciences 24, 445–451.

Whitworth, J.W., Whitehead, E.E., 1991. Guayule Natural Rubber: A Technical Publication with Emphasis on Recent Findings. Guayule Administrative Management Committee and USDA Cooperative State Research Service, Office of Arid Lands Studies, The University of Arizona, Tucson, AZ, USA.

Wood, D.F., Cornish, K., 2000. Microstructure of purified rubber particles. International Journal of Plant Sciences 161, 435–445.

PERGAMON

Phytochemistry 57 (2001) 1135–1148

PHYTOCHEMISTRY

www.elsevier.com/locate/phytochem

Review

Structure–function characterization of cellulose synthase: relationship to other glycosyltransferases

Inder M. Saxena[a], R. Malcolm Brown Jr.[a,*], Thomas Dandekar[b]

[a]*Section of Molecular Genetics and Microbiology, School of Biological Sciences, University of Texas at Austin, Austin, TX 78712, USA*
[b]*European Molecular Biology Laboratory, Postfach 102209, D-69012 Heidelberg, Germany*

Received 18 September 2000; received in revised form 2 February 2001

Abstract

A combined structural and functional model of the catalytic region of cellulose synthase is presented as a prototype for the action of processive β-glycosyltransferases and other glycosyltransferases. A 285 amino acid segment of the *Acetobacter xylinum* cellulose synthase containing all the conserved residues in the globular region was subjected to protein modeling using the genetic algorithm. This region folds into a single large domain with a topology exhibiting a mixed alpha/beta structure. The predicted structure serves as a topological outline for the structure of this processive β-glycosyltransferase. By incorporating new site-directed mutagenesis data and comparative analysis of the conserved aspartic acid residues and the QXXRW motif we deduce a number of functional implications based on the structure. This includes location of the UDP–glucose substrate-binding cavity, suggestions for the catalytic processing including positions of conserved and catalytic residues, secondary structure arrangement and domain organization. Comparisons to cellulose synthases from higher plants (genetic algorithm based model for cotton CelA1), data from neural network predictions (PHD), and to the recently experimentally determined structures of the non-processive SpsA and β4-galactosyltransferase retest and further validate our structure-function description of this glycosyltransferase. © 2001 Published by Elsevier Science Ltd. All rights reserved.

Keywords: Cellulose; Cellulose synthase; *Acetobacter xylinum*; Glycosyltransferases; Genetic algorithm

Contents

1. Introduction 1136
   1.1. Sequence relationship between cellulose synthases and other glycosyltransferases 1136
   1.2. Functional analysis of conserved residues in cellulose synthase and other glycosyltransferases 1137
   1.3. Architecture of the active site of cellulose synthase: a structural model for the active-site region of processive β-glycosyltransferases 1140
   1.4. Relationship of the predicted structure of cellulose synthase with structures of other β-glycosyltransferases 1142
   1.5. Possible mechanisms for synthesis of cellulose and other polysaccharides 1144

2. Significance 1146

Acknowledgements 1146

References 1146

* Corresponding author. Tel.: +1-512-471-3364; fax: +1-512-471-3573.
E-mail address: rmbrown@mail.utexas.edu (R.M. Brown).

0031-9422/01/$ - see front matter © 2001 Published by Elsevier Science Ltd. All rights reserved.
PII: S0031-9422(01)00048-6

1. Introduction

Cellulose is an abundant polysaccharide produced most notably by plants and in varying degrees by several other organisms including algae, bacteria, social amoeba, and tunicates. The polymerization reaction is catalyzed by the enzyme cellulose synthase, a glycosyltransferase that uses UDP–glucose as the substrate. Most glycosyltransferases transfer monosaccharides from a nucleotide sugar donor to hydroxyl groups of acceptor carbohydrates. A glycosyltransferase may catalyze the transfer of a single sugar residue to an acceptor (non-processive) or transfer more than one sugar residue to the acceptor (processive). Glycosyltransferases exhibit specificity for both the donor and the acceptor molecules and are involved in making a specific linkage (α- or β-linkage) between specific atoms of the sugar and the acceptor molecule. Since each linkage is catalyzed by a specific glycosyltransferase, most compounds that either have different kinds of sugars and/or different linkages would require a number of glycosyltransferases for their synthesis. Alternatively, a single enzyme may recognize more than one sugar donor and catalyze more than one type of linkage (for example, hyaluronan synthase in the synthesis of hyaluronic acid). Based upon the linkage at the anomeric carbon, glycosyltransferases can be classified as retaining glycosyltransferases or inverting glycosyltransferases. Since the catalytic mechanism in the two types (retention or inversion) of glycosyl transfer reactions is different, it is generally believed that the two classes of glycosyltransferases would have different sequence and structure characteristics.

The catalytic machinery of glycosyltransferases involves a general acid-base catalysis mechanism that involves acidic residues (aspartate and/or glutamate) whose side chains have the property to act as the general base for acceptor activation or as the nucleophile for formation of a glycosyl–enzyme intermediate. These acidic residues are also involved in the catalytic mechanisms of glycosyl hydrolases where once again they act either as a general base or as a nucleophile (Davies and Henrissat, 1995). Active site glutamate residues have also been shown to be essential for the ADP-ribosyltransferase activity of certain bacterial toxins (Barth et al., 1998) as well as the glycosylphosphatidylinositol (GPI)-anchored and secretory ADP–ribosyltransferases of eucaryotic cells (Okazaki and Moss, 1998). The carboxylate group of an aspartic acid residue (Asp 100) in the active site of T4 β-glucosyltransferase has been shown to be in a position where it activates the 5-hydroxymethyl group on the DNA for nucleophilic attack on the glucose of the donor UDP–glucose (Moréra et al, 1999). Enzymes that catalyze the different glycosyl transfer reactions and that use NDP–sugar as substrates were classified into 26 families based upon sequence similarity (Campbell et al., 1997) and the list now includes 47 families (http://afmb.cnrs-mrs.fr/~pedro/CAZY/gtf.html). Family 2 β-glycosyltransferases include both the processive and the non-processive enzymes. The processive enzymes (for example, cellulose synthase, chitin synthase, hyaluronan synthase, NodC protein) are generally membrane-proteins that synthesize a polysaccharide/oligosaccharide chain. None of these proteins have been characterized and compared structurally; however, the different proteins are related based on sequence characteristics (especially identification of putative catalytic residues). The presence of the conserved catalytic residues in members of the same glycosyltransferase family suggests that they catalyze glycosyl transfer reactions by similar mechanisms and in all likelihood have very similar active-site architecture. Processive glycosyltransferases stay attached to the growing end of a glucan chain, and there is considerable interest in identifying the amino acid residues and the structure of the region that is involved in holding the glucan chain.

Cellulose biosynthesis offers a simple and elegant system for studies on the synthesis of polysaccharides, especially as studied in the bacterium *A. xylinum*. Although the detailed features of cellulose biosynthesis may not be common to the synthesis of other polysaccharides, the structure of the catalytic region of cellulose synthase and other glycosyltransferases may show some conserved features. A prediction of the structure of the globular region of cellulose synthase based on the available data will therefore be helpful in understanding the structure and function of glycosyltransferases, especially the processive β-glycosyltransferases. Moreover it will be important to confirm the relevance of the conserved residues in these glycosyltransferases and to determine their spatial relationship within the three-dimensional structure. More recently the structures of a few β-glycosyltransferases have been determined experimentally (Vrielink et al., 1994; Charnock and Davies, 1999; Gastinel et al., 1999). Although these structures show some similarities, they also exhibit sufficient variations making it all the more important to predict or determine the three-dimensional structures of as many glycosyltransferases for understanding the catalytic properties of this group of enzymes (Breton and Imberty, 1999).

1.1. Sequence relationship between cellulose synthases and other glycosyltransferases

Genes for cellulose synthase were first cloned from the bacterium *A. xylinum* (Saxena et al., 1990; Wong et al., 1990). Sequence comparisons of the derived amino acid sequence of the bacterial cellulose synthase with other proteins revealed the presence of conserved aspartic acid residues and a QXXRW motif in the processive β-glycosyltransferases (Saxena et al., 1995). Since the catalytic machinery of glycosyltransferases is likely to involve residues whose side chains have the proper reactivity to act as

a general base or a nucleophile, the conserved aspartic acid residues are predicted to be involved in the catalytic reaction as acid-base catalysts. The QXXRW motif is present in all the processive β-glycosyltransferases analyzed so far, and this sequence motif is believed to be involved in the processivity function of the enzyme, possibly required for holding the growing glycan chain in the active site. The 'D, D, D35QXXRW' motif has also been identified in a large number of transmembrane proteins involved in the synthesis of a variety of polysaccharides/oligosaccharides (Saxena and Brown, 1997). This motif is present in a large and contiguous globular region that is predicted to be localized in the cytoplasm. Apart from the identification of this motif in proteins whose functions are known (for example, cellulose synthase, chitin synthase, hyaluronan synthase, NodC protein) this motif has been identified in a number of other sequences in the sequence databases. The precise function of a number of these proteins remains to be determined, as in the case of the *E. coli* YhjO polypeptide (Sofia et al., 1994) whose sequence is very similar to the sequence of the *A. xylinum* cellulose synthase.

A substantial number of sequences identified in higher plants also contain the 'D, D, D35QXXRW' motif, and these proteins are characterized either as cellulose synthase or cellulose synthase-like proteins (http://cellwall.stanford.edu/cellwall/). In at least three reports, proteins with the 'D, D, D35QXXRW' motif have been identified as cellulose synthases (CelA1, Rsw1, and Irx3) based on experimental evidence (Pear et al., 1996; Arioli et al., 1998; Taylor et al., 1999). The globular region that contains the 'D, D, D35QXXRW' motif is much larger in these higher plant cellulose synthases (the globular region of CelA1 and Rsw1 is predicted to be 534 and 538 amino acids in length, respectively) in comparison to the globular region of the *A. xylinum* AcsAB cellulose synthase (285 amino acids). Analysis of the regions present between the three conserved aspartic acid residues and the QXXRW motif shows that while the number of amino acids between these residues is similar in the higher plant cellulose synthases, they differ from that of the *A. xylinum* cellulose synthase which is much more similar to the cellulose synthase-like proteins from higher plants and the *E. coli* YhjO polypeptide.

Table 1
Cellulose synthase activity in *Acetbacter xylinum* membrane fractions

Strain (plasmid)	Amino acid substitution	Cellulose synthase specific activity[a]
AY41-34-895 (pIS311-9)	none	1159.72
AY41-34-895 (pIS311-D188P)	D188P	1.16
AY41-34-895 (pIS311-D188N)	D188N	65.29
AY41-34-895 (pIS311-D333R)	D333R	3.46
AY41-34-895 (pIS311-Q369M)	Q369M	1.33
AY41-34-895 (pIS311-R370Q)	R370Q	203.15
AY41-34-895 (pIS311-R370P)	R370P	3.55
AY41-34-895 (pIS311-R372A)	R372A	5.19

[a] Specific activity is defined as picomoles of glucose incorporated into alkali-insoluble product per minute per milligram protein.

1.2. Functional analysis of conserved residues in cellulose synthase and other glycosyltransferases

Although different numbers of amino acids may separate them, the conserved residues in cellulose synthases are predicted to be present at structurally similar positions in the active site. To determine the role of the conserved aspartic acid residues (D189, D236, and D333) and residues in the QXXRW motif (Q369, R370, V371, R372, and W373) of the *A. xylinum* cellulose synthase (AcsAB), we substituted the D189, D236, D333, Q369, R370, and R372 residues with other amino acids using site-directed mutagenesis. Mutants of cellulose synthase with the following non-conservative substitutions- D189Y, D236Y, D333R, Q369M, R370Q, R370P, and R372A were obtained and analyzed for in vitro cellulose synthase activity using *A. xylinum* membrane preparations. The D189Y and D236Y mutations have been described earlier (Saxena and Brown, 1997) and the effect of the remaining mutations on cellulose synthase activity is shown in Table 1. Apart from substitutions in these conserved positions and R370, we also obtained mutations in which the aspartic acid residue at position 188 was replaced with a more conservative (D188N) and a non-conservative (D188P) amino acid. As shown in Fig. 1, cellulose synthase activity in mutants with substitutions at the conserved positions D189, D236, D333, Q369, and R372 was barely detectable, suggesting that these residues are involved in the enzyme activity. Moreover, amino acid substitutions at the non-conserved positions (D188 and R370) adjacent to the conserved residues also led to a reduction in enzyme activity. The level of expression of the mutated cellulose synthase protein in the *A. xylinum* membrane preparations was examined by western blot analysis using antibody raised against the 93 kDa cellulose synthase polypeptide (Chen and Brown, 1996). The 93 kDa cellulose synthase polypeptide was not detected by western analysis in the *A. xylinum* mutant strains AY41-34 and AY41-34-895 (Fig. 2, lanes 1 and 2) (Saxena and Brown, 1995). AY41-34-895 was therefore used as the host strain for expression of the wild-type and mutant cellulose synthase genes cloned in the plasmid pRK311 (Ditta et al., 1985). The amount of cellulose synthase in strains expressing the wild-type protein, and the D188P, D188N, D333R, Q369M, R370Q, R370P, and R372A substitutions was found to be at comparable levels as determined by western analysis (Fig. 2). Cellulose synthase was also detected at similar levels in a strain where

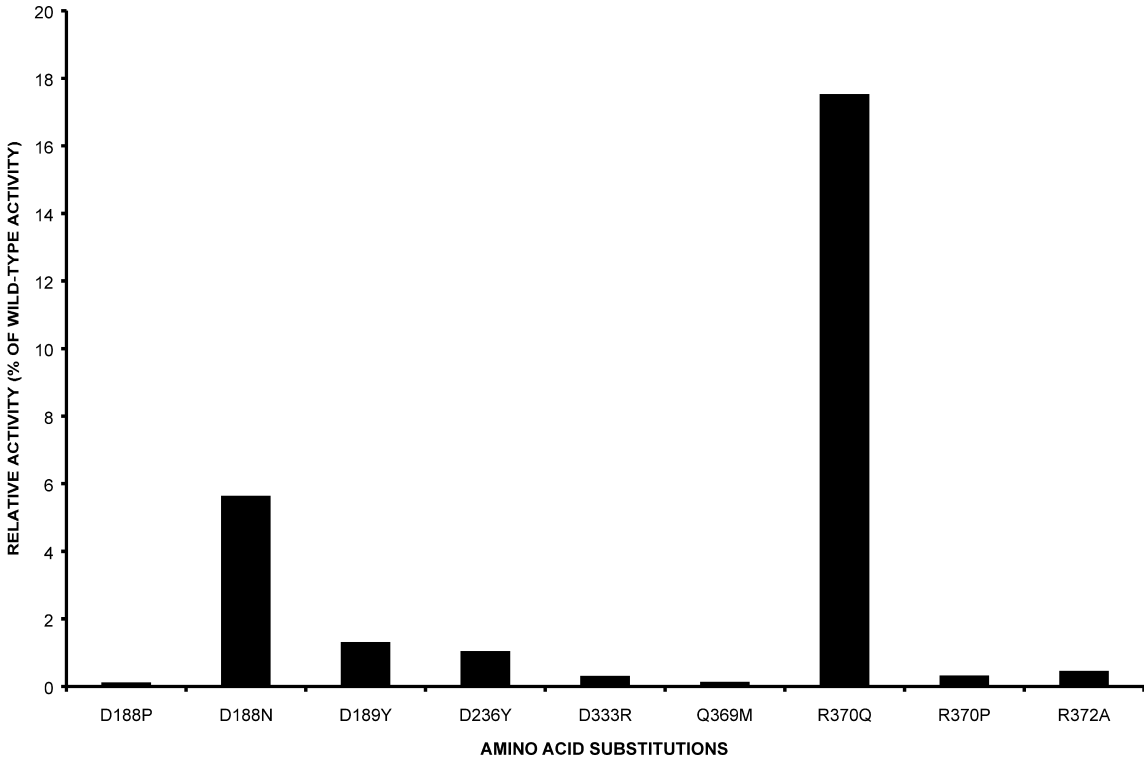

Fig. 1. Effect of amino acid substitutions on the *A. xylinum* cellulose synthase (AcsAB) activity determined in vitro.

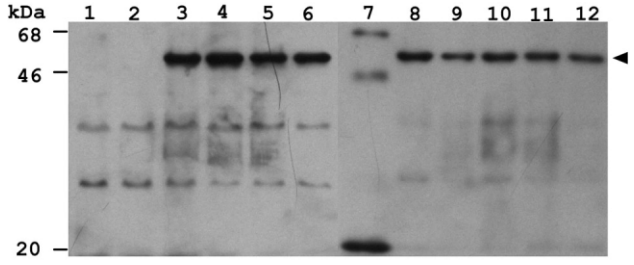

Fig. 2. Western blot analysis of membrane preparations of *A. xylinum* using anti-93 kDa antibody to detect the cellulose synthase. Lanes 1 and 2 contain membrane preparations from *A. xylinum* strains AY41-34 and AY41-34-895 respectively. Lanes 3–6, and 8–12 contain membrane preparations from *A. xylinum* AY 41-34-895 with plasmids expressing wild type cellulose synthase (lane 3), a chimeric cellulose synthase in which the globular region of the *A. xylinum* AcsAB cellulose synthase is replaced by a globular region encoded by *Arabidopsis thaliana* EST T88271 (lane 4), and cellulose synthase with amino acid substitutions D188P (lane 5), D188N (lane 6), D333R (lane 8), Q369M (lane 9), R370Q (lane 10), R370P (lane 11), and R372A (lane 12). Lane 7 contains the molecular weight markers. The cellulose synthase polypeptide fragment detected using the anti-93 kDa antibody is shown by an arrowhead.

the *A. xylinum* AcsAB globular region was substituted with the globular region of an *Arabidopsis thaliana* β-glycosyltransferase (Fig. 2, lane 4).

Whether the conserved residues are involved as catalytic residues, in substrate-binding, in maintaining the architecture of the active site or in some other function has not been determined for the *A. xylinum* cellulose synthase. Support for the idea that the conserved residues function in enzyme activity is also obtained from analysis of a few other glycosyltransferases (Fig. 3). Substrate-binding experiments done using a plasmid construct that expresses the globular region of the cotton CelA1 cellulose synthase in *E. coli* showed that the expressed protein bound to UDP–glucose (Pear et al., 1996). However, when the *N*-terminal part that includes the first conserved aspartic acid residue (corresponding to D189 of the *A. xylinum* AcsAB protein) was missing from this protein, no UDP–glucose binding was observed. These observations suggest that this region, which includes the conserved aspartic acid residue, is essential for binding the substrate. Site-directed mutagenesis experiments using the chitin synthase 2 of yeast showed that the conserved aspartic acid residues and the conserved residues in the QXXRW motif are required for chitin synthase activity (Nagahashi et al., 1995). A conserved aspartic acid residue identified in the β-glycosyltransferases also has been identified in a number of other glycosyltransferases, including the yeast α-1,3-mannosyltransferase (Mnn1p) (Wiggins and Munro, 1998) and large clostridial cytotoxins (Busch et al., 1998). This conserved aspartic acid residue is present in the DXD motif in a variety of glycosyltransferases, and the first aspartic acid in this motif corresponds to D236 of the *A. xylinum* cellulose synthase. In almost all cases the DXD

PROTEIN	REGIONS			
	1	2	3	4
		MOTIFS		
		DXD		QXXRW
	*	*	*	* **
AcsAB	188 D**D**G	231 YILIF**D**CDHV	330 VTE**D**AH	366 HIG**Q**RV**R**WAR
CelA1	DDG	FILNLDCDHY	VTEDIL	RLHQVLRWAL
SacChs2	SDG	VVTLV**D**VGTR	LAE**D**RI	FIS**Q**RR**RW**LN
Mnn1p		EFVFL**D**IDAI		
LT		GGVYL**D**VDIL		
KfiC	D**D**C	FITFQ**D**ADDL		

Fig. 3. Proteins in which the conserved residues identified in β-glycosyltransferases (Saxena et al., 1995) have been analyzed by site-directed mutagenesis- AcsAB, *A. xylinum* cellulose synthase (Saxena and Brown, 1997; this work); SacChs2, *S. cerevisiae* chitin synthase 2 (Nagahashi et al., 1995); Mnn1p, *S. cerevisiae* α-1,3-mannosyltransferase (Wiggins and Munro, 1998); LT, *C. sordellii* lethal toxin (Busch et al., 1998), KfiC, *E. coli* glycosyltransferase (Griffiths et al., 1998), and by assaying a deleted globular region in which one of the conserved residues (conserved aspartic acid in region 1) is missing- CelA1, *G. hirsutum* cellulose synthase (Pear et al., 1996). The regions in which these conserved residues are present and the motifs identified in these regions are indicated. Residue numbers are shown at the start of each amino acid segment for AcsAB. Asterisks indicate the conserved residues identified in the β-glycosyltransferases. Residues analyzed by site-directed mutagenesis for each of the proteins are underlined. Positions in which substitution of the conserved residue resulted in loss of enzyme activity or substrate binding are indicated in bold.

motif is flanked by four hydrophobic residues on the *N*-terminal side, with the third of these often being an aromatic residue (Wiggins and Munro, 1998). Site-directed mutagenesis of the conserved aspartic acid residues and the flanking residues in Mnn1p showed that the aspartic acid residues are essential for α-1,3-mannosyltransferase activity. Furthermore the aspartic acid residues in the DXD motif were shown to have no effect on protein multimerization, and were suggested to be involved in catalysis. Substitution of the aspartic acid residues in the DXD motif of the *Clostridium sordellii* lethal toxin (LT) led to a loss of the binding of the substrate UDP–glucose, suggesting that these residues are important for UDP–glucose binding (Busch et al., 1998). One possible function of the DXD motif in the catalytic site could be in binding a metal ion that is used to coordinate the phosphates of the NDP–sugar in the active site. A DXD motif is also conserved in DNA polymerases where the aspartates are in the active site coordinating manganese and magnesium ions that hold the phosphates of the nucleotide triphosphate substrate (Pritchard and McHenry, 1999).

Although three aspartic acid residues have been identified at conserved positions in the processive β-glycosyltransferases, at present there is insufficient evidence to suggest which of these aspartic acid residues actually functions as a base during the catalytic reaction. Our prediction that at least two glycosidic linkages are formed simultaneously or sequentially during the synthesis of cellulose and a few other polysaccharides would require at least two aspartate residues to function as bases. There is only a single conserved aspartic acid residue in regions 3 and 4 (Fig. 3) present in domain B of the processive β-glycosyltransferases and this aspartic acid residue probably functions as a base. On the other hand, regions 1 and 2 (Fig. 3) present in domain A of both the processive and the non-processive β-glycosyltransferases and a number of other proteins, contains two conserved aspartic acid residues. The catalytic mechanism for glycosyl transfer with inversion of configuration requires a single base and so a single aspartic acid residue is sufficient for this function. However, where glycosyl transfer reaction takes place with retention of configuration, at least two amino acid residues are required, with one residue functioning as a nucleophile and the other as an acid/base. Interestingly, two amino acid residues are conserved in regions 1 and 2 of β-glycosyltransferases, and only one conserved residue is observed in the other proteins, including the α-1,3-mannosyltransferases and α-1,3-fucosyltransferases. Moreover this conserved residue present in region 2 is part of the DXD motif that has been identified in both α- and β- glycosyltransferases. The role of the aspartic acids in the DXD motif is suggested to be in the binding of the NDP–sugar substrate. Therefore, the aspartic acid residue present in region 1 of the β-glycosyltransferases (Fig. 3) may function as a catalytic residue in this group of enzymes. However, in the structure determined for the SpsA protein (Charnock

and Davies, 1999), the conserved aspartic acid residues that align with regions 1 and 2 of the β-glycosyltransferases are shown to contact the UDP portion of the UDP-sugar donor (the nature of the sugar is not known at present). Furthermore, it is speculated that the aspartate that functions as a catalytic base resides about 100 residues C-terminal to the conserved aspartate in region 2. This aspartate could be in a position similar to the aspartate present in region 3 of the β-glycosyltransferases. However, there is no QXXRW motif in the SpsA sequence and not much sequence similarity in the C-terminal portion of SpsA and regions 3 and 4 of the processive β-glycosyltransferases.

1.3. Architecture of the active site of cellulose synthase: a structural model for the active-site region of processive β-glycosyltransferases

Cellulose synthase is a transmembrane protein that has not been sufficiently purified from any source for structural analysis. Since the conserved residues predicted to be involved in catalysis and processivity are present in a globular region, we have attempted to predict the folding of this region from the *A. xylinum* cellulose synthase and determine if this structure is conserved in the other β-glycosyltransferases. To this end, a 285 amino acid segment (residues 128 to 412 of AcsAB) which contained all the conserved amino acid residues in a globular region of cellulose synthase was subjected to modeling. A BLAST search of the PDB protein sequences database using the 285 amino acid segment of *A. xylinum* cellulose synthase as a query did not identify any significant sequence matches in the database, nor did, incidentally, the related sequences YhjO, CelA1, and Rsw1. Similarly, no structural relatives were found applying the PHD server (Rost and Sander, 1996), iterative searches [PSI-BLAST (Altschul et al., 1997)] or sequence-based three dimensional structural homology searches [sophisticated search techniques after Huynen et al. (1998), as well as the direct SCOP blast server (Hubbard et al., 1999)]. Furthermore, there were no similarities to known domains using the latest version of SMART (Schultz et al., 1998) or ProDom (Corpet et al., 1998).

In the absence of any structural information for modeling, we decided to obtain an ab initio model using the genetic algorithm (Dandekar and Argos, 1994). The algorithm evolves protein structure predictions in parallel in a computer evolution, recombining and selecting "fittest" structures according to basic protein building principles. These include heavy selection against structural clashes and globular packing and more complex ones such as cooperative growth of secondary structure and sheet formation. Detailed criteria for these and their respective selection weights have been described previously and validated on a test battery of 20 proteins with known structure and a wide range of topologies, yielding correct topology predictions and an average RMSD error of 4-6 Å (Dandekar and Argos, 1996). As an additional structure selection criterion derived from experimental data (see Dandekar and Argos, 1997 for such selection parameters), catalytic aspartic acid residues were rewarded when being close together. The combination of experimental data with the genetic algorithm model has previously been shown to be an effective modeling tool including blind tests for topology description and prediction (Dandekar and Leippe, 1997; Saxena et al., 1997; Tribble et al., 2000). The algorithm folded the region of the cellulose synthase starting from sequence and secondary structure (using several available standard packages for secondary structure prediction) with the assumption that it has a globular solution structure and is an independent folding unit. The fittest and also the topologically most satisfying structure obtained from all the simulations is shown in Fig. 4a. The less fit structures had similar topologies but were not packed as well. The dimensions of the predicted structure of the globular region of the *A. xylinum* cellulose synthase are roughly 60 × 60 × 70 Å (less than half of this box is filled by the protein) and the topology of the folded structure shows 10 strands and 8 alpha-helices (Fig. 4b). The globular region has a mixed topology of beta-strands and alpha-helices (Table 2) and does not exhibit a true alpha-beta barrel as observed in the structure of some other proteins. As seen in Fig. 4a and b, the helices and strands in the globular region of cellulose synthase as predicted by the genetic algorithm do not alternate regularly and are interrupted by long loop regions. Note that the exact arrangement of the strands is only roughly indicated by the algorithm and has not been refined further (Fig. 4a and b). However the topological sketch is sufficient to indicate and compare their overall connectivity and arrangement (Fig. 6). In a similar way, the nucleotide-binding fold is delineated, but the arrangement of strands is again only approximately given.

The predicted structure of the globular region of the *A. xylinum* cellulose synthase shows the presence of a central cavity between the conserved aspartic acid residues. The distances between the conserved aspartic acid residues are estimated to be 20 Å between D189 and D236, 7 Å between D189 and D333, and 18 Å between D236 and D333. From these estimates, the central, elongated cavity can accommodate two UDP–glucose residues (each UDP–glucose residue having a dimension of about 8 Å) as shown in Fig. 4c and predicted in the model for cellulose biosynthesis (Saxena et al., 1995). We note that a suitable cavity size to accommodate the UDP–glucose was by no means predefined by the selection criteria. For instance, having the three catalytic residues maximally close together would have satisfied best the additional structure selection criterion. However, optimizing among all selection criteria by the genetic

algorithm achieved, nevertheless, the correct, suitable cavity size, indicating one internal control for the prediction. Moreover, the residues in the QXXRW motif are present in a region close to the central cavity that is believed to be the catalytic pocket. Our model suggests that helix H6 with the conserved aspartate D333 is

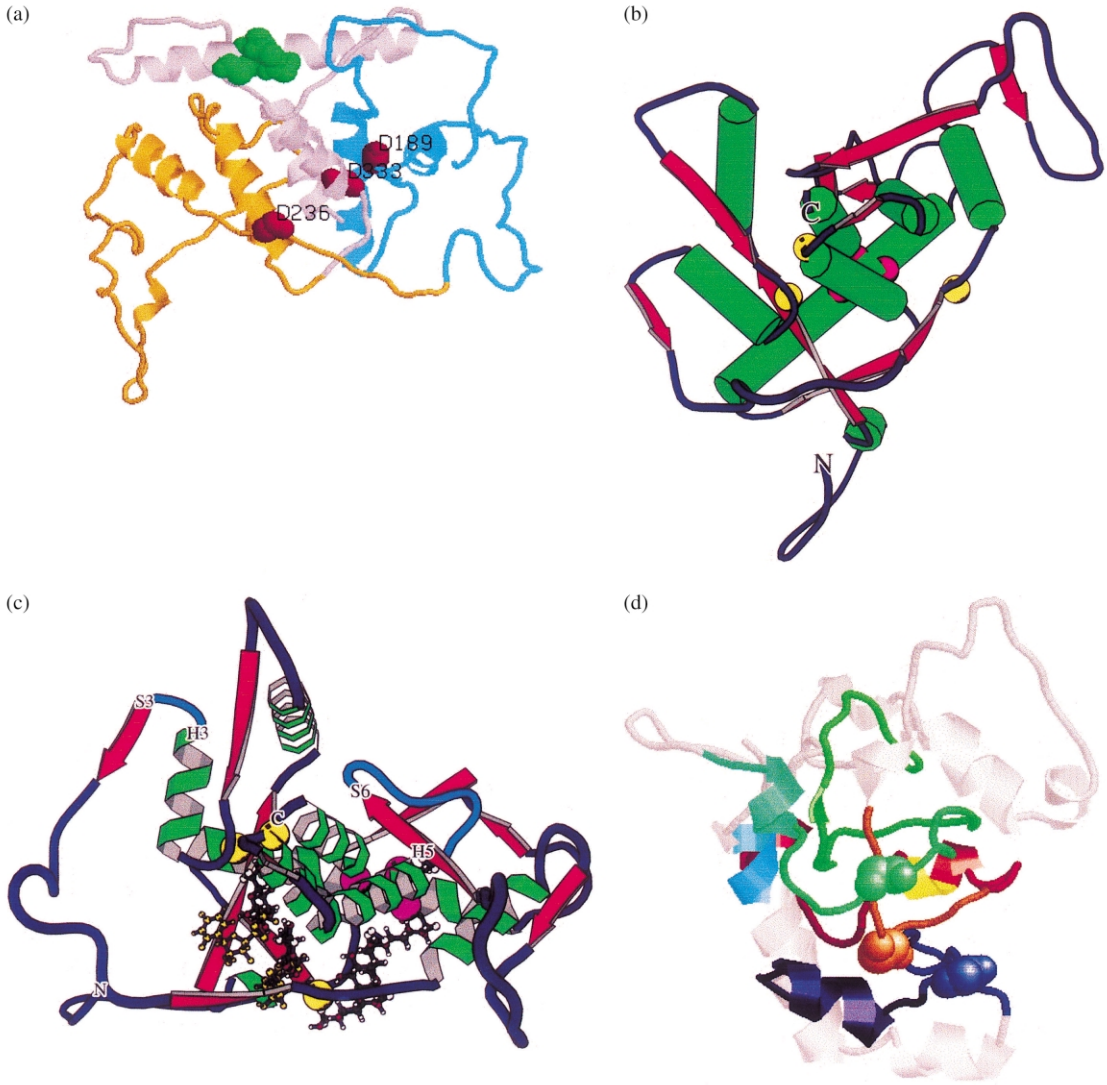

Fig. 4. (a) A ribbon model of the globular region (amino acid residues 128–412) of the *A. xylinum* cellulose synthase (AcsAB) as determined by genetic algorithm. Helical regions are indicated as such. The chain trace of the 285 amino acid globular region is shown starting from cyan (AcsAB residues 128–227) to gold (AcsAB residues 228-327) and grey (AcsAB residues 328–412). The catalytic aspartic acid residues are labeled and shown in red and spacefill representation. The QRVRW conserved motif is shown in green and spacefill. The model was drawn using the program Rasmol by Roger Sayle; (b) a schematic representation of the topology of the globular region of *A. xylinum* cellulose synthase. The alpha-helices are shown as cylinders and the beta-strands as arrows. Small balls indicate the aspartic acid residues (yellow) and the QXXRW motif (purple); (c) ribbon diagram of the globular region of the *A. xylinum* cellulose synthase showing the presence of two UDP-glucose molecules in the central cavity. The conserved aspartic acid residues are shown as yellow balls and the QXXRW region is shown in purple. The loop regions between H3 and S3 and S6 and H5 (shown in cyan) are the regions where insertions are observed in the cellulose synthases from plants. The glucose residues are arranged in a way that they could contact the catalytic aspartic acid residues and would form a cellobiose unit after removal of the UDP moieties during chain initiation. To prevent cluttering of the view in the catalytic cleft, the UDP moieties are a bit more spread out; the position of the right UDP moiety indicates also that the helix with the QXXRW motif can easily be reached (shown as an arrow in the general model in Fig. 7) after further growth of the carbohydrate chain. A glucan chain of 6 glucose residues is shown in the extended catalytic site. The reducing end of the glucan chain is on the top (probably close to the QXXRW motif) and the non-reducing end (the growing end of the glucan chain) is shown close to the second conserved aspartic acid residue (D236CD in the DXD motif); (d) a ribbon model of the globular region (534 residues; amino acids 225-758) of the *G. hirsutum* cellulose synthase (CelA1) as determined by genetic algorithm. This is a coarse model in which every third residue was modeled (a total of 178 residues were modeled) to confirm the general model for processive β-glycosyltransferases. The model depicts the large insertions in the cellulose synthases from plants (shown in white) and the spatial arrangement of the catalytic aspartates (shown thick in spacefill representation) and residues in the QXXRW motif (shown in yellow). The chain trace is color-coded- N-terminus of the chain is blue, C-terminus is red.

Table 2
Secondary structures predicted by genetic algorithm in the globular region of *Acetobacter xylinum* cellulose synthase

Pattern of helices and strands	Amino acid residues[a]	Amino acid sequence
H1	144–146	NPD
S1	150–157	TVDIFVPT
H2	159–173	NEELSIVRLTVLGSL
S2	182–187	VRVHIL
H3	192–201	RPEFAAFAAE
S3	205–208	NYIA
S4	231–235	YILIF
H4	241–251	PTRAFLQLTMG
S5	259–262	IALM
S6	289–295	NLFYGVV
H5	311–323	CAILRRTAIEQIG
S7	327–329	TQT
H6	333–344	DAHTALKMQRLG
S8	348–353	AYLRIP
H7	356–381	GGLATERLILHIGQR VRWARGMLQIF
S9	391–393	GLS
S10	396–401	QRLCYL
H8	402–411	SAMTSFLFAV

[a] The amino acid residues correspond to the complete AcsAB sequence.

central and close to the cleft. Moreover, this helix or helix H7 that contains the QXXRW motif are involved dynamically (perhaps with a structural change) in the enzymatic reaction. The tryptophan residue in the QXXRW motif is perhaps required in glucan binding. Furthermore, the long loop flanked by beta-strands S3 and S4 may help to accommodate the growing glucan chain. Residues making contact with the substrate include the conserved aspartic acid residues. A key region making contact includes residues I234, F235, and D236 while Y231 and I232 are flanking residues. Besides D333, H335 is also in close contact to the substrate. Similarly, besides D189, R191 could also be important. Further away residues I319 to V330 make up the flanking region. The structure determined by the genetic algorithm shows a globular model in accordance to the information from sequence and experiment. The loop regions apparent from the model agree as an independent test well with the accessibility predictions available for the sequence from PHD, an independent prediction algorithm using a neuronal network (Rost and Sander, 1996). Moreover, experiments done with the globular region of the cellulose synthase (CelA1) from plants suggest that the N-terminus of this region is required for UDP–glucose binding (Pear et al., 1996) and the model positions it not far away from the catalytic cleft.

As mentioned earlier, the globular region of cellulose synthases from plants is much larger than the *A. xylinum* cellulose synthase with large insertions between the conserved aspartic acid residues. In CelA1 these regions have been identified as P-CR (plant-conserved region) between the first and the second conserved aspartic acid residues and HVR (hypervariable region) between the second and the third conserved aspartic acid residues (Pear et al., 1996). Similar regions have now been identified in other plant cellulose synthases as well (Arioli et al., 1998; Taylor et al., 1999). The significance of these regions is not known at present. Upon alignment of the globular regions of the *A. xylinum* cellulose synthase (AcsAB), the *E. coli* YhjO polypeptide, and the CelA1 and Rsw1 cellulose synthases from plants, we have determined the position of these regions with respect to the predicted structure of the globular region of the *A. xylinum* cellulose synthase (Fig. 5). These regions are present in loops with the P-CR present between secondary structures H3 and S3 and the HVR between S6 and H5. These loop regions are on the surface and on the other side such that they can easily accommodate additional amino acid residues without interfering with the catalytic activity.

To further examine and compare the structure predicted for the globular region of the *A. xylinum* cellulose synthase, a coarse model of the globular region of cotton (*Gossypium hirsutum*) cellulose synthase CelA1 (Pear et al., 1996) is also predicted. To derive this model, every third residue was modeled by the genetic algorithm (residues in between were assumed to have identical secondary structural state). Despite long sequence insertions, the spatial arrangement of the conserved aspartic acid residues and the neighboring secondary structures in the cellulose synthase from plants (Fig. 4d) was found to be similar to that in the cellulose synthase from *A. xylinum*. Without providing details in resolution, the structure shown in Fig. 4d is another indication from an independent simulation that our model (Fig. 4a) captures the correct general features.

1.4. Relationship of the predicted structure of cellulose synthase with structures of other β-glycosyltransferases

Although the structure and mechanisms for a number of glycosyl hydrolases was known for some time (Davies and Henrissat, 1995), the structure for only a few β-glycosyltransferases have been determined so far. The structure of the T4 β-glucosyltransferase was first determined by Vrielink et al. (1994) and more recently the substrate binding and catalytic mechanism for this enzyme has been proposed (Moréra et al., 1999). This enzyme transfers a glucose residue from UDP–glucose to hydroxymethylcytosine in modified DNA. The sequence of the T4 enzyme does not show similarity to any of the known glycosyltransferases and so far has not been classified into any glycosyltransferase family (Campbell et al., 1997). However, the structure of the T4 enzyme was found to exhibit similarity to the structure of glycogen phosphorylase. Though no sequence similarities were observed between these two proteins, the similarity in the spatial arrangement and in the

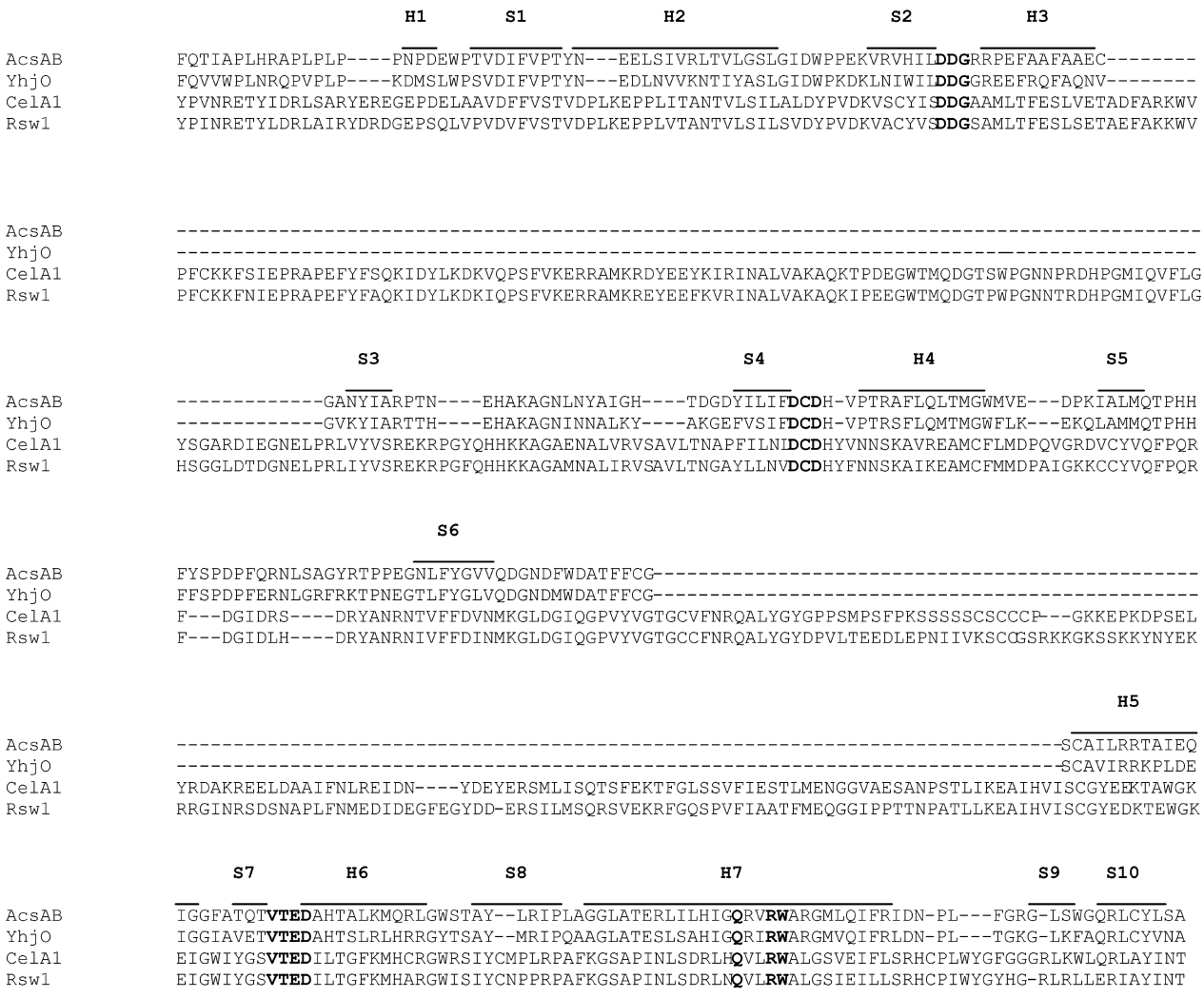

Fig. 5. Multiple alignment of the globular regions of the *A. xylinum* cellulose synthase (AcsAB), *E. coli* YhjO protein, *G. hirsutum* CelA1, and *A. thaliana* Rsw1. The secondary structures identified in the AcsAB globular region by genetic algorithm are shown above the AcsAB sequence.

chemical nature of the substrates suggested an evolutionary relationship between these two proteins based on a structurally conserved catalytic core (Holm and Sander, 1995). The predicted fold of the α-1,3-fucosyltransferases has also been suggested to show similarity to the structure of the T4 β-glucosyltransferase (Breton et al., 1998). Recently, the structures of two more β-glycosyltransferases have been determined experimentally. The structure of SpsA, a glycosyltransferase from *Bacillus subtilis* has been solved (Charnock and Davies, 1999). The substrate and acceptor specificity for this protein is not known, but it is presumably involved in the synthesis of the spore coat. This protein shares sequence homology with the glycosyltransferases in family 2 which includes enzymes that catalyze sugar transfer by an inversion mechanism. This family includes both non-processive as well as processive enzymes. From sequence analysis, SpsA is a non-processive enzyme that transfers a single sugar residue from a nucleotide–diphospho–sugar donor to a specific acceptor. The structure of SpsA shows that it is a two-domain protein with a nucleotide-binding domain and an acceptor binding domain. On the other hand, the structure of β4Gal-T1 reveals a single large domain and the overall fold was found to be different from any fold previously determined (Gastinel et al., 1999).

The modeled topology of the cellulose synthase as a prototype of a processive β-glycosyltransferase fits well in the range of structures experimentally described (Charnock and Davies, 1999; Gastinel et al., 1999) or predicted for other glycosyltransferases (Breton and Imberty, 1999). None of these structures were used for our prediction. They also cannot be used, as there is not sufficient homology for a homology prediction. At the same time, the genetic algorithm prediction is an *ab initio* prediction and does not provide a homology model. The

connectivity of the folds determined for SpsA and β4Gal-T1, and that predicted for cellulose synthase is shown in Fig. 6. Specifically comparing the structure of SpsA (Charnock and Davies, 1999) with the cellulose synthase structure as modeled by the genetic algorithm, we note that the first 100 *N*-terminal residues in SpsA provide the nucleotide binding fold and consist of four parallel β-strands flanked on either side by two helices. In our predicted structure there is a similar arrangement of helix alternating with strand for the first three helices and four strands (no helix was found between strands 3 and 4). Strands 1, 2 and 4 participate in the nucleotide-binding region and strand 8 (later in the chain trace) joins this. Furthermore, in our model strand 3 and helix 3 loop out (which is not the case in the SpsA structure but has been noted for strand 1 and helix 1 of the β4Gal-T1 structure). A more refined model (including refinement of strand positions to each other) may be expected to lead to a better topology of the nucleotide-binding site. On the other hand, re-screening the complete cellulose synthase region modeled here for hidden regular nucleotide-binding domains using IMPALA (Schaffer et al., 1999) showed that none of these are present, indicating by an independent method that cellulose synthase seems to be different in this respect and therefore the need for an *ab initio* model. The C-terminal part of the SpsA structure is a mixed β-sheet flanked by three helices on one side and one helix on the other. In our model of the cellulose synthase, the C-terminal part shows a similar but less regular succession of helices and strands as compared to the N-terminal part. Strands 9, 10 and 6 form a sheet region with helices interspersed and the flanking strand 8 adds to the nucleotide-binding region. The cellulose synthase fold is more integrated than the SpsA structure, which shows a clear split between the N-terminal nucleotide-binding part and the C-terminal part. In fact the compactness of the cellulose synthase is closer in relationship to the β4Gal-T1 structure.

The β4Gal-T1 structure (Gastinel et al., 1999) reveals eleven strands and eight helices (two of them being short 3_{10} helices) in comparison to the cellulose synthase structure that shows ten strands and eight helices. The nucleotide-binding region of β4Gal-T1 is part of the central eight-stranded mixed and twisted β-sheet surrounded by two α-helices on one side and by four α-helices on the other. This bigger sheet is neither predicted for the cellulose synthase nor found in the SpsA structure. However, the sequence of helices and strands in the nucleotide-binding region of β4Gal-T1 looks similar to our predicted cellulose synthase fold and is not as regular as it is in SpsA. The C-terminal part of β4Gal-T1 contains a small sheet region with a similar arrangement as found in our model of cellulose synthase. The β4Gal-T1 fold is again different from the structure of the T4 phage β-glucosyltransferase (Vrielink et al., 1994).

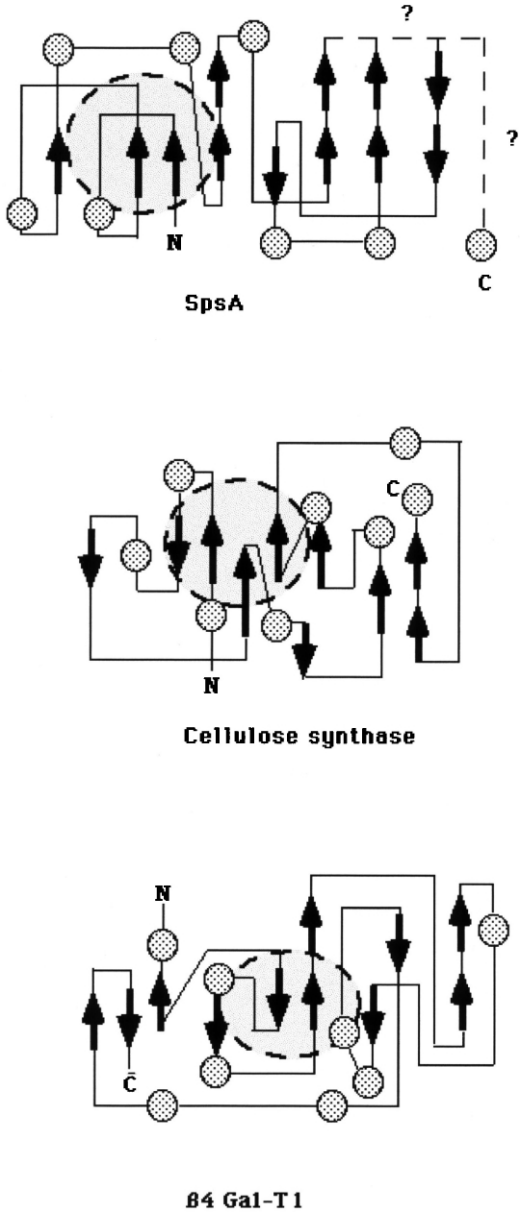

Fig. 6. Topological comparison of the *B. subtilis* SpsA protein, bovine β4Gal-T1 catalytic domain, and the *A. xylinum* cellulose synthase globular region. The circle represents the approximate nucleotide-binding site in each protein.

1.5. Possible mechanisms for synthesis of cellulose and other polysaccharides

Since every glucose unit in the cellulose chain is oriented 180° with respect to its neighbor, we had proposed a model in which two UDP–glucose molecules are positioned in the active site of cellulose synthase at an 180° orientation. Upon catalysis, the glucose units are linked simultaneously or sequentially to extend the cellulose chain two units at a time (Saxena et al., 1995). This model proposed that the active site of the enzyme has an extended region that carries not only the catalytic

residues, but also a region that holds the growing chain (glucan-binding region). Since the catalytic region is predicted to have two UDP–glucose binding sites and as no primer requirement is observed, initiation of cellulose synthesis probably takes place by the formation of a cellobiose unit in the catalytic pocket. In such a case, the UDP-portion of the first UDP-glucose is cleaved, leaving an exposed reducing end in the first glucose (terminal residue) and this glucose is linked via its non-reducing end to the second glucose by a β-1,4–linkage. The cellobiose unit thus formed moves, as it has no bonding in the catalytic pocket, into the glucan-binding region, but does not leave the enzyme because it is in a twisted conformation. In this conformation the cellobiose unit is associated with the glucan-binding region and does not move or slide. In the next step of chain elongation, two new UDP–glucose molecules enter the catalytic pocket and two new β-1,4-linkages are formed either sequentially or simultaneously. The formation of a covalent bond at the non-reducing end of the cellobiose unit present in the glucan-binding region makes this cellobiose unit to adopt an extended conformation and allows it to slide further in the glucan-binding region. This model of the catalytic and glucan-binding region of cellulose synthase is similar to the one proposed, based on direct structural data, for the catalytic domain of CBHI (Divne et al., 1998). Both cellulose synthase and CBHI are processive enzymes that have to be tightly associated with the cellulose chain. In CBHI, the cellulose chain is passaged through a tunnel-like structure in which the protein interacts with at least 10 glucose residues. For the glycosyl hydrolases, the tunnel-like structure probably imposes a steric confinement for the stabilization of a sugar conformation that is able to undergo catalysis, and in this the ring distortion is thought to play an important role (Divne et al., 1998). A similar structure can also be visualized for the cellulose synthase and possibly other processive glycosyltransferases where a glycan chain is passed through a tunnel-like structure where it is held in a conformation that allows both its tight association as well as allows it to slide. The amino acid residues involved in the sugar-protein interaction are usually aromatic residues, such as tryptophan with its indole ring and tyrosine, and we expect them to be conserved in the glucan-binding region of the processive glycosyltransferases.

Is there a need for two catalytic centers in cellulose synthase and possibly other processive β-glycosyltransferases? The requirement for two catalytic centers in these enzymes was proposed to account for the two-fold symmetry of the glucose residues in a cellulose chain where every residue is rotated 180° with respect to its neighbor (Saxena et al., 1995). The absence of duplicated active sites in the cellulose synthase catalytic subunit has led others to suggest that there can be as much as 120° rotation about the β-1,4-linkage. Accordingly all glucose residues can be added in a particular orientation at a single site and the alternating residues can relax into opposing orientations after they have exited the catalytic site (Delmer, 1999). This leads into the nature of the glucan chain in the active site of the enzyme. Do the glucose residues in the glucan chain at this point of synthesis have intramolecular H-bonds to stabilize the chain or do these H-bonds form at a later point? The intramolecular H-bonds between O3′ and O5 exist in crystalline cellulose, and it will be interesting to determine if they are also present in the glucan chain in the active site. In the structure of CBHI from *Trichoderma reesei* bound to cellulose, the cellulose chain has torsion angles at the linkages that are similar to other cellobiosyl linkages (Divne et al., 1998).

The two catalytic centers were also thought to be required for synthesis of polysaccharide chains that have alternating sugar residues that are different and that are linked by different linkages as in the case of hyaluronan (DeAngelis, 2000) and type 3 capsular

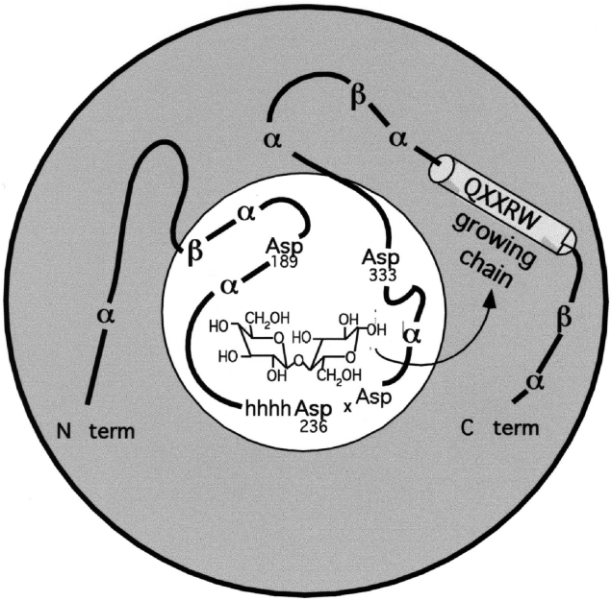

Fig. 7. A cartoon presenting a general model for the globular region of processive glycosyltransferases. The black line represents the main chain trace of the globular region of the *A. xylinum* cellulose synthase. The globular topology of this region is indicated by the grey circle and the globular arrangement of the catalytic residues is shown in the center. The three conserved catalytic residues are indicated by Asp (aspartate, sometimes also glutamate residues; the numbers are only given to identify the corresponding residues in the *A. xylinum* cellulose synthase). α and β indicate stable secondary structure elements that provide a framework for the catalytic residues. The QXXRW motif (alpha-helix with these residues; see text) holds the growing glucan chain (chain itself is only written as text in the cartoon). The processive assembly of the glucan chain takes place by the sequential or simultaneous addition of two glucose residues to the growing end. Functional motifs flank the key catalytic residues (for instance the DXD motif with accompanying *N*-terminal hydrophobic and aromatic residues for Asp 236). h represents hydrophobic residues.

polysaccharide of *Streptococcus pneumoniae* (Cartee et al., 2000). These polysaccharides have a disaccharide repeat and current evidence suggests that the enzymes required for their synthesis are capable of forming all of the glycosidic linkages present in these polysaccharides. Moreover, it is envisaged that a single polypeptide catalyzes the transfer of two distinct sugars in the case of hyaluronan and type 3 capsular polysaccharide. The transfer of the two different sugars to the growing polysaccharide chain is probably catalyzed by a mechanism similar to that proposed for cellulose biosynthesis. Whether catalysis involves a single active site or two independent sites for transfer of the two sugars to the growing chain is not very well understood, although two separate glycosyltransferase activities have been implicated for the synthesis of hyaluronan and other polysaccharides. The *Pasteurella multocida* hyaluronan synthase (PmHasA) shows the presence of duplicated domains A (A1 and A2) instead of domains A and B, and mutational analysis suggests the presence of two relatively independent glycosyltransferase activities on a single polypeptide chain (Jing and DeAngelis, 2000). Moreover, the transfer of sugars by this enzyme has been shown to take place in a sequential manner instead of simultaneous addition of a disaccharide subunit (DeAngelis, 2000).

The similarity between the different β-glycosyltransferases and in their mode of action has been further strengthened by the recent demonstration of the elongation of the growing chain from the non-reducing end as in the case of cellulose (Koyama et al., 1997), chitin (Sugiyama et al., 1999), chitin oligosaccharide (Kamst et al., 1999), hyaluronan (DeAngelis et al., 2000), and type 3 capsular polysaccharide (Cartee et al., 2000). This mechanism of chain growth from the non-reducing end is similar to that observed for the synthesis of starch and glycogen. In all these cases growth occurs by direct polymerization from a nucleotide sugar.

2. Significance

A combination of functional and modeling studies offers an insight into the folding pattern and the arrangement of conserved amino acids in the globular region of the *A. xylinum* cellulose synthase and other processive β-glycosyltransferases. The protein structure calculated by the genetic algorithm was carefully optimized and is the overall fittest from a total of 11 million solution trials. The fitness criteria applied had been validated on 20 proteins with known crystal structure and different topologies (Dandekar and Argos, 1996). The structure calculated is supported by the predicted spatial constraints (size of the UDP–glucose binding pocket; transfer of the growing chain to the QXXRW region), the available experimental data (requirement of the first conserved aspartic acid and *N*-terminus in UDP–glucose binding experiments is supported in the model where the *N*-terminus is flanking the catalytic cleft; requirement of the conserved aspartic acid residues for enzyme activity as determined by site-directed mutagenesis and activity measurements), and sequence analysis (identification of the conserved residues and the QXXRW motif in the globular region). As an independent test, the distribution of accessible loop regions agrees well with that derived by neuronal network prediction (Rost and Sander, 1996). Nevertheless, we suspect the RMSD error in several areas of the model to be still high (higher than 5 Å). However, the structure is useful to get a first approximation view at the spatial arrangement of the catalytic residues, the glucan holding residues (QXXRW region) for the growing cellulose chain and, also importantly, of all the neighboring residues acting in concert with these central ones. These features as well as the alpha/beta mixed topology without a regular succession of helices and strands predict a simplified and general model for the structure and action of processive β-glycosyltransferases (Fig. 7). We hope that this first structure-function characterization of cellulose synthase will stimulate further research and will be an incentive for new studies.

Acknowledgements

This work was supported by grants from the USDA (96-35301-3176) and DOE (DE-FG03-94ER20145) to I.M.S. and R.M.B. T.D. thanks DFG and BMBF for support.

References

Altschul, S.F., Madden, T.L., Schaffer, A.A., Zhang, J., Zhang, Z., Miller, W., Lipman, D.J., 1997. Gapped BLAST and PSI-BLAST: a new generation of protein database search programs. Nucleic Acids Res. 25, 3389–3402.

Arioli, T., Peng, L., Betzner, A.S., Burn, J., Wittke, W., Herth, W., Camilleri, C., Höfte, H., Plazinski, J., Birch, R., Cork, A., Glover, J., Redmond, J., Williamson, R.E., 1998. Molecular analysis of cellulose biosynthesis in *Arabidopsis*. Science 279, 717–720.

Barth, H., Preiss, J.C., Hofmann, F., Aktories, K., 1998. Characterization of the catalytic site of the ADP-ribosyltransferase *Clostridium botulinum* C2 toxin by site-directed mutagenesis. J. Biol. Chem. 273, 29506–29511.

Breton, C., Imberty, A., 1999. Structure/function studies of glycosyltransferases. Curr. Op. Structural Biol. 9, 563–571.

Breton, C., Oriol, R., Imberty, A., 1998. Conserved structural features in eukaryotic and prokaryotic fucosyltransferases. Glycobiology 8, 87–94.

Busch, C., Hofmann, F., Selzer, J., Munro, S., Jeckel, D., Aktories, K., 1998. A common motif of eukaryotic glycosyltransferases is essential for the enzyme activity of large clostridial cytotoxins. J. Biol. Chem. 273, 19566–19572.

Campbell, J.A., Davies, G.J., Bulone, V., Henrissat, B., 1997. A classification of nucleotide-diphospho-sugar glycosyltransferases based on amino acid sequence similarities. Biochem. J. 326, 929–939.

Cartee, R.T., Forsee, W.T., Schutzbach, J.S., Yother, J., 2000. Mechanism of type 3 capsular polysaccharide synthesis in *Streptococcus pneumoniae*. J. Biol. Chem. 275, 3907–3914.

Charnock, S.J., Davies, G.J., 1999. Structure of the nucleotide-diphospho-sugar transferase, SpsA from *Bacillus subtilis*, in native and nucleotide-complexed forms. Biochemistry 38, 6380–6385.

Chen, H.P., Brown Jr., R.M., 1996. Immunochemical studies of the cellulose synthase complex in *Acetobacter xylinum*. Cellulose 3, 63–75.

Corpet, F., Gouzy, J., Kahn, D., 1998. The ProDom database of protein domain families. Nucleic Acids Res. 26, 323–326.

Dandekar, T., Argos, P., 1994. Folding the main chain of small proteins with the genetic algorithm. J. Mol. Biol. 236, 844–861.

Dandekar, T., Argos, P., 1996. Identifying the tertiary fold of small proteins with different topologies from sequence and secondary structure using the genetic algorithm and extended criteria specific for strand regions. J. Mol. Biol. 256, 645–660.

Dandekar, T., Argos, P., 1997. Applying experimental data to protein fold prediction with the genetic algorithm. Protein Engineering 10, 877–893.

Dandekar, T., Leippe, M., 1997. Molecular modeling of amoebapore and NK-lysin: a four-alpha-helix bundle motif of cytolytic peptides from distantly related organisms. Fold Des. 2, 47–52.

Davies, G., Henrissat, B., 1995. Structure and mechanisms of glycosyl hydrolases. Structure 3, 853–859.

DeAngelis, P.L., 2000. Molecular directionality of polysaccharide polymerization by the *Pasteurella multocida* hyaluronan synthase. J. Biol. Chem. 274, 26557–26562.

Delmer, D.P., 1999. Cellulose biosynthesis. Exciting times for a difficult field of study. Annual Review of Plant Physiology. Plant Mol. Biol. 50, 245–276.

Ditta, G., Schmidhauser, T., Yakobson, E., Lu, P., Liang, X., Finlay, D.R., Guiney, D., Helinski, D.R., 1985. Plasmids related to the broad host range vector, pRK290, useful for gene cloning and for monitoring gene expression. Plasmid 13, 149–153.

Divne, C., Ståhlberg, J., Teeri, T.T., Jones, T.A., 1998. High-resolution crystal structures reveal how a cellulose chain is bound in the 50 Å long tunnel of cellobiohydrolase I from *Trichoderma reesei*. J. Mol. Biol. 275, 309–325.

Gastinel, L.N., Cambillau, C., Bourne, Y., 1999. Crystal structure of the bovine β4galactosyltransferase catalytic domain and its complex with uridine diphoshogalactose. EMBO J. 18, 3546–3557.

Griffiths, G., Cook, N.J., Gottfridson, E., Lind, T., Lidholt, K., Roberts, I.S., 1998. Characterization of the glycosyltransferase enzyme from the *Escherichia coli* K5 capsule gene cluster and identification and characterization of the glucuronyl active site. J. Biol. Chem. 273, 11752–11757.

Holm, L., Sander, C., 1995. Evolutionary link between glycogen phosphorylase and a DNA modifying enzyme. EMBO J. 14, 1287–1293.

Hubbard, T.J.P., Ailey, B., Brenner, S.E., Murzin, A.G., Chothia, C., 1999. SCOP: a structural classification of proteins database. Nucleic Acids Res. 27, 254–256.

Huynen, M., Doerks, T., Eisenhaber, F., Orengo, C., Sunyaev, S., Yuan, Y., Bork, P., 1998. Homology-based fold predictions for *Mycoplasma genitalium* proteins. J. Mol. Biol. 280, 323–326.

Jing, W., DeAngelis, P.L., 2000. Dissection of the two transferase activities of the *Pasteurella multocida* hyaluronan synthase: two active sites exist in one polypeptide. Glycobiology 10, 883–889.

Kamst, E., Bakkers, J., Quaedvlieg, N.E.M., Pilling, J., Kijne, J.W., Lugtenberg, B.J.J., Spaink, H.P., 1999. Chitin oligosaccharide synthesis by rhizobia and zebrafish embryos starts by glycosyl transfer to O4 of the reducing-terminal residue. Biochemistry 38, 4045–4052.

Koyama, M., Helbert, W., Imai, T., Sugiyama, J., Henrissat, B., 1997. Parallel-up structure evidences the molecular directionality during biosynthesis of bacterial cellulose. Proc. Natl. Acad. Sci. USA 94, 9091–9095.

Moréra, S., Imberty, A., Aschke-Sonnenborn, U., Rüger, W., Freemont, P.S., 1999. T4 Phage β-glucosyltransferase: Substrate binding and proposed catalytic mechanism. J. Mol. Biol. 292, 717–730.

Nagahashi, S., Sudoh, M., Ono, N., Sawada, R., Yamaguchi, E., Uchida, Y., Mio, T., Takagi, M., Arisawa, M., Okabe, H.Y., 1995. Characterization of chitin synthase 2 of *Saccharomyces cerevisiae*. J. Biol. Chem. 270, 13961–13967.

Okazaki, I.J., Moss, J., 1998. Glycosylphosphatidylinositol-anchored and secretory isoforms of mono-ADP-ribosyltransferases. J. Biol. Chem. 273, 23617–23620.

Pear, J.R., Kawagoe, Y., Schreckengost, W.E., Delmer, D.P., Stalker, D.M., 1996. Higher plants contain homologs of the bacterial *celA* genes encoding the catalytic subunit of cellulose synthase. Proc. Natl. Acad. Sci. USA 93, 12637–12642.

Pritchard, A.E., McHenry, C.S., 1999. Identification of the acidic residues in the active site of DNA polymerase III. J. Mol. Biol. 285, 1067–1080.

Rost, B., Sander, C., 1996. Bridging the protein sequence-structure gap by structure predictions. Ann. Rev. Biophys. Biomol. Str. 25, 113–136.

Saxena, I.M., Brown Jr., R.M., 1995. Identification of a second cellulose synthase gene (acsAII) in *Acetobacter xylinum*. J. Bacteriol. 177, 5276–5283.

Saxena, I.M., Brown Jr., R.M., 1997. Identification of cellulose synthase(s) in higher plants: Sequence analysis of processive β-glycosyltransferases with the common motif 'D,D,D35Q(R,Q)XRW.' Cellulose 4, 33–49.

Saxena, I.M., Brown Jr., R.M., Fevre, M., Geremia, R.A., Henrissat, B., 1995. Multidomain architecture of β-glycosyl transferases: Implications for mechanism of action. J. Bacteriol. 177, 1419–1424.

Saxena, I.M., Lin, F.C., Brown Jr., R.M., 1990. Cloning and sequencing of the cellulose synthase catalytic subunit gene of *Acetobacter xylinum*. Plant Mol. Biol. 15, 673–683.

Saxena, P., Whang, I., Voziyanov, Y., Harkey, C., Argos, P., Jayaram, M., Dandekar, T., 1997. Probing Flp: a new approach to analyze the structure of a DNA recognizing protein by combining the genetic algorithm, mutagenesis and non-canonical DNA target sites. Biochimica et Biophysica Acta 1340, 187–204.

Schaffer, A.A., Wolf, Y.I., Ponting, C.P., Koonin, E.V., Aravind, L., Altschul, S.F., 1999. IMPALA: matching a protein sequence against a collection of PSI-BLAST-constructed position-specific score matrices. Bioinformatics 15, 1000–1011.

Schultz, J., Milpetz, F., Bork, P., Ponting, C.P., 1998. SMART, a simple modular architecture research tool: identification of signaling domains. Proc. Natl. Acad. Sci. USA 95, 5857–5864.

Sofia, H.J., Burland, V., Daniels, D.L., Plunkett III, G., Blattner, F.R., 1994. Analysis of the *Escherichia coli* genome. V. DNA sequence of the region from 76.0 to 81.5 minutes. Nucleic Acids Res. 22, 2576–2586.

Sugiyama, J., Boisset, C., Hashimoto, M., Watanabe, T., 1999. Molecular directionality of β-chitin biosynthesis. J. Mol. Biol. 286, 247–255.

Taylor, N.G., Scheible, W.-R., Cutler, S., Somerville, C.R., Turner, S.R., 1999. The *irregular xylem3* locus of *Arabidopsis* encodes a cellulose synthase required for secondary cell wall synthesis. Plant Cell 11, 769–779.

Tribble, G., Ahn, Y.T., Lee, J., Dandekar, T., Jayaram, M., 2000. DNA recognition, strand selectivity, and cleavage mode during integrase family site-specific recombination. J. Biol. Chem. 275, 22255–22267.

Vrielink, A., Ruger, W., Driessen, H.P.C., Freemont, P.S., 1994. Crystal structure of the DNA modifying enzyme β-glucosyl-

transferase in the presence and absence of the substrate uridine diphosphoglucose. EMBO J. 13, 3413–3422.

Wiggins, C.A.R., Munro, S., 1998. Activity of the yeast MNN1 α1,3-mannosyltransferase requires a motif conserved in many other families of glycosyltransferases. Proc. Natl. Acad. Sci. USA 95, 7945–7950.

Wong, H.C., Fear, A.L., Calhoon, R.D., Eichinger, G.H., Mayer, R., Amikam, D., Benziman, M., Gelfand, D.H., Meade, J.H., Emerick, A.W., Bruner, R., Ben-Bassat, A., Tal, R., 1990. Genetic organization and regulation of the cellulose synthase operon in *Acetobacter xylinum*. Proc. Natl. Acad. Sci. USA 87, 8130–8134.

PERGAMON

Phytochemistry 57 (2001) 1149–1157

PHYTOCHEMISTRY

www.elsevier.com/locate/phytochem

Transcriptional control of lignin biosynthesis by tobacco LIM protein

Akiyoshi Kawaoka *, Hiroyasu Ebinuma

Nippon Paper Industries Co., Ltd, Pulp and Paper Research Laboratory, 5-21-1, Oji, Kita-ku, Tokyo 114-0002, Japan

Received 5 July 2000; received in revised form 1 November 2000

Abstract

Lignin is a complex phenolic plant polymer that is essential for mechanical support, defense, and water transport in higher plants. The AC-rich motif, Pal-box is an important *cis*-acting element for gene expression in phenylpropanoid biosynthesis. We isolated a cDNA clone (*Ntlim1*) encoding a Pal-box binding protein by Southwestern screening. The deduced amino acid sequence of Ntlim1 is highly similar to members of the LIM protein family that contain a zinc finger motif. Moreover, Ntlim1 had a specific DNA-binding ability and transiently activated transcription of a β-glucuronidase reporter gene driven by the Pal-box sequence. The results of transient expression assays with tobacco cultured cells showed that fusion proteins between GFP and Ntlim1 can enter nuclei. Transgenic tobacco plants with antisense Ntlim1 showed low levels of transcripts from some key phenylpropanoid pathway genes such as phenylalanine ammonia-lyase, hydroxycinnamate CoA ligase and cinnamyl alcohol dehydrogenase. Furthermore, a greater than 20% reduction in lignin content was observed in transgenic tobacco with antisense *Ntlim1*. © 2001 Elsevier Science Ltd. All rights reserved.

Keywords: Transcription factor; LIM domain; Gene expression; Lignin; Phenylpropanoid

1. Introduction

Lignin is a complex phenolic polymer that reinforces the walls of certain cells in vascular tissues, and plays an important role in mechanical support, water transport and pathogen resistance in higher plants. In the pulp and paper industry, lignin must be removed by harsh chemical treatments, which is costly both to the mill and the environment. Genetic modification of the lignin content and composition of woody plants is currently receiving considerable attention in forest biotechnological studies and wood formation. In addition, the lignin polymer is intimately associated with cell wall polysaccharides, such as cellulose and hemicellulose of forage. Lignin interferes with the digestibility of these carbohydrates. Thus, the modification of lignin content and monomer composition by biotechnological procedures is of significant commercial interest.

Lignin is derived from the dehydrogenative polymerization of monolignols, *p*-coumaryl alcohol, coniferyl alcohol, and sinapyl alcohol. Based on tracer experiments and subsequent enzymatic analysis of the intermediate steps, it has been shown that monolignols are synthesized through the phenylpropanoid biosynthetic pathway (Higuchi, 1985). The lignin biosynthetic pathway has been relatively well studied, and most genes encoding the enzymes in this pathway have been identified in several plant species (Whetten et al., 1998). The targeted manipulation of specific genes and enzymes has complemented the chemical characterization of lignin mutants in a variety of plant species (Whetten et al., 1998). These studies have exploited a range of different genes encoding enzymes involved in the control of lignification at three levels. The first enzymes are those of the common phenylpropanoid pathway: phenylalanine ammonia-lyase (PAL), cinnamate 4-hydroxylase (C4H) and hydroxycinnamate CoA ligase (4CL). The second group consists of those in the hydroxylation/methylation step of monolignol biosynthesis: caffeate/5-hydroxyferulate-*O*-methyltransferase (COMT), caffeoyl CoA/5-hydroxyferuloyl CoA-*O*-methyltransferase (CCoAOMT) and ferulate-5-hydroxylase (F5H). The third group consists of those in the last steps of monolignol biosynthesis: hydroxycinnamoyl-CoA:NADPH oxidoreductase (CCR) and

* Corresponding author. Tel.: +81-3-3911-5106; fax: +81-3-3914-3350.

E-mail address: akiyoshi.kawaoka@nifty.ne.jp (A. Kawaoka).

0031-9422/01/$ - see front matter © 2001 Elsevier Science Ltd. All rights reserved.
PII: S0031-9422(01)00054-1

cinnamyl alcohol dehydrogenase (CAD). Several attempts to produce transgenic tobacco with antisense or sense-suppression methods have led to the modification of lignin content and monomeric composition (Boudet, 1998).

Most of the genes involved in lignin biosynthesis have been identified and their promoter regions have been studied. The AC rich-element Pal-box is an important *cis*-acting element (Boudet, 1998). The horseradish peroxidase (HRP) encoded by the *prxC2* gene is involved in lignification (Kawaoka et al., 1992). We previously reported the cloning of a cDNA encoding *TFHP1*, which specifically bound to the G-box motif in the *prxC2* promoter (Kawaoka et al., 1994). In a later report, analysis of the regulatory properties of the *prxC2* promoter revealed another positive *cis*-acting element, POP (Pal-box related *cis*-acting element of *prxC2*), which contained a Pal-box like motif between −178 and −136 bp from the translation start site (Kaothien et al., 2000). The Pal-box motif, CCA (C/A) (A/T) A (A/C) C (C/T) CC, is a highly conserved sequence that is involved in the expression of phenylpropanoid biosynthetic genes such as *PAL* (Cramer et al., 1989; Lois et al., 1989; Ohl et al., 1990), *4CL* (Douglas et al., 1987), *CHS* (Dron et al., 1988) and *CAD* (Feuillet et al., 1995). The Pal-box motif appears to be similar to the nucleotide sequence bound by MYB transcription factors. The first evidence for the role of MYB proteins in the regulation of genes in the phenylpropanoid pathway came from the study of a flower-specific MYB from *Antirrhinum*. Overexpression of two *Antirrhinum* MYB genes in transgenic tobacco down-regulated the expression of some genes in phenylpropanoid biosynthesis (Tamagnone et al., 1998). This result suggests that MYB-type transcription factors might be involved in regulating the expression of genes in lignin biosynthesis. However, there are many members of the *MYB* gene family in a plant genome and the DNA-binding specificity of plant MYB proteins varies considerably (Martin and Paz-Ares, 1997). The binding-site performance and affinity of MYB proteins is also likely to be strongly influenced by other protein factors that interact with them (Jin and Martin, 1999). Hence, it is difficult to believe that the MYB-type transcription factors alone play a pivotal role in the expression of lignin biosynthetic genes.

To understand the regulation of lignin biosynthesis, we focused on a transcription factor that controls the expression of genes encoding enzymes in this pathway. We describe here the functional analysis of a tobacco protein, called *Ntlim1*, which specifically bound to the Pal-box sequence. The Ntlim1 protein has two LIM domains which are cysteine-rich polypeptides composed of two special zinc fingers separated by a two-amino acid spacer. Other reports on plant LIM proteins describe sunflower PLIM1 and WLIM1 (Baltz et al., 1992; Mundel et al., 2000). Although the LIM domain is comprised of a double, semi-conservative zinc finger motif, there is still not enough proof for its DNA-binding activity. Furthermore, the LIM domain may function as an interface for protein-protein interaction (Crawford et al., 1992; Sadler et al., 1992). In this report, we show that the Ntlim1 protein acts as a potential transcription factor in lignin biosynthesis by binding to a specific DNA sequence. Moreover, suppression of Ntlim1 caused simultaneous reduction in the transcript levels of some phenylpropanoid pathway genes and a low lignin content in transgenic plants.

2. Results

2.1. Molecular cloning of a cDNA encoding Pal-box binding protein

To investigate the existence of a protein that binds to the Pal-box like motif in tobacco nuclear protein, we prepared a double-stranded oligonucleotide probe P that corresponded to three tandem copies of the Pal-box like motif (-CCACTTGAGTAC-) in the horseradish peroxidase *prxC2* promoter region. The binding of nuclear protein to probe P was tested by a gel retardation assay using the nuclear extracts from tobacco stems. As shown in Fig. 1, several retarded bands appeared in the presence of nuclear extracts from tobacco stems and were maintained even in the presence of poly (dI-dC)·poly (dI-dC) as a non-specific competitor. On the other hand, in the presence of excess amounts of the homologous non-labeled DNA fragment as a specific competitor, the retarded complexes were not observed, confirming the presence of nuclear factors that specifically bind to the Pal-box like motif in tobacco stems.

To isolate cDNAs which encode the Pal-box binding protein, a λgt11 expression library constructed with mRNA from tobacco stems was screened using probe P. From the screening of one million recombinant phages, one positive clone was obtained. The cDNA insert of the positive clone was 1.0 kb in length and contained an open reading frame that encodes a protein of 200 amino acid residues (Fig. 2a). From a GenBank database search, the deduced amino acid sequence of the clone proved to be highly homologous to a plant LIM protein, the PLIM1 of late pollen genes in the sunflower (Baltz et al., 1992) and Arabidopsis L2 (GenBank accession no. X91398). We designated the protein encoded by this cDNA as Ntlim1. The LIM motif defines one class of zinc-binding domains and was originally recognized in, and named after, the protein products of the *lin-11*, *isl-1* and *mec-3* genes (Taira et al., 1995). Furthermore, the results of the motif search showed that the deduced amino acid sequence of the Ntlim1 protein contains two repeats of conserved amino acid sequences of the LIM domain (LIM1 and LIM2; Fig. 2b). To determine the

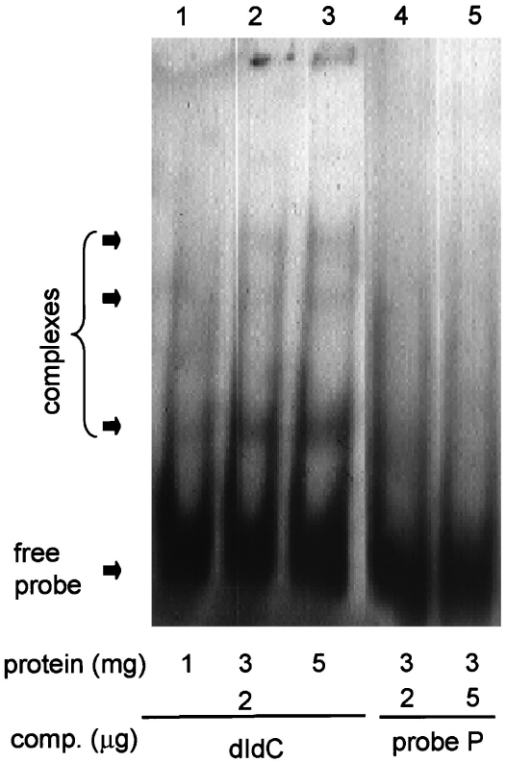

Fig. 1. The Pal-box binding proteins in tobacco. Interaction of nuclear proteins extracted from tobacco stems with a double-stranded synthetic oligonucleotide corresponding to the Pal-box. Various concentrations of nuclear proteins and DIG-labled DNA were incubated with either poly(dI-dC)·poly(dI-dC), 50-, or 100-fold molar excess of non-labeled probe P as a specific competitor.

a

MAFAGTTQKCMACDKTVYLVDKLTA 25
DNRIYHKACFRCHHCKGTVKLGNYN 50
SFEGVLYCRPHFDQLFKQTGSLDKS 75
FEGTPKIVKPQKPIDSEKPQVAKVT 100
SMFGGTREKCFGCKKTVYPTEKVSA 125
NGTPYHKSCFQCSHGGCVISPSNYT 150
AHEGRLYCKHHHI*QLIKEKGNLSKL* 175
EGDHEMNSTTTTEVTAESYTADQVD 200

b

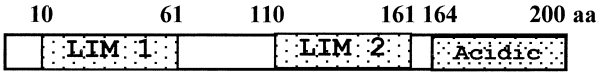

Fig. 2. Amino acid sequence and structural features of Ntlim1. (a) Putative amino acid sequence (DDBJ/GenBank/EMBL accession no. AB023479). The LIM domains are indicated by underlines and the acidic domain is in italics. (b) Schematic drawing showing locations of LIM domains and the acidic region of the Ntlim1 protein.

number of genes in the tobacco genome that are related to the gene for Ntlim1, Southern hybridization was carried out. Three hybridizing bands were obtained with genomic DNA digested with either *Eco*RV or *Dra*I, indicating that there are at least three copies of *Ntlim1* in the tobacco genome (data not shown). Total RNA extracted from tobacco roots, stems and leaves was subjected to electrophoresis, blotted, and the accumulation of *Ntlim1* mRNA in each organ was determined by Northern hybridization. The *Ntlim1* mRNA was abundant in stems and was also detected in leaves and roots (Kawaoka et al., 2000).

2.2. Ntlim1 protein is a transcription factor

To determine whether the Ntlim1 protein indeed binds to the Pal-box like sequence, we prepared protein extracts from *Escherichia coli* carrying the expression vector pGEX-2TK, which produces glutathione-S-transferase (GST) fusion protein, by isopropyl-β-D-thiogalactopyranoside (IPTG) induction. The fusion protein, GST-Ntlim1, was purified through Glutathione-Sepharose 4B resin. After digestion with thrombin protease, the band of purified Ntlim1 protein (24 kDa) was observed by SDS–PAGE. The DNA-binding ability of the purified Ntlim1 was tested by gel retardation assay using radiolabeled probe P (Fig. 3). A retarded band showing DNA-binding activity of Ntlim1, which disappeared in the presence of an excess amount of non-labeled probe P, was observed (lanes 3 and 4). The Pal-box binding specificity of Ntlim1 was also confirmed by a competition assay using an excess amount of another non-labeled Pal-box sequence of bean Pal2 (-CCAC-CAACCCCC-, lanes 5 and 6).

Ntlim1 has three notable domains: the LIM1 domain, the LIM2 domain and the acidic domain (amino acids 164-200). To confirm whether *Ntlim1* functions as a transcription activator in vivo, we constructed an effector plasmid that was a full-length *Ntlim1* cDNA under the control of the cauliflower mosaic virus (CaMV) 35S core promoter, and two kinds of chimeric GUS genes used as reporter plasmids (Fig. 4a). The P reporter plasmid was constructed using double-stranded synthetic oligonucleotides. A three-copy sequence of the Pal-box like motif was ligated to the -90 bp CaMV 35S minimum promoter. Transient expression of GUS in tobacco leaves was measured 24 h after the effector and reporter were co-introduced by particle bombardment. As shown in Fig. 4b, the co-introduction of reporter P with the effector construct led to many blue spots, indicating GUS expression. However, when the reporter plasmid alone was introduced, no blue spots were obtained.

To investigate the localization of the Ntlim1 protein in tobacco cells, two kinds of chimeric genes were constructed between the Ntlim1 protein and Green Fluorescent Protein (GFP) under the control of the 35S

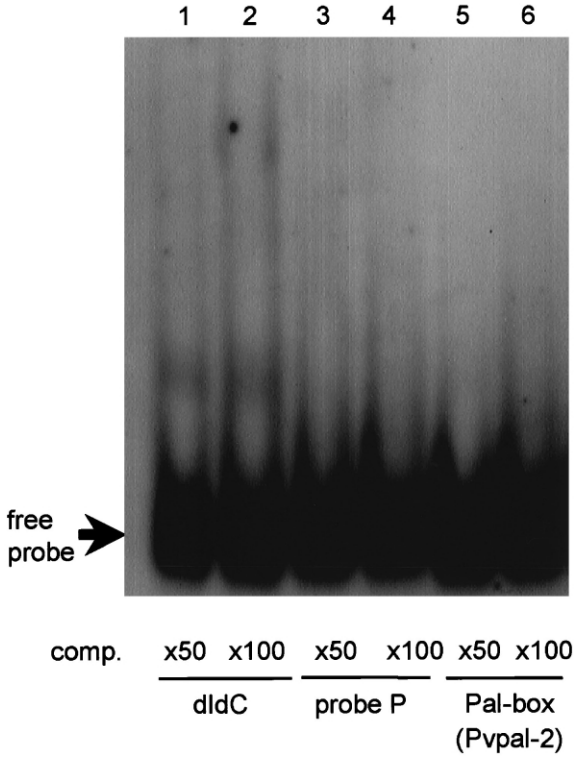

Fig. 3. Gel retardation assay of the Ntlim1 protein expressed in *Escherichia coli*. The purified Ntlim1 was incubated with DIG-labeled probe P in either the presence of excess amounts of non-labeled probe P (lanes 3, 4) or non-labeled double-stranded oligonucleotide corresponding to the Pal-box sequence of the bean *pal2* gene (lanes 5, 6), which were used as competitors, or without an excess of non-labeled probe P (lanes 1, 2).

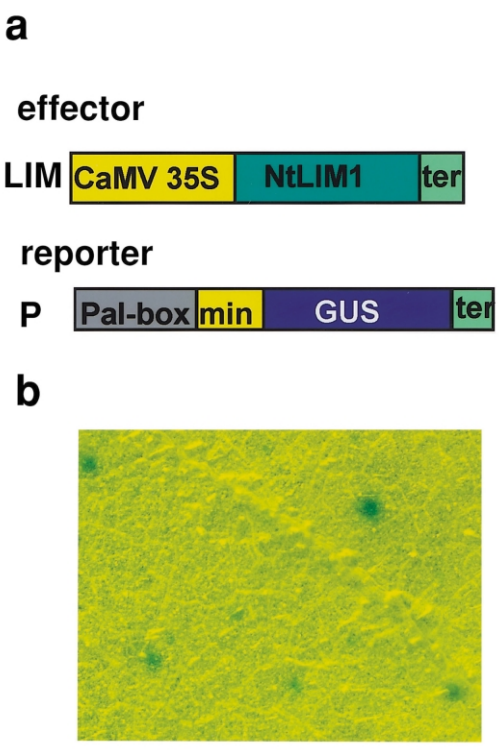

Fig. 4. *trans*-Activation by Ntlim1 in tobacco leaf tissue. (a) Reporter and effector constructs. The construct names are shown at the left side of each construct. Pal-box, three copies of Pal-box like motif; min, 35S promoter truncated at position-90; GUS, uid A coding region; ter, nopaline synthase terminator; CaMV35S, 35S promoter; Ntlim1, sequence encoding full-length Ntlim1. (b) *trans*-Activation of Pal-box sequence by Ntlim1. Effector and reporter constructs were co-introduced into tobacco leaves by particle bombardment, and blue spots indicating GUS activity were measured after 24 h of incubation.

promoter. GFP-LIM and LIM-GFP were translationally ligated to the GFP gene at the N- or C-terminal of Ntlim1, respectively (Fig. 5a). These genes were introduced into tobacco cultured BY-2 cells by particle bombardment. At 48 h after introduction, fluorescence microscopy studies showed both types of fusion proteins at high levels exhibiting bright green mainly in nuclei (Fig. 5b), whereas no green fluorescence was detected in the untransformed BY-2 cells. We also introduced GFP alone into BY-2 cells and strong green fluorescence was observed in the cytoplasm of these cells (data not shown). Ntlim1 appears to be a nuclear protein.

2.3. *Ntlim1* affects gene expression of lignin biosynthesis

To investigate the molecular effects of *Ntlim1* on lignin biosynthesis, a 1.0-kb fragment of *Ntlim1* was inserted in the antisense orientation between the CaMV 35S promoter and the 3′ terminator sequence of the nopaline synthase gene. This construct was introduced into tobacco plants by Agrobacterium-mediated transformation. Twenty independent primary transgenic plants (T1) were produced and all lines contained the respective T-DNA determined by PCR analysis. Subsequently, seven antisense lines were screened by measuring the *Ntlim1* transcript levels in the stems, and were grown to maturity in a greenhouse. Their self-pollinated seeds (T2) were collected and used for further investigation. Ten T2 kanamycin-resistant transgenic plants were grown in a greenhouse. All of them showed a normal growth rate and flowered at similar times. No remarkable abnormal growth or flower color changes were found in the transgenic lines, except that several lines showed a slightly increased stem height. We isolated cDNA clones encoding some of the structural genes, *PAL*, *4CL* and *CAD*, involved in phenylpropanoid biosynthesis from tobacco by PCR. The expression levels of these structural genes, the transgene, and the endogenous *Ntlim1* were estimated by Northern blotting using random-primed probes. Total RNAs were extracted from stems in the kanamycin-resistant T2-transgenic A9 and A19 plants. Signals of the antisense *Ntlim1* gene were not detected in either plant carrying the antisense *Ntlim1*

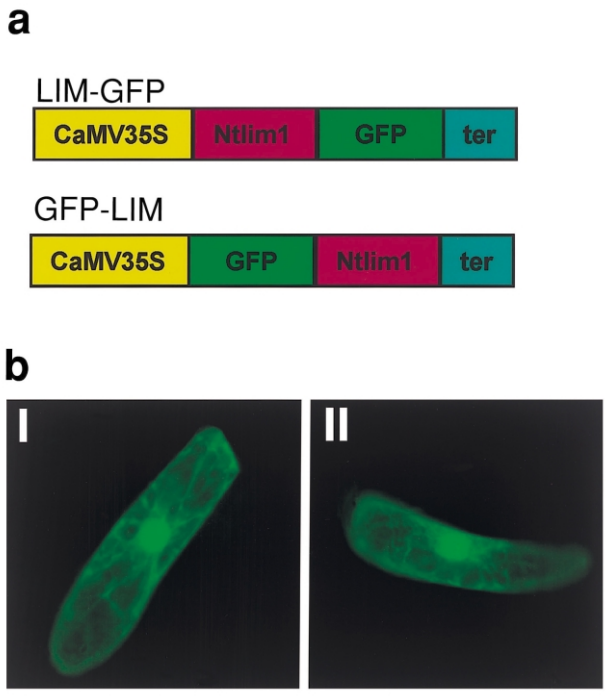

Fig. 5. Localization of the fusion protein between Ntlim1 and GFP. (a) Constructs of the chimeric genes. Two kinds of chimeric plasmids (LIM-GFP and GFP-LIM), under the control of the 35S promoter, were produced. (b) Fluorescence image of LIM-GFP (I) and GFP-LIM (II).

gene. The antisense Ntlim1 transcript is probably unstable in tobacco cells. In antisense plants, endogenous *Ntlim1* (1.2 kb) expression was suppressed and the mRNA levels of *PAL, 4CL* and *CAD* were also lower than those in the wild-type plant (Fig. 6).

To examine the effect of the simultaneous reduction of the transcript levels in many lignin biosynthetic genes, the content and monomeric composition of lignin in transgenic plants were analyzed. The lignin content of the cell wall residue (CWR) of stem xylem tissues was

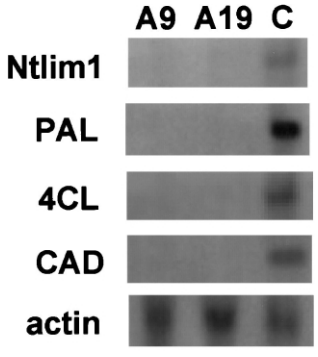

Fig. 6. RNA gel blot analysis showing the expression of genes in the phenylpropanoid biosynthesis pathway. Total RNA was extracted from stems of wild-type (C) and T2-transgenic plants with the antisense (A9 and A19) construct. The transgenic plants were grown in the greenhouse for 10 weeks. Accumulation of the mRNA of *Ntlim1*, *PAL*, *4CL* and *CAD* was investigated.

Table 1
Lignin content in transgenic plants

Line	Lignin content[a]	*S* (μmol/g)[b]	*V* (μmol/g)[b]	*S*/*V*
C	21.2±0.6 (100)	124.4±3.1	157.2±4.8	0.79
A9	15.5±0.3 (73)	31.5±0.9	67.3±3.7	0.47
A19	15.9±0.5 (75)	45.2±4.6	65.7±8.3	0.69

[a] Lignin content is expressed as a percentage (w/w) of cell wall residues (CWR) by Klason lignin.

[b] Syringaldehyde and vanillin were obtained when CWR was treated by the alkaline nitrobenzene oxidation procedure. Values are expressed as μmol per gram of CWR. All values represent the mean ±S.D. of results from the analysis of three to six plants.

measured by the gravimetric Klason procedure. Lignin determinations were carried out on the T2 kanamycin-resistant transgenic line after 10 weeks of growth in a greenhouse. The lignin contents of the basal stem part (5 internodes from the bottom) in the A9, A19 and control plants were measured. Reductions of more than 20% were observed in these antisense plants (Table 1).

To determine the monomeric composition of lignin in the CWR, we examined the CWR from each plant by alkaline nitrobenzene oxidation analysis. Vanillin and syringaldehyde are generated from the non-condensed fraction of lignin by this procedure (Chiang and Funaoka, 1988). Vanillin and syringaldehyde are considered to be derived from guaiacyl and syringyl units in lignin, respectively. The relative abundance of guaiacyl and syringyl units in lignin can be summarized as the S/V ratio (the ratio of the amounts of syringaldehyde and vanillin). The A9 and A19 plants showed lower S/V ratios and decreased amounts of total aldehydes. These results suggest that lignin in the transgenic plants with a decreased expression level of *Ntlim1* contained more condensed units that could not be degraded by oxidation procedures.

3. Discussion

Lignin is the second most abundant polymer on earth after cellulose. Although vital to plant fitness, lignin negatively impacts paper pulp processing and feed for livestock. Much of the cost, complexity and pollution associated with the pulping process is due to the removal of lignin from wood to produce high-quality paper. The regulation of lignin biosynthesis might lead to sizable economic benefits when using woody plants for pulping and forage crops. Transgenic experiments that assess the genes for many steps in this pathway have provided important results indicating the review of this proposal by Whetten et al. (1998).

From the results of transient expression analysis using tobacco protoplasts, the Pal-box like motif has been shown to be a *cis*-acting element for expression of the

basic horseradish peroxidase *prxC2* gene (Kaothien et al., 2000). The Pal-box is a common *cis*-acting element for several phenylpropanoid biosynthetic genes (Boudet, 1998). Antirrhinum *MYB* genes are known to have a Pal-box binding function and to regulate phenylpropanoid biosynthesis (Tamagnone et al., 1998). In this study, we isolated a novel Pal-box binding factor by Southwestern screening from an expression library of tobacco stems. The predicted amino acid alignment of the isolated clone exhibited a high similarity to LIM proteins. The cloned Pal-box motif-binding factor encodes a protein consisting of 200 amino acid residues and shares a 55% identity with sunflower PLIM-1 protein, which is a transcription factor required for the expression of late pollen genes (Baltz et al., 1992). This protein contains a consensus amino acid sequence defined as the LIM domain which is a unique cysteine-rich motif with two zinc fingers connected by a short spacer of invariably two amino acid residues (Dawid et al., 1995). LIM proteins form a diverse group which includes LIM-homeodomain proteins, LIM-only protein and LIM-kinase (Taira et al., 1995). Very little is understood about the function of the LIM proteins in higher plants. The LIM domain may provide an interface for protein-protein interaction (Crawford et al., 1992; Sadler et al., 1992) and the LIM-only protein Lmo2 is part of a sequence-specific DNA-binding complex (Wadman et al., 1997). The sunflower pollen protein PLIM-1 reportedly binds to nucleic acids in vitro, but no specific DNA-binding sequence was described (Baltz et al., 1996). Thus, there is still not enough evidence to suggest that the LIM domain is able to bind to DNA. We have shown that the Ntlim1 protein expressed in *E. coli* binds to a Pal-box like motif in vitro. Furthermore, either the LIM1 or the LIM2 domain was sufficient for its DNA-binding (Kawaoka et al., 2000). The results presented in Fig. 5 indicate that Ntlim1 also bound to the Pal-box motif in vivo. Transient *trans*-activation experiments indicate that *Ntlim1* has a domain that acts as a transcription activator. The most likely candidate for this domain is the C-terminal 37-amino acid acidic polypeptide. No homology to known transcription activation domains has been observed and there are no distinctive features in its amino acid sequence in the C-terminal region of Ntlim1. Random acidic amino acid peptides from *E. coli* have been reported to substitute for the acidic activator domain of Gal4 in yeast (Ma and Ptashne, 1987). The Gal4 activator can activate transcription in tobacco (Ma et al., 1988). Plant transcription factors, such as maize VP1 and Dof1, have acidic domains that function in transcriptional activation in plants (McCarty et al., 1991; Yanagisawa and Sheen, 1998). All of this evidence supports the hypothesis that an acidic domain of Ntlim1 may function in transcriptional activation.

Northern blot analysis showed that at least two genes encoding enzymes of general phenylpropanoid metabolism (*PAL* and *4CL*) and one in the lignin branch (*CAD*) were affected by Ntlim1 at the transcriptional level (Fig. 6). Transgenic plants with the antisense *Ntlim1* showed decreased expression of these genes. Thus, suppression of *Ntlim1* expression could block many steps in phenylpropanoid biosynthesis and Ntlim1 might also regulate the expression of some other genes in this pathway that contain the Pal-box sequence in their promoter regions. The Pal-box has been reported to be a common recognition site of MYB proteins (Grotewold et al., 1994; Douglas, 1996). Overexpression of *AmMYB308* repressed the expression of *C4H*, *4CL* and *CAD* in tobacco, but did not affect the steady-state level of *PAL* transcript (Tamagnone et al., 1998). Different *MYB* factors could coordinately regulate the expression of *PAL* (Tamagnone et al., 1998). Many copies of the *MYB* gene family have been identified in the plant genome and their DNA-binding specificities vary considerably (Martin and Paz-Ares, 1997). From our previous result, the sequence recognized by the Ntlim1 protein is similar to that recognized by MYB proteins, although the last 6 bases in the consensus of the Ntlim1 recognition sequence are not rigid (Kawaoka et al., 2000). Therefore, the discrepancy in the effect on the *PAL* gene expression between Ntlim1 and AmMYB308 protein might result from the smaller difference in their recognition sequences. It is also possible that both Ntlim1 and AmMYB308 proteins are members of the Pal-box binding complex although they compete with each other in binding to the Pal-box. The Ntlim1 may bind to the *PAL* promoter while AmMYB308 does not. To clarify this matter, further analysis of the Pal-box binding complex by an immunological experiment is needed.

The low expression level of *PAL*, *4CL* and *CAD* in the A9 plant with antisense *Ntlim1* resulted in a 27% reduction in its lignin content compared with that in control plants. Several attempts to reduce the lignin content by inhibiting the activity of enzymes in the phenylpropanoid biosynthesis pathway have been reported (Douglas, 1996). Transgenic plants with repressed COMT or CAD activities resulted in a modified lignin structure instead of reduced lignin content, suggesting that neither enzyme limits lignin accumulation (Dwivedi et al., 1994; Halpin et al., 1994). However, a reduced expression of *PAL* or *4CL* has previously been shown to cause lower lignin content and altered lignin composition in transgenic plants (Elkind et al., 1990; Lee et al., 1997). Lignin is an essential component of the plant cell wall and a severe reduction in lignin content ($>40\%$) can cause an abnormal growth phenotype in herbaceous plants. For example, transgenic tobacco with suppression of *PAL* or overexpression of *MYB*-related transcription factors showed an abnormal growth phenotype (Sewalt et al., 1997; Tamagnone et al., 1998). Transgenic tobacco plants with antisense *CCR* showed a 47% reduction in Klason lignin, but normal plant growth was severely

affected (Piquemal et al., 1998). CCoAOMT antisense tobacco plants with up to a 66% reduction in lignin content grew as normally as wild-type plants, but their vessel shape was significantly collapsed (Zhong et al., 1998). However, transgenic aspen trees with down-regulated 4CL and a lignin content reduction of up to 45% exhibited a normal phenotype because the reduction in the lignin content was compensated by an increase in cellulose content (Hu et al., 1999). In this study, we detected no visible abnormal growth in the transgenic tobacco with sense and antisense *Ntlim* and we also found no sign of vessel collapse in the A9 plant with up to 27% reduction in the lignin content. Thus, Ntlim1 may function as a weak activator that helps maintain basal expression of the genes encoding enzymes in the phenylpropanoid biosynthesis pathway which leads to retained basal enzyme activities in lignifying tissues. Our results suggest that genetic engineering of the transcription factor involved in lignin biosynthesis may be an efficient strategy for producing plants with improved pulping characteristics or digestibility.

4. Experimental

4.1. Plant material

Nicotiana tabacum cv Petit Havana SR-1 was used. Tobacco plants were grown in a greenhouse at 25°C under a 16-h light and 8-h dark photo-period.

4.2. Screening of the library and DNA sequencing

Total RNA was isolated from stems of tobacco plants that were grown for 6 weeks in a greenhouse. Using oligo (dT) and random primers, a cDNA library was constructed in λgt11 vector (Stratagene, La Jolla, CA, USA). The amplified library was screened with a digoxigenin (DIG)-labeled double-stranded oligonucleotide fragment that corresponded to a triple repeat of a Pal-box like motif, -CCACTTGAGTAC-. We used essentially the same screening protocol as Singh et al. (1988). An inserted DNA fragment of a positive clone was amplified by polymerase chain reaction using forward and reverse primers for λgt11 vector. The amplified DNA fragment was recloned into pNoTA/T7 vector by PCR Cloner (5 Prime, 3 Prime Inc., Boulder, CO, USA). Sequence analysis was performed on double-stranded DNA templates using a DyeDeoxy™ Terminator Cycle Sequencing Kit (Perkin Elmer, Foster City, CA, USA).

4.3. Expression of Ntlim1 in Escherichia coli

E. coli cells, JM109, carrying the expression vector pGEX-2 TK (Amersham Pharmacia Biotech, Buckinghamshire, UK) containing the cDNA sequence encoding *Ntlim1* were grown to an absorbance at 660 nm of 0.8 in LB broth. IPTG was added to the culture at a final concentration of 1 mM and the cells were cultured at 25°C for an additional 2 h. Cells were harvested by centrifugation and the crude extract was used for purification of the Ntlim1 protein by Glutathione-Sepharose 4B according to the manufacture's instructions (Amersham Pharmacia Biotech).

4.4. Gel retardation assay

The binding reaction was carried out in a 20 μl reaction mixture containing protein, 2 ng of DIG-labeled DNA probe, 10 mM Tris–HCl pH 8.0, 80 mM KCl, 0.016% NP40, 7.5% glycerol, 1 mM DTT, and 1 μg poly (dI-dC)·poly (dI-dC) (Amersham Pharmacia Biotech). The reaction mixtures were pre-incubated at 23°C for 15 min, mixed with radiolabeled DNA probe, and allowed to react for a further 30 min at 23°C. Each sample was applied without dye onto a 5% non-denaturing polyacrylamide gel in 0.5×TBE buffer. Electrophoresis was carried out at 15 V/cm in 0.5×TBE buffer. Following the electrophoresis, the gel was dried and exposed overnight to X-ray film. For a competitive binding assay, excess amounts of non-labeled DNA fragments (competitors) were added to the reaction mixture at the pre-incubation step.

4.5. Plasmid construction of effector

Effector plasmids were constructed under the control of the CaMV 35S promoter in a modified pBI221-mcs plasmid that placed a multi-cloning site into the GUS structural gene. A double-stranded synthetic oligonucleotide based on the synthetic linker III for a multi-cloning site (Malik and Wahab, 1993) was inserted at the *Bam*HI-*Sac*I site in pBI221 (Jefferson et al., 1987). To generate LIM, which has a full-length cDNA of Ntlim1, the *Bam*HI fragment of Ntlim1 was ligated into the same site of pBI221-mcs.

4.6. Construction of reporter plasmids and particle bombardment

The P reporter plasmid was constructed using double-stranded synthetic oligonucleotides. A three-copy sequence of the Pal-box like motif (-CCACTTGAGTAC-) was ligated to the *Eco*RV site at-90 bp of the CaMV 35S promoter. The correctness of orientation of the inserted oligonucleotides was checked by sequencing. Biolistic particle bombardment of the tobacco leaves was carried out following the manufacture's protocol (Bio-Rad, Hercules, CA, USA). GUS activity was assayed by a method described by Jefferson et al. (1987) using X-glucuronide as the substrate.

4.7. GFP fusion plasmids

The GFP coding region was amplified from pbluesGFP(S65T)nos KS (a gift from Yasuo Niwa, University of Shizuoka) using specific primers and transitionally subcloned into the pBI221-mcs with Ntlim1 at the N- or C-terminal. The resulting plasmids, GFP-LIM and LIM-GFP driven by the 35S promoter, were introduced into cultured tobacco BY-2 cells (a gift from Seiichiro Hasezawa and Toshiyuki Nagata, University of Tokyo).

4.8. Transformation of tobacco

Chimeric genes of antisense and sense *Ntlim1* cDNA under the control of the 35S promoter were ligated into the binary vector pBI121 (Clontech, Palo Alto, CA, USA). Tobacco was transformed with *Agrobacterium tumefaciens* LBA4404 (Life Technologies, Rockville, MD, USA) that the binary vector introduced by an electroporation using the leaf disk transformation method (Rogers et al., 1986).

4.9. Isolation of tobacco PAL, 4CL and CAD cDNA clones

Tobacco *PAL*, *4CL* and *CAD* cDNAs were amplified by PCR using the specific primers as described previously (Kawaoka et al., 2000).

4.10. Lignin determinations

Lignin determination was performed on the dried insoluble cell wall residues (CWR) of samples soxhlet-extracted with toluene/ethanol, ethanol, and water. Klason lignin was measured by the method used by Effland (1977). Alkaline nitrobenzene oxidation was performed according to Kajita et al. (1996).

Acknowledgements

We thank Kazuya Yoshida and Pulla Kaothien (Nara Institute of Science and Technology) for their helpful discussions. We are also grateful to Masako Obata, Nippon Paper Industries for her technical advice on lignin analysis.

References

Baltz, R., Domon, C., Pillay, D.T.N., Steinmetz, A., 1992. Characterization of a pollen-specific cDNA from sunflower encoding a zinc finger protein. Plant J. 2, 713–721.

Baltz, R., Evrard, J.-L., Bourdon, V., Steinmetz, A., 1996. The pollen-specific LIM protein PLIM-1 from sunflower binds nucleic acids in vitro. Sex Plant Reprod. 9, 264–268.

Boudet, A.-M., 1998. A new view of lignification. Trends in Plant Sci. 3, 67–71.

Chiang, V.L., Funaoka, M., 1988. The formation and quantity of diphenylmethane type structures in residual lignin during kraft delignification of Douglas-fir. Holzforschung 42, 385–389.

Cramer, C.L., Edwards, K., Dron, M., Liang, X., Dildine, S.L., Bolwell, G.P., Dixon, R.A., Lamb, J., Schuch, W., 1989. Phenylalanine ammonia-lyase gene organization and structure. Plant Mol. Biol. 12, 367–383.

Crawford, A., Michelsen, J.W., Beckerle, M.C., 1992. An interaction between zyxin and α-actinin. J. Cell Biol. 116, 1381–1393.

Dawid, I.B., Toyama, R., Taira, M., 1995. LIM domain proteins. Comptes Rendus heb domadaire des séances de Académie des Sciences, Paris, Science de la Vie/Life Sciences 318, 295–306.

Douglas, C., 1996. Phenylpropanoid metabolism and lignin biosynthesis: from weeds to trees. Trends Plant Sci. 1, 171–177.

Douglas, C., Hoffman, H., Schulz, W., Hahlbrock, K., 1987. Structure and elicitor or UV-light stimulated expression of two 4-coumarate:CoA ligase genes in parsley. EMBO J. 6, 1189–1195.

Dron, M., Clouse, S.D., Dixon, R.A., Lawton, M.A., Lamb, C.J., 1988. Glutathione and fungal elicitor regulation of a plant defense gene promoter in electroporated protoplasts. Proc. Natl. Acad. Sci. USA 85, 6738–6742.

Dwivedi, U.N., Campbell, W.H., Yu, J., Dalta, R.S.S., Bugos, R.C., Chiang, V.L.C., Podila, G.K., 1994. Modification of lignin biosynthesis in transgenic *Nicotiana* though expression of an antisense *O*-methyltransferase gene from Populus. Plant Mol. Biol. 26, 61–71.

Effland, M.J., 1977. Modified procedure to determine acid insoluble lignin in wood and pulp. Tappi 60, 143–144.

Elkind, Y., Edwards, R., Mavandad, M., Hendrick, S.A., Dixon, R.A., Lamb, C.J., 1990. Abnormal plant development and down-regulation of phenylpropanoid biosynthesis in transgenic tobacco containing a heterogous phenylalanine ammonia-lyase gene. Proc. Natl. Acad. Sci. USA 87, 9057–9061.

Feuillet, C., Lauvergeat, V., Deswarte, C., Pilate, G., Boudet, A., Grima-Pettenati, J., 1995. Tissue- and cell-specific expression of a cinnamyl alcohol dehydrogenase promoter in transgenic poplar plants. Plant Mol. Biol. 27, 651–667.

Grotewold, E., Drummoid, B.J., Bowen, B., Peterson, T., 1994. The myb-homologous P gene controls phlobaphene pigmentation in maize floral organs by directly activating flavonoid biosynthetic gene subset. Cell 76, 543–553.

Halpin, C., Knight, M.E., Foxon, G.A., Campbell, M.M., Boudet, A.M., Boon, J.J., Chabbert, B., Tollier, M.-T., Schuch, W., 1994. Manipulation of lignin quality by down regulation of cinnamoyl alcohol dehydrogenase. Plant J. 6, 339–350.

Higuchi, T., 1985. Biosynthesis of lignin. In: Higuchi, T. (Ed.), Biosynthesis and Biodegradation of Wood Components. Academic, pp. 141–160.

Hu, W.-J., Harding, S.A., Popko, J.L., Ralph, J., Stokke, D.D., Tsai, C.-J., Chiang, V.L., 1999. Repression of lignin biosynthesis promotes cellulose accumulation and growth in transgenic trees. Nature Biotech. 17, 808–812.

Jefferson, R.A., Kavanagh, T.A., Bean, M.W., 1987. GUS fusion: β-glucuronidase as a sensitive and versatile gene fusion marker in higher plants. EMBO J. 6, 3901–3907.

Jin, H., Martin, C., 1999. Multifunctionality and diversity within the plant MYB-gene family. Plant Mol. Biol. 41, 577–585.

Kajita, S., Katayama, Y., Omori, S., 1996. Alteration in the biosynthesis in transgenic plants with chimeric genes for 4-coumarate:coenzyme A ligase. Plant Cell Physiol. 37, 957–965.

Kaothien, P., Shimokawatoko, Y., Kawaoka, A., Yoshida, K., Shinmyo, A., 2000. A *cis*-element containing PAL-box functions in the expression of the wound-inducible peroxidase gene of horseradish. Plant Cell Reports 19, 558–562.

Kawaoka, A., Sato, S., Nakahara, K., Matsushima, N., Okada, N., Sekine, M., Shinmyo, A., Takano, M., 1992. Expression and

promoter activity of genes for isozymes of horseradish peroxidase. Plant Cell Physiol. 33, 1143–1150.

Kawaoka, A., Kawamoto, T., Sekine, M., Yoshida, K., Takano, M., Shinmyo, A., 1994. A *cis*-acting element and trans-acting factor involved in the wound-induced expression of a horseradish peroxidase gene. Plant J. 6, 87–97.

Kawaoka, A., Kaothien, P., Yoshida, K., Endo, S., Yamada, K., Ebinuma, H., 2000. Functional analysis of tobacco LIM protein Ntlim1 involved in lignin biosynthesis. Plant J. 22, 289–301.

Lee, D., Meyer, K., Chapple, C., Douglas, C., 1997. Antisense suppression of 4-coumarate:coenzyme A ligase in *Arabidopsis* leads to altered lignin subunit composition. Plant Cell 9, 1985–1998.

Lois, R., Dietrich, A., Hahlblock, K., Schulz, W., 1989. A phenylalanine ammonia-lyase gene from parsley: structure, regulation and identification of elicitor and light responsive *cis*-acting elements. EMBO J. 8, 1641–1648.

Ma, J., Ptashne, M., 1987. Deletion analysis of GAL4 defines two transcriptional activating segments. Cell 48, 847–853.

Ma, J., Prizibilla, E., Hu, J., Bogorad, L., Ptashne, M., 1988. Yeast activators stimulate plant gene expression. Nature 334, 631–633.

Malik, V.S., Wahab, S.Z., 1993. Versatile vector for expressing genes in plants. J. Plant Biochem. Biotech. 2, 69–70.

Martin, C., Paz-Ares, J., 1997. MYB transcription factors in plants. Trends Genet. 13, 67–73.

McCarty, D.R., Hattori, T., Carson, C.B., Vasil, V., Lazar, M., Vasil, I.K., 1991. The viviparous-1 developmental gene of maize encodes a novel transcriptional activator. Cell 66, 895–905.

Mundel, C., Baltz, R., Eliasson, Å, Brooner, R., Grass, N., Kräuter, R., Evrard, J.-L., Steinmetz, A., 2000. A LIM-domain protein from sunflower is located to the cytoplasm and/or nucleus in a wide variety of tissues and is associated with the phragnoplast in dividing cells. Plant Mol. Biol. 42, 291–302.

Ohl, S., Hedrick, S.A., Chory, J., Lamb, C.J., 1990. Functional properties of a phenylalanine ammonia-lyase promoter from *Arabidopsis*. Plant Cell 2, 837–848.

Piquemal, J., Lapierre, C., Myton, K., O'Connell, A., Schuch, W., Grima-Pettenai, J., Boudet, A.-M., 1998. Down-regulation of cinnamoyl-CoA reductase induces significant changes of lignin profiles in transgenic tobacco plants. Plant J. 13, 71–83.

Rogers, S.G., Hoesch, R.B., Fraley, R.T., 1986. Gene transfer in plant: production of transformed plant using Ti plasmid vectors. Meth. Enzymol. 118, 627–640.

Sadler, I., Crawford, A.W., Michelsen, J.W., Beckerle, M.C., 1992. Zyxin and cCRP: two interactive LIM domain proteins associated with the cytoskeleton. J. Cell Biol. 119, 1573–1587.

Sewalt, V.J.H., Ni, W., Blount, J.W., Jung, H.G., Masoud, S.A., Howles, P.A., Lamb, C., Dixon, R.A., 1997. Reduced lignin content and altered lignin composition in transgenic tobacco down-regulated in expression of L-phenylalanine ammonia-lyase or cinnamate 4-hydroxylase. Plant Physiol. 115, 41–50.

Singh, H., Lebowitz, J.H., Baldwin Jr., A.S., Sharp, P.A., 1988. Molecular cloning of an enhancer binding protein: isolation by screening of an expression library with a recognition site DNA. Cell 52, 415–423.

Taira, M., Evrard, J.-L., Steinmetz, A., Dawid, I.B., 1995. Classification of LIM proteins. Trend Genet. 11, 431–432.

Tamagnone, L., Merida, A., Parr, A., Mackay, S., Culianez-Macia, F.A., Roberts, K., Martin, C., 1998. The AmMYB308 and AmMYB330 transcription factors from *Antirrhinum* regulate phenylpropanoid and lignin biosynthesis in transgenic tobacco. Plant Cell 10, 135–154.

Wadman, I.A., Osada, H., Grutz, G.G., Agulnick, A.D., Westphal, H., Foster, A., Rabbitts, T.H., 1997. The LIM-only protein Lmo2 is a bridging molecule assembling an erythroid, DNA-binding complex which includes the TAL1, E47, GATA-1 and Ldb1/NLI proteins. EMBO J. 16, 3145–3157.

Whetten, R.W., MacKay, J.J., Sederoff, R.R., 1998. Recent advances in understanding lignin biosynthesis. Ann. Rev. Plant Physiol. Plant Mol. Biol. 49, 585–609.

Yanagisawa, S., Sheen, J., 1998. Involvement of maize of zinc finger proteins in tissue-specific and light-regulated gene expression. Plant Cell 10, 75–89.

Zhong, R., Morrison, W.H., Negrel, J., Ye, Z.-H., 1998. Dual methylation pathway in lignin biosynthesis. Plant Cell 10, 2033–2045.

PERGAMON

Phytochemistry 57 (2001) 1159–1166

PHYTOCHEMISTRY

www.elsevier.com/locate/phytochem

Antisense and sense expression of cDNA coding for CYP73A15, a class II cinnamate 4-hydroxylase, leads to a delayed and reduced production of lignin in tobacco

Kristopher Blee[a], Joon W. Choi[b], Ann P. O'Connell[a], Steve C. Jupe[a], Wolfgang Schuch[c], Norman G. Lewis[b], G. Paul Bolwell[a,*]

[a]*Division of Biochemistry, School of Biological Sciences, Royal Holloway, University of London, Egham, Surrey, TW20 0EX, UK*
[b]*Institute of Biological Chemistry, Washington State University, Pullman, WA 99164-6340, USA*
[c]*Zeneca Wheat Improvement Centre, Norwich, NR4 7UH, UK*

Received 1 November 2000; received in revised form 30 January 2001

Abstract

A number of plant species contain the class II of genes encoding the cytochrome P450, CYP73, the cognate protein of which cinnamic acid 4-hydroxylase, is the second enzyme of the phenylpropanoid pathway. In order to begin to determine possible functionality, tobacco has been transformed with a truncated French bean class II cinnamate hydroxylase (CYP73A15) in the sense and antisense orientations. Signals for C4H protein could be detected in vascular tissue from wild-type plants using heterologous probes. The transformed plants showed a normal phenotype, even though detectable C4H protein was much reduced in tissue prints. Young propagated transformants displayed a range of reduced C4H activities, as well as either reduced or no phloroglucinol-stainable lignin. However, all mature tobacco plants showed the accumulation of lignin, even though its deposition was apparently delayed. This was not due to induction of tyrosine ammonia-lyase activity, which was not detected, but instead it is presumed due to sufficient C4H residual activity. Analysis of the lignin content of the plants showed reductions of up to 30% with a slightly reduced syringyl to guaiacyl ratio as compared to wild type. This reduction level was favourable in comparison with some other targets in the lignification pathway that have been manipulated including that of class I cinnamate 4-hydroxylase. It is proposed that the class II cinnamate 4-hydroxylase might also function in lignification in a number of species including French bean and tobacco, based on these data. © 2001 Elsevier Science Ltd. All rights reserved.

Keywords: Tobacco; *Nicotiana tabacum*; Solanaceae; Transformation; Cinnamate 4-hydroxylase; Antisense expression; Tyrosine ammonia-lyase; Lignin

1. Introduction

Cinnamate 4-hydroxylase is the second enzyme of the phenylpropanoid pathway and integral to the biosynthesis of the most abundant of the phenolics in vascular plants. It has been identified and classified as a cytochrome P450, CYP73. Molecular cloning of a large number of stress-inducible CYP73 orthologues was achieved initially, but more recently a number of divergent members of the family have appeared in data bases. These divergent members show about 60% sequence similarity to the initially cloned cinnamate 4-hydroxylases enabling them to be classified within the same family. CYP73A15 from French bean falls into this category and was shown to code for a cinnamate 4-hydroxylase following heterologous expression in yeast (Nedelkina et al., 1999). However, it differs from other CYP73s in several domains. It is completely divergent in the N-terminus while three internal domains and the C-terminus are highly divergent. It has thus been classified as a class II C4H. It has not been established hitherto of why there is more than one form of the enzyme. This

Abbreviations: C4H, cinnamate 4-hydroxylase; C4L, cinnamoyl-CoA 4-ligase; CAD, coniferyl alcohol dehydrogenase; CCR, cinnamoyl-CoA reductase; COMT, caffeic acid 3-*O*-methyltransferase; CCOMT, cinnamoyl-CoA *O*-methyltransferase; F5H, ferulate 5-hydroxylase; TAL, tyrosine ammonia lyase

* Corresponding author. Tel.: +44-1784-443553; fax: +44-1784-434326.

E-mail address: uhbc006@vms.rhbnc.ac.uk (G.P. Bolwell).

0031-9422/01/$ - see front matter © 2001 Elsevier Science Ltd. All rights reserved.
PII: S0031-9422(01)00150-9

could be due to multiple forms having evolved to respond to differing developmental and environmental stimuli or it could reflect subtle differences in specificity as has been found for the other cytochrome P450s involved in phenylpropanoid and lignin metabolism (Humphreys et al., 1999; Osakabe et al. 1999).

There is continued interest in modifying lignin content and monomer composition as a means of improving the efficiency of pulp and paper making for quality, economic and environmental reasons (O'Connell et al., 1999). A second target is forage crops since lignin-polysaccharide complexes are anti-nutritional (Boudet et al., 1996).

A considerable number of individual steps in phenylpropanoid and monolignol biosynthesis have now been subjected to antisense and sense supression using tobacco as a model plant with varying results. For example, down-regulation of the class I form CYP73A3 from *Medicago* in tobacco resulted in reduced Klason lignin contents and a decreased syringyl/guaiacyl ratio (Sewalt et al., 1997). In the same study, the preceding enzymatic step, catalysed by phenylalanine ammonia-lyase was also subjected to down-regulation. This also resulted in significant lignin reduction, as well as an increase in the syringyl/guaiacyl (S/G) ratio. Other steps in the phenylpropanoid pathway that have been modified in tobacco include 4CL, COMT, F5H, CCR and CAD. That is, 4-coumarate ligase levels have been genetically manipulated in tobacco (Kajita et al., 1996) and *Arabidopsis* (Lee et al., 1997), as well as with more striking results in aspen (Hu et al., 1999). COMT has also been modified in tobacco where strong down-regulation (Atanassova et al., 1995) led to a drastic reduction of S-units, and detection of 5-hydroxyguaiacyl units but with no overall reduction in lignin. F5H is now believed to act at the level of coniferyl aldehyde (Humphreys et al., 1999; Osakabe et al., 1999, Li et al., 2000) and is responsible for introduction of the final aromatic hydroxyl group for the incorporation of syringyl groups in lignin (Meyer et al., 1996, 1998). CCR has been altered in tobacco (Piquemal et al., 1998), the down-regulation of which led to a reduction in lignin of up to 50% with an increased S/G ratio. CAD, the final enzyme of monolignol biosynthesis, was one of the first to be targetted (Halpin et al., 1994). Manipulation of CAD has been proposed to lead to a type of brown midrib phenomenon due to a reported increase of the incorporation of aldehyde residues into lignin. However, there was no overall reduction in lignin reported.

In order to further evolve such strategies it is necessary to saturate the manipulation of the pathway. Manipulation of several steps have been reported including class I C4H. Preliminary evidence from model systems suggested that the class II C4H might also be related to vascular differentiation rather than stress responses (Nedelkina et al., 1999). This evidence, based on expression in cell cultures undergoing xylogenesis, suggested it was subjected to the same hormonal control thought to be involved in vascular differentiation. In contrast, it was not highly induced by fungal elicitor action, unlike many other CYP73s, particularly, CYP73A2 and A3 which are class I forms. The possible function of the class II enzyme has been investigated in transgenic tobacco by subjecting it to antisense and sense suppression in the present study. Transgenic tobacco already exists expressing antisense CYP73A3. In the latter case, the effects on lignification were significant, considering it resulted in down-regulation of an enzyme early in the pathway (Sewalt et al., 1997). In the case of the class II C4H, lignin analysis has been performed so that its down-regulation may be evaluated in the context of manipulation of other enzymes of the lignin pathway.

2. Results

2.1. Generation of tobacco plants engineered for antisense and partial sense expression of CYP73A15

HD5 is a 1.1 kb clone of CYP73A15 which lacks about 100 amino acids at the N-terminus of the cognate protein including the membrane insertion sequence. Tobacco leaf discs were transformed using *Agrobacterium* strains containing HD5 in antisense or sense orientation inserted into the binary vector pJR1Ri. Initially 24 antisense and 32 partial sense transformants were produced of which 20 of the former and 29 of the latter survived. They were routinely maintained in sterile culture and propagated from cuttings every 3 months. All plants were tested for the presence of the insert using PCR and found to be positive (data not shown). Selected plants were grown through to maturity although all the data in the present work pertains to T_0 transformants.

2.2. Analysis of transgenic tobacco plants

Stems of tobacco plants were analysed at the young plant stage (about 10 cm in height) generated from cuttings and grown under sterile conditions. Mature tobacco was grown under greenhouse conditions for which the stem tissue in the fourth internode was analysed. The young plants were analysed for cinnamate 4-hydroxylase activity (Fig. 1) and for the presence of the enzyme as detected immunologically in tissue prints (Fig. 2). Stem sections from both types of plants were subjected to phloroglucinol and to Mäule staining (Fig. 3). Fig. 1 shows a range of recoverable enzyme activity in young plants or from over 110% to as low as 10%. Although there were no instances of no detectable activity, some lines had a considerable down-regulation of activity.

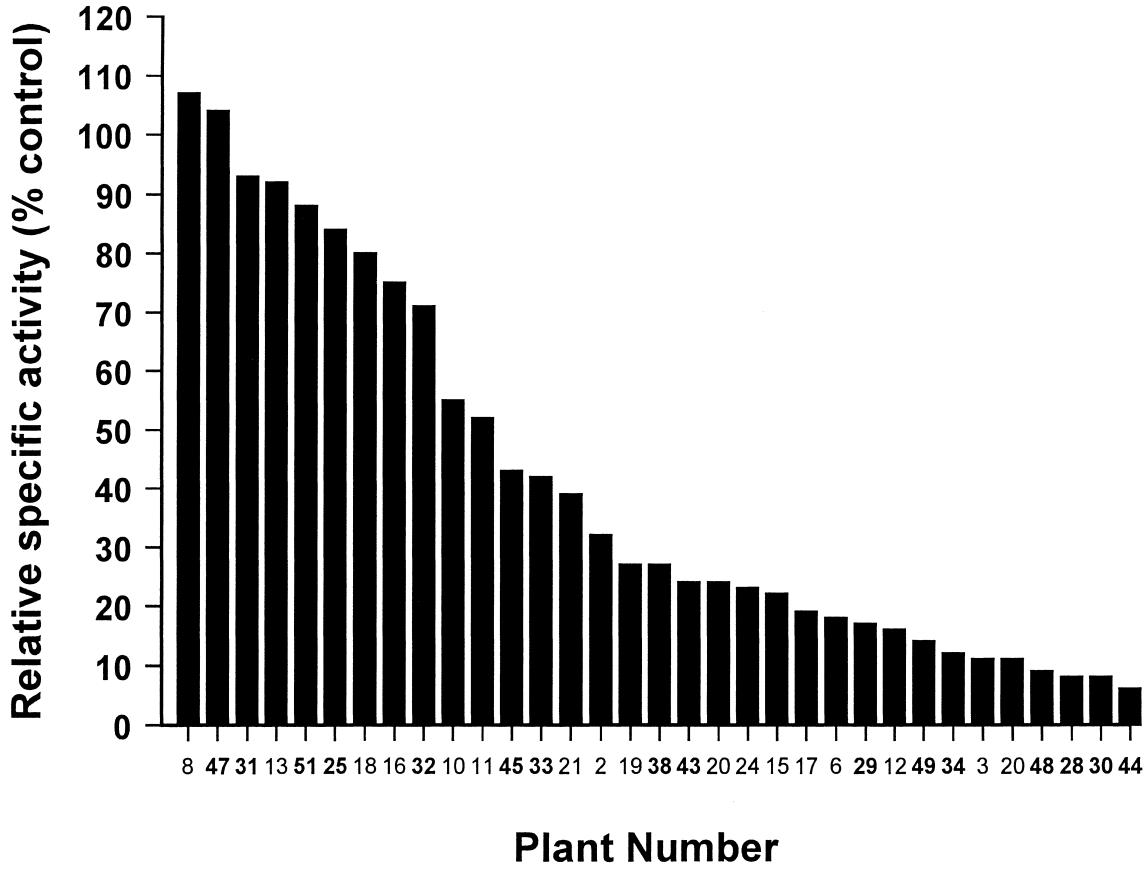

Fig. 1. Range of cinnamate 4-hydroxylase activity in transgenic lines. Activity was determined in stems of regenerated cuttings under sterile conditions. Numbers in plain font are antisense lines; in bold sense lines.

Lines showed activities over the whole range; there was no evidence of clusters or a reduction favoured by antisense or partial sense constructs. Fig. 2 summarises tissue prints of two of these lines, No. 2 (Fig. 2B) and No. 34 (Fig. 2C), which have no immunodetectable C4H subunits even when subjected to extended incubation with substrate compared with wild type (Fig. 2A). However, there is residual activity in these two lines (Fig. 1) so these levels are outside the limits of immunological detection. Some of the young plants showed very low stainable lignin (Fig. 3).

This trend was not found in mature stems. In these samples, enzyme activity was not able to be detected, even though all transgenic lines stained positively for lignin. Compared with young stems there is a delayed accumulation of lignin. In all cases, the red staining in young and mature stems was typical of high syringyl:guaiacyl ratio lignin, which was consistent with the analysis of lignin in these plants.

The possibility that lignin deposition may be due to an induction of tyrosine ammonia-lyase (TAL) activity was examined in young plants and fifth internodes. However, no TAL activity was detected in either the wild type or transgenic plants (data not shown). Hence, even in the down-regulated plants, there must be enough residual C4H activity to allow accumulation of lignin precursors over time and hence synthesis and detection of stainable lignin.

2.3. Analysis of lignin

The total lignin content by the acetyl bromide method (Iiyama and Wallis, 1990) and the syringyl/guaiacyl ratio by thioacidolysis (Lapierre et al., 1986; Rolando et al., 1992) for a number of transgenic lines in comparison with wild type plants is shown for fourth internode sections (Table 1). The wild type lignin is typical for that reported in a number of studies with a lignin content of around 20% and an S/G ratio of 0.85. With the exception of plants Nos. 32 and 45, all transgenic lines showed reduction of lignin content. This was considerable in line No. 30 and compares favourably with other targets for manipulation (Table 2).

3. Discussion

A member of the CYP73 family of plant cytochrome P450s from French bean (CYP73A15) has been identified recently that shows only about 60% sequence similarity

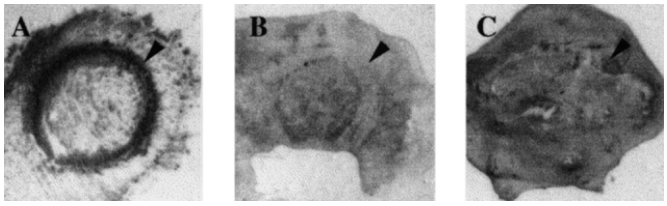

Fig. 2. Tissue prints of control (wild type WT, A) and two transgenic lines (No. 2, B; No. 34, C) using anti-C4H-serum.

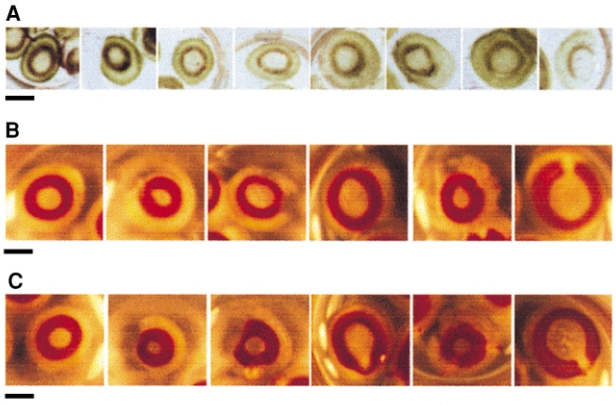

Fig. 3. Lignin staining of control and anti-C4H tobacco. In each case the first image is of WT followed by various lines. A are stems of young seedlings showing reduced lignin staining, B and C are fourth internodes treated with phloroglucinol (B) and the Mäule test (C) reagents respectively. Bar = 400 μm (A), 2500 μm (B and C).

Table 1
Lignin analyses for transgenic tobacco plants: lignin contents and compositions for the fourth internode as determined by acetyl bromide and thioacidolysis methods

Samples, fourth internode of lines	Lignin content (%)	*G* (μmol g^{-1} cell wall residue)	*S* (μmol g^{-1} cell wall residue)	*S*/*G*
C4H WT[a]	20.15±0.12	197.4±25.77	162.1±20.01	0.82
C4H 2	19.04±0.60	219.9±11.85	162.9±11.25	0.74
C4H 10	17.64±0.38	134.2±1.42	130.8±0.49	0.97
C4H 12	18.97±0.67	181.1±8.60	158.2±6.48	0.87
C4H 24	19.22±0.30	205.4±8.87	143.8±5.98	0.70
C4H 30	14.67±0.17	138.6±4.82	114.8±4.34	0.83
C4H 32	20.31±0.36	179.5±6.94	190.2±6.22	1.06
C4H 34	18.36±0.90	176.1±8.89	88.5±4.55	0.50
C4H 38	18.64±0.29	177.8±6.94	148.1±10.38	0.83
C4H 45	20.06±1.22	178.4±7.52	126.7±6.56	0.71
C4H 49	17.87±0.04	150.1±14.62	118.6±13.86	0.79

[a] WT = wild type.

Table 2
Summary of results of manipulations of target enzymes in tobacco

Enzyme	Residual activity (%)	Residual lignin (%)	*S*/*G*	Reference
None (WT)	100	100	0.9	
PAL	16–49	51–83	1–1.5	Sewalt et al., 1997
Class I C4H	33	79	0.6	Sewalt et al., 1997
Class II C4H	10–50	70–90	0.5–1.0	This work
4CL (At)	8–50	65–78	0.5–0.9	Kajita et al., 1996
COMT	2–56	100	0.07–0.5	Atanassova et al., 1995
CCR	10	57	1.7	Piquemal et al., 1998
CAD	10	100	0.4	Halpin et al., 1994
Peroxidase	Isoform only	60–90	0.6–0.9	Blee et al., unpublished data

to class I C4Hs. It is, however, a C4H when expressed in yeast and has been designated a class II C4H (Nedelkina et al., 1999). Although a class I enzyme is also present in tobacco, cross-hybridisation at the stringencies used is unlikely due to lack of sequence similarity. A class II C4H has been identified in tobacco (D. Werck-Reichhart, personal communication). The present work describes successful antisense and sense suppression of C4H activity in tobacco stems in an effort to investigate a possible function of the class II cinnamate 4-hydroxylase in lignification.

Tobacco subjected to expression of the truncated French bean class II C4H regenerated into plants that showed a normal phenotype in common with other targets in lignification (Atanassova et al., 1995; Dwivedi et al., 1994; Halpin et al., 1994; Sewalt et al., 1997) but not all (Piquemal et al., 1998). However, these lines showed reduced activity and immunodetectable C4H, which also somewhat affected lignin content.

Young stems produced by cuttings of T_0 lines and grown under sterile conditions appeared to have a much-reduced lignin content as indicated by staining and in some cases even a lack of phloroglucinol-detectable lignin staining. That is, onset of lignification was apparently developmentally delayed since when plants were transferred to glasshouse conditions, lignin, as exemplified by samples taken from the fourth internode, appeared of normal and near to wild-type composition with respect to colour in the Mäule reaction. However, a detailed analysis of mature stems revealed some lines with reduced lignin content with a slight reduction in S/G ratios, this being similar to the result of manipulating class I C4H with partial sense and antisense CYP73A4 from *Medicago* (Sewalt et al., 1997). Overall the class II C4H proved to be a target for manipulation with similar value to other targets (Table 2).

Inspecting the accumulated data for transformations, it would appear that manipulation of targets in the phenylpropanoid pathway (PAL, C4H and 4CL) in tobacco and *Arabidopsis* reduces the lignin content and, with the exception of PAL, generally shows higher *G* to *S* ratios (Kajita et al., 1996; Sewalt et al, 1997). This may indicate that reduction of flux through the pathway leads to selective depletion of the intermediates that go through to *S* units and *G* units, since there is growing evidence that these pathways may be differentially regulated in different cell types. In contrast, down regulation of enzymes of monolignol biosynthesis (CCR and CAD) leads to limited effects on total lignin but with drastic and opposing changes in S/G ratios (Halpin et al., 1994; Piquemal et al., 1998). However, there is much current debate about the actual flow through the later stages of the pathway and compartmentation. This has centered on CYP84 and its actual substrate, ferulic acid or coniferyl alcohol (Humphreys et al., 1999; Osakabe et al., 1999) and the relative roles of COMT and CCOMT. Since not all these targets have yet been manipulated in tobacco, but rather in *Arabidopsis* and *Populus*, there is not yet one complete inventory of the result of manipulations of all possible targets in one species. The dissection of the polymerization process is complicated by, among other considerations, the number of isoforms of peroxidase and laccase present in any one species. Antisense manipulation of a peroxidase isoform of tobacco did however result in some reduction in lignin (K.R. Blee, J.W. Choi, N.G. Lewis and G.P. Bolwell, unpublished data).

Nevertheless, modest reductions in lignin have commercial and environmental benefits (Baucher et al., 2000). Indeed these studies reveal that the lignin does not need to be reduced to improve significantly the pulping performance as found for CAD and COMT. Furthermore, these results of the present study indicate that in subsequent investigations on manipulation of C4H levels in different species, it will be important to consider that more than one class of C4H may be present. Finally, a combinatorial approach in selection of species for transformation and subsequent manipulation could involve differential targets determining both flux and composition.

4. Experimental

4.1. Materials

[U-^{14}C] tyrosine (16.6 GBq/mmol) and [2-^{14}C] cinnamic acid (2.0 GBq/mmol) were obtained from Amersham. Anti-(cinnamate 4-hydroxylase) serum was obtained as described previously (Smith et al., 1994). The tobacco strain used throughout was *Nicotiana tabacum* cv Samsun.

4.2. Determination of enzyme activity

Phenylalanine ammonia-lyase was determined by the spectrophotometric assay following the production of cinnamic acid at 290 nm. Tyrosine ammonia-lyase activity was determined radiometrically and determination of incorporation into *p*-coumaric acid following separation by TLC. Cinnamate 4-hydroxylase activity was determined radiometrically (Nedelkina et al., 1999).

4.3. Immunological detection of cinnamate 4-hydroxylase

Plant stems were removed and cut transversely with a razor blade and blotted immediately onto nitro-cellulose or nylon membrane pre-wetted with methanol (Cassab and Varner, 1987). The stems were printed for approximately one minute applying some pressure to obtain a good imprint upon the membrane. The prints were then left to air-dry. Immunolocalisation with anti-bean C4H was carried out after first blocking the prints in 25 mM

Tris–HCl (pH 7.5), 0.15 M NaCl (PBS)/4% BSA for 30 min, rinsed in PBS (5×5 min) and then incubated in 1:3000 WGA (Sigma) for 1–2 h. This was followed by further rinses in PBS (5×5 min) and then application of the primary antibody at 1:1000 dilution. The membrane was left shaking overnight followed by rinses in PBS, and then incubated with anti-rabbit IgG-alkaline phosphatase conjugate (2–3 h), followed by washes with PBS/1% Triton. The membrane was colour developed with nitroblue tetrazolium (NBT) and bromo-chloro-indolyl-phosphate (BCIP) in 100 mM Tris–HCl pH 9.5, 100 mM NaCl, 5 mM $MgCl_2$ for 10–30 min.

4.4. Generation of tobacco plants transgenic for *CYP73A15*

The partial CYP73A15 clone HD5 (Nedelkina et al., 1999) was inserted into the binary vector pJR1Ri in antisense and sense orientation. Disarmed *Agrobacterium tumefaciens* LB404 harboring this Bin 19 binary vector was used for all experiments. Within the T-DNA region pBin19 constructs contained kanamycin resistance and, in the reverse orientation with respect to the promoter, the full length HD5 cDNA. CaMV/35S promoter and nopaline synthase terminator were used to regulate expression from the antisense constructs and kanamycin resistance within the T-DNA. The pBin19 also contained a bacterial kanamycin resistance gene for selection. After transformation of *A. tumefaciens* with pBin19 antisense constructs cultures were initiated in 100 ml of Luria-Bertani medium containing 50 μg ml^{-1} kanamycin and allowed to grow 12 h at room temperature with shaking. *A. tumefaciens* cells were collected by centrifugation and resuspended in liquid MS medium. Leaf strips were cut from genetically identical tobacco plants (*Nicotiana tabacum* cv Samsun) generated by vegetative propagation. Leaf strips were incubated in the resuspended *A. tumefaciens* cells for 20 min before being placed on to solid MS medium containing 1 μg ml^{-1} BAP and 0.1 μg ml^{-1} NAA for 2 days. The leaf strips were transferred to solid MS medium containing 1 μg ml^{-1} BAP, 0.1 μg ml^{-1} NAA, 500 μg ml^{-1} carbenicillin, and 100 μg ml^{-1} kanamycin and left for 5 weeks to form shoots. Shoots were excised from the leaf strips and pushed into solid MS medium containing 500 μg ml^{-1} carbenicillin and 100 μg ml^{-1} kanamycin and allowed 4 weeks for rooting. Rooting on selective medium was repeated before transferring rooted plants to solid growth matrix of equal amounts of Minster Economy No3 Compost (Heatherwood Nurseries, Ashington, Wimborne, UK) and Sinclair Growers Potting and Bedding Compost (William Sinclair Horticulture Ltd, Firth Road, Lincoln, UK with 10 ml of Osmocote Plus controlled release fertilizer (Scotts Europe B.V., The Netherlands) in 15 cm pots. The plants were glasshouse grown, watered once daily to field capacity, and received natural lighting.

4.5. Analysis of transgenic plants

DNA was isolated from leaf tissue using the Fast DNA Kit for plants (Bio 101, Carlsbad, CA, USA) and added to Ready to Go PCR beads (Amersham Pharmacia Biotech, Buckinghamshire, UK) with CaMV/35S promoter and nopaline synthase terminator primers 5′-CAATCCCACTATCCTTCGC-3′ and 5′-CATCG-CAAGACCGGCAACAG-3′ respectively. Cycling proceeded after 7 min at 95°C with 40 cycles of 1 min at 95°C, 1 min at 58°C, and 2 min at 72°C.

4.6. Lignin detection

Using a razor blade, 3 freehand sections 2–3 mm in thickness were excised from growing tobacco plant stems approximately 2.5 cm above the soil level, or at agar level for plants still on tissue culture medium. Immediately after being excised, the tissue sections from respective plants were placed in water filled microtiter-plate-wells. Two sets of sections from each plant were collected and then subjected to lignin staining using either the phloroglucinol–HCl or permanganate methodology.

For phloroglucinol–HCl staining, water was first removed and then 0.1% phloroglucinol in 70% ethanol was added. After incubation (15 min), the solution was removed and 18% aqueous HCl was added. The sections remained in this solution until photographs were taken, approximately 50–60 min.

Permanganate staining followed after removal of water from the second set of stem sections to which 0.5% potassium permanganate was added. After incubation for 8 min the sections were rinsed with distilled water and decolorized for 7 min with the addition of 18% aqueous HCl. After removal of the decolorization solution 20% aqueous ammonium hydroxide was added. The sections remained in this solution until photographs were taken, approximately 50–60 min.

4.7. Sample preparation for lignin analysis

The xylem tissues of transgenic tobacco plants were carefully isolated using a scalpel from both the phloem and cortex, respectively, with each ball-milled to a fine powder. The extractives were removed through sequential extraction with water, ethanol and ethanol/toluene (1/1, v/v), using a soxhlet extraction apparatus for each solvent for at least 8 h (Yahiaoui et al., 1998). The resulting extractive-free samples were dried in vacuo and stored in a desiccator until needed.

4.8. Determination of lignin contents by the acetyl bromide method

The method was modified from Iiyama and Wallis, 1990: Samples (4–6 mg) were individually placed in 5 ml

glass vials, containing a solution of 25% (w/w) AcBr in glacial acetic acid (2.5 ml) and perchloric acid (70%, 0.1 ml). Each bottle was sealed with a PTFE-coated silicon cap and placed in an oven at 70°C for 30 min, with each vial swirled gently at 10 min intervals. The resulting solutions were next transferred to volumetric flasks (50 ml), containing 2 M NaOH (10 ml) and glacial acetic acid (12 ml). Each vial was rinsed with a minimum amount of acetic acid, and the solution made up to 50 ml with glacial acetic acid. Each solution was then subjected to UV analysis (280 nm), calibrated against the absorbance of the corresponding blank solution (lacking only sample). Lignin contents were determined by using an absorptivity value for lignin of 20.09 g^{-1} l cm^{-1} for the absorbance at 280 nm. All data were mean values for three determinations.

4.9. Thioacidolysis

S and *G* ratios were determined by thioacidolysis (Lapierre et al., 1986; Rolando et al., 1992): Samples (14–16 mg) were individually dispersed with thioacidolysis reagent (15 ml, 0.2 M BF_3-etherate in a 8.75:1 (v/v) dioxane:ethanethiol) in a 20 ml glass tube fitted with a Teflon-lined screwcap under nitrogen atmosphere. Thioacidolysis was performed by placing each sample in a heating block held at 100°C for 4 h. After cooling the reaction tubes in ice-water, each reaction mixture was individually poured into CH_2Cl_2 (20 ml). Each reaction tube was then rinsed with water (3×5 ml) with the aqueous solutions added to the reaction mixtures. To this was added internal standard (tetracosane C_{24}, ca 0.8 mg) following which, each aqueous phase was adjusted to pH 3–4 with 0.4 M $NaHCO_3$. Each organic phase was next separated by decantation, with the aqueous phases resulting extracted with CH_2Cl_2 (3×30 ml); the combined organic phases were dried (anhydr. Na_2SO_4) and evaporated to dryness.

Each thioacidolysis residue was dissolved in CH_2Cl_2 (2 ml), with an aliquot (20 μl) silylated at room temperature with N,O bis (trimethylsilyl) trifluoroacetamide (BSTFA, 100 μl) in pyridine (40 μl) in a reaction vial (200 μl). The resulting derivatives were applied to a HP 6890 Series GC System equipped with a HP-5 (cross-linked 5% phenyl methyl siloxane, 30 m×0.25 mm× 0.25 μm) column; product identity was established by reference to retention times of authentic silylated standards, and by mass spectrometric analyses using the HP 5973 MS detector (EI mode, 70 eV). Column conditions: 160–250°C at 2°C/min until the final temperature, this being held at 250°C for a further 5 min. For quantitative analyses, authentic standards (G-CHSEt-CHSEt-CH_2SEt and S-CHSEt-CHSEt-CH_2SEt) were used to calculate the response factors for both monomeric *G* and *S* units, respectively. All samples were analyzed in duplicate.

Acknowledgements

We are indebted to Emma Guiney for skillful technical assistance with the transgenic procedures and maintenance of plants used in this study. G.P.B. thanks the BBSRC(UK) for funding; N.G.L. thanks the National Aeronautics and Space Administration (NAG21198) and the United States Department of Energy (DE-FG03-97ER20259) for generous support of this study.

References

Atanassova, R., Favet, N., Martz, F., Chabbert, B., Tollier, M-T., Monties, B., Fritig, B., Legrand, M., 1995. Altered lignin composition in transgenic tobacco expressing *O*-methyltransferase sequences in sense and antisense orientation. The Plant Journal 6, 465–477.

Baucher, M., van Montagu, M., Boerjan, W., 2000. Improvement of wood quality of the pulp and paper industry by genetic modification of lignin biosynthesis in poplar. In: Arencibia, A.D. (Ed.), Plant Genetic Engineering: Towards the Third Millennium. Elsevier, Amsterdam, pp. 215–221.

Boudet, A.M., Goffner, D.P., Grima-Pettenati, J., 1996. Lignins and lignification: recent biochemical and biotechnological developments. Comptes Rendus de l'Académie des Sciences, Séries 3 319, 317–331.

Cassab, G.I., Varner, J.E., 1987. Immunocytolocalization of extensin in developing soybean seed coats by immunogold-silver staining and by tissue printing on nitrocellulose paper. Journal of Cell Biology 105, 2581–2588.

Dwivedi, U.N., Campbell, W.H., Yu, J., Datla, R.S.S., Bugos, R.C., Chiang, V.L., Podila, G.K., 1994. Modification of lignin biosynthesis in transgenic *Nicotiana* through expression of an antisense *O*-methyltransferase gene from *Populus*. Plant Molecular Biology 26, 61–71.

Halpin, C., Knight, M.E., Foxon, G.A., Campbell, M.M., Boudet, A.M., Boon, J.A., Chabbert, B., Tollier, M.-T., Schuch, W., 1994. Manipulation of lignin quality by the down-regulation of cinnamyl alcohol dehydrogenase. The Plant Journal 6, 339–350.

Hu, W.J., Harding, S.A., Lung, J., Popko, J.L., Ralph, J., Stokke, D.D., Tsai, C.J., Chiang, V.L., 1999. Repression of lignin biosynthesis promotes cellulose accumulation and growth in transgenic trees. Nature Biotechnology 17, 808–812.

Humphreys, J.M., Hemm, M.R., Chapple, C., 1999. New routes for lignin biosynthesis defined by biochemical characterization of recombinant ferulate 5-hydroxylase, a multifunctional cytochrome P450-dependent monooxygenase. Proceedings of the National Academy of Science of the United States of America 96, 10045–10050.

Iiyama, K., Wallis, A.F.A., 1990. Determination of lignin in herbaceous plants by an improved acetyl bromide procedure. Journal of Food Science and Agriculture 51, 145–161.

Kajita, S., Katayama, Y., Omori, S., 1996. Alterations in the biosynthesis of lignin in transgenic plants with chimeric genes for 4-coumarate: coenzyme A ligase. Plant Cell Physiology 37, 957–965.

Lapierre, C., Monties, B., Rolando, C., 1986. Thioacidolysis of poplar lignin: identification of monomeric syringyl products and characterization of guaiacyl-syringyl lignin fraction. Holzforschung 40, 113–118.

Lee, D., Meyer, K., Chapple, C., Douglas, C.J., 1997. Antisense suppression of 4-coumarate: coenzyme A ligase activity in *Arabidopsis* leads to altered lignin subunit composition. The Plant Cell 9, 1985–1998.

Li, L., Popko, J.L., Umezawa, T., Chiang, V.L., 2000. 5-hydroxyconiferyl aldehyde modulates enzymatic methylation for syringyl monolignol formation, a new view of monolignol biosynthesis in angiosperms. The Journal of Biological Chemistry 275, 6537–6545.

Meyer, K., Cusumano, J., Somerville, C., Chapple, C., 1996. Ferulate-5-hydroxylase from *Arabidopsis thaliana* defines a new family of cytochrome P450-dependent monoxygenases. Proceedings of the National Academy of Science of the United States of America 93, 6869–6874.

Meyer, K., Shirley, A.M., Cusumano, J.C., Bell-Lelong, D.A., Chapple, C., 1998. Lignin monomer composition is determined by the expression of a cytochrome P-450 monooxygenase in *Arabidopsis*. Proceedings of the National Academy of Science of the United States of America 95, 6619–6623.

Nedelkina, S., Jupe, S.C., Blee, K.A., Schalk, M., Werck-Reichhart, D., Bolwell, G.P., 1999. Novel characteristics and regulation of a divergent cinnamate 4-hydroxylase (CYP73A15) from French bean: engineering expression in yeast. Plant Molecular Biology 39, 1079–1090.

O'Connell, A., Bolwell, G.P., Schuch, W., 1999. The impact of forest tree biotechnology on the pulp and paper-making processes in the 21st century. In: Lindsay, K. (Ed.), Transgenic Plant Research. Harwood, Amsterdam, pp. 175–186.

Osakabe, K., Tsao, C.C., Li, L., Umezawa, T., Carraway, D.T., Smeltzer, R.H., Joshi, C.P., Chiang, V.L., 1999. Coniferyl aldehyde 5-hydroxylation and methylation direct syringyl lignin biosynthesis in angiosperms. Proceedings of the National Academy of Science of the United States of America 96, 8955–8960.

Piquemal, J., Lapierre, C., Myton, K., O'Connell, A., Schuch, W., Grima-Pettenati, J., Boudet, A.M., 1998. Down-regulation of cinnamoyl-CoA reductase induces significant changes of lignin profiles in transgenic tobacco plants. The Plant Journal 13, 71–83.

Rolando, C., Monties, B., Lapierre, C., 1992. Thioacidolysis. In: Methods of Lignin Chemistry. Springer-Verlag, pp. 334–349.

Sewalt, V.J.H., Ni, W., Blount, J.W., Jung, H.G., Masoud, S.A., Howles, P.A., Lamb, C., Dixon, R.A., 1997. Reduced lignin content and altered lignin composition in transgenic tobacco down-regulated in expression of L-phenylalanine ammonia-lyase or cinnamate 4-hydroxylase. Plant Physiology 115, 41–50.

Smith, C.G., Rodgers, M.W., Zimmerlin, A., Ferdinando, D., Bolwell, G.P., 1994. Tissue and subcellular immunolocalisation of enzymes of lignin synthesis in differentiating and wounded hypocotyl tissue of French bean (*Phaseolus vulgaris* L.). Planta 192, 155–164.

Yahiaoui, N., Marque, C., Myton, K.E., Negrel, J., Boudet, A.M., 1998. Impact of different levels of cinnamyl alcohol dehydrogenase down-regulation on lignins of transgenic tobacco plants. Planta 204, 8–15.

PERGAMON

Phytochemistry 57 (2001) 1167–1176

PHYTOCHEMISTRY

www.elsevier.com/locate/phytochem

Repression of *O*-methyltransferase genes in transgenic tobacco affects lignin synthesis and plant growth

Gaëlle Pinçon[a], Stéphane Maury[a], Laurent Hoffmann[a], Pierrette Geoffroy[a], Catherine Lapierre[b], Brigitte Pollet[b], Michel Legrand[a,*]

[a]*Institut de Biologie Moléculaire des Plantes du Centre National de la Recherche Scientifique, Université Louis Pasteur, 12, rue du Général Zimmer, 67084 Strasbourg cedex, France*

[b]*Laboratoire de Chimie Biologique, Institut National Agronomique, 78850 Thiverval-Grignon, France*

Received 17 July 2000; received in revised form 22 January 2001

Abstract

Among the different enzymatic steps leading to lignin biosynthesis, two methylation reactions introduce the methyl groups borne by guaiacyl (G) and syringyl (S) units. Tobacco possesses a complex system of methylation comprising three classes of CCoAOMTs (caffeoyl-CoA-*O*-methyltransferases) and two classes of COMTs (caffeic acid OMTs). Antisense plants transformed with the CCoAOMT sequence alone or fused to COMT I sequence have been produced and compared to ASCOMT I plants in order to study the specific role of each OMT isoform in lignin biosynthesis, plant development and resistance to pathogens. Tobacco plants strongly inhibited in OMT activities have been selected and analyzed. Whereas antisense COMT I plants exhibited no visual phenotype, CCoAOMT repression was shown to strongly affect the development of both single and double transformants: a reduction of plant growth and the alteration of flower development were observed in the most inhibited plants. Lignin analysis performed by Klason and thioacidolysis methods, showed a decrease in the lignin quantity and changes in the lignin structure of ASCCoAOMT and ASCCoAOMT/ASCOMT I transgenics but not in ASCOMT I plants. Inhibition of COMT I in single as well as in double transformed tobacco was demonstrated to decrease S unit synthesis and to provoke the accumulation of 5-hydroxyguaiacyl lignin units. ASCCoAOMT/ASCOMT I tobacco was affected in lignin amount and composition, thus demonstrating additive effects of inhibition of both enzymes. The changes of lignin profiles and the phenotypical and molecular alterations observed in the different transgenic lines were particularly prominent at the later stages of plant development. © 2001 Elsevier Science Ltd. All rights reserved.

Keywords: *Nicotiana tabacum*; Solanaceae; Tobacco; Antisense RNA expression; Lignin; Phenylpropanoid metabolism; *O*-Methyltransferases

1. Introduction

Phenylpropanoid metabolism provides monolignols, the building units of lignin but also a large array of compounds implicated in plant development and interactions of plants with the environment. Among them, there are pigments such as flavonoids, antibiotics (termed phytoalexins) such as isoflavonoids, coumarins and stilbenes, and signals produced by wounded plants that are involved in the recognition of symbionts (*Rhizobium* sp.) and pathogens (*Agrobacterium* sp.). On the other hand, the deposition of phenylpropanoids in the cell wall of resistant hosts has often been implicated in the mechanisms of defense developed by plants toward fungi, bacteria or viruses. In fact, phenolic polymers, esters and amides have been found in increased quantities in the walls of infected cells and participate in cell wall thickening that represents a general response of plants to pathogen attack.

Intense efforts have been made recently aiming at modifying the content and/or the composition of lignin by genetic engineering as a means of improving the pulping process of trees or of increasing digestibility of animal forages (Baucher et al., 1998; Boudet, 1998; Whetten et al., 1998; Grima-Pettenati and Goffner, 1999). The analysis of transgenic plants affected in distinct biosynthetic steps has produced unexpected findings leading to a profound reappraisal of our understanding of the phenylpropanoid metabolic grid (Atanassova et al., 1995; Van Doorsselaere et al., 1995) and suggested the

* Corresponding author. Tel.: +33-3-88-41-72-80; fax: +33-3-88-61-44-42.

E-mail address: michel.legrand@ibmp-ulp.u-strasbg.fr (M. Legrand).

0031-9422/01/$ - see front matter © 2001 Elsevier Science Ltd. All rights reserved.
PII: S0031-9422(01)00098-X

occurrence of alternative pathways (Kajita et al., 1997; Sewalt et al., 1997a,b; Zhong et al., 1998; Hu et al., 1999). In several cases, lignin from transgenic plants was shown to incorporate unusual components, thus demonstrating a certain degree of plasticity in lignin biosynthesis (Halpin et al., 1994; Baucher et al., 1996; Chapple and Carpita, 1998; Ralph et al., 1998; Whetten et al., 1998). Some transgenic plants, affected in lignin biosynthesis, have been reported to display visual phenotypes. For example, transgenic tobacco plants with a strong decrease in phenylalanine ammonia-lyase (PAL) activity had a reduced lignin content and were severely affected in their development (Elkind et al., 1990). Tobacco, poplar and aspen plants depressed in cinnamyl alcohol dehydrogenase (CAD) had a red coloration of the xylem (Halpin et al., 1994; Higuchi et al., 1994; Baucher et al., 1996; Tsai et al., 1998; Lapierre et al., 1999) and tobacco down-regulated for cinnamoyl-CoA reductase (CCR) exhibited an altered development and a reduction of the plant size (Piquemal et al., 1998). In contrast, in transgenic aspen trees transformed with 4-coumarate: CoA ligase (4CL), the reduction of lignin content had no deleterious effect on plant development, perhaps due to a compensatory increase of cellulose synthesis (Hu et al., 1999).

In order to study the impacts of the modification of phenylpropanoid pathway activity, we attempted to repress OMT genes by expressing antisense RNA. Tobacco was transformed with *O*-methyltransferase sequences that had been isolated from cDNA libraries representing transcripts from tobacco leaves infected with tobacco mosaic virus (TMV) (Jaeck et al., 1992; Martz et al., 1998). Lignin of tobacco down-regulated for caffeic acid/5-hydroxyferulic acid *O*-methyltransferase (COMT I) was shown to have a decreased content in S units, an abnormally high content in 5-hydroxy G units and a higher G unit content (Fig. 1). Taken together, these results indicated that COMT I inhibition specifically affected the second methylation step of the pathway and that another enzyme, namely caffeoyl-CoA OMT (CCoAOMT) catalyzed the first methylation reaction leading to G unit synthesis. Tobacco CCoAOMTs have been cloned and shown to belong to a small gene family composed of three distinct classes (Martz et al., 1998; Maury et al., 1999).

Here we report on the production, selection and analysis of tobacco plants transformed by CCoAOMT cDNA alone or by CCoAOMT and COMT I sequences in the antisense orientation. Plant transformation resulted in a strong OMT gene repression whose outcomes were examined at the level of phenylpropanoid gene expression and of whole plant development. It appeared that, whereas the repression of COMT I induced no visual phenotype, the introduction of the antisense CCoAOMT sequence, alone or together with COMT I, provoked important morphological and developmental alterations. Lignin analysis demonstrated that COMT I repression in double transformants induced a profound change in lignin composition with a decreased content of syringyl units and an accumulation of 5-hydroxy G unit, as observed previously in single transformants (Atanassova et al. 1995). CCoAOMT inhibition resulted in lower lignin quantity in transgenics compared to wild plants and had no effect on lignin S unit content. In double antisense tobacco the effects of both gene inhibition on lignin biosynthesis could be observed. In all transgenic lines we have obtained, the consequences of transformation were enhanced when plants aged, thus illustrating the importance of developmental cues in phenyl propanoid metabolism regulation.

2. Results and discussion

2.1. The tobacco system of *O*-methylation

Table 1 schematically presents the *O*-methylation system of tobacco that comprises two classes of COMTs (COMT I and II) and 3 classes of CCoAOMTs, based on sequence analysis of cloned cDNAs (Pellegrini et al., 1993; Jaeck et al., 1996; Martz et al., 1998). The 3 CCoAOMT classes have been recently shown to display different expression patterns and to encode protein isoforms of 27 and 32 kDa (Maury et al., 1999). Concerning COMTs, class I is highly expressed in lignifying tissues whereas COMT II expression is barely detectable in healthy tissues but is strongly induced in leaves hypersensitively reacting to TMV infection (Pellegrini et al., 1993; Jaeck et al., 1996). COMT I is also stimulated by infection but to a lower extent than COMT II (Legrand et al., 1978). Therefore, COMT I is considered primarily involved in lignin biosynthesis and COMT II may be regarded as a pathogenesis-related enzyme that participates in plant defense response to biotic and abiotic stress. Moreover, the promoter of the COMT II gene has been recently shown to be inducible by various chemicals and environmental cues (Toquin, 1999). In vivo, COMT I catalyzes the second methylation step leading to syringyl lignin unit (Fig. 1) and CCoAOMT activity methylates caffeoyl-CoA into feruloyl-CoA.

Fig. 1 summarizes the most striking effects of COMT I inhibition: S unit content was strongly decreased as evidenced by the disappearance of the red coloration observed after Maüle staining of transgenic stem sections and the changes in GC profiles after lignin thioacidolysis (Fig. 1). Recent studies of substrate specificity of tobacco OMTs using recombinant enzymes expressed in *E. coli*, have shown that, in vitro, CCoAOMTs and more surprisingly COMTs, methylate caffeoyl- and 5-hydroxyferuloyl-CoA (Maury et al., 1999). COMT I was also shown to be active with the cognate free acids, aldehydes, and alcohols as substrates, indicating that, in

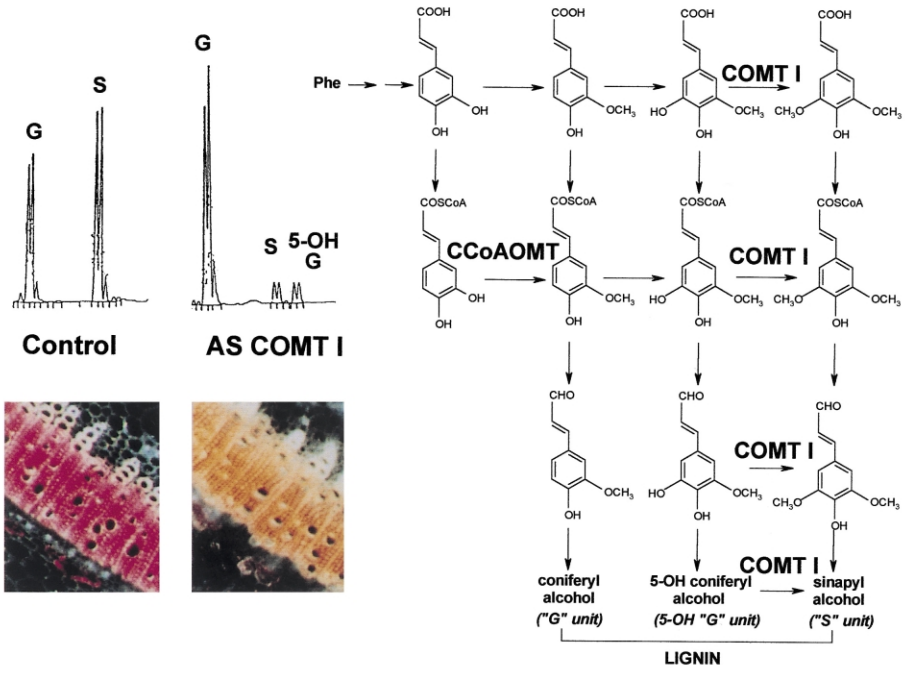

Fig. 1. The role of CCoAOMT and COMT I in lignin synthesis as deduced from the analysis of ASCOMT I tobacco. On the left hand are presented histochemical and chemical analysis data of wild type and transgenic tobacco. The disappearance of the red Maüle coloration of ASCOMT I section compared to control section is due to the decrease of lignin S unit content that is also shown in upper GC profiles obtained after lignin thioacidolysis. The new peaks in transgenic lignin indicate the presence of 5-OH guaiacyl unit. The scheme on the right hand summarizes our current view of the metabolic grid on the basis of recent in vivo and in vitro data.

Table 1
The *O*-methyltransferases of tobacco cDNAs and enzyme isoforms were obtained from TMV-infected tobacco leaves

Class	COMTs		CCoAOMTs		
	I	II	1	2	3
cDNAs	2	1	5	1	1
Isoforms	1	2	1	1	1
Molecular mass (kDa)	39.5	42 + 43	27	27	32

planta, syringyl unit synthesis may operate at the level of free acids, CoA esters, aldehydes or alcohols (Humphreys et al., 1999; Maury et al., 1999; Osakabe et al., 1999). In vitro data showing COMT I activity toward 5-hydroxyconiferyl alcohol were corroborated by the observations of Chen et al, (1999) who demonstrated by in vivo labelling experiments that coniferyl alcohol can be incorporated into the lignin syringyl unit.

2.2. Production of antisense tobacco plants inhibited in OMT gene expression

Agrobacterium tumefaciens was used to transform tobacco plants with the different constructs presented in Fig. 2. The T-DNA of the pBF8 (Atanassova et al., 1995) included between the right (RB) and left (LB) borders, the cloning cassette where the OMT sequence was inserted, the kanamycin resistance gene for transformant selection and the *GUS* gene as a marker of position effects. For the double construct, CCoAOMT and COMT sequences were transcriptionally fused in antisense orientation. Plants transformed with the pFB8 vector without the OMT gene were used as controls. For the different genotypes, populations of in vitro plants were analysed at first and the most strongly inhibited individuals were selected, transferred to the greenhouse and studied further.

2.2.1. Study of the control population

Plants transformed with an empty plasmid (without the OMT gene) constituted the control population. Seventeen 8 week-old in vitro plantlets were tested for CCoAOMT activity and data are presented in Fig. 3A. Large fluctuations in CCoAOMT activity values were recorded, indicating that natural variation of CCoAOMT activity occurs in wild type tobacco as was found previously for COMT I activity (Atanassova et al., 1995). The distribution of enzyme activity values was shown to be normal by Probit analysis, with a mean activity value of 10.7 nkatal/g protein and a standard deviation of 4.4 nkatal/g. The solid line and the two dotted lines in Fig. 3A indicate the mean activity value and standard deviation values of control population, respectively.

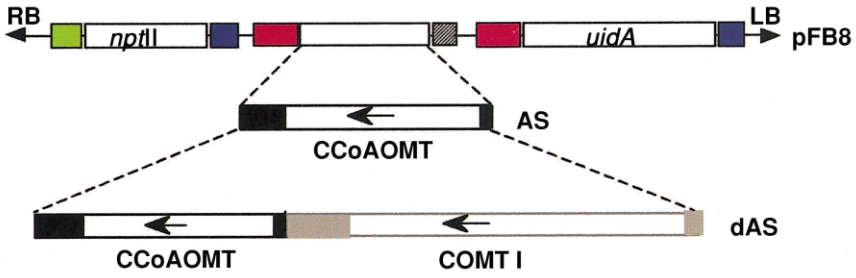

Fig. 2. The pBF8 vector. It contains the *npt* II gene under the control of *nos* promoter (in green) and terminator (in blue) for selection of transformants. The *uid* A (GUS) gene is an internal marker controlled by CaMV 35 S RNA promoter (in red) and the *nos* terminator. Antisense OMT sequences were introduced in the cloning cassette controlled by 35 S RNA promoter and terminator. Untranslated 5 and 3 regions of CCoAOMT and COMT I cDNAs are indicated in black and gray color, respectively. AS: antisense; dAS: double antisense.

2.2.2. Screening of the ASCCoAOMT population

Data of enzyme activity measurements on the population of plants transformed with CCoAOMT are presented in Fig. 3B. Again, some fluctuations were observed, however, 10 individuals had an enzyme activity below the standard deviation of controls indicated by the horizontal dotted line (Fig. 3B). Those particular transformants presented residual activity values of about 20–50% of the mean activity value of controls. In order to check if the decrease of mean CCoAOMT activity in transgenics was due to the repression of CCoAOMT genes, the amounts of enzyme were evaluated in immunoblotting experiments (Fig. 3C). As expected from previous work (Maury et al., 1999) two bands were revealed in control stems (Fig. 3C, control). In the transformants inhibited in CCoAOMT activity the intensity of both bands decreased, indicating that the introduction of one CCoAOMT sequence (member No. 2 of class 1, Martz et al., 1998) in the plant genome repressed the expression of all the members of the tobacco CCoAOMT gene family.

2.2.3. Screening of the ASCCoAOMT/ASCOMT I population

In order to investigate the possibility of obtaining strong and simultaneous inhibitions of both types of OMT in the same tobacco genotype, we transformed plants with the double construct depicted in Fig. 2. Only six double transformants out of 16, rooted and survived on the selection medium. These transformants were tested toward caffeoyl-CoA (Fig. 4B) and caffeic acid (Fig. 4A) as substrates. In vitro substrate specificity studies have shown that caffeic acid is almost exclusively methylated by COMT I but that both CCoAOMT and COMT I accept caffeoyl-CoA as a substrate (Maury et al., 1999). Therefore, enzyme inhibitions were measured at the protein level by western analysis, using antibodies specific for each OMT type (Hermann et al., 1987; Maury et al., 1999). Band intensities were measured by scanning the immunoblots and the relative protein amounts, quantified using imaging software, are presented in Figs. 4C and D. Protein quantities appeared correlated to activity values presented in Fig. 4A and B. Thus, transformation by the double antisense construct proved an efficient means for inhibiting the expression of all the members of CCoAOMT and COMT I gene families of tobacco.

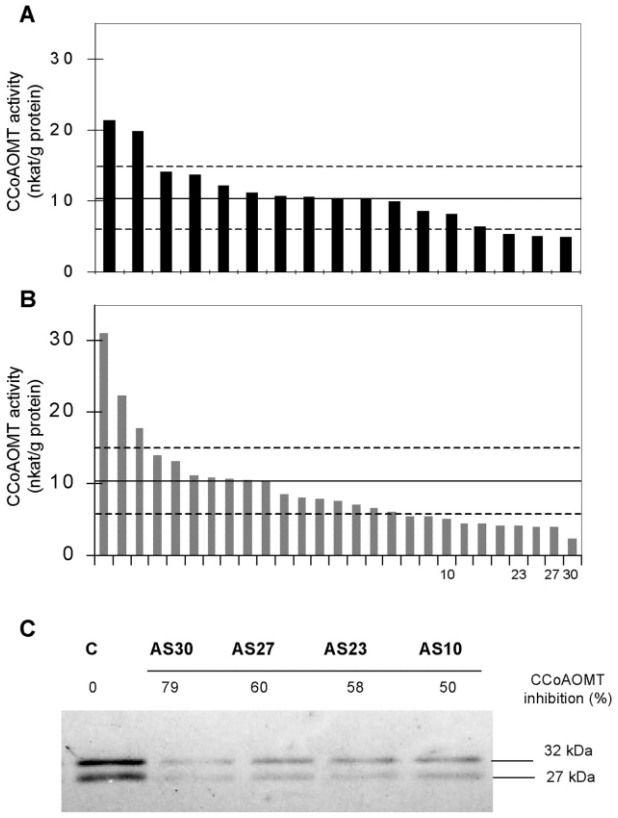

Fig. 3. CCoAOMT expression in control and transgenic population of tobacco plants. The activity value of each individual of control (A) and transgenic (B) population is shown. The solid horizontal line and the dotted lines indicate the mean value and the standard deviation values of control population, respectively. Immunoblotting (C) of controls (c) and of some selected inhibited plants (Nos. 10, 23, 27, 30) revealed 2 bands whose intensity was inversely correlated to CCoAOMT inhibition level.

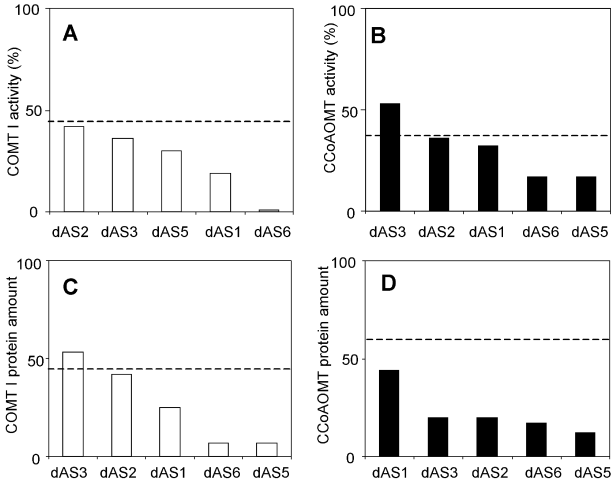

Fig. 4. COMT I and CCoAOMT activity and protein amounts in tobacco plants transformed with the double antisense construct. COMT I; (A) and CCoAOMT; (B) activities were measured with caffeic acid and caffeoyl-CoA as substrate, respectively. Enzyme amounts were calculated from band intensities measured on immunoblots probed with specific antibodies (C) and (D). Values are expressed relative to the mean value of control population taken as 100%. The dotted line in each graph indicates the lower value of standard deviation of control population.

2.3. Impact of OMT gene inhibition on plant development

Transgenic tobacco plants, belonging to the different genotypes and strongly down-regulated in OMT expression, were transferred to the greenhouse for investigating possible impacts of the transformation on plant growth and development. Fig. 5A shows tobacco plants transformed with COMT I, or CCoAOMT or double COMT I/CCoAOMT constructs after three months of growth. Compared to the untransformed controls, B10 (T2) plants which are homozygous for the COMT I transgene, displayed no visible phenotype, in agreement with previous observations carried out on primary transformants (Atanassova et al., 1995). In contrast, a clear reduction of the size of plants transformed with the CCoAOMT sequence alone or the CCoAOMT sequence fused to COMT I sequence, was observed. Growth inhibition was observed for three ASCCoAOMT primary transformants (out of 27) whereas all the six primary double transformants that survived were affected. In fact, the mean stem internode length of these plants was shorter and accounted for their smaller size compared to controls. We noticed that this phenotype was particularly pronounced at the stem extremities i.e. for oldest and youngest tissues of the stem. These effects found in many transformants down-regulated for CCoAOMT are in stark contrast to the results of Zhong et al. (1998) who did not observe any effect of CCoAOMT inhibition in single or double transformants (inhibited for CCoAOMT and COMT I). In those transgenics the important reduction of lignin synthesis did not affect plant growth.

As shown in Fig. 5 leaf and flower development of dAS plants was also affected. Most of the transgenic leaves had a narrower shape (Fig. 5B) and in some cases the stamen of flowers were shorter than those of controls (Fig. 5C). The reduction of stamen size made natural fertilization impossible. However, manual pollination yielded about as many seeds as control flowers, thus indicating that the repression of OMT genes had no impact on fertility.

2.4. Molecular analysis of tobacco transformants

2.4.1. Genetic analysis

To select the primary transformants likely to generate stable transformed lines, we performed genomic analysis of the most inhibited plants by Southern blotting and by analysing the segregation of the kanamycin resistance trait in the progeny obtained by selfing. After plant DNA extraction and digestion with XbaI restriction enzyme, the cut DNA preparations were analyzed by Southern blotting (not shown). Blots were hybridized to an *nptII* probe and the number of radioactive bands measured the number of T-DNA copies integrated into the plant genome. Results obtained for a few ASCCoAOMT primary transformants are presented in Table 2 along with the proportion of plants resistant to kanamycin that were found in the progeny obtained by selfing of those plants. In the three progenies, the ratio was close to 1:3 i.e. the theoretical value expected for the Mendelian segregation of one insertion locus (Table 2). In one case the analysis revealed the presence of two insertions (plant No. 23, Table 2) and for one plant (plant No. 19), resistance trait segregation in the progeny was aberrant and did not allow us to draw any sound conclusion. Genotypes 23 and 30 that were highly inhibited (see Fig. 3) were analysed in the next generation. Analysis of T2 tobacco plants confirmed the presence of one TDNA copy in No. 30 genotype and demonstrated that the two copies detected in transformant No. 23 segregated independently (data not shown). Inhibited monocopy plants have been selected and will be used to produce homozygous seeds.

2.4.2. Enzyme inhibition levels fluctuate during development

Inhibition levels were measured in the 5th internode of stems at the stage of 6 weeks and 12 weeks of development (Fig. 6). Surprisingly enough, at the 6 week developmental stage, CCoAOMT inhibition was lost in transgenic plants which have been selected on the view of their low enzyme activity at the in vitro plantlet stage. When the same genotypes were tested 6 weeks later at the 12 week stage, a high degree of inhibition was recovered (Fig. 6). This was true at the activity and protein levels as evidenced by the decreased intensity of protein bands detected on western blots (not shown). Our data

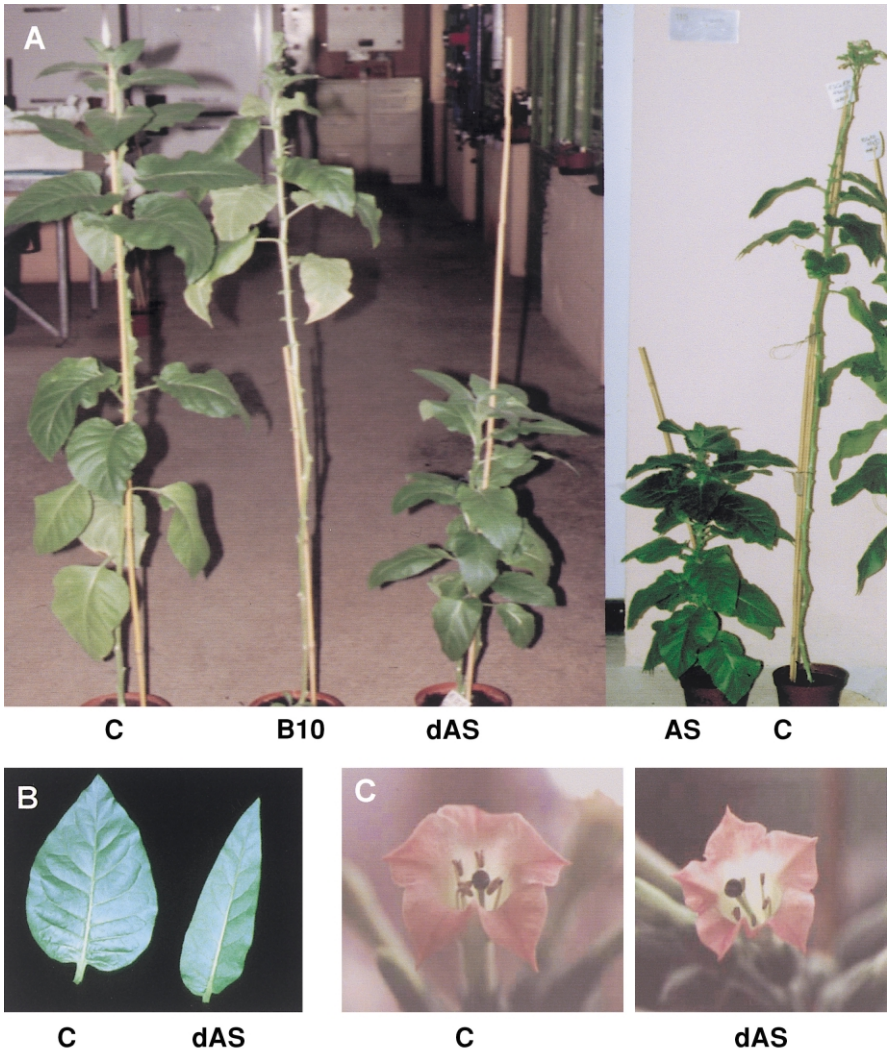

Fig. 5. Phenotypes of tobacco plants inhibited in CCoAOMT or/and in COMT I activity. A: size of transformed and untransformed plants. AS: ASCCoAOMT plants; B10: ASCOMT I plants; dAS: ASCCoAOMT/ASCOMT I plants. B: Effect on leaf shape. C: Effects on flower development.

Table 2
Genetic analysis of ASCCoAOMT plants. The number of inserted T-DNA copies of primary transformants was determined by Southern blotting and the progeny obtained by selfing was analyzed for the segregation of kanamycin resistance

	Plants				
	23	30	27	19	6
Segregation ratio[a]	21/229	82/209	51/164	32/31	67/199
Number of insertions[b]	2	1	1	Nd	1
Number of copies[c]	Nd	1	1	1	1

[a] Number of plants sensitive to kanamycin/number of plants resistant to kanamycin.
[b] Inferred from segregation ratio value; nd: not determined.
[c] Inferred from Southern blot analysis.

illustrate the fact that the molecular analysis of transformants must be performed at different stages of development before sound conclusions can be drawn regarding the relationship between gene expression and any observed phenotype.

2.4.3. CCoAOMT inhibition affects the expression of other phenylpropanoid genes

Previous studies have shown that COMT I repression in antisense tobacco affects CCoAOMT expression (Martz et al., 1998). We investigated whether CCoAOMT inhibition in ASCCoAOMT plants had an effect on the level of expression of COMT I and CAD that are situated downstream in the pathway. To that aim, antisense primary transformants were in vitro propagated and analysed by western blotting. Fig. 7 presents the results obtained for three genotypes that displayed various degrees of CCoAOMT inhibition as illustrated by the

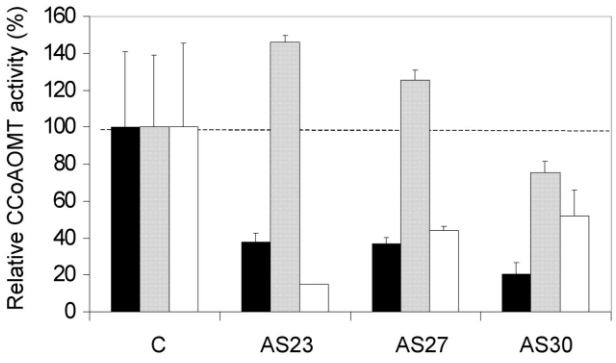

Fig. 6. Variation of inhibition levels during development. CCoAOMT activity is expressed relative to control mean value taken as 100% (c). Enzyme activity was measured in the whole stems of (■) plants grown for 6 weeks in vitro, or in the 5th internode of stems of plants transferred (■) for 6 weeks or for (□) 12 weeks in the greenhouse. Error bars calculated from duplicate values are shown.

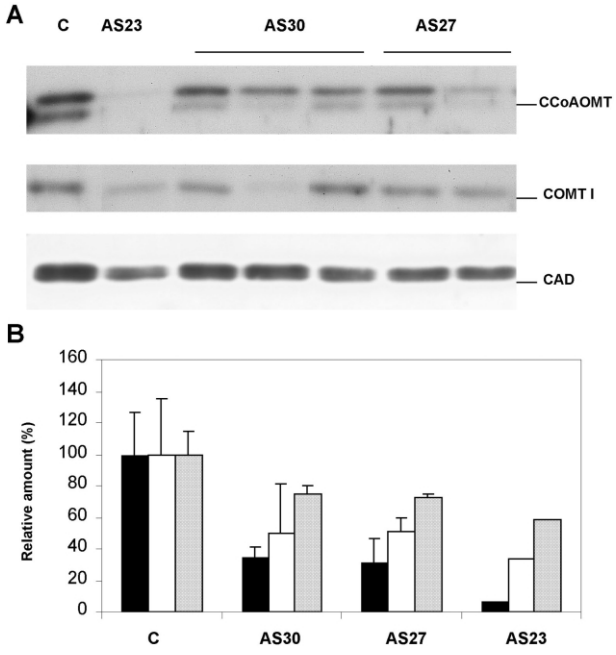

Fig. 7. Effects of CCoAOMT repression on the expression level of other genes of the pathway. Expression levels were estimated after immunoblotting with specific antibodies (A) and relative enzyme quantities were calculated from the band intensity values (B), taking control values (c) as 100%. Controls were assayed in triplicates and one, two or three plants of AS23, AS27 and AS30 genotype respectively, were propagated in vitro and analysed independently. (■) CCoAOMT; (□) COMT I; (■) CAD.

variable intensity of the two CCoAOMT bands detected on the blots probed with specific antibodies (Fig. 7A). In the same samples COMT I and CAD proteins were detected by antibodies raised against COMT I or CAD and their quantities were shown to decrease in plants with low CCoAOMT amounts. This is clearly shown in Fig. 7B, where band intensities were normalized relative to controls (lane c): AS23 genotype that was the most inhibited for CCoAOMT was also the most affected in COMT I and CAD expression. These data indicate that variations of the metabolic flux through the pathway due to the inhibition CCoAOMT affect the expression of COMT I and CAD genes that are downstream in monolignol synthesis. The underlying regulation mechanism is not known and may involve the control of intermediate pool size. Anyhow, the simultaneous repression of several biosynthetic genes would undoubtedly reinforce the effects of the transformation but would also complicate the interpretation of the data. A careful analysis of intermediate pool sizes and of the carbon flow in transgenic plants should bring about new insights into the regulation of phenylpropanoid metabolism.

2.5. Impact on lignin content and composition

Repression of lignin biosynthetic genes has been shown to affect the quantity and/or the quality of the lignin of transgenic plants (for review see Baucher et al., 1998; Boudet, 1998; Whetten et al., 1998). We compared lignin content and composition in untransformed and transformed tobacco genotypes at the age of 12 weeks. As shown in Table 3, CCoAOMT inhibition in single (genotypes 30 and 27) or double transformants (dAS5 plants) resulted in lower Klason lignin amounts. However, the effects on lignin structure were quite different for the two types of transgenics : whereas S unit content and β–*O*–4 bond frequency remained unchanged in ASCCoAOMT plants, the simultaneous inhibition of the two OMTs changed both lignin amount and composition as evidenced by the decrease of S unit and β–*O*–4 bond contents of transgenic lignin (Table 3). The decrease of S unit content in dAS tobacco was accompanied by the accumulation of 5-hydroxyguaiacyl unit (not shown) that is a COMT I inhibition signature (Atanassova et al., 1995; Van Doorsselaere et al., 1995). It is most probably the decrease of lignin synthesis that is responsible for the reduction of growth we observed for these tobacco genotypes (Fig. 5). It is noteworthy that Zhong et al. (1998) obtained tobacco plants displaying 40–60% reduction in lignin content and which grew however normally. In our studies we noticed a reduction of growth rate under greenhouse and in vitro conditions, although lignin content decrease was in about the same range (48% of control value, Table 3). These discrepancies may originate from different growth conditions, the use of different gene vectors or may have another unknown origin. A few cases are known where the diminution of lignin content of transgenic plants has been demonstrated to have negative impacts on the growth rate of transgenic plants (Elkind et al., 1990; Piquemal et al., 1998). Unexpectedly, repression of lignin synthesis in aspen tree transformed with antisense 4-coumarate CoA ligase gene, promoted cellulose accumulation and growth (Hu et al., 1999). This contrasts with what was observed in transgenic tobacco where 4-CoA

Table 3
Lignin analyses for wild type and selected transformants[a]

	Plants	Plant code		
	Control	30	27	dAS5
% Klason lignin	17.4±0.6	16.0±0.7	14.8±0.2	8.4±0.1
% Units only in β–*O*–4 bonds	51.3± 1.4	52.0 ± 3.0	47± 2.0	37.5±1.5
% of S unit in β–*O*–4 bonds	51.3± 1.4	49.6± 3.9	51.3± 1.5	44 ± 1.1

[a] Lignin quantity was evaluated by using the method of Klason and lignin composition was analysed after thioacidolysis. Plants, Nos. 30 and 27 are single transformants (ASCCoAOMT) and dAS5 is a double transformant (ASCCoAOMT/ASCOMT I). Values were calculated from 2 or 3 replicates harvested at the age of 12 weeks.

ligase inhibition provoked the appearance of brownish xylem tissues (Kajita et al., 1997). All these data indicate that phenylpropanoid metabolism repression may have diverse and unpredictable impacts on plant physiology, may be due to the multiple functions of the compounds synthesized through this pathway.

2.5.1. Concluding remarks

We have shown here that the inhibition of CCoAOMT and COMT I gene expression alone or together in transgenic tobacco differently affects lignin synthesis. CCoAOMT inhibition decreases total lignin content whereas COMT I inhibition changes lignin S unit content. In tobacco transformed with a double antisense construct, cumulative effects were observed, both the quantity and the quality of lignin being changed. Changes in lignin composition induced by COMT I inhibition had no impact on plant development in contrast to the multiple effects of CCoAOMT inhibition (Fig. 5).

Lignin has a negative impact on the exploitation of the biomass. Therefore, many attempts have been made recently to modify lignin content and structure by genetic engineering in order to facilitate delignification of paper pulp or to increase digestibility of cattle fodder. CAD inhibition has indeed been shown to change lignin composition (Halpin et al., 1994; Baucher et al., 1996) and in turn to increase lignin extractability (Baucher et al., 1996; Lapierre et al., 1999) and fiber degradability (Bernard-Vailhé et al., 1996a; Sewalt et al., 1997b; Baucher et al., 1999). In contrast, the decrease in S unit content in lignin of COMT I-repressed plants lowered the efficiency of kraft pulping (Lapierre et al., 1999; M. Petit-Conil, personal communication) and increased cell wall degradability (Bernard-Vailhé et al., 1996b).

Phenylpropanoid metabolism is strongly activated upon pathogen attack and participates to the establishment of resistance (Fritig et al., 1972; Legrand et al., 1978; Legrand, 1983; Jaeck et al., 1992). An increased susceptibility toward the fungal pathogen *Cercospora nicotianae* was reported for tobacco repressed in PAL expression, may be due to the inhibition of the developmental accumulation of chlorogenic acid (Maher et al., 1994). However, PAL repressed tobacco was not affected in the hypersensitive response to TMV primary infection (i.e. in lesion development) but did not display systemic acquired resistance toward a secondary TMV infection (Pallas et al., 1996). Transgenic tobacco plants affected in OMT expression displayed variable level of resistance toward virus infection: repression of COMT I or CCoAOMT alone had no detectable impact on antiviral resistance (measured by TMV lesion growth) but double transgenic tobacco developed larger necrotic lesions upon TMV infection (Maury et al., 1999; Hoffmann et al., 2000; Maury, 2000). Analysis of soluble and insoluble phenolic content of healthy or infected tobacco genotypes repressed in different steps of phenylpropanoid synthesis should bring new information about the role of particular phenolics in plant resistance mechanism to a given pathogen.

3. Experimental

3.1. Plant material

Transgenic tobacco plants (*Nicotiana tabacum* cv Samsun NN) were grown in vitro under a light/dark regime of 12 h (24°C)/12 h (20°C) for 6 weeks after germination. The nutritive MS medium contained kanamycin (150 mg/l) as selective agent. The plants were transferred to the greenhouse and cultivated on soil under a light–dark period of 16 h/8 h at 22 ± 2°C.

3.1.1. Vector construction

The binary vector pFB8 was derived from pBI 101 as described by Atanassova et al. (1995) and is shown in Fig. 2. The double construct contained CCoAOMT and COMT I sequences (including 5 and 3 untranslated parts) fused in antisense orientation. The different constructs were introduced into *Agrobacterium tumefaciens* by electroporation and 10 day old tobacco seedlings were transformed by infiltration of agrobacteria (Rossi et al., 1993).

3.1.2. Enzyme assays

Tobacco tissues were ground with a pestle and a mortar in liquid nitrogen and then in 0.1 M sodium phosphate buffer, pH 7.5, 10 mM DTT, containing quartz and polyclar AT (Serva). After centrifugation at

13000 rpm for 15 min at 4°C, the supernatant was filtered on glass wool and tested for OMT activity. COMT I activity was assayed in the presence of 3 mM caffeic acid and 50 μM ^{3}H-SAM (10^5 cpm in 1 ml). After 1 h incubation, 100 μl of 9N H_2SO_4 was added. The reaction product, ferulic acid, was extracted with 5 ml NA scintillation solution (Ready Organic, Beckman) and its radioactivity measured in a Beckman LS 6500 apparatus. For CCoAOMT measurement, 15 μl of enzyme extract was incubated for 15 min at 30°C in the presence of 40 μM caffeoyl-CoA and 40 μM ^{3}H-SAM (40000 cpm in 10 μl). At the end of incubation, ferulic acid was added as a radiochemical carrier and the reaction product, feruloyl-CoA was hydrolyzed with 3 μl of 5 N NaOH for 15 min at 40°C. After the addition of 3 μl of 6 N HCl and 0.2 ml H_2O, ferulic acid was extracted with 0.5 ml EtOAc and counted with MP scintillation solution (Ready Gel, Beckman). Protein was measured by the method of Bradford (1976).

3.1.3. Synthesis of CoA esters

Caffeoyl-CoA and feruloyl-CoA were prepared according to the method of Stöckigt and Zenk (1974) and identified and quantified as described by Lüderitz et al. (1982).

3.1.4. SDS–PAGE and immunoblotting

The basic procedures for electrophoresis under denaturing conditions and for immunoblotting have been described previously (Legrand et al., 1987). Alkaline phosphatase activity was revealed using a chemiluminescent substrate (BioRad CDP-Star). After scanning of the blots with a Argus II AGFA scanner, proteins were quantified using imaging software (MacBAS version 2.2).

3.1.5. Lignin analysis

Lignin quantity was estimated by the Klason method and lignin composition was analysed after thioacidolysis as previously described (Lapierre, 1986).

Acknowledgements

We thank Dr. B. Fritig for continuous support. We are grateful to Dr. C. Halpin (Dundee, UK) for the gift of CAD antibodies. We thank R. Wagner, S. Staerck and M. Kerneis for taking good care of our tobacco plants. This work was supported by the Commission of European Communities (ECLAIR-OPLIGE AGRE 0021 and FAIR-TIMBER CT 95-0424)

References

Atanassova, R., Favet, N., Martz, F., Chabbert, B., Tollier, M.T., Monties, B., Fritig, B., Legrand, M., 1995. Altered lignin composition in transgenic tobacco expressing *O*-methyltransferase sequences in sense and antisense orientation. Plant Journal 8, 465–477.

Baucher, M., Bernard-Vailhé, M.A., Chabbert, B., Besle, J.M., Opsomer, C., Van Montagu, M., Botterman, J., 1999. Down-regulation of cinnamyl alcohol dehydrogenase in transgenic alfalfa (*Medicago sativa L.*) and the effect on lignin composition and digestibility. Plant Molecular Biology 437–477.

Baucher, M., Chabbert, B., Pilate, G., Van Doorsselaere, J., Tollier, M.T., Petit-Conil, M., Cornu, D., Monties, B., Van Montagu, M., Inzé, D., Jouanin, L., Boerjan, W., 1996. Red xylem and higher lignin extractability by down-regulating a cinnamyl alcohol dehydrogenase in poplar. Plant Physiology 112, 1479–1490.

Baucher, M., Monties, B., Van Montagu, M., Boerjan, W., 1998. Biosynthesis and genetic engineering of lignin. Critical Reviews in Plant Science 17 (2), 125–197.

Bernard-Vailhë, M.A., Cornu, A., Robert, D., Maillot, M.-P., Besle, J.-M., 1996a. Cell wall degradability of transgenic tobacco stems in relation to their chemical extraction and lignin quality. Journal of Agricultural and Food Chemistry 44, 1164–1169.

Bernard-Vailhé, M.A., Migné, C., Cornu, A., Maillot, M.P., Grenet, E., Besle, J.M., Atanassova, R., Martz, F., Legrand, M., 1996b. Effect of modification of the O-methyltransferase activity on cell wall composition, ultrastructure and degradability of transgenic tobacco. Journal of the Science of Food and Agriculture 72, 385–391.

Boudet, A.-M., 1998. A new view of lignification. Trends in Plant Science 3 (2), 67–71.

Bradford, M., 1976. A rapid and sensitive method for the quantitation of microgram quantities of protein-dye binding. Analytical Biochemistry 72, 248–254.

Chapple, C., Carpita, N., 1998. Plant cell walls as targets for biotechnology. Current Opinion in Plant Biology 1, 179–185.

Chen, F., Yasuda, S., Fukushima, F., 1999. Evidence for a novel biosynthetic pathway that regulates the ratio of syringyl to guaiacyl residues in lignin in the differentiating xylem of *Magnolia kobus* DC. Planta 207, 597–603.

Elkind, Y., Edwards, E., Mavandad, M., Hedrick, S.A., Ribak, O., Dixon, R.A., Lamb, C.J., 1990. Abnormal plant development and down-regulation of phenylpropanoid biosynthesis in transgenic tobacco containing a heterologous phenylalanine ammonia-lyase gene. Proceeding of the National Academy of Sciences USA 87, 9057–9061.

Fritig, B., Legrand, M., Hirth, L., 1972. Changes in the metabolism of phenolic compounds during the hypersensitive reaction of tobacco to TMV. Virology 47, 845–848.

Grima-Pettenati, J., Goffner, D., 1999. Lignin genetic engineering revisited. Plant Science 145, 51–65.

Halpin, C., Knight, M.E., Foxon, G.A., Campbell, M.M., Boudet, A.M., Boon, J.J., Chabbert, B., Tollier, M.-T., Schuch, W., 1994. Manipulation of lignin quality by down-regulation of cinnamyl-alcohol dehydrogenase. Plant Journal 6, 339–350.

Hermann, C., Legrand, M., Geoffroy, P., Fritig, B., 1987. Enzymatic synthesis of lignin: purification to homogeneity of the three *O*-methyltransferases of tobacco and production of specific antibodies. Archives of Biochemistry and Biophysics 253, 367–376.

Higuchi, T., Ito, T., Umezawa, T., Hibino, T., Shibata, D., 1994. Red-brown color of lignified tissues of transgenic plants with antisense CAD gene: wine-red lignin from coniferyl aldehyde. Journal of Biotechnology 37, 151–158.

Hoffmann, L., Maury, S., Pinçon, G., Geoffroy, P., Fritig, B., Legrand, M., 2000. Impacts of the repression of phenylpropanoid synthesis on development and disease resistance of transgenic tobacco. 6th International Congress of Plant Molecular Biology, Québec, Canada, 18–24 June.

Hu, W.-J., Harding, S.A., Lung, J., Popko, J.L., Ralph, J., Stokke, D.D., Tsai, C.-J., Chiang, V.L., 1999. Repression of lignin biosynthesis promotes cellulose accumulation and growth in transgenic trees. Nature Biotechnology 17, 808–812.

Humphreys, J.M., Hemm, M.R., Chapple, C., 1999. New routes for lignin biosynthesis defined by biochemical characterization of recombinant ferulate 5-hydroxylase a multifunctional cytochrome P450-dependent mono-oxygenase. Proceedings of the National Academy of Sciences of the United States of America 96, 10045–10050.

Jaeck, E., Dumas, B., Geoffroy, P., Favet, N., Inze, D., Van Montagu, M., Fritig, B., Legrand, M., 1992. Regulation of enzymes involved in lignin biosynthesis, induction of *O*-methyltransferase mRNAs during the hypersensitive reaction of tobacco to tobacco mosaic virus. Molecular Plant–Microbe Interactions 5, 294–300.

Jaeck, E., Martz, F., Stiefel, V., Fritig, B., Legrand, M., 1996. Expression of class I *O*-methyltransferase in healthy and TMV-infected tobacco. Molecular Plant–Microbe Interactions 9, 681–688.

Kajita, S., Hishiyama, S., Tomimura, Y., Katayama, Y., Omori, S., 1997. Structural characterization of modified lignin in transgenic tobacco plants in which the activity of 4-coumarate:coenzyme A ligase is depressed. Plant Physiology 114, 871–879.

Lapierre, C., 1986. Thioacidolysis of poplar lignins: identification of monomeric syringyl products and characterization of guaiacyl-syringyl rich fractions. Holzforschung 40, 113–118.

Lapierre, C., Pollet, B., Petit-Conil, M., Toval, G., Romero, J., Pilate, G., Leplé, J.-C., Boerjan, W., Ferret, V., De Nadai, V., Jouanin, L., 1999. Structural alterations of lignins in transgenic poplars with depressed cinnamyl alcohol dehydrogenase or caffeic acid O-methyltransferase activity have an opposite impact on the efficiency of industrial kraft pulping. Plant Physiology 119, 153–163.

Legrand, M, 1983. Phenylpropanoid metabolism and its regulation in disease. In: Callow, J.A. (Ed.), Biochemical Plant Pathology. John Wiley & Sons, Chichester, pp. 367–384.

Legrand, M., Fritig, B., Hirth, L., 1978. *o*-Diphenol *O*-methyltransferases of healthy and tobacco-mosaic-virus infected hypersensitive tobacco. Planta 144, 101–108.

Legrand, M., Kauffmann, S., Geoffroy, P., Fritig, B., 1987. Biological function of pathogenesis-related proteins: four tobacco pathogenesis-related proteins are chitinase. Proceedings of the National Academy of Sciences of the United States of America 84, 6750–6754.

Lüderitz, T., Shatz, G., Grisebach, H., 1982. Enzymic synthesis of lignin precursors: purification and properties of 4-coumarate:CoA ligase from cambial sap of spruce (*Picea albies* L.). European Journal of Biochemistry 123, 583–586.

Maher, E.A., Bate, N.J., Elkind, Y., Dixon, R.A., Lamb, C., 1994. Increase disease susceptibility of transgenic tobacco plants with suppressed levels of preformed phenylpropanoid products. Proceedings of the National Academy of Sciences of the United States of America 91, 7802–7806.

Martz, F., Maury, S., Pinçon, G., Legrand, M., 1998. cDNA cloning, substrate specificity and expression study of tobacco caffeoyl-CoA 3-O-methyltransferase, a lignin biosynthetic enzyme. Plant Molecular Biology 36, 427–437.

Maury, S., 2000. Etude des *O*-méthyltransférases de la voie des Phénylpropanoïdes chez le Tabac et Modulation de leur Expression dans des Tabacs Transgéniques:Conséquences sur la Biosynthèse de la Lignine et d'autres Composés Phénoliques et sur la Résistance aux Agents Pathogénes. Thése de doctorat. Université Louis Pasteur, Strasbourg.

Maury, S., Geoffroy, P., Legrand, M., 1999. Tobacco *O*-methyl transferases involved in phenylpropanoid metabolism: the different CCoAOMT and COMT classes have distinct substrate specificities and expression patterns. Plant Physiology 121, 215–224.

Osakabe, K., Tsao, C.C., Li, L., Popko, J.L., Umezawa, T., Carraway, D.T., Smeltzer, R.H., Hoshi, C.P., Chiang, V.L., 1999. Coniferyl aldehyde 5-hydroxylation and methylation direct syringyl lignin biosynthesis in angiosperms. Proceedings of the National Academy of Sciences USA 96, 8955–8960.

Pallas, J.A., Paiva, N.L., Lamb, C., Dixon, R.A., 1996. Tobacco plants epigenetically suppressed in phenylalanine ammonia-lyase do not develop systemic acquired resistance in response to infection by tobacco mosaic virus. Plant Journal 10, 281–293.

Pellegrini, L.O.G., Geoffroy, P., Fritig, B., Legrand, M., 1993. Molecular cloning and expression of a new class of ortho-diphenol-*O*-methyltransferases induced in tobacco leaves by infection or elictor treatment. Plant Physiology 103, 509–517.

Piquemal, J., Lapierre, C., Myton, K., O'Connell, A., Schuch, W., Grima-Pettenati, J., Boudet, A.M., 1998. Down-regulation of cinnamoyl-CoA reductase induces significant changes of lignin profiles in transgenic tobacco plants. Plant Journal 13, 71–83.

Ralph, J., Hatfield, R., Piquemal, J., Yahiaoui, N., Pean, M., Lapierre, C., Boudet, A.M., 1998. NMR characterization of altered lignins extracted from tobacco plants down-regulated for lignification enzymes cinnamyl alcohol dehydrogenase and cinnamoyl-CoA reductase. Proceedings of the National Academy of Sciences of the United States of America 95, 12803–12808.

Rossi, L., Escudero, J., Hohn, B., Tinland, B., 1993. Efficient and sensitive assay for T-DNA dependent transient gene expression. Plant Molecular Biology Reporter 11, 220–229.

Sewalt, V.J.H., Ni, W., Blount, J.W., Jung, H.G., Masoud, S.A., Howles, P.A., Lamb, C., Dixon, R.A., 1997a. Reduced lignin content and altered lignin composition in transgenic tobacco down-regulated ihn expression of L-phenylalanine ammonia-lyase or cinnamate 4-hydroxylase. Plant Physiology 115, 41–50.

Sewalt, V.J.H., Ni, W., Jung, H.G., Dixon, R.A., 1997b. Lignin impact on fiber degradation: increases enzymatic digestibility of genetically engineered tobacco (*Nicotiana tabacum*) stems reduced in lignin content. Journal of Agricultural and Food Chemistry 45, 1977–1983.

Stöckigt, J., Zenk, M.H., 1974. Enzymatic synthesis of chlorogenic acid from caffeoyl-CoA and quinic acid. FEBS Letters 42, 131–133.

Toquin, V., 1999. Analyse de la Structure et de l'Expression d'un Gène d'O-Méthyltransférase de Tabac. Etude de l'Activité du Promoteur dans des Plantes Transgéniques. Thèse de doctorat. Université Louis Pasteur, Strasbourg.

Tsai, C.-J., Popko, J.L., Mielke, M.R., Hu, W.-J., Podila, G.K., Chiang, V.L., 1998. Suppression of *O*-methyltransferase gene by homologous sense transgene in quaking aspen causes red-brown wood phenotypes. Plant Physiology 117, 101–112.

Van Doorsselaere, J., Baucher, M., Chognot, E., Chabbert, B., Tollier, M.T., Petit-Conil, M., Leplé, J.C., Pilate, G., Cornu, D., Monties, D., Van Montagu, M., Inzé, D., Boerjan, W., Jouanin, L., 1995. A novel lignin in poplar trees with a reduced caffeic acid/5-hydroxyferulic acid *O*-methyltransferase activity. Plant Journal 8, 855–864.

Whetten, R.W., MacKay, J.J., Sederoff, R.R., 1998. Recent advances in understanding lignin biosynthesis. Annual Review of Plant Physiology Plant Molecular Biology 49, 585–609.

Zhong, R., Morrison, W.H., Negrel, J., Ye, Z.H., 1998. Dual methylation pathway in lignin biosynthesis. Plant Cell 10, 2033–2046.

PERGAMON

Phytochemistry 57 (2001) 1177–1185

PHYTOCHEMISTRY

www.elsevier.com/locate/phytochem

Caffeoyl coenzyme A *O*-methyltransferase and lignin biosynthesis

Zheng-Hua Ye[a,*], Ruiqin Zhong[a], W. Herbert Morrison III[b], David S. Himmelsbach[b]

[a]*Department of Botany, University of Georgia, Athens, GA 30602, USA*

[b]*Richard B. Russell Agriculture Research Center, US Department of Agriculture, Agriculture Research Service, Athens, GA 30604, USA*

Received 7 July 2000; received in revised form 3 October 2000

Abstract

Lignin, a complex phenylpropanoid compound, is polymerized from the monolignols *p*-coumaryl alcohol, coniferyl alcohol and sinapyl alcohol. These three monolignols differ only by the 3- and 5-methoxyl groups. Therefore, enzymatic reactions controlling the methylations of the 3- and 5-hydroxyls of monolignol precursors are critical to determine the lignin composition. Recent biochemical and transgenic studies have indicated that the methylation pathways in monolignol biosynthesis are much more complicated than we have previously envisioned. It has been demonstrated that caffeoyl CoA *O*-methyltransferase plays an essential role in the synthesis of guaiacyl lignin units as well as in the supply of substrates for the synthesis of syringyl lignin units. Caffeic acid *O*-methyltransferase has been found to essentially control the biosynthesis of syringyl lignin units. These new findings have greatly enriched our knowledge on the methylation pathways in monolignol biosynthesis. © 2001 Elsevier Science Ltd. All rights reserved.

Keywords: Caffeoyl CoA *O*-methyltransferase; Caffeic acid *O*-methyltranferase; Guaiacyl lignin units; Syringyl lignin units; Lignin biosynthesis

1. Introduction

The ability for plants to make lignin, a complex phenylpropanoid polymer, was thought to evolve when land plants first emerged on the land from aquatic environments (Raven et al., 1999). Lignin provides the mechanical strength to the walls of conducting tracheary elements (TEs) for enduring the negative pressure generated from transpiration. It also renders the walls of maturing TEs undigestible by hydrolytic enzymes released during autolysis of xylogenesis. In addition, deposition of lignin in the walls of sclerenchyma cells, which adds physical toughness and chemical durability to the wall, may deter feeding by herbivores. Lignin is often deposited at the sites of wounding or pathogen invasion, which may provide a physical barrier for protection of adjacent tissues from further damage.

Lignin is polymerized from three monolignols, *p*-coumaryl alcohol, coniferyl alcohol, and sinapyl alcohol, of which the proportions differ among plants. These monolignols are synthesized through the common phenylpropanoid biosynthetic pathway. Since the first elucidation of the pathway through tracer experiments, many enzymes and the corresponding genes involved in the phenylpropanoid pathway have been identified and characterized in detail. These biochemical and molecular analyses confirmed the existence of enzymes carrying out each step in the pathway. However, in the last decade, we have seen some significant modifications of the lignin biosynthetic pathway. It has been found that caffeoyl coenzyme A (CoA) *O*-methyltransferase (CCo AOMT) is essential for lignin biosynthesis (Ye et al., 1994), and caffeic acid *O*-methyltransferase (COMT) controls the synthesis of syringyl lignin units (Atanassova et al., 1995; Van Doorsselaere et al., 1995; Li et al., 2000). It has also been shown that ferulic acid 5-hydroxylase (F5H), which was traditionally thought to use ferulic acid as its substrate, preferentially converts coniferaldehyde and coniferyl alcohol into 5-hydroxyconiferaldehyde and 5-hydroxyconiferyl alcohol, respectively (Humphreys et al., 1999; Osakabe et al., 1999; Li et al., 2000). We have seen breakthroughs in understanding of the process controlling monolignol polymerization. It has been discovered that a group of proteins named dirigents may control the coupling of monolignols in a stereoselective manner (Davin et al., 1997; Davin and Lewis, 2000). All these new findings have greatly enriched our knowledge on the biosynthesis of lignin. It is clear that our quest on lignin biosynthesis

* Corresponding author. Fax: +1-706-542-1832.
E-mail address: ye@dogwood.botany.uga.edu (Z.-H. Ye).

0031-9422/01/$ - see front matter © 2001 Elsevier Science Ltd. All rights reserved.
PII: S0031-9422(01)00051-6

is far from the end. We are still not clear how monolignols are exported from the cytosol to the wall, and once they are in the wall, how they are polymerized into the ordered structure. We know little about the regulatory mechanisms controlling the coordinate expression of genes involved in the lignin biosynthetic pathway. Further study of these issues will not only satisfy our curiosity about the synthesis of lignin, the second most abundant natural product on earth, but also help to develop ideal strategies for genetic engineering of lignin biosynthesis in order to reduce pollution from pulping and increase digestibility of forage crops. In this short review, we will focus on the role of CCoAOMT in the biosynthesis of lignin. One can find some recent comprehensive reviews on lignin by Boudet (1998), Whetten et al. (1998), Lewis (1999), and Sederoff et al. (1999).

2. Early view on the methylation pathway in lignin biosynthesis

Recent biochemical and molecular studies have strongly suggested that methylation of the 3-hydroxyl group of hydroxycinnamates occurs on the CoA ester form, instead of on the free acid form. Although this is an important finding in lignin biosynthesis, this new view can trace back to the early proposed methylation pathway by Neish (1968). Neish put forward a lignin biosynthetic pathway in which the carboxyl group was first activated on cinnamic acid or on *p*-coumaric acid, and the subsequent reactions including methylation occurred on the ester forms. This pathway was proposed based on the following lines of evidence. First, ester forms of *p*-coumaric acid, caffeic acid, and ferulic acid were detected in plants (El-Basyouni et al., 1964; El-Basyouni and Neish, 1966; Brown, 1966, 1969). Second, the free acids would tend to be insoluble in the acidic environment, so the ester forms would be preferred intermediates (Brown, 1969). However, this proposed methylation pathway using the ester forms instead of the acid forms was largely neglected since then. In the subsequent literature, it was proposed that methylation of the 3- and 5-hydroxyl groups occurred at the acid forms of hydroxycinnamates (summarised in Lewis and Yamamoto, 1990). This probably resulted from the identification of the *O*-methyltransferase (OMT) capable of using caffeic acid and 5-hydroxyferulic acid as substrates. The view that COMT was the sole OMT involved in lignin biosynthesis was not challenged until the identification of CCoAOMT using caffeoyl CoA as its substrate.

3. First identification of CCoAOMT in parsley and carrot

CCoAOMT was first identified in parsley and carrot cultured cells challenged with fungal elicitors (Matern et al., 1988; Kühnl et al., 1989; Pakusch et al., 1989). CCoAOMT from parsley and carrot specifically methylates caffeoyl CoA (Fig. 1) but not caffeic acid. Identification of CCoAOMT led Kühnl et al. (1989) to question the conventional view of methylation reactions on the acid forms and they proposed roles of CCoAOMT in the biosynthesis of phenylpropanoid-derived compounds such as lignin. However, this proposal was not immediately recognized due to lack of substantial evidence for the involvement of CCoAOMT in lignin biosynthesis. First, CCoAOMT in the cultured cells induced by fungal elicitors was thought to play a role in defense because no lignin was detected in treated cells (Pakusch et al., 1989). Second, no correlative evidence was available to suggest that CCoAOMT expression was associated with lignification. The importance of CCoAOMT in lignin biosynthesis was not realized until the finding that CCoAOMT was specifically expressed in all lignified cells in Zinnia.

4. Ubiquitous distribution of CCoAOMT in plants

After identification of the elicitor-inducible CCo AOMT in parsley and carrot, Schmitt et al. (1991) purified CCoAOMT, sequenced its peptides, and finally cloned CCoAOMT cDNA from parsley using probes based on the peptide sequence. Based on their homology to the parsley CCoAOMT, CCoAOMT cDNAs and genomic DNAs have been isolated from a number of other plants such as zinnia, quaking aspen, poplar, tobacco, alfalfa, pine, *Arabidopsis*, maize, eucalyptus, rice, *Stellaria longipes*, and *Vitis vinifera*. CCoAOMTs from different plants share high sequence identity at the amino acid level, but they show little sequence similarity to COMT except for the consensus regions involved in *S*-adenosyl-L-methionine and metal binding (Vidgren et al., 1994; Ibrahim et al., 1998). It is interesting to note that CCoAOMTs share significant amino acid similarity to catechol OMT from rat and human (Salminen et al., 1990; Bertocci et al., 1991).

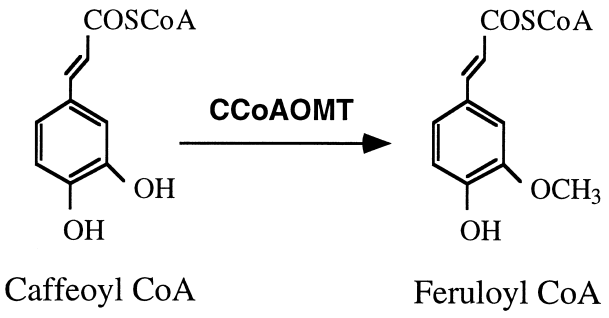

Fig. 1. CCoAOMT catalyzes methylation of caffeoyl CoA to feruloyl CoA. CCoAOMT was first identified in cultured parsley and carrot cells challenged with fungal elicitors.

5. Association of CCoAOMT expression with lignification in Zinnia

During the study of genes expressed in the in vitro-cultured TEs of Zinnia, Ye et al. (1994) have found a close association of CCoAOMT activity with lignification. The Zinnia system used in this study is ideal for biochemical and molecular dissection of enzymes and genes involved in the biosynthesis of polysaccharides and lignin. In this system, single mesophyll cells are mechanically isolated from young leaves, and then cultured in a liquid medium containing an appropriate ratio of auxin and cytokinin (Fukuda, 1996). In general, the cultured cells start to deposit secondary wall materials after 48 h of culture, and lignin deposition is evident between 60 and 72 h. Therefore, the time course of xylogenesis and gene expression can be monitored and used for functional analysis of the genes induced during xylogenesis.

In cultured Zinnia cells, the CCoAOMT gene expression was found to be markedly induced after 48 h induction, and CCoAOMT activity also dramatically increased after 60 h of induction (Fig. 2; Ye et al., 1994). The time course of CCoAOMT induction was coincident with the timing of lignification, and it exhibited an identical pattern to that of cinnamate 4-hydroxylase, a known gene involved in the phenylpropanoid pathway. This clearly indicated that CCoAOMT might play an important role in lignin biosynthesis.

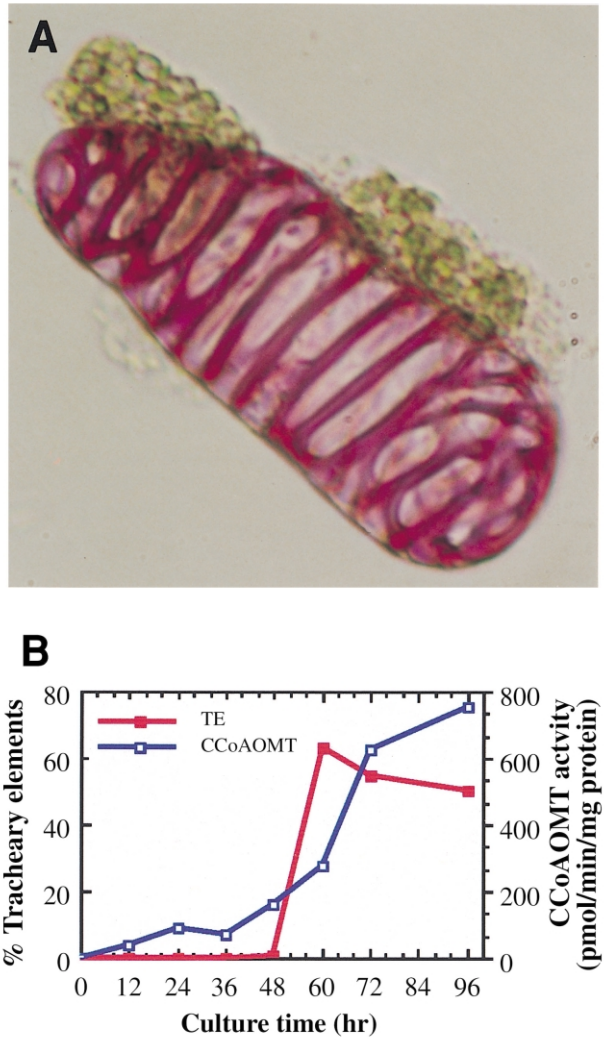

Fig. 2. Induction of CCoAOMT activity during in vitro TE formation in Zinnia. A. TE transdifferentiated from an isolated zinnia mesophyll cell. Lignified secondary wall is stained red with phloroglucinol-HCl. B. Time course of TE formation and CCoAOMT activity in isolated zinnia mesophyll cells. Mesophyll cells were cultured in the TE induction medium and monitored for TE formation and CCoAOMT activity. It is apparent that the dramatic increase of CCoAOMT activity correlates with timing of TE formation.

Examination of the gene expression pattern of CCo AOMT in the Zinnia plant further supported its possible involvement in lignification. It was found that the CCoAOMT gene was specifically expressed in all lignifying tissues in Zinnia including phloem fibers and xylem (Ye et al., 1994; Ye and Varner, 1995). Immunolocalization in Zinnia showed that CCoAOMT was present in TEs, xylary fibers and phloem fibers, and also in xylem ray parenchyma cells (Fig. 3; Ye, 1997). Based on these findings, it was proposed that the CCoAOMT-mediated methylation pathway was essential for lignin biosynthesis (Ye et al., 1994; Ye and Varner, 1995; Ye, 1997), in addition to its proposed role in defense (Matern et al., 1988; Kühnl et al., 1989; Pakusch et al., 1989).

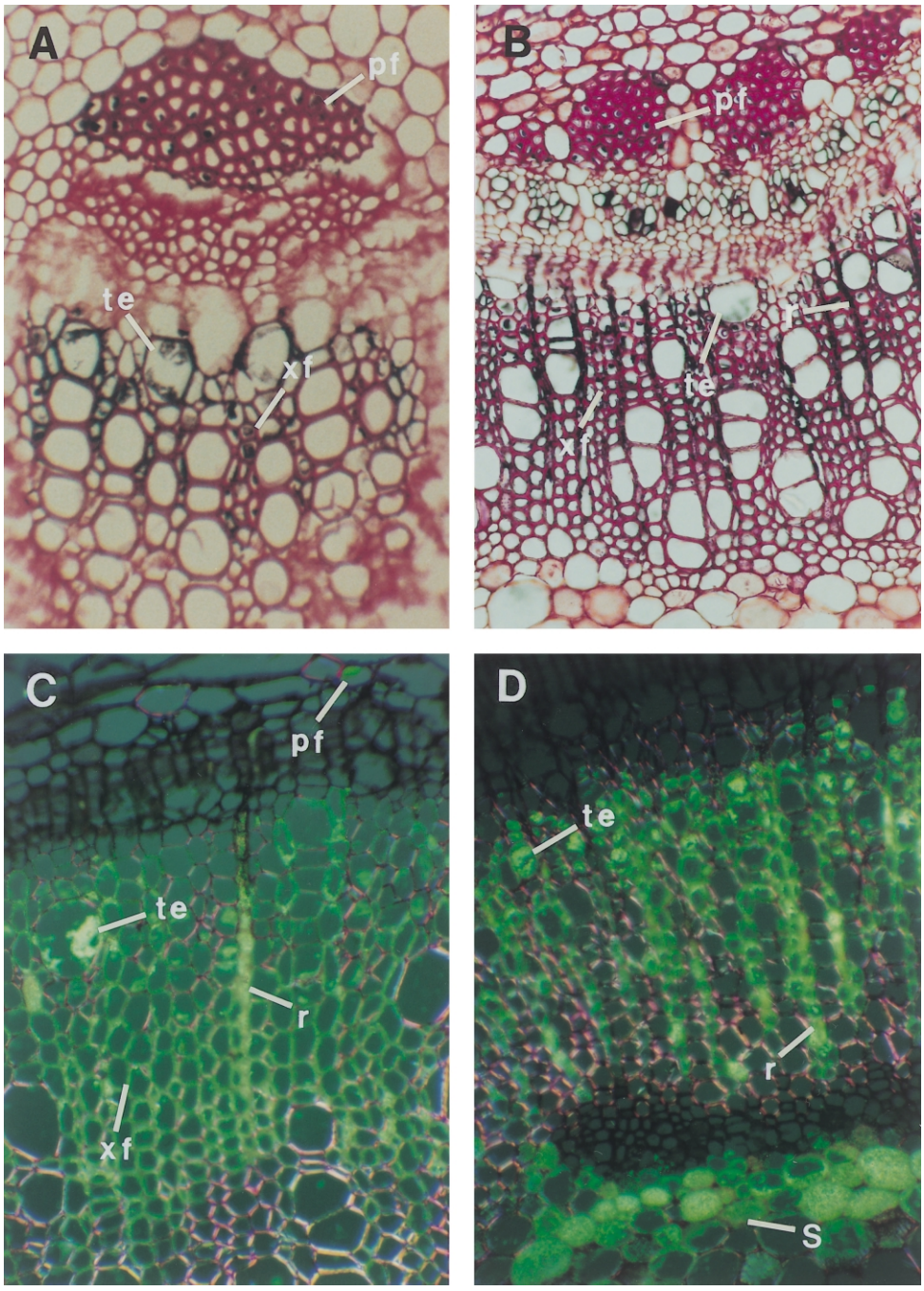

Fig. 3. Association of CCoAOMT with cells undergoing lignification. Stem sections of Zinnia (A), poplar (B), tobacco (C), and forsythia (D) were probed with polyclonal antibodies raised against Zinnia recombinant CCoAOMT and detected with gold-conjugated secondary antibody. The signal was amplified with silver enhancement, and seen either as black under bright field (A and B) or as yellow-green under UV epifluorescence (C and D). It is evident that CCoAOMT signal is present in TEs, xylary fibers, phloem fibers, sclerenchyma cells, and xylem ray parenchyma cells. Abbreviations: pf, phloem fiber; r, ray parenchyma cells; s, sclerenchyma cells; te, tracheary elements; xf, xylary fiber.

6. Ubiquitous association of CCoAOMT expression with lignification in plants

After the finding that CCoAOMT expression was closely associated with lignification in zinnia, the next important issue was to determine whether this expression pattern was common in plants. Localization of CCoAOMT at the protein or mRNA level confirmed that CCoAOMT was expressed in lignifying tissues in both herbaceous plants including parsley, tobacco, tomato, soybean and alfalfa, and woody plants including forsythia and poplar (Ye, 1997; Inoue et al., 1998; Kersey et al., 1999; Chen et al., 2000; Zhong et al., 2001). Similar to that in Zinnia, CCoAOMT was found to be present in TEs, xylary fibers, phloem fibers and xylem ray parenchyma cells in these plants (Fig. 3). Studies of CCoAOMT activity and its gene expression in tobacco, quaking aspen and pine also showed a close correlation with lignification in xylem (Martz et al., 1998; Meng and Campbell, 1998; Li et al., 1999; Maury et al., 1999). Taken together, these results further indicated that association of CCoAOMT with lignification was ubiquitous in both herbaceous and woody plants.

7. Down-regulation of CCoAOMT in transgenic plants reduces lignin content

Along with the demonstration of the close association of CCoAOMT with lignification, results from transgenic studies of COMT also indicated that other OMTs in addition to COMT might be involved in lignin biosynthesis (Dwivedi et al., 1994; Atanassova et al., 1995; van Doorsselaere et al., 1995; Tsai et al., 1998). COMT had long been thought to be the sole OMT involved in lignification. However, down-regulation of COMT expression in both transgenic tobacco and poplar proved that this was not the case. Transgenic plants with down-regulation of COMT showed an almost complete loss of syringyl lignin units but with little effect on guaiacyl lignin units (Atanassova et al., 1995; van Doorsselaere et al., 1995; Tsai et al., 1998; Jouanin et al., 2000; Fig. 4). In addition, no significant reduction in total lignin content was found in these transgenic plants. The only exception was the transgenic poplar plant with no detectable COMT activity, which showed 17% reduction in lignin content (Jouanin et al., 2000). Although these results clearly demonstrated that COMT was probably the sole enzyme responsible for the synthesis of syringyl lignin units, it suggested that COMT was not essential in the synthesis of guaiacyl lignin units. Even if COMT does contribute to guaiacyl lignin synthesis, other OMTs must have compensated for the loss of COMT. One of the best candidates of such OMTs was logically proposed to be CCoAOMT.

The unequivocal demonstration of the essential role of CCoAOMT in lignin biosynthesis came from transgenic studies (Zhong et al., 1998). It was shown that down-regulation of CCoAOMT in transgenic tobacco

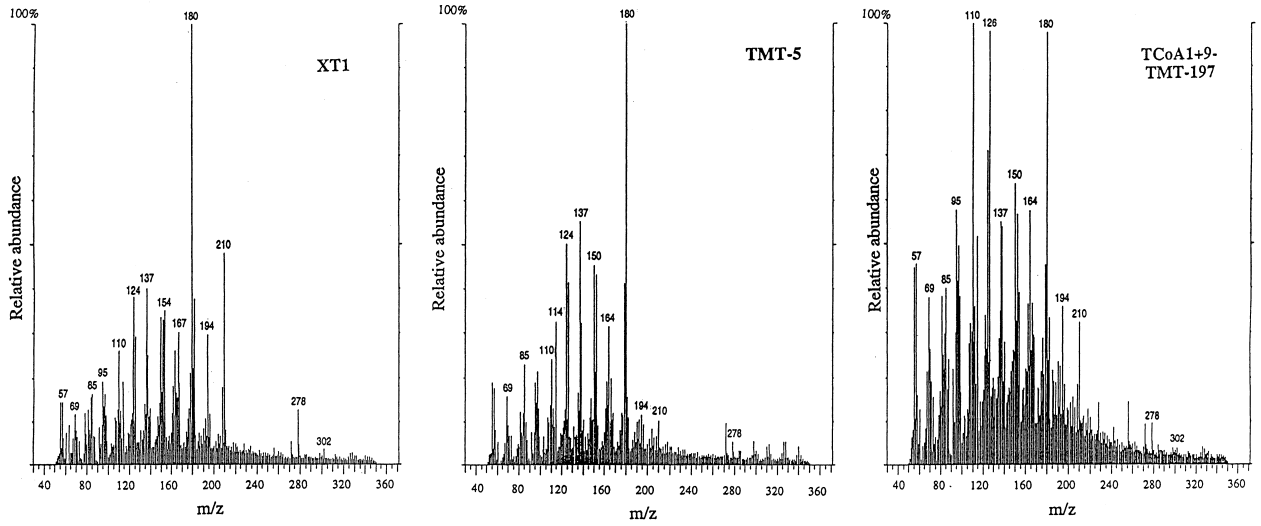

Fig. 4. Down-regulation of CCoAOMT effectively reduces the synthesis of guaiacyl lignin units in transgenic tobacco plants. Cell walls of the wild type (XT1), a transgenic line with down-regulation of COMT (TMT-5), and a transgenic line with down-regulation of both CCoAOMT and COMT (TCoA1 + 9-TMT-197) were analyzed with in-source pyrolysis mass spectrometry. Mass peaks of guaiacyl lignin had m/z values of 124, 137, 138, 150, 152, 164, 166, 178, and 180. Mass peaks of syringyl lignin had m/z values of 154, 167, 168, 180,182, 194, 208, and 210. Mass peaks of cellulose and amylose had m/z values of 57, 60, 73, 85, 86, 96, 98, 100, 102, 110, 112, 126, and 144. Mass peaks of hemicellulose had m/z values of 58, 85, 86, and 114. Down-regulation of COMT (TMT-5) dramatically decreases the syringyl lignin unit as evidenced by a reduction in the relative ratio of mass peaks of m/z 194 and 210 (syringyl lignin unit) over m/z 110 and 126 (polysaccharides) compared with the wild type (XT1). Simultaneous down-regulation of CCoAOMT and COMT (TCoA1 + 9-TMT-197) reduces both guaiacyl and syringyl lignin units as evidenced by a reduction in the relative ratio of mass peaks of m/z of 124, 150 and 180 (guaiacyl lignin unit) and 180, 194 and 210 (syringyl lignin unit) over m/z 110 and 126 (polysaccharides) compared with the wild type (XT1).

plants not only dramatically reduced total lignin content, but also decreased both guaiacyl and syringyl lignin units. The important role of CCoAOMT in the synthesis of guaiacyl lignin units was best exemplified in plants with down-regulation of both CCoAOMT and COMT (Fig. 4). While down-regulation of COMT resulted only in a reduction in syringyl lignin units, further down-regulation of CCoAOMT together with COMT effectively decreased both guaiacyl and syringyl lignin units.

In addition to the essential role of CCoAOMT in lignification in herbaceous tobacco plants, it has also been shown that CCoAOMT plays a similar role in lignin biosynthesis in woody poplar plants (Meyermans et al., in press; Zhong et al., in press). Reduction of CCoAOMT in transgenic poplar plants led to a decrease in both lignin content (Fig. 5) and guaiacyl and syringyl lignin units. Taken together, the transgenic studies in both tobacco and poplar have clearly confirmed the early hypothesis that the CCoAOMT-mediated methylation pathway is essential for lignin biosynthesis under normal plant growth and development. They also demonstrate that the methylation reactions in lignin biosynthesis are catalyzed by both COMT and CCoAOMT.

It is worth noting that although down-regulation of COMT resulted in an almost complete loss of syringyl lignin units, down-regulation of CCoAOMT did not lead to a similar level of reduction in guaiacyl lignin units. There are several possibilities for this insufficient reduction in guaiacyl lignin units. First, antisense repression does not lead to a complete loss of CCoAOMT activity, so the residual activity present in the transgenic plants might be sufficient to sustain the biosynthesis of substantial amount of lignin. Second, CCoAOMT genes are present in a gene family in tobacco and poplar. Some gene members might not share enough nucleotide sequence homology with the gene used for antisense repression, so that their gene expression might not be affected. Third, some novel OMTs capable of methylating caffeoyl CoA such as the multifunctional OMT from pine (Li et al., 1997) might partially compensate for the loss of CCoAOMT. Fourth, it is possible that, when CCoAOMT expression is repressed, COMT might partially compensate for the synthesis of guaiacyl lignin units. It is clear that more work needs to be done to investigate how many different types of OMTs are involved in the biosynthesis of guaiacyl lignin units.

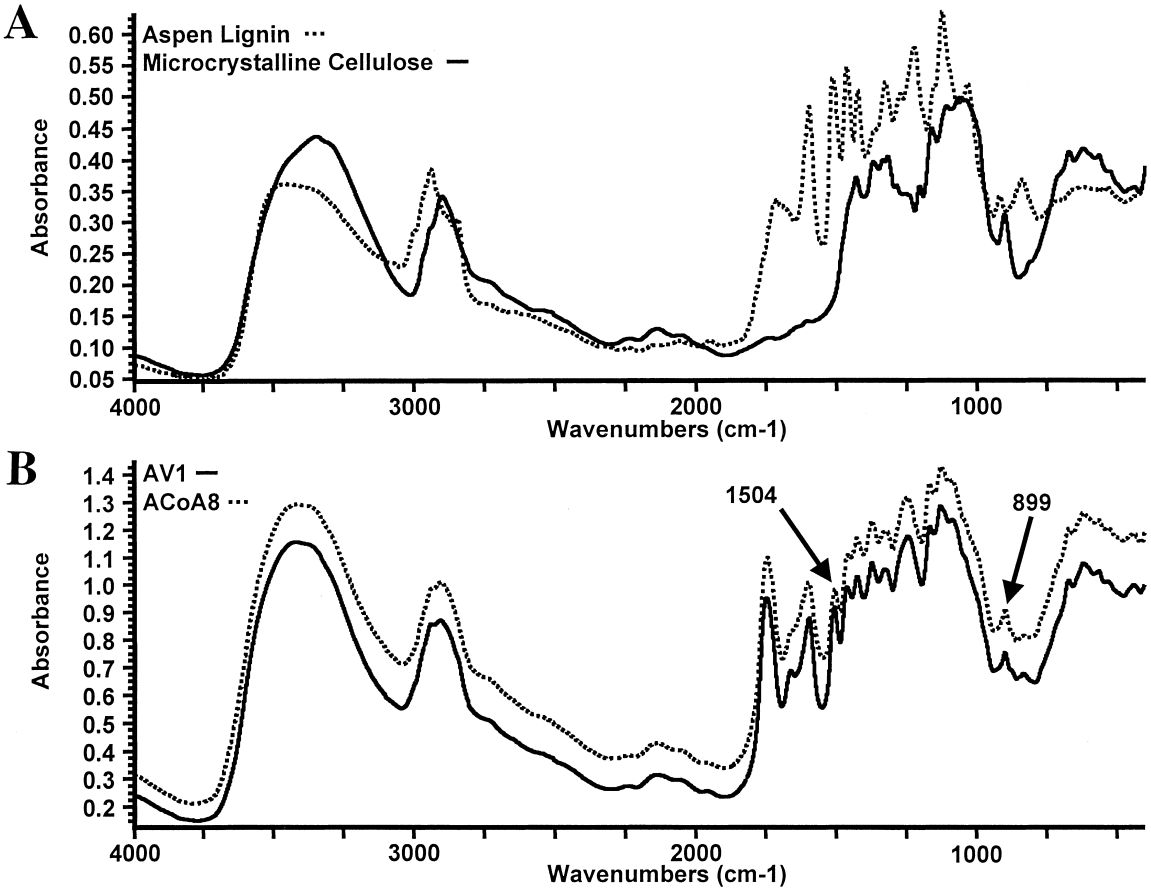

Fig. 5. Down-regulation of CCoAOMT reduces lignin content in woody poplar plants. Cell walls of the wild type (AV1) and a transgenic line with down-regulation of CCoAOMT (AcoA8) were anaylzed with diffuse reflectance infrared fourier transform spectroscopy. A. Spectra of standard lignin and cellulose. B. Spectra of cell walls from transgenic poplar plants. Lignin absorbances at 1504 and 1596 cm^{-1}, and cellulose absorbance at 899 cm^{-1} were used for quantitative analysis, which showed that in ACoA8 lignin was reduced to 56% that of the wild type (AV1).

8. CCoAOMT is induced in the pith of the *elp1* mutants

Genetic analysis of Arabidopsis mutants with ectopic deposition of lignin has further correlated CCoAOMT expression with lignification (Zhong et al., 2000). In the wild-type *Arabidopsis* inflorescence stems, lignin is deposited in the walls of xylem cells and interfascicular fiber cells (Fig. 6). Correspondingly, CCoAOMT is shown to be specifically expressed in these lignifying cells. In the inflorescence stems of the *elp1* mutants, lignin is ectopically deposited in the walls of pith parenchyma cells in addition to it normal deposition in the walls of xylem and fiber cells. In the lignifying pith cells of *elp1*, CCoAOMT is found to be abundantly induced (Fig. 6). The *elp1* mutation was recessive and monogenic. It has been proposed that the *ELP1* locus is involved in the repression of the lignin biosynthetic pathway in the pith. These results further support the conclusion drawn from biochemical and molecular analysis that CCoAOMT is essential for lignin biosynthesis.

9. Recent findings on F5H and COMT

Recently, biochemical characterization of the substrate specificities of F5H and COMT has led to a revolutionary revision of the lignin biosynthetic pathway (Humphreys et al., 1999; Maury et al., 1999; Osakabe et al., 1999; Li et al., 2000). First, the long-held notion that 5-hydroxylation of hydroxycinnamates occurs on the acid form proves not to be correct. Instead, it has been found that F5H preferentially hydroxylates coniferaldehyde and coniferyl alcohol (Humphreys et al., 1999; Osakabe et al., 1999; Li et al., 2000). Second, it has been shown that COMT can efficiently use 5-hydroxyconiferaldehyde and 5-hydroxyconiferyl alcohol as substrates (Humphreys et al., 1999; Maury et al., 1999; Osakabe et al., 1999; Li et al., 2000). Third, radiotracer experiments have proven that wood contains enzymes to convert coniferaldehyde and coniferyl alcohol into sinapaldehyde and sinapyl alcohol, respectively, required for the synthesis of syringyl lignin (Matsui et al., 1994; Chen et al., 1999). These

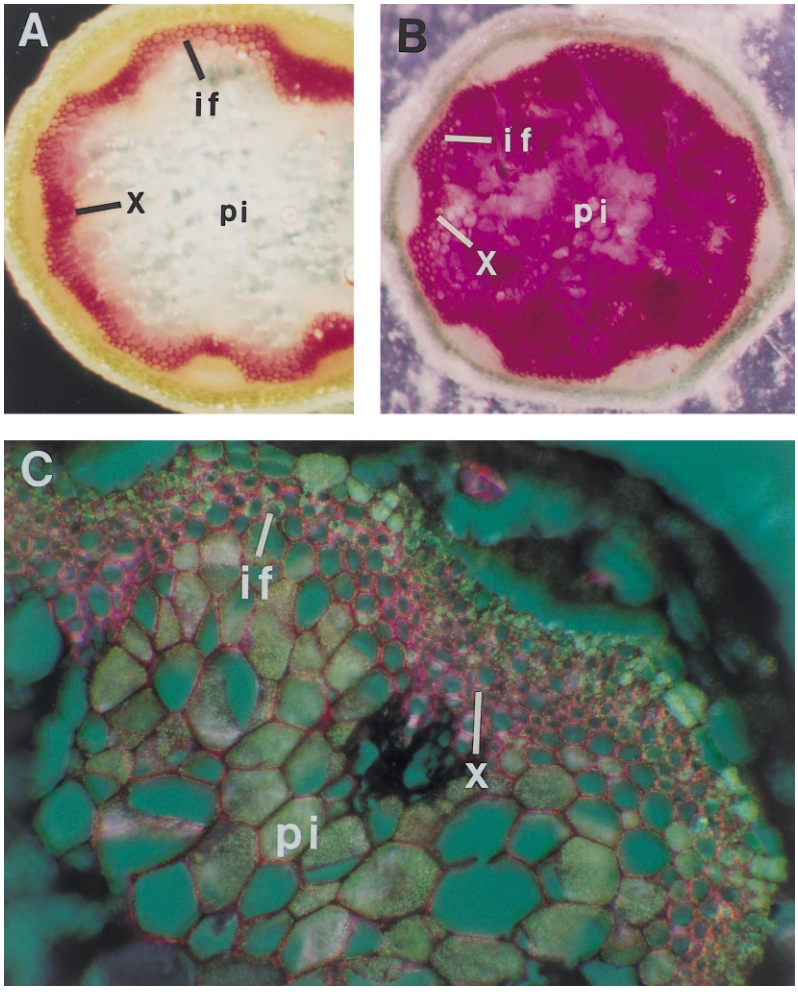

Fig. 6. Ectopic induction of CCoAOMT in the pith cells of *Arabidopsis elp1* mutant. A. Section from the wild-type stem showing lignin staining (red) in xylem and interfascicular fibers. B. Section from the *elp1* mutant stem showing intensive lignin staining in the pith in addition to xylem and interfascicular fibers. C. Immunolocalization of CCoAOMT in the *elp1* stem showing the presence of CCoAOMT signal (yellow-green) in the lignifying pith cells. Abbreviations: if, interfascicular fiber; pi, pith; x, xylem.

results strongly suggest that 5-methoxylation occurs only at the aldehyde and alcohol forms of the phenylpropanoid pathway intermediates. Finally, elegant competitive studies of substrate specificity have demonstrated that COMT does not use caffeic acid as the substrate in the presence of 5-hydroxyconiferaldehyde (Li et al., 2000).

Taken together, these results indicate that CCoAOMT does not contribute to the methylation of 5-hydroxyl groups of hydroxycinnamates because the substrate is not available (Li et al., 2000). This is consistent with the transgenic studies that down-regulation of COMT alone almost completely blocks the biosynthesis of syringyl lignin (Atanassova et al., 1995; van Doorsselaere et al., 1995). These results also suggest that feruloyl CoA is an important intermediate required for the synthesis of both guaiacyl and syringyl lignin units. This conforms with the antisense CCoAOMT results that down-regulation of CCoAOMT, which reduces the production of feruloyl CoA, results in a decrease in both guaiacyl and syringyl lignin units (Zhong et al., 1998).

10. Concluding remarks

The demonstration of the essential role of CCoAOMT in lignin biosynthesis has greatly enriched our knowledge on the biosynthetic pathway of lignin. This finding has also confirmed Neish's early proposal that the intermediates for methoxylation occur on the ester forms (Neish, 1968). The recent novel findings resulted from the study of methoxylation pathways have suggested that the lignin biosynthetic pathway is far more complicated than what we had thought. It appears that our quest on the methylation pathways in lignin biosynthesis has not reached an end. We are still not clear how many different kinds of OMTs participate in the methylation of 3-hydroxyl groups of hydroxycinnamates although CCoAOMT is clearly involved. It seems that the antisense approach may not be able to further address this issue. It is likely that mutational analysis in plants such as *Arabidopsis* would be able to provide conclusive answers on the roles of different OMTs in the methylation of 3-hydroxyl groups of hydroxycinnamates. It is anticipated that further studies of the methylation pathways using biochemical, molecular and genetic approaches will resolve the roles of different OMTs in the biosynthesis of lignin.

References

Atanassova, R., Favet, N., Martz, F., Chabbert, B., Tollier, M.-T., Monties, B., Fritig, B., Legrand, M., 1995. Altered lignin composition in transgenic tobacco expressing *O*-methyltransferase sequence in sense and antisense orientation. Plant Journal 8, 465–477.

Bertocci, B., Miggiano, V., Prada, M.D., Dembic, Z., Lahm, H.-W., Malherbe, P., 1991. Human catechol-*O*-methyltransferase: cloning and expression of the membrane-associated form. Proceedings of the National Academy of Sciences USA 88, 1416–1420.

Boudet, A.M., 1998. A new view of lignification. Trends in Plant Science 3, 67–71.

Brown, S.A., 1966. Lignins. Annual Review of Plant Physiology 17, 223–244.

Brown, S.A., 1969. Biochemistry of lignin formation. Bioscience 19, 115–121.

Chen, C., Meyermans, H., Burggraeve, B., De Rycke, R.M., Inoue, K., Vleesschauwer, V.D., Steenackers, M., Van Montagu, M.C., Engler, G.J., Boerjan, W.A., 2000. Cell-specific and conditional expression of caffeoyl-coenzyme A-3-*O*-methyltransferase in poplar. Plant Physiology 123, 853–867.

Chen, F., Yasuda, S., Fukushima, K., 1999. Evidence for a novel biosynthetic pathway that regulates the ratio of syringyl to guaiacyl residues in lignin in the differentiating xylem of *Magnolia kobus* DC. Planta 207, 597–603.

Davin, L.B., Lewis, N.G., 2000. Dirigent proteins and dirigent sites explain the mystery of specificity of radical precursor coupling in lignan and lignin biosynthesis. Plant Physiology 123, 453–461.

Davin, L.B., Wang, H.-B., Crowell, A.L., Bedgar, D.L., Martin, D.M., Sarkanen, S., Lewis, N.G., 1997. Stereoselective bimolecular phenoxy radical coupling by an auxiliary (dirigent) protein without an active center. Science 275, 362–366.

Van Doorsselaere, J.V., Baucher, M, Chognot, E., Chabbert., B., Tollier, M.-T., Petit-Conil, M., Leplé, J.-C., Pilate, G., Cornu, D., Monties, B., Montagu, M.V., Inzé, D., Boerjan, W., Jouanin, L., 1995. A novel lignin in poplar trees with a reduced caffeic acid/5-hydroxyferulic acid *O*-methyltransferase activity. Plant Journal 8, 855–864.

Dwivedi, U.N., Campbell, W.H., Yu, J., Datla, R.S.S., Bugos, R.C., Chiang, V.L., Podila, G.K., 1994. Modification of lignin biosynthesis in transgenic *Nicotiana* through expression of an antisense *O*-methyltranferase gene from *Populus*. Plant Molecular Biology 26, 61–71.

El-Basyouni, S.Z., Neish, A.C., 1966. Occurrence of metabolically-active bound forms of cinnamic acid and its phenolic derivatives in acetone powders of wheat and barley plants. Phytochemistry 5, 683–691.

El-Basyouni, S.Z., Neish, A.C., Tower, G.H.N., 1964. The phenolic acids in wheat. III. Insoluble derivatives of phenolic cinnamic acids as natural intermediates in lignin biosynthesis. Phytochemistry 3, 627–639.

Fukuda, H., 1996. Xylogenesis: initiation, progression, and cell death. Annual Review of Plant Physiology and Plant Molecular Biology 47, 299–325.

Humphreys, J.M., Hemm, M.R., Chapple, C., 1999. New routes for lignin biosynthesis defined by biochemical characterization of recombinant ferulate 5-hydroxylase, a multifunctional cytochrome P450-dependent monooxygenase. Proceedings of the National Academy of Sciences USA 96, 10045–10050.

Ibrahim, R.K., Bruneau, A., Bantignies, B., 1998. Plant *O*-methyltransferases: molecular analysis, common signature and classification. Plant Molecular Biology 36, 1–10.

Inoue, K., Sewalt, V.J.H., Murray, B.G., Ni, W., Stürzer, C., Dixon, R.A., 1998. Developmental expression and substrate specificities of alfalfa caffeic acid 3-*O*-methyltransferase and caffeoyl coenzyme A 3-*O*-methyltransferase in relation to lignification. Plant Physiology 117, 761–770.

Jouanin, L., Goujon, T., de Nadaï, V., Martin, M.-T., Mila, I., Vallet, C., Pollet, B., Yoshinaga, A., Chabbert, B., Petit-Conil, M., Lapierre, C., 2000. Lignification in transgenic poplars with extremely reduced caffeic acid *O*-methyltransferase activity. Plant Physiology 123, 1363–1373.

Kersey, R., Inoue, K., Schubert, K.R., Dixon, R.A., 1999. Immunolocalization of two lignin O-methyltransferases in stems of alfalfa (*Medicago sativa L.*). Protoplasma 209, 46–57.

Kühnl, T., Koch, U., Heller, W., Wellmann, E., 1989. Elicitor induced *S*-adenosyl-L-methionine:caffeoyl-CoA 3-*O*-methyltransferase from carrot cell suspension cultures. Plant Science 60, 21–25.

Lewis, N.G., 1999. A 20th century roller coaster ride: a short account of lignification. Current Opinion in Plant Biology 2, 153–162.

Lewis, N.G., Yamamoto, E., 1990. Lignin: occurrence, biogenesis and biodegradation. Annual Review of Plant Physiology and Plant Molecular Biology 41, 455–496.

Li, L., Osakabe, K., Joshi, C.P., Chiang, V.L., 1999. Secondary xylem-specific expression of caffeoyl-coenzyme A 3-*O*-methyltransferase plays an important role in the methylation pathway associated with lignin biosynthesis in loblolly pine. Plant Molecular Biology 40, 555–565.

Li, L., Popko, J.L., Umezawa, T., Chiang, V.L., 2000. 5-Hydroxyconiferyl aldehyde modulates enzymatic methylation for syringyl monolignol formation, a new view of monolignol biosynthesis in angiosperms. Journal of Biological Chemistry 275, 6537–6545.

Li, L., Popko, J.L., Zhang, X.H., Osakabe, K., Tsai, C.J., Joshi, C.P., Chiang, V.L., 1997. A novel multifunctional *O*-methyltransferase implicated in a dual methylation pathway associated with lignin biosynthesis in loblolly pine. Proceedings of the National Academy of Science USA 94, 5461–5466.

Martz, F., Maury, S., Pincon, G., Legrand, M., 1998. cDNA cloning, substrate specificity and expression study of tobacco caffeoyl-CoA 3-*O*-methyltransferase, a lignin biosynthetic enzyme. Plant Molecular Biology 36, 427–437.

Matern, U., Wendorff, H., Hamerski, D., Pakusch, A.E., Kneusel, R.E., 1988. Elicitor-induced phenylpropanoid synthesis in Apiaceae cell cultures. Bull. Liaison Group Polyphenols 14, 173–184.

Matsui, N., Fukushima, K., Yasuda, S., Terashima, N., 1994. On the behavior of monolignol glucosides in lignin biosynthesis. II. Synthesis of monolignol glucosides labeled with 3H at the hydroxymethyl group of side chain, and incorporation of the label into magnolia and ginkgo lignin. Holzforschung 48, 375–380.

Maury, S., Geoffroy, P., Legrand, M., 1999. Tobacco *O*-methyltransferases involved in phenylpropanoid metabolism. The different caffeoyl-coenzyme A/5-hydroxyferuloyl-coenzyme A 3/5-*O*-methyltransferase and caffeic acid/5-hydroxyferulic acid 3/5-*O*-methyltransferase classes have distinct substrate specificities and expression patterns. Plant Physiology 121, 215–223.

Meng, H., Campbell, W.H., 1998. Substrate profiles and expression of caffeoyl coenzyme A and caffeic acid *O*-methyltransferases in secondary xylem of aspen during seasonal development. Plant Molecular Biology 38, 513–520.

Meyermans, H., Morreel, K., Lapierre, C., Pollet, B., De Bruyn, A., Busson, R., Herdewijn, P., Devreese, B., Van Beeumen, J., Marita, J.M., Ralph, J., Chen, C., Burggraeve, B., Van Montagu, M., Messens, E., Boerjan, W., in press. Modifications in lignin and accumulation of phenolic glucosides in poplar xylem upon downregulation of caffeoyl-coenzyme A *O*-methyltransferase, an enzyme involved in lignin biosynthesis. Journal of Biological Chemistry.

Neish, A.C., 1968. Monomeric intermediates in the biosynthesis of lignin. In: Freudenberg, K., Neish, A.C. (Eds.), Constitution and Biosynthesis of Lignin. Springer-Verlag, New York, pp. 1–43.

Osakabe, K., Tsao, C.C., Li, L., Popko, J.L., Umezawa, T., Carraway, D.T., Smeltzer, R.H., Joshi, C.P., Chiang, V.L., 1999. Coniferyl aldehyde 5-hydroxylation and methylation direct syringyl lignin biosynthesis in angiosperms. Proceedings of the National Academy of Science USA 96, 8955–8960.

Pakusch, A.-E., Kneusel, R.E., Matern, U., 1989. *S*-Adenosyl-L-methionine: *trans*-caffeoyl-coenzyme A 3-*O*-methyltransferase from elicitor-treated parsley cell suspension cultures. Archives of Biochemistry and Biophysics 271, 488–494.

Raven, P.H., Evert, R.F., Eichhorn, S.E., 1999. Biology of plants, 6th Ed. W.H. Freeman and Company, New York.

Salminen, M., Lundström, K., Tilgmann, C., Savolainen, R., Kalkkinen, N., Ulmanen, I., 1990. Molecular cloning and characterization of rat liver catechol-*O*-methyltransferase. Gene 93, 241–247.

Schmitt, D., Pakusch, A.-E., Matern, U., 1991. Molecular cloning, induction, and taxonomic distribution of caffeoyl-CoA 3-*O*-methyltransferase, an enzyme involved in disease resistance. Journal of Biological Chemistry 266, 17416–17423.

Sederoff, R.R., MacKay, J.J., Ralph, J., Hatfield, R.D., 1999. Unexpected variation in lignin. Current Opinion in Plant Biology 2, 145–152.

Tsai, C.-J., Popko, J.L., Mielke, M.R., Hu, W.-J., Podila, G.K., Chiang, V.-L., 1998. Suppression of *O*-methyltransferase gene by homologous sense transgene in quaking aspen causes red-brown wood phenotypes. Plant Physiology 117, 101–112.

Vidgren, J., Svensson, L.A., Liljas, A., 1994. Crystal structure of catechol *O*-methyltransferase. Nature 368, 354–358.

Whetten, R.W., MacKay, J.J., Sederoff, R.R., 1998. Recent advances in understanding lignin biosynthesis. Annual Review of Plant Physiology and Plant Molecular Biology 49, 585–609.

Ye, Z.-H., 1997. Association of caffeoyl CoA 3-*O*-methyltransferase expression with lignifying tissues in several dicot plants. Plant Physiology 115, 1341–1350.

Ye, Z.-H., Varner, J.E., 1995. Differential expression of two *O*-methyltransferases in lignin biosynthesis in *Zinnia*. Plant Physiology 108, 459–467.

Ye, Z.-H., Kneusel, R.E., Matern, U., Varner, J.E., 1994. An alternative methylation pathway in lignin biosynthesis in *Zinnia*. Plant Cell 6, 1427–1439.

Zhong, R., Morrison III, W.H., Negrel, J., Ye, Z.-H., 1998. Dual methylation pathways in lignin biosynthesis. Plant Cell 10, 2033–2045.

Zhong, R., Morrison, W.H.III, Himmelsbach, D.S., Poole, F.L.II, Ye, Z.-H., 2001. Essential role of caffeoyl CoA *O*-methyltransferase in lignin biosynthesis in woody poplar plants. Plant Physiology, in press.

Zhong, R., Ripperger, A., Ye, Z.-H., 2000. Ectopic deposition of lignin in the pith of stems of two *Arabidopsis* mutants. Plant Physiology 123, 59–69.

PERGAMON

Phytochemistry 57 (2001) 1187–1195

PHYTOCHEMISTRY

www.elsevier.com/locate/phytochem

Two cinnamoyl-CoA reductase (CCR) genes from *Arabidopsis thaliana* are differentially expressed during development and in response to infection with pathogenic bacteria

Virginie Lauvergeat [a], Christophe Lacomme [b], Eric Lacombe [a], Eric Lasserre [b], Dominique Roby [b], Jacqueline Grima-Pettenati [a,*]

[a] *Signaux et Messages Cellulaires chez les Végétaux, UMR CNRS-UPS 5546, Pôle de Biotechnologie Végétale, 24 Chemin de Borde Rouge, Auzeville BP17, 31326 Castanet Tolosan, France*

[b] *Laboratoire de Biologie Moléculaire des Relations Plantes-Microorganismes, UMR CNRS-INRA 215, IFR 40, Pôle de Biotechnologie Végétale, 24 Chemin de Borde Rouge, Auzeville BP17, 31326 Castanet Tolosan, France*

Received 25 July 2000; received in revised form 27 November 2000

Abstract

Cinnamoyl-CoA reductase (CCR ; EC 1.2.1.44) catalyses the conversion of cinnamoyl-CoAs into their corresponding cinnamaldehydes, i.e. the first step of the phenylpropanoid pathway specifically dedicated to the monolignol biosynthetic branch. In previous work, we described the isolation and characterisation of the first cDNA encoding CCR in Eucalyptus (Lacombe, E., Hawkins, S., Van Dorsselaere, J., Piquemal, J., Goffner, D., Poeydomenge, O., Boudet, A.M., Grima-Pettenati, J., 1997. Cinnamoyl CoA reductase, the first committed enzyme of the lignin branch biosynthetic pathway: cloning, expression and phylogenetic relationships. Plant Journal 11, 429–441) and shown the role of this enzyme in controlling the carbon flux into lignins (Piquemal, J., Lapierre, C., Myton, K., O'Connell, A., Schuch, W., Grima-Pettenati, J., Boudet, A.M., 1998. Down-regulation of cinnamoyl-CoA reductase induces significant changes of lignin profiles in transgenic tobacco plants. Plant Journal 13, 71–83). Here, we report the characterisation of two functionally and structurally distinct cDNA clones, AtCCR1 and AtCCR2 (81.6% protein sequence identity) in *Arabidopsis thaliana*. The two recombinant proteins expressed in *Escherichia coli* are able to use the three cinnamoyl-CoAs tested but with different levels of efficiency. AtCCR1 is five times more efficient with feruloyl-CoA and sinapoyl-CoA than AtCCR2. In addition, the two genes are differentially expressed during development and in response to infection. *AtCCR1* is preferentially expressed in tissues undergoing lignification. In contrast, *AtCCR2*, which is poorly expressed during development, is strongly and transiently induced during the incompatible interaction with *Xanthomonas campestris* pv. *campestris* leading to a hypersensitive response. Altogether, these data suggest that *AtCCR1* is involved in constitutive lignification whereas *AtCCR2* is involved in the biosynthesis of phenolics whose accumulation may lead to resistance. © 2001 Elsevier Science Ltd. All rights reserved.

Keywords: *Arabidopsis thaliana*; Brassicaceae; Lignin biosynthesis; Defence; Hypersensitive reaction; Cinnamoyl CoA reductase

1. Introduction

Lignins, which are complex aromatic polymers resulting from the oxidative polymerization of hydroxycinnamyl alcohols (*p*-coumaryl, coniferyl and sinapyl alcohols), have played a major role in the successful land colonisation by plants (Lewis and Davin, 1994). Their deposition occurs in the walls of certain specialised cells such as tracheary elements allowing water and nutrient conduction as well as structural support. In addition, induced lignification is one plant defence response to environmental cues such as wounding, mechanical stress or pathogen attack (Vance et al., 1980; Lewis and Yamamoto, 1990; Moerschbacher et al., 1990; Nicholson and Hammerschmidt, 1992). Increased lignification has often been observed in response to infection and is believed to participate in parasite confinement because lignin represents an undegradable mechanical barrier

* Corresponding author. Tel.: +33-5-62-19-35-13; fax: +33-5-62-19-35-02.

E-mail address: grima@smcv.ups-tlse.fr (J. Grima-Pettenati).

0031-9422/01/$ - see front matter © 2001 Elsevier Science Ltd. All rights reserved.
PII: S0031-9422(01)00053-X

for most micro-organisms (Kimmins and Wuddah, 1977; Vance et al., 1980; Legrand, 1983; Ride, 1983; Lange et al., 1995; Walter, 1992). In most cases, the tissue location and the monomeric composition of defence lignins are different from those of structural lignins (Lange et al., 1995 and references therein). Taken together, these data suggest that lignin biosynthesis is controlled by two signal transduction pathways, one in the development of vascular tissues, and the other in plant defence responses.

The biosynthesis of lignins begins with the common phenylpropanoid pathway starting with the deamination of phenylalanine and leading to the cinnamoyl-CoA esters which are the common precursors of a wide array of end-products playing key roles during plant development and defence such as flavonoids, coumarins, lignins, phlobaphenes and many small phenolic molecules (Hahlbrock and Scheel, 1989; Dixon and Lamb, 1990). Cinnamoyl-CoA esters are then channelled into the lignin branch pathway to produce monolignols *via* two reductive steps i.e. cinnamoyl-CoA reductase (CCR) and cinnamyl alcohol dehydrogenase (CAD).

The organisation and regulation of phenylpropanoid genes, particularly the first and last step of the "general phenylpropanoid" pathway, catalysed by phenylalanine ammonia-lyase (PAL) and cinnamate-CoA ligase (4CL), have been extensively studied. Depending on the species, PAL and 4CL are encoded by several genes which are largely controlled at the level of transcription during development and in response to environmental cues such as infection, UV light (Chappell and Hahlbrock, 1984; Lawton and Lamb, 1987; Hahlbrock and Scheel, 1989; Dixon and Paiva, 1995). In contrast to the considerable amount of data accumulated on the regulation of these genes, little is known about the steps devoted more specifically to the lignin monomer biosynthesis, such as CCR. A rapid and transient increase of feruloyl-CoA reductase and PAL activities was previously reported in cell suspension of spruce treated with cell wall preparation of *Rhizosphaera kalkhoffii* (Messner and Boll, 1993). Concomitant with this increase in enzyme activities, a rapid accumulation of low molecular weight lignin-like material was observed in the medium, resembling gymnosperms' compression wood lignins (Lange et al., 1995). Whether the same *CCR* gene is under the control of both the developmental programs during normal plant growth and the defensive reactions triggered by environmental cues, is still a totally open question.

The cloning and characterisation of the cDNA encoding CCR was first achieved in *Eucalyptus* (Lacombe et al., 1997), enabling us to address this question and to gain an insight into the regulation of the lignin pathway in developmental and defence processes. Consistent with its role in lignin biosynthesis during plant development, expression of the *CCR* gene was shown to be high in tissues undergoing active lignification, i.e. vascular cambium and differentiating xylem (Lacombe et al., 1997, 2001). Moreover, this enzyme, which occupies a key position between the general phenylpropanoid pathway and the lignin specific branch, has been shown to be a control point regulating the carbon flux towards lignins by gene transfer experiments (Piquemal et al., 1998). Through ectopic expression of a homologous antisense gene, significant down-regulation for CCR has been obtained in transgenic tobacco plants leading to both qualitative and quantitative changes in lignins profiles (Piquemal et al., 1998). CCR is apparently encoded by a single gene per haploid genome in *Eucalyptus* (Lacombe et al., 1997), poplar (Leplé et al., 1998) and tobacco (Piquemal et al., 1998) and by two genes in maize (Pichon et al., 1998). According to Northern blot experiments performed on different organs using specific probes for the two maize genes, it was concluded that *ZmCCR1* was involved in lignification whereas the role of *ZmCCR2*, which is expressed only in roots and at a low level, remains to be elucidated.

The systematic sequencing project of *Arabidopsis thaliana* expressed sequence tags (ESTs) allowed us to identify by homology search, two genes exhibiting high homology with *CCR* genes previously isolated from other species and, therefore, putatively encoding CCR in this species. Using the Darwin software (Gonnet et al., 1992), we built a phylogenetic tree showing that AtCCR1 is closer than AtCCR2 to the core of the dicotyledon CCRs involved in lignin biosynthesis. Since these cDNAs initially derived from two different libraries, a library prepared from mRNA of different *Arabidopsis* organs for *AtCCR1*, and from mRNA isolated from a cell suspension culture inoculated by *Xanthomonas campestris* pv. *campestris* for *AtCCR2*, we made the hypothesis that the two genes may play different roles in *Arabidopsis*. In order to gain insight into the respective role of these genes in *Arabidopsis*, we expressed the recombinant proteins in *E. coli* and compared their specific activities towards three hydroxy-cinnamoyl substrates. The expression patterns of the two genes were also assessed during development and upon infection by pathogenic bacteria.

The characterisation of two structurally and functionally distinct *CCR* genes *AtCCR1* and *AtCCR2*, which are differentially expressed during development and in response to a pathogen challenge enable us to show that the two enzymes serve different physiological functions in *Arabidopsis*. Biochemical and in vivo expression analyses provide evidence that *AtCCR1* is associated with lignin biosynthesis during development. On the other hand, *AtCCR2* mRNA is strongly and transiently induced during the incompatible reaction with *Xanthomonas campestris* pv. *campestris* but not in lignifying tissue, suggesting a role for this enzyme in the formation of phenolic compounds associated with the hypersensitive response in *Arabidopsis*.

2. Results

2.1. Sequence analysis of two CCR cDNA clones from Arabidopsis

The *AtCCR1* cDNA is 1269 nucleotides long and has an open reading frame (ORF) of 1032 nucleotides encoding a 344 amino acid protein (Fig. 1) with a predicted molecular mass of 37.5 kDa and a pI of 6.1. The clone is not full length since the 5′ non coding region is missing. The *AtCCR2* cDNA is 1216 nucleotides long and contains an ORF encoding a protein of 332 amino acids (36.6 kDa) with a calculated pI of 6.09 (Fig. 1). Based on the eukaryotic consensus sequence of Kosak (1984), the ATG at position 63 is the initiation codon with an A at position −3. The position +5 is not occupied by a C in contrast with what is frequently observed in plants (Lütcke et al., 1987). No putative polyadenylation signal was found in either cDNAs. The two nucleotide sequences share 78.2 and 44.2% identity in their coding and 3′ untranslated regions, respectively. Because of their high sequence divergence, the 3′ regions were used to generate specific probes relative to *AtCCR1* and *AtCCR2* sequences, respectively (see Experimental).

The protein sequences deduced from the cDNAs *AtCCR1* and *AtCCR2* show 81.6% identity and 18.7% similarity (Fig. 1). The region in the N terminal portion of CCRs involved in the NADP(H) cofactor binding site (Lacombe et al., 1997) is conserved in both AtCCR sequences (Fig. 1). They also exhibit the signature of CCR, a very well conserved motif (KNWYCYGK), which is thought to be involved in the catalytic site of this enzyme (Lacombe et al., 1997). The alignment of these sequences with the predicted amino acid sequence of the *Eucalyptus gunnii* CCR (EuCCR, Lacombe et al., 1997) revealed a slightly higher homology for AtCCR1 (75% identity + 12% similarity) than for AtCCR2 (73% identity + 12.5% similarity). Based on the PAM distances reported on the phylogenetic tree (Fig. 2) built with the sequences of CCRs from different species, both AtCCRs belong to the group of CCRs from dicot origin. Interestingly, AtCCR1 is slightly closer to the other dicots CCRs than AtCCR2.

2.2. Copy number of CCR genes in A. thaliana

In order to evaluate the complexity of the CCR gene family in the *Arabidopsis* genome, genomic DNA was

```
                                                                  I▽
AtCCR1  MPVDVASPA GKTVCVTGAG GYIASWIVKI LLERGYTVKG TVRNPDDPKNT 50
AtCCR2       MLVD GKLVCVTGAG GYIASWIVKL LLERGYTVRG TVRNPTDPKNN 44
               ** ******* *********  ******** * ***** ****
                                                          II▽
AtCCR1  HLRELEGGK ERLILCKADL QDYEALKAAI DGCDGVFHTA SPVTDDPEQMV 100
AtCCR2  HLRELQGAK ERLTLHSADL LDYEALCATI DGCDGVFHTA SPMTDDPETML 94
        ******* * *** *  ***  ***** * * ********** ** ***** *

AtCCR1  EPAVNGAKF VINAAAEAKV KRVVITSSIG AVYMDPNRDP EAVVDESCWSD 150
AtCCR2  EPAVNGAKF VIDAAAKAKV KRVVFTSSIG AVYMNPNRDT QAIVDENCWSD 144
        ********* ****** *** **** ***** *********  ****** ****
           III▽
AtCCR1  LDFCKNTKN WYCYGKMVAE QAAWETAKEK GVDLVVLNPV LVLGPPLQPTI 200
AtCCR2  LDFCKNTKN WYCYGKMLAE QSAWETAKAK GVDLVVLNPV LVLGPPLQSAI 194
        ********* ******* ** * ****** * ********** ********  *

AtCCR1  NASLYHVLK YLTGSAKTYA NLTQAYVDVR DVALAHVLVY EAPSASGRYLL 250
AtCCR2  NASLVHILK YLTGSAKTYA NLTQVYVDVR DVALGHVLVY EAPSASGRYIF 244
        **** **** ********** **** ***** **** ***** *********
                                 IV▽
AtCCR1  AESARHRGE VVEILAKLFP EYPLPTKCKD EKNPRAKPYK FTNQKIKDLGL 300
AtCCR2  AETALDRGE VVEILAKFFP EYPLPTKCSD EKNPRAKPYK FTTQKIKDLGL 294
        ** *  *** ******* ** ******** * ********** ** ********

AtCCR1  ELTSTKQSF YDTVKSLQEK GHLAPPPPPP SASQESVENG IKIGS       344
AtCCR2  EFKPIKQSL YESVKSLQEK GHL-PLPQDS NQNEVIIES            332
        *    ***  *  ******* *** * *           *
```

Fig. 1. Alignment of the deduced amino acid sequences of AtCCR1 (T41765) and AtCCR2 (Z24528). Symbols (*) denote identical amino acids. The shaded amino acids are putative amino acids involved in cofactor binding. The box indicates the putative signature of CCRs. Sequence alignment was performed using the program Multalin (Corpet, 1988). The positions of the introns in AtCCR1 and AtCCR2 are indicated by white and black arrows, respectively.

digested to completion with either *Eco*RI, *Eco*RV, *Pst*I or *Xba*I, which do not cut the cDNA, or *Bam*HI, which has one restriction site in the *AtCCR1* sequence, and subjected to Southern blot analysis (Fig. 3). A 703 bp fragment of the *AtCCR2* cDNA was used as a probe allowing cross hybridisation between the two cDNA sequences. For each restriction digest, one strong and one weak hybridisation signal was observed. The strong intensity signal corresponded to homologous hybridisation to the *AtCCR2* gene whereas the faint band resulted from cross-hybridisation with the *AtCCR1* gene, showing the occurrence of two CCR-related genes in the *Arabidopsis thaliana* genome. This was further confirmed by the presence in *Arabidopsis* database of only two genomic sequences (AC010924 and AC011713) corresponding to *AtCCR1* and *AtCCR2*, respectively. Both genes are localised on chromosome 1. The sequence corresponding to *AtCCR1* gene (located on BAC clone AC010924) contained four introns at identical positions to introns I, II, III, IV from *Eucalyptus CCR* gene (Lacombe et al, 1997). Surprisingly, only three introns were found in the genomic sequence of *AtCCR2* (located on BAC clone AC011713) at similar positions as the introns II, III, IV in *AtCCR1* and *EuCCR* genes indicating that the first intron is missing.

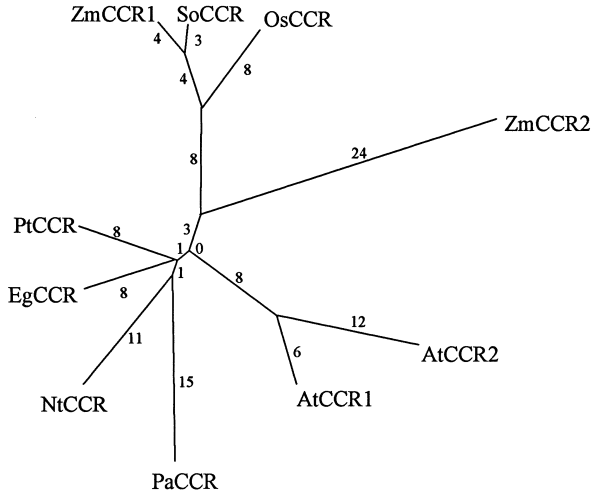

Fig. 2. Phylogenetic tree of AtCCRs and related sequences as obtained using DARWIN (Gonnet et al., 1992). The tree was built using the sequences indexed in EMBL as follows : AtCCR1 (*Arabidopsis thaliana*, T41765) and AtCCR2 (*Arabidopsis thaliana*, Z24528); EgCCR (*Eucalyptus gunnii*, X97433)(Lacombe et al., 1997); ZmCCR1 (*Zea mays*, X98083; Y13734) and ZmCCR2 (*Zea mays*, Y15069) (Pichon et al., 1998); PaCCR (*Picea abies*, Goffner, personal communication); PtCCR (*Populus trichocarpa* x *P. Deltoides*, A47097); NtCCR (*Nicotiana tabacum*, A47101) (Piquemal et al., 1998); OsCCR (*Oriza sativa*, EST D46355); SoCCR (*Saccharum officinarum*, AJ231134).

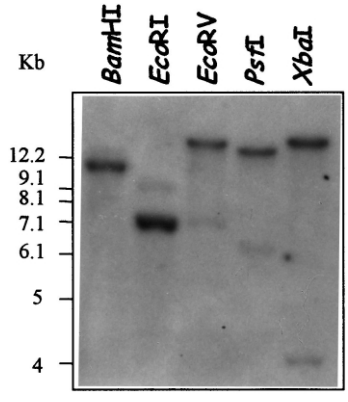

Fig. 3. Southern blot analysis of *Arabidopsis thaliana* genomic DNA. *Arabidopsis thaliana* DNA was digested with *Bam*HI, *Eco*RI, *Eco*RV, *Pst*I and *Xba*I. Hybridization was performed with the *Bgl*II-*Dra*I RaR108 (*AtCCR2*) cDNA fragment. The molecular weight markers are indicated on the left.

2.3. Functional expression of the A. thaliana CCR cDNAs in E. coli

In order to compare the biochemical properties of AtCCR1 and AtCCR2, *E. coli* expressed-GST fusion proteins were purified to 90% homogeneity, as determined by SDS-PAGE (data not shown). Under denaturing electrophoresis conditions, these proteins exhibited a molecular mass of approximately 64 kD, which is in agreement with the size of the fusion proteins GST-AtCCR1 and GST-AtCCR2. Purified fusion proteins were then used to determine the apparent K_m and K_{cat} values for three potential CCR substrates : feruloyl-CoA, sinapoyl-CoA and caffeoyl-CoA (Table 1). Although, the measurements have been performed using fusion proteins and should be confirmed using purified recombinant proteins, the data obtained clearly showed that the two enzymes are able to use the three substrates but with different efficiencies. AtCCR1 exhibited a clear preference for feruloyl-CoA and to a lesser extent for sinapoyl-CoA. AtCCR2 preferentially used feruloyl-CoA but converted sinapoyl-CoA and caffeoyl-CoA with approximately the same lower efficiency. AtCCR1 was 5 times more efficient with feruloyl-CoA and sinapoyl-CoA than AtCCR2 (K_{cat}/K_m). Caffeoyl-CoA, the least favoured substrate, appeared to be used with the same efficiency by both AtCCRs.

2.4. Developmental expression of CCR genes

To investigate the spatial expression of *CCR* genes in *Arabidopsis*, Northern analysis was carried out with RNA extracted from different parts of two month-old plants (Fig. 4). Blots were hybridised with gene-specific probes for *AtCCR1* and *AtCCR2* (see experimental section) corresponding to their 3′ regions. *AtCCR1* specific probe hybridised to a single mRNA species of about 1.6 Kb mainly in stems and at a lower level in leaves and flowers (including petioles and sepals). In contrast, *AtCCR2* mRNA was hardly detectable in these organs by Northern blot analysis, suggesting that the *AtCCR2*

Table 1
Kinetic parameters of AtCCR1 and AtCCR2 fusion proteins

Substrate	K_m (μM)		K_{cat} (min^{-1})		K_{cat}/K_m (min^{-1} μM^{-1})	
	AtCCR1	AtCCR2	AtCCR1	AtCCR2	AtCCR1	AtCCR2
Feruloyl-CoA	0.96	4.7	2.28	2.23	2.37	0.47
Sinapoyl-CoA	6.32	30.7	3.67	3.5	0.58	0.11
Caffeoyl-CoA	12.5	5.16	2.18	0.87	0.17	0.17

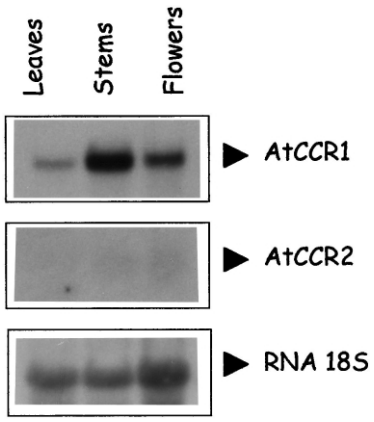

Fig. 4. Northern blot analysis of total RNA (25 μg per lane) from *Arabidopsis thaliana* leaves, stems and flowers, probed with ^{32}P-labeled AtCCR1 and AtCCR2 specific fragments and 18S ribosomal RNA.

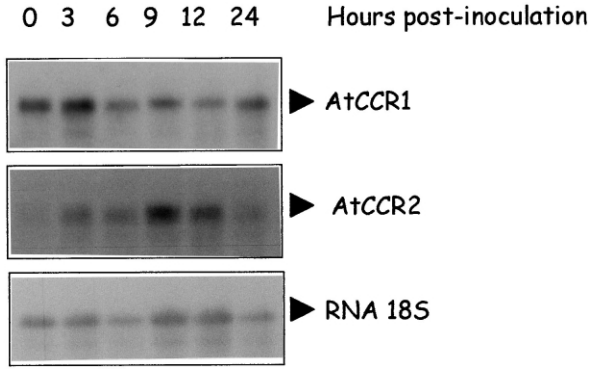

Fig. 5. Northern blot analysis of total RNA from *Arabidopsis* leaves inoculated with *Xanthomonas campestris* pv. *campestris*. Healthy leaves (time O), or leaves from Col-O ecotype (incompatible interaction), inoculated with the *Xanthomonas campestris* pv. *campestris* strain 147, were harvested at different times post-inoculation; RNA was extracted and analysed as described for Fig. 4.

gene is expressed at very low levels in all the organs tested.

2.5. Expression of Arabidopsis CCR upon infection with bacterial pathogens

The fact that the *AtCCR2* cDNA was isolated from *Arabidopsis* cells inoculated with an avirulent isolate of *Xanthomonas campestris* pv. *campestris*, led us to analyse in detail the expression patterns of *AtCCR1* and *AtCCR2* genes during plant-pathogen interactions.

Northern blot analysis was performed from leaf tissues of Col-O ecotype of *Arabidopsis* after challenge by *Xanthomonas campestris* pv. *campestris* isolate 147, an incompatible interaction leading to HR. Total RNA was extracted at different times after pathogen challenge (Fig. 5). In healthy leaves (time 0), a signal corresponding to *AtCCR1* mRNA was observed whereas *AtCCR2* mRNA was virtually undetectable (Fig. 5). At 3 h post inoculation (hpi), the steady-state content of *AtCCR1* mRNA slightly increased, then decreased (6 hpi) and stayed relatively constant (trancripts still being detectable) until 24 hpi). This drop of the *AtCCR1* mRNA level below the basal level (time 0) was consistently observed in independent experiments. In contrast, the level of *AtCCR2* mRNA increased strongly and transiently after inoculation by the pathogen. The hybridisation signal became clearly detectable 3 hpi, reached a maximum at 9 hpi, then decreased to become slightly detectable after 24 hpi. In addition, different compounds known as modulators of stress response in plants such as elicitors, methyl jasmonate, salicylic acid and ethylene were tested on *AtCCR2* expression in *Arabidopsis* plants. An increase of *AtCCR2* transcripts accumulation was detected only in response to exogenous apply of salicylic acid (data not shown).

No significant accumulation of *AtCCR1* and *AtCCR2* mRNA transcripts was seen after infiltration with water nor during a compatible interaction leading to disease (data not shown).

3. Discussion

We report here the functional characterisation of two *CCR* cDNA clones from *Arabidopsis thaliana*, originally obtained from two different cDNA libraries. We have shown that AtCCR1 and AtCCR2 exhibit distinct biochemical properties and that the corresponding genes are differentially expressed during development and in response to pathogen challenge.

Although their deduced protein sequences showed high sequence identity with CCRs previously isolated from other species and shown to be involved in lignin biosynthesis during vascular development (Lacombe et al., 1997; Pichon et al., 1998; Piquemal et al., 1998),

more detailed phylogenetic analysis revealed that AtCCR1 is closer than AtCCR2 to the core of the other dicotyledones CCRs. Taken together with the respective origin of the clones, this result favours the hypothesis that the two genes could play different roles *in planta*.

As a first step towards deciphering their respective functions, we have produced the recombinant fusion proteins in *E. coli* and tested their activities towards three potential CCR substrates. AtCCR1 exhibited a clear substrate preference for lignin-specific substrates (feruloyl-CoA, sinapoyl-CoA) as previously reported for CCR from other species such as *Eucalyptus* (Goffner et al., 1994), spruce (Luderitz and Grisebach, 1981) and poplar (Sarni et al., 1984). The strong preference of AtCCR1 for feruloyl-CoA is consistent with the monomeric composition of lignin in *Arabidopsis* xylem which is mainly composed of guaiacyl G units (Chapple et al., 1992). All together these data suggest that *AtCCR1* might be involved in lignin biosynthesis. On the other hand, AtCCR2 also exhibited a clear preference for feruloyl-CoA but the substrate affinity and the conversion efficiency is 5 times lower as compared to AtCCR1.

In addition to the biochemical analyses, the Northern blot experiments showed that *AtCCR1* is preferentially expressed in stems, this supporting its role in vascular lignification. Further confirmation of the role of *AtCCR1* was provided by antisense experiments performed in parallel to our study leading to *Arabidopsis* plants exhibiting a decreased lignin content (Jouanin, personal communication). In contrast to *AtCCR1*, *AtCCR2* is present only in trace amounts in healthy tissues, suggesting that it is not involved in lignification during development.

Since lignification has been reported as a part of the active mechanisms induced during resistance (Dixon and Lamb, 1990), the question whether the *AtCCR* genes are regulated in response to pathogen infection has been addressed. *AtCCR1* transcript level is not significantly induced during incompatible interaction with *Xanthomonas campestris* pv. *campestris* leading to hypersensitive response (HR). Whereas *AtCCR2* mRNA accumulated strongly and transiently in infected leaves. Therefore it clearly appears that *AtCCR1* and *AtCCR2* genes show a differential expression pattern in response to *Xanthomonas* infection, suggesting a role for *AtCCR2* in the establishment of disease resistance mechanisms. As observed in other pathosystems, lignification can be one important component of the defence response leading to resistance (Fusch and Sacristan, 1996; Tang et al., 1999). Several studies have shown that genes involved in the early or later steps of lignification (phenylpropanoid and monolignols synthesis) are up-regulated in response to pathogen infection (Dong et al., 1991; Buell and Somerville, 1995). For example, an increase in mRNA accumulation of *C4H*, *CAD* and *Eli3* (the latest subsequently identified as a CAD, Logemann et al., 1997) was observed in *Arabidopsis* ecotype Col-O undergoing an HR (Buell and Somerville, 1995). The data presented here are in agreement with these observations suggesting a close relationship between induction of genes of the monolignol pathway and HR-mediated resistance.

Although lignins or "lignin-like material" are known to be synthesised during the hypersensitive reaction to reinforce cell walls, interfering with pathogen penetration, lignification appears only as a late response in the resistance process. In the pathosystem studied here, we would favour the hypothesis that the end products of the *AtCCR2*-mediated pathway may not be lignins or "lignin-like" material but rather intermediary phenolic compounds that could be synthesised more rapidly than the polymer itself and which play a role in defence either by a phytoalexin action or by reinforcing the cell walls, or both. In support to this hypothesis, coniferaldehyde and coniferyl alcohol which are the products of the *CCR* and *CAD*-mediated reactions, respectively, appear to function as phytoalexins in the incompatible interaction between flax and *Melampsora lini* and are involved in the restriction of the fungus growth in the resistant flax leaves (Keen and Littlefield, 1979). Here, we have shown for the first time, the direct implication of a *CCR*-family member, *AtCCR2* in defence responses *via* a strong transcriptional activation during HR. The nature of the phenolic compounds leading to resistance still needs to be addressed. To this end it is worth noting that during plant evolution, the earliest role of intermediary end products of the lignin branch pathway is thought to be related to defence against bacterial, fungal or viral pathogens (Raven, 1977).

In conclusion to this work and in regard to recent data, it seems likely that some members of the gene families encoding enzymes of the monolignol biosynthesis pathway like *AtCCR2*, *COMTII* (Pellegrini et al., 1993), *Eli3* (Logemann et al., 1997 and references therein) are poorly expressed during development and belong to a specifically regulated pathway preceding HR or activated as a consequence of HR establishment.

4. Experimental

4.1. Arabidopsis CCRs

The EST database (dbEST) (Newman et al., 1994; Cooke et al., 1996) was searched using the NCBI GenInfo network BLAST server (Altschul et al., 1990) for CCR-like sequences from *Arabidopsis*, and this resulted in the identification of two cDNAs encoding CCR. The 67e6t7 EST (T41765), initially isolated from a cDNA library prepared from equal portions of poly(A+) mRNA from etiolated seedlings, roots, leaves, and flowering inflorescences (Newman et al., 1994), was obtained from the Arabidopsis Biological Resource Center at

Ohio State University. The RaR108 clone (Z24528) was isolated from an *Arabidopsis* cDNA library prepared from a cell suspension inoculated for one hour with *Xanthomonas campestris* pv. *campestris* in the presence of cycloheximide (Lacomme and Roby, 1996).

4.2. Sequencing and phylogenetic analyses

Nucleotide sequencing was performed automatically, in both directions, using an Applied Biosystems automated sequencer (Perkin Elmer/Applied Biosystems Division). After completion of sequencing of the cDNAs corresponding to the ESTs 67e6t7 and RaR108, they were renamed respectively *AtCCR1* and *AtCCR2*.

Standard sequence analysis was performed using the PCgene software package (IntelliGenetics, Inc.). The phylogenetic tree was obtained using the DARWIN software (Gonnet et al., 1992) with the public server (CBRG@inf.ethz.ch). Multiple alignments were performed using CLUSTAL W (Thompson et al., 1994).

4.3. Plant material

Seeds of *Arabidopsis thaliana* L. (Heynh) ecotypes Col-O were soaked in water for 2 h, then sterilised for 10 min in a 12% Na hypochlorite solution and washed in sterile water. Seeds were spread on MS (Murashige and Skoog, 1962) medium and grown in vitro for one week in a culture chamber (16 h photoperiod, 20°C). The young plantlets were transferred to soil and grown in a growth chamber (9 h photoperiod, 22°C) as described by Lummerzheim et al. (1993).

4.4. Bacterial strain and inoculation procedure

The source and growth conditions of the isolate 147 of *Xanthomonas campestris* pv. *campestris* isolates, as well as the plant inoculation procedure used in this study (manual infiltration of leaves), were as described by Lummerzheim et al. (1993).

4.5. Southern and Northern blot analyses

Genomic DNA was purified from *Arabidopsis* according to the protocol described by Dellaporta et al. (1983), and digested with appropriate restriction enzymes: *Bam*HI, *Eco*RI, *Eco*RV, *Pst*I and *Xba*I, that do not cut *AtCCR2* cDNA. The Southern blot experiment was performed as previously described by Lacomme and Roby (1996), using a *Bgl*II-*Dra*I fragment (position 248 to 951 in *AtCCR2*).

RNA extraction and Northern blot analysis were as previously described by Lummerzheim et al. (1993). Specific probes were generated by PCR: *AtCCR1* specific probe (491bp) was obtained using sense 5AT1 [5′AGCCGAGAGTGCTCGCC3′] and antisense 3AT1 [5′TAAGTGTAATCTATTACATAG3′] primers located respectively at positions 755 and 1246 on the *AtCCR1* cDNA; *AtCCR2* specific probe (402bp) was obtained using 5AT2 [5′GCGCGAGACCGCACT TG3′] and 3AT2 [5′TTTTTAAGAAAGAACAATCA GC3′] primers located respectively at positions 797 and 1191 of the corresponding cDNA. The amplified fragments were gel-purified and radio-labelled by random priming using a Nonaprimer Kit II (Appligene). The absence of cross hybridisation between the two probes was verified on Southern blots.

4.6. Expression in Escherichia coli and purification of fusion proteins

AtCCR1 cDNA was digested with *Eco*RI and *Not*I and ligated into the *Eco*RI-*Not*I linearized pGEX 4T-1 vector (Pharmacia). For convenient cloning of the *AtCCR2* cDNA, an *Eco*RI site was introduced by PCR, fifteen bases downstream from the ATG start codon. PCR reactions were performed using one oligonucleotide 5′ATTGAATTCCTCGTCTGCGTCACC3′ introducing an *Eco*R1 site and the M13 -20 universal primer (Biolabs), located on the pBluescript-SK downstream from the stop codon. The amplified product was digested with *Eco*RI and *Xho*I and ligated into *Eco*RI-*Xho*I linearized pGEX 4T-1 vector. The fidelity of PCR was checked by DNA sequencing. Both constructs were introduced into *E. coli* strain BL21 (DE3) (Studier and Moffat, 1986). Growth and induction of bacterial cells with isopropyl β-D-thiogalactoside at 0.1 mM final concentration were performed as described in Lauvergeat et al. (1995). The fusion proteins CCR-GST were purified from bacterial lysate on a Glutathione Sepharose 4B column (Pharmacia) according to the manufacturer's instructions. Protein concentrations were determined by the Bradford assay (Bradford, 1976).

4.7. CCR activity assay and K_m determination

CCR activity was measured spectrophotometrically and determination of kinetic parameters was performed as previously described in Goffner et al. (1994). The three substrates: feruloyl CoA, sinapoyl CoA and caffeoyl CoA, were synthesised according to the method of Stöckigt and Zenk (1975).

Acknowledgements

The authors are grateful to the *Arabidopsis* Biological Resource Center at Ohio State for DNA material (*AtCCR1* cDNA clone) and to Deborah Goffner for providing the corresponding sequence. We thank François Godard for providing infected plant material used for Northern blot analysis and Saida Danoun for the

synthesis of CCR substrates. This work was financially supported by CNRS, Université Paul Sabatier and INRA funds.

References

Altschul, S.F., Gish, W., Miller, W., Myers, E.W., Lipman, D.J., 1990. Basic local alignment search tool. Journal of Molecular Biology 215, 403–410.

Bradford, M.M., 1976. A rapid and sensitive method for the quantitation of microgram quantities of protein utilizing the principle of protein-dye binding. Analytical Biochemistry 72, 248–254.

Buell, C.R., Somerville, S.C., 1995. Expression of defense-related and putative signalling genes during tolerant and susceptible interactions of Arabidopsis with *Xanthomonas campestris* pv. *campestris*. Molecular Plant-Microbe Interactions 8, 435–443.

Chappell, J., Hahlbrock, K., 1984. Transcription of plant defense genes in response to UV light or fungal elicitor. Nature 311, 76–78.

Chapple, C.C.S., Vogt, T., Ellis, B.E., Somerville, C.R., 1992. An *Arabidopsis* mutant defective in the general phenylpropanoid pathway. Plant Cell 4, 1413–1424.

Cooke, R., Raynal, M., Laudie, M., Grellet, F., Delseny, M., Mooris, P., Guerrier, D., Giraudat, J., Quigley, F., Clabault, G., Li, Y.F., Mache, R., Krivitzky, M., Gy, J.J., Kreis, M., Lecharny, A., Parmentier, Y., Marbach, J., Fleck, J., Clement, B., Phillips, G., Herve, C., Bardet, C., Tremousaygue, D., Lescure, B., Lacomme, C., Roby, D., Jourjon, M.F., Chabrier, P., Charpenteau, J.L., Desprez, T., Amsellem, J., Chiapello, H., Hofte, H., 1996. Further progress towards a catalogue of all *Arabidopsis* genes: analysis of a set of 5000 non-redundant ESTs. Plant Journal 9, 101–124.

Corpet, F., 1988. Multiple sequence alignment with hierarchical clustering. Nucleic Acids Research 16, 10881–10890.

Dellaporta, S.L., Wood, J., Hicks, J.B., 1983. A plant DNA minipreparation: version II. Plant Molecular and Biological Reports 1, 19–21.

Dixon, R.A., Lamb, C.J., 1990. Molecular communication in interactions between plants and microbial pathogens. Annual Review of Plant Physiology and Plant Molecular Biology 41, 339–367.

Dixon, R.A., Paiva, N.L., 1995. Stress-induced phenylpropanoid metabolism. Plant Cell 7, 1085–1097.

Dong, X., Mindrinos, M., Davis, K.R., Ausubel, F.M., 1991. Induction of *Arabidopsis* defense genes by virulent and avirulent *Pseudomonas syringae* strains and by a cloned avirulence gene. Plant Cell 3, 61–72.

Fusch, H., Sacristan, M.D., 1996. Identification of a gene in *Arabidopsis thaliana* controlling resistance to clubroot (*Plasmodiophora brassicae*) and characterization of the resistance response. Molecular Plant-Microbe Interactions 9, 91–97.

Goffner, D., Campbell, M.M., Campargue, C., Clastre, M., Borderies, G., Boudet, A., Boudet, A.M., 1994. Purification and characterization of cinnamoyl-CoA:NADP oxidoreductase in *Eucalyptus gunnii*. Plant Physiology 106, 625–632.

Gonnet, G.M., Cohen, M.A., Benner, S.A., 1992. Exhaustive matching of the entire protein sequence database. Science 256, 1443–1445.

Hahlbrock, K., Scheel, D., 1989. Physiology and molecular biology of phenylpropanoid metabolism. Annual Review of Plant Physiology and Plant Molecular Biology 40, 347–369.

Keen, N.T., Littlefield, L.J., 1979. The possible association of phytoalexins with resistance gene expression in flax to *Melampsora lini*. Physiology and Plant Pathology 14, 265–280.

Kimmins, W.C., Wuddah, D., 1977. Hypersensitive resistance: determination of lignin in leaves with a localized virus infection. Phytopathology 67, 1012–1016.

Kosak, M., 1984. Compilation and analysis of sequences upstream from the translational start site in eucaryotic mRNAs. Nucleic Acids Research 12, 857–872.

Lacombe, E., Hawkins, S., Van Dorsselaere, J., Piquemal, J., Goffner, D., Poeydomenge, O., Boudet, A.M., Grima-Pettenati, J., 1997. Cinnamoyl CoA reductase, the first committed enzyme of the lignin branch biosynthetic pathway: cloning, expression and phylogenetic relationships. Plant Journal 11, 429–441.

Lacombe, E., Van Dorsselare, J., Boerjan, W., Boudet, A.M., Grima-Pettenati, J., 2001. Characterisation of *cis*-elements required for vascular expression of the Cinnamoyl CoA Reductase gene and for protein-DNA complex formation. *Plant Journal*.

Lacomme, C., Roby, D., 1996. Molecular cloning of a sulfotransferase in *Arabidopsis thaliana* and regulation during development and in response to infection with phytopathogenic bacteria. Plant Molecular Biology 30, 995–1008.

Lange, B.M., Lapierre, C., Sandermann Jr., H., 1995. Elicitor-induced spruce stress lignin. Structural similarity to early developmental lignins. Plant Physiology 108, 1277–1287.

Lauvergeat, V., Kennedy, K., Feuillet, C., McKie, J.H., Gorrichon, L., Baltas, M., Boudet, A.M., Grima-Pettenati, J., Douglas, K.T., 1995. Site-directed mutagenesis of a serine residue in cinnamyl alcohol dehydrogenase, a plant NADPH-dependant dehydrogenase, affects the specificity for the coenzyme. Biochemistry 34, 12426–12434.

Lawton, M.A., Lamb, C.J., 1987. Transcriptional activation of plant defense genes by fungal elicitor, wounding and infection. Molecular Cell Biology 7, 335–341.

Legrand, M., 1983. Phenylpropanoid metabolism and its regulation in disease. In: Callow, J.A. (Ed.), Biochemical Plant Pathology. John Wiley and Sons, Chichester, UK, pp. 367–384.

Leplé, J.C., Grima-Pettenati, J., Van Montagu, M., Boerjan, W., 1998. A cDNA encoding cinnamoyl-CoA reductase from *Populus trichocarpa*. Plant Physiology 117, 1126.

Lewis, N.G., Davin, L.B., 1994. Evolution of lignan and neolignan biochemical pathways. In: Nes, D. (Ed.), Evolution of Natural Products. ACS Symposium Series No. 562. American Chemical Society, Washington, DC, pp. 202–246.

Lewis, N.G., Yamamoto, E., 1990. Lignin: occurrence, biogenesis and biodegradation. Annual Review of Plant Physiology and Plant Molecular Biology 41, 455–496.

Logemann, E., Reinold, S., Somssich, I.E., Hahlbrock, K., 1997. Modes of expression and common structural features of the complete phenylalanine ammonia-lyase gene family in parsley. Biological Chemistry 378, 909–913.

Lüderitz, T., Grisebach, H., 1981. Enzymic synthesis of lignin precursors. Comparison of cinnamoyl-CoA reductase and cinnamyl alcohol:NADP dehydrogenase from spruce (*Picea abies* L.) and soybean (*Glycine max* L.). European Journal of Biochemistry 119, 115–124.

Lummerzheim, M., De Oliveira, D., Castresana, C., Miguens, F.C., Louzada, E., Roby, D., Van Montagu, M., Timmerman, B., 1993. Identification of compatible and incompatible interactions between *Arabidopsis thaliana* and *Xanthomonas campestris* pv. *campestris* and characterization of the hypersensitive response. Molecular Plant-Microbe Interactions 6, 532–544.

Lütcke, H.A., Chow, K.C., Mickel, F.S., Moss, K.A., Kern, H.F., Scheele, G.A., 1987. Selection of AUG initiation codons differs in plants and animals. EMBO Journal 6, 43–48.

Messner, B., Boll, M., 1993. Elicitor-mediated induction of enzymes of lignin biosynthesis and formation of lignin like material in cell suspension cultures of spruce (*Picea abies*). Plant Cell Tissue Organ Culture 34, 261–269.

Moershbacher, B., Noll, U., Gorrichon, L., Reisener, H.J., 1990. Specific inhibition of lignification breaks hypersensitive resistance of wheat to stem rust. Plant Physiology 93, 465–470.

Murashige, T., Skoog, F., 1962. A revised medium for rapid growth and bioassays with tobacco tissue cultures. Physiologia Plantarum 15, 473–479.

Newman, T., de Bruijn, F.J., Green, P., Keegstra, K., Kende, H., McIntosh, L., Ohlrogge, J., Raikhel, N., Somerville, S., Thomashow,

M., Retzel, E., Somerville, C., 1994. Genes galore: a summary of methods for accessing results from large-scale partial sequencing of anonymous *Arabidopsis* cDNA clones. Plant Physiology 106, 1241–1255.

Nicholson, R.L., Hammerschmidt, R., 1992. Phenolic compounds and their role in disease resistance. Annual Review of Phytopathology 30, 369–389.

Pellegrini, L., Geoffroy, P., Fritig, B., Legrand, M., 1993. Molecular cloning and expression study of a new class of ortho-diphenol-*O*-methyl transferases induced in tobacco (*Nicotiana tabacum* L.) leaves by infection of elicitor treatment. Plant Physiology 103, 509–517.

Pichon, M., Courbou, I., Beckert, M., Boudet, A.M., Grima-Pettenati, J., 1998. Cloning and characterization of two maize cDNAs encoding cinnamoyl CoA reductase (CCR) and differential expression of the corresponding genes. Plant Molecular Biology 38, 671–676.

Piquemal, J., Lapierre, C., Myton, K., O'Connell, A., Schuch, W., Grima-Pettenati, J., Boudet, A.M., 1998. Down-regulation of cinnamoyl-CoA reductase induces significant changes of lignin profiles in transgenic tobacco plants. Plant Journal 13, 71–83.

Raven, J.A., 1977. The evolution of vascular plants in relation to supracellular transport processes. In: Woolehouse, H. (Ed.), Advances in Botanical Research, Vol. 5. pp. 153–219.

Ride, J.P., 1983. Structural barriers in defense. In: Callow, J.A. (Ed.), Biochemical Plant Pathology. John Wiley and Sons, Chichester, UK, pp. 215–236.

Sarni, F., Grand, C., Boudet, A.M., 1984. Purification and properties of cinnamoyl CoA reductase and cinnamyl alcohol dehydrogenase from poplar stems. European Journal of Biochemistry 1, 259–265.

Stöckigt, J., Zenk, M.H., 1975. Chemical syntheses and properties of hydroxycinnamoyl-coenzyme A derivatives. Zeitschrift für Naturforschung 30, 352–358.

Studier, F.W., Moffat, B.A., 1986. Use the T7 RNA Polymerase to direct selective high-level expression of cloned genes. Journal of Molecular Biology 189, 113–130.

Tang, X., Xie, M., Jin Kim, Y., Zhou, J., Klessing, D.F., Martin, G.B., 1999. Overexpression of pto activates defense responses and confers broad resistance. Plant Cell 11, 15–29.

Thompson, J.D., Higgins, D.G., Gibson, T.J., 1994. Clustal W: improving the sensitivity of progressive multiple sequence alignment through sequence weighting, position-specific gap penalties and weight matrice choice. Nucleic Acids Research 22, 4673–4680.

Vance, C.P., Kirk, T.K., Sherwood, R.T., 1980. Lignification as a mechanism of disease resistance. Annual Review of Phytopathology 18, 259–288.

Walter, M.H., 1992. Regulation of lignification in defense. In: Boller, T., Meins, F. (Eds.), Plant Gene Research Genes Involved in Plant Defense. Springer Verlag, Wien, pp. 327–352.

PERGAMON

Phytochemistry 57 (2001) 1197–1200

PHYTOCHEMISTRY

www.elsevier.com/locate/phytochem

Sesquiterpene lactones from *Smyrnium olusatrum*

Ali A. El-Gamal*

Department of Pharmacognosy, Faculty of Pharmacy, Mansoura University, Mansoura 35516, Egypt

Received in revised form 12 January 2001

Abstract

Fruits of *Smyrnium olusatrum* afforded three sesquiterpene lactones, namely, 1β,8β-dihydroxyeudesman-3,7(11)-dien-8α,12-olide, 1β,8β-dihydroxyeudesman-4(15),7(11)-dien-8α,l2-olide, and 1β,10α,4α,5β-diepoxy-6β-hydroxyglechoman-8α,12-olide. Four related known sesquiterpenes were also isolated and characterized. The structure elucidation of the isolated compounds was based primarily on 1D and 2D NMR analyses. The in vitro cytotoxicity of the extract and isolated compounds against P-388 mouse lymphoma cells will be also discussed. © 2001 Published by Elsevier Science Ltd.

Keywords: *Smyrnium olusatrum*; Apiaceae; Sesquiterpenes; Eudesmen-8α,12-olide; Glechomanolides; Cytotoxic activity

1. Introduction

Several sesquiterpene lactones, furanosesquiterpenes and oxepines have been isolated from members of the genus *Smyrnium* (Ulubelen et al., 1971, 1979, 1984, 1985; Bohlmann and Zdero, 1973; Ulubelen and Abdolmaleky, 1982; Goren et al., 1984; Ulubelen and Oksuz, 1984; Goren and Ulubelen, 1985, 1987a,b; Ulubelen and Goren, 1986; Molleken et al., 1998). The young shoots of *Smyrnium olusatrum* are cultivated and used as pot herb and edible salad in some areas in Libya. The plant is also used as antiscorbutic in Palestine (Jafri and El-Gadi, 1985). This study reports the isolation of three new sesquiterpene lactones **1**, **2** and **5** in addition to four known ones **3**, **4**, **6** and **7** from the fruits of *S. olusatrum* collected from the Libyan desert. The cytotoxicity of the CH_2Cl_2 extract and the isolated compounds is also reported.

2. Results and discussion

Repeated chromatography of the cytotoxic CH_2Cl_2 extract of the fruits of *S. alusatrum* on normal and C18 reversed phase silica gel afforded the new sesquiterpene lactones **1**, **2** and **5**, in addition to the four known sesquiterpenes 1β-acetoxyeudesman-4(15),7(11)-dien-8α,12-olide (**3**), 1β acetoxy, 8β-hydroxyeudesman-4(15),7(11)-dien-8α,12-olide (**4**) (Ulubelen et al, 1985), 1β,10α, 4α,5β-diepoxyglechoman-8α,12-olide (**6**), previously reported as a semi-synthetic derivative (Stahl and Datta, 1972), and 1β,10α, 4α,5β-diepoxy-8α hydroxy-glechoman-8α,12-olide (**7**) (Ulubelen et al., 1985).

The EIMS of **1** displayed a molecular ion peak $[M]^+$ at m/z 264, suggesting the molecular formula $C_{15}H_{20}O_4$ and six degrees of unsaturation. The IR spectrum (KBr) of **1** showed an intense broad absorption band around 3400 cm^{-1}, for hydroxyl groups, 1762 cm^{-1}, for α,β-unsaturated lactone functionality. The ^{13}C and ^1H NMR spectra of **1** (Table 1) were in agreement with a dihydroxy C-8,12 eudesmanolide skeleton for **1** (Ulubelen et al., 1985). The oxygenated doublet of doublets resonating at δ 3.78 ($J = 7.5$ and 7.5) (Table 1), which correlated with the methine carbon resonating at δ 75.2, was assigned to H-1. This was based on the observed ^3J-HMBC coupling between C-1 and the methyl proton singlet resonating at δ 1.59 (H_3-14) (Fig. 1). This was further supported by the observed COSY couplings between H-1 and both proton signals resonating at δ 2.45 and 2.30 (H_2-2). The high $J_{1,2}$ values suggested the α-configuration of H-1 and indicated its axial orientation (Ulubelen et al., 1985). Both H_2-2 also displayed COSY couplings with the broad olefinic singlet resonating at δ 5.40 (H-3) which in turn displayed a ^3J-HMBC coupling with the methyl carbon at δ 21.0 (C-15) (Fig. 1).

The downfield quaternary carbon resonating at δ 105.1 was assigned to C-8. This was suggested by its ^3J-HMBC couplings with both proton signals resonating at δ 2.89 and 2.56 (H_2-6). The carbonyl ester C-12 (δ_C

* Tel.: +20-50-347496; fax: +20-50-347496.
E-mail address: aelgamal00@yahoo.com (A.A. El-Gamal).

0031-9422/01/$ - see front matter © 2001 Published by Elsevier Science Ltd.
PII: S0031-9422(01)00211-4

Table 1
^{13}C and ^{1}H NMR spectral data of compounds **1**[a], **2**[a] and **5**[b]

Position	**1**		**2**		**2**[c]	**5**[b]	
	δ_C	δ_H	δ_C	δ_H	δ_H	δ_C	δ_H
1	75.2, *d*	3.78, *dd* (7.5, 7.5)	78.1, *d*	3.60, *m*	3.35, *dd* (11.5, 4.4)	69.0, *d*	2.74, *brd* (10.3)
2	33.4, *t*	2.45, *m*	31.7, *t*	1.91, *m*	1.70, *m*	22.8, *t*	2.03, *dd* (13.9, 3.2)
		2.30, *m*		1.78, *m*	1.60, *brdd* (12.5, 4.4)		1.40, *dd* (13.9, 10.6, 3.2)
3	122.1, *d*	5.40, *brs*	34.3, *t*	2.35, *m*	2.33, *ddd* (11.5, 5.0, 3.0)	37.1, *t*	2.33, *m*
				2.17, *ddd* (13.8, 5.2, 1.2)	2.00, *brdd* (13.5, 5.2)		1.38, *m*
4	133.5, *s*	–	148.4, *s*	–	–	60.0, *s*	–
5	49.2, *d*	2.10, *brd* (13.3)	50.0, *d*	1.95, *m*	2.1, *brdd* (13.5, 5.2)	65.7, *d*	3.19, *d* (6.5)
6	24.4, *t*	2.89, *dd* (13.1, 3.1)	24.6, *t*	2.75, *m*	2.62, *dd* (13.2, 3.4)	68.8, *d*	4.69, *dd* (6.5, 2.9)
		2.56, *brt* (13.2)			2.45, *btr* (13.2)		
7	162.1, *s*	–	161.8, *s*	–	–	156.6, *s*	–
8	105.1, *s*	–	104.6, *s*	–	–	78.6, *d*	5.44, *dd* (5.4, 1.8)
9	47.9, *t*	3.33, *d* (13.4)	49.0, *t*	3.34, *d* (13.4)	2.74, *d* (13.8)	38.7, *t*	2.97, *dd* (15.9, 1.8)
		1.75, *d* (13.1)		1.81, *d* (13.4)	1.50, *d* (13.8)		1.84, *dd* (15.9, 5.4)
10	39.5, *s*	–	42.1, *s*	–	–	57.8, *s*	–
11	121.6, *s*	–	121.5, *s*	–	–	129.6, *s*	–
12	172.7, *s*	–	172.7, *s*	–	–	172.6, *s*	–
13	8.2, *q*	1.87, 3H, *s*	8.2, *q*	1.83, 3H, *s*	1.80, 3H, *s*	10.2, *q*	1.92, 3H, *d* (1.9)[d]
14	10.5, *q*	1.59, 3H, *s*	11.3, *q*	1.49, 3H, *s*	1.00, 3H, *s*	17.4, *q*	1.08, 3H, *s*
15	21.0, *q*	1.73, 3H, *s*	107.6, *t*	4.96, *d* (1.2)	4.89, *s*	17.4, *q*	1.25, 3H, *s*
				4.77, *d* (1.2)	4.56, *s*		
1-OH	–	6.32, *brs*	–	U		–	–
6-OH	–	–	–	–		–	2.68, *d* (2.9)
8-OH	–	9.42, *s*	–	U		–	–

[a] In pyridine-d_5, 400 MHz for ^{1}H and 100 MHz for ^{13}C NMR. Carbon multiplicities were determined by DEPT135° experiments. *s* = Quaternary, *d* = methine, *t* = methylene, *q* = methyl carbons, coupling constants *(J)* are in Hz, U = unobserved.
[b] In $CDCl_3$, 500 MHz for ^{1}H and 125 MHz for ^{13}C NMR.
[c] In $CDCl_3$, 400 MHz.
[d] Long range with proton number 6 (Ulubelen and Goren, 1986).

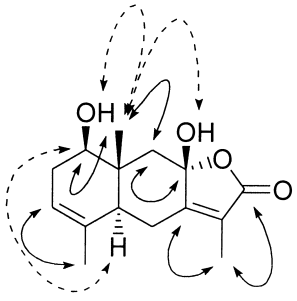

Fig. 1. Important HMBC (solid lines) and NOESY (dashed lines) correlations of **1**.

172.7) displayed a ^{3}J-HMBC coupling with the proton methyl singlet resonating at δ 1.87 (H_3-13).

The assignment of the relative stereochemistry of **1** was further supported by NOESY data (Fig. 1) and the study of Drieding model. Thus, the β-oriented C-14 methyl singlet displayed NOESY correlations with both exchangeable proton singlets at δ 6.32 (C-1 OH) and 9.42 (C-8 OH), confirming their β-orientation. Likewise, the α-oriented H-1 was NOESY-correlated with the broad doublet resonating at δ 2.10 (H-5), suggesting their location on the same face of **1**. Compound **1** was, therefore, identified as the new sesquiterpene 1β,8β-dihydroxyeudesm - 3,7(11) - dien - 8α,12 - olide (**1**). It is worth noting that the C-1 acetoxy derivative of **1** was previously reported from *Smyrnium galaticum* (Ulubelen and Goren, 1986).

The EIMS of **2** displayed a molecular ion peak $[M]^+$ at *m/z* 264, suggesting the same molecular formula of **1** ($C_{15}H_{20}O_4$). The IR spectrum (KBr) of **2** showed a similar pattern to those of **1** with an additional absorption band at 890 cm^{-1}, characteristic for an exocyclic methylene group. The ^{13}C and ^{1}H NMR spectral data of **2** (Table 1) were in agreement with those of **1** with the replacement of the $\Delta^{3,4}$ with $\Delta^{4,15}$ system. The two olefinic proton doublets resonating at δ 4.96 and 4.77 which correlated with the methylene carbon at δ 107.6 were assigned H_2-15. Both protons displayed ^{3}J-HMBC couplings with C-5 (δ 50.0) and C-3 (δ 34.3) and ^{2}J-HMBC coupling with the quaternary olefinic carbon at δ 148.8 (C-4). Therefore, **2** is the deacetylated derivative of compound **4**. In fact, comparing the ^{1}H NMR data of **2** in $CDCl_3$ with those of **4** (Table 1) indicate that having significant difference of H_1 proton being 3.35 (*dd*, J = 11.5, 4.4 Hz) in **2** while it is 4.57 (*dd*, J = 11.6, 4.7 Hz) in **4**. Hence, compound **2** was proved to be 1β,8β-dihydroxyeudesm-4(15),7(11)-dien-8α,12-olide.

The EIMS of **5** displayed a molecular ion peak $[M]^+$ at *m/z* 280, suggesting the molecular formula $C_{15}H_{20}O_5$ and six degrees of unsaturation. The IR spectrum (KBr)

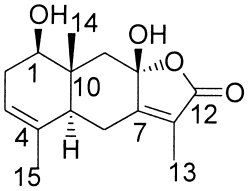

1

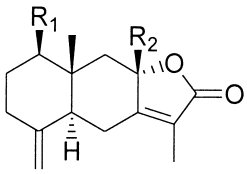

	R_1	R_2
2	OH	OH
3	OAc	H
4	OAc	OH

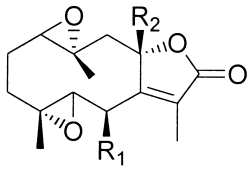

	R_1	R_2
5	OH	H
6	H	H
7	H	OH

of **5** showed an absorption band at 3637 cm^{-1} for hydroxyl group and 1756 cm^{-1} for α,β-unsaturated lactone functionality. The ^{13}C and ^{1}H NMR spectra of **5** (Table 1) suggested a monohydroxy C-8, 12 germacranolide skeleton for **5** (Stahl and Datta, 1972; Ulubelen et al., 1985). The oxygenated doublet of doublets resonating at δ 4.69 ($J=6.5$ and 2.9) (Table 1), which correlated with the methine carbon resonating at δ 68.8, was assigned to H-6. This was based on the observed COSY coupling between H-6 and the proton doublet resonating at δ 3.19 (H-5) and the exchangeable proton doublet at δ 2.68 (C-6 OH). The proton H-6 displayed ^{3}J-HMBC coupling with C-4 (δ 60.0) and C-11 (δ 129.6). A ^{2}J-HMBC coupling was also observed between H-6 and C-7 (δ 156.6). The proton doublet of doublets resonating at δ 5.44 which correlated with the oxygenated methine carbon at δ 78.6 was assigned H-8. This was based on its COSY coupling with the doublet of doublets resonating at δ 2.97 and 1.84 (H_2-9). The methylene H_2-9 displayed a ^{3}J-HMBC coupling with C-14 methyl singlet (δ_C 17.4).

Once again, the assignments of the relative stereochemistry of **5** were based on NOESY data. Thus, the β-oriented C-14 methyl singlet displayed NOESY correlation with the proton doublet of doublets at δ 2.97 (H-9b) which in turn showed cross peak with H-8, confirming their β-orientation. The exchangeable proton doublet at δ 2.68 showed NOESY correlation to the methyl singlet at δ 1.25 (H_3-15), suggesting their β-orientation. Likewise, the α-oriented H-1 was NOESY-correlated with the proton doublet resonating at δ 3.19 (H-5), suggesting their location on the same lower face of **5**. Compound **5** was therefore identified as the new germacranolide 1β, 10α, 4α, 5β-diepoxy-6β-hydroxyglechoman-8α,12-olide.

The CH_2Cl_2 extract of the fruits of *S. olusatrum* exhibited significant in vitro cytotoxicity (IC_{50} 9.0 μg ml^{-1}) against P-388 mouse lymphoma cells. (Carmichael et al., 1987; Twentyman and Luscombe, 1987). However, the isolated compounds (**1**, **2**, **3**, **4**, **6** and **7**) showed marginal activity with IC_{50} 60, 65, 42, 58, 94 and 88 μg ml^{-1}, respectively.

3. Experimental

3.1. General

Mps: uncorrected, Yanagimoto MP-3 micro mp apparatus. ^{1}H and ^{13}C NMR: $CDCl_3$ or pyridine with TMS as int. standard, Bruker AM 400 and Bruker AM 500 2D NMR (COSY, NOESY, HMQC and HMBC), EI–MS: 70 eV, Hitachi M-80 or VG Autospec. IR: KBr on a Jasco A-302 or Perkin Elmer 1710. UV: CH_3OH, Hitachi 557. Prep. HPLC: Rp-18 column (10 μm, 30×2.15 cm i.d.). MPLC Rp-18 column (20 μm, 10×2.15 cm i.d.). Kusano Scientific Co. CC: Kieselgel 60, anal. TLC: silica gel $60F_{254}$ and RP-18 F_{254} (0.25 mm) precoated plates. Spots detection: UV light at 254 and/or spraying with 10% H_2SO_4. Cytoxicity bioassay: Tosoh MPR-A4i microplate reader.

3.2. Plant material

The fruits of *Smyrnium olusatrum* were collected from the moist and shady places of the Gebel Akhdar area in Libya in 1996. The plant was identified by Professor Dr. Elgady, Faculty of Science, El-Faateh University, Tripoli, Libya. A voucher specimen is deposited in the Pharmacognosy Department, Faculty of Pharmacy, Mansoura University, Mansoura, Egypt.

3.3. Extraction and isolation

Air dried powdered fruits (750 g) were extracted to exhaustion by hot 70% methyl alcohol. The methanolic extract was concentrated under reduced pressure to give about 100 g of the total extract ($IC_{50}=10.2$ μg ml^{-1} to P-388 cell line). The extract was treated with a minimum volume of alcohol diluted with water and successively partitioned with pet. ether, CH_2Cl_2 and *n*-butanol. The CH_2Cl_2 extract (13 g, $IC_{50}=9$ μg ml^{-1} to P-388 cell line) was applied to the top of silica gel packed column (390 g) and eluted with pet. ether—EtOAc gradient. Similar fractions were combined and subjected either to direct crystallization or to further chromatographic purifica-

tion on normal and C-18 reversed phase silica (using MPLC and HPLC). The CH_2Cl_2 extract afforded four main fractions, fractions 13–15, fraction 20, fractions 26–29 and fractions 30–35. Direct crystallization of fractions 13–15 and 20 gave compounds **3** (70 mg) and **4** (80 mg) respectively. Fractions 26–29 were further purified by using MPLC with H_2O:CH_3CN gradient to give compound **7** (60 mg). Fractions 30–35 were applied to the top of a silica gel packed column using CH_2Cl_2: MeOH gradient to give three main subfractions. Subfractions 6–8 afforded compound **6** (40 mg) on direct crystallization from MeOH while subfractions 13-16 and 19–22 were further purified using HPLC on Rp-18 column with CH_3CN:H_2O (20:80 and 30:70). Fractions 13–16 gave compound **7** (30 mg) while fractions 19–22 gave compounds **1**, **2** and **5** (20, 30 and 3 mg respectively).

*3.3.1. 1β,8β-Dihydroxy eudesman 3,7(11)-dien 8α,12 olide (**1**)*

White needle crystals from MeOH; mp 193–195°C, UV λ_{max} MeOH, 215 IR *v* KBr 3400, 2976, 2933, 1762, 1898, 1471, 1353, 1323, 1241, 1042, 1007, 946.

EI–MS *m/z* (rel. int.): 264 $[M]^+$ (52) (calc. for $C_{15}H_{20}O_4$), 246 $[M^+–H_2O]$ (50), 228 (40), 213 (27), 194 (21), 166 (52), 126 (100), 121 (45), 105 (28), 91 (38), 69 (59), 53 (37). ^{1}H NMR (400 MHz, pyridine-d_5) and ^{13}C NMR (100 MHz, pyridine-d_5) Table 1.

*3.3.2. 1β,8β-Dihydroxy eudesman 4(15),7(11)-dien 8α,12 olide (**2**)*

White prism crystals from MeOH; mp 178–180°C. UV λ_{max} nm: 218 IR *v* KBr cm^{-1} 3410, 2950, 1758, 1660, 1470, 1386, 1347, 890, 861. EI–MS *m/z* (rel. int.): 264 $[M]^+$ (100) (calc. for $C_{15}H_{20}O_4$), 246 $[M–H_2O]^+$ (55) 236 (75), 218 (38), 203 (47), 189 (37), 175 (52), 163 (81), 145 (56), 105 (47), 91 (60), 55 (62).

^{1}H NMR (400 MHz, pyridine-d_5, $CDCl_3$) and ^{13}C NMR (100 MHz, pyridine -d_5) Table 1.

*3.3.3. 1β,10α;4α,5β-Diepoxy 6-β-hydroxy-glechoman-8α, 12 olide (**5**)*

White needle crystals (3 mg) from MeOH; mp 165–168°C. UV λ_{max} nm: 217. IR *v* $CHCl_3$ cm^{-1}, 3637, 2906, 1756, 1034, 853, 765, 723. EI–MS *m/z* (rel. int.): 280 $[M]^+$ (12) (calc. for $C_{15}H_{20}O_5$), 262 $[M–H_2O]^+$ (50), 251 (7), 233 (13), 205 (11), 181 (31), 150 (26), 126 (52), 111 (35), 97 (63), 83 (37), 69 (100), 53 (37). ^{1}H NMR (500 MHz, $CDCl_3$) and ^{13}C NMR (125 MHz, $CDCl_3$) Table 1.

Acknowledgements

The author would like to thank Professors H. Itokawa and K. Takeya, Tokyo University of Pharmacy and Life Science, for the NMR analyses and Professor H. Abd El Fattah, Faculty of Pharmacy, Mansoura University, Egypt, for providing the plant material.

References

Bohlmann, F., Zdero, C., 1973. Polyacetylenvenbindungen, 220. Über die Inhaltsstoffe von *Smyrnium olusatrum* L. (Polyacetylenic compounds 220 on the constituents of *Smyrnium olusatrum* L. Chem. Ber. 106, 3614–3620.

Carmichael, J., DeGraff, W.G., Gazdar, A.F., Minna, J.D., Mitchell, B., 1987. Evaluation of a tetrazolium-based semiautomated colorimeter assay: assessment of chemosensitivity testing. Cancer Res. 47 (4), 936–942.

Goren, N., Ulubelen, A., 1985. Oxepine derivatives from the roots of *Smyrnium rotundifolium*. Phytochemistry 24 (12), 3051–3052.

Goren, N., Ulubelen, A., 1987a. Glechomanolides and eudesmanolides from *Smyrnium perfoliatum*. Phytochemistry 26 (9), 2585–2587.

Goren, N., Ulubelen, A., 1987b. Sesquiterpene lactones from the fruits of *Smyrnium connatum*. Phytochemistry 26 (9), 2633–2634.

Goren, N., Ulubelen, A., Jakupovic, J., Bohlmann, F., Grenz, M., 1984. Sesquiterpene lactones from the fruits of *Smyrnium rotundifolium*. Phytochemistry 23 (10), 2281–2284.

Jafri, S.M.H., El-Gadi, A., 1985. Flora of Libya. Al-Faateh University, Faculty of Science Publication Tripoli, 117, p. 30.

Molleken, U., Sinnwell, V., Kubeczka, K.-H., 1998. The essential oil composition of the fruits from *Smyrnium perfoliatum*. Phytochemistry 47 (6), 1079–1083.

Stahl, E., Datta, S.N., 1972. Neue sesquiterpenoide Inhaltsstoffe der Gundelrebe (*Glechoma hederacea* L). (New sesquiterpenoides of ground ivy (*Glechoma hederacea* L.). Liebigs Ann. Chem. 757, 23–32.

Twentyman, P.R., Luscombe, M., 1987. A study of some variables in a tetrazolium dye (MTT) based assay for cell growth and chemosensitivity. Br. J. Cancer 56 (3), 279–285.

Ulubelen, A., Abdolmaleky, H., 1982. Istanbulin D and istanbulin E, two new sesquiterpene lactones from *Smyrnium creticum*. Phytochemistry 21 (8), 2128–2129.

Ulubelen, A., Ates, N., Nishida, T., 1979. Istanbulin C, a novel sesquiterpene lactone from *Smyrnium connatum*. Phytochemistry 18, 338.

Ulubelen, A., Goren, N., 1986. Additional sesquiterpenoids from the fruits of *Smyrnium galaticum*. J. Nat. Prod. 49 (6), 1104–1105.

Ulubelen, A., Goren, N., Bohlmann, F., Jakupovic, J., Grenz, M., Tanker, N., 1985. Sesquiterpene lactones from *Smyrnium cordifolium*. Phytochemistry 24 (6), 1305–1308.

Ulubelen, A., Oksuz, S., 1984. Eremophilenolides as oxidative artifacts of furanoeremophilanes. J. Nat. Prod. 47 (1), 177–178.

Ulubelen, A., Oksuz, S., Samek, Z., Holub, M., 1971. Sesquiterpene lactones from *Smyrnium olusatrum* L. roots. Tetrahedron Lett. 46, 4455–4456.

Ulubelen, A., Oksuz, S., Tanker, N., 1984. Furanosesquiterpenes from the fruits of *Smyrnium cordifolium*. Phytochemistry 23 (8), 1793–1794.

PERGAMON

Phytochemistry 57 (2001) 1201–1203

PHYTOCHEMISTRY

www.elsevier.com/locate/phytochem

Monoterpene coumarins from *Ferula ferulago*

Mohamed H. Abd El-Razek[a], Shinji Ohta[b], Ahmed A. Ahmed[c], Toshifumi Hirata[a,*]

[a]*Department of Mathematical and Life Sciences, Graduate School of Science, Hiroshima University, 1-3-1 Kagamiyama, Higashi-Hiroshima 739-8526, Japan*

[b]*Instrument Center for Chemical Analysis, Hiroshima University, 1-3-1 Kagamiyama, Higashi-Hiroshima 739-8526, Japan*

[c]*Department of Chemistry, Faculty of Science, El-Minia University, El-Minia 61519, Egypt*

Received 11 January 2001; received in revised form 27 April 2001

Abstract

Two monoterpene coumarins, designated ferulagol A and B, as well as three known monoterpene coumarins and three sesquiterpene lactones were isolated from the chloroform extract of the roots of *Ferula ferulago*. The structures of ferulagol A and B were determined to be 7-[(*E*)-3′-hydroxy-3′,7′-dimethyl-4′,6′-octadienyloxy]coumarin and 7-[(3′*Z*,5′*E*)-7′-hydroxy-3′,7′-dimethyl-3′,5′-octadienyloxy]coumarin, respectively. © 2001 Elsevier Science Ltd. All rights reserved.

Keywords: *Ferula ferulago*; Umbelliferae; Roots; Monoterpene coumarin

1. Introduction

Members of the genus *Ferula* are widespread throughout Central Asia and Mediterranean area. The gum resins, which are obtained by incision of the roots of several species are used as spices and drugs in many countries and the resins have been reported to cure stomachic, vermifuge and carminative disorders (Boulus, 1983). The extract of the roots of *Ferula ferulago* enjoys a reputation as a folk medicine and is used as an antispasmodic. The chemistry of the genus *Ferula* has been studied by many groups. The widespread compounds in this genus are characteristic sesquiterpenes (Gonzalez and Barrera, 1995; Appendino et al., 1997; Chen et al., 2000), and sesquiterpene coumarins (Murray, 1989; Ahmed, 1999). Only a few monoterpenes (Grag and Agarwal, 1988; Grag et al., 1989) have been detected. Recently, it has been reported that terpene coumarins showed anti-HIV activity (Zhou et al., 2000). Here we report the isolation and structure elucidation of the two new monoterpene coumarins designated ferulagol A (**1**) and B (**2**).

2. Results and discussion

Finely ground dried roots of *F. ferulago* were extracted with chloroform, and the extract was subjected to column chromatography to give ferulagol A (**1**) and ferulagol B (**2**), as well as three known monoterpene coumarins, 6-methoxy-7-geranyloxy coumarin (**3**) (Talapatra et al., 1973), diversinin (**4**) (Kiseleva et al.,1975), and diversin (**5**) (Kir'yalov, 1969; Kiseleva et al., 1975), and three sesquiterpene lactones malafil (**6**), malafilin (**7**), and malafilinin (**8**) (Rychlewska et al., 1985). Compounds **3** and **5** have been reported from *Feronia elephantum* (Talapatra et al., 1973), and *Machaeranthera scabrella* (Bohlmann and Grenz, 1976), respectively. Monoterpene coumarins **4** and **5** were detected in *F. diversivitata* (Kir'yalov, 1969; Kiseleva et al., 1975).

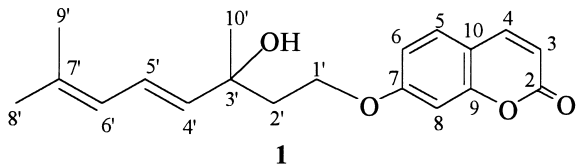

1

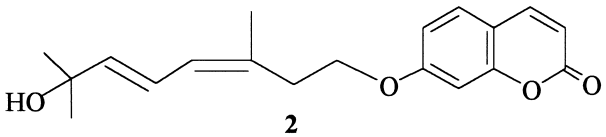

2

* Corresponding author. Tel;+81-824-247435; fax: +81-824-247435.

E-mail address: thirata@sci.hiroshima-u.ac.jp (T. Hirata).

0031-9422/01/$ - see front matter © 2001 Elsevier Science Ltd. All rights reserved.
PII: S0031-9422(01)00246-1

Ferulagol A (**1**) was shown by HRFABMS (*m*/*z* 315.1611 $[M+H]^+$, Δ +1.4 mmu) to have the molecular formula $C_{19}H_{22}O_4$. The UV and IR spectra showed the presence of hydroxyl and carbonyl groups, and carbon–carbon double bonds. Compound **1** was characterized primarily from its ^1H NMR spectrum (Table 1). This revealed a pattern of aromatic protons typical for a coumarin nucleus substituted only at C-7. The ^{13}C NMR spectrum displays nineteen carbon atoms among which were detected nine sp^2 carbon atoms of the coumarin nucleus and the 10 carbons for a side-chain, which included three methyls, one methylene attached to an oxygen function, one sp^3 methylene, one tertiary alcoholic carbon, and four olefinic carbons. After assignment of all protons directly bonded with carbon atoms by the ^1H–^{13}C shift-correlated measurement (HMQC spectrum), it was possible to assume from ^1H–^1H COSY and HMBC that **1** was a monoterpene coumarin. The ^1H–^1H COSY spectrum showed correlations between the downfield shifted olefinic proton at δ_H 6.49 (1H, *dd*) and the other two olefinic protons at δ_H 5.65 (1H, *d*) and 5.85 (1H, *d*). It is clear from the coupling constant that the geometry of the 4′,5′ double bond is *trans*. Geminal dimethyl protons H_3-8′ and H_3-9′ showed HMBC correlations to olefinic carbons at δ_C 135.9 (C-7′) and 124.2 (C-6′). The remaining methyl protons H_3-10′ showed HMBC correlations to sp^3 methylene carbon at δ_C 40.8 (C-2′), the quaternary carbon at δ_C 72.4 (C-3′), and the olefinic carbon at δ_C 136.2 (C-4′). These findings revealed the side chain structure (C-1′–C-10′). Further, the methylene protons at δ_H 4.21, 4.19 (H-1′) showed an HMBC correlation to an aromatic carbon δ_C 161.9 (C-7), indicating that the side chain is attached to C-7 of the coumarin moiety via an ether linkage. Thus, the structure of **1** was 7-[(*E*)-3′-hydroxy-3′,7′-dimethyl-4′,6′-octadienyloxy]coumarin.

The molecular formula of ferulagol B (**2**) is the same as ferulagol A (**1**) and it was determined to be $C_{19}H_{22}O_4$ by HRFABMS. The IR and UV spectra of **2** were almost identical to those of **1**. The ^1H and ^{13}C NMR spectral data are shown in Table 1. The ^{13}C NMR and DEPT spectral data showed 19 carbons including 3 methyls, two methylenes, 8 methines and 6 quaternary carbon atoms. Extensive NMR experiments (^1H–^1H COSY, HMQC and HMBC) indicated that **2** resembled **1**. All of the signals were assigned by a detailed comparison of NMR spectral data with those of **1** and 7-[(*E*)-7′-hydroxy-3′,7′-dimethyl-2′,5′-octadienyloxy]coumarin (Quader et al., 1992), except for resonances due to the monoterpenyloxy side-chain. The ^1H NMR spectrum contained a series of mutually coupled proton signals at δ_H 5.95 (1H, *d*), 6.46 (1H, *dd*), and 5.76 (1H, *d*), that indicate the presence of conjugated double bonds. The ^1H–^1H COSY spectrum of **2** clarified the connection of the carbon bonds at 3–4, 5–6–8, 1′–2′, and 4′–5′–6′. The H_3–8′ and H_3–9′ dimethyl protons showed HMBC correlations to carbon signals of C-7′ (δ_C 70.7, s) and C-6′ (δ_C 140.3, *d*). The ^{13}C chemical shift of C-7′ and the ^1H

Table 1
^1H and ^{13}C NMR spectral data for compounds **1** and **2** ($CDCl_3$)

	1		**2**	
	δ_H (*J* in Hz)	δ_C (Multiplicity)[a]	δ_H (*J* in Hz)	δ_C (Multiplicity)[a]
2		161.2 (C)		161.1 (C)
3	6.24 (9.5 *d*)	112.9[b] (CH)	6.22 (9.5 *d*)	112.3[c] (CH)
4	7.63 (9.5 *d*)	143.2 (CH)	7.62 (9.5 *d*)	143.3 (CH)
5	7.35 (8.5 *d*)	128.7 (CH)	7.34 (8.5 *d*)	128.7 (CH)
6	6.83 (8.5, 2.5 *dd*)	113.7[b] (CH)	6.80 (8.5, 2.5 *dd*)	113.0[c] (CH)
7		161.9 (C)		161.9 (C)
8	6.80 (2.5*d*)	101.5 (CH)	6.76 (2.5 *d*)	101.3 (CH)
9		155.8 (C)		155.8 (C)
10		112.6 (C)		112.4 (C)
1′	4.21 (*m*)	65.6 (CH_2)	4.07 (*m*)	65.8 (CH_2)
	4.19 (*m*)			
2′	2.19 (*m*)	40.8 (CH_2)	2.69 (*m*)	31.8 (CH_2)
	2.03 (*m*)			
3′		72.4 (C)		133.7 (C)
4′	5.65 (15.3*d*)	136.2 (CH)	5.95 (10.7 *d*)	127.5 (CH)
5′	6.49 (15.3, 10.7*dd*)	124.5 (CH)	6.46 (15.0, 10.7 *dd*)	122.1 (CH)
6′	5.85 (10.7*d*)	124.2 (CH)	5.76 (15.0 *d*)	140.3 (CH)
7′		135.9 (C)		70.7 (C)
8′	1.77 (*s*)	26.0 (CH_3)	1.31 (*s*)	29.9 (CH_3)
9′	1.74 (*s*)	18.3 (CH_3)	1.31 (*s*)	29.9 (CH_3)
10′	1.39 (*s*)	29.2 (CH_3)	1.85 (*s*)	24.1 (CH_3)

[a] HMQC allowed assignments of protonated carbons.
[b] Signals may be interchangeable.
[c] Signals may be interchangeable.

resonances attributed to two methyls at δ_H 1.31 suggested that C-7′ should be hydroxylated. Also, the olefinic proton 5′-H (δ_H 6.46) showed HMBC correlations to C-7′ and C-3′ (δ_C 133.7, s). Moreover, there were clear HMBC correlations of H_3-10′ with carbon signals C-2′ (δ_C 31.8, t), C-3′ (δ_C 133.7, s) and C-4′ (δ_C 127.5, *d*). The chemical shift of the C-10′ signal at δ_C 24.1 is typical of a *cis* methyl group with respect to an olefinic proton, which was supported by an NOE experiment. Thus, the structure of **2** was 7-[(3′*Z*,5′*E*)-7′-hydroxy-3′,7′-dimethyl-3′,5′-octadienyloxy]coumarin.

3. Experimental

3.1. Plant material

Roots of *F. ferulago* were obtained from the local market in Egypt, in April 1999. A voucher speciment (A. Ahmed 111) is deposited in the Department of Botany, El-Minia University.

3.2. Isolation and purification

Finely ground dried roots (250 g) of *F. ferulago* was soaked in chloroform for 24 h at room temperature, the extract was concentrated, and the residue (60 g) was subjected to silica gel flash chromatography using a step wise gradient with hexane–ether. The ether fraction was applied to a silica gel column with hexane–chloroform (1:4). Fractions of interest were applied to Sephadex LH-20 (hexane–EtOAc, 1:1), and finally preparative TLC to give new compounds **1** (35 mg) and **2** (27 mg), as well as coumarins, 6-methoxy-7-geranyloxy coumarin (**3**) (20 mg), diversinin (**4**) (17 mg), diversin (**5**) (40 mg), and three known sesquiterpenes lactone and malafil (**6**) (30 mg), malafilin (**7**) (60 mg), and malafilinin (**8**) (49 mg).

3.3. Ferulagol A (*1*)

UV, λ_{max} MeOH 322 nm (log ε 4.70); IR ν_{max} film cm^{-1}: 3433, 1728, 1614; ^1H and ^{13}C NMR (see Table 1); FABMS *m*/*z* 315 $[M+H]^+$; HRFABMS *m*/*z* 315.1611 $[M+H]^+$, calc. for $C_{19}H_{23}O_4$, 315.1597.

3.4. Ferulagol B (*2*)

UV, λ_{max} MeOH 322 nm (log ε 4.65); IR ν_{max} film cm^{-1}: 3433, 1728, 1614; ^1H and ^{13}C NMR (see Table 1); FABMS *m*/*z* 315 $[M+H]^+$; HRFABMS *m*/*z* 315.1611 $[M+H]^+$, calc. for $C_{19}H_{23}O_4$, 315.1597.

References

Ahmed, A.A., 1999. Sesquiterpene coumarins and sesquiterpenes from *Ferula sinaica*. Phytochemistry 50, 109–112.

Appendino, G., Jakupovic, J., Alloatti, S., Ballero, M., 1997. Daucane esters from *Ferula arrigonii*. Phytochemistry 45, 1639–1643.

Bohlmann, F., Grenz, M., 1976. Naturally occuring coumarin derivatives XIII, Two new coumarin derivatives from *Machaeranther scabrella* (Greene) Shinners. Berichte Deusche Chemischen Gesellschaft 109, 1584–1585.

Boulus, L., 1983. Medicinal Plants of North Africa MI: Algonae. p. 183.

Chen, B., Teranishi, R., Kawazoe, K., Takaishi, Y., Honda, G., Itoh, M., Takeda, Y., Kodzhimatov, K.O., 2000. Sesquiterpenoids from *Ferula kuhistanica*. Phytochemistry 54, 717–754.

Gonzalez, A.G., Barrera, J.B., 1995. Chemistry and sources of mono- and bicyclic sesquiterpenes from *Ferula* species. Progress in the Chemistry of Organic Natural Products 64, 1–92.

Grag, S.N., Agarwal, S.K., 1988. New monoterpene diols from essentail oil of *Ferula jaeschkeana*. Phytochemistry 27, 936–937.

Grag, S.N., Misra, L.N., Agarwal, S.K., 1989. Essentail oil from rhizomes of *Ferula jaeschkeana*. Phytochemistry 28, 634–636.

Kir'yalov, N.P., 1969. Coumarin diversin from the roots of Ferula diversivitta. Khimiya Prirodnykh Soedinenii 5, 51–52.

Kiseleva, V.V., Nikonov, G.K., Karryev, M.O., 1975. Structure of diversin and diversinin, coumarins of *Ferula diversivittata*. Khimiya Prirodnykh Soedinenii 11, 344–349.

Murray, R.D.H., 1989. Coumarins. Natural Product Reports 6, 591–624.

Quader, M.A., Et-Turbi, J.A., Armstrong, J.A., Gray, A.I., Waterman, P.G., 1992. Coumarins and their taxonomic value in the genus *Phebalium*. Phytochemistry 31, 3083–3089.

Rychewska, U., Hodgson, D.J., Holub, M., Budesinsky, M., Smitalova, Z., 1985. The structure of 2-oxo-8α-angeloyloxy-11α-acetoxy-5βH,6αH,7αH-guai-1(10),3-dien-6,12-olide, a sesquiterpenic lactone from *Laserpitium prutenicum* L. Revision of the stereostructures of native 2-Oxoguai-1(10),3-dien-6,12-oides from the species of the Umbelliferae family. Collections of Czechoslovak Chemical Communications 50, 2607–2624.

Talapatra, S.K., Chaudhuri, M.K., Talapatra, B., 1973. Coumarins of the root bark of *Feronia elephantum*. Phytochemisty 12, 236–237.

Zhou, P., Takaishi, Y., Duan, H., Chen, B., Honda, G., Itoh, M., Takeda, Y., Kodzhimatov, K.O., Lee, H., 2000. Coumarins and biocoumarins from *Ferula sumbul*: anti-HIV activity and inhibition of cytokin release. Phytochemistry 53, 689–697.

PERGAMON

Phytochemistry 57 (2001) 1205–1208

PHYTOCHEMISTRY

www.elsevier.com/locate/phytochem

Quassinoids from *Eurycoma harmandiana*

Tripetch Kanchanapoom[a,b], Ryoji Kasai[a], Phannipha Chumsri[c], Kazuo Yamasaki[a,*]

[a]*Institute of Pharmaceutical Sciences, Faculty of Medicine, Hiroshima University, 1-2-3 Kasumi, Minami-ku, Hiroshima 734-8551, Japan*
[b]*Department of Pharmaceutical Botany and Pharmacognosy, Faculty of Pharmaceutical Sciences, Khon Kaen University, Khon Kaen 40002, Thailand*
[c]*Department of Pharmacognosy, Faculty of Pharmacy, Mahidol University, Bangkok 10400, Thailand*

Received 21 December 2000; received in revised form 12 April 2001

Dedicated to Professor Vichiara Jirawongse on the occasion of his 83rd birthday

Abstract

Three quassinoids, iandonosides A and B and iandonone, were isolated from the root of *Eurycoma harmandiana,* along with five known quassinoids, casteloside B, 13 β, 21-dihydroeurycomanone, chaparrinone, glaucarubolone and ailanquassin B as well as the coumarin, scopoletin. The structural elucidations were based on analyses of spectroscopic data. © 2001 Elsevier Science Ltd. All rights reserved.

Keywords: Eurycoma harmandiana; Simaroubaceae; Quassinoids, Iandonoside A; Iandonoside B; Iandonone; Iandonol

1. Introduction

Eurycoma harmandiana Pierre is a small Simaroubaceous plant (Thai name: Ian-don) distributed in the border regions between Thailand and Laos. In a previous paper (Kanchanapoom et al., 2001), we reported the isolation and structural elucidation of canthin-6-one and β-carboline alkaloids. Further investigation of the root of the same plant afforded nine compounds (**1**–**9**), which included three new unusual 15α-OH quassinoids (**2**, **3**, **5**) together with five known quassinoids (**1, 4, 6**–**8**) and one known coumarin (**9**). The present paper deals with the structural determination of these compounds.

2. Results and discussion

From the ethanolic extract of the roots of *E. harmandiana,* nine compounds (**1**–**9**) were isolated. Five were identified as known quassinoids; casteloside B (**1**) (Chaudhuri and Kubo, 1992), l3β,21-dihydroeurycomanone (**4**) (Morita et al., 1990), chaparrinone (**6**), glaucarubolone (**7**) (Chaudhuri and Kubo, 1992) and ailanquassin B (**8**) (Aono et al., 1994) together with one known coumarin, scopoletin (**9**) by physical data and spectroscopic evidence.

Iandonoside A was obtained as an amorphous powder and determined as $C_{26}H_{38}O_{13}$ by HR–FAB mass spectrometry. The ^{13}C NMR spectrum revealed the presence of one β-glucopyranosyl unit together with 20 carbon signals for the aglycone, which suggested a C_{20} quassinoid skeleton. DEPT experiments indicated the presence of three methyls, two methylenes, 10 methines, as well as five quaternary carbons in the aglycone moiety. The signals at δ 72.3 (C-20) and 110.9 (C-11) in the ^{13}C NMR spectrum were characteristic of an 11β,20-hemiketal moiety. Comparison of the ^{1}H and ^{13}C NMR spectral data of **2** with those of **1** revealed the same relative arrangement of carbons and protons in rings A and B. The chemical shifts of rings C and D suggested differences in the relative configuration of hydroxyl group at C-15. The complete assignments were established by using HSQC, NOESY, difference NOE spectral experiments (Fig. 1) and the coupling constants in the ^{1}H NMR spectrum (Table 1). Irradiation of the H-20 signal (δ 3.70) gave rise to NOE enhancements at H-13 (δ 2.81), H-14 (δ 2.10) indicating the presence of α-configuration of Me-21 (δ 1.24) and β-configuration of H-14. The coupling constant of H-12 (δ 3.97, *d*, $J=5.0$ Hz) confirmed the α-configuration for the hydroxyl group at C-12. The configuration of the hydroxyl group at C-15 was assigned as α by the coupling constant of H-15 (δ 4.50, *d*, $J=4.6$ Hz), and further support was

* Corresponding author. Tel.: +81-82-257-5285; fax: +81-82-257-5289.

E-mail address: yamasaki@pharm.hiroshima-u.ac.jp (K. Yamasaki).

0031-9422/01/$ - see front matter © 2001 Elsevier Science Ltd. All rights reserved.
PII: S0031-9422(01)00235-7

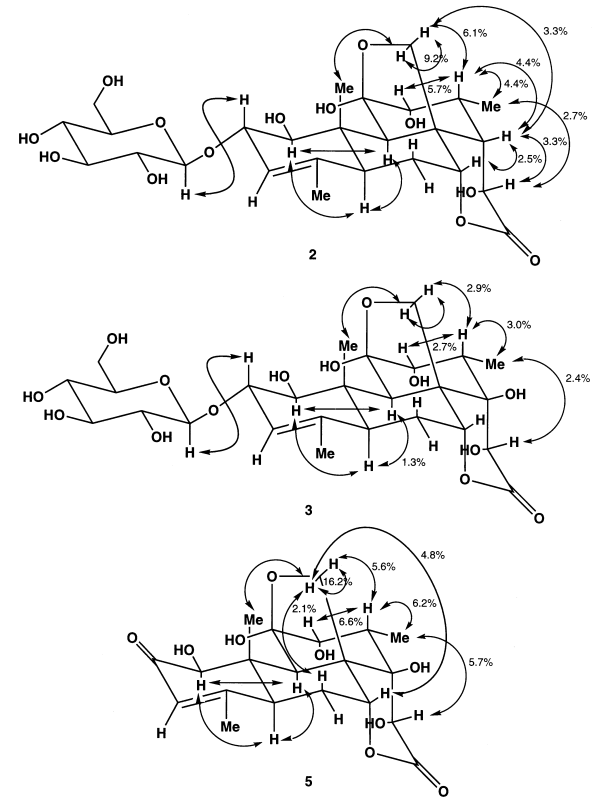

Fig. 1. NOESY and NOE enhancements of **2**, **3** and **5**.

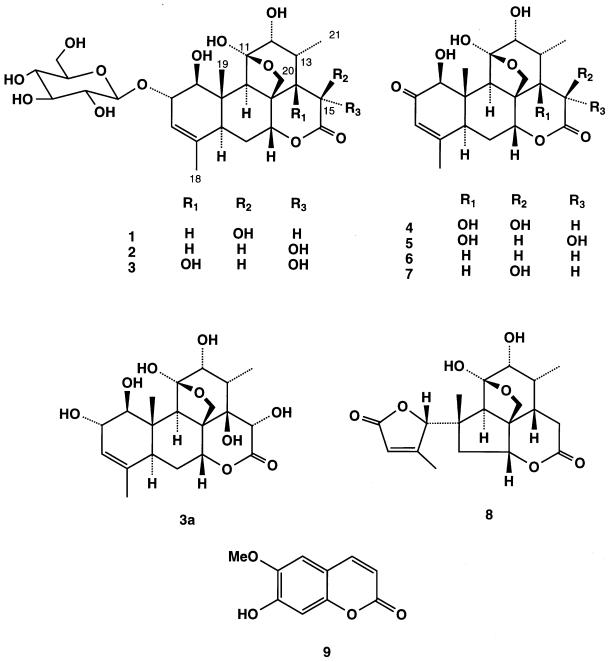

obtained by irradiation of the signal at H-15 which exhibited the NOE enhancements at H-14 and Me-21 but no enhancement at H-9 (δ 3.53). Consequently, the structure of **2** was elucidated as shown.

Iandonoside B (**3**) was obtained as an amorphous powder and determined as $C_{26}H_{38}O_{14}$ by HR–FAB mass spectrometry. Inspection of the ^{13}C NMR spectrum showed the presence of one β-glucopyranosyl unit and 20 carbon signals for the aglycone, which indicated it to be a C_{20} quassinoid glucoside. On enzymatic hydrolysis with crude hesperidinase (Kohda and Tanaka, 1975), **3** gave the new aglycone, named iandonol (**3a**). On going from **3** to **3a**, the chemical shifts were changed for C-2, C-1 and C-3 by +11.2, −1.3 and −2.3 ppm, respectively. This confirmed the location of the glucopyranosyl moiety on C-2. The ^1H and ^{13}C NMR spectral data were similar with those of **2**. However, the signal for H-14 was absent as well as the signal for H-15 (δ 4.73) appeared as singlet. In addition, the carbon signals for C-l4, C-13 and C-15 showed different chemical shifts at δ 76.6, 41.4 and 76.1 (Table 2), respectively, indicating the replacement of a proton (H-14) by a hydroxyl group. The relative configurations were confirmed by using the coupling constants in the ^1H NMR spectrum (Table 1), NOESY and difference NOE spectral experiments (Fig. 1). On irradiation of the signal at δ 2.95 (H-13), the intensity of H-20 (δ 4.53) was enhanced, and irradiation of the H-15 signal (δ 4.73) caused as determined increase in the NOE enhancement at Me-21 only (δ 1.45). Upon irridiation of the H-9 signal (δ 3.88), NOE enhancement was observed for the H-5 a signal (δ 2.76) but not for either the H-12 (δ 4.17) or H-15 (δ 4.73) signals. Thus, the stereochemistry of the hydroxyl groups at C-12 and C-15 were assigned as α, α-configurations, and the also Me-21 has an α-configuration. On the basis of these spectral data, the structure of **3** was determined as the 14β-hydroxy analogue of iandonoside A.

Iandonone (**5**) was obtained as an amorphous powder, with a molecular formula of $C_{20}H_{24}O_9$ by HR–FAB mass spectrometry. The ^{13}C NMR spectrum revealed the presence of 20 carbons, including a δ-lactone carbonyl (δ 171.9), an α,β-unsaturated ketone carbonyl carbon (δ 197.4) and two olefinic carbons (δ 126.2 and 162.2) indicative of a C_{20} quassinoid skeleton. Iandonone showed the same chemical shifts for rings B, C and D with those of **3**, and the chemical shifts of ring A were in full agreement with those of **4**. The stereochemistry of three hydroxyl groups at C-1, C-12 and C-15 were also confirmed by using NOESY difference NOE experiments (Fig. 1) and the coupling constants in the ^1H NMR spectrum (Table 1), led to deduce as β,α,α-configurations, respectively. Therefore, the structure of **5** was elucidated as shown.

3. Experimental

3.1. General

NMR spectra were recorded in C_5D_5N using a JEOL JNM A-400 spectrometer (400 MHz for ^1H NMR and

Table 1
^{1}H NMR spectral data for compounds **2**, **3**, **3a** and **5** (C_5D_5N, 400 MHz)

Proton	**2**	**3**	**3a**	**5**
H-1	4.02, *d*, *J* = 8.0 Hz	4.14, *d*, *J* = 8.0 Hz	4.11, *d*, *J* = 7.8 Hz	4.36, *s*
H-2	4.58, *m*	4.57, *m*	4.62, *m*	–
H-3	5.77, *bs*	5.80, *bs*	5.78, *bs*	6.11, *bs*
H-5	2.67, *bd*, *J* = 14.0 Hz	2.76, *bd*, *J* = 14.0 Hz	2.82, *bd*, *J* = 13.4 Hz	3.15, *bd*, *J* = 14.0 Hz
H-6e	2.02, *dt*, *J* = 14.0, 2.7 Hz	2.13, *dt*, *J* = 140, 2.7 Hz	2.18, *dt*, *J* = 14.0, 2.5 Hz	2.31, *dt*, *J* = 14.0, 2.2 Hz
H-6a	1.86, *td*, *J* = 14.0, 2.7 Hz	1.89, *td*, *J* = 14.0, 2.7 Hz	1.96, *td*, *J* = 14.0, 2.5 Hz	2.04, *td*, *J* = 14.0, 2.2 Hz
H-7	4.46 *t*, *J* = 2.7 Hz	5.06, *t*, *J* = 2.7 Hz	[a]	5.13, *bs*
H-9	3.53, *s*	3.88, *s*	3.94, *s*	4.13, *s*
H-12	3.97, *d*, *J* = 5.0 Hz	4.17, *d*, *J* = 4.9 Hz	4.11, *d*, *J* = 5.5 Hz	4.08, *d*, *J* = 5.1 Hz
H-13	2.81, *m*	2.95, *m*	3.00, *m*	2.97, *m*
H-14	2.10, *dd*, *J* = 7.8, 5.1 Hz	–	–	–
H-15	4.50, *d*, *J* = 4.6 Hz	4.73, *s*	4.75, *s*	4.80, *s*
H-18	1.43, *bs*	1.44, *bs*	1.59, *bs*	1.76, *bs*
H-19	1.54, *s*	1.61, *s*	1.72, *s*	1.57, *s*
H-20	3.70, *d*, *J* = 8.6 Hz	4.03, *d*, *J* = 9.5 Hz	4.03, *d*, *J* = 8.8 Hz	4.04, *d*, *J* = 9.0 Hz
	4.10, *d*, *J* = 8.6 Hz	4.53, *d*, *J* = 9.5 Hz	4.56, *d*, *J* = 8.8 Hz	4.53, *d*, *J* = 9.0 Hz
H-21	1.24, *d*, *J* = 7.1 Hz	1.45, *d*, *J* = 7.1 Hz	1.49, *d*, *J* = 7.3 Hz	1.48, *d*, *J* = 7.1 Hz
H-1′	5.19, *d*, *J* = 7.6 Hz	5.18, *d*, *J* = 7.8 Hz		
H-2′	4.06, *dd*, *J* = 8.1, 7.6 Hz	4.06, *dd*, *J* = 8.5, 7.8 Hz		
H-3′	4.19, *dd*, *J* = 8.5, 8.1 Hz	4.17, *dd*, *J* = 9.0, 8.5 Hz		
H-4′	4.24, *dd*, *J* = 9.1, 8.5 Hz	4.20, *dd*, *J* = 9.0, 8.5 Hz		
H-5′	3.95, *m*	3.94, *m*		
H-6′	4.54, *bd*, *J* = 11.5 Hz	4.51, *dd*, *J* = 12.0, 2.6 Hz		
	4.38, *dd*, *J* = 11.5, 4.7 Hz	4.35, *dd*, *J* = 12.0, 5.1 Hz		

a Interferred signal.

Table 2
^{13}C NMR spectral data for compounds **1**–**3**, **3a** and **5** (C_5D_5N, 100 MHz)

Carbon	**1**	**2**	**3**	**3a**	**5**
1	82.6	82.8	82.8	84.1	84.8
2	84.1	83.7	83.8	72.6	197.4
3	124.6	124.9	124.8	127.1	126.2
4	136.0	135.7	135.5	135.0	162.2
5	41.3	41.6	41.2	41.4	42.5
6	26.0	26.0	25.7	25.9	25.9
7	78.6	79.3	71.5	70.8	70.9
8	47.4	44.8	50.0	50.1	49.9
9	45.5	45.9	44.8	45.0	45.3
10	42.0	42.3	42.3	42.3	45.7
11	111.0	110.9	110.3	110.5	110.1
12	80.5	78.3	78.8	79.1	78.7
13	33.1	31.9	41.4	41.9	41.1
14	49.6	48.5	76.6	76.7	76.6
15	68.7	65.4	76.1	76.5	75.9
16	174.3	171.2	172.0	172.1	171.9
18	21.0	21.1	21.1	21.3	22.4
19	10.3	10.7	10.9	11.1	10.6
20	71.8	72.3	67.9	67.9	67.7
21	16.3	13.0	10.1	10.2	10.1
G-1	106.4	106.3	106.2		
G-2	76.1	76.2	76.3		
G-3	78.6	78.6	78.5		
G-4	71.6	71.6	70.7		
G-5	78.5	78.5	78.5		
G-6	62.7	62.7	62.7		

100 MHz for ^{13}C NMR) with tetramethylsilane (TMS) as internal standard. MS were recorded on a JEOL JMS-SX 102 spectrometer. Preparative HPLC was carried out on columns of ODS (150×20 mm i.d., YMC) and polyamine II (250×20 mm i.d., YMC) with a Tosoh refraction index (RI-8) detector. The flow rate was 6 ml/min. For CC, silica gel G 60 (Merck), RP-l8 (50 mm, YMC) and highly porous copolymer of styrene and divinylbenzene (Mitsubishi Chem. Ind. Co. Ltd) were used. The solvent systems were: (I) EtOAc–MeOH (9:1), (II) EtOAc–MeOH–H_2O (4:1:0.1), (III) EtOAc–MeOH –H_2O (7:3:0.3), (IV) EtOAc–MeOH–H_2O (6:4:1), (V) 30–50% MeOH, (VI) 80% MeCN, (VII) 12% MeCN, (VIII) 10% MeCN, (IX) CH_2Cl_2, (X) CH_2C1_2–MeOH (19:1), (XI) CH_2Cl_2–MeOH (9:1), (XII) CH_2Cl_2–MeOH (4:1), (XIII) 40–100% MeOH, (XIV) 50–100% MeOH.

3.2. Plant material

The root of *Eurycoma harmandiana* was collected in May 1998 from Nong Khai Province, north-eastern Thailand. The identification of the plant was confirmed by Professor Vichiara Jirawongse, Department of Pharmaceutical Botany and Pharmacognosy, Faculty of Pharmaceutical Sciences, Khon Kaen University. A voucher sample (KKU-0017) is kept in the Herbarium of the Faculty of Pharmaceutical Sciences, Khon Kaen University, Thailand.

3.3. Extraction and isolation

The dried root (7.0 kg) of *E. harmandiana* was extracted with 95% EtOH. After removal of the solvent by evaporation, the residue (200 g) was extracted with CH_2Cl_2, EtOAc and *n*-BuOH, successively. The *n*-BuOH extract (45.0 g) was subjected to a column of highly porous copolymer of styrene and divinylbenzene, and eluted with H_2O, MeOH and Me_2CO, successively. The fraction eluted with MeOH was applied to a silica gel column (systems I, II, III and IV, successively) affording nine fractions. Fraction 5 was subjected to a column of RP-18 using system V, then followed by HPLC-polyamine II (system VI) and HPLC–ODS (system VII) to provide compounds **1** (5 mg), **2** (4 mg) and **3** (30 mg). The EtOAc extract (27.5 g) was further separated on a column of RP-18 (system V), and finally purified by HPLC–ODS (system VIII) to give compounds **4** (84 mg) and **5** (21 mg). The CH_2C1_2 extract (90.0 g) was subjected to a column of a silica gel (systems IX, X, XI and XII) affording six fractions. Fraction 2 was repeatedly chromatographed on a silica gel column using gradient system (CH_2Cl_2 to 5% MeOH in CH_2Cl_2) to provide six fractions. Fraction 2-2 was further purified by using a RP- 18 column (system XIII) to afford compounds **9** (53 mg). Fraction 2-4 was similarly purified by using a RP-18 column (system XIV) to give compound **6** (268 mg). Fraction 2-6 was applied to a column of silica gel (system I), this being followed by HPLC–ODS (system VII) to afford compounds **7** (24 mg) and **8** (13 mg).

3.4. Iandonoside A (*2*)

Amorphous powder. $[\alpha]_D^{20}$ +19.1° (MeOH, *c* 0.3); ^{1}H NMR: Table 1; ^{13}C NMR: Table 2; negative HR–FAB–MS, *m*/*z*: 557.2258 $[M-H]^-$ ($C_{26}H_{37}O_{13}$ requires 557.2234).

3.5. Iandonoside B (*3*)

Amorphous powder. $[\alpha]_D^{20}$ +4.1° (MeOH, *c* 0.7); ^{1}H NMR: Table 1; ^{13}C NMR: Table 2; negative HR–FAB–MS, *m*/*z*: 573.2148 $[M-H]^-$ ($C_{26}H_{37}O_{14}$ requires 573.2183).

3.6. Enzymatic hydrolysis of iandonoside B (*3*)

Iandonoside B (**3**) 8 mg was dissolved in 0.5 ml of MeOH. A solution of crude hesperidinase (100 mg in 20 ml of H_2O) was added. After shaking at 37 °C for 24 h, the mixture was extracted with EtOAc. The EtOAc extract was evaporated to provide a new aglycone, iandonol (**3a**) 3 mg. The structure was identified by ^{1}H and ^{13}C NMR spectral analysis.

3.7. Iandonol (*3a*)

Amorphous powder. $[\alpha]_D^{20}$ −72.6° (MeOH, *c* 0.2); ^{1}H NMR: Table 1; ^{13}C NMR: Table 2; positive HR–FAB–MS, *m*/*z*: 411.1691 $[M-H]^-$, ($C_{20}H_{27}O_9$ requires 411.1655).

3.8. Iandonone (*5*)

Amorphous powder. $[\alpha]_D^{20}$ +4.6° (MeOH, *c* 0.4); ^{1}H NMR: Table 1; ^{13}C NMR: Table 2; positive HR–FAB–MS, *m*/*z*: 409.1468 $[M-H]^-$ ($C_{20}H_{25}O_9$ requires 409.1498).

Acknowledgements

We would like to thank the Research Center for Molecular Medicine, Hiroshima University for the use of its NMR facilities.

References

Aono, H., Koike, K., Kaneko, J., Ohmoto, T., 1994. Alkaloids and quassinoids from *Ailanthus malabarica*. Phytochemistry 37, 579–584.

Chaudhuri, S.K., Kubo, I., 1992. Two quassinoid glucosides from *Castela tortuosa*. Phytochemistry 31, 3961–3964.

Kanchanapoom, T., Kasai, R., Chumsri, P., Hiraga, Y., Yamasaki, K., 2001. Canthin-6-one and β-carboline alkaloids from *Eurycoma harmandiana*. Phytochemistry 56, 383–386.

Kohda, H., Tanaka, O., 1975. Enzymatic hydrolysis of ginseng saponins and their related glycosides. Yakugaku Zasshi 95, 246–249.

Morita, H., Kishi, E., Takeya, K., Itokawa, H., Tanaka, O., 1990. New quassinoids from the roots of *Eurycoma longifolia*. Chemistry Letters 749–752.

PERGAMON

Phytochemistry 57 (2001) 1209–1212

PHYTOCHEMISTRY

www.elsevier.com/locate/phytochem

Three clerodane diterpenoids from *Croton eluteria* Bennett

Claire Vigor*, Nicolas Fabre, Isabelle Fourasté, Claude Moulis

Laboratoire Pharmacophores Redox, Phytochimie et Radiobiologie, Faculté des Sciences Pharmaceutiques, 35 chemin des Maraîchers, F-31062 Toulouse, France

Received 13 November 2000; received in revised form 29 March 2001

Abstract

Three furanoid clerodanes have been isolated from the stem bark of *Croton eluteria* Bennett. Their structures have been established by spectroscopic methods. The compounds were named cascarillin B (7α-acetoxy-3,4,15,16-diepoxy-12-oxo-cleroda-13(16),14-dien-20-al), cascarillin C (7α-acetoxy-15,16,12,20-diepoxy-20-hydroxy-cleroda-3,4,13(16),14-triene) and cascarillin D (7α-acetoxy-3,4,15,16-diepoxy-cleroda-13(16),14-dien-20-al). © 2001 Elsevier Science Ltd. All rights reserved.

Keywords: *Croton eluteria* Bennett; Euphorbiaceae; Furanoid diterpene; Clerodane

1. Introduction

Cascarilla bark, obtained from *Croton eluteria* Bennett (Euphorbiaceae) is a shrub or small tree indigenous to the Bahama Islands. It was reported to be balsamic, digestive, hypotensive, narcotic, stomachic and tonic (Greenish, 1924).

It has been used as a traditional medicine for many applications such as for dysentery, dyspepsia, malaria and fever (Duke, 1984).

From the phytochemical point of view, some terpene derivatives were previously reported and specially some *ent*-clerodane furano-diterpenoids: cascallin, cascarillone and cascarillin A (Halsall et al., 1965; Hegnauer, 1966; Claude-Lafontaine et al., 1976; Hagedorn and Brown, 1991). In this paper, we describe the isolation and structural elucidation of three new related compounds from the stem bark of *C. eluteria* Bennett.

2. Results and discussion

The molecular formula $C_{22}H_{28}O_6$ of compound **1** was determined by ESI mass spectrometry mesured in the positive ion mode (*m/z* 389.2 $[M+H]^+$, *m/z* 411.2 $[M+Na]^+$). Its ^{13}C NMR decoupled spectrum (Table 1) showed 22 signals in agreement with the molecular formula. The characteristic NMR signals for a furan ring were present in the ^1H and ^{13}C NMR spectra (δ_H 6.64 *br s,* 7.40 *br s*, 8.03 *br s*; δ_C 108.6, 144.6, 147.5 and 128.9 *Cq*), as were those of an aldehyde group (δ_H 10.18 *s*; δ_C 206.0), an ester carbonyl group (δ_C 170.3) and a keto group (δ_C 193.6). These functional groups account for five of the six oxygens, and the remaining oxygen was involved in an epoxide unit as indicated by a singlet signal at δ_H 2.85 and δ_C 62.0. In addition, four methyl groups were present and were identified from their chemical shifts and coupling patterns as a doublet for C-17 (δ_H 1.01 *d*, $J=7.3$ Hz; δ_C 13.7), two singlets (C-18: δ_H 1.12 *s*; δ_C 19.9 and C-19: δ_H 1.06 *s*; δ_C 19.2) and an acetyl group (δ_H 2.04 *s*; δ_C 21.6).

Considering the quaternary carbons (δ_C 36.3 and 56.0), the C–H group (δ_C 48.5) and their heteronuclear correlations displayed in the HMBC spectrum, these signals could be assigned, respectively, to carbons C-5, C-9 and C-10 of the decalin moiety. The position of the aldehyde group was deduced from the HMBC spectrum which exhibited cross peaks between the aldehyde carbon and H-8, H-11 and the aldehyde proton with C-9, C-11 (Fig. 1). Its chemical shift agrees with an aldehyde group that we assigned to C-9. The location of the epoxide group (C-3–C-4) was deduced from the HMBC spectrum correlations between C-3 (δ_C 62.0) and H-1a, H-2a, H-18 and C-4 (δ_C 65.1) with H-18, H-19, H-6a, H-6b, H-2a; Fig. 1. In the same way, the acetoxy group was located on position C-7 (correlations

* Corresponding author. Tel.: +33-5-6225-6844; fax: +33-5-6155-4330.

E-mail address: vigorcl@hotmail.com (C. Vigor).

0031-9422/01/$ - see front matter © 2001 Elsevier Science Ltd. All rights reserved.
PII: S0031-9422(01)00183-2

between acetate protons (δ_H 2.04 *s*) and C-7), and the keto group in position C-12 (correlations between the quaternary carbon signal at δ_C 193.6 and H-11a, H-11b and H-14; Fig. 1).

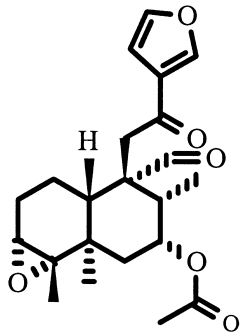

Compound **1**

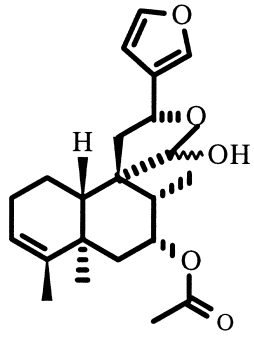

Compound **2**

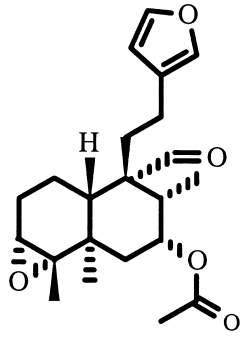

Compound **3**

The ^{13}C NMR signal of the shielded Me-19 (δ_C 19.2) suggested a *trans* A/B ring junction for decalin as previously discussed by Manabe and Nishino (1986). The α orientation for the C-3–C-4 epoxy group was proposed on the basis of the ^1H NMR signals of the shielded Me-19 protons (δ_H 1.06 *s*) (Manabe and Nishino, 1986). Finally, an α orientation for the acetoxy group was proposed on the basis of the *J* value $J_{8\beta-7\beta} = 4$ Hz which is in accordance with axial-equatorial coupling and corresponds to an approximate dihedral angle H-7β–H-8β of 70°. This was supported by the coupling constant values of H-6 (see Table 1) and the values reported in the literature (Bedir et al., 1999; Tori et al., 1999).

Thus, these data allowed us to establish **1**, as 7α-acetoxy-3,4,15,16-diepoxy-12-oxo-cleroda-13(16),14-dien-20-al, which we named cascarillin B.

The positive ESI mass spectrum of compound **2** showed peaks at *m/z* 397.2, *m/z* 413.2 and *m/z* 337.0 corresponding to $[M+Na]^+$, $[M+K]^+$, and $[M-OCOCH_3+Na]^+$ respectively, suggesting a $C_{22}H_{30}O_5$ formula. The acetoxy group was still present as supported by the ESI mass spectral data, the carbon at δ_C 172.4, and three protons at δ_H 2.06 ppm. The HMBC spectrum did not allow us to locate the acetoxy group. But, the ^1H–^1H COSY spectrum showed a cross peak between H-17 (δ_H 1.13, d, $J = 7.3$ Hz) and H-8 (δ_H 1.66, *dd*, $J = 7.3$, 3 Hz). The latter proton ($J = 3$ Hz) correlates with a deshielded proton at δ_H 5.03 ppm (*m*) whose chemical shift is in agreement with a CH-7α-acetoxy as already described for **1**. Both epoxide and aldehyde groups were absent from **2** and replaced by a double bound and a lactol function, respectively. This was shown by the characteristic ^1H and ^{13}C NMR signals at δ_H 5.22 ppm (H-3), δ_C 122.3 (C-3) and δ_C 144.6 (C-4) for the first one, and at δ_H 5.85 ppm (H-20), δ_C 101.6 (C-20) and δ_H 5.08 ppm (H-12), δ_C 73.2 (C-12) for the second one. The spectrum unambiguously revealed the C-3–C-4 unsaturation (cross peaks between H-18/C-4 and H-18/C-3). This was confirmed by the ^1H–^1H COSY correlations (H-18/H3). In the same way, the C-20 carbon (δ_C 101.6), involved in the lactol function, was correlated in the HMBC spectrum with H-8, H-11b and H-12. The correlations of C-9 with H-10, H-17, H-11a, H-11b and H-20, confirmed this result. The methine (C-12) at δ_C 73.2 was correlated with H-11b and H-20, and this proton displayed a cross peak with C-16 and C-20. Thus, the structure of **2** was established as 7α-acetoxy-15,16,12,20-diepoxy-20-hydroxy-cleroda-3,4,13(16),14-triene, which we named cascarillin C.

The molecular formula of compound **3** was determined as $C_{22}H_{30}O_5$ based on ESI mass spectrum $[M+Na]^+$ (*m/z* 397.3) and $[M+K]^+$ (*m/z* 413.3). Comparison of the spectral data of this compound with that of **1** indicated that compound **3** differed from **1** through the lack of a keto group in position C-12. These results led us to propose the structure 7α-acetoxy-3,4,15,16-diepoxy-cleroda-13(16),14-trien-20-al for compound **3**, which we named cascarillin D.

3. Experimental

3.1. Instrumentation

^1H NMR (400 MHz) and *J* mod. ^{13}C NMR (100 MHz) were obtained with CD_3OD or $CDCl_3$ as solvent,

Table 1
^1H and ^{13}C NMR data for compounds **1**, **2** in CD_3OD and **3** in $CDCl_3$ (δ in ppm, multiplicities, J in Hz)

	δ H			δ C		
Position	**1**	**2**	**3**	**1**	**2**	**3**
1a	1.37 *m*	2.04 *m*	1.61 *m*	16.6	23.5	17.1
1b	1.17 *m*		1.38 *m*			
2a	1.95 *m*	2.00 *m*	2.13 *m*	27.6	29.6	29.0
2b	1.42 *m*	1.85 *m*	1.76 *m*			
3	2.85 *s*	5.22 *br s*	3.00 *br s*	62.0	122.3	63.5
4	–	–	–	65.1	144.6	66.7
5	–	–	–	36.3	39.7	37.6
6a	2.09 *dd* (14.6–3.7)	2.17 *dd* (14.6–2.6)	2.13 *m*	39.9	42.1	41.1
6b	1.76 *dd* (14.6–3.7)	1.47 *dd* (14.6–3.4)	1.84 *dd* (14.5–3.7)			
7	5.25 *dd* (3.7-3)	5.03 *ddd* (3.4–3–2.8)	5.29 *dd* (3.6-3)	74.2	77.3	75.9
8	2.63 *dd* (7.3–4)	1.66 *dd* (7.3–3)	2.14 *m*	37.3	47.3	38.5
9	–	–	–	56.0	55.5	54.9
10	2.04 *s*	1.62 *br s*	3.31 *dd* (4.9–3.3)	48.5	52.1	49.9
11a	3.37 *d* (17.8)	2.64 *dd* (13.3–7.2)	1.99 *m*	38.5	45.3	32.2
11b	2.76 *d* (17.8)	1.92 *dd* (13.3–8.9)	1.65 *m*			
12	–	5.08 *dd* (8.9–7.2)	a: 2.35 *dd* (12.5–4.9)	193.6	73.2	18.4
			b: 2.28 *dd* (12.5–4.9)			
13	–	–	–	128.9	131.7	126
14	6.64 *br s*	6.63 *br s*	6.32 *br s*	108.6	111	111.8
15	7.40 *br s*	7.40 *br s*	7.4 *br s*	144.6	144.3	144.3
16	8.03 *br s*	7.45 *br s*	7.32 *br s*	147.5	140.9	140.1
17	1.01 *d* (7.3)	1.13 *d* (7.3)	1.15 *d* (7. 3)	13.7	15.4	13.5
18	1.12 *s*	1.59 *m*	1.19 *s*	19.9	18.5	20.1
19	1.06 *s*	1.27 *s*	1.07 *s*	19.2	22.7	19.5
20	10.18 *s*	5.85 *s*	10.14 *d* (0.7)	206.0	101.6	208.1
$OCO\underline{C}H_3$	2.04 *s*	2.06 *s*	2.07 *s*	21.6	21.4	21.3
$O\underline{C}OCH_3$	–	–	–	170.3	172.4	172.1

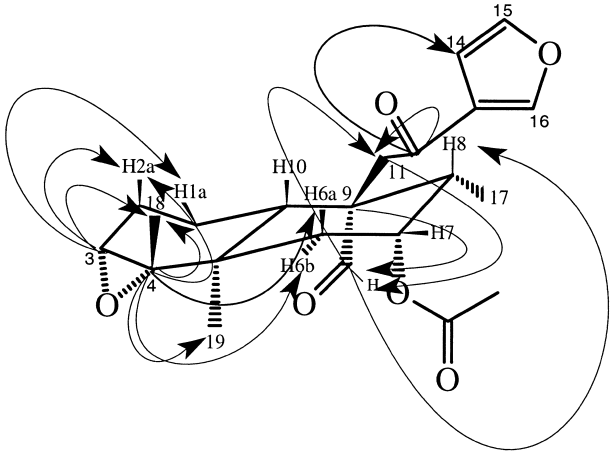

Fig. 1. Significant HMBC couplings of **1**.

on a Brücker ARX-400 spectrometer. Chemical shifts are given in δ (ppm) using the solvent peaks, δ_H 4.87, δ_C 48 ppm and δ_H 7.23, δ_C 77 ppm, respectively, as standards ; ESI–MS: 3.5 kV (MeOH–$CHCl_3$) (Perkin Elmer API Sciex 365 Mass spectrometer); HR–FAB (positive ion mode) mass spectra were recorded on an Autospec 6F mass spectrometer manufactured by Micromass.

3.2. Plant material

Croton eluteria Bennett, collected in Ecuador, was purchased from Richard et Frappa, Aubagne, France. Voucher specimens were identified by Professor Isabelle Fourasté and deposited at the herbarium of the Pharmacognosy Laboratory, Faculty of Pharmacy (Toulouse).

3.3. Extraction and isolation

Air-dried powdered bark (1 kg) of *C. eluteria* Bennett was extracted with Me_2CO at room temperature (24 h). The extract (70 g) was taken up in $CHCl_3$ and chromatographed on silica gel columns eluted with various proportions of $CHCl_3$ and MeOH. The fraction containing the main furanoid diterpenes (revealed on TLC by Ehrlich reagent) was evaporated to dryness and separated on 3 successive silica gel (70–200 μm) columns eluted with a hexane–EtOAc gradient.

Further purification of the crude diterpene by reverse-phase chromatography (Mega Band Elut Varian C18 cartridge: MeOH–H_2O 6:4), followed by medium

pressure (10 bars) silica gel chromatography (silica 60Å, CC chromagel SDS, 6–35 μm) eluted with toluene–EtOAc 95:5 and then another reverse-phase chromatography (C18 cartridge MeOH–H_2O 1:1) gave pure compound **1**.

Concerning compounds **2** and **3**, they were obtained by successive medium pressure (10 bars) silica gel chromatography (silica 60 Å, CC chromagel SDS, 6–35 μm) eluted with a toluene–EtOAc gradient, followed by reverse-phase chromatography (C 18 cartridge: MeOH–H_2O 13:7; 14:6) and preparative HPLC (Varian Dynamax 100 Å, MeOH–H_2O 7:3, 10 ml $min^{-1,}$ 204 nm; MeOH–H_2O 15:5, 10 ml min^{-1}, 204 nm).

*3.3.1. Cascarillin B (**1**)*

$C_{22}H_{28}O_6$; yellow resin (126 mg); mp 68–70° C; $[\alpha]_D^{20}$ −29.1 ($CHCl_3$; *c* 1.65); UV λ_{max} $CHCl_3$ nm (log ε: 275 (3.1); ESI–MS, *m/z*: 389.2 $[M+H]^+$; 411.2 $[M+Na]^+$; HR–FABMS (positive mode) *m/z*: 329.174 $[M-C_2H_4O_2+H]^+$; $C_{20}H_{24}O_4+H$ requires, 329.175; ^1H NMR, ^{13}C NMR: Table 1.

*3.3.2. Cascarillin C (**2**)*

$C_{22}H_{30}O_5$; clear yellowish resin (11 mg); mp 60–62°C; $[\alpha]_D^{20}$ −47.6 ($CHCl_3$; *c* 0.227); UV λ_{max} $CHCl_3$ nm (log ε: 244 (2.9); ESI–MS, *m/z*: 397.2 $[M+Na]^+$; 413.2 $[M+K]^+$; 337.0 $[M-OCOCH_3+Na]^+$; HR–FABMS (positive mode) *m/z*: 357.207 $[M-H_2O+H]^+$; $C_{22}H_{28}O_4+H$ requires, 357.207; ^1H NMR, ^{13}C NMR: Table 1.

*3.3.3. Cascarillin D (**3**)*

$C_{22}H_{30}O_5$; clear yellowish resin (6 mg); mp 64–66°C; $[\alpha]_D^{20}$ −23.6 ($CHCl_3$; *c* 0.356); ESI–MS, *m/z*: 397.3 $[M+Na]^+$; 413.3 $[M+K]^+$; HR-FABMS (positive mode) *m/z*: 375.216 $[M+H]^+$; $C_{22}H_{30}O_5+H$ requires, 275.217; ^1H NMR, ^{13}C NMR: Table 1.

References

Bedir, E., Tasdemir, D., Çalis, I., Zerbe, O., Sticher, O., 1999. Neoclerodane diterpenoids from *Teucrium polium*. Phytochemistry 51, 921–925.

Claude-Lafontaine, A., Ruillard, M., Cassan, J., Azzaro, M., 1976. New terpene derivatives, constituents of the essential oil of Cascarilla. Bull. Soc. Chim. Fr., 88–90.

Duke, J.A., 1984. CRC Handbook of Medicinal Herbs. CRC Press, Boca Raton.

Greenish, H.G., 1924. A Text Book of Materia Medica, 4th Edition. J&A Churchill, London.

Hagedorn, M.L., Brown, S., 1991. The constituents of Cascarilla oil (*Croton eluteria* Bennett). Flavour and Fragrance Journal 6, 193–204.

Halsall, T.G., Oxford, A.W., Rigby, W., 1965. The structure of cascarillin A, an epoxy-furanoid diterpene. Chem. Commun. 11, 218–219.

Hegnauer, R., 1996. Chemotaxonomie der Pflanzen, Vol 4. Bick Läuser, Basel and Stuttgart.

Manabe, S., Nishino, C., 1986. Stereochemistry of *cis*-clerodane diterpenes. Tetrahedron 42, 3461–3470.

Tori, M., Katto, A., Masakazu, S., 1999. Nine new clerodane diterpenoids from rhizomes of *Solidago altissima*. Phytochemistry 52, 487–493.

PERGAMON

Phytochemistry 57 (2001) 1213–1217

PHYTOCHEMISTRY

www.elsevier.com/locate/phytochem

Penicillosides A–C, C-15 oxypregnane glycosides from *Caralluma penicillata*

Essam Abdel-Sattar[a,1], Mohammed Abdul-Aziz A1-Yahya[b], Norio Nakamura[a], Masao Hattori[a,*]

[a]*Institute of Natural Medicine, Toyama Medical and Pharmaceutical University, 2630 Sugitani, Toyama 930-0194, Japan*
[b]*Department of Pharmacognosy, College of Pharmacy, King Saud University, Riyadh 11451, PO Box 2457, Saudi Arabia*

Received 9 November 2000; received in revised form 30 January 2001

Abstract

The chloroform fraction of the defatted ethanol extract from the aerial parts of *Caralluma penicillata* yielded three C-15 oxypregnane glycosides, penicillosides A–C. Their structures were established by a combination of spectroscopic methods. © 2001 Elsevier Science Ltd. All rights reserved.

Keywords: *Caralluma penicillata*; Asclepiadaceae; C-15 Acylated oxypregnane glycosides

1. Introduction

In a continuation of our interest in the chemical composition of the genus *Caralluma,* the aerial parts of *Caralluma penicillata* (defl) M.E. Br. indigenous to the Kingdom of Saudi Arabia were investigated (Collenette, 1985). This plant has been used in Saudi traditional medicine for the treatment of snake and scorpion bites (Al-Yahya et al., 1983). A case of toxicity of *C. penicillata* was reported by Hamadan (1980) and was manifested by the death of 50 sheep over a period of 1 month due to grazing on the plant in the Aseer region of the Kingdom of Saudi Arabia. A study of the plant was undertaken by Al-Yahya and Tariq (1983), to evaluate its toxicity and pharmacological properties, and a phytochemical and biological screening was reported by Mossa et al. (1983).

In a previous study, the isolation of four new pregnane glycosides from *Caralluma russeliana* was reported (Al-Yahya et al., 2000). In the present study, we report on the isolation of three oxypregnane glycosides from *C. penicillata*.

2. Results and discussion

The defatted ethanol extract of the aerial parts of *C. penicillata* was suspended in water and extracted with diethyl ether, $CHCl_3$ and *n*-butanol. The $CHCl_3$ soluble fraction was subjected to repeated chromatography to afford three pregnane glycosides **1–3.** Compounds **1–3** gave positive tests for sterols (Liebermann–Burchard reagent) and sugars and/or glycosides, and a negative test for 2-deoxy sugars (Keller–Killiani).

Compound **1** was isolated as white needles, mp 215–217°C, $[\alpha]_D^{25}$ −30° and had a molecular formula $C_{41}H_{62}O_{15}$ as shown by electrospray ionization mass (ESI–MS; *m*/*z* 793 $[M-H]^+$ and 817 $[M+Na]^+$, in the negative and positive ion modes, respectively) and ^{13}C NMR spectroscopic data (DEPT). The IR spectrum of **1** showed the presence of a hydroxyl group (3400 cm^{-1}) and an ester carbonyl group (1720 cm^{-1}). The acid hydrolysis of **1** yielded two sugars, identified as glucose and digitalose, using TLC by comparison with authentic samples. The ^{13}C NMR (DEPT) spectrum of **1** revealed a total of 41 carbon signals, of which five corresponded to methyl carbons, nine to methylene carbons, 21 to methine carbons, and six to quaternary carbons. The NMR spectral data of **1** were very similar to those of russeliosides A–D, pregnane glycosides isolated from *C. russeliana* (Al-Yahya et al., 2000). In the ^1H and ^{13}C NMR spectra of **1**, the proton and carbon signals due to the sugar portion were

* Corresponding author. Tel.: +81-76-434-7630; fax: +81-76-432-2281.

E-mail address: saibo421@ms.toyama-mpu.ac.jp (M. Hattori).

[1] Present address: Department of Pharmacognosy, College of Pharmacy, Cairo University, Cairo 11562, Egypt.

0031-9422/01/$ - see front matter © 2001 Elsevier Science Ltd. All rights reserved.
PII: S0031-9422(01)00163-7

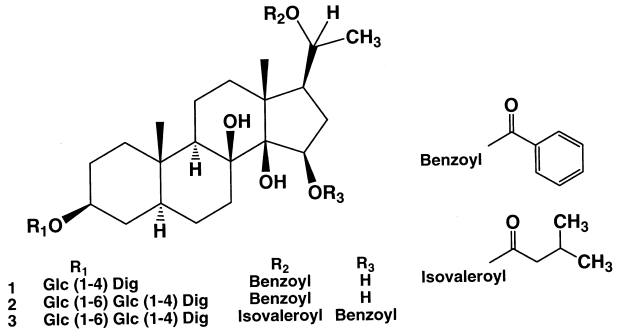

	R_1	R_2	R_3
1	Glc (1-4) Dig	Benzoyl	H
2	Glc (1-6) Glc (1-4) Dig	Benzoyl	H
3	Glc (1-6) Glc (1-4) Dig	Isovaleroyl	Benzoyl

similar to those of russelioside C (Al-Yahya et al., 2000) and hisianthosides (Qiu et al., 1999) and were due to one D-glucose unit and one D-digitalose unit. Two anomeric protons and their carbon signals resonated at δ_H 4.75, 5.16 and at δ_C 102.3, 105.3, in the ^1H and ^{13}C NMR spectra, respectively. D-Digitalose was determined as the inner sugar unit from the observed correlation between H-1′/C-3 and between H-3/C-1′, in the HMBC spectrum. The β-configuration of all of the sugar units was indicated from the large coupling constants of their anomeric protons (Agrawal, 1992). Comparison of the NMR spectral data of the aglycone part of **1** with those of russelioside C (Al-Yahya et al., 2000) revealed that **1** showed the absence of any double bond in the skeleton, the presence of a benzoyl residue, and a hydroxyl group located at C-15. The identification of the benzoyl unit was deduced from the UV spectrum (λ_{max} 228, 272 and 280 nm) and from the proton signals at δ_H 8.20 (2H, *m,* H-3, H-7), 7.52 (1H, *m,* H-5) and 7.45 (2H, *m,* H-4, H-6), which were correlated with the aromatic methine carbons at δ_C 130.2 (C-3, C-7), 133.6 (C-5) and 128.9 (C-4, C-6), in the ^1H and ^{13}C NMR spectra, respectively (Rasoanaivo, 1991; El Sayed et al., 1995; Halim and Khalil, 1996). The position of the benzoyl moiety was identified as at C-20 based on the long-range correlation between its carbonyl group (δ_H 166.2) and H-20 (δ_H 5.76) in the HMBC spectrum, and from the downfield shift of C-20 (δ_C 74.3) relative to the corresponding carbon in russelioside C (δ_C 68.8) (Al-Yahya et al., 2000). The hydroxylation at C-15 was deduced from the direct correlation between the proton signal at δ_H 4.61 (H-15) and H-16α (δ_H 2.5) and H-16β (δ_H 1.8) in the ^1H-^1H COSY spectrum, and by comparison with related compounds (Konda et al., 1992; Warashina and Noro, 2000). In the HMBC spectrum, the correlations between H-15/C-13, H-15/C-14, H-15/C-16 and H-15/C-17, further confirmed the previous assumption. The determination of the α-configuration of H-15 was achieved from the spatial correlation between H-15/H-9α (δ_H 1.16) and H-15/H-12α (δ_H 1.44), in the NOESY spectrum. The side chain at C-17 was assigned as β from the NOESY spectrum, which showed spatial relation between H-17/H-15α and H-17/H-16α, from the splitting pattern of H-17α (*dd*, $J = 13$, 6 Hz) and by comparison with the data of the previously isolated glycosides from the genus *Caralluma* (Lin et al., 1994; Halim and Khalil, 1996; Qiu et al., 1997, 1999; Al-Yahya et al., 2000). The stereochemistry of C-20 was determined as *S* in a similar way as in russeliosides A–D, and was deduced from the observation of the spatial relations between H-20/H-21, H-20/H-18 and H-l6α/H-21 and was further supported from the absence of any correlation between H-21 and H-l8 (Itokawa et al., 1988; Qiu et al., 1997; Al-Yahya et al., 2000). From the foregoing evidence, the structure of compound **1** was established as 20-*O*-benzoyl-(20*S*)-pregnane-3β, 8β, 14β, 15β, 20-pentaol 3-*O*-β-D-glucopyranosyl (1→4) β-D-digitalopyranoside, and named penicilloside A.

Compound **2** was isolated as a white amorphous powder, $[\alpha]_D^{25}$ −35.2° and had a molecular formula $C_{47}H_{72}O_{20}$ as shown from the ESI–MS (*m/z* 955 $[M-H]^-$ and 979 $[M+Na]^+$, in the negative and positive ion modes, respectively) and the ^{13}C NMR spectral data (DEPT). The IR spectrum of **2** showed similar absorption bands to those of **1**. The ESI–MS showed the presence of a quasimolecular ion peak at *m/z* 979 $[M+Na]^+$, which suggested one additional hexose unit relative to **1**. The presence of three sugar units in **2** was deduced from the ^1H and ^{13}C NMR spectra, which showed the presence of three anomeric protons at δ_H 4.36, 4.40, and 4.60, which are connected to carbon signals at δ_C 102.8, 105.1, and 104.2, respectively. Acid hydrolysis revealed the presence of two sugars, identified as D-digitalose and D-glucose by TLC, and by the comparison of the ^1H and ^{13}C NMR spectra of **2** (Table 1) with those of russelioside D (Al-Yahya et al., 2000). The connections of the sugar units were similar to those in **1**, with an additional glucose unit (glucose-2) located at C-6 of glucose-1. The attachment of glucose-2 to C-6 of glucose-1 was deduced from the HMBC spectrum and from the glycosylation shift of C-6″ (+7.8 ppm) relative to the corresponding carbon in glucose-2 (C-6‴) (Agrawal, 1992). The ^1H and ^{13}C NMR spectral data of the aglycone part of **2** (Table 2 and Experimental) were identical with those of **1**, which indicated that both glycosides have the same aglycone. The previous assumption was supported by the result of acid hydrolysis. The presence of the benzoyl moiety and its attachment to C-20, and the configurations of C-15, C-17 and C-20 were deduced as in **1**. Therefore, the structure of compound **2** was elucidated as 20-*O*-benzoyl-(20*S*)-pregnane-3β, 8β, 14β, 25β, 20-pentaol 3-*O*-β-D-glucopyranosyl (1→6) β-D-glucopyranosyl (1→4) β-D-digitalopyranoside, and named penicilloside B.

Compound **3** was isolated as a white amorphous powder, $[\alpha]_D^{25}$ −46.7° and had a molecular formula $C_{52}H_{80}O_2$, as shown from the ESI–MS (*m/z* 1039 $[M-H]^-$ and 1063 $[M+Na]^+$, in negative and positive ion modes, respectively) and ^{13}C NMR spectral data (DEPT). The acid hydrolysis of **3** yielded two sugars, identified as glucose and digitalose, and a different aglycone from that of **1**

Table 1
^1H and ^{13}C NMR spectral data of the sugar part of compounds **1–3** (C_5D_5N, 500 and 125 MHz, respectively)[ab]

	1		**2**[c]		**3**	
	δ_H	δ_C	δ_H	δ_C	δ_H	δ_C
Dig						
1	4.75 (*d*, 7.7)	102.3	4.36 (*d*, 7.7)	102.8	4.72 (*d*, 7.5)	102.3
2	3.42 (*dd*, 8.5, 9.3)	71.3	3.58 (*t*, 8)	71.7	3.39 (*dd*, 8.5, 9.5)	71.2
3	3.57 (*dd*, 2.3, 9.4)	85.4	3.22 (*dd*, 9, 1.3)	85.8	3.51 (*dd*, 3, 9.4)	85.5
4	4.35 (*br s*)	76.2[d]	4.17 (*br s*)	75.0[d]	4.51 (*br s*)	75.4
5	3.75 (*m*)	70.4	3.63 (*m*)[e]	71.4	3.84, (*m*)	70.5
6	1.60 (*d*, 6.5)	17.7	1.28 (*d*, 6.5)	17.6	1.73 (*d*, 6.5)	17.9
MeO	3.67 (*s*)	58.9	3.49 (*s*)	58.7	3.62 (*s*)	58.8
Glc-1						
1	5.16 (*d*, 7.7)	105.3	4.60 (*d*, 7.6)	104.2	5.14 (*d*, 7.7)	104.9
2	3.99 (*t*, 8)	76.0[d]	3.2 (*t*, 8)	75.8	3.94 (*t*, 8.5)	75.7
3	4.24 (*t*, 9)	78.2	3.64 (*m*)[e]	78.0	4.16 (*dd*, 8.5, 9)	78.2[d]
4	4.18 (*t*, 9)	71.7	3.30 (*m*)[e]	71.7[d]	4.02 (*t*, 9)	71.7[d]
5	3.94 (*m*)	78.5	3.44 (*m*)	77.4	4.10 (*t*, 8, 8.5)	77.6
6a	4.55 (*br d*, 12)	62.9	4.14 (*br d*, 11.7)	70.4	4.82 (*br d*, 11)	70.4
6b	4.33 (*dd*, 6, 12)		3.76 (*dd*, 6, 11.7)		4.29 (*dd*, 6, 11)	
Glc-2						
1			4.40 (*d*, 7.7)	105.1	5.17 (*d*, 7.5)	105.6
2			3.18 (*t*, 9)	75.2[d]	4.03 (*t*, 8.5)	75.1
3			3.36 (*t*, 9)	77.8	4.22 (*m*)	78.4[d]
4			3.32 (*m*)[e]	71.9[d]	4.24 (*m*)	71.6[d]
5			3.26 (*m*)[e]	78.2	3.95 (*m*)	78.5[d]
6a			3.86 (*d*, 2, 11.7)	62.8	4.52 (*br d*, 12)	62.6
6b			3.65 (*dd*, 5, 11.7)		4.37 (*dd*, 5, 12)	

[a] Assignments were determined using 2D NMR (^1H–^1H COSY, NOESY, HMQC and HMBC) spectra; Dig, digitalose; Glc, glucose.
[b] Multiplicity was determined by DEPT experiments and *J* values are given in parentheses.
[c] Measured in CD_3OD at 400 (^1H NMR) and 100 MHz (^{13}C NMR).
[d] Interchangeable in the same column.
[e] Overlapping with other signals.

and **2** (TLC). The ^1H and ^{13}C NMR spectral data of **3** (Table 1) showed the presence of three sugar units, which were identified as two glucose units and one digitalose unit. The sugar units were connected in the same sequence as in **2** by comparison of their spectral data (Table 1). Compound **3** showed, in addition to the benzoyl moiety in **1** and **2**, another acyl moiety identified as isovaleric acid. The identification of the isovaleroyl moiety was achieved from the ^1H NMR spectrum, which showed the presence of one methine, one methylene and two methyl proton signals at δ_H 2.14 (1H), 2.18 (2H) and 0.90 (6H), respectively, which correlated with the corresponding carbon signals at δ_C 25.7, 43.9 and 22.2, in the ^{13}C NMR spectrum (Halim and Khalil, 1996; Chen et al., 1999). The position of the benzoyl moiety was determined to be at C-15 from the downfield shift of C-15 (δ_C 76.2) relative to the corresponding carbon in **1,** and from the long-range correlation between the carbonyl group of the benzoyl moiety (δ_C 166.2) and H-15 in the HMBC spectrum. The isovaleroyl moiety was attached to C-20 based on the long-range correlation between the carbonyl group (δ_C 172.2) and H-20 (δ_H 5.48) in the HMBC spectrum. The configuration of the stereocenters in **3** was determined in the same way as in **1**. Therefore, compound **3** was elucidated as 15β-*O*-benzoyl-20-*O*-isovaleroyl-(20*S*)-pregnane-3β, 8β, 14β, 15β, 20-pentao1 3-*O*-β-D-glucopyranosyl (1→6)-β-D-glucopyranosyl (1→4)-β-D-digitalopyranoside, and named penicilloside C.

3. Experimental

Melting points were determined on a Yanagimoto micromelting point apparatus and are uncorrected. Optical rotations were measured using a JASCO DIP-360 automatic polarimeter. UV spectra were measured on Shimadzu UV-2200 UV–VIS spectrophotometer. IR spectra were measured on a JASCO FT/IR-230 IR spectrometer. ^1H and ^{13}C NMR spectra were measured with a JNM-LA400WB Lambada (Jeol) NMR (^1H, 400 MHz; ^{13}C, 100 MHz) or a Varian UNITY 500 spectrometer (^1H, 500 MHz; ^{13}C, 125 MHz), using TMS as internal standard. ESI–MS spectra were measured with Perkin-Elmer SCIEX API III biomolecular mass analyzer. MPLC separations were carried out on LiChroprep RP-18 (Merck, size A) with 5.5 ml flow rate and 4 ml fractions were collected. TLC was carried out on precoated Si gel plates (Kieselgel 60 F_{254}, Merck), using $CHCl_3$–MeOH (9:1), or CH_2Cl_2–MeOH–H_2O (25:8:1) as the developing solvent systems. TLC plates were visualised

Table 2
^{13}C NMR spectral data of the aglycone moiety of compounds **1–3** (C_5D_5N, 125 MHz)[a]

C	1	2[b]	3
1	38.4, *t*	39.2, *t*	38.1, *t*
2	29.5, *t*	30.1, *t*	29.4, *t*
3	77.1, *d*	79.6, *d*	76.9, *d*
4	34.4, *t*	35.0, *t*	34.1, *t*
5	45.2, *t*	46.4, *d*	45.1, *d*
6	25.4, *t*	25.9, *t*	25.1, *t*
7	35.1, *t*	35.5, *t*	35.3, *t*
8	77.2, *s*	78.1, *s*	74.2, *s*
9	51.2, *d*	52.1, *d*	51.4, *d*
10	36.8, *s*	37.6, *s*	36.8, *s*
11	18.1, *t*	18.8, *t*	18.2, *t*
12	42.2, *t*	42.1, *t*	41.6, *t*
13	48.1, *s*	49.9, *s*	47.8, *s*
14	83.7, *s*	84.2, *s*	83.8, *s*
15	72.2, *d*	73.3, *d*	76.2, *d*
16	35.7, *t*	35.9, *t*	32.2, *t*
17	52.4, *d*	53.2, *d*	51.6, *d*
18	18.1, *q*	18.1, *q*	17.6, *q*
19	13.3, *q*	13.5, *q*	13.3, *q*
20	74.3, *d*	75.5, *d*	73.0, *d*
21	19.4, *q*	19.5, *q*	19.0, *q*
Benzoyl			
1	166.2, *s*	166.2, *s*	166.2, *s*
2	130.7, *s*	130.7, *s*	130.7, *s*
3, 7	130.2, *d*	130.2, *d*	130.2, *d*
4, 6	128.9, *d*	128.9, *d*	128.9, *d*
5	133.6, *d*	133.6, *d*	133.6, *d*
Isovaleroyl			
1			172.2, *s*
2			43.9, *t*
3			25.7, *d*
4, 5			22.2, *q*

[a] Multiplicity was determined by DEPT experiments; *s*, quaternary; *d*, methine; *t*, methylene, and *q*, methyl carbons.
[b] Measured in CD_3OD at 100 MHz.

by spraying with anisaldehyde reagent followed by heating.

3.1. Plant materials

The aerial parts of *C. penicillata* were collected from the Aseer region of the Kingdom of Saudi Arabia in April 1996. The plant material was kindly identified by Dr. Sultan Ul-Abedin, College of Pharmacy, King Saud University, Riyadh, Saudi Arabia. A voucher specimen was deposited in the herbarium of the College of Pharmacy, King Saud University, Riyadh, Saudi Arabia (No. 11677B).

3.2. Extraction and isolation

The air-dried aerial parts of *C. penicillata* (1 kg) were defatted with petrol followed by extraction with EtOH (10 l) to give a crude EtOH extract (131 g). The EtOH extract (120 g) was suspended in water and extracted with ether, chloroform and *n*-butanol to give extracts of 8, 20 and 18 g, respectively. A portion of the $CHCl_3$ extract (5 g) was applied to a Si gel column (3.8×16 cm) eluted with MeOH/$CHCl_3$ mixtures (10–20%) with fractions being collected (100 ml), to give three main fractions, fr. A (470 mg), fr. B (195 mg) and fr. C (350 mg). Fr. A (200 mg) was purified on MPLC using RP-18 and MeOH–H_2O (73:27) as the eluent, to give compound **1** (100 mg). Fr. B was subjected to rechromatography on a Si gel column (2×40 cm) using $CHCl_3$-MeOH–H_2O (7:2:0.05) as the solvent system to give compound **2** (28 mg). Fr. C was purified on MPLC using RP-18 and MeOH–H_2O (7.5:2.5) as the solvent system, to give compound **3** (35 mg).

3.3. Acid hydrolysis of compounds *1–3*

Compounds **1–3** were hydrolysed according to procedure described by Halim and Khalil (1996).

*Penicilloside A **(1)***. White needles, mp 215–217°C (uncorr.); $[\alpha]_D^{25}$ −30° (MeOH, *c*. 0.09); UV λ_{max}^{MeOH} nm (log ε): 228 (4.0), 272 (2.9), 280 (2.9); IR ν_{max}^{KBr} cm^{-1}:3400, 1720, 1650, 1455, 1080; ^1H NMR (C_5D_5N, 500 MHz), aglycone moiety: δ 1.07 (3H, *s*, H-19), 1.16 (1H, *m*, H-9α), 1.36 (3H, *d*, *J*=6 Hz, H-21), 1.55 (3H, *s*, H-18), 1.80 (1H, *m*, H-16β), 1.98 (1H, *J*=13, 6 Hz, H-17α), 2.50 (1H, *m*, H-16α), 4.61 (1H, *br t*, *J*=8 Hz, H 15α), 5.76 (1H, *m*, H-20), benzoyl moiety: 7.45 (2H, *m*, H-4, H-6), 7.52 (1H, *m*, H-5), 8.20 (2H, *m*, H-3, H-7), sugar mioety, see Table 1; ^{13}C NMR (C_5D_5N, 125 MHz), see Tables 1 and 2; ESI–MS, *m*/*z* (rel. int.): 793 [M−H] (75), 817 $[M+Na]^+$ (100), in negative and positive ion modes, respectively.

Penicilloside B (***2***). An amorphous white powder; $[\alpha]_D^{25}$ −35.2° (MeOH *c*. 0.075); UV λ_{max}^{MeOH} nm (log ε): 228 (3.1), 272 (2.8), 280 (2.7); IR ν_{max}^{KBr} cm^{-1}: 3400, 1710, 1650, 1460, 1060; ^1H NMR (CD_3OD, 400 MHz), aglycone moiety: δ 0.97 (3H, *s*, H-19), 1.07 (1H, *m*, H-9α), 1.18 (3H, *s*, H-18), 1.26 (3H, *d*, *J*=6 Hz, H-21), 1.55 (1H, *m*, H-16β), 1.86 (1H, *m*, H-17α), 2.32 (1H, *m*, H-16α), 4.28 (1H, t, *J*=8 Hz, H-15α), 5.30 (1H, *m*, H-20), benzoyl moiety: 7.46 (2H, *m*, H-4, H-6), 7.58 (1H, *m*, H-5), 7.97 (2H, *m*, H-3, H-7), sugar moiety, see Table 1; ^{13}C NMR (CD_3OD, 100 MHz), see Tables 1 and 2; ESI–MS, *m*/*z* (rel. int.): 955 $[M-H]^-$ (100), 979 $[M+Na]^+$ (100), in negative and positive ion modes, respectively.

*Penicilloside C (**3**)*. An amorphous white powder, $[\alpha]_D^{25}$ −46.7° (MeOH, *c*. 0.1); UV λ_{max}^{MeOH} nm (log ε): 228 (3.2), 255 (2.7), 261 (3.5), 280 (1.9); IR ν_{max}^{KBr} cm^{-1}: 3400, 1710, 1650, 1460, 1060; ^1H NMR (C_5D_5N, 500 MHz): aglycone moiety: δ 1.07 (3H, *s*, H-19), 1.23 (1H, *m*, H-9α), 1.23 (3H, *d*, *J*=6 Hz, H-21), 1.58 (3H, *s*, H-18), 1.80 (1H, *m*, H-16β), 1.90 (1H, *J*=11, 6 Hz, H-17α), 2.50 (1H, *m*, H-16α), 5.90 (1H, *m*, H-15α), 5.48 (1H, *m*, H-20), benzoyl moiety, 7.38 (2H, *m*, H-4, H-6), 7.52 (1H, *m*, H-5), 8.32 (2H, *m*, H-3, H-7), isovaleroyl moiety: 0.90

(6H, *d*, $J = 6$ Hz, H-4, H-5), 2.14 (1H, *m*, H-3), 2.18 (2H, *m*, H-2), sugar moiety, see Table 1; ^{13}C NMR (C_5D_5N, 125 MHz), see Tables 1 and 2; ESI–MS, *m*/*z* (rel. int.): 1039 $[M-H]^-$ (60), 1063 $[M+Na]^+$ (100), in negative and positive ion modes, respectively.

Acknowledgements

The authors are indebted to Dr. Sultan Ul-Abedin, Pharmacognosy Department, College of Pharmacy, King Saud University, Riyadh, Saudi Arabia, for the identification of the plant material and Dr. C.-M. Ma for measuring the ESI–MS spectra. E.A.S. thanks the Japan Society for the Promotion of Science (JSPS) for financial support (research grant No. L00553).

References

Agrawal, P.K., 1992. NMR spectroscopy in the structural elucidation of oligosaccharides and glycosides. Phytochemistry 31, 3307–3330.

Al-Yahya, M.A., Abdel-Sattar, E., Guittet, E., 2000. Pregnane glycosides from *Caralluma russeliana*. J. Nat. Prod. 63, 1451–1453.

Al-Yahya, M.A., Tariq, M., Khalifa, T.I., Ashraf, I., 1983. Toxicity studies on *Caralluma penicillata* — a poisonous plant from Saudi Arabia. Toxicon (suppl.) 3, 9–12.

Al-Yahya, M.A., Tariq, M., 1983. Studies on *Caralluma penicillata*. Fitoterapia, LIV, 41–46.

Chen, J.-J., Zhang, Z.-X., Zhou, J., Li, B.-T., 1999. New pregnane glycosides from *Sinomarsdenia incisa*. J. Nat. Prod. 62, 829–832.

Collenette, S., 1985. An Illustrated Guide to the Flowers of Saudi Arabia. Scorpion, London, pp. 276–278.

El Sayed, K.A., Halim, A.F., Zaghloul, A.M., McChesney, J.D., Stone, P., Voehler, M., Hayashi, K., 1995. Pregnane glycosides from *Stapelia variegata*. Phytochemistry 39, 395–403.

Halim, A., Khalil, A.T., 1996. Pregnane glycosides from *Caralluma retrospiciens*. Phytochemistry 42, 1135–1139.

Hamadan, K., 1980. Report on the Poisoning Due to *Caralluma penicillara* in Sheep. Ministry of Agriculture, Saudi Arabia.

Itokawa, H., Xu, J., Takeya, K., 1988. Pregnane glycosides from an antitumour fraction *of Periploca sepium*. Phytochemistry 27, 1173–1179.

Lin, L.-J., Lin, L.-Z., Gil, R.R., Cordell, G.A., Ramesh, M., Srilatha, B., Reddy, B., Appa Rao, A.V.N., 1994. Pregnane glycosides from *Caralluma umbellata*. Phytochemistry 35, 1549–1553.

Konda, Y., Toda, Y., Harigaya, Y., 1992. Two new glycosides, hancoside and neohancoside A, from *Cynanchum hancockianum*. J. Nat. Prod. 55, 1447–1453.

Mossa, J.S., Al-Yahya, M.A., Al-Meshal, I.A., Tariq, M., 1983. Phytochemical and biological screening of Saudi medicinal plants: part 4. Fitoterapia, LIV, 75–80.

Qiu, S.-X., Cordell, G.A., Kumar, B.R., Rao, Y.N., Ramesh, M., Kokate, C., Appa Rao, A.V.N., 1999. Bisdesmosidic pregnane glycosides from *Caralluma lasiantha*. Phytochemistry 50, 485–491.

Qiu, S.-X., Lin, L.-Z., Cordell, G.A., Ramesh, M., Kumar, B.R., Radhakrishna, M., Mohan, G.K., Reddy, B.M., Rao, Y.N., Srinivas, B., Thomas, S.N., Appa Rao, A.V.N., 1997. Acylated C-21 steroidal bisdesmosidic glycosides from *Caralluma umbellata*. Phytochemistry 46, 333–340.

Rasoanaivo, P., Kaneda, N., Kinghorn, A.D., Farnsworth, N.R., 1991. Folotsoside A, a new pregnane glycoside from *Folotsia sarcostemmoides*. J. Nat. Prod. 54, 1672–1676.

Warashina, T., Noro, T., 2000. Steroidal glycosides from the aerial part of *Asciepias incarnata*. Phytochemistry 53, 485–498.

PERGAMON

Phytochemistry 57 (2001) 1219–1222

PHYTOCHEMISTRY

www.elsevier.com/locate/phytochem

A steroidal saponin from the seeds of *Allium tuberosum*

Zhong-Mei Zou[a], De-Quan Yu[a,*], Pu-Zhu Cong[b]

[a]*Institute of Materia Medica, Chinese Academy of Medical Sciences and Peking Union Medical College, Beijing 100050, China*
[b]*Institute of Medicinal Plants Developments, Chinese Academy of Medical Sciences and Peking Union Medical College, Beijing 100094, China*

Received in revised form 25 May 1999

Abstract

A steroidal saponin, named tuberoside, together with seven known compounds, were isolated from the seeds of *Allium tuberosum* Rottl. ex Spreng. Its structure was established by spectroscopic data, hydrolysis, and comparison with spectral data of known compounds to be (2α, 3β, 5α, 25*S*)-2,3,27-trihydroxyspirostane 3-*O*-α-L-rhamnopyranoyl-(1→2)-*O*-[α-L-rhamnopyranoyl-(1→4)]-β-D-glucopyranoside. © 2001 Published by Elsevier Science Ltd.

Keywords: *Allium tuberosum*; Liliaceae; Saponin; Spirostanol glycoside; Tuberoside

1. Introduction

Allium tuberosum Rottl. ex Spreng is widely cultivated and used as food in China, whose seeds have been reputedly used as a traditional Chinese medicine for treating both impotence and nocturnal emissions (Jiangsu New Medicinal College, 1979). Species of *Allium* genus are famous for their production of sulfur-containing biologically active natural products. With regard to the saponin constituents of the *Allium* genus, many steroidal saponins have been reported (Zou et al., 1999). However, there has been no exploration of the secondary metabolites of *A. tuberosum* seeds. Our detailed investigation of its seeds has led to the discovery of a new saponin (**1**), together with eight known compounds, gitogenin 3-*O*-α-L-rhamnopyranosyl-(1→2)-β-D-galactopyranoside (Mimaki et al., 1996), S-allylcysteine (**3**), L-tyrosine (**4**), adenosine (**5**), inosine (**6**), allantoin (**7**) and mannitol (**8**). The known compounds were identified by direct comparison with authentic samples (co-TLC, IR, MS, NMR) or with reported spectral and physical data. This paper deals with the isolation and structural elucidation of the new saponin (**1**).

2. Results and discussion

Commercially available seeds of *Allium tuberosum* (9.5 kg) were defatted with petroleum ether followed by extraction with hot 70% EtOH. The concentrated extract was partitioned between $CHCl_3$ and H_2O, then between *n*-BuOH and H_2O. The *n*-BuOH soluble phase was subjected to silica gel column chromatography to give a new compound, named tuberoside (**1**).

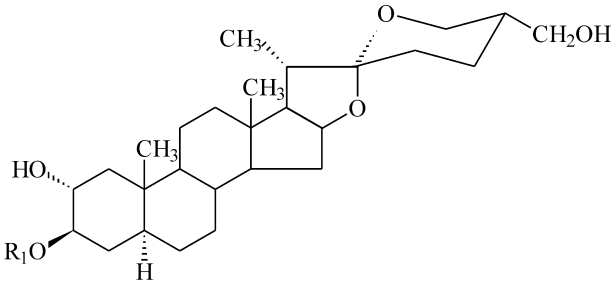

1. R_1=α-L-Rha*p*-(1→2)-[α-L-Rha*p*-(1→4)]-β-D-Glc*p*

Tuberoside (**1**) was obtained as an amorphous powder, with the molecular formula $C_{45}H_{74}O_{18}$, which was deduced from the FAB–mass spectrum showing an $[M+H]^+$ ion at *m*/*z* 903 and the ^{13}C NMR spectrum (Table 1). The IR spectrum of **1** showed the characteristic absorption of hydroxyl groups at 3422 cm^{-1}. The FAB–mass spectrometry of compound **1** showed fragment ion

* Corresponding author. Tel.: +86-10-63036781; fax: +86-10-63017757.
E-mail address: dquanyu@public.bta.net.cn (D.-Q. Yu).

0031-9422/01/$ - see front matter © 2001 Published by Elsevier Science Ltd.
PII: S0031-9422(01)00216-3

peaks at m/z 757 (M + H-146), 611 (M + H-146-146), 449 (M + H-146-146-162), which suggested the sequential loss of two deoxy hexose and one hexose moiety. The NMR spectra (Tables 1 and 2) of **1** also showed the presence of three sugars from the three anomeric protons at δ 5.00 (*d*, $J = 7.3$ Hz), 6.38 (*s*) and 5.38 (*s*) in the ^{1}H NMR spectrum, and the three anomeric carbon signals at δ 102.9, 102.2, 100.9 in the ^{13}C NMR spectrum.

On acid hydrolysis, **1** afforded D-glucose, L-rhamnose, which were identified by co-TLC with authentic samples and aglycone (**1a**). The NMR spectral data (Table 1) indicated **1a** is a spirostanol derivative with three hydroxyl groups, and the base peak at m/z 155 in EI–MS spectrum of **1a** proved a hydroxyl group to be located at the F ring (Cong, 1987). Further analysis of

Table 1
^{13}C NMR spectroscopic data of compounds **1** and **1a** (125 MHz)[a]

C	1	1a
1	45.9	45.0
2	70.6	73.1
3	85.1	76.4
4	33.5	37.4
5	44.6	44.9
6	28.1	27.8
7	32.3	32.1
8	34.6	35.6
9	54.4	54.3
10	36.9	37.6
11	21.5	21.2
12	40.1	39.9
13	40.6	41.7
14	56.4	56.2
15	32.2	32.8
16	81.2	80.9
17	63.1	63.0
18	16.6	16.2
19	15.6	13.6
20	42.1	41.7
21	15.1	14.4
22	109.7	109.2
23	31.6	31.9
24	24.1	24.5
25	39.2	38.2
26	64.1	63.1
27	64.4	63.4
Glc- 1	100.9	
2	78.0	
3	78.0	
4	78.7	
5	77.2	
6	61.1	
Rha- 1	102.2	
2	72.6a[b]	
3	72.7a	
4	73.9b	
5	70.5	
6	18.6	
Rha- 1	102.9	
2	72.5a	
3	72.7a	
4	74.1b	
5	69.6	
6	18.6	

[a] Spectra were measured in pyridine-d_5 (**1**) and chloroform-*d* (**1a**).
[b] a and b signals may be interchangeable.

Table 2
^{1}H NMR spectroscopic data of compound **1** (500 MHz, pyridine-d_5)[a]

Position	δ_H	J (Hz)
H-1α	2.22 *dd*	12.7, 4.7
H-1β	1.16 *m*	
H-2β	4.07 *ddd*	12.1, 11, 4.7
H-3α	3.88 *dd*	11.4, 11.0
H-4α	2.0 overlap	
H-4β	1.39 overlap	
H-5α	1.01 overlap	
H-6	1.20 *m*	
	1.08 *m*	
H-7	0.83 *m*	
	1.48 *m*	
H-8	1.39 overlap	
H-9	0.62 *ddd*	11, 11, 2.5
H-11	1.48 *m*	
	1.23 *m*	
H-12	1.63 overlap	
	1.03 *dd*	11.8, 11.8
H-14	1.00 *m*	
H-15	2.00 overlap	
	1.39 overlap	
H-16	4.54 *m*	
H-17	1.39 overlap	
H-18	0.80 *s*	
H-19	0.94 *s*	
H-20	1.95 *m*	
H-21	1.12 *d*	6.9
H-23	1.74 *m*	
H-23	1.74 *m*	
H-24	1.80 overlap	
	0.96 *m*	
H-25	2.06 *m*	
H-26eq	4.13 *dd*	11.4, 5.2
H-26ax	3.89 *dd*	11.4, 11.1
H-27a	3.71 *dd*	10.7, 5.1
H-27b	3.63 *dd*	10.7, 7.2
Glc H-1	5.00 *d*	7.3
H-2	4.19 *t*	8.9, 7.3
H-3	4.21 *t*	8.9
H-4	4.38 *t*	8.9
H-5	3.75 *d*	8.9
H-6	4.07 *dd*	12.3, 3.6
	4.24 *dd*	12.3, 5.1
Rha H-1	6.38 *s*	
H-2	4.82 *br.s*	
H-3	4.59 *dd*	9.3, 3.3
H-4	4.34 *dd*	9.4, 9.3
H-5	4.92 *dd*	9.4, 6.1
H-6	1.63 *d*	6.1
Rha H-1	5.85 *s*	
H-2	4.66 *brs*	
H-3	4.47 *dd*	9.3, 3.4
H-4	4.32 *dd*	9.4, 9.3
H-5	4.85 *dd*	9.4, 6.3
H-6	1.66 *d*	6.3

[a] All assignments were confirmed by ^{1}H–^{1}H COSY, ^{13}C–^{1}H COSY and DEPT spectra.

the ^1H and ^{13}C NMR spectra of **1a** allowed its identification as (2α, 3β, 5α, 25*S*)-spirostan-2,3,27-triol (crestagenin), isolated previously from the leaves of *Digitalis canariensis* (Dolgado et al., 1969; Gonzalez, et al. 1983).

The ^1H and ^{13}C NMR spectral data assignments of compound **1** were performed via analyses of the ^1H–^1H COSY, ^{13}C–^1H COSY and DEPT spectra. The presence of two terminal α-L-rhmnopyranosyl moieties in the molecule of **1** was demonstrated by the two sets of characteristic six carbon signals at δ 102.2, 72.6, 72.7, 73.9, 70.5, 18.6; 102.9, 72.5, 72.7, 74.1, 69.6, 18.6 in the ^{13}C NMR spectrum. The C-5 signals of two rhamnose units at δ 70.5 and 69.6, respectively, indicated their α-configurations (Seo et al., 1978). Comparison of ^{13}CNMR data of the sugar moieties with the corresponding methyl β-D-glucopyranoside (Agrawal et al., 1985) indicated that the C-2 and C-4 of the glucosyl moiety were shifted downfield to δ 78.0 and 78.7 from 73.7 and 70.3, respectively. The significant glycosylation shifts clearly showed the two terminal rhamnopyranoses were linked to the C-2 and C-4 positions of the inner glucopyranose. The β-configuration of the glucopyranose was further confirmed by the large $J_{1,2}$ couplings of its anomeric proton.

The linkage of the sugar chain was concluded to be at the C-3 hydroxyl position of the aglycone because, in the ^{13}C NMR spectrum of **1**, the signal due to C-3 shifted to a lower field by 8.7 ppm, whereas the signals due to C-2 and C-4 moved to upper fields by 2.5 and 3.9 ppm, as compared with those of **1a**. Accordingly, the structure of **1** was elucidated as (2α, 3β, 5α, 25*S*)-2,3,27-trihydroxyspirostane 3-*O*-α-L-rhamnopyranoyl-(1→2)-*O*-[α-L-rhamnopyranoyl-(1→4)]-β-D-glucopyranoside (**1**).

3. Experimental

3.1. General

Mps were obtained on a Boetius miromelting apparatus and are uncorrected. Optical rotations were measured with Perkin-Elmer 241 polarimeter. IR spectra were recorded on a Perkin-Elmer 683 instrument. EIMS was obtained on a VG Zab-2f and FABMS on a VG Zabspec mass spectrometer. The ^1H NMR spectra (500 MHz) and ^{13}C NMR (125 MHz) were recorded on a Brüker AM-500 spectrometer and the chemical shifts are reported in ppm using the solvent as reference.

3.2. Plant materials.

The seeds of *Allium tuberosum* Rottl. ex Spreng were purchased from Beijing Tong-Ren-Tang Group, China, and were identified by Mr. Wei-Ze Liu, Institute of Materia Medica, Chinese Academy of Medical Sciences and Peking Union Medical College, China.

3.3. Extration and isolation.

Air-dried and powdered seeds of *A. tuberosum* Rottl. Ex Spreng (9.5 kg) were defatted by percolation with petroleum ether followed by extraction with hot 75% EtO. The combined EtOH extracts were filtered, evap. under red. press. and the residue suspended in H_2O and partitioned with $CHCl_3$ and *n*-BuOH, respectively.

The *η*-BuOH extract (62 g) was fractionated on a silica gel column with a gradient mixture of $CHCl_3$–MeOH and finally with MeOH to give five Frs. (A_1–A_5). Fr. A_1 was chromatographied on silica gel, eluting with $CHCl_3$–MeOH (9:1) to give compounds **2** (10 mg) and **5** (176 mg), while Fr. A_2 was repeatedly chromatographied on silica gel to give compounds **6** (15 mg) and **7** (7 mg). Fr.A_3 was subjected to silica gel with $CHCl_3$-MeOH (20:3) to give compounds **1** (31mg) and **8** (38 mg). Fr.A_4 was repeatedly chromatographied on silica gel CC to give compound **3** (162mg). Fr. A_5 was subjected to silica gel CC with $CHCl_3$–MeOH (5:1) to give compound **4** (16 mg).

3.4. Tuberoside A (*1*)

$C_{45}H_{74}O_{18}$, amorphous powder, mp 292–293°, $[\alpha]_D^{25}$ −33°; *c* 0.02, MeOH. IR (KBr) cm^{-1} 3422, 2932, 1452, 1381, 1043, 987, 912. FABMS *m/z* 903 $[M+H]^+$, 757 $[M+H\text{-}146]^+$, 611 $[M+H\text{-}2\times146]^+$, 449 [aglycone + H]$^+$, 431, 413. ^1H and ^{13}C NMR data, see Tables 1 and 2.

3.5. Acid hydrolysis of *1*

Compound **1** (20 mg) was heated with 3% H_2SO_4 (EtOH, 1:1) at 100°C for 3 h. After cooling, the reaction mixture was neutralized with 1 N NaOH and partitioned between AcOEt and H_2O. The AcOEt soluble phase was concentrated and subjected to silica gel CC with $CHCl_3$ to give the known crestaganin **1a**.

Compound **1a**: white powder, EI–MS *m/z* 448 (M^+), 155 (100). ^1H NMR ($CDCl_3$) δ 0.97 (3H, *d*, *J* = 7.8 Hz), 0.86 (3H, *s*), 0.76 (3H, *s*), 3.71 (*dd*, *J* = 10.7, 5.1 Hz, CH_2-27), 3.63 (*dd*, *J* = 10.7, 7.1 Hz, CH_2-27), 3.89 (1H, *dd*, *J* = 11.4, 11.1 Hz, CH_2-26), 4.13 (*dd*, *J* = 11.4, 5.2 Hz, CH_2-26). ^{13}C NMR data, see Table 1.

The H_2O soluble phase was concentrated and examined by comparison with authentic samples through TLC ($CHCl_3$–MeOH–H_2O, 7:3:0.1) to detect D-glucose and L-rhamnose.

Acknowledgements

The authors are grateful to Mr. Wei-Ze Liu, Institute of Materia Medica, CAMS and PUMC, for the identification of plant sample and to Professors Wen-Yi He and

Man Kong, for measurements of NMR spectra. Our thanks are also due to Mr. Li-Jun Li, Institute of Materia Medica, CAMS and PUMC, for measurements of MS.

References

Agrawal, P.K., Jain, D.C., Gupta, R.K., Thakur, R.S., 1985. Carbon -13 NMR spectroscopy of steroidal sapogenins and steroidal saponins. Phytochemistry 24, 2479–2496.

Dolgado, B.J., Velazquez, J.M., Breton Funes, J.L., 1969. Glucosides and aglucones of Scrophulariaceae. XIII. Aglucones of *Digitalis canariensis*. An. Quim. 65, 817–824.

Gonzalez, A.G., Darias, V., Suarez, M.C., Janssen, K., 1983. Preliminary pharmacobilological study of new steroidal saponins. Farmaco (Sci.) 38, 3–8.

Jiangsu New Medicinal College, 1979. The Dictionary of Chinese herbal Medicines, Vol. 2. Shanghai People's Publishing Press, Shanghai, pp. 1646.

Mimaki, Y., Kanmoto, T., Kuroto, M., Sashida, Y., Satomi, Y., Nishino, A., Nishino, H., 1996. Steroidal saponins from *Hosta longipes* and their inhibitory activity on tumor promoter -induced phospholipid. Phytochemistry 42, 1065–1070.

Cong, P.Z., 1987. Application of Mass Spectrometry in Natural Organic Chemistry. Science Publishing Press, Beijing, pp. 786.

Seo, S., Tomita, Y., Tori, K, Yoshimura, Y., 1978. Determination of the absolute configuration of a secondary hydroxy group in a chiral secondary alcohol using glycosidation shifts in carbon-13 nuclear magnetic resonance spectroscopy. J. Am. Chem. Soc. 100 (11), 3331–3339.

Zou, Z.M., Yu, D.Q., Cong, P.Z., 1999. Research progress in the chemical constituents and pharmacological actions of *Allium* species. Acta Pharm. Sinica 34, 395–400.

PERGAMON

Phytochemistry 57 (2001) 1223–1226

PHYTOCHEMISTRY

www.elsevier.com/locate/phytochem

Acylated apigenin glycosides from alfalfa (*Medicago sativa* L.) var. Artal

Anna Stochmal[a,*], Ana M. Simonet[b], Francisco A. Macias[b], Maria A. Oliveira[c], Josi M. Abreu[c], Robert Nash[d], Wieslaw Oleszek[a]

[a]*Department of Biochemistry, Institute of Soil Science and Plant Cultivation, ul. Czartoryskich 8, 24-100 Pulawy, Poland*
[b]*Departamento de Química Orgánica, Facultad de Ciencias, Universidad de Cádiz, C/República Saharaui s/n, Apdo. 40, 11510-Puerto Real, Cádiz, Spain*
[c]*Instituto Superior de Agronomia, Secgco de Produgco Animal, Tapada da Ajuda-, 1349-017 Lisboa, Portugal*
[d]*Institute of Grassland and Environmental Research, Plas Gogerddan, Aberystwyth, Cardiganshire SY23 3EB, UK*

Received 27 February 2001; received in revised form 24 April 2001

Abstract

Three flavones, including 4′-*O*-[2′-*O*-*E*-feruloyl-*O*-β-D-glucuronopyranosyl(1→2)-*O*-β-D-glucuronopyranoside]apigenin, 7-*O*-β-D-glucuronopyranosyl-4′-*O*-[2′-*O*-*E*-feruloyl-*O*-β-D-glucuronopyranosyl(1→2)-*O*-β-D-glucuronopyranoside]apigenin and 7-*O*-β-D-glucuronopyranosyl-4′-*O*-[2′-*O*-*p*-*E*-coumaroyl-*O*-β-D-glucuronopyranosyl(1→2)-*O*-β-D-glucuronopyranoside]apigenin have been identified in alfalfa var. Artal. The known flavone 7-*O*-{2-*O*-E-feruloyl-[β-D-glucuronopyranosyl(1→3)]-*O*-β-D-glucuronopyranosyl (1→2)-*O*-β-D-glucurono-pyranoside} apigenin was also isolated. The structures of these compounds were deduced on the basis of their spectral data. © 2001 Elsevier Science Ltd. All rights reserved.

Keywords: *Medicago sativa*; Aerial parts; Acylated apigenin glucuronides

1. Introduction

Alfalfa is a pasture crop rich in good quality protein. Its nutritional value has been, however, influenced by the presence of secondary metabolites including saponins and flavonoids. While saponins have been extensively studied (Oleszek, 2000), very little is known on alfalfa flavonoids (Bisby et al., 1994). In our preliminary HPLC screening of 50 alfalfa varieties obtained from USDA stocks it was clear that flavonoid profiles of all tested samples contained a number of glycosides and were, with some exceptions, very similar to each other (Stochmal et al., 1999). From the Polish variety Boja several novel, acylated with ferulic and coumaric acids apigenin and luteolin glycosides have been isolated and fully characterized (Stochmal et al., 2001). All these flavonoids had only glucuronic acid in the sugar moiety and the acylation occurred on the sugar attached at C-7 of the aglycone. The HPLC profile of the variety Artal showed some dissimilarities with other cultivars and thus, the aim of the present work was to isolate and chemically characterize the unknown compounds.

2. Results and discussion

Preliminary analyses with HPLC (diode array detection) of flavonoids in the aerial parts of alfalfa var. Artal indicated the presence of several flavones, out of which, the one dominant and two minor compounds had UV spectra identical to apigenin glycosides, but their retention times were different from the others so far characterized. The column chromatography of a purified flavonoid fraction afforded four compounds, which were fully characterized by spectral techniques. Compound **4** was identified as 7-*O*-{2-*O*-*E*-feruloyl-[-*O*-β-D-glucuronopyranosyl(1→3)]-*O*-β-D-glucuronopyranosyl (1→2)-*O*-β-D-glucuronopyranoside}apigenin by comparison of its NMR and FAB-MS spectra with previously reported literature data (Stochmal et al., 2001).

Compound **1** gave a molecular ion (ESI–HRMS, negative ion mode) at *m*/*z* 797.1575, which together with the ^{1}H and ^{13}C NMR spectral data (Tables 1 and 2) was consistent with the empirical formula $C_{37}H_{34}O_{20}$.

* Corresponding author. Tel. +48-81-8863421; fax +48-81-8864547.
E-mail address: asf@iung.pulawy.pl (A. Stochmal).

0031-9422/01/$ - see front matter © 2001 Elsevier Science Ltd. All rights reserved.
PII: S0031-9422(01)00204-7

Table 1
^{1}H NMR data of flavonoids **1–3** (CD_3OD)

H	**1**[a]	**2**	**3**
Apigenin			
3	6.87 *s*	6.61 *s*	6.61 *s*
6	6.19 *d J* = 1.9	6.48 *d J* = 2.0	6.46 *d J* = 2.0
8	6.51 *d J* = 1.9	6.79 *d J* = 2.0	6.78 *d J* = 2.0
2′ and 6′	7.98 *d J* = 8.7	7.84 *d J* = 9.0	7.83 *d J* = 9.0
3′ and 5′	7.10 *d J* = 8.7	7.15 *d J* = 9.0	7.14 *d J* = 9.0
Glucuronic acids			
1	5.32 *d J* = 7.4	5.37 *d J* = 7.1	5.35 *d J* = 6.8
2	3.56 *brdd*	3.74 *dd J* = 7.1, 5.1	3.73 *dd J* = 7.1, 6.8
3	3.40 (o)	3.62 (o)	3.63 (o)
4	3.40 (o)	3.62 (o)	3.63 (o)
5	3.97 *brd*	4.01 *d J* = 9.8	4.06 *d J* = 9.5
1′	4.93 *d J* = 8.2	5.09 *d J* = 7.8	5.07 *d J* = 8.1
2′	4.64 *dd J* = 8.7, 8.2	4.90 *dd J* = 9.0, 7.8	4.92 *dd J* = 8.8, 8.1
3′	3.40 (o)[b]	3.66 *dd J* = 9.0, 9.0	3.68 *dd J* = 9.0, 8.8
4′	3.40 (o)[b]	3.62 (o)	3.63 (o)
5′	3.71 *brd*	3.87 *d J* = 9.5	3.91 *d J* = 9.3
1″		5.18 *d J* = 7.6	5.19 *d J* = 7.6
2″		3.57 *brdd*	3.58 *brdd*
3″		3.62 (o)	3.63 (o)
4″		3.62 (o)	3.63 (o)
5″		4.07 *d J* = 9.0	4.12 *d J* = 9.5
Phenolic acid			
2	7.26 *d J* = 1.9	7.07 *d J* = 2.0	7.40 *d J* = 8.5
3	–	–	6.74 *d J* = 8.5
5	6.77 *d J* = 8.2	6.73 *d J* = 8.3	6.74 *d J* = 8.5
6	7.08 *dd J* = 8.2, 1.9	6.99 *dd J* = 8.3, 2.0	7.40 *d J* = 8.5
7	7.50 *d J* = 15.8	7.53 *d J* = 15.9	7.58 *d J* = 15.9
8	6.41 *d J* = 15.8	6.25 *d J* = 15.9	6.30 *d J* = 15.9
OCH_3	3.80 *s*	3.84 *s*	–

[a] DMSO-d_6.
[b] (o) Overlapped with other signals.

Table 2
^{13}C NMR data of flavonoids **1–3** (CD_3OD)

	Apigenin				Glucuronic acids				Phenolic moiety		
C	**1**	**2**	**3**	**C**	**1**	**2**	**3**	**C**	**1**	**2**	**3**
2	166.1	165.9	166.0	1	99.7	99.1	99.4	1	127.8	127.8	127.3
3	104.8	104.9	105.0	2	82.9	82.6	82.9	2	111.7	111.6	131.2
4	183.9	184.0	184.0	3	76.5	76.4	76.5	3	149.3	149.2	116.7
5	163.2	162.9	162.8	4	72.8	72.9	72.9	4	150.5	150.6	161.2
6	100.2	101.3	101.2	5	76.1	76.2	76.1	5	116.4	116.4	116.7
7	165.5	164.5	164.5	6	172.5	172.6	172.6	6	124.2	124.2	131.2
8	95.1	96.0	95.9	1′	102.7	101.6	102.3	7	147.0	146.9	146.7
9	159.4	158.9	158.9	2′	75.2	75.2	75.2	8	115.7	115.5	115.4
10	105.4	107.3	107.3	3′	75.9	75.9	75.9	9	168.7	168.6	168.7
1′	126.1	125.8	125.8	4′	73.4	73.4	73.4	OCH_3	56.4	56.4	–
2′	129.1	129.2	129.3	5′	75.9	75.9	76.2				
3′	117.9	117.9	117.9	6′	172.5	172.6	172.6				
4′	161.3	161.4	161.4	1″		101.3	101.3				
5′	117.9	117.9	117.9	2″		74.4	74.4				
6′	129.1	129.2	129.3	3″		77.3	77.3				
				4″		73.1	73.0				
				5″		76.6	76.7				
				6″		173.0	172.8				

The downfield region of the ^{1}H NMR spectrum (Table 1) showed two spin systems correlated by ^{1}H–^{1}H shift correlation (COSY): an AA'BB' system at δ 7.98 (*d*, 8.7 Hz, H-2′ and H-6′) and δ 7.10 (*d*, 8.7 Hz, H-3′ and H-5′), and an AB system at δ 6.51 (*d*, 1.9 Hz, H-8) and δ 6.19 (*d*, 1.9 Hz, H-6). These two systems together with a singlet at δ 6.87 (H-3) indicated the presence of an apigenin aglycone in compound **1** (Stochmal et al., 2001). The UV and ^{13}C NMR (Table 2) spectra and the ROE correlations between the H-2′/H-6′ signal and the H-3 signal of the apigenin confirmed this structure.

The other group of signals in the downfield region of the ^{1}H NMR spectrum corresponded to a phenolic acyl moiety. An ABX system at δ; 7.26 (*d*, 1.9 Hz, H-2); δ 7.08 (*dd*, 8.2 Hz, 1.9 Hz, H-6) and δ; 6.77 (*d*, 8.2 Hz, H-5), and two doublets at δ 7.50 (H-7) and δ 6.41 (H-8) with a coupling constant of 15.8 Hz typical of an *E*-double bound were observed. The ROE correlation between a methoxyl group signal at δ 3.80 (*s*) with H-2 and the correlation between the double bound signals and the aromatic protons H-2 and H-6 (Fig. 1) suggested the presence of a ferulic acyl moiety, confirmed with the presence of nine signals in the ^{13}C NMR spectrum (Ibrahim and Barron, 1989) (Table 2).

The sugar region of the ^{1}H NMR spectrum showed the presence of two sugar units, with anomeric proton signals at δ 5.32 (*d*, 7.4 Hz, H-1) and δ 4.93 (*d*, 8.2 Hz, H-1′). The ^{13}C NMR spectrum showed 12 signals for two hexose units. Two typical C-6 signals of carboxyl groups at δ 172.5 suggested two glucuronic acid moieties. Their β-configuration was evident from the coupling constant of the anomeric protons.

The connection between the glucuronyl moieties and apigenin was established as 4′-[glucuronopyranosyl (1→2)glucuronopyranosyl] apigenin, from the observed ROE correlation between H-3′ and H-5′ of apigenin and H-1 of the first glucuronic acid and H-2 and H-1′ of both glucuronic acids. The pronounced downfield shift of H-2′ of the second glucuronic acid (δ 4.64) indicated the linkage between the sugar and the acyl moiety at C-2′, and thus **1** is 4′-*O*-[2′-*O*-*E*-feruloyl-*O*-β-D-glucurono pyranosyl(1→2)-*O*-β-D-glucuronopyranoside]apigenin.

Compound **2** showed a molecular ion (ESI–HRMS, negative ion mode) at *m*/*z* 973.1903 according with a molecular formula $C_{43}H_{41}O_{26}$ and peak at 269.0452 corresponding to the aglycone. The ^{1}H and ^{13}C NMR spectra of **2** (Tables 1 and 2) were very similar to those of compound **1**. The additional signals that appeared in its spectra corresponded to a third glucuronic acid moiety. The observed ROE correlation between H-6 and H-8 of the apigenin moiety and H-1″ of the third glucuronic acid determined the structure of **2** as 7-*O*-β-D-glucuronopyranosyl-4′-*O*-[2′-*O*-*E*-feruloyl-*O*-β-D-glucuronopyranosyl(1→2)-*O*-β-D-glucuronopyranoside]apigenin.

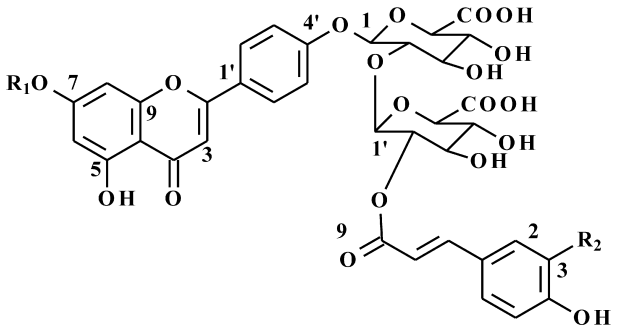

1: R_1=H R_2=OCH_3
2: R_1=glucuronic acid R_2=OCH_3
3: R_1=glucuronic acid R_2=H

Fig. 1. Chemical formula of compounds **1**–**3**.

Compound **3** gave a molecular ion (ESI–HRMS, negative ion mode) at *m*/*z* 943.1765 with a molecular formula $C_{42}H_{40}O_{26}$ and peak at 269.0470 corresponding to the aglycone. The only spectroscopic difference between the spectra of compounds **2** and **3** was in the phenolic moiety signals, the ^{1}H NMR spectrum (Table 1) of **3** had two doublets δ 7.40, *d*, 8.5 Hz, H-2 and H-6 and δ 6.74, *d*, 8.5 Hz, H-3 and H-5) typical of a *p*-coumaroyl moiety. The ^{13}C NMR spectrum (Table 2) was in agreement with the structure of the acyl moiety and the ROE effects observed confirmed an identical connection of apigenin, glucuronic acids and coumaroyl moiety as compound **2**. The structure of **3** was stablished as 7-*O*-β-D-glucuronopyranosyl-4′-*O*-[2′-*p*-*E*-coumaroyl-*O*-β-D-glucuronopyranosyl (1→2)-*O*-β-D-glucuronopyranoside]apigenin.

As far as we know, the three flavone glycosides (**1**, **2** and **3**) are reported here for the first time as natural compounds. They, similarly to previous identified apigenin glycosides in alfalfa (Stochmal et al., 2001), possess glucuronic acid as a sole sugar subunit in the sugar chain, and acylation with ferulic and coumaric acids occurred on the glucuronic acid moieties. However, the difference with previously identified compounds is in the acylation position. The three identified glycosides are acylated on sugars attached at C-4′, while all previously reported compounds were acylated on sugars at C-7. These differences may be specific for this particular variety or they may reflect the influence of environmental conditions. Plant material from which present flavonoids were separated was collected from plants grown in Portugal. The four isolated compounds were tested for their antioxidant activity in β-carotene/linoleic acid heterogenous system (Pratt, 1992), and for radical scavenging activity in methanolic solution of DPPH (Lee et al., 1998). They showed no activity in both tests performed. More research is needed, in order to shed some light on the function of acylated glucuronides in the host plant on their adaptation to environmental conditions.

3. Experimental

3.1. General

Flavonoids were chromatographed on Cellulose (Merck) ready to use plates, developed with 15% AcOH and after drying plates were observed under a UV lamp. High-performance liquid chromatography was performed on an HPLC system (Waters) consisting of 616 pump, a 600 s controller, and a 996 photodiode array detector. The Millenium Chromatography Manager was used to monitor chromatographic parameters and to process the data.

^{1}H, ^{13}C and 2D NMR spectra were recorded in CD_3OD and DMSO-d_6 on a Varian UNITY-400 instrument operating at 400 MHz for ^{1}H NMR and 100 MHz for ^{13}C NMR. Chemical shifts are reported in ppm (δ). ESI–HRMS were recorded in the negative ion mode on a Mariner Biospectrometry Workstation (Per Septive Biosystems). UV spectra were recorded on a HP 8453 UV/vis spectrophotometer. The α values were obtained in MeOH at 20°C on a Jasco P-1020 spectropolarimeter. Melting points were uncorrected.

3.2. Plant material and isolation

The lucerne var. Artal (American variety) was seeded in March 1999 in the north of Portugal, at Vairco (near Porto), and the samples were collected on the 23 August 1999, and they were from a 2nd harvest. The material was freeze dried, powdered and used for extraction.

Powdered plant material was extracted in a Soxhlet with chloroform to remove chlorophyl and fats. After drying it was extracted with 70% MeOH at room temperature. After filtration the extract was evaporated in vacuo (40°C) yielding a brown solid. The solid was suspended in water and loaded onto a C18 filled column (30×70 mm, 60 μm, Baker) equilibrated with water. The column was washed with water to remove carbohydrates, and flavonoids were washed out with 40% MeOH. The 40% MeOH fraction was evaporated to dryness, redissolved in 20% MeOH and loaded onto a C18 column (40 ×300 mm, 25–40 μm, Merck). The column was washed with MeOH-H_2O (linear gradient 20–70% MeOH) and 10 ml fractions were collected with a fraction collector. Fractions showing identical chromatographic characteristics (TLC, HPLC) were combined. Four single flavonoids were obtained.

3.2.1. 4′-*O*-[2′-*O*-*E*-Feruloyl-β-D-glucuronopyranosyl (1→2)-*O*-β-D-glucuronopyranoside]apigenin (**1**)

Amorphous yellow powder (15 mg); mp. 197–198°C; UV λ_{max}^{MeOH} nm: 271 *sh*, 325; $[\alpha]_D^{20}$ −74.2°(MeOH, *c* 0.1); HRMS *m*/*z*: 797.1575 [calc. for $C_{37}H_{33}O_{20}$ $[M\text{-}1]^-$, 797.1560], 269.0457 [M–H–ferulic acid–2GluA]$^-$. For ^{1}H and ^{13}C NMR see Tables 1 and 2, respectively.

*3.2.2. 7-O-β-D-Glucuronopyranosyl-4′-O-[2′-O-E-feruloyl -O-β-D-glucuronopyranosyl (1→2)-O-β-D-glucurono pyranoside]apigenin (**2**)*

Amorphous yellow powder (3 mg); mp. 197–198°C; UV λ_{max}^{MeOH} nm: 270 *sh*, 319; $[\alpha]_D^{20}$ −10.23° MeOH, *c* 0.1); HRMS *m/z*: 973.1903 [calc. for $C_{43}H_{41}O_{26}$ $[M\text{-}1]^-$, 973.1881], 269.0452 [M–H–ferulic acid–3GluA]$^-$. For ^1H and ^{13}C NMR see Tables 1 and 2, respectively.

*3.2.3. 7-O-β-D-Glucuronopyranosyl-4′-O-[2′-p-E-coumaroyl-O-β-D-glucuronopyranosyl (1→2)-O-β-D-glucuronopyranoside]apigenin (**3**)*

Amorphous powder (3 mg); mp. 197–198°C; UV λ_{max}^{MeOH} nm: 272 sh, 314; α_D^{20} −52.45° λ_{max}MeOH *c* 0.1); HRMS *m/z*: 943.1575 [calc. for $C_{42}H_{39}O_{25}$ $[M\text{-}1]^-$, 943.1775], 269.0470 [M–H–coumaric acic–3GluA]$^-$. For ^1H and ^{13}C NMR see Tables 1 and 2, respectively.

*3.2.4. 7-O-{2-E-Feruloyl-[β-D-glucuronopyranosyl(1→3)] -O-β-D-glucuronopyranosyl(1→2)-O-β-D-glucurono pyranoside}apigenin (**4**) (10 mg)*

UV, HRMS and NMR data were in accordance with literature data (Stochmal et al., 2001).

Acknowledgements

The authors are grateful to the Polish Commitee of Science (KBN) for financial support (grant no. 5P06A00718), to the Ministerio de Asuntos Exteriores (Spanish-Polish Joint Cooperation PO-1998) and the Comisión Interministerial de Ciencias y Tecnología (C.I.C.Y.T.; Project No. AGF97-1230-C02-02) Spain.

References

Bisby, F.A., Buckingham, J., Harborne, J.B., 1994. Phytochemical Dictionary of the Leguminosae. Chapmann and Hall, London, UK.

Ibrahim, R., Barron, D., 1989. Phenylpropanoids. In: Dey, P.M., Harborne, J.B. (Eds.), Methods in Plant Biochemistry, Vol. 1. Plant Phenolics. Academic Press, London, UK, pp. 75–111.

Lee, S.K., Mbwambo, Z.H., Chung, H.-S., Luyengi, L., Games, E.J.C., Metha, R.G., Kinghorn, A.D., Pezzuto, J.M., 1998. Evaluation of the antioxidant potential of natural products. Combin. Chem. High Throughput Screen 1, 35–46.

Oleszek, W., 2000. Alfalfa saponins: chemistry and application. In: Bidlack, W.R., Omaye, S.T., Meskin, M.S., Topham, D.K. (Eds.), Phytochemicals as Bioactive Compounds. Technomic Publishing, Lancaster–Basel, pp. 67–88.

Pratt, D.E., 1992. Natural antioxidants from plant material. In: Huang, M.-T., Ho, C.-T., Lee, C.Y. (Eds.), Phenolic Compounds in Food and their Effect on Health. II. Antioxidants and Cancer Prevention. American Chemical Society, Washington, DC, pp. 54–71.

Stochmal, A., Oleszek, W., Leitz, R.E., Di Paola, P., 1999. Saponin and flavonoid profiles of 47 alfalfa varieties of different origin. In: Phytochem. Soc. Europe Meeting, Book of Abstracts, p. 30.

Stochmal, A., Piacente, S., Pizza, C., De Riccardis, F., Leitz, R., Oleszek, W., 2001. Alfalfa (*Medicago sativa* L.) flavonoids. 1. Apigenin and luteolin glycosides from aerial parts. J. Agric. Food Chem. 49, 753–758.

PERGAMON

Phytochemistry 57 (2001) 1227–1230

PHYTOCHEMISTRY

www.elsevier.com/locate/phytochem

Benzopyrans from *Hypericum polyanthemum*

Alexandre B.F. Ferraz[a,b], Sérgio A.L. Bordignon[b], Charley Staats[a], Jan Schripsema[c], Gilsane Lino von Poser[a,*]

[a]*Programa de Pós Graduação em Ciências Farmacêuticas, UFRGS. Av. Ipiranga, 2752, 90610-000 Porto Alegre, RS, Brazil*
[b]*Fundação SOAD-CINCAN-ULBRA, R. Miguel Tostes, 2350, 90610-000 Canoas, RS, Brazil*
[c]*Setor de Química de Produtos Naturais, LCQUI/CCT, Universidade Estadual do Norte Fluminense, Av. Alberto Lamego, 2000, 28015-620 Campos dos Goytacazes, RJ, Brazil*

Received in revised form 22 February 2001

Abstract

From the aerial parts of *Hypericum polyanthemum* Klotzsch ex Reichardt (Guttiferae), three chromenes, 6-isobutyryl-5,7-dimethoxy-2,2-dimethyl-benzopyran; 7-hydroxy-6-isobutyryl-5-methoxy-2,2-dimethyl-benzopyran and 5-hydroxy-6-isobutyryl-7-methoxy-2,2-dimethyl-benzopyran were isolated. Their structures were determined by NMR spectroscopic analyses. © 2001 Elsevier Science Ltd. All rights reserved.

Keywords: *Hypericum polyanthemum*; Guttiferae; Benzopyrans; Chromenes; 6-Isobutyryl-5,7-dimethoxy-2,2-dimethyl-benzopyran; 7-Hydroxy-6-isobutyryl-5-methoxy-2,2-dimethyl-benzopyran; 5-Hydroxy-6-isobutyryl-7-methoxy-2,2-dimethyl-benzopyran

1. Introduction

Plants of the Gutifferae contain several constituents with diverse biological activities (Fuller et al., 1999; Verotta et al., 1999; McKee et al., 1998). Recently, the genus *Hypericum*, which contains about 400 species, has received attention for the antiviral action of hypericin and pseudohypericin on lipid enveloped and non-enveloped DNA and RNA viruses. These polycyclic quinones were isolated from *H. perforatum*, the most well-known species, widely employed as an antidepressive (Sommer and Harrer, 1994; Vorbach et al., 1994). The most common compounds isolated from plants of this genus are xanthones (Bennett and Lee, 1989), flavonoids (Rocha et al., 1995), phloroglucinol and filicinic acid derivatives (Jayasuriya et al., 1991; Rocha et al., 1995) and, less frequently, benzopyrans (Décosterd et al., 1986; Ishiguro et al., 1990).

Among the approximately 20 native *Hypericum* species from South Brazil, only *H. brasiliense* has been investigated. From this plant, xanthones and phloroglucinol derivatives were isolated, and its extracts have been found to inhibit monoamine oxidases (MAO), enzymes important in the regulation of levels of some physiological amines and which are thought to contribute to the management of depression (Rocha et al., 1994; Rocha et al., 1995).

In this paper, we deal with the structural elucidation of three new benzopyrans isolated from the aerial parts of *H. polyanthemum*, another species from South Brazil.

2. Results and discussion

From the chloroform extract of the aerial parts of *H. polyanthemum* three major compounds (**1**, **2** and **3**) were isolated. Compound **1** showed an $[M]^+$ at m/z 290.15181 in the HREIMS, which corresponds to a molecular formula of $C_{17}H_{22}O_4$ (calc. 290.1519). The IR spectrum of this compound showed absorptions which indicated the presence of a *gem*-dimethyl group (1383 and 1366 cm^{-1}) and a benzene ring (1603 and 1469 cm^{-1}). The ^{13}C NMR spectrum showed 15 signals, of which two (δ_C 27.82 and 17.88) corresponded to two methyl groups each. In the ^1H NMR spectrum the appearance of a pair of doublets at δ 6.46 and 5.51 (each 1H, $J = 10$ Hz) together with a six-proton singlet at δ 1.42 indicated the presence of a dimethylpyran ring system in the molecule. A singlet at δ 6.19 indicated the

* Corresponding author.
E-mail address: gilsane@farmacia.ufrgs.br (G.L. von Poser).

0031-9422/01/$ - see front matter © 2001 Elsevier Science Ltd. All rights reserved.
PII: S0031-9422(01)00169-8

existence of a penta-substituted aromatic ring. In the ^{13}C NMR spectrum, the wide disparity in chemical shifts between the oxygenated and non-oxygenated aromatic carbons were indicative of a phloroglucinol oxidation pattern in the aromatic ring. In addition to the IR absorption at 1699 cm^{-1}, attributable to a carbonyl group, the signal at δ 3.03 (1H, *qq*, $J=6.8$, 6.8 Hz) coupled to a six-proton doublet at δ 1.13 in the ^1H NMR spectrum indicated the presence of an isobutyryl substituent in the aromatic ring. Finally, two ^1H signals at δ 3.74 and 3.72 showed the presence of two methoxyl groups attached to the aromatic ring. The resonances of the methoxyl carbons at δ 63.64 and 55.70 indicated that the former was hindered from lying in the plane of the aromatic ring while the latter was substituted *ortho* to the aromatic proton. The structure, 6-isobutyryl-5,7-dimethoxy-2,2-dimethyl-benzopyran, was confirmed by interpretation of HMBC data. Besides the expected cross-peaks for the dimethylbenzopyran moiety (H-3/C-2, C-10, 2-Me_2; H-4/C-2, C-9; 2-Me_2/C-2, C-3), the following correlations were observed: H-8/C-6, C-7, C-9, C-10; H-2′/C-3′, C-4′; H_3-3′ and $H_3$4′/C1′; 5-OMe/C-5; 7-OMe/C-7.

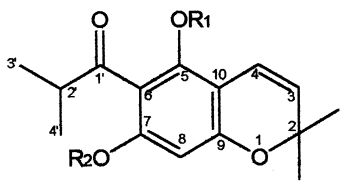

1 R^1=Me, R^2=Me

2 R^1=Me, R^2=H

3 R^1=H, R^2=Me

Compound **2**, also identified as a benzopyran, was obtained as a yellow viscous oil. The UV spectrum revealed a phenolic compound with an extended chromophore. The molecular ion $[M]^+$ at *m/z* 276.13616 (calc. 276.1362) is compatible with the molecular formula of $C_{16}H_{20}O_4$. Major differences in the ^1H NMR spectrum of **2** compared to **1** were the presence of only one methoxyl signal at δ 3.78 and the presence of a signal of an aromatic hydroxyl group at δ 13.09, suggesting that instead of one of the methoxyl groups, a hydroxyl group should be present. This chelated phenolic hydroxyl signal in its ^1H NMR spectrum and a chelated carbonyl group absorption at 1621 cm^{-1} in its IR spectrum demonstrated that the hydroxyl group was at position 5 or 7. The ^{13}C NMR spectroscopic signal of the methoxyl group at δ 63.59 showed that the hydroxyl group should be located at C-7. The placement of the methoxyl and hydroxyl groups (5-OMe, 6-isobutyryl, 7-OH) was confirmed by analysis of the HMBC spectrum which showed the following correlations: 2-Me_2/2-Me_2, C-2, C-3; H-8/C-9, C-10, C-7; H_3-3′ and $H_3$4′/C-3′, C-4′, C-2′, C1′; 5-OMe/C-5; 7-OH/C-7, C-6 and C-8. Further, the NMR spectroscopic data are nearly identical to those of a chromene isolated from *Rhyncholacis penicillata* (Podostemaceae), which only differs in the substituent (methylbutyryl group) at position 6 (Burkhardt et al., 1994).

Compound **3** ($C_{16}H_{20}O_4$) gave rise to a molecular ion $[M]^+$ at *m/z* 276.13616 (calc. 276.1362). As in compound **2**, the UV and IR spectra suggested that an aromatic ring and a chelated hydroxyl group were present. The ^1H NMR spectrum displayed a single methoxyl signal at δ 3.85 and a signal of an aromatic hydroxyl group at δ 14.28. The ^{13}C NMR spectroscopic signal of the methoxyl group appeared at δ 55.59 showing that the hydroxyl should be located at C-5. The NOE effects (7-OMe/H-8; H-8/7-OMe; 2-Me_2/H-3; H-3/H-4; $H_3$3′ and $H_3$4′/H-2′) confirmed the structure to be 5-hydroxy-6-isobutyryl-7-methoxy-2,2-dimethyl-benzopyran.

Chromenes containing an isobutyryl substituent have been previously isolated from *H. revolutum* (Décosterd et al., 1986). The isolated benzopyrans are derivatives of phloroglucinol and thus related to hyperforin. The contribution of these compounds to the pharmacological activity or toxicity of *Hypericum* extracts is still unknown, but will be the subject of future investigations.

3. Experimental

3.1. General procedures

NMR (400 Mhz for ^1H and 100 MHz for ^{13}C), in $CDCl_3$ using the solvent as internal standard; HREIMS: 70 eV; mass spectra were obtained through GC–MS analysis: temp. program 100–270°C (4°/min), injector 250°, transferline 230°, column DB-1, **1** eluted at 27.35 min, **2** at 38.54 min, and **3** at 38.11 min; prep. TLC: 20×20 cm plates coated with 0.5 mm layers of silica gel GF_{254} (Merck); bands were detected in UV light (254 nm).

3.2. Plant material

Plant material of *H. polyanthemum* Klotzsch ex Reichardt (aerial parts) was collected in Guaritas, Caçapava do Sul, Rio Grande do Sul, Brazil, in August, 1998. The voucher specimen is deposited in the Herbarium of the Federal University of Rio Grande do Sul (ICN) (*Hypericum polyanthemum*, Bordignon et al. 1405).

3.3. Isolation procedures

Air dried and powdered plant material (80 g) was extracted in a Soxhlet apparatus with $CHCl_3$ over 12 h and then the extract was evaporated to dryness under reduced pressure. The $CHCl_3$ extract (2.2 g) of *H. polyanthemum* was analyzed by silica gel TLC. Three products were isolated by prep. TLC over silica gel with $CHCl_3$. The compounds **1** (78 mg), **2** (39 mg), and **3** (46 mg) were recovered from the adsorbent using $CHCl_3$.

Table 1
^{1}H NMR chemical shift data for compounds **1**–**3** (δ, in $CDCl_3$, 400 MHz)[a]

	1	2	3
H-3	5.51 (1H, *d*, *J* = 10.0)	5.59 (1H, *d*, *J* = 10.0)	5.44 (1H, *d*, *J* = 10.0)
H-4	6.46 (1H, *d*, *J* = 10.0)	6.49 (1H, *d*, *J* = 10.0)	6.66 (1H, *d*, *J* = 10.0)
H-8	6.19 (1H, *s*)	6.19 (1H, *s*)	5.89 (1H, *s*)
H-2′	3.03 (1H, *qq*, *J* = 6.8, 6.8)	3.76 (1H, *qq*, *J* = 6.7, 6.7)	3.73 (1H, *qq*, *J* = 6.7, 6.7)
H_3-3′, H_3-4′	1.13 (6H, *d*, *J* = 6.8)	1.18 (6H, *d*, *J* = 6.8)	1.15 (6H, *d*, *J* = 6.8)
5-OMe	3.72 (3H, *s*)	3.78 (3H, *s*)	–
7-OMe	3.74 (3H, *s*)	–	3.85 (3H, *s*)
2-Me_2	1.42 (6H, *s*)	1.44 (6H, *s*)	1.44 (6H, *s*)
5-OH	–	–	14.28 (1H, *s*)
7-OH	–	13.09 (1H, *s*)	–

[a] H, multiplicities; coupling constants in Hz.

3.3.1. 6-Isobutyryl-5,7-dimethoxy-2,2-dimethylbenzopyran (*1*)

Viscous oil. R_f 0.45 ($CHCl_3$). EIMS *m*/*z* (rel. int.): 290 [$M^{+\cdot}$] (13), 275 (42), 261(3), 247(100), 217(30), 43 (33). HREIMS: 290.15181 found; calc. for $C_{17}H_{22}O_4$: 290.1519. UV$\lambda MeOH_{max}$ nm: 231, 257 *sh*, 320 *sh*. IR$\nu CHCl_3$ $_{max}$ cm^{-1}: 2973, 2889, 1699, 1603, 1574, 1469, 1418, 1383, 1366, 1028, 891, 824. ^{1}H NMR ($CDCl_3$): Table 1. ^{13}C NMR ($CDCl_3$): Table 2.

3.3.2. 7-Hydroxy-6-isobutyryl-5-methoxy-2,2-dimethylbenzopyran (*2*)

Viscous oil. R_f 0.63 ($CHCl_3$). EIMS *m*/*z* (rel. int.): 276 [$M^{+\cdot}$] (23), 261 (100), 247 (52), 233 (75), 228 (30), 43 (75). HREIMS: 276.13616 found; calc. for $C_{16}H_{20}O_4$: 276.1362. UV$\lambda MeOH_{max}$ nm: 235 *sh*, 263, 295 *sh*, 348. IR$\nu CHCl_3$ $_{max}$ cm^{-1}: 2983, 2889, 1628, 1581, 1472, 1385, 1372, 1236, 1152, 995, 957, 893. ^{1}H NMR ($CDCl_3$): Table 1. ^{13}C NMR ($CDCl_3$): Table 2.

Table 2
^{13}C NMR chemical shift data for compounds **1**–**3** (δ, in $CDCl_3$, 100 MHz)

	1	2	3
C-2	76.65	77.36	78.04
C-3	127.68	128.08	125.29
C-4	116.51	116.55	116.15
C-5	153.96	158.33	162.15
C-6	117.99	107.97	104.82
C-7	157.33	165.85	162.49
C-8	96.11	101.32	91.24
C-9	155.56	160.21	159.77
C-10	107.93	107.31	103.03
CO isobutyryl	208.56	210.62	210.37
CH isobutyryl	42.09	38.61	39.52
CH_3 isobutyryl	17.88	19.65	19.25
5-OMe	63.64	63.59	–
7-OMe	55.70	–	55.59
2-Me_2	27.82	28.23	28.38

3.3.3. 5-Hydroxy-6-isobutyryl-7-methoxy-2,2-dimethylbenzopyran (*3*)

Viscous oil. R_f 0.79 ($CHCl_3$). EIMS *m*/*z* (rel. int.): 276 [$M^{+\cdot}$] (31), 261 (100), 243 (52), 233 (53), 43 (52). HREIMS: 276.13616 found; calc. for $C_{16}H_{20}O_4$: 276.1362. UV$\lambda MeOH_{max}$ nm: 226 *sh*, 272, 295 *sh*, 349. IR$\nu CHCl_3$ $_{max}$ cm^{-1}: 2970, 2900, 1620, 1571, 1508, 1465,1418, 1382, 1368, 1030, 891, 812, 713. ^{1}H NMR ($CDCl_3$): Table 1. ^{13}C NMR ($CDCl_3$): Table 2.

Acknowledgements

We thank M.A. Lima and Dr. N. Zanatta, Departamento de Química, Universidade Federal de Santa Maria, Brazil, for the NMR spectra and to CNPq and FAPERGS for the financial support. The Centro Nacional de Ressonância Magnética Nuclear of the Department of Biochemistry of the UFRJ is gratefully acknowledged for access to the NMR facilities.

References

Bennett, G.J., Lee, H.-H., 1989. Xanthones from Guttiferae. Phytochemistry 28, 967–998.

Burkhardt, G., Becker, H., Grubert, M., Thomas, J., Eicher, T., 1994. Bioactive chromenes from *Rhycholacis penicillata*. Phytochemistry 37, 1593–1597.

Décosterd, L., Stoeckli-Evan, H., Msonthi, J.D., Hostettmann, K., 1986. A new antifungal chromene and a related dichromene from *Hypericum revolutum*. Planta Medica 52, 429.

Fuller, R.W., Westegaard, C.K., Collins, J.W., Cardelina II, J.H., Boyd, M.R., 1999. Vismiaphenones D–G, new prenylated benzophenones from *Vismia cayennensis*. Journal of Natural Products 62, 67–69.

Ishiguro, K., Yamaki, M., Kashihara, M., Takagi, S., Isoi, K., 1990. A chromene from *Hypericum japonicum*. Phytochemistry 29, 1010–1011.

Jayasuriya, H., Clark, A.M., McChesney, J.D., 1991. New antimicrobial filicinic acid derivatives from *Hypericum drummondii*. Journal of Natural Products 54, 1314–1320.

McKee, T.C., Covington, C., Fuller, R.W., Bokesch, L.R., Young, S., Cardellina II, J.H., Kadushin, M.R., Soejarto, D.D., Stevens, P.F.,

Cragg, G.M., Boyd, M.R., 1998. Pyranocoumarins from tropical species of genus *Callophylum*: a chemotaxonomic study of extracts in the National Cancer Institute collection. Journal of Natural Products 61, 1252–1256.

Rocha, L., Marston, A., Kaplan, M.A.C., Stoeckli-Evans, H., Thull, U., Testa, B., Hostettmann, K., 1994. An antifungal gamma-pyrone and xanthones with monoamine oxidase inhibitory activity from *Hypericum brasiliense*. Phytochemistry 36, 1381–1385.

Rocha, L., Marston, A., Potterat, O., Kaplan, M.A.C., Stoeckli-Evans, H., Hostettmann, K., 1995. Antibacterial phloroglucinols and flavonoids from *Hypericum brasiliense*. Phytochemistry 40, 1447–1452.

Sommer, H., Harrer, G., 1994. Placebo-controlled double-blind study examining the effectiveness of an *Hypericum* preparation in 105 mildly depressed patients. Journal of Geriatric Psychiatry and Neuropharmacology S9–S11.

Verotta, L., Appendino, G., Belloro, E., Jakupovic, J., Bombardelli, E., 1999. Furohyperforin, a prenylated phloroglucinol from St. John's Wort (*Hypericum perforatum*). Journal of Natural Products 62, 770–772.

Vorbach, E.U., Hubner, W.D., Arnoldt, K.H., 1994. Effectiveness and tolerance of the *Hypericum* extracts L1 160 in comparison with imipramine: randomized double-blind study with 135 outpatients. Journal of Geriatric Psychiatry and Neuropharmacology S19–S23.

PERGAMON

Phytochemistry 57 (2001) 1231–1235

PHYTOCHEMISTRY

www.elsevier.com/locate/phytochem

Diels–Alder type adducts from *Morus cathayana*

Rui-Chao Shen, Mao Lin*

Institute of Materia Medica, Chinese Academy of Medical Sciences and Peking Union Medical College, 1 Xian Nong Tan Street, Beijing 100050, People's Republic of China

Received in revised form 21 February 2001

Abstract

Two natural Diels–Alder type adducts, cathayanon A (**1**) and cathayanon B (**2**), resembling sanggenon C (**4**) and O (**3**), were isolated from the root bark of *Morus cathayana*. Their structures were elucidated on the basis of spectroscopic evidence. The structure of **1** was confirmed by the results of X-ray crystallographic analysis. The absolute configurations of **1** and **2** were determined as 2*S*, 3*R*,14*S*, 19*S*, 20*R* and 2*S*, 3*R*, 14*R*, 19*S*, 20*R*, respectively. The absolute configurations at C-2 and C-3 of two other known isomeric Diels–Alder adducts sanggenon O (**3**) and C (**4**) were deduced as 2*R*, 3*S*. Pharmacological tests indicated that **1** and **2** exhibited potent activities on the inhibition of HL-60 cell adhesion to BAEC at concentrations of 10^{-5} mol l^{-1}, with inhibitory rates of 44.72 and 39.02%, respectively. © 2001 Elsevier Science Ltd. All rights reserved.

Keywords: *Morus cathayana*; Moraceae; Flavanone; Diels–Alder adduct; Cathayanon A; Cathayanon B

1. Introduction

Numerous isoprenoid-substituted phenolic compounds, including flavonoids have been isolated from the Mulberry tree (Nomura, 1988; Nomura and Hano, 1994). Some of these compounds showed interesting activities such as inhibitory activities against arachidonate 5-lipoxygenase (Reddy et al., 1991). In the course of our studies on the antinflammatory agents, we selected the Chinese mulberry tree, *Morus cathayana* Hemsl. for evaluation. Two new Diels–Alder type adducts, cathyanon A (**1**) and cathayanon B (**2**) having the same skeleton as sanggenons C (**4**) and O (**3**), were isolated from the root bark of *M. cathayana* along with 13 known components which were identified as sanggenons O (**3**; Hano and Nomura, 1985), C (**4**), A, and M (Fukai et al., 1998), moracins C, M, O, and P (Nagao, 1981), mulberroside C (Hirakura et al., 1986), scopoletin, umbelliferone, α-amyrin acetate (Jia et al., 1996), and 4-hydroxy-3,5-dimethoxybenzyl alcohol. Moracin O and 4-hydroxy-3,5-dimethoxybenzyl alcohol were isolated from this source for the first time. This paper deals with the isolation and structural determination of two new Diels–Alder type adducts by spectroscopic methods, including determination of their absolute configurations. The structure of **1** was confirmed by X-ray crystallographic analysis. Previously, a number of flavanones having isoprenyl (geranyl) groups and Diels–Alder type adducts have been reported from the root bark of *M. cathayana*. The absolute configurations of the stereocenters of the methylcyclohexene ring have been elucidated distinctively by Nomura, T. (Nomura, 1988). More recently the structures of sanggenons have been revised (Fukai et al., 1998). However, the sterochemistry of C-2 and C-3 have not been reported. This paper also deals with the deduction of the absolute configurations at C-2 and C-3 of two known Diels–Alder type adducts, sanggenons O (**3**) and C (**4**).

2. Results and discussion

Cathayanon A (**1**), pale yellow crystals, mp 180–181°C (*d*), showed $[\alpha]_D^{19}$ −193.9°. The UV spectrum exhibited maxima at 205, 230 (*sh*), 282 and 310 nm, which were similar to those of sanggenons O (**3**) and C (**4**), two flavanone Diels–Alder adducts. The IR spectrum exhibited maxima at 3427, 1633, 1452 and 1146 cm^{-1} similar to those of **3** and **4**. A molecular formula of $C_{40}H_{36}O_{12}$ was determined by the HRFABMS [*m*/*z* 709.2348, $(M+H)^+$] suggesting that **1** was an isomer of **3** and **4**. These results suggested that **1** is a Diels–Alder adduct such as **3** and **4** which are regarded as cycloaddition products of a chalcone and a dehydroprenyl flavanone derivative. This was substantiated by detailed

* Corresponding author. Tel.: +86-10-63165326; fax: +86-10-63017757.

E-mail address: linmao@imm.ac.cn (M. Lin).

0031-9422/01/$ - see front matter © 2001 Elsevier Science Ltd. All rights reserved.
PII: S0031-9422(01)00171-6

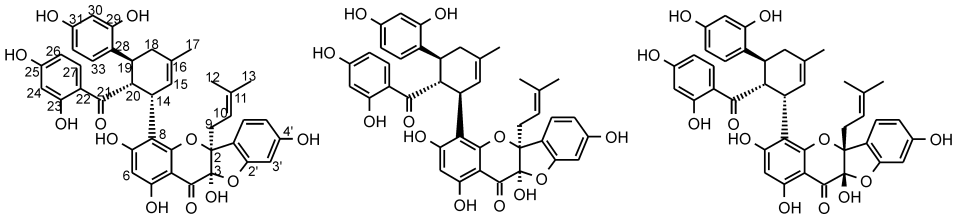

(1) (2) (3)

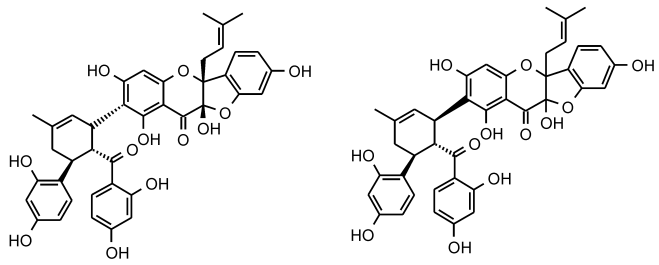

(4) (5)

analyses of ^{1}H NMR, ^{1}H–^{1}HCOSY, ^{13}C NMR and DEPT spectra of **1** and by comparison of the ^{1}H NMR and ^{13}C NMR spectroscopic data of **3** and **4**, obtained from this plant and other *Morus* plants (Nomura et al., 1981). The ^{1}H NMR spectrum of **1** at room temperature showed broad proton signals especially for the protons of H-14, H-19, H-20 of the methylcyclohexene ring. When measured at 90°C in DMSO-*d*, it showed a fairly resolved spectrum as follows: the signals of three sets of ABX type aromatic protons at δ 6.97 (1H, *d*, $J=8$ Hz, 27-H), 6.42 (1H, *dd*, $J=2$, 8 Hz, 26-H), 6.29 (1H, *d*, $J=2$ Hz, 24-H), 6.77 (1H, *d*, $J=8$ Hz, 33-H), 6.22 (1H, *d*, $J=2$ Hz, 30-H), 6.10 (1H, *dd*, $J=2$, 8 Hz, 32-H), 7.39 (1H, *d*, $J=8$ Hz, 6′-H), and 6.00∼6.03 (2H, m, 3′ and 5′-H); the protons of a prenyl group at δ 1.46, 1.67 (each 3H, *s*, 11-CH_3), 2.64 (1H, *dd*, $J=7.5$, 15 Hz, 9-Ha), 2.93 (1H, *dd*, $J=6.9$, 15 Hz, 9-Hb), and 5.23 (2H, *br s*, 10 and 15-H); an aromatic proton at *d* δ 5.65 (1H, *s*, 6-H) and the protons of a trisubstituted methylcyclohexene ring at δ 1.51 (3H, *s*, 16-CH_3), 2.15 (1H, *m*, 18-Ha), 2.48 (1H, *m*, 18-Hb), 4.20 (1H, *br s*, 14-H), 3.82 (1H, *m*, 19-H), and 4.04 (1H, *t*, $J=7$ Hz, 20-H). Both the coupling constants of H-14/H-20, and H-19/H-20, were 7 Hz, suggesting that the relative configurations at C-14, 19, 20 were *cis–trans* adducts, thus resembling those of **3** and **4** (Nomura, 1988). Therefore, the relative configurations of the three substituents on the methylclohexene ring of **1** were the same as **3** and **4**. However, the signal of H-20 at 4.04 ppm of **1** was shifted to high field (−0.57 ppm) compared with **3**. These data led us to presume that the proton of H-20 has been shielded due to the change of chemical environment. The CD curve of **1** showed a positive Cotton effect in the 280–320 nm region. Hence, the absolute configurations of **1** at C-14, 19, 20 were the same as **4** (14*S*, 19*S*, 20*R*) based on the excition chirality theory (Nomura, 1988). The locations of three substituents (methylcyclohexene ring, prenyl, and hydroxy groups) were determined from the ^{13}C-NMR and DEPT spectra as well as being compared with other similar Diels–Alder type adducts, obtained from this plant (Nomura et al., 1981). The ^{13}C NMR spectrum of **1** was similar to those of **3** and **4** (see Table 1). The signal at δ 97.5 was attributed to C-6, indicating that the methylcyclohexene ring was connected to C-8. It has been reported that the Diels–Alder type adducts from *Morus* sp. exhibited positive optical rotation for *cis–trans* adducts. Compound **1** was a *cis–trans* adduct, however its optical rotation was negative, $[\alpha]_D^{19}$ −193.9, indicating that the absolute configurations at C-2 and C-3 of **1** are different from that of **3** and **4**.

The structural determination of **1** was supported by the results of an X-ray crystallographic analysis. The PLUTO drawing and the fractional atomic coordinates of **1** are given in Fig. 1. The determination of the absolute configurations of **1** at C-14, 19, 20 by NMR spectroscopic analysis was identical to the PLUTO drawing as 14*S*, 19*S*, 20*R* and shown in Fig. 1, it can be concluded that Fig. 1 also showed the absolute configuration of **1**. Thus, the absolute configurations of **1** at C-2 and C-3 were determined as 2*S* and 3*R*. Both the C-2 isoprenyl and the C-3 hydroxyl group have an α-orientation. It can be observed from the molecular model of **1** that H-20 was located in the shielding zone of the ring B, and this may account for the high field shift of H-20 in **1**.

There are no previous data concerning the absolute configurations at C-2 and C-3 of **3** and **4**. A positive Cotton effect was observed in the 280–320 nm region in the CD spectrum of **3** as well as in **1** and **4**. This observation indicated that the three chiral centers on the cyclohexenyl ring of **3** have the same absolute configurations as those **1** and **4** (Nomura, 1988). The proton

Table 1
^{13}C NMR chemical shift assignments of compounds **1**–**4**[a]

Carbon	1	2	3	4
2	92.0	92.1	91.8	92.0
3	102.0	102.6	102.2	102.4
4	188.6	187.7	188.2	188.3
4a	99.9	99.8	99.8	99.9
5	163.2	163.2	163.4	163.9
6	97.5	95.6	96.4	109.0
7	167.2	166.5	167.5	167.6
8	108.8	108.4	108.7	96.5
8a	161.0	162.1	161.8	161.9
1′	122.7	122.3	121.9	122.2
2′	160.6	161.5	161.1	161.2
3′	99.1	99.4	99.3	99.5
4′	160.6	161.5	161.1	161.2
5′	110.3	110.2	109.5	109.7
6′	125.6	125.3	125.5	125.6
9	32.5	31.9	31.8	32.0
10	118.6	118.8	118.4	118.5
11	136.3	135.7	136.8	136.7
12	18.2	18.4	18.0	18.1
13	25.9	25.9	25.4	25.9
14	34.7	39.3	35.6	35.9
15	123.1	125.2	122.6	122.8
16	135.0	133.5	135.1	135.0
17	23.7	23.4	23.7	23.7
18	32.5	31.9	33.6	33.8
19	32.1	38.1	32.6	32.8
20	46.9	46.6	47.9	48.3
21	209.2	209.3	208.5	208.8
22	113.5	115.4	113.8	114.0
23	166.0	164.9	165.8	165.8
24	103.5	103.3	103.5	103.8
25	166.4	165.4	166.4	166.8
26	107.3	107.6	107.3	107.6
27	128.5	129.2	128.9	129.0
28	120.8	121.4	121.1	121.3
29	156.0	155.9	156.4	156.5
30	103.2	102.6	103.2	103.5
31	157.8	156.8	157.6	157.8
32	108.0	108.2	108.6	108.7
33	134.8	132.7	134.6	134.7

[a] In acetone-d_6.

H-20 of **3** was not located in the shielding zone of the B ring, because both prenyl and hydroxy groups at C-2 and C-3 have β-orientation by comparing the two molecular models of **1** and **3.** The absolute configurations at C-2 and C-3 of **3** are hence reversed compared with those of **1** and was deduced as 2*R*, 3*S*. In order to confirm the location of the methylcyclohexene group of **3**, a chemical reaction has been employed. An aliquot **4** was treated with 5%K_2CO_3 solution at room temperature (Hano and Nomura, 1985) to give an equilibrium mixture (1:1) of **3** and **4** as determined by HPLC analysis. Thus, the absolute configurations at C-2 and C-3 of **4** were the same as **3** and may be specified as 2*R*, 3*S*.

Cathayanon B (**2**), $[\alpha]_D^{19}$ −733.7°, is a yellow powder. Its UV, IR and FAB–MS spectra were very similar to

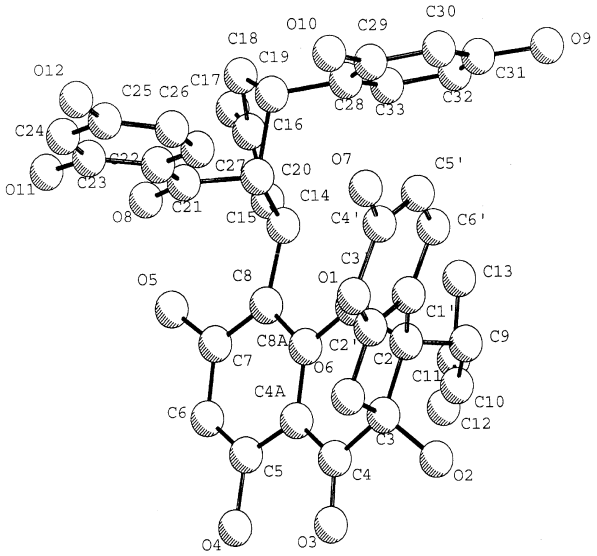

Fig. 1. The PLUTO drawing of **1**.

those of **1**, **3** and **4**. The HRFABMS of **2** revealed an $[M+H]^+$ at *m*/*z* 709.2374 corresponded to the molecular formula $C_{40}H_{36}O_{12}$. The ^{1}H NMR of **2** showed signals corresponding to three sets of ABX type aromatic protons at δ 7.45 (1H, *d*, *J*=8 Hz, 27-H), 5.98 (1H, *dd*, *J*=2, 8 Hz, 26-H), 5.92 (1H, d, *J*=2Hz, 24-H), 6.77 (1H, *d*, *J*=8 Hz, 6′-H), 6.68 (1H, *dd*, *J*=2, 8 Hz, 5′-H), 6.64 (1H, *br s*, 3′-H), 6.31 (1H, *d*, *J*=8 Hz, 33-H), 5.98 (1H, *dd*, *J*=2, 8 Hz, 32-H), and 6.18 (1H, *d*, *J*=2 Hz, 30-H); the protons of a prenyl group at δ 1.52, 1.80 (each 3H, *s*, 11-CH_3), 2.97 (1H, *dd*, *J*=8.4, 15 Hz, 9-Ha), 3.03 (1H, *dd*, *J*=5.6, 15 Hz, 9-Hb) and 5.17 (1H, *m*, 10-H); an isolated aromatic proton at δ 5.74 (1H, *s*, 6-H); and the protons of a trisubstituted methylcyclohexene ring at δ 1.64 (3H, *s*, 16-CH_3), 2.10∼2.20 (2H, *br s*, 18-Ha,b), 5.27 (1H, *br s*, 15-H), 3.75 (1H, *br s*, 19-H), 4.14 (1H, *br s*, 20-H) and 4.21 (1H, *m*, 14-H). The coupling constant of the methylcyclohexene protons H-14/H-20 and that of H-19/H-20 were 11 Hz. Thus, it can be concluded that the relative configurations of the three protons on the trisubstituted methylcyclohexene ring should be an all-*trans* Diels–Alder type adduct, an isomer of **1**, **3** and **4** and of the all-*trans* adduct sanggenon D (**5**; Fukai et al., 1998). Because the CD curve of **2** was similar to that of **5**, which showed a negative Cotton effect in the 280–320 nm region (Nomura, 1988), the absolute configurations at C-14, 19, 20 of **2** were determined as 14*R*, 19*S*, 20*R*. The chemical shift of H-20 of **2** also appeared at a relatively high field (3.96 ppm) resembling compound **1**. The proton H-20 was located in the shielding zone of ring B. This was the same factor that accounted for the shift of H-20 of **2** to high field. Hence, the absolute configurations of **2** at C-2 and C-3 are 2S, 3R. Compared with the ^{13}C NMR spectrum of **1** (see Table 1) the methylcyclohexene ring of **2** would be connected with C-8, similar to **1** and **3** as shown in

Fig. 1. Its absolute configurations at C-2, C-3 would be the same as **1** (2*S*, 3*R*).

The pharmacological tests indicated that the adhesion of HL-60 to BAEC was significantly inhibited by **1** and **2** (1×10^{-5} mol l^{-1}) with inhibitory rates of 44.72 and 39.02%, respectively (Li et al., 2000).

3. Experimental

3.1. General

Melting points were determined on XT4-100X micro-melting point apparatus and are uncorrected. Optical rotations were obtained on a Perkin-Elmer 241 polarimeter. UV spectra were measured on a Shimadzu UV-300 spectrophotometer. IR spectra were recorded on a Perkin-Elmer 683 infrared spectrophotometer. NMR spectra were obtained using an Arian Mercury-300 and Brüker AM-500 spectrophotometers with TMS as internal standard. MS spectra were obtained on an Autospec-Ulma-Tof mass spectrometer. CD spectra were recorded on a JASCO model J-715 spectropolarimeter. HPLC was performed on a Waters 411 equipped with UV-254 detector. Column chromatography was performed using Si gel (Qing Dao Hai Yang Chemical Group Co., Qing Dao, People's Republic of China). Reversed phase column chromatography was performed using Merck Lichroprep RP-8 and RP-18 (40–63 μm) columns, respectively. Analytical column using RP-18(5μm) column (25 cm×4.6 mm) with UV detection at 254 at a mobile phase CH_3CN–H_2O (65:35).

3.2. Plant material

The root bark of *Morus cathayana* was collected at Jiujiang, Jiangxi Province, People's Republic of China in August, 1997 and identified by Professor Ce-Ming Tan. The voucher sample was deposited in our institute (No. 95021).

3.3. Extraction and isolation

The root bark of *M. cathayana* (19 kg) was chipped and extracted with 95% ethanol at room temperature. The resultant extract (820 g) was mixed with silica gel (60–100 mesh) and eluted with $CHCl_3$ and EtOAc sequentially. The $CHCl_3$ solution was concentrated in vacuo and evaporated to yield a residue (229 g), which was submitted to CC on silica gel using cyclohexane-EtOAc (30:1∼7:1) as an eluent to give α-amyrin acetate (6 g), sanggenon M (47 mg) and sanggenon A (17 mg).

Evaporation of the EtOAc solution in vacuo yielded a residue (355 g), which was fractionated over a silica gel column, eluting with $CHCl_3$–MeOH (20:1–6:1) to yield four fractions B-1, B-2, B-3 and B-4. The fraction B-1 (60 g) was applied to a silica gel column eluted with $CHCl_3$–MeOH (20:1), with the fraction of interest being further purified on a RP-18 column with MeOH–H_2O (7:3) as eluent to give scopoletin (10 mg), 4-hydroxy-3,5-dimethoxybenzyl alcohol (46 mg), umbelliferone (73 mg), moracin C (66 mg), moracin P (50 mg) and moracin O (66 mg), respectively. Fraction B-2 (117 g) was fractionated by silica gel CC, RPCC(RP-18) with cyclohexane–EtOAc (5:1) over silica gel, with MeOH–H_2O (7:3) on RP-18 column, with CH_3CN–H_2O (6:4) on RP-8 column to yield **1** (300 mg), **3** (20 mg) and **4** (10 mg). The fraction B-3 (126 g) was separated over silica gel CC with cyclohexane–EtOAc (2:1) and $CHCl_3$–MeOH (20:1) to give sanggenon M (200 mg). Fraction B-4 (150 g) was fractionated in sequence with $CHCl_3$–Me_2CO (10:1∼1:1) over silica gel CC, MeOH–H_2O (6:4) on RPCC(RP-18) column to give **2** (170 mg) and mulberroside (600 mg), respectively.

3.4. Cathayanon A (*1*)

Pale yellow crystal (CH_3OH); mp 180–181°C (d); $[\alpha]_D^{19}$ −193.9° (*c* 0.12, MeOH); UV (MeOH) λ_{max} 205, 230 (sh), 282, 310nm; IR (KBr) ν_{max} 3427, 1633, 1452, 1146 cm^{-1}; ^1H NMR (DMSO-d_6, 300 MHz, 90°C) δ 1.46, 1.67 (each 3H, *s*, 11-CH_3), 1.51 (3H, *s*, 16-CH_3), 2.15 (1H, *m*, 18-Ha), 2.48 (1H, *m*, 18-Hb), 2.64 (1H, *dd*, *J*=7.5, 15 Hz, 9-Ha), 2.93 (1H, *dd*, *J*=6.9, 15 Hz, 9-Hb), 6.97 (1H, *d*, *J*=8 Hz, 27-H), 6.42 (1H, *dd*, *J*=2, 8 Hz, 26-H), 6.29 (1H, *d*, *J*=2 Hz, 24-H), 6.77 (1H, *d*, *J*=8 Hz, 33-H), 6.22 (1H, *d*, *J*=2 Hz, 30-H), 6.10 (1H, *dd*, *J*=2, 8 Hz, 32-H), 7.39 (1H, *d*, *J*=8 Hz, 6′-H), 6.00∼6.03 (2H, *m*, 3′ and 5′-H), 5.65 (1H, *s*, 6-H), 5.23 (2H, *br s*, 10 and 15-H), 4.20 (1H, *br s*, 14-H), 3.82 (1H, *m*, 19-H), 4.04 (1H,*t*, *J*=7 Hz, 20-H); ^{13}C NMR (acetone-d_6, 125 MHz), see Table 1; FABMS *m/z* 709 $[M+H]^+$ (15), 641 (12), 491 (45), 339 (50), 303 (18), 243 (30), 219 (60), 203 (100); HRFABMS calcd for $C_{40}H_{37}O_{12}$, *m/z* 709.2285 $[M+H]^+$, found 709.2348; CD (*c* 7.77×10^{-4}M, MeOH) $[\theta]_{223}$ +4531 (valley), $[\theta]_{237}$ +33243, $[\theta]_{250}$ +4930 (valley), $[\theta]_{276}$ +28178, $[\theta]_{292}$ +12023, $[\theta]_{297}$ +10626, $[\theta]_{305}$ 0, $[\theta]_{328}$ −48820.

3.5. Cathayanon B (*2*)

Yellow powder; $[\alpha]_D^{19}$ −733.7°C (*c* 0.18, MeOH); UV (MeOH) λ_{max} 205, 230 (sh), 282, 310 nm; IR (KBr) ν_{max} 3427, 1633, 1452, 1146 cm^{-1}; ^1H NMR (acetone-d_6, 500 MHz, 20°C) δ 1.52, 1.80 (each 3H, *s*, 11-CH_3), 2.97 (1H, *dd*, *J*=8.4, 15 Hz, 9-Ha), 3.03 (1H, *dd*, *J*=5.6, 15 Hz, 9-Hb), 5.17 (1H, *m*, 10-H), 7.45 (1H, *d*, *J*=8 Hz, 27-H), 5.98 (1H, *dd*, *J*=2, 8 Hz, 26-H), 5.92 (1H, *d*, *J*=2 Hz, 24-H), 5.74 (1H, *s*, 6-H), 6.77 (1H, *d*, *J*=8 Hz, 6′-H), 6.68 (1H, *dd*, *J*=2, 8 Hz, 5′-H), 6.64 (1H, *br s*, 3′-H), 6.31 (1H, *d*, *J*=8 Hz, 33-H), 5.98 (1H, *dd*, *J*=2, 8 Hz, 32-H), 6.18 (1H, *d*, *J*=2 Hz, 30-H), 1.64 (3H, *s*, 16-

CH_3), 2.10∼2.20 (2H, *br s*, 18-Ha,b), 5.27 (1H, *br s*, 15-H), 3.75 (1H, *br s*, 19-H), 4.14 (1H, *br s*, 20-H), 4.21 (1H, *m*, 14-H); ^{13}C NMR (acetone-d_6, 125 MHz), see Table 1; FABMS *m/z* 709 $[M+H]^+$ (40), 641 (30), 625 (11), 491 (24), 353 (5), 203 (15), 137 (100); HRFABMS calcd for $C_{40}H_{37}O_{12}$, *m/z* 709.2285 $[M+H]^+$, found 709.2374; CD (*c* 9.89×10^{-4} M, MeOH) $[\theta]_{223}$ −99485, $[\theta]_{233}$ 0, $[\theta]_{241}$ +16284, $[\theta]_{247}$ 0, $[\theta]_{251}$ −1208, $[\theta]_{253}$ 0, $[\theta]_{270}$ +12840, $[\theta]_{290}$ −28269 (valley), $[\theta]_{294}$ −27329, $[\theta]_{326}$ −61019.

3.6. X-ray crystallographic analysis of **1**

A pale yellow crystal with approximate dimensions of $0.35\times0.35\times0.50$ mm was selected. The following crystallographic data were obtained: monoclinic, space group $P2_1$, lattice constants, $a=10.190$ (1) Å, $b=17.353$ (1) Å, $c=12.557$ (1) Å, $\beta=113.003$ (4)°, $Z=2$. The diffraction data were collected on a MAC DIP-2030K image plate diffractometer with MoK_α radiation ($\lambda=0.71073$ Å), graphite monochromator. A total of 2160 independent reflections were collected in the range of $0°<\theta<25°$ by ω scan technique, of which 2139 reflections ($|F|^2\geqslant10\sigma|F|^2$) were observed and used in structural analysis. The crystal structure was solved by direct methods (SHELXS-86). Forty-six non-hydrogen atoms were located from the E-map. The others were found with successive difference Fourier synthesis. All the non-hydrogen atoms were subjected to anisotropic refinement by full matrix least-squares. The hydrogen atoms were determined with theoretic calculation. The final R_f is 0.058 and the final R_w is 0.065 ($w=1/\sigma^2|F|$), $(\Delta/\sigma)_{max}=0.145$, $(\Delta\rho)_{min}=-0.250$ e/Å^3, $(\Delta\rho)_{max}=0.210$ e/Å^3. The final formula was determined as $C_{40}H_{36}O_{12}(CH_3OH)_3$, which included three molecules of methanol. The corresponding formula weight of **1** was 708.81. The calculated density was 1.303 g/ml. All calculations were carried out with NOMCSDP software.

3.7. Pharmacological tests

HL-60 cells-BAEC (Bovine Arterial Endothalium cells) adhesion assay:

HL-60 cells was labeled with MTT for 2 h and washed (×3) with RPMI 1640 containing 2% FBS (Fetal Bovine Serum). Various numbers of MTT-labeled HL-60 cells were added to BAEC (Bovine Arteroa; Endothalium cells) which were cultured in 96 well multidish and stimulated with 100 U ml^{-1} rh TNF-α for 12 h. After 30 min, all MTT-HL-60 cells accumulated at the bottom of the wells. The supernatants were gently removed and 0.1 ml of DMSO was added. The absorbance at 540 nm was measured (Mean ± S.D, $n=6$). The adhesion of HL-60 to BAEC was significantly inhibited by **1** and **2** (1×10^{-5} mol l^{-1}) with inhibitory rate of 44.72 and 39.02%, respectively.

Acknowledgements

This research program was supported by the National Natural Science Foundation of China (39570836). The authors are grateful for the spectral data afforded by Professor Mitsuo Takasugi (Graduate School of Environmental Earth Sciences, Hokkaido University, Japan) and the literature information provided by Dr. Toshio Fukai (Faculty of Pharmaceutical Sciences, Toho University, Japan). The pharmacological tests were measured by Professor Guifang Chen et al. The Department of Instrumental Analysis in our institute measured the ^1H NMR, ^{13}C NMR, ^1H–^1H COSY, DEPT, ^{13}C ^1H COSY, HMBC, NOE DIF, UV, IR, HRFABMS and X-ray diffraction analysis.

References

Fukai, T., Pei, Y.H., Nomura, T., Xu, C.Q., Wu, L.J., Chen, Y.J., 1998. Isoprenylated flavanones from *Morus cathayana*. Phytochemistry 47, 273–280.

Hano, Y., Nomura, T., 1985. Structure of sanggenon O, a natural Diels-Alder type adduct from Chinese crude drug "Sang-Bai-Pi" (*Morus* root bark). Heterocycles 23, 2499–2503.

Hirakura, K., Fujimoto, T., Fukai, T., Nomura, T., 1986. Two phenolic glycosides from the root bark of the cultivated Mulberry tree (*Morus lhou*). J. Nat. Prod. 49, 218–224.

Jia, L.G., Wu, L.J., Xu, C.Q., Chen, Y.J., Liu, S.Y., Chen, M.D., 1996. A study on chemical constituents of the root bark of *Morus cathayana* Hemsl. Journal of Shenyang Pharmaceutical University 68, 192–195 (in Chinese).

Li, L.C., Cheng, G.F., Zhang, C.Y., 2000. Establishment of a model for adhesion of polymorphonuclear leukocyte tosynovial cell. Acta Pharmaceutica Sinica 35 (2), 103–107 (in Chinese).

Nagao, S., 1981. Dissertation: bio-organic chemical studies on phytoalexins produced in *Mulberry*. Hokkaido University.

Nomura, T., 1988. Phenolic compounds of the Mulberry tree and related plants. In: Herz, W., Grisebach, H., Kirby, G.W. (Eds.), Fortschritte der Chemie Organischer Naturstoffe Vol. 53. Springer, Wien, Ch. Tamm, pp. 87–201.

Nomura, T., Hano, Y., 1994. Isoprenoid-substituted phenolic compounds of *Moraceous* plants. Natural Product Reports 11, 205–218.

Nomura, T., Fukai, T., Hano, Y., Uzawa, J., 1981. Structure of sanggenon C, a natural hypotensive Diels–Alder adduct from Chinese crude drug "Sang-Bai-Pi" (*Morus* root bark). Heterocycles 16, 2141–2148.

Reddy, G.R., Ueda, N., Hada, T., Sackeyfio, A.C., Yamamoto, S., Hano, Y., Aida, M., Nomura, T., 1991. A prenylflavone, artonin E, as arachidonate 5-lipoxygenase inhitor. Biochem. Pharmacal. 41, 115–118.

PERGAMON

Phytochemistry 57 (2001) 1237–1243

PHYTOCHEMISTRY

www.elsevier.com/locate/phytochem

Benzophenone *O*-glucoside, a biogenic precursor of 1,3,7-trioxygenated xanthones in *Hypericum annulatum*

Gerassim M. Kitanov*, Paraskev T. Nedialkov

Department of Pharmacognosy, Faculty of Pharmacy, Medical University of Sofia, Dunav str. 2, 1000 Sofia, Bulgaria

Received 22 January 2001; received in revised form 6 April 2001

Abstract

Two new benzophenones, hypericophenonoside (**1**) and annulatophenone (**2**) were isolated from the methanol extract of the herb of *Hypericum annulatum*. The structures of the benzophenones were established as 2′-*O*-β-D-glucopyranosyl-2,4,5′,6-tetrahydroxy benzophenone (**1**) and 2,3′,5′,6-tetrahydroxy-4-methoxybenzophenone (**2**) based on spectral and chemical evidence. Hypericophenonoside is the second benzophenone *O*-glycoside found in nature. Acid and enzymatic hydrolysis of (**1**) has led directly to the formation of 1,3,7-trihydroxyxanthone (gentisein). This fact confirmed the hypothesis that some xanthones could be formed in plants by dehydration of 2,2′-dihydroxybenzophenones, and the intermediate precursors appear to be benzophenone *O*-glycosides *ortho* to the carbonyl function. © 2001 Elsevier Science Ltd. All rights reserved.

Keywords: *Hypericum annulatum*; Guttiferae; Benzophenones; Annulatophenone; Hypericophenonoside; Transformation to 1,3,7-trihydroxyxanthone

1. Introduction

In previous studies of *Hypericum annulatum* Moris, subsp. *annulatum* (Robson, 1993), also known as *Hypericum degenii* Bornm. (Jordanov and Kožucharov, 1970), the presence of several flavonols, biapigenin, catechins, two hypericins and four xanthones was demonstrated. Total hydrolysis of purified EtOH extract from the aerial parts of this species has led to the isolation of large amounts of 1,3,7-trihydroxyxanthone (gentisein), but only low quantities of its 3-*O*-glucoside (xanthohypericoside) were found in the plant (Kitanov and Akhtardziev, 1979; Kitanov and Nedialkov, 2000).

This paper describes the isolation and structure elucidation of two benzophenones and transformation of one of them (hypericophenonoside) to gentisein by acid and enzymatic hydrolysis.

2. Results and discussion

The dried aerial parts of *H. annulatum* were defatted with *n*-hexan and then extracted with hot MeOH. The crude MeOH residue was dissolved in hot water and partitioned subsequently with $CHCl_3$ and EtOAc. The EtOAc extract was fractionated by CC on polyamide using H_2O and H_2O–EtOH mixtures as eluent. The fraction containing compound **1** was rechromatographed on polyamide and eluted with $CHCl_3$–MeOH mixtures. Sephadex LH-20 was used as final purification step. The fraction rich in compound **2** was subjected to gel filtration on Sephadex LH-20.

Compound **1** was easily dissolved in water and gave a dark brown color with ferric chloride. Quantitative acid hydrolysis with HCl yielded an aglycone and D-glucose in a ratio 1:1 (57.54 and 42.46%, respectively). The aglycone was identified by UV, IR, EI-MS, ^{1}H NMR spectra and co-TLC as 1,3,7-trihydroxyxanthone (gentisein) (**1d**), previously isolated from this species (Kitanov and Akhtardzhiev, 1979). The main mystery was the presence only of one band at 304 nm in the UV spectrum of compound **1**, while the aglycone showed absorption maxima at 236, 260, 310 and 367 nm typical for xanthones. The similar four maxima were also observed for 3-*O*-β-D-glucoside of 1,3,7-trihydroxyxanthone found not so long ago in the same plant (Kitanov and Nedialkov, 2000). Mild acid hydrolysis of **1** with 0.2–0.5 M HCl and TFA and treatment with β-glucosidase similarly led to the obtaining of gentisein and D-glucose. When monitored by TLC, mild and

* Corresponding author. Tel.: +359-2-987-6265; fax: +359-2-987-9874.

E-mail address: gkitanov@mbox.pharmfac.acad.bg (G.M. Kitanov).

0031-9422/01/$ - see front matter © 2001 Elsevier Science Ltd. All rights reserved.
PII: S0031-9422(01)00194-7

enzymatic hydrolysis of **1** showed presence of an intermediate product, which could not be isolated because of its instability.

The IR spectrum of **1** showed absorption bands at 3302 (OH), 1643 (C=O), 1601 and 1516 (C=C) cm^{-1}. The bathochromic shift of the band at 304 nm in the UV spectrum with $AlCl_3$ (+14 nm) and NaOAc (+33 nm) revealed the presence of free hydroxyls *ortho* and *para*, respectively, to the carbonyl function. The HREI-MS of **1** showed the highest peak at *m/z* 244.0383 (rel. int. 100%) corresponding to the molecular formula $C_{13}H_8O_5$ of gentisein **1d**. In the FAB-MS spectrum the $[M+H]^+$ peak at *m/z* 425 was consistent with molecular formula $C_{19}H_{20}O_{11}$, the base peak at *m/z* 263 $[M_{agl}+H]^+$ (rel. int. 100%) with the formula $C_{13}H_{10}O_6$ and an ion peak at *m/z* 245 $[M_{gent}+H]^+$ indicated the gentisein moiety (Fig. 1). Gentisein **1d** was obtained by dehydration of aglycone **1c** ($M_{agl}-M_{gent}=18$). The molecular mass of **1** was also confirmed by elemental analysis data: C = 53.71 and H = 4.82% respectively.

The ^1H NMR spectrum of **1** in acetone-d_6 (Table 1) showed the presence of signals from two chelated

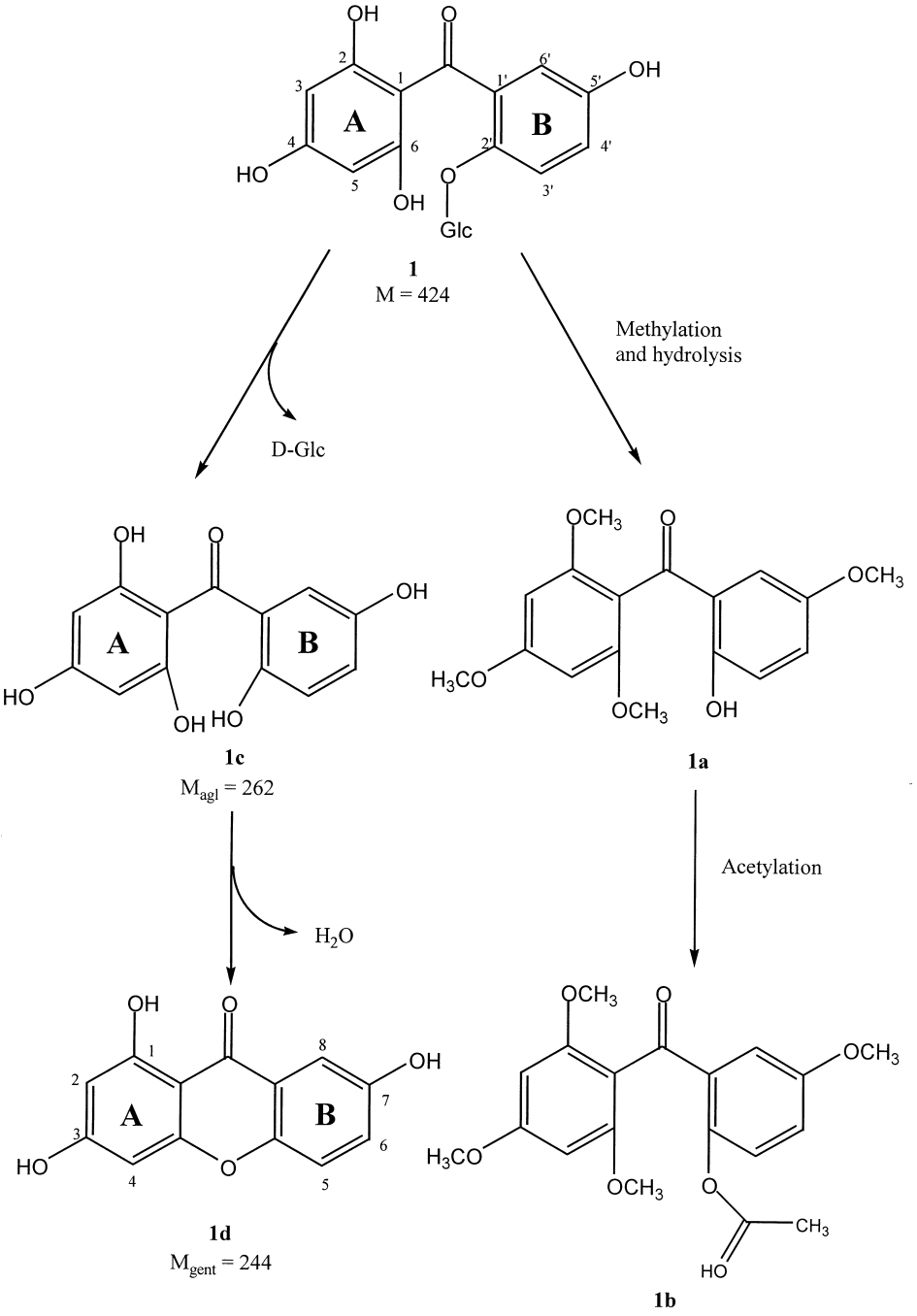

Fig. 1. Transformation of hypercophenonoside (**1**).

Table 1
^{1}H NMR spectral data (300 MHz) for **1**, **1b** and **2**[a]

No.	**1** (acetone-d_6) (*J*)	**1** (DMSO-d_6) (*J*)	**1b** ($CDCl_3$) (*J*)	**2** (acetone-d_6) (*J*)	**2** (DMSO-d_6) (*J*)
1	–	–	–	–	–
2	10.96 *br. s*, OH[b]	11.44 *s*, OH[b]	3.68 *s*, OMe[b]	10.22 *br. s*, OH[b]	9.80 *s*, OH[b]
3	5.91 *s*[b]	5.74 *s*[b]	6.12 *s*[b]	6.02*s*[b]	5.90 *s*[b]
4	8.26 *br. s*, OH[b]	10.38 *s*, OH	3.84 *s*, OMe	3.81 *s*, OMe	3.75 *s*, OMe
5	5.91 **s**[b]	5.74 *s*[b]	6.12 *s*[b]	6.02*s*[b]	5.90 *s*[b]
6	10.96 *br. s*, OH[b]	11.44 *s*, OH[b]	3.68 *s*, OMe[b]	10.22 *br. s*, OH[b]	9.80 *s*, OH[b]
1′	–	–	–	–	–
2′	–	–	2.03 *s*, OAc	6.62 *d*, (2.2)[b]	6.65 *d*, (2.1)[b]
3′	7.08 *d*, (8.8)	7.0 *d*, (8.7)	6.96 *d*, (8.8)	8.40 *br. s*, OH[b]	9.50 *s*, OH[b]
4′	6.81 *dd*, (8.8, 3.0)	6.70 *dd*, (8.7, 2.9)	7.03 *dd*, (8.8, 3.0)	6.49 *t*, (2.2)	6.35 *t*, (2.1)
5′	8.26 *br. s*, OH[b]	9.15 *s*, OH	3.78 *s*, OMe	8.40 *br. s*, OH[b]	9.50 *s*, OH[b]
6′	6.72 *d*, (3.0)	6.51 *d*, (2.9)	7.28 *d*, (3.0)	6.62 *d*, (2.2)[b]	6.65 *d*, (2.1)[b]
1″	4.73 *d*, (7.7)	4.59 *d*, (7.2)	–	–	–
2″	3.23 *m*[c]	3.02–3.67 *m*[c]	–	–	–
3″	3.31 *m*[c]	Sugar	–	–	–
4″	3.45 *m*[c]		–	–	–
5″	3.66 *br. t*[c]	Protons	–	–	–
6″	3.88 *br. d*[c]		–	–	–

[a] The chemical shifts are expressed in ppm and the coupling constants (*J*) in Hz/s. All protons were assigned by ^{1}H–^{1}H and HETCOR experiments.
[b] Overlapping.
[c] Signal patterns are unclear due to overlapping.

hydroxyl protons at δ 10.96 and a broad signal at δ 8.26 (which were much more expressed in DMSO-d_6 at δ 11.44, 10.38 and 9.15) all disappearing after addition of D_2O. The presence of two hydroxyl groups *ortho* to the carbonyl was confirmed by the appearance of signals from two acetyl groups in lower field at δ 2.30 and 2.35 after peracetylation of **1**. The presence of five substituents of aromatic rings of **1** was confirmed by DEPT experiment (Table 2). The signal at δ 5.91 (*s*, 2H) indicated a symmetrical three substituted phloroglucinol ring A, which was confirmed by the presence of the overlapping signals in ^{13}C NMR at 165.86 ppm (C_2 and C_6) and 96.48 ppm (C_3 and C_5) (Table 2). The signals of three aromatic protons from ring B (acetone-d_6) appeared as two doublets and a quadruplet at δ 7.08, 6.72 and 6.81 with $J=8.8$ and 3.0 Hz respectively. This fact pointed to the *ortho* and *meta* positions of the protons and an asymmetrical structure of this ring.

The signal at δ 4.73 (*d*, $J=7.7$ Hz) and a multiplet at δ 3.23–3.88 were assigned to the sugar residue with β-configuration of the anomeric proton. The positions of all protons were assigned by ^{1}H–^{1}H COSY and HETCOR experiments. Results of ^{13}C NMR and DEPT experiments (Table 2) confirmed the structure of aglycone **1c** as 2,2′,4,5′,6-pentahydroxybenzophenone.

The presence of hydroxyl groups *para* to the carbonyl function and the symmetrical structure of ring A suggest the location of sugar moiety in ring B. To determine the position of the glucose, **1** was methylated and the resultant compound was hydrolyzed by HCl (Fig. 1). The bathochromic shift of the bands at 262 and 369 nm in UV spectra of **1a** with $AlCl_3$ (+19 and +70 nm, respectively) indicated the presence of a free hydroxyl group *ortho* to the carbonyl moiety.

Acetylation of **1a** gave **1b** with mp 121.5–123°C. The EI-MS spectrum of this compound showed a molecular ion $[M]^{+\cdot}$ at *m*/*z* 360 corresponding to the formula $C_{19}H_{20}O_7$ and a peak at *m*/*z* 318 $[M-Ac+H]^+$, which indicated **1b** as a monoacetate. The IR spectrum showed an absorption at 1769 cm^{-1} (–OAc group) and an absence of characteristic band for free hydroxyl groups. The ^{1}H NMR spectrum (Table 1) indicated signals for five aromatic protons, four methoxyl groups, two of which are overlapping at δ 3.68, and an acetyl group at δ 2.03 (3H) *ortho* to the carbonyl function.

Thus the structure of **1** was established as 2′-*O*-β-D-glucopyranosyl-2,4,5′,6-tetrahydroxybenzophenone, named hypericophenonoside. It is a new natural compound and the second benzophenone *O*-glycoside found in the plants (Ferrari et al., 2000).

Compound **2** was isolated as pale yellow needles. It reacted with ferric chloride to give a dark brown color. The IR spectrum established the presence of a hydroxyl (3302 cm^{-1}), a conjugated carbonyl (1645 cm^{-1}) and an aromatic system (1582, 1520 cm^{-1}). The bathochromic shift of the UV maximum after addition of aluminum chloride (+33 nm) and the absence of shift upon addition of sodium acetate revealed free hydroxyl substituents *ortho* to the carbonyl group. The presence of four hydroxyls, two of which *ortho* to the carbonyl function, was confirmed by the presence of two sharp singlets at δ 9.80 (2H) and 9.50 (2H) in the ^{1}H NMR

Table 2
^{13}C NMR spectral data (75 MHz) for **1** and **2**[a]

No.	**1**		**1**	**2**		2
	Acetone-d_6	DEPT	DMSO-d_6	Acetone-d_6	DEPT	DMSO-d_6
1	107.09	–	105.04	106.96[b]	–	106.97[b]
2	165.86[b]	–	163.71[b]	163.76[b]	–	158.28[b]
3	96.48[b]	94.99[b]	94.42[b]	95.12[b]	93.62[b]	92.83[b]
4	167.11	–	165.26	167.37	–	161.85
5	96.48[b]	94.99[b]	94.42[b]	95.12[b]	93.62[b]	92.83[b]
6	165.86[b]	–	163.71[b]	163.76[b]	–	158.28[b]
1′	136.81	–	134.66	144.88	–	140.81
2′	148.66	–	146.46	108.17[b]	106.68[b]	108.52[b]
3′	119.95	118.46	117.73	159.56[b]	–	157.52[b]
4′	118.31	116.82	116.18	106.96[b]	105.48	106.97[b]
5′	153.95	–	151.83	159.56[b]	–	157.52[b]
6′	115.38	113.89	113.36	108.17[b]	106.68[b]	108.52[b]
1″	104.93	103.44	102.59	–	–	–
2″	75.51	74.02	73.48	–	–	–
3″	78.15	76.66	76.53	–	–	–
4″	71.83	70.34	69.75	–	–	–
5′	78.22	76.73	76.95	–	–	–
6″	63.32	61.83[c]	60.89	–	–	–
>C=O	199.46	–	197.12	200.11	–	195.67
–OCH_3	–	–	–	56.49	54.97	54.97

[a] The chemical shifts are expressed in (ppm). All carbons were assigned by HETCOR and DEPT experiments.
[b] Overlapping.
[c] Signals are turned upside-down.

spectrum in DMSO-d_6 (Table 1), both disappearing after addition of D_2O.

The HREI-MS spectrum showed $[M]^{+\cdot}$ at m/z 276.0642 consistent with the molecular formula $C_{14}H_{12}O_6$ and ion peaks at m/z 167 [$C_8H_7O_4$] derived from ring A and at m/z 137 [$C_7H_5O_3$] from ring B (Fig. 2). The molecular formula of **2** was confirmed by elemental analysis. The data of ^1H NMR and molecular ions of EI–MS support the presence of two symmetrical hydroxyls and a methoxyl group in ring A (phloroglucinol system) and two symmetrical hydroxyls in ring B (resorcinol system).

^1H NMR exhibits a signal of two protons from phloro glucinol ring A at δ 6.02. A doublet at δ 6.62 (2H, $J=2.2$) and a triplet at δ 6.49 (1H) indicated a symmetric resorcinol structure of ring B. The methoxyl group appeared as a singlet at δ 3.81. The assignment of the signals was confirmed by ^1H–^1H COSY, ^{13}C NMR, HETCOR and DEPT experiments (Table 2). Consequently the structure of **2** was established as 2,3′,5′,6-tetrahydroxy-4-methoxybenzophenone, named annulatophenone.

Up to now, only several benzophenone *C*-glucosides were found in *Mangifera indica* L. (Tanaka et al., 1984) and a benzophenone *O*-glucoside together with a *C*-glucoside was recently reported in *Gnidia involucrata* Steut. Ex A. Rich. (Ferrari et al., 2000). Although prenylated benzophenones often occur in the Guttiferae, simple benzophenones are rare in this family and have not been found in species of genus *Hypericum* (Bennett and Lee, 1989). The presence of simple benzophenones in species of this genus and their co-occurrence with simple xanthones may be of taxonomic and biogenetic value.

The biosynthetic pathways to xanthones in higher plants have been discussed in several reviews (Carpenter et al., 1969; Sultanbawa, 1980; Bennett and Lee, 1989; Peres and Nagem, 1997). It has been shown that polyhydroxybenzophenones could be intermediate precursors in the formation of xanthones. The biosynthesis involves shikimate and acetate pathways formation of intermediate benzophenones, which then react intramolecularly to give xanthones. The mechanism for this intramolecular reaction has been postulated involving four possible pathways.

Two alternative pathways of xanthone biosynthesis in cell cultures of *Centaurium erythraea* Rafn. and *Hypericum androsaemum* L. were recently reported (Beerhues, 1996; Schmidt and Beerhues, 1997). In the first one, the intermediate 2,3′,4,6-tetrahydroxybenzophenone was shown to be intramolecularly coupled to 1,3,5-trihydroxyxanthone, whereas in the second one it was coupled to form the isomeric 1,3,7-trihydroxyxanthone. These regioselective oxidative phenol couplings were catalyzed by xanthone synthases, proposed to be cytochrome P_{450} oxydases (Peters et al., 1998).

One of the pathways is dehydration between the hydroxyl groups of the acetate and shikimate derived rings (2,2′-dihydroxybenzophenones) via intermediates such as

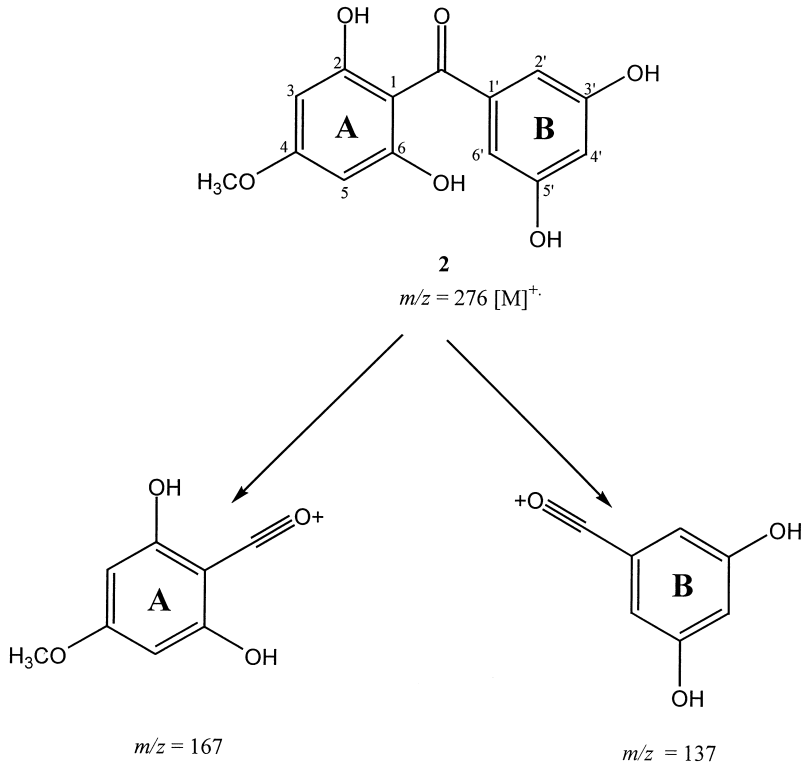

Fig. 2. EI–MS fragmentation of annulatophenone (**2**).

O-pyrophosphates (Carpenter et al., 1969; Sultanbawa, 1980). Up to date however there is no evidence for in vivo formation of polyhydroxyxanthones from benzophenones by dehydration mechanism. The question of the co-occurrence of suitable polyhydroxybenzophenone intermediates and xanthones in plants has not yet found a satisfactory answer.

In our case, in the herb of *Hypericum annulatum* we found the co-occurrence of large amounts of hypericophenonoside **1** (with 2,2′-hydroxyl groups) together with 1,3,7-trihydroxyxanthone (gentisein) **1d**. The benzophenone *O*-glucoside **1** was easily transformed into gentisein by acid or enzymatic hydrolysis. This fact supports the evidence that 2,4,5′,6-tetrahydroxybenzophenone-2′-*O*-glucoside **1** is a precursor of 1,3,7-trihydroxyxanthone. The transformation is realized by elimination of the glucose moiety and subsequent dehydration involving hydroxyls from phloroglucinol ring A and ring B, located *ortho* to the carbonyl group (Fig. 1). These results pointed to the fact, that one of the biosynthetic pathways of xanthone formation in plants is through an intermediate glycosidation at an earlier stage of the benzophenone biosynthesis before cyclization of the two rings.

Finally, it can be concluded that some xanthones are formed in vivo by dehydration of 2,2′-dihydroxybenzophenones. This is a spontaneous reaction which appears to be regulated by deglucosilation of the precursor and the precursors appear to be benzophenones with *O*-glycosilation *ortho* to the carbonyl function.

3. Experimental

3.1. General experimental procedures

Mps uncorr. OR was measured on a Perkin-Elmer 241 polarimeter using MeOH as solvent. UV spectra were run in MeOH and shift reagents on a Specord UV–VIS and IR spectra were recorded in nujol on a Shimadzu FTIR-8101 M instruments. ^{1}H and ^{13}C NMR spectra were obtained on a Bruker ARX 300 apparatus at 300 and 75 MHz, respectively, in acetone-d_6 and DMSO-d_6 (**1** and **2**) and $CDCl_3$ (**1b**), using TMS as internal standard. HREI- and FAB-MS analyses were performed on a Varian MAT 711 mass spectrometer at 70 eV in positive ion mode. Open column chromatography (CC): polyamide S (Woelm, Germany) and Sephadex LH-20 (Pharmacia, Sweden). TLC was performed using silica gel 60 GF_{254} (Merck), $CHCl_3$–MeOH–H_2O (70:20:2) (A), EtOAc–MeCOEt–HCO_2H–H_2O) (25:10:2:4) (B), EtOAc–MeOH–H_2O–AcOH (65:15:15:20) (C) and cellulose (Merck), EtOAc-pyridine–H_2O (12:5:4) (D) mixtures were used as solvents. Hydrolysis of hypericophenonoside **1** was carried out with HCl and TFA (100°C, 2h) and β-glucosidase

(Koch-Light Laboratories) (25°C, 48 h). Methylation of **1** ($Me_2SO_4 + K_2CO_3$ in dry acetone) and acetylation of **1** and **1a** (Ac_2O–pyridine method) were performed by usual procedures. Detection of benzophenones was by spraying with Fast blue salt B (Riedel-De Haën, Germany) in MeOH–H_2O (1:1) and of sugars by anizidine phtalate reagent followed by heating at 110°C for 3–5 min.

3.2. Plant material

The aerial parts of *Hypericum annulatum* (syn. *H. degenii*) were collected during the flowering season from wild habitat at the Central Rhodope Mountains in July 1997. A voucher specimen (No. 144296) has been deposited at the Herbarium of Botany Institute of Sofia (SOM).

3.3. Extraction and isolation

The air dried and powdered herb (1.7 kg) was defatted with *n*-hexan (1 l×6) and extracted with hot MeOH (6 l×8). The crude MeOH residue was dissolved in hot H_2O (2 l), filtered and treated with $CHCl_3$ (300 ml×10). The aq. phase was fractionated with EtOAc (500 ml×7). The EtOAc fraction (52 g) was chromatographed on a polyamide column (150 g), using a 0–60% EtOH linear gradient and gave mixture of **1** and other compounds (H_2O fraction, 5.5 g) and **2** (30–40% EtOH, 2.5 g). The H_2O fraction was rechromatographed (×3) on polyamide (30 g, step gradient $CHCl_3$–MeOH 85:15–80:20). Subsequent Sephadex LH-20 gel filtration (MeOH) gave pure compound **1** (2.1 g). The other fraction, rich in **2**, was further purified on Sephadex LH-20 (MeOH) and by repeated recrystallization from H_2O–EtOH, 383 mg of this compound was obtained.

3.4. Hypericophenonoside (*1*) (2.1 g)

Pale yellow needles (from H_2O), mp 156–158°C. $[\alpha]_D^{20}$ +46.11° (MeOH, *c*1.0300). UV λ_{max}^{MeOH} nm (log ε): 206 (4.327), 225^{sh}, 304 (4.149); +$AlCl_3$ 202, 220, 318; +$AlCl_3$/HCl 202, 220, 315; +NaOAc 337; +NaOAc/H_3BO_3 308. IR ν_{max}^{nujol} cm^{-1}: 3302 (chelated OH); 1643 (>C=O); 1601, 1516 (>C=C<, aromatic). ^1H and ^{13}C NMR: see Tables 1 and 2. HREI–MS *m*/*z* (rel. int.): 244.0383 $[M_{gent}]^{+\cdot}$ $[C_{13}H_8O_5]$ (100), (calcd 244.1993). FAB-MS *m*/*z* (rel. int.): 425 $[M+H]^+$ (42), 263 $[M_{agl}+H]^+$ (100), 245 $[M_{gent}+H]^+$ (16), 163 $[(M_{glu}-H_2O)+H]^+$ (4). Found: C, 53.71; H, 4.82%. $C_{19}H_{20}O_{11}$ requires: C, 53.78; H, 4.75%.

3.5. Acid hydrolysis of *1*

A sample of compound **1** (50 mg) was dissolved in 10 ml of 1 N HCl and refluxed on water bath (100°C). The hydrolysis was monitored by TLC, system A, time interval 5–10 min, for 2 h. After dilution with H_2O and cooling, the aglycone ppt. was filtered and recrystallized from MeOH. The aq. solution was evapd to dryness in vacuo. The residue was dissolved in 50% EtOH and examined for sugar by TLC using solvent systems C and D. The aglycone was identified as 1,3,7-trihydroxyxanthone (gentisein) on the basis of co-TLC, UV, IR, EI–MS and ^1H NMR and the sugar was identified to be D-glucose. The similar procedure was used for mild hydrolysis of **1** with 0.2 M, 0.5 M HCl and 2 M TFA in H_2O–MeOH (1:1).

3.6. Enzymatic hydrolysis of *1*

Compound **1** (15 mg) was dissolved in H_2O and 20 mg of β-glucosidase were added. The solution remained for 48 h at 25°C and then was heated at 80°C for 30 min. The reaction mixture was extracted ×3 with EtOAc to remove the aglycone part and both solutions (H_2O and EtOAc) were evaluated for identification of the components.

3.7. Methylation and hydrolysis of *1*

Compound **1** (200 mg) was refluxed for 46 h with Me_2SO_4 (6 ml) in dry acetone (150 ml), containing dry K_2CO_3 (4 g). After filtration and evapn. to dryness the residue was dissolved in 40 ml MeOH–4% HCl (1:1). The mixture was refluxed on boiling water bath for 3 h and MeOH was removed in vacuo. The aq. solution was extracted with $CHCl_3$ (30 ml×5), dryed and after evapn. of the solvent the residue was purified on Sephadex LH-20 (MeOH). The methylated aglycone was crystallized from MeOH–C_6H_6 to give a solid (76 mg) of **1a**.

3.8. 2′-Hydroxy-2,4,5′,6-tetramethoxybenzophenone (*1a*) (76 mg)

Yellow flakes (from MeOH–C_6H_6), mp 177.5–179°C. UV λ_{max}^{MeOH} nm: 231, 262, 369; +$AlCl_3$ 250^{sh}, 281, 439; +$AlCl_3$/HCl 262^{sh}, 281^{sh}, 369, 439^{sh}; +NaOMe 231^{sh}, 262, 369. IR ν_{max}^{nujol} cm^{-1}: 3300 (w, chelated OH), 1615 (>C=O), 1608, 1587 (>C=C<, aromatic). HREI-MS *m*/*z*: 318.2896 (calcd. 318.3205) $[C_{17}H_{18}O_6]$.

3.9. Acetylation of *1* and *1a*

Samples of **1** (30 mg) and **1a** (20.4 mg) were treated with C_5H_5N (0.6 ml) and Ac_2O (2 ml) and refluxed for 3 h. The reaction mixtures were poured on ice and kept at 4°C for 24 h. The ppts. were filtered, dried and crystallized from EtOH to give 21 mg of **1**-octaacetate and 16 mg of **1a**-monoacetate (**1b**) derivatives.

3.10. 2′-Acetoxy-2,4,5′,6-tetramethoxybenzophenone (**1b**) (16 mg)

Colorless prismatic crystals (from EtOH), mp 121.5–123°C. IR ν_{max}^{nujol} cm^{-1}: 1769 (–OAc), 1659 (>C=O), 1605, 1590 (>C=C<, aromatic). ^1H NMR: see Table 1. EI-MS *m/z* (rel. int.): 360 $[M]^+$ $[C_{19}H_{20}O_7]$ (5), 318 $[M-Ac+H]^+ = [M_{\mathbf{1a}}]^+$ (22), 287 $[M-Ac-OMe]^+ = [M_{\mathbf{1a}}-OMe]^+$ (61), 195 $[M-165]^+$ (7), 168 $[M-192]^+$ (100), 150 $[M-192-H_2O]^+$ (46).

3.11. Annulatophenone (**2**) (383 mg)

Pale yellow needles (from H_2O–EtOH), mp 187–189°C. UV λ_{max}^{MeOH} nm (log ε): 208 (4.371), 222^{sh}, 306 (3.908); $+AlCl_3$ 226^{sh}, 307^{sh}, 339; $+AlCl_3$/HCl 225^{sh}, 303^{sh}, 331; +NaOAc 306; +NaOAc/H_3BO_3 306. IR ν_{max}^{nujol} cm^{-1}: 3302 (chelated OH), 1645 (>C=O), 1582, 1520 (>C=C<, aromatic). ^1H and ^{13}C NMR: see Tables 1 and 2. HREI–MS *m/z*: 276.0642 $[C_{14}H_{12}O_6]$ (calc. 276.241). EI-MS: 276 $[M]^{+\cdot}$ (100), 259 $[M-OH]^+$ (90), 167 $[M-109]^+$ $[C_8H_7O_4]$ (83), 137 $[M-139]^+$ $[C_7H_5O_3]$ (14). Found: C, 60.79; H, 4.47%. $C_{14}H_{12}O_6$ requires C, 60.87; H, 4.38%.

Acknowledgements

The authors are indebted to Professor Ivo Ivanov (Sofia, Bulgaria), Dr. Ulrich Girreser (Kiel, Germany) and to Dr. Joachim Opitz (Stuttgart, Germany) for measurement and providing NMR an MS spectra. This work was supported by a grant 21/1998 from Medicinal Science Council (MSC) at Medical University of Sofia.

References

Beerhues, L., 1996. Benzophenone synthase from cultured cells of *Centaurium erythraea*. FEBS Letters 383, 264–266.

Bennett, G.J., Lee, H.-H., 1989. Xanthones from Guttiferae. Phytochemistry 28, 967–998.

Carpenter, I., Locksley, H.D., Scheinmann, F., 1969. Xanthones in higher plants: biogenetic proposals and a chemotaxonomic survey. Phytochemistry 8, 2013–2026.

Ferrari, J., Terreaux, C., Sahpaz, S., Msonthi, J.D., Wolfender, J.-L., Hostettmann, K., 2000. Benzophenone glycosides from *Gnidia involucrata*. Phytochemistry 54, 883–889.

Jordanov, D., Kožucharov, S., 1970. *Hypericum* L. In: Jordanov, D. (Ed.), Flora of R. P. Bulgaricae, Vol. 4. BAS, Sofia, pp. 224–264.

Kitanov, G., Akhtardzhiev, Ch., 1979. Isolierung von Gentisein aus *Hypericum degenii* Bornm. Pharmazie 34, 447–448.

Kitanov, G.M., Nedialkov, P.T., 2000. Xanthohypericoside, a new xanthone-*O*-glucoside from *Hypericum annulatum*. Pharmazie 55, 397–398.

Peres, V., Nagem, T.J., 1997. Trioxygenated naturally occurring xanthones. Phytochemistry 44, 191–214.

Peters, S., Schmidt, W., Beerhues, L., 1998. Regioselective oxidative phenol couplings of 2,3′,4,6-tetrahydroxybenzophenone in cell cultures of *Centaurium erythraea* and *Hypericum androsaemum*. Planta 204, 64–69.

Robson, N.K.B., 1993. Studies in *Hypericum*: validation of new names. Bulletin of the Natural History Museum of London (Botany) 23, 67–70.

Schmidt, W., Beerhues, L., 1997. Alternative pathways of xanthone biosynthesis in cell cultures of *Hypericum androsaemum*. FEBS Letters 420, 143–146.

Sultanbawa, M.U.S., 1980. Xanthonoids of tropical plants. Tetrahedron 36, 1465–1506.

Tanaka, T., Sueyasu, T., Nonaka, G.I., Nishioka, J., 1984. Tannins and related compounds. XXI. Isolation and characterization of galloyl and *p*-hydroxybenzoyl esters of benzophenone and xanthone *C*-glucosides from *Mangifera indica* L. Chemical and Pharmaceutical Bulletin 32, 2676–2686.

PERGAMON

Phytochemistry 57 (2001) 1245–1248

PHYTOCHEMISTRY

www.elsevier.com/locate/phytochem

Lignan and phenylpropanoid glycosides from *Fernandoa adenophylla*

Tripetch Kanchanapoom[a,b], Ryoji Kasai[a], Kazuo Yamasaki[a,*]

[a]*Institute of Pharmaceutical Sciences, Faculty of Medicine, Hiroshima University, 1-2-3 Kasumi, Minami-ku, Hiroshima 734-8551, Japan*
[b]*Department of Pharmaceutical Botany and Pharmacognosy, Faculty of Pharmaceutical Sciences, Khon Kaen University, Khon Kaen 40002, Thailand*

Received 29 December 2000; received in revised form 19 March 2001

Dedicated to Professor Vichiara Jirawongse on the occasion of his 83rd birthday

Abstract

From the leaves and branches of *Fernandoa adenophylla*, a lignan glycoside (fernandoside) and a phenylpropanoid glycoside (2″-*O*-β-apiosylverbascoside) were isolated together with 12 known compounds. The structural elucidations were based on analyses of physical and spectroscopic data. © 2001 Published by Elsevier Science Ltd.

Keywords: *Fernandoa adenophylla*; Bignoniaceae; Lignan glycoside; Phenylpropanoid glycoside; Fernandoside; 2″-*O*-β-Apiosylverbascoside

1. Introduction

As part of our ongoing study on Thai medicinal plants, we investigated the constituents of *Fernandoa adenophylla* Steenis (Bignoniaceae, Thai name: Khae-hang-khang) collected from the botanical gardens, Faculty of Pharmaceutical Sciences, Khon Kaen University, Thailand. *F. adenophylla* is a tree, 5–13 m high, distributed in south and south-east Asia regions. In Thai traditional medicine, the leaves are used for external treatment of skin diseases. No chemical investigation has been carried out on this genus. The present study deals with the isolation and structural elucidation of 14 compounds (**1**–**14**), including a new lignan glycoside (**8**), a new phenylpropanoid glycoside (**12**) and 12 known compounds (**1**–**7**, **9**–**11** and **13** and **14)** from this plant.

2. Results and discussion

From the methanolic extract of the leaves and branches of *F. adenophylla,* 14 compounds (**1**–**14**) were isolated. Twelve were identified as known compounds; salidroside (**1**) (Schwab and Schreier, 1988), decaffeoylverbacoside (**2**), verbascoside (**3**), isoverbascoside (**4**), leucosceptoside A (**5**) (Miyase et al., 1982), plantaginoside C (**6**) (Miyase et al., 1991), martynoside (**7**) (Sasaki et al., 1978), (6*R*, 9*S*)-oxo-α-ionol glucoside (**9**) (Pabst et al., 1992), hispidulin-7-*O*-β-glucoside (**10**) (Hase et al., 1995), (+)-lyoniresinol 3a-*O*-β-glucoside (**11**) (Achenbach et al., 1992), apigenin-7-*O*-β-glucuronide (**13**) (Hase et al., 1995) and hispidulin-7-*O*-β-glucuronide (**14**) (Subramanian and Nair, 1972) by comparison of physical data with literature values and from spectroscopic evidence.

The molecular formula of compound **8** was determined as $C_{36}H_{44}O_{16}$ by HR–FAB mass spectrometry. The ^{1}H and ^{13}C NMR spectra of **8** were very similar to those of **11**. In addition, the signals of 1,3,4-trisubstituted aromatic ring, one methoxy signal and one ester carbonyl carbon were observed. Comparison of the ^{13}C NMR spectral data of **8** with those of **11** revealed the downfield shift of C-6 (+2.2 ppm) and upfield shift of C-5 (−2.6 ppm) of the glucosyl moiety indicating that the additional unit is an ester located at C-6 of the glucosyl moiety. Moreover, the HMBC spectrum (Fig. 1) revealed the correlation between H-6 (δ 4.56 and 4.33) of the glucosyl moiety and carbonyl carbon (δ 168.0). The methoxyl group of the additional unit was assigned to position C-3″ by a difference NOE experiment in the ^{1}H NMR spectrum. Irradiation of this methoxy signal (δ 3.78) caused an NOE enhancement at H-2″ (δ 7.48, *d*, $J=2.0$ Hz). Consequently, the structure of compound **8**

* Corresponding author. Tel.: +81-82-257-5285; fax: +81-82-257-5289.
E-mail address: yamasaki@pharm.hiroshima-u.ac.jp (K.Y. Yamasaki).

0031-9422/01/$ - see front matter © 2001 Published by Elsevier Science Ltd.
PII: S0031-9422(01)00212-6

was assigned as (+)-lyoniresinol 3a-[6-(4-hydroxy-3-methoxy)-benzoyl]-*O*-β-glucopyranoside, named fernandoside.

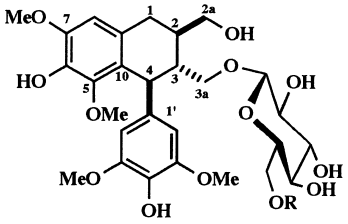

R

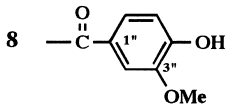

8

11 H

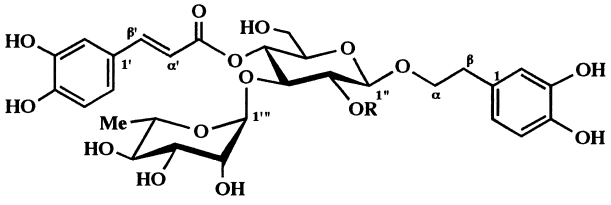

R

3 H

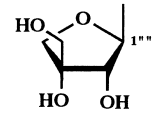

12

The molecular formula of compound **12** was determined as $C_{34}H_{44}O_{19}$ by HR–FAB mass spectrometry. Inspection of the ^{1}H NMR spectrum revealed the presence of two sets of AMX systems [δ 6.66 (*d*, J = 2.0 Hz), δ 6.63 (*d*, J = 8.1 Hz) and δ 6.52 (*dd*, J = 8.1, 2.0 Hz) for the 3,4-dihydroxy-β-phenylethoxyl moiety; and δ 7.01 (*d*, J = 2.0 Hz), δ 6.73 (*d*, J = 8.1 Hz) and δ 6.90 (*dd*, J = 8.1, 2.0 Hz) for the caffeoyl moiety], two *trans*-olefinic protons [δ 7.24 (*d*, J = 15.9 Hz) and δ 6.23 (*d*,J = 15.9 Hz)] together with three anomeric protons δ 4.41 (*d*, J = 7.8 Hz) for β-glucose, δ 5.00 (*d*, J = 1.3 Hz) for α-rhamnose and δ 5.17 (*d*, J = 2.2 Hz) for β-apiose. Acid hydrolysis with 0.2 N H_2SO_4 afforded rhamnose, apiose and glucose (identified by TLC). Comparison of the ^{13}C NMR spectral data with those of verbascoside (**3**) indicated that glucose is the core sugar with the 3,4-dihydroxy-β-phenylethoxyl moiety located at C-1″ as well as the *trans*-caffeoyl moiety linked at C-4″. The complete assignments were based on the results of COSY, HSQC and HMBC. COSY and HSQC experiments were used to determine the sugar protons (Table 2). HMBC correlations were observed between H-1″ (δ 4.41) and CH_2-

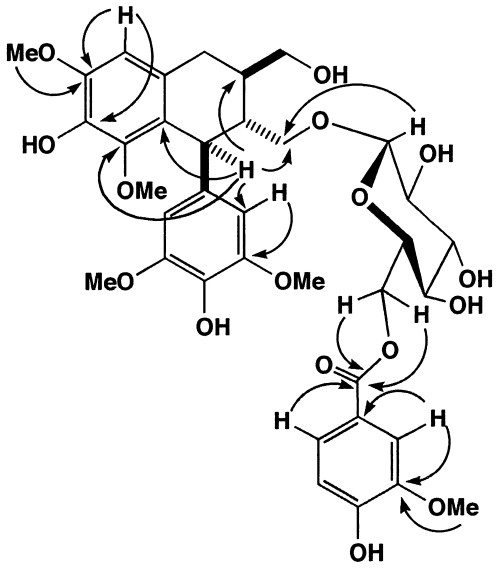

Fig. 1. The HMBC correlations of fernandoside (**8**).

α (δ 72.2); H-2″ (δ 3.47) and C-1″ and C-1‴″ H-3″ (δ 3.87) and C-2″ and C-1‴ as well as H-4″ and a carbonyl carbon (δ 168.3). Also, the reciprocal HMBC correlations were found between H-1‴″ and C-2″; H-1‴ and C-3″. On the basis of the spectral data, the structure of compound **12** was established as 3,4-dihydroxy-β-phenylethoxy - *O* - β - apiofuranosyl - (1→2) - α - rhamnopyranosyl-(1→3)-4-*O*-caffeoyl-β-glucopyranoside (2″-*O*-β-apiosylverbascoside).

3. Experimental

3.1. General

NMR spectral data were recorded in CD_3OD using a JEOL JNM A-400 spectrometer (400 MHz for ^{1}H NMR and 100 MHz for ^{13}C NMR) with tetramethylsilane (TMS) as internal standard. MS were recorded on a JEOL JMS-SX 102 spectrometer. IR were measured with a HORIBA FT 710 infrared spectrometer. UV were recorded on a JASCO V-520 spectrophotometer. Optical rotations were measured with a Union PM-1 digital polarimeter. Preparative HPLC was carried out on columns of ODS (20×150 mm i.d., YMC) and Diol-120 (8.0×300 mm i.d., YMC) with a Tosoh refraction index (RI-8) detector. The flow rates were 6 ml/min for ODS and 3ml/min for Diol-120. For CC, silica gel G 60 (Merck), YMC-gel ODS (50 μm, YMC), polyamide C-200 (Wako) and highly porous copolymer of styrene and divinylbenzene (Mitsubishi Chem. Ind. Co. Ltd) were used. The solvent systems were: (I) EtOAc–MeOH–H_2O (4:1:0.1), (II) EtOAc–MeOH–H_2O (7:3:0.3), (III) 20–70% MeOH, (IV) 10% MeCN, (V) 20% MeCN, (VI) 25% MeCN, (VII) MeCN, (VIII) 15% MeCN and (IX)

100–80% MeCN. The spray reagent used for TLC was 10% H_2SO_4 in 50% EtOH.

3.2. Plant material

The leaves and branches of *Fernandoa adenophylla* Steenis were collected in May 2000 from the botanical gardens, Faculty of Pharmaceutical Sciences, Khon Kaen University, Thailand. The identification of the plant was confirmed by Professor Vichiara Jirawongse, Department of Pharmaceutical Botany and Pharmacognosy, Faculty of Pharmaceutical Sciences, Khon Kaen University. A voucher sample is kept in the Herbarium of the Faculty of Pharmaceutical Sciences, Khon Kaen University, Thailand.

3.3. Extraction and isolation

The dried leaves and branches (2.5 kg) of *F. adenophylla* were extracted with hot MeOH. After removal of the solvent by evaporation, the residue (240.0 g) was defatted with Et_2O. The aqueous layer was subjected to a column of highly porous copolymer of styrene and divinylbenzene and eluted with H_2O, MeOH and Me_2CO, successively. The fraction eluted with MeOH (25.0 g) was subjected to a column of silica gel (systems I and II, respectively) affording three fractions. Fraction 1 (4.8 g) was applied to a RP-18 column using system III to provide 11 fractions. Fraction 1-1 was purified by prep. HPLC–ODS (system IV) to give compounds **1** (43 mg) and **2** (120 mg). Fractions 1-5 and 1-7 were similarly purified by prep. HPLC-ODS (system V) to afford compounds **3** (1 g) and **4** (620 mg). Fractions 1-8 and 1-9 were further purified by prep. HPLC–ODS (system VI) and HPLC–Diol (system VII) to provide compound **5** (32 mg), **6** (38 mg), **7** (17 mg), **8** (24 mg), **9** (9 mg) and **10** (90 mg). Fraction 2 (8.4 g) was applied to a RP-18 column (system III) to afford 13 fractions. Fraction 2-5 was purified by prep. HPLC–ODS (system VIII) to give compound **11** (160 mg). Fractions 2-8, 2-9 and 2-10 were combined and further separated on a column of polyamide (system IX), then followed by prep. HPLC–ODS (system V) to afford compound **12** (24 mg). Fractions 3 was subjected to a RP-18 column of (system III), then

Table 1
^{13}C NMR spectral data of compounds **8** and **11** (100 MHz, CD_3OD)

Carbon no.	**8**	**11**	Carbon no.	**8**	**11**
1	33.7	33.7	Glc-1	104.8	104.7
2	40.9	40.5	2	75.1	75.1
2a	66.2	66.2	3	78.1	77.8
3	46.4	46.6	4	71.9	71.6
3a	71.8	71.5	5	75.5	78.1
4	42.8	42.7	6	65.0	62.8
5	148.9	148.5			
6	138.8	138.8	1″	122.5	
7	147.6	147.5	2″	113.6	
8	107.8	107.8	3″	152.9	
9	130.2	130.1	4″	148.7	
10	126.2	126.3	5″	116.0	
			6″	125.1	
1′	139.4	139.3			
2′	106.9	106.9	MeO-5	60.2	60.1
3′	148.9	148.9	MeO-7	56.6	56.6
4′	134.5	134.4	MeO-3′,5′	56.9	56.9
5′	148.9	148.9	MeO-3″	56.4	
6′	106.9	106.9	-COO-	168.0	

Table 2
NMR spectral data of compounds **3** and **12** (100 MHz for ^1H NMR and 400 MHz for ^{13}C NMR, CD_3OD)

No.	Carbon		Proton
	3	**12**	**12**
Aglycone			
1	131.5	131.6	
2	116.5	116.5	6.66 (*d*, *J* = 2.0 Hz)
3	144.6	144.6	
4	146.1	146.1	
5	117.1	117.2	6.63 (*d*, *J* = 8.1 Hz)
6	121.3	121.3	6.52 (*dd*, *J* = 8.1, 2.0 Hz)
α	72.2	72.2	3.96 (*m*)
			3.70 (*m*)
β	36.5	36.5	2.75 (*t*, *J* = 7.3 Hz)
Caffeoyl moiety			
1′	127.7	127.7	
2′	115.2	115.2	7.01 (*d*, *J* = 2.0 Hz)
3′	149.7	149.7	
4′	146.8	146.8	
5′	116.3	116.3	6.73 (*d*, *J* = 8.1 Hz)
6′	123.2	123.2	6.90 (*dd*, *J* = 8.1, 2.0 Hz)
α′	114.7	114.9	6.23 (*d*, *J* = 15.9 Hz)
β′	148.0	147.9	7.54 (*d*, *J* = 15.9 Hz)
C=O	168.3	168.3	
Glucose			
1″	104.2	103.1	4.41 (*d*, *J* = 7.8 Hz)
2″	76.2	81.0	3.47 (*dd*, *J* = 9.8, 8.8 Hz)
3‴	81.6	82.0	3.87 (*t*, *J* = 9.3 Hz)
4″	70.4	70.8	4.89 (*t*, *J* = 9.3 Hz)
5″	76.0	76.0	3.48–3.52[a]
6″	62.4	62.4	3.50–3.62[a]
Rhamnose			
1‴	103.0	103.5	5.00 (*d*, *J* = 1.3 Hz)
2‴	72.3	72.3	3.90–4.00[a]
3‴	72.0	71.9	3.50–3.60[a]
4‴	73.8	73.8	3.27 (*t*, *J* = 9.6)
5‴	70.6	70.9	3.50–3.60[a]
6‴	18.4	18.4	1.06 (*d*, *J* = 6.1 Hz)
Apiose			
1⁗		111.2	5.17 (*d*, *J* = 2.2 Hz)
2⁗		78.5	3.90 (*d*, *J* = 1.8 Hz)
3⁗		80.4	
4⁗		75.1	3.97 (*d*, *J* = 9.9 Hz)
			3.70 (*d*, *J* = 9.9 Hz)
5⁗		65.5	3.55 (*s*)

[a] Signal pattern unclear due to overlapping.

followed by HPLC–ODS (system IV) to provide compounds **13** (51 mg) and **14** (75 mg).

3.4. Fernandoside (**8**)

Amorphous powder, $[\alpha]_D^{26}$ +25.0° (MeOH, *c* 1.24); UV λ_{max}^{MeOH} (nm): 362, 250; IR: υ_{max}^{KBr} cm^{-1} 3430, 2938, 1698, 1701, 1610, 1515, 1427, 764; ^1H NMR (CD_3OD): δ 7.50 (1H, *dd*, *J* = 8.1, 2.0 Hz, H-6″), δ 7.48 (1H, *d*, *J* = 2.0 Hz, H-2″), δ 6.77 (1H, *d*, *J* = 8.1 Hz, H-5″), δ 6.50 (1H, *s,* H-8), δ 6.37 (2H, *s,* H-2′, 6′), δ 4.56 (1H, (*dd*, *J* = 12.0, 2.1 Hz, H-6 Glc), δ 4.33 (1H, *d*, *J* = 11.5 Hz, H-4), δ 4.31 (1H, (*dd*, *J* = 12.0, 6.3 Hz, H-6 Glc), δ 4.28 (1H, *d*, *J* = 7.8 Hz, H-1 Glc), δ 3.84 (1H, *dd*, *J* = 10.2, 9.3 H-4 Glc), δ 3.79 (3H, *s,* MeO-7), δ 3.78 (3H, *s,* MeO-3″) 3.68 (6H, *s,* MeO-3′, 5′), δ 3.58 (1H, (*dd*, *J* = 11.0, 4.4 Hz, H-2a), δ 3.52 (1H, *m*, H5 Glc), δ 3.48 (1H, *dd*, *J* = 11.0, 6.8 Hz, H-2a), δ 3.41 (1H, *dd*, *J* = 9.8, 4.2 Hz, H-3a), δ 3.37 (2H, *m,* H-3a, 3 Glc), δ 3.30 (3H, *s* MeO-5), δ 3.24 (IH, *dd*, *J* = 7.8, 7.8 Hz, H-2 Glc), δ 2.64 (1H, (*dd*, *J* = 15.1, 4.9 Hz, H-1), δ 2.53 (1H, *dd,* *J* = 15.1, 11.5 Hz, H-1), δ 2.09 (1H, *m,* H-3), δ 1.61 (1H, *m*, H-2); ^{13}C NMR (CD_3OD): Table 1; negative HR–FAB–MS, *m*/*z*: 731.2504 $[M–H]^-$ ($C_{36}H_{43}O_{16}$ requires 731.2551).

3.5. 2″-O-β-Apiosylverbascoside (**12**)

Amorphous powder, $[\alpha]_D^{26}$ −90.7° (MeOH, *c* 1.40); UV λ_{max}^{MeOH} (nm): 355, 250; IR υ_{max}^{KBr} cm^{-1}: 3400, 2936, 1698, 1604, 1518, 1447, 813; ^1H NMR (CD_3OD) and ^{13}C NMR (CD_3OD): Table 2; negative HR–FAB–MS, *m*/*z*: 755.2413 $[M–H]^-$ ($C_{34}H_{43}O_{19}$ requires 755.2398).

3.6. Acid hydrolysis of 2″-O-β-apiosylverbascoside (**12**)

Compound **12** (5 mg) was dissolved in 0.2 N H_2SO_4 (5 ml) and heated at 95°C for 2 h. After cooling, the reaction mixture was extracted with EtOAc. The aqueous layer was neutralized with $NaHCO_3$, concentrated to dryness, and extracted with pyridine. The pyridine extract was then analyzed on silica gel TLC (EtOAc–MeOH–H_2O–AcOH 13:3:3:4), affording rhamnose (R_f 0.63), apiose (R_f 0.49) and glucose (R_f 0.39).

Acknowledgements

We would like to thank the Research Center for Molecular Medicine, Hiroshima University for the use of its NMR facilities.

References

Achenbach, H., Lowel, M., Waibel, R., Gupta, M., Solis, P., 1992. New lignan glucosides from *Stemmadenia minima*. Planta Medica 58, 270–272.

Hase, T., Ohtani, K., Kasai, R., Yamasaki, K., Picheansoonthon, C., 1995. Revised structure for hortensin, a flavonoid from *Millingtonia hortensis*. Phytochemistry 40, 287–290.

Miyase, T., Koizumi, A., Ueno, A., Noro, T., Kuroyanagi, M., Fukushima, S., Akiyama, Y., Takemoto, T., 1982. Studies on the acyl glycosides from *Leucoseptrum japonicum*. Chemical and Pharmaceutical Bulletin 30, 2732–2737.

Miyase, T., Ishino, M., Akahori, C., Ueno, A., Ohkawa, Y., Tanizawa, H., 1991. Phenylpropanoid glycosides from *Plantago asiatica*. Phytochemistry 30, 2015–2018.

Pabst, A., Barron, D., Semon, E., Schreier, P., 1992. Two diastereomeric 3-oxo-α-ionol α-D-glucosides from raspberry fruit. Phytochemistry 31, 1649–1652.

Sasaki, H., Taguchi, H., Endo, T., Yosioka, I., Higashiyama, K., Otomasu, H., 1978. The glycosides of *Martynia louisiana* Mill. A new phenylpropanoid glycoside, martynoside. Chemical and Pharmaceutical Bulletin 26, 2111–2121.

Schwab, W., Schreier, P., 1988. Aryl β-D-glucosides from *Carica papaya* fruit. Phytochemistry 27, 1813–1816.

Subramanian, S.S., Nair, A.G.R., 1972. Flavonoids of the leaves of *Pedalium murex*. Phytochemistry 27, 464–465.

PERGAMON

Phytochemistry 57 (2001) 1249–1253

PHYTOCHEMISTRY

www.elsevier.com/locate/phytochem

Flavonoid ketohexosefuranosides from the leaves of *Crataegus pinnatifida* Bge. var. *major* N.E.Br.

Pei-Cheng Zhang[a,*], Sui-Xu Xu[b]

[a]*Institute of Materia Medica, Chinese Academy of Medical Science and Peking Union Medical College, Beijing 100050, People's Republic of China*
[b]*Department of Phytochemistry, Shenyang Pharmaceutical University, Shenyang 110015, People's Republic of China*

Received 27 November 2000; received in revised form 27 February 2001

Abstract

Four flavonoid ketohexosefuranosides, pinnatifinoside A, pinnatifinoside B, pinnatifinoside C, and pinnatifinoside D were isolated from the leaves of *Crataegus pinnatifida* Bge. var. *major* N.E.Br. Their structures were elucidated by spectroscopic analysis (UV, IR, MS and 1D, 2D NMR) and chemical evidence. © 2001 Elsevier Science Ltd. All rights reserved.

Keywords: *Crataegus pinnatifida* Bge. var. *major* N.E.Br.; Rosaceae; Flavonoid ketohexosefuranosides; Pinnatifinoside A; Pinnatifinoside B; Pinnatifinoside C; Pinnatifinoside D

1. Introduction

Crataegus pinnatifida Bge. var. *major* N.E.Br. (Rosaceae) is widely distributed in the northeast part of China. It is used as a medicinal plant to improve digestion, remove retention of food, promote blood circulation and resolve blood stasis both in traditional and folk medicine (Ammon and Händel, 1981). At the same time, it shows numerous mild, but well documented, pharmacological activities and few side effects. Preparations of *C. pinnatifida* Bge. var. *major* (leaves or fruit) improve the heart function, and there are indications of declining cardiac performance, deficiency of the coronary blood supply and mild forms of arrhythmia (Pöpping et al., 1995; Al Makdessi et al., 1996). To date, more than 50 flavonoids have been isolated from *Crataegus* (Nikolov et al., 1982; Dauguet et al., 1993). Chemical investigation of the leaves of *C. pinnatifida* Bge. var. *major* N.E.Br. led to the isolation of four new compounds, which were named pinnatifinoside A (**1**), pinnatifinoside B (**2**), pinnatifinoside C (**3**), and pinnatifinoside D (**4**).

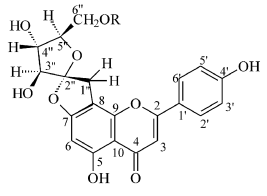

1 R=H
2 R=Acetyl

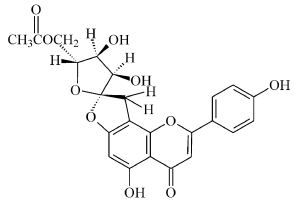

3

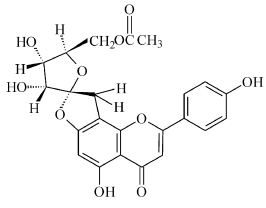

4

2. Results and discussion

Compound **1** was obtained as yellow needles, $[\alpha]_D^{25}$ +79 (MeOH, *c* 0.24) and showed a positive Mg-HCl color reaction. The HRESIMS of **1** indicated the $[M+H]^+$ at *m/z* 415.1099 corresponding to a molecular formula $C_{21}H_{18}O_9$ (calc. 414.1022). The absorption bands at ν_{max} 3370, 1650 and 1606, 1520 cm^{-1} in the IR

* Corresponding author.
E-mail address: pczhang@imm.ac.cn (P.-C. Zhang).

0031-9422/01/$ - see front matter © 2001 Elsevier Science Ltd. All rights reserved.
PII: S0031-9422(01)00170-4

Table 1
^{1}H NMR spectroscopic data for compounds **1**–**4** (DMSO-d_6)[a]

H	1	2	3	4
3	6.84 *s*	6.85 *s*	6.82 *s*	6.82
5-OH	13.20 *s*	13.22 *s*	13.19 *s*	13.20 *s*
6	6.36 *s*	6.36 *s*	6.30 *s*	6.33 *s*
2′,6′	7.95 *d* (8.8)	7.97 *d* (8.8)	7.94 *d* (8.6)	7.95 *d* (8.7)
3′,5′	6.94 *d* (8.8)	6.93 *d* (8.8)	6.92 *d* (8.6)	6.93 *d* (8.7)
4′-OH	10.40 *s*	10.40 *s*	10.38 *s*	10.44 *s*
1″	3.67 *d* (16.7)	3.70 *d* (16.7)	3.69 *d* (16.7)	3.49 *d* (16.7)
	3.13 *d* (16.7)	3.13 *d* (16.7)	3.18 *d* (16.7)	3.30 *d* (16.7)
3″	4.16 *t* (5.1)	4.17 *t* (5.1)	3.96 *t* (5.0)	4.06 (overlap)
3″-OH	5.94 *d* (5.1)	6.07 *d* (5.1)	5.83 *d* (5.0)	5.29 *d* (5.0)
4″	3.83 *m*	3.83 *m*	4.18 *m*	4.09 *m*
4″-OH	5.50 *d*	5.70 *d*	5.48 *d*	5.10 *d*
5″	3.88 *m*	4.05 *m*	4.12 *m*	4.06 (overlap)
6″	~3.45 *m*	4.28 *m*, 4.06 *m*	4.39 *m*, 3.96 *m*	4.19 *m*, 4.00 *m*
6″-OH	4.85 *t* (5.0)			
–CH_3		2.03 *s*	2.02 *s*	2.04 *s*

[a] *J* values are given in Hz.

spectrum were characteristic of hydroxyl, hydrogen bonded carbonyl and aromatic groups, respectively. The UV spectrum of **1** exhibited absorption maxima at 326 (Band I) and 271 nm (Band II; in MeOH), bathochromic shifts of 66, 41, 66 and 66 nm with NaOMe, NaOAc, $AlCl_3$ and $AlCl_3$ + HCl in Band I, respectively, as well as bathochromic shifts of 8 nm with $AlCl_3$ and $AlCl_3$ + HCl, and no shifts with NaOMe and NaOAc in Band II. These data ultimately revealed (see later) that **1** had two free hydroxyl groups at C-5 and 4′ and no free hydroxyl group at C-7 in the flavone skeleton.

Table 2
^{13}C NMR specroscopic data for compounds **1**–**4** (DMSO-d_6)

C	1	2	3	4
2	163.5	163.5	163.6	164.6
3	102.7	102.9	103.0	103.0
4	181.9	182.1	182.1	182.2
5	161.7	161.9	162.0	162.0
6	93.8	94.0	93.9	94.2
7	163.3	163.4	163.3	163.8
8	102.5	102.4	102.3	102.5
9	151.5	151.7	151.8	151.7
10	104.2	104.5	104.5	104.5
1′	120.9	121.0	121.1	121.3
2′	128.4	128.6	128.6	128.8
3′	115.9	116.0	116.1	116.2
4′	161.2	161.3	161.4	161.5
5′	115.9	116.0	116.1	116.2
6′	128.4	128.6	128.6	128.8
1″	31.4	31.6	31.4	33.5
2″	121.6	121.6	121.8	118.5
3″	80.7	80.7	74.4	74.7
4″	76.0	76.8	71.3	69.1
5″	83.9	80.5	81.2	84.3
6″	60.8	63.8	64.4	64.2
–CH_3		20.6	20.7	20.8
–C=O		170.3	170.3	170.5

In the ^{1}H NMR spectrum (Table 1), a downfield proton at δ 13.20 confirmed the presence of the 5-OH, two set of doublets at δ 7.95 (2H, *d*, J = 8.8 Hz) and 6.94 (2H, *d*, J = 8.8 Hz) that were assigned to H-2′,6′ and H-3′,5′, respectively, and two singlets at δ 6.84 and 6.36 that were due to the protons at C-3 and C-6 in rings A and C. These data indicated the aglycone moiety was analogous to apigenin except for the absence of one proton in ring A. In the ^{13}C NMR spectrum (Table 2), 15 carbon signals from the aglycone moiety were similar to those of vitexin (Lin et al., 1999), but the signals of C-6 and C-9 appeared at δ 93.8 and 151.5, shifted upfield by $\Delta\ \delta$ 4.0 ppm compared with those of vitexin. In addition, six carbon signals from a sugar moiety were evident. In the DEPT spectrum, carbon signals from the sugar moiety resonated at δ 121.6 (C), 83.9 (CH), 80.7 (CH), 76.0 (CH), 60.8 (CH_2) and 31.4 (CH_2). Furthermore, the carbon signal at δ 31.4 was directly attached

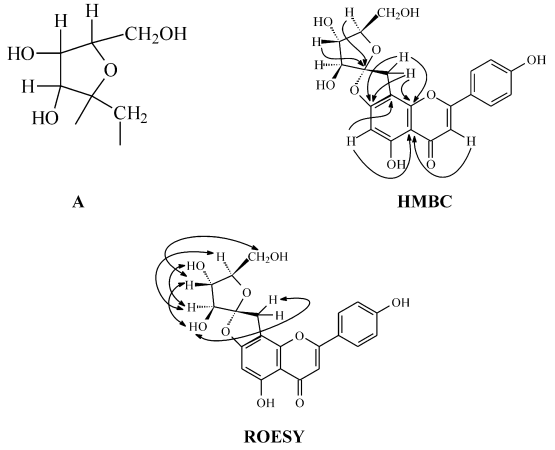

Fig. 1. Structure of fragment A and the key correlation of HMBC and ROESY for **1**.

to the protons at δ 3.67 (1H, *d*, $J=16.7$ Hz, H-1″*a*) and 3.13 (1H, *d*, $J=16.7$ Hz, H-1″*b*) in the HMQC spectrum. In the ^{1}H–^{1}H COSY spectrum, the proton at δ 3.83 (1H, *m*, H-4″) correlated with protons at δ 4.16 (1H, t, $J=5.1$ Hz, H-3″) and 3.88 (1H, *m*, H-5″), while the proton at δ 3.88 (1H, *m*, H-5″) correlated with protons at δ ~3.45 (2H, *m*, H-6″). Consequently, this is taken into consideration of the HMQC and HMBC spectral analyses (Fig. 1), the sugar was a ketohexose skeleton and confirmed the presence of fragment A (Fig. 1). The connectivity of the aglycone and sugar moiety was established on the basis of the following evidence. A downfield quaternary carbon (δ 121.6) of ketohexose C-2″ should be linked to the C-7 oxygen atom due to the absence of a free 7-OH in the UV and ^{1}H NMR spectra, and the signal of C-7 should display an upfield shift compared with the corresponding signals of apigenin (Ternai and Markham, 1976). The downfield chemical shift revealed that C-2″ was at the center of a dioxaspirocycle (Bheemasankara et al., 1988). The signal (δ 31.4) of ketohexose C-1″ was linked to C-8, instead of C-6, of the flavone skeleton, which was confirmed by the HMBC spectrum in which the carbon signals at δ 151.3 (C-9) and δ 163.3 (C-7) were correlated with the protons at δ 3.67 (H-1″*a*), 3.13 (H-1″*b*). The C-8 signal appeared at δ 102.5 (quaternary carbon) in the ^{13}C NMR spectrum. Furthermore, it was essential to clarify the type and relative configuration of the sugar moiety. The ROESY spectrum (Fig. 1) showed cross peaks between protons at δ 4.16 (1H, *t*, $J=5.1$ Hz, H-3) and 3.88 (1H, *m*, H-5), at δ 3.83 (1H, *m*, H-4) and ~3.45 (2H, *m*, H-6), and proton at δ 4.16 (1H, *t*, $J=5.1$ Hz, H-3) and hydroxyl proton at δ 5.50 (1H, *d*, $J=5.1$ Hz, 4-OH), and proton at δ 3.67 (1H, *d*, $J=16.7$ Hz, H-1a) and hydroxyl proton at δ 5.94 (1H, *d*, $J=5.1$ Hz, 3-OH). These data indicated a relative configuration of the sugar moiety as that of α-D-fructofuranose (Agrawal, 1992). Thus, the structure of pinnatifinoside A was elucidated as **1**. It is a new flavonoid.

Compound **2** was obtained as light yellow needles, $[\alpha]_D^{25}$ +58 (MeOH, *c* 0.12). It was identical with **1** in the Mg–HCl color reaction, UV and IR spectra except for the absorption band at 1710 cm^{-1}. The HRESIMS of **2** showed a $[M+H]^+$ at *m*/*z* 457.1167 corresponding to the molecular formula $C_{23}H_{20}O_{10}$ (calc. 456.1128). The ^{1}H and ^{13}C NMR spectra of **2** were analogous to those of **1** (Tables 1 and 2). A methyl singlet at δ 2.03 (*s*) in the ^{1}H NMR spectrum and two carbon signals at δ 20.6 and 170.3 in the ^{13}C NMR spectrum of **2** indicated the presence of an additional acetyl group. Absence of a free hydroxyl group at δ 4.85 of the sugar moiety in the ^{1}H NMR spectrum, a typical downfield shift of C-6″ at δ 63.8 ($\Delta\delta$ 3.0) and an upfield shift of C-5″ at δ 80.5 ($\Delta\delta$ 3.4) in the ^{13}C NMR spectrum, when compared with those of 1, showed acetylation of C-6″-OH. Furthermore, the related stereochemical assignments at the sugar moiety were inferred from 2D NMR spectroscopic studies (^{1}H–^{1}HCOSY, ROESY and HMQC). Alkaline hydrolysis of two with 0.1% KOH afforded **1**. Thus, the structure of pinnatifinoside B was established as **2**, a new compound.

Compound **3** was obtained as yellow needles, $[\alpha]_D^{25}$ −34 (MeOH, *c* 0.16). It was identical with **2** in the Mg–HCl color reaction, UV, ESIMS and IR spectra. The HRESIMS of **3** showed the $[M+H]^+$ at *m*/*z* 457.1178 corresponding to a molecular formula $C_{23}H_{20}O_{10}$ (calc. 456.1128). The ^{1}H and ^{13}C NMR spectra of **3** (Tables 1 and 2) were also analogous to those of **2** except for the signals of the sugar moiety. It was essential to clarify the type and configuration of the sugar moiety. In the DEPT spectrum, carbon signals from the sugar moiety were at δ 121.8 (C), 81.2 (CH), 74.4 (CH), 71.3 (CH), 64.4 (CH_2) and 31.4 (CH_2).

Furthermore, the carbon signal at δ 31.4 was directly attached to the protons at δ 3.69 (1H, *d*, $J=16.7$ Hz) and 3.18 (1H, *d*, $J=16.7$ Hz). Consequently, the sugar was also a ketohexose skeleton. In the ^{1}H–^{1}H COSY spectrum, the proton at δ 4.18 (1H, *t*, $J=5.0$ Hz, H-4″) correlated with the protons at δ 4.12 (1H, *m*, H-5″) and 3.96 (1H, *t*, $J=5.0$ Hz, H-3″), and the proton at δ 4.12 (1H, *m*, H-5″) correlated with the protons at δ 4.39 (1H, *m*, H-6″) and 3.96 (1H, *m*, H-6″). Combined with the HMQC and HMBC spectral data, the presence of fragment A (Fig. 1) was confirmed. Furthermore, cross peaks between protons at δ 3.96 (1H, H-3″) and 4.18 (1H, H-4″) in the NOESY spectrum suggested the relative configuration of sugar moiety as that of β-D-allulofuranose (Yu and Yang, 1999). The connectivity of aglycone and sugar moiety was established using the same method as **1**. Finally, the position of the acetyl group was deduced to be C-6″ in the sugar moiety by the long distance correlations of carbonyl signal at δ 170.3 and the protons at δ 4.39 and 3.96 (H-6″). Thus, the structure of pinnatifinoside C was elucidated as **3**.

Compound **4** was obtained as yellow needles, $[\alpha]_D^{25}$ +25 (MeOH, *c* 0.11). It was identical with **2** and **3** in the Mg–HCl color reaction, UV, ESIMS and IR spectra. The HRESIMS of **4** showed the $[M+H]^+$ at *m*/*z* 457.1170 corresponding to a molecular formula $C_{23}H_{20}O_{10}$ (calc. 456.1128). The ^{1}H and ^{13}C NMR spectra of **4** (Tables 1 and 2) were also analogous to those of **2** and **3** except for the signals of the sugar moiety. The signal of C-1″ and 2″ in the sugar moiety appeared at δ 33.0 and 118.5, which indicated that the configuration of **4** was different from that of **3**. The related stereochemical assignments suggested that the relative configuration of the sugar moiety was the same as that of α-D-allulofuranose (Yu and Yang, 1999). The position of the acetyl group was at C-6″ in the sugar moiety as evidenced by HMBC, HMQC, ^{1}H–^{1}H COSY and NOESY experiments. Thus, the structure of pinnatifinoside D was elucidated as **4**.

3. Experimental

Melting points were taken on an X4 micro-melting point apparatus and are uncorrected. UV spectra were determined with a Hitachi UV-2201 spectrophotometer and IR spectra with a Shimadzu (KBr) IR spectrophotometer. ^{1}H, ^{13}C and 2D NMR spectra were measured on a Brüker ARX at 300 MHz for ^{1}H and 75 MHz for ^{13}C with TMS as an internal standard and coupling constants (J) are given in Hz. Mass spectra were recorded on a Finnigan ESIMS spectrometer. Optical rotations were measured on a Perkin-Elmer 241 digital polarimeter in CH_3OH. HR-mass spectra were recorded on a VG-Autospec-3000 spectrometer.

3.1. Plant material

The leaves of *C. pinnatifida* Bge. var. *major* were collected from Liaoning Province of China, in June 1997. A voucher specimen (970706) was taxonomically identified by Professor Chunquan Xu and deposited in the Herbarium of Department of Traditional Chinese Medicines, Shenyang Pharmaceutical University.

3.2. Extraction and isolation

The leaves (20 kg) were first extracted three times with 80% aq. EtOH under reflux. The extracts were combined and concentrated under reduced pressure. The concentrated extract was suspended in water and was subjected to macroporous resin column chromatography, eluting with 55% EtOH. The solvent was evaporated under reduced pressure to obtain a mixture (120 g). This was applied to a silica gel column eluted with a $CHCl_3$–CH_3OH in gradient to afford Frs, 2, 3 and 4. Fr 2 [1 g, $CHCl_3$–CH_3OH (50:1)] was subjected to polyamide column chromatography with H_2O–EtOH (1:1) to yield **3** (15 mg) and **4** (10 mg). Fr 3 [3 g, $CHCl_3$–CH_3OH (20:1)] was subjected to polyamide column chromatography with H_2O–EtOH (1:1) to yield **2** (19mg). Fr 4 [$CHCl_3$–CH_3OH (10:1)] was applied to a silica gel column eluted with $CHCl_3$–CH_3OH (in gradient) as eluent, with combined fractions [$CHCl_3$–CH_3OH (15:1∼9:1)] being subjected to polyamide column chromatography with H_2O–EtOH (3:2) to yield **1** (24 mg).

3.3. Pinnatifinoside A (*1*)

Yellow needles; mp 185–187°C; $[\alpha]_D^{25}$ +79 (MeOH, *c* 0.24); UV λ_{max} (MeOH) nm: 326, 271; (+MeONa) 392, 271; (+NaOAc) 367, 271; (+$AlCl_3$) 392, 279; (+$AlCl_3$+HCl) 392, 279. IR ν_{max} (KBr) cm^{-1}: 3370, 1650, 1606 and 1520; ESIMS *m/z*: 415 $[M+H]^+$, 397 [415–18], 367 [397–30] and 283 [367–84]; ^{1}H and ^{13}C NMR data Tables 1 and 2.

3.4. Pinnatifinoside B (*2*)

Light yellow needles; mp 240–242°C; $[\alpha]_D^{25}$ +58 (MeOH, *c* 0.12); UV λ_{max} (MeOH) nm: 322, 271; (+MeONa) 393, 271; (+$AlCl_3$) 389, 278; (+$AlCl_3$+HCl) 393, 279; IR ν_{max} (KBr) cm^{-1}: 3370, 1710, 1650, 1606 and 1520; ESIMS *m/z*: 457 $[M+H]^+$, 439 [457–18], 379 [439–60], 351 [379–28], 323 [351–28] and 295 [323–28]; HRESIMS $[M+H]^+$: found 457.1167. Calc. for $C_{23}H_{20}O_{10}$: 456.1128 ^{1}H and ^{13}C NMR data see Tables 1 and 2.

Alkaline hydrolysis of **2**. Compound **2** was heated with 0.1% KOH for 0.5 h at 60°C. The hydrolysate was neutralized with 0.1 N HCl and extracted by EtOAc. The EtOAc extract was evaporated, and the residue was subjected to polyamide TLC using $CHCl_3$: MeOH: MeCOEt (4:1:0.5) and EtOH–H_2O (1:1) as solvent, respectively. The product of hydrolysis was identical with pinnatifinoside A (1) by their R_f values.

3.5. Pinnatifinoside C (*3*)

Light yellow needles; mp 246–248°C; $[\alpha]_D^{25}$ −34 (MeOH, *c* 0.16); UV λ_{max} (MeOH) nm: 324, 270; (+MeONa) 391, 270; (+$AlCl_3$) 390, 278; (+$AlCl_3$+HCl) 390, 279; IR ν_{max} (KBr) cm^{-1}: 3370, 1710, 1650, 1606 and 1520; ESIMS *m/z*: 457 $[M+H]^+$, 439 [457–18], 379 [439–60], 351 [379–28], 323 [351–28] and 295 [323–28]; HRESIMS $[M+H]^+$: found 457.1178. Calc. for $C_{23}H_{20}O_{10}$: 456.1128. ^{1}H and ^{13}C NMR data (Tables 1 and 2).

3.6. Pinnatifinoside D (*4*)

Light yellow needles; mp 248–250°C; $[\alpha]_D^{25}$ +25 (MeOH, *c* 0.11); UV λ_{max} (MeOH) nm: 324, 271; (+MeONa) 391, 270; (+$AlCl_3$) 390, 278; (+$AlCl_3$+HCl) 390, 279; ESIMS *m/z*: 457 $[M+H]^+$, 439 [457–18], 379 [439–60], 351 [379–28], 323 [351–28] and 295 [323–28]; HRESIMS $[M+H]^+$: found 457.1170. Calc. for $C_{23}H_{20}O_{10}$: 456.1128. ^{1}H and ^{13}C NMR data (Tables 1 and 2).

Acknowledgements

The authors wish to thank Wen Li and Yi Sha of Shenyang Pharmaceutical University for running NMR spectra.

References

Agrawal, P.K., 1992. NMR spectroscopy in the structural elucidation of oligosaccharides and glycosides. Phytochemistry 31, 3307–3330.

Al Makdessi, S., Sweidan, H., Müllner, S., Jocob, R., 1996. Myo-

cardial protection by pre-treatment with *Crataegus oxyacantha*. Arzneimittelforschung 46, 25–27.

Ammon, H., Händel, M., 1981. *Crataegus*, Toxikologie und Pharmakologie Teil II: Pharmkodynamik. Planta Medica 43, 209–239.

Bheemasankara Rao, C.H., Ramana, K.V., Venkata Rao, D., Eoin Fahy, Faulkner, J.D., 1988. Metabolites of the gorgonian *Isis hippuris* from India. Journal of Natural Products 51, 954–958.

Dauguet, J.C., Bert, M., Dolley, J., Bekaert, A., Lewin, G., 1993. 8-Methoxy-kaempferol 3-neohesperidoside and other flavonoids from bee pollen of *Crataegus monogyna*. Phytochemistry 33, 1503–1505.

Lin, L., Xie, N., Cheng, Z.H., 1999. Flavonoids from *Cajanus cajan* L. Journal China Pharmaceutical University 30, 21–23.

Nikolov, N., Seligmann, O., Wagner, H., Horowitz, R., Gentili, B., 1982. Neue Flavonoid-Glykoside und *Crataegus monogyna* and *Crataegus pentagyna*. Planta Medica 44, 50–53.

Pöpping, S., Rose, H., Ioneseu, I., Fisher, Y., Kammermeier, H., 1995. Effect of a hawthorn extract on contraction and energy turnover of isolated rat cardiomyocytes. Arzneimittelforschung, 45 Suppl (2) 11, 1157–1161.

Ternai, B., Markham, K.R., 1976. Carbon-13NMR studies of flavonoids — I flavones and flavonols. Tetrahedron 32, 565–569.

Yu, D.Q., Yang, J.S., 1999. Analysis of Nuclear Magnetic Resonance Spectra, 2nd, Enlarged Edition Handbook of Analytical Chemistry, No 7. Chemical Industrial Press: Beijing, PR China. p. 904.

PERGAMON

Phytochemistry 57 (2001) 1255–1258

PHYTOCHEMISTRY

www.elsevier.com/locate/phytochem

Chemical constituents from *Dendrobium densiflorum*

Chengqi Fan, Wei Wang, Yiping Wang, Guowei Qin, Weimin Zhao*

Department of Phytochemistry, Shanghai Institute of Materia Medica, Shanghai Institute of Biological Sciences, Chinese Academy of Sciences, 294 Taiyuan Road, Shanghai 200031, People's Republic of China

Received 27 October 2000; received in revised form 15 February 2001

Abstract

5-[2′-(3″-Hydroxy-5″-methoxyphenyl)-ethyl]-1,3-benzodioxole and 7-hydroxy-2-methoxy-1,4-phenanthrenedione, along with 16 known compounds were identified from the stems of *Dendrobium densifiorum* Lindl. ex Wall. (Orchidaceae). The structure of a previously reported compound dendroflorin obtained from the plant was revised on the basis of spectroscopic analysis. Among the identified compounds, five were found to exhibit anti-platelet aggregation activity in vitro. © 2001 Elsevier Science Ltd. All rights reserved.

Keywords: Orchidaceae; *Dendrobium densiflorum*; Densiflorol A and B; Anti-platelet aggregation activity

1. Introduction

The stems of several *Dendrobium* species (Orchidaceae) are used in traditional Chinese medicine as a Yin tonic to nourish the stomach, promote the production of body fluid and reduce fever (Jiangsu New Medical College, 1986). Several chemical components of this species have been identified before (Jan et al., 1975; Talapatra et al., 1984). We herein report the structural elucidation of a new bibenzyl named densiflorol A (**1**) and a new phenanthrenedione named densiflorol B (**2**) and the structural revision of dendroflorin (**3**), a previously reported compound obtained from *D. densiflorum* Lindl. ex Wall. (Talapatra et al., 1984). Besides the above three compounds, 15 other known compounds (**4**–**16**, oleanolic acid and β-sitosterol) were also identified from the plant. Compounds **6**, **7**, **10**, **14** and **15** were found to exhibit anti-platelet aggregation activity in preliminary pharmacological tests.

2. Results and discussion

The stems of *D. densiflorum* Lindl. ex Wall. were powdered and extracted with CH_2Cl_2, and the filtrate was evaporated to dryness to give CH_2Cl_2 extract. The CH_2Cl_2 extract was subjected to a series of column chromatographic steps on silica gel and filtration through Sephadex LH-20 to yield 18 compounds.

Compound **1** was obtained as a white amorphous powder. HREIMS of **1** exhibited a molecular ion peak at m/z 272.1031 [M^+] (calculated for $C_{16}H_{16}O_4$, 272.1048). In the ^{13}C NMR spectrum of **1**, 16 carbon signals were observed as one methyl, three methylenes, six methines and six quaternary carbons. A bibenzyl skeleton with one methoxy, one hydroxyl and one methylenedioxy group were deduced to the structure of **1** according to ^{13}C NMR spectroscopic data. Proton coupling of **1** revealed a 1,3,4-substituted benzene ring [δ 6.60 (1H, *d,* 1.5), 6.55 (1H, *dd,* 1.5, 7.9), 6.65 (1H, *d,* 7.9)] and a 1,3,5-substituted benzene ring [δ 6.15 (2H, *d,* 1.6) and 6.25 (1H, *d,* 1.6)]. On the basis of above evidence and results of HMQC and HMBC spectra, the structure of **1** was established to be 5-[2′-(3″-hydroxy-5″-methoxyphenyl)-ethyl]-1,3-benzodioxole as shown in Figs. 1 and 2. Compound **1** is a new compound named densiflorol A.

Compound **2** was obtained as a red amorphous powder. HREIMS of 2 exhibited a molecular ion peak at m/z 254.0584 [M^+] (calculated for $C_{15}H_{10}O_4$, 254.0579). In the ^{13}C NMR spectrum of **2**, 15 carbon signals were observed including one methyl, six methines and eight quaternary carbons. Among the eight quaternary carbons, two should be carbonyl carbons according to their chemical shifts at δ 180.2 (*s*) and 188.4 (*s*). One hydroxyl and one methoxy group exist in the structure of **2** according to proton signals at 10.45 (1H, *s*) and δ 3.90

* Corresponding author. Tel.: +86-21-64311833; fax: +86-21-64370269.

E-mail address: wmzhao@mail.shcnc.ac.cn (W. Zhao).

0031-9422/01/$ - see front matter © 2001 Elsevier Science Ltd. All rights reserved.
PII: S0031-9422(01)00168-6

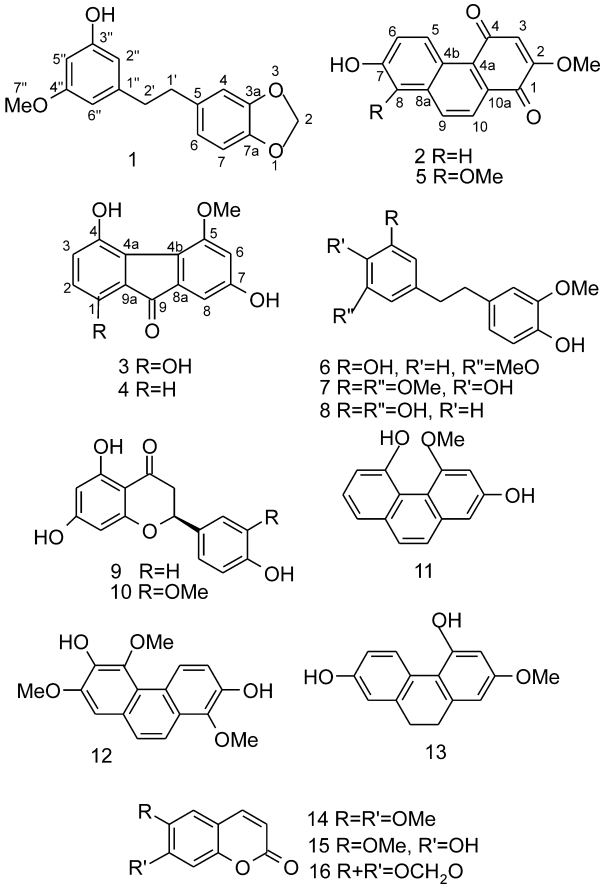

Fig. 1. Structures of compounds **1**–**16**.

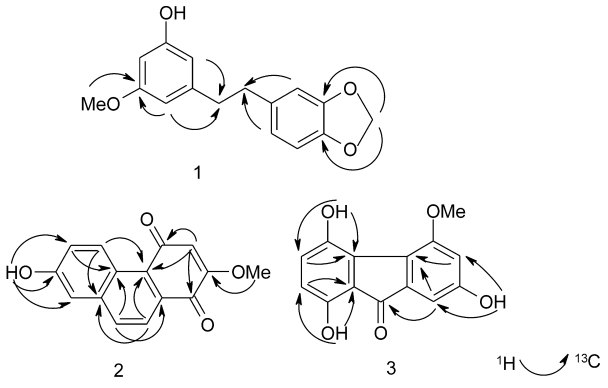

Fig. 2. Main ^{13}C–^{1}H long range correlation signals in HMBC spectra of **1** ($CDCl_3$), **2** and **3** (DMSO-d_6).

(3H, *s*) and downfield carbon signals at δ 158.3 and δ 157.5. Compound **2** was suspected to be an anthrenedione or phenanthrenedione from above NMR spectra data. In ^{1}H NMR spectrum of **2**, three aromatic proton signals at δ 7.25 (*d,* 2.2), 7.30 (*dd*, 2.2, 9.5) and 9.35 (*d,* 9.5) were observed, which enabled the deduction of an aromatic ring with 1,3,4-substitution pattern. Another aromatic ring was suggested to be of 1,2,3,4-substitution pattern according to two coupled protons at δ 7.95 (*d,* 8.6) and 8.10 (*d,* 8.6). NOE correlations were found between proton signals at δ 7.25 and 8.10, between the methoxy proton signal and the proton signal at δ 6.30 (*s*) in a NOESY spectrum. The skeleton of **2** was thus revealed to be phenanthrenedione. According to ^{1}H–^{13}C long range correlation signals in HMBC spectrum of **2**, especially to those between C-4a and H-5 (δ9.35), and between C-4a and H-3 (δ 6.30), the structure was finally established to be 7-hydroxy-2-methoxy-1, 4-phenanthrenedione as shown in Figs. 1 and 2. Compound **2** is a new compound named densiflorol B.

Compound **3** was obtained as a red amorphous powder. HREIMS of **3** exhibited a molecular ion signal at *m*/*z* 258.0515 [M^+] (calculated for $C_{14}H_{10}O_5$, 258.0528). In the ^{13}C NMR spectrum of **3**, 14 carbon signals were observed as one methyl, four methines and nine quaternary carbons, one of which should be a carbonyl carbon (δ 194.6). Three hydroxyl groups and one methoxy group should exist in the structure of **3** according to proton signals at δ 8.70 (1H, *s*), 9.85 (1H, *s*), 10.25 (1H, *s*) and 4.05 (3H, *s*), and methyl carbon at δ 57.0. Aromatic proton signals at δ 6.60 (1H, *d,* 8.9), 6.85 (1H, *d,* 8.9) and 6.65 (1H *d,* 2.0), 6.70 (1H, *d,* 2.0) in ^{1}H NMR spectrum of **3** indicated the existence of two *ortho*-coupled protons and two *meta*-coupled protons. The ^{1}H NMR (acetone-d_6) and MS data of **3** were in accordance to those of a known compound named dendroflorin (1,2,5-trihydroxy-7-methoxy-9*H*-fluoren-9-one) isolated from the same species before (Talapatra et al., 1984; Talapatra et al., 1985). The positions of hydroxy and methoxy groups in the structure of dendroflorin were established by comparing the chemical shifts between dendroflorin and its peracetate. In order to confirm the structure of dendroflorin, NMR spectra of **3** were measured again in DMSO-d_6. In ^{1}H NMR of **3** in DMSO-d_6, three hydroxy proton signals could be clearly observed. A NOESY spectrum of **3** showed correlations not only between the methoxy protons at δ 4.05 (3H, *s*) and proton at δ 6.70 (1H, *d,* 2.0), but also between the methoxy protons and the hydroxy proton at δ 8.70. In addition, NOE correlation signals between the hydroxy proton signal at δ 10.25 and the proton signal at δ 6.65, between the hydroxy proton at δ 8.70 and the proton at δ 6.85, and between the hydroxy proton at δ 9.85 and the proton at δ 6.60, were also observed. On the basis of above evidence and further analysis of its HMBC spectrum, the structure of **3** was established to be 1,4,7-trihydroxy-5-methoxy-9*H*-fluoren-9-one (Figs. 1 and 2). The structure of dendroflorin reported before should thus be revised.

From the CH_2Cl_2 extract of *D. densiflorum,* 11 other known compounds, including cypripedin (**5**; Schmalle and Hausen, 1979), gigantol (**6**; Leslie and Jamieson, 1982), moscatilin (**7**; Majumder and Sen, 1987a), tristin (**8**; Majumder and Pal, 1993), naringenin (**9**; Albach and Redman, 1969), homoeriodictyol (**10**; Liu et al., 1992), moscatin (**11**; Majumder and Sen, 1987b), 2,6-dihydroxy-

1,5,7-trimethoxyphenanthrene (**12**; Tuchinda et al., 1988; Majumder and Sen, 1991), 4,7-dihydroxy-2-methoxy-9, 10-dihydro-phenanthrene (**13**; Shuozo et al., 1983), scopoletin (**15**; Sankar et al., 1982) and ayapin (**16**; Zhu et al., 1992) were identified for the first time from this species. Four other previously reported compounds from this plant, including dengibsin (**4**; Schmalle and Hausen, 1979), scoparone (**14**; Sankar et al., 1982), oleanolic acid and β-sitosterol were also obtained. The structures of all above compounds were identified by spectral analysis and by comparison of spectral data with those reported.

During our investigation of components with anti-platelet aggregation activity from *D. densiflorum,* compounds **6**, **7**, **10**, **14** and **15** were found to exhibit anti-platelet aggregation activity on SD rat platelet aggregation in preliminary pharmacological tests in vitro (Table 1). Among them, scoparone **(14)** has been reported to possess potent anti-platelet aggregation activity before and was used as positive control.

3. Experimental

3.1. Materials and methods

3.1.1. General

IR spectra were obtained using a KBr discs on Perkin-Elmer 599B spectrometer. UV spectra were measured with a Shimadzu UV-3000 spectrometer, whereas NMR spectra were recorded on Bruker AM-400 spectrometer. Chemical shifts were reported in δ (ppm) with residual C_5H_5N signals (7.24/123.5), DMSO signals (2.50/39.5), acetone signals (2.07/30.5) and $CHCl_3$ signals (7.25/77.0) as internal standards. MS spectra were recorded on Finnigan 90 or MAT 95 instruments.

3.1.2. Plant material

Fresh stems of *D. densiflorum* (Orchidaceae) were collected and identified by Professor Ming Zhang from Chongqing Academy of Chinese Materia Medica in April 1999. A voucher specimen (SIMM990418) is deposited in the Herbarium of Shanghai Institute of Materia Medica, Chinese Academy of Sciences.

Table 1
Inhibitory effect of compounds on rat platelet aggregation

Compound	*N*	50 μM		100 μM	
		X±S.D.	Inhibition (%)	X±S.D.	Inhibition (%)
Control	7	42±5	–	42±5	–
6	4	46±8	−10	29±10*	31
7	4	30±4**	29	27±8**	36
10	3	35±1*	17	21±8**	50
14	3	29±19	31	15±11**	64
15	4	40±8	5	33±5*	21

*$P<0.05$.
**$P<0.01$ vs. control.

3.1.3. Extraction and isolation

Fresh stems of *D. densiflorum* (Orchidaceae; 7.5 kg) were powdered and then extracted with CH_2Cl_2 (3×2 l) at reflux and the filtrate was evaporated to dryness to give the extract (18 g). The extract was subjected to column chromatography (CC) on silica gel with petroleum ether-acetone gradient (5:1→4:1→2:1→acetone) to give fractions I–IV. Fractions I–III were further subjected to repeated CC on silica gel eluted with petroleum ether–$CHCl_3$ gradients (1:3→0:1) and on a Sephadex LH-20 column eluted with EtOH. Eighteen compounds were finally obtained. Compounds **1** (12 mg), **11** (14 mg), **12** (23 mg), **14** (156 mg), **16** (117 mg) and β-sitosterol (53 mg) were obtained from fraction I. Compounds **2** (14 mg), **3** (97 mg), **4** (18 mg), **5** (27 mg), **6** (21 mg), 7 (44 mg), **10** (52 mg) and **15** (65 mg) were obtained from fraction II. Compounds **8** (5 mg), **9** (12 mg), **13** (7 mg) and oleanolic acid (15 mg) were obtained from fraction III.

3.1.4. Platelet preparations and aggregations

Blood was removed from venacava inferior of male Sprague–Dawley rats (250–300 g) and mixed with sodium citrate anticoagulant (9:1, v/v). PRP (platelet rich plasma) was obtained by centrifuging blood for 5 min at 200 *g*. For aggregation in PRP, the platelet count was adjusted to 4×10^8 platelets/ml with PPP (platelet poor plasma). Before the addition of ADP at final concentration of 4 μM, platelets were preincubated with the test compounds for 3 min at 37°C. In order to eliminate the effect of the solvent on the aggregation, the final concentration of DMSO was fixed at 5% and vehicle control was used. Platelet aggregations were recorded using Born's method with a MPG-3D aggregometer (Shanghai, China) and percentages of aggregation are presented as means±S.D. (Durand et al., 1996).

3.1.5. Densiflorol A (*1*)

White amorphous powder. EIMS *m/z:* 272 [M^+]; HREIMS *m/z:* 272.1031 [M^+] (calculated for $C_{16}H_{,16}O_4$, 272.1048); IR ν^{KBr} cm^{-1}: 3307 (OH), 1592, 1500 (arom.), 1244 (−OCH_2O−); UV λ_{max}^{MeOH} nm: 281.5; ^{1}H NMR data (400 MHz, $CDCI_3$): δ 6.65 (1H, *d, J*=7.9 Hz, H-7), 6.60 (1H, *d, J*=1.5 Hz, H-4), 6.55 (1H, *dd, J*=1.5 and 7.9 Hz, H-6), 6.25 (1H, *d, J*=1.6 Hz, H-6″), 6.15 (1H, *d, J*=1.6 Hz, H-2″), 6.15 (1H, *d, J*=1.6 Hz, H-4″), 5.85 (2H, *s,* H-2), 3.70 (3H, *s,* H-7″), 2.70 (4H, *m,* H-1′, 2′); ^{13}C NMR data (100 MHz, $CDCl_3$): δ 160.9 (*s,* C-5″), 156.7 (*s,* C-3″), 147.6 (*s,* C-3a), 145.7 (*s,* C-7a), 144.5 (*s,* C-1″), 135.6 (*s,* C-5), 121.3 (*d,* C-6), 109.0 (*d,* C-4), 108.2 (*d,* C-7), 108.1 (*d,* C-2″), 106.8 (*d,* C-6″), 100.8 (*t,* C-2), 99.2 (*d,* C-4″), 55.3 (*q*, C-7″), 38.3 (*t,* C-2′), 37.3 (*t*, C-1′).

*3.1.6. Densiflorol B (**2**)*

Red amorphous powder. EIMS *m/z:* 254 [M^+], 225, 197, 155; HREIMS *m/z:* 254.0584 [M^+] (calculated for $C_{15}H_{10}O_4$, 254.0579); IR ν^{KBr} cm^{-1}: 3384 (OH), 1670, 1643 (C=O), 1621, 1595 (arom.); UV λ_{max}^{MeOH} nm: 390.0, 302.5, 230.5; ^1H NMR data (400 MHz, DMSO-d_6): δ 10.45 (*s,* 7-OH), 9.35 (1H, *d,* $J=9.5$ Hz, H-5), 8.10 (1H, *d,* $J=8.6$ Hz, H-9), 7.95 (1H, *d,* $J=8.6$ Hz, H-10), 7.35 (1H, *dd,* $J=2.2$ and 9.5 Hz, H-6), 7.25 (1H, *d,* $J=2.2$ Hz, H-8), 6.30 (1H, *s,* H-3), 3.90 (3H, *s,* 2-OMe); ^{13}C NMR data (100 MHz, DMSO-d_6): δ 188.4 (*s*, C-4), 180.2 (*s*, C-1), 158.3 (*s,* C-2), 157.5 (*s,* C-7), 138.9 (*s,* C-8a), 132.3 (*d,* C-9), 129.7 (*d,* C-10), 128.3 (*s,* C-10a), 126.8 (*s,* C-4a), 123.3 (*s,* C-4b), 122.4 (*d,* C-6), 121.8 (*d*, C-5), 111.1 (*d*, C-3), 109.7 (*d*, C-8), 56.4 (*q*, 2-OMe).

*3.1.7. Dendroflorin (**3**)*

Red amorphous powder. EIMS *m/z:* 258 [M^+], 243, 215, 187, 137, 129; HREIMS *m/z:* 258.0515 [M^+] (calculated for $C_{14}H_{10}O_5$, 258.0528); IR ν^{KBr} cm^{-1}: 3345 (OH), 1681 (C=O), 1614, 1492 (arom.); UV λ_{max}^{MeOH} nm: 381.5, 258.0; ^1H NMR data (400 MHz, acetone-d_6): δ 6.88 (1H, *d,* $J=9.0$ Hz, H-3), 6.80 (1H, *d,* $J=1.7$Hz, H-8), 6.73 (1H, *d,* $J=1.7$ Hz, H-6), 6.60 (1H, *d,* $J=9.0$ Hz, H-2), 4.10 (311, *s,* 5-OMe); ^1H NMR data (400 MHz, DMSO-d_6): δ 10.25 (*s,* 7-OH), 9.85 (*s,* 1-OH), 8.70 (*s,* 4-OH), 6.85 (1H, *d,* $J=8.9$ Hz, H-3), 6.70 (1H, *d,* $J=2.0$ Hz, H-6), 6.65 (1H, *d,* $J=2.0$ Hz, H-8), 6.60 (1H *d,* $J=8.9$ Hz, H-2), 4.05 (3H, *s,* 5-OMe); ^{13}C NMR data (100 MHz, DMSO-d_6): δ 190.7 (*s,* C-9), 159.8 (*s,* C-7), 152.5 (*s,* C-5), 150.9 (*s,* C-1), 142.8 (*s,* C-4), 136.4 (*s,* C-8a), 127.2 (*d,* C-3), 124.8 (*s,* C-4a), 119.6 (*s,* C-4b), 119.4 (*d,* C-2), 116.9 (*s,* C-9a), 104.8 (*d,* C-6), 104.3 (*d*, C-8), 57.0 (*q*, 5-OMe).

Acknowledgements

The authors wish to thank Shanghai Institute of Biological Sciences, Chinese Academy of Sciences for partial financial support of the research work.

References

Albach, R.F., Redman, G.H., 1969. Composition and inheritance of flavones in citrus fruits. Phytochemistry 8, 127–143.

Durand, P., Bloy, C., Peltier-Pujol, F., Blache, D., 1996. In-vitro and ex-vivo inhibition of blood platelet aggregation by naftazone. Journal of Pharmacy and Pharmacology 48, 566–572.

Jan, D., Kurt, L., Jan, R., 1975. New glycoside, 2-(β-D-glucopyranosyloxy)-4,5-dihydroxy-*trans*-cinnamic acid (densifioroside), from *Dendrobium densiflorum*. Acta Chemica Scandinavica B29, 627–628.

Jiangsu New Medical College, 1986. Dictionary of Chinese Medicines. Shanghai Scientific and Technologic Press, Shanghai, pp. 586.

Leslie, C., Jamieson, S.V., 1982. Dihydrostilbenes of *Cannabis*. Sythesis of canniprene. Journal of Chemical Society, Perkin Trans. 1, 1467–1475.

Liu, Y.L., Ho, K.D., Cassady, J.M., 1992. Isolation of potential cancer chemopreventive agents from *Eriodictyon californicum*. Journal of Natural Product 55, 357–363.

Majumder, P.L., Pal, S., 1993. Cumulatin and tristin, two bibenzyl derivatives from the orchids *Dendrobium cumulatum* and *Bulbophyllum triste*. Phytochemistry 32, 1561–1565.

Majumder, P.L., Sen, R.C., 1987a. Moscatilin, a bibenzyl derivative from the orchid *Dendrobium moscatum*. Phytochemistry 26, 2121–2124.

Majumder, P.L., Sen, R.C., 1987b. Structure of moscatin — a new phenanthrene derivative from the orchid *Dendrobium moscatum*. Indian Journal of Chemistry 26B, 18–20.

Majumder, P.L., Sen, R.C., 1991. Pendulin, a polyoxygenated phenanthrene derivative from the orchid *Cymbidium pendulum*. Phytochemistry 30, 2432–2434.

Sankar, S.S., Gilbert, R.D., Fornes, R.E., 1982. ^{13}C NMR studies of some hydroxycoumarins and related compounds. Organic Magnetic Resonance 19, 222–224.

Schmalle, H., Hausen, B.M., 1979. A new sensitizing quinone from lady slipper (*Cypripedium calceolus*). Naturwissenschaften 66, 527–528.

Shuozo, T., Masae, Y, Keiko, I., 1983. Antimicrobial agents from *Bletilla striata*. Phytochemistry 22, 1011–1015.

Talapatra, S.K., Rose, S., Mallik, A.K., 1984. Dendroflorin, a new fluorenone derivative from *Dendrobium densiflorum*. Journal of Indian Chemistry Society 61, 1010–1012.

Talapatra, S.K., Rose, S., Mallik, A.K., Talapatra, B., 1985. Dengibsin and dengibsinin, the first natural fluorenone derivatives from *Dendrobium gibsonii*. Tetrahedron 41, 2765–2769.

Tuchinda, P., Udchachon, J., Khumtaveeporn, K., Taylor, W.C., Engelhardt, L.M., White, A.H., 1988. Phenanthrenes of *Eulophia nuda*. Phytochemistry 27, 3267–3271.

Zhu, R.Z., Jia, X.Q., Gao, J.S., 1992. Chemical study on *Mai-Luo-Ning* injection. Chinese Traditional Patent Medicine 14, 35.

PERGAMON

Phytochemistry 57 (2001) 1259–1262

PHYTOCHEMISTRY

www.elsevier.com/locate/phytochem

Acylated flavonoid glycosides from *Bassia muricata*

Mohamed S. Kamel[a,*], Khaled M. Mohamed[a], Hashim A. Hassanean[a], Kazuhiro Ohtani[b], Ryoji Kasai[b], Kazuo Yamasaki[b]

[a]*Department of Pharmacognosy, Faculty of Pharmacy, Assiut University, Assiut 71526, Egypt*
[b]*Institute of Pharmaceutical Sciences, Hiroshima University Faculty of Medicine, 1-2-3 Kasumi, Minami-Ku, Hiroshima 734, Japan*

Received 20 October 2000; received in revised form 3 May 2001

Abstract

From the arial parts of *Bassia muricata*, two acylated flavonoid glycosides quercetin-3-*O*-(6″-caffeoyl)-sophoroside and quercetin-3-*O*-(6″-feruloyl)-sophoroside have been isolated together with two known flavonoid glycosides quercetin-3-*O*-sophoroside and quercetin-3,7-*O*-β-diglucopyranoside, as well as four known triterpenoidal saponins, oleanolic acid-3-*O*-β-glucopyranoside, chikusetsusaponin IVa, chikusetsusaponin IVa methyl ester and oleanolic acid-3,28-β-diglucopyranoside. The structures of the isolated compounds were verified by means of MS and NMR spectral analyses. © 2001 Elsevier Science Ltd. All rights reserved.

Keywords: *Bassia muricata*; Chenopodiaceae; Acylated flavonoid glycosides

1. Introduction

Bassia muricata (L.) Murr. (Chenopodiaceae) is a common sandy herb growing in Egyptian deserts (Tackholm, 1974). The plant is used in folk medicine to treat renal and rheumatic diseases (Al-Yahya et al., 1990). The chloroform and ethanolic extracts of the plant produced pilo-erection, significant hypotension, a remarkable decrease in WBCs counts, and a significant increase in prothrombin time besides their significant contractions of isolated guinea pig ileum. Meanwhile, the ether and benzene extracts showed antimicrobial activities (Al-Yahya et al., 1990). Reviewing current literature showed that only a few species of *Bassia* have been investigated and were found to contain triterpenoidal saponins identified as bassic acid glycosides (Rizk, 1986). This work describes the isolation and structural elucidation of two new acylated flavonoid glycosides (**1**) and (**2**) together with two known flavonoid glycosides and four known triterpenoidal saponins.

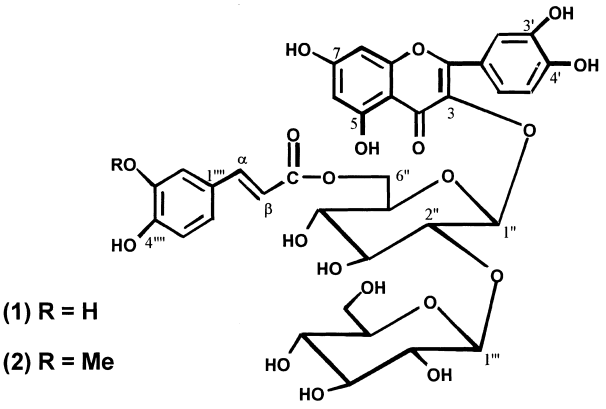

2. Results and discussion

The ethanolic extract of the aerial parts of *B. muricata* was defatted with diethylether and the aqueous layer was subjected to column chromatography on Diaion HP-20. The 50% methanol eluate was repeatedly chromatographed on columns of silica gel and then by MPLC and HPLC to afford eight glycosides.

The molecular formula of compound **1** was deduced as $C_{36}H_{36}O_{20}$ from HR FAB-MS spectrometry (see Experimental). Inspection of the ^{13}C NMR and DEPT spectra of **1** (Table 1) displayed the presence of two β-

* Corresponding author. Tel.: +20-088-333196; fax: +20-088-332776.
E-mail address: mkamel@mailcity.com (M.S. Kamel).

0031-9422/01/$ - see front matter © 2001 Elsevier Science Ltd. All rights reserved.
PII: S0031-9422(01)00240-0

glucopyranosyl units from the anomeric signals at δ 101.5 and 105.6 as well as the other signals characteristic for glucopyranosyl units as shown in Table 1 (Bradbury and Jenkins, 1984). Besides, the spectra showed 15 carbon signals for 3-*O*-glycosylated quercetin (Harborne and Mabry, 1982) and 9 carbon signals for a caffeoyl moiety (Bloor et al., 1998). From ^{1}H NMR spectral data of **1** (Experimental), the doublet at δ 5.11 (J = 7.6 Hz) of the anomeric proton of one of the two glucopyranosyl units indicated its β configuration. The anomeric proton of the second glucosyl unit was obscured by the H_2O signal. However, the β configuration of the glucosyl residues were very obvious from the downfield shifts of their anomeric carbons when compared with those reported for α-anomers in the ^{13}C NMR spectral analysis (Bradbury and Jenkins, 1984). Moreover the coupling constant (15.6 Hz) of the two doublets at δ 5.59 and 7.30 (each 1H) indicated the *trans* configuration of the caffeoyl moiety (Fiasson et al., 1997). In the ^{13}C NMR spectrum of **1**, the downfield shift of C-2″ (δ 82.2) together with the upfield shift of C-1″ (δ 101.5) proved the attachment of the terminal glucosyl unit to this position (Bradbury and Jenkins, 1984). Furthermore, the signal at δ 64.6 was assigned to the C-6 of one of the two glucosyl units to which the caffeoyl moiety is attached (Miyase et al., 1992). To determine the attachment site of the caffeoyl moiety, compound **1** was acetylated and subjected to EI–MS spectral analysis according to the procedure established by Komori et al. (1975) which revealed a characteristic peak at m/z 331 (18%) corresponding to tetraacetylated glucose as a cationic fragment with a molecular formula $(C_{14}H_{19}O_9)^+$ as shown in Fig. 1. This significant peak proved the presence of an unsubstituted terminal glucosyl unit (Komori et al, 1975). Consequently, the attachment site of the caffeoyl moiety must be at C-6 of the internal β-glucosyl unit (C-6) and the structure of compound **1** was assigned as shown.

Table 1
^{13}C NMR spectral data of compounds **1** and **2** (100 MHz, CD_3OD)

C	1	2	C	1	2
2	158.1	158.1	*Terminal*	*sugar*	
3	135.1	135.2	**1‴**	105.6	105.6
4	179.9	179.9	**2‴**	74.7	74.7
5	162.8	162.8	**3‴**	76.7	76.7
6	99.8	99.8	**4‴**	71.7	71.8
7	165.6	165.5	**5‴**	77.7	77.7
8	94.7	94.7	**6‴**	61.7	61.7
9	158.1	158.1			
10	105.9	106.0		*Caffeoyl*	*Feruloyl*
1′	122.7	122.7	α	114.5	114.8
2′	116.3	116.3	β	146.4	146.7
3′	145.8	145.9	**1⁗**	127.4	127.3
4′	149.7	150.3	**2⁗**	115.0	111.1
5′	117.4	117.4	**3⁗**	149.3	149.7
6′	123.8	123.8	**4⁗**	146.9	149.0
Internal	*sugar*		**5⁗**	116.3	116.2
1″	101.5	101.5	**6⁗**	122.8	123.9
2″	82.2	82.4	−COO	169.1	168.9
3″	75.7	75.6	−OMe		56.2
4″	70.0	70.1			
5″	75.8	76.0			
6″	64.6	64.5			

The molecular formula of compound **2** was determined as $C_{37}H_{38}O_{20}$ from HR FAB–MS spectrometry (see Experimental). ^{13}C and DEPT NMR spectra of 2 were almost similar to those of **1**. However, the signal at δ 56.2 in 2 together with the downfield shift of C-4‴ (+2.1 ppm) indicated the presence of a feruloyl moiety instead of the caffeoyl moiety (Miyase et al., 1992). EI–MS of the acetylated derivative of **2** exhibited the same results as **1**. Consequently, the site of attachment of the feruloyl moiety was proved to be at C-6″ of the internal glucosyl unit and the structure of **2** was determined as shown.

On the basis of ^{1}H and ^{13}C NMR, compounds **3**–**8** were identified as follows: compound (**3**) quercetin-3-*O*-sophoroside (Veit et al, 1990), compound (**4**) quercetin-3,7-*O*-β-diglucopyranoside (Harborne et al., 1982), compound (**5**) oleanolic acid-3-*O*-β-glucopyranoside (Mahato et al., 1988), compound (**6**) chikusetsusaponin IVa (Mohamed et al., 1998), compound (**7**) chikusetsusaponin IVa methyl ester, compound (**8**) oleanolic acid-3,28-β-diglucopyranoside (Mahato et al., 1988).

3. Experimental

^{1}H and ^{13}C NMR (TMS as int. standard): 400 MHz and 100 MHz respectively were recorded on a Jeol JNM

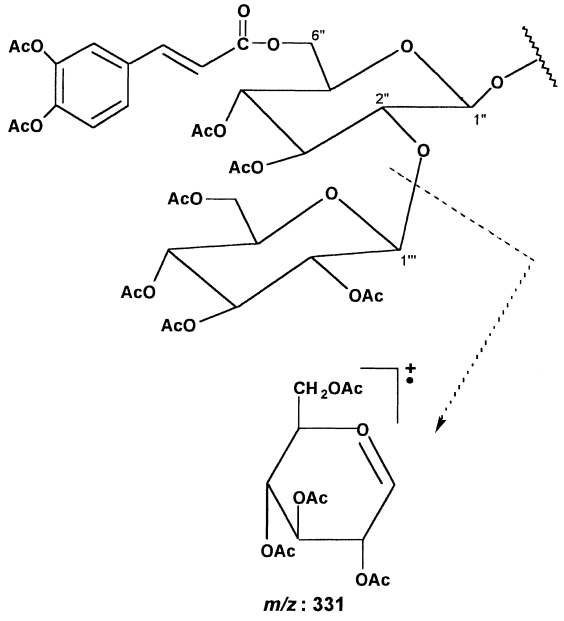

Fig. 1. Results of EI–MS analysis of the acetate derivative of compound **1**.

α-400 spectrometer. MS spectra were recorded on a Jeol JMS-SX 102 spectrometer by direct inlet method at an ionizing voltage of 70 eV. MPLC: RP-18 column (20 mm i.d. ×40 cm); flow rate of mobile phase 3 ml/min. HPLC: D-ODS-5 and polyamine columns (each 20 mm i.d. ×25 cm, YMC) with a Toyo Soda high speed chromatograph HLC-803 D pump and a Tosoh refraction index (RI-8) detector; flow rate of mobile phase 6 ml/min, injection vol. 0.8–1.0 ml. CC: Kieselgel 60 (70-230 mesh, Merck) and Diaion HP 20 (Mitsubishi). TLC: silica gel 60 precoated plates, F-254 and HPTLC using RP-18 precoated plates, F-254 s (Merck).

3.1. Plant material

Aerial parts of *B. muricata* (L.) Murr. were collected from Assiut Valley, Assiut, Egypt, in June 1997. The plant was identified by Professor A. Fayed, Department of Botany, Faculty of Science, Assiut University, Assiut, Egypt. A voucher specimen is deposited at the Herbarium of Department of Pharmacognosy, Faculty of Pharmacy, Assiut University, Assiut, Egypt.

3.2. Extraction and isolation of compounds (*1*–*8*)

The air dried powdered aerial parts of *B. muricata* (2 kg) were extracted with 70% EtOH. The dried ethanolic extract (220 g) was suspended in H_2O and defatted with diethylether. The aq. fr. (115 g) was applied to a column of Diaion HP-20 and eluted with H_2O, 50% MeOH, MeOH and acetone successively. The 50% MeOH eluate (30 g) was chromatographed on silica gel CC using EtOAc–MeOH–H_2O (40:10:1 and 70:30:3) to give 6 fractions. Fraction 4 (4.5 g) eluted with EtOAc–MeOH–H_2O (70:30:3) was subjected to MPLC using ODS column and 40–60% MeOH as a solvent system followed by HPLC using polyamine column and 90% MeCN as solvent to afford compounds **1** (yellow powder, 58 mg), **2** (yellow powder, 42 mg), **3** (yellow powder, 134 mg) and **4** (yellow powder, 97 mg). Fraction 5 (6.7 g) eluted with EtOAc–MeOH–H_2O (70 : 30 : 3) was subjected to MPLC using ODS column and 40–60% MeOH as solvent followed by HPLC using an ODS column and 58% MeOH as solvent to afford compounds **5** (white powder, 137 mg), **6** (white powder, 228 mg), **7** (white powder, 26 mg) and **8** (white powder, 21 mg).

3.2.1. Compound (*1*)

Quercetin-3-*O*-(6″-caffeoyl)-sophoroside. R_t 23 min (polyamine, 90% MeCN). UV λ_{max} MeOH nm: 251, 329 and 295 (sh). HR FAB–MS (negative) *m*/*z*: 787.1736 $[M–H]^-$ $C_{36}H_{35}O_{20}$ (req. 787.1721). ^{13}C NMR (CD_3OD, Table 1). ^1H NMR (CD_3OD): δ 7.65 (1H, *dd*, *J* = 2.0, 8.8 Hz, H-6′), 7.30 (1H, *d*, *J* = 15.6 Hz, H-β), 6.86 (1H, *d*, *J* = 8.8 Hz, H-5′), 6.79 (1H, *bs*, H-2′ or 2‴″), 6.50-6.78 (3H, *m*, H-2‴″, 5‴″, 6‴″), 6.21 (1H, *bs*, H-8), 6.13 (1H, *bs*, H-6), 5.59 (1H, *d*, *J* = 15.6 Hz, H-α), 5.11 (1H, *d*, *J* = 7.6 Hz, H-1″) and H-1″ was obscured by H_2O signal.

3.2.2. Compound (*2*)

Quercetin-3-*O*-(6″-feruloyl)-sophoroside. R_t 21 min (polyamine, 90% MeCN). UV λ_{max} MeOH nm: 253, 330 and 297 (sh). HR FAB–MS (negative) *m*/*z*: 801.1890 $[M–H]^-$ $C_{37}H_{37}O_{20}$ (req. 801.1878). ^{13}C NMR (CD_3OD, Table 1). ^1H NMR (CD_3OD): δ 7.65 (1H, *dd*, *J* = 2.0, 8.5 Hz, H-6′), 7.31 (1H, *d*, *J* = 16.1 Hz, H-β), 6.86 (1H, *d*, *J* = 8.5 Hz, H-5′), 6.79 (1H, *bs*, H-2″), 6.69 (1H, *dd*, *J* = 1.8, 8.1 Hz, H-6‴″), 6.63 (1H, *bs*, H-2‴″), 6.62 (1H, *d*, *J* = 8.1 Hz, H-5‴″), 6.14 (1H, *bs*, H-8), 6.10 (1H, *bs*, H-6), 6.03 (1H, *d*, *J* = 16.1 Hz, H-α), 5.04 (1H, *d*, *J* = 7.6 Hz, H-1″), 4.75 (1H, *d*, *J* = 7.8 Hz, H-1‴) and 3.70 (3H, *s*, −OMe).

3.3. Acetylation of compounds *1* and *2*.

A sample of 10 mg of compounds **1** and **2** was separately dissolved in 2 ml acetic anhydride-dried pyridine (1:1) and left overnight at room temp. The solvents were removed by evaporation under reduced pressure and the residues were subjected to EI–MS spectral analysis.

Acknowledgements

The authors are grateful to the Japan Society for Promotion of Science (JSPS) and a Grant-in-Aid, Ministry of Education and Culture, Japan for the financial support of this work. Also, we would like to thank the Research Center of Molecular Medicine of the Hiroshima University School of Medicine, Japan, for NMR measurements.

References

Al-Yahya, M.A., Al-Meshal, I.A., Mosa, J.S., Al-Badr, A., Tariq, M., 1990. Saudi plants, a phytochemical and biological approach, Vol. 64. King Saud University Press.

Bloor, S.J., Bradley, J.M., Lewis, D.H., Davies, K.M., 1998. Identification of flavonol and anthocyanin metabolites in leaves of *Petunia* 'Mitchill' and its LC transgenic. Phytochemistry 49, 1427–1430.

Bradbury, H., Jenkins, J., 1984. Determination of the structures of trisaccharides by ^{13}C NMR spectroscopy. Carbohydr. Res. 126, 125–156.

Fiasson, K.G., Fiasson, J.L., Waton, H., 1997. Quercetin glycosides from European aquatic *Ranunculus* species of subgenus *Batrachium*. Phytochemistry 45, 1063–1067.

Harborne, J.B., Mabry, T.J., 1982. The Flavonoids: Advances in Research. Chapman & Hall, London, New York.

Komori, T., Ida, Y., Mutou, Y., Miyahara, K., Nohara, T., Kawasaki, T., 1975. Mass spectra of spirostanol and and furostanol glycosides. Biomed. Mass Spectrom. 2, 65–77.

Mahato, S.B., Sarkar, S.K., Poddar, G., 1988. Triterpenoid saponins. Phytochemistry 27, 3037–3067.

Miyase, T., Iwata, Y., Ueno, A., 1992. Tenuifolioses G-P, oligosaccharide multi-esters from the roots of *Polygala tenuifolia* Willd. Chem. Pharm. Bull. 40, 2741–2748.

Mohamed, K.M., Hasanean, H.H., Ohtani, K., Yamasaki, K., 1998. Triterpenoidal saponins from *Kochia indica* Wight. Bull. Pharm. Sci., Assiut University 21 (1), 27–36.

Rizk, A. M., 1986. The Phytochemistry of Flora of Qatar, Vol. 29. King Print of Richmond.

Tackholm, V., 1974. Students Flora of Egypt, 2nd ed. Cooperative Printing Co, Beirut, p. 466.

Veit, M., Geiger, H., Czygan, F-C., Markham, K.R., 1990. Malonylated flavone 5-*O*-glucosides in the barren sprouts of *Equisetum arvense*. Phytochemistry 29, 2555–2560.

PERGAMON

Phytochemistry 57 (2001) 1263–1268

PHYTOCHEMISTRY

www.elsevier.com/locate/phytochem

Isoflavonoid glycosides from *Dalbergia sissoo*

Salwa F. Farag[a,*], Amany S. Ahmed[a], Kenji Terashima[b], Yoshiaki Takaya[b], Masatake Niwa[b]

[a]*Department of Pharmacognosy, Faculty of Pharmacy, Assiut University, Assiut 71526, Egypt*
[b]*Faculty of Pharmacy, Meijo University, Tempaku, Nagoya 468-8503, Japan*

Received 20 October 2000; received in revised form 1 March 2001

Abstract

Two isoflavone glycosides, biochanin A 7-*O*-[β-D-apiofuranosyl-(1→5)-β-D-apiofuranosyl-(1→6)-β-D-glucopyranoside] and tectorigenin 7-*O*-[β-D-apiofuranosyl-(1→6)-β-D-glucopyranoside], were isolated from *Dalbergia sissoo*. Their structures were elucidated on the basis of spectral and chemical evidence. © 2001 Elsevier Science Ltd. All rights reserved.

Keywords: Leguminosae; *Dalbergia sissoo*; Isoflavone glycosides; Isoflavone apioglucosides

1. Introduction

An aqueous extract of the leaves of *Dalbergia sissoo* Roxbg. (Leguminosae) has been used for the treatment of gonorrhea in Arabic countries (El-Dagwy, 1996). Many isoflavonoids and neoflavonoids have been reported from *D. sissoo* (Seshadri, 1972; Sharma et al., 1979, 1980; Ingham, 1983). Our detailed study on the constituents of the above plant led to the isolation of two new isoflavone glycosides (**1**, **3**) together with five known isoflavone glycosides (**2**, **4**–**7**) from the leaves and stem-bark of *D. sissoo* (Kinjo et al., 1987; Ishikura et al., 1989; Rao et al., 1989; Ramesh and Yuvarajan, 1995; Mathias et al., 1998).

2. Results and discussion

The methanol extract of the leaves of *D. sissoo* collected in Egypt was successively partitioned between water and hexane, chloroform, ethyl acetate and *n*-butanol to give the corresponding solubles. The butanol and water soluble fractions were respectively separated to give a new compound **1** and a known compound **2**. The methanol extract of the stem-bark was partitioned between water and chloroform, and between water and *n*-butanol. The *n*-butanol soluble fraction was separated to give a new compound **3** and five known compounds **4**–**7**. These compounds were identified as biochanin A 7-*O*-[β-D-apiofuranosyl-(1→6)-β-D-glucopyranoside] (**2**) (Rao et al., 1989), prunetin 4′-*O*-[β-D-apiofuranosyl-(1→6)-β-D-glucopyranoside] (**4**) (Ramesh and Yuvarajam, 1995), 7-methyltectorigenin 4′-*O*-[β-D-apiofuranosyl-(1→6)-β-D-glucopyranoside] (**5**) (Mathias et al., 1998), genistein 8-*C*-[β-D-glucopyranoside] (**6**) (Kinjo et al., 1987) and prunetin 4′-*O*-[β-D-glucopyranoside] (**7**) (Ishikura et al., 1989) by comparison of the spectral data with the reported data.

Compound **1**, $[\alpha]_D^{25}$ −106.1° (*c* 0.26, MeOH), was found by high-resolution FABMS to have the molecular formula $C_{32}H_{38}O_{18}$. The UV spectrum (λ_{max}^{MeOH} 261 and 327 nm) showed the characteristic absorption of an isoflavone, and a bathochromic shift (271 and 322 nm) on addition of $AlCl_3$ suggested the presence of free 5-OH and substituted 7-OH. The ^{1}H NMR spectrum exhibited one methoxy group [δ 3.8 (3H, *s*)], one set of *meta*-coupled aromatic protons [δ 6.47 (*d*, *J* = 1.8 Hz) and δ 6.63 (*d*, *J* = 1.8 Hz)], two sets of *ortho*-coupled aromatic hydrogens [δ 6.95 (2H, *d*, *J* = 8.4 Hz) and δ 7.46 (2H, *d*, *J* = 8.4 Hz)] and a non-coupled aromatic hydrogen [δ 8.12 (1H, s)] (Table 1). These features are characteristic of a 5,7,4′-trihydroxyisoflavone derivative (Markham and Geiger, 1994). The ^{1}H and ^{13}C NMR spectra (Table 1) revealed three anomeric signals ($\delta_{H\text{-}1''}$ 4.92 (*d*, *J* = 7.3 Hz) and $\delta_{C\text{-}1''}$ 101.5 (*d*), $\delta_{H\text{-}1'''}$ 4.97 (*d*, *J* = 2.6 Hz) and $\delta_{C\text{-}1'''}$ 110.8 (*d*) and $\delta_{H\text{-}1''''}$ 4.96 (*d*, *J* = 2.6 Hz) and $\delta_{C\text{-}1''''}$ 111.9 (*d*)) together with 13 carbon signals in the

* Corresponding author. Tel.: +20-088-333196; fax: +20-088-332776.
E-mail address: farag_s@yahoo.com (S.F. Farag).

0031-9422/01/$ - see front matter © 2001 Elsevier Science Ltd. All rights reserved.
PII: S0031-9422(01)00195-9

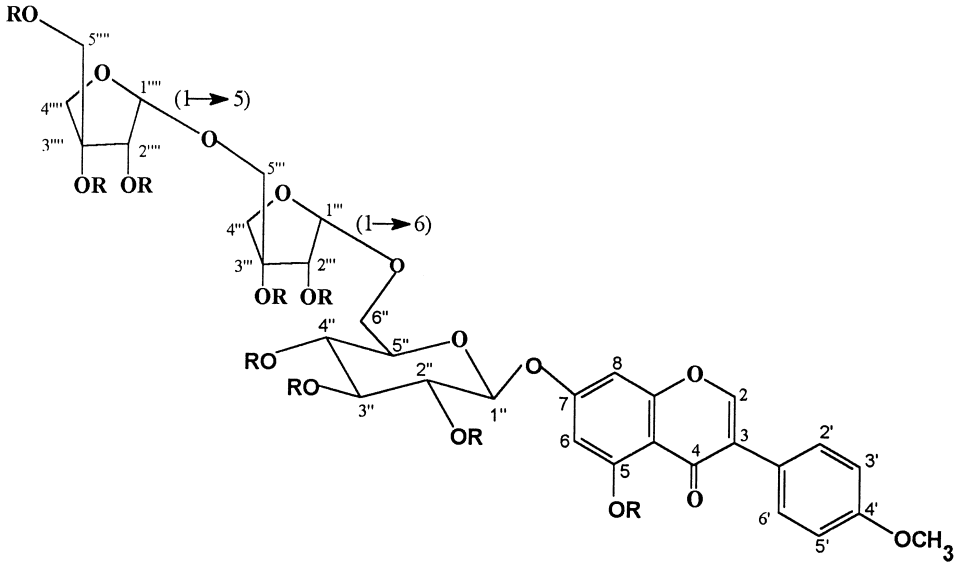

Compound 1 R= H
Compound 8 R= Ac

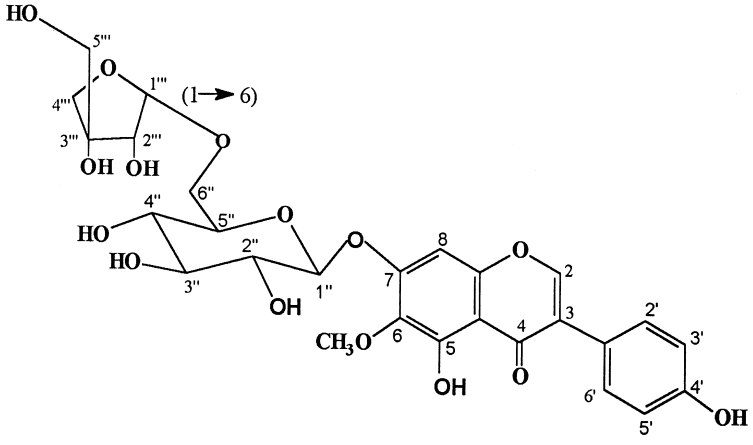

Compound 3

region of sugars indicated **1** to be an isoflavone-*O*-triglycoside (Agrawal, 1992). The ^{13}C NMR shifts of the three sugars are consistent with those corresponding to one glucopyranosyl and one apiofuranosyl moiety (Rao et al.,1989) with an additional apiofuranosyl moiety. The β-configuration of the glycosidic linkages was evident from the observed ^{13}C NMR chemical shifts for the anomeric carbons of glucose ($\delta_{C\text{-}1''}$ 101.5) and apiose ($\delta_{C\text{-}1'''}$ 110.8 and $\delta_{C\text{-}1''''}$ 111.9) (Ramesh and Yuvarajan, 1995; Mathias et al., 1998). The downfield shifts of C-6″ (δ_C 67.6) and C-5‴ (δ_C 69.3) suggesting that the interglycosidic linkages is apiofuranosyl (1⁗→5‴) apiofuranosyl (1‴→6″) glucopyranoside (Ramesh and Yuvarajan, 1995). The heteronuclear multiple bond correlation spectroscopy (HMBC) spectrum (Table 1) showed cross peaks between H-2′ (6′) δ_H 7.52 and C-4′ (δ_C 159.2) and between $C\underline{H}_3O$ (δ_H 3.8) and C-4′, respectively, determined the position of the methoxy group to be 4′. The identity of the three sugars and their sequence were determined by the exhaustive analysis of the NMR spectral data of the corresponding nonaacetate **8**, which was obtained by acetylation of **1** with acetic anhydride and pyridine in the presence of 4-(dimethylamino) pyridine (DMAP). The NMR data of **8** (see Experimental) are in accor-

Table 1
NMR spectral data of compounds **1** and **3** in DMSO-d_6

	1			**3**		
Positions	^{13}C	^{1}H	HMBC	^{13}C	^{1}H	HMBC
2	154.8 CH	8.42 (1H, *s*)		154.6 CH	8.35 (1H, *s*)	
3	122.2 C		2, 2′, 6′	122.0 C		2, 2′, 6′
4	180.4 C			180.8 C		2
5	161.6 C			152.9 C		
6	99.6 CH	6.48 (1H, *s*)	8	132.5 C		8, OMe
7	162.9 C		6	156.5 C		8, 1″
8	94.5 CH	6.72 (1H, *s*)		94.3 CH	6.89 (1H, *s*)	
9	157.2 C		2, 8	152.5 C		2, 8
10	106.1 C		6, 8	106.6 C		8
1′	122.7 C		3′, 5′	121.1 C		2, 3′, 5′
2′, 6′	130.1 CH	7.52 (2H, *d*, *J*=8.4)		130.1 CH	7.38 (2H, *d*, *J*=8.8)	
3′, 5′	113.7 CH	7.01 (2H, *d*, *J*=8.4)		115.1 CH	6.83 (2H, *d*, *J*=8.8)	
4′	159.2 C		2′, 3′, 5′, 6′, OMe	157.5 C		2′, 3′, 5′, 6′
1″	99.8 CH	5.05 (1H, *d*, *J*=7.3)		100.3 CH	5.04 (1H, *d*, *J*=7.3)	3″, 5″
2″	73.0 CH	3.28 (1H, *m*)		73.1 CH	3.34 (1H, *m*)	3″
3″	76.2 CH	3.29 (1H, *m*)		76.7 CH	3.33 (1H, *m*)	2″, 4″
4″	69.7 CH	3.13 (1H, *t*, *J*=8.8)		70.0 CH	3.14 (1H, *t*, *J*=8.8)	3″, 5″
5″	75.5 CH	3.61 (1H, *m*)		75.7 CH	3.62 (1H, *dd*, *J*=8.8, 7.3)	3″, 5″a,b
6″	67.6 CH_2	3.88 (1H, *d*, *J*=11)	1‴	67.8 CH_2	3.88 (1H, *d*, *J*=11)	4″, 1‴
		3.46 (1H, *dd*, *J*=11, 7)			3.47 (1H, *dd*, *J*=11, 7.3)	
1‴	109.0 CH	4.82 (1H, *d*, *J*=2.9)*[a]	6″a, 4‴b, 5‴a,b	109.5 CH	4.81 (1H, *d*, *J*=2.9)	6″a,b, 2‴, 4‴
2‴	76.3 CH	3.74 (1H, *d*, *J*=2.9)		75.9 CH	3.78 (1H, *d*, *J*=2.9)	4‴b, 5‴a
3‴	77.4 C		4‴b, 5⁗a,b	78.7 C		1‴, 5‴a,b, 4‴b
4‴	73.4 CH_2	3.89 (1H, *d*, *J*=9.2)	1‴, 5‴a,b	73.2 CH_2	3.92 (1H, *d*, *J*=9.2)	1‴
		3.62 (1H, *d*, *J*=9.2)			3.60 (1H, *d*, *J*=9.2)	
5‴	69.3 CH_2	3.53 (1H, *d*, *J*=9.9)	1‴,4‴a, 1⁗	63.3 CH_2	3.38 (1H, *m*)	2‴, 4‴a, 4‴b
		3.36 (1H, *d*, *J*=9.9)			3.34 (1H, *m*)	
1⁗	109.0 CH	4.81 (1H, *d*, *J*=2.9)*	4⁗b			
2⁗	75.6 CH	3.75 (1H, *d*, *J*=2.9)	4‴b			
3⁗	78.7 C		4⁗b,5⁗b			
4⁗	73.4 CH_2	3.83 (1H, *d*, *J*=9.5)	1⁗, 5⁗a			
		3.56 (1H, *d*, *J*=9.5)				
5⁗	63.1 CH_2	3.32 (1H, *m*)	2⁗, 4⁗a			
		3.27 (1H, *m*)				
OMe	55.1 CH_3	3.79 (3H, *s*)		60.3 CH_3	3.76 (3H, *s*)	

[a] *The assignments may be interchangeable.

dance with this interpretation. In the HMBC spectrum (see Fig. 1), the anomeric proton signal at δ_H 5.197 (6-substituted glucopyranosyl moiety), δ_H 4.956 (5-substituted apiofuranosyl moiety) and δ_H 4.986 (terminal apiofuranosyl moiety) showed long-range correlations with the ^{13}C signals at δ_C 159.9 (C-7 of aglycone), δ_C 66.3 (C-6″ of 6-substituted glucopyranosyl moiety) and δ_C 67.5 (C-5‴ of 5-substituted apiofuranosyl moiety), respectively. The other correlations are in agreement with the proposed structure. Furthermore, acid-catalysed hydrolysis of **1** gave biochanin A (5,7-dihydroxy-4′-methoxyisoflavone). From the above evidence, the structure of **1** was concluded to be biochanin A 7-*O*-[β-D-apiofuranosyl-(1→5)-β-D-apiofuranosyl-(1→6)-β-glucopyranoside].

Compound **3**, $[\alpha]_D^{25}$ −67.0° (*c* 0.28, MeOH), was assigned the molecular formula C_{27} H_{30} O_{15} from its HRFABMS. The UV spectrum showed a bathochromic shift (264 and 330 nm to 274 and 330 nm) on addition of $AlCl_3$, suggesting the presence of free 5-OH and a substituted 7-OH group. The ^1H NMR spectrum exhibited signals at δ 8.35 (1H, *s*), δ 7.38 (2H, *d*, *J* = 8.8 Hz), and 6.38 (2H, *d*, *J* = 8.8 Hz), attributable to hydrogens at H-2 and two sets of *ortho*-coupled aromatic hydrogens at H-2′, 6′ and H-3′, 5′ of an isoflavone derivative as shown in Table 1. A singlet signal at δ 6.89 (1H, *s*) indicated only one hydrogen to be present on the A-ring of the isoflavone. The ^1H and ^{13}C NMR spectra (Table 1) showed two anomeric signals [$\delta_{H\text{-}1''}$ 5.04 (1H, *d*, *J* = 7.3 Hz) and $\delta_{C\text{-}1''}$ 100.3 (*d*) and $\delta_{H\text{-}1'''}$ 4.81 (1H, *d*, *J* = 2.9 Hz) and $\delta_{C\text{-}1'''}$ 109.5 (*d*)] and 9 carbon signals in the region of sugars, indicating that **3** is an isoflavone having two phenolic hydroxyl groups, one methoxy group [δ_H 3.76 (3H, *s*) and δ_C 60.3 (*q*)] and one *O*-diglycosidic group (Agrawal, 1989, 1992). The ^{13}C NMR chemical shifts were in agreement with one glucopyranosyl and one apiofuranosyl moiety (Rao et al., 1989). The chemical shifts of the anomeric carbons at $\delta_{C\text{-}1''}$ 100.3 and $\delta_{C\text{-}1'''}$ 109.5 recognized the β-configuration of the glycosidic linkages (Ramesh and Yuvarajan, 1995; Mathias et al., 1998). The interglycosidic linkage (1‴→6″) was indicated by the downfield shift of C-6″ at δ_C 67.8 (Ramesh and Yuvarajan, 1995). The identity of the two sugars and their sequence were assigned by the ^1H–^1H COSY and HMBC spectra. The HMBC spectrum (Table 1) showed that the signals due to the disaccharide moiety consisted of one glucopyranosyl and one apiofuranosyl moiety. The anomeric proton signals at [δ_H 5.04 (6-substituted glucopyranosyl moiety) and δ_H 4.81 (terminal apiofuranosyl moiety) showed the correlations with the ^{13}C signals at δ_C 156.5 (C-7 of aglycone) and δ_C 67.8 (C-6″ of 6-substituted glucopyranosyl moiety), respectively. The methoxy group was located at C-6 as follows. In the ^{13}C NMR spectrum, the chemical shift values (δ_C 130.1 and 115.1) were assigned to carbon atoms 2′/ 6′ and 3′/ 5′, respectively, suggesting that **3** contained a 4′-hydroxyphenyl group (δ_C 130.0 and 115.2) as in genistein but not a 4′-methoxyphenyl group (δ_C 131.1 and 114.5) as in biochanin (Agrawal, 1989). Also the HMBC spectrum showed cross peak between the methoxy group signal at δ_H 3.76 and the C-6 signal at δ_C 132.5. Furthermore, acid-catalysed hydrolysis of **3** gave tectorigenin (5,7,4′-trihydroxy-6-methoxyisoflavone). From the above evidence, the structure of **3** was determined to be tectorigenin7-*O*-[β-D-apiofuranosyl-(1→6)-β-D-glucopyranoside].

Apiose sugar is not commonly encountered in glycosides. Three isoflavone apioglucosides have been iso-

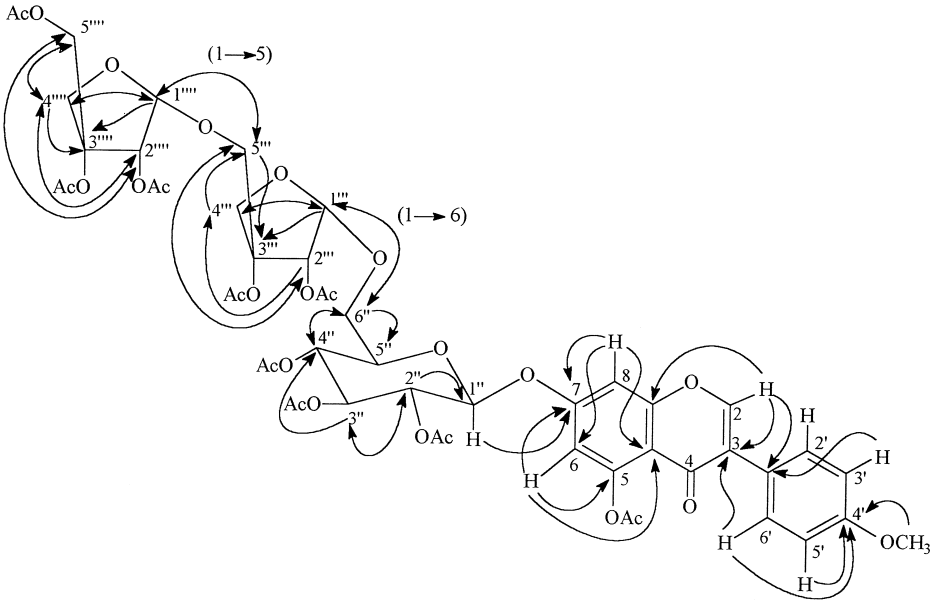

Fig. 1. Significant long range correlations observed in the HMBC spectrum of compound **8**.

lated in three species of *Dalbergia* (Rao et al., 1989; Ramesh and Yuvarajan, 1995; Mathias et al., 1998). In the course of the present work, this is the first report of the occurrence of isoflavone apioglucosides from *D. sissoo* Roxbg. which is of great importance.

3. Experimental

3.1. General

Optical rotations were taken on a JASCO P-1020 polarimeter (cell length 100 mm). UV spectra were measured on a JASCO V-560 UV/VIS spectrophotometer (cell length 10 mm). IR spectra were recorded on JASCO FT/IR-410 infrared spectrophotometer. 1D and 2D NMR spectra were recorded on JEOL A-400 and A-600 spectrometers. FABMS was measured with a JEOL HX-110 spectrometer using *m*-nitrobenzyl alcohol as a matrix. Analytical thin layer chromatography (TLC) was conducted on Si gel GF_{254} (Type 60) (E. Merck) and on precoated aluminium sheets of RP-18 F_{254} (E. Merck). Preparative TLC was performed on Si gel GF_{254} (Type 60) (E. Merck). Column chromatography was performed with Silica gel 60 (E. Merck), Diaion HP-20 AG (75-150 μ, Mitsubishi Chemical Industries Co. Ltd.) and Develosil Lop ODS (30-50 μ, Nomura Chemicals).

3.2. Plant material

The leaves and stem-bark of *D. sissoo* were collected in the campus of Assiut University, Assiut, Egypt, in August 1997. A voucher specimen has been deposited in the Herbarium of the Pharmacognosy Department, Faculty of Pharmacy, Assiut University.

3.3. Extraction and isolation

3.3.1. Extraction and isolation of the leaves

The air-dried leaves (2.0 kg) were powdered and extracted with MeOH (2×15 l) at room temperature. The MeOH extract (100 g) was partitioned between water and *n*-hexane, $CHCl_3$, EtOAc and *n*-BuOH to give the corresponding solubles (40 g), (20 g), (5.0 g), (5.0 g) and H_2O (30.0 g), respectively. The *n*-BuOH soluble fraction (5.0 g) was subjected to column chromatography on Si gel (600 g) and eluted with a stepwise gradient solvent system of $CHCl_3$–MeOH (each 500 ml), to give fractions 1–5, respectively. Fraction 3 (20 mg), eluted with $CHCl_3$–MeOH (7:3), was purified by preparative TLC (EtOAc–acetone–AcOH–H_2O/30:3:1:1) to give compound **2** (5 mg). The water soluble fraction (30.0 g) was chromatographed on Diaion HP-20 using a stepwise gradient solvent system of H_2O–MeOH (H_2O, 50% MeOH, 80% MeOH and MeOH) to give 4 fractions. The fraction eluted with 50% MeOH (8 g) was subjected to column chromatography on Si gel (240 g) and eluted with a stepwise gradient solvent system of $CHCl_3$–MeOH (each 250 ml). The fraction eluted with $CHCl_3$–MeOH (1:1) (70 mg) was purified by reversed-phase column chromatography on ODS (100 g) and eluted with a solvent system of MeOH–H_2O (2:3) to give compound **1** (25 mg).

3.3.2. Extraction and isolation of stem-bark

The air-dried stem-bark (1.0 kg) was ground and extracted with MeOH (2×10 l) at room temperature. The MeOH extract (90 g) was partitioned between $CHCl_3$ and H_2O and *n*-BuOH and H_2O, successively. The *n*-BuOH soluble material (20.0 g) was subjected to column chromatography on Diaion HP-20 using a stepwise gradient solvent system of H_2O–MeOH (H_2O, 50% MeOH, 80% MeOH and MeOH) to give 4 fractions. The second fraction (10.0 g) eluted with 50% MeOH was chromatographed on Si gel using a stepwise gradient solvent system of EtOAc–MeOH. The fraction (2.0 g) eluted with EtOAc–MeOH (7:3) was separated by reversed-phase column chromatography on ODS (250 g) and eluted with MeOH–H_2O (1:3) to give compound **3** (38 mg) and then with MeOH–H_2O (2:3) to give compound **5** (64 mg).The third fraction (1 g) eluted from Diaion HP-20 with 80% MeOH was subjected to column chromatography on Si gel (30 g) and eluted with a stepwise gradient solvent system EtOAc–MeOH (10:0–7:3) (each 100 ml). The fraction (35 mg) eluted with EtOAc–MeOH (9:1) was purified by reversed-phase column chromatography on ODS (100 g) and eluted with a solvent system of MeOH–H_2O (1:1) to give compound **4** (10 mg).

The fourth fraction (5 g) eluted from Diaion HP-20 was subjected to column chromatography on Si gel (150 g) and eluted with a stepwise gradient solvent system EtOAc–MeOH (each 250 ml). The fraction (24 mg) eluted with EtOAc–MeOH (9:1) was purified by reversed-phase column chromatography on ODS (100 g) and eluted with a solvent system of MeOH–H_2O (1:1) to give compound **6** (2.4 mg). The fraction (200 mg) eluted with EtOAc–MeOH (8:2) was purified by reversed-phase column chromatography on ODS (250 g) and eluted with a solvent system of MeOH–H_2O (1:3) to give compound **7** (70 mg).

Compound **1**: yellow amorphous powder. $[\alpha]_D^{25}$ −106.1° (*c* 0.26, MeOH). UV λ_{max}^{MeOH} nm: 261, 327; +$AlCl_3$: 271, 322; +NaOAc : 261, 327. IR (KBr) ν_{max}: 3383, 2930, 2361, 1654, 1613, 1515, 1442, 1291, 1249, 1181, 1070, 835 cm^{-1}. ^1H and ^{13}C NMR spectral data: see Table 1. HRFAB–MS *m*/*z* 711.2163 $[M+1]^+$, *m*/*z* 711.2136 calculated for $C_{32}H_{39}O_{18}$.

Compound **3**: yellow amorphous powder. $[\alpha]_D^{25}$ −67.0° (*c* 0.28, MeOH). UV λ_{max}^{MeOH} nm: 264, 330; +$AlCl_3$: 275, 325; +NaOAc: 264, 330. IR (KBr) ν_{max}: 3372, 2926, 1655, 1613, 1590, 1516, 1460, 1442, 1367, 1319, 1271, 1228,

1177, 1073, 1002, 924, 827 cm^{-1}. ^1H and ^{13}C NMR spectral data: see Table 1. HRFAB–MS m/z 595.1681 $[M+1]^+$, m/z 595.1663 calculated for $C_{27}H_{31}O_{15}$.

4. Acetylation of 1

Compound **1** (9.4 mg) was treated with 0.25 ml of acetic anhydride and 2 mg of DMAP in 0.5 ml of pyridine at room temperature for 24 h. After dilution with 5 ml of water, the reaction mixture was extracted twice with 5 ml of ethyl acetate. The organic layer was washed with water and brine and dried over magnesium sulfate. The crude product obtained by evaporation was purified by Si gel column chromatography using $CHCl_3$–MeOH (98:2) to give the corresponding nonacetate **8** (11.0 mg, yield 76%). Compound **8**: colorless amorphous powder. IR (KBr)ν_{max}: 3400, 1652, 1612, 1165, 1075, 825 cm^{-1}; ^1H NMR (600 MHz, $CDCl_3$) δ 7.927 (1H, *s*: H-2), 7.418 (2H, *d*, $J=8.8$ Hz: H-2′ and H-6′), 6.978 (1H, *d*, $J=2.6$ Hz: H-8), 6.930 (2H, *d*, $J=8.8$ Hz: H-3′ and H-5′), 6.634(1H, *d*, $J=2.6$ Hz: H-6), 5.332 (1H, *s*: H-2‴′), 5.312 (1H, *dd*, $J=9.5$, 9.2 Hz: H-3″), 5.303 (1H, *d*, $J=0.7$ Hz: H-2‴), 5.266 (1H, *dd*, $J=9.5$, 7.7 Hz: H-2″), 5.197 (1H, *d*, $J=7.7$ Hz: H-1″), 5.053 (1H, *dd*, $J=10.3$, 9.2 Hz: H-4″), 4.986 (1H, *s*: H-1‴′), 4.956 (1H, *br.s*: H-1‴), 4.705 (1H, *d*, $J=12.5$ Hz: H-5‴′a), 4.606 (1H, *d*, $J=12.5$ Hz: H-5‴′b), 4.371 (1H, *d*, $J=11.0$ Hz: H-5‴a), 4.242 (1H, *d*, $J=10.6$ Hz: H-4‴′a), 4.194 (1H, *d*, $J=9.9$ Hz: H-4‴a), 4.129 (1H, *d*, $J=10.6$ Hz: H-4‴′b), 4.113 (1H, *d*, $J=9.9$ Hz: H-4‴b), 3.946 (1H, *d*, $J=11.0$ Hz: H-5‴b), 3.922 (1H, *ddd*, $J=10.3$, 7.3, 2.2 Hz: H-5″), 3.807 (3H, *s*:-OC$\underline{H}_3$), 3.777 (1H, *dd*, $J=11.0$, 2.2 Hz: H-6″a), 3.552 (1H, *dd*, $J=11.0$, 7.3 Hz: H-6″b), 2.388, 2.063, 2.058, 2.045, 2.042, 2.025, 2.018, 2.002, 1.956 (each 3H, *s* :-OC$\underline{H}_3$). ^{13}C NMR (150 MHz, $CDCl_3$) : δ152.0 (CH: C-2), 125.8 (C: C-3), 174.7 (C: C-4), 151.1 (C: C-5), 102.2 (CH: C-8), 159.9 (C: C-7), 110.2 (CH: C-6), 158.7 (C: C-9), 113.6 (C: C-10), 123.9 (C: C-1′), 130.5 (CH: C-2′ (6′)), 114.7 (CH: C-3′ (5′)), 159.8 (C: C-4′), 98.3 (CH: C-1″), 71.1 (CH: C-2″), 72.78 (CH: C-3″), 68.6 (CH: C-4″), 73.8 (CH: C-5″), 66.3 (CH_2: C-6″), 106.5 (CH: C-1‴), 76.6 (CH: C-2‴), 84.5 (C: C-3‴′), 73.2 (CH_2: C-4‴), 67.5 (CH_2: C-5‴), 106.0 (CH: C-1‴′), 76.3 (CH: C-2‴′), 83.3 (C: C-3‴′), 72.82 (CH_2: C-4‴′), 63.3 (CH_2: C-5‴′), 55.4 (CH_3:-O$\underline{C}H_3$), 21.2, 20.8, 20.5 (each CH_3:-CO$\underline{C}H_3$), 21.3, 20.72, 20.66 (each $2CH_3$:-CO$\underline{C}H_3$), 170.6, 170.3, 169.9, 169.77, 169.76, 169.5, 169.3, 169.29, 169.0 (each C:-$\underline{C}OCH_3$). FAB-MS $[M+1]^+$, m/z 1089 calculated for $C_{50}H_{57}O_{27}$.

5. Acid-catalyzed hydrolysis of 1

Compound **1** (13 mg) was heated in 1 ml of 2 M HCl at 100°C for 2 h. The reaction mixture was evaporated and then dried in vacuo. The residue was separated by Si gel column chromatography using $CHCl_3$–MeOH (98:2) to give an aglycone (3.0 mg, 58% yield). The aglycone was identified as biochanin A by comparison of its ^1H NMR spectral data with those of an authentic sample (commercially available from Sigma-Aldrich Co).

6. Acid-catalyzed hydrolysis of 3

Compound **3** (17 mg) was treated in the same manner as compound **1** to give an aglycone (3.4 mg, 40% yield). The aglycone was identified as tectorigenin by comparison of its ^1H NMR spectral data with those of an authentic sample derived from tectoridin (Farag et al., 1999).

Acknowledgements

The authors thank Dr. Susumu Teramoto, Faculty of Science, Kumamoto University, Japan for an authentic sample of prunetin 4′-*O*-[β-D-glucopyranoside].

References

Agrawal, P.K., 1989. Carbon-13 NMR of Flavonoids. Elsevier Science, London, p. 196.

Agrawal, P.K., 1992. NMR spectroscopy in the structure elucidation of oligosaccharides and glycosides. Phytochemistry 31, 3307–3330.

El-Dagwy, A.A., 1996. Encyclopedia for Production of Aromatic and Medicinal Plants, Vol. 1. Imprimerie Atlas, Cairo, p. 192.

Farag, S.F., Backheet, E.Y., El-Emary, N.A., Niwa, M., 1999. Isoflavonoids and flavone glycosides from rhizomes of *Iris carthalinae*. Phytochemistry 50, 1407–1410.

Ingham, J. L., 1983. In: Ingham, J. L., Kokinen, A., Lounasmaa, M. (Eds.), Progress in the Chemistry of Natural Organic Products, Vol. 43. Springer, Wien/New York, pp. 1–200.

Ishikura, N., Watanabe, Y., Teramoto, S., 1989. The formation of flavonoids in cell suspension cultures of *Prunus* × *yedoensis* Matsum. Botanical Magazine, Tokyo 102, 547–560.

Kinjo, J., Furusawa, J., Baba, J., Takeshita, T., Yamasaki, M., Nohara, T., 1987. Studies on the constituents of *Pueraria lobata*. III. Isoflavonoids and related compounds in the roots and the voluble stems. Chemical Pharmaceutical Bulletin 35, 4846–4850.

Markham, K. R., Geiger, H., 1994. In: Harborne, J.B. (Ed.), The Flavonoids Advances in Research Since 1986. Chapman & Hall, London, p. 458.

Mathias, L., Vieira, I.J.C., Braz-Filho, R., Rodrigues-Filho, E., 1998. A new isoflavone glycoside from *Dalbergia nigra*. Journal of Natural Products 61, 1158–1161.

Ramesh, P., Yuvarajan, C.R., 1995. Coromandelin, a new isoflavone apioglucoside from the leaves of *Dalbergia coromandeliana*. Journal of Natural Products 58, 1240–1241.

Rao, P.S., Asheervadam, Y., Khalilullah, M., Murti, V.V.S., 1989. A revised structure for the isoflavone lanceolarin. Phytochemistry 28, 957–958.

Seshadri, T.R., 1972. Polyphenols of *Pterocarpus* and *Dalbergia* woods. Phytochemistry 11, 881–898.

Sharma, A., Chibber, S.C., Chawla, H.M., 1979. Caviunin 7-*O*-gentiobioside from *Dalbergia sissoo* pods. Phytochemistry 18, 1253.

Sharma, A., Chibber, S.C., Chawla, H.M., 1980. Isocaviunin 7-gentiobioside, a new isoflavone glycosides from *Dalbergia sissoo*. Phytochemistry 19, 715.

PERGAMON

Phytochemistry 57 (2001) 1269–1271

PHYTOCHEMISTRY

www.elsevier.com/locate/phytochem

Pyrrolizidine alkaloids from *Ageratum houstonianum* Mill

Helmut Wiedenfeld[a,*], Adolfo Andrade-Cetto[b]

[a]*Pharmazeutisches Institut der Universität, Universität Bonn, An der Immenburg 4, D-53121 Bonn, Germany*
[b]*Departamento de Biología, Facultad de Ciencias, Universidad Nacional Autónoma de México, México, DF, Mexico*

Received in revised form 6 April 2001

Dedicated with great compliments to Professor Dr. Dr. h. c. mult. H. Oelschläger on the occasion of his 80th birthday

Abstract

Four pyrrolizidine alkaloids (PA) were isolated from *Ageratum houstonianum* and their structures elucidated by spectroscopical methods. Besides the already known lycopsamine three new PA were found. Their structures are the 2*S*-2-hydroxy-2,3-dimethyl-butanoyl-O^9 as well as the O^7 esters of retronecine and the O^9 derivative of heliotridine. © 2001 Elsevier Science Ltd. All rights reserved.

Keywords: *Ageratum houstonianum* (Mill); Asteraceae; Eupatorieae; Pyrrolizidine alkaloids; Lycopsamine; O^9-(2*S*-2-Hydroxy-2,3-dimethyl-butanoyl)-retronecine; O^9-(2*S*-2-Hydroxy-2,3-dimethyl-butanoyl)-heliotridine; O^7-(2*S*-2-Hydroxy-2,3-dimethyl-butanoyl)-retronecine

1. Introduction

Ageratum houstonianum (Mill) (Asteraceae, tribe Eupatorieae) is a plant widespread in Mexico and southern USA. It is reported that the leaves of this plant show antifungal properties (Pandey et al., 1984). The essential oil contents chromenes and shows antimicrobiotical activities (Menut et al., 1993). Further investigations show the occurence of benzofurans (Anthonsen and Chantarasakul, 1970; Bowers, 1977; Breuer et al., 1987; Siebertz et al., 1988) as well as of flavonoids and methoxyflavones (Minonskowski and Gill, 1973, 1975; Quijano et al., 1982, 1985, 1987). In the Indian medicine of Mexico it is used traditionally. Our own ethnopharmacological studies in the zone of Tlanchinol, Hidalgo, showed that the natives use water decotions of the plant against pain and infections, especially for cleaning external wounds. There the plant is called with its indian (nahuatl) name "Micashihuil". As *A. houstonianum* belongs to the asteraceae family and the tribe eupatorieae the presence of pyrrolizidine alkaloids (PA) could be presumed.

To estimate a possible toxic effect the knowledge of the particular structures of the PA contained is necessary. Therefore aerial parts of the plant *A. houstonianum* were investigated. The plant material was collected in the above mentioned region.

Four PA were isolated and their structures determined by GC–MS and homo- as well as hetero-nuclear 2D NMR correlated spectroscopy. Three of them have not been described previously. The known alkaloid belongs to the retronecine-type and is O^9-(−)-viridifloryl-retronecine (=lycopsamine). The new PA show the structures of the retronecine-O^9- as well as retronecine-O^7-2*S*-2-hydroxy-2,3-dimethyl-butanoic ester and the heliotridine-O^9-2*S*-2-hydroxy-2,3-dimethyl-butanoic ester.

Based on the structure–toxicity relationship (Wiedenfeld and Röder, 1984) for all substances low toxic side effects must be expected.

2. Results and discussion

In our investigation, aerial parts of *A. houstonianum* were extracted as already described (Röder and Wiedenfeld, 1977; Wiedenfeld and Röder, 1979). From the crude alkaloidal extract **1**, **2**, **3** and **4** were isolated (Fig. 1).

The GC–MS spectrum of **1** shows the $[M]^+$ peak at 299 corresponding to the formula $C_{15}H_{25}NO_5$. The further MS fragmentation and also the NMR data are corresponding to those describes earlier (Wiedenfeld and Röder, 1991).

The $[M]^+$ peak in the GC–MS spectrum of **2** occurs at 269 indicating the molecular formula $C_{14}H_{23}NO_4$.

* Corresponding author. Tel.: +49-228-735225; fax: +49-228-737929.

E-mail address: wiedenfeld@uni-bonn.de (H. Wiedenfeld).

0031-9422/01/$ - see front matter © 2001 Elsevier Science Ltd. All rights reserved.
PII: S0031-9422(01)00192-3

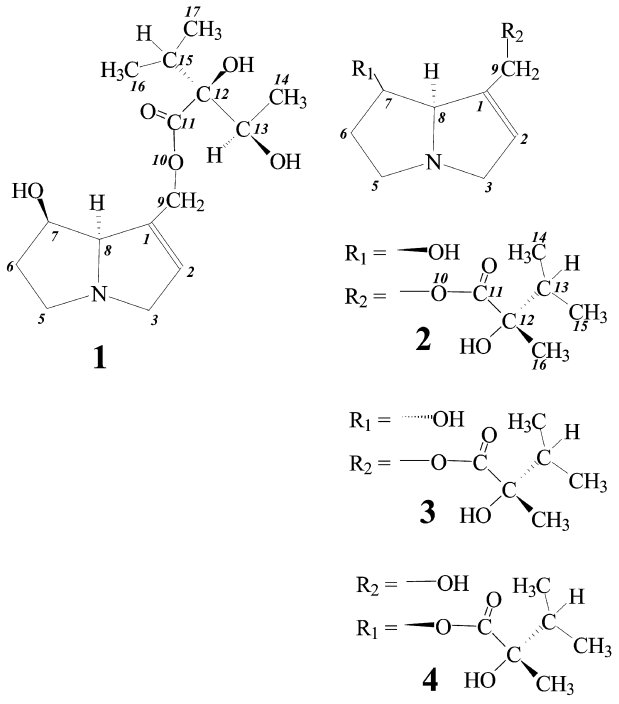

Fig. 1. Structures of the isolated compounds **1**–**4**.

Loss of OH leads to *m*/*z* 252. The ions *m*/*z* 225 and 208 result from $[M]^+ - C_3H_8$ and further loss of OH. The cleavage of the ester function leads to *m*/*z* 138. The fragments *m*/*z* 138, 120, 93 and 80 are typical for retronecine or its isomer heliotridine and are identical with those in **1**. The MS spectra of **3** and **4** are similar to that of **2**; they only differ in the intensities of their fragments.

The ^1H and ^{13}C NMR data of **2**, **3** and **4** are summarized in the experimental part. The assignment was performed by interpretation of H,H- and C,H-correlated spectra. Important structural information is provided by the ^{13}C chemical shift of C-6 (**2**: 35.7; **3**: 33.7; **4**: 34.2 ppm), C-7 (**2**: 70.1; **3**: 73.7; **4**: 74 ppm) and C-8 (**2**: 77.6; **3**: 79.5; **4**: 74.8 ppm) (Jones et al., 1982; Mohanraj and Herz, 1982; Wiedenfeld and Röder, 1991). These signals determine a retronecine-*O*-9 ester **2**, a heliotridine-*O*-9 ester **3** and a retronecine-*O*-7 ester **4**. This is further proofed by the ^1H and ^{13}C shift for C-9: 4.70/61.8 (**2**), 4.67/60.7 (**3**) and 3.97/58.2 (**4**) as well as by the ^1H data for C-7: 4.20 (**2**), 4.16 (**3**) and 5.12 (**4**). The esterifying acid is characterized by the values for C-12 (76 ppm, S), C-13 (1.80 and 35 ppm) and the methyl groups 14/15 (~0.8 and ~17 ppm) as well as for the methyl group 16 (~1.2 and ~23 ppm). The stereochemistry at C-12 can be deduced by interpretation of the shift-difference of the C-9H_2 AB system (Mohanraj and Herz, 1982; Wiedenfeld and Röder, 1991). For this aspect a value near 0 is found indicating the *S*-configuration. These data leads to the structure of a 2*S*-2-hydroxy-2,3-dimethyl-butanoic acid.

Until now, only one report can be found in literature about a PA esterified with a 6-C-acid (Hartmann et al., 1990). There, a *O*-9 and a *O*-7 ester of retronecine with 2-hydroxy-3-methyl-butyric acid is described which were formed after feeding *Creatonotus transiens* butterflies with retronecine.

Our results show that similar structures can occur natively in plant material, too. For the new PA, we propose the names retrohoustine **2**, isoretrohoustine **4** and heliohoustine **3**.

3. Experimental

3.1. General

NMR spectra were measured in $CDCl_3$/DMSO-d_6 at 400 and 100 MHz, respectively. GC–MS: GC: 150 (5 min) –250°C, 10°/min; HP-1, 25 m×0.32 mm; Inj.: 250°C, det.: 280°C; R_t: **1**: 12.94 min, **2**: 10.45 min, **3**: 10.93 min, **4**: 10.72 min; MS: 220°C; interface: 250°C; 2000 emV.

3.2. Plant material

Plants were gathered at several places near Tlanchinol, Hidalgo, Mexico, in the years 1998 and 1999. The material was identified by Enrique Ortíz Bemudes, University of Mexico, a voucher specimen (IMSS14141) was deposited at the herbarium of medicinal plants at the Mexican Institut for Social Security in Mexico City.

3.3. Isolation of alkaloids

Extn of plant material (aerial parts; 500 g) was carried out as described earlier (Röder and Wiedenfeld, 1977; Wiedenfeld and Röder, 1979). Prep. TLC [silica gel F_{254}, CH_2Cl_2–MeOH–NH_4OH (25%), 75:24:1] yielded the alkaloids as oils (4 mg **1**, 12 mg **2** and 8 mg **3** and **4**).

3.4. Retrohoustine 2

GC–MS *m*/*z* (rel. int.): $[M]^+$ $C_{14}H_{23}NO_4$ 269 (0.22); $C_{14}H_{22}NO_3$ 252 (0.65); $C_{11}H_{15}NO_4$ 225 (5.65); $C_{11}H_{14}NO_3$ 208 (1.74); $C_8H_{12}NO$ 138.04 (100); $C_8H_{10}N$ 120 (8.26); C_6H_7N 93 (68.04); C_5H_6N 80 (16.96).

^1H NMR: δ 5.74 (1H, *td*, $J_{2,3a/b}=1.7$ Hz, H-2), 4.70 (2H, *ddt*, $J_{9a,9b}=13.3$ Hz, $J_{9a/b,3a/b}=1.2$ Hz $J_{9a/b,2}=1.0$ Hz, H_2-9), 4.20 (1H, *td*, $J_{7,8}=3.3$ Hz, $J_{7,6}=1.2$ Hz, H-7), 4.10 (1H, *m*, H-8), 3.84 (1H, *dddt*, $J_{3a,3b}=15.6$ Hz, $J_{3a,8}=2.4$ Hz, $J_{3a,2}=1.7$ Hz, $J_{3a,9}=1.2$ Hz, H-3A), 3.33 (1H, *dddd*, $J_{3b,3a}=15.6$, $J_{3b,5b}=5.8$, $J_{3b,8}=1.9$ Hz, $J_{3b,2}=1.7$ Hz, H-3B), 3.17 (1H, *dt*, $J_{5a,5b}=8.5$, $J_{5a,6}=1.7$ Hz, H-5A), 3.1 (2OH), 2.66 (1H, *ddd*, $J_{5b,5a}=8.5$, $J_{5b,3b}=5.8$, $J_{5b,6}=2.9$ Hz, H-5B), 1.88 (1H, *q*, $J_{13,14/15}=6.9$ Hz, H-13), 1.86 (2H, *m*, H_2-6), 1.17 (3H, *s*, H_3-16), 0.85 (3H, *d*, $J_{15,13}=6.9$ Hz, H_3-15), 0.79 (3H, *d*,

$J_{14,13}$ = 6.9 Hz, H_3-14), ^{13}C NMR: δ 179.2 (*s*, C-11), 132.9 (*s*, C-1), 127.8 (*d*, C-2), 77.6 (*d*, C-8), 76.5 (*s*, C-12), 70.1 (*d*, C-7), 62.1 (*t*, C-3), 61.8 (*t*, C-9), 53.3 (*t*, C-5), 35.7 (*t*, C-6), 35.3 (*d*, C-13), 22.7 (*q*, C-16), 16.8 (*q*, C-14), 14.4 (*q*, C-15).

3.5. Isoretrohoustine **4**

GC–MS *m*/*z* (rel. int.): $[M]^+$ $C_{14}H_{23}NO_4$ 269 (0.28); $C_{14}H_{22}NO_3$ 252 (0.13); $C_{11}H_{15}NO_4$ 225 (3.83); $C_{11}H_{14}NO_3$ 208 (0.26); $C_8H_{12}NO$ 138.04 (100); $C_8H_{10}N$ 120 (10.0); C_6H_7N 93 (87.18); C_5H_6N 80 (26.92).

^1H NMR: δ 5.55 (1H, *dd*, $J_{2,3a/b}$ = 1.8 Hz, $J_{2,8}$ = 1.4 Hz, H-2), 5.12 (1H, *ddd*, $J_{7,8}$ = 3.3 Hz, $J_{7,6a}$ = 1.2 Hz, $J_{7,6b}$ = 1.0 Hz, H-7), 4.2 (2OH), 4.18 (1H, *m*, H-8), 3.97 (2H, *dt*, $J_{9a,9b}$ = 11.5 Hz, $J_{9a/b,3a/b}$ = 5.4 Hz, H_2-9), 3.78 (1H, *ddd*, $J_{3a,3b}$ = 14.0 Hz, $J_{3a,8}$ = 6.2 Hz, $J_{3a,9a/b}$ = 5.4 Hz, H-3A), 3.29 (1H, *ddd*, $J_{3b,3a}$ = 14.0, $J_{3b,8}$ = 6.3, $J_{3b,9a/b}$ = 5.0 Hz, H-3B), 3.10 (1H, *dd*, $J_{5a,5b}$ = 9.0, $J_{5a,6}$ = 2.7 Hz, H-5A), 2.66 (1H, *dd*, $J_{5b,5a}$ = 9.1, $J_{5b,3b}$ = 8.2, H-5B), 1.94 (2H, *m*, H_2-6), 1.78 (1H, *q*, $J_{13,14/15}$ = 6.9 Hz, H-13), 1.13 (3H, *s*, H_3-16), 0.81 (3H, *d*, $J_{15,13}$ = 6.9 Hz, H_3-15), 0.73 (3H, *d*, $J_{14,13}$ = 6.9 Hz, H_3-14), ^{13}C NMR: δ 175.3 (*s*, C-11), 139.1 (*s*, C-1), 124.4 (*d*, C-2), 76.2 (*s*, C-12), 74.8 (*d*, C-8), 74.0 (*d*, C-7), 62.7 (*t*, C-3), 58.2 (*t*, C-9), 53.1 (*t*, C-5), 34.7 (*d*, C-13), 34.2 (*t*, C-6), 23.3 (*q*, C-16), 17.2 (*q*, C-14), 15.9 (*q*, C-15).

3.6. Heliohoustine **3**

GC–MS *m*/*z* (rel. int): $[M]^+$ $C_{14}H_{23}NO_4$ 269 (1.09); $C_{14}H_{22}NO_3$ 252 (0.22); $C_{11}H_{15}NO_4$ 225 (4.78); $C_{11}H_{14}NO_3$ 208 (0.11); $C_8H_{12}NO$ 138.04 (100); $C_8H_{10}N$ 120 (5.33); C_6H_7N 93 (81.53); C_5H_6N 80 (19.02).

^1H NMR: δ 5.62 (1H, *t*, $J_{2,3a/b}$ = 1.2 Hz, H-2), 4.67 (2H, *m*(broad), H_2-9), 4.2 (2OH), 4.16 (1H, *t*, $J_{7,8}$ = 2.2 Hz, H-7), 3.98 (1H, *m*, H-8), 3.77 (1H, *ddt*, $J_{3a,3b}$ = 14.6 Hz, $J_{3a,8}$ = 6.6 Hz, $J_{3a,9}$ = 5.2 Hz, H-3A), 3.29 (1H, *dtd*, $J_{3b,3a}$ = 14.6, $J_{3b,5b}$ = 4.1, $J_{3b,8}$ = 2.0 Hz, H-3B), 3.11 (1H, *dm*, $J_{5a,5b}$ = 10.5, H-5A), 2.57 (1H, *ddd*, $J_{5b,5a}$ = 10.6, $J_{5b,3b}$ = 4.8, $J_{5b,6}$ = 1.3 Hz, H-5B), 1.78 (1H, *q*, $J_{13,14/15}$ = 6.7 Hz, H-13), 1.74 (1H, *tm*, $J_{6a,6b}$ = 6.0 Hz, H-6A), 1.62 (1H, *td*, $J_{6b,6a}$ = 6.1 Hz, $J_{6b,5}$ = 5.8 Hz, H-6B), 1.23 (3H, *s*, H_3-16), 0.83 (3H, *d*, $J_{15,13}$ = 6.7 Hz, H_3-15), 0.80 (3H, *d*, $J_{14,13}$ = 6.7 Hz, H_3-14), ^{13}C NMR: δ 175.5 (*s*, C-11), 136.5 (*s*, C-1), 124.4 (*d*, C-2), 79.5 (*d*, C-8), 77.1 (*s*, C-12), 73.7 (*d*, C-7), 61.4 (*t*, C-3), 60.7 (*t*, C-9), 53.7 (*t*, C-5), 35.2 (*d*, C-13), 33.7 (*t*, C-6), 22.8 (*q*, C-16), 17.1 (*q*, C-14), 16.1 (*q*, C-15).

Acknowledgements

We are thankful to Ivan Pérez Samayoa for his great help in collecting and identifying the plant material.

References

Anthonsen, T., Chantarasakul, S., 1970. Ageratone and dihydroageratone, new benzofuran derivatives from *Ageratum houstonianum*. Acta Chem. Scand. 24, 721–722.

Bowers, W.S., 1977. Chromene compounds useful as insecticides with antijuvenile hormone action. Ger. Offen., 25.

Breuer, M., Budzikiewicz, H., Siebertz, R., Proksch, P., 1987. Benzofuran derivatives from *Ageratum houstonianum*. Phytochemistry 26, 3055–3057.

Hartmann, T., Biller, A., Witte, L., Ernst, L., Boppré, M., 1990. Transformation of plant pyrrolizidine alkaloids into novel insect alkaloids by arctiid moths (Lepidoptera). Biochem. Syst. Ecol. 18, 549–554.

Jones, A.J., Culvenor, C.C.J., Smith, L.W., 1982. Pyrrolizidine alkaloids — a carbon-13 NMR study. Aust. J. Chem. 35, 1173–1184.

Menut, C., Lamaty, G., Zollo, P.H.A., Kuiate, J.R., Bessiere, J.M., 1993. Aromatic plants of tropical Central Africa. Part X. Chemical composition of the essential oils of *Ageratum houstonianum* Mill. and *Ageratum conyzoides* L. from Cameroon. Flavour Fragrance J. 8, 1–4.

Minonskowski, H., Gill, S., 1973. Flavonoids from *Ageratum mexicanum*. Acta Pol. Pharm. 30, 105.

Minonskowski, H., Gill, S., 1975. Flavonoids of the herb *Ageratum Mexicanum* Sims. (Compositae). Acta Pol. Pharm. 32, 633–639.

Mohanraj, S., Herz, W., 1982. High resolution proton NMR and carbon-13 NMR spectra of saturated pyrrolizidine monoester alkaloids. J. Nat. Prod. 45, 328–336.

Pandey, D.K., Chandra, H., Tripathi, N.N., Dixit, S.N., 1984. Mycotoxicity in leaves of some higher plants with special reference to that of *Ageratum houstonianum* mill. Mykosen 26, 565–573.

Quijano, L., Calderon, J.S., Gomez, F., Rios, T., 1982. Two polymethoxyflavones from *Ageratum houstonianum*. Phytochemistry 21, 2965–2967.

Quijano, L., Calderon, J.S., Gomez, F., Escobar, E., Rios, T., 1985. Flavonoids from *Ageratum* species. Part 4. Octasubstituted flavones from *Ageratum houstonianum*. Phytochemistry 24, 1085–1088.

Quijano, L., Calderon, J.S., Garibay, F.G., Escobar, E., Rios, T., 1987. Flavonoids from *Ageratum* species. Part 5. Further polysubstituted flavones from *Ageratum houstonianum*. Phytochemistry 26, 2075–2078.

Röder, E., Wiedenfeld, H., 1977. Isolation and structural elucidation of the alkaloid fuchsisenecionine from *Senecio fuchsii*. Phytochemistry 16, 1462–1463.

Siebertz, R., Proksch, P., Wray, V., Witte, L., 1988. A benzofuran from *Ageratum houstonianum*. Phytochemistry 27, 3996–3997.

Wiedenfeld, H., Röder, E., 1979. The pyrrolizidine alkaloid senecionin from *Senecio fuchsii*. Phytochemistry 18, 1083–1084.

Wiedenfeld, H., Röder, E., 1984. Pyrrolizidine alkaloids: structure and toxicity. Dtsch. Apoth. Ztg. 124, 2116–2122.

Wiedenfeld, H., Röder, E., 1991. Pyrrolizidine alkaloids from *Ageratum conyzoides*. Planta Med. 57, 578–579.

PERGAMON

Phytochemistry 57 (2001) 1273–1276

PHYTOCHEMISTRY

www.elsevier.com/locate/phytochem

Indole alkaloids from the seeds of *Centaurea cyanus* (Asteraceae)

Satyajit D. Sarker[a,*], Anuszka Laird[a], Lutfun Nahar[b], Yashodharan Kumarasamy[a], Marcel Jaspars[c]

[a]*School of Pharmacy, The Robert Gordon University, Schoolhill, Aberdeen AB10 1FR, Scotland, UK*
[b]*Japp Laboratory, Department of Chemistry, University of Aberdeen, Meston Walk, Old Aberdeen, Aberdeen AB24 3UE, Scotland, UK*
[c]*Marine Natural Products Laboratory, Department of Chemistry, University of Aberdeen, Meston Walk, Old Aberdeen, Aberdeen AB24 3UE, Scotland, UK*

Received 11 January 2001; received in revised form 22 February 2001

Abstract

Preparative RP-HPLC analysis of a methanol extract of the seeds of *Centaurea cyanus* afforded four indole alkaloids: moschamine, *cis*-moschamine, centcyamine and *cis*-centcyamine, the latter two being new natural products. Structures of these compounds were elucidated by comprehensive spectroscopic analyses. General toxicity of the isolates was determined by Brine Shrimp Lethality bioassay. © 2001 Elsevier Science Ltd. All rights reserved.

Keywords: *Centaurea cyanus*; Compositae; Asteraceae; Indole; Moschamine; Centcyamine; Toxicity; Brine Shrimp Lethality bioassay; *Artemia salina*; NMR

1. Introduction

Centaurea cyanus L. (family: Asteraceae *alt*. Compositae), commonly known as "Cornflower" or "Bachelor's button", is a flowering weed indigenous to Iran, Iraq, Turkey and Pakistan in Asia, and Albania, Bulgaria, Greece, Italy and the former Yugoslavia in Europe, and also cultivated and naturalised in many other parts of the world (GRIN database, 2000). Flower-heads of this plant are well-known crude drugs used in European traditional medicine in the treatment of minor ocular inflammation (Bruneton, 1995), and as diuretic and cholagogic agents (Mashkovskii, 1984; Litvinenko and Bubenchikova, 1988). Antimicrobial (Monya et al., 1968), antiinflammatory and immunological activities (Garbacki et al., 1999) of *C. cyanus* flowers have also been reported. Previous phytochemical studies on *C. cyanus* revealed the presence of various types of plant secondary metabolites, e.g. anthocyanins, flavonoid and their glycosides, phenolcarboxylic acids, sesquiterpenes, coumarins, etc. (Dictionary of Natural Products, 1999; Phytochemical and Ethnobotanical database, 2000; ISI database, 2000). We now report on the isolation, structure determination and general toxicity (in Brine Shrimp Lethality bioassay) of four indole alkaloids from the seeds of *C. cyanus*.

2. Results and discussion

RP-HPLC analysis of the MeOH extract of the seeds of *C. cyanus* yielded four indole alkaloids which, on the basis of extensive spectroscopic analyses (e.g. UV, LSIMS, and 1D and 2D NMR), were characterised as moschamine (**1**), *cis*-moschamine (**2**), *(E) N*-(4-hydroxycinnamoyl)-5-metho xytryptamine (**3**) and *(Z) N*-(4-hydroxycinnamoyl)-5-methoxytryptamine (**4**). Compounds **3** and **4** were found to be new natural products and named, respectively, centcyamine and *cis*-centcyamine.

All four compounds show positive colour reactions with Dragendorff's reagent. Their UV absorption maxima are similar to those of indole alkaloids reported previously from *C. moschata* (Sarker et al., 1997). In fact, the UV absorption maxima of the mixture (45:55) of **1** and **2** are identical to those previously published for moschamine and *cis*-moschamine (Sarker et al., 1997). ^{1}H and ^{13}C NMR data of **1** and **2** also match published data (Sarker et al., 1997). LSIMS and 2D-NMR

* Corresponding author. Tel.: +44-1224-262547; fax: +44-1224-262555.
E-mail address: s.sarker@rgu.ac.uk (S.D. Sarker).

0031-9422/01/$ - see front matter © 2001 Elsevier Science Ltd. All rights reserved.
PII: S0031-9422(01)00084-X

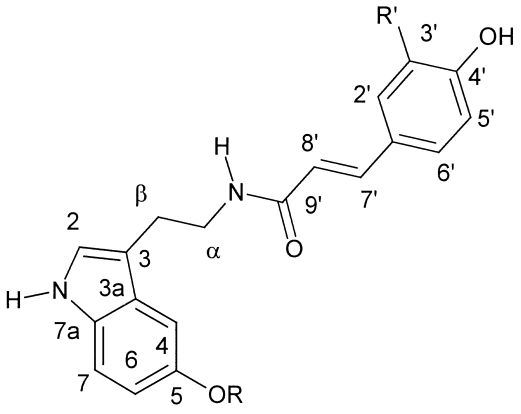

1 R = H R' = OMe

3 R = Me R' = H

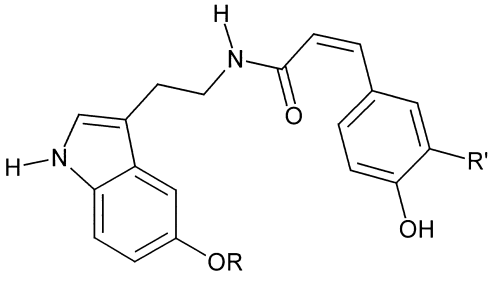

2 R = H R' = OMe

4 R = Me R' = H

experiments, *e.g.* COSY, HSQC and HMBC further confirmed the identities of **1** and **2** as moschamine and *cis*-moschamine respectively.

Compounds **3** and **4** were also isolated as an approximately 45:55 mixture of *cis-trans* isomers. Two well-separated peaks could be observed in the RP-HPLC, but on isolation they readily formed the mixture again. Owing to this unavoidable situation, all spectroscopic analyses on **3** and **4** were performed on the mixture. A LSI mass spectrum revealed $[M+H]^+$ (positive ion mode) ion peak at *m/z* 337, suggesting $M_r = 336$ and solving for $C_{20}H_{20}N_2O_3$. ^1H and ^{13}C NMR spectra (Table 1) for this mixture were similar to those for **1** and **2** with the exception that instead of a 3-methoxy-4-hydroxyphenyl, a 4-hydroxyphenyl moiety was present in **3** and **4**. In addition, instead of a 5-hydroxytryptamine (in **1** and **2**), a 5-methoxytryptamine formed the amide linkage with 4-hydroxycinnamoyl moiety **3** and **4**. ^1H–^1H COSY revealed 4 different spin systems: H-7↔H-6↔H-4, H_2-α↔H_2-β, H-7′↔H-8′ and H-2′ (H-6′)↔H-3′ (H-5′).

Table 1
^1H and ^{13}C NMR data of compounds **3** and **4** (coupling constant J = Hz in parentheses)

Carbon no.	δ_H[a]		δ_C[a]	
	3	**4**	**3**	**4**
2	6.91 *s*	6.99 *s*	123.0	122.8
3	–	–	111.1	111.1
3a	–	–	128.0	128.0
4	6.92 *d* (2.3)	6.93 *d* (2.3)	102.2	102.0
5	–	–	148.8	148.8
5-MeO	3.81 *s*	3.79 *s*	55.1	55.0
6	6.64 *dd* (2.3, 8.6)	6.62 *dd* (2.3, 8.6)	111.0	111.0
7	7.12 *d* (8.6)	7.10 *d* (8.6)	111.2	111.2
7a	–	–	132.0	132.0
α-CH_2	3.53 *t* (7.1)	3.45 *t* (7.1)	40.1	39.9
β-CH_2	2.89 *t* (7.1)	2.82 *t* (7.1)	25.0	24.8
1′	–	–	127.0	127.1
2′	7.35 *d* (8.2)	7.32 *d* (8.2)	129.8	133.6
3′	6.74 *d* (8.2)	6.66 *d* (8.2)	114.6	115.1
4′	–	–	160.0	159.5
5′	6.74 *d* (8.2)	6.66 *d* (8.2)	114.6	115.1
6′	7.35 *d* (8.2)	7.32 *d* (8.2)	129.8	133.6
7′	7.42 *d* (15.7)	6.58 *d* (12.7)	140.5	136.7
8′	6.36 *d* (15.7)	5.78 *d* (12.7)	117.5	120.4
9′	–	–	167.8	169.0

[a] δ in ppm.

All methyl, methylene and methine carbons were unambiguously assigned from ^1H–^{13}C direct correlation observed in HSQC spectrum. The most crucial ^1H–^{13}C long-range correlation observed in HMBC (Fig. 1) was the ^3J correlation from the methoxyl protons (δ_H 3.81/3.79) to the oxygenated aromatic carbon C-5 (δ_C 148.8) which was related (^3J) to H-7 (δ_H 7.12/7.10). The amide linkage was confirmed from the ^3J correlation from H_2-α (δ_H 3.53/3.45) to the carbonyl carbon (C-9′, δ_C 167.8/169.0). Thus a combination of 1D and 2D NMR techniques allowed the unambiguous characterisation of compounds **3** and **4**. Compounds **1** and **2** were previously isolated from another species, *C. moschata*, but to our knowledge, **3** and **4** are new natural products. Compounds arising from the amide formation between tryptamine (or serotonin) and cinnamic acid (or derivatives) have also been observed in few other species of the family Compositae (Dictionary of Natural Products, 1999). The co-occurence of moschamine (**1**) and *cis*-moschamine (**2**) both in *C. cyanus* and *C. moschata* might be significant from chemotaxonomic viewpoint

Both mixtures, **1** and **2**, and **3** and **4** showed significant toxicity in Brine Shrimp (*Artemia salina*) Lethality bioassay (Meyer et al., 1982). The LD_{50}s for these geometrical isomeric mixtures **1** and **2**, and **3** and **4** were determined, respectively, 21.65 and 14.43 μg/ml. The observed lethality induced by these compounds is comparable to that published for berberine chloride (LD_{50} = 22.5 μg /ml) (Meyer et al., 1982), and both the mixtures

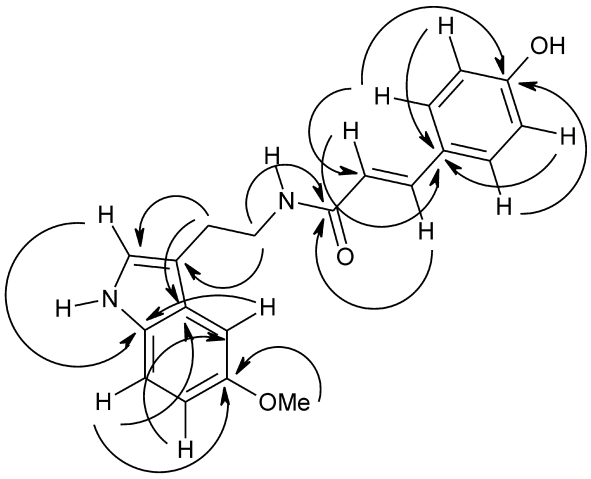

Fig. 1. ^{1}H–^{13}C long-range correlations observed in HMBC of **3**.

are more than 3 times more toxic than strychnine sulfate ($LD_{50} = 77.2$ μg/ml).

3. Experimental

3.1. General

UV spectra were obtained in MeOH. NMR spectra were recorded in CD_3OD using a Varian Unity INOVA 400 MHz NMR Spectrometer. LSIMS (positive ion mode); glycerol matrix using a Cs^+ primary ion beam on a VG Quattro triple quadrupole mass spectrometer (VG Biotech. Altrincham, UK). HPLC separation was performed in the Dionex prep-HPLC System coupled with Gynkotek GINA50 autosampler and Dionex UVD340S Photo-Diode-Array detector. RP stands for reversed-phase C_{18} column. Sep-Pak Vac 35 cc (10 g) C_{18} cartridge (Waters) was used for pre-HPLC fractionation.

3.2. Plant material

Seeds of *C. cyanus* L. (catalogue no: 304 A) were purchased from commercial source (Chiltern Seeds, Bortree Stile, Ulverston, Cumbria LA12 7PB, UK), and a voucher specimen (CA2000005) representing this purchase has been generated in the School of Pharmacy, The Robert Gordon University, Aberdeen, UK.

3.3. Extraction

Ground seeds (11.0 g) of *C. cyanaus* were Soxhlet-extracted successively with *n*-hexane, dichloromethane and MeOH. All these extracts were separately concentrated using a rotary evaporator at a maximum temperature of 45°C.

3.4. Isolation of compounds

The MeOH extract was fractionated on a Sep-Pak, using 20, 40, 60, 80 and 100% MeOH–water mixture (150 ml each) as eluent. Preparative RP-HPLC (isocratic, 32% MeOH in water, 15 ml/min) of the Sep-Pak fraction (40% MeOH in water) yielded compounds **1** and **2** as a mixture (45:55, 3.5 mg), and **3** and **4** also as a similar mixture (45:55, 2.1 mg).

3.5. Moschamine [(E) N-(3-methoxy-4-hydroxycinnamoyl)-5-hydroxytryptamine, **1**] + cis-moschamine [(Z) N-(3-methoxy-4-hydroxycinnamoyl)-5-hydroxytryptamine, **2**]

Amorphous. UV, ^{1}H and ^{13}C NMR (Sarker et al., 1997). LSIMS (positive ion mode) m/z 353 $[M+H]^+$.

3.6. Centcyamine [(E) N-(4-hydroxycinnamoyl)-5-methoxytryptamine, **3**] + cis- centcyamine [(Z) N-(4-hydroxycinnamoyl)-5-methoxytryptamine, **4**]

Amorphous. UV λ_{max} nm: 224, 287, 296, 312. ^{1}H- and ^{13}C NMR (Tables 1). LSIMS (positive ion mode) m/z 337 $[M+H]^+$.

3.7. Brine Shrimp (Artemia salina) Lethality bioassay

Brine shrimp eggs were purchased from Pet Shop, Kittybrewster, Aberdeen, UK. The bioassay was conducted following the procedure published previously (Meyer et al., 1982). LD_{50}s were determined from the 24 h counts using the probit analysis method (Finney, 1971). Percentage mortalities were adjusted relative to the natural mortality rate of the control, following Abbots formula $P = Pi - C/1 - C$, where P denotes the observed non-zero mortality rate and C represents the mortality rate of the control.

Acknowledgements

We thank Russell S. Gray (Department of Chemistry, University of Aberdeen, Aberdeen, UK) for NMR analyses.

References

Bruneton, J., 1995. Pharmacognosy, Phytochemistry, Medicinal Plants. Tec-Doc Lavoisier, Paris, New York, pp. 310.

Dictionary of Natural Products (DNP) on CD-ROM, 1999. release 8:1, Chapman and Hall, Boca Raton, FL.

Finney, D.J., 1971. Probit Analysis, 3rd Edition. Cambridge University Press, Cambridge.

Garbacki, N., Gloaguen, V., Damas, J., Bodart, P., Tits, M., Angenot, L., 1999. Antiinflammatory and immunological effects of *Centaurea cyanus* flower heads. J. Ethnopharmacology 68, 235.

GRIN database, 2000. USDA, ARS, National Genetic Resources Program. Germplasm Resources Information Network (GRIN), National Germplasm Resources Laboratory, Beltsville, Maryland, USA. Available on-line at: http/www.ars-grin.gov/cgi-bin/npgs/html/tax_search.pl?Centaurea+cyanus.

ISI database, 2000. Institute for Scientific Information, UK. Available on-line through Web of Science at: http://wos.mimas.ac.uk.

Litvinenko, V.I., Bubenchikova, V.N., 1988. Phytochemical study of *Centaurea cyanus*. Khimiya Prirodnykh Soedinenii 6, 792.

Mashkovskii, M.D., 1984. Medicinal Plants, Vol. 1. Meditsina, Moscow, 499 pp.

Meyer, B.N., Ferrigni, N.R., Putnam, J.E., Jacobson, L.B., Nicholas, D.E., McLaughlin, J.L., 1982. Brine shrimp: a convenient general bioassay for active plant constituents. Planta Medica 45, 31.

Monya, K., Sabau, M., Racz, G., 1968. Antibiotic effect of extracts from *Centaurea*. Planta Medica 16, 58.

Phytochemical and Ethnobotanical Database, 2000. USDA-ARS-NGRL, Bletsville Agricultural Research Center, Beltsville, Maryland, USA. Available on-line at: http://www.ars-grin/cgi-bib/duke/pharmacy2.pl.

Sarker, S.D., Savchenko, T., Whiting, P., Sik, V., Dinan, L., 1997. Moschamine, *cis*-moschamine, moschamindole and moschamindolol: four novel indole alkaloids from *Centaurea moschata*. Nat. Prod. Lett. 9, 189.

PERGAMON

Phytochemistry 57 (2001) 1277–1280

PHYTOCHEMISTRY

www.elsevier.com/locate/phytochem

Haplophytin-A and B: the alkaloidal constituents of *Haplophyllum acutifolium*

Muhammad Shaiq Ali[a,*], Muhammad Kashif Pervez[a], Muhammad Saleem[a], Rasool Bakhsh Tareen[b]

[a]*H.E.J. Research Institute of Chemistry, University of Karachi, Karachi-75270, Pakistan*
[b]*Department of Botany, Baluchistan University, Quetta (Baluchistan), Pakistan*

Received 13 September 2000; received in revised form 30 November 2000

Dedicated to my PhD research supervisor, Professor Viqar Uddin Ahmad on his retirement

Abstract

During the phytochemical investigation of *Haplophyllum acutifolium*, two alkaloids named haplophytin-A (**1**) and B (**2**) have been obtained. In addition, some known constituents: flindersine (**3**), kusunokinin (**4**), β-sitosterol, oleanolic acid, cholesterol and hexadecanoic acid, have also been obtained. The known constituents have never been obtained from this source. The structures of all the isolated constituents were elucidated by spectroscopic means. However, the structures of constituents **1** and **2** were further confirmed through HMBC technique. © 2001 Elsevier Science Ltd. All rights reserved.

Keywords: *Haplophyllum acutifolium*; Rutaceae; Haplophytin-A; Haplophytin-B; Structure elucidation; Spectroscopy

1. Introduction

The genus *Haplophyllum* belongs to the family Rutaceae having about 70 species distributed in the Mediterranean countries. Out of 70, seven are found in Pakistan. Chemical literature survey reveals the presence of lignans (Gozler et al., 1996; Evcium et al., 1986; Gozler and Gozler, 1984), lignan-glycosides (Gozler et al., 1994), coumarins (Ulubelen et al., 1993), sterols, flavonoids (Yuldasher et al., 1987), several classes of alkaloids [furoquinoline (Gozler et al., 1996), quinoline (Sheriha et al., 1987), pyranoquinoline (Ulubelen, 1985) and tetrahydrofuroquinoline (Rozsa et al., 1986)] in various species of the genus *Haplophyllum*. Several biologically active secondary metabolites have been detected from various *Haplophyllum* species (Sheriha et al., 1987).

The presence of variety of biologically active chemical constituents form the members of the genus *Haplophyllum* motivated us to start our phytochemical investigation on *H. acutifolium*. In the present communication, we wish to describe the isolation and characterization of two alkaloids named haplophytin-A and B, and several known constituents [flindersine (**3**), kusunokinin (**4**), β-sitosterol, oleanolic acid, cholesterol and hexadecanoic acid] from the titled source.

2. Results and discussion

Haplophytin-A (**1**) was isolated from the methanol soluble part of *Haplophyllum acutifolium*. Lack of optical rotation means that there is probably no chirality in the molecule. The compound **1** gave positive response with UV light (254 nm) and Dragendroff's reagent confirming the presence of conjugated/aromatic system and nitrogen atom, respectively. The presence of unsaturation was further determined through infra-red spectrum which showed an absorption at 1500 cm^{-1} (C=C) together with other absorption bands at 3260 and 1660 cm^{-1} due to the N–H and conjugated amide-carbonyl, respectively. The molecular weight of **1** was confirmed with the help of FDMS and found 257 a.m.u. The formula of the corresponding peak was depicted from HR–EIMS as $C_{15}H_{15}NO_3$.

The proton NMR of **1** showed the presence of three quaternary methyl signals, out of them one appeared at δ 3.90 and the remaining two at δ 1.51 as a common signal of six protons. The spectrum did not contain any

* Corresponding author. Tel.: +92-21-496-8497; fax: +92-21-496-3373.
E-mail address: shaiq303@super.net.pk (M.S. Ali).

0031-9422/01/$ - see front matter © 2001 Elsevier Science Ltd. All rights reserved.
PII: S0031-9422(01)00188-1

methylene however, the same spectrum showed five downfield methine signals at δ 7.26 (*dd*, $J=8.8$, 2.8 Hz, H-6), 7.10 (*d*, $J=8.8$ Hz, H-7), 7.25 (*dd*, 8.8, 2.8 Hz, H-8), 5.54 (*d*) and 6.76 (*d*). The two upfield methine signals at δ 5.54 and 6.76 having the same magnitude of coupling constant ($J=9.9$ Hz) confirming the vicinal orientation attested for C-11 and C-12. The chemical shifts of remaining three methine signals at δ 7.26, 7.10 and 7.25 concluded the presence of aromatic ring in the molecule. The multiplicities of these three methine signals and their corresponding coupling constants showed that they are arranged in the manner that the H-6 and H-8 are *ortho* to H-7. The methoxyl moiety could be fixed either at C-5 or C-8 which was partially confirmed through HMBC experiment (Fig. 1) and finally, by compression with the data of closely related published compounds (Huffman and Hau, 1972).

The broad-band spectrum of **1** displayed 15 carbon signal which were sorted out into three methyls, five methines and remaining seven quaternary carbons. The chemical shift of methoxyl moiety (δ 55.7) inferred the direct attachment of this moiety to aromatic ring. The position of this methoxyl moiety at C-5 was determined through NOE experiment. Upon irradiation at δ 1.51 (H-14, H-15), a 33 and 16% NOE effect of the signals of H-12 and OMe, respectively, was observed. This 16% NOE effect would not have been observed if the methoxyl moiety had been situated at C-8. The other two quaternary methyls (C-14 and C-15) appeared at δ 28.0, found to be attached with a quaternary carbon connected to the electron withdrawing hetero-atom and thus assigned to C-13 (δ 79.0). The most downfield signal at δ 162.4 was due to the conjugated amide whereas the second quaternary downfield signal at δ 155.0 was due to the carbon at which methoxyl moieties is attached (C-5). The two methine signals of the ring having the oxygen as an hetero-atom appeared at δ 126.2 and 117.5 due to C-11 and C-12, respectively. The remaining three aromatic methine signals were observed in the carbon spectrum at their usual positions (δ 103.5, 120.5 and 117.4).

With the help of spectral evidences given earlier, the structure of the discussed compound was assigned as **1**

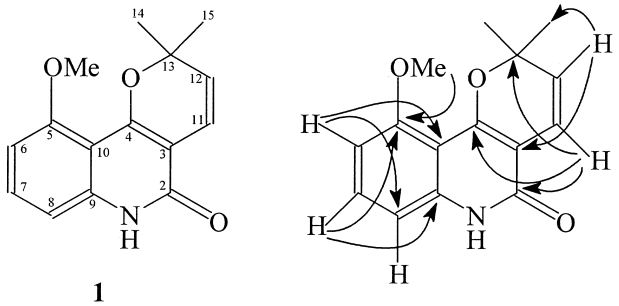

1

Fig. 1. HMBC connectivities.

and named haplophytin-A which is a new addition in the alkaloidal constituents of *Haplophyllum acutifolium*. Although similar types of compounds are already reported in the literature (Huffman and Hau, 1972) but having no methoxyl at C-5.

Haplophytin-B (**2**) was obtained from the same extract with the elution of 45% ethyl acetate in hexane. It showed positive UV response confirming the presence of conjugated/aromatic system in the molecule. The presence of unsaturation was supported by the absorption at 1500 cm^{-1} (C=C) in the IR spectrum which also showed an intense absorption band at 3320 cm^{-1} due to the hydroxyl function in the molecule. The molecular mass of **2** was determined through FDMS and found 347 a.m.u. The formula of this peak was observed as $C_{18}H_{21}NO_6$ with the aid of HRMS.

The proton spectrum of **2** exhibited four methyl resonances, out of them two at δ 4.47 and 4.10 due to the methoxyl moieties and their chemical shifts suggested direct attachment to the aromatic system. The remaining two quaternary methyl signals appeared at δ 1.29 and 1.25 (H-4′ and H-5′). The molecule contains only one methylene appeared as two separate sets of double-doublets at δ 4.13 ($J=9.9$, 8.0 Hz, Ha-′1) and 3.81 ($J=8.0$, 2.5 Hz, Hb-′1). The same spectrum showed four downfield methine signals at δ 8.01 (*d*, $J=9.4$ Hz, H-5), 7.34 (*d*, $J=9.4$ Hz, H-6), 7.73 (*d*, $J=2.8$ Hz, H-α) and 7.30 (*d*, $J=2.8$ Hz, H-β) and an upfield carbinylic proton at δ 4.49 (H-′2) as a double-doublet ($J=9.9$, 2.5 Hz). The signals at δ 8.01 and 7.34 and their same coupling constant confirmed their *ortho* arrangement and thus assigned to H-5 and H-6, respectively. The methine signal at δ 7.73 showed the presence of an electron withdrawing hetero-atom in the vicinity and attested for H-α. With the help of coupling constant of H-α ($J=2.8$ Hz) the H-β was located in the spectrum at δ 7.30.

The broad-band spectrum of haplophytin-B exhibited 18 carbon signals which were resolved into four methyls, one methylene, five methines and remaining eight quaternary carbon atoms. Out of four methyl signals, two were at δ 60.0 and 61.9 due to the methoxyl moieties in the molecule and their positions were fixed through HMBC experiment (Fig. 2) and literature values (Bessonova and Yunusov, 1986; Rasulova et al., 1987). The remaining two methyl signals appeared at δ 25.0 and 26.9 due to the C-4′ and C-5′, respectively. The only one methylene (C-1′) present in the molecule resonated at δ 72.5. An upfield methine signal resonated at δ 77.8 corresponded to the carbinylic carbon. The molecule contains four downfield methine signals at δ 119.5 (C-5), 114.0 (C-6), 144.3 (C-α) and 106.5 (C-β). The most downfield methine signal at δ 144.3 was due to the direct attachment to an hetero-atom (oxygen). A hydroxyl function attached to the quaternary carbon at which two quaternary methyls are attached appeared at δ 72.8.

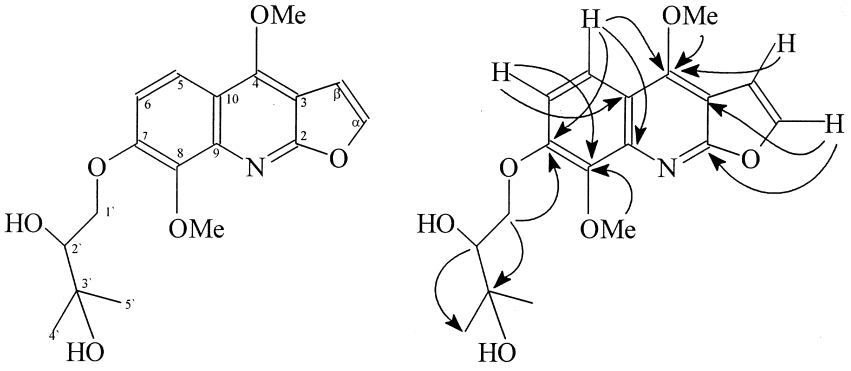

2

Fig. 2. HMBC connectivities.

Three more quaternary carbons resonated at δ 153.9 (C-4), 142.1 (C-8) and 142.9 (C-7) were due to the two methoxyl and a side chain containing carbons, respectively. The position of side chain at C-7 was determined through HMBC connectivities (Fig. 2) and n.O.e measurements. Upon irradiation at δ 4.10 (C-8 OMe), a 29 and 13% NOE effect of the signals of H-2′ and H-1′, respectively, was observed suggested the attachment of side chain at C-3. Such a type of skeleton is already reported in literature with either different side chains or sugar units (Bessonova and Yunusov, 1986; Rasulova et al., 1987) and therefore, the previously discussed compound is assigned as **2** and named haplophytin-B. This compound is also a new addition in the alkaloidal constituents of *H. acutifolium*.

In addition to **1** and **2**, six more known constituents have been detected which have never been reported so far from our investigated source and their data are given in Section 3. The new constituents, haplophytin-A and B were found totally inactive against various tested bacteria and fungi.

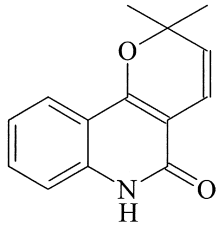

3

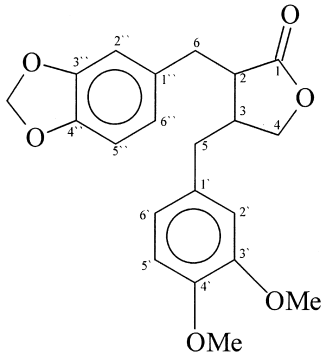

4

3. Experimental

3.1. General

The ^{1}H and ^{13}C NMR spectra were recorded at 500, 400, 300 and 75,100, 125 MHz, respectively, on Brüker AM-500, AM-400 and AM-300 in $CDCl_3$.

3.2. Collection and identification

The plant material was collected from Quetta (Pakistan) in May 1999 and identified by Dr. R.B. Tareen, Department of Botany, Baluchistan University, Quetta (Baluchistan), where the voucher specimen has been deposited in the herbarium.

3.3. Extraction and isolation

The collected plant material (15 kg) was dried under shade and chopped into small pieces. The dried and chopped material (8 kg) was soaked in MeOH (14 l) for a period of 10 days. The percolation was repeated three times. The MeOH was evaporated under reduced temperature (28°C) and the gummy material thus obtained (276 g) was subjected to silica gel column chromatography using hexane, hexane–ethyl acetate, ethyl acetate, ethyl acetate–methanol and finally, pure methanol as mobile phase.

The fraction obtained with 15% ethyl acetate in hexane showed a strong UV-active spot on TLC with some minor impurities which on washing with methanol yielded **1** as a white powder (13 mg). The same UV active spot on spraying with Dragendroff's reagent changed into an orange spot confirming the presence of nitrogen in the molecule.

Haplophytin-A (**1**): m.p.: 209–210.5°C; $[\alpha]_D$: 0 ($CHCl_3$, *c* 0.506); UV $\lambda_{max}^{CHCl_3}$ nm (log ε): 244 (7.92); IR ($CHCl_3$): 3260 (N–H), 1660 (C=O), 1500 (C=C) cm^{-1}; EI–MS: *m/z* 257 $[M^+]$, 242 $[M–Me]^+$ (100%), 199, 121, 106; FDMS: *m/z* 257; HR–MS: *m/z* 257.9968 ($C_{15}H_{15}NO_3$ requires *m/z* 257.10518); ^1H NMR ($CDCl_3$, 400 MHz): δ 7.26 (1H, *dd*, *J* = 8.8, 2.8 Hz, H-6), 7.25 (H, *dd*, *J* = 8.8, 2.8 Hz, H-8), 7.10 (1H, *d*, *J* = 8.8 Hz,H-7), 6.76 (1H, *d*, *J* = 9.9 Hz, H-12), 5.54 (1H, *d*, *J* = 9.9 Hz, H-11), 3.90 (3H, *s*, OMe) and 1.51 (6H, s, H-14, 15); ^{13}C NMR ($CDCl_3$, 100 MHz): δ 162.4 (C-2), 115.7 (C-3), 156.0 (C-4), 155.0 (C-5), 103.5 (C-6), 120.5 (C-7), 117.4 (C-8), 132.9 (C-9), 106.5 (C-10), 126.2 (C-11), 117.5 (C-12), 79.0 (C-13), 28.0 (C-14, 15) and 55.7 (OMe); HMBC: see Fig. 1.

Elution with 45% ethyl acetate in hexane from the same column afforded another UV and Dragendroff's reagent positive sample as a dirty white powder (16.5 mg) which on washing with a 1:1 mixture of chloroform and hexane yielded **2**.

Haplophytin-B (**2**): mp: 151.5–153°C; $[\alpha]_D$: +63.6° (MeOH, *c* 0.33); UV λ_{max} CD_3OD nm (log ε): 251 (5.16); IR (KBr): 3320 (OH), 1500 (C=C) cm^{-1}; EI–MS: *m/z* 347 $[M]^+$, 287, 227 [M–side chain$^+$] (100%), 216; FDMS: *m/z* 347; HR–MS: *m/z* 347.13711 ($C_{18}H_{21}N$ O6 requires *m/z* 347.13687); ^1H NMR (CD_3OD, 500 MHz): δ 8.01 (1H, *d*, *J* = 9.4 Hz, H-5), 7.73 (1H, *d*, *J* = 2.8 Hz, H-α), 7.34 (1H, *d*, *J* = 9.4 Hz, H-6), 7.30 (1H, *d*, *J* = 2.8 Hz, H-β), 4.49 (1H, *dd*, *J* = 9.9, 2.5 Hz, H-′2), 4.47 (3H, s, C-4 OMe), 4.13 (1H, *ds*, *J* = 9.9, 8.0 Hz, Ha-′1), 4.10 (3H, *s*, C-8 OMe), 3.81 (1H, *ds*, *J* = 8.0, 2.5 Hz, Hb-′1), 1.29 (3H, s, H-′4), 1.25 (3H, s, H-′5); ^{13}C NMR (CD_3OD, 125 M Hz): δ 165.8 (C-2), 115.9 (C-3), 153.9 (C-4), 119.5 (C-5), 114.0 (C-6), 142.9 (C-7), 142.1 (C-8), 159.0 (C-9), 103.3 (C-10), 144.3 (C-α), 106.5 (C-β), 61.9 (C-8 OMe), 60.0 (C-4 OMe), 72.5 (C-′1), 77.8 (C-′2), 72.8 (C-′3), 25.0 and 26.9 (C-′4, C-′5); HMBC: see Fig. 2.

References

Bessonova, I.A., Yunusov, S.Yu., 1986. Alkaloids of the roots of the *Haplophyllum obtusifolium*. Chemistry of Natural Products 22 (6), 684–686.

Evcium, U., Gozler, B., Freyer, A.J., Shamma, M., 1986. Haplomyrtin and (−) haplomyrfolin: two lignans from *Haplophyllum myrtifolium*. Phytochemistry 25, 1949–1951.

Gozler, B., Gozler, T., Saglam, H., Hesse, M., 1996. Minor lignans from *Haplophyllum cappadocicum*. Phytochemistry 42 (3), 689–693.

Gozler, B., Onur, M.A., Gozler, T., Kadan, G., Hesse, M., 1994. Lignans and lignan glycosides from *Haplophyllum cappadocicum*. Phytochemistry 37 (6), 1693–1998.

Gozler, B., Rentsch, D., Gozler, T., Unver, N., Hesse, M., 1996. Lignans, alkaloids and coumarins from *Haplophyllum vulcanicum*. Phytochemistry 42 (3), 695–699.

Gozler, T., Gozler, B., 1984. Konyanin: a new lignan from *Haplophyllum vulcanicum*. Tetrahedron 40, 1145–1150.

Huffman, J.W., Hsu, T.M., 1972. A one step synthesis of flindersine. Tetrahedron Lett., 141–143.

Rasulova, Kh.A., Bessonova, I.A., Yagudaev, M.R., Yunusov, S.Yu, 1987. Haplosinine — a new furanoquinoline glycoalkaloid. Chemistry of Natural Products 23 (6), 731–734.

Rozsa, Zs., Rabik, M., Szendrei, K., Kalman, A., Argay, Gy., Pelczer, I., Aynechi, M., Meste, M., Reisch, J., 1986. Dihydroperfamine, an alkaloid from *Haplophyllum glabrinum*. Phytochemistry 25 (8), 2005–2007.

Sheriha, G.M., Abouamer, K., Elshtaiwi, B.Z., Ashour, A.S., Abed, F., Alhallaq, H.H., 1987. Quinoline alkaloids and cytotoxic lignans from *Haplophyllum tuberculatum*. Phytochemistry 26, 3339–3341.

Ulubelen, A., Mericli, A.H., Mericli, F., Sonhez, U., Ilarslan, R., 1993. Alkaloids and coumarins from *Haplophyllum thesioides*. Nat. Prod. Lett. 1 (4), 269–272.

Ulubelen, A., 1985. Alkaloids from *Haplophyllum buxbaumii*. Phytochemistry 24 (2), 372–374.

Yuldasher, M.P., Batirov, E.Kh., Malikov, V.M., 1987. Flavonoids of some plants of the genus *Haplophyllum*. Kim. Prir. Soendin 3, 452–453.

PERGAMON

Phytochemistry 57 (2001) 1281–1285

PHYTOCHEMISTRY

www.elsevier.com/locate/phytochem

Minor cytotoxic and antibacterial compounds from the rhizomes of *Amomum aculeatum*

Jörg Heilmann[a,*], Reto Brun[b], Stefan Mayr[a], Topul Rali[c], Otto Sticher[a]

[a]*Department of Applied BioSciences, Institute of Pharmaceutical Sciences, Swiss Federal Institute of Technology (ETH) Zurich, CH-8057 Zurich, Switzerland*

[b]*Swiss Tropical Institute, Socinstr. 57, CH-4002 Basel, Switzerland*

[c]*PNG Biodiversity PTY Ltd., Port Moresby, Papua New Guinea*

Received 11 January 2001; received in revised form 27 March 2001

Abstract

A new cytotoxic 1,7-dioxa-dispiro[5.1.5.2]pentadeca-9,12-dien-11-one derivative, aculeatin D, and a new alkenone, 5-hydroxy-hexacos-1-en-3-one, have been isolated as minor compounds from the rhizomes of *Amomum aculeatum*. Their structures have been determined mainly by NMR spectroscopy and mass spectrometry. Aculeatin D showed high cytotoxicity against the KB and the L-6 cell line with IC_{50} of 0.38 μg/ml and 1 μg/ml, respectively. Additionally, it revealed remarkable activity against two *Plasmodium falciparum* strains, as well as against *Trypanosoma brucei rhodesiense* and *Trypanosoma cruzi*. 5-Hydroxy-hexacos-1-en-3-one exhibited neither cytotoxic nor antiprotozoal activity, whereas antibacterial testing against *Bacillus cereus*, *Escherichia coli* and *Staphylococcus epidermidis* showed moderate to strong activity for both compounds. © 2001 Published by Elsevier Science Ltd. All rights reserved.

Keywords: Amomum aculeatum; Zingiberaceae; 1,7-Dioxa-dispiro[5.1.5.2]pentadeca-9,12-dien-11-one; Aculeatin D; Cytotoxicity; Antiprotozoal activity

1. Introduction

Recently we isolated three novel dioxa-dispiroketals as main compounds from the petroleum ether extract of the rhizomes of *Amomum aculeatum* (Heilmann et al., 2000), a plant used in the folk medicine of Papua New Guinea against fever and malaria (Holdsworth and Mahana, 1983). These compounds, which we named aculeatins A–C, represent a novel class of natural products exhibiting high cytotoxicity against the KB cell line and promising activity against the *Plasmodium falciparum* strains K1 and NF54. Further investigation on the petroleum ether extract led to the isolation of two new minor compounds: the first one was established as *rel*-(2*R*,4*S*,6*S*)-4-hydroxy-2-tridecyl-1,7-dioxa-dispiro[5.1.5.2]pentadeca-9,12-dien-11-one (= aculeatin D, **1**) another dioxa-dispiroketal with differing stereochemistry at C-4. The second compound, the alkenone 5-hydroxy-hexacos-1-en-3-one (**2**), is possibly a precursor or a degradation product during the biosynthesis or the metabolism of these dispiroketals.

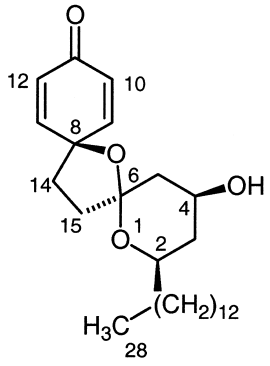

1

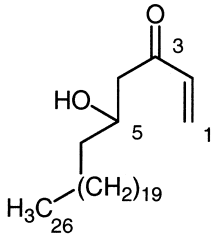

2

2. Results and discussion

HRESIMS of compound **1** revealed a pseudomolecular ion $[M+Na]^+$ at m/z 441.2970 which strongly

* Corresponding author. Tel.: +41-1-635-60-49; fax: +41-1-635-68-82.

E-mail address: heilmann@pharma.ethz.ch (J. Heilmann).

0031-9422/01/$ - see front matter © 2001 Published by Elsevier Science Ltd. All rights reserved.
PII: S0031-9422(01)00174-1

suggested that **1** was a stereoisomer of the 1,7-dioxa-dispiro[5.1.5.2]pentadeca-9,12-dien-11-one derivatives aculeatin A and B. In accordance the ^{13}C NMR experiments (including DEPT 135 and DEPT 90) showed the typical signals of the 1,7-dioxa-dispiro[5.1.5.2]pentadeca-9,12-dien-11-one skeleton: Four methine and one quaternary carbons at δ 184.9 (C-11, *s*), 151.7 (C-9, *d*), 148.7 (C-13, *d*), 127.7 (C-12, *d*) and 127.2 (C-10, *d*) characteristic of a dienone moiety, two quaternary carbons at δ 109.3 (C-6) and 78.1 (C-8) corresponding to the spiro centres as well as 8 signals of methylene carbons between δ 29.3 and 29.6 belonging to the alkyl side chain. The ^1H NMR spectrum resembled those of aculeatin A and B except of remarkable upfield shifts between 0.5 and 1 ppm for protons H-2 (δ 2.93) and H-4 (δ 3.38) indicating different stereochemistry in this part of the molecule (for ^1H and ^{13}C NMR data, see Table 1). ^1H, ^1H-COSY, HSQC and HMBC experiments established identical correlations as for aculeatin A and B confirming again the assumption that all three are stereoisomers. An ROESY experiment revealed strong NOEs between H-2 and H-4 as well as between H-15 (δ 1.78 and 1.13) and H-2/H-4 for compound **1** which confirmed that this compound is the hitherto unknown *rel*-(2*R*,4*S*,6*S*)-4-hydroxy-2-tridecyl-1,7-dioxa-dispiro[5.1.5.2]pentadeca-9,12-dien-11-one. Therefore aculeatin D (**1**) constitutes the fourth representative of the novel class of 1,7-dioxa-dispiro[5.1.5.2]pentadeca-9,12-dien-11-ones.

Aculeatin D (**1**) was evaluated for its cytotoxicity and antiprotozoal activity (see Table 2). Compared to aculeatin B [*rel*-(2*R*,4*R*,6*S*)-4-hydroxy-2-tridecyl-1,7-dioxa-dispiro[5.1.5.2]pentadeca-9,12-dien-11-one], inversion of stereochemistry at C-4 led to a doubled cytotoxicity against the KB cell line (IC_{50} 0.38 μg/ml (**1**) versus 0.82 μg/ml (aculeatin B)). In contrast, activity against the *Plasmodium falciparum* strains K1 and NF54 decreased significantly from aculeatin B to aculeatin D (**1**) (0.18 versus 0.42 μg/ml for *P. falciparum* strain K1 and 0.26 versus 0.47 μg/ml for *P. falciparum* strain NF54). Ongoing studies focus now on the discovery of the hitherto unknown mechanisms of cytotoxicity and anti-

Table 1
^1H (500 MHz) and ^{13}C (75.5 MHz) NMR data of compounds **1** (in C_6D_6) and **2** (in $CDCl_3$). Chemical shifts in ppm, *J* in Hz

C/H	**1** ^1H	**1** ^{13}C[a]	**2** ^1H	**2** ^{13}C[a]
1			6.28, *dd* (*J* = 0.8, 17.7) 5.93, *dd* (*J* = 0.8, 10.5)	119.2 *t*
2	2.93, *m*	71.4 *d*	6.38, *dd* (*J* = 10.5, 17.7)	136.7 *d*
3	1.60, *m* 1.05, *m*	41.2 *t*		202.0 *s*
4	3.38, *m*	66.6 *d*	2.82, *dd* (*J* = 2.7, 17.5) 2.70, *dd* (*J* = 9, 17.5)	45.7 *t*
5	1.843, *ddd* (*J* = 1.5, 4, 9.8) 1.75 *m*	44.0 *t*	4.13, *m*	67.6 *d*
6		109.3 *s*	1.55, *m* 1.45, *m*	36.5 *t*
7			1.35–1.25, *m*	29.3–29.6 *t*
8		78.1 *s*	1.35–1.25, *m*	29.3–29.6 *t*
9	6.90, *dd* (*J* = 2.9, 10)	151.7 *d*	1.35–1.25, *m*	29.3–29.6 *t*
10	6.07, *dd* (*J* = 2, 10)	127.2 *d*	1.35–1.25, *m*	29.3–29.6 *t*
11		184.9 *s*	1.35–1.25, *m*	29.3–29.6 *t*
12	6.04, *dd* (*J* = 2, 10)	127.7 *d*	1.35–1.25, *m*	29.3–29.6 *t*
13	6.20, *dd* (*J* = 2.9, 10)	148.7 *d*	1.35–1.25, *m*	29.3–29.6 *t*
14	1.88, *m* 1.42, *m*	35.1 *t*	1.35–1.25, *m*	29.3–29.6 *t*
15	1.78, *m* 1.13, *m*	33.0 *t*	1.35–1.25, *m*	29.3–29.6 *t*
16	1.55, *m* 1.31, *m*	36.2 *t*	1.35–1.25, *m*	29.3–29.6 *t*
17	1.35–1.25, *m*	26.2 *t*	1.35–1.25, *m*	29.3–29.6 *t*
18–23	1.35–1.25, *m*	29.3–29.6 *t*	1.35–1.25, *m*	29.3–29.6 *t*
24	1.35–1.25, *m*	29.3–29.6 *t*		31.9 *t*
25	1.35–1.25, *m*	29.3–29.6 *t*		22.7 *t*
26	1.35–1.25, *m*	32.3 *t*	0.91, *t* (*J* = 6.9)	14.1 *q*
27	1.35–1.25, *m*	23.1 *t*		
28	0.92, *t* (*J* = 6.9)	14.4 *q*		

[a] Multiplicities determined by DEPT 135 and DEPT 90.

Table 2
Cytotoxicity, antiprotozoal and antibacterial activity of compounds **1** and **2** (values given as IC_{50} in μg/ml or as MIC (antibacterial activity) in μg/ml, cytotoxicity $n=4$, other $n=3$)

	1	2	Reference compounds
Cytotoxicity			
KB cells	0.38	Not active	Podophyllotoxin, 0.01
L-6 cells	1.00	Not active	
Antiprotozoal activity			
P. falciparum K1	0.42	Not active	Chloroquine, 0.09
P. falciparum NF54	0.47	Not active	Chloroquine, 0.004
T.b. rhodesiense	0.20	Not active	Melarsoprol, 0.0007
T. cruzi	0.49	Not active	Benznidazole, 2.1
Antibacterial activity			
B. cereus	16	32	Chloramphenicol, 4
E. coli	16	64	Chloramphenicol, 2
St. epidermidis	8	16	Chloramphenicol, 4
Antifungal activity			
C. albicans	Not active	Not active	Miconazole nitrate, 32

plasmodial activity to find analogous structures with more specific biological effects.

5-Hydroxy-hexacos-1-en-3-one (**2**) exhibited a molecular ion at m/z 394 in the positive DEIMS. ^{13}C NMR experiments sorted 26 C-atoms into one quaternary, two methines, 22 methylenes and one methyl and led to a molecular formula of $C_{26}H_{50}O_2$ for **2** (for ^{13}C NMR data see Table 1). A carbonyl carbon resonating at δ 202.0, a methylene carbon at δ 119.2 and a methine carbon at δ 136.7 suggested the presence of a 1-en-3-one substructure. Twelve methylene signals between δ 29.3 and 29.6 revealed the presence of an alkyl chain and a methine carbon at δ 67.6 indicated an additional hydroxyl group. The suggestions from the ^{13}C NMR were confirmed by the ^1H NMR spectrum which showed signals at δ 6.28 (*dd*, $J=0.8$, 17.7) and δ 5.93 (*dd*, $J=0.8$, 10.5) for H-1, and at δ 6.38 (*dd*, $J=10.5$, 17.7) for H-2, as well as by a multiplet at δ 4.13 corresponding to H-5. ^1H, ^1H-COSY, HSQC and HMBC experiments established the structure and allowed the connection of the substructures as well as the assignment of all ^1H and ^{13}C NMR signals outside the region δ 1.25–1.35 and δ 29.3–29.6, respectively. 5-Hydroxy-hexacos-1-en-3-one (**2**) is also a new compound to the best of our knowledge. Due to the same number of C-atoms and the 5-hydroxy-1-en-3-one substructure, it seemed reasonable to assume that this compound represents possibly a precursor or a degradation product of the aculeatins what has to be clarified in further studies.

5-Hydroxy-hexacos-1-en-3-one (**2**) showed neither cytotoxic nor antiprotozoal activity. The antibacterial testing against *Bacillus cereus*, *Escherichia coli* and *Staphylococcus epidermidis* revealed moderate activity in the same range compared to the aculeatins A-C (unpublished results) but somewhat lower compared to aculeatin D (**1**) (see Table 2).

3. Experimental section

3.1. General

^{13}C NMR spectra were measured on a Bruker AMX-300 spectrometer (operating at 300.13 MHz for ^1H and 75.47 for ^{13}C) at 295 K. All other NMR spectra were recorded on a Bruker DRX-500 spectrometer (operating at 500.13 MHz for ^1H and 125.77 for ^{13}C) at 295 K. Spectra were measured in $CDCl_3$ and C_6D_6 and referenced against residual $CHCl_3$ (^1H δ 7.27) and $CDCl_3$ (^{13}C δ 77.0) or residual C_6H_6 (^1H δ 7.16) and C_6D_6 (^{13}C δ 128.0). DEI-MS (at 70 eV) were measured on a Hitachi-Perkin Elmer-RMUGM mass spectrometer and HRESIMS were recorded on a 4.7T-FT/ICR IonSpec Ultima mass spectrometer. A description of the other instruments used in this study has been provided in previous reports (Quadri-Spinelli et al., 2000; Winkelmann et al., 2000).

3.2. Collection and extraction

Rhizomes and roots of *Amomum aculeatum* Roxb. were collected in the Central Province of Papua New Guinea in September 1996. A voucher specimen is deposited in the Rijksherbarium (Leiden, The Netherlands) with the identification number ETH 96/1. Air dried plant material (659 g) was extracted successively with petroleum ether, CH_2Cl_2, MeOH, MeOH-H_2O 7:3 and H_2O. The extracts were stored under nitrogen at−20°C.

3.3. Isolation

The petroleum ether extract (11.1 g) was subjected to VLC on silica gel (35–70 μm) using a step gradient of hexane, hexane-CH_2Cl_2, CH_2Cl_2, CH_2Cl_2-ethyl acetate, ethyl acetate, ethyl acetate-MeOH and MeOH. The fraction CH_2Cl_2-ethyl acetate 4:6, yielding a mixture of aculeatin B,C and D (**1**), was separated twice by CC on silica gel (60–200 μm) using methyl–*tert*–butylether–diethylether–*n*-hexane 7.5:24.1:0.9 as eluent. Fractions containing aculeatin D were combined and purified on Sephadex LH-20 (cyclohexane–CH_2Cl_2–MeOH 7:4:1) yielding 5.3 mg pure **1**. The CH_2Cl_2-ethyl acetate 8:2 VLC fraction (1.23 g) was subjected to open column chromatography on silica gel (60-200 μm) using diisopropylether-diethylether-*n*-hexane 14.3:36.6:49.1 as eluent. Fractions containing **2** were pooled and further separated on silica gel (60–200 μm) with cyclohexane-CH_2Cl_2-MeOH 7:4:1 as eluent. Fractions containing **2**

were purified with prep. TLC and *n*-hexane-diethylether 1:1 as eluent yielding pure 5-hydroxy-hexacos-1-en-3-one (1.5 mg, **2**).

3.4. rel-(2R,4S,6S)-4-Hydroxy-2-tridecyl-1,7-dioxa-dispiro[5.1.5.2]pentadeca-9,12-dien-11-one (= aculeatin D, **1**)

Yellow oil (5.3 mg). $[\alpha]_D^{20}+46.5$ ($c=1$, $CHCl_3$); UV (MeOH) λ_{max} (lgε) 230 (4.15); positive DEI-MS (rel. intensity) m/z 418 $[M]^+$ (<1), 400 $[M\text{-}H_2O]^+$ (<1), 372 (<1), 281 (1), 235 (6), 165 (19), 107 (100); HRESIMS m/z 441.2970 $[M+Na]^+$ for $C_{26}H_{42}O_4$ (cal. 441.2980).

3.5. 5-Hydroxy-hexacos-1-en-3-one (**2**)

White waxy solid (1.5 mg). $C_{26}H_{50}O_2$; unstable; $[\alpha]_D^{20}-7$ ($c=0.1$, $CHCl_3$,). DEI–MS (pos. mode) m/z 394 $[M]^+$ (2); 339 (14), 297 (11), 98 (58), 97 (100), 55 (95).

3.6. Antiprotozoal activity

3.6.1. Plasmodium falciparum

Antiplasmodial activity was determined using two strains of *P. falciparum*: NF54 (sensitive to all known drugs) and K1 (resistant to chloroquine and pyrimethamine). A modification of the [^{3}H]-hypoxanthine incorporation assay was used (Matile and Pink, 1990). Briefly, infected human red blood cells were exposed to serial drug dilutions in microtiter plates for 48 h. Viability was assessed by measuring the incorporation of [^{3}H]-hypoxanthine by liquid scintillation counting. From the sigmoidal inhibition curves IC_{50} values were calculated.

3.6.2. Trypanosoma cruzi

Rat skeletal myoblasts (L-6 cells) were seeded in 96-well microtiter and infected with trypomastigotes of *T. cruzi* (Tulahuen strain C2C4) containing the β-galactosidase (Lac Z) gene. A serial drug dilution was added and the plates incubated for 4 days. The substrate CPRG/Nonidet was added to the wells and the colour reaction which developed was read photometrically at 540 nm. From the sigmoidal inhibition curves IC_{50} values were calculated.

3.6.3. Trypanosoma b. rhodesiense

Serial drug dilutions in Minimum Essential Medium supplemented according to Baltz et al. (1985) were added to microtiter plates. Trypomastigotes of *T.b.rhodesiense* STIB 900 were added to each well and the plates incubated for 72 h. Viability was assessed by Alamar Blue leading to a colour reaction which was read in a fluorescence scanner (Millipore Cytofluor 2300) (Räz et al., 1997). Fluorescence development was expressed as percentage of the control, and IC_{50} values were determined.

3.7. Cytotoxic activity

The screening for activity against the KB cell line (ATCC CCL 17) was performed as described previously (Ankli et al., 2000).

Activity against L-6 cells (rat skeletal myoblasts) was determined with the Alamar Blue assay using the same protocol as for *T. b. rhodesiense*.

3.8. Antibacterial and antifungal activity

The antimicrobial activity testing against *Bacillus cereus*, *Escherichia coli, Staphylococcus epidermidis* and *Candida albicans* followed the instructions published in Ankli et al. (2000).

Acknowledgements

Special thanks are given to Dr. O. Zerbe (Institute of Pharmaceutical Sciences, ETH Zurich) for recording NMR spectra and many helpful discussions. Mr. M. Wasescha (Institute of Pharmaceutical Sciences, ETH Zurich) is gratefully acknowledged for performing the KB cell assay. The authors are indepted to Dr. W. Amrein, Mr. R. Häflinger and Mr. O. Greter (Institute of Organic Chemistry, ETH Zurich) for recording mass spectra, and Dr. E. Zass (Institute of Organic Chemistry, ETH Zurich) for performing literature searches. Furthermore we wish to express our thanks to P. Piskaut (University of Papua New Guinea), Dr. M. Baltisberger (Geobotanical Institute, ETH Zurich) and Dr. M. M. J. van Balgooy (Rijksherbarium, Leiden, The Netherlands) for identification of plant material. A grant from the Studienstiftung des deutschen Volkes to Stefan Mayr is gratefully acknowledged.

References

Ankli, A., Heilmann, J., Heinrich, M., Sticher, O., 2000. Cytotoxic cardenolides and antibacterial terpenoids from *Crossopetalum gaumeri*. Phytochemistry 54, 531–537.

Baltz, T., Baltz, D., Giroud, C., Crockett, J., 1985. Cultivation in a semi-defined medium of animal infective forms of *Trypanosoma brucei*, *T. equiperdum*, *T. evansi*, *T. rhodesiense* and *T. gambiense*. EMBO Journal 4, 1273–1277.

Heilmann, J., Mayr, S., Brun, R., Rali, T., Sticher, O., 2000. Antiprotozoal activity and cytotoxicity of novel 1,7-dioxa-dispiro[5.1.5.2]-pentadeca-9,12-dien-11-one derivatives from *Amomum aculeatum*. Helvetica Chimica Acta 83, 2939–2945.

Holdsworth, D.K., Mahana, P., 1983. Traditional medicinal plants of Huon Peninsula, Morobe province, Papua New Guinea. International Journal of Crude Drug Research 21, 121–133.

Matile, H., Pink, J.R.L., 1990. *Plasmodium falciparum* malaria parasite cultures and their use in immunology. In: Lefkovits, I., Pernis,

B. (Eds.), Immunological Methods, Vol. IV. Academic Press, San Diego, pp. 221–234.

Räz, B., Iten, M., Grether-Bühler, Y., Kaminsky, R., Brun, R., 1997. The Alamar Blue® assay to determine drug sensitivity of African trypanosomes (*T. b. rhodesiense* and *T. b. gambiense*) in vitro. Acta Tropica 68, 139–147.

Quadri-Spinelli, T., Heilmann, J., Rali, T., Sticher, O., 2000. Bioactive coumarin derivatives from the fern *Cyclosorus interruptus*. Planta Medica 66, 728–733.

Winkelmann, K., Heilmann, J., Zerbe, O., Rali, T., Sticher, O., 2000. New phloroglucinol derivatives from *Hypericum papuanum*. Journal of Natural Products 63, 104–108.

PERGAMON

Phytochemistry 57 (2001) 1287–1291

PHYTOCHEMISTRY

www.elsevier.com/locate/phytochem

An ellagic compound and iridoids from *Cornus capitata* root cultures

Norie Tanaka[a,*], Takashi Tanaka[b], Toshihiro Fujioka[c], Hiroko Fujii[c], Kunihide Mihashi[c], Koichiro Shimomura[d], Kanji Ishimaru[a]

[a]*Department of Applied Biological Sciences, Faculty of Agriculture, Saga University, 1 Honjo, Saga 840-8502, Japan*
[b]*Faculty of Pharmaceutical Sciences, Nagasaki University, 1-14 Bunkyo-chou, Nagasaki 852-8521, Japan*
[c]*Faculty of Pharmaceutical Sciences, Fukuoka University, 8-19-1 Nanakuma, Jonan-ku, Fukuoka 814-0180, Japan*
[d]*Tsukuba Medicinal Plant Research Station, National Institute of Health Sciences, 1 Hachimandai, Tsukuba, Ibaraki 305-0843, Japan*

Received 1 December 2000; received in revised form 2 March 2001

Abstract

An ellagic acid derivative, 3,3′-di-*O*-methylellagic acid 4-(5″-acetyl)-α-L-arabinofuranoside, and two iridoid glucosides, 6α-dihydrocornic acid and 6β-dihydrocornic acid, were isolated from *Cornus capitata* adventitious roots cultured in Murashige–Skoog (Murashige, T., Skoog, F., 1962. A revised medium for rapid growth and bioassays with tobacco tissue cultures. Physiol. Plant. 15, 473–487) liquid medium containing 10 μM $CuSO_4$. Three known related metabolites, i.e. stenophyllin H1, dihydrocornin and cornin were also produced in the root cultures. The chemical structures were characterized by analysis of spectroscopic data. © 2001 Elsevier Science Ltd. All rights reserved.

Keywords: *Cornus capitata*; Cornaceae; Adventitious root; Ellagic acid; Iridoid

1. Introduction

The genus *Cornus* is well known to contain a large amount of polyphenols such as tannins (especially hydrolyzable tannins) (Okuda et al., 1984; Hatano et al., 1989a,b, 1990; Lee et al., 1989) and iridoid compounds (Bate-Smith et al., 1975; Jensen et al., 1973a,b, 1975; Nishino et al., 1988; Stermitz and Krull, 1998). *Cornus capitata,* often decorating the mountainsides in the Himalayas with its bright yellow four bracts, is used as a source of tannin constituents. Recently, polyphenol production in adventitious roots of *C. capitata* was reported (Tanaka et al., 1997, 1998), and high concentrations of galloylglucoses accumulated in the presence of copper ions (Cu^{2+}) in the culture medium (Tanaka et al., 1998). In the course of those studies, a new ellagic acid derivative and two new iridoid glucosides were isolated from the cultures. This paper describes the characterization of the new constituents, together with related known compounds (ellagic compound and iridoids), isolated from the cultures.

* Corresponding author. Tel.: +81-0952-28-8753; fax: +81-0952-28-8753.
E-mail address: norie@cc.saga-u.ac.jp (N. Tanaka).

2. Results and discussion

2.1. Isolation of metabolites and characterization of known compounds

The aqueous acetone extract of the lyophilized adventitious roots of *C. capitata* cultured in MS medium containing 30 g/l maltose instead of sucrose, 3 mg/l IAA and 10 μM $CuSO_4$ was purified by column chromatography with Sephadex LH-20 and preparative C_{18} gel to afford compounds **1**–**6.** Compounds **2**, **5** and **6** were identified as an ellagic acid derivative, stenophyllin H1 (Nishimura, 1985), iridoid glucosides, dihydrocornin (Jensen et al., 1973a,b; Damtoft et al., 1981) and cornin (Miller, 1928; Jensen et al., 1980; Franzyk et al., 1998), respectively, by comparing their ^{1}H, ^{13}C NMR spectral data and the physical properties with those reported in the literature.

2.2. Characterization of new ellagic compound

Compound **1** was obtained as an off-white amorphous powder. Positive-ion fast atom bombardment mass spectroscopy (FAB–MS) of **1** gave a quasi-molecular ion peak at m/z 527 $[M+Na]^+$, which corresponded to

0031-9422/01/$ - see front matter © 2001 Elsevier Science Ltd. All rights reserved.
PII: S0031-9422(01)00179-0

the molecular formula of $C_{23}H_{20}O_{13}$. The ^1H NMR spectrum of **1** showed two aromatic protons at δ 7.73 (*s*) and δ 7.52 (*s*), and two methoxyl (δ 4.06 and δ 4.09) and one acetyl (δ 2.04) groups, together with six protons arising from a sugar moiety (Table 1). The ^{13}C NMR spectrum of **1** exhibited 12 signals (Table 2, C-1–6 and C-1′–6′) together with two carbonyl carbons at δ 158.4 and δ 158.5 due to α,β-unsaturated lactones, two methoxyl carbons (δ 60.8 and δ 61.5), one acetyl carbon (δ 20.6 and δ 170.3), and five sugar carbons (Table 2, C-1″–5″) whose chemical shifts were identical with those of arabinofuranose. The ^1H and ^{13}C NMR spectra suggested a di-*O*-methylellagic acid structure by comparison of their chemical shifts with those of a reference (Khac et al., 1989). The two methoxyl groups were concluded to be at C-3 and C-3′ positions by their low-field ^{13}C NMR chemical shifts (δ 60.8 and δ 61.5). The position of the arabinose moiety was also concluded to be at C-4 by the NOE spectrum observed between H-5 and arabinose anomeric protons (Fig. 1). The configuration of the anomeric carbon was concluded to be α from the *J*-value (1.5 Hz) in the ^1H NMR spectrum. The position of the acetyl group was also characterized to be at C-5″ by the analysis of the HMBC spectrum (Fig. 1). Therefore, **1** was identified as 3,3′-di-*O*-methylellagic acid 4-(5″-acetyl)-α-L-arabinofuranoside.

Table 1
^1H NMR spectral data of **1** and **2** (in DMSO-d_6[a], δ values)

H	1	2
5	7.73 (*s*)	7.76 (*s*)
8 (OCH_3)	4.09 (*s*)	4.09 (*s*)
5′	7.52 (*s*)	7.55 (*s*)
8′ (OCH_3)	4.06 (*s*)	4.06 (*s*)
Arabinose		
1″	5.68 (*d*, 1.5)	5.66 (*d*, 1.5)
2″	4.26 (*dd*, 1.5, 4)	4.24 (*dd*, 1.5, 4)
3″	3.88 (*dd*, 4, 6)	3.95 (*dd*, 4, 6)
4″	4.17 (*dt*, 3, 6, 7)	3.50 (*dt*, 3, 6, 5)
5″	4.12 (*dd*, 7, 11)	3.60 (*dd*, 7, 11)
	4.28 (*dd*, 3, 11)	3.85 (*dd*, 3, 11)
Ac	2.04 (*s*)	

[a] TMS was used as the internal standard. Coupling constants (*J* in Hz) in parentheses.

Table 2
^{13}C NMR spectral data of **1** and **2** (in DMSO-d_6, δ values)

C	1	2
1	111.6	111.7
2	140.8	140.5
3	142.1	142.1
4	150.3	150.7
5	112.1	112.7
6	114.4	114.2
7 (COO)	158.5	158.5
8 (OCH_3)	61.5	61.4
1′	110.4	111.2
2′	141.6	141.6
3′	140.4	140.4
4′	153.8	153.0
5′	111.9	111.8
6′	112.7	112.8
7′ (COO)	158.4	158.4
8′ (OCH_3)	60.8	61.0
Arabinose		
1″	107.6	107.5
2″	81.7	82.1
3″	77.0	76.5
4″	82.7	86.1
5″	63.6	61.0
CO	170.3	
CH_3	20.6	

2.3. Characterization of new iridoids

Compounds **3** and **4** were obtained as yellow amorphous powders, both exhibiting a $[M–H]^-$ ion peak at *m/z* 483 ($C_{16}H_{24}O_{10}$) upon negative FAB–MS. The ^1H (Table 3) and ^{13}C (Table 4) NMR spectra of **3** and **4** were almost identical to those of the iridoid glucoside, dihydrocornin (**5**) (Damtoft et al., 1981), except for the disappearance of the signal of the carboxyl methyl group (COOMe) which generally is observed in cornaceous iridoid derivatives. From the spectral data mentioned above, **3** and **4** were identified as epimeric constituents of C-6 dihydrocornic acid. The configuration at C-6 position of compounds **3** and **4** was supposed to be β and α, respectively, by the chemical shifts (δ 75.1 and δ 78.8) of C-6 in the ^{13}C NMR (Table 4) (Damtoft et al., 1981). This configuration was also supported by NOE correlations observed between H-5 and H-6 in **3** (Fig. 2), and H-5 and H-7α in **4** (Fig. 3), respectively. The configuration of the anomeric center of **3** and **4** was concluded to be β from the *J*-value (8 Hz) of the H-1′ signals (Table 3). Therefore, **3** and **4** were characterized as 6α-dihydrocornic acid and 6β-dihydrocornic acid, respectively. Although the existence of dihydrocornic acid, an intermediate in the biosynthetic pathway of iridoid metabolism, has been proposed (Bate-Smith et al., 1975), this is the first example of the isolation of dihydrocornic acid from plant material.

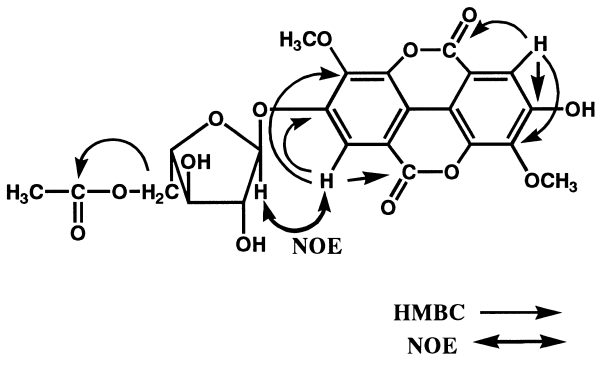

Fig. 1. HMBC and NOE correlation in **1**.

Table 3
^{1}H NMR spectral data of **3**, **4** and **5** (δ values)

H	**3**[a]	**4**[a]	**5**[b]
1	5.21 (*d*, 9)	5.25 (*d*, 5)	5.65 (*d*, 5)
3	7.62 (*s*)	7.41 (*s*)	7.95 (*s*)
5	2.82 (*dd*, 4, 9)	2.79 (*t*, 6)	3.28 (*m*)
6	4.47 (*t*, 4)	4.05 (*m*)	4.51 (*q*, 6)
7	1.38 (*ddd*, 4, 10, 13)	1.25 (*m*)	1.48 (*m*)
	1.92 (*dd*, 8, 13)	2.17 (*m*)	2.23 (*m*)
8	2.30 (*m*)	1.96 (*q*, 7)	2.10 (*q*, 7)
9	1.70 (*dt*, 4, 8)	2.03 (*dt*, 5, 6, 7)	2.34 (*m*)
10	1.12 (*d*, 8)	1.15 (*d*, 7)	1.03 (*d*, 7)
OCH_3	–	–	3.60 (*s*)
Glucopyranose			
1′	4.70 (*d*, 8)	4.65 (*d*, 8)	5.38 (*d*, 8)
2′	3.24 (*dd*, 8, 9)	3.20 (*t*, 8)	4.06 (*t*, 8)
3′	3.40 (*t*, 9)	3.37 (*m*)	4.28 (*t*, 8)
4′	3.31 (*m*)	3.37 (*m*)	4.26 (*t*, 8)
5′	3.29 (*m*)	3.30 (*m*)	4.00 (*m*)
6′	3.67 (*dd*, 6, 12)	3.67 (*dd*, 6, 12	4.37 (*dd*, 6, 12)
	3.86 (*dd*, 2, 12)	3.89 (*dd*, 2, 12)	4.54 (*dd*, 3, 12)

[a] In CD_3OD.
[b] In C_5D_5N. Coupling constants (J in Hz) in parentheses.

Table 4
^{13}C NMR spectral data of **3**, **4**, **5** and **6** (δ values)

C	**3**[a]	**4**[a]	**5**[b]
1	101.2	97.5	97.2
3	155.9	153.6	152.1
4	107.4	110.8	111.4
5	43.5	43.7	43.6
6	75.1	78.8	78.0
7	43.2	42.7	42.3
8	35.2	34.3	33.5
9	47.0	47.9	47.5
10	21.9	21.1	21.1
COO	171.1	171.0	171.6
OCH_3	–	–	49.6
Glucopyranose			
1′	100.4	100.2	100.8
2′	74.9	74.8	74.8
3′	78.1	78.1	78.5
4′	71.7	71.7	71.5
5′	78.5	78.4	78.8
6′	63.0	62.8	62.7

[a] In CD_3OD.
[b] In C_5D_5N.

3. Experimental

3.1. General

^{1}H and ^{13}C NMR spectral data were measured at 500 and 125 MHz, respectively. Column chromatography was performed on Sephadex LH-20 (Pharmacia Fine Chemical), MCI-gel CHP 20P (Mitsubishi Chemical Industries) and preparative C_{18} 125 Å (Waters) column-gels. TLC analysis was performed on silica-gel plates (Merck, Kieselgel 60F254), with the mobile solvent benzene–ethylformate–formic acid (1:7:1). Spots of compounds on TLC plates were visualized by exposure to UV (254 nm).

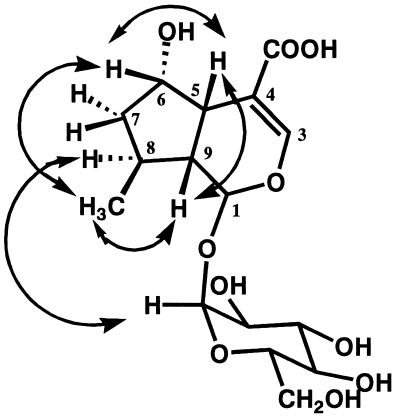
OH
COOH
H
H
H

was concentrated to approximately 60 ml in vacuo at 40°C and was subjected to column chromatogaraphy with Sephadex LH-20 (Pharmacia) using H_2O–MeOH (1:0–0:1) as the eluant to afford four fractions (Fr. 1–4). Fr. 1 was applied to Sephadex LH-20 and preparative C_{18} 125 Å, both using H_2O–MeOH (1:0–0:1) elution solvent, to afford three subfractions (Fr. 11–13). Fr. 11 was further re-applied to preparative C_{18} 125 Å (H_2O–MeOH, 1:0–17:3) and MCI-gel (H_2O–MeOH, 1:0–4:1) chromatography to afford compound **3** (51.4 mg) and subfraction Fr. 111. Fr. 111 was purified by preparative C_{18} 125 Å (H_2O–MeOH, 1:0–7:3) and Sephadex LH-20 (EtOH) to give compound **5** (30.2 mg) and **6** (17.2 mg). Fr. 2 was subjected to preparative C_{18} 125 Å (H_2O–MeOH, 1:0–1:0) to afford compound **4** (4.4 mg). Fr. 3 was applied to preparative C_{18} 125 Å (H_2O–MeOH, 1:0–1:0) and Sephadex LH-20 (EtOH) to give compounds **1** (12.0 mg) and **2** (8.8 mg).

*3.3.1. 3, 3′-di-O-Methylellagic acid 4-(5″-acetyl)-α-L-arabinofuranoside (**1**)*

An off-white amorphous powder, $[\alpha]_D^{28}$ −180.0° (DMSO; *c* 0.13); ^1H and ^{13}C NMR spectral data of **1**, see Tables 1 and 2; positive FABMS *m*/*z* (rel. int.); 527 $[M+Na]^+$ (12.8). (Found: C, 52.53; H, 4.01. $C_{23}H_{20}O_{13}$ H_2O requires: C, 52.87; H, 4.21%).

*3.3.2. Stenophyllin H-1(**2**)*

A yellow amorphous powder, $[\alpha]_D^{28}$ −72.2° (DMSO; *c* 0.09); ^1H and ^{13}C NMR spectral data of **2**, see Tables 1 and 2.

*3.3.3. 6α-Dihydrocornic acid (**3**)*

A yellow amorphous powder, $[\alpha]_D^{28}$ −67.9° (MeOH; *c* 1.34); ^1H and ^{13}C NMR spectral data of **3**, see Tables 3 and 4. Negative FABMS *m*/*z* (rel. int.); 375 $[M-H]^-$ (27.8). (Found: C, 48.59; H, 6.32. $C_{16}H_{24}O_{10}$ H_2O requires: C, 48.73; H, 6.60%).

*3.3.4. 6β-Dihydrocornic acid (**4**)*

A yellow amorphous powder, $[\alpha]_D^{28}$ −271.6° (MeOH; *c* 0.18); ^1H and ^{13}C NMR spectral data of **4**, see Tables 3 and 4. Negative FABMS *m*/*z* (rel. int.); 375 $[M-H]^-$ (27.8). (Found: C, 48.62; H, 6.48. $C_{16}H_{24}O_{10}$ H_2O requires: C, 48.73; H, 6.60%).

*3.3.5. Dihydrocornin (**5**)*

A yellow amorphous powder, $[\alpha]_D^{28}$ −134.0° (MeOH; *c* 0.21); ^1H and ^{13}C NMR spectral data of **5**, see Tables 3 and 4.

*3.3.6. Cornin (**6**)*

An off-white amorphous powder; ^1H NMR (CD_3OD): δ 1.22 (*d*, *J* = 6.7 Hz, H-10), 1.98 (*m*, H-7b), 2.19 (*dt*, *J* = 7.8, 3.0 and 3.8 Hz, H-9), 2.51 (*m*, H-7a), 2.60 (*m*, H-8), 3.51 (*m*, H-5), 3.68–3.62 (*m*, 4H, H-2′, H-3′, H-4′, H-5′), 3.72 (*s*, 11-OCH_3), 3.87 (*m*, H-6b′), 3.91 (*m*, H-6a′), 4.65 (*d*, *J* = 7.8 Hz, H-1′), 5.25 (*d*, *J* = 6.8 Hz, H-1), 7.46 (*s*, H-3); ^{13}C NMR (CD_3OD) : δ 20.57 (C-10), 29.90 (C-8), 43.56 (C-7), 43.72 (C-5), 45.54 (C-9), 51.94 (OCH_3), 62.76 (C-6′), 71.59 (C-4′), 74.67 (C-2′), 77.98 (C-3′), 78.38 (C-5′), 97.10 (C-1), 100.60 (C-1′), 105.52 (C-4), 153.77 (C-3), 168.82 (COO), 215.74 (C-6).

Acknowledgements

This work was supported by research fellowships of the Japan Society for the Promotion of Science for young scientists.

References

Bate-Smith, E.C., Ferguson, I.K., Hutson, K., Jensen, S.R., Nielsen, B.J., Swan, T., 1975. Phytochemical interrelationships in the Cornaceae. Biochem. Syst. Ecol. 3, 79–89.

Damtoft, S., Jensen, S.R., Kjaer, A., Nielsen, B.J., 1981. ^{13}C and ^1H NMR spectroscopy as a tool in the configuration analysis of iridoid glucosides. Phytochemistry 20, 2717.

Franzyk, H., Jensen, S.R., Stermitz, F.R., 1998. Iridoid glucosides from *Penstemon secundiflorus* and *P. grandiflorus*: revised structure of 10-hydroxy-8-epihastatoside. Phytochemistry 49, 2025–2030.

Hatano, T., Ogawa, N., Kira, R., Yasuhara, T., Okuda, T., 1989a. Tannins of cornaceous plants I. Cornusiins A, B and C, dimeric, monomeric and trimeric hydrolyzable tannins from *Cornus officinalis*, and orientation of valoneoyl group in related tarinins. Chem. Pharm. Bull. 37, 2083–2090.

Hatano, T., Yasuhara, T., Abe, R., Okuda, T., 1990. A galloylated monoterpene glucoside and a dimeric hydrolysable tannin from *Cornus officinalis*. Phytochemistry 29, 2975–2978.

Hatano, T., Yasuhara, T., Okuda, T., 1989b. Tannins of cornaceous plants II. Cornusiins D, E and F, new dimeric and trimeric hydrolyzable tannins from *Cornus officinalis*. Chem. Pharm. Bull. 37, 2665–2669.

Jensen, S.R., Kjaer, A., Nielsen, J., 1973a. Glucosides in *Cornus capitata* and *C. kousa*. Phytochemistry 12, 2301.

Jensen, S.R., Kjear, A., Nielsen, J., 1973b. Dihydrocornin, a novel natural iridoid glucoside. Acta Chem. Scand. 27, 2581–2585.

Jensen, S.R., Kjaer, A., Nielsen, B.J., 1975. The genus *Cornus*: nonflavonoid glucosides as taxonomic markers. Biochem. Syst. Ecol. 3, 75–78.

Jensen, S.R., Kjaer, A., Nielsen, B.J., 1980. Iridoid glucosides in *Griselinia*, *Aralidium* and *Toricellia*. Phytochemistry 19, 2685–2688.

Khac, D.D., Tran-Van, S., Campos, A.M., Lallemand, J.Y., Fetizon, M., 1990. Ellagic compounds from *Diplopanax stachyanthus*. Phytochemistry 29, 251–256.

Lee, S.H., Tanaka, T., Nonaka, G., Nishioka, I., 1989. Sedoheptulose digallate from *Cornus officinalis*. Phytochemistry 28, 3469–3472.

Lloyd, G., McCown, B., 1980. Commercially-feasible micropropagation of mountain laurel, *Kalmia latifolia*, by use of shoot-tip culture. Int. Plant Prop. Soc. 30, 421–427.

Miller, E.R., 1928. Cornin: a glucoside from *Cornus florida* L. J. Am. Pharm. Assoc. 17, 744–750.

Nishimura, H., 1985. Phytochemical study on tannins and related compounds of *Quercus stenophylla*. Doctoral thesis, Kyushu University, p. 80.

Nishino, C., Kobayashi, K., Fukushima, M., 1988. Halleridone, a cytotoxic constituent from *Crunus controversa*. J. Nat. Prod. 51, 1281–1282.

Okuda, T., Hatano, T., Ogawa, N., Kira, R., Matsuda, M., 1984. Cornusiin A, a dimeric ellagitannin forming four tautomers, and accompanying tannins in *Cornus officinalis*. Chem. Pharm. Bull. 32, 4662–4665.

Stermitz, F.R., Krull, R.E., 1998. Iridoid glycosides of *Cornus canadensis*: a comparison with some other *Cornus* species. Biochem. Syst. Ecol. 26, 845–849.

Tanaka, N., Shimomura, K., Kamiya, T., Kayano, T., Ishimaru, K., 1997. Tannin and related compounds in callus and root cultures of *Cornus capitata*. Plant Biotechnol. 14, 59–62.

Tanaka, N., Kamiya, T., Shimomura, K., Ishimaru, K., 1998. Polyphenols in adventitious root cultures of *Cornus capitata*. Nat. Med. 52, 510–517.

Tanaka, N., Shimomura, K., Ishimaru, K., 1999. Antioxidative and radical scavenging activities of *Cornus capitata* adventitious roots. Jpn. J. Food Chem. 6, 48–52.

Phytochemistry, 2001, **57**, 149

Inhibition of polygalacturonase from *Verticillium dahliae* by a polygalacturonase inhibiting protein from cotton

Jacinda T. James, Ian A. Dubery

Department of Chemistry and Biochemistry, Rand Afrikaans University, PO Box 524, Auckland Park, 2006, South Africa

The inhibition of *Verticillium dahliae* extracellular endo-PGase by salicylic acid-induced PGIP purified from cotton, is reported.

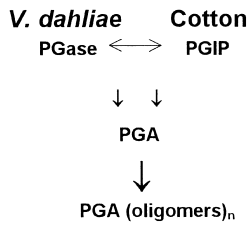

Phytochemistry, 2001, **57**, 157

Cell-wall proteins from Sitka spruce xylem are selectively insolubilised during formation of dehydrogenation polymers of coniferyl alcohol

Gordon J. McDougall

Unit of Plant Biochemistry, Biochemistry and Cell Biology Division, Scottish Crop Research Institute, Invergowrie, Dundee DD2 5DA, Scotland, UK

Extracts from Sitka spruce xylem that are enriched in cell-wall proteins readily produce dehydrogenation polymers from coniferyl alcohol and hydrogen peroxide. Certain polypeptides are insolubilised with the DHPs. The mechanism and selectivity of their insolubilisation is discussed.

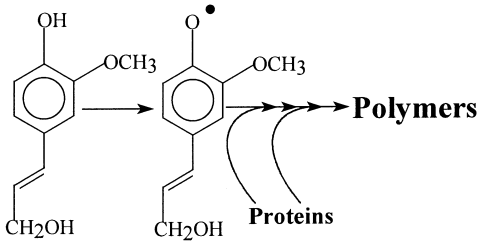

Phytochemistry, 2001, **57**, 165

Biosynthesis of diaporthin and orthosporin by *Aspergillus ochraceus*

Jonathan P. Harris, Peter G. Mantle

Biochemistry Department, Imperial College of Science, Technology and Medicine, London SW7 2AY, UK

Co-occurrence of diaporthin (**1**) and orthosporin (**2**) as growth-associated metabolites of an isolate of *Aspergillus ochraceus* in submerged fermentation facilitated radiochemical demonstration of the biosynthesis of diaporthin from acetate and methionine-derived *O*-methylation of orthosporin. In contrast to diaporthin, orthosporin occurring in fermentation broth was affected by the methylation inhibitor ethionine, implying that it arose by de-*O*-methylation of diaporthin.

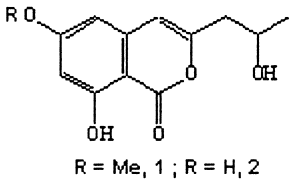

R = Me, 1 ; R = H, 2

Phytochemistry, 2001, **57**, 171

Accumulation of 6-deoxocathasterone and 6-deoxocastasterone in *Arabidopsis*, pea and tomato is suggestive of common rate-limiting steps in brassinosteroid biosynthesis

Takahito Nomura[a], Tatsuro Sato[b], Gerard J. Bishop[c], Yuji Kamiya[d], Suguru Takatsuto[e], Takao Yokota[a]

[a]*Department of Biosciences, Teikyo University, Utsunomiya 320-8551, Japan*
[b]*Center for Research on Wild Plants, Utsunomiya University, Utsunomiya 321-8505, Japan*
[c]*Institute of Biological Sciences, University of Wales Aberystwyth, Aberystwyth SY23 3DD, UK*
[d]*The Institute of Physical and Chemical Research (RIKEN), Wako-shi, Saitama 351-0198, Japan*
[e]*Department of Chemistry, Joetsu University of Education, Joetsu-shi, Niigata 943-8512, Japan*

In *Arabidopsis* seedlings, pea shoots and tomato shoots, brassinosteroids in the late C-6 oxidation pathway were predominant and high levels of 6-deoxocastasterone and 6 deoxocastasterone were commonly observed. Based on these findings, biosynthetic control points are discussed.

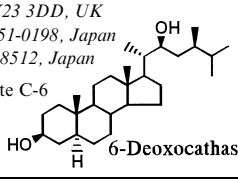

6-Deoxocathasterone

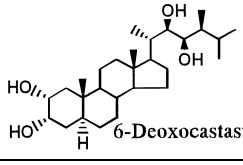

6-Deoxocastasterone

Phytochemistry, 2001, **57**, 179

Metabolism of indole-3-acetic acid by orange (*Citrus sinensis*) flavedo tissue during fruit development

Jesús Chamarro[a], Anders Östin[b], Göran Sandberg[b]

[a]*Instituto de Biología Molecular y Celular de Plantas, UPV-CSIC, Avda. de los Naranjos, s/n, 46022, Valencia, Spain*
[b]*Department of Forest Genetics and Plant Physiology, The Swedish University of Agricultural Sciences, S901 83, Umeå, Sweden*

The metabolism of indole-3-acetic acid by orange flavedo tissue is studied, in relation to the homeostatic control of the levels of this PGR, at different stages of fruit development. The main metabolites have been positively identified.

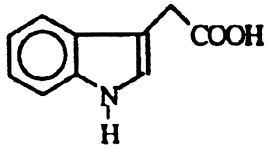

indole-3-acetic acid

Phytochemistry, 2001, **57**, 189

The uptake and speciation of various Al species in the *Brassica rapa pekinensis*

Tjaša Bantan Polak[a], Radmila Milačič[a], Boris Pihlar[b], Bojan Mitrović[c]

[a]*Department of Environmental Sciences, Jožef Stefan Institute, Jamova 39, 1000 Ljubljana, Slovenia*
[b]*Faculty of Chemistry and Chemical Technology, University of Ljubljana, Aškerčeva 5, 1000 Ljubljana, Slovenia*
[c]*Lek Pharmaceutical and Chemical Company d.d., Celovška 135, 1000 Ljubljana, Slovenia*

Uptake and speciation of Al was investigated in the *Brassica rapa pekinensis*. Speciation analysis indicated that Al^{3+} added to the nutrient solution was not transformed in the growth media, but in the roots transformation to Al-malate occurred. Al was transported from roots to the upper parts of the plant as Al-malate (70%) and Al^{3+} (30%). Al-citrate or Al-malate added to the nutrient solution were transferred to the upper parts of the plant without transformation of their chemical forms.

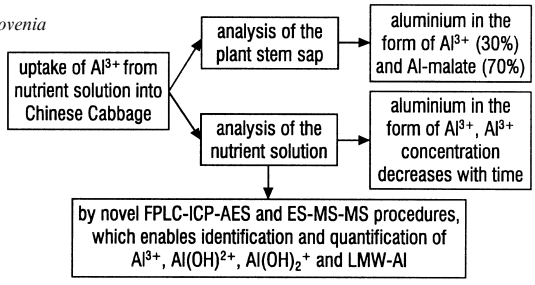

Phytochemistry, 2001, **57**, 199

Biotransformation of (*R*)-(+)- and (*S*)-(−)-limonene by fungi and the use of solid phase microextraction for screening

Jan C.R. Demyttenaere, Kristof Van Belleghem, Norbert De Kimpe

Department of Organic Chemistry, Faculty of Agricultural and Applied Biological Sciences, Ghent University, Coupure Links 653, B-9000 Ghent, Belgium

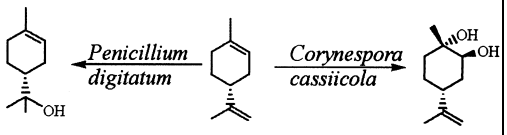

The biotransformation of (*R*)-(+)- and (*S*)-(−)-limonene by fungi was studied. (*R*)-(+)- and (*S*)-(−)-limonene were converted to (*R*)-(+)- and (*S*)-(−)-α-terpineol resp., by *Penicillium digitatum*, and to (1*S*,2*S*,4*R*)- and (1*R*,2*R*,4*S*)-*trans*-limonene-1,2-diol resp., by *Corynespora cassiicola*. Solid phase microextraction was used as screening and monitoring technique for bioconversion experiments.

Phytochemistry, 2001, **57**, 209

Comprehensive chemical profiling of gramineous plant root exudates using high-resolution NMR and MS

Teresa W.-M. Fan[a], Andrew N. Lane[b], Moshe Shenker[c], John P. Bartley[d], David Crowley[e], Richard M. Higashi[f]

[a]*Department of Land, Air and Water Resources, University of California, One Shields Avenue, Davis, CA 95616, USA*
[b]*Division of Molecular Structure, National Institute for Medical Research, Mill Hill, London NW71AA, UK*
[c]*Department of Soil and Water Sciences, Faculty of Agricultural, Food and Environmental Quality Sciences, The Hebrew University of Jerusalem, Rehovot 76-100, Israel*
[d]*School of Physical Sciences, Queensland University of Technology, GPO Box 2434, Brisbane 4001, Queensland, Australia*
[e]*Department of Soil and Environmental Sciences, University of California, Riverside, CA 92521-0424, USA*
[f]*Crocker Nuclear Laboratory, University of California, One Shields Avenue, Davis, CA 95616, USA*

Metal ion ligands in root exudates of different plant types were examined using multinuclear 2-D NMR and high-resolution MS. Uptake of nutrient transition metals was related to the mugineic acid phytosiderophores while uptake of pollutant Cd appeared to be mediated by a different mechanism.

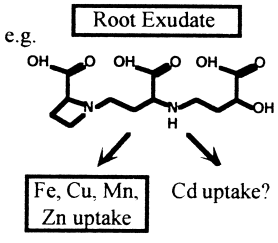

Phytochemistry, 2001, **57**, 223

Phytoalexins from *Pinus strobus* bark infected with pinewood nematode, *Bursaphelenchus xylophilus*

Fujinori Hanawa, Toshihiro Yamada, Tadakazu Nakashima

Forestry and Forest Products Research Institute (FFPRI), PO Box 16, Tsukuba, Ibaraki 305-8687, Japan

From the bark of *Pinus strobus* infected with pinewood nematode, 3-*O*-methyldihydropinosylvin (**1**) and (2*S*)-pinocembrin (**2**) were isolated as inducibly produced antimicrobial compounds. Compound **1** was proved to be nematocidal and time course accumulation of **1** and **2** were analyzed.

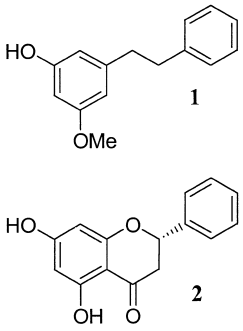

Phytochemistry, 2001, **57**, 229

Synergism between the potato glycoalkaloids α-chaconine and α-solanine in inhibition of snail feeding

David B. Smith[a], James G. Roddick[a], J. Leighton Jones[b]

[a]*School of Biological Sciences, University of Exeter, Washington Singer Laboratories, Perry Road, Exeter EX4 4QG, UK*
[b]*Campden and Chorleywood Food Research Association, Chipping Campden, GL55 6LD, UK*

The potato glycoalkaloids, solanine and chaconine, individually deterred feeding by the snail, *Helix aspersa*, with chaconine being the more active. In combination the two glycoalkaloids produced a synergistic effect. Antifeedant activities of extracts of tuber peel from three potato varieties were compared with equivalent authentic glycoalkaloid solutions.

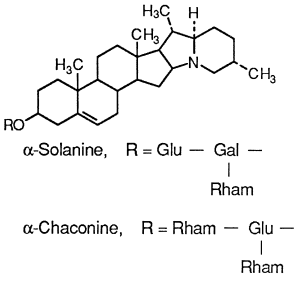

Phytochemistry, 2001, **57**, 235

A chemotaxonomic investigation of volatile constituents in *Stachys* subsect. Swainsonianeae (Labiatae)

Helen D. Skaltsa[a], Anna Mavrommati[a], Theophanis Constantinidis[b]

[a]*Division of Pharmacognosy, School of Pharmacy, University of Athens, Panepistimiopolis, Zografou, GR-157 71, Athens, Greece*
[b]*Botanical Institute, Department of Biology, University of Patras, GR-265 00, Patras, Greece*

The composition of the previously unknown essential oils of *Stachys* subsect. Swainsonianeae (Labiatae) are investigated by GC–MS analyses. Eighteen populations were analyzed and more than two hundred components were identified. The results are subject to statistical analyses and discussed in relation to the taxonomy of the subsection.

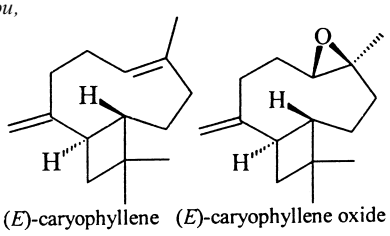

Phytochemistry, 2001, **57**, 245

Essential oils from Azorean *Laurus azorica*

Luis G. Pedro[a], Pedro A.G. Santos[a], Jaime A. da Silva[a], A. Cristina Figueiredo[a], José G. Barroso[a], Stanley G. Deans[b], Anja Looman[c], Johannes J.C. Scheffer[c]

[a]*Centro de Biotecnologia Vegetal, Departamento de Biologia Vegetal, Faculdade de Ciências de Lisboa, Bloco C2, Campo Grande, 1749-016 Lisbon, Portugal*
[b]*Department of Food Science and Technology, SAC, Auchincruive, Ayr KA6 5HW, Scotland, UK*
[c]*Division of Pharmacognosy, LACDR, Leiden University, Gorlaeus Laboratories, PO Box 9502, 2300 RA Leiden, The Netherlands*

The essential oils isolated from the leaves of ten and from unripe berries of eight populations of *Laurus azorica* (Seub.) Franco, collected on five islands of the Azorean archipelago, were analyzed. Cluster analysis of the enantiomeric composition of α- and β-pinene in the leaf oils clearly showed two groups.

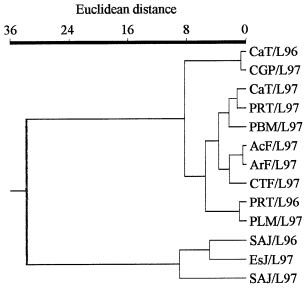

Phytochemistry, 2001, **57**, 251

Cyclolinopeptides F–I, cyclic peptides from linseed

Teruki Matsumoto, Akira Shishido, Hiroshi Morita, Hideji Itokawa, Koichi Takeya

School of Pharmacy, Tokyo University of Pharmacy and Life Science, 1432-1 Horinouchi, Hachioji, Tokyo 192-0392, Japan

Four cyclic peptides, cyclolinopeptides F–I, have been isolated from the seeds of *Linum usitatissimum*.

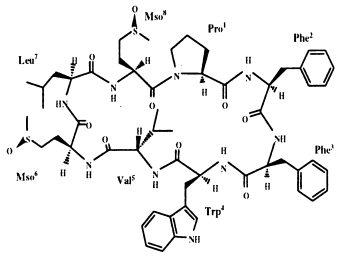

Structure of cyclolinopeptide F (1)

Phytochemistry, 2001, **57**, 261

Jesterone and hydroxy-jesterone antioomycete cyclohexenone epoxides from the endophytic fungus *Pestalotiopsis jesteri*

J.Y. Li, Gary A. Strobel

Department of Plant Sciences, Montana State University, Bozeman, MT, 59717, USA

Jesterone and hydroxy-jesterone are antifungal metabolites from an endophytic fungus.

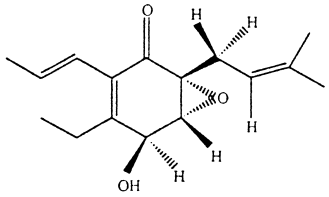

Phytochemistry, 2001, **57**, 267

Sesquiterpene lactones and a myoinositol from glandular trichomes of *Viguiera quinqueremis* (Heliantheae; Asteraceae)

Otmar Spring[a], Reinhard Zipper[a], Sabine Reeb[b], Bernhard Vogler[b], Fernando B. Da Costa[c]

[a]*Institut für Botanik, Universität Hohenheim, D-70599 Stuttgart, Germany*
[b]*Institut für Chemie, Universität Hohenheim, D-70599 Stuttgart, Germany*
[c]*Faculdade de Ciências Farmacêuticas de Ribeirão Preto, Universidade de São Paulo, Av. do Café s/n°, 14040-903, Ribeirão Preto, SP, Brazil*

HPLC analysis and LC NMR experiments revealed the occurrence of 15 germacranolides and a myoinositol derivative in glandular trichome extracts of *Viguiera quinqueremis*. Their structures were determined by spectral analysis.

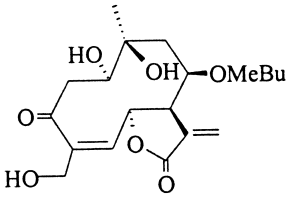

Phytochemistry, 2001, **57**, 273

Benzopyran derivatives from *Mallotus apelta*

Tian-Ying An, Li-Hong Hu, Xiao-Fang Cheng, Zhong-Liang Chen

National Center for Drug Screening, Shanghai Institute of Materia Medica, Shanghai Institutes for Biological Sciences, Chinese Academy of Sciences, Shanghai, 200031, People's Republic of China

Benzopyran compounds were obtained from the leaves of *Mallotus apelta*. One showed moderate antibiotic activity against *Micrococcus lutens*.

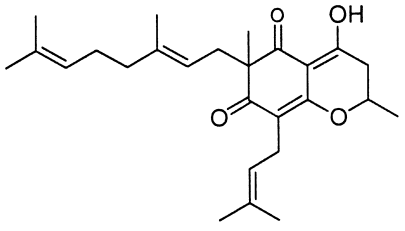

Phytochemistry, 2001, **57**, 279

Nemorosone, the major constituent of floral resins of *Clusia rosea*

Osmany Cuesta-Rubio[a], Herman Velez-Castro[b], Bernardo A. Frontana-Uribe[c], Jorge Cárdenas[c]

[a]*Instituto de Farmacia y Alimentos, Universidad de la Habana, Ave. 23 No. 21425, Lisa, C. Habana, 13600, Cuba*
[b]*Centro de Química Farmacéutica, Calle 200 esq. 21, C. Habana, 13600, Cuba*
[c]*Instituto de Química, Universidad Nacional Autónoma de México, Circuito Exterior, Ciudad Universitaria, Coyoacán C.P. 04510, México DF*

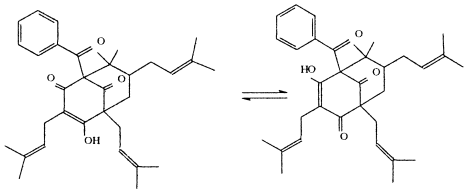

Nemorosone, the major constituent of the floral resin of *Clusia rosea* was isolated after exhaustive chromatography. A keto–enol equilibrium can be observed in this product. The previously announced structure for methyl-nemorosone was corrected on the basis of high field 2D NMR spectroscopic techniques and NOE difference spectroscopy experiments.

Phytochemistry, 2001, **57**, 285

Minor constituents of *Spigelia anthelmia* and their cardiac activities

Harald Hübner[a], Wolfgang Vierling[b], Wolfgang Brandt[b], Melchior Reiter[b], Hans Achenbach[a]

[a]*Department of Pharmaceutical Chemistry, University of Erlangen, D-91052 Erlangen, Germany*
[b]*Institute of Pharmacology and Toxicology, Technical University, D-80802 München, Germany*

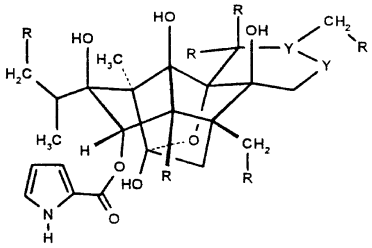

The isolation and structure elucidation of 20 spiganthine and ryanodine like compounds from the aerial parts of *Spigelia anthelmia* L. is reported. Their cardiac and insect antifeedant activities are discussed.

Phytochemistry, 2001, **57**, 297

Flavonoid glucuronides from *Helicteres isora*

Kohei Kamiya[a,b], Yasuhisa Saiki[a], Takao Hama[a], Yasuo Fujimoto[c], Hanani Endang[d], Mansur Umar[d], Toshiko Satake[a,b]

[a]*Faculty of Pharmaceutical Sciences, Kobe Gakuin University, Nishi-ku, Kobe 651-2180, Japan*
[b]*High Technology Research Center, Kobe Gakuin University, Nishi-ku, Kobe 651-2180, Japan*
[c]*College of Pharmacy, Nihon University, 7-7-1, Narashinodai, Funabashi, Chiba 274-8555, Japan*
[d]*Department of Pharmacy, Faculty of Mathematics and Natural Sciences, University of Indonesia, Depok-Jawa Barat, Indonesia*

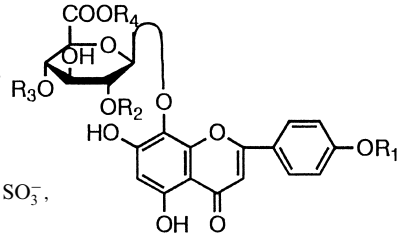

Five flavonoid glucuronides (**1**–**5**) were isolated from the fruit of *Helicteres isora*. These structures were determined by spectroscopic methods and chemical evidence. **1**: $R_1 = CH_3$, $R_2 = R_3 = R_4 = H$; **2**: $R_1 = CH_3$, $R_2 = R_3 = H$, $R_4 = n$–Bu; **3**: $R_1 = CH_3$, $R_2 = SO_3^-$, $R_3 = R_4 = H$; **4**: $R_1 = CH_3$, $R_2 = R_3 = SO_3^-$, $R_4 = H$; **5**: $R_1 = H$, $R_2 = R_3 = SO_3^-$, $R_4 = H$

Phytochemistry, 2001, **57**, 303

Rapid detection of chlorinated bisbibenzyls in *Bazzania trilobata* using MALDI-TOF mass spectrometry

Andreas Speicher[a], Klaus Hollemeyer[b], Elmar Heinzle[b]

[a]*Institut für Organische Chemie, Universität des Saarlandes, PO Box 151150, 66041 Saarbrücken, Germany*
[b]*Institut für Technische Biochemie, Universität des Saarlandes, PO Box 151150, 66041 Saarbrücken, Germany*

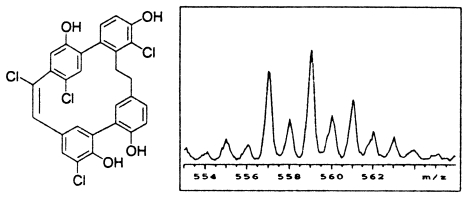

Chlorinated bisbibenzyls of the isoplagiochin C/D type are detected in crude bryophyte plant extracts of *Bazzania trilobata* from different locations using MALDI-TOF mass spectrometry.

Phytochemistry, 2001, **57**, 307

Pacifigorgianes and tamariscene as constituents of *Frullania tamarisci* and *Valeriana officinalis*

Claudia Paul[a], Wilfried A. König[a], Hermann Muhle[b]

[a]*Institut für Organische Chemie, Universität Hamburg, Martin-Luther-King-Platz 6, D-20146 Hamburg, Germany*
[b]*Abteilung Spezielle Botanik, Universität Ulm, D-89091 Ulm, Germany*

Several sesquiterpenes were isolated from liverworts and the angiosperm investigated.